

Wireless Communications and Mobile Computing

Machine Learning for Energy Efficient Wireless Communications and Mobile Computing

Lead Guest Editor: Alireza Souri

Guest Editors: Mu-Yen Chen and Nima Jafari Navimipour





Machine Learning for Energy Efficient Wireless Communications and Mobile Computing

Wireless Communications and Mobile Computing

Machine Learning for Energy Efficient Wireless Communications and Mobile Computing

Lead Guest Editor: Alireza Souri


Guest Editors: Mu-Yen Chen and Nima Jafari
Navimipour



Copyright © 2023 Hindawi Limited. All rights reserved.

This is a special issue published in “Wireless Communications and Mobile Computing.” All articles are open access articles distributed under the Creative Commons Attribution License, which permits unrestricted use, distribution, and reproduction in any medium, provided the original work is properly cited.

Chief Editor






















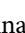

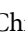


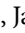





Zhipeng Cai , USA

Associate Editors

Ke Guan , China
Jaime Lloret , Spain
Maode Ma , Singapore

Academic Editors

Muhammad Inam Abbasi, Malaysia
Ghufran Ahmed , Pakistan
Hamza Mohammed Ridha Al-Khafaji ,
Iraq
Abdullah Alamoodi , Malaysia
Marica Amadeo, Italy
Sandhya Aneja, USA
Mohd Dilshad Ansari, India
Eva Antonino-Daviu , Spain
Mehmet Emin Aydin, United Kingdom
Parameshchhari B. D. , India
Kalapraveen Bagadi , India
Ashish Bagwari , India
Dr. Abdul Basit , Pakistan
Alessandro Bazzi , Italy
Zdenek Becvar , Czech Republic
Nabil Benamar , Morocco
Olivier Berder, France
Petros S. Bithas, Greece
Dario Bruneo , Italy
Jun Cai, Canada
Xuesong Cai, Denmark
Gerardo Canfora , Italy
Rolando Carrasco, United Kingdom
Vicente Casares-Giner , Spain
Brijesh Chaurasia, India
Lin Chen , France
Xianfu Chen , Finland
Hui Cheng , United Kingdom
Hsin-Hung Cho, Taiwan
Ernestina Cianca , Italy
Marta Cimitile , Italy
Riccardo Colella , Italy
Mario Collotta , Italy
Massimo Condoluci , Sweden
Antonino Crivello , Italy
Antonio De Domenico , France
Floriano De Rango , Italy

Antonio De la Oliva , Spain
Margot Deruyck, Belgium
Liang Dong , USA
Praveen Kumar Donta, Austria
Zhuojun Duan, USA
Mohammed El-Hajjar , United Kingdom
Oscar Esparza , Spain
Maria Fazio , Italy
Mauro Femminella , Italy
Manuel Fernandez-Veiga , Spain
Gianluigi Ferrari , Italy
Luca Foschini , Italy
Alexandros G. Fragkiadakis , Greece
Ivan Ganchev , Bulgaria
Óscar García, Spain
Manuel García Sánchez , Spain
L. J. García Villalba , Spain
Miguel Garcia-Pineda , Spain
Piedad Garrido , Spain
Michele Girolami, Italy
Mariusz Glabowski , Poland
Carles Gomez , Spain
Antonio Guerrieri , Italy
Barbara Guidi , Italy
Rami Hamdi, Qatar
Tao Han, USA
Sherief Hashima , Egypt
Mahmoud Hassaballah , Egypt
Yejun He , China
Yixin He, China
Andrej Hrovat , Slovenia
Chunqiang Hu , China
Xuexian Hu , China
Zhenghua Huang , China
Xiaohong Jiang , Japan
Vicente Julian , Spain
Rajesh Kaluri , India
Dimitrios Katsaros, Greece
Muhammad Asghar Khan, Pakistan
Rahim Khan , Pakistan
Ahmed Khattab, Egypt
Hasan Ali Khattak, Pakistan
Mario Kolberg , United Kingdom
Meet Kumari, India
Wen-Cheng Lai , Taiwan

Jose M. Lanza-Gutierrez, Spain
Pavlos I. Lazaridis , United Kingdom
Kim-Hung Le , Vietnam
Tuan Anh Le , United Kingdom
Xianfu Lei, China
Jianfeng Li , China
Xiangxue Li , China
Yaguang Lin , China
Zhi Lin , China
Liu Liu , China
Mingqian Liu , China
Zhi Liu, Japan
Miguel López-Benítez , United Kingdom
Chuanwen Luo , China
Lu Lv, China
Basem M. ElHalawany , Egypt
Imadeldin Mahgoub , USA
Rajesh Manoharan , India
Davide Mattera , Italy
Michael McGuire , Canada
Weizhi Meng , Denmark
Klaus Moessner , United Kingdom
Simone Morosi , Italy
Amrit Mukherjee, Czech Republic
Shahid Mumtaz , Portugal
Giovanni Nardini , Italy
Tuan M. Nguyen , Vietnam
Petros Nicolitidis , Greece
Rajendran Parthiban , Malaysia
Giovanni Pau , Italy
Matteo Petracca , Italy
Marco Picone , Italy
Daniele Pinchera , Italy
Giuseppe Piro , Italy
Javier Prieto , Spain
Umair Rafique, Finland
Maheswar Rajagopal , India
Sujan Rajbhandari , United Kingdom
Rajib Rana, Australia
Luca Reggiani , Italy
Daniel G. Reina , Spain
Bo Rong , Canada
Mangal Sain , Republic of Korea
Praneet Saurabh , India

Hans Schotten, Germany
Patrick Seeling , USA
Muhammad Shafiq , China
Zaffar Ahmed Shaikh , Pakistan
Vishal Sharma , United Kingdom
Kaize Shi , Australia
Chakchai So-In, Thailand
Enrique Stevens-Navarro , Mexico
Sangeetha Subbaraj , India
Tien-Wen Sung, Taiwan
Suhua Tang , Japan
Pan Tang , China
Pierre-Martin Tardif , Canada
Sreenath Reddy Thummaluru, India
Tran Trung Duy , Vietnam
Fan-Hsun Tseng, Taiwan
S Velliangiri , India
Quoc-Tuan Vien , United Kingdom
Enrico M. Vitucci , Italy
Shaohua Wan , China
Dawei Wang, China
Huaqun Wang , China
Pengfei Wang , China
Dapeng Wu , China
Huaming Wu , China
Ding Xu , China
YAN YAO , China
Jie Yang, USA
Long Yang , China
Qiang Ye , Canada
Changyan Yi , China
Ya-Ju Yu , Taiwan
Marat V. Yuldashev , Finland
Sherali Zeadally, USA
Hong-Hai Zhang, USA
Jiliang Zhang, China
Lei Zhang, Spain
Wence Zhang , China
Yushu Zhang, China
Kechen Zheng, China
Fuhui Zhou , USA
Meiling Zhu, United Kingdom
Zhengyu Zhu , China

Contents

Retracted: SM-PageRank Algorithm-Based User Interest Model for Mobile Smart Tourism Platform

Wireless Communications and Mobile Computing

Retraction (1 page), Article ID 9850362, Volume 2023 (2023)

Retracted: Design and Implementation of Node of Wireless Network Environment Monitoring System Based on Artificial Intelligence

Wireless Communications and Mobile Computing


Retraction (1 page), Article ID 9757606, Volume 2023 (2023)

Retracted: Research on Automobile Assembly Line Optimization Based on Industrial Engineering Technology and Machine Learning Algorithm

Wireless Communications and Mobile Computing


Retraction (1 page), Article ID 9890274, Volume 2023 (2023)

ML-DDoSnet: IoT Intrusion Detection Based on Denial-of-Service Attacks Using Machine Learning Methods and NSL-KDD

Mona Esmaeili, Seyedamiryousef Hosseini Goki, Behnam Hajipour Khire Masjidi, Mahdi Sameh, Hamid Gharagozlou , and Amin Salih Mohammed

Research Article (16 pages), Article ID 8481452, Volume 2022 (2022)

Design of Shared Internet of Things System for English Translation Teaching Using Deep Learning Text Classification

Lin He, Jiaqi Guo, and Jiaxin Lin 

Research Article (10 pages), Article ID 3576419, Volume 2022 (2022)

Blockchain-Based Crowdsourcing Makes Training Dataset of Machine Learning No Longer Be in Short Supply

Haitao Xu , Wei Wei , Yong Qi , and Saiyu Qi 


Review Article (13 pages), Article ID 7033626, Volume 2022 (2022)

Application of Kohonen Neural Network in Sports Cluster

Youwen Mao 



Research Article (11 pages), Article ID 2266702, Volume 2022 (2022)

Sports Video Motion Direction Detection and Target Tracking Algorithm Based on Convolutional Neural Network

Long Liu 


Research Article (10 pages), Article ID 5760758, Volume 2022 (2022)

Inventory Management Optimization of Green Supply Chain Using IPSO-BPNN Algorithm under the Artificial Intelligence

Ying Guan , Yingli Huang , and Huiyan Qin


Research Article (14 pages), Article ID 8428964, Volume 2022 (2022)

Interaction Design of Wellness Building Space by Deep Learning and VR Technology in the Context of Internet of Things

Mei Yang  and Xinyu Wang


Research Article (10 pages), Article ID 6567431, Volume 2022 (2022)

The Influence of Robot-Assisted Industry Using Deep Learning on the Economic Growth Rate of Manufacturing Industry in the Era of Artificial Intelligence

Ziyu Xu 

Research Article (12 pages), Article ID 4594858, Volume 2022 (2022)

Constructing a Music Network Teaching System by Using Neural Network Model with Wireless Audio Transmission

Weiming Liu 



Research Article (11 pages), Article ID 2805117, Volume 2022 (2022)

ObjectDetect: A Real-Time Object Detection Framework for Advanced Driver Assistant Systems Using YOLOv5

Jamuna S. Murthy, G. M. Siddesh, Wen-Cheng Lai , B. D. Parameshachari , Sujata N. Patil, and K. L. Hemalatha


Research Article (10 pages), Article ID 9444360, Volume 2022 (2022)

Mobile Sink-Based Path Optimization Strategy in Heterogeneous WSNs for IoT Using Pigeon-Inspired Optimization Algorithm

Zhengzong Wang, Yinggao Yue , and Li Cao 

Research Article (18 pages), Article ID 2674201, Volume 2022 (2022)

Visual Design of Brand Image by Marine Bionic System in the Environment of Internet of Things and Machine Learning

Minghui Niu and Joung Hyung Cho 


Research Article (16 pages), Article ID 2153770, Volume 2022 (2022)

Predicting the Investment Risk in Supply Chain Management Using BPNN and Machine Learning

Lan Li 


Research Article (11 pages), Article ID 4340286, Volume 2022 (2022)

Industrial Internet of Things Anti-Intrusion Detection System by Neural Network in the Context of Internet of Things for Privacy Law Security Protection

Di Teng 

Research Article (17 pages), Article ID 7182989, Volume 2022 (2022)

Classification of Diabetic Retinopathy Based on Multiscale Hybrid Attention Mechanism and Residual Algorithm

Yue Miao  and Siyuan Tang

Research Article (11 pages), Article ID 5441366, Volume 2022 (2022)

Contents


Development Policy of the International Trade Industry under the Background of Cloud Computing and Internet of Things

Liang Wu, Jianhua Zhou , Honglei Tang, and Hanjie Xiao
Research Article (12 pages), Article ID 6313339, Volume 2022 (2022)


Energy-Aware Intrusion Detection Model for Internet of Vehicles Using Machine Learning Methods

Lu Lihua 
Research Article (8 pages), Article ID 9865549, Volume 2022 (2022)


The Core Cluster-Based Subspace Weighted Clustering Ensemble

Xuan Huang, Fang Qin , and Lin Lin
Research Article (17 pages), Article ID 7990969, Volume 2022 (2022)

Psychological Quality of Piano Players Based on Big Data Algorithm

Rui Li , Rasa Kirliauskienė, Yixin Sun, Shixue Dong, and Li Zhang
Research Article (12 pages), Article ID 7237099, Volume 2022 (2022)

Implementation of Embedded Microprocessor in Optimal Teaching of Physical Health in the Internet Era

Juan Liu 
Research Article (15 pages), Article ID 4193644, Volume 2022 (2022)




Remote Monitoring and Management System of Intelligent Agriculture under the Internet of Things and Deep Learning

Meirong Zhu  and Jie Shang 
Research Article (13 pages), Article ID 1206677, Volume 2022 (2022)

Using the Neutrosophic DEMATEL Method to Determine the Effect of Internet Finance and Big Data Risk Control Monitoring

Lin Tian and Hongmei Gu 
Research Article (7 pages), Article ID 9395567, Volume 2022 (2022)

Home Based Monitoring for Smart Health-Care Systems: A Survey

J. Anu Shilvya, S. Thomas George , M. S. P. Subathra, P. Manimegalai, Mazin Abed Mohammed ,
Mustafa Musa Jaber, Afsaneh Kazemzadeh, and Mohammed Nasser Al-Andoli 
Review Article (10 pages), Article ID 1829876, Volume 2022 (2022)


Gathering Contextual Data with Power Information Using Smartphones in Internet of Everything

Umar Mahmud , Shariq Hussain , and Ibrahima Kalil Toure 
Research Article (14 pages), Article ID 4445751, Volume 2022 (2022)

[Retracted] Design and Implementation of Node of Wireless Network Environment Monitoring System Based on Artificial Intelligence






Pinghui Zou and Gaoqing Ji 
Research Article (9 pages), Article ID 5911476, Volume 2022 (2022)

Brand LOGO Image Recognition and Inquiry Creative Teaching Design Based on Deep Learning

Xin Gao  and Wenjing Chen



Research Article (10 pages), Article ID 5396468, Volume 2022 (2022)

Autoencoder for Design of Mitigation Model for DDOS Attacks via M-DBNN

Ankit Agrawal , Rajiv Singh , Manju Khari , S. Vimal , and Sangsoon Lim 


Research Article (14 pages), Article ID 9855022, Volume 2022 (2022)

The Mathematical Model of Marine Engine Room Equipment Based on Machine Learning

Ji Zeng , Bowen Jin , He Zhang, Songyan Mai, Bo Yuan, Hui Jiang, Mengkai Yang, and Chaochun Huang

Research Article (8 pages), Article ID 8366670, Volume 2022 (2022)


Empirical Analysis of Machine Learning Algorithms for Multiclass Prediction

Umar Ishfaq, Danial Shabbir, Jumshaid Khan, Hikmat Ullah Khan, Salman Naseer, Azeem Irshad ,

Muhammad Shafiq , and Habib Hamam


Research Article (12 pages), Article ID 7451152, Volume 2022 (2022)

Bank Green Credit Risk Assessment and Management by Mobile Computing and Machine Learning Neural Network under the Efficient Wireless Communication

Yuan Feng 


Research Article (11 pages), Article ID 3444317, Volume 2022 (2022)

Research on Dynamic Spectrum Allocation Algorithm Based on Cyclic Neural Network

Xiaomo Yu, Yonghua Cai , Wenjing Li, Xiaomeng Zhou, and Ling Tang

Research Article (14 pages), Article ID 7928300, Volume 2022 (2022)

Development Model of Enterprise Green Marketing Based on Cloud Computing

Dian Jia and Zhaoyang Wu 


Research Article (10 pages), Article ID 4931374, Volume 2022 (2022)

Adaptive Control System of Intelligent Lower Limb Prosthesis Based on 5G Virtual Reality

Gongxing Yan, Jialing Li , Hui Xie, and Minggui Zhou


Research Article (12 pages), Article ID 4572503, Volume 2022 (2022)

Modeling of Residential Environment Artistic Design Based on Multisensor Data Fusion

Yang Yu 

Research Article (18 pages), Article ID 4961698, Volume 2022 (2022)


Application of Neural Network Based on Multisource Information Fusion in Production Cost Prediction

Biaowen Wei 

Research Article (13 pages), Article ID 5170734, Volume 2022 (2022)


Contents

Financial Asset Risk Measurement Based on Smart Sensor Big Data Security Analysis and Bayesian Posterior Probability Model

Zixin Lu 


Research Article (12 pages), Article ID 8303555, Volume 2022 (2022)

Superresolution Reconstruction of Remote Sensing Image Based on Generative Adversarial Network

Qiaoliang Zhou 

Research Article (10 pages), Article ID 9114911, Volume 2022 (2022)

Optimal Design of Ecological Landscape Spatial Structure Based on Edge Computing of Internet of Things

Ru An 


Research Article (9 pages), Article ID 9303327, Volume 2022 (2022)

Multiobjective Optimization of Structure and Robustness of a Split Parallel Multicomponent Strain Sensor

Peng Kong, Xiaoqiang Peng, and Zhenzeng Lian 


Research Article (12 pages), Article ID 6387919, Volume 2022 (2022)

A Hybrid Convolutional Neural Network and Relief-F Algorithm for Fault Power Line Recognition in Internet of Things-Based Smart Grids

Zhang Yuqing 

Research Article (7 pages), Article ID 4911553, Volume 2022 (2022)

Design and Implementation of Artwork Display System Based on Internet of Things Technology

Qian Zhao and Chenglin Wu 


Research Article (17 pages), Article ID 7180462, Volume 2022 (2022)

Design and Implementation of Fully Convolutional Network Algorithm in Landscape Image Processing

Yinan Pan , Yuan Li , and Jing Jin 

Research Article (9 pages), Article ID 7387363, Volume 2022 (2022)

Application Research of Manuscript Writing Robot Based upon Laser Sensor in News Dissemination Field

Lijia Huang 


Research Article (12 pages), Article ID 4372527, Volume 2022 (2022)

Evaluation of Rural Tourism Carrying Capacity Based on Ecological Footprint Model

Lei Li , Xiaojuan Ye, and Xilong Wang


Research Article (10 pages), Article ID 4796908, Volume 2022 (2022)

Realization of Wireless Sensors and Intelligent Computer Aided Teaching in Physical Education and Training

Guang Wu and Xuezheng Zhang 


Research Article (12 pages), Article ID 6415352, Volume 2022 (2022)

Application of Computer Data Mining Technology Based on AKN Algorithm in Denial of Service Attack Defense Detection

Xiang Huang 


Research Article (12 pages), Article ID 4729526, Volume 2022 (2022)

Reliability and Life Prediction Algorithms of Insulated Cables Based on Wireless Network Communication

Jianguo Sun , Zhonghua Ni, and Yanxin Liu


Research Article (12 pages), Article ID 5672349, Volume 2022 (2022)

PSE and ISE Based E-Commerce Model Design of Sharing Enterprises

Suhong Yang , Mohammed k. Hassan, and Vinay kumar

Research Article (9 pages), Article ID 7134861, Volume 2022 (2022)

Assembly Sequence Planning Based on Hierarchical Model

Chunxi Li  and Wenjun Hou


Research Article (19 pages), Article ID 9461794, Volume 2022 (2022)

IAMnet: Presentation of Parallelization Approach for Repetitive Mining on Network Topologies with an Improved Apriori Method

Hooman Bavarsad Salehpour, Parvaneh Asghari , Hamid Haj Seyyed Javadi , and Mohammad Ebrahim Shiri


Research Article (14 pages), Article ID 8217774, Volume 2022 (2022)

A Rapid Combined Model for Automatic Generating Web UI Codes

Wei Zhang , Shangmin Luan, and Liqin Tian


Research Article (10 pages), Article ID 4415479, Volume 2022 (2022)

A Blockchain-Based Key-Revocation Access Control for Open Banking

Khaled Riad  and Mohamed Elhoseny


Research Article (14 pages), Article ID 3200891, Volume 2022 (2022)

Interactive Art Design Based on Intelligent Sensors and Information Fusion Technology

Yanming Zhu, Tingting Qiu, and Wei Miao 


Research Article (13 pages), Article ID 6777620, Volume 2022 (2022)

Digital Development Strategy of Agricultural Planting and Breeding Enterprises Based on Intelligent Sensors

Jincheng Zhang 

Research Article (14 pages), Article ID 6495191, Volume 2022 (2022)

Application of Artificial Intelligence Recognition Technology in Digital Image Processing

Xi Zhang 


Research Article (10 pages), Article ID 7442639, Volume 2022 (2022)

Contents

A Novel Highway Routing Protocol in Vehicular Ad Hoc Networks Using VMaSC-LTE and DBA-MAC Protocols

Edris Khezri , Esmail Zeinali , and Hadi Sargolzaey
Research Article (11 pages), Article ID 1680507, Volume 2022 (2022)


China's Energy Demand Forecasting Based on the Hybrid PSO-LSSVR Model

Yifei Yang, Lu Han, Yarong Wang, and Jianzhong Wang 
Research Article (12 pages), Article ID 7584646, Volume 2022 (2022)

Sports Event Model Evaluation and Prediction Method Using Principal Component Analysis

Weiwei Yu and Jinming Xing 
Research Article (10 pages), Article ID 9351522, Volume 2022 (2022)






[Retracted] SM-PageRank Algorithm-Based User Interest Model for Mobile Smart Tourism Platform

Hua Li  and Tao Su
Research Article (12 pages), Article ID 6034500, Volume 2022 (2022)


Anomaly Recognition Algorithm for Human Multipose Motion Behavior Using Generative Adversarial Network

Nan Zhang, Jie Ren, Qixiao Xu , Hao Wu, and Meng Wang
Research Article (9 pages), Article ID 2656001, Volume 2022 (2022)



Security-Aware Routing Protocol Based on Artificial Neural Network Algorithm and 6LoWPAN in the Internet of Things

Jiangdong Lu , Dongfang Li , Penglong Wang , Fen Zheng , and Meng Wang 
Research Article (8 pages), Article ID 8374473, Volume 2022 (2022)

Design and Practice of Aerobics Teaching Design Based on Data Fusion Algorithm

Chuanqi Ma 
Research Article (14 pages), Article ID 1275508, Volume 2022 (2022)


Applying Knowledge Graph to Analyze the Historical Landscape Based on CiteSpace

Youping Teng, Yue Huang , and Shuai Yang 
Research Article (12 pages), Article ID 3867541, Volume 2022 (2022)

The Effect of 3D Image Virtual Reconstruction Based on Visual Communication

Li Xu, Ling Bai, and Lei Li 
Research Article (8 pages), Article ID 6404493, Volume 2022 (2022)

A Multipath Payment Scheme Supporting Proof of Payment


Hanguan Qian  and Lin You 
Research Article (7 pages), Article ID 9911915, Volume 2022 (2022)

Load Balancing Routing Algorithm of Low-Orbit Communication Satellite Network Traffic Based on Machine Learning

Tie Liu , Chenhua Sun, and Yasheng Zhang


Research Article (14 pages), Article ID 3234390, Volume 2021 (2021)

An Empirical Study Based on the Impact of Smart Sensor System on Rural Relative Poverty

Tian Luan and Xiaoyan Liu 


Research Article (14 pages), Article ID 3635382, Volume 2021 (2021)

Financial Management Early-Warning Mechanism Construction and Decision Analysis Research Based on Wireless Sensor Network and Data Mining

Zeyuan Chang and Heran Yang 

Research Article (13 pages), Article ID 6047798, Volume 2021 (2021)

[Retracted] Research on Automobile Assembly Line Optimization Based on Industrial Engineering Technology and Machine Learning Algorithm

Xiaorui Shi, Wei Cui, Ping Zhu, and Yanhua Yang 


Research Article (9 pages), Article ID 2658090, Volume 2021 (2021)

Computer Digital Technology-Based Educational Platform for Protection and Activation Design of Ming Furniture

Zhe Peng  and Yichen Du

Research Article (8 pages), Article ID 3000011, Volume 2021 (2021)

Real-Time Capture of Snowboarder's Skiing Motion Using a 3D Vision Sensor

Zhipeng Li, Jun Wang, Tao Zhang, Dave Balne, Bing Li, Ruizhu Yang, Wenli Song , and Xingfu Zhang

Research Article (11 pages), Article ID 8517771, Volume 2021 (2021)

Retraction

Retracted: SM-PageRank Algorithm-Based User Interest Model for Mobile Smart Tourism Platform

Wireless Communications and Mobile Computing

Received 11 July 2023; Accepted 11 July 2023; Published 12 July 2023

Copyright © 2023 Wireless Communications and Mobile Computing. This is an open access article distributed under the Creative Commons Attribution License, which permits unrestricted use, distribution, and reproduction in any medium, provided the original work is properly cited.

This article has been retracted by Hindawi following an investigation undertaken by the publisher [1]. This investigation has uncovered evidence of one or more of the following indicators of systematic manipulation of the publication process:

- (1) Discrepancies in scope
- (2) Discrepancies in the description of the research reported
- (3) Discrepancies between the availability of data and the research described
- (4) Inappropriate citations
- (5) Incoherent, meaningless and/or irrelevant content included in the article
- (6) Peer-review manipulation

The presence of these indicators undermines our confidence in the integrity of the article's content and we cannot, therefore, vouch for its reliability. Please note that this notice is intended solely to alert readers that the content of this article is unreliable. We have not investigated whether authors were aware of or involved in the systematic manipulation of the publication process.

Wiley and Hindawi regrets that the usual quality checks did not identify these issues before publication and have since put additional measures in place to safeguard research integrity.

We wish to credit our own Research Integrity and Research Publishing teams and anonymous and named external researchers and research integrity experts for contributing to this investigation.

The corresponding author, as the representative of all authors, has been given the opportunity to register their agreement or disagreement to this retraction. We have kept a record of any response received.

References

- [1] H. Li and T. Su, "SM-PageRank Algorithm-Based User Interest Model for Mobile Smart Tourism Platform," *Wireless Communications and Mobile Computing*, vol. 2022, Article ID 6034500, 12 pages, 2022.

Retraction

Retracted: Design and Implementation of Node of Wireless Network Environment Monitoring System Based on Artificial Intelligence

Wireless Communications and Mobile Computing

Received 11 July 2023; Accepted 11 July 2023; Published 12 July 2023

Copyright © 2023 Wireless Communications and Mobile Computing. This is an open access article distributed under the Creative Commons Attribution License, which permits unrestricted use, distribution, and reproduction in any medium, provided the original work is properly cited.

This article has been retracted by Hindawi following an investigation undertaken by the publisher [1]. This investigation has uncovered evidence of one or more of the following indicators of systematic manipulation of the publication process:

- (1) Discrepancies in scope
- (2) Discrepancies in the description of the research reported
- (3) Discrepancies between the availability of data and the research described
- (4) Inappropriate citations
- (5) Incoherent, meaningless and/or irrelevant content included in the article
- (6) Peer-review manipulation

The presence of these indicators undermines our confidence in the integrity of the article's content and we cannot, therefore, vouch for its reliability. Please note that this notice is intended solely to alert readers that the content of this article is unreliable. We have not investigated whether authors were aware of or involved in the systematic manipulation of the publication process.

Wiley and Hindawi regrets that the usual quality checks did not identify these issues before publication and have since put additional measures in place to safeguard research integrity.

We wish to credit our own Research Integrity and Research Publishing teams and anonymous and named external researchers and research integrity experts for contributing to this investigation.

The corresponding author, as the representative of all authors, has been given the opportunity to register their

agreement or disagreement to this retraction. We have kept a record of any response received.

References

- [1] P. Zou and G. Ji, "Design and Implementation of Node of Wireless Network Environment Monitoring System Based on Artificial Intelligence," *Wireless Communications and Mobile Computing*, vol. 2022, Article ID 5911476, 9 pages, 2022.

Retraction

Retracted: Research on Automobile Assembly Line Optimization Based on Industrial Engineering Technology and Machine Learning Algorithm

Wireless Communications and Mobile Computing

Received 11 July 2023; Accepted 11 July 2023; Published 12 July 2023

Copyright © 2023 Wireless Communications and Mobile Computing. This is an open access article distributed under the Creative Commons Attribution License, which permits unrestricted use, distribution, and reproduction in any medium, provided the original work is properly cited.

This article has been retracted by Hindawi following an investigation undertaken by the publisher [1]. This investigation has uncovered evidence of one or more of the following indicators of systematic manipulation of the publication process:

- (1) Discrepancies in scope
- (2) Discrepancies in the description of the research reported
- (3) Discrepancies between the availability of data and the research described
- (4) Inappropriate citations
- (5) Incoherent, meaningless and/or irrelevant content included in the article
- (6) Peer-review manipulation

The presence of these indicators undermines our confidence in the integrity of the article's content and we cannot, therefore, vouch for its reliability. Please note that this notice is intended solely to alert readers that the content of this article is unreliable. We have not investigated whether authors were aware of or involved in the systematic manipulation of the publication process.

Wiley and Hindawi regrets that the usual quality checks did not identify these issues before publication and have since put additional measures in place to safeguard research integrity.

We wish to credit our own Research Integrity and Research Publishing teams and anonymous and named external researchers and research integrity experts for contributing to this investigation.

The corresponding author, as the representative of all authors, has been given the opportunity to register their

agreement or disagreement to this retraction. We have kept a record of any response received.

References

- [1] X. Shi, W. Cui, P. Zhu, and Y. Yang, "Research on Automobile Assembly Line Optimization Based on Industrial Engineering Technology and Machine Learning Algorithm," *Wireless Communications and Mobile Computing*, vol. 2021, Article ID 2658090, 9 pages, 2021.

Research Article

ML-DDoSnet: IoT Intrusion Detection Based on Denial-of-Service Attacks Using Machine Learning Methods and NSL-KDD

Mona Esmaeili,¹ Seyedamiryousef Hosseini Goki,² Behnam Hajipour Khire Masjidi,³ Mahdi Sameh,⁴ Hamid Gharagozlou ,⁵ and Amin Salih Mohammed^{6,7}

¹Department of Electrical & Computer Engineering, University of New Mexico, Albuquerque, NM 8731, USA

²Department of Computer Science, University of Victoria, Victoria, BC, Canada

³Department of Computer, Faculty of Electricity and Computer, Islamic Azad University, North Tehran Branch, Tehran, Iran

⁴Department of Computer Engineering, Sabzevar Branch, Islamic Azad University, Sabzevar, Iran

⁵Department of Mathematics and Computer Science, Amirkabir University of Technology, Tehran, Iran

⁶Department of Computer Engineering, College of Engineering and Computer Science, Lebanese French University, Kurdistan Region, Iraq

⁷Department of Software and Informatics Engineering, Salahaddin University, Kurdistan Region, Iraq

Correspondence should be addressed to Hamid Gharagozlou; hamid.gh@aut.ac.ir

Received 3 February 2022; Revised 1 March 2022; Accepted 7 July 2022; Published 21 August 2022

Academic Editor: Ashish Bagwari

Copyright © 2022 Mona Esmaeili et al. This is an open access article distributed under the Creative Commons Attribution License, which permits unrestricted use, distribution, and reproduction in any medium, provided the original work is properly cited.

The Internet of Things (IoT) is a complicated security feature in which datagrams are protected by integrity, confidentiality, and authentication services. The network is protected from external interruptions and intrusions. Because IoT devices run with a range of heterogeneous technologies and process data over time, standard solutions may not be practical. It is necessary to develop intelligent procedures that can be used for multiple levels of data flow in the system. This study examines metainnovations using deep learning-based IDS. Per the findings of the earlier tests, BiLSTMs are better for binary (regular/attacker) classification; however, sequential models (LSTM or BiLSTM) are better for detecting some brutal attacks in multiclass classifiers. According to experts, deep learning-based intrusion detection systems can now recognize and select the best structure for each category. However, specific difficulties will need to be solved in the future. Two topics should be studied further in future attempts. One of the researchers' concerns is the impact of various data processing techniques, such as artificial intelligence or metamethods, on IDS. The BiLSTM approach has chosen the safest instances with the highest accuracy among the models. According to the findings, the most reliable and suitable solution for evaluating DDoS attacks in IoT is the BiLSTM design.

1. Introduction

As the secure network architecture transitions to open connectivity, the network becomes more adaptable, omnipresent, and cognitive. These advancements have accelerated the development of next-generation Internet technologies, including big data, cloud computing, the Internet of Things, and programmable networks. However, with software-defined network architecture, the potential of a DDoS attack brought on by centralized control becomes more apparent [1]. IDS are divided into two categories. Vulnerability assess-

ment, which finds attacks based on recognized signatures, and anomaly detection, which detects aberrant attacks based on usual usage patterns, are the two types. At the same time, it is difficult to find unknown threats using abuse detection and anomaly detection benefits in finding them. Nevertheless, because defining a range of typical use patterns is complex, anomaly detection has a high rate of false alerts [2]. DDoS attacks are presently one of the most challenging network attacks to recognize [3]. The goal is to deplete the target platforms or network capabilities, making the victim unable to perform routine tasks. There are two types of

DDoS attacks: resource bandwidth-consuming attacks and system resource-consuming attempts. Many zombie hosts are used in resource bandwidth attacks to swiftly produce a significant volume of traffic that converges on the victim's server and entirely consumes its network bandwidth resources. Sending a high number of UDP, TCP, and ICMP packets repeatedly, for example, might trigger a flooding attack, resulting in UDP flooding, TCP flooding, and ICMP flooding. Amplification attacks, such as DNS reflection amplification attacks, can also be performed via reflection. Protocol vulnerabilities are commonly used in system resource attacks to use the victim's host resources (TCP-SYN half-connection attack employing TCP three-way handshake, for example [4]).

Conventional network approach checking and data analytics confront various obstacles and issues in such networks, such as reliability and practical real-time analysis of massive data. Furthermore, due to varied factors such as device mobility and network heterogeneity, the pattern of network traffic, particularly in cellular networks, shows exceptionally complicated behavior. Deep learning has been successfully used in large data systems to aid analytics and knowledge discovery by recognizing hidden and complex patterns. Researchers in the field of networking are using deep learning techniques for network traffic monitoring and analysis applications, such as traffic categorization and prediction, as a result of these results [5]. Conceptual designs based on traditional machine learning, based on manually and expert-generated features, are outmoded and unable to keep up with the rapidly increasing collection of applications and the moving target nature of mobile traffic [6].

As cyberattacks grow more intelligent, it is becoming increasingly challenging to find advanced cyberattacks in many industries, including industry, national defense, and healthcare. Traditional intrusion detection systems can no longer detect sophisticated attacks with unusual patterns. Attackers get around recognized signatures by impersonating regular users. Deep learning is a potential solution to these problems [2]. Deep learning (DL) intrusion detection does not require much malicious activity or a list of typical activities to create detection rules. Through empirical data learning, DL defines incursion characteristics on its own. Since machine learning is widely used in IDS research, KDD has been used as a dataset in many of them. Most of these research studies use binary categorization to divide the KDD into the attack and benign categories. They also use multiclass classification to divide the KDD into four distinct groups. Even though the large-scale CNN algorithm has produced impressive results in detecting attacks, few people consider keeping good detection performance with limited resources. Deploy the learned CNN model in the SD-IoT controller, for example. As more IoT devices are installed in the system, the likelihood of the network being attacked by unsecured IoT devices grows, needing the development of a defense mechanism. Deep learning can dynamically extract high-level characteristics from low-level ones, allowing for sophisticated representation and reasoning.

Standard solutions may not be practical since IoT devices employ various heterogeneous technologies and ana-

lyze data over time. Intelligent processes that can be used for various levels of data flow in the system must be developed. The IDS, based on deep learning, is used to investigate metainnovations in this work. BiLSTMs are better for binary (regular/attacker) classification. At the same time, sequential models (LSTM or BiLSTM) are better for finding some harsh attacks in multiclass classifiers, according to the results of prior testing. Deep learning-based intrusion detection systems, according to experts, can now recognize and pick the best structure for each category. On the other hand, specific problems will need to be resolved in the future. In future attempts, two things should be investigated further. The influence of various data processing techniques, such as artificial intelligence or metamethods, on IDS is one of the researchers' concerns. The BiLSTM technique has found the safest examples with the maximum accuracy among the models. According to the findings, the BiLSTM design is the most reliable and proper choice for analyzing DDoS attacks in IoT. MLP, LSTM, BiLSTM, KNN, SVM, LDA, DT, and RF are among the eight machine learning algorithms used in this study to find DDoS attacks in IoT. NSL-KDD is the process dataset, with 1 and 0 labels denoting normal and abnormal behaviors, respectively. A confusion matrix is used to display the classification findings.

This paper includes the following sections. (1) Introduction supplies the main problem statement and importance, contribution, and novelty of the presented method. (2) Literature Review represents the background of both the method and the problem of recent years' research. (3) Methods and Material illustrates the approach characteristics and introduction to supplied machine learning techniques. (4) Results and Discussion also presents the classification and diagnosis outcomes. And finally, (5) Conclusion presents the overall results and future works.

2. Literature Review

DDoS attacks are presently the most common and effective dangers to businesses, becoming increasingly tempting [7]. GitHub, for instance, was the target of one of the most significant DDoS attacks ever in 2018 [8]. This devastating attack is one of the most well-publicized attacks of the modern era, shattering the foundations of one of the CIA security triad's pillars (presence). Thousands of dump terminals, computers, and botnets are used by attackers to perform DDoS attacks simultaneously, exhausting the target system's significant resources and rendering all services inaccessible. There are many legitimate and effective technologies available that may be used to conduct DDoS attacks on both big sizes and small sizes. Another DDoS attack occurred recently [8]; the lawful Memcached utility, whose primary task is to lessen the load on the supporting Internet services, was abused by the attackers. The attacker used Memcached items and fake IP addresses, allowing Memcached answers to be routed to the target addresses at a rate of 126.9 million packets per second, using a significant amount of target capacity. Furthermore, the use of fake IPs makes tracing DDoS attacks nearly hard [9].

Numerous publications have been written on IDS. IDS based on software-defined networks is proposed by Manso et al. [10]. DDoS attacks are detected by the proposed IDS, which alerts the sensor nodes. Karim et al. [11] investigated the performance of Snort-based IDS on a network. Xu et al. [12] proposed a deep forest-based distributed denial-of-service detection and defense model. They concentrate on attacks on smart nodes and the significant data context. Anomaly detection approaches for commercial sensor networks based on machine learning have also been studied [13]. According to Lv et al. [14], solving the security problems of CITS Digital Twins (DTs) using deep learning (DL) is possible. Chen et al. [15] have concluded that motorcycle bans reduce traffic accident deaths by a significant amount, and their effectiveness doesn't diminish over time due to the diversity of their policies. A proposed study by Lv et al. [16] examines the application of Digital Twins in manufacturing intelligent equipment and further optimizes its fault diagnosis effect. In Liu et al. [17], a framework has been proposed for analyzing lung and colon histopathological images. Sun et al. [18] describe a lightweight remote control communication scheme. The authors believe that analyzing the scheme's performance shows that it is practical and appropriate for non-time-sensitive scenarios that require high anonymity. Naive Bayes, random forests, and logistic regression were proposed as machine learning approaches to detect fake identity attacks by Mehbodniya et al. [19]. According to Cao et al. [20], an optimization model based on SAGIN-IoV service requirements is constructed and an improved algorithm is proposed. A lifelong learning framework called the Generalized Lifelong Spectral Clustering (GL22SC) has been explored by Sun et al. [21]. According to Ahmadi et al. [22], deep-Q-reinforcement learning ensembles can choose a subset of devices in each communication round by using a combined deep-Q-reinforcement learning ensemble based on spectral clustering (DQRE-SCnet). According to Sun et al. [23], Flexible Clustered Lifelong Learning (FCL3) comprises two knowledge libraries: a feature learning library and a model knowledge library. According to Liu et al. [24], the SFERNN was optimized by minimizing the cross-entropy loss on the source branches and the distributional discrepancy between the source branches and the target branches. Using the modified Lamport Merkle Digital Signature method, Mehbodniya et al. [25] developed a framework for generating and verifying digital signatures. An improved gray wolf optimization (IGWO) algorithm was used by Zhang et al. [26] to develop a charging safety early-warning model for electric vehicles (EV). It is a pioneering attempt to distinguish transferable or untransferable knowledge across domains with the Knowledge Aggregation-induced Transferability Perception (KATP) developed by Dong et al. [27]. According to Yang et al. [28], aggregated vehicle fuel consumption data can be protected against time series-based differential attacks using a negative survey approach. An algorithm combining interactive machine learning and active learning for HBR prediction was proposed by Wu et al. [29]. Using local

differential privacy (LDP) and elliptic curve cryptography (ECC), Khaliq et al. [30] describe parking recommender systems with research gaps. Recent SBR prediction models have performed poorly due to mislabeled instances in five publicly available datasets, according to Wu et al. [31]. Kim et al. employed several KDD computer vision experiments to divide the dataset into four groups or two or more independent variables, attack and benign. Instead of concentrating on primary groups, they focus on specific attacks within the same area. They also looked at the DoS category in both databases and created a DL model for detecting DoS [2]. In a software-defined Internet of Things setting, Wang et al. suggested a DDoS attack detection system to safeguard in real time. They used an updated firefly method to find DDoS attacks to enhance the convolutional neural network (CNN). The findings showed that the proposed technique could detect innocuous traffic and DDoS activities with more than 99 percent [4]. Depending on the information entropy and deep learning, Liu et al. suggested a two-level DDoS attack detection approach. First, the information entropy detection technique found suspicious elements and ports with coarse granularity. The convolutional neural network (CNN) model used a fine-grained packet-based detection technique to find regular traffic from suspect traffic. The controller implemented the defense strategy to thwart the onslaught. The testing findings reveal that the suggested method's detection accuracy is 98.98 percent, indicating that it can successfully identify DDoS attack traffic in an SDN context [1]. Based on their analysis of the impact of class imbalance on SBR prediction, Zheng et al. [32] found that it had a negative impact on prediction accuracy. A random forest classifier was used by Zhang et al. [33] to train a Just-in-Time defect prediction model based on six open source projects. A DeepBAN communication framework was proposed by Liu et al. [34]. The results showed that it can improve the energy efficiency of dynamic WBANs by 15% over stochastic scheduling schemes. The dominant feature set was extracted using a novel dominant feature selection algorithm developed by Gera et al. [35]. Smart contract vulnerability detection using graph neural networks and expert knowledge was explored by Liu et al. [36]. The proposed solution by Zhang et al. [37] is aimed at achieving rapid video prefetching and traffic reduction. With their new detection method, Zong et al. [38] applied a multiscale grouping (MSG) structure to a 3D point cloud tunnel dataset and applied a 3D-BoNet instance segmentation model. An optimization of energy consumption in dynamic wireless sensor networks using fog computing and fuzzy multiattribute decision-making was proposed by Varmaghani et al. [39]. According to Zong and Wan [40], a 3D scanner can be used to acquire 3D data. The method's validity and reliability have been further verified. As a result of sophisticated fuzzy logic, Singh et al. [41] develop algorithms for mobility and traffic management that are as flexible as possible while retaining high performance. Xie et al. [42] have proposed many heuristic or metaheuristic algorithms/methods to solve this NP-hard problem. Using the traditional undesired multiuser

interference and the interference caused by imperfect hardware components, Li et al. [43] summarize constructive interference (CI) and explain how it can benefit the 1-bit signal design. As a future multichannel communication application for terahertz (THz), Feng et al. [44] presented a 220 GHz four-channel, noncontiguous, and manifold-coupled waveguide multiplexer.

Ghanbari upgraded the VFD and devised feature extraction methods with a mother wavelet to boost detection. For DDoS attacks, the adoptive mother wavelet was designed to reach the best similarity and flexibility to the input data for a specific purpose. Because Internet traffic data with DDoS-ITD is a long-range-dependent signal, a variational technique is used to extract the hidden properties of each DDoS-ITD scale. This study employs and advances an online variance fractal dimension approach. Then, a CNN-based IDS was created to improve the sensitivity of DDoS attack detection. As a result, a weighted cost function was designed for assessing the artificial neural network and CNN structure. The suggested structure of the polyscale CNN about policy gradient-based deep reinforcement learning was used to develop and execute the IDS for unlabeled data to get a more real IDS. The IDS discovered the irregularities with 93 percent accuracy [45]. A 220 GHz multicircuit integrated front end based on solid-state circuits was presented by NIU et al. [46]. The knowledge-based VQA (Visual Question Answering) module developed by Zheng et al. [47] is designed to extend the versatility of knowledge-based VQA. Ramtin et al. [48] analyzed the maximum damage that a DDoS attacker can make without being detected by a detection system at the network edge. They considered two classical classifiers based on hypothesis testing, whether the detector knows the distribution of attack traffic or not. The authors theoretically proved that the maximum damage follows a square root law. They also illustrated their results using empirical data. The study by Zheng et al. [49] proposes a detailed visual reasoning model as a theoretical and experimental basis for introducing different levels of knowledge representation into deep learning. Zheng et al. [50] developed a multilayer semantic representation network for sentence representation. In a side-channel attack using an off-the-shelf smartphone, Yu et al. [51] demonstrated the feasibility of inferring keystrokes on touch screens. The concept of user authentication was advanced by Kong et al. [52] in order to protect user privacy and to provide personalized services to users. According to Hajipour et al. [53], the Breast Cancer Ultrasound Dataset is used as the input image for a two-dimensional contourlet. A fog-based smart grid scheme with sensible pricing and packing was presented by Zhao et al. [54]. In a study by Meng et al. [55], they propose a method for adaptive neural tracking control of an uncertain two-link rigid-flexible manipulator under vibration amplitude constraints. In earlier papers, Ghanbari and Kinsner have described an abnormality detector for enhancing the detection rate of a DDoS attack in a smart grid. Increased categorization of the training and testing stages was used to carry out this improvement. A full version of the variance fractal dimension trajectory (VFDTv2) was applied to extract intrinsic charac-

teristics from the stochastic fractal input data. A discrete wavelet transform was applied to the input data during data preprocessing. The VFDTv2 removed critical differentiating features (see Table 1).

Mishra and Pandya analyzed and contrasted intrusion detection and prevention methods for minimizing DDoS attacks, emphasizing detection approaches. In addition, the categorization of intrusion detection systems, numerous anomaly detection approaches, different intrusion detection systems patterned on datasets and various machine learning methods, and pattern recognition algorithms for data preprocessing and malware detection were covered. Finally, a more significant viewpoint was imagined while reviewing research obstacles, possible answers, and future aspirations [67]. According to Ahmadi and Abadi [68], the expert can access and develop the system without knowing the underlying code by using the object orientation properties of C++. For selecting the optimal BFTIs, Zhou et al. [69] proposed a multiobjective function consisting of a BFTI's smallest occlusion and its largest facade texture area. Ahmadi et al. [70] used deep neural networks with fuzzy wavelets to predict Iranian energy demand. Among the innovative studies presented by Zhou et al. [71], one focuses on the design of airborne-oriented supercontinuum laser hyperspectral (SCLaHS) LiDARs with 50 bands but with a 20 nm spectral resolution and a 0.5-meter ground sampling distance (GSD). A case study method was used by Tondro et al. [72] to gather in-depth data timeline attributes of all ICT-based enterprises and academic institutions within Alborz province in Iran. This paper presents a generalized buffering algorithm (GBA), which considers all instances within a buffer zone in terms of geometric distance and attribute characteristics [73]. For a comprehensive review of relevant research, Liang et al. [74] used bibliometric mapping, text mining, and qualitative analysis. In a study by Zhao and Wang [75], they have improved lightweight mobile networks based on YOLOv3 for pedestrian detection. For visual tracking, Zhu et al. [76] developed the Siamese-ORPN (Siamese Oriented Region Proposal Network). Li et al. [77] proposed a novel neural network architecture for encoding and synthesizing 3D shapes. The authors discussed transfer learning-based neural network models for the identification of butterfly species in Rajeena et al. [78]. Ghayvat et al. suggested a strategy that combines a blockchain-based nondisclosure method with a two-step authentication architecture and an elliptic curve cryptography-based cryptographic signature framework. Furthermore, a process was designed to protect the ecosystem from DoS and DDoS-based attack methods [79]. Mirsky et al. proved a plug-and-play network intrusion detection system that can autonomously and efficiently train to find attacks on the local network. Kitsune's main algorithm collaboratively used autoencoders to distinguish between the normal and anomalous traffic patterns. Kitsune was shown to be capable of detecting a variety of attacks at a rate equivalent to that of offline anomaly trackers, even on a Raspberry Pi [80]. Additionally, Bovenzi et al. suggested a two-stage hierarchical technique for detecting attacks. It detected

TABLE 1: The summary of the research in the field of IoT intrusion detection.

Author	Year	Feature extraction	Attack	Classification
Wang et al. [4]	2022	(i) Per networking flow, the number of packets (ii) The amount of data transferred each networking flow in bytes (iii) Each networking flow's duration (iv) Networking flow rate (v) The communication flow's source IP addresses (vi) The IP addresses of the networking flow's source	DDoS	Firefly and CNN
Liu et al. [1]	2022	Source IP address, destination IP address, source port, destination port, packet length, and packet protocol	DDoS	Information entropy, CNN
Najafimehr et al. [56]	2022	CICFlowMeter features	DDoS SDN flood, reflection, Portmap reflection, MSSQL reflection, NetBIOS reflection amplification	CLSTMNet, CNN-LSTM
Prasad and Chandra [57]	2022	COLS_WONA features	Volumetric DDoS	Defensive fast detection mode
Xu et al. [58]	2022	Automatic spatial feature extraction	DoS attack	CNN, LSTM
Tsogbaatar et al. [59]	2021	Time Series Benchmark Suite	Very short intermittent DDoS	CNN
Tang et al. [60]	2021	Multifeature fusion	Low-rate denial-of-service attack	CNN
Alkahtani and Aldhyani [61]	2021	Properties of switch device port replication in IoT scenarios	Botnet attack	CNN, LSTM
Mendonca et al. [62]	2021	User features of HTTP, HTTPS, FTP, SSH, and email protocols	DDoS	Fast hierarchical deep CNN, tree CNN
Ghanbari and Kinsner [63]	2021	Adaptive mother wavelet	DDoS	CNN, genetic neural network
Liu et al. [64]	2019	NetFlow images	DDoS, DoS	SVM, CNN, ANN
Cheng et al. [65]	2020	Grayscale matrix feature	DDoS	Multiscale CNN
Cil et al. [66]	2021	(i) In the reverse direction, the average number of the bulk rate (ii) In the rearward order, the average number of bytes of the bulk rate (iii) In the reverse direction, total bytes used for headers (iv) The total number of bytes delivered in the backward order in the first window (v) In the backward direction, the maximum size of a packet (vi) In the reverse order, the smallest packet size (vii) In the backward direction, the standard deviation of the packet size	DDoS	Feedforward-based deep neural network

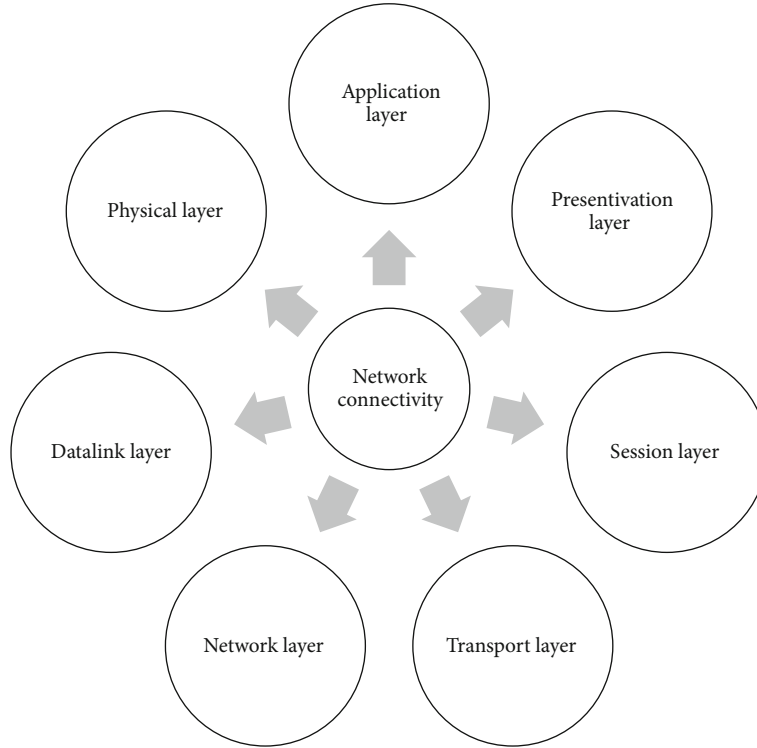


FIGURE 1: The 7-layer conceptual framework for describing network connectivity.

and classified attacks using a unique lightweight method based on a multimodal deep autoencoder and soft-output classifications. Apart from the performance benefits, their approach is well suited for dispersed and privacy-preserving deployments while minimizing the need for retraining, which is necessary for the high speed and durability needed in IoT applications [81].

For data postprocessing, a support vector machine (SVM) was used. The solution correctly identified the DDoS attack with an accuracy of 87.35 percent [82]. Zhang et al. [83] proposed updating a particle swarm template (PST) to accelerate the randomized search. This is a set of uniformly sized particles in the 6D space of the camera pose that are presampled within the unit sphere. According to Zhang et al. [84], orthogonal processing on compression (orthogonal POC) can efficiently support text analytics irrespective of how the data is processed. Fouladi et al. suggested a continuous wavelet transform and CNN-based detection and countermeasure technique. To distinguish attack data from baseline characteristics, the approach employed CWT characteristics as the input for the CNN algorithm. The suggested system has a high detection rate against DNS amplification, NTP, and TCP-SYN flood attacks, with a low false alarm rate, according to the empirical observations [85].

3. Methods and Material

3.1. Distributed Denial-of-Service (DDoS) Attack. DDoS attacks stand for distributed denial-of-service attacks. This form of attack takes advantage of network resource ability restrictions, such as the infrastructure that supports a com-

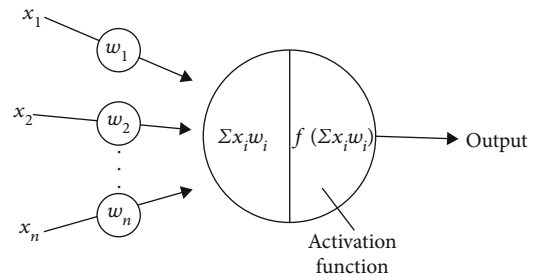


FIGURE 2: The leading architecture of the MLP method.

pany's website. The DDoS attack will make many requests to the targeted online resource to overwhelm the website's ability to handle multiple demands and prevent it from operating correctly. In a DDoS attack, the incoming traffic that floods the target comes from various places. It makes stopping the attack by blocking a single source difficult [86]. A DoS or DDoS attack is like a mob of people surrounding a shop's entrance door, making it difficult for genuine companies to visit and disrupting business. Numerous attack machines can create more attack traffic than a single attack machine. Multiple attack machines are more difficult to switch off than a single attack machine. Each attack machine's activity can be stealthier, making it more difficult to detect and shut down. Because the received signal overwhelming the target comes from various sources, using ingress filtering alone may not be enough to halt the attack. It is also difficult to distinguish between regular user traffic and DoS attacks when dispersed over numerous places of origin [87].

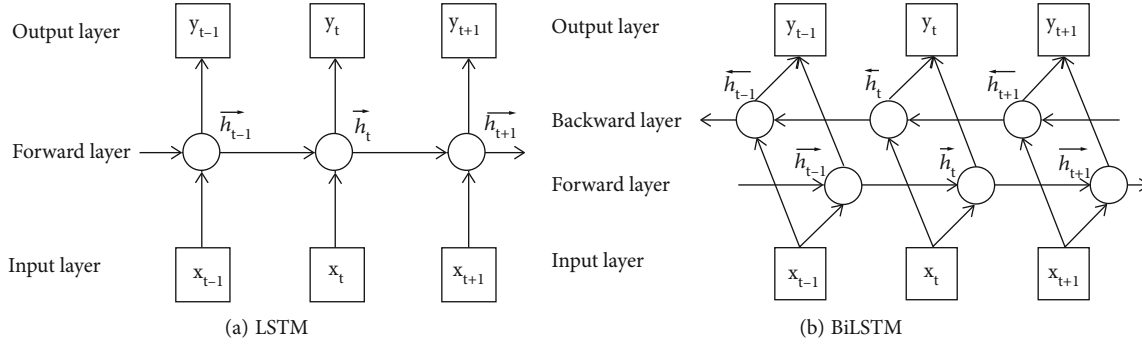


FIGURE 3: The architecture of the LSTM and BiLSTM methods.

TABLE 2: The correlation coefficient for IoT intrusion detection.

Correlation value	Categorical value
(-0.1, 0.1)	Very weak
(-0.3, -0.1) or (0.1, 0.3)	Weak
(-0.5, -0.3) or (0.3, 0.5)	Moderate
(-1, -0.5) or (0.5, 1)	Strong

Computer networks connected to the Internet are used to conduct DDoS attacks. Malware-infected PCs and other devices (such as the Internet of Things equipment) form these networks, run remotely by an intruder. Bots (or zombies) are standalone devices, while a botnet refers to a collection of bots. To conduct an offensive using a botnet, the attacker can send remote commands to each bot. Each bot in a botnet queries the IP address of the victim's server or network. Overburdening the server or network could result in a denial-of-service attack against ordinary traffic. As each bot is an actual Internet node, it can be difficult to distinguish attack traffic from regular traffic [88]. DDoS attacks target various parts of a network connection. Before you can understand how other DDoS attacks work, you must first understand how a network connection is made. A networking line on the Internet forms numerous components or "layers." Each layer in the model has a distinct function, like how each layer in a home carries out a specific goal. The OSI model is a seven-layer theoretical framework for explaining network connections (see Figure 1).

While virtually all DDoS attacks include flooding a target device or network with traffic, there are three types of attacks. In response to the target's defenses, an intruder may utilize one or more alternative attack vectors or cycle possible attacks [86–88].

3.2. Feature Extraction. The three significant processes are data preprocessing, training, and validation. The data preparation stage's primary purpose is to turn raw data into a well-formatted dataset with suitable properties and labels. Data is acquired from various sources for network traffic categorization, including recorded network traffic, checked network information, and sampled packet data. The preprocessing is then completed [89]. Based on the parameters of the chosen machine learning technique and the prob-

lem's knowledge domain, the primary method may vary. After data processing, feature extraction, an essential part of a classification model, is performed. The feature extraction is aimed at enhancing the classification model's performance by removing unnecessary features and speeding up the training process by lowering the number of attributes in the dataset. The final dataset, which has the proper collection of features, is divided into separate sets for training and test data. The chosen learning approach employs the movement set to automatically learn the model parameters and produce a classifier during the training phase.

It must be emphasized that the human setting of a collection of hyperparameters is needed for most learning algorithms. Decide the proper hyperparameter values for a model for a particular circumstance. The rule of thumb, earlier experiences, values used in other successful applications, and validation techniques have all been used to select suitable hyperparameters. The training set can train separate classifiers targeting diverse groups of hyperparameters using the specified learning method. The performance of the classifiers developed is then estimated using a validation set that does not overlap with the training set. The finished classifier is constructed using the same hyperparameters that supply the best performance. The performance of the finished classifier is assessed in the testing step based on the predictions it makes using the activity that can be defined [90].

3.3. Multilayer Perceptron. An ANN is inspired by the form and functionality of biological neural networks. Artificial neurons, a collection of nodes stacked into layers and linked by weighted edges, make up the system. Figure 2 depicts a primary artificial neuron. The received signals are weighted and aggregated. Then, using an activation function for each neuron, they were converted into an output signal. The output signals are passed on to the next layer [91]. This procedure is repeated until the final and output layers are reached. Between the input and output levels are hidden layers that do processing and calculations. The weights of coupled neurons are initially randomly given during the training phase. Then, the underlying learning algorithm is perfected. Back-propagation with gradient descent is the most widely used learning approach for perfecting edge weights. ANN comes in a variety of shapes and sizes. A simple ANN consists of a feedforward network link devoid of cycles [91].

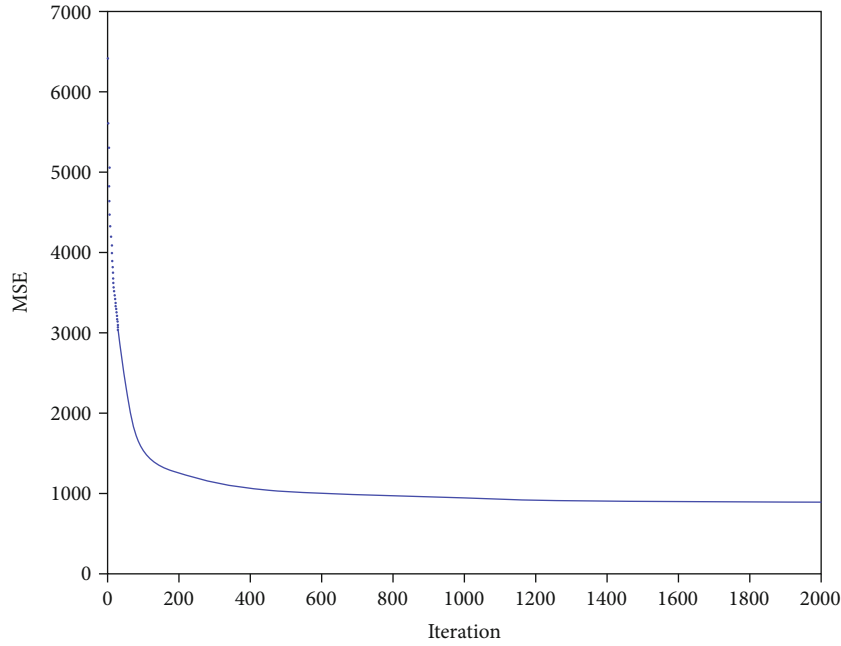


FIGURE 4: The training process of the MLP method.

3.4. Long Short-Term Memory (LSTM). Long short-term memory (LSTM) is a paradigm first suggested in 1997. Bidirectional LSTM expands the LSTM model, a gated recurrent neural network. The crucial aspect is that these networks may keep data for future cell processing. We may conceive of LSTM as an RNN with two key vectors and a memory pool [92]:

- (1) The output stays at the present step in a short-term condition
- (2) The long-term state, while moving across the network, saves, retrieves, and refuses things intended for the long-term

As shown in Figure 3, the choice to read, store, or write is dependent on some perceptron. The result of the activation functions is a number between 0 and 1 (0, 1). The forget and output gates decide whether fresh material should be kept or discarded. The model choice is made using the LSTM block's storage and the output gate's situation. The output is then sent again into the network as an input, resulting in a recurrent sequence. When categorizing texts, the LSTM model may be used to resolve the challenges that typical machine learning methods struggle to extract high-level meaning [93]. This model takes as input a content matrix made up of pretrained distributed word vectors and then uses its unique memory structure to extract feature expressions forming context information (see Figure 3). Figure 3(a) depicts the LSTM modeling approach. A conventional LSTM network may use only the historical context. The lack of future context, on the other hand, may result in an insufficient grasp of the compound word. A forward LSTM layer and a backward LSTM layer are combined in BiLSTM. The correlation method may be used entirely by

summing the knowledge of two ideates before and after the word. Figure 3(b) depicts the model's architecture [93].

4. Results and Discussion

4.1. Data Collection. NSL-KDD is a database suggested to address some of the KDD dataset's profound contradictions [94]. The definitive collection of data to be examined is contained in this database, which forms a wide range of simulated intrusions in a military network environment. However, McHugh's issues stay in this latest version of the KDD dataset. The natural network structure may not be completed. It can still be used as a collection due to the absence of public datasets for network-based systems. Researchers can employ user data to compare different intrusion detection technologies. Furthermore, the NSL-KDD training and test suites have a reasonable quantity of records. This edge can save money by allowing you to do tests on the complete set without having to pick a tiny section at random. As a result, the assessment outcomes of various research projects will be similar and consistent [94]. The NSL-KDD dataset offers benefits over the original KDD dataset: the learning suite lacks more information. Therefore, classifiers will not be biased toward more records. Because the testing sets have no history of duplicating, training performance is not influenced by approaches with higher detection capability in repeating data [95]. The proportion of records in the primary KDD dataset is inversely linked to the number picked from each category. As a result, the recognition accuracy of various machine learning methods varies across a more excellent range, making a correct assessment of different learning strategies more efficient. The training and test suites have a considerable number of records, making them cost-effective to run the tests in their

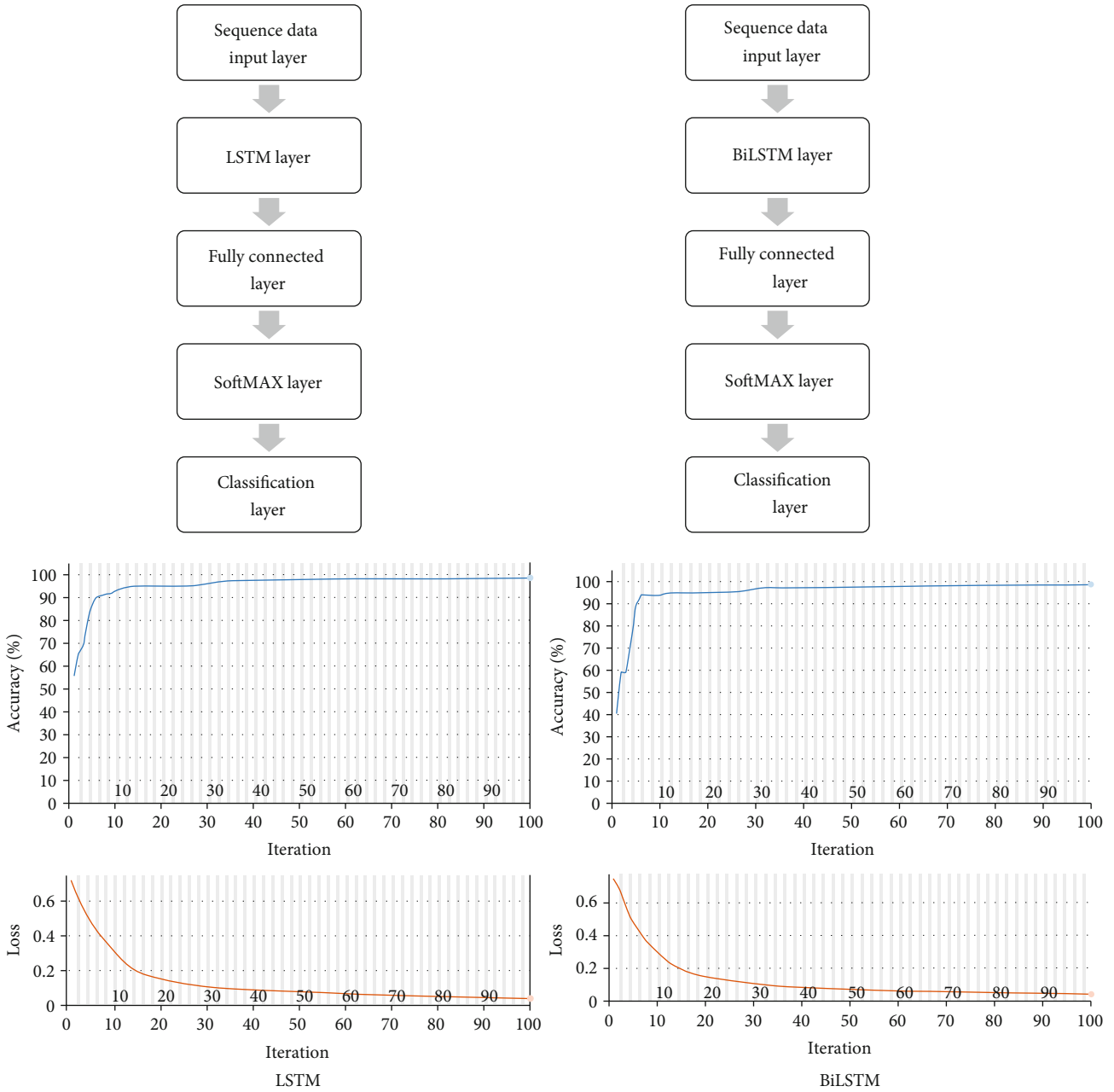


FIGURE 5: The architecture and the training process of the LSTM and BiLSTM networks.

entirety rather than selecting a tiny part at random. As a result, the outcomes of various research paper assessments will be uniform and similar. One of the critical drawbacks of KDD datasets is the enormous quantity of extra records, which causes pattern recognition to learn duplicate entries, which is typically destructive to networks such as U2R and R2L attacks. Furthermore, these repeated data in the test suite skew the assessment findings since approaches with superior detection rates in repeating records influence the outcome [94].

4.2. Results of Feature Extraction. Network traffic is often collected by DDoS detection techniques using passive net-

work monitoring. The bought data is then analyzed to check whether there is any attack traffic. There are two basic methods for scanning an inactive network. For instance, packet capture intercepts and records network data packets. Wireshark and TCP dump are two tools that can gather data packets. Network flow monitoring supplies aggregated traffic data for a flow between two endpoints. Consequently, DDoS detection systems' effectiveness is assessed using two feature sets: packet-level and flow-level characteristics. Table 2 summarizes the packet- and flow-level characteristics. This study describes a flow as a one-way series of packages with identical 5-tuple values, including the source IP address, source port number,

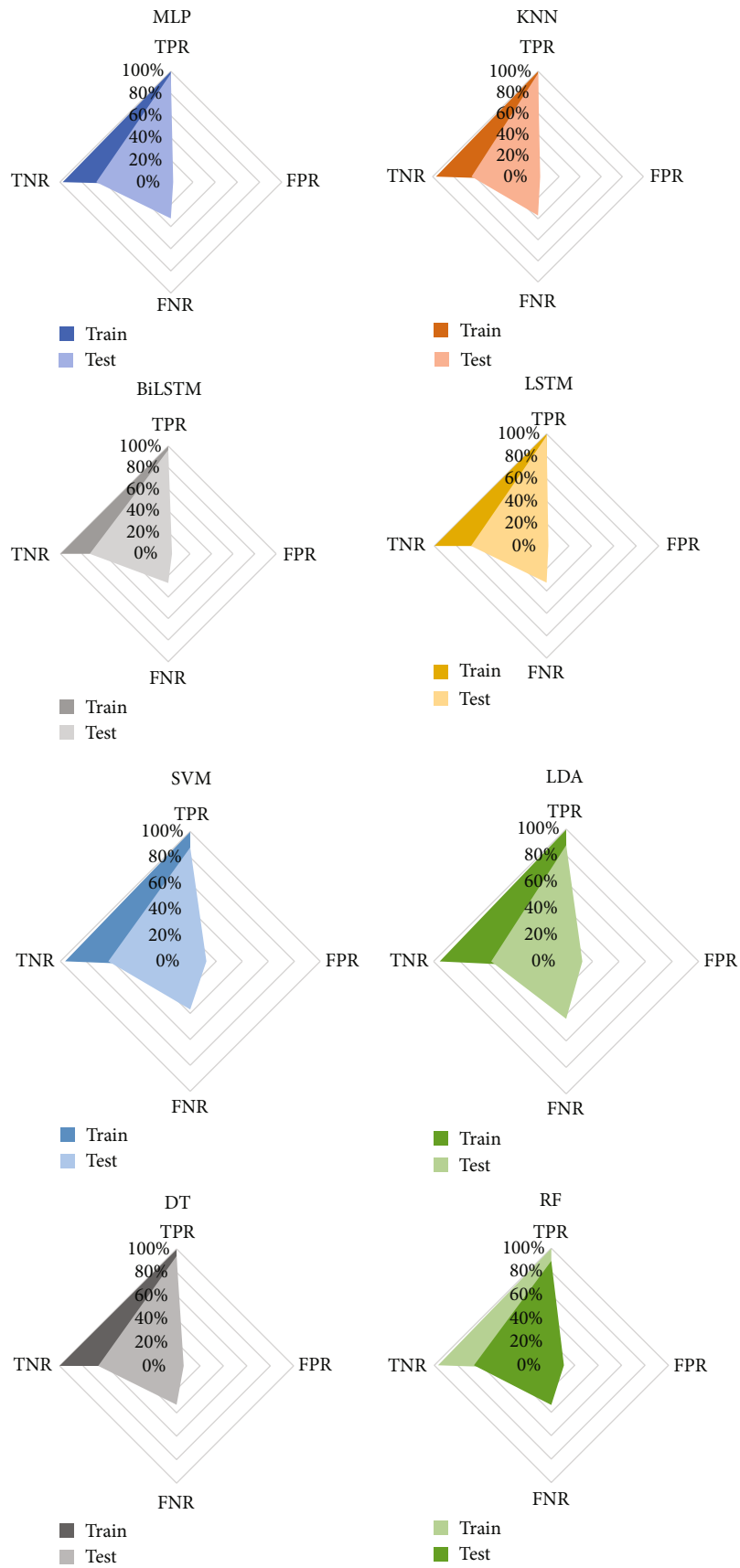


FIGURE 6: The confusion plots of the used ML methods.

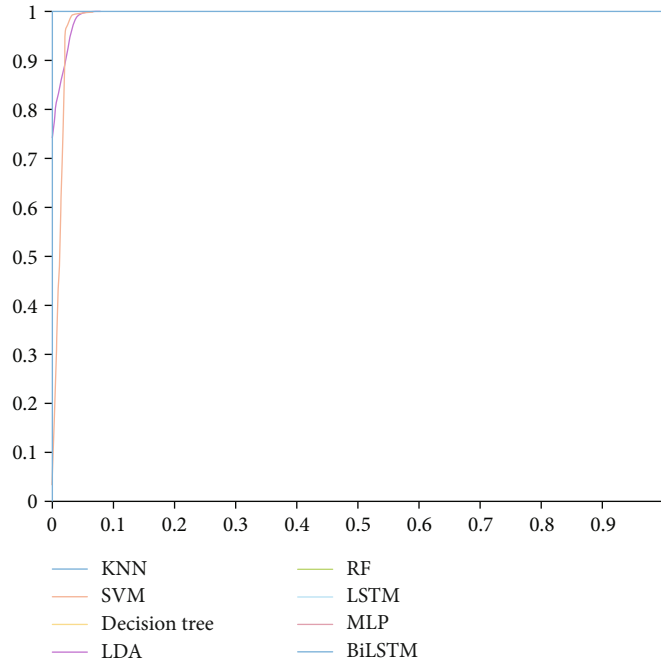


FIGURE 7: The ROC curve of the proposed methods.

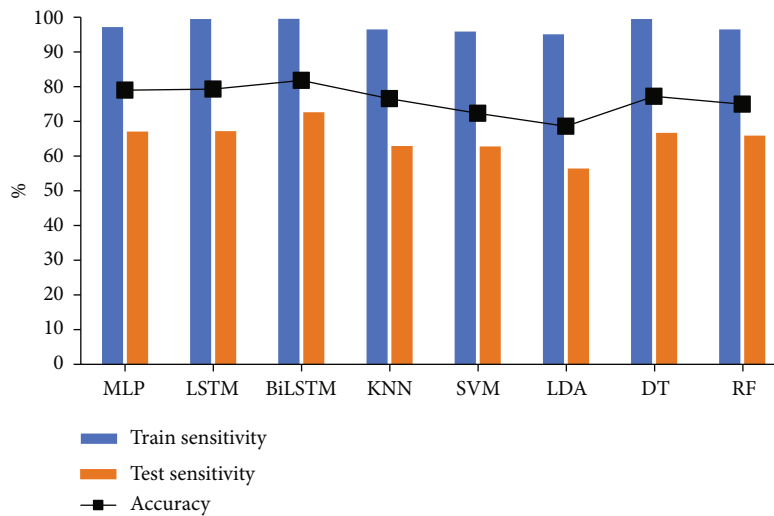


FIGURE 8: The accuracy, train sensitivity, and test sensitivity of the proposed approach.

destination IP address, port number, and protocol ID. This research investigates the detection performance of ML-based algorithms on both specified characteristics.

4.3. Classification Results. Various DDoS detection techniques have been presented. Many of them rely on a simple ANN using the backpropagation algorithm. The significant distinction between such designs is the structure of the recommended ANN in proportion to the number of neurons in each layer and the number of hidden layers. The majority of ANNs that have been evaluated have only one hidden layer. Neurons in the input layer reflect the gathered features from network traffic. In contrast, neurons in the output layer

show the needed labels. Neurons in the buried layer typically range from 3 to 50 in number. ANNs are used to perform a wide range of detection tasks.

An ANN is used to decide the number of zombies engaged in a DDoS attack in this research. The system generates a regular profile in advance and continuously analyzes network traffic to detect an attack. A DDoS attack is recorded when the entropy of flow size deviates from a usual preset threshold. The deviation value is given into the ANN model to calculate the number of zombies. An ensemble detection strategy was developed to find DDoS attacks, which combines multiple ANN classifiers. The training dataset was first partitioned into two groups, attack and routine

traffic, in the proposed way. The dataset for each class was further separated into n subgroups. The data was divided into k distinct groups in each subset. k training sets were reconstructed using these disjoint sets by omitting one of the disjoint sets. As a result, k and n ANN classifiers were created for each class. After then, a fresh instance is put through its paces with all the classifiers. Weighted majority voting is used to make decisions over n subsets in each class. In contrast, a weighted product rule is used to make decisions across distinct classes.

Eight machine learning algorithms are employed in this article to diagnose DDoS attacks in IoT. The process dataset is NSL-KDD, with 1 and 0 labels showing normal and anomalous behaviors, respectively. The MLP network is the first way of diagnosis. The ANN network is designed with two hidden layers, each having 19 and 10 neurons. 70% of the dataset is trained, with the remaining 30% used for validation and testing. Iteration continues until the MSE of numerical labels is fixed. Figure 4 shows the outcomes of the MLP network.

The categorization results are shown in the form of a confusion matrix (see Figure 5). Figure 6 shows the results of the training confusion matrix, which show that 99.9% of the attacks are effectively found. To put it another way, out of 12109 anomaly nodes, 12098 (99.9%) are discovered and trained; however, 11 are misdiagnosed. As a result, the training procedure has a sensitivity of 99.9%. Furthermore, specificity is the opposite side of the diagnostic. This measure depicts the frequency of bad outcomes. Based on these findings, 8115 (97.6%) normal nodes are appropriately categorized, while 199 (2.4%) are misdiagnosed. Finally, the accuracy metrics showed the true-positive rate as a percentage of all diagnostic positives. In this case, 98.4 percent of the 12297 nodes used in DDoS attacks are indeed positive nodes or attacks. Finally, the training procedure is 99 percent correct. The findings of the testing dataset, on the other hand, confirm the networks that were used. According to the results, the testing samples' accuracy for 30% of the data is 79.5 percent. Furthermore, the sensitivity, specificity, and accuracy scores are 97.9 percent, 67.3 percent, and 66.5 percent, respectively. If we use the overfitting metrics (OF) to measure the difference between the two accuracies, the OF is 19.5 percent. The lower value of this OF confirms the categorization findings. The LSTM and BiLSTM architectures are depicted in Figure 5. The accuracy value of the LSTM and BiLSTM for the training procedure is 99.9% and 100%, respectively, based on their results. Furthermore, the OF values are 20.1 percent and 17.7 percent, respectively. MLP, LSTM, BiLSTM, KNN, SVM, LDA, DT, and RF are among the eight machine learning algorithms used to verify the classification findings in this study. The LSTM and BiLSTM approaches surpass other methods in terms of test accuracy.

The ROC is illustrated in Figure 7 to compare the provided machine learning approach for diagnosing DDoS attacks. The horizontal axis of the ROC curve is the rate of the false-positive index depending on the anomaly class. The vertical axis shows the actual positive rate. The best classifier has the highest rate of true positives and the lowest

number of false positives. The BiLSTM approach appears to be the best classifier for the supplied characteristics based on the findings. Figure 8 shows the accuracy of the machine learning classifiers. MLP, LSTM, BiLSTM, KNN, SVM, LDA, DT, and RF accuracy values are 79.5 percent, 80 percent, 82.3 percent, 77 percent, 82.8 percent, 69 percent, 77.7 percent, and 75.4 percent, respectively, according to the data. Using the provided strategy, the BiLSTM architecture with the maximum accuracy is more correct and suitable for diagnosing DDoS attacks in IoT.

5. Conclusion

This study uses eight machine learning algorithms to diagnose DDoS attacks in IoT, including MLP, LSTM, BiLSTM, KNN, SVM, LDA, DT, and RF. The process dataset is NSL-KDD, with 1 and 0 labels showing normal and anomalous behaviors, respectively. The categorization results are shown in the form of a confusion matrix. According to the findings of MLP's training confusion matrix, 99.9% of attacks are effectively recognized. Furthermore, specificity is the opposite side of the diagnostic. This measure depicts the frequency of bad outcomes. Based on these findings, 8115 (97.6%) normal nodes are appropriately categorized, while 199 (2.4%) are misdiagnosed. Finally, the accuracy metrics showed the true-positive rate as a percentage of all diagnostic positives. The accuracy value of the LSTM and BiLSTM for the training procedure is 99.9% and 100%, respectively, based on their results. Furthermore, the OF values are 20.1 percent and 17.7 percent, respectively. The LSTM and BiLSTM approaches surpass other methods in terms of test accuracy. The ROC is shown to compare the provided machine learning algorithm for diagnosing DDoS attacks. Based on the findings, the BiLSTM process appears to be the best classifier for the supplied characteristics. MLP, LSTM, BiLSTM, KNN, SVM, LDA, DT, and RF test accuracy values are 79.5 percent, 80 percent, 82.3 percent, 77 percent, 82.8 percent, 69 percent, 77.7 percent, and 75.4 percent, respectively. Using the provided strategy, the BiLSTM architecture with the maximum accuracy is more correct and suitable for diagnosing DDoS attacks in IoT. For future works, we suggest that other methods like GRU also can result in high accuracy like LSTM methods.

Acronyms

ANN:	Artificial neural network
BiLSTM:	Bidirectional long short-term memory
CNN:	Convolutional neural network
CWT:	Continuous wavelet transform
DL:	Deep learning
DNS:	Domain name system
DT:	Decision tree
ICMP:	Internet control message protocol
DDoS:	Distributed denial of service
DoS:	Denial of service
IDS:	Intrusion detection system
IoT:	Internet of Things
KNN:	k -nearest neighbor algorithm

LDA:	Linear discriminant analysis
LSTM:	Long short-term memory
MLP:	Multilayer perceptron
NSL-KDD:	Network-based intrusion detection system dataset
NTP:	Network time protocol
OSI:	Open system interconnection
R2L:	Remote to user
RF:	Random forest
RNN:	Recurrent neural network
ROC:	Receiver operating characteristic
SDN:	Software-defined networking
SVM:	Support vector machine
SYN:	Synchronize
TCP:	Transmission control protocol
U2R:	User to root
UDP:	User datagram protocol
VFDT:	Variance fractal dimension trajectory.

Data Availability

Data is available and can be provided over the emails querying directly to the corresponding author (hamid.gh@aut.ac.ir).

Conflicts of Interest

The authors declare that they have no conflicts of interest.

References

- [1] Y. Liu, T. Zhi, M. Shen, L. Wang, Y. Li, and M. Wan, "Software-defined DDoS detection with information entropy analysis and optimized deep learning," *Future Generation Computer Systems*, vol. 129, pp. 99–114, 2022.
- [2] J. Kim, J. Kim, H. Kim, M. Shim, and E. Choi, "CNN-based network intrusion detection against denial-of-service attacks," *Electronics*, vol. 9, no. 6, pp. 916–921, 2020.
- [3] F. O. Catak and A. F. Mustacoglu, "Distributed denial of service attack detection using autoencoder and deep neural networks," *Journal of Intelligent Fuzzy Systems*, vol. 37, no. 3, pp. 3969–3979, 2019.
- [4] J. Wang, Y. Liu, H. Feng, and National Engineering Laboratory on Interconnection Technology for Next Generation Internet, Beijing Jiaotong University, Beijing, China, "IFACNN: efficient DDoS attack detection based on improved firefly algorithm to optimize convolutional neural networks," *Mathematical Biosciences and Engineering*, vol. 19, no. 2, pp. 1280–1303, 2021.
- [5] M. Abbasi, A. Shahraki, and A. Taherkordi, "Deep learning for network traffic monitoring and analysis (NTMA): a survey," *Computer Communications*, vol. 170, pp. 19–41, 2021.
- [6] G. Aceto, D. Ciuonzo, A. Montieri, and A. Pescapé, "Mobile encrypted traffic classification using deep learning: experimental evaluation, lessons learned, and challenges," *IEEE Transactions on Network and Service Management*, vol. 16, no. 2, pp. 445–458, 2019.
- [7] K. S. Sahoo, S. K. Panda, S. Sahoo, B. Sahoo, and R. Dash, "Toward secure software-defined networks against distributed denial of service attack," *The Journal of Supercomputing*, vol. 75, no. 8, pp. 4829–4874, 2019.
- [8] S. Kottler, "February 28th DDoS incident report," *GitHub*, pp. 1–3, 2018, <http://githubengineering.com/ddos-incident-report/>.
- [9] S. Haider, A. Akhuzada, I. Mustafa et al., "A deep CNN ensemble framework for efficient DDoS attack detection in software defined networks," *IEEE Access*, vol. 8, pp. 53972–53983, 2020.
- [10] P. Manso, J. Moura, and C. Serrão, "SDN-based intrusion detection system for early detection and mitigation of DDoS attacks," *Information*, vol. 10, no. 3, p. 106, 2019.
- [11] I. Karim, Q. T. Vien, T. A. Le, and G. Mapp, "A comparative experimental design and performance analysis of Snort-based intrusion detection system in practical computer networks," *Computers*, vol. 6, no. 1, p. 6, 2017.
- [12] R. Xu, J. Cheng, F. Wang, X. Tang, and J. Xu, "A DRDoS detection and defense method based on deep forest in the big data environment," *Symmetry (Basel)*, vol. 11, no. 1, p. 78, 2019.
- [13] D. Ramotsoela, A. Abu-Mahfouz, and G. Hancke, "A survey of anomaly detection in industrial wireless sensor networks with critical water system infrastructure as a case study," *Sensors (Switzerland)*, vol. 18, no. 8, p. 2491, 2018.
- [14] Z. Lv, Y. Li, H. Feng, and H. Lv, "Deep learning for security in digital twins of cooperative intelligent transportation systems," *IEEE Transactions on Intelligent Transportation Systems*, pp. 1–10, 2021.
- [15] J. Chen, Q. Wang, J. Huang, and X. Chen, "Motorcycle ban and traffic safety: evidence from a quasi-experiment at Zhejiang, China," *Journal of advanced transportation*, vol. 2021, Article ID 7552180, 13 pages, 2021.
- [16] Z. Lv, J. Guo, and H. Lv, "Safety Poka yoke in zero-defect manufacturing based on digital twins," *IEEE transactions on industrial informatics*, p. 1, 2022.
- [17] X. Liu, J. Zhao, J. Li, B. Cao, and Z. Lv, "Federated neural architecture search for medical data security," *IEEE transactions on industrial informatics*, vol. 18, no. 8, pp. 5628–5636, 2022.
- [18] Q. Sun, K. Lin, C. Si, Y. Xu, S. Li, and P. Gope, "A secure and anonymous communicate scheme over the Internet of Things," *ACM Transactions on Sensor Networks*, vol. 18, no. 3, pp. 1–21, 2022.
- [19] A. Mehbodniya, J. L. Webber, M. Shabaz, H. Mohafez, and K. Yadav, "Machine learning technique to detect Sybil attack on IoT based sensor network," *IETE Journal of Research*, pp. 1–9, 2021.
- [20] B. Cao, J. Zhang, X. Liu et al., "Edge-cloud resource scheduling in space-air-ground integrated networks for Internet of Vehicles," *IEEE Internet of Things Journal*, vol. 9, no. 8, pp. 5765–5772, 2021.
- [21] G. Sun, Y. Cong, J. Dong, Y. Liu, Z. Ding, and H. Yu, "What and how: generalized lifelong spectral clustering via dual memory," *IEEE transactions on pattern analysis and machine intelligence*, vol. 44, no. 7, pp. 3895–3908, 2021.
- [22] M. Ahmadi, A. Taghavirashidzadeh, D. Javaheri, A. Masoumian, S. J. Ghoushchi, and Y. Pourasad, "DQRE-SCnet: a novel hybrid approach for selecting users in federated learning with deep-Q-reinforcement learning based on spectral clustering," *Journal of King Saud University-Computer and Information Sciences*, 2021.
- [23] G. Sun, Y. Cong, Q. Wang, B. Zhong, and Y. Fu, "Representative task self-selection for flexible clustered lifelong learning," *IEEE transaction on neural networks and learning systems*, vol. 33, no. 4, pp. 1467–1481, 2020.


- [24] F. Liu, G. Zhang, and J. Lu, "Multi-source heterogeneous unsupervised domain adaptation via fuzzy-relation neural networks," *IEEE Transactions on Fuzzy Systems*, vol. 29, no. 11, pp. 3308–3322, 2020.
- [25] A. Mehbodniya, J. L. Webber, R. Neware, F. Arslan, R. V. Pamba, and M. Shabaz, "Modified Lamport Merkle Digital Signature blockchain framework for authentication of Internet of Things healthcare data," *Expert Systems*, p. e12978, 2022.
- [26] L. Zhang, T. Gao, G. Cai, and K. L. Hai, "Research on electric vehicle charging safety warning model based on back propagation neural network optimized by improved gray wolf algorithm," *Journal of Energy Storage*, vol. 49, p. 104092, 2022.
- [27] J. Dong, Y. Cong, G. Sun, Z. Fang, and Z. Ding, "Where and how to transfer: knowledge aggregation-induced transferability perception for unsupervised domain adaptation," *IEEE Transactions on Pattern Analysis and Machine Intelligence*, p. 1, 2021.
- [28] W. Yang, X. Chen, Z. Xiong, Z. Xu, G. Liu, and X. Zhang, "A privacy-preserving aggregation scheme based on negative survey for vehicle fuel consumption data," *Information Sciences*, vol. 570, pp. 526–544, 2021.
- [29] X. Wu, W. Zheng, X. Chen, Y. Zhao, T. Yu, and D. Mu, "Improving high-impact bug report prediction with combination of interactive machine learning and active learning," *Information and Software Technology*, vol. 133, p. 106530, 2021.
- [30] A. Khaliq, A. Anjum, A. Ajmal, J. Webber, A. Mehbodniya, and S. Khan, "A secure and privacy preserved parking recommender system using elliptic curve cryptography and local differential privacy," *IEEE Access*, vol. 10, 2022.
- [31] X. Wu, W. Zheng, X. Xia, and D. Lo, "Data quality matters: a case study on data label correctness for security bug report prediction," *IEEE Transactions on Software Engineering*, vol. 48, no. 7, pp. 2541–2556, 2021.
- [32] W. Zheng, Y. Xun, X. Wu, Z. Deng, X. Chen, and Y. Sui, "A comparative study of class rebalancing methods for security bug report classification," *IEEE Transactions on Reliability*, vol. 70, no. 4, pp. 1658–1670, 2021.
- [33] W. Zheng, T. Shen, X. Chen, and P. Deng, "Interpretability application of the Just-in-Time software defect prediction model," *Journal of Systems and Software*, vol. 188, article 111245, 2022.
- [34] K. Liu, F. Ke, X. Huang et al., "DeepBAN: a temporal convolution-based communication framework for dynamic WBANs," *IEEE Transactions on Communications*, vol. 69, no. 10, pp. 6675–6690, 2021.
- [35] T. Gera, J. Singh, A. Mehbodniya, J. L. Webber, M. Shabaz, and D. Thakur, "Dominant feature selection and machine learning-based hybrid approach to analyze android ransomware," *Security and Communication Networks*, vol. 2021, Article ID 7035233, 22 pages, 2021.
- [36] Z. Liu, P. Qian, X. Wang, Y. Zhuang, L. Qiu, and X. Wang, "Combining graph neural networks with expert knowledge for smart contract vulnerability detection," *IEEE Transactions on Knowledge and Data Engineering*, p. 1, 2021.
- [37] X. Zhang, Y. Wang, M. Yang, and G. Geng, "Toward concurrent video multicast orchestration for caching-assisted mobile networks," *IEEE Transactions on Vehicular Technology*, vol. 70, no. 12, pp. 13205–13220, 2021.
- [38] C. Zong, H. Wang, and Z. Wan, "An improved 3D point cloud instance segmentation method for overhead catenary height detection," *Computers & electrical engineering*, vol. 98, article 107685, 2022.
- [39] A. Varmaghani, A. Matin Nazar, M. Ahmadi, A. Sharifi, S. Jafarzadeh Ghouschi, and Y. Pourasad, "DMTC: optimize energy consumption in dynamic wireless sensor network based on fog computing and fuzzy multiple attribute decision-making," *Wireless Communications and Mobile Computing*, vol. 2021, Article ID 9953416, 14 pages, 2021.
- [40] C. Zong and Z. Wan, "Container ship cell guide accuracy check technology based on improved 3D point cloud instance segmentation," *Brodogradnja*, vol. 73, no. 1, pp. 23–35, 2022.
- [41] R. Singh, A. Mehbodniya, J. L. Webber et al., "Analysis of network slicing for management of 5G networks using machine learning techniques," *Wireless Communications and Mobile Computing*, vol. 2022, Article ID 9169568, 10 pages, 2022.
- [42] Y. Xie, Y. Sheng, M. Qiu, and F. Gui, "An adaptive decoding biased random key genetic algorithm for cloud workflow scheduling," *Engineering applications of artificial intelligence*, vol. 112, article 104879, 2022.
- [43] A. Li, C. Masouros, A. L. Swindlehurst, and W. Yu, "1-bit massive MIMO transmission: embracing interference with symbol-level precoding," *IEEE Communications Magazine*, vol. 59, no. 5, pp. 121–127, 2021.
- [44] Y. Feng, B. Zhang, Y. Liu et al., "A 200–225-GHz manifold-coupled multiplexer utilizing metal wave guides," *IEEE Transactions on Microwave Theory and Techniques*, vol. 69, no. 12, pp. 5327–5333, 2021.
- [45] M. Ghanbari, "Adaptive machine learning and signal processing detection schemes for DDoS attacks," 2022.
- [46] Z. Niu, B. Zhang, B. Dai et al., "220 GHz multi circuit integrated front end based on solid-state circuits for high speed communication system," *Chinese Journal of Electronics*, vol. 31, no. 3, pp. 569–580, 2022.
- [47] W. Zheng, L. Yin, X. Chen, Z. Ma, S. Liu, and B. Yang, "Knowledge base graph embedding module design for visual question answering model," *Pattern Recognition*, vol. 120, p. 108153, 2021.
- [48] A. R. Ramtin, P. Nain, D. S. Menasche, D. Towsley, and E. D. S. E Silva, "Fundamental scaling laws of covert DDoS attacks," *Performance Evaluation*, vol. 151, p. 102236, 2021.
- [49] W. Zheng, X. Liu, X. Ni, L. Yin, and B. Yang, "Improving visual reasoning through semantic representation," *IEEE Access*, vol. 9, pp. 91476–91486, 2021.
- [50] W. Zheng, X. Liu, and L. Yin, "Sentence representation method based on multi-layer semantic network," *Applied Sciences*, vol. 11, no. 3, p. 1316, 2021.
- [51] J. Yu, L. Lu, Y. Chen, Y. Zhu, and L. Kong, "An indirect eavesdropping attack of keystrokes on touch screen through acoustic sensing," *IEEE Transactions on Mobile Computing*, vol. 20, no. 2, pp. 337–351, 2021.
- [52] H. Kong, L. Lu, J. Yu, Y. Chen, and F. Tang, "Continuous authentication through finger gesture interaction for smart homes using WiFi," *IEEE Transactions on Mobile Computing*, vol. 20, no. 11, pp. 3148–3162, 2021.
- [53] B. Hajipour Khire Masjidi, S. Bahmani, F. Sharifi, M. Peivandi, M. Khosravani, and A. Hussein Mohammed, "CT-ML: diagnosis of breast cancer based on ultrasound images and time-dependent feature extraction methods using contourlet transformation and machine learning," *Computational Intelligence and Neuroscience*, vol. 2022, Article ID 1493847, 15 pages, 2022.

- [54] S. Zhao, F. Li, H. Li et al., "Smart and practical privacy-preserving data aggregation for fog-based smart grids," *IEEE Transactions on Information Forensics and Security*, vol. 16, pp. 521–536, 2021.
- [55] Q. Meng, X. Lai, Z. Yan, C. Su, and M. Wu, "Motion planning and adaptive neural tracking control of an uncertain two-link rigid-flexible manipulator with vibration amplitude constraint," *IEEE Transactions on Neural Networks and Learning Systems*, vol. 33, no. 8, pp. 3814–3828, 2021.
- [56] M. Najafimehr, S. Zarifzadeh, and S. Mostafavi, "A hybrid machine learning approach for detecting unprecedented DDoS attacks," *The Journal of Supercomputing*, vol. 78, no. 6, pp. 8106–8136, 2022.
- [57] A. Prasad and S. Chandra, "VMFCVD: an optimized framework to combat volumetric DDoS attacks using machine learning," *Arabian Journal for Science and Engineering*, vol. 47, pp. 1–19, 2022.
- [58] X. Xu, J. Sun, C. Wang, and B. Zou, "A novel hybrid CNN-LSTM compensation model against DoS attacks in power system state estimation," *Neural Processing Letters*, vol. 54, no. 3, pp. 1597–1621, 2022.
- [59] E. Tsogbaatar, M. H. Bhuyan, D. Fall et al., "A 1D-CNN based deep learning for detecting VSI-DDoS attacks in IoT applications," in *International Conference on Industrial, Engineering and Other Applications of Applied Intelligent Systems*, vol. 12798 of *Advances and Trends in Artificial Intelligence. Artificial Intelligence Practices*, pp. 530–543, Springer, Cham, 2021.
- [60] D. Tang, L. Tang, W. Shi, S. Zhan, and Q. Yang, "MF-CNN: a new approach for LDoS attack detection based on multi-feature fusion and CNN," *Mobile Networks and Applications*, vol. 26, no. 4, pp. 1705–1722, 2021.
- [61] H. Alkahtani and T. H. H. Aldhyani, "Botnet attack detection by using CNN-LSTM model for Internet of Things applications," *Security and Communication Networks*, vol. 2021, 23 pages, 2021.
- [62] R. V. Mendonca, A. A. M. Teodoro, R. L. Rosa et al., "Intrusion detection system based on fast hierarchical deep convolutional neural network," *IEEE Access*, vol. 9, pp. 61024–61034, 2021.
- [63] M. Ghanbari and W. Kinsner, "Detecting DDoS attacks using an adaptive-wavelet convolutional neural network," *Canadian Conference on Electrical and Computer Engineering*, 2021, pp. 1–7, ON, Canada, September 2021.
- [64] X. Liu, Z. Tang, and B. Yang, "Predicting network attacks with CNN by constructing images from NetFlow data," in *2019 IEEE 5th Intl Conference on Big Data Security on Cloud (Big-DataSecurity), IEEE Intl Conference on High Performance and Smart Computing (HPSC) and IEEE Intl Conference on Intelligent Data and Security (IDS)*, pp. 61–66, Washington, DC, USA, May 2019.
- [65] J. Cheng, Y. Liu, X. Tang, V. S. Sheng, M. Li, and J. Li, "DDoS attack detection via multi-scale convolutional neural network," *Computers, Materials & Continua*, vol. 62, no. 3, pp. 1317–1333, 2020.
- [66] A. E. Cil, K. Yildiz, and A. Buldu, "Detection of DDoS attacks with feed forward based deep neural network model," *Expert Systems with Applications*, vol. 169, p. 114520, 2021.
- [67] N. Mishra and S. Pandya, "Internet of Things applications, security challenges, attacks, intrusion detection, and future visions: a systematic review," *IEEE Access*, vol. 9, pp. 59353–59377, 2021.
- [68] M. Ahmadi and M. Q. H. Abadi, "A review of using object-orientation properties of C++ for designing expert system in strategic planning," *Computer Science Review*, vol. 37, p. 100282, 2020.
- [69] G. Zhou, X. Bao, S. Ye, H. Wang, and H. Yan, "Selection of optimal building facade texture images from UAV-based multiple oblique image flows," *IEEE Transactions on Geoscience and Remote Sensing*, vol. 59, no. 2, pp. 1534–1552, 2021.
- [70] M. Ahmadi, M. Soofiabadi, M. Nikpour, H. Naderi, L. Abdullah, and B. Arandian, "Developing a deep neural network with fuzzy wavelets and integrating an inline PSO to predict energy consumption patterns in urban buildings," *Mathematics*, vol. 10, no. 8, p. 1270, 2022.
- [71] G. Zhou, X. Zhou, Y. Song et al., "Design of supercontinuum laser hyperspectral light detection and ranging (LiDAR) (SCLaHS LiDAR)," *International journal of remote sensing*, vol. 42, no. 10, pp. 3731–3755, 2021.
- [72] M. Tondro, M. Jahanbakht, S. B. Rabbani, and M. Zaber, "Does immergence of ICT focused institutions increase the pace of urban development? A provincial case study in Iran using data from the ground and above," in *I2022 IEEE Conference on Technologies for Sustainability (SusTech)*, pp. 219–223, Corona, CA, USA, April 2022.
- [73] G. Zhou, R. Zhang, and S. Huang, "Generalized buffering algorithm," *IEEE Access*, vol. 9, pp. 27140–27157, 2021.
- [74] X. Liang, L. Luo, S. Hu, and Y. Li, "Mapping the knowledge frontiers and evolution of decision making based on agent-based modeling," *Knowledge-Based Systems*, vol. 250, p. 108982, 2022.
- [75] L. Zhao and L. Wang, "A new lightweight network based on MobileNetV3," *KSII Transactions on Internet and Information Systems (TIIS)*, vol. 16, no. 1, pp. 1–15, 2022.
- [76] H. Zhu, M. Xue, Y. Wang, G. Yuan, and X. Li, "Fast visual tracking with Siamese oriented region proposal network," *IEEE Signal Processing Letters*, vol. 29, p. 1437, 2022.
- [77] J. Li, K. Xu, S. Chaudhuri, E. Yumer, H. Zhang, and L. Guibas, "GRASS: generative recursive autoencoders for shape structures," *ACM Transactions on Graphics (TOG)*, vol. 36, no. 4, pp. 1–14, 2017.
- [78] P. P. F. Rajeeva, R. Orban, K. S. Vadivel et al., "A novel method for the classification of butterfly species using pre-trained CNN models," *Electronics*, vol. 11, no. 13, p. 2016, 2022.
- [79] H. Ghayvat, S. Pandya, P. Bhattacharya et al., "CP-BDHC: blockchain-based confidentiality-privacy preserving big data scheme for healthcare clouds and applications," *IEEE Journal of Biomedical and Health Informatics*, vol. 26, no. 5, pp. 1937–1948, 2021.
- [80] Y. Mirsky, T. Doitshman, Y. Elovici, and A. Shabtai, "Kitsune: an ensemble of autoencoders for online network intrusion detection," 2018, <http://arxiv.org/abs/1802.09089>.
- [81] G. Bovenzi, G. Aceto, D. Ciunzio, V. Persico, and A. Pescapé, "A hierarchical hybrid intrusion detection approach in IoT scenarios," in *2020 IEEE Global Communications Conference, GLOBECOM 2020- Proceedings*, pp. 1–7, Taipei, Taiwan, December 2020.
- [82] M. Ghanbari and W. Kinsner, "Detecting DDoS attacks using polyscale analysis and deep learning," *International Journal of Cognitive Informatics and Natural Intelligence*, vol. 14, no. 1, pp. 17–34, 2020.
- [83] J. Zhang, C. Zhu, L. Zheng, and K. Xu, "ROSEfusion: random optimization for online dense reconstruction under fast

- camera motion,” *ACM transactions on graphics*, vol. 40, no. 4, pp. 1–17, 2021.
- [84] F. Zhang, J. Zhai, X. Shen, O. Mutlu, and X. Du, “POCLib: a high-performance framework for enabling near orthogonal processing on compression,” *IEEE transactions on Parallel and Distributed Systems*, vol. 33, no. 2, pp. 459–475, 2022.
- [85] R. F. Fouladi, O. Ermiş, and E. Anarim, “A novel approach for distributed denial of service defense using continuous wavelet transform and convolutional neural network for software-defined network,” *Computers & Security*, vol. 112, p. 102524, 2022.
- [86] Y. Cui, Q. Qian, C. Guo et al., “Towards DDoS detection mechanisms in software-defined networking,” *Journal of Network and Computer Applications*, vol. 190, p. 103156, 2021.
- [87] R. Doshi, N. Apthorpe, and N. Feamster, “Machine learning DDoS detection for consumer Internet of Things devices,” in *Proceedings -2018 IEEE Symposium on Security and Privacy Workshops, SPW*, pp. 29–35, San Francisco, CA, USA, May 2018.
- [88] R. M. A. Ujjan, Z. Pervez, K. Dahal, A. K. Bashir, R. Mumtaz, and J. González, “Towards sFlow and adaptive polling sampling for deep learning based DDoS detection in SDN,” *Future Generation Computer Systems*, vol. 111, pp. 763–779, 2020.
- [89] Z. Liu, X. Yin, and Y. Hu, “CPSS LR-DDoS detection and defense in edge computing utilizing DCNN Q-learning,” *IEEE Access*, vol. 8, pp. 42120–42130, 2020.
- [90] J. Hou, P. Fu, Z. Cao, and A. Xu, “Machine learning based DDoS detection through NetFlow analysis,” in *Proceedings-IEEE Military Communications Conference MILCOM*, pp. 565–570, Los Angeles, CA, USA, October 2018.
- [91] Y. N. Soe, P. I. Santosa, and R. Hartanto, “DDoS attack detection based on simple ANN with SMOTE for IoT environment,” in *Proceedings of 2019 4th International Conference on Informatics and Computing, ICIC*, pp. 1–5, Semarang, Indonesia, October 2019.
- [92] Y. Li and Y. Lu, “LSTM-BA: DDoS detection approach combining LSTM and Bayes,” in *Proceedings -2019 7th International Conference on Advanced Cloud and Big Data, CBD*, pp. 180–185, Suzhou, China, September 2019.
- [93] W. Huang, X. Peng, Z. Shi, and Y. Ma, “Adversarial attack against LSTM-based DDoS intrusion detection system,” in *Proceedings-International Conference on Tools with Artificial Intelligence, ICTAI*, pp. 686–693, Baltimore, MD, USA, November 2020.
- [94] M. Tavallae, E. Bagheri, W. Lu, and A. A. Ghorbani, “A detailed analysis of the KDD CUP 99 data set,” in *IEEE Symposium on Computational Intelligence for Security and Defense Applications, CISDA*, pp. 1–6, Ottawa, ON, Canada, July 2009.
- [95] R. Rama Devi and M. Abualkibash, “Intrusion detection system classification using different machine learning algorithms on KDD-99 and NSL-KDD datasets - a review paper,” *International Journal of Computer Science & Information Technology (IJCSIT)*, vol. 11, no. 3, pp. 65–80, 2019.

Research Article

Design of Shared Internet of Things System for English Translation Teaching Using Deep Learning Text Classification

Lin He,¹ Jiaqi Guo,² and Jiaxin Lin ³

¹School of Foreign Languages, Southwest Medical University, Luzhou 646000, China

²Graduate School, The University of Melbourne, Victoria 3010, Australia

³School of Foreign Studies, Northwestern Polytechnical University, Xi'an 710129, China

Correspondence should be addressed to Jiaxin Lin; jasonlin@gdufe.edu.cn

Received 26 March 2022; Revised 17 May 2022; Accepted 7 July 2022; Published 30 July 2022

Academic Editor: Mu-Yen Chen

Copyright © 2022 Lin He et al. This is an open access article distributed under the Creative Commons Attribution License, which permits unrestricted use, distribution, and reproduction in any medium, provided the original work is properly cited.

The purpose is to adapt to the current social development and promote the English translation teaching reform. Based on the theories of deep learning (DL), text classification (TC), and the Internet of Things (IoT), this work analyzes the current situation of English translation teaching. Additionally, 100 text categories are selected from the English text corpus of Northwestern Polytechnic University as the research objects. The data are classified by the DL-based TC method and analyzed by introducing the simulated annealing algorithm. Finally, the storage and security performance of the shared IoT system are described. The results show that the proposed TC method can overcome the performance loss caused by the function extraction method, greatly reducing the training time and function space. The storage and security performance of the shared IoT system to encrypt English text will increase with the number of model iterations. Therefore, this work designs the English translation teaching-oriented shared IoT system using a DL-based TC. The finding plays an important role in subsequent English translation and enriching the theory of IoT.

1. Introduction

China's cultural, political, and ideological exchanges extend globally with domestic development and further opening up. Thus, as the demand for composite multilingual talents spikes, the importance of college English translation teaching also increases. Reforming college English translation and improving students' comprehensive English quality are keys to translation teaching. This has attracted all stakeholders in English education and international communication [1].

Amin et al. [2] proposed the deep learning- (DL-) based Word2Vec model to convert words into vectors, didimensionalized the high-dimensional sparse vectors, and judged the semantic similarity between words through the word distances. Then, the Doc2vec mode was used to represent sentence vectors and text vectors. Meanwhile, the similarity between sentences/texts was judged through the sentence/text vector distance. Although Word2Vec could lend well to lexical analysis, it effectively failed to use global lexical

information. Shen et al. [3] designed the glove method by learning word vectors based on global vocabulary information, and the representation of word vectors has indeed been improved. Wang et al. [4] constructed a FastText structure similar to Word2Vec, only with different tasks. FastText accelerated the training speed while maintaining high accuracy. It could be as accurate as the DP classifier by using n -grams to narrow the linear and DL models' accuracy gap. Kim et al. [5] utilized a hierarchical attention model to classify long text and represent text features. Compared with other traditional models, the hierarchical attention model performed better in document classification tasks. Zeng et al. [6] applied DL to the text classification (TC) model and greatly improved the classification effect. These research findings had strong research significance in the TC field. With the emergence of artificial intelligence (AI) and boosting series algorithm models, many researchers used the boosting algorithm for TC and achieved good results. Mahdi et al. [7] applied the DL-based TC algorithm to English translation teaching and improved students' classroom

enthusiasm and understanding of English words and grammar. Following the above literature review, this work tries to distinguish itself by further exploring the possible combination of DL-based TC algorithm with the Internet of Things (IoT), Word2Vec, Doc2vec, and attention mechanism (AM). Meanwhile, this work starts from the overall situation in the English translation types without a specific division of poetry, novels, and narrative. Thus, the findings have a certain universality.

DL, TC, and IoT technology are being integrated into English translation teaching in this context. Then, it classifies the English text corpus of Northwestern Polytechnic University using the TC method. The translation results are analyzed by considering the IoT system storage and safety factor. The purpose is to provide effective methods for English translation teaching in the future. Figure 1 displays the theoretical framework.

2. Basic Concept and Technical Route

2.1. TC. Text representation, the primary task of TC, converts text information into a computer-understandable form and then uses various algorithms to complete natural language processing (NLP). TC divides a text into multiple categories according to the subject and content of a given document. In the late 1950s, word frequency statistics, probability models, and factor decomposition algorithms promoted the rapid development of TC technology. Since then, many researchers have carried out extensive research in TC [8].

Latent Dirichlet Allocation (LDA), an unsupervised machine learning (ML) technology, can extract topic information hidden in large-scale document sets or corpora. LDA introduces word exchange by representing each document as a word frequency vector. Then, hard-to-model texts are digitalized [9] to reduce complexity by ignoring the relationship and order among words, thus improving the model. The formation process of LDA is as follows.

- (1) For each document, a topic is extracted from the topic distribution
- (2) Then, a word is extracted from the word distribution of the topic
- (3) The process iterates until each word in the document is traversed

In English translation, the keywords are the text features reflecting the content. The keywords and word frequency differ from document to document. Thus, they are good metrics for distinguishing documents. The words can be extracted through word segmentation. So far, multiple mature English thesauruses are available for word segmentation, such as the data thesaurus [10].

The research on Chinese TC technology starts late and is thus relatively shallow. In developed countries where TC technology has seen much early development, relevant algorithms are mainly used in English TC. Researchers have improved the existing algorithms for Chinese TC. Some

have found mature applications, which have accelerated the development of TC technology in China. Although several ML models have been used in TC, the processing method is relatively simple [11]. It is not robust enough for complex practical problems, such as multicategory medical TC and unevenly distributed texts. Moreover, shallow ML models and integrated classifiers have limited the generalization ability. Fortunately, DL can lend well to TC tasks by scientifically organizing and managing big data. It can also mitigate text information overload. Besides, the DL model has unique advantages in feature extraction and semantic mining. Therefore, the DL-based TC model is the general trend and worth further exploration [12].

2.2. DL. DL, a research hotspot in ML, is a general term for learning methods based on the artificial neural network (ANN). Proposed in the 1940s, DL can simulate the cognitive mechanism of the human brain [13]. Figure 2 is the DL theoretical model.

DL algorithm observes the neural network (NN)'s error function gradient descent and corrects the weight and deviation according to the gradient descent. The specific calculation is given in Equation (1).

$$A_{a+1} = A_a - c_a d_a. \quad (1)$$

In (1), A_{a+1} represents the weight and deviation of the neuron layer. A_a is the weight and deviation after iterative calculation. c_a represents the learning rate of the neural network, and d_a is the gradient of the error function.

Equation Equation (2) is the specific calculation method of the space size of the convolution kernel after the cavity.

$$B = (n - 1) * b + 1. \quad (2)$$

In (2), B represents the size of the convolution kernel space, n is the size of the original convolution kernel, and b is the void rate. Equation Equation (3) calculates the image size after convolution.

$$C = \frac{(l - K + 2P)}{T + 1} \quad (3)$$

In (3), C represents the image size after convolution, and l and K are input and output image sizes, respectively. P is the filling size of the image, and T means the step size.

Nonnegative matrix factorization (NMF), another DL method, can regenerate output as similar as to the original matrix by finding two or more nonnegative matrices to reduce the nonlinear data dimension. Equation (4) calculates the norm cost function based on matrix difference.

$$\min_{P, W, Q} \|Y - LWQ^T\|_F^2. \quad (4)$$

In (4), Q^T is the transpose of matrix Q . $\|\cdot\|_F$ represents the norm of matrix difference. L , W , Q , and Y represent different matrices. Common DL models are as follows.

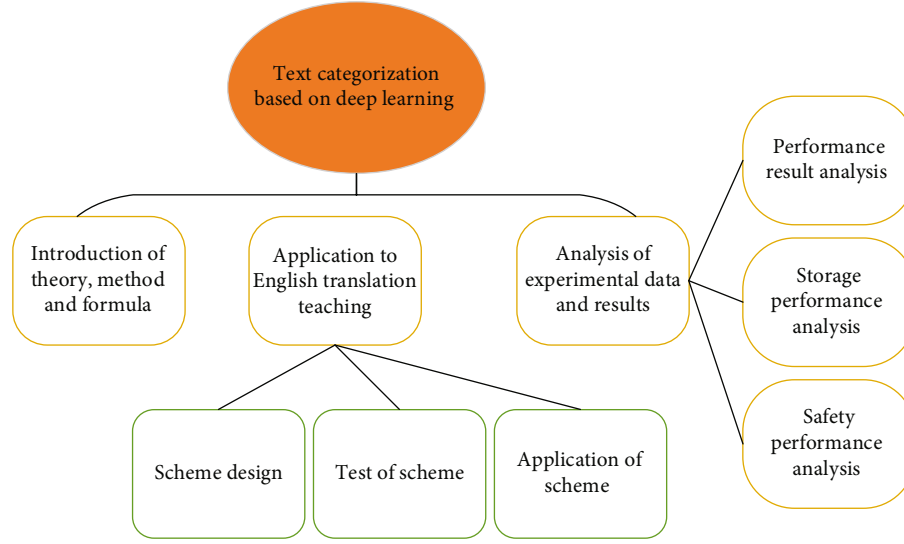


FIGURE 1: Theoretical research structure.

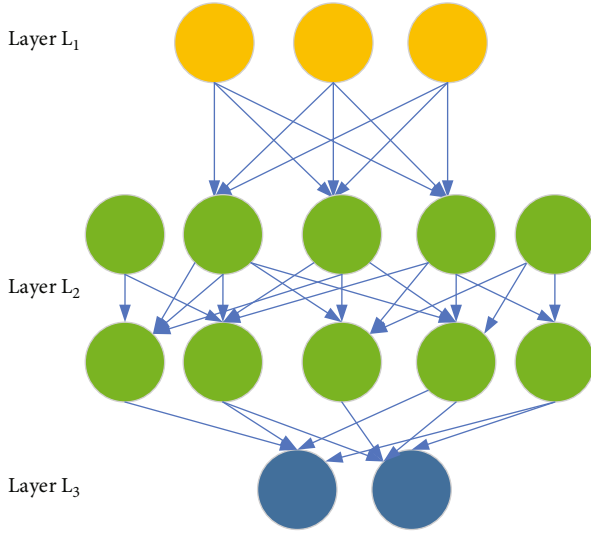


FIGURE 2: DL model.

- (1) Convolutional neural networks (CNN): CNN includes convolution calculation and calculates the feedforward neural network with depth structure. It is mainly divided into the input, convolution, pooling, and fully connected layers. It is one of the representative DL algorithms of DL. Figure 3 shows the CNN model

Equation Equations (5) and (6) give the specific calculation.

$$R_t = \mathfrak{F}(B_t[b_{t-1}, x_t] + P_f), \quad (5)$$

$$Y_t = \mathfrak{F}(A_t \cdot [b_{t-1}, x_t] + P_I). \quad (6)$$

R_t represents the forget gate, \mathfrak{F} is the hidden layer neuron, and B_t is the model output. b_{t-1} represents the hidden

layer information at time $t-1$, x_t is the input at time t , and Y_t is the input gate. P_f and P_I represent the activation functions of the forget gate and input gate, respectively.

- (2) The autoencoder (AE): NN based on multilayer neurons includes autoencoder and sparse coding, which have recently attracted extensive attention. Figure 4 is an AE
- (3) Deep belief networks (DBN): it is pretrained in the way of a multilayer AE and then combined with identification information to further optimize the network weight. The model can lend to both unsupervised and supervised learning [14]. Figure 5 reveals the DBN model

2.3. IoT Technology. IoT realizes the omniconnection of in and between things and people and between the real and virtual worlds. Data acquisition and object perception are key to IoT, supported by advanced technologies and communication networks. Finally, the collected data can be processed and analyzed to help humans make decisions. The technical means used to realize IoT is called IoT technology [15]. It has many applications involving optical, mechanical, electrical, information, communication, materials, and chemistry fields. Usually, an IoT system is based on the Internet, using sensors, radio frequency identification (RFID), Global Positioning System (GPS), and communication technology. It can provide multiple communication channels [16].

Professor Ashton from the United States first proposed the concept of connecting all sensors to the Internet, making communication between machines possible, and connecting items to the Internet according to the pre-defined protocol. Data are collected on the IoT with RFID and sensor technology for intelligent identification, positioning, and monitoring [17]. Then, IoT combines the physical, virtual, and

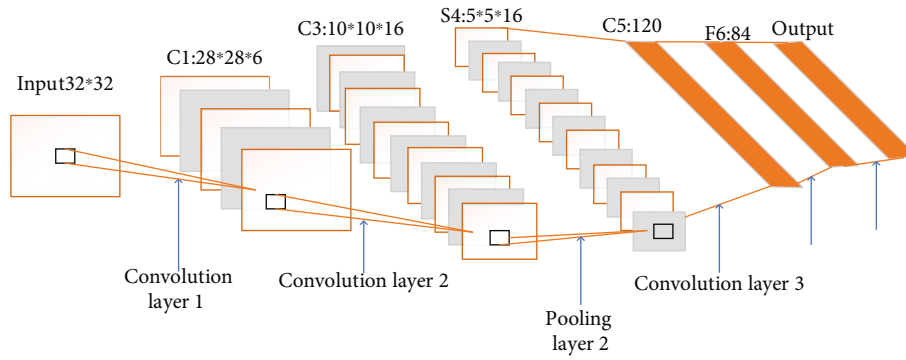


FIGURE 3: CNN model.

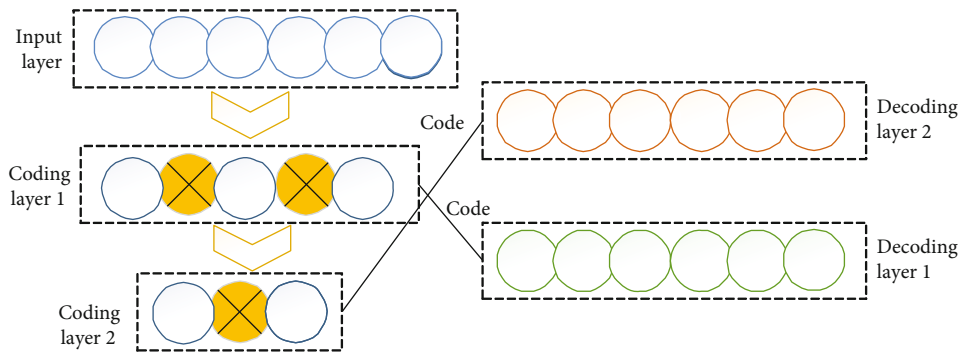


FIGURE 4: AE model.

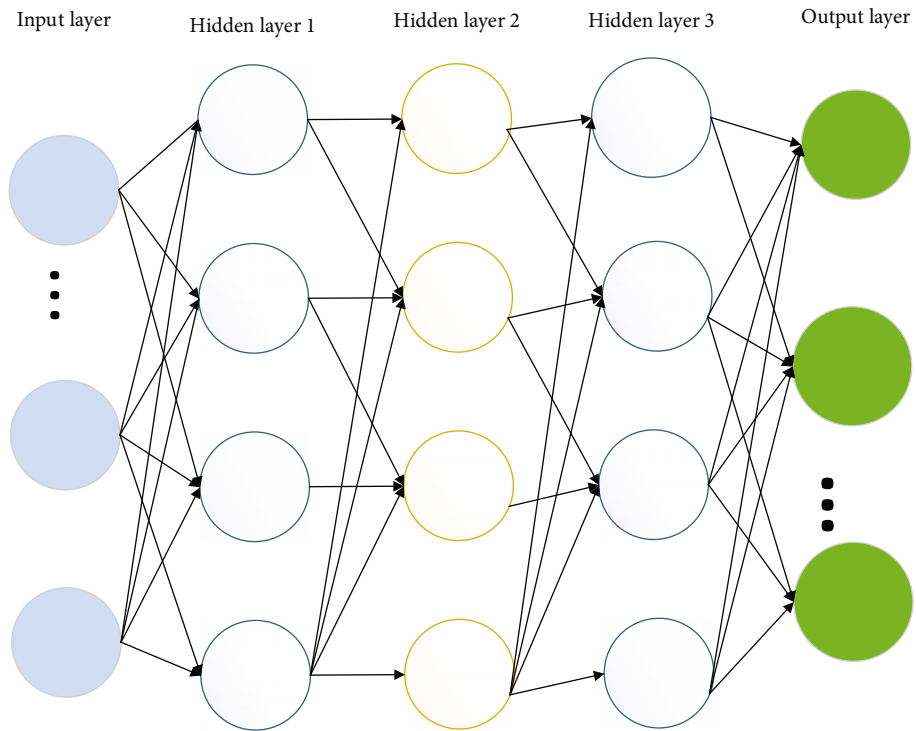


FIGURE 5: DBN model.

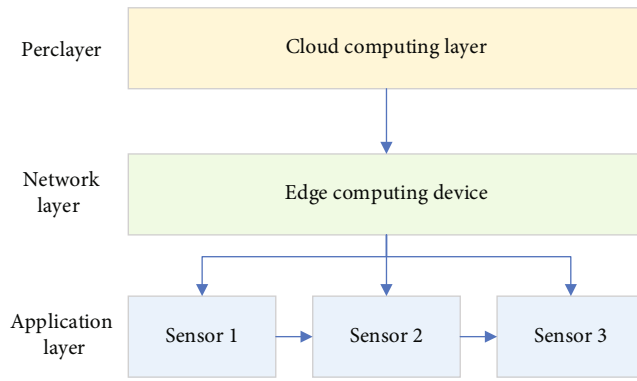


FIGURE 6: Shared IoT architecture.

digital worlds with human society closely through simple and timely interactions. IoT technology aims to bridge the gap between enterprise big data and individual-user data in the trading platforms [18]. Large enterprises often recruit technical personnel to deal with data transaction business. Most enterprise-level data are not patented, attracting many data peddlers to use data as a resource effectively. Besides, the third-party data trading platform is convenient for individual operators to grasp data [19] comprehensively, even though risks are inevitable, such as data leakage.

2.4. Current Situation of English Translation Teaching. Cultivating students' comprehensive English quality has been put on the agenda in higher education. Traditionally, exam-oriented education focuses on listening, reading, writing, and academic scores while ignoring students' practical skills [20]. In particular, translation is a science with a strong local flavor. In other words, second language learners tend to translate the source language into the target language word-to-word, with poor wording and sentence structures, leading to some misunderstanding. Thus, proper context-based translation is in high demand, especially as China encourages more and more international companies into domestic markets. English translation ability is becoming a basic skill for social talents, just as driving and computer proficiencies. This is where College English must improve its teaching quality in translation, help cultivate multi-linguistic talents, and promote China's revitalization. There is a need for higher institutions to offer various English translation practices and introduce English translation methods into classroom teaching. English translation is the main manifestation of students' comprehensive English proficiency and evaluation of their English practical abilities [21]. Most importantly, more opportunities should be provided for students to practice translation outside the classroom, cultivate their interest in learning, and improve their learning enthusiasm.

3. Scheme and Test of IoT System in English Translation Teaching

3.1. Shared IoT Design. As an emerging trading market in recent years, the data trading platform is in the early stage of development. IoT-based data trading platform mostly adopts centralized architecture, completing data storage and transmission through a central control [22], which has

some problems. For example, centralized services cannot catch up with the dynamic needs of data multiplication. Thus, shared IoT provides a new solution and is chosen here for studying the big data-based English translation. Share IoT has a unique structure, as explained below [23].

The perception layer acquires the front-end data using RFID to obtain electronic tags and using Beidou to obtain longitude and latitude, and environmental monitoring temperature, and humidity sensors.

Network layer servers as the background server that transmits information through telecommunication networks and the Internet. It can transmit and process the information from the perception layer. Its key technology is long-distance, high-fidelity transmission, and data processing.

The application layer processes the information from the front-end perception layer and realizes specific applications, such as autonomous driving (AD), environmental monitoring, and health management. It analyzes and processes information, makes correct decisions, or controls behavior to achieve intelligent management and service.

IoT devices need to connect to the Internet to realize remote control. Mobile phones or computers can issue control commands through the Internet. Communication is divided into uplink and downlink, which are the two directions of communication. Transmitting the data on the device end to the cloud is called uplink, and downlink is to send control commands to the user terminal devices, such as the mobile phone or computer. Figure 6 displays the architecture of the Shared IoT.

This section selects the English text corpus of Northwestern Polytechnic University for analysis based on the text encryption algorithm. English text corpora include several categories: agriculture, art, communication, computer, economy, education, electronics, energy, environment, and history. Computers and wireless networks are used as the hardware environment. These data are collected by a computer and then preprocessed, mainly through text retrieval. Finally, according to the needs of this experiment, the text is classified and sorted out. Some categories are relatively few and unrepresentative. Thus, 100 representative text categories are selected for the experiment. Figure 7 gives the flowchart of the text encryption algorithm.

3.2. IoT in English Translation Teaching. With the popularization of the 5G network, IoT sees broader applications. In particular, there are three main application forms to English translation teaching:

- (1) Basic application: text monitoring: IoT technology can give an alarm in selecting English translation texts once the text number exceeds the preset threshold and help administrators control texts through remote monitoring
- (2) Intermediate application: text statistics: IoT systems can analyze the collected text data from different dimensions and types and visualize them through a chart on the screen. As such, administrators can quickly and intuitively understand the operation status of the whole IoT device

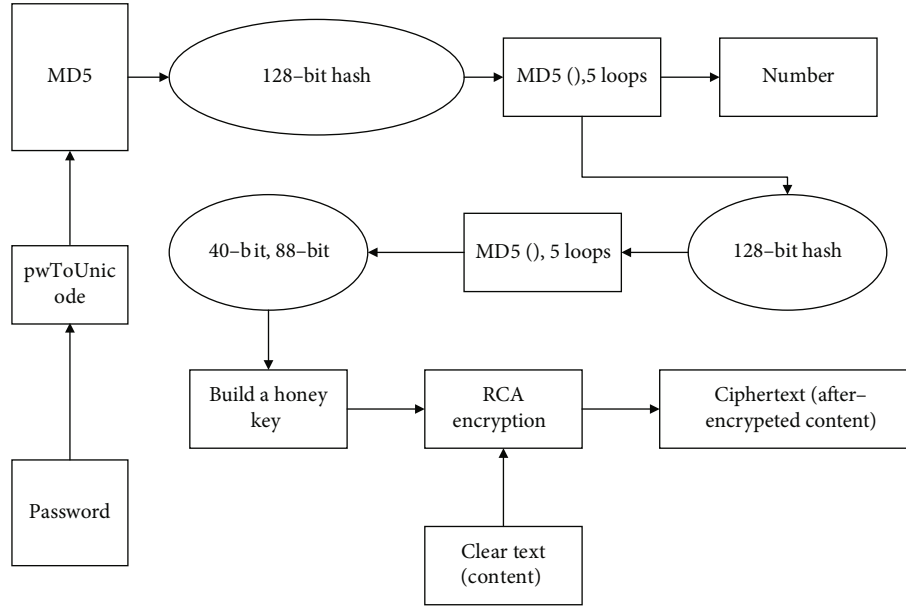


FIGURE 7: Flow chart of text encryption algorithm.

TABLE 1: Experimental data set.

Type	Training set		Test set	
	Type	Number	Type	Number
Agriculture		500	Education	500
Art		500	Electronics	500
Signal communication		500	Energy	500
Computer		500	Environment	500
Economics		500	History	500

TABLE 2: Required experimental environment.

Project	Model
Outward expansion flash	512 K*16
Led liquid crystal display	\
JTAG simulator interface	\
TMS320VC5402@100MHzDSP Main controller	\
Outward expansion SRAM	256 K*16

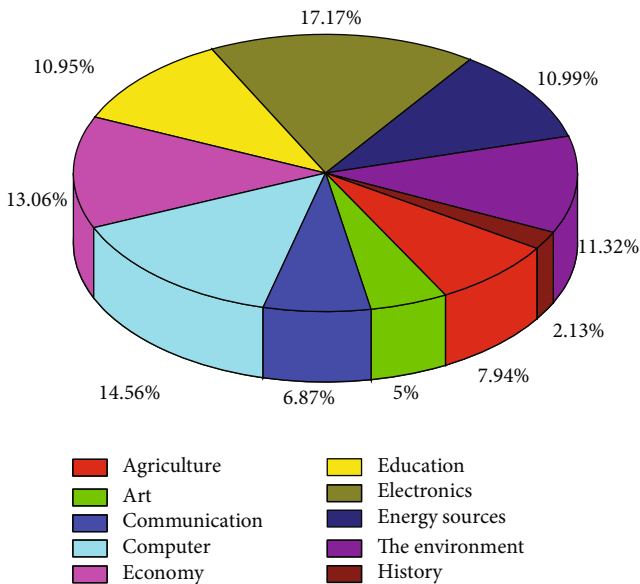


FIGURE 8: Test results of English translation text.

(3) Advanced applications: data mining: IoT can mine useful things from the database. For example, according to students' information retrieval history, teachers can classify, track, and analyze the English text during translation teaching and provide personalized teaching schemes.

3.3. Verifying the Shared IoT Design. The public's archive utilization needs are very much personalized and diversified. Intelligent and accurate file classification is based on professional knowledge and creativity and employs virtual space and knowledge maps. The archives are mapped from the physical space to the network space based on the Internet and cloud platforms.

In particular, the card in file classification uses an encryption mechanism to encrypt teaching documents. The single key-based encryption has a deadly defect that is prone to attack. The attack is based on password guessing. Each guess is compared with the real user password to calculate the initialization vector. Then, the initialization vector is checked for correctness: the guess and attack do not stop until the vector is correct, and the correct password is returned.

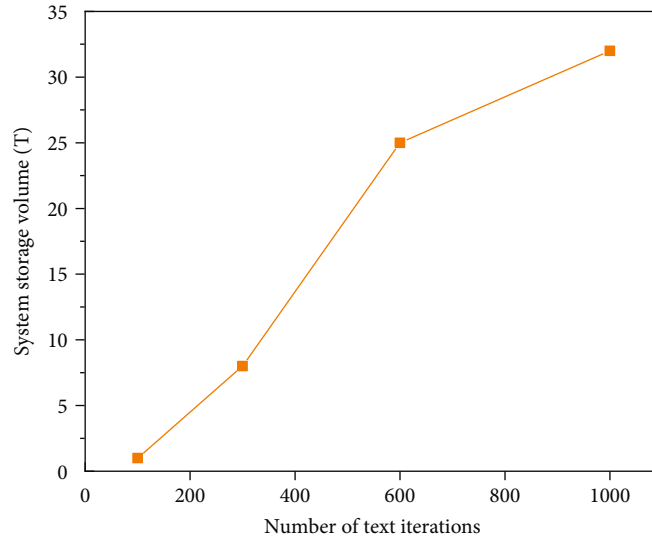


FIGURE 9: Storage performance analysis of shared IoT.

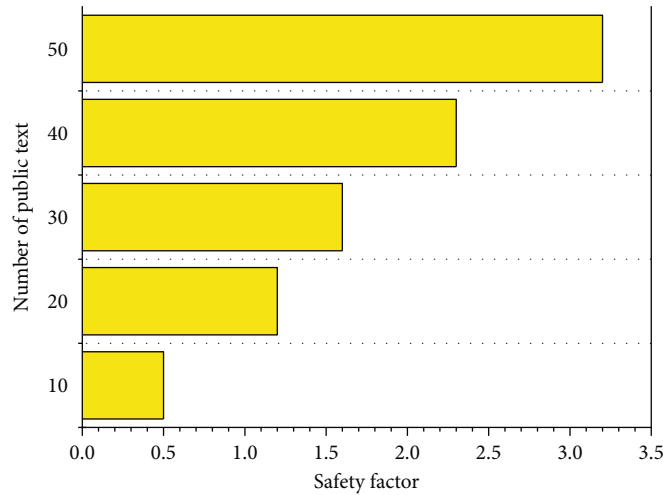


FIGURE 10: Analysis of the safety factor of shared IoT maintenance.

4. Experimental Results and Analysis

4.1. Experimental Dataset and Collection. This section takes the English text corpus of Northwestern Polytechnic University as the research object. It uses a text encryption algorithm to analyze the data. The specific experimental data set is shown in Table 1.

Firstly, the IoT system is used to classify the English text corpus of Northwestern Polytechnic University, delete the wrong words, sentences, and grammar, and then train the DL model. Finally, the TC method is introduced to classify the text. Figure 8 gives the details.

In Figure 8, English texts of agricultural, artistic, social, computer, economic, education, electric power, energy, environment, and historical type account for 7.94%, 5%, 6.87%, 14.56%, 13.06%, 10.95%, 17.17%, 10.99%, 11.32%, and 2.13%, respectively. Obviously, the proposed TC method overcomes the performance loss caused by the function extraction method, avoids the problem that the

function extraction method does not consider the semantic relationship between words, greatly reduces the function space, and reduces the training time. Experiments show that the classification effect is basically unchanged, and the TC method is better than the function extraction method.

4.2. Experimental Environment and Storage Analysis of Shared IoT System. The specific experimental environment is shown in Table 2.

Figure 9 analyzes the storage performance of the shared IoT.

In Figure 9, the storage analysis curve of the IoT shows a rising trend as a whole. The shared IoT system consumes 1 T, 8 T, 25 T, and 32 T storage capacity to encrypt the text through 100, 300, 600, and 1,000 iterations. Thus, the storage of the shared IoT system increases with the number of iterations to encrypt a text.

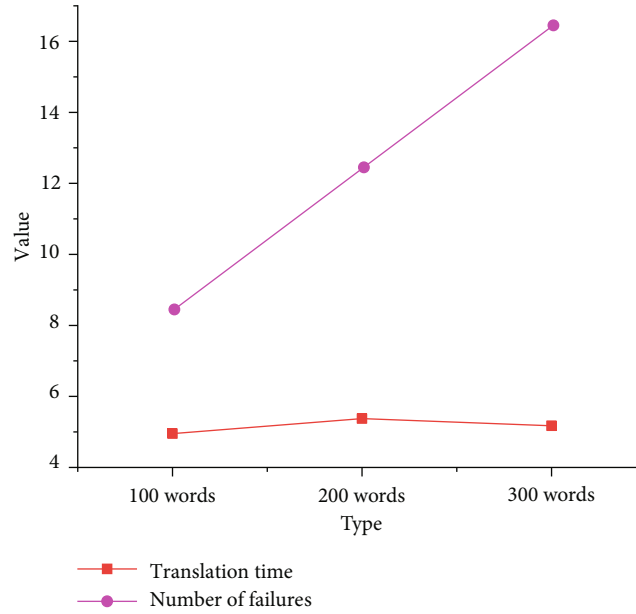


FIGURE 11: Translation time and failure times under different word numbers.

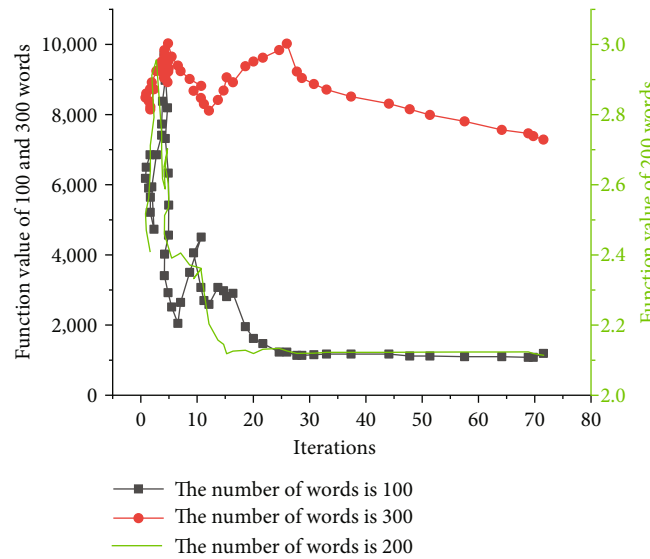


FIGURE 12: Iterations under different word numbers.

4.3. Analysis of Security Factor of Shared IoT Maintenance.

Figure 10 analyzes the safety factor of shared IoT maintenance. The security factor of the shared IoT system is 0.5, 1.6, and 3.0 to encrypt 10, 30, and 50 texts. Thus, the shared IoT system’s security factor increases with the number of encrypted texts.

In order to analyze the performance of the TC more accurately, the simulated annealing algorithm (SAA) is now introduced. Then, 100, 200, and 300 English words are selected as the research data. The specific experimental results are shown in Figure 11.

According to Figure 11, when the number of translated words is 100, 200, and 300, the translation time and failure times are 4.953 seconds and 8, 5.375 seconds and 12 and

5.172 seconds and 16, respectively. Thus, the translation time does not significantly increase with the increase in word number, maintained at around 5 seconds on average. At the same time, translation failures increase with the number of translated words.

The iteration times of SAA under a different number of translated words are shown in Figure 12.

Apparently, SAA’s translation speed declines less obviously with the increase of translated words. The algorithm iteration is stable no matter how many words. Specifically, when translating 100, 200, and 300 words, SAA reaches the optimal solution at around the 30th iteration. Thus, the number of translated words has a small impact on the algorithm iterations.

5. Discussion

English translation is one of the critical contents of English teaching. Here, 100 text categories are selected from the English text corpus of Northwestern Polytechnical University and are analyzed by integrating DL, TC, and IoT. The result shows that the TC method can reduce the training time and speed up model convergence. The storage and security performance of IoT encrypted text will increase with the number of English texts. Cherif et al. [24] proposed a TC model based on semantic enhancement and feature fusion. The model obtained the enhanced semantic features of the CNN model through the attention layer and then fused them with the local features extracted by the convolution layer. Then, experiments were conducted to show its effectiveness. Lee et al. [25] constructed a new word vector model for Chinese text based on the structure of Word2Vec. They found that the partial radicals of Chinese characters contain certain semantic information and introduced the partial radical information into the text representation. Experiments showed that the model had a good classification effect for classifying Chinese news headlines. Luo [26] proposed a DL CNN model to enrich the text generalization and memory information, giving the word vectors richer stylistic features. Compared with the theories and methods proposed by the three scholars, the proposed DL-based TC is simpler and easier to use in practice. The TC algorithm has been applied in many fields, providing rich references. Additionally, IoT technology is one of the most key technologies. The continuous promotion of the 5G network greatly facilitates IoT development. Thus, applying IoT in English translation teaching is the development trend of the times. Finally, there are not many theories of applying DL and TC to the field of the English translation, where this work bridges the gap.

6. Conclusion

The purpose is to design shared IoT to classify, translate, and search English texts efficiently, accurately, and quickly. This work first selects 100 text categories from the English text corpus of Northwestern Polytechnic University and analyzes them using the DL-based TC. Then, it describes the storage and security performance of the IoT system. The main conclusions are as follows. The storage capacity of the shared IoT system increases with the encrypted text iterations, and the security coefficient storage of the shared IoT system also increases with the number of encrypted text. The result proves that the designed IoT system is safe and effective. Additionally, using the proposed DL-based ANN method in classifying the English corpus can reduce the model training time.

The deficiency is summarized. Certain limitations exist in the collected text types. Research on other fields is lacking, such as Chinese TC. The future research direction is to improve the retrieval speed of massive amounts of TC encryption in the shared IoT system. Then, the shared IoT system should be optimized further, ensure against data duplication and resell transactions of the third-party platform, and reduce user risk.

Data Availability

The raw data supporting the conclusions of this article will be made available by the authors, without undue reservation.

Consent

Informed consent was obtained from all individual participants included in the study.

Conflicts of Interest

All authors declare that they have no conflict of interest.

Acknowledgments

This work was supported by the Research on Ideological and Political Path of College English Teaching Course supported by Joint Foreign Language Project of Hunan Social Science Fund (20WLH3) and Hunan Provincial Educational Teaching Reform Project (Grant No. HNJG-2021-1149).





References

- [1] D. Kwesiga, C. Tawiah, M. A. Imam et al., "Barriers and enablers to reporting pregnancy and adverse pregnancy outcomes in population-based surveys: EN-INDEPTH study," *Population Health Metrics*, vol. 19, no. S1, pp. 1–14, 2021.
- [2] S. U. Amin, M. Alsulaiman, G. Muhammad, M. A. Mekhtiche, and M. S. Hossain, "Deep learning for EEG motor imagery classification based on multi-layer CNNs feature fusion," *Future Generation Computer Systems*, vol. 101, no. 4, pp. 542–554, 2020.
- [3] C. Shen, G. Song, X. Zhu et al., "An in-depth study of heteroatom boosted anode for potassium-ion batteries," *Nano Energy*, vol. 89, no. 78, article 105294, 2020.
- [4] S. Wang, B. Kang, J. Ma et al., "A deep learning algorithm using CT images to screen for Corona virus disease (COVID-19)," *European Radiology*, vol. 12, no. 1, pp. 12–15, 2021.
- [5] D. W. Kim, G. Lee, S. Y. Kim et al., "Deep learning-based algorithm to detect primary hepatic malignancy in multiphase CT of patients at high risk for HCC," *European Radiology*, vol. 3, no. 18, pp. 1–11, 2021.
- [6] X. Zeng, Z. Jiang, W. Luo et al., "Efficient and accurate identification of ear diseases using an ensemble deep learning model," *Scientific Reports*, vol. 11, no. 1, p. 10839, 2021.
- [7] F. P. Mahdi, K. Motoki, and S. Kobashi, "Optimization technique combined with deep learning method for teeth recognition in dental panoramic radiographs," *Scientific Reports*, vol. 10, no. 1, pp. 22–30, 2020.
- [8] A. Dhar, H. Mukherjee, N. S. Dash, and K. Roy, "Text categorization: past and present," *Artificial Intelligence Review*, vol. 54, no. 4, pp. 3007–3054, 2021.
- [9] L. Xia, R. Zhao, Y. Wu, and X. Tong, "Intentional control of type I error over unconscious data distortion: a Neyman-Pearson approach to text classification," *Journal of the American Statistical Association*, vol. 116, no. 533, pp. 68–81, 2021.
- [10] S. Minaee, N. Kalchbrenner, E. Cambria, N. Nikzad, M. Chenaghlu, and J. Gao, "Deep learning-based text classification," *ACM Computing Surveys (CSUR)*, vol. 1, no. 1, p. 42, 2020.

- [11] C. Tsigkanos, M. Garriga, L. Baresi, and C. Ghezzi, "Cloud deployment tradeoffs for the analysis of spatially distributed Internet of Things Systems," *ACM Transactions on Internet Technology (TOIT)*, vol. 20, no. 2, pp. 1–23, 2020.
- [12] Y. Liang, H. Li, B. Guo et al., "Fusion of heterogeneous attention mechanisms in multi-view convolutional neural network for text classification," *Information Sciences*, vol. 548, pp. 295–312, 2021.
- [13] C. Chang and M. Masterson, "Using word order in political text classification with long short-term memory models," *Political Analysis*, vol. 28, no. 3, pp. 395–411, 2019.
- [14] J. Xu and Q. Du, "Adversarial attacks on text classification models using layer wise relevance propagation," *International Journal of Intelligent Systems*, vol. 35, no. 9, pp. 1397–1415, 2020.
- [15] M. A. Ibrahim, M. U. Khan, F. Mehmood, M. N. Asim, and W. Mahmood, "GHS-NET a generic hybridized shallow neural network for multi-label biomedical text classification," *Journal of Biomedical Informatics*, vol. 116, no. 1, article 103699, 2021.
- [16] F. Kanavati, G. Toyokawa, S. Momosaki et al., "Weakly-supervised learning for lung carcinoma classification using deep learning," *Scientific Reports*, vol. 10, no. 1, pp. 26–30, 2020.
- [17] N. Koroniotis, N. Moustafa, and E. Sitnikova, "A new network forensic framework based on deep learning for Internet of Things networks: a particle deep framework," *Future Generation Computer Systems*, vol. 110, no. 8, pp. 91–106, 2020.
- [18] P. Lam, A. Zhu, L. Salminen, S. Thomopoulos, N. Jahanshad, and P. Thompson, "Comparison of deep learning methods for brain age prediction," *Biological Psychiatry*, vol. 87, no. 9, pp. 374–S375, 2020.
- [19] X. Kong, Y. Xu, Z. Jiao, D. Dong, X. Yuan, and S. Li, "Fault location technology for power system based on information about the power Internet of Things," *IEEE Transactions on Industrial Informatics*, vol. 16, no. 10, pp. 6682–6692, 2020.
- [20] A. Smerdin, G. Ermachkov, V. Nezevak, O. Sidorov, and A. Golubkov, "Use of sensor networking technology to build a power transformer monitoring system," *E3S Web of Conferences*, vol. 224, no. 4, article 02021, 2020.
- [21] S. Moon, M. Y. Kim, and D. Iacobucci, "Content analysis of fake consumer reviews by survey-based text categorization," *International Journal of Research in Marketing*, vol. 38, no. 2, pp. 343–364, 2021.
- [22] L. Enamoto, L. Weigang, and G. P. R. Filho, "Generic framework for multilingual short text categorization using convolutional neural network," *Multimedia Tools and Applications*, vol. 80, no. 9, pp. 13475–13490, 2021.
- [23] T. Wang, Y. Cai, H. Leung, R. Y. K. Lau, H. Xie, and Q. Li, "On entropy-based term weighting schemes for text categorization," *Knowledge and Information Systems*, vol. 63, no. 9, pp. 2313–2346, 2021.
- [24] W. Cherif, A. Madani, and M. Kissi, "Supervised classification by thresholds: application to automated text categorization and opinion mining," *Concurrency and Computation: Practice and Experience*, vol. 34, no. 4, 2022.
- [25] Y. H. Lee, P. J. H. Hu, W. J. Tsao, and L. Li, "Use of a domain-specific ontology to support automated document categorization at the concept level: method development and evaluation," *Expert Systems with Applications*, vol. 174, no. 8, article 114681, 2021.
- [26] X. Luo, "Efficient english text classification using selected machine learning techniques," *Alexandria Engineering Journal*, vol. 60, no. 3, pp. 3401–3409, 2021.

Review Article

Blockchain-Based Crowdsourcing Makes Training Dataset of Machine Learning No Longer Be in Short Supply

Haitao Xu ¹, Wei Wei ², Yong Qi ¹ and Saiyu Qi ¹

¹Department of Computer Science and Technology, Xi'an Jiaotong University, Xi'an 710049, China

²School of Computer Science and Engineering, Xi'an University of Technology, Xi'an, China

Correspondence should be addressed to Yong Qi; qiy@mail.xjtu.edu.cn

Received 13 April 2022; Accepted 6 June 2022; Published 26 July 2022

Academic Editor: Alireza Souri

Copyright © 2022 Haitao Xu et al. This is an open access article distributed under the Creative Commons Attribution License, which permits unrestricted use, distribution, and reproduction in any medium, provided the original work is properly cited.

Recently, machine learning has become popular in various fields like healthcare, smart transportation, network, and big data. However, the labelled training dataset, which is one of the most core of machine learning, cannot meet the requirements of quantity, quality, and diversity due to the limitation of data sources. Crowdsourcing systems based on mobile computing seem to address the bottlenecks faced by machine learning due to their unique advantages; i.e., crowdsourcing can make professional and nonprofessional participate in the collection and annotation process, which can greatly improve the quantity of the training dataset. Additionally, distributed blockchain technology can be embedded into crowdsourcing systems to make it transparent, secure, traceable, and decentralized. Moreover, truth discovery algorithm can improve the accuracy of annotation. Reasonable incentive mechanism will attract many workers to provide plenty of dataset. In this paper, we review studies applying mobile crowdsourcing to training dataset collection and annotation. In addition, after reviewing researches on blockchain or incentive mechanism, we propose a new possible combination of machine learning and crowdsourcing systems.

1. Introduction

In recent years, machine learning (ML) techniques have made a lot of achievements in many fields [1–4]. However, a large number of labelled training dataset is one of the most cores of the technology. The quality, quantity, and diversity of training dataset have significant effects on the generalization capability and accuracy of trained models. Unfortunately, those data mainly originate from web crawlers or are provided by hired workers that leads to two main concerns. First, data originated from web, which may be not reliable, cause some issues on copyright [5] and privacy. Second, the service fee for hiring workers to collect special dataset or annotate dataset may be high. These bottlenecks hinder the further development of machine learning.

Thanks to the development of wireless technology and the popularity of mobile computing, crowdsourcing [6] appeared and the technology has gained great interest and adoption like Upwork [7], Amazon Mechanical Turk [8], and UBER [9]. Meanwhile, crowdsourcing systems are pop-

ular in environmental monitoring [10], smart transportation [11, 12], healthcare [13], and online marketplace [14]. The main idea of the technology is to find solutions of problems publicly, and it can easily increase energetic efficiency [3, 15, 16]. In addition, crowdsourcing in mobile computing domain is named mobile crowdsourcing (MCS). In particular, MCS systems dedicate to collecting data with sensors embedded on mobile devices. This technique provides a new idea for solving the problems above.

Now, we introduce a traditional MCS system. A naive MCS system mainly consists of three parties: task requesters, workers, and MCS system. Figure 1 shows the workflow, and the detail is introduced as follows: (1) the task requesters post tasks with payments by MCS system. (2) Workers choose the tasks which they are interested in by MCS system. (3) Workers work for the tasks and submit the results to MCS system. (4) The task requesters receive the results, and MCS system sends the payments to the workers.

In order to overcome the bottlenecks we introduced before, we can replace the above tasks with training dataset

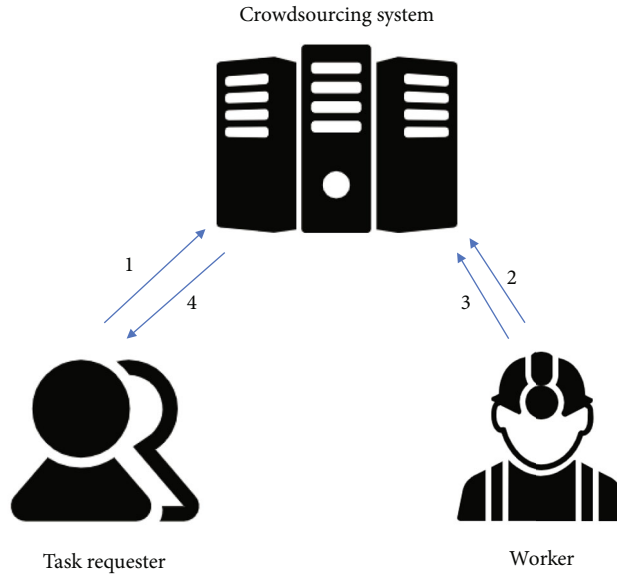


FIGURE 1: Workflow of traditional crowdsourcing system.

collection tasks or training dataset annotation tasks. If the function of MCS system is to collect training dataset, which we named TDCMCS system (training dataset collection mobile crowdsourcing system), workers need to collect data and annotate them before submitting the results. Otherwise, in the TDAMCS system (training dataset annotation mobile crowdsourcing system), task requesters need to submit the dataset which need workers to annotate. Fortunately, these two types of system already exist in recent years [17, 18], and we will introduce them in Section 3.

In fields of machine learning (ML), the training dataset consists of image dataset [19, 20], video dataset [17], text dataset [21], and other dataset [22]. The corresponding MCS systems have existed, and we will introduce them in Section 3.

However, traditional MCS systems are almost implemented on cloud servers; the detailed researches are shown in Section 3. Unfortunately, centralized platforms face many problems. First, centralized cloud servers inherently suffer from single point of failure and cannot ensure transparent operation, which will result in misbehavior. The order of passengers cannot be stopped at the end of services in April 17, 2015, as a service outage appeared because of hardware failure in Uber Technologies, China [23]. Second, the data (if the system is a crowdsensing system) produced by workers should belong to workers themselves, but when the data is stored on cloud servers, problems like unclear copyright [24] and information leakage [25, 26] will appear, which obviously does not meet the requirements of General Data Protection Regulation (GDPR) [5]. In December 2015, the Office of the Australian Information Commissioner (OAIC) reported that freelancer broke the Privacy Act by revealing true identity of users which included dummy accounts, IP addresses, and active account [27]. Third, centralized cloud servers are easy to be remotely hijacked and suffer mischief attacks and DDoS attacks, which leads to

the unavailable services. In May 2014, Elance and oDesk is out of services for many workers because of DDoS attacks [28]. Fourth, the service fee of the centralized crowdsourcing system is usually high; for example, the sliding service fee for five percent to twenty percent is necessary for most of the crowdsourcing systems [7].

To overcome the challenges above, decentralized crowdsourcing systems [29], usually combined with blockchain [30] technology and cryptographic algorithms [24, 31], become a great idea. Blockchain-based CS system often regards smart contracts as a trusted third-party broker, which can automatically execute codes of smart contract, and the whole process is public and traceable, so that various functions can be realized in distributed ways. In fact, the distributed crowdsourcing system based on blockchain has applications in many fields like court processing of adjudication, posting and assigning tasks, data collection, copyright protection, data transactions, mobile health, and energy trading. Even so, there are still some problems existing when combining blockchain-based CS system with machine learning. The core problem is that the quality and quantity of training labelled dataset cannot be guaranteed. To ensure the quality of training data, building reputation systems is a great proposal. In the TDCMCS system, after receiving the training labelled dataset, the task requester can give a feedback for the dataset. The feedback influences the reputation of worker, which is positively related to the payments. Hence, worker will prefer to offer high quality of training labelled dataset. In the TDAMCS system, the task requester should give a feedback on the quality of annotation. Meanwhile, truth discovery [32], one of the carefully designed algorithms [33–35] based on mathematical theory [36], can enhance the quality of annotation. Truth discovery (TD) algorithm is a method to discover truth among unreliable users' information. In order to collect satisfactory quantity of training dataset, incentive method is necessary. The price

of training dataset in the marketplace or the payments of hiring workers determines how many workers can be attracted to provide the dataset or annotate the dataset.

Recent researches make it possible to break through the bottlenecks of training dataset mentioned above. Note that, this is not the first survey on crowdsourcing and machine learning. Survey of Alenezi and Faisal [37] used either machine learning, crowdsourcing, or both of them in the proposed solutions which were aimed at surveying the current learning and e-learning schemes. Ørting et al. [38] reviewed studies published until July 2018 which combine crowdsourcing with analysis of the medical images. Jin et al. [39] surveyed the past quality control research of collect knowledge about various types of data items. Konečný et al. [40] described the types of annotation computer vision that researchers have collected using crowdsourcing in their survey.

Different from them, our contributions are shown as follows: (1) we review studies which combine crowdsourcing systems with the analysis of training dataset collection and annotation. (2) We also review some researches on blockchain, incentive mechanism, PPTD, etc., and extract some available techniques and methods which can break through the bottleneck of quality, quantity, and diversity of training dataset. (3) We summarize future development directions, and we propose an implementation of a decentralized (i.e., blockchain) MCS system that has the functions of collecting training datasets and annotating datasets.

Table 1 shows the summary of important abbreviations in our paper. In the rest of paper, we introduce the preliminaries in Section 2, and then, we introduce the related applications in Section 3. Section 5 provides future scope of machine learning with crowdsourcing technology. Next, the paper is concluded in Section 6.

2. Preliminaries

This section introduces all the core technologies and methods mentioned in this paper.

2.1. Machine Learning. Machine learning is designed to simulate human intelligence by learning among the surroundings which is a developing branch of computational algorithms. The core problem of ML is how to construct computers that automatically improve by learning experience [41]. ML is considered to be the core in the new age of big data. In addition, techniques based on ML have been utilized successfully in various fields ranging among computer vision, pattern recognition, finance, biomedical, computational biology, entertainment, medical applications, and spacecraft engineering [42].

In ML, a common task is to study and construct the algorithms which can be learned from data and then make predictions [43]. The algorithms make data-driven predictions or decisions by building mathematical models from input data [44]. These input data are commonly divided in multiple datasets. Particularly, three types of datasets (i.e., training datasets, validation datasets, and test datasets) are

TABLE 1: Summary of abbreviations.

Machine learning	ML
Federated learning	FL
Crowdsourcing	CS
Mobile crowdsourcing	MCS
Training dataset collection mobile crowdsourcing	TDCMCS
Training dataset annotation mobile crowdsourcing	TDAMCS
General data protection regulation	GDPR
Office of the Australian Information Commissioner	OAIC
Truth discovery	TD
Privacy-preserving truth discovery	PPTD
Short message service	SMS

usually utilized in different phases of the generation of the model.

Training dataset is very important in fields of machining learning, but its development is limited because constructing a well-annotated and large-scale dataset is very difficult as the expensive fee of data acquisition and annotation [45].

2.2. Blockchain. A blockchain [46] can be defined as a database which is shared among the users. Blockchain allows its users to trade valuable assets in a pseudonymous and public setup without relying on any central authority or intermediary [47]. A blockchain system consists of three core elements: the block, the chain, and the activity.

Concretely, blocks are storage carriers based on consensus agreements by all validators or stakeholders. The storage contents also capture the interactions of the various parties, such as Bitcoin transactions. Activities can be represented in a service manner in the blockchain system. For instance, digital transactions can be the service contents in Bitcoin. In addition, the chain is the connection of all blocks and is one-way growing. The one-way chain growth is a core property of tamper-resistant.

2.3. Smart Contracts. Szabo [48] initially introduced smart contract in the 1990s. Smart contract originated from the idea to create a technological legal framework which can help businesses, reducing disputes and costs. Smart contracts allow any user to define and execute smart contracts on the blockchain which can maintain the balance and data storage of them. In addition, the access is completely controlled by its code. However, all contract data and balances are public on the blockchain. The program code captures the logic terms of the contract between multiple parties and then defines triggers and response actions. The functions are executed in a smart contract when triggered by events or times. For example, when transactions are added to the blockchain. The creation of autonomous agents is allowed on smart contracts, and their behaviors are completely dependent on the transactions sent to them and their code. Hence, contracts are transparent and decentralized. The financial transaction rules can be enforced without any trusted third-party through the smart contracts.

2.4. Crowdsourcing. Crowdsourcing [49] is a novel model where organizations or individuals obtain services or goods from a relatively open, large, and often rapidly growing group of participants. The services mainly include voting, ideas, finances, and microtasks.

Until 2021, crowdsourcing generally involves using the network (however, online is not always necessary) to attract and assign works between participants and then achieve cumulative results. The word “crowdsourcing” was allegedly created in 2005 [50–52]. Compared with outsourcing, crowdsourcing usually involves a more public and less-specific group [53–55].

Improving costs, speed, flexibility, quality, diversity, or scalability is the advantage of crowdsourcing [56, 57]. A general crowdsourcing method usually includes virtual labor markets, competitions, and public online collaboration. Some crowdsourcing give organizations ways which go beyond the ideas provided just by their employees like LEGO ideas [58, 59]. Amazon Mechanical Turk is one of the crowdsourcing where monotonous “microtasks” are performed by large, paid crowds at the same time. Some unprofitable organizations like Wikipedia have utilized crowdsourcing technology to develop common goods [60].

2.5. Crowdsensing. Crowdsensing [61], which can be called mobile crowdsensing sometimes, is a technology where a large number of crowd share and extract information collectively via their mobile devices (such as smartphones, wearables, and tablet computers). In conclusion, it means crowdsourcing of sensing data from mobile devices.

Raghu et al. coined “mobile crowdsensing” (MCS) in 2011 [62]. MCS belongs to three main types: social (like tracking personal exercise data in a community), infrastructure (like locating potholes), and environmental (like monitoring pollution). Current CS applications operate based on the core assumption that all participants submit the sensing data voluntarily which results in extensive user participation [63]. Also, it can indicate the way users who carry mobile devices form microcrowds based on specific CS activities [64].

2.6. Truth Discovery. In order to achieve the aim of solving conflicts from multiple data sources with noises, truth discovery (TD) is widely utilized in various areas [65]. Although differences exist in the algorithm to compute weights of users and ground truths, the procedure of existing TD algorithms can be concluded as follows: a TD algorithm commonly initializes a random number of ground truths (According to [66, 67], the ground truth value of each object can be also initialized as the average of the sum of the sensory values of the object by different users.) and then conducts truth update and weight update iteratively until convergence. Current TD algorithms almost follow two principles: (1) the data of the user who holds a higher weight has more effect in the execution. (2) The user who provides a more accurate data item will have a higher weight (i.e., it is closer to the aggregated truth).

Due to the concerns of privacy, privacy-preserving truth discovery (PPTD) algorithm appears in recent years. Weight of data provider, data provided by provider, and truth need

to be preserved in cipher domain. Weight can be usually used to infer whether the provider is rich or poor. For instance, if a provider has a high weight, it can always provide more accurate data, and accurate data is usually collected by sensors embedded in high-end devices, so the provider is usually a wealthy person who can buy high-end mobile devices. Besides, data and truth belong to individuals and therefore need to be encrypted, and only a few people can decrypt them. By combination with homomorphic cryptographic algorithm or perturbation algorithm, PPTD algorithm implements the TD algorithm calculation in the cipher domain.

3. Related Applications

As shown in Table 2, we introduce papers in different fields with the aim of extracting suitable methods and techniques to make the combination of MCS and machine learning possible. Note that, we focus on the researches of training dataset collection or annotation. Hence, federated learning (FL) is not in our consideration. At the same time, we discuss the weaknesses and advantages of each type of system in Tables 3 and 4.

In fact, crowdsourcing systems can be divided into traditional crowdsourcing [68], mobile crowdsourcing (MCS) [69], vehicle crowdsourcing (VCS), and so on according to the tools used to complete the task. On the other hand, crowdsourcing systems can be divided into centralized crowdsourcing and decentralized crowdsourcing according to the environment in which the system is deployed. Decentralized crowdsourcing can be further divided into blockchain-based crowdsourcing and non-blockchain-based crowdsourcing. In addition, crowdsourcing systems can also be divided according to the task types or application fields, which we will not elaborate here.

3.1. Centralized Crowdsourcing System. The general steps of machine learning are as follows: (1) getting the dataset and preprocessing, (2) selecting the algorithm in machine learning and determining the model, (3) training the model and cross-validation, (4) verification curve and learning curve, (5) training dataset multiple times, (6) testing data test model, and (7) predicting new outcomes. We focus on crowdsourcing systems which can help to get various training dataset.

Swearngin and Yang [70] proposed a centralized crowdsourcing system to collect large-scale data of interface tappability on a variety of mobile applications.

Kuldeep et al. [71] proposed a centralized crowdsourcing system called SMSAssassin, which was aimed at collecting spam mails. The system is effective to filter email spams.

Amini and Yang [72] proposed a centralized crowdsourcing framework named CrowdLearner, which was aimed at generating recognizers by using mobile sensors input automatically. At the same time, the framework assigns the annotation tasks to the crowd.

Trivedi et al. [73] proposed a centralized crowdsourcing system which can assign the sensing tasks to workers. Workers sense the text datasets of mobile phone battery temperature via their mobile devices, and the system can infer ambient temperature.

TABLE 2: Summary of literatures on various fields.

Item	Related work	Key points
Centralized MCS system with dataset collection or annotation	[70–74]	[70] Training dataset collection of interface tappability [71] Training dataset collection of spam SMSes [72] Training dataset annotation [73] Training dataset collection of temperature [74] Training dataset collection and trading of images [17] Training dataset collection of videos [75] Training dataset collection of images with labels [76] Training dataset collection of audios
Centralized traditional CS system with dataset collection or annotation	[17, 18, 75–87]	[18] Training dataset annotation with three criteria to ensure high quality [77] Training dataset annotation with high quality and low costs [78–87] Other systems for training dataset annotation
Decentralized CS systems without blockchain	[88–91]	[88–91] Task completion in a distributed way but need a centralized system or trusted third-party servers [92] Court processing of adjudication [93] A general blockchain-based decentralized framework [94] Collaboratively building and updating a dataset [95] Copyright-preserving data trading [96] Data trading based on reverse auction [97] Task-worker matching [98] Healthcare remedy evaluation system [99] Novel mobile health applications [100, 101] Peer-to-peer energy trading platform
Decentralized CS systems with blockchain	[92–101]	[102] Blockchain-based MCS system with reputation system
Reputation system with blockchain	[102]	[102] Blockchain-based MCS system with reputation system
PPTD	[65, 67, 103–114] [115–118]	[65, 67, 103–114] PPTD systems implemented on cloud servers [115–118] PPTD systems implemented on blockchain

TABLE 3: Advantages and weakness of the systems.

Item	Transparency	Suffer single point of failure	Suffer remote hijacking	Suffer mischief attacks	Suffer DDoS attacks
Centralized traditional CS system with dataset collection or annotation	No	Yes	Yes	Yes	Yes
Centralized MCS system with dataset collection or annotation	No	Yes	Yes	Yes	Yes
Decentralized CS systems without blockchain	No	Yes/no	Yes/no	Yes/no	Yes/no
Decentralized CS systems with blockchain	Yes	No	No	No	No
Decentralized CS systems with blockchain and PPTD	Yes	No	No	No	No

TABLE 4: Advantages and weakness of the systems.

Item	Service fee	Data privacy protection	Data quality	Data quantity	Data diversity
Centralized traditional CS system with dataset collection or annotation	High	No	Low	Small	Low
Centralized MCS system with dataset collection or annotation	High	No	Low	Medium	Low
Decentralized CS systems without blockchain	High	No	Low	Small	Low
Decentralized CS systems with blockchain	Low	Yes	Low	Large	High
Decentralized CS systems with blockchain and PPTD	Low	Yes	High	Large	High

Lan et al. [74] proposed a centralized crowdsourcing system named CrowdBuy. It is a privacy-preserving image dataset trading system where a buyer can purchase desired image dataset from available mobile users efficiently, while quality is guaranteed and data ownership and privacy of users are respected.

Next, we introduce some researches on traditional crowdsourcing systems which were aimed at collecting training dataset or annotating dataset. In fact, we can easily convert these systems to MCS systems due to the development of mobile computing.

Sigurdsson et al. [17] proposed a data collection approach named the Hollywood in Homes. The corresponding crowdsourcing system was aimed at collecting dataset of videos, and the annotation works are assigned by workers.

Law and Ahn [75] proposed a research dataset, and it contains one hundred thousand images with English labels, which was generated from a crowdsourcing game named TagATune.

Orlandic et al. [76] presented a centralized CS system which was aimed at collecting dataset of audios. About 3,000 recordings of coughs are labelled by 4 experienced doctors to help diagnosing medical abnormalities. It is one of the largest dataset of cough which is annotated by experts currently.

Hsueh et al. [18] evaluated annotation data from both unprofessional workers hired from the Internet and professional workers in research laboratories. Meanwhile, the impact of noisy annotations on sentiment classification model performance and the utility of annotation selecting on classification efficiency and accuracy are examined.

Chang et al. [77] proposed a centralized crowdsourcing approach named Revolt, the idea of which is to convert expert annotation to crowd-based annotation. Experiments evaluated by them compare traditional crowdsourcing annotation with Revolt and proved that the approach can produce high-quality label with lower financial cost.

Other scholars [78–87] proposed their own crowdsourcing systems for annotate datasets, which will not be described in detail here.

In conclusion, there have been a lot of researches on MCS systems or traditional CS systems for collecting various types of training datasets or annotation. However, these systems often do not take incentives into account. We next focus on the traditional crowdsourcing systems which embed incentives for collecting datasets or some methods of hiring workers.

Zheng et al. [119] proposed a mobile crowdsensing data trading system named ARETE, where the data seller can obtain profit by offering data services after acquiring raw data, while data buyer can buy data services through queries. Additionally, reward sharing and the price design of online data are studied in depth.

Gao et al. [120] proposed a scheme in MCS, which was aimed at solving the recruitment problems of unknown workers. In the scenario, the prior sensing qualities of workers are unknown. Meanwhile, a combined multiarmed bandit problem was modeled to find an optimal solution algorithm.

Hu et al. [121] presented an incentive scheme based on dynamic demand in a mobile crowdsensing systems which is location-dependent. The mechanism changes the payment of sensing tasks dynamically to balance their popularity and demand at each round.

Liu et al. [122] aimed at the problem of online recruitment under the time and budget constraints and proposed a dynamic worker hiring strategy under truthful pricing. In addition, the worker hiring strategy contains an online pricing mechanism based on reverse auction which achieves individual rationality and truthfulness.

It can be seen that if we want to use the MCS system to collect the training data (or hire workers to annotate training dataset) needed for machine learning, incentives are essential. The crowdsourcing trading system or worker recruiting system are feasible. We need to model the specific scenarios (e.g., limited budget, limited time to recruit workers, or unknown quality of workers) by combining specific game theory methods, which will result in reasonable benefits for all parties. As a result, enough workers will participate in the works.

The quality, quantity, and diversity of training dataset have significant effects on the generalization capability and accuracy of trained models. Applying ML in crowdsourcing can easily overcome the bottleneck of the quantity and diversity of training dataset and make it no longer be in short supply.

3.2. Decentralized Crowdsourcing System. Because of the problems of centralized systems we mentioned in Section 1, distributed crowdsourcing systems come into being. As far as we know, few researchers proposed decentralized crowdsourcing systems which were aimed at collecting training dataset or hiring workers to annotate training dataset. Most researches that combine decentralized systems with machine learning focus on training models, i.e., federated learning [40, 123–126]. We first introduce some traditional decentralized crowdsourcing systems without combining blockchain technology.

Ryabinin and Gusev [88] proposed a software library to enable traditional mobile crowdsourcing applications to increase privacy of users without affecting the overall quality of crowdsourcing dataset. Additionally, they proposed Fougere, a decentralized approach, which can send data samples to third-party servers from user devices.

Zhang et al. [89] proposed a protocol named D2, which can help to design a DTN- (delay-tolerant network-) based distributed crowdsourcing system. The goal of them is completing calculation tasks collaboratively and minimizing time consumption.

Yang et al. [90] proposed a task assignment approach scheme that exploits social relations in the crowdsourcing systems. Their approach focused on load balancing in distributed environment.

Cheung et al. [91] proposed a distributed and asynchronous task assignment in the MCS.

Researches above focused on task completion in a distributed way, but they actually utilized a centralized system (or trusted third-party servers) to support services, which runs in the opposite direction of building the crowdsourcing system in a decentralized way.

3.3. Blockchain-Based Crowdsourcing System. The emerging blockchain technology is unique among distributed systems due to its unique advantages. Next, we introduce the decentralized CS systems which is based on blockchain.

Ast and Sewrjugin [92] presented a blockchain-based crowdsourcing application named CrowdJury, which court used to process adjudication. However, they did not provide the details of the crowdsourcing protocols design.

Li et al. [93] presented CrowdBC, a decentralized CS framework based on blockchain, where the tasks can be resolved by a group of workers without relying on any third trusty institution. In addition, privacy of users can be guaranteed, while low transaction fee is required.

Harris and Waggoner [94] presented a decentralized framework for users to build datasets collaboratively and use smart contracts to host updated models continuously. In order to keep the model accurate on some test sets, they proposed both nonfinancial and financial incentive structures to provide good data.

Sheng et al. [95] proposed a blockchain-based crowdsourcing data trading framework called CPchain, which was aimed at preserving copyright. Without any truthful broker, it can construct credible and truthful data trading between mutually untrusted users while guaranteeing the copyright and quality of data.

An et al. [96] presented a blockchain-based CS data trading system. Their highlight is that the system was the path-breaking work which utilized both blockchain and reverse auction to guarantee the truthfulness and fairness of the whole data transaction process.

Meanwhile, due to the existence of unique nonfungible tokens in the blockchain, we advise to combine it with digital copyright to protect data copyright.

Zhang et al. [97] presented a blockchain-based platform named PFCrowd, which performs matching algorithm of encrypted task-worker between different crowdsourcing systems without any trustful third-party institution. The core of their approach is to covert the task recommendation algorithm into a credible smart contract.

J. Park et al. [98] proposed CORUS, a healthcare remedy evaluation system utilizing blockchain-based CS and cloud computing platform. The system is an efficient and effective alternative scheme to the expensive clinical trials and objective evaluation on the remedies.

By combining crowdsourcing with mobile computing, cloud computing, Internet of Things (IoT), and blockchain, Fernández-Caramés et al. [99] proposed a system which stores data of patient and develops novel mobile health applications. The application supports diagnosing, public health actions, studying, and monitoring. In addition, it can help people to control diseases and increase global awareness on popularity of diabetes.

Shen et al. [100] presented a blockchain-based architecture and an optimization model. The goal of the architecture is to manage the operation of crowdsourcing energy systems which enables P2P energy trading. Users on Internet can easily and seamlessly trade energy on the system.

Jamil et al. [101] proposed an energy transaction platform built on blockchain which can provide day-ahead controlling, generation scheduling, and real-time support.

Hence, we recommend emerging blockchain technology to combine with the MCS system to collect training dataset or hire workers to label the dataset.

3.4. Reputation System and Privacy-Preserving Truth Discovery. As we mentioned in Section 1, to ensure high quality of training data, building reputation system is a great idea. Feedback of task requesters is the core of reputation system [127, 128].

K. Zhao et al. [102] proposed BC-MCS, an efficient and credible blockchain-based mobile crowdsensing system, which combined edge computing with the emerging blockchain technology in the MC scenario. The privacy-preserving reputation management approach is the key idea of the proposed system which can resist malicious users.

On the other hand, aggregating multiple annotations, which can make the annotations more accurate, is a great method. Truth discovery is an algorithm which stands out from the crowd.

An et al. [104] presented a light blockchain-based model which can assess quality of data. A couple of quality assessment processes on data are presented in their model. One of them is implemented in data quality assessment, and the other is implemented in the selection of users. Meanwhile, the service fee is low as smart contracts and consensus mechanism are carefully redesigned to be suitable for CS.

Miao et al. [65] proposed a PPTD framework for CS systems on cloud, which can protect the privacy of both sensory data and reliability scores generated by the TD algorithm of users. Their work was achieved by using homomorphic cryptographic scheme and threshold Paillier cryptosystem. By optimizing the algorithm, Zheng et al. [105] greatly reduces the communication and computing overhead. Compared with Miao, Zheng's designs achieved at least 30x and 10x savings on communication and computation of users, respectively.

Works of Cai et al. [106] are on stream data. They presented a CS system which enables PPTD algorithm and blockchain-based full-fledged knowledge monetization. Two noncollusion cloud servers were used to execute PPTD algorithm, and blockchain was used to construct a fair data trade market that does not need trusted third parties.

Tang et al. and Xu et al. [107, 108] presented the noninteractive PPTD systems which did not need users to be online all the time and guaranteed the privacy strongly.

Zheng et al., Xue et al., and Miao et al. [67, 109, 110] proposed novel PPTD systems, which can protect both sensory data and reliability scores of users. Miao's work is on both batch data and stream data.

Gao et al. [111] proposed an efficient and novel location-based PPTD mechanism, which can aggregate data accurately with both data privacy and location privacy of users protecting. In addition, superincreasing sequence techniques are used to guarantee efficiency and feasibility.

Xu et al. [112] presented the first verifiable and PPTD protocol in CS systems named V-PATD. Their openly verifiable approach lets any entity verify whether the aggregated truths returned from the cloud server are correct. Their verification approach is scalable and efficient as the cloud server carries most of the computation burdens.

Wang et al. [103] proposed a CS system which can execute a private and fair truth discovery (PFTD). The system is based on two noncollusion cloud servers and Paillier

cryptosystem. Their goal is to not only protect the privacy of each workers but also guarantee the fairness in crowdsourcing.

PPTD algorithm mentioned above is all by using homomorphic cryptographic scheme, as Zhang et al. and Sun et al. [113, 114] utilized the method of adding perturbation to the data to protect privacy. This method greatly reduces the computational cost of PPTD.

The above work is based on the centralized cloud server to realize the PPTD algorithm. Due to the problems of centralization (mentioned in the Section 1), some distributed solutions have emerged one after another.

Liang et al. [115] presented a blockchain-based novel CS model which can control quality of crowdsensing data. In the model, TD algorithm and fuzzy theories are utilized.

By combining zero-knowledge proof, trusted hardware, and differential privacy, Duan et al. [116] presented a blockchain-based CS ecosystem which support data aggregation services which completely guarantee data aggregation correctness, differential privacy, confidentiality, and robustness.

Tian et al. [117] presented a blockchain-based framework which is secure and reliable while supporting PPTD algorithm. Without any central servers, the framework assigns the data processing tasks to decentralized workers, whose behaviors are forced and verified by using the novel smart contract technology. At the same time, because the blockchain cannot protect the privacy of on-chain data, they combined privacy-preserving solution with blockchain for protecting privacy.

Wang [118] proposed PrivSTD, a PPTD mechanism based on edge computing, which can gain high accuracy of truth aggregated by streaming crowdsourcing data with the privacy protection of workers.

There are a large amount of researches on blockchain-based PPTD algorithm. It is an innovative idea to combine with annotating training dataset.

4. Challenges for Combining Machine Learning with Crowdsourcing Technology

In this paper, we focus on crowdsourcing help to supply training dataset and annotate dataset, which lead to many challenges.

4.1. Quality of Training Dataset. Although the combination of ML and crowdsourcing can easily solve the problem of the diversity and quantity of training dataset, the quality of the datasets is difficult to guarantee because the workers in crowdsourcing may be professional or nonprofessional.

4.2. Incentives. If the reward for labeling tasks and collecting datasets is too low, no workers will participate in the work, and if it is too high, the employer's benefits will decrease. How to set the rational reward is a challenge.

In addition, crowdsourcing can help train the models of machine learning, i.e., federated learning (FL), which brings some new challenges.

4.3. Privacy and Security. As an efficient privacy-preserving method, FL can train a lossless ML model through local training and parameter transfer of the participants without directly obtaining the data source. However, there are also many security risks in FL. The main security threats include poisoning attacks, adversarial attacks, and privacy leaks.

4.4. Communication Efficiency. ML algorithms, especially complex deep learning algorithms, need to train a large number of parameters during the training process. For instance, CNN may need to train millions of parameters, and each update process needs to update millions of parameters. In addition, the state of network communication may also lead to high communication costs. For example, unstable network conditions and inconsistent speeds during parameter uploading and downloading will lead to excessive model training costs for the entire algorithm.

4.5. Heterogeneity. In FL system, another challenge is the heterogeneity among the client devices, including differences in storage, CPU computing power, and network transmission. The heterogeneity makes the computing time of the devices different and even cause individual devices to drop directly.

5. Future Scope of Machine Learning with Crowdsourcing Technology

The researchers believe that it has immense potential in many fields when machine learning meets crowdsourcing. We consider that there are two types of blockchain-based systems that hold great promise: TDCMCS system (training dataset collection crowdsourcing system) and TDAMCS system (training dataset annotation crowdsourcing system).

In the TDCMCS system, task requesters post dataset collection tasks on blockchain. Workers receive the tasks and collect training dataset by their sensors embedded on mobile devices. After annotating the training dataset, workers submit the results on blockchain. Finally, task requesters receive the result and give the feedback on the training labelled dataset. A good feedback will enhance the reputation of the worker. By combining reputation system, the quality of datasets can be improved, because the reputation directly affects rewards and whether the workers can be assigned tasks. To attract workers to the tasks, we advise set payment when posting tasks or build an auction system. If the incentive mechanisms are reasonable, the number of dataset will grow explosively. Game theory is an analytical tool which can ensure the rationality of the reputation system and the fairness of the trading system. Truth discovery is a great data aggregation algorithm that can make annotation of training dataset more accurate. In addition, blockchain-based crowdsourcing systems can solve problems such as single points of failure.

In the TDCMCS system, the workflow is a little different from in TDCMCS system. First, task requesters post dataset annotation tasks on blockchain with their dataset public online (e.g., IPFS [129] or NFS [130]). Second, workers get the dataset and annotate it. Third, the annotations will be uploaded on blockchain, and the smart contract will execute PPTD algorithm to make the annotations more accurate.

Finally, the feedback and quality of annotations jointly determine the change in reputation.

Such systems could shine in a large number of domains like environmental monitoring, smart transportation, and healthcare [131]. There will be an explosion of all kinds of high-quality datasets in many domains, leading to rapid advances in machine learning.

6. Conclusion

In this paper, we survey the researches on crowdsourcing systems, machine learning, truth discovery, etc., and propose the possible combination of machine learning and MCS systems. The goal of this survey is to provide a possible guide for combination of crowdsourcing and machine learning to explore potential research directions in related fields and may lead to exciting results.

Conflicts of Interest

The authors declare that they have no conflicts of interest.

Acknowledgments

This study was supported by the Ministry of Education of the People's Republic of China under Grant No. 2020KJ010801.

References

- [1] W. Wang, X. Zhao, Z. Gong, Z. Chen, N. Zhang, and W. Wei, "An attention-based deep learning framework for trip destination prediction of sharing bike," *IEEE Transactions on Intelligent Transportation Systems*, vol. 22, no. 7, pp. 4601–4610, 2021.
- [2] D. Poap, M. Woniak, W. Wei, and R. Damaeviius, "Multi-threaded learning control mechanism for neural networks," *Future Generation Computer Systems*, vol. 87, pp. 16–34, 2018.
- [3] A. Zielonka, A. Sikora, M. Woźniak, W. Wei, Q. Ke, and Z. Bai, "Intelligent internet of things system for smart home optimal convection," *IEEE Transactions on Industrial Informatics*, vol. 17, no. 6, pp. 4308–4317, 2021.
- [4] J. H. Wu, W. Wei, L. Zhang et al., "Risk assessment of hypertension in steel workers based on LVQ and fisher-SVM deep excavation," *IEEE Access*, vol. 7, pp. 23109–23119, 2019.
- [5] P. Voigt and A. Von dem Bussche, "The eu general data protection regulation (gdpr)," in *A Practical Guide*, vol. 10, no. 3152676pp. 10–5555, Springer International Publishing, Cham, 1st edition, 2017.
- [6] H. Jeff, "The rise of crowdsourcing," *Wired magazine*, vol. 14, no. 6, pp. 1–4, 2006.
- [7] UpworkFebruary 2022, <https://www.upwork.com/>.
- [8] Amazon mechanical turkFebruary 2022, <https://www.upwork.com/>.
- [9] UberFebruary 2022, <https://www.uber.com/>.
- [10] M. Stevens and E. D'Hondt, "Crowdsourcing of pollution data using smartphones," in *Workshop on ubiquitous crowdsourcing*, pp. 1–4, ACM, 2010.
- [11] W. Wang, F. Xia, H. Nie, Z. Chen, and W. Wei, "Vehicle trajectory clustering based on dynamic representation learning of internet of vehicles," *IEEE Transactions on Intelligent Transportation Systems*, vol. 22, no. 6, pp. 3567–3576, 2021.
- [12] C. H. Liu, Z. Dai, H. Yang, and J. Tang, "Multitask-oriented vehicular crowdsensing: a deep learning approach," in *IEEE INFOCOM 2020 -IEEE Conference on Computer Communications*, Toronto, ON, Canada, 2020.
- [13] P. McCartney, "Crowdsourcing in healthcare," *MCN: The American Journal of Maternal/Child Nursing*, vol. 38, no. 6, p. 392, 2013.
- [14] S. Gaikwad, D. Morina, R. Nistala et al., "Daemo: a self-governed crowdsourcing marketplace," in *Adjunct proceedings of the 28th annual ACM symposium on user interface software & technology*, pp. 101–102, 2015.
- [15] Y. Liu, X. Sun, W. Wei, and W. Jing, "Enhancing energy-efficient and QoS dynamic virtual machine consolidation method in cloud environment," *IEEE Access*, vol. 6, pp. 31224–31235, 2018.
- [16] H. Dou, Y. Qi, W. Wei, and H. Song, "Carbon-aware electricity cost minimization for sustainable data centers," *IEEE Transactions on Sustainable Computing*, vol. 2, no. 2, pp. 211–223, 2017.
- [17] G. A. Sigurdsson, G. Varol, X. Wang, A. Farhadi, I. Laptev, and A. Gupta, "Hollywood in homes: crowdsourcing data collection for activity understanding," in *European Conference on Computer Vision*, pp. 510–526, Cham, 2016.
- [18] P.-Y. Hsueh, P. Melville, and V. Sindhwani, "Data quality from crowdsourcing: a study of annotation selection criteria," in *Proceedings of the NAACL HLT 2009 workshop on active learning for natural language processing*, pp. 27–35, 2009.
- [19] G. Chen, C. Li, W. Wei, W. Jing, and R. Damaeviius, "Fully convolutional neural network with augmented atrous spatial pyramid pool and fully connected fusion path for high resolution remote sensing image segmentation," *Applied Sciences*, vol. 9, no. 9, p. 1816, 2019.
- [20] Q. Ke, J. Zhang, W. Wei, R. Damaševičius, and M. Woźniak, "Adaptive independent subspace analysis of brain magnetic resonance imaging data," *IEEE Access*, vol. 7, pp. 12252–12261, 2019.
- [21] L. Gao, S. Biderman, S. Black et al., "The pile: an 800gb dataset of diverse text for language modeling," 2020, <https://arxiv.org/abs/2101.00027>.
- [22] M.-C. Yuen, I. King, and K.-S. Leung, "A survey of crowdsourcing systems," in *2011 IEEE third international conference on privacy, security, risk and trust and 2011 IEEE third international conference on social computing*, pp. 766–773, Boston, MA, USA, 2011.
- [23] Uber china statement on service outageFebruary 2022, <http://shanghaiist.com/2015/04/18/uber/chinese/operations/recently/hacked.php/>.
- [24] W. Wei, M. Woniak, R. Damasevicius, X. Fan, and Y. Li, "Algorithm research of known-plaintext attack on double random phase mask based on WSNs," *Journal of Internet Technology*, vol. 20, no. 1, pp. 39–48, 2019.
- [25] W. Wei, S. Liu, W. Li, and D. Du, "Fractal intelligent privacy protection in online social network using attribute-based encryption schemes," *IEEE Transactions on Computational Social Systems*, vol. 5, no. 3, pp. 736–747, 2018.
- [26] S. W. Chen, D. L. Chiang, C. H. Liu et al., "Confidentiality protection of digital health records in cloud computing," *Journal of Medical Systems*, vol. 40, no. 5, pp. 1–12, 2016.

- [27] FreelancerFebruary 2022, <http://www.smh.com.au/business/freelancer-contests-20000-privacy-breach-finefrom-oaic-20160112-gm4aw2.html>.
- [28] Elance and odesk hit by ddosFebruary 2022, <https://gigaom.com/2014/03/18/elance-hit-by-major-ddosattack-downing-service-for-many-freelancers/>.
- [29] D. Guo, J. Xie, X. Zhou, X. Zhu, W. Wei, and X. Luo, "Exploiting efficient and scalable shuffle transfers in future data center networks," *IEEE Transactions on Parallel and Distributed Systems*, vol. 26, no. 4, pp. 997–1009, 2015.
- [30] S. Nakamoto, "Bitcoin: a peer-to-peer electronic cash system," *Decentralized Business Review*, no. article 21260, 2008.
- [31] S. Qi, Y. Lu, W. Wei, and X. Chen, "Efficient data access control with finegrained data protection in cloud-assisted IIoT," *IEEE Internet of Things Journal*, vol. 8, no. 4, pp. 2886–2899, 2021.
- [32] X. Yin, J. Han, and S. Yu Philip, "Truth discovery with multiple conflicting information providers on the web," *IEEE Transactions on Knowledge and Data Engineering*, vol. 20, no. 6, pp. 796–808, 2008.
- [33] W. Wei, H. Song, H. Wang, and X. Fan, "Research and simulation of queue management algorithms in ad hoc networks under DDoS attack," *IEEE Access*, vol. 5, pp. 27810–27817, 2017.
- [34] J. Chen, D. Chenglie, Y. Zhang, P. Han, and W. Wei, "An adaptive clustering-based algorithm for automatic path planning of heterogeneous UAVs," *IEEE Transactions on Intelligent Transportation Systems*, pp. 1–12, 2021.
- [35] S. Xia, D. Peng, D. Meng et al., "A fast adaptive k-means with no bounds," *IEEE Transactions on Pattern Analysis and Machine Intelligence*, vol. 44, no. 1, pp. 1–99, 2020.
- [36] H. M. Srivastava, Y. Zhang, L. Wang, P. Shen, and J. Zhang, "A local fractional integral inequality on fractal space analogous to Anderson's inequality," *Abstract and Applied Analysis*, vol. 2014, 7 pages, 2014.
- [37] H. S. Alenezi and M. H. Faisal, "Utilizing crowdsourcing and machine learning in education: literature review," *Education and Information Technologies*, vol. 25, no. 4, pp. 2971–2986, 2020.
- [38] S. Ørting, A. Doyle, A. van Hilten et al., "A survey of crowdsourcing in medical image analysis," 2019, <https://arxiv.org/abs/1902.09159>.
- [39] Y. Jin, M. Carman, Y. Zhu, and Y. Xiang, "A technical survey on statistical modelling and design methods for crowdsourcing quality control," *Artificial Intelligence*, vol. 287, article 103351, 2020.
- [40] J. Konečný, H. B. McMahan, F. X. Yu, P. Richtárik, A. T. Suresh, and D. Bacon, "Federated learning: strategies for improving communication efficiency," 2016, <https://arxiv.org/abs/1610.05492>.
- [41] M. I. Jordan and T. M. Mitchell, "Machine learning: trends, perspectives, and prospects," *Science*, vol. 349, no. 6245, pp. 255–260, 2015.
- [42] I. El Naqa and M. J. Murphy, *What Is Machine Learning?*, Springer International Publishing, Cham, 2015.
- [43] F. Provost and R. Kohavi, "Glossary of terms," *Journal of Machine Learning*, vol. 30, no. 2/3, pp. 271–274, 1998.
- [44] C. M. Bishop and N. M. Nasrabadi, *Pattern Recognition and Machine Learning*, vol. 4, Springer, 2006.
- [45] C. Tan, F. Sun, T. Kong, W. Zhang, C. Yang, and C. Liu, "A survey on deep transfer learning," in *Artificial Neural Networks and Machine Learning – ICANN 2018*, V. Kurková, Y. Manolopoulos, B. Hammer, L. Iliadis, and I. Maglogiannis, Eds., pp. 270–279, Springer International Publishing, Cham, 2018.
- [46] S. Nakamoto, *Bitcoin: A Peer-to-Peer Electronic Cash System*, Technical report, Manubot, 2019.
- [47] M. Risius and K. Spohrer, "A blockchain research framework," *Business & Information Systems Engineering*, vol. 59, no. 6, pp. 385–409, 2017.
- [48] N. Szabo, "Smart contracts: building blocks for digital markets," *EXTROPY: The Journal of Transhumanist Thought*, vol. 18, no. 2, 1996.
- [49] CrowdsourcingFebruary 2022, <https://en.wikipedia.org/wiki/Crowdsourcing/>.
- [50] E. Estellés-Arolas and F. G.-L.-d. Guevara, "Towards an integrated crowdsourcing definition," *Journal of Information Science*, vol. 38, no. 2, pp. 189–200, 2012.
- [51] M. Hirth, T. Hoßfeld, and P. Tran-Gia, "Anatomy of a crowdsourcing platformusing the example of microworkers.com," in *2011 Fifth international conference on innovative mobile and internet services in ubiquitous computing*, pp. 322–329, Seoul, Korea (South), 2011.
- [52] E. Schenk and C. Guittard, "Crowdsourcing: what can be outsourced to the crowd, and why," in *Workshop on open source innovation*, vol. 72, p. 3, Strasbourg, France, 2009.
- [53] D. C. Brabham, *Crowdsourcing*, Mit Press, 2013.
- [54] D. C. Brabham, "Crowdsourcing as a model for problem solving," *Convergence*, vol. 14, no. 1, pp. 75–90, 2008.
- [55] J. Prpic and P. Shukla, "Crowd science: measurements, models, and methods," in *2016 49th Hawaii International Conference on System Sciences (HICSS)*, pp. 4365–4374, Koloa, HI, USA, 2016.
- [56] R. Buettner, "A systematic literature review of crowdsourcing research from a human resource management perspective," in *2015 48th Hawaii International Conference on System Sciences*, pp. 4609–4618, Kauai, HI, USA, 2015.
- [57] J. Prpić, A. Taeihagh, and J. Melton, "The fundamentals of policy crowdsourcing," *Policy & Internet*, vol. 7, no. 3, pp. 340–361, 2015.
- [58] W. Liu, J. Moultrie, and S. Ye, "The customer-dominated innovation process: involving customers as designers and decision-makers in developing new product," *The Design Journal*, vol. 22, no. 3, pp. 299–324, 2019.
- [59] D. Schlagwein and N. Bjorn-Andersen, "Organizational learning with crowdsourcing: the revelatory case of lego," *Journal of the Association for Information Systems*, vol. 15, no. 11, pp. 754–778, 2014.
- [60] A. Taeihagh, "Crowdsourcing, sharing economies and development," *Journal of Developing Societies*, vol. 33, no. 2, pp. 191–222, 2017.
- [61] CrowdsensingFebruary 2022, <https://en.wikipedia.org/wiki/Crowdsensing/>.
- [62] R. K. Ganti, F. Ye, and H. Lei, "Mobile crowdsensing: current state and future challenges," *IEEE Communications Magazine*, vol. 49, no. 11, pp. 32–39, 2011.
- [63] Y. Wang and J. Ma, *Mobile Social Networking and Computing: A Multidisciplinary Integrated Perspective*, CRC Press, 2014.
- [64] A.-S. K. Pathan, *Crowd Assisted Networking and Computing*, CRC Press, 2018.
- [65] C. Miao, W. Jiang, L. Su et al., "Cloud-enabled privacy-preserving truth discovery in crowd sensing systems," in

- Proceedings of the 13th ACM Conference on Embedded Networked Sensor Systems*, pp. 183–196, 2015.
- [66] Q. Li, Y. Li, J. Gao et al., “A confidence-aware approach for truth discovery on long-tail data,” *Proceedings of the VLDB Endowment*, vol. 8, no. 4, pp. 425–436, 2014.
- [67] Y. Zheng, H. Duan, and C. Wang, “Learning the truth privately and confidently: encrypted confidence-aware truth discovery in mobile crowdsensing,” *IEEE Transactions on Information Forensics and Security*, vol. 13, no. 10, pp. 2475–2489, 2018.
- [68] X. Liu, P. Zou, W. Zhang et al., “CPSFS: a credible personalized spam filtering scheme by crowdsourcing,” *Wireless Communications and Mobile Computing*, vol. 2017, 9 pages, 2017.
- [69] Y. Qiao, J. Zhang, Q. He et al., “Truthful profit maximization mechanisms for mobile crowdsourcing,” *Wireless Communications and Mobile Computing*, vol. 2022, 13 pages, 2022.
- [70] A. Swearngin and L. Yang, “Modeling mobile interface tappability using crowdsourcing and deep learning,” in *Artificial Intelligence for Human Computer Interaction: A Modern Approach*, pp. 73–96, Springer, 2021.
- [71] K. Yadav, P. Kumaraguru, A. Goyal, A. Gupta, and V. Naik, “SMSAssassin: Crowdsourcing driven mobile-based system for SMS spam filtering,” *12th Workshop on Mobile Computing Systems and Applications*, pp. 1–6, 2011.
- [72] S. Amini and L. Yang, “Crowdlearner: rapidly creating mobile recognizers using crowdsourcing,” *26th annual ACM symposium on User interface software and technology*, pp. 163–172, 2013.
- [73] A. Trivedi, P. Bovornkeeratiroj, J. Breda, P. Shenoy, J. Taneja, and D. Irwin, “Phone-based ambient temperature sensing using opportunistic crowdsensing and machine learning,” *Sustainable Computing: Informatics and Systems*, vol. 29, article 100479, 2021.
- [74] Z. Lan, Y. Li, X. Xiang, X. Y. Li, and L. Qiang, “Crowdbuy: privacy-friendly image dataset purchasing via crowdsourcing,” in *IEEE INFOCOM 2018 - IEEE Conference on Computer Communications*, Honolulu, HI, USA, 2018.
- [75] E. Law and L. Von Ahn, “Input-agreement: a new mechanism for collecting data using human computation games,” in *Proceedings of the SIGCHI Conference on Human Factors in Computing Systems*, pp. 1197–1206, 2009.
- [76] L. Orlandic, T. Teijeiro, and D. Atienza, “The coughvid crowdsourcing dataset, a corpus for the study of large-scale cough analysis algorithms,” *Scientific Data*, vol. 8, no. 1, pp. 1–10, 2021.
- [77] J. C. Chang, S. Amershi, and E. Kamar, “Revolt: collaborative crowdsourcing for labeling machine learning datasets,” in *Proceedings of the 2017 CHI Conference on Human Factors in Computing Systems*, pp. 2334–2346, 2017.
- [78] T. Finin, W. Murnane, A. Karandikar, N. Keller, J. Martineau, and M. Dredze, “Annotating named entities in twitter data with crowdsourcing,” in *Proceedings of the NAACL Workshop on Creating Speech and Text Language Data With Amazon’s Mechanical Turk*, 2010.
- [79] H. Fromreide, D. Hovy, and A. Sjøgaard, “Crowdsourcing and annotating NER for Twitter# drift,” *LREC*, pp. 2544–2547, 2014.
- [80] S. Park, P. Shoemark, and L.-P. Morency, “Toward crowdsourcing micro-level behavior annotations: the challenges of interface, training, and generalization,” in *Proceedings of the 19th international conference on Intelligent User Interfaces*, pp. 37–46, 2014.
- [81] M. Lease, “On quality control and machine learning in crowdsourcing,” in *Workshops at the Twenty-Fifth AAAI Conference on Artificial Intelligence*, 2011.
- [82] T. W. Cenggoro, F. Tanzil, A. H. Aslamiah, E. K. Karuppiah, and B. Pardamean, “Crowdsourcing annotation system of object counting dataset for deep learning algorithm,” *IOP Conference Series: Earth and Environmental Science*, vol. 195, no. 1, article 012063, 2018.
- [83] B. M. Good, M. Nanis, C. Wu, and A. I. Su, “Microtask crowdsourcing for disease mention annotation in PubMed abstracts,” in *Pacific Symposium on Biocomputing Co-Chairs*, pp. 282–293, World Scientific, 2014.
- [84] J. Yang, J. Fan, Z. Wei, G. Li, T. Liu, and X. du, “Cost-effective data annotation using game-based crowdsourcing,” *Proceedings of the VLDB Endowment*, vol. 12, no. 1, pp. 57–70, 2018.
- [85] S. Hantke, Z. Zhang, and B. W. Schuller, “Towards intelligent crowdsourcing for audio data annotation: Integrating active learning in the real world,” *Interspeech*, pp. 3951–3955, 2017.
- [86] P. Roit, A. Klein, D. Stepanov et al., “Controlled crowdsourcing for highquality qa-srl annotation,” 2019, <https://arxiv.org/abs/1911.03243>.
- [87] S. Hao, J. Deng, and L. Fei-Fei, “Crowdsourcing annotations for visual object detection,” in *The 4th Human Computation Workshop, HCOMP@AAAI 2012*, vol. WS-12-08 of AAAI Technical Report, Toronto, Ontario, Canada, 2012.
- [88] M. Ryabinin and A. Gusev, “Towards crowdsourced training of large neural networks using decentralized mixture-of-experts,” *Advances in Neural Information Processing Systems*, vol. 33, pp. 3659–3672, 2020.
- [89] S. Zhang, J. Wu, and S. Lu, “Minimum makespan workload dissemination in DTNs: making full utilization of computational surplus around,” *The fourteenth ACM international symposium on Mobile ad hoc networking and computing*, pp. 293–296, 2013.
- [90] P. Yang, Q. Li, Y. Yan et al., ““Friend is treasure”: exploring and exploiting mobile social contacts for efficient task offloading,” *IEEE Transactions on Vehicular Technology*, vol. 65, no. 7, pp. 5485–5496, 2016.
- [91] M. H. Cheung, R. Southwell, F. Hou, and J. Huang, “Distributed time-sensitive task selection in mobile crowdsensing,” *The 16th ACM International Symposium on Mobile Ad Hoc Networking and Computing*, pp. 157–166, 2015.
- [92] F. Ast and A. Sewrjugin, *The crowdjury, a crowdsourced justice system for the collaboration era*, Technical report, 2015, August 2015, <https://www.http://weusecoins.com/assets/pdf/library/The>.
- [93] M. Li, J. Weng, A. Yang et al., “Crowdbc: a blockchain-based decentralized framework for crowdsourcing,” *IEEE Transactions on Parallel and Distributed Systems*, vol. 30, no. 6, pp. 1251–1266, 2019.
- [94] J. D. Harris and B. Waggoner, “Decentralized and collaborative AI on blockchain,” in *2019 IEEE international conference on blockchain (Blockchain)*, pp. 368–375, Atlanta, GA, USA, 2019.
- [95] D. Sheng, M. Xiao, A. Liu, X. Zou, and S. Zhang, “Cpchain: a copyright-preserving crowdsourcing data trading framework based on blockchain,” in *2020 29th International Conference on Computer Communications and Networks (ICCCN)*, Honolulu, HI, USA, 2020.

- [96] B. An, M. Xiao, A. Liu, G. Gao, and H. Zhao, "Truthful crowdsensed data trading based on reverse auction and blockchain," in *Database Systems for Advanced Applications*, G. Li, J. Yang, J. Gama, J. Natwichai, and Y. Tong, Eds., pp. 292–309, Springer International Publishing, Cham, 2019.
- [97] C. Zhang, Y. Guo, H. Du, and X. Jia, "Pfcrowd: privacy-preserving and federated crowdsourcing framework by using blockchain," in *2020 IEEE/ACM 28th International Symposium on Quality of Service (IWQoS)*, Hang Zhou, China, 2020.
- [98] J. Park, S. Park, K. Kim, and D. Lee, "Corus: blockchain-based trustworthy evaluation system for efficacy of healthcare remedies," in *2018 IEEE International Conference on Cloud Computing Technology and Science (CloudCom)*, pp. 181–184, Nicosia, Cyprus, 2018.
- [99] T. M. Fernández-Caramés, I. Froiz-Míguez, O. Blanco-Novoa, and P. Fraga-Lamas, "Enabling the internet of mobile crowdsourcing health things: a mobile fog computing, blockchain and IoT based continuous glucose monitoring system for diabetes mellitus research and care," *Sensors*, vol. 19, no. 15, p. 3319, 2019.
- [100] W. Shen, A. F. Taha, J. Wang, K. Kvaternik, and A. Hahn, "Energy crowdsourcing and peer-to-peer energy trading in blockchain-enabled smart grids," *IEEE Transactions on Systems, Man, and Cybernetics: Systems*, vol. 49, no. 8, pp. 1612–1623, 2019.
- [101] F. Jamil, N. Iqbal, S. Ahmad, and D. Kim, "Peer-to-peer energy trading mechanism based on blockchain and machine learning for sustainable electrical power supply in smart grid," *IEEE Access*, vol. 9, pp. 39193–39217, 2021.
- [102] K. Zhao, S. Tang, B. Zhao, and Y. Wu, "Dynamic and privacy-preserving reputation management for blockchain-based mobile crowdsensing," *IEEE Access*, vol. 7, pp. 74694–74710, 2019.
- [103] Z. Wang, X. Cheng, S. Sen, and L. Wang, "Achieving private and fair truth discovery in crowdsourcing systems," *Security and Communication Networks*, vol. 2022, 15 pages, 2022.
- [104] J. An, J. Cheng, X. Gui et al., "A lightweight blockchain-based model for data quality assessment in crowdsensing," *IEEE Transactions on Computational Social Systems*, vol. 7, no. 1, pp. 84–97, 2020.
- [105] Y. Zheng, H. Duan, X. Yuan, and C. Wang, "Privacy-aware and efficient mobile crowdsensing with truth discovery," *IEEE Transactions on Dependable and Secure Computing*, vol. 17, no. 1, pp. 121–133, 2020.
- [106] C. Cai, Y. Zheng, and C. Wang, "Leveraging crowdsensed data streams to discover and sell knowledge: a secure and efficient realization," in *38th IEEE International Conference on Distributed Computing Systems, ICDCS 2018*, pp. 589–599, Vienna, Austria, 2018.
- [107] X. Tang, C. Wang, X. Yuan, and Q. Wang, "Non-interactive privacy-preserving truth discovery in crowd sensing applications," in *2018 IEEE Conference on Computer Communications, INFOCOM 2018*, pp. 1988–1996, Honolulu, HI, USA, 2018.
- [108] G. Xu, H. Li, and R. Lu, "Practical and privacy-aware truth discovery in mobile crowd sensing systems," in *Proceedings of the 2018 ACM SIGSAC Conference on Computer and Communications Security*, pp. 2312–2314, 2018.
- [109] K. Xue, B. Zhu, Q. Yang, N. Gai, D. S. Wei, and N. Yu, "Inpptd: a lightweight incentive-based privacy preserving truth discovery for crowdsensing systems," *IEEE Internet of Things Journal*, vol. 8, no. 6, pp. 4305–4316, 2021.
- [110] C. Miao, W. Jiang, L. Su et al., "Privacy-preserving truth discovery in crowd sensing systems," *ACM Transactions on Sensor Networks (TOSN)*, vol. 15, no. 1, pp. 1–32, 2019.
- [111] J. Gao, F. Shaojing, Y. Luo, and T. Xie, "Location privacy-preserving truth discovery in mobile crowd sensing," in *29th International Conference on Computer Communications and Networks, ICCCN 2020*, pp. 1–9, Honolulu, HI, USA, 2020.
- [112] G. Xu, H. Li, S. Xu et al., "Catch you if you deceive me: verifiable and privacy-aware truth discovery in crowdsensing systems," in *ASIA CCS '20: The 15th ACM Asia Conference on Computer and Communications Security*, pp. 178–192, Taipei, Taiwan, 2020.
- [113] C. Zhang, C. Xu, L. Zhu, Y. Li, and H. Wu, "An efficient and privacy-preserving truth discovery scheme in crowdsensing applications," *Computers Security*, vol. 97, article 101848, 2020.
- [114] P. Sun, Z. Wang, Y. Feng, L. Wu, and Z. Wang, "Towards personalized privacy-preserving incentive for truth discovery in crowdsourced binarychoice question answering," in *IEEE International Conference on Computer Communications (INFOCOM 2020)*, Toronto, ON, Canada, 2020.
- [115] D. Liang, J. An, J. Cheng, Y. He, and R. Gui, "The quality control in crowdsensing based on twice consensus of blockchain," in *Proceedings of the 2018 ACM International Joint Conference and 2018 International Symposium on Pervasive and Ubiquitous Computing and Wearable Computers, UbiComp/ISWC 2018 Adjunct*, pp. 630–635, Singapore, 2018.
- [116] H. Duan, Y. Zheng, Y. Du, A. Zhou, C. Wang, and M. H. Au, "Aggregating crowd wisdom via blockchain: a private, correct, and robust realization," in *2019 IEEE International Conference on Pervasive Computing and Communications (PerCom)*, pp. 1–10, Kyoto, Japan, 2019.
- [117] Y. Tian, J. Yuan, and H. Song, "Secure and reliable decentralized truth discovery using blockchain," in *7th IEEE Conference on Communications and Network Security, CNS 2019*, pp. 1–8, Washington, DC, USA, 2019.
- [118] C. Wang, *Privacy-Preserving Truth Discovery in Mobile Crowdsensing: Challenges, Solutions, and Opportunities*, 2018.
- [119] Z. Zheng, Y. Peng, F. Wu, S. Tang, and G. Chen, "Arete: on designing joint online pricing and reward sharing mechanisms for mobile data markets," *IEEE Transactions on Mobile Computing*, vol. 19, no. 4, pp. 769–787, 2020.
- [120] G. Gao, J. Wu, M. Xiao, and G. Chen, "Combinatorial multi-armed bandit based unknown worker recruitment in heterogeneous crowdsensing," in *IEEE INFOCOM 2020 - IEEE Conference on Computer Communications*, Toronto, ON, Canada, 2020.
- [121] J. Hu, Z. Wang, J. Wei et al., "Towards demand-driven dynamic incentive for mobile crowdsensing systems," *IEEE Transactions on Wireless Communications*, vol. 19, no. 7, pp. 4907–4918, 2020.
- [122] W. Liu, Y. Yang, E. Wang, and J. Wu, "Dynamic user recruitment with truthful pricing for mobile crowdsensing," in *IEEE INFOCOM 2020 - IEEE Conference on Computer Communications*, Toronto, ON, Canada, 2020.
- [123] P. Kairouz, H. B. McMahan, B. Avent et al., "Advances and open problems in federated learning," *Foundations and Trends® in Machine Learning*, vol. 14, no. 1–2, pp. 1–210, 2021.
- [124] T. Li, A. K. Sahu, A. Talwalkar, and V. Smith, "Federated learning: challenges, methods, and future directions," *IEEE Signal Processing Magazine*, vol. 37, no. 3, pp. 50–60, 2020.

- [125] K. Bonawitz, H. Eichner, W. Grieskamp et al., “Towards federated learning at scale: system design,” *Proceedings of Machine Learning and Systems*, vol. 1, pp. 374–388, 2019.
- [126] Q. Yang, Y. Liu, Y. Cheng, Y. Kang, T. Chen, and H. Yu, “Federated learning,” *Synthesis Lectures on Artificial Intelligence and Machine Learning*, vol. 13, no. 3, pp. 1–207, 2019.
- [127] J. Yang, H. Wang, Z. Lv et al., “Multimedia recommendation and transmission system based on cloud platform,” *Future Generation Computer Systems*, vol. 70, pp. 94–103, 2017.
- [128] Z. Ji, H. Pi, W. Wei, B. Xiong, M. Wozniak, and R. Damasevicius, “Recommendation based on review texts and social communities: a hybrid model,” *IEEE Access*, vol. 7, pp. 40416–40427, 2019.
- [129] J. Benet, “Ipfs-content addressed, versioned, p2p file system,” 2014, <https://arxiv.org/1407.3561>.
- [130] S. Shepler, B. Callaghan, D. Robinson et al., *Rfc3530: Network File System (Nfs) Version 4 Protocol*, 2003.
- [131] J. Li, G. Deng, W. Wei, H. Wang, and Z. Ming, “Design of a real-time ECG filter for portable mobile medical systems,” *IEEE Access*, vol. 5, pp. 696–704, 2017.

Research Article

Application of Kohonen Neural Network in Sports Cluster

Youwen Mao 

School of Physical Education, Anyang Normal University, Anyang 455000, China

Correspondence should be addressed to Youwen Mao; 00852@aynu.edu.cn

Received 9 April 2022; Revised 7 June 2022; Accepted 8 June 2022; Published 12 July 2022

Academic Editor: Alireza Souri

Copyright © 2022 Youwen Mao. This is an open access article distributed under the Creative Commons Attribution License, which permits unrestricted use, distribution, and reproduction in any medium, provided the original work is properly cited.

People's physical fitness is directly linked to the national physique of a country. It is an important analysis indicator of the country's comprehensive national strength and economic level. Moreover, students' physical and mental health is in a stage of rapid development. Their physical health is not only directly related to their study and life at this stage but it will also have a profound impact on the physical level, health status, and work ability of adults. Starting from the cluster analysis of sports, this article explores the communication effects of sports, communication strategies, and the relationship between sports and the development of users' healthy habits by defining concepts and types and combining quantitative and qualitative analysis. Study the relationship and then analyze whether sports applications bring people the effect of promoting healthy behavior. This article retrieved documents about the application of Kohonen neural network in sports cluster analysis in domestic literature databases such as Weipu, Wanfang data, and CNKI. A total of 144 documents were retrieved from the database, and the retrieved documents were collected for sports activities. The study of class analysis can avoid human subjective factors and obtain clustering results quickly and objectively, thus providing an ideal clustering method for comprehensive evaluation of sports. The experiment proves the cluster analysis of the impact of sports on people's physical fitness, the heterogeneity test results are 0% (boys) and 3% (girls), it is believed that there is no statistical heterogeneity in the physical fitness of middle school boys in each study, and $P < 0.001$, indicating that the influence of sports on people's physical fitness is significantly different between the experimental group and the control group. This shows that the application of Kohonen neural network clustering analysis method has great practical value for comprehensively evaluating people's physical functions and physical fitness. It is an objective, reasonable, effective, and rapid quantitative evaluation method.

1. Introduction

Sports cluster analysis came into being. It improved the user experience with the help of big data, informatization, and neural network technology. At the same time, it has not only been recognized and loved by the public but it has also promoted the national sports boom and also conveyed the sports belt. There is positive energy coming. Research and analysis on the communication effects of the emerging media of sports applications and people's sports conditions are not only helpful to help people improve their physical conditions but also a positive response to national policies, and it is important for the development of sports and the participation of the people. The sports industry cluster is the product of the integration process of the global economy,

which is produced and gradually deepened. It is the application and innovation of the industry cluster theory in the field of sports. As a new force in the rising sports industry, the sports industry cluster has broad development prospects and huge development space.

The application of cluster analysis in sports in foreign countries is much earlier than that in China, and the rapid development and update of Kohonen neural network technology has made the methods and types of cluster analysis greatly improved and developed. I believe that in the near future, the clustering analysis method that introduces the Kohonen neural network technology will become an efficient clustering method. Kalini explores how virtual communities have a positive impact on the development of a healthy lifestyle in reality through the characteristics of information

sharing, interaction, and common interest gathering [1]. Shadloo proposed that the factors that affect college students' physical exercise behavior mainly include sports awareness, sports knowledge and methods, exercise atmosphere and sports expertise, and sports consumption behaviors which have a clear correlation with college students' physical exercise behaviors [2]. Li started from the analysis of the existing misunderstandings in sports and the negative effects they produced and proposed the basic model and planning of sports cluster analysis [3].

The cluster analysis method originated in western countries. Compared with the western countries, the cluster analysis method started late and its development is relatively slow. With the continuous development of information and communication and the maturity of computer network technology, the use of cluster analysis methods can predict the activity space and development trends of various sports. Bodyanskiy proposes that health education for college students should focus on combining physical exercise and health and help college students develop good physical exercise habits by introducing the impact of physical exercise on human health, the principles that physical exercise should follow, and common physical fitness methods [4]. Bodyanskiy proposed that the cognition and feeling of sports behavior are related to sports behavior, sports persistence, and sports experience and can directly affect sports behavior [5]. Watanabe proposes to use sports to make people come out of busy work, improve their physical health and find a communication partner, obtain spiritual comfort, and achieve the optimization of the social support network [6].

Through the cluster analysis of sports, this article explores the ways in which sports affect people's healthy living habits, which can not only make people pay more attention to their own health but also promote people to increase their physical fitness. This paper also uses the Kohonen neural network to iteratively optimize the objective function to perform a cluster analysis of sports, avoiding many subjective factors, statistically surveying the related data of the types of sports that people participate in daily, and analyzing its relationship with people's behavior habits. The relationship between cultivation and promotion provides a fast and novel cluster analysis method for similar research in the future.

2. Application of Kohonen Neural Network in Sports Cluster

2.1. Neural Networks

2.1.1. Neural Networks. Artificial neural network is composed of a large number of neurons. Its main function is to imitate the functions of the human brain to process information. Its processing ability is very powerful, and its learning ability is also super strong, capable of processing very complex nonlinearities. Transformed into an easy-to-understand form of expression, artificial neural network can be referred to as neural network [7, 8]. By designing a comprehensive neural network evaluation model that combines BP network and self-organizing competition network,

the evaluation results of 28 provinces and regions are fitted and ranked, and the development stage of regional high-tech industrial clusters can be defined.

(1) Neuron Model. Generally, the neuron of a neural network is composed of many inputs and one output. The input of the neuron is $x_1 \cdots x_n$, w_{ij} represents the weight of the j input, the threshold of the neuron is represented by θ_j , the self-information and external information of the neuron are, respectively, u_i and s_i denoted, the output is denoted by y_i , and its model can be represented by

$$\tau \frac{du_i}{dt} = -u_i(t) + \sum w_{ij}x_j(t) - \theta_i, \quad (1)$$

$$y_i = f[u_i(t)]. \quad (2)$$

The expression formula of the model is a first-order differential, so it can mimic the function of human neural network processing information well. In addition, its output can be expressed in the following three forms [9].

Linear type:

$$f(u_i) = \begin{cases} 1, & u_i \geq u_2, \\ au_i + b, & u_i \leq 0 < u_2, \\ 0, & u_i < u_1. \end{cases} \quad (3)$$

Step type:

$$f(u_i) = \begin{cases} 1, & u_i \geq 0, \\ 0, & u_i < 0. \end{cases} \quad (4)$$

Type S:

$$f(u_i) = \frac{1}{1 + \exp(-u_i/c)}. \quad (5)$$

Among them, a is the proportional coefficient, b is the variable value, and c is the fixed value.

(2) Types of Neural Networks. Forward network refers to the connection between layers, but there is no connection between each layer. The network is always moving forward, and the network of the last layer is not connected to the first layer network, which is the beginning and the end of the network. There is no connection between the networks, and the networks are lined up. This is the forward network feedback network. On the basis of the forward network, the last layer of the network is connected to the first layer of network; that is, the output is introduced to the first the input of the layer is on [10, 11]. If there is no feedback, the network within the layer has a one-way connection. This form is conducive to strengthening the influence within the same layer and promoting network learning. The intralayer interconnection network is also under the condition that all or not all neurons in the same layer are connected to each other under

the condition that all or not all neurons in the same layer are connected to each other. This interconnection method promotes the activity in the same layer, whether it is strong or strong or weak both are weak [12]. Existing studies have analyzed industrial clusters and their performance from different research aspects through the methods of AHP, DEA, location quotient, principal component analysis, multiple regression statistics, and summarization. The neural network method is mainly used in the theoretical stage.

2.1.2. Kohonen Neural Network Algorithm Steps. For the input vector $Y = \{y_1, y_2, \dots, y_n\}$, if there are c fuzzy subsets forming a fuzzy c partition of the input vector Y , then the membership of these fuzzy subsets should meet the following conditions:

$$0 \leq r_{ik} \leq 1, \quad \sum_i r_{ik} = 1. \quad (6)$$

The objective function of cluster Y is generally expressed in the following form:

$$J(R, Z, Y) = \sum_i \sum_k (r_{ik})^\lambda (\|Y_k - Z_i\|)^2, \quad (7)$$

where λ is the power exponent of the membership function r , $Z = (z_1, z_2, \dots, z_c)$ is the cluster center of a given input sample, and R is a fuzzy c partition of the input sample Y . The above formula is the core optimization goal of Kohonen neural network algorithm [13, 14].

Select a learning sample $Y = \{y_1, y_2, \dots, y_n\}$ with correct data, where the number of samples in the learning sample is n , each sample vector is a p -dimensional vector, and the initial value $c (1 \leq c \leq n)$ and the feature distance used for cluster analysis are given.

Step 1. Initialize the cluster center vector $Z = (z_1, z_2, \dots, z_c)$, each vector in this cluster center vector set is also a p -dimensional vector, and initialize the number of training $T = 0$, the maximum number of training is T_{\max} , and the initial weighted power exponent of the degree of membership is $K_0 (K_0 > 1)$. Set the termination error of the iteration as $\varepsilon > 0$ [15, 16].

Step 2. Calculate the membership degree of each sample belonging to the $i (2 \leq i \leq c)$ type in the input mode and mark it as r_{ik} . The membership degree calculation function is as follows:

$$r_{ik} = \frac{1}{\sum_{j=1}^c (\|Y_k - Z_i\| / \|Y_k - Z_j\|)^{2/(\lambda-1)}}. \quad (8)$$

After the membership degree r_{ij} is calculated, use this membership degree to calculate the iteratively updated learning rate a of the weight value, and the calculation learning rate a function is as follows:

$$a_{ik}(T) = r_{ik}^\lambda, \quad (9)$$

$$\lambda = \frac{K_0 - T(K_0 - 1)}{T_{\max}},$$

where K_0 is a normal number greater than 1, when $T = T_{\max}$, $\lambda = 1$.

Step 3. Adjust the cluster center vector, and update the vector formula according to the previous cluster center vector and the learning rate as follows:

$$Z_i(t) = Z_i(T-1) + \frac{\sum_{k=1}^N a_{ik}(Y_k - Z_i(T-1))}{\sum_{k=1}^N a_{ik}}, \quad i = 1, 2, \dots, c. \quad (10)$$

Step 4. Calculate the energy function and the correction error of the clustering center vector Z . If formula (19) is satisfied, the algorithm stops iterating.

$$\|Z(T) - Z(T-1)\|^2 = \sum_{i=1}^c \|Z_i(T) - Z_i(T-1)\|^2 \leq \varepsilon. \quad (11)$$

When the number of iterations is greater than the initially set maximum number of iterations T_{\max} , it will also cause the iteration to terminate; otherwise, it will move to the second step to continue the calculation iteration.

2.2. Metrics and Criterion Functions in Cluster

2.2.1. Measurement Methods in Cluster Analysis. In cluster analysis, we need to select appropriate indicators as the basis for clustering. Commonly used measures are similarity and dissimilarity measures, which quantitatively describe the degree of similarity or dissimilarity between two data objects or clusters. Or the greater the similarity between clusters, the smaller the dissimilarity; conversely, the smaller the similarity, the greater the dissimilarity [17, 18]. However, most existing clustering algorithms often use dissimilarity to represent the similarity measure and use it as a measure of computing data objects. We introduce the following commonly used standardization methods.

(1) Min-Max Standardization.

$$(x_{jl})' = \frac{x_{jl} - \min(x_{.l})}{\max(x_{.l}) - \min(x_{.l})}. \quad (12)$$

Among them, x_{jl} represents the value of the j data object under the l attribute; $\max(x_{.l})$ and $\min(x_{.l})$, respectively, represent the maximum and minimum values of the l attribute in the data set, making $(x_{jl})' \in [0, 1]$.

(2) *Z-Score Standardization*.

$$(x_{jl})' = \frac{x_{jl} - x_l}{S_j}. \quad (13)$$

Among them, x_l represents the mean $x_l = (1/n_j) \sum_{j=1}^{n_j} x_{jl}$ of the l attribute, and the standard deviation $S_j = (1/n_j) \sum_{j=1}^{n_j} (x_{jl} - x_l)^2$.

(3) *Decimal Scaling Standardization*. Standardization is carried out by moving the decimal point position of the attribute value. The number of decimal points moved depends on the maximum absolute value in the attribute value. The calculation method is

$$x' = \frac{x}{10^j}. \quad (14)$$

2.2.2. *Criterion Function in Cluster Analysis*. After determining the similarity measurement method, in order to complete the clustering, the corresponding criterion function needs to be determined. The commonly used clustering criterion function is as follows.

(1) *Criterion Function*. This kind of clustering criterion function is mostly used for clustering problems where data objects are densely distributed, the number of data objects is small, and there are significant differences between data objects between different classes [19, 20]. Assuming that the distance between any data object x in class c_i and class center m_i is represented by $d(x, m_i)$, the error sum of squares function is defined as follows:

$$J_c = \sum_{i=1}^k \sum_{x \in c_i} d(x - m_i)^2. \quad (15)$$

Among them, k is the number of clusters, c_i is the cluster set of class i , x is the data object in class c_i , and m_i is the class center in class c_i , which is generally obtained by calculating the average value of all data objects in class c_i . The calculation formula is

$$m_i = \frac{1}{n_i} \sum_{x \in c_i} x, \quad i = 1, 2, \dots, k. \quad (16)$$

The more compact, the better the clustering effect.

(2) *Weighted Average Square Distance and Criterion Function*.

$$J_i = \sum_{i=1}^k P S_i^*. \quad (17)$$

P represents the weighted prior probability, which is calculated from the number n_i of data objects in class c_i and the total number n of all data objects in the data set. The calculation formula is as follows:

$$P = \frac{n_i}{n}. \quad (18)$$

Among them, S_i^* represents the average squared distance between data objects in the class, and its calculation formula is

$$S_i^* = \frac{2}{n_i(n_i - 1)} \sum_{x \in c_i} \sum_{x' \in c_i} x - x'^2. \quad (19)$$

(3) *Interclass Distance and Criterion Function*. This clustering criterion function is used to describe the degree of separation between different categories, and there are usually two definitions.

General distance between classes and function definitions:

$$J_{b1} = \sum_{i=1}^k (m_i - m)^T (m_i - m). \quad (20)$$

Weighted interclass distance and function definition:

$$J_{b2} = \sum_{i=1}^k P (m_i - m)^T (m_i - m). \quad (21)$$

Among them, m_i represents the mean vector of class c_i , m represents the mean vector of the entire data set, and P is the weighted prior probability. Construct industrial cluster organization neural network. Build an industrial cluster network architecture, and use the newff() function to establish a preliminary neural network function. The four input elements of the function are an $R \times 2$ -dimensional matrix composed of the maximum and minimum values in the R -dimensional input samples, the number of network neurons in the layer, the transfer function used by each layer of network neurons, and the type of function used for training.

3. Experimental Design of Sports Cluster

3.1. *Cluster Experiment Object*. Retrieving literature about the application of Kohonen neural network in sports clustering analysis using Weipu, Wanfang data, CNKI, and other domestic literature databases. The search terms are Kohonen neural network, sports cluster analysis, etc. A total of 144 articles were retrieved from the database, the inclusion and exclusion criteria were strictly set, and the quality of the final included research articles was evaluated.

Inclusion criteria: the subjects are nonprofessional sports people; the literature that studies the application of Kohonen neural network in sports cluster analysis; experimental research, the number of experimental group and control group, the indicators of the experimental group and control group before and after intervention documents with clear

TABLE 1: Data sheet of evaluation index system for index reliability testing.

	Very clear	Clear	General	Not clear	Chaotic	Alpha
Body shape	4.37	3.42	4.21	3.01	3.24	0.8567
Body function	4.06	3.57	4.39	3.10	3.01	0.8233
Physical fitness	3.39	3.76	4.35	3.46	3.50	0.7369
Willing to participate in sports	3.84	3.37	4.08	3.14	3.44	0.7419

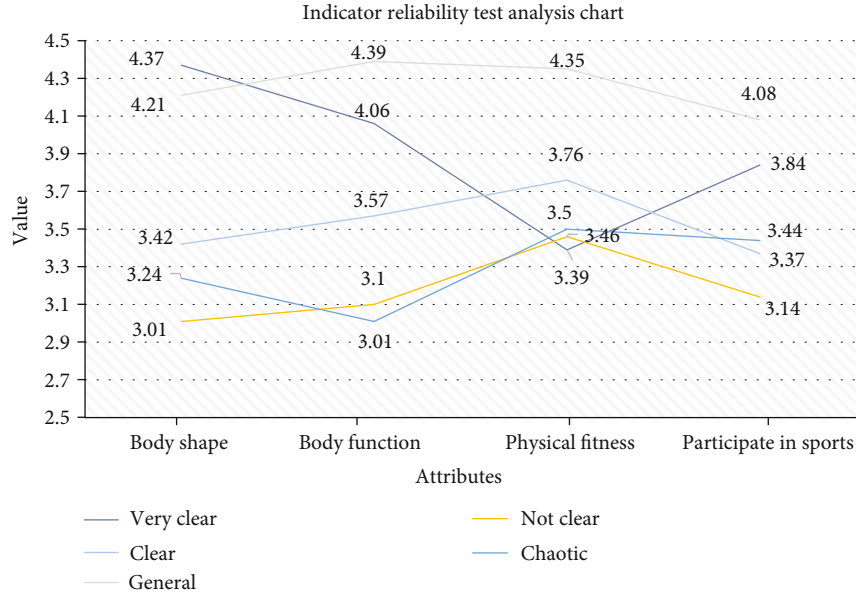


FIGURE 1: Indicator reliability test analysis chart.

TABLE 2: Statistical data table of published years of included literature.

Years	Journal literature	Degree literature	Conference documents	Patent literature
2001-2005	5	9	1	0
2006-2010	7	16	3	0
2011-2015	13	19	6	2
2016-2020	18	31	9	5

descriptions of changes; for studies of the same population by the same researcher, only the most recently published one is selected.

Exclusion criteria: the subjects are professional sports people; the study before the experiment is not comparable to the baseline of the experimental group and the control group; nonexperimental research; the number of the experimental group and the control group, the changes in the experimental group and the control group before and after the intervention are not described enough in clear documents; documents published by different authors with exactly the same content, documents published after deletion.

3.2. Learning and Training of Neural Networks. In the Kohonen neural network, the weight represents the components of each cluster center, and the number of nodes in the output layer represents the number of clusters. In the network training process, since the selection of the initial weight will not have much impact on the training result, we randomly select 5 numbers between 0 and 1 as the initial weight. There are 12 groups of network training samples, and each group of sample vectors contains 5 components (5 indicators). The training times of the selected network is 2000 times.

3.3. Statistical Data Processing Methods. SPSS 23.0 was used to process the data, and the numbers are expressed in percent (%), where K is the number of data in this experiment, the variance of all survey results, and $P < 0.05$ indicates that the difference is statistically significant. The formula for calculating reliability is shown in

$$a = \frac{k}{k-1} \left(1 - \frac{\sum \sigma_i^2}{\sigma^2} \right). \quad (22)$$

4. Experimental Sports Cluster

4.1. Evaluation Index System Based on Index Reliability Testing. A coefficient alpha of 0.8 or higher indicates that the indicator is very good, while a coefficient alpha of 0.7 or higher is also acceptable. Reliability is analyzed here for

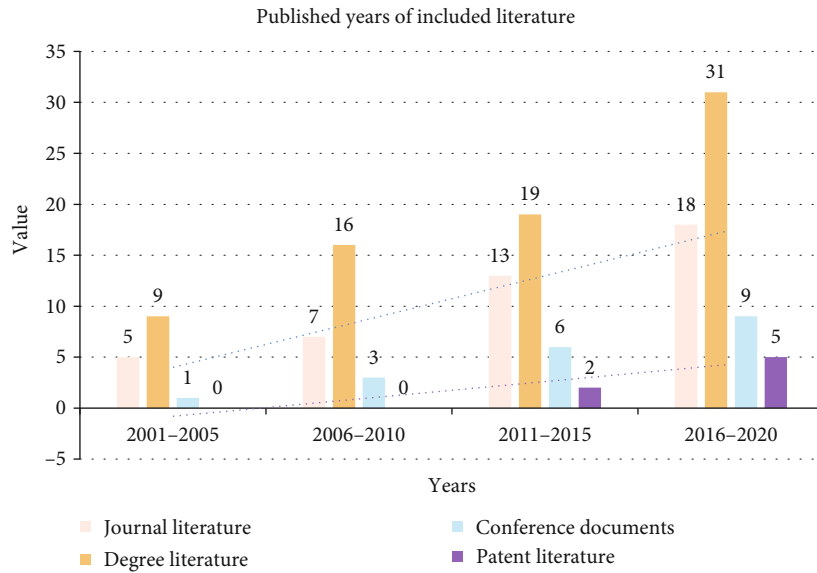


FIGURE 2: Statistical analysis chart of published years of included literature.

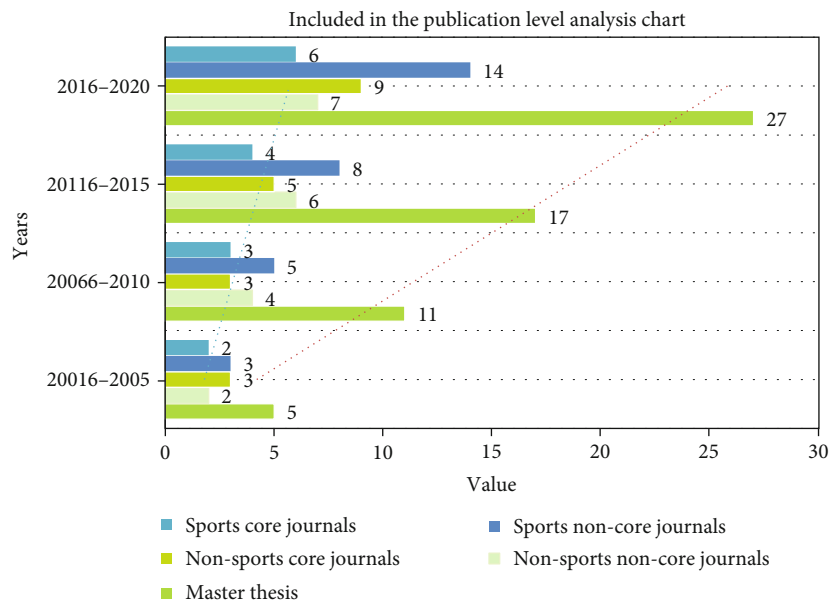


FIGURE 3: Included in the publication level analysis chart.

TABLE 3: Data table of the impact of sports on people’s body shape.

Index	Publication bias	Heterogeneity	Total effect	P	Weight mean difference	95% confidence interval	
Male	Height	No	19%	0.75	0.47	-0.42	0.73
	Weight	No	24%	0.20	0.79	0.17	0.56
	Shape	No	21%	0.66	0.47	0.25	-0.27
Female	Height	No	19%	1.07	0.26	-0.63	0.55
	Weight	No	53%	0.63	0.68	-0.41	0.53
	Shape	No	21%	0.72	0.41	0.17	-0.50

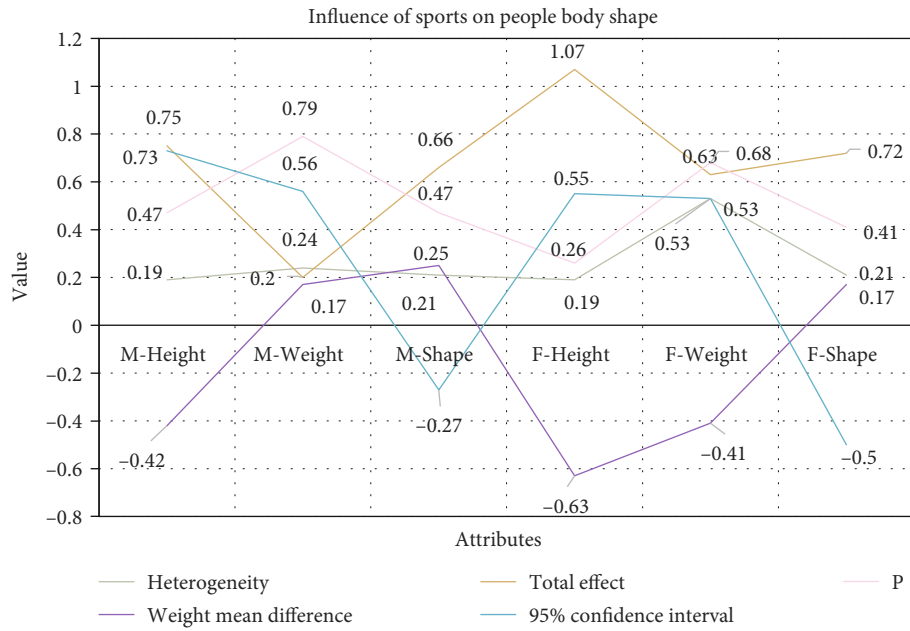


FIGURE 4: Analysis of the influence of sports on people’s body shape.

TABLE 4: Data sheet on the impact of sports on people’s physical function.

Index	Publication bias	Heterogeneity	Total effect	P	Weight mean difference	95% confidence interval
Male	Vital capacity	Yes	10%	8.62	<0.001	-23.65
	Step test index	No	48%	4.35	<0.001	-2.73
Female	Vital capacity	Yes	43%	6.71	<0.001	-28.76
	Step test index	No	67%	4.39	<0.001	-5.29

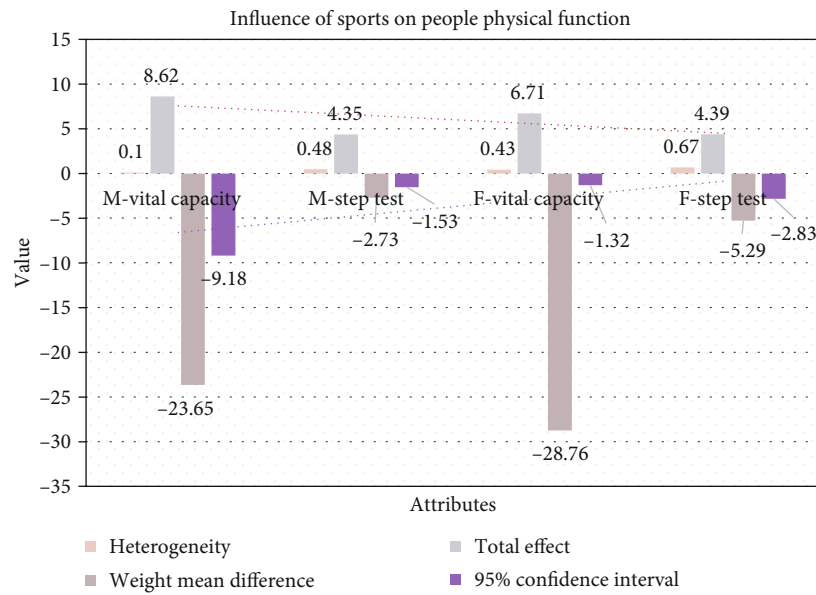


FIGURE 5: Analysis of the influence of sports on people’s physical functions.

TABLE 5: Data table of the impact of sports on people’s physical fitness.

Index		Publication bias	Heterogeneity	Total effect	P	Weight mean difference	95% confidence interval
Male	50 meters	No	0%	5.95	<0.001	0.49	0.62
	Endurance running	No	54%	3.16	<0.001	9.57	1.25
	Standing long jump	Yes	67%	3.22	<0.001	-0.27	-4.41
	Sitting forward bending	Yes	0%	1.73	0.11	-0.55	0.16
Female	50 meters	No	3%	2.84	<0.001	0.46	0.64
	Endurance running	No	42%	4.33	<0.001	9.65	9.19
	Standing long jump	Yes	0%	7.61	<0.001	-8.59	-7.36
	Sitting forward bending	Yes	0%	5.23	<0.001	-0.96	-0.59

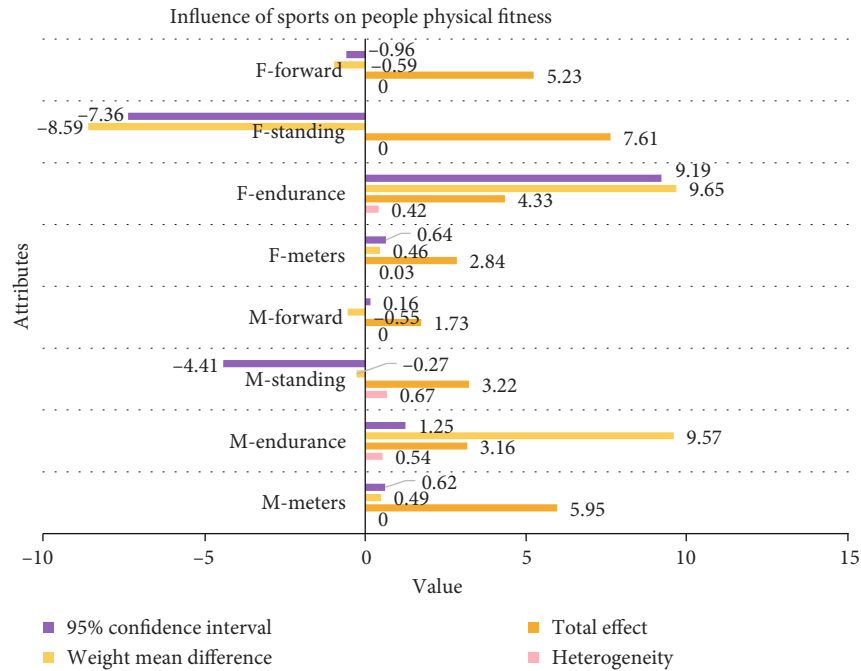


FIGURE 6: Analysis of the influence of sports on people’s physical fitness.

TABLE 6: Data table of the impact of sports on people’s physical fitness.

Age	Very clear	Clear	General	Not clear	Chaotic
6-12	3.37	3.58	4.19	4.06	4.48
12-18	2.92	3.61	3.93	4.18	4.22
18-30	3.21	3.81	3.95	4.43	4.30
30-50	3.33	3.45	3.73	4.41	4.44
50-65	3.58	3.51	3.62	4.48	4.34

each task type, but the reliability coefficients chosen for each task type are slightly different. The results are presented in Table 1 and Figure 1.

4.2. *Publication Time and Publication of the Included Literature.* The time of literature research and the level of publications can show the research status of related research fields from one aspect. Table 2 shows the publication years

and publication status of the 144 research articles included in this article.

It can be seen from Figure 2 that since 2000, the literature on sports cluster analysis research has shown an increasing trend, which also reflects from the side that sports researchers are paying more and more attention to people’s physical health, especially since 2016. A total of 63 research documents were included, accounting for 43.75% of the total included documents, which also shows the increase in research on physical fitness levels in recent years. Using “Internet +” new technology, through cloud computing and big data platform, develop modern medical information service industry and sports intelligence industry.

It can be seen from Figure 3 that the number of research literatures on sports and people’s physical health by Chinese sports researchers has been increasing year by year, but the research quality is generally low, reflecting that sports researchers are paying more and more attention to this field, but their research capabilities need to be further improved.

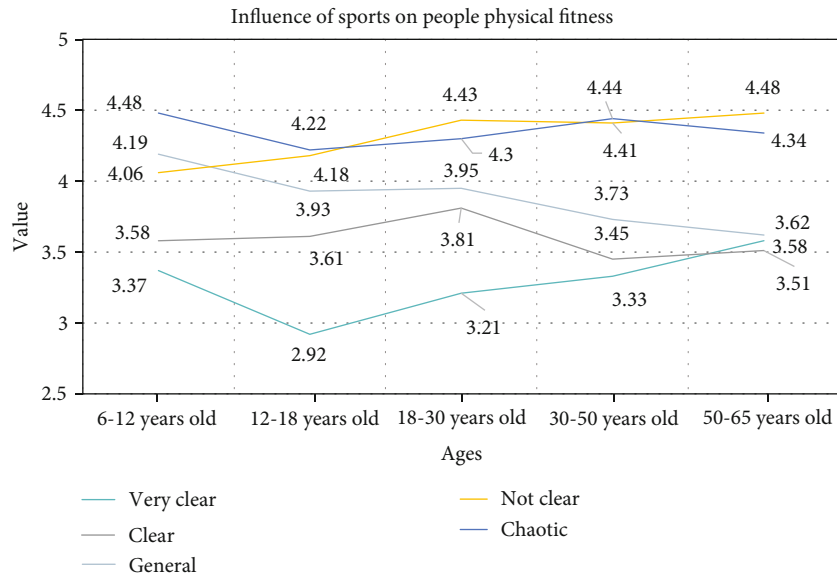


FIGURE 7: Analysis of the influence of sports on people’s physical fitness.

4.3. Cluster Results of Test Indicators

4.3.1. *The Impact of Sports on People’s Body Shape.* Showing body shape indicators in the form of data is a necessary method to study the law of human growth and development, physical fitness, and nutritional status. Through the cluster analysis of the included 144 research documents, the data of physical fitness index of sports are obtained. The specific results are shown in Table 3.

It can be seen from Figure 4 that the weighted average weight difference of boys is 0.20 kg, which is a positive value, indicating that the weight decreased after the experiment. Naturally, the weight is increasing, but here it decreases, indicating that physical exercise still has a certain positive effect on weight control. On the other hand, the weighted mean difference of girls’ weight is -0.41 kg, which is a negative value, indicating that the weight is still increasing after the experiment. Taking into account the heterogeneity of girls’ weights between studies, the result is 53% > 24%, which exceeds that of boys. There is too much heterogeneity in weight between various studies, indicating that there is obvious statistical heterogeneity, so the results may appear such deviations. The specific results are shown in Table 4.

From Figure 5, it can be seen the result of cluster analysis on the effect of sports on the vital capacity of middle school boys, the heterogeneity test result is 10%, the obtained value of the overall effect is 8.62, the weighted mean difference is -23.65, $P < 0.001$, which means that sport has an effect on the vital capacity of boys, and there is a significant statistical difference between the experimental group and the control group. In cluster analysis of the effect of sports on girls’ vital capacity in gymnastics, the heterogeneity test score is 45%, the overall effect size is 6.71, and the weighted mean difference is -28.76, $P < 0.001$, indicating that the effect of sports on girls’ vital capacity in the experimental group is statistically significantly different from the control group. There is

also a significant statistical difference between the experimental group and the control group in the effect of sports on the human step test index.

4.3.2. *The Impact of Sports on People’s Physical Fitness.* Physical fitness is an important aspect of evaluating the level of sports and generally includes strength, endurance, flexibility, and other qualities. In this study, four evaluation indicators, including 50-meter running, endurance running, standing long jump, and sitting forward bending, were selected as the research objects of cluster analysis. The specific results are shown in Table 5.

It can be seen from Figure 6 the cluster analysis of the impact of sports on people’s physical fitness, the heterogeneity test results are 0% (boys) and 3% (girls), and it is believed that there is no statistical difference in the physical fitness of middle school boys in each study. It is qualitative and $P < 0.001$, indicating that the influence of sports on people’s physical fitness is statistically different between the experimental group and the control group. There was no statistical difference between the experimental group and the control group without exercise intervention in the sitting position of boys in the seated forward bending ($P = 0.11 > 0.05$), while there was a significant statistical difference in girls ($P = 0.11 > 0.05$, $P < 0.001$). The flexibility of boys itself is worse than that of girls, and the plasticity is not as strong as that of girls. There may be no statistically different results. But generally speaking, physical exercise intervention has improved the flexibility of middle school students, but the improvement is not great.

4.3.3. *The Impact of Sports on Whether People Are Willing to Participate in Sports.* People’s willingness to participate in sport is an important indicator of how they assess the extent to which sport will develop in the future. By testing the questionnaire using methods commonly used in sociological research, making additions and modifications based on the

test results, and conducting cluster analyses of the recorded research data, we could obtain information about whether people want to participate in sports. The specific results are listed in Table 6.

It can be seen from Figure 7 that with the promotion of sports, people are willing to take the initiative to participate in sports, which increases sports consumption in disguise and promotes the development of the sports industry. It shows that sports intervention can significantly improve people's willingness to participate in sports.

5. Conclusions

This paper uses the Kohonen neural network to study the impact of sports on students' body shape, physical function, physical fitness, and whether they are willing to participate in sports. Five indicators are selected for cluster analysis. After the intervention of sports, people's vital capacity and the step test index increased significantly and have significant statistical significance, which shows that the application of Kohonen neural network clustering analysis method has great practical value for the comprehensive evaluation of people's physical function and physical fitness. There is objective, reasonable, effective, and rapid quantitative evaluation of people's physical functions and physical fitness methods.

In recent years, the literature on physical health research has shown an increasing trend, which also reflects from the side that sports researchers are paying more and more attention to people's physical health. Traditional literature reviews will be affected by the author's different subjective views and interests. This will produce different results, and cluster analysis has certain procedures and rules to follow, which can enhance the objectivity and accuracy of the results. It can be seen from the research in this article that the application of cluster analysis to the field of sports research can not only avoid the huge projects brought about by sports tests but also expand the research sample size by comprehensively analyzing the relevant research results to obtain more accurate research. The results provide possibilities and methods.

In the domestic research literature in recent years, there are many studies on physical health, the intervention methods are not consistent, and the choice of exercise methods is various. This also has a certain impact on the research results of this article, making the research results of this article unable to meet expectations. In addition, due to issues such as search methods and database permissions, some related studies may be missed, which will affect the results of the research. However, because of the higher the quality of the cluster analysis method itself, the more uniform the literature inclusion criteria, the stronger the objectivity of the results, and the more convincing it is to solve the problem of inconsistent research results, so the conclusions obtained in this article are still objective.

Data Availability

No data were used to support this study.

Conflicts of Interest

The author declares that there are no conflicts of interest regarding the publication of this article.

Acknowledgments

This work was supported by the Humanities and Social Science Research General Project of the Education Department of Henan Province 2019, Research Title: Research on the Codevelopment of National Fitness and Sports Industry under the Background of "Healthy China" (2019-ZDJH-419).

References

- [1] H. Kalini, H. Mihanovi, S. Cosoli, M. Tudor, and I. Vilibić, "Predicting ocean surface currents using numerical weather prediction model and Kohonen neural network: a northern Adriatic study," *Neural Computing and Applications*, vol. 28, no. S1, pp. 611–620, 2017.
- [2] F. F. Razi and N. Shadloo, "Portfolio selection using hybrid algorithm of data envelopment analysis based on Kohonen neural network and cuckoo algorithm," *Journal of Information & Optimization Sciences*, vol. 37, no. 4, pp. 549–567, 2016.
- [3] Y. Li, G. Cheng, X. Chen, and C. Liu, "Coal-rock interface recognition based on permutation entropy of LMD and supervised Kohonen neural network," *Current Science*, vol. 116, no. 1, pp. 96–103, 2019.
- [4] Y. V. Bodyanskiy, A. O. Deineko, and F. M. Eze, "Kernel fuzzy Kohonen's clustering neural network and its recursive learning," *Automatic Control and Computer Sciences*, vol. 52, no. 3, pp. 166–174, 2018.
- [5] Y. V. Bodyanskiy, A. O. Deineko, and Y. V. Kutsenko, "Online kernel clustering based on the general regression neural network and T. Kohonen's self-organizing map," *Automatic Control and Computer Sciences*, vol. 51, no. 1, pp. 55–62, 2017.
- [6] E. S. J. Gontijo, C. H. Watanabe, A. S. C. Monteiro et al., "Effects of Fe(III) and quality of humic substances on As(V) distribution in freshwater: use of ultrafiltration and Kohonen neural network," *Chemosphere*, vol. 188, pp. 208–217, 2017.
- [7] A. Guo, A. Jiang, J. Lin, and X. Li, "Data mining algorithms for bridge health monitoring: Kohonen clustering and LSTM prediction approaches," *Journal of Supercomputing*, vol. 76, no. 2, pp. 932–947, 2020.
- [8] A. A. Pastukhov and A. A. Prokofiev, "Kohonen self-organizing map application to representative sample formation in the training of the multilayer perceptron," *St. Petersburg Polytechnical University Journal Physics & Mathematics*, vol. 2, no. 2, pp. 134–143, 2016.
- [9] H. T. Thanh, N. Q. Hung, and T. D. Thanh, "Applying topic model combined with Kohonen networks to discover and visualize communities on social networks," *Science & Technology Development Journal - Economics - Law and Management*, vol. 3, no. 3, pp. 311–326, 2019.
- [10] D. Zaborski, K. M. Kavetska, W. Grzesiak, K. Królaczyk, and E. Dzierzba, "The use of selected statistical methods and Kohonen networks in the revision and redescription of parasites," *Annals of Parasitology*, vol. 62, no. 4, pp. 285–293, 2016.
- [11] I. Hammami, G. Mercier, A. Hamouda, and J. Dezert, "Kohonen's map approach for the belief mass modeling," *IEEE Transactions on Neural Networks & Learning Systems*, vol. 27, no. 10, pp. 2060–2071, 2016.

- [12] T. M. Tatarnikova and E. D. Poymanova, "Model of multi-level data storage system," *Scientific and Technical Journal of Information Technologies Mechanics and Optics*, vol. 19, no. 2, pp. 271–279, 2019.
- [13] P. Lisiak, I. Rojek, and P. Twardowski, "Evaluating the reliability of groove turning for piston rings in combustion engines with the use of neural networks," *Archives of Mechanical Technology & Materials*, vol. 37, no. 1, pp. 35–40, 2017.
- [14] M. Allamehzadeh, S. Durudi, and L. Mahshadnia, "Pattern recognition of seismogenic nodes using Kohonen self-organizing map: example in west and south west of Alborz region in Iran," *Science*, vol. 30, no. 3, pp. 145–155, 2017.
- [15] J. Garcia-Perez and R. Riano, "Optimum seismic zoning using an artificial neural network," *Earthquake Spectra*, vol. 32, no. 2, pp. 1187–1207, 2016.
- [16] L. R. Clovis, C. A. Scapim, R. J. B. Pinto, M. Vivas, J. E. de Almeida Filho, and A. T. do Amaral Júnior, "Yield stability analysis of maize hybrids using the self-organizing map of Kohonen," *Euphytica*, vol. 216, no. 10, pp. 1–10, 2020.
- [17] T. Li, "Sports mental behaviours of college students based on cluster analysis," *Journal of Discrete Mathematical Sciences & Cryptography*, vol. 21, no. 6, pp. 1299–1304, 2018.
- [18] F. J. Lanferdini, R. R. Bini, P. Figueiredo et al., "Differences in pedaling technique in cycling : a cluster analysis," *International Journal of Sports Physiology and Performance*, vol. 11, no. 7, pp. 959–964, 2016.
- [19] M. Konchev, "Application of cluster analysis for the development of distance learning in national sport academy 'vasil levski'," *Oxidation Communications*, vol. 42, no. 1, pp. 101–110, 2019.
- [20] F. Damas, K. Nosaka, C. Libardi, T. C. Chen, and C. Ugrinowitsch, "Susceptibility to exercise-induced muscle damage: a cluster analysis with a large sample," *International Journal of Sports Medicine*, vol. 37, no. 8, pp. 633–640, 2016.

Research Article

Sports Video Motion Direction Detection and Target Tracking Algorithm Based on Convolutional Neural Network

Long Liu 

Chongqing Preschool Education College, WanZhou 404100, Chongqing, China

Correspondence should be addressed to Long Liu; 20221005@hncj.edu.cn

Received 20 April 2022; Revised 26 May 2022; Accepted 4 June 2022; Published 11 July 2022

Academic Editor: Nima Jafari Navimipour

Copyright © 2022 Long Liu. This is an open access article distributed under the Creative Commons Attribution License, which permits unrestricted use, distribution, and reproduction in any medium, provided the original work is properly cited.

In order to effectively detect and monitor athletes and record various motion data of targets, the study suggests a study of target tracking algorithms to detect the direction of motion video sports movement based on the neural network. A class of feedforward neural networks with convolutional computation and deep structure is one of the representative algorithms of deep learning. Firstly, the athlete image is obtained from the video frame; combined with the nonathlete image to construct the training set, use the bootstrapping algorithm to train the convolutional neural network classifier. In the case of input picture frames, pyramids of different scales are then constructed by subsampling, and the location of many candidate athletes is detected by a neural network of disruption. Finally, these centers calculate the center of gravity of the athletes, find the athlete to represent the candidate, and determine the location of the final athlete through a local search process. The results of the experiment show that the proposed scheme of 6000 frames in the two game videos is compared with the AdaBoost scheme, and the detection rate of the proposed scheme is 75.41% to calculate the average detection accuracy and false alarm speed of all players. The detection rate is higher than the AdaBoost scheme. Therefore, this scheme has a high detection rate and low false positives.

1. Introduction

Moving target tracking is a core subject in the field of computer vision. Its core idea is to capture moving targets quickly and accurately by comprehensively using technical means such as image processing and video analysis [1]. In recent years, with the continuous improvement of science and technology, the technology of moving target detection and tracking has also become mature. It has wide application prospects in medical research, traffic monitoring, passenger flow statistics, astronomical observation, visual monitoring, sports, and other fields. Monitoring dynamic scenes through cameras has long been widely used in all aspects of social life. Safety monitoring of public and vital facilities to control traffic on cities and highways, from the detection of military targets to intelligent weapons, cameras play a very important role as an extension of human vision [2, 3]. In sports videos, however, the athletes' colors and backgrounds are similar, and athletes can block each other out. The uniqueness of sports video poses significant challenges to object detection

and tracking technology. Mobile target tracking technology plays an important role in the field of sports video analysis. By tracking athletes in real time, we can analyze athletes' motion trajectory and judge the standardization of their actions. For example, in the diving competition, through the analysis of the athletes' diving action track, judge whether the athletes' take-off, somersault, entering the water, and other actions are correct and consistent. In weightlifting training, we can help athletes analyze the essentials of movement by tracking the movement track of barbell. Therefore, the purpose of this paper is to devise a plan to enable objective detection and tracking of heritage devices and to establish a simulation system to verify the accuracy of the algorithm. The goal of the motion detection and tracking system is to gain experience in digital imaging, modeling, computer vision, and other technologies (see Figure 1). This system can be widely used in related fields such as traffic control, astronomical observations, biomedical research, passenger traffic statistics, and sports [4–6]. In the analysis of sports video, moving target detection and

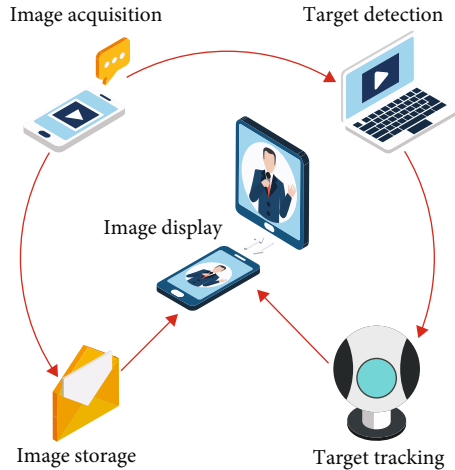


FIGURE 1: Sports video motion direction detection and tracking system based on convolutional neural network.

tracking technology has played an important role, which is convenient to correct the subtle movement differences that cannot be detected by human eyes in training or competition, thereby improving the training and competition results of the athletes. Therefore, together with the research topics of this paper, the research and application of technology in video game equipment were researched and discussed, combined with the research topic of this article, which will be of great theoretical importance and will have a positive impact on other areas based on mobile target tracking practical value [7, 8]. Detection and removal of moving objects in video games: detection and removal of moving objects are important for tracking of the target later, and the quality of the deleted image will be directly affected.

2. Literature Review

As a comprehensive application technology that plays an extremely important role in many fields, the research of video tracking theory started earlier. The research and application of multitarget detection, recognition, and tracking technology have been paid great attention [9]. Gardini and others proposed a color-based particle filter tracking algorithm, which uses the color histogram as the feature to track the moving target. Color histogram has the advantages of stable features, antipartial occlusion, simple calculation method, and small amount of calculation. The disadvantage is that when the distribution of background color is similar to that of target color, it is easy to mistake the background as a moving target. In particular, when the size of the tracked target is small, it is difficult to judge the exact position of the target according to the color histogram, and the convolution neural network depends on the number of sample points. When there are few samples, the accuracy of the algorithm will be reduced [10]. Wang and others believe that because the moving speed of the moving target is fast in sports video and the moving speed often changes greatly, it is difficult for the general motion model to accurately predict the approximate position of the moving target [11]. Kumar and others proposed a novel tracking algorithm based on target con-

tour, which uses the optical flow method to track the target contour. However, the optical flow method has complex calculation, low accuracy, and poor anti-interference and is vulnerable to noise [12]. Shang and others proposed a kernel-based mean shift algorithm, which has low computational complexity and high precision. By continuously calculating the mean shift vector, the search position can be updated iteratively until it converges to the optimal matching point. However, due to the limitation of convergence, the algorithm can achieve good results only if the difference between the predicted position and the real position of the target is small [13]. Véstias introduced a more general moving object detection and event recognition system. Objects are found by detecting interframe image changes, and a prediction and nearest neighbor matching technology is used in tracking [14]. Hidayat and others introduced a visual monitoring system. It uses multiple cooperative cameras to continuously track people and vehicles in complex environments and analyzes target categories and behaviors [15]. Gan and others proposed many algorithms for target tracking. According to the types of tracking targets, they can be divided into two categories: rigid object tracking and non-rigid object tracking. According to the number of targets, it can be divided into single target tracking and multitarget tracking [16]. Li and others estimated the motion of the object by calculating the motion of the brightness of the moving object table. In general, the motion of the object corresponds to the motion of the optical flow. Therefore, the relative motion of the object relative to the background can be obtained by calculating the optical flow field on the surface of the object. However, in practical application, due to the complexity of optical flow calculation and inaccurate estimation, it is less used [17].

Based on this research, this paper presents a sports video guidance research and goal tracking algorithm based on neural network connectivity. The bootstrapping algorithm is used to train the convolutional neural network classifier. For the input detection image frame, multiple candidate athlete positions are detected by convolutional neural network, and then, the candidate athlete positions are fused to determine the final athlete position. Experiments are carried out on some football game videos. Compared with the AdaBoost algorithm, the planning strategy achieves the best performance of the detection rate and alarm, and the search is faster.

3. Research Methods

3.1. Convolutional Neural Network Architecture. The convolution neural network is composed of six different types of convolution layers, as shown in Figure 2. The input layer receives the gray image of 21×43 , and the C1 layer convolutes the input image using a 5×5 acceptance domain. This layer consists of 4 feature maps that share the receiving area and the deviation. Layer S1 performs subsampling and local averaging operations on the map, creating four feature maps [18]. Subsampling reduces both input dimensions and improves image translation, scale, and deformation stability. In addition, the map output of hybrid functions combines

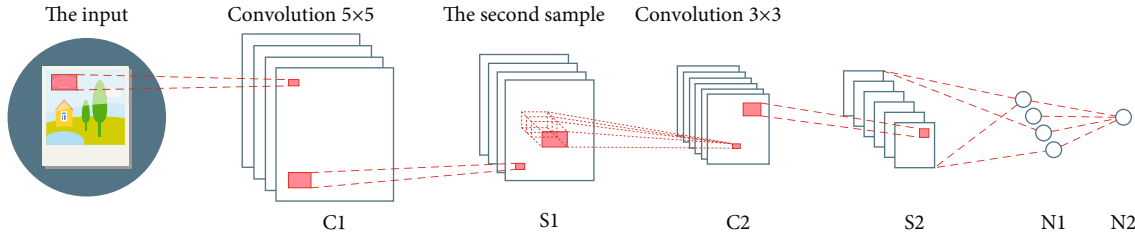


FIGURE 2: Basic structure of convolutional neural network.

different functions, which helps to extract more complex information. Layer C2 is not fully connected to layer S1, and the output map of layer S1 is converted to a 3×3 receiving area to create 14 feature maps. Layer S2 has the same function as layer S1 and consists of 14 feature maps. The role of layers N1 and N2 is to sort after the front section has been disassembled and the input size reduced. The output of a neuron in the N2 layer determines whether the input image is an athlete or not an athlete; -1 is not an athlete, and +1 is an athlete. In addition, for the training of network, this paper adopts the classical back-propagation algorithm with improved momentum method.

3.2. Proposed Athlete Detection Scheme

3.2.1. Training of Convolutional Neural Networks. For the training of the network, the bootstrapping strategy is adopted. It is a self-expanding method that initializes a learner with seed information and seed templates and expands new knowledge and improves learning performance by automatically learning the training set. Apply a neural network on a sample set containing nonathlete images and iteratively enhance the negative training sample set based on the resulting false positives. The algorithm steps are shown in Table 1.

Bootstrapping algorithm mainly has the following steps. (1) Establish a test data set composed of athlete images (positive samples) and nonathlete images (negative samples). The test set remains unchanged in the bootstrapping iteration. On the contrary, the training set needs to be updated continuously. (2) For the neurons in N1 and N2 layers, a back-propagation algorithm with increasing momentum term is used to train the network. In the iteration, ThrFa gradually decreases to 0, which can avoid the redundancy of some training sets. (3) Select the samples whose false alarm result of network classification is greater than ThrFa, generate a new model, and add it to the negative sample training set so that the network will focus on the decision boundary of current athlete classification in the next iteration. After 6 iterations, the learning process stops when the number of false positives remains approximately constant.

3.2.2. Detection of Athletes. This paper is based on the trained convolution neural network to detect athletes. The specific process is mainly divided into the following five steps.

Step 1. In order to detect athletes with multiscale size, repeat the secondary sampling operation with a factor of 1.2 on the input image to generate a pyramid composed of images with different sizes and scales.

Step 2. For each image of the pyramid, complete convolution is carried out through the convolution neural network to obtain an image containing the output results of the network. The positive pixels in the output image are the detected candidate athlete positions.

Step 3. This paper observes that real athlete images usually give a continuous scale value of positive response, while nonathlete images will not occur. In order to eliminate false positives to real athletes, this paper determines the distribution based on the volume of the positive solution (the positive value of the positive solution) in the local pyramid. If its volume is more than that of the original ThrVol, the athlete is classified as an athlete; otherwise, he is a nonathlete [19, 20].

3.3. Overview of Object Detection Methods

3.3.1. Image Preprocessing Method. For the collected original pictures, due to noise, light, and other reasons, which often cannot be directly used for tracking and detection, so first we need to carry out the relevant preprocessing work of the original image. Preprocessing includes image processing, file encoding and transmission, edge sharpening, and more. Preprocessing not only effectively removes images and improves image quality and sharpness but also ensures good processing for target processing, such as targeted detection, extraction, and timely monitoring of target time. It is more suitable for computer analysis, image comprehension, and recognition. In sports video target detection and monitoring system, many conventional algorithms related to image processing are usually used. Generally speaking, these auxiliary technologies are often used before the core processing technology, and their purpose is to improve the performance of the system. The image preprocessing technology used in this paper mainly includes image enhancement, ordinary filtering, and morphological filtering.

(1) Gray Processing. Color images are generally divided into three types: black and white, grayscale, and color. In general engineering applications, it is often necessary to convert color images into grayscale shapes to solve problems. Digital video recordings captured by digital cameras are all color

TABLE 1: Training network based on bootstrapping algorithm.

-
1. Randomly selected 50 positive and 50 negative samples from the initial training to develop the test procedure. It will be used to select the recommended weight in grades 3 and 8
 2. Set momentum parameter $BIter = 0$ and false alarm threshold $ThrFa = 0.7$
 3. Iterate the training network 50 times, and use the same number of positive and negative samples in each iteration. Set $BIter = BIter + 1$
 4. From 100 video frames, collect samples whose detection false-positive results exceed $ThrFa$, and collect up to 3000 new samples
 5. Add the newly collected samples to the negative sample training set
 6. If $ThrFa \geq 0.2$, set $ThrFa = ThrFa - 0.2$
 7. If $BIter < 6$, go to step 3
 8. Iterate 50 times and exit
-

images; in order to facilitate fast processing, it is necessary to replace the printed images' color in gray. The process of converting color images to a gray image is called grayscale processing. The description of the grayscale image, like the color image, also shows the total and local distribution and the characteristics of chromaticity and brightness of the whole image. Typically, each pixel of the color image is represented by 3 bytes, each byte corresponds to the brightness of the RGB component, and each pixel of the converted image is represented by one byte. The higher the brightness, the brighter; the lower the value, the darker the light. The relationship between conversions usually uses the following model:

$$\text{gray}(i, j) = 0.11r(i, j) + 0.48g(i, j) + 0.2b(i, j). \quad (1)$$

Gray conversion can also take the maximum, minimum, or arithmetic average of the three components, respectively. Gray processing first reads the image and copies it to the memory and then makes each color component equal and equal to $\text{gray}(i, j)$, which completes the process of converting the original color image into gray image.

(2) *Image Enhancement.* The purpose of image enhancement is to enhance the information that users are interested in the image, such as edge and contour, expand the difference between different object features in the image, and provide a good foundation for the extraction of image information and the application of other analysis technologies. The general formula for the conversion of grays is shown in

$$s = T(r). \quad (2)$$

In the formula, r and s represent the pixel values before and after processing, respectively, and T is a transformation that maps from the original definition domain $[r_0, r_k]$ to the new definition domain $[s_0, s_k]$.

Different definitions of T can get different transformation results. The commonly used grayscale transformations include linear inversion transformation, logarithmic transformation, contrast stretching, and histogram equalization. The function formula of contrast stretching is (3), where e is the parameter given by the control slope and M is the

mean value of pixel gray. The output of the narrow frame is a high-contrast image.

$$s = T(r) = \frac{1}{1 + (m/r)^E}. \quad (3)$$

Histogram averaging changes the input gray level according to formula $(x \cdot x)$ to obtain the output gray level s , as shown in

$$s = T(r) = \int_0^1 p_r(w) dw. \quad (4)$$

In the formula, $p_r(w)$ is a function of the probability density of the gray level in a given figure and w is the dummy variable of the integral [21]. Then, as shown in Equation (5), the probability density function of the output gray level is uniform:

$$p_s(s) = \begin{cases} 1, & 0 \leq s \leq 1, \\ 0. & \end{cases} \quad (5)$$

After histogram equalization, the gray level of the image is more balanced, and the final result is an image with extended dynamic fan Tian, which has high contrast.

3.3.2. *Commonly Used Moving Target Detection Methods.* Detecting moving objects in the sequence of images is a difficult and very important field of study. In general, object detection in sports video mainly identifies and analyzes moving objects in the video stream and filters out moving objects in the image from the scene. Commonly used detection methods are the range difference method, the background removal method, the statistical method, and the optical flow method.

(1) *Frame Difference Method.* The range difference method is an algorithm that uses sequential frame image differences in a video sequence for target detection and resolution. This is a very common method. Threshold processing plays a key role in the application of frame difference method, because if the threshold is too low, it will suppress the effective changes in the image. The selection of threshold usually depends on the specific external environmental conditions

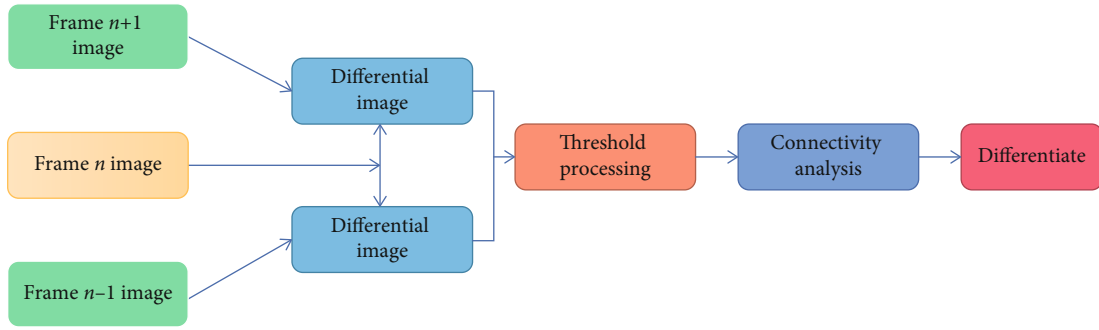


FIGURE 3: Schematic diagram of the frame difference method.

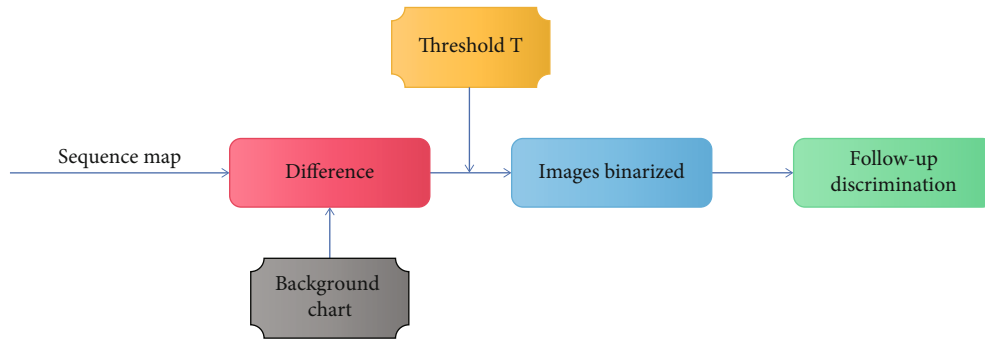


FIGURE 4: Background subtraction method.

such as scene and camera. The selection of threshold can choose either global threshold or local threshold, because the noise caused by the image under different illumination is not necessarily the same, so the use of local threshold can better suppress the noise.

The algorithm of frame difference method is simple and does not consider the update of background, and its shortcomings are also very obvious. The number of frames taken by the algorithm is high, and the moving speed of the target is also required. If the target moves too fast and the selection time interval is long, there will be no coverage area between frames, resulting in the inability to segment the moving target. On the contrary, Figure 3 is a schematic diagram of the frame difference method.

(2) *Cut the Background.* The background removal method is also a common algorithm for detecting moving targets. Its principle is to exclude algorithms that use current images and background images to achieve moving targets (see Figure 4), used to remove the current frame and background pattern. If the background pattern is chosen correctly, moving objects can be segmented more accurately. The background subtraction method is generally based on a fixed camera. In principle, if the background is still, the pixels of the video image with moving targets other than the moving targets should be unchanged, and only the moving target area changes. How to get this invariant region to meet the dynamic changes of the scene is a difficulty in the background subtraction method. Considering that background subtraction is a changing process, it is necessary to update

the background model at any time according to different situations, that is, to increase the adaptability of the algorithm itself. Background subtraction is the process of subtracting each frame in the image sequence with a fixed background model. Its mathematical expression is shown in

$$R(i, j) = F(i, j) - G(i, j), \quad (6)$$

where $R(i, j)$ is the moving target to be detected; $F(i, j)$ is a video sequence image; $G(i, j)$ is the background model image.

(3) *Optical Flow Method.* The optical flow method analyzes the motion field of each point in the sequence image to find out the motion of the corresponding point on the image plane caused by spatial motion. Optical flow method usually assumes that the interval between adjacent times is very narrow, which is generally considered to be within tens of milliseconds, so the difference between images at adjacent times is also very small. The optical flow method does not need to process the image and extract its eigenvalues first, but directly process the image itself.

3.4. Multitarget Tracking Algorithm Based on Camera Motion Estimation

3.4.1. *Global Motion Estimation.* Global motion is usually caused by the movement of the camera. If the camera moves during shooting and the objects in the frame have their own motion, then the background and foreground have their

own motion. In the video sequence, the sound of the background is caused by the sound of the camera that is called global motion. The goal of global forecasting is to find the right camera sound system that allows the world to move through the video on a regular basis. In video segmentation of moving objects, you can first calculate global motion, then compensate for camera movement between calculated frames to align the background between frames, and then separate the front object and background according to the motion zone information. When generating panorama, the correlation of corresponding pixels between frames is obtained by global motion estimation. Then, the panorama can be obtained by stitching the adjacent frames according to the motion parameters. Encoding is the use of panoramas to predict and compensate, which greatly improves the compression ratio. Therefore, the analysis of the law of motion of the camera, which leads to a change in the image, or the analysis of the motion of the front object, is the basis for the analysis of the motion of the world. Methods for estimating global motion parameters are generally divided into differential methods and point-to-point methods. In this paper, the six-parameter affine model is used to model the camera motion causing the scene change between frames, and the differential method is used to solve the global motion parameters. Since the above conditions can be met between adjacent frames during video capture, such a model can reasonably depict the movement of the camera between adjacent frames.

The motion of the earth on the background due to the motion of the chamber can be expressed by a model of affine motion with 6 parameters, as shown in

$$\begin{cases} x_i = ax_i' + by_i' + e, \\ y_i = cx_i' + dy_i' + f. \end{cases} \quad (7)$$

Among them, $p = (x_i, y_i)$ is the coordinate of the current frame I_k , $p'' = (x_i', y_i')$ is the adjacent frame, the coordinates of the point corresponding to P in I_k .

3.4.2. Camera Model and Camera Calibration. The camera design simplifies and approximates the geometry of the optical image. Camera design is usually defined by a number of parameters called camera parameters, and the process of resolving camera parameters is called camera adjustment. The perforated model is the most suitable model for the camera. It defines the descriptive process as the central process of perspective planning. The intersection of the line connecting the point on the scene with the optical center and the plane of the image is the point of projection of the point on the image. Perspective is characterized by “near is big, far is small.” Also, the points on the line do not change the ratio of the intersections during the projection. Figure 5 shows the projection process of a camera simulated by computer graphics. We call the joint location as the camera joint, and the joint design with the camera as the center location and as the direction of the camera is called the control camera. The image control system is an integrated system created by two-dimensional images, which generally acts as

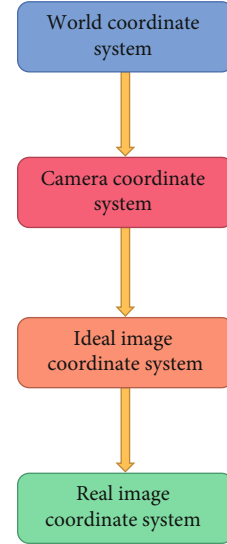


FIGURE 5: The process of projecting a point in the world coordinate system to an image.

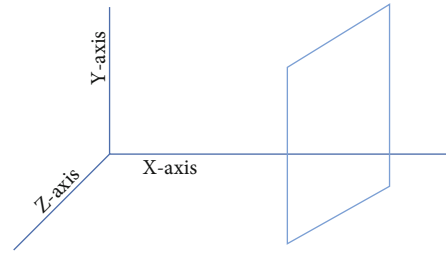


FIGURE 6: Pinhole camera model.

a camera control system. Figure 6 is a schematic diagram of the model of the pinhole camera.

3.4.3. Sports Vision’s Many Target Trajectory Tracking Algorithm. Multitarget monitoring is the focus of current computer visual research, especially human tracking, which is the current research hotspot. Current multitarget control algorithms are roughly divided into two types: model-based multitarget control systems, a multitarget monitoring system based on the integration of information from multiple sources. The model-based multitarget control algorithm mainly uses multitarget motion models to create a multitarget motion model using the relationships between tracks and then uses the corresponding tracking algorithm to search for the state position space to obtain the target position. It is mainly used to track people. A multisource target tracking algorithm is usually used to melt information obtained from multiple sensors and then uses a neural network or latent Markov model to integrate the information. This type of algorithm is mainly used in radar signal processing and other fields.

This article uses rotating neural networks and camera motion algorithms to analyze football and hockey videos, track athletes’ treadmills, obtain athletes’ movement calculations and movement speeds, and assist coaches in tactical

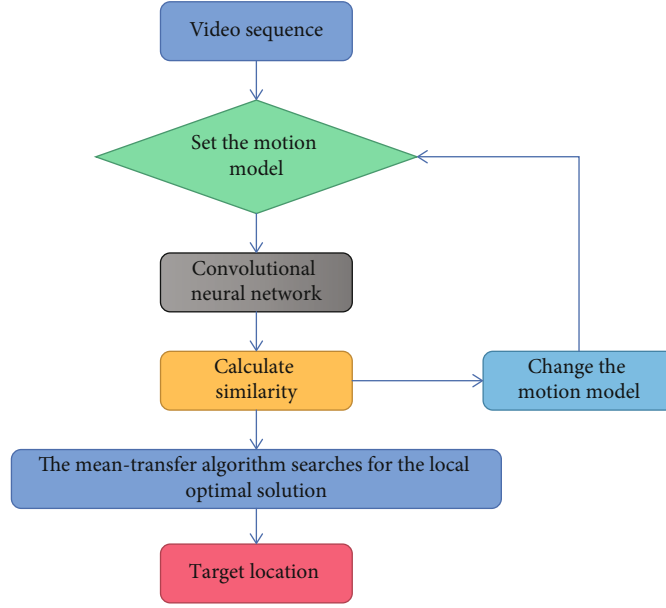


FIGURE 7: Algorithm flowchart.

analysis. Traditional multitarget tracking algorithms are usually based on a static background, and this type of algorithm cannot be useful because it is not possible to obtain real-time target movement information because it is only possible to obtain the target speed and trajectory compared to the camera information for coaches. The flow of algorithms in this article is shown below.

- (1) Use the camera calibration algorithm to obtain the mapping relationship between the site model and the first video image, as shown in

$$\begin{cases} x' = \frac{a_{11}x + a_{12}y + a_{13}}{a_{31}x + a_{32}y + a_{33}}, \\ y' = \frac{a_{21}x + a_{22}y + a_{23}}{a_{31}x + a_{32}y + a_{33}}, \end{cases} \quad (8)$$

where point (x', y') is the coordinate on the site model and point (x, y) is the coordinate on the first video image

- (2) Using convolution neural network and mean shift hybrid tracking algorithm, the coordinate point (x_k'', y_k'') of the player on the current video frame is obtained
- (3) $(x_i, y_i)^T$ is the position of a pixel point in the current frame image and $(x_i', y_i')^T$ is the position of the point in the previous frame image. The relationship between the two is shown in

$$\begin{pmatrix} x_i' \\ y_i' \end{pmatrix} = A \begin{pmatrix} x_i \\ y_i \end{pmatrix} + T, \quad (9)$$

where

$$A = \begin{pmatrix} a_2 & a_3 \\ a_4 & a_5 \end{pmatrix} \quad (10)$$

represents scaling, rotation, and stretching motion; $T = (a_0, a_1)^T$ represents translational motion. The camera motion parameter

$$\begin{pmatrix} a_{k0} & a_{k2} & a_{k3} \\ a_{k1} & a_{k4} & a_{k5} \end{pmatrix} \quad (11)$$

is obtained by using the global motion estimation algorithm

- (4) Solve that the coordinate point (x_k'', y_k'') of the tracked target on the current frame corresponds to the coordinate point $(\tilde{x}_k, \tilde{y}_k)$ under the image coordinate system of the first frame, as shown in

$$(x_k'', y_k'')^T = \prod_{j=1}^k \begin{pmatrix} a_{j0} & a_{j2} & a_{j3} \\ a_{j1} & a_{j4} & a_{j5} \end{pmatrix} \begin{bmatrix} 1 \\ \tilde{x}_k \\ \tilde{y}_k \end{bmatrix}, \quad (12)$$

where

$$A = \prod_{j=1}^k \begin{pmatrix} a_{j0} & a_{j2} & a_{j3} \\ a_{j1} & a_{j4} & a_{j5} \end{pmatrix} = \begin{pmatrix} a_0 & a_2 & a_3 \\ a_1 & a_4 & a_5 \end{pmatrix}, \quad (13)$$

$$\begin{pmatrix} a_{j0} & a_{j2} & a_{j3} \\ a_{j1} & a_{j4} & a_{j5} \end{pmatrix}$$

TABLE 2: Technical parameters.

Test video	Resolving power	Number of frames	Number of color blocks of color histogram	Number of samples of convolutional neural network	Mean shift average iteration	Calculation time (MS)
Table tennis	251×177	74	$3 * 3 * 3$	100	5	2431
Horizontal bar	450×270	76	$7 * 7 * 3$	100	3	4063
6142 football	241×177	70	$7 * 7 * 7$	300	4	6142
Weightlifting	610×465	67	$7 * 7 * 7$	300	3	11820

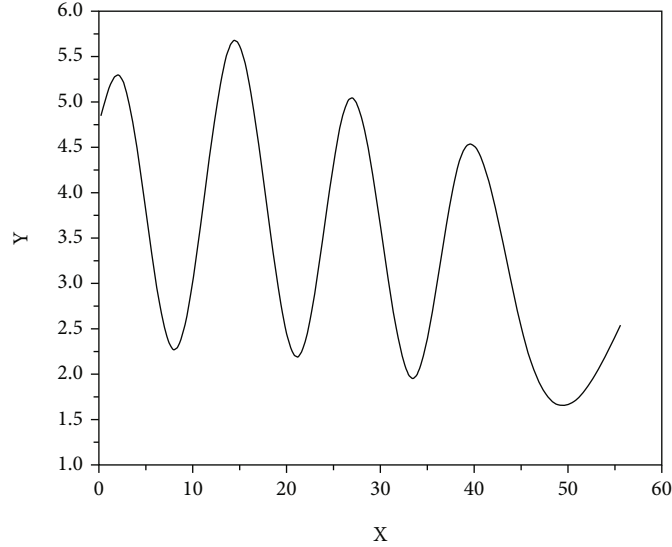


FIGURE 8: Schematic diagram of table tennis motion tracking trajectory.

TABLE 3: Comparison of the average detection rate and false alarm rate of the two schemes for each team's player detection.

Team	Paper scheme		AdaBoost scheme	
	Detection rate (%)	False-positive rate (%)	Detection rate (%)	False-positive rate (%)
England	76.81	1.10	63.61	7.68
Portugal	83.14	1.04	88.55	1.15
France	87.77	0.41	83.27	1.14
Italy	73.36	1.83	72.40	1.47
Average value	80.07	1.08	74.30	1.60

is the global motion estimation parameter from frame $J - 1$ to frame J of the video. The flowchart of this algorithm is shown in Figure 7. Table 2 is the technical data obtained during the testing of this document, and Figure 8 is a schematic diagram of the table tennis track control

4. Discussion of Results

The proposed method is compared with the detection method based on AdaBoost algorithm. The video set used for training and testing is recorded by a fixed position mobile camera. In the video frame, the player position of a specific party is manually marked and represented by a rect-

TABLE 4: Comparison of the average detection rate and false alarm rate of the two schemes for all player detection.

	Detection rate (%)	False-positive rate (%)
Paper scheme	75.41%	1.62%
AdaBoost scheme	70.02%	1.34%

angular box. Then, these athlete images are extracted with a size of 12×24 pixels [22].

4.1. Detection of Specific Athletes. In the first experiment, the specific players in the game video were detected. Extract video samples from two matches of FIFA World Cup. Among them, each team wears different colors of team

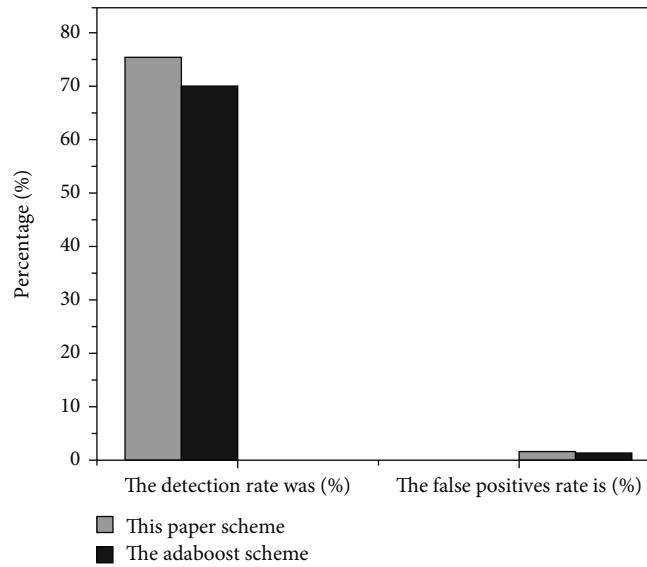


FIGURE 9: Comparison of the average detection rate and false alarm rate for all players detected by the two schemes.

uniforms, so as to form a different contrast compared with the background. For each team, 250 samples containing negative samples were extracted to form a training set, and four independent detectors corresponding to four teams were trained and tested on each team. Compare this scheme with AdaBoost scheme on 6000 frames of the above two game videos, and calculate the average accuracy and false-positive rate of player detection of each team. The results are shown in Table 3. Among them, the accuracy rate is the proportion of the number of athletes detected as the team in one frame to the number of all athletes of the team. The false-positive rate is the proportion of the number of athletes in the team to the number of nonathletes in the team.

4.2. Testing of All Athletes. In the second experiment, all players on the game video were detected. In this paper, 450 samples are extracted from the above two games as training sets to train the detectors corresponding to the two games. Compare this scheme with AdaBoost scheme on 6000 frames of the above two game videos (see Table 4), and calculate the average accuracy and false-positive rate of all players. The detection accuracy of this scheme is 75.41%, which is much higher than that of AdaBoost scheme. The results are shown in Figure 9.

5. Conclusion

The complexity of sports itself brings many difficulties to the actual detection and tracking of moving objects. In order to detect and track athletes effectively, this paper improves the commonly used single tracking algorithm and further improves the effect of sports target detection and tracking. To identify the benefits of an algorithm, this paper uses Matlab to simulate and provide examples of discovery and tracking effects. The main research results are as follows. Detection and removal of moving objects in video games:

detection and removal of moving objects are important for tracking of the target later, and the quality of the deleted image will be directly affected, effect after tracking. In view of the difficult problem in video game, this paper compares the advantages and disadvantages of different processes, background deletion process and streamer process, and also compares medium, medium, morphological filtering, and other filtration algorithms. Video games move the extraction target based on convolutional neural network with experimental quality.

In this paper, some main problems related to sports video moving target tracking technology are studied, and the corresponding research results are obtained. However, the relevant video processing technology still needs further research in the following aspects. At present, video-based target tracking algorithms can only deal with the visual information from a single angle and cannot obtain the omnidirectional information of the whole tracked target as a whole. Therefore, this kind of algorithms are often difficult to achieve good results when dealing with blocking, heavy prosperity, and other phenomena. If the visual information from multiple angles can be fused, the stereo feature model of the tracked target can be established, and the correlation between cameras can be used to track the motion of the target; the robustness and stability of the algorithm will be greatly improved. Therefore, the future multitarget tracking algorithm will develop in the direction of multisource information fusion.

Data Availability

No data were used to support this study.

Conflicts of Interest

The author declares that there are no conflicts of interest regarding the publication of this article.

Acknowledgments

This work was supported by the 2022 Projects of Science and Technology in Henan Province: Algorithm and Application of Movement Image Based on Convolutional Neural Network (Grant Number: 222102320063).

References

- [1] A. N. Gorban, E. M. Mirkes, and I. Y. Tugin, "How deep should be the depth of convolutional neural networks: a backyard dog case study," *Cognitive Computation*, vol. 12, no. 2, pp. 388–397, 2020.
- [2] Z. Huang, J. Zhu, J. Lei, X. Li, and F. Tian, "Tool wear monitoring with vibration signals based on short-time Fourier transform and deep convolutional neural network in milling," *Mathematical Problems in Engineering*, vol. 2021, Article ID 9976939, 14 pages, 2021.
- [3] H. Ali, G. Mubeen, T. S. Ali, Z. Tehseen, and A. Waqas, "High efficiency video coding (hevc)-based surgical telementoring system using shallow convolutional neural network," *Journal of Digital Imaging*, vol. 32, no. 6, pp. 1027–1043, 2021.
- [4] S. Qin, R. V. Lehn, V. Zavala, and T. Jin, "Predicting critical micelle concentrations for surfactants using graph convolutional neural networks," *The Journal of Physical Chemistry B*, vol. 125, no. 37, pp. 10610–10620, 2021.
- [5] K. C. Burak, M. K. Baykan, and H. Uuz, "A new deep convolutional neural network model for classifying breast cancer histopathological images and the hyperparameter optimisation of the proposed model," *The Journal of Supercomputing*, vol. 77, no. 3, pp. 1–17, 2021.
- [6] Y. Cheng, K. Hu, J. Wu, H. Zhu, and X. Shao, "A convolutional neural network based degradation indicator construction and health prognosis using bidirectional long short-term memory network for rolling bearings," *Advanced Engineering Informatics*, vol. 48, no. 1, pp. 101247–101251, 2021.
- [7] K. Marek, E. Micha, S. Marcin, K. Józef, and M. Roman, "Cell nuclei segmentation in cytological images using convolutional neural network and seeded watershed algorithm," *Journal of Digital Imaging*, vol. 33, no. 1, pp. 231–242, 2021.
- [8] W. Cotrim, L. B. Felix, V. Minim, R. C. Campos, and L. A. Minim, "Development of a hybrid system based on convolutional neural networks and support vector machines for recognition and tracking color changes in food during thermal processing," *Chemical Engineering Science*, vol. 240, no. 4, pp. 116679–116683, 2021.
- [9] S. Baroud, S. Chokri, S. Belhaous, and M. Mestari, "A brief review of graph convolutional neural network based learning for classifying remote sensing images," *Procedia Computer Science*, vol. 191, no. 1, pp. 349–354, 2021.
- [10] E. Gardini, M. J. Ferrarotti, A. Cavalli, and S. Decherchi, "Using principal paths to walk through music and visual art style spaces induced by convolutional neural networks," *Cognitive Computation*, vol. 13, no. 2, pp. 570–582, 2021.
- [11] Y. Wang, J. Peng, and Z. Jia, "Brain tumor segmentation via c-dense convolutional neural network," *Progress in Artificial Intelligence*, vol. 10, no. 2, pp. 147–156, 2021.
- [12] A. Kumar, A. R. Tripathi, S. C. Satapathy, and Y. D. Zhang, "Sars-net: covid-19 detection from chest X-rays by combining graph convolutional network and convolutional neural network," *Pattern Recognition*, vol. 122, no. 11, article 108255, 2021.
- [13] R. Shang, Y. Meng, W. Zhang, F. Shang, and S. Yang, "Graph convolutional neural networks with geometric and discrimination information," *Engineering Applications of Artificial Intelligence*, vol. 104, no. 1, article 104364, 2021.
- [14] M. Véstias, "Efficient design of pruned convolutional neural networks on fpga," *Journal of Signal Processing Systems*, vol. 93, no. 5, pp. 531–544, 2021.
- [15] A. A. Hidayat, T. W. Cenggoro, and B. Pardamean, "Convolutional neural networks for scops owl sound classification," *Procedia Computer Science*, vol. 179, no. 4, pp. 81–87, 2021.
- [16] H. Gan, M. Ou, F. Zhao, C. Xu, and Y. Xue, "Automated piglet tracking using a single convolutional neural network," *Biosystems Engineering*, vol. 205, no. 1, pp. 48–63, 2021.
- [17] J. Li and D. Liu, "Information bottleneck theory on convolutional neural networks," *Neural Processing Letters*, vol. 53, no. 2, pp. 1385–1400, 2021.
- [18] C. P. George, "Convolutional neural networks: alternate drivers' visual perception," *IEEE Potentials*, vol. 39, no. 1, pp. 19–24, 2020.
- [19] J. Wang, T. T. Hormel, Q. You, Y. Guo, and Y. Jia, "Robust non-perfusion area detection in three retinal plexuses using convolutional neural network in oct angiography," *Biomedical Optics Express*, vol. 11, no. 1, pp. 330–345, 2020.
- [20] Y. Xu, H. Cui, B. Fan, B. Zou, and L. Wang, "Integrative model of CT imaging and clinical features using attentional multi-view convolutional neural network (AM-CNN) for prediction of esophageal fistula in esophageal cancer," *International Journal of Radiation Oncology • Biology • Physics*, vol. 108, no. 3, pp. e637–e638, 2020.
- [21] W. Walid, M. Awais, A. Ahmed, G. Masera, and M. Martina, "Real-time implementation of fast discriminative scale space tracking algorithm," *Journal of Real-Time Image Processing*, vol. 18, no. 6, pp. 2347–2360, 2021.
- [22] Z. Cheng, Z. Yang, and Y. Gangui, "A novel frequency regulation strategy for a pv system based on the curtailment power-current curve tracking algorithm," *IEEE Access*, vol. 8, pp. 77701–77715, 2020.

Research Article

Inventory Management Optimization of Green Supply Chain Using IPSO-BPNN Algorithm under the Artificial Intelligence

Ying Guan ^{1,2}, Yingli Huang ¹ and Huiyan Qin¹

¹School of Economics & Management, Northeast Forestry University, Harbin 150000, China

²School of Software and Microelectronics, Peking University, Beijing, China

Correspondence should be addressed to Yingli Huang; xhzhang@nefu.edu.cn

Received 27 January 2022; Revised 23 May 2022; Accepted 28 May 2022; Published 28 June 2022

Academic Editor: Mu-Yen Chen

Copyright © 2022 Ying Guan et al. This is an open access article distributed under the Creative Commons Attribution License, which permits unrestricted use, distribution, and reproduction in any medium, provided the original work is properly cited.

This exploration is aimed at reducing the waste of resources in the supply chain inventory management and provide better services for green supply chain management. It mainly proposes a backpropagation neural network (BPNN) model based on improved particle swarm optimization (IPSO) (IPSO-BPNN) and applies it to inventory management prediction. First, the important technologies of green supply chain and intelligent supply chain are analyzed from the perspective of the ecological environment. Next, the particle swarm optimization (PSO) algorithm is optimized based on the adaptive improvement of the learning factor and the addition of the speed mutation operator. Then, it is applied to the learning and training of BPNN. Finally, the simulation experiment of the combination model is conducted. The application fields of the combination model are analyzed. The results show that a single BPNN model will produce large errors in the training process. The final error of BPNN using the traditional PSO algorithm is 0.0259, while the error of BPNN optimized by IPSO is 0.0163. The optimized combination model has higher accuracy, better performance, and the lowest error rate. The classification error rate of its training set and test set is 1.51 and 2.16, respectively. The mean square error of the training set is 0.0163 and that of the test set is 0.0229. Under 6 ~ 12 different hidden nodes, the daily measurement model error and monthly measurement model error are both low when the number of nodes is 11. Moreover, the training set is always better than the test set. Finally, the network structure of the combination model is determined as the structure of 6-11-1. This prediction module will provide purchase volume suggestions and inventory volume suggestions to provide a feasible direction for the green development of inventory management.

1. Introduction

This exploration will study green supply chain management from the sustainable development perspective. Since the second half of the 20th century, due to the progress of science and technology, mankind's ability to use nature has increased rapidly and the scale of developing nature has expanded unprecedentedly. It creates unprecedented wealth and high-speed economic growth in human history. With the deterioration of the ecological environment and the further aggravation of the natural resource shortage, enterprises begin to think about how to realize the sustainable development of energy [1]. The increasingly serious environmental problems have forced enterprises to reexamine their production mode and increase the capital investment in green production to reduce

the damage to the environment [2]. As the final end of the supply chain, consumers need to supervise and report enterprises' products. Paying attention to the green degree of the enterprise's products in real time is responsible for itself and the whole society [3]. Present consumers pay more attention to environmental issues and green production than ever before. As one of the crucial sustainable development strategies, remanufacturing has attracted extensive attention. The most critical product recycling problem in remanufacturing process needs to be solved in combination with a green supply chain [4]. A green supply chain requires all enterprises in the supply chain to pay attention to the impact on the environment [5]. Green supply chain management is a new concept combining supply chain management with environmental protection. Its core idea is to comprehensively consider and

optimize manufacturing resource utilization and environmental protection in the supply chain management's key business circulation process [6].

The rise of the green supply chain is to meet the needs of more and more consumers for green products and sustainable development. "Green" requires producing recyclable products to reduce environmental pollution in use. More importantly, it is essential to focus on effective resource utilization in the production process [7]. Therefore, the green supply chain requires all member enterprises in the supply chain, from the procurement of raw materials to recycling recyclable waste, to focus on the impact on the environment. The research on the coordination of a green supply chain can increase enterprises' economic and social benefits, improve their competitiveness, save resources, and protect the environment [8]. Inventory management in the green supply chain is the third profit source of enterprises. This exploration takes inventory management in the green supply chain as the starting point. The economic value of inventory includes increasing customer satisfaction, preventing various losses caused by the shortage, and increasing the market share of products. However, inventory also brings pressure from huge costs and resource reuse to enterprises [9]. Thereby, a reasonable control strategy and inventory management will bring greater economic and environmental benefits to enterprises. Green supply chain management is proposed as a new concept combining environmental protection with supply chain management. Its core idea is to comprehensively consider environmental protection and optimal utilization of manufacturing resources in the key business circulation process of the supply chain management. It ensures the realization of the added green value of products and plays a positive role in promoting green consumption [10].

With the rapid progress of computer technology, green supply chain management has entered the intelligent stage. In recent ten years, neural network theory and practice have made remarkable progress, which once again expands the connotation of the computing concept [11]. Major companies in technologically developed countries have a special preference for neural network chips and biochips. The neural network has successfully solved some problems that other methods cannot solve because of its characteristics of parallel processing, distributed storage, and adaptation [12]. The neural network was originally applied to pattern recognition. Now, it has been extended to many fields, and the most common is prediction [13]. It can also be used to solve various classification problems, such as pattern recognition, translation, bank credit risk assessment, and signature recognition [14]. The neural network technology has the characteristics of distributed information storage, large-scale parallel processing, good self-organization, and self-learning ability. Hence, it is widely used in the field of supply chain management [15]. The backpropagation neural network (BPNN) is the most widely used. However, the BPNN learning algorithm is based on gradient descent, which has some problems, such as slow convergence speed, easy to fall into a local minimum, and long training time [16]. Particle swarm optimization (PSO), which has the characteristics of

fast convergence and simple calculation, is introduced as the learning algorithm of BPNN to optimize its parameters to improve the model's performance. However, the algorithm has the phenomenon of premature and slow speed in the later stage of evolution [17]. This exploration will optimize the algorithm. The optimization idea includes adding mutation operator and adaptive adjustment of learning factor.

Under the background of sustainable development, based on the idea of improving the inventory management level in green supply chain management, this exploration introduces an artificial intelligence (AI) algorithm and PSO algorithm to predict inventory management. First, green supply chain technology and inventory management background are introduced. Next, the PSO algorithm is improved, and two improved methods are proposed: adding mutation operator and adaptive adjustment of learning factor. Finally, the improved PSO (IPSO) algorithm is combined with BPNN and applied to inventory management prediction, and simulation experiments and empirical analysis are carried out. The research innovation is to apply AI technology based on the PSO algorithm to the field of the green supply chain. This exploration provides a reference for the sustainable development of the supply chain.

2. Literature Review

Supply chain management in the ecological environment is proposed in 1996, namely, green supply chain management [18]. The initial research on green supply chain management believes that it includes the whole production process, product composition and product use. It is the combination of the original supply chain thought and environmental protection thought. Finally, the green supply chain must form a long-term and stable strategic relationship within the supply chain [19]. After the 21st century, researchers believe that a green supply chain should include inventory, strategy, and environment. Recently, the definition of green supply chain management is mainly based on the product and production environment [20]. American scholars define it as the setting of supply chain management policies and environmental problems in designing, distributing, and using products and services [21]. Scholars in China define it as the supply chain management that considers the overall environmental benefit optimization [22]. Based on previous studies, a conceptual model of the green supply chain is proposed here. It comprises four subsystems: the consumption system, production system, environmental system, and social system. The model reflects the circular movement of knowledge flow, logistics, capital flow, and information flow in the whole green supply chain [23].

With the progress of AI, the management information system is gradually introduced for intelligent supply chain management. The traditional enterprise management information system is built based on the database and can only provide statistical query functions [24]. At the end of the 20th century, the new enterprise management system closely connected the enterprise's resources with the business process. Moreover, it lays a certain foundation for improving

the enterprise's competitive advantage and efficiency [25]. The enterprise information system in the 21st century can provide decision-makers with auxiliary decision-making information and business data processing capacity. AI brings more convenience to supply chain management [26]. Decision-making technology is the research hotspot of multiple scholars and enterprise management developers. The supporting technologies of decision technology include metaheuristic algorithms and neural network technology [27]. Metaheuristic algorithms have good performance in problem solving and optimization. At present, they mainly include the PSO algorithm, monarch butterfly optimization (MBO), moth swarm algorithm (MSA), Hunger Games Search (HGS), and Runge-Kutta (RUN).

Jha et al. predicted India's GDP based on a multivariable fuzzy time series model and MBO combination algorithm. The results show that the proposed combination algorithm is better than the existing prediction methods [28]. Ramaporselvi and Geetha proposed an adaptive MSA optimization algorithm and applied it to the congestion management for a power system transmission line. Experimental results show that the algorithm's performance is better than the existing technology [29]. Mehta et al. applied HGS to automotive engineering design and optimization. The experimental results show that the algorithm has good robustness in obtaining the best global optimal solution [30]. Yousri et al. proposed an interactive variant of the RUN optimization algorithm to determine the reliable parameters of the single-diode and double-diode model parameters of different photovoltaic cells/modules. The results show that this method provides highly competitive results compared with other well-known parameter extraction methods [31].

AI can solve incomplete, fuzzy, and complex problems by simulating behavior [32]. Artificial neural network technology was born in the middle of the last century and developed rapidly at the end of the 20th century [33]. Because of the large-scale parallel computing ability, neural network technology is widely used in prediction, such as weather prediction, pattern recognition, and statistical calculation [34].

A PSO algorithm is used to solve the problems of the slow convergence speed of BPNN [35]. It was proposed at the end of the 20th century and was originally used to study the foraging behavior of birds [36]. It is widely adopted in pattern classification, neural networks, and function optimization. It is one of the optimization algorithms with superior performance because of its simple operation, easy implementation, and fast convergence speed [37]. It has attracted the attention of multiple scholars, and many researchers have done a lot of research on improving the optimization ability of the PSO algorithm. Thakkar and Chaudhari (2021) discussed existing methods' limitations and potential future research directions to enhance stock market prediction based on the PSO algorithm [38]. At present, the decision-making mechanism based on the PSO algorithm is easy to fall into the premature convergence problem of local optimization. Moreover, there is less research on applying the PSO algorithm in the ecological environment. Hence, this exploration combines it with deep learning and applies

it to green supply chain management to fill the research gap in this field.

Based on the definition of green supply chain management in previous studies, this exploration defines it as follows. It is a management mode with sustainable development as the goal. Its activities cover the whole life cycle of products, and its actors include the government, the public, and all supply chain members. The research content here is green supply chain management. There is less research on the combination of the PSO algorithm and neural network and their application in green supply chain management in the previous research. BPNN has good prediction performance, and the PSO algorithm can solve the problems of slow neural network convergence. Therefore, this exploration will combine the two algorithms to study green supply chain management. The scope of supply chain management is wide. Previous studies regard the supply chain as a whole, and there is less research on the details of specific supply chain management. Hence, this exploration takes inventory management in supply chain management as the research object to optimize supply chain inventory management. It focuses on inventory management prediction in supply chain management based on an IPSO algorithm and BPNN. It is aimed at achieving the purpose of green supply chain management finally.

3. Intelligent Inventory Management in the Green Supply Chain

Based on the above research background and the analysis of relevant existing literature, this section mainly constructs the green supply chain management model, analyzes the contents and characteristics of inventory management in the supply chain, and introduces the relevant theories of BPNN and PSO. PSO defects are improved, and the IPSO algorithm is put forward. IPSO is used to optimize the traditional BPNN, and the optimization algorithm is applied to the prediction of green supply chain inventory management to verify the model's performance.

3.1. Construction of Green Supply Chain Management Model. Green supply chain management focuses on the sustainable development of the whole product cycle, including the impact on the environment in procurement, material management, logistics, production, manufacturing, and treatment [39]. It promotes resource reduction, recovery, and reuse in the supply chain's upstream, middle, and downstream activities [40]. It provides a solution to improve the environmental impact caused by supply chain management. Figure 1 presents the overall model of green supply chain management.

Figure 1 displays that the green supply chain management model here includes green procurement, green processing, green marketing, and recycling. After green purchases to suppliers, enterprises will carry out inventory management. Inventory management in green supply chain management is mainly studied. The design of green supply chain management considers the impact of procurement, logistics, material management, production, manufacturing, and processing processes on the environment. In fact, it will

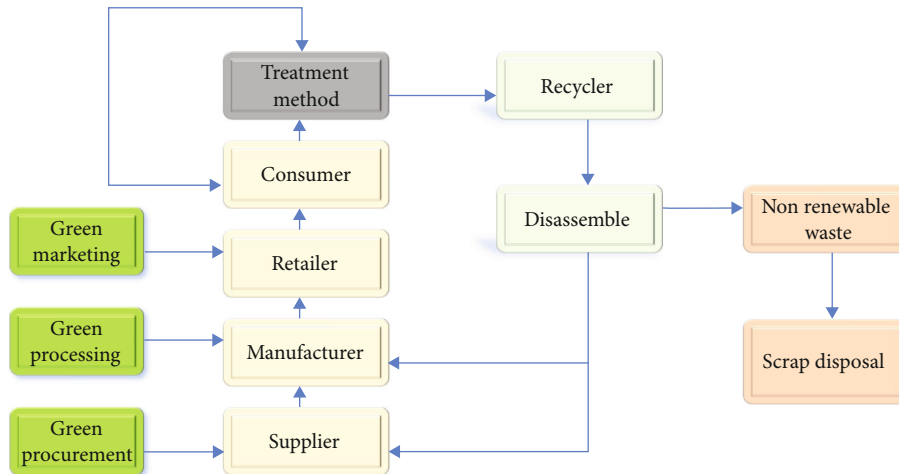


FIGURE 1: Overall model of green supply chain management.

promote the reduction, reuse, and recycling of resources in the upstream, middle, and downstream activities of the supply chain. Environmental supply chain management provides a new perspective, including a two-way supplier of products or services or even a cyclical perspective.

3.2. Contents and Characteristics of Inventory Management.

Inventory in supply chain management includes the materials in the production process, parts or raw materials that have not been used in the enterprise, and the finished products in the production process before they are delivered to customers. Inventory level is crucial for the development and survival of enterprises.

Inventory management functions in enterprise supply chain management mainly include stabilizing the production and operation scale to obtain economies of scale, balancing the time difference between supply and demand, and buffering the impact of uncertain factors. Therefore, inventory plays a vital role in enterprise management and cutting huge costs. Excessive costs make the current costs less and increase storage expenses, taxes, insurance, and the economic burden of enterprises. Due to product aging and other problems, inventory management directly affects the sustainable development of enterprise resources. Besides, excessive inventory will cause great risks to enterprises [41]. Inventory affects the green development of supply chain management and enterprise budget. It should be controlled within a reasonable range to ensure the sustainable development of inventory resources at the lowest cost.

The ultimate goal of inventory control is to reduce inventory costs as much as possible and meet customer needs. There are multiple influencing factors of inventory cost, as shown in Figure 2 [42].

Figure 2 shows that the main influencing factors of inventory cost are storage, ordering, replenishment, and out-of-stock cost. Out-of-stock cost is an opportunity cost. It refers to the expenses incurred by failing to provide services to customers for some reason, or failing to obtain the predetermined profit due to the loss of sales to customers. Besides, it also includes the adverse consequences caused

by the loss of reputation due to some difficult factors [43]. For suppliers, out of stock means losing sales opportunities, reducing profits that could have been obtained, or violating contracts and treaties. If they are punished heavily, they will lose credibility, important customers, and market competitiveness. For manufacturers, out of stock will increase the procurement cost. More seriously, it will stop the work and wait for materials, which will affect the normal production operation [44]. Ordering cost refers to all expenses incurred in the ordering process, including two expenses. One is the fixed cost of ordering expenses, including travel expenses, ordering handling fees, communication expenses, entertainment expenses, and relevant expenses of the person in charge of ordering. The ordering fee is related to the order times, but not to the order quantity. The other is the cost of the ordered goods, which is related to the order quantity. Storage cost refers to the cost invested in maintaining inventory. It mainly includes inventory investment and storage costs. For example, it includes the interest payable on the funds occupied by the goods, the insurance and taxes paid for the goods, and the expenses for using the warehouse, keeping the goods, damage, and deterioration of the goods. Replenishment means that when the customer comes to purchase, there is no stock in the warehouse; however, to avoid losing sales opportunities, the enterprise still persuades the customer to order here, promises to purchase immediately, and then replenishes the goods to the customer. Replenishment has obvious benefits for enterprises. It can occupy fewer funds and less inventory and reduce storage costs, and it is impossible to incur shortage expenses. However, to realize replenishment, replenishment costs often occur [45].

Based on the above, it is found that the problems to be solved for inventory control are divided into three categories in Figure 3.

Figure 3 shows that the inventory control strategy's implementation should meet the demanders' needs, the selection of appropriate control methods, and the supplier's operation mode. The control method is the core of inventory management. The traditional inventory control model

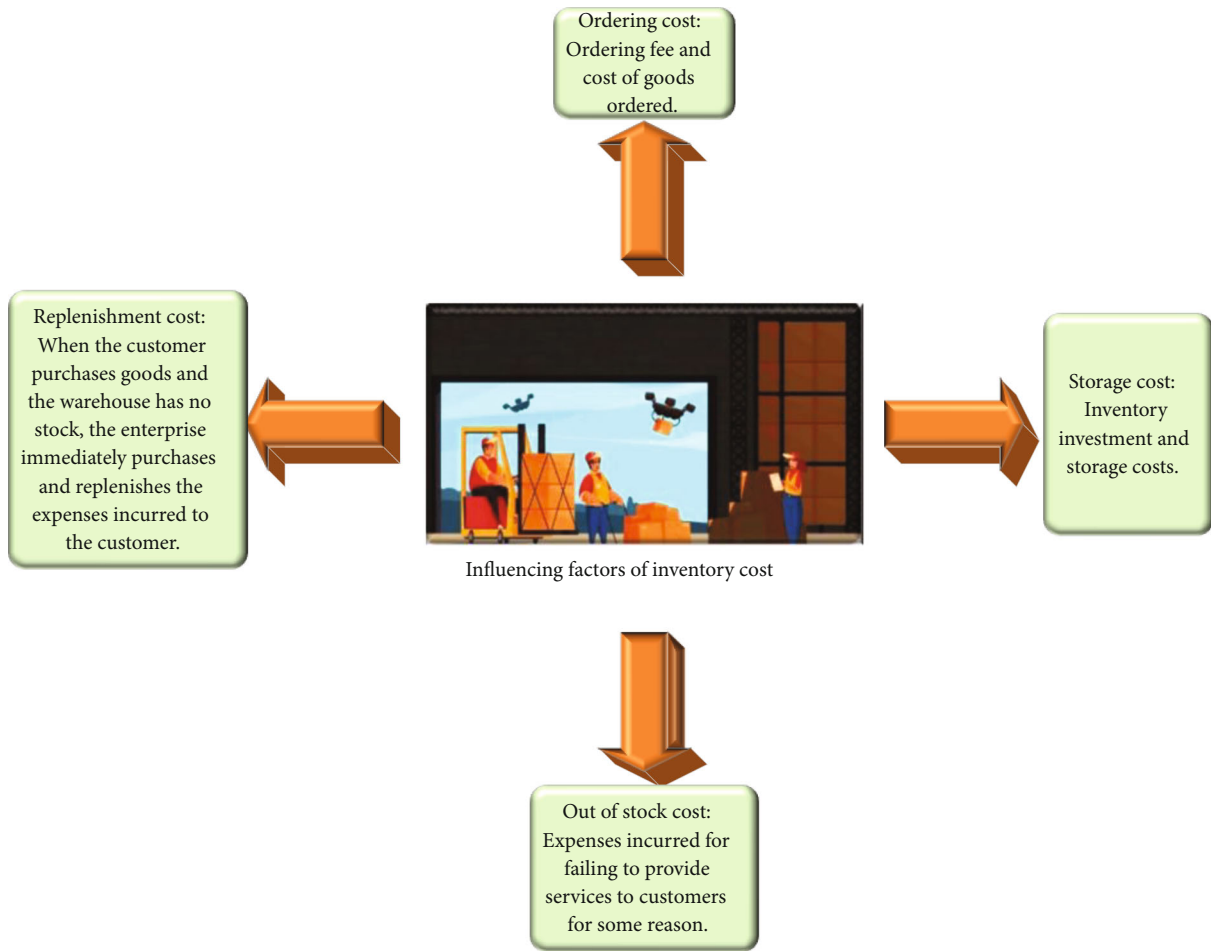


FIGURE 2: Influencing factors of inventory cost.

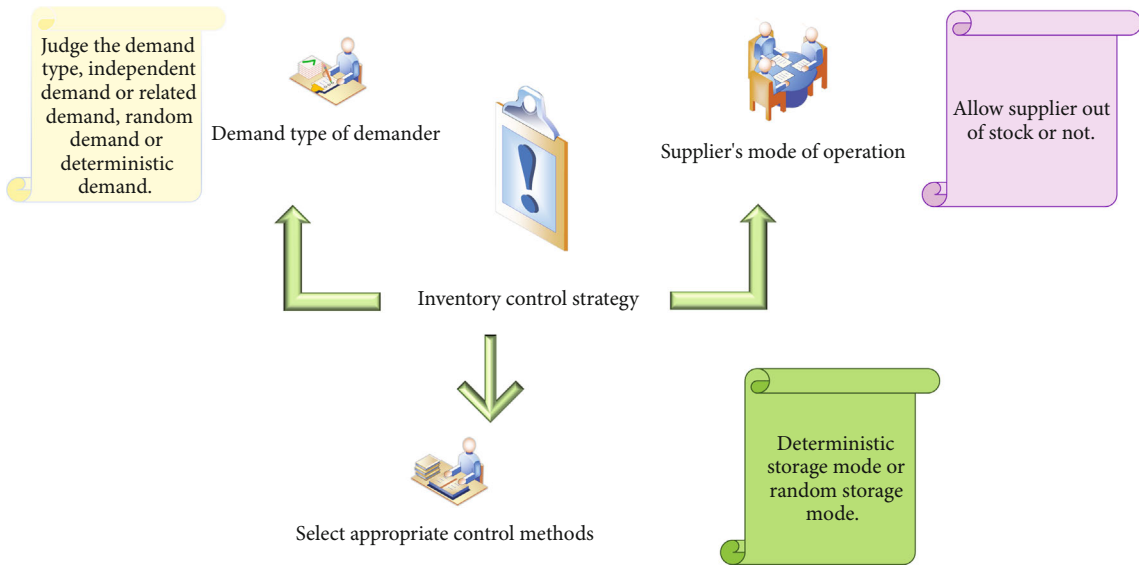


FIGURE 3: Categories of inventory control.

includes random and deterministic storage models. A new inventory control model suitable for green supply chain management is proposed based on the traditional inventory control model.

The problems to be solved in inventory management under green supply chain management focus more on the communication between enterprises. It includes strengthening the accurate transmission of information among enterprises

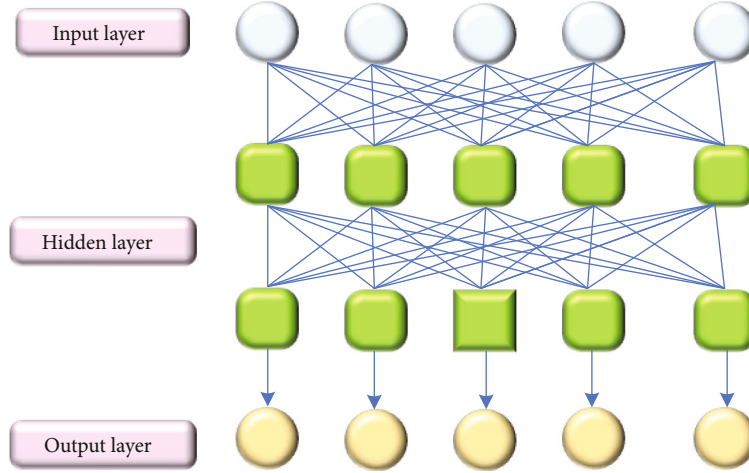


FIGURE 4: BPNN model.

and the smooth transmission of information flow, handling of uncertain problems, and reducing unnecessary waste by strengthening information exchange.

3.3. Basis of BPNN. BPNN is the most widely used neural network at present. Figure 4 is its structural model.

Figure 4 shows that BPNN is a feedforward neural network. Neurons accept the input of the previous layer and output to the next layer. The first layer of the whole model is the input layer, the middle layer is the hidden layer, and the last layer is the output layer. The hidden layer neurons of BPNN use sigmoid differentiable functions like the transfer functions [46].

The parallel processing of BPNN makes it one of the most widely used algorithms. The advantages of BPNN include having strong fault tolerance, dealing with uncertain systems through adaptive and self-learning, and coordinating various input relationships. However, it also has some disadvantages, such as long training time, a large amount of computation, and slow convergence speed. Therefore, a PSO algorithm is introduced because it is easy to operate.

3.4. Introduction to PSO. The mathematical description of PSO is as follows. First, it is to determine the search space and the number of particles in the population. Then, it is to use vectors to represent the particle position and the optimal position in the particle “flight.” Next, it is to mark all particles’ position and most valuable position. Finally, it is to present the position change rate of particles [47]. The change of particle position is calculated using equations (1) and (2).

$$v_{id}(t+1) = \omega * v_{id}(t) + m_1 * \text{rand}() * (p_{id}(t) - x_{id}(t)) + m_2 * \text{rand}() * (p_g(t) - x_{id}(t)), \quad (1)$$

$$x_{id}(t+1) = x_{id}(t) + v_{id}(t+1). \quad (2)$$

In (1) and (2), m_1 and m_2 are the accelerated factors. ω is the inertia factor, and t is the current iteration times. p_g is

the current global optimal position of the particle swarm. p_{id} is the optimal individual, and v_{id} indicates the position change rate. d is the spatial dimension, and i is the particle serial number.

The initial velocity and position of the particle swarm are generated randomly. Then, they iterate according to the above two equations until the conditions are finally met.

Figure 5 reveals the PSO flow.

Figure 5 shows the flow of PSO. It includes initializing the particle swarm, calculating the fitness value of each particle, comparing the fitness value of each particle with extreme individual value and extreme global value, and determining whether to change the iteration times.

The parameters of PSO include inertia weight, learning factor, maximum, particle dimension, population size, and termination condition. The adaptive adjustment in the inertia weight is determined by

$$\omega = \omega_{\max} - \frac{\omega_{\max} - \omega_{\min}}{h_{\max}} * h. \quad (3)$$

In (3), h_{\max} is the maximum number of iterations, h represents the current number of iterations, and ω is the weight.

In the inertia weight setting, the general practice is to set the initial value of ω to 0.9 and make it decrease linearly to 0.3 with the increase of iteration times. It can achieve the desired purpose of optimization. In the PSO algorithm, two acceleration coefficients control the influence of “cognitive” part and “social” part on particle velocity. In the population-based optimization method, it is always hoped that the individual can search in the whole optimization space in the initial stage, so as not to fall into the local value too early. In this way, in the end stage, it can improve the convergence speed and accuracy of the algorithm. Besides, it can effectively find the optimal global solution. According to previous studies, it is better if the acceleration coefficient is less than 4. The selection of the maximum speed should not exceed the particle width range. If the maximum velocity is too high, the particle may fly over the position of the optimal solution. If it is too small, it may reduce the global

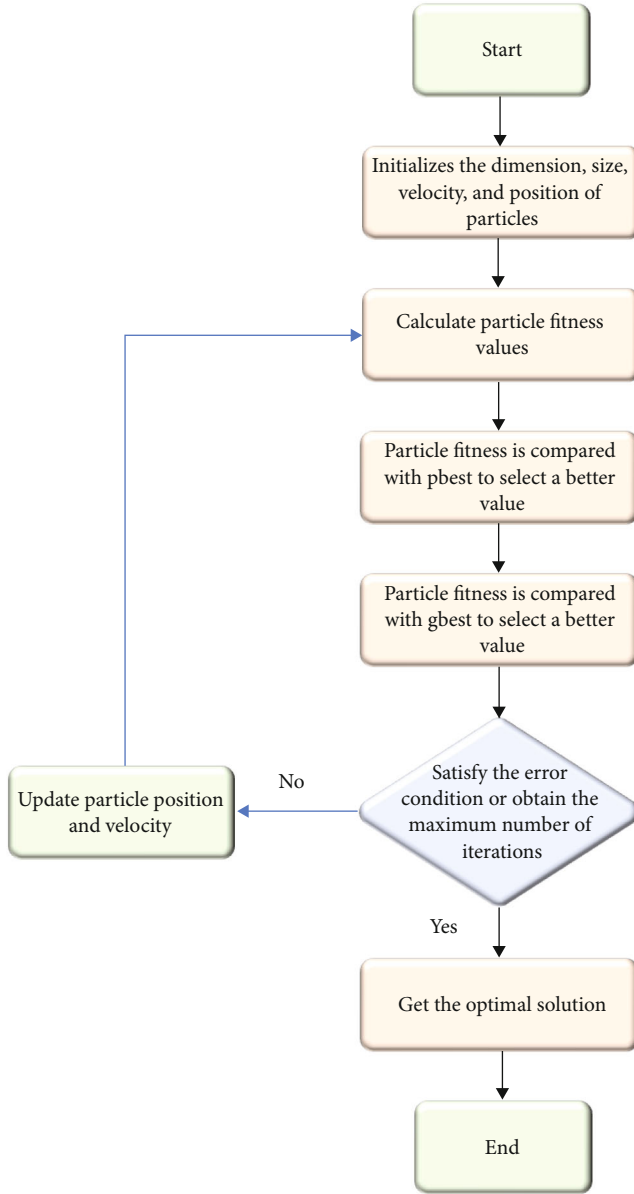


FIGURE 5: Flow of PSO.

retraction ability of particles. Generally, the population size does not need to be too large. Dozens of particles are enough. More particles can be selected for some special problems. The number of particles can be up to 100~200. The particle dimension is determined by the solution space dimension of the optimization problem. The suspension conditions are specified according to specific problems after reaching the maximum number of iterations or meeting the minimum error requirements. Therefore, Table 1 is a summary of parameter settings for the PSO algorithm.

The traditional PSO algorithm easily falls into the optimal local solution during its operation, so it is necessary to take some measures to improve it [48]. The improvement strategy of the algorithm is to add a speed mutation operator and improve the adaptability of learning factors. Adding speed mutation operator can further search particles

TABLE 1: Parameter setting of PSO.

Parameters types	Parameter settings
Inertia weight	The initial value is set to 0.9 and then iterated to 0.3
Learning factor	The sum of acceleration coefficients is less than 4
Maximum speed	Not exceeding the particle width range
Particle dimension population size	The particle dimension is determined by the solution space dimension; the group size ranges from dozens to 200
Termination conditions	Meet the minimum error requirements or reach the maximum iteration times

through the mutation of particle swarm speed when the PSO algorithm has not obtained the optimal solution to avoid falling into the optimal local solution. Learning factors mainly affect the optimization speed and accuracy of the algorithm. Improving its adaptability is of great help to improve the algorithm's overall performance. Therefore, PSO is optimized, including adding mutation operators and improving the adaptive ability to learn factors. A population use variance is adopted to add a mutation operator, as shown in equation (4).

$$\sigma^2 = \sum_{i=1}^n \left(\frac{f_i - f'}{f} \right)^2, \quad (4)$$

where n represents the number of particles, f' is the average fitness of particles, and σ^2 is the variance of population fitness. f is the normalized calibration factor.

The convergence degree of population fitness variance can be defined by

$$f = \max \{ 1, |f_i - f'| \}. \quad (5)$$

Based on the above, mutation operation is performed when PSO does not obtain the fully optimal solution. By mutation of particle swarm velocity, the particles can be further searched. The particle velocity can be calculated by

$$\begin{aligned} v_{id}(t+1) = & \omega * v_{id}(t) + m_1(t) * \text{rand}() \\ & * (p_{id}(t) - x_{id}(t)) + m_2(t) \\ & * \text{rand}() * (p_g(t) - x_{id}(t)) \\ & + \text{flag} * \delta * v_{\max}, \end{aligned} \quad (6)$$

where $\text{flag} * \delta * v_{\max}$ represents the mutation operator and μ is the influence degree of the mutation operator on velocity. The value of δ reads

$$\delta = \min \left\{ \left| \frac{f_g(t) - f_t}{f_t} \right|, 1 \right\}. \quad (7)$$

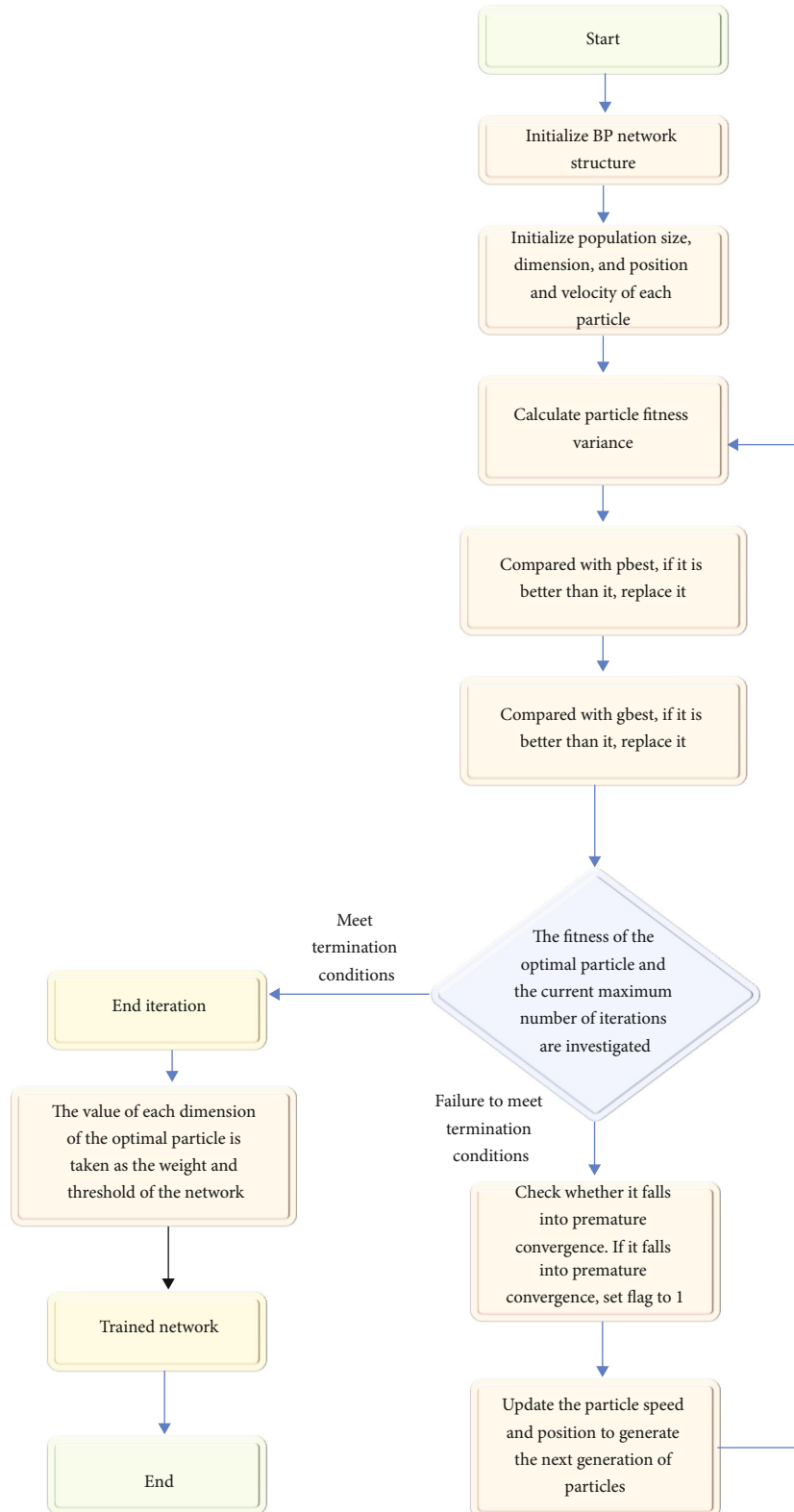


FIGURE 6: Flow chart of IPSO training BPNN.

In (7), $f_g(t)$ is the fitness value of the globally optimal particle and f_t represents the empirical optimal value.

The acceleration coefficient in learning factors is adjusted in the adaptive adjustment of learning factors. Equations (8) and (9) show the value of the acceleration coefficient.

$$\begin{cases} m_1(t) = 4 * \frac{|f_a(t) - f_g(t)|}{f_a(t)}, \\ m_2(t) = 4 - m_1(t), \end{cases} \quad (8)$$

$$f_a(t) = \frac{1}{N} \sum_{i=1}^N f_i(t). \quad (9)$$

In (8) and (9), $f_a(t)$ is average fitness. N indicates the number of fitness.

Equation (1) is improved, as shown in equation (10).

$$\begin{aligned} v_{id}(t+1) = & \omega * v_{id}(t) + m_1(t) * \text{rand} \\ & * (p_{id}(t) - x_{id}(t)) + m_2(t) * \text{rand} \\ & * (p_g(t) - x_{id}(t)). \end{aligned} \quad (10)$$

3.5. BPNN Based on IPSO. BPNN is trained with the IPSO and its performance and generalization ability are improved.

Figure 6 displays the flow of BPNN based on IPSO.

Figure 6 shows that when IPSO trains BPNN, the threshold and connection weight of the neural network correspond to the dimension component of each particle in the particle swarm. The fitness function combined with the algorithm is borne by the mean square error of the neural network.

The training sample's output value deviation and particle fitness are calculated by equations (11) and (12), respectively.

$$I_i = \sum_j (Q_{ij} - q_{ij})^2, \quad (11)$$

$$R = \frac{1}{n} \sum_{i=1}^n R_i. \quad (12)$$

In (11) and (12), Q_{ij} is the expected output value, q_{ij} is the actual output value, I is the output deviation, and R is the particle fitness.

3.6. Model Simulation. The sample set used in the simulation of BPNN based on IPSO is the Iris dataset. Iris is an Iris tectorum Maxim plant. It is divided into three types: Setosa, Versicolor, and Virginica. Iris database is a widely used pattern classification example system. Pattern classification will distinguish three plants according to four attribute values. The dataset is a commonly used classification experimental dataset, which can be directly downloaded from the website <http://archive.ics.uci.edu/ml/datasets/iris>. The experimental data are directly selected from the dataset, so there is no data preprocessing.

TABLE 2: Experimental environment.

Category	Specific model
Operating system	Windows XP Professional
Development language	C language
Development platform	MS VS. NET
Grid training	Matlab 6.5
Database	SQL Server 2000
Memory	512 MB DDR
CPU	Pentium (R) 4 2.80 GHz

In the simulation test of BPNN and BPNN based on the traditional PSO algorithm, the network structure is 4-4-3. The PSO scale is 20. The dimension is 35, the maximum number of iterations is 7000, the maximum particle velocity is 0.5, and the minimum error is 0.01. The BPNN structure includes 7 thresholds and 25 weights [49]. The parameter setting of BPNN [50] is $\omega = 0.73$ and $c_1 = c_2 = 1.49$. Equation (13) is the BPNN parameter setting based on the traditional PSO algorithm.

$$\omega = \omega_{\max} - \frac{\omega_{\max} - \omega_{\min}}{\text{iter}_{\max}} * \text{iter}, \quad (13)$$

where iter_{\max} is the maximum number of iterations and iter is the current number of iterations. $\omega_{\max} = 0.9$ and $\omega_{\min} = 0.3$. c_1 and c_2 adjust themselves. The flag in the mutation operator is initially 0, which is further adjusted in the iterative process. In the mutation condition, $\lambda = 0.0001$.

The network structure of the IPSO algorithm is 6 input nodes and 1 output node, and the hidden nodes are 6, 8, 11, and 12, respectively. The PSO scale is 40, and the network structure determines the particle dimension [51]. Besides, the maximum particle velocity is 0.5, the maximum number of iterations is 7000, and the minimum error is 0.1. The inertia weight is adjusted adaptively: $\omega_{\max} = 0.9$ and $\omega_{\min} = 0.3$, mutation operator flag = 0, $\lambda = 0.0001$.

The network performance evaluation indexes used in the simulation include the classification error rate (E_X) of the training set, the classification error rate (E_C) of the test set, the mean square error (MSE_X) of the training set, and the mean square error (MSE_C) of the test set. Equations (14) and (15) are calculation equations of the mean square error of the training set and the mean square error of the test set.

$$\text{MSE}_X = \frac{1}{2d} \sum_{t=1}^d \sum_{k=1}^n (a_{kl} - t_{kl})^2, \quad (14)$$

$$\text{MSE}_C = \frac{1}{2q} \sum_{i=1}^q \sum_{k=1}^n (a_{kl} - t_{kl})^2. \quad (15)$$

In (14) and (15), d is the number of training set samples, t_{kl} represents the desired output of the output neuron, and a_{kl} is the actual output of the output neuron.

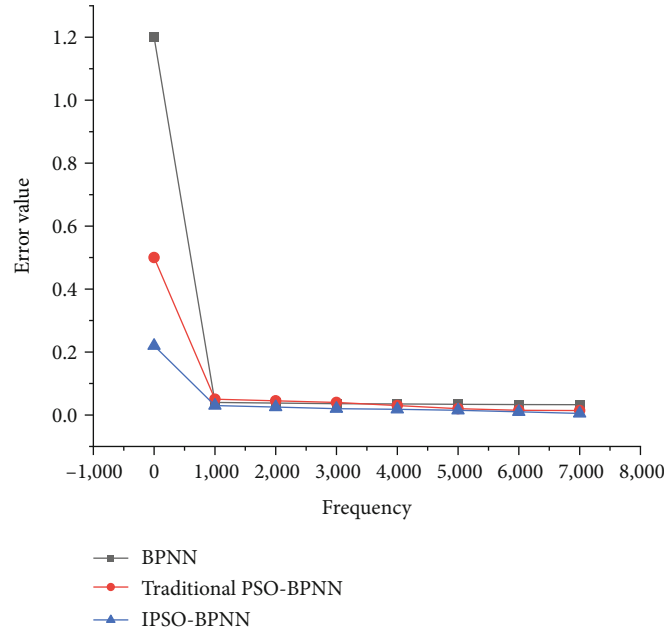


FIGURE 7: Training errors of BPNN.

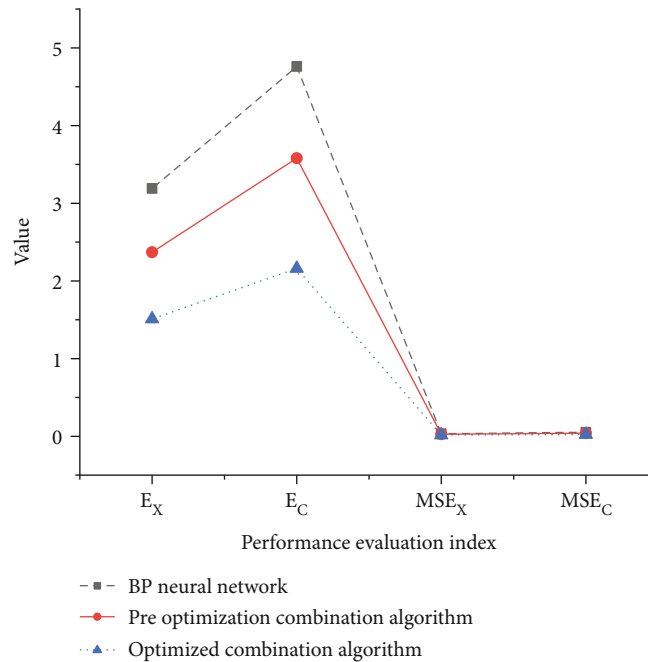


FIGURE 8: Performance comparison of different algorithms.

3.7. Application of the Combined Algorithm in Supply Chain Management. The inventory management in an enterprise’s supply chain management system is taken as the research object. The enterprise’s supply chain management is divided into three layers: appearance, business, and data. As one of the subsystems of supply chain management, the overall inventory management process includes raw material purchase receipt, picking an issue, movement, and inventory counting.

The combined algorithm proposed in the full text is used to predict the inventory in inventory management to meet the requirements of green supply chain management. The

use network is a 3-layer network, and the input nodes are 6. The number of hidden layer nodes adopts 11 nodes with good convergence and generalization. The particle swarm size of the prediction model is 40. The maximum particle velocity is 0.5, the minimum error is 0.01, and the maximum number of iterations is 7000. The mutation operator is 0.0001, the maximum value in the adaptive adjustment of inertia weight is 0.9, and the minimum value is 0.3. The enterprise data are selected from 2018 to 2021 for network training, and the daily test results are compared with the monthly test results in terms of network performance with 6~12 nodes.

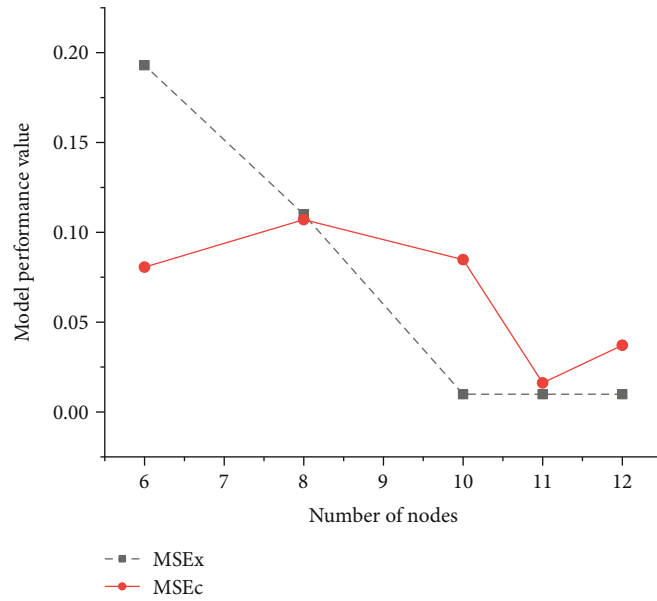


FIGURE 9: Comparison of daily test results of inventory forecast performance of networks with different numbers of nodes.

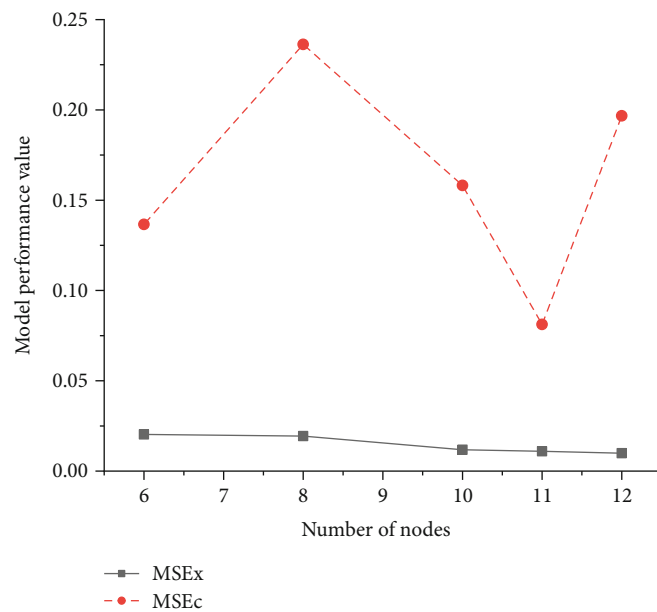


FIGURE 10: Comparison of monthly test results of inventory forecast performance of networks with different numbers of nodes.

Table 2 displays the operating environment of the experiment.

4. Result Analysis of Intelligent Supply Chain Management

4.1. Comparative Analysis of Simulation Results. Figure 7 displays the error results in the training process of BPNN, traditional PSO-BPNN, and IPSO-BPNN.

Figure 7 shows that the training error of a single BPNN reaches the minimum value of 0.033 after 7000 times of training, and the BPNN error using traditional PSO is 0.0259. The BPNN error optimized by IPSO is 0.0163, which

shows that the BPNN model based on the IPSO algorithm has higher accuracy and better performance, and the improvement effect of the PSO algorithm is remarkable. Moreover, the errors of the two combined algorithms are lower than that of a single BPNN, which shows that the PSO algorithm can improve the convergence speed and accuracy of BPNN to a certain extent. After further improving the PSO algorithm, the performance improvement effect of BPNN is more obvious.

Figure 8 displays the performance comparison results of the three algorithms based on the performance indexes.

Figure 8 shows that the generalization error rate and the training error rate of the three algorithms are low and that of

the optimized algorithm is the lowest. The classification error rate of the optimized combination algorithm is 1.51 for the training set, 2.16 for the test set, 0.0163 for the training set, and 0.0229 for the test set. The error rate of BPNN is the highest. It suggests that the performance of the optimized model is better, although the Iris dataset is relatively simple.

4.2. Analysis of the Inventory Forecast Performance of Networks. Figures 9 and 10 are the daily and monthly test results of inventory forecast performance of networks with the different numbers of nodes.

Figures 9 and 10 show that under 6 ~ 12 different hidden nodes, both the daily measurement error rate and monthly measurement error rate show that when the number of nodes is 11, the error rate is low, and the training set is always better than the test set. The minimum value of daily measurement training error appears in the training set when the number of nodes is 11. The minimum value of monthly measurement error is also 0.0099, which appears in the training set when the number of nodes is 11. It shows that when the number of hidden nodes is 11, the model's generalization ability is good and its training error is small. Hence, the network structure of the final combined model is 6-11-1. The inventory control auxiliary module is developed on the VS.NET platform based on the above model. The prediction module can give purchase volume suggestions and inventory volume suggestions, providing a feasible direction for the green development of inventory management.

5. Discussion

The training error of BPNN is large, and the training error of BPNN combined with the PSO algorithm is small. It indicates that the performance of the combined model is better than that of the single model, which is consistent with Li et al.'s research [52]. Using a combined model to study problems has become an important theoretical research method, the IPSO algorithm combined with BPNN has the best performance. It shows that the proposed two optimization methods can improve the adaptive ability of the learning factors, increase the speed mutation operator, and make the particles that have fallen into local optimization jump out of the local solution. In the final comparison of the generalization error rate and training error rate, the BPNN combined with the IPSO algorithm performs best. It proves once again the correctness of the optimization algorithm used. The advantage of this research method is to use the improved algorithm for network learning. Simulation results show that the improved algorithm can effectively shorten the training time of neural networks and enhance the generalization performance of the neural network. The research disadvantage is that only BPNN is selected as a single model in the model comparison, so the results are not comprehensive enough.

6. Conclusion

Nowadays, it is easy to waste resources in supply chain management. Therefore, in response to the green development

policy in supply chain management, this exploration uses AI technology to study inventory management in supply chain management. The traditional PSO algorithm is mainly improved by improving the adaptive ability to learn factors and adding the speed mutation operator. The IPSO algorithm is proposed and applied to the learning and training of BPNN, and a combination model with high accuracy is obtained. The research results will provide a reference for the intelligent development of inventory management. They are expected to be applied to major supply chain management to improve supply chain management efficiency. However, there are still some research deficiencies. Due to the limited ability, the performance of the algorithm constructed in inventory management prediction has not been deeply studied. The real-time transmission of supply chain management is not discussed. This exploration only selects two models to compare with the optimal combination algorithm proposed, and only verifies the performance of the improved algorithm after adding two mechanisms. It does not verify the algorithm's performance when adding only one mechanism, nor compare it with other business intelligence tools. Therefore, the follow-up research will focus on applying the combined algorithm constructed in inventory management prediction. It will strengthen the analysis of real-time transmission, select more relevant models for comparative analysis, and provide customers with various optional intelligent decision-making models according to different needs to provide a reference for green supply chain management development.

Data Availability

The raw data supporting the conclusions of this article will be made available by the authors, without undue reservation.

Consent

Informed consent was obtained from all individual participants included in the study.

Conflicts of Interest

All authors declare that they have no conflict of interest.

Authors' Contributions

All authors listed have made a substantial, direct, and intellectual contribution to the work and approved it for publication.

Acknowledgments

This work was supported by type D project of the special fund for basic scientific research of central colleges and universities "The model, path and experimental demonstration of natural resources capitalization taking the forest ecological bank as an example" (No. 2572020DZ09) and "Sustainable development mechanism to release resource advantages from the perspective of green finance" (No. 2572020DY06).

References

- [1] S. Seuring, S. Aman, B. D. Hettiarachchi, F. A. de Lima, L. Schilling, and J. I. Sudusinghe, "Reflecting on theory development in sustainable supply chain management," *Cleaner Logistics and Supply Chain*, vol. 3, article 100016, 2022.
- [2] S. Gawusu, X. Zhang, S. A. Jamatutu, A. Ahmed, A. A. Amadu, and E. Djam Miensah, "The dynamics of green supply chain management within the framework of renewable energy," *International Journal of Energy Research*, vol. 46, no. 2, pp. 684–711, 2022.
- [3] H. F. Lin, "IT resources and quality attributes: the impact on electronic green supply chain management implementation and performance," *Technology in Society*, vol. 68, article 101833, 2022.
- [4] H. Sri, "Analysis supply chain management factors of lecturer's turnover phenomenon," *International Journal of Supply Chain Management*, vol. 9, no. 1, pp. 582–591, 2020.
- [5] H. Birkel and J. M. Müller, "Potentials of industry 4.0 for supply chain management within the triple bottom line of sustainability - a systematic literature review," *Journal of Cleaner Production*, vol. 289, article 125612, 2021.
- [6] D. J. Ketchen Jr. and C. W. Craighead, "Research at the intersection of entrepreneurship, supply chain management, and strategic management: opportunities highlighted by COVID-19," *Journal of Management*, vol. 46, no. 8, pp. 1330–1341, 2020.
- [7] S. Bag, P. Dhamija, D. J. Bryde, and R. K. Singh, "Effect of eco-innovation on green supply chain management, circular economy capability, and performance of small and medium enterprises," *Journal of Business Research*, vol. 141, pp. 60–72, 2022.
- [8] L. Jum'a, M. Ikram, Z. Alkalha, and M. Alaraj, "Factors affecting managers' intention to adopt green supply chain management practices: evidence from manufacturing firms in Jordan," *Environmental Science and Pollution Research*, vol. 29, no. 4, pp. 5605–5621, 2022.
- [9] C. W. Craighead, D. J. Ketchen Jr., and J. L. Darby, "Pandemics and supply chain management research: toward a theoretical toolbox," *Decision Sciences*, vol. 51, no. 4, pp. 838–866, 2020.
- [10] R. A. Rupa and A. N. M. Saif, "Impact of green supply chain management (GSCM) on business performance and environmental sustainability: case of a developing country," *Business Perspectives and Research*, vol. 10, no. 1, pp. 140–163, 2022.
- [11] S. M. Wu, F. T. Chan, and S. H. Chung, "A study on green supply chain under capital constraint considering time-varying salvage value," *International Journal of Production Research*, vol. 60, no. 1, pp. 8–24, 2022.
- [12] C. Liu, "Risk prediction of digital transformation of manufacturing supply chain based on principal component analysis and backpropagation artificial neural network," *Alexandria Engineering Journal*, vol. 61, no. 1, pp. 775–784, 2022.
- [13] W. Fu, H. Zhang, and F. Huang, "Internet-based supply chain financing-oriented risk assessment using BP neural network and SVM," *PLoS One*, vol. 17, no. 1, article e0262222, 2022.
- [14] M. B. Faasolo and E. Sumarliah, "An artificial neural network examination of the intention to implement blockchain in the supply chains of SMEs in Tonga," *Information Resources Management Journal (IRMJ)*, vol. 35, no. 1, pp. 1–27, 2022.
- [15] S. A. R. Khan, Z. Yu, H. Golpira, A. Sharif, and A. Mardani, "A state-of-the-art review and meta-analysis on sustainable supply chain management: future research directions," *Journal of Cleaner Production*, vol. 278, article 123357, 2021.
- [16] D. Asamoah, B. Agyei-Owusu, F. K. Andoh-Baidoo, and E. Ayaburi, "Inter-organizational systems use and supply chain performance: mediating role of supply chain management capabilities," *International Journal of Information Management*, vol. 58, article 102195, 2021.
- [17] B. Esmaeilian, J. Sarkis, K. Lewis, and S. Behdad, "Blockchain for the future of sustainable supply chain management in industry 4.0," *Resources, Conservation and Recycling*, vol. 163, article 105064, 2020.
- [18] L. J. R. Nunes, T. P. Causer, and D. Ciolkosz, "Biomass for energy: a review on supply chain management models," *Renewable and Sustainable Energy Reviews*, vol. 120, article 109658, 2020.
- [19] U. Mishra, J. Z. Wu, and B. Sarkar, "Optimum sustainable inventory management with backorder and deterioration under controllable carbon emissions," *Journal of Cleaner Production*, vol. 279, article 123699, 2021.
- [20] A. Chakraborty, S. Maity, S. Jain, S. P. Mondal, and S. Alam, "Hexagonal fuzzy number and its distinctive representation, ranking, defuzzification technique and application in production inventory management problem," *Granular Computing*, vol. 6, no. 3, pp. 507–521, 2021.
- [21] C. N. Wang, T. T. Dang, and N. A. T. Nguyen, "A computational model for determining levels of factors in inventory management using response surface methodology," *Mathematics*, vol. 8, no. 8, p. 1210, 2020.
- [22] S. K. Das, M. Pervin, S. K. Roy, and G. W. Weber, "Multi-objective solid transportation-location problem with variable carbon emission in inventory management: a hybrid approach," *Annals of Operations Research*, vol. 31, pp. 1–27, 2021.
- [23] Y. S. Huang, C. C. Fang, and Y. A. Lin, "Inventory management in supply chains with consideration of logistics, green investment and different carbon emissions policies," *Computers & Industrial Engineering*, vol. 139, article 106207, 2020.
- [24] A. P. Piotrowski, J. J. Napiorkowski, and A. E. Piotrowska, "Population size in particle swarm optimization," *Swarm and Evolutionary Computation*, vol. 58, article 100718, 2020.
- [25] E. S. El-Kenawy and M. Eid, "Hybrid gray wolf and particle swarm optimization for feature selection," *International Journal of Innovative Computing Information and Control*, vol. 16, no. 3, pp. 831–844, 2020.
- [26] D. Sedighzadeh, E. Masehian, M. Sedighzadeh, and H. Akbaripour, "GEPSO: a new generalized particle swarm optimization algorithm," *Mathematics and Computers in Simulation*, vol. 179, pp. 194–212, 2021.
- [27] M. P. Ha, M. Nazari-Heris, B. Mohammadi-Ivatloo, and H. Seyedi, "A hybrid genetic particle swarm optimization for distributed generation allocation in power distribution networks," *Energy*, vol. 209, article 118218, 2020.
- [28] V. V. Jha, K. S. Jajoo, B. K. Tripathy, and S. Durai, "An improved monarch butterfly optimization based multivariate fuzzy time series approach for forecasting GDP of India," *Evolutionary Intelligence*, vol. 26, pp. 1–15, 2022.
- [29] R. Ramaporselvi and G. Geetha, "Congestion management in deregulated power system using adaptive moth swarm optimization," *COMPEL-The international journal for computation and mathematics in electrical and electronic engineering*, vol. 29, 2021.
- [30] P. Mehta, B. S. Yildiz, S. M. Sait, and A. R. Yildiz, "Hunger games search algorithm for global optimization of engineering

- design problems,” *Materials Testing*, vol. 64, no. 4, pp. 524–532, 2022.
- [31] D. Yousri, M. Mudhsh, Y. O. Shaker et al., “Modified interactive algorithm based on Runge Kutta optimizer for photovoltaic modeling: justification under partial shading and varied temperature conditions,” *IEEE Access*, vol. 10, pp. 20793–20815, 2022.
- [32] Y. Hu, Y. Zhang, and D. Gong, “Multiobjective particle swarm optimization for feature selection with fuzzy cost,” *IEEE Transactions on Cybernetics*, vol. 51, no. 2, pp. 874–888, 2021.
- [33] M. Ahmad, I. A. Khaja, A. Baz, H. Alhakami, and W. Alhakami, “Particle swarm optimization based highly non-linear substitution-boxes generation for security applications,” *IEEE Access*, vol. 8, pp. 116132–116147, 2020.
- [34] P. K. Das and P. K. Jena, “Multi-robot path planning using improved particle swarm optimization algorithm through novel evolutionary operators,” *Applied Soft Computing*, vol. 92, article 106312, 2020.
- [35] T. R. Farshi, J. H. Drake, and E. Özcan, “A multimodal particle swarm optimization-based approach for image segmentation,” *Expert Systems with Applications*, vol. 149, article 113233, 2020.
- [36] M. Shafipour, A. Rashno, and S. Fadaei, “Particle distance rank feature selection by particle swarm optimization,” *Expert Systems with Applications*, vol. 185, article 115620, 2021.
- [37] N. B. Shaik, S. R. Pedapati, S. A. A. Taqvi, A. R. Othman, and F. A. A. Dzubir, “A feed-forward back propagation neural network approach to predict the life condition of crude oil pipeline,” *PRO*, vol. 8, no. 6, p. 661, 2020.
- [38] A. Thakkar and K. Chaudhari, “A comprehensive survey on portfolio optimization, stock price and trend prediction using particle swarm optimization,” *Archives of Computational Methods in Engineering*, vol. 28, no. 4, pp. 2133–2164, 2021.
- [39] A. Mukherjee, D. K. Jain, P. Goswami, Q. Xin, L. Yang, and J. J. Rodrigues, “Back propagation neural network based cluster head identification in MIMO sensor networks for intelligent transportation systems,” *IEEE Access*, vol. 8, pp. 28524–28532, 2020.
- [40] M. M. Almalki, E. S. Alaidarous, D. A. Maturi, M. A. Z. Raja, and M. Shoaib, “A levenberg–marquardt backpropagation neural network for the numerical treatment of squeezing flow with heat transfer model,” *IEEE Access*, vol. 8, pp. 227340–227348, 2020.
- [41] V. Geetha, K. S. Aprameya, and D. M. Hinduja, “Dental caries diagnosis in digital radiographs using back-propagation neural network,” *Health information science and systems*, vol. 8, no. 1, pp. 1–14, 2020.
- [42] A. Yusuf and D. Soediantono, “Supply chain management and recommendations for implementation in the defense industry: a literature review,” *International Journal of Social and Management Studies*, vol. 3, no. 3, pp. 63–77, 2022.
- [43] S. A. S. Salari, H. Mahmoudi, A. Aghsami, F. Jolai, S. Jolai, and M. Yazdani, “Off-site construction three-echelon supply chain management with stochastic constraints: a modelling approach,” *Buildings*, vol. 12, no. 2, p. 119, 2022.
- [44] M. I. Majumder and M. M. Habib, “Supply chain management in the banking industry: a literature review,” *American Journal of Industrial and Business Management*, vol. 12, no. 1, pp. 10–20, 2022.
- [45] X. Zhao and J. Hou, “Applying the theory of constraints principles to tourism supply chain management,” *Journal of Hospitality & Tourism Research*, vol. 46, no. 2, pp. 400–411, 2022.
- [46] Y. Zhong and X. Wu, “Effects of cost-benefit analysis under back propagation neural network on financial benefit evaluation of investment projects,” *PLoS One*, vol. 15, no. 3, article e0229739, 2020.
- [47] I. Khan, M. A. Z. Raja, M. Shoaib et al., “Design of neural network with Levenberg-Marquardt and Bayesian regularization backpropagation for solving pantograph delay differential equations,” *IEEE Access*, vol. 8, pp. 137918–137933, 2020.
- [48] B. O. P. Soepangkat, R. Norcahyo, M. K. Effendi, and B. Pramujati, “Multi-response optimization of carbon fiber reinforced polymer (CFRP) drilling using back propagation neural network-particle swarm optimization (BPNN-PSO),” *Engineering Science and Technology, an International Journal*, vol. 23, no. 3, pp. 700–713, 2020.
- [49] S. Song, X. Xiong, X. Wu, and Z. Xue, “Modeling the SOFC by BP neural network algorithm,” *International Journal of Hydrogen Energy*, vol. 46, no. 38, pp. 20065–20077, 2021.
- [50] J. Tian, Y. Liu, W. Zheng, and L. Yin, “Smog prediction based on the deep belief - BP neural network model (DBN-BP),” *Urban Climate*, vol. 41, article 101078, 2022.
- [51] Y. Cui, H. Liu, Q. Wang et al., “Investigation on the ignition delay prediction model of multi-component surrogates based on back propagation (BP) neural network,” *Combustion and Flame*, vol. 237, article 111852, 2022.
- [52] F. Li, J. P. Hughes, K. Hemming, M. Taljaard, E. R. Melnick, and P. J. Heagerty, “Mixed-effects models for the design and analysis of stepped wedge cluster randomized trials: an overview,” *Statistical Methods in Medical Research*, vol. 30, no. 2, pp. 612–639, 2021.

Research Article

Interaction Design of Wellness Building Space by Deep Learning and VR Technology in the Context of Internet of Things

Mei Yang¹ and Xinyu Wang²

¹*School of Architecture, Planning & Surveying, University of Technology MARA, Kuala Lumpur 59200, Malaysia*

²*School of New Media Art, Chongqing Finance and Economics College, Chongqing, China 401320*

Correspondence should be addressed to Mei Yang; 2020625604@student.uitm.edu.my

Received 26 March 2022; Revised 18 May 2022; Accepted 30 May 2022; Published 25 June 2022

Academic Editor: Mu-Yen Chen

Copyright © 2022 Mei Yang and Xinyu Wang. This is an open access article distributed under the Creative Commons Attribution License, which permits unrestricted use, distribution, and reproduction in any medium, provided the original work is properly cited.

This study explores the application of deep learning theory and virtual reality (VR) technology to the interactive behavior design of building space according to the interaction behavior of wellness building space in the context of the Internet of Things (IoT). Firstly, VR theory is made into an image-based 3-dimensional (3D) modeling process. Secondly, the interactive behavior information data is analyzed according to the theory of deep learning and edge computing. Finally, the particle swarm optimization (PSO) is used to analyze the predicted temperature with the wellness building space model, as well as to make a study based on the changes in the user's psychological indicators. The results show that the model predictions of deep learning-edge computing are most like the actual environmental settings. Both PSO and deep learning algorithms have varying degrees of influence on the final prediction results. The average temperature of the wellness building space established by deep learning and edge computing is 24.58 degrees, the average measured value of the actual environment is 24.49 degrees, and the predicted values of the two are similar. While users experienced the interactive design of the health building, their heart rate dropped from 73.17 to 68.79 and gradually became stable. There is no obvious change in the user's heart rate, which reflects the comfort of the wellness building space designed based on deep learning and VR interaction.

1. Introduction

A wide variety of building components are included in the architectural space, and the building components have only changed in terms of styles and materials during hundreds or decades of development [1]. If each building component is not in the same position, it is physically connected by the relationship between each other. If these large numbers of building components can be intelligently transformed through the Internet of Things (IoT), then the physical connections between them can be upgraded to communication and information connections, thus forming the overall space with intelligent properties. These structures make it a space of interconnected intelligent building components that can be controlled remotely, managed on-site, collected data feedback from sensors, stored status information in the cloud, and analyzed and managed big data [2–5]. This will lead to dramatic changes in buildings, making them more comfortable, energy-efficient, convenient, and

safe. Meanwhile, it can reduce various energy consumption losses through intelligent adjustment to achieve a fantastic life experience and maximize the function of energy-saving and emission reduction [6, 7]. Virtual reality (VR) technology can reconstruct multidimensional cultural spaces and provide the possibility of immersion in the digital world and has increasingly become an important tool for cultural heritage research, protection, and dissemination. Regarding VR development in Europe, especially in the research of distributed parallel processing, auxiliary equipment design, and application, the intersection of VR application should focus on the overall comprehensive technology. The technology mainly includes VR reconstruction problems and architectural and scientific visualization computing [8–10].

Firstly, a three-dimensional model of the building must be constructed to simulate the building environment space. Viewing through the monitor can only be from one angle or one side [11]. Previously, the way of browsing animation

is mainly adopted. For example, when a spline curve is established as a browsing path, a camera simulating a “human eye” is set up on this path to obtain a dynamic change in the architectural environment space. However, this animation has poor operability and human-computer interaction [12]. 3D Studio MAX is used to generate the design of the 3D architectural virtual space. This software system provides a camera plug-in. It consists of two cameras set horizontally. It is set at the appropriate position of the building scene and can obtain still pictures of buildings or browse animations simultaneously. Two pictures of the same target object are obtained [13–15]. However, the previous architectural design was based on the interaction between space and behavior. The three-dimensional spatial structure of the architectural space cannot be dynamically demonstrated, and there is a patterned architectural design behavior. Deep learning includes computational vision, natural language processing, and deep reinforcement learning. These address the problem of identification and decision-making concerning different types of data [16, 17]. At present, edge computing of operators is mainly in the pre-commercial stage of technical research, laboratory testing, and relatively simple scenarios [18]. Deep generative models are becoming the foundation of modern machine learning. Research on conditional generative adversarial networks (CGAN) shows the learning complex high-dimensional distributions on natural images [19]. While state-of-the-art models can generate high-fidelity, diverse natural images at high resolution, they rely on many annotated data [20].

Based on the IoT background, the deep learning theory and VR technology are applied to the interactive behavior design of building space according to the interaction behavior of wellness building space. Firstly, VR theory is made into an image-based 3D modeling process. Secondly, the interactive behavior information data is analyzed according to the theory of deep learning and edge computing. Finally, particle swarm optimization is used to predict temperature analysis with the wellness building space model, as well as make research based on changes in user psychological indicators. Technological development is taken as the premise; the comfort of health building is taken as the foundation. In the context of IoT, an interactive space for healthcare buildings based on VR and deep learning is designed. The design breaks through the traditional interactive design concept of healthcare buildings and has certain reference significance for the rational and scientific space design of healthcare buildings. The innovation lies in IoT and deep learning to supervise and control the equipment data of healthcare building space, which is different from the previous model of the design of healthcare building space. Additionally, VR technology is used for spatial interaction design to avoid the weak sense of interactive experience caused by relying on two-dimensional images for design and establish a dynamic interactive design of health building space.

Section 1 discusses the background of building space design for healthcare and the current status of building space and deep learning. Section 2 describes the production process, technical principles, and technical characteristics of the VR technology environment and explains the modeling process of VR technol-

ogy on images. This part also discusses the workflow of deep learning and the principle of edge computing, which provides the technical and theoretical basis. Finally, the interactive design process of health building space based on VR and deep learning in IoT is designed. Section 3 mainly conducts temperature prediction and experience analysis of the designed health building space. Section 4 discusses based on the analysis results. Section 5 summarizes the research.

2. Method

2.1. Exploration of VR Technology Theory. Virtual reality (VR) is a new technology in the computer field developed as a comprehensive computer graphics, multimedia, sensor, human-computer interaction, network, stereoscopic display and simulation, and other technologies. At present, the research and application fields involved have included military, medicine, psychology, education, scientific research, commerce, film and television, entertainment, manufacturing, and engineering training. VR is a computer system that can create and experience virtual worlds (virtual worlds are a general term for all virtual environments). The VR system is established as multidimensional cyberspace that contains various kinds of information, and it is no longer purely digital cyberspace. Human perceptual cognition and rational cognition ability can be brought into full play in this multidimensional cyberspace [21]. Creating a VR system that allows participants to have an immersive sense of reality and a perfect interaction ability requires high-performance computer hardware and software, various advanced sensors, and a toolset that can generate virtual environments. The production process of the VR technology environment is shown in Figure 1.

In Figure 1, the VR technology environment applies the limitations of existing digital computers to process purely digital information. It builds cyberspace to accommodate various information sources such as images, sounds, and chemical smells. The information space can not only observe the results of information processing from the outside but also participate in the information processing environment through visual, auditory, olfactory, password, gesture, and other forms. Such an information processing environment is called a virtual environment. The virtual environment is generated by a computer and acts on the user through sight, hearing, touch, etc., to produce an immersive interactive visual simulation. VR uses “immersion,” “interaction,” and “imagination” to describe its characteristics, and the three are indispensable. The technical characteristics of VR are shown in Table 1.

In Table 1, immersive technologies have changed, to a certain extent, the way consumers, businesses, and the digital world interact. Users expect a greater shift from the 2-dimensional (2D) interface to the more immersive 3D world. They can capture richer, smoother pictures and experiences in 3D. Augmented reality (AR) is a field extended by the development of VR technology. It organically “superimposes” computer-generated virtual images or other information into real-world scenes with the help of computer vision and interactive technologies, including

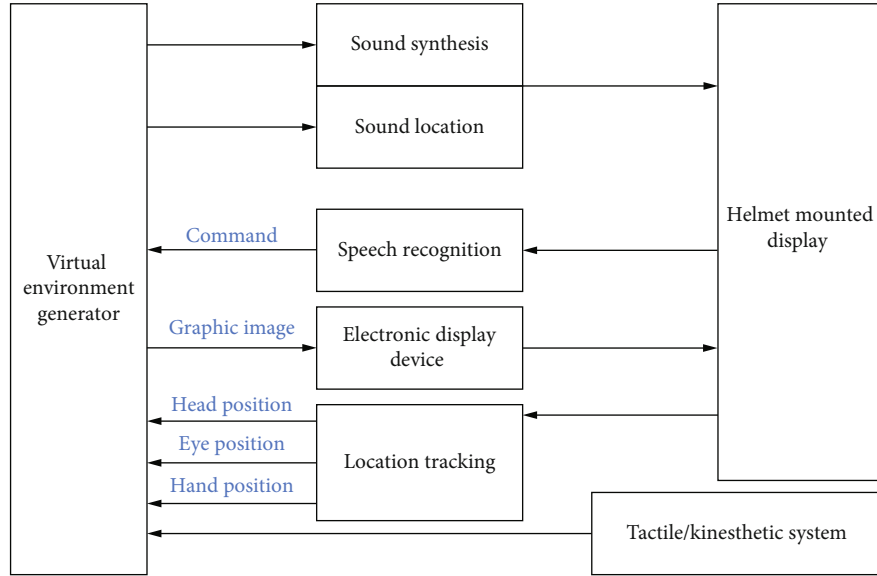


FIGURE 1: The generation process of the VR technology environment.

TABLE 1: Features of VR technology.

Feature	Equipment used
Immersion	Helmet display and data headset
Interaction	Computer keyboard, mouse, etc.
Imagination	Equipped with visual, auditory, tactile sensing, and reaction devices

visual, auditory, olfactory, and tactile information. AR achieves a sensory experience “beyond” reality. The foundation of AR technology lies in tracking and positioning, user interaction, virtual fusion, and system display technology. VR technology uses computer simulation to generate a virtual world of 3D space, providing users with simulations of visual, auditory, tactile, and other senses. It allows users to observe things in 3D space in a timely and unlimited manner as if they were in the real world. When the user moves the position, the computer can immediately perform complex calculations and transmit the precise 3D world image to produce a sense of presence. It can substitute human consciousness into a virtual world. When people look at the world around them, they get slightly different images due to the different positions of the two eyes. This difference allows people to perceive depth and makes things appear 3D. VR technology also uses this visual difference to arrange different pictures for the eyes so that the observer can feel the three-dimensionality of the picture. VR is a 360-degree panoramic interaction. It not only has a strong sense of immersion and three-dimensionality but also allows users to interact with the virtual world [22]. The principle of VR core technology is shown in Figure 2.

In Figure 2, VR technology is a computer technology that can create and experience virtual worlds. It can use a computer to generate a simulation environment, a system simulation of multisource information fusion interactive

three-dimensional dynamic scene and entity behavior. This technology can use professional equipment such as sensor helmets to allow users to enter the virtual space and perceive and operate various objects in the virtual world in real time to get a real immersive experience. The image-based modeling process of VR technology is shown in Figure 3.

Figure 3 expresses the scene in different forms, such as panoramic images and light fields, with photo data taken in different directions and positions. Secondly, the new view of image synthesis is used to compose a new virtual environment. The all-seeing function is used to perform a set of all environment mappings for a given scene [23]. The all-seeing function is defined as

$$u = \text{Plenoptic}(\theta, \phi, \lambda, V_x, V_y, V_z, t). \quad (1)$$

(V_x, V_y, V_z) represents the position of the viewpoint in space. ϕ represents the elevation angle for the field of view direction and range. θ is the azimuth angle. λ represents the wavelength perceived by the human eye. t stands for time. The brightness of each point on the image reflects the intensity of light at a certain point on the surface of an object in space. The position of the point on the image is related to the geometric position on the surface of the space object. The reference coordinate system of the camera model

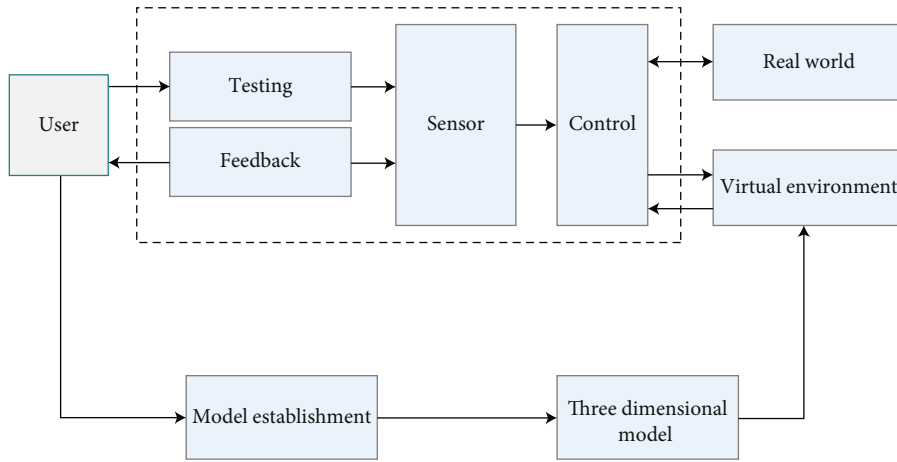


FIGURE 2: The principle of VR core technology.

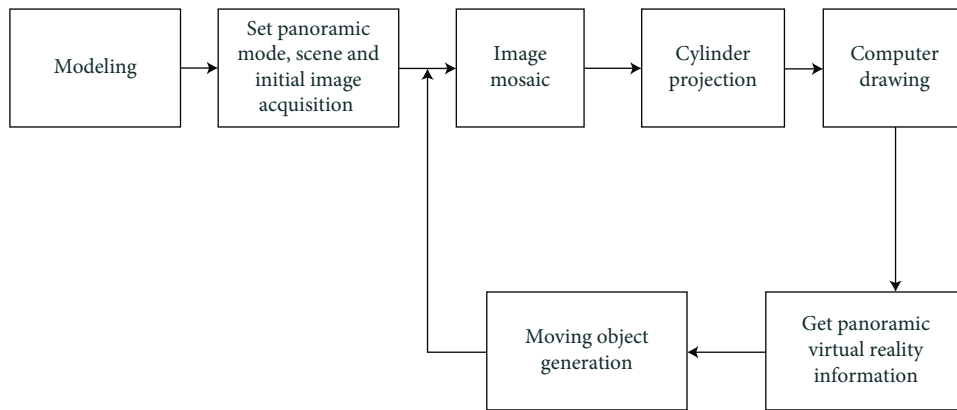


FIGURE 3: The modeling process of VR technology image-based.

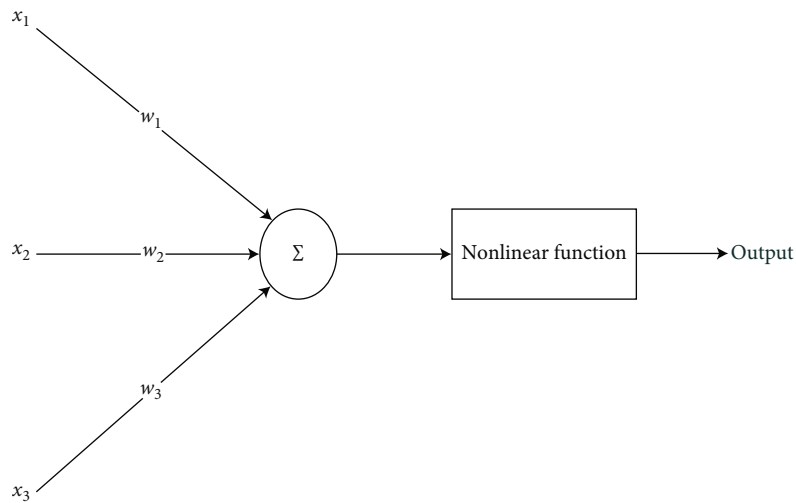


FIGURE 4: Deep learning neural network.

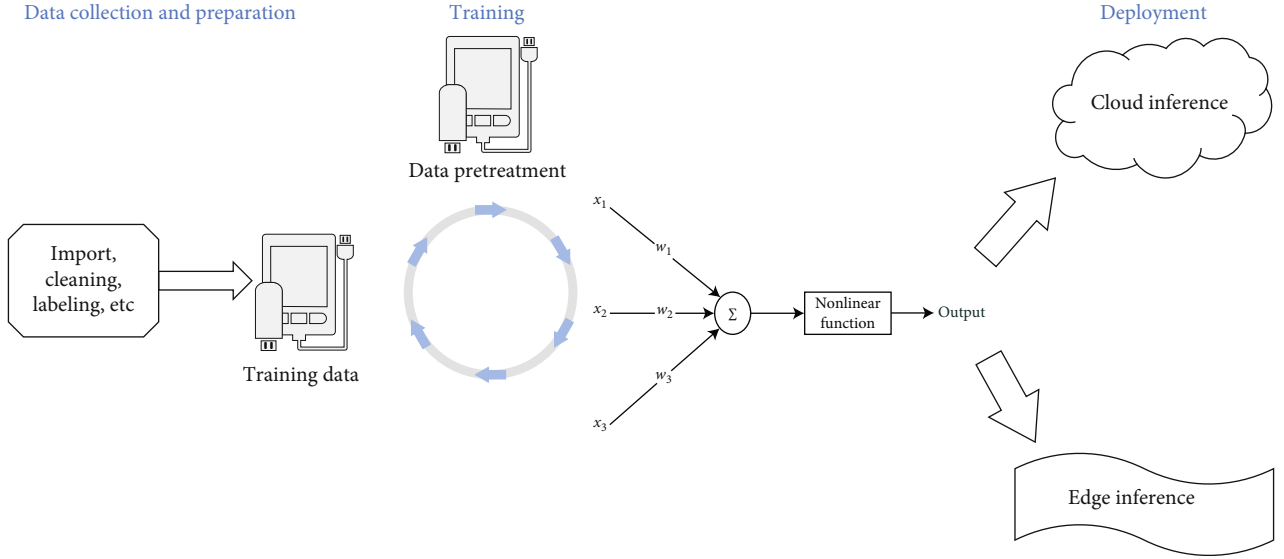


FIGURE 5: Workflow of deep learning.

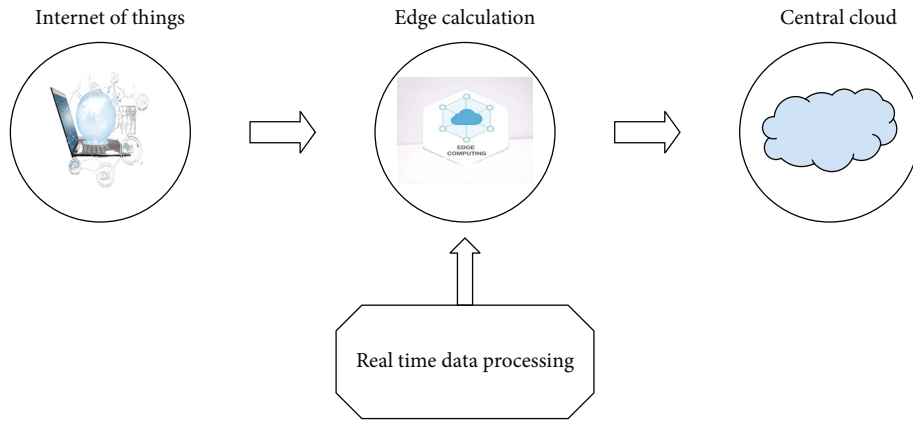


FIGURE 6: Principles of edge computing.

is used to solve for each coordinate, as shown in

$$\begin{bmatrix} u \\ v \\ 1 \end{bmatrix} = M \begin{bmatrix} X_w \\ Y_w \\ Z_w \\ 1 \end{bmatrix}, \quad (2)$$

$$Z_c \begin{bmatrix} u \\ v \\ 1 \end{bmatrix} = M_1 M_2 X_w = M X_w. \quad (3)$$

(u, v) is expressed as the coordinates of the computer image in pixel units. (X_w, Y_w, Z_w) are the coordinates of the actual image in physical units. M is the camera calibration. The internal parameters of the camera are marked as M_1 , and the external parameters are marked as M_2 . The original image data is converted into stitched image data according to the requirements of panoramic vision consistency and maintaining the spatial constraints in the actual scene. The feature points

are selected as Harris corners on the image, and the theoretical description is shown in

$$C = \begin{bmatrix} \left(\frac{\partial I}{\partial x}\right)^2 & \left(\frac{\partial I}{\partial x}\right)\left(\frac{\partial I}{\partial y}\right) \\ \left(\frac{\partial I}{\partial x}\right)\left(\frac{\partial I}{\partial y}\right) & \left(\frac{\partial I}{\partial y}\right)^2 \end{bmatrix}. \quad (4)$$

$I(x, y)$ represents the grayscale value. If the two eigenvalues of the matrix C at a point are large, a small movement of the point in any direction will cause a large change in the gray value. The function of corner detection is shown in

$$R = \det C - k(\text{trance}C)^2. \quad (5)$$

The k parameter is set to 0.04. The point in the local area corresponding to the maximum value of the corner function is the corner. Determine a threshold, and select the point whose R -value is greater than the threshold as the corner point.

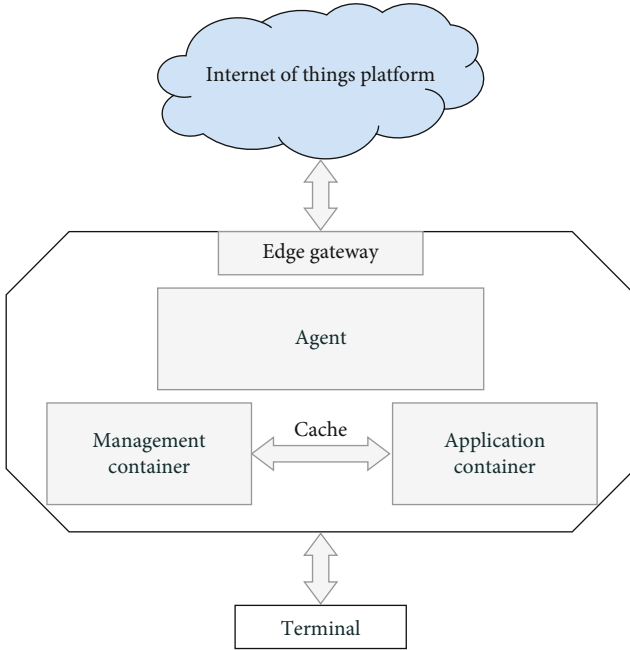


FIGURE 7: Data processing of edge computing in the context of IoT.

2.2. Principles of Deep Learning and Edge Computing. As an emerging technology in machine learning algorithms, deep learning is to build a neural network that simulates the human brain for analysis and learning. Its essence is to perform hierarchical feature representation on observation data and realize the further abstraction of low-level features into a high-level feature representation. This is all performed through neural networks [24]. The deep learning neural network is shown in Figure 4.

In Figure 4, deep learning uses neural network technology. The most basic unit of a neural network is a neuron. x_1 , x_2 , and x_3 are the input values of deep learning. w_1 , w_2 , and w_3 are weights. When the network adds a computing layer, it can not only solve the exclusive OR (XOR) problem but also have a perfect nonlinear classification effect. Theoretically, a two-layer neural network can approximate any continuous function infinitely. The deep learning workflow is shown in Figure 5.

In Figure 5, firstly, the definition is questioned, and the dataset is collected to ensure that the dataset is feature-rich enough to make predictions. Secondly, model prediction performance metrics are defined. Finally, the model evaluation method is determined, and the model is built for verification. Edge computing supports a hierarchy of end devices, edge computing nodes, and cloud data centers. It can provide computing resources and scale according to the number of clients, avoiding network bottlenecks in a central location. The principle of edge computing is shown in Figure 6.

In Figure 6, edge computing does not need to transmit data to the cloud when processing data. It is suitable for data analysis and intelligent processing and has the advantages of safety, speed, and easy management. Edge computing can better support real-time intelligent processing and execution of local data and meet the real-time requirements of IoT [25]. The image-based two-dimensional partial differential

equations are shown in

$$\frac{\partial f(x, y)}{\partial x} = \lim_{\epsilon \rightarrow 0} \frac{f(x + \epsilon, y) - f(x, y)}{\epsilon}, \quad (6)$$

$$\frac{\partial f(x, y)}{\partial y} = \lim_{\epsilon \rightarrow 0} \frac{f(x, y + \epsilon) - f(x, y)}{\epsilon}. \quad (7)$$

In Equations (6) and (7), the gradient of the image is the partial derivative of the current pixel (x, y) concerning the x -axis and the y -axis. Therefore, the gradient can be understood as the speed at which the gray value of the pixel changes. After the image has been computed, nonmaximum suppression can help suppress all gradient values except local maxima to 0.

2.3. Establishment of a Spatial Interaction Design Model of the Healthy Building in the Context of the IoT. A deep neural network is a complex, nonlinear, and nonconvex function. This function is then used to fit the patterns in various types of input data so that patterns in these data can be identified. Ultimately, it can align the model's prediction with the ground-truth label. The data processing of edge computing in the context of IoT is shown in Figure 7.

Figure 7 applies a software development kit (SDK) by providing devices adapted to different access protocols. Edge nodes can uniformly manage and monitor different devices, making device access simple and fast. Nodes can process data reported by devices in real time, clear and filter data, and authenticate devices online. It supports offline nodes to store and encrypt local data and supports the deployment of custom applications to edge nodes in container mode. The cloud can manage, monitor, and operate images and container applications unified.

Wisdom combines technical means and IoT and technical means to connect all traceable intelligent device data to the Internet. User data is stored in a decentralized way of IoT, and the public key and private key cannot be tampered with to complete the verification and confirmation. Wellness is the application direction and scenario-based on big data artificial intelligence, applying IoT unmanned intelligent terminal equipment to build smart cities and communities. The design is simple, pays attention to the shape of the volume, and emphasizes the contrast between the virtual and the real. The design is simple, focusing on the shape of the volume, emphasizing the contrast between virtual and real. The main building complex of beige paint is appropriately matched with warm red brick walls and a bell tower in length and height. This highlights the modern fashion but does not lose elegant, warm temperament, in line with children and the elderly physical and psychological needs [26]. The wellness building space interaction is shown in Table 2.

In Table 2, the interaction design process of VR wellness building space in an IoT context based on deep learning and edge computing is shown in Figure 8.

In Figure 8, the interaction design of the wellness building space is designed by combining VR technology with deep learning [27]. According to the selected wellness building design scheme, it is operated through the client software

TABLE 2: Interaction behavior of wellness building space.

Various spaces	Interactive behavior
Living space	Family visits, indoor walks, window sill viewing, balcony activities, watching TV, and chatting
Bed living space	Sleep, nursing, and family visits
Traffic contact space	A simple walk, rest at corridor rest, visit friends, and stop for communication
Public event space	Recreational activities, leisure communication, rehabilitation and fitness, laundry and bathing, consultation, and prescription

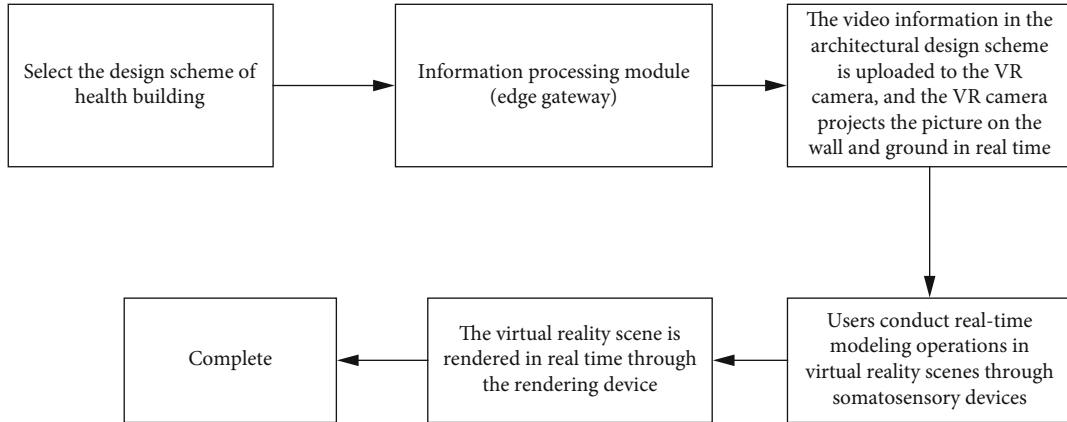


FIGURE 8: The interaction design process of wellness building space-based on VR and deep learning in the context of IoT.

installed on the smart mobile terminal (Android phone or iPad) device. The wellness building design scheme has different decoration materials, including wall color, floor selection, sofa style, and door and window style. The somatosensory device captures the posture of the human body and obtains the skeleton data and motion trajectory of the human body. The device uploads the data to the VR camera, calibrates, and obtains the coordinates of the user's head position or eye position in the VR scene. Finally, the coordinate parameters are corrected, and the interaction design of the Wellness building space is completed. Table 3 shows the qualified range of healthcare building environmental indicators and user physiological indicators.

3. Results and Discussion

3.1. Comparison of Temperature Prediction Results in Wellness Building Space under Different Models. According to VR technology and deep learning theory, the model parameter weight w_i in deep learning is 0.4~0.9. The value of edge computing ε is 0.0001. In the information processing data, 500 groups of data are selected as the sample set, and 25 groups are selected as the interactive behavior data set to predict wellness building space by different models—prediction of the interaction behavior of wellness building space-based on deep learning-edge computing and PSO. The number of model iterations is 200. Figure 9 shows the prediction results of the wellness building space interaction design under different models.

TABLE 3: Qualified range of healthcare building environmental indicators and user physiological indicators.

Index	Indicator normal range
Building temperature	24-25°C
Body temperature	36-37°C
Systolic blood pressure	140~90 (mmHg)
Diastolic blood pressure	90~60 (mmHg)
Heart rate	60~100 (min)

In Figure 9, the model prediction of deep learning-edge computing is most like the actual environment setting value. Both particle swarm optimization and deep learning algorithms have varying degrees of influence on the final prediction results. The average temperature of the wellness building space established by deep learning and edge computing is 24.58 degrees. The average value of the actual environmental measurement value is 24.49 degrees. The two predictions are similar. The prediction of the model is successful. The wellness building space of the PSO studied as a comparative study predicts an average temperature of 23.60 degrees, which is quite different. As the number of iterations increases, the average error rate of PSO increases from 10.56% to 13.45%. The average error rate for deep learning-edge computing is 6.40%.

3.2. Physiological Index Analysis of User Experience in Wellness Building Space. The advantage of the wellness building industry is that it can realize the remote supply of

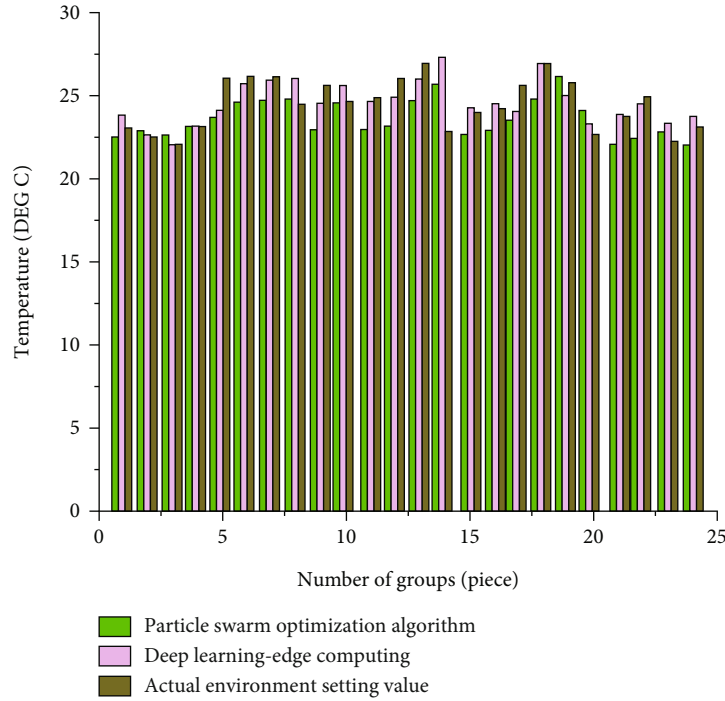


FIGURE 9: Prediction results of wellness building space interaction design under different models.

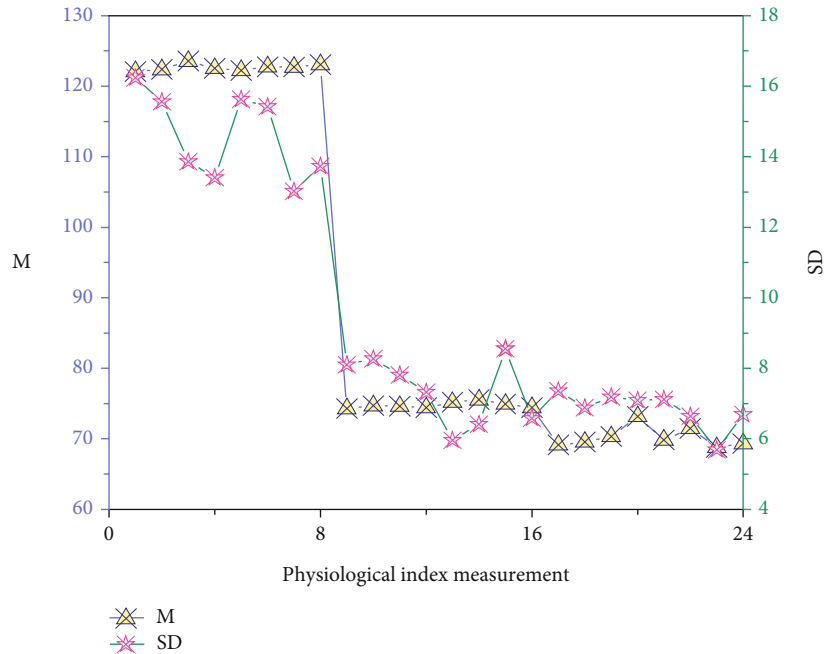


FIGURE 10: Analysis of physiological indicators of user experience in wellness building space.

resources. Unlike traditional industries, wellness is an industry that can easily achieve long-distance supply. The elderly and subhealthy people have become the main target groups of the wellness industry. However, according to incomplete estimates, the current annual supply of products for the wellness life of the elderly is between 500 billion and 700 billion yuan. Product demand continues to be strong, but effective supply is insufficient. The interaction design experience

of wellness building space is studied and analyzed according to the user's physiological indicators. Physiological indicators are divided into three categories, 1-8 are systolic blood pressure measurement indicators, 9-16 are diastolic blood pressure physiological measurement indicators, and 17-24 are physiological measurement indicators. Figure 10 shows the analysis of user physiological indicators in the wellness building space-based on deep learning and VR technology.

In Figure 10, while the user experiences the wellness building interactive design, the mean systolic blood pressure is 122.65, and the standard deviation is 14.60. The diastolic blood pressure mean is 74.76, and the standard deviation is 7.37. The mean heart rate is 70.19, with a standard deviation of 6.83. And the mean of systolic blood pressure is much larger than the standard deviation of systolic blood pressure. While the user experiences the interaction design of the wellness building, the heart rate drops from 73.17 to 68.79 and gradually becomes stable. There is no significant change in the user's heart rate. These data reflect the comfort of the wellness building space-based on deep learning and VR interaction design.

4. Discussion

The healthcare building space is predicted by building temperature, and the user experience physiological indicators are analyzed. The model based on deep learning-edge computing predicted that the average temperature of the healthcare building space is 24.58°C. The average value of the actual environmental measurement value is 24.49°C, and the predicted value of the two is similar. These values correspond to the appropriate temperature values for building dwellings. The data reflects the effectiveness and feasibility of the design from the side. In addition, when users experience the health building space, the physiological indicators conform to the normal physiological index range. In the interactive design of healthcare building space based on VR emotion measurement, the rationality of the design of elderly care institutions is directly proportional to the results of the emotional index scale (physiological and psychological) of the elderly. This result is beneficial in promoting the expression of positive emotions in the elderly. This is consistent with the physiological indicators of user experience in the research of healthcare building space in this paper, which shows the rationality of the research results, and reflects the comfort of healthcare building space based on deep learning and VR interactive design.

5. Conclusion

The interaction design of wellness building space is studied based on VR technology and deep learning theory and edge computing. The results show that the average temperature of the health building space established by deep learning and edge computing is 24.58°C; the average measured value of the actual environment is 24.49°C. The two predicted values are similar, and the model prediction is successful. The average temperature of the health building space predicted by the particle swarm algorithm as a comparative study is 23.60°C, which is quite different. As the number of iterations increases, the average error rate of PSO increases from 10.56% to 13.45%. The average error rate for deep learning-edge computing is 6.40%. While users experience the interactive design of healthcare buildings, the mean value of systolic blood pressure is 122.65, and the standard deviation is 14.60. The diastolic blood pressure mean was 74.76, and the standard deviation was 7.37. The mean heart rate was 70.19, with a standard deviation of 6.83. The mean of systolic blood pressure is

much larger than the standard deviation of systolic blood pressure. This study has certain reference significance for the virtual interaction design of healthcare building space in the context of IoT. However, according to the development of modern healthcare buildings, more and more intelligent equipment may have a certain impact on the design. It is hoped that this study can optimize the interactive design of the health building space with the advancement of technology. And there is no description of the services provided by the healthcare building. In the future, effective resources will be used for intelligent healthcare building service design.

Data Availability

The raw data supporting the conclusions of this article will be made available by the authors, without undue reservation.

Ethical Approval

This article does not contain any studies with human participants or animals performed by any of the authors.

Consent

Informed consent was obtained from all individual participants included in the study.

Conflicts of Interest

All authors declare that they have no conflict of interest.

Acknowledgments

The authors acknowledge the help from the university colleagues.

References

- [1] E. Elbailuomy, I. Hegazy, and S. Sheta, "The impact of architectural spaces' geometric forms and construction materials on the users' brainwaves and consciousness status," *International Journal of Low-Carbon Technologies*, vol. 14, no. 3, pp. 326–334, 2019.
- [2] M. S. Jalali, J. P. Kaiser, M. Siegel, and S. Madnick, "The internet of things promises new benefits and risks: a systematic analysis of adoption dynamics of IoT products," *IEEE Security & Privacy*, vol. 17, no. 2, pp. 39–48, 2019.
- [3] R. Lowe, "Networked and integrated sustainable urban technologies in Internet of Things-enabled smart city governance," *Geopolitics, History, and International Relations*, vol. 12, no. 2, pp. 75–85, 2021.
- [4] D. Li, "Analysis on the monitoring system of energy conservation and comfort in office buildings based on Internet of Things," *International Journal of Low-Carbon Technologies*, vol. 15, no. 3, pp. 351–355, 2020.
- [5] S. Wan, J. Hu, C. Chen, A. Jolfaei, S. Mumtaz, and Q. Pei, "Fair-hierarchical scheduling for diversified services in space, air and ground for 6g-dense internet of things," *IEEE Transactions on Network Science and Engineering*, vol. 8, no. 4, pp. 2837–2848, 2021.

- [6] X. Yao, G. Li, J. Xia et al., "Enabling the big earth observation data via cloud computing and DGGs: opportunities and challenges," *Remote Sensing*, vol. 12, no. 1, p. 62, 2020.
- [7] S. Singh, I. H. Ra, W. Meng, M. Kaur, and G. H. Cho, "SH-BlockCC: a secure and efficient Internet of Things smart home architecture based on cloud computing and blockchain technology," *International Journal of Distributed Sensor Networks*, vol. 15, no. 4, Article ID 155014771984415, 2019.
- [8] D. Bogusevski, C. Muntean, and G. M. Muntean, "Teaching and learning physics using 3D virtual learning environment: a case study of combined virtual reality and virtual laboratory in secondary school," *Journal of Computers in Mathematics and Science Teaching*, vol. 39, no. 1, pp. 5–18, 2020.
- [9] H. Zhao, Q. H. Zhao, and B. Ślusarczyk, "Sustainability and digitalization of corporate management based on augmented/virtual reality tools usage: China and other world IT companies' experience," *Sustainability*, vol. 11, no. 17, p. 4717, 2019.
- [10] B. Wu, X. Yu, and X. Gu, "Effectiveness of immersive virtual reality using head-mounted displays on learning performance: a meta-analysis," *British Journal of Educational Technology*, vol. 51, no. 6, pp. 1991–2005, 2020.
- [11] M. H. E. M. Browning, F. Saeidi-Rizi, O. McAnirlin, H. Yoon, and Y. Pei, "The role of methodological choices in the effects of experimental exposure to simulated natural landscapes on human health and cognitive performance: a systematic review," *Environment and Behavior*, vol. 53, no. 7, pp. 687–731, 2021.
- [12] T. D. Glover, S. Munro, I. Men, W. Loates, and I. Altman, "Skateboarding, gentle activism, and the animation of public space: CITE—a celebration of skateboard arts and culture at the Bentway," *Leisure Studies*, vol. 40, no. 1, pp. 42–56, 2021.
- [13] Y. P. Ma, "Extending 3D-GIS district models and BIM-based building models into computer gaming environment for better workflow of cultural heritage conservation," *Applied Sciences*, vol. 11, no. 5, p. 2101, 2021.
- [14] M. Matthys, L. De Cock, J. Vermaut, N. Van de Weghe, and P. De Maeyer, "An "animated spatial time machine" in co-creation: reconstructing history using gamification integrated into 3D city modelling, 4D web and transmedia storytelling," *ISPRS International Journal of Geo-Information*, vol. 10, no. 7, p. 460, 2021.
- [15] E. D. Aydın and T. Tong, "Enhancing architectural representations in 3D virtual reality: building denotative and connotative meanings," *Megaron*, vol. 14, no. 2, p. 185, 2019.
- [16] B. H. Kann, D. F. Hicks, S. Payabvash et al., "Multi-institutional validation of deep learning for pretreatment identification of extranodal extension in head and neck squamous cell carcinoma," *Journal of Clinical Oncology*, vol. 38, no. 12, pp. 1304–1311, 2020.
- [17] J. C. Rayan, N. Reddy, J. H. Kan, W. Zhang, and A. Annapragada, "Binomial classification of pediatric elbow fractures using a deep learning multiview approach emulating radiologist decision making," *Radiology: Artificial Intelligence*, vol. 1, no. 1, article e180015, 2019.
- [18] S. Guo, Y. Dai, S. Guo, X. Qiu, and F. Qi, "Blockchain meets edge computing: Stackelberg game and double auction based task offloading for mobile blockchain," *IEEE Transactions on Vehicular Technology*, vol. 69, no. 5, pp. 5549–5561, 2020.
- [19] L. Cross, J. Cockburn, Y. Yue, and J. P. O'Doherty, "Using deep reinforcement learning to reveal how the brain encodes abstract state-space representations in high-dimensional environments," *Neuron*, vol. 109, no. 4, pp. 724–738.e7, 2021.
- [20] H. Liu and Y. Zhang, "Deep learning based crack damage detection technique for thin plate structures using guided lamb wave signals," *Smart Materials and Structures*, vol. 29, no. 1, article 015032, 2020.
- [21] Y. C. Huang, S. J. Backman, K. F. Backman, F. A. McGuire, and D. W. Moore, "An investigation of motivation and experience in virtual learning environments: a self-determination theory," *Education and Information Technologies*, vol. 24, no. 1, pp. 591–611, 2019.
- [22] N. Ahmadpour, M. Keep, A. Janssen, A. S. Rouf, and M. Marthick, "Design strategies for virtual reality interventions for managing pain and anxiety in children and adolescents: scoping review," *JMIR Serious Games*, vol. 8, no. 1, article e14565, 2020.
- [23] J. Song, Q. Li, H. Wang, and L. Sun, "Under the concealing surface: detecting and understanding live webcams in the wild," *Proceedings of the ACM on Measurement and Analysis of Computing Systems*, vol. 4, no. 1, pp. 1–25, 2020.
- [24] K. A. Hasenstab, N. Yuan, T. Retson et al., "Automated CT staging of chronic obstructive pulmonary disease severity for predicting disease progression and mortality with a deep learning convolutional neural network," *Radiology: Cardiothoracic Imaging*, vol. 3, no. 2, article e200477, 2021.
- [25] J. Li, B. Mei, H. Liu et al., "In situ X-ray absorption near-edge structure calculation and machine learning analysis of the structural evolution in lithium-ion battery cathode materials," *The Journal of Physical Chemistry C*, vol. 125, no. 34, pp. 18979–18987, 2021.
- [26] A. Carver, A. Lorenzon, J. Veitch, A. Macleod, and T. Sugiyama, "Is greenery associated with mental health among residents of aged care facilities? A systematic search and narrative review," *Aging & Mental Health*, vol. 24, no. 1, pp. 1–7, 2020.
- [27] B. Surya, D. N. A. Ahmad, H. H. Sakti, and H. Sahban, "Land use change, spatial interaction, and sustainable development in the metropolitan urban areas, South Sulawesi Province, Indonesia," *Land*, vol. 9, no. 3, p. 95, 2020.

Research Article

The Influence of Robot-Assisted Industry Using Deep Learning on the Economic Growth Rate of Manufacturing Industry in the Era of Artificial Intelligence

Ziyu Xu 

Business School, Nanfang College Guangzhou, Guangzhou 510970, China

Correspondence should be addressed to Ziyu Xu; xuzy@nfu.edu.cn

Received 26 March 2022; Revised 17 May 2022; Accepted 30 May 2022; Published 25 June 2022

Academic Editor: Mu-Yen Chen

Copyright © 2022 Ziyu Xu. This is an open access article distributed under the Creative Commons Attribution License, which permits unrestricted use, distribution, and reproduction in any medium, provided the original work is properly cited.

The arrival of the era of artificial intelligence (AI) impacts a country's economic growth. This work was aimed at helping a country achieve high-quality economic growth through AI. First, the penetration effect, boundary extension effect, knowledge creation effect, and self-deepening effect of AI in the process of penetration into the economy and society are analyzed. Then, the labor factors, capital factors, and production technology factors affecting economic growth are discussed. Furthermore, three channels through which AI affects economic growth are proposed: the labor channel, capital channel, and productivity channel. Finally, relevant verifications are carried out. The verification results demonstrate that AI will promote an increase in economic growth rate in the long run but have a specific inhibitory effect in a short time. According to the research results, sound policy suggestions are put forward for the positive impact of AI technology on economic growth, the negative effect on labor employment and income distribution, capital accumulation and capital structure, and the effect on production efficiency. This work has certain reference significance for the research on the economic growth rate of the national manufacturing industry in the era of AI.

1. Introduction

Since the 21st century, artificial intelligence (AI) technology has made breakthrough progress worldwide with the rapid progress of the Internet and information technology. It has accelerated penetration and integration into economic society and promotes human culture to quickly enter the intelligence era. AI is the most significant innovation in a new generation of technology. AI products are extensively used in all fields of production and life of human society, including intelligent robots, smart homes, AI doctors, unmanned factories, and autonomous vehicles. They have a profound impact on the economic community and have gradually become the focus of major countries [1]. Based on this, governments worldwide have launched a new round of competition around AI. The United States, Japan, Germany, France, and other countries have successively promulgated a series of policies and measures to support the development

of the AI industry to seize the dominant position in international competition in the new period [2].

At present, countries have taken measures to seize the development opportunities of AI to accelerate the penetration of AI into the economy and society. In this context, it is essential to systematically analyze the impact channels of AI on economic growth and explore the potential problems and risks of AI in the process of infiltrating into the economy and society. These measurements are of great significance for effectively preventing and responding to the potential dangers of AI and seizing the development opportunities of AI. Acemoglu and Restrepo argue that AI affects the wages of low-skilled workers, causing their wages to stagnate [3]. Polusmakova and Glushchenko believe that although AI can bring sustained returns to capital, it does not have the potential to enable long-term economic growth because income is the only source of investment, and the automation brought about by AI inhibits income [4]. Yee

and You found that AI can significantly improve productivity; however, the economic growth rate has slowed down significantly. The authors explain it with four possible explanations: estimation error, measurement error, reallocation, and execution lag [5]. Scholars usually consider the substitution effect of AI on labor, the complementary effect, and the productivity effect of creating new tasks when studying the impact of AI on the economy. Nevertheless, they generally only introduce a single effect into the constructed model for analysis and demonstration and cannot fully reflect the impact mechanism of AI on the economy. Therefore, this work introduces multiple effects into the model for research to help countries achieve high-quality economic growth driven by innovation.

The impact of the robot-assisted industry based on deep learning on economic growth is studied here to help the countries achieve high-quality economic development. Firstly, this work analyzes the four primary effects of AI in infiltrating into the economy and society and explores three factors affecting economic growth. Then, an analysis framework of the impact of AI on economic growth is proposed, which is composed of labor channels, capital channels, and productivity channels. Then, the influence of AI on economic development through three media is examined. The test results indicate that AI has a tremendous impact on economic growth. Finally, policy recommendations are put forward for the effects. This work has particular reference significance for the research on the effects of the robot-assisted industry on the manufacturing economy in the context of AI.

2. Impact of AI on the Economic Growth Rate of the Manufacturing Industry

2.1. Economic Effects of AI. As the most representative technological innovation in the new round of technological progress, AI has a wide range of penetration, almost into all industries and links of economic society. Moreover, with the continuous expansion of AI applications, the emergence of new industries, departments, and occupations has accelerated the adjustment and upgrading of the industry [6]. In addition, AI can realize self-learning and self-renewal and upgrading through machine learning and DL to realize the self-deepening of capital and trigger all-around changes from natural science to social science. AI has four economic effects: penetration effect, boundary extension, knowledge creation, and self-deepening effect [7].

Penetration effect refers to the potential of innovative technology to integrate and penetrate all sectors of economic society and all links of production and life and to change the economic operation mode. As a new universal purpose technology, AI technology can directly affect the production activities of human society, presenting strong permeability. Unlike traditional technological innovation, AI penetration shows the characteristics of intelligence and can penetrate almost all industries and links of economic society. Firstly, AI is broadly used in the industrial sector, which directly affects the production and management of the industrial sector. Secondly, AI has the characteristics of intelligence, accel-

erating its penetration and integration with the service industry. Finally, unlike modern technological innovation, AI also directly affects the agricultural sector [8]. Figure 1 displays the penetration scope of AI technology in the economic society.

According to the China Robot Industry Alliance statistics, the application scope of domestic industrial robots in 2017 had affected 37 big industrial categories and 102 middle industrial categories of the national economy, covering three major industries, and the scope of influence was still expanding. AI and machine learning have penetrated into almost any field. The intelligent penetration process of AI is reflected in the substitution of AI capital for traditional capital and the direct substitution of AI capital for labor factors [9].

Boundary extension refers to the potential of expanding the boundaries of social work tasks and improving the work tasks through some innovative technologies and economic and social integration. It is another primary effect of universal purpose technology. In terms of the whole economic and social scope, the continuous penetration and integration of AI into the economic society will continue to give birth to new products, technologies, business forms, and industries. In addition, some traditional backward industries will be eliminated from the market to realize the transformation and upgrading of traditional industries. For the enterprises or industry, AI can expand into new businesses, new markets, and new products and eliminate obsolete products and traditional production jobs. In general, the boundary extension effect of AI is as follows: (1) AI dramatically extends and supplements human physical and mental strength, expanding the range of tasks that humans can complete and the upper limit of work tasks; (2) AI gradually eliminates the old low-end production tasks for old products; (3) AI raises the lower limit of work tasks, adjusting and improving the production tasks of the entire society or industry [10, 11].

AI is a representative of creative technology in the novel era. Its knowledge creation effect is far greater than traditional technological innovation, opening a new stage of knowledge production from natural science to social science. First, it promotes progress in natural science and improves the research efficiency of natural science such as physics and medicine. AI has innovated the method of natural science knowledge production and created a substantial driving force for the development of natural science. Moreover, while expanding the research content of social sciences, it has changed the traditional knowledge production methods, means, and tools of social sciences, providing a massive impetus for the development of social sciences [12, 13].

In recent years, significant breakthroughs have been made in the new generation of information technologies, such as mobile Internet and cloud computing. This progress guarantees the computing power of machine learning and deep learning. The rapid development of big data has offered massive learning data for machine learning and deep learning. Consequently, machine learning has made significant progress, breaks through the dependence of AI on human programmers to a certain extent, and realizes self-learning

Artificial intelligence type	Artificial neural networks	Expert system	Robot
Agriculture	Classification and evaluation of agricultural product characteristics; Agricultural forecasting and modeling analysis.	Crop pest management, animal and plant nutrition management, farm management, greenhouse environmental monitoring.	Agricultural farming, sowing, irrigation, and harvesting tasks.
Industry	Product manufacturing, mining detection, signal analysis, etc.	Scientific production in manufacturing; Intelligent management.	Intelligent production is accelerating the transformation and upgrading of traditional manufacturing industries.
Service industry	Face recognition, disease analysis and identification in the medical industry, monitoring of crowding in subway stations, weather forecast, and risk assessment and profit forecast analysis in the financial industry	Auxiliary medical diagnosis, education, science, military, etc.	Sweeping robot, learning robot, escort robot, etc.

FIGURE 1: Penetration scope of AI technology in economic society.

and self-renewal. Then, the self-deepening effect of AI gradually plays a role. The self-deepening effect is mainly manifested in two aspects. First, through machine learning and deep learning, various computer technologies have achieved breakthroughs as “learning results,” giving AI more functions and expanding the range of tasks that AI products can accomplish, such as intelligent machines, algorithms, or software. Second, the intelligent, robotized efficiency of work tasks is improved through self-learning [14].

2.2. Factors Affecting Economic Growth. The analysis of economic growth theory suggests that both the classical Cobb-Douglas (C-D) and various economic growth models regard labor, capital investment, and production technology level as important variables affecting economic growth. Therefore, discussing a country’s economic growth is inseparable from analyzing production factors, let alone the technical analysis [15]. Equation (1) indicates the economic output described in the model studied by predecessors.

$$Y_{it} = A_{it}F(L_{it}, K_{it}). \quad (1)$$

In Equation (1), i denotes the industry; t stands for the year; Y represents the output level; A refers to the production technology level; L signifies the labor factor input; K represents the capital factor input. The production function of C-D can be written as

$$Y_{it} = A_{it}L_{it}^{\alpha}K_{it}^{\beta}. \quad (2)$$

Equation (3) can be obtained by sorting out Equation (2).

$$g_Y = \alpha g_L + \beta g_K + g_A. \quad (3)$$

In Equation (3), g_Y , g_L , g_K , and g_A are the growth rate of output, labor, capital input, and production technology, respectively. α and β represent the share of labor and capital factors, respectively. Equation (3) shows that economic growth results from the comprehensive action of various factors, such as labor factors, capital factors, and production technology levels.

2.3. Channels of AI Affecting the Economy. The theories related to AI and economic growth suggest that the intelligent penetration effect of AI is the substitution of intelligent machines for labor and the substitution of traditional capital. Therefore, the intelligent penetration effect will directly affect labor and capital [16]. The boundary extension effect manifests in the continuous birth of new production tasks in society or industry and the gradual demise of low-end, backward production. These changes will affect labor employment and capital investment. Knowledge creation and self-deepening effects affect production efficiency by affecting the level of production technology but do not immediately affect labor employment and capital investment. Hence, this work does not consider the impact of knowledge creation and self-deepening on labor and capital. Figure 2 shows the overall framework of AI and economic growth:

Among the four basic effects of AI, intelligent penetration and boundary extension can affect the labor factors in the production process, which are indispensable for economic growth. AI affects labor employment and labor income by exerting the effect of intelligent penetration. On the one hand, AI penetrates and integrates into the economy and society. On the other hand, AI affects the quantity and structure of labor employment by increasing intelligent

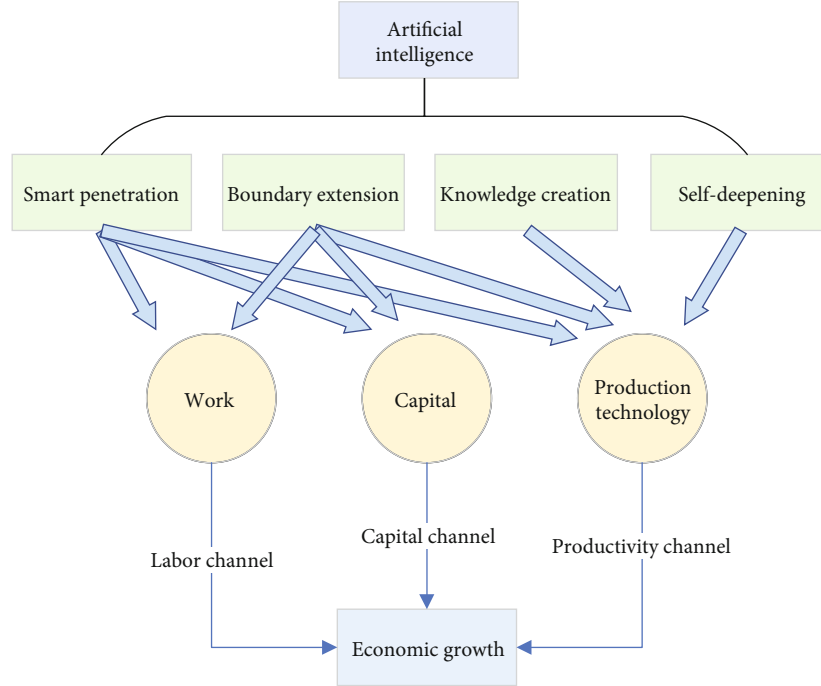


FIGURE 2: Overall framework of AI affecting economic growth.

automation and the income effect of intelligent penetration. In addition, AI affects labor employment by creating new industries, products, and tasks, called the boundary extension employment effect. The effect of boundary extension on labor income level is called the income effect of boundary extension [17, 18]. Figure 3 illustrates the influence on economic growth due to AI's intelligent penetration effect and boundary extension effect on labor employment and income.

Capital is the key factor to achieving economic growth. AI usually affects economic growth through intelligent penetration and boundary extension effects acting on capital accumulation and capital structure [19, 20]. Figure 4 is a visual display.

Increased productivity can generate additional resources. Production efficiency contains two parts: technological progress and technological efficiency. Based on this, the productivity channels of AI affecting economic growth can be divided into two impact paths: affecting technological progress and affecting technological efficiency. First, under the influence of the intelligent penetration effect, AI may affect production efficiency by replacing the labor force and traditional capital or by affecting the fit of connection and cooperation, among other factors. Second, the boundary extension effect creates new jobs for the economy and society, along with the disappearance of traditional backward production capacity and the escalation of social tasks, affecting production efficiency. The role of knowledge creation refers to the influence of intelligent machines on scientific knowledge. The intelligent automation of production has been realized with the progress of scientific knowledge. Knowledge production efficiency will increase exponentially and create a large amount of scientific knowledge for society. Scientific knowledge may affect production efficiency

through guiding research and development practice or knowledge transformation and application. Finally, the self-deepening effect is manifested in the continuous self-renewal and upgrading of intelligent machines through machine learning, especially DL. It can further improve the production efficiency of intelligent machines and promote the continuous reform of the management mode of micro subjects, society, and economic and social organizations [21, 22]. Figure 5 presents the four economic effects of AI on economic growth by affecting technological progress and efficiency.

3. Research Methodology and Framework

Figure 6 displays the main framework of this research.

This work investigated labor force education in various industries in recent years. Table 1 shows the industry and corresponding serial numbers.

Figure 7 shows the education situation of workers in various industries.

The following primary hypotheses are made based on the survey data:

Hypothesis 1. In a closed economy, there are two sectors: manufacturers and households. The production department is in a completely competitive market, and only one manufacturer is producing the final product in the whole society. The elasticity of substitution of factor is $\sigma \in (1, \infty)$. Equation (4) indicates the production function:

$$Y = A \left(\int_{N-1}^N y(x)^{\sigma-1/\sigma} dx \right)^{\sigma/\sigma-1}. \quad (4)$$

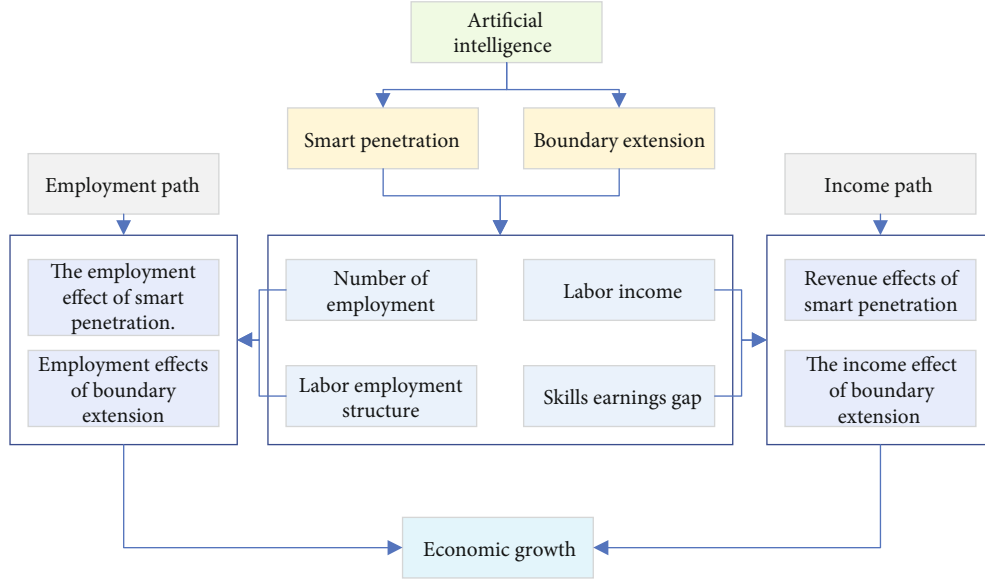


FIGURE 3: Labor channels of AI affecting economic growth.

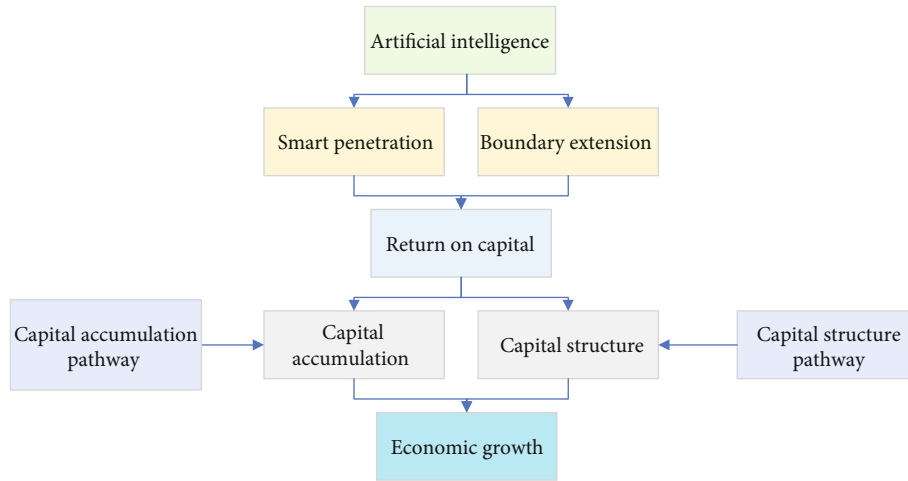


FIGURE 4: AI's capital channels affecting economic growth.

In Equation (4), x represents the work task, and $x \in [N - 1, N]$ represents the number of work tasks standardized to 1 in economic society. It is even more difficult to produce from production task $N - 1$ to N . $y(x)$ represents the output of task x . If the price of the final product is standardized as 1, Equation (5) describes the utility preference of the family under the static model.

$$u(t) = \frac{(Ce^{-v(L)})^{1-\theta} - 1}{1-\theta}. \quad (5)$$

In Equation (5), C represents consumption, and L indicates the labor supply of the household sector. The labor supply meets the conditions $v'(L) = W/C > 0$ and $v''(L) < 0$. The consumption level is $C = RK + WL$. K represents the capital provided by the household sector. If capital is

inelastic to changes in intelligent automation, the equilibrium labor supply satisfies

$$L = L^s \left(\frac{W}{RK} \right). \quad (6)$$

Suppose that $w = W/RK$, indicating the salary level after standardization.

Hypothesis 2. Based on the impact of AI on labor employment structure and referring to existing studies, labor heterogeneity is divided into the high-skilled labor force and low-skilled labor force. The high-skilled labor force is engaged in work tasks with low repeatability and relatively high creativity. The low-skilled labor force is

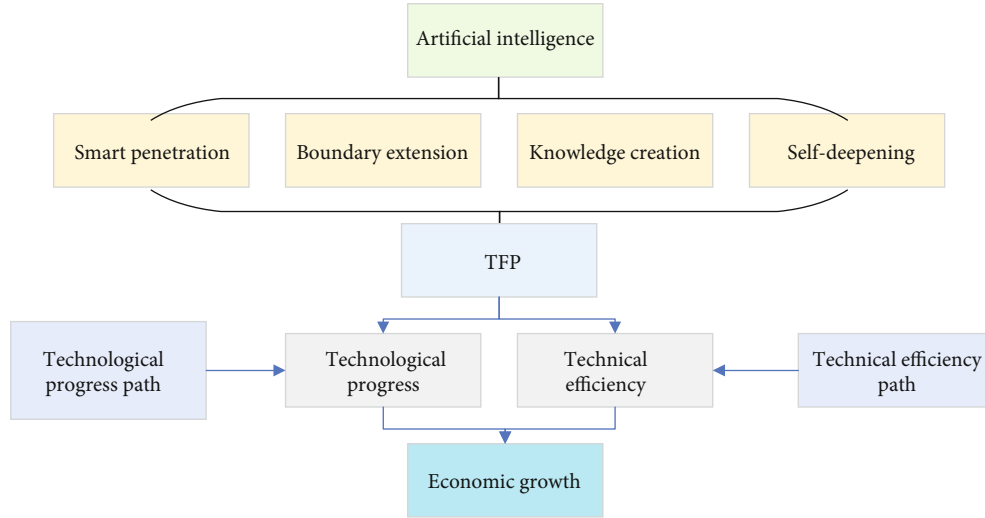


FIGURE 5: AI affecting economic growth through productivity channels.

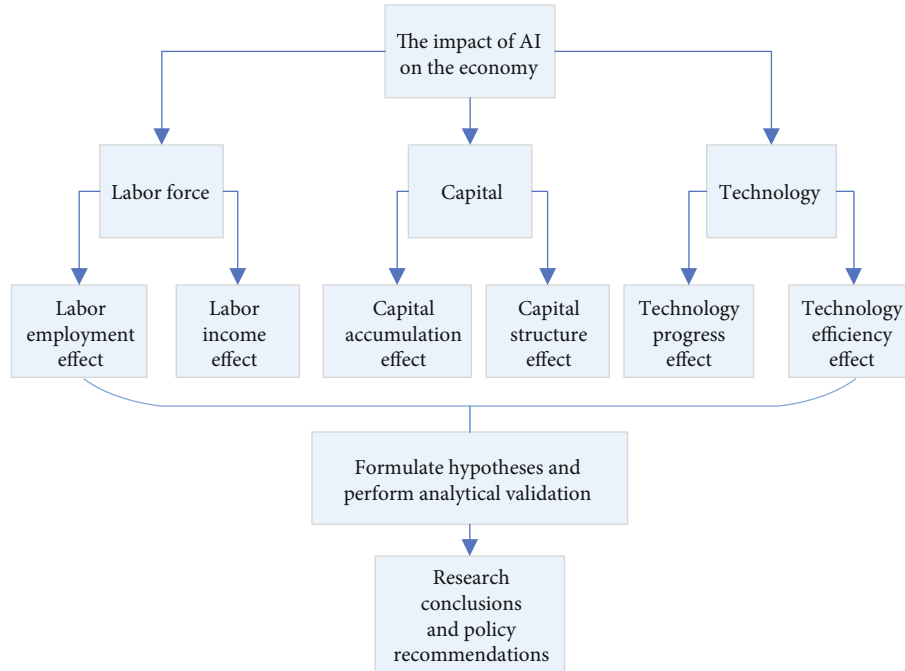


FIGURE 6: Research framework.

engaged in tasks with high repeatability and relatively low creativity [23].

Hypothesis 3. In terms of the intelligent penetration effect, AI involves both intelligent penetration I of low-end work tasks and intelligent penetration I' of high-end work tasks when integrating with the economic society. $I \in [N-1, N]$ is the upper bound of low-end task intelligent penetration. When $x \leq I$, the work task can be completed by an intelligent machine or labor force. $M \in [I, N]$ is set as the upper bound of low-skilled work tasks. When $I < x \leq M$, the work task can be completed by both low-skilled and high-skilled labor force. $I' \in [M, N]$ is set as the upper bound of intelligent pen-

etration of high-end tasks. When $M < x \leq I'$, the work task can be completed by both intelligent machines and highly skilled labor. When $I' < x \leq N$, work tasks can only be completed by highly skilled labor [24]. In terms of the boundary extension effect, the development of AI will give birth to new work tasks. The industry's work task boundary will be expanded, the upper bound N will be improved, and the industrial structure will be optimized and upgraded.

Hypothesis 4. The improvement difficulty of intelligent penetration I of low-end work tasks is greater than that of high-end work tasks I' due to the difficulty of work tasks. Hence, $\Delta I > \Delta I'$, and $N - I' > M - I$.

TABLE 1: Industry and the corresponding number.

Industry	Serial number
Agriculture, forestry, animal husbandry, and fishery	A
Mining industry	B
Manufacturing industry	C
Production and supply industry of electricity, heat, gas, and water	D
Construction industry	E
Wholesale and retail	F
Transportation, storage, and postal services	G
Accommodation and catering	H
Information transmission, software, and information technology services	I
Finance	J
Real estate	K
Leasing and business services	L
Scientific research and technology services	M
Water conservancy, environment, and public facilities management	N
Residential services, repair, and other services	O
Education	P
Health and social work	Q
Culture, sports, and entertainment	R
Public administration, social security, and social organizations	S

Hypothesis 5. Production efficiency $\gamma_L(x)$ of low-skilled labor on $(I, M]$ is equal to production efficiency $\gamma_H(x)$ of the highly skilled labor force on $(I', M]$, and the labor force has comparative advantages in complex production tasks. Then, production efficiency $\gamma_M(x)$ of intelligent machines is constant at 1.

Hypothesis 6. Since the penetration of AI in the economic society is still in its infancy, AI will improve labor productivity [25].

Based on the basic theoretical assumptions, a model is established for analysis to further explore the impact of AI on economic growth through the number of employed workforce and employment structure. Equation (7) is derived by sorting out and solving the objective function equation of the final output.

$$\begin{aligned}
Y = A & \left[(I - N + 1 + I' - M)^{1/\sigma} K^{(\sigma-1)/\sigma} \right. \\
& + \left(\int_I^M \gamma_L(x)^{\sigma-1} dx \right)^{1/\sigma} L_L^{(\sigma-1)/\sigma} \\
& \left. + \left(\int_{I'}^N \gamma_H(x)^{\sigma-1} dx \right)^{1/\sigma} L_H^{(\sigma-1)/\sigma} \right]^{\sigma/(\sigma-1)}. \quad (7)
\end{aligned}$$

In Equation (7), L_H and L_L are the numbers of high-skilled and low-skilled labor forces, respectively. Equation (8) can be obtained according to Equation (7).

$$\begin{aligned}
\frac{\partial Y}{\partial N} = \frac{1}{\sigma-1} \gamma_H(N)^{\sigma-1} & \left(\int_{I'}^N \gamma_H(x)^{\sigma-1} dx \right)^{(1/\sigma)-1} L_H^{(\sigma-1)/\sigma} Y^{1/\sigma} \\
& - \frac{1}{\sigma-1} (I - N + 1 + I' - M)^{(1/\sigma)-1} K^{(\sigma-1)/\sigma} Y^{1/\sigma}. \quad (8)
\end{aligned}$$

Capital income is used to standardize the wage income of two types of the labor force to analyze the impact of AI on labor income. Then, Equation (9) holds.

$$\frac{dlnw}{dI} = -\frac{1}{\sigma + \varepsilon} (I - N + 1 + I' - M)^{-1} - \frac{1}{\sigma + \varepsilon} \frac{\gamma(I)}{\int_I^N \gamma(x)^{\sigma-1} dx}. \quad (9)$$

Equation (9) shows that because $\sigma + \varepsilon_H > 0$ and $(I - N + 1 + I' - M) > 0$, $dlnw_H/dI = -(1/\sigma + \varepsilon_H)(I - N + 1 + I' - M)^{-1} < 0$. The intelligent penetration of AI in work tasks makes the standardized labor wage level show a downward trend. It is because intelligent penetration brings intelligent machines to replace skilled labor, the return on capital increases, and the relative income level of skilled labor shows a downward trend. The impact of intelligent penetration on the income gap between high- and low-skilled labor is explored and analyzed. Equation (10) describes the labor skill premium.

$$\ln \left(\frac{W_H}{W_L} \right) = \ln \left(\frac{W_H}{RK} \right) - \ln \left(\frac{W_L}{RK} \right). \quad (10)$$

The labor force with high education level has higher working time elasticity and labor participation elasticity, that is, $\varepsilon_H > \varepsilon_L$. Therefore, Equation (11) can be obtained by sorting Equation (10).

$$\begin{aligned}
d \ln \left(\frac{w_H}{w_L} \right) = & \left(\frac{1}{\sigma + \varepsilon_L} - \frac{1}{\sigma + \varepsilon_H} \right) (I - N + 1 + I' - M)^{-1} \\
& \cdot (dI + dI') + \frac{1}{\sigma + \varepsilon_L} \frac{\gamma_L(I)^{\sigma-1}}{\int_I^M \gamma_L(x)^{\sigma-1} dx} dI \\
& - \frac{1}{\sigma + \varepsilon_H} \frac{\gamma_H(I')}{\int_{I'}^N \gamma_H(x)^{\sigma-1} dx} dI'. \quad (11)
\end{aligned}$$

Equation (11) indicates the impact of intelligent penetration on the income gap between high- and low-skilled labor forces. w_L and w_H represent the wage level of low-skilled and high-skilled labor force, respectively. The equation shows that intelligent penetration will expand the income gap between high- and low-skilled labor forces. On the impact of the level of intelligent penetration on the return of capital relative factors, after the objective function equation is

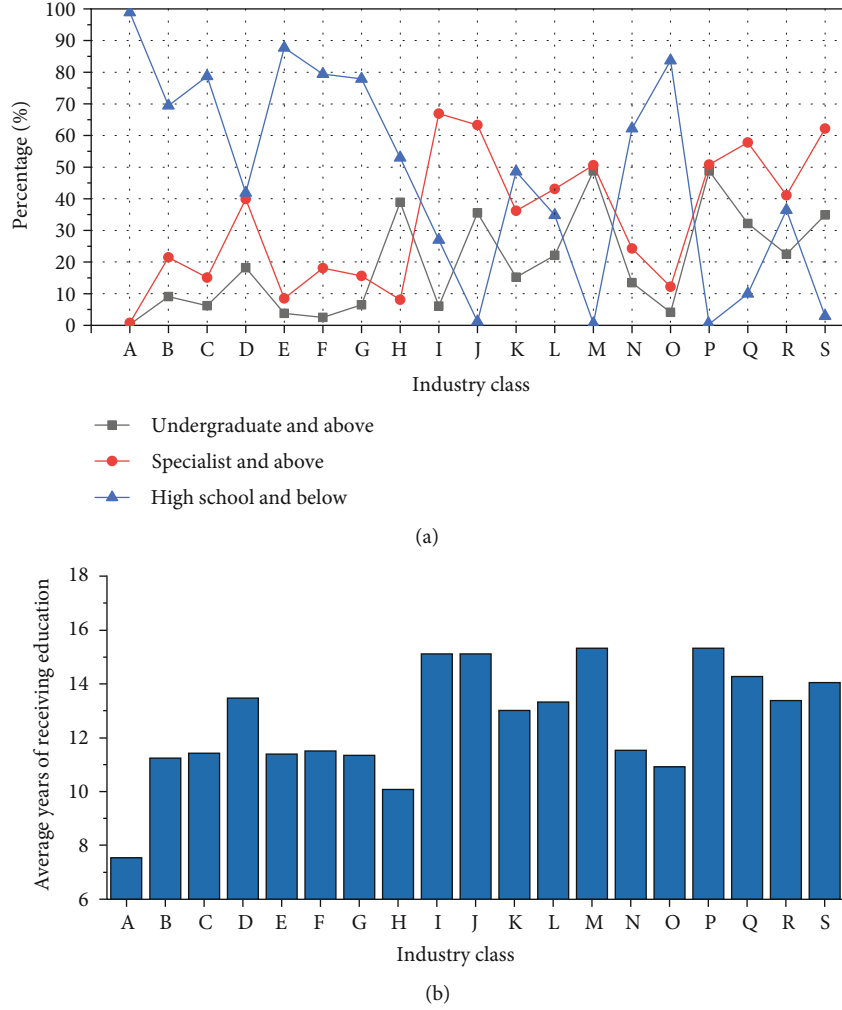


FIGURE 7: Education level of workers in various industries ((a) the proportion of different academic qualifications in each industry and (b) the average years of receiving education in each industry).

sorted and solved, Equation (12) can be obtained:

$$\frac{d \ln w}{dI} = -\frac{\varphi(\varepsilon - \sigma)}{1 - \sigma} \cdot \frac{\gamma(I)^{\sigma-1}}{\int_I^N \gamma(x)^{\sigma-1} dx} - \frac{\varphi(\varepsilon - \sigma)}{1 - \sigma} \cdot \frac{\gamma_M(I)^{\sigma-1}}{\int_{N-1}^I \gamma_M(x)^{\sigma-1} dx} \quad (12)$$

Equation (12) suggests that as intelligent penetration deepens, the relative return of capital increases. While attracting AI capital investment, it will crowd out traditional capital investment. AI capital has cost advantages over labor and traditional capital, resulting in a decline in the growth rate of relative return of capital. When the increased AI capital is difficult to make up for the squeezed out traditional capital, the capital accumulation shows a downward trend. Equation (13) indicates the effect of the extension effect on capital accumulation by affecting the relative factor price.

$$\frac{d \ln K}{dN} = \frac{d \ln K}{d \ln w} * \frac{d \ln w}{dN} = \frac{\varphi(\varepsilon - \sigma)^2}{(1 - \sigma)^2} \cdot \left[\frac{\gamma(N)^{\sigma-1}}{\int_I^N \gamma(x)^{\sigma-1} dx} + \frac{\gamma_M(N-1)^{\sigma-1}}{\int_{N-1}^I \gamma_M(x)^{\sigma-1} dx} \right] \quad (13)$$

Equation (13) shows the rise in the relative return of capital and the capital accumulation under the boundary extension effect of AI. Equations (12) and (13) illustrate that the impact of AI on capital accumulation is lagging, which makes capital accumulation decline first and then rise.

4. Research Results and Policy Recommendations

4.1. *Research Results.* It comes to the following conclusions through the basic assumptions based on survey data and analysis, as well as the support of theory and equations.

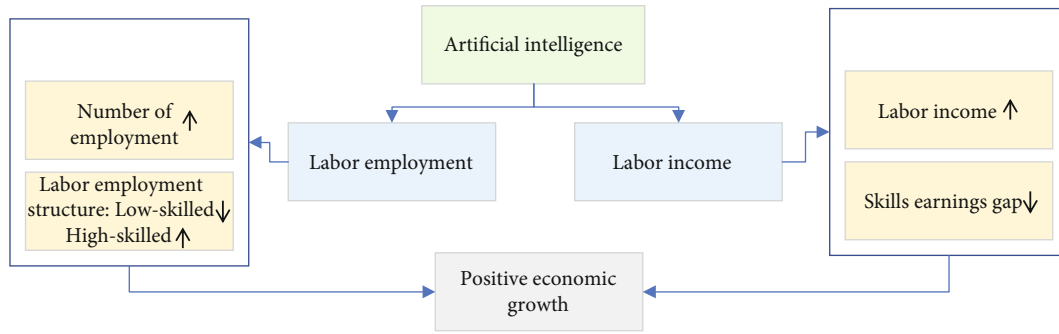


FIGURE 8: Schematic diagram of action direction of labor channel.

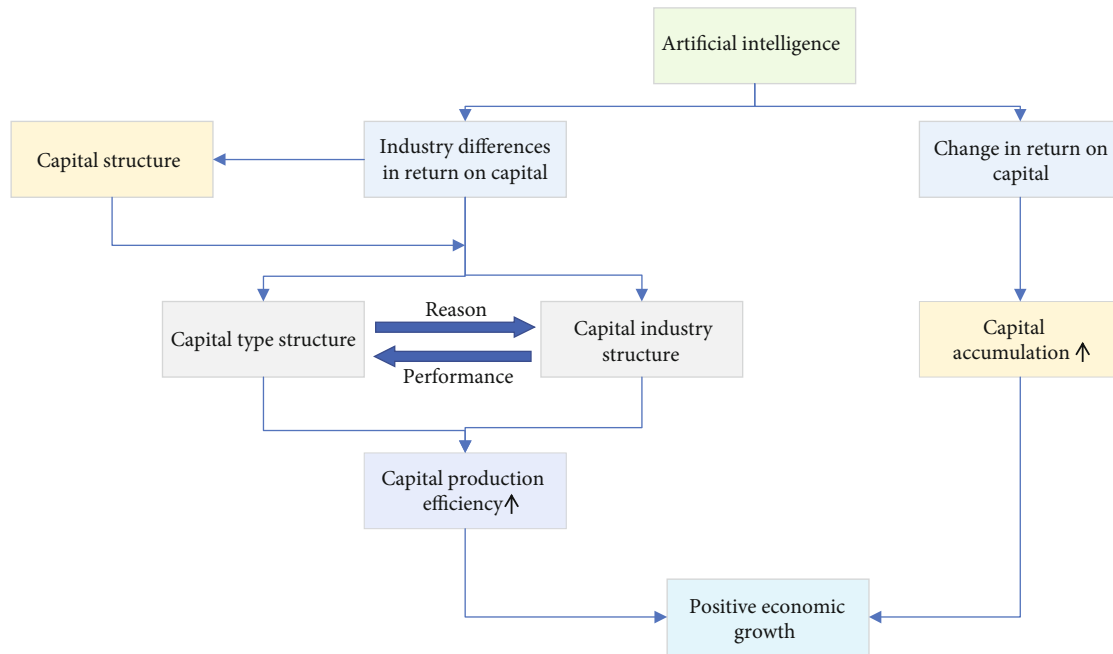


FIGURE 9: Schematic diagram of the action direction of capital effect.

Conclusion 1. AI affects economic growth through labor employment and labor income. (1) The impact of AI on labor employment has a lag, making the labor employment level first fall and then rise. It is primarily manifested in the decline of the employment level of the low-skilled labor force and the rise of the employment level of the high-skilled labor force, driving the economy to decline first and then rise. (2) The impact of AI on the level of labor income lags. The level of labor income decreases first and then rises, promoting the economy to decline first and then rise. (3) The impact of AI on the skill income gap also lags. The skill income gap first expands and then narrows in time, making the economic growth decline first and then rise by acting on the labor income gap. Figure 8 shows the details.

Conclusion 2. AI affects economic growth through capital accumulation and capital structure. (1) AI has a lagging impact on capital accumulation, making capital accumulation decline first and then rise; consequently, economic growth declines first and then rises. (2) AI promotes eco-

nomical growth by acting on capital structure. Figure 9 presents the details.

Conclusion 3. AI affects economic growth through technological progress and technological efficiency. (1) AI can boost economic growth by promoting the progress of cutting-edge technology. (2) AI can stimulate economic growth by improving technical efficiency. Figure 10 shows the specific contents.

4.2. Policy Proposals. Based on the above conclusions, the specific policy recommendations are as follows.

Recommendation 1. It is necessary to increase support for basic research on AI-related technologies to give full play to its positive role in economic; it is essential to adhere to the AI technology innovation as the breakthrough of economic growth, accelerate the improvement of the top-level design and industry norms for the development of AI industry, and expand the scale of AI industry and AI industry chain. In addition, AI, employment, and income distribution need to be incorporated into the statistical monitoring system to

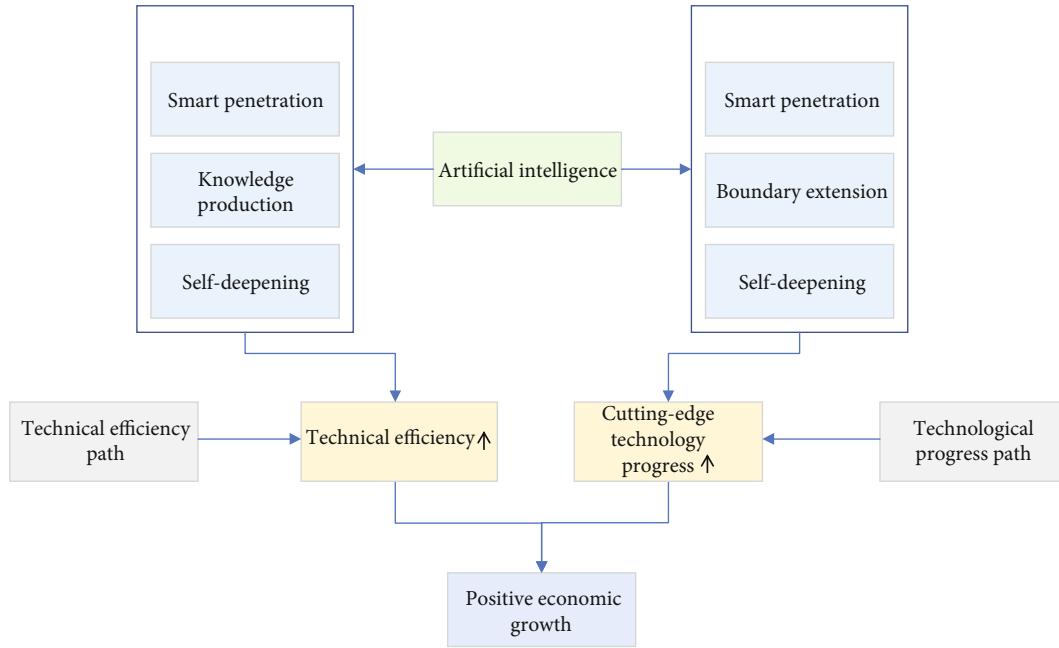


FIGURE 10: Effect orientation of AI.

promote the deep integration of AI and industry in stages and with emphasis.

Recommendation 2. Given the negative effect of AI technology on labor employment and income distribution, it is necessary to expand the coverage of social security policies, sincerely implement the unemployment insurance and assistance policies, and reduce the unstable factors caused by unemployment and wage decline. In addition, it is essential to deepen the reform of AI-oriented curriculum and skills in higher education and accelerate the improvement of labor market-oriented education. The scale of automation in low-skilled sectors needs to be appropriately controlled to prevent large-scale unemployment in low-skilled sectors due to AI penetration.

Recommendation 3. The supply-side structural reform shall advance for the effect of AI technology on capital accumulation and capital structure; it is also necessary to accelerate the improvement of the market exit mechanism to remove inefficient and backward production capacity from the market as soon as possible. According to the characteristics of different industries, the penetration and integration of AI into industries should be promoted in a focused and targeted manner. Besides, capital allocation and production efficiency in the industry need to be improved. It is essential to improve the construction of high-skilled talents, such as optimizing the talent training mechanism based on key colleges, strengthening the construction of innovative talent teams, and introducing more high-level overseas talents.

Recommendation 4. Regarding the effect of AI technology on production efficiency, it is essential to promote the continuous development of strategic emerging industries such as new materials and new energy. Besides, active exploration is required for the possible penetration fields of AI and promotes the deep integration of AI with industries such as new materials and new energy. The production

and research and development process of enterprises related to new materials and new energy can be used as a testing ground for AI to promote the continuous upgrading of AI and give full play to its efficiency. Attention should be paid to the application of AI technology such as machine learning in scientific research. Besides, enterprises and scientific research institutions in the field of AI should be encouraged to strengthen exchanges and cooperation with overseas advanced technical teams to realize the deep application of AI technology in the research process of various fields.

5. Conclusion

This work studies the impact of the DL-based robot-assisted industry on the economic growth rate. First, an analysis is conducted on the intelligent penetration effect, boundary extension effect, knowledge creation effect, and self-deepening effect of AI in economic and social penetration. Besides, the labor factors, capital factors, and production technology factors affecting economic growth are discussed. Then, the analysis framework of AI's impact on economic growth is proposed, consisting of the labor channel, capital channel, and productivity channel. Finally, AI's impact on economic growth through three channels is tested. The test results show that AI technology can promote long-term economic growth and even exponential growth. Meanwhile, the labor force was liberated from mechanized, low-knowledge, and creative work and turned into programmed, open-ended mental work. New jobs have continuously increased the demand for high-skilled labor, raised real wages, and promoted high-quality economic growth. Moreover, the rapid penetration of AI in the economic society will attract more capital accumulation, increase capital investment, improve capital production efficiency, and support macro-economic growth. In addition, it can significantly improve

technical efficiency, reflected in the growth of total factor productivity, and provide more power for economic growth. Finally, the research conclusions are summarized, and corresponding policy recommendations are put forward.

Compared with previous studies, this work more comprehensively demonstrates the influence mechanism of AI on the economy by introducing four effects into the model for analysis. Due to limited capacity, this work does not consider the impact of AI on economic growth under the background of the declining supply of the right-age labor force and the aging population simultaneously. The follow-up research will be optimized from this aspect. This work has particular reference significance for the research on the impact of the robot-assisted industry on the manufacturing economy in the AI era.

Data Availability

The raw data supporting the conclusions of this article will be made available by the authors, without undue reservation.

Ethical Approval

This article does not contain any studies with human participants or animals performed by any of the authors.

Consent

Informed consent was obtained from all individual participants included in the study.

Conflicts of Interest

The author declares no conflict of interest.

Acknowledgments

This work is supported by the fund of Department of Education of Guangdong Province in China (ID: 2019WQNCX156).

References

- [1] R. Abdulov, "Artificial intelligence as an important factor of sustainable and crisis-free economic growth," *Procedia Computer Science*, vol. 169, pp. 468–472, 2020.
- [2] A. Micu, A. E. Micu, M. Geru, A. Căpățină, and M. C. Muntean, "The impact of artificial intelligence use on the E-commerce in Romania," *Amfiteatru Economic*, vol. 23, no. 56, pp. 137–154, 2021.
- [3] D. Acemoglu and P. Restrepo, "The race between man and machine: implications of technology for growth, factor shares, and employment," *American Economic Review*, vol. 108, no. 6, pp. 1488–1542, 2018.
- [4] N. Polusmakova and M. Glushchenko, "Impact of artificial intelligence and industrial automation on territorial development: strategic guidelines," *IOP Conference Series: Materials Science and Engineering*, vol. 828, no. 1, p. 7, 2020.
- [5] D. H. Yee and Y. Y. You, "The impact of awareness of new artificial intelligence technologies on policy governance on risk," *Research in World Economy*, vol. 11, no. 2, p. 152, 2020.
- [6] C. Ye, Z. Zhao, and J. Cai, "The impact of smart city construction on the quality of foreign direct investment in China," *Complexity*, vol. 2021, Article ID 5619950, 9 pages, 2021.
- [7] A. A. Dashkov and Y. O. Nesterova, "Research on the impact of artificial intelligence on the business model of an organization," *E-Management*, vol. 3, no. 4, pp. 26–36, 2021.
- [8] L. Cavaliere, R. Rajan, and R. Setiawan, "The impact of E-recruitment and artificial intelligence (AI) tools on HR effectiveness: the case of high schools," *Product Management*, vol. 26, no. 1, pp. 322–343, 2021.
- [9] Q. Zhang, "A literature review of foreign studies on the impact of CALL on second language acquisition from 2015," *English Language Teaching*, vol. 14, no. 6, p. 76, 2021.
- [10] R. Solaimani, F. Rashed, S. Mohammed, and W. W. ElKelish, "The impact of artificial intelligence on corporate control," *Corporate Ownership and Control*, vol. 17, no. 3, pp. 171–178, 2020.
- [11] H. Jiang, "Impact of heterogeneous FTA on service trade in the context of smart economy," *Journal of Physics: Conference Series*, vol. 1533, no. 4, p. 042063, 2020.
- [12] K. Joamets and A. Chochia, "Artificial intelligence and its impact on labour relations in Estonia," *Slovak Journal of Political Sciences*, vol. 20, no. 1, pp. 255–277, 2020.
- [13] M. A. Hannan, A. Q. Al-Shetwi, P. J. Ker et al., "Impact of renewable energy utilization and artificial intelligence in achieving sustainable development goals," *Energy Reports*, vol. 7, no. 2020, pp. 5359–5373, 2021.
- [14] N. M. Tri and D. T. Nhe, "Impact of Industrial Revolution 4.0 on the labor market in Vietnam," *Research in World Economy*, vol. 12, no. 1, p. 94, 2021.
- [15] H. Feng, "The impact of artificial intelligence on vocational education and countermeasures," *Journal of Physics Conference Series*, vol. 1693, no. 1, article 012124, 2020.
- [16] C. Li, H. Song, and M. Fu, "Research on the impact of artificial intelligence technology on accounting," *Journal of Physics: Conference Series*, vol. 1486, no. 3, p. 032042, 2020.
- [17] H. Androschuk, "Artificial intelligence: economy, intellectual property, threats," *Theory and Practice of Intellectual Property*, vol. 2, no. 2, pp. 56–74, 2021.
- [18] N. N. Arief and A. Gustomo, "Analyzing the impact of big data and artificial intelligence on the communications profession: a case study on public relations (PR) practitioners in Indonesia," *International Journal on Advanced Science Engineering and Information Technology*, vol. 10, no. 3, p. 1066, 2020.
- [19] J. Mookerjee and O. Rao, "A review of the impact of disruptive innovations on markets and business performance of players," *International Journal of Grid and Distributed Computing*, vol. 14, no. 1, pp. 605–630, 2021.
- [20] C. Chen, Y. Hu, M. Karupiah, and P. M. Kumar, "Artificial intelligence on economic evaluation of energy efficiency and renewable energy technologies," *Sustainable Energy Technologies and Assessments*, vol. 47, no. 3, article 101358, 2021.
- [21] J. Yue, "Research on the reform of accounting teaching mode under the impact of artificial intelligence," *Journal of Physics Conference Series*, vol. 1651, no. 1, article 012003, 2020.
- [22] X. Zhou, "The usage of artificial intelligence in the commodity house price evaluation model," *Journal of Ambient Intelligence and Humanized Computing*, vol. 5, pp. 1–8, 2020.
- [23] N. A. Aziz, N. Adnan, D. A. Wahab, and A. H. Azman, "Component design optimisation based on artificial intelligence in support of additive manufacturing repair and restoration:

current status and future outlook for remanufacturing,” *Journal of Cleaner Production*, vol. 296, article 126401, 2021.

- [24] J. Zhao, X. Xi, Q. Na, S. Wang, S. N. Kadry, and P. M. Kumar, “The technological innovation of hybrid and plug-in electric vehicles for environment carbon pollution control,” *Environmental Impact Assessment Review*, vol. 86, p. 106506, 2021.
- [25] P. Sandner, A. Lange, and P. Schulden, “The role of the CFO of an industrial company: an analysis of the impact of blockchain technology,” *Future Internet*, vol. 12, no. 8, p. 128, 2020.

Research Article

Constructing a Music Network Teaching System by Using Neural Network Model with Wireless Audio Transmission

Weiming Liu 

College of Music and Dance, Hunan City University, Yiyang 413000, China

Correspondence should be addressed to Weiming Liu; liuweiming@hncu.edu.cn

Received 29 January 2022; Revised 21 February 2022; Accepted 27 May 2022; Published 18 June 2022

Academic Editor: Mu-Yen Chen

Copyright © 2022 Weiming Liu. This is an open access article distributed under the Creative Commons Attribution License, which permits unrestricted use, distribution, and reproduction in any medium, provided the original work is properly cited.

The purpose is to solve the problems that the traditional teaching methods limit the openness and extension of the music classroom, the interaction between teachers and students, the environment of students' autonomous learning, and the music teaching situation. Wireless local area networks, Bluetooth, and intelligent transmission channels based on specific frequency can replace wired audio transmission and are widely used in the digital music classroom. Moodle system is used to build a music teaching network system based on the analysis of previous studies and the existing music teaching network platform. The system combines with Convolutional Neural Network (CNN) structure based on cloud computing to effectively identify and create music scores. The system effectiveness is further proved by analyzing the learning effect of the students and teaching effect of teachers in the conservatory of music. The results show that the system makes the experience of teachers and students in the teaching system different from before, and students can freely choose the time and place of class. In addition, the teaching method is flexible, and the teaching methods and resources are real-time. Therefore, in the music teaching network course, it overcomes some shortcomings of the traditional teaching mode. The music class is open and flexible. Teachers and students can have more interactive behavior and realize the students' self-study and music teaching environment. This exploration can provide a theoretical basis and practical experience for music-related teaching.

1. Introduction

Today, cloud computing is not a strange word. Cloud computing is a service model related to the Internet [1]. In general, it is a calculation of dynamic virtual resources. This resource is provided by the Internet [2], so the cloud is the name of this resource-providing network. Like clouds in the sky, the amount of resources in these "clouds" is infinite and can be accessed at any time. Access costs are also quite low [3]. The access method is also very convenient. It only needs a computer or a mobile phone. Cloud computing is very fast, and it can reach 100,000 computing cycles per second, which allows users to use this computing power to meet their needs. For example, cloud computing can be used to simulate the changing trend of the market economy. Then, according to the simulation results, people can take certain business actions, such as buying or selling stocks [4]. The advancement of network and multimedia technology has

provided new support for education reform and development [5]. The purpose is to satisfy the different conditions of educational reform for different disciplines, diversify the teaching form, and make the teaching resources more vibrant and colorful. It can meet the needs of different types of students and different classes and improve teaching efficiency and teacher-student satisfaction. The Moodle teaching platform is deeply studied based on traditional disciplines with modern network technology and cloud computing technology. Moreover, the traditional teaching model of music discipline is analyzed [6]. Based on the actual curriculum of the music subject, the two are innovatively integrated by integrating the constructivist learning theory to satisfy the actual creation conditions of the music curriculum in this system [7]. Based on the basic functions of the Moodle platform, the functional modules are redeveloped to expand the functional modules of their learning activities [8]. An effective music teaching system based on

the Moodle platform is developed. It provides a reference for the development of Moodle platform online course, education information, and music education.

Specific operations are as follows. First, cloud computing technology is used to summarize and analyze the current music teaching situation in all colleges. For example, how do teachers teach and what music students like? Then, the data of online music playing, downloading, and online karaoke songs from computers, TV, mobile phones, and other media are analyzed using cloud computing technology. Then, the data and all kinds of data information obtained from the analysis are input into the online music education curriculum system and used for reference to enrich teaching resources and teaching forms. For example, exercises in class can adopt the form of karaoke songs, which can systematically input the songs sung by students. Then, the songs can be compared with those previously recorded in cloud computing data to summarize the advantages and disadvantages of students' singing performance and evaluate the system scores.

E-learning is an educational model that establishes new communication mechanisms and interactions between people through the support of the network [9]. The research can promote the birth of the online teaching platform to promote the development of new learning methods of online learning [10]. Therefore, some shortcomings of the traditional teaching model are overcome in the network course of music education. The network teaching platform supplements the shortcomings of the traditional teaching mode and enriches the teaching activities. In traditional teaching, teachers talk more, and the teaching form is single. Compared with traditional teaching, online learning has more diversified teaching modes and abundant teaching resources, effectively improving students' sense of participation and teaching efficiency. It will become an indispensable teaching method and application in future teaching [11].

The informationization of music education is the inevitable requirement of improving music teaching and innovating music classroom teaching mode. The digital construction of the music classroom is the performance of the close combination of music discipline and educational informatization. Unlike traditional wireless systems, such as Wireless Local Area Networks and Bluetooth, the intelligent transmission channel based on a specific frequency can send a series of low-power pulses on broadband. The interference caused by a wider spectrum, lower power, and impulsive data is less than that caused by traditional wireless solutions. Hence, it can meet all the applications of traditional wireless in the digital music classroom and provide comparable performance with wired in the indoor wireless environment.

Learning resources are the support of network teaching. All kinds of excellent learning resources are integrated. Constructing the teaching resource library has become the development trend of online education. The open-source network teaching platform comes into being under this demand [12]. Open source is an abbreviation for open source code. In the open-source agreement, the developer's rights are guaranteed. Meanwhile, users can enjoy the right to copy, distrib-

ute, and modify freely. The Moodle platform is one of the open-source teaching platforms.

2. State of the Art

Chinese educationists' teaching ideas and practices unconsciously contain the idea of effective teaching. They are mainly embodied in the teaching aims, methods, and principles [13]. Exploration of teaching efficiency starts from a primitive tribe in China and has a long history. Confucian ideology about the teaching of students according to their aptitude and western-style schools reflects Chinese' pursuit for teaching efficiency. It is embodied in many ways [14]. The basic principles of the effective teaching idea are applied in practical teaching and learning, including the humanities and social sciences. It has achieved some success. Many studies abroad apply the effective teaching idea to music teaching.

These research theories are tightly integrated with the practice of music teaching. First, the teaching theory is enriched by it. Then, it has instructive significance for the content and method of the music. There is a strong criticism of the past teacher education model in modern western countries [15]. It thinks that it only focuses on imparting the principles of education and teaching content, which is far from reality. For example, German scholar Hart believes that the former teaching philosophy still plays a major role in nurturing teachers. In other words, the teaching material of the theory can hardly be reflected in the actual examination [16]. The discussion of teaching theory is relatively isolated from each other and stands in their respective positions. They ignore reality and work without thinking. In the reform of teacher education, the western developed countries have always been in a leading position, but the effect is not so obvious. There is a contradiction. First, multiple scholars are actively engaged in studying the effective teaching idea. Then, they engage in a rigid and unrealistic educational model [17–19]. Compared with the domestic, although the application of the effective teaching idea in the music has not been mature in the teaching of music, the attention of this kind of research is still very high. In addition, the application research of the effective teaching idea in music only stays in the superficial change, and there are no deeper research results. In the practice of music teaching, it is difficult to put forward an excellent suggestion. Quite a few countries have applied the effective teaching idea widely in the practice of music research [20–23]. Learning is the process of students' self-construction cognition. The perfect knowledge system is just a repository of theories, so learners should build up their own knowledge of the real world. There are many studies on the practical behavior of music teaching as an experimental method of the effective teaching idea, and they also draw good conclusions.

The achievement of efficient teaching needs certain conditions. This condition is the method and approach for effective teaching. The educators and practitioners attach importance to teaching efficiency and actively explore and seek effective teaching methods and ways. At present, the research on the effective teaching idea is mainly

concentrated in the psychology and educational circles in China. If the application of the effective teaching idea in music is taken as the keyword, there are only six papers in this field. Among them, half of the main content is to analyze and study the curriculum system, and the other three are to study music teaching in teacher's college. Moreover, few citations and download times show that few people pay attention to it [24–26]. From the above analysis, the importance of the effective teaching idea is not emphasized in music teaching in China. The students' curiosity and thirst for knowledge should be used in music teaching. In this way, students' enthusiasm and initiative can be greatly inspired, and students can achieve an efficient combination of theory and performance in music learning. The effectiveness of teaching idea of teacher education is a scientific and advanced concept in the world, but it has not been widely applied. Therefore, in order to achieve the expected teaching effect, it is necessary to influence students through teachers' routine teaching behavior, thus obtaining satisfactory learning effect [27].

According to the practical problems, such as high maintenance costs, delayed updates, and insufficient teaching resources in colleges, scholars analyzed the related concepts of CCAI (Cloud Computing and Artificial Intelligence) and discussed the materialization of cloud computing. In addition, cloud platform status and cloud service modes of PaaS, SaaS, and IaaS are also analyzed. Combined with the teaching design and the organization of teaching resources, the access technology of the domestic typical cloud platform and the Google App Engine "public cloud" platform is discussed, and the cloud software supporting CCAI and the performance of CCAI under different cloud services are discussed [28, 29].

To sum up, music teaching has gradually developed towards the direction of music education informatization. While realizing the new reform of music teaching, it also leads the new concept of music teaching and effectively promotes the development of music teaching. However, there is a lack of a mature teaching system according to the characteristics of music teaching. Based on this, from the perspective of actual needs, this thesis will introduce a neural network model to improve the recognition efficiency of the music score and then realize a set of network teaching systems that makes full use of teaching resources.

3. Methodology

3.1. Research Subjects. Six teachers and 100 students of music performance major in Northeast Petroleum University are selected as the research subjects. The students and teachers are divided into experimental and control groups, with three teachers and 50 students in each group. Before the experiment, the scores of 100 students are basically the same. Teachers spend the same amount of time preparing lessons, effectively attending classes, correcting homework after class, and evaluating grades.

Teachers in the experimental group take the music teaching system under the Moodle platform for classes. Students attend classes on time, complete the homework

assigned by teachers on time, and submit it on the system. Teachers in the control group take the traditional teaching form. Students attend classes on time and complete homework assigned by teachers on time.

After half a semester, the six teachers are interviewed about preparing lessons, reviewing homework, and evaluating their grades in class and after class. Besides, in the experimental group, the curriculum design, curriculum resource design, curriculum activity design, curriculum interface design, and curriculum evaluation design of the system are required to be evaluated by teachers. In addition, five professional achievements of 100 students are compared, including vocal music, the theoretical basis of music, rhythm training, Chinese and foreign music history, and songwriting.

3.2. Analysis of Music Teaching Needs under Moodle Platform. The Moodle platform is developed based on constructivist theory. The functional view of the Moodle platform, which is emphasized by the constructivist theory, is also basically satisfied. There are five functional modules in the platform. They are user management, course development, teaching activities, evaluation management, and management of learning process tracking. Based on Moodle platform, as for the teaching system design, specific curriculum in the music discipline should be involved to analyze the requirements of the music teaching system, as shown in Figure 1.

As for the system of music teaching based on Moodle platform, the role of a system administrator, teacher, course creator, a teacher without editorial authority, students, and visitors should be included in the design of the user role. The course creator creates a new course for others on the platform, authorizes the teacher's authority, and approves the student's admission. Teachers can conduct all activities within the course. Teachers without edit rights can participate in all activities in the course but cannot edit or change activities.

The use of system administrators, teachers, and students is mainly analyzed. System administrator application: the system administrator controls the highest authority in the system and authorizes other user role permissions in the system, as shown in Figure 2.

In the Moodle platform music teaching system, the realization of the system is also an achievement of the change of teacher's role. The teacher is transferred from the traditional knowledge-teacher, mainly composed of "teaching", to the leader, organizer, and evaluator of teaching activities. When systematic teaching is carried out, the problems and teaching objectives to be solved are clearly defined by teachers to create an online learning environment. According to the transformation of the teacher's role, the functional module design for the teacher is shown in Figure 3.

Students are the subject of knowledge learning. In the Moodle platform music teaching system, all the teaching contents are always carried out around the students' learning. They are system users and the main participants, collaborators, and evaluators in the learning activities. Students complete the various functions for the student function module by using a computer connected to the Internet.

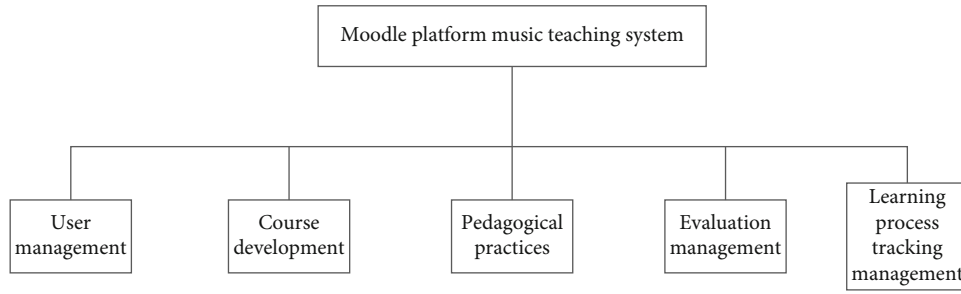


FIGURE 1: Functional block diagram of the music teaching system on the basis of Moodle platform.

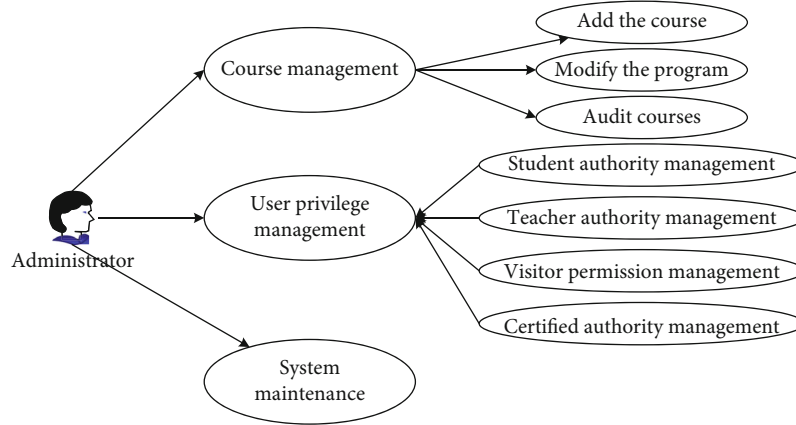


FIGURE 2: Application permissions of system administrators.

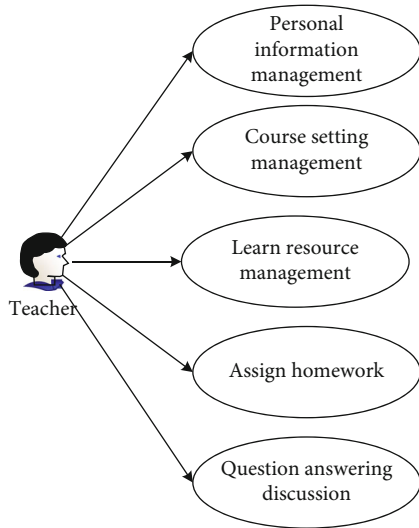


FIGURE 3: Application permissions of teacher.

Through research and analysis, the student-oriented functional modules in the system are listed in detail, as shown in Figure 4.

In the online music teaching platform, the wireless transmission equipment needs to support the synchronous access of multiple devices to realize the cable replacement between traditional musical instruments and electronic musical instruments and tuning equipment. The musical instruments in students' hands are wirelessly connected with the tuning equipment through wireless communication technol-

ogy. Hence, students can hold musical instruments and move freely in the classroom. They can also plug and play to simplify the steps of using musical instruments. After the wireless transmission of the device, teacher management is also particularly important. The wireless device is connected to the network transceiver through integration. The teacher monitors the working status of all wireless transmitting devices in real-time through the teacher control software under the transmission network to realize the effective audio output under the one-to-many management mode. The tuning interface is open for teachers to realize the effect management of digital mixer. Teachers simulate the best tuning effect by choosing different performance modes and complete the unity of teaching and learning through the interaction between teachers and students provided by digital music management software.

3.3. System Specific Design. According to the system requirements analysis, the music teaching system based on Moodle platform is constructed. The aim is to conduct online teaching of music subjects through the Moodle platform and realize the integration of teaching and learning on the network environment platform. This thesis was aimed at scientifically combining the music course teaching with the Moodle open-source teaching platform and strives to develop and design a music teaching system based on the Moodle platform. The shortcomings of traditional music classes are supplemented. Students study music in the online environment. It provides a reference for music educators and promotes the development of music teaching.

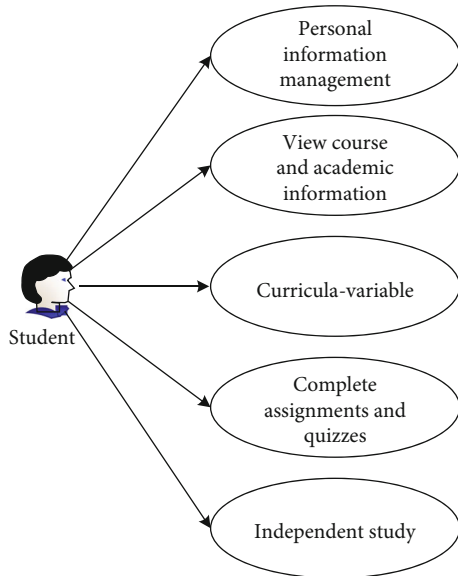


FIGURE 4: Application permissions of student.

The Moodle platform itself is a way of constructivist theory. In the Moodle platform, various common social software is integrated, such as blogs (weblogs), wikis (multiperson collaborative writing tools), and RSS (online news). Various social software is integrated to achieve a diversity of teaching activities and learning evaluation methods. In the Moodle platform, the role of the teacher has been changed. In the Moodle platform, the teacher's task is the design of teaching resources and teaching activities, rather than the design of teaching content in traditional teaching. Therefore, the design of the music teaching system under the Moodle platform should be guided by constructivist learning theory and teaching system design theory. Music lessons' flexibility, openness, and interactivity based on the Moodle platform are realized.

The music teaching system based on the Moodle platform adopts the modular structure system design. System engineering perspectives and methods are applied. The modular design of the system emphasizes learning-centered. The modular structure is used as a guiding ideology. The overall platform system is designed. Figure 5 shows the flow chart of the design method of the music teaching system in the Moodle platform.

3.4. Audio Transmission Technology of Digital Music Classroom. Wireless transmission equipment needs to support synchronous access of multiple devices to realize cable replacement among traditional musical instruments, electronic musical instruments, and tuning equipment [30, 31]. Through wireless communication technology, the musical instruments in students' hands are wirelessly connected with tuning equipment. It enables students to hold musical instruments and move freely in the classroom. Besides, it can achieve the plug-and-play function, simplifying the steps of using musical instruments [32]. Low-power pulses are sent over a wide frequency through a specific frequency intelligent transmission channel. This transmission mode

has a wide spectrum, low power, and nerve impulse, so the interference in the transmission process is relatively small, and the transmission efficiency can be comparable with that of a wired digital music classroom. In a complete digital music classroom, when configuring the receiving end and transmitting end of wireless audio transmission, the number of transmitting ends is configured according to the number of students' synchronous performance needs, and the receiving end is connected to the active speaker or mixer [33]. In the network environment, teachers control the switch of any transmitter and equalize the timbre on the management software of digital music classrooms to realize the effect management of digital mixer. Teachers can simulate the best tuning effect by choosing the current performance mode. The unity of teaching and learning is realized through the interaction between teachers and students provided by digital music management software.

The audio transmission system is connected with the computer display platform. The performance process of sound effects of musical instruments can be directly displayed on the screen through the spectrum-making software. Then, students can intuitively and audiovisual synchronously understand the sound generation mode of music theory and the location of different high and low audio frequencies.

3.5. Music Recognition Method Based on Neural Network. Due to the complex structure and great implementation difficulty of traditional music score recognition algorithms and the low accuracy of existing commercial recognition software, it is necessary to study an easy-to-implement and high-precision algorithm. According to the previous research, a music recognition method based on a neural network is proposed. Figure 1 shows the principle of the identification method. First, the height of the input music score image is fixed to 128 pixel, and the width is scaled up and down. Then, the noise is added to simulate all kinds of unsatisfactory music score images in the real environment. Next, a five-layer residual Convolutional Neural Network (CNN) is used to extract different levels of features from the note information in the image. Meanwhile, the deep semantic feature information is fused with the shallow detail feature information in multiscale. Through the cross supplementation of multilevel information, more perfect feature information is provided for the next stage of note recognition. Finally, the dimension transformation of the extracted feature sequence is performed and used as the input of the note recognition part. Bisru completes the recognition of the note sequence. The Connectionist Temporal Classification (CTC) function is adopted, with no forced alignment requirements on the dataset. Figure 6 shows the specific structure.

In the score image, the notes are discrete and evenly distributed, mainly composed of straight lines or curves in multiple directions, solid or hollow near circle graphics. The convolutional layer in CNN has local connection and weight sharing characteristics, which is conducive to extracting the edge features and position information of notes. Therefore, CNN is used to extract the features of notes in the music score image. The activation function layer can enhance the

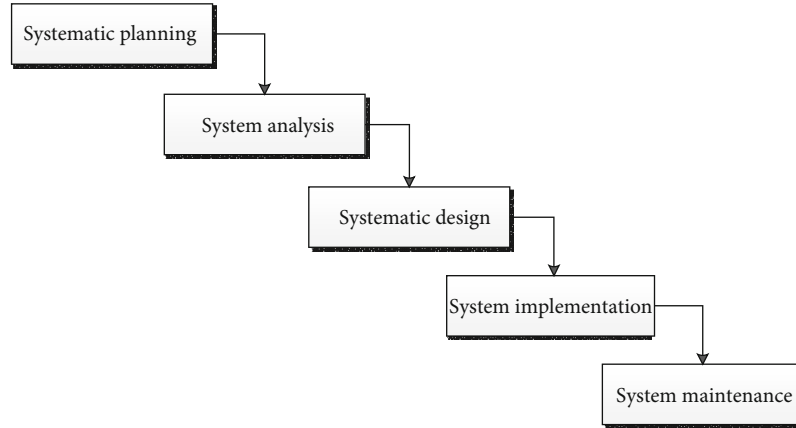


FIGURE 5: System design diagram.

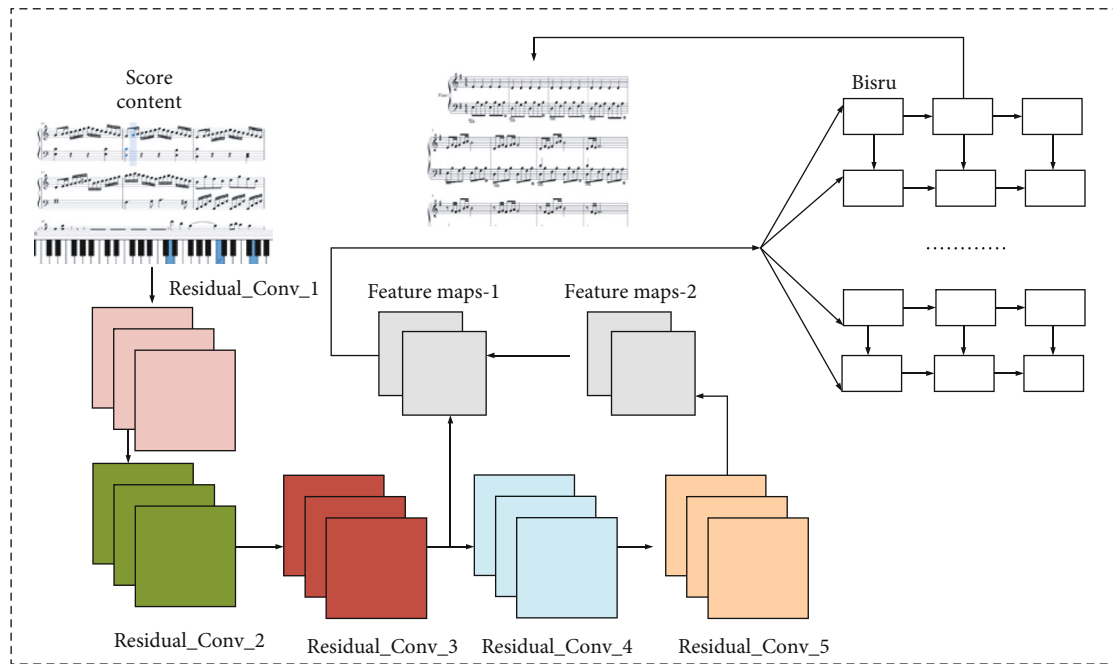


FIGURE 6: Music recognition method based on neural network.

expression ability of CNN and make CNN have differentiability to realize the nonlinear mapping of music score image from low dimensional simple features to high dimensional complex features. On the premise of retaining the main features of the convolutional layer, the pooling layer reduces the amount of weight parameters, speeds up the calculation speed, and prevents overfitting problems. It is usually necessary to increase the layer width or depth of CNN to improve the detection accuracy of the model. However, in the process of parameter updating, the gradient disappearance/explosion problem is easy to occur, leading to the model's nonconvergence.

When using CNN to extract note features, the convolutional layer increases, making the model extract features of different levels of information. Shallow features generally include note location and edge information. Although the resolution is small, deep features have rich semantic infor-

mation, which can help the network to recognize notes better. However, due to the lack of detailed features in the shallow network, the recognition accuracy of notes may be affected. Therefore, in note recognition, the deep semantic information and shallow detail information of CNN are fused in multiscale. Figure 7 shows the specific process.

Many kinds of networks can effectively recognize the notes in the music score image. The note type and order in each score are fixed due to the note sequence. Moreover, the notes at the current moment have a strong correlation with the notes before and after. In the experiment, recurrent neural networks (RNN) are used to recognize notes. RNN is prone to gradient disappearance in the training process due to the large data length. Therefore, it is necessary to control the information flow through the long short-term memory (LSTM) network with "gate mechanism" or gated unit to alleviate the potential problem of gradient disappearance.

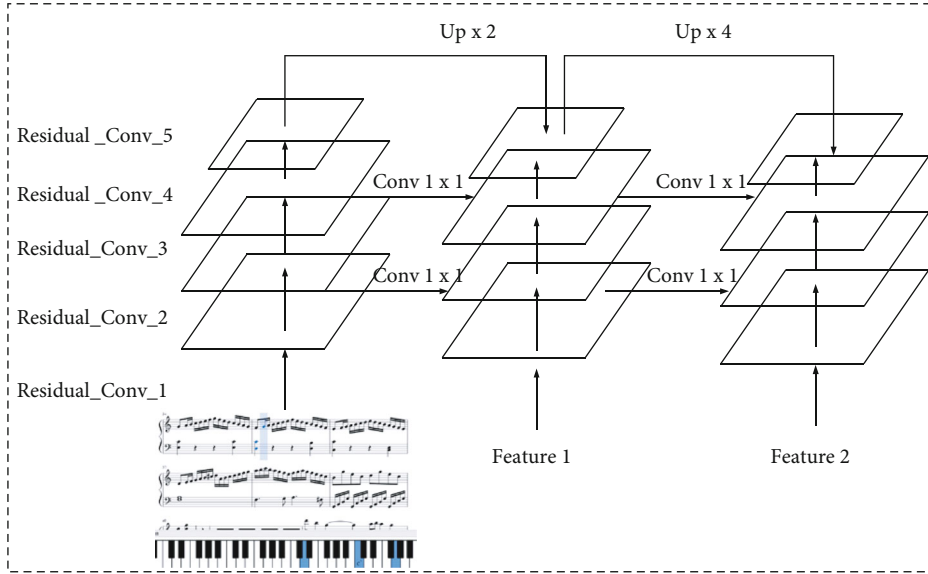


FIGURE 7: Schematic diagram of multiscale feature fusion.

However, the forget gate, input gate, and unit state of LSTM network or gated unit still need the output of the hidden unit at the previous time in addition to the input at the current time, which greatly limits the speed of parallel operation. Therefore, the simple cycle unit module is used to remove the constraint between the states at the continuous time. The weak circularity and high parallelism make the calculation of gate state only depend on the input information at the current time.

3.6. Experimental Design and Dataset Selection. MuseScore data are selected as the dataset of music score note detection. MuseScore is a free music annotation software that allows its users to upload their music scores to their websites and share them with others. It can be downloaded in the form of MuseScore file (mscz), PDF, MusicXML, MIDI, and MP3. MuseScore Compressed Music Score (MSCZ) and Music XML (MXL) files are downloaded from MuseScore, and the tag format required is generated by parsing these files. The whole training process is completely end-to-end, and the music score image is directly input. Through the model, the loss function is calculated. Finally, the model parameters are optimized by the loss function. Data enhancement is applied during training, and different training samples are presented to the network model each time. The batch size of the training model through the stochastic gradient descent optimizer is 32, the initial learning rate is 0.001, and the learning rate is constant attenuation.

4. Results and Discussion

4.1. Note Recognition Results. The model tests a total of 1500 music score images converted by MuseScore. These music score images do not have any data enhancement. Finally, the overall recognition results' average symbol accuracy (mAP) is 0.92, the accuracy of note pitch is 0.98, and the accuracy of time value is 0.96. Table 1 displays the average

TABLE 1: Note recognition results of neural network model.

Class	Sharp	Flat	Natural	clefG	clefF
AP	0.96	0.93	0.91	0.98	0.97
Class	clefC	Barline	Timesig	Note	Rest
AP	0.88	0.91	0.82	0.93	0.92

mean precision (AP) for each class. The results show that the neural network model here performs well in note recognition, and the accuracy of time value and pitch is higher than 0.9.

4.2. Implementation of Music Teaching System Integrating Wireless Audio Transmission. The music teaching system based on Moodle platform is based on "constructivism." The music discipline is supported explicitly by the curriculum. The use of the platform has subverted the traditional teaching model. As for the subject and object of teaching, personalization and intelligent learning navigation are considered. Meanwhile, it should be emphasized that teachers and members of student groups must help each other. The scientific knowledge curriculum system is studied, and the music teaching classroom is transplanted to the network. The fast and distributed information exchange characteristics of the network make the teaching advantages and effects more prominent. Humanized, intelligent, dynamic, and scientific learning programs are gradually adopted, which promotes the improvement of learners' learning effects and effectively reduces learning costs. The site is currently named "Magic Light" music.

The system is composed of multiple wireless music box playing systems, and wireless resource sharing between small systems is realized through WiFi. Through the design of wireless mode, resource sharing is realized. Each music box wirelessly transmits its own stored audio files or shared audio files in other music boxes in the wireless environment

TABLE 2: Evaluation and feedback of the music teaching system.

	Teacher1	Teacher2	Teacher3	Average score
Course objective design	10	9	10	9.66
Course resource design	9	9	9	9
Course activity design	10	10	9	9.66
Course interface design	9	9	9	9
Course evaluation design	9	9	10	9.33

to the wireless speaker for playback. Playback control is realized through mobile terminal devices such as mobile phones, pads, or PC. The wireless audio transmission module of the system is Nordic company's nRF24L01 wireless module and adopts 2.4 GHz short-range wireless transmission technology. In the transmitting part, the main control module transmits the sound source data through the 2.4 GHz band of nRF24L01 module. In the receiving part, the MCU controller receives audio data from the 2.4 GHz of wireless module nRF24L01 through the SPI interface. Then, the audio data are transmitted to the audio output module through the SPI interface to play music.

The system of network music teaching is mainly built based on the Moodle platform. For music teaching, modern network technology is used to combine the network platform with traditional teaching to realize new applications. The system can be used to enrich the deficiencies in traditional teaching. It can also be used as an independent online learning course in a self-directed way. The current four basic courses in the system can meet the basic learning of music subjects. All these courses are designed effectively based on the guidance of constructivist theory. It is completely different from traditional music teaching.

In the research of the subject, Moodle is redeveloped and practiced for the specific needs of the music subject course. New plug-ins have been developed, and new learning activity modules have been expanded to meet the specific needs of the discipline. The complete construction of the course is realized, which lays a foundation for the learner's knowledge and cognitive construction. Based on the generation of dynamic and characteristic learning programs under the constructivist theory, the introduction and application of a personalized intelligent learning platform in music learning fully combine the Moodle platform with online music teaching.

4.3. Application Analysis of System Administrator. Based on the music teaching system of Moodle platform, the teaching process design of three teachers in the experimental group after using the system is evaluated. The evaluation content includes the curriculum, resource, activity, interface, and evaluation designs. The evaluation standard is 10 points. Ten points represent total satisfaction, and no shortcomings. Nine points show great satisfaction and means that the system can be improved. Eight points show general satisfaction, and there are many areas needing improvement. A score of 7-5 indicates a general effect. 5 points below indicate dissatisfaction, and the system should be perfected if it is going to be used. The feedback results can be clearly seen in Table 2.

Table 2 reveals the specific scores of five evaluations of the teaching process design of the music teaching system. The total score is 46.65, which reaches the excellent level of teaching design. It also suggests that in the experimental group, teachers are satisfied with the music teaching system. There is no evaluation below 9 points. However, the scores of five indicators indicate that the system needs further improvement in curriculum resource design and curriculum interface design. The system has been modified and improved according to the corresponding scoring standards.

In addition, the teaching process of the teachers in the experimental group and the control group is interviewed. As for the experimental group, teachers say that after using the teaching system, the time spent in various teaching links is much shorter than before, and class efficiency is significantly improved. As the system effectively records the students' homework submission and classroom performance, the performance evaluation can be automatically generated, which is quite convenient and fast.

As for the control group, teachers say that the time spent in each teaching link has not changed. Preparing lessons still requires a lot of reading materials. Therefore, more time is spent. In class, students are easily distracted and a lot of time is needed to maintain classroom discipline, resulting in less effective class time. Reviewing homework after class also wastes a lot of time, which reduces private time after class. Grade evaluation is also relatively slow. It needs to read massive classroom records and check past classroom performance to evaluate scores comprehensively.

The teachers' average time spent in preparing lessons, effectively attending classes, reviewing homework after class, and evaluating their achievements is compared. Table 3 reveals the results.

Table 3 suggests that the teachers in the experimental group spend only 0.5 hours preparing lessons, which is 0.4 hours less than the teachers in the control group. The effective class time of the teachers in the experimental group is 1.4 hours, which is 0.3 hours more than that of the teachers in the control group. Teachers in the experimental group spend 1.5 hours reviewing homework after class, which is one hour less than those in the control group. Teachers in the experimental group spend 2 hours on performance evaluation, which is 2 hours less than that in the control group.

These data suggest that the teachers in the experimental group spend less time preparing lessons, correcting homework assignments, and assessing the scores than the teachers in the control group. However, the effective class time of the experimental group teachers is higher than that of the control group. Thus, through the analysis of the results, it is

TABLE 3: Comparisons of the time spent in the teaching process between the experimental group and the control group.

Time (h)	Experimental group	Control group
The average time spent on preparing lessons	0.5 h	1.3 h
The average effective class time	1.4 h	1.1 h
The average time spent on correcting homework after class	1.5 h	2.5 h
The average time spent on performance appraisal	2 h	4 h

considered that using the system can effectively shorten the time of teaching links, improve the effective class time and the work efficiency of teachers, and reduce the burden of teachers in all aspects.

4.4. Application Analysis of Students. The practicality of the course content of the online teaching platform, the rationality of the course structure, and the effect of music learning are studied. 100 professional students from the experimental and control groups are collected to prove the system effectiveness after half a semester, including vocal music, the theoretical basis of music, rhythm training, Chinese and foreign music history, and songwriting. Then, the average scores of the five professional courses of the experimental group and the control group are compared. Table 4 suggests the results.

Table 4 reveals that in the vocal music class, the average score of the experimental group students is 9 points higher than the scores of the control students. In the course of the theoretical basis of music, the average score of the experimental group students is 8 points higher than the average score of the control students. In the rhythm training class, the experimental group is 8 points higher than the control group's average. In the course of Chinese and foreign music history, the experimental group is 9 points higher than the average score of the control group. In songwriting, the experimental group is 6 points higher than the average score of the control group. It reveals that the average scores of the five courses of the students in the experimental group are higher than the average scores of the students in the control group. It fully demonstrates the effectiveness of the use of the music teaching system.

In addition, 50 students from the experimental group are also surveyed for their satisfaction with the use of the system. The full score is 10 points. 10 points mean that they are very satisfied, have no shortcomings, and are willing to continue using it. 8-9 points mean that they are very satisfied, there is a shortcoming, and they are willing to continue using it. 6-7 points indicate general satisfaction, some defects need improvement, and they are willing to continue using it. 4-5 points suggest that they are generally satisfied, many shortcomings need improvement, and they are willing to use them after improvement. 2-3 is not satisfied, but the system can be used after improvement. 1 point means very dissatisfaction and they are unwilling to use it again. Table 5 presents the results of the student satisfaction score.

Table 5 shows that all the students are satisfied with the music teaching system, while the degree of satisfaction is different. More than 90% of students are willing to use the Moodle platform to learn more courses. This system can effectively improve their learning efficiency and academic

TABLE 4: Comparison of the average scores of 5 professional courses in the experimental group and the control group of students.

Courses	Average score of students in the experimental group	Average score of students in the control group
Vocal music	89	80
Theoretical basis of music	95	83
Rhythm training	93	85
Chinese and foreign music history	96	87
Song writing	87	81

TABLE 5: Satisfaction results of the use of the music teaching system by the experimental group students.

Score	The number of the students	Proportion of students (%)
1	0	0%
2-3	0	0%
4-5	2	4%
6-7	3	6%
8-9	40	80%
10	5	5%

performance. Therefore, the effectiveness of the system has also been verified.

The music module based on the Moodle platform has been implemented in the expected functional modules through the application analysis and summary of specific roles. When using functional modules, the principle of "learning" is followed as much as possible. The advantages of the module function are effectively combined with the actual course as much as possible. Curriculum construction comes from the guidance of constructivist theory. The teaching methods under the direction of the constructivist theory are integrated into the specific curriculum. The unification of theory and practice is realized, and the system construction of the curriculum is completed. Teaching resources are rich. Course resource content can meet the needs of the actual course. Music teaching content is presented on the platform in various ways, which is in line with the actual needs of students. The secondary development guarantees the implementation of the course. According to the particularity of the music discipline, the effective secondary

development satisfies the original intention of the design and realizes the full implementation of the course.

5. Conclusion

First, the wireless transmission technology in the digital music classroom environment is analyzed. On this basis, the neural network model is applied to music score recognition, which lays a foundation for the subsequent construction of the network curriculum system for music education. The main functions, relative advantages, and development status of the Moodle platform are introduced in detail. The constructivist theory is applied to study its significance for music teaching. The importance of the reform of music education is explored. The music curriculum guided by constructivism theory is built on the Moodle platform, and the music teaching system based on Moodle platform is designed. However, there are also some research deficiencies. Due to the limited music data input of the system, the music types in the music teaching system are not comprehensive enough. In the follow-up research, corresponding measures will be taken to collect more music data to further improve the music teaching system.

Data Availability

The raw data supporting the conclusions of this article will be made available by the authors, without undue reservation.

Ethical Approval

This article does not contain any studies with human participants or animals performed by any of the authors.

Consent

Informed consent was obtained from all individual participants included in the study.

Disclosure

A preprint has previously been published in 2021 IEEE International Conference on Advances in Electrical Engineering and Computer Applications (AEECA).

Conflicts of Interest

The author declares no conflict of interest.

Authors' Contributions

The author has made a substantial, direct, and intellectual contribution to the work and approved it for publication.

References

- [1] J. O. Connelly and P. Miller, "Improving learning outcomes for higher education through smart technology," *International Journal of Conceptual Structures and Smart Applications (IJCSSA)*, vol. 6, no. 1, pp. 1–17, 2018.
- [2] V. Kumar and D. Sharma, "Creating collaborative and convenient learning environment using cloud-based Moodle LMS," *International Journal of Web-Based Learning and Teaching Technologies (IJWLTT)*, vol. 11, no. 1, pp. 35–50, 2016.
- [3] M. Gupta, S. Marsden, T. Oluka, R. Sharma, and H. Lucas, "Lessons learned from implementing E-learning for the education of health professionals in resource-constrained countries," *Electronic Journal of e-Learning*, vol. 15, no. 2, pp. 144–155, 2017.
- [4] B. Gan, T. Menkhoff, and R. Smith, "Enhancing students' learning process through interactive digital media: new opportunities for collaborative learning," *Computers in Human Behavior*, vol. 51, pp. 652–663, 2015.
- [5] L. Johnson, S. Adams Becker, and C. Hall, "NMC technology outlook for Australian tertiary education: a horizon project regional report," The New Media Consortium. Cover image courtesy of Open Universities Australia ISBN, Austin, Texas, 2015.
- [6] C. D. Dziuban and A. G. Picciano, "What the future might hold for online and blended learning research," in *In Conducting Research in Online and Blended Learning Environments: New Pedagogical Frontiers*, vol. 173, Routledge, 2015.
- [7] T. S. Hew and S. L. S. A. Kadir, "Predicting the acceptance of cloud-based virtual learning environment: the roles of self determination and channel expansion theory," *Telematics and Informatics*, vol. 33, no. 4, pp. 990–1013, 2016.
- [8] E. M. Mocanu and A. Deaconu, "The use of information and communication technology (ICT) as a teaching method in vocational education and training in tourism," *Acta Didactica Napocensia*, vol. 10, no. 3, pp. 19–34, 2017.
- [9] B. L. M. Harasim, "Online Education," *American Journal of Nursing*, vol. 107, no. 5, p. 74, 2019.
- [10] Y. U. Lasheng, W. U. Xu, and Y. Yu, "An online education data classification model based on Tr_MAdaBoost algorithm," *Chinese Journal of Electronics*, vol. 28, no. 1, pp. 21–28, 2019.
- [11] O. Odena, "Multicultural dialogues in post-conflict music education settings," in *In Advancing multicultural dialogues in education*, pp. 215–233, Palgrave Macmillan, Cham, 2018.
- [12] M. C. Moore, "Reflections on traditional African American music: its function and relevance in contemporary music education," in *In Traditional musics in the modern world: Transmission, evolution, and challenges*, Springer, Cham, 2018.
- [13] D. Sirek, "Our culture is who we are! "Rescuing" Grenadian identity through musicking and music education," *International Journal of Music Education*, vol. 36, no. 1, pp. 47–57, 2018.
- [14] M. K. Hedgecoth and M. Major, "Revisioning and reinstating: music education after the great recession," *Arts Education Policy Review*, vol. 120, pp. 1–10, 2019.
- [15] A. Fung, "Transgenerational father-son resistance: a phenomenological inquiry of a music education professor's learning and parenting," *Music Education Research*, vol. 20, no. 5, pp. 616–626, 2018.
- [16] L. B. Horodyskyj, C. Mead, Z. Belinson, S. Buxner, S. Semken, and A. D. Anbar, "Habitable worlds: delivering on the promises of online education," *Astrobiology*, vol. 18, no. 1, pp. 86–99, 2018.
- [17] L. Feng and M. Suzhen, "Bounds for nonisotropic Marcinkiewicz integrals associated to surfaces," *Journal of the Australian Mathematical Society*, vol. 99, no. 3, pp. 380–398, 2015.

- [18] T. Fabio, A. A. Elsadany, X. Baogui, and H. N. Agiza, "Local stability of the Cournot solution with increasing heterogeneous competitors," *Nonlinear Analysis-Real World Applications*, vol. 26, pp. 150–160, 2015.
- [19] C. Yujun and Z. Yumei, "Monotone iterative technique for $(k, n-k)$ conjugate boundary value problems," *Differential Equations*, vol. 69, no. 69, pp. 1–11, 2015.
- [20] "on observability and detectability of continuous-time stochastic Markov jump systems," *Journal of Systems Science & Complexity*, vol. 28, no. 4, pp. 830–847, 2015.
- [21] Y. Zhiguo, Z. Guoshan, W. Jiankui, and Z. Weihai, "State and output feedback finite-time guaranteed cost control of linear it stochastic systems," *Journal of Systems Science & Complexity*, vol. 28, no. 4, pp. 813–829, 2015.
- [22] M. Xinzhu, L. Rui, and Z. Tonghua, "Adaptive dynamics for a non-autonomous Lotka-Volterra model with size- selective disturbance," *Nonlinear Analysis-Real World Applications*, vol. 16, pp. 202–213, 2014.
- [23] "Stochastic linear quadratic optimal control with constraint for discrete-time systems," *Applied Mathematics and Computation*, vol. 228, pp. 264–270, 2014.
- [24] J. Tang, H. Guoping, and F. Liang, "A new non-interior continuation method for second-order cone programming," *Journal of Numerical Mathematics*, vol. 21, no. 4, pp. 301–323, 2013.
- [25] X. Zhou, X. Shi, and H. Cheng, "Modelling and stability analysis for a tuberculosis model with healthy education and treatment," *Computational and Applied Mathematics*, vol. 32, no. 2, pp. 245–260, 2013.
- [26] S. Pang, T. Li, F. Dai, and M. Yu, "Particle swarm optimization algorithm for multi-salesman problem with time and capacity constraints," *Applied Mathematics & Information Sciences*, vol. 7, no. 6, pp. 2439–2444, 2013.
- [27] J. Wang and Q. Zhan, "Visualization analysis of artificial intelligence technology in higher education based on SSCI and SCI journals from 2009 to 2019," *International Journal of Emerging Technologies in Learning (IJET)*, vol. 16, no. 8, pp. 20–33, 2021.
- [28] D. Wang, X. Lv, S. Zhang, and T. Zhu, "Role of network cloud platform-based and progressive health education in postoperative rehabilitation of patients with tibial fracture," *American Journal of Translational Research*, vol. 13, no. 5, pp. 4819–4824, 2021.
- [29] Y. Ding, Y. Li, and L. Cheng, "Application of Internet of Things and virtual reality technology in college physical education," *IEEE Access*, vol. 8, pp. 96065–96074, 2020.
- [30] V. Caputo, "Add technology and stir: music, gender, and technology in today's music classrooms," *Visions of Research in Music Education*, vol. 16, no. 5, p. 10, 2021.
- [31] P. J. da Silva and M. R. Voelzke, "Digital technology and musical instruments as methodology of teaching sound waves in physics," *Brazilian Journal of Development (ISSN)*, vol. 7, no. 9, pp. 89593–89601, 2021.
- [32] P. R. Webster and D. B. Williams, "Technology's role for achieving creativity, diversity and integration in the American undergraduate music curriculum: some theoretical, historical and practical perspectives," *Journal of Music, Technology & Education*, vol. 11, no. 1, pp. 5–36, 2018.
- [33] A. M. Hart, "The tablet as a classroom musical instrument," *Athens Journal of Education*, vol. 5, no. 3, pp. 299–324, 2018.

Research Article

ObjectDetect: A Real-Time Object Detection Framework for Advanced Driver Assistant Systems Using YOLOv5

Jamuna S. Murthy,¹ G. M. Siddesh,² Wen-Cheng Lai ,^{3,4} B. D. Parameshachari ,⁵
Sujata N. Patil,⁶ and K. L. Hemalatha⁷

¹Department of Computer Science and Engineering, M S Ramaiah Institute of Technology, India

²Department of Information Science Engineering, M S Ramaiah Institute of Technology, India

³Bachelor Program in Industrial Projects, National Yunlin University of Science and Technology, Taiwan

⁴Department of Electronic Engineering, National Yunlin University of Science and Technology, Taiwan

⁵Department of TCE, GSSS Institute of Engineering and Technology for Women, Mysuru, Karnataka 570016, India

⁶Department of Electronics and Communication Engineering, KLE Dr. M.S. Sheshgiri College of Engineering and Technology, Belagavi, 590008 Karnataka, India

⁷Department of ISE, Sri Krishna Institute of Technology, Bengaluru, India

Correspondence should be addressed to Wen-Cheng Lai; wenlai@mail.ntust.edu.tw

Received 22 February 2022; Revised 25 March 2022; Accepted 3 May 2022; Published 14 June 2022

Academic Editor: Alessandro Bazzi

Copyright © 2022 Jamuna S. Murthy et al. This is an open access article distributed under the Creative Commons Attribution License, which permits unrestricted use, distribution, and reproduction in any medium, provided the original work is properly cited.

In the recent times, there has been a lot of speculation related to advanced driver-assistance system (ADAS) which provides best driving experience for the drivers. ADAS technology helps to detect the unhealthy driving conditions which lead to road accidents today. Road accidents are basically caused due to distracted driving, over speeding, drink and drive, foggy weather, no proper headlights, or due to some object which suddenly trespasses the vehicle. Today the major advancements in ADAS include parking assistance, road traffic detection, object detection on highways, and lane detection. But the major risk limitation in ADAS system is the speed and time at which the object is detected and tracked. Several algorithms such as R-CNN, Fast R-CNN, and YOLO were used for effective object detection and tracking earlier, but sometimes, the system do fail to detect due the speed factor. Hence, the proposed work presents a novel approach called “A Real-Time Object Detection Framework for Advanced Driver Assistant Systems” by implementing the state-of-the-art object detection algorithm YOLOv5 which improves the speed in detection of object over real-time. This paper provides a comparison between other state-of-the-art object detectors such as YOLOv3 and YOLOv4. Comparison is done based on mean average precision (mAP) and frames per second (FPS) on three benchmark datasets collected as a part of research findings. YOLOv5 proves to be faster and 95% accurate than the other object detection algorithms in the comparison. This framework is used to build a mobile application called “ObjectDetect” which helps users make better decisions on the road. “ObjectDetect” consists of a simple user interface that displays alerts and warnings.

1. Introduction

According to the WHO, approximately 1.3 million people die each year due to road traffic crashes [1]. With a rise in accidents and with the increase in the number of vehicles, ADAS has become a vital part of the driving experience. Prior warnings seconds before an incident can help the driver handle the situation in a better manner. ADAS has

emerged as an extremely vital tool with respect to safety in the automobile industry. Notable automotive giants such as MG Astor, BMW, and Mahindra XUV700 have stepped in to integrate ADAS into their models [2]. Existing ADAS technologies operate on visual cameras [3], RADARs [4, 5], and LiDARs [6] for the object detection. ADAS mainly depends on features such as high speed, high accuracy, low cost, and low power consumption. Apart from these factors

ADAS should effectively work at three situations, i.e., traveling in rural roads, urban roads, and in highways. By using sensor technology, the goal of object detection is achieved; higher rate sensors are too costly and consume more power. Also, sensors become weak based on continuous operation. Hence, by realizing the importance of speed and cost factor, our state-of-the-art methodology included deep learning approach to address this issue by implementing system called “A Real-Time Obstacle Detection Framework for Advanced Driver Assistant Systems” by implementing the state-of-the-art object detection algorithm YOLOv5.

The ADAS is one of these technologies. It allows the autonomous car to get real-time support in particular traffic circumstances and detect threats from nearby objects using on-board sensors. The development of ADAS technology has accelerated the transition to autonomous driving. Based on visual data collected from sophisticated sensors like cameras, a TSR system may detect one or more traffic signs. Similarly, a greater grasp of road sceneries leads to a better awareness of the surroundings, which relates to the driving space of cars on the side of the road terrain. For example, employing on-board sensors, ADAS allows an autonomous car to get real-time support in certain traffic situations and detect risks related to adjacent objects. ADAS technology has facilitated the rapid evolution of autonomous driving. An object detection system may identify one or more traffic lights based on visual input from sophisticated sensors such as cameras. Similarly, a better understanding of road scenes leads to a better understanding of the surrounding environment, which is relevant to vehicle driving space on the side of the road terrain.

Major advancements in the creation of revolutionary advanced technologies, as well as the widespread deployment of fixed and mobile sensors, such as image sensors, have aided their usage in the road traffic management and monitoring process. Because of advancements in computer vision research, intelligent transportation systems (ITS) have undergone a significant transformation in order to lessen the effect of human lives lost as a consequence of road accidents and rising traffic congestion [7]. Furthermore, significant progress in the computer vision domain has been made due to the rapid evolution of machine learning algorithms, particularly with the enormous growth in traffic data volumes (big data), the emergence of deep neural networks (DNNs), and the development of powerful computers with graphics processors, such as graphics processing units (GPUs). However, some vision-based applications, such as real-time embedded systems, need a significant quantity of memory and fast processing rates. Indeed, segmentation-based road recognition is one of the most difficult problems in computer vision [8], which entails investigating and detecting the vehicle’s surroundings. Unlike traditional approaches that rely on hand-crafted features such as edges and corners, deep learning models are trained incrementally using enormous amounts of data, automating the process of obtaining and training hierarchical feature representations.

Proposed framework consists of three major modules, object extraction, object detection-tracking, and object visualization. Visualization module is applied to build an

interactive mobile application called “ObjectDetect” which assists the user by notifying them with unique alerts and warnings. ObjectDetect is aimed towards providing alerts and warnings a few seconds prior based on the real-time data. In order to build proposed “ObjectDetect” framework, a survey was conducted on multiple object detection algorithms such as R-CNN, Fast-RCNN, Faster RCNN, YOLOv3, and YOLOv4. Since the research work is aimed at improving the speed and accuracy factors which were the limitations on previous works, finally, YOLOv5 was chosen. The proposed model is not a per-trained model and is aimed at including a system that will be able to assist drivers in compromising situations by giving a heads up with significant speed and accuracy.

The article is organized in the following manner. Section 2 discusses about the recent studies on autonomous vehicles and object detection methodologies. Section 3 presents the proposed ObjectDetect mechanism on obstacle detection and driver assistance using YOLOv5 model. Section 4 details the experiment configuration and results evaluated for the ObjectDetect method. And Section 5 concludes the contribution of research and advantages of method; then, Section 6 discusses the future extension of ObjectDetect model.

2. Literature Review

Numerous researches are done on different aspects of ADAS and Autonomous vehicles. The IoT-based occlusion technique called multiple targets tracking in occlusion area with interacting object models in urban environments was used for autonomous vehicles to solve the problem of object detection by Chen et al. by using a laser scanner [9]. The different observed shapes on each laser scan made it difficult to identify the object. Hence, proposed system is developed using machine learning approach using YOLOv5 which reduces the occlusion issue. ADAS also includes driver monitoring systems. Driver monitoring system (DMS) helps in keeping track of various facial features of the driver like eyelid and mouth movement. One such system was proposed by Kato et al. [10].

There is a lot of research done in object detection since it plays a crucial role in many of the technologies, to get a better understanding of state-of-the-art object detection techniques and models, cloud-based. Liu et al. conducted a survey of most of the research that provides a clear picture of these techniques. The main goal of this survey was to recognize the impact of deep learning techniques in the field of object detection that has led to many ground breaking achievements. This survey covers many features of object detection ranging from detection frameworks to evaluation metrics [11, 12].

For many region-based detectors, like Fast R-CNN [13], a costly per-region subnetwork is applied several times. In order to address this, Girshick introduced R-FCN by proposing location-sensitive score maps to address a dilemma between translation-invariance in image classification and translation-variance in object detection [14]. One of the major challenges of object detection was to detect and localize multiple objects across a large spectrum of scales and

locations, due to which the pyramidal feature representations were introduced. In this, an image is represented with multiscale feature layers. Feature pyramid network (FPN), one such model to generate pyramidal feature representations for object detection, presents no difficulty and as well as effective but may not be the optimal architecture design. For image classification in a vast search space, the neural architecture search (NAS) algorithm demonstrates favorable results on the productive discovery of outstanding architectures. Hence, inspired by the modularized architecture proposed by Zoph et al., Dai et al. proposed the search space of scalable architecture that generates pyramidal representations. They proposed architecture, called NAS-FPN, which provides a lot of flexibility in building object detection architecture and is adaptable to a variety of backbone models, on a wide range of accuracy and speed tradeoffs [15].

Various detection systems repurpose classifiers by taking a classifier for an object and evaluating it at multiple locations and scales in a test image. For example, R-CNN uses region proposal methods to first produce bounding boxes that are likely to appear in an image and then, on these suggested boxes, run a classifier. These intricate pipelines were slow and hard to optimize. Hence, Ghiasi et al. proposed you only look once (YOLO), an algorithm that is a single convolutional network that simultaneously predicts multiple bounding boxes and class probabilities for those boxes. Unlike R-CNN and other similar algorithms, YOLO is found to be extremely fast and sees the entire image during training and testing, hence making fewer background errors. When trained on natural images and tested on the artwork, YOLO outperforms other algorithms by a wide margin. But YOLO was yet found to lag behind state-of-the-art detection systems in accuracy and struggled to localize some objects precisely [16]. Redmon et al. by focusing mainly on improving recall and localization while maintaining classification accuracy, proposed YOLOv2. It was then found that detection methods are constrained to a small set of objects; hence, they as well proposed a joint training algorithm that allows one to train object detectors on both detection and classification data, using which they trained the YOLO9000 algorithm which was built by modifying YOLOv2 [17].

The majority of the accurate CNN-based object detectors required high GPU power and training in order to achieve their optimal accuracy. High GPU power is essential for achieving accuracy and speed in real-time since it is vital in a car collision or obstacle warning model. Redmon and Farhadi proposed a modified version of the state-of-the-art object detection models, YOLOv5, with significant improvement in the speed and accuracy of the models. An impressive aspect of this model is that it can operate in real-time on a conventional GPU and training as well requires only a single GPU. Hence, using conventional GPUs such as 1080Ti or 2080 Ti, we can train an accurate and extremely fast object detector [18]. Since YOLOv5 outperforms other frameworks, our proposed framework is based on it.

Traditionally, traffic sign identification has been based on colour and form patterns, with two associated stages: detection and classification [19, 20]. After many preprocessing processes, such as data transformation and normalisa-

tion, which consists of identifying areas of interest (ROI) based on colour segmentation and “sliding window” manner, traffic signs are detected in the image. Following the pattern recognition step, the classification stage involves classifying each sign feature into categories such as “speed restrictions” and “pedestrian crossing.” The template-matching technique was used to improve the feature classification process in [19]. The probable traffic indicators are then classified using a shallow neural network (i.e., a multi-layer perceptron (MLP)). Hmida et al. [20] suggested a hardware design that uses a template-matching approach to classify traffic indicators. Similarly, for successful feature extraction and classification, some studies have used shallow classifiers, such as support vector machines (SVMs) or random forests, in combination with local descriptors like the histogram of oriented gradient (HOG), such as [21]. Hmida et al. [22], for example, presented a traffic sign identification system based on linear SVMs and the MNIST dataset. Gecer et al. [23] used a high-performance technique for traffic sign identification based on blob detectors and SVM classifiers, which increased the model’s colour discriminating capacity by obtaining an accuracy rate of 98.94 percent. However, because of the broad variety of road signs in unexpected locations, obscured and tiny road signs, and fluctuating weather conditions (e.g., shadows and lightning), it is difficult to distinguish them using conventional approaches, which is why deep learning techniques are used.

Many studies have applied facial features and convolution network-based object detection models for the autonomous assistance of drivers based on obstacle detection. These models do not possess optimal architecture design and region identification mechanism. The existing methods provide better accuracy of detection of objects with speed of detection as a trade-off metric. Pipelining of existing detectors was unable to detect the larger object spaces. Hence, the proposed solution comes with utilization of conventional GPU power-based pipelined and accurate YOLOv5 framework for obstacle detection on a higher speed.

3. Proposed Work

ADAS is developed with the help of YOLOv5 model with efficient obstacle detection mechanism and faster speed. The object detection is done with the help of mobile application and alerts to the user. Car processing unit detects the real time video of the driver’s view and fed to the model for the accurate and fast detection of objects in urban roads. The input video is processed as frames; each of which acts as input to the object recognition and detection algorithm (YOLOv5). Each frame is processed along three stages in the algorithm, namely, backbone, neck, and head as shown in Figure 1.

- (i) Backbone [24]: CSPDarknet53
- (ii) Neck: concatenated path aggregation networks (PANet) with spatial pyramid pooling (SPP) additional module
- (iii) Head: YOLO layer

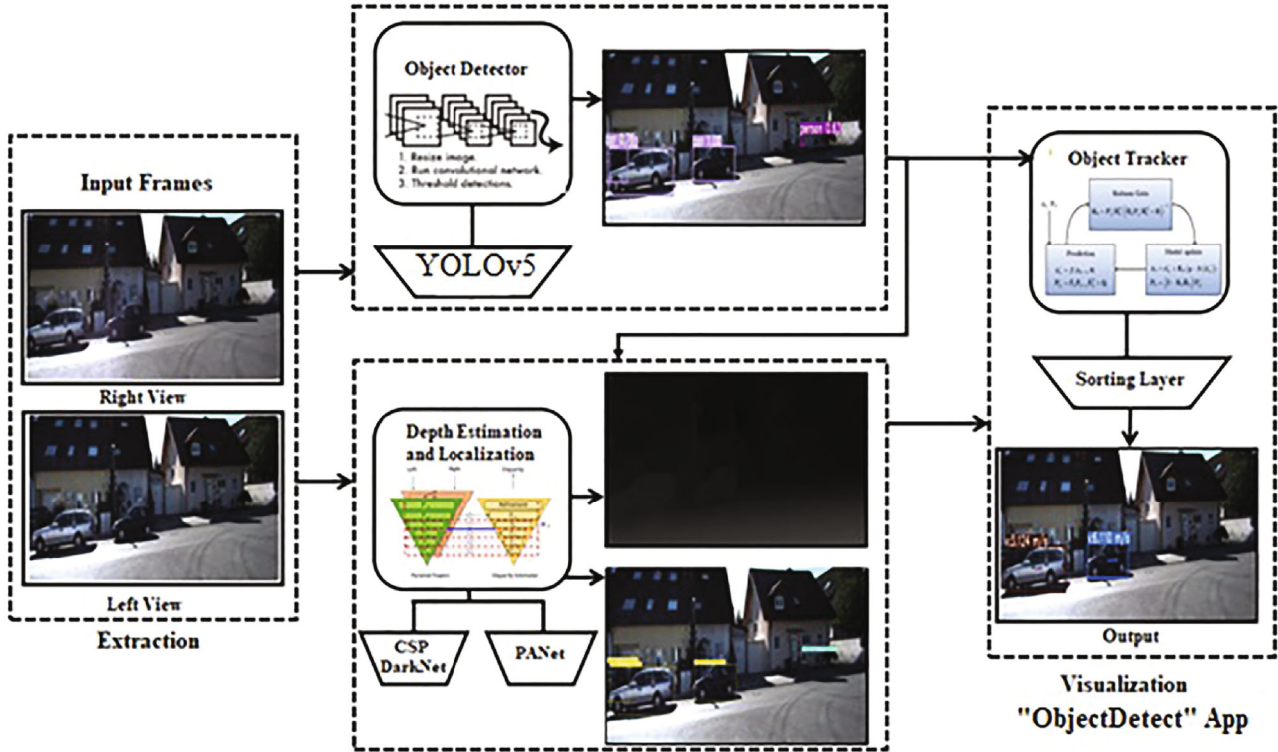


FIGURE 1: Proposed “ObjectDetect” framework for object detection and tracking.

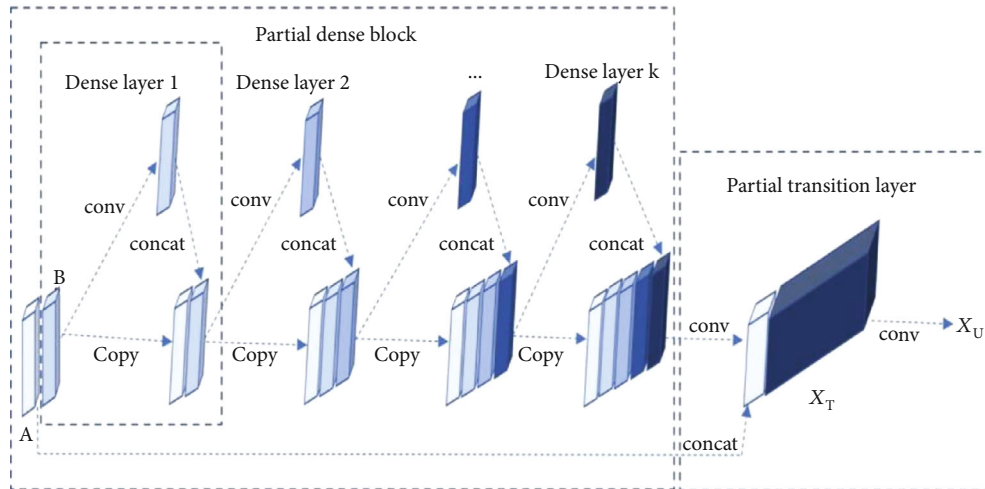


FIGURE 2: The overview of CSPDenseNet.

Proposed system comprises three major modules. These 3 modules are

- (i) Object extraction (backbone and neck)
- (ii) Object detection and tracking (head)
- (iii) Object visualization

3.1. *Object Extraction.* The backbone and neck take images (each of the frames) as input to extract the feature maps using CSPDarknet53 and SPP, PANet path-aggregation.

Darknet53 comprises 53 convolutional layers. For detection tasks, 53 layers stacked on to the original architecture of 53 layers give us 106 layers of architecture.

Step 1. Input: the video input is processed frame by frame

Step 2. CSPDarknet53: cross-stage-partial-connections are concerning used to eliminate duplicate gradient information that occurs while using conventional DenseNet [25]

- (i) In CSPDenseNet, the base layer is divided into 2 parts; here, part A and part B

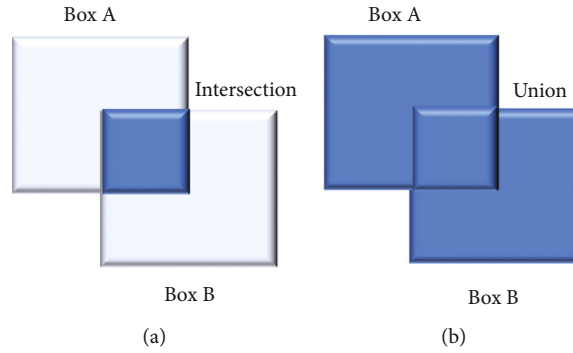


FIGURE 3: (a) The intersection of bounding boxes. (b) The union of bounding boxes.

- (ii) One part will go into the original dense block and is processed accordingly; here, part B is processed in the dense block
- (iii) The other part will directly skip to the transition stage

As a result of this, there is no duplicate gradient information; it also reduces a lot of computations, as shown in Figure 2.

Step 3. Additional layers are added between the backbone and the head using the neck. To aggregate the information, the YOLOv5 algorithm applies a modified path aggregation network [26] with a modified spatial attention module and a modified SPP (spatial pyramid pooling) [27]. Concatenated path aggregation networks [28] with spatial pyramid pooling (SPP) additional modules [26] are used to increase the accuracy of the detector

3.2. Object Detection. Each frame processed in the backbone and neck is then transferred to the head which involves the YOLOv5 algorithm which works using the following techniques:

Step 1. Residual blocks: initially, the input frame is divided into grids. Each grid cell is responsible for detecting the objects present in its cell

Step 2. Bounding box regression: the YOLO algorithm runs such that bounding boxes and confidence scores are predicted around every object present in that particular grid

Every bounding box consists of these attributes: width (bw), height (bh), bounding box center (x, y), and confidence score (c). The confidence score represents how confident and accurate the algorithm is of a particular object in that bounding box. Together with these attributes, YOLO uses a single bounding box regression to predict the probability of an object appearing in the bounding box. Figure 3 shows the YOLOv5 algorithm being run in real-time on a webcam. The algorithm detected objects in the frames by indicating the classes they belong to and the confidence scores representing how sure it is of the objects.

Step 3. Intersection over union (IoU): if no object exists in a grid cell, then the confidence score is zero; else, the confidence score must be equal to the intersection over union (IoU) between the predicted box and ground truth. Here, the ground truth boxes are manually predefined by

the user; hence, greater IoU means greater confidence score, which means higher accuracy of prediction by the algorithm. Filtration of those boxes with no objects is done based on the probability of objects in that box. Nonmax suppression processes eliminate the unwanted bounding boxes, and the box with the highest probability or confidence score will remain [29]

$$\text{IoU} = \frac{\text{Area of } (\text{BoxA} \cap \text{BoxB})}{\text{Area of } (\text{BoxA} \cup \text{BoxB})}. \quad (1)$$

The above Equation (1) IoU calculation is used to measure the overlap between two proposals.

Nonmax suppression [30]: this is used to find the appropriate bounding box among the predicted bounding boxes by the algorithms based on the confidence scores. This is represented in Algorithm 1 below.

Step 4. Final detection: the algorithm detects the object and class probabilities with confidence scores. This is depicted in Figures 4(a)–4(c)

4. Visualization

The final module of the proposed system involves an android-based application. The application inputs a real-time video stream from the device; camera runs an object detection algorithm on it and notifies the user under any case of any condition that requires to be brought to the user's attention and needs to be acknowledged [31]. These conditions could be any obstacle or collision ahead or the user being in close contact with respect to the user's position. With the YOLOv5 algorithm, the system is powerful enough to run object detection in various weather conditions. The alerts are of 3 categories:

- (i) The green alert is shown when there are no threats detected
- (ii) The yellow alert is shown when the threat detected is of low priority, such as stationary objects in front of the vehicle, like animals or pedestrians crossing
- (iii) The red alert is shown when the threat detected is of the highest priority such as objects approaching the car at high speeds

```

Input: Set of proposal boxes  $A$ , corresponding confidence scores  $C$  and overlap threshold  $T$ .
Output: A list of filtered proposals  $F$ .
procedure Sup( $A, m$ )
   $A_{sup} \leftarrow \emptyset$ 
  for  $a_i \in A$  do
    remove  $\leftarrow false$ 
    for  $a_j \in A$  do
      if  $match(a_i, a_j) > \alpha_{sup}$  then
        if  $value(m, a_j) > value(m, a_i)$  then
          remove  $\leftarrow true$ 
      else remove then
         $A_{sup} \leftarrow A_{sup} \cup a_i$ 
  return  $A_{sup}$ 

```

ALGORITHM 1: Non_Max_Suppression (Sup).

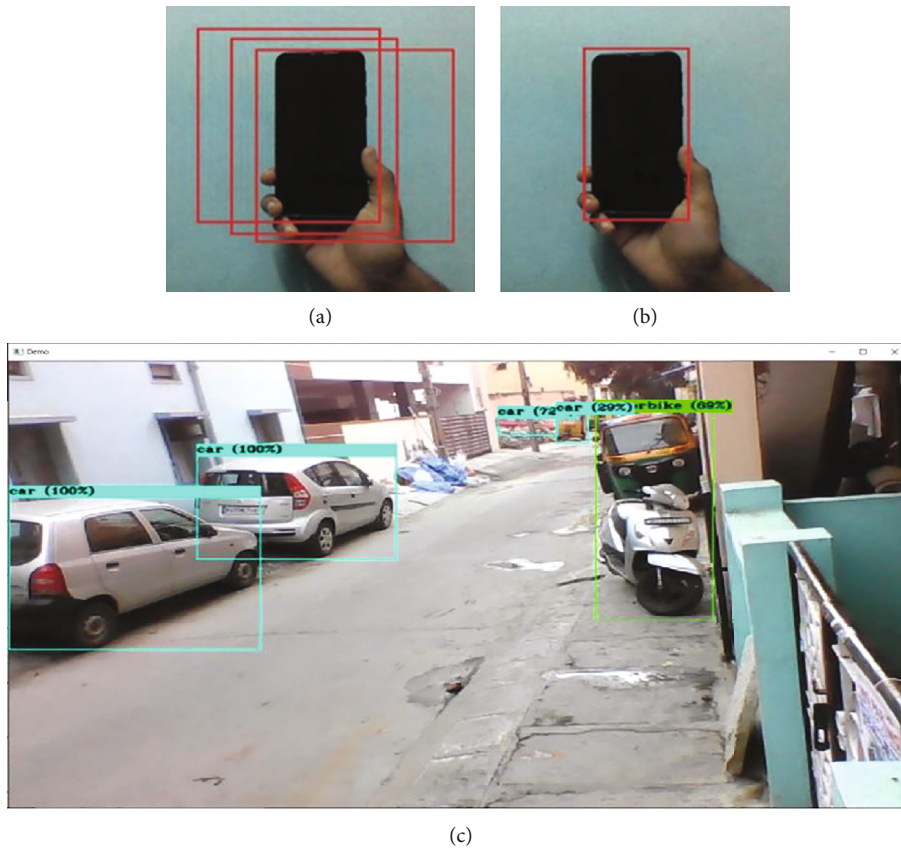


FIGURE 4: (a, b) Bounding boxes and class predictions. (c) Confidence scores around the objects when the algorithm is run on a webcam in real-time.

5. Evaluation Results

With the aim of creating a CNN for real-time operation on a conventional GPU, YOLOv5 was introduced. In the process of doing so, various training improvement methods on the accuracy of the classifier on the ImageNet dataset were tested, and their influence was noted along with the accuracy

of the detector on the MS COCO dataset with the following configuration.

PC specification:

Central processing unit: 11th generation Intel® Core™ i7

Graphic processing unit: NVIDIA®, 16 GB graphic card

Hard disk capacity: 1 TB

OS requirement: iOS/Windows 10/Ubuntu 18



FIGURE 5: YOLOv5 on rural road dataset.



FIGURE 7: YOLOv5 on highway dataset.



FIGURE 6: YOLOv5 on urban road dataset.

Random access memory: 16-32 GB
 Car computing unit specification:
 NVIDIA Jetson Xavier NX 16 GB
 Central processing unit: ARM®v8.2
 Graphic processing unit: NVIDIA®, CUDA®
 Hard disk capacity: 1 TB
 OS requirement: iOS/Windows 10/Ubuntu 18
 Random access memory: 16-32 GB

While comparing YOLOv5 with other state-of-the-art object detectors, it was found that YOLOv5 improved YOLOv4's AP by 10% and FPS by 12%, and within comparable performance, YOLOv5 ran twice faster than Efficient-Det [32]. It was found that the classifiers' accuracy was enhanced by proposing features such as CutMix and Mosaic data augmentation, class label smoothing, and Mish activation [33, 34].

In order to evaluate the proposed framework, 3 different types of datasets based on three categories such as rural roads, urban roads, and highways were used. The 3 datasets were created by labelled annotations of images which were captured as a novel part of research work. 8% of the collected data consisted of blurry images and images with low visibility. An example of each dataset is shown in Figures 5–7. The 3 different datasets were categorized as explained in Table 1.

TABLE 1: Datasets.

Sl. no.	Datasets	Number of images
1	Rural roads	1,20,000
2	Urban roads	1,24,000
3	Highways	1,50,000

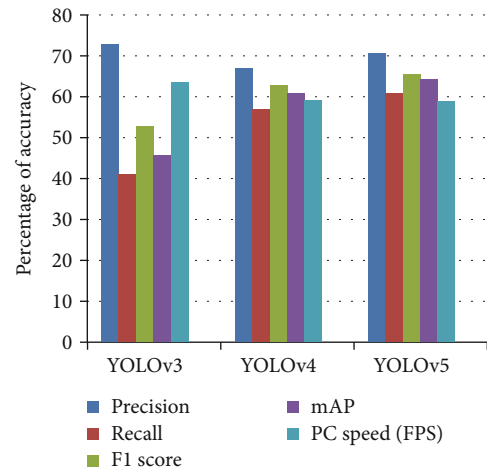


FIGURE 8: Comparative analysis of state-of-the-art models of rural road dataset.

The main goal of the research work is to reduce and increase the accuracy and speed at which the objects are detected; hence, here, the mAP (mean of average precision) and FPS (frames per second) play a very important role. The measures such as precision, recall, F -measure, PC speed (FPS), and Jetson speed (FPS) are used to compare the proposed model against two classic algorithms such as YOLOv3 [35, 36] and YOLOv4. The measures are listed below.

$$mAp = \sum_{q=1}^Q \frac{AveP(q)}{Q}, \quad (2)$$

$$F1score = 2 * \frac{(Precision * Recall)}{(Precision + Recall)}, \quad (3)$$

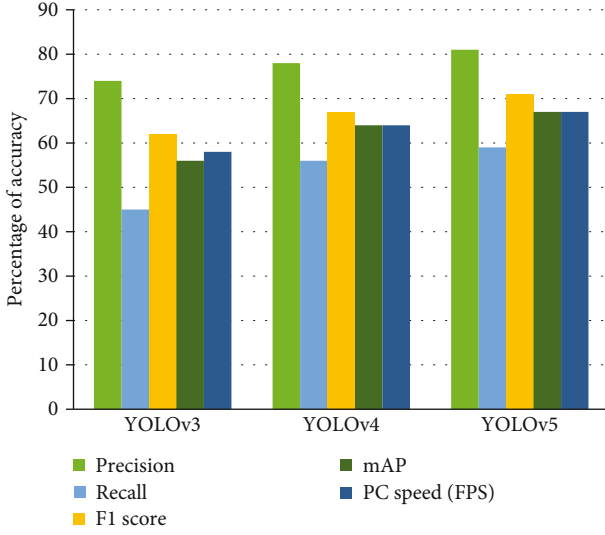


FIGURE 9: Comparative analysis of state-of-the-art models of urban road dataset.

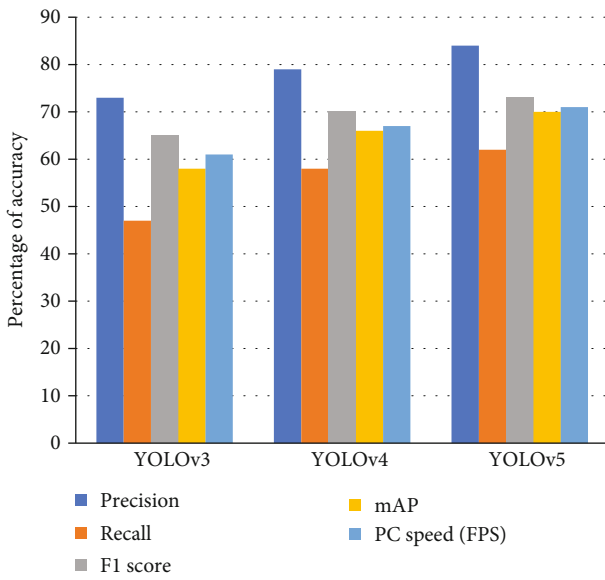


FIGURE 10: Comparative analysis of state-of-the-art models of highway dataset.

$$\text{Precision} = \frac{(\text{True Positive})}{(\text{True Positive} + \text{False Positive})}, \quad (4)$$

$$\text{Recall} = \frac{(\text{True Positive})}{(\text{True Positive} + \text{False Negative})}. \quad (5)$$

Figures 8–10 present the comparative analysis of YOLOv5 against other state-of-the-art models in rural roads, urban roads, and highway datasets. Here, YOLOv3 has good precision but has very bad recall and F -measure. Also, the mAP and FPS are very low. But YOLOv4 and YOLOv5 comparatively has balanced scores, but YOLOv5 outperforms other two algorithms because since the proposed works are

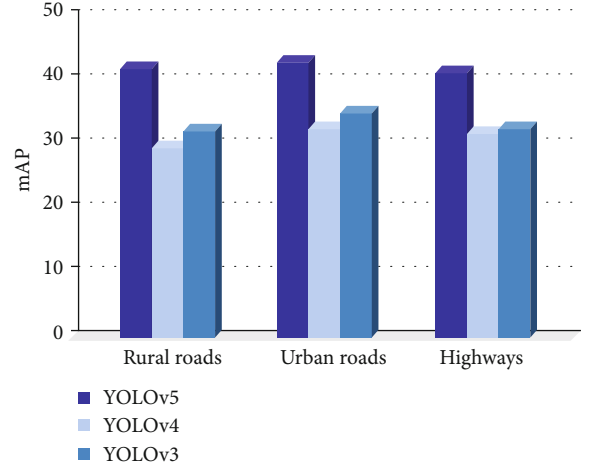


FIGURE 11: Comparison of state-of-the-art object detectors on the custom dataset.

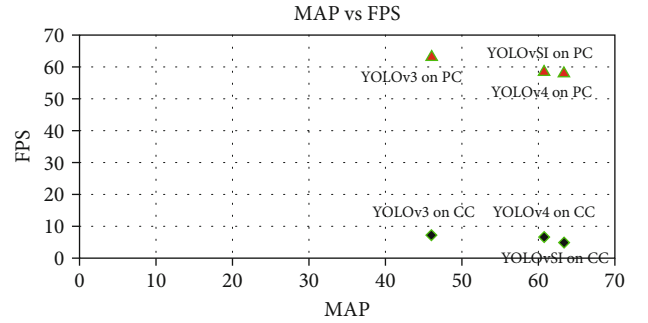


FIGURE 12: Graphical analysis of mAP vs. FPS with PC and CC specifications.

aimed at increasing speed and accuracy, YOLOv5 is the best fit state-of-the-art model for problem definition.

The mAP of the state-of-the-art object detectors such as YOLOv3, YOLOv4, and YOLOv5 was compared using the three datasets, i.e., rural roads, urban roads, and highway datasets given below. The results of this comparison are represented in Figure 11. With respect to mAP, it is clearly seen that YOLOv5 outperforms the other two by a significant margin.

Figure 12 represents a comparative analysis of YOLOv5 with other state-of-the-art object detection algorithms regarding mean average precision (y -axis) and frames per second (x -axis) for PC and CC specifications as listed below in table. From Figure 12, it can be inferred that the YOLOv5 algorithm performs better than others in real-time detection. It achieves an average precision between 67 and 70 and frames per second between 65 and 124.

6. Conclusions

The proposed framework is intended to provide real-time object detection with optimal speed and accuracy to assist the driver. This framework is achieved by implementing the state-of-the-art YOLOv5 algorithm. The whole framework is implemented in the form of three major modules, namely, extraction, detection, and visualization. The first

module, extraction, is used to obtain the feature map of the given input. The detection module identifies and localizes the object present in the input. The last module is used to provide an interface that comprises alerts and warnings. The proposed framework is applied to build the android application called “ObjectDetect” which assists the user by notifying them of significant events that require the user to analyze and decide based on it. The proposed application, “ObjectDetect,” relies majorly on a camera. With the help of some sophisticated cameras, this system can operate under challenging weather conditions. Hence, in the future, we can integrate this system with other sensors, such as LIDAR, to enhance speed and accuracy. The visualization can be improved by integrating “ObjectDetect” with other driver assistance technologies, such as Google Maps and voice assistant. In the future, with the help of a cloud-based approach, the processes can be recorded and analyzed. The cloud-based approach also helps in increasing the accessibility of the application. Raspberry pi can also be used in order to have a smooth flow in the processes and increased efficiency. In the future, the proposed framework can be integrated with the electronic control unit (ECU) present inside the vehicles.

Data Availability

No data were used to support this study.

Conflicts of Interest

The authors declare that they have no conflicts of interest.

References

- [1] “National motor vehicle crash causation survey,” *National Highway Traffic Safety Administration Technical Report DOT HS*, vol. 811, 2008.
- [2] <https://www.newsbytesapp.com/news/auto/most-affordable-ad-as-equipped-cars-available-in-india/story>.
- [3] P. Kiran, B. D. Parameshachari, J. Yashwanth, and K. N. Bharath, “Offline signature recognition using image processing techniques and back propagation neuron network system,” *SN Computer Science*, vol. 2, no. 3, pp. 1–8, 2021.
- [4] L. Wang, Y. Zhang, and J. Wang, “Map-based localization method for autonomous vehicles using 3D-LIDAR,” *IFAC-Papers OnLine*, vol. 50, no. 1, pp. 276–281, 2017.
- [5] Q. Zou, H. Jiang, Q. Dai, Y. Yue, L. Chen, and Q. Wang, “Robust lane detection from continuous driving scenes using deep neural networks,” *IEEE Transactions on Vehicular Technology*, vol. 69, no. 1, pp. 41–54, 2020.
- [6] S. N. Shivappriya, M. Priyadarsini, A. Stateczny, C. Puttamadappa, and B. D. Parameshachari, “Cascade object detection and remote sensing object detection method based on trainable activation function,” *Remote Sensing*, vol. 13, no. 2, p. 200, 2021.
- [7] Q. Cabanes and B. Senouci, “Objects detection and recognition in smart vehicle applications: point cloud based approach,” in *2017 Ninth International Conference on Ubiquitous and Future Networks (ICUFN)*, pp. 287–289, Milan, Italy, 2017.
- [8] P. Jagannathan, S. Rajkumar, J. Frnda, P. B. Divakarachari, and P. Subramani, “Moving vehicle detection and classification using Gaussian mixture model and ensemble deep learning technique,” *Wireless Communications and Mobile Computing*, vol. 2021, 15 pages, 2021.
- [9] J. F. Chen, C. C. Wang, and C. F. Chou, “Multiple target tracking in occlusion area with interacting object models in urban environments,” *Robotics and Autonomous Systems*, vol. 103, pp. 68–82, 2018.
- [10] S. Kato, E. Takeuchi, Y. Ishiguro, Y. Ninomiya, K. Takeda, and T. Hamada, “An open approach to autonomous vehicles,” *IEEE Micro*, vol. 35, no. 6, pp. 60–68, 2015.
- [11] S. Shaily, S. Krishnan, S. Natarajan, and S. Periyasamy, “Smart driver monitoring system,” *Multimedia Tools and Applications*, vol. 80, no. 17, pp. 25633–25648, 2021.
- [12] L. Liu, W. Ouyang, X. Wang et al., “Deep learning for generic object detection: a survey,” *International Journal of Computer Vision*, vol. 128, no. 2, pp. 261–318, 2020.
- [13] Z. Zou, Z. Shi, Y. Guo, and J. Ye, “Object detection in 20 years: a survey,” 2019, <http://arxiv.org/abs/1905.05055>.
- [14] R. Girshick, “Fast r-cnn,” in *Proceedings of the IEEE international conference on computer vision*, pp. 1440–1448, 2015.
- [15] J. Dai, Y. Li, K. He, and J. Sun, “R-fcn: object detection via region-based fully convolutional networks,” in *Advances in neural information processing systems*, vol. 29, pp. 379–387, 2016.
- [16] G. Ghiasi, T. Y. Lin, and Q. V. Le, “Nas-fpn: learning scalable feature pyramid architecture for object detection,” in *Proceedings of the IEEE/CVF Conference on Computer Vision and Pattern Recognition*, pp. 7036–7045, 2019.
- [17] J. Redmon, S. Divvala, R. Girshick, and A. Farhadi, “You only look once: unified, real-time object detection,” in *Proceedings of the IEEE conference on computer vision and pattern recognition*, pp. 779–788, 2016.
- [18] J. Redmon and A. Farhadi, “YOLO 9000: better, faster, stronger,” in *Proceedings of the IEEE conference on computer vision and pattern recognition*, pp. 7263–7271, 2017.
- [19] A. Hechri, R. Hmida, and A. Mtibaa, “Robust road lanes and traffic signs recognition for driver assistance system,” *International Journal of Computational Science and Engineering*, vol. 10, no. 1/2, pp. 202–209, 2015.
- [20] R. Hmida, A. Ben Abdelali, and A. Mtibaa, “Hardware implementation and validation of a traffic road sign detection and identification system,” *Journal of Real-Time Image Processing*, vol. 15, no. 1, pp. 13–30, 2018.
- [21] J. Greenhalgh and M. Mirmehdi, “Real-time detection and recognition of road traffic signs,” *IEEE Transactions on Intelligent Transportation Systems*, vol. 13, no. 4, pp. 1498–1506, 2012.
- [22] R. Hmida, A. B. Abdelali, and A. Mtibaa, “Speed limit sign detection and recognition system using SVM and MNIST datasets,” *Neural Computing and Applications*, vol. 31, no. 9, pp. 5005–5015, 2019.
- [23] B. Gecer, G. Azzopardi, and N. Petkov, “Color-blob-based COSFIRE filters for object recognition,” *Image and Vision Computing*, vol. 57, pp. 165–174, 2017.
- [24] C. L. Su, W. C. Lai, J. Y. Wu, and P. Y. Wang, “Design and implementation of edge computing for detection on embedded electromobility,” in *4th International Conf. on Artificial Intelligence for Industries (AII)*, Laguna Hills, CA, USA, 2021.
- [25] A. Bochkovskiy, C. Y. Wang, and H. Y. M. Liao, “YOLOv5: optimal speed and accuracy of object detection,” 2020, <http://arxiv.org/abs/2004.10934>.

- [26] C. Y. Wang, H. Y. M. Liao, Y. H. Wu, P. Y. Chen, J. W. Hsieh, and I. H. Yeh, "CSPNet: a new backbone that can enhance learning capability of CNN," in *In Proceedings of the IEEE/CVF conference on computer vision and pattern recognition workshops*, pp. 390-391, 2020.
- [27] S. Liu, L. Qi, H. Qin, J. Shi, and J. Jia, "Path aggregation network for instance segmentation," in *In Proceedings of the IEEE conference on computer vision and pattern recognition*, pp. 8759-8768, 2018.
- [28] K. He, X. Zhang, S. Ren, and J. Sun, "Spatial pyramid pooling in deep convolutional networks for visual recognition," *IEEE Transactions on Pattern Analysis and Machine Intelligence*, vol. 37, no. 9, pp. 1904-1916, 2015.
- [29] H. Rezatofighi, N. Tsoi, J. Gwak, A. Sadeghian, I. Reid, and S. Savarese, "Generalized intersection over union: a metric and a loss for bounding box regression," in *In Proceedings of the IEEE/CVF Conference on Computer Vision and Pattern Recognition*, pp. 658-666, 2019.
- [30] A. Amidi and S. Amidi, *VIP cheatsheet: convolutional neural networks*, 2018.
- [31] J. Redmon, *YOLOv3: an incremental improvement*/Joseph Redmon, Ali Farhadi-University of, Washington, 2018.
- [32] Y. H. Lee and Y. Kim, "Comparison of CNN and YOLO for object detection," *Journal of the semiconductor & display technology*, vol. 19, pp. 85-92, 2020.
- [33] S. Ren, K. He, R. Girshick, and J. Sun, "Faster r-cnn: towards real-time object detection with region proposal networks," *Advances in Neural Information Processing Systems*, vol. 28, pp. 91-99, 2015.
- [34] C. Lee, H. J. Kim, and K. W. Oh, "Comparison of faster R-CNN models for object detection," in *In 2016 16th international conference on control, automation and systems (iccas)*, pp. 107-110, Gyeongju, Korea (South), 2016.
- [35] C.-L. Su, W.-C. Lai, and C. Te Li, "Pedestrian detection system with edge computing integration on embedded vehicle," in *International Conf. on Artificial Intelligence in Information and Communication (ICAIIIC)*, Jeju Island, Korea (South), 2021.
- [36] C. L. Su, W. C. Lai, Y. K. Zhang, T. J. Guo, Y. J. Hung, and H. C. Chen, "Artificial intelligence design on embedded board with edge computing for vehicle applications," in *IEEE 3rd International Conf. on Artificial Intelligence and Knowledge Engineering (AIKE)*, Laguna Hills, CA, USA, 2020.

Research Article

Mobile Sink-Based Path Optimization Strategy in Heterogeneous WSNs for IoT Using Pigeon-Inspired Optimization Algorithm

Zhengzong Wang, Yinggao Yue , and Li Cao 

School of Intelligent Manufacturing and Electronic Engineering, Wenzhou University of Technology, Wenzhou 325035, China

Correspondence should be addressed to Li Cao; caoli198723@163.com

Received 26 January 2022; Revised 21 April 2022; Accepted 16 May 2022; Published 11 June 2022

Academic Editor: Alireza Souri

Copyright © 2022 Zhengzong Wang et al. This is an open access article distributed under the Creative Commons Attribution License, which permits unrestricted use, distribution, and reproduction in any medium, provided the original work is properly cited.

Data collection is the basic purpose of deploying in heterogeneous WSNs for Internet of things, and the problem of data collection is the key problem that needs to be solved in heterogeneous WSNs. How to collect energy-efficient and reliable data is one of the key technologies of heterogeneous WSNs. Collecting the sensor node data by mobile sink is an effective measure to solve data collection efficiency. To this end, a data collection strategy of mobile sink for heterogeneous WSNs based on pigeon-inspired optimization by PSO algorithm is proposed. The proposed algorithm uses the improved pigeon-inspired optimization by particle swarm optimization algorithm to select the best dwell point and then regards the construction of the moving path based on the dwell point as a traveling salesman problem to optimize the moving path and solve the optimal moving path. The experimental analysis and simulation results show that, compared with other algorithms, the algorithm proposed in this paper can effectively prolong the lifetime of the network and reduce the delay of data collection, increasing the amount of data collection.

1. Introduction

With the rapid development of information technology and Internet of things, wireless sensor networks (WSNs) have been widely used in environmental monitoring, industrial production, intelligent agriculture, intelligent transportation systems, rehabilitation medicine, and other applications [1–3]. As a key technology in the field of data collection, it is now also the basis for big data and artificial intelligence technologies. In traditional heterogeneous WSNs, the data forwarding between sensor nodes usually adopts a multihop approach [4, 5]. However, due to the large amount of data forwarded from other nodes, the sensor nodes near sink are prone to die due to excessive energy consumption, resulting in the interruption of the network link [6, 7]. At the same time, these sensing nodes are micronodes, which are generally powered by batteries. Their node energy is limited, and the transmission of sensing data requires multiple hops, which limits the application of WSNs [8]. To avoid this problem, researchers propose a mobile sink data collection method [9]. The mobile sink moves according to a cer-

tain path in the monitoring area. It is not advisable to move the sink to visit every sensor node [10]. How to plan the path of moving sinks in the sensing area of heterogeneous WSNs, so that the sensing data passes through fewer hops and is collected to sink nodes within a limited delay, becomes a challenge.

The core problem of this paper is how to use the mobile sink to collect data efficiently and reliably for heterogeneous WSNs [11]. In order to better achieve the goal, we need to save network energy, extend the network life cycle, and reduce network latency [12]. To this end, the following two algorithms according to the number of mobile sinks are proposed. A data collection strategy for heterogeneous WSNs is based on a single mobile sink. The main work of this paper is as follows: A data collection algorithm based on a single sink is proposed. The algorithm is divided into two different stages: clustering and path planning. (1) In the clustering stage, the average residual energy of network nodes and the distribution density of neighbor nodes are considered. (2) In the path planning stage, for the selected number of N cluster head nodes, the mobile sink will traverse the

position of each cluster head according to the planned path to collect data. The mobile sink adopts pigeon-inspired optimization by PSO algorithm for path planning. The Euclidean distance between cluster heads is used as the weight, and the optimal path is found on the basis of the minimum spanning tree formed by all cluster heads. Since some nodes of the obtained minimum spanning tree have multiple connection paths, the idea of the PSO-PIO algorithm is to delete multiple branches of a node and reconnect all nodes. There is only one path in the entire area, and each cluster head is only passed through once, so as to obtain the shortest path for moving the sink, so that the network has the shortest delay in data collection.

In traditional heterogeneous WSNs, usually adopts a multihop approach. However, due to the massive forwarding of data from other nodes, the nodes located near the sink are prone to die due to excessive energy consumption, resulting in network link interruption. At the same time, these sensing nodes are micronodes, which are generally powered by batteries. Their node energy is limited, and the transmission of sensing data requires multiple hops, which limits the application of WSNs. To avoid this problem, a mobile sink-based data collection method of heterogeneous WSNs is proposed. The mobile sink starts from a certain point, visits each node, and completes the task of data collection. Such a process can generally be viewed as the traveling salesman problem. Solving the path planning strategy of moving sink is an NP-hard problem. The PIO algorithm performs search calculation and problem solving according to the unique homing behavior of the pigeon flock. Through the experimental analysis of the heterogeneous WSNs data collection method of the PSO-PIO algorithm and the comparison with other algorithms, the algorithm can effectively prolong the lifetime of the network and reduce the delay of data collection.

2. Related Work

In traditional heterogeneous WSNs, the nodes transmit data to a fixed base station in a multihop manner, which easily causes nodes near the base station to participate in excessive data forwarding. The researchers propose a data collection scheme of mobile sink. The coordination network formed between UAVs and WSNs helps to improve the quality and coverage. Combined with the UAV maneuverability model, a data collection model combining UAVs and wireless sensor networks is established. The model considers the importance of topology and strategic location to determine UAV waypoints and determine data transfer patterns. Sayeed et al. proposed a new maneuverability of attraction factor of UAV moving waypoints [13]. Data loss and latency in cluster heads are caused by energy consumption and duplication of work. Cluster members send data from the threshold model to the cluster head. Cluster heads collect data from mobile sinks and report to receivers when data arrives nearby [14].

The data collection scheme of heterogeneous WSNs based on the mobile sink mainly includes fixed movement, random movement, and controlled movement.

2.1. Random Movement. In random movement, the path of moving the sink is not set in advance. For example, if the node is placed on an animal, the movement trajectory of the animal is random, although this scheme is easy to implement [14, 15]. The remaining energy and position of nodes are the main parameters for selecting cluster heads. A control strategy for mobile receivers to collect data from cluster heads is designed [16]. Movement trajectory planning of mobile agents has been receiving much attention. Based on the traversal sequence, the mobile agent uses the particle swarm algorithm to select anchor nodes for each CHs within the communication range. The communication range is dynamically adjusted, and anchor nodes are merged in duplicate coverage areas to further improve performance [17]. In MWSN, the nodes enter and exit the network randomly, and due to the limited resources in WSNs, the link quality of the path used for data transmission and the time consumed by data forwarding must be tested [18].

2.2. Fixed Movement. In fixed movement, mobile sinks visit some prespecified locations along a fixed route and collect data from groups of sensor nodes. Kumar et al. proposed an efficient algorithm to improve the data collection process, using a network flow approach to achieve efficient data forwarding [19, 20]. According to the traveling salesman problem (TSP), the mobile actor tour program passes through these rendezvous points. We also propose a new rendezvous node rotation scheme to equitably utilize all nodes [21]. In resource-constrained wireless sensor networks, energy saving is a key issue. The use of mobile receivers to transmit sensory data has become a common method to save the limited energy of sensors. Agrawal et al. proposed a mesh round-robin routing protocol (GCRP), which aims to minimize the overhead of updating the latest location of mobile receivers. A set of sharing rules is also proposed to govern when and with whom mobile sinks share the latest location information of receivers [22].

2.3. Controlled Movement. Controllable movement means that path planning can be performed according to the information fed back by the path [23]. Ren et al. proposed a mobile sink reliable data acquisition algorithm; this method greatly improves the efficiency of network work. [24].

In summary, solving the mobile sink path planning strategy is an NP-hard problem, such as node energy and node density. The pigeon flock algorithm performs search calculation and problem solving according to the unique homing behavior of the pigeon flock, and the PIO algorithm provides an effective approach.

3. Mathematical Model of Data Collection

The data collection of heterogeneous WSNs is mainly based on clustering data method, and its main content is to divide the network hierarchically. The entire network is divided into several cluster heads, and adjacent nodes are in one cluster [25]. Each cluster will choose a node as the cluster head, and all communications in the network are transmitted in the backbone network [26]. Compared with other

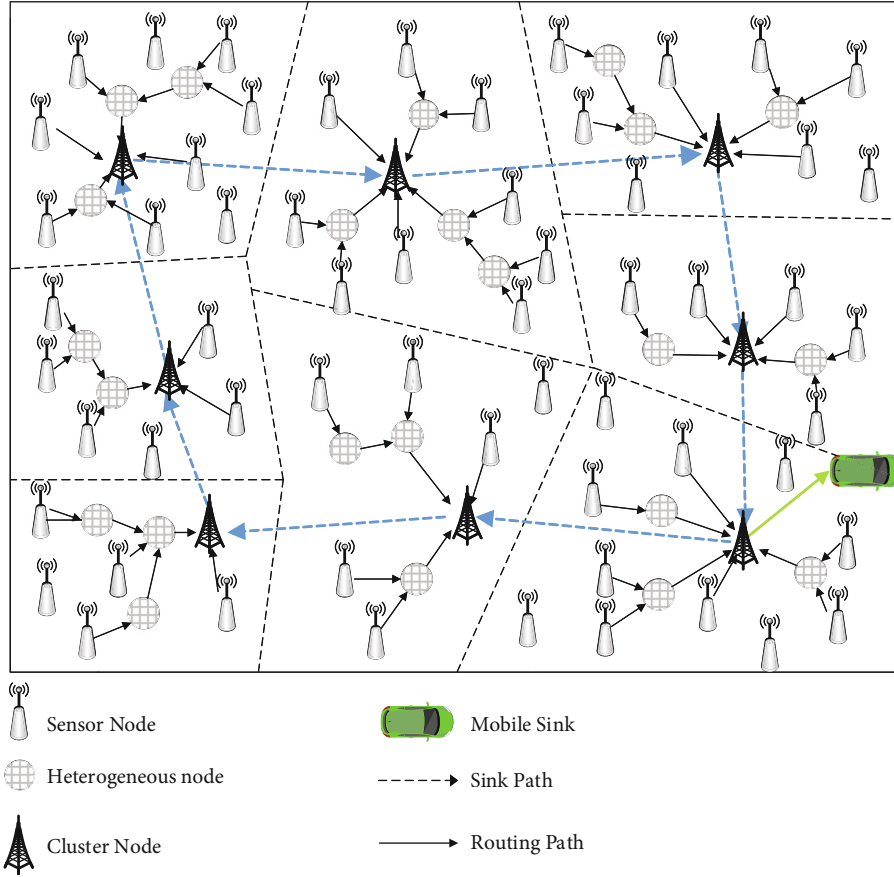


FIGURE 1: Data collection process of mobile sink based on RPs.

routing protocols, the clustering algorithm pays more attention to balancing the energy consumption, avoiding hotspot problems.

Although the mobile sink scheme can effectively improve the data collection rate, there is still a problem that must be solved in this scheme: the planning of the moving path of the sink. Obviously, with different moving paths, the data collected by nodes may be different, and the network energy consumption will also be different. Therefore, how to plan the movement of the sink is the key technology of the data collection scheme based on the mobile sink.

At present, there are two strategies to plan the movement path of the sink: (1) The mobile sink traverses the entire area within the network. (2) Moving sink only traverses some preset positions; these positions are called resident point rendezvous points (RPs). Compared with the first strategy, the path planning strategy citing RPs is more efficient and consumes less energy. The collection process of mobile sink based on RPs heterogeneous WSNs is shown in Figure 1. Mobile sinks form data collection paths by traversing RPs.

Mathematical model of mobile sink data collection for heterogeneous WSNs based on resident points rendezvous points (RPs):

The number of n nodes $\{s_1, s_2, s_3, \dots, s_n\}$ is deployed in the monitoring area of $l \times l$. Let s_i denote the i -th sensing

node, and $1 \leq i \leq n$. Each moving path of MS consists of the number of κ RPs, where $\kappa < n$. κ RPs constitute the set of RPs $Q = \{q_1, q_2, q_3, \dots, q_\kappa\}$.

Let the parameter T_p denote a moving path of the MS, which consists of K RPs. The sequence of paths T_p is $T_p = \{q_1, q_2, q_3, \dots, q_\kappa\}$. Use the following formula to calculate the length of the path T_p :

$$L(T_p) = d_{12} + \dots + d_{\kappa 1}, \quad (1)$$

where the parameter d_{ij} represents the distance between q_i and q_j traversed in the path.

The data collection method for heterogeneous WSNs aims to minimize the path T_p length and satisfy the constraints of data transmission delay and data volume. Let the parameter D_p^T denote the time delay for the sink node to collect data along the path T_p , and define the parameter D_p^T by D_{\max} . That is where the parameter D_{\max} represents the maximum delay allowed. Furthermore, let the parameter B denote the maximum data capacity allowed by the channel. The data transmitted by RP to the sink node each time should be less than B . Therefore, $W_k^{\text{out}} \leq B$, where the parameter W_k^{out} represents the amount of data transmitted by the k -th RP to the sink node in each round.

Finally, the objective function for establishing the data collection of heterogeneous WSNs based on path planning is as follows:

$$\min L(T_p), \quad (2)$$

$$\text{s.t. } D_p^T \leq D_{\max}, \quad (3)$$

$$W_k^{\text{out}} \leq D_{\max}, 1 \leq k \leq \kappa. \quad (4)$$

However, solving the mobile sink path planning strategy for RPs is an *NP*-hard problem, which is affected by multiple factors, such as node energy and node density. The pigeon flock algorithm performs search calculation and problem solving; according to the unique homing behavior of the pigeon flock, the pigeon-inspired optimization algorithm provides an effective new approach. Therefore, a mobile sink data acquisition algorithm based on PIO optimization by PSO algorithm is proposed, and the sink moves according to these resident points to form the optimal data transmission path.

4. Pigeon-Inspired Algorithm Optimization by Particle Swarm Optimization

4.1. Pigeon-Inspired Optimization Algorithm. Pigeon-inspired optimization (PIO) algorithm was proposed by Duan Haibin [27]. The design inspiration of the pigeon flock algorithm comes from the unique homing behavior of the pigeon flock [28, 29]. The algorithm mainly finds the global optimal solution of the optimization problem by simulating the navigation behavior of the pigeon flock. According to the behavior of pigeons in the process of homing, there are three key reference factors for their main navigation, which are [30] as follows: (1) the influence of the sun on the pigeon's homing and its navigation ability depend on the position of the sun; (2) the influence of geomagnetic field on pigeons [31]; the upper beak of pigeons contains a magnetic induction structure, which plays an important role in indicating the flight of pigeons. and (3) the influence of terrain landmarks on pigeon navigation and similar terrain will speed up the homing process of pigeons [32].

The homing navigation of the pigeon flock is mainly carried out in two ways. At different flight positions, pigeons will use different navigation tools. They should refer to the geomagnetic field to determine the direction [33]. Use iconic landmarks to navigate when they close to the destination [34].

Initialize a pigeon group with M individuals in the D -dimensional space; the position of the i -th ($i = 1, 2, 3, \dots, M$) pigeon in the population is represented by $X_i = (X_i^1, X_i^2, X_i^3, \dots, X_i^N)$; the speed of the i -th pigeon is represented by $V_i = (V_i^1, V_i^2, V_i^3, \dots, V_i^N)$; and the fitness of the pigeon is represented by the function $\text{fitness}(X_i^N)$, the geomagnetic compass operator is marked as N_{MAX1} , and the landmark operator is marked as N_{MAX2} . Each pigeon is based on the geomagnetic compass operator [35, 36]:

$$V_i^N = V_i^{N-1} * e^{-RN} + \text{rand} (X_G - X_i^{N-1}), \quad (5)$$

$$X_i^N = X_i^{N-1} + V_i^N, \quad (6)$$

$$X_C^N = \frac{\sum_{i=1}^{M^{(N)}} X_i^N F(X_i^N)}{M^{(N)} \sum_{i=1}^{M^{(N)}} F(X_i^N)}, \quad (7)$$

$$X_i^N = X_i^{N-1} + \text{rand} (X_C^{N-1} - X_i^{N-1}), \quad (8)$$

$$F(X_i^N) = \begin{cases} \frac{1}{\text{fitness}(X_i^N) + \varepsilon}, \text{Min-os} \\ \text{fitness}(X_i^N), \text{Max-os} \end{cases}, \quad (9)$$

$$M^{(N)} = \frac{M^{(N-1)}}{2}, \quad (10)$$

where the parameter X_C^N is the center position after the N -th iteration, which is identified as a landmark. $F(X_i^N)$ is the fitness function. For solving Min-os (minimum optimal solution), Max-os (maximum optimal solution) has two different forms, and $M^{(N)}$ is the number of pigeons remaining after the N -th iteration [37, 38]. After the above iteration loop reaches N_{MAX2} , the landmark operator stops working and outputs the optimal solution adapted at this time [39].

4.2. Pigeon-Inspired Algorithm Optimization by PSO. The PSO algorithm is a novel optimization algorithm proposed in recent years. There are not many studies on it at present. The advantage of PSO-PIO algorithm is that the PSO algorithm with fast convergence speed in the early stage can quickly lock the region where the optimal solution is located and sets up diversity monitoring. After the diversity drops to a certain level, the PIO algorithm performs a locked area search to quickly find the optimal solution.

4.2.1. The PSO Algorithm. The mathematical model of article swarm optimization (PSO) is as follows [40]: Assuming that there are S particles in a random distribution state in the D -dimensional space, let the coordinates of the i -th particle in the population be

$$x_i^N = [x_{i1}^N, x_{i2}^N, x_{i3}^N, \dots, x_{iD}^N]^T. \quad (11)$$

After N iterations, the optimal coordinate of the i -th particle is

$$p_i^N = (p_{i1}^N, p_{i2}^N, p_{i3}^N, \dots, p_{iD}^N). \quad (12)$$

The optimal coordinates of the swarm particles are

$$P_{g\text{best}}^N = (P_{g\text{best}1}^N, P_{g\text{best}2}^N, P_{g\text{best}3}^N, \dots, P_{g\text{best}D}^N). \quad (13)$$

The velocity of the i -th particle is

$$v_i^N = [v_{i1}^N, v_{i2}^N, v_{i3}^N, \dots, v_{iD}^N]^T. \quad (14)$$

After $N + 1$ iterations of the particle, its own velocity and

position are updated as

$$v_{id}^{N+1} = \omega^N v_{id}^N + c_1 r_1 (p_{id}^N - x_{id}^N) + c_2 r_2 (p_{gbest,d}^N - x_{id}^N), \quad (15)$$

$$x_{id}^{N+1} = x_{id}^N + v_{id}^N, \quad (16)$$

$$\omega^N = (\omega_{MAX} - \omega_{MIN}) \left(\frac{v_{max}^N - N}{v_{max}^N} \right) + \omega_{MIN}, \quad (17)$$

where ω is the dynamic inertia factor, c_1 and c_2 are the learning factors, r_1 and r_2 are random numbers between $[0,1]$, ω_{MAX} is the maximum value of the factor, ω_{MIN} is the minimum value, and v_{max} is the speed [41].

4.2.2. Particle Swarm Algorithm with Jump Operator. In the later iteration of particle swarm optimization, the optimal coordinates will be limited to the local area. To this end, an adaptive jump operator is added to compare the similarity between the optimal coordinates of individual particles and the optimal coordinates of group particles. Given the particles of different jump probabilities, after the N -th iteration, the probability formula and jump formula for the i -th particle to jump out of the current position are

$$p = \exp \left(f(p_{gbest}^N) - f(p_i^N) \right), \quad (18)$$

$$x_i^N = x_i^N + \text{rand} \times (\text{ub} - \text{lb}), \quad (19)$$

where the parameter rand is between $[0,1]$ and parameters ub and lb are upper and lower limits.

4.2.3. Pigeon Flock Algorithm with Interference Operator. In practical problems, the PIO algorithm also has a limited number of iterations that are prone to local optimal solutions. This phenomenon is particularly serious when solving optimization problems of complex functions. An interference operator is introduced:

$$\text{pert}(N) = 0.1 \times \text{rand} \times \left(1 - \frac{N}{N_{max}} \right), \quad (20)$$

$$X_i^N = X_i^N + \text{pert}(N) \times (\text{ub} - \text{lb}) \times (r_1 - r_2), \quad (21)$$

where the parameters rand , r_1 , and r_2 are random numbers on $[0,1]$ and the parameter $\text{pert}(N)$ is the interference operator.

4.2.4. Particle Swarm and Pigeon Swarm Hybrid Optimization Algorithm (PSO-PIO). The PSO-PIO algorithm redefines a diversity function.

$$\text{div}(N) = \frac{\sigma^N}{\sigma_{max}}, \quad (22)$$

$$\sigma^N = \frac{1}{m} \sum_{i=1}^m \left(l_i^N - l_{ave}^N \right)^2, \quad (23)$$

$$\sigma_{max} = \max_{j \in \{1,2,\dots,N\}} \{ \sigma_j \}, \quad (24)$$

where the parameter j is the j -th iteration. The parameter σ_j is the variance of the j -th generation population. The parameter l_i^N is the distance between the population particle, and the optimal particle after N iterations, $l_i^N = \sqrt{\sum_{d=1}^D (X_i^N - p_{gbest}^N)^2}$, the parameter D is the dimension. The parameter l_{ave}^N is the average Euclidean distance between the population particle and the optimal particle after N iterations, $l_{ave}^N = 1/m \sum_{i=1}^m l_i^N$.

The solution process of the PSO-PIO algorithm mainly includes two steps: The first step uses the particle swarm algorithm with a jump operator to perform a preliminary search, and when the diversity function drops to a certain threshold, it goes to the second step. Further optimal solutions are performed using the landmark operator of the pigeon colony algorithm with disturbance operator. The algorithm adopts the PSO algorithm with fast convergence speed in the early stage to quickly lock the region where the optimal solution is located and sets up diversity monitoring. After the diversity drops to a certain level, the interference algorithm PIO algorithm is used to search the locked area to quickly find the optimal solution. The implementation process is shown in Figure 2.

The basic steps of PSO-PIO algorithm are as follows:

Step 1. Initialization algorithm parameters. The population m , the space dimension D , the inertia factors ω_{MAX} and ω_{MIN} , the learning factors c_1 and c_2 , and the maximum number of iterations N_{MAX} .

Step 2. According to the fitness function, mark the individual optimal solution p_i and the current global optimal solution p_{gbest} .

Step 3. According to the PSO algorithm, gradually calculate the new position and new speed of each particle, compare the similarity between the particle's p_i and p_{gbest} , and calculate the particle's jump probability p , and set the random number $p_0 \in [0, 1]$. If $p > p_0$, the particle jumps out of the current position according to the jump formula; otherwise, it stays at the current position to calculate p_i and p_{gbest} for the next round.

Step 4. Use the diversity function to evaluate the diversity level of the population, and judge whether the diversity $\text{div}(N)$ is less than the set diversity threshold. If it is less than the set diversity threshold, terminate the PSO algorithm, enter the pigeon flock algorithm, and go to step 5; otherwise, go to step 3.

Step 5. Enter the landmark operator of the PIO algorithm with interference operator, and calculate the center position x_C of the population through the center position calculation formula (3).

Step 6. Update the center position x_C of the population and the position of each individual according to the landmark operator of the PIO algorithm, and calculate the probability pert according to the interference operator, determine the update position, and repeatedly calculate the particle position for the next iteration.

Step 7. Whether N is greater than N_{MAX} , if so, terminate the algorithm and output the result, otherwise go to step 6.

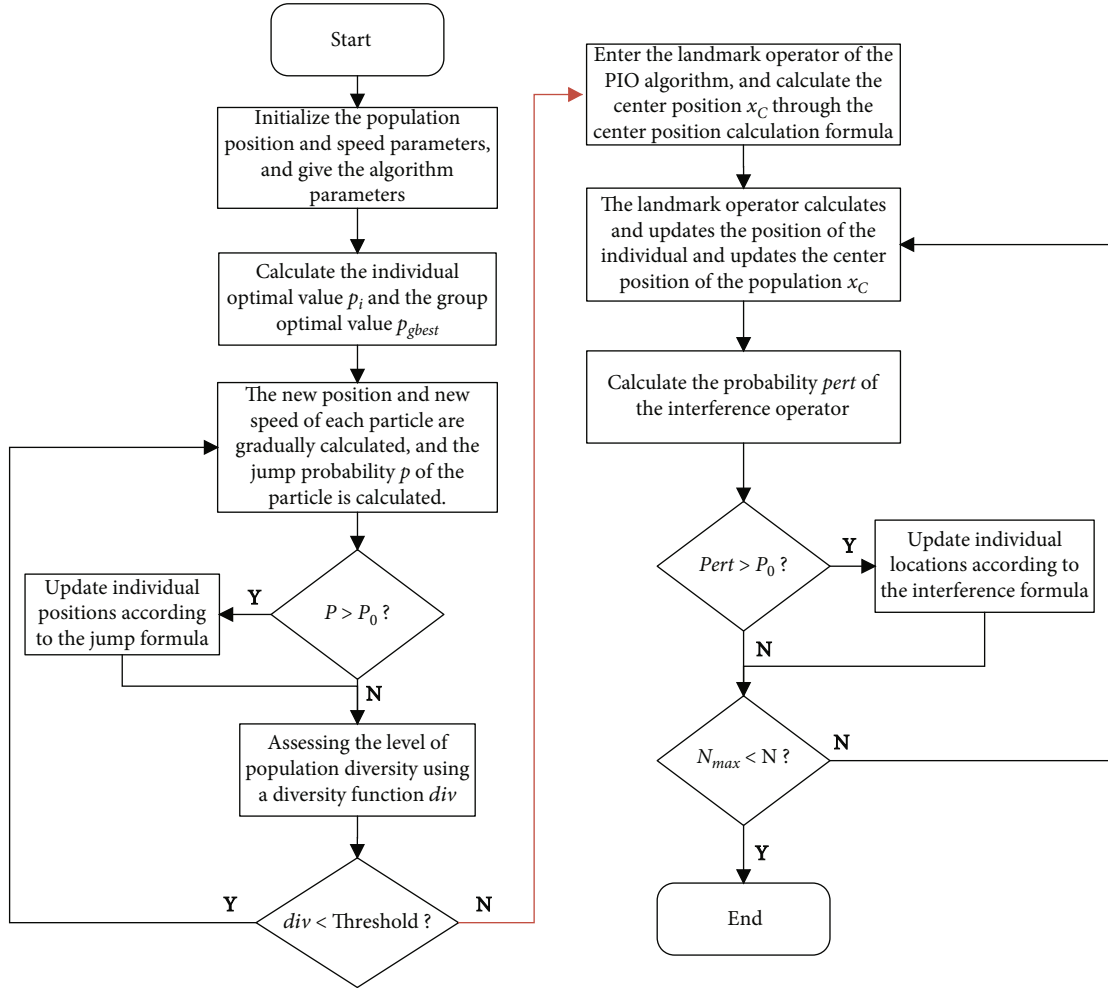


FIGURE 2: The workflow of the PSO-PIO algorithm.

5. Data Collection Strategy of HWSNs Based on PSO-PIO

The main process of the data collection method of heterogeneous WSNs based on the PSO-PIO algorithm is as follows:

5.1. Improvement of SEP Clustering Algorithm. The traditional SEP clustering algorithm is improved, and the threshold function is optimized based on the average residual energy factor and the distribution density factor of neighbor nodes.

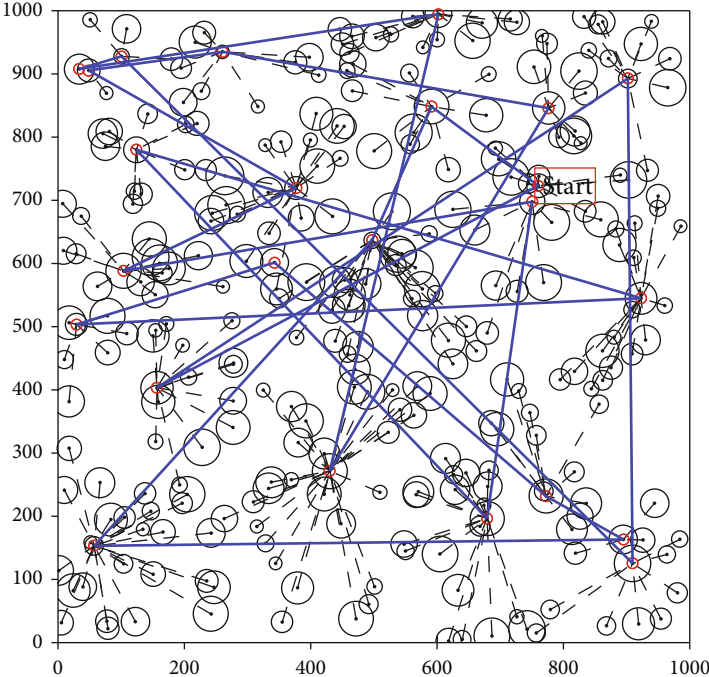
5.2. Path Planning Strategy Based on PSO-PIO Algorithm. After clustering in the first section and selecting cluster heads (residence points RPs), the mobile sink will traverse the positions of each cluster head according to the planned path to collect data. The minimum spanning tree of the backbone network composed of the entire nodes. Once the resident point RPs are selected, constructing the movement trajectory according to the RPs is a traveling salesman problem (TSP).

In order to ensure that the moving path of sink is optimal, that is, the mobile sink moves from the first cluster head to the last one, and each cluster head passes through only once during the movement. The proposed PSO-PIO algorithm can obtain the optimal mobile sink path planning

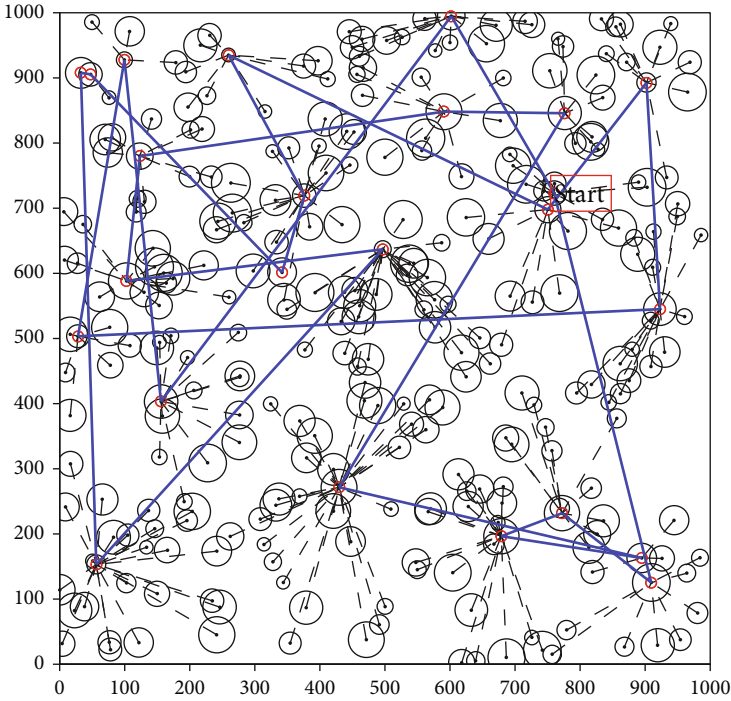
TABLE 1: Simulation environment parameter setting.

Parameter	Value
Network range	$1000 \times 1000 \text{ m}^2$
Number of nodes	300
Common node communication radius	50 m
Heterogeneous node communication radius	60 m
V_{Sink}	5 m/s
Initial energy of common node	1 J
Initial energy of heterogeneous node	2 J
E_{elec}	50 nJ/bit
E_{fs}	10 pJ/bit/m ²
E_{mp}	0.0013 pJ/bit/m ⁴
l	4,000 bits
d_0	$\sqrt{E_{\text{fs}}/E_{\text{mp}}} = 87 \text{ m}$

strategy, and the PSO-PIO algorithm optimizes the edges and nodes in the minimum spanning tree, so as to obtain the optimal path of sink.

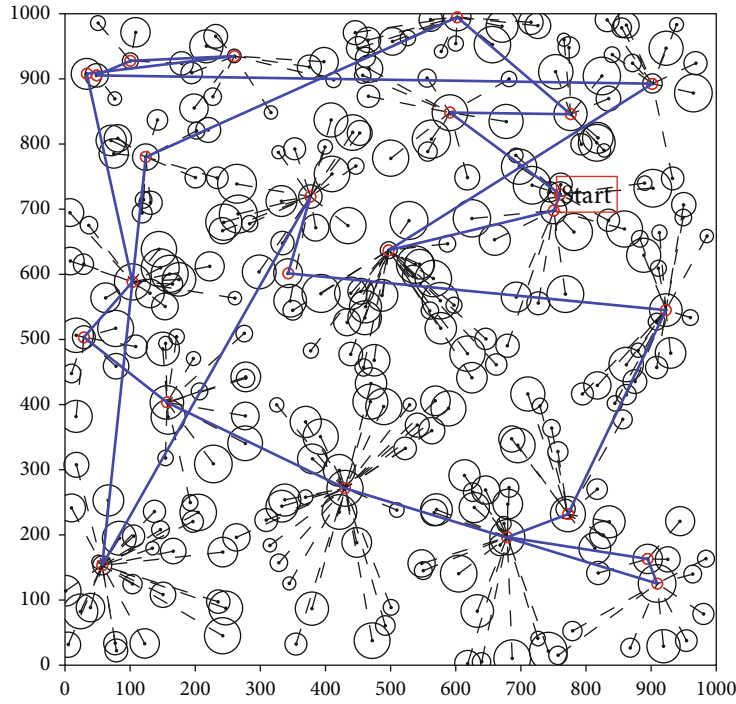


(a) Random walk

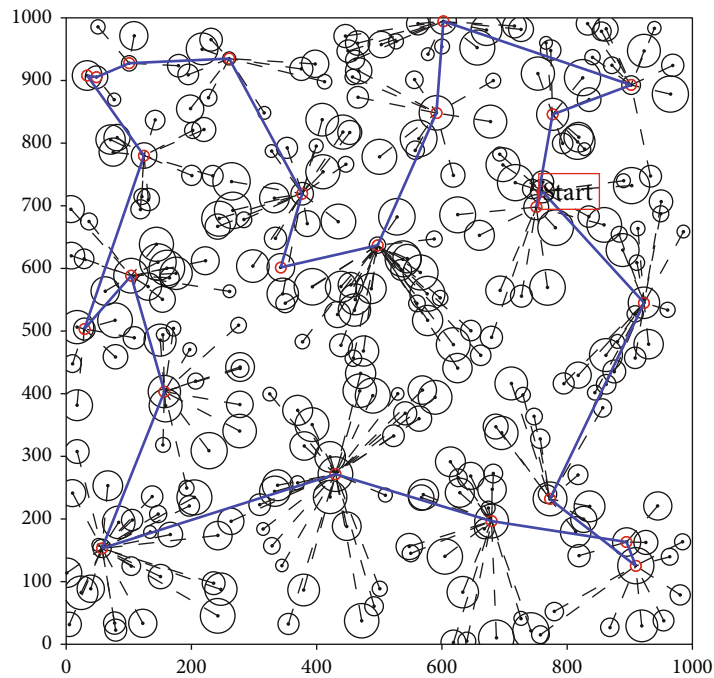


(b) PSO

FIGURE 3: Continued.



(c) PIO



(d) PSO-PIO

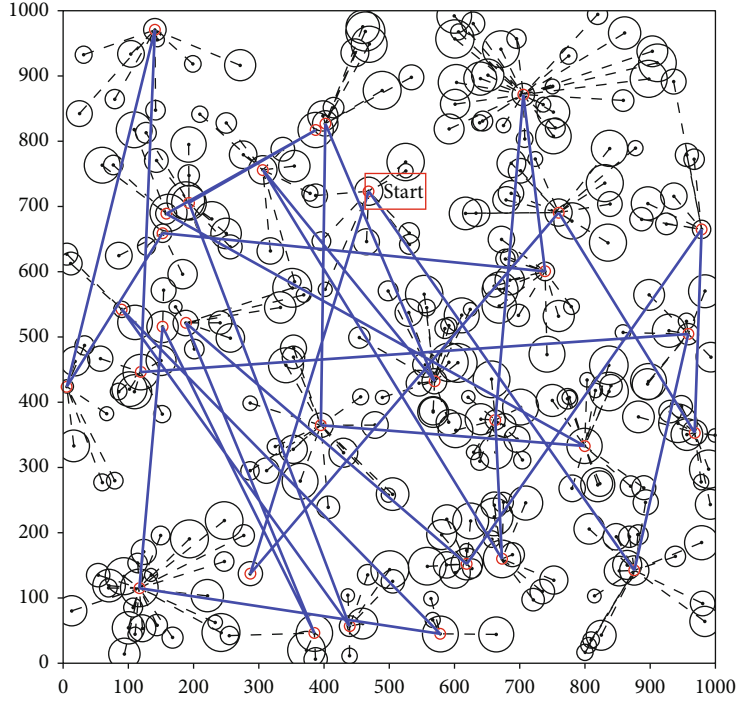
FIGURE 3: Comparison of mobile sink path planning for 24 nodes.

5.3. Data Collection

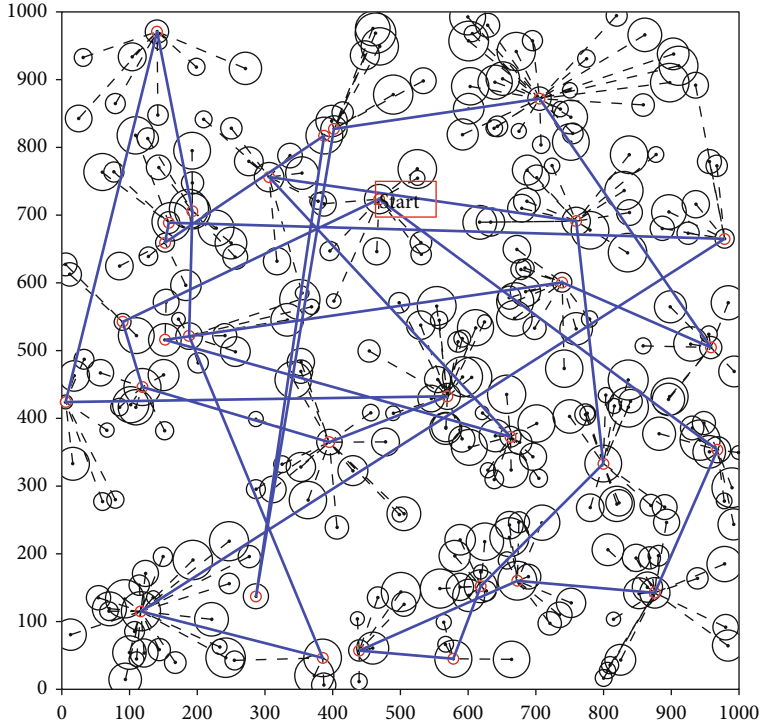
5.3.1. Intracluster data collection. Step 1: After the cluster head node of each cluster is successfully selected, the cluster head broadcasts information such as its ID number, location, and remaining energy within its maximum propagation radius.

Step 2: After the nodes receive the information from cluster head, they record the information.

Step 3: The member nodes perform data transmission according to the divided clusters. The cluster head node uses the TDMA strategy to allocate time slots for the nodes in the cluster, and all ordinary nodes perform data transmission in the allocated time slots.



(a) Random walk



(b) PSO

FIGURE 4: Continued.

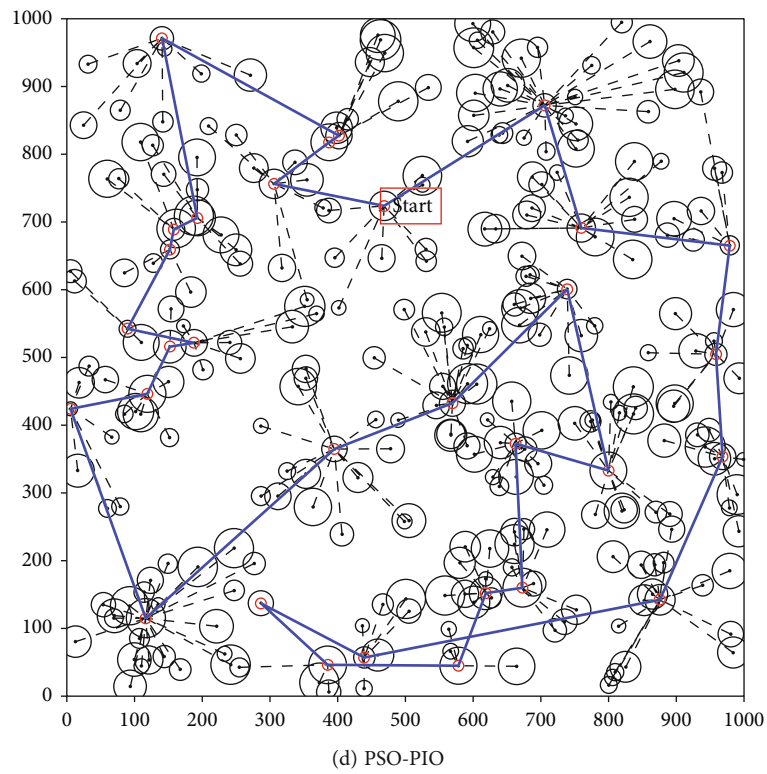
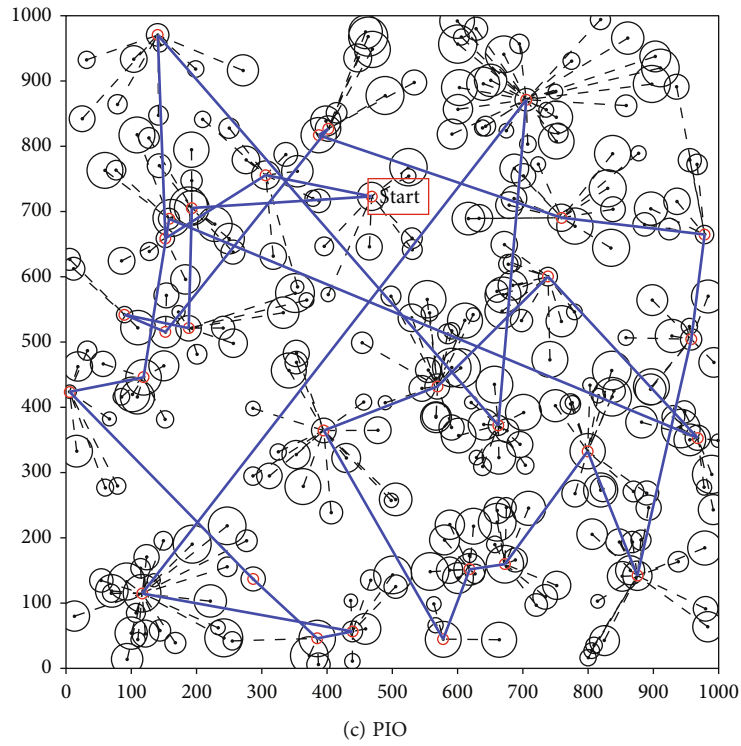


FIGURE 4: Comparison of mobile sink path planning for 32 nodes.

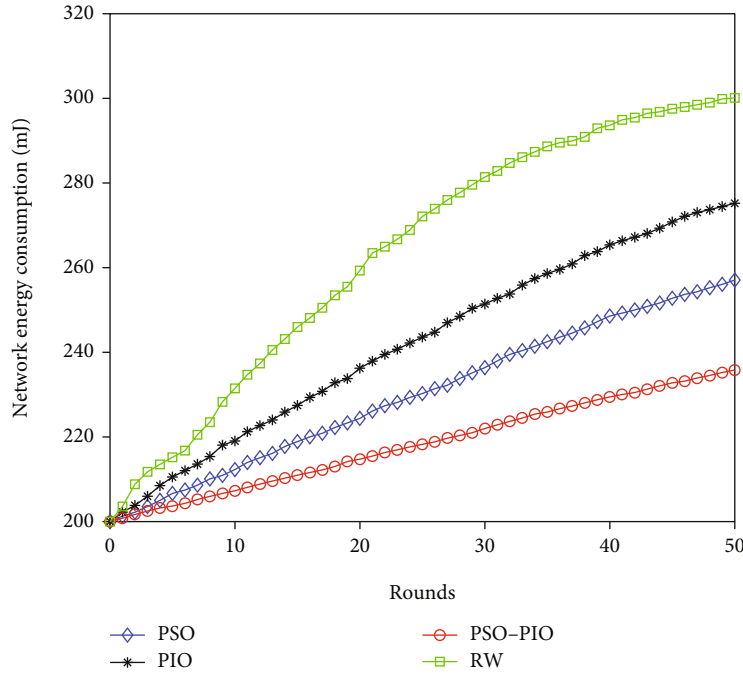


FIGURE 5: Comparison of network energy consumption.

5.3.2. *Mobile Sink to Collect Data.* The cluster head node processes the received data and then forwards it to the base station to complete the data collection of heterogeneous WSNs.

6. Algorithm Comparison and Performance Analysis

This paper compares four data collection strategies, which are the random walk method, the movement strategy of the PSO algorithm, the movement strategy of the PIO algorithm, and the PSO-PIO algorithm. In the mobile strategy, four algorithms are compared. In the experiment, the number of populations are 30, the iterations are 50, and the best and average values of 30 independent runs were used as the final test results. The population size of the pigeon colony algorithm is 30, the number of iterations of the map and compass operator is 40, the number of iterations of the compass operator is 10, and the factor of the map and compass is 0.2. The parameter settings of the heterogeneous wireless sensor network are shown in Table 1.

6.1. *Comparison of Mobile Path Planning.* In order to visually see the movement process of the mobile sink node of heterogeneous WSNs, this paper describes its movement path in detail and gives the movement paths of two different network architectures with 24 resident points and 32 resident points, respectively. The moving path of the algorithm is shown in Figures 3 and 4.

From the network simulation of 24 RPs in Figure 3, the simulation area in this paper is large, and the total movement path is relatively long, so the movement path planning strategies of the four algorithms are relatively long. Among them, in the movement mode of random walk, its moving

path is disordered, and the path is the longest. Particle swarm optimization is a little better than random movement; it has less chaotic movement. Compared with random movement and the PSO algorithm, the PIO algorithm has a relatively shorter movement path, and the strategy of the movement path is relatively better, but it is not the optimal one.

Figure 4 shows the mobility of 32 resident nodes, which can be compared by path planning. Due to the large scope of simulation in this paper, there are many RPs. The relative effects of the proposed four algorithms are not the best, but from the perspective of the four current literature methods, this paper proposes its moving path compared with the other three methods. Obviously shorter, the strategy is better.

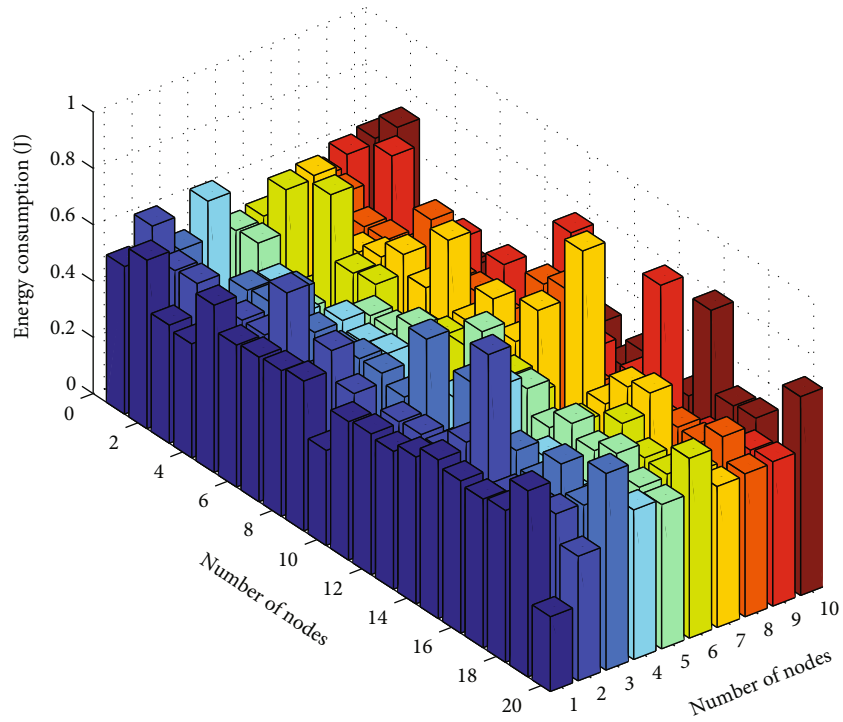
6.2. *Comparison of Network Energy Consumption.* The energy consumption comparison of the four algorithms is shown in Figure 5. The RW method in the figure is an abbreviation for the random walk method.

From the perspective of the growth rate of the network, the method of random movement consumes the most energy. The PIO algorithm optimization by PSO algorithm has the smallest network energy consumption, and the smaller the growth rate, the lowest network energy consumption.

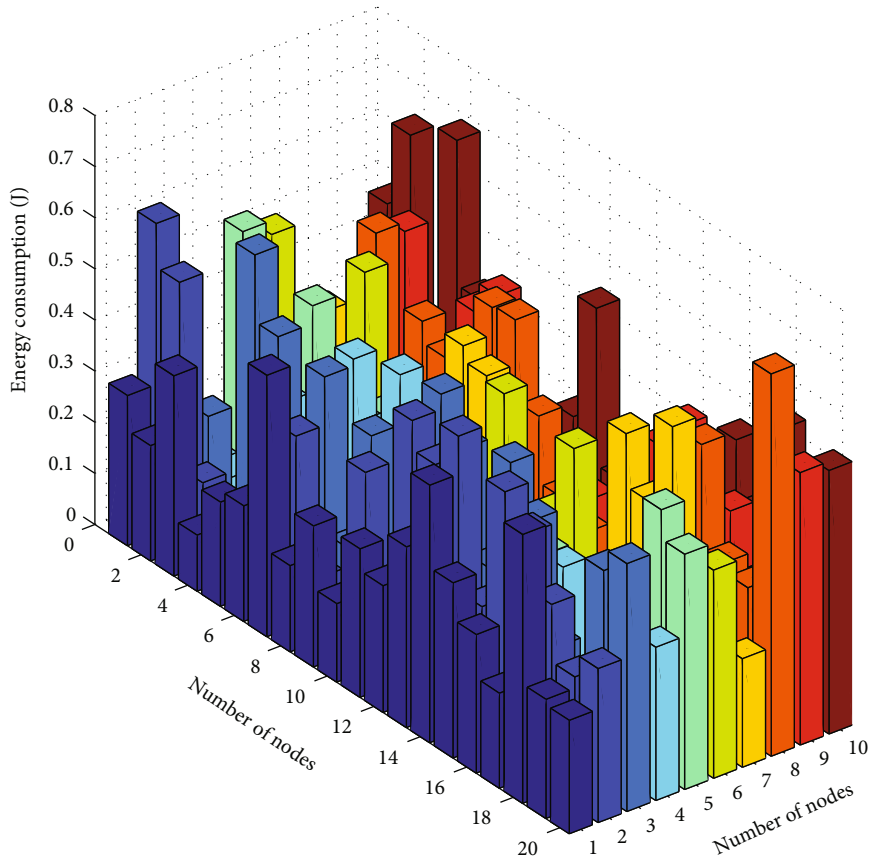
Moreover, we add a comparison of the three-dimensional energy consumption of the algorithms, as shown in Figure 6.

Similarly, through the energy consumption comparison of the three-dimensional network, it can be seen that the energy consumption of this paper is the smallest.

6.3. *Comparison of the Number of Packets Received by Sink.* The comparison of the number of packets collected by the four algorithms is shown in Figure 7.

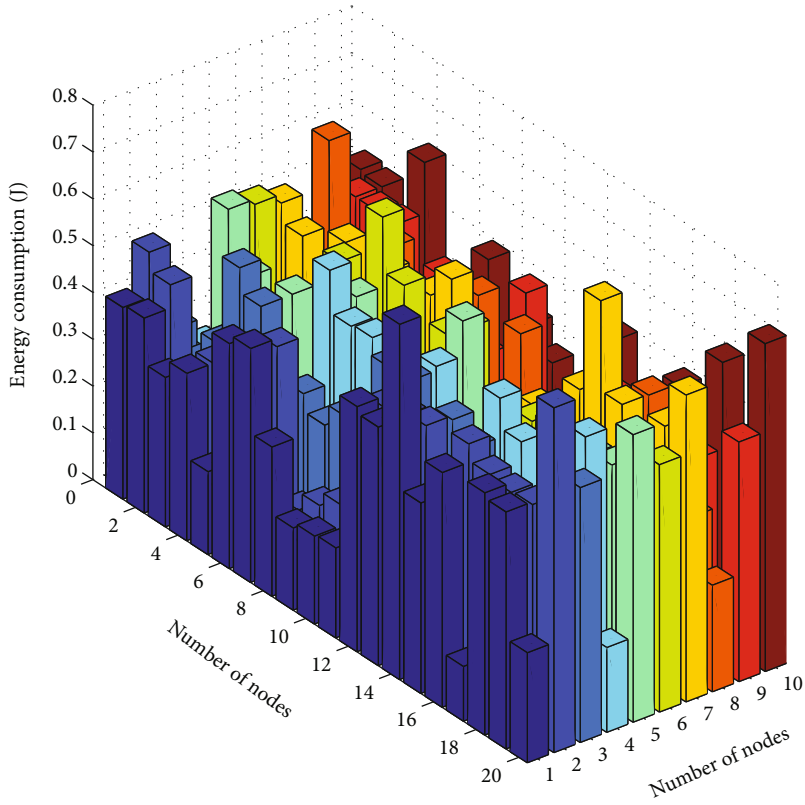


(a) Random walk

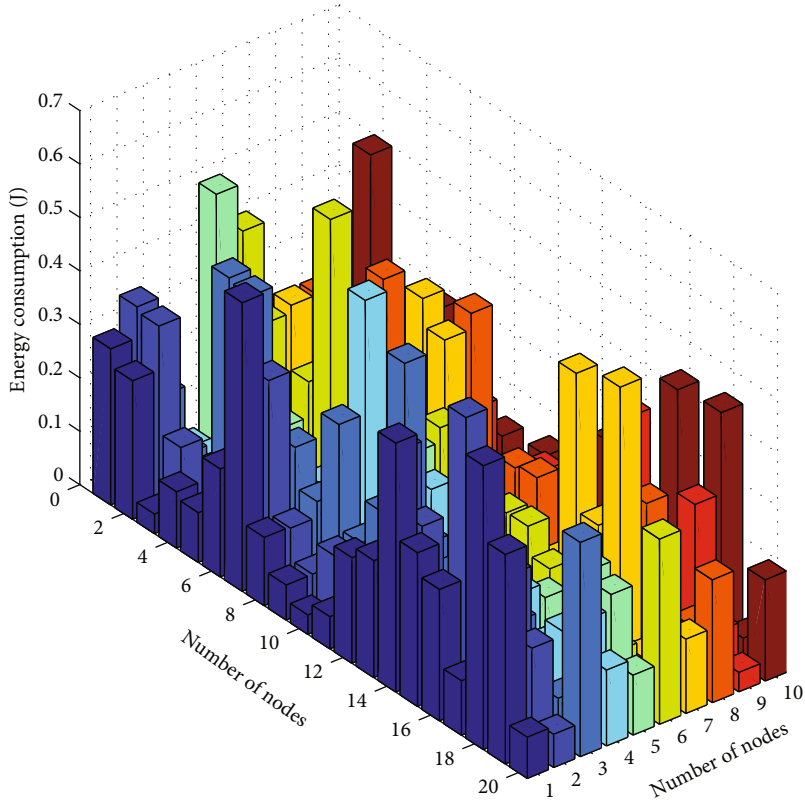


(b) PSO

FIGURE 6: Continued.



(c) PIO



(d) PSO-PIO

FIGURE 6: Comparison of 3D network energy consumption.

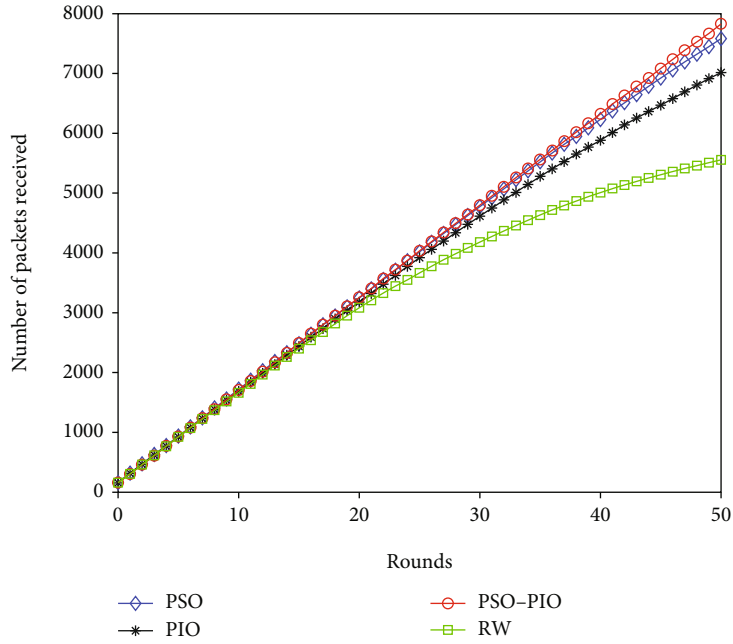


FIGURE 7: Comparison of the number of packets received by the sink.

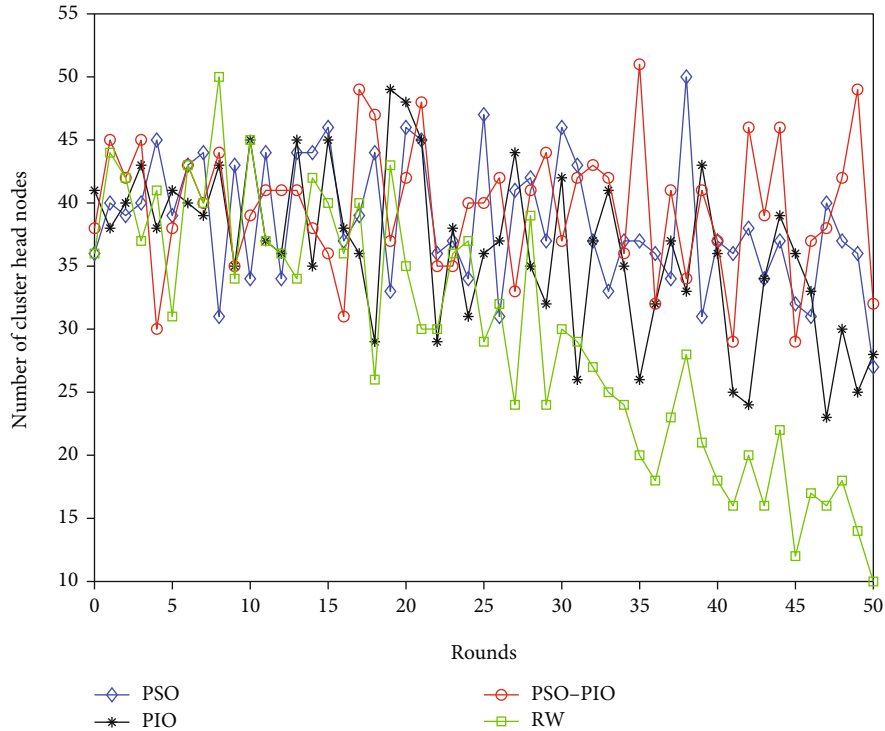


FIGURE 8: Comparison of the number of cluster head nodes.

The number of received data packets for the four algorithms is the same, and as the simulation progresses, the gap gradually emerges. The number of datagrams collected by random walk gradually decreases. With the progress of the simulation, the network energy consumption of random walk is relatively large, resulting in the death of some nodes, resulting in a small number of data packets accepted by the sink. The number of received packets of the other three types

is not much different. The improved PIO algorithm proposed in this paper receives the most packets, but compared with the PSO algorithm and the basic PIO algorithm, the difference is not so obvious.

6.4. Comparison of the Number of Cluster Head Nodes. The comparison of the number of cluster head nodes is shown in Figure 8.

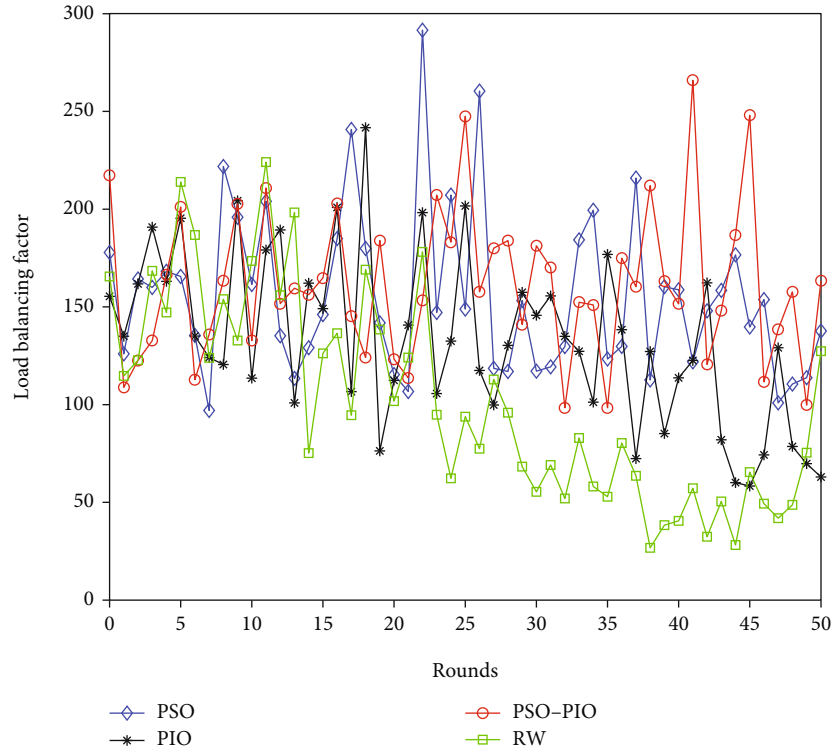


FIGURE 9: Comparison of network load balancing.

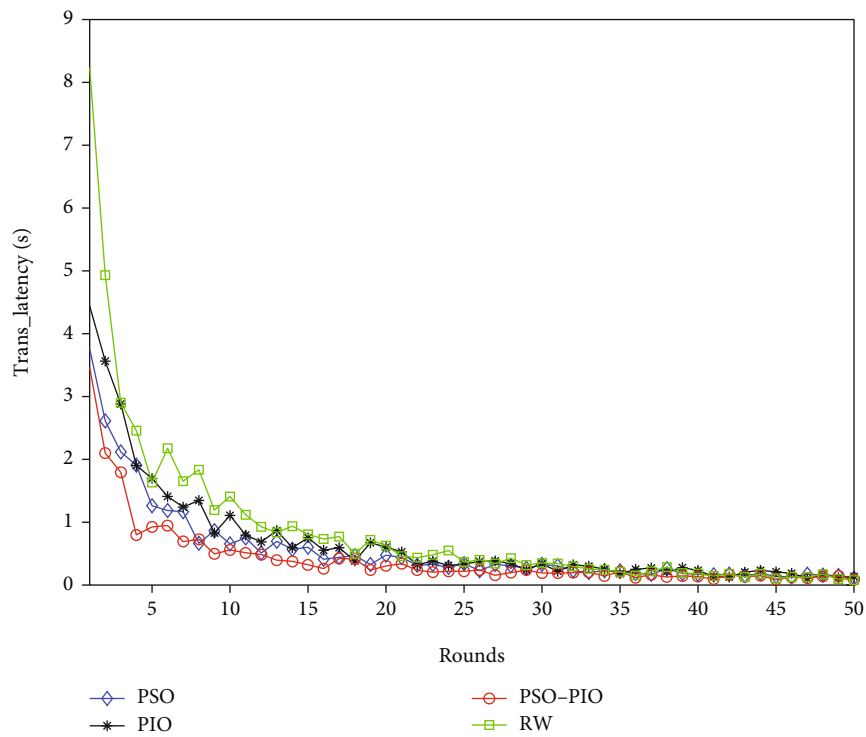


FIGURE 10: Comparison of network transmission delays.

With the simulation progresses, the number of cluster head nodes in the random walk movement method fluctuates greatly. The number of cluster head nodes gradually decreased and finally dropped to 10. The number

of cluster head nodes of the other three intelligent optimization algorithms is not much different, and the number of cluster head nodes is relatively balanced, with little difference.

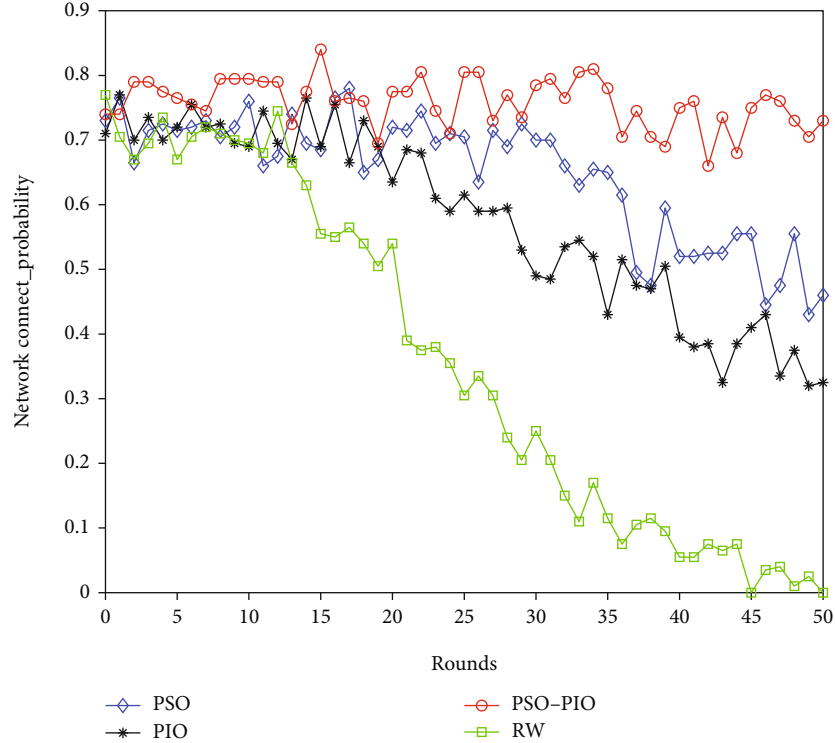


FIGURE 11: Comparison of network connectivity.

6.5. Comparison of Network Load Balance. The calculation formula of network load balancing is in reference [5]. According to the calculation in reference [5], we can obtain the network load balancing performance of the four algorithms. Figure 9 shows the simulation results.

From the comparison of network load balance in Figure 9, it can be seen that in the first 25 times of polling, the network load balance of the four methods has little difference. After 25 times of polling, the network load balance of the random walk method is sharp. The main reason is that the network energy consumption of the random walk method is too large, the energy of the nodes is exhausted in a large area, and its load balance fluctuates greatly. The other three methods are relatively balanced.

6.6. Comparison of Network Transmission Delay. The transmission delay measures the real-time performance of different data collection methods by the transmission time of successfully received data packets. The calculation formula of network transmission delay is in reference [5]. According to the calculation of reference [5], we can obtain the network transmission delay of four algorithms. The network delays of the three algorithms are shown in Figure 10.

At the beginning of the network transmission delay, the network delay is long, mainly because the algorithm needs to perform a lot of operations at the beginning, and it takes some calculation time to find the optimal moving path. As the iterative operation of the intelligent optimization algorithm progresses, it gradually gains an advantage in finding the optimal path, and gradually finds a relatively optimal path plan, so that the transmission time is gradually shortened. From the perspective of the transmission delay of the

entire network, the random walk method takes the longest time, the basic PIO algorithm has a longer delay, and the PSO algorithm has a shorter transmission delay. The PSO-PIO algorithm has the shortest transmission delay. The main benefit is that the path it calculates is optimal, so the transmission delay is the shortest.

6.7. Network Connectivity Comparison. The network connectivity generally adopts the method of continuous motion discretization to calculate the network connectivity. The calculation formula of network connectivity is in reference [5]. The network connectivity comparison is shown in Figure 11.

The connectivity of the network is an important indicator to be considered in the data collection process, which directly affects the working stability and reliability of heterogeneous WSNs. From the comparison of network connectivity in Figure 11, except for the huge fluctuation of random walk, the network connectivity of the other three algorithms is relatively good. The PSO-PIO algorithm has the best moving path planning, and its network connectivity performance is also the best. In this way, the phenomenon of data congestion and large area packet loss that is easy to occur in the data transmission process is avoided, and the stability of the network operation is improved.

7. Conclusions

In this paper, an efficient data collection method based on path optimization is proposed in heterogeneous WSNs for Internet of things. Aiming at the path problem of mobile sinks in heterogeneous WSNs, a path optimization strategy based on the PSO-PIO algorithm is proposed. The PSO-

PIO algorithm considers the network energy consumption, data transmission delay, and network work efficiency when collecting data when selecting the resident point, and uses the PSO algorithm to select some nodes as the resident point, and then constructs the optimal mobile path. Compared with the PSO and PIO algorithms, the algorithm can ensure the balance of energy consumption, effectively reduce the transmission delay, and greatly prolong the network life. In addition, the algorithm can overcome the fatal impact of unreliable links on multihop data collection and ensure the algorithm's energy-saving and efficient data collection in the actual environment.

The current work does not consider the reliability and data redundancy in the process of data transmission. The next step is to further improve the efficiency of heterogeneous WSNs data collection and the reliability of the network, expand the mobile path of multiple sink and achieve the goal of multiple sink to complete data collection together.

Data Availability

The data used to support the findings of this study are included in the article.

Conflicts of Interest

The authors declare that they have no conflicts of interest.

Acknowledgments

This work was supported in part by the Natural Science Foundation of Hubei Province under Grant 2020CFB304, in part by Wenzhou basic scientific research project under Grant R20210030 and the talent introduction project of Wenzhou University of Technology, scientific research project of Wenzhou University of Technology of Yinggao Yue and Li Cao, Wenzhou intelligent Image Processing and Analysis Key Laboratory Construction Project under Grant 2021HZSY007105, in part by open project of Wenzhou Key Laboratory of intelligent image processing and analysis under Grant ZY2019020, and major scientific and technological innovation projects of Wenzhou science and technology plan under Grant ZG2021021, major project of Zhejiang Natural Science Foundation under Grant LD21F020001.

References

- [1] M. A. M. Sadeeq and S. Zeebaree, "Energy management for internet of things via distributed systems[J]," *Journal of Applied Science and Technology Trends*, vol. 2, no. 2, pp. 59–71, 2021.
- [2] S. Sicari, A. Rizzardi, and A. Coen-Porisini, "5G In the internet of things era: an overview on security and privacy challenges," *Computer Networks*, vol. 179, no. 10, article 107345, 2020.
- [3] L. U. Khan, W. Saad, Z. Han, E. Hossain, and C. S. Hong, "Federated learning for internet of things: recent advances, taxonomy, and open challenges[J]," *IEEE Communications Surveys & Tutorials*, vol. 23, no. 3, pp. 1759–1799, 2021.
- [4] J. Liang, Z. Xu, Y. Xu, W. Zhou, and C. Li, "Adaptive cooperative routing transmission for energy heterogeneous wireless sensor networks," *Physical Communication*, vol. 49, no. 12, article 101460, 2021.
- [5] Y. Bai, L. Cao, S. Wang, H. Ding, and Y. Yue, "Data collection strategy based on OSELM and gray wolf optimization algorithm for wireless sensor networks," *Computational Intelligence and Neuroscience*, vol. 2022, 18 pages, 2022.
- [6] H. Kumar and P. K. Singh, "Enhancing network lifetime and throughput in heterogeneous wireless sensor networks[J]," *Wireless Personal Communications*, vol. 120, no. 4, pp. 2971–2989, 2021.
- [7] R. Almesaeed and A. Jedidi, "Dynamic directional routing for mobile wireless sensor networks," *Ad Hoc Networks*, vol. 110, no. 1, p. 102301, 2021.
- [8] G. Kadiravan, P. Sujatha, T. Asvany et al., "Metaheuristic clustering protocol for healthcare data collection in mobile wireless multimedia sensor networks[J]," *Computers, Materials & Continua*, vol. 66, no. 3, pp. 3215–3231, 2021.
- [9] B. Khalifa, Z. Al Aghbari, and A. M. Khedr, "A distributed self-healing coverage hole detection and repair scheme for mobile wireless sensor networks," *Sustainable Computing: Informatics and Systems*, vol. 30, no. 6, article 100428, 2021.
- [10] J. Sumathi and R. L. Velusamy, "A review on distributed cluster based routing approaches in mobile wireless sensor networks[J]," *Journal of Ambient Intelligence and Humanized Computing*, vol. 12, no. 1, pp. 835–849, 2021.
- [11] L. Fan, L. Liu, H. Gao, Z. Ma, and Y. Wu, "Secure K-nearest neighbor queries in two-tiered mobile wireless sensor networks," *Digital Communications and Networks*, vol. 7, no. 2, pp. 247–256, 2021.
- [12] L. Cao, Y. Yue, and Y. Zhang, "A data collection strategy for heterogeneous wireless sensor networks based on energy efficiency and collaborative optimization," *Computational Intelligence and Neuroscience*, vol. 2021, Article ID 9808449, 13 pages, 2021.
- [13] M. Sayeed and R. Kumar, "An efficient mobility model for improving transmissions in multi-UAVs enabled WSNs[J]," *Drones*, vol. 2, no. 3, pp. 31–43, 2018.
- [14] V. Saranya, S. Shankar, and G. R. Kanagachidambaresan, "Energy efficient data collection algorithm for mobile wireless sensor network," *Wireless Personal Communications*, vol. 105, no. 1, pp. 219–232, 2019.
- [15] A. Pang, F. Chao, H. Zhou, and J. Zhang, "The method of data collection based on multiple mobile nodes for wireless sensor network[J]," *IEEE Access*, vol. 8, no. 1, pp. 14704–14713, 2020.
- [16] J. Wang, Y. Cao, B. Li, H. J. Kim, and S. Lee, "Particle swarm optimization based clustering algorithm with mobile sink for WSNs," *Future Generation Computer Systems*, vol. 76, no. 11, pp. 452–457, 2017.
- [17] Y. Gao, J. Wang, W. Wu, A. Sangaiah, and S. J. Lim, "A hybrid method for mobile agent moving trajectory scheduling using ACO and PSO in WSNs[J]," *Sensors*, vol. 19, no. 3, pp. 575–584, 2019.
- [18] A. H. F. Farzana and S. Neduncheliyan, "Ant-based routing and QoS-effective data collection for mobile wireless sensor network[J]," *Wireless Networks*, vol. 23, no. 6, pp. 1697–1707, 2017.
- [19] N. Kumar and D. Dash, "Flow based efficient data gathering in wireless sensor network using path-constrained mobile sink [J]," *Journal of Ambient Intelligence and Humanized Computing*, vol. 11, no. 3, pp. 1163–1175, 2020.

- [20] S. Mahmoudzadeh, D. M. W. Powers, and A. Atyabi, "UUV's hierarchical DE-based motion planning in a semi dynamic underwater wireless sensor network," *IEEE transactions on cybernetics*, vol. 49, no. 8, pp. 2992–3005, 2019.
- [21] S. D. Trapasiya and H. B. Soni, "Path scheduling for multiple mobile actors in wireless sensor network[J]," *International Journal of Electronics*, vol. 104, no. 5, pp. 868–884, 2017.
- [22] A. Agrawal, V. Singh, S. Jain, and R. K. Gupta, "GCRP: Grid-cycle routing protocol for wireless sensor network with mobile sink," *AEU-International Journal of Electronics and Communications*, vol. 94, pp. 1–11, 2018.
- [23] J. Lee, S. Oh, S. Park, Y. Yim, S. H. Kim, and E. Lee, "Active data dissemination for mobile sink groups in wireless sensor networks," *Ad Hoc Networks*, vol. 72, no. 4, pp. 56–67, 2018.
- [24] G. Ren, J. Wu, and F. Versonnen, "Bee-based reliable data collection for mobile wireless sensor network[J]," *Cluster Computing*, vol. 22, no. S4, pp. 9251–9260, 2019.
- [25] S. Zafar, A. Bashir, and S. A. Chaudhry, "Mobility-aware hierarchical clustering in mobile wireless sensor networks[J]," *IEEE Access*, vol. 7, no. 2, pp. 20394–20403, 2019.
- [26] A. A. Baradaran and K. Navi, "HQCA-WSN: high-quality clustering algorithm and optimal cluster head selection using fuzzy logic in wireless sensor networks," *Fuzzy Sets and Systems*, vol. 389, no. 6, pp. 114–144, 2020.
- [27] Z. Cui, J. Zhang, Y. Wang et al., "A pigeon-inspired optimization algorithm for many-objective optimization problems[J]," *SCIENCE CHINA Information Sciences*, vol. 62, no. 7, pp. 1–3, 2019.
- [28] H. Alazzam, A. Sharieh, and K. E. Sabri, "A feature selection algorithm for intrusion detection system based on pigeon inspired optimizer," *Expert Systems with Applications*, vol. 148, no. 6, p. 113249, 2020.
- [29] A. Q. Tian, S. C. Chu, J. S. Pan, H. Cui, and W. M. Zheng, "A compact pigeon-inspired optimization for maximum short-term generation mode in cascade hydroelectric power station [J]," *Sustainability*, vol. 12, no. 3, pp. 767–779, 2020.
- [30] G. Chen, J. Qian, Z. Zhang, and S. Li, "Application of modified pigeon-inspired optimization algorithm and constraint-objective sorting rule on multi-objective optimal power flow problem," *Applied Soft Computing*, vol. 92, no. 7, p. 106321, 2020.
- [31] Y. Zhong, L. Wang, M. Lin, and H. Zhang, "Discrete pigeon-inspired optimization algorithm with metropolis acceptance criterion for large-scale traveling salesman problem," *Swarm and Evolutionary Computation*, vol. 48, no. 8, pp. 134–144, 2019.
- [32] H. Qiu and H. Duan, "A multi-objective pigeon-inspired optimization approach to UAV distributed flocking among obstacles," *Information Sciences*, vol. 509, no. 1, pp. 515–529, 2020.
- [33] Y. Wang, G. Zhang, and X. Zhang, "Multilevel image thresholding using tsallis entropy and cooperative pigeon-inspired optimization bionic algorithm[J]," *Journal of Bionic Engineering*, vol. 16, no. 5, pp. 954–964, 2019.
- [34] X. Hai, Z. Wang, Q. Feng et al., "Mobile robot ADRC with an automatic parameter tuning mechanism via modified pigeon-inspired optimization[J]," *IEEE/ASME Transactions on Mechatronics*, vol. 24, no. 6, pp. 2616–2626, 2019.
- [35] D. Zhang and H. Duan, "Social-class pigeon-inspired optimization and time stamp segmentation for multi-UAV cooperative path planning," *Neurocomputing*, vol. 313, no. 11, pp. 229–246, 2018.
- [36] W. Ruan and H. Duan, "Multi-UAV obstacle avoidance control via multi-objective social learning pigeon-inspired optimization[J]," *Frontiers of Information Technology & Electronic Engineering*, vol. 21, no. 5, pp. 740–748, 2020.
- [37] A. L. Bolaji, F. Z. Okwonu, P. B. Shola, B. S. Balogun, and O. D. Aduhisi, "A modified binary pigeon-inspired algorithm for solving the multi-dimensional knapsack problem[J]," *Journal of Intelligent Systems*, vol. 30, no. 1, pp. 90–103, 2021.
- [38] H. Duan, M. Huo, and Y. Shi, "Limit-cycle-based mutant multiobjective pigeon-inspired Optimization," *IEEE Transactions on Evolutionary Computation*, vol. 24, no. 5, pp. 948–959, 2020.
- [39] T. Li, C. Zhou, B. Wang, B. Xiao, and X. Zheng, "A hybrid algorithm based on artificial bee colony and pigeon inspired optimization for 3D protein structure prediction[J]," *Journal of Bionanoscience*, vol. 12, no. 1, pp. 100–108, 2018.
- [40] Z. Cui, J. Zhang, D. Wu et al., "Hybrid many-objective particle swarm optimization algorithm for green coal production problem," *Information Sciences*, vol. 518, no. 5, pp. 256–271, 2020.
- [41] Y. Cao, H. Zhang, W. Li, M. Zhou, Y. Zhang, and W. A. Chaovalitwongse, "Comprehensive learning particle swarm optimization algorithm with local search for multimodal functions," *IEEE Transactions on Evolutionary Computation*, vol. 23, no. 4, pp. 718–731, 2019.

Research Article

Visual Design of Brand Image by Marine Bionic System in the Environment of Internet of Things and Machine Learning

Minghui Niu and Joung Hyung Cho 

Department of Marine Design Convergence Engineering, Pukyong National University, Busan 612022, Republic of Korea

Correspondence should be addressed to Joung Hyung Cho; 202056731@pukyong.ac.kr

Received 15 March 2022; Revised 17 May 2022; Accepted 23 May 2022; Published 11 June 2022

Academic Editor: Mu-Yen Chen

Copyright © 2022 Minghui Niu and Joung Hyung Cho. This is an open access article distributed under the Creative Commons Attribution License, which permits unrestricted use, distribution, and reproduction in any medium, provided the original work is properly cited.

Based on the environment of economic globalization, many clothing companies have increased the requirements for clothing design styles to diversify them, thereby increasing the interest of consumers. The main purpose and motivation are to explore the pattern design of children's clothing with the marine bionic environment as the design source. Firstly, the collaborative business concept of IoT machine learning is introduced into the field of clothing design. Design styles and elements related to marine bionic environments are introduced. A set of questionnaires about the visual design preferences of children in different families on marine style clothing patterns are designed to examine differences in the cognitive level of color patterns among children of different age groups. Through the sorting, statistics, and analysis of the questionnaire results, different families have a stronger interest in clothing with warm colors as the color style and lines and ordinary paintings as the pattern drawing style. This provides a certain degree of design ideas for related clothing design work and provides unique insights into the visual design of brand image based on the marine bionic system in the Internet of Things (IoT) and machine learning environment.

1. Introduction

With the formation of the global economic integration trend, the quality of life continues to rise, and the requirements for clothing from children to adults have long ceased to be comfortable and warm [1]. Humans have gradually increased their requirements for fashion and viewing. At present, in order to expand the interests of many manufacturers, the pattern design of clothing is too simple, there is a serious follow-up phenomenon, and it is easy to cause visual fatigue [2]. The natural marine world is a source of original design ideas. Humans can simulate marine life, extract inspiration, and imitate colors to design trendy clothing [3]. The Internet of Things (IoT) technology can coordinate the visual design of brand clothing in the clothing industry, and machine learning can be used to innovate the visual design [4].

The brand visual design of clothing is a very important part. The style and pattern of clothing are the only way to

capture consumer interest. Bhatt et al. (2019) used the multifactor line regression method to study the design of clothing. In the results, there is a significant positive correlation between the upgrading of clothing and the fashion style of environmental concern. Environmental protection and creative clothing can stimulate the interest of consumers [5]. Kim and Lee (2019) also believed that most consumers' purchasing interests focus on the detailed visual stimuli of models or clothing. This is a very important point in clothing sales [6]. Pu and Meng (2019) pointed out that marine resources can play a great role in many current visual designs and hope to achieve rational and comprehensive optimization of resource development and promote the development of marine resources [7]. Varol (2021) believed that many icons from movies, music, design, politics, and sports had influenced the clothing styles of different periods. This further proves that the design of clothing style is an important link [8]. As for the brand design of IoT

enterprises, Nguyen et al. (2021) [9] used the IoT and enterprise data to design the system of data-driven and customer emotion monitoring. By designing the framework of data-driven decision support system, the framework proposed a practical workflow for end users. The results showed that combining the IoT and enterprise data could improve the prediction results and simplify troubleshooting. In addition, with regard to the establishment and research of high-performance IoT virtualization framework, Al-Azez et al. (2019) [10] studied the high-energy IoT structure with point-to-point networking and processing. The research results presented that the hybrid scenario could process up to 77% of task requests, but the energy consumption was higher than other scenarios. Ju et al. (2021) [11] studied the IoT-assisted multiple fuzzy-enhanced energy scheduling method in the intelligent scheduling system. The results suggested that this method was superior to the traditional system design, which improved the system accuracy and reduced the execution time. With the increasingly fierce competition in the apparel industry market, the style of design is the focus for consumers to choose. Section 1 describes the concept and application of machine learning in the IoT. In Section 2, the concept of collaborative business of machine learning and elements and functions of the marine bionic environment is supplemented and explained in the IoT environment. The visual structure of marine bionic elements is designed based on IoT machine learning. In Section 3, the data results are obtained through the research on the color degree of clothing design. Section 3 draws the research data results through the study of clothing design color. Section 4 summarizes the research conclusions. The contribution is to take the color and overall pattern of marine creatures as the evaluation standard and analyze children's preference for a specific pattern to give the design standard of clothing.

2. Related Work

With the development of the IoT and machine learning technology, the rapid development of hardware, software, and communication technology promotes the emergence of sensing equipment connected to the Internet. These devices provide observations and data measurements from the physical world. Machine learning technology is widely used in the development analysis model. These models are integrated into different service applications and clinical decision support systems. Samie et al. (2019) [12] researched IoT machine learning and reviewed the role of machine learning from the cloud to embedded equipment in the IoT. They studied the use of machine learning in application data processing and management tasks. These are guiding significance for the development of IoT machines in various fields of society. Zolanvari et al. (2019) [13] analyzed machine learning for industrial Internet network vulnerabilities. The use of machine learning in response to this sensitivity is discussed through network vulnerability. Subsequently, the available intrusion detection solution is described using the machine learning model. Tahsien et al. (2020) [14] reviewed and studied IoT security solutions based on machine learning and conducted the most advanced review of possible security solutions for IoT devices.

TABLE 1: Recent related work on IoT and machine learning.

Author	Year	Content
Samie et al.	2019	Overview of IoT machine learning
Zolanvari et al.	2019	Industrial internet network vulnerability
Tahsien et al.	2020	IoT security solution
Kishor et al.	2021	Random forest machine learning method

They discussed the challenge of machine learning-based IoT system security, indicating that machine learning techniques can respond to various Internet access. Kishor et al. (2021) [15] studied fog computing intelligent medical data separation scheme based on IoT and machine learning. They used a random forest machine learning method to isolate patient data and improve delays using fog intelligently. This model achieves 92%-95% of the overall delay reduction to the existing working techniques. In summary, the IoT, machine learning neural networks have been applied in multiple fields, and the construction of the model can be fully borrowed from the reference experience. A disadvantage is that the accuracy and precision of the current model are not high, and it is necessary to further optimize and improve in later work. The list of literature research is shown in Table 1:

3. Methods

3.1. The Concept of Machine Learning Collaborative Business in the IoT Environment. A lot of studies have been done on the microstructure coating of marine bionic functional surface, but there are still many practical problems. The real biological epidermis is easy to change under the influence of the environment. For the problems of long time and high cost of completely replicating the epidermis structure in a large area, the IoT brand is used for system engineering design, including the Internet, communication protocol, signal detection and processing, information fusion, database management and development, and software development [16]. Based on the current IoT technology, the system covers different aspects of the circulation of brand clothing and the whole sales process, including personalized services for members and customers. The machine learning collaborative e-commerce structure in the IoT environment can further improve the business efficiency of supply chain management. The framework structure of brand collaborative business is shown in Figure 1.

In Figure 1, the intelligentization of brand clothing store sales and the realization of the coordination and interoperability of various links can reduce inventory stock, reduce costs, and strengthen personalized services for member customers. Additionally, it can also improve the efficiency of the enterprise, grasp the sales situation in time, and provide a reliable basis for enterprise decision-making. This collaborative business structure is generally improved by a collaborative filtering algorithm (CFA) [17]. The structure of the collaborative filtering algorithm is shown in Figure 2.

In Figure 2, the research purpose of CFA is to analyze the degree of college students' access to commodities in the daily network. For example, for a group of students with the same or similar hobbies, there is a certain degree of similarity in

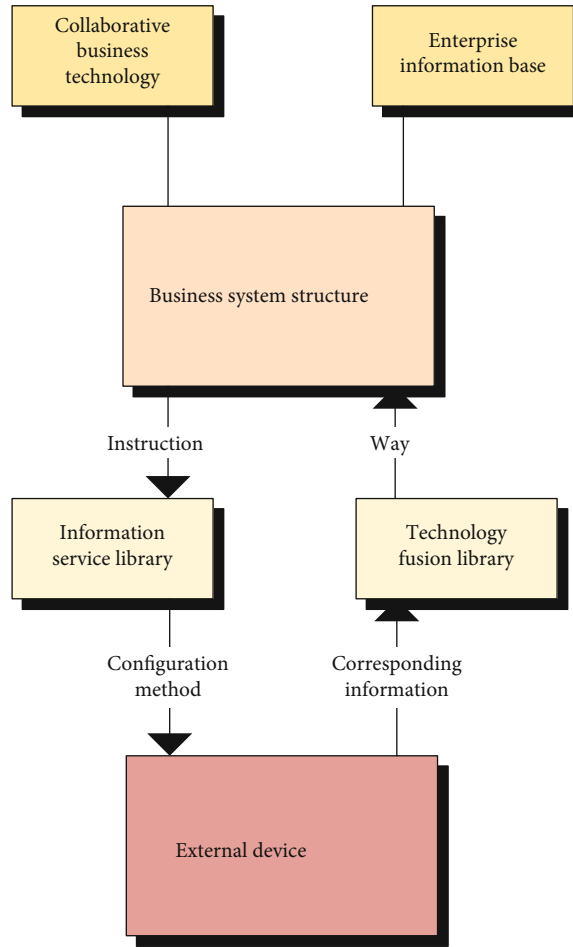


FIGURE 1: Structure of collaborative commerce.

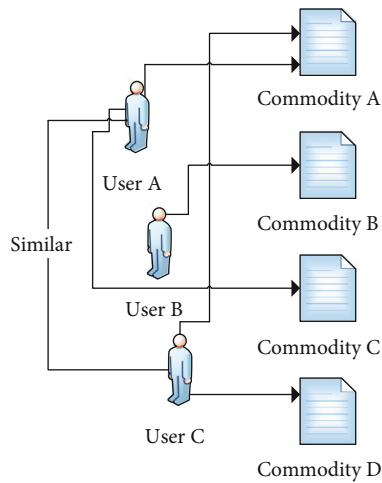


FIGURE 2: CFA structure.

the software used when accessing goods. The item A used by user A will also be the item frequently used by user B, and the material A frequently referenced by user C will also be the material frequently used by user D for reference.

Traditional CFA analysis of user similarity generally uses three methods:

- (1) Jaccard index [18]. The purpose of the coefficient is to judge the relevance of binary data, as shown in

$$\text{sim}(i, j) = \frac{|R_i \cap R_j|}{|R_i \cup R_j|}, \quad (1)$$

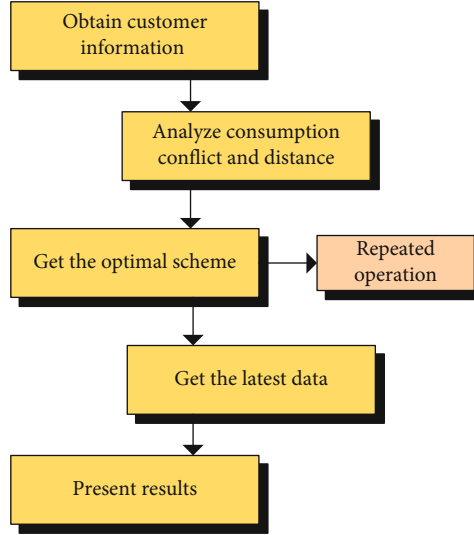


FIGURE 3: Analysis of member consumption.

where $R_i \cap R_j$ represents a common thing for users i and j . $R_i \cup R_j$ represents everything for users i and j . The Jaccard index is widely used to compare users' online shopping carts.

- (2) Cosine similarity [19]. The user score is a vector on an n -dimensional matrix, and the similarity of users i and j is calculated by the cosine angle between the vectors, as shown in

$$\text{sim}(i, j) = \cos(i, j) = \frac{i \cdot j}{\|i\| \cdot \|j\|}, \quad (2)$$

$$\cos(i, j) = \frac{\sum_{c=1}^n R_{i,c} R_{j,c}}{\sqrt{\sum_{c=1}^n R_{i,c}^2} \cdot \sqrt{\sum_{c=1}^n R_{j,c}^2}}, \quad (3)$$

where $\sum_{c=1}^n R_{i,c} R_{j,c}$ represents the user's score vector inner product. $\sqrt{\sum_{c=1}^n R_{i,c}^2} \cdot \sqrt{\sum_{c=1}^n R_{j,c}^2}$ represents the product of the modulus of the user vector. $R_{i,c}$ and $R_{j,c}$ represent the user's evaluation score for item j . However, different users have different ratings for the same product. Therefore, this method cannot accurately calculate the similarity. The analysis process that CFA is used to analyze members' consumption intention is shown in Figure 3.

- (3) Modified cosine similarity. This method can fill the gap of no scoring standard in cosine similarity, using the average of user scores for analysis, as shown in

$$\text{sim}(i, j) = \frac{\sum_{c=1}^n (R_{i,c} - R_i^-) (R_{j,c} - R_j^-)}{\sqrt{\sum_{c=1}^n (R_{i,c} - R_i^-)^2} \cdot \sqrt{\sum_{c=1}^n (R_{j,c} - R_j^-)^2}}, \quad (4)$$

where $R_{i,c}$ and $R_{j,c}$ represent user i and j 's evaluation of item c . R_i^- and R_j^- represent the average of the ratings. In the current membership service, the process of purchasing clothing, which does not need to guide customers, is shown in Figure 4.

In Figure 4, the technical solution adopted in the intelligent display and matching part of the member user is that the member customer walks in front of the member experience device and can choose clothing according to their preferences. In corresponding scenarios, the technology can recommend matching clothing to customers, and users can arbitrarily match clothing according to their own preferences.

3.2. Elements and Functions of Marine Bionic Environment. The application of marine bionic form design to the brand image design of children's clothing enriches the formal language of the product and embodies the unique aesthetic feeling [20]. The characteristics of marine bionic environment are shown in Figure 5.

In Figure 5, the inspiration of marine bionic design includes not only the real form of the marine world directly derived from nature, but also the abstract form and subjective image form extracted from rational thinking.

Most marine plants use bright colors to convey messages of friendliness, hostility, excitement, threat, or deception. Its ultimate purpose is to survive [21]. These beautiful and bright colors are used in children's products with unexpected results. The benefits of marine elements on children's attractiveness are shown in Figure 6.

In Figure 6, bright colors can beautify and enrich the color language of children's products, making the products more beautiful and beautiful. The bionics of biological structure and texture is a commonly used method in modern design. The use of biological structure or texture effects in product design can make the audience feel the novelty and uniqueness of creativity [22] and will bring tactile and visual

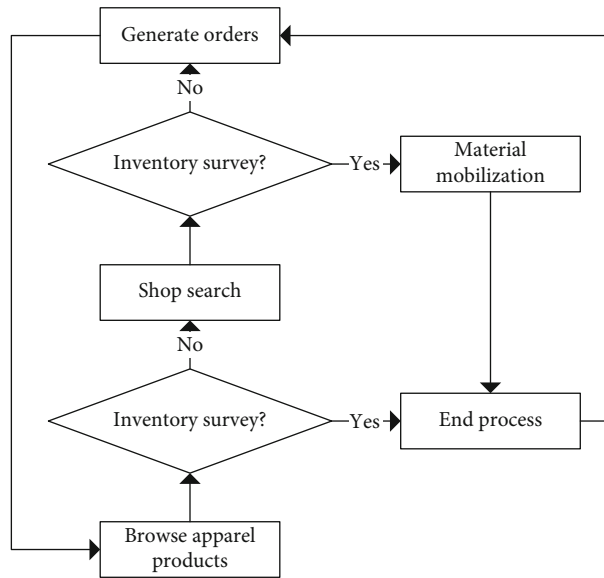


FIGURE 4: The flow of membership-style clothing purchases.

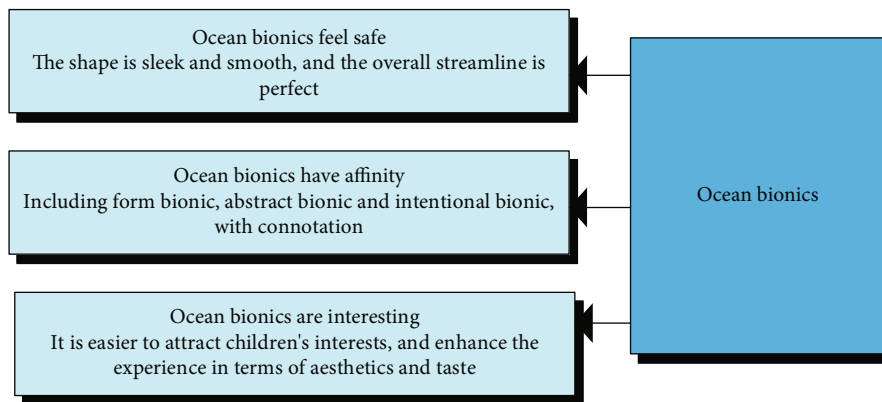


FIGURE 5: Features of the marine biomimetic environment.

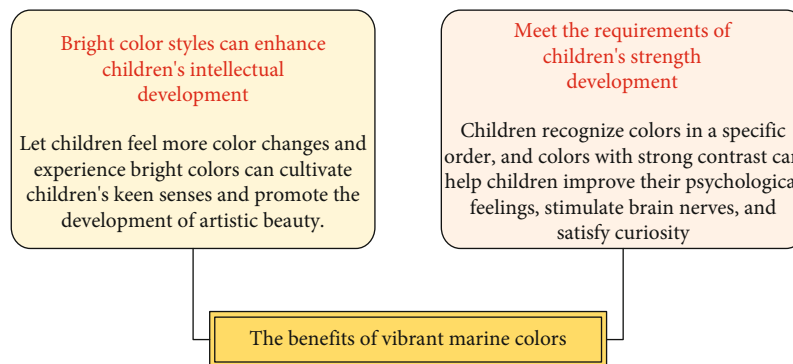


FIGURE 6: Marine elements enhance children's senses.

impact to people. Several marine bionic design results are shown in Figure 7.

In Figure 7, the process of bionic design is the process of imitating a creature in the ocean. Its design process is shown in Figure 8.

In Figure 8, in the design field, natural elements have been fully utilized as a valuable resource. Designers often look for design inspiration in natural things, solve the root of the problem by drawing on the modeling structure of natural ecology, and use their professional quality and



FIGURE 7: Results of marine bionic design.

professional skills to reconstruct it to form a certain aesthetic sense [23]. A notable example of reproduction in natural design is the graphic patterns and colors of animal fur. The color tone of marine life can generally be divided into five types as shown in Figure 9.

In Figure 9, the marine life has high color saturation and strong contrast and has a strong visual impact. Its own color and pattern form have certain inspirations for textile design, clothing design, environmental design, and graphic design. When the marine life color of clothing design is adopted [24], it can help summarize the ideas in the color style design of clothing and use it in the design of children's clothing.

3.3. Children's Cognition of Color in Different Age Groups. The color style visual design of children's clothing needs to be carried out for children of different ages. The marine bionic environment gives people the feeling of being smart. When designing patterns, an innovative design process from shape resemblance to spiritual resemblance is required, and emotional factors need to be incorporated [25]. Children of

different ages have different perceptions of different colors in their hearts. Children's psychological and cognitive development is divided into four stages, as shown in Table 2.

Children around the age of 14 gradually have their own aesthetic ability. When choosing clothes and other things, they begin to follow their own choices and oppose their parents' choices. At this stage, there are five aspects of clothing selection criteria that parents give their children, as shown in Figure 10.

In Figure 10, the comfort and safety of clothing are equally important when parents consider purchasing children's clothing. Comfortable clothing is conducive to the healthy growth of children.

At this stage, biological children have entered the best period of memory. The development of children's intelligence and the education of knowledge are of great concern to parents. They will cultivate children to accumulate knowledge and enhance the learning atmosphere in any way and by any means.

With people's pursuit of healthy life and high-quality life, environmental protection has become a hot topic.

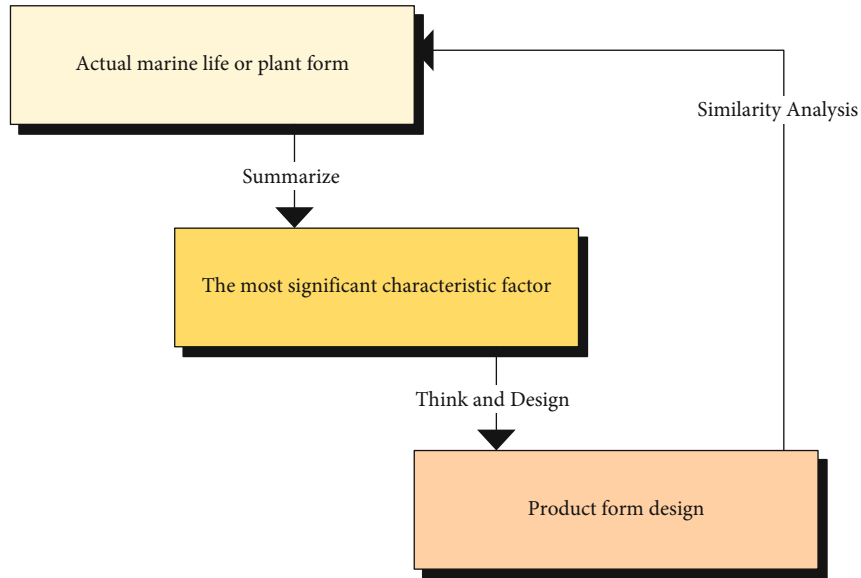


FIGURE 8: The design process of marine bionics.

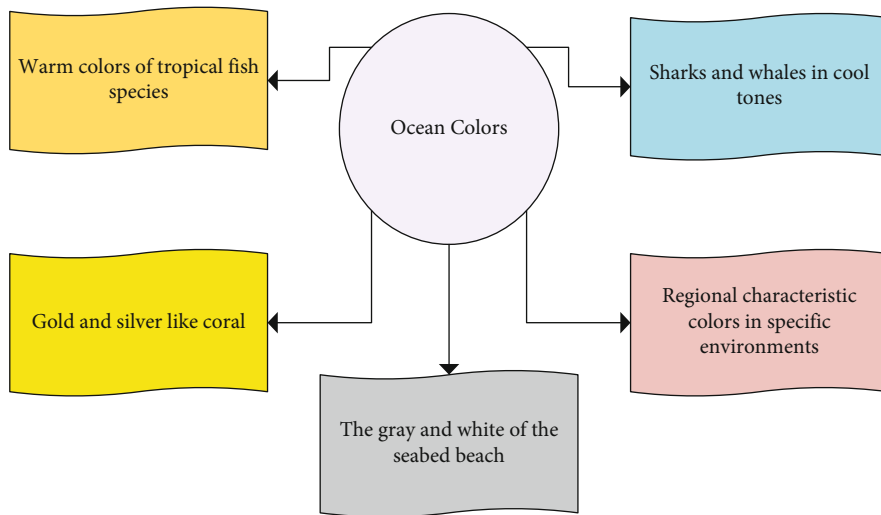


FIGURE 9: The tone of marine bionic colors.

Green, eco-friendly clothing has the least negative impact on the environment and human health. When parents buy clothing products for children, they pay special attention to the quality of clothing.

Based on attaching importance to safety, modern parents advocate freedom, pursue individuality, and pay attention to taste. Children mainly consider the attractiveness and fun of the product. Based on ensuring the health, safety, greenness, environmental protection and other qualities of children’s clothing, there are further requirements for the value of the additional spiritual level.

According to relevant data records, children aged 8-15 are the main component of the children’s clothing market. Most of the children at this stage will have their own right to choose when buying clothing, and they will be the main players in future consumer spending by choosing products

through their own aesthetic wishes. Figure 11 shows the main structure and players in the consumer market for children of this age group.

In Figure 11, the reason for this structure is that children in this age group begin to switch from passive consumption to active choice consumption, and children’s curiosity makes their market potential unprecedented and high commercial value. The root of these lies in their pursuit of fashion and individuality.

3.4. Wireless Sensor Communication and Mobile Computing. Wireless sensor network (WSN) is self-organized by a large number of small, low-cost, and resource-constrained sensor nodes deployed in specific monitoring areas with the ability of environmental parameter sensing, information processing and storage, and wireless communication. It is an important

TABLE 2: Color psychological cognition of children of different ages.

Generation	Cognitive ability
Infants and toddlers aged 0-3	Children at this stage are still at the stage of preliminary exploration of the world, and their cognitive level is relatively elementary, so they should focus on guidance and enlightenment. Their understanding of natural forms is only at a preliminary stage, and they have not yet formed their own consciousness. Therefore, the clothing at this stage still has the guardian's aesthetic decision.
4-6-year-old children	This stage is mostly preschool. Children currently have excellent imitation ability and show great curiosity and thirst for knowledge about the things around them. Bright colors and prominent features can attract children's attention well. At this time, children are very easily influenced, have low self-control, are prone to emotional fluctuations, and have a certain aesthetic foundation. The design choices of clothing can have their own choices, but most of them still depend on their parents.
Children aged 7-12	Children at this stage begin to mature in their understanding of patterns and colors, have unique personality development, and are more sensitive to aesthetic abilities. At this time, children have strong expressiveness, their pursuit of unique personality begins to surge, they have their own understanding of aesthetics, and the choice of clothing can be chosen by themselves.
Children 13-16	Children at this stage begin to develop a more mature consumption concept and have their own brand awareness. After accumulating a lot of knowledge, their ability to understand color has a unique trait, and they began to show opposition to their parents' choices. They matured in their consumption concepts. They broke away from the naive style of childhood and began to imitate the adult style.

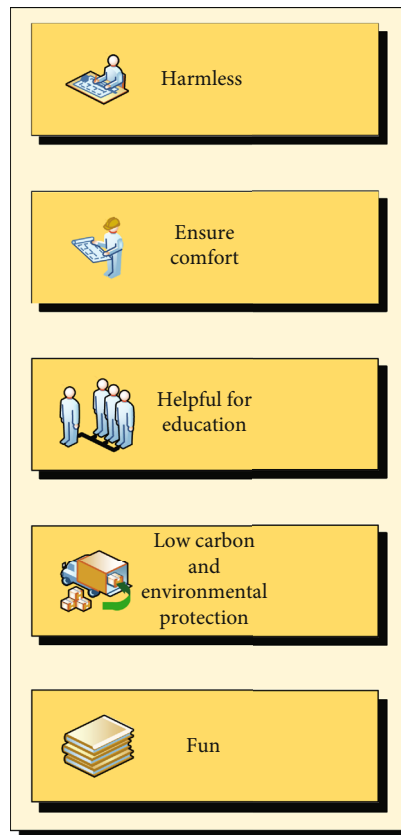


FIGURE 10: Parents' clothing selection criteria.

emerging technology for information sensing and data collection in the twenty-first century. WSN is a new network form integrating sensor technology, semiconductor manufacturing technology, microelectromechanical system, embedded computing technology, radio communication technology, distributed processing technology, and modern

network technology. Generally, when designing the pattern style of clothing, the general pattern design can be composed of points, lines, and surfaces. In fact, points can have many different shapes, so points are the basis of some graphics. It can have different characters and color elements [26], become abstract points, and form different patterns. Based

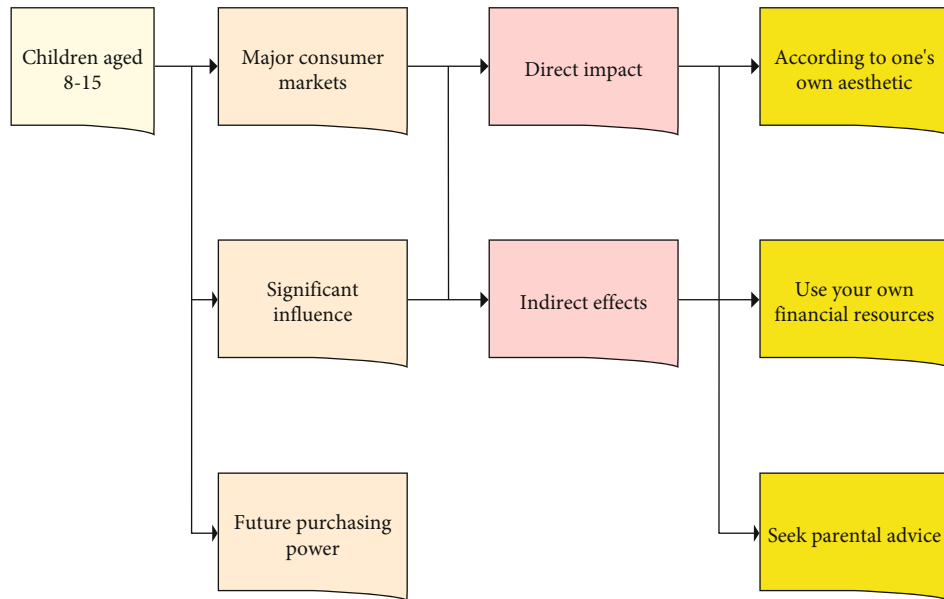


FIGURE 11: The structure of children in the consumer market.

on the IoT machine learning, the visual structure of marine bionic elements is optimized and designed. The pattern of grid points is shown in Figure 12.

In Figure 12, when extracting and applying graphic elements, the shape of the graphic can be adjusted appropriately without changing the basic shape. After the pattern is extracted, it is arranged into two-sided continuous and four-sided continuous graphics. Through repetition, reconstruction, gradual change, and concretization, new patterns are formed and applied to the packaging design of brand image to bring good visual effect.

3.5. Feedback Questionnaire Design for children’s Clothing Design with Marine Bionic Elements. With people’s pursuit of healthy life and high-quality life, environmental protection has become a hot topic. Green, eco-friendly clothing has the least negative impact on the environment and human health. When parents buy clothing products for children, they pay special attention to whether the quality of clothing, the material, and the shape of the products are beneficial to children’s health. Incorporating the design concept of “happy, healthy, green and environmental protection” into the product plays a vital role in the future development of children and has certain educational significance for children. The marine environment gives people a pure, green, and natural feeling, which is in line with parents’ expectations for their children’s inner world. Marine element brands are the first choice for parents.

A questionnaire on the effect of marine bionic elements on children’s visual design was designed, and the color and pattern making style of visual patterns were investigated in the environment of high-energy IoT. The data collected in the questionnaire mainly includes the description of the cognitive and structural characteristics of marine bionic elements. In addition, the age distribution of children’s parents is also investigated in the daily clothing purchase.

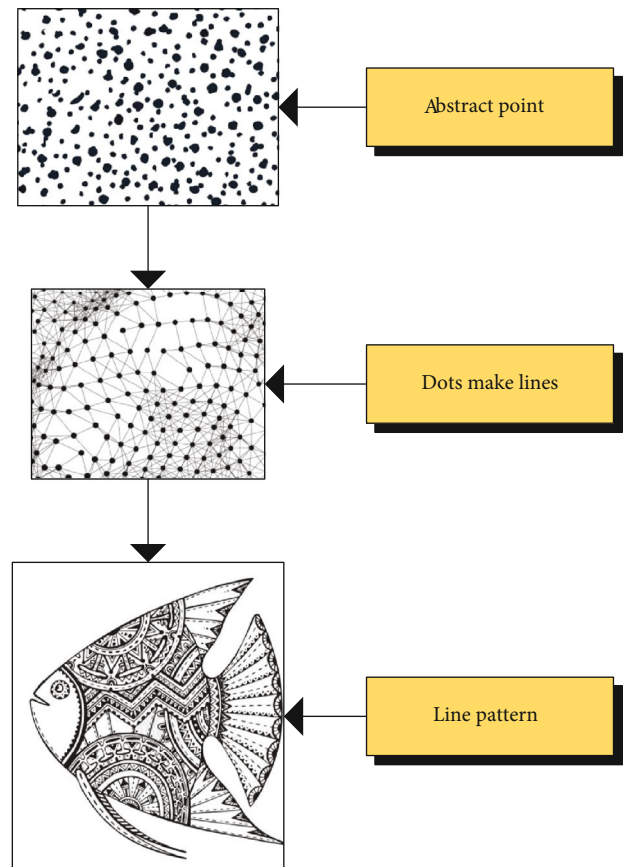


FIGURE 12: Construction of a common pattern.

The data on age and options are automatically collected and evaluated in the system by the high-energy IoT framework. The questionnaire designed by relevance concept is shown in Table 3.

TABLE 3: Questionnaire for the visual design of marine bionic clothing.

Basic information:

Parent's age:

- A. 27-30
- B. 31-36
- C. 37-40
- D. Above 41

Your gender:

- A. Male
- B. Female

Questionnaire questions and options:

How many outfits are typically bought for a child in a one-month period:

- A. 1-3
- B. 4-6
- C. 7-9
- D. More than 10

When shopping for clothing, who chooses:

- A. The child chooses by himself
- B. The parent makes the choice
- C. Appropriately listen to the child's opinion

Before buying clothing, how do you know clothing information:

- A. Other people's clothes packaging
- B. Advertising
- C. Familiar brand
- D. Recommend by friends
- E. Other ways

When choosing to clothe for children, will you pay special attention to the brand benefits of clothing:

- A. I care a lot
- B. I will choose brand
- C. I do not care

You generally choose foreign brands or domestic brands:

- A. Foreign brands
- B. Domestic brands
- C. Do not care

What is your child's favorite color in this marine environment-inspired costume:

- A. Bright colors
- B. Deep colors
- C. Black and white gray

Which pattern do children like the most in the visual design of such marine bionic clothing:

- A. Line drawing
- B. Paper cut
- C. Ink painting
- D. Paste type
- E. Ordinary painting

Which shade does your child prefer:

- A. Warm colors

TABLE 3: Continued.

- B. Cool colors
- C. It does not matter

Which presentation style does your child prefer:

- A. Realism that is more in line with facts
- B. Abstraction that is more exaggerated
- C. It does not matter

Other additions:

TABLE 4: Test results of questionnaire validity.

Sampling suitability quantity	.943	
	Chi-square read	3204.042
Sphericity test	Degrees of freedom	407
	Significance	.000

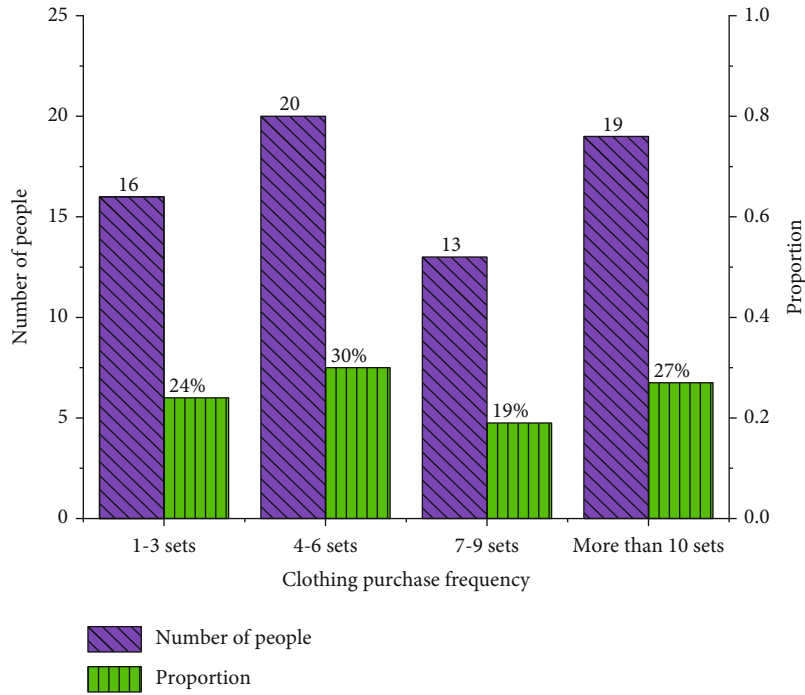
The validity of the questionnaire is tested after designing the questionnaire. SPSS statistical software is used to analyze the questionnaire, as shown in Table 4.

The suitable sampling number is 0.943, which is greater than 0.9, and the significance is 0.000. The validity of the questionnaire is good, and the results can be used and adopted. The experimental data set of the study is obtained by means of a questionnaire survey. Questionnaires are distributed to 80 families to investigate the influence of children's clothing on marine bionic visual design and ask their opinions. A total of 73 questionnaires are returned after completing the survey. There are 68 valid questionnaires, and the survey results will be statistically analyzed in the results.

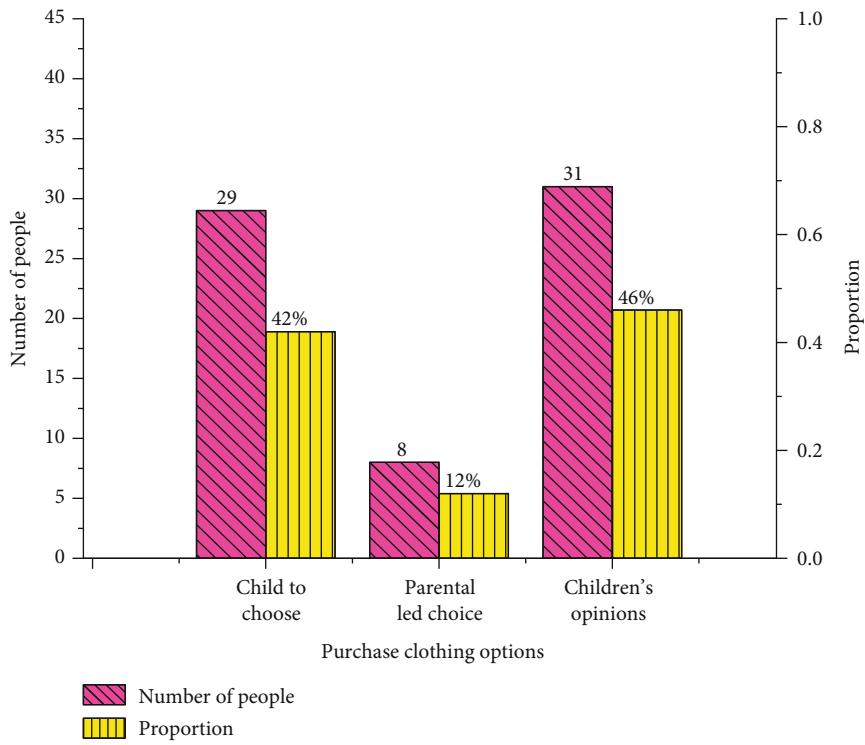
4. Results

4.1. Discussion on the Color Degree of General Families for Marine Bionic Visual Clothing Design. In this link, firstly, statistics and analysis of the pattern and color results of the visual design of marine bionic clothing are carried out in general families. Additionally, other factors affecting clothing purchases in the family are also analyzed, including purchase volume, choice of clothing purchased, choice of clothing brand, and access to clothing information. The survey results are drawn as a statistical map to judge the factors and degrees of influence of these factors on the design of marine bionic clothing and give some suggestions for discussion. The statistical results are shown in Figure 13.

In Figure 13(a), most families purchase clothes for their children within a month, and the frequency is relatively average. Among them, 20 and 19 families purchased 4-6 pieces and more than ten pieces, accounting for 30% and 27%, respectively. In Figure 13(b), when buying children's clothing for children, most families will consider their children's opinions, and eight families, accounting for 12%, are completely dominated by parents. In Figure 13(c), 33 of the 68 families will first consider domestic brands when

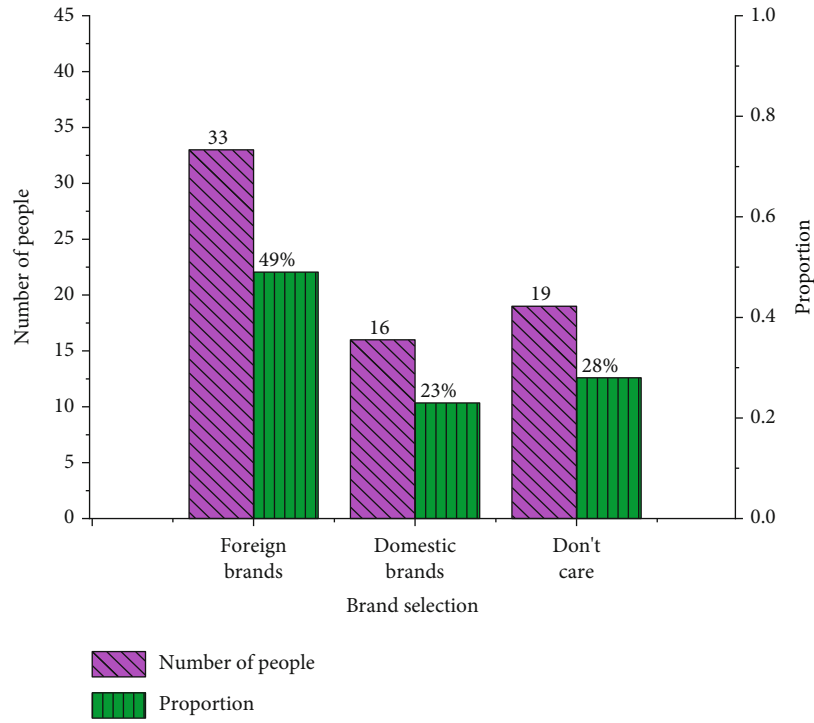


(a)

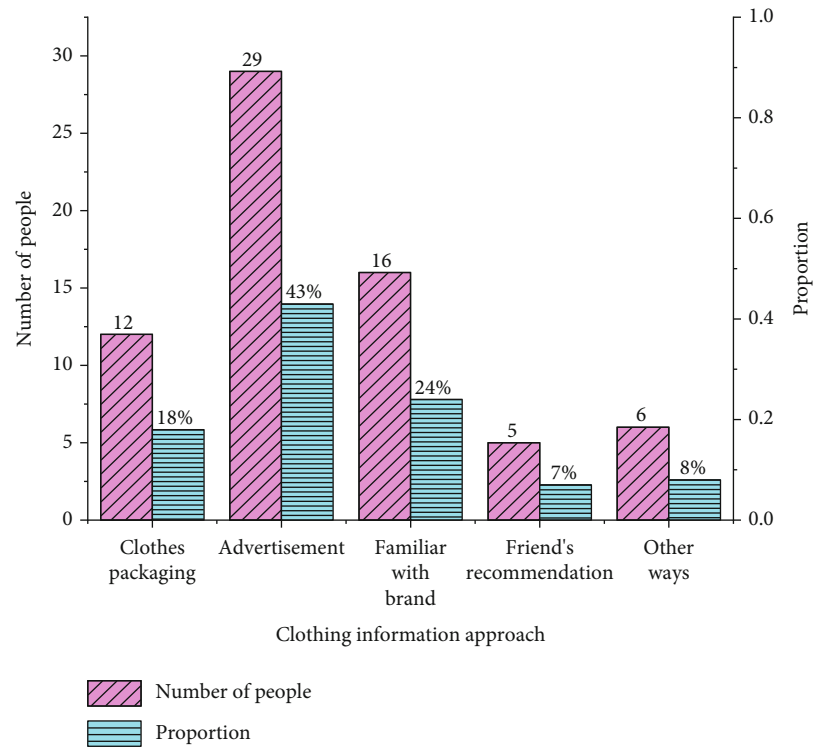


(b)

FIGURE 13: Continued.



(c)



(d)

FIGURE 13: Continued.

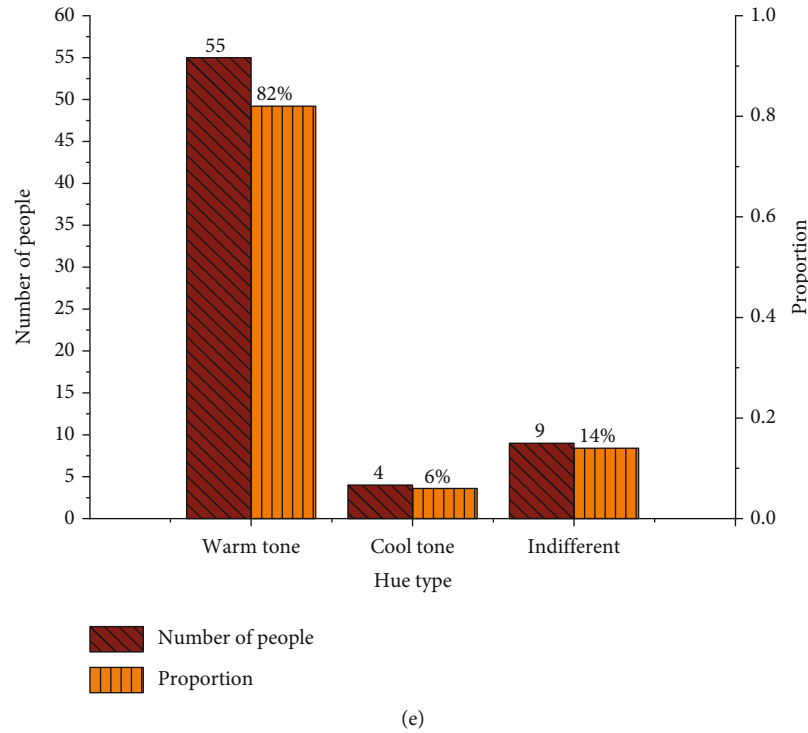


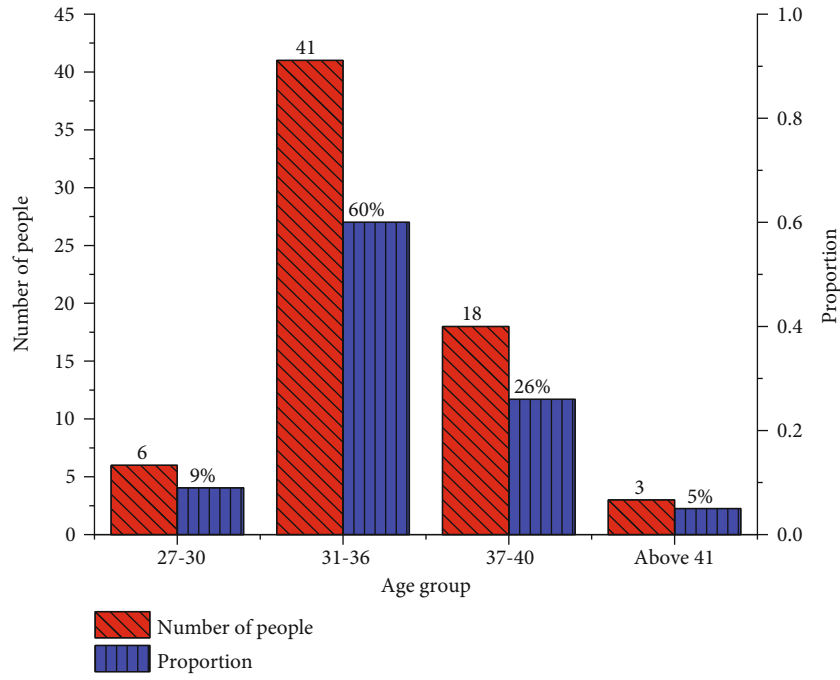
FIGURE 13: Statistics on clothing color and purchase situation ((a) is the purchase frequency of clothing; (b) is the source of choice when purchasing clothing; (c) is the brand selection of clothing; (d) is the way to obtain clothing information; and (e) is the evaluation of the color of the marine biomimetic pattern).

purchasing children's clothing, 16 of the remaining families will consider foreign brands first, and 19 will not care about the influence of brands. In Figure 13(d), 29 families obtained information from advertisements when purchasing clothing, accounting for 43%, and 16 families obtained information from friends' recommendations. Finally, in Figure 13(e), children in 55 families prefer the visual style of clothing in warm colors, and only 4 prefer cool colors. Therefore, when using the marine bionic environment to design clothing styles, designers should first consider starting with warm colors, which can better attract children's attention and choose to buy. Additionally, designers should also properly consider cool-toned clothing to meet the needs of all consumers.

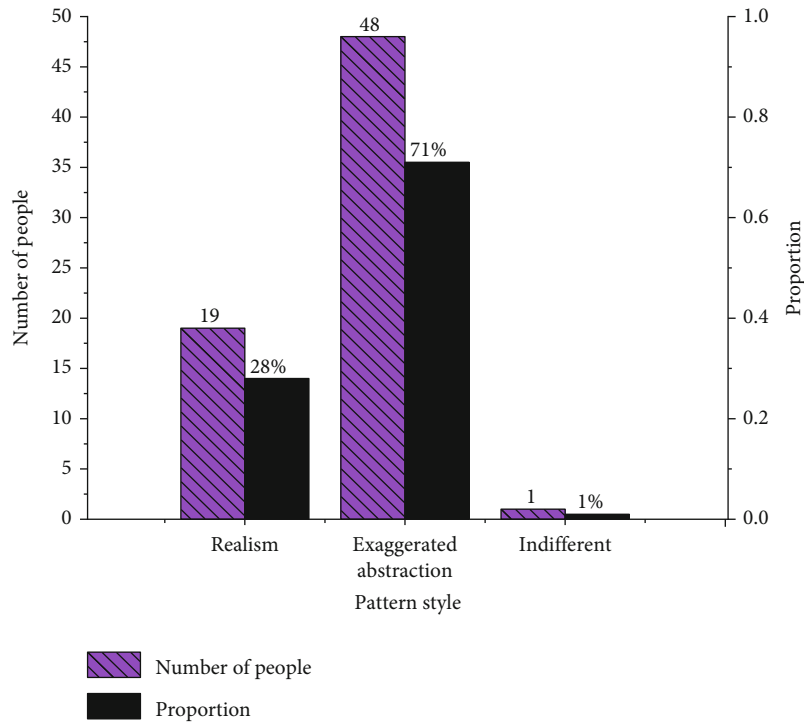
4.2. The Pattern Style Evaluation of the General Family for the Visual Design of Marine Bionic Clothing. Aesthetic preference is the personal preference and appreciation of the aesthetician for the structure, shape, color, material, and other aspects of things. Children of different ages have different aesthetic styles and tastes. Noble aesthetic sentiment can make the aesthetic person get spiritual pleasure and satisfaction and finally get the perfection of personality. The influence of the marine bionic environment on the visual design of children's clothing is discussed. A questionnaire is used to rate 68 families for different styles of color visual design clothing. This link will evaluate the design style and style of clothing patterns in the bionic environment, and the data results are shown in Figure 14.

In Figure 14(a), in the 68 surveyed households, most of the parents are concentrated in the age group of 31-40. Among them, parents aged 31-36 are the most, with 41 accounting for 60%. In Figure 14(b), 48 parents aged 31-36, and 71% of the families prefer the exaggerated abstract pattern style in clothing. Most of these patterns are anthropomorphic animated characters based on marine animals. Therefore, it is also loved by most children. In Figure 14(c), the line drawing and ordinary drawing are the most popular, with 17 and 19 families, accounting for 25% and 27%, respectively, followed by the sticker type, with 12 people, accounting for 18%. Finally, the same number of people who like paper-cut shapes and ink paintings are ten people, accounting for 15%, respectively. When carrying out the visual design of marine simulation-style patterns, it is necessary to focus on line drawing and ordinary painting, and most people who like ordinary pattern style design still occupy the majority.

To sum up, through the concept description of machine learning collaborative e-commerce under the concept of IoT and the analysis of elements and functions of the marine bionic environment, the visual structure of marine bionic elements is designed and optimized based on the cognition of color by children of different age groups. The survey results of marine bionic visual clothing design showed that children from 55 families preferred the visual style of clothing in warm colors, and children from only four families preferred cool colors. In addition, in the evaluation of pattern style, line painting and ordinary painting are the most

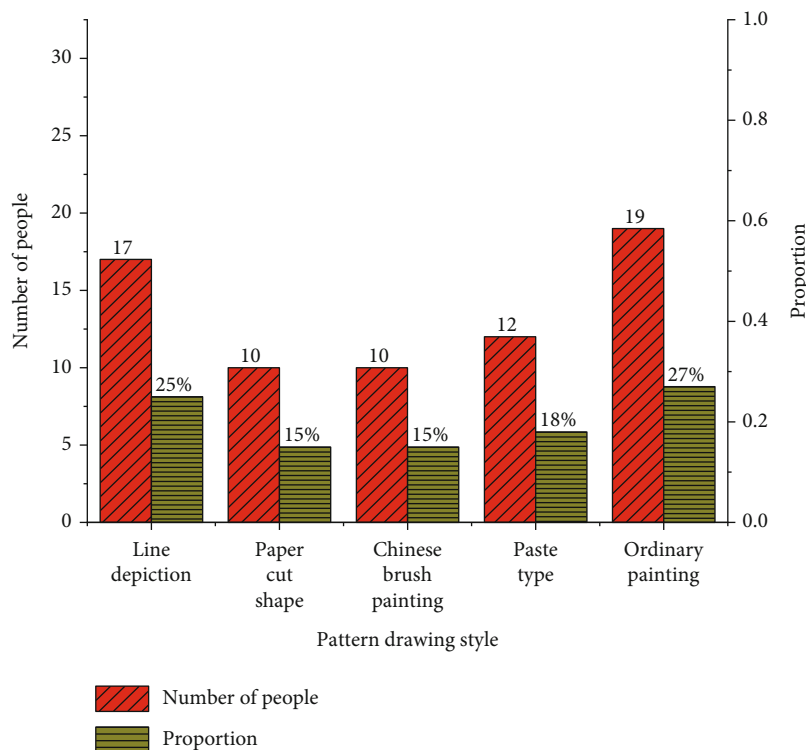


(a)



(b)

FIGURE 14: Continued.



(c)

FIGURE 14: Visual style evaluation of pattern style ((a) is the age group distribution of parents in the family; (b) is the genre style of the visual pattern; and (c) is the drawing method of the pattern).

popular, with 17 and 19 families, accounting for 25% and 27%, respectively, followed by sticker type, with 12 families, accounting for 18%. Research shows that different families have different needs for clothing color and clothing design style, and the design direction should be adjusted according to the actual situation.

5. Conclusion

At present, given the diversification of clothing styles, major children’s clothing companies urgently need to seize the children’s mainstream aesthetic style and improve their sales performance. Therefore, they try to apply new network technologies in children’s wear design. Based on the IoT and machine learning method, the bionic system factors of marine organisms are studied in children’s wear pattern design. Firstly, in the large environment of the IoT, machine learning is a synergistic business concept with technology that summarizes the design process of clothing. Secondly, examples and methods of marine bionic elements in style design are set forth. A set of marine-style apparel visual questionnaires for different family children are designed combined with the difference in color and pattern cognitive ability in four different ages. Children in 68 families have surveyed various styles and colors of clothing patterns and home environments. The questionnaire results have been summarized, and most children are more interested in warm-tone patterns and colors and the pattern drawn in bylines and ordinary paintings. Therefore, in the clothing

style design, the above three factors should be used as the main design style. The main shortcomings of research are that the investigation of sample data is 68, less than a normal survey, and the result is limited. Hence, in subsequent work, to improve the advantages of the proposed work, the number of survey samples will be further expanded, and the data will be further collected to improve the operational efficiency of the model.

Data Availability

The raw data supporting the conclusions of this article will be made available by the authors, without undue reservation.

Ethical Approval

This article does not contain any studies with human participants or animals performed by any of the authors.

Consent

Informed consent was obtained from all individual participants included in the study.

Conflicts of Interest

All Authors declare that they have no conflict of interest.

Acknowledgments

The authors acknowledge the help from the university colleagues. This work was supported by a grant from Brain Korea 21 Program for Leading Universities and Students (BK21 FOUR) MADEC Marine Designing Education Research Group.

References

- [1] T. Tang and P. Hu, "Quantitative standard of promotion strategy and analysis on the influence of consumer purchase behavior," *Cluster Computing*, vol. 22, no. S2, pp. 4949–4955, 2019.
- [2] A. Omwami, H. Lahti, and P. Seitamaa-Hakkarainen, "The variation of the idea development process in apparel design: a multiple case study," *International Journal of Fashion Design, Technology and Education*, vol. 13, no. 3, pp. 341–351, 2020.
- [3] A. F. B. A. Jawhar and S. S. H. M. Salem, "Aesthetic values of free drawing style on women eveningwear using decorations inspired by marine," *International Design Journal*, vol. 11, no. 2, pp. 179–184, 2021.
- [4] D. Wei, Y. Nagai, L. Jing, and G. Xiao, "Designing comfortable smart clothing: for infants' health monitoring," *International Journal of Design Creativity and Innovation*, vol. 7, no. 1-2, pp. 116–128, 2019.
- [5] D. Bhatt, J. Silverman, and M. A. Dickson, "Consumer interest in upcycling techniques and purchasing upcycled clothing as an approach to reducing textile waste," *International Journal of Fashion Design, Technology and Education*, vol. 12, no. 1, pp. 118–128, 2019.
- [6] D. J. Kim and S. Lee, "A study of consumer perception on fashion show using big data analysis," *Journal of Fashion Business*, vol. 23, no. 3, pp. 85–100, 2019.
- [7] J. Pu and Y. Meng, "Application of visual design in the development of marine tourist resources," *Journal of Coastal Research*, vol. 98, no. sp1, pp. 125–128, 2019.
- [8] E. Varol, "Being a style icon in fashion world: iris Apfel," *Global Journal of Arts Education*, vol. 11, no. 1, pp. 89–101, 2021.
- [9] A. Nguyen, S. Foerstel, T. Kittler et al., "System design for a data-driven and explainable customer sentiment monitor using IoT and enterprise data," *IEEE Access*, vol. 9, pp. 117140–117152, 2021.
- [10] Z. T. Al-Azez, A. Q. Lawey, T. E. H. El-Gorashi, and J. M. H. Elmighani, "Energy efficient IoT virtualization framework with peer to peer networking and processing," *IEEE Access*, vol. 7, pp. 50697–50709, 2019.
- [11] H. Ju, Y. Chen, V. Sivakumar, and C. B. Sivaparthipan, "Energy optimised IoT assisted multiple fuzzy aggravated energy scheduling approach for smart scheduling systems," *Enterprise Information Systems*, vol. 15, no. 7, pp. 951–965, 2021.
- [12] F. Samie, L. Bauer, and J. Henkel, "From cloud down to things: an overview of machine learning in Internet of Things," *IEEE Internet of Things Journal*, vol. 6, no. 3, pp. 4921–4934, 2019.
- [13] M. Zolanvari, M. A. Teixeira, L. Gupta, K. M. Khan, and R. Jain, "Machine learning-based network vulnerability analysis of industrial Internet of Things," *IEEE Internet of Things Journal*, vol. 6, no. 4, pp. 6822–6834, 2019.
- [14] S. M. Tahsien, H. Karimipour, and P. Spachos, "Machine learning based solutions for security of internet of things (IoT): a survey," *Journal of Network and Computer Applications*, vol. 161, article 102630, 2020.
- [15] A. Kishor, C. Chakraborty, and W. Jeberson, "Intelligent healthcare data segregation using fog computing with internet of things and machine learning," *International Journal of Engineering Systems Modelling and Simulation*, vol. 12, no. 2/3, pp. 188–194, 2021.
- [16] S. Sehnem, A. A. F. S. L. Queiroz, S. C. F. Pereira, G. Santos Correia, and E. Kuzma, "Circular economy and innovation: a look from the perspective of organizational capabilities," *Business Strategy and the Environment*, vol. 31, no. 1, pp. 236–250, 2022.
- [17] X. Yu, F. Jiang, J. Du, and D. Gong, "A cross-domain collaborative filtering algorithm with expanding user and item features via the latent factor space of auxiliary domains," *Pattern Recognition*, vol. 94, pp. 96–109, 2019.
- [18] M. Ayub, M. A. Ghazanfar, T. Khan, and A. Saleem, "An effective model for Jaccard coefficient to increase the performance of collaborative filtering," *Arabian Journal for Science and Engineering*, vol. 45, no. 12, pp. 9997–10017, 2020.
- [19] R. H. Singh, S. Maurya, T. Tripathi, T. Narula, and G. Srivastav, "Movie recommendation system using cosine similarity and KNN," *International Journal of Engineering and Advanced Technology*, vol. 9, no. 5, pp. 556–559, 2020.
- [20] Y. Zhou, "Brand design of coastal eco-tourism products based on cultural creativity," *Journal of Coastal Research*, vol. 112, no. sp1, pp. 306–310, 2020.
- [21] X. Zhang and M. Yang, "Color image knowledge model construction based on ontology," *Color Research & Application*, vol. 44, no. 4, pp. 651–662, 2019.
- [22] S. M. Hosseini, M. Mohammadi, A. Rosemann, T. Schröder, and J. Lichtenberg, "A morphological approach for kinetic façade design process to improve visual and thermal comfort: review," *Building and Environment*, vol. 153, pp. 186–204, 2019.
- [23] H. Huang, C. Lin, and D. Cai, "Enhancing the learning effect of virtual reality 3D modeling: a new model of learner's design collaboration and a comparison of its field system usability," *Universal Access in the Information Society*, vol. 20, no. 3, pp. 429–440, 2021.
- [24] M. Fakhraee, N. J. Planavsky, and C. T. Reinhard, "The role of environmental factors in the long-term evolution of the marine biological pump," *Nature Geoscience*, vol. 13, no. 12, pp. 812–816, 2020.
- [25] D. Zhang, "Color versus form: which matters more in children's preferences of package design?," *Journal of International Consumer Marketing*, vol. 31, no. 1, pp. 39–52, 2019.
- [26] C. J. He, B. A. Ying, X. F. Wang, and J. Qi, "Construction and application of clothing pattern design model based on directed graph method," *Journal of Fiber Bioengineering and Informatics*, vol. 14, no. 1, pp. 41–51, 2020.

Research Article

Predicting the Investment Risk in Supply Chain Management Using BPNN and Machine Learning

Lan Li 

School of Management, Hubei University of Education, Wuhan, Hubei, China 430205

Correspondence should be addressed to Lan Li; lilan@hue.edu.cn

Received 25 January 2022; Revised 14 April 2022; Accepted 25 April 2022; Published 8 June 2022

Academic Editor: Mu-Yen Chen

Copyright © 2022 Lan Li. This is an open access article distributed under the Creative Commons Attribution License, which permits unrestricted use, distribution, and reproduction in any medium, provided the original work is properly cited.

The present work is aimed at solving the investment risks in the supply chain management (SCM) process of enterprises. Therefore, the Back Propagation Neural Network (BPNN) algorithm, logistic regression analysis, and other related theories are used for the risk prediction analysis of supply chain samples. Firstly, 40 pieces of supply chain training data are collected as research samples. Secondly, the examples are trained using the BPNN algorithm. Meanwhile, a logistic regression model is constructed based on Principal Component Analysis (PCA). Finally, the two models conduct risk prediction on the test samples. The results indicate that the BPNN model can effectively predict various risks in the SCM process. It achieves an excellent evaluation effect of single risks, consistent with the actual results. Still, there are some deviations between the prediction results and the actual results of mixed risks. When the significance P value is more than 0.5, the sample is predicted to be of high risk. When it is less than 0.5, the sample is predicted to be of low risk. The prediction accuracy of the logistic regression model is as high as 92.8%, demonstrating brilliant applicability and popularization in the investment risk prediction of the supply chain. The BPNN algorithm and logistic regression model can precisely predict the investment risk in SCM and provide a reference for the improved SCM and the sustainable and stable development of enterprises in the supply chain.

1. Introduction

1.1. Research Background. With the development of science and technology, market competition is becoming even more dynamic and globalized. The supply chain faces increasingly fierce competition in the modern market [1]. However, the supply chain of each industry is affected by a variety of factors. The risk prediction in the supply chain management (SCM) process can offer vital information for the regular operation of the supply chain [2]. Rapid and efficient risk prediction and analysis of the SCM process will help supply chain managers accurately identify and judge the risks faced by the supply chain. It is also practicable to adopt corresponding risk control strategies to optimize enterprise management and workflow and reduce risks in the process of enterprise investment, guaranteeing the virtuous development cycle of the supply chain [3, 4].

1.2. Literature Review. Some scholars have employed the Back Propagation Neural Network (BPNN) to evaluate the

risk of specific links in the supply chain. Jeong et al. believed that the BPNN risk prediction model dramatically improved the work efficiency in product logistics transmission and ameliorated problems, such as missed and wrong shipments [5]. Shao et al. analyzed fruit and vegetable production, logistics, and sales risk indicators through the BPNN model. They suggested that the sales were a precarious link, which significantly impacted the overall management process of the supply chain; there were also certain risks in the logistics link [6]. Jiang et al. established a risk index evaluation system by sampling the supply chain data of enterprises. They also built a logistic regression model based on PCA to predict the risk of supply chain variables faced by enterprises [7]. Zheng et al. used the primary effect model to evaluate the influencing factors of logistics enterprises. They deemed that the logistic regression analysis results would be affected by the deviation of sample data [8]. Liu et al. reported that the additives added to product processing could seriously increase the risk to the supply chain. Hence, the authors established a corresponding BPNN model for risk prediction

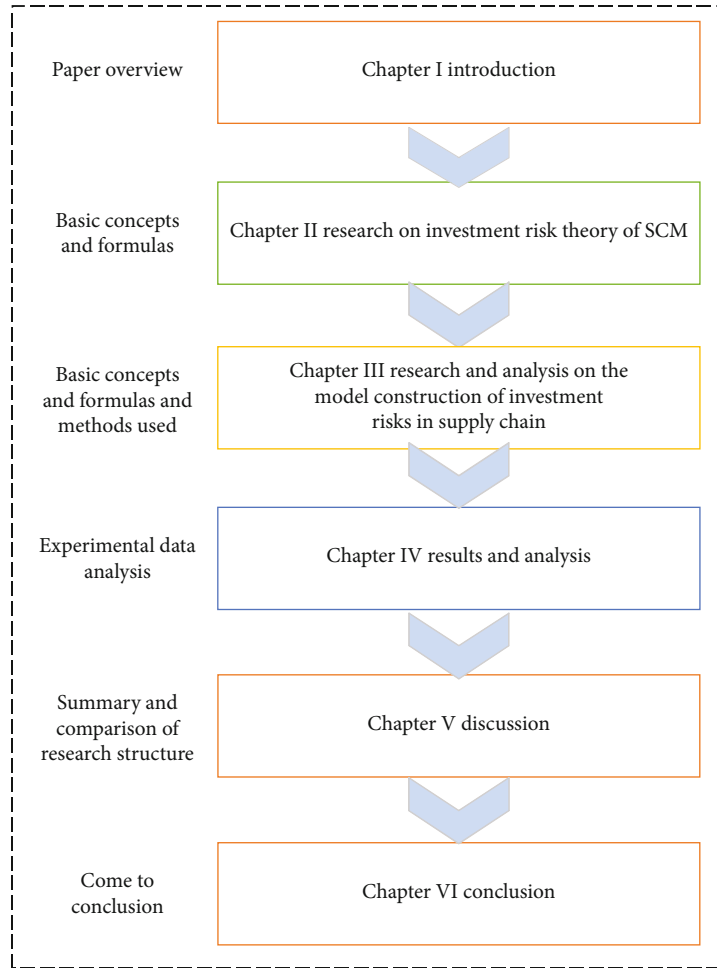


FIGURE 1: Organizational structure.

[9]. The existing works reflect many factors forming the investment risk of SCM and a remarkably high correlation between various factors, resulting in a lot of overlapping information. The BPNN structure and logistic regression model have advantages in analyzing complex data of a large volume and poor independence. In the related studies listed above, the first few authors mainly studied the industrial SCM from the perspective of logistics enterprises. The latter scholars applied the BPNN and logistic regression model to discuss investment management risks. They all put forward individual opinions from different angles with a certain systematicness. The downside of these studies is that they are limited to a small range of industries and lack certain universality. In addition, the research results are generally more descriptive in words than in data.

1.3. Research Questions and Objectives. This paper collects forty groups of supply chain training samples and ten groups of supply chain test samples for risk forecasting. Specifically, the principal indicators are selected for screening and analysis; the logistic regression model is established based on PCA to optimize the risk indicators; the BPNN model implements risk prediction on these indexes. Risk identification and evaluation of various risk indicators in the SCM process could

clearly understand different risk types and levels. It can help enterprises involved in the supply chain improve their awareness of risk management and provide a reference basis for risk prediction and evaluation. It can also provide an effective early warning plan for SCM to reduce investment risks in the supply chain. Figure 1 reveals the organizational structure of the research reported here.

2. Research on Investment Risk Theory of SCM

2.1. SCM. SCM originates from logistics management. As the logistics industry develops, the vertical integration model has become the logistics industry's trend, yet it does not expand the research scope of logistics management. The value chain concept gradually appears under enterprises' collectivized and globalized advancement. On this basis, supply chain theory has gradually formed combined with resource sharing and information interaction among enterprises [10–12]. Scholars worldwide have done many studies on the risk prediction of the supply chain and proposed some common risk evaluation methods. (1) Fuzzy comprehensive evaluation method: it calculates the fuzzy relationship based on the weight of each index and the fuzzy matrix of the prediction object and judges the prediction

object using a specific evaluation model combined with the function of each index [13]. (2) Analytical hierarchy process: it decomposes the relevant factors affecting the prediction results into different levels such as objectives, methods, and criteria, then makes qualitative and quantitative analysis, and finally obtains the decision-making method [14]. (3) Grey system theory: aiming at the sample system with low information accuracy, it comprehensively evaluates the risk indicators during SCM by determining the standard weight, evaluation standard, sample matrix, the grey evaluation coefficient, grey evaluation weight matrix, and other methods or steps. (4) Rough set theory: this method mainly uses the correlation among multitudes of historical data to reflect the importance of target attributes. (5) Regression analysis: it refers to a process where a scholar needs to collect a large number of sample data, calculate the regression function among dependent and independent variables based on mathematical statistics, and analyze the relationship between two or more variables. (6) BPNN: this model is established through sample data acquisition and repeatedly trained via the self-learning characteristics to correct the weight and reduce the model error. Then, the connection weight of each layer of the network is analyzed, and a conclusion is drawn [15, 16].

Ricardo Saavedra et al. believed that SCM could systematically coordinate the relationship between departments within the enterprise and related enterprises and improve the work efficiency of departments and economic benefits of enterprises [17]. Kerkkamp et al. reported that SCM was a management mode connecting raw material suppliers, product manufacturers, distributors in goods transportation, logistics personnel, and customers. Besides, information and material flow were continuously repeated [18]. Chkanikova and Sroufe believed that SCM was often a time-based competitive strategy compared with the role of enterprises in a single link. Besides, improving information communication and material turnover efficiency could connect different enterprises, increase cooperation and closeness, and enhance group competitiveness [19]. Pan et al. expounded that from the perspective of overall function, SCM was a comprehensive functional network chain structure mode focusing on the core enterprise using the control of information flow, logistics, and capital flow. It involved the procurement of raw materials, the manufacturing of intermediate products, the manufacturing of final products, and the final product delivery to consumers by the sales network [20].

In short, unlike the visualization concept of the supply chain, SCM is a management mode characterized by strategic cooperation among enterprises at each node. It effectively integrates various resources and maximizes the profits of the whole supply chain system. Because the supply chain system involves multiple participants, links, and objectives, the system is greatly affected by internal and external change factors and often faces management risks.

2.2. Management Risks in Supply Chain. There are many risks in the management process of the supply chain, roughly divided into three categories. (1) Environmental risk: it refers to the risks caused by the external environmen-

tal factors of the supply chain, including natural conditions, financial policies, and national laws. (2) Operational risk: it refers to the factors affecting the cohesion and destroying the cooperation of enterprises in the operation process, including information processing, agreement risk, and profit priority. (3) Internal management risk: it indicates the possible problems of each link and enterprise involved in the operation of the whole supply chain and the impact on the whole network chain, including supply link, manufacturing link, logistics link, and customer demand [21]. This paper only analyzes the internal management risk.

Many influencing factors of investment risk exist because SCM involves multiple enterprises or departments. Risk management of the supply chain is aimed at reducing the risk of the supply chain in general by identifying and managing the risk factors existing in the supply chain links and external risk factors [22, 23].

SCM's structure and involved aspects primarily determine the potential risks. Four leading risk indicators are selected here, and three secondary indexes are chosen for each dimension. The secondary indexes of the supply risk are the order satisfaction rate, on-time delivery rate, and quality qualification rate; those of the manufacturing risk are order completion rate, on-time delivery rate, and product qualification rate; those of the demand risk are product return rate, customer churn rate, and order change rate; those of the transportation risk are interactive inventory rate, safe delivery rate, and on-time delivery rate [24].

Figure 2 displays the SCM process and risk classification.

In Figure 2, there are four main links in the SCM process: suppliers, manufacturers, logistics and transportation, and final customers. Each link involves multiple aspects. Correspondingly, the operation process in each part faces corresponding risks, which will ultimately affect the regular operation of the entire supply chain and increase the risk of investment.

Risk management, an essential part of SCM, refers to the management process of identifying, evaluating, and analyzing various possible index risks. Efficiently predicting, preventing, and controlling risks help accurately deal with hidden dangers, ensure enterprises' regular operation, and minimize economic losses. Enterprises can carry out conventional risk management with detailed overall planning and prejudice to avoid SCM risks. Figure 3 demonstrates the main links.

As shown in Figure 3, the risk management process of the supply chain mainly includes five links: risk awareness, risk identification, risk assessment, risk treatment, and final inspection and evaluation. Firstly, employees and managers in the supply chain must have a degree of risk awareness and consciously predict and estimate risks in advance. Secondly, they need to investigate and identify the risks and analyze the reasons for the formation of risks through classification. Thirdly, they provide a reference for subsequent processing by quantitatively calculating the risk factors. A series of corresponding measures are taken to control the risk within an acceptable range. Finally, the whole process of risk management is scientifically checked and evaluated. Of course, in the entire process, each link is indispensable

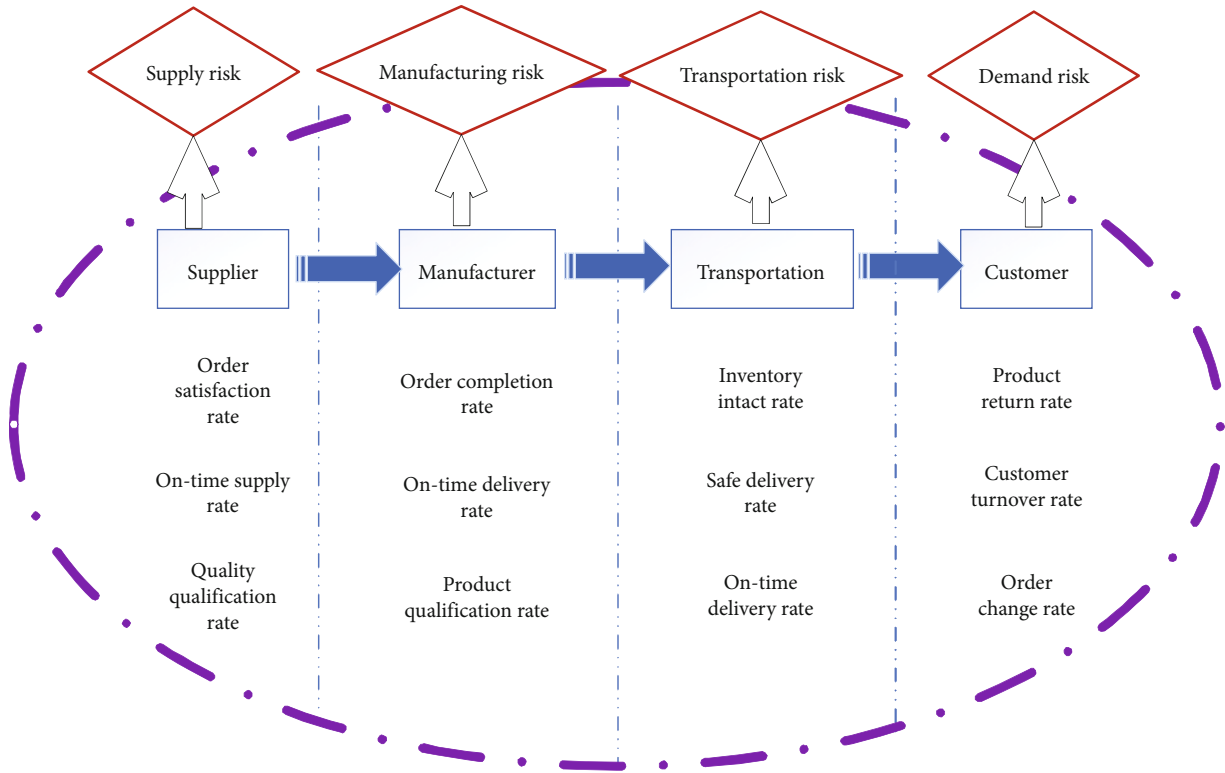


FIGURE 2: SCM process and risk classification.

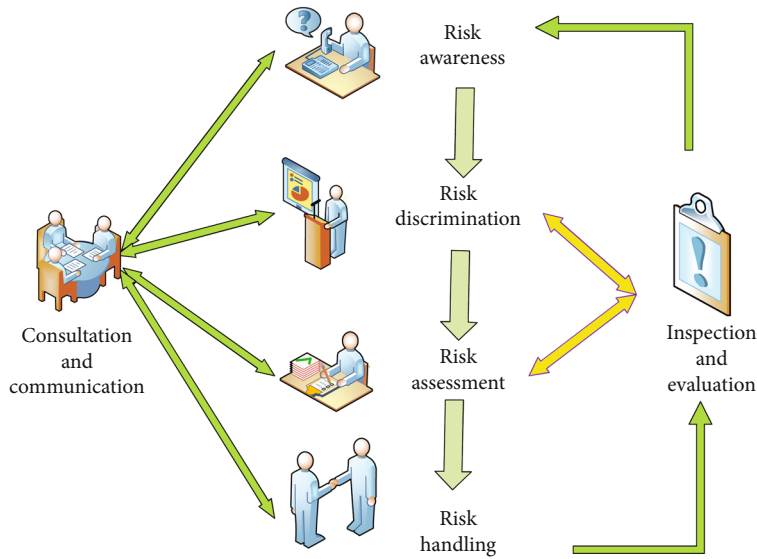


FIGURE 3: Procedures of risk management in supply chain.

for a complimentary consultation and information communication to form a complete closed loop to deal with the risks of SCM.

2.3. *BPNN Algorithm.* BPNN is used to conduct risk evaluation. In principle, the network is trained with several evaluation samples representing the sudden risks in a supply chain with known risk types and levels. In this way, it can obtain the empirical knowledge of risk types and levels and

the tendency of risk evaluation indicators in the supply chain from the training samples [25]. After the training, the new samples with unknown risks should be input into the network. The network can automatically diagnose the risk types and levels of the new samples according to experience and memory [26].

Here, the standard BPNN with a three-layer topology is used to analyze and evaluate the risks in a supply chain. Figure 4 describes the topology of BPNN.

In Figure 4, the input layer has i neuron inputs; $X = (x_1, x_2, \dots, x_i)^T$ expresses their signals; there are m neurons in the hidden layer, and $O = (O_1, O_2, \dots, O_m)^T$ means their signals as well as the input signals of the output layer; the output layer has k neurons, and $Y = (y_1, y_2, y_k)^T$ represents their signals.

Equation (1) denotes the function of the input layer, i.e., the hidden layer of BPNN.

$$o_m = f\left(\sum_{i=1}^n v_{im}x_i\right). \quad (1)$$

In Equation (1), f and v represent the activation function and weight of the hidden layer, respectively. Similarly, the relational expression between the output and implicit layers can be expressed as

$$y_k = f\left(\sum_{i=1}^n w_{mk}o_m\right). \quad (2)$$

In Equation (2), the meaning of the letters is the same as that in Equation (1). The error between BPNN training prediction and expectation is calculated according to

$$E = \frac{1}{2} \sum_{k=1}^m e_k^2 = \frac{1}{2} \sum_{k=1}^m (d_k - o_k)^2. \quad (3)$$

In Equation (3), d denotes the expected value, o stands for the predicted value, and e refers to the difference between expected mean value and the target value. The gradient method is used in the training optimization process of BPNN to quickly decrease the weight and reach the optimum:

$$\begin{aligned} \Delta w_{jk} &= \eta \delta_k^0 y_j = \eta (d_k - o_k)^2 o_k (m - o_k) y_j, \\ \Delta v_{jk} &= \eta \delta_k^y x_i = \eta \left(\sum_{k=1}^m \delta_k^0 w_{jk} \right) y_j (m - y_i) x_i, \end{aligned} \quad (4)$$

where η and δ represent the learning rate of BPNN and error signal factor, respectively. The remaining letters have the same meaning as in the above equations.

2.4. Logistic Regression Analysis. The logistic regression model is extensively used and has penetrated the fields of medicine, economics, biology, and engineering technology. On the one hand, the logistic regression model can mine the internal information hidden in the data and measure the dependence between explanatory and response variables. On the other hand, it can predict or provide a priori information for decision-makers to make accurate decisions [27].

Let the distribution function of random variable X be

$$F(x, \mu, \sigma) = \frac{1}{1 + e^{-(x-\mu)/\sigma}}, \quad -\infty < x < \infty. \quad (5)$$

In Equation (5), when $-\infty < \mu < \infty$ and $\sigma > 0$, X is said to obey a univariate logistic distribution with parameters μ, σ . μ is called the location parameter of the distribution, and σ is called the scale of the distribution parameter. At this time, the density function of X is defined as

$$f(x, \mu, \sigma) = \frac{e^{-(x-\mu)/\sigma}}{\sigma(1 + e^{-(x-\mu)/\sigma})^2}, \quad -\infty < x < \infty. \quad (6)$$

The variable Y is set to be a random variable of two categories. $Y = 1$ and $Y = 0$ indicate the occurrence and nonoccurrence of the events, respectively. The binary logistic regression model is used to describe the relationship between Y and covariate $X = (X_1, X_2, \dots, X_m)^T$. Equation (6) illustrates the form of the binary logistic regression model.

$$P(Y = 1 | \mathbf{x}) = \frac{e^{g(\mathbf{x})}}{1 + e^{g(\mathbf{x})}}. \quad (7)$$

In Equation (7), there is

$$g(\mathbf{x}) = \beta_1 x_1 + \beta_2 x_2 + \dots + \beta_m x_m, \quad (8)$$

where β denotes the risk probability of the supply chain. The present work mainly adopts the logistic regression model with two classifications shown in Equation (7).

PCA tries to regroup many original indicators with specific correlations (such as P indicators) into a new set of unrelated comprehensive indicators to replace the original indicators [28]. It is a multivariate statistical method to investigate the correlation between multiple variables. It explores how to reveal the internal structure of various variables through a few principal components. In other words, it derives a few main features from the original variables to retain as much information of the original variables as possible and keep them independent. Mathematically, a linear combination of the original P indexes is usually used as a new comprehensive index [29].

3. Research and Analysis on the Model Construction of Investment Risks in Supply Chain

3.1. Model Construction Based on the BP Neural Network. Here, 40 supply chain training samples are used to repeatedly test the BPNN model. There are i ($i = 12$) secondary indexes under the top four leading risk assessment indicators in the input layer and m secondary indexes in the hidden layer, which is finally determined by the test results. The output layer has five main risk evaluation indicators: supply, manufacturing, demand, transportation, and risk levels. Based on the BPNN algorithm, Equation (9) illustrates the relationship between the number of training samples and the number of neurons in each topology layer, i.e., the number of layers.

$$N = 1 + O_m \times \frac{x_i + y_k + 1}{y_k}. \quad (9)$$

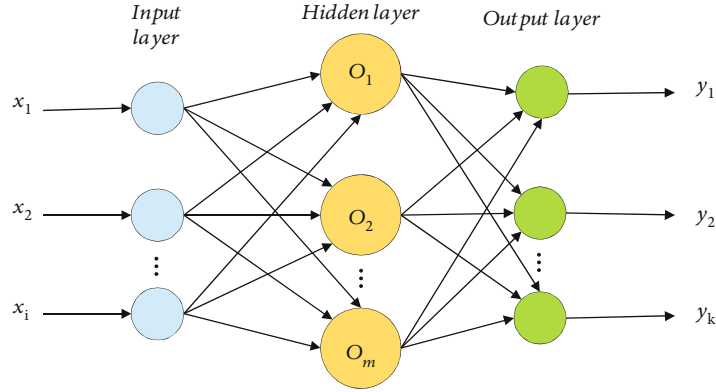


FIGURE 4: Topology structure of BPNN.

TABLE 1: Sample variable regression analysis.

Project	Main indicators	Intercept
Regression coefficient (B)	1.257	-1.446
Standard error (S.E.)	0.632	0.693
Wald	4.332	4.361
Degree of freedom	1	1
Significance (P)	0.035	0.028
OR	3.421	0.256
Confidence interval (E.N.) 95%		
Lower limit	1.045	
Upper limit	11.769	

In Equation (9), N denotes the number of training samples, x_i refers to the number of input layer nodes, y_k stands for the number of output layer nodes, and O_m represents the number of hidden layer nodes.

Symbols represent the output results of indicators in the BPNN model. Among the top four indicators, 1 represents risks, and 0 represents nonrisks; among the risk level indexes, 0 represents the level with nonrisks, and 1, 2, and 3 indicate low-, medium-, and high-risk levels, respectively.

3.2. Construction of Logistic Regression Model. Forty supply chain training sets are selected as the data samples. The logistic prediction model is constructed according to these samples. The contribution of its risk indicators to the supply chain is scored, with the range set to 0-100. 0 represents that the leading indicators are not at risk, 1 means that the leading indicators are at risk; 100 demonstrates that the risk is exceptionally high. The greater the value, the higher the risk level. Besides, classified forecasting is conducted on ten supply chain test samples. The logistic prediction model is designed as Equation (10), and the significance segmentation point is 0.5. When the significance P value is larger than 0.5, the sample prediction is of high risk; when the significance P value is less than 0.5, the sample is predicted as low risk.

SPSS analysis is conducted on the data of four main risk indicators (supply risk, manufacturing risk, demand risk, and logistics risk). The analysis results demonstrate that

the risk probability of the main indicators exceeds 85% of the total risk. The logistic model analyzes the values of the main indicators. The significance of the result variables is summarized in Table 1.

Table 1 illustrates that the P value of the main indicators is 0.035 and the P value of the intercept is 0.028, both meeting the test criteria, i.e., less than 0.05. Equation (10) manifests the logistic regression prediction model.

$$P = \frac{e^{(-1.453+1.248F_1)}}{1 + e^{(-1.453+1.248F_1)}}. \quad (10)$$

In Equation (10), F_1 represents the contribution rate of the main index to the sample risk.

4. Results and Analysis

4.1. Risk Evaluation and Analysis of BPNN Model for Training Samples. The MATLAB platform is adopted to train the BPNN model. After repeated training data convergence, the actual system error is the same as the target error, reaching 0.002. Five supply chain training samples, A, B, C, D, and E, are selected for regression simulation. The expected values are represented by A_q , B_q , C_q , D_q , and E_q . The output results are shown in Figure 5. The BPNN model values are represented by A_m , B_m , C_m , D_m , and E_m , and Figure 6 provides the output results.

Figures 5 and 6 denote that the supply, transportation, and demand risks of training sample A are normal in the expected output A_q and the network output A_m . However, the output results of the manufacturing risk are abnormal, indicating a threat with a low-risk level and an error of 0.001. The two output results B_q and B_m of the supply risk indicator of sample B show that there is a risk with a high level and an error of 0.0015. C_q and C_m of the demand risk indicator of sample C are abnormal, and the risk level is medium, with an error of 0.00017. D_q and D_m of the five indicators of sample D are completely consistent, and the error is 0. E_q and E_m of the demand risk indicator of sample E are abnormal, the risk level is low, and the error is 0.0012. It can be concluded that the final result output by the network model is basically the same as the expected result,

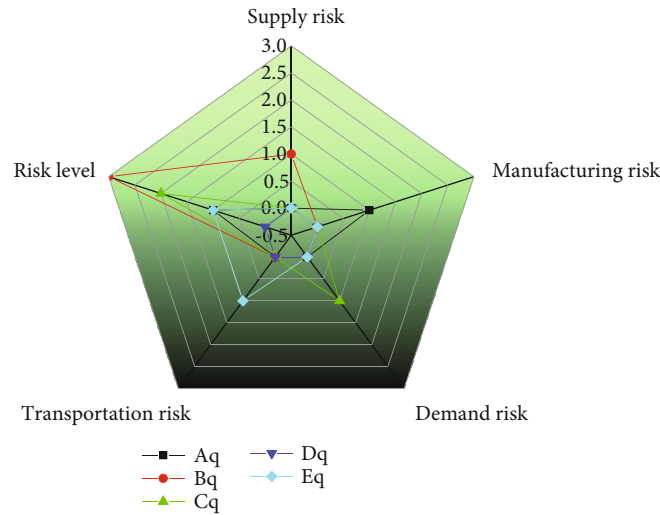


FIGURE 5: Expected output of supply chain training samples.

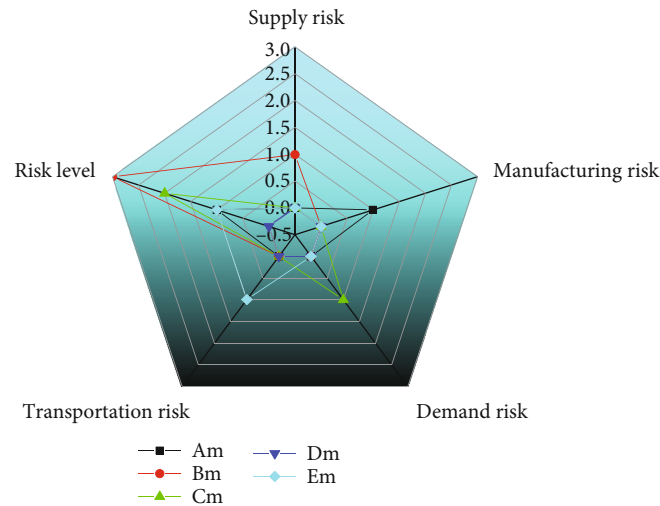


FIGURE 6: BPNN output of supply chain training samples.

and the error is within the set range. In other words, the BPNN model can test the supply chain well.

4.2. Risk Evaluation and Analysis of the BPNN Model for Test Samples. Twelve indicator values of ten test samples, A-1, B-1, C-1, D-1, E-1, F-1, G-1, H-1, I-1, and J-1, are shown in Figures 7 and 8. The BPNN model is used to compare and analyze the actual results and the predicted results of all indicators, and the results are shown in Figures 9 and 10.

The customer churn rate is the ratio of the number of customers lost to the number of customers for all consumer products or services. Figure 7 suggests that the return rate, customer churn rate, and order change rate of sample E-1 are significantly higher than those of other samples. The customer churn rate is up to 60%. The order change rate of sample J-1 is up to 91%, which has obvious demand risk. The on-time delivery rate of sample D-1 is as low as 40%, and the on-time delivery rate of sample G-1 is as low as 30%. There are proven obvious logistics risks.

Figure 8 denotes that the return rate, customer churn rate, and order change rate of sample E-1 are significantly higher than those of other samples, the customer churn rate has reached 60%, the order change rate of sample J-1 has reached 91%, and there is obvious demand risk. The on-time delivery rate of sample D-1 is as low as 40%, and the on-time delivery rate of sample G-1 is as low as 30%, both of which have apparent logistics risks.

Figures 9 and 10 demonstrate that the BPNN model has a brilliant evaluation effect on the single risk, consistent with the actual results. Still, there are some deviations in the evaluation of mixed risks. The real risk type of sample C-1 is that both supply and manufacturing risks exist simultaneously, and both risks are predicted during the model evaluation. However, the supply risk is at a high level, and the manufacturing risk is at a medium level. The model obtains results that both risks are at a high level. This situation may result from the lack of samples with both supply and manufacturing risks in the training samples, leading to

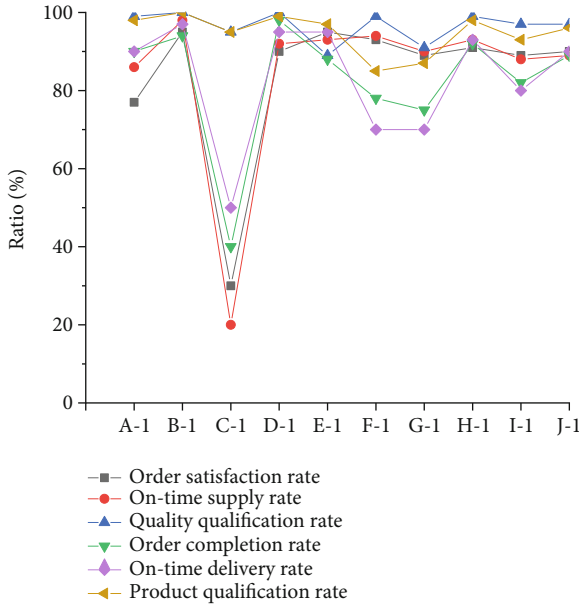


FIGURE 7: Analysis indicators of supply chain test samples.

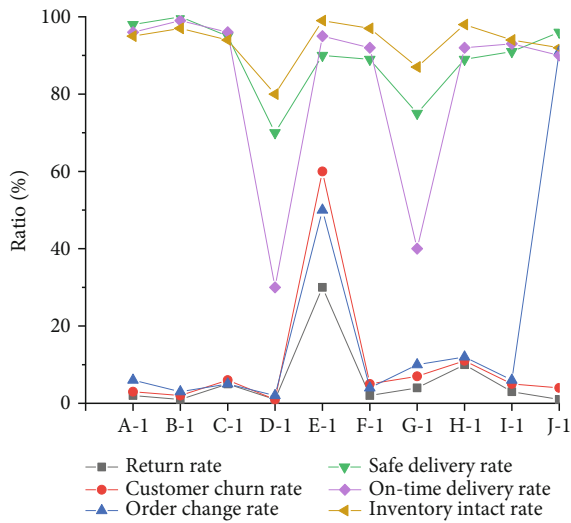


FIGURE 8: Analysis indicators of supply chain test samples.

insufficient model training and imperfect data collection. The demand risk of sample E-1 is very high, and the model makes a proper judgment, consistent with the expected result. For sample G-1, manufacturing and logistics risks exist concurrently, and the predicted risk is at a high level, but the analysis result of the model is a medium risk level. Analyzing the sample index data suggests that the manufacturing and logistics risks in the G-1 samples are inconsistent, and the model deviates in judgment, resulting in inconsistent judgment results. However, the overall model can effectively predict the risk level of each index of the supply chain.

4.3. Risk Evaluation Analysis of Logistic Regression Model of Test Samples. The logistic regression model in Section 3.2 predicts the investment risk of 10 test samples in SCM. Table 2 displays the results.

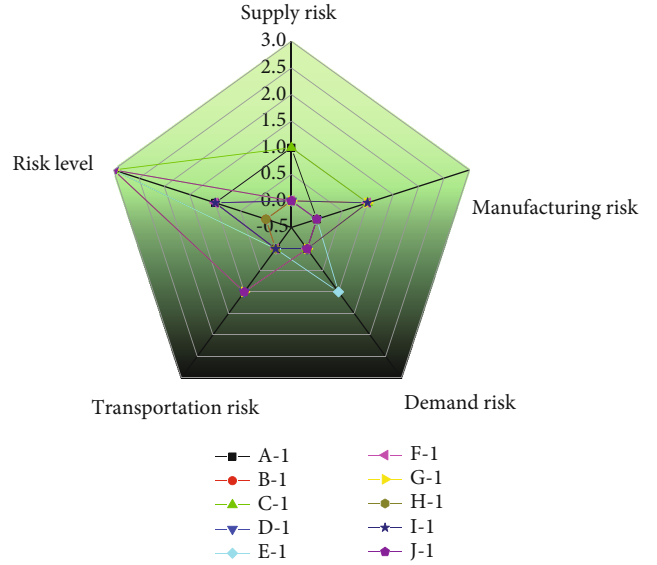


FIGURE 9: Actual evaluation results of supply chain test samples.

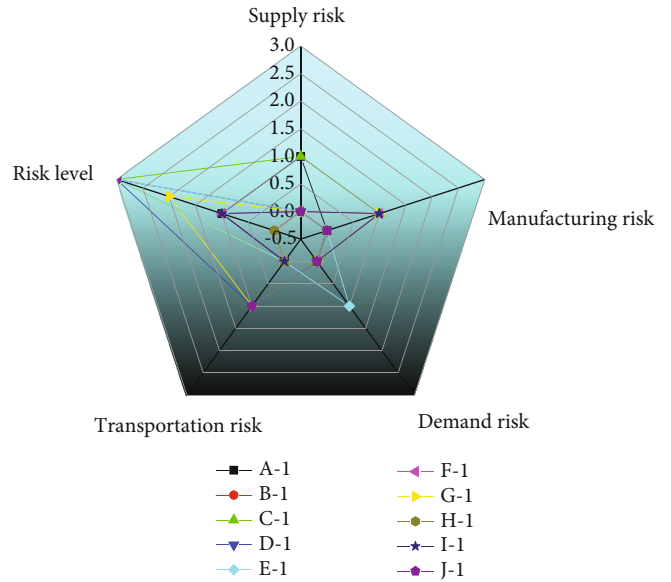


FIGURE 10: Risk evaluation results of the BPNN model for test samples.

Table 2 indicates that when the expected risk is 0, the prediction accuracy of the logistic model reaches 85.7%; when the expected risk is 1, the prediction accuracy of the logistic model is very high, reaching 100%. For ten prediction samples, the overall prediction accuracy has gained 92.8%. The results show that the logistic model has excellent applicability and promotion in investment risk prediction of the supply chain and can provide strong data support for the development of the industry. Mentzer used the risk questionnaire method to study the investment risk of SCM. He found that SCM was systematic and strategic coordination of the functions of traditional enterprises departments within an enterprise and between enterprises from the entire supply chain. The aim was to improve the long-term

TABLE 2: Supply chain sample forecast results.

Expected value	Estimated value		Number of samples	Correct rate (%)	Total accuracy (%)
	0	1			
0	6	1	7	85.7	92.8
1	0	3	3	100	

performance of the supply chain and each enterprise [30]. From the perspective of environmental analysis, Ma used the financial statement method to predict the risks existing in the supply chain. Ma thought that SCM was based on the core enterprise, through the control of information flow, logistics, and capital flow, starting from the procurement of raw materials, making intermediate products, and final products. Finally, the product was delivered to consumers by the sales network, which connected suppliers, manufacturers, distributors, retailers, and end-users into a whole functional network chain structure model [31].

5. Discussion

The issues of risk investment and risk sharing in SCM are critical, especially for industries with extended supply chains and increasingly uncertain supply and demand. Firstly, this paper collects 40 pieces of supply chain data as research samples and carries out corresponding sample training via the BPNN algorithm. Secondly, the data samples are simulated and trained based on PCA. Finally, the risk prediction is simulated to verify the performance of the models reported here. The main conclusions are as follows. (1) The BPNN model can precisely predict a single risk, and there will be some deviation in evaluating mixed risk. (2) The prediction accuracy of the logistic model is high, about 92.8%. It has good applicability and popularization in investment risk prediction of the supply chain. Bandyopa considered the unequal relationship among enterprises in the supply chain and divided the supply chain enterprises into two categories: core enterprises and partner enterprises. They also utilized the Stackelberg model to discuss the investment decision game between them and compared the results with those of the Cournot model. They concluded that different types of enterprises had different degrees of investment and information sharing, which provided a judgment basis for the investment of supply chain enterprises [32]. Yu et al. constructed the net present value model, internal rate of return model, and Gordon lobar model of investment based on the cost-benefit analysis method and the principle of marginal income. The authors emphasized the use of multiple economic models to study investment problems from different angles [33]. Compared with the conclusions drawn by these two scholars, this paper applies the BPNN and logistic regression models to forecast investment risks of SCM and draws the corresponding conclusions through continuous test and sample training. The achievements reported here have specific effectiveness. In addition, the current mainstream neural network algorithm and a regression model are applied, sorting out the theoretical con-

text for the future research on enterprise supply chain and presenting a new research perspective.

6. Conclusion

The investment risk in the process of enterprise SCM is a problem that all companies have to face. The BPNN analysis and logistic regression analysis are carried out on the risk prediction in the process of SCM. The main conclusions are as follows. (1) After a mass of supply chain training samples is collected, the BPNN model is trained using the MATLAB platform by setting four risk indicators (supply risk, manufacturing risk, demand risk, and logistics risk). After repeated training and data convergence, the risk prediction is performed on ten test samples. The results indicate that the BPNN model can effectively predict various risks in the SCM process. The evaluation effect of a single risk is perfect, consistent with the actual results. Still, there are some gaps between predicted and actual results when evaluating mixed risks. (2) A logistic regression model is constructed based on the PCA with 40 training samples. When the significance P value is more than 0.5, the sample is predicted to be at high risk. When it is less than 0.5, the sample is predicted to be at low risk. (3) After analyzing ten prediction samples, the prediction accuracy of the logistic model is very high, attaining 92.8%. In conclusion, the model has excellent applicability and popularization in the investment risk prediction of the supply chain.

Due to limited energy, the range of data is relatively small. Besides, SCM's environmental and overall operational risks are ignored in this experiment. The future study will expand the data size and investigate the risk assessment of environmental factors and operational factors to improve reference value for assessing investment risks in the SCM process.

Data Availability

The raw data supporting the conclusions of this article will be made available by the author, without undue reservation.

Ethical Approval

This article does not contain any studies with human participants or animals performed by any of the authors.

Consent

Informed consent was obtained from all individual participants included in the study.

Conflicts of Interest

The author declares that there is no conflict of interest.

Authors' Contributions

All authors listed have made a substantial, direct, and intellectual contribution to the work and approved it for publication.

Acknowledgments

The authors acknowledge the help from the university colleagues.

References

- [1] K. Govindan, T. C. E. Cheng, N. Mishra, and N. Shukla, "Big data analytics and application for logistics and supply chain management," *Transportation Research*, vol. 114, pp. 343–349, 2018.
- [2] M. Bhutta, A. Muzaffar, G. Egilmez, F. Huq, M. N. Malik, and M. A. Warraich, "Environmental sustainability, innovation capacity, and supply chain management practices nexus: a mixed methods research approach," *Sustainable Production and Consumption*, vol. 28, pp. 1508–1521, 2021.
- [3] A. Arasteh, "Supply chain management under uncertainty with the combination of fuzzy multi-objective planning and real options approaches," *Soft Computing*, vol. 24, no. 7, pp. 5177–5198, 2020.
- [4] S. Muneer, "The information system management and its infrastructure for supply chain management as antecedents of financial performance," *Journal of Asian Finance Economics and Business*, vol. 7, no. 1, pp. 229–238, 2020.
- [5] H. Jeong, R. A. Karim, H. L. Sieverding, and J. J. Stone, "An application of GIS-linked biofuel supply chain optimization model for various transportation network scenarios in Northern Great Plains (NGP), USA," *Bioenergy Research*, vol. 14, no. 2, pp. 612–622, 2021.
- [6] B. Shao, C. Ni, J. Wang, and Y. Wang, "Research on venture capital based on information entropy, BP neural network and CVaR model of digital currency in Yangtze River Delta," *Procedia Computer Science*, vol. 187, pp. 278–283, 2021.
- [7] F. Jiang, Z. Guan, Z. Li, and X. Wang, "A method of predicting visual detectability of low-velocity impact damage in composite structures based on logistic regression model," *Chinese Journal of Aeronautics: English version*, vol. 34, no. 1, pp. 296–308, 2021.
- [8] J. Zheng, Y. Y. Li, G. Bao, and X. Zou, "A new result for global existence and boundedness of solutions to a parabolic-parabolic Keller-Segel system with logistic source," *Journal of Mathematical Analysis & Applications*, vol. 462, no. 1, pp. 1–25, 2018.
- [9] Y. Liu, X. Wang, X. Zhu, and Y. Zhai, "Thermal error prediction of motorized spindle for five-axis machining center based on analytical modeling and BP neural network," *Journal of Mechanical Science and Technology*, vol. 35, no. 1, pp. 281–292, 2021.
- [10] H. Yong, H. Huang, and L. Dong, "Inventory and pricing decisions for a dual-channel supply chain with deteriorating products," *Operational Research*, vol. 20, no. 3, pp. 1–43, 2020.
- [11] S. Xu, "Retracted article:BP neural network-based detection of soil and water structure in mountainous areas and the mechanism of wearing fatigue in running sports," *Arabian Journal of Geosciences*, vol. 14, no. 11, pp. 1–15, 2021.
- [12] S. Tang and F. Yu, "Construction and verification of retinal vessel segmentation algorithm for color fundus image under BP neural network model," *The Journal of Supercomputing*, vol. 77, no. 4, pp. 3870–3884, 2021.
- [13] B. Feng, K. Sun, Z. Zhong, and M. Chen, "The Internal Connection Analysis of Information Sharing and Investment Performance in the Venture Capital Network Community," *International Journal of Environmental Research and Public Health*, vol. 18, pp. 22–11943, 2021.
- [14] W. D. Lopes, D. F. M. Monte, C. M. G. C. de Leon et al., "Logistic regression model reveals major factors associated with total bacteria and somatic cell counts in goat bulk milk," *Small Ruminant Research*, vol. 198, article 106360, 2021.
- [15] C. Haiyun, H. Zhixiong, S. Yüksel, and H. Dinçer, "Analysis of the innovation strategies for green supply chain management in the energy industry using the QFD-based hybrid interval valued intuitionistic fuzzy decision approach," *Renewable and Sustainable Energy Reviews*, vol. 143, no. 1, article 110844, 2021.
- [16] L. Xiao, Q. Zhu, X. Xu, and C. Wäger, "Time lag effect of supply chain management on firm performance," *Journal of Systems Science and Systems Engineering*, vol. 30, no. 3, pp. 321–338, 2021.
- [17] M. M. Ricardo Saavedra, C. H. D. O. Fontes, and F. G. M. Freires, "Sustainable and renewable energy supply chain: a system dynamics overview," *Renewable and Sustainable Energy Reviews*, vol. 82, Part 1, pp. 247–259, 2018.
- [18] R. Kerckamp, W. Heuvel, and A. Wagelmans, "Two-echelon supply chain coordination under information asymmetry with multiple types," *Omega*, vol. 76, pp. 137–159, 2018.
- [19] O. Chkanikova and R. Sroufe, "Third-party sustainability certifications in food retailing: certification design from a sustainable supply chain management perspective," *Journal of Cleaner Production*, vol. 282, article 124344, 2021.
- [20] S. Pan, D. Trentesaux, D. McFarlane, B. Montreuil, E. Ballot, and G. Q. Huang, "Digital interoperability in logistics and supply chain management: state-of-the-art and research avenues towards physical Internet," *Computers in Industry*, vol. 128, article 103435, 2021.
- [21] S. Dellana, W. J. Rowe, and Y. Liao, "A scale for measuring organizational risk management maturity in the supply chain," *Benchmarking: An International Journal*, vol. 29, no. 3, pp. 905–930, 2022.
- [22] S. Chen, Q. Jiang, Y. He et al., "A BP neural network based hierarchical investment risk evaluation method considering the uncertainty and coupling for the power grid," *IEEE Access*, vol. 8, no. 99, pp. 110279–110289, 2020.
- [23] S. Tian, N. Dai, L. Li, W. Li, Y. Sun, and X. Cheng, "Three-dimensional mandibular motion trajectory-tracking system based on BP neural network," *Mathematical Biosciences and Engineering*, vol. 17, no. 5, pp. 5709–5726, 2020.
- [24] Z. Zhang, V. Trevino, S. S. Hoseini et al., "Variable selection in logistic regression model with genetic algorithm," *Annals of Translational Medicine*, vol. 6, no. 3, p. 45, 2018.
- [25] P. Schober and T. R. Vetter, "Logistic regression in medical research," *Anesthesia & Analgesia*, vol. 132, no. 2, pp. 365–366, 2021.

- [26] H. Birkel and J. M. Muller, "Potentials of industry 4.0 for supply chain management within the triple bottom line of sustainability - a systematic literature review," *Journal of Cleaner Production*, vol. 289, no. 10, article 125612, 2021.
- [27] R. Toorajipour, V. Sohrabpour, A. Nazarpour, P. Oghazi, and M. Fischl, "Artificial intelligence in supply chain management: a systematic literature review," *Journal of Business Research*, vol. 122, no. 8, pp. 502–517, 2021.
- [28] A. Talukder and M. Z. Hossain, "Prevalence of diabetes mellitus and its associated factors in Bangladesh: application of two-level logistic regression model," *Scientific Reports*, vol. 10, no. 1, 2020.
- [29] X. Mo and Y. Zeng, "The relationship between ovarian endometriosis and clinical pregnancy and abortion rate based on logistic regression model," *Saudi Journal of Biological Sciences*, vol. 27, no. 1, pp. 561–566, 2020.
- [30] M. Mentzer, "Research on supply chain management and talent assurance of emergency logistics personnel under public health emergencies," *American Journal of Industrial and Business Management*, vol. 11, no. 1, pp. 60–75, 2021.
- [31] I. Ma, "Opportunities for implementation of non-cash transactions of supply chain management of village-owned business agencies," *Uncertain Supply Chain Management*, vol. 56, no. 42, pp. 69–78, 2021.
- [32] J. Bandyopa, "The zero trust supply chain: managing supply chain risk in the absence of trust," *International Journal of Production Research*, vol. 59, no. 11, pp. 3430–3445, 2020.
- [33] H. Yu, Y. Zhao, Z. Liu et al., "Research on the financing income of supply chains based on an E-commerce platform," *Technological Forecasting and Social Change*, vol. 169, no. 45, article 120820, 2021.

Research Article

Industrial Internet of Things Anti-Intrusion Detection System by Neural Network in the Context of Internet of Things for Privacy Law Security Protection

Di Teng 

Department of Law, Harbin Finance University, Harbin 150000, China

Correspondence should be addressed to Di Teng; 2009035@hrbfu.edu.cn

Received 2 April 2022; Revised 12 May 2022; Accepted 13 May 2022; Published 6 June 2022

Academic Editor: Mu-Yen Chen

Copyright © 2022 Di Teng. This is an open access article distributed under the Creative Commons Attribution License, which permits unrestricted use, distribution, and reproduction in any medium, provided the original work is properly cited.

Today, the Industrial Internet of Things (IIoT) and network technology are highly developed, and network data breaches occur every year. Therefore, an anti-intrusion detection system has been established to improve the privacy law security protection of IIoT. In the adversarial network, the security performance requirements and structural system of the Internet of Things have high-strength requirements. The network system must adopt a system with strong stability and a low data loss rate. After comparing a large number of network structures, the initial network technology in deep learning is adopted. The Convolutional Neural Network (CNN) technology for handwritten character recognition optimizes and upgrades the LeNet-5 network, and the new LeNet-7 is built. Additionally, three network technologies are combined, and an IIoT anti-intrusion detection system is constructed. The performance of the system is tested and verified. The model has high data accuracy, detection rate, and low false-positive rate. The model's generality on high-performance data is validated and compared with privacy-aware task offloading methods, achieving the best performance. Therefore, the system can be applied to the data privacy law security protection of IIoT.

1. Introduction

Due to the rapid development of the Internet of Things (IoT) and 5th-Generation Mobile Network (5G) technologies, the data generated by network users across the country have gathered into a vast network, and it has penetrated any corner of work and life. This significantly improves the convenience and work efficiency of people's lives. Renewable energy has become one of the main resources to help the world protect the environment from pollution and provide people with new energy [1]. Because of the rapid development of the IoT, each section of data in the network contains private data such as the user's personal information and location information, the enterprise's business secrets, and the state secrets of the government. In recent years, data breaches have occurred frequently. For example, in 2010, diplomatic mails from the United States were leaked through WikiLeaks [2]. In 2016, the LinkedIn network platform spread to nearly 500 million users [3]. The economic losses

caused by data breaches averaged 3.6 million U.S. dollars each year, according to the report released by IBM in 2020 [4]. The news all show that today's networks face serious security threats, and network attacks occasionally occur, especially in the field of the Industrial Internet of Things (IIoT). It is precisely because of the increased occurring IoT security issues that some scholars have emphasized the need to pay attention to the privacy protection of network data and the accountability of data leakage [5]. In recent years, many professionals have researched the security issues of IIoT. Hui et al. used the N-shift encryption scheme and Lyapunov stability theory to establish a chaotic secure communication scheme to solve the security risks in data transmission [6]. Wei proposed a MAGAN model that is less affected by the data loss rate than the baseline comparison model. It shows better results than traditional processing methods [7]. Sharmeen et al. concluded that IIoT working environment is complex, malicious programs increase, and it is not easy to be found, and attacks from criminals are

the main reasons for IIoT security threats [8]. Therefore, ensuring the integrity, privacy, effectiveness, controllability, and anti-attack of data in IIoT is the main work of current IIoT security technology research. And strengthening confidentiality measures, user authentication technology, and anti-intrusion detection technology are specific research projects. In the *Global Industrial Internet of Things Network Security Report*, anti-intrusion detection technology ranks third among current IIoT security protection measures [9], which shows that IIoT anti-intrusion measures can improve IoT security protection performance from the source. Balakrishnan et al. argued that since IoT involves many different entities and different applications, the vulnerability to unauthorized access is much higher. Today's cyberattacks facing communication networks are very powerful and very worrying [10]. Wei et al. proved that mobile smart terminals had become prominent targets of cyberattackers. Security vulnerabilities and privacy leaks seriously restrict the application development of IoT [11]. The IoT vulnerability situation is getting worse by the day. Therefore, the anti-intrusion technology of IIoT is studied. Bovenzi et al. [12] studied the hierarchical hybrid intrusion detection method in the IoT scenario and proposed a two-stage hierarchical network intrusion detection method. Their novel lightweight solution based on multi-modal deep autoencoders performs anomaly detection. In addition to the performance advantages, the proposed system is suitable for distributed and privacy-preserving deployments. Additionally, the system limits the necessity of retraining, in line with the high efficiency and flexibility required for IoT scenarios.

This study will comprehensively analyze the initial network and IIoT anti-intrusion detection methods in deep learning and optimize them for the LeNet-5 network. Section 1 introduces and explains the background of the IIoT and mobile network technology. Section 2 carries out the performance test of the Internet of Things security protection system by introducing the Internet of Things mobile smart devices, combined with the structural analysis of the information technology industry. Section 3 tests the performance of the anti-intrusion detection model by using an improved Convolutional Neural Network (CNN). Section 4 draws experimental conclusions through the inductive arrangement and systematic summary of the data results, analysis, and discussion. The innovation is that the initial network and CNN are combined in deep learning to establish an anti-intrusion detection model. Deep neural networks are built to enhance the representational power of the model. The network successfully uses the ReLU activation function as the activation layer of the cellular neural network, which alleviates the gradient disappearance problem of the sigmoid activation function, and the convergence speed is faster. Smaller convolution kernels and smaller sliding strides are used. Compared with ordinary neural networks, the initial network has only two convolution kernel sizes. Therefore, the network can be further deepened. Furthermore, multiple small convolution kernels are introduced to reduce the total network parameters. Simple average pooling is used instead of fully connected layers as the output of

the convolution operation. Characteristic patterns may appear in different locations in the image.

2. Methods

2.1. IIoT

2.1.1. The Concept of IIoT. IIoT is the abbreviation for the combination of IoT and industrial manufacturing to improve the efficiency of industrial automation products. IIoT can perceive the system, has the advantages of reliable transmission and processing intelligence, and is commonly used in transportation, power grids, factories, and environmental monitoring. There are generally four implementation stages [13–16]

For the first stage, intelligent control is shown in Figure 1. This node combines sensors, wireless sensor networks, and other modules through intelligent sensing to achieve industry data collection and control equipment

In Figure 1, communication technologies such as local networks or the Internet are used to connect sensors, controllers, machines, people, things, to form the connection between people and things and things and things and realize informatization, remote management control, and intelligent network. The IoT is an extension of the Internet. It includes the Internet and all resources on the Internet and is compatible with all applications on the Internet. But all elements in IoT (all devices, resources, communications, etc.) are personalized and privatized. For the second stage, the comprehensive exchange is shown in Figure 2. IIoT uses sensors and other modules to collect data and integrates information technology and features through communication technologies such as the Internet, mobile networks, wide area networks, or radio and transmits the data in real time and quickly.

In Figure 2, the communication protocol is the language of the networked world. But the industrial network world is often not as open and unified as the Internet, due to industries, application scenarios, network topology, and mutual games between major industrial enterprises and countries. With the advent of emerging concepts such as the Industrial Internet, traditional industrial protocols are underdeveloped in terms of security and future-proofing. Industrial control security has become an important part of national infrastructure security. IoT technology is the integration of the Internet and the idea of intelligent data analysis. The construction of an integrated system where hardware entities and software entities are placed is very important [17]. The deep application of the third stage is shown in Figure 3. Cloud computing, big data, and other platforms are used for modeling, analysis, and optimization to develop multi-source heterogeneous data and find valuable information at a high speed and accuracy through data mining, data storage, and other technologies.

In Figure 3, the technological revolution is at some stage before the digital industrial revolution is truly revolutionized. After the invention of new technologies, industry professionals find their own internal technology gaps and choose new technologies that are suitable for them. Then,

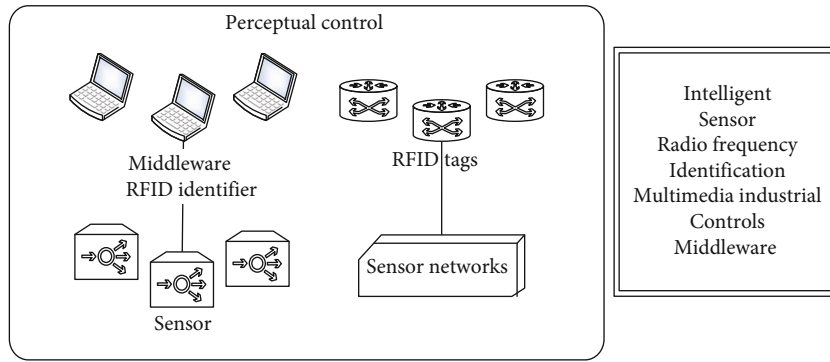


FIGURE 1: IIoT intelligent control stage.

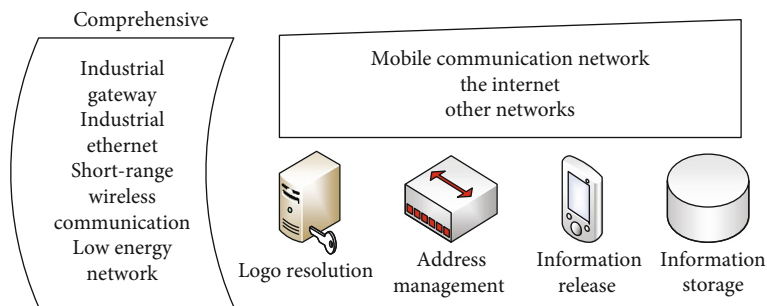


FIGURE 2: IIoT full communication stage.

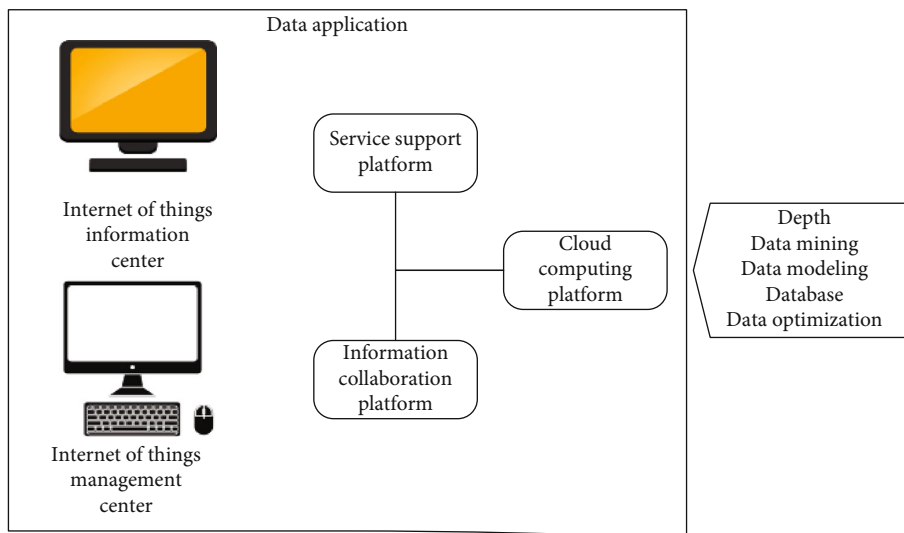


FIGURE 3: Deep application stage of IIoT.

the technology is further configured for each industry. However, technology generally remains the same. Different industries have different application scenarios, resulting in different requirements. Replacing the kernel of the network (i.e., the search machine) by spiral search and bubble net search can improve the accuracy and reduce the execution time to achieve the goal achieved by the retrieval function [18]. For the fourth stage, service innovation is shown in Figure 4. Through intelligent equipment, platform integration, and other technologies, it can provide users with inno-

vative services, including smart logistics and competent medical care, and establish a new ecological model of IIoT in all aspects to improve service levels.

In Figure 4, the innovation stage of the IIoT is divided into three stages. Step 1 is cognitive innovation. The cognition of the Industrial Internet has gradually evolved and made breakthroughs, extending from the interconnection of equipment to the interconnection of people, machines, and things and then to the comprehensive link of all elements, the entire industrial chain, and the entire value chain.

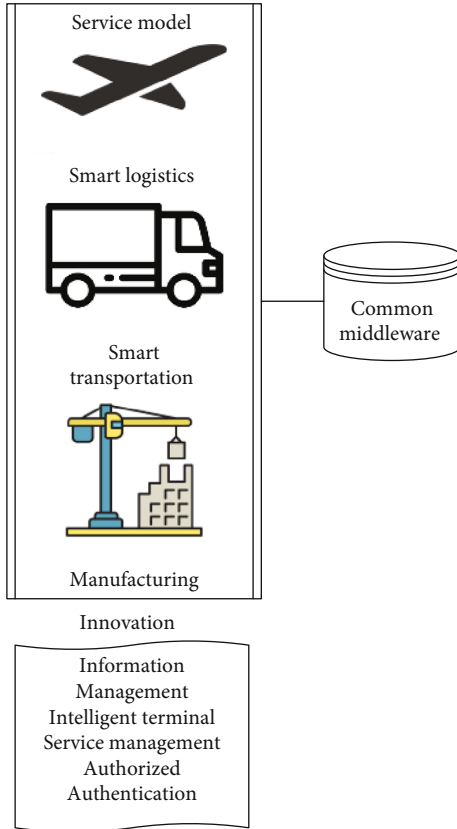


FIGURE 4: IIoT innovative service stage.

The Industrial Internet is an important cornerstone of the fourth industrial revolution. It is the deep integration of a new generation of network information technology and manufacturing. It can form a new industrial manufacturing and service system and promote the high-quality development of the real economy represented by advanced manufacturing.

Step 2 is idea innovation. The development law and mechanism of the Industrial Internet should be correctly grasped. The Industrial Internet is not a simple copy of the consumer Internet in the field of production, but a comprehensive expansion and leap of information network technology from virtual to physical, from life to production. This is not the connection extension of the consumer Internet from people to things, but the complete creation of a networked and intelligently upgraded infrastructure that expands from manufacturing to various industrial fields.

Step 3 is pattern innovation. The world today is going through a new round of major development, transformation, and adjustment, and the economic and social development of various countries is increasingly linked. Open cooperation is a realistic requirement to promote the stable recovery of the world economy. The development of the Industrial Internet is not limited to one country and one place. It must provide new impetus for the global economy to get out of the recession cycle in the process of “bringing in” and “going out.” The development of the IIoT is not just to catch up and improve the development level of the country but also to

provide an important breakthrough for global network governance to break the monopoly deadlock and move towards multiparty cogovernance based on new elements, new fields, and new forms.

2.1.2. The Structure of IIoT. Starting from the system and automation control, IIoT can be divided into four structures, comprehensive perception, network transmission, intelligent processing, and integrated application, as shown in Figure 5 [19–22].

In Figure 5, the key technologies of IIoT mainly include comprehensive perception, information transmission, intelligent processing, and information feedback. Comprehensive perception refers to the collection and acquisition of information on objects anytime and anywhere by using modern information collection and collection techniques. Information transmission is the reliable exchange and sharing of information anytime and anywhere through various communication networks and the Internet. Intelligent processing is to analyze and process the collected massive data and information, improve the insight into the industrial production environment and market, and realize intelligent decision-making and control. Information feedback means that the processed information is communicated to each production link in the form of program instructions to optimize the production structure and complete the production plan. In comprehensive perception, data collection equipment includes instruments and sensors. Its primary function is to realize the exchange of IIoT information. The most used control device is the Programmable Logic Controller (PLC). Its role is to issue commands to the control device. Field equipment includes complex collection equipment responsible for collecting on-site process data to achieve accurate control and management.

In network transmission, data transmission is a collection of multiple communication networks. Its function is to connect the network of various devices on-site, is a bridge between data collection and postprocessing, and integrates multiple connection methods such as 5G, Bluetooth, and Wi-Fi. In IIoT, a variety of connection technologies must be used to ensure the connection of many sensors and processors.

Intelligent processing includes communicator, manager and historical data server, remote control, and other equipment. Generally, cloud computing is used as a platform for large-scale data processing to ensure data security. Comprehensive application is a service based on practical application. It provides personalized assistance to users through information control, authentication, authorization, etc., and it is necessary to ensure the safe access and privacy protection of users.

2.2. Current Status of IIoT Security Testing. At present, the safety protection system used in actual production is subject to design constraints, causing the problem of incomplete analysis of the system’s learning of data characteristics. It mainly exists in the following categories [23]:

Unable to extract the characteristics of multiple data: IIoT is more advanced than the current security protection

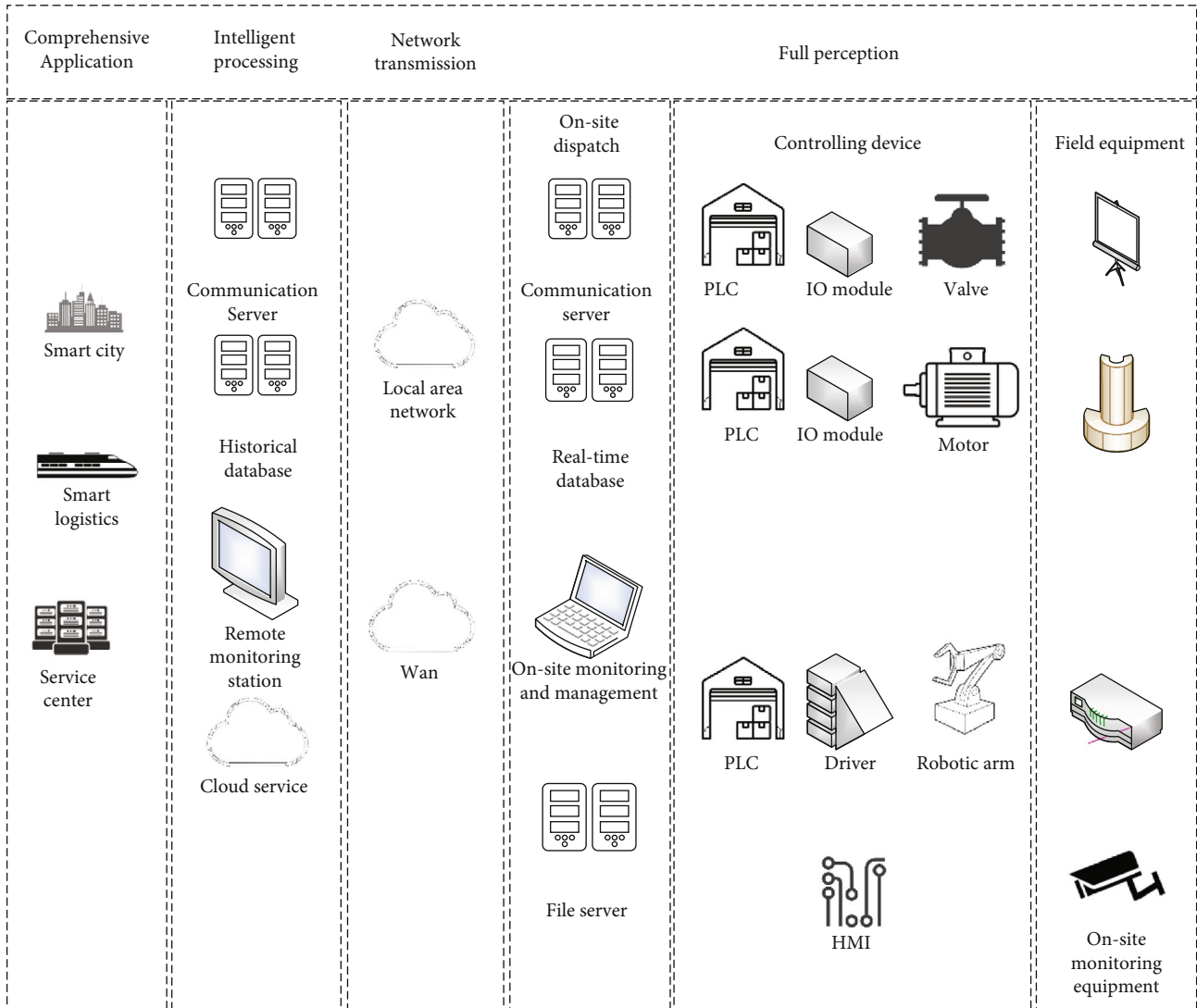


FIGURE 5: Four structures of IIoT.

system. Various new types of intrusion methods continue to appear. There is endless emergence of old protection systems that cannot process new high-latitude data and cannot extract the characteristics of the data, resulting in excessive energy consumption and inability to complete the work.

Detection accuracy is low: when computing many multi-dimensional data features, various calculation equations and parameters will be used, which requires high model processing performance. The current detection system cannot use these equations to cause the problem of low detection accuracy.

High false alarm rate: in the actual IIoT production process, there will be a variety of data exchanges involving multiple device communications. Due to loopholes in the traditional detection system, regular data access is judged as an intrusion, causing the device to fail to receive data usually.

What is designed here is an IIoT-IDS. According to the security requirements of IIoT [24], the detection system needs to have the following functions, as shown in Table 1.

The deeper integration of key elements of IIoT will boost traditional industries to develop faster, create better value, and improve productivity and production efficiency. There are also two sides to the deep application of IIoT. While it improves industrial efficiency and promotes the development of social processes, the security risks caused by the complexity and uncertainty of the network will affect the location of network value.

2.3. IDS

2.3.1. Basic Concepts. In James P. Anderson's Computer Security Monitoring and Surveillance in 1980, the concept of anti-intrusion detection was first proposed [25]. In 1986, Peter Neumann and Dorothy Denning established the real-time model of IDS [26]. They applied this model to computer security defense work for the first time. The IDS is essentially a network security management system, and its function diagram is shown in Figure 6. The working principle is to collect and analyze data information in the network

TABLE 1: Functional requirements of the detection system.

Functional requirements	Describe
Stability	Because the IIoT keeps running for a long time and almost does not allow the system to restart or rest, it is necessary to ensure the long-term operation of the system.
High precision	Distinguishing between targeted intrusions and regular user access requires a high degree of identification.
Timeliness	In the long-term work, it is necessary to ensure the accuracy of the data, no packet loss phenomenon can occur, and intrusion behavior can be detected in time.
Versatility	Because IIoT work types are divided into multiple systems, they need to be highly adaptable and easy to deploy.

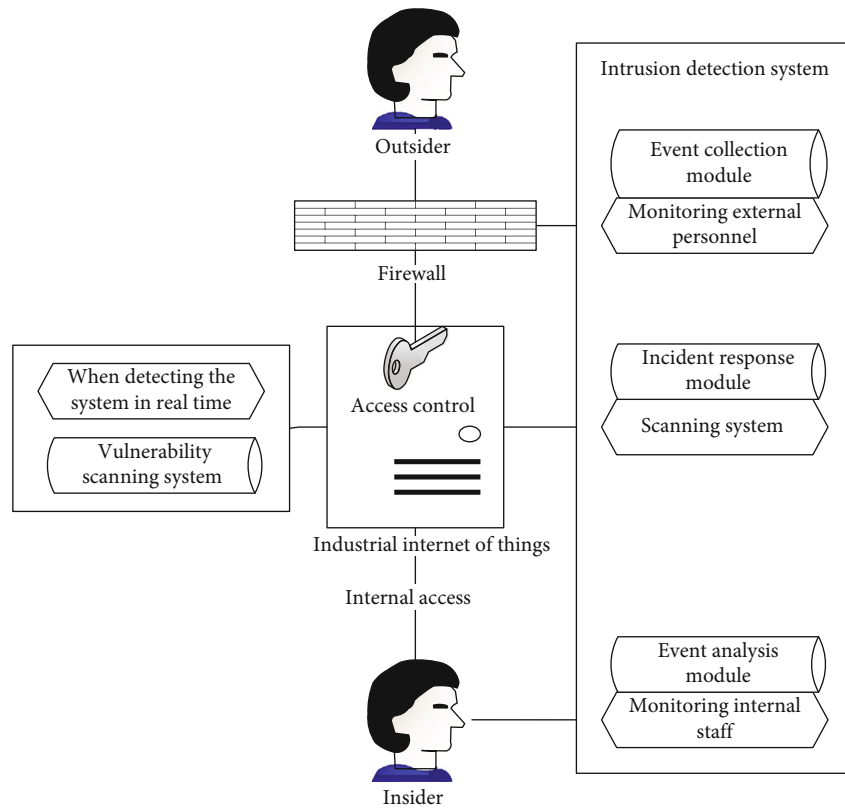


FIGURE 6: Schematic diagram of the role of IDS.

to extract offensive details and behaviors to determine whether the data has intrusions. Unauthorized or abnormal access behavior in the network is judged [27].

In Figure 6, since the system cannot be completely prevented from being attacked or intruded, the intrusion detection system becomes a system that can detect attacks or intrusions in time and provide valuable security alerts to security managers. As the actual harm of intrusion events is increasing, people pay more and more attention to intrusion detection systems. Intrusion detection system has become an important link in the network security architecture. The IDS can effectively judge abnormal network phenomena and protect the system, equipment, and machinery. The IDS extends the firewall, which usually includes the behavior subject, resource objects, audit records, behavior files, abnormal records, and processing

rules [28]. The general detection process is shown in Figure 7.

In Figure 7, the first steps of professional business process management include process design, analysis, and optimization. Design includes documenting the actual state of existing processes. The relevant knowledge held by the employees of the process is collected and integrated, which not only improves the transparency of the process but also allows for a more in-depth analysis of the process. Structured and process-organizational models can reflect the complexity of business operations and simplify them into manageable terms. The IDS needs to identify abnormal behaviors accurately and efficiently. When designing the structure, it must have all the mentioned functions. Therefore, referring to the general process of the IDS, the basic flow of the IIoT-IDS is shown in Figure 8.

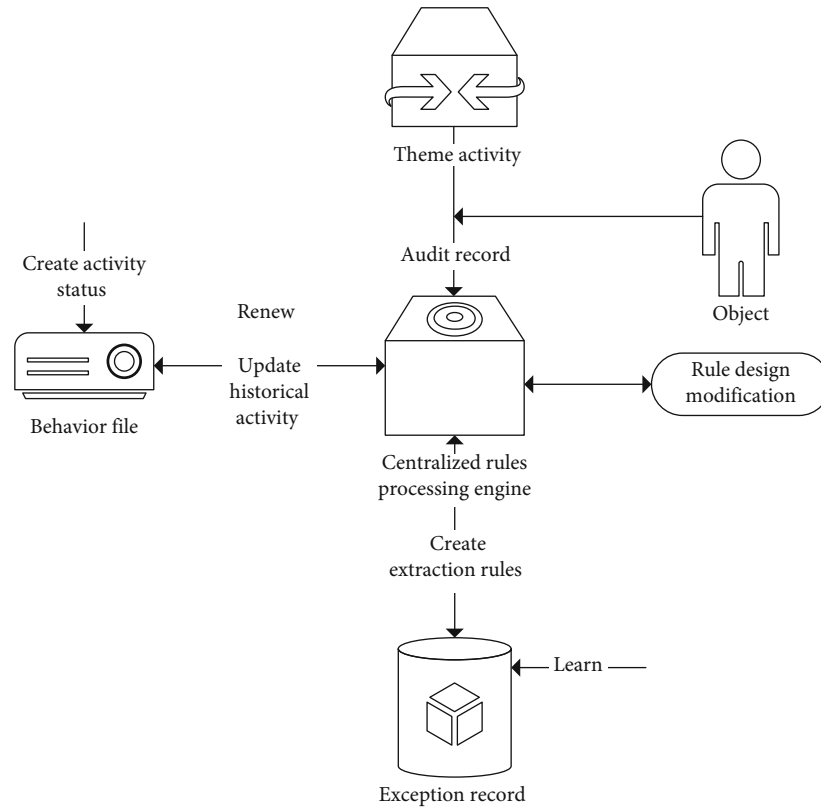


FIGURE 7: General IDS process.

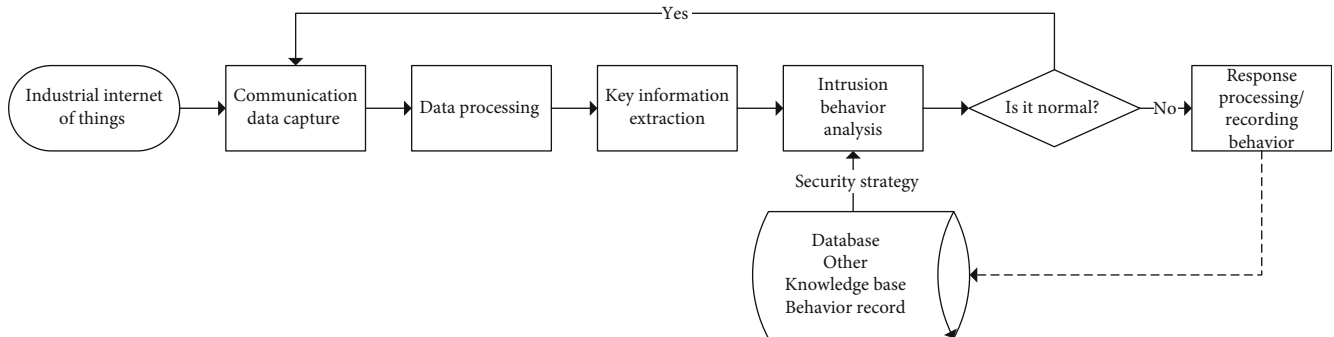


FIGURE 8: The basic flow of IDS.

In Figure 8, this stage is the core stage of the entire intrusion detection system. The purpose of the system is to detect anomalies or to detect system vulnerabilities or application bugs for intrusion. According to the purpose of the system, it can be divided into abnormal behavior and misuse detection. The report and response phase responds to the judgments made in the previous phase. If it is judged that an intrusion has occurred, the system will take corresponding response measures or notify the management personnel that an intrusion has occurred so that measures can be taken. Recently, people’s requirements for intrusion detection and response are increasing, especially for their tracking functions.

2.3.2. *IDS Category.* According to the data source to classify [29], the standard classification method is the object and

detection technology. The general classification is shown in Figure 9. In addition, it can be divided into the centralized type and distributed type according to the model system. The operational mode of the tool can be divided into connection and offline types.

According to the classification of detection technology [30], the IDS can be divided into three types: anomaly detection, misuse detection, and hybrid detection. The principle of anomaly check is to determine whether it is an intrusion by the proportion of network users’ daily behaviors and operations to system resources. The working principle of misuse detection is to establish a database through the recorded intrusion behavior. When an access behavior occurs, it is compared with the intrusion behavior recorded in the database to judge the intrusion behavior. Traditional anomaly detection can identify attacks from unknown users.

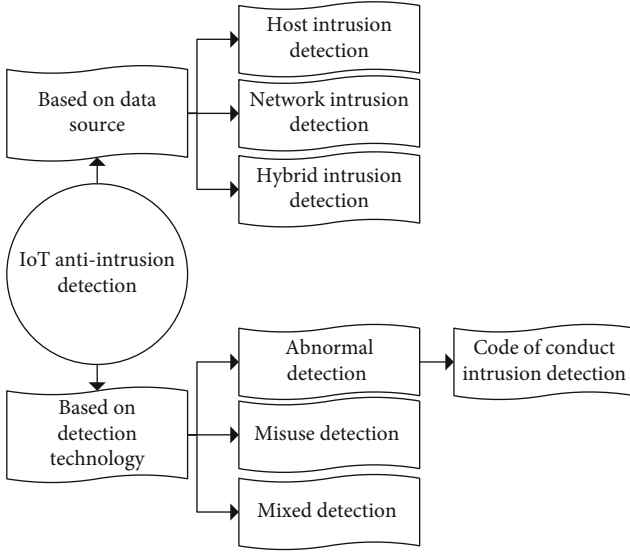


FIGURE 9: Classification of IDS.

In actual applications, false positives occur from time to time. The detection rate of misuse detection is high, and the false-negative rate is also high. Therefore, a hybrid detection is produced after the two are comprehensively optimized. The frame is shown in Figure 10.

In Figure 10, intrusion detection technology is a technology designed and configured to ensure the security of computer systems that can timely detect and report unauthorized or abnormal phenomena in the system. It is a technology used to detect violations of security policies in computer network technology. In addition to firewalls and antivirus systems, intrusion detection technology has become an effective way to resist hacker attacks and has become the third wave of network security. IDS is primarily used to monitor and analyze user and system activity, identify activity patterns that reflect known attacks, and alert relevant individuals. For abnormal behavior patterns, IDS performs statistical analysis in the form of reports.

2.3.3. Anti-Intrusion Detection Method. In the IIoT-IDS, each connection point instance is taken as a point in the feature space, and the training set T is given as follows:

$$T = \{(X_i, y_i), \dots, (X_n, y_n)\} \in R^N \times \{-1, 1\}^N. \quad (1)$$

N is the number of connection points of the input space network, (X_i, y_i) is the output feature vector, and the binary variable $y \in \{-1, 1\}$. The hyperplane is defined as shown in the following equation:

$$\omega^T x + b = 0. \quad (2)$$

ω is the hyperplane weight, and b is the bias value. The classification decision function can be obtained through ω and b , as shown in the following equation:

$$f(x) = \text{sign}(\omega^T x + b). \quad (3)$$

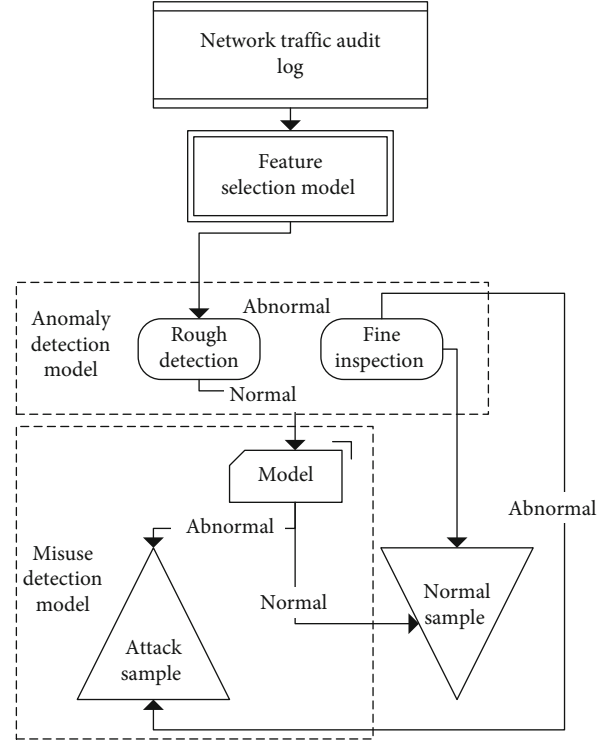


FIGURE 10: Hybrid anti-intrusion detection structure.

The objective function of the linearly separable constrained optimization problem is shown in the following equation:

$$\begin{aligned} \min_{\omega, b} \frac{1}{2} \|\omega\|^2 \\ \text{s.t. } y_i(\omega^T x_i + b) \geq 1, \quad i = 1, \dots, N \end{aligned} \quad (4)$$

Lagrange multiplier is introduced, as shown in the following equation [31]:

$$\alpha = (\alpha_1, \dots, \alpha_n), \quad \alpha \geq 0, i = 1, \dots, N. \quad (5)$$

Therefore, Equation (6) is obtained:

$$L(\omega, b, \alpha) = \frac{1}{2} \|\omega\|^2 + \sum_{i=1}^N \alpha_i - \sum_{i=1}^N \alpha_i y_i (\omega^T x_i + b). \quad (6)$$

Equation (6) is minimized, and Equation (7) is obtained:

$$\max_{\alpha} \min_{\omega, b} L(\omega, b, \alpha). \quad (7)$$

Therefore, it is necessary to find the minimum value of ω, b in L and the maximum value of α , which can further transform the problem of solving the convex quadratic

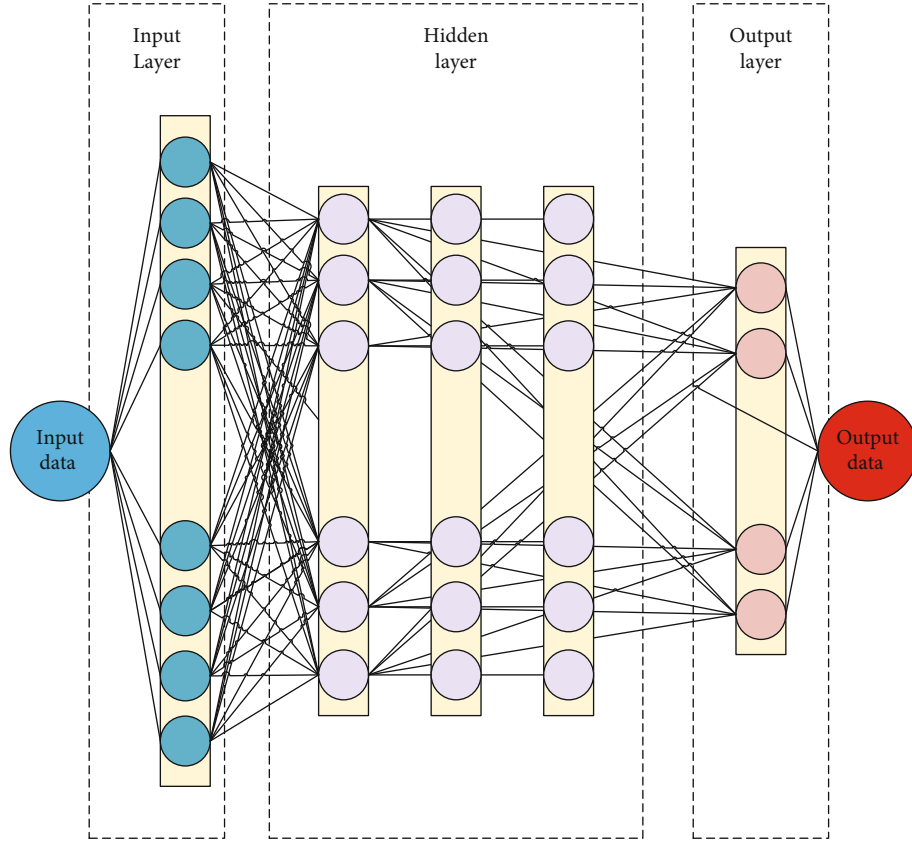


FIGURE 11: Multilevel structure of the neural network.

programming of the support vector machine (SVM) into a dual problem, such as shown in Equations (8) and (9):

$$\max_{\alpha} \sum_{i=1}^N \alpha_i - \frac{1}{2} \sum_{i=1}^N \sum_{j=1}^N \alpha_i \alpha_j y_i y_j x_i^T x_j \quad (8)$$

$$\text{s.t. } \sum_{i=1}^N \alpha_i y_i = 0, \quad \alpha \geq 0, i = 1, \dots, N \quad (9)$$

Solving again can get the value of the Lagrange multiplier α_i . Turn to find the optimal hyperplane ω, b . Finally, the hyperplane and the classification decision function are obtained. These are the current mainstream algorithms for solving.

2.3.4. Arrangement of Anti-Intrusion Detection Algorithms Combined with Artificial Neural Networks. The Artificial Neural Network (ANN) is a processing algorithm proposed by research experts inspired by neural signals in human nerves. It can be explained by multilevel sensors [32], and the basic model is shown in Figure 11.

The increase in the number of hidden layers can reduce network error and improve accuracy. Still, it also complicates the network, thereby increasing the training time of the network and the tendency of “overfitting.” The design of a neural network should give priority to a 3-layer network. Increasing the number of hidden layer nodes to obtain lower errors makes the training effect easier to achieve than increasing the number of hidden layers. A neural network

model without hidden layers is a linear or nonlinear regression. Therefore, the network model without hidden layers is included in the regression analysis. The technology is so mature that it is unnecessary to discuss it in neural network theory. Choosing the number of hidden layer nodes in a neural network is significant. It has a great impact on the performance of the established neural network model and is the direct cause of “overfitting” during training. At present, there is no scientific and universal determination method in theory. The calculation formulas proposed in most literature to determine the number of hidden layer nodes are aimed at arbitrarily many training samples and for the most unfavorable situation. It is difficult to satisfy in general engineering practice and should not be used. The neural network comprises an input layer, a hidden layer, and an output layer. When using an ANN as an IDS, assume that the connection data X of the input network is a $\mathbf{m} \times n$ -dimensional classification sample. Then, the neurons of the input layer are as shown in the following equation:

$$X = \{X_1, X_2, \dots, X_n\}, \quad X_i \in \{0, 1\}. \quad (10)$$

The hidden layer analyzes whether the input data is an intrusion, and the output layer is responsible for making decisions. For the input neuron X , it is mapped to the hidden layer, as shown in the following equation:

$$H = \{H_1, H_2, \dots, H_n\}, \quad H_i \in \{0, 1\}. \quad (11)$$

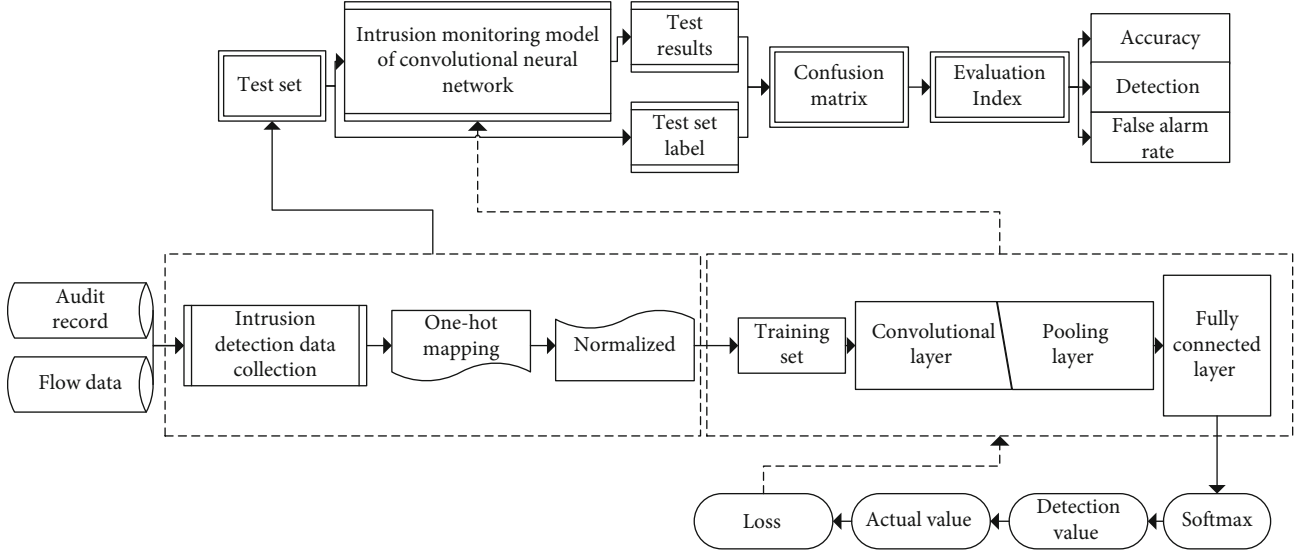


FIGURE 12: CNN-IIoT anti-intrusion detection model structure.

The output result is as shown in the following equation:

$$H = \sigma(f(x)) = \sigma(W * X_i + b_i). \quad (12)$$

Use the output result of the hidden layer as the input to map to the output layer, as shown in the following equation:

$$Y = \sigma(g(H)) = \sigma(W^T * H_i + b_i). \quad (13)$$

σ is the nonlinear activation function mapping [33]. An ANN is a representative method of artificial intelligence (AI) in deep learning. Since it was proposed, it has been applied to different scenarios, and many new structures have evolved. Deep learning can efficiently handle high-latitude nonlinear problems and is widely used in many fields. The anti-intrusion detection is a multiclassification problem, and the neural network structure in deep learning is used for research.

2.4. IIoT-IDS by LeNet-5CNN

2.4.1. Basic Structure. In IIoT, devices are always connected to the Internet. Therefore, security protection should be established in IIoT. The autonomy of deep learning is used. The constructed IIoT-IDS model structure is shown in Figure 12, which is used to identify intrusion data.

In Figure 12, intrusion detection is accomplished by performing tasks: (1) monitor and analyze user and system activities; (2) audit system structures and weaknesses; (3) identify patterns of activity that reflect known attacks and alert relevant individuals; (4) statistical analysis of abnormal behavior patterns; (5) evaluate the integrity of important systems and data files; and (6) audit trail management of operating systems, and identify user behaviors that violate security policies.

2.4.2. IIoT Anti-Intrusion Model by LeNet-5. CNN was first proposed in 1990. In 1998, Lecun established a LeNet-5

model for handwritten digit recognition [34], one of CNN's earliest representative models. It contains one input layer, one output layer, two convolutional layers, two pooling layers, and one fully connected layer. The convolutional and pooling layers can be changed to change the structure of the entire network.

Although the LeNet5 network is small, it contains the basic modules of deep learning: convolutional layers, pooling layers, and fully connected layers. This is the basis for other deep learning models. The input image is subjected to the first convolution operation (using six convolution kernels of size $5 * 5$) to obtain 6 C1 feature maps (6 feature maps of size $28 * 28$, $32 - 5 + 1 = 28$). The size of the convolution kernel is $5 * 5$, and there is a total of $6 * (5 * 5 + 1) = 156$ parameters. Among them, +1 means that grain has a bias. For the convolutional layer C1, each pixel in C1 is connected to $5 * 5$ pixels in the input image and one tendency. So there are $156 * 28 * 28 = 122304$ connections in total. There are 122304 connections, but only 156 parameters need to be learned, mainly through weight sharing. The most used LeNet-5 currently has a 7-layer structure, as shown in Figure 13.

Among them, the convolutional layer is the core component of CNN, and there are two primary responsibilities. One uses several convolution kernels to extract data features, and the other uses activation functions to process data results. The input data of the convolution layer comes from the pooling layer, and the obtained data is subjected to the convolution operation. The result is obtained through the corresponding activation function [35]. The process is shown in Equations (14) and (15):

$$x_i^l = f(h_j^l), \quad (14)$$

$$h_j^l = \sum_{i \in M_j} h_j^{l-1} \otimes W_{ij}^l + b_j^l. \quad (15)$$

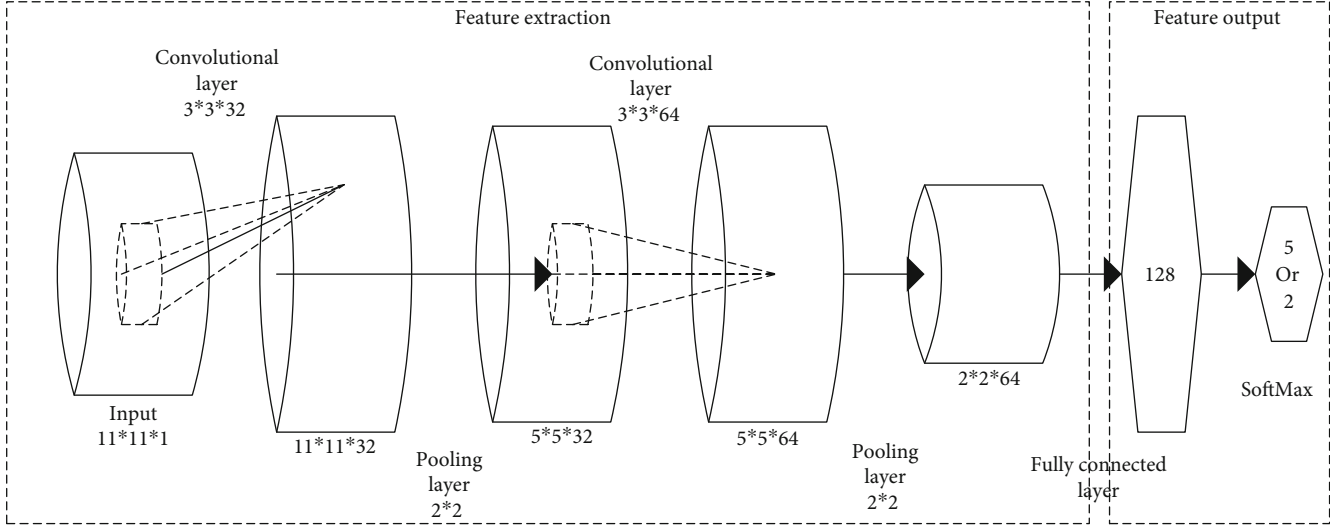


FIGURE 13: The basic structure of LeNet-5 networks.

h_j^l is the activation output of the j th nerve in the l th layer, h_j^{l-1} represents the i th two-dimensional output matrix of the $l-1$ layer, W_{ij}^l is the convolution kernel, \otimes is the convolution operation, and b_j^l is the bias value.

After the convolution calculation, the dimensionality of the data is still very high. A pooling operation is needed. The data output by the convolution is sampled and compressed to reduce the feature dimensionality, as shown in the following equation:

$$h_j^l = \beta_j^l \text{upsample}(x_i^{l-1}) + b_j^l. \quad (16)$$

x_i^{l-1} is the output feature of the upper layer, β_j^l is the pooling coefficient, and upsample is the pooling function.

The fully connected layer changes the pooled two-dimensional data features into one-dimensional data features, like multilayer sensors, such as Equations (17) and (18):

$$x_j^l = f(h_j^l), \quad (17)$$

$$h_j^l = \sum_{i \in M_j} x_i^{l-1} * W_{ij}^l + b_j^l. \quad (18)$$

CNN is divided into two stages for training. One is forward propagation, and the other is reverse fine-tuning. The overall training process is shown in Figure 14.

The main steps and content are shown in Table 2.

This part is aimed at protecting data and preventing breaches in the network. Any exploitation of malware can cause a lot of damage to the company. Safely maintaining a network is the goal of all system administrators. Here, there are several important open source network intrusion detection tools. In today's world, data breaches, threats, attacks, and intrusions are becoming very sophisticated.

Cybercriminals and hackers have come up with new ways to gain access to business and home networks, making a multilayered approach to cybersecurity an urgent need. Therefore, the intrusion detection system is the most important tool used to defend the network from the high-tech attacks that occur on a daily basis. IDSs are network security tools used to detect exploits against targeted applications or computers. It is considered a high-end network device or software application that assists network or system administrators to monitor various malicious activities or threats in the network or system. A security information and event management system is used to report any unusual activity to administrators.

In Figure 14, the convolutional network is essentially an input-to-output mapping. It can learn a large number of mapping relationships between input and output without any precise mathematical expression between input and output. As long as the convolutional network is trained with known patterns, the network has input and output pairs. Convolutional networks perform supervised training, so their sample set consists of pairs of input vectors and ideal output vectors. All of these vector pairs should be derived from the actual "running" results of the system that the network is about to simulate. They can be collected from the actual operating system. Before starting training, all weights should be initialized with some different small random numbers. "Small random numbers" can be used to ensure that the network does not saturate due to too large weights, resulting in training failure. "Different" can be used to ensure that the network can learn properly. In fact, if the weight matrix is initialized with the same number, the network cannot learn.

2.4.3. Improved LeNet-5 Model. The traditional activation functions are saturated nonlinear, sigmoid, and tanh. A saturated nonlinear function will take longer to converge than a nonsaturated nonlinear function ReLU model. For large datasets, a faster learning process means more time savings.

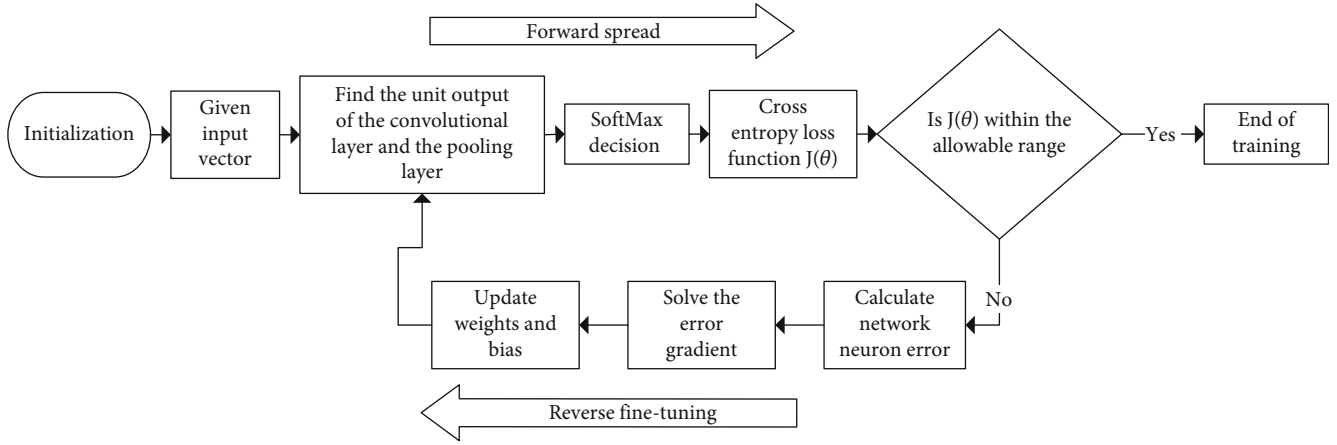


FIGURE 14: The training process of CNN.

TABLE 2: Training process steps.

Step number	Step content
Step 1	Initialize network weights
Step 2	Input data through convolutional layer, sampling layer, and fully connected layer to get the output value
Step 3	Use the crossentropy function to compare the error between the output value and the target value
Step 4	If the error is greater than the actual value, input the error into the network and calculate the total error
Step 5	Update according to the error; repeat the second item

In addition, ReLU also introduces a certain sparsity. In the category of feature representation, the data has a certain sparsity. Some of the data is redundant. This sparsity can be simulated to preserve the characteristics of the data in a maximum approximation manner by introducing ReLU. In addition, the data collected by the LeNet-5 network also has the shortcomings of too light fitting degree and single response mode. Standard LeNet-5 networks are flawed. When convolutional layers are used for data feature extraction, and pooling layers are used for dimensionality reduction, data features become sparse. The data processing by the two-layer convolutional layer of the LeNet-5 network model will cause incomplete data extraction. The characteristic information of the data will be lost when the subsequent pooling layer of the convolutional layer processes the data.

The feature information of anti-intrusion detection data is unevenly distributed. The feature attributes of some data have a more significant impact on the recognition of detection results during network model processing. Part of the attribute feature information contains a small amount of data, which will cause the phenomenon that the data feature has nothing to do with intrusion behavior. When processing these data in the convolutional and pooling layers, it will cause a waste of redundant resources, which will interfere with the detection of intrusion behavior. In LeNet-5's anti-intrusion detection, the input data is different from the original image data because the convolutional layer and the pooling layer are alternately used. One-dimensional data mapping will become blurred after two-dimensional space, making the entire model unable to describe the characteris-

tic behavior accurately, and the model's anti-intrusion performance is not ideal. Therefore, the traditional LeNet-5 [36] model will be optimized. The two convolutional layers are subjected to a pooling operation, and suitable parameters are used to extract the abnormal features of the data fully. The optimized model is the LeNet-7 model, and the structure is shown in Figure 15. There are four convolutional layers in the improved LeNet-7 network, two pooling layers, and one fully connected layer.

In Figure 15, as the depth of the network increases, the accuracy of the network should increase synchronously, and the overfitting problem needs to be paid attention to. But one problem with increasing network depth is that these added layers signal parameter updates. The gradient is propagated from the back to the front. After increasing the depth of the network, the gradient of the earlier layers will be very small, which means that the learning of these layers is basically stagnant. This is the vanishing gradient problem. The second problem with deep networks is training. When the network is deeper means the parameter space is larger and the optimization problem becomes harder. Therefore, simply increasing the network depth leads to higher training errors. Although the deep network converges, the network begins to degenerate; that is, increasing the number of network layers leads to greater errors.

2.5. IIoT-IDS by Inception-CNN. The improved LeNet-7 is improved compared to LeNet-5, but it is not enough to process the complex data in IIoT. The Inception network in the field of deep learning combined with CNN is used; the IIoT-IDS is established.

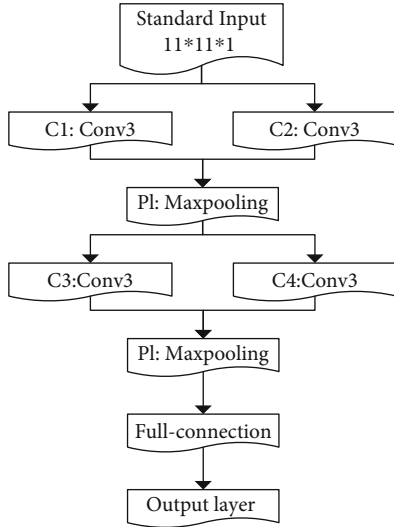


FIGURE 15: Improved LeNet-7 model structure diagram.

2.5.1. Inception Network. To specifically solve the severe high-energy problem caused by the parameter hierarchy in the neural network, people have proposed deep learning combined with the CNN Inception network [37].

There are currently 4 Inception networks, of which Inception V4 can be combined with residual connections to build a deeper Inception-ResNet network. The Inception network can sparse the network structure and produce dense data. Multiple channels and multiple levels can be set in the network, and various convolution kernels and pooling can be used to operate. The basic structure of Inception is shown in Figure 16.

In order to increase the nonlinear model and reduce the parameter settings, the Inception model is expanded. The calculation amount of the model is increased, its structure is modified, the amount of convolution parameters is reduced, and the network nonlinearity is appropriately deepened. Combining different channels can extract more data features.

2.5.2. The Detection Method of Inception-CNN. The modified pooling method can scale and move data features undistorted. And it can reduce the load on the network. Therefore, an adaptive pooling algorithm is proposed. It can assign pooling weights to the dynamic elements of different pooling cores and more comprehensively express data characteristics, as shown in Equations (19) and (20):

$$S_{ij} = \mu_{ij} \max_{i=1, j=1}^c (F_{ij}) + b, \quad (19)$$

$$\mu_{ij} = \frac{2}{c^2 \left(1 + e^{-(F_{ij}/F_{sum})\sigma^2} \right)}. \quad (20)$$

μ_{ij} is the pooling factor, F_{sum} is the total element of the pooling core, and σ is the standard deviation. This algorithm can overcome the limitation of maximum pooling and obtain more accurate feature information.

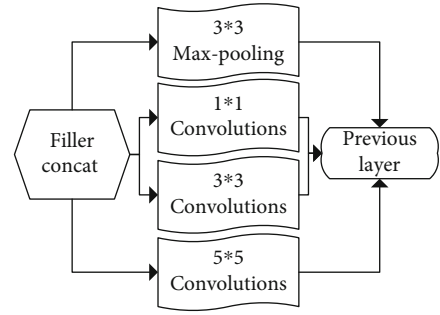


FIGURE 16: The basic structure of Inception.

2.5.3. IIoT-IDS Solution by Inception-CNN. Integrating the detection method of Inception and the improved LeNet-7 network, the model flow chart of the built Inception-CNN IIoT-IDS and the training structure of the model are shown in Figure 17.

Data preprocessing: the data used here comes from the MNIST dataset, and the mobile network data in the dataset is screened. Then, the information is normalized. Because the dimensionality of the original data is high, it must be reduced. Data with greater influence on the result is selected, and no influence data is removed. After that, the abnormal data part is adaptively manipulated. The detection algorithm flow of this model is shown in Table 3.

Model training: the data obtained by preprocessing is converted into a two-dimensional format to adapt it to the CNN format. Extract rich and diverse characteristics of intrusion behavior; adjust parameters until convergence.

Data output: after completing the training, use the test set to evaluate the model's performance. If it meets the requirements, stop training. Otherwise, repeat the above steps to check the accuracy of the model.

2.5.4. The Limitations of the Anti-Intrusion Detection Algorithm of the Inception-CNN Network. At present, IDS technology is still regarded as a state that has not been fully completed. From a technological point of view, the technology does have some shortcomings and distances. People expect the functionality that IDS brings, but there are still bottlenecks that cannot be fully overcome in current commercial IDS suites. The amount of information generated by IDS is excessive, but the skills and ability to effectively filter, sift, and correlate data are lacking. Although IDS can bring various advantages, it should be emphasized here that the establishment of IDS is not foolproof for enterprises to strengthen information security. Before enterprises have mature basic concepts and processing procedures for information security, they will face more difficulties when building an IDS. IDS detects attack events based on the characteristic data of intrusion attacks rather than the way of using behavior. Therefore, intrusion detection is limited to predefined system events. In addition, the management console cannot effectively manage an unlimited number of monitoring devices, nor does it support intercorrelation of data from multiple different information sources. Currently, most of the data-related returns provided by IDS are based

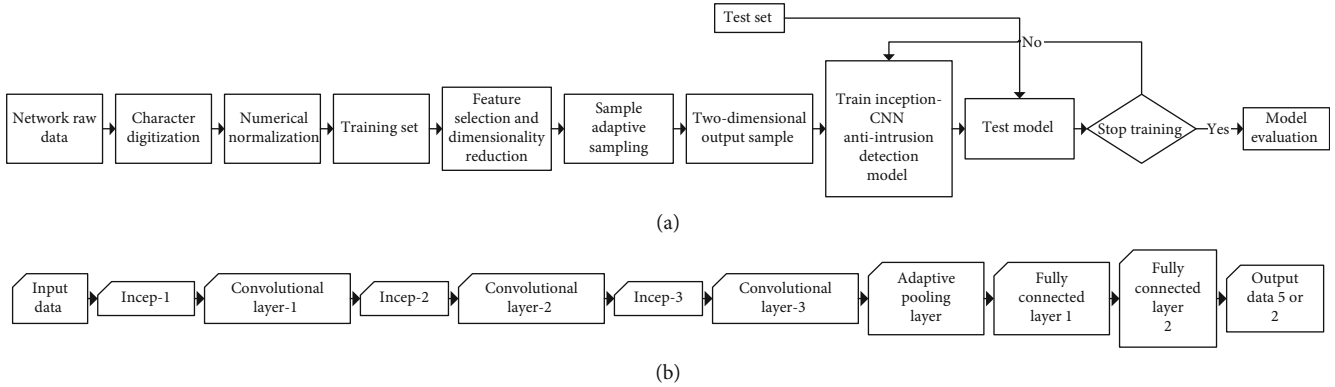


FIGURE 17: Inception-CNN IIoT-IDS structure diagram. (a) Shows the detection flow chart of the entire system. (b) Shows the model training structure diagram.

TABLE 3: The process of the anti-intrusion detection algorithm of Inception-CNN.

Number	Content
1	Lookup packet netDevice = pcap_lookupdev(errbuf)
2	Create capture criteria p = pcap_open_live(netDevice, 3000, 1, 440, errbuf)
3	Set filter conditions pcap_compile(p, &fcode, filter_string, 0, netmask)
4	Enter loop condition while((ptr = (char *) (pcap_next(p, &hdr))) = NULL)
5	Format the captured data eth = (struct libnet_ethernet_hdr *)ptr
6	Close the capture standard and initialize the signal processing function pcap_close if(eth->ether_type = ntohs(ETHERTYPE_ARP))
7	End

on predesigned templates. Such reward schemes are helpful, but limited.

3. Results

3.1. Inception-CNN IIoT Anti-Intrusion Detection Model Performance Test. The three performances of a single CNN, a traditional Inception network, and an improved Inception-CNN network are tested, and the performance of the three models is compared. This proves the applicability of the established Inception-CNN model, and the result is shown in Figure 18.

In Figure 11, the data accuracy rate of the improved Inception-CNN model is 99%, the detection rate is 97%, the data accuracy rate is 99%, and the data false alarm rate is only 1%. This shows that its performance is entirely beyond the other two traditional models. This model has a high autonomous learning ability and can adapt to network data monitoring in a complex environment. Network security requires the management of a multilayered system. The goal of cybersecurity is to protect the integrity of core assets, minimize possible losses, maximize return on investment, and ensure business continuity. The occurrence of

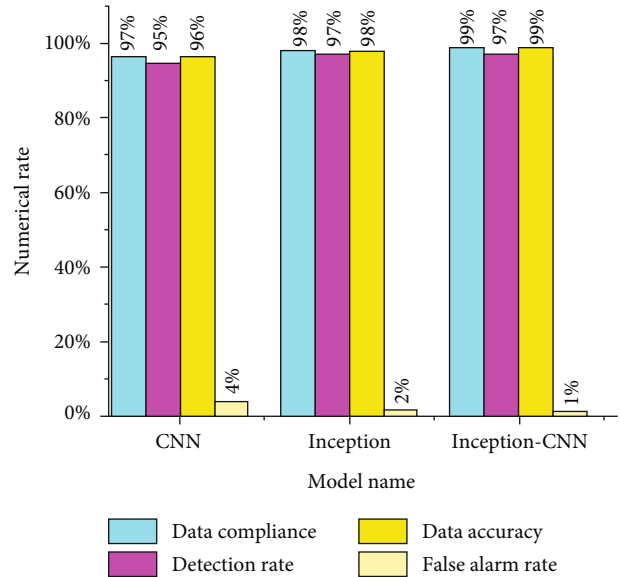


FIGURE 18: Comparison of the performance values of the three networks.

network intrusion has increased people’s management of network security. This can help users establish a dynamic defense-in-depth system and grasp network security as a whole and is also the development direction of network security.

3.2. Inception-CNN IIoT Anti-Intrusion Detection Model Performance Change Trend. After the improvement, the Inception-CNN model is better than the traditional two monitoring models. It is necessary to analyze the accuracy of the data and the trend of the loss value to determine whether the model’s high performance is accidental. The test and training set are analyzed uniformly, and the result is shown in Figure 19.

In Figure 19, the data accuracy of the improved Inception-CNN model and the training set test set can maintain a gradual upward trend and finally stabilize. At the beginning of the test, the loss value of the data is more significant than one in the training set of the test set. As the experiment progresses, the loss value gradually decreases,

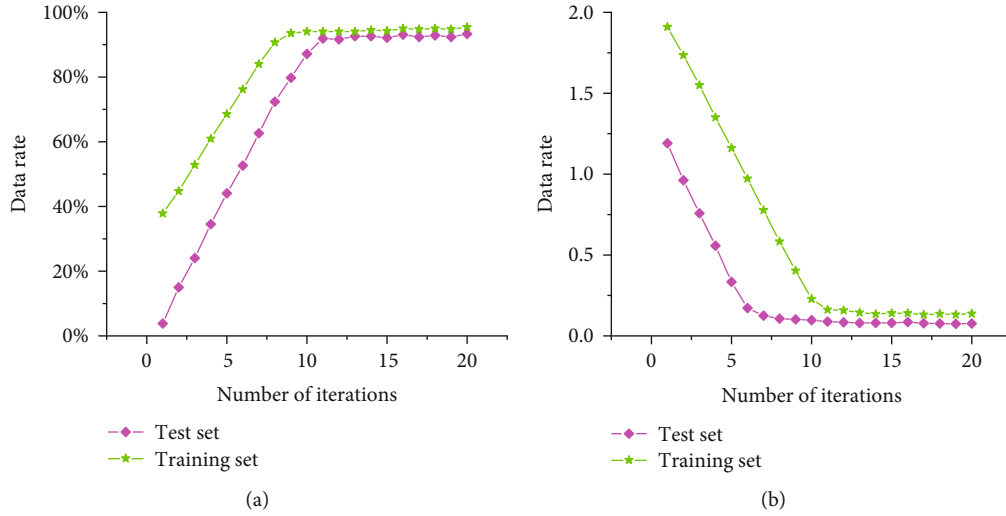


FIGURE 19: Inception-CNN model accuracy and loss value change trend. (a) Shows the accuracy change curve of the training set test set. (b) Shows the loss value change curve of the training set test set.

TABLE 4: Comparison of research methods.

Method comparison	Lenet-7	A privacy-aware task offloading method
Main technology used	Neural networks	Cloud computing
Preprocessing technology	Neural network pooling layer	Gan training
Type of data	Network intrusion data	Network intrusion data
Evaluation measures	Detection accuracy and loss values	Benchmark performance experiments
Advantage	High detection accuracy and small loss value	Low network load
Shortcoming	Unable to detect in a complex network environment	Vulnerable to leaks when targeting multiple targets

approaches 0, and remains stable. These two result curves show that the improved Inception-CNN model has good stability, and the high accuracy and high precision are not due to accidental factors. Therefore, the model can be applied to the actual IIoT-IDS. The network environment is also becoming more and more complex. Various complex devices need to be constantly upgraded and patched, which makes the work of network administrators continue to increase. The negligence of network administrators may cause major security risks. Therefore, the intrusion detection system has become a new hot spot in the security market, not only attracting more and more attention but also beginning to play its key role in various environments.

4. Discussion

Starting with the security of the IIoT, the requirements for security performance are learned from the literature. The structure system of IIoT is introduced, and the corresponding security protection technology is analyzed. The IDS of IIoT is built based on the Inception network and the convolutional neural LeNet-5 network in deep learning. The LeNet-5 network is modified according to actual requirements. A new LeNet-7 network structure is constructed. IDS has the advantages of high accuracy, high data accuracy, high detection, and low false-positive rate. This kind of sys-

tem has high detection accuracy for single intrusion behavior of simple data. However, the established LeNet-7 detection network system has insufficient detection ability for larger databases. Secondly, the detection performance in a specific complex network environment will be affected by various objective factors, which will lead to the degradation of the detection performance. Xu et al. developed a privacy-aware task offloading method. Firstly, the strength Pareto evolutionary algorithm is well studied and improved to obtain offloading strategies that synergistically improve training performance and privacy protection [38]. A comparison of the method with the method used is shown in Table 4.

Then, the most balanced offloading policy is trained. Finally, systematic experiments show that the method achieves the best performance among other representative benchmark methods. The new network technology proposes a privacy protection model, which can demonstrate the security of using the technology, the importance of privacy protection, and the necessity of using new technologies for privacy protection research.

5. Conclusion

With the development of information technology and industrial technology, IIoT takes up an increasing proportion of

manufacturing, which provides excellent convenience for industrial control and inspection. However, the hidden dangers of IIoT that threaten private data and security have also increased. In recent years, network data breaches have emerged one after another. The design of security and anti-intrusion systems for IIoT has also become the end-point of research. Starting from the safety of IIoT, the security performance requirements are learned from the literature. The structural system of IIoT is introduced. The corresponding security protection technology is analyzed. By the Inception network and the convolutional neural LeNet-5 network in the field of deep learning, an IDS for IIoT has been established. According to actual requirements, the LeNet-5 network is improved, and the new LeNet-7 network structure is built. Integrating Inception, LeNet-5, and LeNet-7 technologies, the Inception-CNN IIoT IDS is established, and its performance is tested. Experimental results show that this model has the advantages of high accuracy, high data accuracy, high detection, and low false alarm rate. Therefore, this model can be used in IIoT data privacy protection work. However, the research here is only tested in a single network environment, not used in large-scale industrial processes, nor has the model been validated multiple times in a more complex, multi-interaction network environment. In addition, Nascita et al. [39] conducted research on AI techniques for mobile traffic classification by understanding and improving multimodal deep learning architectures. AI-based techniques investigate trustworthiness and interpretability, and the behavior of state-of-the-art multimodal deep learning traffic classifiers is explained and improved. The research has important reference value for the reform of network traffic patterns. However, this study is not very representative. Afterwards, the performance of the built model in the actual IIoT will be verified.

Data Availability

The raw data supporting the conclusions of this article will be made available by the authors, without undue reservation.

Conflicts of Interest

The author declares that there is no conflict of interest.

References

- [1] S. Al-Janabi, A. F. Alkaim, and Z. Adel, "An innovative synthesis of deep learning techniques (DCapsNet & DCOM) for generation electrical renewable energy from wind energy," *Soft Computing*, vol. 24, no. 14, pp. 10943–10962, 2020.
- [2] A. Hallsby, "Psychoanalysis against WikiLeaks: resisting the demand for transparency," *Review of Communication*, vol. 20, no. 1, pp. 69–86, 2020.
- [3] S. Al-Janabi and A. F. Alkaim, "A nifty collaborative analysis to predicting a novel tool (DRFLLS) for missing values estimation," *Soft Computing*, vol. 24, no. 1, pp. 555–569, 2020.
- [4] C. Makridis and B. Dean, "Measuring the economic effects of data breaches on firm outcomes: challenges and opportunities," *Journal of Economic and Social Measurement*, vol. 43, no. 1-2, pp. 59–83, 2018.
- [5] D. Khubalkar, "Data protection and privacy in cyberspace-national and international perspective," *Psychology and Education Journal*, vol. 57, no. 9, pp. 5243–5246, 2020.
- [6] H. Hui, C. Zhou, S. Xu, and F. Lin, "A novel secure data transmission scheme in industrial internet of things," *China Communications*, vol. 17, no. 1, pp. 73–88, 2020.
- [7] H. W. Wei, "MAGAN: a masked autoencoder generative adversarial network for processing missing IoT sequence data," *Pattern Recognition Letters*, vol. 138, pp. 211–216, 2020.
- [8] S. Sharmeen, S. Huda, J. H. Abawajy, W. N. Ismail, and M. M. Hassan, "Malware threats and detection for industrial mobile-IoT networks," *IEEE Access*, vol. 6, pp. 15941–15957, 2018.
- [9] T. D. Diwan, "An experimental analysis of security vulnerabilities in industrial internet of things services," *Information Technology in Industry*, vol. 9, no. 3, pp. 592–598, 2020.
- [10] N. Balakrishnan, A. Rajendran, D. Pelusi, and V. Ponnusamy, "Deep belief network enhanced intrusion detection system to prevent security breach in the Internet of Things," *Internet of Things*, vol. 14, article 100112, 2021.
- [11] F. Wei, P. Vijayakumar, N. Kumar, R. Zhang, and Q. Cheng, "Privacy-preserving implicit authentication protocol using cosine similarity for Internet of Things," *IEEE Internet of Things Journal*, vol. 8, no. 7, pp. 5599–5606, 2021.
- [12] G. Bovenzi, G. Aceto, D. Ciuonzo, V. Persicoand, and A. Pescapé, "A hierarchical hybrid intrusion detection approach in IoT scenarios," in *GLOBECOM 2020-2020 IEEE Global Communications Conference*, pp. 1–7, New York, 2020.
- [13] M. Hadipour, J. F. Derakhshandeh, and M. A. Shiran, "An experimental setup of multi-intelligent control system (MICS) of water management using the Internet of Things (IoT)," *ISA Transactions*, vol. 96, pp. 309–326, 2020.
- [14] W. Z. Khan, M. H. Rehman, H. M. Zangoti, M. K. Afzal, N. Armi, and K. Salah, "Industrial internet of things: Recent advances, enabling technologies and open challenges," *Computers & Electrical Engineering*, vol. 81, article 106522, 2020.
- [15] H. Naeem, F. Ullah, M. R. Naeem et al., "Malware detection in industrial internet of things based on hybrid image visualization and deep learning model," *Ad Hoc Networks*, vol. 105, article 102154, 2020.
- [16] W. Chen, "Intelligent manufacturing production line data monitoring system for industrial internet of things," *Computer Communications*, vol. 151, pp. 31–41, 2020.
- [17] S. Al-Janabi, A. Alkaim, E. Al-Janabi, A. Aljeboree, and M. Mustafa, "Intelligent forecaster of concentrations (PM_{2.5}, PM₁₀, NO₂, CO, O₃, SO₂) caused air pollution (IFCsAP)," *Neural Computing and Applications*, vol. 33, no. 21, pp. 14199–14229, 2021.
- [18] S. Al-Janabi and A. Alkaim, "A novel optimization algorithm (Lion-AYAD) to find optimal DNA protein synthesis," *Egyptian Informatics Journal*, vol. 12, 2022.
- [19] H. A. Khattak, M. A. Shah, S. Khan, I. Ali, and M. Imran, "Perception layer security in Internet of Things," *Future Generation Computer Systems*, vol. 100, pp. 144–164, 2019.
- [20] D. Zhang, C. C. Chan, and G. Y. Zhou, "Enabling industrial internet of things (IIoT) towards an emerging smart energy system," *Global Energy Interconnection*, vol. 1, no. 1, pp. 39–47, 2018.
- [21] X. Huang, "Intelligent remote monitoring and manufacturing system of production line based on industrial Internet of Things," *Computer Communications*, vol. 150, pp. 421–428, 2020.

- [22] S. Al-Janabi, A. Patel, H. Fatlawi, K. Kalajdzic, and I. Al Shourbaji, "Empirical rapid and accurate prediction model for data mining tasks in cloud computing environments," in *2014 international congress on technology, communication and knowledge (ICTCK)*, pp. 1–8, Mashhad, 2014.
- [23] M. Zolanvari, M. A. Teixeira, L. Gupta, K. M. Khan, and R. Jain, "Machine learning-based network vulnerability analysis of Industrial Internet of Things," *IEEE Internet of Things Journal*, vol. 6, no. 4, pp. 6822–6834, 2019.
- [24] K. A. Abuhasel and M. A. Khan, "A secure Industrial Internet of Things (IIoT) framework for resource management in smart manufacturing," *IEEE Access*, vol. 8, pp. 117354–117364, 2020.
- [25] S. Hussin, A. Alguttar, K. Alashik, and R. Yildirim, "An observation of intrusion detection techniques in cyber physical systems," *Avrupa Bilim ve Teknoloji Dergisi*, vol. 34, pp. 277–284, 2020.
- [26] M. A. Mahdi and S. Al_Janabi, "A novel software to improve healthcare base on predictive analytics and mobile services for cloud data centers," in *Big Data and Networks Technologies. BDNT 2019*, Y. Farhaoui, Ed., vol. 81 of Lecture Notes in Networks and Systems, pp. 320–339, Springer, Cham, 2019.
- [27] P. Wang, M. Zhou, and Z. Ding, "A two-layer IP hopping-based moving target defense approach to enhancing the security of mobile ad-hoc networks," *Sensors*, vol. 21, no. 7, p. 2355, 2021.
- [28] S. He, W. Ren, T. Zhu, and K.-K. R. Choo, "BoSMoS: a blockchain-based status monitoring system for defending against unauthorized software updating in Industrial Internet of Things," *IEEE Internet of Things Journal*, vol. 7, no. 2, pp. 948–959, 2020.
- [29] M. A. Sulaiman, "Evaluating data mining classification methods performance in Internet of Things applications," *Journal of Soft Computing and Data Mining*, vol. 1, no. 2, pp. 11–25, 2020.
- [30] L. Fu, W. Zhang, X. Tan, and H. Zhu, "An algorithm for detection of traffic attribute exceptions based on cluster algorithm in industrial Internet of Things," *IEEE Access*, vol. 9, pp. 53370–53378, 2021.
- [31] E. Baraneetharan, "Role of machine learning algorithms intrusion detection in WSNs: a survey," *Journal of Information Technology*, vol. 2, no. 3, pp. 161–173, 2020.
- [32] X. Li, J. Shu, W. Gu, and L. Gao, "Deep neural network for plasmonic sensor modeling," *Optical Materials Express*, vol. 9, no. 9, pp. 3857–3862, 2019.
- [33] L. Xiao, K. Li, Z. Tan et al., "Nonlinear gradient neural network for solving system of linear equations," *Information Processing Letters*, vol. 142, pp. 35–40, 2019.
- [34] T. Saleem and M. Chishti, "Assessing the efficacy of logistic regression, multilayer perceptron, and convolutional neural network for handwritten digit recognition," *International Journal of Computing and Digital Systems*, vol. 9, no. 2, pp. 299–308, 2020.
- [35] H. Zhu, H. Zeng, J. Liu, and X. Zhang, "Logish: a new nonlinear nonmonotonic activation function for convolutional neural network," *Neurocomputing*, vol. 458, pp. 490–499, 2021.
- [36] H. Yang and F. Wang, "Wireless network intrusion detection based on improved convolutional neural network," *IEEE Access*, vol. 7, pp. 64366–64374, 2019.
- [37] J. Kim, J. Moon, E. Hwang, and P. Kang, "Recurrent inception convolution neural network for multi short-term load forecasting," *Energy and Buildings*, vol. 194, pp. 328–341, 2019.
- [38] X. Xu, X. Liu, X. Yin, S. Wang, Q. Qi, and L. Qi, "Privacy-aware offloading for training tasks of generative adversarial network in edge computing," *Information Sciences*, vol. 532, pp. 1–15, 2020.
- [39] A. Nascita, A. Montieri, G. Aceto, D. Ciuonzo, V. Persicoand, and A. Pescapé, "XAI meets mobile traffic classification: understanding and improving multimodal deep learning architectures," *IEEE Transactions on Network and Service Management*, vol. 18, no. 4, pp. 4225–4246, 2021.

Research Article

Classification of Diabetic Retinopathy Based on Multiscale Hybrid Attention Mechanism and Residual Algorithm

Yue Miao  and Siyuan Tang

Department of Computer Science and Technology, Baotou Medical College, Inner Mongolia University of Science and Technology, Baotou 014040, China

Correspondence should be addressed to Yue Miao; 102007036@btmc.edu.cn

Received 16 January 2022; Revised 4 May 2022; Accepted 9 May 2022; Published 2 June 2022

Academic Editor: Mu-Yen Chen

Copyright © 2022 Yue Miao and Siyuan Tang. This is an open access article distributed under the Creative Commons Attribution License, which permits unrestricted use, distribution, and reproduction in any medium, provided the original work is properly cited.

The key of classification diagnosis of diabetic retinopathy lies in the recognition of the features of small lesions, and it is difficult to extract the features of too small lesions by general extraction methods. In order to solve the problem that it is difficult to extract small focus, a hybrid attention mechanism combined with residual convolutional neural network model algorithm is proposed to improve the classification accuracy of diabetic retinopathy. Firstly, a multiscale deep learning network model with hybrid attention is designed, and then, the high-level features of images are extracted by using the network model; finally, after balancing different types of samples by sampling algorithm, the spatial attention and channel attention of the extracted features are enhanced; small-step learning strategy, loss function, and initial parameters are used to optimize the performance of the network model. The classifier based on multiscale hybrid attention network is used to judge the five classifications. Experimental results show that the proposed algorithm can learn more features of small targets and can effectively improve the classification performance of diabetic retina. An experimental test was performed on Kaggle's publicly available dataset of diabetic retinas, and the classification accuracy was 93.8%, compared to some existing classification models; the method proposed in this paper can achieve better classification results for diabetic retinopathy.

1. Introduction

With the improvement of economic level and the change of lifestyle, the incidence of diabetes is increasing year by year. Retinopathy is one of the complications of diabetes, mainly due to the long-term deterioration of small blood vessels in the retinal area. According to the degree of vascular lesions, it can be divided into two categories: nonhyperplasia and hyperplasia. Nonhyperplasia is the early stage of diabetic retinopathy (DR), which can be divided into symptomless, mild, moderate, and severe levels [1], as shown in Figure 1.

The clinical symptoms of nonproliferative DR lesions mainly include microaneurysms, hemorrhage, and soft and hard exudates. The development of the disease may enter the stage of pathological proliferation, mainly due to vascular obstruction resulting in retinal vascular hyperplasia.

In the early stage of the disease, patients cannot detect symptoms, such as symptoms, which has entered the serious stage and missed the best detection and treatment period. Therefore, early detection and intervention play a significant role in preventing vision loss or blindness caused by diabetes [2]. Regular screening can lead to early detection and treatment and slow the progression of the disease and prevent it from happening. Traditional screening mainly relies on ophthalmologists to manually grade and screen retinal images, and its screening intensity is far from meeting the needs of the present stage. The main reasons are as follows: first, there are fewer experienced ophthalmologists; second, manual screening time is long and the result feedback is slow; third, the number of diabetes in China is large. In view of the above situation, there is an urgent need for a high-precision DR automatic recognition and hierarchical diagnosis system to solve the current problems.

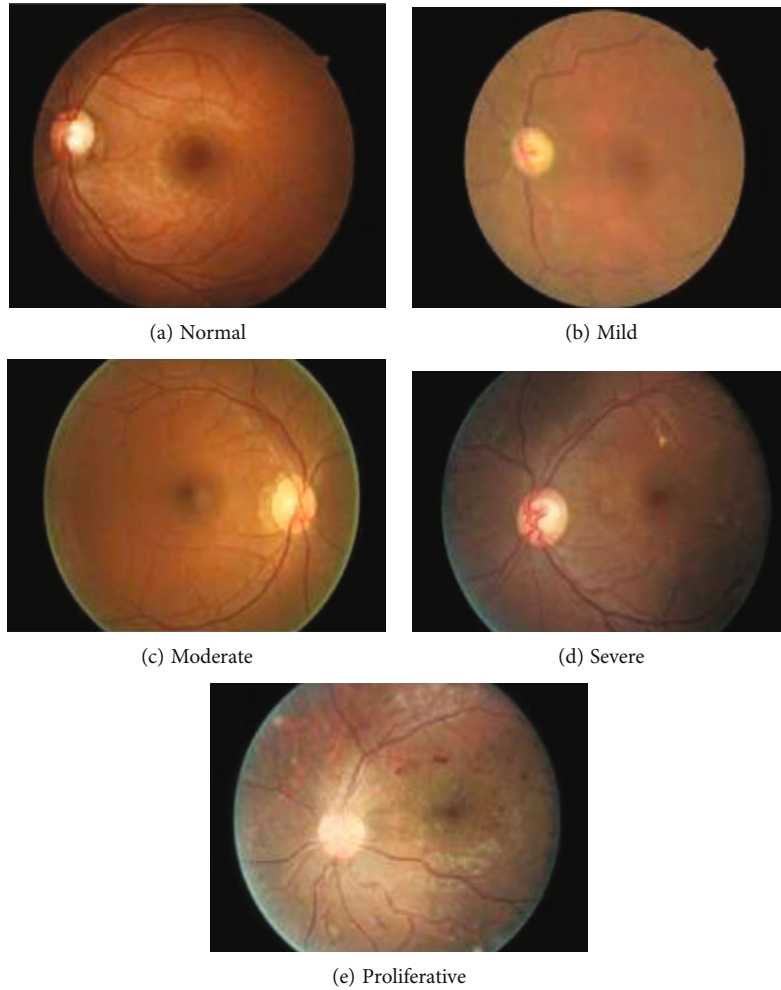


FIGURE 1: Examples of retinal images.

Early diabetic retinopathy is characterized by microaneurysms and exudation, but these symptoms are difficult to extract. This paper mainly solves the problem that small features are difficult to extract, which can be used for early screening and provide some help for doctors. The purpose of this paper is to extract enough small features from retinal fundus color images of diabetes mellitus by deep learning and try to apply them to the early diagnosis of diabetes mellitus, so as to assist doctors to make a reasonable diagnosis and treatment plan, improve the accuracy of classification of diabetic retinopathy, and reduce the burden on doctors.

2. Related Research

In the past few years, many researchers have made great progress in automatic diagnosis of DR using various algorithms, mainly using traditional machine learning algorithms. Basic operations include image preprocessing, feature extraction, and classification [3]. Feature information such as texture, color, and size of image is extracted manu-

ally, and the extracted features are input to support vector machine or random forest and other classifiers for classification and detection. Selecting the right and effective features requires expertise and adjustment of various parameters. These manually extracted features are limited and inaccurate, which will lead to wrong classification, thus affecting the classification performance of lesions and prone to misdiagnosis and missed diagnosis.

Sinthanayothin et al. [4] used Principal Component Analysis (PCA) and edge detection (EDT) to segment the blood vessels and remove background information such as optic disc. Hard exudates were detected by region growth. Sensitivity and specificity were 80.21% and 70.66%, respectively. After binarization of the image, Haloi et al. [5] used morphology to remove the blood vessel, extracted 22 features, and classified them by the support vector machine system. The hard exudates with different sizes could be recognized with a sensitivity of 96.54% and a specificity of 98.35%.

Zhang et al. [6] removed the complex background structure information such as vessels and optic disc, 27 features

were used, and the hard exudate was detected by random forest algorithm (RFA). The AUC is 0.935.

Quellec et al. [7] adopted the wavelet transform algorithm to detect the microhemangioma without removing the optic disc and blood vessel and used the template matching method for the fundus image; by detecting microhemangioma in color fundus image, green component fundus image, and vascular imager image, it is easy to mistake a small lesion for a microhemangioma. The sensitivity and specificity of the algorithm are 89.2% and 89.50%, respectively.

These algorithms are to detect a single disease; using the removal of background and other factors, using different algorithms to extract feature information, the extracted features are entered into a classifier such as a support vector machine or a random forest for classification and detection. How to select suitable and effective features depends on professional knowledge and the adjustment of various parameters. These manually extracted features are limited and inaccurate, which will lead to wrong classification, thus affecting the classification performance of lesions, prone to misdiagnosis and missed diagnosis.

In recent years, with the development of medical image processing and deep learning, deep learning technology has been applied to the detection and diagnosis of DR lesions. Deep convolutional neural network (CNN) can solve the problem of machine learning manual extraction of features which is not accurate and deep features cannot be extracted, while CNN realizes automatic extraction of deeper and more valuable features. Compared with traditional learning methods, its deep learning ability can approximate very complex functions, and its end-to-end characteristics, high accuracy, and robustness are favored by current researchers [8]. Automatic recognition and hierarchical diagnosis system based on deep learning can analyze image information more safely, accurately, efficiently, and noninvasively and can detect, locate, and classify diseases. Therefore, it is necessary to accelerate the application of deep learning in ophthalmic diagnosis, which can contribute to large-scale screening of DR patients, greatly improve clinical efficiency, and alleviate the relative shortage of medical resources [3].

In view of the above problems, under the influence of transfer learning [9], multiscale, attention, and weak supervision mechanisms [10–15], this study improved on the basis of CNN model and proposed a classification model based on residual double-attention mechanism [16], which can be a good solution to the small target difficult to extract the problem. Its main contributions are as follows. ① This paper uses a fusion of attention mechanism and inception module for the DR classification network model algorithm [17], which can strengthen the weight of small lesions and improve the accuracy of classification by modifying the loss function of model training. ② The residual mechanism is added [18]. The core of the residual mechanism uses cross-connection mode to avoid the loss of information transmitted in the layer and the disappearance of gradient, which can greatly accelerate the training of the deep neural network and improve the accuracy of the model.

3. DR Classification Method

The classification of DR lesions based on deep learning is mainly divided into three stages, as shown in Figure 2: image pretreatment stage, classification model training stage, and detection classification stage.

3.1. Image Preprocessing and Data Enhancement. RGB images collected from hospitals have many problems, so data preprocessing is needed before network training. Good and bad image quality has a great influence on the results of retinopathy classification. Prior to feature extraction, preprocessing is crucial to help identify lesions and distinguish the extent of actual lesions, thus improving the accuracy of DR lesion detection. Compared with the blue and red channels, the green channel has the most image information, the largest gap between the green channel and the background, the best contrast and the lowest noise. Green channel images are more conducive to image segmentation and classification, and the Contrast Limited Adaptive Histogram Equalization (CLAHE) method is adopted to enhance contrast. There is better detection of exudates and blood vessels. Illumination correction is for illumination irregularity to improve lumen and brightness of the image. Gaussian filtering and other denoising methods are used to smooth the image, and threshold method is used to delete meaningless black borders. However, network training requires a lot of data, and data enhancement is achieved by image mirroring, rotation, resizing, and clipping.

3.2. Loss Functions Deal with the Problem of Unbalanced Dataset Classes. The dataset used in this study has the problem of category imbalance, which will affect the accuracy of the model. When the sample number of a certain category is small, the proportion of the loss value generated is also small, which does not conform to the characteristics of good performance of all classification categories in the multiclassification model. To solve this problem, the common strategy is resampling the dataset. The problem caused by resampling is oversampling or undersampling, which makes some data lack or reuse problems. Therefore, in this study, the improved loss function is mainly used to punish the classification learning model and modify the learning cost of samples to optimize the network model. On the basis of the original multiclassification focal loss function, regular terms are added to form a loss function suitable for this problem. Formula (1) is the multiclassification focal loss function.

$$L_{\text{MCFL}} = - \sum_{i=1}^n \alpha y' (1-y)^y \log(y'). \quad (1)$$

Formula (2) is the improved multiclassification DR-focal loss function

$$L_{\text{DR-MCFL}} = - \sum_{i=1}^n \alpha y' (1-y)^y \log(y') + \lambda \|y' - y\|_2^2. \quad (2)$$

The regular term is added on the basis of the original loss function, which can solve the problem of the influence of

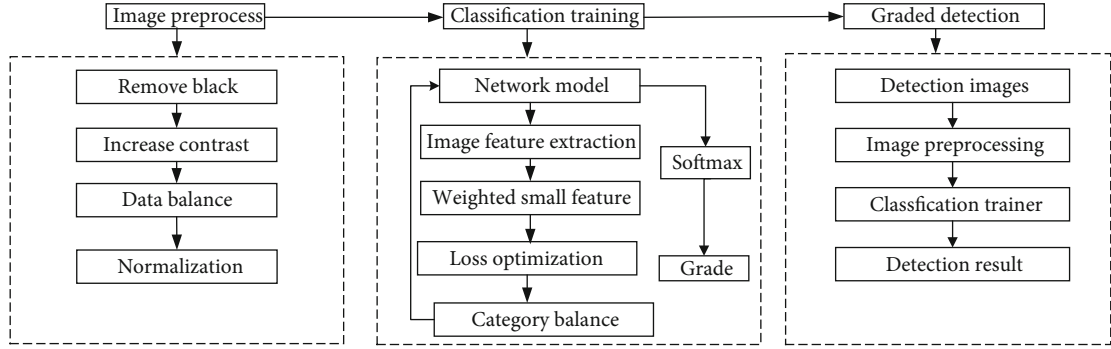


FIGURE 2: DR classification framework.

class imbalance on classification network learning. n is the total number of categories, i indicates a certain category, y' is the predicted result, y is the label value of the sample, α is the equilibrium factor, and λ is the coefficient of the weight of the regular term. The loss function can also accelerate the convergence of the network by adding a second norm as a regular term.

3.3. Related Principles and Mechanisms. DR lesions in the nonhyperplasia stage mainly show symptoms such as hemangioma, fundus hemorrhage, vitreous hemorrhage, and exudate, and the characteristic information of these symptoms is sparse. The traditional network model is not ideal for the detection of small lesions, and the accuracy and performance need to be further improved. In view of sparse lesion areas, attention mechanism can be used to better highlight the information of small lesion feature images, so as to extract richer features. In the network model, residual blocks were added and the information of the front output layer was used as the input of the back layer to prevent the loss of the features of the lesion region and further improve the detection ability of the features of small retinal lesions. Finally, multiclassification is carried out by the Softmax function to accurately achieve the classification of diabetic fundus images at five levels (healthy, mild, moderate, severe, and proliferation).

Based on the above reasons, this study added inception and attention modules on the basis of the basic deep learning network model and combined with the residual thought of ResNet [18]. The core of ResNet uses a cross-connection approach that avoids the loss of information and gradient disappearance problems transmitted in layers, which can greatly speed up training for deeper networks and improve the accuracy of the model. This model can extract more important features under the same amount of computation, so as to improve the training results and make more efficient use of computing resources.

3.3.1. Attention Mechanism. Human perception of the world does not process everything it sees, but rather makes sense of the world around it by capturing the parts that stand out. It is based on human's understanding of the world that this principle is applied to deep learning. Attention mechanism

is widely used in natural image and natural language processing. There are two attention mechanisms, namely, spatial domain and channel. The channel mechanism focuses on the importance of the channel, while the spatial attention mechanism focuses on the importance of different positions on the same channel. If the two mechanisms are combined, the channel can be paid attention to, and the weight of different features on the channel can be given, and the problem of difficult extraction of small features can be solved by increasing the feature weight of small features, so as to improve the classification accuracy of the model [15].

3.3.2. Channel Attention Mechanism. For the natural image in the input convolutional neural network, there are two attributes, in which length and width are the scale space of the image, and the other attribute is the channel. The principle of channel attention mechanism is to firstly reduce channel dimension. After obtaining feature information through maximum pooling and average pooling, respectively, the two parts are splicing together to form a feature map by sharing multilayer perceptron, and then, the weight value is normalized to 0-1 by the sigmoid function. After the calculated weight matrix value is weighted by multiplying the original channel image, the importance of different channels can be finally learned [19], as shown in Figure 3.

- (1) The algorithm flow of the channel attention mechanism principle is as follows
- (2) Feature input: assuming that the feature graph of the input is represented by $F(H, W, C)$, H is height, W is width, and C is channel
- (3) Cycle processing: for $w = 1, 2, \dots, W$, for $h = 1, 2, \dots, H$, and for $c = 1, 2, \dots, C$. Repeat the following operations to perform global average pooling and maximum pooling. Global pooling reduces dimension and maximum pooling extracts more influential channels, as shown in

$$F_{\text{channel avg}}^C = \frac{\sum_{h=1}^H \sum_{w=1}^W (F^{C,H,W})}{H \times W}, \quad (3)$$

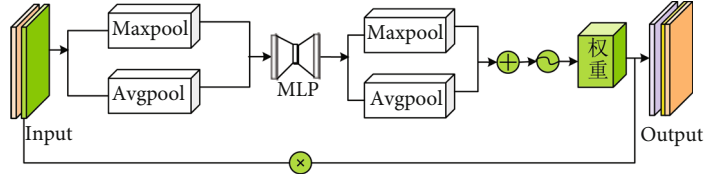


FIGURE 3: Channel attention mechanism diagram.

$$F_{\text{channel max}}^C = \frac{\sum_{h=1}^H \sum_{w=1}^W (F^{C,H,W})}{H \times W}. \quad (4)$$

- (4) Generate channel attention weight value: after adding the maximum pooling layer and average pooling layer through multilayer perceptron operation containing two fully connected layers, the sigmoid function is used to calculate channel attention weight value, as shown in

$$M_c(F) = \text{sigmoid} \left(\text{MLP} \left(F_{\text{channel avg}}^C \right) + \text{MLP} \left(F_{\text{channel max}}^C \right) \right). \quad (5)$$

- (5) Formula (6) is used to calculate the final channel attention graph F' :

$$F' = F \times M_c(F). \quad (6)$$

3.3.3. Attention Mechanics in Space. In the aspect of space domain, it mainly deals with feature dimension. After the channel attention mechanism, the contribution degree of image features on each channel is also different; that is, the importance degree of each channel is different, and the importance of features on each channel is also differentiated. Through the spatial attention mechanism, features with high contribution on this channel can be found. The specific principle is that global average pooling and global maximum pooling are also used to obtain two feature graphs, and then, a convolution kernel is used to form a new feature graph after convolution. More critical and important feature information can be obtained by multiplying the weight value of the feature graph by the weight of the original image through the normalization of the sigmoid function. The attention mechanism can focus more attention on more important features, which is helpful to extract smaller and more difficult feature information [20], as shown in Figure 4.

3.4. Residual Principle of the Module. With the increase of the layers of the deep learning network model, the gradient explosion or gradient disappearance will occur. The main reason is that in the process of network backpropagation, the gradient value may be infinite or zero due to the nonlinear change, which makes the network model either in the state of training stagnation or you are in a state where the

parameter value keeps increasing indefinitely. The overall training stability of the network will become very poor. In order to solve this problem, residual module is adopted in this research. The basic principle is to superimpose the output of shallow layer network on the output of deep layer network to protect the primitiveness and integrity of the characteristic information; learning the difference between its input and output simplifies the difficulty of network training. The strategy is illustrated in Figure 5.

Let X be the output of shallow layer, $H(x)$ is the deep output, $F(x)$ is the transformation represented by the middle two layers of the two, and then, the formula is $H(x) = x + F(x)$.

According to the above formula, when the output of the shallow network is superimposed on the output of deep network, when the network converges to the global optimal solution, the mapping of output layer reestablishes a new channel relational mapping of input to output, and the mapping of original layer is set to 0. After the characteristic information contained in shallow layer X was fully learned through the network, if the parameter adjustment of the back layer made the loss function tend to increase after the change of X , the loss function tended to be 0 through the residual connection channel, and x continued to be transported to the next hidden layer from the identity mapping. In the forward propagation of the network, the training speed of the shallow network layer is faster and easier than that of the layer network layer. Therefore, the training speed of the deep network layer can be accelerated by mapping the features learned at the shallow network layer to the corresponding positions of the deep network layer. In network backpropagation, gradient propagation is faster in the deep network layer due to residual connection branches, and gradient upward can be transmitted by an activation function with the help of residual connection paths. The introduction of residual connection will reduce the parameter values in the module layer and make the parameters in the network more sensitive to the loss function under reverse propagation. Therefore, the convergence of loss function in the network can be accelerated so that the training time of the network is shorter and the training efficiency is higher. Residual connection also regularizes the network.

3.5. Residual Double Attention Module Principles. The residual double attention module is mainly composed of residual, channel attention, and space attention [20]. Deep learning problems often encountered in the explosion problem are gradient disappear or gradient; the usual solution is to initialize the data standardization and batch, at the same time also can bring when depth deepening and the network

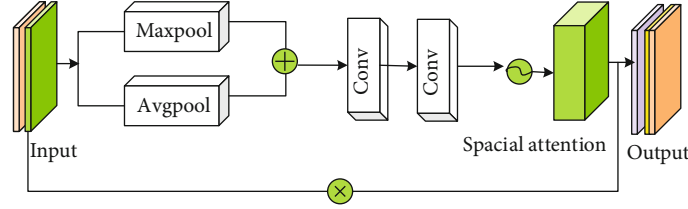


FIGURE 4: Spatial attention mechanism diagram.

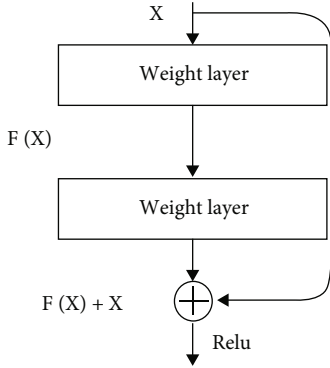


FIGURE 5: Residual schematic diagram.

performance problems, and the residual is mainly used to solve the problem of gradient and also can improve network performance and reduce the error rate; the specific formula is

$$H_{i,d}(x) = (1 + M_{i,c}(x)) \times F_{i,c}(x). \quad (7)$$

H is the feature of the output of residual attention, M is the feature of the attention mechanism, and F is the attention function. Different functions will extract different attention fields. F in Formula (8) stands for attention in the mixed domain.

$$F_{i,c}(x) = \frac{1}{1 + \exp(-x_{i,c})}. \quad (8)$$

F in Formula (9) stands for attention in the channel domain.

$$F_{i,c}(x) = \frac{x_{i,c}}{\|x_i\|}. \quad (9)$$

F in Formula (10) stands for attention in the spatial domain.

$$F_{i,c}(x) = \frac{1}{1 + \exp(-(x_{i,c} - \text{mean}_c)/\text{std}_c)}. \quad (10)$$

3.6. Model Structure. Through the combination of attention mechanism and residuals, the problem of difficult extraction of small features in focus was solved. In the experiment, using the dual attention mechanism of channel and space, not only the features on the important channel can be extracted but also the small features in different spaces can

be focused. In addition, the residual parameter module is used in the model, which can not only reuse the low-order features of the image but also generate new high-order composite features continuously. There are two main modules in the model: inception module and attention module, as shown in Figure 6.

IRCSB has inception module and attention module [21], as shown in Figure 7. The three different scale convolutional layers used in the inception module can capture more locally diverse information, which is then fused, and finally, features are extracted by using a 1×1 convolutional layer for perception of different scales. The inception module main multi-scale extraction feature, first through a 1×1 convolution extraction feature, the convolution of two 3×3 s, a 3×3 convolution, a pool, and a 1×1 convolution are concatenated into the later attention module, thus paying attention to both the important information in the channel and the characteristic information in the space, to ensure the integrity of the information. The different scale convolutions used in the inception module can capture more local and diverse information and then fuse this information, combined with the attention mechanism to increase the weight of small features, which can extract smaller features. In the attention module, there are channel attention (CA) and space attention (SA); CA is mainly used to extract the importance of different channels, as shown in Figure 4. SA is mainly used to focus on areas with high-frequency information and calculate the importance of different areas. The structure of SA is shown in Figure 6.

4. Network Model Training and Testing

The research of this paper is to implement the training and testing of the whole model in Python programming language and PyTorch framework, as shown in Figure 8. The hardware environment of the experiment is as follows: CPU: Intel core i9-9980XE @ 3.00 GHz \times 362; graphics card: NVIDIA GeForce RTX 2080 Ti \times 4; memory: 128 GB.

The data used in the experiment came from the public dataset of Kaggle Competition [18–20]. The dataset is a large number of high-resolution retinal images taken under various imaging conditions, with a total of 35,126 images, with resolutions of 1440×960 , 2240×1488 , and 2304×1536 , respectively. There are many problems in the image, such as artifacts, lack of focus, underexposure, or overexposure. In addition, there are also problems of data imbalance in different levels of images. The dataset was graded by the clinician on each DR lesion image, which was divided into five scales, with an integer 0-4 to represent the severity of the

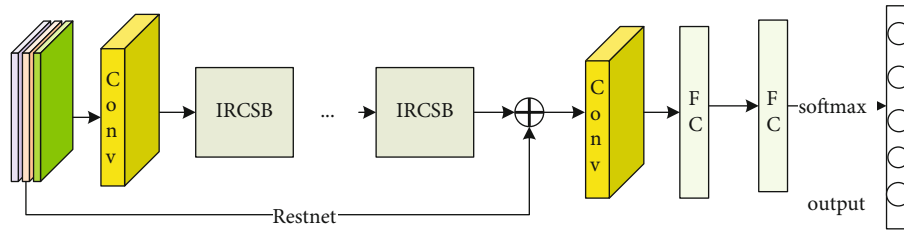


FIGURE 6: Model network structure chart.

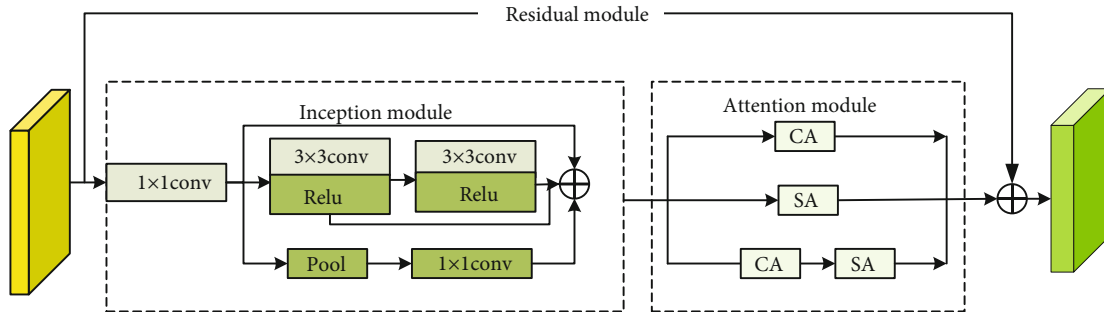


FIGURE 7: IRCSB network structure chart.

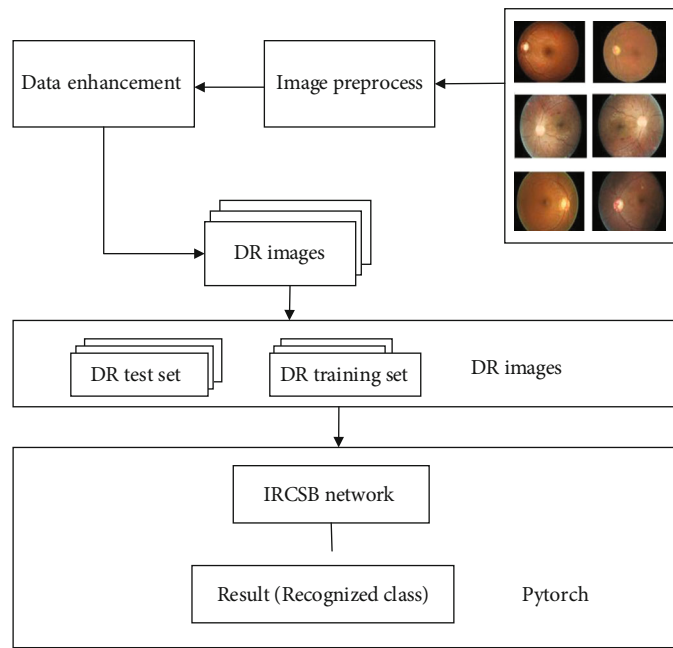


FIGURE 8: DR diagnosis technique using IRCSB network structure.

lesion, namely, asymptomatic, mild, moderate, severe, and proliferative. There were 35,126 images in the test dataset, including 25,810 without DR symptoms, 2443 mild NPDR, 5292 moderate NPDR, 873 severe NPDR, and 708 proliferation maps. There is a serious imbalance between different categories, and image enhancement is used for categories with relatively little data. The details are shown in Table 1.

4.1. *Image Preprocessing.* After histogram equalization, remove black borders from all images. Because images have

different tones and lighting, color and lighting should be balanced to improve the robustness of the model. Otherwise, feature extraction of lesions will be affected in the later stage. Image denoising is to remove the noise in the image without blurring the edges, as shown Figure 9. Median filter is used to remove noise and retain some image features such as discontinuity, edge, or line.

4.2. *Image Cutting Processing.* The common lesions in eye images mainly include microhemangioma, hard exudate,

TABLE 1: Results of datasets.

Lesion level	Quantity (sheet)
Normal	25,810
Slight	2443
Average	5292
Serious	873
Proliferation	708
Total	35,126

hemorrhagic spots, cotton patch, and neovascularization. These small lesion areas are difficult to extract features. For the features of small lesion areas in the eyes are not easy to extract, it is necessary to do some cutting processing on the image. Firstly, the original high-resolution image was scaled to a suitable size (480×480) to extract the global features of the image. Then, the original image is scaled to get a subimage with a size of 1000×1000 , which is cut into four parts. Then, the four images are scaled to 480×480 . Local features of the image can be extracted by using these four small images. Finally, five 480×480 images will be obtained as the input data of the network. The network can extract both global information and local small features so that the convolutional network can fully extract more useful image features. In the experiment, in order to speed up the training of convolutional network, data were normalized, as follows:

$$X = \frac{X - X_{\min}}{X_{\max} - X_{\min}}. \quad (11)$$

5. Experimental Results and Analysis

5.1. Experimental Parameter Settings. The SGD optimizer is adopted, the initial learning rate $lr = 2e - 3$, the learning rate is adjusted dynamically according to the change of loss, and the $l1$ regularization is added. Different activation functions such as Sigmoid, Tanh, ReLU, and LReLU are used to test the accuracy of the network. Finally, LReLU activation function is selected to accelerate the convergence of the network, epochs = 100, batch size = 32, and the learning strategy is step. Four activation functions, Sigmoid, Tanh, ReLU, and LReLU, are used to compare the experimental results, which are shown in Table 2.

5.2. Evaluation Index. For multiclassification problems, the evaluation criteria of sensitivity, specificity, and precision, three indicators, were used to evaluate the experimental results. True positive rate (TPR) refers to the probability of being correctly predicted in actual positive samples, and true negative rate (TNR) refers to the probability of being correctly predicted in actual negative samples, also known as recall rate. Precision is the probability of being correctly predicted in positive samples of predicted results. The AUC is the area under the curve; it is a kind of performance index to measure the classification quality.

$$\text{Accuracy(ACC)} : \text{ACC} = \frac{(\text{TP} + \text{TN})}{(\text{TP} + \text{FP} + \text{TN} + \text{FN})}, \quad (12)$$

the proportion of the number of samples correctly classified by the model to the total number of samples.

$$\text{True positive rate(TPR)} : \text{TPR} = \frac{\text{TP}}{(\text{TP} + \text{FN})}, \quad (13)$$

the percentage of positive samples that are correctly classified among all positive samples.

$$\text{True negative rate(TNR)} : \text{TNR} = \frac{\text{TN}}{(\text{FP} + \text{TN})}, \quad (14)$$

the percentage of negative class samples that are correctly classified among all negative class samples.

$$\text{Precision(precision)} : P = \frac{\text{TP}}{\text{TP} + \text{FP}}, \quad (15)$$

the proportion of positive samples in positive examples determined by the classifier.

$$\text{F1 score} : F1 = \frac{(2 \times P \times \text{TNR})}{P + \text{TNR}},$$

$$\text{AUC(area under the curve)} : \text{AUC} = \frac{1}{2} \sum_{i=1}^{m-1} (x_{i+1} - x_i)(y_i + y_{i+1}). \quad (16)$$

The vertical axis of the receiver operating characteristic curve is the true positive rate (TPR), the horizontal axis is the false positive rate (FPR), and the AUC is the area under the curve; it is a kind of performance index to measure the classification quality.

5.3. Experimental Results. When training the network, the learning rate has a certain impact on the convergence of the model. The learning rate is set to 0.002, 0.05, 0.1, and 0.5, respectively. After continuous test and comparison, it is determined that the initial learning rate is 0.002, and the total number of iterations tends to converge when it is about 1400, which not only ensures the convergence of the loss function but also makes the classification accuracy reach the highest, and the accuracy reaches 93.8%.

5.4. Experimental Comparison. This paper compares the classification performance of multiscale mixed attention model with several traditional models, other deep learning models, and approximate structure models and further verifies the effectiveness of the classification model proposed in this paper.

5.4.1. Compared with Machine Learning Algorithm. Machine learning algorithm method is useful for industry [22, 23] and medical field. Power tools can be diagnosed using the developed method. In the study of recognition of diabetic retinopathy using BP neural network algorithm, the main factors that affect the classification result of neural network are the number of hidden layers and the selection of excitation function. The BP neural network has 8 layers; it consists of an

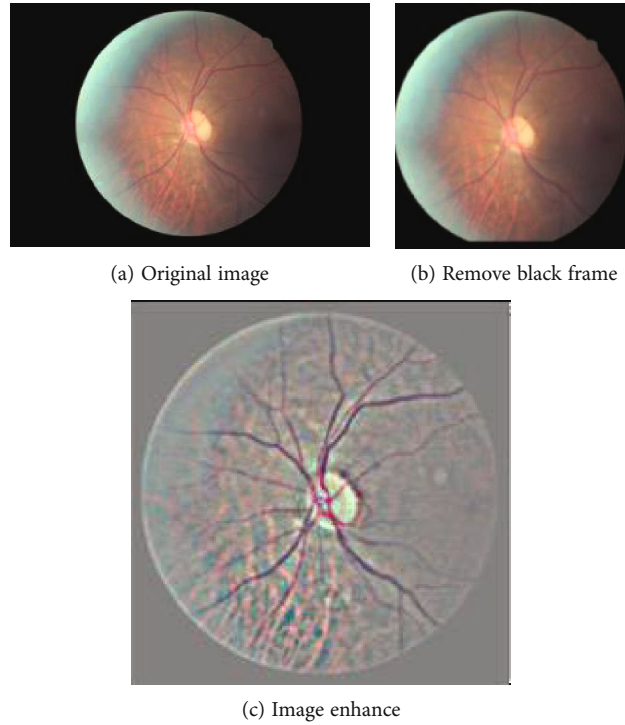


FIGURE 9: DR image preprocess result.

TABLE 2: Experimental results of different activation functions.

Activation function	Accuracy (%)	AUC
Sigmoid	89.5	0.87
Tanh	90.3	0.88
ReLU	92.8	0.91
LReLU	93.0	0.93

TABLE 3: Results of different network models on datasets.

Evaluation results	BP	SVM	Proposed
SE	0.85	0.86	0.934
SP	0.84	0.85	0.962
ACC	0.87	0.88	0.938

input layer, six hidden layers, and an output layer. The full connection between layers is used, and three different excitation functions, hyperbolic tangent function, sigmoid function, and quasilinear function, are used to test the results. Finally, the sigmoid function was chosen, and its prediction accuracy was up to 87%.

In SVM, kernel function is the final classification effect. Kernel function mainly includes polynomial kernel, radial basis kernel, and sigmoid kernel. These functions were tested, respectively, repeated 100 times, the final selection of radial basis function kernel, the error is the smallest, and the accuracy is 88%.

TABLE 4: Results of different network models on datasets.

Model	SP	SE	AUC	ACC
AlexNet	89.07%	79.01%	0.7988	81.76%
LeNet	86.32%	82.45%	0.88.52	87.02%
GoogleNet	90.34%	88.46%	0.9188	92.01%
Proposed	96.2%	93.40%	0.9205	93.80%

This experiment is compared with the traditional machine learning algorithm classifier, and the experimental results are shown in Table 3. The results show that the accuracy rate, true positive rate, and false positive rate of classification have been improved by using the network model of this scheme, and the misclassification rate has been effectively reduced, further confirming the feasibility of this scheme.

5.4.2. Comparison with Other Deep Learning Algorithms.

This paper makes an experimental comparison with LeNet, AlexNet, and GoogleNet. LeNet contains two convolution layers and two full connection layers, with a total of 60,000 learning parameters. The accuracy rate on this dataset is 87.02%. In the AlexNet network model, there are 5 convolution pooling layers, 3 full connection layers, and 1000 neurons in the output layer. The first convolution uses a larger core size of 11×11 with a step size of 4. The core size of the subsequent convolution layer is relatively small, 5×5 or 3×3 , with a step size of 1. The accuracy on this dataset is 81.76%. GoogleNet won the first place in the 2014

ImageNet challenge. Through the concept multiscale structure, it not only expands the depth and width but also improves the utilization of computing resources. This experiment compares with the three network structures of LeNet, AlexNet, and GoogleNet. The comparative experiment shows that the accuracy of the multiscale hybrid attention network proposed in this paper is higher than that of the other three network structures, and the convergence speed is much faster than that of the other two network structures. The overall effect is the best. The results are shown in Table 4.

6. Conclusions

Due to the increasing number of diabetic population and cases of retinopathy, there is an increasing demand for automated DR diagnostic systems. However, there are still some problems in the direct application of these DR systems in clinical practice, so it is urgent to develop a more reliable and practical automatic DR diagnostic grading system to help clinicians do auxiliary examinations [24]. We propose an automatic DR classification system based on attention and residual parameter mechanism. Combined with inception multiscale module feature extraction, the problem of small feature extraction is solved. Finally, it achieves the effect of 5 classification with an accuracy of 93.8%, which is greatly improved compared with the traditional machine classification algorithm. The results show that the algorithm used in the model is superior to the other two algorithms in the recognition of diabetic retinopathy. The contribution of this study is that the diabetic retina can be early screened; it can not only reduce misdiagnosis caused by human factors but also greatly shorten the time of diabetic retinopathy diagnosis, which is of great clinical significance in preventing visual loss and treatment.

The shortage of this study is the use of less external datasets to verify, which needs to use multicenter data to verify the results of this model, so there is a certain gap in clinical application. What we can do on the basis of this study is to use more general data to verify the results of this model. In the future, we can also use multimodal data to realize the study, use multimodel integration or fusion method to train the model, and further improve the classification accuracy.

Data Availability

The raw data supporting the conclusions of this article will be made available by the authors, without undue reservation.

Ethical Approval

This article does not contain any studies with human participants or animals performed by any of the authors.

Consent

Informed consent was obtained from all individual participants included in the study.

Conflicts of Interest

All authors declare that they have no conflict of interest.

Authors' Contributions

All authors listed have made a substantial, direct, and intellectual contribution to the work and approved it for publication.

Funding

This work was supported by No. 2021MS06010. This work was also supported by No. NJZY21068.

Acknowledgments

The authors acknowledge the help from the university colleagues.

References

- [1] R. Ma and Z. Lu, "The value of ophthalmological imaging in the early diagnosis and treatment of diabetic retinopathy," *Imaging Research and Medical Application*, vol. 1, no. 12, 2017.
- [2] L. Yin and H. Peng, "Progress in the treatment of diabetic retinopathy," *Modern Medicine and Health*, vol. 33, no. 1, pp. 80–83, 2017.
- [3] S. K. Somasundaram and P. Alli, "A machine learning ensemble classifier for early prediction of diabetic retinopathy," *Journal of Medical Systems*, vol. 41, no. 12, p. 201, 2017.
- [4] C. Sinthanayothin, V. Kongbunkiat, S. Phoojaruenchanachai, and A. Singalavanija, "Automated screening system for diabetic retinopathy," in *Proceedings of the 3rd International Symposium on Image and Signal Processing and Analysis*, pp. 915–920, Rome, Italy, 2003.
- [5] M. Haloi, S. Dandapat, and R. Sinha, "A Gaussian scalespace approach for exudates detection, classification and severity prediction," *Computer Science*, vol. 56, no. 1, pp. 3–6, 2015.
- [6] X. Zhang, G. Thibault, E. Decencière et al., "Exudate detection in color retinal images for mass screening of diabetic retinopathy," *Medical Image Analysis*, vol. 18, no. 7, pp. 1026–1043, 2014.
- [7] G. Quéllec, M. Lamard, P. M. Josselin, G. Cazuguel, B. Cochener, and C. Roux, "Optimal wavelet transform for the detection of microaneurysms in retina photographs," *IEEE Transactions on Medical Imaging*, vol. 27, no. 9, pp. 1230–1241, 2008.
- [8] F. Meng, W. Yin, and J. He, "Detection of bleeding points in fundus images based on deep learning," *Journal of Shandong University (Science Edition)*, vol. 55, no. 9, pp. 62–71, 2020.
- [9] X. Li, T. Pang, B. Xiong, W. Liu, P. Liang, and T. Wang, "Convolutional neural networks based transfer learning for diabetic retinopathy fundus image classification," in *2017 10th International Congress on Image and Signal Processing, BioMedical Engineering and Informatics (CISP-BMEI)*, Shanghai, China, 2017.
- [10] Y. LeCun and Y. Bengio, "Convolutional networks for images, speech, and time series," in *The Handbook of Brain Theory and Neural Networks*, p. 3361, MIT Press, 1995.

- [11] A. Krizhevsky, I. Sutskever, and G. E. Hinton, "ImageNet classification with deep convolutional neural networks," *Communications of the ACM*, vol. 60, no. 6, pp. 84–90, 2017.
- [12] S. Wang, Y. Yin, G. Cao, B. Wei, Y. Zheng, and G. Yang, "Hierarchical retinal blood vessel segmentation based on feature and ensemble learning," *Neurocomputing*, vol. 149, pp. 708–717, 2015.
- [13] P. Ding, Q. Li, Z. Zhang, and F. Li, "Deep neural network classification method for diabetic retina images," *Computer Applications*, vol. 37, no. 3, pp. 699–704, 2017.
- [14] K. Simonyan and A. Zisserman, "Very deep convolutional networks for large-scale image recognition," 2014, Computer Science, <http://arxiv.org/abs/1409.1556v6>.
- [15] C. Szegedy, W. Liu, Y. Jia et al., "Going deeper with convolutions," in *IEEE 2015 IEEE Conference on Computer Vision and Pattern Recognition (CVPR)*, pp. 1–9, Boston, MA, USA, 2015.
- [16] C. Szegedy, S. Ioffe, V. Vanhoucke, and A. A. Alemi, "Inception-v4, inception-resnet and the impact of residual connections on learning," 2017, Thirty-First AAAI Conference on Artificial Intelligence, <http://arxiv.org/abs/1602.07261>.
- [17] S. Wan, Y. Liang, and Y. Zhang, "Deep convolutional neural networks for diabetic retinopathy detection by image classification," *Computers and Electrical Engineering*, vol. 72, pp. 274–282, 2018.
- [18] K. He, X. Zhang, S. Ren, and J. Sun, "Deep residual learning for image recognition," in *IEEE Conference on Computer Vision & Pattern Recognition*, IEEE Computer Society, 2016.
- [19] K. Xu, J. Ba, R. Kiros et al., "Show, attends and tells: neural image caption generation with visual attention," in *Proceedings of the 32nd International Conference on Machine Learning. PMLR 37*, pp. 2048–2057, New York, 2015.
- [20] S. Woo, J. Park, J. Y. Lee, and I. Kweon, "Clam: convolutional block attention module," *Proceedings of the European conference on computer vision (ECCV)*, vol. 63, pp. 3–19, 2018.
- [21] Y. Miao, S. Tang, P. Du, and Z. Li, "Research on deep learning in the detection and classification of diabetic retinopathy," in *2021 IEEE International Conference on Computer Science, Electronic Information Engineering and Intelligent Control Technology (CEI)*, pp. 107–113, Fuzhou, China, 2021.
- [22] A. Glowacz, "Ventilation diagnosis of angle grinder using thermal imaging," *Sensors*, vol. 21, no. 8, p. 2853, 2021.
- [23] A. Glowacz, "Thermographic fault diagnosis of ventilation in BLDC motors," *Sensors*, vol. 21, no. 21, p. 7245, 2021.
- [24] M. Chen and D. Gong, "Discrimination of breast tumors in ultrasonic images using an ensemble classifier based on Tensor Flow framework with feature selection," *Journal of Investigative Medicine*, vol. 67, Suppl 1, p. A3, 2019.

Research Article

Development Policy of the International Trade Industry under the Background of Cloud Computing and Internet of Things

Liang Wu,^{1,2} Jianhua Zhou ,¹ Honglei Tang,¹ and Hanjie Xiao¹

¹School of Economics and Management, Huzhou University, Huzhou, 313000 Zhejiang, China

²Institute of “Two Mountains” Theory, Huzhou University, Huzhou, 313000 Zhejiang, China

Correspondence should be addressed to Jianhua Zhou; 02834@zjhu.edu.cn

Received 18 April 2022; Accepted 10 May 2022; Published 2 June 2022

Academic Editor: Alireza Souri

Copyright © 2022 Liang Wu et al. This is an open access article distributed under the Creative Commons Attribution License, which permits unrestricted use, distribution, and reproduction in any medium, provided the original work is properly cited.

With the continuous development of Internet technology, new opportunities and challenges have emerged in international trade. If it does not seize new opportunities and take measures to meet challenges, it will cause the development of international trade to enter a state of stagnation, especially when the current domestic demand has not shown a strong recovery. The emergence of cloud computing and the Internet of Things (CCIoT) has provided new technologies and means for the development of international trade. In order to accurately analyze the development policy of the international trade industry and provide strong technical support for the development of the international trade industry under the Internet of Things environment, this paper studies the development policy of the international trade industry in the context of CCIoT. This paper borrows the method of cloud computing and collects relevant data provided by development policies through the perception Internet layer. It is transmitted through the network layer, processed through the high-performance computing cloud, and finally transformed into useful information for the international trade industry. The test results show that the use of cloud computing technology can analyze the existing development policies, promote the development of the international trade industry, and improve the trade efficiency by 3.84%. This reduces the impact of various factors on international trade, while providing strong and good services to users in international trade.

1. Introduction

With the in-depth implementation of the “One Belt, One Road” policy, the current development of international trade is showing a positive trend. However, due to the influence of various factors, there are still many practical problems in the development of the international trade industry. In order to solve these problems, many experts have conducted research on the development policy of international trade, but few have considered the introduction of cloud computing IoT into the development policy of the international trade industry. This paper introduces CCIoT technology into the research of the international trade industry development policy, which plays an important role in solving practical problems. The international trade industry is an important support for the development of the national economy. The development of the international trade industry can provide a solid foundation for the development of the national economy. In order to improve the efficiency of international

trade, many teams have conducted research on this. Hu et al. established an analysis framework based on a knowledge view for international trade enterprises. This is to better cultivate the innovation ability of the overall thinking process of domestic trade enterprises, and timely adjustment of the process can allow information capital to improve the performance of enterprises in the international trade industry [1]. In order to solve the problems faced by the international trade of traditional Chinese medicine, Cheng et al. used the Michael Porter diamond model to analyze the international competitiveness of the traditional Chinese medicine industry [2]. Chang examined the impact of disasters on international trade through the gravity equation model [3]. Rijesh examined the impact of international trade on Indian manufacturing productivity through the effects of economies of scale, reallocation, competition, and spillover channels [4]. Smith et al. proposed a multilevel network approach as an alternative framework for analyzing international organizations in the industrial sector of international

trade [5]. Guliyev et al. discussed the current situation and related issues regarding the development of the oil refining industry worldwide [6]. Ishii studied firm dumping and anti-dumping duties by modeling international industries in which developed and developing country firms trade differentiated goods with each other under incomplete internalization of global pollution and pollution externalities [7]. Many teams have conducted research on the development of the international trade industry, but few teams have conducted research on the international trade industry in the context of cloud computing. For solving this problem, this paper introduces cloud computing into the international trade industry for research and analysis.

The advantages of cloud computing make it used in various fields. To give full play to the advantages of cloud computing, many teams have conducted research on this. To address the inefficiency of retrieving localized data from remote clouds, Deng et al. leveraged cloud computing. They deployed localized computing facilities on the premise of users, prestored cloud data, and distributed it to mobile users with fast local connections [8]. Considering the competitive nature of multitenant environments in cloud computing, Wei et al. proposed a cloud resource allocation model using Hidden Markov Models in cloud computing environments based on incomplete information games [9]. Yi et al. chose to study how to improve the virtual machine sharing strategy from different perspectives to make it harder for intruders to attack the target [10]. Stergiou and Psannis have based on mobile cloud computing and IoT combined with big data technology to examine their common characteristics [11]. To alleviate the problem of long response times for workers that take a long time to process subtasks, Hirai et al. modeled the task scheduling server as a single-server queue [12]. Wang et al. proposed an efficient file-level attribute-based encryption scheme in cloud computing [13]. To improve scalability, availability, and durability, Barsoum and Hasan proposed a map-based provable multicopy dynamic data ownership (MB-PMDDP) scheme [14]. Xia et al. proposed a scheme that supports CBIR on encrypted images without leaking sensitive information to cloud servers. The feature vector is extracted to represent the corresponding image, and the prefiltering table is constructed by a local sensitive hash to improve the search efficiency. Security analysis and experiments prove the security and effectiveness of the proposed scheme [15]. Cloud computing studied by many teams does not involve the international trade industry. To promote the development of the international trade industry, this paper combines cloud computing and Internet of Things technology and introduces it into the study of its development policy.

As the development of the international trade industry is closely related to people's lives, people pay more and more attention to the development of the international trade industry. However, there are many problems in the development process of the international trade industry, which affect the development of the international trade industry. In order to solve various problems in the development of the international trade industry, this paper studies the development policies of the international trade industry under the

background of CCIoT. The results showed that the introduction of CCIoT technology into the international trade industry can effectively reduce the impact of various factors on international trade, alleviate the blocking effect of various problems on its development, and improve trade efficiency. The Internet of Things refers to the realization of the ubiquitous connection between things and people and between things and people through various possible network accesses, and the realization of intelligent perception, identification, and management of objects and processes. The Internet of Things is an information carrier based on the Internet, traditional telecommunication networks, etc. It enables all common physical objects that can be independently addressed to form an interconnected network.

2. Cloud Computing IoT System

2.1. IoT Sensor Network System. The sensor network system [15] includes end nodes, router nodes, coordination nodes, and monitoring centers. The end nodes are located in the industrial exit zone. The location and number of end nodes and cameras can be placed according to actual needs. The system can handle all kinds of accidents in a timely manner and ensure the safe and rapid growth of the trade industry. The system block diagram is shown in Figure 1.

The end nodes send the collected data to other end nodes and process the data at the coordinating node. The wireless sensor monitoring system consists of end nodes, wireless router nodes, coordination nodes, data acquisition centers, and servers. The end nodes are placed high in the industrial area and can collect relevant data and transmit the data on the wireless network through wireless router nodes. First, they are sent to the coordinator and then to the scanner server via the serial port. Then the scanner server transmits the data to the monitoring center through the radio module, and finally, the monitoring center further completes the processing and storage of the data. As soon as the parameters deviate from normal conditions, an alarm is issued immediately. This allows employees and managers to take immediate action to prevent incidents of all kinds, thereby reducing the frequency of incidents. At the same time, the administrator can know from the network address from which site the data is sent. This helps employees and managers to take appropriate measures in a timely manner to improve work efficiency.

2.2. Cloud Computing Platform Management Technology. The cloud computing system is composed of a large number of servers and serves a large number of users at the same time. Therefore, the cloud computing system uses distributed storage to store data and redundant storage to ensure the reliability of data.

A large number of cloud servers are distributed in different industrial export regions. In order to ensure that the entire cloud system [16] can provide services continuously, the international trade industry must make reasonable use of these export zone servers. Cloud computing platform management technology ensures that many servers work together. It also enables users to easily operate and control applications, and to detect and repair faults in a timely

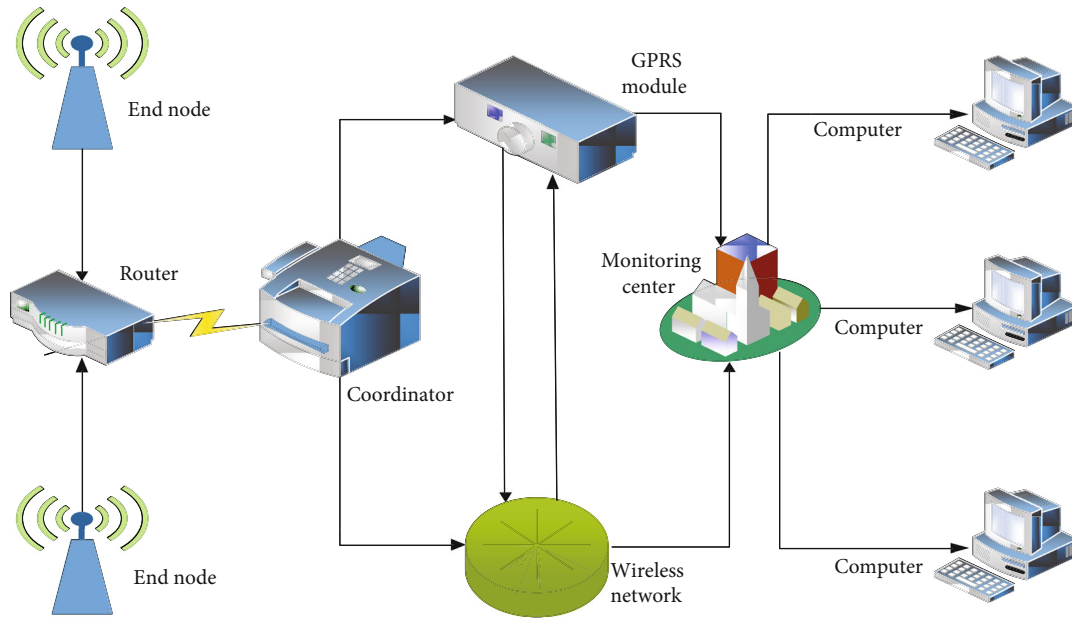


FIGURE 1: The overall framework of the system.

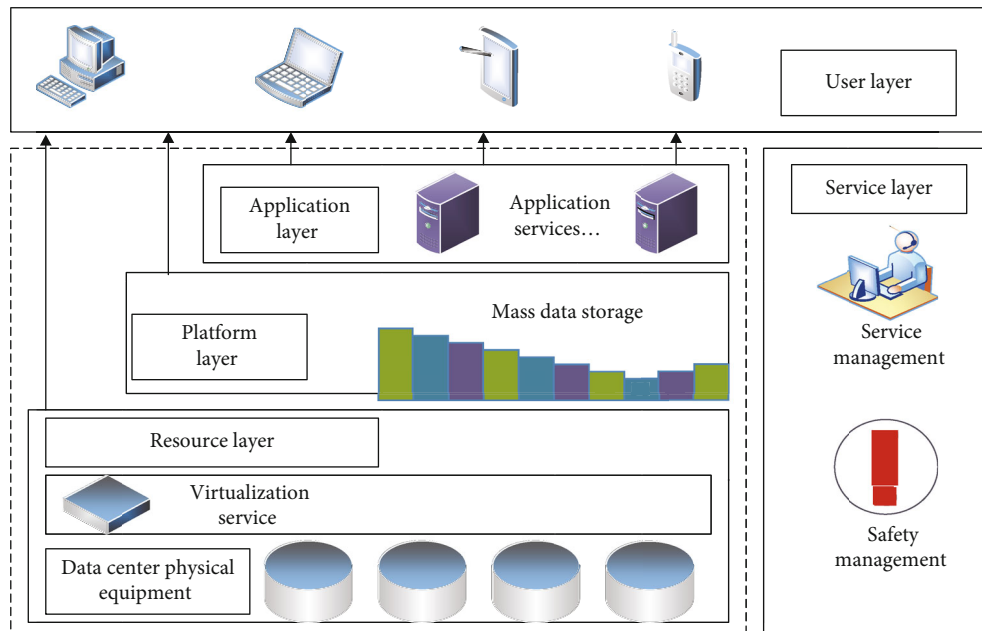


FIGURE 2: Cloud system framework diagram.

manner. The cloud computing platform management architecture is shown in Figure 2.

As shown in Figure 2, the user layer provides relevant hardware configuration resources for the cloud computing service of the data layer by building a super-large-scale data center. At the same time, with the support of virtualization technology, it provides users with powerful computing power and other resources. It is especially convenient for users to publish applications. Users can intelligently select network components and set application publishing parameters without having to understand and manage the basic software and hardware facilities of cloud computing. As the middle layer of the three-layer core

service, the data layer plays a role in linking the previous and the next. It not only undertakes the resource scheduling and management at the bottom of the system but also supplies the distributed programming framework to management software or applications. Due to the popularity of centralized data software applications and the increasing size of data, the data layer must have the ability to handle large data read and write operations that can adapt to the needs of modern applications.

2.3. *GFS System.* GFS is a data management system developed based on data center research and development and hosting network software applications [17]. The GFS system

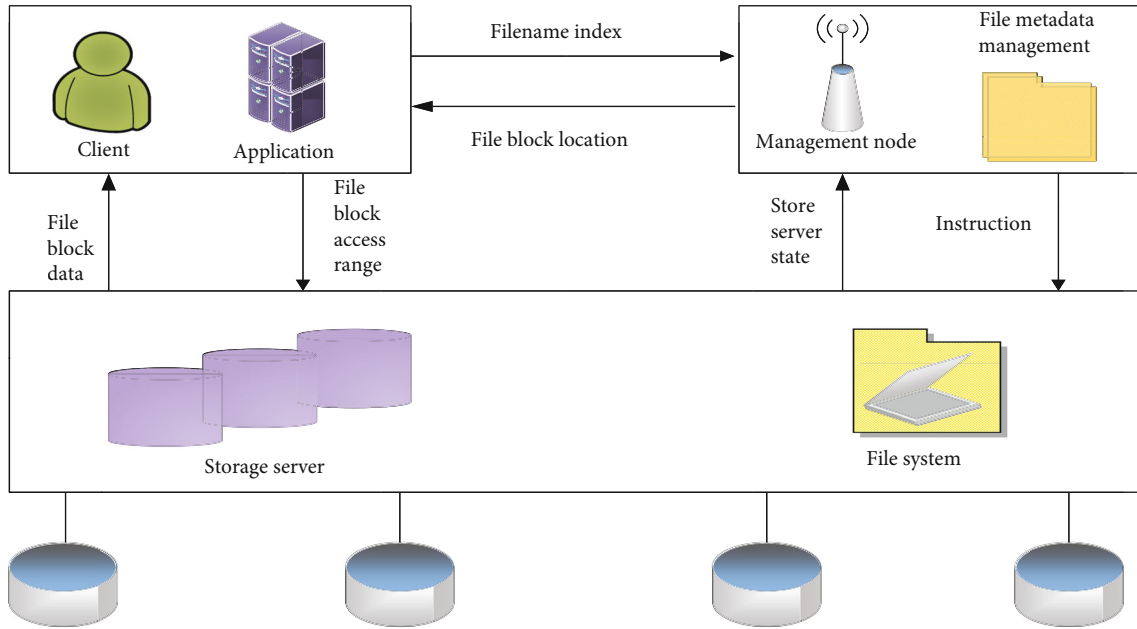


FIGURE 3: GFS system framework.

can meet the needs of the international trade industry to publish and operate network applications developed by enterprises. In addition, GFS is designed with the idea of storing files in blocks. Each block has a fixed size and is copied to multiple block servers simultaneously. It is located at the bottom of the core technology, which provides massive storage space for the international trade industry to facilitate large-scale trade in the international trade industry. The GFS architecture is shown in Figure 3.

As can be seen from Figure 3, the user logs in to the GFS client through the application and can input the file name to be searched into the management node. The file meta management center converts the transmitted data into instruction information through the node and transmits it to the storage server. After that, the storage server will return the data queried in the file system and its own status information to the file meta management center. The file element management center then returns the file location information to the user. After the whole process, users can easily and quickly obtain the files they want.

GFS is a scalable distributed file system for large, distributed applications that access large amounts of data. It runs on inexpensive commodity hardware and provides fault tolerance. It can provide services with high overall performance to a large number of users.

By traditional standards, the files are very large. Files up to several gigabytes in length are not uncommon. Each file usually contains many application objects. When frequently dealing with rapidly growing datasets of terabytes in length containing tens of thousands of objects, it is difficult to manage tens of thousands of kilobytes of file blocks, even if the underlying file system supports it. Therefore, the operating parameters and block size in the design must be reconsidered. The management of large files must be efficient, and it must also support small files, but it does not need to be optimized.

2.4. Data Flow Diagram of the International Trade Industry.

A data flow graph [18] uses a graphical tool to describe the flow of data input and output in an application. It uses a set of graphics or arrows to identify the input and output of the application, which can briefly and comprehensively describe the transmission process of information flow in the system. A data flow diagram treats the system as a complete entity. After the user inputs their own request information, the system processes the information and then outputs it to the user. The data flow diagram of the international trade industry is shown in Figure 4.

As can be seen from Figure 4, the user can add, delete, modify, and check the six functional modules. The six functional modules also send commands to the database. After that, the database will return the data to the function module, and the function module will return the query result to the user. These six functional modules can meet the needs of users to a large extent.

2.5. Cloud Computing Task Scheduling Module. Cloud service management [19] usually consists of two processes: One is the source-based conference management direction, and the other is the user service query analysis center. The cloud computing components are shown in Figure 5.

As can be seen from Figure 5, after the user submits the service request, the user service analysis company collects and analyzes the access functions. It sorts the queue according to the user's deadline, finds available resources, and calculates the execution of the corresponding work queue resources. Cloud source management has two main functions. One is to regularly check and update any source information to the cloud proxy server, and the other is to hold meetings of relevant sources to perform tasks. The pheromone is updated every time when the task is completed. The computing source corresponding to the component is periodically sent to the cloud source directory for storage.

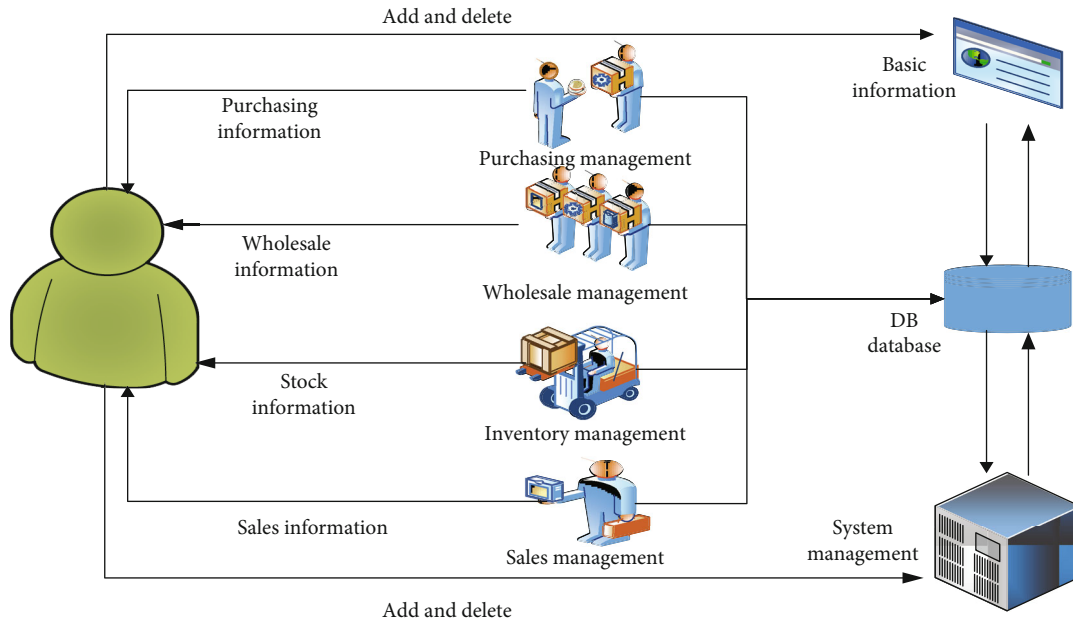


FIGURE 4: Data flow diagram of the international trade industry.

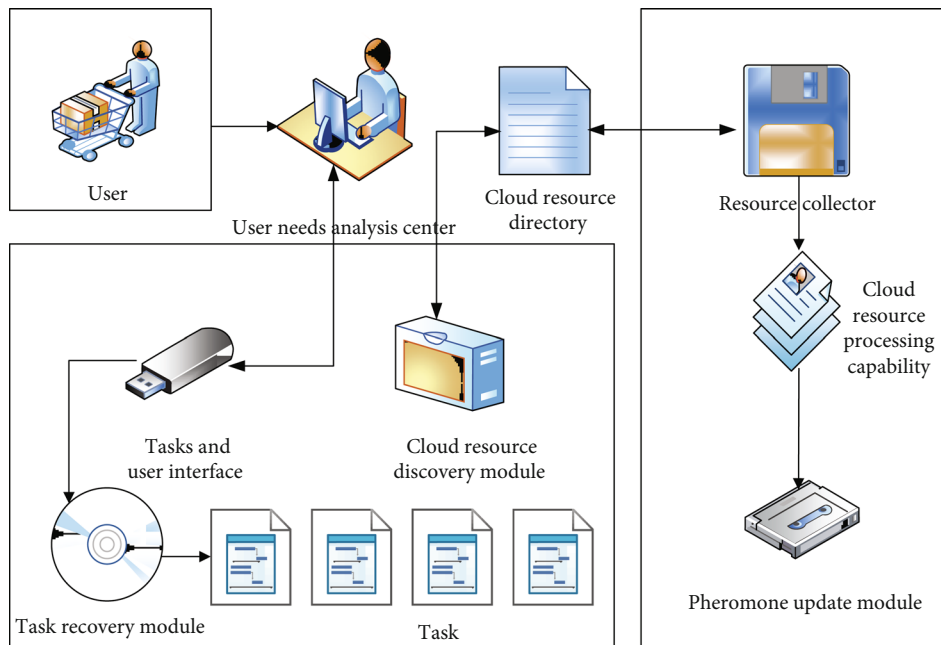


FIGURE 5: Cloud computing task scheduling module diagram.

3. Algorithm Research of the International Trade Industry Based on Cloud Computing and Internet of Things

3.1. Network Throughput. The data in the network is composed of data packets, and the processing of each data packet by the firewall consumes resources. Throughput is the maximum rate a device can accept without frame loss. The test method is as follows: send a certain number of

frames at a certain rate during the test, and calculate the frames transmitted by the device under test. If the number of frames sent is equal to the number of frames received, then the sending rate and retest are increased; if the frame is received, if there are fewer than sending frames, reduce the sending rate and retest until the final result is obtained. Throughput test results are expressed in bits per second or bytes per second.

Network throughput [20] is an important metric used in many grid experiments. It represents the sending process

from the beginning of sending data information to the destination node in the continuous process of a node or unit in the running mode. It is shown in the following:

$$th = \frac{pkt_byte_sum[x]}{end_time[x] - time[x-1]} \times 8/100. \quad (1)$$

Among them, th is the throughput of the network, $pkt_byte_sum[x]$ is the size of the data packet sent by process x , $end_time[x]$ is the time when process j receives the data packet, and $end_time[j-1]$ is the time of the last received packet.

3.2. Membership. In the normal cloud model, the degree of membership obeys a normal distribution with expected entropy En and farsightedness He as standard deviations, i.e., $N[En, (He)2]$, which satisfies the degree of participation from x to C .

$$\mu(x) = \exp \left[-\frac{(x - Ex)^2}{2(E_n')^2} \right]. \quad (2)$$

x is the actual value, E_n' obeys the $E_n' \sim N[En, (He)2]$ distribution, and the value of He is smaller than the value of En . Therefore, when calculating $\mu(x)$, En can be used instead of E_n' .

3.3. Combinatorial Optimization Problem. Combinatorial optimization [21] is an optimization problem that studies different variables. The knapsack problem is an important part of the overall optimization, and it is also the most studied problem in the current overall optimization problem. The knapsack problem is how to choose within a limited total volume to maximize the total value of items. It can be formulated as a linear program as follows:

$$KP \begin{cases} \max \sum_{m=1}^n p_m x_m \\ s, t \begin{cases} \sum_{m=1}^n w_m x_m \leq c \\ x_m \in \{0, 1\} x = 1, \dots, n. \end{cases} \end{cases} \quad (3)$$

n is the number of items, and p_i , w_i , and $m \in N = \{1, \dots, n\}$ are the value and weight of item m , respectively. c is a positive integer and is the capacity of the knapsack.

3.4. Wavelet Transform Function. Wavelet transform is a new transform analysis method. It inherits and develops the idea of localization of short-time Fourier transform, at the same time, overcomes the shortcomings of window size that does not change with frequency, can provide a "time-frequency" window that changes with frequency, and is an ideal tool for signal time-frequency analysis and processing.

$$E_{a,b}(t) = \frac{1}{\sqrt{a}} E \left(\frac{t-b}{a} \right). \quad (4)$$

E is the wavelet function.

3.5. Wavelet Packet Function.

$$C_E = 2\pi \int_{-\infty}^{+\infty} \frac{|E(\varphi)|^2}{|\varphi|} dt < \infty. \quad (5)$$

3.6. Continuous Wavelet Transform (CWT) Function. The CWT function is a transformation method proposed on the basis of the short-time Fourier transform. Its definition is shown in the following formula.

$$CWT(a, b) = \int_{-\infty}^{+\infty} f(t) E_{a,b}(t) dt. \quad (6)$$

3.7. Continuous Wavelet Inverse Transform. The continuous inverse particle transform can reconstruct the time domain signal with the particle transform coefficients. Its calculation formula is as follows.

$$f(t) = \frac{1}{C_\varphi} \int_{-\infty}^{+\infty} \int_{-\infty}^{+\infty} CWT(a, b) E_{a,b}(t) \frac{dad b}{a^2}. \quad (7)$$

3.8. Discrete Wavelet Function. Because the continuous wavelet transform has continuity, it needs to be discretized in the practical application of the computer. The calculation formula of the discretized wavelet function is shown below.

$$E_{j,k}(t) = a^{-j/2} E \left(\frac{t - ka_0^j}{a_0^j} \right). \quad (8)$$

3.9. Split Index. The SPRINT algorithm uses the Gini index as the segmentation criterion. For attribute selection criteria, the Gini index algorithm takes the purity of the dataset as the attribute selection criteria. The formula for calculating the Gini index of node t is

$$G(t) = 1 - \sum_{i=0}^{G-1} [P(i|t)]^2. \quad (9)$$

3.10. Cluster Head Algorithm. In the cluster head selection step, a random number between 0 and 1 is the basis of the cluster head node n . The threshold T is

$$T(n) = \begin{cases} \frac{P}{1 - p \times (m(1/p))} n \in G \\ 0. \end{cases} \quad (10)$$

3.11. Classification of Intelligence Level. According to the heterogeneous characteristics of IoT nodes, it classifies the intelligence level of nodes. It treats a high-intelligence node as the sum of multiple low-intelligence nodes, increasing the probability of a high-intelligence node becoming the head. The intelligence level of the node is defined in the randomly distributed interval $[W, amaxW]$. $amax$ is a multiple of the ratio of the nodes with the highest intelligence level to

the nodes with the lowest intelligence level. For any node s_i , its intelligence is $\alpha_i W$. So the total intelligence is

$$W = \sum_{j=1}^N \partial_j W. \quad (11)$$

3.12. Detection Probability Model.

$$p(x, y) = e^{-ad}. \quad (12)$$

a is the physical property of the sensor. IoT is assumed to be a wireless sensor network with n sensors. The weighting factors for each sensor are W_1, W_2, \dots . Here, $x = 1, 2, 3 \dots n$, $y = 1, 2, 3 \dots m$, and m is the similarity algorithm for the number of monitoring targets.

$$S = \frac{\sum_{i=1}^a A_i B_i}{\sqrt{\sum_{i=1}^a A_i^2} \sqrt{\sum_{i=1}^a B_i^2}}. \quad (13)$$

3.13. *Hash Algorithm.* The hash algorithm has the advantage of fast lookup time, and the formula is shown in (14).

$$H[i] = H[i - 1] \times x + s[i]. \quad (14)$$

3.14. Classical Information Theory.

$$w = p \times \log_2 \frac{1}{p} + q \times \log_2 \frac{1}{p}. \quad (15)$$

Among them, p is the probability that a given item identifier obeys the rules, and q is the probability that it does not conform to the rules.

3.15. Signal Strength Algorithm.

$$S = \frac{1}{n} \sum_{i=1}^n S_i. \quad (16)$$

Among them, S_i represents the signal strength of each node, and n represents the number of hops. S represents the average signal degree on the entire path, and the larger the S of the path, the more reliable the path is.

3.16. Signal Gap Algorithm.

$$D^2 = \frac{1}{n} \sum_{i=1}^n \left(S_i - \frac{\sum_{i=1}^n S_i}{n} \right)^2. \quad (17)$$

The formula represents the size of the gap between the signal strengths of each node on a path. The smaller D^2 is, the better the signal strength distribution of the nodes on the path is.

3.17. Fitness Function.

$$F(y_i) = \frac{1}{n} \sum_{j=1}^n (O_i - T_j)^2. \quad (18)$$

In the formula, O_i, T_i is the j th predicted output and actual output, and n is the total amount of data.

3.18. *ACO Algorithm.* The ACO algorithm is a swarm intelligence algorithm. When simulating foraging ants, the ants choose the walking direction according to the pheromone concentration and plan the optimal path.

$$y_i = \frac{1}{m} \sum_{j=1}^m (O_j - T_j)^2. \quad (19)$$

4. International Trade Industry Development Policy Process

Since this paper is a research on the development policy of the international trade industry based on the background of cloud computing and the Internet of Things, it is difficult to conduct questionnaire surveys and interviews in the field to obtain specific survey data. The main research method of this paper is to conduct relevant data queries on the Internet. With the proposal and continuous construction of the "One Belt, One Road" plan, the international trade industry is constantly faced with opportunities and challenges. The various development policies proposed in the Belt and Road Initiative to seize opportunities and meet challenges also apply to the development of international trade. It inquired about the "Belt and Road" construction and development policies and searched for the fiscal policy, financial policy, investment and trade cooperation policy, customs policy, and transportation policy in the past seven years. It integrates data, conducts research on the development policy of the international trade industry, and conducts a summary analysis [22, 23].

5. Results of the International Trade Industry Development Policies

Today is the era of cloud computing, and international business still faces some challenges. Only by constantly researching and developing policies can we seize opportunities and anticipate challenges and make the international market invincible. In addition, in the context of the Internet of Things, if the international trade industry wants to develop better, it must learn to analyze and use the relevant development policy data provided by cloud computing [24]. In order to better study development policies in the context of cloud computing and the Internet of Things, this paper studies and analyzes international trade data from 2015 to 2021.

5.1. *Fiscal and Tax Payment Policies in the Context of Cloud Computing and IoT.* In the construction of the international trade industry, the fiscal policy can play a very key positive role, and the fiscal and tax payment policy is an important

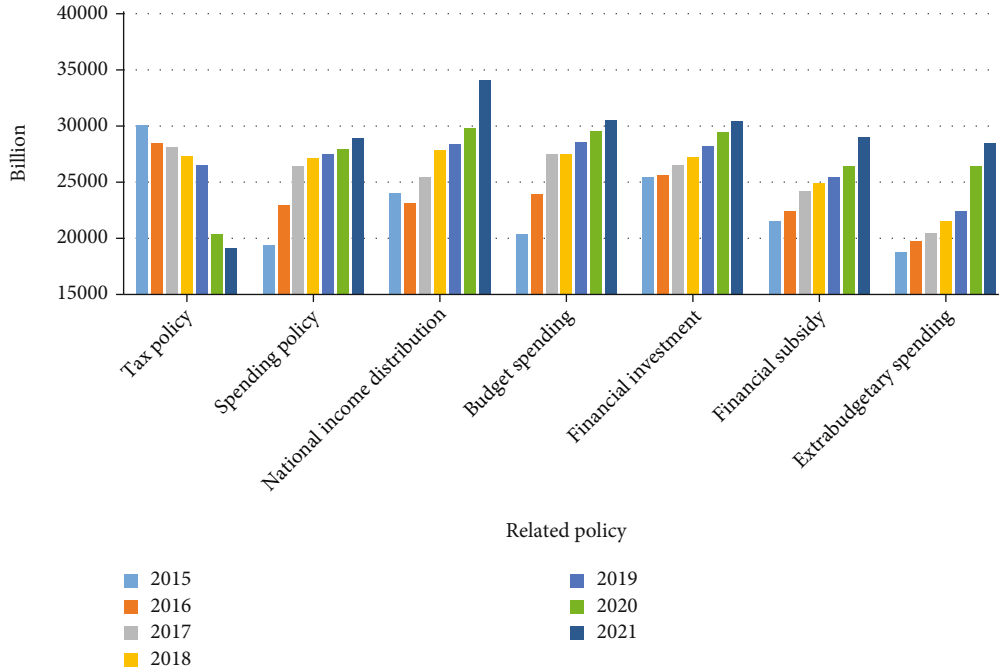


FIGURE 6: Fiscal and tax payment policies in the context of cloud computing and IoT.

part of the fiscal policy [25]. In order to examine the effect of fiscal and tax payment policies on the international trade industry, this paper selects relevant data from 2015 to 2021. The specific data is shown in Figure 6.

As can be seen from Figure 6, from 2015 to 2021, in order to support the development of the international trade industry, the amount of government taxes on it has decreased year by year, while the amount of expenditure and national income distribution has continued to increase. In addition, in order to strengthen the infrastructure construction of the international trade industry, its budgetary and extrabudgetary expenditures on international trade are also increasing. The biggest purpose of increasing financial investment and financial subsidies is to promote the prosperity and development of the international trade industry [26]. Through data analysis, it can be seen that the fiscal and tax payment policy in the context of cloud computing and the Internet of Things can greatly promote the economic development of the international trade industry.

5.2. Financial Payment Policy in the Context of Cloud Computing and IoT. The construction of the international trade industry requires a lot of financing support, and cooperation with other countries will also form a large amount of currency circulation [27]. The financial payment policy in the context of cloud computing and the Internet of Things provides strong support for the financing of the international trade industry. The specific data is shown in Figure 7.

As can be seen from Figure 7, in the financial payment policy in the context of cloud computing and the Internet of Things, in order to better support the financing of the international trade industry, the statutory reserve ratio continues to decrease. The proportion of open market business has increased year by year, and the exchange rate has fluctuated

and developed with the changes in the international situation. In addition, the interest rate of demand deposits in recent years has been significantly lower than the interest rate of time deposits. It increases household savings and increases financing for the international trade industry. Through data analysis, it can be seen that the financial payment policy in the context of cloud computing and the Internet of Things plays an important role in industrial financing [28, 29].

5.3. Investment and Trade Cooperation Policies in the Context of Cloud Computing and IoT. Investment and trade cooperation is an important means to promote the construction of the international trade industry and plays a very important role. Investment and trade cooperation requires all parties to study and solve investment and trade facilitation issues, eliminate investment and trade barriers, build a good business environment, jointly negotiate the construction of free trade zones, stimulate and release cooperation potential, and promote trade development. The investment and trade cooperation policy in the context of cloud computing and IoT is shown in Figure 8.

It can be seen from Figure 8 that the investment and trade cooperation policy in the context of cloud computing IoT can provide the international trade industry with trade information of various neighboring countries. It allows the industry to choose partners independently. Among them, Singapore and Russia are countries that can cooperate deeply. India and Thailand are countries that can accelerate cooperation. The Philippines and Poland are countries that can gradually expand cooperation. Countries to be strengthened are like Mongolia and Egypt. However, a higher cooperation index does not mean a higher trade potential and level. Factors such as trade environment and risks should also be considered. The investment and trade cooperation policy in the context of

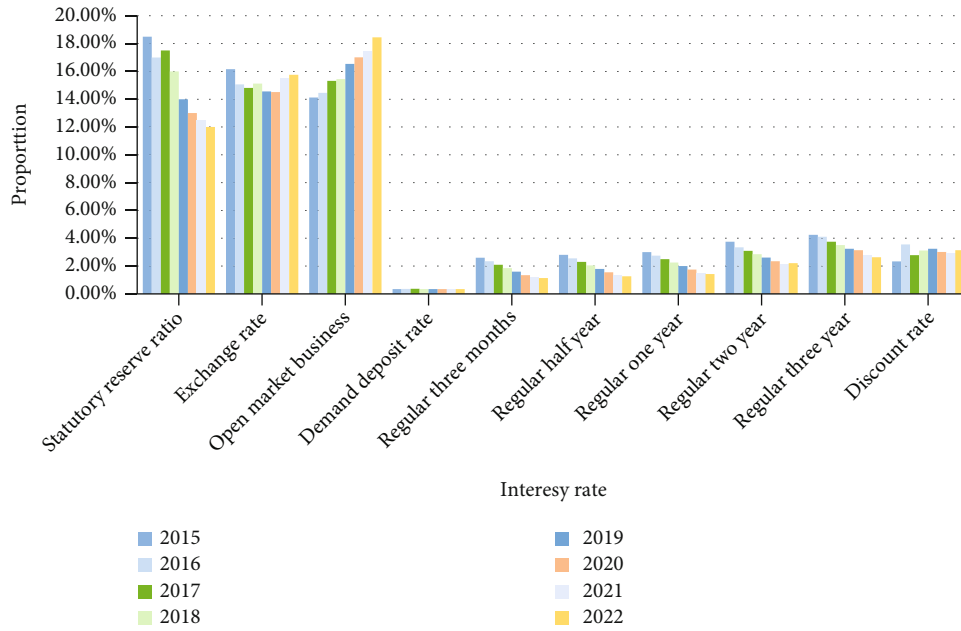


FIGURE 7: Financial payment policies in the context of cloud computing and IoT.

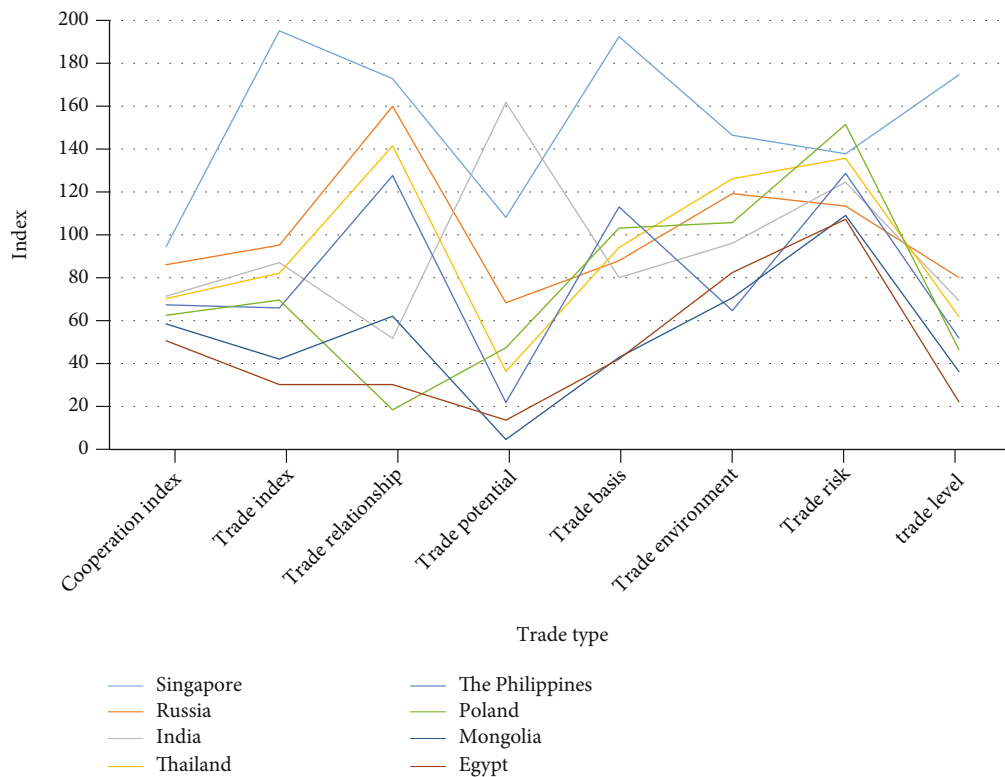


FIGURE 8: Investment and trade cooperation policies in the context of cloud computing and IoT.

cloud computing and IoT can reasonably avoid trade risks for the international trade industry, strengthen international cooperation, and promote trade development.

5.4. Customs Support Policies in the Context of Cloud Computing and IoT. The proposal of the customs support policy also has a very important role and significance for

the development of the international trade industry. The comparative data before and after the customs payment policy is shown in Figure 9.

As can be seen from Figure 9, the data comparison before and after the customs payment policy is very obvious. Before the customs payment policy was proposed, the processing efficiency of the annual trial plan of the international

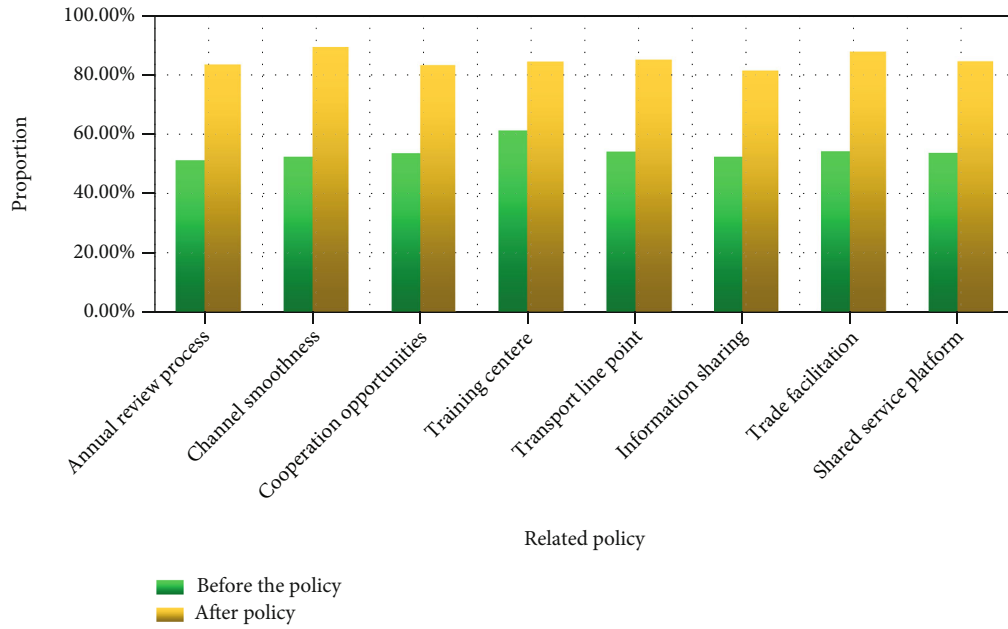


FIGURE 9: Comparative data before and after the customs payment policy.

trade industry was only about 50%. After the policy was proposed, the handling efficiency of the annual trial plan can reach more than 80%, which greatly facilitates the handling of the annual trial plan of the international trade industry. In addition, smooth channels, cooperation opportunities, and the construction of training centers have all been greatly improved after the customs payment policy was proposed, which has promoted the facilitation of international trade.

5.5. *Transportation Support Policies in the Context of Cloud Computing and IoT.* Supporting transportation is key to the rapid development of the international trade industry. Only by continuously developing and paying for transportation and proposing special transportation support policies can international trade really play a role in promoting economic development along the coast. The specific data is shown in Figure 10.

It can be seen from the data in Figure 10 that from 2015 to 2021, the construction rate of railways and highways has been increasing. This shows that today’s transportation infrastructure is constantly being improved, greatly improving the transportation efficiency of the international trade industry. In addition, in the transportation support policy in the context of cloud computing and the Internet of Things, the prediction accuracy of direction is as high as 60%. It can facilitate the international trade industry to choose the mode of transportation according to their needs.

6. Results of the International Trade Industry Development Policy

With the continuous development of the economy, cloud computing and the Internet of Things are getting more and more attention. Due to the multiple advantages of cloud

computing and the Internet of Things, they have also been widely used in China and are suitable for use in various industries. Especially in the process of international trade development, the application of cloud computing and Internet of Things technology can make development policies meet the needs of the international trade industry to the greatest extent. Accordingly, this paper examines the development policies of the international trade industry in the context of cloud computing and the Internet of Things. The investigation has certain practical significance.

- (1) Fiscal and taxation support policies in the context of cloud computing and the Internet of Things. Through the transportation support policy, a tax-related information sharing platform covering various regions, customs, economic, and trade departments can be established. It strengthens the monitoring of tax sources, timely reminds the trade industry of abnormal water wading, and helps the industry to reasonably avoid tax risks. At the same time, it increases investment and subsidies for the construction of the international trade industry through expansionary fiscal policies, expands the scale of international trade, and promotes economic development
- (2) Financial support policies in the context of cloud computing and IoT. Financial support policies can not only play a fundamental and decisive role in the allocation of market resources but also respond to the financial needs of the international trade industry during the development process. Making good use of the financial support policy in the context of cloud computing and the Internet of Things can provide strong financial support for the international trade industry

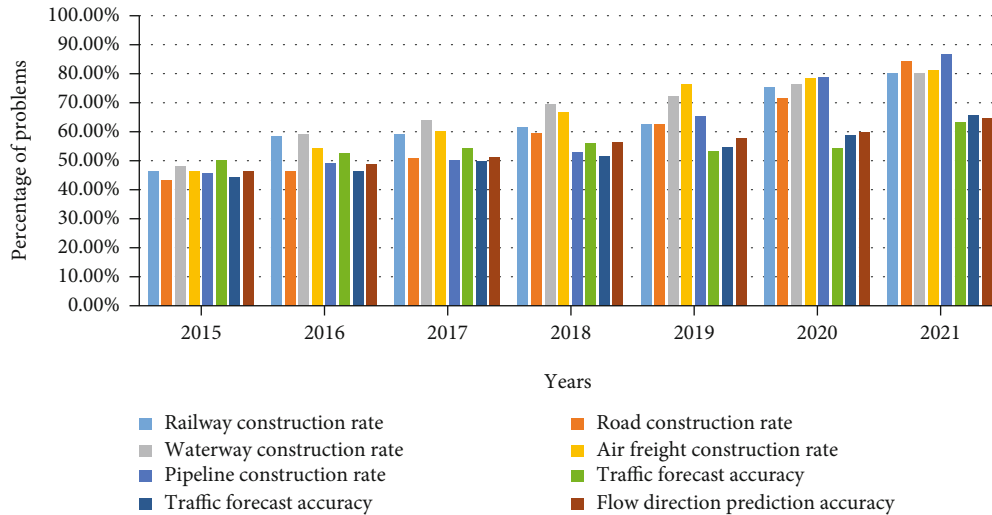


FIGURE 10: Construction results of transportation support policies.

- (3) Supporting policies for investment and trade cooperation in the context of cloud computing and Internet of Things. Investment and trade cooperation support policies play an important role in improving the level of trade liberalization and facilitation. It strengthens cooperation on supply chain security and facilitation, reduces nontariff barriers, and lays a solid foundation for deepening bilateral and multilateral cooperation
- (4) Customs support policy in the context of cloud computing IoT. The customs support policy can further strengthen the cooperation between international customs, realize the interconnection between international customs, effectively promote trade facilitation, and promote the process of regional economic development. In addition, the customs support policy also gives priority to the annual trial plan of the regions along the international trade route. This facilitates the international trade industry to innovate and enrich cooperation mechanisms and strengthen security cooperation with customs of countries along the route
- (5) Transportation support policies in the context of cloud computing and the Internet of Things. Transportation plays a key role in supporting economic development. The proposal of the transportation support policy has laid a strong foundation for promoting the construction of interconnected transportation infrastructure and the construction of the Maritime Silk Road Corridor. In addition, transportation policy supports the internationalization and integration of transportation services in addition to supporting large transportation projects and node construction. It actively develops transport service trade and promotes the development of international trade economy

trade. It plays an important role in promoting the development of the national economy and enhancing the regional economic capacity of the region. This paper studies the industrial development policy of international trade in the context of cloud computing and the Internet of Things and actively explores effective measures to promote the development of global trade. By promoting the development policy of high-tech enterprises, it will transform the development of the international trade industry from small-scale development to large-scale development and comprehensively transform the economic system in the field of international trade. Actively building the development policy of the international trade legal system is the most basic condition to ensure the smooth flow of international trade. Only by actively building an international trade legal system can we create opportunities for global business development and create a better environment for the global market. In addition, development policies that formulate trade strategies can promote healthy and rapid growth in international trade. If it is to trade globally, it must comply with international standards. It is necessary to study global trade rules, improve the quality of certain services according to customs, and actively explore new markets for international trade. At the same time, it is necessary to deepen economic exchanges between countries through regional cooperation, strengthen relations between countries, and lay a solid foundation for long-term cooperation. Through its many regional partners, it can continue to open its markets to international trade, which to a certain extent diversifies international trade. In the future international trade, in addition to actively participating in global trade, it is necessary to formulate environmental trade standards, expand interregional cooperation, and maintain cooperation with developing countries in the region.

7. Conclusion

The development policy of the international trade industry is directly related to the overall development of international

Data Availability

The data that support the findings of this study are available from the corresponding author upon reasonable request.

Conflicts of Interest

The authors declared no potential conflicts of interest with respect to the research, authorship, and/or publication of this article.

References

- [1] Y. P. Hu, I. C. Chang, and W. Y. Hsu, "Mediating effects of business process for international trade industry on the relationship between information capital and company performance," *International Journal of Information Management*, vol. 37, no. 5, pp. 473–483, 2017.
- [2] M. Cheng, G. Yang, X. L. Chi, and M. T. Xin, "Research on competitiveness of traditional Chinese medicine industry's international trade based on diamond theory," *Zhongguo Zhong Yao Za Zhi*, vol. 44, no. 1, pp. 199–203, 2019.
- [3] H. O. Chang, "How do natural and man-made disasters affect international trade? A country-level and industry-level analysis," *Journal of Risk Research*, vol. 20, no. 2, pp. 195–217, 2017.
- [4] R. Rijesh, "International trade and productivity growth in Indian industry: evidence from the organized manufacturing sector," *Journal of South Asian Development*, vol. 14, no. 1, pp. 1–39, 2019.
- [5] M. Smith, S. Gorgoni, and B. Cronin, "International production and trade in a high-tech industry: a multilevel network analysis," *Social Networks*, vol. 59, no. 7, pp. 50–60, 2019.
- [6] I. A. Guliyev, E. T. Mekhdiev, and I. Litvinyuk, "Global refining industry in retrospect, and evaluation of Russia-EU petroleum products' trade perspectives," *International Journal of Energy Economics and Policy*, vol. 7, no. 5, pp. 209–216, 2018.
- [7] Y. Ishii, "Dumping in a product differentiated reciprocal trade industry emitting global pollution," *Journal of International Trade & Economic Development*, vol. 26, no. 2, pp. 195–208, 2017.
- [8] R. Deng, R. Lu, and C. Lai, "Optimal workload allocation in fog-cloud computing toward balanced delay and power consumption," *IEEE Internet of Things Journal*, vol. 3, no. 6, pp. 1171–1181, 2017.
- [9] W. Wei, X. Fan, H. Song, X. Fan, and J. Yang, "Imperfect information dynamic Stackelberg game based resource allocation using hidden Markov for cloud computing," *IEEE Transactions on Services Computing*, vol. 11, no. 1, pp. 78–89, 2018.
- [10] H. Yi, J. Chan, and T. Alpcan, "Using virtual machine allocation policies to defend against co-resident attacks in cloud computing," *IEEE Transactions on Dependable & Secure Computing*, vol. 14, no. 1, pp. 95–108, 2017.
- [11] C. Stergiou and K. E. Psannis, "Recent advances delivered by mobile cloud computing and internet of things for big data applications: a survey," *International Journal of Network Management*, vol. 27, no. 3, pp. 1–12, 2017.
- [12] T. Hirai, H. Masuyama, and S. Kasahara, "Performance analysis of large-scale parallel-distributed processing with backup tasks for cloud computing," *Journal of Industrial & Management Optimization*, vol. 10, no. 1, pp. 113–129, 2014.
- [13] S. Wang, J. Zhou, J. K. Liu, J. Yu, J. Chen, and W. Xie, "An efficient file hierarchy attribute-based encryption scheme in cloud computing," *IEEE Transactions on Information Forensics and Security*, vol. 11, no. 6, pp. 1265–1277, 2016.
- [14] A. Barsoum and M. A. Hasan, "Provable multicopy dynamic data possession in cloud computing systems," *IEEE Transactions on Information Forensics & Security*, vol. 10, no. 3, pp. 485–497, 2015.
- [15] Z. Xia, X. Wang, L. Zhang, Z. Qin, X. Sun, and K. Ren, "A privacy-preserving and copy-deterrence content-based image retrieval scheme in cloud computing," *IEEE Transactions on Information Forensics & Security*, vol. 11, no. 11, pp. 2594–2608, 2016.
- [16] A. M. R. Ulil, S. S. Fiannurdin, A. Tjahjono, and D. K. Basuki, "The vehicle as a mobile sensor network base IoT and big data for pothole detection caused by flood disaster," *Science*, vol. 239, no. 1, article 012034, 2019.
- [17] I. A. Alameri and G. Radchenko, "Development of student information management system based on cloud computing platform," *Journal of Applied Computer Science & Mathematics*, vol. 11, no. 2, pp. 9–14, 2017.
- [18] J. Yin and X. Zhan, "Impact of bias-correction methods on effectiveness of assimilating SMAP soil moisture data into NCEP global forecast system using the ensemble Kalman filter," *IEEE Geoscience and Remote Sensing Letters*, vol. 15, no. 5, pp. 659–663, 2018.
- [19] D. R. Ganesh, "Determination of internet banking usage and purpose with explanation of data flow diagram and use case diagram," *International Journal of Management and Humanities*, vol. 4, no. 7, pp. 52–58, 2020.
- [20] S. Mostafavi and V. Hakami, "A stochastic approximation approach for foresighted task scheduling in cloud computing," *Wireless Personal Communications*, vol. 114, no. 1, pp. 901–925, 2020.
- [21] I. Dimitriou and N. Pappas, "Stable throughput and delay analysis of a random access network with queue-aware transmission," *IEEE Transactions on Wireless Communications*, vol. 17, no. 5, pp. 3170–3184, 2018.
- [22] E. L. Lawler, "Erratum: the traveling salesman problem: a guided tour of combinatorial optimization," *Journal of the Operational Research Society*, vol. 37, no. 6, pp. 655–655, 1986.
- [23] Y. Zhang, H. Huang, L. X. Yang, Y. Xiang, and M. Li, "Serious challenges and potential solutions for the industrial internet of things with edge intelligence," *IEEE Network*, vol. 33, no. 5, pp. 41–45, 2019.
- [24] Z. Lv and H. Song, "Mobile internet of things under data physical fusion technology," *IEEE Internet of Things Journal*, vol. 7, no. 5, pp. 4616–4624, 2020.
- [25] I. Cvitić, D. Peraković, M. Periša, and M. D. Stojanović, "Novel classification of IoT devices based on traffic flow features," *Journal of Organizational and End User Computing*, vol. 33, no. 6, pp. 1–20, 2021.
- [26] B. Zhang, K. Wen, J. Lu, and M. Zhong, "A top-K QoS-optimal service composition approach based on service dependency graph," *Journal of Organizational and End User Computing*, vol. 33, no. 3, pp. 50–68, 2021.
- [27] O. I. Khalaf and G. M. Abdulsahib, "Optimized dynamic storage of data (ODSD) in IoT based on blockchain for wireless sensor networks," *Peer-to-Peer Networking and Applications*, vol. 14, no. 5, pp. 2858–2873, 2021.
- [28] H. Zhao, P.-L. Chen, S. Khan, and O. I. Khalafe, "Research on the optimization of the management process on internet of things (IoT) for electronic market," *The Electronic Library*, vol. 39, no. 4, pp. 526–538, 2021.
- [29] S. Bharany, S. Sharma, S. Badotra et al., "Energy-efficient clustering scheme for flying ad-hoc networks using an optimized LEACH protocol," *Energies*, vol. 14, no. 19, p. 6016, 2021.

Research Article

Energy-Aware Intrusion Detection Model for Internet of Vehicles Using Machine Learning Methods

Lu Lihua 

School of Computer Science, Northwest Polytechnic University, Xi'an, 710129 Shaanxi, China

Correspondence should be addressed to Lu Lihua; lihua1812@yahoo.com

Received 30 March 2022; Accepted 12 May 2022; Published 26 May 2022

Academic Editor: Nima Jafari Navimipour

Copyright © 2022 Lu Lihua. This is an open access article distributed under the Creative Commons Attribution License, which permits unrestricted use, distribution, and reproduction in any medium, provided the original work is properly cited.

With increasing development of Internet of Things (IoT) technology, wireless communications, big data, and smart applications, vehicular communications have become ubiquitous in smart cities, smart transportation systems, and Internet of Vehicles (IoV) environments. In this paper, a new Energy-aware Intrusion Detection System (EIDS) based on intelligent two-phase contract management model is presented for vehicle-to-vehicle (V2V) strategy in the IoV environments. In this strategy, the proposed EIDS predicts safe and energy-efficient end-to-end points for communication between existing vehicles in the IoV. The contract management process shows how the vehicles are connected together with a safe condition to transfer information. For prediction phase, a regression algorithm is applied to evaluate the proposed EIDS according to NSLKDD data set in the IoV environments. Simulation experiments show that the proposed regression-based EIDS strategy can effectively improve the accuracy and precision factors with 90% and 84%, respectively, and greatly minimize execution time by 4 seconds with respect to other machine learning algorithms.

1. Introduction

Today, vehicular communications have developed emerging topics on intelligent transportation systems with respect to wireless distribution and smart devices in the Internet of Things (IoT) environments [1, 2]. In the IoT, smart devices perform communication at different locations by providing a level of transparency among users and maintained an interconnected smart network. According to the main concept of the IoT [3], vehicular communications have wide collaboration between smart devices and big data on new intelligent concept of Internet of Vehicles (IoV) [4–6]. In the IoV environments, the communication model is divided into three statuses including vehicle to vehicle (V2V) [7, 8], vehicle to infrastructure (V2I) [9], and vehicle to people (V2P) [8, 10]. In these models, data transmission as an important problem statement has usually applied smart sensors and intelligent applications with minimum energy consumption to exchange and transfer the information between safety of vehicles [11], applications, devices, sensors, and peoples [12]. In this problem statement, Intrusion Detection Systems (IDS) have critical and emerging issues for support-

ing safety [13, 14], security [15], and privacy of data transmission [16] and information retrieval of intelligent transportation systems in the IoV [17]. The data transmission accumulated by V2V, V2I, and V2P case studies [8, 18, 19] can be managed securely to provide various cloud-edge services such as road safety, smart parking reservations, traffic management, vehicular routing management, and emergency issues [20].

According to the above critical problem statements on the IoV environments, this paper presents a new Energy-aware Intrusion Detection System (EIDS) to provide safety conditions for data transmission between vehicles as a V2V case study to avoid the existing attacks and critical points. In this paper, a machine learning method is presented to predict optimal energy consumption between vehicles to transfer data with safe and secured infrastructure in the IoV environments. The main contributions of this research are shown as follows:

- (i) Proposing an energy-aware intrusion detection model for managing a safe data transmission method for V2V scenarios in IoV

- (ii) Applying regression algorithm as the machine learning method to predict optimal secured infrastructure in the IoV environments
- (iii) Increasing accuracy and precision factors for predicting existing attacks and critical points in the EIDS

The organization of the paper is presented as follows: Section 2 illustrates a comprehensive literature review for security-aware and energy consumption models in the IoT and intelligent transportation systems. Section 3 shows a conceptual model of the proposed energy-aware intrusion detection model based on regression algorithm. Section 4 presents simulation parameters and experimental results based on comparison of existing machine learning algorithms and discussion on evaluation factors, respectively. Finally, Section 5 provides a brief discussion on the experimental results, conclusion, and future works.

2. Related Work

In this section, some new relevant case studies are discussed and analyzed as a literature review for intrusion detection strategies using machine learning and evolutionary algorithms in the IoV, IoT, and vehicular ad hoc network (VANET). Many research studies have evaluated security-based cloud-edge service scheduling and allocation for energy-aware IoV systems [21–24].

Subba et al. [25] provided a theory and algorithm using the IDS framework for VANET security. VANETs have sensors and On-Board Units (OBUs). OBUs use Road Side Units (RSUs) and IEEE 802.11p for connecting vehicles. VANETs are susceptible to diverse kinds of network attacks so they used Intrusion Detection Systems (IDSs) to solve them. Some IDS properties are not suitable for VANET such as IDS traffic volume, bandwidth limitation, dynamic network topology, communication overhead, and scalability which need to be fixed. They presented a new clustering algorithm that produced constant vehicular clusters using vehicular data. The proposed Cluster Head (CH) selection algorithm is based on the Vickrey-Clarke-Groves method. They suggested a game theory-based multilayered intrusion detection framework for VANET to detect different kinds of attacks in VANET. They used NS3 and Simulation of Urban Mobility (SUMO) for simulation. Simulation of the interaction between the IDS and the malicious vehicle reduces the size of IDS traffic by embracing a probabilistic IDS showing strategy based on the Nash equilibrium of the game. The problem is that the proposed algorithm is for vehicles that stop or move slowly. Their future work is to present a dynamic clustering algorithm and also improve components and develop the project.

Kang et al. [26] and his team have proposed an extremely impressive accidental confirmation protocol that contains homomorphic encryption to permit any personal vehicle to self-produce every number of confirmed personalities to get complete obscurity in VANETs. The suggested protocol barricades vehicles by detecting every prohibited

person and increasing traceability. The purpose of this paper has been to propose an extremely effective accidental confirmation order in VANETs, the name of RAU+. The results of this paper show that their suggested RAU+ protocol is rather effective than another protocol and can efficiently decrease the network overhead. The disadvantage of this paper is that it requires more testing in the future to improve their protocol which can be spread to IoT schedules.

In [27], an authentication scheme has been proposed that has led to a complete summary of VANET, and it has been seen that this scheme meets VANET security requirements via security analysis. The signal phase is divided into two stages, and the previous calculation method is used to reduce the calculation cost in the signal stage. Road Side Unit (RSU) has been able to collect multiple signatures in a single unit, and the total length of the signature is a fixed size, which significantly reduces the transmission between the RSU and the application server and improves the verification efficiency for the application. In the next work, to reduce the cost of calculations and communications, the use of a lighter signature plan is considered.

Chen et al. [28] and his colleagues presented a new model based on barriers, and link performance on the highway is presented using the obstacle-based channel model. In this research, the authors have used Markov chain realistic channel model and dual-slop path loss model to evaluate this. Assessment measures can be referred to reliability and time. Evaluation and model of empirical results indicate that this system has effectiveness through security analysis and is also used to evaluate the end-end performance. The advantages of this project are using the real channel simulator, and its drawbacks can be pointed to the long-term connection time.

Zhang et al. [29] suggested a new design for the dissemination of safety messages for quality-based urban IoV provided for accurate estimation of connection probability among vehicles. In this model, the CFs algorithm is used. Simulation results represent a good approximation of the model and the superiority of this protocol. To evaluate the research, time and probability factors have been used. The advantages of this paper are the superiority of it is performing compared to similar studies, and its disadvantages can be referred to as delay.

In [30], the Media Access Control (MAC) program is deliberately based on multilateral cooperation to eliminate delays and data interference in the automotive network. The protocol transmits security data with the corresponding sensors installed along the road and sends the DA search packet in the SCHI gap to obtain RSU-covered car data. When transferring this data, the vehicle node, which has a security message for sending or receiving CCH gap subscribers and transferring nonaccident data, is obtained using the multifaceted reservation mechanism in the SCHI gap. With RSU coordination, security information is tracked by each node in order. To achieve the VANET terminal, RSU has played the role of wireless energy absorption, which has led to uninterrupted channel transmissions, reduced channel delays, and improved channel efficiency.

Yaqub et al. [31] provided a method named cooperative video retrieval scheme (CoRe). Streaming media has become a significant factor to satisfy VANET users, while downloading videos with proper qualities causes bandwidth consumption and may leave insufficient bandwidth for quality of service. To avoid such issues, the authors suggested a communicative system in which vehicles can request more bandwidth in case of sharing. They can ask another vehicle for bandwidth sharing, downloading a part of media, or forwarding the demanded video via a link. The system actually chooses a nearby neighbor vehicle to request, in order to preserve the V2V connection, and it must have sufficient bandwidth to share. Based on the results, CoRe helped users to obtain a better quality of the video. They decided to involve 5G and ICN technologies with a CoRe system in the future.

3. Proposed Method

In this section, a new energy-based vehicle-to-vehicle collaboration is presented. Then, a new IDS approach is applied for the proposed V2V strategy to check and analyze performance of the IoV environments using machine learning methods. In the IoV environments, vehicles collaborate together in a secured end-to-end capacity using IoT application smart devices, sensors, and interconnection methods. On existing interconnection and intraconnection methods, the security is a significant challenge for a safe condition on data transmission between vehicles in the IoV environments. On the other hand, energy consumption of IoT nodes is a critical issue that represents the performance evaluation of vehicular communications in IoV applications. Certainly, in this section, we present a new energy-aware intrusion detection method with respect to minimizing energy consumption of vehicles as a fundamental parameter in the IoV environments.

In the IoV environment, some important factors such as traffic road scheduling, the moving speed of vehicles [32], the density of vehicles movements, and the infrastructure of the network change dynamically. Based on the abovementioned factors, each data transmission strategy between two or more than three vehicles should be examined with energy consumption, delay, and response time metrics. According to the V2V strategy, each vehicle has a communication range for collaboration with other vehicles in the IoV environment. For creating a data transmission connection, energy consumption between two vehicles should be examined before the intraconnection protocol [33]. According to Equation (1), the earned energy factor for transmitting information between two vehicles is evaluated as follows [34, 35]:

$$EV_{ij} = (ET_i \times N_O) + (ET_j \times N_I), \quad (1)$$

where ET is the energy consumption for transmitting data in vehicles i and j , N_O is the number of transmission packets that is sent for each communication round, and N_I is the number of transmission packets that is received in each communication round [36, 37].

Also, the energy consumed in the data transmission between a vehicle and wireless server is calculated as follows according to the following equation [38]:

$$EW = (ET_i \times M) + (ES_j \times K), \quad (2)$$

where M is the number of sent or received packets for each communication round to the wireless server, ES_j is the energy consumption for transmitting data to the vehicle j , and K is the number of sent packets for each communication round.

The total energy consumption metric for one communication round between existing vehicles and servers is computed according to the following equation [39]:

$$ET = \left(\sum EV_{ij} \times NV \right) + \left(\sum EW \times NS \right), \quad (3)$$

where NV is the number of existing vehicles and NS is the number of existing wireless servers in a communication round.

To create a data transmission round, each vehicle as an active node in the IoV sends a request to the neighbors with a broadcast mode. Each other vehicle receives existing request and checks with information for all available candidates to transfer data between activated nodes. According to Figure 1, if a communication distance is higher than the communication range or there is no an activated vehicle in circle of requested vehicle, then targeted node sends request to the wireless server. After finding an appropriate and alive transmission link between existing vehicles and servers according to the V2V strategy [40], link establishment is considered to finalize data transmission link. Then, energy consumption of the established link is examined to check minimum energy consumption between all nodes including activated vehicles and wireless servers. According to Equation (1), the produced energy factor for transmitting information between two vehicles is evaluated. Also, based on Equation (2) [41], the energy consumed in the data transmission between the vehicle and wireless server is calculated. Finally, Equation (3) calculates the total energy consumption metric for one communication round between existing vehicles and the IoV servers. If there is an optimized energy-efficient established link for data transmission, then the intrusion detection method is applied. Otherwise, system reassigns finding transmission link between available vehicles and servers. When an optimized energy-efficient link is selected, the proposed intrusion detection method (EIDS) is activated [42, 43]. In this step, the regression algorithm as the proposed machine learning method selects applied data set for training process for detecting the malicious behaviors and attacks. The existing data set is divided into two sides; the first content is applied for train process as %70, and the other content %30 is evaluated for test process. In the train process, if intrusion detection has safe result for a transmitted link, then real data transmission and packets are transferred in this link. Otherwise, the selected link is unsafe for communication.

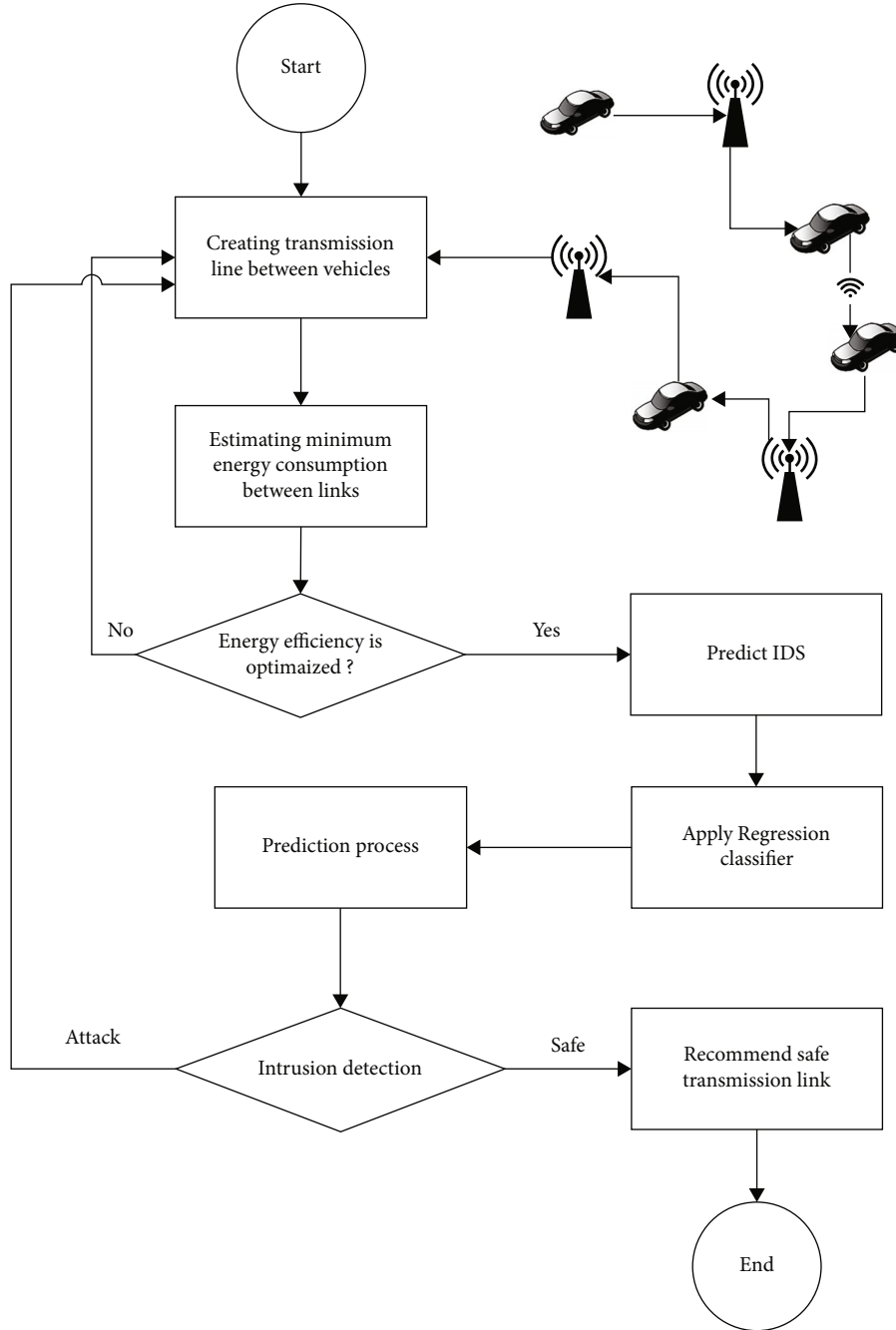


FIGURE 1: The EIDS flowchart based on regression prediction algorithm in IoV.

TABLE 1: Data set parameters.

Description	Train set	Test set
Attacks	3,925,650	250,436
Normal	972,781	60,591

According to the above mentioned framework, the proposed regression-based EIDS method checks minimum energy consumption for each selected transmission link and then proceeds intrusion detection process for existing data set.

4. Experimental and Simulation Results

This section proposes performance evaluation and comparison for the proposed EIDS with regression algorithm and other algorithms including the Support Vector Machine (SVM) [44], Random Forest (RF) algorithm [45], Multilayer Perceptron (MLP) algorithm [46], and Decision Tree (DT) algorithm [47]. We have applied the existing algorithms on the NSLKDD data set [48] as our case study (<https://www.unb.ca/cic/datasets/nsl.html>) with existing information. Also, WEKA toolkit [49] as simulation environment was used to evaluate the proposed EIDS case study using a

TABLE 2: Simulation parameters.

Description	Values (default)
Number of vehicles	10
Communication range between each vehicle	100, 200, 300, 400, 500
Environment dimension	50 * 50 * 50
Transmission rate (Mbps)	100

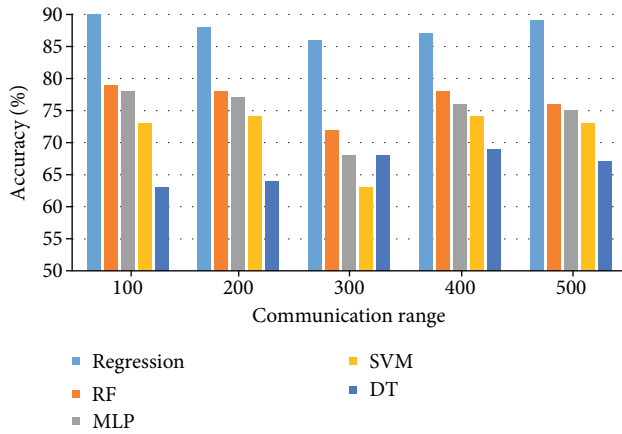


FIGURE 2: Evaluation of accuracy factor for energy-aware intrusion detection strategy in IoV.

TABLE 3: Prediction factors.

Prediction factor	Description
Accuracy	$\frac{TP + TN}{TP + TN + FP + FN}$
Precision	$\frac{TP}{TP + FP}$

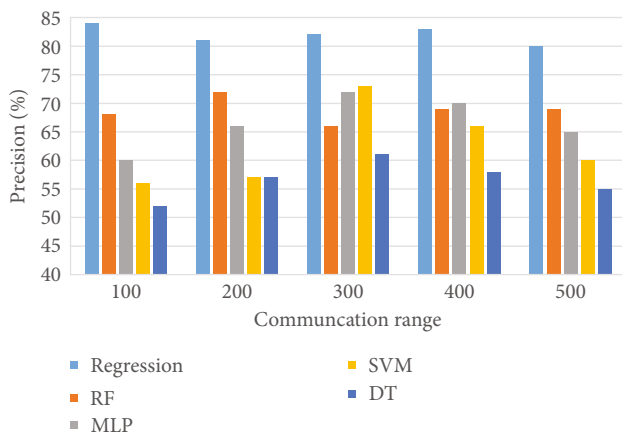


FIGURE 3: Evaluation of precision metric for energy-aware intrusion detection strategy in IoV.

system with Windows 10, Intel i5 3.10 GHz, 8 GB RAM. Also, a brief illustration about the applied NSLKDD data set is shown in Table 1 [50]. Then, the performance metrics used in the evaluation are introduced in Table 2.

According to the proposed Energy-aware IDS approach, we have presented a new regression-based prediction approach to detect minimum energy consumption for a data transmission procedure. For evaluating this procedure, some important prediction factors such as accuracy, precision, and execution time have been analyzed based on existing machine learning algorithms [51]. The experimental results evaluate important prediction factors including accuracy, precision, and execution time on the results of existing machine learning algorithms [52]. Table 3 shows prediction factors with respect to the following training parameters: True Positive (TP), True Negative (TN), False Positive (FP) [53], and False Negative (FN) metrics [54].

4.1. Simulation Results. We have simulated the proposed regression-based EIDS case study with respect to other algorithms in MATLAB environment that simulates the proposed prediction method for V2V strategy in the IoV environment. To evaluate the performance of the proposed algorithm, we considered five communication ranges between each vehicle for V2V strategy as 100, 200, 300, 400, and 500 in the IoV environment.

Figure 2 represents evaluation of accuracy factor with respect to each communication range step. According to the observed diagram, it can be achieved that the proposed regression-based EIDS has optimal score for the accuracy of prediction. The results obtained from the proposed regression-based EIDS method in the IoV were compared with other machine learning algorithms. This comparison on accuracy evaluation shows that the proposed regression-based EIDS has achieved a maximum accuracy factor of 90% for 10 vehicles. Moreover, another optimized machine learning algorithm is the RF algorithm that has approximately 78% accuracy higher than SVM, MLP, and DT prediction algorithms.

According to Figure 3, the proposed regression-based EIDS method has achieved higher precision metric for existing communication ranges between 80% and 85%. But the RF method has achieved only 74% just for communication range 200 with high precision, the SVM algorithm has shown 74% just for communication range 300, and the MLP algorithm has performed 71% of precision just for communication range 300 as best results for each prediction method. This evaluation illustrates that the DT algorithm has only a small amount of precision lower than 55% for detecting attacks in the IoV scenarios. With respect to this comparison, we conclude that the precision factor has different evaluation results with different communication ranges in other algorithms. However, the proposed regression-based EIDS method has attained maximum precision for the overall communication ranges.

Finally, to assess execution time of this prediction, we can observe that the proposed regression-based EIDS has gained 4.5 s for communication range 100, 6.2 s for communication range 200, 14.8 s for communication range 300, 18.9 s for communication range 400, and 20.2 s of execution time for communication range 500 according to Figure 4. So, the proposed method significantly has minimum execution time for the overall communication ranges. On the other

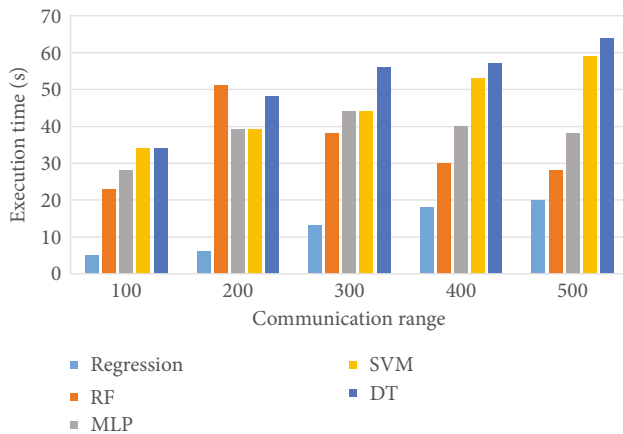


FIGURE 4: Execution time evaluation for the proposed EIDS strategy in the IoV environment.

hand, the execution time of DT algorithm is 69.8 s for communication ranges 300 and 500.

5. Conclusion

In this paper, a new Energy-aware Intrusion Detection System (EIDS) was presented for managing safe transitions and information in the IoV environments. Since the EIDS is based on prediction approach, machine learning techniques were applied to enhance quality of prediction for malicious and existing attacks according to train and test data sets with respect to low energy consumption for each vehicle. The experimental results have shown the efficiency performance of the proposed machine learning algorithms with minimum energy consumption, high accuracy, and maximum precision in the IoV environments. Also, the prediction time of the EIDS with the regression algorithm is lower than that of the other machine learning algorithms. Finally, the proposed algorithm guaranteed safe data transactions between the maximum numbers of vehicles in the IoV environments. In the future work, a new feature selection method for the effective predictable model in machine learning approach can be presented to optimize efficient accuracy and energy consumption with a high-quality priority in the vehicular communications.

Data Availability

The data that support the findings of this study are available from the NSLKDD data set as follows: <https://www.unb.ca/cic/datasets/nsl.html> [48].

Conflicts of Interest

The author declares that there are no conflicts of interest.

References

- [1] S. Babu and A. P. Raj Kumar, "A comprehensive survey on simulators, emulators, and testbeds for VANETs," *International Journal of Communication Systems*, vol. 35, no. 8, article e5123, 2022.
- [2] Z. Lv, L. Qiao, and I. You, "6G-enabled network in box for internet of connected vehicles," *IEEE Transactions on Intelligent Transportation Systems*, vol. 22, no. 8, pp. 5275–5282, 2021.
- [3] P. Sudhakaran, "Energy efficient distributed lightweight authentication and encryption technique for IoT security," *International Journal of Communication Systems*, vol. 35, no. 2, article e4198, 2022.
- [4] B. Cao, Z. Sun, J. Zhang, and Y. Gu, "Resource allocation in 5G IoV architecture based on SDN and fog-cloud computing," *IEEE Transactions on Intelligent Transportation Systems*, vol. 22, no. 6, pp. 3832–3840, 2021.
- [5] C. Zheng, Y. An, Z. Wang et al., "Knowledge-based engineering approach for defining robotic manufacturing system architectures," *International Journal of Production Research*, pp. 1–19, 2022.
- [6] H. Kong, L. Lu, J. Yu, Y. Chen, and F. Tang, "Continuous authentication through finger gesture interaction for smart homes using WiFi," *IEEE Transactions on Mobile Computing*, vol. 20, no. 11, pp. 3148–3162, 2021.
- [7] M. Shurrab, S. Singh, H. Otrok, R. Mizouni, V. Khadkikar, and H. Zeineldin, "An efficient vehicle-to-vehicle (V2V) energy sharing framework," *IEEE Internet of Things Journal*, vol. 9, no. 7, pp. 5315–5328, 2022.
- [8] A. R. Khan, M. F. Jamlos, N. Osman et al., "DSRC technology in Vehicle-to-Vehicle (V2V) and Vehicle-to-Infrastructure (V2I) IoT system for Intelligent Transportation System (ITS): a review," *Recent Trends in Mechatronics Towards Industry*, vol. 730, pp. 97–106, 2022.
- [9] P. Liu and W. D. Fan, "Exploring the impact of connected and autonomous vehicles on mobility and environment at signalized intersections through vehicle-to-infrastructure (V2I) and infrastructure-to-vehicle (I2V) communications," *Transportation Planning and Technology*, vol. 44, no. 2, pp. 129–138, 2021.
- [10] C. Zheng, Y. An, Z. Wang et al., "Hybrid offline programming method for robotic welding systems," *Robotics and Computer-Integrated Manufacturing*, vol. 73, article 102238, 2022.
- [11] J. Chen, Q. Wang, and J. Huang, "Motorcycle ban and traffic safety: evidence from a quasi-experiment at Zhejiang, China," *Journal of Advanced Transportation*, vol. 2021, 13 pages, 2021.
- [12] W. Zhou, J. Liu, J. Lei, L. Yu, and J. N. Hwang, "GMNet: graded-feature multilabel-learning network for RGB-thermal urban scene semantic segmentation," *IEEE Transactions on Image Processing*, vol. 30, pp. 7790–7802, 2021.
- [13] S. Khan, K. Kifayat, A. Kashif Bashir, A. Gurtov, and M. Hassan, "Intelligent intrusion detection system in smart grid using computational intelligence and machine learning," *Transactions on Emerging Telecommunications Technologies*, vol. 32, no. 6, article e4062, 2021.
- [14] J. Yu, L. Lu, Y. Chen, Y. Zhu, and L. Kong, "An indirect eavesdropping attack of keystrokes on touch screen through acoustic sensing," *IEEE Transactions on Mobile Computing*, vol. 20, no. 2, pp. 337–351, 2021.
- [15] M. Zhang, Y. Chen, and J. Lin, "A privacy-preserving optimization of neighborhood-based recommendation for medical-aided diagnosis and treatment," *IEEE Internet of Things Journal*, vol. 8, no. 13, pp. 10830–10842, 2021.
- [16] S. Zhao, F. Li, H. Li et al., "Smart and practical privacy-preserving data aggregation for fog-based smart grids," *IEEE*

- Transactions on Information Forensics and Security*, vol. 16, pp. 521–536, 2021.
- [17] Z. Lv, Y. Li, H. Feng, and H. Lv, “Deep learning for security in digital twins of cooperative intelligent transportation systems,” *IEEE Transactions on Intelligent Transportation Systems*, pp. 1–10, 2021.
- [18] J. Chen, Y. Liu, Y. Xiang, and K. Sood, “RPPTD: robust privacy-preserving truth discovery scheme,” *IEEE Systems Journal*, pp. 1–8, 2021.
- [19] Z. Li, L. Chen, L. Nie, and S. X. Yang, “A novel learning model of driver fatigue features representation for steering wheel angle,” *IEEE Transactions on Vehicular Technology*, vol. 71, no. 1, pp. 269–281, 2022.
- [20] B. Cao, W. Zhang, X. Wang, J. Zhao, Y. Gu, and Y. Zhang, “A memetic algorithm based on two_Arch2 for multi-depot heterogeneous-vehicle capacitated arc routing problem,” *Swarm and Evolutionary Computation*, vol. 63, article 100864, 2021.
- [21] B. Cao, J. Zhang, X. Liu et al., “Edge-cloud resource scheduling in space-air-ground-integrated networks for internet of vehicles,” *IEEE Internet of Things Journal*, vol. 9, no. 8, pp. 5765–5772, 2022.
- [22] H. Cheng, M. Shojafar, M. Alazab, R. Tafazolli, and Y. Liu, “PPVF: privacy-preserving protocol for vehicle feedback in cloud-assisted VANET,” *IEEE Transactions on Intelligent Transportation Systems*, pp. 1–13, 2021.
- [23] L. Zhang, H. Zheng, G. Cai, Z. Zhang, X. Wang, and L. H. Koh, “Power-frequency oscillation suppression algorithm for AC microgrid with multiple virtual synchronous generators based on fuzzy inference system,” *IET Renewable Power Generation*, 2022.
- [24] W. Yang, X. Chen, Z. Xiong, Z. Xu, G. Liu, and X. Zhang, “A privacy-preserving aggregation scheme based on negative survey for vehicle fuel consumption data,” *Information Sciences*, vol. 570, pp. 526–544, 2021.
- [25] B. Subba, S. Biswas, and S. Karmakar, “A game theory based multi layered intrusion detection framework for VANET,” *Future Generation Computer Systems*, vol. 82, pp. 12–28, 2018.
- [26] J. Kang, D. Lin, W. Jiang, and E. Bertino, “Highly efficient randomized authentication in VANETs,” *Pervasive and Mobile Computing*, vol. 44, pp. 31–44, 2018.
- [27] H. Zhong, S. Han, J. Cui, J. Zhang, and Y. Xu, “Privacy-preserving authentication scheme with full aggregation in VANET,” *Information Sciences*, vol. 476, pp. 211–221, 2019.
- [28] R. Chen, Z. Zhong, V. C. M. Leung, and D. G. Michelson, “Link connectivity under more realistic channel model for vehicle-to-vehicle communications,” *International Journal of Ad Hoc and Ubiquitous Computing*, vol. 22, no. 1, pp. 35–47, 2016.
- [29] X. Zhang, Q. Miao, and Y. Li, “An adaptive link quality-based safety message dissemination scheme for urban VANETs,” *IEEE Communications Letters*, vol. 22, no. 10, pp. 2104–2107, 2018.
- [30] H. Zhao, M. Zhang, K. Gao, T. Mao, and H. Zhu, “A multi-channel cooperative demand-aware media access control scheme in vehicular ad-hoc network,” *Wireless Personal Communications*, vol. 104, no. 1, pp. 325–337, 2019.
- [31] M. A. Yaqub, S. H. Ahmed, and D. Kim, “Asking neighbors a favor: cooperative video retrieval using cellular networks in VANETs,” *Vehicular Communications*, vol. 12, pp. 39–49, 2018.
- [32] Z. Liu, L. Fang, D. Jiang, and R. Qu, “A machine-learning based fault diagnosis method with adaptive secondary sampling for multiphase drive systems,” *IEEE Transactions on Power Electronics*, vol. 37, no. 8, pp. 8767–8772, 2022.
- [33] F. Meng, S. Yang, J. Wang, L. Xia, and H. Liu, “Creating knowledge graph of electric power equipment faults based on BERT-BiLSTM-CRF model,” *Journal of Electrical Engineering & Technology*, pp. 1–10, 2022.
- [34] J. Mou, P. Duan, L. Gao, X. Liu, and J. Li, “An effective hybrid collaborative algorithm for energy-efficient distributed permutation flow-shop inverse scheduling,” *Future Generation Computer Systems*, vol. 128, pp. 521–537, 2022.
- [35] B. Li, Y. Feng, Z. Xiong, W. Yang, and G. Liu, “Research on AI security enhanced encryption algorithm of autonomous IoT systems,” *Information Sciences*, vol. 575, pp. 379–398, 2021.
- [36] B. Cao, Y. Zhang, J. Zhao, X. Liu, L. Skonieczny, and Z. Lv, “Recommendation based on large-scale many-objective optimization for the intelligent internet of things system,” *IEEE Internet of Things Journal*, 2021.
- [37] Q. Sun, K. Lin, C. Si, Y. Xu, S. Li, and P. Gope, “A secure and anonymous communicate scheme over the Internet of Things,” *ACM Transactions on Sensor Networks (TOSN)*, vol. 18, no. 3, pp. 1–21, 2022.
- [38] L. Zhang, T. Gao, G. Cai, and K. L. Hai, “Research on electric vehicle charging safety warning model based on back propagation neural network optimized by improved gray wolf algorithm,” *Journal of Energy Storage*, vol. 49, article 104092, 2022.
- [39] K. Wang, H. Wang, and S. Li, “Renewable quantile regression for streaming datasets,” *Knowledge-Based Systems*, vol. 235, article 107675, 2022.
- [40] C. Zhao, F. Liao, X. Li, and Y. du, “Macroscopic modeling and dynamic control of on-street cruising-for-parking of autonomous vehicles in a multi-region urban road network,” *Transportation Research Part C: Emerging Technologies*, vol. 128, article 103176, 2021.
- [41] B. Li, J. Yang, Y. Yang, C. Li, and Y. Zhang, “Sign language/gesture recognition based on cumulative distribution density features using UWB radar,” *IEEE Transactions on Instrumentation and Measurement*, vol. 70, pp. 1–13, 2021.
- [42] Z. Lv, D. Chen, and H. Lv, “Smart city construction and management by digital twins and BIM big data in COVID-19 scenario,” *ACM Transactions on Multimedia Computing Communications and Applications*, 2022.
- [43] Z. Wu, J. Cao, Y. Wang, Y. Wang, L. Zhang, and J. Wu, “hPSD: a hybrid PU-learning-based spammer detection model for product reviews,” *IEEE transactions on cybernetics*, vol. 50, no. 4, pp. 1595–1606, 2020.
- [44] Y. Zhang, F. Liu, Z. Fang, B. Yuan, G. Zhang, and J. Lu, “Learning from a complementary-label source domain: theory and algorithms,” *IEEE Transactions on Neural Networks and Learning Systems*, pp. 1–15, 2021.
- [45] Z. Lv, D. Chen, H. Feng, W. Wei, and H. Lv, “Artificial intelligence in underwater digital twins sensor networks,” *ACM Transactions on Sensor Networks (TOSN)*, vol. 18, no. 3, pp. 1–27, 2022.
- [46] Z. Wu, C. Li, J. Cao, and Y. Ge, “On scalability of association-rule-based recommendation,” *ACM Transactions on the Web (TWEB)*, vol. 14, no. 3, pp. 1–21, 2020.
- [47] L. Liao, L. Du, and Y. Guo, “Semi-supervised SAR target detection based on an improved faster R-CNN,” *Remote Sensing*, vol. 14, no. 1, p. 143, 2022.

- [48] M. Tavallae, E. Bagheri, W. Lu, and A. A. Ghorbani, "A detailed analysis of the KDD CUP 99 data set," in *2009 IEEE symposium on computational intelligence for security and defense applications*, Ottawa, ON, Canada, 2009.
- [49] C. Liu, D. Wu, Y. Li, and Y. du, "Large-scale pavement roughness measurements with vehicle crowdsourced data using semi-supervised learning," *Transportation Research Part C: Emerging Technologies*, vol. 125, article 103048, 2021.
- [50] X. Wu, W. Zheng, X. Chen, Y. Zhao, T. Yu, and D. Mu, "Improving high-impact bug report prediction with combination of interactive machine learning and active learning," *Information and Software Technology*, vol. 133, article 106530, 2021.
- [51] W. Zheng, Y. Xun, X. Wu, Z. Deng, X. Chen, and Y. Sui, "A comparative study of class rebalancing methods for security bug report classification," *IEEE Transactions on Reliability*, vol. 70, no. 4, pp. 1658–1670, 2021.
- [52] G. Sun, Y. Cong, J. Dong, Y. Liu, Z. Ding, and H. Yu, "What and how: generalized lifelong spectral clustering via dual memory," *IEEE Transactions on Pattern Analysis and Machine Intelligence*, vol. PP, p. 1, 2021.
- [53] W. Zheng, J. Y. Cheng, X. Wu, R. Sun, X. Wang, and X. Sun, "Domain knowledge-based security bug reports prediction," *Knowledge-Based Systems*, vol. 241, article 108293, 2022.
- [54] L. Zhong, Z. Fang, F. Liu, B. Yuan, G. Zhang, and J. Lu, "Bridging the theoretical bound and deep algorithms for open set domain adaptation," *IEEE Transactions on Neural Networks and Learning Systems*, pp. 1–15, 2021.

Research Article

The Core Cluster-Based Subspace Weighted Clustering Ensemble

Xuan Huang,^{1,2} Fang Qin ,³ and Lin Lin⁴

¹Chengdu College of University of Electronic Science and Technology of China, Chengdu 611731, China

²The School of Information Science and Technology Southwest Jiaotong University, Chengdu 610031, China

³School of Information Science and Technology, Dalian University of Science and Technology, Dalian 116052, Liaoning, China

⁴College of Information Engineering, Chengdu Aeronautic Polytechnic, Chengdu 610100, China

Correspondence should be addressed to Fang Qin; qinfang@dlust.edu.cn

Received 24 January 2022; Accepted 18 April 2022; Published 24 May 2022

Academic Editor: Nima Jafari Navimipour

Copyright © 2022 Xuan Huang et al. This is an open access article distributed under the Creative Commons Attribution License, which permits unrestricted use, distribution, and reproduction in any medium, provided the original work is properly cited.

In recent years, the Internet of Things (IoT) technology has developed rapidly and is widely used in various fields. It is of great research significance to uncover underlying patterns and insights from the high-dimensional data of IoT, to excavate valuable information to guide people's production and life. Clustering can explore the natural cluster structure of the data, which is conducive to further understanding of the data, and is an essential preprocessing step for data analysis. However, clustering is highly dependent on the data. In order to reduce the complexity of the model, reduce the computational cost, and obtain a more robust clustering solution, we combine subspace clustering and ensemble learning to propose a novel subspace weighted clustering ensemble framework for high-dimensional data. The proposed framework first combines random feature selection and unsupervised feature selection to generate a set of base subspaces. Clustering is performed on each base subspace to achieve a set of subspace clustering solutions that generate a set of adaptive core clusters. The size of the core cluster is between the sample and the cluster. In the ensemble process, the core clusters are viewed as the basic unit, and the stability of the cluster is evaluated by measuring the distance between the core cluster pairs, and the similarity between the core clusters and the clusters in the base subspace, and then weighting the subspace clustering solution. Under this framework, we propose four subspace ensemble approaches based on core cluster to improve the accuracy of consensus clustering solutions. Extensive experiments are conducted on multiple real-world high-dimensional datasets, demonstrating that the proposed framework can process high-dimensional data for the IoT, and the proposed subspace clustering ensemble approaches are superior to the state-of-the-art clustering approaches.

1. Introduction

The Internet of Things is a network platform that combines various information collection devices and the Internet, which facilitates the sharing of information between various devices. Data acquisition devices are widely used in various application fields, and their collected data has the characteristics of high dimension. The impact of high-dimensional data on data mining is twofold. On the one hand, as the data dimension grows, there are more features that describe the sample from different perspectives, which brings richer and more comprehensive information to data analysis; on the other hand, high-dimensional data increases the complexity of the model and make data analysis difficult.

Clustering is an unsupervised learning technique that partitions unlabeled samples into clusters according to the specific criteria. Clustering can reveal the intrinsic properties of the study object and discover its underlying patterns. In the field of data mining and pattern recognition, clustering is often used as data preprocessing, which is the basis for subsequent data analysis. Clustering has always been an active research direction, and in different fields, there are existing multiple clustering algorithms and they achieve satisfactory results. But with the popularity of high-dimensional data, they pose a huge challenge to clustering.

Existing clustering approaches for high-dimensional data can initially be roughly divided into two categories: dimensionality reduction, and then clustering and subspace

clustering. The former typically uses feature selection or feature extraction techniques to extract features from a high-dimensional space that are relevant to subsequent clustering criteria, thereby reducing the dimensionality of the sample. Then, we performed the clustering in the lower-dimensional space. Subspace clustering assumes that the clusters of high-dimensional data are located in low-dimensional subspaces [1], and the goal is to find the clusters hidden in large dimensions.

Clustering is highly dependent on the data. As the dimensions increase, there are a large number of redundant and irrelevant features in the data. This makes the model more complex and the computational complexity grows exponentially. Different clustering algorithms are designed for different types of data, and they can discover the underlying structure of a particular data set, not valid for all types of data. Even with the same clustering algorithm, setting different parameters can group samples into different clusters. As a result, more researchers are focusing on clustering ensemble, trying to achieve better and more robust clustering results by merging multiple base clustering solutions. Recently, spectral clustering [2] has become one of the popular clustering approaches. It first calculates the similarity of the samples to construct an affinity matrix and then decomposes the Laplace vector of the affinity matrix to obtain the eigenvector associated with the feature values. The samples are then mapped to the lower-dimensional space for a final clustering solution.

Spectral clustering [3] can find clusters for complex samples, which is simple to implement and can achieve better results compared to traditional clustering approaches. Recently, some researchers have proposed clustering high-dimensional data through subspace clustering ensemble approaches [4–7]. Some of these employ spectral clustering approach [4, 5]. Cai et al. proposed the spectral clustering approach based on random subspace and graph fusion, termed SC-SRGF [5]. It combines the affinity graph of each subspace with the iterative similarity network fusion scheme and performs spectral clustering on the fusion matrix to obtain the final clustering solution. Huang et al. proposed multidiversified ensemble clustering (MDEC) [4], and under the proposed framework, consistent clustering solutions are obtained by performing spectral clustering, bipartite graph, and hierarchical clustering-based consensus function. These approaches [4–7] use random feature selection to generate a set of subspaces, that is, a certain proportion of features are randomly extracted from the original feature set to generate feature subset. The clusters of each subspace are ensemble to achieve the final clustering solution. However, these approaches [4–6] do not take into account the contributions of different feature subspaces during integration. Literature [7] considers the contribution of each subspace clustering solution in the ensemble process, but it selects members with larger contributions to participate in ensemble. This ensemble selection strategy ignores the feature subspace of small contributions, which is easy to bias the clustering results.

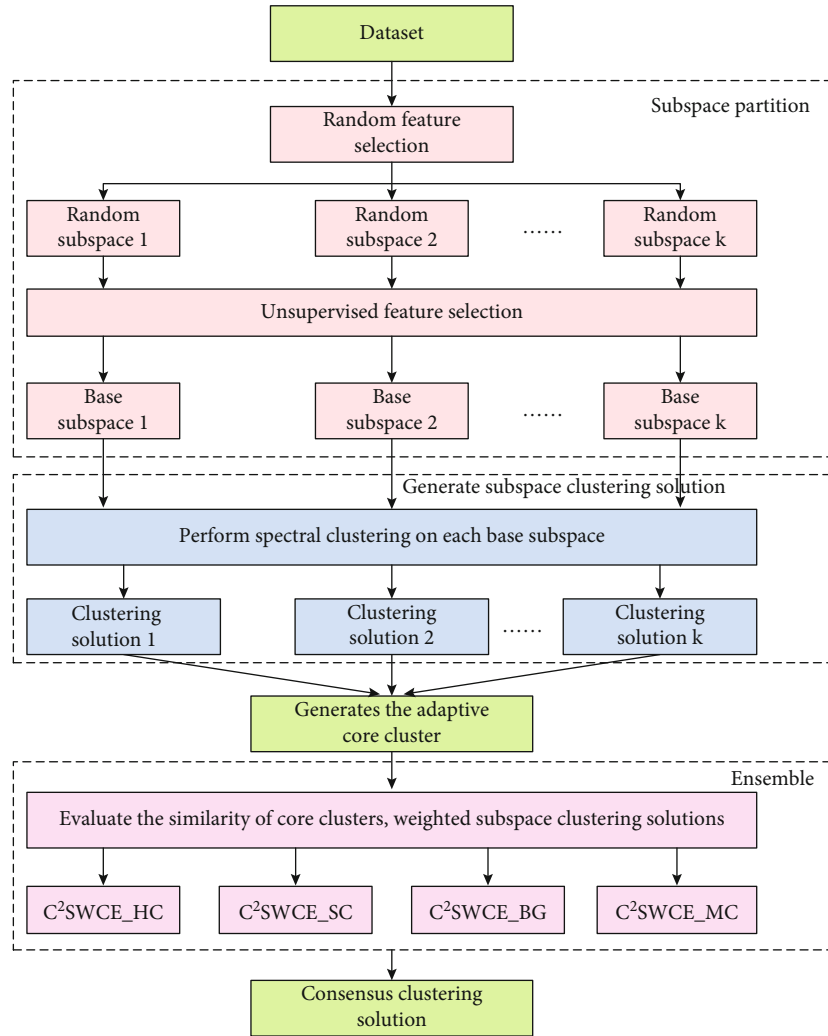
To the abovementioned problem, this paper proposes a novel adaptive core cluster-based subspace weighted clustering ensemble approach, termed C^2 SWCE, which considers

the similarity of clusters in subspaces in the ensemble process, and the weighted subspace clustering solution helps to improve the accuracy of consensus clustering result. The overall process of C^2 SWCE is shown in Figure 1. The proposed framework first uses a combination of random feature selection and unsupervised feature selection to generate a set of base subspaces. Then, spectral clustering is performed in the base subspace to achieve the clustering solution for each base subspace, further generating a set of adaptive core clusters. The core cluster is viewed as the basic unit of clustering ensemble, and the clustering solution of the subspace is weighted by calculating the distance between the core clusters in the subspace, the similarity of the core cluster and the cluster. Finally, we propose four consensus functions under this framework, which combine the locally weighted subspace clustering solutions to achieve the consensus clustering solutions.

The main contributions of our approaches are summarized as follows:

- (1) We combine random feature selection and unsupervised feature selection to generate a set of base subspaces. Random feature selection generates a set of random subspaces, and then, unsupervised feature selection is performed on random subspaces, and the features that retain the local structure of random subspaces are selected, which further reduces the dimensionality of random subspaces. This joint feature selection strategy ensures the diversity of feature subspaces and improves the computational efficiency.
- (2) We introduce the concept of the core cluster, which is a collection of samples that are grouped into the same cluster in all subspaces. In this paper, the core cluster is viewed as the basic unit of the clustering ensemble, which improves the computational efficiency of the integration process
- (3) We propose locally weighted subspace clustering ensemble framework, which evaluates the stability of clusters by calculating the distance of core clusters in each subspace, and the similarity of core clusters and clusters. We further propose four weighted ensemble approaches based on core clusters, which fuse clusters in base subspace and obtain the consensus clustering solution
- (4) The experimental results on several real high-dimensional datasets show that the comprehensive performance of our approaches in clustering accuracy and time complexity is significantly better than that of the state of the art clustering approaches

The rest of this paper is organized as follows: We review the related work in Section 2, the locally weighted subspace clustering ensemble approaches are proposed in Section 3, experimental settings and related results and analysis in Section 4, and finally, in Section 5, we conclude this paper.

FIGURE 1: Flow diagram of the C²SWCE.

2. Related Work

Clustering ensemble, also known as cluster integration, combines multiple base clustering solutions to obtain better and more robust consensus clustering result. The cluster integration process consists of two stages: the base clustering generation and the ensemble of clusters. In the first stage, different clustering algorithms are performed on the dataset, or different parameters are set by the same clustering algorithm to partition samples, and the goal of this stage is to generate diverse clustering solutions. In the second stage, the input base clustering solutions are fused by the consensus function to obtain the final clustering result.

The subspace clustering technique can explore the nature cluster structure of high-dimensional data in different low-dimensional spaces. Subspace clustering ensemble is a method that combines subspace clustering and ensemble learning, which fuses clusters in different feature subspaces to achieve consensus clustering solutions. Among the recently proposed subspace clustering ensemble approaches, Huang et al. proposed a multivariate subspace clustering ensemble framework, termed MDEC [4], in which random

sampling was used to generate a set of feature subspaces. The novelty of this approach is that the randomizing a scaled exponential similarity kernel is used to get a large number of multivariate measures for each random subspace, forming a metric-subspace pairs. Perform spectral clustering on the similar matrix in each metric-subspace pair to obtain a clustering solution for each subspace, use the entropy criterion to weight the clusters of the subspace, and then use spectral clustering, bipartite graph and hierarchical clustering approaches to get a consensus clustering solution.

Cai et al. proposed a novel spectral clustering approach based on subspace, termed SC-SRGF [5], which first generates a set of random feature subspaces, uses the local structures information of each subspace to form the KNN affinity graph, and then use an iterative similarity network fusion scheme to fuse the affinity graphs of each subspace to obtain a unified affinity graph, and obtain the final clustering solution by performing spectral clustering on a unified affinity graph.

Shankar proposed subspace clustering integration framework AP²CE [6], which uses the affinity propagation to produce a representative subset of features and employs

multiple distance function metric objects to produce diverse subspace clustering solutions and use the Ncut to partition the consensus matrix to get the final result.

Verma et al. proposed double weighting semisupervised ensemble clustering based on selected constraint projection, termed DCECP [7], which treats prior knowledge of experts as pairwise constraints and assigned different subsets of pairwise constraints to different integration members. In addition, an adaptive integration member weighting process is designed to associate different weight values with different integration members. Finally, the final clustering result is obtained using the weighted normalized cut algorithm.

Although many successful subspace ensemble clustering approaches have been developed, most existing approaches [4–6] treat each subspace clustering solution equally during the ensemble process. How to weigh the clustering solution according to the contribution of different feature spaces is worth considering in subspace ensemble.

3. Proposed Framework

In this section, we describe the overall process of the locally weighted subspace clustering ensemble approach. First, we give a brief overview of the proposed methods and then detail the proposed algorithm from three aspects: subspace generation, subspace clustering, and fusion of clusters in subspace.

3.1. Overview. In this paper, we introduce a locally subspace weighted clustering ensemble framework. First, we randomly select k feature subset from the original feature set to generate k random subspaces, and then selecting features representing the local structure from each random subspace to generate base subspace. Then, spectral clustering is performed on each base subspace to achieve subspace clustering solutions. The adaptive core clusters are generated from the base subspace clustering solution, which is a set of samples that are grouped into the same cluster in all subspaces. Then, by calculating the distance of the core cluster in different subspaces, the stability of the clusters is evaluated and weighted the base subspace clustering solution. Finally, in order to integrate the clustering solutions of the base subspaces and get the consensus results, in the C²SWCE framework, we propose four adaptive core cluster-based consensus functions, to achieve the final clustering solutions.

Let $X \in R^{n \times m}$ be the input dataset that contains n samples, each with m features. Let x_i ($i = 1, \dots, n$) denotes the i th sample, which corresponds to the i th row of X , so that the input data can be represented as $X = (x_1, x_2, \dots, x_n)$. Let f_j ($j = 1, \dots, m$) denotes the j th feature of the sample, which corresponds to the j th column of the X ; therefore, matrix X can also be represented as $X = (f_1, f_2, \dots, f_m)$.

3.2. Generate Subspaces. The natural cluster structure of high-dimensional data is hidden in low-dimensional subspaces [8]. Subspace clustering explores the possibility of grouping samples in different feature sets. Subspace clustering ensemble fuses clusters in different subspaces to obtain the final clustering solution, which is an effective method

for clustering high-dimensional data. The recently proposed subspace clustering ensemble approaches [5, 9], which uses random feature selection to generate a set of random subspaces. Random subspace has diversity; it explored the potential cluster of high-dimensional dataset from the perspective of different features to achieve diverse subspace clustering solutions. Literature [10] uses stratified sampling method to generate feature groups and verifies that this method is superior to random sampling. This paper uses the random feature selection to obtain a variety of subspaces, and unsupervised feature selection is performed again on the random subspace to select the features that retain the local structure of random subspace.

The specific procedure of feature subspace segmentation is as follows. The original feature set f_1, f_2, \dots, f_m is randomly sampled according to the sampling ratio r , the original features are classified into k feature groups $\mathcal{G}_1, \mathcal{G}_2, \dots, \mathcal{G}_k$, where \mathcal{G}_i ($i = 1, \dots, k$) represents the features contained in the i th random subspace. Let $\widetilde{X}_i \in R^{n \times |\mathcal{G}_i|}$ denotes the matrix corresponding to the i th random subspace, n is the number of samples, and $|\mathcal{G}_i|$ ($i = 1, \dots, k$) is the number of features in the i th random subspace. Obviously, it holds that $\forall \mathcal{G}_i \neq \phi$ ($i = 1, \dots, k$) and $|\mathcal{G}_i| = m \cdot r$.

A set of base subspaces is generated by calculating the Laplace score [11] of features in each random subspace and selecting the important features in random subspace. Then, we construct the KNN graph for each random subspace, which represents the local structure of the random subspace. The KNN graph of the i th subspace is defined as follows:

$$G^i_{\text{KNN}} = \{V^i, E^i\}, \quad (1)$$

where $V^i = \{v_1, v_2, \dots, v_n\}$ is the set of nodes corresponding to the samples x_1, x_2, \dots, x_n in the i th subspace and E^i is the edge set of the i th subspace. We use the Gaussian kernel function to calculate the weights of the edges between the nodes in the subspace and their corresponding KNN nodes. E^i is defined as

$$E^i = \left\{ e_{\alpha\beta}^i \right\}_{n \times n}, \quad (2)$$

where

$$e_{\alpha\beta}^i = \begin{cases} \exp\left(-\frac{\|x_\alpha^i - x_\beta^i\|^2}{2\sigma^2}\right), & \text{if } x_\alpha^i \in \text{KNN}(x_\beta^i) \text{ or } x_\beta^i \in \text{KNN}(x_\alpha^i), \\ 0, & \text{otherwise.} \end{cases} \quad (3)$$

In Equation (3), x_α^i and x_β^i are the two samples in the i th subspace, respectively. $\|x_\alpha^i - x_\beta^i\|^2$ is the Euclidean distance between x_α^i and x_β^i , and $\text{KNN}(\cdot)$ is the K -nearest neighbor (KNN) operator, and σ is the mean of Euclidean distance between the sample and its KNN.

Let $D^i = \text{diag}(E^i 1)$ be the degree matrix of the i th subspace, where $1 = [1, \dots, 1]^T$. The Laplacian of the graph is calculated as follows:

$$L^i = D^i - E^i. \quad (4)$$

In the i th subspace, the Laplace score of f_l^i ($l = 1, \dots, |\mathcal{G}_i|$) is

$$L_{f_l^i}^i = \frac{\tilde{f}_l^{i\top} L^i \tilde{f}_l^i}{\tilde{f}_l^{i\top} D^i \tilde{f}_l^i}, \quad (5)$$

where

$$\tilde{f}_l^i = f_l^i - \frac{f_l^{i\top} D^i 1}{1^\top D^i 1} 1. \quad (6)$$

We calculate the Laplace score for each feature in the subspace and arrange them in descending order to select the top d features. We determine the number of second selected features based on the number of features in random subspace. Let \tilde{r} represents unsupervised feature selection ratio in the random subspace, that is, from each random feature group \mathcal{G}_i ($i = 1, \dots, k$), select important features that represent the local structure of the random subspace to generate $\tilde{\mathcal{G}}_i$ ($i = 1, \dots, k$), it holds that $\tilde{\mathcal{G}}_i \subset \mathcal{G}_i, |\tilde{\mathcal{G}}_i| = |\mathcal{G}_i| \cdot \tilde{r} (i = 1, \dots, k)$, and $\sum_{i=1}^k |\tilde{\mathcal{G}}_i| \ll m$. For convenience, let $S_i \in R^{n \times |\tilde{\mathcal{G}}_i|}$ ($i = 1, \dots, k$) represent the matrix of the i th base subspace, where n is the number of samples and \mathcal{G}_i is the number of features.

3.3. Generate Subspace Clustering Solution. Let S_1, S_2, \dots, S_k represent the base subspaces generated by the joint feature selection strategy, where $S_i \in R^{n \times d_i}$ ($i = 1, \dots, k$) is the i th base subspace, and $d_i = |\tilde{\mathcal{G}}_i|$. Let $P^{(S_i)}$ ($[i = 1, \dots, k]$) be the clustering solution for S_i , formally, the clustering solution for the base subspace is $P^{(S_i)} = \{P^{(S_i)}(x_1), P^{(S_i)}(x_2), \dots, P^{(S_i)}(x_n)\}$, where $P^{(S_i)}(x_j)$ ($j = 1, \dots, n$) is a cluster that contains x_j in S_i . Let $C_l^{(S_i)}$ ($l = 1, \dots, K_{S_i}$) denote the l th cluster in the S_i , then for $\forall x_j \in C_l^{(S_i)}$, it holds that $P^{(S_i)}(x_j) = C_l^{(S_i)}$. Thus, the clustering solution of S_i also be denoted as

$$P^{(S_i)} = \{C_1^{(S_i)}, C_2^{(S_i)}, \dots, C_{K_{S_i}}^{(S_i)}\}, \quad (7)$$

where K_{S_i} is the number of clusters in S_i . Then, we can get the clustering solution set of k base subspace, which is represented as $\mathcal{P} = \{P^{(S_1)}, P^{(S_2)}, \dots, P^{(S_k)}\}$. Subspace clustering ensemble is the fusion of clustering solutions from multiple subspaces to achieve consistent results \mathcal{P}^* .

In the clustering process, most approaches view input samples as base units and group them into different clusters. However, when there are more samples, the computational complexity also increases significantly. Huang et al. introduce the concept of superobject [12], which is defined as in the base clustering ensemble where two samples are partitioned into the same cluster, the two samples are in the same original superobject. The size of superobject is between clus-

ters and samples, and it has been proven that viewing superobject as base units when integrated can significantly improve the scalability of data size and simplify the calculation.

Inspired by the concept of the superobject [12], this paper groups samples in base subspaces to achieve a set of base subspace clustering solutions \mathcal{P} and then generates the adaptive core clusters. The core clusters in high-dimensional space are defined as follows.

$$(1) \forall x_\alpha, x_\beta \in X, \quad \forall S_i (1 \leq i \leq k), \quad P^{(S_i)}(x_\alpha) = P^{(S_i)}(x_\beta), \\ \text{then } x_\alpha, x_\beta \in o$$

$$(2) \forall x_\alpha \in o, x_\beta \notin o, \exists S_i (1 \leq i \leq k), P^{(S_i)}(x_\alpha) \neq P^{(S_i)}(x_\beta)$$

Definition 1. Let X be the input dataset and \mathcal{P} be set of base subspace clustering solutions. Samples that simultaneously satisfying the following two conditions are core clusters, which are denoted as o .

Let $O = \{o_1, o_2, \dots, o_\gamma\}$ be the set of core clusters in a high-dimensional space, where γ is the number of core clusters. It holds that $\forall o_i \neq \emptyset, o_i \cap o_j = \emptyset (\forall i \neq j, i, j = 1, 2, \dots, \gamma)$, and $\bigcup_{i=1}^\gamma o_i = n$.

We provide examples of samples clustering in different subspaces. Given a dataset $X = \{x_1, \dots, x_7\}$, where x_i is the i th sample. These samples are grouped into clusters in subspaces, and the relationships between the samples, core clusters, and clusters are described in Table 1. In subspace S_1 , samples are grouped into two clusters, and in S_2 and S_3 , they are grouped into three clusters, respectively.

According to Definition 1, there are four core clusters are generated in the above example. The relationship between the core cluster and the samples is shown in Table 1, namely, $x_1, x_2 \in o_1, x_3 \in o_2, x_4, x_5 \in o_3$, and $x_6, x_7 \in o_4$. The core cluster is viewed as the basic units of cluster in subspace, for example in base subspace $S_1, o_1, o_2 \subset C_1^{(S_1)}, o_3, o_4 \subset C_2^{(S_1)}$.

In the conventional subspace clustering approaches, samples are basic units. However, samples correspond to different features in different feature subspaces, so the implicit relationship between samples in different subspaces is also different. A core cluster is a set of samples that are grouped into the same clusters in all subspaces. In the process of subspace ensemble, we view the core cluster as the basic unit, that is, each cluster in subspace is composed of core clusters. We evaluate the stability of clusters in subspace by measuring the distance of core clusters pairs contained in the cluster.

Definition 2. $\forall S_i (1 \leq i \leq k), \forall o_\alpha, o_\beta (\alpha, \beta = 1, \dots, \gamma)$, the distance between the core clusters pairs is defined as

$$\text{CCS}^{(S_i)}(o_\alpha, o_\beta) = \frac{1}{|o_\alpha| |o_\beta|} \sum_{x_a \in o_\alpha} \sum_{x_b \in o_\beta} d^{(S_i)}(x_a, x_b), \quad (8)$$

where $|o_\alpha|$ and $|o_\beta|$ are the number of samples contained in o_α and o_β , respectively. $d^{(S_i)}(\cdot, \cdot)$ is a distance metric

TABLE 1: Correspondence between samples, core clusters, and clusters in subspace.

X	x_1	x_2	x_3	x_4	x_5	x_6	x_7
S_1	$C_1^{(S_1)}$	$C_1^{(S_1)}$	$C_1^{(S_1)}$	$C_2^{(S_1)}$	$C_2^{(S_1)}$	$C_2^{(S_1)}$	$C_2^{(S_1)}$
S_2	$C_1^{(S_2)}$	$C_1^{(S_2)}$	$C_2^{(S_2)}$	$C_2^{(S_2)}$	$C_2^{(S_2)}$	$C_3^{(S_2)}$	$C_3^{(S_2)}$
S_3	$C_1^{(S_3)}$	$C_1^{(S_3)}$	$C_1^{(S_3)}$	$C_2^{(S_3)}$	$C_2^{(S_3)}$	$C_3^{(S_3)}$	$C_3^{(S_3)}$
O	o_1	o_1	o_2	o_3	o_3	o_4	o_4

function between samples in S_i , which can be selected as the Euclidean distance, the Manhattan distance, the Cosine distance, and so on. If the distance between the core clusters pairs is smaller, the more stable the clusters in the corresponding subspace, and vice versa. Clusters are evaluated by the average distance between core clusters.

For $\forall S_i$ ($1 \leq i \leq k$), there are a total of K_{S_i} clusters, and each cluster $C_j^{(S_i)}$ ($1 \leq j \leq K_{S_i}$) contains $\tilde{n}_j^{(S_i)}$ core clusters. Obviously, it holds that $\tilde{n}_j^{(S_i)} \geq 1$ and $\sum_{j=1}^{K_{S_i}} \tilde{n}_j^{(S_i)} = \gamma$.

Definition 3. For $\forall C_j^{(S_i)}$ ($1 \leq i \leq k, 1 \leq j \leq K_{S_i}$), the average distance of the core clusters is defined as

$$ACS_j^{(S_i)} = \begin{cases} \frac{2}{\tilde{n}_j^{(S_i)}(\tilde{n}_j^{(S_i)} - 1)} \sum_{a=1}^{\tilde{n}_j^{(S_i)}} \sum_{b=a+1}^{\tilde{n}_j^{(S_i)}} CCS^{(S_i)}(o_a, o_b), & \tilde{n}_j^{(S_i)} > 1, \\ 0, & \tilde{n}_j^{(S_i)} = 1. \end{cases} \quad (9)$$

In Equation (9), $CCS^{(S_i)}(\cdot)$ is a distance metric function of core clusters pairs in S_i and $\tilde{n}_j^{(S_i)}$ is the number of core clusters in $C_j^{(S_i)}$.

The smaller the average distance between the core clusters in a cluster, the denser the cluster, that is, the greater the probability that the core clusters will be grouped into clusters in the base subspace, the higher the stability of the clusters. We introduced the cluster stability index (CSI) to describe this relationship.

Definition 4. For $\forall C_j^{(S_i)}$ ($1 \leq i \leq k, 1 \leq j \leq K_{S_i}$), its cluster stability index is defined as

$$CSI_j^{(S_i)} = e^{-MCS_j^{(S_i)}}, \quad (10)$$

where $MCS_j^{(S_i)}$ is the average distance between the core clusters in $C_j^{(S_i)}$. For $MCS_j^{(S_i)} \in [0, +\infty)$, the range of the cluster stability index is $CSI_j^{(S_i)} \in (0, 1]$.

The CSI is an indicator that describes clusters in a subspace. If the cluster has only one core cluster, the distance

between the core cluster is 0, and the stability index of the corresponding cluster is 1; the cluster can no longer be divided and is stable. If there are multiple core clusters in a cluster, the greater the average distance between the core clusters, the worse the stability of the clusters, and vice versa.

Thus, for $\forall S_i$ ($1 \leq i \leq k$), the average of the stability index for all clusters is

$$CSI^{(S_i)} = \frac{1}{K_{S_i}} \sum_{j=1}^{K_{S_i}} CSI_j^{(S_i)} \quad (1 \leq j \leq K_{S_i}). \quad (11)$$

When fusing the clustering solutions of base subspace, we weight the subspace by the stability of the clusters in the corresponding base subspace. The weight of each base subspace is calculated by

$$\omega^{(S_i)} = \frac{CSI^{(S_i)}}{\sum_{i=1}^k CSI^{(S_i)}}, \quad (12)$$

where

$$\sum_{i=1}^k \omega^{(S_i)} = 1. \quad (13)$$

3.4. Subspace Clustering Ensemble. Clustering ensemble is an effective way to improve robustness and stability of clustering solution [13]. We propose four core cluster-based consensus functions that ensemble clustering solutions for each base subspace to achieve the final clustering results.

Define the core cluster similarity matrix in base subspace based on whether any two core clusters in the subspace are grouped into the same cluster.

Definition 5. For $\forall S_i$, the core cluster similarity matrix is defined as

$$A^{(S_i)} = \left\{ a_{\alpha\beta}^{(S_i)} \right\}_{\gamma \times \gamma} \quad (\alpha, \beta \in [1, \gamma], i \in [1, k]), \quad (14)$$

where

$$a_{\alpha\beta}^{(S_i)} = \begin{cases} CCS^{(S_i)}(o_\alpha, o_\beta), & \text{if } P^{(S_i)}(o_\alpha) = P^{(S_i)}(o_\beta), \\ 0, & \text{otherwise.} \end{cases} \quad (15)$$

In Equation (15), $P^{(S_i)}(o_\alpha)$ and $P^{(S_i)}(o_\beta)$ represent clusters containing o_α and o_β in S_i , respectively. Unlike normal similarity matrices, we define the core cluster similarity matrices rather than similar matrices between samples. At the same time, we achieve the weighted core cluster similarity matrix based on the weights of base subspace, which is represented as

$$A = \frac{1}{k} \sum_{i=1}^k \omega^{(S_i)} \cdot A^{(S_i)}. \quad (16)$$

3.4.1. Hierarchical Clustering Based on the Core Cluster. In this section, we propose the consensus function for hierarchical clustering based on the core clusters, termed C²SWCE_HC. The proposed method views the core cluster as the basic unit and constructs a dendrogram by the core cluster, where the root of the tree corresponds to the dataset and its leaves correspond to all the core clusters in \mathcal{P} . Each level of the dendrogram represents the clustering results of different numbers of core clusters, and the final clustering solution can be achieved by specifying a specific level of the dendrogram.

The specific steps of integration are as follows: First, the γ core clusters in \mathcal{P} as the initial region, which is represented as

$$\Theta^{(0)} = \{\Theta_1^{(0)}, \dots, \Theta_\gamma^{(0)}\}. \quad (17)$$

In Equation (17), $\Theta_i^{(0)} = \{o_i\}$ denotes the i th initial region, which corresponds to the i th core cluster. Let $M^{(0)}$ be the initial similar matrix. Merge the two most similar core clusters in $M^{(0)}$ into one larger cluster and update the similar matrix according to the average link for the next merge of core clusters. Repeat merge the two most similar regions of the similar matrix that were updated in the previous iteration. After each merge, the number of regions is reduced by 1, and after the i th iteration, the merged regions are represented as $\Theta^{(i)} = \{\Theta_1^{(i)}, \dots, \Theta_{\gamma-i}^{(i)}\}$, and the corresponding similar matrix is updated as follows:

$$M^{(i)} = \left\{ \frac{1}{|\Theta_i^{(i)}| |\Theta_j^{(i)}|} \sum_{o_\alpha \in \Theta_i^{(i)}, o_\beta \in \Theta_j^{(i)}} a_{\alpha\beta}^{(i)} \right\}_{(\gamma-i) \times (\gamma-i)}, \quad (18)$$

where $|\Theta_i^{(i)}|$ is the number of core clusters contained in the i th region after the i th iteration, and the maximum number of iterations of the dendrogram is $\gamma - 1$.

For clarity, C²SWCE_HC is summarized in Algorithm 1.

3.4.2. Spectral Clustering Based on the Core Cluster. In this section, we introduce the core cluster-based spectral clustering consensus function to ensemble subspace clustering solutions. First, we build the affinity graph that treats the core clusters as graph nodes and the weighted core cluster similarity matrix as the adjacency matrix. The graph is defined as

$$G = (V, E), \quad (19)$$

where $V = O$ is the nodes set and E is the edge set. The weights of the edge between the nodes v_i and v_j is determined by matrix A , that is, $E_{ij} = A_{ij}$. Let $D \in R^{\gamma \times \gamma}$ be the degree matrix of E , the normalized graph Laplacian is computed as

$$L = D - E = I - D^{-1/2} E D^{-1/2} = I - D^{-1/2} A D^{-1/2}. \quad (20)$$

We perform eigendecomposition on L to achieve the first K eigenvalues, and matrix $\Xi \in R^{\gamma \times K}$ is constructed by corresponding K eigenvectors and perform K -means on the row vectors of the matrix.

For clarity, the C²SWCE_SC algorithm is summarized in Algorithm 2.

3.4.3. Bipartite Graph Partition Based on the Core Clusters. Under the C²SWCE framework, we propose the bipartite graph clustering ensemble based on the core clusters, termed C²SWCE_BG. In ensemble process, we use the core clusters and clusters as graph nodes to construct the bipartite graph. The specific steps are described below.

In different base subspaces, the core clusters are grouped into a set of clusters. In all base subspaces, the set of clusters is

$$\mathcal{C} = \{C_1, C_2, \dots, C_{n_c}\}, \quad (21)$$

where $n_c = \sum_{i=1}^k K_{S_i}$ is the number of clusters in \mathcal{P} . We view both the core cluster and cluster as graph nodes, and construct the bipartite graph. That is:

$$G_{BG} = (U_{BG}, V_{BG}, E_{BG}), \quad (22)$$

where $U_{BG} = OUC$ is the node set corresponding to the core cluster and the cluster; $V_{BG} = \mathcal{C}$ is the node set corresponding to the cluster in \mathcal{P} ; it holds that $|U_{BG}| = \gamma + n_c$, $|V_{BG}| = n_c$. E_{BG} is the edge set.

In \mathcal{C} , clusters in the same subspace contain different core clusters, while clusters in different subspaces may contain the same core cluster. Therefore, we use the Jaccard coefficient to measure the similarity of clusters. The core clusters are viewed as base units; the similarity matrix between clusters is defined as

$$Z = \{z_{ij}\}_{n_c \times n_c}, \quad (23)$$

where

$$z_{ij} = J(C_i, C_j) = \frac{|C_i \cap C_j|}{|C_i \cup C_j|} \quad (i, j \in [1, n_c]). \quad (24)$$

Clusters in the same base subspace do not intersect, so the Jaccard coefficient between clusters in the same subspace is 0. The similarity between clusters pairs is calculated by Equation (24) and the clusters are weighted based on similarity.

The similarity matrix between clusters and the core clusters is constructed as

$$\tilde{Z} = \{\tilde{z}_{ij}\}_{\gamma \times n_c}, \quad (25)$$

where

$$\tilde{z}_{ij} = \begin{cases} \omega^{(S_i)} \cdot \text{CSI}_j, & \text{if } o_i \subseteq C_j, \\ 0, & \text{otherwise.} \end{cases} \quad (26)$$

Input: S_1, S_2, \dots, S_k, K
Output: \mathcal{P}^*

1. Performed clustering on each base subspace to generate a set of subspace clustering ensemble \mathcal{P}
2. Generate the adaptive core clusters according to Definition 1
3. Calculates the average distance between core clusters according to Equations (8) and (9)
4. Calculates the CSI of the cluster according to Equation (10), and $\omega^{(S_i)}$ is achieved according to Equation (11)–(13)
5. Construct the core cluster similarity matrix $A^{(S_i)}$ ($i = 1, \dots, k$) according to Equations (14) and (15), and the weighted core cluster similarity matrix A according to Equation (16).
6. Initialize $\Theta^{(0)} = \{\Theta_1^{(0)}, \dots, \Theta_\gamma^{(0)}\}$, $M(0) = A$
7. Construct the dendrogram
 - for $l = 1$ to $\gamma - 1$ do
 - According to $M^{(l-1)}$, merge the two most similar regions to achieve $\Theta^{(l-1)}$
 - Update $\Theta^{(l)}$, and achieve $M^{(l)}$
8. Select the level of the dendrogram according to K , and achieve K clusters
9. Map the labels of core cluster to the samples.

ALGORITHM 1

Input: S_1, S_2, \dots, S_k, K
Output: \mathcal{P}^*

1. Performed clustering on each base subspace to generate a set of subspace clustering ensemble \mathcal{P}
2. Generate the adaptive core clusters according to Definition 1
3. Calculates the average distance between core clusters according to Equations (8) and (9)
4. Calculates the CSI of the cluster according to Equation (10), and $\omega^{(S_i)}$ is achieved according to Equations (11)–(13)
5. Construct the core cluster similarity matrix $A^{(S_i)}$ ($i = 1, \dots, k$) according to Equations (14) and (15), and the weighted core cluster similarity matrix A according to Equation (16).
6. Build the graph $G = (V, E)$ with $V = O, E = A$
7. Constructed the normalized graph Laplacian L according to Equation (20).
8. Perform eigendecomposition on L to achieve the first K eigenvalues and corresponding eigenvectors to build Ξ
9. After normalizing Ξ , perform K -means to categorized the core clusters
10. Map the labels of core cluster to the samples

ALGORITHM 2

In Equation (26), CSI_j is the cluster stability index of C_j in S_i , $\omega^{(S_i)}$ is the weight of C_j in S_i ($l \in [1, k], i \in [1, \gamma], j \in [1, n_c]$).

Connect the matrix \tilde{Z} and matrix Z to generate matrix $E_{BG} \in R^{(\gamma+n_c) \times n_c}$, that is,

$$E_{BG} = \{e_{ij}\}_{(\gamma+n_c) \times n_c} \quad (27)$$

The entry of E_{BG} corresponds to the weight of the edge between the two nodes in G_{BG} , denoted as

$$e_{ij} = \begin{cases} \omega^{(S_i)} \cdot \text{CSI}_j, & \text{if } u_i \in \mathcal{C}, v_j \in O, v_j \subseteq u_i, \\ J(u_i, v_j), & \text{if } \tilde{u}_i \in \mathcal{C}, \tilde{v}_j \in \mathcal{C}, \\ 0, & \text{otherwise.} \end{cases} \quad (28)$$

In Equation (28), CSI_j is the cluster stability index of the j th cluster. $J(\cdot, \cdot)$ is the Jaccard coefficient operator, which is calculated according to Equation (24). In G_{BG} , there are no edges between cluster nodes or between the core cluster

nodes, only edges between cluster nodes and core cluster nodes.

According to the corresponding features in different base subspaces, we use the weight of the subspace corresponding to the cluster to which the core cluster belongs as the weight of the edges of the core cluster and the cluster. The higher the stability of the cluster, the greater its impact during integration and the greater the weights assigned.

Finally, we use Tcut [14] to segment G_{BG} . All nodes are partitioned into K disjoint groups. The samples contained in the core clusters and cluster of the same group are partitioned in the same cluster.

The specific steps of $C^2\text{SWCE_BG}$ are summarized in Algorithm 3.

3.4.4. Metacluster-Based Ensemble Clustering. Under the proposed $C^2\text{SWCE}$ framework, we propose the metacluster-based consensus clustering algorithm, termed $C^2\text{SWCE_MC}$. In the proposed approach, clusters are regarded as the basic units that use the similarities between them to divide clusters into

Input: S_1, S_2, \dots, S_k, K

Output: \mathcal{P}^*

1. Performed clustering on each base subspace to generate a set of subspace clustering ensemble \mathcal{P}
2. Generate the adaptive core clusters according to Definition 1
3. Calculated the similarity of the cluster according to Equations (23) and (24)
4. Calculate the similarity of clusters and core clusters according to Equations (25) and (26)
5. Construct the bipartite graph according to Equation (22) with $U = \text{OUC}$, $V = \mathcal{C}$
6. Combine matrix \tilde{Z} and matrix Z to generate E_{BG}
7. Segment the G_{BG} by Tcut
8. Map the labels of core cluster to the samples

ALGORITHM 3

different groups, and the samples of the same group are divided into the same cluster.

$C^2\text{SWCE_MC}$ first treats all clusters as nodes and constructs the similar graph, which is defined as:

$$G_M = (V_M, E_M), \quad (29)$$

where $V_M = \mathcal{C}$ is the node set for all clusters in \mathcal{P} and E_M is the edge set. The weights of the edges between nodes are defined by the similarity matrix Z of the clusters by Equations (23) and (24).

$$E_M = \{e_{ij}\}_{n_c \times n_c}, \quad (30)$$

where $e_{ij} = z_{ij}$.

Finally, we adopt Ncut [15] to partition nodes into K disjoint sets of nodes, which denotes as

$$\text{MC} = \{\text{MC}_1, \dots, \text{MC}_K\}, \quad (31)$$

where MC_i ($i \in [1, k]$) represents the i th metacluster, which is the set of clusters. The core clusters are treated as base units in the ensemble. In each subspace, o_i ($i \in [1, \gamma]$) is partitioned into a cluster. o_i may appear multiple times in MC. Define the discriminant function δ to represent the relationship:

$$\delta = \begin{cases} 1, & \text{if } o_i \subseteq C_\beta, \\ 0, & \text{otherwise.} \end{cases} \quad (32)$$

The probability that o_i ($i \in [1, \gamma]$) is grouped into metacluster is

$$\phi(o_i, \text{MC}_j) = \frac{1}{|\text{MC}_j|} \sum_{C_\beta \in \text{MC}_j} \delta \quad (j \in [1, n_c]), \quad (33)$$

where $|\text{MC}_j|$ is the number of clusters in the j th metacluster.

Finally, o_i is assigned to the metacluster with the highest probability, namely,

$$\arg \max_{\text{MC}_j \in \text{MC}} \phi(o_i, \text{MC}_j). \quad (34)$$

We summarize $C^2\text{SWCE_MC}$ in Algorithm 4.

4. Experiments

In this section, we conduct experiments on eight high-dimensional datasets to compare the proposed four subspace clustering ensemble algorithms against several clustering approaches. All the experiments in this paper are conducted in MATLAB R2016a on a PC with 8 Intel 3.40 GHz processors and 8 GB of RAM.

4.1. Datasets. In our experiments, we use eight high-dimensional datasets, which including four cancer gene expression datasets and four image datasets. The 4 gene expression datasets, namely, Yeoh02v1¹, Yeoh02v2¹, Bhattacharjee2001¹, and Golub1999v1¹. The Yeoh02v1 dataset and Yeoh02v2 dataset are the pediatric acute lymphoblastic leukemia dataset, in which Yeoh02v1 dataset contains 2 categories of genes expressed in leukemic blasts, and Yeoh02v2 dataset contains 6 categories of genes expressed in leukemic blasts. Bhattacharjee2001 is the lung tumor samples dataset, which contains 186 lung tumor samples and 17 normal lung tissues. Golub1999v1 is the leukemia dataset, which contains acute myeloid leukemia samples and acute lymphoblastic leukemia samples. The other 4 image datasets, including COIL_20³, USPS², Semeion⁴ and Multi Featureples⁴. The COIL_20 dataset is an image dataset containing 20 item objects, and the other 3 image datasets are all handwritten digit datasets. The USPS dataset contains a total of 10 categories and 11,000 samples. For facilitating comparison, we randomly selected 10% of the samples from each category of the USPS dataset to form a dataset containing 1,100 samples, which is represented as USPS_10P.

To simplify the description, the 8 datasets will be abbreviated as D1 to D8, respectively. The details of the datasets are given in Table 2.

- (1) <https://schlieplab.org/Supplements/CompCancer/>
- (2) <http://www.cad.zju.edu.cn/home/dengcai/Data/MLData.html>
- (3) <https://www.cs.columbia.edu/CAVE/software/softlib/coil-20.php>
- (4) <http://archive.ics.uci.edu/ml/index.php>

4.2. Evaluation Criterion. We use the normalized mutual information (NMI) and the clustering accuracy (ACC) to

<p>Input: S_1, S_2, \dots, S_k, K Output: \mathcal{P}^*</p> <ol style="list-style-type: none"> 1. Performed clustering on each base subspace to generate a set of subspace clustering ensemble \mathcal{P} 2. Generate the adaptive core clusters according to Definition 1 3. Calculate the similarity matrix of clusters in \mathcal{C} according to Equation (23) and (24) 4. Build the graph G_M according to Equations (29)–(31) 5. Partition the graph nodes into K disjoint groups by Tcut, generating MC 6. The core clusters are treated as the base unit, the metaclusters corresponding to the core clusters are determined according to Equations (32), (34), and (35) 7. Map the labels of core cluster to the samples

ALGORITHM 4

TABLE 2: Description of the datasets.

Dataset	Abbreviation	Sample	Dimension	Class
Yeoh02v1	D1	248	2526	2
Yeoh02v2	D2	248	2526	6
Bhattacharje2001	D3	203	1543	5
Golub99v1	D4	72	1868	2
USPS_10P	D5	1100	256	10
COIL_20	D6	1440	1024	20
Semeion	D7	1593	256	10
Multiple features	D8	2000	649	10

evaluate the quality of clustering results. The NMI metrics measure the accuracy of the clustering results according to the shared information of the ground-truth clustering solution and the test clustering solution. Let P denote the clustering solution of the proposed method, and P^G denote the groundtruth clustering solution. The NMI score of P with respect to P^G is calculated as

$$\text{NMI}(P, P^G) = \frac{\sum_{i=1}^{n^P} \sum_{j=1}^{n^G} n_{ij} \log \left(n_{ij} n / n_i^P n_j^G \right)}{\sqrt{\sum_{i=1}^{n^P} n_i^P \log \left(n_i^P / n \right) \sum_{j=1}^{n^G} n_j^G \log \left(n_j^G / n \right)}}, \quad (35)$$

where n^P and n^G are the number of clusters in P and P^G , respectively. n_i^P is the number of samples for the i th cluster in P , and n_j^G is the number of samples for the j th cluster in P^G ; n is the number of input samples, and n_{ij} is the number of samples that the i th cluster in P and the j th cluster in P^G jointly contain.

The ACC measures the ratio of the number of samples that are correctly classified to the number of all samples. The ACC is an indicator that evaluates the accuracy of the clustering result, which is defined as

$$\text{ACC}(P, P^G) = \frac{\sum_{i=1}^n \delta(P^G(x_i), \text{map}(P(x_i)))}{n}, \quad (36)$$

where $P^G(x_i)$ is the groundtruth label corresponding to x_i ,

and $P(x_i)$ is the test clustering labels corresponding to x_i in proposed approach. $\text{map}(\cdot)$ is the relabel mapping function that aligns the test clustering label with the groundtruth label. $\delta(\cdot)$ is an indicator function, which is defined as

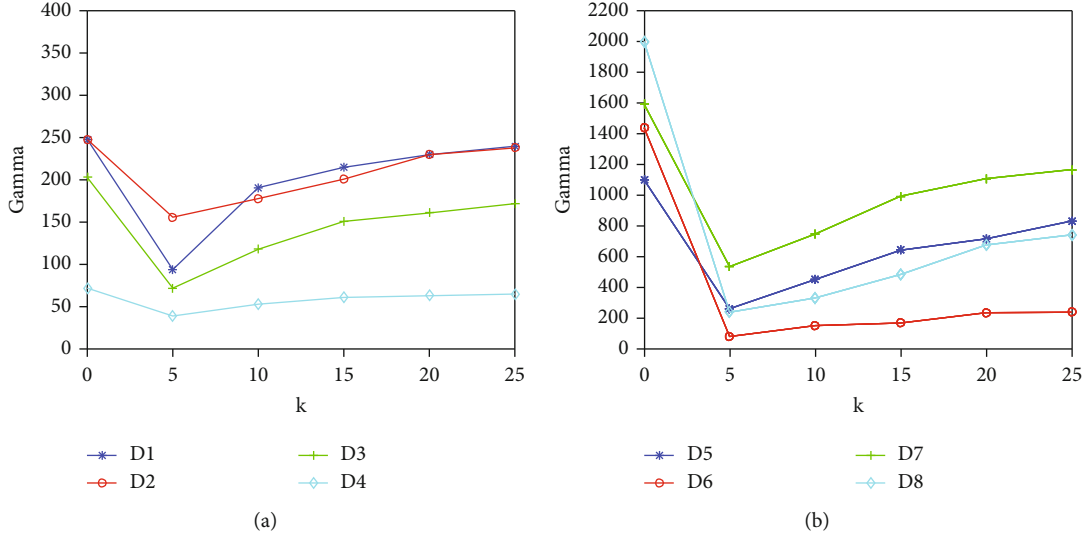
$$\delta(x, y) = \begin{cases} 1, & \text{if } x = y, \\ 0, & \text{otherwise.} \end{cases} \quad (37)$$

The value interval for ACC and NMI score is $[0, 1]$, and a higher ACC score or NMI score indicates a better clustering effect.

4.3. Discussion of the Parameter Selection. There are several parameters in proposed C²SWCE, where k is the number of subspaces, r is the random feature selection ratio, \tilde{r} is the unsupervised feature selection ratio, and K is the number of clusters. To increase the diversity of ensemble members, each subspace randomly generates a different number of clusters within range $[2, \sqrt{n}]$. We set the random feature selection ratio to $r = 0.5$, and the number of generated random subspaces is in the range of $[5, 25]$, with the increment of 5. For each parameter setting, we run the spectral clustering methods 10 times in each random subspace, generating core clusters according to Definition 1 at each time. The average number of generated core clusters is shown in Figure 2.

(1) The relationship between k and γ

In the proposed C²SWCE framework, the core cluster is the basic unit of integration.

FIGURE 2: The correspondence between k and γ ($r = 0.5$).

In Figure 2, k is the number of generated random subspaces, $k = 0$ corresponds to the number of input samples, and s_{ij} is the number of core clusters. It is observed from Figure 2 that in the corresponding dataset, as the number of subspaces increases, so does the number of generated core clusters. For the image datasets (Figure 2(b)), even if the number of subspaces is set to $k = 25$, the number of core clusters is still much smaller than the number of input samples, and this trend is most pronounced on the D6 and D8 datasets. For the gene express datasets (Figure 2(a)), due to the small number of input samples, when the number of subspaces is set to $k = 25$, the number of generated core clusters is close to the number of input samples.

- (2) The influence of parameters k and \tilde{r} on clustering accuracy

In this section, we will compare the effect of the number of a random subspace k and the unsupervised feature selection ratio \tilde{r} on the accuracy of clustering ensemble. We set the value interval of parameter k to $[5, 25]$ and the increment to 5. For each random subspace, the unsupervised feature selection ratio \tilde{r} is set in range of $[0.3, 0.8]$, with increments set to 0.1. For each parameter setting of k and \tilde{r} , we run the proposed methods 10 times, and the average of the NMI scores is shown in Figure 3.

As shown in Figure 3, for the image datasets (D5-D7), parameters k and \tilde{r} are insensitive to clustering results. When \tilde{r} is fixed, the number of subspaces has little effect on the consensus clustering solutions. When k is fixed, the NMI score is relatively high in the range of $[0.6, 0.8]$. For the D1-D3 datasets, as shown in Figures 3(a)–3(c), the higher NMI scores are distributed in parameter k in an interval of $[10, 20]$ and parameter \tilde{r} in an interval of $[0.5, 0.8]$ region. For the D4 dataset, it can be clearly observed that when $\tilde{r} = 0.8$, the corresponding NMI score is higher.

For each dataset, the more base subspaces is divided, the more adaptive core clusters are generated, which adds computational complexity and algorithm runtime. As observed

from Figure 2 that the number of core clusters generated by parameter k in range $[10, 20]$ is moderate. At the same time, when $r = 0.5$ and \tilde{r} is set in the range of 0.5, 0.8, the ensemble result has a higher NMI score. Therefore, in subsequent experiments, we set $k = 10$, $r = 0.8$, and $\tilde{r} = 0.8$ in experiments on all datasets.

4.4. Compare the Effects of Feature Selection and Weighted Strategies on Ensemble Results. In this section, we first compare the impact of the hybrid feature selection strategies on consensus clustering solutions. For each dataset, the proposed four ensemble methods are run on random subspaces and base subspaces generated by mixed feature selection strategies and compare their clustering results. For fair comparison, each ensemble approach runs 10 times in the unweighted manner, recording the average of its NMI scores. The comparison results are recorded in Table 3, with the notation “N” corresponding to the clustering result on random subspace, and the notation “Y” corresponding to the result of clustering result on the base space.

As shown in Table 3, the clustering effect of the proposed clustering ensemble approaches on the base subspace is differently better than that in the random subspace. Therefore, in subsequent experiments, we use the hybrid feature selection strategy, perform unsupervised feature selection on random subspace, generate a set of base subspaces, and then generate ensemble members by performing the clustering on the base subspace.

The proposed four ensemble approaches treat the core cluster as the base unit. The base subspace clustering solutions are weighted by calculating the distance between the core clusters pairs contained in the cluster, or the similarity of core clusters to each cluster. To verify the effect of the weighted clustering integration method, we compared the results of the weighted integration method and the unweighted integration method on the base subspace, respectively. Each ensemble method is run 10 times, and the average NMI of the proposed methods is recorded in Table 4. In Table 4, the notation “N” corresponds to the unweighted clustering results of the

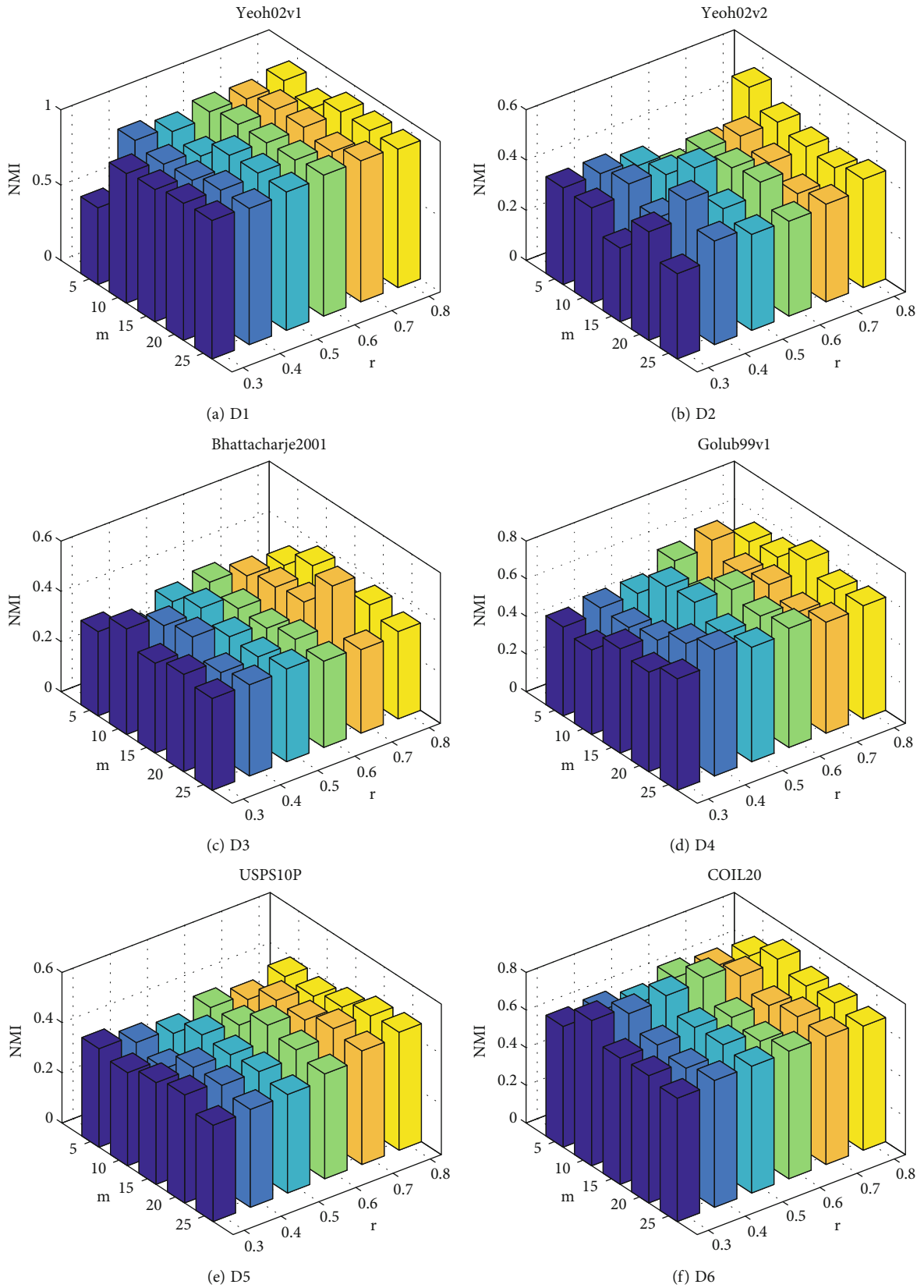


FIGURE 3: Continued.

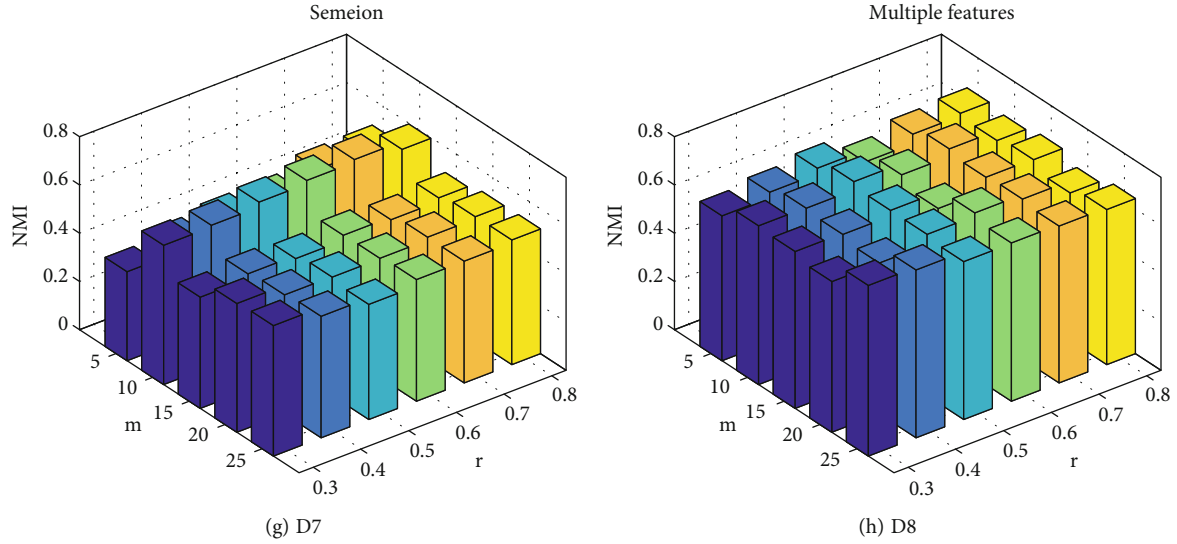

 FIGURE 3: The parameters k and \bar{r} correspond to clustering results (NMI).

TABLE 3: Comparison of clustering results for random subspaces with clustering results for base subspaces (NMI).

Datasets	C ² SWCE_HC		C ² SWCE_SC		C ² SWCE_BG		C ² SWCE_MC	
	N	Y	N	Y	N	Y	N	Y
D1	0.6625	0.8270	0.6381	0.8449	0.7823	0.8436	0.8041	0.8808
D2	0.3322	0.4081	0.3524	0.3845	0.4312	0.4899	0.5202	0.5302
D3	0.4179	0.5209	0.2324	0.3533	0.3502	0.4598	0.4190	0.4948
D4	0.7593	0.8257	0.8203	0.8955	0.8203	0.8955	0.9477	0.8203
D5	0.4377	0.6152	0.5133	0.5815	0.4358	0.6118	0.4374	0.6123
D6	0.8177	0.9113	0.7621	0.7818	0.8082	0.9006	0.8083	0.9104
D7	0.4742	0.6596	0.5331	0.6412	0.5318	0.6704	0.4913	0.6402
D8	0.7417	0.8881	0.7515	0.9324	0.7663	0.8967	0.7865	0.9015

TABLE 4: Comparison of weighted ensemble manner and unweighted ensemble manner (NMI).

Datasets	C ² SWCE_HC		C ² SWCE_SC		C ² SWCE_BG		C ² SWCE_MC	
	Y	N	Y	N	Y	N	Y	N
D1	0.9449	0.8270	0.8943	0.8449	0.8821	0.8436	0.8809	0.8808
D2	0.5386	0.4081	0.5666	0.3845	0.5638	0.4899	0.5211	0.5302
D3	0.5855	0.5209	0.4919	0.3533	0.5514	0.4598	0.5078	0.4948
D4	0.9101	0.8257	0.8955	0.8955	0.8955	0.8955	0.8203	0.8203
D5	0.6675	0.6152	0.5859	0.5815	0.5669	0.6118	0.5460	0.6123
D6	0.9224	0.9113	0.8780	0.7818	0.9277	0.9006	0.8956	0.9104
D7	0.7588	0.6596	0.6597	0.6412	0.6800	0.6704	0.6458	0.6402
D8	0.9099	0.8881	0.9446	0.9324	0.9363	0.8967	0.9021	0.9015

proposed methods, and the notation “Y” corresponds to the weighted clustering results of the proposed methods.

As observed from Table 4, on the other datasets except D4, the fusion results of the proposed four ensemble methods under the weighted ensemble manner are better than the ensemble results of the unweighted ensemble manner. For the D4 dataset, the NMI score of the weighted

ensemble manner of the proposed C²SWCE_HC is 0.9101, which is higher than the NMI score of 0.8257 corresponding to the unweighted ensemble manner. However, on the D4 dataset, there are no significant advantages in the clustering results obtained by the other three ensemble methods using a weighted ensemble manner. For other datasets, the consensus clustering results achieved by the weighted ensemble

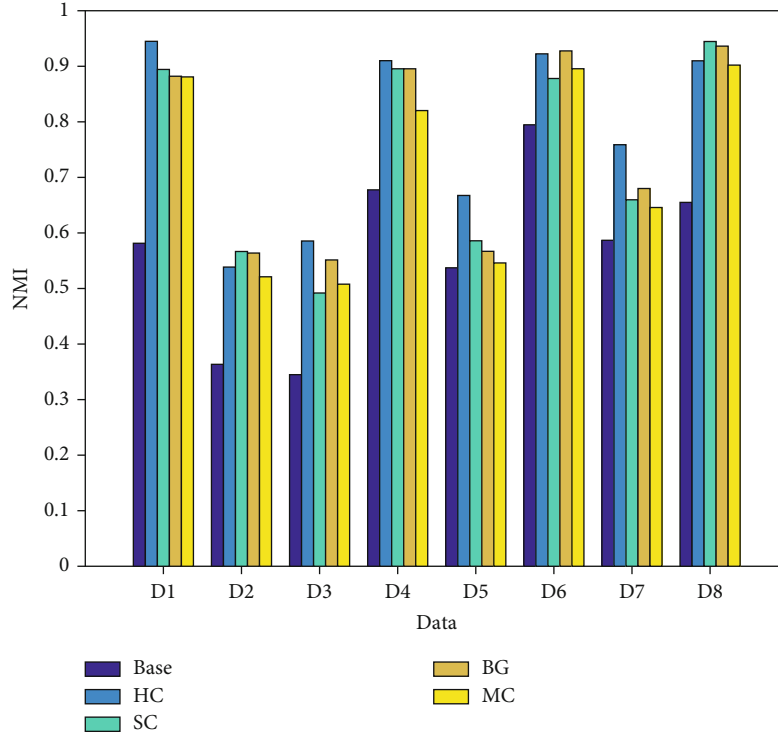


FIGURE 4: Performance comparison of the proposed approaches with the base clustering.

manner are better than those obtained by the unweighted ensemble manner. This illustrates the effectiveness of the proposed weighted ensemble strategies.

4.5. Comparison with Base Clustering. Subspace clustering ensemble can fuse multiple subspace clustering solutions to obtain a better accuracy, more robust consensus solution. In this section, we compare the clustering effects of the proposed locally weighted subspace clustering ensemble approaches, namely, C^2SWCE_HC , C^2SWCE_SC , C^2SWCE_BG , and C^2SWCE_MC against spectral clustering approach. Each method runs 20 times, and their average NMI scores are described in Figure 4.

In Figure 4, “base” corresponds to base clustering results, and “HC,” “SC,” “BG,” and “MC” correspond to the clustering results of C^2SWCE_HC , C^2SWCE_SC , C^2SWCE_BG , and C^2SWCE_MC , respectively. As can be seen from Figure 4, on each experimental dataset, the proposed approaches can achieve better and more robust consensus clustering results than the spectral clustering approach. In particular, on the D1, D2, D3, D6, D7, and D8 datasets, the performance of the proposed 4 clustering integration approaches are significantly better than that of the spectral clustering approach.

4.6. Comparison with Other Clustering Methods. In this section, we compare the proposed consensus clustering approaches with the state-of-the-art clustering approaches to evaluate their effectiveness. Among comparative clustering approaches, K -means and GNMF [16] are classic clustering methods and SSC [17] and LSC [2] are the

clustering methods based on spectral clustering. In the contrasting ensemble methods, MDEC_SC [4], MDEC_HC [4], and MDEC_BG [4] all use spectral clustering to generate the clustering ensemble members, and then, they use spectral clustering, hierarchical clustering, and bipartite graph partition to fuse base clustering solutions, respectively. SC_SRGF [5] adopts spectral clustering to obtain clustering solutions for each subspace; however, ECPCS-HC [18], ECPCS-MC [18], WEAC-AL [19], GP-MGLA [19], LWGP [20], and LWEA [20] all use K -means to generate base clustering solutions. All parameters of the comparison approaches are set as suggested by the corresponding papers.

For a fair comparison, we run each clustering approach 20 times on each dataset and the average performance in terms of NMI and ACC are summarized in Tables 5 and 6, respectively. In Tables 5 and 6, the highest score is highlighted in bold; the symbol “_” indicating that the algorithm cannot be performed.

The landmark-based spectral clustering (LSC) [2] approach is not suitable for datasets with number of features greater than the number of samples, so there are no corresponding clustering results on D1-D4 datasets. As shown in Table 5, the SSC achieves the best average performance in terms of NMI on D3 dataset. For the remaining datasets, the clustering ensemble approaches yield better average performance than the traditional clustering approaches. This also confirms the previous conclusion that the clustering ensemble approaches are more suitable than the traditional clustering approaches for high-dimensional data clustering scenarios.

As can be seen from Tables 5 and 6, the proposed C^2SWCE_HC achieves the highest average NMI scores on

TABLE 5: Average performance in terms of NMI over 20 runs by different clustering methods.

	D1	D2	D3	D4	D5	D6	D7	D8
<i>K</i> -means	0.2481	0.2238	0.3487	0.5222	0.4575	0.7470	0.5219	0.7152
GNMF	0.5962	0.3369	0.3485	0.7223	0.5572	0.8803	0.5885	0.9216
SSC	0.2938	0.3461	0.5916	0.1276	0.4283	0.8640	0.6042	0.8640
LSC	–	–	–	–	0.6646	0.8852	0.6189	0.9266
MDEC_SC	0.8831	0.4938	0.4843	0.7352	0.5922	0.8896	0.6562	0.9385
SC_SRGF	0.2371	0.1931	0.3621	0.5853	0.5524	0.8870	0.5947	0.8460
C ² SWCE_SC	0.8943	0.5666	0.4919	0.8955	0.5859	0.8780	0.6597	0.9446
ECPCS-HC	0.0044	0.2483	0.5141	0.5264	0.5192	0.7751	0.6329	0.7976
MDEC_HC	0.8855	0.4661	0.5284	0.7853	0.6501	0.9177	0.7072	0.8822
WEAC_AL	0.2994	0.3764	0.2886	0.2240	0.4962	0.7921	0.5959	0.7009
LWEA	0.9447	0.2511	0.3533	0.5974	0.5081	0.7636	0.5999	0.7953
C ² SWCE_HC	0.9449	0.5386	0.5855	0.9101	0.6675	0.9224	0.7588	0.9099
MDEC_BG	0.8863	0.5584	0.5079	0.6923	0.5882	0.9162	0.6775	0.9331
GP_MGLA	0.2794	0.3542	0.2847	0.2194	0.4808	0.7974	0.5315	0.6814
LWGP	0.8620	0.3152	0.3630	0.5974	0.5246	0.7924	0.6193	0.8736
C ² SWCE_BG	0.8821	0.5638	0.5514	0.8955	0.5669	0.9277	0.6800	0.9363
ECPCS-MC	0.0816	0.3178	0.4256	0.5660	0.5451	0.8048	0.6600	0.8580
C ² SWCE_MC	0.8809	0.5211	0.5078	0.8203	0.5460	0.8956	0.6458	0.9021

TABLE 6: Average performance in terms of ACC over 20 runs by different clustering methods.

	D1	D2	D3	D4	D5	D6	D7	D8
<i>K</i> -means	0.8182	0.4286	0.5655	0.8597	0.4225	0.5944	0.0411	0.7334
GNMF	0.9395	0.5524	0.7783	0.9444	0.5931	0.8118	0.6390	0.9625
SSC	0.8508	0.5565	0.8177	0.6528	0.4418	0.7821	0.6109	0.8200
LSC	–	–	–	–	0.6505	0.7972	0.6309	0.9675
MDEC_SC	0.9899	0.5395	0.7320	0.9583	0.5031	0.7698	0.0210	0.9713
SC_SRGF	0.7766	0.4097	0.5448	0.9458	0.4911	0.7990	0.0657	0.8465
C ² SWCE_SC	0.9899	0.6109	0.7433	0.9861	0.5423	0.8583	0.0135	0.9793
ECPCS-HC	0.8161	0.4762	0.7695	0.8944	0.4692	0.6307	0.0485	0.8244
MDEC_HC	0.9899	0.5548	0.7744	0.9611	0.6229	0.8543	0.0157	0.8539
WEAC_AL	0.6774	0.5000	0.3693	0.2639	0.4509	0.7063	0.0232	0.6295
LWEA	0.9960	0.4194	0.5419	0.9167	0.5218	0.6076	0.0308	0.7820
C ² SWCE_HC	0.9859	0.6109	0.6133	0.9861	0.5423	0.8583	0.0135	0.9693
MDEC_BG	0.9899	0.6129	0.7488	0.9417	0.4951	0.8460	0.0239	0.9682
GP_MGLA	0.7097	0.4960	0.3596	0.2639	0.4364	0.7354	0.0113	0.5565
LWGP	0.9879	0.4879	0.4975	0.9167	0.5255	0.6764	0.0797	0.9360
C ² SWCE_BC	0.9899	0.6532	0.6552	0.9861	0.5341	0.8358	0.0135	0.9788
ECPCS-MC	0.8363	0.5258	0.6384	0.9069	0.5117	0.6729	0.0207	0.9260
C ² SWCE_MC	0.9899	0.6210	0.7414	0.9722	0.4696	0.8333	0.0546	0.9115

all datasets among the comparative hierarchical clustering ensemble approaches. Especially on the D1-D4 datasets, the performance of the C²SWCE_HC is significantly better than that of WEAC_AL and ECPCS-HC, and it also achieves the highest average ACC score on the D2, D4, D6, and D8 datasets. Comparing the ensemble approaches based on spectral clustering, the average performance in terms of NMI of C²SWCE_SC is significantly higher than that of

other methods on the D1-D4 dataset. For example, on the D1 and D2 datasets, the average NMI scores of SC_SRGF are 0.2371 and 0.1931, respectively, while the average NMI scores of C²SWCE_SC are 0.8943 and 0.5666, respectively, which increased by about 4 times. In addition, compared with the other bipartite graph partitioning ensemble methods, the proposed C²SWCE_BG achieves the highest average NMI score on 6 datasets and the highest average

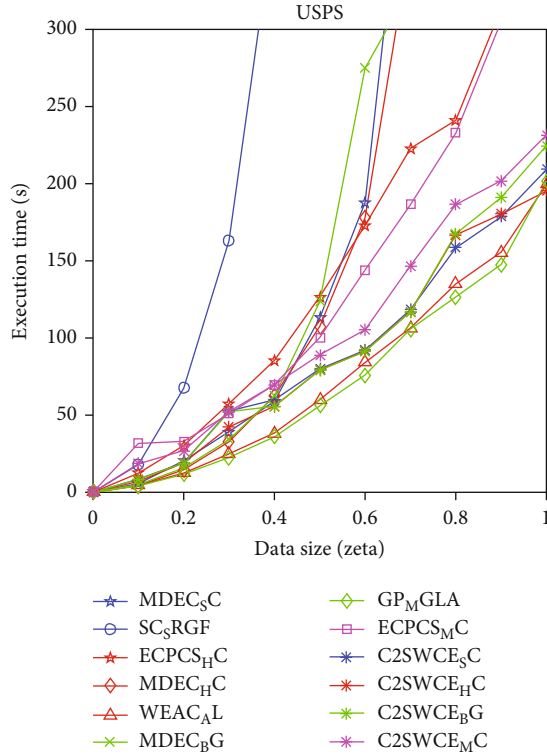


FIGURE 5: Execution time of clustering ensemble approaches with different data sizes.

ACC score on 5 datasets. Its performance is significantly better than MDEC_BG, GP_MGLA, and LWGP. In particular, on the D1, D3, and D4 datasets, the average NMI scores of the C²SWCE_BG are 0.8821, 0.5514, and 0.8955, respectively, significantly exceeding the corresponding NMI scores of 0.2794, 0.2847, and 0.2194 for the GP_MGLA. Finally, the metacluster-based ensemble clustering proposed in this paper is significantly better than that of the ECPCS-MC method on all datasets except D7.

4.7. Execution Time. In this section, we compare the execution times of different clustering ensemble approaches at the integration phase on the USPS dataset. The USPS dataset contains 10 categories with a total of 11,000 samples. To compare the clustering effects of different ensemble approaches on datasets of different sizes, first, according to the method described in Section 4.1, samples of different proportions are randomly selected for each category of the input dataset, to generate the USPS dataset of different sizes. In the experiment, the sample sampling ratio ζ is set in interval of $[0, 1]$, and the increment set to 0.1. That is, the generated dataset contains $n\zeta$ samples, where n is the number of samples in the USPS dataset. Running various ensemble approaches on the USPS datasets of different sizes, Figure 5 compares their execution time during the integration phase.

As can be seen from Figure 5, the execution time of all ensemble approaches increases significantly as the size of the USPS dataset increases, with SC_SRGF and MDEC_SC

approaches increasing the fastest. When clustering all samples of the USPS dataset, the proposed C²SWCE_HC, C²SWCE_SC, C²SWCE_BG, and C²SWCE_MC approaches are 195.23 s, 209.15 s, 220.72 s, and 231.65 s, respectively. Compared with other ensemble methods, the proposed methods have obvious advantages, especially the computational efficiency of C²SWCE_SC is higher than that of the contrasting spectral clustering ensemble methods MDEC_SC and SC_SRGF. The results show that the spectral clustering method based on the core clusters can reduce the complexity of the spectral clustering method to a certain extent. Further, compared with other hierarchical clustering ensemble methods, the execution time of C²SWCE_HC is comparable to that of the WEAC_AL, but much faster than that of ECPCS-HC and MDEC_HC. At the same time, we also observed that the execution time of the C²SWCE_BG is slightly higher than that of the GP_MGLA, but it has a significant advantage over MDEC_BG.

In summary, the proposed approaches have a modest computational cost for ensemble tasks on USPS datasets of different sizes. Compared with the same type of ensemble approaches, the execution time of the proposed 4 approaches have advantages.

5. Conclusion

In this paper, we propose a novel locally weighted subspace clustering ensemble framework, termed C²SWCE. It first uses the hybrid feature selection strategy that combines random feature selection and unsupervised feature selection to generate a set of base subspaces. The strategy combines the diversity of random feature selection to select representative features from each random subspace in an unsupervised manner, continuously reducing the dimensionality of the random subspace. To increase the diversity of subspace ensemble members, in addition to using random feature selection to generate feature subspaces, we also randomly group the samples into different numbers of clusters. Furthermore, we introduce concept of the core cluster. In the ensemble process, the core cluster is viewed as the base unit, which improves the ensemble efficiency to a certain extent. The subspace clustering solution is weighted by evaluating the stability of the cluster. Last but not least, under the proposed framework, four weighted ensemble approaches are proposed to integrate the clustering solutions of the base subspace to achieve the final clustering result. Extensive experiments are conducted on 8 real-world datasets to verify the effectiveness of the proposed ensemble approaches. Experimental results show that compared with the state-of-the-art ensemble methods, our methods have stronger robustness, and the comprehensive performance of clustering accuracy and efficiency has advantages.

Data Availability

Data sharing is not applicable to this article as no new data were created or analyzed in this study.

Conflicts of Interest

The author states that this article has no conflict of interest.

References

- [1] E. Elhamifar and R. Vidal, "Sparse subspace clustering: algorithm, theory, and applications," *IEEE Transactions on Pattern Analysis and Machine Intelligence*, vol. 35, no. 11, pp. 2765–2781, 2013.
- [2] X. Chen and D. Cai, "Large scale spectral clustering with landmark-based representation," *In Proceedings of AAAI Conference on Artificial Intelligence*, vol. 25, no. 1, pp. 313–318, 2011.
- [3] W. Y. Chen, Y. Song, H. Bai, C. J. Lin, and E. Y. Chang, "Parallel spectral clustering in distributed systems," *IEEE Transactions on Pattern Analysis and Machine Intelligence*, vol. 33, no. 3, pp. 568–586, 2011.
- [4] D. Huang, C.-D. Wang, J.-H. Lai, and C.-K. Kwoh, "Toward multidiversified ensemble clustering of high-dimensional data: from subspaces to metrics and beyond," *IEEE Transactions on Cybernetics*, pp. 1–14, 2021.
- [5] X. Cai, D. Huang, C.-D. Wang, and C.-K. Kwoh, "Spectral clustering by subspace randomization and graph fusion for high-dimensional data," in *Pacific-Asia Conference on Knowledge Discovery and Data Mining*, pp. 330–342, Springer, Cham, 2020.
- [6] K. Shankar, "Fuzzy clustering and classification based iris recognition: a medical application," *American Journal of Business and Operations Research*, vol. 1, no. 1, pp. 19–27, 2020.
- [7] S. Verma and S. Gain, "Mitigating hot spot problem in wireless sensor networks using political optimizer based unequal clustering technique," *Journal of Cybersecurity and Information Management*, vol. 8, no. 2, pp. 42–50, 2021.
- [8] H.-P. Kriegel, P. Kröger, and A. Zimek, "Clustering high-dimensional data," *ACM Transactions on Knowledge Discovery from Data*, vol. 3, no. 1, pp. 1–58, 2009.
- [9] Z. Yu, P. Luo, J. You et al., "Incremental semi-supervised clustering ensemble for high dimensional data clustering," *IEEE Transactions on Knowledge and Data Engineering*, vol. 28, no. 3, pp. 701–714, 2016.
- [10] L. Jing, K. Tian, and J. Z. Huang, "Stratified feature sampling method for ensemble clustering of high dimensional data," *Pattern Recognition*, vol. 48, no. 11, pp. 3688–3702, 2015.
- [11] X. He, D. Cai, and P. Niyogi, "Laplacian score for feature selection," *In Proceedings of International Conference on Neural Information Processing Systems*, pp. 507–514, 2005.
- [12] D. Huang, J. Lai, and C.-D. Wang, "Ensemble clustering using factor graph," *Pattern Recognition*, vol. 50, pp. 131–142, 2016.
- [13] C. Domeniconi and M. S. Al-Razgan, "Weighted cluster ensembles," *ACM Transactions on Knowledge Discovery from Data*, vol. 2, no. 4, pp. 1–40, 2009.
- [14] Z. Li, X.-M. Wu, and S.-F. Chang, "Segmentation using superpixels: a bipartite graph partitioning approach," in *Proceedings of IEEE Conference Computer Vision Pattern Recognition*, pp. 789–796, Providence, RI, USA, June 2012.
- [15] J. Jianbo Shi and J. Malik, "Normalized cuts and image segmentation," *IEEE Transactions on Pattern Analysis and Machine Intelligence*, vol. 22, no. 8, pp. 888–905, 2000.
- [16] D. Cai, X. He, J. Han, and T. S. Huang, "Graph regularized nonnegative matrix factorization for data representation," *IEEE Transactions on Pattern Analysis and Machine Intelligence*, vol. 33, no. 8, pp. 1548–1560, 2011.
- [17] S. Matsushima and M. Brbic, "Selective sampling-based scalable sparse subspace clustering," *In Proceedings of Advances in Neural Information Processing Systems*, pp. 12416–12425, 2019.
- [18] D. Huang, C.-D. Wang, H. Peng, J. Lai, and C.-K. Kwoh, "Enhanced ensemble clustering via fast propagation of cluster-wise similarities," *IEEE Transactions on Systems, Man, and Cybernetics: Systems*, vol. 51, no. 1, pp. 508–520, 2021.
- [19] D. Huang, J. H. Lai, and C. D. Wang, "Combining multiple clusterings via crowd agreement estimation and multi-granularity link analysis," *Neurocomputing*, vol. 170, pp. 240–250, 2015.
- [20] D. Huang, C.-D. Wang, and J.-H. Lai, "Locally weighted ensemble clustering," *IEEE Transactions On Cybernetics*, vol. 48, no. 5, pp. 1460–1473, 2018.

Research Article

Psychological Quality of Piano Players Based on Big Data Algorithm

Rui Li ¹, Rasa Kirliauskienė,¹ Yixin Sun,² Shixue Dong,³ and Li Zhang⁴

¹Education Academy, Vytautas Magnus University, Kaunas 44248, Lithuania

²Department of Informatics, King's College London, London WC2B 4BG, UK

³Chinese International College, Dhurakij Pundit University, Bangkok 10210, Thailand

⁴Academy of Arts, Shangqiu University, Shangqiu, 476000 Henan, China

Correspondence should be addressed to Rui Li; rui.li@vdu.lt

Received 18 April 2022; Revised 3 May 2022; Accepted 6 May 2022; Published 24 May 2022

Academic Editor: Alireza Souri

Copyright © 2022 Rui Li et al. This is an open access article distributed under the Creative Commons Attribution License, which permits unrestricted use, distribution, and reproduction in any medium, provided the original work is properly cited.

Piano performance has been around for hundreds of years, and piano performance is currently on the rise. As a pianist, better presentation and performance skills are necessary as a player. And in the process of playing, people must also have a calm psychological quality in order to play the piano perfectly and bring beautiful enjoyment to the audience. This is also the basis for the smooth progress of the performance. The better the psychological quality of the performer, the better the performance will be. This paper analyzes the influence of the psychological quality of piano performance based on the big data algorithm and finds that under the influence of the big data algorithm, the psychological quality of the performers is enhanced by 18%. As for the richness of on-site experience and the stable performance of technology, it is about 20% higher than normal in all aspects, which can provide reference for related research.

1. Introduction

Two hundred years ago, the piano has been popular in Europe. At this time, the piano can only make monotonous pronunciation, but it is still in the stage of development. Among them, there is a piano enthusiast who made a reasonable modification of the piano mechanism, so that the strings can be struck multiple times to produce different sounds. At this point, music began to develop from simple to complex. On this basis, it was slowly used in other musical instruments, and since then, it has entered the era of musical instruments. After 40 years, enthusiasts changed the strings and combined the three elements to achieve the basic model of the modern piano, which is also the origin of the shape of the modern piano. For the next hundred years, the string structure has not changed.

The current piano literature occupies a place in the genre of quyi. It has an extremely important position in the contemporary cultural world. It contains all kinds of rich knowl-

edge, playing techniques, psychological adjustment, and so on. It also has a thought-provoking philosophy and serves as a guiding light for modern players. It is explained from many aspects, combined with some contemporary musical concepts, showing its special vitality. When playing with a piece, it will pay more attention to the inner meaning. In this paper, we pay attention to the analysis of real-time data, which is of reference significance to a certain extent, and can reduce tension as much as possible for piano players when playing, making the performance more stable, and the audience can also be pleasing to the eyes, providing piano players with certain benefits. The uniqueness of this article is that the data often processed by big data algorithms are more realistic have the right to speak.

The paper is mainly divided into 4 parts. The first section of the third chapter mainly describes the psychological influence factors of the piano players. The second section mainly describes the methods of cultivating and adjusting a good performance mentality. The third section mainly

describes the psychological obstacles of the piano players., the fourth section is the big data algorithm used, the fifth section is about the skills of piano players, and the sixth section is the current thinking about music education.

2. Related Work

On big data algorithms, evolutionary algorithms (EA) have recently been suggested as candidate methods for solving big data optimization problems that involve a large number of variables and require analysis in a short time. However, EA faces scalability issues when dealing with big data problems. To address these challenges, Sabar et al. proposed a heterogeneous framework that combines cooperative coevolutionary methods with various types of meme algorithms to improve the efficiency of the solution process [1]. With the rapid development of information technologies such as the Internet and the Internet of Things, big data usually exists in cyberspace in the form of data streams. It brings enormous benefits to the information society. At the same time, it also brings severe challenges to big data mining in data flow. Recently, various university circles have developed a strong interest in massive data mining, and Pradeep and Naveen launched an analysis and discussion on this [2]. Big data (BD) approaches have had a major impact on the development and expansion of supply chain network management and design. In the BD environment, it is very challenging to face these problems and greatly affects the efficiency of SCN. Optimizing the right network with the right batch can minimize the overall carbon footprint in the SCN. It plays a key role in this. In response, Goodarzi et al. developed a production-transport-order-inventory, which is a mixed integer nonlinear programming (MINLP) model [3]. In modern medicine, medical imaging has come a long way, with the ability to capture several biomedical images from a patient. It can use and train these images in intelligent systems. By analyzing these images, different diseases can be identified. Tchapgaa et al. described how to use the Spark framework to apply these algorithms to big data architectures. And he further proposed a classification-based workflow [4].

Among the pianists, Viktor Syriatsky is a contemporary leader. During his 35 years of work at the I. P. Kotlyarevsky State University of Arts in Kharkiv, he trained several generations of famous musicians. Syriatska revealed the fundamental principles of Viktor Syriatska's performance style and the nature of his artistic aspirations. In order to reveal the chosen theme, he used sophisticated music analysis methods [5]. Vsevolod Vladimirovich Topilin (1908–1970) was a pianist and teacher. He played an important role in the development of Ukrainian piano culture. Tragic events of the twentieth century disrupted his life and career and kept him out of public life. Pinchuk introduced the particulars of the pianist's life and work and his works, as well as his place in the musical, and the society's complete evaluation of it [6]. Meitner was a brilliant composer, a brilliant pianist of the twentieth century, and a thoughtful philosopher. Danilova analyzed the relationship between creative reflection in his literary heritage and the author's performance inter-

pretation, revealing that there is an inevitable connection between the master composer's thinking and playing style in the creative process [7]. There are also some pianists who have suffered from osteoarthritis of the thumb, wrist, and metacarpal joints because of playing for a long time. Pianists also hurt their fingers when playing is shown in Table 1.

3. Calculation of the Psychological Quality of Piano Players Based on Big Data Algorithms

3.1. Psychological Influencing Factors of Piano Players. Piano playing has a history of hundreds of years. The piano is also dubbed the master of musical instruments by contemporary people. Because of its special playing style and tone, it is worshipped by many piano lovers. The piano is also the most popular at the moment, and it is also the most studied. In the use of the piano, it is mainly divided into two categories, as shown in Figure 1. No matter what kind of player, most of them will show different degrees of performance in the performance. This is mainly related to the psychological quality of the player. Among them, the way of thinking, behavior, and self-feeling are all related to the performer, and only those who have a certain talent can learn. Moreover, it is necessary to focus on the cultivation of psychology in order to ensure a complete performance [8].

3.1.1. Quality Factors. Psychological quality also has a huge impact on the performer. It is affected by many external factors, and it is also related to the training time in the later stage, and it is also the embodiment of the player's emotions in the performance process. If the player makes a little mistake in the performance, it may lead to a failed performance in the end [9]. When mistakes are made, they are prone to a blank brain, uncontrolled body, rapid heartbeat, weakness of limbs, and various discomforts. However, if the players have a strong ability to withstand pressure, they will generally return to normal through self-regulation. This is a qualified pianist. And it will also determine the response time according to the different reaction speed of the person. If there are gaps in the performance, it will be fatal, and these problems will not easily occur with high quality. Because each person's own ability to bear is different, it also leads to different degrees of panic after playing and attracting attention from everyone, which is not qualified for a piano player.

3.1.2. Technical Factors. If the psychological factor is the soul of the performer, then the technical factor is the body of the performer, and the two are indispensable. If there is no problem with the psychological state, there are two kinds of problems with technology. If the psychology is tough, but the technology is not at home, it will be useless. For the audience, it may be a spit game. For the psychological quality, there are many factors that affect it. For example, the individual's innate ability to accept psychology, pressure, and technical factors are completely related to the individual. It requires unremitting perseverance, training, and also needs to reflect their own perceptions in it. If they truly feel

TABLE 1: The relationship between creative reflection and author's performance interpretation.

Name	Sabar N R	Pradeep K R	Goodarzia F	Tchapga C T	Syriatska T	Pinchuk O	Danilova O S
Question	Scalability issues	Big data mining	Supply chain network management and design have an impact	Use the Spark framework	Reveal selected topic	Learn about pianist works and status	The relationship between creative reflection and author's performance interpretation
Method	Heterogeneous framework	Expand analysis and discussion	Developed a model for nonlinear programming	Classification-based workflow	Using sophisticated music analysis methods	Introduction to the role of musicians in development	Reveals the inevitable connection between thinking and playing style

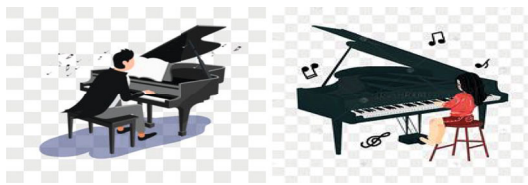


FIGURE 1: Pianist.

that the music is in their hearts and they are within their grasp, they will be able to play with ease, so that they can truly become a qualified pianist and bring joy to the audience [10]. Although diligent practice is also the main work, the technique also requires one's own familiarity with the piano. Only by training each tone and rhythm many times, and really integrating the movements of the fingertips into the heart, there will be few panic and blank situations, and they can have a perfect piano performance. The psychological quality of the piano player will be improved in the technical and psychological quality under the big data algorithm, and the player's heart will be affirmed.

3.1.3. On-the-Spot Experience. Many performers will experience stage fright in different environments, not to say that they are afraid to play, and they are afraid of making mistakes in performance [11]. Because of the difference in their own psychological abilities, the surrounding environment, the touch between their fingers, and the presence of thousands of people watching, they will also involuntarily put pressure on themselves. This results in the player being unable to resonate with the surrounding environment and mood. This makes them unable to play good tunes. They play the piano in the piano room and in the public venue, and their mood is different. In the piano room, most people have no psychological pressure and can play well. But in the open room, there will be pressure, and it is easy to generate tension. Although this reflects the player's ability to be present to a certain extent, it is really unqualified. Although their technical or psychological abilities are qualified, errors occur when they are on the spot. This requires players to try on-the-spot performances many times, so that they can break through themselves and improve their ability to play the piano [12].

3.2. Methods of Cultivating and Regulating a Good Playing Mentality

3.2.1. Relax, Self-Encouragement. The best way to cultivate and adjust a good playing attitude is 1 to 2 hours before the scene, which is conducive to the player's better performance. The main reason why pianists are prone to problems is psychological. They are prone to panic, blanks, etc. As a pianist, they need to adjust themselves before the competition. If there is a bad mentality, they will easily lead to normal thinking disorder and affect the normal performance. As for clear purpose, building confidence is also a must as a pianist. The mentality is not calm, just like water in a glass, shaking left and right, and the brain's speculative operation is suspended. This affects the performance of the pianist. They need to devote themselves wholeheartedly to the performance and to create in their own music without being influenced by the outside world [13].

3.2.2. Accumulation and Cohesion of Aesthetic Feelings. Before participating in the performance, the performers will be well prepared, familiar with the skills, perceive the environment, and achieve the desired effect from the part to the whole through continuous training, so that they can play with ease [14]. There are two difficult points. At the technical level, it takes a long time for the pianist to become familiar with the new repertoire. At the level of accumulating the feeling of the beauty of music, this needs to be cultivated and not achieved overnight. Among them, on the one hand, it is necessary to break through a difficult problem in technique, and on the other hand, it is necessary to further accumulate and condense aesthetic feelings and feelings. It is these accumulations and condensations that will arouse the performers' creative passion and form a huge desire to express before the performance. The on-the-spot tension and cramped emotions before the performance should be transformed into passion rather than tension. This kind of excitement makes people have a strong desire to perform. Only when the performer himself concentrates his thoughts into the music can he express the contagious music with enthusiasm.

3.2.3. Accumulation of Stage Practical Experience. Before the performance, they can usually train outside. They can also

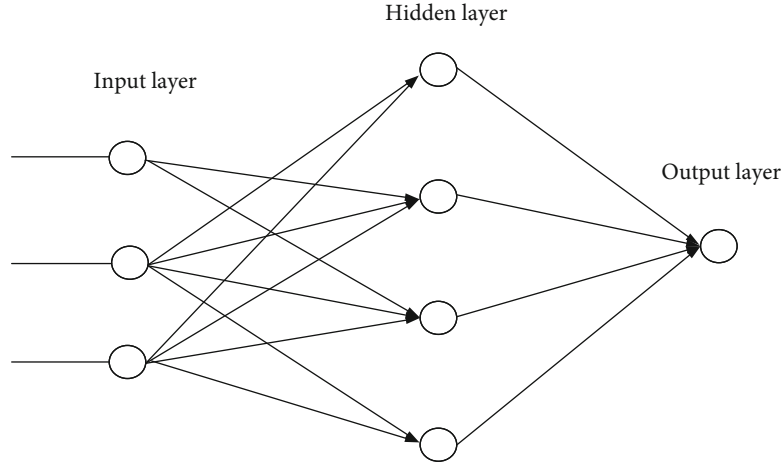


FIGURE 2: Neural network algorithm structure.

perform performances under the watchful eyes of their friends, familiarize themselves with the operating environment in advance, and understand the connection between them. This can also make subsequent performances smoother and smoother. Performers can play directly to people they know, such as colleagues or relatives and friends, to build a platform for psychological communication between performers and the audience [15]. At the same time, they pay special attention to the internal environment such as the sound reflection and the brightness of the light and then adapt to the new piano and try the piano carefully to master the tone and volume of the new piano accompaniment and check whether the keyboard tone is consistent. If there is a problem, they should immediately call a technician to adjust.

3.3. Psychological Disorders of Piano Players

3.3.1. Tension. For some beginner performers, or professional performers, they are more or less in a state of panic before stepping onto the high-profile stage. Their mental state before the performance was full of confidence, and as soon as they got to the stage, their palms were sweaty and nervous. Although there will be relatives and friends around to cheer and encourage, there will be tension caused by some psychological factors, which will lead to mistakes.

3.3.2. Arrogance. For some performers who feel good about themselves, their appearances may be partly nervous and arrogant, feeling that their performances are unmatched and blindly confident. And the usual training is not as good as that of other performers, and they do not communicate with other people very much and live in their own world. Although it is not good to be too nervous, it should not be too arrogant, and there is no pressure at all. This is destined to be eliminated and even more serious consequences.

3.3.3. Negative. There are also some people because of bad performances during the performance give up and deny themselves, resulting in negative emotions and loss of motivation. Some of them are caused by being forced to learn to play the piano, or they do not like it, and they are caused involuntarily. If there is no encouragement in this situation,

it will only develop in a bad direction, or even become reversed, causing more bad results. Because it can be summarized through the neural algorithm of big data, so as to analyze the influence of the players' psychological quality on their performance.

3.4. Big Data Algorithms

3.4.1. Neural Network Algorithm. Neural network algorithm is a relatively traditional computing method, and its network formation is similar to neurons. Each neural unit constitutes a set, and finally a population is formed by synaptic connections. Each neuron is connected to each other, and they have a separate activation or inhibition state [16]. They can combine the information they have or perform one-to-one transmission. Each unit will have a limit function on it. If there are too many transmitted signals, they will play a limiting role. These are built-in neurons and do not need to be trained and learned. They will be trained and learned through each transmission of information by neurons, which means they are mastered, and they are not programming.

However, it is not easy to express this form in a computer program, and it works best in the field of special effects networks. The processing method of neurons is similar to that of our human brain. They are connected through thousands of neurons, and then they always have computing power of an order of magnitude more complex than that of the brain. In order to train them, thousands of cycles need to occur, and these problems that are difficult to solve by programming are input into this training activity. The feature is also because the knowledge of the dynamic system and parameters is included, and the neural network mainly has three layers, which process and transmit information, respectively [17]. According to the layering of the neural network algorithm, a schematic diagram of the algorithm structure is drawn, as shown in Figure 2.

In the neural network algorithm, the input layer mainly stores the original data and the symbol M-input layer dataset. The expressions are as follows:

$$M = \{m_1, m_2, \dots, m_n\}. \quad (1)$$

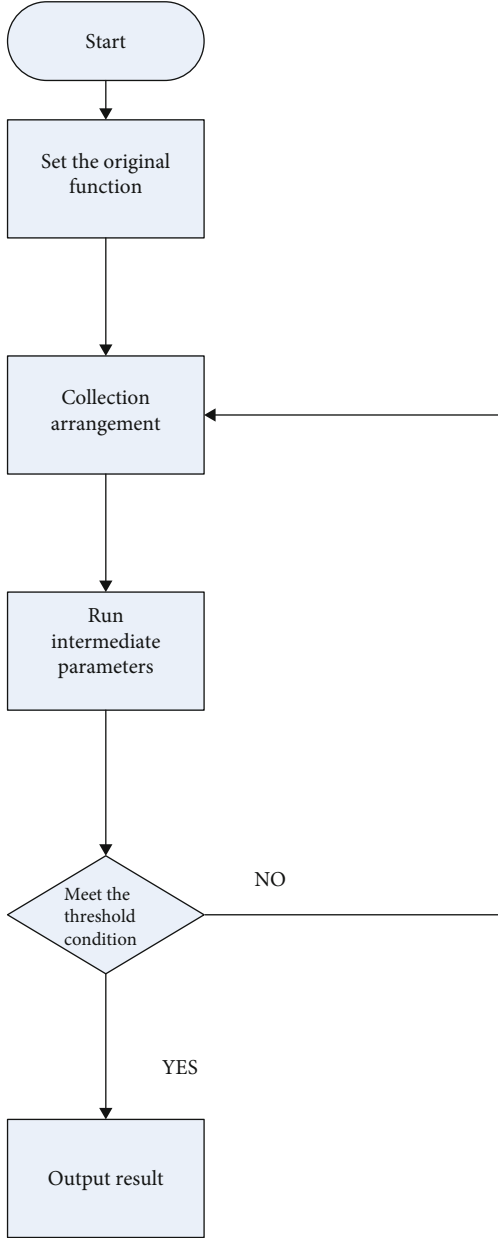


FIGURE 3: Neural network algorithm flow.

After going through the following formula, the two are related.

$$u = \sum_{i=1}^n w_i m_i - \theta = m^T w - \theta. \quad (2)$$

u is the weight relationship between the input data. w is the weight and, θ is the threshold. The startup method between them is as follows:

$$y = \frac{1}{1 + e^{-\lambda u}}. \quad (3)$$

Steps in between are as follows: it first sets up the original

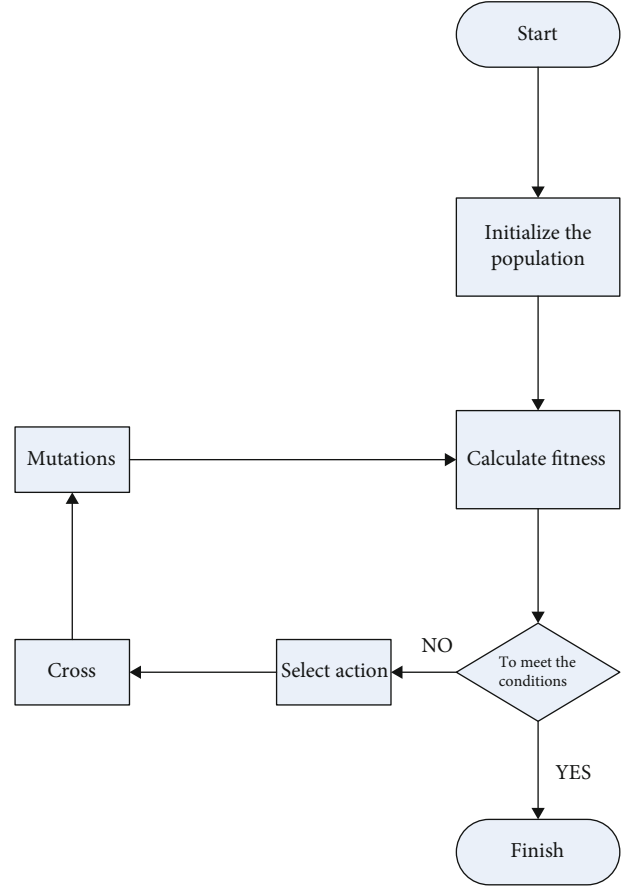


FIGURE 4: Genetic algorithm flow.

function and organizes it into a collection. It calculates the intermediate parameters according to the calculation formula of the correlation relationship and then outputs the results obtained by each layer and performs the function error operation. If it is within reasonable parameters, it outputs the result; otherwise, it reruns the operation until it outputs the result [18]. It is shown in Figure 3.

3.4.2. Genetic Algorithm. Genetic algorithm is an optimization method that performs a global search in parallel and dynamically in the solution space through the transformation, iteration, and mutation of a large number of candidate solutions. Because the genetic algorithm has a relatively complete mathematical model and theory, it has good performance in solving many NP-hard problems.

Genetic algorithms are designed according to Darwin's theory of evolution. Genetic algorithm individuals refer to a certain number of binary strings in a simulated chromosome. The numbering is done in binary, and the encoding method is as follows:

$$g(x_t^t, k) = u_k + \frac{u_k - v_k}{2^l - 1} \left(\sum_{j=1}^t x_t^{i(kl+j)} \times 2^{j-1} \right). \quad (4)$$

u_k means k is the number limit, and v_k means the minimum number of k . The drift point number means that there

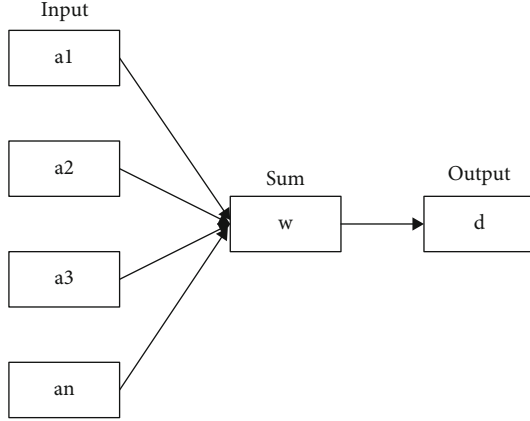


FIGURE 5: Word vector operation process.

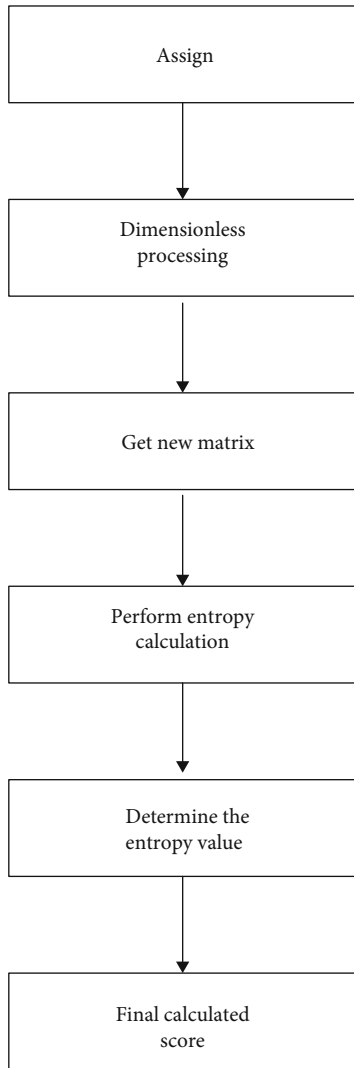


FIGURE 6: Weight division flowchart.

are n data in the hypothesis, and x_1^t is used to represent the t th chromosome of the first generation, where t can be expressed as

TABLE 2: Key points of pianist skills.

Musical skills	Scale	Chromatic scale	Arpeggio	Octave
Relaxation training	0	1	1	1
Skill training	1	1	1	0
Listening training	0	1	1	0

$$t = \{1, 2, \dots, n\}. \quad (5)$$

The quantitative information of each chromosomal gene is represented by $L = m$, and the drift number can be represented as follows:

$$X_0 \in (x_0^1, x_0^2, \dots, x_0^n)^T. \quad (6)$$

The genetic algorithm process is shown in Figure 4.

3.4.3. Word Vector Technology. Natural language understanding can be transformed into a problem of instrument learning. By constructing word vectors, the similarity score and distance are finally obtained, and the minimum number of edits is required to convert one character into another character. The conversion here can be said to be replacement or deletion. The following formula is obtained by finding the minimum number of edits, and this idea is called dynamic programming. The two strings are:

$$a = a_1, a_2 \dots a_n. \quad (7)$$

The formula for recursive calculation of edit distance is as follows:

$$d_{i0} = \sum_{k=1}^i w_{del}(b_k), i \in (1 \sim m), \quad (8)$$

$$d_{0j} = \sum_{k=1}^j w_{ins}(a_k), j \in (1 \sim n), \quad (9)$$

$$d_{ij} = \begin{cases} d_{i-1, j-1}, a_j = b_j, \\ \min(d_{i-1, j} + w_{del}(b_i), d_{i, j-1}), & a_j \neq b_j, \\ w_{ins}(a_j), d_{i-1, j-1} + w_{sub}(a_j, b_j). \end{cases} \quad (10)$$

where w represents the weight of the operation, such as adding, deleting, and changing:

$$w = \begin{cases} 1, & \text{have operation,} \\ 0, & \text{no action.} \end{cases} \quad (11)$$

Its logical relationship is more complex, and the algorithm time complexity is high [19]. The operation flow is shown in Figure 5:

3.4.4. Weight Division. As an objective assignment method, weight planning is to reduce the subjectivity of weights, and it also conforms to the logical thinking in mathematics.

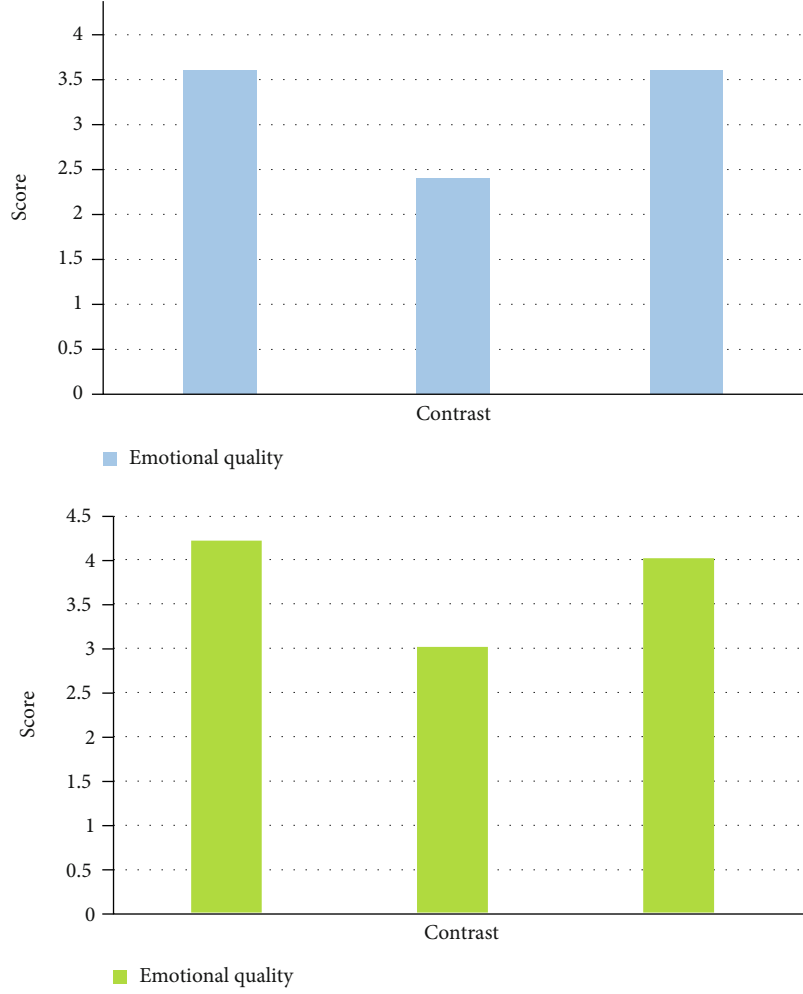


FIGURE 7: Emotional quality comparison.

Considering that in the assignment method, the difference between the original data and the output data will be relatively large, and the tempering treatment is generally performed first [20]. There are the following methods.

The dimensionless processing formula of the positive index is

$$a_{ij} = \frac{x_{ij} - \min_j \{x_{ij}\}}{\max_j \{x_{ij}\} - \min_j \{x_{ij}\}}. \quad (12)$$

The formula for dimensionless processing of negative indicators is

$$a_{ij} = \frac{\max_j \{x_{ij}\} - x_{ij}}{\max_j \{x_{ij}\} - \min_j \{x_{ij}\}}. \quad (13)$$

A new matrix can be obtained by operation. When calculating the index entropy value, the calculation method is

$$h_j = -T \sum_{i=1}^n p_{ij} \ln(p_{ij}). \quad (14)$$

Here $T = 1/\ln n$, $p_{ij} = (a_{ij} + 1)/\sum_{i=1}^n (a_{ij} + 1)$. The value of each indicator is determined as

$$w_j = \frac{1 - h_j}{\sum_{j=1}^m (1 - h_j)}, j = 1, 2, \dots, m. \quad (15)$$

It calculates the final score:

$$S = \sum_{i=1}^n \sum_{j=1}^m W_j A_{ij}. \quad (16)$$

Its operation flow is shown in Figure 6.

3.5. Pianist Skills. There are four types of piano playing techniques, scale, chromatic scale, arpeggio, and octave [21, 22]. This is also a relatively conventional four techniques. In the performance of musical instruments, musical elements are also the basic knowledge of music theory. In the process of

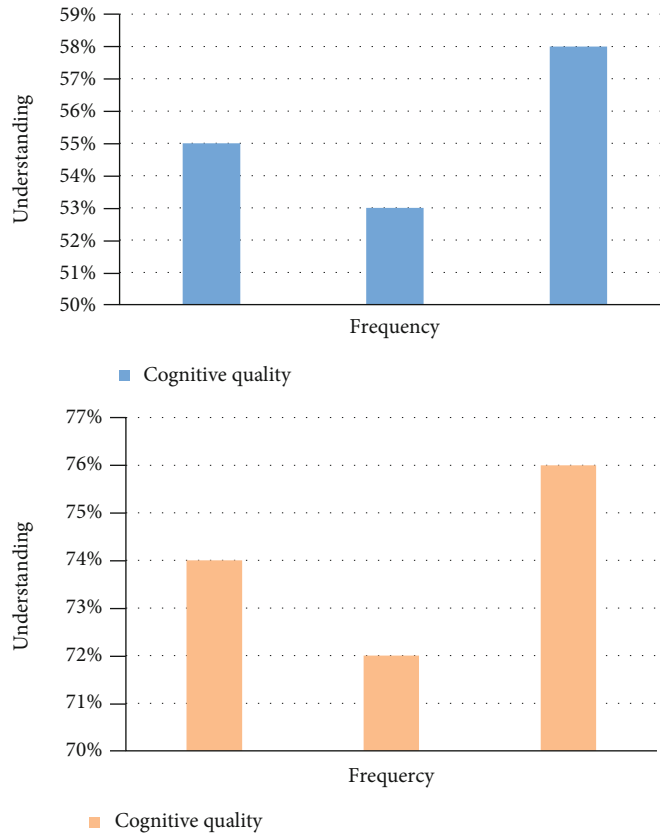


FIGURE 8: Cognitive quality comparison.

musical instrument performance, it is necessary to have strong emotions and perceptions of art. Playing the piano is also the most basic content. Music is inseparable from the piano, and the piano is also inseparable from the music. Generally, piano performance is mainly reflected in the emotional or emotional expression of music, and it is also its main expression method. The two are interdependent. For a perfect piano performance, the two must be inseparable. Music sense can give the piano a better timbre, and the timbre of the piano is not found in other instruments. One of the people’s favorite artistic expressions is piano performance, which has extremely high artistic value and reference significance [23, 24].

If they can play a more beautiful melody, then they must have mastered some basic skills. Taking advantage of the different points and advantages of playing these techniques, the application in piano performance can improve the timbre performance and the intuitive influence of timbre in piano research and can also improve the basic skills of playing. It plays an important and decisive role in understanding the basic piano knowledge and improving the subsequent performance [25, 26].

As the basic method of piano performance, what he needs to do is to integrate the elements, melody, and rhythm in the music and finally interpret the music better. However, this process requires a lot of time and effort. These elements are fused to achieve a situation where they can be retracted freely. Moreover, in the process of learning, they will have

a better understanding of the elements of music, which is quite a training exercise to exercise the skills of the piano player, and it will also allow the player to slowly integrate the skills between the fingers. In training, these three mainstream trainings need to be strengthened [27]. The songs played by some performers will make the audience feel the inner world of the performers in the music, so that the music can be integrated with the spiritual world, directly hit the soul, and give people the enjoyment of the beauty of the spiritual world [28].

From another point of view, the style, charm, melody, and emotion represented by music also determine its particularity and appreciation. Its tone determines the player’s technical ability, as well as the emotional expression of the piano performance, and they restrict and coexist with each other. Without the skill of the pianist, the sound of the piano is meaningless, and vice versa. The tune of the piano player can also prove that the player’s heart is gentle and spreading, and the player’s heart is like the Yangtze River, flowing calmly. The tune is high-pitched and loud, indicating that the performer’s heart is full of passion at this moment, and the blood is bursting [29].

The performance of the tune is related to many aspects, and the tone is also used as a conveyor belt or listening tree for people’s emotional sustenance, conveying the inner emotions of the listener. Different timbres are affected by the player’s skills, finger coordination, flexibility, strength, etc. There are many factors, such as these three aspects,

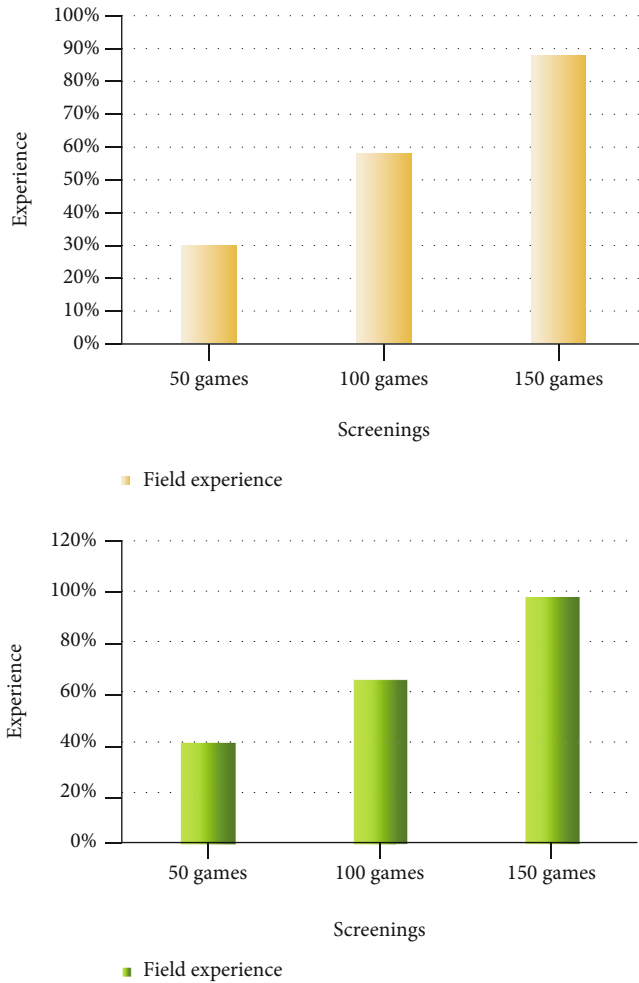


FIGURE 9: Field experience comparison.

keystroke ability, finger coordination, and finger strength control. The key table of piano skills is shown in Table 2 (0 means nonessential key points, and 1 means essential key points).

3.6. Current Situation and Countermeasures of Music Teaching. The education of contemporary music for students should not be left unchecked. It should be people-oriented, cultivate students' interests, focus on students, mutual respect between students and teachers, and advocate independent exploration. It should not be limited to books and can discover more about life. Finding the shadow of music in life is mainly in the cultivation of students' ability, not just letting it go, which is unqualified for teachers. Any kind of skill or ability is acquired under the precipitation of time.

The cultivation of students' musical quality also requires time conversion. Constantly improving and optimizing can only have a solid foundation, so that it will be easier to learn profound knowledge in the follow-up. At the beginning, it is necessary to sort out the structure of music knowledge. As for letting students have a basic understanding of music, only on the basis of understanding music knowledge can they slowly develop their musical literacy and appreciation

ability. This is the focus of music education, the knowledge of teacher education, and the knowledge learned in life, and sorting is the student's own ability and skills.

Modern music education has produced the problem of de-intellectualization, and there are roughly two types. Some teachers have made music class a more professional class, and students do not understand it at all. Without a basic knowledge of music, they are laymen. Another is that music class teachers regard music class as a course for students' daily leisure and relaxation, so that the reformers interpret it as not teaching knowledge. The music class also needs practice, and it is impossible to really understand it only at the knowledge level. At the teaching level, it is actually best to set up some music clubs and let students participate in this kind of activities more, so that students can understand and form their own understanding of music, which is also a basic path for students to understand themselves and the world. With the progress of the times, a lot of one-sided knowledge will be improved, and it will also allow students to develop more comprehensively. Music literacy is related to personal literacy and knowledge. It needs to train interested students into professional music talents and teach students in accordance with their aptitude. As for interested students, they can be trained completely. If they are not interested in music but are interested in other courses, then they can develop other courses. It is unrealistic to train every student in accordance with professional talents.

To cultivate students' interest in music, first of all, students need to be able to understand music. After a period of training, if students find their interest, they will gradually enter their favorite emotions and gradually become more interested in music. The accumulation of knowledge forms a special understanding of music and improves one's own music literacy and appreciation level.

4. Comparison of Psychological Influencing Factors of Performers

Through the big data algorithm, the player's psychology can be obtained from an intuitive data, because the inner activity is indescribable, and the improvement of the player's psychological quality is to convert the natural language into machine learning and then read the obtained data. The word vector is calculated by a recursive algorithm to obtain the weight ratio data. In the comparison between the neural network algorithm and the genetic algorithm in the analysis, the prediction is the neural network algorithm, but the comparison of the genetic algorithm has shortcomings, and it is not easy to compare in terms of cognitive quality.

With the development of science and technology, the psychological quality of piano players is gradually analyzed using big data algorithms. The piano is a keyboard instrument derived from ancient Western music. Among many musical instruments, the piano also has its own unique characteristics. After hundreds of years of circulation and introduction to China, the sound and timbre of the music have gradually formed a unique form, which is loved by the Chinese people.

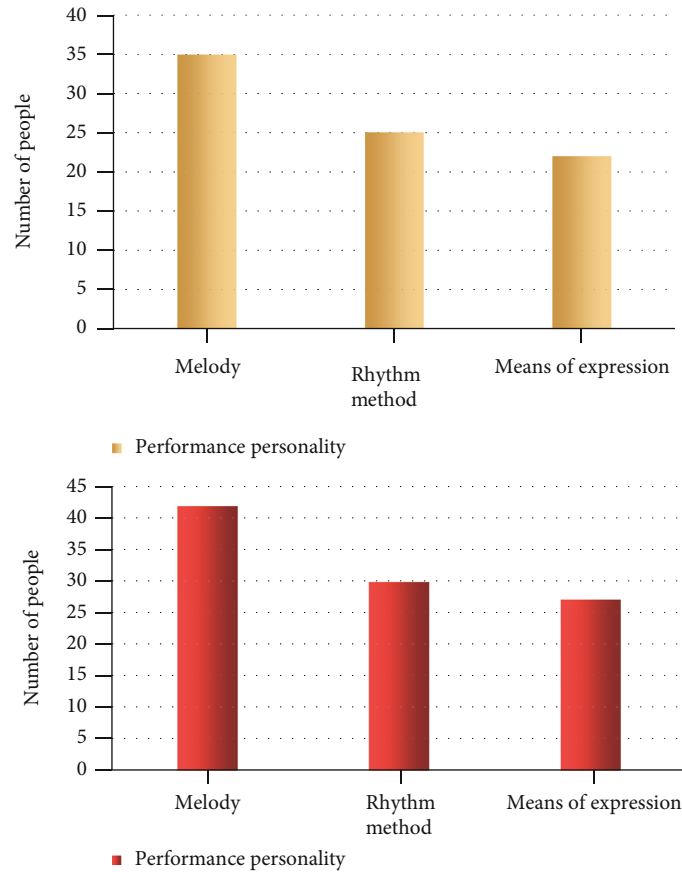


FIGURE 10: Comparison of the number of performers.

This paper mainly compares the four aspects of the pianist's emotional quality, cognitive quality, performance personality, and role adaptability, because in the performance, the emotional quality of the piano player is related to the emotional expression of the performance and the emotional expression of the audience. Through the comparison and analysis of the experiment, the evaluation method under the big data algorithm is compared with the artificial emotional evaluation, as shown in Figure 7.

Through the comparison of the two sets of data, it can be seen that the score of the emotional quality of the piano players under the big data operation will be about 16% higher than the conventional score. It also shows that under the operation of big data, the emotional expression of the piano player will be more familiar to the audience, and it is easy to resonate with the emotion. The music brought to the audience by the pianist under the operation of big data will also become clearer, and the audience can also understand the emotion that the pianist wants to express.

Contemporary music listeners also gradually gain self-awareness, understanding of music, and self-feelings. The listeners will have a self-perception based on the emotions or moods conveyed by the performer and finally come to their own inner feelings. Figure 8 is a comparison of the cognitive qualities of piano players.

Through this set of data comparison charts, it is not difficult to see that in the case of big data operations, the cog-

nitive quality of piano players has improved by about 20%. It also makes players more aware of their own performance. And the concerts expressed in this way bring more intuitive emotional enjoyment to the audience, which is also a big improvement for the performers themselves, because self-awareness is the beginning of progress. Cognitive quality is also a challenge for performers.

Every famous pianist has experienced ups and downs. There is a lot of on-the-spot experience, and on-the-spot experience is indispensable for players. The lack of live experience may affect the performance and even lead to the loss of reputation and no one cares. Experienced players will be at ease. The following figure is a comparison of on-the-spot experience under big data, as shown in Figure 9.

Through comparison, it is found that under the operation and analysis of big data, the experience improvement of live experience to the performers in the same session is not the same. In the case of using big data, the experience improvement is about 10%. It also shows that under the operation of big data, compared with traditional performance, the player will improve faster, and it will be more helpful to the player, which is conducive to adjusting their mentality and overcoming their psychological state. In the case of the state, it will also bring a musical feast.

Modern performances also have a unique performance style and personality, which is also to make the performance more full, and some even exaggerated performances to

achieve the effect expected by the audience. In the case of big data operations, the performers have also become richer in their own unique personalities, as shown in Figure 10.

Through the comparison of the two sets of data, it can be seen that on the basis of big data operations, the number of people who play the piano with individuality has increased by about 20%. Personalized performance also shows that new styles of piano performance will gradually emerge. It is not a single black silent style. More and more excellent piano players express their true self in their personalized performances, expressing different personalities and playing emotions. The performance will be more distinct, with new features and vitality.

5. Discussion

Although the spiritual enjoyment brought by the piano is short-lived, in the long river of time, people will spread this sound. It is sealed in the form of a network, so that it will remain in our hearts forever, and we can play it if we want to listen, pursue the best sound quality, and restore the sound of live performances as much as possible. For music lovers, it is food for the soul; but for those who do not love piano, it means nothing; on the contrary, it may cause major problems, especially for newbies, who are only interested. Only then can they lead them to get started, and they must not act arbitrarily. It is necessary to teach students according to their aptitude and cultivate more musical talents. In the future, it may come into contact with more people, and it will gradually push the performance to a new height. This is what piano performance enthusiasts are looking forward to.

6. Conclusion

The full text mainly describes the analysis of the psychological factors of piano players under the big data and analyzes the influence of emotional quality, cognitive quality, performance personality, and role adaptability on the players. It uses methods such as big data calculation to explain in essence and how to make players play more smoothly. It supplements some skills that piano players need to use. It is found that the piano players under the big data algorithm are more energetic and vital than the original group of piano players, and the performance will be smoother and more stable. Using algorithms in big data for analysis, it tells what factors will be affected by players and how to adjust them, as well as simple playing knowledge and some thoughts on future musical instrument performance. It also shows that piano players under the big data will have more advantages, which will promote the subsequent development. Subsequent piano performances will also bring more excellent and high-quality works to the audience.

Data Availability

This article does not cover data research. No data were used to support this study.

Conflicts of Interest

The authors declare that they have no conflicts of interest.

References

- [1] N. R. Sabar, J. Abawajy, and J. Yearwood, "Heterogeneous cooperative co-evolution memetic differential evolution algorithm for big data optimization problems," *IEEE Transactions on Evolutionary Computation*, vol. 21, no. 2, pp. 315–327, 2017.
- [2] K. R. Pradeep and N. C. Naveen, "A collective study of machine learning (ML) algorithms with big data analytics (BDA) for healthcare analytics (HcA)," *International Journal of Emerging Trends & Technology in Computer Science*, vol. 47, no. 3, pp. 149–155, 2017.
- [3] F. Goodarzi, V. Kumar, and A. Abraham, "Hybrid meta-heuristic algorithms for a supply chain network considering different carbon emission regulations using big data characteristics," *Soft Computing*, vol. 25, no. 11, pp. 7527–7557, 2021.
- [4] C. T. Tchapga, T. A. Mih, and A. T. Kouanou, "Biomedical image classification in a big data architecture using machine learning algorithms," *Journal of Healthcare Engineering*, vol. 2021, no. 2, Article ID 9998819, pp. 1–11, 2021.
- [5] T. Syriatska, "The performing principles of the Ukrainian pianist and teacher Viktor Syriatsky," *Aspects of Historical Musicology*, vol. 23, no. 23, pp. 171–184, 2021.
- [6] O. Pinchuk, "Vsevolod Topilin is a legendary pianist, but... unknown," *Aspects of Historical Musicology*, vol. 23, no. 23, pp. 159–169, 2021.
- [7] O. S. N. K. Danilova, "N. K. Metner – reflecting artist: composer, pianist, teacher," *Musical Art and Education*, vol. 8, no. 1, pp. 73–89, 2020.
- [8] A. James, "When is a chair not a chair?: big data algorithms, disparate impact, and considerations of modular programming," *The computer & internet lawyer*, vol. 34, no. 8, pp. 6–10, 2017.
- [9] M. S. Lingam and A. M. Sudhakara, "A brief account of iterative big data clustering algorithms," *International Journal of Computer Sciences and Engineering*, vol. 5, no. 10, pp. 292–301, 2017.
- [10] T. S. Kowalski, "Kris Shaffer data versus democracy. How big data algorithms shape opinions and alter the course of history," *Studia Medioznawcze*, vol. 21, no. 1, pp. 491–494, 2020.
- [11] Y. O. Serdiuk, "Amanda Maier: a violinist, a pianist, a composer – the representative of Leipzig romanticism," *Aspects of Historical Musicology*, vol. 17, no. 17, pp. 232–248, 2019.
- [12] I. A. Hatipova, "Mikhail Vasilyevich Sechkin – pianist, conductor, teacher," *Aspects of Historical Musicology*, vol. 18, no. 18, pp. 155–170, 2019.
- [13] O. V. Serdiuk, "Maria Szymanowska as a recital pianist-composer of the romantic epoch," *Aspects of Historical Musicology*, vol. 17, no. 17, pp. 180–194, 2019.
- [14] C. Breunig, "Daniel Barenboim conductor and pianist," *Hi-Fi news*, vol. 64, no. 5, pp. 76–77, 2019.
- [15] M.-P. Ivan, "Platelet-rich plasma for thumb carpometacarpal joint osteoarthritis in a professional pianist: case-based review," *Rheumatology International*, vol. 39, no. 12, pp. 2167–2175, 2019.

- [16] D. M. Ponton, "Gregory Haimovsky: a pianist's odyssey to freedom," *Journal of Contemporary European Studies*, vol. 26, no. 4, pp. 474–476, 2018.
- [17] C. Breunig, "Leonard Bernstein composer, conductor, pianist," *Hi Fi News*, vol. 63, no. 9, pp. 74–75, 2018.
- [18] E. Karen and K. E. McAulay, "A dictionary for the modern pianist," *Reference Reviews*, vol. 32, no. 2, pp. 23–24, 2018.
- [19] V. V. Kalitsky, "The performing art of concertmaster: the methodological principles for ensemble pianist training," *Observatory of Culture*, vol. 14, no. 6, pp. 686–693, 2017.
- [20] C. Breunig, "Vladimir Ashkenazy pianist/conductor," *Hi-Fi news*, vol. 62, no. 13, pp. 74–75, 2017.
- [21] C. L. El, "avance hacia la idiomatización del lenguaje pianístico a través de la edición de Clementi de las sonatas de D. Scarlatti. Anuario Musical, 72, 117-130. ISSN: 0211-3538," *Anuario Musical*, vol. 72, no. 72, pp. 117–130, 2018.
- [22] L. Naie, *National University of Arts from Iași, Romania. 4. The Enescian Pianistic Notes and Commentaries (2stpart)*, vol. 19, no. 1, 2020Review of Artistic Education, 2020.
- [23] "Music-making piano droid [the big picture]," *IEEE Spectrum*, vol. 54, no. 8, pp. 16–17, 2017, None..
- [24] Z. Lv, A. Halawani, S. Feng, S. ur Réhman, and H. Li, "Touchless interactive augmented reality game on vision-based wearable device," *Personal and Ubiquitous Computing*, vol. 19, no. 3–4, pp. 551–567, 2015.
- [25] D. R. Kanniga, M. Gurusamy, and P. Vijayakumar, "An efficient cloud data center allocation to the source of requests," *Journal of Organizational and End User Computing (JOEUC)*, vol. 32, no. 3, pp. 23–36, 2020.
- [26] X. Xue and Y. Wang, "Optimizing ontology alignments through a memetic algorithm using both MatchFmeasure and unanimous improvement ratio," *Artificial Intelligence*, vol. 223, pp. 65–81, 2015.
- [27] X. Xue and Y. Wang, "Using memetic algorithm for instance coreference resolution," *IEEE Transactions on Knowledge and Data Engineering*, vol. 28, no. 2, pp. 580–591, 2016.
- [28] H. Chen, Y. Lu, and L. Tu, "Fault identification of gearbox degradation with optimized wavelet neural network," *Shock and Vibration*, vol. 20, no. 2, pp. 247–262, 2013.
- [29] Y. Zeng, G. Chen, K. Li, Y. Zhou, X. Zhou, and K. Li, "M-skyline: taking sunk cost and alternative recommendation in consideration for skyline query on uncertain data," *Knowledge Based Systems*, vol. 163, pp. 204–213, 2019.

Research Article

Implementation of Embedded Microprocessor in Optimal Teaching of Physical Health in the Internet Era

Juan Liu 

School of Physical Education, Hunan City University, Yiyang, 413000 Hunan, China

Correspondence should be addressed to Juan Liu; liujuan@hncu.edu.cn

Received 6 April 2022; Revised 27 April 2022; Accepted 30 April 2022; Published 23 May 2022

Academic Editor: Nima Jafari Navimipour

Copyright © 2022 Juan Liu. This is an open access article distributed under the Creative Commons Attribution License, which permits unrestricted use, distribution, and reproduction in any medium, provided the original work is properly cited.

The emergence of the online media environment has made the social environment faced by contemporary students more complicated. How to adapt to the rapid development of the network media environment, correctly grasping yourself in the complicated network world, not indulging in the network, is one of the focuses of many families and schools. As a media environment, the network has the advantages of rapid dissemination, large amount of information, strong interactivity, and rapid release. Especially through the integration with traditional media and new mobile media, it has become an important source of people's access to massive information. It has had a profound impact. For college sports health science, how to guide students to use online sports health resources for independent learning is an important topic in the reform of college sports health education in the new era. How the university sports health science under the Internet environment can help the development goals of the healthy China in the new era becomes the theoretical problem of the in-depth study of sports health care in colleges and universities in China. This paper studies the optimization and implementation of the teaching principles of sports health in the Internet era. It integrates all the teaching principles of sports health since the reform and opening up and then produces questionnaires. The professors of the teaching of health education are the subjects of the survey. They conducted three rounds of questionnaire survey on the integrated teaching principles of 51 sports health education and analyzed the statistics of each round by mathematical statistics and logic analysis. After the logic unit consumption optimization, the microprocessor performance has been greatly improved and the critical path delay performance optimization maximum value has been increased from 4.69 to 8.24.

1. Introduction

Sports health is a conscious, purposeful, and organized social activity that uses physical activity as the most basic means to follow the scientific methods and techniques to improve the physical fitness and skill level of the practitioner. At the same time, sports health as a cultural phenomenon needs to be widely disseminated in order to be popularized and improved [1–3]. This has created a close connection between sports health and the media. With the advent of online media, the advantages of large information content and fast spread speed have broken the monopoly of traditional Internet on the dissemination of information. The information about sports health care spreads through the network and makes the relationship between the Internet and sports health science. Closeness also provides a broader platform

for the rapid development of sports health-related industries. At this stage, the number of professional sports health education websites in China is increasing [4, 5], such as Tigers Sports Health, Sina Sports Health, Live, Octopus TV, 310 Live, 7M Live, A Live, Snow Mart, LeTV Sports health care, wow sports health, 24 live broadcast, and daily live broadcast. The content covers all aspects of sports health. It enables people to watch sports health education games anytime and anywhere through the mobile Internet and can also learn more about domestic and international sports health education information more quickly and accurately. You can also use the online event playback feature to watch sports health games that you do not see when people miss an exciting event. By browsing the Sports Health Science website [6–9], you can quickly and easily get the news information about sports health care. The rich sports

health network information resources can provide users with a variety of sports health science knowledge, sports health care, sports health lectures, sports health education reviews, sports health star introductions, and so on [10–13]. Principles of physical education refer to the criteria that physical education must follow, which reflects the objective laws of physical education. The basic principles are as follows: the principles of consciousness and enthusiasm, the principle of intuition, the principle of starting from the actual departure, the principle of step-by-step progress, the principle of comprehensive development of the body, and the principle of rational use of exercise load, consolidation, and improvement principles.

The processor under the single-core architecture executes multiple instructions concurrently, not in parallel, so only one process or thread runs at the same time, which cannot fundamentally improve computer performance. One of the most important advantages of multicore processors over single-core processors is that they are easy to optimize and expand. Embedded microprocessors have a wide range of applications in industrial control, personal consumer electronics, communications, and military industries. Many early computers adopted the von Neumann structure, which is not commonly used now. Modern processors widely use the Harvard structure to meet the increasing demand for performance. Among them, the ARM series microprocessor occupies the largest market share in the mobile market and is in a leader position [14–16].

The Internet has entered the education industry. The concept of “Internet +” has pointed out the direction for the development of our traditional education industry. Yang Zhiyong pointed out in his book that the Internet has provided new development opportunities for the development of traditional education because of the traditional secondary vocational position. The teaching method of sports health education in schools has been unable to meet the personality development of students, and students’ ability to learn independently is also limited. We need to provide new development channels for traditional education development and indicate new directions for development. Similarly, Li Yanqin also coincides with Yang Zhiyong’s views in his work. He also supports the “big data era” opened up by the Internet to bring new vitality to our traditional education [17]. Therefore, digital education gradually changes traditional education. At the same time, Sun Quan also analyzed the various shortcomings of traditional secondary vocational schools in his works and Zhu [18]. Their “experiential” teaching methods can also improve classroom efficiency and cultivate students’ individuality and self-learning ability. The study found that the traditional methods of education and teaching have limited students’ ability to learn independently. The overall teaching quality of traditional teaching methods has retreated or stopped, students’ ability to innovate has been limited, and students’ personality development has been restricted [19]. Li Yanqin, Wang Yingna, Shen Chenglin, and other scholars in response to these existing problems [20, 21], according to the development and reform of traditional secondary vocational schools in the context of “Internet +”, also

proposed “creation teaching method,” “reverse thinking teaching method,” “situation Set teaching methods,” “inspired teaching methods,” and other reform methods for traditional secondary vocational schools [22–27]. The emergence of the “Internet +” era has completely changed the traditional sports health education teaching model, making up for the technical defects and deficiencies of the traditional sports health education teaching, bringing more free sports health education teaching space and more convenient sports health learning methods. Make a technical change in the original boring sports health education teaching. As an important Internet and carrier for optimizing the teaching of traditional sports health education [28–31], Internet technology not only improves the effectiveness of teachers’ sports health education but also improves the efficiency of students’ sports health learning. More importantly, digital sports health education breaks the shackles of traditional teaching [32, 33], gets rid of time and space restrictions and regional imprisonment, truly pays attention to students’ individualized differences, cultivates students’ awareness of lifelong sports health training, and stimulates students’ inner existence. The interests and appeals of sports health care meet the diverse needs of students in sports health education and improve the quality of sports health education. At the same time, it also provides technical support for the reform and innovation of sports health education in China and better promotes the development of school education. With the advancement of science and technology and the increasing level of living standards, the per capita life expectancy has become increasingly extended. Information and medical technology are supported by computer technology, and the family can enjoy the professional-level monitoring of the hospital at home with the family as the core.

The lifestyle of students in the Internet age is itself a special group lifestyle, which is different from the lifestyles of other social groups in contemporary society and the lifestyles of students in history. The widespread use of the Internet has made the digital network culture a new cultural trait in the Internet age. The Internet environment in the Internet era has attracted students with diversity, complexity, entertainment, interaction, and virtuality; quickly became their main channel for understanding the outside world; and profoundly affected their behavioral habits [34, 35]. While the Internet brings convenience to students’ life and communication and the improvement of their understanding, their negative influence cannot be ignored. For example, the reality and virtual coexistence of the Internet can easily lead to the imbalance of interpersonal relationships and the alienation of network personality; indulging in the network has a negative impact on the physical and mental health of students; some violent, pornographic, and superstitious information in the Internet causes information pollution to the campus environment [36–38]. These problems affect the normal socialization process of students and need to be highly valued by us. The general microprocessor contains three main registers, one test control register (TCR) is used to provide microprocessor instruction operating code when test mode, a linear feedback shift register (LF-SR) and a multilosing feedback feedback the displacement registers

(MISR) are used to generate random data and compressed test responses, respectively.

Enhance the storage protection ability of the embedded microprocessor for important data through the expansion design, and at the same time have the acceleration engine function of the specific algorithm. Due to the influence of everyone's understanding and experience, the different perspectives lead to the existing teaching principles of sports health education. However, there are fewer studies on the teaching principles of sports health under the new curriculum standards, and fewer papers. Individuals have personal opinions, but they all have limitations. Which one we use when choosing is more appropriate, which requires us to explore, so it is very important to seek better teaching principles of physical education to guide teaching practice. This paper mainly integrates all the teaching principles of sports health education from the reform and opening up to the present through the literature and data method and then produces a questionnaire. Through the expert survey method, the professors in the field of sports health education are studied in the university, and the integration of 51 teaching principles of sports health education was conducted in 3 rounds of questionnaires, and the data obtained from each round were analyzed and counted by mathematical statistics and logic analysis, and expert opinions were collected. Finally, 8 sports health education with the highest concentration of expert opinions were obtained. The main research content of the paper includes the following: the hardware composition of the hardware constitutes the connection method of the hardware of the development board to introduce the connection methods of each functional module and the microprocessor. The system software focuses on analyzing the embedded system guidance program and was finally tested on the hardware platform. Application software is based on designing embedded medical care terminal application software.

2. Proposed Method

2.1. "Internet Plus." "Internet Plus" is a new form under the development of the Internet driven by Innovation 2.0. It combines the Internet with traditional economic industries, makes full use of modern information technology and Internet information platform, promotes a new model of traditional industry economic development, and realizes the tradition. Due to the special technical characteristics of the Internet and the special business management mode of Internet companies, Internet sports health learning has some differences from traditional sports. The new wave of sports led by the Internet New Wave has its new features [2]. "Internet +" is mainly user-oriented, combined with the latest technology, not only forms an "iron triangle" with sports, innovation, venture capital but also provides technical support and thinking innovation for traditional industry updates. Sports has the characteristics of strong derivative and has more extensive cooperation space with traditional industries. For example, Vipshop, Taobao, Dangdang, Alipay, and Applepay are traditional department store purchases, traditional bank counters, traditional cash payment

methods, etc. Effective combination of the Internet "big data platform" is a new model of sports innovation. This multi-component combination of Internet sports and traditional business not only shortens the distance between enterprises and users but also accelerates the pace of innovation of enterprises and makes sports people directly contact with users to meet The various needs of users, the "extra function" brought about by the "Internet" has greatly promoted the cultivation of the innovative spirit of sportsmen and promoted the development of China's market economy. Thus, simply speaking, "Internet +" refers to relying on Internet information technology to promote the deep integration of the Internet and traditional industries, give full play to the advantages of Internet big data, achieve industrial product structure upgrades, improve economic productivity, and ultimately achieve an increase in social wealth.

2.2. "Four-Segment" Sports Health Education Teaching. The traditional "four-stage" sports health education emphasizes the key points of teaching in every aspect of the actual teaching operation, including the work focus of the sports health education teachers and the learning priorities that students need to understand. At the beginning of the "four-segment," more emphasis is placed on the declaration of this course, teaching the content and work of this sports health course. Sports health teachers are often elaborated based on the teaching content of the original prepared teaching plan. At this stage, students have almost no interest in learning, and they have not yet entered the state of learning because they are already familiar with what their teachers will emphasize in this class. In the actual motor skills transfer course, this "beginning part" is more "notification content," that is, "reading" and "sending" the main possible content in this sports health course, it has no real meaning. Guide students and attract students to participate actively in the classroom. Generally speaking, this part is very important, paying attention to the guidance of the course, and the correct way of guiding, will definitely make the teaching work of sports health-care workers very easy and achieve twice the result with half the effort. In the "four-stage" preparation section, more emphasis is placed on the preparations required for this course in this sports health project. The PE teacher will divide the lecture content of this sports health education project into different class hours, and each class will be taught step by step according to the teaching tasks planned in the teaching plan. The narrow understanding is that in the actual "preparation part," the sports health education teachers need to prepare the course for this sports health education course at the beginning of each course: for example, through language, or the introduction of the general action, to introduce this course, let the students have a basic understanding of the content of the course, and can intuitively understand the difficulty of the course. This part can have two levels of meaning, on the one hand, the end of the summary of the sports health project, and on the other hand, the final exam and assessment of this sports health project. The narrow sense is that in the actual traditional sports health education teaching, the end of the course is the end of this course. The sports health teachers make a

brief summary of this course and point out the difficulty of this sports health course. In order to test the student's grasp of the situation, the final test is conducted by arranging the test. This traditional "four-stage" sports health teaching method can also pass the teaching content to students. However, this "pre-emptive" and "passive cramming" learning approach not only brings heavy and repetitive tasks to the sports health teachers themselves but also hinders the individualized and active thinking development of the students. It has slowed down the reform of sports health education.

2.3. Digital Sports Health Education. The concept of digitization is applied to the classroom of sports health care, mainly through the teaching of sports health knowledge through various information resources, which makes the whole sports health education teaching process more intelligent and standardized. Informatization resources include not only various hardware information resources provided by computers, mobile phones, projections, etc. but also various software management resources such as various teaching management software, course monitoring app, and multimedia network materials. In the process of modern digital sports health education, using the convenience of various information resources, the boring, cumbersome, single, and one-sided written physical education teaching content will be displayed through animation, video, audio, and other methods. It is the most popular and most effective teaching method available today. In the process of digital sports health education, we can make use of the convenience of network resources to build a network digital management platform, so that the sports health teachers can supervise and manage the teaching courses and manage the students' learning effects, so that students can independently carry out sports health courses. Difficult learning allows sports health teachers to improve management efficiency and teaching efficiency. It also enables students to master the key and difficult points in the sports health curriculum more vividly and improve the learning efficiency.

The teaching of digital sports health education has gradually surpassed the traditional sports health education teaching mode in the era of "Internet +". More and more colleges, especially those with more time-honored secondary vocational education, have begun to use the digital education methods of the information age to conduct course teaching, especially the sports health courses that focus on student experience, interaction, and participation. Students not only need to learn the basic knowledge of the course in the sports health course but also many different courses in sports health courses, such as the "three-step hurdles" of basketball training courses and the "soccer positioning" of football training courses. The training content requires a certain amount of accumulated practice. Due to various factors such as the time of the course, the course venue, and the weather of the class, it is difficult for students to grasp the essentials of the "three-step hurdle" in the true sense. It is difficult for students to grasp whether their actions are standardized or not. Therefore, through digital teaching methods, sports health teachers can provide students with various related videos, animations, etc. for multimedia indoor teaching.

TABLE 1: Multiplier parameters.

	Average value	Variance
External arrival interval	23.094	0.217
Area 1	8.173	0.2668
Area 2	8.346	0.157
Area 3	11.357	0.289

TABLE 2: Calculation results.

Average throughput rate	0.0246
Average response time	26.3182
Calculated	121.2765
After imitating	109.3901
Error percentage	3.21%

They can also communicate online with students through online management platforms to timely master students' courses on sports health. The degree of mastery allows students to study sports health courses in a variety of different ways and in different ways participate in the study of sports health courses. Users can send appointment requests to the center website at any time to return the appointment for consultation time according to the doctor's time arrangement. Of course, the user also has the permission to cancel the appointment. If the appointment is successful, the appointment time, users and the attending doctors can conduct remote video consultation.

2.4. Internet Sports Health Information. A considerable part of the Internet information bears the role of the government. Generally speaking, in the process of students' socialization, the role and value of guidance is unquestionable. Due to the rich and varied social life, the personality differences of the student groups are becoming more and more obvious, and the effectiveness of Internet information in guiding students is facing enormous challenges. Because of the economic interests and the diversification of economic composition, social organization, and lifestyle, students' differences in material life, spiritual life, working environment, and ideological realm are more and more obvious, and the influence of one-way thinking guidance can be covered. Faces will gradually shrink as the individual differences become more apparent, and the effect will continue to decline. In this context, the guiding function of Internet information can only effectively play its role by continuously deepening the theme and innovative forms. At the same time, communication is the primary task of Internet information. Because students are the key period for the formation of world outlook, outlook on life and values, Internet information needs to disseminate correct and comprehensive information to students. In particular, it is necessary to deal with several relationships, that is, the media also needs to carry forward the excellent traditional sports health culture when spreading the modern sports health culture to students. In the content of Internet information reporting, sports health education is an important source of news and content of Internet

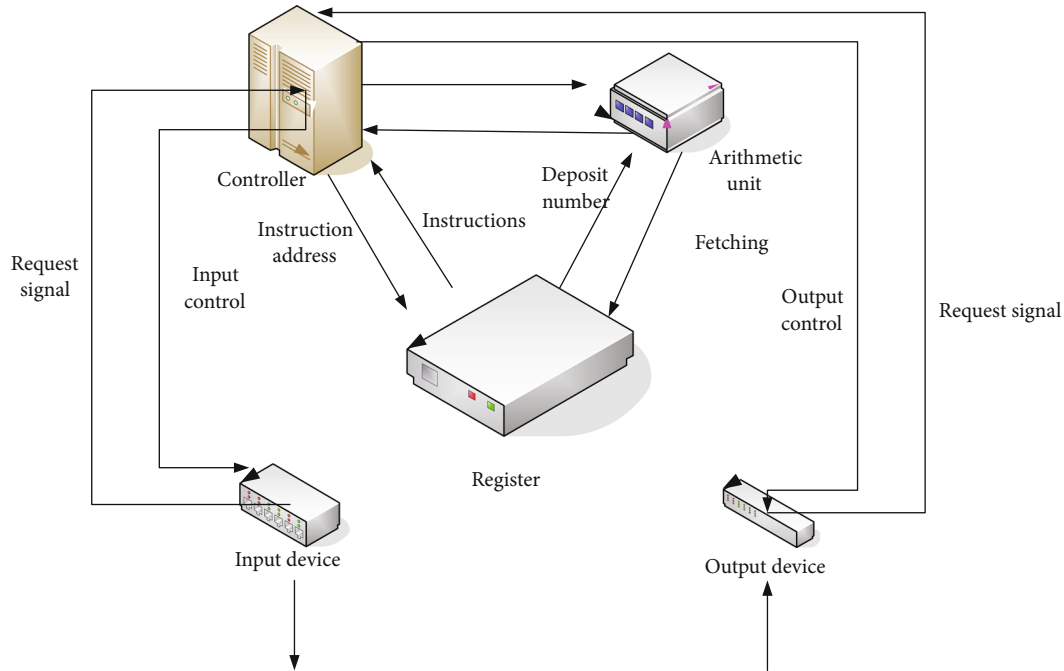


FIGURE 1: Microprocessor structure.

information. Because it will have a huge impact on people’s sports health lifestyle and the development of sports health science, Internet information is especially comprehensive. Influential Internet information must be reported in the field of sports health. However, the main role of determining the specific mode of communication and reporting content is the law of the operation of the news media itself. Indeed, the lives of modern people are closely linked to Internet information. In modern society, especially the popularity of electronic Internet, it has brought a new cultural environment and a broader vision of the observing society. The Internet gives people a world that cannot be described and experienced by language alone, so that they can acquire education, edification, cultural knowledge, morality, aesthetics, behavioral norms, interpersonal relationships, etc., and understand the society they are going to enter. Overview: the Internet has become a teacher to guide students in social learning. Students observe and imitate social behavior through the Internet, which is a study that relies on indirect experience. Many athletes on the Internet are heroes of student worship, and it is easy to stimulate their imitation behavior. In general, students first observe the behavior and consequences of Internet characters, then imitate, and observe the consequences of their imitating behavior. If it can be accepted by society, this temporary imitation may develop into its fixed behavior pattern. The influence of Internet information on students’ interest in sports health care and idol worship is far more than the interpersonal influence of teachers, classmates, and parents. The introduction of various sports health education events and related knowledge in the society reflected by the Internet has inspired their new curiosity and is the basis for their own hobbies.

TABLE 3: Access strategy test parameters.

From the core Test data	Core 1	Core 2
20 times	45%	55%
50 times	68%	32%
100 times	92%	8%

TABLE 4: Performance test parameters.

Code Test data	Shared variable access	In total
1	1	200
2	20	200
3	100	200

2.5. *Embedded Microprocessor.* Since the beginning of the century, the upgrading of digital integrated circuit products has accelerated, especially in the field of consumer electronics. China’s research on embedded microprocessors is relatively backward, and there is still a big gap between related third-party compilation and development tools, manufacturing processes, and software support compared with foreign countries. Embedded systems are widely used in various fields today in the pursuit of portability, low power consumption, and highly integrated digital circuits. As the core of embedded systems, embedded processors have also gained rapid development in both design methods and manufacturing processes. Embedded microprocessors have limited hardware resources, so a branch prediction that not only has low hardware overhead but also has high

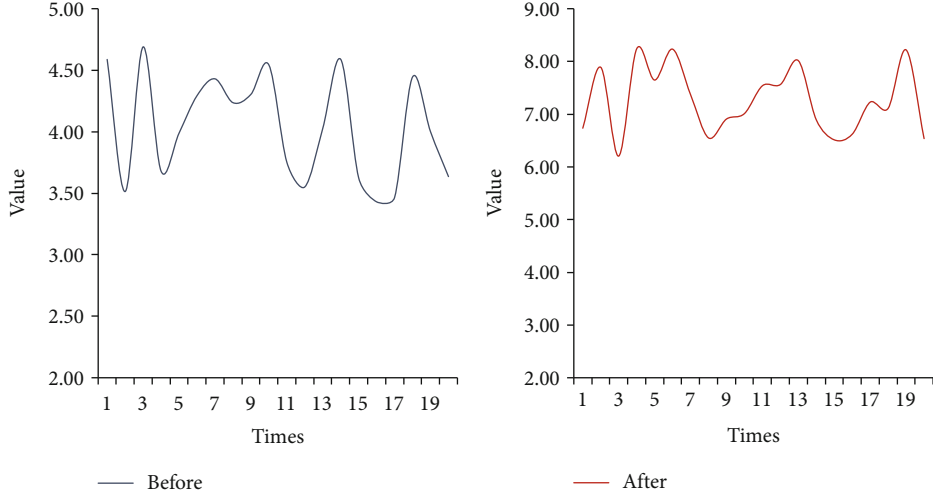


FIGURE 2: Results before and after critical path delay optimization.

execution efficiency is needed to achieve a higher cost performance. Combined with the current reality, the embedded operating system is a multiuser, friendly interface; can perform multiple tasks at the same time; is a widely used, low-cost system, especially with high reliability and development efficiency; and can shorten the development cycle. Embedded real-time operating system. As integrated circuits enter the stage of deep submicron and nanolevel processes, the power consumption of embedded microprocessors is becoming more and more serious, and power consumption has become one of the most important factors restricting the development of a new generation of microprocessors. Since the data transmission rate of the external bus is much lower than the internal bus of the processor, the communication cost of data transmission will greatly reduce the efficiency of cryptographic services. The bypass unit of the processor is an important unit responsible for the correct scheduling of data at all levels. The combination of the central control module and the bus can perfectly manage the entire microprocessor core. That is, the central control module sends a signal to the bus, and the bus reads or writes data from the corresponding component according to the control command. Calculate the expansion function of the embedded microprocessor, expressed as

$$S = -s_i * 2^i + \sum_{i=1}^{i-1} s_{i-1} * 2^i = \sum_{i=0}^{I+1/2-1} [2^{2i}(-2s_{2i+1})], \quad (1)$$

$$S * R = \sum_{i=1} (i-1)/(2-I) [t_h \otimes R \bullet 2^{2i}], \quad (2)$$

where S and R are the complement numbers, S_i is the binary bit, and i is the bit width. Starting from the specific situation of the hardware structure of the designed multicycle multiplier, considering the requirements of layout and speed, structural optimization is required.

$$U_{i+} = \lim_{r \leftrightarrow \infty} \frac{1}{r} + \sum_{i=1}^r \forall_{i+}, k, \quad (3)$$

$$v : 1 \leftrightarrow i+, v : 0 \leftrightarrow i-. \quad (4)$$

Due to the direct mapping method, the memory dedicated to storing page address information and related control bits is tag memory U_{i+} . Page address information is reflected in some high bits of the address bus for calculation, there are

$$C = \left[(i_1, \dots, i_n) \mid i_1 \geq 1, \sum_{i=0}^n r_i = h \right], \quad (5)$$

$$\|C\| = [R + N]^{i2} + 1/(n-1). \quad (6)$$

In the process of synchronous integrated circuit design, each design step h will analyze and optimize the circuit. Utilize the structure $\|C\|$ of multiple storage subarrays in the current memory; that is,

$$\alpha(i_1, \dots, i_{m-1}) = \frac{1}{w} \prod_{i=1}^{n-1} S_i(r_i - 1), \quad (7)$$

$$s_i(i_{n+1}) = v_i^{r_i} / \prod_{a=1}^{r_i-1} \chi_i(a-1), \quad (8)$$

$$H = \sum_{w \in R} \prod_{i=0}^n S_i(r_i + (r * (i-1))). \quad (9)$$

There are many kinds of embedded applications, ranging from audio w , video codec v , image recognition to scientific computing. Store multiple arrays without data relevance into different subarrays, add auxiliary instructions, and use the formula to express

$$v_i = f_{a,b} + \sum_{i=1}^{n=0} v_{a,r} f_{a,b}, i = 1, \dots, M, \quad (10)$$

$$f_a^{i+1} = f_a^b + (f_a^b - h_{i-1}) \bullet v_i f_{i,1} / v_i (1 - f_{ab}), \quad (11)$$

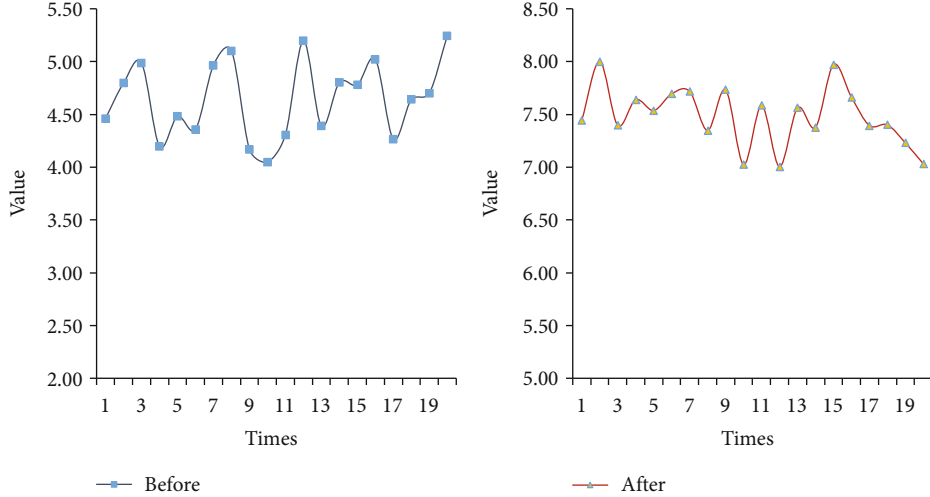


FIGURE 3: Logic unit consumption before and after optimization.

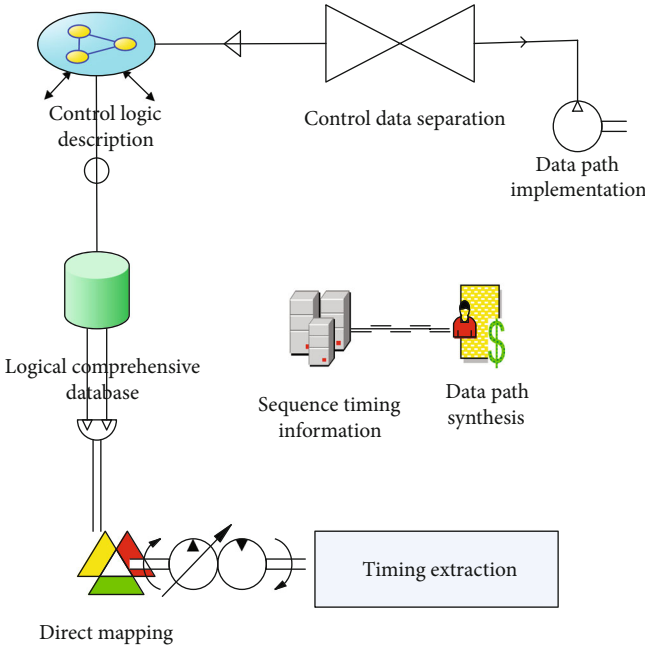


FIGURE 4: Embedded microprocessor used in health-care system.

$$f(i) = -\sum_{s_i \in S} i(S_i) \ln \sqrt{f(s_{i-1})}. \quad (12)$$

Since the data set size $f_{a,b}$, code length, and time and space locality of data and program $f(i)$ of various applications are very different, information entropy can be used to describe the uncertainty of the system state.

$$\prod_{s_i} f_i(s(i-1))f(s_i) = \{f_i\}, \quad (13)$$

$$f(a_{i-1}) = \frac{1-o}{\delta} \exp \left\{ -\sum_{o=1}^n \delta_i f_i(s_i) \right\}, \quad (14)$$

$$\delta = \exp(\chi_o) = \left\{ -\sum_{i=1}^{o-1} \delta_{i-1} f_i(s_{i+1}) \right\}. \quad (15)$$

It is very difficult to measure the arrival interval f_l and service time χ_o of the actual system. Only parameters such as the average value and variance can be accurately measured. Use the multiplier parameters to calculate the data.

$$\varphi(v_{i+1}) = \min_{s_{i-1} \in \delta} \varphi v_{i+1} + f(l+1), \quad (16)$$

$$\bar{\delta}(a, b, i) = \lim_{i \notin \infty} \frac{1}{o-1} \sum_{i=0}^{n-1} \varphi s_{i-1}(a, b, i). \quad (17)$$

The implementation of changes will lead to changes in the distribution of marker φv in the network. Simplify the system into a simpler system, while keeping the properties of the system to be analyzed $\bar{\delta}(a, b, i)$ unchanged; then,

$$m-1(i-1) \geq (S^{-1})^{s-1} f(l), \quad (18)$$

$$r \geq b_i^{m-1} (S^{-1})^{i-1} f(l) / a_i^{n-1} n_{o-1}, \quad (19)$$

$$r_{\max} \geq \left\{ b_i^{m-1} (S^{-1})^{i-1} f(l) / a_i^{n-1} n_{o-1} \right\} / \min_r. \quad (20)$$

The dynamic behavior of the model will be affected by the time parameter, and the behavior of the concurrent uncertain order $m-1^{-\infty}$ in the original system will have a sequence due to the influence of the time parameter. The experimental parameters and calculated results are shown in Table 1 and Table 2.

3. Experiments

This paper selects 15 professors who study the teaching theory of sports health in colleges and universities as the survey object. Through the search engines such as databases, China Knowledge Network, and libraries, we can research the

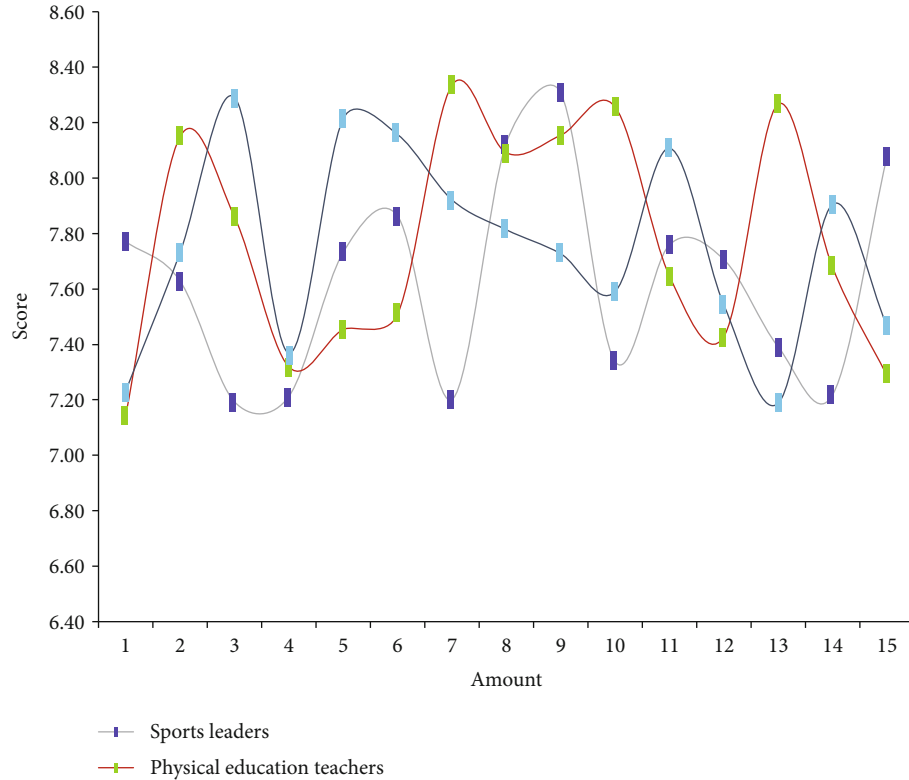


FIGURE 5: Questionnaire score.

research results of domestic and foreign students' sports health lifestyles, study excellent master's and doctoral thesis on sports health care lifestyles, and study on students' sports health lifestyles. The paper reviewed the related books on sports health sociology, sports health psychology, sports health lifestyle, and sports health education. In addition, I borrowed books, statistical software books, and analytical technical materials related to the sports health lifestyle from the Library of the School of Sports and Health Sciences. The collected data were statistically analyzed, organized, and tabulated using Excel and statistical software and multivariate analysis of variance.

4. Discussion

4.1. Embedded Microprocessor-Related Data. Embedded application development debugging environment is a kind of remote cross-debugging software based on the debugging support of embedded microprocessor. It is necessary for embedded application development. Embedded microprocessors are designed for the embedded application environment, and the specific hardware platforms of the applications can be described as vastly different. During the development of specific applications of the chip, the debugging and running of the application program has therefore become very complicated. The embedded microprocessor's support for software debugging will directly affect the application and promotion of the processor. The performance improvement of general-purpose processors greatly enhances the functions of the software, pro-

viding strong support for ultralarge-scale chip testing. The structure of the microprocessor constructed in this experiment is shown in Figure 1.

Functional testing is measured by running results. The design is generally performed during functional testing at level or gate-level simulation. The access strategy testing parameters of this experiment are shown in Table 3.

When developing such complex applications, debugging methods are directly related to the efficiency and progress of the development and determine the quality of the application. Testing its performance, the data is shown in Table 4.

A highly optimized, compact-embedded type is formed after miniaturization. Although its size is small, most of the advantages that are still retained are stable, excellent transplantation, complete network functions, and rich support and standards for various file systems. The simulator developed for the target computer can guarantee the basic correctness of the software, that is to say, the software that cannot run correctly on the simulator will definitely not run correctly on the target computer. Through simulation experiments, we recorded the data before and after the critical path delay optimization, as shown in Figure 2.

The data in the above figure shows that the maximum value of critical path delay performance optimization has increased from 4.69 to 8.24. Analyze the data before and after the logic unit consumption optimization, as shown in Figure 3.

The data in the figure shows that after the logic unit consumption is optimized, the performance of the

TABLE 5: Questionnaire distribution.

Questionnaire type	Leadership questionnaire	Teacher questionnaire	Teacher questionnaire
Number of issues	30	30	60
Number of collections	28	28	59
Effective number	28	28	59
Efficient	94%	94%	98%

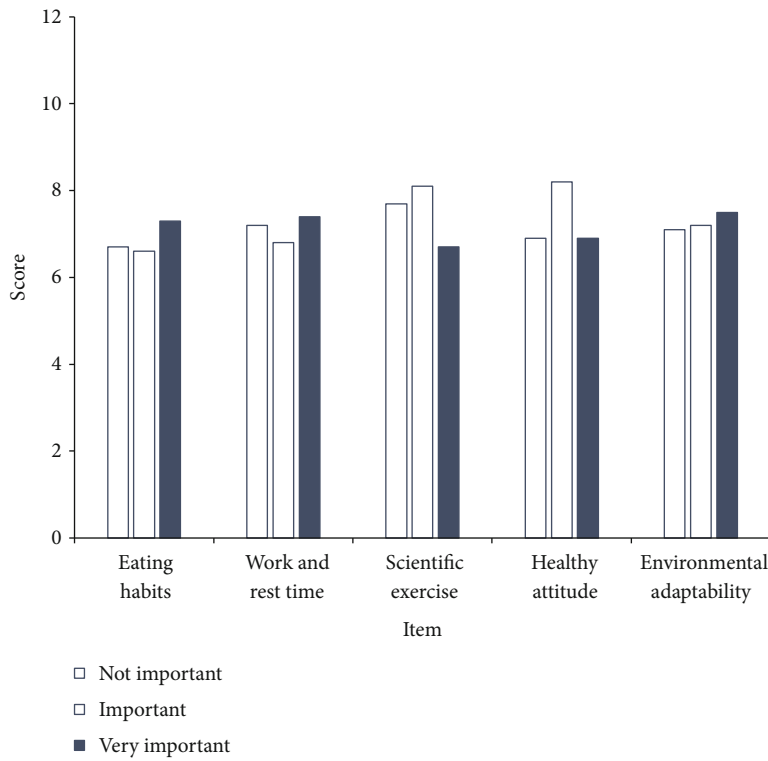


FIGURE 6: Students' cognition.

microprocessor has been greatly improved. The debugging protocol is based on the characteristics of the on-chip hardware debugging support logic and the characteristics of the debugging interface, while the communication protocol can be very flexible, and various communication interfaces can be designed according to the needs to improve the speed and efficiency of debugging.

4.2. *Internet Application and Sports Health Attitude.* With the reform of the college enrollment system and the advancement of quality education, a large number of disadvantaged students in sports have appeared in colleges and universities across the country.

The teaching content and organization form adopt a “one size fits all” method, which lacks pertinence and practicability and fails to reflect the teaching principle of “differentiated treatment and individual teaching.” The student performance evaluation process is mostly result evaluation, ignoring process evaluation. This has greatly affected the enthusiasm of sports-disadvantaged students to participate in sports. The embedded microprocessor is applied to

TABLE 6: Teaching content of physical education and health care.

Teaching content	Quantity	The proportion
National traditional sports	17	99%
Sport dancing	5	22.3%
Ball games	7	31.2%
Sports fun games	3	17.4%
Theory lectures	3	17.4%

the health-care class system, the structure diagram is shown in Figure 4. The real-time operating system module can ensure the real-time and reliability of the program’s execution, thereby reducing development time and ensuring software quality. The embedded system is combined with the specific application, and its upgrade and replacement are also synchronized with specific applications. Therefore, embedded system products have a long-life cycle. Software of the embedded system is solidified in the storage chip or single-chip microcomputer, not stored in the disk and other

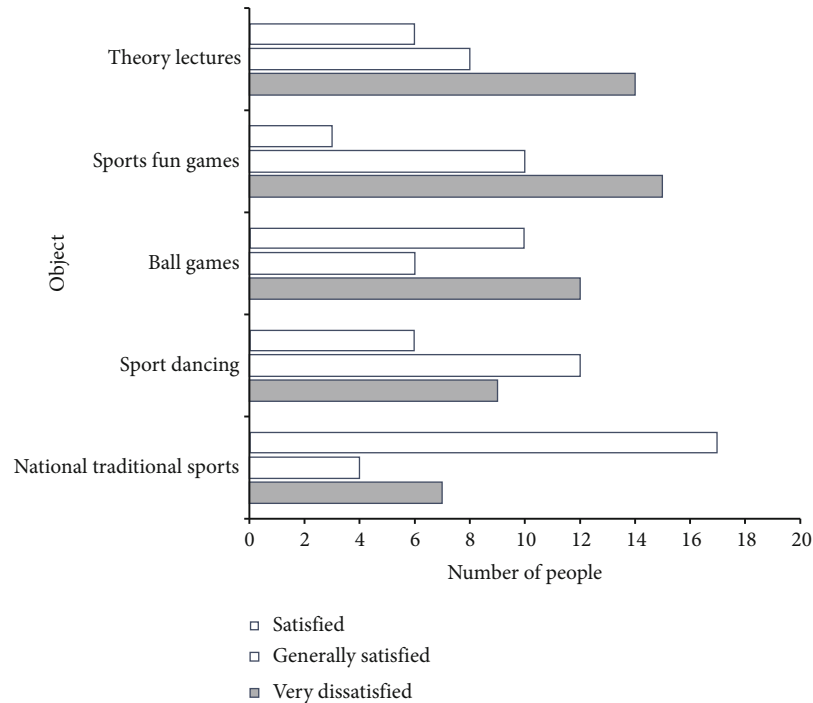


FIGURE 7: Overall evaluation of the health section.

carriers, so it can improve the execution speed and reliability of the program.

At present, the physical health education of disadvantaged students in China lacks a universal teaching guideline, and there is no clear guidance to the curriculum goals, curriculum content, etc., which makes the curriculum design of various colleges and universities more random. The theoretical teaching content lacks pertinence and practicability and cannot effectively teach the related theoretical knowledge of sports health care, rehabilitation exercise prescription, and rehabilitation evaluation. The questionnaire scoring data of this experiment is shown in Figure 5. Disclaimer: the data has no other interest relationship, which is obtained based on the actual situation.

From the data in the above figure, we can see that the reliability of the questionnaire in this experiment is very good. The distribution of the questionnaire is shown in Table 5.

The content of the questionnaire is mainly to investigate students' perceptions of their own physical health. The results of the survey are shown in Figure 6.

Obviously, sports-disadvantaged students believe that a good lifestyle is closely related to their own health and is the most fundamental condition to ensure their health. So we have carried out relevant data statistics for its teaching content, as shown in Table 6.

Generally speaking, the school does not pay much attention to the teaching of physical education and health care. Colleges and universities should expand the scope of practical teaching content, expand with the popular fitness content in the society, and make an effective transition to social sports. The students summarized the overall evaluation of participating in the health-care class, as shown in Figure 7.

For the time being, most students are not very satisfied with the health class. In order to improve the teaching satisfaction of students, we design the tutorial goal of embedded microprocessor application and teaching process and normalize the health data related to the health-care class. As far as the data is concerned, the comparison results of the data integrity before and after are as follows, as shown in Figure 8.

In the physical education work of sports-disadvantaged students, more efforts should be made in the guidance of mental health, and the physical and mental education of health should be carried out. The attention of university leaders is the basic prerequisite for the development of school sports education for disadvantaged students in sports, and it is also an important guarantee for accelerating the construction of sports health-care courses. Emotion regulation physical education teaching model has important practical significance to promote the overall development of students' quality. Inferiority complex, anxiety, fear, weariness, and other negative emotions in health class students affect their learning enthusiasm and then affect the formation and development of students' healthy personality. The data source of this phenomenon is shown in Figure 9.

Physical exercise not only improves people's physical health but also promotes mental health. The emotional regulation of physical exercise is a constructive behavior, which is very popular among students of special groups. The relationship between emotion regulation mode and teaching procedures and teaching strategies is shown in Figure 10.

The use of the Internet requires hardware and software, hardware is the terminal, that is, student handheld devices, such as mobile phones and computers. Data surveys can reflect that 94% of students use smartphones, and 86%

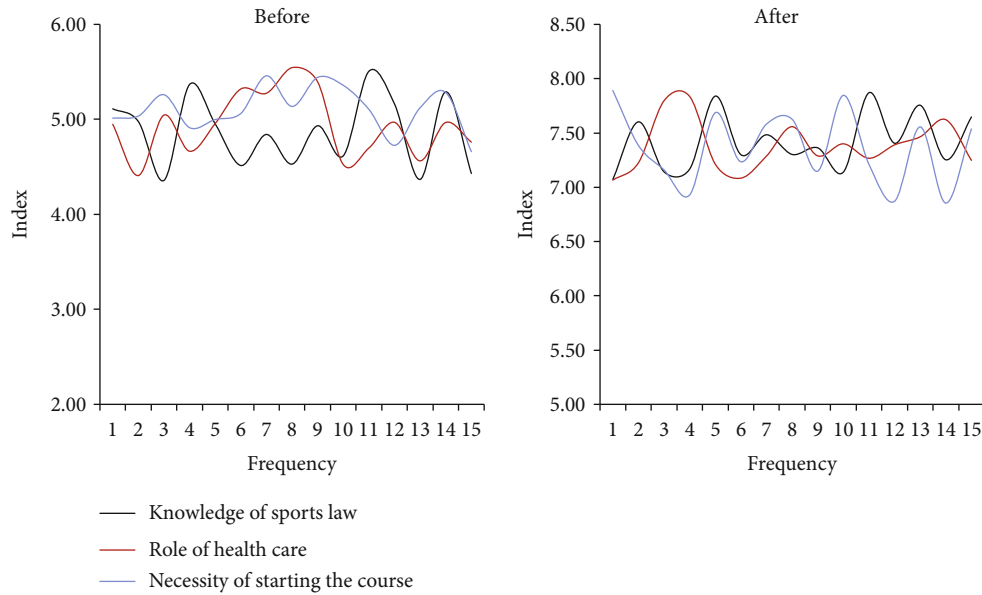


FIGURE 8: Data integrity results.

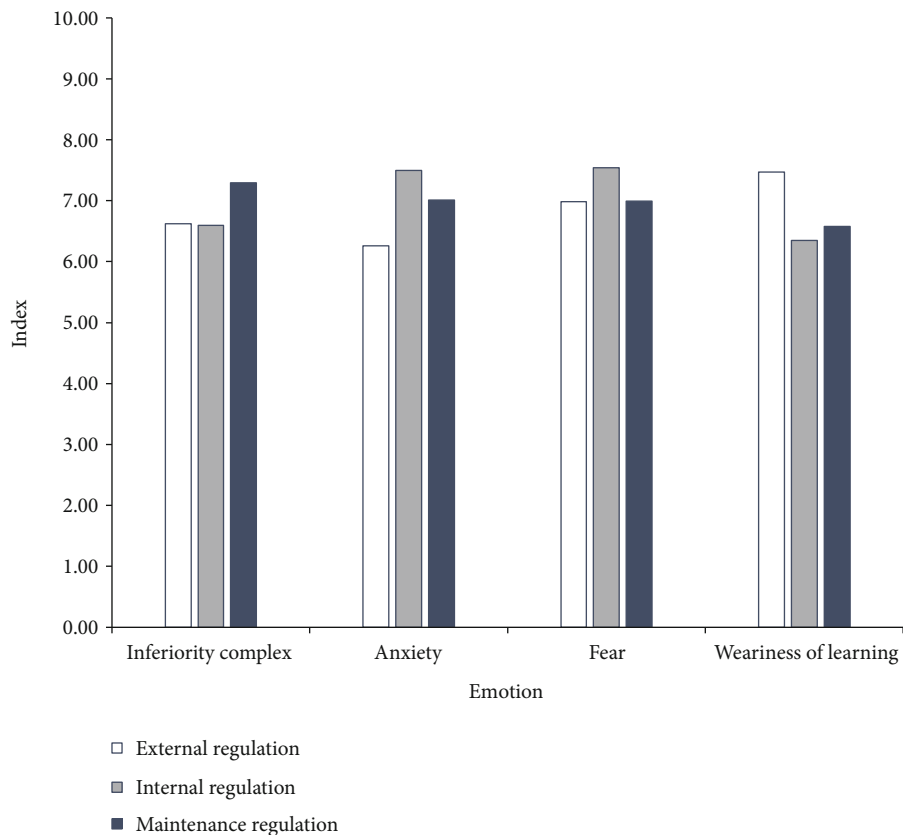


FIGURE 9: Negative sentiment index.

of students have computers, as shown in Figure 11. The data shows that Internet terminals such as mobile phones and computers are already very popular among student groups.

Students' attitudes towards sports health activities are related to their enthusiasm for participating in sports health

activities. Attitude can show people's evaluation and behavioral tendencies toward something. Attitude does not have genetic characteristics but an inherent psychological tendency formed under the influence of social environment. The attitude of sports health care is to make a psychological tendency to participate in sports health activities

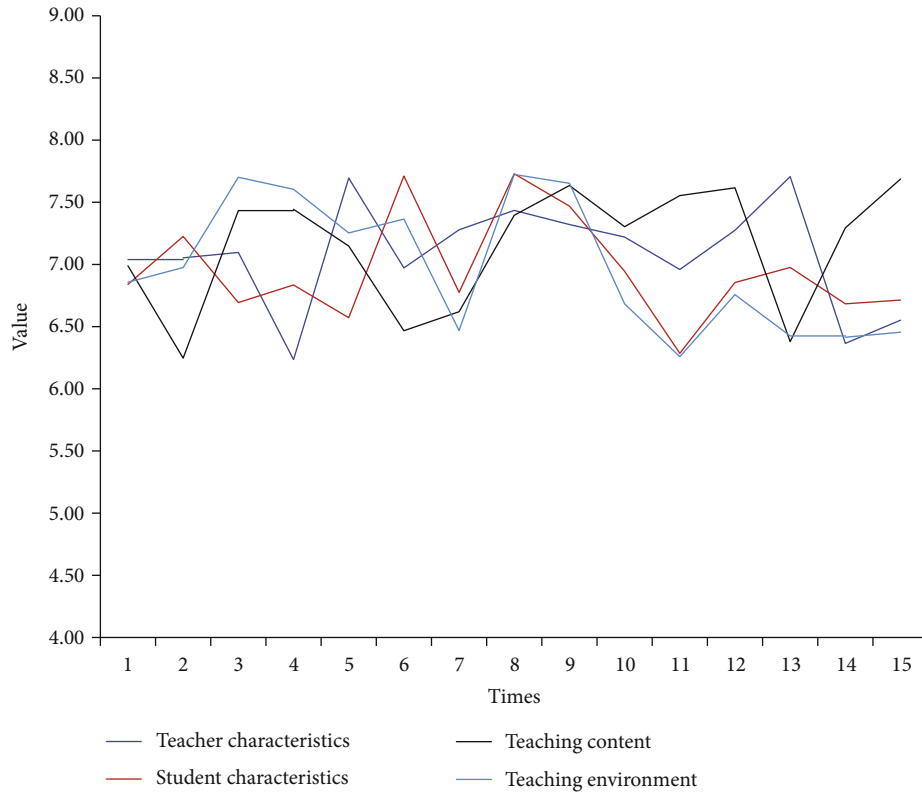


FIGURE 10: Correlation analysis.

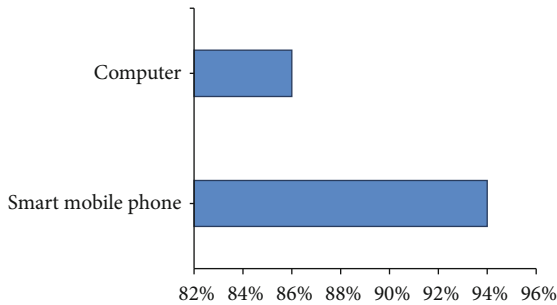


FIGURE 11: Internet terminal equipment survey proportion comparison.

through the value judgment of individuals under the influence of external conditions. The students' participation in the sports health education movement has great directionality and motivation for their participation in the sports health education movement. Students' attitudes towards the participation of sports health education can influence their enthusiasm for sports health training. Figure 12 shows the attitude of students towards the participation of sports health education.

Among them, 46.5% of the students have a favorite attitude towards participating in sports health training; 19.6% of students hold a preferred attitude; the average attitude is 16.3%; the less like and dislike, respectively, account for 12.5% and 5.1%. Overall, the ratio of likes and preferences is 66.1%. It shows that most students' attitude towards the participation of sports health education is preferred.

Students' attitude towards participation in sports health education

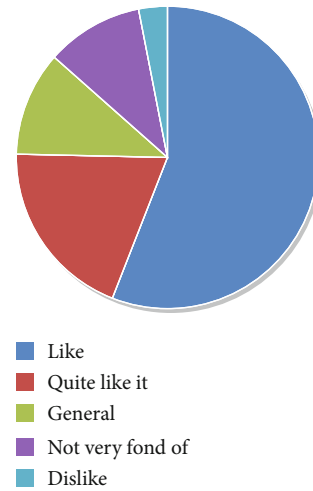


FIGURE 12: Students' attitude towards participation in sports health education.

B3 carries out the principles of collective education in collective activities, B4 raises the principles of sports cognition and inheritance sports culture, and B7 lays down the basic principles of lifelong sports. The concentration of opinions is lower than 7.0, and the degree of coordination of expert opinions is high, so it is directly deleted.

TABLE 7: The first round of the optimization of sports health teaching principles.

Principles of physical education	Opinion concentration M_j	Standard deviation S_j
B1: the holistic principle of teaching	8.00	1.0445
B2: the principles of education, development and purpose of education in teaching	7.17	1.3371
B3: principles of collective education in collective activities	6.50	0.9045
B4: improve sports cognition and inherit the principles of sports culture	5.67	1.9695
B5: principles of reasonable arrangement of physical activity	8.00	1.5954
B6: the principle of promoting continuous improvement of sports skills	8.17	1.0299
B7: lays the foundation principles for lifelong sports	6.67	2.0597
B8: humanistic aesthetic principle	7.50	1.2432

TABLE 8: The second round of the optimization of sports health teaching principles.

Principles of physical education	Opinion concentration M_j	Standard deviation S_j
The holistic principle of C1 teaching	7.83	1.3371
C2: the purpose principle of physical education	3.00	0.0000
C3: humanistic aesthetic principle	8.00	1.3484
C4: principles of reasonable arrangement of physical activity	5.67	0.9847
C5: principles of promoting continuous improvement of motor skills	8.33	0.9847
C6: lays the foundation principles for lifelong sports	4.67	0.7785
C7: healthy lifelong principle	8.67	1.1547

It can be seen from Table 7 and Table 8 that in this round of questionnaires, the objective principle of C2 education, the principle of reasonable physical activity of C4, and the basic principle of C7 lifelong sports are less than 7.0, and the degree of coordination of experts is relatively high. The remaining four decibels are the following: C1. the overall principle of teaching; C3. the principle of humanistic aesthetics; C5. the principle of promoting the continuous improvement of motor skills; and C7. the principle of lifelong health. The purpose principle of C2 education is too general and the scope is too large. It does not highlight the key requirements of sports health education under the new curriculum standard, so it is deleted.

The subjective interest principle refers to the fact that students are the main body of physical education in the process of physical education. Interest is an important driving force of physical education. All activities of teachers should be arranged around the students' interests, needs, and physical and mental characteristics. The main interest of students should be under the leadership of teachers, they actively participate in the learning activities and then cultivate students' fun and interest in sports to show students' autonomy, initiative, and creativity.

5. Conclusions

People's pursuit of improving the computing performance of microprocessors is endless, especially with the further development of multimedia, database, scientific computing, and artificial intelligence applications, the requirements for the computing performance of microprocessors are bound to become higher and higher. In view of the current practice

of sports health education curriculum and teaching reform in China, through the screening and analysis of the principles of physical education teaching principles, the current Chinese sports health teaching principles system should cover the following eight teaching principles, namely, the principle of subjective interest, the principle of safety and hygiene, the principles of humanistic aesthetics, the principle of promoting the improvement of motor skills, the principle of health and lifelongness, the principle of gradual and orderly progress, the principle of teaching students in accordance with their aptitude, and the principle of holistic teaching. The overall view of the sports health teaching process: the vertical view of the sports health teaching process is based on the semester plan, and the horizontal view of the sports health teaching principle is composed of the teaching process. Therefore, we should take a holistic view of sports health education, starting from the overall situation, focusing on the big aspect, to understand sports. Formulate effective and practical teaching objectives, promote students' all-round development, optimize teaching content, adapt to student development, comply with the requirements of the new curriculum standards, and choose effective teaching methods to enable students to accept teaching knowledge and skills. From the overall perspective, it is necessary to look at sports health education in order to maximize the benefits of teaching. Conduct physical education classes with holistic thinking. Pay attention to the integrity of the teaching materials, the development of sports health education should focus on the teaching objectives and the difficulty of teaching; pay attention to the integrity of the physical education curriculum, design the overall teaching situation, run through the physical education class, each part of the

activities must be interlocked. The value of the equipment is fully utilized. With the rapid development of science and technology, the embedded microprocessor has become increasingly becoming the focus topic of continuous attention in the field of computer application research, focusing on the issue of inquiry. Based on this, this article focuses on the teaching resources and design of embedded microprocessor application technology project courses. I hope that the analysis of this article can provide some reference for practitioners.

Data Availability

The data that support the findings of this study are available from the corresponding author upon reasonable request.

Conflicts of Interest

The author declared no potential conflicts of interest with respect to the research, authorship, and/or publication of this article.

References

- [1] S. R. Ramsey, K. L. Thompson, M. McKenzie, and A. Rosenbaum, "Psychological research in the Internet age: the quality of web-based data," *Computers in Human Behavior*, vol. 58, pp. 354–360, 2016.
- [2] L. Xuan and P. Wu, "The optimization and implementation of iptables rules set on Linux," in *International Conference on Information Science & Control Engineering*, pp. 988–991, Shanghai, China, April 2015.
- [3] Y. Q. Huang, "The application of information technology in the fine arts teaching and implementation," *Applied Mechanics and Materials*, vol. 599–601, pp. 2022–2025, 2014.
- [4] Q. Wang, "Design and implementation of recommender system based on Hadoop," in *IEEE International Conference on Software Engineering & Service Science*, pp. 295–299, Beijing, China, August 2017.
- [5] J. Untiedt, "Health professional educators' needs regarding strategies in the implementation of a learning management system," 2014.
- [6] J. M. Mochere, "The future of music education in Kenya: implementation of curriculum and instructional teaching strategies," *Journal of Education & Practice*, vol. 8, no. 7, pp. 171–180, 2017.
- [7] M. N. Hawkey, *Roles and relationships in learning and teaching: a case study of the development and worldwide implementation of a new religious curriculum*, Brigham Young University, United States, 2014.
- [8] J. M. Vesapogu, S. Peddakotla, and S. R. A. Kuppa, "Harmonic analysis and FPGA implementation of SHE controlled three phase CHB 11-level inverter in MV drives using deterministic and stochastic optimization techniques," *Springerplus*, vol. 2, no. 1, pp. 1–16, 2013.
- [9] A. Ahluwalia, A. M. Bassi, and P. Milazzo, "Inauguration of the Centro 3R for the promotion of 3Rs principles in teaching and research," *The Journal of Antimicrobial Chemotherapy*, vol. 35, pp. 260–261, 2018.
- [10] A. Milenin, P. Kustrá, D. Byrska-Wójcik et al., "Numerical optimization and practical implementation of the tube extrusion process of Mg alloys with micromechanical analysis of the final product," *Key Engineering Materials*, vol. 716, no. 8, pp. 55–62, 2016.
- [11] S. Rajendran, O. I. Khalaf, Y. Alotaibi, and S. Alghamdi, "MapReduce-based big data classification model using feature subset selection and hyperparameter tuned deep belief network," *Scientific Reports*, vol. 11, no. 1, p. 24138, 2021.
- [12] N. O. García, M. D. Velásquez, C. T. Romero, J. O. Monedero, and O. Khalaf, "Remote academic platforms in times of a pandemic," *International Journal of Emerging Technologies in Learning*, vol. 16, no. 21, pp. 121–131, 2021.
- [13] I. K. Osamh and G. M. Abdulsahib, "Energy efficient routing and reliable data transmission protocol in WSN," *International Journal of Advances in Soft Computing and its Application*, vol. 12, no. 3, pp. 45–53, 2020.
- [14] S. A. Woreta, Y. Kebede, and D. T. Zegeye, "Knowledge and utilization of information communication technology (ICT) among health science students at the University of Gondar, North Western Ethiopia," *BMC Medical Informatics and Decision Making*, vol. 13, no. 1, article 31, 2013.
- [15] M. Glassman and J. Burbidge, "The dialectical relationship between place and space in education: how the Internet is changing our perceptions of teaching and learning," *Educational Theory*, vol. 64, no. 1, pp. 15–32, 2014.
- [16] C. D. Scott, "Trademark strategy in the Internet age: customer hijacking and the doctrine of initial interest confusion," *Journal of Retailing*, vol. 89, no. 2, pp. 176–189, 2013.
- [17] M. Adil, H. Song, J. Ali et al., "EnhancedAODV: a robust three phase priority-based traffic load balancing scheme for Internet of Things," *IEEE Internet of Things Journal*, 2021.
- [18] F. Zhu, C. Zhang, Z. Zheng, and A. Farouk, "Practical network coding technologies and softwarization in wireless networks," *IEEE Internet of Things Journal*, vol. 8, no. 7, pp. 5211–5218, 2021.
- [19] H. Ko, K. Rim, and I. Praa, "Influence of features on accuracy of anomaly detection for an energy trading system," *Sensors*, vol. 21, no. 12, article 4237, 2021.
- [20] H. Ko, L. Mesicek, J. Y. Hong, S. S. Yeo, S. B. Pan, and P. Kim, "Blog reliability analysis with conflicting interests of contexts in the extended branch for cyber-security," *IEEE Access*, vol. 7, pp. 143693–143698, 2019.
- [21] L. I. Guan-Yi, X. U. Cong-Cai, and S. O. Business, "Circulation organization innovation in the Internet age—based on the perspective of evolution tendency, structural optimization and efficiency of border," *Journal of Business Economics*, 2016.
- [22] B. Agger, "Oversharing: the eclipse of privacy in the Internet age," *International Encyclopedia of the Social & Behavioral Sciences*, pp. 439–445, 2015.
- [23] J. M. P. González, C. P. Saiz, and I. C. Markina, "Health information and youth: challenges in the Internet age," in *Proceedings of the Second International Conference on Technological Ecosystems for Enhancing Multiculturality*, Salamanca, Spain, October 2014.
- [24] J. Abdi, H. Eftekhari, M. Mahmoodi, D. Shojayzadeh, and R. Sadeghi, "Physical activity status and position of governmental employees in changing stage based on the trans-theoretical model in Hamadan, Iran," *Journal of Health Science*, vol. 7, no. 5, article 23, 2015.
- [25] S. V. Gompel, "Copyright formalities in the Internet age: filters of protection or facilitators of licensing. Social science," *Electronic Publishing*, vol. 28, article 1425, 2014.

- [26] B. Bonikowski, "Digitally enabled social change: activism in the Internet age by Jennifer Earl and Katrina Kimport The MIT Press," *Contemporary Sociology A Journal of Reviews*, vol. 93, no. 3, pp. 332-333, 2015.
- [27] W. Aspray, G. Royer, and M. G. Ocepek, *Food in the Internet age*, Springer International Publishing, New York, 2013.
- [28] M. Burri, "Cultural diversity in the Internet age: in search of new tools that work. Social Science," *Electronic Publishing*, vol. 101, article 63, 2016.
- [29] Y. M. Mesfin and K. T. Kibret, "Assessment of knowledge and practice towards hepatitis B among medical and health science students in Haramaya University, Ethiopia," *PLoS One*, vol. 8, no. 11, article e79642, 2013.
- [30] N. Bakir, "Technology and teacher education: a brief glimpse of the research and practice that have shaped the field," *Tech-Trends*, vol. 60, no. 1, pp. 21-29, 2016.
- [31] P. Vega-Villaamil, M. Salve-Bouzo, J. Cubiella et al., "Evaluation of the implementation of Galician Health Service indications and priority levels for colonoscopy in symptomatic patients: prospective, cross-sectional study," *Rev Esp Enferm Dig*, vol. 105, no. 600, article 8, 2013.
- [32] *Revista espanola de enfermedades digestivas: organo oficial de la Sociedad Espanola de Patologia Digestiva*, pp. 600-608, 2014.
- [33] M. Ghassemi, L. A. Celi, and D. J. Stone, "State of the art review: the data revolution in critical care," *Critical Care*, vol. 19, no. 1, p. 118, 2015.
- [34] S. Bharany, S. Sharma, S. Badotra et al., "Energy-efficient clustering scheme for flying ad-hoc networks using an optimized LEACH protocol," *Energies*, vol. 14, no. 19, p. 6016, 2021.
- [35] N. A. Khan, O. I. Khalaf, C. A. T. Romero, M. Sulaiman, and M. A. Bakar, "Application of Euler neural networks with soft computing paradigm to solve nonlinear problems arising in heat transfer," *Entropy*, vol. 23, no. 8, p. 1053, 2021.
- [36] G. Suryanarayana, K. Chandran, O. I. Khalaf, Y. Alotaibi, A. Alsufyani, and S. A. Alghamdi, "Accurate magnetic resonance image super-resolution using deep networks and Gaussian filtering in the stationary wavelet domain," *IEEE Access*, vol. 9, pp. 71406-71417, 2021.
- [37] P. Singh and R. Agrawal, "A customer centric best connected channel model for heterogeneous and Iot networks," *Journal of Organizational and End User Computing*, vol. 30, no. 4, pp. 32-50, 2018.
- [38] H. Kim, "Investigating the mediating role of social networking service usage on the big five personality traits and on the job satisfaction of Korean workers," *Journal of Organizational and End User Computing*, vol. 31, no. 1, pp. 110-123, 2019.

Research Article

Remote Monitoring and Management System of Intelligent Agriculture under the Internet of Things and Deep Learning

Meirong Zhu  and Jie Shang 

School of Economics and Management, Northeast Forestry University, Harbin 150040, China

Correspondence should be addressed to Meirong Zhu; zhumer@nefu.edu.cn

Received 25 January 2022; Revised 23 April 2022; Accepted 29 April 2022; Published 23 May 2022

Academic Editor: Mu-Yen Chen

Copyright © 2022 Meirong Zhu and Jie Shang. This is an open access article distributed under the Creative Commons Attribution License, which permits unrestricted use, distribution, and reproduction in any medium, provided the original work is properly cited.

Based on the Internet of Things (IoT) technology and deep learning algorithm, a greenhouse intelligent agriculture management system was established to analyse the application value of the intelligent agriculture remote monitoring management system in the greenhouse planting industry. Based on the analysis of greenhouse planting demand and environmental factors, the intelligent agriculture monitoring system is established based on the IoT, and the greenhouse system controller is designed based on the adaptive proportion integration differentiation (PID) algorithm. The noise data removal method is established based on the furthest priority strategy k -means (FPKM) algorithm, and the greenhouse data management system is established mainly by the business platform and management platform. The data set of air temperature during the cultivation of *Flammulina velutifolia* in a factory from October 2020 to January 2021 was selected as the research data to analyse the ability of the IoT-based IARMM system to collect greenhouse temperature, carbon dioxide, and light data. In addition, the application of the greenhouse data management system in greenhouse data monitoring and control is analysed. The processing capability of agricultural environment monitoring data based on the FPKM algorithm is analysed. The results show that the intelligent agriculture monitoring system based on IoT and machine learning can effectively monitor the data on greenhouse temperature, carbon dioxide, light, and other environmental factors, and the greenhouse data management system can effectively ensure the normal operation of equipment and data storage. After being processed by the FPKM algorithm, outliers are identified and effectively removed. Under random seeds, the iteration times of the FPKM algorithm and the k -means algorithm are significantly different. The iteration number of the FPKM algorithm is basically stable at approximately 2 times, while the iteration number of the k -means algorithm obviously fluctuates. Based on the IoT and FPKM algorithm, the intelligent agriculture monitoring system covering the user monitoring center, data center module, and mobile phone client module is established. This work establishes a practical remote monitoring and management system for intelligent agriculture based on the IoT and machine learning algorithm, which provides a new idea for intelligent agricultural management.

1. Introduction

Agriculture is the foundation of a country's development, especially for such a large population. Agriculture is the lifeblood of our survival and economic development. Since the founding of new China, we have been looking for ways to solve the problem of food and clothing [1]. In recent years, with the growth of population and social development, the scale of agricultural production has been continuously improved. The traditional agricultural production mode

cannot meet people's demand for crops in different seasons and quality levels [2]. Besides, due to China's vast territory and complex conditions of climate and terrain, there are many regional restrictions on the growth of crops, so the quality and yield of crops cannot be guaranteed [3]. To solve these effects on crops and ensure yield and quality, greenhouses are introduced into agricultural production so that the yield and quality of crops are guaranteed. However, there are still some problems, such as farmers' difficulties in planting, poor control of temperature and water, and pollution

caused by improper implants. Then, there are some poor agricultural products, resulting in an obvious decrease in sales [4, 5].

The Internet of Things (IoT) is a comprehensive adoption of new information technology, including sensors, communication, and automatic control. Currently, it is widely used in agriculture, industry, transportation, and medical treatment [6–8]. The combination of IoT technology and modern agriculture has gradually brought smart agriculture into people's lives, thus improving crop yield and work efficiency, saving resources, and ensuring the quality of crops [9]. Intelligent agriculture systems based on IoT mainly include agricultural production information collection, data storage and management, information analysis, and corresponding decision execution [10]. Intelligent agriculture based on IoT combines advanced science and technology with agricultural production, which can scientifically monitor the growth of crops, changes in the soil and air environment, temperature, humidity, and the soil environment, thereby improving the comprehensive benefits of agricultural production [11]. Through the artificial construction of crop growth environments and intelligent control to optimize the living conditions of crops in greenhouses, greenhouses can make crops in different growth stages in the best environmental conditions [12]. The combination of greenhouses and IoT technology can achieve real-time monitoring of crops, improve the management level of agricultural production, and save labor resources and production costs [13]. The research and application of smart agriculture in planting mainly consists of real-time collection of environmental elements of planting crops through an automated network monitoring system and automatic opening or closing of designated equipment through system settings, which is still in the initial stage [14]. Al-Qurabat et al. [15], based on IoT technology, adopted compression and minimum description length technology in data transmission received by sensors to establish a remote monitoring system for smart agriculture, and the results showed that this method can significantly reduce the data transmission speed and provide a better method for real-time monitoring. Intelligent agriculture started late in China, and intelligent agriculture based on IoT is still in the primary stage. Hence, there are few relevant investigations, and all the requirements for the development of intelligent agriculture cannot be satisfied. The pervasiveness of agriculture towards intelligence and automation has been severely restricted. Besides, there is still a certain gap between China and Western countries in terms of levels of technology and intelligence [16], which needs to be further optimized. On the other hand, the current intelligent agriculture system has collected a large amount of data, which seems to be chaotic but contains great value. If data analysis is conducted without necessary preprocessing, the probability of failure will greatly increase [17]. To ensure accurate and effective information and improve the efficiency of data analysis, it is necessary to add a data preprocessing module before data analysis. The effective processing of these data can provide a scientific basis for the automatic control and intelligent management of the environment.

In summary, there are still some shortcomings in the research of intelligent agriculture systems, and a large number of studies are still needed based on the characteristics of crops and geographical conditions. First, the greenhouse planting requirements and environmental control factors are analysed in this work. Then, a modular greenhouse controller is designed based on the adaptive proportion integration differentiation (PID) algorithm, and the data noise is removed by using the furthest priority strategy for the k -means (FPKM) algorithm. Finally, the intelligent agriculture system and data management system are established based on IoT and are analysed using the test set data. In addition, the intelligent agriculture system is established based on machine learning and IoT. The alarm system and remote control system are added to the data management system and applied to the monitoring of greenhouse crops. The value of intelligent agriculture systems in the greenhouse planting industry under the background of the IoT is discussed to provide a guiding ideology and an experimental basis for the development of intelligent agriculture in the future.

2. Methodology

2.1. Analysis of Greenhouse Planting Requirements. Before establishing the IoT greenhouse system, the detection and related platforms for greenhouse planting need to be analysed. Based on the research results of Al-Qurabat and Kadhum [18], this work further analyses the greenhouse planting demand. First, the data that the greenhouse needs to detect, including temperature, humidity, light, carbon dioxide, and other external environments, need to be determined, and real-time monitoring of the external environment of crop growth needs to be conducted. Then, the obtained information is stored and transmitted so that the obtained data can be shared in a timely manner and sent to farmers in a timely manner so that the internal situation of the greenhouse at all times is understood, and corresponding countermeasures are made according to the situation. After that, the display screen should be installed in the greenhouse to obtain a comprehensive understanding of the greenhouse situation. The most important thing in a greenhouse is the regulation of temperature, which is an important factor for the growth of crops. A temperature evaluation system should be established to monitor whether the current temperature is suitable for the growth of crops to automatically adjust the temperature or manually control the temperature in the later period to ensure the optimal temperature of crops. The remote control system is established to enable farmers to understand the environment in the greenhouse even in the field and make corresponding adjustments to the greenhouse environment to meet the growth of crops. Finally, an early warning and energy-saving device can be set up to issue a remote early warning when abnormalities occur in the greenhouse. At the same time, the installation of farmers can remotely control the relevant equipment in the greenhouse so that it can be shut down in time when it is not needed. The specific greenhouse planting requirements are shown in Figure 1.

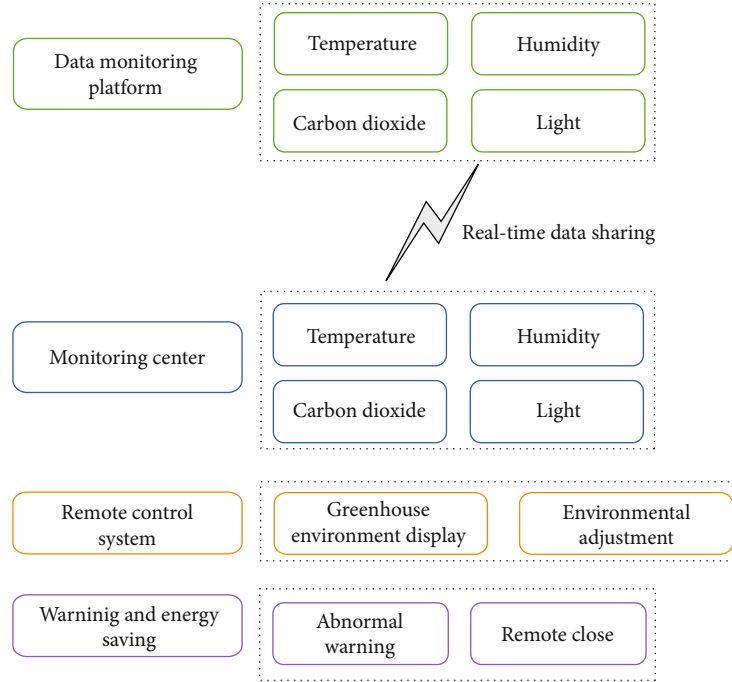


FIGURE 1: Frame diagram of greenhouse planting demand.

2.2. Factor Control of the Greenhouse Environment. The greenhouse environment problem is the root of planting, and too high or too low of a temperature and humidity can stunt crops. Serious conditions may lead to the death of crops. However, the traditional method of carbon dioxide delivery is not only inconvenient but also harmful to the human body [19]. Using the IoT system to control greenhouse factors is now necessary to cultivate better products and reduce the burden on farmers. The greenhouse environmental factor control device is constructed according to the obtained greenhouse information to make the relevant flowchart to design the steps and design a scheme needed for greenhouse environmental factor control. Hot water pipes, hot air heating, and heaters are generally adopted for greenhouse temperature control, while ventilation is generally adopted for cooling. If natural ventilation is not ideal, relevant equipment should be introduced for ventilation and cooling treatment. Humidity is generally divided into dehumidification and humidification. Natural ventilation is used for dehumidification. The wet curtain or spray needs to be introduced for humidification. For light, internal and external sunshade nets can be used. For greenhouse carbon dioxide concentrations, chemical methods can be applied, such as burning coal, drying ice, and biogas fertilizer. The above devices are combined with the IoT system to make an automatic mode.

The greenhouse is a semiclosed system that constantly exchanges energy and matter with the outside world. The heat obtained from the outside of the greenhouse is in a state of thermal balance with that emitted to the outside [20]. In the actual energy calculation of the greenhouse, photosynthesis and respiration can be ignored because the energy costs between them are minimal compared with the others. Then, Equation (1) expresses the environmental heat balance model of the greenhouse:

$$Q_h = Q_s + Q_r - Q_l - Q_c - Q_t - Q_w - Q_e. \quad (1)$$

In Equation (1), Q_s represents the energy obtained from solar radiation in the greenhouse, Q_r represents the heat generated by a heating device in the greenhouse, Q_l represents the heat loss from ventilation inside and outside the greenhouse, Q_c represents the heat loss from the greenhouse covering and the external exchange, Q_t represents the heat absorbed by transpiration, Q_w represents the heat exchanged between surface water vapor and indoor air, and Q_e represents the heat exchanged between crops and indoor air.

According to the change in atmospheric pressure and density in the greenhouse, Q_h can be expressed:

$$Q_h = \rho CH \frac{dT_i}{dt}. \quad (2)$$

In Equation (2), ρ expresses the density of air at standard atmospheric pressure, C expresses the air specific heat capacity at standard atmospheric pressure, H expresses the height of the greenhouse, t expresses the time, and T_i expresses the air temperature in the greenhouse.

Equation (3) shows the heat produced by solar radiation in a greenhouse:

$$Q_s = \vartheta R_0. \quad (3)$$

In Equation (3), ϑ represents the average light transmittance of greenhouse mulch and R_0 represents the external solar radiation intensity.

Equation (4) shows the calculation of the heat generated by the heating device in the greenhouse:

$$Q_r = \frac{\alpha W}{E_s}. \quad (4)$$

In Equation (4), α expresses the heat utilization rate of the greenhouse heating device, W expresses the heat power supplied by the greenhouse heating device, and E_s expresses the floor area of the greenhouse.

The rate of exchange between the air inside and outside the greenhouse affects the amount of heat consumed during ventilation. Equation (5) shows the calculation method for the heat loss of ventilation inside and outside the greenhouse:

$$Q_l = \rho C B \frac{1}{E_s} (T_i - T_0). \quad (5)$$

In Equation (5), B represents the ventilation rate of the greenhouse ventilation device and T_0 represents the air temperature outside the greenhouse.

Equation (6) shows the calculation of heat exchange between greenhouse cover and the outside world:

$$Q_c = g(T_i - T_0) \frac{E_{s1}}{E_s}. \quad (6)$$

In Equation (6), g expresses the heat exchange coefficient of the energy exchange of the covering layer and E_{s1} expresses the area of the greenhouse covering layer.

Equation (7) is the calculation of Q_t :

$$Q_t = F G_x + \frac{\varepsilon \beta T_i}{\eta} - \frac{h_t P \beta_i}{8.03 \eta}. \quad (7)$$

In Equation (7), F represents the heat coefficient of the heat exchange loss between the greenhouse and its covering layer, G_x represents the solar radiation absorbed by crops, ε represents the pressure of saturated water vapor in the greenhouse air when the air temperature is 20°C, β represents the effect coefficient of temperature on saturated water vapor in the greenhouse, η represents the coefficient constant of the hygrometer, h_t represents the coefficient of the heat transfer between the air in the greenhouse and the crops, P represents the standard atmospheric pressure, and β_i represents the absolute indoor humidity.

Equation (8) shows the calculation of Q_w :

$$Q_w = \frac{(T_i - T_l)}{R} \rho C. \quad (8)$$

In Equation (8), R denotes the dynamic impedance of air around crops and T_l denotes the temperature of the plant's own leaves.

The transpiration of crops in the greenhouse, the evaporation of surface water vapor, and the variation in air water vapor caused by the humidifier in the greenhouse can all

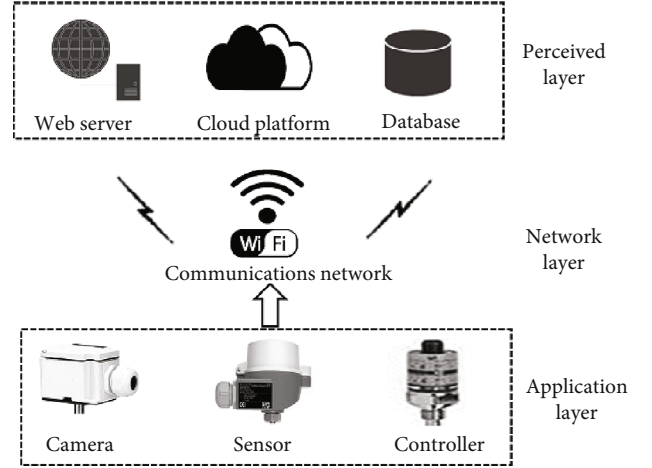


FIGURE 2: The overall framework of the IoT-based intelligent agriculture system.

cause changes in the overall air humidity in the greenhouse [21]. If the distribution of water evaporation in the greenhouse is uniform, the greenhouse air humidity can be expressed as shown in

$$H = J + JT - G_s + R_l. \quad (9)$$

In Equation (9), J denotes the transpiration rate of crops in a greenhouse, JT denotes the transpiration rate of surface water vapor in a greenhouse, G_s denotes the variation quantity of water vapor caused by ventilation exchange in a greenhouse, and R_l denotes the variable quantity of water vapor caused by the greenhouse humidifier.

2.3. The Design of an Intelligent Agriculture System Based on IoT. The IoT mainly includes the perception layer, network layer, and application layer [22]. Consequently, the intelligent agriculture system based on IoT mainly includes these three layers. The perception layer mainly consists of data acquisition control and a real-time video signal monitoring module composed of multisensors, cameras, and controllers deployed in the greenhouse. The involved sensors mainly include a temperature sensor, humidity sensor, light sensor, carbon dioxide sensor, soil temperature and humidity sensor, and soil pH sensor. The sensor collects data through the network layer to the cloud server. The controller relay mainly refers to the control of the greenhouse's environmental regulation electrical equipment. As the middle layer of the intelligent agricultural greenhouse monitoring system, the network layer mainly transmits the environmental data collected from the perception layer to the application layer. Simultaneously, the general command of the application layer is delivered to the controller in the awareness layer. The application layer is the highest layer of the system, and it is a cloud platform service system to realize application functions and data visualization, which is mainly composed of a web server, database, and third-party access cloud platform. Figure 2 shows the overall framework of the IoT-based intelligent agriculture system.

2.4. Design of a Greenhouse System Controller Based on the Fuzzy Adaptive PID Algorithm. In practical engineering adoptions, the most commonly used controller design is the PID controller [23]. The PID controller generally takes the difference (deviation) between the system set value and the measured value as the input value of the system. Equation (10) shows the calculation of the deviation:

$$\varepsilon(t) = p(t) - q(t). \quad (10)$$

Equation (11) shows the output expression of the PID controller:

$$\mu(t) = C_p \varepsilon(t) + C_i \int_0^1 \varepsilon(t) dx + C_d \frac{d\varepsilon(t)}{dt}. \quad (11)$$

In Equations (10) and (11), C_p represents the proportional gain, C_i represents the integral gain, C_d represents the differential gain, $p(t)$ represents the setting value of the system, and $q(t)$ represents the actual value measured by the system.

A fuzzy controller generally consists of two input variables and three output variables [24]. When the temperature factor of the greenhouse is controlled, it is necessary to adjust the parameters of the fuzzy adaptive PID controller online to ensure that the parameter values meet the requirements of temperature control.

Equations (12)–(14) represent the parameter setting calculation method of the fuzzy adaptive PID controller:

$$C_p = C_p^* + \Delta C_p, \quad (12)$$

$$C_i = C_i^* + \Delta C_i, \quad (13)$$

$$C_d = C_d^* + \Delta C_d. \quad (14)$$

In Equations (12)–(14), C_p^* , C_i^* , and C_d express the initial value of the PID controller parameters. ΔC_p , ΔC_i , and ΔC_d express the variable quantity of PID controller parameters.

2.5. Noise Data Removal Based on the Furthest Priority Strategy for the k -Means (FPKM) Algorithm. The original data often have problems such as data inconsistency, duplication, and missing, abnormal, and redundant information [25]. If data mining is performed directly without processing the data, the probability of mining task failure increases significantly [26]. Hence, to ensure the accuracy of mining data and improve mining efficiency, data preprocessing is necessary before data mining. Presently, data preprocessing mainly includes data cleaning, data integration, data transformation, and data specification [27]. The data detected by intelligent agriculture systems need to be removed and processed. The clustering method can not only group the data with large similarity into the same cluster but also isolate outliers in the data and delete them [28]. The k -means algorithm is a classical clustering algorithm based on distance [29]. For the input parameters, m objects can be randomly classified into k clusters. If a cluster is a set of s_{ij} ,

the mean value of a cluster can be expressed as shown in

$$\sigma = \frac{1}{m} \sum_{j=1}^m s_{ij}. \quad (15)$$

Equation (16) shows the criterion function of the k -means algorithm:

$$A = \sum_{i=1}^k \sum_{x \in C_i} |x - \bar{\sigma}|^2. \quad (16)$$

In Equation (16), A denotes the sum of squares of the distances among all the objects in a data set and the mean center of the cluster to which they belong, and x denotes the given data object. $\bar{\sigma}$ is the mean value center of cluster C_i .

The k -means algorithm is simple and can effectively preprocess data. Nonetheless, the algorithm is easily affected by the initial cluster center and is sensitive to “noise” and outlier data while searching for nonconvex clusters [30]. As a result, the adoption scope of the k -means algorithm is limited. The farthest priority strategy k -means (FPKM) algorithm uses the farthest priority strategy to select the center of the cluster, and it introduces the farthest priority strategy and threshold value to judge whether the data contain noise, which can effectively avoid the shortcomings of the k -means algorithm [31].

2.6. Establishment of the Data Management System. The key to crop planting still depends on artificial regulation. If the information is collected in the greenhouse, the corresponding background management system must be set up to observe the data and make corresponding adjustments. The application of the IoT is to facilitate people in managing the production of crops more conveniently and accurately. An artificial intelligence service system is added to the background. Two platforms are mainly designed: business platform and management platform. The overall diagram of the data management system is shown in Figure 3. The business platform mainly includes the timely release of information, remote control of the greenhouse by farmers, timely viewing of the greenhouse and understanding of the internal conditions, disposal of the alarm system by farmers, and setting of all condition thresholds. The management platform is mainly for the management of users and data, timely viewing and management of equipment, and information sharing and release. At the same time, a mobile phone client is set up so that farmers can timely query the situation in the greenhouse from the mobile phone and can conduct remote control.

2.7. The Data Set of the Test. The data set of air temperature during the cultivation process of *Flammulina velutipes* in a factory from October 2020 to January 2021 is used as the research data. The data set includes air temperature data, air humidity data, soil temperature data, and soil humidity data. All four kinds of data are collected every minute. A total of 1,200 groups of complete cycle data are collected,

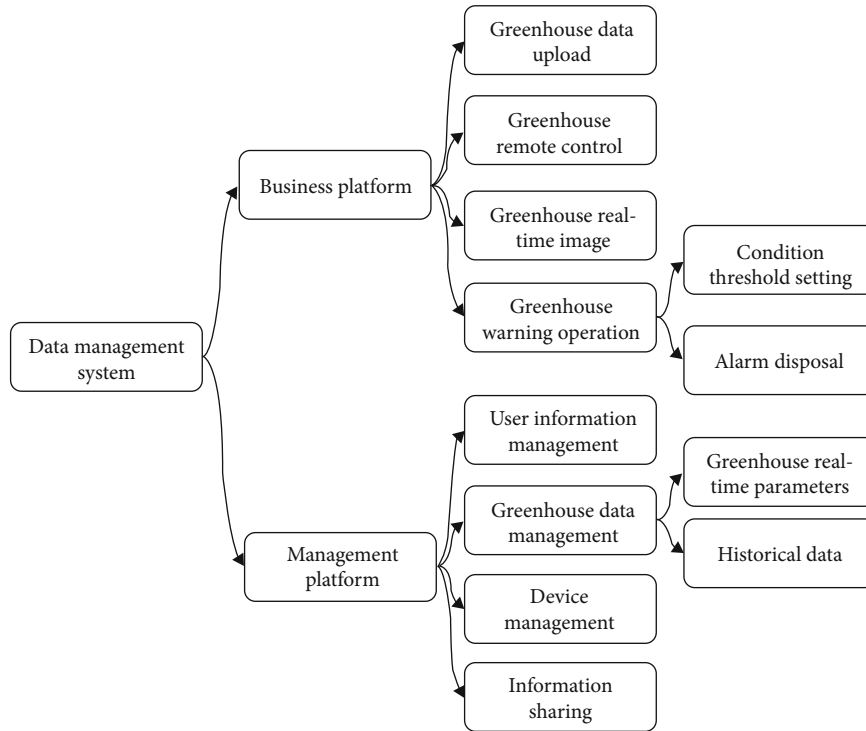


FIGURE 3: The overall frame diagram of the data management system.

1,000 of which are used as the training samples and 200 as the test samples.

3. Results and Discussion

3.1. Analysis of the Results of Noise Data Removal Based on the FPKM Algorithm. The FPKM algorithm is used to denoise the data in the data set (Figure 4). Before the denoising processing of the FPKM algorithm, there are 7 abnormal values in the data. The abnormal values are identified and effectively removed after the processing of the FPKM algorithm.

The denoising efficiency of the algorithm can be represented by the number of iterations. The lower the number of iterations is, the higher the efficiency of the algorithm is [32]. Under the effect of different and random seeds, the iteration times of the FPKM algorithm and the k -means are compared (Figure 5). Under the random seed, the iteration times of the FPKM algorithm and the k -means algorithm are obviously different, and the iteration times of the FPKM algorithm are stable, basically at approximately 2 times. The number of iterations of the k -means algorithm fluctuates obviously. The number of iterations of the k -means algorithm is more than that of the FPKM algorithm under partial random seeds. Hence, the number of iterations of the k -means algorithm is greatly affected by the initial clustering center. The efficiency of the FPKM algorithm is obviously improved.

3.2. Greenhouse Planting Demand Analysis. The greenhouse planting demand is divided into two parts. The first part is the demand for crops in the greenhouse, and the second part

is the backstage management operation of farmers, which is used to comprehensively manage the growth of crops in the greenhouse. We visited and investigated the conditions required in the greenhouse to provide the corresponding data support for the subsequent model establishment and application. Table 1 shows the temperature requirements of various vegetables. According to the figure, the most suitable temperature for different vegetables is shown. Therefore, the temperature is adjusted in the greenhouse by combining the temperature demand of different vegetables with the external environmental temperature. According to the different temperatures that vegetables can tolerate, vegetables can be classified into cold-resistant vegetables, semi-cold-resistant vegetables, warm vegetables, and heat-resistant vegetables. Among them, cold-resistant vegetables are very strong in frost resistance. Some vegetables can survive even at only 10°C. The universal cold-resistant vegetables are leek, spinach, radish, onion, and garlic. Semi-cold-resistant vegetables grow best at 17-20°C, which can withstand the short-term low temperature of -1~-3°C. Common semi-cold-resistant vegetables include Chinese cabbage, radish, carrot, cabbage, pea, and broad bean. Warm vegetables grow at temperatures of 20-30°C and are not resistant to frost. It is easy to cause falling flowers below 15°C. Above 35°C, there will be poor growth and fruit. Warm vegetables mainly include cucumber, tomato, pepper, bean, and eggplant. Heat-resistant vegetables grow better at approximately 30°C, which can still grow normally and bear fruit at 35-40°C, including winter melon, pumpkin, watermelon, cowpea, bean, amaranth, and water spinach.

Figure 6 shows the amount of water required by farmers for growing vegetables, and Figure 7 shows the water use

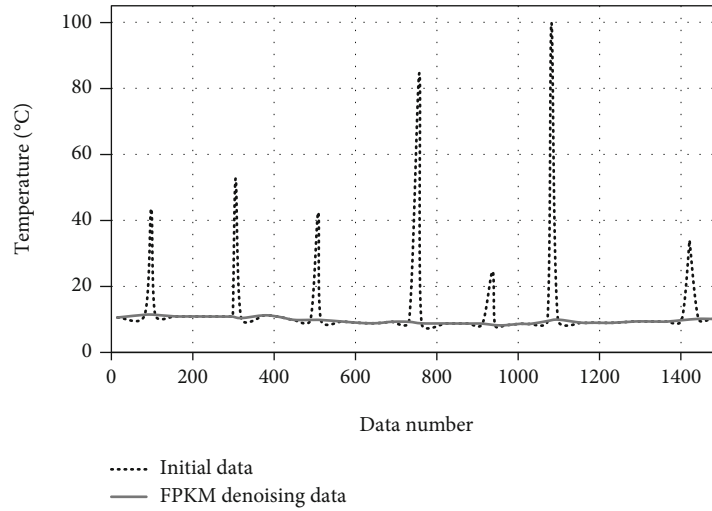


FIGURE 4: The results of noise data removal of the FPKM algorithm.

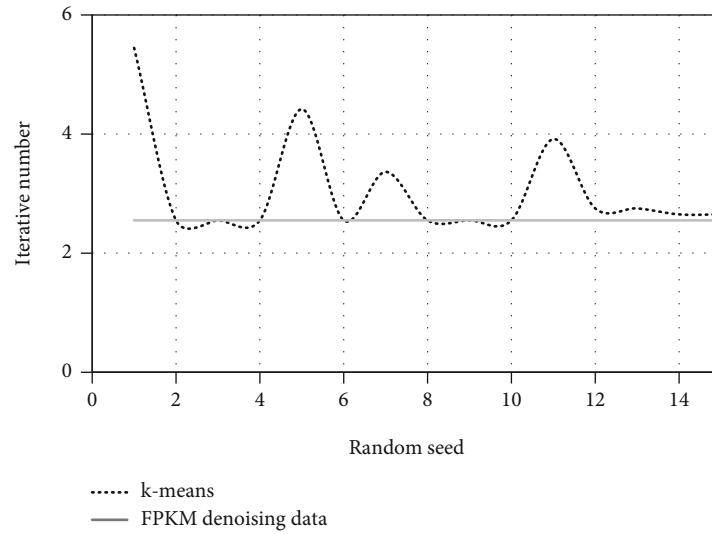


FIGURE 5: Comparison of the iteration times of the different algorithms under random seeds.

TABLE 1: Temperature requirements of different vegetables.

	Growth temperature (°C)			Average monthly temperature during cultivation (°C)		
	Lowest temperature	Most comfortable temperature	Highest temperature	Lowest temperature	Most comfortable temperature	Highest temperature
Hardy vegetables	6-8	16-21	21-27	6	11-19	25
Semihardy vegetable	6-11	16-21	21-27	8	16-21	27
Thermophilic vegetables	11	22-31	32-36	16	18-25	31
Heat-resistant vegetables	11-16	26-31	35-42	17	21-32	34

efficiency of different vegetables. As seen from the figure, the water consumption and transpiration efficiency of different kinds of vegetables vary greatly. The traditional planting mode cannot control the amount of water needed for vegetables, and the transpiration rate cannot be accurately

measured and regulated. Therefore, it is necessary to make use of IoT technology for detection and regulation. In the second part, the background management of farmers is analysed. Farmers need to conduct real-time supervision of the temperature, humidity, carbon dioxide, and other factors

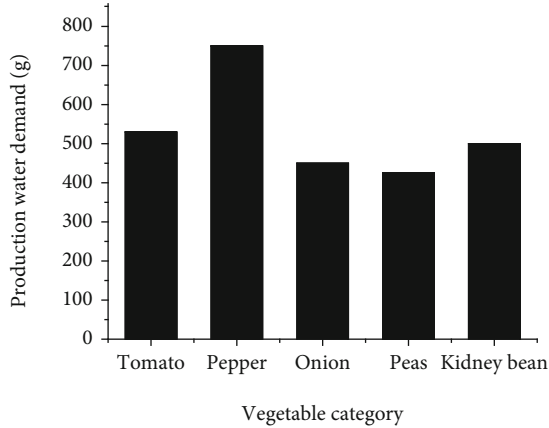


FIGURE 6: Water requirements of different vegetables during the growing process.

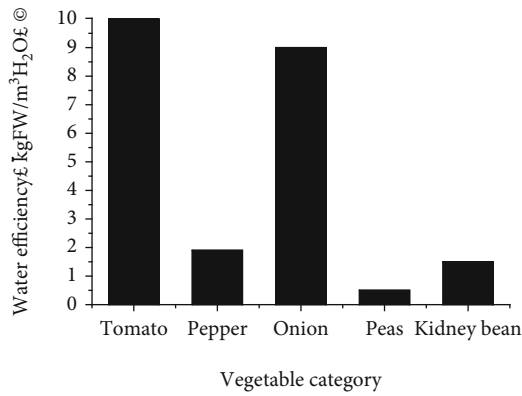


FIGURE 7: Water use efficiency of different vegetables.

in the greenhouse and adjust the environment in the greenhouse in a timely manner.

Figure 8 is the frame of the greenhouse system. As seen from the figure, an overall plan is made for the demand of the greenhouse. The temperature and humidity sensors in the greenhouse can evaluate and adjust the environment in a timely manner. Meanwhile, all the obtained video, weather, and other conditions can be recorded and fed back to the terminal, which can also adjust and monitor the data. This system enables farmers to know all aspects of the greenhouse and automatic irrigation and lighting system, which can be monitored and adjusted by farmers at any time.

3.3. Greenhouse Environmental Factor Control Device. There are many kinds of agricultural products in China. The difference in temperature between the north and south is large, so it is impossible to give a unified agricultural operation mode and path selection [33]. Hot water pipes, hot air, heaters, and other devices are used to increase the greenhouse temperature. An outer sunshade or spray is used to lower the temperature inside the greenhouse. The results showed that the spray was much more effective in lowering the greenhouse temperature. Skylights for the greenhouse are designed to achieve the effect of dehumidification; natural

ventilation is used to achieve the purpose of dehumidification, and a wet curtain and spray are used to achieve the effect of increasing humidity. The results show that both of these methods can effectively increase the moisture in the greenhouse. In the greenhouse, an internal and external sunshade net is used to promote the growth of crops by increasing the ambient light intensity in the farmers' opinion. The result shows that this device can effectively increase the light intensity so that the crops can obtain sufficient light even in rainy weather and avoid direct sunlight at the same time. A carbon dioxide gas production device is used to control the concentration of CO₂ in the greenhouse. Ammonium bicarbonate is placed under the device, sulfuric acid is dripped into the linkage device, and the valve containing the liquid is controlled with the automatic control system to produce carbon dioxide. This method can effectively produce carbon dioxide to meet the needs of crop production. Figure 9 is a flowchart of a greenhouse control system. As seen from the figure, the combination of relevant material devices and the IoT are used to control greenhouse conditions. The design of the background operation management and data control center meets the farmers' overall management of the greenhouse and achieves the functions of mobile phones and PC. Combined with the existing network technology and data technology, the control of greenhouse temperature, humidity, and carbon dioxide is achieved. Then, wireless sensor technology and a monitoring network are adopted to collect environmental and meteorological data back to the data center. Finally, it is presented to farmers in the form of charts.

3.4. Background Design and Database Analysis. A background management system is set up for farmers so that farmers can use mobile phones and other terminals to grasp the situation in the greenhouse in a timely manner. User permission management, database operation, and user management are set to protect the management privacy of farmers. At the same time, the establishment of the data module gives farmers a timely understanding of the relevant data. Figure 10 shows a sample diagram of the user monitoring center and data center module. The information monitored by users including the information of each area in the greenhouse, the early warning information of the specific situation of the greenhouse, the monitoring and viewing of the equipment at any time, and the relevant videos in the greenhouse over time are shown in the figure. Meanwhile, a system supervisor is set up to collect and analyse the data of the data center to comprehensively master the data information in the production of farmers. The mobile phone client model is established. Figure 11 is the greenhouse mobile phone login operation flowchart. It shows the control of the greenhouse system by the mobile phone client. Farmers can use the phone to check the history data and manually control the greenhouse environment at the same time. Through this convenient method, the manpower material resources in agricultural production are greatly reduced, and a precise control system can increase crop production, which provides a design plan used in other crop production for the IoT.

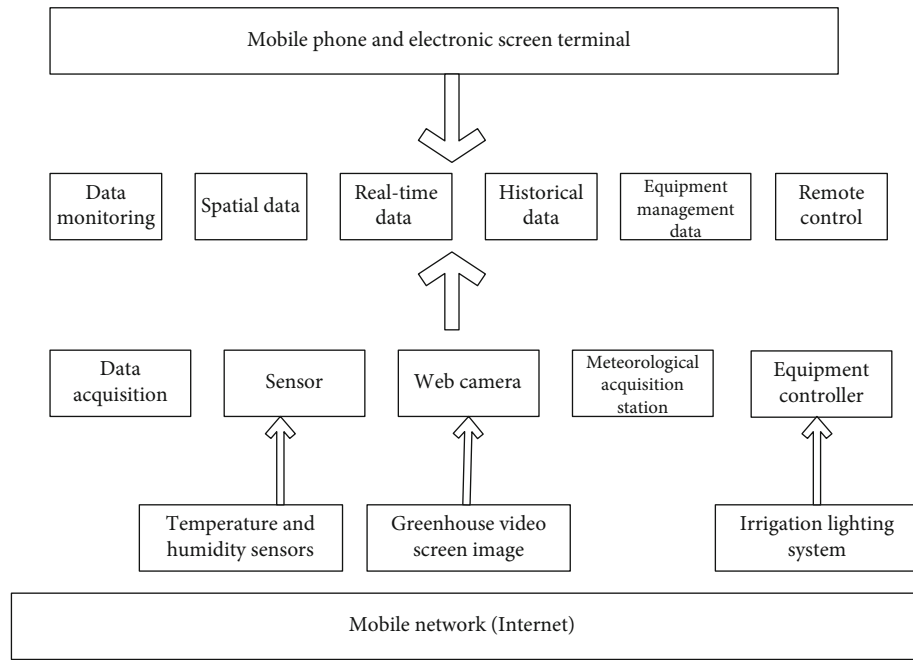


FIGURE 8: Greenhouse IoT detection system.

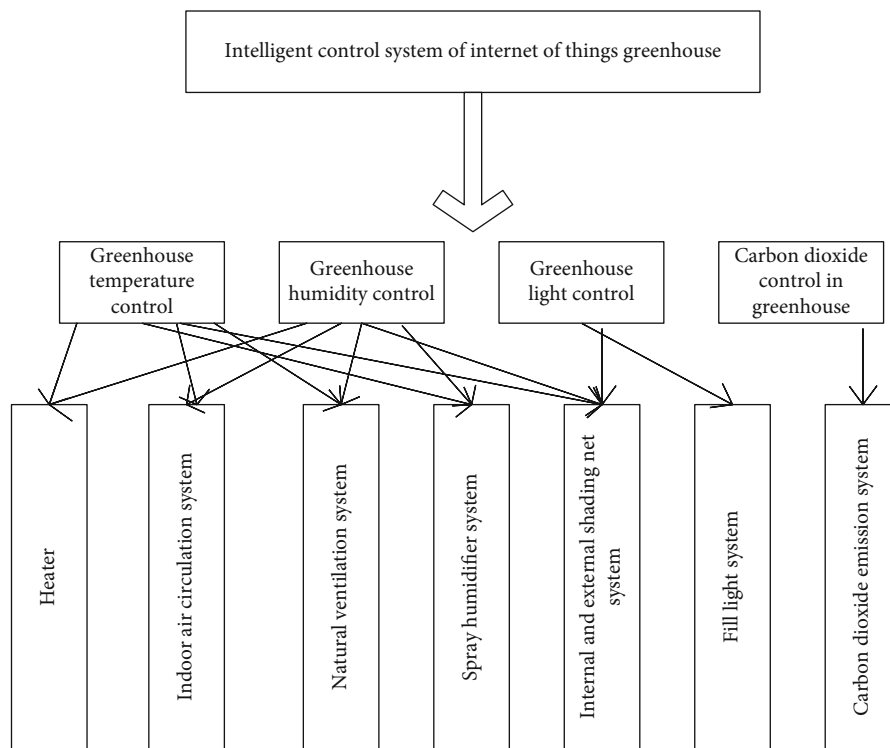


FIGURE 9: Flowchart of the greenhouse control system.

3.5. *Performance Analysis of the Greenhouse System Controller.* The performance of the greenhouse system controller based on the fuzzy adaptive PID algorithm is analysed (Figure 12). Within 2 hours of monitoring, the temperature outside the greenhouse gradually increases, the temperature value in the greenhouse has always remained in the range of

18.0°C~21.0°C, and the error range between the change trend of indoor temperature and the set value is maintained within 3°C. The results show that the greenhouse system controller based on the fuzzy adaptive PID algorithm can effectively maintain the stable state of the temperature in the greenhouse.

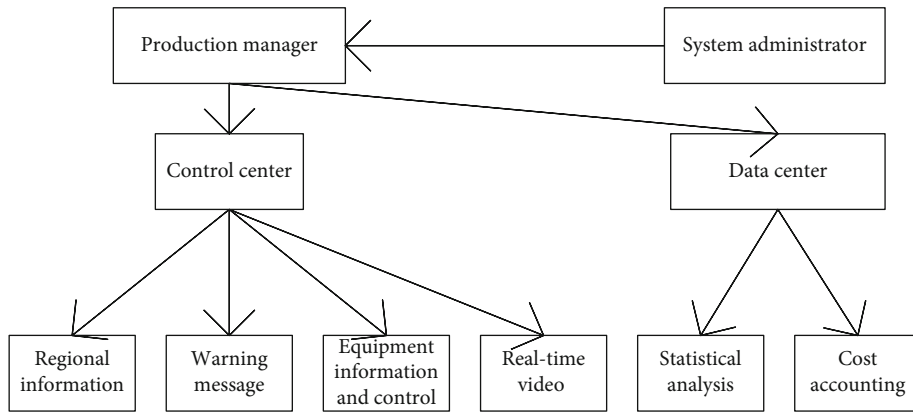


FIGURE 10: Background management system of the greenhouse IoT system.

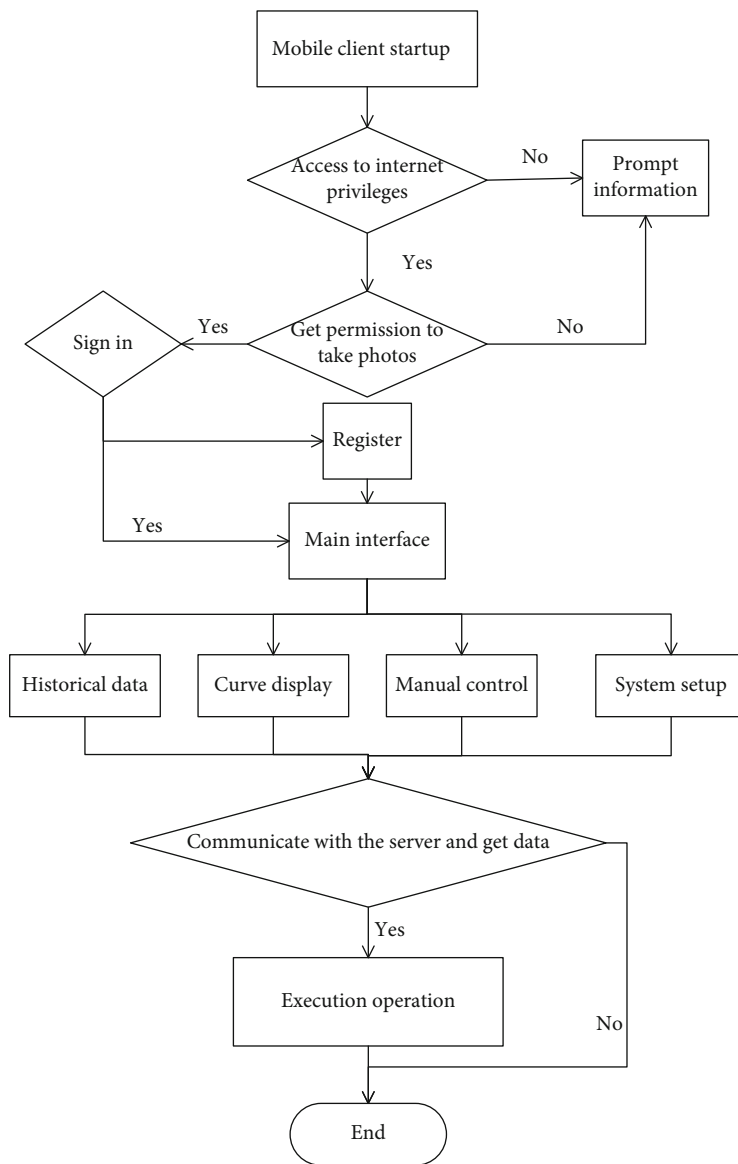


FIGURE 11: Mobile client management process.

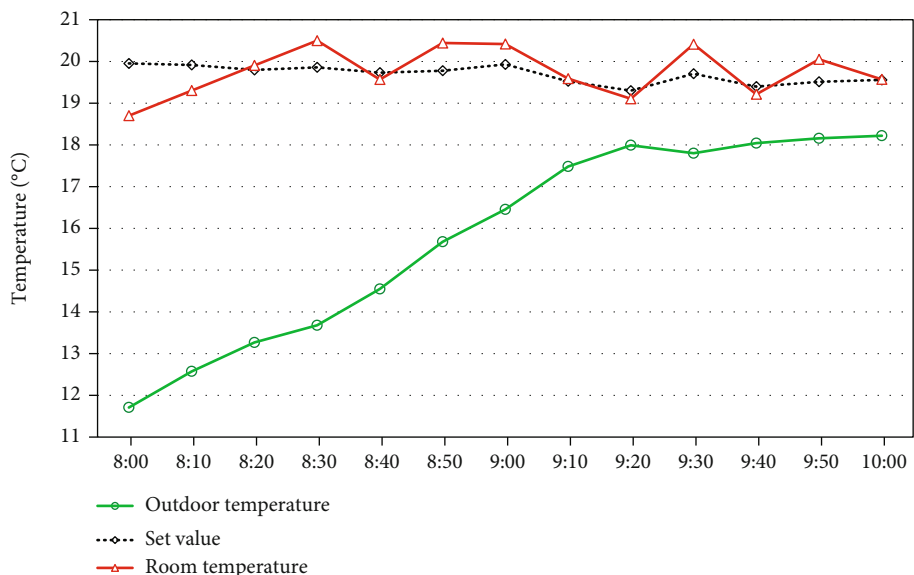


FIGURE 12: Variation curve of temperature inside and outside the greenhouse.

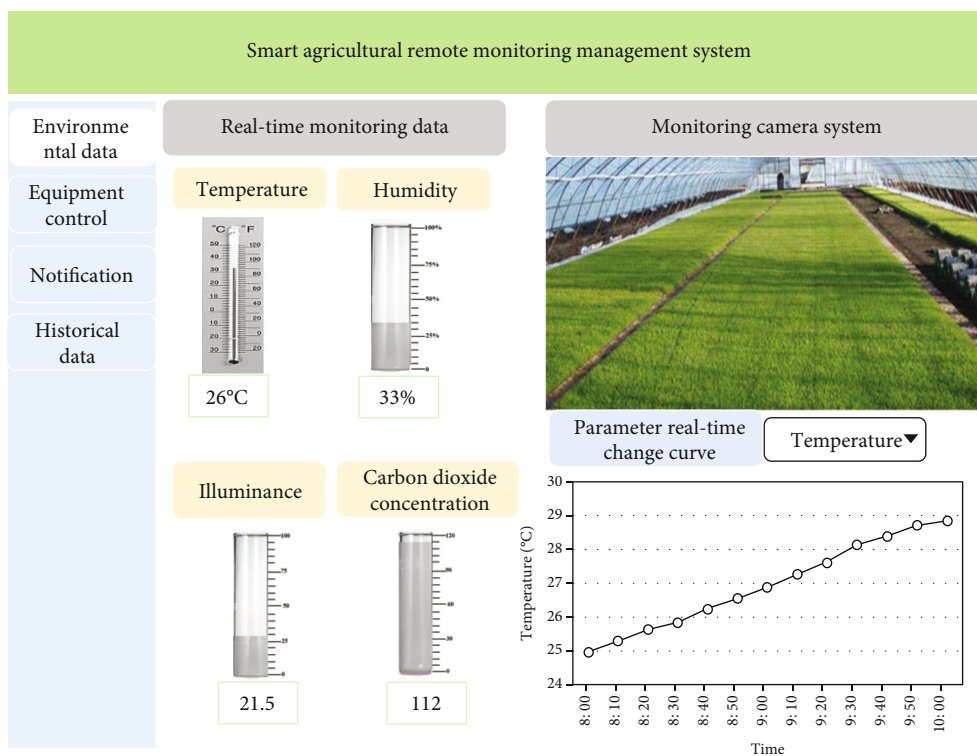


FIGURE 13: The data display page of the intelligent agriculture system.

3.6. *The Data Display and Remote Control Interface of the Intelligent Agriculture System.* The data monitoring part of the intelligent agriculture system can display the specific values of temperature, humidity, carbon dioxide concentration, and light in the greenhouse in real time, which is a real and comprehensive record of the plant growth environment in the greenhouse. At the same time, the situation inside the

greenhouse can be recorded in real time through video monitoring images. The data display page of the intelligent agriculture system is shown in Figure 13.

The remote equipment operation module of the intelligent agricultural system can display the real-time operation and configuration of the equipment and remotely control the greenhouse environmental parameters through real-

Smart agricultural remote monitoring management system						
Environmental data	Parameter settings			Equipment control		
Equipment control		Upper limit	Lower limit	Skylight	Outer shading	
Notification	Temperature	20 ▼	30 ▼	<input checked="" type="checkbox"/>	<input checked="" type="checkbox"/>	
Historical data	Humidity	35 ▼	50 ▼	Inner shade	Humidifier	
				<input checked="" type="checkbox"/>	<input checked="" type="checkbox"/>	
	Illuminance	3000 ▼	7500 ▼	Blower	Heater	
				<input checked="" type="checkbox"/>	<input checked="" type="checkbox"/>	
	Carbon dioxide concentration	200 ▼	700 ▼	CO2 generator	Fill light	
				<input checked="" type="checkbox"/>	<input checked="" type="checkbox"/>	
	Save	Reply to default settings		Save	Implement	

FIGURE 14: The display page of remote equipment operation of the intelligent agricultural system.

time data changes. The display page for remote equipment operation of the intelligent agricultural system is shown in Figure 14.

4. Conclusion

In this work, an effective remote monitoring and management system for intelligent agriculture is established based on the IoT and machine learning algorithm. However, there are still some shortcomings. Only the temperature monitoring in the system is optimized, while the humidity and other environmental factors are not optimized and analysed. In future work, the system will be further improved to increase its application range. In conclusion, it establishes an intelligent agriculture system based on the IoT and machine learning algorithm, which provides guidance and an experimental basis for the development of intelligent agriculture.

Data Availability

The data used to support the findings of this study are available from the authors upon request.

Conflicts of Interest

The authors declare that they have no conflicts of interest.

Acknowledgments

This work was supported by the Heilongjiang Provincial Postdoctoral Science Foundation: Research on the transition of the recycling agriculture industry chain in Heilongjiang Province: dynamic mechanism, upgrading path and development countermeasures (No. LBH-Z14019) and Postdoc-

toral Science Foundation of Heilongjiang Province: Research on the mechanism and realization path of digital technology enabling agricultural green development in Heilongjiang Province (No. LBH-Q21053).

References

- [1] Y. R. Jin and S. Ji, "Mapping hotspots and emerging trends of business model innovation under networking in Internet of Things," *EURASIP Journal on Wireless Communications and Networking*, vol. 2018, no. 1, 2018.
- [2] X. Deng, R. Sun, H. Yang, J. Nie, and W. Wang, "Data transmission method of pasture internet of things based on opportunistic network," *Transactions of the Chinese Society for Agricultural Machinery*, vol. 48, no. 2, pp. 208–214, 2018.
- [3] Y. X. Wei, "Study on the application of internet of things-based intelligent microscope in blood cell analysis," *Journal of Computational and Theoretical Nanoscience*, vol. 14, no. 2, pp. 1199–1203, 2017.
- [4] P. M. Kumar, U. Gandhi, R. Varatharajan, G. Manogaran, R. Jidhesh, and T. Vadivel, "Intelligent face recognition and navigation system using neural learning for intelligent security in internet of things," *Cluster Computing*, vol. 22, no. 4, pp. 7733–7744, 2017.
- [5] L. Jie, Y. Wei, Z. Nan, X. Yang, H. Zhang, and Z. Wei, "A survey on internet of things: architecture, enabling technologies, security and privacy, and applications," *IEEE Internet of Things Journal*, vol. 4, no. 5, pp. 1125–1142, 2017.
- [6] Z. Lv, Y. Han, A. K. Singh, G. Manogaran, and H. Lv, "Trustworthiness in industrial IoT systems based on artificial intelligence," *IEEE Transactions on Industrial Informatics*, vol. 17, no. 2, pp. 1496–1504, 2021.
- [7] Z. Lv, "Security of internet of things edge devices," *Software: Practice and Experience*, vol. 51, no. 12, pp. 2446–2456, 2021.

- [8] M. D. Alshehri, F. K. Hussain, and O. K. Hussain, "Clustering-driven intelligent trust management methodology for the internet of things (CITM-IoT)," *Mobile Networks & Applications*, vol. 23, no. 3, pp. 419–431, 2018.
- [9] J. Wan, S. Tang, Q. Hua, L. Di, C. Liu, and J. Lloret, "Context-aware cloud robotics for material handling in cognitive industrial internet of things," *IEEE Internet of Things Journal*, vol. 4, pp. 2272–2281, 2017.
- [10] P. Sundaravadivel, E. Kougiyanos, S. P. Mohanty, and M. K. Ganapathiraju, "Everything you wanted to know about smart health care: evaluating the different technologies and components of the internet of things for better health," *IEEE Consumer Electronics Magazine*, vol. 7, no. 1, pp. 18–28, 2018.
- [11] J. J. P. C. Rodrigues, X. Wang, A. K. Sangaiah, and M. Sheng, "Guest editorial special issue on integrated computing: computational intelligence paradigms and internet of things for industrial applications," *IEEE Internet of Things Journal*, vol. 5, no. 3, pp. 1572–1574, 2018.
- [12] L. Yuqing, L. S. Jiajia, C. Shouqi, and X. Bowen, "Design and application of monitoring system for crab breeding base based on internet of things," *Transactions of the Chinese Society of Agricultural Engineering*, vol. 34, no. 16, pp. 205–213, 2018.
- [13] C. Man, L. Guo, Y. Gao, and Y. Zhang, "Wisdom farm internet of things software design and selection program," in *International Conference in Communications, Signal Processing, and Systems*, pp. 791–798, Singapore, 2020.
- [14] I. D. I. Saeedi and A. K. M. Al-Qurabat, "Perceptually important points-based data aggregation method for wireless sensor networks," *Baghdad Science Journal*, vol. 35, p. 0875, 2022.
- [15] A. K. M. Al-Qurabat, Z. A. Mohammed, and Z. J. Hussein, "Data traffic management based on compression and MDL techniques for smart agriculture in IoT," *Wireless Personal Communications*, vol. 120, no. 3, pp. 2227–2258, 2021.
- [16] J. Lin, Z. Shen, A. Zhang, and Y. Chai, "Blockchain and IoT based food traceability for smart agriculture," in *Proceedings of the 3rd International Conference on Crowd Science and Engineering*, pp. 1–6, Singapore, 2018.
- [17] I. D. I. Saeedi and A. K. M. Al-Qurabat, "A systematic review of data aggregation techniques in wireless sensor networks," *Journal of Physics: Conference Series. IOP Publishing*, vol. 1818, no. 1, article 012194, 2021.
- [18] M. Al-Qurabat and A. Kadhum, "A lightweight Huffman-based differential encoding lossless compression technique in IoT for smart agriculture," *International Journal of Computing and Digital System*, vol. 11, no. 1, pp. 117–127, 2022.
- [19] A. K. M. Al-Qurabat and A. K. Idrees, "Distributed data aggregation protocol for improving lifetime of wireless sensor networks," *Qalaai Zanist Scientific Journal*, vol. 2, no. 2, pp. 204–215, 2017.
- [20] C. Baglivo, D. Mazzeo, S. Panico et al., "Complete greenhouse dynamic simulation tool to assess the crop thermal well-being and energy needs," *Applied Thermal Engineering*, vol. 179, article 115698, 2020.
- [21] H. G. Mobtaker, Y. Ajabshirchi, S. F. Ranjbar, and M. Matloobi, "Simulation of thermal performance of solar greenhouse in north-west of Iran: an experimental validation," *Renewable Energy*, vol. 135, pp. 88–97, 2019.
- [22] N. Ahmed, D. De, and I. Hussain, "Internet of Things (IoT) for smart precision agriculture and farming in rural areas," *IEEE Internet of Things Journal*, vol. 5, no. 6, pp. 4890–4899, 2018.
- [23] X. Jin, K. Chen, Y. Zhao, J. Ji, and P. Jing, "Simulation of hydraulic transplanting robot control system based on fuzzy PID controller," *Measurement*, vol. 164, article 108023, 2020.
- [24] J. Zhang and L. Guo, "Theory and design of PID controller for nonlinear uncertain systems," *IEEE Control Systems Letters*, vol. 3, no. 3, pp. 643–648, 2019.
- [25] M. Garuti, M. Langone, C. Fabbri, and S. Piccinini, "Monitoring of full-scale hydrodynamic cavitation pretreatment in agricultural biogas plant," *Bioresource Technology*, vol. 247, pp. 599–609, 2018.
- [26] M. Mafa, S. Malgas, A. Bhattacharya, K. Rashamuse, and B. I. Pletschke, "The effects of alkaline pretreatment on agricultural biomasses (corn cob and sweet sorghum bagasse) and their hydrolysis by a termite-derived enzyme cocktail," *Agronomy*, vol. 10, no. 8, p. 1211, 2020.
- [27] C. Nitsos, L. Matsakas, K. Triantafyllidis, U. Rova, and P. Christakopoulos, "Investigation of different pretreatment methods of Mediterranean-type ecosystem agricultural residues: characterisation of pretreatment products, high-solids enzymatic hydrolysis and bioethanol production," *Biofuels*, vol. 9, no. 5, pp. 545–558, 2018.
- [28] M. Amer, M. Nour, M. Ahmed, S. Ookawara, S. Nada, and A. Elwardany, "The effect of microwave drying pretreatment on dry torrefaction of agricultural biomasses," *Bioresource Technology*, vol. 286, article 121400, 2019.
- [29] N. Kumar, S. K. Yadav, and D. S. Yadav, *An Approach for Documents Clustering Using K-Means Algorithm, Innovations in Information and Communication Technologies (IICT-2020)*, Springer, Cham, 2021.
- [30] C. Li and B. Niu, "Design of smart agriculture based on big data and Internet of things," *International Journal of Distributed Sensor Networks*, vol. 16, no. 5, 2020.
- [31] O. Wilkins, C. Hafemeister, A. Plessis et al., "EGRINs (Environmental Gene Regulatory Influence Networks) in rice that function in the response to water deficit, high temperature, and agricultural environments," *The Plant Cell*, vol. 28, no. 10, pp. 2365–2384, 2016.
- [32] P. Nie, T. Dong, Y. He, and F. Qu, "Detection of soil nitrogen using near infrared sensors based on soil pretreatment and algorithms," *Sensors*, vol. 17, no. 5, p. 1102, 2017.
- [33] J. Yue, G. Yang, and H. Feng, "Comparative of remote sensing estimation models of winter wheat biomass based on random forest algorithm," *Transactions of the Chinese Society of Agricultural Engineering*, vol. 32, no. 18, pp. 175–182, 2016.

Research Article

Using the Neutrosophic DEMATEL Method to Determine the Effect of Internet Finance and Big Data Risk Control Monitoring

Lin Tian¹ and Hongmei Gu ²

¹College of Accounting and Finance, Xi'an Peihua University, Xi'an, 710000 Shaanxi, China

²Information Technology and Cultural Management Institute, Hebei Institute of Communications, Shijiazhuang, Hebei, China

Correspondence should be addressed to Hongmei Gu; guhm@hebic.edu.cn

Received 8 March 2022; Accepted 11 April 2022; Published 17 May 2022

Academic Editor: Nima Jafari Navimipour

Copyright © 2022 Lin Tian and Hongmei Gu. This is an open access article distributed under the Creative Commons Attribution License, which permits unrestricted use, distribution, and reproduction in any medium, provided the original work is properly cited.

Internet financial (IF) is an exchanged of goods and pays money over the Internet. The IF plays a critical role in financial fields. The IF is an innovation in the market and financial. The IF is better than the traditional financial. The IF has many criteria and subcriteria. Because there are so many different types of Internet-related financial risks, it is important for the institutions that deal with them to have effective risk prevention, control, monitoring, and management systems in place and to alert the public to any new threats. The goal of this paper is to determine the impacts of IF and big data risk control monitoring. The concept of multicriteria decision-making proposed in this paper deals with four main criteria and seventeen subcriteria. This paper proposed a Decision-Making Trial and Evaluation Laboratory (DEMATEL) method for computing the influence of the IF. The DEMATEL method is integrated with neutrosophic sets for overcoming incomplete and vague information. The applications are proposed to show the outcomes of the proposed methodology.

1. Introduction

Internet financial plays an essential role in the market and growth of countries. The IF presents a significant role in the development of countries. The IF hybrid has many technologies like big data, information technology (IT), and cloud computing. The IF includes many functions and transactions over the Internet, like paying and buying goods online. The IF can reduce financial risks by integrating with many technologies such as IT. The IF can improve the efficiency of resources. The IF can be built in the market-based system using credits. The IF is better than traditional financial. There are many papers in this field [1–9].

Since natural resources are depleting at an alarming rate, the need for energy efficiency in this period has never been greater. A variety of economic factors are significantly influenced by increased energy efficiency as well. Operations research has a subfield known as multicriteria decision-making (MCDM) (OR). Although MCDM could improve

engineering decision-making throughout the entire process of design and manufacture, it is particularly beneficial in high Internet financials where product differentiation and competitive advantage are often achieved by just a few millimeters of improvement in the performance of a given material. When it comes to solving complicated material selection challenges, MCDM approaches have the capacity to examine material, process, and form simultaneously. MCDM approaches must thus be used for a wide range of engineering applications, and the expertise gained should be used to enhance the selection of materials. When selecting and designing materials, it is important to be able to manipulate data ranges effectively in order to make better use of MCDM. If there is ambiguity or compromise, this must be done.

There are two ways to categorize MCDM, based on the weighting mechanism used for each choice. Firstly, a compensatory choice is a judgement that takes into account all of the criteria, including the criteria's strengths as well as

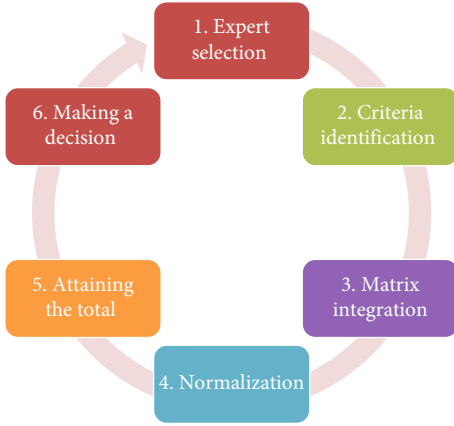


FIGURE 1: The general neutrosophic DEMATEL framework.

TABLE 1: The opinion of the first decision-makers.

	GBC	IC	IFP	MB
GBC	1	0.9	0.8167	0.283
IC	1.111111	1	0.283	0.9
IFP	1.22444	3.533569	1	0.8167
MB	1.111111	1.22444	3.533569	1

TABLE 2: The opinion of the second decision-makers.

	GBC	IC	IFP	MB
GBC	1	0.8167	0.383	0.9
IC	1.22444	1	0.383	0.8167
IFP	2.610966	2.610966	1	0.9
MB	1.22444	2.610966	1.111111	1

their weaknesses, so that the strong aspects of each criteria may compensate for the weak parts. If you are looking for an example of a compensating decision-making tool, look no further than the analytical hierarchy process (AHP). It is used to compare difficult-to-quantify factors. Secondly, an outranking decision-making strategy analyses criteria in couples to decide, based on the comparisons, which criterion ranks higher than the other criteria. Elimination and choice expressing reality (ELECTRE) is an example of an outranking decision-making approach, which is used to choose, rank, and sort options to solve a problem.

The IF can contain many criteria and subcriteria. So, the MCDM methods are proposed to deal with various and conflict criteria. The MCDM is used in problems of decision-making. This paper introduces the DEMATEL method to present the effects of IF in many criteria. The DEMATEL method is an MCDM method. The DEMATEL was used to present the importance of main and subcriteria [10–16].

This paper proposes the DEMATEL method with the neutrosophic sets to overcome incomplete information and uncertainty. The neutrosophic set is a better tool to deal with uncertainty. Neutrosophic sets are better than the fuzzy system. Because the fuzzy system cannot consider the

TABLE 3: The opinion of the second decision-makers.

	GBC	IC	IFP	MB
GBC	1	0.383	0.283	0.8167
IC	2.610966	1	0.8167	0.383
IFP	3.533569	1.22444	1	0.283
MB	2.610966	3.533569	1.22444	1

TABLE 4: The combined opinion of the decision-makers.

	GBC	IC	IFP	MB
GBC	1	0.6999	0.494233	0.666567
IC	1.648839	1	0.494233	0.6999
IFP	2.456325	2.456325	1	0.666567
MB	1.648839	2.456325	1.956373	1

TABLE 5: The normalized opinion of the decision-makers.

	GBC	IC	IFP	MB
GBC	0.141612	0.099114	0.069989	0.094394
IC	0.233496	0.141612	0.069989	0.099114
IFP	0.347846	0.347846	0.141612	0.094394
MB	0.233496	0.347846	0.277046	0.141612

TABLE 6: The total relation matrix.

	GBC	IC	IFP	MB
GBC	0.052029	0.013863	0.017078	0.051229
IC	0.119876	0.039593	0.006365	0.042396
IFP	0.146066	0.182016	0.046716	0.000348
MB	-0.01023	0.129815	0.157892	0.03889

TABLE 7: The criteria's weights.

	Weights
GBC	-0.17355
IC	-0.15706
IFP	0.147095
MB	0.183509

indeterminacy value in its calculations, neutrosophic sets do it. This paper used the single-valued neutrosophic sets (SVNSs), which contain three values: truth, indeterminacy, and falsity values [17–20].

The main contribution in this paper is the first time we introduce the DEMATEL method to determine the effects of Internet financial and big data risk control monitoring under neutrosophic sets to overcome the uncertainty information.

The rest of this paper is presented as follows: Section 2 presents the neutrosophic DEMATEL method, and Section 3 presents the proposed method's application and results. Section 4 presents the conclusions and future work.

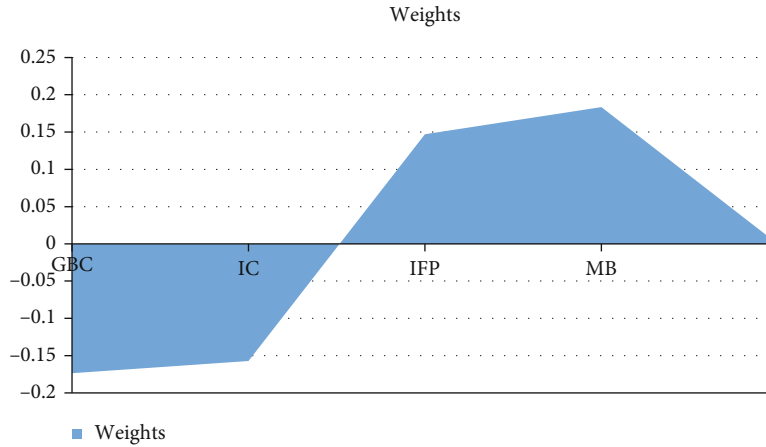


FIGURE 2: The criteria's weights.

TABLE 8: The opinion of the first decision-makers for GBC.

	GBC ₁	GBC ₂	GBC ₃
GBC ₁	1	0.8167	0.9
GBC ₂	1.22444	1	0.383
GBC ₃	1.111111	2.610966	1

TABLE 11: The combined opinion of the decision-makers.

	GBC ₁	GBC ₂	GBC ₃
GBC ₁	1	0.6999	0.488667
GBC ₂	1.648839	1	0.555333
GBC ₃	2.726083	2.111014	1

TABLE 9: The opinion of the second decision-makers.

	GBC ₁	GBC ₂	GBC ₃
GBC ₁	1	0.9	0.283
GBC ₂	1.111111	1	0.383
GBC ₃	3.533569	2.610966	1

TABLE 12: The normalized opinion of the decision-makers.

	GBC ₁	GBC ₂	GBC ₃
GBC ₁	0.171318	0.119905	0.083717
GBC ₂	0.282476	0.171318	0.095139
GBC ₃	0.467027	0.361655	0.171318

TABLE 10: The opinion of the second decision-makers.

	GBC ₁	GBC ₂	GBC ₃
GBC ₁	1	0.383	0.283
GBC ₂	2.610966	1	0.9
GBC ₃	3.533569	1.111111	1

TABLE 13: The total relation matrix.

	GBC ₁	GBC ₂	GBC ₃
GBC ₁	0.068999	0.048545	0.043625
GBC ₂	0.141257	0.07369	0.038893
GBC ₃	0.204848	0.18174	0.068463

2. The Neutrosophic DEMATEL Method

In this section, the MCDM DEMATEL method is proposed to determine the importance of the criteria and subcriteria. Figure 1 provides schematic diagram for DEMATEL in neutrosophic environment. The following steps of DEMATEL method are the following:

- Step 1. Define the goal from this study.
- Step 2. Collect a group of decision-makers and criteria.
- Step 3. Evaluate the criteria by opinions of decision-makers.
- Step 4. Combine the opinions of experts into one matrix.
- Step 5. Normalize the opinions of decision-makers.

TABLE 14: The criteria's weights.

	Weights
GBC ₁	-0.25394
GBC ₂	-0.05013
GBC ₃	0.30407

Step 6. Use the MATLAB software for obtaining the total relation matrix.

3. The Application and Outcomes

This section presents the outcome of the proposed method. First, the goal of this paper is to determine the importance

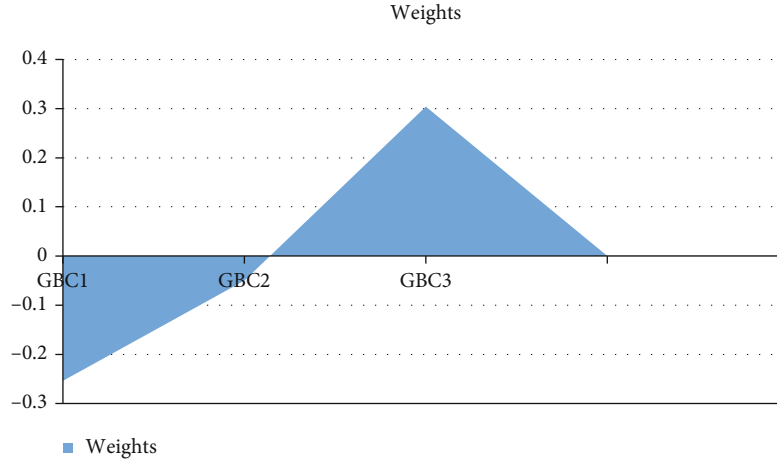


FIGURE 3: The criteria's weights for GBC.

TABLE 15: The opinion of the first decision-makers for GBC.

	IC ₁	IC ₂	IC ₃	IC ₄
IC ₁	1	0.8167	0.9	0.383
IC ₂	1.22444	1	0.8167	0.283
IC ₃	1.111111	1.22444	1	0.9
IC ₄	2.610966	3.533569	1.111111	1

TABLE 18: The combined opinion of the decision-makers.

	IC ₁	IC ₂	IC ₃	IC ₄
IC ₁	1	0.6999	0.666567	0.494233
IC ₂	1.648839	1	0.6999	0.522
IC ₃	1.956373	1.648839	1	0.666567
IC ₄	2.456325	2.418549	1.956373	1

TABLE 16: The opinion of the second decision-makers.

	IC ₁	IC ₂	IC ₃	IC ₄
IC ₁	1	0.9	0.8167	0.283
IC ₂	1.111111	1	0.383	0.9
IC ₃	1.22444	2.610966	1	0.8167
IC ₄	3.533569	1.111111	1.22444	1

TABLE 19: The normalized opinion of the decision-makers.

	IC ₁	IC ₂	IC ₃	IC ₄
IC ₁	0.127694	0.089373	0.085116	0.06311
IC ₂	0.210546	0.127694	0.089373	0.066656
IC ₃	0.249816	0.210546	0.127694	0.085116
IC ₄	0.313657	0.308833	0.249816	0.127694

TABLE 17: The opinion of the second decision-makers.

	IC ₁	IC ₂	IC ₃	IC ₄
IC ₁	1	0.383	0.283	0.8167
IC ₂	2.610966	1	0.9	0.383
IC ₃	3.533569	1.111111	1	0.283
IC ₄	1.22444	2.610966	3.533569	1

TABLE 20: The total relation matrix.

	IC ₁	IC ₂	IC ₃	IC ₄
IC ₁	0.051512	0.029137	0.039625	0.033791
IC ₂	0.113541	0.053168	0.031975	0.028738
IC ₃	0.114989	0.108162	0.050044	0.033578
IC ₄	0.106121	0.149331	0.131718	0.049744

TABLE 21: The criteria's weights.

	Weights
IC ₁	-0.2321
IC ₂	-0.11237
IC ₃	0.053411
IC ₄	0.291062

and effects of IF and big data risk control monitoring. The three experts were collected to evaluate the criteria and sub-criteria. This paper used the four main criteria and seventeen subcriteria as GBC: government-based credit (GBC1: outline planning, GBC2: licensee issue, and GBC3: commercial institution), IC: individual credit (IC1: transaction, IC2: business condition, IC3: record payment, and IC4: investment), IFP: Internet financial platform (IFP1: cost of platform, IFP2: creditworthiness of customer, IFP3: index of credit, IFP4: risk management, and IFP5: supply chain), and MB: market-based credit system (MB1: cost market system, MB2: customer verifying, MB3: information about

market, MB4: big data process, and MB5: security). First, decision-makers evaluated the four criteria in Tables 1–3. Then, Table 4 presents their combined opinions. Then,

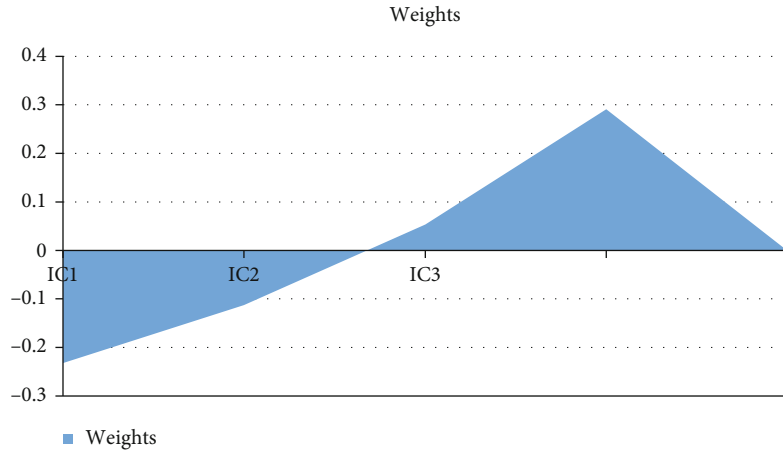


FIGURE 4: The criteria's weights for IC.

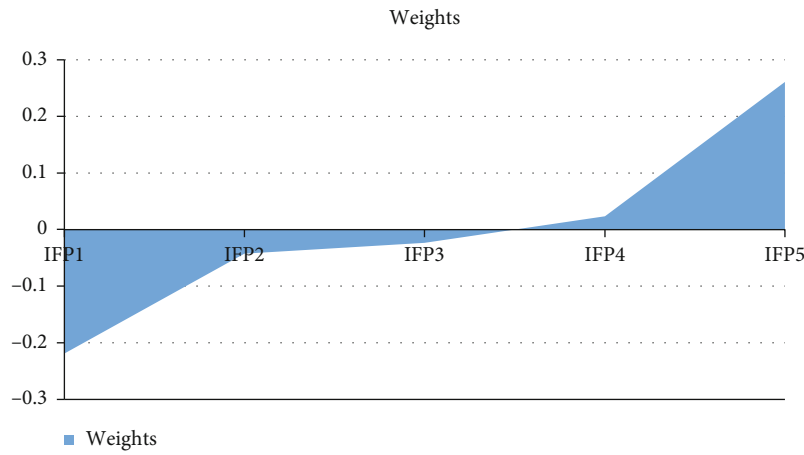


FIGURE 5: The criteria's weights of IFP.

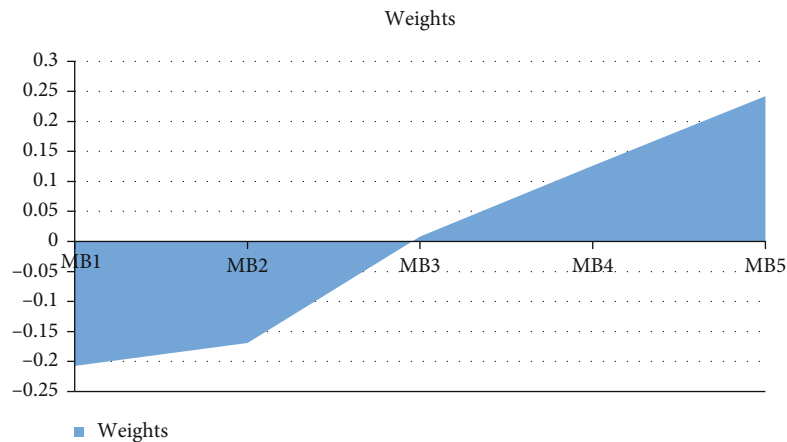


FIGURE 6: The criteria's weights of MB.

Table 5 presents the normalization matrix. Then, the total relation matrix is in Table 6. The criteria's weights are in Table 7. In this step, each criterion's objective weight is obtained by the removal effects (E_j). In what follows, w_j refers to the weight of the j th criterion. The following equation is utilized for generating w_j :

$$w_j = \frac{E_j}{\sum_k E_k} \tag{1}$$

Figure 2 presents the criteria's weights. MB is the highest importance, and GBC is the lowest importance in the IF.

Then, determine the subcriteria's weights for GBC. First, decision-makers' criteria are in Tables 8–10. Then, Table 11 presents their combined opinions. Then, Table 12 presents the normalization matrix. Then, the total relation matrix is in Table 13. The criteria's weights are in Table 14. Figure 3 presents the criteria's weights. GBC3 is the highest importance, and GBC1 is the lowest importance in the IF.

Then, determine the subcriteria's weights for IC. First, decision-makers' criteria are in Tables 15–17. Then, Table 18 presents their combined opinions. Then, Table 19 presents the normalization matrix. Then, the total relation matrix is in Table 20. The criteria's weights are in Table 21. Figure 4 presents the criteria's weights. IC4 is the highest importance, and IC1 is the lowest importance in the IF.

In the IFP, IFP5 is of the highest importance, and IFP1 is of the lowest importance in the IF. In the MB, MB5 is the highest importance, and MB1 is the lowest importance in the IF. Figure 5 presents the weights of IFP. Figure 6 presents the weights of MB.

4. Conclusions

When it comes to making decisions, there is a growing corpus of study in the subject of “many criteria decision analysis” (MCDA), also known as “multiple criteria decision-making,” which analyses the benefits and drawbacks of different possibilities in diverse settings. It is a decision-making tool that is used in a broad variety of industries. It is possible to analyze the suitability of each criterion in terms of how well it fits within the context of the application. For the decision-maker to arrive at an educated judgement on the optimal course of action, this criterion is compared to all other available criterion options. These factors can be examined in a variety of ways.

In this paper, we introduce a new hybrid methodology from the DEMATEL method and neutrosophic sets to determine the effects the Internet financial and big data risk control monitoring. The DMATEL method is used to show the importance and weights of criteria. The four main criteria and seventeen subcriteria are used in this paper. We used the SVNS scale to present the numbers of neutrosophic. The results have many advantages for return on investment (ROI) because energy efficiency initiatives may have both societal and private advantages, and it shows that a platform is in place that leverages and mobilizes commercial-based funding to finance energy efficiency projects. In the future, we will use a hybrid method for neutrosophic sets with metaheuristics algorithms for providing more accurate results.

Data Availability

Data sharing is not applicable to this article as no new data were created or analyzed in this study.

Conflicts of Interest

The authors state that this article has no conflict of interest.

References

- [1] X. Hou, Z. Gao, and Q. Wang, “Internet finance development and banking market discipline: Evidence from China,” *Journal of Financial Stability*, vol. 22, pp. 88–100, 2016.
- [2] P. Xie, C. Zou, and H. Liu, “The fundamentals of Internet finance and its policy implications in China,” *China Economic Journal*, vol. 9, no. 3, pp. 240–252, 2016.
- [3] P. Xie, C. Zou, and H. Liu, *Internet Finance in China: Introduction and Practical Approaches*, Routledge, 2015.
- [4] C. Luo, M. Li, P. Peng, and S. Fan, “How does Internet finance influence the interest rate? Evidence from Chinese financial markets,” *Dutch Journal of Finance and Management*, vol. 2, no. 1, p. 1, 2018.
- [5] W. U. Xiaoqi, “Internet finance: the logic of growth,” *Finance Trade Econ*, vol. 2, pp. 5–15, 2015.
- [6] D. Yang, P. Chen, F. Shi, and C. Wen, “Internet finance: its uncertain legal foundations and the role of big data in its development,” *Emerging Markets Finance and Trade*, vol. 54, no. 4, pp. 721–732, 2018.
- [7] R. Xu, C. Mi, R. Mierzwiak, and R. Meng, “Complex network construction of Internet finance risk,” *Physica A: Statistical Mechanics and its Applications*, vol. 540, article 122930, 2020.
- [8] S. Qi, K. Jin, B. Li, and Y. Qian, “The exploration of Internet finance by using neural network,” *Journal of Computational and Applied Mathematics*, vol. 369, article 112630, 2020.
- [9] Z. Chen, Y. Li, Y. Wu, and J. Luo, “The transition from traditional banking to mobile Internet finance: an organizational innovation perspective—a comparative study of Citibank and ICBC,” *Financial Innovation*, vol. 3, no. 1, pp. 1–16, 2017.
- [10] W.-W. Wu, “Choosing knowledge management strategies by using a combined ANP and DEMATEL approach,” *Expert Systems with Applications*, vol. 35, no. 3, pp. 828–835, 2008.
- [11] H.-S. Lee, G.-H. Tzeng, W. Yeih, Y.-J. Wang, and S.-C. Yang, “Revised DEMATEL: resolving the infeasibility of DEMATEL,” *Applied Mathematical Modelling*, vol. 37, no. 10–11, pp. 6746–6757, 2013.
- [12] C.-L. Lin and G.-H. Tzeng, “A value-created system of science (technology) park by using DEMATEL,” *Expert Systems with Applications*, vol. 36, no. 6, pp. 9683–9697, 2009.
- [13] S.-L. Si, X.-Y. You, H.-C. Liu, and P. Zhang, “DEMATEL technique: a systematic review of the state-of-the-art literature on methodologies and applications,” *Mathematical Problems in Engineering*, vol. 2018, 33 pages, 2018.
- [14] B. Chang, C.-W. Chang, and C.-H. Wu, “Fuzzy DEMATEL method for developing supplier selection criteria,” *Expert Systems with Applications*, vol. 38, no. 3, pp. 1850–1858, 2011.
- [15] W.-W. Wu and Y.-T. Lee, “Developing global managers' competencies using the fuzzy DEMATEL method,” *Expert Systems with Applications*, vol. 32, no. 2, pp. 499–507, 2007.
- [16] J.-I. Shieh, H.-H. Wu, and K.-K. Huang, “A DEMATEL method in identifying key success factors of hospital service quality,” *Knowledge-Based Systems*, vol. 23, no. 3, pp. 277–282, 2010.
- [17] P. Majumdar and S. K. Samanta, “On similarity and entropy of neutrosophic sets,” *Journal of Intelligent Fuzzy Systems*, vol. 26, no. 3, pp. 1245–1252, 2014.

- [18] S. A. Alblowi, A. A. Salama, and M. Eisa, *New Concepts of Neutrosophic Sets*, Infinite Study, 2014.
- [19] S. Broumi, F. Smarandache, and M. Dhar, *Rough Neutrosophic Sets*, Infinite Study, 2014.
- [20] H. Wang, F. Smarandache, Y. Zhang, and R. Sunderraman, *Single Valued Neutrosophic Sets*, Infinite Study, 2010.

Review Article

Home Based Monitoring for Smart Health-Care Systems: A Survey

J. Anu Shilvya,¹ S. Thomas George ,¹ M. S. P. Subathra,² P. Manimegalai,¹ Mazin Abed Mohammed ,³ Mustafa Musa Jaber,^{4,5} Afsaneh Kazemzadeh,⁶ and Mohammed Nasser Al-Andoli ⁷

¹Department of Biomedical Engineering, Karunya Institute of Technology & Sciences, Coimbatore, India

²Department of Robotics Engineering, Karunya Institute of Technology & Sciences, India

³College of Computer Science and Information Technology, University of Anbar, 31001 Ramadi, Anbar, Iraq

⁴Department of Computer Science, Dijlah University College, Baghdad, Iraq

⁵Department of Medical Instruments Engineering Techniques, Al-Farahidi University, Baghdad 10021, Iraq

⁶Shabakeh Pardaz Azarbaijan, Tabriz, Iran

⁷Department of Computer Science and Information Systems, Faculty of Science, Sa'adah University, Sa'adah, Yemen

Correspondence should be addressed to S. Thomas George; thomasgeorge@karunya.edu and Mohammed Nasser Al-Andoli; mnalandoli@saada-uni.edu.ye

Received 26 February 2022; Revised 8 April 2022; Accepted 11 April 2022; Published 12 May 2022

Academic Editor: Alireza Souri

Copyright © 2022 J. Anu Shilvya et al. This is an open access article distributed under the Creative Commons Attribution License, which permits unrestricted use, distribution, and reproduction in any medium, provided the original work is properly cited.

Internet of Things (IoT) is one of the greatest advancements in technology especially in the medical field. The interconnection of medical devices with the internet makes it easier to identify problems and adapts with patient conditions. The sophisticated devices may either be worn or implanted in the users' bodies to continually examine their wellbeing. But due to the availability of several sensors and communication systems, standardization has become a key issue. This survey paper presents the state-of-art research relating to the various sensors and communication models that are used to provide home based monitoring. The small sensor nodes with IoT and its influence on every patient's life in reducing their anxiety of risk when they are inaccessible to medical support are studied. This study helps the researchers in choosing the best available protocols to implement in health-care devices. The contribution to the development of smart cities and data from home or at work for smart health care is discussed. The key findings of this study are the benefits of 5G technology for smart health care, as the most often utilized communication method in the literature to date is 4G. Also, the challenges faced in implementing the models in real time are discussed with the options of future scope mentioned.

1. Introduction

In today's era of digitalization, smart health care has become one of the major advancements in the health field. With the advancement of technology and scientific theory, traditional medicine, which is based on bioengineering, has gradually begun to digitalize and informationize [1]. The Internet of Things is one such technological innovation (IoT). The Internet of Things refers to the interconnection of devices, applications, sensors, and network connections that improves these entities' ability to collect and share data. The differentiating

feature of the Internet of Things in the health-care system is the continuous monitoring of a patient by examining numerous parameters and inferring a favorable outcome from the history of such continual monitoring [2]. This is frequently used in hospitals to continually monitor patients in intensive care units (ICUs) and communicate the data with clinicians. This assists in the early diagnosis of anomalies in patients and the provision of prompt assistance.

In the same way, IoT is utilized in homes to monitor patients remotely. IoT allows for real-time monitoring, which saves lives from a variety of ailments such as diabetes,

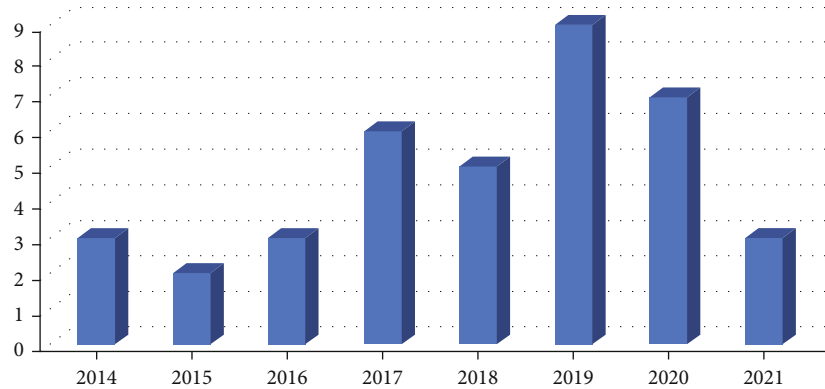


FIGURE 1: Distribution of the review articles based on year of publication [1].

heart failure, asthma attacks, and high blood pressure. Smart medical gadgets link to a smartphone to seamlessly send needed health information to clinicians. These devices also capture information such as oxygen levels, blood pressure, weight, and blood sugar levels [3]. The motivation to this study is that home-based monitoring can save lives by eliminating the time required for patients to travel to hospitals for checkups. This can also diagnose several diseases at an earlier stage. During these difficult times of pandemic, it is necessary that health monitoring can be done at home with ease. To support this technology, highly robust and reliable standards need to be followed. There is lack of standardization and awareness about new technologies in the society which this paper will cover.

Several prior studies have examined certain topics and technology linked to IoT health care. However, there is a lack of standardization due to the availability of many protocols and sensors. This paper provides a detailed study about various IoT methods that can be used at homes for health care. This research based on the literature could help experts in deciding the best methods for home-based monitoring with IoT. This literature survey covers papers published between 2014 and 2021. Papers were collected journals and conferences published in reputed cites such as IEEE Xplore and PubMed. The keywords applied in the search were “IoT AND Smart Healthcare,” “wireless AND sensors,” and “communication models”. Figure 1 shows the distribution of chosen articles based on their year of release.

The main contributions of this study are:

- (i) It provides a detailed review on the various body sensors that are used for remote health-care monitoring is discussed
- (ii) This study focuses on the different models of temperature sensors, heart rate, and blood pressure sensors that are available at low cost and are presented along with their limitations
- (iii) This study also has a major contribution towards the communication models that can be used for remote health care. It mainly focuses on the short-range and long-range communication systems. This

study also highlights the usage of 5G communication model over 4G

- (iv) A comparative analysis is presented for 4G, 5G, and Wi-Fi with the characteristic features of communication system - latency, reliability, throughput, speed, energy and density of connections

The paper is structured as follows: Section 2 begins with the study of various health sensors that is being used predominantly in IoT-based health care. Followed by that the same section includes a detailed investigation on the communication models involving short-range, long-range, and 5G-based communication. Section 3 discusses on the need for the society to incorporate a home-based monitoring system. It also elaborates the limitations in usage of such devices focusing on the communication models. Section 4 wraps up the paper by encapsulating the important findings and providing future directions for the research.

2. Methods and Materials

Smart health care enables individuals from diverse types of backgrounds (e.g., doctors, health workers, physician caregivers, older relatives, and patients) to obtain the proper information and discover the right solutions, with the goal of minimizing medical errors, improving efficiency, and lowering costs at the proper moment in the health-care profession [4]. Smart health care employs a variety of techniques, including the use of mobile phones, computers, and televisions, as well as the use of different networks, including wide area networks, local area networks, and body area networks. Body temperature, pulse rate, blood pressure, and motion detection are the most often monitored metrics. In this part, we will look at the several sensors that are used to measure physical characteristics.

2.1. Body Temperature Sensor. The body temperature is an important measure for identifying different disorders such as hyperthermia, fever, and cold. RTD, thermocouple, semiconductor, and infrared temperature sensors are the most common. The resistance temperature detector (RTD) sensor detects the varying resistance value of metal through which

TABLE 1: Comparison of various temperature sensors [6].

Temp. Sensor type	Temp. Range	Advantages	Disadvantages
RTD Sensors [6]	-196°C +850°C	(i) Incredibly accurate (ii) Stable (iii) Reliability (iv) Consistent (v) High temperature ranges	(i) Costly (ii) Less robust than thermocouple (iii) Requires a constant power supply
Thermocouples [7]	95°C-1260°C	(i) Wide temperature range (ii) Highly rugged (iii) Best for high temperatures	(i) Nonlinear (ii) Low voltage (iii) Least stable
NTC Thermistors [8]	-40°C to 125°C	(i) Extremely sensitive (ii) Ideal for tiny temperature variations (iii) Simple to use (iv) Quick reaction (v) Standard two-wire interface	(i) Fragile (ii) Current source required (iii) Self-heating (iv) Limited temperature range (v) Nonlinear
IR sensors [9]	-20 to 350°C	(i) Hand-held and simple to use (ii) Highly precise and accurate (iii) Fast reaction time (vi) No need to touch with target item	(i) Debris, pollutants, and blackbody radiation all have a negative impact on accuracy

an electrical signal passes. The resistance is then translated into temperature. The thermocouple sensor is made up of two distinct metals that come together to form a junction. The junction output voltage varies as the junction temperature varies. The voltage is then translated into temperature. A semiconductor sensor is a single-chip integrated circuit (IC) that contains a variety of circuits. The temperature of a bipolar junction transistor is determined using the base-emitter voltage and collector current (BJT).

The infrared temperature sensor is a type of noncontact sensor [5]. The infrared photons generated by the human body are converted into electrical energy by the light sensors in the IR sensor. The input impulse is then transferred to the detector, which converts it to temperature. In [5] DS18B20, a 1-wire programmable temperature sensor is designed to evaluate temperature of the body for the Thai people and produced good results. Table 1 presents a comparison of various temperature sensors.

2.2. Heartbeat Sensors. Heartbeat rate is a vital parameter that is measured which can help in the identification of several underlying diseases. Heartbeat sensors are used widely in all smart health-care devices. They are mostly used in wearable devices. [2] uses a microcontroller-based heartbeat sensor. It uses infrared (IR) radiation and operates on the idea of light alteration by blood circulation through thumb or finger for every pulse [10].

The module contains a light detector and bright LED of red color. The device is placed at the fingertip, and when the reflected light falls on the light detector, a signal is produced. This signal varies when blood flows through the vessels because the finger gets opaquer. This variation in the signals is used to determine the heartbeat rate. Working of heartbeat sensor presented in Figure 2.

2.3. Blood Pressure Sensors. Blood pressure is helpful to detect various ailments like hypertension, heart attacks, and stroke. Controlling or reducing blood pressure can aid

in the prevention or postponement of significant health issues such as renal disease, cardiac arrest, cardiovascular disease, brain hemorrhage, and perhaps Alzheimer's disease. Among all the signals acquired by the detectors, the blood pressure signal provides critical information on heart rate, blood vessel flexibility, and biological variation [11]. Narasimhan et al. [12] developed a finger wearable blood pressure measuring system that contains a 30-element capacitive tactile sensor array for measuring contact stress with the thumb, a pump-driven pneumatic bladder for steadily pressing the tactile array and the finger towards one another, and a wristband that encloses the sensing system and bladder. A finger wearable blood pressure sensor is showed in Figure 3.

The result of this device has also satisfied the global standard-specified accuracy criteria. Other low-cost MEMS pressure sensors are also used in various IoT-enabled health monitoring systems. Body temperature, pulse rate, blood pressure, and motion detection are the most often monitored metrics, and these sensors are used to measure physical characteristics. The sensors data can be transferred to the hospitals through latest communication models for analyzing the data and providing immediate support in case of emergency.

P. A. Shaltis et al. developed a wearable noninvasive blood pressure (NIBP) sensor based on photoplethysmography (PPG) approach. The authors have taken into consideration that the sensor not only must be compact and power efficient, but also it has to be attached to the skin stably and comfortably without requiring a large pressure [13]. So, a compact device which can be worn at the finger base is developed which requires less than 5 V power for operation. The experiments were conducted in controlled environments which leads to the drawback that measurements may become unreliable in environments with varying temperatures.

2.4. Body Fat Sensor. With the increase in growth of fitness tracking devices, one important development is the body

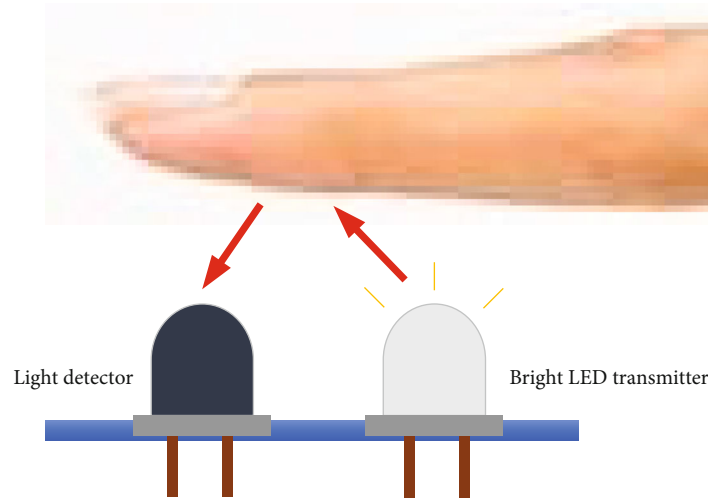


FIGURE 2: Working of heartbeat sensor [2].



FIGURE 3: Finger wearable blood pressure sensor [12].

fat sensor. This helps the individual to keep track of the body composition on a daily basis. It provides an early detection of improper balance in the body composition. These sensors are embedded in measuring scales and also in smart watches. Body fat sensor works on the principle of bioelectric impedance analysis (BIA) which is when electric current is allowed to pass through the body, there is resistance caused due to the body tissues and fluids. This resistance is used to calculate body fat. Tissues that contain large amounts of fluid and electrolytes, such as blood, have high conductivity, but fat and bone slow the signal down.

Some of the limitations of this sensor are that, though BIA is said to be harmless it is advised not to be used by pregnant women and also people having other electronic medical devices inside the body such as pacemakers are recommended not to use it, so incorporating body fat sensor in smart health-care devices along with other sensors is a challenge.

2.5. Body Water Sensor. North Carolina State University researchers have created a wearable, wireless sensor that can monitor a person's skin hydration for use in applications that require identifying dehydration before it becomes a health issue. The technology is light, flexible, and stretchy, and it has already been put into model wristbands and chest patches. Two electrodes constructed of an elastic polymer combination with conductive silver nanowires make up the sensor. The electrical characteristics of the skin are monitored by these electrodes. The readings from the electrodes can indicate how hydrated the skin is because the skin's electric characteristics fluctuate in a predictable way depending on an individual's moisture.

In addition to that, there are also other body hydration detection sensors which work on near-infrared spectroscopy. The effect of water on tissue reflectance at specific wavelengths is used in near-infrared spectroscopy to determine the water content of human tissue.

2.6. Pulse Oximetry Sensor. More medical experts are testing blood oxygen saturation after assessing pulse rate, respiration rate, body temperature, and blood pressure. It is also referred to as the fifth vital sign. Pulse oximetry is a noninvasive way to check one's oxygen saturation. Pulse oximetry sensors assess deoxygenated and oxygenated hemoglobin using red and infrared LEDs. More infrared light is absorbed by oxygenated hemoglobin, allowing more red light to flow through. Deoxygenated hemoglobin, on the other hand, absorbs more red light while allowing more infrared light through.

The oxygen saturation (SPO₂) may be measured using two different approaches. The transmission and reflectance methods are the two options. The LED transmitter and the photodetector receiver are situated on opposite sides of the finger in the transmission technique. This finger will be put between the LEDs and the photodetector, which is often used in hospitals, in this manner. The LED and photodetector are arranged on the same side, adjacent to each other, in the reflectance technique. This approach is perfect for

monitoring at home because it is already utilized in many smartwatches and fitness trackers.

2.7. Nasal Sensor. The respiratory rate is usually measured in breaths per minute or the number of times the chest rises. These breathing rates may be affected by external elements such as temperature, humidity, pressure, and chemical composition. When a patient is at rest, their respiration rate must be examined. The average person's breathing rate is between 15 and 20 breaths per minute. A breathing rate of less than 12 is considered bradypnea, whereas a respiratory rate of more than 30 is considered tachypnea. The condition of sleep apnea occurs when a person's respiratory rate is zero. Monitoring breathing might help with early detection of such illnesses.

The use of a thermistor-based nasal sensor to monitor breathing rate is a highly cost-effective technology. It operates on the principle that exhaled air is warmer than ambient air. A stretch sensitive device worn to the torso is another form of respiratory sensor that measures the relative amount of expansion that happens during respiration (breathing). Breathing causes the rib cage to expand, stretching the device. The stretch relaxes as users exhale, and the sensor returns to its neutral position. On the screen, the resultant waveform is presented, and the respiratory rate is determined.

2.8. Communication Model. IoT has made doctors and patients communication easier. With the help of smart health care today even during this pandemic period, patients are able to carry out their consultation with doctors in an easy way. For this few communication models are responsible. They can be broadly classified into short-range and long-range communication systems. Wireless neighborhood area network (WNAN) is a medium-range network (5-10 km), with Wi-SUN and WM-Bus as examples. Long-distance (up to 100 km) technologies include both authorized (2G/3G/4G, LTE, and soon 5G) and nonlicensed networks, such as low-power wide area network (LPWAN), which encompasses but is not limited to long range (LoRa), Sigfox, narrowband Internet of Things (NB-IoT), and others [14, 15].

2.8.1. Short-Range Communication. Communication protocols are classified into three categories as short-range protocols [16], medium-range protocols, and long-range protocols [17]. Sakina Elhadi [18] focus on the Short-range protocols, namely, Bluetooth, Zigbee, and NFS.

Bluetooth, which is widespread in handsets and desktops, is getting popular in remote monitoring technologies. BLE (also known as Bluetooth smart) was launched in 2010 with the purpose of broadening Bluetooth's application for usage in power-constrained portable devices such as mobile sensors and wireless controllers [19]. Not only does the use in sensors and controllers necessitate low-energy consumption, but also the quantity of data transmitted is minimal, and communications occur infrequently. However, the idea of reduced power and a small form factor raises the difficulty of meeting confidentiality needs while relying on unreliable, low bandwidth wireless connections and restricted computational power and storage [20, 21].

The ZigBee protocol was developed by the ZigBee Alliance and is centered on the IEEE802.15.4 low-power wireless communication benchmark [22]. ZigBee is designed to be a standard for high-level, low-cost communication systems that enable the creation of personal area networks using tiny, low-power digitized devices that transport data over extended distances. Simultaneously, it will be employed in applications requiring less data usage, greater battery capacity, and private network connections. Also, ZigBee may handle a variety of configurations such as mesh, star, and tree networking topology.

NFC (near-field communication) is a form of advancement that includes a set of rules that enable radio recurrence correspondence between two gadgets within a close proximity of 10 cm or less. It operates at a frequency of 13.56 MHz and transfers data at a rate of 424 Kilobits per second. This is widely used in home-based automation to control devices across a short distance. Vagdevi et. al [23] presented an IOT-based home automation system based on NFC. However, NFC is subject to a variety of networking vulnerabilities, such as tag manipulation, as discussed in [24].

2.8.2. Long-Range Communication. In this section, long-range communication protocols available such as Sigfox, long-range (LoRa)-low-power wide area network (LoRaWAN), and narrowband Internet of Things (NB-IoT) are discussed.

SigFox technology is a member of the LPWAN (low-power wide area networks) group of advanced technology that is mainly used for the evolution of the internet networks whenever the volume of data sent from sensory modules is negligible, the operating frequency is wide, and energy consumption rates are very. This protocol is designed in the first four levels of the OSI model. The encryption between linked terminal and the Sigfox cloud offers an end-to-end authentication solution that relies on a cryptographic key maintained in nonaccessible storage and paired with a recognizable and specific ID saved in ROM (read-only memory) on the end devices [14]. Messages delivered by end devices employ the secret key to produce a code that is distinct for every message, primarily for the purpose of authenticating the sender. This code would have a sequence number, which is added into radio frames so as to prevent them from being replayed.

Semtech Corporation invented LoRa technology [14]. It is a patented wireless communication technology. It utilizes spread spectrum encoding in the sub-GHz band to provide long-range service, high-energy efficiency (up to a decade battery lasts), higher bandwidth (higher than or equal to one million nodes), robust connectivity, and localization features. It is being utilized to connect sensors to cloud and provide live data analysis exchange. LoRa wireless technology employs a low-powered broadcast of tiny data packages (0.3 kbps to 37.5 kbps) over a large distance to a receiver. A gateway may manage several of devices in one go [25]. LoRa wireless technology employs the LoRa wide area network (LoRaWAN) protocol, which was designed to provide wireless-powered devices by the LoRa Alliances. The LoRaWAN Network design may be built in a star topology, with bidirectional end to end communication between nodes and

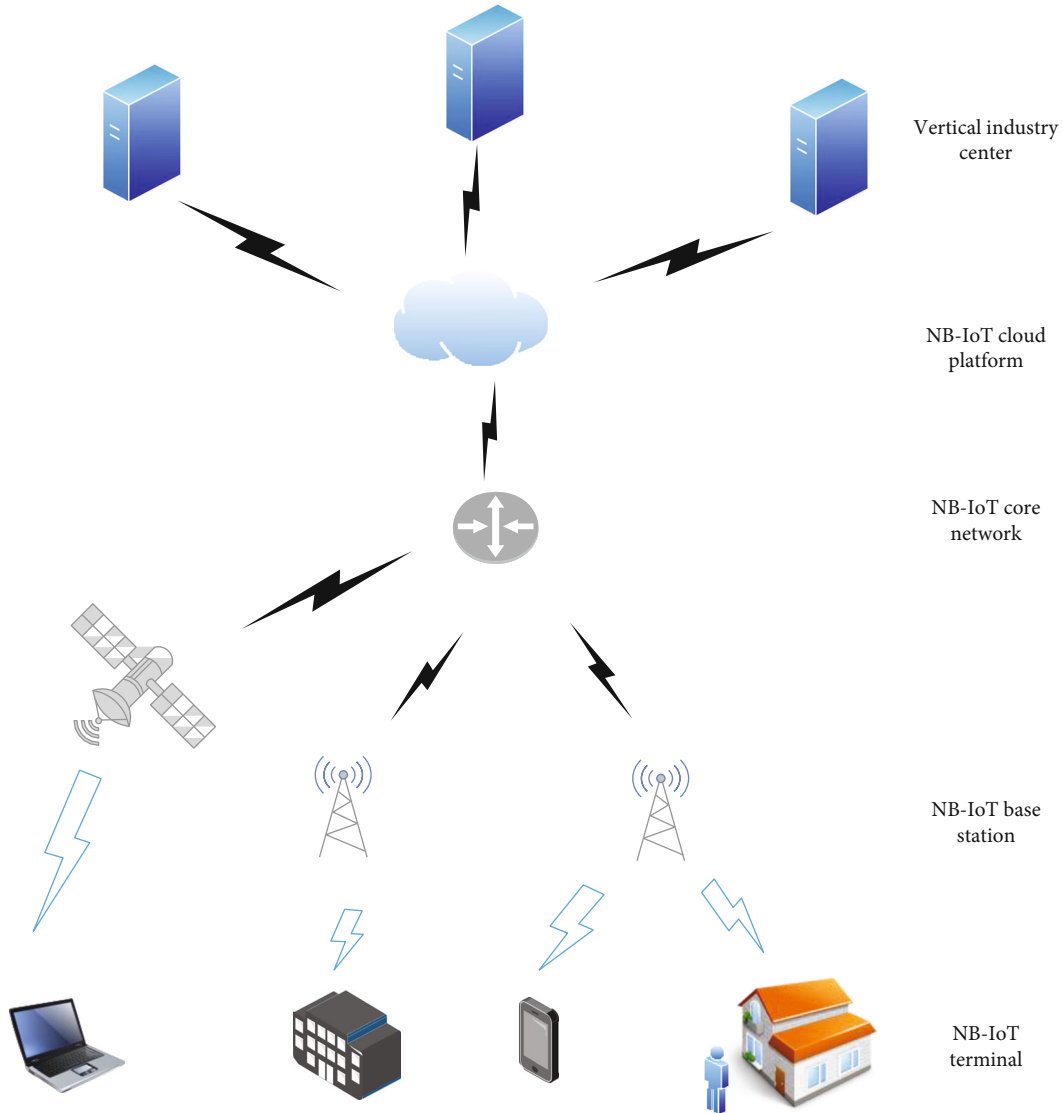


FIGURE 4: NB-IoT network [14].

connector. As terminal nodes transfer data to the gateway, this is referred to as “Uplink,” and when the gateway transmits information to end node, this is referred to as “Downlink.” Parts of LoRaWAN packets can be signed and encrypted using the LoRaWAN protocol. Before an end device can connect with a network server, it must first be enabled. However, there are certain things to think about when it comes to LoRa/LoRaWAN [26], such as the necessity of cloud system to manage stream from low bandwidth connectivity.

The narrowband Internet of Things (NB-IoT) is a large-scale low-power wide area (LPWA) technology suggested by 3GPP for information detection and acquisition in smart low data rate systems. Two common applications are adaptive monitoring and proactive environmental sensing [27]. Huge interconnections, super energy usage, large distance availability, and bidirectional activation between the signaling and information planes [28] are all supported by NB-IoT. Figure 4 represents the NB-IoT network architecture

which has 5 layers from NB-IoT terminal through vertical industry center. Furthermore, it is backed up by an efficient cellular communication network. As a result, NB-IoT is an exciting technology. LTE protocols are used for NB-IoT encrypting data [14]. Encryption is done within the NB-IoT network, but it is accessible to other entities after it exits the NB-IoT network.

2.8.3. 5G Network Communication. WBAN networks are the most prominent ones. Sensors are either wearable or attachable to the body. Ahad [29] discusses about the 5G-based smart health care. He presents the network challenges in IoT that can be overcome through 5G networks which can meet the majority of needs like ultralow latencies, large bandwidth, hyper reliability, high density, and low-energy consumption. Future intelligent health-care systems are predicted to include a hybrid of 5G and IoT devices that will improve phone reception, signal strength, and solve security breaches [29–31].

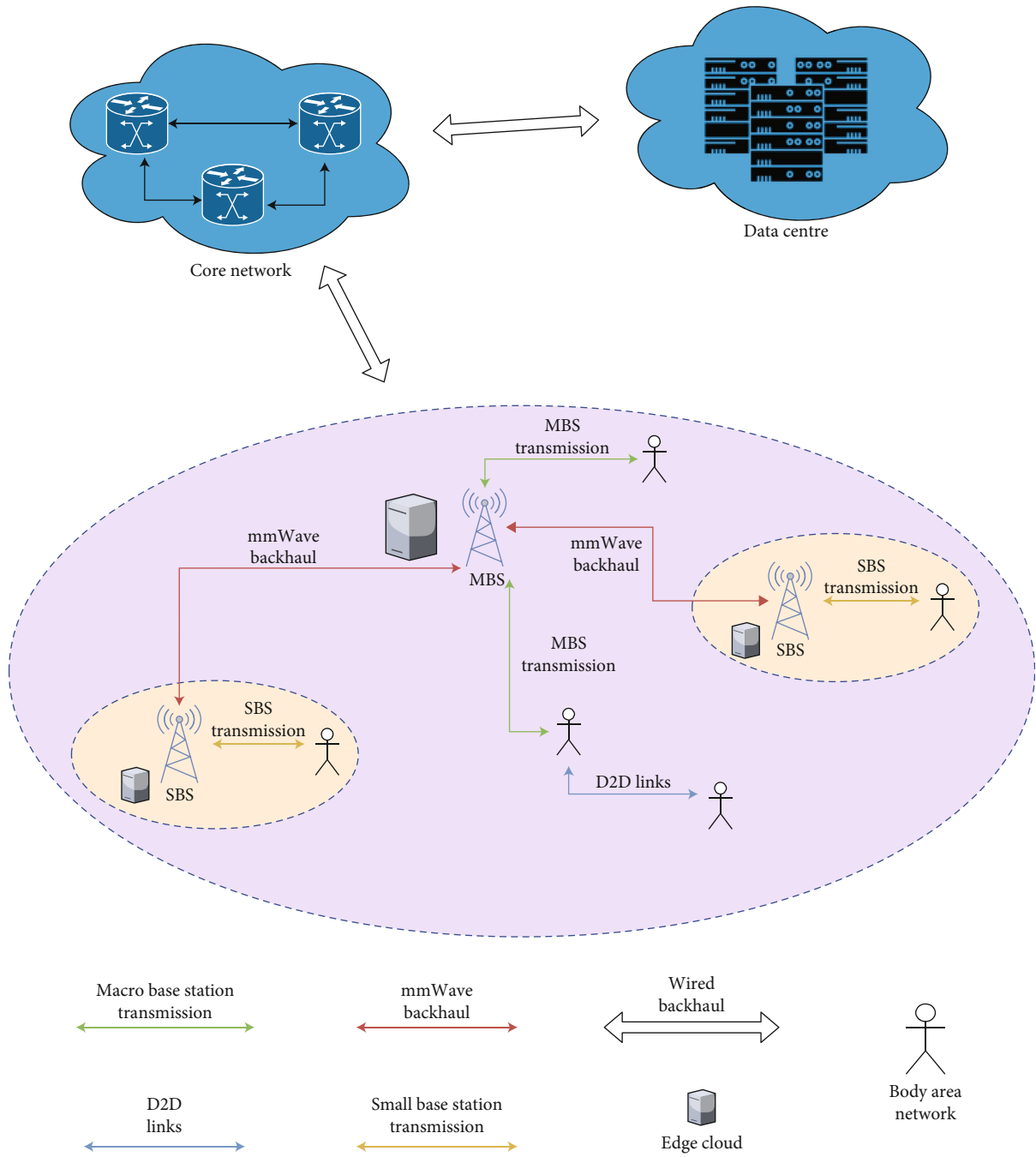


FIGURE 5: 5G smart health-care architecture [29].

Figure 5 shows the architecture of 5G smart health care. D2D is device-to-device direct communication between in the network without engaging base station (BS) or the core network. High path loss problem can be reduced by using millimeter waves (mmWaves) communication that has a band of spectrum between 20 GHz and 300 GHz. mmWaves are millimeter wave communication having spectrum band between 20 GHz and 300 GHz [29], and they work the best in reducing high path loss problems. Edge cloud or edge computing is an advanced networking technology in which the information is analyzed at the edge of network, close to the source of origin. It has the advantage of proving reduced

decision time so it can be used in health devices in the future where the response time is a crucial factor [32]. Some of the major requirements of smart health care for home-based monitoring are low delay, high throughput, high dependability, and better battery life.

5G has the ability to achieve bandwidth that are nearly 100 times faster than 4G while still managing significantly more interconnections [33, 34]. These benefits are bolstered by ultralow delay, or the amount of time it takes for the system to execute a query [35]. Table 2 represents a comparison between Wi-Fi6 and 4G and 5G networks against various measurement criteria. The delay between transmission and

TABLE 2: Comparison of network models [36].

Feature	Wi-Fi6	4G	5G
Latency	20 ms	30–50 ms	1–10 ms
Reliability/availability	99.99%	99.99%	99.99%
Throughput	9.6 Gbps	300 mbps–1 Gbps	10 Gbps
Speed	1 Gbps	20–50 mbps	Up to 1 Gbps
Density of connections	8 per part	12 per part	100 per part
Energy	Medium	High	Medium

reception of information is referred to as latency. As a result, the shorter the latency, the more “real time” the event experience will be. The delay of 5G is between 1 and 10 milliseconds [36]. The efficiency of the network in transmitting data between the transmitter and receiver without loss of data packet is referred to as reliability. The availability of all three networks under review is 99.99 percent. The absolute maximum quantity of information transferred between a location and another in a particular period is called throughput. From source to destination, 5G may transport 10 GB per second. Connection density refers to the number of connected devices per unit area, which may reach 1 Gbps in 5G networks but only 20–50 Mbps in 4G networks. In addition, with a 5G connection, the comparative power consumption levels are medium.

3. Discussion

As mentioned, the IoT is one technological innovation. The Internet of Things refers to the interconnection of devices, applications, sensors, and network connections that improves these entities’ ability to collect and share data [37–42]. In this survey, the various technologies available for smart health care in home-based monitoring are discussed. A number of systems are available in health care with IoT that has made life easier and healthier. Quality health care is very crucial especially during these tough days of pandemic. So IoT and smart health care can be the best choice to maintain good health while being at home.

Different kinds of detectors capable of detecting physiological characteristics of human body have been discussed. There are a variety of heart rate sensor choices available, with thermistor-type temperature sensors being the most precise and dependable. One major issue faced in usage of thermistor is that it has high resistance which requires shielded power cables. There are a variety of blood pressure sensors that may be integrated into an IoT system, but just a few models, such as the finger wearable pressure sensor and MEMS pressure sensor, have been proven to be the most effective. The finger wearable [12] type of blood pressure sensor has brought a truly comfortable device due to its low weight and design structure. Body temperature is the third most often measured physiological parameter. This is one of the most important parameters evaluated in most home-based health-care studies. The most reliable and effective temperature sensors have been discovered to be infrared temperature sensors. It also has the advantage of being con-

tactless which aids during this pandemic time [43]. However, studies show that there is more accuracy in contact-based temperature sensor than the contactless sensors. This brings to the fact that home-based monitoring devices using IoT should not be shared with other individuals.

All the sensors are connected to a controller like Raspberry Pi or Arduino which is interconnected with mobile devices through Wi-Fi [44]. This provides the measured data to be displayed on the mobile phone for patients view. Also, the data can be transferred to the hospitals for analyzing the data and providing immediate support in case of emergency [45]. In terms of short-range communications standards, Bluetooth was discovered to be the most efficient for health care, and many devices have also implemented Bluetooth technology. It is of low cost and versatile among all hardware devices. While in the long-range communication models, NB-IoT was identified to be more appropriate for health care due its ability of having huge interconnections. This makes it suitable to be implemented in large hospitals which keeps account of many users.

Existing communication technologies are incapable of meeting the complex and dynamic demands placed on communication networks by a wide range of smart health-care applications [46, 47]. As a result, the upcoming 5G network is projected to serve smart health-care applications that meet the majority of the requirements, including ultralow latency, high bandwidth, ultrahigh reliability, high density, and high-energy efficiency. Future smart health-care networks are predicted to include a hybrid of 5G and IoT devices that will improve cellular coverage, network performance, and solve security problems.

4. Conclusion

In this study, the significance and beneficial effects of implementing IoT in remote health monitoring systems is discussed. A systematic overview of every sensor that is used for home-based monitoring system is presented. Also, the emerging 5G technology is discussed with a comparison across 4G and Wi-Fi models. It is also shown that there is very little implementation of proposed 5G architecture which can be taken as a future research suggestion. The small sensor nodes with IoT will have a significant influence on every patient’s life, reducing their anxiety of risk even while they are away from family and friends and physician. They also greatly contribute to the development of smart cities. The sensory data might be collected at home or at work.

Also discussed are the problems in sensing, analytics, and illness prediction, which may be overcome to create a smooth interconnection into the medical industry.

The limitations identified in this research are that cloud-based 5G communication models pose the threat of security vulnerability. Hence, strong security protocols and encryptions need to be developed in order to overcome the security threats. The personal patient data has to be encrypted during communication and storage to comply with the medical ethics. This is an area identified as future work to develop systems that are more secure and does not pose any security threats. This would ensure the person's privacy and confidence in the usage of home-based monitoring devices. Limitations of this research include the absence of the usage of artificial intelligence or deep learning in smart health care. These new technical advancements are taking shape leading to a practical AI-based smart health-care system. Machine learning is a vast area in medical field for diagnosis of several illness. It is identified as a future research area to develop systems that are capable of diagnosing diseases at home with minimal intervention of physicians which may be big boon to the personalized health care.

Data Availability

Data sharing not applicable to this article as no datasets were generated or analyzed during the current study.

Conflicts of Interest

The authors declare that there is no conflict of interest.

References

- [1] S. Tian, W. Yang, J. M. Le Grange, P. Wang, W. Huang, and Z. Ye, "Smart healthcare: making medical care more intelligent," *Global Health Journal*, vol. 3, no. 3, pp. 62–65, 2019.
- [2] S. Banka, I. Madan, and S. S. Saranya, "Smart healthcare monitoring using IoT," *International Journal of Applied Engineering Research ISSN 0973-4562*, vol. 13, no. 15, pp. 11984–11989, 2018.
- [3] M. Javaid and I. H. Khan, "Internet of Things (IoT) enabled healthcare helps to take the challenges of COVID-19 pandemic," *Journal of Oral Biology and Craniofacial Research: version*, vol. 11, no. 2, pp. 209–214, 2021.
- [4] A. Ullah, M. Azeem, H. Ashraf, A. A. Alaboudi, M. Humayun, and N. Jhanjhi, "Secure healthcare data aggregation and transmission in IoT a survey," *IEEE Access*, vol. 9, pp. 16849–16865, 2021.
- [5] S. Nookkhaio, V. Thananant, and T. Khunkhao, "Development of IoT heartbeat and body temperature monitoring system for community health volunteer," in *2020 Joint International Conference on Digital Arts, Media, and Technology with ECTI Northern Section Conference on Electrical, Electronics, Computer and Telecommunications Engineering (ECTI DAMT & NCON)*, Pattaya, Thailand, 2020.
- [6] <https://www.variohm.com/news-media/technical-blog-archive/temperature-sensor-comparison>.
- [7] G. Wang, W. Wang, K. Li, and H. Liu, "A digital thermometer with fast response and high precision," in *2014 7th International Conference on Biomedical Engineering and Informatics*, pp. 504–510, Dalian, China, 2014.
- [8] B. A. Kuzubasoglu, E. Sayar, and S. K. Bahadir, "Inkjet-printed CNT/PEDOT: PSS temperature sensor on a textile substrate for wearable intelligent systems," *IEEE Sensors Journal*, vol. 21, no. 12, pp. 13090–13097, 2021.
- [9] G. Gabor, G.-C. Pintilie, A.-T. Plesca, and M. Cardasim, "Temperature monitoring system using an infrared temperature sensor connected to a PLC," *International Conference on Electromechanical and Energy Systems (SIEMEN)*, vol. 2019, pp. 1–4, 2019.
- [10] P. A. Pawar, "Heart rate monitoring system using ir base sensor & Arduino Uno," in *2014 Conference on IT in business, Industry and Government (CSIBIG)*, Indore, India, 2014.
- [11] P. Kaushik and P. Sethi, "A comprehensive study on blood pressure measurement techniques," in *4th International Conference on Computing Communication and Automation (ICCCA)*, Greater Noida, India, 2019.
- [12] R. Narasimhan, T. Parlikar, G. Verghese, and M. V. McConnell, "Finger-wearable blood pressure monitor," in *40th Annual International Conference of the IEEE Engineering in Medicine and Biology Society (EMBC)*, Honolulu, HI, USA, 2018.
- [13] P. A. Shaltis, A. Reisner, and H. H. Asada, "Wearable, cuff-less PPG-based blood pressure monitor with novel height sensor," *International Conference of the IEEE Engineering in Medicine and Biology Society*, vol. 2006, pp. 908–911, 2006.
- [14] W. Anani, A. Ouda, and A. Hamou, "A survey of wireless communications for IoT echo-systems," *IEEE Canadian Conference of Electrical and Computer Engineering (CCECE)*, vol. 2019, pp. 1–6, 2019.
- [15] F. Muheidat and A. T. Lo'Ai, "In-home floor based sensor system-smart carpet- to facilitate healthy aging in place (AIP)," *IEEE Access*, vol. 8, pp. 178627–178638, 2020.
- [16] B. Tamás and Z. Gál, "Overview of the internet of things short range communication technologies," *Proceedings of the 9th International Conference on Applied Informatics*, 2015, Eger, Hungary, 2015, 2015.
- [17] A. Lavric, A. I. Petrariu, and V. Popa, "Long range SigFox communication protocol scalability analysis under large-scale, high-density conditions," *IEEE Access*, vol. 7, pp. 35816–35825, 2019.
- [18] S. Elhadi, A. Marzak, and N. Sael, "Operating models of network protocols IoT: short-range protocols," *International Symposium on Advanced Electrical and Communication Technologies (ISAECT)*, vol. 2020, pp. 1–6, 2020.
- [19] K. Chang, "Bluetooth: a viable solution for IoT? Industry perspectives," *IEEE Wireless Communications*, vol. 21, no. 6, pp. 6–7, 2014.
- [20] A. R. Chandan and V. D. Khairnar, "Bluetooth low energy (BLE) crackdown using IoT," *International Conference on Inventive Research in Computing Applications (ICIRCA)*, vol. 2018, pp. 1436–1441, 2018.
- [21] F. Albert, I. I. Harris, H. Sundaram, and R. Kravets, "Security and privacy in public IoT spaces," in *25th International Conference on Computer Communication and Networks (ICCCN)*, Waikoloa, HI, USA, 2016.
- [22] S. Al-Sarawi, M. Anbar, K. Alieyan, and M. Alzubaidi, "Internet of Things (IoT) communication protocols: review," in *8th International Conference on Information Technology (ICIT)*, pp. 685–690, Amman, Jordan, 2017.

- [23] P. Vagdevi, D. Nagaraj, and G. V. Prasad, "Home: IOT based home automation using NFC," in *International Conference on I-SMAC (IoT in Social, Mobile, Analytics and Cloud) (I-SMAC)*, pp. 861–865, Palladam, India, 2017.
- [24] A. Asaduzzaman, S. Mazumder, S. Salinas, and M. F. Mridha, "A security-aware near field communication architecture," in *International Conference on Networking, Systems and Security (NSysS)*, pp. 33–38, Dhaka, Bangladesh, 2017.
- [25] R. Sinha, W. Yiqiao, and S.-H. Hwang, "A survey on LPWA technology: LoRa and NB-IoT," *ICT Express*, vol. 3, no. 1, pp. 14–21, 2017.
- [26] J. Yi, T. H. Clausen, W. M. Townsley, and C. Systems, "A study of LoRa: long range & low power networks for the Internet of Things," *Sensors*, vol. 16, no. 9, 2016.
- [27] M. Chen, Y. Miao, Y. Hao, and K. Hwang, "Narrow band internet of things," *IEEE Access*, vol. 5, pp. 20557–20577, 2017.
- [28] C. Hoymann, D. Astely, M. Stattin et al., "LTE release 14 outlook," *IEEE Communications Magazine*, vol. 54, no. 6, pp. 44–49, 2016.
- [29] A. Ahad, M. Tahir, and K.-L. A. Yau, "5G-based smart healthcare network: architecture, taxonomy, challenges and future research directions," *IEEE Access*, vol. 7, pp. 100747–100762, 2019.
- [30] D. Pal, S. Funilkul, N. Charoenkitkarn, and P. Kanthamanon, "Internet-of-Things and smart homes for elderly healthcare: an end user perspective," *IEEE Access*, vol. 6, pp. 10483–10496, 2018.
- [31] A. Alelaiwi, "Multimodal patient satisfaction recognition for smart healthcare," *IEEE Access*, vol. 7, pp. 174219–174226, 2019.
- [32] S. U. Amin and M. Shamim Hossain, "Edge intelligence and internet of things in healthcare: a survey," *IEEE Access*, vol. 9, pp. 45–59, 2021.
- [33] E. Kapassa, M. Touloupou, A. Mavrogiorgou et al., "An innovative ehealth system powered by 5G network slicing," in *Sixth International Conference on Internet of Things: Systems, Management and Security (IOTSMS)*, pp. 7–12, Granada, Spain, 2019.
- [34] A. Osseiran, F. Boccardi, V. Braun et al., "Scenarios for 5G mobile and wireless communications: the vision of the METIS project," *IEEE Communications Magazine*, vol. 52, no. 5, pp. 26–35, 2014.
- [35] A. C. Jiménez and J. P. Martínez, "5G networks in eHealth services in Spain: remote patient monitoring system," *IEEE Engineering International Research Conference (EIRCON)*, vol. 2020, pp. 1–4, 2020.
- [36] <https://www.pwc.com/gx/en/industries/tmt/5g/pwc-5g-in-healthcare.pdf>.
- [37] M. N. Al-Mhiqani, R. Ahmad, Z. Z. Abidin, W. Yassin, A. Hassan, and A. N. Mohammad, "New insider threat detection method based on recurrent neural networks," *Indones. J. Electr. Eng. Comput. Sci.*, vol. 17, no. 3, pp. 1474–1479, 2020.
- [38] M. N. Al-Mhiqani, R. Ahmad, Z. Z. Abidin et al., "A new taxonomy of insider threats: an initial step in understanding authorised attack," *International Journal of Information Systems and Management*, vol. 1, no. 4, pp. 343–359, 2018.
- [39] S. S. Bafjaish, M. S. Azmi, M. N. Al-Mhiqani, A. R. Radzid, and H. Mahdin, "Skew detection and correction of Mushaf Al-Quran script using hough transform," *International Journal of Advanced Computer Science and Applications*, vol. 9, no. 8, pp. 402–409, 2018.
- [40] A. Lakhan, M. A. Mohammed, S. Kadry, K. H. Abdulkareem, F. T. Al-Dhief, and C. H. Hsu, "Federated learning enables intelligent reflecting surface in fog-cloud enabled cellular network," *PeerJ Computer Science*, vol. 7, article e758, 2021.
- [41] S. A. Mostafa, S. S. Gunasekaran, A. Mustapha, M. A. Mohammed, and W. M. Abdullallah, "Modelling an adjustable autonomous multi-agent internet of things system for elderly smart home," *International conference on applied human factors and ergonomics*, vol. 953, 2020.
- [42] A. Lakhan, Q. U. A. Mastoi, M. Elhoseny, M. S. Memon, and M. A. Mohammed, "Deep neural network-based application partitioning and scheduling for hospitals and medical enterprises using IoT assisted mobile fog cloud," *Enterprise Information Systems*, pp. 1–23, 2021.
- [43] O. Taiwo and A. E. Ezugwu, "Smart healthcare support for remote patient monitoring during covid-19 quarantine," *Informatics in medicine unlocked*, vol. 20, p. 100428, 2020.
- [44] A. Kumar, R. Krishnamurthi, A. Nayyar, K. Sharma, V. Grover, and E. Hossain, "A novel smart healthcare design, simulation, and implementation using healthcare 4.0 processes," *IEEE Access*, vol. 8, 2020.
- [45] M. Naghshvarianjahromi, S. Kumar, and M. Jamal Deen, "Brain-inspired intelligence for real-time health situation understanding in smart e-health home applications," *IEEE Access*, vol. 7, pp. 180106–180126, 2019.
- [46] S. B. Baker, W. Xiang, and I. Atkinson, "Internet of things for smart healthcare: technologies, challenges, and opportunities," *IEEE Access*, vol. 5, pp. 26521–26544, 2017.
- [47] M. Sathya, S. Madhan, and K. Jayanthi, "Internet of things (IoT) based health monitoring system and challenges," *International Journal of Engineering & Technology*, vol. 7, no. 1.7, pp. 175–178, 2018.

Research Article

Gathering Contextual Data with Power Information Using Smartphones in Internet of Everything

Umar Mahmud ¹, Shariq Hussain ¹ and Ibrahima Kalil Toure ²

¹Department of Software Engineering, Foundation University Islamabad (FUI), Pakistan

²Department of Computer Science, Gamal Abdel Nasser University, Conakry, Guinea

Correspondence should be addressed to Ibrahima Kalil Toure; ikalil@msn.com

Received 30 January 2022; Revised 15 April 2022; Accepted 16 April 2022; Published 6 May 2022

Academic Editor: Alireza Souri

Copyright © 2022 Umar Mahmud et al. This is an open access article distributed under the Creative Commons Attribution License, which permits unrestricted use, distribution, and reproduction in any medium, provided the original work is properly cited.

The advent of smart devices, interacting with each other as well as remote services, has paved the way for the Internet of Everything (IoE). IoE is a direct successor of Internet of Things (IoT), composed of smart devices interacting with remote services. The devices in an IoE environment are power constrained. At the core of an IoE environment, there is a context-aware system that gathers the context and classifies it. Various datasets have been published by authors for context-aware systems. This paper presents a mechanism that gathers a dataset of contextual information along with power information using smartphones. An Android application “PowerIpsum” is developed for gathering contextual information, power information, and user input activity labels. The dataset includes the sensor data as the contextual data, timestamps, average current, and average voltage as well as user activity labels. Time elapsed and power consumption is forecasted using Monte Carlo method. The results provide useful insights and demonstrate the advantages of power information within a context-aware system.

1. Introduction

The fourth industrial revolution has paved the way for establishing smart environments in mundane places [1]. Statista estimates that in 2019, almost 27 billion devices were connected globally [2]. This number reduced to 12.3 billion in 2021, due to COVID, with over a \$160 billion industry [3]. Statista forecasted the total number of devices to be more than 75 billion in 2025. Cisco estimates there would be a trillion devices by 2025 [4, 5]. The International Data Corporation (IDC) predicts 40 billion connected devices generating 80 zettabytes of data by 2025 [6].

The dawn of smart, inexpensive, handheld, seamlessly integrated, and universally available devices have expanded the horizons of human potential [7, 8]. Over the years, the devices have become smaller, have more computation power, communicate seamlessly, and facilitate human

activity recognition [9, 10]. Smart devices communicate not only among themselves but with remote services over the cloud. The smart devices gather sensor data for a users’ activity classification. This helps in facilitating service discovery, delivery, and adaptation. Activity classification requires gathering contextual information about the users, remote services, and the environment [11, 12]. The contextual information includes both the sensor data as well as deduced data from remote services. The context is gathered, transformed, stored, and classified for activity [13, 14]. The prime challenge of a smart environment is the ability of the system to react appropriately to changing perceptions. For example, a change in brightness and orientation of a smartphone with the change in orientation and ambient light is an example of context-awareness. This is possible using an ambient light sensor and accelerometer in a smartphone. In an IoE environment, data is

gathered from the sensors and remote services, stored, and inferred based on historical information. The inference is termed as context inference engine (CIE) and is used to classify the current context as an activity [15].

A context-aware system gathers sensor data and interacts with remote services for service discovery or delivery [12]. A context-aware system is composed of interacting modules. These modules include context gathering module; which gathers data from intrinsic sensors and sensor services as well as deduced data, context history module; that records the history of interactions, a context inference module; which classifies the current context with a degree of confidence using a machine learning algorithm, and an adaptation module; that interacts with remote services.

The task of a context-aware system is to gather context and map it to a correct activity label. This requires communication, storage, and classification process. The proliferation of devices increases connectivity and introduces new challenges in establishing a context-aware system. The prime concern is power as the handheld devices are battery operated. The effect of battery use has been profiled by researchers. A simple 1-2 mW sensor can consume up to 180-300 mW power when the data is sensed and processed [16, 17] showing inefficiency of power consumption. Furthermore, the power consumed is dependent on the combustion of fossil fuels which leads to an increase in carbon emissions.

Context is the collection of attributes describing a state or situation [11]. These attributes are gathered from sensors and sensor services. The sensor data can be deduced to generate more information as part of the context [7]. Context is given activity labels that correspond to the activity or situation. Power information includes the voltage and current used by a context-aware system. This voltage and current can be used to deduce power consumption [18]. The power information includes all attributes that describe the power consumption.

Thus, there is a need to explore a power-conserving context-aware system that provides acceptable activity classification while consuming less power. A power-conserving context-aware system is also termed as green context-awareness (GCx). To develop this system, an appropriate data set is required for the training of classification algorithms. Many datasets are available for activity recognition; however, there is a need to include the power or battery drain information in the data sets. The authors have compiled a data set that includes context information as well as power information by using a smartphone interacting in IoE environments. This also includes the deduced contextual information via remote services and the activity label set by the user. An Android app is developed using MIT AI2 App Inventor [19]. The dataset compiled is useful for measuring the effectiveness of a power conserving context aware system and enables GCx.

The rest of the paper is organized as follows. Section 2 presents contemporary related work and highlights the motivation of this work. Section 3 introduces the concept of smartphone and its relationship with remote services within an IoE environment. Section 4 presents the concept

of power awareness and its phases. Section 5 outlines how power and energy are measured. Section 6 presents how power can be profiled using models and real-time measurement as found in the literature. Section 7 presents how context and power information is gathered using a smartphone as a prelude to the compilation of a dataset. Section 8 discusses the results, and the paper concludes in Section 9.

2. Related Work

Over the years, many researchers have gathered and published data sets that aid in developing context-aware applications. These data sets have been based on wearable devices as well as smartphones. The recent advancements in the design and development of smartphones have embedded a large variety of sensors previously worn on the body. The authors of this paper have selected recent data sets to identify their limitations thus highlighting the significance of the current work. These are discussed in subsequent paragraphs.

Ilarri et al. have reviewed contemporary data sets for context-aware systems [20]. The contextual information gathered in the focus datasets is used by content delivering services including Netflix and Amazon. The datasets reviewed by Ilarri et al. include contextual information that can be harvested using a smartphone, history of interaction, and remote services. Different subsets of these datasets are used for trip planning, movie recommendation, and music recommendation. Some of the contextual attributes include location, time, mood, temperature, sleepiness, crowd information, and nearby family and friends. However, none of these data sets maintain power consumption information or even the battery level of the smartphone. While these datasets are useful in developing smart applications, the application would not consider power as a constraint.

Recently, the concept of the smart grid has been advanced to include energy systems. This has resulted in energy 4.0, a standard where renewable energy resources are managed in smart grids. Shahinzadeh et al. have proposed the concept of Internet of Energy where smart grids are developed for energy management [21]. This is a useful concept for managing energy resources from the perspective of smart cities [22].

Sariaslani has published a Python-based context-aware system for tourists who want to visit attractions in a city [23]. This system uses location through latitude and longitude, history of visits, and the user's context to recommend visit locations in a city. The attractions are selected using an image set of attractions and tourist locations in London. The images are used to extract the owner, occupation, tags, number of favorites, and location. This information is matched with the contextual data to generate recommendations for tourists. This dataset uses the clock and GPS sensor to compile contextual information but lacks power-related information that could aid in the development of a power-conserving context-aware system.

Morgan et al. have developed a prefiltering and heuristic-based context recommendation system tested on LDOS-CoMoDa and DePaul datasets [24]. However, there

is no power information in the datasets selected to test the effectiveness of the proposed techniques.

Chang et al. have developed a tree-based recommender model as a context-aware system using AmazonBooks and Taobao User Behavior dataset [25]. The mechanism for context-based recommendation is promising; however, the datasets used neither consider power information nor the proposed technique consider power as a constraint.

Jeong and Kim have recently used deep learning to enhance the performance of context-aware systems while minimizing the effect of data sparsity [26]. The deep learning model learns contextual information based on multiple data sets. However, the deep learning model still does not consider power information as a contextual feature, mainly because it is beyond the scope of work by the authors.

The closest power information is part of the CARS dataset compiled by Unger et al. using smartphones to gather contextual information [27]. The datasets include battery level, battery temperature, and battery status, i.e., plugged or unplugged. However, this battery information is not suitable to ascertain the amount of power consumed during context gathering. The battery level is just the remaining percentage at the time of context gathering. This cannot be used to develop power constraint context-aware systems. Furthermore, the battery level is dependent on the type, capacity, and wear-and-tear of the battery and is not a good measure of power consumption during context gathering. The newer smartphones do not show a change in battery level when the context is gathered because the process takes fractions of a second. It is necessary to measure average voltage and average current to effectively know the power consumed as wattage.

The related work shows that the main focus has been gathering sensor data and deduced data. The complete power information is missing in the compiled data sets. The authors have compiled a dataset that overcomes this limitation by recording power information including voltage, current, and power with each record. This not only introduces the concept of power as a part of the context but also provides a means to establish the effectiveness of a power-conserving context-aware system, interacting in an IoE environment.

2.1. Comparison of Contemporary Datasets. Table 1 presents a comparison of contemporary datasets based on context information, use of smartphones to collect data, and power information. The statistics of the dataset are not presented as this paper is concerned with the type of data rather than the quantity of data.

2.2. Motivation. While the contemporary datasets are rich in contextual information, they simply ignore the power information. This entails that the context-aware systems developed using these datasets would assume that context awareness is not power constrained. To learn the effect of power on context-aware processing, the power information must be logged with each record in the dataset. Logging battery level is not suitable since this is a misleading ratio. In newer batteries, the level does not change even when the

TABLE 1: Comparison of datasets based on contextual and power information.

Authors	Year	Smart phone	Contextual information	Power information		
				Battery level	Current	Voltage
[20]	2018	✓	✓	×	×	×
[27]	2018	✓	✓	✓	×	×
[23]	2020	✓	✓	×	×	×
[24]	2020	✓	✓	×	×	×
[25]	2021	✓	✓	×	×	×
[26]	2022	✓	✓	×	×	×

smartphone is in use. It is appropriate to measure the voltage and current to calculate power consumption.

3. Smartphones in an IoE Environment

A smart environment is composed of sensors, devices, and remote services. At the heart of a smart ecosystem is a smart device that polls sensors and communicates with remote services. A smart device polls the sensors and remote services and gathers contextual data or context. This context is then transformed, stored, and recognized which is termed as context processing.

A smart personal space is a collection of devices owned or temporarily controlled by a user. A user may own multiple smart devices including wearable and handheld devices. Since these devices are controlled by a user, they are termed as a smart personal space. In addition, a smart personal space includes the private and public data of the user. This data can be maintained within the space or remotely accessed via the Internet.

A smart environment consists of multiple smart spaces interacting with the appliances and remote services [28]. This is analogous to multiple patients in a hospital, multiple persons in a house, engineers in a lab, or colleagues in an office. Within a smart environment, multiple smart personal spaces interact with each other as well as appliances and remote services. Since multiple personal spaces interact with the services using a common channel, conflicts in access can arise. A conflict resolution mechanism is provided in a distributed fashion where remote services and appliances can prioritize service delivery. Figure 1 shows a model of a smart ecosystem.

With the development of system on chip (SoC) based fog environments, IoT has become IoE where devices, sensors, and appliances are all connected, and computation is carried out within the fog. With a higher dependency on fog for computation, mapping, or learning tasks, the IoT world has transformed into artificial intelligence of things (AIoT). The difference between IoE and AIoT is the localized computation and decreased use of bandwidth for cloud storage. AIoT is relatively smarter and can provide abstractions for machine learning and big-data. Hassani et al. have proposed the context to be implemented as a service within a smart environment [29]. The context is processed by a context

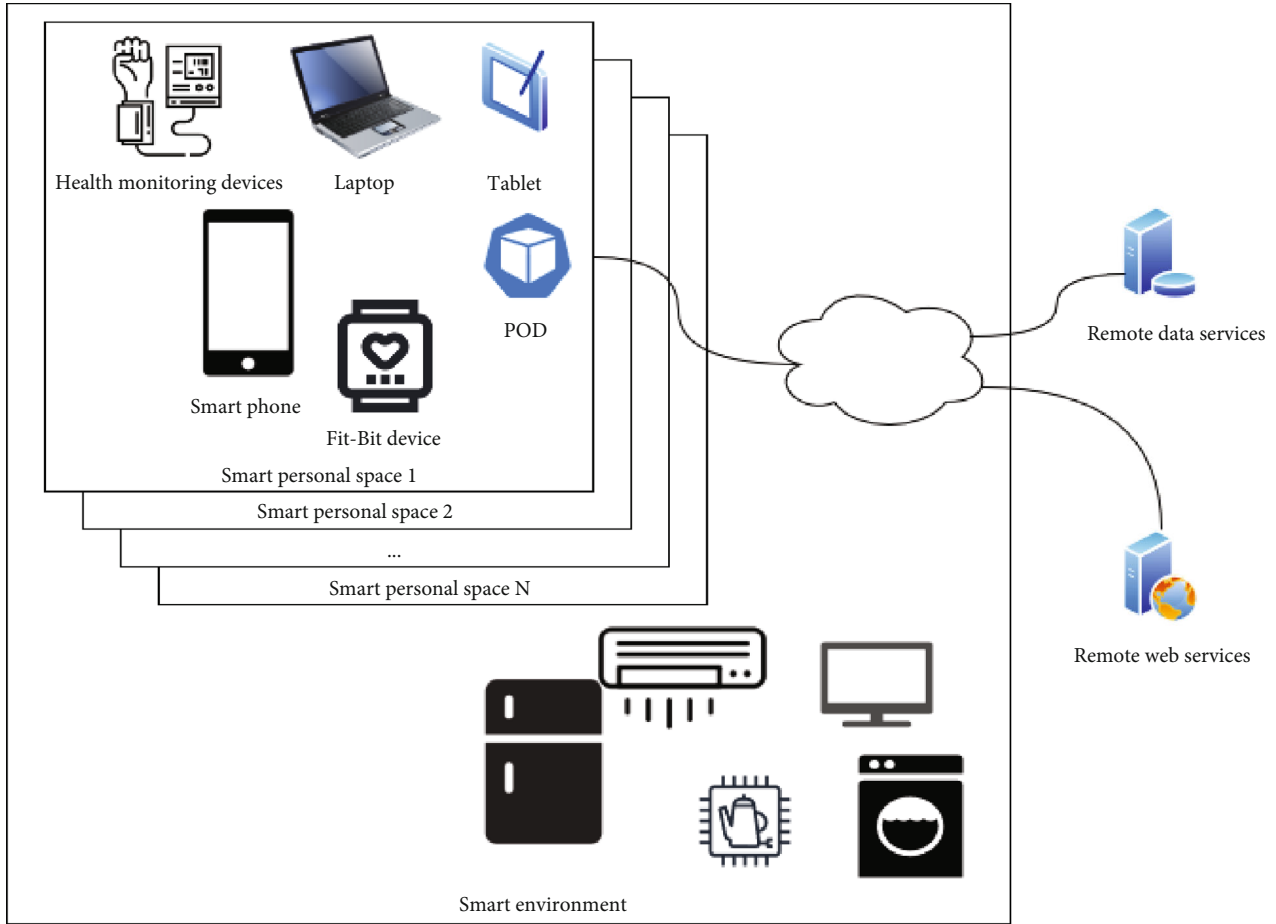


FIGURE 1: A smartphone in an IoE environment.

management platform (CMP), which is responsible for context processing and its provision to context consumers.

4. Power Awareness

Power awareness is the ability of a computer system to provide the same service albeit reduced performance while conserving power. An efficient system might not be a power-aware system as the efficiency parameters would not consider power conservation. Power awareness can also be viewed as a metric for cost of context (CoC) in an IoE environment [30]. The CoC is based on quality of context (QoC) which provides quality parameters to each contextual information. Power consumption can be considered as a cost parameter that could be used for triggering context processing. Power awareness is a combination of two closely linked concepts discussed below:

4.1. Power Consumption and Profiling. Power consumption is the energy consumption by a computation machine to provide a service. The energy is in the form of electrical power distributed through AC mains or DC batteries. A battery-based system needs to be charged regularly while a mains-based system is dependent on the supply of electrical current. Smart handheld devices are mostly battery

operated and use lithium-ion (Li-ion) as the implementation technology [31, 32].

The energy capacity of a battery is represented in watt-hours (Wh) while the operating voltage is 3.8 V. Another method is to use milliampere-hour (mAh) to represent the energy stored in the battery. It is interesting to note that a discharging battery would also lose voltage though for most of the operation it remains above 3.5 V.

The total consumption measured over a period is termed power profiling. The profile can be measured as a simulation as well as in real-time measurement [33]. Power profiling is mostly measured at the device or the OS level but can be fine-grained at the application level. Specialized hardware installed on the chip allows fine-grained measurement; however, the mundane device can use battery drain measures over a period to identify power consumed.

As the first step in power awareness, the power profile needs to be measured over a period [34, 35]. This allows the identification of the power consumption characteristics of a device or an application [36, 37]. Within a smart device, the power is consumed in the communication, storage, and computation phases of a context-aware application. Depending on the environment and the application focus, the profiles can be different. However, a general profile can be formed which can be fine-tuned over time.

TABLE 2: Description of tasks in the BPMN model of PowerIpsum.

Task	Actor	Description
Poll sensors and record timestamp, current, and battery level.		This task records the current timestamp and polls the sensor embedded on the device. For the missing sensors, a null value or zero value is recorded. Furthermore, the average current, voltage, and battery level are also recorded.
Access weather service		The weather service is accessed using latitude and longitude provided by the GPS sensor.
Receive weather data		The weather information is received and appended to the recorded sensor data. This includes the current weather report.
Access map service		The location service is accessed using latitude and longitude provided by the GPS sensor.
Receive map data	Smart device	The location information is received and appended to the recorded contextual information. This includes the current location.
Record timestamp, current, and battery level		The timestamp is recorded again so that elapsed time can be measured. The average current and battery level are again recorded. It has been observed that for the latest smartphones and using newer batteries, the battery level remains unchanged. Also, the average current is the same because the elapsed time is a fraction of seconds.
Get user label		The user types in the activity label to complete the context record. The record is then appended to the context file, which can be shared through email, messaging, or file transfer for postprocessing.
Weather service	OpenWeatherMap	This is a free and online web service that provides the current weather report based on latitude and longitude. The weather report includes weather outlook, temperature, precipitation chances forecast, and other attributes. The service is accessed using the HTTPS/GET method.
MAP service	MAPQUEST	This is a free and online web service that provides location information based on latitude and longitude. The information includes nearby places as well as location tags including street name, locality, and city. This service is accessed using the HTTPS/GET method.

4.2. *Power Conservation.* The final step in power awareness is power conservation. Power conservation is the ability of a system or application to provide the same service while conserving power. Power conservation is a nonfunctional requirement like time and space efficiency. Greener systems are power efficient in addition to time and space efficiency. Consider a case of a supercomputer that is time and space-efficient and consumes power of the order of megawatts (MW). Such computation does not conserve power and increases the carbon footprint as a byproduct.

A system that can measure the power profile and predict battery life needs to provide conservation to increase battery life while providing the same service. Researchers have proposed many techniques that are presented in the next section. The means to measure conservation also needs to be established to ascertain the effectiveness of a power conservation technique.

5. Power and Energy Measurement

Power and energy have been used interchangeably in the literature. Power is the product of voltage and current, measured in watts while energy is the capacity of doing work measured in Joules. Energy can also be measured in watt-hours, by multiplying power with elapsed time. Since it is easier to measure power using a multimeter, and through

power profiling apps, this work considers power in watts and energy in watt-hours. Equation (1) gives the power equation with power (P) measured in watts (W) as a product of voltage (V) and current (I).

$$P = V \times A. \quad (1)$$

Equation (2) represents the electrical energy (E) measured in watt-hours (Wh) as a product of power (P) and time (t).

$$E = P \times t. \quad (2)$$

A watt in terms of energy is when the energy of a Joule (J) passes through an electrical device for a second. Watts can then be measured in Joules per second (J/s). Energy potential is measured in Joules by replacing P with J/s in equation (2). A variation of electrical energy can be represented by combining Ohm's Law in Equation (2). Equation (3) shows the dissipated electrical energy as a product of the square of the current (I), time (t), and resistance (R). This is also measured in Wh .

$$E = I^2 \times R \times t. \quad (3)$$

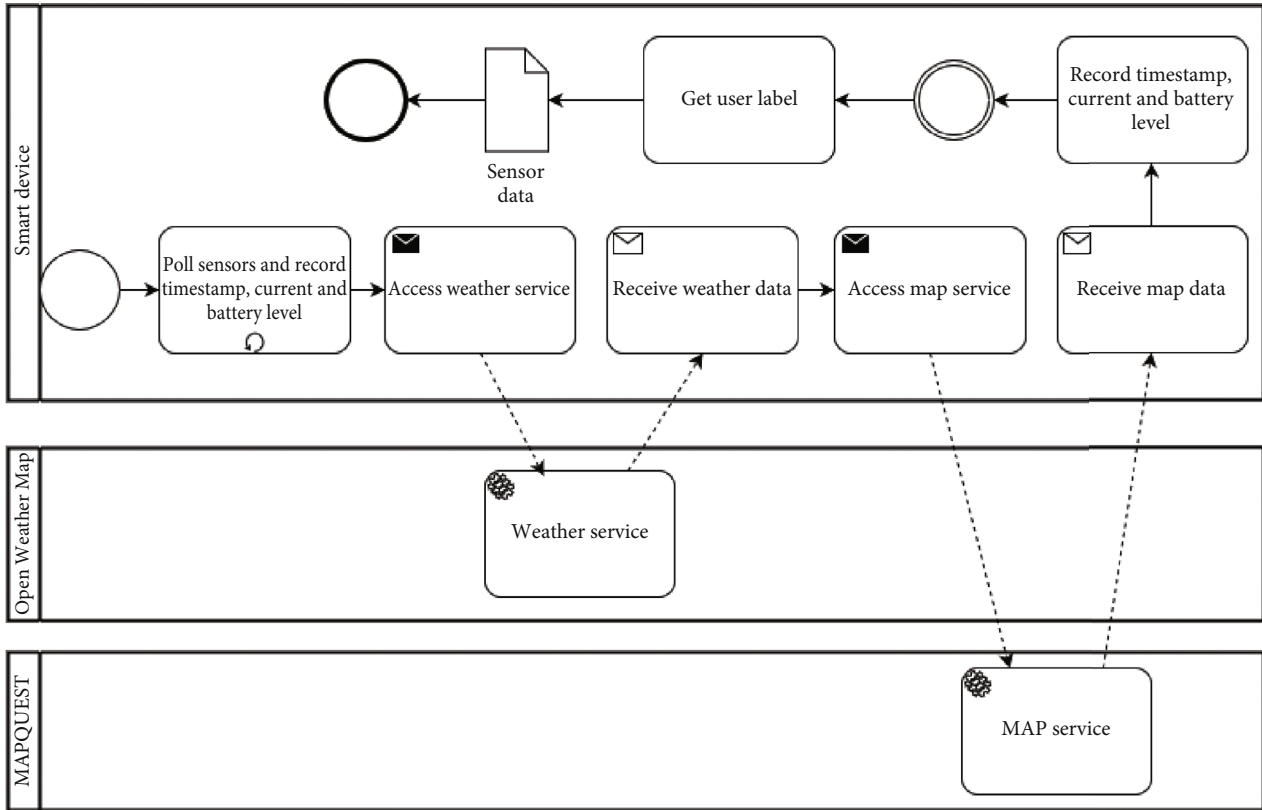


FIGURE 2: Design of PowerIpsum App using BPMN.

6. Power Profiling and Optimization

Power profiling refers to the measurement of power consumption over time. Power profiling is a useful tool to monitor the battery usage of mobile devices. All modern OS support power profiling at the OS level and rank power-draining applications [38]. A human can then tweak applications based on their power profile. Profilers measure the current draw over time and share their results in the form of plots. Jofri et al. have surveyed profiler applications for smartphones [39].

Tsao et al. have modeled the power consumption of I/O operations by implementing a power profiling [40]. This system monitors I/O operations on communication modules and touch screens. Sathyamoorthy et al. have focused on the power profiling of data communication by smartphones in a smart environment [41]. Both authors have reported that the communication modules consume more power, especially in noisy networks. Bolla et al. and Celenlioglu et al. have surveyed power consumption in networks, independently [42, 43]. Brienza et al. carried out power consumption of file-sharing P2P networks [44]. The major power consumer is the communication module. Ismail et al. point out that multimedia applications and screens consume a high amount of power [45]. This can be adjusted based on battery drain. Asnani et al. have recommended that contrast enhancement can reduce power consumption by OLED-based screens [46]. Vasile et al. have reported that the front-end applications consume

more power when compared with back-end components and external web services that are invoked by the back-end components [47]. The authors have profiled power consumption in Windows phones.

Power is a constraint for battery-operated devices. Contemporary technology has paved the way for reducing the size and weight of smart devices. However, power consumption remains a pressing issue in the design and development of smart devices. Both hardware and software need to be optimized for power consumption [48]. While energy-efficient hardware has been designed, there is a need to address power constraints in algorithm design and software development [49]. The optimization of software applications for power usage is a requirement for green computing [50, 51].

Duan et al. have outlined a power estimation model across three layers. These include the hardware layer, the OS layer, and the application that is in the running state [52].

Chang et al. have proposed residual power as the unit of forecast and optimization. Residual power gives the estimated battery life of smartphones and power banks [53]. Lee et al. have profiled the power consumption of context-aware applications [54]. The authors report power is consumed in two stages. First, when the context is gathered through the sensor and then when it is processed. Context processing is more power-intensive based on the algorithm used to classify context. Rault et al. point out that the continuous sampling of real-time sensor data drains the battery quickly [55].

STEP #	pseudocode
1	int numberOfAttributes; //total number of attributes
2	double sensorData[numberOfAttributes]; //array for sensor data
3	URL weatherURL;
4	URL mapURL;
5	file contextFile;
6	procedure init() {
7	mapURL = new URL("https://developer.mapquest.com/");
8	weatherURL = new URL("https://api.openweathermap.org");
9	contextFile = new file("contextualData.Txt");
10	}
11	procedure powerIpsum (){
12	double timestampBefore = getCLK();
13	double avgCurrentBefore = getAverageCurrent();
14	double batteryLevelBefore = getBatteryLevel();
15	for (int i=0; i < numberOfAttributes; i++) {
16	sensorData[i] = attributeValue; //value of attribute
17	}
18	URLConnection con1 = weatherURL.openConnection();
19	string weatherRep = con1.setRequestMethod("GET", lat, long);
20	URLConnection con2 = mapURL.openConnection();
21	string mapRep = con2.setRequestMethod("GET", lat, long);
22	double timestampAfter = getCLK();
23	double avgCurrentAfter = getAverageCurrent();
24	double batteryLevelAfter = getBatteryLevel();
25	string activityLabel = inputUserLabel(); //user types data
26	contextFile.Append(timestampBefore, avgCurrentbefore, batterylevelbefore, sensordata[], weatherRep, mapRep, timestamp- After, avgCurrentafter, batteryLevelafter, activityLabel, "endLine");
27	}

PSEUDOCODE 1: Pseudocode of PowerIpsum process.

Abkenar et al. have proposed a power measurement method during group activity recognition. This is carried out by measuring the current draw of a smartphone from the battery [56]. Bernal et al. have outlined energy consumption reduction strategies based on power profiling [57]. These strategies can potentially optimize battery life in context-aware applications. Similar techniques can be utilized for BEV [58].

Power profiling can be used to optimize device behavior and conserve power. Devices can reduce screen intensity, turn off Wi-Fi/5G/4G modules, and shift to power-saving modes as required. Devices can also inform the users on which applications are consuming more power and can be suspended based on users' input. The optimization is carried out at the device and OS level and has little adaptability. This scheme lacks application-level power conservation. The measurement of power consumption is the basis of power profiling [33].

6.1. Model-Based Profiling. In model-based profiling, software models are used to measure power consumption. This method is useful at design times where the power considerations can be incorporated at the device or OS level. Application development can also utilize this method to improve the development constraints.

An implication of model-based profiling is the comparison of different algorithm approaches based on their power

profiling, like time and space complexity. An algorithm that consumes less power and produces acceptable results is greener. A greener algorithm can be selected for development by engineers to reduce power consumption.

6.2. Real-Time Measurement-Based Profiling. In contrast to model-based power profiling, real-time measurement-based profiling, measure power consumption in real-time. This method has the added advantage of live measurements and can be used by the OS to identify applications that consume less power. González-Pérez et al. have listed guidelines for reliable measurements using Android-based devices [59].

UPower is used in Linux distributions to measure power consumption, voltage level, energy, and battery level [60]. The battery manager extension is provided for use on Android devices [61]. Battery manager extension provides voltage, current, health, temperature, and level information. Both these mechanisms are software-based. This method requires may require hardware support to accurately measure the power consumption. Datta et al. have developed an application that monitors the power consumption of smartphones and logs the usage patterns [62, 63].

The hardware-based measurement uses Summit SMB347 or Maxim MAX17050 for Nexus devices. An external power monitor can also be attached to a Nexus device for real-time profiling [64]. Mukherjee and Chantam have developed a device-level mechanism to measure the total power

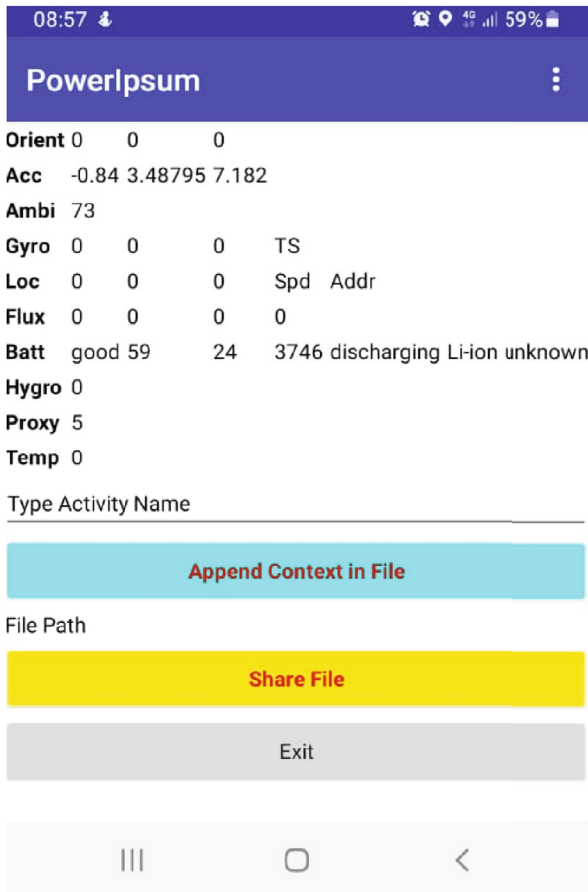


FIGURE 3: PowerIpsum application.

consumption of a Nexus 6 smartphone [65]. Hardware-based approaches are expensive and not available in mundane and widely distributed devices. Tsao et al. focused on I/O operations in mobile devices and profiled power consumption during these operations [40]. In contrast, a software-based mechanism approximates power consumption and is easily available in mundane devices [66].

Schwartz et al. have proposed the use of floating-point operations (FPO) as the measurement method for power consumption [67]. This mechanism is expensive and requires fine-tuned measurements.

7. Gathering Contextual Data and Power Information

The context data is first gathered from the sensor services present in the environment. The data is acquired by accessing the internal sensors as well as remote sensor services. For example, a smartphone can use the internal pedometer, gyroscope, accelerometer, light sensor, etc., as internal sensors while it could access a weather service over the cloud as a remote sensor service. Traditionally, the context congregator module or the context aggregator module of a context-aware system gathers and stores the contextual data [14]. The contextual data can be stored using RDF, XML, and OWL and can be organized in many ways

[13]. There is no context processing at this level. Context processing classifies the activity of the contextual data and history of context using a machine learning algorithm [12, 15]. The first step is to gather data and store it on a device. The user should supply the context label, to aid in classification. The context label of context is the user's label assigned to the context. The label could be on a macro level or micro level, e.g., "Driving" is the context label at the macro level, while "Driving to Carrefour to Buy Groceries" is a label at the microlevel.

7.1. An Example Case. An example case of using PowerIpsum is the data collection of mundane and daily tasks performed by a user. The device captures the sensor data through the sensors embedded in the users' smartphones. This information can be used to access remote services. For example, GPS data is used to get weather and location information through two web services. In addition to contextual data through the sensors, the device also records the elapsed time, average voltage, and average power. For example, a user when going to work uses the app to record the contextual information. The sensor data is recorded, and the remote services are accessed through 4G connectivity. The power consumption is dependent on the signal strength of the network. Remote services are also accessible through Wi-Fi; however, more power is consumed in retransmissions due to low signal strength or noisy channels. The power is calculated in a postprocessing fashion.

7.2. Context Gathering App: "PowerIpsum." To gather contextual data, the authors of this paper have developed an application for Android platforms using MIT App Inventor. MIT App Inventor provides a quick way of developing Android applications and provides a visual component-based interface. A developer needs to drag and drop components and develop their logic around the components. MIT App Inventor has reduced development time, is suitable for use by all ages, and is free to use. The developed application is called as PowerIpsum and is available for download on GitHub under GNU GPL v3.0 License for public use [68]. MIT App Inventor provides a wide array of sensors that may be installed on Android phones. These include clock, gyroscope, accelerometer, ambient light sensor, proximity sensor, GPS, temperature, battery info, orientation, and magnetometer. The testbed is Samsung A03s, Google Nexus 6, Samsung A51, and Samsung S20 are used for application testing purposes, and limited data is collected from these devices. All phones run Android OS. Google Nexus 6 has a built-in power management chip installed that facilitates real-time power measurement, while Samsung A03s, and A51, approximate the power usage using software tools. The data from some of the sensors is raw and needs to be deduced using an online web service to make it meaningful. For example, the GPS sensor returns GPS coordinates in the form of the latitude and longitude of the device. This GPS data can be used to access a weather service and a map service to get the weather information and address information simultaneously. OpenWeather and MapQuest are used as web

TABLE 3: Description of sensor data attributes.

Sensor	Attribute	Value type	Description
CLK	Timestamp	Long	This timestamp is a label to record the time at the start of the process. This timestamp is a long number depicting a nanosecond. The timestamp is also recorded after the processing has been completed and the elapsed time is measured in picoseconds, postprocessing.
Orientation sensor	Azimuth	+ve double	It is used to measure the azimuth for the orientation of the device.
	Pitch	Double	It is used to measure the pitch for orientation of the device.
	Roll	Double	It is used to measure the roll for orientation of the device.
Accelerometer	X acceleration	Double	It measures the acceleration along the x -axis.
	Y acceleration	Double	It measures the acceleration along the y -axis.
	Z acceleration	Double	It measures the acceleration along the z -axis.
Ambiance	Lux	+ve integer	It measures the ambient illuminance in lux.
	X angular velocity	Double	It measures the angular velocity of the device's rotation along the x -axis.
	Y angular velocity	Double	It measures the angular velocity of the device's rotation along the y -axis.
Gyroscope	Z angular velocity	Double	It measures the angular velocity of the device's rotation along the z -axis.
	Latitude	+ve double	Gives the latitude of the device.
	Longitude	+ve double	Gives the longitude of the device.
Location sensor	Altitude	+ve integer	Gives the altitude of the device.
	X strength	Double	Gives the magnetic field strength along the x -axis.
	Y strength	Double	Gives the magnetic field strength along the y -axis.
Magnetometer	Z strength	Double	Gives the magnetic field strength along the z -axis.
	Absolute strength	Double	Gives the absolute strength of the magnetic field.
	Health	String	The health status of the battery.
Battery extension	Level	+ve integer	Gives the battery level as a percentage of total capacity. The before and after battery level is recorded.
	Temperature	Integer	Gives the temperature in Celsius.
	Voltage	+ve integer	Gives the voltage in millivolts (mV).
	Status	String	Gives the status, i.e., charging or discharging.
	Technology	String	The technology of the battery, e.g., lithium-ion, or nickel cadmium.
Hygrometer	Current draw	Integer	Measures the current draw in milliAmperes (mA). The current draw is negative when the device is discharging. This is recorded for both before and after processing.
	Humidity	Integer	Measures the humidity in the environment.
	Near field communication sensor	Distance	+ve integer
Weather web service	Weather	String	Gives the outlook of the weather. The location is the latitude and longitude measured using a location sensor.
Location web service	Address	String	Gives the address of the location. The location is the latitude and longitude measured using a location sensor.

services since both are free for use [69, 70]. Table 2 describes the tasks, shown as a rounded rectangle, of the BPMN model of PowerIpsium. Pseudocode 1 shows the pseudocode of the PowerIpsium process. Since each sensor provides multiple attribute-value pairs, there could be more attributes than the total number of sensors embedded in a smart device. If the number of attributes is n , then, the time complexity of the pseudo code given in

Table 2 is $O(n)$. This shows that the data gathering process has a linear time complexity.

The design is presented using business process model and notation (BPMN 2.0) in Figure 2. BPMN is a standard used to design a business model of interacting services. Since PowerIpsium is envisaged as a service that uses other services, a BPMN is suitable for design. Figure 2 shows that there are three interacting entities or services. The smart

TABLE 4: Statistics of Monte Carlo method on time elapsed and power consumed on different smart phones.

	A03s		A51		S20	
	Time (psec)	P (μW)	Time (psec)	P (μW)	Time (psec)	P (μW)
Average	11.84	30.09	6.79	2.97	6.5	1.57
Median	12	30	7	3	6.5	2
Mode	11	27	7	3	7	2
Max	26	55	12	6	10	3
Min	0	12	3	0	4	1
Std dev	4.83	6.58	1.41	0.95	0.91	0.5

device is the user’s device and interacts with two web services. At the start, the timestamp and battery information are taken and then the internal sensors are polled. After that, the web services are called sequentially via message passing using the HTTP GET method. MIT App Inventor is a single-threaded, sequential app development system. There are no threads and no concurrent execution. The application developed is executed sequentially, as a constraint. The response by the services and the sensor data is stored as a record temporarily, as an intermediate event. The user then inputs the label in the application, and the record is stored in a comma-separated value (CSV) file. The process then completes. The saved file can also be shared via social applications. This aids in data collection purposes.

Figure 3 shows the front end of the PowerIpsium application. The sensor data is arranged in a grid and shown in a row for each sensor. The columns correspond to data values. This is shown to confirm that data is read by the sensors. Once the user types the activity name and presses append context in file, the sensor data is read and appended to a text file. The file can then be shared using social applications by the user. A user can exit the application by pressing the exit button. The application can run in the background with the measurements taken and stored only when the append context in file button is pressed. Depending on the sensor availability, the data is flushed on the application as well as appended to the file. However, it is not easy to confirm whether the data appended in the file is the same as the one flushed on the screen, as some sensors are sensitive and keep on reading data constantly. The timestamps and battery information are recorded when the user presses append context in file. This button gathers and stores context as well as a timestamp, battery information, and average current. Battery information includes battery level and voltage. Voltage and average current draw can be used to measure power as shown in equation (1). Timestamps can be used to find elapsed time and energy can be measured using power and elapsed time as shown in equation (2).

7.3. Data Fields of Contextual Data Set. The data fields or attributes of contextual data include the complete data provided by sensors, APIs, and web services that are accessed by the PowerIpsium application. Table 3 describes the attributes of the contextual data set and the sensors associated

with it. The absence of a sensor on a smartphone shows a null value or 0 in the data record.

The postprocessing computations are carried out using both equations (1) and (2). Time elapsed is measured by subtracting the timestamps. The recorded data is exported to a spreadsheet using MS Excel. The postprocessing of the data set is performed using MS Excel and on a desktop. The time and power used for processing are not considered as this paper is concerned with the time and power consumed in data sensing and storing. The computations required are the time elapsed, power, and energy consumed. Among the targets is the correlation between time elapsed and power conservation. It is interesting to note that time elapsed and power consumption are both random variables that occur with an underlying and undiscovered probability distribution in a context-aware world. Similarly, the context label is also a random variable assigned by a user to a context.

7.4. Using Monte Carlo Method on Contextual Data. The data collection of sensor data for context purposes is a tiresome and time-consuming process. It also depends on the availability of test subjects who would wholeheartedly participate in the project. The privacy concerns of users become a hindrance in data collection. Furthermore, noise can also distort the data and lead to an incorrect conclusion. Since the variables of interest are random variables, an obvious question is what would be the correlation among them? Furthermore, can the power consumption be predicted, based on the time elapsed, with a degree of probability? In the absence of abundant and noise-free data, and a requirement to forecast the outcome, Monte Carlo method can be utilized on the gathered contextual data [71, 72]. The mean and standard deviation of time elapsed, power consumption, and energy computation are taken, and Monte Carlo Method is run to 500 and more instances.

8. Results and Discussion

The sensor data collection is an ongoing task. It is envisaged that the data would be gathered by willing subjects for over a year. Given that a subject provides 10 instances per day, this would collect 3500+ records in a year. An increase of subjects would simply increase the dataset. The collected data set has been uploaded on our institute web page and is regularly updated. Each record is checked for missing attributes, duplication, or null values, and all such records are discarded. Currently, the data set has records of a willing person who uses Samsung A03s for data collection. The same person has used multiple smartphones for testing and evaluation purposes; however, only one is used for extended data collection.

Monte Carlo method is selected for forecasting and modeling the behavior of stochastic processes. Monte Carlo method is widely used, is reliable, and computationally inexpensive [73]. It is also suitable when there is limited empirical data [74]. The collected data set is subject to Monte Carlo method to forecast time elapsed and power consumed. Mean, standard deviation, mode, max, and min after

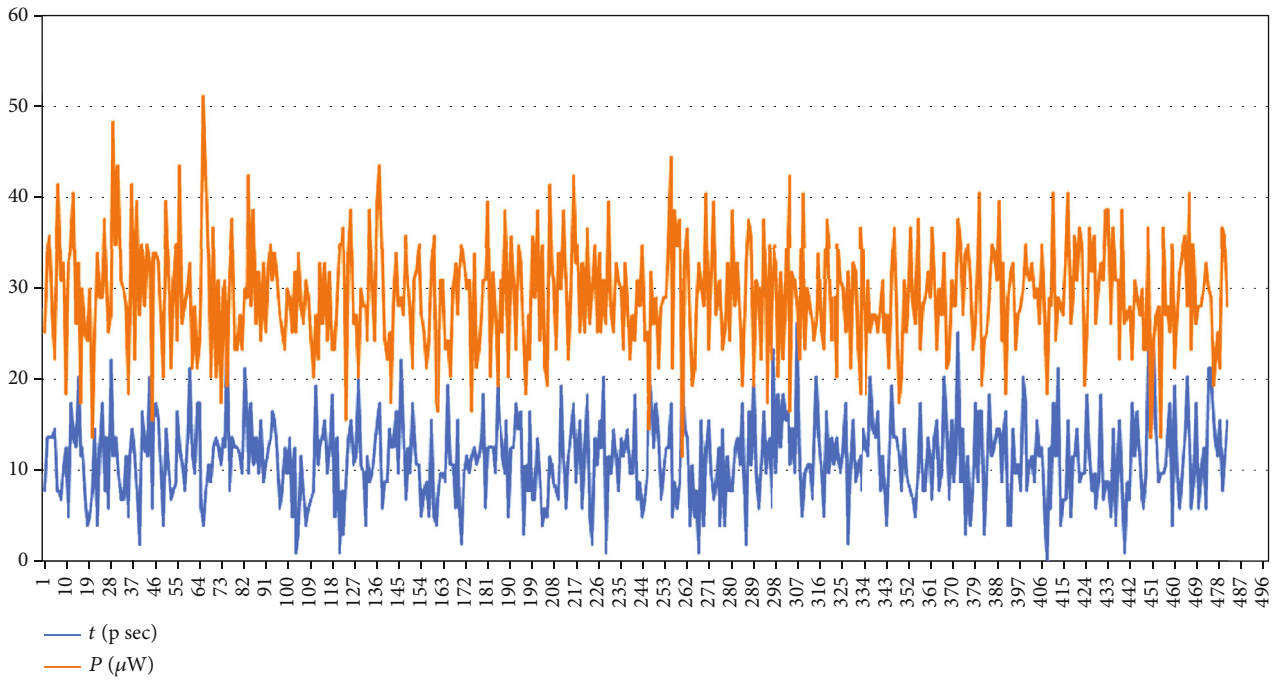


FIGURE 4: Plot of time elapsed and power consumed using Monte Carlo method using Samsung A03s.

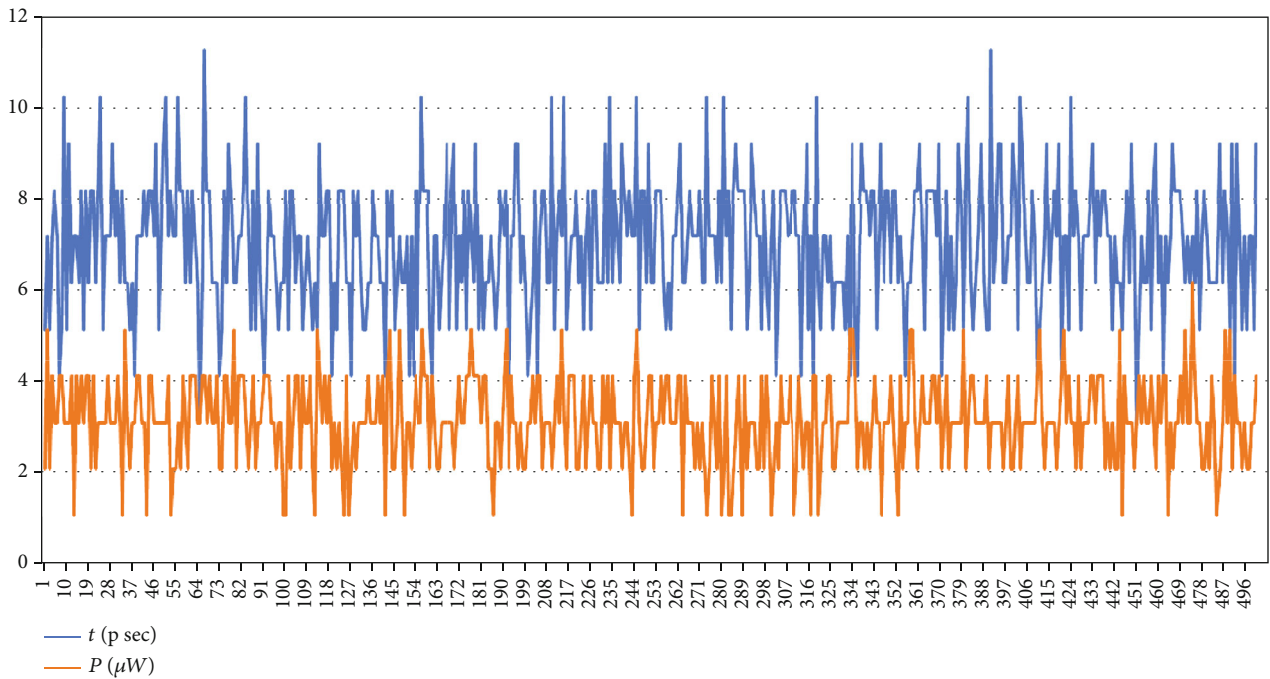


FIGURE 5: Plot of time elapsed and power consumed using Monte Carlo method using Samsung A51.

executing Monte Carlo method are recorded as well. The Monte Carlo method can produce negative numbers which are illogical in this case as time elapsed and power consumption are positive numbers. Absolute value is used to control illogical cases. Table 4 shows some statistics performed on running Monte Carlo method for time elapsed and power

consumed, using 200+ records on Samsung A03s, and 20+ records on A51 and S20.

Figure 4 shows the plot of time elapsed and power consumed after running Monte Carlo method on data collected using A03s. Figure 5 shows the plot of time elapsed and power consumed after running Monte Carlo method on data

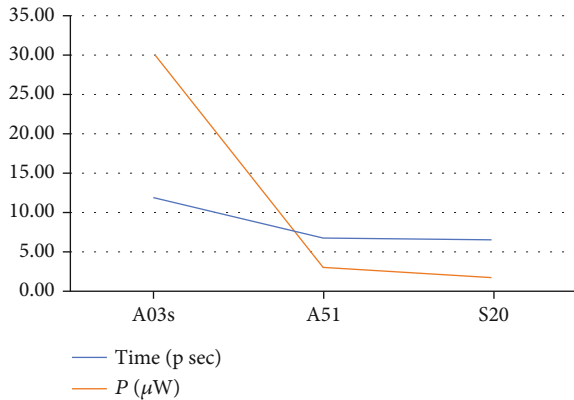


FIGURE 6: Comparison of time elapsed and power consumed after running Monte Carlo method for different smart phones.

collected using A51. While the data collection is less, the Monte Carlo method is executed 500 times in both cases.

The results show that while the time elapsed is similar, the power consumption is different for different data sets. This is because of the smartphone being used and the activities performed. The smartphones being used are of varying performance, which is evident in the power consumption. The power consumption is the average current draw from a smartphone. Since the gathering is performed for fraction of seconds, power as a measure is suitable. Figure 6 compares the time elapsed and power consumed for all three smartphones. It is interesting to note that the expensive and efficient phones took less amount of time and consumed less power. However, the smartphone that has lesser sensors and weaker performance took more time and consumed more power. One of the reasons is the underlying architecture and mobile usage. The data used in Figure 6 is derived from Table 2.

9. Conclusion

There is no information on power or battery usage in the datasets accessible on the UCI Machine Learning Repository or Google Research. Furthermore, the datasets that are used for context awareness are composed of sensor-based data and associated high-level activity. This research aims to collect contextual data as well as power information to help in the creation of a power-conserving context-aware system. The research domain is limited to users' mundane activities performed with a smartphone in an IoE setting. The authors used MIT App Inventor to create PowerIpsum, an Android application that captures sensor data as well as battery information including current and voltages. After that, a user tags the records with activity labels. The dataset is then inspected, compiled, and regularly updated. Monte Carlo method is used on the dataset to determine the correlation between time elapsed and power consumption when contextual data is gathered and stored. The results show that on average the power consumption is higher for older devices while the time elapsed is almost the same. Future work will entail increasing the dataset size and employing various machine learning algorithms for context awareness.

Data Availability

The authors confirm that the data generated or analyzed and supporting the findings of this study are available within the article.

Conflicts of Interest

The authors declare that they have no conflicts of interest.

References

- [1] World Economic Forum, "Fourth industrial revolution," 2021, <https://www.weforum.org/focus/fourth-industrial-revolution>.
- [2] Statista, "Internet of Things (IoT) connected devices installed base worldwide from 2015 to 2025," 2020, <https://www.statista.com/statistics/471264/iot-number-of-connected-devices-worldwide/>.
- [3] K. L. Lueth, "IoT analytics," 2022, <https://www.mdpi.com/2078-2489/5/4/612>.
- [4] AlliedTelesis, "Designing networks for IoT," 2021, <https://www.alliedtelesis.com/en/blog/designing-networks-iot>.
- [5] Cisco, "Internet of things," 2016, <https://www.cisco.com/c/dam/en/us/products/collateral/se/internet-of-things/at-a-glance-c45-731471.pdf>.
- [6] S. Rizvi, R. Pipetti, N. McIntyre, J. Todd, and I. Williams, "Threat model for securing internet of things (IoT) network at device-level," *Internet of Things*, vol. 11, pp. 100240–100252, 2020.
- [7] N. A. Malik, U. Mahmud, and M. Y. Javed, *Future Challenges in Context Aware Computing*, VillaReal, 2007.
- [8] B. Schilit, N. Adams, and R. Want, "Context-aware computing applications," in *Proceedings of the 1994 First Workshop on Mobile Computing Systems and Applications*, pp. 85–90, Washington, DC, 1994.
- [9] U. Mahmud, N. Iltaf, and F. Kamran, "Context congregator: gathering contextual information in CAPP," in *Proceedings of the International Conference on Frontiers of Information Technology*, Islamabad, Pakistan, 2007a.
- [10] S. Hussain, U. Mahmud, and S. Yang, "Car e-talk: an IoT-enabled cloud-assisted smart fleet maintenance system," *IEEE Internet of Things Journal*, vol. 8, no. 12, 2021.
- [11] G. D. Abowd, A. K. Dey, P. J. Brown, N. Davies, M. Smith, and P. Steggle, "Towards a better understanding of context and context-awareness," in *Proceedings of the 1st international symposium on Handheld and Ubiquitous Computing*, pp. 304–307, Karlsruhe, Germany, 1999.
- [12] U. Mahmud and M. Y. Javed, "Context inference engine (CiE)," *International Journal of Advanced Pervasive and Ubiquitous Computing (IJAPUC)*, vol. 4, no. 3, pp. 13–41, 2012.
- [13] U. Mahmud, "Organizing contextual data in context aware systems: a review," in *Handbook of Research on Human-Computer Interfaces, Developments, and Applications*, J. Rodrigues, P. Cardoso, J. Monteiro, and M. Figueiredo, Eds., pp. 273–303, IGI Global, Hershey, PA, 2016.
- [14] U. Mahmud, N. Iltaf, A. Rehman, and F. Kamran, *Context-Aware Paradigm for a Pervasive Computing Environment (CAPP)*, VillaReal, Portugal, 2007.
- [15] U. Mahmud and M. Y. Javed, "Context inference engine (CiE): classifying activity of context using Minkowski distance and standard deviation-based ranks," in *Systems and Software*

- Development, Modeling, and Analysis: New Perspectives and Methodologies*, pp. 65–112, IGI Global, 2014.
- [16] S. L. Kiani, A. Anjum, N. Antonopoulos, and M. Knappmeyer, “Context-aware service utilisation in the clouds and energy conservation,” *Journal of Ambient Intelligence and Humanized Computing*, vol. 5, no. 1, pp. 111–131, 2014.
- [17] O. Yuryur, “Energy efficient context-aware framework in mobile sensing,” in *University of South Florida, Electrical Engineering*, University of South Florida, Florida, 2013.
- [18] U. Mahmud, S. Hussain, and S. Yang, “Power profiling of context aware systems: a contemporary analysis and framework for power conservation,” *Wireless Communication and Mobile Computing*, vol. 2018, article 1347967, pp. 1–15, 2018.
- [19] MIT, “MIT app inventor,” 2012, <https://appinventor.mit.edu/>.
- [20] S. Ilarri, R. Trillo-Lado, and R. Hermoso, “Datasets for Context-Aware Recommender Systems: Current Context and Possible Directions,” in *2018 IEEE 34th International Conference on Data Engineering Workshops (ICDEW)*, pp. 25–28, Paris, 2018.
- [21] H. Shahinzadeh, J. Moradi, G. B. Gharehpetian, H. Nafisi, and M. Abedi, “Internet of energy (IoE) in smart power systems,” in *2019 5th Conference on Knowledge Based Engineering and Innovation (KBEI)*, pp. 627–636, Tehran, 2019a.
- [22] H. Shahinzadeh, J. Moradi, G. B. Gharehpetian, H. Nafisi, and M. Abedi, “IoT Architecture for Smart Grids,” in *2019 International Conference on Protection and Automation of Power System (IPAPS)*, pp. 22–30, Iran, 2019b.
- [23] A. Sariaslani, “Context-aware recommender,” 2020, <https://www.kaggle.com/amiralisa/context-aware-recommender/>.
- [24] C. Morgan, I. Paun, and N. Ntarmos, “Exploring Contextual Paradigms in Context-Aware Recommendations,” in *2020 IEEE International Conference on Big Data (Big Data)*, pp. 3079–3084, Atlanta, 2020.
- [25] D. Chang, J. Liu, Z. Xu, H. Li, H. Zhu, and X. Zhu, “Context-aware tree-based deep model for recommender systems,” *DLP-KDD 2021*, Singapore, 2021.
- [26] S.-Y. Jeong and Y.-K. Kim, “Deep learning-based context-aware recommender system considering contextual features,” *Applied Sciences*, vol. 12, no. 1, pp. 45–52, 2022.
- [27] M. Unger, B. Shapira, L. Rokach, and A. Livne, “Inferring contextual preferences using deep encoder-decoder learners,” *New Review of Hypermedia and Multimedia*, vol. 24, no. 3, pp. 262–290, 2018.
- [28] U. Mahmud, S. Hussain, A. J. Malik, S. Farooqui, and N. A. Malik, “Realizing IoE for smart service delivery: case of museum tour guide,” in *smart systems design, applications, and challenges*, J. M. Rodrigues, P. J. Cardoso, J. Monteiro, and C. M. Ramos, Eds., IGI global, 2020.
- [29] A. Hassani, A. Medvedev, P. D. Haghghi et al., “Context-as-a-Service Platform: Exchange and Share Context in an IoT Ecosystem,” in *2018 IEEE International Conference on Pervasive Computing and Communications Workshops (PerCom Workshops)*, pp. 385–390, Athens, 2018.
- [30] K. S. Jagarlamudi, A. Zaslavsky, S. W. Loke, A. Hassani, and A. Medvedev, “Towards measurable efficient and effective metrics for quality and cost of context,” *Modeling and Using Context*, vol. 4, no. Special Issue, pp. 1–6, 2021.
- [31] D. Ferreira, A. K. Dey, and V. Kostakos, “Understanding human-smartphone concerns: a study of battery life,” in *pervasive computing. Pervasive 2011. LNCS*, K. Lyons, J. Hightower, and E. M. Huang, Eds., Springer, 2011.
- [32] M. Ue, K. Sakaushi, and K. Uosaki, “Basic knowledge in battery research bridging the gap between academia and industry,” *Materials Horizons*, vol. 7, no. 8, pp. 1937–1954, 2020.
- [33] Y.-F. Chung, C.-Y. Lin, and C.-T. King, “ANEPROF: Energy Profiling for Android Java Virtual Machine and Applications,” in *2011 IEEE 17th International Conference on Parallel and Distributed Systems (ICPADS)*, pp. 372–379, Tainan, Taiwan, 2011.
- [34] J. Kulk and J. Welsh, “A low power walk for the NAO robot,” in *Proceedings of the 2008 Australasian conference on Robotics & Automation (ARCA-2008)*, pp. 1–7, Canberra, Australia, 2008.
- [35] C. Seo, G. Edwards, S. Malek, and N. Medvidovic, “A framework for estimating the impact of a distributed software system’s architectural style on its energy consumption,” in *Seventh Working IEEE/IFIP Conference on Software Architecture, 2008. WICSA 2008*, pp. 277–280, Vancouver, BC, Canada, 2008.
- [36] Y. Li, H. Chen, and W. Shi, “Power behavior analysis of mobile applications using bugu,” *Sustainable Computing: Informatics and Systems*, vol. 4, no. 3, pp. 183–195, 2014.
- [37] N. Vallina-Rodriguez, J. Shah, A. Finamore et al., “Breaking for commercials: characterizing mobile advertising,” in *Proceedings of the 2012 Internet Measurement Conference IMC '12*, pp. 343–356, Boston, 2012.
- [38] J. Wang, L. Feng, W. Xue, and Z. Song, “A survey on energy-efficient data management,” *ACM SIGMOD*, vol. 40, no. 2, pp. 17–23, 2011.
- [39] M. H. Jofri, M. F. Fudzee, and N. M. Ismail, “A survey on energy-aware profiler for mobile devices,” in *Computational Intelligence in Information Systems.*, pp. 295–305, Springer, 2015.
- [40] S.-L. Tsao, C.-K. Yu, and Y.-H. Chang, “Profiling energy consumption of I/O functions in embedded applications,” in *Architecture of Computing Systems – ARCS 2013*, H. Kubátová, C. Hochberger, M. Daněk, and B. Sick, Eds., pp. 195–206, Springer, 2013.
- [41] P. Sathyamoorthy, E. C.-H. Ngai, X. Hu, and V. C. Leung, “Profiling energy efficiency and data communications for mobile internet of things,” *Wireless Communications and Mobile Computing*, vol. 2017, Article ID 6562915, 15 pages, 2017.
- [42] R. Bolla, R. Bruschi, F. Davoli, and F. Cucchietti, “Energy efficiency in the future internet: a survey of existing approaches and trends in energy-aware fixed network infrastructures,” *IEEE Communications Surveys & Tutorials*, vol. 13, no. 2, pp. 223–244, 2011.
- [43] M. R. Celenlioglu, D. Gözüpek, and H. A. Mantar, “A survey on the energy efficiency of vertical handover mechanisms,” in *International Conference on Wireless and Mobile Networks (WiMoN)*, Lyon, 2013.
- [44] S. Brienza, S. E. Cebeci, S. S. Masoumzadeh, H. Hlavacs, Ö. Özkasap, and G. Anastasi, “A survey on energy efficiency in P2P systems,” *ACM Computing Surveys*, vol. 48, no. 3, pp. 1–37, 2016.
- [45] M. N. Ismail, R. Ibrahim, and M. F. Fudzee, “A survey on content adaptation systems towards energy consumption awareness,” *Advances in Multimedia*, vol. 2013, Article ID 871516, 8 pages, 2013.
- [46] S. Asnani, M. G. Canu, L. Farinetti, and B. Montrucchio, “On producing energy-efficient and contrast-enhanced images for

- OLED-based mobile devices,” *Pervasive and Mobile Computing*, vol. 75, article 101384, 2021.
- [47] C. V. Vasile, C. Pattinson, and A.-L. Kor, “Mobile phones and energy consumption,” in *Green It Engineering: Social, Business and Industrial Applications*, V. Kharchenko, Y. Kondratenko, and J. Kacprzyk, Eds., pp. 243–271, Springer, 2018.
- [48] J. Flinn, “Extending mobile computer battery life through energy-aware adaptation,” in *Carnegie Mellon University, Computer Science Department, Carnegie Mellon University, Pittsburgh, PA*, 2001.
- [49] O. Landsiedel, K. Wehrle, and S. Gotz, “Accurate prediction of power consumption in sensor networks,” in *The second IEEE workshop on embedded networked sensors, 2005*, pp. 37–44, Sydney, 2005.
- [50] A. Kansal, F. Zhao, J. Liu, N. Kothari, and A. A. Bhattacharya, “Virtual Machine Power Metering and Provisioning,” in *Proceedings of the 1st ACM symposium on Cloud computing SoCC*, vol. 10, pp. 39–50, Indianapolis, Indiana, 2010.
- [51] A. Pathak, Y. C. Hu, and M. Zhang, “Where Is the Energy Spent inside my App?: Fine Grained Energy Accounting on Smartphones with Eprof,” in *Proceedings of the 7th ACM european conference on Computer Systems EuroSys '12*, pp. 29–42, Bern, Switzerland, 2012.
- [52] L.-T. Duan, B. Guo, Y. Shen, Y. Wang, and W.-L. Zhang, “Energy analysis and prediction for applications on smartphones,” *Journal of Systems Architecture*, vol. 59, no. 10, pp. 1375–1382, 2013.
- [53] H.-C. Chang, C.-K. Chung, M.-W. Hung, J.-Y. Lai, and Y.-S. Su, “A power-managed method for mobile devices,” *Recent Patents on Computer Science*, vol. 6, no. 1, pp. 41–46, 2013.
- [54] M. Lee, D.-K. Kim, and J.-W. Lee, “Analysis of characteristics of power consumption for context-aware mobile applications,” *Information*, vol. 5, no. 4, pp. 612–621, 2014.
- [55] T. Rault, A. Bouabdallah, Y. Challal, and F. Marin, “A survey of energy-efficient context recognition systems using wearable sensors for healthcare applications,” *Pervasive and Mobile Computing*, vol. 37, no. 2017, pp. 23–44, 2017.
- [56] A. B. Abkenar, S. W. Loke, W. Rahayu, and A. Zaslavsky, “Energy Considerations for Continuous Group Activity Recognition Using Mobile Devices: The Case of GroupSense,” in *2016 IEEE 30th International Conference on Advanced Information Networking and Applications (AINA)*, pp. 479–486, Crans-Montana, Switzerland, 2016.
- [57] J. F. Bernal, L. Ardito, M. Morisio, and P. Falcarin, “Towards an efficient context-aware system: problems and suggestions to reduce energy consumption in mobile devices,” in *2010 Ninth International Conference on Mobile Business and 2010 Ninth Global Mobility Roundtable (ICMB-GMR)*, Athens, 2010.
- [58] Q. Fang, X. Wei, and H. Dai, “A remaining discharge energy prediction method for lithium-ion battery pack considering SOC and parameter inconsistency,” *Energies*, vol. 12, no. 6, pp. 987–1024, 2019.
- [59] A. González-Pérez, M. Matey-Sanz, C. Granell, and S. Casteleyn, “Using mobile devices as scientific measurement instruments: reliable android task scheduling,” *Pervasive and Mobile Computing*, vol. 81, pp. 101550–101619, 2022.
- [60] R. Hughes, “UPower,” 2007, <https://upower.freedesktop.org/>.
- [61] Pura Vida Apps, “Battery manager extension,” 2010, <https://puravidaapps.com/battery.php>.
- [62] S. K. Datta, C. Bonnet, and N. Nikaein, “Minimizing Energy Expenditure in Smart Devices,” in *2013 IEEE Conference on Information & Communication Technologies*, pp. 712–717, Thuckalay, India, 2013.
- [63] S. K. Datta, C. Bonnet, and N. Nikaein, “Personalized power saving profiles generation analyzing smart device usage patterns,” in *2014 7th IFIP Wireless and Mobile Networking Conference (WMNC)*, pp. 1–8, Vilamoura, Portugal, 2014.
- [64] Mostly-Tech, “Power monitor,” 2015, <https://mostly-tech.com/tag/nexus-6/>.
- [65] A. Mukherjee and T. Chantem, “Energy management of applications with varying resource usage on smartphones,” *IEEE Transactions on Computer-Aided Design of Integrated Circuits and Systems*, vol. 37, no. 11, pp. 2416–2427, 2018.
- [66] K. Naik, *A Survey of Software Based Energy Saving Methodologies for Handheld Wireless Communication Devices*, ASO, 2010.
- [67] R. Schwartz, J. Dodge, N. A. Smith, and O. Etzioni, “Green AI,” *Communications of the ACM*, vol. 63, no. 12, pp. 54–63, 2020.
- [68] U. Mahmud and S. Hussain, “PowerIpsum,” 2022, <https://github.com/umarmahmud5/PowerIpsum>.
- [69] MAPQUEST Developer Network, “MAPQUEST,” 2021, <https://developer.mapquest.com/>.
- [70] Open Weather, “OpenWeather,” 2012, <https://openweathermap.org/>.
- [71] D.-G. Chen and J. D. Chen, *Monte-Carlo Simulation-Based Statistical Modeling*, Springer, 2017.
- [72] N. Chopin and O. Papaspiliopoulos, *An Introduction to Sequential Monte Carlo*, Springer, 2020.
- [73] M. Sabouri and M. Darbandi, “Numerical study of species separation in rarefied gas mixture flow through micronozzles using DSMC,” *Physics of Fluids*, vol. 31, no. 4, article 042004, 2019.
- [74] H. Y. Guo, Y. C. Ding, Q. Chang, C. P. Zhu, Y. Zhao, and Q. Zhang, “The coordinated development between the internal audit guidance by the government audit departments and internal audit units: applying the principal component analysis and Monte-Carlo simulation,” *Journal of Physics: Conference Series*, vol. 1419, no. 1, p. 012040, 2019.

Retraction

Retracted: Design and Implementation of Node of Wireless Network Environment Monitoring System Based on Artificial Intelligence

Wireless Communications and Mobile Computing

Received 11 July 2023; Accepted 11 July 2023; Published 12 July 2023

Copyright © 2023 Wireless Communications and Mobile Computing. This is an open access article distributed under the Creative Commons Attribution License, which permits unrestricted use, distribution, and reproduction in any medium, provided the original work is properly cited.

This article has been retracted by Hindawi following an investigation undertaken by the publisher [1]. This investigation has uncovered evidence of one or more of the following indicators of systematic manipulation of the publication process:

- (1) Discrepancies in scope
- (2) Discrepancies in the description of the research reported
- (3) Discrepancies between the availability of data and the research described
- (4) Inappropriate citations
- (5) Incoherent, meaningless and/or irrelevant content included in the article
- (6) Peer-review manipulation

The presence of these indicators undermines our confidence in the integrity of the article's content and we cannot, therefore, vouch for its reliability. Please note that this notice is intended solely to alert readers that the content of this article is unreliable. We have not investigated whether authors were aware of or involved in the systematic manipulation of the publication process.

Wiley and Hindawi regrets that the usual quality checks did not identify these issues before publication and have since put additional measures in place to safeguard research integrity.

We wish to credit our own Research Integrity and Research Publishing teams and anonymous and named external researchers and research integrity experts for contributing to this investigation.

The corresponding author, as the representative of all authors, has been given the opportunity to register their

agreement or disagreement to this retraction. We have kept a record of any response received.

References

- [1] P. Zou and G. Ji, "Design and Implementation of Node of Wireless Network Environment Monitoring System Based on Artificial Intelligence," *Wireless Communications and Mobile Computing*, vol. 2022, Article ID 5911476, 9 pages, 2022.

Research Article

Design and Implementation of Node of Wireless Network Environment Monitoring System Based on Artificial Intelligence

Pinghui Zou¹ and Gaoqing Ji² 

¹School of Artificial Intelligence, Shenzhen Polytechnic, Shenzhen, 518000 Guangdong, China

²College of Electrical Engineering, Hebei University of Architecture, Zhangjiakou, 075000 Hebei, China

Correspondence should be addressed to Gaoqing Ji; jgq1941@hebiace.edu.cn

Received 4 January 2022; Accepted 16 February 2022; Published 26 April 2022

Academic Editor: Nima Jafari Navimipour

Copyright © 2022 Pinghui Zou and Gaoqing Ji. This is an open access article distributed under the Creative Commons Attribution License, which permits unrestricted use, distribution, and reproduction in any medium, provided the original work is properly cited.

In order to effectively solve the problem of traditional environmental monitoring system due to high sensor cost, difficult deployment, and high maintenance cost, the node design and implementation of a wireless sensor network-based environmental monitoring system are proposed. Simulation experiments show that the time-consuming running time is 14.210361 s. After adding the action force of the grid point on the node, the running time is 11.257740 s, and the operation efficiency of the algorithm is significantly improved. The improved virtual force algorithm optimization improved node coverage by 5.2%. The system is easy to deploy, reduces the development and maintenance cost, and can obtain data or monitor through wireless communication. It is convenient to use and maintain.

1. Introduction

To create a content instrumentation and network monitoring system and to provide users with remote indoor environment monitoring information services, modern science and technology involves various fields, and the interdisciplinary intersection between various fields constructs new technologies. WSN is a perfect combination of sensor technology, embedded system, wireless communication technology, and other fields, which can maximize human vision and help people monitor the changes of external things [1]. WSN has the ability of self-organization and long-distance communication and is widely used in all walks of life [2–5]. The traditional environment detection system has certain limitations. It needs to initialize the sensor network and can only understand the environmental changes through local accuracy. In addition, the monitoring range of wired sensor network is small, there is a monitoring blind area, and the fault-tolerant performance of the network system is also poor [6, 7].

The main categories include RF technology, infrared technology, and Bluetooth technology, which have been common in mobile phones and other devices in the past

decade. These technologies have different characteristics and different costs. The acquisition node in wireless sensor network is one of the most basic elements of the network. It is used to collect, preprocess, store, and transmit the data in the covered area in a multihop manner. Various types of sensors can be installed on the acquisition node, and the soil temperature, soil humidity, noise, light intensity pressure, air humidity, air temperature, and many other material phenomena of interest to us [8, 9]. At the same time, it may have the characteristics of simple, easy to use, reliable work, and low price, and Zigbee advantage lies in the interconnection between equipment in a certain environment and low power consumption; obvious advantages is shown in Figure 1. Wireless sensor network has several remarkable features: first is the high node density, a wide range of distribution. Due to the large number of sensor nodes, the maintenance of the wireless sensor network is more difficult than the traditional wireless network, and the software and hardware of the sensor network must be high robustness and fault tolerance: second is the strong network dynamic. Since the nodes in the network are randomly distributed, the three elements of sensor, perception object, and observer may be

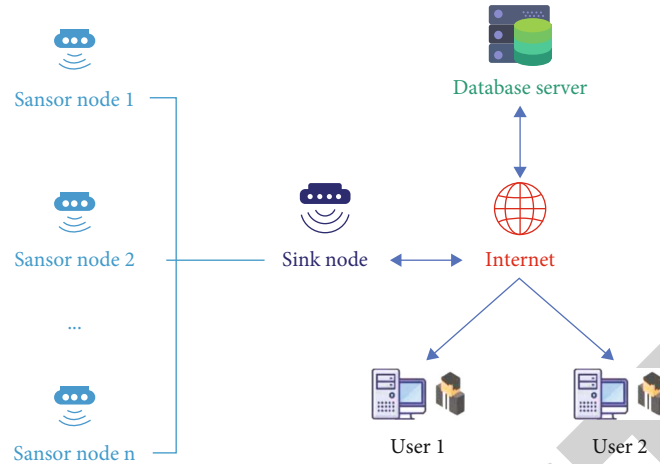


FIGURE 1: Wireless sensor network system architecture.

mobile, and often new nodes join or existing nodes fail, resulting in the sensor network is very dynamic: third is that the node energy is limited. Sensor nodes are mostly distributed in sparsely populated areas and harsh environment, making the energy problem, so sensor nodes are mostly microembedded devices, whose processing capacity, storage capacity, communication bandwidth, and carrying energy are very limited: fourth is low cost. Sensor nodes should be cheap, because a large sensor network often consists of hundreds of sensor nodes, so each node should be low cost, low price: fifth is wireless transmission. Sensor nodes transmit data wirelessly: sixth is node self-organization. Wireless sensor network system is mostly distributed in areas where people cannot or cannot reach, and the deployment of nodes is implemented in a random manner. This requires the communication protocol of the wireless sensor network system to complete the automatic network: the seventh, multihop. A sensor node may not have direct access to the base station, so the data should be transmitted to the base station in a multihop manner. In WSN, the deployment of nodes is usually random. WSN with random layout has some problems, such as low node utilization and small network coverage. Due to the consistency between the virtual force algorithm (VFA) and the network coverage problem, the algorithm is widely used in WSN [10, 11].

Sensor nodes are often a miniature-embedded system that have weak processing, storage, and communication power due to volume, price, and power supply, usually exchanging data only with neighbor nodes within the white body communication range, powered by carrying batteries with limited energy. To access nodes outside the communication range, you must use multihop routes. In order to ensure that the collected data information can be multiple jumped to the converged nodes, the distribution of the nodes should be quite dense. In terms of network function, each sensor node has the dual function of information collection and routing. In addition to local information collection and data processing, they should also store, manage, and integrate the data forwarded by other nodes, while cooperating with other nodes to complete some specific tasks. Convergent nodes usually have strong processing capacity,

storage capacity, and communication capabilities. They can be either a sensor node with enhanced function, sufficient energy supply and memory and computing resources, or a special gateway device without a monitoring function and only a wireless communication interface. The convergence nodes connect the sensor network with the external networks such as the Internet to realize the communication protocol transformation of the two networks, send the detection tasks of the management nodes, and forward the collected data to the external network. Compared to traditional single-sensor devices, the sensor network can change the control objectives and monitoring content to suit the researcher's interests. Users can send instructions to the sinking node via the Internet, and the sinking node is very flexible as it can change the function of the node in the network by providing these instructions to the sensor network. The receiving node is responsible for collecting all the collected data, sending it to the Internet, and storing the collected data in the sensor database. The database provides remote data services and allows users to connect to the Internet and view data.

2. Literature Review

Microsensor technology and the wireless communication capability of node inquiry give broad application prospects for the wireless sensor network. Not having the application fields of wire sensor network include military investigation, environmental monitoring, medical treatment, and building monitoring. With the continuous development and improvement of sensor technology, wireless communication technology, and computer technology, various sensor networks will be spread at all levels of life, especially in areas such as environmental monitoring. Modern environmental control systems usually adopt a line control system. There are two defects in such systems: on the one hand, the wiring control system is highly dependent on the line, and the layout of the system will affect the wiring. On the other hand, in the wired way, the node distribution is fixed; the distribution density is not high; and when some nodes fail, it will lose the local control function. This article collects ambient temperature and humidity

information using a wireless sensor network and transmits this information to the monitoring center in a timely manner. The use of wireless sensor networks compared to traditional monitoring methods has three important advantages: (1) The number of sensor network nodes is high, the distribution density is high, and each node can monitor the details of the local environment. To the information center, therefore, the sensor networks are characterized by high data collection and high accuracy. (2) Because the size of the sensor node is small and the entire network needs to be deployed only once, the deployment of the sensor network has little human impact on the controlled environment. (3) Wireless sensors have the ability to monitor, self-calculate, and store in more complex ways. The sensor may not be desired to connect to physical changes, monitoring, or control. The order is being executed. This topic aims to help protect forests and disrupt traditional methods of environmental monitoring. Environmental monitoring aims to take advantage of a stationary sensor network to provide environmental monitoring information [12]. Mohapatra, H. and others used different filtering methods for different scenes. The data processing of temperature, humidity, and light intensity sensors adopts the amplitude limiting average filtering method, and the data processing of particle concentration sensors with large sampling variation adopts the first-order lag average filtering method [13]. Li, P. and others proposed correlation based data coding mode, distributed algorithm for determining node location in wireless sensor networks and method for reconstructing sensor node location, and developed an operating system based on wireless sensor networks [14]. Li, J. and others developed a wireless sensor network simulation system to study the problems in wireless sensor networks [15]. Y Jia. and others studied methods and technologies for ultralow power wireless sensor networks. According to the particularity of wireless sensor network communication protocols, new routing protocols based on negotiation protocols, directional release protocols, energy sensitive protocols, multipath protocols, and propagation routing protocols are proposed [16]. Watt, A. J. and others believe that wireless sensor network system can also play a great role in traffic. Through various sensors on the node, vehicle speed and traffic flow can be monitored, providing strong support for traffic management departments to better manage urban traffic [17]. Rahman, G. and others conducted data fusion processing on the collected data, and the reliability has been enhanced, but the fusion algorithm is complex, and the real-time performance is not strong [18]. Sharma, H. and others improved wireless sensor network routing protocol algorithm and reduced node power consumption [19]. Li, K. and others established a wireless sensor network test group, specializing in the research on the hardware implementation of wireless sensor networks [20]. Ranjan, A. and others believe that the wireless sensor network system can also be used for forest environmental monitoring and fire alarm. The nodes are randomly densely distributed in the forest and regularly report environmental data under normal conditions. In case of fire, the nodes will transmit the specific address of the fire source, fire size, and other information to relevant departments in a very short time through cooperation [21, 22].

Based on this research, we propose a node design and implementation of an environmental monitoring system for a wireless sensor network based on artificial intelligence. The WSN environmental monitoring system based on ZigBee can be well applied in various environmental monitoring fields such as clean plant and is an effective solution. The traditional environment detection system has certain limitations. It needs to initialize the sensor network and can only understand the environmental changes through local accuracy.

3. Research Methods

3.1. Sensor Node Design. First, wireless sensor node is the way and means to realize the connection of things. Internet of Things is the extension of wireless sensor node to the connection of things in the real world, which is an important basis and component of the realization of this technology. Second, data exchange and transmission are carried out between any objects with the function of signal exchange. The range of network and goods involved is extensive. The Internet of Things is not only a network but also a product of the in-depth development of wireless sensor nodes. It is a brand new innovation in the application of wireless sensor nodes. All kinds of terminals create brand new forms of use and bring more industrial revolution with better operation experience to users.

3.1.1. Design Principles of Sensor Nodes. The device driver is the interface between the operating system kernel and the machine hardware. It protects the software hardware details. In general, Linux device drivers must perform the following functions: start and remove the device, and transfer data from the kernel. Read data from hardware and hardware; read the data sent by the application to the device file; and return the requested data to the application; check. Measure and resolve errors during equipment operation. Networking is a necessary module for many embedded systems, and Ethernet is a high-speed, open, wide-ranging communication interface that plays an important role in the development, debugging, and use of installed systems. An important role is that in order to enable the designed wireless sensor node to form a wireless sensor network with long service life, stability, reliability and superior performance, the node design must consider the following aspects:

- (1) Miniaturization. Miniaturization is the ultimate goal of sensor networks. Only when the size of the node itself is small enough can it ensure that it will not affect the target system environment or the impact can be ignored. In addition, in some special occasions, it is even required that the target system can be small enough to be imperceptible
- (2) Low-power consumption. Due to the particularity of wireless sensor network application environment, it is difficult to replace the power supply, and the requirements for node power consumption are very strict. During normal operation, the power consumption of wireless transceiver is the main part of

node power consumption, so advanced algorithms and protocols must be adopted as far as possible to shorten the duration of wireless transceiver working state

- (3) High stability. In order to meet the requirements of service life in applications, each node must have high stability. The method of modular system design can reduce the mutual interference of circuits and improve the stability of nodes. To coexist with other wireless systems, wireless sensor network nodes must also be able to adapt to external interference. The method to improve the anti-interference performance of nodes is to use multichannel wireless transceiver. This wireless transceiver can make the system work in multiple frequency bands to avoid mutual interference of multiple wireless systems due to sharing a certain frequency [23, 24].
- (4) Rapid development of market economy and the development strategy of "Internet +" also for the new period of production start-up provide a good platform and make the informatization, digitalization, and intelligence, and the network is gradually applied to all walks of life of entrepreneurship development; for all kinds of production environment to implement intelligent real-time monitoring, low cost, and easy operation, business can effectively improve production quality and efficiency. With open market space, this is the subject to adapt to market demand, according to the development of the starting point

3.1.2. Design Concept of Wireless Sensor Node. The chip integrates a radio frequency transmitter and controller to provide high-performance, complex functions.

This kind of communication control is only applicable to power systems, as long as there are wires, data can be transmitted, so this kind of transmission technology is already widely used. The pin description is shown in Table 1.

3.1.3. Calculation of Humidity. The sensor developed from the energy gap material PTAT (proportional to absolute temperature) has excellent linearity, which can be used as follows:

Convert the digital output to the temperature value, as shown in

$$T = d_1 + d_2 \times SO_T, \quad (1)$$

where d_1 and d_2 are specific coefficients, the value of d_1 is related to the working voltage of SHT10, and the value of d_2 is related to the resolution adopted by the internal A/D converter of SHT10.

Since the digital output characteristic of relative humidity is nonlinear, in order to compensate the nonlinearity of humidity sensor, the humidity value can be corrected according to the following formula, as shown in

$$AW_{\text{linear}} = T_1 + T_2 \times CO_{AW} + T_3 \times CO_{AW}^2, \quad (2)$$

TABLE 1: Pin description.

Pin	Name	Notes
1	GND	Land
2	DATA	Serial data, bidirectional
3	SKC	Serial clock, input
4	VDD	Power supply 2.2~5.5 V
5~8	NC	The remaining pins are not connected

where AW_{linear} is the humidity value after linear compensation, AW_{true} is the measured value of humidity, and T_1, T_2, T_3 are the linear compensation coefficients.

The compensation formula is as follows:

$$AW_{\text{true}} = (D - 25) \times (d_1 + d_2 \times CO_{RH}) + AW_{\text{linear}}, \quad (3)$$

where AW_{true} is the humidity value after linear compensation and temperature compensation, D is temperature, and d_1 and d_2 are the compensation coefficients.

3.2. Overall System Scheme Design. In the indoor environment combined with simple equipment to achieve the required environmental quality data collection function. Figure 2 shows the overall block diagram of the system.

The improved VFA is used to optimize the node layout and obtain high network coverage, which provides a reference for the placement position of practical engineering application nodes. The gateway module transmits the data to the external network and gives an early warning of the equipment operation.

3.3. System Hardware Design

3.3.1. Sensor Module. According to the design specifications of the clean workshop, the selected sensor model and its parameters are shown in Table 2, taking volume and cost into consideration.

Figure 3 shows a design flow chart of the hardware structure of the sensor module.

The sensor of digital output is directly connected with STM32 microprocessor, and the sensor of analog output is connected with STM32 microprocessor.

3.3.2. Zigbee Networking Module. Figure 4 shows the design diagram of the hardware structure of the ZigBee network module.

ZigBee networking module consists of CC2530 processor, antenna unit, and power module. Coordinator nodes are connected to gateway modules through serial ports.

3.3.3. Hardware Design of Gateway Module. Figure 5 shows the hardware design structure of the gateway module.

The gateway module includes STM32 microprocessor, serial port, and esp8266 serial port to WiFi module. The module is connected to the coordinator node through serial port.

3.4. Wireless Sensor Network Environmental Monitoring. The ARM processor as the core of coordinated processing and the measured data are recorded and the managed by

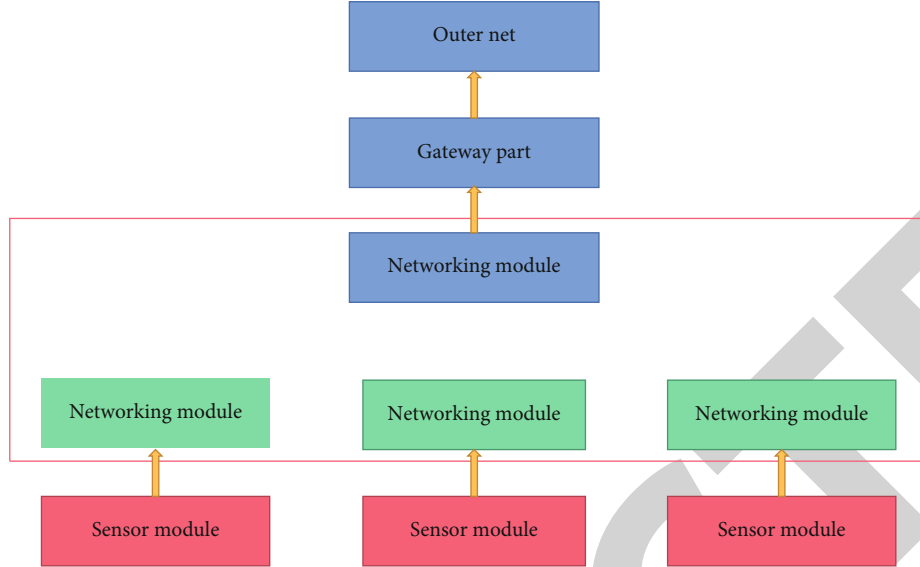


FIGURE 2: Overall system block diagram.

TABLE 2: Model and parameters of sensor.

Sensor	Model	Measuring range
Temperature and humidity	DHT10	0~40°C; 10%~85%~
Pressure	BMP160	300~1000 hPa
PM2.5	DSL-02	0~999.9 $\mu\text{g}/\text{g}^3$

database technology. Figure 6 shows the flow chart of the environmental monitoring.

3.4.1. Sensor Module. Figure 7 shows the flow chart of the design of the sensor module software.

Firstly, the temperature, humidity, dust concentration, and air pressure in the environment are collected and cached in a queue. To effectively remove the interference of various factors on the collected data, the data were processed by a combination of median filtering and sliding mean filtering algorithm. The filtering algorithm flow is shown in Figure 8.

3.5. ZigBee Networking Module. Its application in life is very common; there are a lot of assemblies in display equipment, light sensing equipment, and food image acquisition equipment.

3.6. Sensor Network Node Layout Optimization Algorithm

3.6.1. Traditional VFA. Due to the consistency between VFA and node coverage technology, VFA is used to optimize the node layout. The specific virtual force modeling is as follows: set any two nodes s_i and s_j , and the force of node s_i by node s_j meets the following force relationship, as shown in

$$F_{ij} = \begin{cases} k_1/d_{ij}^{\alpha_1}, & 0 < d_{ij} < r_s; \\ 0, & d_{ij} = r_s \text{ or } d_{ij} > d_{th}; \\ k_2/d_{ij}^{\alpha_2}, & \text{otherwise,} \end{cases} \quad (4)$$

where k_1 and k_2 are gain coefficients; d_{ij} is the distance between nodes s_i and s_j ; d_{th} is the distance threshold between nodes; and r_s is the best distance between nodes.

Each sensor node will update the node position according to the total resultant force. The update formula is shown in

$$x_{\text{new}} = \begin{cases} x_{\text{old}}, & F_{xy} = 0; \\ x_{\text{old}} + \frac{F_x}{F_{xy}} \times d_m \times e^{\frac{-1}{F_{xy}}}, & F_{xy} \neq 0, \end{cases} \quad (5)$$

$$y_{\text{new}} = \begin{cases} y_{\text{old}}, & F_{xy} = 0; \\ y_{\text{old}} + \frac{F_y}{F_{xy}} \times d_m \times e^{\frac{-1}{F_{xy}}}, & F_{xy} \neq 0, \end{cases} \quad (6)$$

where d_m is the maximum moving distance of the sensor node; F_{xy} is the resultant force of the virtual force acting on the node; and F_x and F_y are the x -axis and y -axis components of F_{xy} .

3.6.2. Improvement of VFA. Traditional VFA only considers the force between nodes. In order to reduce the time loss of nodes in the process of location update, the force of grid points on nodes is added, and its definition is shown in

$$F_{\text{grid}} = \begin{cases} \omega d_{ig}, & r < d_{ig} < R; \\ 0, & \text{other} \end{cases}, \quad (7)$$

where ω is the gain coefficient; r is the perceived radius; R is the communication radius; and d_{ig} is the distance between the node and the grid point.

In the actual environmental monitoring process, nodes will gather on the boundary, as shown in Figure 9.

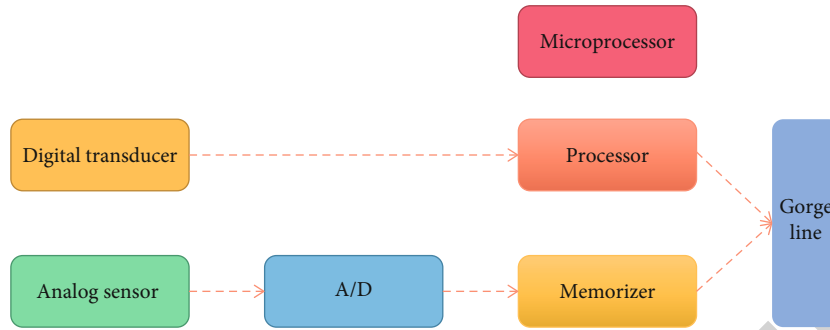


FIGURE 3: Hardware structure design of sensor module.

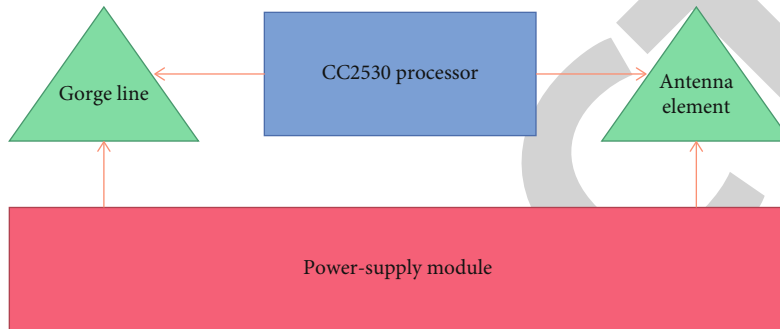


FIGURE 4: Hardware structure design diagram of ZigBee networking module.

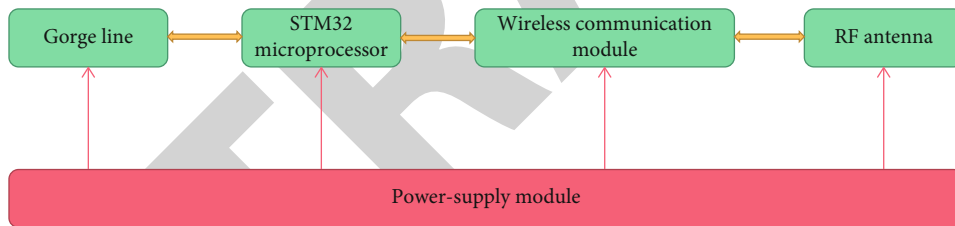


FIGURE 5: Hardware structure design of gateway module.

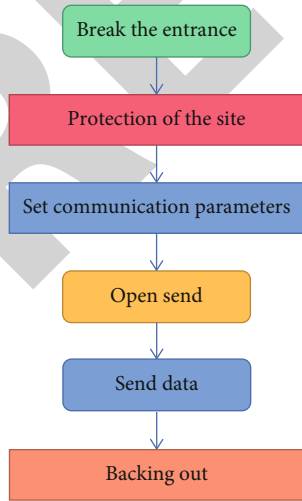


FIGURE 6: Environmental monitoring flow chart.

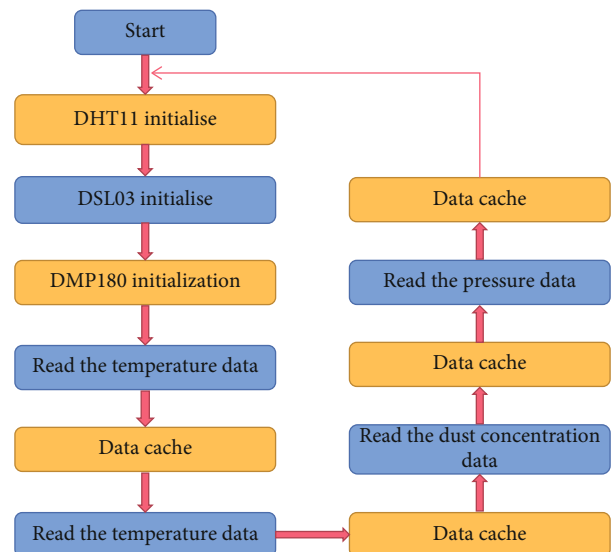


FIGURE 7: Data acquisition software design.

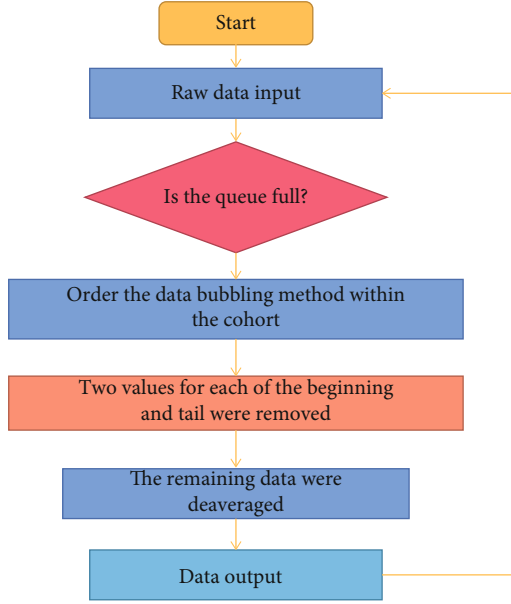


FIGURE 8: Software design of digital filtering algorithm.

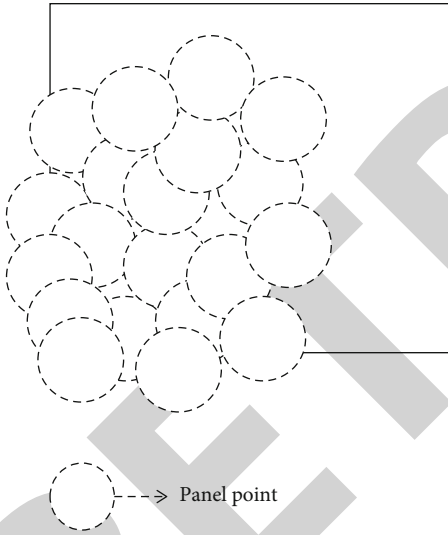


FIGURE 9: Case of a large number of boundary nodes.

In this case, if the nodes move according to the above rules, some nodes will be excluded from the boundary, resulting in the weakening of node coverage of wireless sensor networks.

Let the boundary of the region of interest also have a constraint F_b on the node, so that the node will not be “excluded” outside the region. The expression of the force is shown in

$$F_b = \begin{cases} \frac{\phi d_i}{d_i^3}, & d_i \geq d_{bth} \\ +\infty, & d_i < d_{bth} \end{cases} \quad (8)$$

TABLE 3: Android APP data receiving information.

Ambient temperature	25
Ambient humidity	47
PM2.5	40
Pressure	988
Air conditioning box	Normal operation
Filter screen	Normal operation
Fan coil unit	Fault

where d_i is the distance from the sensor node i to the boundary; ϕ is the gain coefficient; and d_{bth} is the boundary distance threshold.

3.7. Gateway Module Software Design. The WiFi module loads the smart cloud firmware, establishes corresponding data points on the smart cloud platform, and realizes the data interaction between the gateway module, smart cloud server, and applications. Firstly, the gateway module receives the data from the coordinator node through the serial port, then gives an early warning on the operation of the clean equipment, and finally sends the data to the WiFi module through the serial port to the external network.

4. Result Discussion

4.1. System Practicability Test. Conduct a complete test on the data sending and receiving in the environmental monitoring system, and the data receiving information is shown in Table 3. The system can normally display the monitored environmental parameter information, and can make a judgment on the operation status of various components in the fresh air and air conditioning system, which greatly saves the consumption time of manual investigation, troubleshooting in a very short time, and making the normal operation of the equipment.

4.2. Effectiveness Test of Filtering Algorithm. The data detection module is related to the final embodiment of the data collected by each sensor, storing the core data of the environmental quality monitoring system as shown in Figure 10.

The simulation test is carried out on matlabr2013b, and the relevant parameters are set as follows: the monitoring area of wireless sensor network is $800\text{ m} \times 700\text{ m}$; the grid size is set to $2\text{ m} \times 2\text{ m}$; the number of sensor nodes is $n = 36$; under the action of grid points, the sensing radius is $r = 90\text{ m}$; the maximum step is $d_{th} = 2.5\text{ m}$; and under the action of sensor nodes, the maximum step is $d_m = 3.5\text{ m}$. When there is no grid point force, the operation takes 14.210361 s . After adding the force of grid points on nodes, the running time is 11.257740 s , and the operation efficiency of the algorithm is significantly improved. The improved virtual force algorithm improves the node coverage by 5.2%. As can be seen from Figure 10, compared with the initial random distribution of nodes, the nodes are evenly distributed by using this filtering algorithm, and the task of overall regional monitoring is well completed.

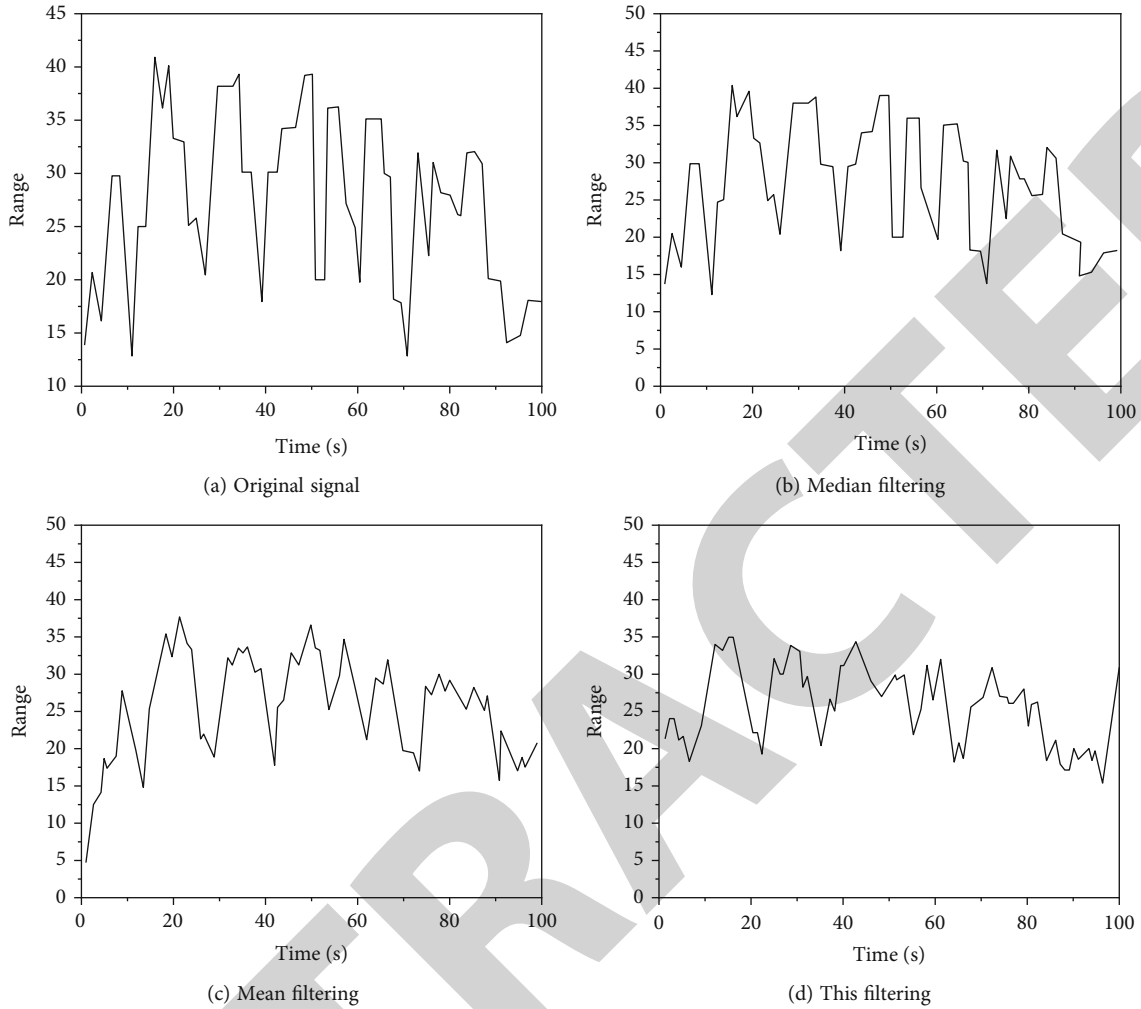


FIGURE 10: Filtering effect.

5. Conclusion

Through the research and the analysis of wireless sensor network, the system designed the sensor module, ZigBee networking module, gateway module, and Android APP monitoring interface and studied the accuracy of the system data collection and the coverage rate of the wireless sensor network. The environmental data collected by the sensor module was filtered, the improved virtual force algorithm was used to optimize the network module layout, and finally the system was tested. The experimental results show that the system has good communication and the signal is stable and can be widely used in various environmental monitoring fields. Wireless sensor network technology has a very broad application prospect, which will profoundly change people's lives. With the further research of wireless sensor network technology, it can be predicted that the products based on wireless sensor network technology will enter more and more into people's lives in the near future.

Data Availability

No data were used to support this study.

Conflicts of Interest

There are no potential competing interests in our paper.

Authors' Contributions

All authors have seen the manuscript and approved to submit to your journal.

Acknowledgments

This study was supported by the Science and Technology Planning Project of Guangdong Province (KTP20210180); the Basic Scientific Research Project in Hebei Province (No. 2021QNJS13, No. 2021QNJS06); and the Project of Zhangjiakou Science and Technology Bureau (No. 1911002B).

References

- [1] T. Yang, W. Yin, W. Zhang, Y. Zhao, C. Ktistis, and A. J. Peyton, "A very-low-frequency electromagnetic inductive sensor system for workpiece recognition using the magnetic polarizability tensor," *IEEE Sensors Journal*, vol. 17, no. 9, pp. 2703–2712, 2019.

Research Article

Brand LOGO Image Recognition and Inquiry Creative Teaching Design Based on Deep Learning

Xin Gao  and Wenjing Chen

Information Engineering Institute, Yellow River Conservancy Technical Institute, Kaifeng, 475000 Henan, China

Correspondence should be addressed to Xin Gao; gaoxin@yrcti.edu.cn

Received 30 January 2022; Accepted 1 March 2022; Published 8 April 2022

Academic Editor: Mu-Yen Chen

Copyright © 2022 Xin Gao and Wenjing Chen. This is an open access article distributed under the Creative Commons Attribution License, which permits unrestricted use, distribution, and reproduction in any medium, provided the original work is properly cited.

In order to develop more reasonable and scientific teaching equipment and software and improve the diversity of teaching process, LOGO image recognition technology is used to build a development environment in experiment, with Unity 3D as the development platform and Vuforia AR SDK as the development tool. LOGO image recognition technology is applied to the case study of high school inquiry teaching. By the way of classroom teaching practice and teacher-student interview, the application effect of LOGO image recognition technology in teaching is evaluated, and the effectiveness of this technology in inquiry teaching practice is verified by practical data. The results show that compared with YOLO (You Only Look Once), R-CNN (Region-CNN), and Faster R-CNN, image recognition algorithms based on deep learning theory, LOGO image recognition ability is stronger and the result is more accurate. Using this teaching mode can significantly improve students' academic performance, and this method is correct, reasonable, and scientific. The application of LOGO image recognition technology based on deep learning in teaching can provide research ideas for the combination of AI and education.

1. Introduction

With the continuous progress of society in recent years, more and more image recognition techniques have been developed, and the most common is to match different algorithms according to the principle of feature extraction (SIFT features, HOG features, and LBP features). According to the gradient of each pixel in each region or the characteristics of the edge histogram, image recognition can be realized [1–3]. Secondly, using the neural network method and the VGGNet network structure and selecting smaller network convolution kernel can significantly improve the expression ability of the network [4]. Microsoft proposed the ResNet algorithm, and the residual learning structure can be used to solve the problem of shallow network gradient dispersion in deep network neural network, so that deep learning can be more widely used in image recognition [5]. The LOGO image recognition technology study has also been reported in many articles; among them, Tang and Peng proposed that better matching results could be achieved by using unique topological constraint algorithms and feature selection

methods [6]; Yuxin and Peifeng used convolutional neural network (CNN) to design a highway entrance vehicle sign recognition system for real-time detection and classification of vehicle signs [7]; Shou-xian and Fang used LOGO system that could better identify the logo in life, in the premise of certain accuracy, and could guarantee real-time performance [8]; and the proposed CNN method based on transfer learning can effectively identify vehicle information [9]. The application of this image recognition technology is mostly used in intelligent transportation system, but not in teaching research.

In the field of education, the teaching of knowledge is mostly the principle of direct teaching, and the students are indoctrinated by language [10, 11]. In the foreign teaching model, the inquiry learning method is often used, that is, to produce association from real life, to use it in teaching, and to improve students' ability and interest in autonomous learning by creating situations [12–14]. The inquiry teaching method study has also been reported in many articles; among them, Aktamiş et al. found that compared with traditional teaching methods, inquiry learning methods could

significantly improve students' academic performance in science education [15]; Andriani found that inquiry teaching methods not only cultivated students' learning intelligence and ability but also improved students' potential emotions and skills [16]; and Zhai found that educational philosophy and teaching model-based inquiry had obvious advantages in college English teaching and could significantly improve students' comprehensive ability and professional quality [17]. The current teaching methods have changed from the original indoctrination to diversified learning methods [18]. It is a hot topic in modern teaching to apply new technology in teaching to improve students' cognitive ability.

Data on LOGO image recognition technology is collected through literature research, and the feasibility of LOGO image recognition technology in teaching is analyzed. The advantages of this technology are studied by combing the requirements, development process, module training, etc. of this technology in teaching application and by comparing it with other algorithms. The purpose is to apply the LOGO image recognition technology supported by machine learning (ML) to the teaching and to conduct a field investigation on the application effect, which will provide theoretical support and practical basis for the further integration of image recognition technology and educational measures.

2. Methods

2.1. Design of LOGO Image Recognition Teaching Mode Based on Deep Learning

- (1) Demand analysis: the traditional shallow learning (focusing on the interpretation of knowledge points, theoretical derivation, students often through imitation to complete the more independent, and discrete action skills) had not satisfied the requirements of the times, so in the teaching design, learners' deep learning ability of "adaption, innovation" should be focused on the cultivation
- (2) Flow chart: as shown in Figure 1, the flow chart of teaching pattern LOGO image recognition based on deep learning was divided into three parts. The first part was that students could take picture and upload pictures of interest; the second part was the training of brand LOGO recognition, which was carried out in the way of network computing and divided into three levels: the shared network algorithm module, the long short-term memory neural network module, and the biasing algorithm module; and the third part was the output of the results; both the teacher and student could get the final results of the data from the client
- (3) Module training: the basic of deep learning was the continuous training of each module, and training in experiment was also through improved algorithms. Firstly, the network information was shared through the module of information sharing. The image data was compressed into $256 * 256 * 3$ tensor and then input to the student client, and the recogni-

tion result was obtained according to the network curve. Next, through LSTM processing images, protobuf was used to serialize the acquired ckpt file, so as to realize the fine classification of images. Finally, in order to improve the recognition ability of the network model to the target image, the bias algorithm was introduced

2.2. Framework of Long Short-Term Memory Neural Networks. Long short-term memory (LSTM) was a kind of neural network based on deep learning [19], because the design architecture of this network was very suitable for processing and predicting important events of time series interval and delay. LSTM image processing efficiency was better than ordinary models such as the hidden Markov model [20, 21], which was similar to the RNN structure. The main frame structure is shown in Figure 2.

LSTM could be divided into two parts: inside and outside. The internal contained input gate (under f -cell), forgetting gate (g/h) and output gate (above f -cell). These gates represented specific vectors, each vector element ranged from 0 to 1, approaching 0 indicated that this gate was closed and approaching 1 indicated that this gate was open. The input door determined the information content that needed to be entered at a certain time, and the specific equation was calculated as follows:

$$f_i = \delta(W_f \cdot [h_{t-1}, x_t] + b_f). \quad (1)$$

The forgetting door determined the information content of that needed to be forgotten at a certain time, and the specific equation was calculated as follows:

$$i_t = \delta(W_i \cdot [h_{t-1}, x_t] + b_i). \quad (2)$$

The output door determined the information content that needed to be output at a certain time, and the specific equation was calculated as follows:

$$o_t = \delta(W_o \cdot [h_{t-1}, x_t] + b_o), \quad (3)$$

where f_i , i_t , and o_t represented the vector values' size of different doors at different moments, respectively; h_{t-1} , x_t represented the input vector values' size at time t and the output state at time $t-1$; W_f , W_i , and W_o represented the parameters of different doors, respectively; and b_f , b_i , and b_o represented the bias parameters of different doors, respectively. On the basis of the above expression, the cell state of each time node could be calculated, and the C_i and the state of the hidden layer h_i equations were as follows:

$$\widetilde{C}_t = \tanh(W_c \cdot [h_{t-1}, x_t] + b_i), \quad (4)$$

$$C_t = f_t * C_{t-1} + i_t * \widetilde{C}_t, \quad (5)$$

$$h_t = o_t * \tanh(C_t), \quad (6)$$

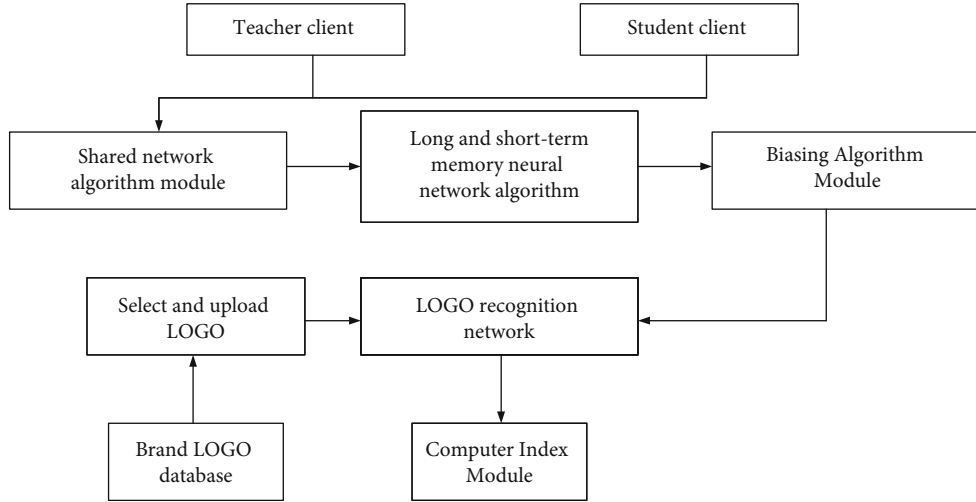


FIGURE 1: Teaching mode flow chart of LOGO image recognition based on deep learning.

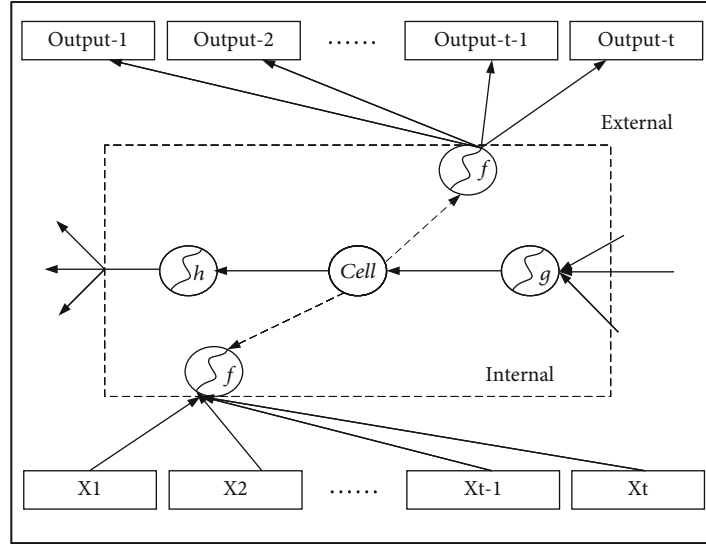


FIGURE 2: Diagrammatic sketch of LSTM model frame structure.

where \widetilde{C}_t represented the variable of the cell state at time t in the LSTM model, C_t represented the cell state at time t , and h_t represented the state of the hidden layer at time t .

The dataset used by LSTM is the MNIST dataset. The MNIST dataset includes images of handwritten digits and corresponding labels, including training data, test data, and validation data. During the network training process, at the beginning, some necessary dependencies and datasets are imported first, and some constants are declared. Next, batch-size = 128 and num-units = 128, placeholders, weights, and bias variables are set, and the network is defined to generate predictions. Then, after defining the loss function, optimizer, and accuracy, run the network.

2.3. Shared Network Algorithm Module and Biasing Algorithm Module. The shared network algorithm module was adopted in this experiment, with specific reference to

Jiang et al.'s method [22]. The ResNet-t and ResNet-s of teacher network and student network both used residual shared network algorithm module to improve the depth of neural network. After introducing the residual module into the deep neural network, the gradient generated by the loss function would not be rapidly dispersed during the back propagation process, so the shallow part of the deep neural network could also adjust the parameters of this layer through the generated loss, and then the shallow part could be well trained. With the increase of network depth, the recognition ability of neural network would be stronger and stronger.

The biasing algorithm module was adopted in this experiment, specifically referring to Fu et al.'s method [23]. The biased CNN was introduced to improve the recognition accuracy of target LOGO, and it was applied to the teacher and student network. Furthermore, it could make the recognition accuracy of the student network close to the level of

TABLE 1: Teaching resource development system of brand LOGO image recognition technology based on deep learning theory.

Resource type	Model	
Development PC	Model	ASUS X555YI
	Operating system	Windows 10 Home Chinese Edition
	Processor	AMD E2-7110 APU with AMD Radeon R2 Graphics
	RAM	6G
	System type	64-bit operating system
	Type	USB interface camera
Camera	Pixel	1.69 million
	Output resolution	150 * 150
	Tool name	Unity 3D
Development engine	Version	2017.2.0f3
	Script editor	Visual Studio 2017
	Compiled language	C/C#
	AR SDK	Vuforia
Test terminal	Surroundings	Android 5.0

the teacher's network on the bias class and make up for the disadvantage of reducing the recognition accuracy caused by the network compression on some target classes.

2.4. Laboratory Development Environment Setting. The development environment of this time is shown in Table 1. The implementation frame was Unity platform, and the AR SDK and Vuforia AR SDK in Unity 3D 2017.2.0f3 were used.

2.5. Comparative Study of Image Recognition Technology. For the purpose of displaying the difference between the LOGO image recognition technology based on deep learning and the network teaching mode built by other algorithms, the commonly used network image recognition algorithms were specially selected, which included Darknet network extraction YOLO (You Only Look Once) algorithm based on noncandidate frame [24], R-CNN (Region-CNN) algorithm based on CaffeNet [25] using Selective Search to obtain target candidate frame, Faster R-CNN algorithm based on VGG16 network [26], and ContextNet algorithm based on LSTM model, and they were named Q1, Q2, Q3, and Q4, respectively.

- (1) YOLO algorithm: it was a CNN operation, which included end-to-end prediction framework, and whose running speed was greatly improved by adding real-time module. The basic goal was to transform the detection problem into an image classification problem. The basic principle was to use windows of different sizes and proportions (aspect ratio) to slide on the whole picture in a certain step size and then classify the image corresponding to the areas of these windows, so that the entire picture could be detected
- (2) R-CNN algorithm: it was an image recognition algorithm that extracted the feature frame according to the image and used the neural network system to realize its operation. It first selected fixed regions on each image by searching and then constructed

training and test samples based on these fixed regions. Nonmaximum suppression (NMS) was used for this score output during the test, which meant the process of removing the duplicate box. At the same time, a regression for each category was trained to achieve high-precision image recognition. However, there were many processes of R-CNN, including region selection, training of CNN, and training of support vector machines (SVM), which made the training time very long and took up a large proportion of space

- (3) Faster R-CNN algorithm: it was to add Faster algorithm to the original CNN network, Faster R-CNN-integrated feature extraction, feature frame extraction, bounding box regression, and image classification into a network, which greatly improved the overall performance, especially in detection speed
- (4) ContextNet algorithm: it was a target context detection network based on LSTM model. ResNet was used as the image feature extraction network, and the improved multiscale target candidate region extraction network was used to extract the target candidate frame. Furthermore, the LSTM model and target context information were used to classify the candidate frame. By using the context information of different scales as the input of the LSTM model, and using the output of the last layer of LSTM as the result of the classification of the entire candidate frame, the context information of multiple different scales was effectively combined to classify the candidate frame

Different pictures were adopted from two different datasets, among which the LOGO dataset contained more than 50 logos, each logo contained 2,000 pictures of different scenes. The other dataset was Pascal VOC, which was the

international authoritative dataset in the field of computer vision. In total, it contained 15,000 different pictures, including multiple pictures with different semantic features. They were named A1 and A2, respectively. Datasets related to education were mainly studied in experiment, such as pictures of chemical equations, pictures of biological experiments, and pictures of physical space. The purpose was to investigate the appropriate image recognition algorithm, which could be applied to practical teaching activities, and improve the efficiency of teaching and students' enthusiasm.

2.6. Algorithm Performance Evaluation Indexes. Generally, the evaluation of the performance of a target detection algorithm was mainly measured in terms of time complexity and detection accuracy [27]. Time complexity was evaluated by the detecting frequency in target detection, which was the number of images that the algorithm could detect per second. As to the accuracy, precision, recall, and mean average precision (mAP) were referred to. These indexes were important reference indicators widely used in the field of algorithm recognition to measure the recognition performance. Currently, it was widely used in the performance evaluation of various target detection algorithms. Precision referred to the proportion of the correct number of detected targets among all detected targets. Recall referred to the ratio of the number of retrieved related targets and the number of all related documents in the image database. The mAP represented the average value of average precision (AP) values for each category. The PR curve of each category was drawn by changing the detected intersection over union (IoU) threshold. According to the PR curve, the AP value of each category could be calculated, and then, the mAP value of the secondary target detection algorithm was obtained through calculating the average value of the AP values of all categories. The AP value was the area enclosed by the PR curve and the x and y axes. In target detection, the calculation equations of precision and recall were the same as the original calculation, but the statistical positive examples were determined by calculating the IoU of the detection frame and the standard frame. If the IoU was greater than a certain threshold, the detection frame was considered as a positive sample; otherwise, the candidate frame was considered as a negative sample.

2.7. Teaching Effect Evaluation of LOGO Image Recognition Based on Deep Learning. The method of evaluating the effect of developed system was based on the method of field investigation, and 8 classes of high school in a certain city were randomly selected as 240 students in different schools and different regions. Four science and technology classes (K1, K2, K3, and K4) and four regular classes (C1, C2, C3, and C4) were designed. The number of students in each class was 30. The difference between students was not very big and there was no significant difference. On the premise of not informing the students of the content, the two classes were taught independently, and the same teacher taught the students. Besides the different teaching resources, other

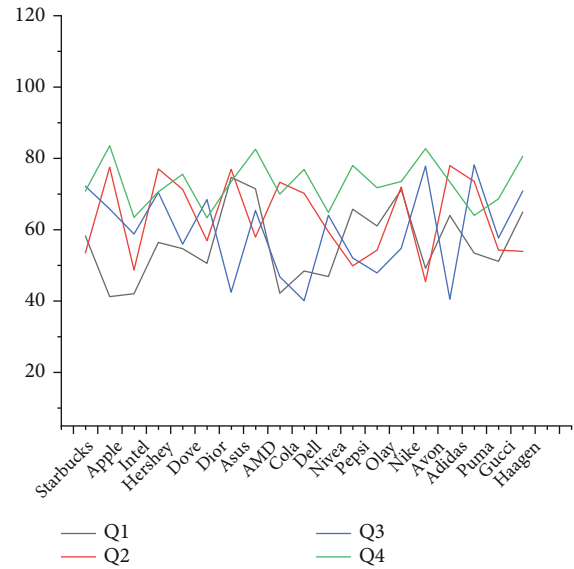


FIGURE 3: Comparison of accuracy performance of different image recognition algorithms.

external factors such as learning environment and teaching time were required to be the same, which effectively controlled the variables. For the students in the science and technology class, the LOGO image recognition technology based on deep learning was used in the teaching, while for the students in the regular class, the common teaching method was adopted. Excel 2019 software was used for data statistics, SPSS 20.0 was used for data significance analysis (multifactor analysis of variance was used), and Origin 9.1 and Visio 2013 software were used for drawing.

3. Results and Discussion

3.1. Performance Comparison of Different Image Recognition Algorithms. The results of the experimental example of the image recognition through the system are shown in Figure 3, and it could be clearly observed that the used ContextNet algorithm was superior to the YOLO algorithm, R-CNN algorithm, and Faster R-CNN algorithm in LOGO image detection. Especially in the case of small LOGO detection, for example, when detecting DELL and GUCCI, two relatively small logos, ContextNet algorithm detected the targets successfully, while the other three algorithms did not detect the targets. At the same time, in terms of the accuracy of the frame detection, the ContextNet algorithm was better than the other three algorithms. For the detection of Starbucks and Apple targets, the target frame obtained by the ContextNet algorithm was more accurate than the other three algorithms.

The performance comparison of recall rates for different image recognition algorithms could be seen in Figure 4; the YOLO network extraction algorithm had no deep learning or other special network structures, so compared with Faster R-CNN, R-CNN, and ContextNet algorithms, its recall rate was the worst, with an average recall rate of 35.56%. Since

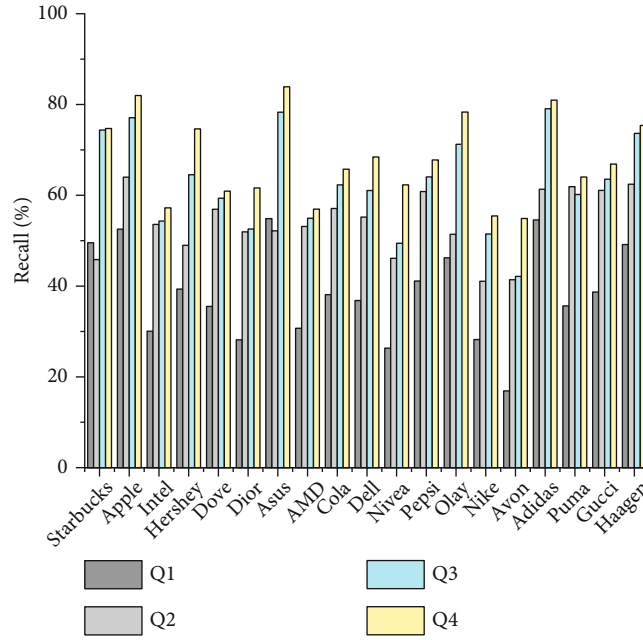


FIGURE 4: Comparison of recall performance of different image recognition algorithms.

the RNN network and Faster R-CNN network had the neural network learning process, the accuracy of the two algorithms was greatly improved, and their average recall rates were 54.03% and 62.82%. Moreover, due to the target context detection network with LSTM model, the Context-Net algorithm was able to extract image feature frame well, with an average recall rate of 68.01%. Based on the above results, the brand LOGO image recognition algorithm based on the proposed deep learning had better recall performance.

The results of the comparison and analysis of the average detection accuracy of different image recognition technologies could be seen from Table 1 and Figure 5. The part-based target detection framework performed very well in the LOGO image dataset. However, although the detection speed of the YOLO algorithm was fast, the noncandidate frame-based Darknet algorithm performed poorly in detecting small targets. The detecting performance of R-CNN was a bit worse than Faster R-CNN, but the operation time and test time consumed by the R-CNN algorithm was much higher than all other methods, which was not practical for algorithms with relatively high requirements. In addition, the R-CNN algorithm used the traditional Selective Search method when obtaining candidate frames. The detecting quality of the R-CNN algorithm was also much worse than the Faster R-CNN algorithm. The main reason was that the R-CNN algorithm used the Selective Search method to extract candidate frames for the target. The Faster R-CNN algorithm used the candidate region extraction network to extract the candidate frame for the target. Selective Search was much less effective than the candidate frame extraction network in acquiring the LOGO image target candidate frame. However, the ContextNet algorithm not only surpassed the other three methods in detection quality but also greatly improved detecting efficiency. Therefore, the

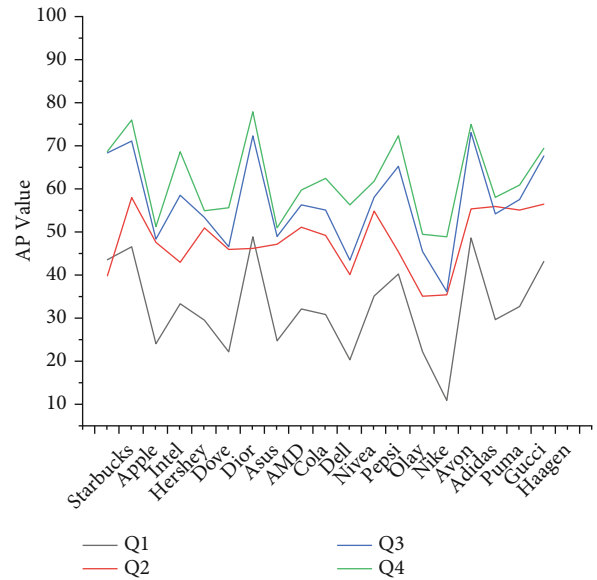


FIGURE 5: Comparative analysis results of AP of different image recognition algorithms.

teaching method based on deep learning LOGO image recognition technology constructed was correct, reasonable, and scientific; it is shown in Table 2.

3.2. Teaching Effect Evaluation Results of LOGO Image Recognition Based on Deep Learning. After the end of the teaching experiment, the difference of teaching effect between the experimental group and the control group was analyzed by the classroom test results. The statistical results are shown in Figure 6, and the results showed that the four classes taught with LOGO image recognition technology

TABLE 2: Results of different algorithms.

Algorithm (model)	mAP (%)	Total train time (min)	Test time (ms)/image	Hyperparameters
YOLO algorithm	32.7	706	22	mp, s = 0.8, 0.2
R-CNN algorithm	50.9	1285	25685	Pixels of the image: 32×32 , 96×96 , and 224×224 Convolution kernel: 3×3 , 5×5 Step size: 1 The number of convolution kernels: 64
Faster R-CNN algorithm	56.9	822	167	The number of convolution kernels: 128 λ : 1 (λ controls the balance between the two task losses) RoI (region proposal): 64
ContextNet algorithm	62.5	1058	198	Stride: 16 Backbone: Xception65

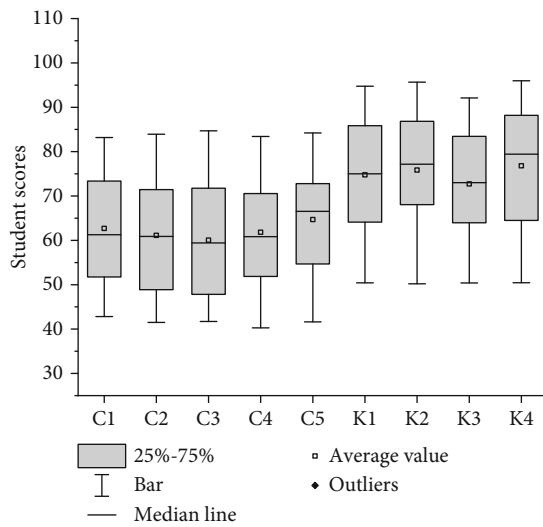


FIGURE 6: Comparison and analysis results of different image recognition techniques.

had a higher average score of 75, 76, 73, and 77, respectively, while the average scores in the four classes of traditional teaching methods were 63, 61, 60, and 62, respectively. It showed that inquiry creative experiment teaching could improve students' achievement significantly compared with traditional teaching, it can be in Figure 7.

The above data were used for independent sample T test by SPSS, and the results are shown in Table 3. The standard deviations of the grades of the classes taught with LOGO image recognition technology were 12.56, 12.72, 12.06, and 14.37, respectively, while the standard deviations of the traditional teaching methods were 12.01, 13.50, 13.84, and 11.54, respectively.

As shown in Table 3, it was tested by the Levene method. When the variance was assumed to be equal, F was 0.032, indicating that the value had a significant difference ($F < 0.05$), while assuming that the variance was not equal, t was 2.014, df was 78, and $p = 0.047 < 0.05$, also indicating that significant level has been reached. Through the test of the two independence, it showed that there was a significant difference between the experimental group and the control

group in the ordinary class, which further proved that inquiry creative experimental teaching had certain superiority compared with the traditional teaching.

4. Discussion

Zhang et al. indicated that an image target feature extraction and recognition model based on a deep CNN was established by using two deep learning algorithms—mask R-CNN algorithm and fast R-CNN algorithm [28]. First of all, aiming at the problem of identifying multiscale targets in LOGO image detection, an improved multiscale LOGO candidate region extraction network is proposed. Different from the original candidate region extraction network, the multiscale target detection is realized by the feature pyramid method. As to the character that the size of the LOGO image is relatively small compared to the ordinary target, the k-means algorithm is applied to the multiscale clustering of the LOGO image target to obtain the distribution of the LOGO target scale. In this way, the priori parameters required by the multiscale candidate region extraction network to extract the candidate frame of the LOGO image target are obtained. The multiscale candidate region extraction network uses the scale features existing between the layers of the CNN and the composition of the feature pyramid to achieve the purpose of extracting the image feature pyramid using the neural network, which is consistent with the findings of Huang et al. [29].

Second, in view of the problem that the target of the LOGO image detection is relatively small and difficult to identify, a target context classification network based on the LSTM model is proposed. The final classification result is obtained by using the target context features of different scales as the input of the LSTM model. This connection method makes full use of the different effects of target context information of different scales on target classification. Furthermore, in order to improve the accuracy of the frame, a suitable method for small target frame regression is used, and the detection accuracy is once again improved. Compared with the traditional target detection methods, the method based on target context features can improve the

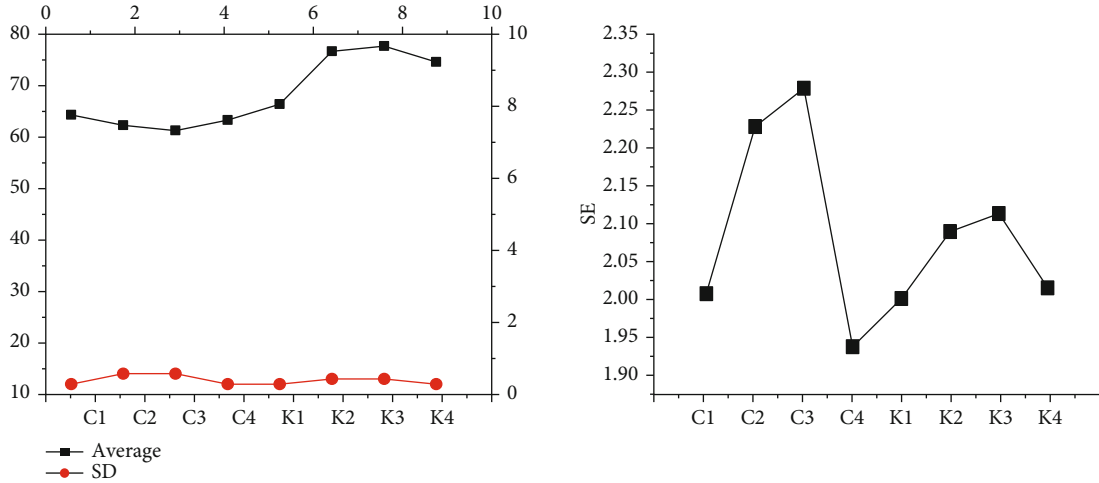


FIGURE 7: The independent T test of LOGO image recognition technology teaching performance based on deep learning.

TABLE 3: Levene test of LOGO image recognition technology teaching performance based on deep learning.

	Levene test of variance equation				T test of mean equation			95% confidence interval	
	f	Sig.	t	df	Sig. bilateral	Mean difference	Standard error	Upper limit	Lower limit
Assuming equal variances	.0032	.790	2.014	78	.047	7.30000	3.62454	.08409	14.51591
Score Assume that the variances are not equal			2.014	77.877	.047	7.30000	3.62454	.08391	14.51609

performance of target detection in image dataset, which is consistent with the findings of Bai et al. [30].

Moreover, the LOGO recognition algorithm is applied to the actual teaching design and added a shared network algorithm module. Compared with the traditional knowledge algorithm, it can well share some parameter layers of the teacher-student network and transform the traditional teacher and student network independent training into simultaneous training. This optimization method has brought about an increase in the accuracy of the student's network and has improved the ability of the student's network model to identify and express. This is consistent with the results of Nie et al. [31]. After the network parameters are shared between teachers and students, it is beneficial to update the bias of the subsequent biased network frequently, and the parameters of the sharing layer are not required to be trained from the beginning, so they can be directly invested in the basic feature extraction of the new biased network. Meanwhile, it also reduces the traditional training time, which greatly saves the cost of training time and is conducive to the continuous iteration and update of the model.

In addition, in view of the unique teaching scene of brand LOGO, the algorithm needs to adopt different strategies according to different classes. In different teaching periods, there are different scene requirements for different target LOGOS. Hence, a biased neural network is designed. By setting the biased vector and the loss function of the student network, without changing the original network size, the recognition accuracy on the target LOGO can be customized and improved, and the recognition accuracy

difference between the biased neural network and the CNN with larger network can be limited in the range of 1% to 5%, and its network expression ability has improved significantly. A brand LOGO recognition creative teaching system based on deep learning neural network is designed and implemented, which incorporates the advanced deep learning method to extract image extraction features. Compared with the previous traditional ML algorithms, it realizes end-to-end automatic feature extraction, greatly reduces the consumption of storage space, and has a higher recognition and expression ability, which is consistent with the research results of Zhang et al. [32].

5. Conclusion

Through collecting a large number of literatures on LOGO image recognition technology, the feasibility of the application of LOGO image recognition technology in teaching is analyzed. By combing the process, development process, and project realization of this technology in teaching application, the application value of this technology is explored by focusing on the individual cases of high school teaching. Finally, through the application and the actual teaching process, through the form of actual investigation, the application effect is studied. The application of LOGO image recognition technology in teaching can significantly improve students' academic performance and effectively drive their interest in learning. Hence, the teaching method of LOGO image recognition technology based on deep learning is correct, reasonable, and scientific. Compared with YOLO,

R-CNN, and Faster R-CNN, LOGO image recognition algorithm method based on deep learning theory has stronger image recognition ability and more accurate results. Primary school English teaching method based on LOGO image recognition can significantly improve students' learning interest and classroom participation, and inquiry creative experimental teaching based on LOGO image recognition has certain superiority compared with traditional teaching. The brand LOGO image recognition and inquiry creative teaching methods of deep learning theory proposed in experiment also have some defects: because the LOGO area occupies a small area in the image, the resolution of the input image is only 28×28 when designing the neural network. The resolution of the input layer directly affects the number of layers that the CNN can contain, thus affecting the training and prediction effect of the network. Hence, in the future work, in order to make up for the simple structure of CNN caused by low resolution of LOGO samples, more samples with higher resolution need to be collected, so as to design CNN that can better extract target features and distinguish different targets.

Data Availability

The raw data supporting the conclusions of this article will be made available by the authors, without undue reservation.

Ethical Approval

This article does not contain any studies with human participants or animals performed by any of the authors.

Consent

Informed consent was obtained from all individual participants included in the study.

Conflicts of Interest

All authors declare that they have no conflict of interest.

Authors' Contributions

All authors listed have made a substantial, direct, and intellectual contribution to the work and approved it for publication.

References

- [1] P. Yang, "Implementation of Chinese character extraction from pictures based on the neural network," in *Big Data Analytics for Cyber-Physical System in Smart City*, pp. 1809–1814, Springer, Singapore, 2019.
- [2] B. Sharma and A. Agarwal, "Evaluation of character recognition algorithm based on feature extraction," in *Communication Networks and Computing*, pp. 76–88, Springer, Singapore, 2018.
- [3] S. Raghunath, D. S. Rajendra, and V. Venkatesh, "Dynamic feature extraction based face recognition using sequential model," *International Journal of Pure and Applied Mathematics*, vol. 119, no. 18, pp. 2029–2037, 2018.
- [4] S. K. Zisserman, "A very deep convolutional networks for large-scale image recognition," *Computer Science*, vol. 79, no. 23, pp. 1409–1556, 2014.
- [5] S. L. Do and J. Haberl, "Development procedure of an air-source heat pump base-case simulation model for a code-compliant residential building," *Energy and Buildings*, vol. 107, pp. 11–25, 2015.
- [6] P. Tang and Y. Peng, "Exploiting distinctive topological constraint of local feature matching for logo image recognition," *Neurocomputing*, vol. 236, pp. 113–122, 2017.
- [7] M. Yuxin and H. Peifeng, "A highway entrance vehicle logo recognition system based on convolutional neural network," in *2019 2nd International Conference on Artificial Intelligence and Big Data (ICAIBD)*, pp. 282–295, Chengdu, China, 2019.
- [8] L. Shou-xian and W. Fang, "Logo recognition system on mobile terminal," *Computer Engineering & Software*, vol. 2, pp. 25–36, 2016.
- [9] W. Zhao, "Research on the transfer learning of the vehicle logo recognition," *AIP Conference Proceedings*, vol. 1864, pp. 020058–0200112, 2017.
- [10] G. Sui, "Reverse ekphrasis: teaching poetry-inspired Chinese brush painting workshops—in English," *International Journal of Art & Design Education*, vol. 38, no. 1, pp. 125–136, 2019.
- [11] G. Zhou, S. W.-Y. Ho, Y. Li, M. Luo, H. Freedman, and J. Luo, "Reciprocal learning between Canadian and Chinese schools through the 24 nature notes project," *Journal of Teaching and Learning*, vol. 13, no. 1, pp. 7–24, 2019.
- [12] A. O. O. Bamidele, H. U. Babaji, S. A. Alome, and A. Taiye, "Effect of guided inquiry teaching method on students academic performance in electrical installation and maintenance work in technical colleges in Gombe state," *ATBU Journal of Science, Technology and Education*, vol. 7, no. 4, pp. 343–352, 2020.
- [13] R. Evans and J. Dolin, "Taking advantage of the synergy between scientific literacy goals, inquiry-based methods and self-efficacy to change science teaching," in *Professional Development for Inquiry-Based Science Teaching and Learning*, pp. 105–120, Springer, 2018.
- [14] X. Jia, W. Hu, F. Cai et al., "The influence of teaching methods on creative problem finding," *Thinking Skills and Creativity*, vol. 24, pp. 86–94, 2017.
- [15] H. Aktamiş, E. Hiğde, and B. Özden, "Effects of the inquiry-based learning method on students' achievement, science process skills and attitudes towards science: a meta-analysis science," *Journal of Turkish Science Education*, vol. 13, no. 4, pp. 248–261, 2016.
- [16] V. S. Andriani, "The effectiveness of inquiry learning method to enhance students' learning outcome: a theoretical and empirical review," *Journal of Education and Practice*, vol. 7, no. 3, pp. 38–42, 2016.
- [17] L. Zhai, "A inquiry teaching mode based on STEM education," *International Journal of Emerging Technologies in Learning (iJET)*, vol. 14, no. 17, pp. 44–58, 2019.
- [18] R. Yuan and L. J. Zhang, "Exploring student teachers' motivation change in initial teacher education: a Chinese perspective," *Teaching and Teacher Education*, vol. 61, pp. 142–152, 2017.
- [19] K. Greff, R. K. Srivastava, J. Koutník, B. R. Steunebrink, and J. Schmidhuber, "LSTM: a search space odyssey," *IEEE*

- transactions on neural networks and learning systems.*, vol. 28, no. 10, pp. 2222–2232, 2017.
- [20] S. Han, J. Kang, H. Mao et al., “Ese: efficient speech recognition engine with sparse lstm on fpga,” in *Proceedings of the 2017 ACM/SIGDA International Symposium on Field-Programmable Gate Arrays*, pp. 75–84, 2017.
- [21] Z. Zhao, W. Chen, X. Wu, P. C. Chen, and J. Liu, “LSTM network: a deep learning approach for short-term traffic forecast,” *IET Intelligent Transport Systems*, vol. 11, no. 2, pp. 68–75, 2017.
- [22] J. Jiang, H. Xu, S. Zhang, Y. Fang, and L. Kang, “FSNet: a target detection algorithm based on a fusion shared network,” *IEEE Access*, vol. 7, pp. 169417–169425, 2019.
- [23] H. Fu, X. Shao, C. Chipot, and W. Cai, “Extended adaptive biasing force algorithm. An on-the-fly implementation for accurate free-energy calculations,” *Journal of chemical theory and computation*, vol. 12, no. 8, pp. 3506–3513, 2016.
- [24] R. Z. Heimer, K. R. Myrseth, and R. S. Schoenle, “YOLO: mortality beliefs and household finance puzzles,” *The Journal of Finance*, vol. 74, no. 6, pp. 2957–2996, 2019.
- [25] Z. Cai and N. Vasconcelos, “Cascade R-CNN: delving into high quality object detection,” in *Proceedings of the IEEE conference on computer vision and pattern recognition*, pp. 6154–6162, 2018.
- [26] H. Jiang and E. Learned-Miller, “Face detection with the faster R-CNN,” in *2017 12th IEEE International Conference on Automatic Face & Gesture Recognition*, pp. 650–670, Washington, DC, USA, 2017.
- [27] E. J. Hwang, S. Park, K.-N. Jin et al., “Development and validation of a deep learning-based automatic detection algorithm for active pulmonary tuberculosis on chest radiographs,” *Clinical Infectious Diseases*, vol. 69, no. 5, pp. 739–747, 2019.
- [28] D. Zhang, J. Zhan, L. Tan, Y. Gao, and R. Župan, “Comparison of two deep learning methods for ship target recognition with optical remotely sensed data,” *Neural Computing and Applications*, vol. 33, no. 10, pp. 4639–4649, 2021.
- [29] W. Huang, G. Li, Q. Chen, M. Ju, and J. Qu, “CF2PN: a cross-scale feature fusion pyramid network based remote sensing target detection,” *Remote Sensing*, vol. 13, no. 5, p. 847, 2021.
- [30] D. Bai, Y. Sun, B. Tao et al., “Improved single shot multibox detector target detection method based on deep feature fusion,” *Concurrency and Computation: Practice and Experience*, vol. 34, no. 4, article e6614, 2022.
- [31] W. Y. Nie, “Construction of network open teaching platform of analytical chemistry based on facial recognition and artificial intelligence,” *Journal of Intelligent & Fuzzy Systems*, vol. 40, no. 4, pp. 7435–7445, 2021.
- [32] Y. Zhang, L. Yu, Z. Fang, N. N. Xiong, L. Zhang, and H. Tian, “An end-to-end deep learning model for robust smooth filtering identification,” *Future Generation Computer Systems*, vol. 127, pp. 263–275, 2022.

Research Article

Autoencoder for Design of Mitigation Model for DDOS Attacks via M-DBNN

Ankit Agrawal ¹, Rajiv Singh ¹, Manju Khari ², S. Vimal ³ and Sangsoo Lim ⁴

¹Department of Computer Science, Banasthali Vidyapith, Banasthali, 304022 Rajasthan, India

²School of Computer and System Sciences, Jawaharlal Nehru University, New Delhi, India

³Department of AI & DS, Ramco Institute of Technology, North Venganallur Village, Rajapalayam, 626117 Tamilnadu, India

⁴Department of Computer Engineering, Sungkyul University, Anyang 14097, Republic of Korea

Correspondence should be addressed to Sangsoo Lim; slim@sungkyul.ac.kr

Received 15 January 2022; Revised 3 March 2022; Accepted 7 March 2022; Published 7 April 2022

Academic Editor: Nima Jafari Navimipour

Copyright © 2022 Ankit Agrawal et al. This is an open access article distributed under the Creative Commons Attribution License, which permits unrestricted use, distribution, and reproduction in any medium, provided the original work is properly cited.

Distributed Denial of Service (DDoS) attacks pose the greatest threat to the continued and efficient operation of the Internet. It can lead to website downtime, lost time and money, disconnection and hosting issues, and website vulnerability. Conventional machine learning methodologies are being harmed by reduced recognition rates and greater false-positive rates due to the emergence of new threats. As a result, high-performance machine learning classifiers with low false-positive rates and high prediction accuracy are required for the DDoS detection system. Here, a deep belief neural network is preferred, upgraded to the modified deep neural network (M-DBNN) to accurately detect DDoS attacks from the network. Enable the database to change a specific format and range, which helps the M-DBNN classifier easily predict the class. An advanced Chimp Optimization Algorithm (ChOA) is used to minimize the error to find the best weight of the M-DBNN classifier; this leads to accurate DDoS attack detection and predict the classes effectively. The proposed method is evaluated for CAIDA “DDoS Attack 2007” dataset. The accuracy of the proposed method is 0.87%, and the outcome is compared with those of other existing methods of deep neural network (DNN), support vector machine (SVM), artificial neural network (ANN), and neural network (NN). The proposed method demonstrates great detection accuracy with a low error.

1. Introduction

Distributed Denial of Service (DDoS) attacks are presently the most common and sophisticated danger to enterprises, and they are becoming progressively difficult to overcome. For example, GitHub became a victim of one of the greatest DDoS attacks ever in 2018 [1]. In February, attacks on eBay, Amazon, and Yahoo were undertaken [2]. In July 2008, a DDoS attack on the Georgian.gov website brought down multiple Georgian servers. The attack on Register.com in January 2001 was carried out by abusing Domain Name System (DNS) servers as reflectors [3]. Previous software protection techniques and intrusion detection systems (IDSs) can recognize and block the attack or intrusion which is happening or already has to a specified extent. However, with the arrival of an era of big data and the resulting

problem of uninterrupted huge data flow, previous software protection techniques and IDSs have been faced with new dares. For today’s high-speed networks, classic network intrusion detection systems (NIDS) have a high rate of packet loss and a high rate of missed detection [4].

Conventional machine learning algorithms are based on shallow learning. Usually, emphasize feature engineering and selection models, making them unable to properly deal with the challenge of a dynamically growing huge amount of data, resulting in erroneous detecting attacks. Shallow learning is not suited for intelligent systems to predict malevolent behaviour in huge amounts of data in particular [5]. Deep learning has advanced quickly in recent years, overcoming many of the shortcomings of conventional machine learning models and providing a model that is well fitted for IDS [6]. It is commonly utilized in various

applications, including speech recognition, picture recognition, machine translation, and a variety of others. It can analyze vast amounts of data once again. Because deep learning approaches can extract high-dimensional features from original data by numerous nonlinear transformations, and the features collected have a hierarchical structure, there is a movement put on them in the construction of novel intrusion detection algorithms [7].

A comprehensive literature assessment on deep learning approaches for intrusion detection has been published. Some of the deep learning approaches for intrusion detection is DNN-based DDoS detection in software-defined networks [8], and CNN-based IDS against DDoS [9]. In the proposed technique, a Modified Deep Belief Neural Network (M-DBNN) [10], like most classical deep learning systems, uses a multilayer restricted Boltzmann machine (RBM) to recognize the DDoS attack. To make the network better fit the training data and increase efficiency in intrusion detection, optimization is employed to identify a suitable weight of M-DBNN. The M-DBNN classifier predicts whether the class is an attack or not attack from the dataset. Whenever a network is attacked and M-DBNN is detected, the user receives an alert notification. On the other hand, the network is secure, and the dataset can be fed into the auto-encoder [11], which compacts the income data into a latent-space format and then restructured this data to give an output. The outcome data of the autoencoder is stored in cloud storage [12].

1.1. Main Contribution. Detect intrusion or DDOS attacks from the network to protect users' personal information. The key contribution of the paper is given below:

- (i) A deep learning system based on Modified Deep Belief Neural Network (M-DBNN) is utilized to detect malicious behaviours in cyber environments and classify them based on attack types
- (ii) Attributes of the dataset are preprocessed to convert a specified format, making the detection process easy. There are three steps to preprocessing the data: Min-Max normalization, Equal Width Discretization, and Correlation-based Feature Selection
- (iii) The preprocessed data are separate for the training and testing process fed in the Modified Deep Belief Neural Network (M-DBNN) classifier, which predicts the input data to either attack or not attack class. The performance of M-DBNN is improved by using the Chimp Optimization Algorithm
- (iv) For DDoS is detected, an alert message is forwarded to the user. Otherwise, the data are allowed to be stored in cloud storage via an autoencoder
- (v) With the help of a ChOA-based M-DBNN classifier, the CAIDA "DDoS assault 2007" dataset is used to detect DDoS attacks. The proposed technique is very sensitive to detecting DDoS attacks, giving 87% accuracy. In addition, the outcome of the pro-

posed technique is compared with previous techniques of DNN, SVM, ANN, and NN

The rest of the paper contains the following: Section 2 presents the literature review related to detecting DDoS attacks. In Section 3, the methodology and architecture of the proposed part are discussed. Section 4 presents the result and discussion of the proposed outcome and compares the proposed and previous techniques. At last, Section 5 contains the conclusion of the paper.

2. Literature Review

Numerous techniques are introduced to detect DDoS attacks or intrusion in networks. A few techniques are discussed below.

Sahoo et al. [13] suggested that the detection of attack traffic is possible by using the SDN's centralized control feature. Various machine learning (ML) approaches were utilized in the STN sector to prevent anomalous traffic. However, the system had an open question about choosing the right features and precise classifiers to detect the attack. The dimension of feature vectors was reduced using SVM-based KPCA, and different SVM parameters were optimized using GA. An enhanced kernel function (N-RBF) was employed to decrease the noise produced by feature discrepancies. Compared to single SVM, the experimental results demonstrated that the model achieves greater generalization and more accurate classification.

Liu [14] had presented a multiscale convolutional neural network with Grayscale Matrix Feature- (GMF-) based DDoS assault detection. The seven-tuple was distinct from characterizing the flow of network characteristics and translated into a grayscale feature via binary, based on the distinct features of the normal flow and the attack flow in the IP protocol. The convolution kernel of various spatial scales was employed to enhance the precision of feature segmentation and local and global features of the network flow, which were recovered based on the network flow Grayscale Matrix Feature (GMF). A DDoS attack classifier was built using a multiscale convolution neural network.

Tuan et al. [15] had suggested a botnet DDoS attack detection using machine learning approaches. Estimation of the method was based on the UNBS-NB 15 and KDD99 publicity datasets, which were well-known for detecting Botnet DDoS attacks. Various machine learning methods like artificial neural network (ANN), support vector machine (SVM), Naïve Bayes (NB), Unsupervised Learning (USML), and Decision Tree (DT) were used for examining the dataset's False Alarm Rate (FAR), accuracy, specificity, AUC, false positive rate (FPR), Matthews correlation coefficient (MCC), and sensitivity.

Doriguzzi-Corin et al. [16] suggested a LUCID, a light-weight deep learning DDoS detection system that used the features of convolutional neural networks (CNNs) to distinguish between malware and benign traffic flows. LUCID was compared to previous state-of-the-art recognition accuracy while delivering a 40x reduction in processing time when

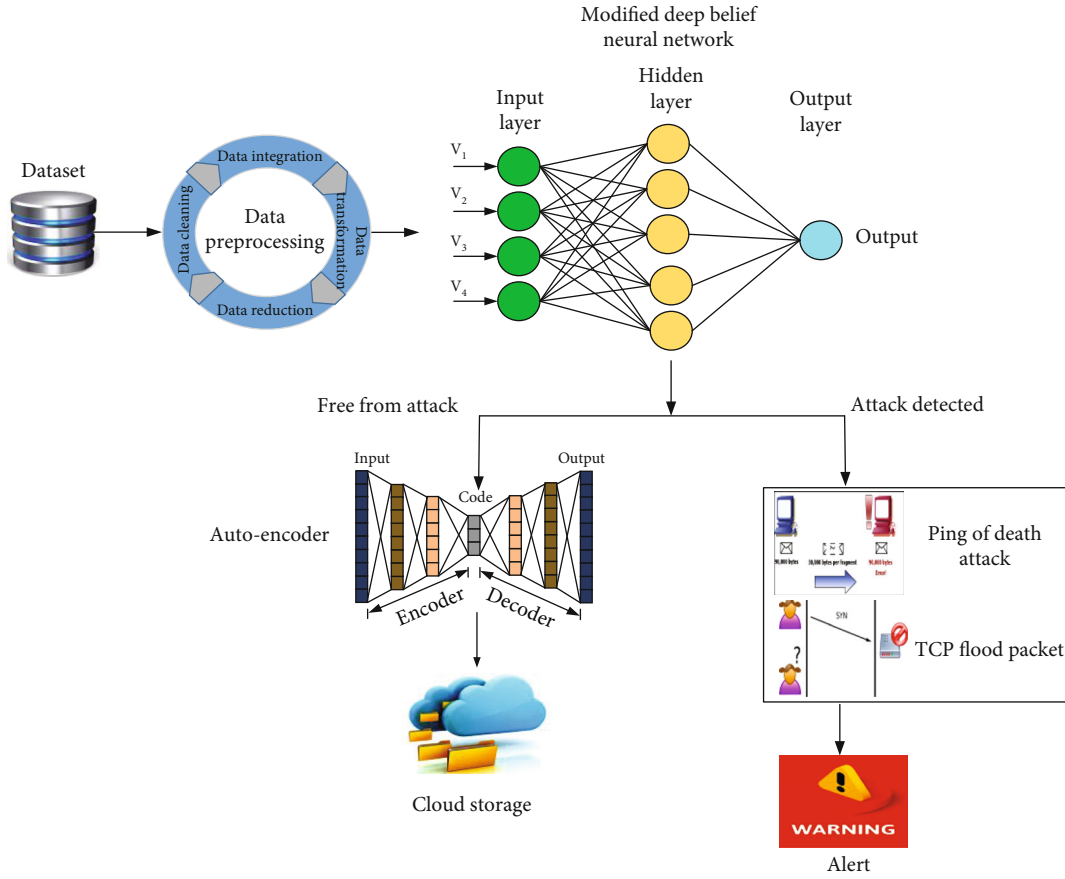


FIGURE 1: Architecture of planned system.

compared to the state-of-the-art, using the most recent datasets. LUCID’s output had the same representation.

Çakmakçı et al. [17] had suggested a multivariate data-friendly online, sequential DDoS detection system. A kernel-based learning method, the Mahalanobis distance, and the chi-square test were all used in the learning algorithm. As detection metrics, extract four entropy-based features and four statistical-based features from network traffic every minute. Then, utilize the entropy features to deploy the kernel-based learning technique to recognize suspicious DDoS input vectors. In every minute, the Mahalanobis distance was calculated among the distribution of dictionary members and suspicious vectors. The Mahalanobis distance was then calculated using the chi-square test. The CICIDS2017 dataset was used to evaluate the DDoS detection strategy.

Dong and Sarem [18] had suggested an SDN technique, and there are two methods for detecting DDoS attacks. To recognize a DDoS assault, one way was to use the severity of the attack, i.e., when a DDoS attack assaulted the SDN controller, four features were examined first. The upgraded K -Nearest Neighbor (KNN) algorithm based on machine learning (ML) was used in other techniques to detect the DDoS attack. A novel notion called the degree of attack was introduced and presented for the first time to detect DDoS attacks.

Hussain et al. [19] had suggested an enabled early detection for distributed denial-of-service (DDoS) assaults coordinated via a botnet that controls malevolent devices and used real network data and deep convolutional neural networks (CNNs). To generate a pooled DDoS assault in a cell that can interrupt CPS operations, the puppet device independently performs quiet call, SMS spamming, or a blend of these attacks targeting call, Internet, SMS, signaling, or a combination of these serviced, alternately.

Alzahrani [20] had suggested an attack prevention system of CS-ANN that combines a Cuckoo Search (CS) approach with an artificial neural network (ANN) approach to identify DDoS attacks and allow the server side to be more attentive. As a nature-inspired method, the cloud user features and the attacker features were optimized using CS. These improved features were then sent to the ANN structure. Features that were trained were saved in the database and used at the testing phase to match the test features with the taught features, resulting in results for both attackers and typical cloud users.

In Ref. [13], the authors explained SDN’s centralized control feature to detect DDoS attacks. However, the method has some disadvantages by the rapid development of new malware, which would necessitate collecting samples at regular intervals to assess performance. In Ref. [14], the novelist explained a multiscale convolutional neural network

(CNN) to recognize DDoS attacks. But the method has several limitations and assumptions, and the method does not include the packet payload; so the data acquired might be sampled. In Ref. [15], the novelists explained a machine learning approach to detecting botnet DDoS attacks. However, there were scalability limits, and the solution was not ideal. In Ref. [16], the authors describe a method of a LUCID system for DDoS detection. The method is not apposite for online systems due to some flow-level statistics. In Ref. [17], the authors explained a multivariate data-friendly online, sequential DDoS detection system. The method gives high accuracy and detects accurate attacks. Yet the method is not suitable for huge datasets. In Ref. [18], the novelists explained the SDN technique to recognize DDoS attacks. But the solution of the method is inefficient and complex owing to the necessity to discern the packet protocol. In Ref. [19], the novelists explain early detection for distributed denial-of-service (DDoS) via CNN. The outcome is good and also predicts accurate class. Owing to its content-based recognition nature, it is computationally expensive, which is the only drawback of this method. In Ref. [20], the authors explained a CS-ANN-based DDoS attack detection technique. The drawback of the method is that it does not predict an accurate class, so alarm rate and accuracy are less in this approach.

3. Proposed Methodology

DDoS attacks disrupt normal server traffic and overburden the target network or service. Money is lost, fraudulent traffic is generated, reputation is harmed, and clients are harmed when a DDoS attack occurs. Intrusion detection is an important process for system security, as it prevents server attacks and network traffic manipulation. In addition, it improves network data security and determines, detects, and recognizes unapproved program usage, data framework destruction, alteration, and copying. Intrusion or DDoS attacks are detected in the proposed study using a Modified Deep Belief Neural Network (M-DBNN). The dataset is first preprocessed to arrive at a numerical value. The value is then fed into M-DBNN, with numerous invisible, hidden layers, a visible input layer, and a visible output layer. Although the range of the input layer is [0, 1], the values of the buried layer are binary numbers. The modified DBNN classifies the input dataset to determine whether or not it has been subjected to a DDoS attack. The advanced algorithm detects and alerts the user if an attack is detected. Data is supplied to an autoencoder, an encoder, and a decoder after the dataset is free of any attacks or difficulties. The modified DBNN classifies the input dataset to assess whether it has been subjected to a DDoS attack. The advanced algorithm detects and warns the user if an attack is detected. When the dataset is clear of attack challenges, it is sent to the autoencoder, with both an encoder and a decoder. The architecture of the proposed system is given in Figure 1, and pseudocode of the overall system is given in Pseudocode 1.

3.1. Preprocessing. The data is not in a specific range, so the preprocessing technique is used to fit the dataset in an exact

```

Pseudocode
Input raw dataset = X
{
For all data in dataset
# Pre-processing
Re-range the dataset using Eq. (1)
Convert numerical value using Eq. (2)
Redundancy using Eq. (3)
Pre-processing data  $\implies$  Pre-data
# M-DBNN
Data splitting
{
Training data
Testing data
Actual class
}
# Training ChOA optimizer
For all in input dataset
{
Initialization = weight using Eq. (8)
Fitness function using Eq. (9)
Update the solution using Eq. (10)
Best solution
}
#Testing the dataset
}
}
End
Outcome:
Predict the class to detect the server is normal or attack

```

PSEUDOCODE 1: Pseudocode of overall system.

range. Several approaches are available for the normalization of the dataset. Among them, Min-Max normalization is more efficient. The normalization approach converts a value from σ to σ^* that is suitable in the range of [A, B]. Its mathematical expression is given below.

$$\sigma^* = \frac{\sigma - \sigma_{\min}}{\sigma_{\max} - \sigma_{\min}}. \quad (1)$$

The data is normalized to give an equal weight of all attributes. After the normalizing process, discretization takes place. The discretization process transfers the domain of the continuous feature to an insignificant domain in the form of a finite number. Equal Width Discretization (EWD) is preferred to transfer the continuous field to a finite number that creates several bins. Moreover, this approach improves the performance in large datasets, where K is used for evaluating the bin quantity. Every bin is allied in a distinct, discrete value. EWD split the number lines among V_{\max} and V_{\min} at the interval of k . Generally, the value of k is set as 10. It is known as a user predefined variable. Interval's width is evaluated by

$$W = \frac{B - A}{N}, \quad (2)$$

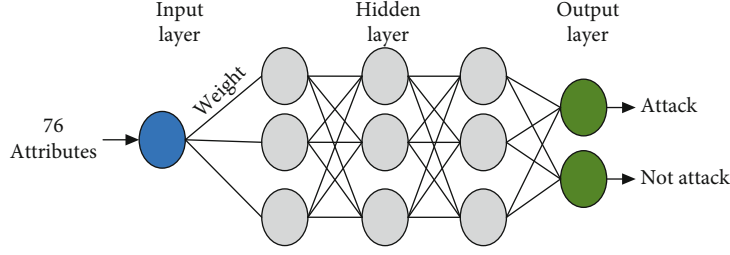


FIGURE 2: Schematic structure of M-DBNN.

where N denotes the interval and B and A are the highest and lowest values of attributes.

Finally, select the feature. In this process, irrelevant and redundant features present in the dataset are eliminated, thus enhancing the accuracy and decreasing the running cost. Here, Correlation-based Feature Selection (CFS) is used. The evaluation role favours subsets with attributes that are substantially correlated with the class but uncorrelated with one another. The feature of irrelevance in the dataset is needed to eliminate since it links to the class. In addition, the fired feature was also eliminated because it was highly linked with the leftover feature. The evaluation of subset in CFS is given below:

$$\text{Merit}_s = \frac{k \overline{\text{rcf}}}{\sqrt{k + k(k-1)r_{\overline{\text{ff}}}}} \quad (3)$$

MS is the average feature-feature inter-correlation, $\overline{\text{rcf}}$ is the mean feature-class correlation, and $r_{\overline{\text{ff}}}$ is the average feature-feature intercorrelation of a feature subset containing k features.

3.2. Modified Deep Belief Neural Network (M-DBNN). Deep belief neural network is a growing approach. DBNN contains a layer by layer arrangement of restricted Boltzmann machine (RBM) [21]. RBM trains the data in greedy layer-wise to accomplish the unsupervised filed solid execution. The significant usage of RBMs is likely to be because there is a lack of labelled data, and RBMs and autoencoders can be pre-trained on unlabeled data and fine-tuned on a small portion labelled data. Greedy layer-wise techniques are utilized for training the data of DBN each layer at each time. The schematic structure of M-DBNN is shown in Figure 2.

Moreover, the method optimizes a layer with a greedy time. Next, the completion of unsupervised training supervised training technique is the whole access layer; the name of this process is fine-tune stage. This stage is a combination of two notions: (a) an initial factor presents an effect of major standardizing, and (b) an input distribution study will help the study of input to outcome mapping. For the process of pretraining, the dataset unsupervised is trained by a greedy layer-wise approach. And the supervised layer is trained by the fine-tuning stage from the first layer to improve the labelled sample feature.

TABLE 1: Parameters of M-DBNN classifier.

Parameters	Ranges
Number of iteration	500
Batch size	14109
Step ratio	0.1
Dropout rate	0.9

For RBM, h and v represent hidden and visible layers, respectively. Here, three variables are needed for system decision, namely,

$$\theta = \{W, A, B\}. \quad (4)$$

Let $A = \{a_i \in R^m\}$ and $A = \{b_j \in R^n\}$.

Here, A denotes an element of visible layer, W denotes weight matrix, and B denotes an element of the hidden layer. a_i represent the i^{th} visible layer threshold, and b_j represent j^{th} hidden layer threshold.

The layer of hidden and visible follows Bernoulli distribution; RBM energy equation is stated as

$$E(v, h \setminus \theta) = - \sum_{i=1}^n a_i v_i - \sum_{j=1}^m b_j h_j - \sum_{i=1}^n \sum_{j=1}^m v_i W_{ij} h_j, \quad (5)$$

where $\theta = W_{ij}, a_i, b_j$. The energy function displayed the energy value for separately visible node and hidden layer node valuation. The overall hidden layer node set is expressed as

$$P(v \setminus \theta) = \frac{1}{z(\theta) a} \sum_h e^{-E(v, h \setminus \theta)}, \quad (6)$$

where $z(\theta)$ is a standardized factor.

The RBM is linked in a way biphasic. The possibility of the beginning of neurons in the visible layer and hidden layer is expressed as

$$P(h_j = 1 | v) = \sigma \left(b_j + \sum_i v_i W_{ij} \right), \quad (7)$$

$$P(v_i = 1 | h) = \sigma \left(a_i + \sum_j h_j W_{ij} \right).$$

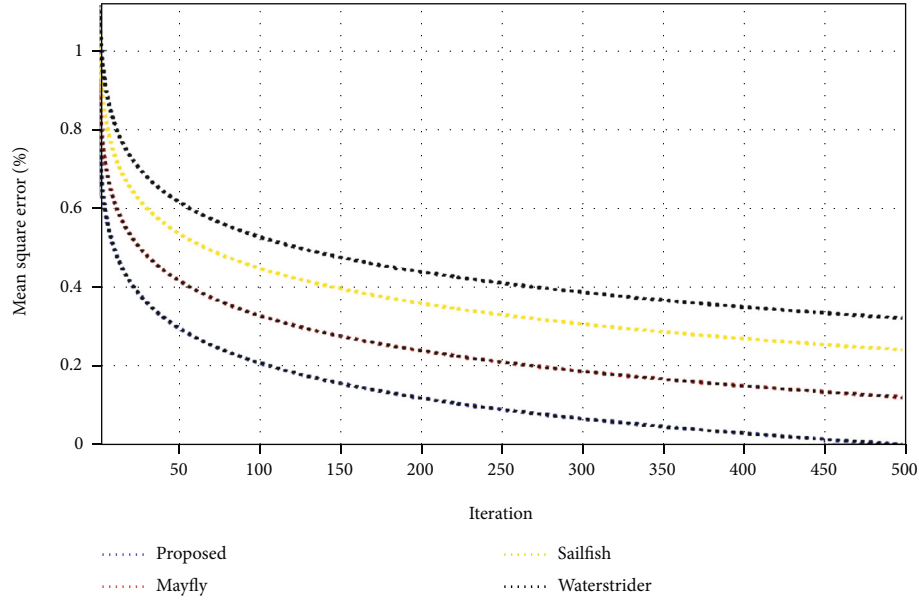


FIGURE 3: Comparison of mean square error in proposed approach and existing approaches.

3.2.1. Training Data. Chimp Optimization Algorithm (ChOA) is used for weight optimization. Weight is defined as the connection between the hidden and visible layers. A suitable weight is used to enhance the performance of the system. ChOA is a group hunting optimization that is a lifestyle of chimpanzees. Four entitled chimps are a group to attack the prey. They are drivers, barriers, chasers, and attackers. The driver follows the prey, while the barrier blocks the prey to move in a different direction, and the chaser moves suddenly to catch the prey. Finally, the attacker attacks the prey.

Step 1. Initialize the weight as an input,

$$\text{Weight} = \{W_1, W_2, \dots, W_n\}. \quad (8)$$

Step 2. Find the fitness function. Here, the error between the real and given outcomes is evaluated to find the fitness function.

$$\frac{\partial E}{\partial w_{ij}^{t-p}} = \frac{\partial E}{\partial y_j} \cdot [1 - y_j] \cdot y_i^{t-p}, \quad (9)$$

where y_i^{t-p} is the output of input unit i , w_{ij}^{t-p} is the weight between input unit i and hidden unit j at time $t - p$, $\partial E/\partial y_j$ can be calculated by standard BP algorithm, and y_j is the output of hidden unit j .

Step 3. Update the outcome to find the best solution. The best solution is not to find, but to repeat the process as Step 2.

$$X_{\text{chimp}}(t+1) = \begin{cases} X_{\text{prey}}(t) - a \cdot d, & \text{if } \mu < 0.5, \\ \text{chaotic}_{\text{value}}, & \text{if } \mu \geq 0.5, \end{cases} \quad (10)$$

$$a = 2fr_1 - f,$$

$$d = |cX_{\text{prey}}(t) - mX_{\text{chimp}}(t)|,$$

$$c = 2r_2, m = \text{chaotic}_{\text{value}},$$

where t indicates the number of the current iteration, X_{chimp} is the position vector of a chimp, X_{prey} is the vector of prey position, and a, m, c represent the coefficient vector. Through the iteration process, f is lowered nonlinearly from 2.5 to 0, m a chaotic vector intended based on several chaotic maps, and r_1 and r_2 are random vectors in the range of $[0, 1]$.

Step 4. The last step is to stop the process. When the best solution is captured, the process goes to an end.

3.2.2. Testing Data. In the proposed work, only 80% dataset is trained; the remaining 20% of the dataset are tested. The test data are correctly predicted for being free from either attack class or attack class. When the attack is recognized, a notification is generated to alert the user.

3.3. Autoencoder. The term autoencoder (AE) is defined as an artificial network system that contains both a decoder and an encoder. The autoencoder compresses the data and encodes the input data and reconstructs the data as near to the original data [22]. The part encoder minimizes the dimensionality of the given data; besides, the decoder decompresses stage to reduce the noise of the given data and create the new data. The key objective of the autoencoder is to reduce the error during reconstruction among input data and reconstructed data. The loss of reconstruction is expressed as L_p distance.

$$\mathcal{L}_{AE}(\theta, \phi) = \min E(x, \hat{x}) = \min \|x - \hat{x}\|_p, \quad (11)$$

where x denotes data of input and \hat{x} represents the data of reconstructed. In other words, the loss of reconstruction is also defined as entropy.

$$\mathcal{L}_{AE}(\theta, \phi) = - \sum_{i=1}^D \hat{x}_i \log(x_i), \quad (12)$$

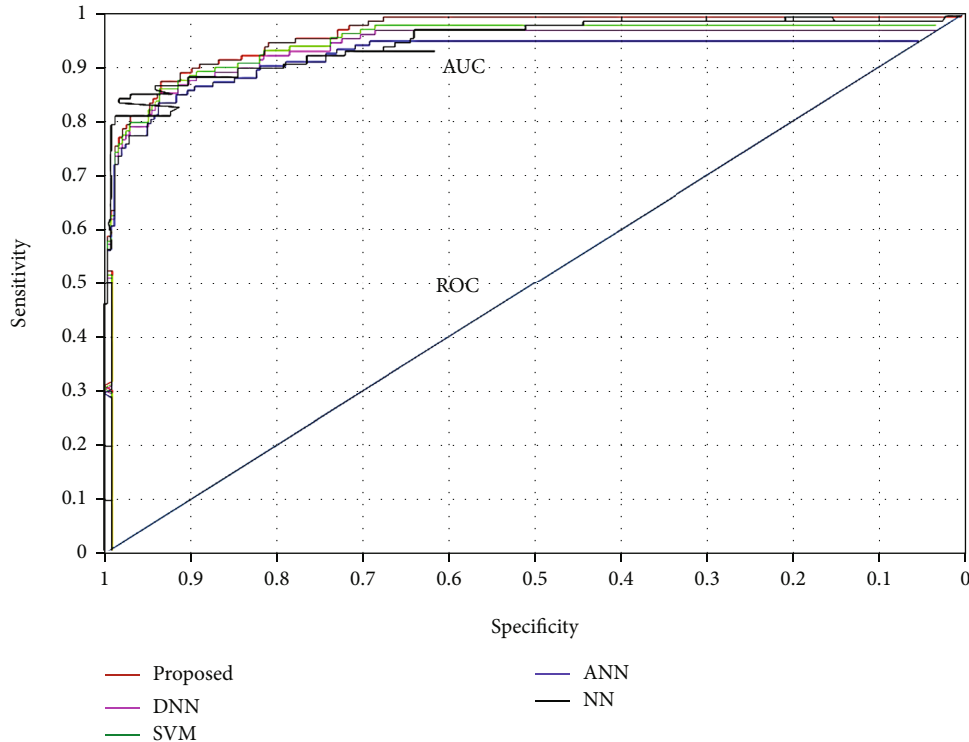


FIGURE 4: Comparison of AUC and ROC curve.

where D is the raw data x dimensionality. The encoder $q_\phi(z|x)$ is the next function of the probability that is utilized to estimate inflexible function $p_\theta(z|x)$. Let us assume $p_\theta(z)$ is Gaussian of multivariate in the covariance matrix of diagonal. Sample point z is randomly selected from $p_\theta(z)$. The function of a decoder is $p_\theta(z|x)$ which is a mapping from the latent space to the raw sample.

3.4. Cloud Storage. Cloud storage is amorphous, with no clear range of abilities or infrastructure. Many conventional hosted or managed service providers (MSP) provide block or file storage in addition to standard remote management protocols or virtual or physical server hosting, so there are plenty of options. Other options have emerged, such as the Amazon S3 service, which mimics flat databases built to store huge things. Some advantages of cloud storage are cost-effectiveness, disaster preparedness, ease of management, and lower influence outages and upgrades [23].

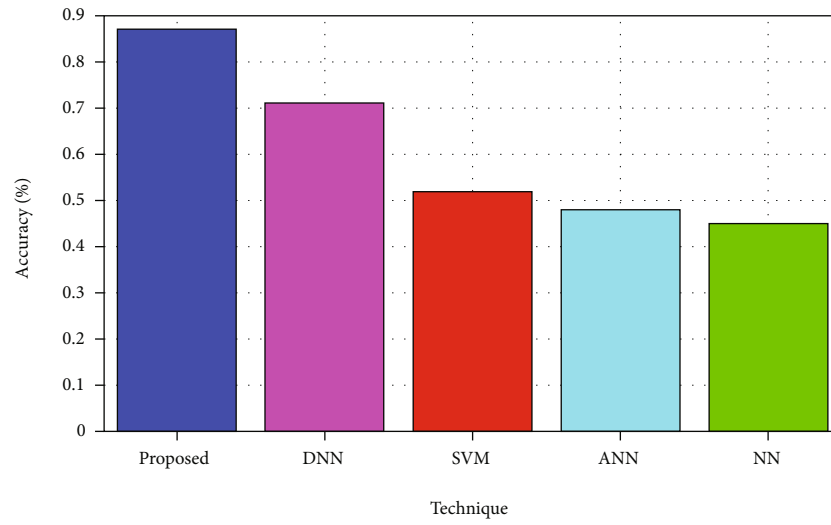
4. Result and Discussion

The ChOA-based M-DBNN is developed to predict the DDoS attack in a network environment. The proposed ChOA-based DBN is implemented and evaluated using MATLAB 2020b in Windows x64 bit platform with Intel Core i5 processor and 8GB Ram. CAIDA “DDoS Attack 2007” [24] is considered the benchmark dataset to analyze the proposed techniques. The proposed technique includes three phases such as preprocessing, M-DBNN training, and testing.

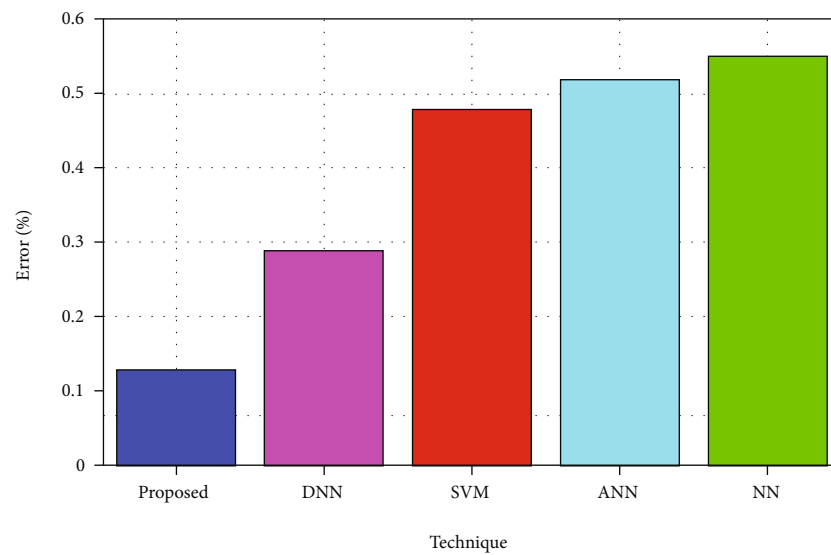
TABLE 2: Confusion matrix of the proposed and existing techniques.

Techniques	Actual class	Predicted class	
		True	False
M-DBNN	Positive	37008	6228
	Negative	62300	7336
SVM	Positive	50074	4407
	Negative	9352	49039
ANN	Positive	32539	37097
	Negative	17356	25880
NN	Positive	32548	25843
	Negative	17399	37084
DNN	Positive	10864	7587
	Negative	18683	3986

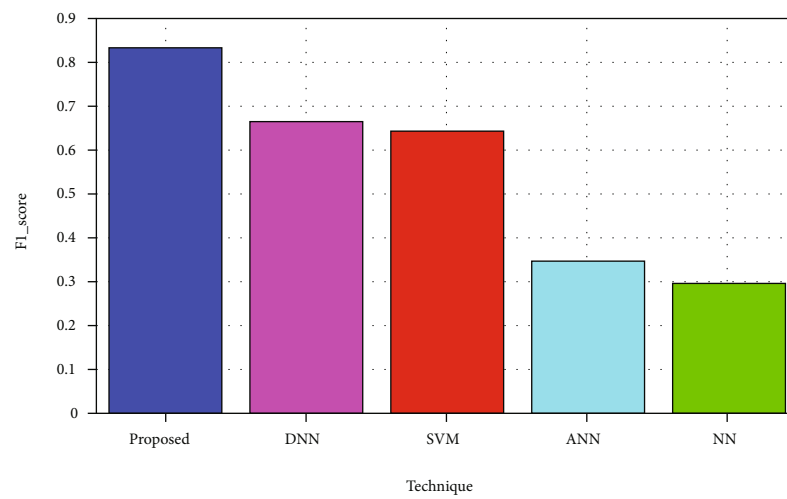
First, the database is taken in *pcap* file format; then extract the *pcap* file to convert to *csv* file format. The database contains 225746 models and 79 attributes, including IP, source IP, source port, protocol type, and destination port. The attributes of the database were preprocessed in which the undesirable variables were removed from the database. There are three steps to preprocessing a database: normalization, discretization, and feature selection. The dataset is first measured to fit within a given range using the Mini-Max normalization. All properties are given equal weight in the data, which is normalized. After that, equal width discrimination occurs, converting successive domain



(a)



(b)



(c)

FIGURE 5: Continued.

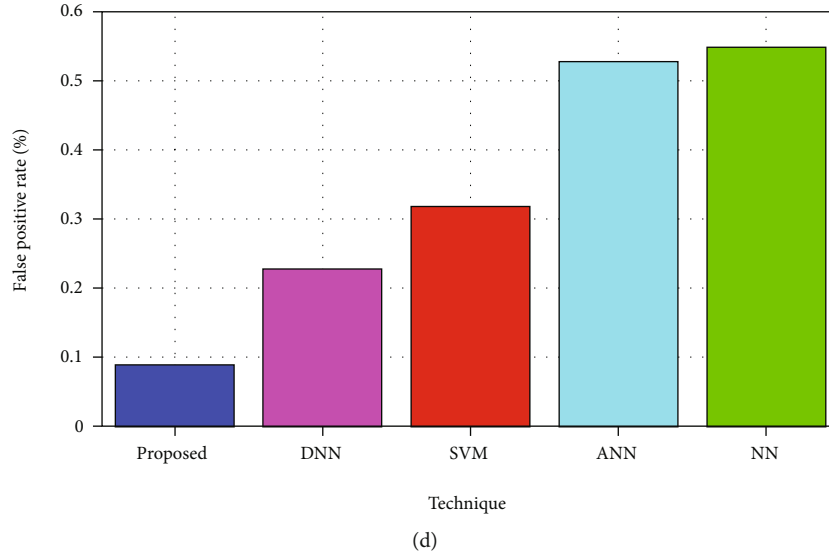


FIGURE 5: Comparison of proposed and existing approaches. (a) Accuracy. (b) Error. (c) F1_score. (d) False positive rate.

features to normal domain features with a limited number. It leads to improved performance on larger databases. The final stage is feature selection, an important preprocessing stage in network traffic classification. Here, correlation-based feature selection is used to remove unnecessary and irrelevant information from the database to improve accuracy and reduce computation costs. Among these 225745 samples, only 80% dataset is trained; i.e., 180596 samples are trained, and the remaining 20% dataset is tested; i.e. 45149 samples are tested. These samples are predicted for either two classes like DDoS attack or not attack

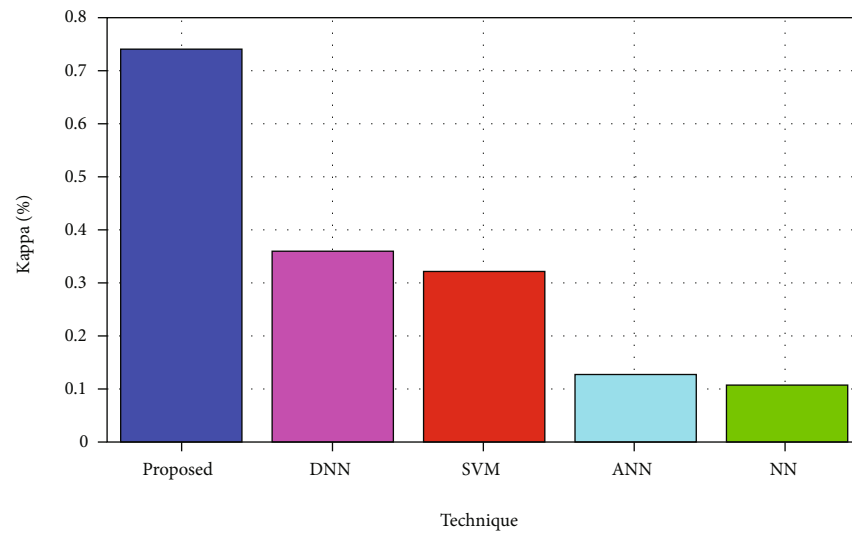
For M-DBNN, the weight parameters are fine-tuned using a supervised backpropagation algorithm, and the tuning step employs supervised learning to fine tune the network structure's weight. The term weight is defined as the interconnection of the input layer and hidden layers. Here, the weight of the M-DBNN is selected for the Chimp Optimization Algorithm. The Chimp Optimization Algorithm (ChOA) is a new metamorphic that has just been introduced. Surprisingly, this reflects the chimp's social status relationships and hunting activity. Using the Chimp Optimization Algorithm (ChOA) to improve the appropriate weight system to reduce error, the M-DBNN trains the input of 79 attributes to detect an intrusion or DTOS attacks. Table 1 contains the parameters of the M-DBNN classifier. The optimal problem is solved up to 500 iteration levels in the proposed and existing techniques. The batch size refers to the sample used to train a model before modifying its trainable model variables, weights, and biases. Here, 14109 batch sizes are used in the M-DBNN for attack detection.

The fitness function of the created chimps is measured using mean square error (MSE) which is dependent on measuring the difference between both the intended and observed values by the generated search agents for all of the training sets. Comparison of mean square error versus iteration graphical model of the proposed and existing approach like mayfly, sailfish, and water strider is sketched

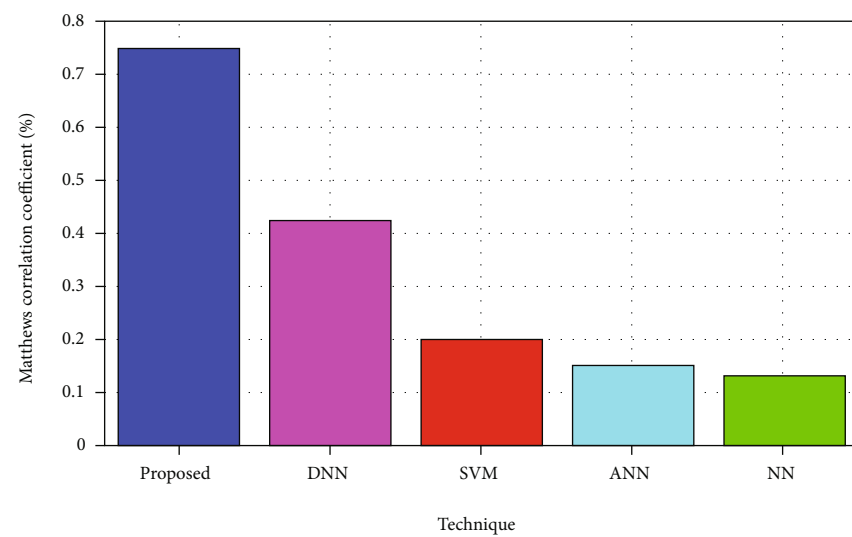
in Figure 3. Among these four approaches, the proposed ChOA give the best outcome; that is, in the first iteration, the value of the mean square is 1%; then the error is reduced to reach 0% at the 500th iteration. Mayfly optimization starts from a 1% error on 1st iteration, which reached a 0.13% error on the 500th iteration. Another Sailfish optimization starts with a 1% error on the 1st iteration, and it reduced the error to reach 0.22% on the 500th iteration. The final approach is to reduce the error value to 1% on the 1st iteration of the water striker, reducing the error to 0.33% on the 500th repeat. This graphical model demonstrates that the proposed ChOA gives 0% error, so the computation time of the approach is reduced.

Area Under the Curve- (AUC-) Receiver Operating Characteristic (ROC) curves seem to be a performance statistic for classification issues at variable threshold levels, which is shown in Figure 4. AUC represents the measure or degree of separation, whereas ROC is a probability curve. Generally, the curve of AUC is reached at 1; the performance of the system's measure is good. But the curve is in 0 value, the system's measure is very poor. The curve AUC gradually reaches 1 in 0.68 specifications in the proposed techniques. Calculating and displaying the true positive ratio instead of the false-positive ratio for classification at different thresholds give the ROC curve. Low training capability, sophisticated network attack detection, and local optimization are all M-DBNN problems. The optimal weights and dependencies of the M-DBNN classifier are determined by the ChOA algorithm.

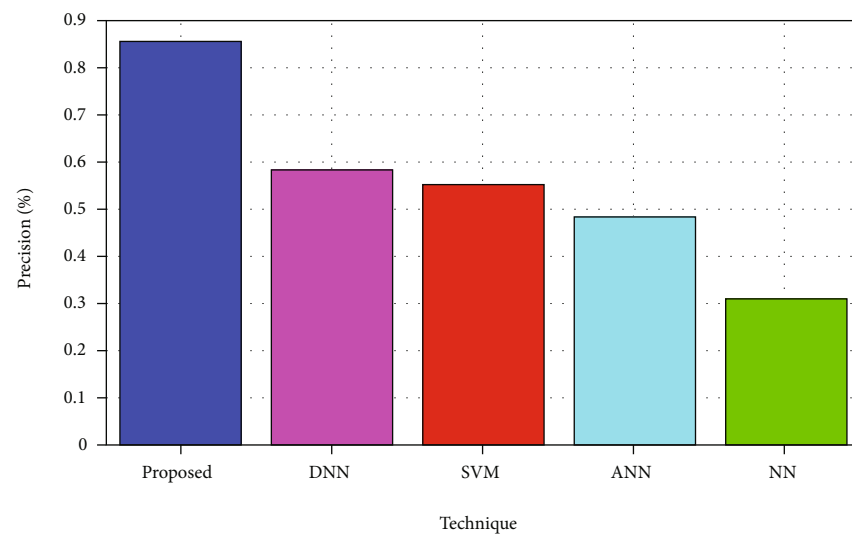
A confusion matrix and performance measures like accuracy, detection rate, and are used to produce analysis assessment. The projected class is represented by each column in the confusion matrix, whereas the actual class is represented by each row. For two or more class matrices, a confusion matrix can be employed. The variables True, False, Negative, and Positive are formulated as follows: True Negative—the number of negative instances is identified



(a)



(b)



(c)

FIGURE 6: Continued.

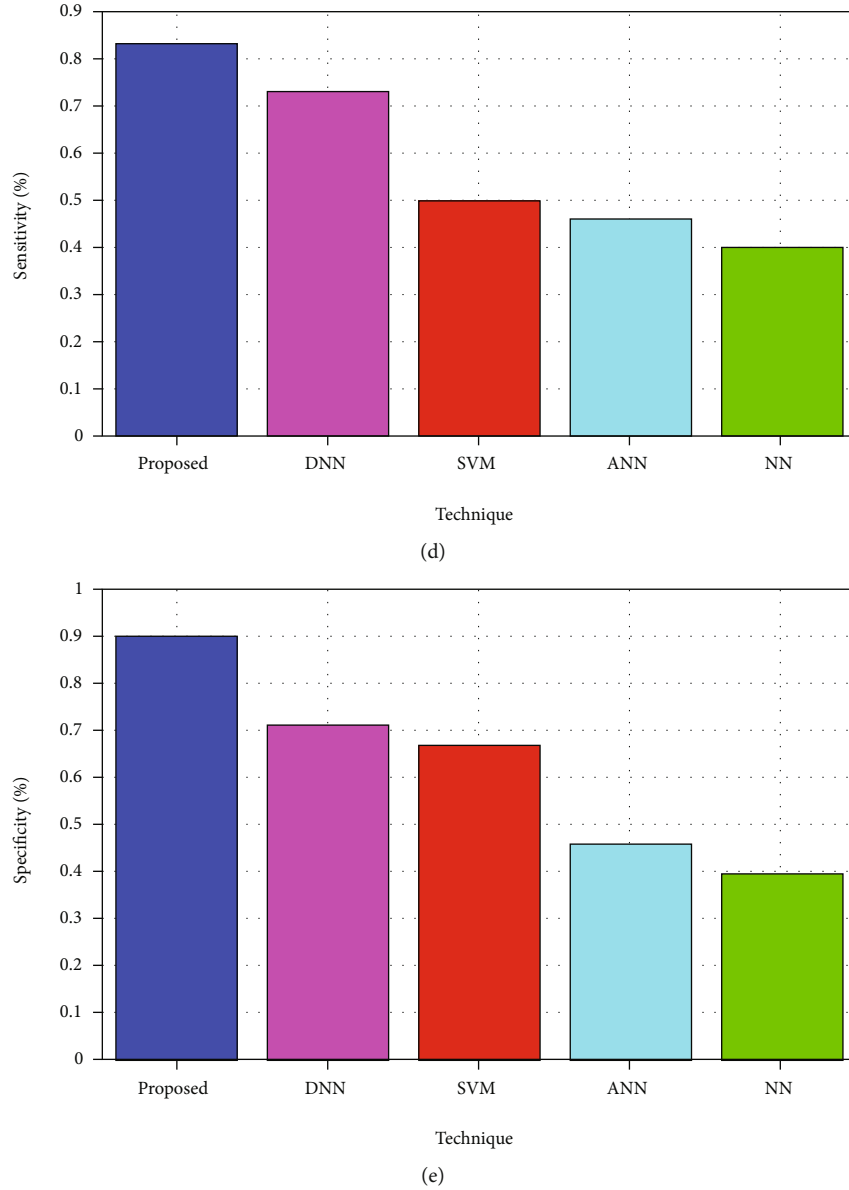


FIGURE 6: Comparison of proposed and existing approaches. (a) Kappa. (b) The Matthews correlation coefficient. (c) Precision. (d) Sensitivity. (e) Specificity.

correctly as ordinary; True Positive—the total number of positive instances is correctly categorized as an attack; False Positive—the number of nonattacking incidents has been incorrectly labelled as attacks; and False Negative—the number of assault instances is labelled as normal when they are not. Table 2 contains the confusion matrix of proposed and existing techniques.

The accuracy of a statistic refers to how close it is to the actual true value. This is significant since inaccuracies in results might be caused by faulty equipment, human error, or inadequate data processing. The accuracy of the proposed and existing approaches is sketched in Figure 5(a). The proposed M-DBNN provides 0.87% accuracy, while the existing DNN, SVM, ANN, and NN techniques give accuracies of 0.71%, 0.52%, 0.48%, and 0.45%, respectively. This is clearly demonstrated, and the proposed approach is more favour-

able than existing techniques. Similarly, the error is analyzed for the proposed and existing approaches that are shown in Figure 5(b). The discrepancy between the calculated value and the actual value is referred to as “error” in statistical analysis. The error of the proposed techniques is 0.13%, and the current techniques of DNN, SVM, ANN, and NN are 0.29% error, 0.48% error, 0.52% error, and 0.55% error, respectively. Then, the F1_score is analyzed and sketched in Figure 5(c). The F1 score is a machine learning metric that was used to calculate the system’s binary categories and quantify the dataset’s accuracy. The precision and recall models have a well-defined harmonic mean. The value of F1_score in the proposed approach is 0.84. And the values of F1_score of DNN, SVM, ANN, and NN are 0.67, 0.65, 0.35, and 0.30, respectively. Then, false positive rate is analyzed. That is, the likelihood of rejection of the null

TABLE 3: Overall performance of proposed and existing approaches.

Performance	Proposed M-DBNN	DNN	SVM	ANN	NN
Accuracy	0.87	0.71	0.52	0.48	0.45
Error	0.13	0.29	0.48	0.52	0.55
F1_score	0.84	0.67	0.65	0.35	0.30
False positive rate	0.09	0.28	0.32	0.53	0.55
Kappa	0.74	0.36	0.32	0.13	0.11
Matthews correlation coefficient	0.74	0.42	0.20	0.15	0.12
Precision	0.85	0.58	0.55	0.48	0.31
Sensitivity	0.83	0.73	0.50	0.45	0.40
Specificity	0.90	0.71	0.67	0.46	0.40

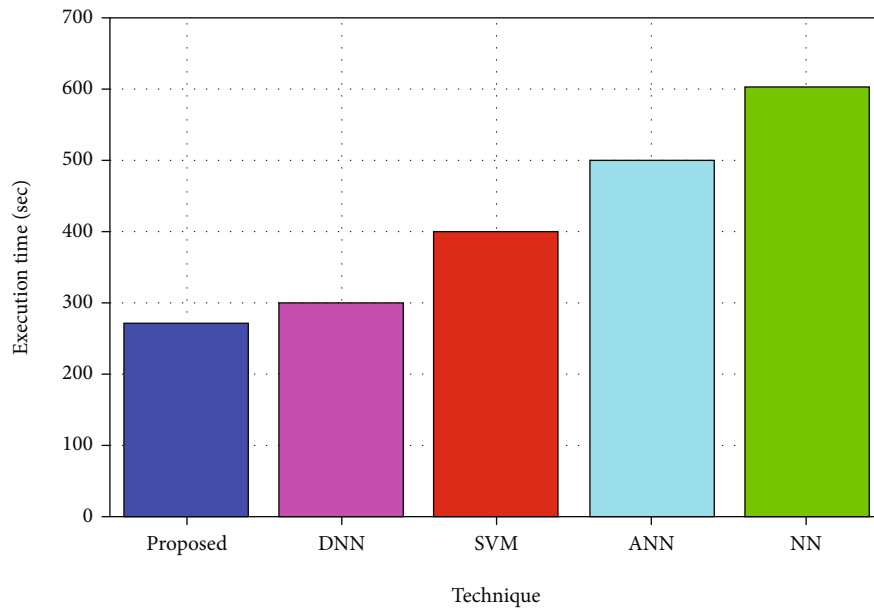


FIGURE 7: Comparison of proposed and existing techniques execution time.

hypothesis incorrectly for a test item is known as the false-positive ratio. The relationship between the number of negative events incorrectly classified as positive and the total number of true negative events is used to compute the false positive rate. The false positive rates of the proposed approach, DNN, SVM, ANN, and NN are 0.09%, 0.28%, 0.32, 0.53%, and 0.55%, respectively.

The statistical analysis of kappa is described as comparing the observed values of a training dataset to the expected value. In the proposed techniques, the value of kappa is 0.74%, 0.36% in DNN techniques, 0.32% in SVM techniques, 0.13% in ANN techniques, and 0.11% in NN techniques. The Matthews correlation coefficient is then analyzed, and in machine learning, the Matthews correlation coefficient (MCC) is used to estimate the validity of two binary classifications. The Matthews correlation coefficient value of the planned techniques is 0.74%, but those of the existing DNN, SVM, ANN, and NN techniques are 0.42%, 0.20%, 0.15%, and 0.12%, respectively. Next, precision is analyzed, which is presented in Figure 6(c). Precision is a labelling

strategy for the positive dataset. The split of true positives into the addition of genuine positives and false positives yields precision. The value of precision in proposed techniques is 0.85%, and those of the existing techniques of DNN, SVM, ANN, and NN contain 0.58%, 0.55%, 0.48%, and 0.31%, respectively. When compared to those of existing techniques, the precision values of the projected techniques is extremely high.

Moreover, the sensitivity of the proposed and existing techniques is analyzed and sketched in Figure 6(d). Sensitivity is critical for sensing network traffic since it precisely measures the positive dataset. The proposed technique is more sensitive, and it is utilized to detect minute variations in the network of a server. In comparison to the proposed techniques, the previous techniques are less sensitive. The sensitivity of the proposed techniques is 0.83%, and the sensitivity values of existing techniques such as DN, SVM, ANN, and NN are 0.73%, 0.50%, 0.45%, and 0.40%, respectively. Specificity is one of the statistical methods for correctly recognizing a negative dataset. Compared to the

current techniques, the planned method identifies the negative energy as 0.90%, which is very positive. Previous techniques of DNN, SVM, ANN, and NN contain 0.71%, 0.67%, 0.46%, and 0.40%, respectively. Table 3 contains the overall performance of the proposed and present approaches.

The suggested and existing approaches' execution times were also examined. The operating time of the approach refers to the time it takes to detect an intrusion or attack on the network. The proposed techniques detect the attack within 270 seconds. The current approaches DNN, SVM, ANN, and NN are 300 seconds, 400 seconds, 500 seconds, and 600 seconds, respectively, as described in Figure 7.

Experimental results have shown that the optimal configuration of M-DBNN techniques can be detected, which increases feature exposure performance, resulting in a much larger detection rate and shorter detection time than the system without reducing the dimension. As a result, the recommended ChOA-based M-DBNN classifier is best suited for DDoS detection and should be used in real-time applications.

5. Conclusion

An enhanced ChOA based M-DBNN is utilized to recognize DDoS attacks in the network. The main aim of the proposed technique is to extract representative features from the CAIDA "DDoS Attack 2007" dataset, reduce classification error, and correctly detect DDoS attacks. The preprocessing of the dataset is to remove redundant and irrelevant features from the dataset and to convert it to a finite number of values. The predata are fed to the M-DBNN to predict the class. An enhancement of M-DBNN is used for ChOA optimization, which reduces the error to select the best weight that is interconnected between the input and hidden layer, so the advanced M-DBNN very accurately predicts the classes. The proposed ChOA based M-DBNN gives high diagnostic accuracy which was demonstrated. Many performance measures of the proposed technique show a significant improvement when compared to the previous technique. The suggested technique had a detection accuracy of 87% and a false positive rate of 0.09% on the CAIDA "DDoS Attack 2007" dataset. In the future, advanced hybrid optimization will be used to predict the class more effectively. In addition, high-speed machine learning is used to detect anomalies in the network.

Data Availability

The dataset used to support the findings of this study is available from the corresponding author upon request.

Conflicts of Interest

The authors declare that there is no conflict of interest regarding the publication of this paper.

Acknowledgments

This work was supported by the National Research Foundation of Korea (NRF) grant funded by the Korea Government (MSIT) (No. 2021R1F1A1063319).

References

- [1] S. Haider, A. Akhuzada, I. Mustafa et al., "A deep CNN ensemble framework for efficient DDoS attack detection in software defined networks," *IEEE Access*, vol. 8, pp. 53972–53983, 2020.
- [2] R. R. Brooks, L. Yu, J. Oakley, and N. Tusing, "Distributed Denial of Service (DDoS): a history," *IEEE Annals of the History of Computing*, p. 1, 2021.
- [3] K. Kumar and S. Behal, "Distributed denial of service attack detection using deep learning approaches," in *2021 8th International Conference on Computing for Sustainable Global Development (INDIACom)*, New Delhi, India, 2021.
- [4] H. Zhang, Y. Li, Z. Lv, A. K. Sangaiyah, and T. Huang, "A real-time and ubiquitous network attack detection based on deep belief network and support vector machine," *IEEE/CAA Journal of Automatica Sinica*, vol. 7, no. 3, pp. 790–799, 2020.
- [5] A. A. Diro and N. Chilamkurti, "Distributed attack detection scheme using deep learning approach for Internet of Things," *Future Generation Computer Systems*, vol. 82, pp. 761–768, 2018.
- [6] A. Manimaran, D. Chandramohan, S. G. Shrinivas, and N. Arulkumar, "A comprehensive novel model for network speech anomaly detection system using deep learning approach," *International Journal of Speech Technology*, vol. 23, no. 2, pp. 305–313, 2020.
- [7] Q. Tian, D. Han, K. C. Li, X. Liu, L. Duan, and A. Castiglione, "An intrusion detection approach based on improved deep belief network," *Applied Intelligence*, vol. 50, no. 10, pp. 3162–3178, 2020.
- [8] A. Makuvaza, D. S. Jat, and A. M. Gamundani, "Deep neural network (DNN) solution for real-time detection of distributed denial of service (DDoS) attacks in software defined networks (SDNs)," *SN Computer Science*, vol. 2, no. 2, pp. 1–10, 2021.
- [9] J. Kim, J. Kim, H. Kim, M. Shim, and E. Choi, "CNN-based network intrusion detection against denial-of-service attacks," *Electronics*, vol. 9, no. 6, p. 916, 2020.
- [10] I. Sohn, "Deep belief network based intrusion detection techniques: a survey," vol. 167, Article ID 114170, *Expert Systems with Applications*, 2020.
- [11] K. Yang, J. Zhang, Y. Xu, and J. Chao, "Ddos attacks detection with autoencoder," in *NOMS 2020-2020 IEEE/IFIP network operations and management symposium*, pp. 1–9, Budapest, Hungary, 2020.
- [12] P. Yang, N. Xiong, and J. Ren, "Data security and privacy protection for cloud storage: a survey," *IEEE Access*, vol. 8, pp. 131723–131740, 2020.
- [13] K. S. Sahoo, B. K. Tripathy, K. Naik et al., "An evolutionary SVM model for DDOS attack detection in software defined networks," *IEEE Access*, vol. 8, pp. 132502–132513, 2020.
- [14] Y. Liu, "Ddos attack detection via multiscale convolutional neural network," *Computers, Materials & Continua*, vol. 62, no. 3, pp. 1317–1333, 2020.
- [15] T. A. Tuan, H. V. Long, R. Kumar, I. Priyadarshini, and N. T. K. Son, "Performance evaluation of botnet DDoS

- attack detection using machine learning,” *Evolutionary Intelligence*, vol. 13, no. 2, pp. 283–294, 2020.
- [16] R. Doriguzzi-Corin, S. Millar, S. Scott-Hayward, J. Martinez-del-Rincon, and D. Siracusa, “LUCID: a practical, lightweight deep learning solution for DDoS attack detection,” *IEEE Transactions on Network and Service Management*, vol. 17, no. 2, pp. 876–889, 2020.
- [17] S. D. Çakmakçı, T. Kemmerich, T. Ahmed, and N. Baykal, “Online DDoS attack detection using Mahalanobis distance and Kernel-based learning algorithm,” *Journal of Network and Computer Applications*, vol. 168, article 102756, 2020.
- [18] S. Dong and M. Sarem, “DDoS attack detection method based on improved KNN with the degree of DDoS attack in software-defined networks,” *IEEE Access*, vol. 8, pp. 5039–5048, 2020.
- [19] B. Hussain, Q. Du, B. Sun, and Z. Han, “Deep learning-based DDoS-attack detection for cyber–physical system over 5G network,” *IEEE Transactions on Industrial Informatics*, vol. 17, no. 2, pp. 860–870, 2021.
- [20] A. S. Alzahrani, “An optimized approach-based machine learning to mitigate DDoS attack in cloud computing,” *International Journal of Engineering Research and Technology*, vol. 13, no. 6, pp. 1441–1447, 2020.
- [21] F. Li, J. Zhang, C. Shang, D. Huang, E. Oko, and M. Wang, “Modelling of a post-combustion CO₂ capture process using deep belief network,” *Applied Thermal Engineering*, vol. 130, pp. 997–1003, 2018.
- [22] S. Wang, H. Chen, L. Wu, and J. Wang, “A novel smart meter data compression method via stacked convolutional sparse auto-encoder,” *International Journal of Electrical Power & Energy Systems*, vol. 118, article 105761, 2020.
- [23] M. Skafi, M. M. Yunis, and A. Zekri, “Factors influencing SMEs’ adoption of cloud computing services in Lebanon: an empirical analysis using toe and contextual theory,” *IEEE Access*, vol. 8, pp. 79169–79181, 2020.
- [24] http://205.174.165.80/CICDataset/CICDDoS2019/Dataset/PCAPs/01-12/PCAP-01-12_0750-0818.zip.

Research Article

The Mathematical Model of Marine Engine Room Equipment Based on Machine Learning

Ji Zeng ¹, Bowen Jin ², He Zhang,² Songyan Mai,² Bo Yuan,² Hui Jiang,² Mengkai Yang,² and Chaochun Huang²

¹Ocean Science and Engineering College, Shanghai Maritime University, Shanghai 201306, China

²Merchant Marine College, Shanghai Maritime University, Shanghai 201306, China

Correspondence should be addressed to Ji Zeng; zengji@shmtu.edu.cn and Bowen Jin; 201940110017@stu.shmtu.edu.cn

Received 25 January 2022; Revised 22 February 2022; Accepted 14 March 2022; Published 4 April 2022

Academic Editor: Mu-Yen Chen

Copyright © 2022 Ji Zeng et al. This is an open access article distributed under the Creative Commons Attribution License, which permits unrestricted use, distribution, and reproduction in any medium, provided the original work is properly cited.

This study is aimed at reducing the occurrence of oil spill accidents in the engine room of ships and carries out risk prevention for the equipment of the port ships, thereby reducing pollution to the marine ecological environment. Firstly, the concepts and principles of cluster analysis and ship automatic identification system are expounded. Secondly, the data information collected by the ship's automatic identification system (AIS) is combined with density-based cluster analysis. The accident area and extent at different stages of the ship's engine room equipment are classified. Finally, cluster analysis is used to evaluate the risk of equipment of the port ship engine room. The results show that there are 43000 ship operation information points in port a, the average operating speed of ships is 9 kilometers, and the fastest operation speed is 16.9 kilometers. In addition, many ship routes in port a need to take risk prevention measures to minimize the impact between ships and reduce the risk of oil leakage in the engine room. The proposed cabin model can easily and quickly analyze the orientation information of the ship and classify all the data into different types according to the surrounding information points. AIS can realize the information transfer between ships and between ship and shore. Information such as the position, speed, and direction of the ship needs to be accurately known to ensure safety at sea. These data need to relate to some terminals and networks to form a maritime monitoring network. The ship AIS based on cluster analysis can cluster the areas where the ship's speed and direction change significantly in the port area, effectively preventing accidents. Scientific risk prevention measures can effectively reduce the oil leakage risk of ship engine room equipment, improve the working efficiency of marine engines, and provide a strong foundation for the entire marine ecological environment protection.

1. Introduction

Since the 20th century, with the use of super large commercial ships, the pollution of the marine ecological environment caused by oil leakage in ship work has become more and more serious, which has also attracted the attention of all countries in the world. Since 1924, the United States promulgated the regulations on marine oil pollution caused by the ship oil spill. Most governments have also enacted conventions and rules on marine oil pollution. These laws and regulations have significantly reduced the oil pollution of the marine ecological environment, and the measures taken for the oil pollution of ships have changed from control to protection.

The marine oil spill is very harmful to the ocean, not only to the organisms in the sea but also to the restoration of the whole marine ecological environment. Therefore, the risk assessment of ship oil leakage equipment is also concerned by all countries [1]. At present, various electronic information devices have been used in the risk assessment of ship oil leakage equipment globally, such as GPS (global positioning system) and ship self-intelligent identification system [2]. At present, there are various ways to evaluate the risk of the data collected by electronic information devices. Analyzing the collected data is also a problem to be solved. Therefore, the clustering analysis of information mining [3] is born globally. It classifies the initially collected data and analyzes the meaning of these data.

The cluster analysis of ship engine room equipment risk assessment techniques is introduced, and the purpose and main motivation are to describe the concept and analysis method of cluster analysis. The main finding of the study is to implement a mathematical system model with an automatic ship identification function, which provides strong technical support for the entire marine ecological environment protection. This is also the main innovation point. The main problem is that there is too little detailed data on oil spills in ship engine rooms. Data can only be obtained through experimental simulation, which is also the fundamental problem of this discussion. The solution is to implement a mathematical model of ship engine room risk assessment by optimizing and improving machine learning-related algorithms combined with cluster analysis algorithms.

The overall structural logic is the following: Section 1 introduces commercial ships, and the theme is introduced through the introduction of the hazards of marine oil spills to the ocean related to the background. Section 2 implements a mathematical model for automatic identification of ship data by using the cluster analysis method combined with artificial intelligence technology. Section 3 takes port a as an example, the risk assessment level is constructed, and the corresponding measures should be taken through the case analysis of ship engine room equipment accidents. Section 4 introduces the experimental environment and the main data collection process and collects the main datasets. Section 5 draws conclusions by systematically analyzing the experimental results and expounds the content of marine ecological environment analysis. These research contents can provide the basis and direction for the risk assessment of ship engine rooms.

2. Recent Related Work

Many related studies have been carried out by scholars on ship engine room equipment and digital modeling technology. Yunlong et al. [4] conducted 3D design and research on ship engine room equipment based on knowledge engineering. Based on the knowledge engineering module, they studied the 3D layout design of the multipurpose cargo ship engine room. They established the classification rules of the ship engine room to improve the efficiency of knowledge acquisition. The result is as expected. The feasibility and effectiveness of knowledge engineering are verified in the 3D layout design of the ship engine room. Zhang et al. [5] designed and researched the virtual ship engine room system based on the Unity3D platform. The mathematical model of the rudder is established based on the introduction of the related concepts of the ship system. Their proposed method enhances the operating experience with the same working environment in the cabin. Park [6] used transfer learning to classify marine engine room machines. The results show that the ship's engine room has improved automation systems. Wang et al. [7] studied the condition monitoring method of marine engine room equipment based on machine learning and proposed a condition monitoring method based on manifold learning and isolation forest. They introduced the isolation forest algorithm to train and build multiple state models using standard condition data. The model has a significant reference value for detecting and

repairing marine engine room equipment. Jou et al. [8] studied the bonded discrete element method of ship-ice interaction in sea ice fields. They conducted icebreaking studies on continuous horizontal ice sheets by loading a single-degree-of-freedom model of the icebreaker. The experimental simulation results verify the effectiveness of the proposed model. Cheng et al. [9] studied the data-driven modeling method of ship motion based on a neural network. They present a global sensitivity analysis method that combines artificial neural networks and sparse polynomial chaos expansion techniques. The findings can provide technical support for high-dimensional sensor data collected from ship motion. Liu et al. [10] conducted research on ship collision risk modeling based on the cloud model and developed an inference engine system based on the cloud model to assess ship collision risk. The results are used to verify the feasibility of the proposed ship collision risk modeling. Compared with the traditional ship collision risk model, the proposed ship collision risk model has the advantages of simple implementation, accurate results, and short time required to generate the risk model.

In summary, to avoid collisions with key objects during navigation, many scholars have constructed a cloud model of ship navigation based on global sensitivity and uncertainty. The model can be used in ship collision risk analysis to reduce the dimension of risk parameters and reveal the main factors of unstable collision risk [11–13]. However, these results are insufficient for evaluating the uncertain results in hazard calculations, making it challenging to predict accidents accurately. Therefore, the proposed risk assessment model of ship engine room combined with clustering analysis and AI can provide reasonable suggestions for basic navigation safety. In this way, marine pilots can make timely and correct decisions to reduce or avoid collisions.

3. Mathematical Model of Room Risk Assessment of Ship Engine Combined with Cluster Analysis and AI

During the navigation of the ship, the condition of the ship's engine room directly affects the navigation risk of the ship. To assess the risk of the ship's voyage, firstly, the data from the ship's engine room is analyzed in detail. During the voyage of the ship, the dimension and total amount of data in the engine room will increase exponentially. Manual processing of all the data in the dataset is difficult to accomplish. Therefore, through the clustering method, the data with the same characteristics in the data is gathered in a group and analyzed and evaluated as a whole.

3.1. Cluster Analysis. Cluster analysis [14] divides the data information into relatively similar groups and then analyzes the data information of these groups. Cluster analysis is a kind of thinking mode of human beings. Its purpose is to gather and analyze information based on a comparable basis. There are many types of clustering, including digital-related data, computer information, statistical information, biological information, and economic-related information. Although they are all in different fields, they are all similar analyses of data, and similar data information is gathered. From the perspective of

machine learning, clustering analysis is unsupervised learning. It depends on a predefined group or part of the data information that has been analyzed. Cluster analysis is also learning with observation property and exploration significance. At the beginning of cluster analysis, there is no need for a clustering basis model. Cluster analysis can analyze and classify according to the most original data information, and the beginning and end of clustering must be the same. Clustering analysis can be used as a feature task of data mining, which can aggregate the scattered data information and then analyze it.

At present, clustering analysis includes system clustering, decomposition, addition, dynamic clustering, ordered sample clustering, overlapping clustering, and fuzzy clustering [15]. The clustering analysis calculation method is shown in Figure 1.

3.2. AIS. Firstly, the AIS [16] is a piece of information and maritime safety intercommunication system between ships and between ships and shore. It consists of VHF (very high frequency) communication equipment, GPS, ship display equipment, sensor equipment, and other devices that can communicate. The equipment realizes the information between ships and between ships and the shore and accurately grasps the ship's position, sailing speed, direction, and other information. The AIS in the vessel can send data to the outside. The VHF equipment can accept similar information from other ships so that the ship can automatically answer. AIS is an information dissemination system that communicates with the outside world. It can connect some terminals and networks to form a marine monitoring network. In the absence of radar, AIS can effectively reduce ship traffic accidents. Among them, the main body of AIS equipment is composed of shore-based (base station) facilities and ship-borne equipment. With the help of the global positioning system, dynamic ship data such as ship position, ship speed, course change rate, and heading can be transmitted to nearby waters through high-frequency digital signals. The test information of AIS is shown in Figure 2.

In Figure 2, if the data of the automatic identification system (AIS) are similar or close to the same level, the similar data is filtered, and only the data points with the same feature in the center of the set are retained. The rest of the data information will be packed and compressed [17]. If the distance between two ship track points is less than 1/2 of the ship length, lossless data compression can be adopted to compress data signals by converting the values of all attributes of the same column in the storage column into binary groups to improve the efficiency of data transmission. The information compression process is shown in Figure 3.

Through preliminary analysis of the information of the AIS, the service identification code, operation address, and operation track point of each ship's waterborne mobile communication are known, as shown in Table 1.

The information in Table 1 is initially analyzed. Then, the form of the data is analyzed. After the data features are extracted, the similarity between the data is calculated [18]. If the extracted information is N , the calculation method is as shown in

$$N = \begin{bmatrix} x_{or} \cdots x_{1d} \\ x_{e1} \cdots x_{ed} \end{bmatrix}. \quad (1)$$

x_{or} represents the r -dimensional information of the 0th data. 1_d represents the number of samples.

The basic equations are used to calculate ship distance:

$$Q_{op} = (d_o, d_r) = \left[\sum_{ior}^h |x_{oi} - x_{ri}|^m \right]^{1/m}, \quad (2)$$

$$Q_{op} = (d_o, d_r) = \left[\sum_{ih1}^h |x_{oi} - x_{ri}|^2 \right]^{1/2}, \quad (3)$$

$$Q_{op} = \sum_{ih1}^d |x_{oi} - x_{ri}|. \quad (4)$$

Equations (2)–(4) denote different representations of the space position coordinates of the ship's distance. (d_o, d_r) represents the distance between two ships during the voyage. The calculation of the spatial position Q_{op} and the angle θ_{op} of the ship's sailing distance from the port is shown in

$$\begin{cases} Q_{op} = \frac{1 - \theta_{op}}{2}, \\ \theta_{op} = \sum_{ih1}^d \frac{x_{oi}x_{ri}}{\left[\sum_{ih1}^d x_{oi}^2 \sum_{ih1}^d x_{ri}^2 \right]^{1/2}}. \end{cases} \quad (5)$$

Finally, the density-based clustering algorithm is selected according to the information characteristics [19]. This clustering algorithm uses the path between the information to analyze whether the information is a unit. It can analyze the orientation information easily and quickly and significantly reduce noise to the analysis results. In the density-based clustering algorithm, information points can divide all information into three types under the information points around them, including center points, edge points, and noise points. Its distribution is shown in Figure 4.

How to judge the area described by the information point mainly depends on two coefficients. One is the area of the information point, which is determined by the radius of the circular area. The other is the total number of other information points. The center point refers to the information point in the radius field of the circular area that exceeds the initial range value of the area, as point c shown in Figure 4. The edge point refers to the information point in the radius field of the circular area that cannot meet the initial range value of the area, as point b showed in Figure 4. The noise point refers to the information point collected that does not meet the above two situations, as point a shown in Figure 4.

3.3. Accident Analysis of Ship Engine Room Equipment: Taking Port a as an Example. Firstly, the general situation of the accident of the engine room equipment of the ship

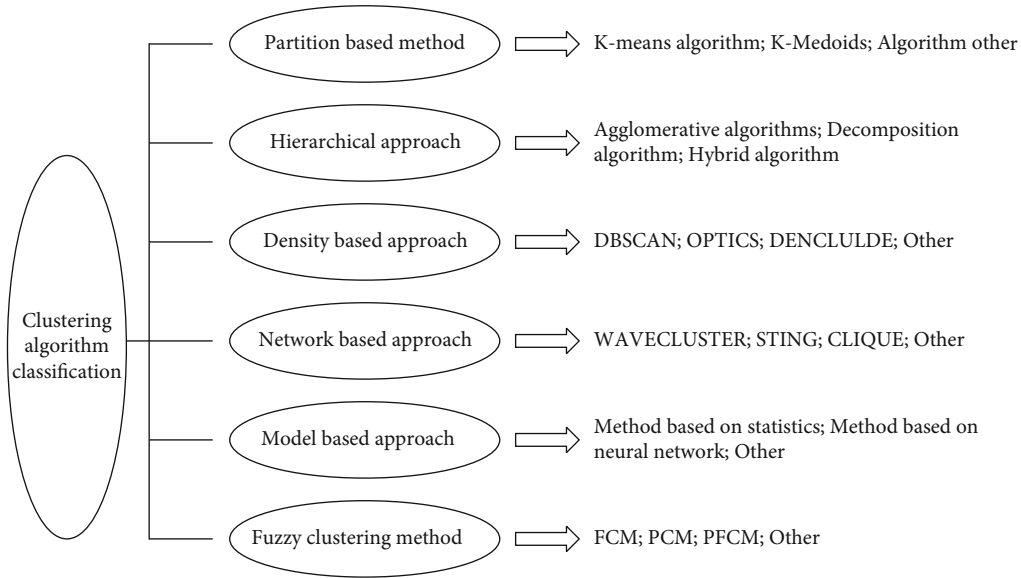


FIGURE 1: General clustering algorithms.

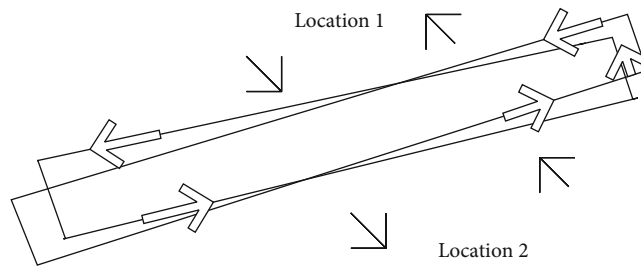


FIGURE 2: Multi-round-trip ship automatic identification data.

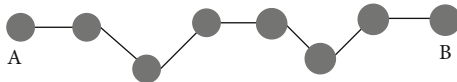


FIGURE 3: Information compression.

TABLE 1: Track composition.

Water mobile communication service identification code (m)	Address	Track point
M ₁	I1	(I11, Y11), (I12, Y12) ...
M1	I2	(I21, Y21), (I22, Y22) ...
M1	I3	(I31, Y31), (I32, Y32) ...
M1	I4	(I41, Y41), (I42, Y42) ...
M2	I5	(I51, Y51), (I52, Y52) ...

is the oil leakage accident [20]. According to the number and area of the oil leakage, the measures taken are also different. It is necessary to prepare the actions to be taken in the face of emergencies to reduce the risk of accidents. The international marine management organization has formulated a

unified risk specification for ships' engine rooms [21]. The scope and quantity of all risks can be represented by a matrix, including the probability matrix and the resultant impact matrix. Different engine room accidents lead to different risk levels. The risk levels of varying engine rooms are analyzed.

Firstly, the base level of the matrix represents the risk of an accident in the ship's engine room, which is minimal, and the threat it poses is relatively tiny. Therefore, preventive measures are not needed.

Secondly, the upper part next to the base layer is the middle part of the matrix. This part has a medium probability of engine room accidents. Therefore, specific prevention measures are needed to reduce the possibility of risk.

Thirdly, the section close to the upper level has the most significant probability of accidents in the ship's engine room. Moreover, this type of accident has a significant impact on the ocean, causing severe pollution and the slow recovery of the sea. For the risk of this kind of level, reduce the risk of the upper deck to the middle tier by preventing it in advance. If the means of prevention cannot downgrade this kind of risk, it should be analyzed from the source of this kind of accident.

According to different risk levels, the required solutions are shown in Table 2.

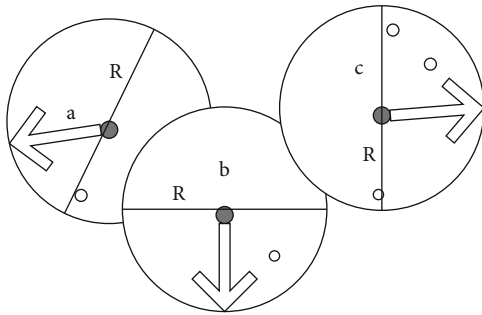


FIGURE 4: Density-based clustering analysis points.

Secondly, judge the critical areas in port a where accidents may occur.

Step 1. Judge the navigation speed of the ship. If there is a potential safety hazard, the ship will change the navigation speed. According to the specific technology, the operating rate of vessels in port a is analyzed, as shown in Figure 5.

According to the analysis of the figure, there are 43000 ship operation information points in port a. The average operation speed of the ship is 9 km, and the fastest operation speed is 16.9 km.

Step 2. Judge the ship's direction of navigation. The vessel has seven recommendations in total, and there is a 45-degree difference in each order.

3.4. Density-Based Cluster Analysis Method to Process Data.

The density-based clustering method can better identify the same feature of the data and can ensure that all the data in the database can be processed. Therefore, the density-based cluster analysis method is used to process the data during the ship's voyage. Through the analysis of AIS data and information, port a is basically from south to north and from east to west. Density-based cluster analysis is employed. Step 1: find a relatively close information point and increase the density of the central area. Step 2: calculate the information by density-based cluster analysis—the high-density range where the speed and direction of ships in port a change rapidly are obtained. The navigation channels are complex in the above measurements compared with other areas. Firstly, the threshold is fixed. The threshold is generally derived from the specific ship performance of the ship sailing, and the speed and direction of the ship are regulated by the threshold [22]. After the threshold is specified, the information points of the ship's operating route that need to be calculated can be obtained. Then, density-based cluster analysis is used to perform calculations on the data to remove noise points. Clustering data for port a is obtained.

In Figure 6, the A sea area is the gathering point of ship speed and direction changes. There are many berthing areas in this sea area, these areas are scattered on the edge of the sea area, and collision accidents are very likely to occur in the process of ships entering and leaving the sea area. Therefore, ships entering and leaving the sea should reduce their speed, pay attention to changes in direction, and assess risks promptly to avoid collisions.

3.5. *Risk Prevention Measures.* From the result of cluster analysis on the data obtained from the AIS of ships, it is known that many ship routes in port need to take risk prevention measures, thus minimizing the impact between vessels and reducing the risk of oil leakage in the engine room. According to the data results of the above analysis, the prevention of oil leakage accidents in the engine room of the ship can be carried out from the following aspects:

- (1) The computer network and radar are used to monitor the ship and provide helpful information for the vessel in motion, thus improving the ship's safety. During the ship's operation, the communication between the vessels and the working post in the port shall be strengthened to form a real-time intelligent management system [23]
- (2) When the total oil volume of ships in the port exceeds 3000 tons, the port should set up prompt signal devices in the water area with high ship density, making the ships passing by or ready to stop pay attention to the current port conditions. Additionally, the silt at the border of the port shall be removed. In extreme weather, the port shall timely inform the ship of a lower speed or prohibit the vessel from passing
- (3) Scientific berthing specifications shall be formulated in the port's ship berthing area and anchoring water area, and the berthing application shall be made before the ship enters the port, as well as the traveling speed after entering the port. In the case of many vessels, separation measures should be taken [3] to avoid collision and oil leakage between ships, thus causing pollution to the marine ecological environment
- (4) The ships entering and leaving should be supervised with antipollution measures. Spot check the antipollution equipment of the vessel and prohibit the vessels with weak antipollution equipment from entering and leaving the port. The ship's antipollution equipment is mainly divided into complicated and soft equipment [24]. The hard equipment specifically includes the oil filtering device, degreasing agent, and water-oil separation device in the ship. The supervision of this equipment must be subtle and careful. The soft equipment is mainly related to norms and systems. According to different risk prevention, different prevention and solution measures are developed, reducing the risk rate of oil leakage. The international standards include *Oil Pollution Prevention Certificate* and *Oil Pollution Emergency Plan on Board*

4. Risk Assessment of Ship Engine Room Equipment

4.1. *Experimental Environment.* The sea area in ports is divided into grids, and the average speed of ships in ports is calculated to study the behavior characteristics of vessels in ports. After the data is analyzed, the grid width is defined

TABLE 2: Risk level and corresponding measures taken.

Risk level	Risk resolution
Low level	In the basic situation, no measures should be taken, but the problem should be prevented from expanding. For example, the oil leakage in the ship's engine room is less than ten tons.
Medium level	Take risk reduction measures, and the funds needed to be considered when using the standards, which shall not exceed the budget. For example, the amount of oil leakage in a ship's engine room is between ten and fifty tons.
High level	Take all feasible measures to reduce the risk level until it reaches the medium level. For example, the amount of oil leakage in a ship's engine room is more than fifty tons.

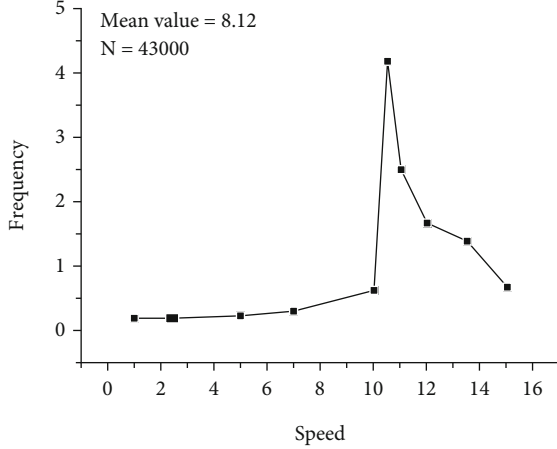


FIGURE 5: The speed of ships at port a.

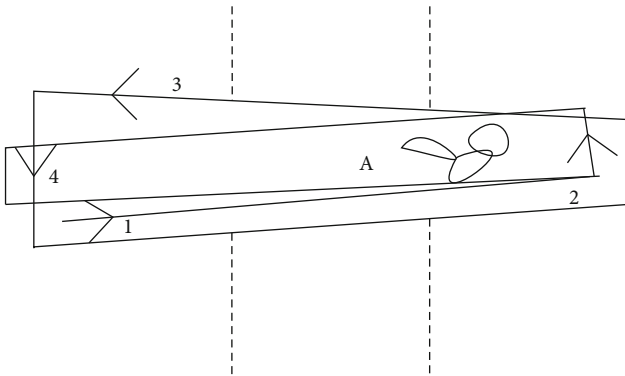


FIGURE 6: Regional clustering analysis of ship speed and direction changes.

as 100 m. The overall grid division of the study area is carried out with a grid of 100 m * 100 m. According to the grid width, the sea area to be studied is divided into 11457 grids. The experimental equipment adopted is a navigation simulator experimental platform. Firstly, data on the hydrological conditions of Tianjin Port are collected. Ship navigation conditions are modeled by simulating ship operations.

4.2. Dataset Collection and Data Preprocessing. The experimental dataset is from the Maritime Comprehensive Database. When the ship is sailing, the intelligent sensors installed on the waterway will transmit the on-site ship data to the data

acquisition unit through standard signals. The standard digitized signal is loaded into the server via the communication network. In addition, the data receiving equipment on the ship will be connected through the cloud server of communication network language. The processed data will be sent to the coast center server. The data is subjected to preprocessing operations. The data collected in the experiment are divided into a training set, validation set, and test set according to the ratio of 6:3:1. The data in the training set can enhance the model training, while only the data in the test set is used to obtain the final model output. The experimental dataset includes ship number, driving speed, heading, system reporting time, and ship navigation coordinates. A sample example of the dataset is shown in Table 3.

4.3. Parameter Setting. In traditional model training, elements in the dataset with significant numerical differences may make model training difficult. For this purpose, the ship data is subjected to data tagging. The route trajectory of each ship is interpolated and smoothed. The state values of all trajectories are placed between [0, 1]. In the spatial network of nonlinear function mapping, the number of hidden nodes in each layer is set to 128. The number of iterations is set to 500, and the batch size is set to 1024. The ship's trajectory data is used for model testing. The initial learning rate is 0.001, and the learning rate decay factor is 0.95.

4.4. Performance Metrics. Mean absolute error (MAE) and root mean square error (RMSE) are used to evaluate the performance of the proposed model algorithm. The smaller the MAE and RMSE values and the smaller the quotient of the within-group variation and the degrees of freedom of error in the analysis of variance, the smaller the sample standard deviation difference between the predicted and observed values (called residuals). To illustrate the degree of dispersion of the samples, in nonlinear fitting, the smaller the RMSE and MAE, the better.

4.5. Performance Evaluation and Discussion. The performance evaluation results of the model are analyzed and discussed. After cluster analysis divides all ship navigation data into information, an AI algorithm constructs ship navigation AIS. The service identification code, operation address, and operation tracking point of each ship's water mobile communication are recorded through the preliminary analysis of AIS data. Additionally, ship engine room accidents are analyzed by measuring ship speed and distance. Port a is used as an example, and the density-based cluster analysis method is used

TABLE 3: Sample examples of research datasets.

Ship number	x	y	Speed	Heading	System reporting time
1102	39123	12013	3	12.1	12.21 09:00
1258	22581	32478	5	14.4	08.11 14:00

TABLE 4: Performance evaluation and comparison of different algorithms.

Method	MAE	RMSE
EKF	0.006	0.016
BPNN	0.051	0.008
LSTM	0.005	0.002

to process the data. The results can provide necessary references for ship navigation risk prevention. Furthermore, the model prediction errors of the LSTM algorithm, EKF, and BPNN algorithms on the test dataset are compared. The data results show that both the mean absolute error and the root mean square error of the LSTM algorithm are the smallest. Among them, the mean absolute error is 0.005, and the root mean square error is 0.002. The specific parameters of each performance index are shown in Table 4. Therefore, the prediction error of the proposed LSTM algorithm is smaller than the other two algorithms, and the model prediction accuracy is higher.

5. Conclusion

Marine pollution damage caused by oil spills in ship engine rooms is not only persecution of aquatic life but also massive harm to the entire marine ecological environment. This contamination requires a very long recovery time. Effective measures must be taken to prevent oil spills in engine rooms and reduce pollution to the marine environment. Cluster analysis and artificial immune systems are presented and analyzed. Density-based cluster analysis is combined with data information collected by AIS. The risk of ship engine room accidents is classified through cluster analysis. Additionally, the speed and direction of the ships in port are analyzed. Ships in a port are subject to accident risk management. Finally, the corresponding risk prevention measures are proposed. Port a is used as an example to assess the risk of ship engine room equipment. The results show that the adjustment of the ship's running speed and direction by the threshold significantly impacts the occurrence of oil leakage accidents in the ship's engine room. Therefore, ships should pay attention to changes in ship speed and direction when entering and leaving the sea. The risk assessment of ship engine room accidents has high value for protecting the marine ecological environment. However, some shortcomings are unavoidable. Some vessels are operating illegally in port waters, and these vessels with abnormal behavior need further behavior detection. In future research, the features of ship data in different ports are extracted to strengthen the monitoring of ship behavior.

Data Availability

The raw data supporting the conclusions of this article will be made available by the authors, without undue reservation.

Ethical Approval

This article does not contain any studies with human participants or animals performed by any of the authors.

Consent

Informed consent was obtained from all individual participants included in the study.

Conflicts of Interest

All authors declare that they have no conflict of interest.

Authors' Contributions

All authors listed have made a substantial, direct, and intellectual contribution to the work and approved it for publication.

Acknowledgments

The authors acknowledge the help from the university colleagues.

References

- [1] Y. P. Li, Z. J. Liu, C. Yao, and Z. G. Zheng, "Analysis of maritime traffic characteristics based on AIS data constraint clustering," *Ship & Ocean Engineering*, vol. 47, no. 1.
- [2] T. R. Zhou, Z. P. Shao, J. C. Pan, and Z. M. Zhang, "A study on the dynamic field of ships in confined waters based on AIS data mining," *Journal (NATURAL SCIENCE EDITION)*, vol. 23, no. 1, pp. 33–38, 2018.
- [3] F. L. Meng, "Using AIS data mining to build ship arrival rule model?," *Ship science and technology*, vol. 38, no. 10, pp. 28–30, 2016.
- [4] W. Yunlong, J. Yunbo, and G. Guan, "Design of three-dimensional layout of ship engine room equipment based on knowledge based engineering," *Journal of Shanghai Jiaotong University*, vol. 55, no. 10, p. 1219, 2021.
- [5] Q. Zhang, N. Chang, and K. Shang, "Design and exploration of virtual marine ship engine room system based on Unity3D platform," *Journal of Intelligent & Fuzzy Systems*, vol. 38, no. 2, pp. 1241–1247, 2020.
- [6] K. M. Park, "Machine classification in ship engine rooms using transfer learning," *Journal of the Korean Society of Marine Environment & Safety*, vol. 27, no. 2, pp. 363–368, 2021.
- [7] R. Wang, H. Chen, and C. Guan, "Condition monitoring method for marine engine room equipment based on machine learning," *CHINESE JOURNAL OF SHIP RESEARCH*, vol. 16, no. 1, 2021.
- [8] O. Jou, M. A. Celigueta, S. Latorre, F. Arrufat, and E. Oñate, "A bonded discrete element method for modeling ship–ice interactions in broken and unbroken sea ice fields," *Computational Particle Mechanics*, vol. 6, no. 4, pp. 739–765, 2019.

- [9] X. Cheng, G. Li, R. Skulstad, S. Chen, H. P. Hildre, and H. Zhang, "A neural-network-based sensitivity analysis approach for data-driven modeling of ship motion," *IEEE Journal of Oceanic Engineering*, vol. 45, no. 2, pp. 451–461, 2020.
- [10] H. Liu, L. Zhang, and S. Liu, "Modeling of ship collision risk based on cloud model," *IEEE Access*, vol. 8, pp. 221162–221175, 2020.
- [11] I. Adhita and M. Furusho, "Ship-to-ship collision analyses based on functional resonance analysis method," *Journal of ETA Maritime Science*, vol. 9, no. 2, pp. 102–109, 2021.
- [12] M. K. Lee, Y. S. Park, S. Park, E. Lee, M. Park, and N. E. Kim, "Application of collision warning algorithm alarm in fishing vessel's waterway," *Applied Sciences*, vol. 11, no. 10, p. 4479, 2021.
- [13] Z. Liu, Y. Li, S. Dong, and Z. Zhang, "Spatial logical relationship analysis model of ship encounter space," *Ocean Engineering*, vol. 239, p. 109912, 2021.
- [14] Q. H. Tian, Y. Y. Mei, Y. X. Du, and X. G. Zhou, "Research on task planning of large capacity coupling design based on cluster analysis," *Mechanical engineering*, vol. 29, no. 5, pp. 544–551, 2018.
- [15] W. Y. Ma, Z. L. Wu, W. F. Li, and J. X. Yang, "Identification of single ship handling mode in AIS data," *China navigation*, vol. 40, no. 4, pp. 51–55, 2017.
- [16] Z. J. Liang, W. Chen, and F. C. Jiang, "A study on AIS based early warning modeling of ship grounding risk," *Zhujiang water transport*, vol. 6, pp. 63–65, 2017.
- [17] Z. Jiao, J. X. Liu, C. Xiao, and H. H. Li, "Track based behavior pattern mining of inland river ships," *Traffic information and safety*, vol. 35, no. 3, 2017.
- [18] S. B. Zhou and W. X. Xu, "Research progress of ship trajectory anomaly detection method," *Journal of electronic measurement and instrumentation*, vol. 31, no. 3, pp. 329–337, 2017.
- [19] B. C. Jiang, W. Z. Key, and H. You, "Mining and identifying abnormal behavior of ships in maritime traffic," *Computer simulation*, vol. 34, no. 6, pp. 329–334, 2017.
- [20] Y. B. Wang, G. C. Pan, L. Xin, and Y. Xiang, "Risk assessment of oil spill accident of ships in the tidal sea," *Marine Limnology bulletin*, vol. 2, pp. 24–29, 2016.
- [21] X. Zhe, C. J. Shi, Q. Y. Hu, and Y. Chun, "A method for planning safe routes using massive AIS data China work safety section science and technology," *Journal of Jimei University*, vol. 12, no. 10, pp. 160–164, 2016.
- [22] L. H. Jiang, Z. Y. Zheng, and Q. Le, "Extraction method of ship encounter information in AIS data," *Chinese science and technology paper*, vol. 12, no. 7, pp. 802–805, 2017.
- [23] J. H. Wu, W. Chen, L. Wen, and J. W. Guo, "Automatic detection and repair algorithm for AIS trajectory anomaly of ship," *China navigation*, vol. 40, no. 1, 2017.
- [24] J. J. Tian, S. F. Tian, and T. Rong, "Impact analysis of offshore oil spill based on GIS," *Surveying and mapping equipment*, no. 1, 2006.

Research Article

Empirical Analysis of Machine Learning Algorithms for Multiclass Prediction

Umar Ishfaq,¹ Danial Shabbir,¹ Jumshaid Khan,¹ Hikmat Ullah Khan,¹ Salman Naseer,² Azeem Irshad ,³ Muhammad Shafiq ,⁴ and Habib Hamam^{5,6,7,8}

¹Department of Computer Science, COMSATS University Islamabad, Wah Campus, Wah Cantt 470040, Pakistan

²Department of Information Technology, University of the Punjab Gujranwala Campus, Gujranwala 52250, Pakistan

³Department of Computer Science and Software Engineering, International Islamic University Islamabad, Pakistan

⁴Department of Information and Communication Engineering, Yeungnam University, Gyeongsan 38541, Republic of Korea

⁵Faculty of Engineering, Uni de Moncton, E1A3E9, Moncton, NB, Canada

⁶International Institute of Technology and Management, Commune d'Akanda, BP, Libreville 1989, Gabon

⁷School of Electrical Engineering, Department of Electrical and Electronic Engineering Science, University of Johannesburg, Johannesburg 2006, South Africa

⁸Spectrum of Knowledge Production & Skills Development, Sfax 3027, Tunisia

Correspondence should be addressed to Muhammad Shafiq; shafiq@ynu.ac.kr

Received 4 January 2022; Revised 21 February 2022; Accepted 11 March 2022; Published 30 March 2022

Academic Editor: Alireza Souri

Copyright © 2022 Umar Ishfaq et al. This is an open access article distributed under the Creative Commons Attribution License, which permits unrestricted use, distribution, and reproduction in any medium, provided the original work is properly cited.

With the emergence of big data and the interest in deriving valuable insights from ever-growing and ever-changing streams of data, machine learning has appeared as an effective data analytic technique as compared to traditional methodologies. Big data has become a source of incredible business value for almost every industry. In this context, machine learning plays an indispensable role of providing smart data analysis capabilities for uncovering hidden patterns. These patterns are later translated into automating certain aspects of the decision-making processes using machine learning classifiers. This paper presents a state-of-the-art comparative analysis of machine learning and deep learning-based classifiers for multiclass prediction. The experimental setup consisted of 11 datasets derived from different domains, publicly available at the repositories of UCI and Kaggle. The classifiers include Naïve Bayes (NB), decision trees (DTs), random forest (RF), gradient boosted decision trees (GBDTs), and deep learning-based convolutional neural networks (CNN). The results prove that the ensemble-based GBDTs outperform other algorithms in terms of accuracy, precision, and recall. RF and CNN show nearly similar performance on most datasets and outperform the traditional NB and DTs. On the other hand, NB shows the lowest performance as compared to other algorithms. It is worth mentioning that DTs show the lowest precision score on the Titanic dataset. One of the main reasons is that DTs suffer from overfitting and use a greedy approach for attribute relationship analysis.

1. Introduction

The rapid development in web technologies resulted in the creation of immense volume of data, which requires efficient data extraction and intelligent data analysis for identifying relevant information. Machine learning (ML) is a relatively new domain of data analysis which plays an important role in emulating human intelligence in electronic devices. Resultantly, these devices can learn and progressively improve their performance on specific tasks without explicit programming [1]. A

recent report suggests that ML will be the center of innovation in near future [2]. ML techniques have been successfully employed in web search [3], recommendation systems [4], email filtering [5], ad placement [6], fraud detection [5], credit scoring [7], stock trading [8, 9], and many other applications.

ML techniques are mainly divided into four categories: (1) supervised, (2) unsupervised, (3) semisupervised, and (4) reinforcement learning. In supervised learning, the classifiers are trained through examples. The classifier identifies patterns from the labeled data and learns from the

observations till achieving a certain level of performance. On the contrary, unsupervised learning interprets the structure of data and uses this information for organizing the data into groups or clusters. Unsupervised ML does not use data labels or any information about the desired outcome in advance. Similarly, semisupervised learning uses a combination of both labeled and unlabeled data for mining meaningful patterns. Research identifies that accuracy can improve significantly when unlabeled data is used in conjunction with labeled data [10]. Finally, reinforcement learning is a new area in ML that is concerned with achieving an optimal outcome through trial and error [11].

The objective of the paper is to present a comprehensive performance analysis of various classification algorithms for multiclass prediction using multiple datasets. The algorithms include Naïve Bayes (NB), decision trees (DTs), random forest (RF), gradient boosted decision trees (GBDTs), and DL-based convolutional neural networks (CNN). NB and DTs are classic ML algorithms. NB is one of the simplest and oldest classifiers which is based on Bayesian theorem. NB is particularly suited in situations where input dimensions are relatively high. Similarly, DTs present the decision results in a tree-like graph with all possible consequences, including chance event outcomes. DTs are mostly applied in decision analysis and operation research for identifying an effective strategy. On the other hand, RF [12] and GBDTs [12] are ensemble-based techniques. An ensemble technique uses multiple base algorithms for better classification results that could be obtained through any of the constituent base algorithm alone. GBDT is a stochastic prediction method that represents an ensemble or collection of single regression trees which are combined (i.e., mean) to give a final prediction. Similarly, RF takes multiple samples of training data, creates models for each data sample, and takes an average of these sample models for making a better estimate of true outcome. Finally, CNN [13] is a recently developed neural network-based classification approach. CNNs are like traditional neural network with neurons having learnable weights and biases. A neuron can receive many inputs, performs a weighted sum, and passes it to an activation function for the final output.

This study is inspired by some recent machine learning and deep learning-based studies in information technology, biology, and medicine. For instance, the study of Amiri et al. [14] employs six popular machine learning classifiers for examining radiomic features which are based on the computed tomography for predicting the risk of chronic kidney illness, particularly in patients undergoing radiation therapy for diseases such as abdominal cancer. Similarly, the study of Loreto et al. [15] addresses the challenge of discharge of patients from Intensive Care Units as ICU readmissions are linked to unfavorable outcomes such as lengthy expenses and high morality rates. The study shows that improving risk stratification for identifying patients highly susceptible of clinical deterioration might enhance the situation for chronically ill patients who are under hospital care.

This study is aimed at exploring the behavior of well-established ML and DL-based algorithms and presents a

performance analysis of simple as well as ensemble-based ML algorithms against convolutional neural networks on multiple small and large datasets. The experimental setup consisted of thirteen datasets derived from different domains, publicly available at the repositories of UCI and Kaggle. The classifiers are evaluated using standard ML measures, i.e., accuracy, precision, and recall. In addition, we separately analyze the training and prediction time of DL and other established classifiers.

The key contributions of this study are summarized as follows:

- (i) This study explores the behavior of well-established ML and DL-based algorithms for multiclass predictions
- (ii) This study presents a performance analysis of simple as well as ensemble-based ML algorithms against convolutional neural networks on multiple small and large datasets
- (iii) The study evaluates the performance of the classifiers using statistical measures such as accuracy and precision and concludes that gradient boosting decision trees (GBDTs) outperform other classifiers. This study also enlightens the researchers in choosing a baseline algorithm or proposing an ensemble-based technique using any of the examined classifiers

The rest of the paper is organized as follows: Section 2 presents the most relevant work to this study. Section 3 presents a brief introduction of the classifiers to be compared and discuss their underlying techniques. Section 4 presents the details of experimental setup including datasets and performance evaluation measures. Section 5 presents the results and discussion based on the experimental setup, and finally, Section 6 concludes the study based on the research findings.

2. Related Works

Several studies have been proposed in literature for empirically comparing the performance analysis of different classification algorithms. However, these studies do not fully analyze the classifier performance on datasets with varying attributes, types of attributes, and sizes.

In StatLog project, Caruana and Niculescu-Mizil [16] compare the performance of nine classifiers on large-scale datasets. The classifiers are selected from different branches of supervised classification including symbolic learning (using C4.5), statistics (using linear regression (LR), NB, and k -nearest neighbor (kNN)), and neural networks (NN). The findings of the study indicate that the performance of classifiers is solely dependent on the characteristics of datasets under investigation. Class imbalance is one of the leading reasons of performance degradation for classifiers, even for well-established classifiers such as latent Dirichlet allocation (LDA), support vector machine (SVM), and classification trees. Traditional

classifiers show serious deficiencies in predicting the instances of minority class [17].

Similarly, Brown and Mues [18] empirically evaluate the predictive power of eight supervised classifiers by gradually increasing class imbalance through random under-sampling. The results of the study prove that RF and GBDTs perform significantly better on credit scoring datasets with pronounced class imbalances as compared to other classifiers. Research identifies that in credit scoring, data quality issues pose a challenge in scorecard development and risk measurement. However, with specific domain knowledge, the accuracy of credit scoring models can be significantly enhanced [19]. In addition, the predictive nature of data such that the captured characteristics are directly associated to the customer defaulting or not poses a serious challenge.

Surprisingly, over the past decade, DL has shown remarkable success in various research domains of artificial intelligence. DL-based techniques show superior performance [20] as compared to other ML methods in areas such as natural language processing, image, and voice recognition, among others. Luo et al. [21] present a performance analysis of Deep Belief Networks (DBN) against popular credit scoring methods such as LOGREG, multilayer perceptron (MLP), and SVM on a credit scoring dataset and identified that DBN outperforms other classifiers. However, the experiments conducted are restricted to Boltzmann machines only. Similarly, Sewak et al. [22] compared the performance of deep neural networks (DNN) against RF for malware classification using different sets of features. Though RF shows better performance as compared to DNN, however, the performance difference is negligible which requires further testing on complex datasets.

On the other hand, Abellán and Castellano [23] identify that a simple classifier with imprecise probabilities, when used as a base classifier in an ensemble scheme, can enhance the performance of other more complex classifiers for predicting credit risks. However, the study did not specify a standard criterion for selecting a base classifier. In this context, Lessmann et al. [24] proposed an ensemble-based approach which creates various noise-free balanced segments from large-scale raw datasets and builds multiple classifiers on these segments using a specific classification technique. The model combines results from multiple classifiers using specific ensemble rules. The results of the study from forty-six imbalanced datasets identify that the ensemble rule MaxDistance performs better with data balancing methods of SplitBal and ClusterBal as compared to other ensemble rules. In addition, the proposed ensemble-based approach outperforms the conventional external data balancing methods.

In addition to proposing a novel ensemble approach, a review of relevant literature identifies several studies which present a performance analysis of existing ensemble-based techniques. The work of Lorena et al. [25] identifies that RF shows better performance as compared to other classifiers through modelling the potential distribution of plant species using nine supervised ML classifiers. Each classifier extracted a different representation of relations between the

distribution profile of plant species and environmental conditions. However, performance analysis was based only on image data with no multiclass attributes. Li et al. [26] investigate the performance of DTs, RF, and SVM. The authors have modeled the potential distribution of various local forest communities in New York State's Huntington Wildlife Forest (HWF). The results of the study indicate that RF and SVM produce better multitemporal predictions as compared to DTs. In addition, RF and SVM reflect changes in forest type much more effectively. On the other hand, Macià and Bernadó-Mansilla [27] presented the design of a mindful repository with properly characterized ML datasets. Consequently, the design of the repository lays the foundation of a well-supported methodology which can effectively assess a learner and provides a rich set of artificial benchmarks.

Similarly, automatic extraction of keywords is significant for text mining, information retrieval, and natural language processing. The study of Onan et al. [28] empirically analyzes effectiveness of the statistical keyword extraction approaches in conjunction with the ensemble learning methods. On the other hand, the study of Onan [29] proposed a recurrent neural network-based approach for opinion mining on instructor review database using an ensemble of classical text representation and word-embedding schemes. The results show the superiority of deep learning-based techniques over conventional machine learning-based algorithms. In sentiment analysis, sarcasm is a form of nonliteral language where users usually express negative emotions by using words having positive literal meanings. The study of Onan [30] presents a deep learning-based model for detecting sarcasm by comparing the predictive performance of topic-based word-embedding schemes against conventional word-embedding approaches. In addition, the study incorporates several implicit and explicit word-embedding-based features. Similarly, in their study [31], Onan and Toçoğlu presented an inverse gravity-based term weighted framework of word embedding with trigrams. The study assigns higher priority to critical words by considering word-ordering information. In addition, the authors introduce a three-layered architecture based on an efficient stacked bidirectional memory scheme. Finally, the study of Onan [32] presented supervised hybrid clustering that is based on k -means and cuckoo search algorithm for partitioning data samples from each class into different clusters resulting in higher diversity of training subsets.

Diagnostic classification of fatal diseases such as cancer can greatly improve the surveillance and treatment procedures for patients. The study of Ma et al. [33] proposed an extreme gradient boosting-based classification model by employing dense multiomics data for segregating early and late stages of cancer. On the other hand, predicting PPI (protein-protein interaction) sites can be significant for getting an insight into the biological activity. The study of Wang et al. [34] proposes a machine learning algorithm that employs eXtreme gradient boosting enhancing the prediction of PPI sites and alleviating heavy expenses associated with running costly and time taking biological experiments.

3. Performance Analyses of ML Algorithms

This study is aimed at presenting the performance analysis of well-established ML techniques against newly developed DL-based algorithms for multiclass prediction; thereby assessing to what extent these classifiers are affected by increasing the complexities of the datasets in terms of size, attributes, and types of attributes. A brief explanation of each of the techniques applied in this study is given in the following.

3.1. Machine Learning-Based Classifiers. ML-based algorithms range from classic Naive Bayes (NB) to ensemble-based decision trees (DTs), random forest (RF), and gradient boosted trees (GBDTs).

3.1.1. Naïve Bayes (NB). Naïve Bayes (NB) is a supervised ML technique which uses probabilistic Bayesian rule for classification. The probabilistic rule allows representing the uncertainty about the model by determining the probabilities of outcome. Given the class label, NB assumes that the features of a dataset are conditionally independent. In [35], the Bayes theorem is given as

$$P() = P()P(h)P(D), \quad (1)$$

where $P(h)$ and $P(D)$ are prior probabilities of hypothesis h and training data D , respectively. On the other hand, $P(h/D)$ represents probability of hypothesis h given the training data D . Similarly, $P(D/h)$ represents the probability of training data D given the hypothesis h . NB is among the most practical models because of speed and space efficiency. It is widely used in text classification, diagnostic, and predictive problems. However, in datasets where the features are not conditionally independent, such as gene expression data due to coregulation, NB suffers performance deficiencies.

3.1.2. Decision Trees (DTs). A DT generates a tree structured decision rule from a large input sample and extracts knowledge to classify the sample input into one of its possible classes. The existing literature presents various DT-based algorithms. However, this paper uses C4.5 as the underlying DT algorithm for classifying the input datasets. C4.5 [36] is an extended version of Iterative Dichotomiser 3 (ID3). ID3 starts from the given set of attributes (S) as the root node. And, for each of the iterations, it computes the information gain and entropy of every unused attribute of the set (S). The attributes with maximum information gain (or minimum entropy) are selected, and the set (S) is partitioned based on the selected attributes resulting in subsets of data. The algorithm continues by considering only the attributes never selected before on the subsets of data and stops when there are no more attributes left for selection or each element in the subset belongs to same class thereby turning into a leaf node. ID3 is based on greedy search. Using the concept of information gain, ID3 selects a test and

avoids other possible choices. Information gain is computed as in [36]

$$\text{Gain}(S, A) = \text{entropy}(S) - \sum_v \frac{|S_v|}{|S|} \text{entropy}(S_v), \quad (2)$$

where S represents the training set, A indicates a specific attribute, v denotes all possible values of attribute A , and $|S|$ and $|S_v|$ are number of elements in S and S_v , respectively. Similarly, C4.5 works in the same manner as ID3. However, the splitting is based on normalized information gain (NIG) which effectively solves overfitting problem. DTs offer many advantages such as the ability to classify numerical, nominal, and textual input types. DTs can handle datasets with missing values and are available in different data mining packages or platforms.

3.1.3. Gradient Boosted Trees (GBDTs). Gradient boosting [37, 38] is an ensemble approach for classification and regression problems, which employs forward-learning mechanism. GBDT produces a prediction result through an ensemble of weak prediction models, mostly decision trees. Weak learners are iteratively integrated into a single and strong prediction model. The algorithm begins by training a decision tree where each observation is given an equal weight. After evaluating the first tree, the weights are increased for those observations which are difficult to classify and decreased for the observations which can be easily classified. The second tree is grown upon the improved predictions of the first tree and computes the classification error from this 2-tree ensemble model. Similarly, the algorithm continues to grow a third decision tree for predicting the revised residuals. This process continues to repeat for a specified number of iterations. Therefore, the final prediction of GBDT is based on the weighted sum of predictions made by the previous trees resulting in improved classification of observations which are not well classified earlier. Gradient boosting can be easily explained in terms of least-squares regression setting where the aim is to “teach” a model F for predicting values of the form $\hat{y} = F(x)$ by minimizing mean square error given as

$$\text{Mean square error} = \frac{1}{n} (\hat{y}_i - y_i)^2, \quad (3)$$

where i is an index over some training dataset of size n and y is the response or output variable. At each iteration m such that $1 \leq m \leq M$, it is assumed that there exists some weak learner F_m and each subsequent learner F_{m+1} is an improvement to its predecessor F_m by adding an estimator h given as in [38]

$$F_{m+1}(x) = F_m(x) + h(x). \quad (4)$$

In [38], we can also find the perfect value of h :

$$F_{m+1}(x) = F_m(x) + h(x) = y \quad (5)$$

or equivalently,

$$h(x) = y - F_m(x). \quad (6)$$

Finally, GBDTs fit h to the remaining $y - F_m(x)$. These remaining or residuals for a given model $F(x)$ represent the negative gradients of squared error loss function given as under

$$\text{Squared error loss function} = \frac{1}{2} (y - F(x))^2. \quad (7)$$

Therefore, GBDTs are, in fact, gradient descent functions. Gradient boosting is simple and effective, particularly, for learning nonlinear functions. One of the biggest advantages of GBDTs is that it decreases human interpretability. However, GBDTs take longer time to produce classifier outcome.

3.1.4. Random Forest (RF). Random forest (RF) consists of multiple DTs which operate as an ensemble [12]. Each individual tree in RF produces a class prediction, and the class with maximum votes is selected as the model's prediction. The algorithm performs an implicit feature selection using a small subset of "strong variables" which leads to superior performance on high-dimensional data [39]. The results of feature selection can be visualized through Gini index [40] which indicates the importance or feature relevance.

Gini index measures an attribute's impurity with respect to each class. At each node within binary trees of the random forest, the optimal split is achieved using Gini impurity which is computationally efficient as compared to entropy. Gini impurity measures how well a potential split is separating samples of the two classes at a particular node. In addition, Gini impurity indicates the frequency of selecting a specific feature for a split and the extent of its overall discriminative score for the given classification problem. Let T be a given training dataset, selecting an attribute at random and checking whether it belongs to some class C_i ; Gini index is computed as in [40]

$$\sum_{j \neq i} \left(\frac{f(C_j, T)}{|T|} \right) \left(\frac{f(C_i, T)}{|T|} \right), \quad (8)$$

where $(f(C_i, T))/|T|$ represents the probability with which the selected attribute belongs to the class C_i . RF selects the best feature among the random subset of features while splitting a node, and it has only two parameters to adjust, i.e., number of variables in a random subset at each node and number of DTs in the forest. RF has many advantages over other ensemble methods. It works well for a large range of items and shows less variance as compared to a single DT. In addition, RF are flexible and output higher accuracy even without scaling of data. However, generating RF is much harder and time-consuming as it requires more computational resources.

3.2. Deep Learning-Based Classifiers. Conventional ML methods are limited in their ability for processing natural

data in raw form. DL-based methods are representation learning methods which allow a machine to be fed with the raw data and automatically discover the representations required for classification. In addition, DL exploits simple but nonlinear modules for transforming the representation at raw input level into a representation at higher or abstract level. Several deep learning techniques have been developed so far; however, this study analyzes only convolutional neural network (CNN) given as follows.

3.2.1. Convolutional Neural Network (CNN). DL has proven to be an outstanding classification technique in image/speech recognition and other relevant applications [13]. The classification process in DL begins by training large multilayer neural networks (MLPs), also called deep neural networks (DNN). MLPs are, in fact, feedforward networks which are trained with standard backpropagation algorithm.

Currently, several DL-based techniques have been proposed. However, this paper employs convolutional neural network (CNN) which is a type of DNN. CNNs utilize multiple layers for multiclass predictions such as one or more pairs of max-pooling layer, a convolutional layer, and one or more fully connected hidden layers. These layers use neurons with tanh, maxout, and rectifier functions for the purpose of identifying a set of locally connected neurons. CNNs continuously extract several low-level characteristics into compressed high-level abstractions and representations.

One of the advantages of CNNs includes fewer parameters and easier training as compared to other deep neural networks. In addition, CNNs show higher accuracy using advance features such as adaptive learning, momentum training, rate annealing, dropout, and L1 or L2 regularization techniques. DL has become a popular research domain in recent years. Therefore, a comprehensive performance analysis is required against well-established machine learning techniques. Table 1 presents a comparison between the machine learning algorithms discussed in the study.

4. Experimental Setup

The choice of an appropriate algorithm in response to a specific classification problem is based not only on prior knowledge about the classifiers' performance but also on systematic evaluation in order to replicate and generalize the results. The recent progress in publicly available datasets has led the machine-learning community to effectively validate and share the experimental results. The experiments were performed on Intel Quad-Core i5-8250U at 1.8 GHz with 8 GB RAM, running 64-bit Windows 10 Home Edition. The datasets were partitioned using 10-fold cross-validation.

In this study, 10-fold cross-validation technique [41] is utilized for measuring accuracy of the classifiers. In this setting, the training dataset is divided into ten equal-sized subsets such that each of these ten subsets is tested using the classifier that has been trained on the remaining nine subsets. The advantages of tenfold cross-validation include reduced computation cost as the process is repeated only ten times. In addition, 10-fold cross-validation results in less biasness as compared to other validation techniques where

TABLE 1: Comparison of ML- and DL-based classifiers.

Classifier	Underlying methodology	Classifier applicability	Nature of prediction/label class	Advantage(s)	Disadvantage(s)
Naïve Bayes [35]	Bayes theorem	Classification	Categorical	Less parameter tuning, less data learning requirements, computationally fast	Conditional independence between attributes
Decision trees [36]	Iterative Dichotomiser 3 (ID3)	Classification, regression	Categorical, continuous	Simple to interpret, shows higher accuracy	Target attribute must have discrete values; dataset must not have complex and many attributes (i.e., imbalance); uses greedy approach for generating DTs; prone to overfitting
Random forest [12]	Aggregation of (decision) trees using bagging with C4.5 algorithm	Classification, regression	Categorical, continuous	Not susceptible to overfitting, reduces error rate while generating DTs	Generates parallel DTs, computationally slow on large and complex datasets
Gradient boosted trees [37, 38]	Adaptive boosting using C4.5 algorithm	Classification, regression	Categorical, continuous	Boosting reduces error by reducing bias and to some extent variance sequential tree generation with improved learning in each iteration	Uses shallow weak learner trees, computationally faster than RF, harder parameter tuning
Deep learning [13]	Convolutional neural networks	Classification, regression	Categorical, continuous	Higher accuracy sometimes exceeds human-level performance; DL algorithms scale with data; CNNs require relatively little preprocessing	Requires large amounts of labeled data and substantial computing power

each data point is tested for exactly once and is utilized in training (10-1) times.

4.1. Datasets. The performance analysis of the classifiers is visualized on eleven datasets from the popular UCI [42] and Kaggle [43] repositories. Table 2 summarizes the characteristics of the datasets. The datasets can be divided into three categories: small, medium, and large based on number of instances and type of attributes. Datasets having less than 10,000 instances are taken as small datasets. Thus, Horse Colic, Titanic, CTG, Spambase, and NYS Dept. of State Business Filings fall under the category of small datasets. On the other hand, datasets with a number of instances between 10,000 and 50,000 are considered as medium datasets. Therefore, Avila, WHO Suicide Statistics, and Adult datasets are categorized as medium-sized datasets. Finally, datasets with a number of instances between 50,000 and 250,000 are taken as large datasets. The study includes TripAdvisor Restaurant, NYS Nyserda, and Black Friday as the large datasets.

4.2. Performance Evaluation Measures (PEMs). The performance of the classifiers is evaluated using the widely used confusion matrix-based metrics, namely, accuracy, precision, and recall. The confusion matrix represents the relation

between predicted values and actual values. Therefore, accuracy, precision, and recall play a significant role in determining an algorithm's strength.

4.2.1. Accuracy. The accuracy of a classifier is computed as the number of correctly predicted instances divided by total number of predictions. In other words, accuracy is the overall percentage of correctly predicted values given as

$$\text{Accuracy} = \frac{\text{TP} + \text{TN}}{\text{TP} + \text{TN} + \text{FP} + \text{FN}}, \quad (9)$$

where TP and TN represent true positive and true negative, respectively. Similarly, FP and FN represent false positive and false negative, respectively. TP and TN show that model predictions agree with the original class values whereas FP and FN indicate the incorrect prediction of the model as compared to original class values.

4.2.2. Precision. Precision represents exactness, and it shows the percentage of correctly predicted positive results (i.e., TP) from all positive predictions given as

$$\text{Precision} = \frac{\text{TP}}{\text{TP} + \text{FP}}. \quad (10)$$

TABLE 2: Characteristics of selected datasets.

Dataset	No. of attributes	No. of instances	Attribute types	No. of prediction classes	Dataset library
Small datasets					
Horse Colic [42]	27	368	Categorical, integer, real	02	UCI
Titanic [43]	12	891	Categorical, integer, real	02	Kaggle
CTG [42]	23	2126	Real	03	UCI
Spambase [42]	57	4601	Integer, real	02	UCI
NYS Dept. of State Business Filings [43]	24	9745	Categorical, integer	10	Kaggle
Medium-sized datasets					
Avila [42]	10	20867	Real	10	UCI
WHO Suicide Statistics [43]	6	43800	Categorical, integer	06	Kaggle
Adult [42]	14	48842	Categorical, integer	02	UCI
Large-sized datasets					
TripAdvisor Restaurant [43]	11	126000	Categorical, integer, real	07	Kaggle
NYS Nysesda [43]	23	223000	Categorical, integer, real	06	Kaggle
Black Friday [43]	11	234000	Categorical, integer	10	Kaggle

Precision is an effective measure to determine the cost associated with false positives. For example, detecting spam emails, a false positive indicates the number of nonspam emails which are identified as spam.

4.2.3. *Recall*. Recall answers what percent of positive cases is predicted correctly. Recall is also referred to as the true-positive rate given as

$$\text{Recall} = \frac{\text{TP}}{\text{TP} + \text{FN}}. \quad (11)$$

5. Results and Discussion

The section presents results of the classifiers discussed in this study using the performance measures of accuracy, precision, and recall. Figure 1 presents the accuracy of the classifiers. NB shows more than 80% accuracy on the Adult dataset and more than 60% accuracy on NYS Nysesda, Horse Colic, CTG, and Spambase datasets. However, the accuracy results of NB are below 50% on Avila, TripAdvisor Restaurants Info, and Titanic datasets, respectively. A possible explanation of such behavior could be that Adult dataset is primarily created for binary classification whereas NYS Nysesda, Horse Colic, CTG and Spambase datasets have multiple types of attributes and these datasets are mainly designed for multiclassification. On the other hand, Avila and TripAdvisor Restaurants Info are complex datasets with several prediction classes and multiple types of attributes. Surprisingly, NB shows lower accuracy on the Titanic dataset. One of the key reasons is that the Titanic dataset has

different proportions of missing values in different attributes.

The accuracy of DTs on Titanic, Spambase, and NYS Dept. of State Business Filings datasets is above 90%. Similarly, DTs show more than 80% accuracy on the Adult dataset and more than 70% accuracy on Horse Colic and Black Friday datasets, respectively. However, the accuracy of DTs is below 60% on Avila and WHO Suicide Statistics datasets. DTs effectively analyze the statistical relationship between a given input and output. Therefore, DTs show higher accuracy overall as compared to NB on multiclass datasets and datasets with missing values.

On the other hand, ensemble-based GBDTs show more than 70% on Horse Colic and WHO Suicide Statistics datasets and above 80% accuracy on CTG and Adult datasets. Similarly, the accuracy of GBDTs is above 90% on Titanic, Spambase, Avila, and Black Friday datasets, respectively. GBDT employs bootstrap bagging to integrate weak learners for overall improvement. Therefore, GBDT shows higher accuracy as compared to DTs, particularly on complex and multiclass datasets such as Avila.

Similarly, RF is another ensemble approach which shows more than 90% accuracy on Titanic, Spambase, and NYS Dept. of State Filings datasets; more than 80% accuracy on Adult and Black Friday datasets; and more than 70% accuracy on the Horse Colic dataset, respectively. However, accuracy results are below 65% on Avila, CTG, and WHO Suicide Statistics. While comparing with DTs, RF shows small improvements on Avila, CTG, and WHO Suicide Statistics datasets. However, on datasets having noisy classification or regression, RF shows overfitting tendency and in the

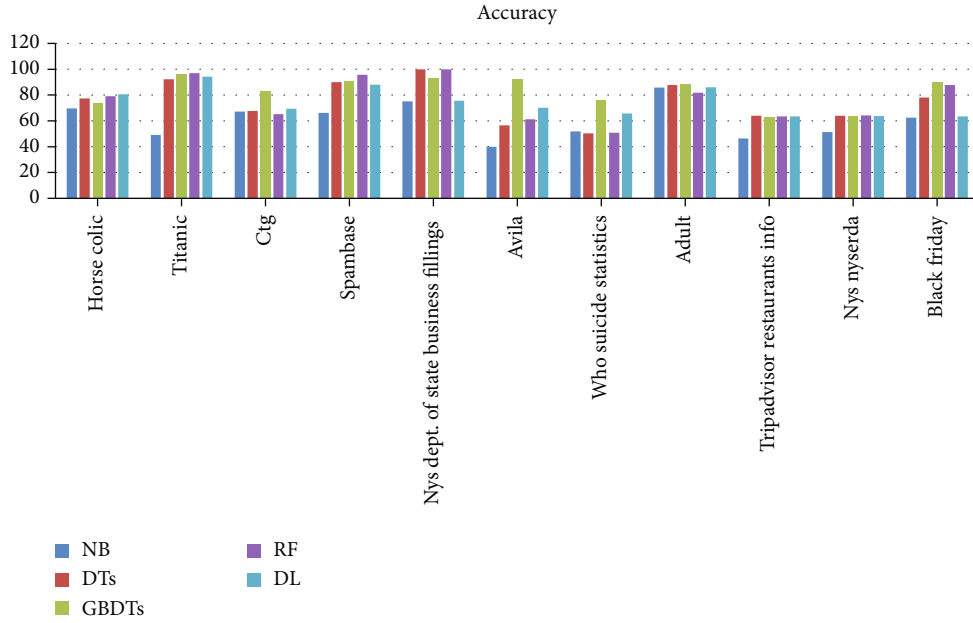


FIGURE 1: Accuracy of the classifiers.

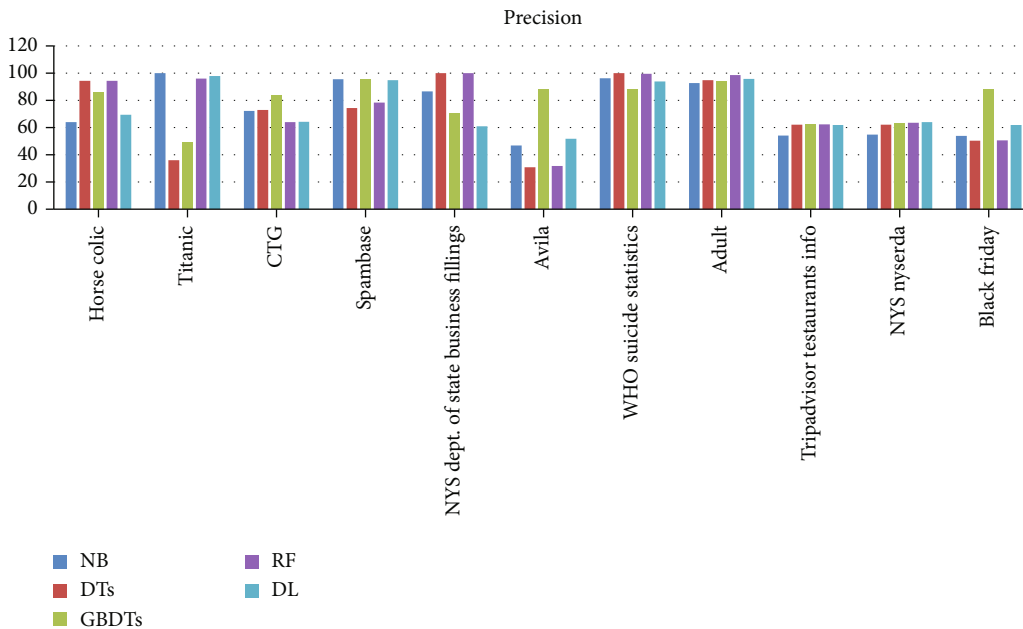


FIGURE 2: Precision of the classifiers.

case of categorical attributes with different numbers of levels, RF favors those attributes having more levels. This behavior is evident on Avila, CTG, and WHO Suicide Statistics datasets where GBDT shows higher accuracy as compared to RF.

Finally, convolutional neural networks (CNN) show more than 90% accuracy on the Titanic dataset; more than 80% accuracy on Horse Colic, Spambase, and Adult datasets; and more than 70% accuracy on NYS Dept. of State Fillings and Avila datasets, respectively. On small datasets, the performance of CNN suffers as DL-based classifiers are slow to train [44]. On the other hand, RF requires tuning of fewer

hyperparameters which makes RF a faster algorithm. Therefore, on small datasets such as Horse Colic and NYS Dept. of State Fillings, RF outperforms CNN in terms of accuracy. One of the drawbacks of RF is that it often yields suboptimal performance on large-scale datasets using the greedy approach of tree construction [45]. Therefore, on Avila and Black Friday datasets, RF shows lower accuracy results as compared to CNN.

Surprisingly, GBDTs outperform all other classifiers discussed in this study in terms of accuracy, particularly, on datasets with multiclassification and missing values. A

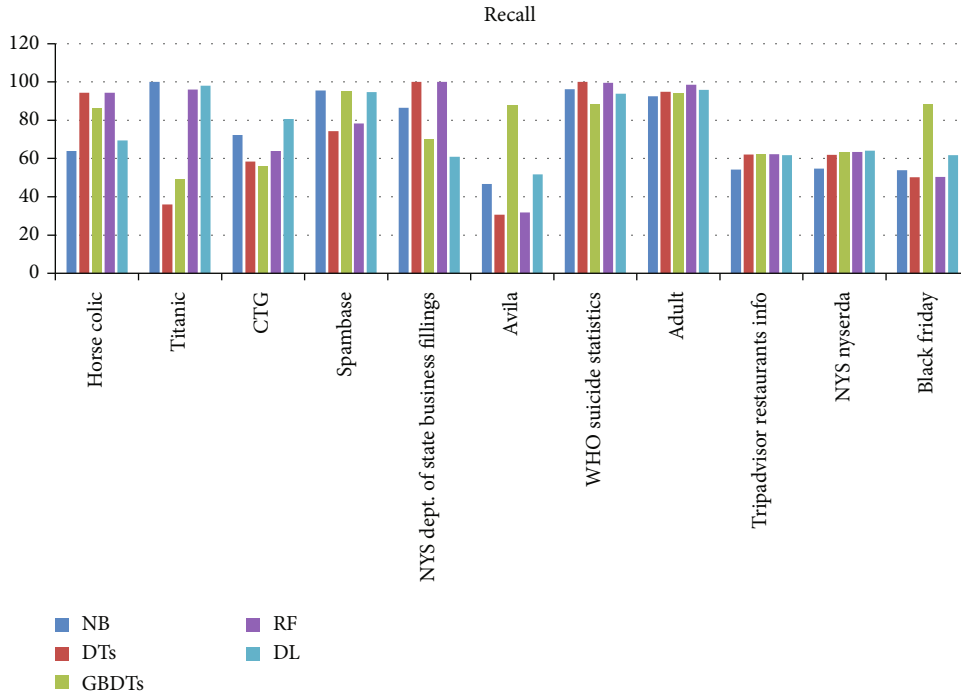


FIGURE 3: Recall score of the classifiers.

possible explanation of such phenomena could be that GBDTs utilize the concept of boosting to shallow the classification trees which results in model simplicity and tuning is limited to the parameters of the gradient boosting algorithms itself. GBDT performs optimization in function space that results in flexible use of custom loss function. In addition, boosting is computationally efficient as compared to deep learning [46–48].

Figure 2 presents the precision results of the classifiers. NB shows more than 90% precision on Titanic, Spambase, and WHO Suicide Statistics; more than 80% precision on NYS Dept. of State Fillings; more than 70% precision on CTG; and below 60% precision on the rest of the datasets. The precision results are different from the accuracy results as shown in Figure 1. This is because precision is independent of accuracy and is concerned with the fraction of positive predictions which are identified as positive in actual. On the other hand, accuracy is simply the fraction of total sample that is correctly identified.

The precision of DTs on Horse Colic, NYS dept. of State Fillings, WHO Suicide Statistics, and Adult datasets is above 90%. Similarly, DTs show more than 70% precision on CTG and Spambase datasets and below 50% precision on Titanic, Avila, and Black Friday datasets, respectively.

It is worth mentioning that DTs show more than 90% accuracy on the Titanic dataset. However, the precision results of DTs on the Titanic dataset are below 40%. On the other hand, NB shows more than 90% precision on the Titanic dataset. However, the accuracy of NB on the Titanic dataset is below 50%. One of the prime reasons is that NB is a simple algorithm less prone to overfit.

On the other hand, DTs suffer from the inability to grasp the relationship between features of the dataset and utilize the greedy learning approach which leads to suboptimal model [38]. Overall, DTs efficiently predict the true positives; therefore, precision results on DTs are higher on most datasets as compared to NB.

On the other hand, GBDTs show more than 60% precision on NYS Dept. of State Fillings, TripAdvisor, and NYS Nysedra datasets and more than 80% precision on Horse Colic, CTG, Avila, WHO Suicide Statistics, and Black Friday datasets. Similarly, precision results are above 90% on Spambase and Adult datasets. The precision results are below 50% on the Titanic dataset. GBDTs show higher precision on complex datasets such as Avila and Black Friday and datasets with missing values such as Titanic as compared to DTs. Similarly, ensemble-based RF shows almost the same behavior as DTs, except on Titanic and Black Friday datasets where RF shows higher precision. Comparing with GBDTs, RF shows lower precision results which show that GBDT classifies the true positives efficiently as compared to RF on complex datasets and datasets with missing values.

Finally, CNN shows more than 60% precision on Horse Colic, CTG, NYS Dept. of State Fillings, TripAdvisor, and Black Friday datasets. Similarly, precision results are above 90% on Titanic, Spambase, and WHO Dept. of State Fillings datasets. However, CNN shows below 50% precision on the Avila dataset. Comparing with RF, CNN shows mixed performance results. On the Horse Colic dataset, CNN shows significantly lower precision results. However, precision results of CNN are significantly higher on the Spambase dataset. Comparing with GBDTs, CNN shows significantly

lower overall precision which indicates that GBDTs can output higher precision as compared to CNN on large, multiclass datasets.

Figure 3 presents the recall of the classifiers. The recall of NB, DTs, GBDTs, RF, and CNN is almost similar to their precision results as shown in Figure 2. A possible explanation of this phenomenon is that both precision and recall are concerned with correctly identified positive predictions. The difference lies in that in precision, the correctly identified positive predictions are from the total positive predictions whereas in recall, the correctly identified positive predictions are from actual positive values. Overall, GBDTs shows higher recall as compared to other classifiers. DTs show more than 90% recall on Horse Colic, NYS Dept. of State Fillings, WHO Suicide Statistics, and Adult datasets. The recall is above 60% on Spambase, TripAdvisor, and NYS Nyserda datasets. However, the classifier shows below 40% recall on Avila and Titanic datasets, respectively. The recall results of DTs are almost similar to the precision results on the datasets analyzed in this study.

The recall of GBDTs on Spambase and Adult datasets is above 90%. The classifier shows more than 80% recall on Horse Colic, Avila, WHO Suicide Statistics, and Black Friday datasets. On NYS Dept. of State Fillings, TripAdvisor, and NYS Nyserda, the recall is above 60%. However, GBDTs shows below 50% recall on the Titanic dataset. The recall results of GBDTs are nearly similar to its precision on the datasets discussed in this study.

RF shows nearly similar recall results as precision on the datasets used for experimental setup. For instance, on Horse Colic, Titanic, NYS Dept. of State Fillings, WHO Suicide Statistics, and Adult datasets, the recall is above 90%; more than 60% recall on CTG, Spambase, Trip Advisor, and NYS Nyserda datasets; and below 40% recall on the Avila dataset, respectively.

Similarly, the recall results of CNN are almost similar to its precision results on the datasets tested. For example, on Titanic, Spambase, and WHO Dept. of State Fillings datasets, the recall is above 90%. CNN shows more than 60% recall on Horse Colic, CTG, NYS Dept. of State Fillings, TripAdvisor, and Black Friday datasets. On the other hand, recall is below 50% on the Avila dataset. As the ML-based NB and DTs, ensemble-based GBDTs and RF and DL-based CNN show nearly similar recall results; therefore, the recall of GBDTs is higher than that of the other classifiers.

6. Conclusions

The study presents a state-of-the-art comparative analysis of machine learning and deep learning-based algorithms for multiclass prediction. The study can serve as a guideline for new researchers in selecting a baseline algorithm or proposing an ensemble-based technique using any of the classifiers examined in this study. The study evaluates the performance of the classifiers using statistical measures such as accuracy, precision, and recall and shows that gradient boosting decision trees (GBDTs) outperform other classifiers discussed in this study. Similarly, decision trees (DTs) show significantly better performance as compared to classic

Naïve Bayes (NB). On small datasets, random forest (RF) shows higher accuracy, precision, and recall scores as compared to convolutional neural networks (CNN). However, on large and regression-based datasets, CNN outperforms RF. The results show that DTs and RF suffer serious performance issues in the case of large and complex datasets due to the underlying greedy approach and overfitness. In the future, we plan to extend this work to include other classifiers and evaluate their performance on significantly large text datasets and image data.

In future work, we plan to apply diverse deep learning (DL) algorithms on larger datasets in addition to the datasets mentioned above. We plan to compare the performance of DL algorithms such as Long Short-Term Memory Networks, Recurrent Neural Networks, and Generative Adversarial Networks using multiple evaluation metrics.

Data Availability

Since the funding project is not closed and related patents have been evaluated, the simulation data used to support the findings of this study are currently under embargo, while the research findings are commercialized. Requests for data, upon the approval of patents after project closure, will be considered by the corresponding author.

Disclosure

The granting agencies did not contribute in the design of the study and collection, analysis, and interpretation of data.

Conflicts of Interest

The authors declare that they have no conflicts of interest.

Acknowledgments

The authors thank the Natural Sciences and Engineering Research Council of Canada (NSERC) and New Brunswick Innovation Foundation (NBIF) for the financial support of the global project. These granting agencies did not contribute in the design of the study and collection, analysis, and interpretation of data.

References

- [1] Z. Chen and B. Liu, "Lifelong machine learning," *Synthesis Lectures on Artificial Intelligence & Machine Learning*, vol. 10, no. 3, pp. 1–145, 2016.
- [2] V. Grover, R. H. Chiang, T.-P. Liang, and D. Zhang, "Creating strategic business value from big data analytics: a research framework," *Journal of Management Information Systems*, vol. 35, no. 2, pp. 388–423, 2018.
- [3] B. Zou, V. Lampos, and I. Cox, "Multi-task learning improves disease models from web search," *World Wide Web*, pp. , 201887–96, 2018.
- [4] D. Geol, J. M. Khandelwal, and R. Tiwari, "Intelligent and integrated book recommendation & best price identifier system using machine learning," in *Intelligent Engineering Informatics*, pp. 397–412, Springer, Berlin/Heidelberg, Germany, 2018.

- [5] L. Buczak and E. Guven, "A survey of data mining and machine learning methods for cyber security intrusion detection," *IEEE Communications Surveys & Tutorials*, vol. 18, no. 2, pp. 1153–1176, 2016.
- [6] P. Chahuaara, N. Grislain, G. Jauvion, and J.-M. Renders, "Real-time optimization of web publisher RTB revenues," in *Proceedings of the 23rd ACM SIGKDD International Conference on Knowledge Discovery and Data Mining*, pp. 1743–1751, New York, United States, 2017.
- [7] S. Bhatia, P. Sharma, R. Burman, S. Hazari, and R. Hande, "Credit scoring using machine learning techniques," *International Journal of Computer Applications*, vol. 161, no. 11, pp. 1–4, 2017.
- [8] D. Nawrocka, *Machine learning for trading and portfolio management using Python*, 2018, Hochschulbibliothek HWR Berlin.
- [9] B. Huang, Y. Huan, L. D. Xu, L. Zheng, and Z. Zou, "Automated trading systems statistical and machine learning methods and hardware implementation: a survey," *Enterprise Information Systems*, vol. 13, pp. 1–13, 2018.
- [10] J. Mata, I. de Miguel, R. J. Duran et al., "Artificial intelligence (AI) methods in optical networks: a comprehensive survey," *Optical Switching and Networking*, vol. 28, pp. 43–57, 2018.
- [11] T. O. Ayodele, "Types of machine learning algorithms, in new advances in machine learning," Portsmouth, United Kingdom, 2010.
- [12] L. Breiman, "Random forests," *Machine Learning*, vol. 45, no. 1, pp. 5–32, 2001.
- [13] Y. Bengio, "Learning deep architectures for AI," *Machine Learning*, vol. 2, no. 1, pp. 1–127, 2009.
- [14] S. Amiri, M. Akbarabadi, F. Abdolali, A. Nikoofar, A. J. Esfahani, and S. Cheraghi, "Radiomics analysis on CT images for prediction of radiation-induced kidney damage by machine learning models," *Computers in Biology and Medicine*, vol. 133, article 104409, 2021.
- [15] M. Loreto, T. Lisboa, and V. P. Moreira, "Early prediction of ICU readmissions using classification algorithms," *Computers in Biology and Medicine*, vol. 118, article 103636, 2020.
- [16] R. Caruana and A. Niculescu-Mizil, "An empirical comparison of supervised learning algorithms," in *Proceedings of the 23rd international conference on Machine learning*, pp. 161–168, Pittsburgh, Pennsylvania, USA, 2006.
- [17] A. Cieslak and N. V. Chawla, "Learning decision trees for unbalanced data," in *Joint European Conference on Machine Learning and Knowledge Discovery in Databases*, pp. 241–256, Springer, Berlin, Heidelberg, 2008.
- [18] I. Brown and C. Mues, "An experimental comparison of classification algorithms for imbalanced credit scoring data sets," *Expert Systems with Applications*, vol. 39, no. 3, pp. 3446–3453, 2012.
- [19] L. Thomas, J. Crook, and D. Edelman, "Credit scoring and its applications," in *Society for industrial and Applied Mathematics*, vol. 2, Siam, Philadelphia, USA, 2017.
- [20] J. Howard, "The business impact of deep learning," in *Proceedings of the 19th ACM SIGKDD international conference on Knowledge discovery and data mining*, pp. 1135–1135, August 2013.
- [21] D. W. Luo, D. Wu, and D. Wu, "A deep learning approach for credit scoring using credit default swaps," *Engineering Applications of Artificial Intelligence*, vol. 65, pp. 465–470, 2017.
- [22] M. Sewak, S. K. Sahay, and H. Rathore, "Comparison of deep learning and the classical machine learning algorithm for the malware detection," in *International Conference on Software Engineering, Artificial Intelligence, Networking and Parallel/Distributed Computing*, pp. 293–296, Busan, Korea, June 2018.
- [23] J. Abellán and J. G. Castellano, "A comparative study on base classifiers in ensemble methods for credit scoring," *Expert Systems with Applications*, vol. 73, pp. 1–10, 2017.
- [24] S. Lessmann, B. Baesens, H.-V. Seow, and L. C. Thomas, "Benchmarking state-of-the-art classification algorithms for credit scoring: an update of research," *European Journal of Operational Research*, vol. 247, no. 1, pp. 124–136, 2015.
- [25] A. C. Lorena, L. F. Jacintho, M. F. Siqueira et al., "Comparing machine learning classifiers in potential distribution modelling," *Expert Systems with Applications*, vol. 38, no. 5, pp. 5268–5275, 2011.
- [26] J. I. Li and C. Beier, "Machine learning approaches for forest classification and change analysis using multi-temporal Landsat TM images over Huntington Wildlife Forest," *GIScience & Remote Sensing*, vol. 50, no. 4, pp. 361–384, 2013.
- [27] N. Macià and E. Bernadó-Mansilla, "Towards UCI+: a mindful repository design," *Information Sciences*, vol. 261, pp. 237–262, 2014.
- [28] S. K. Onan and H. Bulut, "Ensemble of keyword extraction methods and classifiers in text classification," *Expert Systems with Applications*, vol. 57, pp. 232–247, 2016.
- [29] A. Onan, "Mining opinions from instructor evaluation reviews: a deep learning approach," *Computer Applications in Engineering Education*, vol. 28, no. 1, pp. 117–138, 2020.
- [30] A. Onan, "Topic-enriched word embeddings for sarcasm identification," in *Computer Science On-line Conference*, pp. 293–304, Springer, Cham, 2019.
- [31] A. Onan and M. A. Toçoğlu, "A term weighted neural language model and stacked bidirectional LSTM based framework for sarcasm identification," *Access*, vol. 9, pp. 7701–7722, 2021.
- [32] A. Onan, "Hybrid supervised clustering-based ensemble scheme for text classification," *Kybernetes*, vol. 46, no. 2, pp. 330–348, 2017.
- [33] F. Ma, G. Meng, H. Yan, B. C. Yan, and F. Song, "Diagnostic classification of cancers using extreme gradient boosting algorithm and multi-omics data," *Computers in Biology and Medicine*, vol. 121, article 103761, 2020.
- [34] X. Wang, Y. Zhang, B. Yu et al., "Prediction of protein-protein interaction sites through eXtreme gradient boosting with kernel principal component analysis," *Computers in Biology and Medicine*, vol. 134, article 104516, 2021.
- [35] A. McCallum and K. Nigam, "A comparison of event models for naive Bayes text classification," *AAAI-98 workshop on learning for text categorization*, vol. 752, pp. 41–48, 1998.
- [36] J. R. Quinlan, "Induction of decision trees," *Machine Learning*, vol. 1, no. 1, pp. 81–106, 1986.
- [37] J. H. Friedman, "Stochastic gradient boosting," *Computational Statistics & Data Analysis*, vol. 38, no. 4, pp. 367–378, 2002.
- [38] J. Ye, J.-H. Chow, J. Chen, and Z. Zheng, "Stochastic gradient boosted distributed decision trees," in *Proceedings of the 18th ACM conference on Information and knowledge management*, pp. 2061–2064, November 2009.
- [39] R. Genuer, J.-M. Poggi, and C. Tuleau-Malot, "Variable selection using random forests," *Pattern Recognition Letters*, vol. 31, no. 14, pp. 2225–2236, 2010.

- [40] A. Liaw and M. Wiener, "Classification and regression by random forest," *R news*, vol. 2, pp. 18–22, 2002.
- [41] T. G. Dietterich, "Approximate statistical tests for comparing supervised classification learning algorithms," *Neural Computation*, vol. 10, no. 7, pp. 1895–1923, 1998.
- [42] K. T. Dheeru, *Machine Learning Repository*, School of Information and Computer Sciences, University of California Irvine, 2017.
- [43] *Kaggle dataset library*, 2021, <http://www.kaggle.com/>.
- [44] J. Schmidhuber, "Deep learning in neural networks: an overview," *Neural Networks*, vol. 61, pp. 85–117, 2015.
- [45] Z.-H. Zhou and J. Feng, "Deep forest: towards an alternative to deep neural networks," pp. 3553–3559, 2017, <http://arxiv.org/abs/1702.08835>.
- [46] E. B. Sudakov and D. Koroteev, "Driving digital rock towards machine learning: predicting permeability with gradient boosting and deep neural networks," *Computers & Geosciences*, vol. 127, pp. 91–98, 2019.
- [47] X. Wang, S. Yin, M. Shafiq et al., "A new V-net convolutional neural network based on four-dimensional hyperchaotic system for medical image encryption," *Networks*, vol. 2022, pp. 1–14, 2022.
- [48] T. Shahwar, J. Zafar, A. Almogren et al., "Automated detection of Alzheimer's via hybrid classical quantum neural networks," *Electronics*, vol. 11, no. 5, p. 721, 2022.

Research Article

Bank Green Credit Risk Assessment and Management by Mobile Computing and Machine Learning Neural Network under the Efficient Wireless Communication

Yuan Feng 

Northeastern University, Boston, MA 02115, USA

Correspondence should be addressed to Yuan Feng; feng.yuan2@northeastern.edu

Received 25 January 2022; Revised 23 February 2022; Accepted 26 February 2022; Published 29 March 2022

Academic Editor: Alireza Souri

Copyright © 2022 Yuan Feng. This is an open access article distributed under the Creative Commons Attribution License, which permits unrestricted use, distribution, and reproduction in any medium, provided the original work is properly cited.

The study is aimed at assessing and managing the green credit risk of banks, reduces the systemic risk in the financial industry, and improves the efficiency of the use of bank funds. With the development and evolution of efficient wireless data communication and transmission technology, the study combines theoretical and empirical green credit analysis to analyze listed companies in different industries quantitatively. The index system of credit risk assessment is established through wireless data transmission technology combined with mobile computing and machine learning neural networks. A backpropagation neural network (BPNN) model is confirmed by principal component analysis and factor analysis, and the performance of the model is verified with example data. The results show that the BPNN-based credit risk assessment model can provide 95% accuracy. In addition, 99% of the sample companies have low risk and no green credit risk. However, most companies in the coal industry are at greater risk. Overall, medium and high-risk companies accounted for 11.5%. Compared with other state-of-the-art models, the machine learning neural network adopted here has better data fitting and prediction accuracy, higher learning efficiency, and higher accuracy. The model established inefficient wireless communication is suitable for bank credit risk assessment and has good reference value and practical significance for bank credit risk assessment and management in different industries.

1. Introduction

As ecological civilization and city construction develop rapidly in China, many companies and individuals have begun to change their concepts and attitudes toward green, environmentally-friendly, and energy-saving industries [1]. Economic growth is the core of social development; however, how to achieve high-quality, sustainable, and healthy development has become a social problem worldwide [2]. To improve the environment and achieve sustainable economic development, the Chinese government vigorously promotes green civilization construction [3]. In the financial sector, banks are actively launching the green credit business, that is, increasing the financing costs of high-polluting industries and companies, increasing investment in environmental protection companies and industries, and guiding the upgrading and replacement of industries. This has funda-

mentally regulated and restricted the industries [4]. Credit business is the source of bank revenue. While this approach brings income to the bank, it also brings huge risks. When banks handle green credit business, various companies must be audited, and environmentally-friendly companies often have problems such as a single source of income and meager profits, creating difficulties for banks in dealing with such businesses [5]. Banks must investigate a company's environmental protection work, operating status, and qualifications, as well as the status of the industry. They also need to establish and review appropriate loan lines for companies with poor capabilities. Therefore, assessing and managing banks' green credit risks play a very prominent role in promoting the upgrading of industries in China and ensuring the stability of the financial market [6].

Backpropagation neural network (BPNN) has complex classification capabilities and good multidimensional

function mapping capabilities. Compared with traditional linear analysis approaches, BPNN can solve nonlinear problems and has been better applied in different scenarios [7]. Wang et al. (2017) designed a BPNN model with air temperature as the input parameter and established the association between the data and solar radiation error and air temperature. This method could provide good performance, proving that BPNN had a powerful nonlinear fitting function. Thus, BPNN was very suitable for monitoring wireless sensor air temperature [8]. Cui et al. (2019) developed a BPNN analysis platform based on the engineering geological database. They established a geotechnical parameter prediction model based on analyzing the characteristics of geotechnical materials and the distribution of geotechnical sediments and geotechnical parameters. Results found that BPNN could improve model prediction accuracy [9]. Yuan et al. (2019) proposed a fingerprint activity detection method based on BPNN. The proposed method could provide higher classification efficiency and better detection performance [10]. The above works can prove the advantages of BPNN in analyzing nonlinear problems. There are many reports on applying BPNN to financial risk assessment; however, the accuracy is maintained at about 85%, which cannot meet the ever-increasing requirements of financial risk assessment [11]. Therefore, proposing an adequate green credit risk assessment and management model has become a hot topic.

Therefore, back propagation neural network (BPNN) is used to build a risk assessment and management model for bank green credit risk. The data of listed companies in different industries are used to optimize the parameters and test the model's performance. Principal component analysis and factor analysis are used to determine the main optimization parameters of the back-propagation neural network model. The results have practical value for promoting the green and healthy development of the financial industry and industrial upgrading. The innovations are as follows: (1) the current problems of banks' green credit risk and the factors affecting green credit are analyzed in detail. (2) BPNN is applied to green credit, and a risk assessment and management model is established. (3) The parameters and process of BPNN are optimized. The predictive and analytical capabilities of the model are significantly improved.

There are five sections in total. Section 1 highlights the importance of exploring banks' green credit risk control and management and determines the research ideas. Section 2 clarifies recent works on BPNN in green finance and financial credit risk models and determines the research gaps. Section 3 proposes the green credit risk assessment model for banks based on BPNN and elaborates the modeling details, parameters, and datasets. Section 4 analyzes the model performance using sample data, derives the version and advantages of the model, and compares the proposed model with other algorithms. Section 5 gives conclusions, including the actual contributions, limitations, and prospects.

2. Related Work

2.1. Green Credit Risk Assessment. Green credit risk assessment is the cornerstone of sustainable socioeconomic devel-

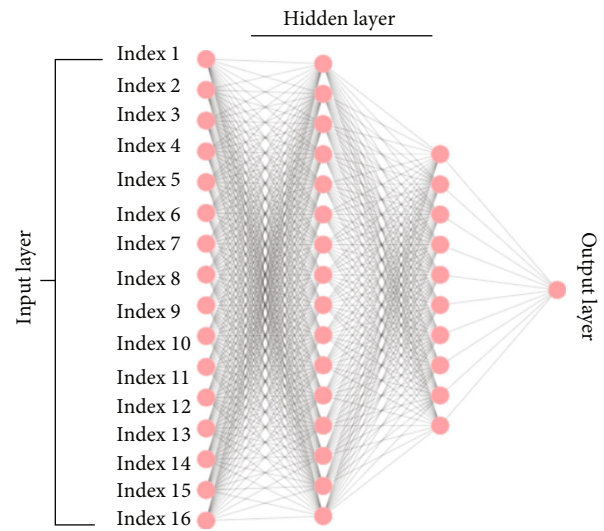


FIGURE 1: Bank risk assessment model based on BPNN.

opment. It can increase banks' profits and income, reduce banks' credit risks, and promote industrial upgrading [12]. There have been many reports on green credit risks. Cui et al. (2018) practiced least squares regression and random effect panel regression based on a five-year dataset of 24 Chinese banks to test whether a higher green credit ratio would reduce banks' nonperforming loan ratio. Results showed that allocating more green loans to the total loan portfolio would reduce banks' nonperforming loan ratio [13]. Taking 150 listed renewable energy companies in China as examples, He et al. (2019) constructed a threshold effect model and studied the nonlinear correlation between renewable energy investment and green economic development. Results found that the impact of renewable energy investment on the green economy development index had a double threshold effect. Increasing environmental pollution control expenditures and adjusting the industrial structure were conducive to improving the green economy development index. Taghizadeh and Yoshino (2019) found that increasing the proportion of green credit could reduce the risk of green finance, increase the rate of return of green energy projects, and increase the transparency of green finance and investment [14]. Song et al. (2019) established a dynamic panel model for 12 Chinese commercial banks and seven international commercial banks. They adopted the generalized moment method to study the impact of green credit on commercial banks' profitability and clarified the differences between China and other countries. Results demonstrated that the project financing ratio of international banks positively impacted banks' profitability. In contrast, the green credit ratio of Chinese commercial banks was inversely proportional to its profitability. The profitability of Chinese banking was positively affected by the growth rates of asset size, management expense ratio, cash ratio, and Gross Domestic Product (GDP) [15].

2.2. BPNN to Assess Credit Risks. BPNN implements a mapping function from input to output and can approximate

TABLE 1: Variables and their numbers.

First-level indicators	References	Second-level indicators	Abbreviations	Numbers
Profitability $\times 1$	Le et al. (2020) [24]	Return on equity	ROE	$\times 11$
		Return on assets	ROA	$\times 12$
		Sales margin	SM	$\times 13$
		Current ratio	CR	$\times 21$
Solvency $\times 2$	Guerini et al. (2020) [25]	Quick ratio	QR	$\times 22$
		Assets and liabilities	AAL	$\times 23$
		Interest coverage ratio	ICR	$\times 24$
		Cash coverage ratio	CCR	$\times 25$
		Earnings per share	EPS	$\times 31$
Development capacity $\times 3$	Ika et al. (2017) [26]	Net assets growth rate	NAGR	$\times 32$
		Total assets growth rate	TAGR	$\times 33$
		Inventory turnover	IT	$\times 34$
		Accounts receivable turnover rate	ARTR	$\times 35$
		Total assets turnover	TAT	$\times 41$
Competency $\times 4$	Maksymchuk et al. (2020) [27]	Cost of sales	QC	$\times 42$
		Management cost	MC	$\times 43$
		Waste gas emissions	WGE	$\times 51$
Environmental quality $\times 5$	Ali et al. (2019) [28]	Wastewater discharge	WD	$\times 52$
		Solid waste emissions	SWE	$\times 53$

any nonlinear continuous function with arbitrary precision. It can automatically extract the “reasonable rules” between output and output data by learning and adaptively memorizing the network weights. Nevertheless, there is little research on BPNN applications in credit risks. Zhou et al. (2019) proposed a BPNN-big data mining method based on particle swarm optimization (PSO). Results suggested that the parallel risk management model had fast convergence speed, predictive solid ability, and screen default behaviors. Simultaneously, the distributed implementation on the big data cluster significantly reduced the processing time used for model training and testing [16]. Shen et al. (2019) put forward an integrated model based on comprehensive minority oversampling technology and BPNN classifier optimization technology for personal credit risk assessment. They found that this model was more effective in processing credit data than other classification models in China [17]. Guo (2020) proposed a loan risk assessment algorithm based on BPNN. Results found that the algorithm based on BPNN was better than traditional logistic regression, which could effectively reduce investors’ risk [18]. Du et al. (2021) established a BPNN credit risk early-warning model. Trained by 450 data samples from 90 companies in 5 years, the network output rate could reach 85%. The genetic algorithm (GA) was employed for optimization so that warnings were more accurate and errors were more minor. Afterward, the accuracy rate could reach 97%. Therefore, using BPNN to warn and assess the internet credit risks had excellent accuracy and computational efficiency, which could expand BPNN applications in internet finance and provide a new development direction for early financial warning [19].

TABLE 2: Factor analysis results.

	Kaiser-Meyer-Olkin	0.763
	Chi-square value	2989.004
Bartlett’s spherical test	Df	182
	Sig.	0.000

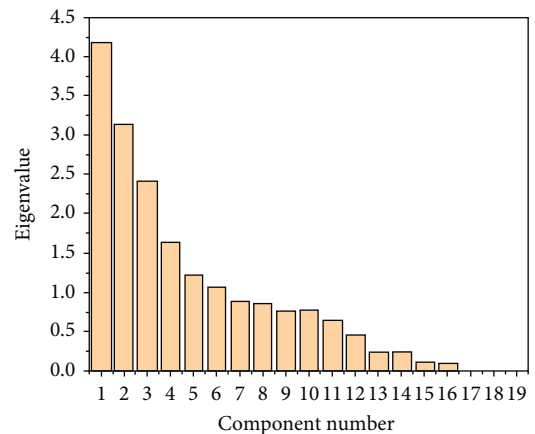


FIGURE 2: Gravel experiment results of factor analysis.

2.3. *A Summary of Research Problems.* In summary, green financial tools have been quite mature worldwide. Among the works on credit risk assessment, scholars have focused on improving and perfecting the assessment methods, including big data, artificial intelligence, and vector machines. There are very few reports assessing green

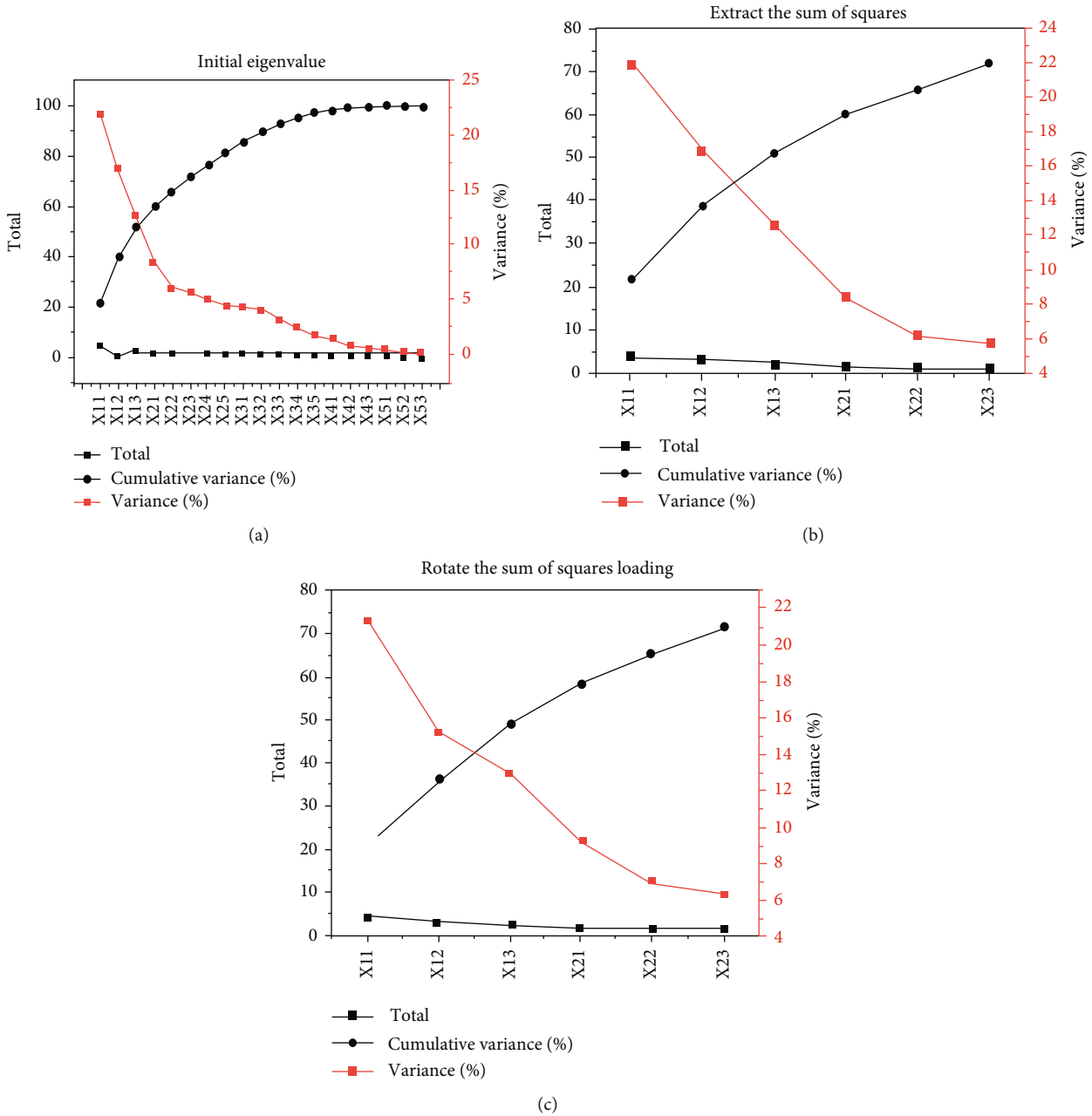


FIGURE 3: Variance analysis results.

credit risks because environmental credit financing uses bonds, funds, and equity. The research and practice of green credit in China have started late, and green credit has only been implemented for about ten years. In China, works on credit risks focus on Analytical Hierarchy Process (AHP), information entropy weighting, data mining, and fuzzy evaluation, with limited tools for assessing and using green credit risks. Moreover, there are a few types of companies involved in green credit risk assessment. Therefore, BPNN, a deep learning approach, will be applied for assessing and predicting the green credit risks of different companies in China, proposing comprehensive management and control recommendations for green credit risks.

3. Research Methodology

3.1. Risk Assessment Model. BPNN has good classification and prediction functions. Assessing banks' green credit risks is classifying companies with similar credit risks. BPNN can learn the relationships between the companies' financial and environmental indicators and the corresponding risks to discover the laws and nonlinear functions. Then, it extracts the valuable information of the test data through the functional relationship found above to judge and analyze the green credit risks of companies [20]. BPNN emphasizes the depth of the model structure, usually up to 10 hidden layers. Figure 1 shows the constructed BPNN bank risk assessment model. The model contains four layers: the input layer, the

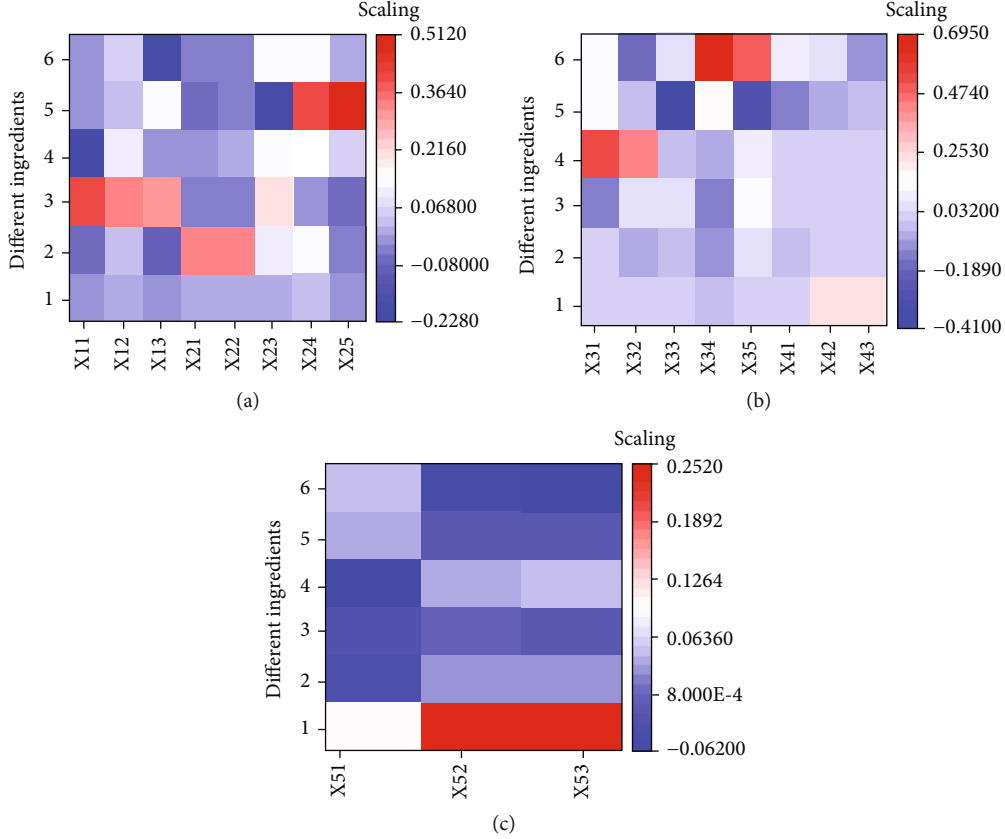


FIGURE 4: Rotation component matrix.

node layer, the output layer, and the hidden layer. The input layer inputs all indicator data and is constructed as per the details of the subsequently constructed indicator system. The node layer learns data as per the corresponding indicators. The calculation process uses the error of each node layer as the evaluation factor. Finally, the evaluation result for a company can be output. Compared with other models, BPNN can provide more hierarchical results, present a better performance in data modeling or exploration, and simulate more complex models. Therefore, unlike recent works, deep learning algorithms are applied to study the green credit risks.

4. Indicator System Construction

Indicators are selected referring to previous documents [21–23]. Two indicators, company finance and environment, are selected. Sixteen financial indicators are selected from profitability, solvency, development capacity, operating capacity, and performance environment. The environmental indicators include waste gas emissions, wastewater discharge, and solid waste emissions. Details of indicator definitions and variables are summarized in Table 1. As per the recent works on green credit risk assessment, the indicator particularity and the data availability can be considered. Hence, the selected 19 evaluation indicators conform to the construction principles of the indicator system.

5. Model Parameter Settings

(1) Input and output layers are as follows: the input layer has 19 neurons, which is determined by 19 corporate financial and environmental indicators. The output layer has 1 neuron, which is determined by the default risk level indicator of the green credit companies. (2) Hidden layer is as follows: according to previous experiments and references, the learning efficiency and prediction accuracy of multiple hidden layers are significantly higher than that of a neural network with only one hidden layer. Therefore, a neural network with two hidden layers is utilized. It is imperative to determine the number of hidden layer neurons. There are three empirical methods to determine the best number of neurons [29]:

$$\sum_{j=0}^n C_{nj}^j > m, j \in [0, n], \quad (1)$$

$$n_1 = \sqrt{n+m} + \alpha, \alpha \in [1, 10], \quad (2)$$

$$n_2 = \log_2^n. \quad (3)$$

In Eqs. (1)–(3), m indicates the number of samples, n_j indicates the number of hidden layer neurons, n represents the number of input units, and n_1 represents the number of output layer neurons. Since the input layer has 19 neurons and the output layer has one neuron, the best value range of hidden layer neurons can be obtained by combining the

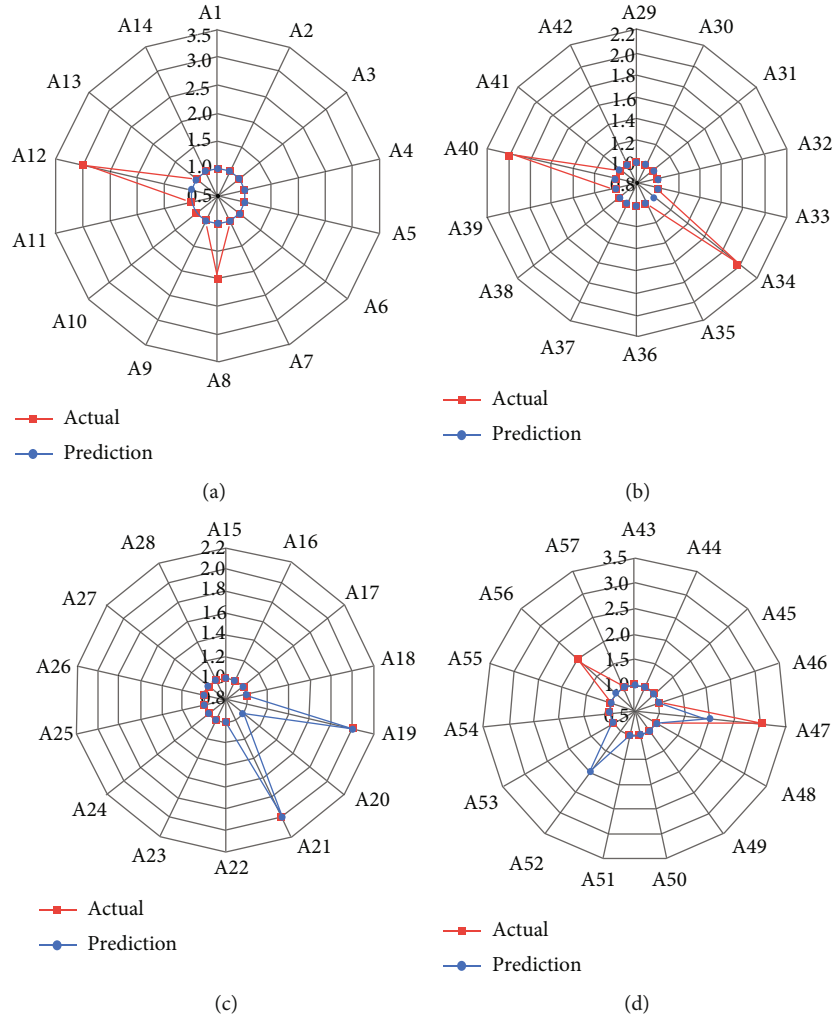


FIGURE 5: BPNN prediction results.

above empirical equations [4, 15]. The optimal neuron distribution is defined according to minimizing neural network errors. The RStudio software is employed for cyclic calculation programming. The number of neurons in each hidden layer should be controlled within [4, 15]. Once the error reaches the minimum, the system stops the calculation.

(3) Learning rate is as follows: a learning rate of 0.01 is determined according to the experience [30]. Threshold is as follows: according to the equation of the hidden layer and the output layer, Eq. (4) can be obtained:

$$H_i = f\left(\sum_{i=1}^n \omega_{ij}x_i - \alpha_j\right), j = 1, 2, \dots, l. \quad (4)$$

In (4), H_i represents the output of the hidden layer, ω_{ij} indicates the connection weight between the input layer and the hidden layer, f denotes the activation function of the hidden layer, l represents the number of hidden layer neurons and α_j indicates the threshold.

$$o_k = \sum_{i=1}^n H_j \omega_{jk} - b_k, k = 1, 2, \dots, m \quad (5)$$

In (5), o_k represents the output of the output layer, ω_{jk} represents the connection weight between the hidden layer and the output layer, and b_k represents the threshold. The above calculation process suggests that both the outputs of the hidden layer and the output layer must be thresholded. According to the data of the input layer, the threshold is set to 0.01, meaning that only when the sum of the input layer values is greater than 0.01, the hidden layer and the output layer can calculate and have outcome.

6. Data and Performance Analysis

China's energy-saving and environmentally friendly companies and coal mining companies are selected as the green credit risk evaluation objects to compare the influence of environmental risks on green credit defaults [31]. Data of 164 listed companies of "energy-saving and environmental protection" and 26 "coal mining companies" are selected.

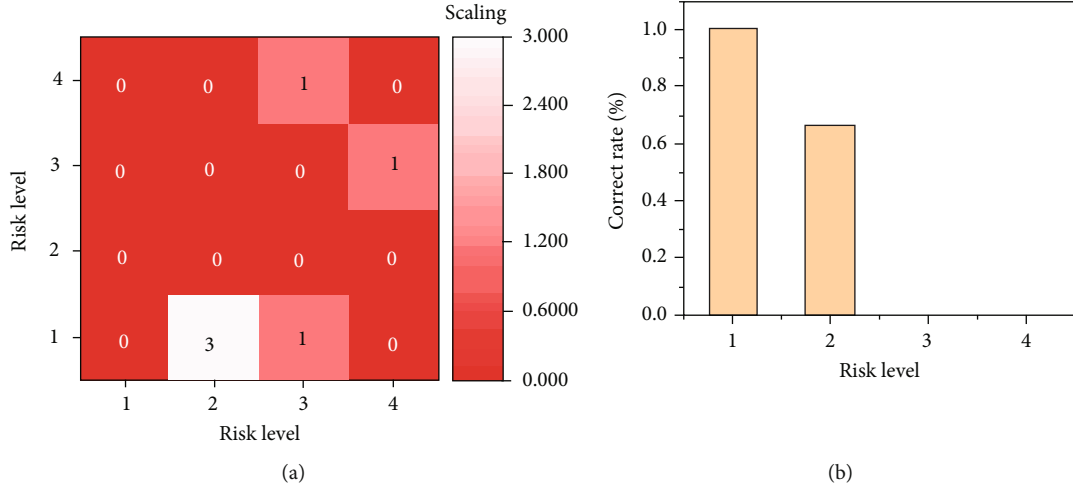


FIGURE 6: The risk prediction results of green credit.

The deadline for data reporting is December 31, 2019. Data sources include the RESSET financial database and the annual reports, social responsibility reports, and environmental information disclosure reports of various companies. The missing environmental information of some companies is calculated using the output value method [32]. Factor analysis [33] screened the above indicators and reduced the data dimension. The financial indicators and environmental indicators of the companies are the input data, and the risk indicators of the companies are the output data. The data are standardized first. Here, the maximum-minimum method normalizes all the data to the interval [0, 1], as shown in Eq. (6)

$$x = \frac{x_{ij} - \min x_{ij}}{\max x_{ij} - \min x_{ij}}, i = 1, 2, \dots, n, j = 1, 2, \dots, m. \quad (6)$$

According to experience, 70% of the sample data are determined as the training set; that is, data of 133 companies consist of the training set. The remaining 30% of the sample data are defined as the test set; that is, data of 57 companies constitute the test set. Both the training set and the test set are selected randomly. The factor analysis equation is shown in Eq. ((7)):

$$\begin{cases} X_1 = b_{11}f_1 + b_{12}f_2 + \dots + b_{1m}f_m + \varepsilon_1 \\ \dots \\ X_p = b_{p1}f_1 + b_{p2}f_2 + \dots + b_{pm}f_m + \varepsilon_p \end{cases} \quad (7)$$

In (7), X_p indicates p explanatory variables, and f_m demonstrates m principal components. This equation represents the linear combination relationship between each variable and the principal components. Before factor analysis, the data applicability should be tested. Here, the Kaiser-Meyer-Olkin (KMO) and Bartlett's spherical test are adopted to test the structure validity.

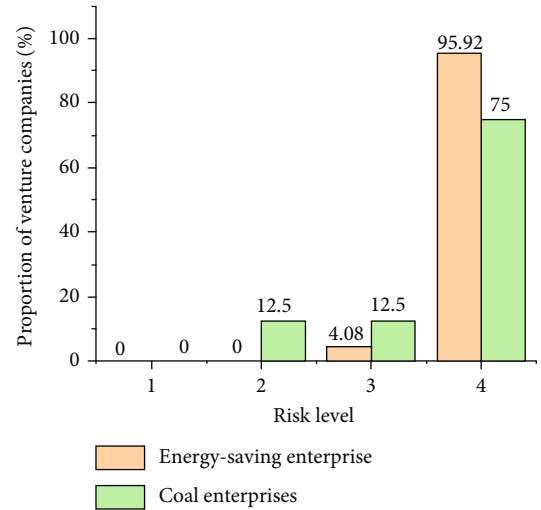


FIGURE 7: Classification of prediction results.

7. Result Analysis

7.1. Factor Analysis Results. As shown in Table 2, the KMO coefficient is 0.763, indicating that the data can be subjected to factor analysis. The chi-square of Bartlett's spherical test is 2989.004, and the P value of corresponding adjoint probability is 0.000, which is significant at the 99% confidence level. The null hypothesis is rejected, and the correlation matrix between variables is not independent. Hence, the selected 19 indicators can undergo factor analysis.

In Figure 2, the common factor is extracted from the data given that the feature root is greater than 1. The gravel experiment results indicate that when the number of principal components exceeds 6, changes in the total information in the feature root tend stable, and the sixth feature root is still greater than 1. Hence, it is most appropriate to extract six principal components.

Figure 3(a) is the result of the initial feature, Figure 3(b) is the loaded result of the extracted sum of squares, and Figure 3(c) is the rotated sum of squares. The cumulative

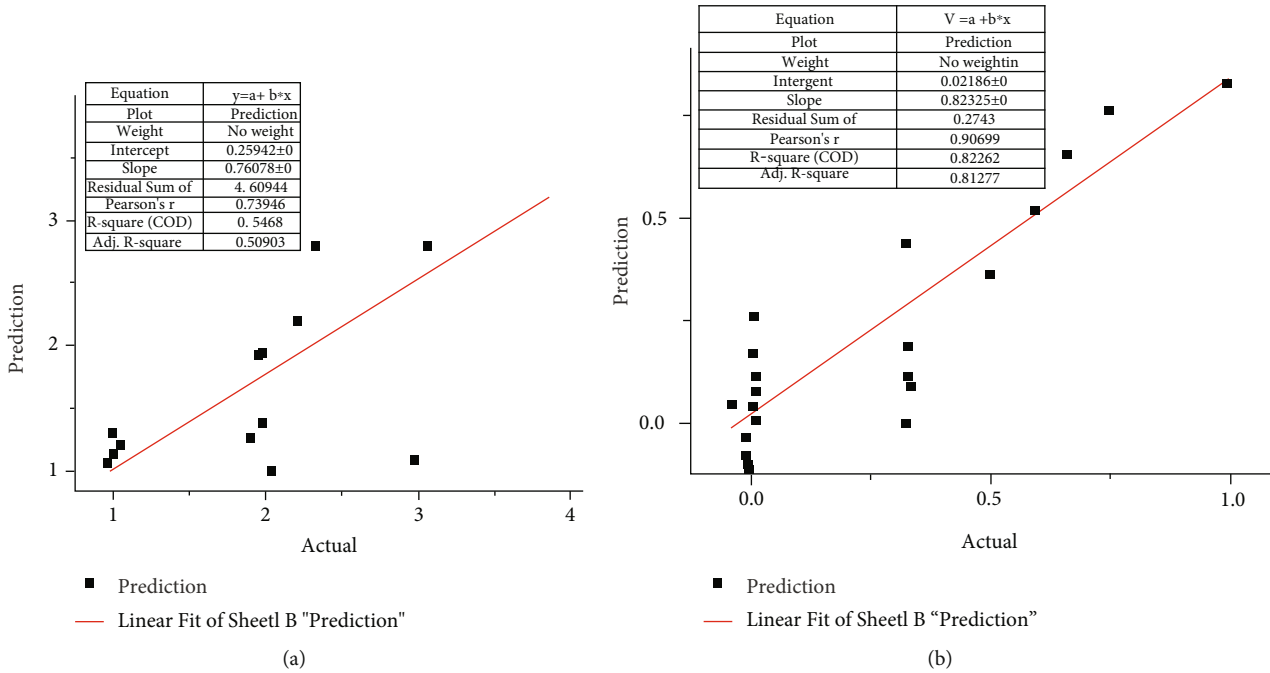


FIGURE 8: Fitting of actual values and predicted values ((a) simple linear regression; (b) BPNN).

variance of these six eigenvalues reaches 71.496%, indicating that the first six principal components explain more than 70% of the original variables. Therefore, these concentrated factors can be used for principal component analysis.

Figure 4(a) displays the rotation component matrix results of profitability and solvency, Figure 4(b) displays the rotation component matrix results of development capacity, and Figure 4(c) displays the rotation component matrix results of environmental performance. The PCA results unquestionably show how each principal component concentrates the original information.

8. Risk Prediction

In Figure 5, green credit risk is divided into four categories (1-4), represented by different numbers to indicate the risk level of other companies. Figure 5(a) is the A1-A14 risk prediction result of the environmental protection company. Figure 5(b) is the A29-A42 risk prediction result of the environmental protection company. Figure 5(c) is the A15-A28 risk prediction result of the coal company, and Figure 5(d) is the A43-A57 risk prediction result of the chemical company result. Among them, Figure 5(a) shows that in the A1-A14 risk prediction results of the environmental protection company, the predicted values of A8 and A12 have a significant deviation from the actual value results. The forecasts of the remaining companies are not too far from the actual results. In Figure 5(b), the predicted value of the two groups of data A34 and A40 deviates greatly from the actual value. In Figure 5(c), the predicted value of the two groups of data A19 and A21 has a large deviation from the actual value. In Figure 5(d), the deviation of the predicted value results of A47, A52, and A56 from the actual value exceeds the estimated range. Among them, the difference between

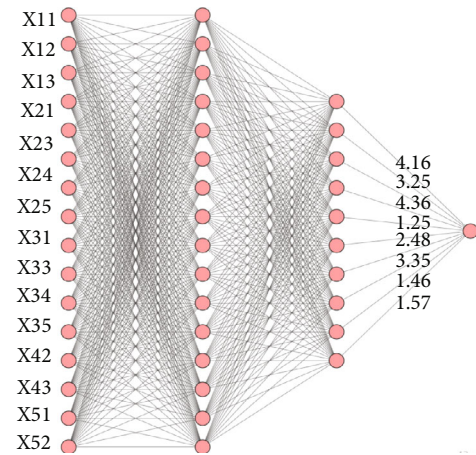


FIGURE 9: BPNN structure with a single hidden layer.

the predicted value of the experimental data of the A47 group and the predicted value of the other groups is too significant, which may be because the BPNN is not adjusted accurately, resulting in a significant error in this group of experiments. The results showed that five companies' green credit risk forecasts were incorrect. The overall prediction accuracy of the model reaches 91.23%. Therefore, BPNN can provide conservative results on banks' green credit risk.

Figure 6(a) shows the matrix of different risks, and Figure 6(b) shows the correct prediction rate. According to the classification of neural network's prediction results, among the 47 energy-saving and environmental protection companies predicted, there are no high-risk and medium-risk companies and only two low-risk companies. A total of eight coal companies are predicted, including one medium-risk company and one low-risk company.

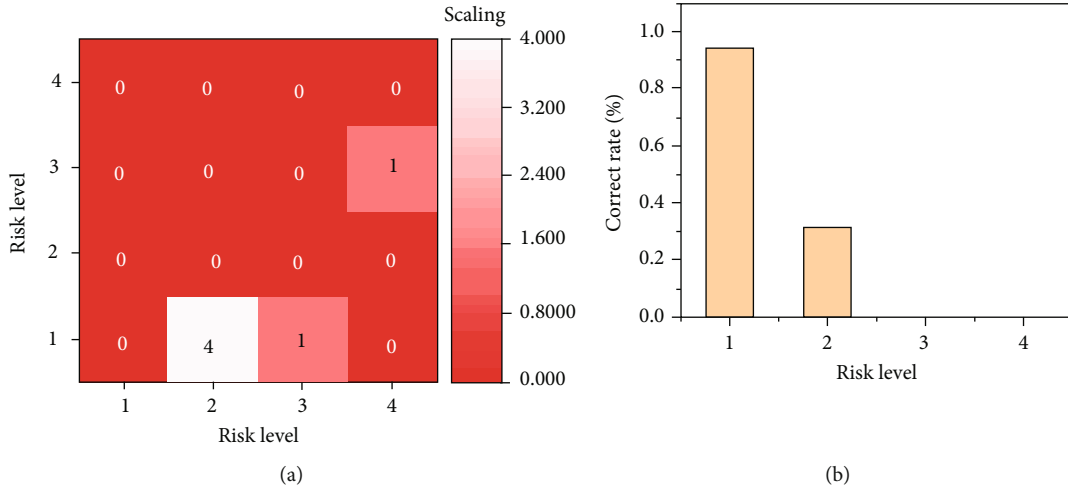


FIGURE 10: Prediction results of green credit risks.

Chongzhou Coal has a medium risk due to its high three-waste emissions.

In Figure 7, low-risk companies account for 4.08% of all 146 energy-saving and environmental protection companies, and 95.92% are risk-free. There are no high-risk companies in coal mining companies; however, medium-risk and low-risk companies account for 25%, while risk-free companies account for only 75%. This result can reflect that the green credit risks of coal mining companies are generally much more significant than those of energy-saving and environmental protection companies.

9. Model Performance Comparison

Figure 8(a) displays the prediction results using the simple linear regression method, and Figure 8(b) displays the proposed method’s results. The error rate of simple linear regression is 2.471839878, and the error rate of BPNN is 0.1308943154. The error of simple linear regression is about 18.88 times that of the BPNN. Hence, the predicted value of BPNN is closer to the fitted line, while the expected value of simple linear regression has more considerable white noise than the fitted line.

According to Figure 9, BPNN with a single hidden layer is adopted to predict and assess banks’ green credit risks to test the advantages of BPNN over the single-layer neural networks. Given one hidden layer, BPNN’s threshold and learning rate are 0.01. The number of neurons with the minor error found through cyclic calculation is 7. At this point, the model error rate is 0.1391539131, more significant than that of BPNN with double hidden layers.

Figure 10(a) presents the matrix of different risks obtained by a single-layer network, and Figure 10(b) presents the correct prediction rate of a single-layer network. There are 57 predicted sample companies in total, while the green credit risk predictions of 6 companies are incorrect. Precisely, the four low-risk companies are mistakenly predicted as being risk-free, one medium-risk company is mistakenly predicted as being risk-free, and one high-risk company is incorrectly expected as medium-risk. Compared

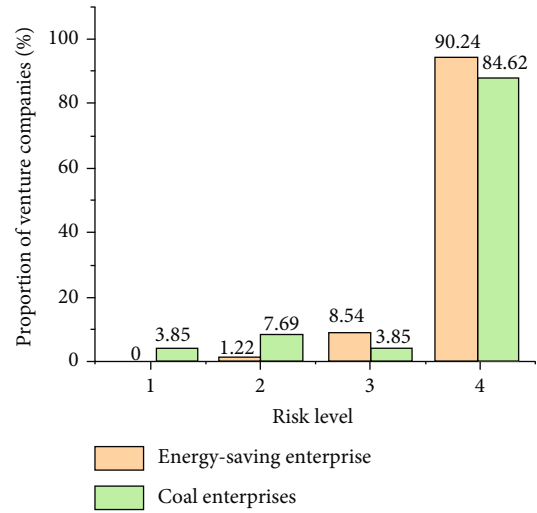


FIGURE 11: Comparison of risks in different industries.

with BPNN, the single-layer network has more false predictions for low-risk companies. The overall prediction accuracy is lower than BPNN. Both the simple linear regression and the single hidden layer network have weaker prediction effects than BPNN. Therefore, the established green credit risk assessment model is scientific and practical.

10. Credit Risk Assessment

There is one high credit risk company in the coal industry, accounting for 3.85% of the total. Due to the increased emission of “three wastes,” the company has a very high credit risk due to environmental factors. The credit risk of coal mining companies is significantly greater than that of energy conservation and environmental protection companies. Therefore, companies with large emissions of “three wastes” such as coal are more prone to credit defaults. There are no high-risk companies in the energy conservation and environmental protection industry. Two energy-saving and environmental protection companies have medium credit risk,

accounting for 1.22%. Two coal mining companies have medium credit risk, accounting for 7.69%. The number of high-risk companies in the coal industry is greater than that of energy-saving and environmental protection companies, indicating that environmental problems have seriously affected the company's credit assessment. The penalties imposed by the regulatory authorities on the company's environmental pollution problems can directly affect its business development, which indirectly affects its ability to repay when due. In addition, the credit risk assessment uses a logistic regression model to score underlying credit. Credit accounts are classified at different levels by managing the account life cycle and possible account cancellation periods. Credit scores and risk levels are used for risk assessment. These variables help to establish a sound credit risk assessment system. The true value of green credit risk is to evaluate the risk level of bank customers and to improve the stability of customer fund storage while ensuring the bank's operating performance. The risk assessment models for different industries are shown in Figure 11.

11. Conclusions

Factors affecting the green credit risks are analyzed. Nineteen indicators covering six dimensions of profitability, solvency, development capacity, operating capacity, performance environment, and environmental quality are summarized, and an indicator system for green credit risk assessment is established. BPNN is employed to evaluate and predict green credit risks, and the results are compared with those of BPNN with a single hidden layer and simple linear regression. Results suggest that the proposed model has better performance and higher prediction accuracy. Although the research builds the contribution evaluation model, there are still some weaknesses. (1) Due to data collection limitations, when determining a company's environmental protection indicators, only the information of "three wastes" can be collected. Other environmental protection data cannot be obtained or used because there is no uniform statistical caliber. Therefore, proper screening should be carried out when selecting research data, focusing on the validity of data collection. (2) When choosing an industry, only considering the energy-saving and environmental protection industry and the coal mining industry is limited to a certain extent. In the future, these two aspects will be analyzed to improve the green credit risk assessment model further.

Data Availability

The raw data supporting the conclusions of this article will be made available by the author, without undue reservation.

Consent

Informed consent was obtained from all individual participants included in the study.

Conflicts of Interest

The author declares that he/she has no conflict of interest.

Authors' Contributions

The author listed has made a substantial, direct, and intellectual contribution to the work and approved it for publication.

Acknowledgments

The author acknowledges the help from the university colleagues.

References

- [1] H. Maoxing and Y. Qi, "The Marxist green development concept and green development in contemporary China: comment on incompatibility theory between environment and development," *Economic Research Journal*, vol. 52, no. 6, pp. 17–30, 2017.
- [2] M. E. Kruk, A. D. Gage, C. Arsenault et al., "High-quality health systems in the sustainable development goals era: time for a revolution," *The Lancet Global Health*, vol. 6, no. 11, pp. e1196–e1252, 2018.
- [3] R. Wang, R. Qi, J. Cheng, Y. Zhu, and P. Lu, "The behavior and cognition of ecological civilization among Chinese university students," *Journal of Cleaner Production*, vol. 243, pp. 118464–118473, 2020.
- [4] L. He, L. Zhang, Z. Zhong, D. Wang, and F. Wang, "Green credit, renewable energy investment and green economy development: empirical analysis based on 150 listed companies of China," *Journal of Cleaner Production*, vol. 208, pp. 363–372, 2019.
- [5] W. Yin, Z. Zhu, B. Kirkulak-Uludag, and Y. Zhu, "The determinants of green credit and its impact on the performance of Chinese banks," *Journal of Cleaner Production*, vol. 286, pp. 124991–124998, 2021.
- [6] H. Wen, C.-C. Lee, and F. Zhou, "Green credit policy, credit allocation efficiency and upgrade of energy-intensive enterprises," *Energy Economics*, vol. 94, pp. 105099–105099, 2021.
- [7] J. C. Li, D. L. Zhao, B. F. Ge, K. W. Yang, and Y. W. Chen, "A link prediction method for heterogeneous networks based on BP neural network," *Physica A: Statistical Mechanics and its Applications*, vol. 495, pp. 1–17, 2018.
- [8] B. Wang, X. Gu, L. Ma, and S. Yan, "Temperature error correction based on BP neural network in meteorological wireless sensor network," *International Journal of Sensor Networks*, vol. 23, no. 4, pp. 265–278, 2017.
- [9] K. Cui and X. Jing, "Research on prediction model of geotechnical parameters based on BP neural network," *Neural Computing and Applications*, vol. 31, no. 12, pp. 8205–8215, 2019.
- [10] C. Yuan, X. Sun, and Q. J. Wu, "Difference co-occurrence matrix using BP neural network for fingerprint liveness detection," *Soft Computing*, vol. 23, no. 13, pp. 5157–5169, 2019.
- [11] X. Huang, X. Liu, and Y. Ren, "Enterprise credit risk evaluation based on neural network algorithm," *Cognitive Systems Research*, vol. 52, pp. 317–324, 2018.
- [12] P. Monnin, *Integrating Climate Risks into Credit Risk Assessment-Current Methodologies and the Case of Central*

- Banks Corporate Bond Purchases*, Council on Economic Policies, 2018.
- [13] Y. Cui, S. Geobey, O. Weber, and H. Lin, "The impact of green lending on credit risk in China," *Sustainability*, vol. 10, no. 6, pp. 2008–2015, 2018.
- [14] F. Taghizadeh-Hesary and N. Yoshino, "The way to induce private participation in green finance and investment," *Finance Research Letters*, vol. 31, pp. 98–103, 2019.
- [15] X. Song, X. Deng, and R. Wu, "Comparing the influence of green credit on commercial bank profitability in China and abroad: empirical test based on a dynamic panel system using GMM," *International Journal of Financial Studies*, vol. 7, no. 4, pp. 64–71, 2019.
- [16] H. Zhou, G. Sun, S. Fu, J. Liu, X. Zhou, and J. Zhou, "A big data mining approach of PSO-based BP neural network for financial risk management with IoT," *IEEE Access*, vol. 7, pp. 154035–154043, 2019.
- [17] F. Shen, X. Zhao, Z. Li, K. Li, and Z. Meng, "A novel ensemble classification model based on neural networks and a classifier optimisation technique for imbalanced credit risk evaluation," *Physica A: Statistical Mechanics and its Applications*, vol. 526, pp. 121073–121083, 2019.
- [18] Y. Guo, "Credit risk assessment of P2P lending platform towards big data based on BP neural network," *Journal of Visual Communication and Image Representation*, vol. 71, pp. 102730–102736, 2020.
- [19] G. Du, Z. Liu, and H. Lu, "Application of innovative risk early warning mode under big data technology in internet credit financial risk assessment," *Journal of Computational and Applied Mathematics*, vol. 386, p. 113260, 2021.
- [20] D. Zheng, Z. D. Qian, Y. Liu, and C. B. Liu, "Prediction and sensitivity analysis of long-term skid resistance of epoxy asphalt mixture based on GA-BP neural network," *Construction and Building Materials*, vol. 158, pp. 614–623, 2018.
- [21] Y. Changwei, L. Zonghao, G. Xueyan, Y. Wenying, J. Jing, and Z. Liang, "Application of BP neural network model in risk evaluation of railway construction," *Complexity*, vol. 2019, 12 pages, 2019.
- [22] X. Deng, T. Xu, and R. Wang, "Risk evaluation model of highway tunnel portal construction based on BP fuzzy neural network," *Computational Intelligence and Neuroscience*, vol. 2018, 16 pages, 2018.
- [23] X. Cai, Y. Qian, Q. Bai, and W. Liu, "Exploration on the financing risks of enterprise supply chain using Back propagation neural network," *Journal of Computational and Applied Mathematics*, vol. 367, pp. 112457–112463, 2020.
- [24] T. D. Q. Le and T. Ngo, "The determinants of bank profitability: a cross-country analysis," *Central Bank Review*, vol. 20, no. 2, pp. 65–73, 2020.
- [25] M. Guerini, L. Nesta, X. Ragot, and S. Schiavo, "Firm liquidity and solvency under the Covid-19 lockdown in France," *OFCE Policy Brief*, vol. 76, pp. 1–20, 2020.
- [26] L. A. Ika and J. Donnelly, "Success conditions for international development capacity building projects," *International Journal of Project Management*, vol. 35, no. 1, pp. 44–63, 2017.
- [27] B. Maksymchuk, T. Matviichuk, V. Solovyov et al., "Developing healthcare competency in future teachers," *Revista Romaneasca Pentru Educatie Multidimensionala*, vol. 12, no. 3, pp. 24–43, 2020.
- [28] H. S. Ali, V. Zeqiraj, W. L. Lin et al., "Does quality institutions promote environmental quality?," *Environmental Science and Pollution Research*, vol. 26, no. 11, pp. 10446–10456, 2019.
- [29] Y. J. Song, B. Y. Song, Z. S. Zhang, and Y. W. Chen, "The satellite downlink replanning problem: a BP neural network and hybrid algorithm approach for IoT internet connection," *IEEE Access*, vol. 6, pp. 39797–39806, 2018.
- [30] S. Chen, G. Fang, X. Huang, and Y. Zhang, "Water quality prediction model of a water diversion project based on the improved artificial bee colony-back-propagation neural network," *Water*, vol. 10, no. 6, pp. 806–813, 2018.
- [31] T.-T. Feng, X.-L. Gong, Y.-H. Guo, Y.-S. Yang, and J. Dong, "Regulatory mechanism design of GHG emissions in the electric power industry in China," *Energy Policy*, vol. 131, pp. 187–201, 2019.
- [32] B. Miranda and A. C. Mohan, "The correlation between TQM implementation and trade financial performance," *Journal of Economic & Management Perspectives*, vol. 11, no. 4, pp. 1626–1629, 2017.
- [33] M. Sellbom and A. Tellegen, "Factor analysis in psychological assessment research: common pitfalls and recommendations," *Psychological Assessment*, vol. 31, no. 12, pp. 1428–1441, 2019.

Research Article

Research on Dynamic Spectrum Allocation Algorithm Based on Cyclic Neural Network

Xiaomo Yu,^{1,2} Yonghua Cai ,³ Wenjing Li,^{1,2} Xiaomeng Zhou,¹ and Ling Tang⁴

¹Department of Logistics Management and Engineering, Nanning Normal University, Nanning, 530001 Guangxi, China

²Guangxi Key Lab of Human-Machine Interaction and Intelligent Decision, Nanning Normal University, Nanning, 530001 Guangxi, China

³School of Mathematics and Computer Science, Hebei Normal University for Nationalities, Chengde, 067000 Hebei, China

⁴Arts Institute, Guangxi University for Nationalities, Nanning, 530001 Guangxi, China

Correspondence should be addressed to Yonghua Cai; caiyonghua@st.btbu.edu.cn

Received 12 January 2022; Accepted 19 February 2022; Published 23 March 2022

Academic Editor: Nima Jafari Navimipour

Copyright © 2022 Xiaomo Yu et al. This is an open access article distributed under the Creative Commons Attribution License, which permits unrestricted use, distribution, and reproduction in any medium, provided the original work is properly cited.

Due to the wide application of cognitive wireless network, the network structure is becoming more and more complex. It is difficult to establish the corresponding mathematical model to simulate the high complexity network environment. The algorithm based on recurrent neural network in deep reinforcement learning can effectively solve this problem. In addition, with the rise of deep learning in recent years, the combination of reinforcement learning and deep learning shows excellent ability in dealing with complex problems and data operation. This paper is aimed at studying dynamic spectrum allocation based on cyclic neural network. This paper briefly introduces MATLAB, sets up the network environment of algorithm simulation, then analyzes the overall performance of the improved genetic algorithm, and explores the influence of genetic algorithm-related parameters and network environment-related parameters on the performance of the algorithm. The results show the improved genetic algorithm. The network efficiency can be improved by about 2%, but the spectrum switching frequency can be reduced by 69%. When the number of primary users in the network is large, the network benefit of improving the genetic algorithm is superior to the other two algorithms. In addition, when the crossover probability is 0.6 and 0.1, the fitness value is higher than the crossover probability of 0.9 and 0.5; the interference of authorized users in the network initially has less impact on the secondary user.

1. Introduction

The “object” in the Internet of Everything, that is, the sensor and other intelligent objects in the Internet, is used to detect various kinds of data that are artificially needed and timely guide the changes of various states and parameters in the current situation. It can be seen that the significance of sensor network for the era of Internet of all things is extraordinary [1, 2]. The wireless sensor network is an important part of the Internet of Things. It plays a role similar to the “sensor” and directly affects the Internet of Things to make the next judgment. The wireless sensor network is a multihop network formed by a large number of sensor nodes disposed

in the detection area through self-organization. Its main function is data collection, processing, and transmission. When establishing a wireless sensor network, it can be manually deployed or directly use the flight device to scatter the sensor nodes to the monitoring area, and then, the nodes self-organize into a network [3, 4]. The main task of the wireless sensor network is to collaboratively sense and collect data between nodes and report the monitoring information to users; its advantages include rapid deployment, self-organizing into the network, and good concealment, so it is in intelligent transportation and battlefield targets. Applications in areas such as rapid positioning, physiological data collection systems, and marine data detection have excellent

performance, but the limitations are that the energy of the sensor is limited and the communication capacity between nodes is limited [5, 6].

At the same time, with the wide application of wireless communication in various industries, the number of various forms of wireless communication has increased dramatically, while the spectrum resources are very limited, and the frequency band becomes more and more crowded. Of course, scientists are constantly trying new wireless communication technology theory to alleviate this situation. Therefore, for traditional communication systems, scientists have proposed link adaptive technology and multiantenna technology to coordinate the contradiction between the high demand of wireless communication services and the scarcity of spectrum resources [7, 8]. However, due to the satisfaction of Shannon's theorem, the transmission efficiency of the spectrum cannot be improved without limit, and the contradiction is not improved. The utilization of spectrum resources is still very unbalanced, although the spectrum resources at this stage have been saturated. The information transmission between wireless sensor network nodes adopts IEEE802.15.4 protocol. The IEEE802.15.4 protocol is the basis of Zigbee, MiWi, and Thread specifications. It works in the ISM frequency band and has the lowest transmission power, the smallest transmission distance, and short operation time and is easy to be subject to other communication system and noise interference characteristics. The ISM band is an unlicensed band and is used by many types of networks because it has no authorized use restrictions. Currently, at least three kinds of wireless communication protocols use this frequency band, which are IEEE802.11b/g protocol, Bluetooth, and IEEE802.15.4 protocol [9, 10]. Along with the wider application range of wireless sensor networks, the possibility of multiple wireless sensor networks in the same area is increasing, so the wireless sensor network itself will also cause interference, affecting the performance of both. Therefore, it is necessary to apply the dynamic spectrum allocation technology in cognitive radio to wireless sensor networks to solve the problem of imbalance in spectrum utilization [11, 12].

Zhang proposed a new dynamic spectrum allocation method for hybrid accessed cognitive femtocell. In this method, a macro base station (BS) allocates a portion of the subchannels to a femto access point (FAP) to motivate the FAP to serve macro users (MUS). The FAP then allocates subchannels and power to maximize femtocell network utility while guaranteeing the throughput of the served MUS. In addition, we attribute the corresponding resource allocation problem to a utility maximization problem and propose a method to solve by the dual decomposition method. The simulation results show that the method has good effects on wireless service providers and femtocells [13, 14]. Touzri proposed a game-based design method for dynamic spectrum allocation mechanism of cognitive radio networks. The secondary user (SU) detects when channels can be used without disturbing any primary users and attempts to opportunistically use them. When the SU detects an idle channel, it estimates its capacity and sends its estimate to the central manager. The manager calculates the

conflict-free allocation by implementing a real mechanism. SUS must pay the amount allocated, depending on a set of valuations, which are expressed as profit maximizers. Touzri proposed and tests two mechanisms for realizing this idea, which are proven to be real and easy to handle and approximately effective. We show the flexibility of these mechanisms and show how they can be modified to achieve other goals, such as fairness, and how they can run without actually charging SUS [15, 16]. In dynamic spectrum allocation (SA) of elastic optical networks (EONS), spectral fragmentation will have a significant impact on spectrum utilization. In order to reduce the segmentation, the SA algorithm should fully consider various factors to achieve the purpose of optimization. Prasan studied the SA problem with long-term awareness in dynamic scenarios. First, Prasan designed a new metric that considers the effects of debris from the perspective of occupied frequency slots (FSS) and idle frequency slots (FSS), measuring the fragmentation in the path. Using this metric, a hold time sensing algorithm is proposed, which considers the different overall fragment states in the network and selects the optimal spectrum allocation method. The performance of the algorithm is verified by simulation. Compared with the traditional algorithm, the algorithm has lower blocking probability and can better utilize network resources [17, 18]. The service provider and the D2D service group solved the user spectrum allocation problem by using Bertrand game theory. The utility functions of the D2D service group and the cellular service provider are improved, respectively. Hoffmann also proposed optimal pricing for cellular service providers and dynamic price adjustment strategies for D2D service groups. In addition, the existence of the Nash equilibrium state and the convergence of the algorithm are proved. Through simulation and experiment, the influence of different cellular users and different learning factors on the performance of the scheme is analyzed. Compared with the existing scheme, this scheme not only improves the spectrum utilization rate but also improves the system fairness [19, 20].

The purpose of this paper is to study dynamic spectrum allocation based on cyclic neural network. This paper introduces several models of dynamic spectrum allocation. The improved genetic algorithm is simulated on MATLAB platform to verify the performance of the algorithm. The influences of network environment parameters on the network revenue are compared with CSGC, traditional genetic algorithm, and improved genetic algorithm. The conclusion is drawn that the improved genetic algorithm can guarantee the network revenue and reduce the energy loss caused by the spectrum switching frequency.

2. Proposed Method

2.1. Overview of Dynamic Spectrum Allocation. Dynamic spectrum allocation is a method of saving spectrum. The system assigns an idle channel to the mobile station in real time according to the call application of the mobile station. After the users are used, they will be redistributed by the system recycling channel.

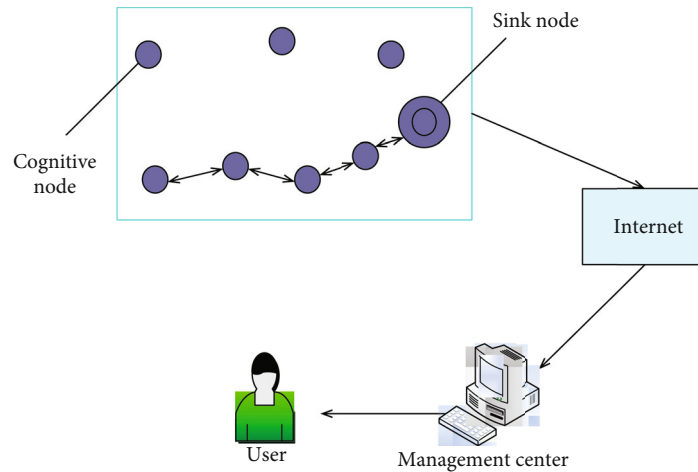


FIGURE 1: Wireless sensor network structure.

2.1.1. Wireless Sensor Network. Wireless sensor network (WSN) is a distributed sensor network, whose end is a sensor that can sense and check the outside world. Sensors in WSN communicate wirelessly, so the network settings are flexible, the location of devices can be changed at any time, and they can also be connected with the Internet in wired or wireless way. A multihop ad hoc network is formed by wireless communication. As a key field of Internet of Things applications, the task of wireless sensor network is to cooperate among nodes to sense and collect data. Its architecture is generally composed of three parts: cognitive node, sink node, and user management center. Its structure is shown in Figure 1.

The transmission of wireless sensor networks is based on the spectrum resources in the network. However, in the process of the development of wireless communication technology, the limited spectrum resources are used by various wireless communication methods, and the problem of resource shortage is becoming more and more serious. In order to improve the utilization of spectrum resources and solve the problem of unbalanced spectrum utilization, various dynamic spectrum allocation methods are proposed.

2.1.2. The Concept of Dynamic Spectrum Allocation. There are two types of basic users in cognitive radio networks, authorized users and unauthorized users, which are also called primary user (PU) and secondary users (SU), respectively. At present, the fixed spectrum allocation policy is to allocate the licensed spectrum to the main users, so they have the absolute priority to use the licensed spectrum. Secondary users have the ability to detect spectrum holes in real time (spectrum holes are frequency bands not occupied by PU in the spectrum domain), that is, when the authorized spectrum is idle at a certain moment and not occupied by the primary users, secondary users can access this spectrum and then use this spectrum for data transmission.

Dynamic spectrum allocation technology is a cognitive radio-based spectrum switching technology. The two most important features of cognitive radio systems are the spec-

trum sensing and spectrum reconfiguration of the physical layer. The dynamic spectrum allocation technology can detect which channel frequency band is idle in the current state and record and share all the busy and idle states. In each cycle, the system parameters are adjusted in real time, and when there is a free frequency band, assign authorized users in a timely manner. When spectrum allocation is performed on cognitive users, it is necessary to dynamically detect whether there is a free spectrum or whether the authorized user is in a free time state. The spectrum allocation is based on the above-mentioned allocation method, and the frequency band resources are dynamically utilized to maximize the utilization of the spectrum and the transmission rate. The cognitive radio theory topology is shown in Figure 2.

As can be seen from Figure 2, cognitive radio theory in other words is to use the spectrum for secondary utilization, that is, in the case where the spectrum resources are scarce, and the cognitive user and the authorized user need to occupy the channel information at the same time, the authorization is realized. Users and cognitive users can share spectrum resources fairly and efficiently with each other, maximizing the occupation of spectrum information and reducing waste of spectrum resources. Dynamic spectrum allocation follows the principle of authorized users, and the cognitive user is supplemented by the dynamic and flexible allocation of spectrum. In the cognitive wireless sensor network system, the bandwidth, user location, and number of channels are not fixed. Dynamic spectrum allocation can adaptively adjust the spectrum allocation strategy according to user requirements or the system's own indicators, thereby improving system flexibility and avoiding waste of spectrum holes, so dynamic spectrum allocation has a great advantage over the static spectrum allocation method in solving the problem of spectrum resource sharing. According to the network structure, spectrum allocation is divided into centralized and distributed. The centralized allocation method collects spectrum resources by a dedicated network coordinator and establishes a schedule, broadcasts to the secondary users, and performs spectrum allocation according to the

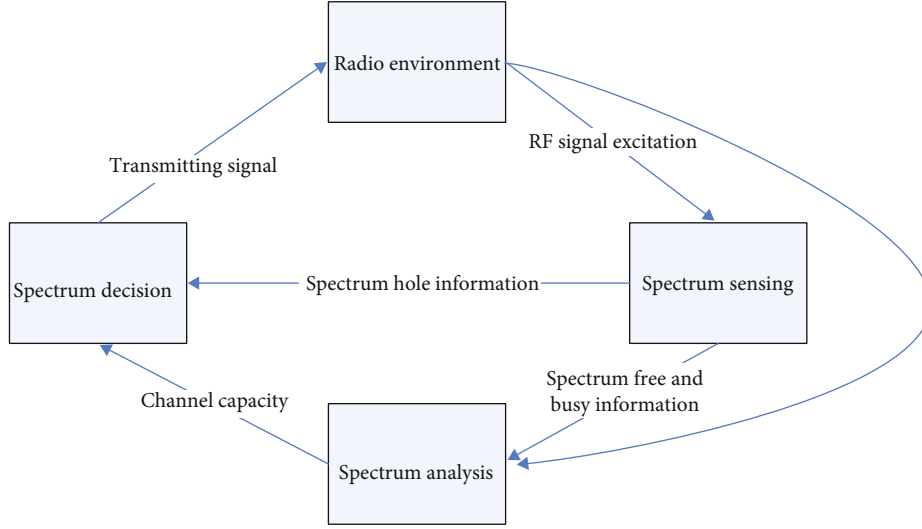


FIGURE 2: Cognitive radio theory topology.

wireless environment monitoring information uploaded by the secondary users, and the cognitive users assigned to the spectrum start to transmit data. The centralized allocation method can take into account the different needs of different users. The network coordinator is responsible for coordinating the spectrum configuration of each user to avoid mutual interference. The information exchange causes a large amount of scheduling overhead and energy consumption. When the network scale is large, the disadvantage is as follows. Once the network coordinator fails or is damaged, the entire network will be partially or even completely paralyzed. Distributed requires each sensor node to have the ability to perceive global or local spatially available spectrum and compete for spectrum allocation based on monitoring information between local and neighbors. It is suitable for nonfixed networks with low complexity, but distributed allocation due to each node participates in the allocation and is more susceptible to wireless environments such as channel fading.

2.1.3. Dynamic Spectrum Allocation Model. The current models for dynamic spectrum allocation mainly include interference temperature, auction bidding, graph theory coloring, and game theory. The game theory model and the auction bidding model are mainly used in the distributed spectrum allocation model, while the graph theory coloring model and the interference temperature model are mostly used in centralized spectrum allocation. The four spectrum allocation models are briefly described below.

(1) Interference Temperature Model. The interference temperature model is an underlay spectrum access method, which means that the power of the receiver is reduced to the extent that the primary user can withstand by adjusting the power of the transmitter, as long as the transmission power of the secondary user does not exceed that set by the primary user. Interfering with temperature, you can coexist with authorized users, wherein the interference tem-

perature is quantized as the ratio of the interference power to the bandwidth, and the representation method is

$$T_I(f_c, B) = \frac{P_I(f_c, B)}{kB}. \quad (1)$$

In formula (1), T_I is the interference temperature, $P_I(f_c, B)$ is the average noise power (unit W) of the receiving device with f_c as the center frequency, B is the bandwidth, k is the Boltzmann constant, and $1.38 * 10^{-23} J/^{\circ}C$ is received by the main user. The sum of the temperature corresponding to the transmission power of the secondary user and the interference temperature T_I is less than the threshold T_L , that is, according to

$$T_I + \frac{P_S^I}{kB} \leq T_L. \quad (2)$$

This means that the secondary user can use the same frequency within the same communication range as the primary user without affecting the primary user.

(2) Auction Bidding Model. The auction bidding model performs spectrum allocation based on the bidding idea of the most profitable person in economics. The auction bidding model is usually applied to the centralized spectrum allocation. Each secondary user passes its own network revenue to the BS, and there is no information transmission between the secondary users. Therefore, the centralized allocation method can reduce the overhead and be closer to the principle of wireless sensor network energy saving. When using the auction bidding model for spectrum allocation, the auctioneers in the auction are usually simulated by the base station or the fusion center, and each cognitive node is a bidder. For each auction, the cognitive node will price and bid on the demand for spectrum resources, and the auctioneer will determine the spectrum allocation scheme for the purpose of

maximizing network revenue. In the auction bidding model, the network can formulate rules according to its own needs, such as maximum throughput, time fairness, and fairness of opportunity. The bidder obtains the relevant spectrum allocation scheme according to the rules.

(3) *Graph Theory Coloring Model*. Graph theory is a mathematical model function in discrete mathematics. First, the specific practical problems are abstracted into graphs, and the constructed graphs are discussed and studied. Shading a graph means that all the vertices of the graph are colored, but adjacent nodes must use different colors and then the minimum number of colors to use. This is the research background of the graph theory coloring model. Figure 3 is a schematic diagram of a graphing coloring model. In the figure, the A area is adjacent to the B area and the C area, and the B area is adjacent to the D area so that the colors of the three areas A, B, and C are different, and the color of the B area and the D area are also different, which can satisfy the requirements of different colors of adjacent areas in the graph coloring. In a distributed network, the graph theory coloring model maps the network distribution of authorized cognitive radios to cognitive users, as shown in Figure 3.

As can be seen from Figure 3, the topology diagram shown in Figure 2 shows the network structure in which the primary and secondary users coexist in cognitive radio. If two network common channels A, B, and C are assumed, we use the aggregate symbol channel $\{A, B, C\}$ to represent the user. The symbol of -IV is used to indicate, and the authorized users occupy channels A, B, C, and C, respectively. The range within the circle indicates that the authorized users cannot share the same channel, and the spectrum occupancy of the cognitive user cannot affect the normal spectrum usage of the authorized user. For example, in the topology diagram, if the channel occupied by the authorized user IV is channel C, the cognitive user cannot use channel C within the coverage of the authorized user IV, so the available channel set is channel5 $\{A, B\}$; other cognitive users and authorized users should also follow such rules. The line in Figure 2 indicates that there is interference at two points of the line segment, that is, if the two vertices in the figure are connected by a common line, it means that the two lines share the same frequency band. At the same time, each vertex exists in a set, which represents the spectrum resources that can be used in the area, because the spectrum usage information of the authorized users changes in real time. As the network environment changes, each node in the network topology updates the network topology information in the database in each cycle of the system through interaction and exchange of information.

2.2. Dynamic Spectrum Allocation Algorithm Based on Cyclic Neural Network. The main problems caused by channel allocation in available spectrum space are adjacent channel interference and cochannel interference. For adjacent channel interference, nonoverlapping channels can be used to eliminate it. For cochannel interference, it is necessary to carry out optimal channel allocation in cognitive wireless

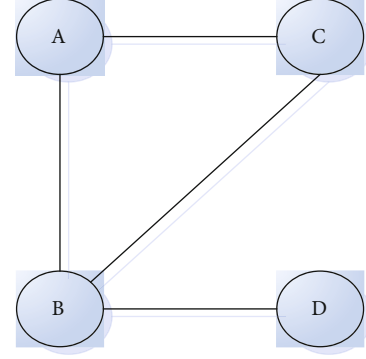


FIGURE 3: Graph coloring model.

networks to avoid conflicts caused by selecting the same channel. Aiming at the joint problem of dynamic power control and channel allocation, in order to overcome the large amount of computation caused by the large space state and partial observability of complex problems, a joint algorithm of dynamic power control and channel allocation based on cyclic neural network is proposed. So that the secondary users can successfully access the channel, make the best use of the optimal power control strategy, avoid harmful interference to the primary users, and improve the overall performance of cognitive wireless networks and the utilization of spectrum resources.

2.2.1. Long- and Short-Term Memory Cycle Neural Network. Long-term and short-term memory is a special cyclic neural network, which mainly includes forgetting stage, selective memory stage, and output stage. It is realized through forgetting gate, input gate, and output gate, respectively. The core of long-term and short-term memory is to control the unit state through three interactive gating states, remember the information that needs to be remembered for a long time, and forget the unimportant information. Therefore, it shows excellent performance in solving the problems of gradient disappearance and gradient explosion in the process of long sequence training.

(1) *Forgetting Stage*. The first stage of long-term and short-term memory is the forgetting stage, which is mainly to selectively forget the input transmitted from the previous node, which is determined by the sigmoid activation function of the forgetting gate, as shown in the following formula.

$$f = \sigma(W_f n[h_{t-1}, x_t] + b_f). \quad (3)$$

(2) *Selective Memory Stage*. It is mainly to memorize and select the input value and determine the new information that should be stored in the unit state. Firstly, the sigmoid function layer determines the updated value, and then, the tanh function layer creates the candidate value vector \tilde{C} to help adjust the neural network and then creates the state combined with the updated value and the candidate value, as shown in the following formula.

$$i_t = \sigma(W_i n[h_{t-1}, x_t] + b_i), \quad (4)$$

$$\tilde{C} = \tanh(W_C n[h_{t-1}, x_t] + b_C). \quad (5)$$

(3) *Output Phase.* In this stage, the results of forgetting stage and selective memory stage are summed, and the output value is obtained by sigmoid function and tanh function, as shown in the following formula. The new cell state and the new hidden state are then transferred to the next step.

$$C = f_t * C_{t-1} + i_t * \tilde{C}, \quad (6)$$

$$o_t = \sigma(W_o n[h_{t-1}, x_t] + b_o), \quad (7)$$

$$h_t = o_t * \tanh(C). \quad (8)$$

2.2.2. *Algorithm Flow.* We consider using long-term and short-term memory combined with deep Q network to integrate some known observation information collected and obtain the optimal control strategy through online learning and distributed methods. The unique network structure of long-term and short-term memory can better estimate the state of the channel and improve the probability of successful access to the channel, as shown in Figure 4.

2.3. Research on Dynamic Spectrum Allocation Algorithm Based on Genetic Algorithm

2.3.1. *Characteristics and Processes of Traditional Genetic Algorithms.* The genetic algorithm performs search calculation and problem-solving according to the law of natural selection. In recent years, through in-depth research by scholars at home and abroad, many problems that cannot be solved by traditional mathematics have been solved. The advantages of genetic algorithms are as follows:

- (1) Searching in units of populations, multiple individuals simultaneously comparing with inherent parallelism
- (2) The search ability size has nothing to do with the problem to be solved
- (3) It has strong scalability and can be combined with other models and algorithms to optimize the performance of the algorithm
- (4) The evaluation function mechanism is adopted in the search process to reduce the complexity
- (5) Iteratively using the probability mechanism, the randomness is strong

Genetic algorithm as a classical evolutionary algorithm also has its own drawbacks:

- (1) The initial population has a great influence on the performance of the algorithm, which can be improved by adding some prior knowledge
- (2) The three operations of selecting, crossing, and mutating in the algorithm involve multiple parameters, such as crossover probability and mutation

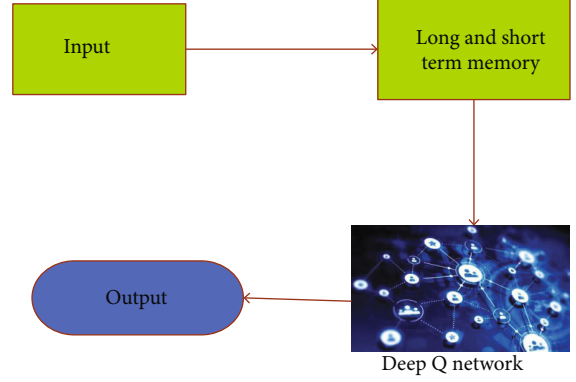


FIGURE 4: Structure of long-term and short-term memory depth Q network.

probability. The difference of these parameters will affect the performance of the algorithm. In practical applications, multiple tests are needed to find the optimal parameters

- (3) The genetic algorithm does not use the feedback information of the network in time, so it takes a lot of training to get an accurate solution, but this reduces the efficiency of the algorithm
- (4) It is prone to “premature” phenomenon

2.3.2. *Adaptive Genetic Algorithm.* Adaptive genetic algorithm means that some parameters in the genetic algorithm can change with the evolution process, which increases the diversity of the algorithm population. The adaptive genetic algorithm is a derivative algorithm based on traditional genetic algorithm. It inherits the advantages of traditional genetic algorithm and abandons the shortcomings of traditional genetic algorithm so that the algorithm performs crossprobability and mutation probability in the process of implementing adaptive genetic algorithm. It will change with the increase of evolutionary algebra and the change of population fitness value, so it fills the inadequacies of traditional genetic algorithm to some extent. Adaptive genetic algorithm can be adaptive from various angles, such as fitness function, crossover probability, mutation probability, selection probability, and population size. The most commonly used are crossover probability and mutation probability. Generally, in the early stage of evolution, crossover can produce individuals with high fitness values. Therefore, increasing the probability of crossover and reducing the probability of mutation can speed up the optimization process. In the later stage of evolution, crossover cannot produce better individuals, and mutation operation is required for global optimization, so reduce the crossover probability, reduce the probability of mutation, reduce the amount of redundant operations, continue to enhance the diversity of the population, and avoid the phenomenon of “premature.”

2.4. Improved Genetic Algorithm

2.4.1. *Improve the Background Proposed by Genetic Algorithm.* The routing protocol or any algorithm in the

wireless sensor network should be based on energy conservation. The cognitive radio and the wireless sensor network are combined to make the spectrum resources be used in a rational and balanced manner. The wireless sensor network can transmit data more smoothly. However, this combination also invisibly adds to the WSNS, the burden of nodes detecting spectrum holes and increasing traffic. At the same time, in the process of dynamic spectrum allocation, the nodes continuously switch the frequency to gain greater bandwidth gain, which makes the energy consumption problem more serious. In terms of reducing energy consumption, domestic and foreign experts and scholars have done research on reducing the number of transmission nodes and node dormancy and reducing the number of secondary user perceptions and achieved certain results. In terms of dynamic spectrum allocation, many domestic and foreign research scholars have carried out research and proposed model algorithms such as game theory model, graph theory coloring model, and interference temperature model to allocate spectrum. Later, many scholars used the improved intelligent optimization algorithm to distribute. The intelligent optimization algorithm has the characteristics of simple and easy to use, multi-issue, and robust, among which quantum genetic algorithm, leapfrog algorithm, and immune cloning algorithm have achieved good results. As a mature search-based heuristic algorithm used in computational science to solve optimization problems, genetic algorithm also has a good performance in spectrum allocation. Because wireless sensor networks have limited energy characteristics and spectrum switching will bring about data packet collision, data transmission failure retransmission, redetection of spectrum holes and spectrum allocation, the algorithm proposed in this paper is aimed at maximizing network benefits and minimizing the frequency of spectrum switching to ensure that the entire network consumes the least amount of energy in spectrum allocation. The improved genetic algorithm has improved in coding, crossover, mutation, and fitness function. The simulation results show that the algorithm improves the network revenue, reduces the energy consumption caused by the spectrum switching process, and avoids the genetic algorithm convergence too fast.

2.4.2. Algorithm Theory Model. Solving problems in the field of computing often comes down to a model that uses models to describe specific problems. The establishment of the theoretical model requires specific analysis of specific problems. The models used in different problems are different, and the problems applied by different models are different. There is no fixed match between the two. The model chosen is not good or bad, only suitable and inappropriate; there is no universal model for all problems. When using the search optimization algorithm to solve the dynamic spectrum allocation problem, based on the existing model, the optimal solution obtained by the optimization algorithm is replaced by the optimization algorithm, which is the allocation scheme for the spectrum allocation. For the centralized spectrum allocation method, the graph theory coloring model or the interference temperature model is adopted, and the

graph theory coloring model itself has the advantage of avoiding mutual interference between cells. The dynamic spectrum allocation problem channel assignment model is mathematically described, then the objective function is formulated according to the actual network conditions, and the genetic algorithm is used to find the optimal solution under the objective function.

2.4.3. Encoding. Coding is the first step of the genetic algorithm. It is the bridge between the genetic algorithm and the problem to be solved. It has a decisive influence on the performance of the algorithm. If the coding method is not properly selected, the algorithm search space will be greatly increased, and the coding will be increased. And the amount of computation of the decoding process would take up too much memory. The purpose of the encoding process is to construct the chromosome according to certain rules and follow the process in the genetic algorithm with the chromosome as the basic unit. When the algorithm initializes the network environment, the primary user and the secondary user position are randomly determined. The algorithm obtains the benefit matrix B , the available channel matrix L , and the interference constraint matrix C in the graph theory coloring model according to the location information of the two. The operation of the genetic algorithm is based on chromosomes. If the chromosomes are represented by S and each chromosome S represents a conflict-free and feasible spectrum allocation scheme, then the chromosome S should correspond to the element $a_{n,m}$ in the distribution matrix $A = \{a_{n,m} | a_{n,m} \in \{0, 1\}\}_{N \times M}$. This coding method will generate a lot of redundant bits in the chromosome S , which makes the algorithm search space increase, and it is more difficult to find the optimal solution and reduce the performance of the algorithm. At the position where the available channel matrix L is 0, the channel is definitely not allocated to the user, so the allocation matrix is A definitely 0 at the corresponding position. Since there is such a relationship between the available channel matrix L and the distribution matrix A , we can only use the chromosome S to record the allocation matrix elements at the position where the available channel L element is 1. The chromosome S length $L(S)$ obtained after such mapping is shown in formula (3), which is the number of nonzero elements in the available channel matrix L .

$$L(S) = \sum_{l_{n,m}=1} l_{n,m}, \quad (9)$$

$$L = \begin{bmatrix} 1 & 0 & 1 & 0 & 0 & 1 \\ 0 & 0 & 0 & 1 & 1 & 0 \\ 0 & 1 & 0 & 0 & 0 & 1 \\ 0 & 0 & 0 & 1 & 0 & 0 \\ 1 & 0 & 0 & 0 & 0 & 0 \end{bmatrix}, \quad (10)$$

$$S = [0\ 1\ 1\ 0\ 1\ 1\ 0\ 1\ 0]A = \begin{bmatrix} 0 & 0 & 1 & 0 & 0 & 1 \\ 0 & 0 & 0 & 0 & 1 & 0 \\ 0 & 1 & 0 & 0 & 0 & 0 \\ 0 & 0 & 0 & 1 & 0 & 0 \\ 0 & 0 & 0 & 0 & 0 & 0 \end{bmatrix}. \quad (11)$$

The mapping relationship between the chromosome S and the available channel matrix L and the distribution matrix A is as shown in Figure 5, and the elements of the distribution matrix corresponding to the nonzero position in the available channel matrix A are recorded in the chromosome S . Since the available channel matrix L for each allocation process is unchanged and the location of the nonzero elements in the channel matrix L is determined, the chromosomes do not change the number of bits due to the different allocation scheme. It should also be noted that the interference constraint matrix $C = \{c_{n,k,m} | c_{n,k,m} \in \{0, 1\}\}_{N \times N \times M}$ specifies that when the user $c_{n,k,m} = 1$ and the user n jointly use the channel k when m , interference may occur. If $a_{n,m} = a_{k,m}$ is satisfied in the allocation matrix A , $a_{n,m}$ or $a_{k,m}$ need to be randomly set to zero. That is, the channel m is not allowed to be simultaneously allocated to user n and user k , and only one of the users can be assigned to channel m . At this time, the corresponding position in the chromosome S should also be set to zero.

2.4.4. Cross and Variation. Crossover and mutation operations are the core of the whole genetic algorithm. Since both crossover and mutation are random operations, there may be disadvantages to the performance of the convergence efficiency of the algorithm. Crossover is a kind of local optimization process. It is suitable for individuals with higher fitness in the early stage of evolution. When the population is large, the mutation operation can optimize the problem globally. It is suitable for the late evolution and the population fitness value is universal. It is too high, and the difference between individuals is very small, which is close to the optimal solution. At this time, the cross process can no longer produce better individuals, so the mutation process is needed to produce individuals closer to the optimal solution. The crossover probability and the mutation probability are fixed constants in the traditional genetic algorithm and are independent of each other. Their size needs to be determined empirically. The crossover probability ranges from 0.40 to 0.99, and the variation probability is a constant between 0.0001 and 0.1. Fixed crossover probability and mutation probability often reduce the convergence rate of the algorithm, causing the algorithm to “prematurely mature” and reduce the efficiency of the algorithm to find the optimal solution. This section adds adaptive crossover probability and mutation probability to the traditional genetic algorithm so that the crossover probability and mutation probability can be adjusted in real time according to the chromosome being operated. Appropriately increasing the crossover probability and reducing the mutation probability in the early stage of evolution can shorten the

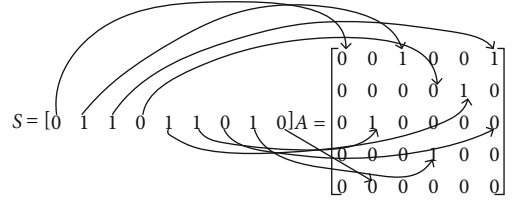


FIGURE 5: Mapping process of chromosomes.

process of finding the optimal solution by using the cross process and reduce the calculation amount. In the later stage of evolution, it is suitable to reduce the calculation amount of the cross operation, and the crossover probability should be reduced to increase the mutation probability. It can avoid the algorithm falling into local optimum, prevent the genetic algorithm from converge too fast, and speed up the search for the global optimal solution. We assume that the crossover probability and the mutation probability are represented by pc and pm , respectively. The adaptive mathematical expressions for pc and pm are

$$pc = \begin{cases} pc_1 * \frac{(pc_1 - pc_2)(f - f_{avg})}{f_{max} - f_{avg}} & f \geq f_{avg}, \\ pc_1 & f < f_{avg}, \end{cases} \quad (12)$$

$$pm = \begin{cases} pm_1 * \frac{(pm_1 - pm_2)(f_{max} - f')}{f_{max} - f_{avg}} & f' \geq f_{avg}, \\ pm_1 & f' < f_{avg}. \end{cases} \quad (13)$$

In equations (6) and (7), f_{max} is the maximum value of the fitness value in the current population, f_{avg} is the average value of the fitness values in the current population, and f is the larger fitness value of the two individuals to be crossed. f' is the fitness value of the individual to be mutated; pc_1 , pc_2 , pm_1 , and pm_2 are constants. The individual's crossover probability and mutation probability are linearly transformed between the average fitness and the maximum fitness value according to the individual's fitness value. In order to ensure that the superior individuals of each generation do not participate in the crossvariation process, the genetic algorithm proposed in this paper adopts adaptive crossover probability and mutation probability. If the optimal individual fitness value of the current population is better than the optimal individual fitness value of the next generation population, then all the individuals whose fitness value is greater than the optimal fitness value of the next generation are directly replaced by the individuals whose fitness value is the worst in the next generation. When the individual's fitness value is greater than the group average fitness value, the individual's crossover probability and mutation probability will be reduced so that the solution can be protected into the next generation; when the individual fitness value is less than the group average fitness value, both take larger values, making the solution easier to

eliminate, ensuring population diversity and avoiding “premature” phenomena.

2.4.5. Fitness Function. In genetic algorithms, the pros and cons of an individual are represented by the size of the fitness value. The fitness value has a certain mapping relationship with the objective function in the actual problem. In some problems, the objective function can be directly used as the fitness function, but the fitness function must be non-negative and continuous and needs to consider the complexity of the overall algorithm, convergence time, etc., and then, the target function needs to be processed accordingly to achieve adaptation, meeting the requirements of fitness function. The fitness function of the improved genetic algorithm proposed in this paper is determined by the special conditions of wireless sensor network energy limitation. In the wireless sensor network, the sensor as a network node has the characteristics of difficulty in replacing the battery and limited energy. In addition, the cognitive radio technology is added to the wireless sensor network, and the node needs to constantly perceive the spectrum hole to maintain the network system. The revenue frequently switches the spectrum, and the switching spectrum is bound to bring problems such as packet transmission failure and retransmission. These additional functions greatly increase the node energy consumption. The node energy imbalance is easy to cause the node to fail. After the node fails, it needs to be restarted. Building a network topology and reallocating the spectrum put a heavier burden on the nodes. From this point of view, it is necessary to reduce the overall spectrum switching frequency for the network, so the minimum spectrum switching frequency is added to the objective function. The current spectrum allocation strategy makes the spectrum utilization low, and the generation of cognitive radio technology solves this problem. In order to avoid the imbalance of spectrum allocation, the network function is maximized in the objective function. In a conflict-free allocation case, the user n return is r_n , and the network system revenue is represented by U , and its size is related to the distribution matrix and the benefit matrix. The mathematical expression is shown in equation (8).

$$U = \sum_{n=1}^N r_n = \sum_{n=1}^N \sum_{m=1}^M a_{n,m} \cdot b_{n,m}. \quad (14)$$

Assuming that the spectrum allocation scheme before the spectrum allocation is the initial allocation matrix A_1 , the switching frequency is determined by the current allocation matrix A and the initial allocation matrix A_1 , and h_{im} is used to indicate the frequency switching frequency of the node i on the spectrum m , and then, h_{im} mathematical expression is shown in (9).

$$h_{im} = 1 - a1_{i,m} \cdot b_{n,m}, \quad i \in N, m \in M. \quad (15)$$

Then, the mathematical expression of the frequency switching frequency H of the overall spectrum allocation system of the WSNS is shown in equation (10).

$$H = \sum_i^N \sum_{m=0}^M h_{im}, \quad i \in N, m \in M. \quad (16)$$

For each spectrum allocation, the larger the H value, the more users need to switch the frequency compared with the original allocation scheme, and the smaller the H value, the smaller the number of users who need to switch frequency, the more in line with the principle of low switching frequency. If the objective function itself meets the requirements of the fitness function, it can be directly used as the fitness function. The objective function is represented by Obj_F . The mathematical expression of Obj_F is as shown in formula (11). The larger the network gain, the larger the objective function close to the demand; because the switching frequency takes the minimum value, it should be negative to ensure that the fitness value is larger, and the chromosome is closer to the optimal solution to be searched.

$$Obj_F = U - H = \sum_{n=1}^N \sum_{m=1}^M a_{n,m} \cdot b_{n,m} - \sum_{i=1}^{N-1} \sum_{m=0}^{M-1} h_{im}. \quad (17)$$

Shown in Figure 6 is a flowchart to improve the hybrid algorithm of genetic algorithm and recurrent neural network.

3. Experiments

3.1. Experimental Methods. The improved genetic algorithm is simulated on the MATLAB platform to verify the performance of the algorithm. The experimental process mainly includes the deployment of the network environment, experimental parameter setting, simulation of the algorithm, obtaining relevant data, and finally analyzing the data to obtain conclusions. For parameter setting, refer to the parameters recognized by many people in previous studies.

3.2. Experimental Environment and Parameters. In the experiment, a square network area of 10 m * 10 m is constructed. In this network area, all interference factors such as noise are ignored. All users use the same transmit power, and the coverage radius and interference radius are the same. The node position of the wireless sensor network does not change substantially, ensuring that the network topology does not change during the primary spectrum allocation process. The benefit matrix B , the available matrix L , and the interference constraint matrix C in the graph theory coloring model do not change. In terms of network environment parameters, it is assumed that the primary and secondary user transmission distance is a minimum of 1 m, the maximum value is 4 m, and the primary user's coverage radius is 2 m, that is, the primary user is the center, within 2 m radius, and the secondary user shall not use the same spectrum as the primary user to transmit data. In the experiments in this paper, in order to avoid the existence of accidental errors, the average of 40 experimental results was taken for each set of data. In addition to studying the effects of primary users, secondary users, and available channels on algorithm performance, other experiments were set to 15 primary users, 10 secondary users, and 10 available channels.

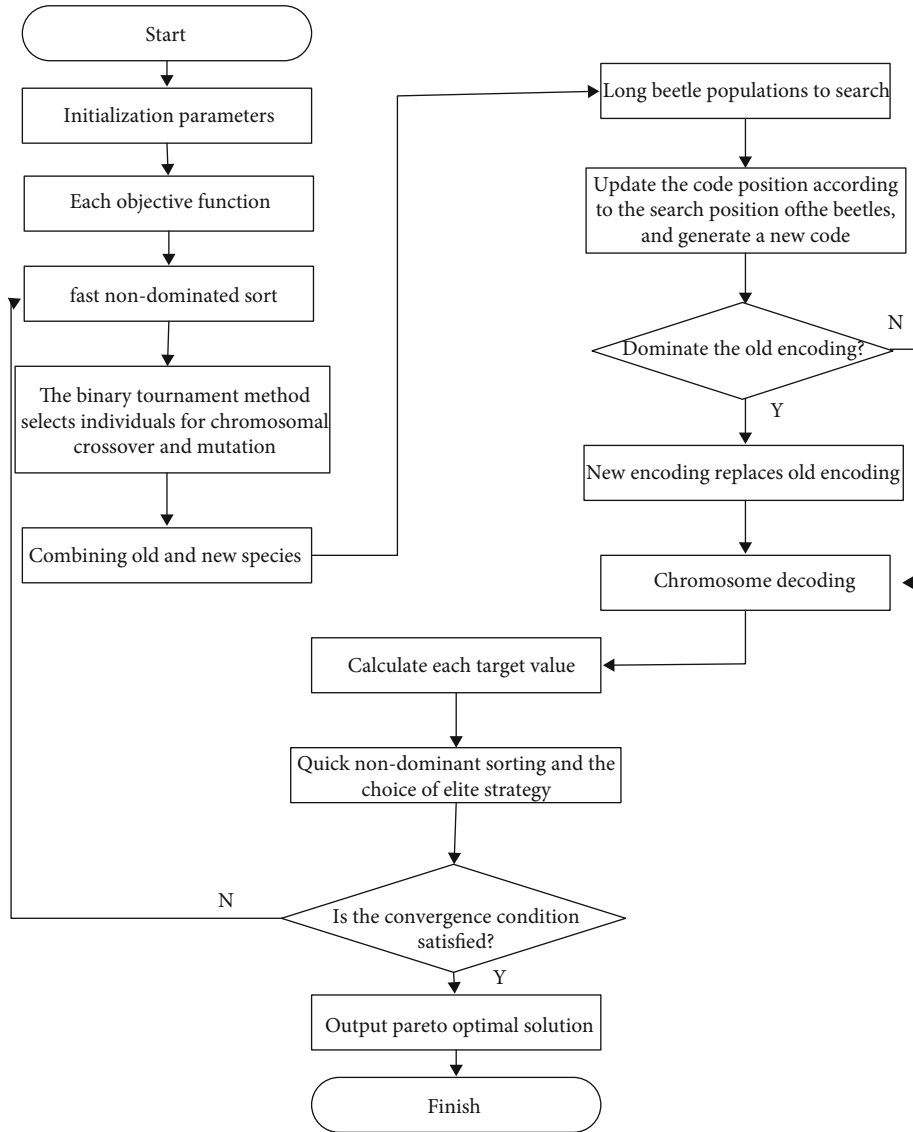


FIGURE 6: Hybrid algorithm of improved genetic algorithm and recurrent neural network.

3.3. *Improve the Overall Performance Simulation of Genetic Algorithm.* The improved genetic algorithm will be compared with the color-sensitive coloring algorithm in the traditional genetic algorithm and graph theory coloring model in terms of switching frequency, network benefit, and fitness value. Color-sensitive graph theory coloring is an important branch of the graph theory shading model algorithm. It can set whether the relationships between users are coordinated and can also set six different labeling criteria as needed. Since the fitness value is only set in the genetic algorithm, the color-sensitive coloring algorithm only compares the network revenue and the switching frequency and does not involve the comparison of the fitness values. The fitness value is limited to the genetic algorithm for comparison.

4. Discussion

4.1. *Overall Performance Simulation of Improved Genetic Algorithm.* The comparison results of fitness values of two

genetic algorithms in the same network environment are shown in Figure 7.

The abscissa in the figure is the evolution algebra, and the ordinate is the fitness value. It can be seen from Figure 7 that with the continuous increase of evolution algebra, the fitness value of the improved genetic algorithm is not much different from that of the traditional genetic algorithm before the 18th generation, but the whole process of the improved genetic algorithm is constantly searching for the optimal solution, while the optimization speed of the traditional genetic algorithm is relatively slow; there are only some changes around the 63rd and 148 generations. Compared with the traditional genetic algorithm, the performance of the improved genetic algorithm is improved. The traditional genetic algorithm is easy to fall into the local optimal, but cannot find the global optimal solution.

4.2. *Influence of Genetic Algorithm Parameters on the Performance of Improved Genetic Algorithm.* The improved

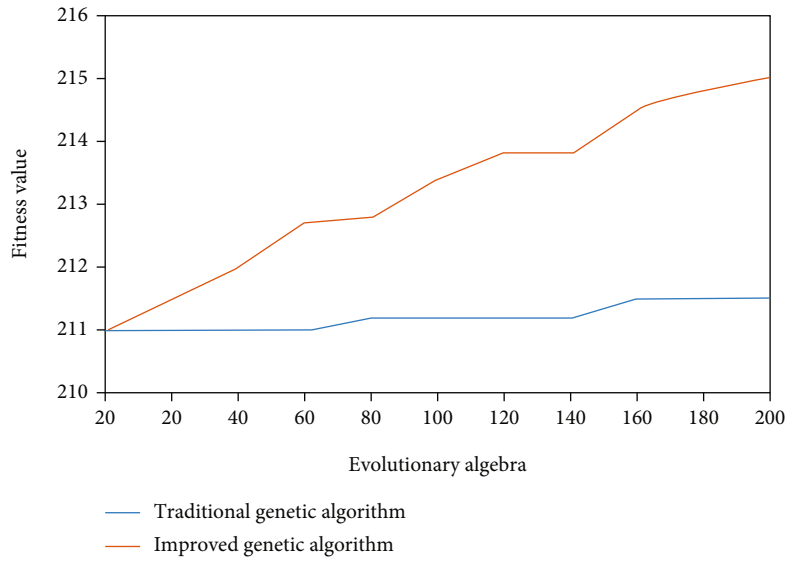


FIGURE 7: Comparison of fitness values of two genetic algorithms.

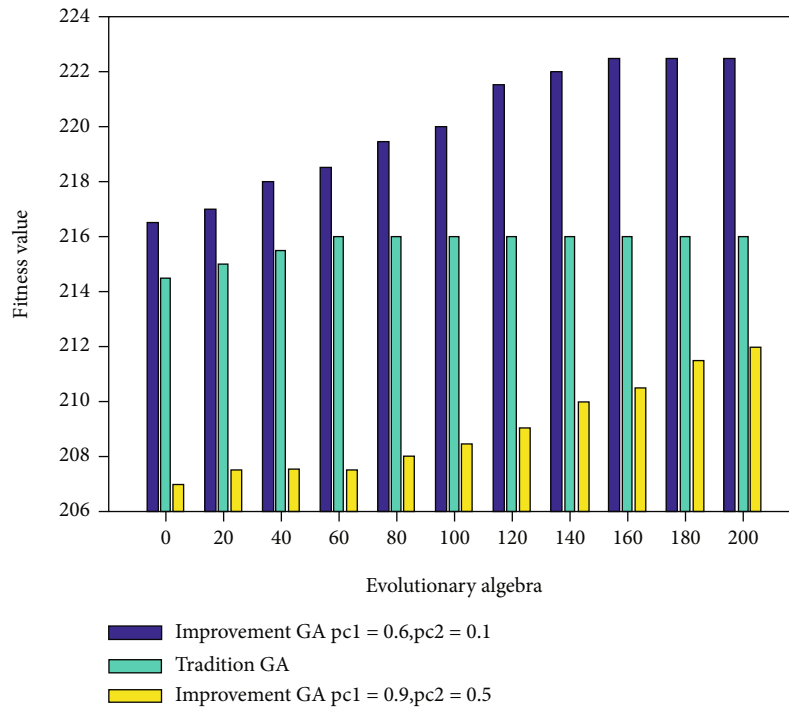


FIGURE 8: Comparison of fitness values when pc1 and pc2 take different values.

genetic algorithm with two sets of crossover probability is compared with the traditional genetic algorithm, comparing its optimization ability, and the results are shown in Figure 8. The abscissa is the evolutionary algebra, and the ordinate is the fitness value.

It can be seen from Figure 5 that when $pc1 = 0.9$ and $pc2 = 0.5$, the fitness value is even lower than that of traditional genetic algorithm, while when $pc1 = 0.6$ and $pc2 = 0.1$, the fitness value is much higher than that of traditional genetic algorithm, the optimization ability of traditional genetic algorithm is relatively poor, and the optimal solution is not much differ-

ent from the initial solution. Comprehensive comparison shows that when the crossprobability is 0.6 and 0.1, the fitness value is higher than that when the crossprobability is 0.9 and 0.5, while the traditional genetic algorithm is between them, so when the crossprobability is not selected, the performance of the improved genetic algorithm is not as good as that of the traditional genetic algorithm, but the optimization ability of the improved genetic algorithm of the two groups of crossprobability is worth affirming. Therefore, it can be seen that the network allocation efficiency has been significantly improved when the number of household users is different.

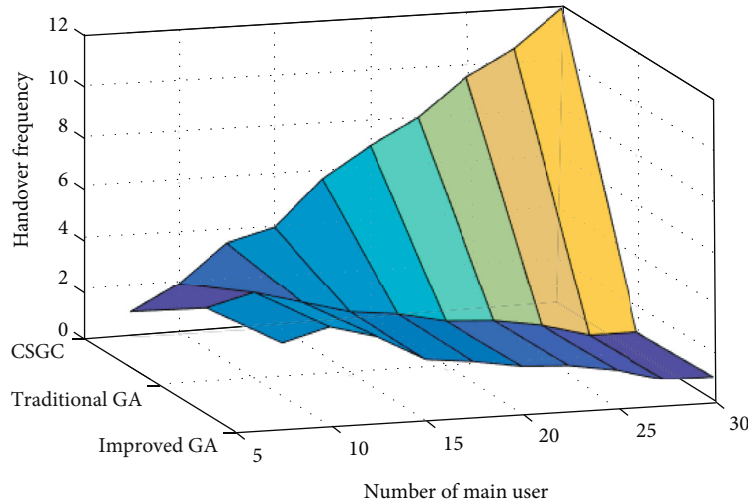


FIGURE 9: Relationship between switching frequency and number of main households.

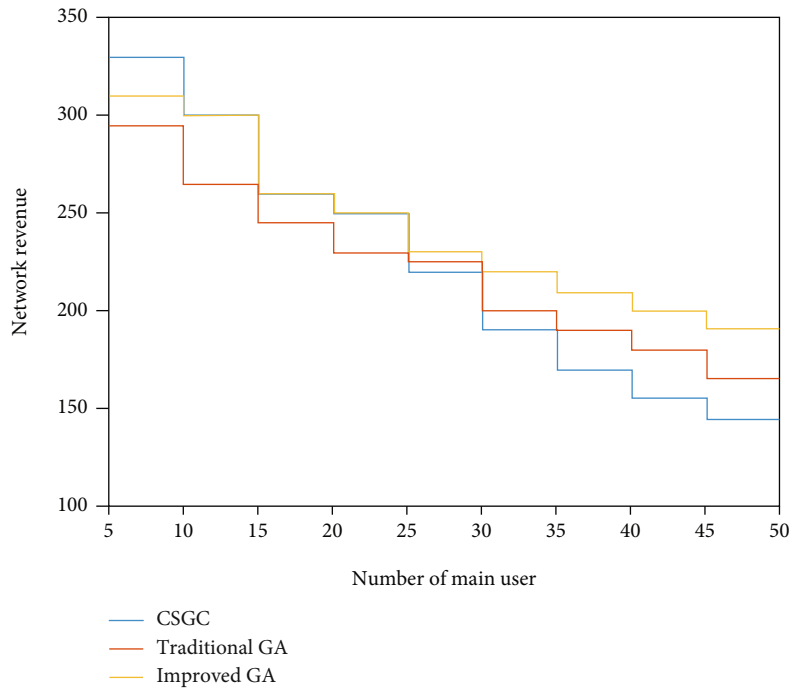


FIGURE 10: Relationship between network revenue and number of main users.

4.3. Influence of Network Environment Parameters on Performance of Improved Genetic Algorithm

4.3.1. Influence of Network Environment Parameters on Switching Frequency. The change of switching frequency in the process of increasing the number of main households from 5 to 50 is shown in Figure 8. In the figure, the abscissa is the main number of users, and the ordinate is the switching frequency.

As can be seen from Figure 9, with the increase of the number of main users, the switching frequency of CSGC algorithm shows an overall upward trend, while the switching frequency of the two genetic algorithms tends to decline after a short rise in 5-10 main users. The interference of authorized users in the network has little effect on the sec-

ondary users at first, but the number of primary users is increasing, but the available channels are not increasing, which leads to less and less channels that the secondary users can allocate. Genetic algorithm, considering that it wants to switch less frequency, wants to find a stable and assignable channel to allocate to the secondary users, and the switching frequency is also becoming smaller and smaller.

4.3.2. The Influence of Network Environment Parameters on Network Revenue. The relationship between network revenue and the number of primary users is shown in Figure 10. The abscissa is the number of users, and the ordinate is the network revenue.

As can be seen from Figure 7, with the increase of the number of main users, the overall trend of network revenue

of the three algorithms is declining. It can be seen from the descending slope that CSGC algorithm declines the fastest, while the two genetic algorithms are relatively slow. When the number of primary users is less than 10, the network income of CSGC algorithm is the highest; when the number of primary users is between 10 and 18, the network income from high to low is improved genetic algorithm, CSGC algorithm, and traditional genetic algorithm; when the number of primary users is greater than 18, the network income of improved genetic algorithm is the highest, followed by traditional genetic algorithm. The network income of CSGC algorithm is the least. It can be seen that the improved genetic algorithm can improve the network efficiency by about 2%, but the spectrum switching frequency can be reduced by 69%. When the number of main users in the network is large, the improved genetic algorithm has advantages over the other two algorithms. In the follow-up experiments, the calculation time of the algorithm is also compared, and the result is very similar to that of Figure 9, so I will not explain it too much.

5. Conclusions

In recent years, with the rapid development of wireless communication technology, the scarcity and low utilization of wireless spectrum resources become more and more prominent. With the increasing density of network systems, intelligent algorithms that can be adjusted quickly are needed for the management of spectrum resources. With the continuous development and technical maturity of cyclic neural network, it has gradually become an effective solution.

In this paper, MATLAB is briefly introduced, the network environment of algorithm simulation is set up, then the overall performance of the improved genetic algorithm is analyzed, and the relevant parameters of genetic algorithm and the suitable network environment are explored. The performance of the improved genetic algorithm with different crossover probability and mutation probability is compared with that of the traditional genetic algorithm, and the influence of the number of main users on the network revenue and switching frequency of the improved genetic algorithm, the traditional genetic algorithm, and the CSGC algorithm is explored. The simulation results show that the improved genetic algorithm can improve the network revenue and reduce the switching frequency, which is more suitable for small networks with more primary users or networks with more primary users but less node density.

In view of the scarcity of wireless spectrum resources, it can now be strengthened by networking technology. Therefore, for this research, the Internet of Things technology will be deeply discussed in the follow-up research.

Data Availability

No data were used to support this study.

Conflicts of Interest

The authors declare that they have no conflicts of interest.

Acknowledgments

This work was supported by the National Natural Science Foundation of China (No. 62066032 and No. 61866006), Natural Science Foundation of Guangxi Province (No. 2021GXNSFAA075019), Project of National Ethnic Affairs Commission of China (No. 2020-GMI-010), Philosophy and Social Science Foundation of Guangxi (No. 21FYJ041), Guangxi Innovation-Driven Development of Special Funds Project (Gui Ke AA17204091), Vocational Education Teaching Reform Research Project of Guangxi (No. GXGZJG2019A045), Middle-Aged and Young Teachers' Basic Ability of Scientific Research Promotion Project of Guangxi (No. 2021KY0130), and Higher Education Undergraduate Teaching Reform Project of Guangxi (No. 2021JGA243 and No. 2020JGA240). This study acknowledges the support of the Guangxi Key Lab of Human-Machine Interaction and Intelligent Decision, the Logistics Engineering Innovation Laboratory, Logistics Engineering Technology Laboratory and Smart Logistics Exhibition Center of Nanning Normal University. The authors gratefully acknowledge the support of construction project of practice conditions and practice base for industry-university cooperation of the Ministry of Education (No. 202102079139).

References

- [1] I. Khan, F. Belqasmi, R. Glitho, N. Crespi, M. Morrow, and P. Polakos, "Wireless sensor network virtualization: a survey," *IEEE Communications Surveys & Tutorials*, vol. 18, no. 1, pp. 553–576, 2016.
- [2] S. K. F. A. R. Z. A. N. A. Begum, P. Vigneshwari, and S. Rekha, "Wireless sensor networks for condition monitoring in the railway industry: a survey," *IEEE Transactions on Intelligent Transportation Systems*, vol. 16, no. 3, pp. 1088–1106, 2015.
- [3] H. Xu and T. Zhang, "Performance analysis of mobile wireless sensor network system under n-rayleigh fading channels," *Chinese Journal of Sensors and Actuators*, vol. 28, no. 2, pp. 265–270, 2015.
- [4] H. Sinan Kurt and U. Yildiz, "Packet size optimization in wireless sensor networks for smart grid applications," *IEEE Transactions on Industrial Electronics*, vol. 64, no. 3, pp. 2392–2401, 2017.
- [5] P. Tang and T. W. S. Chow, "Wireless sensor-networks conditions monitoring and fault diagnosis using neighborhood hidden conditional random field," *IEEE Transactions on Industrial Informatics*, vol. 12, no. 3, pp. 933–940, 2016.
- [6] R. K. Sharma, T. Duda, and C. L. Makino, "Integrative signaling networks of membrane guanylate cyclases: biochemistry and physiology," *Frontiers in Molecular Neuroscience*, vol. 9, p. 83, 2016.
- [7] E. Arutyunov, M. de Leeuw, and S. J. van Tongeren, "The exact spectrum and mirror duality of the $(AdS_5 \times S^5)$ η superstring," *Theoretical and Mathematical Physics*, vol. 182, no. 1, pp. 23–51, 2015.
- [8] M. Gury-Ben Ari, C. A. Thaiss, and N. Serafini, "The spectrum and regulatory landscape of intestinal innate lymphoid cells are shaped by the microbiome," *Cell*, vol. 166, no. 5, pp. 1231–1246.e13, 2016.
- [9] K. Yui, A. Sato, and G. Imataka, "Mitochondrial dysfunction and its relationship with mTOR signaling and oxidative

- damage in autism spectrum disorders,” *Mini Reviews in Medicinal Chemistry*, vol. 15, no. 5, pp. 373–389, 2015.
- [10] W. Zhang, Y. Sun, L. Deng, C. K. Yeo, and L. Yang, “Dynamic spectrum allocation for heterogeneous cognitive radio networks with multiple channels,” *IEEE Systems Journal*, vol. 13, no. 1, pp. 53–64, 2019.
- [11] A. H. Hadjahmadi and M. M. Homayounpour, “Robust feature extraction and uncertainty estimation based on attractor dynamics in cyclic deep denoising autoencoders,” *Neural Computing and Applications*, vol. 31, no. 11, pp. 7989–8002, 2019.
- [12] S. Hellerman, D. Orlando, S. Reffert, and M. Watanabe, “On the CFT operator spectrum at large global charge,” *Journal of High Energy Physics*, vol. 2015, no. 12, pp. 1–34, 2015.
- [13] C. Bao, P. Yifei, and Y. Zhang, “Fractional-order deep back-propagation neural network,” *Computational Intelligence and Neuroscience*, vol. 2018, Article ID 7361628, 10 pages, 2018.
- [14] L. M. Rasdi Rere, M. I. Fanany, and A. M. Arymurthy, “Meta-heuristic algorithms for convolution neural network,” *Computational Intelligence and Neuroscience*, vol. 2016, Article ID 1537325, 13 pages, 2016.
- [15] T. Touzri, M. B. Ghorbel, and B. Hamdaoui, “Efficient usage of renewable energy in communication systems using dynamic spectrum allocation and collaborative hybrid powering,” *IEEE Transactions on Wireless Communications*, vol. 15, no. 5, pp. 3327–3338, 2016.
- [16] L. Sboui, H. Ghazzai, Z. Rezki, and M.-S. Alouini, “On green cognitive radio cellular networks: dynamic spectrum and operation management,” *IEEE Access*, vol. 4, no. 3/4, pp. 4046–4057, 2016.
- [17] P. K. Sahoo, S. Mohapatra, and J.-P. Sheu, “Dynamic spectrum allocation algorithms for industrial cognitive radio networks,” *IEEE Transactions on Industrial Informatics*, 2017.
- [18] I. Balapuwaduge, F. Y. Li, and V. Pla, “Dynamic spectrum reservation for CR networks in the presence of channel failures: channel allocation and reliability analysis,” *IEEE Transactions on Wireless Communications*, vol. 17, no. 2, pp. 882–898, 2017.
- [19] H. Hoffmann, P. Ramachandra, I. Z. Kovács, L. Jorgueski, F. Gunnarsson, and T. Kürner, “Potential of dynamic spectrum allocation in LTE macro networks,” *Advances in Radio Science*, vol. 13, no. 2, pp. 95–102, 2015.
- [20] A. Kumar, A. Sengupta, R. Tandon, and T. C. Clancy, “Dynamic resource allocation for cooperative spectrum sharing in LTE networks,” *IEEE Transactions on Vehicular Technology*, vol. 64, no. 11, pp. 5232–5245, 2015.

Research Article

Development Model of Enterprise Green Marketing Based on Cloud Computing

Dian Jia¹ and Zhaoyang Wu² 

¹*School of Economics and Management, Qinghai Minzu University, Xining 810007, Qinghai, China*

²*School of Economics and Management, Qinghai Normal University, Xining 810016, Qinghai, China*

Correspondence should be addressed to Zhaoyang Wu; 2018130@qhnu.edu.cn

Received 18 January 2022; Accepted 22 February 2022; Published 22 March 2022

Academic Editor: Nima Jafari Navimipour

Copyright © 2022 Dian Jia and Zhaoyang Wu. This is an open access article distributed under the Creative Commons Attribution License, which permits unrestricted use, distribution, and reproduction in any medium, provided the original work is properly cited.

Internet-based cloud computing is currently an important core technology for computer development in China. It can be used not only in marketing but also in various industries. At the same time, people-oriented and green projects and products that focus on the development of the ecological environment and green consumption dominate the current market trend. The purpose of this paper is at studying the development model of enterprise green marketing based on cloud computing. This article compares and analyzes enterprise green marketing systems through big data algorithms and statistical methods. It starts with the basic characteristics of cloud computing, studies the opportunities and challenges that cloud computing brings to enterprises' green marketing efforts, describes the green marketing processes and characteristics of enterprises, and analyzes cloud. The feasibility of the construction of the computing system, the basic architecture of the cloud computing system, and the construction of a complete cloud computing data processing flow are proposed. The research data found that the combination of the green marketing development model and cloud computing in the enterprise operating system is conducive to the development of the enterprise; it improves the discovery efficiency of the enterprise and reduces the pollution in the production of the enterprise; the cloud computing can greatly improve the work efficiency of the employees. Cloud computing can improve employees' speed to complete tasks by about 20% and reduce the error rate by about 50%. The cloud computing enterprise green marketing development model has guiding significance for the long-term development of the enterprise.

1. Introduction

The meaning of green marketing is that the company takes “protect the environment, start with me” as its work purpose and uses “green ecology” as its guiding core and “reduces the damage to the global ecological environment” as its service center, positioning the starting point as a new marketing model that “meets consumers' green consumption.” Since then, the company's green marketing model has been rapidly promoted in developed countries and some developing countries [1].

In today's Chinese society, sustainable development has become an important theme in a new era [2]. In order to enhance market competitiveness, enterprises have established a good corporate image, controlled pollution, saved energy, and reduced consumption and improved efficiency has

become an urgent need for an enterprise to succeed [3]. At the same time, the wave of Internet development has also provided some convenient conditions for companies to implement a series of measures. Therefore, we propose the “cloud computing-based enterprise green marketing development model” [4]. At the same time, China's existing market is fiercely competitive and most companies place too much emphasis on micro- and near-term interests. In addition, the current legal system is not sound and the system is not relatively speaking [5]. It is perfect, which has caused many problems and obstacles for the company's green marketing. As a new type of computing model, cloud computing is used in many fields. People are willing and looking forward to cloud computing to achieve interconnection, collaborative work, and knowledge sharing. People also urgently need reliable and efficient technical means and implementation models.

Well, we are also thinking about whether we can combine cloud computing and enterprise green marketing to achieve the “cloud computing enterprise green marketing development model” [6, 7].

Cloud computing is changing information technology [8]. As information and processes are being migrated to the cloud, this is not only a place where computing is done, but fundamentally, how is it done? As a result, more and more companies and academia are investing in this technology, which will also greatly change the way IT professionals work. Cloud computing solves many problems of conventional computing, including handling peak loads, installing software updates, and redundant computing cycles. However, new technologies also bring new challenges, such as data security, data ownership, and transcode data storage. Arora discussed the cloud computing security problem mechanism, the challenges that cloud service providers are facing in cloud engineering, and proposed a metaphorical study of various security algorithms [9, 10]. In addition, companies that undertake a large number of batch-oriented tasks with Armbrust can obtain results as soon as their programs are scaled up, because the cost of using one server for 1,000 hours is only 10% higher than the cost of using one server for 1,000 hours [11]. This flexibility of resources does not have to pay a high price for large-scale purchases, which is unprecedented in IT history.

Cloud computing is an important prerequisite for long-term green development of enterprises [12]. The purpose of this paper is to study the development model of enterprise green marketing based on cloud computing. This article compares and analyzes enterprise green marketing systems through big data algorithms and statistical methods. It starts with the basic characteristics of cloud computing, studies the opportunities and challenges that cloud computing brings to enterprises' green marketing efforts, describes the green marketing processes and characteristics of enterprises, and analyzes cloud. The feasibility of the construction of the computing system, the basic architecture of the cloud computing system, and the construction of a complete cloud computing data processing flow are proposed. The use of cloud computing for green marketing in practice serves the purpose of changing the traditional way of developing the use of structures and exploring a more effective marketing model in the modern sense from the perspective of cloud computing business marketing.

2. Programs Method

2.1. The Connotation of Cloud Computing. Cloud computing is a relatively new form of supplement, consumption, and delivery implemented by Internet technology. It mainly takes virtual resources as the object of service and has dynamic scalability [13]. It can use the Internet to calculate data and use the underlying server, storage, and network technology architecture as a computing resource in an abstract way. And it can access the configurable computing resource sharing space through the network to achieve a certain degree of management, so as to quickly provide computing resources to demand users in [14].

2.1.1. Characteristics of Cloud Computing. The main characteristics of cloud computing include the following aspects: first, it can provide self-service; according to the needs of users to allocate, users can operate freely on the interface, so as to achieve the smooth application of resources and in the process of use can also be adjusted and released various resources [15]. The second point is that the time period of network access in cloud computing is very free and not limited by the location [16]. The service platform provided by cloud computing can be accessed in various ways, which greatly facilitates users. Third, cloud computing can reach the state of resource pooling. In this way, the physical resources of the computer do not belong to a specific individual and will be occupied only when they are needed; otherwise, there is no need to occupy them. Fourth, it has a large elastic space, can timely adjust and allocate resources to meet the needs of customers, and has strong shrinkage and expansion performance [17, 18]. We have a general understanding of the main features of cloud computing, which is a way to make our lives more convenient and our businesses more successful. Time is free, resources are shared, there is a lot of flexibility, and the characteristics of cloud computing determine its position in enterprise applications.

2.1.2. Cloud Computing Architecture. Cloud computing has a huge architecture, including five major structural layers, which are organically unified, as shown in Figure 1, namely, cloud client, cloud application, cloud platform, cloud infrastructure, and service layer [19]. This study uses a B2B model.

- (1) The cloud client, also known as the cloud terminal or cloud computer, is the part that connects with the customer most closely. The composition of the cloud client mainly includes computer hardware and computer software. Among them, hardware is necessary, while the existence and use of software are largely determined by the specific application degree of cloud computing. The design of software should meet the standards of cloud services to play an effective role [20]. Currently, the main cloud clients are mobile phones (Linux-based Palm, Android, iPhone, etc.), fat clients (Cherrpal, Wyse, etc.), and thin clients [21]
- (2) Requirements for cloud application foundation: the first is that cloud infrastructure is a kind of commercial software that is easy to manage and operate under the premise of network access. The second point is the reasonable and scientific control of the software through the server. Only in this way can the client use the form of Web to access the application system remotely and achieve the desired effect [22]. Third, in the delivery of cloud applications, the main pattern is one-to-many, in terms of architecture, price, and partners [23]. Fourth, the functionality of cloud applications is centralized when they are updated, which means that there is no need to download patches and upgrade packages from the

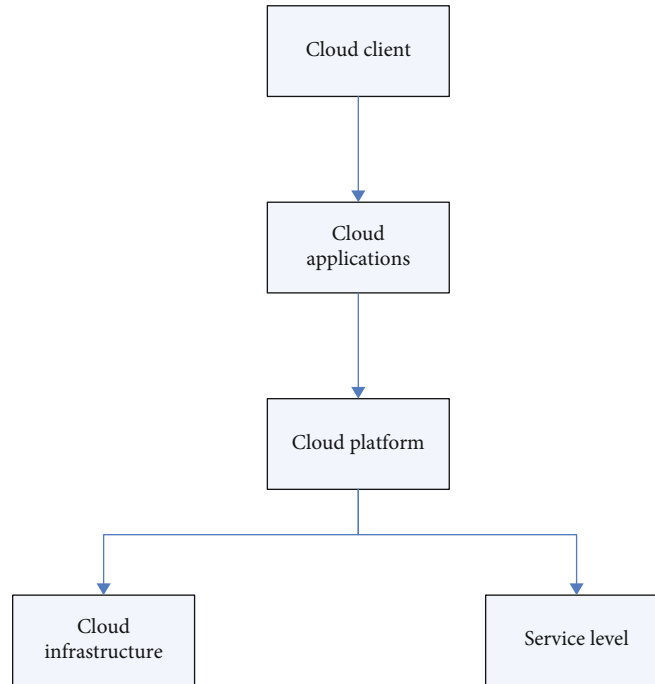


FIGURE 1: The composition of the cloud computing.

cloud client. At present, the types of cloud applications mainly include “Web applications,” “software as a service,” and “software + services” [24, 25]. In the cloud computing market, SaaS services account for about 58% of the total. The growing maturity of cloud computing and the gradual growth of the industry chain are driving the rapid development of SaaS services

- (3) The cloud platform is usually referred to as platform as a service; the main feature is the computer platform or it could be multiple solutions as a specialized service, it mainly plays the function of its service program on the basis of cloud infrastructure, so you do not have to process more complex procurement activities, also can reduce the underlying hardware and software of the corresponding management program of computing time, and improve the ability of system application deployment [26, 27]. The main types of cloud platforms currently in use include solution stacks and structured storage. Solution stack, for example, Google App Engine, is mainly designed by combining the convenient environment of cluster development with the platform of hosting Web applications; currently, the programming languages adopted mainly include Python and Java. The database types of structured storage are all cloud-based databases, including the Amazon-distributed database and BigTable database system, which generally do not directly provide relevant business services to the outside world. The types of storage on the basis of cloud files mainly include

the Amazon online storage service, which is fee based and targeted at the public. In the process of using the Web, various digital data can be saved through this online storage method, which is also very convenient to look up

- (4) Cloud infrastructure is usually also an example of infrastructure as a service, which is the delivery of computer infrastructure, usually through the creation of a platform-virtualized environment to achieve the desired purpose. Major types include the use of physical machines and virtual machines, physical host rent is usually provided by different kinds of IDC, the virtual machine is on the basis of the operating system virtualization, the virtual to physical machine can have multiple parallel operation systems, each system has a relatively independent operation, and between its types are mainly Amazon EC2. Rackspace improves the utilization efficiency of the server. GoGrid is used for Cloud computing. In particular, Amazon EC2 is also called the horse into play, can have very high flexibility in strengthening the self-recovery system, reduce artificial maintenance features of cloud computing, and can be calculated according to the customer’s resources for expansion and contraction of the corresponding use of virtualization technology; it will be an independent virtual machine, as an example, its function and virtual dedicated servers at the same equipment
- (5) The composition of the server layers mainly includes computer hardware and, when necessary, computer software. The design and application process of

software and hardware is consistent with the delivery process of cloud services and has the coordination and unity of architecture

The application of cloud computing to green marketing and wireless networks is mainly attributed to the advantages of on-demand deployment, flexibility, reliability, and cost effectiveness of cloud computing.

2.2. Enterprise Green Marketing Development Mode. In order to comply with the requirements of environmental protection and sustainable economic development in China, the 18th national congress of the communist party of China (CPC) advocated “green” development. Under the background of ecological civilization, the enterprise green marketing development model has become a new marketing model and gradually developed in China. The development mode of green marketing is relatively slow in China due to its late start and the insufficient understanding of some enterprises. At the same time, the growth of national economy and the improvement of people’s material level will be restricted by resources and the environment. Therefore, it is necessary to speed up the intensity and process of the development mode of green marketing, so as to promote the green management of enterprises into a normal track.

2.2.1. Conduct Objective Quantitative Analysis and Evaluation on the Efficiency of the Enterprise Collaborative Network. Objective quantitative analysis and evaluation of the efficiency of the enterprise collaborative network are an important link to ensure and promote the optimization of the collaborative business chain. The network optimization is realized based on the multilevel and multistage complex random analysis of the collaborative business chain. On the basis of the proof of the phase type for a randomly distributed system, a computational method of complex coordination and a quantitative expression of the system efficiency are presented in this paper. This method has the advantages of wide application range and easy to parse.

- (1) In the network cooperative organization of enterprises following pH distribution (network organization U): U_i is the i th unit of the organization, U_2 , U_3 is the intermediate unit, and U_4 is the task termination unit

$$U = \sum_{i=1}^4 U_i, \quad (1)$$

$$y[n] = \sum_{i=1}^N \sum_{l=1}^L w_i(l) S_i(n-l),$$

$$\rho_j = \rho_i \frac{j e_t + (j-1) e_r}{i e_t + (i-1) e_r}$$

- (2) S_{mn} is the state transition probability, that is, the probability of successful task delivery between units. Satisfy, according to the image,

$$\sum_{U_i} S u_i = 1, \quad (2)$$

$$E_C = N C V_{dd}^2$$

2.2.2. Based on the Enterprise Efficiency Monitoring System. The energy consumption of the monitoring network node based on enterprise efficiency is mainly concentrated on the data transmission unit. The energy consumption at the transmitting end is mainly generated by the transmitting circuit and the power amplifier circuit, while the energy consumption at the receiving end is mainly generated by the receiving circuit. Energy consumption at the transmitting end is shown in formula (3), while energy consumption at the receiving end is shown in formula (4):

$$E_{tr}(k, d) = \begin{cases} k E_{elec} + k E_{apm1} d^2, & (d < d_0), \\ k E_{elec} + k E_{amp2} d^4, & (d \geq d_0), \end{cases} \quad (3)$$

$$E_{rx}(k) = k E_{elec}, \quad (4)$$

Where E is the number of bits of data sent or received, k is the distance between two nodes, d is a constant, and the value is related to the network environment:

$$d_0 = \sqrt{\frac{E_{apm1}}{E_{amp2}}}, \quad (5)$$

$$\frac{d \rho_i e}{i d \lambda \cdot e_t + (i-1) \lambda d \cdot e_r} = \beta,$$

$$A(\delta) = 1 + \alpha_{i1} \delta^{-1} + \alpha_{i2} \delta^{-2} + \dots + \alpha_{in} \delta^{-n}.$$

Sustainable supply chain management and green marketing have become key themes in academic research and management practice since the concept of sustainability was transformed into the mainstream of business. Great progress has been made in both areas. It has been recognized that green marketing and sustainable supply chain management should be seamlessly integrated to better meet the needs of green customers through supply chain functions. Existing research has explored point-to-point integration methods. Liu proposed a new hub-and-center integration model that integrates green marketing and sustainable supply chain management from six dimensions (product, promotion, plan, process, people, and project (called 6P)). Empirical studies have been conducted with the industry to test the 6P integration model. This paper presents the empirical research results on the driving factors and obstacles of integration dimension, integration strategy, and multidimensional integration, as well as the significance of management. The new integrated model allows the flow of resources such as information, materials, and capital between green

marketing and sustainable supply chain management through a variety of direct channels. According to the triple bottom line goal, it is possible to achieve better overall business performance.

2.2.3. Sustainable Industrial Chain Management. As global warming intensifies, both developed and developing countries are committed to sustainable development. Committed to sustainable development, it has been in the form of thematic study of sustainable supply chain collaborative management and is based on the traditional theory to explore how to synergize in order to promote the sustainable development of the world's stakeholders, one of the characters of economic man hypothesis, which has the self-interest preference, always in its own interests, for maximum core concerns, to determine how to build and implement sustainable global supply chain collaborative management. As a decision criterion, it does not take into account the psychological factors and their behavior. In 1965, the American strategic management expert H. Igor Ansoff first applied the idea of collaboration in this field. Behavioral economic research shows that a large number of scientific experiments and empirical studies have confirmed the advantages of the application of writing ideas in management but the current research collaborative management concept has no unified behavioral tendency and does not have realistic objectivity.

The government supervision of sustainable supply chain collaborative management is the mainstream direction of supply chain collaborative management research. In response to global warming, countries have issued a series of policies, which has set off a research upsurge in the academic circles and has triggered everyone's thinking and exploration of the future. Before companies bear part of the losses, most of the existing research is to guide macro-recommendations or government subsidies, etc. In the supply chain management of enterprises, in addition to considering economic issues, it is also necessary to promote the development of sustainable supply chain collaborative management from the perspective of government supervision, as well as environmental and social factors. In other words, companies are subject to government regulation. However, the goal of sustainable supply chain collaborative optimization seldom considers the maximum social welfare. The future can be based on government regulation management which refers to the economic, environmental, and social impact of enterprises based on the product life cycle.

2.2.4. Integration Model of Central Radiation. With the continuous development of information technology, data types and data storage are constantly increasing and the construction of enterprise informatization is accelerating. Due to the inconsistency of data standards, the difficulty of data communication between enterprises and enterprises is increasing and the number of data islands increases sharply. How to make good use of the acquired data to effectively support the business activities and decisions of enterprises has become a crucial issue in the process of enterprise informatization. In the face of the increasingly complex data environment, it is the primary task of enterprise

informatization construction to establish exchanges among multiple data islands. By analyzing the distribution, heterogeneity, and autonomy of data sources in the data center construction of downhole operation branch, this paper studies the virtual data integration model and its realization technology, proposes the virtual data integration architecture, constructs the virtual data integration metadata model, and realizes the data integration among information islands based on the model. We set up a data source layer for data source dispersion. A metamodel of virtual data integration is established by using metadata technology, through the metamodel to realize the logical integration of multiple scattered data sources to form the unified data access logical interface. In order to effectively solve the problem of low data source access efficiency, the data access layer is constructed by data segmentation technology. The granularity of the accessed data is refined to improve the efficiency of data access.

2.2.5. Analysis of the Path for Enterprises to Build Green Marketing

- (1) Change the concept of the environment and establish a "green" consumer culture. Enterprises should change the misconception of "polluting first, then treating," establish an environmental concept, condense environmental protection awareness into the values of each employee, strengthen the concept of green marketing, and establish a "green" corporate culture. Enterprises should use a variety of publicity methods and publicity methods to continuously publicize environmental protection and green consumption knowledge to help consumers establish green consumption awareness. Enterprises should guide consumers in a variety of ways to consume reasonably and moderately, put an end to comparison consumption and show off consumption, and promote the awareness of green consumption in the society by promoting the knowledge of green consumption and forming an atmosphere of green consumption
- (2) Improve the green management organization and establish green rules and regulations. To implement green marketing, enterprises must rely on effective organization and management. First of all, the enterprise should set up a special green management organization, which is responsible for the green design, green production, and green marketing of the company. Establish full-time environmental protection functional departments at all levels, implement internal hierarchical management, integrate corporate resources, and jointly complete ecological environmental protection and construction. Secondly, we should carry out green education activities for employees, help employees understand basic environmental protection knowledge and master specific environmental protection skills, and improve the teaching effect by establishing a corresponding reward and punishment system. Finally,

through strengthening management and technological innovation, enterprises must strive to obtain green environmental label certification and international environmental standard system certification in developed countries in Europe and America, establish a green image of the enterprise, enhance the competitiveness of the enterprise, and break through the restrictions of green barriers in developed countries. In addition, enterprises should construct a green evaluation index system to monitor their green marketing behavior

The core elements of the development model based on workflow efficiency mainly include the following aspects:

Roles: different configurations of roles under different organisational structures, with clear correspondence between roles and people.

Responsibilities: definitions of responsibilities for different roles, used to clarify the stages and timing of intervention in the process.

Processes: definition of the sequence of nodes in the corresponding process according to the scenario, e.g. development, testing, deployment.

Nodes: clear definition of roles in different nodes, as enablers for the orderly completion of the nodes.

A rational process management mechanism that facilitates efficient work; in order to avoid excessive complexity in process collaboration, collaboration rules are also established.

3. The Experiments

3.1. Experimental Settings

3.1.1. Experimental Background. In response to the requirements of the green marketing development model of the enterprise, this experiment investigated the speed of completing the operational tasks of 40 enterprises across the country, the time required for multilevel managers to hand over tasks, and the accuracy and superiority of the assigned tasks to reduce environmental pollution. From the perspective of improving safety production and monitoring accuracy, test the advantages and popularity of cloud computing in the green operation model of enterprises and combine cloud computing with the green development model of enterprises to make it play the greatest role in enterprise management and development.

3.1.2. Experimental Setup Process. The experiment sets up a control group and an experimental group. The control group adopted the traditional enterprise marketing model, and the experimental group adopted the human-computer interactive cloud computing green marketing model. Because cloud computing is a relatively large concept, we conduct research through specific tasks, give full play to the advantages of enterprise personnel, and get results.

3.2. Experimental Steps

3.2.1. Data Accuracy of Human-Computer Interaction Adjustment in the Enterprise Green Marketing System. Using

human power to transmit data, 40 companies are divided into four groups, each group of 10 companies, named A, B, C, and D groups. Traditionally, four sets of data are used to transmit data and the efficiency of manpower in transmission is detected based on the time required to complete the given task plan.

3.2.2. Meetings and Tasks Are Performed by Manpower throughout the Day. Divide 40 companies into eight groups of 5 companies, 4 groups of experimental groups, and 4 groups of control groups, using manual testing as the control group, and the experimental group uses the cloud computing submethod, using Internet thinking for testing, and treat each process as each node, and each node can be detected, and time is used as the main observation parameter to detect the accuracy of the data obtained. In turn, these datasets are often entered as parameters and analyzed by the necessary algorithms to produce the final result.

3.2.3. Convenience of Detection Using Cloud Computing. Use artificial detection as a control group to collect data on the cloud computing of the nodes. Through multiple experiments and integrations, the time and workflow are planned to obtain the optimal combination ratio.

3.2.4. Feasibility of Cloud Computing in the Development Model of Corporate Green Marketing. According to the monitoring plan given by the cloud computing and the monitored parameters of the enterprise's green marketing model, the simulation parameter estimation scheme through the simulation database is feasible.

4. Discussion

4.1. Comparative Analysis of Two Different Schemes

- (1) From Table 1 and Figure 2, it can be seen that the four sets of situation data indicate that the data of pure human resources in the enterprise operating system are compared with the data measured through cloud computing. It can be clearly seen that the efficiency of the nodes based on cloud computing is significantly higher than the efficiency of manual work. By comparing the entire work, it is found that the error rate has been greatly reduced and the working time has been reduced. When the error rate is 33.2%, the node's efficiency is 44.8%. The working efficiency is increased by about 20% compared with that of the control group. It can be seen that the marketing model under the cloud computing situation is conducive to the conservation of corporate resources and has a promoting effect on the green development model of the enterprise
- (2) Table 2 and Figure 3 are the results of research on the use of cloud computing to set the nodes of enterprise resources. Enterprise work detects people's work errors every two hours, and compares the data

TABLE 1: Degree of reduction of the experimental group compared with the control group (unit%).

	Error rate	Operating hours	Work efficiency
Comparison between group A and the control group	34.2	45.8	44.8
Comparison between group B and the control group	33.2	48.2	53.8
Comparison between group C and the control group	26.7	45.1	56.8
Comparison between group D and the control group	36.8	50.1	49.3

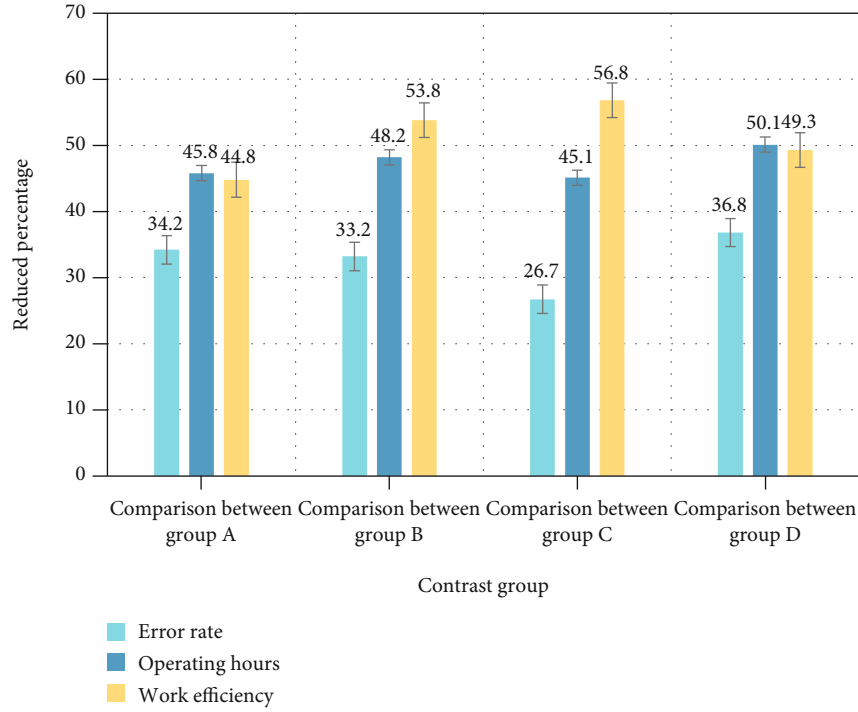


FIGURE 2: Degree of reduction of the experimental group compared with the control group (unit%).

TABLE 2: Number of errors in the comparison between the two groups.

	In the case of cloud computing	Professional inspector	Degree of error reduction (%)
7 to 9 o'clock	4	8	0.50
9 to 11 o'clock	2	6	0.33
13:00 to 15:00	5	12	0.58
15:00 to 17:00	8	16	0.50
17:00 to 19:00	5	9	0.44
19:00 to 21:00	6	11	0.45

of cloud computing and professional manual detection, from 7:00 am to 11:00 am. There is a slight error; the temperature data of human-computer interaction detection measured from 13:00 noon to 21:00 pm is compared with the data of manual detec-

tion. The experimental results show that the error of each working line in cloud computing is much smaller than that of professional manual measurement. From the data shown in Table 2 and Figure 3, it can be seen that the number of errors of each working line is higher than that of the professional work. The number of errors is small, and the number of errors in the experimental group is about 50% lower than that of the control group on average. This shows that if the company wants to develop a marketing model from green, the combination with cloud computing is essential

4.2. Advantages of Using Cloud Computing in the System of Enterprise Green Marketing

- (1) The data shows that after excluding some experimental errors, the data obtained by professional manual testing and cloud computing testing are basically the same. Before the cloud computing measuring instrument, the number of labor used was 22 ± 1 people, and after the various parameters of enterprise green marketing obtained by cloud computing detection assistance, the number of labor used was

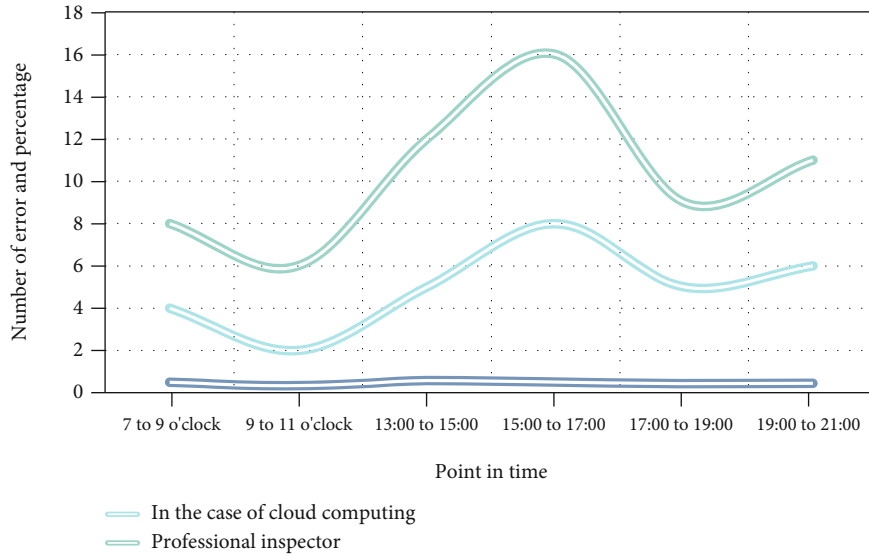


FIGURE 3: Number of errors in the comparison between the two groups.

TABLE 3: Comparison of cloud computing and control.

	Number of people saved	Economic cost savings (%)	Time saving (%)
Comparison between group A and the control group	8	34.4	33.4
Comparison between group B and the control group	10	25.7	48.5
Comparison between group C and the control group	5	13.5	52.1
Comparison between group D and the control group	8	15.3	45.7

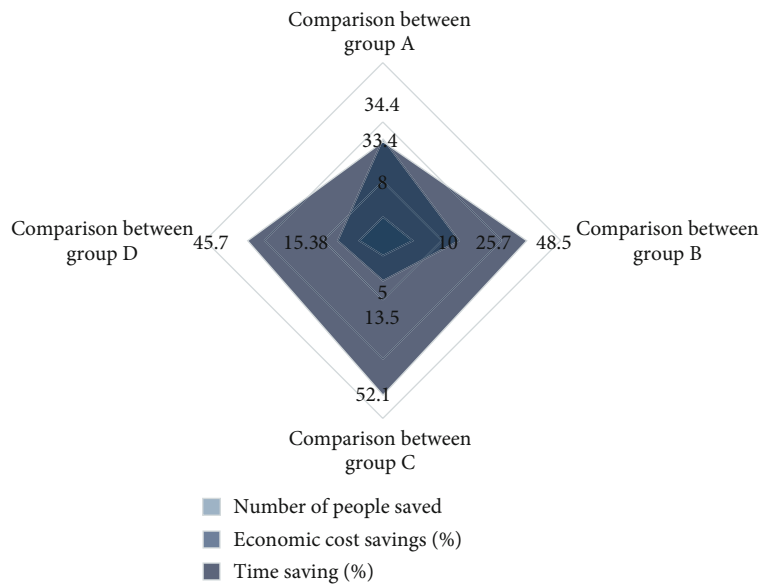


FIGURE 4: Comparison of cloud computing and control.

greatly reduced and the number was 5 ± 1 . For individuals, their labor costs have been greatly reduced by nearly 80% and the working speed has been increased by 60%. As shown in Table 3 and Figure 4, it can be seen that the number of people in each work line has been greatly reduced. Four groups of enterprises were randomly selected. In

the same type of work, it was found that after using the cloud computing node strategy to improve the work, its number has been significantly reduced, the economic cost has been saved by about 20%, and the average working time of a batch of the entire work line has been saved by about 45%. It can be seen from this that the combined application of

TABLE 4: Comparison of advantages of using cloud computing.

	Speed of capital return (%)	Fast storage improvement rate	Duty cycle improvement rate
Group A enterprise	46.4	47.2	54.2
Group B enterprises	55.3	52.1	48.3
Group C enterprises	48.6	55.6	47.2
Group D enterprise	55.8	56.6	48.5

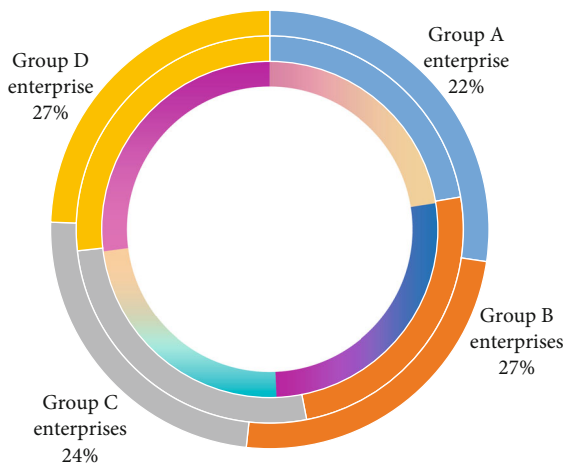


FIGURE 5: Comparison of the advantages of using cloud computing.

enterprise green marketing methods and cloud computing networks is conducive to the development of enterprises

- (2) It can be seen in Table 4 and Figure 5 that after the four groups of enterprises experimented with working lines, they switched to cloud computing storage and program operations. Because the safe use of the program and the entire process reduce excessive manual intervention, this not only frees people's hands and brains but also greatly saves the length of the enterprise's operating capital chain. On the other hand, because it is fast and easy, the characteristics of short-term storage can reduce the company's entire data and operation and storage costs. From the comparison of the company's three-month work data with the traditional job issuance, the company's work efficiency in safe operation and enterprise storage, as well as the cost of funds, is clear. The recovery speed has been greatly improved. From this aspect, it can be seen that the green marketing model of cloud computing enterprises can quickly recover the funds of the enterprise, which is beneficial to the development of the enterprise

5. Conclusions

Enterprises are not only the subject of economic activities but also consumers of productive resources and creators of products. They are also the subjects and entities of industrial development and technological use, which play a very important role in the sustainable development of the society. For the enterprise, the green economy promotes the transformation of the company's business model into resource conservation or intensive transformation. It uses cloud computing to promote enterprises to meet consumers' green needs as the starting point to organize production, emphasizes environmental protection, and seeks economic, social, and ecological aspects. Benefits are unified. More and more companies will use cloud computing as the basic operating model.

Sound laws and regulations can effectively promote the implementation of green marketing and also promote the development of green product production. Although China has formulated relevant laws and regulations on environmental protection and sustainable development, these systems are not complete and there are some shortcomings, which can no longer meet the development needs of the market economy. The cloud computing enterprise green marketing development model can speed up the company's capital recovery rate, reduce the loss caused by unnecessary manual interference, improve the company's work efficiency, make the office convenient, and operate the network, which greatly saves the company's operating costs. This has greatly promoted the development of enterprises.

Based on the trend of the Internet, the research is based on cloud computing to reform the original traditional methods of enterprises to achieve higher accuracy and superiority. This article is aimed at studying cloud computing-based enterprise green marketing development models. This article compares and analyzes enterprise green marketing systems through big data algorithms and statistical methods. It starts with the basic characteristics of cloud computing, studies the opportunities and challenges that cloud computing brings to enterprises' green marketing efforts, describes the green marketing processes and characteristics of enterprises, and analyzes cloud. The feasibility of the construction of the computing system, the basic architecture of the cloud computing system, and the construction of a complete cloud computing data processing flow are proposed. The research data found that the combination of the green marketing development model and cloud computing in the enterprise operating system is conducive to the development of the enterprise; it improves the discovery efficiency of the enterprise and reduces the pollution in the production of the enterprise; the cloud computing can greatly improve the work efficiency of the employees. Cloud computing can improve employees' task completion speed by about 20% and reduce the error rate by about 50%. Cloud computing has guiding significance for the long-term development of the company's green marketing development model.

Data Availability

This article does not cover data research. No data were used to support this study.

Conflicts of Interest

The authors declare that they have no conflicts of interest.

References

- [1] C. Li, S. Zhang, P. Liu, F. Sun, J. M. Cioffi, and L. Yang, "Overhearing protocol design exploiting Intercell interference in cooperative green networks," *IEEE Transactions on Vehicular Technology*, vol. 65, no. 1, pp. 441–446, 2016.
- [2] Y. Yu, "Research on the evaluation algorithm of social capital influence of enterprise network marketing," *Security and Communication Networks*, vol. 2021, Article ID 7711322, 8 pages, 2021.
- [3] A. F. S. Devaraj, M. Elhoseny, S. Dhanasekaran, E. L. Lydia, and K. Shankar, "Hybridization of firefly and Improved multi-objective particle swarm optimization algorithm for energy efficient load balancing in cloud computing environments," *Journal of Parallel and Distributed Computing*, vol. 142, pp. 36–45, 2020.
- [4] Y. Zhao, "Sports enterprise marketing and financial risk management based on decision tree and data mining," *Journal of Healthcare Engineering*, vol. 2021, Article ID 7632110, 8 pages, 2021.
- [5] H. Hwangbo, Y. S. Kim, and K. J. Cha, "Use of the smart store for persuasive marketing and immersive customer experiences: a case study of Korean Apparel Enterprise," *Mobile Information Systems*, vol. 2017, Article ID 4738340, 17 pages, 2017.
- [6] R. Arora, A. Parashar, and Cloud Computing Is Transforming, "Secure user data in cloud computing using encryption algorithms," *International Journal of Engineering Research and Applications*, vol. 3, no. 4, pp. 1922–1926, 2017.
- [7] K. Shizuma, W. I. Nursal, and Y. Sakurai, "Long-term monitoring of radiocesium concentration in sediments and river water along five rivers in Minami-Soma city during 2012–2016 following the Fukushima Dai-ichi Nuclear Power Plant accident," *Applied Sciences*, vol. 8, no. 8, pp. 1319–1329, 2018.
- [8] X. Li, H. Jianmin, B. Hou, and P. Zhang, "Exploring the innovation modes and evolution of the cloud-based service using the activity theory on the basis of big data," *Cluster Computing*, vol. 21, no. 1, pp. 907–922, 2018.
- [9] R. Arora, "A study of consumers' attitude towards environment friendly products," *Asian Social Science*, vol. 8, no. 12, 2018.
- [10] L. Qi, X. Chang, and J. Guan, "The application of pump intelligent condition monitoring technology in nuclear power station IOP Conference Series: Earth and Environmental Science," no. 3, Article ID 032006, 2019.
- [11] M. Armbrust, "Research contributions in human-computer interaction," *Interactions*, vol. 23, no. 3, pp. 38–44, 2016.
- [12] L. Chen and X. Yin, "Low-power pest monitoring model based on cloud computing," *Revista Científica-Facultad de Ciencias Veterinarias*, vol. 29, no. 2, 2019.
- [13] S. Sun, M. Kadoch, L. Gong, and B. Rong, "Integrating network function virtualization with SDR and SDN for 4G/5G networks," *IEEE Network*, vol. 29, no. 3, pp. 54–59, 2015.
- [14] V. Agarwal, J. W. Buttles, L. H. Beaty, J. Naser, and B. P. Hallbert, "Wireless online position monitoring of manual valve types for plant configuration management in nuclear power plants," *IEEE Sensors Journal*, vol. 17, no. 2, pp. 311–322, 2017.
- [15] S. Namasudra and P. Roy, "PpBAC," *Journal of Organizational and End User Computing*, vol. 30, no. 4, pp. 14–31, 2018.
- [16] B. Huang, J. Wei, Y. Tang, and C. Liu, "Enterprise risk assessment based on machine learning," *Computational Intelligence and Neuroscience*, vol. 2021, Article ID 6049195, 6 pages, 2021.
- [17] M. Peng, H. Wang, S. Chen et al., "An intelligent hybrid methodology of on-line system-level fault diagnosis for nuclear power plant," *Nuclear Engineering and Technology*, vol. 50, no. 3, pp. 396–410, 2018.
- [18] K. Hirose, "Long-term monitoring of radiocesium deposition near the Fukushima Dai-ichi nuclear power plant: effect of interception of radiocesium on vegetables," *Journal of Radio Analytical and Nuclear Chemistry*, vol. 318, no. 1, pp. 65–70, 2018.
- [19] E. I. Sobeh, N. S. Donia, A. M. Abd el Salam, and M. N. ELSayed, "Design of a sensor network node for air quality monitoring in nuclear installations," *Journal of Environmental Science*, vol. 45, no. 3, pp. 69–85, 2019.
- [20] L. Zhu, M. Li, and N. Metawa, "Financial risk evaluation Z-score model for intelligent IoT-based enterprises," *Information Processing & Management*, vol. 58, no. 6, article 102692, 2021.
- [21] J. Aparna, S. Philip, and A. Topkar, "Thermal energy harvester powered piezoresistive pressure sensor system with wireless operation for nuclear reactor application," *Review of Scientific Instruments*, vol. 90, no. 4, pp. 044705–044747, 2019.
- [22] H. Chen, H. Chen, W. Zhang, C. Yang, and H. Cui, "Research on marketing prediction model based on Markov prediction," *Wireless Communications and Mobile Computing*, vol. 2021, Article ID 4535181, 9 pages, 2021.
- [23] B. Yang and Y. M. Liao, "Research on enterprise risk knowledge graph based on multi-source data fusion," *Neural Computing and Applications*, vol. 34, no. 4, pp. 2569–2582, 2022.
- [24] M. Raza, N. Aslam, H. le-Minh, S. Hussain, Y. Cao, and N. M. Khan, "A critical analysis of research potential, challenges, and future directives in industrial wireless sensor networks," *IEEE Communications Surveys & Tutorials*, vol. 20, no. 1, pp. 39–95, 2017.
- [25] H. Yetgin, K. T. K. Cheung, M. el-Hajjar, and L. Hanzo, "A survey of network lifetime maximization techniques in wireless sensor networks," *IEEE Communications Surveys & Tutorials*, vol. 19, no. 2, pp. 828–854, 2018.
- [26] P. C. S. Rao, P. K. Jana, and H. Banka, "A particle swarm optimization based energy efficient cluster head selection algorithm for wireless sensor networks," *Wireless Networks*, vol. 23, no. 7, pp. 2005–2020, 2017.
- [27] S. Kurt, H. U. Yildiz, M. Yigit, B. Tavli, and V. C. Gungor, "Packet size optimization in wireless sensor networks for smart grid applications," *IEEE Transactions on Industrial Electronics*, vol. 64, no. 3, pp. 2392–2401, 2017.

Research Article

Adaptive Control System of Intelligent Lower Limb Prosthesis Based on 5G Virtual Reality

Gongxing Yan,^{1,2} Jialing Li ,³ Hui Xie,¹ and Minggui Zhou¹

¹School of Intelligent Construction, Luzhou Vocational and Technical College, Luzhou, 646000 Sichuan, China

²Science and Technology Division, Chongqing Creation Vocational College, Chongqing 402160, China

³Chongqing Modern Prosthetic Technology Service Center, Chongqing 400021, China

Correspondence should be addressed to Jialing Li; ygx8303@lzy.edu.cn

Received 5 January 2022; Accepted 16 February 2022; Published 18 March 2022

Academic Editor: Alireza Souri

Copyright © 2022 Gongxing Yan et al. This is an open access article distributed under the Creative Commons Attribution License, which permits unrestricted use, distribution, and reproduction in any medium, provided the original work is properly cited.

With the rapid development of computer science and technology in our country, especially the advent of the 5G network era, the emergence of smart prostheses makes it possible for disabled, injured, or amputee people with lower limbs to walk and exercise like normal people. However, due to the different selection of prosthetic materials, the final lower limb prostheses produced will also have different performance differences. How to select prosthetic materials to optimize the performance of the intelligent lower limb prosthesis is the focus of extensive discussion in the medical community. For this reason, this article takes the research of the adaptive control system of intelligent lower limb prosthesis based on 5G virtual reality as the research object. By using the current advanced 5G communication technology and virtual reality technology, a high-performance intelligent lower limb prosthesis is produced. Provide assistance with basic walking and motor abilities in daily life of patients with lower limb disabilities. This article first gives a systematic theoretical introduction to 5G virtual reality technology, expounds the current status of patients with lower limb disabilities, and proposes to use intelligent lower limb prosthetics to replace healthy lower limbs to solve the basic walking and sports needs of disabled patients in daily life and then use 5G virtual reality technology. The selection of human knee joints and ankle joints and structural system design were carried out. Finally, it was decided to use the four-bar linkage structure as the knee joint structure of the three-dimensional modeling of the intelligent lower limb prosthesis. At the end of this article, the application and simulation of the intelligent lower limb prosthesis to the human body were also carried out. The results of the experiment found that after 45 weeks of wearing exercises, the gait of the intelligent lower limb prosthesis is consistent with the expected effect whether it is walking on level ground and up and down the stairs or uphill. Due to the strong adaptiveness of the intelligent lower limb prosthesis sexual control, it can well assist the basic life movement ability of patients with lower limb disabilities.

1. Introduction

1.1. Background and Significance. In recent years, with the acceleration of the aging of our country's population, a considerable part of the elderly population suffers from cerebrovascular diseases and neurological diseases which have caused midwind and hemiplegia, resulting in lower limb damage. In addition, more and more people suffer from physical or neurological injuries caused by accidental traffic accidents and natural disasters. These patients with lower limb disabilities are suffering from physical pain and psychological economic pressure at the same time, and it has

become a multilateral appeal to quickly find an effective rehabilitation treatment method and means.

Intelligent lower limb prosthesis is a human prosthetic product developed in recent years. It is a bioelectronic device based on 5G virtual reality technology and biomimetic technology to imitate the gait, posture, and habits of human walking. Most people still retain motor nerves at the end of the thigh after amputation and have certain motor functions. Connecting a smart prosthesis to the stump of the thigh instead of a healthy limb can meet the basic activities of patients in daily life. And through 5G virtual reality technology, the interaction between the smart prosthesis and the

human brain nerves can be realized, so that the smart prosthesis can promptly and effectively listen to the instructions sent by the human brain and make corresponding actions quickly, so that people with lower limb disabilities can live like normal people. New research shows that virtual reality technology has the potential to help amputees “feel” the sensation of touch from prosthetic limbs. Teach their brains to believe that the prosthesis belongs to their body. Many amputees choose to stop using prosthetics after a period of time because they feel uncomfortable. On the one hand, the patient feels that the missing limb seems to remain. That is, there are so-called phantom limbs; on the other hand, prosthetics on the market usually do not provide tactile feedback, and patients need to combine observation to use them correctly. Virtual reality technology cleverly combines vision and touch to enhance a patient’s experience with a prosthetic limb, allowing the brain to “believe” that the prosthetic limb is a natural extension of the body. The device used in the trial is portable and could one day be a therapy to help patients permanently implant prostheses.

1.2. Related Work. Early on, people put forward experimental ideas for human lower limb prostheses and made prosthetic models. Wen et al. proposed a novel application of adaptive dynamic programming (ADP), which can optimize lower limb prosthetics. This is a wearable robot that can help amputees recover their motor functions. However, the current control of these robotic devices usually relies on finite state impedance control (FS-IC), which lacks adaptability to the user’s physical condition. And they also found that manually and heuristically customizing joint impedance settings in the clinic greatly hindered the widespread use of these advanced medical devices. Their simulation study proved the feasibility of ADP to automatically adjust the impedance parameters of twelve knee joints to achieve balanced walking during the complete gait cycle. Since it is difficult to obtain an accurate model of human walking dynamics, they considered a model-free ADP control algorithm. First, direct heuristic dynamic programming (DHDP) is applied to the control problem, and its performance is evaluated on the frequently used dynamic walking simulator Open Sim. For comparison, they chose another established ADP algorithm, Neural Fitting Q with Continuous Action (NFQCA). In both cases, the ADP controller learned to control the right knee joint and achieved a balanced walk, but in the 200-gait-based test, DHDP performed better than NFQCA in this application [1]. In addition, Su et al. have also pointed out that the electric intelligent lower limb prosthesis can drive the knee and ankle joints, so that transfemoral amputees can seamlessly transition between motion states with the help of the intention recognition system. However, previous intent recognition studies usually install multiple sensors on the prosthesis, and they use machine learning techniques to analyze time series data with empirical characteristics. In this regard, they proposed a novel method of training an intent recognition system that provides a natural transition between horizontal walking, stairs up/down, and ramp up/down. Since the transition between

two adjacent states is driven by movement intention, their purpose is to explore the mapping between the movement state of the healthy leg and the movement intention of the amputee before the transition of the prosthesis occurs. They use an inertial measurement unit (IMU) and place it on the healthy leg of a lower extremity amputee to monitor their movement status. They analyze the IMU data in the early swing phase of healthy legs and input the data into a convolutional neural network (CNN) to learn feature maps without the involvement of experts. The method they proposed can predict the movement intentions of unilateral amputees and able-bodied persons and help to adaptively precalibrate the control strategies used to drive the dynamic intelligent prosthesis [2]. In short, research and reports on intelligent lower limb prostheses are not uncommon. This article is based on the research of predecessors and proposes to use the emerging 5G virtual reality technology to optimize the adaptive control system of intelligent lower limb prostheses so that people with lower limb disabilities can be better. It adapts well to the intelligent lower limb prosthesis to meet the needs of daily life activities and even sports.

1.3. Innovations in This Article. The innovations of this paper are mainly reflected in the following aspects: (1) Based on the high coverage of lower limb disabilities in China, this paper proposes the use of intelligent lower limb prosthetics to assist in solving the basic sports needs of patients with lower limb disabilities in daily life. (2) This article introduces and elaborates the 5G virtual reality technology and the gait characteristics of human lower limbs in detail, which provides sufficient theoretical support for the subsequent simulation design and 3D modeling of intelligent lower limb prostheses. The article consists of the technical introduction of the 5G virtual reality intelligent lower limb prosthesis adaptive control system, the prosthetic structure design and the adaptive control experiment, and other parts.

2. Intelligent Artificial Limb Adaptive Control System

2.1. 5G Virtual Reality Technology

2.1.1. 5G Technology. Figure 1 is a schematic diagram of 5G virtual reality technology; 5G technology is a new generation of advanced mobile communication technology after 2G, 3G, and 4G. It is an extension and sublimation of the previous three generations of system technology. The performance of 5G is more optimized, it reduces the delay in the processing and transmission of data, the rate is more efficient and rapid, and the new energy technology is adopted, which greatly reduces the cost and increases the system capacity and large-scale equipment connections. The application and promotion of 5G technology will greatly change people’s production and life. The advent of the 5G era will push people into a more efficient and convenient social environment [3, 4].

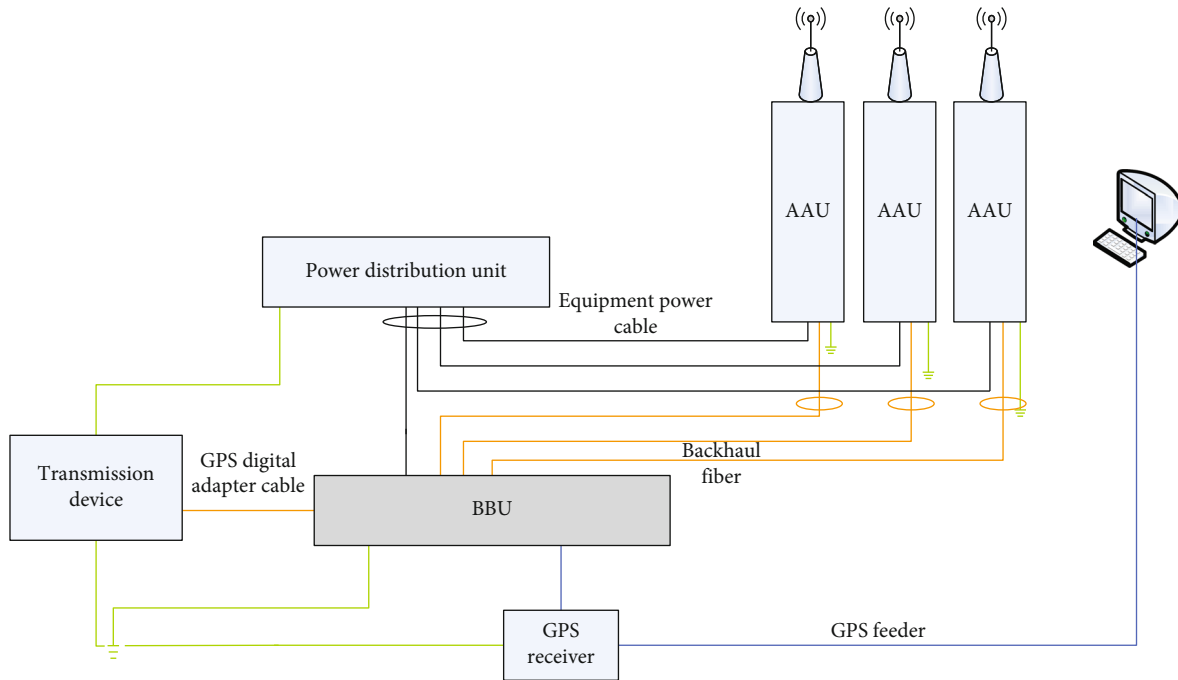


FIGURE 1: 5G virtual reality technology.

5G is different from the previous generations of mobile communication technologies. It has more distinctive network characteristics, as shown in the following:

- (1) 5G has a higher peak network speed standard, which can meet the transmission of large amounts of data such as high-definition video and virtual reality
- (2) 5G technology can be specifically applied to the autonomous driving of unmanned vehicles and the guidance of telemedicine surgery to realize information docking in the air
- (3) 5G has a huge network capacity and super device link capability, which can simultaneously meet the transmission of massive information resources and the connection of many devices, and has extremely high mobile IoT communication capabilities
- (4) The spectrum efficiency of 5G is also more than 10 times higher than the general long-term evolution technology
- (5) 5G can give users a higher sense of experience. Its network area communication coverage is extremely high, it is extremely mobile, and it can quickly receive and reply to messages
- (6) Compared with 2G, 3G, and 4G, the traffic density and connection density of 5G have been greatly improved
- (7) The level of coordination and intelligence of the 5G network system has been significantly improved,

and the internal self-adjustment of the network is also more flexible and convenient

2.1.2. Virtual Reality Technology. Virtual reality (virtual reality) technology, referred to as VR technology, is also called spiritual technology in our country. It is a way to project images and environments of the real world into the virtual world in a three-dimensional dynamic form by using computer and multimedia technology. And under the premise of wearing some professional sensing equipment such as data gloves and sensor helmets, people can perceive and operate any object in the virtual world in real time with their own sense of sight, hearing, touch, and smell and give users a sense of reality in the real environment [5, 6].

2.1.3. Characteristics of Virtual Reality Technology. Virtual reality technology mainly exhibits three basic characteristics: interactive, immersive, and conceptual, as follows:

- (1) *Interactivity.* It means that the user can get feedback on the perception and operation of the object in the virtual environment. In other words, when the user moves the object touched and grasped, the object in the hand will move with the movement of the hand movement; it has a very strong operability.
- (2) *Immersion.* Whether the user can reach the state of immersion in the virtual world and the degree of immersion determine the success of the modeling of this virtual environment model. When the user is in the virtual world, with the assistance of professional sensing appliances, he perceives all objects in the virtual world through his eyes, ears, nose, and

fingers. When the user is fully engaged in the virtual environment, it is difficult to distinguish. When the illusion of true and false, then it highlights the immersion of virtual reality technology [7, 8].

- (3) *Conceptual*. In the virtual world, users continuously learn to improve themselves by acquiring the required information and materials, and on this basis, they produce new ideas, thereby deepening the concept, improving their perceptual and rational understanding, continuously acquiring new knowledge, and forming a learning-creation-re-learning-re-creation process.

2.1.4. Classification of Virtual Reality Technology

- (1) *Immersive Virtual Reality Technology*. It incorporates virtual reality hardware equipment and software technology, has the characteristics of large investment and obvious effects, and is suitable for network settings of large- and medium-sized enterprises [9].
- (2) *Distributed Virtual Reality Technology*. This technology connects users and virtual environments distributed in different locations through digital networks, enabling them to share information and coordinate work to save energy and reduce costs [10].
- (3) *Desktop Virtual Reality Technology*. Use simple and basic virtual reality hardware and software equipment to achieve the minimum requirements for virtual reality technology, which has the characteristics of low investment and large returns.
- (4) *Pure Software Virtual Reality Technology*. It refers to the pure use of computer systems and networks and virtual reality software environments to realize virtual reality technology without having virtual reality hardware and software facilities and equipment. This development method of realizing virtual reality technology has the least investment, the effect is also very obvious, and it is the most economical.
- (5) *Augmented Virtual Reality Technology*. This development method is to superimpose the information of the real world with the information of the virtual world. The user can superimpose the graphics model of the real world and the virtual world drawn by the computer with the help of the head-mounted display to realize the virtual reality technology. The development cost of this method is high, and the calculation process is cumbersome and complicated and is generally suitable for advanced and sophisticated technical fields [11, 12].

2.2. *Intelligent Lower Limb Prosthesis and Its Adaptive Control System*. The lower limb of the human body is an important part of the human body structure [13, 14]. It is the basic movement joint for people to walk, run, jump, and stand [15]. The movement process is very complicated. Therefore, if you want to control the human lower limb prosthesis, you must first understand the human lower limb.

2.2.1. *Human Lower Limb Gait*. To understand the gait of the lower limbs of the human body is mainly to understand the gait cycle, step length, and pace of the lower limbs of the human body, including the following aspects [16, 17]:

- (1) *The Gait Cycle*. The gait cycle of the human walking is the process from the heel of one side to the ground to the heel of the other side. It includes two parts: support period and swing period. The support period accounts for about 60% of the entire gait cycle, and the swing period accounts for about 40% [18].
- (2) *Step Length*. The length of the human step length is related to the height, age, and gender of the human body [19]. Usually, after a step is taken on the heel or toe on the same side, the distance walked by the heel or toe is the step length.
- (3) *Pace*. It is also called the frequency of pace and refers to the number of steps the human body walks per unit time during walking. The walking speed of the human body is also affected by age and height.
- (4) *The Human Body Joint Angle*. The human body joint angle includes three aspects, namely, the hip joint angle, the knee joint angle, and the ankle joint angle. The angle of the hip joint refers to the angle between the longitudinal axis of the human trunk and the longitudinal axis of the thigh, where the counterclockwise direction is curling and the clockwise direction is stretching; the knee joint angle refers to the angle formed between the parallel longitudinal direction of the calf and the longitudinal direction of the thigh [20, 21].

2.2.2. *Adaptive Control Method of Intelligent Lower Limb Prosthesis*. With the development of our country's economy and the improvement of people's living standards, the performance and quality requirements of lower limb prostheses for the disabled have become higher and higher. Traditional lower limb prostheses are gradually being replaced by new intelligent lower limb prostheses. The intelligent lower limb prosthesis can realize the interaction with the human body through the use of virtual reality technology and has an adaptive control function. There are three adaptive control methods for intelligent lower limb prostheses:

- (1) *Behavior-Based Control Method*. When a part of the human body is stimulated by the external environment, the intelligent prosthesis can obtain the current gait information of the human body through external sensors and make action judgments based on it, so as to realize the control of the lower limb prosthetic movement and then synthesize and adjust the simple movement into the overall movement of the lower limb prosthesis, so as to complete the response to external information.
- (2) *Control Method Based on the Human Neural Network System*. The neural network system in the human brain is the basic structure for controlling

human activities. For the human body, simple horizontal walking can be applied to the control of intelligent lower limb prostheses by building a neural network model.

- (3) *Model-Based Control Method*. This control method is currently the most widely used control method. Through accurate mathematical modeling of the lower limbs of the human body and then use the existing data for artificial planning to formulate the best motion trajectory of the prosthesis, collect the motion information of the prosthesis through the motion test of the prosthesis, and compare it with the expected result to obtain the deviation information, and then continuously adjust the gait of the intelligent lower limb prosthesis based on this, and finally realize the adaptive control of the intelligent lower limb prosthesis [22, 23].

2.3. Combination of 5G Virtual Reality Technology and Lower Limb Rehabilitation Technology. A large number of studies have found that repeated exercise rehabilitation training will have a good exercise effect on the patient's cerebral cortex. For the motion simulation learning technology of rehabilitation sports, the best rehabilitation effect must be achieved after repeated training and completion of a series of tasks. In the treatment process of rehabilitation sports training, the patient's visual and auditory perception and the body's self-perception are used to judge the effect of the training and complete the feedback on the results of the rehabilitation training. Usually, this rehabilitation process is long and boring, and patients must be fully psychologically prepared [24].

Virtual reality technology is a product of the development of network technology. The virtual reality scenes it creates are realized through computer systems. There is no need to worry about and consider the workload and intensity of work, and there is enough time and ability to meet patients for repeated rehabilitation training. At the same time, in the virtual reality environment, due to its performance characteristics such as immersion and interactivity, it can give patient rehabilitation information feedback based on the patient's training state through the patient's sense organs such as sight, hearing, smell, touch, and taste. And during training, patients can perceive any training scene and object in the virtual environment with the help of sensors, which increases the interest of the patient's training process, which is of great help to improve the patient's enthusiasm for participating in rehabilitation training [25].

3. Experiment of Adaptive Control for Prosthetic Structure Design

The realization of the movement of the lower limbs of the human body should fully consider the dynamic system of each joint, and the most important structure for the intelligent lower limb prosthesis is the knee joint. Therefore, to design a smart lower limb prosthesis, the choice of the knee joint structure is very important. The excellent knee joint structure not only gives the prosthesis enough stable support when it is in the support period but also gives it flexible

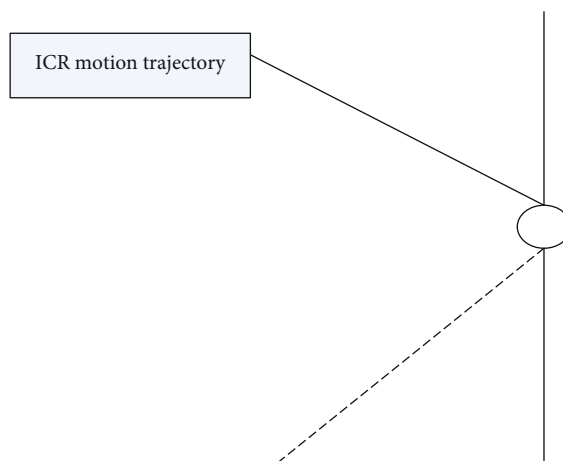


FIGURE 2: Schematic diagram of the instant center of rotation of a single knee joint.

movement during the swing period of the prosthesis. This article has carried out the structure design experiment of the intelligent lower limb prosthesis and analyzed its adaptive control according to its sports training effect.

3.1. Design of Dynamic Knee Joint Structure

3.1.1. Selection of Knee Joint Structure. As the most important joint structure of the intelligent lower limb prosthesis, the selection of the knee joint is very important, and it is directly related to the success of the final modeling of the intelligent lower limb prosthesis. To select the knee joint, we must first understand the internal structure of the human knee joint and grasp the functional characteristics of the knee joint. Only on the basis of real understanding of the motion function of the human knee joint can the design of the prosthetic structure be better realized. The knee joint is the largest and most complex joint of the human body. It is mainly composed of the tibia, the inner and outer calf ankle, the humerus, the inner and outer thigh, and the patella. The knee joint between the thigh and the calf mainly has 6 moving parts, namely, the tibial plateau, meniscus, femur, femoral ankle, patella, and the ligaments, that connect each part. The movement process of the knee joint is the process of the femoral ankle, that is, the thigh sliding on the surface of the meniscus under the restraint of the connecting ligaments, thereby forming a special pulley structure between the meniscus and the femoral ankle. In this way, it appears that the structure of the knee joint is extremely complicated, and its movement process is not simple rotation. Therefore, the knee joint structure of the intelligent lower limb prosthesis cannot be simply designed as a pure roller rotation. The contact surface between the tibia, the calf, and the meniscus not only has roller-type rotation but also sliding, and the instantaneous time should be selected as the center of rotation and designed as a uniaxial knee joint, as shown in Figure 2. The rotation trajectory of the instantaneous rotation center ICR of the knee joint is actually a J-shaped curve. This design structure is simpler and more durable; the calculation is convenient, and the production cost is low. But at the same time, this single-axis knee joint structure cannot satisfy the

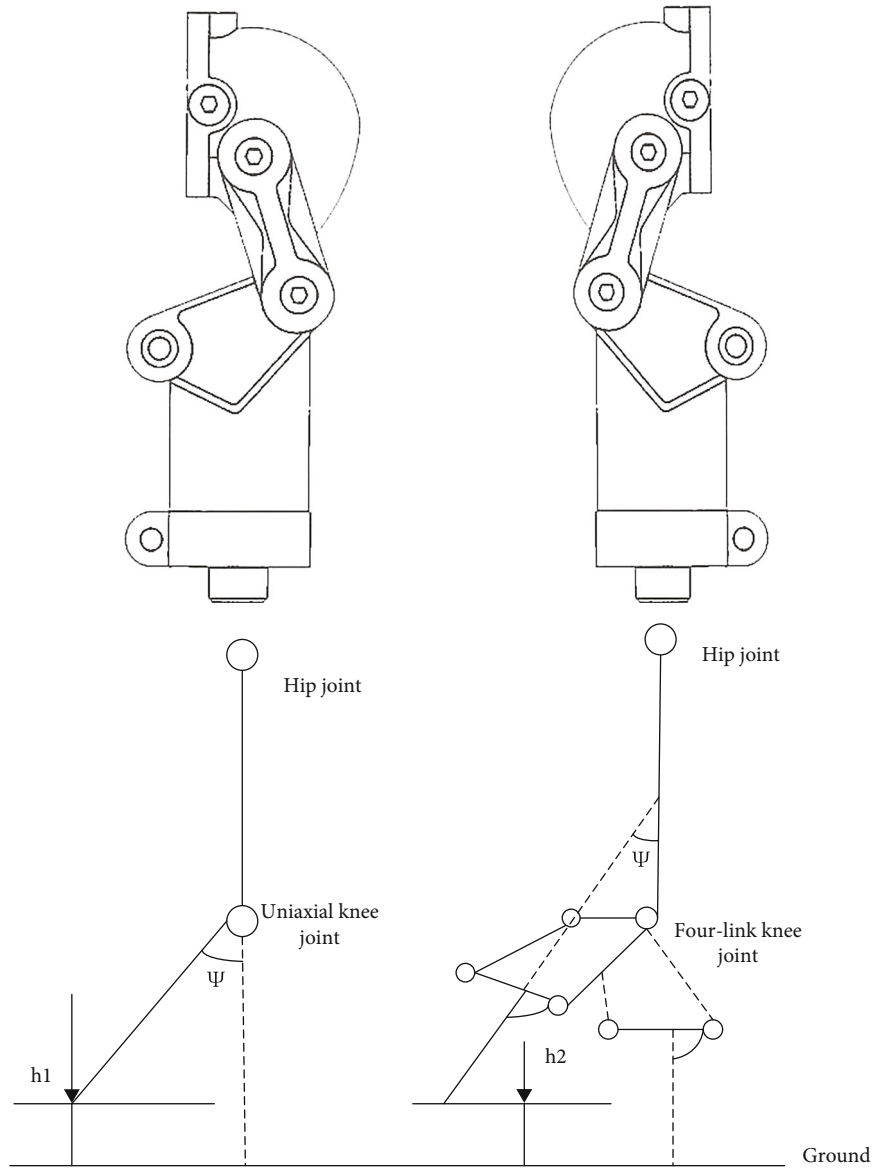


FIGURE 3: Comparison of single-axis knee joint and four-link knee joint flexion.

instantaneous rotation of the prosthesis, and this structure makes it difficult for the prosthesis to raise the height of the foot from the ground. In contrast, multiaxis knee joints can well simulate the motion of human knee joints, but the more the number of multiaxis knee joints, the worse the stability will be, which is not conducive to the balance of the human body structure when the prosthesis is in the support period. And the more the number of axes, the more complicated it is to optimize the design of the prosthesis structure. Therefore, in this experiment, we finally use the four-bar mechanism as the main structure of the knee joint.

The following Figure 3 shows the structure of a four-link knee joint. It can be seen from the figure that, compared with a single-axis knee joint structure, the height of the heel of the four-link knee joint mechanism from the ground is significantly higher, which is more conducive to walking on the prosthesis. It can avoid obstacles autonomously at

all times, thereby improving the performance advantages of intelligent lower limb prosthetics.

3.1.2. Selection of Knee Joint Drive System. Passive knee joints are also called cushioned knee joints. Generally, they have no active power and rely only on the residual limb of a single leg to provide power. The passive knee joint can continuously adjust the buffer force according to the external environment and the gait of the prosthetic walking. Because of its simple structure and easy control, it becomes the mainstream design of the prosthetic knee joint. Active knee joints rely on external force driving as their own power source. Active intelligent lower limb prostheses mainly include pneumatic drive, hydraulic drive, and motor drive. The external force drive of active knee joints relies on motor drive. Although the active knee joint can provide power for extension and flexion of the lower limb prosthesis, its small

battery capacity and heavy weight often lead to a short battery life. Based on the advantages and disadvantages of these two types of knee joint driving, this article attempts to combine the two driving methods to implement hybrid driving.

Hybrid drive uses motor drive as the active driving force and damping as the power of the passive knee joint; hybrid drive can not only meet the walking form under active driving but also the driving form of passive walking. The patient wears intelligent lower limbs equipped with a hybrid drive system. After the prosthesis, the active driving force when climbing and stair climbing can greatly reduce the consumption of the patient's physical energy by the exercise, and the passive driving mode can be activated on flat ground or when the battery power is low can maximize energy saving and extend battery life ability. Usually in daily life, it is recommended that patients adopt a driving form of active and passive at the same time. This not only allows the patient to achieve a walking gait like a healthy limb but also looks beautiful and does not consume too much physical energy when walking.

3.2. Selection and Design of Ankle Joint. When the human body is standing normally, the angle between its calf and the sole of the foot is a right angle, that is 90° , perpendicular to the ground, and the sole of the foot is parallel to the ground. In the process of walking, the angle between the sole of the foot and the calf will swing back and forth between $10^\circ \sim 20^\circ$ and $-30^\circ \sim -50^\circ$. The functions of the ankle joint during human walking include assisting the movement of the lower limbs and reducing vibration and antiskid.

By investigating the gait of the ankle joint when walking, we found that the ankle joint mainly presents two states when walking: standing state and swing state. The ankle joint is mainly in the form of pure rolling motion during the whole walking process, so for the design of the ankle joint, we adopt a uniaxial knee joint structure. Since the driving form of the knee joint is hybrid drive, and there is already active driving force here, but the ankle joint needs to be powered to cooperate with it to complete the whole walking process of the knee joint, so it is necessary to add flow damping, by using the flow damping current to change the size of the damping.

3.3. Optimization Design of Four-Bar Linkage Knee Joint Structure. According to the previous article, the increase in the number of axes of the multiaxis knee joint will cause the stability of the prosthesis to decrease. Therefore, in order to make the movement of the four-bar structure more in line with the movement of the knee joint, we will compare the four-bar length, and its initial angle is optimized. The

instantaneous coordinates of the knee joint will change with the rotation of its bending angle, so the four-bar linkage can be used as a known condition. Suppose the lengths of the four bars of the four links are $L_1, L_2, L_3,$ and $L_4,$ and the angles between them and the coordinate axis are $\theta_1, \theta_2, \theta_3,$ and $\theta_4,$ and the four bars are represented by CF, DE, CD, and EF, respectively. The CF rod is connected to the thigh, the DE rod is connected to the calf, and the intersection of the extension lines of the other two rods is set as $P,$ which is the instantaneous rotation center of the knee joint.

First of all, we need to determine the design variables and use the four-bar lengths $L_1, L_2, L_3,$ and L_4 as the design variable parameters. When the four-bar lengths are known, the angle degrees of $\theta_1, \theta_3,$ and θ_4 can be obtained directly through the variable formula. The variable formula is

$$X = [x_1, x_2, x_3, x_4, x_5]^T = [l_1, l_2, l_3, l_4, \theta_2]^T. \quad (1)$$

After that, the objective function is established. A total of 12 variables are involved in the optimization experiment of the four-bar linkage structure. It is required to minimize the error between the actual trajectory and the ideal trajectory, so the expression is

$$\min f(X) = \sqrt{\frac{1}{2} \sum_{i=1}^{12} [(x_{pi} - x_{p'i})^2 + (y_{pi} - y_{p'i})^2]}. \quad (2)$$

Among them, x_{pi} and y_{pi} represent the coordinates of the four-link trajectory, and $x_{p'i}$ and $y_{p'i}$ represent the coordinates of the actual trajectory of the knee joint. The projection formula of the four bars of the four-bar linkage on the coordinate axes X and Y is as follows:

$$\left\{ \begin{array}{l} l_6 \cos \theta_1 + l_3 \cos \theta_4 = l_4 \cos \theta_3 + l_5 \cos \theta_2 \\ l_6 \sin \theta_1 + l_3 \sin \theta_4 = l_4 \sin \theta_3 + l_5 \sin \theta_2 \end{array} \right\}. \quad (3)$$

According to point P of the center of rotation:

$$\left\{ \begin{array}{l} \frac{x_c}{y_c} = \frac{x_p - x_c}{y_p - y_c} \\ \frac{x_f - x_e}{y_f - y_e} = \frac{x_p - x_e}{y_p - y_e} \end{array} \right\}. \quad (4)$$

Combine formula (3) and formula (4) and substitute the coordinates of each point to obtain:

$$\left\{ \begin{array}{l} x_p = \frac{x_c (y_e x_f - x_e y_f)}{x_c (y_e - y_f) - y_c (x_e - x_f)} = \frac{l_5 \cos \theta_1 [l_6 \sin (\theta_2 - \theta_1) + l_3 \sin (\theta_2 - \theta_4)]}{l_5 \sin (\theta_2 - \theta_1) + l_3 \sin (\theta_1 - \theta_4)} \\ y_p = \frac{y_c (y_e x_f - x_e y_f)}{x_c (y_e - y_f) - y_c (x_e - x_f)} = \frac{l_5 \sin \theta_1 [l_6 \sin (\theta_2 - \theta_1) + l_3 \sin (\theta_2 - \theta_4)]}{l_5 \sin (\theta_2 - \theta_1) + l_3 \sin (\theta_1 - \theta_4)} \end{array} \right\}. \quad (5)$$

Since the knee joint moves back and forth within a certain angle instead of periodic movement, the CD rod is the main power rod, and the other three rods are passive rods, so the four-link knee joint is a double rocker structure, which needs to meet the conditions:

$$\left\{ \begin{array}{l} l_4 > \max \{l_3, l_5, l_6\} \\ l_3 < \min \{l_4, l_5, l_6\} \end{array} \right\}. \quad (6)$$

The length of the four bars and the range of instantaneous center coordinates are as follows:

$$\left\{ \begin{array}{l} 35 < l_6 < 55 \\ 30 < l_5 < 55 \\ 40 < l_4 < 60 \\ 20 < l_3 < 40 \\ 0 < x_p < 40 \\ 0 < y_p < 150 \end{array} \right\}. \quad (7)$$

According to the above calculation process, the final optimization results of the four-link knee joint are $l_3 = 22$ mm, $l_4 = 50$ mm, $l_5 = 35$ mm, $l_6 = 44$ mm, and $\theta_2 = 28^\circ$. After optimization, the coordinates of each point obtained after optimization and the expected coordinates of each point are drawn into a graph for comparison, and it can be obtained: After optimization, the trajectory of the four-bar linkage is consistent with the expected trajectory, indicating that the optimized four-bar linkage structure meets the requirements of simulating the instantaneous change of the human lower limb prosthetic knee joint.

3.4. Construction of the Three-Dimensional Model of the Ankle Joint. According to the selection of the prosthetic knee and ankle joints, we finally established the three-dimensional model of the knee and ankle joint with the optimized four-bar linkage structure. The main body is mainly designed as a frame structure that reduces weight. It can also increase the rigidity of the structure and save costs. A magnetic current damper is installed between the upper plate and the lower plate. It is the lower leg part of the prosthesis, and the installation position of the magnetic current damping must meet the following conditions:

- (1) When the knee joint rotation angle is 0 degrees, the magnetic current damping is in a fully expanded state
- (2) When the knee joint is bent, it can effectively expand and contract and provide sufficient damping force in the stroke
- (3) The axis of the shock absorber cannot be collinear with the axis of rotation of the knee joint. The electromagnetic damper is installed between the top plate and the lower part of the lower leg position. A variety of drive motors must be installed on the

TABLE 1: Initial values of CPG network parameters.

Oscillator	Parameter value	Angular frequency	Phase
1	2.2361	0	0
2	3.2315	6.4574	19.4236
3	1.6247	13.4987	31.4587
4	1.3529	19.3649	36.4579
5	0.6354	26.4538	50.1246

thigh. One is because the calf does not have enough space to accommodate it, and the other is that the weight of the motor device is too large. If it is installed on the calf, the calf will continue to bend and stretch when walking. The reciprocating motion of the drive motor will affect the flexibility of the prosthesis, and it will also consume more energy from the human body

The calf is mainly composed of the sole of the foot, the calf connecting frame, and the damping buffer system. For aesthetics and simulation, the size of the sole is mainly based on the actual size of the human body. After putting on shoes, it can also have the flexibility and practicality of ordinary soles. The calf support is mainly connected to the thigh and sole, and the thigh is welded. The shaft is connected to the shaft base so that it can rotate around the shaft. Adjust the calf support and cushioning at the back of the foot to connect the shaft to the shaft seat. Although the axle seat is installed on the back of the foot, the actual expansion distance of the shock absorber is reduced, which will not be convenient for the effective use of the formation, but in order to achieve the coordination, aesthetics, and compactness of the equipment, it is best to install and fix the sole of the foot. The drive system also includes a stepper motor and a reduction gear. Due to the flexibility of the calf, the motor does not take up much space. Therefore, the motor is installed parallel to the lower leg. After the reduction gear changes speed and direction with a certain transmission ratio, the power is connected to the ankle. In this way, the three-dimensional modeling of the ankle joint is completed.

4. Application and Simulation Analysis of Intelligent Lower Limb Prosthesis

In the third part of this article, we selected and designed the structural system of the human knee and ankle joints by using 5G virtual reality technology and established a three-dimensional model of the intelligent lower limb prosthesis and found that the intelligent lower limb prosthesis is adaptive performance advantages in sexual control. In this chapter, we will conduct a simulation experiment of intelligent lower limb prosthesis and apply it to the human body. And we will analyze and discuss the great help of intelligent lower limb prosthesis for disabled people according to the different synchrony of human walking (including walking on flat ground and going up and down stairs).

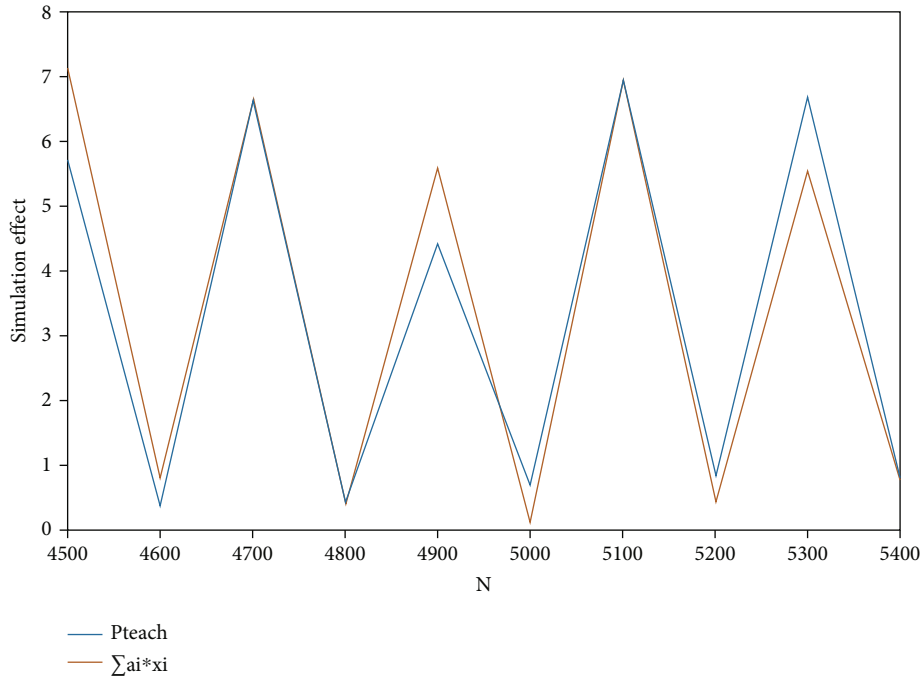


FIGURE 4: Simulation effect of smart lower limb prosthesis walking on the ground.

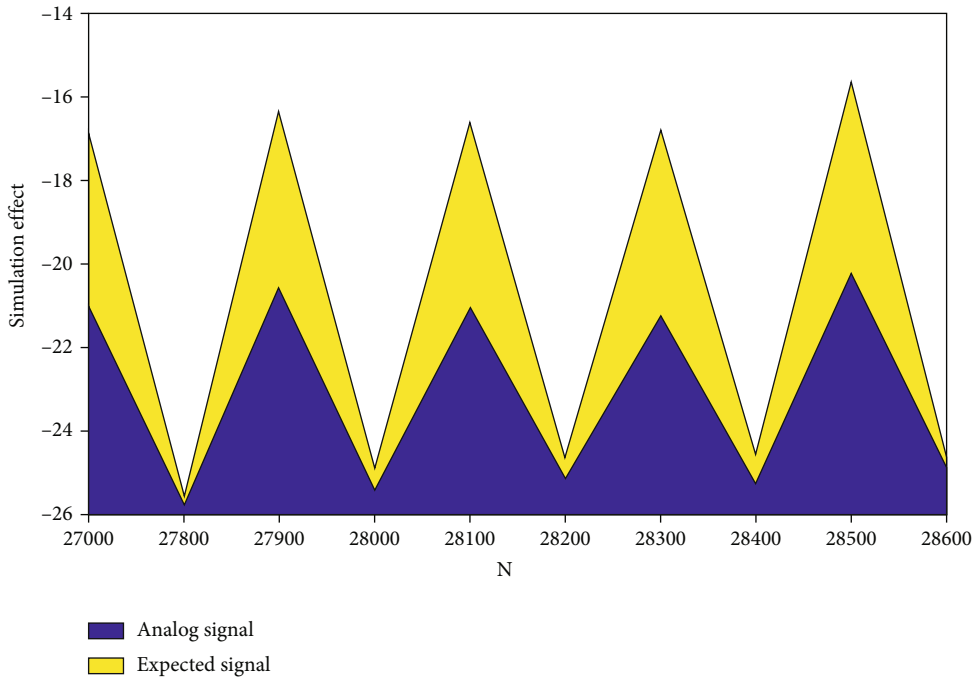


FIGURE 5: Gait simulation effect when going up the stairs.

4.1. Analysis of Gait Simulation Effect When Walking on Level Ground. The two-layer CPG neural network is composed of a neural network and a CPG neuron layer. Since the neuron layer has no input of feedback information, the entire control network does not form a closed loop. Therefore, the researchers introduced a new network layer-neural network layer on the CPG neuron layer. The neurons in this layer can receive the input of sensory feedback infor-

mation from the external environment, and at the same time, the neurons can be optimized and solved, and further obtain the optimal value of each parameter in the network.

In order to explore the simulation effect of the intelligent lower limb prosthesis on human gait when walking on flat ground, here we introduce the CPG oscillator and use the CPG oscillator to test the simulation effect of the prosthesis on the gait signal. The initial values of the main parameters

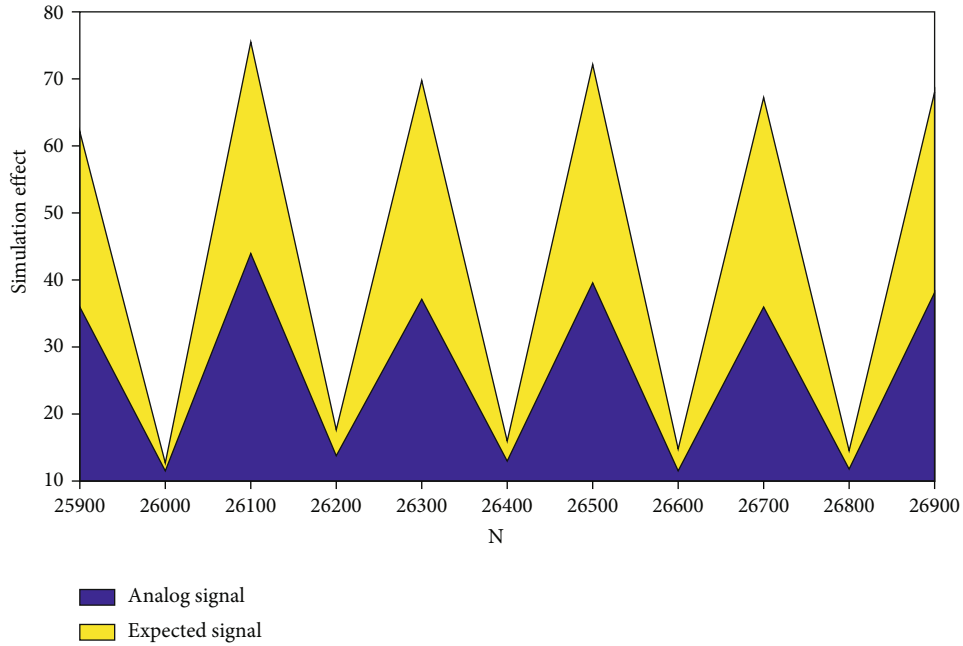


FIGURE 6: Gait simulation when going down the stairs.

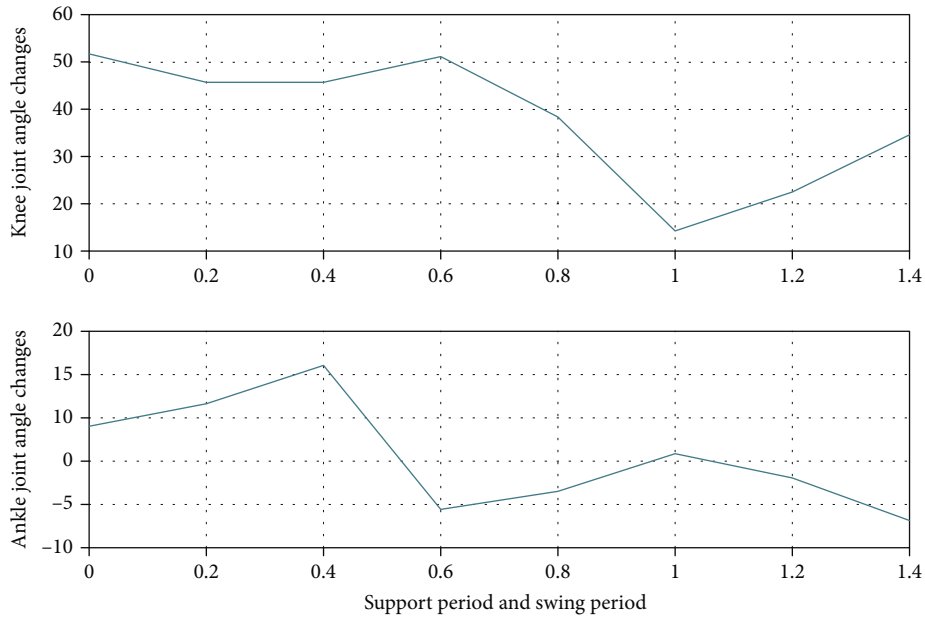


FIGURE 7: Simplified diagram of finite state machine model of knee-ankle integrated.

of the CPG oscillator are shown in Table 1. Figure 3 shows the gait signal simulation effect of the knee joint when walking on the ground.

It can be seen from Table 1 and Figure 4 that after 45 weeks of practice, the frequency, amplitude, and phase of the output signal of the oscillator network have achieved convergence, and the overall output signal of the oscillator network is close to the signal during actual practice, which is very good.

4.2. Analysis of Gait Simulation Effect When Going Up and Down Stairs. The simulation experiment was carried out to

simulate the gait of the human body when going up and down the stairs. The simulation effect is shown in Figures 5 and 6.

According to the gait simulation effect of Figures 4 and 5, it can be seen that when the intelligent lower limb prosthesis goes up and down the stairs, its gait structure is basically the same as our expected human gait structure, and the intelligent lower limb prosthesis adopts a four-link knee joint structure; it shows a greater performance advantage when walking; through the combination of active and passive driving force, it greatly saves the energy consumption of the human body when walking and provides great help to the disabled.

4.3. Knee-Ankle Integrated Finite State Machine Control. The main driving force of the knee and ankle joints is provided by the stepper motor accelerometer, which can use angle changes to control its own motion state. Here, we take the state of walking on flat ground as an example. Because the gait is simple and easy to control, there is no need to divide the state too much. According to the finite state machine control principle, the knee joint control can be divided into four states. Since the body needs stable support, the support period is divided into three states, and the swing period has little effect on the stability of the body, so only one state is needed during the swing period. Similarly, the movement of the ankle joint is divided into four states accordingly, and try to make the points of the four states at the same time point, so that the same starting state can be used to control the four states, so as to realize the knee and ankle joints. The specific situation is shown in Figure 7.

5. Conclusions

The development of society and the improvement of living standards will also increase the demand for prostheses by the disabled, and the performance requirements for the intelligence, aesthetics, and adaptability of the prostheses are also increasing. Therefore, the research on smart prostheses in related fields will be more in-depth. On the basis of analyzing the characteristics of virtual reality technology, system characteristics, and virtual hardware equipment, this paper proposes to participate in virtual reality rehabilitation scenarios in the lower limb exoskeleton rehabilitation system that has been designed in the laboratory and build a more reasonable humanized rehabilitation training. The system can better serve the lower limb rehabilitation training.

At present, rehabilitation training for patients with lower limb disabilities is mainly reciprocating passive training. This training is not only inefficient and slow in effectiveness but also easily affects the patient's psychology. Long-term repetitive training not only wears down the patient's rehabilitation patience but also reduced its enthusiasm for receiving rehabilitation treatment. To this end, this research introduces an active collaborative stimulation training method based on 5G virtual reality technology.

By establishing a three-dimensional model of the intelligent lower limb prosthesis, it simulates the three-dimensional virtual scene of the patient's sports rehabilitation training and stimulates and maintains the enthusiasm of the patient to actively receive the rehabilitation training to promote the patient's rehabilitation process. Facilitate the patient's recovery process. The design of this article focuses on the construction of virtual roaming scenes, and it is necessary to formulate scientific and perfect rehabilitation evaluation strategies to carry out rehabilitation planning for patients at different rehabilitation stages. Visualized remote network virtual scene is a new direction of rehabilitation medicine. Relying on network technology to realize remote communication between rehabilitation patients and doctors, this distributed virtual reality technology is also an urgent problem to be solved.

Data Availability

This article does not cover data research. No data were used to support this study.

Conflicts of Interest

The authors declare that they have no conflicts of interest.

Acknowledgments

This work was supported by the Luzhou Science and Technology Planning Project (2021-SYF-44), the Scientific Research and Innovation Team Construction Project of Luzhou Vocational and Technical College (2021YJTD07), and the Special Project for Technological Innovation and Application Development in Yongchuan District (2021yc-cxfz30011).

References

- [1] Y. Wen, J. Si, X. Gao, S. Huang, and H. H. Huang, "A new powered lower limb prosthesis control framework based on adaptive dynamic programming," *IEEE Transactions on Neural Networks and Learning Systems*, vol. 28, no. 9, pp. 2215–2220, 2017.
- [2] B. Y. Su, J. Wang, S. Q. Liu, M. Sheng, J. Jiang, and K. Xiang, "A CNN-based method for intent recognition using inertial measurement units and intelligent lower limb prosthesis," *IEEE Transactions on Neural Systems and Rehabilitation Engineering*, vol. 27, no. 5, pp. 1032–1042, 2019.
- [3] Y. Zhang, L. Liu, J. Tian, and Q. E. Wu, "Intent recognition of a lower limb prosthesis based on multi-source information and general regression neural network," *Journal of Computational and Theoretical Nanoence*, vol. 13, no. 11, pp. 8956–8962, 2016.
- [4] M. Sheng, W.-J. Wang, T.-T. Tong, Y.-Y. Yang, H.-L. Chen, and S. Ben-Yue, "Motion intent recognition in intelligent lower limb prosthesis using one-dimensional dual-tree complex wavelet transforms," *Computational Intelligence and Neuroscience*, vol. 2021, Article ID 5631730, 15 pages, 2021.
- [5] G. Sorin, G. Pasquier, E. Drumez, A. Arnould, H. Migaud, and S. Putman, "Reproducibility of digital measurements of lower-limb deformity on plain radiographs and agreement with CT measurements," *Orthopaedics & Traumatology, Surgery & Research*, vol. 102, no. 4, pp. 423–428, 2016.
- [6] R. Cameron, M. M. Wernke, H. M. Powell et al., "Elevated vacuum suspension preserves residual-limb skin health in people with lower-limb amputation: randomized clinical trial," *Journal of Rehabilitation Research and Development*, vol. 53, no. 6, pp. 1121–1132, 2016.
- [7] N. Thatte, T. Shah, and H. Geyer, "Robust and adaptive lower limb prosthesis stance control via extended Kalman filter-based gait phase estimation," *IEEE Robotics and Automation Letters*, vol. 4, no. 4, pp. 3129–3136, 2019.
- [8] N. Thatte and H. Geyer, "Toward balance recovery with leg prostheses using neuromuscular model control," *IEEE Transactions on Biomedical Engineering*, vol. 63, no. 5, pp. 904–913, 2016.
- [9] A. B. Wanamaker, R. R. Andridge, and A. M. Chaudhari, "When to biomechanically examine a lower-limb amputee,"

- Prosthetics and Orthotics International*, vol. 41, no. 5, pp. 431–445, 2017.
- [10] S. Pandit, A. Godiyal, A. Vimal, U. Singh, D. Joshi, and D. Kalyanasundaram, “An affordable insole-sensor-based trans-femoral prosthesis for normal gait,” *Sensors*, vol. 18, no. 3, p. 706, 2018.
- [11] D. L. Crouch and H. H. Huang, “Musculoskeletal model-based control interface mimics physiologic hand dynamics during path tracing task,” *Journal of Neural Engineering*, vol. 14, no. 3, p. 036008, 2017.
- [12] A. Mutlu, M. D. Kharooty, and Y. Yakut, “The effect of segmental weight of prosthesis on hemodynamic responses and energy expenditure of lower extremity amputees,” *Journal of Physical Therapy Science*, vol. 29, no. 4, pp. 629–634, 2017.
- [13] A. Sawers, J. Kim, and B. Hafner, “Practice-effects in performance-based balance tests limit their application among lower-limb prosthesis users,” *Archives of Physical Medicine and Rehabilitation*, vol. 100, no. 10, article e24, 2019.
- [14] I. Batzianoulis, N. E. Krausz, A. M. Simon, L. Hargrove, and A. Billard, “Decoding the grasping intention from electromyography during reaching motions,” *Journal of Neuroengineering and Rehabilitation*, vol. 15, no. 1, p. 57, 2018.
- [15] J. Loughran, “News briefing - mobile world congress: virtual reality - 5G headset coupled with full-body suit promises complete virtual immersion,” *Engineering and Technology*, vol. 12, no. 3, pp. 13–13, 2017.
- [16] N. Shawen, L. Lonini, C. K. Mummidisetty et al., “Fall detection in individuals with lower limb amputations using mobile phones: machine learning enhances robustness for real-world applications,” *Jmir Mhealth & Uhealth*, vol. 5, no. 10, article e151, 2017.
- [17] P. K. Kumar, M. Charan, and S. Kanagaraj, “Trends and challenges in lower limb prosthesis,” *IEEE Potentials*, vol. 36, no. 1, pp. 19–23, 2017.
- [18] G. Fiedler and M. S. Johnson, “Correlation of transtibial prosthetic alignment quality and step-by-step variance of gait,” *JPO: Journal of Prosthetics and Orthotics*, vol. 29, no. 1, p. 1, 2017.
- [19] Z. Chunlin, “Multidisciplinary cooperation and active development of limb salvage treatment for patients with osteosarcoma around the knee joint,” *Chinese Journal of Bone and Joint*, vol. 6, no. 6, pp. 401–403, 2017.
- [20] L. Min, “Research on intelligent gesture recognition based on neural network and virtual reality technology% research on intelligent gesture recognition based on neural network and virtual reality technology,” *Journal of Changchun Normal University (Natural Science Edition)*, vol. 37, no. 3, pp. 69–74, 2018.
- [21] Z. Yongliang, Z. Guangchao, and C. Xilang, “Research on the key technology of command and control system intelligent decision making based on knowledge,” *Microcomputer Applications*, vol. 36, no. 2, pp. 56–59, 2017.
- [22] C. Xiang and B. Li, “Research on ship intelligent manufacturing data monitoring and quality control system based on industrial Internet of Things,” *The International Journal of Advanced Manufacturing Technology*, vol. 107, no. 3-4, pp. 983–992, 2020.
- [23] W. Cao, H. Yu, W. Zhao, J. Li, and X. Wei, “Target of physiological gait: realization of speed adaptive control for a prosthetic knee during swing flexion,” *Technology and Health Care*, vol. 26, no. 1, pp. 1–12, 2018.
- [24] Q. Wang, “Research on the improved CNN deep learning method for motion intention recognition of dynamic lower limb prosthesis,” *Journal of Healthcare Engineering*, vol. 2021, Article ID 7331692, 5 pages, 2021.
- [25] Z. Liu, W. Lin, Y. Geng, and P. Yang, “Intent pattern recognition of lower-limb motion based on mechanical sensors,” *Acta Automatica Sinica (English Edition)*, vol. 4, no. 4, pp. 651–660, 2017.

Research Article

Modeling of Residential Environment Artistic Design Based on Multisensor Data Fusion

Yang Yu 

Academy of Fine Arts, Weifang University, Weifang, 261061 Shandong, China

Correspondence should be addressed to Yang Yu; 20110898@wfu.edu.cn

Received 29 December 2021; Accepted 4 March 2022; Published 16 March 2022

Academic Editor: Alireza Souri

Copyright © 2022 Yang Yu. This is an open access article distributed under the Creative Commons Attribution License, which permits unrestricted use, distribution, and reproduction in any medium, provided the original work is properly cited.

The development of a 3D city model is accompanied by the continuous progress of technical knowledge, the continuous increase of public interest in it, and the rapid progress of national knowledge. The use of a 3D city model has become the common concern of academia, enterprises, and most users. The article takes the community as an example to summarize the research overview and basic knowledge of the 3D model. From the aspects of 3D city location data collection technology, 3D city model technology, 3D exhibition, etc., the advanced technology in 3D city model, 3D GIS software system, and other issues are discussed and studied, and the current state-of-the-art technology development level is summarized and analyzed. The article first introduces the purpose and importance of the 3D town model and further analyzes the development context, research background, and research content at home and abroad. Secondly, the theoretical basis of the 3D data model, study location data characteristics, location data model configuration, location data survey structure, and location data model construction requirements were put forward. Then, 3DMax software was used to build a house model and finally find it in OpenGL software. The effective distance of the detector is 0.4–3.5 m, and the maximum resolution is 640×480 . It also introduces the realization of 3D architectural model storage and the visual expression of 3D city modeling. The article uses the Kinect depth sensor to recreate a simple static dimensional scene.

1. Introduction

In the process of modernization, 3D modeling of cities is an admirable and challenging task. Exploration and surveying are important measures to build the national economy and national security. In the process of social development, the geographical knowledge obtained through testing provides an important foundation to analyze, express, and explain global changes, and it is also an important platform and guarantee for urban modeling. Based on the analysis of different types of information on the subject, through the city's comprehensive system research, various types of data are exchanged and integrated. The city 3D model is a high-tech computer network model system. It can not only create a virtual computer city but also enable each city to allocate resources. Most importantly, it will encourage cities to support various industries, through digital procurement, integrated computer storage, and management. With the advancement of computer technology, the rapid development of remote sensing technology, photogrammetry tech-

nology, and related technologies can realize the rapid three-dimensional structure of spatial information [1].

Experts at home and abroad also have a lot of research on environmental art design modeling. Ziedan believes that the advancement of 3D mapping and the availability of 3D city models have promoted the development of new technologies for mitigating multipath. He proposed several algorithms that use all available multipath and non-line-of-sight signals to improve the accuracy of city positioning [2]. Meyer et al. proposed an algorithm to track an unknown number of targets based on the measured values provided by multiple sensors. The algorithm achieves scalability with low computational complexity by running propagation on a properly designed factor graph. The redundant formula of data association uncertainty and the "enhanced target state" including binary targets make it possible to use statistical independence to greatly reduce its complexity [3]. AHC believes that the main advantage of 3D is that it can alleviate the degradation problem when training a deep network, so that it can make full use of the performance improvement

obtained by increasing the network depth [4]. Singla and Padia feel that the virtual 3D city model is a digital representation of terrain surfaces, sites, buildings, roads, waterways, etc. Usually, these models are used to present, explore, and analyze urban areas. These models are also used in areas such as smart cities, virtual reality, infrastructure planning, telecommunications, disaster management, real estate services, education, tourism, and change detection [5]. Xie and Lu feel that 3D modeling algorithms include modules that preprocess point clouds, extract tunnel axes, perform coordinate transformation, perform noise reduction, and generate 3D models. The measurement results of TLS were compared with the results of total station and numerical simulation, which confirmed the reliability of TLS [6]. Peronato et al.'s 3D model-based method simulates the solar radiation on all building surfaces, while also taking into account mutual reflections. Therefore, the 3D model is discretized by calculating the solar sensor grid [7].

With the rapid development of science and technology today, nature and creative art must be able to fully meet the needs of the development of the digital age, and new technical forces are needed to enrich and expand the content and density of the environment. It opens up a new way of environmental design, and the 3D application research of art design has jumped out of ordinary horizontal, vertical, and cross-sections. The location and design were observed and tested from different angles to make the work more meticulous and perfect, thereby enhancing the designer's competitiveness. The use of modeling to participate in the display of the program can enrich the means of display, mobilize the enthusiasm of the visitors, increase the value of the design project, and bring prosperity to the related industries of environmental technology design [8].

2. Three-Dimensional Spatial Data Model Analysis and Point Cloud Data Acquisition and Preprocessing

2.1. Spatial Data Management. In the current three-dimensional GIS field, how to effectively manage three-dimensional spatial data is a difficult problem. Most of the 3D geographic information system data is still managed by design visualization. For the three-dimensional representation of spatial entities, a two-dimensional system is used, and only part of the model basically manages and expresses three-dimensional spatial data in a three-dimensional manner. Comprehensive comparison of the feasible data management methods of 3D GIS can be summarized as the following.

2.1.1. File Method. Texture image data and multimedia data, spatial data, attribute data, etc., are all stored in the file system. The file format is organized by custom developer data, such as Arc/Info, MapInfo, and other software stored in custom files. This management method is easier to understand and implement. If the amount of data is not very large and the data does not include simultaneous operations, etc., it can play an active role in a wide range of data. As the amount of data increases, new forms of data types and data

applications will release new functions to computers. This management method can no longer meet the requirements of spatial data management. It is difficult to integrate geometric data management, data attribution, image texture data, etc., which makes 3D GIS software unsuitable [9].

2.1.2. Relational Database. Even if the existing general commercial relational database is used to manage multiple types of spatial data, there are usually two ways to achieve it: using binary data types, such as BLOB. All geometric objects are considered to have points, and X , Y , and Z of each point are stored as a line. The collection of spatial data is a joint operation. No matter which method is adopted, users must modify the spatial data structure, construct, and manage the corresponding spatial index, and the operation is very complicated. At the same time, in terms of spatial data objects, there is still a big gap between binary and correlation tables [10].

2.1.3. Mixed Management. The original data is still controlled by the two-dimensional GIS, in which the geometric data is controlled by the file system, and the quality data is controlled by the business-related database system. In addition, image files are also included in the data. This control method is very common in 3D architectural images and is usually used to create simple simulated scenes. It is expressed with a new data structure from the two-dimensional geographic information system database, which gives the file a new data structure. The reconstruction method is most suitable for expressing images and data files and then using software to create landscape models. The main disadvantage of this method is the lack of effective integrated data management in 3D data management [11].

2.1.4. Object-Oriented Database. Most object-oriented models are the English expression and control of spatial data. It not only supports records of different lengths but also supports knowledge legacy and nesting. Compared with traditional relational databases, object-oriented spatial database management systems have many advantages, such as allowing users to define objects and the structure and operations of objects; increasing the ability to manage internal dynamic data, data connections, and so on; and supporting complex data types, language compatibility, etc. Other object-oriented library systems have been withdrawn and are not used in GIS. However, with the continuous advancement of its theory and technology, object-based databases can become the main management method of GIS spatial data [12]. The performance comparison of database systems is shown in Table 1.

2.2. Three-Dimensional Spatial Data Acquisition Method. Nowadays, three-dimensional geographic information systems are widely used, such as mountainous areas, oceans, mines, and other fields. This is not much different from a two-dimensional geographic information system. The workload of 3D geographic information system is relatively large, and the costly part is data collection, which is an important part of a smoothly running 3D geographic information system. The 3D city model includes many objects, such as

TABLE 1: To compare the performance of the database system.

Project	Oracle	Sybase	Infomix	DB2	MS SQL server
Ease of operation	Relatively high	High	Generally	Generally	High
Stability	High	High	High	High	Relatively high
Compatibility	High	High	Generally	Generally	High
Speed	Highest	High	High	High	Relatively high
Network performance	Good	Good	Difference	Generally	Good
Performance under massive data	The best	Good	Good	Good	Generally
Spatial database structure	Have	Without	Have	Without	Have
Spatial data indexing speed	High	Without	Generally	Without	Generally
Data security	High	High	Generally	Generally	High
Support three operating systems	Yes	Yes	Yes	Yes	Windows only
Support Chinese	Good	Generally	Good	Good	Good
Windows client	Have	Have	Have	Have	Have
Annotation data interface	ODBC, ADO, OLEDB	ODBC, ADO	ODBC	ODBC	ODBC, ADO, OLEDB

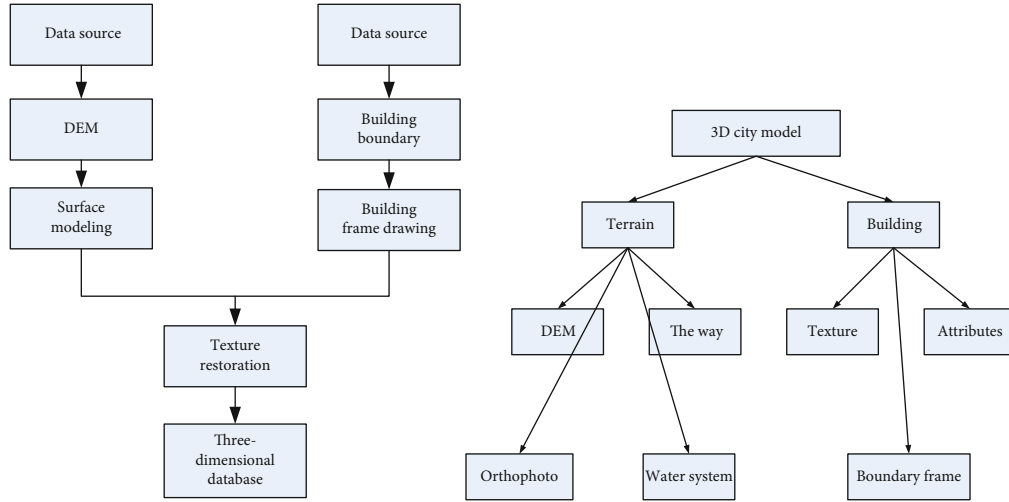


FIGURE 1: The 3D GIS data acquisition process and the 3D city model.

buildings, landscapes, water systems, roads, and plants, but there are two main types of 3D data collection: one is to control the underlying soil trend and soil moisture. Due to the need for in-depth urban management, digital elevation models are usually used to visualize the landscape in 3D GIS and provide users with ground elevation information. The other part is the most important part of the city, and it is often the building that people care about most. The collection methods of these two parts of spatial data are also different, as shown in Figure 1. Surface features such as roads are attached to the terrain DEM for display; shown in Figure 1 is a simple three-dimensional GIS data collection flowchart and three-dimensional city model [13].

2.3. Registration of Point Cloud Data. In the process of Kinect data collection, due to the limitations of the environment and the equipment itself, only the local depth information of the scene can be obtained from one angle. In order to obtain global point cloud data, it is necessary to collect data

on the surface of a certain object model from multiple angles. In order to obtain the complete model surface point cloud data, the point cloud data obtained from different angles should be unified to the camera coordinate system through matrix transformation. This process is called point cloud registration, and finally, these data are merged into one piece to generate the final point cloud model [14].

The relationship between the two sets of point cloud data in different coordinate systems can be represented by a conversion matrix. For a point $X = [x y z]$ in the point cloud, its homogeneous coordinates can be written as

$$X = [xyz]. \quad (1)$$

Given the transformation matrix H , the transformation relationship between the data point X and its corresponding point X' is as follows:

$$X' = HX. \quad (2)$$

Among them, the transformation matrix H can be written as follows:

$$H = \begin{bmatrix} a_{11} & a_{12} & a_{13} & t_x \\ a_{21} & a_{22} & a_{23} & t_y \\ a_{31} & a_{32} & a_{33} & t_z \\ v_x & v_y & v_z & s \end{bmatrix}. \quad (3)$$

H can be abbreviated as follows:

$$H = \begin{bmatrix} A & T \\ V & S \end{bmatrix}. \quad (4)$$

In formula (4),

$$A = \begin{bmatrix} a_{11} & a_{12} & a_{13} \\ a_{21} & a_{22} & a_{23} \\ a_{31} & a_{32} & a_{33} \end{bmatrix} \quad (5)$$

is the rotation transformation matrix, $T = [t_x, t_y, t_z]^T$ is the translation vector, $V = [v_x, v_y, v_z]$, and S are the overall scale factor.

In the process of Kinect obtaining point cloud data, there will be rotation or translation transformations between point cloud data from different perspectives. The matrix transformation here refers to the rigid body transformation; that is, there is no deformation. The problem of point cloud registration is transformed into the point cloud data alignment with the help of translation or rotation transformation of the point cloud data under specific criteria. The Euclidean transformation matrix can be written in the following form:

$$R = \begin{bmatrix} \cos \beta \cos \gamma & \cos \beta \sin \gamma & \sin \beta \\ -\cos \alpha \sin \gamma - \sin \alpha \sin \beta \cos \gamma & \cos \alpha \cos \gamma - \sin \alpha \sin \beta \sin \gamma & \sin \alpha \cos \beta \\ \sin \alpha \sin \gamma - \cos \alpha \sin \beta \cos \gamma & -\sin \alpha \cos \gamma - \cos \alpha \sin \beta \sin \gamma & \cos \alpha \cos \beta \end{bmatrix}. \quad (10)$$

The article is mainly aimed at the registration of rigid objects, so after determining the Euclidean transformation, the above 6 parameters $\alpha, \beta, \gamma, t_x, t_y, t_z$ can be calculated.

2.4. Number of Control Points. According to the transformation formula of formula (2), if several groups of control points in the point cloud data can be found, then the parameters of the rotation matrix H can be calculated. From the formula of the transformation matrix of formula (3), it can be seen that there are 15 degrees of freedom in the formula, and 3 linear formulas can be obtained from a set of corresponding points of the point cloud data in accordance with formula (2):

$$H = \begin{bmatrix} A_{3 \times 3} & T_{3 \times 3} \\ 0_{1 \times 3} & 1 \end{bmatrix}. \quad (6)$$

In the above formula, $A_{3 \times 3}$ is the rotation transformation matrix. When the point cloud rotates by an angle α around the x axis, $Ax(\alpha)$ can be expressed as

$$Ax(\alpha) = \begin{bmatrix} 1 & 0 & 0 \\ 0 & \cos \alpha & \sin \alpha \\ 0 & -\sin \alpha & \cos \alpha \end{bmatrix}. \quad (7)$$

When the angle of rotation around the y axis is β , the rotation matrix $Ay(\beta)$ is

$$Ay(\beta) = \begin{bmatrix} \cos \beta & 0 & \sin \beta \\ 0 & 1 & 0 \\ -\sin \beta & 0 & \cos \beta \end{bmatrix}. \quad (8)$$

When the angle of rotation around the z axis is γ , the rotation matrix $Az(\gamma)$ is

$$Az(\gamma) = \begin{bmatrix} \cos \gamma & \sin \gamma & 0 \\ -\sin \gamma & \cos \gamma & 0 \\ 0 & 0 & 1 \end{bmatrix}. \quad (9)$$

If the point cloud rotates around the $x, y,$ and z axes in turn, the transformation matrix of the point cloud can be expressed as $R = A_x(\alpha)A_y(\beta)A_z(\gamma)$:

$$\begin{bmatrix} x' \\ y' \\ z' \\ 1 \end{bmatrix} = \begin{bmatrix} a_{11} & a_{12} & a_{13} & t_x \\ a_{21} & a_{22} & a_{23} & t_y \\ a_{31} & a_{32} & a_{33} & t_z \\ v_x & v_y & v_z & s \end{bmatrix} \begin{bmatrix} x \\ y \\ z \\ 1 \end{bmatrix}. \quad (11)$$

According to formula (11), to obtain 15 parameters of matrix H , at least 5 sets of corresponding points are needed. Because it is the registration of rigid objects, the coordinate transformation between point clouds is Euclidean transformation, and the transformation relationship is

$$X' = HX \begin{bmatrix} A_{3 \times 3} & T_{3 \times 1} \\ 0_{1 \times 3} & 1 \end{bmatrix}_{4 \times 4} X. \quad (12)$$

It can be seen from formula (12) that at least three sets of control points are needed to find the unique solution of the six parameters of matrix H , but the three sets of corresponding points must not be collinear. Therefore, in order to achieve the registration of point cloud data, it is necessary to find at least three pairs of corresponding points from the point clouds obtained from different angles, which is the key to obtaining the transformation matrix.

2.5. Transformation Matrix Solution. Changing the coordinate transformation of the point cloud data into a nonhomogeneous way, then formula (12) becomes

$$X' = R_{3 \times 3}X + T_{3 \times 1}. \quad (13)$$

In order to eliminate the influence of nonlinear formulas, it is necessary to transform the nonlinear formula system into a linear formula system; then, the Euclidean transformation relationship of the coordinates of the space point becomes

$$\begin{bmatrix} x'_i \\ y'_i \\ z'_i \end{bmatrix} = \begin{bmatrix} a_{11} & a_{12} & a_{13} \\ a_{21} & a_{22} & a_{23} \\ a_{31} & a_{32} & a_{33} \end{bmatrix} \begin{bmatrix} x_i \\ y_i \\ z_i \end{bmatrix} + \begin{bmatrix} t_x \\ t_y \\ t_z \end{bmatrix}. \quad (14)$$

It can be seen from the above formula that to obtain the rotation matrix A and the translation vector T in the above formula, it is necessary to find at least 4 sets of corresponding points. If the angle of rotation between the two point clouds is small, then the matrix of its rotation around the x , y , and z axes can be written as

$$A_x(\alpha) = \begin{bmatrix} 1 & 0 & 0 \\ 0 & 1 & \alpha \\ 0 & -\alpha & 0 \end{bmatrix} A_y(\beta) = \begin{bmatrix} 1 & 0 & \beta \\ 0 & 1 & 0 \\ -\beta & 0 & 1 \end{bmatrix} A_z(\gamma) = \begin{bmatrix} 1 & \gamma & 0 \\ -\gamma & 1 & 0 \\ 0 & 0 & 1 \end{bmatrix}. \quad (15)$$

Therefore, the rotation transformation formula of formula (10) can be changed to

$$R_{3 \times 3} = \begin{bmatrix} 1 & \gamma & \beta \\ -\gamma & 1 & \alpha \\ -\beta & -\alpha & 1 \end{bmatrix}. \quad (16)$$

Then, the Euclidean transformation relation of formula (13) can be written as

$$\begin{bmatrix} x'_i \\ y'_i \\ z'_i \end{bmatrix} = \begin{bmatrix} 1 & \gamma & \beta \\ -\gamma & 1 & \alpha \\ -\beta & -\alpha & 1 \end{bmatrix} \begin{bmatrix} x_i \\ y_i \\ z_i \end{bmatrix} + \begin{bmatrix} t_x \\ t_y \\ t_z \end{bmatrix}. \quad (17)$$

Therefore, the above formula can approximate the 6 parameters of the transformation matrix through 2 sets of control points: $\alpha, \beta, \gamma, t_x, t_y, t_z$. Since the corresponding points between the two-point cloud sets we get are not particularly accurate, there will be errors when the transformation matrix is solved by the least-point linear solution. In order to reduce this error, it is usually necessary to find as many control points as possible to limit this conversion relationship, so as to better solve the transformation matrix.

2.6. Objective Function. If N sets of corresponding point pairs are obtained from two sets of point cloud data obtained from different perspectives, the two sets of corresponding points are represented as $Q = \{Q_1, Q_2, Q_3, \dots, Q_N\}$. The transformation matrix between the point cloud data is solved by the relationship between the corresponding point sets, that is, the European transformation matrix H described above, so that the two sets of point sets undergo coordinate transformation, and the registration error between the point sets is minimized. Assuming that the mean square error between the two sets of corresponding points P and Q is $f(H)$, then the problem of solving the nonlinear formula system is transformed into solving the transformation matrix H that minimizes the value of the objective function $f(H)$.

$f(H)$ is what we call the objective function. The objective function has many forms. According to different error measurement requirements, the solution of $f(H)$ is also different. The common forms are as follows.

The distance from point to point and

$$f(H) = f(R, T) = \sum_{i=1}^N Q_i - RP_i - T_2. \quad (18)$$

The sum of squared distances from point to point:

$$f(H) = f(R, T) = \sum_{i=1}^N Q_i - RP_i - T_2^2. \quad (19)$$

Normalized sum of squared point-to-point distances:

$$f(H) = f(R, T) = \frac{1}{N} \sum_{i=1}^N Q_i - RP_i - T_2^2. \quad (20)$$

Point-to-surface distance and

$$f(H) = f(R, T) = \sum_{i=1}^N n_i^T (Q_i - RP_i - T)_2. \quad (21)$$

Among them, n_i represents the unit normal vector of Q_i surface.

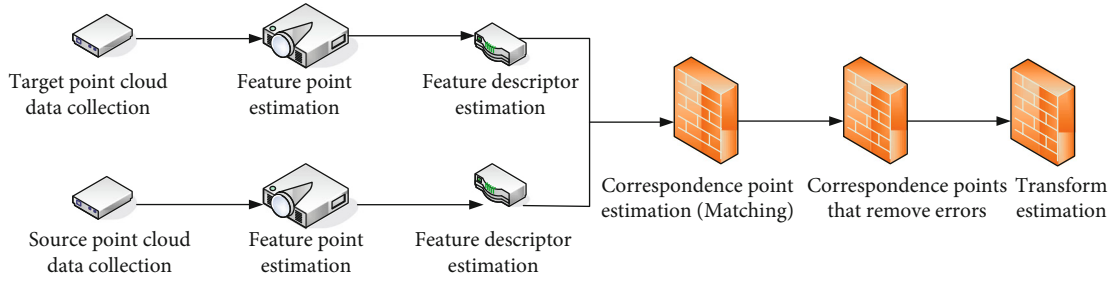


FIGURE 2: Block diagram of the point cloud data coarse registration process.

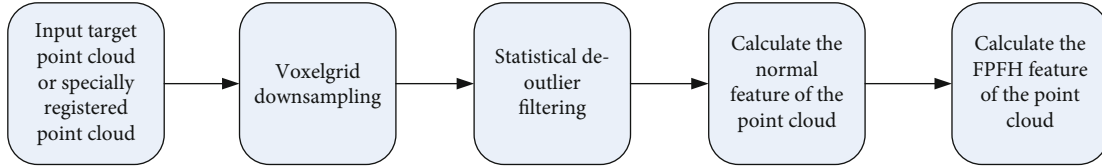


FIGURE 3: Schematic diagram of FPFH calculation process.

2.7. Initial Registration Based on Sampling Consensus Algorithm. The purpose of the initial registration is to estimate the initial transformation parameters between the point clouds under different viewing angles, make them initially aligned, and provide a good initial value for the ICP fine registration. In this paper, the sampling consistent initial registration algorithm (SAC-IA) is used. The main principle is to first calculate the normal of the surface and then estimate the fast point feature histogram (FPFH) descriptor of the surface. Then, according to the feature descriptors, the feature matching and the selection of matching points are performed, so that the transformation parameters between the point cloud data can be obtained quickly and more accurately. The initial registration process of point cloud data is shown in Figure 2.

To achieve SAC-IA registration, first, we need to estimate the fast point feature histogram (FPFH) of the point cloud surface. On the premise of not affecting the detailed features of the point cloud surface, in order to reduce the amount of calculation, the data needs to be processed by downsampling and filtering. Figure 3 shows the flow chart of extracting FPFH descriptors.

The normal vector is an important attribute of the geometric surface, and many operations on the point cloud data will use the normal vector information. For example, when lighting and rendering the surface of a point cloud model, the normal information of the point cloud surface is required to produce an effect that conforms to people's visual habits. The calculation methods of the surface normal of point cloud data are roughly divided into two types: the first one is to reconstruct the surface mesh of the collected point cloud data and then to solve the surface normal vector according to the reconstructed surface. Since the surface global meshing needs to be performed first, the solution of the normal vector will become more complicated; the second method does not need to perform surface meshing on the point cloud data but directly estimates its surface based on the point cloud data. For the normal vector, the latter

method is adopted here. The normal vector approximation of a certain point on the surface can be replaced by the normal of the tangent plane of the surface at this point, which becomes the problem of least squares plane fitting estimation. The least squares method is an optimization algorithm whose purpose is to minimize the mean squared error between the objective function and the data to be measured. Therefore, the normal vector of the estimated surface can be transformed into the eigenvectors and eigenvalues of the covariance matrix between a point on the surface and its neighboring points.

On the basis of Kinect-based 3D reconstruction research, using PCL point cloud library and OpenNI framework, programming in VC++, design a 3D reconstruction system. The system can realize the rapid reconstruction of simple, small-scale scenes. The system is divided into several functional modules. The main functional modules are shown in Figure 4.

The specific functions of each module are as follows:

- (1) *Image Information Acquisition Module.* After Kinect obtains the depth image, it is read into the computer memory through the OpenNI interface and then copied to the video memory.
- (2) *Preprocessing Module.* This module filters the original depth image. The calculation process of each point in the filtering process is independent of the calculation process of other points, and the GPU can be used for parallel calculation. The implementation code of preprocessing is written as a CUDA Kernel function, and each thread calls the Kernel function to process a pixel
- (3) *Point Cloud Computing Module.* First, the module calculates the three-dimensional coordinates of each point according to the depth image collected. The three-dimensional coordinate calculation process of each point has no dependence on the coordinate

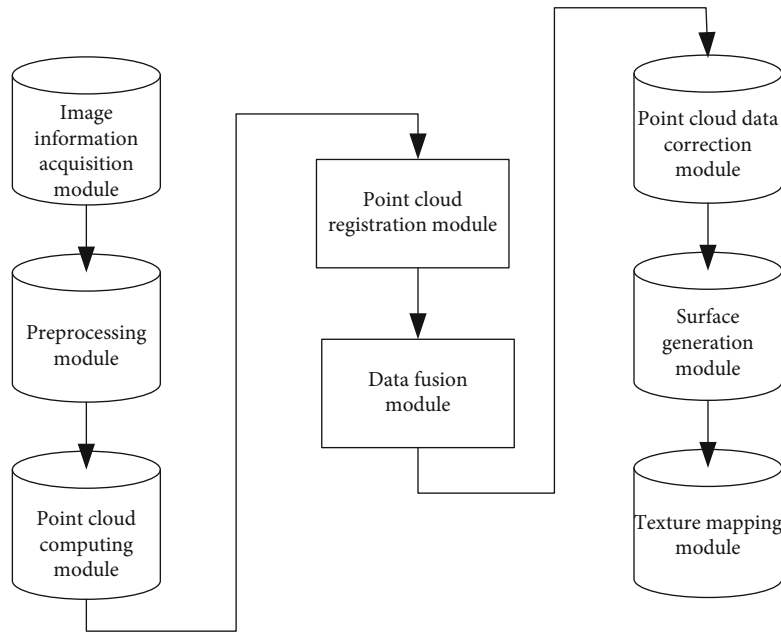


FIGURE 4: Function module diagram.

calculation results of other points, and the GPU can be used for parallel calculation. The code for calculating the coordinates is written into the Kernel function, and each thread calls the Kernel function to calculate the three-dimensional coordinates of a point. Then, the module calculates the normal vector of each point according to the coordinate data. The normal vector calculation process of each point does not depend on the normal vector calculation results of other points. The GPU can be used for parallel calculation, and the normal vector calculation code is written as a Kernel function. Each thread calls the Kernel function to calculate the normal vector of a point.

- (4) *Point Cloud Registration Module*. Firstly, find the corresponding point pair between the point cloud of the current frame and the point cloud of the previous frame, and construct the equation. In this step, GPU parallel computing can be used, and the code for finding corresponding points is written as a Kernel function, and each thread is responsible for finding the corresponding point of a point in the point cloud of the current frame in the point cloud of the previous frame. After constructing the equation, the coefficient matrix of the equation is copied back to the memory, and the transformation parameters are solved in the CPU.

The program module diagram of the 3D reconstruction system is shown in Figure 5.

As shown in Figure 5, the CPU is mainly responsible for the main process of executing the program and the serial calculation part, and the GPU is mainly responsible for parallel acceleration operations. In the process from point cloud pre-

processing to data correction, GPU participates. The parallel computing of GPU can increase the speed of data calculation, so as to meet the real-time requirements of model reconstruction.

3. Workflow of Residential Environment Art Design Modeling

The current mainstream development technology of 3D models has two categories, one is to model stereo images through high-precision aerial photography, and the other is to model stereo images based on low-altitude oblique photography. In order to save costs, considering the existing high-precision aerial photography and 1:500 topographic map data, the project adopts the first method [15]. The main workflow is shown in Figure 6.

The detailed workflow is shown in Figure 7.

3.1. Building Element Modeling. The three standard accuracies of low, medium, and high modeling accuracy of objects are 1 meter, 0.8 meters, and 0.5 meters, respectively.

In the process of community modeling, building model modeling is an indispensable part. The architectural model is between the plan view and the actual three-dimensional space, which closely connects the two to form a three-dimensional model. Building modeling can intuitively reflect the design intent for customers' reference and make up for the limitations of drawings in performance. It is not only a form of design but also a link in the designer's design process, and it is widely used in real estate development, urban construction, design bidding, commercial housing sales, and investment cooperation. The building element model includes the following:

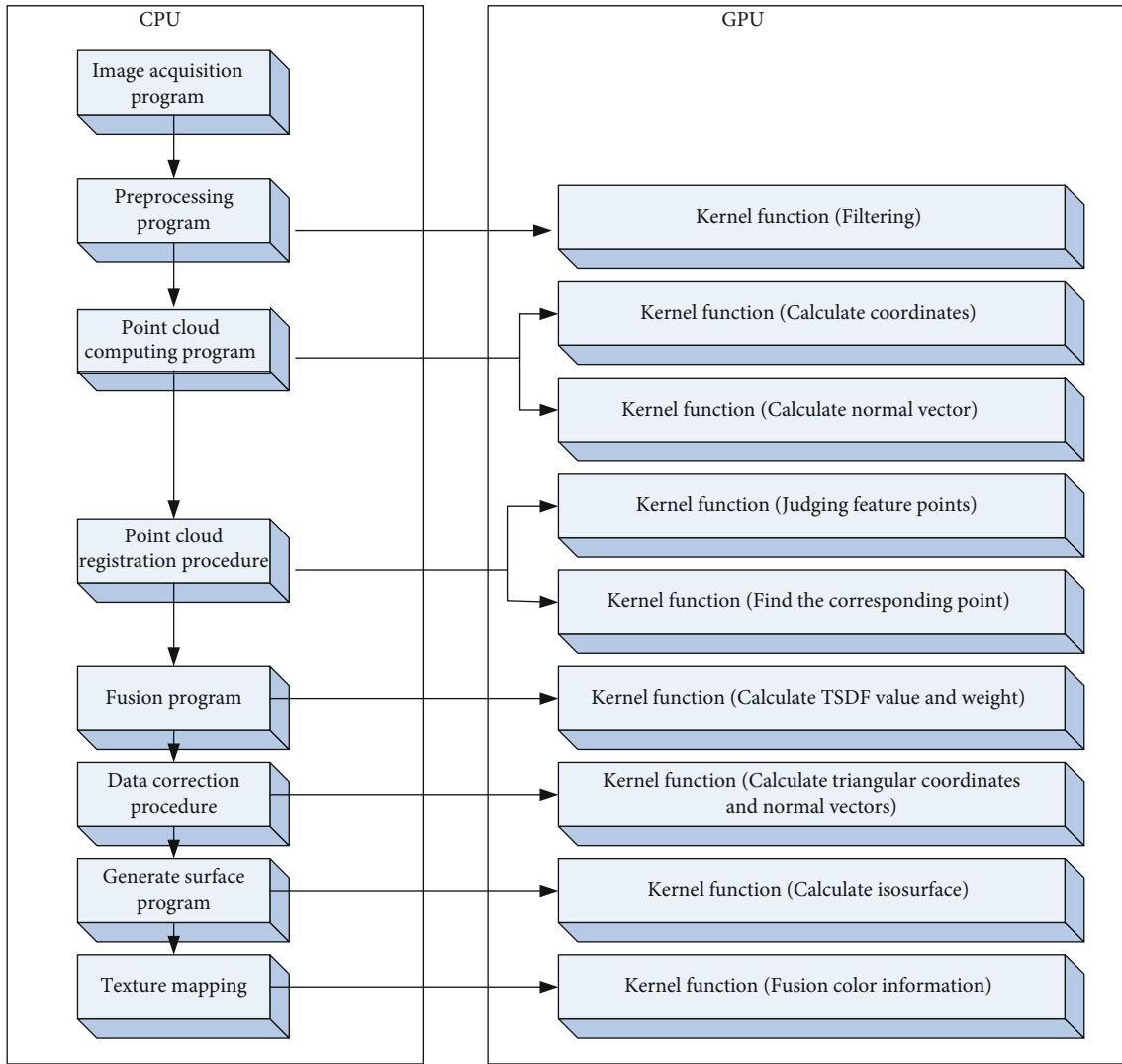


FIGURE 5: Program module.

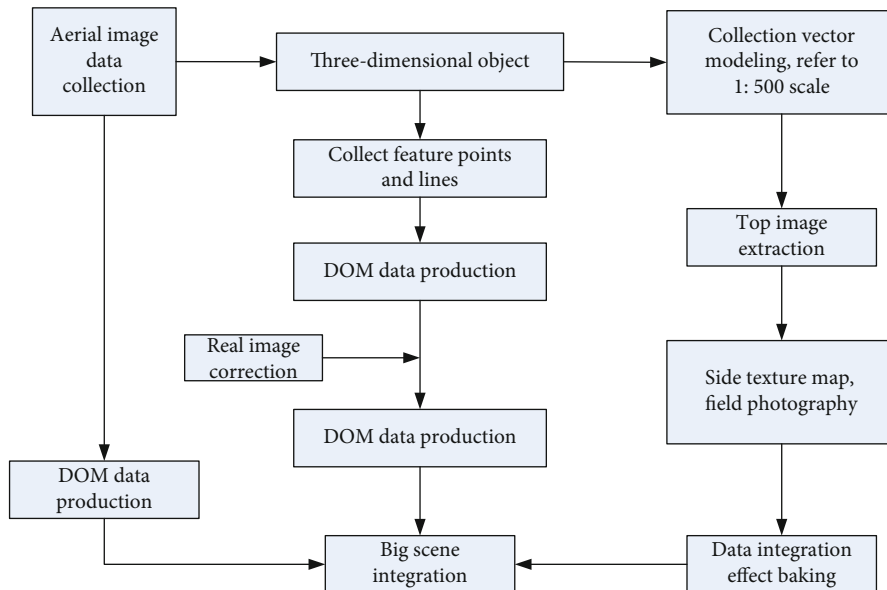


FIGURE 6: Workflow chart.

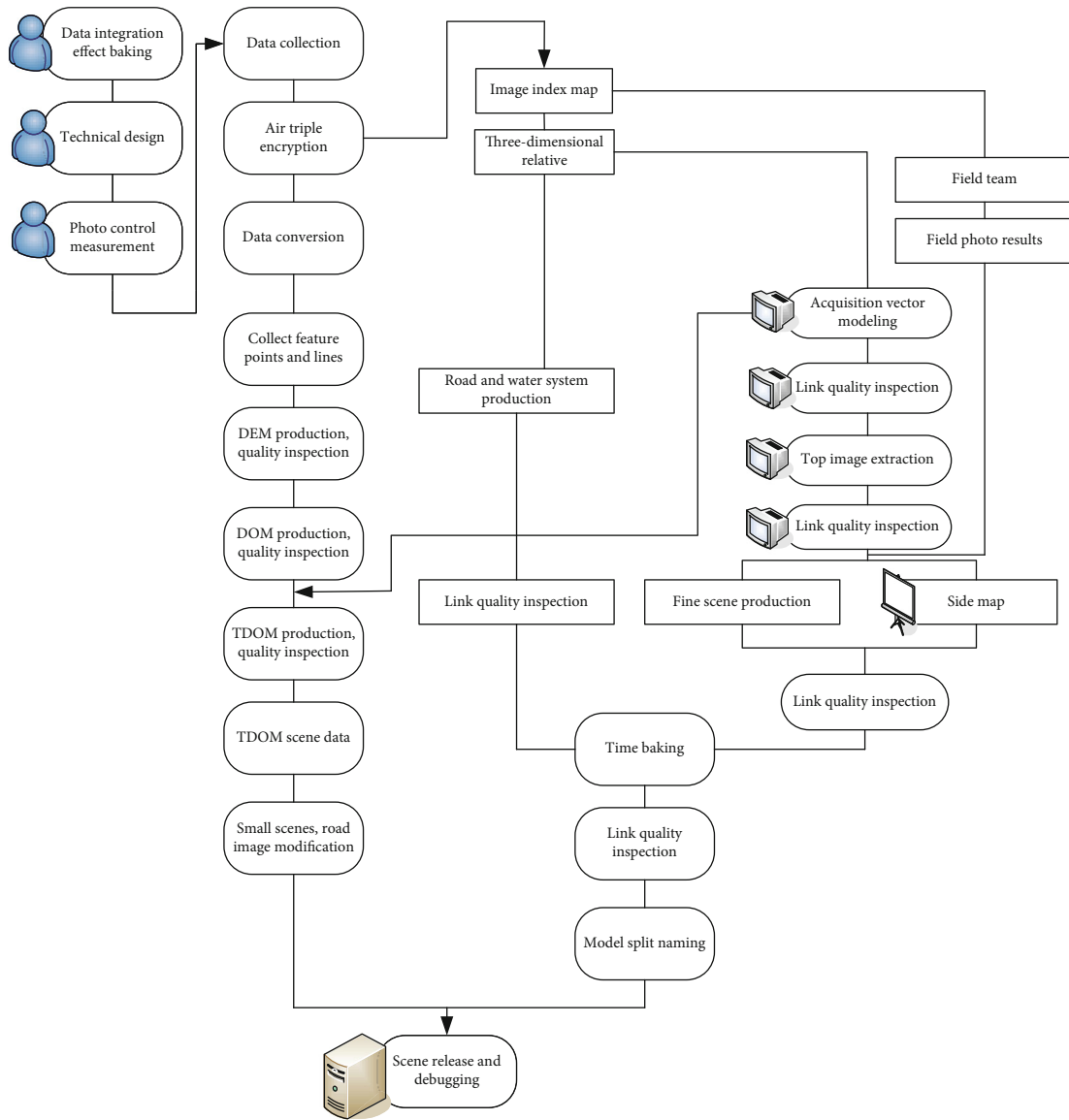


FIGURE 7: The detailed workflow chart.

Building: according to the complexity of the building, location distribution characteristics, and shape, it is divided into the following aspects:

- (1) Simple independent buildings
- (2) Multistorey buildings: this type of building is higher than all types of buildings
- (3) Auxiliary building: it must be determined that it is a building and that it is connected to the main building. There are two situations, one is that both sides are connected to other buildings, and the other is that one side is connected to the main building
- (4) Inner courtyard: it is divided into complex inner courtyard and simple inner courtyard. The complex inner courtyard refers to the open space enclosed by various eaves; the simple inner courtyard refers

to the open space in the flat roof house. Figure 8 shows the accuracy and quantity of buildings and roads

For the model that reflects the modeling object, any size changes such as length, width, height, and other details should not be less than 50 cm. Individual iconic antique buildings should reflect the size change details not less than 20 cm, such as changing the corners of the building's appearance, eaves shapes, door frame styles, windows and balconies, etc. The building model modeling method must meet the following requirements:

Building model production regulations: it is suitable to use technical means such as photogrammetry, laser scanning, or interactive CAD to obtain geometric information, add different types of geometric textures according to its modeling level, and then perform geometric modeling.

Building models must meet the following requirements:

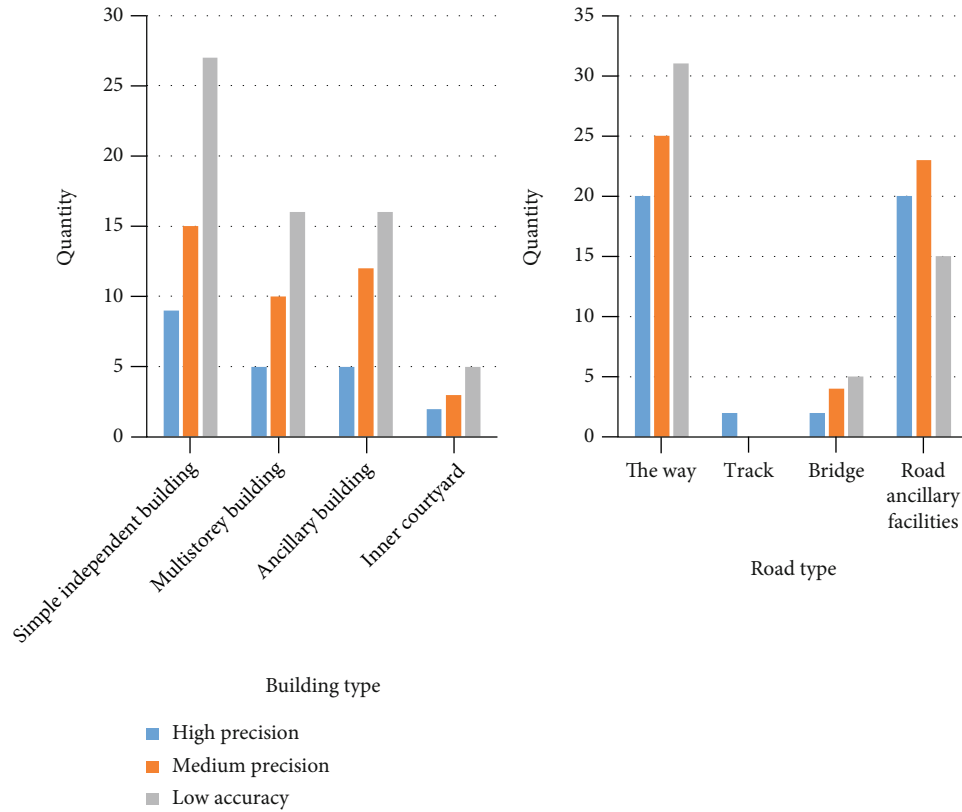


FIGURE 8: Accuracy and quantity of buildings and roads.

- (1) The model should be made according to the architectural design data or the measurement structure of fine instruments
- (2) The roof of the model should reflect details such as accessory equipment and roof structure
- (3) The height accuracy of the model should be better than 1 meter
- (4) The base of the model should be consistent with the topography and be on the same level as the topography
- (5) For more complex buildings whose main body includes a variety of other types of buildings, it can be divided into different types of buildings first and then modeling
- (6) The texture used in the model should be consistent with the appearance of the building; reflect the transparency, color, image, etc., that meet the actual situation; and distinguish the different textures of wood, glass, bricks, etc. Except for the objects modeled in the texture image, there should not be any objects. The changing details of the roof and the facade of the object should be clearly visible
- (7) The complex buildings, arcs, spheres, or folded surfaces whose main body contains a variety of geometric shapes should reflect the main geometric characteristics of the building
- (8) The model should truly reflect the appearance details of the model object. All types of accessory equipment, windows, balconies, and billboards must be clearly marked on the side, and the side contour line should reflect the details of the change on the model. When walking along the modeled object, it can clearly observe every detail of the modeled object, and the original object is consistent with the model [16]. The accuracy of the model in the construction elements should meet the requirements of Table 2

Under normal circumstances, the terrain planning is mostly a large area, which can be a large area of community or the terrain of schools, factories, and so on. Due to the large area of planning terrain, when creating the model, the strict modeling idea is first determined; otherwise, some structures will be missed in the modeling process. The general planning type of terrain contains many different structures, and the model is established according to a certain order of modeling, so as not to miss the actual needs of any structure in the production process. Here, from low to high, the height of the bottom of the model is created in order of space. These models include the underground garage, the surface (including the entrance to the underground cavity that needs to be reserved), the underground garage and the water surface, sidewalks and urban green space, roads and various shops, some steep slopes or steps that vary widely (including pavilions), equipment such as water dock areas, platforms and ramps in places, sports venues, and paving within the community. The modeling

TABLE 2: Model accuracy performance of building elements.

Content	First level	Level 2	Level 3	Level 4	Quantity
Roof	Subject modeling effect	Detailed modeling effect	Subject modeling effect	Subject modeling effect	55
Underwear structure	Subject modeling effect	Detailed modeling effect	No need to show	Subject modeling effect	25
Eaves	Subject modeling effect	Detailed modeling effect	No need to show	No need to show	45
Parapet	Subject modeling effect	Detailed modeling effect	No need to show	Subject modeling effect	14
Open balcony	Subject modeling effect	Detailed modeling effect	No need to show	Subject modeling effect	88
Important roof decoration	Subject modeling effect	Detailed modeling effect	No need to show	No need to show	52
Building	Detailed modeling effect	Detailed modeling effect	Subject modeling effect	Subject modeling effect	75
Large steps	Subject modeling effect	Detailed modeling effect	No need to show	Subject modeling effect	53
Eaves	More than 1 meter detailed modeling effect	More than 0.5 meters detailed modeling effect	No need to show	Subject modeling effect	78
Water tank	Symbolic effect	Subject modeling effect	No need to show	Symbolic effect	41
Queti	Symbolic effect	Subject modeling effect	No need to show	No need to show	14
Bottom quotient	Subject modeling effect	Detailed modeling effect	No need to show	No need to show	5
Porch	Subject modeling effect	Detailed modeling effect	No need to show	Subject modeling effect	41
Ordinary steps	Subject modeling effect	Subject modeling effect	No need to show	No need to show	25
Launch tower	Symbolic effect	Subject modeling effect	No need to show	No need to show	25
Pillar (pier)	Subject modeling effect	Detailed modeling effect	No need to show	Subject modeling effect	4
Facade protrusions or important decorations	More than 1 meter detailed modeling effect	More than 0.5 meters detailed modeling effect	No need to show	Subject modeling effect	75
Flagpole	Symbolic effect	Subject modeling effect	No need to show	No need to show	23
Skylight	Subject modeling effect	Subject modeling effect	No need to show	Subject modeling effect	53
Kiss beast	Symbolic effect	Subject modeling effect	No need to show	No need to show	69
Outdoor stairs	Subject modeling effect	Detailed modeling effect	No need to show	Subject modeling effect	87
General population	Subject modeling effect	Detailed modeling effect	No need to show	Subject modeling effect	53
Door decorations	Symbolic effect	Subject modeling effect	No need to show	No need to show	12
Chimney	Symbolic effect	Subject modeling effect	No need to show	No need to show	36
Hanging corridor	Subject modeling effect	Detailed modeling effect	No need to show	Subject modeling effect	58
Unit inscription	Symbolic effect	Subject modeling effect	No need to show	No need to show	78

method of the extrusion modifier is used to extract line segments using CAD drawings and add closed lines to make terrain models, which greatly improves the efficiency of use. The extraction of lines and closed lines requires care and patience to successfully complete the modeling of the cells.

Other special requirements: all buildings should be based on the height of the parapet wall. Sidewalks, small bridges, and barns do not need to be collected in the construction area. For the roof decoration, the geometric shape must be modeled on the highest side not less than 2 meters, or the projection surface is not less than 2 square meters. Collect basic houses with building height not less than 2 meters and not less than 2.5 square meters and houses higher than 2 meters and longer than 2.5 square meters. When the length of the structure is too large, it should be divided accordingly. The height of the building usually exceeds 60 meters. In the case of maintaining the appearance of the original house, the height difference shall not exceed 0.5 meters, and the horizontal angle and the house with a level of not more than 0.5 meters can be assembled appropriately according to the situation. Modeling areas of level 4 do not need to model fences and walls. Modeling areas above level 3 should model fences and walls. For shopping malls, enterprises and institutions, government schools, hospitals, high-end residential buildings, and other buildings along both sides of the street, where the height of the parapet wall is not less than 0.5 meters and the width is not less than 0.5 meters, it should be reflected separately. There are parapets on the roof, and in a residential area, the height of the parapets is the standard. For shopping malls, enterprises and institutions, government schools, hospitals, high-end residences, and industrial and mining buildings along both sides of the street, where the height of the parapet is not less than 1.5 meters, except for billboards, the parapet needs to be reflected separately. The parapet wall always needs to be in the form of the house on top of the house, except for the iron fence [17].

3.2. Modeling of Traffic Elements. The community adopts a loop-through road layout. Cars and pedestrians are unblocked, and the arterial roads are clearly demarcated. The road from east to west is a main road in the community, integrating landscape and arterial traffic. Other community-level roads are clearly divided into groups and connected to main roads. Community-level roads have various forms, some of which are responsible for greening or parking. Road modeling can make it more convenient and accurate for customers to see the internal structure of the community on the map, bringing more convenience to customers. Modeling of traffic elements includes the following main contents [18].

- (1) Roads, including urban roads, intercity highways, and rural roads
- (2) Rail transit on the ground, including light rail and railway
- (3) Bridges, including pedestrian bridges, vehicle bridges, and viaducts

- (4) Road ancillary facilities, including roadsides, road traffic signs and markings, fences and vegetation isolation belts, etc.

The modeling method of the traffic element model should meet the following requirements:

- (1) The base of the model should be on the same level as the terrain position and should be consistent with the terrain undulations
- (2) It should accurately reflect the structural characteristics of traffic facilities and auxiliary facilities. Structural features with any dimensional change of more than 1 meter should be 3D geometric modeling
- (3) The texture should have clear details and accurately reflect the material characteristics of the modeled object. The difference and separation between different materials or paving forms should be clearly reflected
- (4) The linear model of the road and its ancillary facilities should be drawn based on the road centerline in the topographical map and should be consistent with the road centerline. The curved line sections can be smoothly processed
- (5) The base contour line should be consistent with the topographical map or design drawing. The curved line can be smoothly processed, and the height of the model can be measured on-site or interpreted by on-site photos

The accuracy of the traffic element model should meet the requirements of Table 3.

3.3. Modeling of Vegetation Elements. Although flowers and trees are not the main buildings in the three-dimensional geographic information system of the community, they play an irreplaceable role in the simulation of the community. There are two types of vegetation models: one is lawn-like area vegetation; the other is flower, wood grain, and other point models. The vegetation element model includes the following main contents: street trees and green spaces planted in rows on both sides of the road and landscape plants grown in communities, parks, and courtyards [19]. Figure 9 shows the relationship between the calculation speed and the number of vegetation. When the number of calculation speeds of the point model is small, the calculation speed is 218k/s, while the running speed of lawn-like vegetation is stable at 100-200k/s. The relationship between the number of parts and the speed is mainly evaluated for water objects and buildings in the modeling software.

The modeling method of vegetation elements should meet the following requirements:

One or several methods of CAD, fractal, and other modeling techniques can be used to model.

For example, the process of CAD modeling is as follows:

- (1) Data processing, including field data collection, standard texture production, data distribution, etc.

TABLE 3: Traffic factor model precision performance grading.

Content	First level	Level 2	Level 3	Level 4	Quantity
Road barrier	Terrain effect or no performance	Subject modeling effect	Detailed modeling effect	Main body modeling effect or terrain effect	25
Roadbed	Terrain effect or no performance	Main body modeling effect or terrain effect	Main body modeling effect or terrain effect	Main body modeling effect or terrain effect	42
Road noise barrier	No need to show	Subject modeling effect	Subject modeling effect	No need to show	42
Sidewalk	Terrain effect or no performance	Subject modeling effect	Detailed modeling effect	Subject modeling effect	52
Ground road	Main body modeling effect or terrain performance	Main body modeling effect or terrain performance	Detailed modeling effect or terrain effect	Main body modeling effect or terrain performance	34
Road traffic marking	No need to show	Main body modeling effect or terrain performance	Detailed modeling effect	Terrain effect or no performance	19
Road, railway tunnel	No need to show	Subject modeling effect	Detailed modeling effect	No need to show	25
Vehicle bridge	Symbolic effect	Subject modeling effect	Detailed modeling effect	Subject modeling effect	86
Bus station	No need to show	Symbolic effect	Detailed modeling effect	Terrain effect or no performance	38
Train platform	Terrain effect or no performance	Subject modeling effect	Detailed modeling effect	Main body modeling effect or terrain effect	72
Footbridge	Symbolic effect	Subject modeling effect	Detailed modeling effect	Subject modeling effect	25
Rail	Terrain effect or no performance	Main body modeling effect or terrain effect	Main body modeling effect or terrain effect	Main body modeling effect or terrain effect	42
High-speed road	Symbolic effect	Subject modeling effect	Detailed modeling effect	Subject modeling effect	24
Overpass	Symbolic effect	Subject modeling effect	Detailed modeling effect	Subject modeling effect	53
Round the island	No need to show	Subject modeling effect	Subject modeling effect	Symbolic effect	25
Traffic barrier	No need to show	Subject modeling effect	Subject modeling effect	Subject modeling effect	42

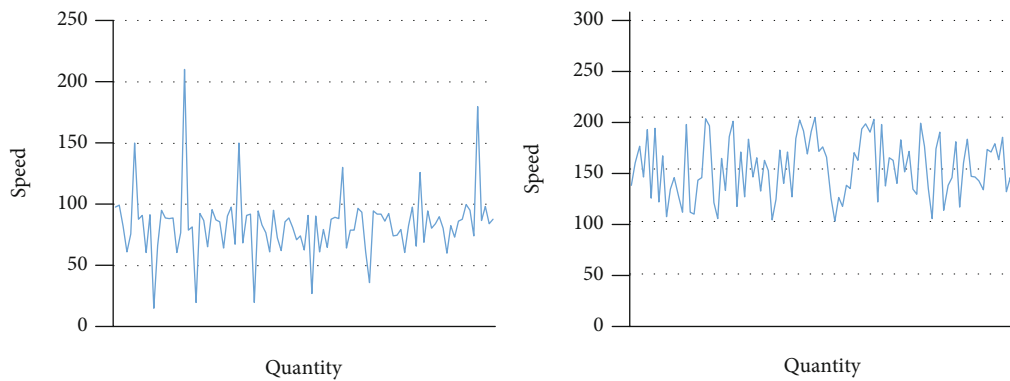


FIGURE 9: The relationship between computing speed and quantity.

- (2) Field research and data collection, collecting information such as shape, location, tree species, distribution, tree height, color, etc.
- (3) Optimization of plant element model data; according to performance and application requirements, the model

- is optimized by reducing the number of geometric faces in the model and reducing the texture resolution
- (4) The model is made to make the model equivalent to the level according to performance requirements and site survey conditions

TABLE 4: Vegetation factor model precision performance grading.

Content	First level	Level 2	Level 3	Level 4	Quantity
Greenbelt fence	Symbolic effect	Subject modeling effect	No need to show	No need to show	54
Flower garden	Main body modeling effect or terrain effect	Subject modeling effect	No need to show	Terrain effect or no performance	24
Hedgerow	Main body modeling effect or terrain effect	Subject modeling effect	No need to show	Terrain effect or no performance	14
Nursery	Main body modeling effect or terrain effect	Main body modeling effect or terrain effect	Terrain effect or no performance	Terrain effect or no performance	55
Grassland	Main body modeling effect or terrain effect	Main body modeling effect or terrain effect	Terrain effect or no performance	Main body modeling effect or terrain effect	35
Forest	Symbolic effect or terrain effect	Symbolic effect	No need to show	Terrain effect or no performance	85
Tree protection facilities	Symbolic effect	Subject modeling effect	No need to show	No need to show	54
Greenbelt fence	Symbolic effect	Subject modeling effect	No need to show	No need to show	42
Flower stand	Symbolic effect	Subject modeling effect	No need to show	No need to show	35
Striped greening tree	Symbolic effect	Subject modeling effect	No need to show	Terrain effect or no performance	23



FIGURE 10: Hydrological model.

The modeling plant element model must meet the following requirements:

- (1) The geographic location of plants should be based on topographic maps or DOMs at scales such as 1 : 500, 1 : 1000, and 1 : 2000
- (2) The texture must be true and accurate, can reflect the texture, pattern, and color of each component part of the plant and be clearly distinguishable
- (3) Realizing the fine modeling effects of specific modeling such as landscape plants, small landscapes, cultural relics, and tree species
- (4) It is suitable for the complete element modeling of branches, leaves, and trunks and the modeling of plant elements. It can use wooden models or can use fractal techniques in architecture
- (5) The collocation and positioning of landscape plants must conform to reality

The model accuracy of vegetation elements should meet the requirements of Table 4.

3.4. Water System Element Modeling. The water system is an important part of physical geography, and it is of great significance to hydrological research. Under natural conditions, water flows to low places; the initial distribution of the water system can be obtained from the water flow lines in digital topographic maps or other graphics. The water system component model mainly includes rivers, water surfaces, river banks, small bridges, and guardrails. The content is shown in Figure 10 [20].

The modeling method of the water system element model should meet the following requirements:

- (1) The water system element model can be made according to the centerline of the water system in the topographic map, and the curved water system can be smoothly processed. One or several other methods of CAD and other modeling techniques can also be used for modeling
- (2) The water system and its auxiliary facilities must have modeling performance
- (3) The water surface can be represented or modeled by terrain as required, and the water surface texture can

TABLE 5: Hydrological model precision performance grading.

Content	First level	Level 2	Level 3	Level 4	Quantity
Embankment	Main body modeling effect or terrain effect	Terrain effect or no performance	Main body modeling effect or terrain effect	Main body modeling effect or terrain effect	52
Bed	Main body modeling effect or terrain effect	No need to show	Main body modeling effect or terrain effect	The effect of the terrain or no performance	41
Reef	Symbolic effect	No need to show	Main body modeling effect or terrain effect	The effect of the terrain or no performance	25
Breakwater	Main body modeling effect or terrain effect	Terrain effect or no performance	Main body modeling effect or terrain effect	Main body modeling effect or terrain effect	36
Boiled terrier	The modeling effect of the subject	No need to show	The modeling effect of the subject	The modeling effect of the subject	29
Water surface	Main body modeling effect or terrain effect	Terrain effect or no performance	Main body modeling effect or terrain effect	Main body modeling effect or terrain effect	42
Guardrail	The modeling effect of the subject	No need to show	Detailed modeling effect	No need to show	53
Hydrophilic step	The modeling effect of the subject	Terrain effect or no performance	Detailed modeling effect	Terrain effect or no performance	25
Pier	Main body modeling effect or terrain effect	Terrain effect or no performance	Main body modeling effect or terrain effect	Main body modeling effect or terrain effect	45
Sluice	The modeling effect of the subject	Terrain effect or no performance	The modeling effect of the subject	Symbolic effect	39
Flood wall	The modeling effect of the subject	No need to show	The modeling effect of the subject	The modeling effect of the subject	42
Dam	The modeling effect of the subject	No need to show	The modeling effect of the subject	The modeling effect of the subject	32
Parking lot	Main body modeling effect or terrain effect	Terrain effect or no performance	Main body modeling effect or terrain effect	Main body modeling effect or terrain effect	53
Hydrophilic platform	The modeling effect of the subject	Terrain effect or no performance	Detailed modeling effect	Main body modeling effect or terrain effect	23
Tidal flat	Main body modeling effect or terrain effect	No need to show	Main body modeling effect or terrain effect	Terrain effect or no performance	11

be represented as dynamic, static animation effects, or translucent effects according to its specific needs

- (4) When modeling auxiliary facilities such as flood walls, guardrails, and river banks, in order to match the display effect of the three-dimensional scene, the DEM should be changed to match the three-dimensional model
- (5) The geographic location of the water system and its ancillary facilities should be based on a topographic map with a scale of 1:2000 or above and can also be determined based on the DOM. The water depth should be interpreted and extracted based on the DEM model, the images obtained by aerial photography, or on-site surveys [21]

The accuracy of the water system element model should meet the requirements of Table 5. Figure 11 shows the relationship between the number and accuracy of water system elements.

The category of visualization technology discussed in this article is to express the indicated cell in the form of a graph or image. In fact, for a large area of the cell model, if an image

is used to express, it is difficult to grasp the layout of tall buildings without specific houses, and if the community model is divided into small units, although it reflects the local topography, it is difficult to grasp the overall situation. A better solution is to use computer animation technology to enable people to swim in the real environment, so as to understand the community environment from both the whole and the local aspects. The so-called animation is actually to release a group of continuous images at a fast enough speed to give people a feeling of continuous movement. That is to say, to form an animation, it is necessary to generate a sequence of consecutive patterns in advance, play them continuously when needed, and store the pattern in the computer. At present, according to the difference between the storage and the hour of each frame, the animation technology is divided into two types: frame animation and graphic array animation. Each image is just a full-screen graphic of a box, saving more memory and getting faster runtime performance.

4. Discussion

The scope of the visualization technology discussed above is to express the cell that is about to be represented in the form

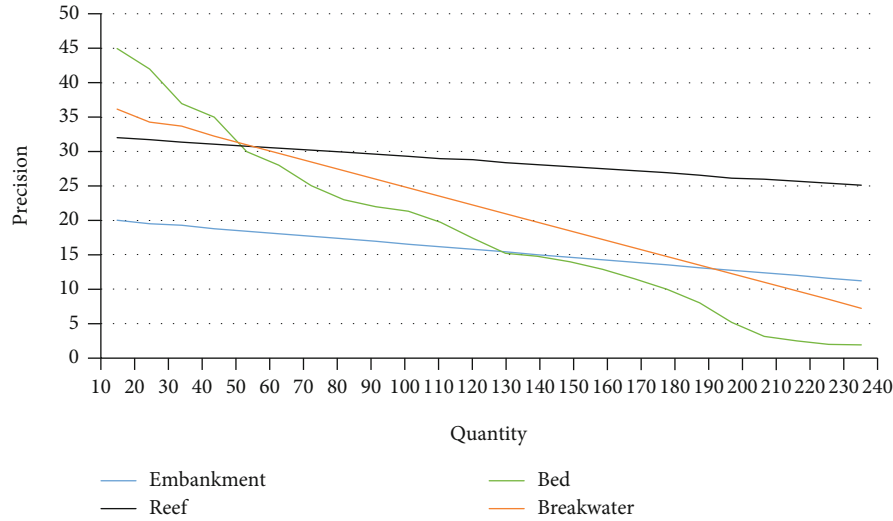


FIGURE 11: The relationship between quantity and accuracy.

of a graph or image. In fact, for a large-area cell model, if using an image to express, it can only see the high-rise buildings but not the specific houses, and it is difficult to grasp the layout. If the community model is divided into small units, it is difficult to grasp the overall situation although it reflects the local terrain. A better solution is to use computer animation technology to enable people to swim in the real environment, so as to understand the community environment from both the overall and the local aspects. The so-called animation is actually to release a group of continuous images at a fast enough speed to give people a feeling of continuous movement. That is to say, in order to form an animation, it is necessary to generate a set of continuous code sequences in advance, play them continuously when needed, and store the graphics in the computer. At present, according to the difference between the storage and the hour of each frame, the animation technology is divided into two types: frame animation and graphic array animation. Each picture is just a full-screen cuboid graphic, which saves more memory and can achieve faster runtime performance [22].

In particular, the constructed three-dimensional spatial data model should meet the following requirements as much as possible: as far as the real performance of the real world is concerned, the accuracy of the description is of course the highest. From the unilateral observation of the application as a whole, meeting actual needs is the most important. From the perspective of database management, the higher the level of detailed real-world description, the greater the amount of geometry and attribute data required and the greater the management difficulty [23]. The description ability of spatial relationship can express the mutual relationship between geographic objects. This is the characteristic of three-dimensional geographic information data model which is different from other data models. Complete and accurate description of spatial relationship is also the basic principle of spatial analysis. In order to make 3D GIS not only a demonstration tool but also a practical tool, the data model must include the description of the spatial relation-

ship. Three-dimensional GIS systems not only deal with some simple single objects but also cover all the characteristics of a given geographic area, and the amount of data is often very large. The speed of data retrieval, which is closely related to this, must also be considered at the same time, which also includes retrieval of geometric information and retrieval of attribute information [24].

Attribute description ability is a means to simulate and reproduce the real world as much as possible. The spatial three-dimensional data model should not only observe the characteristic attributes of things but also pay attention to other manifestations of geometric characteristics. Attributes can be divided into social attributes and physical attributes. The first refers to the inherent properties of the feature, such as ownership, name, and type; the latter refers to the external performance of the feature, such as material, texture, and color. Once this information is available at the same time, the 3D GIS system can satisfy the reproduction of the real world, as well as the repair and query needs in practical applications. The speed and difficulty of 3D imaging visualization are important applications that affect 3D spatial data models. The scale and data model of 3D display are closely related to aesthetics and data structure. For example, the display vector structure data model is better than the grid structure data model, and the effect is more beautiful. At the same time, as the amount of data in the display scene model increases, the 3D rendering speed will also decrease. Therefore, as far as possible, to speed up the effective speed of 3D model display and the degree of appearance, under certain hardware resource conditions, it is also one of the issues that must be considered when establishing a data model. In order to ensure the current nature of the data and serve other systems or projects, the data model has the ability to transform other systems' models, which can not only accept the transfer of other data but also realize the transfer of other data. And to ensure that, during this mutual conversion, the information loss should be reduced to a minimum, and there should be a higher degree of convenience [25].

5. Conclusion

Through the analysis of the development of 3D city modeling at home and abroad, the construction and visualization of the community 3D modeling have been researched, mainly analyzing the meaning and purpose of 3D city modeling; further study its background, combined with domestic and foreign development, to further understand the necessity of 3D city modeling. The theoretical basis of the three-dimensional spatial data model is explained, the nature and distribution of spatial data are studied, the acquisition of three-dimensional spatial data is studied, and the acquisition process and method are carefully summarized. Using 3DMax software to build a residential building model, import the 3ds file into OpenGL, and model the building; finally, use OpenGL software to visualize the model. Research on the theory and foundation of city 3D modeling and visualization, put forward the matters needing attention in the process of texture matching, explain the importance of viewport transformation in visualization, and finally realize the visualization of the district. In terms of three-dimensional data acquisition, although there are many methods to obtain three-dimensional information from the urban landscape, they cannot fully meet the requirements of speed and convenience. Most methods are inefficient and difficult to obtain, and accuracy cannot be guaranteed in engineering operations. From the perspective of landscape modeling, the current data model description items are mainly focused on geographic entities, and there is no general description of the urban landscape in terms of human thinking concepts, nature, and social semantics. In terms of 3D landscape visualization, in order to improve the speed of mass data roaming, landscape, and other aspects, further research is needed to establish a better realism and aesthetic database.

Data Availability

No data were used to support this study.

Conflicts of Interest

The author declares that there is no conflict of interest with any financial organizations regarding the material reported in this manuscript.

References

- [1] A. P. Patil and N. Chakrabarti, "A review into the evolution of HIPAA in response to evolving technological environments," *Journal of Cybersecurity and Information Management*, vol. 4, no. 2, pp. 5–15, 2020.
- [2] N. I. Ziedan, "Urban positioning accuracy enhancement using 3d buildings model and accelerated ray tracing," in *In Proceedings of the 30th International Technical Meeting of The Satellite Division of the Institute of Navigation (ION GNSS+ 2017)*, pp. 3253–3268, Portland, Oregon, 2017.
- [3] F. Meyer, P. Braca, P. Willett, and F. Hlawatsch, "A scalable algorithm for tracking an unknown number of targets using multiple sensors," *IEEE Transactions on Signal Processing*, vol. 65, no. 13, pp. 3478–3493, 2017.
- [4] H. Chen, Q. Dou, L. Yu, J. Qin, and P. A. Heng, "VoxResNet: deep voxelwise residual networks for brain segmentation from 3D MR images," *NeuroImage*, vol. 170, pp. 446–455, 2018.
- [5] J. G. Singla and K. Padia, "A novel approach for generation and visualization of virtual 3D city model using open source libraries," *Journal of the Indian Society of Remote Sensing*, vol. 2020, no. 49, pp. 1–6, 2002.
- [6] X. Xie and X. Lu, "Development of a 3D modeling algorithm for tunnel deformation monitoring based on terrestrial laser scanning," *Underground Space*, vol. 2, no. 1, pp. 16–29, 2017.
- [7] G. Peronato, E. Rey, and M. Andersen, "3D model discretization in assessing urban solar potential: the effect of grid spacing on predicted solar irradiation," *Solar Energy*, vol. 176, no. DEC., pp. 334–349, 2018.
- [8] C. Pang and Z. Guan, "Community environmental detection and community outdoor space health promotion based on cloud resource scheduling mechanism," *Journal of Healthcare Engineering*, vol. 2022, Article ID 4454447, 11 pages, 2022.
- [9] P. Tsai, Y. Lin, Y. Ou, E. T. H. Chu, and J. W. S. Liu, "A framework for fusion of human sensor and physical sensor data," *IEEE Transactions on Systems Man & Cybernetics Systems*, vol. 44, no. 9, pp. 1248–1261, 2014.
- [10] M. P. Couper, "The future of modes of data collection," *Public Opinion Quarterly*, vol. 75, no. 5, pp. 889–908, 2011.
- [11] M. Dong, K. Ota, and A. Liu, "RMER: reliable and energy-efficient data collection for large-scale wireless sensor networks," *IEEE Internet of Things Journal*, vol. 3, no. 4, pp. 511–519, 2016.
- [12] S. Biswas, D. Devi, and M. Chakraborty, "A hybrid case based reasoning model for classification in internet of things (IoT) environment," *Journal of Organizational and End User Computing*, vol. 30, no. 4, pp. 104–122, 2018.
- [13] A. Tzikas, D. R. Holmes, S. Gafoor et al., "Percutaneous left atrial appendage occlusion: the Munich consensus document on definitions, endpoints, and data collection requirements for clinical studies," *EuroIntervention*, vol. 12, no. 1, pp. 103–111, 2016.
- [14] J. D. Miller, M. Crowe, B. Weiss, J. L. Maples-Keller, and D. R. Lynam, "Using online, crowdsourcing platforms for data collection in personality disorder research: the example of Amazon's Mechanical Turk," *Personality Disorders: Theory, Research, and Treatment*, vol. 8, no. 1, pp. 26–34, 2017.
- [15] N. Biyani, R. D. Righetto, R. Mcleod et al., "Focus: the interface between data collection and data processing in cryo-EM," *Journal of Structural Biology*, vol. 198, no. 2, pp. 124–133, 2017.
- [16] C. E. Rouse, L. O. Eckert, I. Babarinsa et al., "Spontaneous abortion and ectopic pregnancy: case definition & guidelines for data collection, analysis, and presentation of maternal immunization safety data," *Vaccine*, vol. 35, no. 48, pp. 6563–6574, 2017.
- [17] A. Capponi, C. Fiandrino, D. Kliazovich, P. Bouvry, and S. Giordano, "A cost-effective distributed framework for data collection in cloud-based mobile crowd sensing architectures," *IEEE Transactions on Sustainable Computing*, vol. 2, no. 1, pp. 3–16, 2017.
- [18] S. Stieglitz, M. Mirbabaie, B. Ross, and C. Neuberger, "Social media analytics - challenges in topic discovery, data collection, and data preparation," *International Journal of Information Management*, vol. 39, pp. 156–168, 2018.

- [19] M. L. Galas and T. I. Pak, "Methodology of stratification research of modern civil society in Russia," *Proceedings of the National Academy of Sciences of the United States of America*, vol. 99, no. 3, pp. 7280–7287, 2018.
- [20] A. T. Peterson, M. Pape, and J. Soberón, "Rethinking receiver operating characteristic analysis applications in ecological niche modeling," *Ecological Modelling*, vol. 213, no. 1, pp. 63–72, 2008.
- [21] A. Sariga and J. Uthayakumar, "Type 2 fuzzy logic based unequal clustering algorithm for multi-hop wireless sensor networks," *International Journal of Wireless and Ad Hoc Communication*, vol. 1, no. 1, p. 33, 2020.
- [22] H. Elsayy, A. Sultan-Salem, M. S. Alouini, and M. Z. Win, "Modeling and analysis of cellular networks using stochastic geometry: a tutorial," *IEEE Communications Surveys & Tutorials*, vol. 19, no. 1, pp. 167–203, 2017.
- [23] S. J. Marshall and G. Clarke, "Modeling north American fresh-water runoff through the last glacial cycle," *Quaternary Research*, vol. 52, no. 3, pp. 300–315, 2017.
- [24] S. Niksa, "FLASHCHAIN theory for rapid coal devolatilization kinetics. 8. Modeling the release of sulfur species from various coals," *Energy & Fuels*, vol. 31, no. 5, pp. 4925–4938, 2017.
- [25] J. Simunek and J. W. Hopmans, "Modeling compensated root water and nutrient uptake," *Ecological Modelling*, vol. 220, no. 4, pp. 505–521, 2017.

Research Article

Application of Neural Network Based on Multisource Information Fusion in Production Cost Prediction

Biaowen Wei 

Zhejiang Industry Polytechnic College, Shaoxing, 312000 Zhejiang, China

Correspondence should be addressed to Biaowen Wei; 2004016@fjxu.edu.cn

Received 31 December 2021; Accepted 22 February 2022; Published 15 March 2022

Academic Editor: Nima Jafari Navimipour

Copyright © 2022 Biaowen Wei. This is an open access article distributed under the Creative Commons Attribution License, which permits unrestricted use, distribution, and reproduction in any medium, provided the original work is properly cited.

Production cost forecasting is an important basis for cost accounting, cost decision-making, and cost planning. It is the scale necessary to reduce product costs and an important way to enhance enterprise competitiveness and improve system benefits. A neural network based on multisource information fusion is a manifestation of integrated internal knowledge. By learning to integrate multiple sources of information, it is easier to understand cognitive thinking and integrate the complex relationships of uncertain regions into regular signals. Fusion prediction does not need to understand the specific mechanism of the process but can fully approximate various nonlinear functional relationships determined by input and output with the continuous update of its internal weights. This paper mainly studies the application of neural network based on multisource information fusion in production cost prediction, analyzes the technology of multisource information fusion, and proposes a method of applying multisource information fusion theory to BP neural network and RBF network. Experiments have proved that through the comparison of the results of the BP neural network and the RBF network, for the six cost categories, compared with the BP neural network, the prediction results of the RBF network are closer to the true value, and they all show higher prediction capabilities. Among them, the error of the RBF network in predicting the total salary of the current month is 0.01004. The performance of the RBF network model is better than that of the BP neural network model.

1. Introduction

China is in a period of in-depth development of industrial growth, information development, urban promotion, and agricultural renewal, and product demand will see new growth. Multisource information fusion is a multilevel, multistep process, with the characteristics of availability, compatibility, and aggregation of multisource data, so as to regularly improve status and identity analysis. Due to its high availability, good scale, high reliability, and low cost of information retrieval, it has been widely used in modern military and civilian environments, promoting the development of modern technology and the improvement of human life. In recent years, multisensor information fusion technology has received extensive attention and applications. Information fusion is a new research direction of generating information, which solves the specific problem of using multiple sensors (multiple or multiple types) in the system. If an enterprise wants to obtain and maintain long-term competi-

tion, it must face the problem of insufficient production cost control to improve its system performance and competitiveness. However, in today's relatively saturated market, market prices are the decisive factor in the market, and market prices are severely restricted by market costs. Therefore, deepening corporate cost control, lowering market prices, and ensuring corporate profit growth are the keys to the survival and development of the industry. Pricing forecast is also the primary link and foundation for enterprises to achieve greater economic benefits and pursue primary goals.

Although the use of deep learning and neural network technologies is becoming more and more popular, there are still some challenges when it comes to combining multiple sources of information and data. Bayesian reasoning provides a rigorous method for the quantification of uncertainty in decision-making. The uncertainty quantification using Bayesian inference takes into account the uncertainty related to the model parameters and the uncertainty of combining multiple data sources. Chandra and Kapoor proposed a

Bayesian framework for transfer learning using neural networks, which considers single and multiple data sources. They used the existence of the prior distribution to define the dependence between different data sources in the multisource Bayesian transfer learning framework and used the Markov chain Monte Carlo method to obtain samples from the posterior distribution. The results show that the framework provides a robust probabilistic method for decision-making, but the experimental data is not clear [1]. Recently, self-centered activity recognition has attracted considerable attention in the pattern recognition and artificial intelligence community because it is widely applicable to human systems, including the evaluation of diet and physical activity, as well as the monitoring of patients and the elderly. Yu et al. proposed a knowledge-driven multisource fusion framework to identify self-centered activities (ADL) in daily life and designed a simple likelihood table to provide everyone with regular ADL information. Then, a well-trained convolutional neural network is used to generate a set of text labels, together with regular information and other sensor data, which are used to identify ADL based on statistics and support vector machines based on information theory. Experiments show that the proposed method accurately recognizes 15 predefined ADL categories, including various sedentary activities that were previously difficult to recognize. When applied to real-life data recorded using self-built wearable devices, the method is better than previous methods. The average accuracy of 15 ADLs reached 85.4%, but this research has not yet been widely used [2]. Recently, artificial neural networks (ANN) have been applied to various robotics-related research fields due to their powerful spatial feature abstraction and temporal information prediction capabilities. ANNs are connectionist models, which means that they are naturally weak in long-term planning, logical reasoning, and multistep decision-making. Zuo et al. proposed an improved ANN (SANN) model of State Calculator and Result (SOAR), which simultaneously utilizes the long-term cognitive planning capabilities of SOAR and the powerful feature detection capabilities of ANN. It imitates the cognitive mechanism of the human brain and uses an additional logical planning module to improve the traditional ANN. In addition, they also built a data fusion module to combine the probability vector obtained by SOAR planning with the original data feature array. The experimental results show the efficiency and high accuracy of the proposed architecture, and it also has great potential for more complex tasks that require robust classification, long-term planning, and fast learning. Some potential applications include recognizing the grabbing sequence in a multiobject environment and multiobject cooperative grabbing, but the practicality is not strong [3]. With the development of the Industrial Internet of Things, diagnosis based on data fusion is attractive for effective use of multisource monitoring information of motors. Following the paradigm of multimodal deep learning (MDL), Fu et al. proposed a new multisensory fusion model called multimodal neural network based on dynamic routing (DRMNN). Specifically, they studied the fusion of vibration and stator current signals and designed a multimodal feature extraction scheme for

dimensionality reduction and invariant feature capture based on multisource information. Since it is necessary to determine the importance of each mode, a dynamic routing algorithm is introduced in the decision-making layer to adaptively assign appropriate weights to different modes. The effectiveness and robustness of the developed DRMNN have been proven in an experimental study conducted on a motor test platform. However, the experimental subjects are somewhat one-sided and cannot be used in real life [4]. In order to solve the problem of complicated robot assembly and learning process and high requirements for programming technology, Wang et al. proposed an implicit interaction method based on forearm sEMG (surface electromyography) and inertial multisource information fusion to realize robot demonstration programming. Based on the assembly experience gained by the demonstrator's demonstration and learning, they proposed a multiple depth deterministic strategy gradient (M-DDPG) algorithm to modify assembly parameters to improve the adaptability to assembly objects and environmental changes. In the demonstration programming experiment, they proposed an improved PCNN (Parallel Convolutional Neural Network), namely, one-dimensional PCNN (1 D-PCNN); the feature inertia and EMG are automatically extracted through one-dimensional convolution and pooling, which improves the generalization performance and accuracy of gesture recognition to a certain extent, but the experimental operation is too complicated [5]. Previous literature has shown that the prior sharing of imperfect demand information by retailers will harm retailers, benefit manufacturers, and reduce the total profit of the supply chain. Zhao and Li extend the research of information sharing to include that manufacturers may have the ability to invade and may face uneconomical or economic production. When the manufacturer's production costs are not considered, the expropriation of manufacturers encourages retailers to share demand information with manufacturers and improve supply chain performance. In addition, manufacturers may have incentives to encourage retailers to improve the accuracy of demand forecasts. When the manufacturer infringes and faces production diseconomy, information sharing is beneficial to the retailer, and it is beneficial to the manufacturer and the supply chain when the production diseconomy is relatively small. When the demand becomes more volatile or the retailer's demand signal becomes more accurate, the retailer will get more benefits from the following aspects, but the specific quantitative relationship has not been studied in depth [6]. An educational publishing industry usually builds up large inventories for "on-demand production"; however, frequent revisions can lead to obsolescence problems. Lee and Liang proposed two models to solve different but related problems, inventory scrap, and contract design. The industry uses predictive models to forecast demand and manage inventory of various printed products. This model was developed to improve the accuracy of demand forecasts and reduce inventory obsolescence. In addition, there is information asymmetry in a two-side supply chain, and contract design is conducive to educational publishing retailers. Therefore, the profit margin of the entire supply chain has not been maximized, and the

manufacturer's profit is also very limited. The research suggests encouraging retailers to provide real information to improve the profitability of the entire supply chain. An empirical study of leading education publishers in Taiwan validated the proposed model. The results show that the proposed printing decision model improves the prediction accuracy by 3.7% and reduces the cost by 8.3%. The contract design improves the profitability of the overall supply chain and the manufacturer by 0.5% and 2.7%, respectively, but the initial capital investment is too large [7]. The above research makes a detailed analysis on the application of neural network and multisource information fusion. It is undeniable that these studies have greatly promoted the development of corresponding fields. We can learn a lot from methods and data analysis. However, there is relatively little research on the prediction of production cost in the field of neural network. It is necessary to fully apply these algorithms to the research in this field. This paper combines neural network and information fusion system and proposes two information fusion algorithms based on neural network. Combining the advantages of multisource signals and neural networks, embed the multisource information processing mechanism into the neural network. Through the learning of BP neural network and RBF network, the ability of neural network to process information is broadened, and it proves the superiority of multisource information fusion compared with single information fusion. After training, the neural network does not need any additional information; it can fuse multisource information and conduct experiments on it.

2. Application Method of Neural Network Based on Multisource Information Fusion in Production Cost Prediction

The basic neurons in the neural network are similar to the neurons in the neural network in the human body, because the artificial neural network model is an imitated biological neuron. The neuron model system is shown in Figure 1. The neuron unit consists of multiple inputs $p_i, i = 1, 2, \dots, n$, and one output q_j . The intermediate state is represented by the weighted sum and correction value of the input signal, and the output is

$$Q_j(t) = f \left(\sum_{i=1}^n w_{ji} p_i - \phi_j \right) \quad (1)$$

The threshold of the neuron is expressed as ϕ_j , w_{ij} is the connection weight coefficient, n is the number of input signals, Q_j is the output of the neuron, t is the time, and f is the output transformation function, as shown in Figure 2; there are three transformation function forms of f , which can be seen from the figure which are continuous and non-linear [8].

The basic neuron model of neural network has three basic principles:

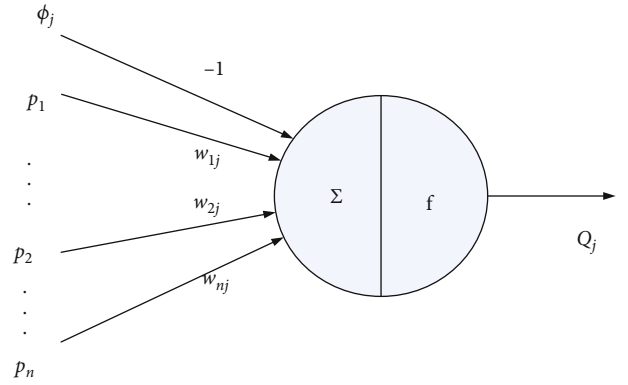


FIGURE 1: Neuron model.

- (1) The connection function is required. The connection strength is expressed by the weight on the connection. When the weight is positive, it means activation, and negative value means inhibition
- (2) A summation unit that calculates the sum of the magnitude (average line) of each input signal
- (3) An activation function whose main purpose is to map and limit the size of neurons [9]

In fact, the process of human understanding of many realities is the process of compiling multisource information. People first perceive existing objects from multiple angles and places through sense organs such as the fingers, eyes, ears, and nostrils; then, the cognitive information that can be confirmed and matched with each other is released to the brain to improve the cognitive process in the brain and then obtain an accurate description of the factors, to the point of understanding [10]. This process of first visualizing and then developing knowledge is the process of human fusion of multisource information. Figure 3 roughly shows the basic flow of human information processing.

Multisensor information fusion using neural networks does not require any a priori information compared with the traditional fusion methods based on probability theory; it overcomes the defects of difficult-to-obtain and computationally intensive evidence in evidence-theoretic fusion methods. It not only broadens the ability of neural network to process information, so that it can handle both precise and imprecise or fuzzy information, but also, the trained neural network can fuse multisensor information without additional information, which improves the fusion capability of the fusion system as well as the accuracy of fusion. Here are the two neural networks used in this article.

2.1. BP Neural Network. BP (back propagation) network is a multilayer feedthrough neural network trained according to error generation algorithm, and it is one of the most widely used neural models [11]. Its main idea is to compare the results of receiving stimuli (weighting effect) with the expected results of receiving errors through training samples. It can be calculated that the error is caused by the influence of the input size and boundary, and then, we calculate

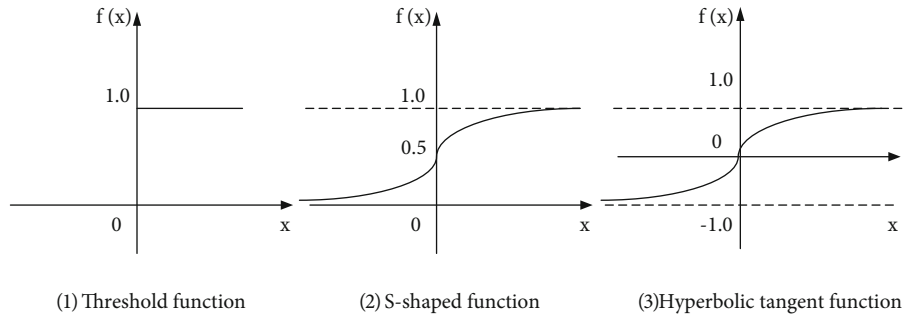


FIGURE 2: Common transformation (excitation) functions in neurons.

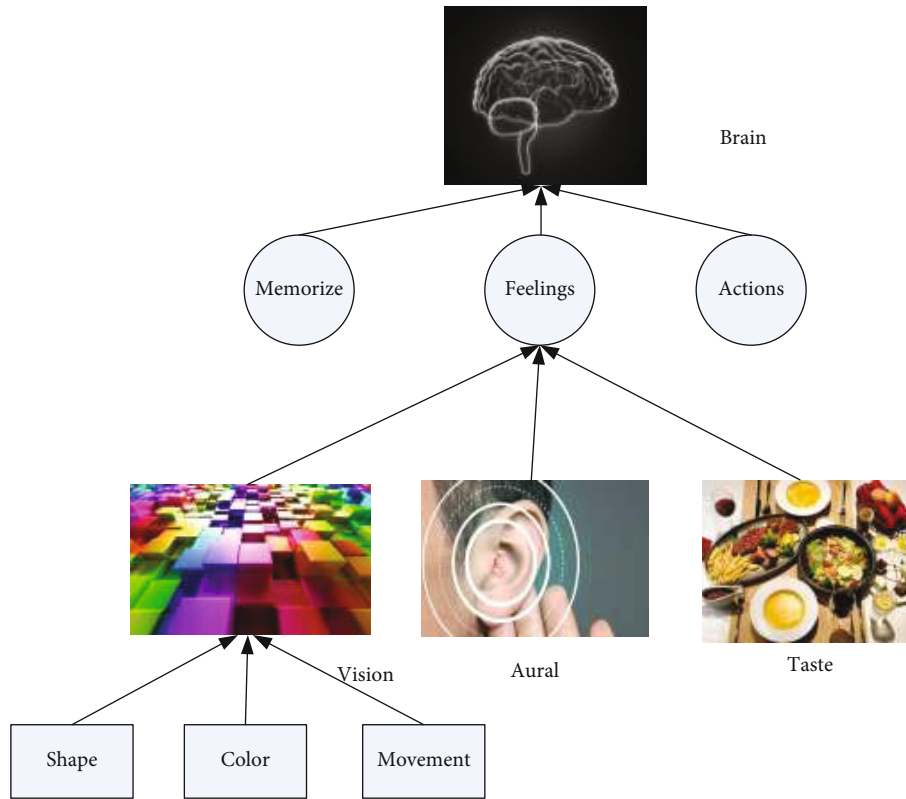


FIGURE 3: The way the cranial nervous system receives and processes signals.

the dimension and threshold of each layer in the network to adjust and correct until the result is as close as possible to the expected vector to end the training. This learning process is referred to as reverse spread [12]. After the propagation is completed, the weights and thresholds are determined, and the functional relationship between input and output is also determined. At this time, the neural network has the function of memory and prediction.

2.2. RBF Network. RBF neural network has only one hidden layer, so it can be regarded as a three-layer network structure, which belongs to the forward neural network model. The input layer is in the first layer of the network structure; the implicit layer is in the second layer, and the radial basis function is used for the transform function of the implicit layer; the last layer is the output layer, which does not do

the same work as the implicit layer and has a different learning strategy. In the RBF network learning algorithm, there are three sets of parameters to be adjusted: the center of the basis function in the implicit layer, the variance, and the connection weights from the implicit layer units to the output units.

The RBF network mainly generates a hidden layer space in the basic structure. When the network starts to input, the input can be converted into the hidden layer space through the functional relationship, which avoids the connection function. Because as long as the center point of the RBF network is determined, the functional relationship is also determined, and the conversion of the input to the hidden layer space is linear; the output only needs to add the value of each hidden space; sigmoid is often used for the output of hidden layers [13]. On the whole, although the input to output of

the neural network is not linear, the weight of the network is artificially controllable, which improves the training efficiency and avoids the problem of local minima. The generalization ability of RBF is better than BP network in many aspects, but the structure of BP network is simpler than RBF network when solving the problems with the same accuracy requirements. RBF network can approximate any nonlinear function with any accuracy and has the ability of global approximation. In theory, RBF network and BP network can approach any nonlinear function with arbitrary accuracy. The multisource information fusion in research is to simulate the complex process of human brain processing multisource data. In a system with multiple sensors, due to the different physical characteristics of the sensors, using these sensors to measure the same object will obtain measurement information under different systems. The multisensor fusion system can convert the measurement information under these different systems into the same coordinate system and then combine them according to the optimal signal to obtain comprehensive information of the object [14]. Multisource information aggregation, also called multisensor information fusion, is the process of processing data for multiple sensors or multiple data sources. It has the advantages of strong survivability, wide area, high reliability, high search performance, and low data collection cost, which is suitable for machine production [15]. Therefore, it is of great significance to broaden and deepen the scientific research of multisource data integration and the design of related algorithms based on multisource information fusion to solve existing problems.

In practical applications, in order to obtain more accurate results, multiple sensors can be used to measure the same object. However, due to the different physical characteristics of sensors, it is likely to cause differences in accuracy between sensors [16]. In this case, it can consider the process of measuring data by proportionally distributing the data of each sensor to obtain more accurate measurement values. The specific derivation process of the proportional distribution of sensor accuracy is as follows: first, consider two different sensors measuring the same object at time t ; the results are, respectively,

$$\begin{aligned} U_{t_1} &= s_t + v_{t_1}, \\ U_{t_2} &= s_t + v_{t_2} \end{aligned} \quad (2)$$

Among them, t represents the time parameter, s_t represents the true value of the target, v_{t_1} and v_{t_2} represent the random error, and the random error satisfies $v_{t_1} \sim (0, F_{t_1})$, $v_{t_2} \sim (0, F_{t_2})$, and the measured values of the two sensors are independent of each other [17]. Assuming that the estimated value \hat{s}_t of s_t has a linear relationship with the measured values z_{t_1} and z_{t_2} , since the estimated value \hat{s}_t is an unbiased estimate of s_t , there is

$$\hat{s}_t = f_{t_1} z_{t_1} + f_{t_2} z_{t_2}. \quad (3)$$

f_{t_1} and f_{t_2} indicate the weight of the measured value of

each sensor. At this time, the estimated error is

$$\tilde{s}_t = s_t - \hat{s}_t. \quad (4)$$

Using the cost function G to represent the root mean square error of \tilde{s}_t , then we have

$$G = E(\tilde{s}_t^2) = E\left[s_t - f_{t_1}(s_t + v_{t_1}) - f_{t_2}(s_t + v_{t_2})\right]^2. \quad (5)$$

Since \hat{s}_t is an unbiased estimate of s_t , we can get

$$E(\tilde{s}_t) = E\left[s_t - f_{t_1}(s_t + v_{t_1}) - f_{t_2}(s_t + v_{t_2})\right] = 0. \quad (6)$$

Because of $E(v_{t_1}) = E(v_{t_2}) = 0$, $E(s_t) = E(\hat{s}_t)$, it can get

$$f_{t_2} = I - f_{t_1}. \quad (7)$$

Among them, I is the proper-dimensional identity matrix. The cost function G can be rewritten as

$$G = E\left[\left(f_{t_1}\right)^2 (v_{t_1})^2 + \left(I - f_{t_1}\right)^2 (v_{t_2})^2 + 2\left(f_{t_1}\right)\left(I - f_{t_1}\right)(v_{t_1})(v_{t_2})\right]. \quad (8)$$

From $v_{t_1} \sim (0, F_{t_1})$, $v_{t_2} \sim (0, F_{t_2})$, and v_{t_1} and v_{t_2} which are independent of each other, we can get

$$\begin{aligned} E\left[(v_{t_1})^2\right] &= F_{t_1}, \\ E\left[(v_{t_2})^2\right] &= F_{t_2}, \\ E\left[(v_{t_1})(v_{t_2})\right] &= 0. \end{aligned} \quad (9)$$

Then,

$$G = E(\tilde{s}_t^2) = \left(f_{t_1}\right)^2 F_{t_1} + \left(I - f_{t_1}\right)^2 F_{t_2}. \quad (10)$$

In order to find the smallest cost function G , let $\phi = (f_{t_1}, f_{t_2})$ and derivate ϕ .

$$\frac{\partial G}{\partial \phi} = 0. \quad (11)$$

Solve the optimal weight:

$$\begin{aligned} f_{t_1} &= \frac{F_{t_2}}{F_{t_1} + F_{t_2}}, \\ f_{t_2} &= \frac{F_{t_1}}{F_{t_1} + F_{t_2}}. \end{aligned} \quad (12)$$

The best estimate is

$$\hat{s}_t = \frac{F_{t_2}}{F_{t_1} + F_{t_2}} z_{t_1} + \frac{F_{t_1}}{F_{t_1} + F_{t_2}} z_{t_2} = \frac{F_{t_1} F_{t_2}}{F_{t_1} + F_{t_2}} \left(\frac{1}{F_{t_1}} z_{t_1} + \frac{1}{F_{t_2}} z_{t_2} \right). \quad (13)$$

The error covariance matrix after fusion is

$$F_t = \frac{F_{t_1} F_{t_2}}{F_{t_1} + F_{t_2}} = \left(\frac{1}{F_{t_1}} + \frac{1}{F_{t_2}} \right)^{-1}. \quad (14)$$

By analogy, if there are Q sensors, the corresponding measurement set and measurement noise matrix set are $\{z_{t_q}\}$ and $\{v_{t_q}\}$, respectively; $q = 1, 2, \dots, Q$ is Gaussian white noise, which satisfies $v_{t_q} \sim (0, F_{t_q})$; and the noises are not correlated. According to the limit theory of multivariate function, the weighting coefficient corresponding to the measured value of each sensor under the minimum mean square error can be obtained.

$$f_{t_q} = \frac{1/F_{t_q}}{\sum_{q=1}^Q (1/F_{t_q})}. \quad (15)$$

The error covariance matrix after fusion is

$$F_t = \left(\frac{1}{F_{t_1}} + \frac{1}{F_{t_2}} + \dots + \frac{1}{F_{t_q}} \right)^{-1}. \quad (16)$$

The multisensor optimal estimate is

$$\hat{s}_t = F_t \left(\frac{1}{F_{t_1}} z_{t_1} + \frac{1}{F_{t_2}} z_{t_2} + \dots + \frac{1}{F_{t_q}} z_{t_q} \right). \quad (17)$$

Consistency fusion is an effective algorithm under a distributed structure. It refers to the interaction of information between each subject and neighboring subjects in a multi-agent system. As a result, they influence each other, making the subjects gradually converge over time [18]. For research on consistency weighted fusion, graph theory is an important analysis tool. In a wireless sensor network, there are Q wireless sensors, which can be expressed as $H = (W, E)$. Among them, $W = \{1, 2, \dots, Q\}$ represents the sensor node set, and $E \subset W \times W$ is the edge set. If the sensor node i and sensor node j can communicate, then

$$E_{ij} \subset E, \quad i = 1, 2, \dots, Q; j = 1, 2, \dots, Q. \quad (18)$$

According to whether the edges are directed, the network topology can be divided into directed graphs and undirected graphs. $\Omega_i = \{j : (i, j) \in E\}$ represents the set of communicable neighbors of sensor node i . The communication conditions between all nodes can be represented by Laplacian matrix A , and the elements of Laplacian matrix are expressed in the following form:

When $i = j$,

$$a_{ij} = \sum_j c_{ij}. \quad (19)$$

When $i \neq j$,

$$a_{ij} = -c_{ij}. \quad (20)$$

If $E_{ij} \subset E$, then $c_{ij} > 0$; otherwise, $c_{ij} = 0$. If the network topology is an undirected graph, then $c_{ij} = c_{ji}$; at this time, A is a symmetric matrix, all its eigenvalues are real numbers, and there is only one zero eigenvalue α_1 . The algebraic connectivity of the network is closely related to the nonzero minimum eigenvalue α_2 . The larger the α_2 is, the better the connectivity between sensor nodes in the network structure, and the faster the system will converge. The form of consistency weighted fusion is shown below [19].

$$s_{(t+1)_i} = s_{t_i} + \beta \sum_{j \in \Omega_i} c_{ij} (s_{t_j} - s_{t_i}). \quad (21)$$

Among them, $0 < \beta < 1/\Delta$ is the step size, $\Delta = \max_i (\sum_{j \neq i} c_{ij})$. It can be seen from the above formula that if the topological structure is always the same and the network connection is an undirected graph, then each subject in the system will evolve toward the state of the neighboring subject. The information of each subject is transferred and transformed according to the consensus algorithm. When $t \rightarrow \infty$ and $(s_{t_j} - s_{t_i}) \rightarrow 0, \forall i \neq j$, then all subjects in the system will eventually converge, reaching the weighted average of the initial value.

In wireless sensor networks, a large number of wireless sensors are used to measure the same object, and then, the measurement data is combined by a central or distributed system to achieve the purpose of accurate tracking [20]. However, due to the limitations of the sensor's own application conditions, traditional centralized systems are not suitable for wireless sensor networks to optimize services in complex environments. In an integrated system, all sensor components in the network are information processing centers, and only the sensor components exchange information with neighboring components. Compared with centralized systems, distributed systems have obvious advantages in terms of network communication and computational complexity, and integrated systems can better adapt to interference such as packet loss and long delay.

The neural structure based on the multisource information fusion system used in this paper is shown in Figure 4 [21]. Production cycle, factory scale, production complexity, production efficiency, etc. can be measured offline and have an extremely close relationship with product cost, which is used as the input of the neural network.

The hierarchical modular neural network fusion model is composed of multisensor unit MSU (multisensor unit), task decomposition unit (TDU), neural network submodule SMNNU (submodular neural network), and fusion

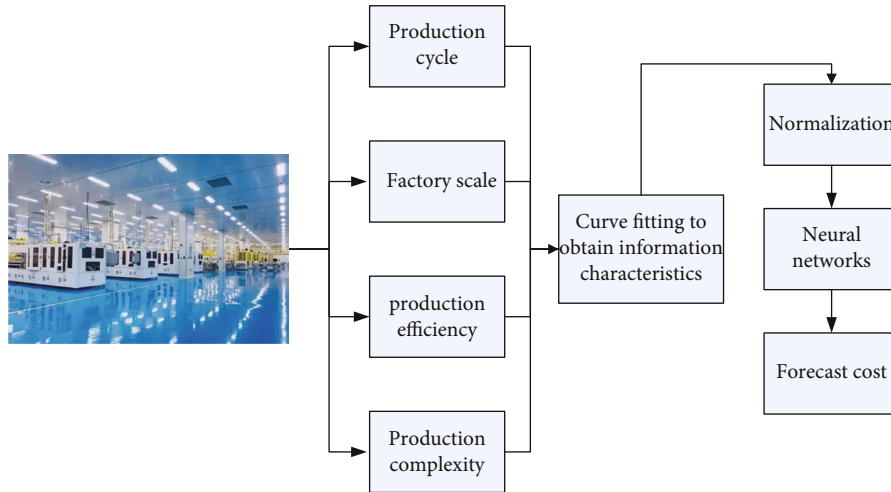


FIGURE 4: Multi-information fusion structure diagram based on neural network.

synthesis unit (fusion synthesis unit), as shown in Figure 5 [22]. Among them, the neural network submodule SMNNU can be integrated by a small neural network composed of multiple neural networks in parallel. The basic idea is that in the learning phase, the sensor unit will preprocess the detected signal and send it to the TDU, where the learning sample space is decomposed into several sample subspaces; an SMNNU is constructed for each subspace, and learning is performed. In the working stage, TDU is used to determine the degree of membership of the data to each subspace. FSU dynamically selects some or all of the SMNNUs to work according to the degree of membership and integrates the processing results of the selected SMNNUs in a weighted sum [23].

2.3. Production Cost Forecast

2.3.1. The Concept of Production Cost. Production cost refers to the cost of manufacturing services, that is, the cost incurred by an enterprise to produce a product. For each product price, production costs belong to all related costs that occur in a specific production stage, as shown in Figure 6. Compared with the cost of other steps, the entire production process includes uncertain factors of raw materials, technological processes, and labor. Therefore, the calculation and prediction of production costs will become complicated and important [24].

Because the object of production is generally a product, a product is a combination of related behaviors or interactions that transform inputs into production. We can see that the meaning of products is very broad. For different companies, product cost allocation and manufacturing processes are also very different. As far as traditional manufacturing is concerned, the main characteristics of its production are multi-step, medium-scale production; a large proportion of simulation work in the manufacturing process; and low automation. Compared with other automated production lines such as automobile production lines, it has more complex uncertainties.

Cost forecasting is very important to enterprises and to a certain extent determines the efficiency and knowledge of market pricing, cost analysis, and management. At present, the main cost estimation methods include parameter method, comparison method, and analysis method. Parametric methods use experience and statistics to decompose each key feature of the product, analyze the functional relationship between each key parameter and cost, and then use dynamic analysis to make cost forecasts. This method is simple and fast, but the accuracy rate is not very high [25]. The main manifestations of the comparative method are cluster analysis and case-based thinking methods, which are most suitable for forecasting and estimating with rich historical data and significant similarity. Compared with the above two methods, the analysis method is mainly through the analysis and modeling of the basic elements of the product and market capabilities and further enhances the resulting cost forecast results.

2.3.2. Principles of Production Cost Forecasting. For the special time-space relationship of each product, it is required that the prediction of production cost must comprehensively consider time factors, space factors, and related policy factors, and with the development of science and technology, the production of various products will gradually mature. The purpose of forecasting production costs is to strengthen cost management, pay attention to cost forecasts, and strengthen the study of cost forecasting theory, so as to reduce production costs and improve economic benefits of enterprises. In order to make the predicted results more reasonable, the production cost forecast should follow the following basic principles [26].

2.3.3. Scientific Principles. In the calculation of production cost, the choice of cost factors must be scientific, the definition and extension must be refined, and the corresponding response must also appear in the forecasting system. If the cost object is determined incorrectly or inaccurate cost calculation tools are used, the problem of cost calculation will be greatly increased.

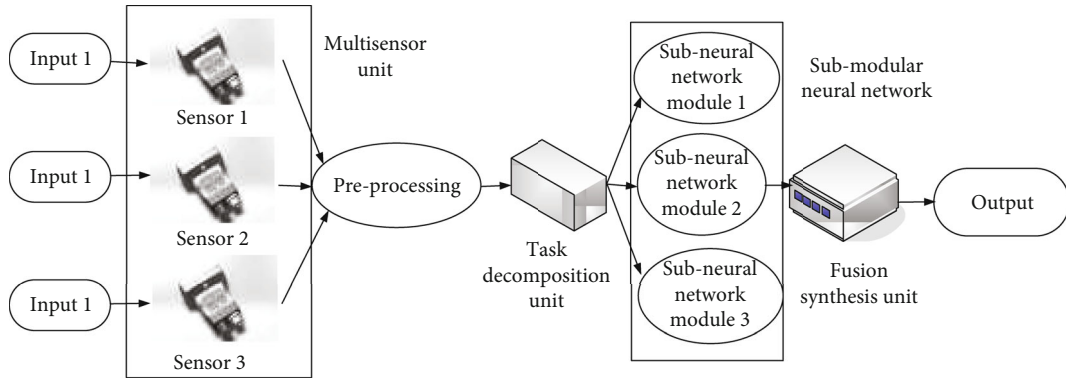


FIGURE 5: Information fusion model of modular neural network integration.

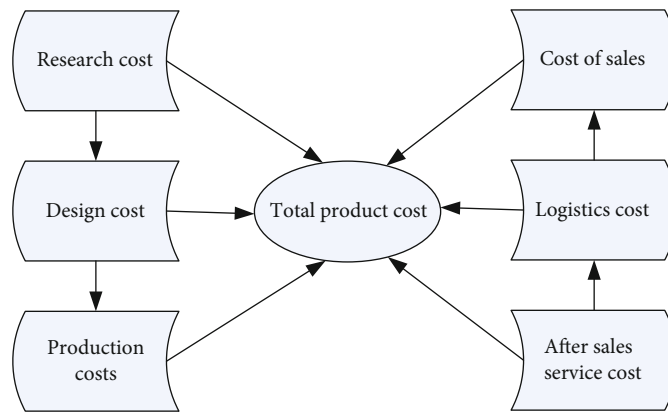


FIGURE 6: Description of total product cost and total production cost.

TABLE 1: Classification of production cost items.

Serial number	Main influencing factors	Production cost item	Cost proportion
1	Time and space factors	Expenditure on raw materials, electricity, repair, and production site	35%~50%
2	Time factor	Wages and benefits, depreciation	30%~45%
3	Policy factors	Quality inspection fee and maintenance fee	5%~10%
4	Other factors	Other expenses	5%~10%

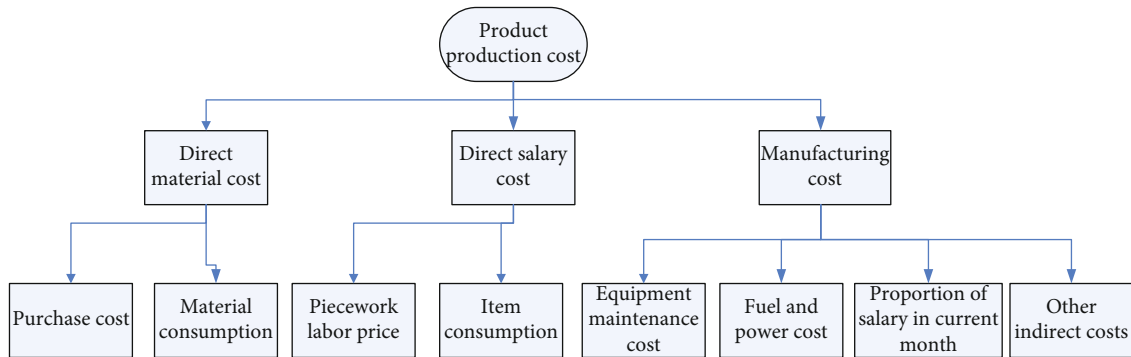


FIGURE 7: Qualitative structure diagram of product production cost prediction model.

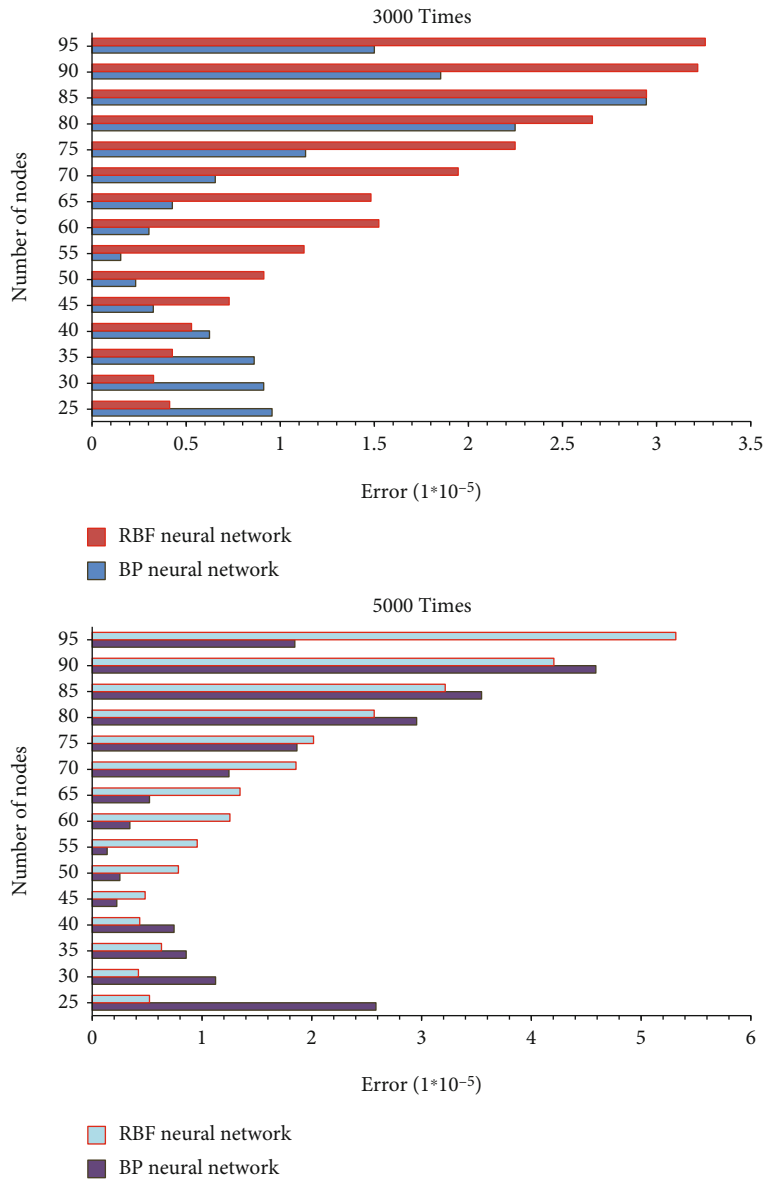


FIGURE 8: The influence of hidden nodes on the training error of the number of nodes.

2.3.4. *The Principle of Comprehensive Rationality.* In order to be more comprehensive and better reflect the value of the product in the manufacturing process, the selection of materials requires comprehensive thinking and requirements, so that cost analysis can provide relatively rich information. When designing a forecasting system, it is necessary not only to calculate the total cost and individual cost of the product but also to distinguish the total cost according to the reason to reflect the summary and system of market value. In this way, it is not only easy to manage production costs but also easy to analyze the system benefits in production and calculate the production department [27].

2.3.5. *The Principle of Feasibility.* The cost objects listed in the feasibility requirements must be realized. The first is to keep the selection of objects consistent with the relevant departments, and the maximum extent of statistical data

should be used. Secondly, the selected indicators must be measurable and quantifiable.

2.3.6. *Coordination Principle.* The manufacturing process is complex, and there is always more than one purpose to make a budget, more than one product is produced, and more than one material for cost accounting. Therefore, after payment, it is usually not directly and completely credited to the account of the identification project, and a system is required to allocate the cost to several things. At the same time, the system must also consider the cost difference of the same product on the production line and the cost difference of different types on the same production line. In this way, the correction system is also reduced to facilitate the application of prediction and maintain the degree of freedom of the same level of objects. This process cannot be

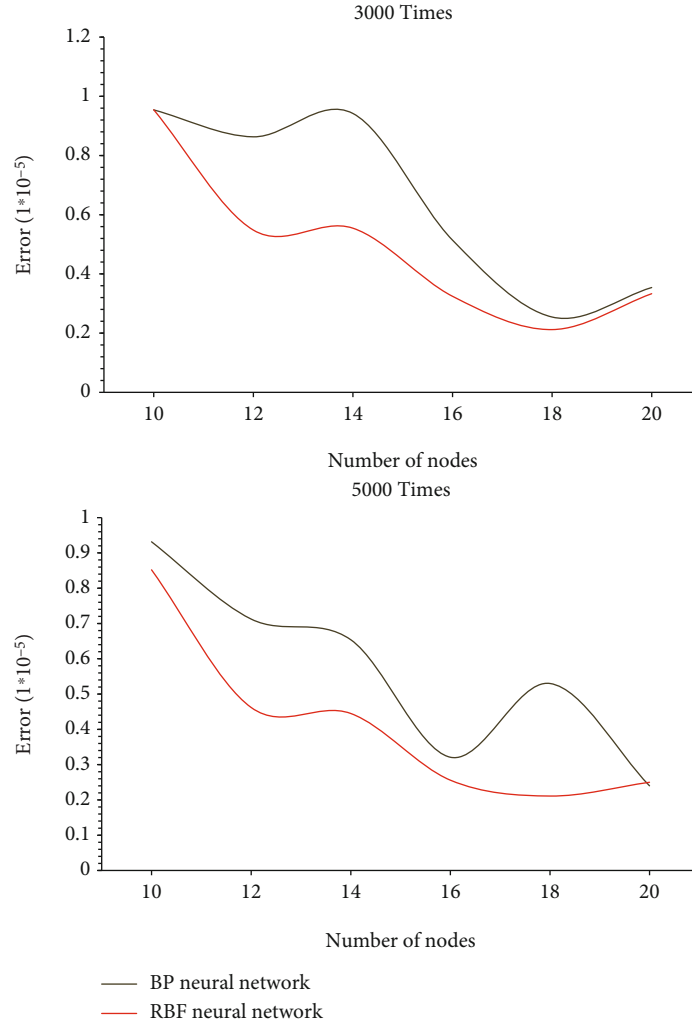


FIGURE 9: The influence of the number of training sample sets on the model prediction error.

TABLE 2: The true value of various costs in the production model.

Costs spent on items	Cost actual value (million yuan)	Costs spent on items	Cost actual value (million yuan)
Direct material cost	10.23	Total wage	25.31
Stuff consume price	12.45	Living expenses	0.5
Cost of fix	0.23	Indirect cost	1

considered in isolation, but it must be planned together with the probability model.

2.3.7. *The Principle of Associativity.* The principle of integration should combine qualitative analysis and quantitative analysis and plan production costs according to different companies and different regions. Since the locations of several companies are very different, it is impossible to have a

unified model for specific charging calculation methods. After a long process, many commonly used cost accounting methods have been formed, namely, the variety method, the batch method, and the step method. If the company's products are not produced in stages, but only one step, all product varieties can be directly used as cost accounting tools. This is the variety method. If the product is divided into several steps or several batches, it is a batch method. If the intermediate is a semifinished product and the product is mass-produced, the finished product and the completion of each step are for the cost calculation object; this method is called the step-by-step method. When the production cost is only for forecasting, it should be planned according to the characteristics of the company to be effective.

3. Establishment of Production Cost Prediction Model

3.1. *Establishment and Quantification of Index System.* There are many factors that affect production costs. To sum up, production cost is the cost down a series of production activities and consists of three components: direct materials,

TABLE 3: Comparison of BP neural network and RBF network total production cost prediction results.

	True value	Predicted value	
		BP neural network	RBF networks
Total production cost	49.72	48.25	49.12
Predicted difference	0	1.47	0.6
Prediction error	0	0.0296	0.0121

TABLE 4: Comparison of prediction results of total production cost of BP neural network and RBF network.

	Average accuracy rate	Highest accuracy rate	Time (s)
BP neural network	0.7785	0.8724	864
RBF networks	0.8512	0.9201	852

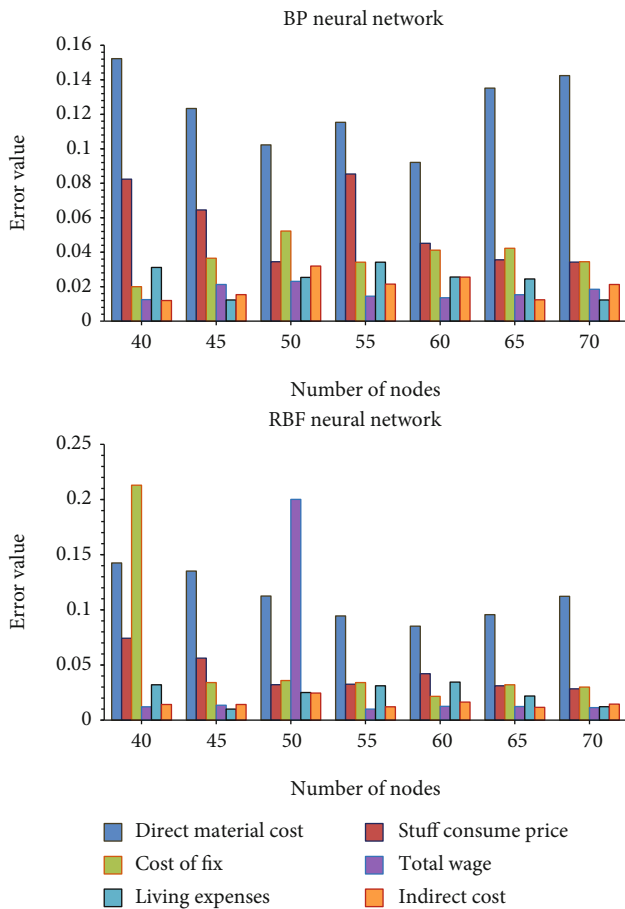


FIGURE 10: BP neural network and RBF network production cost prediction results.

direct labor, and manufacturing overhead; the forecast of production costs mainly considers space and time factors that affect production costs. Regarding the time factor, due

to the very complicated impression factors in different periods, coupled with the human factor of historical data, we do not specifically analyze the time influencing factors. The spatial factors of production costs mainly include location conditions and natural disasters. The unascertained evaluation model is used to determine the complexity coefficients of these influencing factors in product production, so as to analyze the influence of spatial factors. The policy factors are directly calculated according to the current financial system. Therefore, the cost items can be classified according to the main influencing factors, as shown in Table 1.

Among them, type 1 cost items consider not only the impact of space factors but also time factors; type 2 cost items mainly consider the impact of time; type 3 cost items are determined according to the financial policies of the country and the enterprise.

3.2. *Cost and Quality Relationship System and Impact.* With the passage of time and the development of the company, there will also be manufacturing cost factors that cannot be controlled as the primary control, or from uncontrollable to controllable, which can meet industry growth needs and cost forecasts. In summary, the current production cost and quality relationship system and influencing variables of the manufacturing industry are shown in Figure 7.

The parameters and formulas of the model are described as follows:

- (1) Product production cost prediction model variables
 - (i) Direct material cost (DMC) = material purchase price (MPP) * material consume (MC)
 - (ii) Item consumption cost, stuff consume price (SCP)
 - (iii) Equipment maintenance cost, cost of fix (CF)
 - (iv) Total salary for the month, total wage (TW)
 - (v) Living expenses (LE)

According to the above description, the above are uncontrollable variables, and the remaining are indirect cost (IC).

- (2) Based on the above forecast model variable analysis and cost accounting system, a cost forecast model can be obtained

$$W = \sum DMC_n + \sum SCP_n + \sum CF_n + \sum TW_n + \sum LE_n + IC \quad (22)$$

Among them, $\sum LC_n$ is the sum of labor wages for manufacturing the product.

BP network is the most widely used in neural network, and there have been many successful application examples of BP network. This article will use the BP network and the RBF network to integrate the multisource information that affects the production cost.

4. Neural Network Based on Multisource Information Fusion in Production Cost Prediction

The selection of the number of hidden layer nodes has a certain impact on the learning and performance of the BP network, but there is no certain principle or law to follow in the selection of the number of nodes. It is necessary to obtain a suitable number of hidden layer nodes through continuous attempts. Use the training sample set to train the neural network with different hidden layer nodes, and the training error based on the same training times (3000, 5000 times) is shown in Figure 8. Applying the trained prediction model to the test sample set, the prediction result shown in Figure 9 can be obtained.

It can be seen from Figure 8 that when the number of nodes is too few or too many, the error obtained by training the number of model nodes is relatively large, and the highest value has reached $5.3162e^{-5}$. When the number of training sample sets increases, the prediction errors of the BP neural network model and the RBF network model both show a downward trend, and the performance of the RBF network model is better than that of the BP neural network model. In order to further explore the quantitative relationship between the various cost prediction results and the true value in the production model, a neural network with 40 to 75 nodes is selected for exploration. Among them, Table 2 is the true value of various costs in the production model; the influencing factors of different cost categories are different. Through the comparison of the prediction results of six main production cost categories, the most suitable neural network is judged. Table 3 is the comparison of the production cost prediction results of the BP neural network and the RBF network, and Table 4 is the comparison of the total production cost prediction results. Figure 10 is the production cost prediction results of BP neural network and RBF network.

$$\text{Forecast error} = \frac{\text{true value} - \text{forecast result}}{\text{true value}}. \quad (23)$$

From Figure 10, it can be found that for the six cost categories, the RBF network is closer to the true value than the BP neural network, and it shows a higher predictive ability. Among them, the error of the RBF network in predicting the total salary of the current month is 0.01004. The prediction result of the RBF network is slightly better than that of the BP network, and the training process is much simpler, which is more suitable for realizing multisource information fusion. And the two kinds of neural networks have large errors in direct material costs, item consumption costs, living expenses, and other indirect costs. For example, in the direct material cost prediction, the error of the prediction result of the BP neural network is 0.1523, and the error of the prediction result of the RBF network is 0.1425. The source of large errors is related to the large fluctuations in direct material costs, because the cost of direct materials is uncontrollable in many aspects, such as commodity prices

and customer purchases which are important factors that lead to changes in direct material costs. The neural network has powerful training and customization capabilities, strong resilience, and fault tolerance, and the neural network adopts a parallel structure and distributed storage, which can quickly realize the nonlinear mapping of system input to output. According to a certain learning method and a specific topological structure, the neural network can quickly grasp the knowledge of the sample through offline learning of a large number of samples. The connection weights and thresholds are stored, and the trained neural network can be used to quickly realize the fusion of the input information of the system and output the fusion results in a timely manner. Modern technology is becoming more and more complex, and the information provided by multiple sensors can effectively improve the accuracy requirements of a single sensor for target estimation.

5. Conclusion

The development of multisensor information fusion technology has improved people's ability to obtain various information. How to comprehensively process the obtained information to obtain accurate and reasonable estimates and decisions has become a practical problem that people urgently need to solve. Information fusion technology is a comprehensive information processing technology born to meet this social demand. Product cost prediction is of vital importance to enterprises and to a certain extent determines the effectiveness and scientificity of product pricing, cost analysis, and management. With the development of modern technology, multisource data fusion will surely become an important means of intelligent control and data processing for complex production equipment and advanced weapon systems in the future. Since information fusion is an emerging discipline, its development and application have just begun, coupled with the complexity of theory and technology, so there is no comprehensive performance test and evaluation method at present; the establishment of the design and evaluation method of the information fusion system and the correct evaluation of the results of multisource data fusion are of great significance to the application of information fusion. It should be said that this is the future development direction of information fusion technology. In practical applications, it is also necessary to add neural network modules as needed to improve tracking and prediction capabilities.

Data Availability

No data were used to support this study.

Conflicts of Interest

The author declares that there are no conflicts of interest regarding the publication of this article.

References

- [1] R. Chandra and A. Kapoor, "Bayesian neural multi-source transfer learning," *Neurocomputing*, vol. 378, pp. 54–64, 2020.
- [2] H. Yu, W. Jia, Z. Li et al., "A multisource fusion framework driven by user-defined knowledge for egocentric activity recognition," *EURASIP Journal on Advances in Signal Processing*, vol. 2019, no. 1, 23 pages, 2019.
- [3] G. Zuo, T. Pan, T. Zhang, and Y. Yang, "SOAR improved artificial neural network for multistep decision-making tasks," *Cognitive Computation*, vol. 13, no. 3, pp. 612–625, 2021.
- [4] P. Fu, J. Wang, X. Zhang, L. Zhang, and R. X. Gao, "Dynamic routing-based multimodal neural network for multi-sensory fault diagnosis of induction motor," *Journal of Manufacturing Systems*, vol. 55, no. 4, pp. 264–272, 2020.
- [5] W. Fei, Q. Huan, Z. Xingqun, and W. Jianhui, "Demonstration programming and optimization method of cooperative robot based on multi-source information fusion," *Robot*, vol. 40, no. 4, pp. 551–559, 2018.
- [6] D. Zhao and Z. Li, "The impact of manufacturer's encroachment and nonlinear production cost on retailer's information sharing decisions," *Annals of Operations Research*, vol. 264, no. 1-2, pp. 499–539, 2018.
- [7] C. Y. Lee and C. L. Liang, "Manufacturer's printing forecast, reprinting decision, and contract design in the educational publishing industry," *Computers & Industrial Engineering*, vol. 125, pp. 678–687, 2018.
- [8] F.-P. Pai, L.-J. Yang, and Y.-C. Chung, "Multi-layer ontology based information fusion for situation awareness," *Applied Intelligence*, vol. 46, no. 2, pp. 285–307, 2017.
- [9] H. Xu and B. Lian, "Fault detection for multi-source integrated navigation system using fully convolutional neural network," *IET Radar, Sonar & Navigation*, vol. 12, no. 7, pp. 774–782, 2018.
- [10] L. Li, F. Zhu, H. Sun, Y. Hu, Y. Yang, and D. Jin, "Multi-source information fusion and deep-learning-based characteristics measurement for exploring the effects of peer engagement on stock price synchronicity," *Information Fusion*, vol. 69, no. 3, pp. 1–21, 2021.
- [11] H. Li, R. Nie, J. Cao, X. Guo, D. Zhou, and K. He, "Multi-focus image fusion using U-shaped networks with a hybrid objective," *IEEE Sensors Journal*, vol. 19, no. 21, pp. 9755–9765, 2019.
- [12] G. Notton, M. L. Nivet, C. Voyant et al., "Intermittent and stochastic character of renewable energy sources: consequences, cost of intermittence and benefit of forecasting," *Renewable and Sustainable Energy Reviews*, vol. 87, pp. 96–105, 2018.
- [13] K. Mwanalushi, "Maintaining props," *Low Cost & Regional Airline Business*, vol. 13, no. 1, pp. 40–43, 2018.
- [14] A. Couto, P. Costa, L. Rodrigues, V. V. Lopes, and A. Estanqueiro, "Impact of weather regimes on the wind power ramp forecast in Portugal," *IEEE Transactions on Sustainable Energy*, vol. 6, no. 3, pp. 934–942, 2014.
- [15] C. Y. Lee and M. Tuegeh, "Optimal optimisation-based micro-grid scheduling considering impacts of unexpected forecast errors due to the uncertainty of renewable generation and loads fluctuation," *IET Renewable Power Generation*, vol. 14, no. 2, pp. 321–331, 2020.
- [16] H. Thieblemont, F. Haghighat, R. Ooka, and A. Moreau, "Predictive control strategies based on weather forecast in buildings with energy storage system: a review of the state-of-the-art," *Energy and Buildings*, vol. 153, pp. 485–500, 2017.
- [17] J. Chen, L. Chen, and M. Shabaz, "Image fusion algorithm at pixel level based on edge detection," *Journal of Healthcare Engineering*, vol. 2021, no. 7, 10 pages, 2021.
- [18] F. Lei, X. Liu, Z. Li, Q. Dai, and S. Wang, "Multihop neighbor information fusion graph convolutional network for text classification," *Mathematical Problems in Engineering*, vol. 2021, no. 1, 9 pages, 2021.
- [19] A. A. Cire, A. Diamant, T. Yunes, and A. Carrasco, "A network-based formulation for scheduling clinical rotations," *Production & Operations Management*, vol. 28, no. 5, pp. 1186–1205, 2019.
- [20] G. Xue and O. F. Offodile, "Integrated optimization of dynamic cell formation and hierarchical production planning problems," *Computers & Industrial Engineering*, vol. 139, article 106155, 2020.
- [21] S. Guo, B. Zhang, T. Yang, D. Lyu, and W. Gao, "Multitask convolutional neural network with information fusion for bearing fault diagnosis and localization," *IEEE Transactions on Industrial Electronics*, vol. 67, no. 9, pp. 8005–8015, 2020.
- [22] R. K. Vemuri, P. C. S. Reddy, P. Kumar, J. Ravi, S. Sharma, and S. Ponnusamy, "Deep learning based remote sensing technique for environmental parameter retrieval and data fusion from physical models," *Arabian Journal of Geosciences*, vol. 14, no. 13, pp. 1–10, 2021.
- [23] Y. Liang, H. Li, B. Guo et al., "Fusion of heterogeneous attention mechanisms in multi-view convolutional neural network for text classification," *Information Sciences*, vol. 548, no. 2021, pp. 295–312, 2020.
- [24] A. Jakoplić, D. Franković, V. Kirinčić, and T. Plavšić, "Benefits of short-term photovoltaic power production forecasting to the power system," *Optimization and Engineering*, vol. 22, no. 1, pp. 9–27, 2021.
- [25] M. Botz and J. Marsden, "Heap leach production modeling: a spreadsheet-based technique," *Mining, Metallurgy & Exploration*, vol. 36, no. 6, pp. 1041–1052, 2019.
- [26] S. Roth, V. Kalchschmid, and G. Reinhart, "Development and evaluation of risk treatment paths within energy-oriented production planning and control," *Production Engineering*, vol. 15, no. 3, pp. 413–430, 2021.
- [27] Y. Wu, X. Li, and Z. Cao, "Effective DOA estimation under low signal-to-noise ratio based on multi-source information meta fusion," *JOURNAL OF BEIJING INSTITUTE OF TECHNOLOGY*, vol. 30, no. 4, pp. 377–396, 2021.

Research Article

Financial Asset Risk Measurement Based on Smart Sensor Big Data Security Analysis and Bayesian Posterior Probability Model

Zixin Lu 

School of Business, Shandong Normal University, Jinan, 250358 Shandong, China

Correspondence should be addressed to Zixin Lu; lzx@sdsu.edu.cn

Received 11 January 2022; Accepted 23 February 2022; Published 12 March 2022

Academic Editor: Alireza Souri

Copyright © 2022 Zixin Lu. This is an open access article distributed under the Creative Commons Attribution License, which permits unrestricted use, distribution, and reproduction in any medium, provided the original work is properly cited.

Following the speeding up of a process of financial globalization, the risks faced by financial markets have become more complex and diversified. Correlated patterns among financial assets exhibit characteristics of nonlinearity, asymmetry, and tail correlation. The original linear correlation analysis method is no longer suitable, but relevant information describing financial risks. In order to confirm whether an asset is safe, the key is to study and master its volatility, and this is based on our mastery of volatility measurement skills. This article is based on smart sensor big data security analysis and Bayesian analysis. The risk measurement of financial assets based on the empirical probability model is studied. The GARCH- t (1,1) model is selected according to the Akaike information criterion (AIC) after the generalized autoregressive conditional heteroskedasticity (GARCH) model is established by the EViews software. According to the results of probability integral transformation, a series of correlation coefficients and degrees of freedom of t -copula are obtained by the maximum likelihood estimation method. This paper uses the risk-adjusted return on capital (RAROC) method to evaluate the risk performance of financial assets. Financial institutions can only retain and absorb the financial market risks that cannot be avoided and transferred. The edge user node sends the service request to the edge server node. The edge server uses the model proposed in this paper to evaluate the user's trust and selects the corresponding service level according to the trust level corresponding to the calculated credibility results. The data show that the edge calculation takes 0.2581 seconds, while the linear search takes about 64 seconds. The results show that intelligent edge computing improves the accuracy and efficiency of financial asset risk measurement.

1. Introduction

For nearly half a century, the world's financial and economic markets have developed rapidly, and the basic characteristics of financial and economic markets have been gradually replaced by economic globalization and financial integration. With the increasingly destructive power of financial risks to the financial system, many high-risk financial derivatives have been born, making the possibility of financial turbulence continue to increase, which has led financial institutions, investors, regulators, and academia to pay close attention to financial risk measurement. The Bayesian posterior method is a method that integrates the prior information about the unknown parameters with the sample information, then obtains the posterior information according to the Bayesian formula, and then infers the unknown parameters according to the posterior information.

Currently, big data is widely used in all walks of life, with the big data era gradually taking shape. Being the irreplaceable information technology, which has created great advantages that provide a strong guarantee for market development and change the traditional business model to improve the economic benefits of enterprises, it has created great advantages for all industries. Also, big data technology has changed the behavior of consumers, which can provide better services for consumers, optimize and improve product quality, improve economic benefits for corporations, reduce the inventory of corporate products, and use big data technology. It forecasts changes in the market and provides a more important guarantee for enterprises. Big data analysis technology would be developing faster and faster in China, and it is believed that in the near and distant future, it will be widely used in various industries and can effectively control the technology of big data analysis.

The risk measurement of financial assets can improve the balance of information in the financial market. Liu et al. believe that in recent years, with the explosive development of smart cities, green energy management systems have received extensive research, with their focus on engineering web-based power generation systems using edge infrastructure including deep reinforcement learning. First, they gave an overview of energy management based on the Internet of Things in smart cities. Then they proposed a framework and software model of an IoT system based on edge computing. After that, they proposed an effective energy-dispatching scheme with deep reinforcement learning for the proposed framework. Their research lacks a certain degree of innovation [1]. According to Cao et al., as a complement to existing remote cloud centers, multi-access edge computing (MEC) configured for deployment proximal to mobile user terminals as a promising technology for 5G heterogeneous networks has been identified. To adapt to stochastic and changeable environments, augmented intelligence (AI) is introduced in MEC with a view to making intelligent fashions. They introduced the basic concepts and main applications of MEC and reviewed the existing basic work using various ML-based methods. In addition, they also discussed some potential problems of AI in MEC for future work. Their research is not accurate enough [2]. Xu et al. believe that edge caches are vulnerable to cache pollution attacks (CPAttacks), leading to interruption of content delivery. To solve this problem, they proposed a CPAttack-detection scheme based on the hidden Markov model (HMM). According to the CPAttack model, the cache status of edge devices is characterized by two parameters: content request rate and cache loss rate. Then, using the observation sequence constructed by the cache state, they developed a detection algorithm based on HMM to distinguish CPAttack in the time-invariant content request process. In order to cope with the lack of training data and the dynamic change of the cache state, they designed an algorithm based on adaptive HMM (AHMM) to detect CPAttack during the time-varying content request process. Their research lacks necessary data [3]. Luo et al. believe that vehicle edge computing (VEC) integrates mobile edge computing (MEC) into the vehicle network, which can provide more functions to execute resource-constrained applications and reduce the waiting time for connected vehicles. First, they proposed a dual importance (DI) evaluation method to reflect the relationship between vehicle priority (PoV) and content priority (PoC). Then, they proposed a method based on fuzzy logic to select the most appropriate content replication tool (CRV) to assist the content distribution and redefine the number of content request tools in each segment. They proposed an algorithm based on immune cloning to solve this problem. Their research method has certain flaws [4].

According to the inference node allocation algorithm proposed based on the edge computing idea, different rule sets and conditions of different simulation environments are designed in the simulation environment, and the two evaluation parameters designed for its real-time performance and resource balance are observed to verify the performance of the proposed algorithm. Both real-time performance and resource balance have been greatly improved. This article uses the CCA method to analyze the risk level of the insurance sec-

tor and the securities sector and combines the analysis results of the banking sector and the overall financial sector to explore the specific risk situation of my country's financial system. The financial system covers a wider range. Bayesian networks can combine prior information or expert knowledge with sample data to solve problems in related fields. When modeling with less sample data, prior information and domain knowledge play an important role.

2. Intelligent Edge Computing and Bayesian Posterior Probability Model

2.1. Intelligent Edge Computing. Each mobile device in the edge node contains a trusted execution environment to store pseudonyms, and malicious adversaries cannot tamper with the stored information. When the key generation center traces a single point of failure of the malicious vehicle, the edge node assists the key generation center to complete the dual traceability of the malicious vehicle. The vehicle migrates multi-tasking to the mobile device for processing. Before receiving the processed message, the vehicle should check the integrity of the message obtained from the mobile device and share data with vehicles in the same area through edge nodes, reducing system redundancy and reducing system overhead [5].

Therefore, the wireless access network has the ability of low-latency, high-bandwidth transmission, and wireless network information perception and opening, avoiding bottlenecks and system failures. At the same time, computing tasks and data sinking, that is, localized deployment, can effectively reduce the computing load and storage load of mobile systems, thereby achieving the goal of optimizing mobile network operating costs [6]. In addition, mobile operators can use mobile edge computing platforms to form a new industry chain that will benefit from the cooperation of mobile cloud platforms, application developers, and network equipment manufacturers. Mobile edge computing can be applied to the business model of some specific applications, which can benefit from both application service providers and application service users [7].

Based on the real-time information of the wireless access network, the degree of congestion of the wireless cellular network and the occupancy of network bandwidth can be estimated, which will assist such applications to make decisions to improve the quality of service. In the same-frequency networking mode, the task migration system adopts a full spectrum reuse mode to improve the utilization of the spectrum, but this method will introduce interference between cells. Compared with the same-frequency networking, the cells in the interfrequency networking mode use different frequency band resources [8]. Although the spectrum efficiency of this method is lower, the resource management algorithm is simple, and cell users under the same frequency have higher transmission efficiency. From the perspective of edge servers, based on the strong computing and communication capabilities of edge servers, edge computing system managers expect to be able to share information related to road safety and popular content uploaded by vehicles with other vehicles in real time, thereby improving road traffic safety and obtaining more benefits [9].

In order to realize the rapid and efficient diffusion of traffic information, vehicles and edge servers need to obey the following calculation migration rules. Through tree search, MCTS obtains the optimal decision of each mobile device on the offload rate, computing resource rate, and communication resource rate. The optimal decision obtained by MCTS is to jointly simulate the future state trajectory and output the best strategy for the current and future moments. DNN is used to generate prior probability distribution that guides MCTS search to accelerate the convergence of MCTS. In order to train DNN, this paper collects training data and labels from the iterative results of MCTS [10].

2.2. Bayesian Posterior Probability Model. The parameters of the Bayesian network are the probability distribution corresponding to each node variable, which are usually obtained by training and learning from the training sample data set. However, when the fault relationship is simple and clear, sometimes the corresponding network parameters can be given directly by analyzing the characteristics of the problem. Bayesian theory is a very effective modeling method for evaluating chemical abnormal events with low probability and high risk [11]. Directional energy is defined as

$$OE_{\theta,s} = (I \times f_{\theta,s}^e)^2 + (I \times f_{\theta,s}^o)^2. \quad (1)$$

Among them, $f_{\theta,s}^e$ and $f_{\theta,s}^o$ are odd-even symmetric orthogonal filter banks in the direction θ and the scale s . The expression of the likelihood function is as follows:

$$p(\theta | X) = \prod_{i=1}^n p(\theta | x_i). \quad (2)$$

According to the nature of exchangeability and conditional probability:

$$p(y, \phi) = p(y)p(\phi | y), \quad (3)$$

$$p(\phi, y) = p(\phi)p(y | \phi), \quad (4)$$

$$p(\phi | y) = \frac{p(\phi)p(y | \phi)}{p(y)} \propto p(\phi)p(y | \phi). \quad (5)$$

The prior information is updated through historical data, and the posterior probability density function $f(x | data)$ is obtained. Its expression is as follows:

$$f(x | data) = \frac{g(x | data)f(x)}{\int g(x | data)f(x)dx} \propto g(x | data)f(x). \quad (6)$$

The probability density function of Beta (a, b) prior distribution is as follows:

$$f(x) = \frac{\Gamma(a+b)}{\Gamma(a)\Gamma(b)} x^{a-1}(1-x)^{b-1} \propto x^{a-1}(1-x)^{b-1}, a > 0, b > 0. \quad (7)$$

The expectation and variance of Beta (a, b) are

$$E(x) = \frac{a}{a+b}, \quad (8)$$

$$V(x) = \frac{ab}{(a+b)^2(a+b+1)}. \quad (9)$$

Use the sample reflected by the probability density function to estimate the expected value of the distribution:

$$E(x) = \lim_{N \rightarrow \infty} \frac{\sum_{i=1}^N x_i f(x_i)}{\sum_{i=1}^N f(x_i)}. \quad (10)$$

Among them, N is the number of iterations.

Define the texture gradient as the distance between these two histograms:

$$\chi^2(g, h) = \frac{1}{2} \sum \frac{(g_i - h_i)^2}{g_i + h_i}. \quad (11)$$

In order to ensure stability, the improved characteristics are defined as

$$\hat{f}(x) = f(x) \left(\frac{-f''(x)}{|f'(x) + \lambda|} \right). \quad (12)$$

Among them, λ is a parameter used to optimize features.

The Bayesian framework combines the prior probability and the posterior probability, that is, the observation likelihood probability obtains the final pixel-level saliency detection result:

$$f(sal | I) = \frac{f(sal)f(I | sal)}{f(sal)f(I | sal) + f(b)f(I | b)}, \quad (13)$$

$$f(b) = 1 - f(sal). \quad (14)$$

Among them, $f(sal)$ and $f(b)$ represent the prior distribution of the target and background, respectively. An efficient and scalable feature extraction algorithm for time-series filters available features in the early stages of the machine learning pipeline to obtain features that are meaningful for classification or regression, while controlling the selection of unrelated features as far as possible.

The Bayesian network model construction process is shown in Figure 1. The failure prediction method is based on the failure physical model, through the analysis of the failure of the equipment, mining the relevant characteristic parameters when the failure occurs, and establishing the failure model of the equipment on the basis of studying the operating principle and physical nature of the equipment; this method is generally applicable for simple equipment with simple system composition and simple operating principle, and the data collected from the sensor is combined with the failure model to predict the potential failure of the equipment, so as to achieve the purpose of reducing the number of maintenance and maintenance costs, and

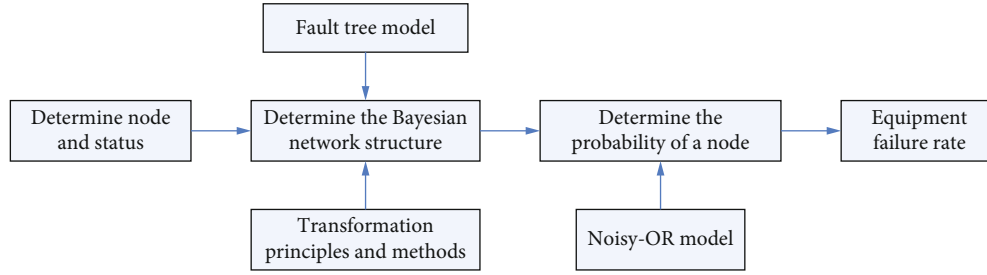


FIGURE 1: Bayesian network model construction process.

extending the maintenance cycle of the equipment. And it is not suitable for equipment with a complex structure, such as the complex electronic information system and mechanical equipment system. Generally, fault prediction technology based on data and statistics is used. After the Bayesian network model is constructed in this paper, according to the given prior probability, the corresponding posterior probability of each fault node factor at the time of failure can be inferred [12, 13].

As shown in Figure 1, the state of node and model evaluation should be determined first, and then the probability of node occurrence and equipment failure rate should be determined by using the Bayesian network structure, while the principle and method of Noisy-OR model transformation is lag behind.

2.3. Financial Asset Risk Measurement. When investors make investment decisions, they only pay attention to the returns and risks of the asset portfolio. At the same time, for investors, the mean and variance can truly describe the returns and risks of the portfolio. And the risk preference of all investors in the market is risk aversion, that is, the investment preference of investors follows the principle of second-order random dominance. Because the object of venture capital is new projects or startups, there are a lot of uncertainties in its market prospects and investment income, so venture capital is a veritable high-risk investment behavior [14].

In order to reduce the risk and ensure the realization of the expected return, venture capitalists must use scientific methods to measure the risks of the projects or enterprises they invest in. Because of the insufficient sample size and the nonrepeatability of single-period investment, the historical data needed for venture capital measurement cannot be obtained accurately, and the required historical data can only be obtained from similar projects. After the financial risk status is identified, it is necessary to quantitatively measure the more important risks. Risk measurement is the core of risk management, which directly determines the effectiveness of risk management [15, 16].

The Bayesian network is established based on a bow-tie model. Risk source and failure of control measures in advance are mapped to root event, intermediate nodes are built from root event to risk event, the leaf node is mapped from risk event, safety barrier node is mapped from postaccident control measures, and the result node is mapped from accident consequence to establish the risk Bayesian network of evaluation object. The main methods measure the market risk such as

interest rate sensitivity analysis, volatility analysis, VaR, stress test, and extreme value theory. Because duration only measures the linear relationship between a bond price change and yield change, but the actual market situation shows that the change between a bond price and interest rate is nonlinear, especially when the yield changes greatly, duration cannot accurately measure the interest rate sensitivity of bond price. Therefore, the second-order estimation of the interest rate sensitivity of bond price, namely convexity, must be used to correct the error of duration estimation [17].

3. Financial Asset Risk Measurement Experiment

3.1. Experimental Parameters. In a distributed D2D-ECN network, the primary user MD and the auxiliary user SD are randomly distributed within the coverage of the local base station LBS. D2D-ECN is a powerful and user-friendly trading platform that uses proven and mature technology to help traders reach a higher level of forex trading. Traders get guaranteed execution without requotes as long as there is depth available in the market. When the distance between the primary user and the auxiliary user is less than the preset distance threshold, MD and SD can establish a data transmission link through the device through technology. The channel model not only considers the path loss based on distance but also considers small-scale fading [18, 19]. The international financial mechanism refers to the general term for the rules, conventions, policies, mechanisms, and organizational arrangements for the regulation of international payment, settlement, exchange, and transfer of various currencies. The specific simulation parameters are shown in Table 1.

3.2. Data Selection. Due to the limited data of personal housing mortgage loans contained in the database and a large part of the sample index that is incomplete, plus the factors of the bank, this paper samples the data in the database; part of the sample is extracted from the database for empirical analysis. In this paper, the daily closing prices of energy stocks in Shanghai Stock Exchange and Shenzhen Stock Exchange are selected by using a risk control strategy. The data comes from DaWisdom software [20].

3.3. Model Parameter Estimation. After establishing the GARCH model with EViews software, according to the AIC criterion, select the GARCH- t (1,1) model. The advantage of AIC is that it has a commercial bank background,

TABLE 1: Simulation parameters.

Energy arrival rate	[10,1517] (J/cm ² /day)
Available computing resources	[2.5,5] (GHz)
Maximum transmit power of the main user	0.130 W
Calculation period required for unit bit	735 cycles/bit
Calculated size of the task	[100,300] (Kbits)
Shadow fading	PL (dB) = 62.3
System bandwidth	5 MHz
Discount factor	0.9
Time-varying learning rate	1/t

natural resource information advantages, and a low cost of obtaining high-debt and high-quality corporate information. Then establish the corresponding GARCH- t (1,1) models for SH and SZ, respectively, so that the respective mean values of the two sequences and the relevant parameter values and the degrees of freedom of t distribution can be obtained, and then use the MATLAB2010 software to calculate the heteroscedasticity $h(t)$. The iterative formula calculates $h(t)$ sequences and converts them into probability integrals. According to the result of the probability integral conversion, the maximum likelihood estimation method is used to obtain a series of correlation coefficients and degrees of freedom of t -Copula [21, 22].

3.4. Image Edge Pixel Distribution. For each image, we calculate the proportion of background pixels whose edges are within 10% of the image size from the four edges of the image. The pixels within 10% of the image size are selected to be consistent with the parameter selection of the background reference set in the method. The edge user node sends a service request to the edge server node, and the edge server uses the model proposed in this paper to evaluate the user's credibility and selects the corresponding service level according to the credibility level corresponding to the calculated credibility result [23, 24].

3.5. Performance Evaluation. This article uses the RAROC method to evaluate the risk performance of financial assets. Financial institutions can only retain and absorb financial market risks that cannot be avoided and transferred. For this reason, financial institutions and their business departments must prepare a part of special capital to resist risk losses to ensure the normal operation of the institution. The model is highly conservative, and the choice of confidence level should also consider the constraints of sample data. The higher the confidence level is chosen, the less likely the actual loss will exceed VaR [25].

3.6. Data Analysis. Reduce the low degree of relevance through dimensionality reduction and centralized processing of data, thereby reducing the workload of data processing. This article uses principal component analysis to reduce the dimensionality of the collected data. The analysis principle of PCA is to remove the components with small variances and retain the components with large variances.

In this way, the dimensionality of the data set is reduced. Therefore, when using principal component analysis to study complex signals, some components can be ignored to improve research efficiency. After the principal component model is established, the statistics of the test sample can be completed through the principal component model. Whether there is a fault can be assessed according to how much the value of the statistic differs from the control limit. CPV determines the retention of the number of principal elements, and the PCA analysis is used to model the sample set [26]. Big data is the term for big data sets. Big data sets are those that have grown beyond the simple database and data processing architectures used in the early days, when big data was more expensive and less feasible.

3.7. Bayesian Model Test. After obtaining the inductive strength of the conclusion and the similarity between categories, the Bayesian model can be tested. The Bayesian model test is divided into two parts: firstly, the average value of all subjects is used for testing; secondly, the test is conducted by using single-subject data to test whether the model can cope with individual differences, that is, whether it can make personalized predictions. At the same time, the outlier detection and the determination of the membership degree of the sample points in this paper are all carried out in the feature space. In order to ensure the accuracy of the outlier detection and the membership degree of the sample points obtained, it is also necessary to find a suitable mapping feature space for the training set [27]. No matter how the Bayesian model test establishes the hypothesis, it does not need to give the significance level. As long as the posterior distribution of the parameters is given, by calculating the posterior probability of each hypothesis, and comparing the posterior probability of the hypothesis, the desired value can be obtained by the test results.

4. Financial Asset Risk Measurement Analysis

4.1. Edge Computing Simulation Analysis. The problems faced by the edge computing platform in its promotion are analyzed. Then, the typical edge computing platform is analyzed from the perspective of architecture, and the demand parameters of edge computing application scenarios are listed. Finally, a classification model of the edge computing platform is proposed. We use 5 users and 1 edge server,

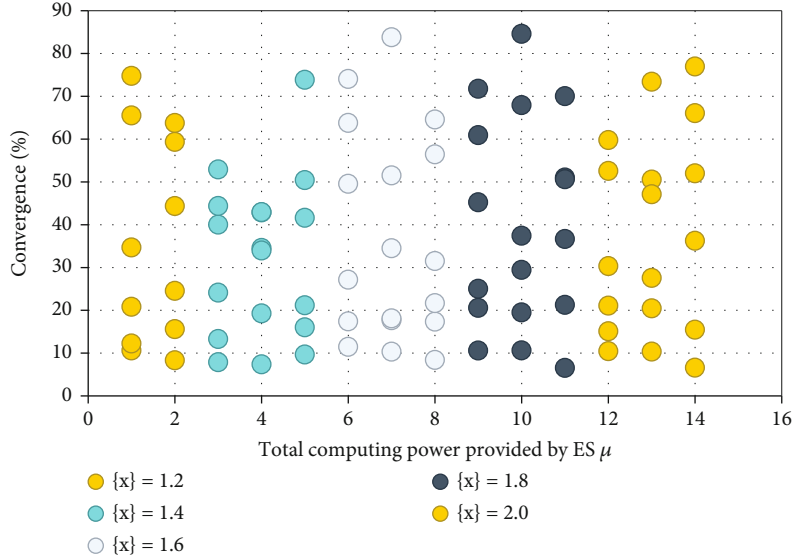
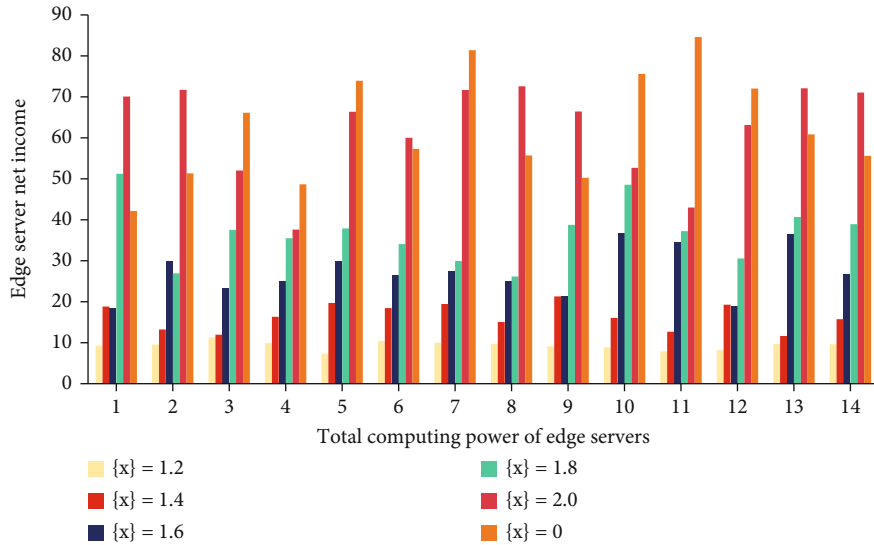


FIGURE 2: Convergence of the edge computing technology.

FIGURE 3: The trend of edge server net income with different μ .

where the cost of computing power provided by the edge server can be shown as $C(x) = px$, and we set $p = 10$ in this chapter. The local computing power of 5 smart terminals is set to $\{x\} = \{1.2, 1.4, 1.6, 1.8, 2.0\}$. The convergence of the edge computing technology is shown in Figure 2. μ represents the total computing power obtained by all smart terminals from the edge server. When μ increases, the total net income increases first, and then when μ exceeds a certain threshold, v gradually decreases. When μ reaches a certain threshold, the user's net income does not increase. This is in line with our expectations, because the benefits of blockchain-based digital currencies (such as Bitcoin) within a fixed period of time are limited, and the benefits will not continue to grow when the user's computing power is large enough. The change trend of edge server net income with different μ is shown in Figure 3. First, it increases with the increase of μ and then begins to decrease after passing the

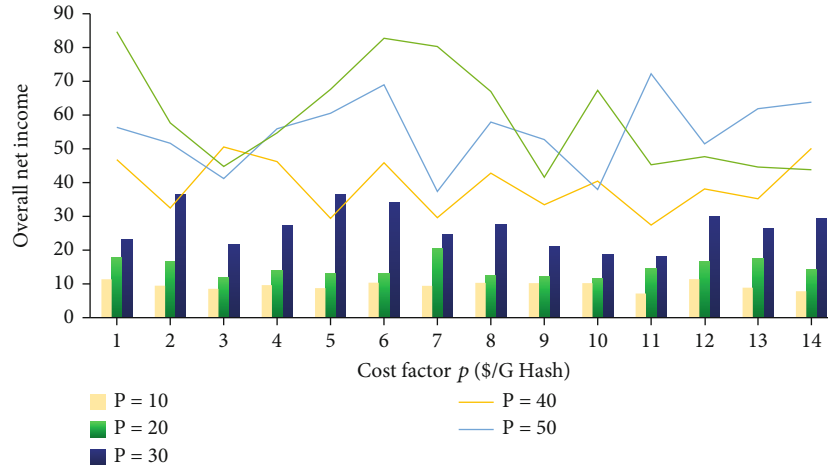
TABLE 2: The calculation results of each smart terminal i .

5 users-1 edge server scenario	X_1	X_2	X_3	X_4	X_5
CVX results	0.69	0.49	0.29	0.09	0
Sum $\{x\}$	1.56				
Intelligent edge computing results	0.69	0.49	0.29	0.09	0
Sum $\{x\}$	1.56				

threshold. This result is also correct, starting to provide users with computing resources to increase the probability of users gaining benefits, and at the same time, it can also increase the shared benefits they receive. When μ continues to increase, the revenue of digital currency will not increase, the cost of providing computing resources increases, and the net revenue decreases. In summary, the trend of the total net income in Figure 3 is correct.

TABLE 3: Calculation results of intelligent edge computing.

5 users-1 edge server scenario	γ_1	γ_2	γ_3	γ_4	γ_5
CVX results	0.4937	0.4944	0.4950	0.4956	0.4962
Time-consuming			57880.2 s		
Linear search results	0.4937	0.4944	0.4950	0.4956	0.4962
Time-consuming			64.8359 s		
Intelligent edge computing results	0.4937	0.4944	0.4950	0.4956	0.4962
Time-consuming			0.2581 s		

FIGURE 4: First the relationship between the cost coefficient p and the overall net income.

Compare the result of intelligent edge calculation with the calculation result of the MATLAB convex optimization toolbox CVX. The calculation results of each smart terminal i are shown in Table 2. Observation shows that smart edge computing is consistent with CVX, which verifies the correctness of the design algorithm. The calculation results of intelligent edge computing are shown in Table 3. First, the numerical edge calculation is consistent with the CVX and linear search calculation results, and the edge calculation takes 0.2581 seconds in the calculation time, while the linear search takes about 64 seconds. The CVX calculation tool takes about 5788 seconds. This comparison reflects the design of only edge computing based on correctness while taking into account computational efficiency.

First of all, the relationship between the cost coefficient p and the overall net income is shown in Figure 4. At this time, the block capacity is set to $t = 1$ Mbit. The result can show that when the cost coefficient increases, the overall net income decreases. The relationship between the cost coefficient p and the sharing ratio is shown in Figure 5. At this time, the block capacity is set to $t = 1$ Mbit. Observation shows that when p increases, the self-revenue ratio of all smart terminals i decreases. The explanation of this phenomenon is as follows. When p increases, the edge server needs more costs. In order to ensure the fairness of the income and maximize the overall net income, the proportion of the income allocated to the edge server will inevitably increase, and the result is consistent with our expectations.

The effect of block capacity t on the sharing ratio is shown in Figure 6. At this time, the cost coefficient is set to $p = 10$ USD/G Hash. It can be found that when t increases, the self-revenue ratio of all smart terminals i will also increase. This is because the increase in block capacity increases the variable revenue and thus the overall revenue. In order to ensure the fairness of revenue sharing when the edge server needs to bear the cost, the proportion of users will be appropriately increased. It should be noted that the overall return does not increase linearly with t . When t is too large, the probability of winning P will decrease.

4.2. Nonparametric Bayesian Dynamic Asset Allocation and Empirical Analysis. Taking the daily income data of three types of assets as samples, they are China stock funds (Harvest CSI 300 ETF (159919) and Harvest CSI 500 ETF (159922), China bond funds (Cathay Pacific SSE 5-year Treasury ETF, 511010), and Gold funds (Huaan Gold Easy ETF, 518880). All data comes from the WONDER database. This section assumes that the risk-free interest rate is zero. In order to cover a more comprehensive scale and have a good representation in the market, which can better reflect the situation of China's stock market, we use Harvest CSI 300 ETF and Harvest CSI 500 ETF as research samples. In addition, because gold is naturally a currency, has a high value, and is an independent resource, investing in gold can usually help investors avoid problems that may occur in the economic environment, so this article uses the representative Huaan Gold Easy ETF as a research sample. In

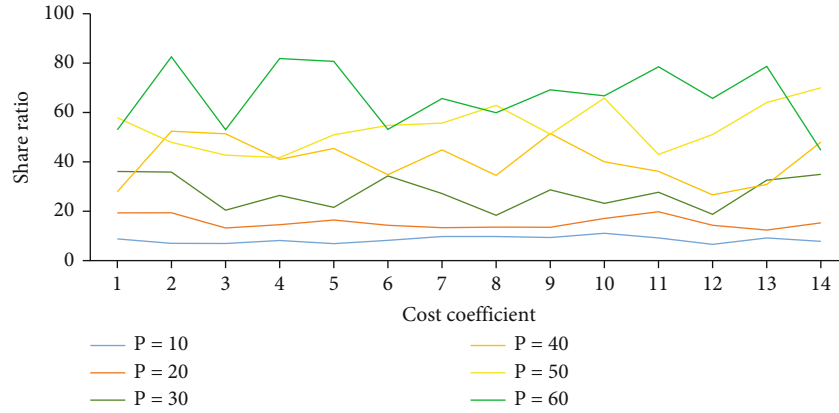


FIGURE 5: The relationship between the cost coefficient p and the share ratio.

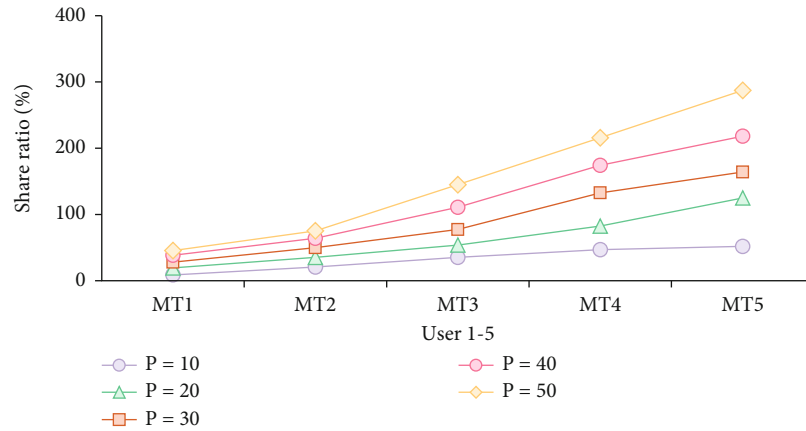


FIGURE 6: The effect of block capacity t on the share ratio.

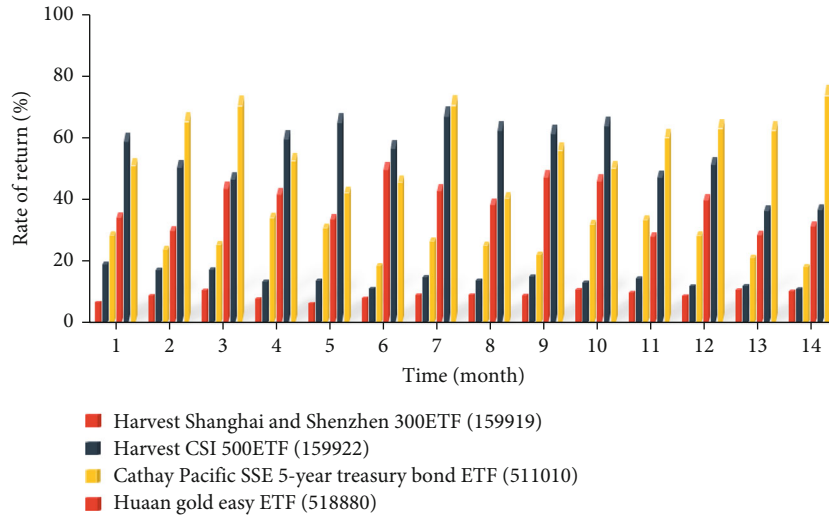


FIGURE 7: The sequence of the cumulative returns of the four assets in the past 3 years.

asset allocation, bond assets can play the role of asset allocation stabilizer, so this article uses more stable national debt for the sample, the Cathay Pacific SSE 5-year Treasury Bond ETF [28].

The sequence of the cumulative returns of the four assets in the past three years is shown in Figure 7. It can be seen that the stock market has experienced a substantial rise in the past three years, but then there has been a substantial rise

TABLE 4: Descriptive statistics of the daily return rate of assets.

Statistics	Harvest Shanghai and Shenzhen 300 ETF	Harvest CSI 500 ETF	Cathay Pacific SSE 5-year Treasury Bond ETF	Huaan Gold Easy ETF
Minimum	-10.545	-10.536	-1.691	-3.800
Median	0.045	0.187	0.013	0.017
Max	9.165	9.412	2.285	4.622
Mean	0.077	0.064	0.016	0.015
Standard deviation	1.543	1.782	0.214	0.847
Skewness	-0.847	-1.242	0.472	0.562
Kurtosis	13.338	11.792	26.134	7.372
Sharpby	0.032	0.020	0.352	0.021

TABLE 5: Correlation of assets.

Harvest Shanghai and Shenzhen 300 ETF	Harvest Shanghai and Shenzhen 300 ETF	Harvest CSI 500 ETF	Cathay Pacific SSE 5-year Treasury Bond ETF	Huaan Gold Easy ETF
Harvest Shanghai and Shenzhen 300 ETF	1	0.694	-0.016	0.036
Harvest CSI 500 ETF	0	1	-0.012	-0.007
Cathay Pacific SSE 5-year Treasury Bond ETF	0	0	1	0.107
Huaan Gold Easy ETF	0	0	0	1

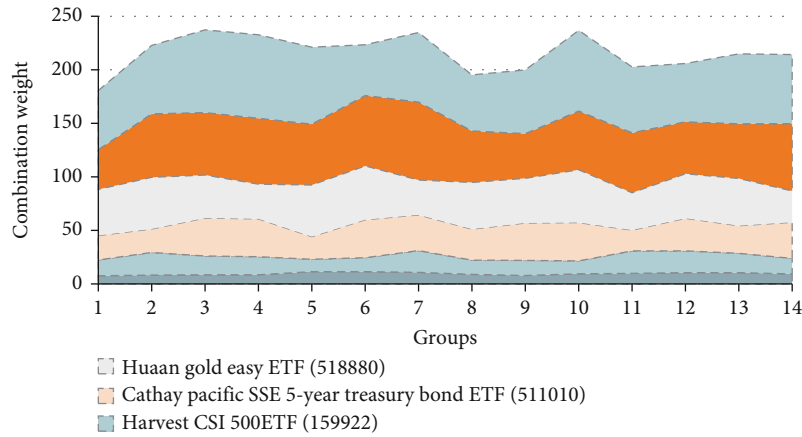


FIGURE 8: Four characteristics of data construction of four assets in the past three year-portfolio weight.

and fall during the two years. In fact, this round of Chinese stock market changes is completely independent of the stock markets of other countries, and the fluctuation range is very large. Bonds have basically maintained a stable upward trend. There are certain fluctuations in the gold market, but the overall trend is rising. The descriptive statistics of the daily return rates of the 4 assets are shown in Table 4. It can be seen from Table 4 that the total average daily return rate of the 4 asset return rate series is positive, and the ARCH test shows that the 4 asset return rate series have significant heteroscedasticity.

The correlation of the 4 assets is shown in Table 5. From Table 5, the unconditional correlation between assets during the sample investment period can be seen. Harvest CSI 300

ETF (159919) and Harvest CSI 500 ETF (159922) have a strong positive correlation. Harvest CSI 300 ETF (159919) and Huaan Gold Easy ETF (518880) have a certain positive correlation, while Cathay Pacific SSE 5-year Treasury Bond ETF (511010), Harvest CSI 300 ETF (159919), and Cathay Pacific SSE 5-year Treasury Bond ETF (511010) have a negative correlation with Harvest CSI 500 ETF (159922).

The four characteristics of the data construction of the four assets in the past 3 year-portfolio weights are shown in Figure 8. Both the driving weights and the Cathay weights represent their overall ratings. The return sequence is converted to the main component. As the explanatory power of data changes declines, the first main component explains the total data 68.64% of the change, while the other principal

TABLE 6: Model prediction effect evaluation.

Characteristic portfolio	1	2	3	4
LPS				
TSVL-DPM	2.03	2.10	2.13	2.09
TSV-DPM	2.04	2.14	2.15	2.14
SV-N	2.08	2.15	2.16	2.15
LPS _{0.05}				
TSVL-DPM	2.96	3.13	3.16	3.06
TSV-DPM	3.00	3.16	3.19	3.13
SV-N	3.05	3.18	3.21	3.12

TABLE 7: Forecast model Sharpby.

Model LPS	TSVL-DPM	TSV-DPM	SV-N
Sharpby	3.54	3.37	2.82

components explained 25.52%, 0.05%, and 0.01% of the data changes, respectively. The first principal component explains most of the data changes. Among them, the weight of Harvest CSI 300 ETF (159919) and Harvest CSI 500 ETF (159922) are positive, and that of Cathay Pacific SSE 5-year Treasury ETF (511010) and Huaan Gold Easy ETF (518880) is negative, as shown in the figure. In the dynamic asset allocation model, the construction of feature portfolios is not fixed, because during the investment period, the covariance of assets will change over time, so the weight of each asset in each feature portfolio will also change with time, that is, according to changes in investment opportunities and changes in the covariance matrix of assets, the feature-investment portfolio is dynamically constructed.

4.3. Comparative Analysis of Model Effects. The model prediction effect evaluation is shown in Table 6. The Sharp prediction model is shown in Table 7. In order to evaluate the accuracy of the predictions of different asset return generation models, this paper uses the logarithmic prediction score (LPS) and logarithmic prediction tail score (LPTS) evaluation methods to compare the model prediction effects, that is, the log prediction score and the log prediction tail. The smaller the score, the better the prediction effect of the model. In order to measure the investment performance of the asset allocation model, the model can be used to predict the expected portfolio return rate and volatility to evaluate the model. Specifically, the Sharpe ratio is used to compare the models. It is generally believed that the larger the Sharpe ratio value, the model investment performance the better. Because this kind of economic evaluation relies on the assumption of the investor's utility function, this kind of evaluation is not reliable in a statistical sense. However, the economic impact of the model will give investors a strong incentive to use this method.

It can be seen from Table 6 that the logarithmic prediction scores (LPS) of several models are relatively similar, indicating that these models have good fitting effects on the sample data, and the logarithmic prediction tail score (LPTS) value is compared. It is found that the TSVL-DPM

model has the smallest score value, which is significantly smaller than the SV-N model, indicating that the TSVL-DPM model has the best effect in extreme event prediction. It can be seen from Table 7 that the Sharpe ratio of the TSVL-DPM model is the largest, indicating that the TSVL-DPM model performs best in the dynamic asset allocation strategy model.

5. Conclusions

For all current social enterprises, in the financial investment project system, doing a good job of risk control has more significant application significance. The important goal of social enterprise management and development is to maximize the benefits, and financial investment activities themselves have income uncertainty. In this case, if each enterprise wants to achieve the goal of maximizing benefits, it needs to conduct a comprehensive risk analysis of financial investment activities and eliminate its risks as much as possible to ensure that the project can obtain the corresponding benefits. This paper chooses the EGARCH model to describe the volatility of financial assets, adopts the extreme value theory on the sample residual sequence after parameter estimation, constructs the EGARCH-GPD model, and finally realizes the dynamic value-added reseller (VaR) estimation of financial assets. In the empirical analysis of the combination model, the comparison with other classic models and the return test results of VaR estimation show that the combination model is indeed more accurate and effective in estimating financial risk VaR. Through the denoising, normalization, power spectrum analysis of these three vibration signal sets, and the analysis of the vibration signal in the normal state, the normal state standard threshold is set. The training sample data set is obtained by comparing the vibration signal set in the state of broken teeth with the normal standard threshold, and the verification sample data set is obtained by comparing the vibration signal in the worn state with the normal standard threshold.

When financial institutions measure the market risk of overseas financial assets, even if they use the VAR model, they simply consider the risk of the price fluctuation of financial assets in the country where they are located, and there is no effective management of the exchange rate risk after translation. This paper proposes to improve the traditional VAR model based on continuous time, which not only considers the respective volatility of securities return and exchange rate. VaR's risk calculation method for financial assets or investment portfolios is based on a statistical analysis of the past return characteristics to predict the volatility and correlation of their prices, thereby estimating the maximum possible loss. Therefore, it is not the whole of systematic risk management based solely on the objective probability of losses that the risk may cause, and only focusing on the statistical characteristics of the risk. Because the probability cannot reflect the willingness or attitude of the economic subject to the risks it faces, it cannot determine the share of the risk that the economic subject is willing to bear and should avoid when faced with a certain amount of risk. In the sensitivity analysis of the new VAR model,

their relative and absolute VaR values are monotonically increasing, and VaR is more sensitive to the correlation coefficient than the volatility of financial asset prices and exchange rates. In this paper, a fast numerical method is proposed, and the vectorization analytical expression of the objective function is derived. The parallel calculation of tmcmc is realized, and the efficiency of model parameter correction is greatly improved.

Data Availability

The data that support the findings of this study are available from the corresponding author upon reasonable request.

Conflicts of Interest

The author declares no conflicts of interest.

Acknowledgments

This work was supported by the National Social Science Foundation of China (14BTQ049), Shandong Natural Science Foundation (ZR2020MG003), and Special Project for Internet Development of Social Science Planning Special Program of Shandong Province (17CHLJ23).

References

- [1] Y. Liu, C. Yang, L. Jiang, S. Xie, and Y. Zhang, "Intelligent edge computing for IoT-based energy management in smart cities," *IEEE Network*, vol. 33, no. 2, pp. 111–117, 2019.
- [2] B. Cao, L. Zhang, Y. Li, D. Feng, and W. Cao, "Intelligent off-loading in multi-access edge computing: a state-of-the-art review and framework," *IEEE Communications Magazine*, vol. 57, no. 3, pp. 56–62, 2019.
- [3] Q. Xu, Z. Su, K. Zhang, and P. Li, "Intelligent cache pollution attacks detection for edge computing enabled mobile social networks," *IEEE Transactions on Emerging Topics in Computational Intelligence*, vol. 4, no. 3, pp. 241–252, 2020.
- [4] Q. Luo, C. Li, T. H. Luan, and W. Shi, "EdgeVCD: intelligent algorithm-inspired content distribution in vehicular edge computing network," *IEEE Internet of Things Journal*, vol. 7, no. 6, pp. 5562–5579, 2020.
- [5] R. Dautov, S. Distefano, D. Bruneo et al., "Metropolitan intelligent surveillance systems for urban areas by harnessing IoT and edge computing paradigms," *Software: Practice and Experience*, vol. 48, no. 8, pp. 1475–1492, 2018.
- [6] G. Jia, G. Han, H. Rao, and L. Shu, "Edge computing-based intelligent manhole cover management system for smart cities," *IEEE Internet of Things Journal*, vol. 5, no. 3, pp. 1648–1656, 2018.
- [7] D. Sivaganesan, "Design and development AI-enabled edge computing for intelligent-IOT applications," *Journal of Trends in Computer Science and Smart technology (TCSST)*, vol. 2019, no. 2, pp. 84–94, 2019.
- [8] T. Wang, H. Luo, X. Zheng, and M. Xie, "Crowdsourcing mechanism for trust evaluation in CPCS based on intelligent mobile edge computing," *ACM Transactions on Intelligent Systems and Technology*, vol. 10, no. 6, pp. 1–19, 2019.
- [9] M. Usman, A. Jolfaei, and M. A. Jan, "RaSEC: an intelligent framework for reliable and secure multilevel edge computing in industrial environments," *IEEE Transactions on Industry Applications*, vol. 56, no. 4, pp. 4543–4551, 2020.
- [10] S. Chen, H. Wen, J. Wu et al., "Radio frequency fingerprint-based intelligent mobile edge computing for internet of things authentication," *Sensors*, vol. 19, no. 16, pp. 12–15, 2018.
- [11] J. M. Hung, X. Li, J. Wu, and M. F. Chang, "Challenges and trends in developing nonvolatile memory-enabled computing chips for intelligent edge devices," *IEEE Transactions on Electron Devices*, vol. 67, no. 4, pp. 1444–1453, 2020.
- [12] X. Wang, Y. Han, V. C. M. Leung, D. Niyato, X. Yan, and X. Chen, "Convergence of edge computing and deep learning: a comprehensive survey," *IEEE Communications Surveys & Tutorials*, vol. 22, no. 2, pp. 869–904, 2020.
- [13] I. Nazarenko and A. Oriekhova, "Diagnostics of monetary assets of Ukrainian agribusiness entities: relevance, peculiarities, and the process of algorithm construction," *Journal of Environmental Management and Tourism*, vol. 8, no. 7, pp. 1373–1381, 2017.
- [14] M. D. Flood and P. Monin, "Form PF and the systemic risk of hedge funds: risk-measurement precision for option portfolios," *Journal of Alternative Investments*, vol. 18, no. 4, pp. 125–147, 2016.
- [15] E. Mordecki, A. R. Pena, and A. Sosa, "Exchange credit risk: measurement and implications on the stability of partially dollarized financial systems," *SSRN Electronic Journal*, vol. 3, no. 2, pp. 523–531, 2016.
- [16] Y. Sandoval, R. Nowak, C. R. Defilippi et al., "Myocardial infarction risk stratification with a single measurement of high-sensitivity troponin ihigh-sensitivity," *Journal of the American College of Cardiology*, vol. 74, no. 3, pp. 271–282, 2019.
- [17] M. O. Morais, A. C. F. Pinto, and M. C. Klotzle, "Scenario analysis in the BNDES experience: integrating operational risk management with the measurement of capital," *Revista Contabilidade & Finanças*, vol. 29, no. 77, pp. 283–296, 2018.
- [18] R. Daza and K. M. Hargiss, "Factors comprising effective risk communication, decision-making, and measurement of IT and IA risk," *International journal of strategic information technology and applications*, vol. 9, no. 1, pp. 23–40, 2018.
- [19] G. Peters, P. V. Shevchenko, B. Hassani, and A. Chapelle, "Should the advanced measurement approach be replaced with the standardized measurement approach for operational risk?," *Journal of Operational Risk*, vol. 11, no. 3, pp. 1–49, 2016.
- [20] X. Zhu, J. Li, and D. Wu, "Should the advanced measurement approach for operational risk be discarded? Evidence from the Chinese banking industry," *Review of Pacific Basin Financial Markets and Policies*, vol. 22, no. 1, 2019.
- [21] F. Piacenza and C. Belloni, "Standardized measurement approach extension to integrate insurance deduction into operational risk capital requirement," *Journal of Operational Risk*, vol. 12, no. 4, pp. 31–49, 2017.
- [22] Z. Xu, G. Zhu, N. Metawa, and Q. Zhou, "Machine learning based customer meta-combination brand equity analysis for marketing behavior evaluation," *Information Processing & Management*, vol. 59, no. 1, article 102800, 2022.
- [23] A. A. M. Jamal, W. M. R. W. Ahmad, A. Esa, and N. A. A. Jalil, "Risk management outdoor education for instructors and students: application using Rasch measurement," *Journal of Computational and Theoretical Nanoscience*, vol. 24, no. 11, pp. 7974–7976, 2018.

- [24] N. Szumilo, P. Gantenbein, W. Gleissner, and T. Wiegelmann, "Predicting uncertainty: the impact of risk measurement on value of real estate portfolios," *Journal of Property Research*, vol. 33, no. 1, pp. 1–17, 2016.
- [25] E. Wulandari, D. Supyandi, and E. Ernah, "The risk measurement of horticultural price: a comparison based on financial access in West Java, Indonesia," *Sains Malaysiana*, vol. 49, no. 3, pp. 713–719, 2020.
- [26] H. Kim, "Application to the stochastic modelling of risk measurement in bunker price and foreign exchange rate on the maritime industry," *Journal of Korea Port Economic Association*, vol. 34, no. 1, pp. 99–110, 2018.
- [27] N. Georgiopoulos, "The use of the triangular approximation for some complicated risk measurement calculations," *Journal of Risk Model Validation*, vol. 11, no. 3, pp. 69–98, 2017.
- [28] R. Hoffmann, J. Napiórkowski, T. Protasowicki, and J. Stanik, "Measurement models of information security based on the principles and practices for risk-based approach," *Procedia Manufacturing*, vol. 44, no. 1, pp. 647–654, 2020.

Research Article

Superresolution Reconstruction of Remote Sensing Image Based on Generative Adversarial Network

Qiaoliang Zhou 

School of Information Engineering, JinZhou University, JinZhou 434000, China

Correspondence should be addressed to Qiaoliang Zhou; zhouqiaoliang@cumt.edu.cn

Received 1 November 2021; Revised 5 December 2021; Accepted 29 December 2021; Published 10 March 2022

Academic Editor: Mu-Yen Chen

Copyright © 2022 Qiaoliang Zhou. This is an open access article distributed under the Creative Commons Attribution License, which permits unrestricted use, distribution, and reproduction in any medium, provided the original work is properly cited.

To recreate high-resolution, more detailed remote sensing images from existing low-resolution photos, this technique is known as remote sensing image superresolution reconstruction, and it has numerous uses. As an important research hotspot of neural networks, generative adversarial network (GAN) has made outstanding progress for image superresolution reconstruction. It solves the computational complexity and low reconstructed image quality of standard superresolution reconstruction algorithms. This research offers a superresolution reconstruction strategy with a self-attention generative adversarial network to improve the quality of reconstructed superresolution remote sensing images. The self-attention strategy as well as residual module is utilized to build a generator in this model that transforms low-resolution remote sensing images into superresolution ones. It aims to determine the discrepancy between a reconstructed picture and a true picture by using a deep convolutional network as a discriminator. For the purpose of enhancing the accuracy, content loss is used. This is done to obtain accurate detail reconstruction. According to the findings of the experiments, this approach is capable of regenerating higher-quality images.

1. Introduction

People's expectations for image quality have risen in tandem with scientific and technological advancements and the widening of practical application domains. Image resolution is the key basis for measuring image accuracy and clarity, and the level of image resolution is positively correlated with image clarity. As a result, meeting the public's desire for high-quality photographs is now a top priority for image processing researchers.

In remote sensing imaging, people can use the acquired remote sensing data for military target identification, environmental monitoring, disaster research, and timely understanding and tracking of changes on the ground. A high-resolution remote sensing image can provide more detailed texture information and higher resolution. The richer feature information contained in the image provides a favorable basis for the various research and application of remote sensing images. However, in the remote sensing imaging process, the distance between the target and the imaging system is relatively long, and it is also affected by some other

factors. The quality of the obtained remote sensing image is often low, which makes the local area in the image blurred, part of the information is lost, and the target recognition is low, which cannot meet people's data requirements [1–5].

Improving the hardware conditions of imaging equipment is the most direct and effective way to obtain superresolution images. This method is mainly divided into two kinds: improving the manufacturing process of the sensor to reduce the pixel size. However, as the pixel size continues to decrease, the amount of light it obtains becomes smaller, and shot noise will eventually be introduced. This leads to reduced image quality. The second is to increase the number of photosensitive elements on the sensor to increase the number of pixels. This approach will lead to a significant increase in economic costs and limit the development and application of high-resolution image technology through hardware methods.

Image superresolution reconstruction is a software technique that reconstructs a high-resolution image from a series of lower-resolution photos. As a result of this method's ability to overcome the limits of current hardware technology, it

is inexpensive and easy to implement and can be used with any current picture system. Economic, practical, and extremely viable are all attributes of superresolution reconstruction technology. This technology is not just useful for image processing in remote sensing. Medical imaging and video surveillance are two examples of where it might be used. It offers major theoretical significance and vast application potential to use software technologies to improve the resolution of remote sensing images [6–10].

Scholars in the United States and elsewhere have used cutting-edge artificial intelligence algorithms in the field of image superresolution reconstruction, thanks to the rapid growth of AI, machine learning, computer vision, and other technologies. A new area of machine learning called deep learning enables computers to build more complex notions from simpler ones. In deep learning, it is possible to improve the quality of the rebuilt image while also reducing the computation time. There are numerous academic benefits and potential applications for using the network model of deep learning to rebuild satellite picture resolution [11–15].

The following are the paper’s innovations: (1) Using a self-attention generating adversarial network, a technique for recovering the texture features from a rebuilt superresolution remote sensing image is presented to address this challenge. (2) In order to enhance the quality of superresolution image reconstruction, optimize content and perceptual loss. (3) Many experiments have proven that the proposed method is reliable and correct, and it performs better on common datasets.

Our paper is organized as follows: Section 1 is an introduction. In Section 2, the related work is introduced. In Section 3, the proposed method is explained in detail. In Section 4, extensive experiments are conducted to verify the effectiveness of the proposed method. Section 5 is a conclusion.

2. Related Work

The interpolation-based superresolution method used different interpolation functions to fit the known pixel values of the surrounding neighborhood and then calculated the pixel for the position which is needed to be interpolated. Literature [16] used the geometric duality of images with different resolutions to estimate the pixels to be interpolated by calculating the local covariance for low-resolution images. Literature [17] proposed an image interpolation algorithm combining soft decision estimation and piecewise autoregressive reconstruction model. Each interpolation process could estimate a group of pixels at the same time, which effectively improved the edge and texture structure for interpolated images. Literature [18] proposed an adaptive interpolation algorithm, which first estimated high-resolution image gradient from low-resolution picture, and then used it as a constraint, which could reconstruct the high-resolution picture. Literature [19] introduced new model parameters on the basis of moving least square interpolation to recover more image details.

The reconstruction-based superresolution method analyzed factors such as downsampling, blur, and noise that cause image degradation, established a physical model for

image degradation, and estimated the original high-resolution picture by optimizing the objective function. Literature [20] proposed a convex set projection method to achieve superresolution reconstruction and used the intersection of convex sets generated by the solution space under different constraints to obtain high-resolution images. Literature [21] proposed an iterative back-projection method, which substitutes the initially estimated high-resolution picture to the degradation model to generate the degraded image. That iteratively updated the reconstructed image by optimizing the error between it and the actual low-resolution image. Literature [22] utilized the maximum posterior probability estimation method to estimate high-resolution pictures when posterior probability is the largest. Literature [23] proposed a regional spatial adaptive full variational reconstruction model and added the processing process of spatial information filtering and information weight clustering. While restoring the edge details of the image, the interference of noise is suppressed. Literature [24] proposed a superresolution reconstruction algorithm with adaptive regularization parameters, which used the particle swarm optimization algorithm to solve appropriate regularization parameters for different image regions, which improved the quality of image reconstruction. Literature [25] estimated the high-resolution target picture with maximizing the likelihood, and the reconstructed image had obvious edge and texture features.

In the learning-based superresolution method, a large number of training samples were used to understand the mapping relationship between high-resolution and low-resolution images. The high-resolution image that corresponds to the low-resolution image could then be obtained by using this mapping relationship. Literature [26] suggested an instance learning-based strategy for superresolution reconstruction building a Markov network to learn the mapping from low-resolution picture block sizes to high-resolution image block sizes. After that, you could perform superresolution reconstruction using the network model you learned before. Literature [27] built a Markov random field using the maximum posterior probability and then used the belief propagation technique to maximize the estimate of model parameters. This enhanced the rebuilt image’s edge sharpness and texture details. In the literature, a neighborhood embedding reconstruction algorithm based on local linear embedding was proposed by literature [28]. The approach leveraged the local linear embedding of manifold learning to rebuild high-resolution images when the associated low-resolution image blocks had similar local manifold structures. Literature [29] had shown that using a binary tree complex wavelet transform to extract the image’s feature information allows for superresolution reconstruction while still preserving the image’s rich features. Literature [30] showed that only the final layer uses subpixel convolution for image upsampling, which minimized the computational complexity of the network model. Reconstruction networks with 20 convolutional layers were proposed in literature [31], and residual learning and gradient clipping were used to ensure the efficiency and stability of the networks’ convergence. Deep networks had fewer training parameters

because literature [32] employed a recursive structure to share weight parameter values. Literature [33] employed an adversarial network to generate a superresolution image reconstruction and recovered more image texture information. A single network model was presented in literature [34] for achieving arbitrary scale superresolution reconstruction. The network's upsampling module accepted the superresolution reconstruction multiple as an input parameter, and the weight of the convolutional layer is dynamically predicted, and upsampling in various proportions was performed on that anticipated weight. Literature [35] introduced the superresolution reconstruction network with a feedback mechanism and used the feedback's in-depth data for guidance in expressing the network appropriately, improving picture reconstruction.

3. Method

Using a self-attention generative adversarial network, this chapter provides a paradigm for superresolution reconstruction (SAGAN). The discriminator employs a deep convolutional neural network and adversarial loss to optimize the training of the superresolution model, while the generator uses a deep residual network that combines an attention mechanism with a residual network module. The content loss function of the model is based on the Charbonnier loss function. While this is going on, the feature value before activation for the VGG network is applied to generate perceptual loss, which can obtain precise texture detail reconstruction.

3.1. Overall Framework. To estimate the superresolution image from a low-resolution image, the superresolution reconstruction problem uses a low-resolution image. This image is as close as possible to the original superresolution photograph. A generator network G must be trained to solve this problem, and the parameters of the network can be represented by the symbol θ for the network. Low-resolution images are fed into the generator network, and the output is rebuilt superresolution images, namely,

$$\hat{I}_S = G_\theta(I_L), \quad (1)$$

where \hat{I}_S is the reconstructed superresolution image, I_L represents the low-resolution image, and θ should satisfy

$$\theta = \arg \max_{\theta} \sum L(\hat{I}_S, I_S), \quad (2)$$

where L is loss and I_S is the true superresolution image.

Superresolution picture reconstruction requires training a generator network and a discriminator network to tackle the task effectively. Generators and discriminators make up the system's overarching framework. To begin, the generator tries to make the low-resolution picture look like a true superresolution picture, while the discriminator looks for differences between the two. Figure 1 depicts the overall model's block diagram.

Ultimately, the goal of this research is to develop a generator network that can produce superresolution images that

are as close to actual ones as feasible. The self-attention layer as well as residual self-attention is introduced and embedded to accomplish this. It is capable of superior superresolution picture reconstruction by utilizing global feature information. Our method replaces the standard BatchNorm layer for the generator with an instance normalization layer. Additionally, the resemblance between generated picture and the original picture can be assessed further thanks to the use of content loss optimization techniques. The perception loss is also optimized, and perception loss is calculated using features before activation of the VGG19 network.

3.2. Self-Attention Mechanism Layer. Deep learning researchers originally advocated using the attention mechanism for natural language processing. It is capable of removing regions from the global area that are not as important, which is crucial for jobs like natural language processing. Internal correlation in the data distributions can be captured better with this technique, and the need for external information is reduced. To focus on a specific location, the human eye quickly analyzes the entire image. The primary objective of the self-attention model is also to choose from a big amount of information that is more critical for the current aim.

It is more efficient to simulate the multilevel dependencies between picture regions when using the self-attention mechanism module in deep learning. The self-attention mechanism is critical in models that must account for global interdependencies. The majority of GAN-based picture generating models now use convolutional layers to create their convolutions. However, because convolution only processes local information, modeling global image dependencies with just the convolution layer is computationally inefficient. With the self-attention mechanism, the image's long-range and multilevel dependencies can be dealt with more effectively, and the generation for near and far details in the picture may be coordinated. To better reconstruct superresolution picture's texture details, consider adding the self-attention layer to the generator's residual module as well as using global information. Figure 2 depicts the hypothesized self-attention mechanism's structural diagram.

As a result of applying two convolutional layers on top of the residual block's second feature map, we can get the two feature spaces $a(x)$ and $b(x)$, respectively. Pixel features are extracted using $a(x)$, and global features are extracted using $b(x)$. The attention map is created by taking $a(x)$ and $b(x)$ and translating them into the following:

$$\alpha_{ji} = \frac{\exp(\beta_{ij})}{\sum_{i=1}^N \exp(\beta_{ij})}, \quad (3)$$

$$\beta_{ij} = a(x_i)b(x_j), \quad (4)$$

where α_{ji} represents the model's attention for the i th position while processing the j th area; then, the output is

$$\varepsilon_i = \sum_{i=1}^N \alpha_{ji} c(x_i). \quad (5)$$

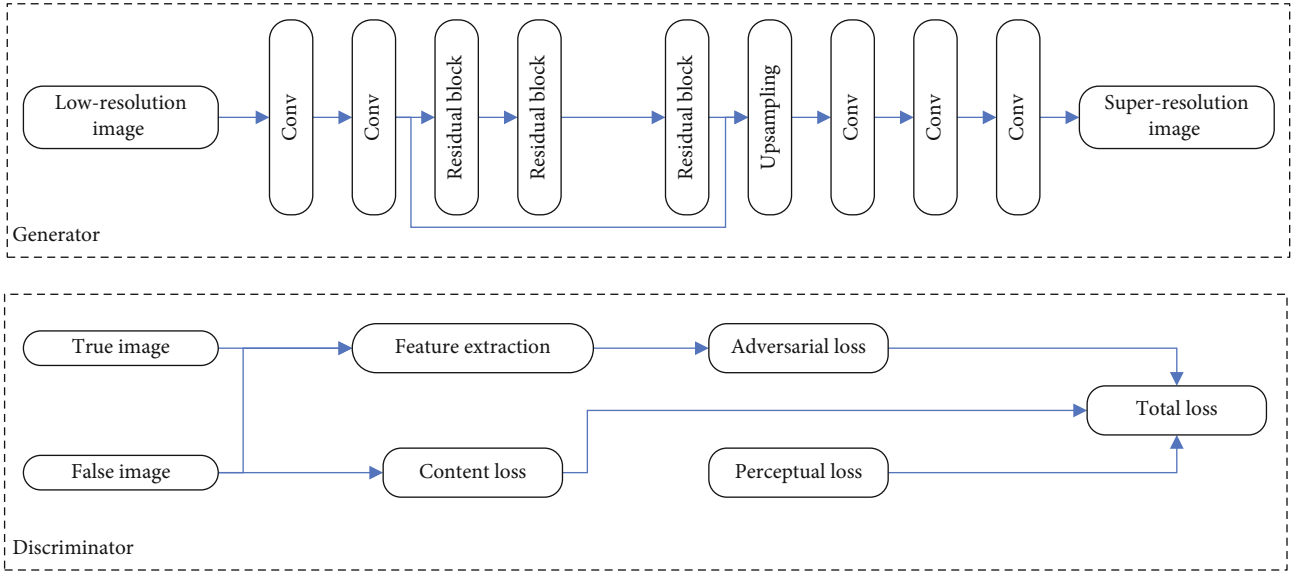


FIGURE 1: The structure of SAGAN.

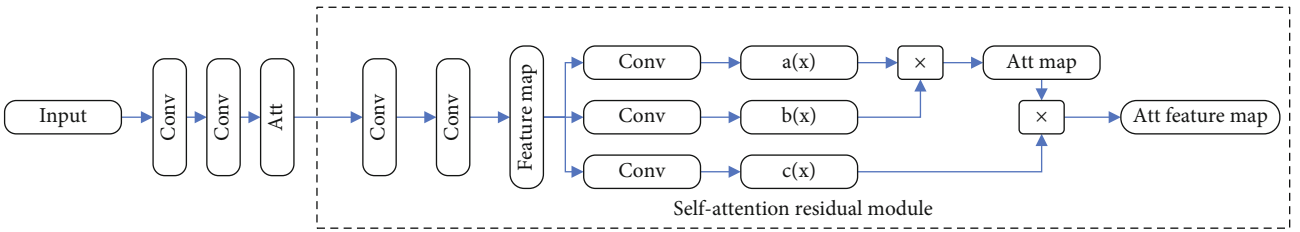


FIGURE 2: Self-attention schematic.

Add the output from the attention layer back to the input feature map after multiplying it by the scale parameter. As a result, here is what we have:

$$y_i = \gamma \varepsilon_i + x_i, \quad (6)$$

where y_i is the final output and the initial value of γ is set as zero. The extracted feature map will be fed into the next attention mechanism network, and the feature extraction and learning process will be repeated. Adding a self-attention layer to the generator's residual module improves image reconstruction by making greater use of global feature data. This aids in the recovery of high-resolution photos' texture information.

3.3. Instance Normalization. In many image classification tasks, batch normalization is proved to be efficient. Nevertheless, this normalizing strategy reduces the performance. Instance normalization was first proposed in image style conversion. The instance normalization layer allows instance-specific contrast information to be removed from content images. This simplifies the generation process and can greatly improve image quality.

Instance normalization itself is a very simple algorithm, especially suitable for scenes where the batch size is small and each pixel is considered separately, because it calculates the normalized statistics without mixing the data between

batches and channels. For this kind of application scenario, it is generally considered to use instance normalization. In image applications, the value on each channel is relatively large, so a more appropriate normalized statistic can be obtained. When doing picture style conversion, this is employed to greatly improve the end result. SAGAN's picture superresolution reconstruction model considers using an instance normalizing layer in place of the generator's batch normalization layer in order to increase speed. One way to generate a single picture instance is by doing instance normalization on a single image. Using this example regularization formula, we may express as

$$y_{tcmn} = \frac{x_{tcmn} - \mu_{tc}}{\sqrt{\sigma_{tc}^2 + \nu}}, \quad (7)$$

$$\mu_{tc} = \frac{\sum_{h=1}^H \sum_{w=1}^W x_{tchw}}{HW}, \quad (8)$$

$$\sigma_{tc}^2 = \frac{\sum_{h=1}^H \sum_{w=1}^W (x_{tchw} - \mu_{tc})^2}{HW}, \quad (9)$$

in which H and W denote the image's height and width and x_{tcmn} denotes the tc mnth image in the batch, where m and n are the image's spatial dimensions, c is the input feature channel, and t is the batch's index.

3.4. Loss Function. SAGAN uses adversarial loss in the loss function to reconstruct images with crisp textures at high resolution. The discriminator network is deceived as much as possible by the superresolution image rebuilt by the generator network. The adversarial loss is

$$L(G, D) = E_{I_S \sim \tilde{I}_S} [\log D_\theta(I_S)] + E_{I_L \sim \tilde{I}_L} [\log (1 - D_\theta(G_\theta(I_L)))], \quad (10)$$

where $D_\theta(I_S)$ represents the reconstructed superresolution picture, I_S is the true superresolution picture, and I_L represents the low-resolution image.

GANs have traditionally used JS divergence as a way to gauge how far real-world data differs from the generated data's probability distribution. There are no valid gradients for training if you use JS divergence to estimate the probability distribution. Because the distance between the generated sample and the real sample is discontinuous in high-dimensional space, the created sample cannot be compared to the genuine sample. GAN cannot practice because there are not any junction points. The distance between two distributions is calculated using the Wasserstein distance rather than the JS divergence in this article. The lowest gap between the real sample distribution and the produced sample distribution is used to calculate the Wasserstein distance. In theory, the Wasserstein distance is differentiable almost everywhere. Therefore, it can quickly and effectively guide the training of the GAN model. In the adversarial training process, the adversarial loss based on the Wasserstein distance is

$$L_w(G, D) = E_{I_S \sim \tilde{I}_S} D_\theta(I_S) - E_{I_L \sim \tilde{I}_L} D_\theta(G_\theta(I_L)). \quad (11)$$

When all samples are considered, the generator loss and discriminator loss are both defined as

$$L_G = -\sum D_\theta(G_\theta(I_L)), \quad (12)$$

$$L_D = \sum (D_\theta(I_S) - D_\theta D_\theta(G_\theta(I_L))). \quad (13)$$

To determine how comparable reconstructed superresolution picture and target superresolution picture are, a loss must be built between the two images during the experimental training procedure. As long as the difference between the reconstructed and target superresolution images is being measured with MSE, model training will have a much smaller impact, because the reconstructed image will be excessively smooth and lack realism if only pixel-level reconstruction is used. In most image superresolution reconstruction techniques, the difference between reconstructed and target images is calculated using perceptual loss at the moment. Contrary to popular belief, perceptual loss has been extensively studied and exploited in image superresolution reconstruction methods.

When using a pretrained deep network, perceptual loss is often embedded on the activation layer, and associated loss function is derived using the activated feature value. However, as the network depth increases, the number of

activated features decreases, making it difficult to keep track of everything. As a result, SAGAN calculates perceptual loss using feature value, and feature value before activation better represents the image's feature information. It is capable of keeping an eye on the reconstructed image's texture and comparing it to the original. Prior to applying an activation layer, a trained VGG19 is applied to get the feature value. Perceptual loss is computed by comparing Euclidean distance between superresolution picture feature map generated and image's initial feature:

$$L_P = \sum (V(I_S) - V(G_\theta(I_L)))^2, \quad (14)$$

where V is the VGG19 module.

A content loss function must be incorporated into the model to guarantee that the generated superresolution picture and original picture have similar content. SAGAN replaces the usual L2 loss with Charbonnier loss to increase the network's performance. Charbonnier loss is

$$L_C = \sum (\rho(I_S - (G_\theta(I_L))), \quad (15)$$

where ρ is the Charbonnier penalty function. For this reason, it has stronger supervision capabilities than other types of losses and is more robust for Charbonnier's loss. Adding up all of the above losses, the generator network model has a total loss of

$$L = L_P + \lambda_1 L_G + \lambda_2 L_C, \quad (16)$$

where λ_1 and λ_2 are two weights for loss.

3.5. Generator and Discriminator Structure. The generator's primary job during training is to produce images with a high level of resemblance to real high-resolution images. In order to discriminate between a reconstructed and true superresolution image, the discriminator must be used. After training the generator and discriminator, the generated network is the needed network for superresolution picture reconstruction. Different convolution kernels, downsampling, self-attention residuals, and picture reconstruction via upsampling all make up the generator network. The generator structure is shown in Figure 3.

An image can be reconstructed using three distinct convolution kernel sizes (3×3 , 5×5 , and 7×7) and then convolved across three different receptive fields (3×3 , 5×5 , and 7×7). Next, a 1×1 convolutional layer is applied with a PReLU activation function on the convolved feature map and the original picture, and the results are delivered to the Concat layer. Convolutional layers and self-attention layer are employed in a single self-attention residual module. Next comes the instance normalization layer, followed by the convolutional layer. The activation strategy makes use of PReLU, and the jump connection is inserted. An additional jump connection is embedded to the last output layer for the self-attention residual block. It is utilized for image pixel amplification. At the same time,

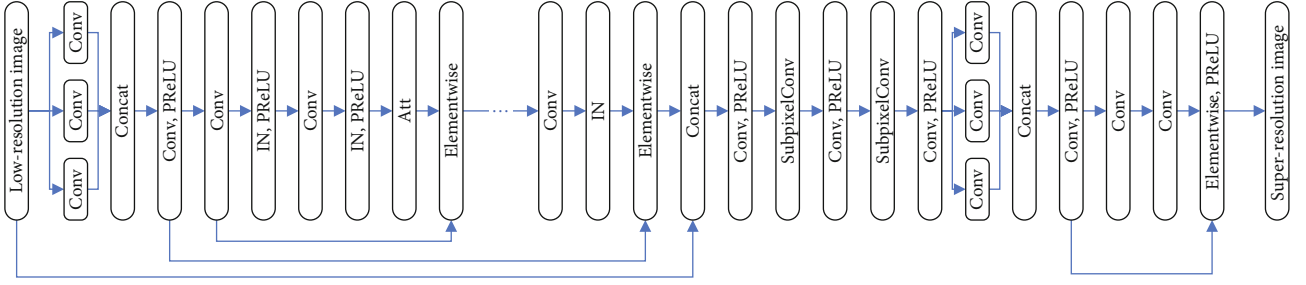


FIGURE 3: Generator network.

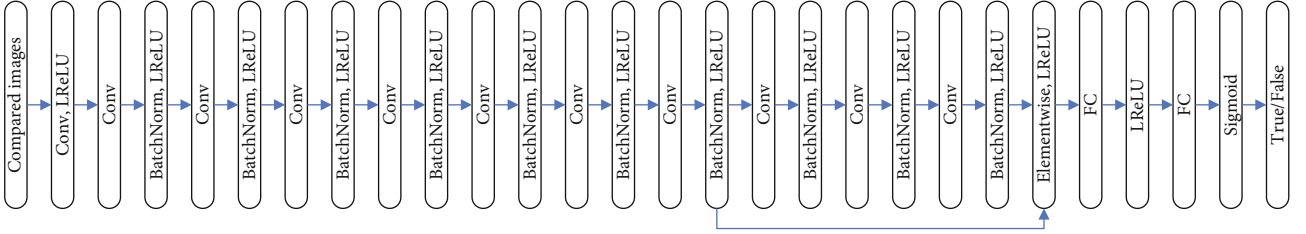


FIGURE 4: Discriminator network.

TABLE 1: The dataset details.

Dataset	Scenes	Size	Total	Training	Testing	Resolution
UC	21	256 × 256	2100	1680	420	0.3
NW	45	256 × 256	31500	4500	450	0.2-30

TABLE 2: Comparison with other methods on UC.

Method	Bicubic	SRCNN	ESPCN	MSRN	SAGAN
PSNR	26.8	29.7	31.5	34.8	35.4
SSIM	0.64	0.78	0.82	0.93	0.94

TABLE 3: Comparison with other methods on NW.

Method	Bicubic	SRCNN	ESPCN	MSRN	SAGAN
PSNR	27.9	30.8	32.5	34.9	35.6
SSIM	0.67	0.82	0.85	0.93	0.95

massive deep network layers are increased to improve image reconstruction in the image upsampling part.

A deep convolutional neural network is utilized in the discriminator network. BatchNorm is still employed in the discriminator network because of its efficacy in image classification tasks, while LReLU is utilized as the activation function. The structure is illustrated in Figure 4.

With the convolutional layer, the feature map is sent to the fully connected layer, where it is classified using the sigmoid activation function. Generator and discriminator minimization leads to better visual quality while generating high-resolution photos.

4. Experiment and Discussion

4.1. Dataset. Three remote sensing picture datasets are used in this article. UC Merced’s land use dataset (UC) is the first

one to use [36]. The training picture set has 80 photos chosen at random, whereas the testing image set contains 20 images chosen at random from the training image set. NWPU-RESISC45 (NW) is the second [37]. The dataset consists of 45 different types of scenes, each of which has 700 photos. The dataset’s size is the same as the UC dataset, and all of the images are 256 × 256 pixels. A random sample of 100 photographs from each type of scene is chosen at random and added to the training image set. Then, from the rest of the photos, randomly select 10 images from each scene type to include in the testing set. The dataset is shown in Table 1.

In this work, peak the signal-to-noise ratio (PSNR) and structural similarity (SSIM) are utilized to evaluate the performance. These are two different performance indicators, and the performance of the algorithm can be evaluated from different aspects.

4.2. Comparison with Other Methods. SAGAN proposed in this paper is compared with Bicubic [38], SRCNN [39], ESPCN [30], and MSRN [40]. To ensure fairness, all methods are all retrained and tested from the same set of remote sensing images. Experimental details are illustrated in Tables 2 and 3.

There is a 3 dB to 5 dB difference in PSNR between SAGAN and SRCNN/ESPCN for both datasets. The outcomes of image superresolution reconstruction have been greatly improved as a result of significant advancements. SRCNN and ESPCN, on the other hand, are only capable of extracting a few features. Deep networks like SAGAN and MSRN outperform SRCNN and ESPCN in terms of performance. The approach in this research has higher objective indicators PSNR and SSIM on the two datasets for the deep network MSRN when compared to the SAGAN method. Here is a way to demonstrate how much better SAGAN is than the alternatives.

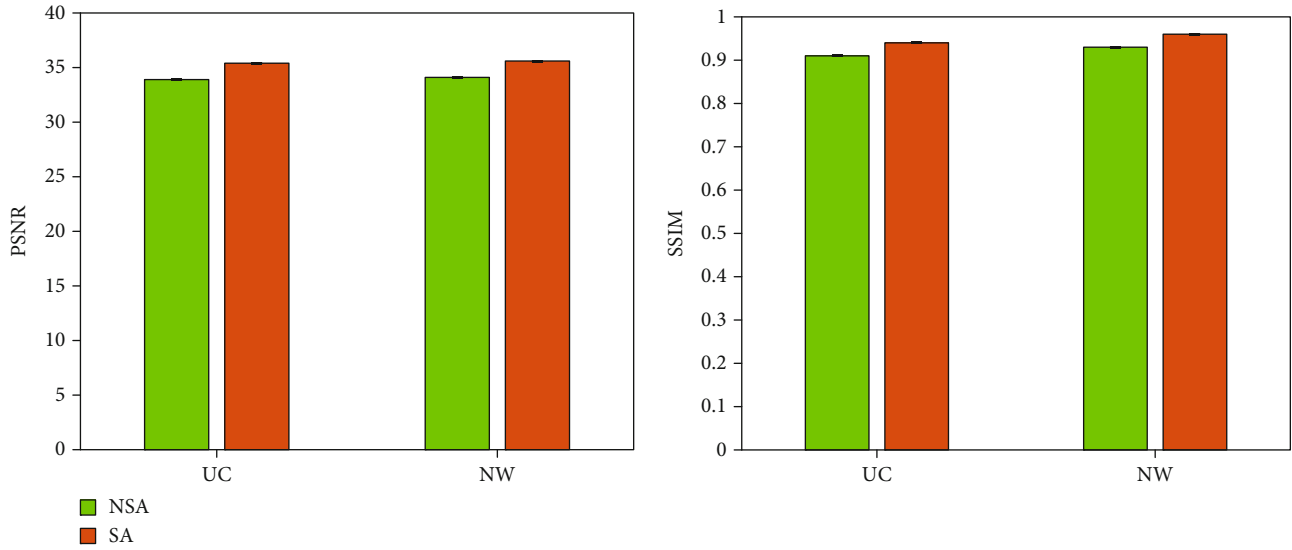


FIGURE 5: Evaluation on self-attention mechanism layer.

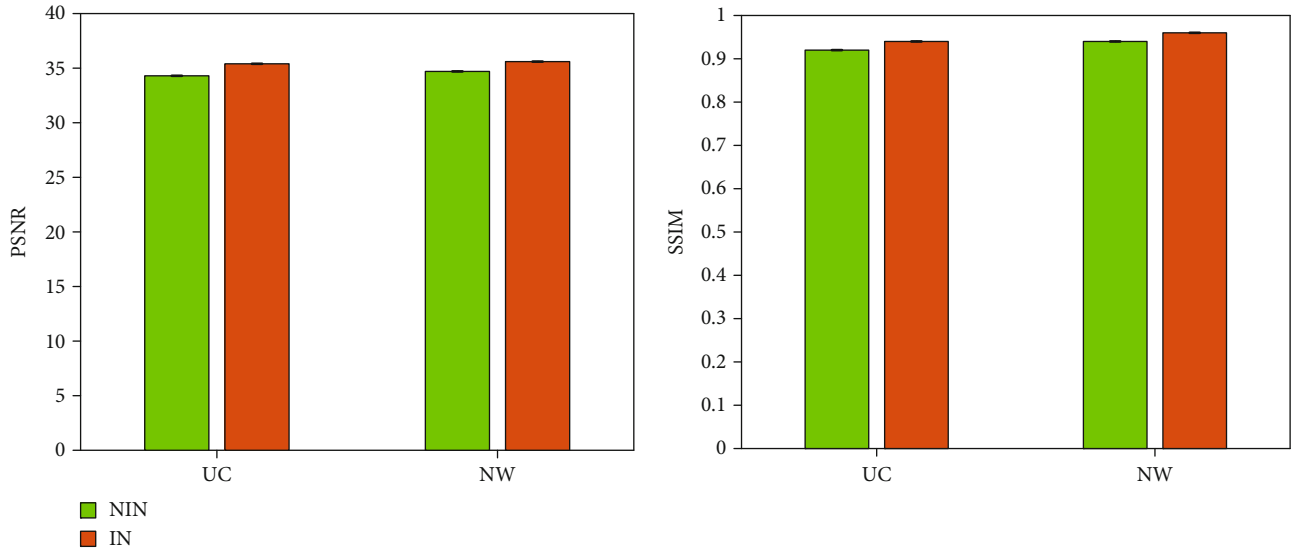


FIGURE 6: Evaluation of instance normalization layer.

4.3. Evaluation on Self-Attention Mechanism Layer. Self-attention mechanisms are used to extract more discriminatory features from the pipeline in this study. We conduct a comparative experiment to examine the model's performance with and without a self-attention mechanism layer to demonstrate the strategy's efficacy. Experimental results on two datasets are illustrated in Figure 5. NSA represents having no self-attention layer. SA represents having a self-attention layer.

Obviously, with the introduction of the self-attention layer, both the PSNR and SSIM for the model can be improved. On the UC dataset, the gains of PSNR and SSIM are 1.5% and 0.03. On the NW dataset, the gains of PSNR and SSIM are also 1.5% and 0.03. These data can verify the correctness of using the self-attention mechanism layer.

4.4. Evaluation on Instance Normalization Layer. In this work, an instance normalization layer is embedded in the pipeline to normalize features. To verify the effectiveness of this strategy, a comparative experiment is conducted to compare the performance for the model with and without an instance normalization layer. The experimental results on two datasets are illustrated in Figure 6. NIN represents having no instance normalization layer. IN represents having an instance normalization layer.

Obviously, with the introduction of the instance normalization layer, both the PSNR and SSIM of the model can be improved. On the UC dataset, the gains of PSNR and SSIM are 1.1% and 0.02. On the NW dataset, the gains of PSNR and SSIM are also 0.9% and 0.02. These data can verify the correctness of using the instance normalization layer.

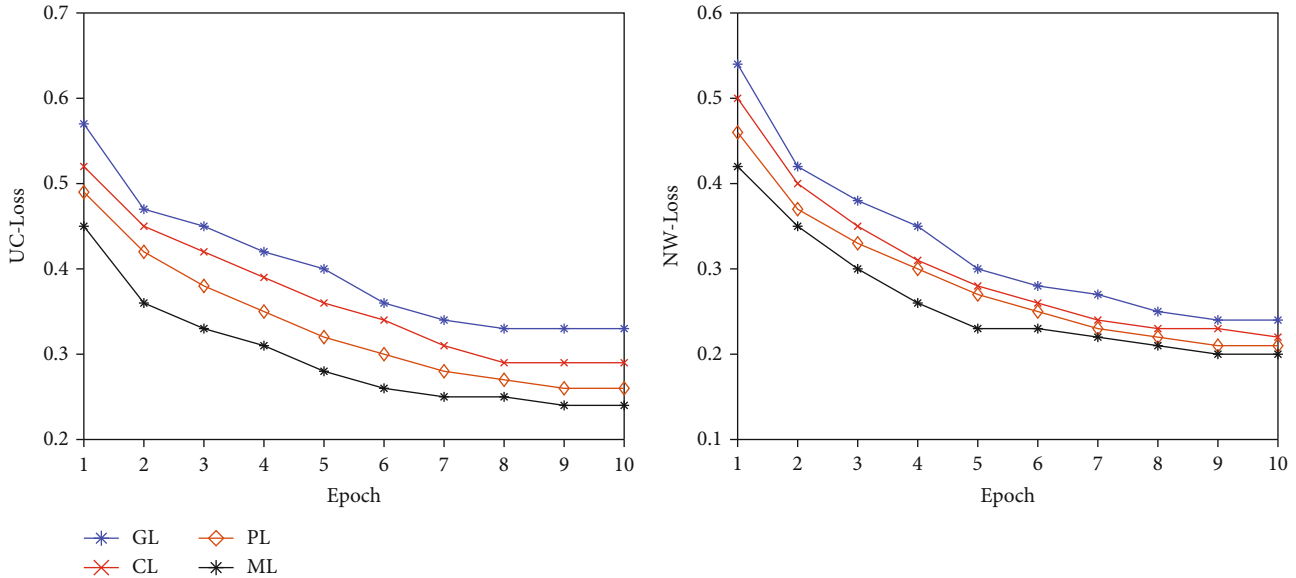


FIGURE 7: The training loss on two datasets.

TABLE 4: Evaluation on different losses.

Loss	UC		NV	
	PSNR	SSIM	PSNR	SSIM
GL	33.2	0.89	34.1	0.91
CL	33.5	0.90	34.3	0.91
PL	33.7	0.91	34.5	0.92
GL+CL	34.6	0.92	34.6	0.93
GL+PL	34.8	0.92	34.8	0.93
CL+PL	35.1	0.93	35.2	0.94
ML	35.4	0.94	35.6	0.95

4.5. Evaluation on Loss. In this work, a mixed loss consisting of generator loss, content loss, and perceptual loss is proposed to optimize the network. To prove the effectiveness of this strategy, we first conducted a comparative experiment to compare the training loss of the model with different losses. Experimental results are illustrated in Figure 7. GL is generator loss. CL is content loss. PL is perceptual loss. ML is mixed loss proposed in this work.

As the number of iterations increases, the loss value for the network gradually decreases and finally converges steadily. But it should be noted that, compared with other individual loss functions, the combined loss proposed in this paper has the lowest corresponding loss in any iteration. This can effectively prove the reliability and correctness of the loss in this article.

To further verify the effectiveness of this loss combination strategy in this article, this article also conducts another set of comparative experiments to compare the effects of different loss combinations on model performance. Experimental results on two datasets are illustrated in Table 4.

It can be seen that compared with any single loss, the loss of our combination is higher than their performance. In addition, with the gradual introduction of losses, the performance of the model is gradually increasing. This shows

that combining different losses can effectively make network learning more discriminative features. And compared with the loss of any other pairwise combination, the best performance can be obtained by combining three kinds of losses. This also further proves the correctness and reliability of the loss proposed in this article.

5. Conclusion

Superresolution reconstruction technology can use software algorithms to effectively improve the resolution of remote sensing images without being restricted by hardware devices. This method has low cost and high universality. Vigorous development on deep learning technology has made image superresolution reconstruction technology a research hotspot. Among them, the generative adversarial network, as a classic algorithm in deep learning, has developed rapidly in superresolution reconstruction, and many excellent and effective algorithm models have emerged. However, most networks are for general images, and there are still many deficiencies and room for improvement in the reconstruction methods of remote sensing images. This thesis studies the generative countermeasure network, focusing on super-resolution reconstruction with a generative adversarial network on remote sensing images. This paper proposes a superresolution reconstruction algorithm with a self-attention strategy. The first step is to add a self-attention layer to the generator network so that global features may be efficiently utilized when reconstructing high-resolution images. Replace the BatchNorm layer with the instance normalization layer based on the deep network structure. Once you have optimized the content loss, compare the reconstructed superresolution image to the original to see how closely they compare in terms of resolution. The final step is to optimize and generate perception loss based on the feature value prior to activation of the VGG19 network. Prior to activation, the features provide a more accurate

representation of the image's feature information. It is now possible to examine the texture consistency in order to confirm that the reconstructed image is accurate. According to results from experiments, the suggested approach improves PSNR and SSIM scores compared to existing algorithms, while also providing greater realism and clarity in the reconstructed image's textures.

Data Availability

The datasets used are available from the corresponding author on reasonable request.

Conflicts of Interest

The author declares that they have no conflict of interest.

Acknowledgments

The project is sponsored in part by the Science Foundation of JinZhou University, Project No. 2020KY05.

References

- [1] X.-L. Chen, H.-M. Zhao, P.-X. Li, and Z.-Y. Yin, "Remote sensing image-based analysis of the relationship between Urban Heat Island and land use/cover changes," *Remote Sensing of Environment*, vol. 104, no. 2, pp. 133–146, 2006.
- [2] J. Ma, H. Zhou, J. Zhao, Y. Gao, J. Jiang, and J. Tian, "Robust feature matching for remote sensing image registration via locally linear transforming," *IEEE Transactions on Geoscience & Remote Sensing*, vol. 53, no. 12, pp. 6469–6481, 2015.
- [3] A. Romero, C. Gatta, and G. Camps-Valls, "Unsupervised deep feature extraction for remote sensing image classification," *IEEE Transactions on Geoscience & Remote Sensing*, vol. 54, no. 3, pp. 1349–1362, 2016.
- [4] J. Cheng, H. Liu, T. Liu, F. Wang, and H. Li, "Remote sensing image fusion via wavelet transform and sparse representation," *Isprs Journal of Photogrammetry & Remote Sensing*, vol. 104, no. 6, pp. 158–173, 2015.
- [5] Y. Chang, L. Yan, and H. Fang, "Anisotropic spectral-spatial total variation model for multispectral remote sensing image destriping," *IEEE Transactions on Image Processing*, vol. 24, no. 6, pp. 1852–1866, 2015.
- [6] E. Michael and D. Dmitry, "Example-based regularization deployed to super-resolution reconstruction of a single image," *Computer Journal*, vol. 1, pp. 15–30, 2018.
- [7] S. Zhao, L. Zehua, and L. Hu, "A mixed non-local prior model for image super-resolution reconstruction," *Chinese Journal of Electronics*, vol. 26, no. 4, 2017.
- [8] W. Guo, Y. Tong, and Y. Huang, "A high-efficiency super-resolution reconstruction method for ultrasound microvascular imaging," *Applied Sciences*, vol. 8, no. 7, p. 1143, 2018.
- [9] J.-w. Zhao, Q.-p. Yuan, J. Qin, X.-p. Yang, and Z.-h. Chen, "Single image super-resolution reconstruction using multiple dictionaries and improved iterative back-projection," *Optoelectronics Letters*, vol. 15, no. 2, pp. 156–160, 2019.
- [10] S. Liu and X. Li, "A novel image super-resolution reconstruction algorithm based on improved GANs and gradient penalty," *International Journal of Intelligent Computing and Cybernetics*, vol. 12, no. 3, pp. 400–413, 2019.
- [11] Y. Li, X. Fan, and F. Zhang, "DLBI: deep learning guided Bayesian inference for structure reconstruction of super-resolution fluorescence microscopy," *Bioinformatics*, vol. 34, no. 13, pp. i284–i294, 2018.
- [12] W. Wang, Y. Hu, and Y. Luo, "Brief survey of single image super-resolution reconstruction based on deep learning approaches," *Sensing and Imaging*, vol. 21, no. 1, 2020.
- [13] J. Pei, K. Zhong, and J. Li, "ECNN: evaluating a cluster-neural network model for city innovation capability," *Neural Computing and Applications*, pp. 1–13, 2021.
- [14] C. Im, S. Jung, and C. Eom, "A deep learning-based super-resolution RF map reconstruction for indoor fingerprint positioning," *Journal of the Institute of Electronics and Information Engineers*, vol. 57, no. 1, pp. 9–14, 2020.
- [15] M. Kawulok, P. Benecki, S. Piechaczek, K. Hrynchenko, D. Kostrzewa, and J. Nalepa, "Deep learning for multiple-image super-resolution," *IEEE Geoscience and Remote Sensing Letters*, vol. 17, no. 6, pp. 1062–1066, 2020.
- [16] X. Li and M. T. Orchard, "New edge-directed interpolation," *IEEE Transactions on Image Processing*, vol. 10, no. 10, pp. 1521–1527, 2001.
- [17] X. Zhang and X. Wu, "Image interpolation by adaptive 2-D autoregressive modeling and soft-decision estimation," *IEEE Transactions on Image Processing*, vol. 17, no. 6, pp. 887–896, 2008.
- [18] L. Wang, S. Xiang, and G. Meng, "Edge-directed single-image super-resolution via adaptive gradient magnitude self-interpolation," *IEEE Transactions on Circuits and Systems for Video Technology*, vol. 23, no. 8, pp. 1289–1299, 2013.
- [19] Y. J. Lee and J. Yoon, "Image zooming method using edge-directed moving least squares interpolation based on exponential polynomials," *Applied Mathematics and Computation*, vol. 269, pp. 569–583, 2015.
- [20] H. Stark and P. Oskoui, "High-resolution image recovery from image-plane arrays, using convex projections," *Journal of the Optical Society of America A*, vol. 6, no. 11, pp. 1715–1726, 1989.
- [21] M. Irani and S. Peleg, "Improving resolution by image registration," *CVGIP: Graphical Models and Image Processing*, vol. 53, no. 3, pp. 231–239, 1991.
- [22] R. R. Schultz and R. L. Stevenson, "A Bayesian approach to image expansion for improved definition," *IEEE Transactions on Image Processing*, vol. 3, no. 3, pp. 233–242, 1994.
- [23] Q. Yuan, L. Zhang, and H. Shen, "Regional spatially adaptive total variation super-resolution with spatial information filtering and clustering," *IEEE Transactions on Image Processing*, vol. 22, no. 6, pp. 2327–2342, 2013.
- [24] R. M. Bahy, G. I. Salama, and T. A. Mahmoud, "Adaptive regularization-based super resolution reconstruction technique for multi-focus low-resolution images," *Signal Processing*, vol. 103, pp. 155–167, 2014.
- [25] K. Tan, W. Li, and J. Pei, "An I/Q-channel modeling maximum likelihood super-resolution imaging method for forward-looking scanning radar," *IEEE Geoscience and Remote Sensing Letters*, vol. 15, no. 6, pp. 863–867, 2018.
- [26] W. T. Freeman, T. R. Jones, and E. C. Pasztor, "Example-based super-resolution," *IEEE Computer Graphics and Application*, vol. 22, no. 2, pp. 56–65, 2002.
- [27] T. Zhang, K. Gao, and G. Ni, "Spatio-temporal super-resolution for multi-videos based on belief propagation," *Signal Processing: Image Communication*, vol. 68, pp. 1–12, 2018.

- [28] H. Chang, D. Y. Yeung, and Y. Xiong, "Super-resolution through neighbor embedding," in *IEEE Conference on Computer Vision and Pattern Recognition*, pp. 275–282, Washington, USA, 2004.
- [29] Y. Deng and F. Liu, "Hallucinating faces based on adaptive neighborhood selection and dual tree complex wavelet transform," *Optik*, vol. 127, no. 2, pp. 525–534, 2016.
- [30] W. Shi, J. Caballero, and F. Huszár, "Real-time single image and video super-resolution using an efficient sub-pixel convolutional neural network," in *IEEE Conference on Computer Vision and Pattern Recognition*, pp. 1874–1883, Las Vegas, USA, 2016.
- [31] J. Kim, J. K. Lee, and K. M. Lee, "Accurate image super-resolution using very deep convolutional networks," in *IEEE Conference on Computer Vision and Pattern Recognition*, pp. 1646–1654, Las Vegas, USA, 2016.
- [32] J. Kim, J. K. Lee, and K. M. Lee, "Deeply-recursive convolutional network for image super-resolution," in *IEEE Conference on Computer Vision and Pattern Recognition*, pp. 1637–1645, Las Vegas, USA, 2016.
- [33] C. Ledig, L. Theis, and F. Huszár, "Photo-realistic single image super-resolution using a generative adversarial network," in *IEEE Conference on Computer Vision and Pattern Recognition*, pp. 105–114, Honolulu, USA, 2017.
- [34] X. Hu, H. Mu, and X. Zhang, "Meta-SR: a magnification-arbitrary network for super-resolution," in *IEEE Conference on Computer Vision and Pattern Recognition*, pp. 1575–1584, Long Beach, USA, 2019.
- [35] Z. Li, J. Yang, and Z. Liu, "Feedback network for image super-resolution," in *IEEE Conference on Computer Vision and Pattern Recognition*, pp. 3862–3871, Long Beach, USA, 2019.
- [36] Y. Yang and S. Newsam, "Bag-of-visual-words and spatial extensions for land-use classification," in *SIGSPATIAL International Conference on Advances in Geographic Information Systems*, pp. 270–279, San Jose, USA, 2010.
- [37] G. Cheng, J. Han, and X. Lu, "Remote sensing image scene classification: benchmark and state of the art," *Proceedings of the IEEE*, vol. 105, no. 10, pp. 1865–1883, 2017.
- [38] R. G. Keys, "Cubic convolution interpolation for digital image processing," *IEEE Transactions on Acoustics, Speech, and Signal Processing*, vol. 29, no. 6, pp. 1153–1160, 1981.
- [39] C. Dong, C. C. Loy, and K. He, "Learning a deep convolutional network for image super-resolution," in *European Conference on Computer Vision*, pp. 184–199, Zurich, Switzerland, 2014.
- [40] J. C. Li, F. M. Fang, and K. F. Mei, "Multi-scale residual network for image super-resolution," in *European Conference on Computer Vision*, pp. 517–532, Munich, Germany, 2018.

Research Article

Optimal Design of Ecological Landscape Spatial Structure Based on Edge Computing of Internet of Things

Ru An 

School of Fine Arts, Xinxiang University, Xinxiang, 453001 Henan, China

Correspondence should be addressed to Ru An; anru1989@xxu.edu.cn

Received 19 January 2022; Revised 21 February 2022; Accepted 22 February 2022; Published 7 March 2022

Academic Editor: Nima Jafari Navimipour

Copyright © 2022 Ru An. This is an open access article distributed under the Creative Commons Attribution License, which permits unrestricted use, distribution, and reproduction in any medium, provided the original work is properly cited.

Ecological landscape space refers to a whole composed of many different ecosystems in a larger area. The spatial structure of the ecological landscape is the spatial arrangement and combination of the components and elements of the landscape. With the sustainable development of today's world, the procedure of urbanization is also accelerating. The urbanization procedure has significantly changed the types of urban landscapes and the spatial structure of urban landscapes, which will also produce corresponding ecological effects. No matter how good or bad the ecological effect is, it will have a certain impact on people's lives. Therefore, continuously promoting the majorization of the spatial structure of urban ecological landscape is a significant method to promise the healthy improvement of the city. This article is aimed at studying the optimal design of urban ecological landscape spatial structure based on edge computing of the Internet of Things. This paper uses city A as the experimental object to design a space structure majorization experiment of urban ecological landscape based on the edge computing of the Internet of Things, and the experiment draws a conclusion. The urban ecological landscape structure majorization plan based on the edge computing of the Internet of Things increases the biodiversity index of city A by 1.2, indicating that the method of optimizing the structure of the ecological landscape based on the edge computing of the Internet of Things has a better effect of optimizing the structure of the ecological landscape.

1. Introduction

Cities have always been places where mankind lives and seeks development and are also the center of technological innovation, economic development, and social development. It can be said that cities are the most important living environment for mankind. In the procedure of urban development, various problems are usually encountered, and the ecological problem is one of the most important problems. The problems of urban ecological environment are often caused in the space of urban ecology landscape. With the continuous acceleration and deepening of contemporary urbanization, the types and structures of urban ecological landscapes have also undergone significant changes. However, changes in the spatial structure of the urban ecological landscape will inevitably have a certain impact on the urban ecological environment.

In the procedure of urbanization, more and more natural landscapes and agricultural land in urban areas are continu-

ously transformed into urban construction land, which has led to the continuous increase in urban greenhouse gas emissions. The development of urban industry has led to an increase in emissions of fossil combustion exhaust gas in urban areas. Moreover, due to the sustained growth of urban building land, the urban ecology type of land is reduced, which leads to aggravation of urban landscape fragmentation and destroys the original ecological function and landscape function of urban ecological landscape. The destruction of the ecological functions and functions of the urban ecological landscape will cause the material and energy circulation in the urban ecological system to be hindered in time and space, which will cause a huge adverse impact on the urban regional ecological system. At the same time, the destruction of the spatial structure of the urban ecological landscape will also lead to other global ecological and environmental problems. For example, severe weather such as urban heat island effect, air pollution, water pollution, greenhouse effect, smog, and sandstorms has increased.

The aggravation of such environmental problems will undermine the sustainable development of the global ecological environment. It has destroyed the living environment of human beings all over the world and threatened the survival and development of all human beings on the earth. Therefore, the research on how to promote the continuous majorization of the dimensional structure of urban ecological landscape and protect the urban ecological environment has extremely important practical significance.

Edge computing refers to the use of an open platform that integrates network, computing, storage, and application core capabilities on the side close to the source of objects or data to provide the nearest end service. The innovation of this article lies in the idea that combining with the edge computing of the Internet of Things, it discusses a beneficial method to promote the optimal design of urban ecological landscape spatial structure.

2. Related Work

Because the research on how to promote the continuous majorization of the spatial structure of urban ecological landscape has extremely important practical significance. In recent years, more and more researches on how to promote the continuous majorization of the spatial structure of urban ecological landscape have emerged in the academic circles. Among them, Min et al.'s main content is the study of forest ecological landscape structure in urban ecological landscape. They conducted a quantitative analysis of the urban forest ecological landscape structure in the built-up area of Jinan and proposed a majorization strategy for the forest ecological landscape structure through RS and GIS technology [1]. The research of Chao et al. mainly analyzed the relationship between the urban green space ecological landscape structure and social economic variables in different cities in the Munich region of southern Germany. They combined the multicity dynamic scenario modeling method to compare and evaluate the impact of different urban green space ecological landscapes on social and economic development [2]. Cui et al. found that rapid urbanization led to more fragmentation of urban green space and at the same time reduced the connectivity of urban green space. Therefore, they use a geographic information system and remote sensing technology to solve the problem of a green space ecological source through landscape spatial pattern analysis and ecological connection index analysis method [3]. The research of Oehrlein et al. mainly focuses on the total scale and accessibility of urban green spaces. They proposed a new method that takes a linear algorithm as the core to evaluate the scale and accessibility of urban green space in a comprehensive manner and can calculate the optimal distribution ratio between urban residential areas and green space [4]. Dobbs and others believe that vegetation is one of the main resources for cities to participate in ecosystem functions and provide ecosystem services. They studied the relationship between the landscape structure of more than one hundred cities in the world and factors such as population, socioeconomic, and climate and concluded that the best description of the urban landscape is the number, fragmen-

tation, and spatial distribution of vegetation [5]. Soltanifard and Jahari's research evaluated the spatial characteristics of the ecological quality of urban green spaces. Through spatial analysis and correlation testing, they made a thorough inquiry of the connection between the ecological landscape and ecological quality of the green space and reached a conclusion. If the scope and continuity of urban green space are too low, it will not be able to effectively support some key ecological services [6].

3. Majorization Method of Ecological Landscape Spatial Structure

The urban ecological landscape space refers to the urban ecological whole composed of many different ecological systems in the entire urban area. The spatial structure of urban ecological landscape is the spatial arrangement and combination of important components of the urban ecological environment system. The urban ecological landscape structure can be shown in Figure 1.

3.1. Edge Computing of the Internet of Things. Due to the accelerated popularization and development of mobile network technology and Internet of Things technology, today's world has entered a new era of Internet technology where everything can be connected. In this context, the number of mobile verge devices on the Internet will increase dramatically. The massive amount of data generated at the bottom of the Internet of Things perception will cause the number of cloud computing transmission loads to increase rapidly, which will also easily lead to relatively long Internet delays [7]. As a new technology to improve the experience of using network resources, the edge computing technology of the Internet of Things can be used for computing and storage services at the verge of the Internet due to its proximity to the data source. And it can provide users with a task transfer platform, which effectively reduces the delay of Internet data transmission. The edge computing technology of the Internet of Things refers to providing users with nearby network resource services on an open platform with network transmission, computing, and storage functions on the side closest to the source of things or data. Edge computing applications are launched at the verge of the network, and its service response speed is relatively fast, which can meet the basic needs of various industries in real-time processing, intelligent computing, and privacy protection. The edge computing of the Internet of Things is located between the physical entity and the industrial connection, and it is located on the top of the physical entity, which is completely different from the traditional cloud computing technology. Cloud computing technology can still access historical data generated by edge computing. In fact, people can regard edge computing as the eyes, ears, and limbs of the entire computer intelligent system. Although the core server of the computer intelligent system can make the intelligent system have relatively strong artificial intelligence, it will not be able to function if it lacks edge computing capabilities. And various big data procedureing applications often encounter the difficulty of not being able to collect suitable data, and

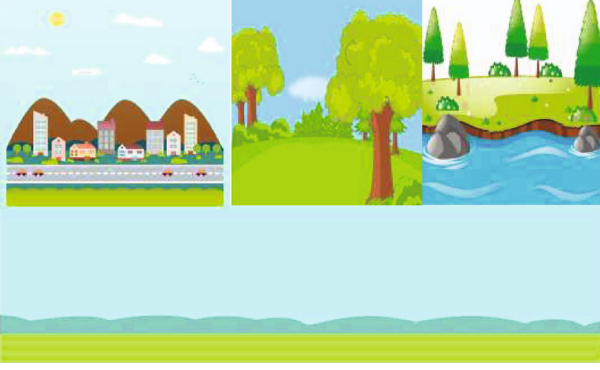


FIGURE 1: Urban ecological landscape structure.

edge computing can solve this problem for the big data algorithm of the core server. It can be drawn that the edge computing of the Internet of Things not only compensates for the transmission delay of the cloud computing platform but also meets the needs of core server computing expansion [8]. The basic framework of IoT edge computing is shown in Figure 2.

As a new architecture, IoT edge computing has its own unique characteristics [9]. The main difference between it and cloud computing lies in its service location, resource performance, and service quality [10]. The main features of IoT edge computing are as follows: first, relative to cloud computing, IoT edge computing is physically closer to the ground, as shown in Figure 3.

Second, the service node of edge computing is relatively low. Traditional cloud computing services are driven by ultra-high-performance infrastructure, but mobile edge computing only needs to process a small range of data in advance to provide real-time response functions. Finally, edge computing obeys multiple communication protocols. The edge computing of the Internet of Things can not only realize the short-distance transmission of the Internet of Things center but also support the connection of the cloud computing data center to realize the long-distance network transmission of the Internet [11]. They are the main distinguishing features between edge computing and cloud computing of the Internet of Things.

All in all, IoT edge computing is a network service technology that can achieve low latency, fast transmission, and link capacity improvement and energy efficiency.

3.2. The Edge Computing Resource Distribution Algorithm of the Internet of Things. The edge computing resource distribution algorithm of the Internet of Things is an algorithm that can reduce the cost of small- and medium-sized base stations in the local area network, so as to satisfy the energy depletion limits in the enduring majorization procedure and finally achieve network resource load balancing [12]. This algorithm first establishes a task load model, analyzes the total amount of tasks received by the base station, and then establishes a calculation model to predict and analyze the cost of local calculation and offload calculation of tasks from the perspective of time delay and energy depletion. Then, establish a credit model to conduct risk assessment on the

offload target selected by the base station. Finally, a marginal cost model is established, and the way to complete the task is selected through this model [13].

The first is the task load model. Assuming that the upload of user terminal s tasks follow the Poisson distribution and its average task upload rate in the time interval t is i , the average task load rate on the base station is

$$\vartheta_i = \sum_s \pi_s^i. \quad (1)$$

Next, establish a calculation model. First, the calculation energy depletion of the base station is linearly related to the task load, so the local calculation energy depletion can be shown as follows:

$$E_i^s = k\omega_i^2 \beta^i. \quad (2)$$

Among them, k is the energy depletion of one CPU cycle. Because of the limited computing power of the base station, the task load needs to be procedured in order [14]. Therefore, the average calculation postponement for a task to be completed on the base station is

$$D_k^i(\beta^i) = \frac{1}{u_i} - \omega_i. \quad (3)$$

Among them, A represents the amount of tasks that has to be programmatic on the base station per unit time. Similar to the calculation delay, with the aim of facilitating the calculation, the average transmission delay can be obtained by modeling the $M/M/1$ queuing system as

$$D^{si} \beta^i = \frac{1}{\gamma^i} \beta. \quad (4)$$

Namely,

$$D^{si} \beta^i = \frac{\nu}{1 - \gamma^i}. \quad (5)$$

Among them, ν represents the time that the network broadband serves a task. In summary, in each time interval t , the sum of the time delays for the completion of tasks on the base station is

$$D^t \beta = \gamma_i^j D^{it} \beta^i + \sum_{it} \beta^t. \quad (6)$$

The total energy depletion of the base station is

$$E_i^t(\beta^t) = E^{it}. \quad (7)$$

Next is the trust model: since base stations are deployed by SBSs by users, compared to task local proceduring or offloading to cloud proceduring, offloading to other base stations may have a higher risk of security and privacy leakage. Therefore, when selecting peer-to-peer offloading

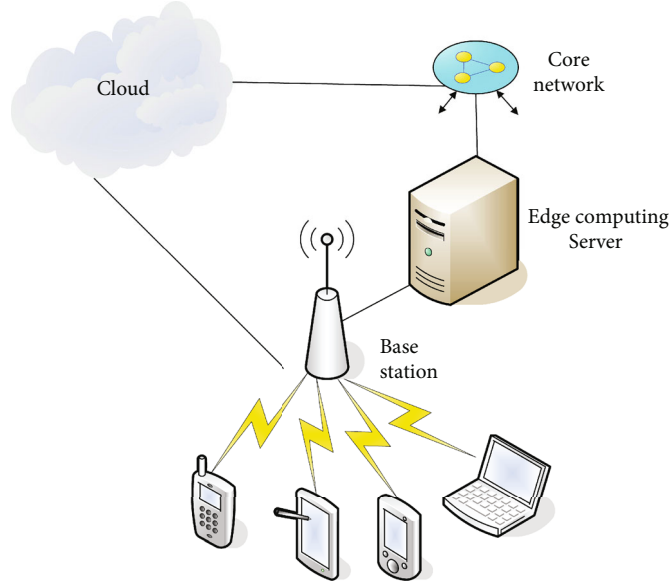


FIGURE 2: The basic framework of IoT edge computing.

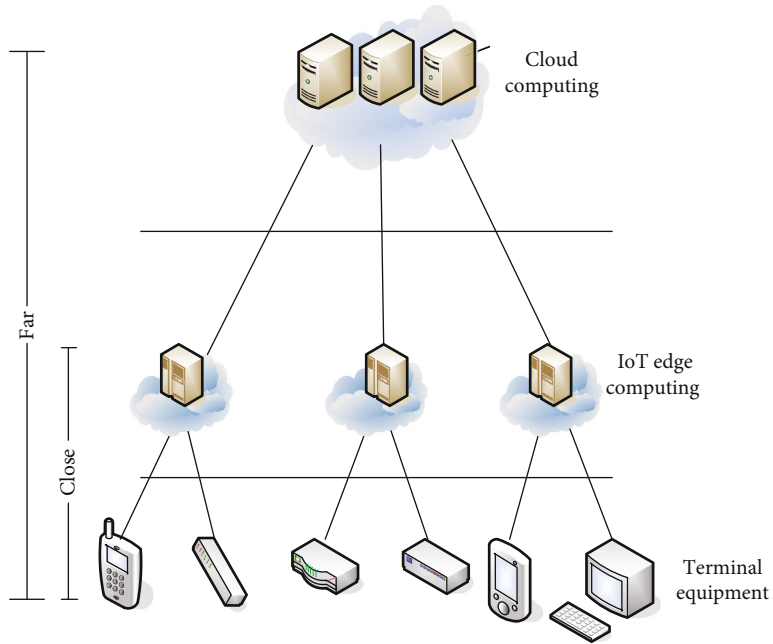


FIGURE 3: The relative position of cloud computing and edge computing.

objects, the trust issue between base stations needs to be considered [15]. Assume that the trust value between the base stations is

$$T_t^i = \frac{d_i}{\sum_e d_i} * \beta_i. \quad (8)$$

Among them, T_t^i is the trust value between the base stations, and when the trust values of the two base stations are both 0, $T_t^i=1$. Using the social trust network, the security risk cost of transferring the computing task of one base station to other base stations is modeled as follows:

$$R_t^i = \sum_e \beta_{it} R_{it}. \quad (9)$$

Namely,

$$R_t^i = \sum_e \omega_i \beta_{it} (I - T_i). \quad (10)$$

Among them, A is the conversion of security risks into a value equivalent to currency costs and B is the amount of offloading calculations between each base station. Next, in order to more intuitively show the difference in cost between local calculation and offload calculation, four auxiliary

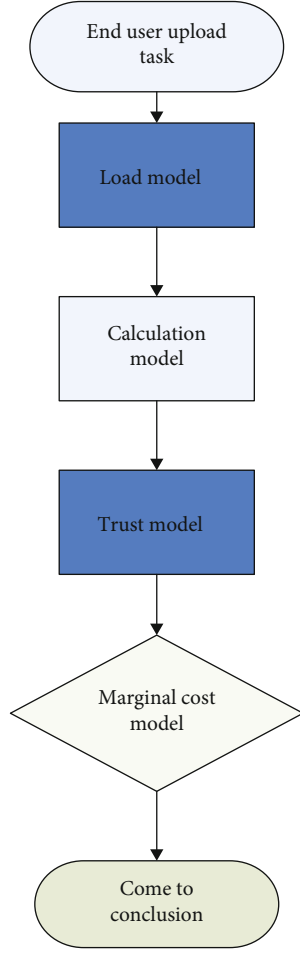


FIGURE 4: The algorithm flow of IoT edge computing resource distribution.

functions are set using the concept of marginal cost [16], as shown in the following:

Marginal calculation delay function:

$$d_{it}(\beta_{it}) = \frac{1}{u_i} + \beta_{it}. \quad (11)$$

Namely,

$$d_{it}(\beta_{it}) = \frac{u_{it}}{\beta_{it}}. \quad (12)$$

Marginal transmission delay function:

$$g_i(\gamma_i) = \frac{v}{(\gamma - v\gamma_{it})}. \quad (13)$$

Marginal uninstall risk function:

$$r_i = \frac{\partial(\beta_i)R}{\partial\gamma_t}. \quad (14)$$

The marginal function of cost required to complete the task:

$$\aleph_{it} = w_c(\beta_{it}) + w_r. \quad (15)$$

In the procedure, the unit is unified in the calculation model and the trust model; that is, operating expenses and risk expenses are converted into corresponding costs. This concludes the basic flow of the entire algorithm. The basic procedure of the edge computing resource distribution algorithm of the Internet of Things can be shown in Figure 4.

Among them, the trust model refers to the model of finding and traversing the trust path when establishing the trust relationship and verifying the certificate. The trust model of urban landscape spatial structure refers to a model that finds and facilitates the trust path when establishing the trust relationship for urban landscape spatial structure data.

4. Majorization Experiment of Ecological Landscape Spatial Structure Based on Edge Computing of Internet of Things

4.1. Experimental Method. The experimental method of this experiment is as follows: first, select any city (city A) as the experimental object and data source of this experiment. Next, by analyzing the urban landscape structure data of city A from 2017 to 2019, the biodiversity of city A from 2017 to 2019 is obtained. We use biodiversity as the standard to determine the degree of majorization of the city's ecological landscape structure. Next, we will combine the edge computing of the Internet of Things and edge computing resource distribution algorithms to further analyze and procedure the ecological landscape structure data of city A from 2017 to 2019 and calculate the biodiversity of city A to judge the rationality of the urban landscape spatial structure of city A. Then, combined with the obtained biodiversity results of city A from 2017 to 2019, the majorization plan for the ecological landscape structure of city A is summarized. Finally, under the guidance of the majorization plan, the changes in the urban ecological landscape structure of city A from 2020 to 2021 and the corresponding biodiversity are obtained. Based on this, it is judged whether the urban ecological landscape structure majorization method based on the edge computing of the Internet of Things is effective [17].

4.2. Selection and Analysis of Urban Ecological Landscape Structure Data for City A from 2017 to 2019. First of all, city A is a small urban area located in Zhejiang Province. The location and transportation conditions of this area are convenient. Nowadays, the procedure of urbanization has been speeding up, but at the same time, environmental problems have become more and more serious. Therefore, the selection of city A as the object of this experimental analysis has certain practical reference significance. The urban ecological landscape structure data of city A selected in this experiment from 2017 to 2019 are shown in Table 1.

From Table 1, we can see that the urban ecological landscape structure of city A is not balanced, and the land for gardens and water areas is small; the distribution of land use in other areas is also uneven. Affected by this structure,

TABLE 1: Landscape ecological structure of city A in 2017-2019.

Years	Arable land	Garden land	Other agricultural land	Urban land	Waters
2017	33.56%	3.86%	20.9%	21%	13.98%
2018	34.8%	3.9%	18.2%	30.1%	15.2%
2019	33.86%	4.22%	40%	28.6%	15.14%

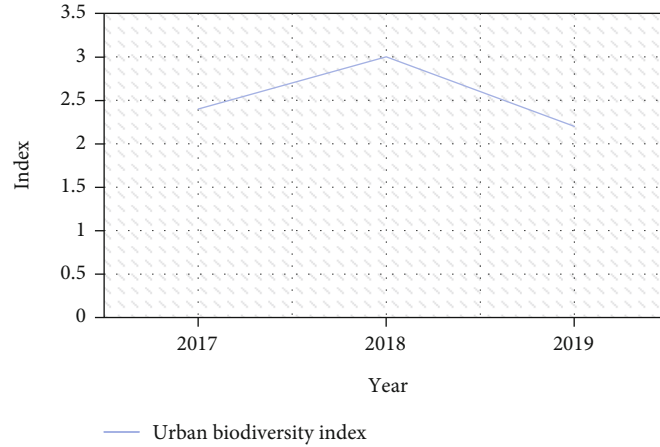


FIGURE 5: 2017-2019 biodiversity index of city A.

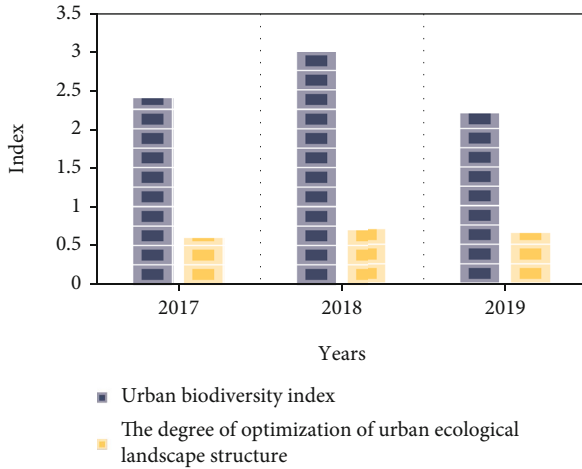


FIGURE 6: The relationship between the urban biodiversity and the majorization degree of urban ecological landscape structure in city A from 2017 to 2019.

we analyze the biodiversity results of city A from 2017 to 2019, as shown in Figure 5.

From Figure 5, we can see that the biodiversity index of city A has changed significantly from 2017 to 2019, from 2.4 in 2017 to 2.2 in 2019. Although the biodiversity index of city A increased in 2018, it dropped sharply in 2019. It shows that the overall biodiversity trend of city A in 2017-2019 has declined. After analysis, we believe that this is mostly been brought about by the improper planning of the urban ecological landscape structure of city A from 2017 to 2019. The connection between the urban biodiversity and the urban ecological landscape structure of city A from 2017 to 2019 can be shown in Figure 6.

TABLE 2: 2020-2021 preset ecological landscape structure of city A based on IoT edge computing.

	2020	2021
Arable land	20%	25%
Garden land	30%	25%
Other agricultural land	20%	10%
Urban land	10%	10%
Waters	20%	30%

4.3. 2020-2021 Urban Ecological Landscape Structure Majorization of City A Based on Edge Computing of the Internet of Things. After analyzing the urban ecological landscape structure and biodiversity of city A from 2017 to 2019, we combined the edge computing of the Internet of Things and the resource distribution algorithm based on edge computing to further procedure and analyze the urban ecological landscape data of city A from 2017 to 2019. Combined with the analysis of the factors affecting the changes in biodiversity of city A from 2017 to 2019, this experiment created a new urban ecological landscape structure majorization plan for city A [18]. Under the guidance of new urban ecological landscape structure majorization plan for city A created based on reasonable analysis, the preset land use planning for city A can be shown in Table 2.

According to Table 2, in order to better regulate the balance of the ecosystem of city A and increase biodiversity, the 2020-2021 urban ecological landscape structure majorization plan of city A that we created adds planning for garden land and water area on the original basis. The changes in city A's urban biodiversity 2019-2021 and the comparison with city A's 2017-2019 biodiversity under the guidance of this

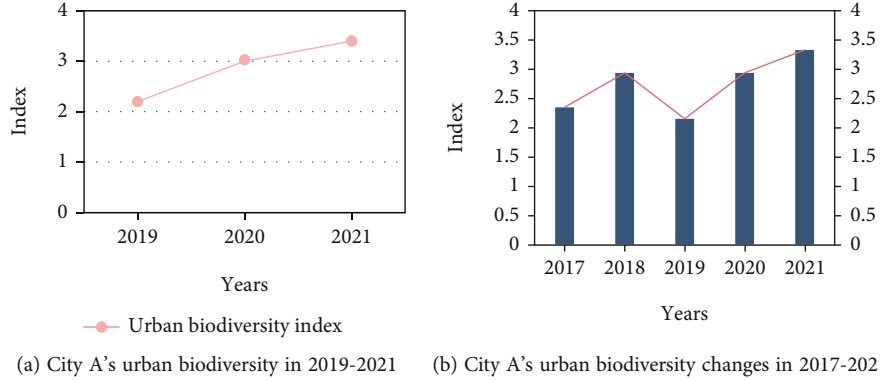


FIGURE 7: Biodiversity changes in city A based on edge computing of the Internet of Things.

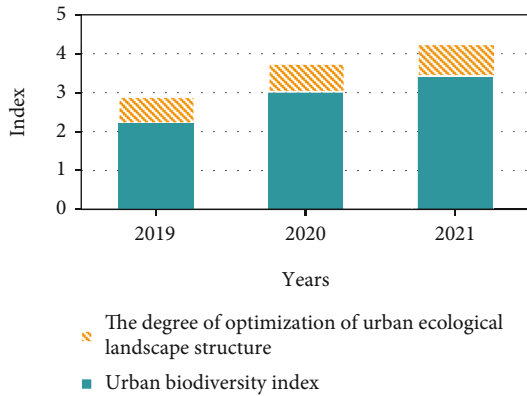


FIGURE 8: The relationship between the urban biodiversity and the majorization degree of urban ecological landscape structure in city A from 2019 to 2021.

set of IoT edge computing-based majorization plan for urban ecological landscape structure in city A are shown in Figure 7.

From Figure 7 we can see that under the guidance of the urban ecological landscape structure majorization scheme based on the edge computing of the Internet of Things, the biodiversity index of city A has increased from 2.2 in 2019 to 3.4 in 2021, an increase of 1.2 in total. This shows that the urban ecological landscape structure majorization effect based on edge computing of the Internet of Things is better, which makes the biodiversity of city A have a greater increase. The relationship between the biodiversity and the degree of landscape majorization in city A from 2019 to 2021 can be shown in Figure 8.

4.4. Experiment Summary. At this point, the whole experiment is over. Next, we will make a summary of this experiment. First of all, the subject of this experiment is city A, and the original data selected in the experiment are the urban ecological landscape structure data of city A from 2017 to 2019. In the first step of the experiment, we analyzed the urban ecological landscape structure data of city A from 2017 to 2019 and obtained the degree of majorization of city A's biodiversity and urban ecological landscape structure. In the second step, it combines the edge computing of the Internet of Things and the resource distribution plan based

on edge computing to obtain the urban ecological landscape structure data, biodiversity, and urban ecological landscape structure majorization degree of city A from 2017 to 2019. It did further data proceduring and analysis. On this basis, it designed a new urban ecological landscape structure majorization plan for city A. In the final step of the experiment, we will compare the degree of majorization of the 2020-2021 biodiversity and landscape structure of city A under the guidance of the new city A urban ecological landscape structure majorization plan with the relevant data of city A in 2017-2019. It judges the effectiveness of the urban ecological landscape structure majorization scheme based on edge computing of the Internet of Things. The experiment concluded that the urban ecological landscape structure majorization scheme based on edge computing of the Internet of Things increased the biodiversity index of city A by a total of 1.2. It shows that the majorization design of urban ecological landscape structure based on the edge computing of the Internet of Things has a good majorization effect [19–21].

5. Discussion

As an important center for human survival and development, cities have always played an important role in social development. The development of a city can not only affect social and economic development but also affect the environment in which people live. With the improvement of the level of urban development, the environmental problems of the city have become increasingly prominent. Most of the environmental problems start from the destruction of the urban ecological landscape structure to varying degrees [22]. The urban ecological landscape space refers to the urban ecological whole composed of many different ecological systems in the entire urban area. The spatial structure of urban ecological landscape is the spatial arrangement and combination of important components of the urban ecological environment system. Urban ecological landscape plays an important role in regulating the balance of the entire city's ecosystem and maintaining biodiversity. The majorization of urban ecological landscape structure is a significant method to protect the urban ecological landscape and protect the human living environment [23].

Scientific and effective majorization methods are indispensable to optimize the structure of urban ecological landscape. Therefore, this paper combines the edge computing of the Internet of Things and the resource distribution algorithm based on edge computing to conduct a research on the majorization of urban ecological landscape structure [24]. This paper designs a majorization experiment of urban ecological landscape structure based on edge computing of the Internet of Things. In the experiment, city A, a small city in Zhejiang Province, was chosen as the experimental object and data source. Next, this article analyzes the urban landscape structure data of city A from 2017 to 2019 to obtain the biodiversity of city A from 2017 to 2019. It uses biodiversity as the standard to determine the degree of majorization of the city's ecological landscape structure. Then, this paper will analyze and procedure the ecological landscape structure data of city A from 2017 to 2019 based on the edge computing and edge computing resource distribution algorithm of the Internet of Things. Afterwards, this paper designs an optimized plan for the ecological landscape structure of city A based on the biodiversity results obtained. Finally, this article analyzes the degree of majorization of the urban ecological landscape structure of city A in 2020–2021 under the guidance of the majorization plan and the corresponding biodiversity. Based on this, this article judges whether the urban ecological landscape structure majorization method based on the edge computing of the Internet of Things is effective [25]. The results show that the ecological landscape spatial structure of smart cities in the IoT environment has been optimized to a certain extent.

6. Conclusions

Cities have always been important environmental bases for human survival and development, as well as centers of socioeconomic development and technological innovation. In today's era, the entire society is constantly developing, and cities are also constantly developing. In the procedure of urban development, not only economic and cultural development problems will be encountered but also various ecological and environmental problems will be encountered. The urban ecological environment problems often start from the destruction of urban ecological landscape and ecological landscape structure. The majorization of the spatial structure of urban ecological landscape is bound to be inseparable from scientific and effective majorization methods. Therefore, this paper uses city A as the experimental object to design an urban ecological landscape spatial structure majorization experiment based on the edge computing of the Internet of Things. The research conclusions drawn in this paper are of great significance for promoting the spatial structure of urban ecological landscape and also have certain reference value for promoting the application of edge computing of the Internet of Things in the majorization of the spatial structure of ecological landscape; at the same time, it can also promote the construction process of a smart city. However, due to the limited research level and conditions, the research in this article also has certain limitations. It is believed that more researches on the majorization of the spa-

tial structure of ecological landscape will appear in the academic circles in the future, so as to continuously promote the continuous majorization and development of the spatial structure of social ecological landscape.

Data Availability

No data were used to support this study.

Conflicts of Interest

The author declares that he has no competing interests.

References

- [1] X.-N. Min, Y. H. Wang, X. Gao, and G. H. Liu, "Ecological pattern of urban forest landscape of Ji'nan City, China," *The journal of applied ecology*, vol. 30, no. 12, pp. 117–126, 2019.
- [2] X. Chao, D. Haase, D. O. Pribadi, and S. Pauleit, "Spatial variation of green space equity and its relation with urban dynamics: a case study in the region of Munich," *Ecological Indicators*, vol. 93, no. 10, pp. 512–523, 2018.
- [3] L. Cui, J. Wang, L. Sun, and C. Lv, "Construction and majorization of green space ecological networks in urban fringe areas: a case study with the urban fringe area of Tongzhou District in Beijing," *Journal of Cleaner Production*, vol. 6, no. 2, pp. 124–266, 2020.
- [4] J. Oehrlin, B. Niedermann, and J. H. Haunert, "Analyzing the supply and detecting spatial patterns of urban green spaces via optimization," *PFG Journal of Photogrammetry, Remote Sensing and Geoinformation Science*, vol. 87, no. 4, pp. 137–158, 2019.
- [5] C. Dobbs, C. Nitschke, and D. Kendal, "Assessing the drivers shaping global patterns of urban vegetation landscape structure," *Science of the Total Environment*, vol. 592, no. 8, pp. 171–177, 2017.
- [6] H. Soltanifard and E. Jafari, "A conceptual framework to assess ecological quality of urban green space: a case study in Mashhad City, Iran," *Environment, Development and Sustainability: A Multidisciplinary Approach to the Theory and Practice of Sustainable Development*, vol. 21, no. 4, pp. 1781–1808, 2019.
- [7] R. Salvati, F. Ranalli, M. Carlucci, A. Ippolito, A. Ferrara, and P. Corona, "Forest and the city: a multivariate analysis of peri-urban forest land cover patterns in 283 European metropolitan areas," *Ecological Indicators*, vol. 73, pp. 369–377, 2017.
- [8] A. Baker and B. Marques, "Out of place: rewriting the signatures of a landscape," *Spaces and Flows: An International Journal of Urban and ExtraUrban Studies*, vol. 8, no. 4, pp. 1–12, 2017.
- [9] S. Cao, D. Hu, Z. Hu, W. Zhao, S. Chen, and C. Yu, "Comparison of spatial structures of urban agglomerations between the Beijing-Tianjin-Hebei and Boswash based on the subpixel-level impervious surface coverage product," *Journal of Geographical Sciences*, vol. 28, no. 3, pp. 306–322, 2018.
- [10] W. Yin, Y. Liu, W. Yi, X. Lu, X. Zhao, and L. Zhao, "Ecological and low-carbon technology in urban decentralized treatment and reclamation of wastewater," *Journal of Landscape Research*, vol. 10, no. 3, pp. 79–83, 2018.
- [11] H. K. Heo, D. K. Lee, J. H. Park, and J. H. Thorne, "Estimating the heights and diameters at breast height of trees in an urban

- park and along a street using mobile LiDAR,” *Landscape and Ecological Engineering*, vol. 15, no. 3, pp. 253–263, 2019.
- [12] L. Inostroza, Z. Hamstead, M. Spyra, and S. Qureshi, “Beyond urban-rural dichotomies: measuring urbanisation degrees in central European landscapes using the technomass as an explicit indicator,” *Ecological Indicators*, vol. 96, no. 1, pp. 466–476, 2019.
- [13] A. Tomao, L. Secondi, G. Carrus, P. Corona, L. Portoghesi, and M. Agrimi, “Restorative urban forests: exploring the relationships between forest stand structure, perceived restorativeness, and benefits gained by visitors to coastal *Pinus pinea* forests,” *Ecological Indicators*, vol. 90, no. 7, pp. 594–605, 2018.
- [14] C. Arnaiz-Schmitz, M. F. Schmitz, C. Herrero-Jauregui, J. Gutiérrez-Angonese, F. D. Pineda, and C. Montes, “Identifying socio-ecological networks in rural-urban gradients: diagnosis of a changing cultural landscape,” *Science of the Total Environment*, vol. 612, no. 15, pp. 625–635, 2018.
- [15] D. L. Fraser, K. Ironside, R. K. Wayne, and E. E. Boydston, “Connectivity of mule deer (*Odocoileus hemionus*) populations in a highly fragmented urban landscape,” *Landscape Ecology*, vol. 34, no. 5, pp. 1097–1115, 2019.
- [16] J. Kim, “Subdivision design and landscape structure: case study of the Woodlands, Texas, US,” *US Urban Forestry & Urban Greening*, vol. 38, no. 8, pp. 232–241, 2019.
- [17] K. Borowiak, M. Lisiak, J. Kanclerz et al., “Relations between rare earth elements accumulation in *Taraxacum officinale* L. and land use in an urban area - a preliminary study,” *Ecological Indicators*, vol. 94, no. 11, pp. 22–27, 2018.
- [18] C. D. Yu and D. Nan, “Analysis of landscape ecological planning based on the high-order multiwavelet neural network algorithm,” *Computational Intelligence and Neuroscience*, vol. 2021, Article ID 9420532, 8 pages, 2021.
- [19] O. Soydan, “Effects of landscape composition and patterns on land surface temperature: urban heat island case study for Nigde, Turkey,” *Turkey Urban Climate*, vol. 34, no. 12, pp. 100688–100688, 2020.
- [20] Y. Luo and J. Wu, “Linking the minimum spanning tree and verge betweenness to understand arterial corridors in an ecological network,” *Landscape Ecology*, vol. 36, no. 5, pp. 1549–1565, 2021.
- [21] J. Steenberg, P. N. Duinker, and S. A. Nitoslawski, “Ecosystem-based management revisited: updating the concepts for urban forests,” *Landscape and Urban Planning*, vol. 186, no. 86, pp. 24–35, 2019.
- [22] F. Ding, “The transformation and governance of urban villages with historic culture: a case study of Xiaxifang, Yongfeng County, Ji’an City,” *Jiangxi Province Journal of Landscape Research*, vol. 10, no. 5, pp. 122–124, 2018.
- [23] M. Su, Z. Ying, H. Yan et al., “The influence of landscape pattern on the risk of urban water-logging and flood disaster,” *Ecological Indicators*, vol. 92, no. 9, pp. 133–140, 2017.
- [24] F. Ungaro, I. Zasada, and A. Piorr, “Turning points of ecological resilience: geostatistical modelling of landscape change and bird habitat provision,” *Landscape and Urban Planning*, vol. 157, pp. 297–308, 2017.
- [25] D. Wan and S. Yin, “Construction of ecological environment information system based on big data: a case study on Dongting Lake ecological area,” *Mobile Information Systems*, vol. 2021, Article ID 3885949, 2021.

Research Article

Multiobjective Optimization of Structure and Robustness of a Split Parallel Multicomponent Strain Sensor

Peng Kong,^{1,2} Xiaoqiang Peng,¹ and Zhenzeng Lian ²

¹Laboratory of Science and Technology on Integrated Logistics Support, National University of Defense Technology, Changsha, 410073 Hunan Province, China

²China Aerodynamics Research and Development Center, Mianyang, 621000 Sichuan Province, China

Correspondence should be addressed to Zhenzeng Lian; liansky2020@163.com

Received 29 November 2021; Accepted 26 January 2022; Published 7 March 2022

Academic Editor: Alireza Souri

Copyright © 2022 Peng Kong et al. This is an open access article distributed under the Creative Commons Attribution License, which permits unrestricted use, distribution, and reproduction in any medium, provided the original work is properly cited.

A novel split parallel multicomponent strain sensor structure layout is proposed based on the special requirements of the helicopter rotor airfoil wind tunnel test for measuring aerodynamic sensors. The sensor consists of two splits with the same configuration; the performance of the sensor not only depends on the split structure of the sensor but also depends on the assembly relationship between the splits. Three steps have been performed so as to enhance the technical performance of the sensor. First, the RBF neural network approximate model and the second-generation nondominated sorting genetic algorithm are used to optimize the split of sensor deterministically; secondly, the rotor airfoil wind tunnel test model and the sensor finite element system model are established, and the 6σ robustness analysis is carried out; finally, the 6σ robust multiobjective optimization has been carried out considering the sensor split processing errors and the assembly errors. The results show that, compared to initial designed sensors, the sensitivity of the three components of the sensor is increased by 285.46%, 284.95%, and 151.5%, respectively, and the maximum equivalent stress is reduced by 28.4%; the interference to the three components is reduced by 97.82%, 92.83%, and 99.8%, respectively, and the quality is reduced by 25.74%. Meanwhile, the quality level of the sensor was promoted, and the sensitivity of the response to assembly and manufacturing errors were reduced. These results exhibit that the structural layout, optimized path, and method in this strain sensor are suitable for the needs of helicopter rotor airfoil wind tunnel test.

1. Introduction

Helicopter rotor dynamic stall is a serious unsteady aerodynamic phenomenon with complex mechanisms, especially the airfoil dynamic stall. Hence, in-depth understanding of the rotor airfoil dynamic stall characteristics is of great importance to investigate the ways to improve rotor performance, predict the rotor aerodynamics more accurately, and thereby promote the development of advanced helicopters.

The wind tunnel test is the main means to understand the dynamic stall characteristics and flow mechanism of the rotor blade airfoil recently. It is necessary to develop a multicomponent strain-type force sensor to support the model through the left and right sides in parallel and accurately measure the model resistance, lift, and pitch moments during the wind tunnel test of the helicopter rotor airfoil.

While in the conventional wind tunnel test, the aircraft model, sensors, and supporting test device are connected in series and connected at a single point, whose precision and accuracy are mainly rely on the performance of the sensor, that is, the sensor's own sensitivity, stiffness, strength, and mutual interference between components [1–4].

Therefore, a novel split parallel multicomponent strain sensor structure layout is proposed consisting of two components, A and B, to meet the needs of the rotor-wing wind tunnel test, on the basis of conventional three-piece beam load cells. A and B are three-component strain sensors with the same configuration, supporting the rotor airfoil wind tunnel test model from both sides in parallel to complete the model aerodynamics and torque measurement. The development of the sensor must consider not only the sensitivity, stiffness, strength, and mutual interference between

the components but also the impact of assembly errors between the A and B components on the overall performance of the sensor.

The following design and optimization approaches are proposed to improve the sensor split and its overall technical performance. Firstly, a finite element analysis model is established with the sensor split as the object to analyze separately its strain under the action of resistance, lift, and pitch moment cloud map and to determine the location of strain gauges and the way of group bridges; secondly, the RBF neural network approximate model and NSGA-II multiobjective optimization algorithm are utilized to deterministically optimize the sensor split performance and obtain the Pareto optimal solution and excellent monomer performance [5]; thirdly, a finite element system model of the rotor airfoil wind tunnel test model and sensor was established. Based on the RSM response surface approximation model and the Monte Carlo simulation technology, the quality level of the system was tested, and the robustness optimization technology was introduced to improve the robustness of the sensor.

2. Materials and Methods

2.1. Geometry. The geometry and main parameters of the sensor splits are shown in Figures 1 and 2. The left and right ends of the split use single-piece beam-type elastic elements (serial number 1) of the same geometric size to bear resistance F_x . The length, width, and height of the single-piece beam-type elastic elements are expressed as $L2$, $B3$, and $H3$; the middle of the split body is a three-beam elastic element; the middle main beam (serial number 2) of the three-beam elastic element bears the lift force F_y ; the front and rear side beams (serial number 3) bear the pitching moment M_z ; the length, width, and height of the middle main beam are expressed as $L1$, $B1$, and $H1$; the front and rear side beams have the same geometric dimensions, and their length, width, and height are, respectively, $L1$, $B2$, and $H2$; the thickness of the front and rear flange sensors is $S2$; and the thickness of the middle flange $S1$ plays the role of connection.

Each measurement of the elastic element of this layout is independent of the load measurement, that is, it is sensitive to the load of the measured component and insensitive to the load of other components, so it is easy to obtain the required sensitivity and less mutual interference.

2.2. Key Technical Requirements. The split structure of the sensor requires high sensitivity, sufficient strength, rigidity, and small interference between the components.

Sensitivity is an important factor of sensor design which can be improved for the strain-type force sensor by increasing the design strain value of the measuring element. And the design strain value of the general wind tunnel sensor is selected ranging 300~600 $\mu\epsilon$ [6].

Sufficient strength under the maximum external load is necessary to ensure the safety of the wind tunnel test. The rotor airfoil wind tunnel test's heave motion frequency can reach 5, while the first-order natural frequency of the system composed of strain-type force sensor and rotor airfoil wind tunnel test model must be 10 times than its motion frequency [7].

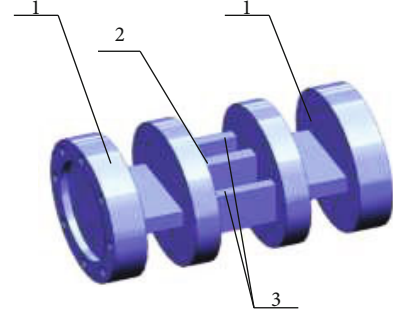


FIGURE 1: The geometric structure of the sensor split.

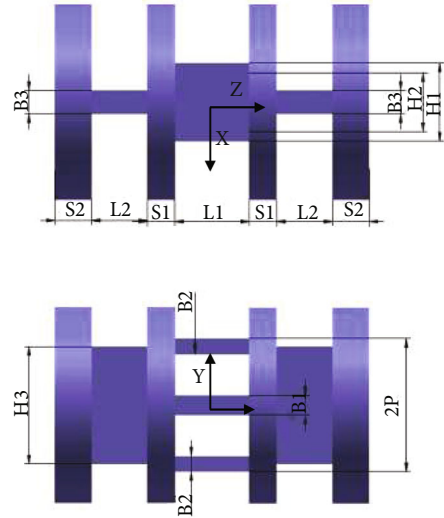


FIGURE 2: The main geometric parameters of the sensor split.

In the structural design, due to mutual interference between the components, it is necessary to allocate the stiffness reasonably to ensure proper deformation in the load direction of the measured component and reduce its deformation in other components. Generally, the amount of interference between the components of the strain sensor should be controlled below 10% [6].

2.3. Analysis of Split Finite Element Model

2.3.1. Geometry Simplification. The original structure of the model is simplified, especially some local details without affecting the calculation accuracy of the device. These simplifications will not affect the overall analysis results of the original structure but can significantly improve the speed and quality of the finite element analysis and sometimes improve the accuracy and reliability of calculation results.

2.3.2. Meshing. In order to ensure the accuracy of the calculation results, second-order grid elements are used. In order to reasonably arrange the density of the grid, the dimensional functions proximity and curvature are used. The mesh is refined in the place where the stress gradient is large. The quality of the grid has a greater impact on the calculation accuracy. Through the finite element-preprocessing software, the mesh

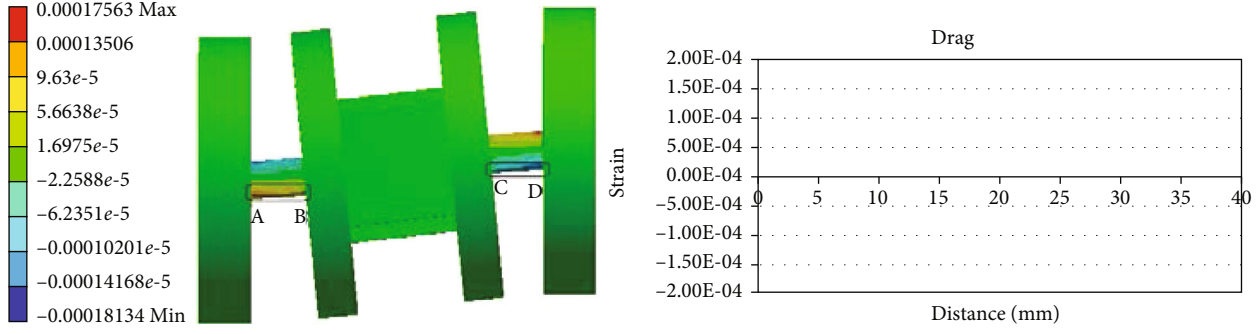


FIGURE 3: Strain cloud diagram and strain distribution of maximum resistance.

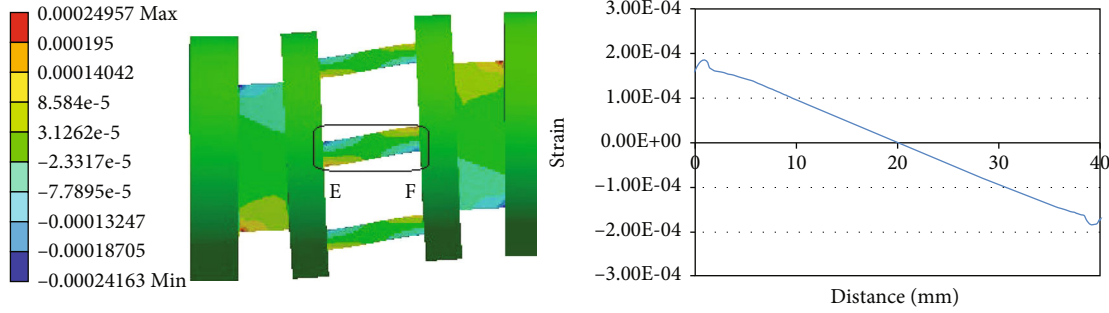


FIGURE 4: Strain cloud diagram and strain distribution of maximum lift.

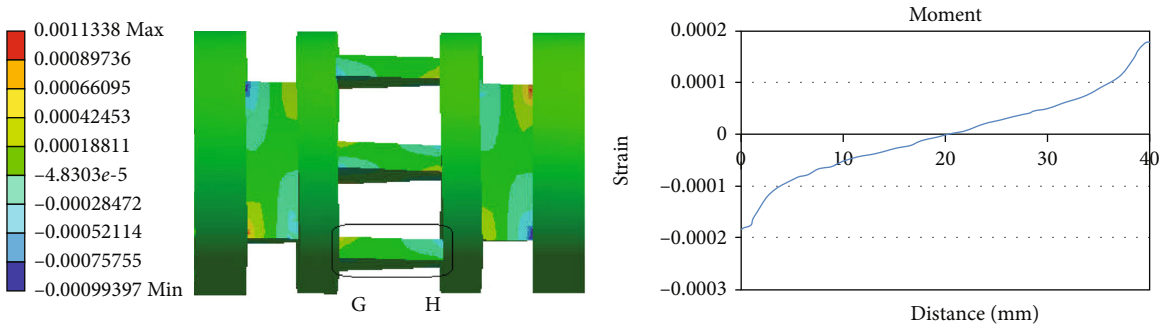


FIGURE 5: Strain cloud diagram and strain distribution of maximum pitching moment.

quality is checked and modified until the finite element model fully meets the high-precision requirements. In actual calculations, the calculation results of two different mesh densities are compared. If the calculation results are very different, you can continue to increase the grid until the calculation results are not much different and the grid size is appropriate.

2.3.3. Definition of Material Properties and Boundary Conditions. The material used in the design is with elastic modulus $E = 200GPa$ and yield strength $\sigma_S = 2020MPa$. According to the impact factor $n_c = 1.5$ and safety factor $n_a = 2$ selected in [8], the allowable stress can be obtained $[\sigma] = 673MPa$.

The following loads were applied for static calculations: (1) maximum resistance F_X , (2) maximum lift F_Y , (3) maximum pitch moment M_Z , (4) maximum lateral force F_Z , (5)

maximum yaw moment M_Y , (6) maximum roll moment M_X , and (7) maximum load of six components under test conditions.

2.3.4. Static Analysis and Results. Figures 3–5 are the strain cloud diagrams of strains under the action of maximum resistance F_X , maximum lift F_Y , and maximum pitch moment M_Z , as well as the distribution diagrams along \overrightarrow{DC} , \overrightarrow{BA} , \overrightarrow{EF} , and \overrightarrow{HG} , respectively. It can be seen from the figure that the maximum strain is close to the endpoint of the elastic measuring element, the best choices for strain gauges, and the maximum strain values at each position are $175.63 \mu\epsilon$, $249.57 \mu\epsilon$, and $113.38 \mu\epsilon$, which cannot meet the sensitivity requirements.

From Figure 6, the maximum equivalent stress value of the model is $\sigma_r = 575MPa$, which is less than the allowable stress of the material.

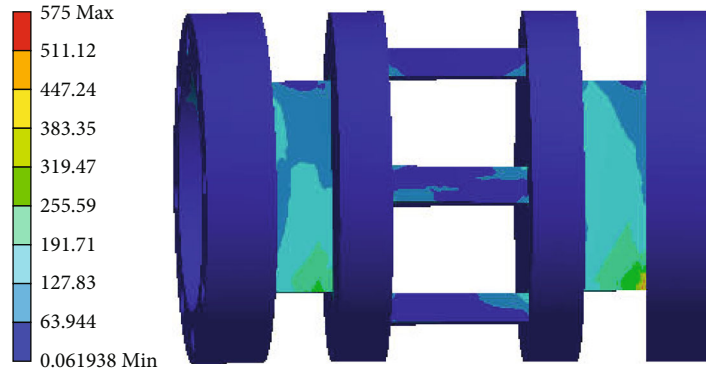
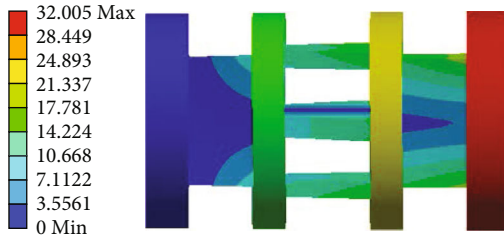


FIGURE 6: Strain cloud diagram of maximum load.

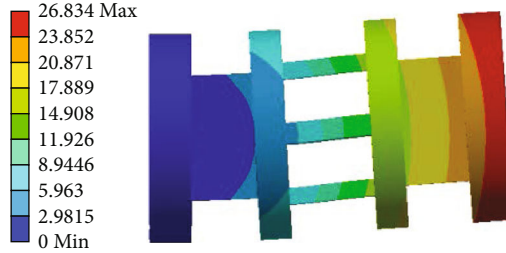
F: Model
Total deformation
Type: Total deformation
Frequency: 202.01 HZ
Unit: mm
2020/5/7 14:01



F: Model
Total deformation 3
Type: Total deformation
Frequency: 761.67 HZ
Unit: mm
2020/5/7 14:04



F: Model
Total deformation 2
Type: Total deformation
Frequency: 670.71 HZ
Unit: mm
2020/5/7 14:03



F: Model
Total deformation 4
Type: Total deformation
Frequency: 1197.9 HZ
Unit: mm
2020/5/7 14:05



FIGURE 7: The shape of the first 4th-order splitting mode.

2.3.5. Modal Analysis and Results. In terms of resonance, all the modes whose natural frequency is in the range of the external load frequency should be maintained, and it must be calculated to be more than 10 times the operating frequency in this study. Therefore, the first 4 natural frequencies were selected to verify if they are in the resonance zone. The change of the first 4th-order mode shape of splitting is shown in Figure 7, and the natural frequency of each order is shown in Table 1.

2.4. Strain Gauge Position and Group Bridge. According to the strain cloud diagram and strain value distribution diagram [9–11], the installation position of the strain gauge is

TABLE 1: Result of mode analysis.

Mode	1	2	3	4
Frequency	202.01	670.71	761.67	1197.9

determined by comprehensively considering the paste technique and sensitivity requirements of the strain gauge. Wheatstone bridge was designed reasonably to achieve the largest possible output for the measured component [8] and the smallest possible output signal for other components, as well as achieve the electrical decomposition of force and torque. The final distribution of strain gauges and bridge formation are shown in Figures 8 and 9.

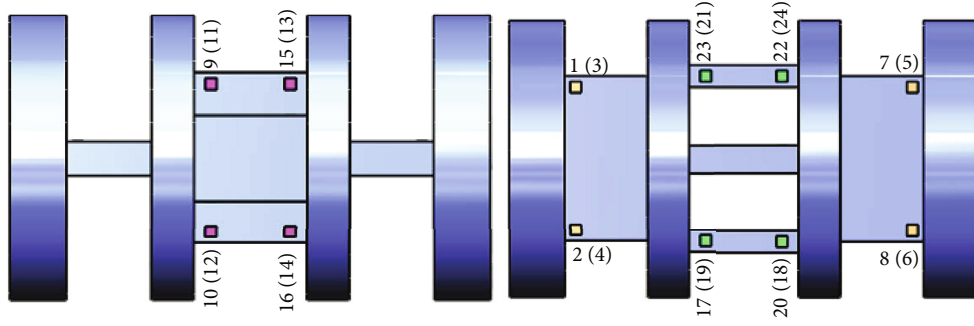


FIGURE 8: Layout of strain gauges.

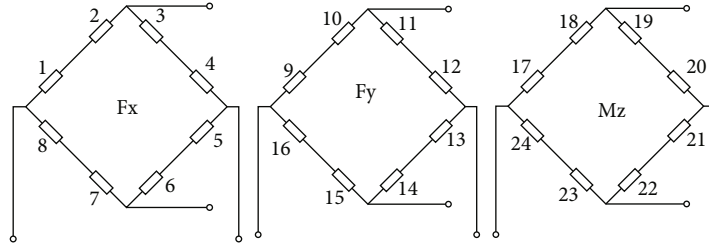


FIGURE 9: Wheatstone bridge diagram of each component.

3. Optimized Design of Sensor Split Structure

Parameter optimization is needed as the finite element analysis of the initial design of the sensor split proved that it cannot meet the sensitivity requirements. Appropriate design variables and output responses for experimental design were selected, and a sufficient number of finite element analysis sample points were generated to fit the approximate model; the optimization problem was defined, and the sensor parameters were optimized based on the NSGA-II multiobjective optimization algorithm.

3.1. Approximate Model and Verification. The RBF neural network approximate model is used in simulating the input-output relationship of the finite element model to solve the problem of huge time cost during calculation. The establishment of approximate models mainly is as follows:

- (1) The input parameters were defined as x_i (x_i are the geometric parameters B1, B2, B3, H1, H2, H3, L1, L2, S1, S2, and P, $1 \leq i \leq 11, i \in N$) with a total of 11 input variables whose initial value and range of values are shown in Table 2
- (2) The output parameters were defined as y_j , with the maximum equivalent stress s_{\max} and the maximum deformation displacement value d_{\max} under the maximum load of six components under test conditions, first-order natural frequency $freq1$; the average strain values ($\epsilon_{xx1} \sim \epsilon_{xx8}$, $\epsilon_{xy1} \sim \epsilon_{xy8}$, $\epsilon_{xz1} \sim \epsilon_{xz8}$, $\epsilon_{xmx1} \sim \epsilon_{xmx8}$, $\epsilon_{xmy1} \sim \epsilon_{xmy8}$, and $\epsilon_{x mz1} \sim \epsilon_{x mz8}$) of strain gauges 1-8 are under maximum resistance F_X , maximum lift F_y , maximum lateral force F_z , maximum roll moment M_x , maximum yaw moment M_y , and maximum pitch moment M_z ; average strain

TABLE 2: Design parameters and value range.

Parameters	Lower bound	Value	Upper bound
B1	5	10	10
B2	4	8	8
B3	5	12	15
H1	25	40	45
H2	20	30	40
H3	50	60	80
L1	20	40	60
L2	10	30	40
S1	5	15	15
S2	12.5	20	22.5
P	30	34	50

values ($\epsilon_{yx1} \sim \epsilon_{yx8}$, $\epsilon_{yy1} \sim \epsilon_{yy8}$, $\epsilon_{yz1} \sim \epsilon_{yz8}$, $\epsilon_{ymx1} \sim \epsilon_{ymx8}$, $\epsilon_{y my1} \sim \epsilon_{y my8}$, and $\epsilon_{y mz1} \sim \epsilon_{y mz8}$) of strain gauges 9-16 are under maximum resistance F_X , maximum lift F_y , maximum lateral force F_z , maximum roll moment M_x , maximum yaw moment M_y , and maximum pitch moment M_z ; average strain values ($\epsilon_{mzx1} \sim \epsilon_{mzx8}$, $\epsilon_{mzy1} \sim \epsilon_{mzy8}$, $\epsilon_{mzz1} \sim \epsilon_{mzz8}$, $\epsilon_{mzmx1} \sim \epsilon_{mzmx8}$, $\epsilon_{mzmy1} \sim \epsilon_{mzmy8}$, and $\epsilon_{mzmz1} \sim \epsilon_{mzmz8}$) of the serial number 17-24 strain gauges are under maximum resistance F_X , maximum lift F_y , maximum lateral force F_z , maximum roll moment M_x , maximum yaw moment M_y , and maximum pitch moment M_z . A total of 148 output responses are set as output parameters

TABLE 3: The error calculation results of an approximate model.

Index	R^2	Index	R^2	Index	R^2
s_{\max}	0.93	$\epsilon_{xmy1} \sim \epsilon_{xmy8}$	0.94~0.95	$\epsilon_{mzx1} \sim \epsilon_{zx8}$	0.97~0.98
d_{\max}	0.95	$\epsilon_{xmx1} \sim \epsilon_{xmx8}$	0.93~0.94	$\epsilon_{mzy1} \sim \epsilon_{mzy8}$	0.91~0.92
$freq1$	0.988	$\epsilon_{yx1} \sim \epsilon_{yx8}$	0.97~0.98	$\epsilon_{mzz1} \sim \epsilon_{mzz8}$	0.97~0.98
$mass$	1	$\epsilon_{yy1} \sim \epsilon_{yy8}$	0.97~0.98	$\epsilon_{mzmx1} \sim \epsilon_{mzmx8}$	0.97~0.98
$\epsilon_{xx1} \sim \epsilon_{xx8}$	0.94~0.95	$\epsilon_{yz1} \sim \epsilon_{yz8}$	0.96~0.97	$\epsilon_{mzmy1} \sim \epsilon_{mzmy8}$	0.94~0.95
$\epsilon_{xy1} \sim \epsilon_{xy8}$	0.97~0.98	$\epsilon_{ymx1} \sim \epsilon_{ymx8}$	0.94~0.95	$\epsilon_{mzmx1} \sim \epsilon_{mzmx8}$	0.97~0.98
$\epsilon_{xz1} \sim \epsilon_{xz8}$	0.94~0.95	$\epsilon_{yzy1} \sim \epsilon_{yzy8}$	0.94~0.96		
$\epsilon_{xmx1} \sim \epsilon_{xmx8}$	0.96~0.97	$\epsilon_{ymz1} \sim \epsilon_{ymz8}$	0.96~0.97		

(3) The optimal Latin hypercube test design method was used to obtain a sufficient number of sample points, and an approximate model of RBF neural network was established

(4) The cross-validation method was used to detect the accuracy of the approximate model. If the accuracy is insufficient, the approximate point is added to increase the approximate model to a sufficient accuracy

The credibility index R^2 was utilized as the evaluation index to detect the global and local approximation accuracy of the approximation model with a lower limit of 0.9. The closer the R^2 to 1, the more accurate.

From the approximate model error calculation results (shown in Table 3), it can be seen that the radial basis neural network approximate model exhibits good performance in fitting the sensor split finite element model.

3.2. Multiobjective Optimization. Taking the input parameters x_i of the above approximate model as the design variables, the average strain value $\epsilon_1 \sim \epsilon_{24}$ as the constraint, the minimizing of maximum equivalent stress s_{\max} , the maximum displacement value d_{\max} , the maximizing of first-order natural frequency $freq1$, and the minimizing of interference η_x , η_y , and η_{mz} of the components of F_x , F_y , and M_z are the goal of optimizing. Then, the optimization problem was defined as below [12–15].

$$\left\{ \begin{array}{l} \text{Minimize : } d_{\max}, Mass \\ \text{Minimize : } \eta_x, \eta_y, \eta_{Mz} \\ \text{Minimize : } s_{\max} \\ \text{Maximize : } freq1 \\ \text{s.t } 300\mu m \leq \epsilon_j \leq 600\mu m, j \in [1, 24] \& \& j \in N \\ s_{\max} \leq 673 MPa \\ D.v. \quad x_i^{(L)} \leq x_i \leq x_i^{(U)} \\ \quad \quad i \in [1, 11] \& \& i \in N. \end{array} \right. \quad (1)$$

According to the principle of Wheatstone bridge, for resistance bridge, when $R \gg \Delta R$

$$U_o = \frac{U_i K}{8} (\epsilon_1 + \epsilon_2 - \epsilon_3 - \epsilon_4 + \epsilon_5 + \epsilon_6 - \epsilon_7 - \epsilon_8), \quad (2)$$

where U_o is the output voltage of the bridge, U_i is the supply voltage of the bridge, and K is the sensitivity coefficient of the strain gauge.

When the sensor is under the maximum load of each component, the output voltage of the resistance bridge is

$$\begin{aligned} U_o^{xx} &= \frac{U_i K}{8} (\epsilon_{xx1} + \epsilon_{xx2} - \epsilon_{xx3} - \epsilon_{xx4} + \epsilon_{xx5} + \epsilon_{xx6} - \epsilon_{xx7} - \epsilon_{xx8}), \\ U_o^{xy} &= \frac{U_i K}{8} (\epsilon_{xy1} + \epsilon_{xy2} - \epsilon_{xy3} - \epsilon_{xy4} + \epsilon_{xy5} + \epsilon_{xy6} - \epsilon_{xy7} - \epsilon_{xy8}), \\ U_o^{xz} &= \frac{U_i K}{8} (\epsilon_{xz1} + \epsilon_{xz2} - \epsilon_{xz3} - \epsilon_{xz4} + \epsilon_{xz5} + \epsilon_{xz6} - \epsilon_{xz7} - \epsilon_{xz8}), \\ U_o^{xmx} &= \frac{U_i K}{8} (\epsilon_{xmx1} + \epsilon_{xmx2} - \epsilon_{xmx3} - \epsilon_{xmx4} + \epsilon_{xmx5} + \epsilon_{xmx6} - \epsilon_{xmx7} - \epsilon_{xmx8}), \\ U_o^{xmy} &= \frac{U_i K}{8} (\epsilon_{xmy1} + \epsilon_{xmy2} - \epsilon_{xmy3} - \epsilon_{xmy4} + \epsilon_{xmy5} + \epsilon_{xmy6} - \epsilon_{xmy7} - \epsilon_{xmy8}), \\ U_o^{xmxz} &= \frac{U_i K}{8} (\epsilon_{xmxz1} + \epsilon_{xmxz2} - \epsilon_{xmxz3} - \epsilon_{xmxz4} + \epsilon_{xmxz5} + \epsilon_{xmxz6} - \epsilon_{xmxz7} - \epsilon_{xmxz8}), \\ \eta_{xy} &= abs[(U_o^{xy})/U_o^{xx}], \\ \eta_{xz} &= abs[(U_o^{xz})/U_o^{xx}], \\ \eta_{xmx} &= abs[(U_o^{xmx})/U_o^{xx}], \\ \eta_{xmy} &= abs[(U_o^{xmy})/U_o^{xx}], \\ \eta_{xmxz} &= abs[(U_o^{xmxz})/U_o^{xx}], \\ \eta_x &= \eta_{xy} + \eta_{xz} + \eta_{xmx} + \eta_{xmy} + \eta_{xmxz}. \end{aligned} \quad (3)$$

η_{yx} , η_{yz} , η_{ymx} , η_{yzy} , η_{ymz} , η_y , η_{mzx} , η_{mzy} , η_{mzz} , η_{mzmx} , η_{mzmy} , and η_{mz} can be obtained based on the same process.

Based on the established RBF neural network approximate model, the Pareto optimal solution (shown in Figure 10) was obtained by using the NSGA-II optimization algorithm after repeated experiments with a population size of 100, a cross-distribution index of 100, and a cross-probability of 0.9 in 6001 calculation steps.

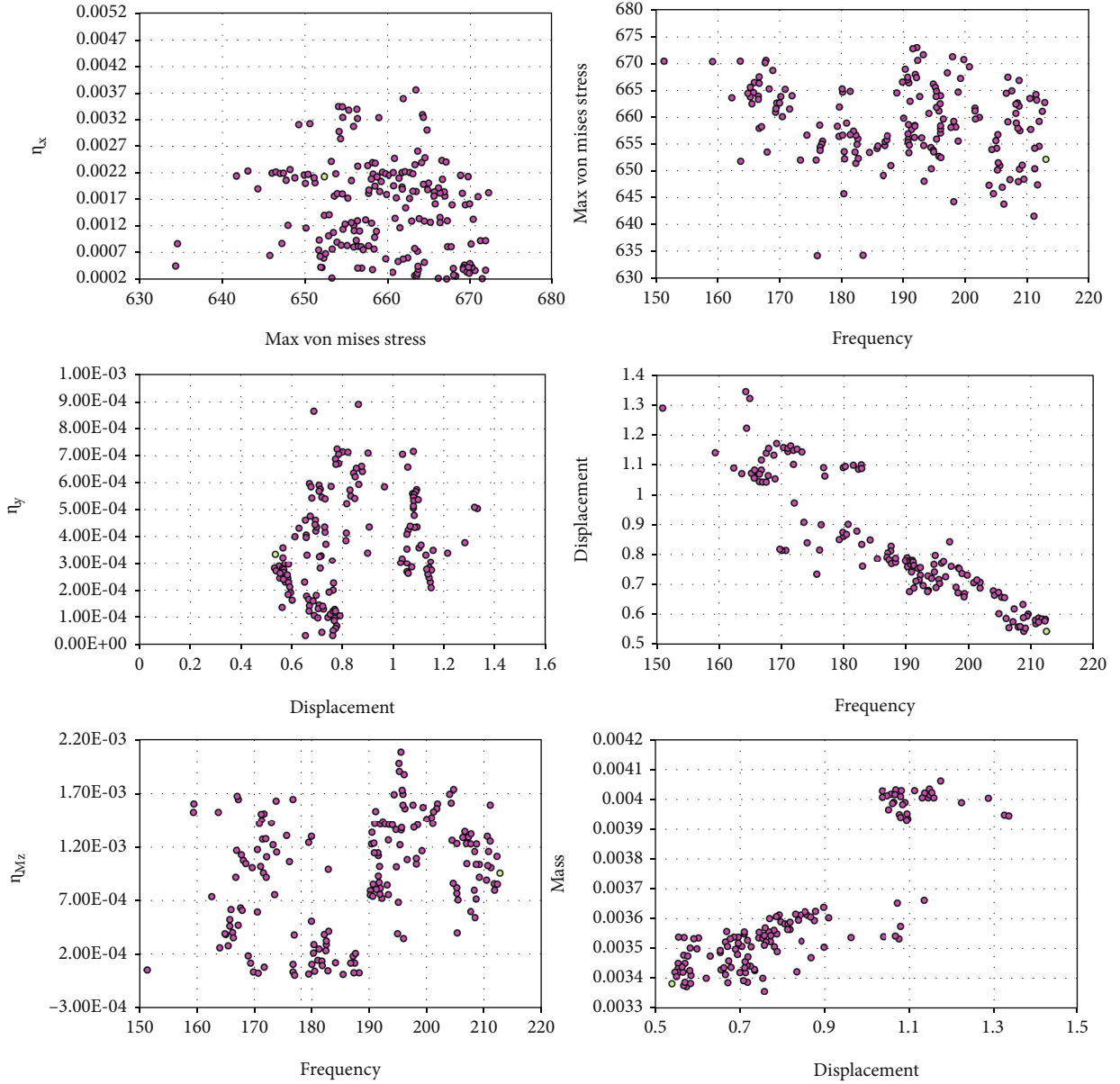


FIGURE 10: Pareto optimal solution.

After sorting the above solution sets, the 1896th is determined to be the optimal solution whose comparative analysis of the results is shown in Table 4.

In initial design, the initial interference η_x on the resistance F_X and the interference on the pitching moment M_Z are relatively large, reaching 4.26% and 5.12%, respectively; the strain values under the action of the maximum resistance F_X , the maximum lift F_y , and the maximum pitching moment M_Z are 81.6 $\mu\epsilon$, 115.1 $\mu\epsilon$, and 167.7 $\mu\epsilon$, respectively, which cannot meet the technical requirements of the sensor split. After optimization, the strain values under the action of the maximum resistance F_X , the maximum lift F_y , and the maximum pitching moment M_Z are increased by 271%, 408%, and 227%, respectively, and the interference of the component is reduced by 95%, 94.4%, and 98.1%;

the first-order natural frequency is increased by 5%, and the quality is reduced by 28.1%.

4. Robustness Analysis and Optimization

Some uncertain factors, such as the processing error of the sensor split and the assembly error between the sensor splits, are inevitable to encounter during the execution of the actual rotor blade wind tunnel test project. Without considering the influence of these uncertain factors in the deterministic optimization of the sensor split, the optimization result may present lower reliability or robustness and greater technical risks in practice [16, 17].

Therefore, it is necessary to further perform robust analysis and even optimization on the split parallel

TABLE 4: Optimization results.

Optimization goal	Initial value (mm)	Optimization value (mm)	Percent changed
s_{\max}	575	652.33	13.45%
d_{\max}	0.7413	0.5399	-27.17%
$freq1$ (Hz)	202.49	212.628	5%
Mass	0.0047	0.00338	28.1%
ε_x	81.6	302.6	271%
ε_y	115.1	585.19	408%
ε_{Mz}	167.7	548.62	22%
η_x	4.26%	0.214%	-95.0%
η_y	0.6125%	0.034%	-94.4%
η_{mz}	5.12%	0.098%	-98.1%

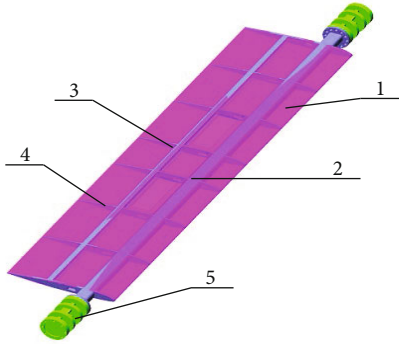


FIGURE 11: Three-dimensional diagram of the system. (a) Test model skin. (b) Test model front beam. (c) Test model rear beam. (d) Test model longitudinal beam. (e) Sensor split.



FIGURE 12: Grid division diagram.

TABLE 5: Mechanical parameters of T800 carbon fiber-reinforced composites.

Elastic modulus, GPa			Shear modulus, GPa			Poisson's ratio		
E_1	E_2	E_3	G_{12}	G_{13}	G_{23}	ν_{12}	ν_{13}	ν_{23}
195	8.58	8.58	4.6	4.6	2.9	0.33	0.33	0.48
Tensile strength, MPa			Compression strength, MPa			Shear strength, MPa		
X_T	Y_T	Z_T	X_C	Y_C	Z_C	S_{12}	S_{13}	S_{23}
3071	88	88	1747	271	271	143	143	143

TABLE 6: Material properties.

Material	Modulus (GPa)	Poisson's ratio	Density (kg m^{-3})
7075	72	0.33	2810

multicomponent strain sensor considering the interference of uncertain factors.

4.1. System Finite Element Model Analysis

4.1.1. Geometric Model. The scheme of analysis system is shown in Figure 11, consisting of main components such as front and rear beams, longitudinal beams, and skin with a total length of 1950 mm and a chord length of 300 mm. The binary model of OA309 airfoil is used in characterizing cross-section.

4.1.2. Pretreatment. Firstly, the model is simplified as below without affecting the calculation accuracy of the device.

- (1) The fine process holes for nonconnections with little effect on the overall performance of the structure are ignored
- (2) Small chamfers and rounded corners are removed
- (3) The quality unit is used for the parts that do not participate in the analysis
- (4) Quadrilateral shell elements are used to divide the grid after extracting the corresponding shell

Secondly, 4-node quadrilateral elements divided each component and were combined with the aforementioned sensor split grid to form an assembly (Figure 12) so as to ensure the accuracy and efficiency of the calculation, using the wind tunnel test model.

Finally, the material properties and boundary conditions are defined. The material of the front beam of the test model is 7075, and the rest of the test model is made of T800 carbon fiber-reinforced composite material. The material properties are shown in Tables 5 and 6. The applied loads and constraints are mainly composed of three aspects that are inertial load and aerodynamic load, the last one is one sensor split that is fixedly connected through the screw hole, and the other is applied with 6 degrees of freedom through the screw hole assembly error (Δx , Δy , Δz , $\Delta \alpha$, $\Delta \beta$, and $\Delta \gamma$).

4.1.3. Finite Element Static Analysis and Results. The von Mises stress is employed for strength evaluation according to the fourth strength theory. In Figure 13, the maximum equivalent stress value of the sensor $\sigma_r = 600.9 \text{ MPa}$ is smaller than the allowable stress of the material. Hence, the model is applicable.

4.1.4. Modal Analysis and Results. The first-order natural frequency of the system must be greater than 50 Hz. Figure 14 shows the first-order vibration mode of the system with natural frequency of 54.17 Hz.

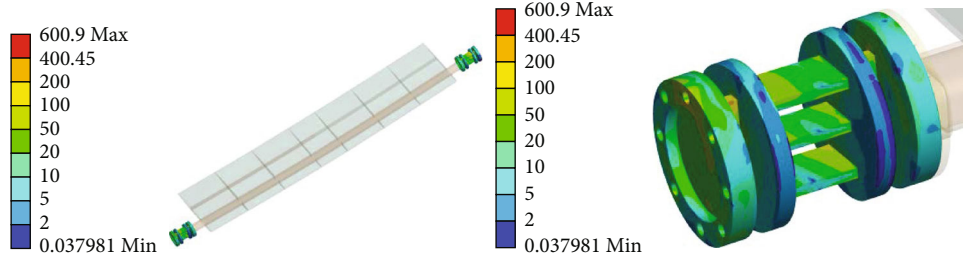


FIGURE 13: Stress contours of the model.

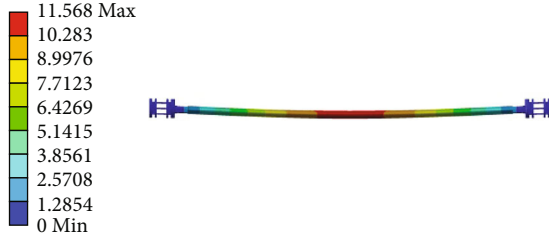


FIGURE 14: The first-order natural frequency of the system.

TABLE 7: Input parameters and value range.

Input parameters	Lower bound	Upper bound	Output parameters
$B1$	5	8	s_{\max}
$B2$	4	8	$freq1$
$B3$	5	15	$mass$
$H1$	25	45	
$H2$	20	40	
$H3$	50	80	
$L1$	20	60	
$L2$	10	40	
$S1$	5	15	
$S2$	12.5	22.5	
P	30	50	
Δx	0	0.3	
Δy	0	0.5	
Δz	0	0.2	
$\Delta \alpha$	0	0.15	
$\Delta \beta$	0	0.15	
$\Delta \gamma$	0	0.15	

TABLE 8: The error calculation results of an approximate model.

Index	R^2
s_{\max}	0.985
$freq1$	0.964
$mass$	0.992

4.2. *System Approximate Model.* The optimal Latin hypercube test design method is used to obtain a certain number of sample points, and a fourth-order polynomial response surface (RSM) approximate model is established. Input parameters and output parameters are shown in Table 7.

Credibility indicators (R^2) are taken as evaluation indicators. It can be seen from the calculation results of the approximate model error (Table 8) that the approximate model has good performance in fitting the system.

4.3. *Robustness Analysis.* The 6σ robustness analysis, the basis of the robustness optimization, is to evaluate the quality level of the deterministic optimization plan by disturbing the current design point, generating a set of sample points around its average value, and then estimating the quality level reliability failure rate and million defective rate of the output response index at a single design point through statistical analysis. At the same time, the average and standard deviation of each output response index are counted. The 6σ robustness analysis assumes that the product performance distribution is a normal distribution, and the distance between the mean value of the performance index and the quality constraint is $\pm 6\sigma$.

$$\left\{ \begin{array}{l}
 \text{Minimize : } \mu(Mass) + 6\sigma \\
 \text{Minimize : } \mu(\eta_x, \eta_y, \eta_{Mz}) + 6\sigma \\
 \\
 \mu(\eta_x, \eta_y, \eta_{Mz}) + 6\sigma \leq 0.01 \\
 s.t \quad \mu(\varepsilon_j) - 6\sigma \geq 300\mu\varepsilon \\
 \mu(\varepsilon_j) + 6\sigma \leq 600\mu\varepsilon \\
 \\
 \mu(s_{Max}) + 6\sigma \leq 673MPa \\
 \mu(freq1) - 6\sigma \leq 50Hz \\
 j \in [1, 24] \&\& j \in N \\
 j \in [1, 24] \&\& j \in N \\
 \\
 D.v. \quad x_i^{(L)} \leq x_i \leq x_i^{(U)} \\
 i \in [1, 17] \&\& i \in N.
 \end{array} \right. \quad (4)$$

TABLE 9: Random noise variables and values of probability density function (distribution type, average, and coefficient of variation).

Input parameter	Distribution type	Average	Coefficient of variation
<i>B1</i>	Normal	5.76	1%
<i>B2</i>	Normal	5.29	1%
<i>B3</i>	Normal	7.59	1%
<i>H1</i>	Normal	33.56	0.1%
<i>H2</i>	Normal	29.38	0.1%
<i>H3</i>	Normal	65.18	0.1%
<i>L1</i>	Normal	43.33	0.1%
<i>L2</i>	Normal	12.62	0.5%
<i>S1</i>	Normal	13.59	0.5%
<i>S2</i>	Normal	15.94	0.5%
<i>P</i>	Normal	40.18	0.1%

TABLE 10: Random noise variables and values of probability density function (distribution type and range).

Input parameter	Distribution type	Range
Δx	Uniform	[0,0.3]
Δy	Uniform	[0,0.5]
Δz	Uniform	[0,0.2]
$\Delta \alpha$	Uniform	[0, 0.1°]
$\Delta \beta$	Uniform	[0, 0.1°]
$\Delta \gamma$	Uniform	[0, 0.1°]

Based on the results of the deterministic optimization of the above sensor splits and the assembly errors between the splits, the sensor split approximate model and the system approximate model are combined. The Monte Carlo sampling is used to evaluate the quality level of the deterministic optimization plan, and 11 design variables and assembly error variables (the relative displacement and angular error between the two sensor splits: three displacement errors, Δx , Δy , and Δz , and three angular errors, $\Delta \alpha$, $\Delta \beta$, and $\Delta \gamma$) are selected as the noise factor (Tables 9 and 10). Based on the combined approximation model, the sample points were collected by descriptive sampling method with 100 sampling times to obtain the quality level of the deterministic optimization plan. As shown in Table 11, the quality levels of maximum equivalent stress s_{\max} , first-order natural frequency $freq1$, and the strain ϵ_x and ϵ_{Mz} , under the action of the maximum resistance F_X , and the maximum pitching moment M_Z are 1.414 σ , 1.636 σ , and 1.31 σ , which cannot reach the level of robustness quality, and robustness optimization is required. The robustness optimization of the split-parallel multicomponent strain-type force sensor is still based on the approximation model established above. The descriptive sampling method is used to collect sample points. The value ranges of design variables and noise factors are shown in Tables 9, 10,

TABLE 11: Comparison of robustness before and after optimization.

Input parameter	Deterministic optimization value		Robust optimization value	
	Solution	6 σ analysis	Solution	Quality level
<i>B1</i>	5.76	8	5.97	8
<i>B2</i>	5.29	8	5.86	8
<i>B3</i>	7.59	8	7.35	8
<i>H1</i>	33.56	8	33.78	8
<i>H2</i>	29.38	8	34.30	8
<i>H3</i>	65.18	8	64.78	8
<i>L1</i>	43.33	8	41.60	8
<i>L2</i>	12.62	8	15.04	8
<i>S1</i>	13.59	8	12.67	8
<i>S2</i>	15.94	8	14.85	8
<i>P</i>	40.18	8	35.49	8
Δx	0	8	0	8
Δy	0	8	0	8
Δz	0	8	0	8
$\Delta \alpha$	0	8	0	8
$\Delta \beta$	0	8	0	8
$\Delta \gamma$	0	8	0	8
ϵ_x	302.65	1.516	314.54	8
ϵ_y	585.19	8	443.08	8
ϵ_{Mz}	548.62	1.31	421.79	8
η_x	0.214%	8	0.093%	8
η_y	0.034%	8	0.0439%	8
η_{mz}	0.098%	8	0.008%	8
s_{\max}	600.9	1.414	419.3035	8
$freq1$	54.713	1.636	53.27	8
$mass$	0.00338		0.00349	

TABLE 12: Design variables and value ranges.

Input parameter	Lower bound	Upper bound
<i>B1</i>	5	8
<i>B2</i>	4	8
<i>B3</i>	5	15
<i>H1</i>	25	45
<i>H2</i>	20	40
<i>H3</i>	50	80
<i>L1</i>	20	60
<i>L2</i>	10	40
<i>S1</i>	5	15
<i>S2</i>	12.5	22.5
<i>P</i>	30	50

TABLE 13: Comparison of results before and after two optimizations.

Optimization goal	Initial value	Optimization value	Percent changed
Mass	0.0047	0.00349	-25.74%
ε_x	81.6	314.54	285.46%
ε_y	115.1	443.08	284.95%
ε_{Mz}	167.7	421.79	151.5%
η_x	4.26%	0.093%	-97.82%
η_y	0.6125%	0.0439%	-92.83%
η_{mz}	5.12%	0.008%	-99.8%

and 12. Algorithm NSGA-II is used for robust optimization. Through robust multiobjective optimization, the sensor output parameters can reach a quality level above 6 sigma (Table 11). By comparing the parameters before and after the robustness optimization (Table 13), it is found that the sensitivity of the three components increases by 14.73%, 21.2%, and 29.3%, respectively, when the quality of the sensor increases slightly and the amount of interference changes little.

5. Conclusions

- (1) A split parallel multicomponent strain sensor structure layout is proposed to satisfy the special requirements for the measurement of aerodynamic sensors by the helicopter rotor airfoil wind tunnel test
- (2) A finite element analysis model is established with the sensor split as the object to analyze separately its strain under the action of resistance, lift, and pitch moment cloud map and to determine the location of strain gauges and the way of group bridges
- (3) The RBF neural network approximate model and NSGA-II multiobjective optimization algorithm are utilized to deterministically optimize the sensor split performance and obtain excellent monomer performance. Satisfying the strength and rigidity, the strain values under the action of the maximum resistance F_x , the maximum lift F_y , and the maximum pitching moment M_z of the sensor split structure are increased by 271%, 408%, and 227%, respectively, and the interference of the component is reduced by 95%, 94.4%, and 98.1%; the first-order natural frequency is increased by 5%, and the quality is reduced by 28.1%
- (4) Based on the above deterministic optimization, the split manufacturing error and the assembly error between the splits are introduced, and the sensor and rotor airfoil test model-integrated finite element system model and RSM approximate model are successively established by using the Monte Carlo sampling method to check the quality level of the system and 6σ robustness optimization to improve

the robustness of the sensor and reduce the sensitivity of the response to assembly and manufacturing errors

- (5) Through 6σ robustness analysis based on deterministic optimization, the robustness of the sensor was improved, and the sensitivity of the response to assembly and manufacturing errors were reduces
- (6) After these two optimizations, satisfying the strength and rigidity and considering the random noise effect of the split manufacturing error and the assembly error between the splits, the strain value of the maximum resistance F_x , the maximum lift F_y , and the maximum pitching moment M_z of the sensor were increased by 285.46%, 284.95%, and 151.5%, respectively, the interference to the three components was reduced by 97.82%, 92.83%, and 99.8%, respectively, and the quality was reduced by 25.74%. At the same time, the sensor quality level reached 6σ

Data Availability

No data were used to support this study.

Conflicts of Interest

The authors declare no conflict of interest.

References

- [1] A. R. Tavakolpour-Saleh, A. R. Setoodeh, and M. Gholamzadeh, "A novel multi-component strain-gauge external balance for wind tunnel tests: simulation and experiment," *Sensors & Actuators A Physical*, vol. 247, pp. 172–186, 2016.
- [2] L. Zhao, Y. Yan, X. Yan, and L. Zhao, "Structural parameters optimization of elastic cell in a near-bit drilling engineering parameters measurement sub," *Sensors*, vol. 19, no. 15, 2019.
- [3] R. P. Ubeda, S. C. Gutiérrez Rubert, R. Z. Stanisic, and Á. P. Ivars, "Design and manufacturing of an ultra-low-cost custom torque sensor for robotics," *Sensors*, vol. 18, no. 6, 2018.
- [4] V. Grosu, S. Grosu, B. Vanderborght, D. Lefeber, and C. Rodriguez-Guerrero, "Multi-axis force sensor for human-robot interaction sensing in a rehabilitation robotic device," *Sensors*, vol. 17, no. 6, p. 1294, 2017.
- [5] X.-L. Zhang, T. Wu, Y. Shao, and J. Song, "Structure optimization of wheel force transducer based on natural frequency and comprehensive sensitivity," *Journal of Sound and Vibration*, vol. 30, no. 4, pp. 973–981, 2017.
- [6] D. He, *Wind tunnel balance*, National Defense Industry Press, 1999.
- [7] R. A. B. Almeida, D. C. Vaz, A. P. V. Urgueira, and A. R. Janeiro Borges, "Using ring strain sensors to measure dynamic forces in wind-tunnel testing," *Sensors and Actuators A: Physical*, vol. 185, pp. 44–52, 2012.
- [8] Y. Li, Y. Zhao, J. Fei et al., "Design and development of a three-component force sensor for milling process monitoring," *Sensors*, vol. 17, no. 5, 2017.

- [9] Y. Sun, Y. Liu, T. Zou, M. Jin, and H. Liu, "Design and optimization of a novel six-axis force/torque sensor for space robot," *Measurement*, vol. 65, pp. 135–148, 2015.
- [10] S. Hu, H. Wang, Y. Wang, and Z. Liu, "Design of a novel six-axis wrist force sensor," *Sensors*, vol. 18, no. 9, p. 3120, 2018.
- [11] J. Ma and A. Song, "Fast estimation of strains for cross-beams six-axis force/torque sensors by mechanical modeling," *Sensors*, vol. 13, no. 5, pp. 6669–6686, 2013.
- [12] A. Witoniowski and A. Bar, "Parametrical excitement vibration in tandem mills—mathematical model and its analysis," *Journal of Materials Processing Technology*, vol. 134, no. 2, pp. 214–224, 2003.
- [13] A. Batish, A. Bhattacharya, M. Kaur et al., "Hard turning: parametric optimization using genetic algorithm for rough/finish machining and study of surface morphology," *Journal of Mechanical Science & Technology*, vol. 28, no. 5, pp. 1629–1640, 2014.
- [14] G. Huang, D. Zhang, S. Guo, and H. Qu, "Design and optimization of a novel three-dimensional force sensor with parallel structure," *Sensors*, vol. 18, no. 8, p. 2416, 2018.
- [15] D. D. Nguyen and C. H. Kuo, "Design and optimization of a joint torque sensor for lightweight robots," *IEEE Sensors Journal*, vol. 21, no. 8, pp. 9788–9797, 2021.
- [16] C. L. Fu, Y. C. Bai, C. Lin, and W. W. Wang, "Design optimization of a newly developed aluminum-steel multi-material electric bus body structure," *Structural & Multidisciplinary Optimization*, vol. 60, no. 5, pp. 2177–2187, 2019.
- [17] X. Hu, R. Bao, W. Chen, and H. Wang, "Robust optimal design of strain-gauge-based force sensors using moving morphable components method: enhanced sensitivity and reduced cross-interference," *Structural and Multidisciplinary Optimization*, vol. 64, no. 3, pp. 1439–1455, 2021.

Research Article

A Hybrid Convolutional Neural Network and Relief-F Algorithm for Fault Power Line Recognition in Internet of Things-Based Smart Grids

Zhang Yuqing 

Tianjin Key Laboratory of Optoelectronic Detection Technology and Systems, School of Electronic and Information Engineering, Tiangong University, Tianjin 300387, China

Correspondence should be addressed to Zhang Yuqing; z.191092@yahoo.com

Received 18 January 2022; Accepted 21 February 2022; Published 5 March 2022

Academic Editor: Nima Jafari Navimipour

Copyright © 2022 Zhang Yuqing. This is an open access article distributed under the Creative Commons Attribution License, which permits unrestricted use, distribution, and reproduction in any medium, provided the original work is properly cited.

Today, energy management based on the digitalization of smart grids by the Internet of Things (IoT) is an emerging paradigm for power line systems. There are several environmental hazards to break down high-voltage power cables such as lightning, severe voltage fluctuations, and incorrect design of electric field distribution. So, identifying faulty high-voltage power lines is one of the most emerging challenges in smart grids to avoid disruption of the power distribution networks. This paper presents a new hybrid Convolutional Neural Network and Relief-F (CNN-RF) algorithm for an energy-aware collaborative learning approach to detect power line systems in smart grids. This hybrid approach ensures the stability and reliability of the defective power line system and improves the energy efficiency of the smart grids. This approach can detect the defective power line recognition using damaged power line images concerning automatic monitoring using Unmanned Aerial Vehicle (UAV) control system and IoT communications. By applying UAV control system and IoT communications on gathering damaged power line images, human faults and environmental hazards for extra data transmission are avoided. Experimental results show that the proposed CNN-RF model represents a high accuracy rate of 92.2% for recognizing damaged power lines. Also, the precision of damaged line detection ratio is higher than other prediction methods by the rate of 92.5%. Finally, the performance of the damaged line prediction approach in the CNN-RF method has a daily minimum cost in the IoT-based smart grids.

1. Introduction

Today, by increasing information technology and computer science paradigms on Internet of Things (IoT) [1, 2], wireless communications, and 5G technologies, smart environments can apply these paradigms to improve and facilitate resource management, optimized services, and energy efficiency factors [3, 4]. Smart grid network is one of important smart environments that energy efficiency and fault tolerant methods are considering to manage optimized services using the IoT and intelligent applications [5, 6].

In smart grid network, power cables have many dynamic modules for improving industrial power management and smart environments to create and support a safe condition for power lines in electricity flow networks [7, 8]. Today,

high-voltage power cable examination is a critical manner for getting time and human side effects [9]. On the other hand, the IoT smart devices can help to control, trace, and detect power line systems by applying intelligent aspects and technical applications for avoiding damaged cables and power lines and energy failures in smart grids [10, 11].

Due to limited time, energy saving resources, and highly cost of checking damaged and faulty power lines, Unmanned Aerial Vehicle (UAV) control systems can help to gather and select existing optimal power line detection methods [12, 13]. So, smart grids with the help of IoT applications and smart devices can increase the accuracy of prediction methods with respect to the key solutions of machine learning and smart monitoring in smart grids [14–16]. On the other hand, capturing and gathering high-

resolution information is a critical task for detecting damaged power lines in grid networks. By using UAV control systems, a managed and collected procedure is established for power lines in smart grids [17–19].

To solve these problem statements correctly, this paper presents a new hybrid Convolutional Neural Network and Relief-F (CNN-RF) algorithm to analyze damaged and faulty power line systems in smart grids based on energy consumption factor. The proposed power line detection system includes three phases consist of collecting the image data from Unmanned Aerial Vehicle (UAV) control system and IoT communications, featuring selection method, including two main smart power grid environments such as urban and mountain, and predicting damaged cables to forward for empirical analysis and improvement procedures. The proposed CNN-RF algorithm is employed to show how on-time failure influences the power consumption and energy flow delay in smart grid network.

The main contributions of this technical research are shown as follows:

- (i) Proposing a hybrid Convolutional Neural Network and Relief-F (CNN-RF) algorithm to analyze both accuracy of prediction approach and finding failures and damaged cables
- (ii) Selecting optimal operators that are applied to the prediction stage using RF algorithm
- (iii) Facilitating modifiability and energy management according to predicted damaged power lines in smart power grid network

The structure of this paper is shown as follows: the literature related to the fault detection methods using artificial intelligence in the smart grid and IoT industry is reviewed in Section 2, the proposed methods for detection of damaged and crashed power lines are introduced in Section 3, the experimental results are discussed in Section 4, and the discussion and conclusions are shown in Section 5.

2. Related Work

This section discusses a brief motivation about existing case studies on fault detection methods using artificial intelligence in the smart grid and IoT industry. For example, this work [20] presented a power cable model with sets of essential points for power cable discovery. The offered design of discovery is short and precise since the endpoints and the curve equation per cable are contained in the classified essential points. Moreover, a new model based on the CNN algorithm model was presented to forecast classes of points on power cables in the visual image instantly. In this study, a new positive instance checking procedure was instructed to discover the unique idea of cable essential point's discovery by applying the pixels along each power cable as positive instances for essential points voting and forecast.

Another work [21] presented a generalized focal loss function established on the Matthews correlation coefficient

to handle the class inequality issue in PL segmentation while using a generic deep segmentation structure. The loss function was assessed by enhancing the vanilla U-Net model with an extra convolutional auxiliary classifier head for more suitable learning and quick model conjunction. The evaluation of two PL datasets demonstrated that the presented loss function outperforms the famous BBCE loss in PL dice scores on both the datasets, accuracy, and false detection rate values.

Mukherjee et al. [22] presented a relative analysis of three separate deep learning standards with a traditional machine learning standard to define the most useful multilabel classifier for the recognition of data intrusion areas has been done. Analysis results showed that the power flow correlation characteristics and locational recognition of FDIA can be proposed as a multilabel classification issue. Comprehensive assessments have been performed to specify the parameter sensitivity over the presented structure. Tian et al. [23] offered a new mixed deep learning instrument to determine the damages in the communication cables. This structure included CNN and SVM that CNN is used for the category of damaged power cables pictures, and SVM is for the recognition and estimating the intensity of damaged power cables using statistical information. The importance of this study contains no additional communication cables control and checkup fees.

Xia et al. [24] suggested a collaborative detection instrument for false data attacks. A trust-based compromised PMU recognition method was proposed to determine negative PMUs by scanning manners of PMUs in a process. Moreover, a voting-based discovery strategy was presented based on physical directions to catch FDIA collaboratively. This strategy enhanced the recognition speed while decreasing the computational charge at the control center. The empirical outcomes using the PowerWorld simulator demonstrated the efficiency and usefulness of the presented mechanism and strategies. Zhang et al. [25] designed an objective power cable discovery approach employing convolutional and modeled components. A convolutional neural network was constructed to receive hierarchical reactions from a separate layer. Moreover, the rich component maps are combined to build a fusion outcome, and the modeled information consists of length, width, orientation, and the area received from the most unsophisticated component map. Eventually, the fusion outcome is combined with modeled information to reach an outcome with obvious experience.

According to the above-related works, there are some limitations to enhancing the prediction of damaged power lines and cables in smart grids. With respect to the above limitations, the next section presents a new hybrid model to predict damaged and faulty points of power lines using the information of UAV control systems in IoT-enabled power grids.

3. Proposed Method

Detection of damaged and crashed power lines is an important way to check and modify various faults in smart grids. It



FIGURE 1: Applied correlation method on an image sample of power lines in the urban dataset.

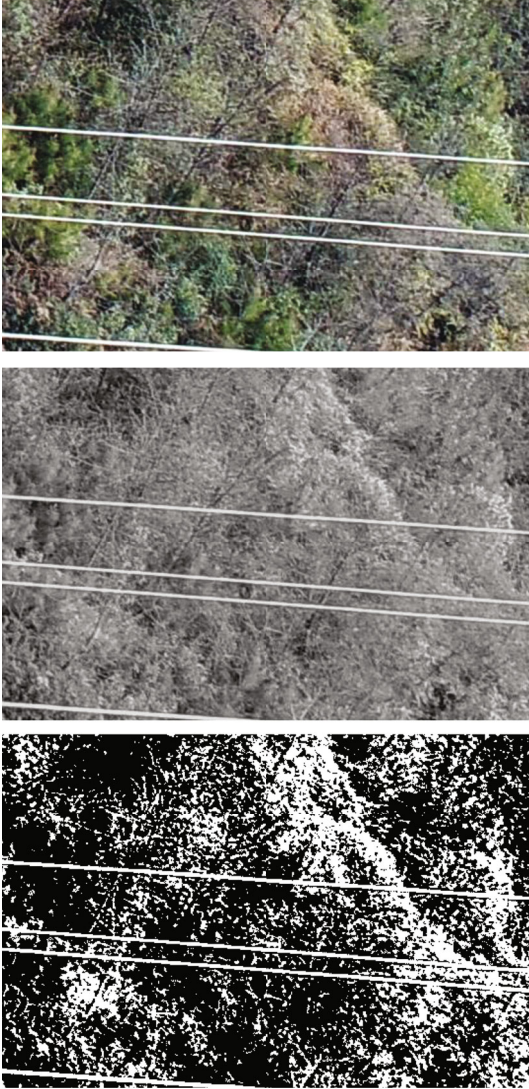


FIGURE 2: Image sample example with applied correlation method in the power lines mountain dataset.

is particularly suitable for evaluating urban and mountain power lines with respect to the UAV data collections. Our ideal to detect edge-based UAV pictures is based on a smart model that UAV control systems collect all images and map according to existing variables including L as a set of m rows and m columns of pixels. We define A as the number of edge lines, and M is a set of colors in the edge lines that show $(m_1, m_2, m_3 \dots m_k)$ a real-time safety critical system [26].

According to power line detection, we present a new hybrid Convolutional Neural Network and Relief-F (CNN-RF) algorithm that we used CNN algorithm based on the classification and recognition procedures in [20, 27, 28].

The proposed CNN algorithm has a set of 4-tuple structure $N = (E, D, O, C)$ variables that are mainly reflected to cluster image parameters of the existing samples where [29, 30]

- (i) E is an encoding platform with 7 layers to cluster scattered important points of power lines
- (ii) D is a decoder for classifying key points of power lines from UAV images directly to the detailed pixels of damaged cables
- (iii) O is a set of operators that are applied to the prediction stage with three functional subnets to train procedures in power line detection
- (iv) C is a final clustering function to show damaged and faulty positions of power lines and cables in smart grid images

For optimizing the matching method for existing pixels along power lines as applied samples and train existing pixels with sets of m rows and m columns as encoded vectors, we apply the Relief-F algorithm [31]. The Relief-F algorithm was defined and applied to many research topics [32]. The algorithm is applied for classifying continuous values in images. The Relief-F algorithm mainly includes three main levels: intratraining distribution, intertraining distribution, and update features. In this procedure, the Relief-F algorithm can extend a random sample R as a targeted image from the set of training samples. After choosing a random sample, this algorithm selects a set of neighbors as R number of samples to update the weight of each pixel value as a targeted feature according to Equation (1) [33, 34].

$$F(A) = F(A) - \sum_j^k \Delta(L, R, H_j) + \sum_{\text{class}(R)}^n \frac{P(K)}{1 - p(\text{class}(R))}. \quad (1)$$

According to Equation (1), function $F(A)$ is defined as updated feature selection and previous features where $\Delta(L, R, H_j)$ represents the difference between sample R_i as new feature selection and sample R_j as previous features on the characteristic L , and as shown in Equation (2), H_j represents the j nearest neighbor sample in class K [35]. Final value of the H is categorized into three types

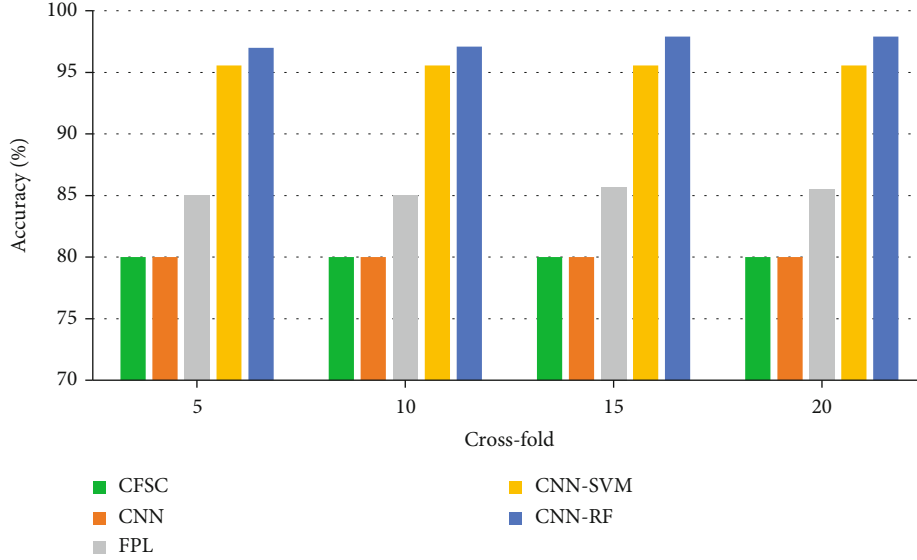


FIGURE 3: Accuracy evaluation on cross-folds 5, 10, 15, and 20 in the PLDU dataset.

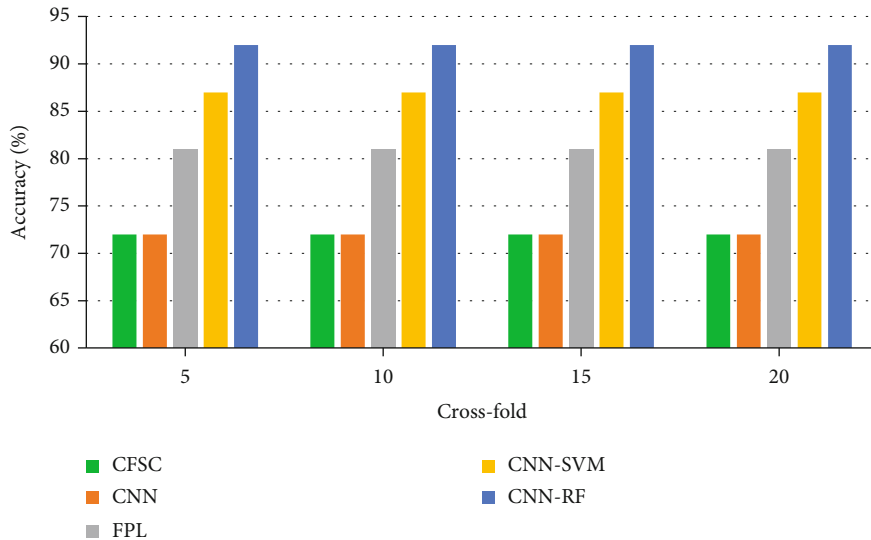


FIGURE 4: Accuracy evaluation on cross-folds 5, 10, 15, and 20 in the PLDM dataset.

including a continuous value, 0, and 1 according to Equation (1) [34].

$$\Delta(L, R, H_j) = H, \quad (2)$$

$$H = \begin{cases} \frac{|R_i[L] - R_j[L]|}{\max(L) - \min(L)}, & \text{if } L \text{ is a continuous value,} \\ 0 & R_i[L] = R_j[L], \\ 1 & R_i[L] \neq R_j[L]. \end{cases} \quad (3)$$

For enhancing the effectiveness of the proposed hybrid CNN-RF algorithm, we calibrate the assigned classes to each set of targeted pixels in the sample power line images. In real images, there exist millions of different

pixels, and we can calibrate targeted pixels with an approximate evaluation to divide the entire sample area into $k \times m$ detection regions C_{km} . The size of each image C_i was defined as follows [36]:

$$C_i = (\text{width} = 100\text{pix} \approx 100\text{m}, \text{height} = 100\text{pix} \approx 100\text{m}). \quad (4)$$

According to the above technical aspects, the proposed CNN-RF algorithm can perfectly select important key features based on targeted pixels in the UAV images.

4. Experimental Results

In this section, a series of experimental results are evaluated to validate the proposed method's efficiency. For analyzing the proposed CNN-RF prediction model, we

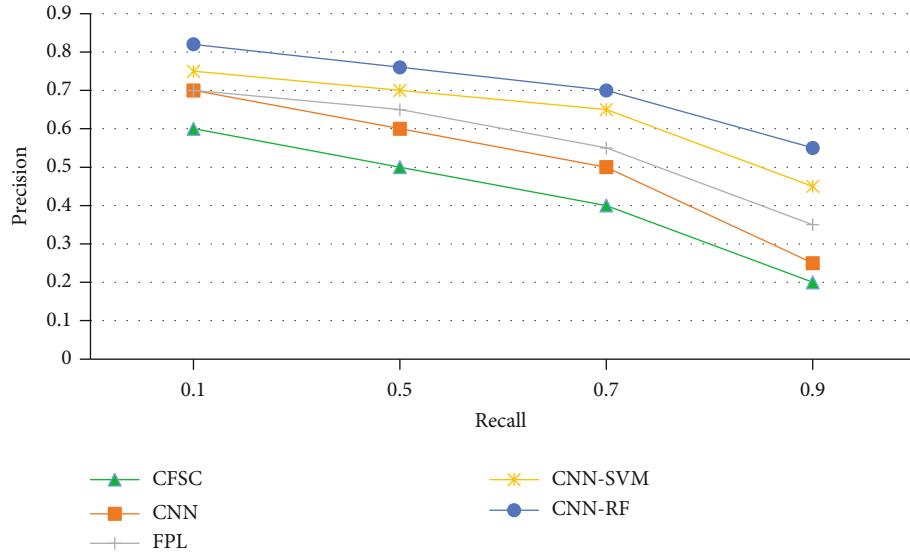


FIGURE 5: Precision-recall curves on the PLDU dataset.

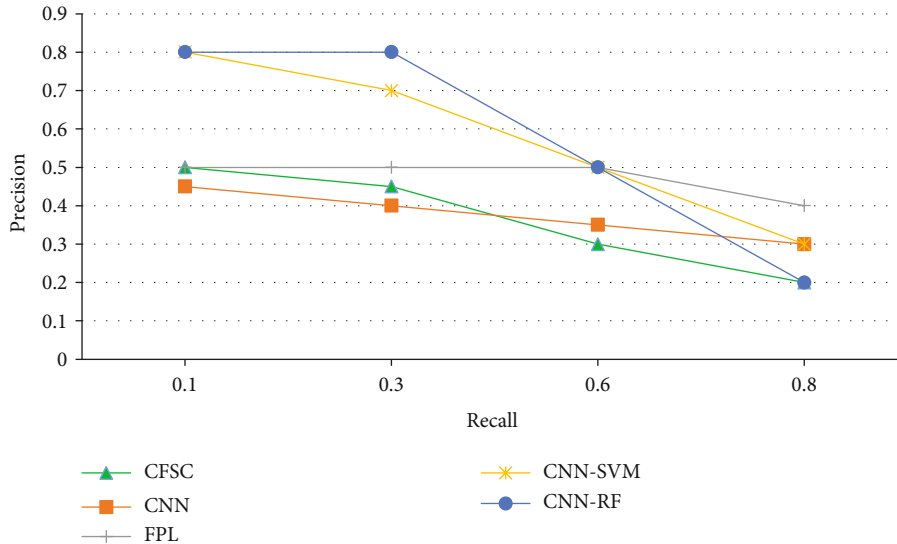


FIGURE 6: Precision-recall curves on the PLDM dataset.

used two popular power line detection datasets (<https://github.com/SnorkerHeng/PLD-UAV>) with high-pixel observations in urban locations (Power Line Detection in Urban (PLDU)) and mountain-desert locations (Power Line Detection in Mountain (PLDM)) as shown in Figures 1 and 2. To capture the damaged and disrupted power line images in the PLDU and PLDM datasets, UAV control systems have flown above the power line locations within ten and thirty meters, respectively. For achieving optimal prediction results, we categorized 453 samples of images for training and 120 samples for testing methods in the PLDU dataset. Also, from 287 total samples of images in the PLDM dataset, we divided 237 samples for training and 50 samples for testing methods. The experimental results are performed on NVIDIA 4-

Plus-1 ARM Cortex-A15 CPU, 192 CUDA core, and 16 DDR4 memory in MATLAB R2021a.

According to the prediction evaluation, the proposed CNN-RF method is compared to some newly released mechanisms to detect damaged power lines with UAV and the IoT technologies including Convolutional Neural Network (CNN) [20], CNN [37] and Support Vector Machine (CNN-SVM) [23], Focal Phi Loss (FPL) [21, 38], and convolutional features and structured constraints (CFSC) [25, 39].

Our research is based on the results of feature selection and finally completes the diagnosis of breast masses through the classifier. To evaluate and compare the performance of feature selection techniques using the two-stage feature selection method and other algorithms, three performance

measures, namely, accuracy, precision, and recall, are shown in Equation (5).

$$\begin{aligned} \text{Accuracy} &= \frac{\text{true positive} + \text{true negative}}{\text{true positive} + \text{true negative} + \text{false positive} + \text{false negative}}, \\ \text{Precision} &= \frac{\text{true positive}}{\text{true positive} + \text{false positive}}, \\ \text{Recall} &= \frac{\text{true positive}}{\text{true positive} + \text{false negative}}. \end{aligned} \quad (5)$$

Figure 3 shows the comparison of accuracy factors for existing prediction models in the PLDU dataset. The red line in the figure indicates the estimated latency equals the ground truth. That is, the prediction model accurately estimates the actual latency. The blue line shows the accuracy of the CNN-RF method to detect damaged power line images in cross-folds 5, 10, 15, and 20 that have better estimation performance of the prediction model than other methods. It can be seen that as compared with benchmarking prediction models, our prediction model can estimate the damaged power lines in urban images more accurately.

Figure 4 illustrates the accuracy evaluation with recent works and the proposed CNN-RF method in the PLDM dataset, where our method realizes substantially better performance than CNN, CNN-SVM, FPL, and CFSC.

Figure 5 suggests the percentage of precision-recall curves using different machine learning algorithms and the number of cross-folds, respectively. The proposed CNN-RF method has the highest ratio than other CNN, CNN-SVM, FPL, and CFSC algorithms to detect damaged power lines in urban environments. Also, Figure 6 depicts the percentage of precision-recall curves using different machine learning algorithms and the number of cross-folds for PLDM dataset, respectively. The proposed CNN-RF method has the highest ratio than other algorithms to select damaged power lines in environments.

5. Conclusion

This paper presented a hybrid CNN-RF method for IoT-enabled fault power line detection to find the optimum prediction performance among crashed and damaged power cables and lines. Two important different datasets, namely, PLDM and PLDU concerning UAV control systems, were compared. This comparison has shown rather varying behaviors of the two datasets to support the optimum prediction performance. The experimental results show that the proposed CNN-RF method has a maximum accuracy ratio for predicting damaged power lines up to 97% for power line recognition in urban environments. Also, we observed that the proposed CNN-RF method illustrated optimum accuracy performance for detecting damaged cables in the mountain and out of cities with 92% better than other recent case studies including CNN, CNN-SVM, FPL, and CFSC. Finally, the proposed CNN-RF method has a better precision-recall ratio than other algorithms. However, our proposed method has

some limitations. First, we approximate the proposed model just to check power lines in a static environment after gathering the UAV control system as offline mode. Second, we discovered some problems of urban power lines that technical secretaries have modified damaged power lines in an on-time schedule. So, there are some gaps between damaged images and real fixed cables in urban environments. In future works, some other powerful metaheuristic algorithms can be applied to find optimal feature selection method and increasing accuracy of damaged fault prediction in power lines.

Data Availability

The experiment data supporting this experiment evaluation are from the following reported studies, which were cited and are included within the articles: Jaffari et al. [21]: A Novel Focal Phi Loss for Power Line Segmentation with Auxiliary Classifier U-Net (Sensors, 21(8), 2803) and Dai et al. [20]: Fast and Accurate Cable Detection Using CNN (Applied Intelligence, 50(12), 4688-4707).

Conflicts of Interest

The author declares that there are no conflicts of interest regarding the publication of this paper.

References

- [1] G. Prasad and L. Lampe, "Full-duplex power line communications: design and applications from multimedia to smart grid," *IEEE Communications Magazine*, vol. 58, no. 2, pp. 106–112, 2020.
- [2] T. Sui, D. Marelli, X. Sun, and M. Fu, "Multi-sensor state estimation over lossy channels using coded measurements," *Automatica*, vol. 111, 2020.
- [3] Z. Zhang, R. Deng, D. K. Yau, and P. Chen, "Zero-parameter-information data integrity attacks and countermeasures in IoT-based smart grid," *IEEE Internet of Things Journal*, vol. 8, no. 8, pp. 6608–6623, 2021.
- [4] H. Zhou, C. Xu, C. Lu et al., "Investigation of transient magnetolectric response of magnetostrictive/piezoelectric composite applicable for lightning current sensing," *Sensors and Actuators A: Physical*, vol. 329, 2021.
- [5] C. Mi, J. Chen, Z. Zhang, S. Huang, and O. Postolache, "Visual sensor network task scheduling algorithm at automated container terminal," *IEEE Sensors Journal*, p. 1, 2021.
- [6] A. Yan, Z. Wu, J. Guo, J. Song, and X. Wen, "Novel double-node-upset-tolerant memory cell designs through radiation-hardening-by-design and layout," *IEEE Transactions on Reliability*, vol. 68, no. 1, pp. 354–363, 2019.
- [7] Z. Lv, L. Qiao, and H. Song, "Analysis of the security of Internet of Multimedia Things," *ACM Transactions on Multimedia Computing, Communications, and Applications*, vol. 16, no. 3, pp. 1–20, 2020.
- [8] Z. Li, Y. Liu, P. Yin et al., "Constituting abrupt magnetic flux density change for power density improvement in electromagnetic energy harvesting," *International Journal of Mechanical Sciences*, vol. 198, 2021.
- [9] C. Guo, C. Ye, Y. Ding, and P. Wang, "A multi-state model for transmission system resilience enhancement against short-

- circuit faults caused by extreme weather events,” *IEEE Transactions on Power Delivery*, vol. 36, pp. 2374–2385, 2020.
- [10] J. Li, J. Dai, A. Issakhov, S. F. Almojil, and A. Souri, “Towards decision support systems for energy management in the smart industry and Internet of Things,” *Computers & Industrial Engineering*, vol. 161, 2021.
- [11] J. Tian, Y. Liu, W. Zheng, and L. Yin, “Smog prediction based on the deep belief-BP neural network model (DBN-BP),” *Urban Climate*, vol. 41, 2022.
- [12] M. M. Rezinkina, Y. I. Sokol, A. O. Zaporozhets, O. G. Gryb, I. T. Karpaliuk, and S. V. Shvets, “Monitoring of Energy Objects Parameters with Using UAVs,” in *Control of Overhead Power Lines with Unmanned Aerial Vehicles (UAVs)*, pp. 1–8, Springer, 2021.
- [13] Y. Lin, H. Song, F. Ke, W. Yan, Z. Liu, and F. Cai, “Optimal caching scheme in D2D networks with multiple robot helpers,” *Computer Communications*, vol. 181, pp. 132–142, 2022.
- [14] A. Souri, M. Y. Ghafour, A. M. Ahmed, F. Safara, A. Yamini, and M. Hoseyninezhad, “A new machine learning-based healthcare monitoring model for student’s condition diagnosis in Internet of Things environment,” *Soft Computing*, vol. 24, no. 22, pp. 17111–17121, 2020.
- [15] A. Yan, Z. Fan, L. Ding et al., “Cost-effective and highly reliable circuit components design for safety-critical applications,” *IEEE Transactions on Aerospace and Electronic Systems*, pp. 1–1, 2022.
- [16] J. K. Gupta and S. K. Guptab, “Iot based statistical approach for human crowd density estimation-design and analysis,” *Advances In Industrial Engineering And Management (AIEM)*, vol. 8, pp. 10–14, 2019.
- [17] Z. Lv, D. Chen, R. Lou, and H. Song, “Industrial security solution for virtual reality,” *IEEE Internet of Things Journal*, vol. 8, pp. 6273–6281, 2020.
- [18] G. Luo, Q. Yuan, H. Zhou et al., “Cooperative vehicular content distribution in edge computing assisted 5G-VANET,” *China Communications*, vol. 15, no. 7, pp. 1–17, 2018.
- [19] L. Guo, C. Ye, Y. Ding, and P. Wang, “Allocation of centrally switched fault current limiters enabled by 5G in transmission system,” *IEEE Transactions on Power Delivery*, vol. 36, pp. 3231–3241, 2020.
- [20] Z. Dai, J. Yi, Y. Zhang, B. Zhou, and L. He, “Fast and accurate cable detection using CNN,” *Applied Intelligence*, vol. 50, pp. 4688–4707, 2020.
- [21] R. Jaffari, M. A. Hashmani, and C. C. Reyes-Aldasoro, “A novel focal phi loss for power line segmentation with auxiliary classifier U-Net,” *Sensors*, vol. 21, no. 8, p. 2803, 2021.
- [22] D. Mukherjee, S. Chakraborty, and S. Ghosh, “Deep learning-based multilabel classification for locational detection of false data injection attack in smart grids,” *Electrical Engineering*, vol. 104, 2022.
- [23] Y. Tian, Q. Wang, Z. Guo et al., “A hybrid deep learning and ensemble learning mechanism for damaged power line detection in smart grids,” *Soft Computing*, pp. 1–9, 2021.
- [24] Z. Xia, G. Long, and B. Yin, “Confidence-aware collaborative detection mechanism for false data attacks in smart grids,” *Soft Computing*, vol. 25, no. 7, pp. 5607–5618, 2021.
- [25] H. Zhang, W. Yang, H. Yu, H. Zhang, and G.-S. Xia, “Detecting power lines in UAV images with convolutional features and structured constraints,” *Remote Sensing*, vol. 11, no. 11, p. 1342, 2019.
- [26] A. Souri and M. Norouzi, “A new probable decision making approach for verification of probabilistic real-time systems,” in *2015 6th IEEE International Conference on Software Engineering and Service Science (ICSESS)*, pp. 44–47, Beijing, China, 2015.
- [27] Z. Lv, J. Guo, and H. Lv, “Safety poka yoke in zero-defect manufacturing based on digital twins,” *IEEE Transactions on Industrial Informatics*, p. 1, 2022.
- [28] W.-F. Lai and W.-T. Wong, “Use of graphene-based materials as carriers of bioactive agents,” *Asian Journal of Pharmaceutical Sciences*, vol. 16, no. 5, pp. 577–588, 2021.
- [29] X. Xiang, N. Lv, X. Guo, S. Wang, and A. El Saddik, “Engineering vehicles detection based on modified faster R-CNN for power grid surveillance,” *Sensors*, vol. 18, no. 7, p. 2258, 2018.
- [30] B. Cao, W. Zhang, X. Wang, J. Zhao, Y. Gu, and Y. Zhang, “A memetic algorithm based on two_Arch2 for multi-depot heterogeneous-vehicle capacitated arc routing problem,” *Swarm and Evolutionary Computation*, vol. 63, 2021.
- [31] I. Kononenko, “Estimating attributes: analysis and extensions of RELIEF,” in *in European conference on machine learning*, pp. 171–182, Springer, 1994.
- [32] J. Dou, Y. Song, G. Wei, and Y. Zhang, “Fuzzy information decomposition incorporated and weighted Relief-F feature selection: when imbalanced data meet incompleteness,” *Information Sciences*, vol. 584, pp. 417–432, 2022.
- [33] J. Hou, Y. Wu, A. S. Ahmad, H. Gong, and L. Liu, “A novel rolling bearing fault diagnosis method based on adaptive feature selection and clustering,” *IEEE Access*, vol. 9, pp. 99756–99767, 2021.
- [34] H. Chen, Y. Miao, Y. Chen, L. Fang, L. Zeng, and J. Shi, “Intelligent model-based integrity assessment of nonstationary mechanical system,” *Journal of Web, Engineering*, vol. 20, 2021.
- [35] M. B. Abdulrazaq, M. R. Mahmood, S. R. Zeebaree, M. H. Abdulwahab, R. R. Zebari, and A. B. Sallow, “An analytical appraisal for supervised classifiers’ performance on facial expression recognition based on relief-F feature selection,” *Journal of Physics: Conference Series*, vol. 1804, no. 1, 2021.
- [36] L. Yang, Z. Xiong, G. Liu, Y. Hu, X. Zhang, and M. Qiu, “An analytical model of page dissemination for efficient big data transmission of C-ITS,” *IEEE Transactions on Intelligent Transportation Systems*, 2022.
- [37] L. Zhang, T. Gao, G. Cai, and K. L. Hai, “Research on electric vehicle charging safety warning model based on back propagation neural network optimized by improved gray wolf algorithm,” *Journal of Energy Storage*, vol. 49, 2022.
- [38] L. Zhong, Z. Fang, F. Liu, B. Yuan, G. Zhang, and J. Lu, “Bridging the theoretical bound and deep algorithms for open set domain adaptation,” *IEEE Transactions on Neural Networks and Learning Systems*, 2021.
- [39] W. Zhou, Q. Guo, J. Lei, L. Yu, and J.-N. Hwang, “IRFR-Net: interactive recursive feature-reshaping network for detecting salient objects in RGB-D images,” *IEEE Transactions on Neural Networks and Learning Systems*, 2021.

Research Article

Design and Implementation of Artwork Display System Based on Internet of Things Technology

Qian Zhao^{1,2} and Chenglin Wu³ 

¹Guangzhou Academy of Fine Arts, Guangzhou, 510006 Guangdong, China

²Graduate Institute of Creative Industries, College of Management, Shih Chien University, Taipei 10001, Taiwan

³School of Computer Science, Huanggang Normal College, Huanggang, 438000 Hubei, China

Correspondence should be addressed to Chenglin Wu; wuchenglin@hgnu.edu.cn

Received 15 November 2021; Accepted 18 January 2022; Published 27 February 2022

Academic Editor: Nima Jafari Navimipour

Copyright © 2022 Qian Zhao and Chenglin Wu. This is an open access article distributed under the Creative Commons Attribution License, which permits unrestricted use, distribution, and reproduction in any medium, provided the original work is properly cited.

The IoT brings digital and intelligent changes, which can change many ways of seeing the world. Among them, the display of rare works of art is easily overlooked. This paper studies the artwork display system based on the IoT technology and uses the Spring framework under the uRLLC communication protocol to design the artwork display system through the design of the database and the controller. This article takes the artistic work display system as the research object, studies the operating mode of the system model, conducts system testing in an indoor environment, and compares communication with traditional distributed computing technology. Based on the experimental results, it can be seen that the real-time performance of this system is far superior to traditional cloud computing systems.

1. Introduction

The Internet of Things (IoT) has been applied in many fields. In the field of visualization, there are often higher standards for the reliability and real-time performance of IoT devices. In addition, as there are more and more IoT devices, and these devices are usually heterogeneous, how to manage these devices will be an urgent problem to be solved. And edge computing provides a new way to solve these problems. Edge computing can realize on-site processing of IoT device data, provide the system with high real-time performance, and ensure the reliability of communication.

Zhu et al. applied augmented reality technology to the exhibition of cultural relics and developed a cultural relic display system that supports the interaction of flashlight light [1]. Levin et al. used augmented reality technology to achieve a restoration display of the frescoes in St. Clement's Church [2]. Chakraborty et al. combine the outdoor AR system with the Yuanmingyuan Ruins to realize the digital res-

toration of ancient images such as water viewing method, east-west water tower, and big water method [3]. Taking the world cultural heritage Dujiangyan as an example, Zou et al. use digital technology to attract the audience to understand water conservancy knowledge and historical stories based on the characteristics of Dujiangyan's regional protection. In addition, digital technology is used to improve the existing wasteland in the Dujiangyan Scenic Area and promote Dujiangyan tourism [4]. Zou et al. used AR technology to carry out a digital display and experience project of material cultural heritage ARCHEOGUIDE on mobile devices, with the purpose of recreating cultural heritage scenes for tourists through visual display methods [5]. Wei et al. use digital animation, virtual reality, and other technologies to digitally display representative European culture and superimpose virtual information on the cultural relics of the ancient city through AR technology [6]. Jian et al. elaborated on the protection methods of cultural heritage in the new era and proposed that the combination of cultural heritage and AR will become the inevitable trend of cultural heritage protection [7].

Li uses AR technology to visualize the three-dimensional model of outdoor cultural heritage sites and provides users with cultural heritage information through the object panoramic visualization system [8]. Xuanyuan et al. use augmented reality technology to develop the Byblos system, through which users can visit the image structure of the Roman theater to understand the cultural background [9]. Based on mobile augmented reality technology (Mobile Augmented Reality, MAR for short) combined with the digital protection of intangible cultural heritage taking Longquan celadon as an example, Riliang et al. have researched and designed a system applied on a smartphone platform [10]. Sinha et al. use AR technology and somatosensory interaction technology to study how national orchestral instruments can perform virtual performance. His research makes people enjoy the fun of virtual combination when enjoying musical instruments. This application has successfully attracted people's interest in national musical instruments [11].

This article introduces the system architecture, database, edge computing server, and data processing flow are designed and explained in detail, and edge computing is combined with the display of artworks to provide users with smart electricity usage. In the future, we will continue to observe the stability of the system, improve the system's ability to process concurrency, and lay a firm foundation for building edge computing IoT systems.

2. IoT Technology and Art Exhibition Architecture

2.1. Hierarchical Architecture of Art Display System Based on AIIoT Technology. With the further integration and application of AIIoT technology in smart images, especially in its artwork display system, "artificial intelligence" has gradually developed to "applied intelligence," and smart images with image energy efficiency management and smart IoT applications as the core are especially developed. Green smart images have quietly become the development trend of future images, so it is very important to actively construct and carry out theoretical and applied research on "AIIoT+smart images" [12], in order to improve the feasibility and scalability of intelligent image artworks during system development and the safety and reliability of the system during actual operation [13]. On the basis of the original three-tier system architecture of the intelligent image art display system, combined with the actual fusion application of AIIoT technology, the overall hierarchical structure of the intelligent image art display system based on AIIoT is finally formed, that is, a total of 5 layers from bottom to top. The terminal equipment layer, the intelligent perception layer, the network communication layer, the AI cloud brain control layer, and the application scenario layer are composed. This system architecture can make the structure of the largest and most complex artwork display system in the intelligent image clearer and the division of labor. Among them, the terminal equipment layer is located at the bottom of the architecture and is the ultimate bearer of green smart images to achieve "green" and "intelligence," generally including building system smart

terminals that implement various specific functions [14]. The intelligent perception layer refers to all kinds of intelligent devices with communication capabilities in the green intelligent image, as well as smart sensors and controllers, which can perform preliminary information processing and provide basic data for the application scenario layer and mainly carry the information transfer obtained from the perception layer. The AI cloud brain control layer is equivalent to an artificial intelligence control decision-making platform; that is, through AI intelligent units, intelligent algorithms and information technology to complete the mining, calculation, analysis, statistics, classification, and integration of real-time data and information of each subsystem can finally be achieved. The autonomous learning and control, intelligent decision-making and organization, and personalized customization are the functions used; the application scenario layer is to establish a system integration platform for each module system of specific users according to the different requirements of different users [15].

In recent years, with the continuous deepening of the country's new urbanization process, the country, provinces, prefectures, cities, and related industries have successively issued "green policies," related industry standards and regulations, which have strongly promoted the construction and development of smart images. Globalization, especially the 30 years of digitalization in our country, is model era→PC interconnection era→mobile internet era→IoT→smart IoT evolving, especially with the rapid development and integration of AI technology and IoT technology. While information and data provide vitality to AI, AI is also creating all possibilities for IoT. The AIIoT technology has become an effective way and the best way to intelligently upgrade major traditional industries represented by the image industry in the next ten years. Smart image is an ideal combination of "AI+smart image." Its core is "artificial intelligence platform," that is, "AI cloud brain." The overall architecture of the system composed of intelligent image "AI cloud brain" is composed of perception layer, transmission layer, and control layer. It has the characteristics of high precision, low cost, complete functions, and strong automation [16]. The transport layer generally refers to a comprehensive technical system composed of 5G and AI computing; the control layer is mainly composed of clusters such as control, decision-making, execution, and management. The Chinese name of "AIIoT" is intelligent IoT, that is, "AI+IoT," which is based on the organic combination, effective combination, and application integration of artificial intelligence and IoT [17]. In fact, the concept of AIIoT was proposed as early as 2017 and was first popularized by the industry. In recent years, it has become a hot vocabulary and industry hotspot in the IoT industry and the image industry [18].

2.2. NB-IoT Technology. The smart art display system based on NB-IoT uses the following technologies: sensor technology, IoT wireless remote communication technology, and cloud platform technology, so that terminal managers can remotely monitor the temperature and humidity data of the art display system and take corresponding measures [19]. This system is composed of temperature and humidity

sensor module, GPS module, NB-IoT module, and transparent cloud platform module. The temperature and humidity module adopts the industrial-grade temperature and humidity sensor SHT20, and the GPS module model adopts the L70-R which supports low power consumption mode [20]. The temperature and humidity sensor collects the temperature and humidity of the indoor system environment, and the GPS sensor collects the geographic location [21]. The visual engineering measurement platform based on IoT technology and cloud computing combines the characteristics of engineering measurement and is divided into three levels: data acquisition layer, data analysis and storage layer, and management and application layer on the basis of IoT application mode [22].

2.2.1. Data Collection Layer. The data collection layer covers the perception layer and network layer of the IoT system architecture and is responsible for collecting measurement data and uploading the data to the designated server [23]. The IoT is responsible for connecting numerous devices, computers, and built-in sensors in a dynamic network and continuously receiving and exchanging information from the external environment [24]. In engineering surveys, the total station and GPS-RTK-integrated machine can complete most of the survey tasks, so the platform is mainly designed for the data networking of these two types of equipment [25]. The GPS-RTK-integrated machine adopts relative positioning measurement method to eliminate errors such as ephemeris, ionosphere, and troposphere; combined with carrier phase measurement technology, cm-level high-precision measurement can be achieved, which can meet the requirements of engineering measurement. The data transmission uses the 5G IoT module. Compared with the traditional radio transmission method, the data transmission method of the 5G IoT module is not easily affected by the surrounding environment and transmission power, and the transmission distance is not limited. The measurement data can be directly uploaded to the server. Relative positioning measurement requires the use of two satellite receivers, a base station and a mobile station. The base station is placed in a location with stable geological conditions and known three-dimensional coordinates. During the measurement, the base station collects satellite observation information and sends the observation data and its own three-dimensional coordinates to the mobile station through the 5G IoT module. While the measuring station obtains the measurement information sent from the base station, it also collects the satellite observation information, and the information is calculated in real time, and then, the calculated data with a positioning accuracy of cm level is obtained. Finally, the 5G IoT module is used to upload the calculated data to the server. Considering that the current smart phones are equipped with Bluetooth communication function, an Android-based uRLLC communication terminal is designed, which uses the Bluetooth communication function of the mobile phone to establish a connection with the total station to realize wireless control of the total station and at the same time uses the mobile phone network

communication function to communicate with the server to realize data transmission.

2.2.2. Data Analysis and Storage Layer. The data analysis and storage layer use cloud computing technology to analyze the raw data measured by the equipment and store the data for subsequent use.

2.2.3. Management and Application Layer. The management and application layer adopts the B/S architecture, that is, the general browser/server architecture on the Internet. The back end adopts Spring, SpringMVC, Mybatis, and other frameworks, and the front end adopts Vue, Axios, and Element-ui frameworks; the front and back ends use very lightweight and language-independent JSON for data interaction. The B/S architecture uses the HTTP protocol for communication, and business processing is performed on the server. There is no need to develop and maintain client programs, and cross-platform operations can be easily realized, ensuring the security of the platform and data to the greatest extent. In order to facilitate the internal collaborative measurement in engineering measurement, the platform is designed to implement a management platform and a measurement platform. The management platform runs in the browser on the PC side to provide personnel with functions such as data management, measurement task management, and report management; the measurement platform runs on the browser of the mobile device (smart phone); a visual measurement interface is provided for the measurement personnel to improve the efficiency of the measurement operation. The entire measurement platform application layer design is divided into management platform and measurement platform.

Considering that engineering measurement operations are mainly divided into known point stakeout and unknown point measurement, the platform designs a set of internal collaborative measurement operations process based on these two measurement operation methods and corresponding operation procedures, combined with the platform application mode. Create a measurement task on the management platform and assign it to the surveyor. The surveyor can select the available measurement equipment on the platform to start the visual measurement operation. After the measurement is completed, it will be submitted to the staff for review. The task that passes the review can be exported to the report, and the review is not passed. The task needs to be reassigned to the surveyor for measurement. Through the powerful storage and computing capabilities of the cloud computing center, the requirements of the system can be met.

2.3. SAS Logical Structure Model Based on Improved Hypergraph. "Super network" is used to describe a system with many nodes and nested networks in the network. Hypergraph theory is one of the methods with a relatively complete mathematical definition. A hypergraph is a two-tuple V is a finite set of nodes, satisfying the formula:

$$G = G_w + G_{nb} + G_t, \quad (1)$$

$$G = \frac{\sum_{j=1}^k \sum_{h=1}^k \sum_{t=1}^{n_j} \sum_{r=1}^{n_h} |y_{ij} - y_{hr}|}{2n^2 u}. \quad (2)$$

A hypergraph can be regarded as a generalization of graph theory. Its edges can include any number of nodes. The finite set of nodes with the same attributes is the hyper-edge of the hypergraph. The definition of hypergraph ignores the connection relationship between nodes. However, whether in the definition of weights in hypernetworks or in the study of flows, the connection relationship between nodes is of great significance. Improve the definition of hypergraph by increasing the connection relationship between nodes, so that it includes both the definition of nodes and edges in basic graph theory and the definition of super edges in hypergraph theory:

$$u_h \leq u_j \leq \dots \leq u_k, \quad (3)$$

$$G_{jj} = \frac{1/2 u_j \sum_{i=1}^{n_j} \sum_{r=1}^{n_j} |y_{ji} - y_{jr}|}{n_j^2}, \quad (4)$$

$$Gw = \sum_{j=1}^k G_{jj} p_j s_j. \quad (5)$$

Combined with the introduction of the characteristics of commonly used centrality indicators in related literature, the actual T1-1 network is investigated, and the neighbor-based node centrality and the path-based node subgraph centrality are selected as indicators to evaluate the importance of nodes. At the same time, these two centrality indicators are easy to extend to the hypergraph, and the definition in the hypergraph is equally clear. Logical nodes are ranked according to relative (super) degree centrality, and the top three LNs are the same, namely, IHMI (human machine interaction), TCTR, and TVTR. In terms of (super) degree centrality, they are the most important, because they have more connections with other nodes, and they also appear more frequently in different functions:

$$G_{jh} = \frac{\sum_{z=1}^{h_j} \sum_{r=1}^{n_h} |y_{ji} - y_{hr}|}{n_j n_h (u_j + u_h)}, \quad (6)$$

$$G_{nb} = \sum_{j=2}^k \sum_{h=1}^{j-1} G_{jh} (p_j s_h + p_h s_j) D_{jh}, \quad (7)$$

$$G_t = \sum_{j=2}^k \sum_{h=1}^{j-1} G_{jh} (p_j s_h + p_h s_j) D_{jh} (1 - D_{jh}). \quad (8)$$

In the SAS-improved hypergraph modeling process, the logical nodes in the SAS logical structure are defined as the nodes of the SAS-improved hypergraph model, the logical connections between logical nodes are defined as edges, and the logical function composed of several logical nodes is defined as super side. Take the T1-1 type substation in IEC61850 as an example to carry out the improved hyper-

graph modeling and related analysis of SAS. Each logical node (LN) is a subfunction located in a physical node, and only data in the LN can interact. There may be a logical connection between two LNs, and each functional super edge contains multiple LNs:

$$D_{jh} = \frac{d_{jh} - P_{jh}}{d_{jh} + P_{jh}}, \quad (9)$$

$$d_{jh} = \int_0^{\infty} dF_j(y) \int_0^y (y-x) dF_h(x), \quad (10)$$

$$d_{jh} = \int_0^{\infty} dF_h(y) \int_0^y (y-x) dF_j(x). \quad (11)$$

The improved hypergraph model of SAS logical structure is a triplet. The node set V in the triplet is combined with the edge set GE and the hyperedge set HGE, respectively, which can form the SAS graph model GG=VE and the hypergraph model HG=VE:

$$f(x) = \frac{1}{Nh} \sum_{i=1}^N k \left(\frac{X_i - x}{h} \right), \quad (12)$$

$$k(x) = \frac{1}{\sqrt{2\pi}} \exp \left(-\frac{x^2}{2} \right), \quad (13)$$

$$h_t = \tanh (w_c x_t + u_c (r_t \Theta h_{t-1}) + b_c), \quad (14)$$

$$h_t = z_t \Theta h_{t-1} + (1 - z_t) \Theta h_t. \quad (15)$$

In the graph structure, the objects appearing in pairs are related to a certain degree. Among them, objects are abstracted into nodes in the graph, and the "association" between two objects is called an edge. Graph models have advantages when analyzing networks or complex networks. Based on the mathematical definition of the graph and some basic parameters used to describe the graph, some commonly used parameters to measure the topological structure characteristics of the graph model can be derived. The definitions of these parameters are as follows:

$$\sigma t = \frac{\sqrt{1/n \sum_{i=1}^n (FI_{it} - FI_{it})^2}}{FI_{it}}, \quad (16)$$

$$u_{(j|i)} = w_{ij} A_i, \quad (17)$$

$$s_j = \sum_i c_{ij} u_{(j|i)}. \quad (18)$$

Using the definitions and formulas of these parameters, the basic parameter values of the T1-1 SAS logic graph model can be calculated. The position of a node in the network topology determines its criticality and scope of influence. Structural centrality is the most commonly used indicator for evaluating the importance of nodes. They measure the criticality of nodes themselves by influencing the capabilities of other nodes. The neighbor-based centrality indicators and path-based centrality indicators are two

commonly used centrality indicators:

$$\ln\left(\frac{FI_{it}}{FI_{it}-1}\right) = \alpha + \beta \ln FI_{it} - 1 + v_i + \mathfrak{F}_t, \quad (19)$$

$$c_{ij} = \frac{e^{b_{ij}}}{\sum_k e^{b_{ik}}}. \quad (20)$$

The degree centrality index is a typical neighbor-based centrality index, which is defined as the number of adjacent nodes of a node. According to the degree centrality index, the more direct neighbors of a node, the more critical it is. When considering the information dissemination process, when the path through the node can spread information faster and more widely, the node is more critical, and this can be calculated by the centrality index based on the path, and the centrality of the subgraph is a typical. The path-based centrality index is as follows:

$$r = \frac{\alpha}{1-\beta}, \quad (21)$$

$$\theta = -\frac{1}{T} \ln(1+\beta), \quad (22)$$

$$\tau = \frac{\ln(2)}{\theta}. \quad (23)$$

They are the most vulnerable nodes based on degree centrality. Once they fail, they can have a significant impact on SAS. For other LNs, the ranking of superdegree and degree is quite different. For example, ITCI is ranked fourth in the ranking of relative hyper centrality, but it is not yet ranked in the top ten in relative hyper centrality. This shows that there is a logical connection between ITCI and fewer LNs, but it appears in more super edges:

$$\ln\left(\frac{FI_{it}}{FI_{it}-1}\right) = \alpha + \beta \ln FI_{it} - 1 + \phi X_{it} - 1 + v_i + \tau_t, \quad (24)$$

$$k_{t1}[i] = \sum_j \cos(w_i^1, w_j^2). \quad (25)$$

Logical nodes are sorted according to relative (super) subgraph centrality. As shown in (25), the ordering of each LN according to relative subgraph centrality and relative hypersubgraph centrality is very different. PDIS has the greatest hypersubgraph centrality, which means that the closed loop of PDIS passes through more super edges and has more short closed paths than other LNs, and data deviations will propagate faster.

3. Artwork Display System Design

3.1. System Hardware and Software Support

3.1.1. Work of Art Data Analysis Server. The work of art data analysis service is based on the Spring framework, and the dependencies between objects are handed over to Spring to reduce the coupling between components; use nonblocking

input/output (NIO) to solve high concurrency downloading artwork data transmission problem and improve server data processing capacity. The automated deployment of services is realized by writing shell scripts and combining with the maven packaging tool. The data analysis service is highly available and easy to expand. It can automatically handle client connections and deal with abnormal situations accordingly to ensure data security and accuracy.

3.1.2. uRLLC Communication Terminal. uRLLC communication terminal is based on the Android operating system and is responsible for data forwarding between the total station and the server. During the measurement, the server issues measurement instructions to the uRLLC communication terminal, and the uRLLC communication terminal sends the received measurement instructions to the total station and obtains the measurement data returned by the total station and finally sends the measurement data to the server. In this process, the mobile phone acts as an intermediary for data transmission and is responsible for data forwarding, and the data processing will be carried out by the server.

3.1.3. Artwork Information Management Platform. The management platform is divided into 6 modules according to functions, and each module will carry out authority control to ensure the security of the platform and data. The user management module is responsible for the management of platform users and the corresponding role authority management. The equipment management module manages the communication parameters of the total station and the GPS-RTK-integrated machine and the server. The parameter management module is responsible for the basic parameters in engineering measurement such as projection parameters and coordinate systems. The basic control points and other parameters are stored and changed. The job management module is responsible for task creation, dispatch, audit, and report export. The operation log module records all logs of the platform to ensure that all user operations on the platform are traceable and commonly used the tool module provides common calculation tools such as coordinate conversion, seven-parameter calculation, four-parameter calculation, and geodetic calculation.

3.1.4. Visual Measurement Platform. The visual measurement platform is mainly divided into 3 modules. The surveyor can select the equipment being used in the equipment selection module, then select the task assigned to him in the construction measurement module, and enter the visualization interface for measurement; the custom module provides temporary operation functions. Surveyors can create tasks and complete measurements according to the on-site environment and assist or supplement the tasks assigned to them.

3.2. System Design Steps

3.2.1. Control Function. In order to complete the distributed access control decision, operations such as the decision-making authorization of the access control authority of the IoT device and the setting of the access control strategy

and the management of user information are completed by four smart contracts deployed in the hyperledger, namely, the PIP contract, PAP contract, PDP contract, and PEP contract. In this section, we will introduce the contracts and functions that implement access control functions. In the PIP contract, the resource owner manages the access control authority of the IoT device and the identity of the registered user through this contract. The PIP contract contains the following functions:

- (i) AddResource() function. This function is triggered when the resource owner uploads the access control authority of the IoT device
- (ii) AddResource() function. This function writes the access control authority information of the device into the blockchain. A legal access control authority information requires four parameters
- (iii) DeleteResource() function. Under certain circumstances, the resource owner no longer continues to share the access control authority of the device. Through this function, enter the resource ID to be revoked, and the system deletes the corresponding resource information in the blockchain to complete the resource cancellation; the resource applicant will not be able to search for information about the resource on the blockchain.
- (iv) UserRegister() function. The user enters the user name and user ID in the user registration page; the system registers the user identity information through this function and saves it in the blockchain for subsequent system operations.

The PDP contract is responsible for judging whether the resource requester matches the access control policy of the applied device and judging whether the current resource requester is an authorized user of the device. The functions included in the contract are as follows: The MatchPolicy() function is mainly responsible for comparing the attribute information of the resource requester with the attribute information in the access control policy of the requested IoT device to determine whether it can obtain the access control authority of the device. This function is called by the GetPermission() function in the PEP contract when the resource requester applies for resource access control permissions.

The JudgeUser() function is responsible for judging whether the current resource requester is one of the authorized users of the device and passing the judgment result to the PEP contract. The judgment process is similar to the MatchPolicy() function, so I will not repeat it.

In the PEP contract, the contract is responsible for receiving the results returned by the PDP contract and executing corresponding actions based on the results. The PEP contract contains the following four functions:

- (i) The ShowResource() function displays the obtained access control authority according to the entered user name

- (ii) The UseResource() function determines whether the device is included in the user's available resource list according to the result returned by the JudgeUser() function in the PDP contract
- (iii) The FindResourceByRes_ID() function is called by the system when the resource requester searches for available equipment, and the corresponding search result is displayed according to the input resource ID
- (iv) The GetPermission() function grants the access control permission of the device to the resource requester according to the result returned by the MatchPolicy() function in the PDP contract and uploads the permission information obtained by the resource requester to the blockchain.

3.2.2. Construction of BIM Core Database. The monitoring data is used for the construction of the BIM database, which mainly includes the data collection and transmission layer, the data processing and analysis layer, and the data storage layer. In the demonstration of real-time monitoring functions, the monitoring data and evaluation results need to be reflected in the BIM three-dimensional model for visual warning display, which is realized through the user interaction layer. The basis of monitoring visualization is the image model of the tunnel, including the positioning of the tunnel structure axis, the detailed structure, and the positioning of the sensors. In addition, the model and parameter information of equipment operation and maintenance and pipeline installation management are also applied to the BIM module, and the import interface is set to integrate the monitoring data in the database with the BIM 3D model. The technical realization is shown in Figure 1.

4. Artwork Display System

4.1. System Hardware Analysis. As shown in Figure 2, the landslide monitoring data collection system constructed by the wireless sensor network in this article is composed of two parts: a short-range wireless sensor network and a remote monitoring center. The wireless sensor network is the basis for building the IoT architecture, including sensor nodes, routing nodes, and assemble nodes, using the ZigBee protocol to build a clustered network structure, so as to realize mutual communication and information transfer between nodes.

As shown in Table 1, the choice of data transmission protocol determines the reliability and stability of data transmission in wireless sensor networks, compared with other transmission protocols such as Bluetooth, WiFi802.11, WirelessUSB, Bluetooth, Cellular, and ZigBee802.15.4. The transmission rate is low, but it can meet the small-capacity monitoring data transmission, the power consumption is low, the transmission distance can be expanded, and the overall implementation is easier.

The data transmission process is shown in Figure 3. Based on the IoT technology, this platform connects the GPS-RTK-integrated machine and the total station, two

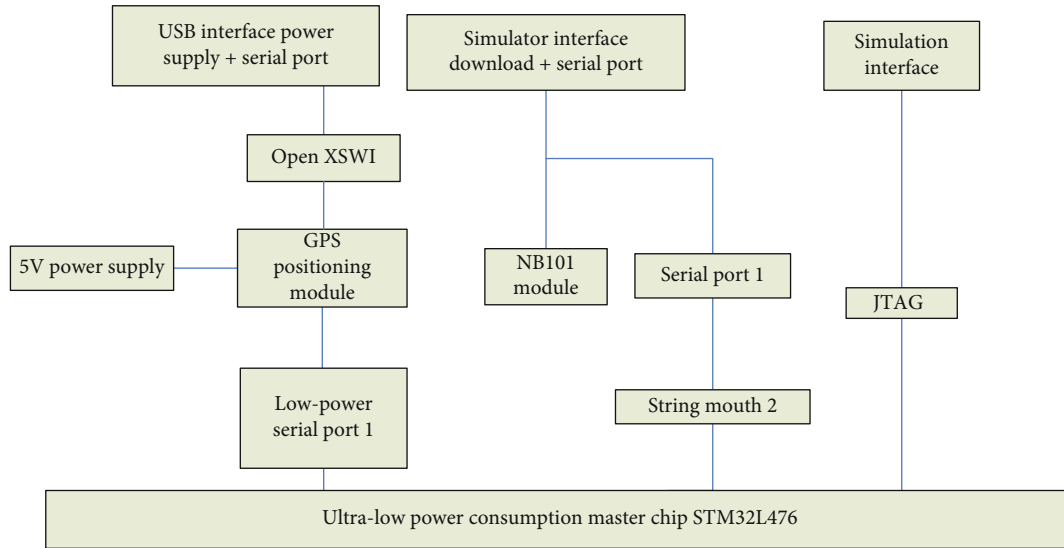


FIGURE 1: Integration of monitoring data in database with BIM 3D model.

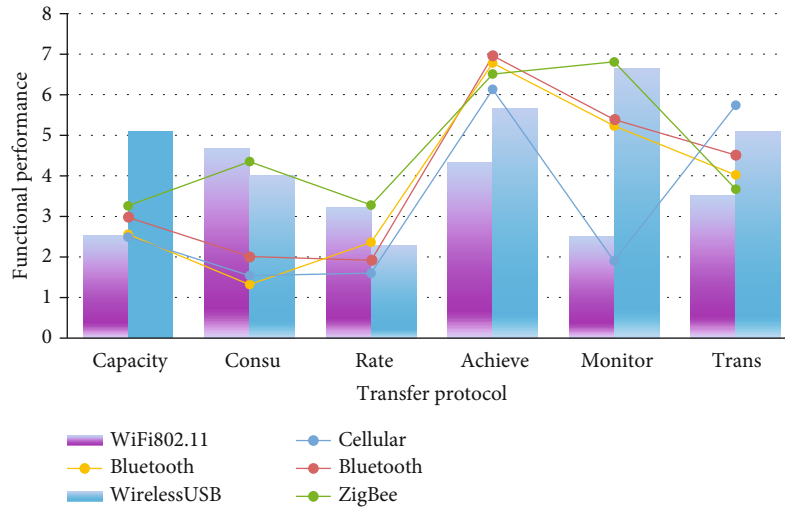


FIGURE 2: Reliability and stability of data transmission in the network.

TABLE 1: Reliability and stability of data transmission in wireless sensor networks.

Item	Bluetooth	WiFi802.11	WirelessUSB	Bluetooth	Cellular	ZigBee
Capacity	2.98	2.53	5.1	2.56	2.49	3.26
Consu	2.01	4.67	4	1.32	1.54	4.35
Rate	1.92	3.22	2.28	2.36	1.6	3.28
Achieve	6.96	4.34	5.65	6.78	6.13	6.51
Monitor	5.39	2.5	6.65	5.23	1.9	6.81
Trans	4.51	3.51	5.1	4.02	5.74	3.67

commonly used measurement equipment in engineering surveys, so that it can safely communicate with the server to achieve measurement data. At the same time, the platform is based on cloud computing technology and B/S architecture and has designed a management platform and measurement platform that can be operated across platforms. The

stored measurement data is used to achieve internal collaborative measurement. The management platform provides unified management functions for engineering measurement data and work processes. The measurement platform realizes the visual measurement operation. The platform realizes the unification of online management and measurement,

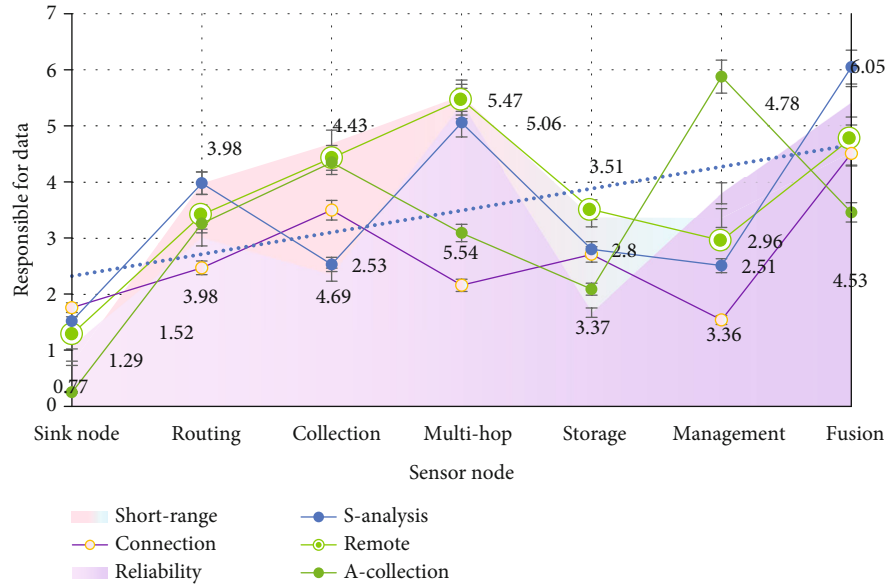


FIGURE 3: Artwork information data transmission process.

which can effectively improve the efficiency of engineering measurement and greatly reduce the overall cost of construction.

As shown in Table 2, this article mainly accesses two measuring devices, a total station and a GPS-RTK-integrated machine. When measuring with a total station device, it is highly dependent on the measurement function of the total station. What the platform does is to control the total station for measurement and then read and store the measurement results of the total station. The platform itself cannot improve the measurement accuracy of the total station. There are many factors affecting the measurement accuracy of GPS-RTK-integrated equipment. Therefore, the GPS-RTK all-in-one device was tested during the platform test, and the projection parameters are shown in Table 3.

As shown in Figure 4, the user authenticates his identity through the security authentication interface provided by the cloud computing layer and obtains a security token. The user uses the security token to issue control instructions to the edge layer through the device control channel of cloud computing and submit this control information to the system. If it is found through the network inspection that the user and the edge server are in the same local area network, the user is allowed to establish a secure connection with the edge server through a security token, and the user submits this control information to the system through the edge layer device. After receiving the control instruction, the edge layer device encapsulates the instruction through the conversion relationship and sends it to the target perception layer device. The sensing layer device executes the instruction and returns the result. The return process is consistent with the device upload process.

The selected plane coordinates of the known points are as follows: After creating the coordinate stakeout task, select the GPS-RTK all-in-one device for measurement, record 8 sets of measurement data, and obtain the measurement

result graph, as shown in Figure 5. It is expressed in plane coordinates and normal height format. Compare the measured data in the figure with the original coordinates of the known points, and perform the difference calculation on X, Y, and H to obtain the deviation table, as shown in Table 4. The direction from a point on the ground to a point in the sky or another point on the ground is represented by the angle between the projection of the line connecting the two points on the horizontal plane and the reference direction. This representation is also called azimuth, which is one of the ways to measure the angular difference between objects on a plane. It is the horizontal included angle from the north direction line of a point to the target direction line in a clockwise direction. The analysis shows that when the GPS-RTK-integrated machine is used for measurement, it can ensure the measurement error within 1 cm in the horizontal direction and 2 cm in the elevation direction, which meets the engineering measurement requirements.

As shown in Figure 6, a monitoring terminal of this system is equipped with NB-IoT communication module, temperature and humidity sensor, photoresistor sensor, ethanol sensor, air quality sensor, etc. Turn on the power, the monitoring terminal will initialize the hardware, monitor the NB-IoT network attachment status, and access the cloud platform. Then, the monitoring terminal enters the normal environmental monitoring stage.

As shown in Table 5, in order to ensure the practicability of the system, this article tests the accuracy and completeness of its functions, including data collection, LCD display, abnormal alarm and remote data reporting, management, display, and other functions. The test is mainly through the indoor field test of the monitoring terminal and the remote test of the indoor monitoring management platform. The monitoring terminal is placed in the room for field test.

The LCD display screen of the monitoring terminal 1 is shown in Figure 7. This article separately displays the

TABLE 2: Highly dependent on total station equipment measurement.

Item	Short range	Remote	Reliability	Connection	S-analysis	A-collection
Sink node	0.77	1.29	1.08	1.76	1.52	0.25
Routing	3.98	3.42	3.01	2.47	3.98	3.26
Collection	4.69	4.43	2.35	3.5	2.53	4.35
Multihop	5.54	5.47	5.4	2.16	5.06	3.09
Storage	3.37	3.51	1.67	2.71	2.8	2.09
Management	3.36	2.96	3.8	1.54	2.51	5.88
Fusion	4.53	4.78	5.43	4.51	6.05	3.46

TABLE 3: Physical equipment test projection parameters.

Item	Communication module	Data analysis	Packaging module	Data calculation	Response module	Data storage
Edge	4.23	3.34	2.86	3.93	3.67	2.59
Storage	2.31	3.91	3.18	2.92	1.43	4.28
Traditional	1.58	1.19	1.65	3.36	1.79	6.28
Centralized	4.48	4.52	1.67	2.87	6.15	4.73
Cloud	2.22	6.17	6.28	2.22	5.77	4.77
Model	5.34	6.09	4.89	6.04	2.92	2.41

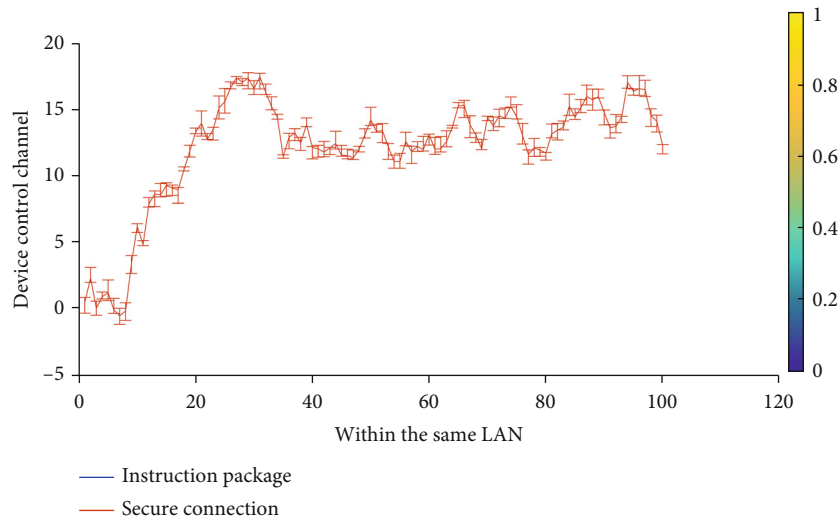


FIGURE 4: Security authentication interface authentication identity.

temperature, humidity, light intensity, ethanol concentration, air quality, voltage, and real-time time data collected by the monitoring terminal and their status. The normal temperature range is 10~16°C, and the light intensity is normally less than 100lx, and the actual values are all outside the normal range. Therefore, the LCD displays that its status is abnormal, and the terminal activates a buzzer to alarm.

As shown in Figure 8, the indoor environment monitoring management platform built by the OneNET IoT cloud platform realizes the management of 30 monitoring terminals. At the same time, abnormal alarms can be viewed through the status display icon of each monitoring terminal.

At the same time, you can view the detailed data of each monitoring terminal through the view detail function. As

shown in Table 6, the detailed data display interface of the monitoring terminal can be used to view the temperature, humidity, light intensity, ethanol concentration, air quality, and values such as voltage, and at the same time, you can view its changing trend through the graph. After the above tests, the monitoring terminal data collection, data display, abnormal alarm, and other functions are normal and meet the design requirements. At the same time, the interactive function of the monitoring terminal and the cloud platform is accurate and stable. The system completes one data collection, data display, abnormal judgment, and data reporting time, no more than 20 seconds, indicating that the functionality of the indoor environment monitoring system meets the expected requirements and is practical.

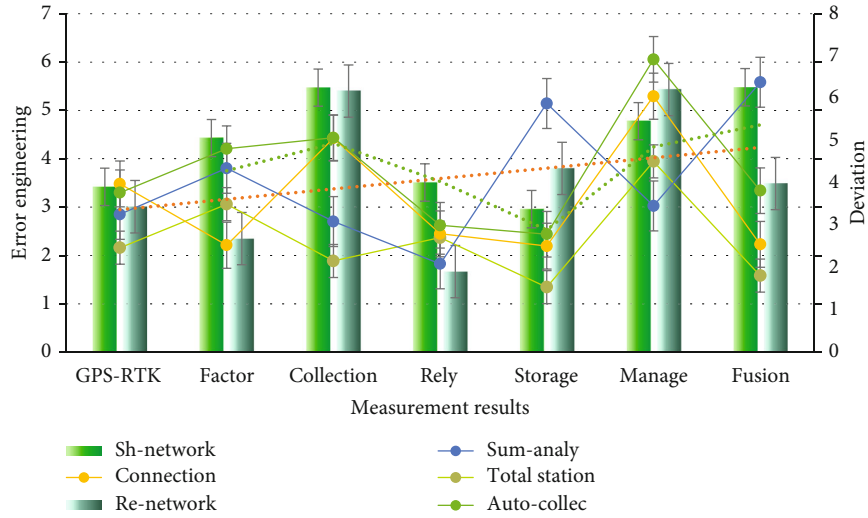


FIGURE 5: All-in-one machine 8 sets of data measurement results.

TABLE 4: Difference calculation comparison deviation.

Item	Sh-network	Re-network	Total station	Connection	Sum-analy	Auto-collec
GPS-RTK	3.42	3.01	2.47	3.98	3.26	3.77
Factor	4.43	2.35	3.5	2.53	4.35	4.81
Collection	5.47	5.4	2.16	5.06	3.09	5.07
Rely	3.51	1.67	2.71	2.8	2.09	3
Storage	2.96	3.8	1.54	2.51	5.88	2.79
Management	4.78	5.43	4.51	6.05	3.46	6.92
Fusion	5.48	3.49	1.81	2.55	6.38	3.82



FIGURE 6: The monitoring terminal enters the normal environmental monitoring stage.

As shown in Figure 9, compared with the traditional centralized cloud computing model, this system adds an edge computing layer close to the sensing layer device and quickly processes the data of the sensing layer device through the computing and storage capabilities of the edge

layer. The following article describes the design of the edge server. As shown in Table 7, the four functional modules of the edge server are as follows: communication module, data analysis and packaging module, data operation and response module, and data storage module.

TABLE 5: Functional accuracy and completeness testing.

	Sink node	Routing node	Collection	Storage	Management	Fusion
Capacity	3.74	2.58	4.76	3.61	5.28	2.73
Consumpt	3.8	3.6	5.75	4.88	4.55	5.23
Rate	1.91	4.65	3.09	4.76	4.42	3.5
Achieve	2.96	1.49	5.07	6.82	5.37	4.88
Monitor	2.67	1.62	2.28	5.23	5.84	4.66
Transmis	2.92	3.32	5.97	5.55	4.06	3.72

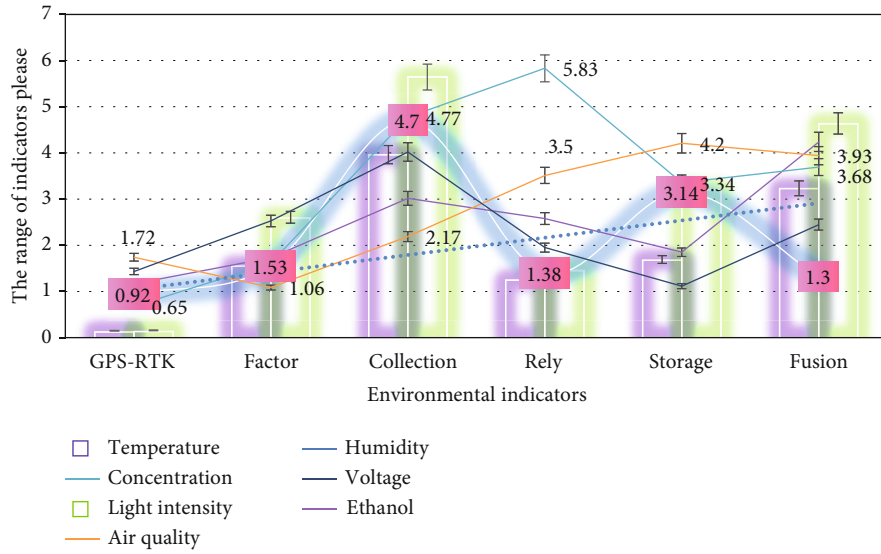


FIGURE 7: LCD display of monitoring terminal 1.

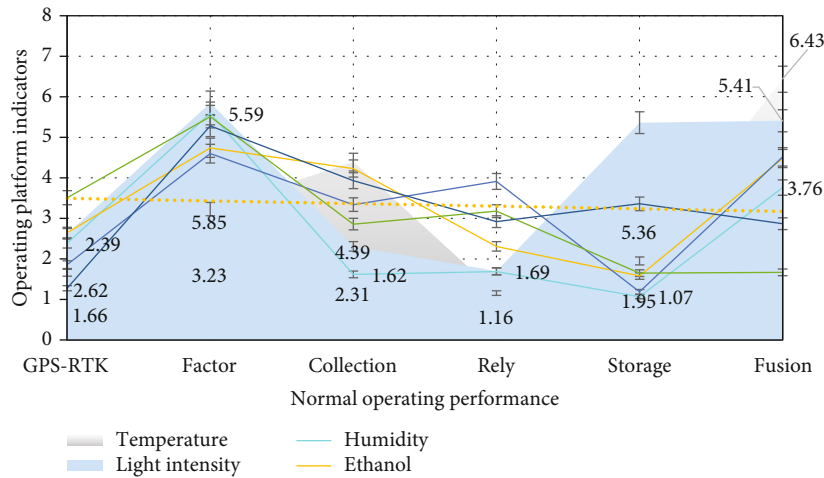


FIGURE 8: Remote monitoring indoor environment monitoring management platform.

As shown in Figure 10, through the communication layer, the system edge server can perceive the communication status of IoT devices and their communication status, obtain communication links, and provide access ports for new devices. At the same time, ensure smooth communication between the edge server and the cloud computing center, and ensure a smooth data flow channel. The

equipment behavior in this system refers to the measurement and regulation of external monitoring variables and equipment variables.

As shown in Figure 11, when the sensing layer device generates data, it is uploaded to the edge layer device. The edge layer converts the data through the conversion relationship and, according to the data type, stores the data in the

TABLE 6: Detailed data of each monitoring terminal.

Item	Temperature	Humidity	Light intensity	Ethanol	Concentration	Air quality	Voltage
GPS-RTK	1.66	2.39	2.62	2.65	1.86	3.51	1.28
Factor	3.23	5.59	5.85	4.74	4.6	5.51	5.28
Collection	4.39	1.62	2.31	4.23	3.34	2.86	3.93
Rely	1.16	1.69	1.7	2.31	3.91	3.18	2.92
Storage	1.95	1.07	5.36	1.58	1.19	1.65	3.36
Fusion	6.43	3.76	5.41	4.48	4.52	1.67	2.87

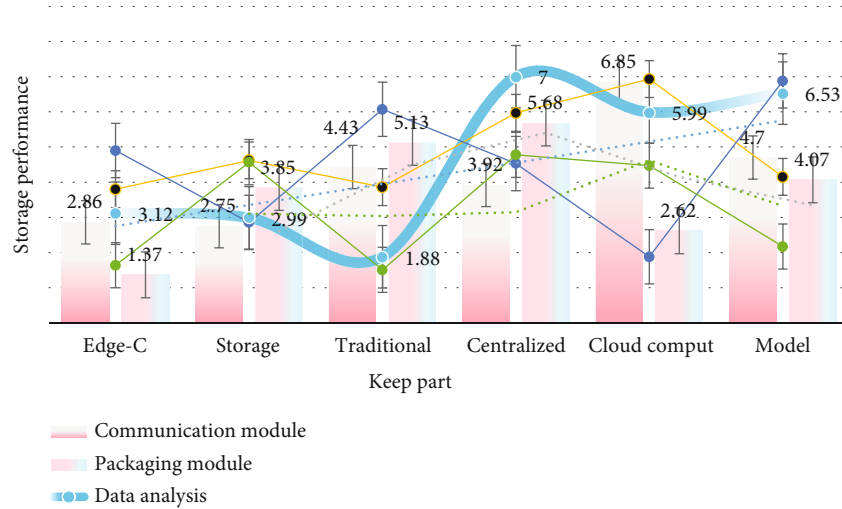


FIGURE 9: Computing layer close to the sensing layer device.

TABLE 7: Communication module provides device awareness for edge servers.

	Communication module	Data analysis	Packaging module	Data calculation	Response module	Data storage
Edge computing	2.86	3.12	1.37	3.8	4.9	1.64
Storage	2.75	2.99	3.85	4.62	2.86	4.57
Traditional	4.43	1.88	5.13	3.86	6.07	1.51
Centralized	3.92	7	5.68	5.97	4.53	4.78
Cloud computing	6.85	5.99	2.62	6.93	1.88	4.47
Model	4.7	6.53	4.07	4.15	6.88	2.17

Redis storage and time series database in turn and indicates the synchronization priority of the data. According to the priority of data synchronization, the data is synchronized to the cloud computing layer in real time or regularly through the communication layer, and the data storage server of the cloud computing layer is updated. As shown in Table 8, according to the results of data processing, it is judged whether it is necessary to control the corresponding IoT devices to perform corresponding operations to obtain operating performance data.

The IoT devices in this system are mainly smart controllers and smart meters connected in series in the power circuit, as shown in Figure 12, deployed in each exhibition hall. Due to the deployment of more wireless access points on the exhibition hall floor, the campus network covers a

wide range, and the signal is strong; smart controller devices use wireless communication protocols for communication, while smart meters use more stable wired communication. The most important equipment behavior of the intelligent controller is the on-off control of the power circuit and the power safety protection. The intelligent controller provides 10 branch circuit channels, which means that after the main circuit flows into the intelligent controller, multiple branch circuits can be separated, and through internal relays and control algorithms, different branch circuits can be controlled at the same time.

The smart controller replaces the traditional single-function wall switch. The user can control the on-off of the channel through the panel channel buttons of the smart controller and the corresponding APP, as shown in Table 9. The

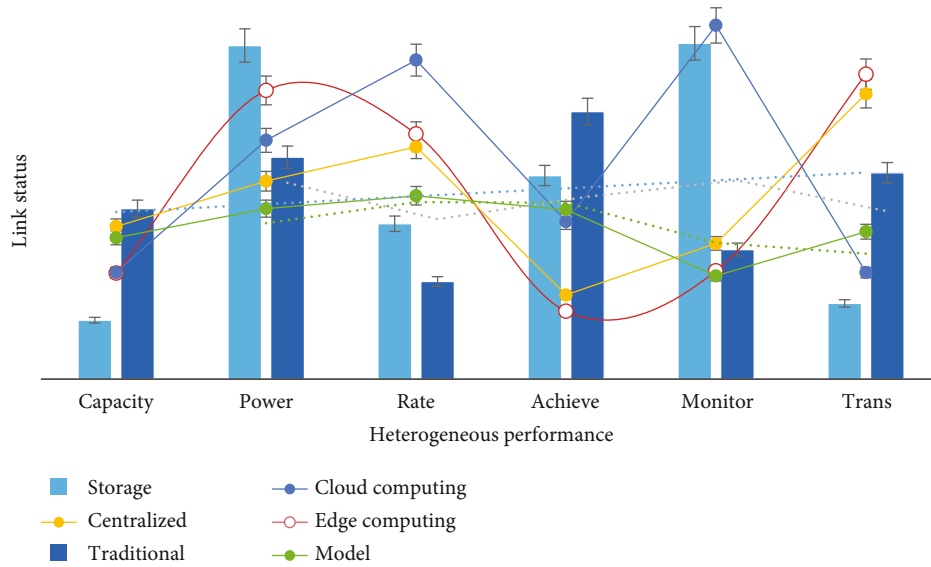


FIGURE 10: Perceive IoT devices and their communication status.

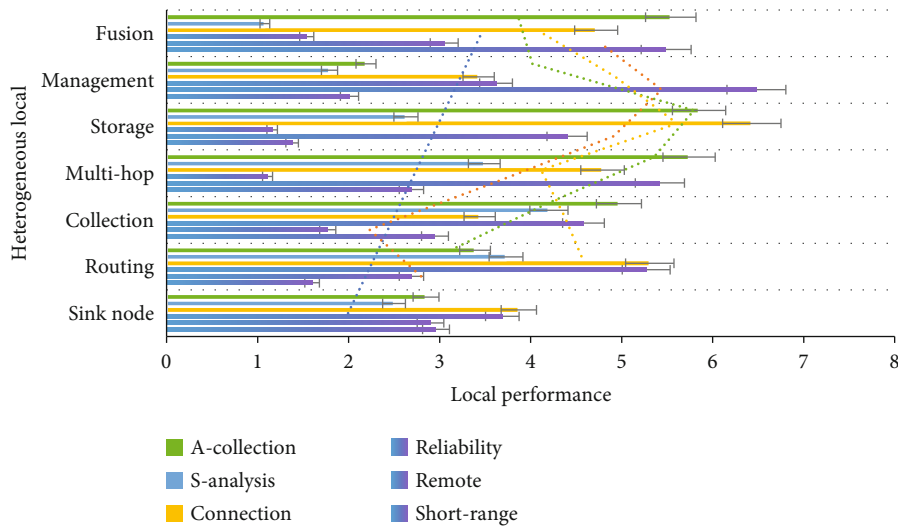


FIGURE 11: The communication layer synchronizes data to the cloud computing layer.

TABLE 8: Device control channel through cloud computing.

Item	Short range	Remote	Reliability	Connection	S-analysis	A-collection
Sink node	2.96	2.9	3.69	3.87	2.5	2.85
Routing	1.6	2.69	5.27	5.31	3.73	3.39
Collection	2.95	1.77	4.58	3.44	4.2	4.97
Multihop	2.69	5.42	1.11	4.79	3.49	5.74
Storage	1.38	4.4	1.16	6.43	2.63	5.85
Management	2.01	6.48	3.62	3.43	1.79	2.19
Fusion	5.49	3.05	1.54	4.72	1.08	5.54

system uses the first 6 channels of the intelligent controller, of which the first three channels are lighting channels, the fourth channel is socket channel, and the fifth and sixth channels are spare channels. Figure 8 shows the usage of each channel in Hall 1101 within one month. Among them,

the use of the first three channels of the intelligent controller accounted for 79% of the daily use, and its use is greatly related to the life of the visitors. The types of exhibits in this system include graphic design, painting design, fashion design, industrial design, film and television animation,

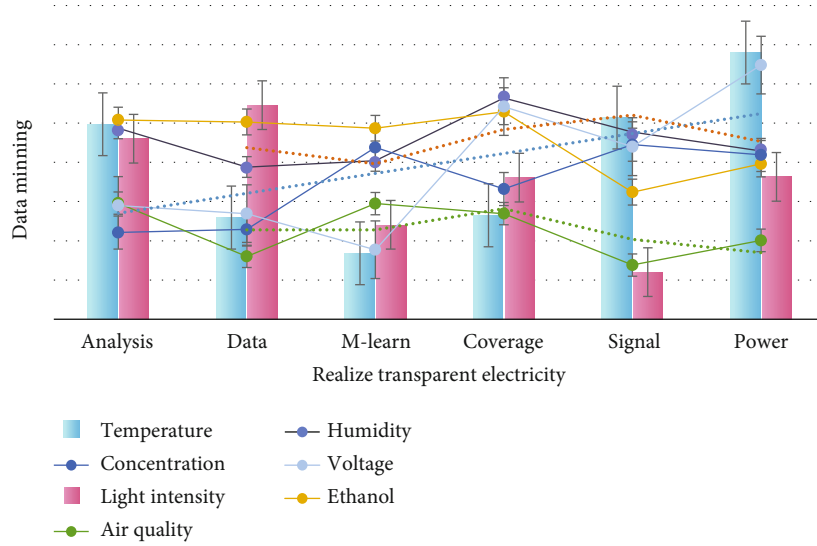


FIGURE 12: Smart controllers and smart meters in the loop.

TABLE 9: Panel channel buttons of smart controller.

Item	Short range	Remote	Reliability	Connection	S-analysis	A-collection
Sink node	5.31	3.73	3.39	5.03	2.68	2.08
Routing	3.44	4.2	4.97	3.14	4.78	2.87
Collection	4.79	3.49	5.74	1.42	2.46	1.78
Multihop	6.43	2.63	5.85	4.9	2.6	3.22
Storage	3.43	1.79	2.19	3.02	1.64	2.33
Management	4.72	1.08	5.54	4.77	3.37	4.37
Fusion	2.95	6.13	2.49	1.08	2.09	6.3

architectural environment, art synthesis, digital photography, graduation design, and other types; exhibit formats include four types: video, audio, picture, and text. The management of the exhibits in this article can be realized from various presentation layer pages and back-end java source files. According to different management directions and user rights, under the premise of unified art, the front-end output of different types and formats of exhibits can be realized.

The main equipment behaviors of smart meters are electrical energy measurement and monitoring of voltage, current, and power. Through the measurement of the electric energy value, this article calculates the electricity consumption of the exhibition hall per hour, and this figure is usually directly related to the exhibition hall electricity bill. The histogram of electricity consumption in an exhibition hall within 3 months is shown in Figure 13. The electricity consumption includes fluorescent lamps, long-arm spotlights, LED lamps, air conditioners, sockets, and temperature and humidity control, and data is obtained through smart meters. Through clear electricity consumption data, transparent electricity consumption is realized and users' awareness of energy saving is enhanced. These data are uploaded to the cloud server, and the corresponding user energy consumption model is established through data analysis, data

mining, machine learning, and other technologies, and the corresponding energy saving suggestions are given.

In this system, this article uses two indicators of communication round-trip delay and communication jitter to compare the traditional cloud computing system with this system. Among them, this article uses average deviation to define communication jitter, as shown in Table 10.

Figure 14 shows the result of the communication round-trip delay between the traditional cloud computing system and this system. In traditional cloud computing systems, the communication round-trip delay time of the intelligent controller is mainly distributed between 80 ms and 260 ms, with an average delay of 350 ms. In the "direct connection" mode of this system, the communication round-trip delay time is mainly distributed between 65 ms and 80 ms, and the average delay is 73.5 ms. Through the calculation of the experimental results, it can be known that in the traditional cloud computing system, the communication jitter is 290 ms, while in this system, the communication jitter is 16 ms, which is about 1/4~1/5 of the main communication delay interval. Based on the experimental results, it can be seen that the real-time performance of this system is far superior to the traditional cloud computing systems. The online display system of the artworks facilitates the college's

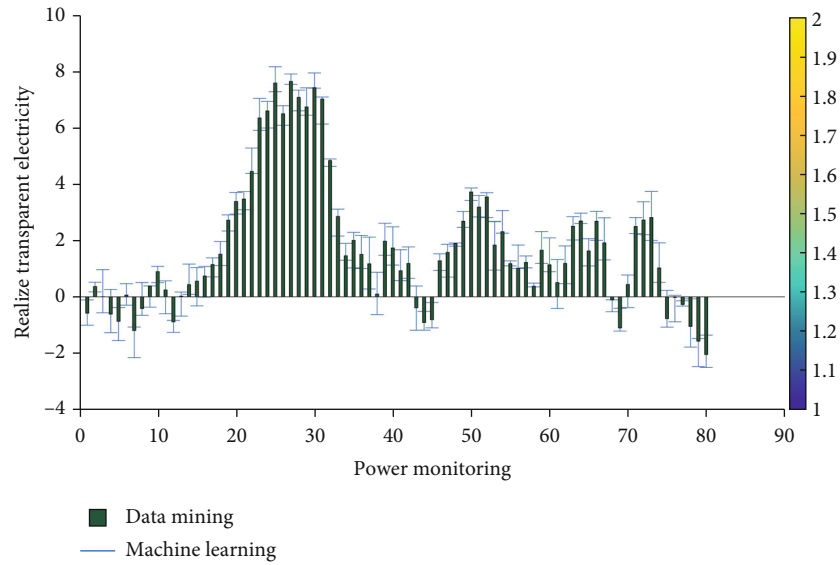


FIGURE 13: Electricity consumption of exhibition hall per hour.

TABLE 10: Mean deviation to define communication jitter.

Item	Temperature	Humidity	Light intensity	Ethanol	Concentration	Air quality	Voltage
Analysis	4.97	4.87	4.6	5.08	2.21	2.96	2.9
Data	2.59	3.88	5.46	5.03	2.29	1.6	2.69
M-learn	1.68	4.04	2.41	4.87	4.38	2.95	1.77
Coverage	2.65	5.64	3.61	5.29	3.32	2.69	5.42
Signa	5.14	4.77	1.2	3.24	4.45	1.38	4.4
Power	6.8	4.29	3.63	3.96	4.19	2.01	6.48

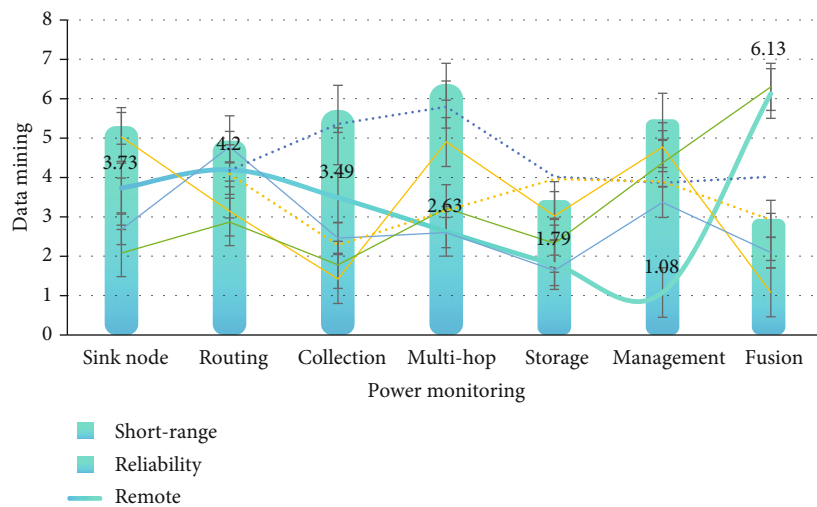


FIGURE 14: Traditional cloud computing system and the system.

management of exhibits, exhibitions, and topics; facilitates users' inquiries and statistical analysis; standardizes the review process of exhibits; improves the quality and efficiency of exhibit information management; and is in line with the online exhibit management function, a practical

online work information management platform. After the system is perfected, it will run successfully on the Internet platform. The system has intuitive interface and simple and easy-to-use functions, reduces a lot of manpower and time for exhibit management, and enhances efficiency.

5. Conclusions

The equipment model of the artwork display system is a collection of equipment behaviors and an abstraction of IoT equipment. Usually, a device model contains multiple device behaviors. In the artwork display system, because the communication protocols of the connected perception layer devices are different, the same device behavior often has many different expressions under different device models, which is easy to cause errors. The system converts the device information in the form of “many-to-one” to unify the data format, facilitate server data processing, and write the conversion relationship into the system configuration table. When the data is sent from the edge server to the perception layer device, the data can be correctly distributed through the conversion relationship for data packaging. As long as the conversion relationship is filled in correctly, the system does not need to pay attention to the heterogeneity among IoT devices, reducing the difficulty of system development.

When data is sent from the edge layer to the cloud computing layer, Google’s open source protocolbuffer protocol (protolbuf for short) is used to encapsulate the data. The protolbuf protocol has a certain encryption capability for information, and when the amount of information is constant, the information transmission efficiency is higher and the communication flow is reduced. The data processing and response module is the core part of the edge server. This module determines the priority of data processing by identifying the source and type of data. For high-priority data, it often seizes the server’s computing resources, obtains the results, and executes the tasks in accordance with the established procedures to improve the real-time performance of the system. Different from cloud computing storage, due to limited storage resources, edge servers only include Redis storage and time series data databases.

This article introduces the design of the artwork display system in detail, focusing on the use of the knowledge of the Internet of Things, but it can be found that there are many deficiencies in the article, mainly reflected in the inadequacy of data processing. In response to this problem, in the follow-up research, in-depth analysis of big data processing technology will be carried out. Combined with the Internet of Things technology, the system can be made more intelligent and more powerful.

Data Availability

The data that support the findings of this study are available from the corresponding author upon reasonable request.

Conflicts of Interest

The authors declare that they have no conflicts of interest.

References

[1] J. H. Zhu, J. Wu, and Y. Tao, “Sensor optimal placement algorithm based on coverage rate,” *Computer Engineering*, vol. 36, no. 3, pp. 94–96, 2020.

[2] L. Levin, M. Segal, and H. Shpungin, “Cooperative data collection in ad hoc networks,” *Wireless Networks*, vol. 19, no. 2, pp. 145–159, 2013.

[3] S. Chakraborty, S. Chakraborty, S. Nandi, and S. Karmakar, “ADCROSS: adaptive data collection from road surveilling sensors,” *IEEE Transactions on Intelligent Transportation Systems*, vol. 15, no. 5, pp. 2049–2062, 2014.

[4] C. Zou, W. Jiang, and F. Tsung, “A LASSO-based diagnostic framework for multivariate statistical process control,” *Technometrics*, vol. 53, no. 3, pp. 297–309, 2011.

[5] C. Zou, Z. Wang, X. Zi, and W. Jiang, “An efficient online monitoring method for high-dimensional data streams,” *Technometrics*, vol. 57, no. 3, pp. 374–387, 2019.

[6] Q. Wei, W. Huang, W. Jiang, and W. Zhao, “Real-time process monitoring using kernel distances,” *International Journal of Production Research*, vol. 54, no. 21, pp. 6563–6578, 2016.

[7] L. E. Jian, L. I. U. Yongyan, Y. E. Xi, Z. H. O. U. Wu, and L. I. Zhiwei, “Market-oriented operation pattern of regional power network integration with high penetration level of distributed energy resources,” *Proceedings of the CSEE*, vol. 36, no. 12, pp. 3343–3354, 2016.

[8] L. I. Rui, “Comprehensive benefit evaluation method of distributed generation microgrid projects based on different business models,” *Power System Technology*, vol. 41, no. 6, pp. 1748–1758, 2017.

[9] W. A. N. G. Xuanyuan, L. I. U. Dunnann, and L. I. U. Zhen, “Operation mechanism and key technologies of virtual power plant under ubiquitous IoT,” *Power System Technology*, vol. 43, no. 9, pp. 3175–3183, 2019.

[10] L. I. U. Riliang, L. I. U. Haitao, and X. I. A. Shengfeng, “IoT technology application and prospects in distribution transformer service area management,” *High Voltage Engineering*, vol. 45, no. 6, pp. 1707–1714, 2019.

[11] R. S. Sinha, Y. Wei, and S.-H. Hwang, “A survey on LPWA technology: LoRa and NB-IoT,” *ICT Express*, vol. 3, no. 1, pp. 14–21, 2017.

[12] Y.-P. E. Wang, X. Lin, A. Adhikary et al., “A primer on 3GPP narrowband Internet of Things,” *IEEE Communications Magazine*, vol. 55, no. 3, pp. 117–123, 2017.

[13] F. Liang, L. H. Yin, and Y. C. Guo, “A survey of key technologies in attribute-based access control scheme,” *Chinese Journal of Computers*, vol. 40, no. 7, pp. 1680–1698, 2017.

[14] A. Ouaddah, A. Abou Elkalam, and O. A. Ait, “FairAccess: a new blockchain-based access control framework for the Internet of Things,” *Security & Communication Networks*, vol. 9, no. 18, pp. 5943–5964, 2016.

[15] A. Ouaddah, A. A. Elkalam, and A. A. Ouahman, “Towards a novel privacy-preserving access control model based on blockchain technology in IoT,” in *Europe, Middle East and North Africa Conference on Technology and Security to Support Learning, EMENA-TSSL 2016*, vol. 5no. 6, pp. 523–533, Saidia, Oujda, Morocco: Springer Verlag, 2017.

[16] A. Outchakoucht, H. Es-Samaali, and J. Philippe, “Dynamic access control policy based on blockchain and machine learning for the IoT,” *International Journal of Advanced Computer Science and Applications*, vol. 8, no. 7, pp. 417–424, 2017.

[17] D. D. F. Maesa, P. Mori, and L. Ricci, “Blockchain based access control,” in *IFIP international conference on distributed applications and interoperable systems*, vol. 8no. 5, pp. 206–220, Neuchâtel, Switzerland: Springer, Cham, 2017.

- [18] S. Ding, J. Cao, C. Li, K. Fan, and H. Li, "A novel attribute-based access control scheme using blockchain for IoT," *IEEE Access*, vol. 7, no. 45, pp. 38431–38441, 2019.
- [19] J. S. Shi and R. Li, "Survey of blockchain access control in IoT," *Journal of Software*, vol. 30, no. 6, pp. 1632–1648, 2019.
- [20] A. Z. Ourad, B. Belgacem, and K. Salah, "Using blockchain for IoT access control and authentication management," in *International Conference on IoT*, vol. 7no. 6, pp. 150–164, Seattle, WA, United states: Springer Verlag, 2018.
- [21] I. Riabi, Y. Dhif, and H. K. B. Ayed, "A blockchain based access control for IoT," in *2019 15th international wireless communications and mobile computing conference (IWCMC)*, vol. 7no. 32, pp. 2086–2091, Tangier, Morocco: Institute of Electrical and Electronics Engineers Inc, 2019.
- [22] K. Košťál, P. Helebrandt, M. Belluš, M. Ries, and I. Kotuliak, "Management and monitoring of IoT devices using blockchain," *Sensors*, vol. 19, no. 4, pp. 856–868, 2019.
- [23] E. Adi, A. Anwar, Z. Baig, and S. Zeadally, "Machine learning and data analytics for the IoT," *Neural Computing and Applications*, vol. 32, no. 20, pp. 16205–16233, 2020.
- [24] H. Gao, Z. Ma, S. Luo, Y. Xu, and W. Zheng, "BFR-SE: a blockchain-based fair and reliable searchable encryption scheme for IoT with fine-grained access control in cloud environment," *Wireless Communications and Mobile Computing*, vol. 2021, 21 pages, 2021.
- [25] Z. H. A. N. G. Liang, L. I. U. Baixiang, Z. H. A. N. G. Ruyi, J. I. A. N. G. Binxin, and L. I. U. Yijiang, "Overview of blockchain technology," *Computer Engineering*, vol. 45, no. 5, pp. 1–12, 2019.

Research Article

Design and Implementation of Fully Convolutional Network Algorithm in Landscape Image Processing

Yinan Pan ¹, Yuan Li ², and Jing Jin ²

¹College of Landscape Architecture and Art, Northwest A&F University, Yangling 712100, Shaanxi, China

²Architectural Environment Art, Xi'an Academy of Fine Arts, Xian 710065, Shaanxi, China

Correspondence should be addressed to Yuan Li; 28018@xafa.edu.cn

Received 7 December 2021; Revised 18 January 2022; Accepted 26 January 2022; Published 26 February 2022

Academic Editor: Mu-Yen Chen

Copyright © 2022 Yinan Pan et al. This is an open access article distributed under the Creative Commons Attribution License, which permits unrestricted use, distribution, and reproduction in any medium, provided the original work is properly cited.

With the gradual improvement of the quality of life, taste, and ecological and environmental awareness of urban residents in China, the environmental landscape of residential areas has gradually become a hot spot. At present, the level of the residential environmental landscape has become a necessary means for real estate developers to publicize products and improve economic benefits. Although many residential areas have invested a high cost in constructing environmental landscapes, there are always some deficiencies and defects in the design and implementation of environmental landscapes in residential areas due to various reasons. Therefore, to ameliorate the low efficiency and high cost of manual processing of landscape images, a Fully Convolutional Network (FCN) model based on the traditional Convolutional Neural Network (CNN) is designed for semantic segmentation of landscape images to deal with the excessive amount of landscape elements in landscape image processing. The deconvolution method is utilized to realize pixel-level semantic segmentation. Besides, the image preprocessing method enhances the data to prevent overfitting from commonly occurring in FCN. Moreover, the model two-stage training method ameliorates long training time and complex convergence in deep learning. Finally, three upsampling network structures, i.e., FCN-32s, FCN-16s, and FCN-8s, are selected for a comparative experiment to determine the most suitable network. The experimental results demonstrate that the FCN-8s upsampling network structure is the most prominent; it attains a pixel accuracy of more than 90%, an average accuracy of 88%, and an average Image Understanding of 75%. The three values are the highest among the three upsampling structures, indicating that the FCN-8s can realize accurate landscape image processing. Besides, the recognition accuracy of FCN for landscape elements reaches 90%, 25% higher than that of CNN. This method is effective and accurate in classifying landscape elements, improves the classification accuracy intelligently, and significantly reduces the cost of landscape element classification, which is feasible.

1. Introduction

With the application of computer science to landscape architecture, landscape architecture design method tends to be of high-efficiency, fast, accurate, variegated, and easy to modify, bringing the science of landscape architecture to a new era [1]. Natural landscape photos are the most common and widely used image data in people's daily life, and there are increasing landscape images on the Internet. In addition to the role of appreciation and adjustment, such data are also widely used in the planning and design and landscape classification of landscape architecture. Therefore, it is essential to correctly classify the landscape elements in natural

landscape images to improve landscape architects' reading and search speed [2]. So far, the primary image classification technology is limited to the underlying visual features of images [3].

Nowadays, the continuous innovation of science and technology, especially computer technology, has brought hope for large-scale image data processing by computers [4]. Digital image recognition technology is an innovative technology that can identify experimental content by computer based on digital image processing technology [5]. Image recognition technology appeared in the middle of the 20th century and was first applied in aerospace exploration. It mainly went through three growth stages: text recognition,

digital image processing/recognition, and object recognition [6]. In the late 1980s, this kind of technology appeared in different fields. The landscape design in many residential areas in China does not accord with the people-oriented view in many aspects. For example, some communities' road network design excessively pursues artistry, leading to complex road bends and loss of convenience, increasing walking distance. Residents often fall on rainy and snowy days because the pavement materials are polished granite or nonslip floor tiles. For another instance, there is no special access or facilities for people with disabilities in the community. Some residential areas do not open unique activity venues for the elderly and young children; sometimes, they have to awkwardly watch young couples do a public display of affection. Some residential areas have no outdoor space for shelter, and residents cannot go out on rainy or hot days. To achieve a people-oriented landscape, the designers should perform a thoughtful and humane design by fully understanding the residents' age structure, occupation, life, work habits, and physical requirements. In this way, residential landscaping and leisure facilities can respect and consider every detail of human activities and enable the residents to feel the comfort of a humane space.

Performance evaluation indicators, also known as evaluation factors or evaluation items, refer to the aspects from which to measure or evaluate the work performance of the evaluation object, determining what to evaluate. The evaluation indicators involve all aspects of the evaluated person's performance in the performance evaluation process. Performance evaluation indicators measure whether the actual behavior results of the evaluated person have reached the performance objectives or to what extent. Establishing relevant evaluation indicators for a specific performance goal is essential, including quantity, quality, timeliness, cost, and outcome. Therefore, the performance evaluation indicator is not a single index but an evaluation index system composed of multiple relevant evaluation indexes. Performance evaluation indicator is the critical factor affecting the objectivity and accuracy of evaluation results. It is necessary to establish a set of scientific and comprehensive performance evaluation indicator systems for accurately and scientifically evaluating the performance of the public sector. In recent years, innovative deep learning (DL) technology has been popular in the context of big data. Convolutional Neural Network (CNN) is a representative DL network, which contains unique processing methods and has participated in many fields and scenarios. Here, the Fully Convolutional Network (FCN) model based on the traditional CNN is adopted to classify the landscape elements in the landscape image, and a comparative experiment is performed to prove the model's validity. The FCN model for landscape element recognition reported here has the advantages of a high degree of automation, fast speed, and wide application range, which is conducive to the digital information of landscape architecture and can facilitate the promotion of digital landscape. Most previous studies have studied and improved the garden design concept from actual situations or psychology. This study intends to combine neural network technology with the garden design method

and use the design concept to improve the garden design defects fundamentally. This innovative scheme can fundamentally improve the work in this field. Therefore, the research results can provide a new perspective judgment and basis for the garden design criteria. Firstly, this paper theoretically expounds on the image recognition technology, introduces some key technologies to reduce noise and remove miscellaneous information, and leads to the related concepts of image and processing. Then, the operation mode of FCN illustrates the advantages of CNN. The segmentation technology process is introduced to illustrate the design process of the garden. The FCN model is trained and tested to obtain the training data results, thus drawing the research conclusion.

2. Literature Review

Zhang et al. [7] studied wavelet analysis and applied this method to image decomposition and reconstruction, indicating that the image analysis method has made a significant breakthrough in mathematics. Setti and Wanto [8] proposed a backpropagation algorithm to predict the most significant number of Internet users globally, meaning that the research on neural networks is gradually maturing. At present, image processing technology is developing rapidly. For example, Agrawal and Jayaswal [9] used a support vector machine to learn network diagnosis and classify bearing faults.

The landscape element classification belongs to image recognition. As a classical recognition application of high-dimensional big data sets, image recognition regards the image to be tested as a high-dimensional random vector, maps the obtained data to the low-dimensional feature space through linear or nonlinear methods, and finds the dimensional structure in the hidden low-dimensional high-dimensional data. Ding et al. [10] collected 1,257 gardeners' social capital perception questionnaires. The authors applied factor analysis and regression analysis in the statistical analysis stage to analyze the role and relative importance of different factors and social capital. They found that the social capital level was significantly influenced by the integration with green infrastructure, accessibility, scale, visual openness, planting form, barren landscape, agricultural infrastructure, and intelligent infrastructure. From the psychology perspective, Zhang and Li [11] identified the influencing factors of residents' sense of security and comfort of the public garden landscape and put forward some countermeasures to improve public garden landscape design. They suggested that landscape designers should focus on increasing the attraction of public landscapes and comprehensively consider landscape's ornamental, living, and leisure. The previous studies lay a theoretical foundation for improving public landscape design and residents' quality of life.

3. Research Method

3.1. Image Recognition Technology. Human beings primarily obtain external information from images. With the development of computer science, digital image processing

technology has been widely used in various fields such as industrial production, physical health, and traffic safety [12]. The information in the landscape image is input into the landscape element recognition system through computer programming to automatically recognize landscape elements [13]. The core part of digital image processing is image recognition. The specific image recognition process contains feature extraction of landscape images after preprocessing, some standards (such as Bag-of-Words models and neural networks) used to classify landscape elements on images, and completing the task of identifying landscape elements [14]. Figure 1 illustrates the general composition of the landscape image recognition system.

In Figure 1, image preprocessing aims to show image information more clearly, reduce noise, remove redundant information, and provide high-quality images for subsequent operations [15]. The function of image feature extraction is to study how to extract more efficient features from the original image and realize a precise mapping relationship between images in a particular feature vector or spatial vector. The advantages, disadvantages, and stability of feature extraction directly impact the recognition system's performance. Therefore, choosing images with features such as concentration and robustness is essential to better adapt to changes in environment, space, and scale [16]. Classifier design and training map an image feature to a feature vector or space and then use some decision rules to classify the low-dimensional feature space to obtain the most accurate classification results [17]. The trained classifier predicts the landscape image and identifies the categories of landscape elements in the landscape image to get the recognition results [18].

3.2. Image Preprocessing. The purpose of image preprocessing is to improve the data intensity of the whole model during training. Improving data intensity refers to using some methods or techniques to increase the number of training samples and enhance the richness of training samples [19]. Especially for DL, improving data intensity is an indispensable technical means. The advantage of improving data intensity is that, in model training, the growth of data amount and data richness will significantly reduce the overfitting of model training [20].

There are many ways to improve data intensity, among which translation, rotation, scaling, and flipping are commonly used [21]. These four methods are used to train the network structure to complete classifying landscape elements in images. The label of the input landscape image is the category of the landscape element. While increasing the data intensity, the label of the landscape element will not change, so the operation order is not irrelevant. The actual operation order in the experiment is rotation, translation, scaling, and flipping. After increasing the data intensity, it is necessary to perform sample randomization processing on the landscape images ready to be input to the model for training. Specifically, an experimental sample is randomly selected from the training set as the input. The following section designs the structure of FCN reported here.

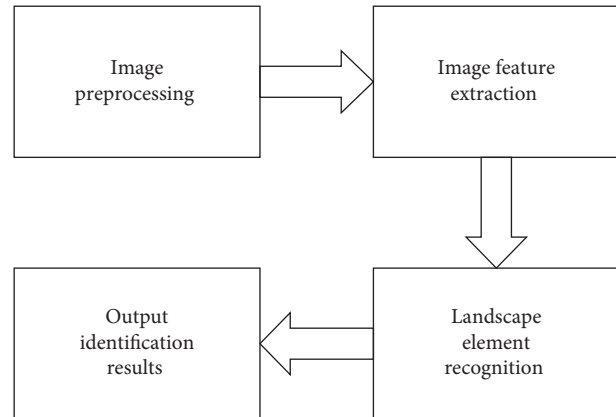


FIGURE 1: General composition of the landscape image recognition system.

3.3. Structure of FCN

3.3.1. Convolution. Unlike the traditional CNN, including AlexNet [22] and LeNet [23], which require input images to meet their set conditions, FCN has no strict requirements on the size of the input image. Figure 2 reveals the traditional CNN structure. The first layer to the fifth layer is the convolution layer, and the last three layers are one-dimensional vectors. The length of the sixth and seventh layers is 4,096, and the length of the eighth layer is 1,000, representing the category's probability value.

The difference between FCN and CNN is that FCN aims to classify pixels in landscape images [24]. CNN and FCN are also different in structure, mainly the network's last layer. After the convolutional layer of CNN is connected to the fully connected layer, a one-dimensional vector with a fixed size is finally obtained and normalized by softmax [25]. However, the last layer of FCN is the convolutional layer, so the final output result is an image with labels. The network structure shown in Figure 2 is modified to replace the last three layers by the convolution layers with convolution kernels of (4096, 1, 1), (4096, 1, 1), and (1000, 1, 1), respectively, to constitute the corresponding FCN, as presented in Figure 3.

The process of replacing the last three fully connected layers with convolution layers is the convolution mentioned above. The structure of the fully connected layer is similar to that of the convolution layer. However, the neurons in the convolution layer can only accept the data of a specific region in the previous layer, and the neurons in the same layer can only use one parameter [26]. The similarity of the two layers is to use the dot product calculation method and have the same function expression. In this way, the fully connected and convolution layers can be converted to each other to find the fully connected layer corresponding to each convolution layer. However, in practical applications, the fully connected layer plays a more significant role because the convolution operation of the convolution layer on the image is equivalent to an operation of the fully connected layer, which will make the calculation more convenient.

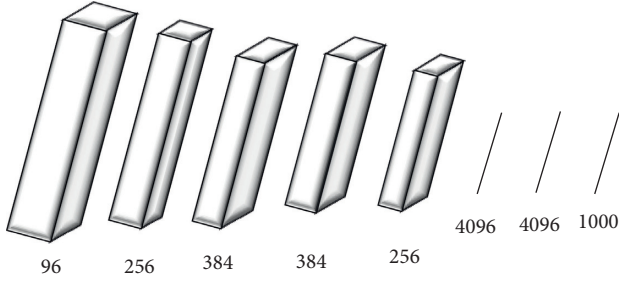


FIGURE 2: Structure of traditional CNN.

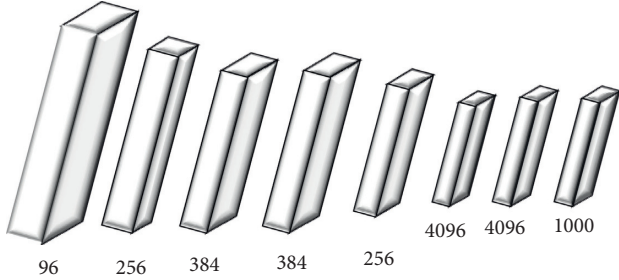


FIGURE 3: Structure of FCN.

3.3.2. Upsampling. Upsampling is also called deconvolution. Deconvolution is calculated by addition and multiplication, the same as the convolution network. The difference is that deconvolution derives multiple pixels from one pixel, while the convolution network is the opposite [27]. The forward propagation and backward propagation of deconvolution are opposite to the propagation direction of the convolution network, but they have the same optimization method [28]. Figure 4 displays the comparison between the convolution network and the deconvolution network.

As mentioned above, FCN does not impose restrictions on the size of the input image. However, after several operations of pooling the convolution kernel in the network, the scale of the landscape image will decrease, and the resolution of the horizontal image will gradually decrease. For example, suppose the size of the input image is $h \times w$. After several convolution pooling operations, an image with the size of $h/32 \times w/32$ may be generated, which is also the smallest layer. This layer is called the thermal image, a high-dimensional feature map [29]. Figure 5 reveals the convolution of FCN.

Then, FCN adopts upsampling, namely, deconvolution, to continuously enlarge the landscape image to the same size as the original image, to realize the classification of pixels in the landscape image. The final input result is an image after upsampling, and then each pixel in the output landscape image can be predicted. This method aims to obtain the maximum value of the corresponding position of the landscape image pixels in all the obtained images. The maximum value of this position is the probability that judges the category.

3.3.3. Jumping Structure. The semantic segmentation of landscape images under FCN is basically completed after the convolution and sampling. However, the upsampling

operation will excessively reduce the resolution of the landscape image, which makes the final structure rougher and rougher. Therefore, the obtained segmentation results cannot meet the standard requirements.

As shown in Figure 6, the size of the original input image will become very small after the pooling operation of convolution kernels. For example, after the third convolution pooling, the image will become 1/8 of the original image size. After the fourth convolution pooling, the image size will become 1/16 of the original image. After the fifth convolution pooling, the image size will become 1/32 of the original image. However, after the sixth and seventh convolution pooling, the image will not become smaller, but the number of feature maps will be reduced. At this time, the image is called the thermal image.

The feature obtained after the fifth-layer convolution pooling performs deconvolution operation on a 1/32-size thermal image to restore its original size. The reason is that the thermal image cannot accurately express the characteristics of the original image due to the limitation of accuracy. Therefore, the forward iteration method is employed here to refill the details of the image with the convolution kernel in the fourth layer as the deconvolution, which is equivalent to an interpolation operation. The convolution kernel in the third layer can further supply the details to restore the whole image. The above process is named jumping structure, aiming to optimize semantic segmentation results [30].

3.4. Process Framework of the Segmentation Technology. It provides the test results of the functions of the semantic segmentation model of landscape elements in landscape images based on FCN.

From Figure 7, the core part of the simple model is the FCN of DL; it is also the core part of the algorithm reported here. Firstly, the model directly reads the landscape image and then preprocesses the image. Finally, it classifies the landscape elements in the image through FCN and outputs semantic segmentation results. The image reading steps are implemented using Python's third-party library function [31].

3.5. Training of the Semantic Segmentation Model Based on FCN

3.5.1. Pretraining. Due to the complexity of FCN of DL, it takes a long time to train the model. Moreover, FCN has deep network layers. On the one hand, when conducting specific experiments, the final results of the model may remain near the optimal solution, which may affect the experimental results. On the other hand, the whole model may take a long time for convergence.

Therefore, in the concrete training of the FCN model, the model parameters with good convergence are usually used to initialize the parameters of the new model [32]. The pre-training method has been widely used in the deep execution and automatic coding networks. Firstly, relatively few training samples train the parameters of each layer in the

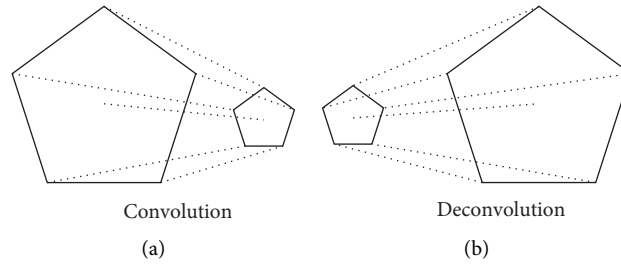


FIGURE 4: Comparison between the (a) convolution network and the (b) deconvolution network.

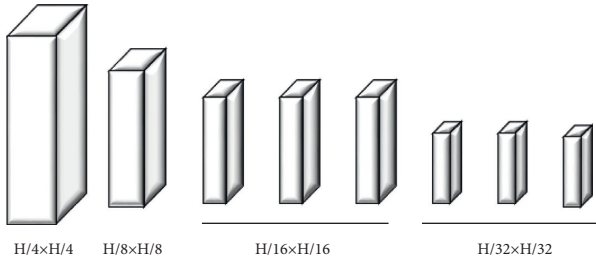


FIGURE 5: Convolution of FCN.

training network. Then, these parameters initialize the training model. Finally, the formal model is trained. The random initialization method may lead to the local minimum rather than the global minimum [33]. However, the pretraining method can make the model obtain better performance here, which the existing CNN models adopt. Inspired by pretraining, the two-stage training method is also used to train the model.

3.5.2. Two-Stage Training of the Model. For the two-stage training of the model, a pretrained model is used to initialize the model that needs to be trained, to share the parameters of the convolution layer, and to improve the effect of using random initialization alone. The optimization steps for training in the experiment are as follows.

Step 1: 500 simple images are manually selected. First, the model is trained on these 500 images. After the model converges, the parameters in the model are saved and downloaded. Because the selected images are simple, the convergence rate of the model is speedy.

Step 2: the second training of the model is executed on all training sets. The parameters obtained in Step 1 are used to initialize the model parameters so that all network weights and parameters are updated. This step significantly reduces the model's training time, improves the model's performance, and speeds up the convergence speed of the model. Finally, an improved model is obtained.

After training, these models will generate multiple Caffemodel files. These model files represent the parameters of the FCN model saved under different iterations. Ultimately, these models are used to segment the landscape elements in the landscape image to gain the final result map. Figure 8 denotes the two-stage training process of the model.

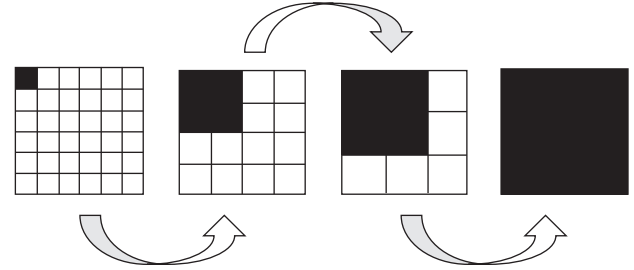


FIGURE 6: Convolution operation.

3.6. Experimental Data Source. In the first experimental stage, 500 training set images are selected as the pretraining data set using the two-stage training model in Figure 8. Then, the second-stage training is performed. The loss and iterative performances of the model are proved by comparing the result data of two-stage training.

In the second experimental stage, different single scene elements are taken as the main scene landscape images to train the model to compare the performance of three different upsampling structures in different landscape element classification in the training process. The landscape element as the central scene in each landscape image must occupy 60% of the landscape image, and each scene element prepares 100 pictures to train the model. The garden landscape images are divided into three categories: waterscape, landscape, and vegetation in the experiment.

4. Experimental Results of Two-Stage Training and Different Upsampling Methods

4.1. Results of Two-Stage Training of the Model. After repeated experiments, the learning rate of the weight parameter is determined as 10^{-10} , and the weight attenuation coefficient is 0.005. Figure 8 displays the model after the second-stage training. The models before and after the two-stage training are compared. In the process of two-stage training, 500 images of the training set are selected as the data set of pretraining, and then the model two-stage training is carried out. Figure 9 illustrates the relationship between loss and iteration of the model with and without two-stage training.

In Figure 9, the longitudinal coordinates represent the value of the loss function, which is responsible for measuring the probability that the test data belongs to a specific category; the lower the loss function, the faster the network

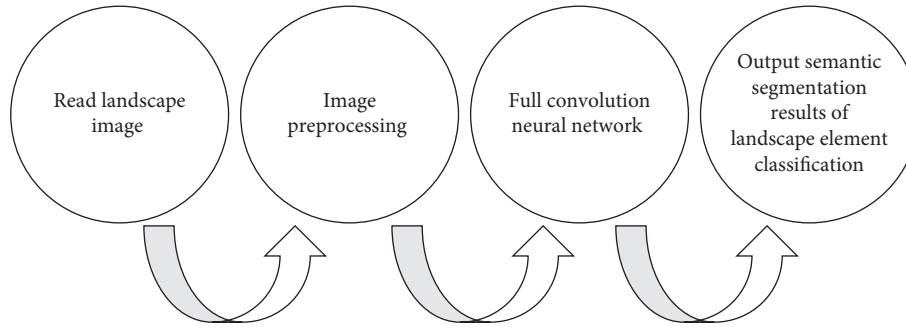


FIGURE 7: Functions of the semantic segmentation model.

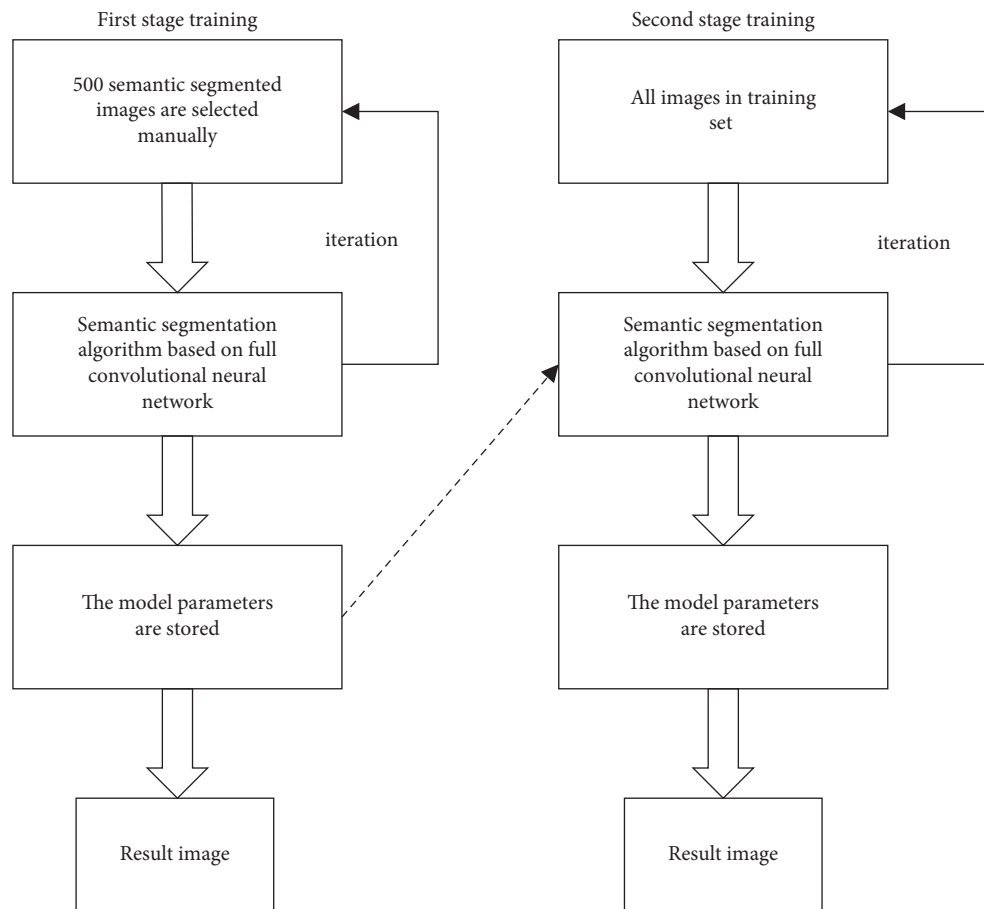


FIGURE 8: Two-stage training process of the model.

convergence. From Figure 9, the loss values of the model before and after the two-stage training decrease rapidly during 300 to 500 iterations. However, after 500 iterations, the loss value of the model after two-stage training reaches 0.43 at 700 iterations, but the loss value of the model before two-stage training only is 0.47. The convergence speed of the model after two-stage training is faster than that of the model before two-stage training, indicating a better effect. With the iteration, the two models are in a relatively stable state ultimately. The loss value of the model after two-stage training is stable at about 0.41, while the loss value of the model before the two-stage training is stable at about 0.45. This result indicates that the convergence speed of the model

after the two-stage training is more and more gentle. The experimental results show that the two-stage training method can effectively accelerate the convergence speed in the training process of the landscape image semantic segmentation model, and the data proves that the method is feasible. Therefore, the two-stage training method is adopted to train the model in the subsequent experiments.

4.2. Experimental Results of Three Kinds of Upsampling on Images. From Figure 10, among the three detection factors, the FCN-8s network achieves higher pixel accuracy, average accuracy, and average IU compared to the other two

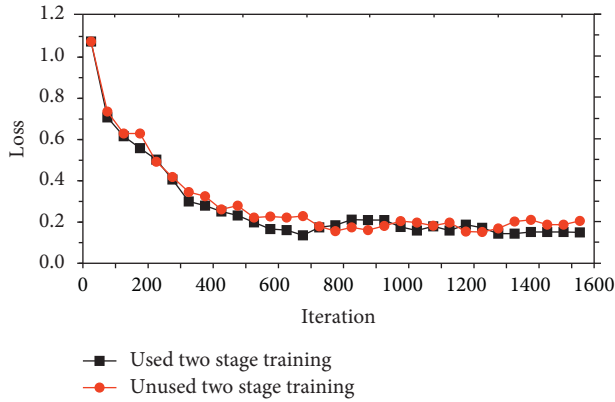


FIGURE 9: Comparison of the model before and after the two-stage training.

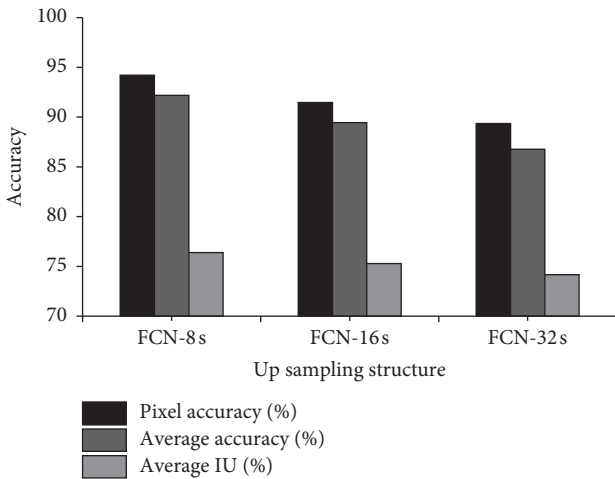


FIGURE 10: Experimental results of three different upsampling methods on waterscape images.

networks. The sampling accuracy of pixels in waterscape images reaches 92%, the average accuracy reaches 89%, and the average IU attains 75%. The pixel sampling accuracy of FCN-16s in landscape images is 90%, the average accuracy is 89%, and the average IU is 76%. The pixel sampling accuracy of FCN-32s in vegetation images is 94%, the average accuracy is 92%, and the average IU is 76%. The accuracy of the other two neural networks is relatively lower. Figures 10–12 provide the accuracy comparison among FCN-8s, FCN-16s, and FCN-32s, from the perspective of pixel accuracy, average accuracy, and average IU value. Among these three upsampling structures, the FCN-8s structure achieves the highest pixel accuracy, average accuracy, and average IU value. The pixel accuracy is more than 90%, the average accuracy is more than 88%, and the average IU value is more than 75%. This model has good adaptability and high accuracy for various landscape elements in landscape images. Its average accuracy is lower than pixel accuracy because the average accuracy is calculated by combining the information of all categories in the image. At the same time, too much test set data can also lead to low average accuracy and average IU value.

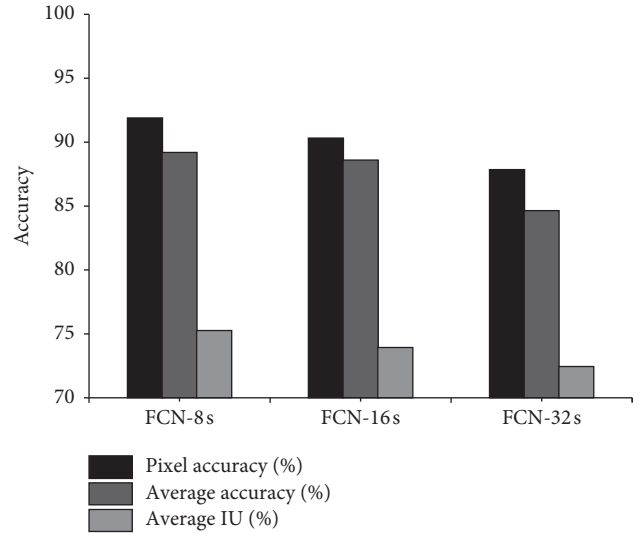


FIGURE 11: Experimental results of three different upsampling methods on landscape images.

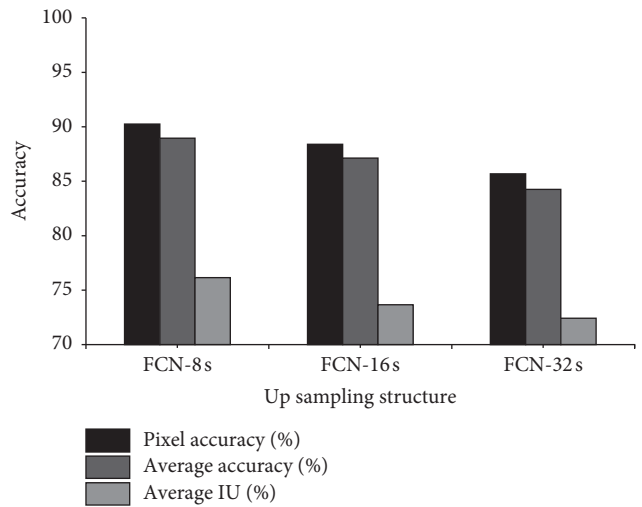


FIGURE 12: Experimental results of three different upsampling methods on vegetation images.

Figures 10–12 show that the FCN-8s structure is more prominent than the other two upsampling structures. The disadvantage of the final output image of FCN-32s is that the edge segmentation effect is not good, and there is a lack of some detailed information, failing to achieve excellent detail processing results. Therefore, the jump layer method is adopted to reduce the step size of the shallow upsampling and fuse the results with the results obtained at a higher level. Then, the upsampling output is carried out. Finally, deconvolution is used to complete the semantic segmentation of the whole landscape image. It can be seen that the FCN-16s structure has a significant improvement over FCN-32s, and the FCN-8s structure is more detailed than FCN-16s in image processing. Therefore, the FCN-8s structure is selected as the optimal upsampling structure for classifying landscape elements in landscape images.

5. Discussion

Given the problems of low efficiency and high cost of artificial processing of landscape images, this paper uses the FCN technology under DL to construct the element classification model for landscape images. Besides, semantic segmentation technology is adopted to edit and train the model, which verifies the effectiveness of the FCN method. A two-stage training is carried out on the FCN model to reduce training time. Three upsampling structures, namely, FCN-32s, FCN-16s, and FCN-8s area, are used for a comparative experiment to verify the effect of the whole model on image processing. Finally, the FCN-8s upsampling structure with the best pixel accuracy, average accuracy, and average IU value is selected, and these three values reach 90%, 88%, and 75%, respectively. At the same time, the pixel accuracy of each object is more than 86%, which shows that the model is very suitable for the classification of landscape elements in garden landscape images. Yang [34] analyzed the application of computer simulation in urban landscape design and value analysis and established computer-aided design of green space. They provided suggestions on the practical application of technical measures to save square: innovation of space design and application of newly constructed wetland system and garden rainwater in the design of regulation and storage system. The relationship between the design of the new square rainwater storage system and the urban landscape environment is consistent with the research results reported here, which can effectively optimize the concept of garden design [35].

6. Conclusion

The completion of pixel classification of landscape images is only a tiny step in landscape architecture evaluation. This method can evaluate the weight of different landscape elements after classifying landscape elements in landscape images to ultimately complete the intelligent landscape evaluation of the whole landscape image, which is worth being applied and promoted. This scientific approach improves objectivity, scientificity, and persuasion of the results of landscape evaluation and promotes future landscape evaluation. This paper achieves satisfactory results in the semantic segmentation of landscape element classification and realizes the semantic segmentation model based on FCN. For landscape images containing multiple landscape element categories, this method has the advantages of high accuracy, less time-consuming, and good robustness. This method can also process multiple complex landscapes simultaneously, dramatically reducing image processing time, saving time, and providing technical support for the automatic classification of landscape images. The research also lays a good foundation for landscape evaluation in the future with intelligent processing of landscape images. However, there are still some problems. The model is still not accurate enough in detail processing. Some element categories in the garden landscape image occupy a small area. In this case, the model may ignore them, resulting in incorrect classification. The follow-up study will try different deconvolution algorithms to extract more accurate details.

Data Availability

The raw data supporting the conclusions of this article will be made available by the authors, without undue reservation.

Ethical Approval

This article does not contain any studies with human participants or animals performed by any of the authors. Informed consent was obtained from all individual participants included in the study.

Conflicts of Interest

All authors declare that they have no conflicts of interest.

Authors' Contributions

All authors listed have made a substantial, direct, and intellectual contribution to the work and approved it for publication.

Acknowledgments

The authors acknowledge the help from the university colleagues.

References

- [1] I. Kim, S. Hong, J.-H. Lee, and J.-C. Bazin, "Overlay design methodology for virtual environment design within digital games," *Advanced Engineering Informatics*, vol. 38, no. 1, pp. 458–473, 2018.
- [2] A. La Notte, D. D'Amato, H. Mäkinen et al., "Ecosystem services classification: a systems ecology perspective of the cascade framework," *Ecological Indicators*, vol. 74, pp. 392–402, 2017.
- [3] F. Huang, Y. Yu, and T. Feng, "Hyperspectral remote sensing image change detection based on tensor and deep learning," *Journal of Visual Communication and Image Representation*, vol. 58, no. 1, pp. 233–244, 2019.
- [4] X. Xing, F. Shen, Y. Yang, T. S. Heng, and L. Xuelong, "Learning discriminative binary codes for large-scale cross-modal retrieval," *IEEE Transactions on Image Processing*, no. 5, p. 1, 2017.
- [5] Y. Shu, Y. Chen, and C. Xiong, "Application of image recognition technology based on embedded technology in environmental pollution detection," *Microprocessors and Microsystems*, vol. 75, no. 6, Article ID 103061, 2020.
- [6] C. Hyun-Woo, Y. Hyuk-Jin, and Y. Jae-Chan, "Analysis of crack image recognition characteristics in concrete structures depending on the illumination and image acquisition distance through outdoor experiments," *Sensors*, vol. 16, no. 10, p. 1646, 2016.
- [7] Z. Zhang, C. Sun, R. Bridgelall, and M. Sun, "Road profile reconstruction using connected vehicle responses and wavelet analysis," *Journal of Terramechanics*, vol. 80, pp. 21–30, 2018.
- [8] S. Setti and A. Wanto, "Analysis of backpropagation algorithm in predicting the most number of internet users in the world," *Jurnal Online Informatika*, vol. 3, no. 2, pp. 110–115, 2019.
- [9] P. Agrawal and P. Jayaswal, "Diagnosis and classifications of bearing faults using artificial neural network and support vector

- machine,” *Journal of the Institution of Engineers (India):Series*, vol. 101, no. 1, pp. 61–72, 2020.
- [10] X. Ding, Y. Zhang, J. Zheng, and X. Yue, “Design and social factors affecting the formation of social capital in Chinese community garden,” *Sustainability*, vol. 12, no. 24, Article ID 10644, 2020.
- [11] X. Zhang and S. Li, “Application of psychological elements in landscape design of public gardens,” *Revista Argentina de Clinica Psicologica*, vol. 29, no. 2, pp. 142–149, 2020.
- [12] X. Chen, J. Zhang, X. Wang, and Y. Zhu, “State-of-the-art review on asphalt mixture distribution uniformity based on digital image processing technology,” *IOP Conference Series: Earth and Environmental Science*, vol. 638, no. 1, Article ID 012074, 2021.
- [13] M. Zhao, S. Pan, X. Shang, and Y. Minmin, “Classification and recognition of regional landscape elements of highway in guangdong province,” *IOP Conference Series: Earth and Environmental Science*, vol. 358, no. 4, p. 4, 2019.
- [14] Z. Chen and J. Gu, “A time-domain computing accelerated image recognition processor with efficient time encoding and nonlinear logic operation,” *IEEE Journal of Solid-State Circuits*, vol. 54, no. 11, pp. 3226–3237, 2018.
- [15] Y. G. Kim, Y. S. Lee, and S. W. Chung, “Signal strength-aware adaptive offloading with local image preprocessing for energy efficient mobile devices,” *IEEE Transactions on Computers*, vol. 69, no. 1, pp. 99–111, 2020.
- [16] W. Zhao and S. Du, “Spectral-spatial feature extraction for hyperspectral image classification: a dimension reduction and deep learning approach,” *IEEE Transactions on Geoscience and Remote Sensing*, vol. 54, no. 8, pp. 4544–4554, 2016.
- [17] S. Heisel, T. Kovačević, H. Briesen, G. Schembecker, and K. Wohlgemuth, “Variable selection and training set design for particle classification using a linear and a non-linear classifier,” *Chemical Engineering Science*, vol. 173, pp. 131–144, 2017.
- [18] N. Yoshikatsu and S. Hideo, “Simultaneous object segmentation and recognition by merging CNN outputs from uniformly distributed multiple viewpoints,” *IEICE - Transactions on Info and Systems*, vol. 101, no. 5, pp. 1308–1316, 2018.
- [19] T. R. Luana, J. S. Brad, and P. D. O. Erick, “Is there sufficient evidence to supplement omega-3 fatty acids to increase muscle mass and strength in young and older adults?” *Clinical Nutrition*, vol. 39, no. 1, pp. 23–32, 2020.
- [20] W. Fangling, L. Yuchang, Y. Gang, and Z. Yuanmin, “Respiratory muscle training improves strength and decreases the risk of respiratory complications in stroke survivors: a systematic review and meta-analysis,” *Archives of Physical Medicine and Rehabilitation*, vol. 101, no. 11, pp. 1991–2001, 2020.
- [21] L. Mottron, “Should we change targets and methods of early intervention in autism, in favor of a strengths-based education?” *European Child & Adolescent Psychiatry*, vol. 26, no. 7, pp. 815–825, 2017.
- [22] W. Nawaz, S. Ahmed, A. Tahir, and A. K. Hassan, “Classification of breast cancer histology images using ALEXNET,” in *Proceedings of the 16th IEEE International Bhurban Conference on Applied Sciences and Technology*, Islamabad, Pakistan, June 2018.
- [23] L. Dan, X. Shen, and H. Zhang, *Improved Convolutional Neural Network Based on Lenet-5*, Computer Era, Shanghai, China, 2016.
- [24] P. Bing, W. Liu, and Z. Zhang, “DeepCEDNet: an efficient deep convolutional encoder-decoder networks for ECG signal enhancement,” *IEEE Access*, vol. 9, p. 1, 2021.
- [25] F. Wang, J. Cheng, and W. Liu, L. Haijun, Additive margin softmax for face verification,” 2018, <https://arxiv.org/abs/1801.05599>.
- [26] J. Tang, H. Xia, J. Zhang, and J. Qiao, “Deep forest regression based on cross-layer full connection,” *Neural Computing and Applications*, vol. 33, pp. 1–22, 2021.
- [27] E. A. Pnevmatikakis, D. Soudry, Y. Gao et al., “Simultaneous denoising, deconvolution, and demixing of calcium imaging data,” *Neuron*, vol. 89, no. 2, pp. 285–299, 2016.
- [28] A. G. Meresescu, M. Kowalski, F. Schmidt, and F. Landais, “Water residence time estimation by 1D deconvolution in the form of a l2-regularized inverse problem with smoothness, positivity and causality constraints,” *Computers & Geosciences*, vol. 115, no. 1, pp. 105–121, 2018.
- [29] D. López-Sánchez, J. M. Corchado, and A. González Arrieta, “Data-independent random projections from the feature-map of the homogeneous polynomial kernel of degree two,” *Information Sciences*, vol. 436, pp. 214–226, 2018.
- [30] V. A. Boldinov, V. A. Bukhalev, and A. A. Skrynnikov, “Game-theoretic control of the object’s random jump structure in the class of pure strategies,” *Journal of Computer and Systems Sciences International*, vol. 59, no. 4, pp. 494–503, 2020.
- [31] M. Newville, T. Stensitzki, D. B. Allen, and A. Ingargiola, “LMFIT: nonlinear least-square minimization and curve-fitting for python,” 2016, <https://arxiv.org/abs/1212.1916>.
- [32] Z. Yan, Z. Qiu, S. Huo, W. Wei, and Y. Fei, “RGB-DI images and full convolution neural network-based outdoor scene understanding for mobile robots,” *IEEE Transactions on Instrumentation and Measurement*, vol. 68, no. 1, pp. 27–37, 2019.
- [33] Y. Chen, Y. Chi, J. Fan, and C. Ma, “Gradient descent with random initialization: fast global convergence for nonconvex phase retrieval,” *Mathematical Programming*, vol. 176, pp. 5–37, 2019.
- [34] L. Yang, “Computer simulation of urban garden landscape design based on FPGA and neural network,” *Microprocessors and Microsystems*, vol. 83, Article ID 103988, 2021.
- [35] B. Hu, “Deep learning image feature recognition algorithm for judgment on the rationality of landscape planning and design,” *Complexity*, vol. 2021, Article ID 9921095, 15 pages, 2021.

Research Article

Application Research of Manuscript Writing Robot Based upon Laser Sensor in News Dissemination Field

Lijia Huang 

School of Culture and Media, Xichang University, Xichang 615000, Sichuan, China

Correspondence should be addressed to Lijia Huang; xcc02600051@xcc.edu.cn

Received 24 December 2021; Revised 26 January 2022; Accepted 27 January 2022; Published 17 February 2022

Academic Editor: Nima Jafari Navimipour

Copyright © 2022 Lijia Huang. This is an open access article distributed under the Creative Commons Attribution License, which permits unrestricted use, distribution, and reproduction in any medium, provided the original work is properly cited.

Under the background of the information and data age, intelligent technology has had a large and profound impact on the production field of each industry, and the field of news dissemination has inevitably become one of them. With the rapid development of new media technologies, the traditional news production model has been impacted by the development of the times. Out of the needs of the transformation and upgrading of its own industry and the further development of laser sensor smart technology, a manuscript writing robot based on laser sensors came into being. Manuscript writing robot is the first time in the history of the development of news dissemination that the main body of news manuscripts has been changed from a natural person to a machine, realizing the transformation of the news production process from semifixed to completely relying on machine automation. This paper first briefly introduces the manuscript writing robot's working principle and work characteristics, analyzes its influence on other aspects, then models the machine hardware system, and finally conducts a quality comparison test between the manuscript writing robot and traditional artificial news production. Through the analysis of experimental data, the language organization ability of the manuscript writing robot is generally inferior to the traditional artificial language organization ability. However, the quality of manuscript writing robot data is 1.1 times that of traditional humans, and the speed of producing news is also 1.3 times faster than traditional humans. In terms of the depth and breadth of the scope of news, the overall average value of writing robots is 0.475 higher than that of traditional humans. Generally speaking, manuscript writing robots have clear advantages compared with traditional manual labor in news production and have a large room for development.

1. Introduction

In recent years, science and technology represented by artificial intelligence and information sensing technology have been developed rapidly, and many industries have realized the transformation and improvement of the times under the support of these intelligent technologies. The field of news communication has also profoundly changed its future development direction due to the development of the times, and the competition among news media has become increasingly fierce. Catering to the requirements of the times, seizing the opportunities of the times, and seizing development opportunities have become the necessary means for news media to win the battle for survival.

As a new type of measuring instrument, the laser sensor has the advantages of noncontact long-distance measurement, fast speed, high precision, large range, and strong

antilight and electrical interference. It is also often used in the field of robot manufacturing. Robots based on laser sensor technology can quickly process a large amount of information, make highly accurate judgments, and have extremely superior data and information processing capabilities.

At present, systems or robots developed based on laser sensing technology have received extensive attention from scholars. In his article, Daniel studied how to build a robot sensor control board and put it into practical use. He believes that the interpretation of sensor data can be achieved by using robot neural network algorithms, fuzzy logic algorithms, and artificial intelligence algorithms. This process is called sensor fusion or sensor interpretation in the field of artificial intelligence. Such algorithms can also be used for advanced signal processing in image processing, pattern recognition, MRI, ultrasound, and interpretation of sonar

and radar signals [1]. Villagrossi et al. have developed an intelligent system that uses a single-point laser displacement sensor and combines the robot sensor information to synchronize the handshake communication process. This system can use the robot as a measuring instrument, allowing the rapid reconstruction of extremely robust 3D images under difficult working conditions. They used a two-stage method to compare the reconstructed 3D point cloud with the nominal 3D point cloud and found that the system can automatically adjust the robot's deburring trajectory. This experiment proves the feasibility and effectiveness of the proposed solution [2]. Yanbiao and Xiangzhi proposed a hand-eye calibration method based on semidefinite programming (SDP) for arc welding robots and laser vision sensors. They established the conversion relationship between the pixel coordinate system and the laser plane coordinate system based on the mathematical model of the laser vision sensor's three-dimensional measurement. In addition, the conversion relationship between the arc welding robot coordinate system and the laser vision sensor measurement coordinate system was established based on the hand-eye calibration model. They used ordinary least squares (OLS) to calculate the rotation matrix and used SDP to identify the direction vector of the rotation matrix to ensure their orthogonality. In the feasibility appraisal, it is proved that this method can reduce the calibration error and ensure the orthogonality of the calibration results [3]. Liu and Tian researched a new method of robot welding path planning based on laser scanning for nonideal tube intersection curves. They used a laser displacement sensor to scan and identify the weld seam and analyzed the direction and posture of the spatial weld seam to give the laser sensor scan trajectory. After sampling and filtering the distance data obtained by the laser sensor, they proposed a new type of welding spot recognition algorithm suitable for the mentioned scanning trajectory. Finally, the ADAMS simulation experiment proves that the scheme can effectively avoid the adverse effects of up-and-down welding on the welding quality [4]. Ge et al. proposed and constructed a robot welding seam online grinding system based on a laser vision sensor. They developed welding seam tracking software and applied the online interaction method to grinding system data based on XML (Extensible Markup Language) files. They first established a hand-eye calibration model to convert the data into the robot coordinate system. Then, they extracted the weld contour information, stored it in the data buffer, and transmitted the coordinates of the robot grinding point through the self-developed weld grinding software. They integrated a vision system and a self-made grinding system at the end of the robot. Finally, the reliability and practicability of the system and the proposed online method of data interaction are verified through experiments [5]. Pachkawade V proposed a manufacturing method based on laser sensing technology to develop transducers based on microsized capacitive gaps suitable for various applications. He produced a low-cost prototype using fast and advanced laser micromilling technology. It achieved a parallel cut width (capacitor gap) of approximately 60 microns on a piece of aluminum and a piece of stainless steel, with

thicknesses of 1 and 2 mm, respectively. This device has been shown to facilitate driving and sensing changes in capacitance on its electrodes through electrostatic means. He conducted experiments on aluminum structures and provided results, including analytical modeling, manufacturing, and electrical characteristics. It proved the applicability of the device as a two-degree-of-freedom resonant mode positioning sensor using weak electrostatic coupling. The sensor has sensitivity based on vibration amplitude to respond to relative changes in stiffness and can solve the order of least stiffness perturbation [6]. Laser sensor technology has been created and used in many fields, but its integration with the news dissemination field has not yet received widespread attention. Laser sensors with high accuracy, high processing efficiency, and large dynamic range can be integrated with high effect in the field of new production.

The manuscript writing robot based on laser sensor is the product of the fusion of the news communication industry and science and technology, and it has a strong contemporary character. Manuscript writing robots only began to enter people's sight after 2015. In an era when new media is prevalent, most scholars are studying the combination of the Internet and traditional news dissemination. Few scholars have combined news dissemination and smart sensor technology for research. However, with the rapid development of science and technology nowadays, the traditional news dissemination field can only achieve deeper development if it is combined with the characteristics of the times [7]. As a part of intelligent science and technology, manuscript writing robots play a very special and important role in improving the efficiency of news production and advancing the process of intelligent news dissemination. This paper studies the application of laser sensor-based manuscript writing robots in the field of news dissemination, which is of innovative significance for filling the current gaps in news dissemination research and promoting the continuous development of manuscript writing robot technology.

This paper conducts a study on the application of a laser sensor-based manuscript writing robot in the field of news communication. The working principle of the handwriting robot is introduced in detail, the impact on the news industry is analyzed, and a comparison experiment between the manuscript writing robot and the traditional manual handwriting is conducted. The paper is organized as follows:

Section 1 introduces the current status of research development in the field of news communication and laser sensor technology and provides a brief description of the current research results at home and abroad.

Section 2 mainly introduces the working principle, working characteristics of the manuscript robot, and its impact on the news communication industry.

Section 3 uses the manuscript writing robot hardware system for system modeling and probabilistic modeling of the selected LiDAR and compares and tests the manuscript writing robot news production model with the traditional manual news production model.

Section 4 analyzes the experimental results of this paper and concludes that the quality of news edited by the manuscript writing robot is inferior to that of traditional manual editing. However, in terms of news processing efficiency, the manuscript writing robot outperforms traditional humans.

Section 5 provides an overview of the paper, describing the main topics addressed in this paper and the future of manuscript writing robots.

2. Manuscript Writing Robot Based on Laser Sensor

2.1. The Working Principle of the Manuscript Robot. Manuscript bots are artificial intelligence software that can automatically generate manuscripts based on algorithms in the first place, instantly output analysis and research, and deliver important information and interpretations to users. The production method of manuscript robot news is slightly different from the traditional news production method. In traditional news writing, the formal completion of a news article needs to go through the following links: news information collection, news information collation, manuscript writing and editing, review and proofreading, and final issuance and push, as shown in Figure 1. The content of each link is a completely manual operation [8].

In the writing process of the manuscript robot, the entire news generation process needs to go through four links: information collection, information analysis and processing, news content generation according to preset semantic processing templates, and review push release, as shown in Table 1. The whole process is the result of the prewritten algorithm program and big data, the whole process can be automated, and the time from the news event to the final draft is very short [9].

The functional requirements of the robot usually involve four modules: information collection module, data processing module, signal input and output I/O module, and power management and electrical protection module. Each module needs to be implemented independently in terms of a function, and there are dependencies between the modules. According to the functional requirements of each module, the corresponding electrical components are selected, and the type and number of electrical components are determined based on the mechanical structure of the body and the control strategy of the software. Figure 2 shows the relationship between the four modules.

The key to improving the response time of a writing robot lies in the robot's core component, the servo motor. The robot is driven by the servo motor to realize the multi-degree-of-freedom movement during operation. If high speed and accuracy are required for robot operation, the actual requirement is that the response speed and control accuracy of the servo motor should be high enough.

2.1.1. Information Collection. Information gathering is the first step for the writing robot to complete news editing work. The information collection of news writing here is

roughly the same as that of the reporter's previous news interviews. Through the sensory information processing technology, the effective mass data related to the report theme is captured from the database in cooperation with the media organization, as shown in Figure 3. Machine news writing is currently mainly used in the field of phenomenon reports. The distinguishing feature of this type of news report is that its content is mainly supported by data, and the complete news report can only be produced by machine news writing relying on the processing results of the target data. Therefore, the primary link of using machine news writing to produce news content is data capture. Therefore, some people call machine news writing "data porters." The rapid development of big data technology makes machine news writing present the advantages of wide information sources and accurate capture in the data capture stage [10].

2.1.2. Information Analysis and Processing. Information analysis and processing is the second step of the manuscript writing robot to complete the news editing work. Through the screening and analysis of the captured data, the process of selecting data that meets the news value is shown in Figure 4. In this process, the robot first excludes illegal data, such as sensitive words and clearly wrong data. Then, according to the present news point, select the data that coincides with the news value, and combine the news report model that has been set manually to measure the "news" in the data. This process is similar to the conception process of journalists in the traditional news production process: determining the theme, screening useful materials, arranging the structure of the article, and so on.

2.1.3. Generate News Content according to the Preset Semantic Processing Template. After collecting and analyzing the news information in the first two links, in the third step, the robot must match the most appropriate language template model based on the best news angle selected by the algorithm and the filtered data. Then, it fills the selected key data into the language template model to automatically generate the main body of the manuscript. First of all, the search system searches out all relevant news from the news database according to the user's intention and performs preprocessing, including word segmentation and sentence processing. Next, the importance of sentences is sorted based on a series of algorithms, among which are graph-based sorting and feature-based sorting algorithms [11]. The graph sorting algorithm will build a graph network model, as shown in Figure 5. Each sentence of the document is regarded as a node in the graph network. The similarity between sentences is used as the edge weight between the nodes. The calculation formula for the similarity between sentences is

$$\text{similarity}(s_i, s_j) = \frac{|\{w_k | w_k \in s_i \ \& \ w_k \in s_j\}|}{\log(|s_i|) + \log(|s_j|)}. \quad (1)$$

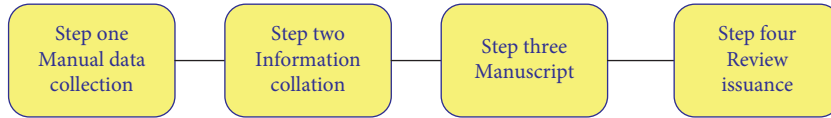


FIGURE 1: Schematic diagram of news production process.

TABLE 1: Main content of news production steps.

Procedure	Traditional news production	Robot news production method
News source	Journalists selectively compile and edit the content of mass communication	Data from massive databases on the Internet
News gathering	Manual information search, screening, or on-site interview	Computer program for automatic data collection
News production	Journalists participate in the work of collecting, writing, editing, arranging, and proofreading	Computers rely on “machines” to automatically write articles
Press releases	Man-manipulated works are mainly text	Released after manual review

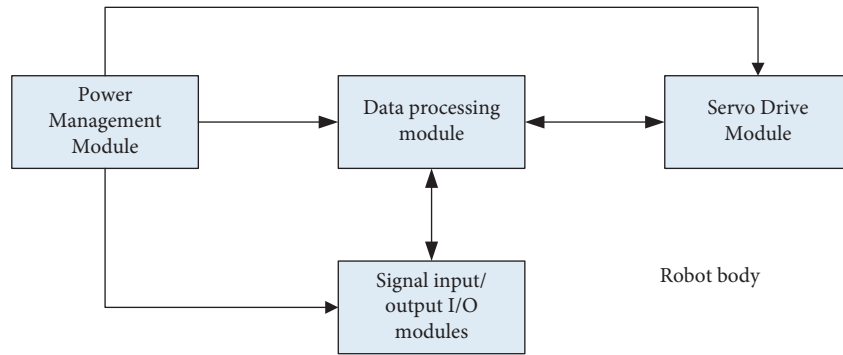


FIGURE 2: Relationship diagram modules.

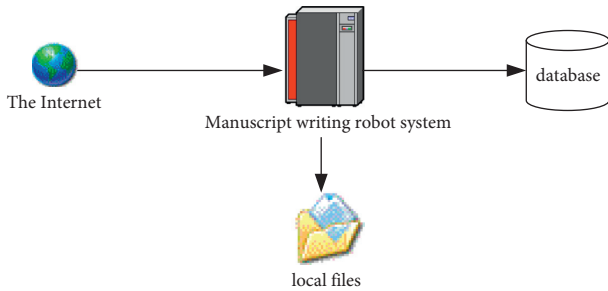


FIGURE 3: Principles of information collection by manuscript robots.

Using the principle to iteratively spread the weight to calculate the score of each sentence, as an important parameter for generating short summaries, the graph model formula is as follows [12]:

$$S(V_i) = (1 - d) + d * \sum_{j \in \ln(V_i)} \frac{1}{|\text{out}(V_j)|} S(V_j). \quad (2)$$

2.1.4. Review Push Release. The review push release is the last step of the manuscript writing robot to complete the news work. The difference from the previous three steps is that this step cannot be separated from the manual “review

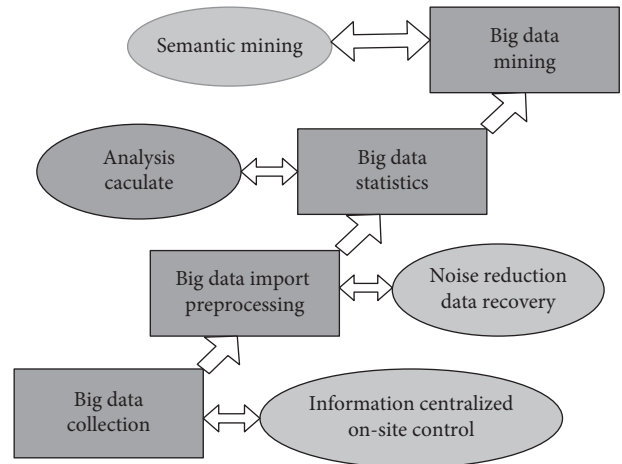


FIGURE 4: Schematic diagram of data analysis by manuscript robot.

push,” that is, the manual review and release of the automatically generated news manuscript. After all, the manuscript robot algorithm system is just a program. Although its own algorithms can be used to improve the accuracy of news content in some fields of news production, the current algorithms have not yet reached the level of checking and judging the correctness of information like the human brain. It is still necessary for the media to modify the robot’s manuscript based on its own news positioning and other

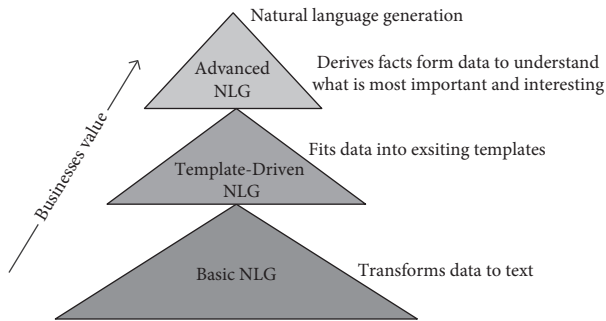


FIGURE 5: Text generation processing.

factors. Manually review the manuscript and distribute it to various channels for push after confirming that it is correct [13]. With the improvement of the algorithm technology of manuscript robots, some media have begun to try to make manuscript robots realize the full automation of news production. In the future, with the development of this technology, the participation of manual editorial review in specific reporting areas is expected to gradually decrease.

2.2. Work Characteristics of Manuscript Robots. The manuscript writing robot based on laser sensor technology has overturned the traditional mode of news production and has unique working characteristics compared to the traditional news production mode. An American media once did an experiment in which a reporter from National Public Radio and a writing robot simultaneously edited a brief report of sports news, which was faster and more recognized than trying to write a report. The experimental results are shown in Table 2.

It can be seen from Table 2 that the superiority of the manuscript writing robot in terms of speed cannot be surpassed by human journalists, but the journalist outperforms the manuscript writing robot in terms of manuscript quality and reader acceptance. It can be seen from the experiment that the manuscript writing robot has the characteristics of fast speed and good at comprehensive information processing [14].

This paper summarizes and analyzes the characteristics of the news production of the manuscript robot from three aspects: the main body of the news production of the manuscript robot, the content of news production, and the cost of news production.

2.2.1. Intelligent Mechanization of the Main Body of News Production. The most essential difference between the news production of the manuscript robot and the news production under the traditional mode is that the main body of the news production in the traditional mode is humans, while the main body of the news production of the manuscript robot is the mechanical program. News production in the traditional mode is similar to the manual assembly line, with semiautomatic and semifixed nature. The news editor can only proceed after the reporter has conducted the actual investigation and interview. With the progress of the times,

computer-assisted news that has appeared only collects data and information through computers. Even if it later develops into data journalism, computers only play the role of supplementary information in the news, appearing as supplementary background material for news content. However, the manuscript writing robot is not just like an auxiliary role in data journalism; it has the feature of fully automating every program from the beginning to the end of news production [15]. In this respect, the use of manuscript writing robots has transformed the work of journalists from complex and boring information gathering to a more creative direction. This changing trend is both an opportunity and a challenge for those engaged in the news industry.

2.2.2. Personalized and Accurate News Production Content. In the era of big data where new media is prevalent, users receive a large amount of information every day. How the media uses this information push channel to select the most interesting news information from the mass data stream has become the primary link in news production. It is impossible for such extremely complex tasks to be completed by humans alone, which has become the advantage of robot news production. The manuscript writing robot can produce news information that is most closely connected to the audience and users while ensuring that the news production meets the quantity requirements. Moreover, the manuscript writing robot can also use the powerful information acquisition and discrimination capabilities of its own system to reduce the probability of error to an extremely low level, thereby improving the accuracy of news articles. From the perspective of news sources, if it only relies on manual screening to obtain such complex news information, the probability of reporting errors will greatly increase. However, the manuscript writing robot directly uses the system information sensing technology to process the original data, which is much lower than the manual method to report the error, thus ensuring the accuracy of the news source [16].

2.2.3. Economical News Production Costs. The impact of the Internet on the traditional news dissemination industry puts it under tremendous economic pressure. The adjustment of the internal structure of the industry, the external transformation and upgrading, the improvement of news production efficiency, and the reduction of production costs are inevitable measures for the sustainable development of the entire news dissemination industry. Although the manuscript writing robot needs to invest a lot of money in the initial use of the system, in the long run, the production cost of the manuscript robot is much lower than the production cost of news based on manual labor alone.

According to statistics, the cost of writing different types of news reports by writing robots used by the British news communication industry is much lower than the cost of manual production of news, as shown in Table 3. Although the application of manuscript writing robots has not yet reached a mature level, its cost-effectiveness in the field of news production in the future will become higher and higher [17].

TABLE 2: Experimental comparison results.

Reporter	VS	Manuscript robot
8 minutes	Writing time	3 minutes
9813 readers recognized	Manuscript quality	932 readers recognized
Deduction and association	Competitive advantages	Induction and synthesis
Depth and character theme	Areas of expertise	News manuscripts

TABLE 3: Different types of news writing costs.

News type	Labor cost (€)	Cost of writing robot (€)
Financial news	10	5
Sports news	12	5
Political news	16	6
Life news	9	4

2.3. Impact Analysis of Manuscript Robots. There are four main aspects to the impact of writing robots, including the impact on people engaged in the news industry, the impact on news consumers, the impact on the news media, and the impact on society as a whole. Dividing it into the coordinate axes of the four-quadrant graph, as shown in Figure 6. The horizontal axis is on the news-public basis, and the vertical axis is on the micro-macro basis. News media and society are at the macroend, and the news industry, personnel, and news audiences are at the microend. From another perspective, people in the news industry and news media have news attributes, while readers and society have public attributes. Journalists, news consumers, news media, and society are all closely related to the development of writing robots [18].

2.3.1. Impact on Personnel Engaged in the News Industry. The invention of the manuscript robot has realized a fundamental change in news production methods. Its emergence will replace part of the work of people in the news industry, which will cause changes in the structure of the news industry. Manuscript writing robots liberated some journalists from their pipeline-like work, but at the same time as the liberation, the development of the industry also posed more arduous challenges to them. In the follow-up news production process using manuscript robots, the focus of manual operation will soon focus more energy on improving the quality of news products so that the original more “informative” news will become more high-quality news. Some research scholars also emphasized that the main purpose of introducing machines (algorithms) is to weaken the labor of journalists so that they can extract more time and energy to get rid of the trouble of processing data and spend more time on making good news. In the future, human reporters will work together with robot news writers [19].

2.3.2. Impact on News Consumers. In the context of the era of big data, news consumers, that is, readers, have extremely high requirements for the quality of news content and the aesthetics of arrangement. The production level of news has a profound impact on news audiences. The quality of news produced by the manuscript robot is not inferior to the

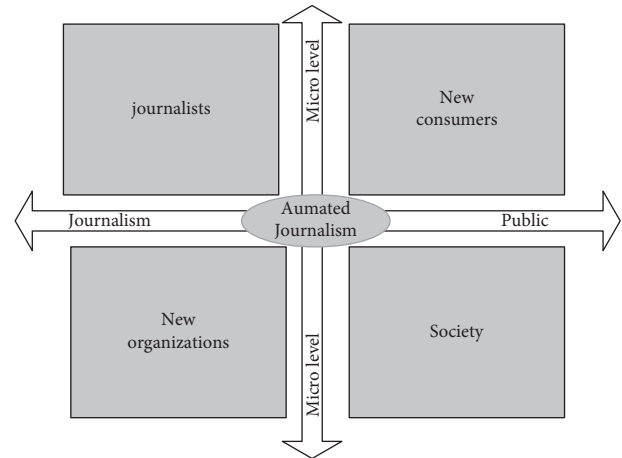


FIGURE 6: The writing robot and the four actors related to it.

quality of the news produced by humans, and the manuscript robot can also judge the user’s preferences by analyzing user data to produce and deliver more personalized news to readers. In this regard, writing robots still have a relatively ideal development trend in terms of the breadth of user audiences in the future.

2.3.3. Impact on News Media. The decline of the traditional news dissemination industry forces the industry to adjust its internal structure by introducing new media technical talents and reducing the number of traditional journalists. However, news production is indispensable to the demand for labor, and the reduction of the number of personnel will cause the number of news productions to fail to meet the development requirements. The cost of new media technical personnel is relatively high, and the labor return time is long. For the entire industry facing a development crisis, this method cannot quickly solve the problem, but the writing robot can effectively alleviate this situation. Manuscript writing robots can produce news that meets the development requirements with relatively low production costs and fast and efficient information processing technology, speeding up the pace of industrial production of news [20].

2.3.4. Impact on Society. There is no doubt that the writing robot has the advantage of being able to use large-scale industrial production of news, and its development status in the news dissemination industry in the future will gradually increase. This development trend has met the increasing demand of modern people for news and information. However, because the information processing algorithm system of the manuscript robot is more willing to push news

content that matches the interests of users, the probability of user groups seeing news content that does not conform to their opinions will become less and less. This will put the user group in a highly homogeneous speech background, and it will also bring a certain degree of public opinion risk to the society.

3. Experimental Research on the Application of Manuscript Robots in the Field of News Communication

This paper firstly carries on the systematic modeling of the selected manuscript writing robot hardware system, carries on the probabilistic modeling of the chosen laser radar, then carries on the pinhole camera principle analysis of the chosen camera, and introduces its image alignment and calibration principle. Later, the manuscript writing robot news production mode and the traditional manual news production mode were compared and tested [21].

3.1. Laser Modeling. The two-dimensional LiDAR emits laser pulses through its transmitter. When the laser touches the object, part of the laser light is reflected back to the laser receiver, the time difference between the transmission and reception is settled, and the ranging function can be realized. The performance parameters of the laser rangefinder used in this paper are shown in Table 4.

When the laser radar establishes its mathematical model, it mainly establishes the Bayesian observation model $p(A_t | B_t, m)$ of its scan data. The standard established by the observation model is that $p(A_t | B_t, m)$ has a smooth corresponding relationship with the pose B_t of the manuscript writing robot. That is, the change of the pose B_t is small, and the change of the observation model $p(A_t | B_t, m)$ is correspondingly small.

A single frame of scan data contains data after one week of LiDAR opening angle scanning. At this time, assuming that there is a total of scan data, the scan data A_t can be expressed as

$$A_t = \{A_t^1, A_t^2, \dots, A_t^n\}. \quad (3)$$

Use A_t^k to represent the k observation value in the observation data at t time (A_t^k represents a specific value). It is assumed that the scan data in the laser scan data of a single frame are all independent. At this time, the value of $p(A_t | B_t, m)$ can be expressed as the product of n scan data:

$$p(A_t | B_t, m) = \prod_{k=1}^n p(A_t^k | B_t, m). \quad (4)$$

When the laser scanning data is used in practice, the independent assumption performs well, so this Bayesian observation model can be used as the laser radar mathematical model.

The camera used in this paper uses TOF (time of flight) technology. It can perform depth imaging, and the imaging efficiency is higher. Table 5 shows the main parameters of the camera.

TABLE 4: LiDAR main parameters.

The main parameters	Performance
Opening angle	260°
Scanning frequency	18°/HZ
Angle resolution	1°
Work area	0.04 m–10°m
Power consumption	4°W

TABLE 5: The main parameters of the camera.

The main parameters	Performance
Color camera resolution	2120 × 960 30FPS
Depth camera resolution	515 × 424
Infrared resolution	515 × 424
Depth distance	0.4 m–4.8 m
Horizontal field of view	80°
Vertical field of view	60°

The difference between the depth camera and the ordinary monocular camera is that it is equipped with two cameras. The color camera and the depth camera obtain color RGB images and depth images, respectively. For this paper, the pinhole camera model is adopted, as shown in Figure 7.

It can be seen from Figure 6 that there are three coordinate systems $X_d, Y_d,$ and Z_d in the camera imaging process of the pinhole model, which are represented as the camera coordinate system, the physical plane coordinate system, and the pixel coordinate system. Among them, the geometric correspondence between the point $P(X_d, Y_d, Z_d)^t$ of the camera coordinate system and the point $[X_p, Y_p, F]^t$ of XOY on the physical plane under the pinhole camera model can be expressed as [22]

$$\begin{cases} X_p = F \frac{X_d}{Z_d}, \\ Y_p = F \frac{Y_d}{Z_d}. \end{cases} \quad (5)$$

The relationship between the imaging point $[X_p, Y_p, F]^t$ and the pixel coordinate $[u, v]^t$ on the physical plane XOY is

$$\begin{cases} u = \alpha X_p + d_x, \\ v = \beta Y_p + d_y. \end{cases} \quad (6)$$

Through the joint transformation of the three coordinate system transformation formulas (5) and (6), the relationship between the pixel coordinates and the points of the camera coordinate system can be obtained, expressed as

$$\begin{cases} u = F_x \frac{X_d}{Z_d} + d_x, \\ v = F_y \frac{X_d}{Z_d} + d_y. \end{cases} \quad (7)$$

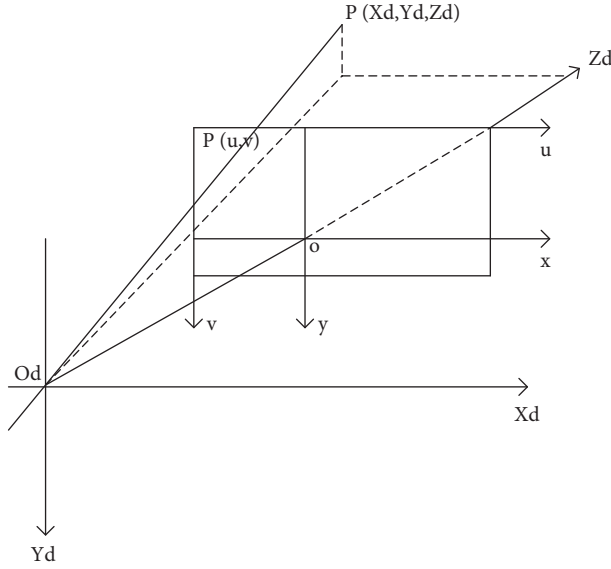


FIGURE 7: Pinhole model camera points are expressed in each coordinate system.

Among them,

$$\begin{aligned} F_x &= \alpha F, \\ F_y &= \beta. \end{aligned} \quad (8)$$

At the same time, formula (6) can be expressed as [23]

$$Z_d \begin{bmatrix} u \\ v \\ 1 \end{bmatrix} = \begin{bmatrix} F_x & 0 & d_x \\ 0 & F_y & d_y \\ 0 & 0 & 1 \end{bmatrix} \begin{bmatrix} X_d \\ Y_d \\ Z_d \end{bmatrix}, \quad (9)$$

where $K = \begin{bmatrix} F_x & 0 & d_x \\ 0 & F_y & d_y \\ 0 & 0 & 1 \end{bmatrix}$ is the internal parameter matrix of the camera.

The vision camera must be calibrated before use to calibrate its internal camera parameters to get the best effect. The camera used in this paper needs to calibrate the internal parameters of its two cameras, namely, calibrate the color camera and the depth camera. Depth cameras are different from ordinary cameras in that they can directly obtain depth information while observing without additional calculations. The key point to realize this feature is that each pixel of the color image has the gray value of the depth image; that is, the depth information corresponds to it. Therefore, in the process of calibrating the two cameras, it is necessary to align the color image and the depth image while obtaining the camera internal parameters. This paper mainly analyzes the principle of color and depth image alignment of the RGB-D camera.

The internal parameter matrix obtained by the internal parameter K_{rgb} of the color camera after calibration is shown in formula (9). At this time, according to the camera pinhole

model, the mapping relationship between the homogeneous coordinate $P = [u, v, 1]^t$ of the pixel point in the imaging plane and the three-dimensional space coordinate ($P = [X, Y, Z, 1]^t$) of the point in the camera coordinate system is shown in formulas (10) and (11) [24]:

$$K_{rgb} = \begin{bmatrix} F_{x,rgb} & 0 & d_{x,rgb} \\ 0 & F_{y,rgb} & d_{y,rgb} \\ 0 & 0 & 1 \end{bmatrix}, \quad (10)$$

$$Z_{rgb} P_{rgb} = K_{rgb} [I|0] P_{rgb}. \quad (11)$$

Expand formulas (10) and (11) to get

$$Z_{rgb} \begin{bmatrix} u_{rgb} \\ v_{rgb} \\ 1 \end{bmatrix} = \begin{bmatrix} F_{x,rgb} X_{rgb} + d_{x,rgb} Z_{rgb} \\ F_{y,rgb} Y_{rgb} + d_{y,rgb} Z_{rgb} \\ Z_{rgb} \end{bmatrix}, \quad (12)$$

$$Z_{rgb} \begin{bmatrix} u_{rgb} \\ v_{rgb} \\ 1 \end{bmatrix} = \begin{bmatrix} F_{x,rgb} & 0 & d_{x,rgb} & 0 \\ 0 & F_{y,rgb} & d_{y,rgb} & 0 \\ 1 & 0 & 0 & 0 \end{bmatrix} \begin{bmatrix} X_{rgb} \\ Y_{rgb} \\ Z_{rgb} \\ 1 \end{bmatrix}. \quad (13)$$

The homogeneous coordinates $P_{rgb} = [X_{rgb}, Y_{rgb}, Z_{rgb}, 1]$ in the formula are expressed as $P_{rgb} = [X_{rgb}, Y_{rgb}, Z_{rgb}]$ with nonhomogeneous coordinates. At this time, formula (12) can be transformed into formula (14). The coordinate change of the internal reference K_{ir} of the depth camera can be expressed in the same way as formula (15):

$$Z_{rgb} P_{rgb} = K_{rgb} \overline{P_{rgb}}, \quad (14)$$

$$Z_{ir} P_{ir} = K_{ir} \overline{P_{ir}}. \quad (15)$$

Since the transformation relationship of the entire camera is considered, the relative relationship R_{rgb}, T_{rgb} of the color camera and the relative relationship R_{ir}, T_{ir} of the depth camera need to be subjected to rigid body transformation. The transformation process is shown in formula (16) and formula (17) [25]:

$$R_{ir2rgb} = R_{rgb} R_{ir}^{-1}, \quad (16)$$

$$T_{ir2rgb} = T_{rgb} - R_{ir2rgb} T_{ir}. \quad (17)$$

The consideration is the relative transformation relationship between the cameras. At the same time, it is necessary to establish the relationship between the inhomogeneous three-dimensional space coordinates P_{rgb} and $\overline{P_{rgb}}$ of the two cameras in their respective coordinate systems, as shown in formula (18). At this time, substituting the two transformation formulas into it, it can get formula (19):

$$\overline{P_{rgb}} = R_{ir2rgb} \overline{P_{ir}} + T_{ir2rgb}, \quad (18)$$

$$Z_{rgb} P_{rgb} = K_{rgb} R_{ir2rgb} K_{ir}^{-1} Z_{ir} P_{ir} + K_{rgb} T_{ir2rgb}. \quad (19)$$

At this time, P_{rgb} and P_{ir} in the imaging planes of the two cameras can be connected so that $R = K_{rgb} R_{ir2rgb} K_{ir}^{-1}$ and $T = K_{rgb} T_{ir2rgb}$ in formula (17) can be simplified formula (20), where R and T are the external camera parameters in camera calibration.

$$Z_{rgb} P_{rgb} = R Z_{ir} P_{ir} + T. \quad (20)$$

3.2. Evaluation Method of Manuscript Quality. The method of assessing the quality of the manuscript can be done using metaheuristic algorithms. The metaheuristic algorithm is a modification of the heuristic algorithm, which is the product of combining a stochastic algorithm with a local search algorithm. It is proposed relative to an optimization algorithm, which can find the optimal solution of a problem, while a metaheuristic algorithm is an intuitively or empirically constructed algorithm that can give a feasible solution to a problem at an acceptable expense (mean computational time and space), and the degree of deviation of that feasible solution from the optimal solution is not necessarily predictable in advance.

This paper first modeled the hardware of the manuscript robot system, introduced the selected LiDAR parameters and its probability model, analyzed the principle of the pinhole model of the camera used in this paper, and introduced its calibration method at the same time, and the method of assessing the quality of manuscripts is introduced. It laid the foundation for the follow-up comparison experiment between the manuscript writing robot and the traditional artificial news production.

3.3. Comparative Experiment. In this controlled experiment, four major news articles on sports, finance and economics, politics, and entertainment were selected as samples. It mainly compares the pros and cons of manuscript writing robots with traditional humans from these four aspects. They are the comparison of news production language (readability and vividness), data comparison (objectivity and credibility), publication time comparison (publishing speed), and coverage comparison (depth and breadth).

3.3.1. News Language Comparison. To evaluate whether the news language of a news article has its distinctive personality and is different from literature or other professional languages, it mainly depends on its readability and vividness of language organization. The experiment selects the mentioned four categories of topics to analyze the manuscript writing robots and traditional artificially produced news language samples. The experimental data is shown in Figure 8.

As shown in Figure 8, the average readability of the manuscript-written robot news language is 7.95, and the vividness of the language organization is 7.425; the average

readability of the traditional artificial news language is 8.65, and the vividness of the language organization is 8.325.

3.3.2. News Data Comparison. News data refers to data capture, statistics, analysis, and visualization based on news content. Nowadays, news of any subject matter will quote the data, and the quotation of data can promote the determination of news topics and show news points through the characteristics of the data. It plays an essential role in the reporting stage of news. The objectivity and credibility of data as a whole also determine the objectivity and credibility of news. The experiment selects four types of topics to analyze the new data samples of writing robots and traditional manual production. The experimental data is shown in Figure 9.

It can be seen from Figure 9 that the average objectivity of the news data of the manuscript writing robot is 9.275, and the credibility of the news data is 9.1; the average objectivity of the traditional artificial news data is 8.45, and the credibility of the news data is 8.2.

3.3.3. Comparison of News Release Time. The most important thing for news articles is to highlight the timeliness, which is one of the important criteria for evaluating the value of a news article. The experiment selects the manuscript writing robot and traditional manual production to compare the speed (min/piece) and release speed (min/piece) of the four types of news topics. The experimental data is shown in Figure 9.

It can be seen from Figure 10 that the average news acquisition speed of the manuscript writing robot is 5.55 min/piece, and the news release speed is 10.575 min/piece; the average traditional manual news acquisition speed is 7.875 min/piece, and the news release speed is 13.45 min/piece.

3.3.4. Comparison of News Coverage. The scope of a news report is the combination of all report objects, including the depth and breadth of the report. It stipulates which people and events are to be reported and how large the coverage is. It is the most basic part of the news reporting process. In this paper, test experiments are carried out on the depth and breadth of the four types of reports. The results are shown in Figure 11.

It can be seen from Figure 11 that the average depth of the range of news writing robots is 8.675, and the breadth of the news range is 8.65; the average depth of the range of traditional artificial news is 8.575, and the range of traditional artificial news is 8.275.

4. Discussion

By comparing the experimental data, the following conclusions can be drawn:

- (1) The average readability of news produced under the traditional manual mode is 0.7 higher than that produced under the news production mode of the

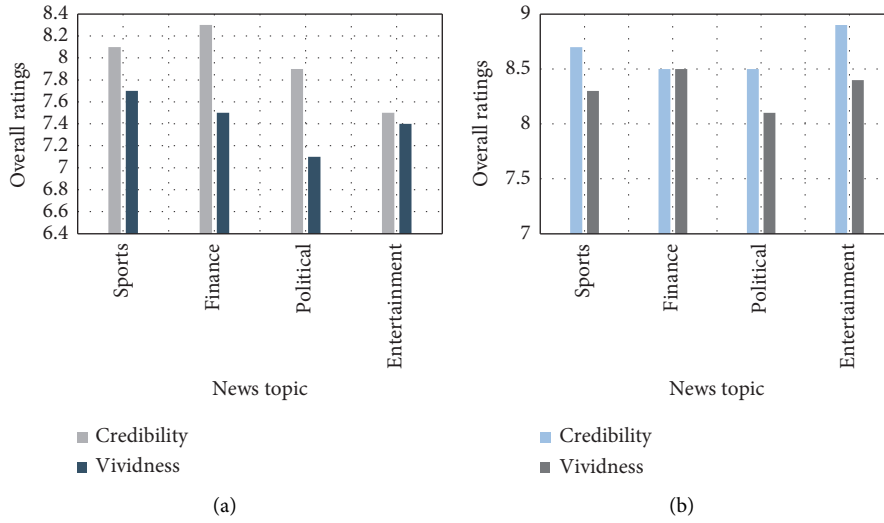


FIGURE 8: Comparison of the readability and vividness of news language. (a) The readability and vividness of the new language of the manuscript robot. (b) The readability and vividness of traditional artificial news language.

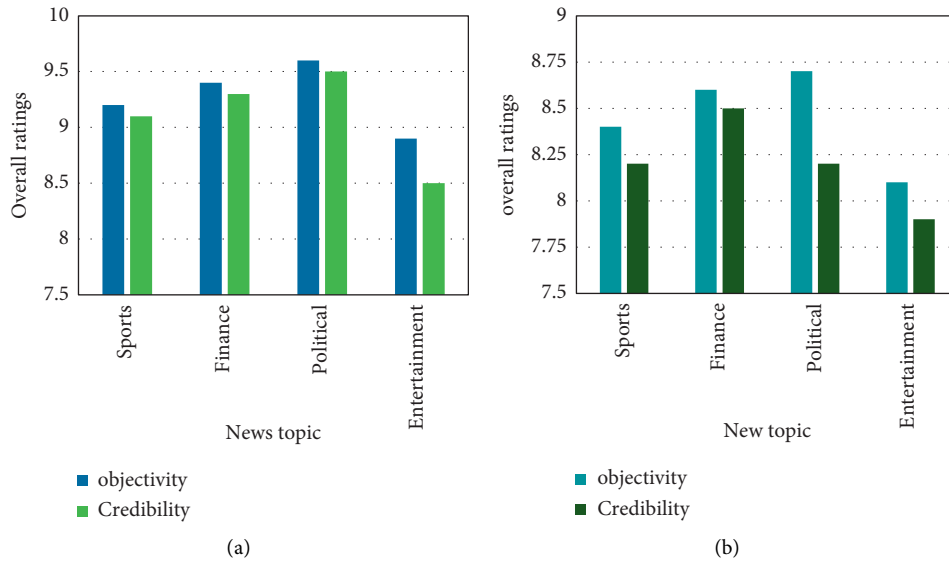


FIGURE 9: Comparison of objectivity and credibility of news data. (a) The objectivity and credibility of the news data of the writing robot. (b) The objectivity and credibility of traditional artificial news data.

manuscript robot. The average vividness of the news language organization produced under the traditional manual mode is 0.9 higher than the vividness of the news language organization produced under the news writing robot news production mode.

- (2) The average value of objectivity of manuscript-written robot news data is 0.825 higher than that of traditional artificial news data, and the average value of credibility of manuscript writing robot news data is 0.9 higher than that of traditional artificial news data.
- (3) The average speed of manuscript writing robot news is 2.325 min/piece faster than that of traditional manual news, and the speed of manuscript writing

robot news release is 2.875 min/piece faster than that of traditional manual news.

- (4) The average depth of the coverage of the news coverage of the manuscript robot is 0.1 greater than that of the traditional manual news coverage, and the coverage of the news coverage of the manuscript robot is 0.375 larger than the coverage of the traditional manual news.

The entire comparative data shows that, in terms of news language, the news quality of manuscript writing robot editors is not as good as that of traditional manual editors. However, in terms of news data, news acquisition, publishing speed, and news coverage, manuscript writing robots are superior to traditional humans.

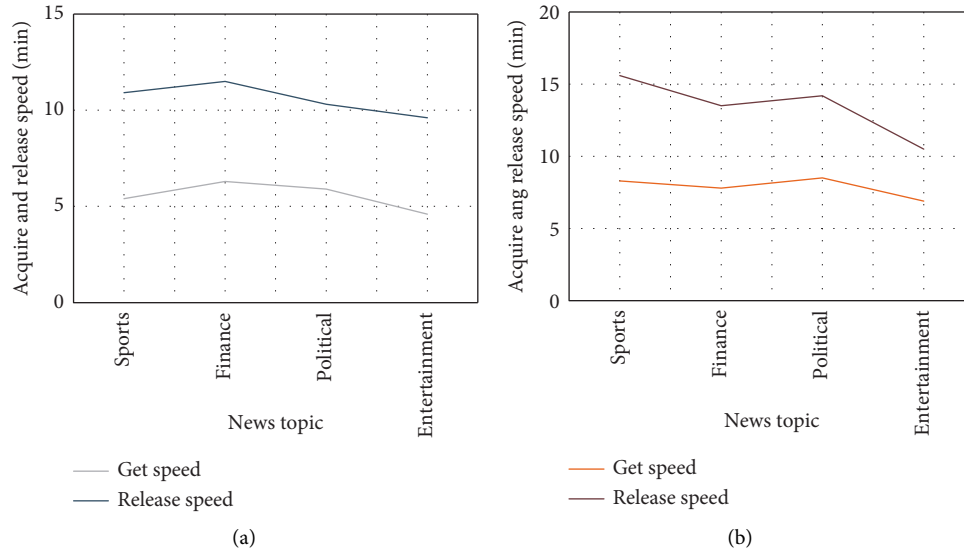


FIGURE 10: Comparison of news acquisition and publication time. (a) The time when the manuscript robot news is obtained and released. (b) The acquisition and release time of traditional artificial news.

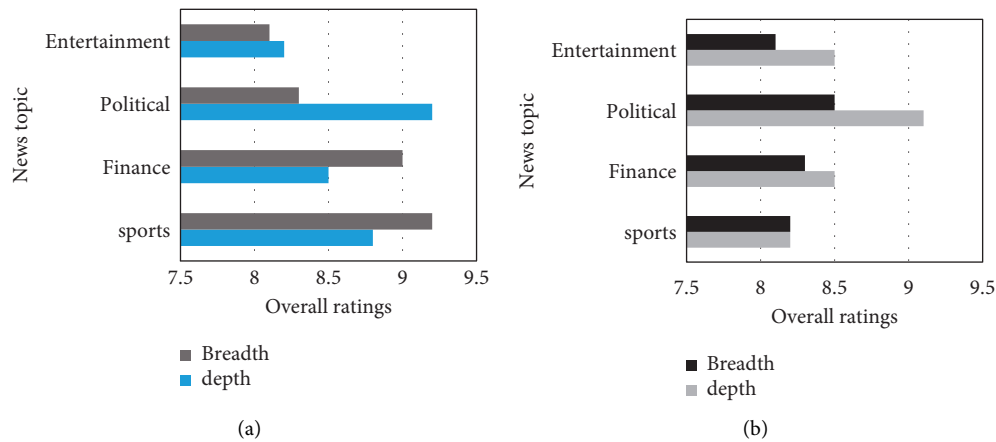


FIGURE 11: News coverage comparison. (a) The depth and breadth of the scope of the manuscript robot news. (b) The depth and breadth of the scope of traditional artificial news.

5. Conclusion

Due to the limited level of technological development, this is related to the sensors that create the robotic system, and manuscript writing robots are currently only used in news production by a few media. And after comparing and analyzing the news articles produced by manuscript writing robots and those edited by human reporters, it is found that machine news writing lacks the readability and vividness of language organization. In the era of big data, it may also cause data security problems. However, even so, it is the general trend that the news dissemination industry caters to the development of the times. The application of the laser sensor-based manuscript writing robot to the field of news communication is by no means a flash in the pan; it is a product with strong characteristics of the times. As the level of information technology continues to improve, the news production capacity of writing robots will be further

improved. And the sensors are secure and cannot fully represent the writing of the manuscript but are only able to capture snapshots of the writing. Robotic writing is a more complex concept that also has temporal characteristics, for example. Moreover, the selected sensors are only able to represent some features of the conceptual dimension of writing. The quality of the currently weak language organization will be further improved with the development of technology. Writing robots and journalism will undergo a more comprehensive and in-depth integration. The applicable fields of robot production news will become more extensive. The news articles produced by it will appear in front of the audience in large numbers. Its significance to the field of news dissemination is not only to innovate news production methods but also to promote the transformation and upgrading of the entire industry. Therefore, the manuscript writing robot still has a very ideal development prospect.

Data Availability

No data were used to support this study.

Conflicts of Interest

The authors declare that they have no conflicts of interest.

References

- [1] R. Daniel, "Robot sensor controller board," *Circuit cellar*, vol. 50, 2017.
- [2] E. Villagrossi, C. Cenati, and N. Pedrocchi, "Flexible robot-based cast iron deburring cell for small batch production using single-point laser sensor," *International Journal of Advanced Manufacturing Technology*, vol. 92, no. 5, pp. 1–14, 2017.
- [3] Z. Yanbiao and C. Xiangzhi, "Hand-eye calibration of arc welding robot and laser vision sensor through semidefinite programming," *Industrial Robot: An International Journal*, vol. 45, no. 5, pp. 597–610, 2018.
- [4] Y. Liu and X. Tian, "Robot path planning with two-axis positioner for non-ideal sphere-pipe joint welding based on laser scanning," *The International Journal of Advanced Manufacturing Technology*, vol. 105, no. 1-4, pp. 1295–1310, 2019.
- [5] J. Ge, Z. Deng, and Z. Li, "Robot welding seam online grinding system based on laser vision guidance," *The International Journal of Advanced Manufacturing Technology*, vol. 116, no. 5, pp. 1737–1749, 2021.
- [6] V. Pachkawade, D. Cerica, S. Dricot, S. Stoukatch, and M. Kraft, "Direct laser writing to fabricate capacitively transduced resonating sensor," *Microsystem Technologies*, vol. 26, no. 2, pp. 547–562, 2020.
- [7] Y. Pang, B. K. Chen, W. Liu, S. F. Yu, and S. N. Lingamanaik, "Development of a non-contact and non-destructive laser speckle imaging system for remote sensing of anisotropic deformation around fastener holes," *NDT & E International*, vol. 111, no. Apr., pp. 102219.1–102219.14, 2020.
- [8] J.-Y. Park and J.-R. Lee, "Application of the ultrasonic propagation imaging system to an immersed metallic structure with a crack under a randomly oscillating water surface," *Journal of Mechanical Science and Technology*, vol. 31, no. 9, pp. 4099–4108, 2017.
- [9] W. Lee, D. B. Kim, M. H. Song, and D. K. Yoon, "Optofluidic ring resonator laser with an edible liquid laser gain medium," *Optics Express*, vol. 25, no. 13, pp. 14043–14048, 2017.
- [10] R. L. Kiscaden, "Know thy customers' preferences and give them the gift of choice," *Air conditioning, Heating & Refrigeration News*, vol. 265, no. 3, p. 22, 2018.
- [11] S. M. Bueno and Trenchless Technology, vol. 28, no. 7APP., p. 6, 2019.
- [12] Plastics News Group, "Ube, MHI complete merger of injection machine businesses," *Plastics News*, vol. 109, no. 1, p. 24, 2017.
- [13] G. Pirlo, R. Plamondon, and E. Anquetil, "Guest editorial special issue on drawing and handwriting processing for user-centered systems," *IEEE Transactions on Human-Machine Systems*, vol. 47, no. 2, pp. 165–168, 2017.
- [14] T. J. Froehlich, "The role of pseudo-cognitive authorities and self-deception in the dissemination of fake news," *Open Information Science*, vol. 3, no. 1, pp. 115–136, 2019.
- [15] J. Iqbal and Z. H. Khan, "The potential role of renewable energy sources in robot's power system: a case study of Pakistan," *Renewable and Sustainable Energy Reviews*, vol. 75, no. 75, pp. 106–122, 2017.
- [16] L. Chang, E. L. Shengbo, and H. Karl, "Measurement dissemination-based distributed bayesian filter using the latest-in-and-full-out exchange protocol for networked unmanned vehicles," *IEEE Transactions on Industrial Electronics*, vol. 64, no. 11, pp. 8756–8766, 2017.
- [17] R. K. Kaliyar, A. Goswami, and P. Narang, "EchoFakeD: improving fake news detection in social media with an efficient deep neural network," *Neural Computing & Applications*, vol. 33, pp. 8597–8613, 2021.
- [18] C. Rémi, R. David, M. Guillaume, M. Pierre, and V. Marie-Aude, "Precisely positioning the tip of an instrument inserted through an orifice with a free wrist robot: application to prostate biopsies," *International Journal of Computer Assisted Radiology and Surgery*, vol. 13, no. 5, pp. 611–618, 2018.
- [19] K. Sharma and R. Doriya, "Coordination of multi-robot path planning for warehouse application using smart approach for identifying destinations," *Intelligent Service Robotics*, vol. 14, no. 2, pp. 313–325, 2021.
- [20] R. Wang, Y. Wei, H. Song et al., "From offline towards real-time verification for robot systems," *IEEE Transactions on Industrial Informatics*, vol. 14, no. 4, pp. 1712–1721, 2018.
- [21] G. Carriere, M. Benoussaad, and V. Wagner, "Off-line correction method suitable for a machining robot application to composite materials," *The International Journal of Advanced Manufacturing Technology*, vol. 110, no. 9-10, pp. 1–15, 2020.
- [22] L. Jill, "DeVries. Know when a SCARA robot is the right choice for your application," *Assembly*, vol. 61, no. 3 Suppl., pp. 48-49, 2018.
- [23] S. Manoharan and R. Senthilkumar, "An intelligent fuzzy rule-based personalized news recommendation using social media mining," *Computational Intelligence and Neuroscience*, vol. 2020, Article ID 3791541, 10 pages, 2020.
- [24] T.-Y. Kim, S.-H. Kim, and H. Ko, "Design and implementation of BCI-based intelligent upper limb rehabilitation robot system," *ACM Transactions on Internet Technology*, vol. 21, no. 3, 2021.
- [25] C. Romero-González, J. Martínez-Gómez, I. García-Varea, and L. Rodríguez-Ruiz, "On robot indoor scene classification based on descriptor quality and efficiency," *Expert Systems with Applications*, vol. 79, no. Aug., pp. 181–193, 2017.

Research Article

Evaluation of Rural Tourism Carrying Capacity Based on Ecological Footprint Model

Lei Li ¹, Xiaojuan Ye,¹ and Xilong Wang²

¹College of Tourism, Xinyang Normal University, Xinyang 464000, Henan, China

²College of Management, Ocean University of China, Qingdao 266100, Shandong, China

Correspondence should be addressed to Lei Li; 2020261709@xynu.edu.cn

Received 27 December 2021; Revised 19 January 2022; Accepted 27 January 2022; Published 17 February 2022

Academic Editor: Nima Jafari Navimipour

Copyright © 2022 Lei Li et al. This is an open access article distributed under the Creative Commons Attribution License, which permits unrestricted use, distribution, and reproduction in any medium, provided the original work is properly cited.

The evaluation of the environmental carrying capacity of tourism resources has important guiding significance for the sustainable development of tourism. This study uses the ecological footprint index to construct the evaluation model of rural tourism environmental carrying capacity and quantitatively analyzes the impact of rural tourism ecological footprint on the environment, ecological pressure, and the maximum carrying capacity of tourists in Nanyang City (China) from 2011 to 2020, so as to provide a reference basis for local rural tourism planning and ecological environment management. The empirical analysis results show that (1) during the decade 2011–2020, the overall ecological footprint increased by 31.47%; however, the per capita ecological footprint showed a downward trend year by year; (2) in the ten years from 2011 to 2020, although the environmental carrying capacity was in surplus, it showed a downward trend year by year, and the ecological pressure index initially appeared; (3) taking the number of tourists in 2020 as the reference value, the prediction of the ecological pressure of rural tourism environment and the carrying capacity of tourists shows that although the ecological pressure is in a relatively safe state, it will show an unsafe state with the increase of the number of tourists. Based on the above results, it is suggested that local governments and tourism planning and management departments should pay full attention to the adverse impact of tourism development on the environment, strengthen the construction of green transportation, balance the development of tourism resources, scientifically control the number of tourists, improve tourists' awareness of environmental protection, protect the ecological environment of Nanyang City, and realize the sustainable development of rural tourism.

1. Introduction

Tourism is the main way of relaxation and entertainment for modern people. Because of its beautiful natural scenery, strong local flavor, and rich folk culture, rural tourism is sought after by tourists all over the world. With the vigorous development of rural tourism, some scenic spots or tourist destinations operate in the pursuit of short-term interests, saturated or super environment carrying capacity, and it leads to the destruction of ecological environment, the decline in the humanistic environment, the waste of social resources, and the decline of tourists' satisfaction, which seriously affects the long-term and stable development of rural tourism. With the popularization of the concept of sustainable development, in order to realize the sustainable development of the tourism environment, the carrying

capacity of tourism resources and environment has become one of the criteria to judge the sustainable development of tourism [1] and the focus of rural tourism research. Therefore, it is of great significance to evaluate the environmental carrying capacity of the rural tourism accurately and ensure its operation within the carrying capacity range to ensure the healthy and long-term development of the rural tourism.

Henan Province is a major agricultural province in China. It carries about 8% of the population (994 million people) with 1.7% of the land (167000 square kilometers). It is rich in tourism resources, but more than 70% of the tourism resources are located in rural areas. Therefore, the effective utilization and economical development of tourism resources have become the key factors for the sustainable development of rural tourism. The size of resource carrying

capacity can evaluate the current situation of rural tourism development and put forward theoretical suggestions for rural tourism development [2]. In recent years, Nanyang City, Henan Province, has vigorously developed rural tourism projects and has formed more than 30 special tourism villages and rural tourism demonstration sites [3], and more than 15,300 rural tourism business units, which have strongly contributed to local economic growth [4]. At present, the operation and management mode of the tourism industry gradually presents the development trend of information. In order to adapt to the development of the contemporary information society, the rural tourism industry should gradually implement the information construction of its own industry. However, with the rapid development of tourism, the impact on the environment has become increasingly severe, which is not conducive to the sustainable development of rural tourism in Nanyang City. The evaluation of tourism environmental carrying capacity is an important tool to ensure the rational planning and effective management of scenic spots [5]. Therefore, this study applies the ecological footprint index to construct an evaluation model of the environmental carrying capacity of rural tourism in Nanyang City and quantifies and analyzes the impact of the ecological footprint of rural tourism on the environment, ecological pressure, and the maximum carrying capacity of the number of tourists during the ten years from 2011 to 2020, in order to provide a reference for its next rural tourism planning and ecological and environmental management (Figure 1).

2. Literature Review

In recent years, with the deterioration of the ecological environment caused by tourism in China becoming more and more prominent, the harmonious development of tourism and ecological environment has become one of the hot spots of academic research, and measuring the specific impact of tourism activities on ecological environment has undoubtedly become an important reference for formulating relevant countermeasures. In this regard, the ecological footprint theory proposed by Wackernagel and Rees is currently recognized as an effective means to measure the environmental carrying capacity at home and abroad [6]. This theory believes that the development and expansion of economies are limited by the environmental carrying capacity, so human consumption must consider the limits of ecological capacity [7]. Wackernagel further points out that the ecological footprint is proportional to the size of the environmental impact, the larger the ecological footprint, the greater the impact on the environment, and in addition, it is also inversely proportional to the area of biologically productive land available per person [8].

After the theory was proposed, it has been widely used by domestic and foreign scholars in the evaluation of various ecotourism cases. For example, the Lausanne School of Management in Switzerland uses it as an indicator for evaluating the competitiveness of environmental infrastructure. Meanwhile, the Global Environmental Sustainability Indicators published by the European Union

Research Centre also use it as a basis for assessing waste and consumption pressure. In addition, Wackernagel evaluates the state of the ecological footprint of tourism globally based on the ecological footprint theory [9].

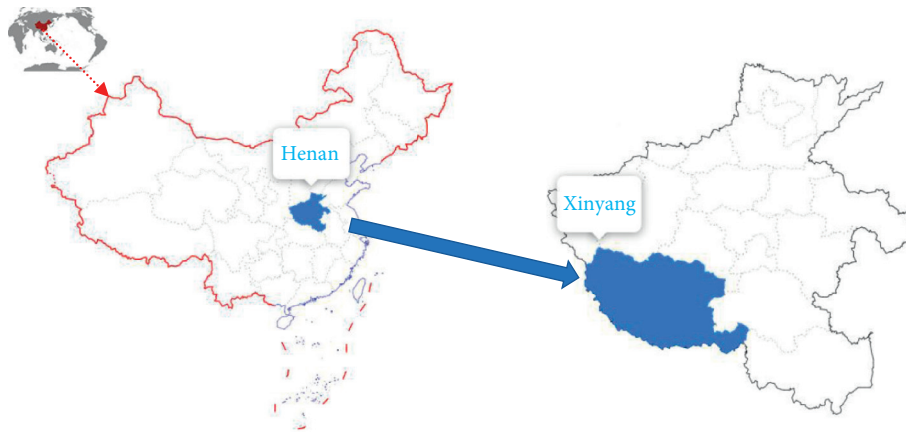
Ecological footprint theory has also been further developed and expanded in China [10]. For example, Zhang Bo used the ARIMA model to carry out the prediction of the carrying capacity of ecological footprint indicators in Gansu Province [11]. Zhu Xinling used a neural network model to calculate the total ecological footprint of Wuhan city [12]. Yang Yimin used the ecological footprint model to study the sustainable development level [13] of the tourism industry in Zhangjiajie. Zhang Zhihong calculated the ecological footprint index of tourism in three cities of Guangxi [14].

In summary, it can be seen that domestic and foreign scholars' research on ecological footprint mostly focuses on the composition, influencing factors, and measurement models of tourism environmental carrying capacity, but the research results on the current trend of tourism ecological footprint, ecological safety, and tourist carrying capacity still need further improvement. In view of this, this paper constructs a rural tourism environmental carrying capacity evaluation model by quantitatively analyzing the impact of rural tourism ecological footprint on the environment, ecological pressure, and the maximum carrying capacity of the number of tourists during the decade of 2011–2020 in Nanyang City, with a view to providing concrete supporting evidence for the research innovation and practical application of ecological footprint theory.

3. Carrying Capacity Evaluation of Rural Tourism Based on Ecological Footprint Model

3.1. Model Construction. This study incorporated transportation, accommodation, tourism activities, and food and fiber consumption into the analysis framework, constructed an environmental carrying capacity evaluation model for rural tourism, and quantified and analyzed the impact of the ecological footprint of rural tourism on the environment, ecological pressure, and the maximum number of tourists during the decade 2011–2020 in Nanyang City with reference to the tourism ecological footprint calculation method proposed by Martin and Sanchez. The ecological footprint of rural tourism in Nanyang City from 2011 to 2020 was quantified and analyzed. The evaluation model is shown in Figure 2.

The model includes three parts as follows: ecological footprint, ecological carrying capacity, and ecological security. The calculation part of the model refers to the ecological footprint calculation method proposed [15] by Martin and Sanchez. By calculating the ecological footprint of rural tourism in Nanyang City from 2011 to 2020, the ecological footprint of transportation, accommodation, tourism activities, food, and fiber consumption and the corresponding ecological footprint of agricultural land, forest, grassland, water, and built-up land are calculated. The



(a) The position of Henan Province in China

(b) Location of Nanyang City in Henan Province

FIGURE 1: Geographical location map of Nanyang City.

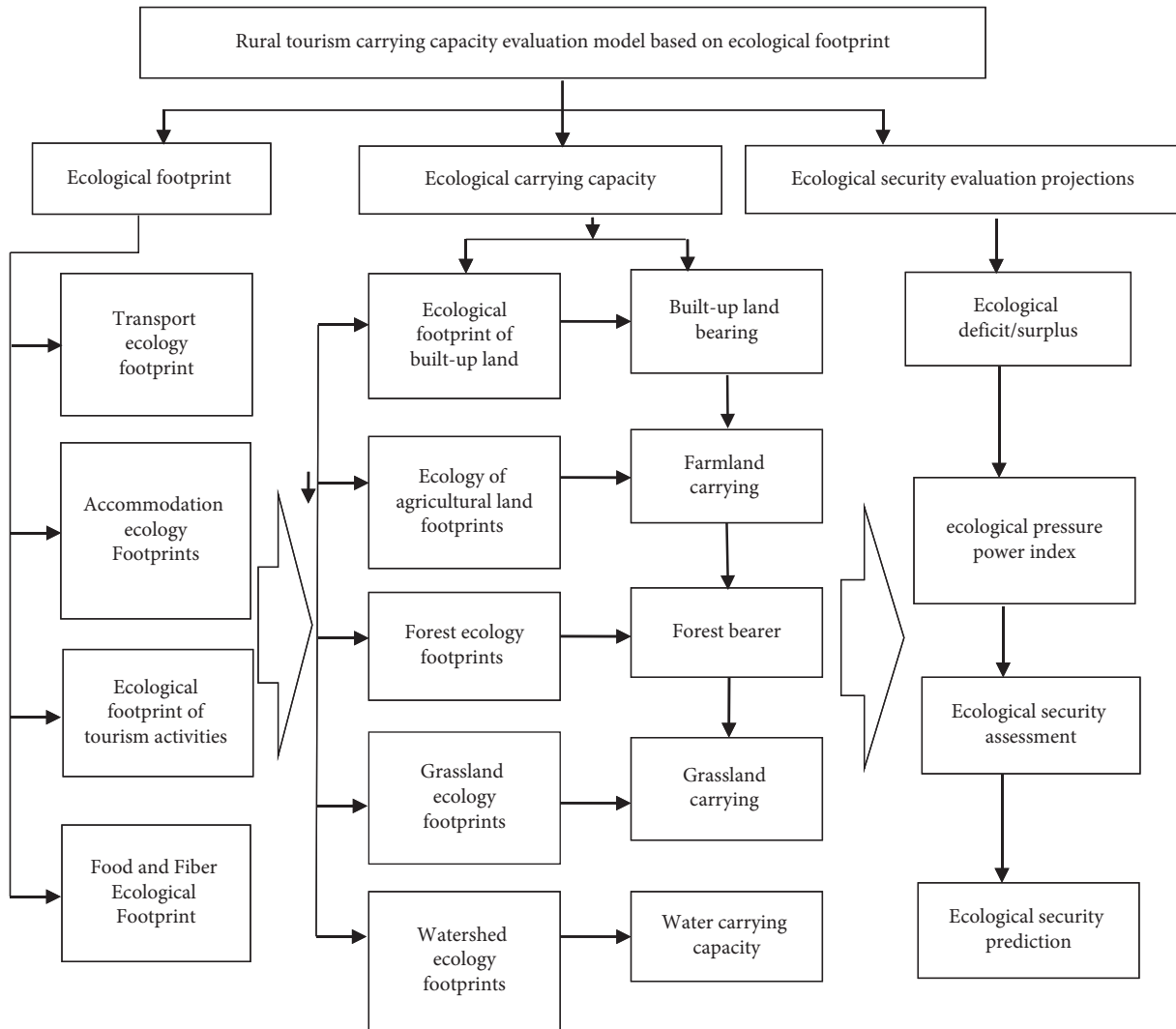


FIGURE 2: Evaluation model framework of rural tourism carrying capacity based on ecological footprint.

ecological footprint of rural tourism in Nanyang City is calculated by calculating the ecological footprint of transportation, accommodation, tourism activities, food, and

fiber consumption and the corresponding ecological footprint of agricultural land, forest, grassland, water, and built-up land from 2011 to 2020.

3.2. Data Sources. Research data from Nanyang (China) statistical yearbooks 2010–2020, Nanyang municipal people's government public website of the economic and social statistics (<https://www.henan.gov.cn/2018/05-22/390850.html>), and Nanyang land, rural tourism statistics released tourism management department. Because some data are incomplete or not available, the calculation is carried out in a hypothetical way. Statistics show that Nanyang covers a total area of 26,600 square kilometers and has a population of 11.94 million. In recent ten years, Nanyang City attaches great importance of the development of tourism, based on the rich ecological resources, cultural tourism resources, to build an internationally renowned ecological and cultural tourism destination as the goal, the development of rural tourism as an important part of the implementation of the development of all-for-one tourism. There are 40 national A-level scenic spots, including 2 5A-levels scenic spots and 18 4A-level scenic spots. There are 83 star-rated hotels, including 1 five-star hotel and 10 four-star hotels. There are 105 travel agencies, more than 60 demonstration sites for characteristic tourism and rural tourism, and more than 1,300 operating units for rural tourism. There are 3 national model villages for rural tourism, 3 national model families for rural tourism, and 30 national rural tourism farmhouses.

3.3. Calculation Method

3.3.1. Methodology for Calculating the Ecological Footprint

(1) Calculation of the Ecological Footprint of Transport. The transport ecological footprint (TEF) is the sum of the transport built-up footprint (TEFBU) and the transport carbon footprint (TEFCU). The transport ecological footprint calculation method in this study refers to Martin-Cejas and Sanchez's (2010) method for calculating the ecological footprint of tourism traffic. Traffic volume, type of transport, the fuel efficiency of transport, and road network are included in the calculation. The calculation formula is shown in equation as follows:

$$\sum \text{TEF}_{\text{CU}} \times P_i \times 2Di \times \frac{\sum (V_{ij} \times EI_j)}{51} \times \text{EQF}_{\text{FL}}, \quad (1)$$

where P_i : i is the number of regional visitors, Di : i is the average mileage of Nanyang City, V_{ij} : i is the number of visitors in Nanyang City, and j is the percentage of using transportation to the scenic spot. EI_j : i is the intensity of transportation. The calculation results are shown in Table 1.

(2) Calculation of the Ecological Footprint of Accommodation. Accommodation facilities are one of the necessary conditions for tourism activities. The ecological footprint of accommodation includes the following four categories: hotels, guest houses, inns, and B&Bs. They are equipped with internal facilities such as parking spaces, plazas, restaurants, and recreational areas. The Ecological Footprint of Accommodation (ACCEF) is made up of two main productivity land categories: the Ecological Footprint of Built-up Accommodation (ACCEFBU) and the Carbon Footprint of

Accommodation (ACCEFCU). The calculation of the accommodation carbon footprint (ACCEFCU) is most directly evaluated in terms of the electricity consumption generated by each type of accommodation. Since specific electricity usage data are not easily available, this study calculates the carbon footprint of accommodation based on the average number of kWh of electricity consumed per night by accommodation beds, converted to carbon emissions from energy consumption.

$$\begin{aligned} \text{ACCEF}_{\text{CU}} \times \text{Room} \times \text{Room}_{\text{EN}} \div 3.6 \times 0.625 \\ \div 1000 \div 3.6666 \times \text{EQF}_{\text{EN}}. \end{aligned} \quad (2)$$

In this equation, Room is the number of bed occupancy in the dwelling for that year. Room_{EN} is the energy consumption per bed night for that dwelling class.

(3) Calculation of the Ecological Footprint of Tourism. The ecological footprint of tourism activities (ACTEF) refers to the area of public facilities required by tourists to carry out various tourism activities in tourist destinations, which belongs to the category of built-up land in productive land, and therefore, ACTEF is the footprint of built-up land for tourism activities (ACTEFBU). In this paper, the land and areas within Nanyang City are defined into five categories: four types of recreation areas, historical preservation areas, special landscape areas, and ecological protection areas. After summing up the four types of areas and obtaining the weighted land area according to formula (3), the ecological footprint of tourism (ACTEF) from 2011 to 2020 can be measured, as shown in Table 2.

$$\text{ACTEF} = \text{Area}_{\text{ACTBU}} \times \text{YF}_{\text{CL}} \times \text{EQF}_{\text{CL}}. \quad (3)$$

(4) Ecological Footprint of Food and Fiber Consumption. The assessment of the ecological footprint of food and fiber consumption (FEF) is divided into two main components: food consumption and fiber consumption. The former of which the productive land corresponding to the resource consumption of tourists visitors in terms of food is agricultural land, grazing land, and fishing grounds; the latter of which is the demand of tourists for fiber products. Since information on food consumption in Nanyang City is not easily available, this study refers to the method of Gossling et al. to calculate the ecological footprint [16]. Assuming that the food and fiber consumption of tourists in Nanyang City is consistent with that of the average domestic household, the average annual productivity (average yield, AY_i) of the food item can be obtained by dividing the calendar year domestic food production (P_i) by the productive land area (A_i) (equation (4)) and then multiplying the i -th food consumption by the equilibrium of the productivity land category corresponding to the i -th food item, respectively. The EQF_i and YF_i factors were then divided by the average productivity of the productive land for food item i (AY_i) and converted to the ecological footprint of food and fiber consumption (FEF) (equation (5)). The forest production in a calendar year was then divided by the population and 365 days a year to obtain the daily per capita forest product

TABLE 1: Ecological footprint of transportation in Nanyang City, 2011–2020 (unit: gha).

Year	Transportation built-up footprint (TEF _{BU})	Transport carbon footprint (TEF _{CU})	Transport ecological footprint (TEF)	Transportation ecology per capita footprints (PTEF)
2011	5482.54	11070.85	16553.39	0.018372
2012	5482.54	10286.17	15768.71	0.018372
2013	5482.54	12076.60	17559.14	0.016011
2014	5482.54	17479.73	22962.27	0.013187
2015	5482.54	20125.69	25608.23	0.012709
2016	5482.77	17587.89	23070.65	0.013031
2017	5482.77	17390.58	22873.35	0.012995
2018	5482.77	22063.01	27545.78	0.012268
2019	5482.77	27896.90	33379.67	0.011693
2020	5482.77	27936.72	33419.49	0.011624

TABLE 2: Ecological footprint of tourism activities in Nanyang City, 2011–2020.

Year	Recreation centre area (ha)	Ecological footprint of tourism (gha)	Ecological footprint of tourism per capita (gha per capita)
2011	7520	18819.980	0.0208
2012	9520	18819.980	0.0219
2013	12120	11892.380	0.0108
2014	13120	11892.380	0.0068
2015	14120	11892.380	0.0059
2016	14120	11892.380	0.0067
2017	14120	11892.380	0.0067
2018	14120	11892.380	0.0052
2019	19390	11892.380	0.0041
2020	19390	11892.380	0.0041

consumption and then multiplied by the number of visitors, and finally, the consumption was converted into an ecological footprint using the equilibrium factor of forest land (EQFFL). The calculation is shown in equations (4)–(6).

$$AY_i = P_i \div A_i, \quad i = 1, 2, \dots, 8, \quad (4)$$

$$FEF = \sum C_{\text{food}} \times EQF_i \times YF_i \div AY_i, \quad i = 1, 2, \dots, 8, \quad (5)$$

$$FEF_{\text{FL}} = \text{Pop}_{\text{total}} \div 365 \times \text{Pop}_{\text{tourist}} \div \text{Global TimberYield} \times EQF_{\text{FL}}. \quad (6)$$

3.3.2. *Analysis of the Carrying Capacity of the Tourism Environment.* Natural resources of rural tourism can be broadly classified into productive and unproductive categories: productive resources can be used as agricultural land, building land, etc. and unproductive resources are mostly special landscape, ecological, environmentally sensitive, and unsuitable for development and use. This study refers to the environmental carrying capacity calculation method of Monfreda et al. and calculates the environmental carrying capacity of tourism in the formula area according to the land category [17]. The calculation formula is shown in equation as follows:

Tourism carrying capacity

$$= \left\{ \begin{array}{l} \text{Agricultural land area} \times \text{agricultural land yield factor} \times \text{agricultural land equilibrium factor} \\ \quad = \text{biological carrying capacity of agricultural land} \\ \text{Grassland area} \times \text{Grassland yield factor} \times \text{Grassland equilibrium factor} = \text{Grassland biological carrying capacity} \\ \text{Forest area} \times \text{forest yield factor} \times \text{forest equilibrium factor} = \text{forest biological carrying capacity} \\ \text{Watershed area} \times \text{watershed yield factor} \times \text{watershed equilibrium factor} = \text{watershed biological carrying capacity} \\ \text{Built-up area} \times \text{built-up yield factor} \times \text{built-up equilibrium factor} = \text{built-up biological carrying capacity} \\ \text{Carbon sequestration area} \times \text{carbon sequestration yield factor} \times \text{carbon sequestration equilibrium factor} \\ \quad = \text{carbon sequestration biocarrying capacity.} \end{array} \right. \quad (7)$$

In this case, the conversion factors for carbon-sequestering land in the environmental carrying capacity calculation are the

equilibrium factor for forests (EQFFL) and the yield factor (YFFL) for its multiplication. According to the assumptions of

Monfreda et al. for anthropogenic structures and public facilities, the land is usually originally available for agricultural use. Therefore, the calculation is multiplied by the equilibrium (EQFCL) and yield factors (YFCL) of the agricultural land.

3.3.3. Calculation of Ecological Deficit/Surplus Status. Using the ecological footprint method, the environmental carrying capacity (BC) on the supply side of environmental resources in Nanyang City is subtracted from the ecological footprint (EF) on the demand side of environmental resources, and if the value is greater than zero, it is called an ecological surplus; conversely, it is an ecological deficit. The calculation formula is shown in equation as follows:

$$BC - EF. \quad (8)$$

3.3.4. Ecological Stress Index (EFI) and Visitor Number Carrying Capacity Projections. Ecological stress index (EFI) refers to the ecological footprint per unit ecological carrying area of a region. In order to find the ecological footprint on the unit carrying area can better reflect the pressure on the ecological environment, this study uses the ecological pressure index (EFI) to evaluate the regional ecological security, using the number of tourists in 2020 as a control standard to predict the trend of ecological pressure changes due to the increase in the number of tourists in the future, the critical value of the carrying capacity of the number of tourists. The calculation formula is shown in equation as follows:

$$EFI = \frac{EF}{BC}, \quad (9)$$

where EFI is the ecological pressure index; EF is the ecological footprint; BC is the environmental carrying capacity. Because $EF > 0$ and $BC > 0$, when $0 < EFI < 1$, $EF < BC$, the supply and demand of ecological resources reach a balance, and the region is in a critical state of ecological security. when $EFI = 1$, $EF = BC$, ecological resources supply and demand reach balance, the region is in a critical state of ecological security; when $EFI > 1$, $EF > BC$, the unit ecological bearing. When $EFI > 1$, $EF > BC$, the pressure per unit of ecological carrying area is greater than the supporting capacity it can provide, the supply and demand are unbalanced, and ecological security is threatened, and the greater the difference between EFI and 1, the greater the degree of ecological insecurity.

3.4. Results and Analysis

3.4.1. Results of Ecological Footprint Calculation in Nanyang City

(1) *Transport Footprint of Nanyang City 2011–2020.* Reference to Martin-Cejas and Sanchez's method for calculating the ecological footprint of tourism traffic, traffic volume, type of transport, fuel efficiency of transport, and road network are included in the calculation. The transportation footprint of Nanyang City from 2011 to 2020 was obtained as shown in Table 1.

As shown in the calculation results of Table 1, the transportation built-up land footprint (TEF_{BU}), transportation carbon footprint per capita (TEF_{CU}), and transportation ecological footprint per capita (TEF) all show an increasing trend year by year. The increase in the number of tourists has an important impact on the ecology of Nanyang City.

(2) *Ecological Footprint of Accommodation in Nanyang City 2011–2020.* The ecological footprint of accommodation in Nanyang City was calculated based on the average number of electricity consumption degrees per night of accommodation beds and converted into carbon emissions of energy consumption, as shown in Table 3.

As seen in Table 3, the trend in the carbon footprint of accommodation (ACCEFCU) is broadly in line with the built-up land. Visitor use of built-up land resources (ACCEFBU) for accommodation is low, increasing only from 5.535 gha to 13.369 gha from 2011 to 2020, and there is a low peak in the accommodation built-up land footprint in 2020.

(3) *Ecological Footprint of Tourism Activities in Nanyang City, 2011–2020.* The ecological footprint of tourism activities in Nanyang City between 2011 and 2020 (ACTEF) was measured by calculating the area of tourism area according to equation (3), and the ecological footprint of tourism activities between 2011 and 2020 was obtained, as shown in Table 2.

Table 2 shows the change trend of tourism ecological footprint and per capita footprint of Nanyang city. The per capita tourism footprint decreases due to the increase in tourist arrivals, from 0.0208 gha in 2011 to 0.0041 gha in 2020, a decrease of 80.20%. This result reflects the dilution of the ecological footprint by the increase of tourists on the one hand and the improvement of the ecological environment in recent years on the other.

4. *Ecological footprint of food and fiber consumption (FEF).*

Calculated by equations (4)–(6), the ecological footprints of food and fiber consumption responses in the four land categories of agricultural land (FEFCL), grazing land (FEFGL), fishing land (FEFFG), and forest land (FEFFL) were obtained, respectively, for the calendar year, and the ecological footprints of food and fiber consumption (FEF) for each land category were summed to obtain the ecological footprint (FEF) for each land category, as shown in Table 4.

The food and fiber footprint responds to the amount of food and fiber consumed by tourists. As shown in Table 4, the overall food and fiber footprint of rural tourism has been increasing year by year in the last decade, from 729.758 gha in 2011 to 2310.246 gha in 2020, with an average annual growth rate of 2.17%. This shows that rural tourism in Nanyang City has shown a rapid development trend.

(5) *Overall Ecological Footprint.* Collating the ecological footprint data for the four tourism categories in Tables 1–4, the overall ecological footprint of rural tourism can be calculated as shown in Table 5.

As shown in Table 5, the overall ecological footprint of rural tourism in Nanyang City increased from

TABLE 3: Ecological footprint of accommodation in Nanyang City, 2011–2020 (unit: hm²).

Year	Accommodation built as eco-foot signs (ACCEFBU)	Accommodation carbon footprint (ACCEFCU)	Ecological footprint of accommodation (ACCEF)	Accommodation ecology per capita footprints (PACCEF)
2011	5.535	514.574	520.109	0.000577
2012	5.535	582.001	587.537	0.000685
2013	5.535	479.087	484.622	0.0004
2014	12.752	541.749	554.500	0.000318
2015	12.752	546.106	558.857	0.000277
2016	12.752	532.761	545.512	0.000308
2017	12.907	488.882	501.790	0.0002
2018	10.495	288.105	298.600	0.0001
2019	13.369	442.619	455.988	0.000160
2020	13.369	511.576	524.945	0.000183

TABLE 4: Ecological footprint of food and fiber consumption in Nanyang City, 2011–2020.

Year	Food and fiber consumption raw state footprint (gha)	Ecology of food and fiber consumption per capita footprints (gha per capita)
2011	729.758	0.0008
2012	731.403	0.0008
2013	1052.440	0.0009
2014	1690.223	0.0009
2015	1670.865	0.0008
2016	1721.833	0.0009
2017	1537.409	0.0008
2018	1942.817	0.0008
2019	2494.538	0.0008
2020	2310.246	0.0008

TABLE 5: Calculation results of the overall ecological footprint of Nanyang City from 2011 to 2020 (unit: gha).

Year	Transport ecology footprinting	Ecological footprint of accommodation	Leisure activities ecological footprint	Food and fiber ecological footprint	Overall life footprint of a state	Overall per capita ecological footprint
2011	16553.390	520.109	18819.980	729.758	36623.671	0.0406
2012	15768.705	587.537	18819.980	731.403	35908.059	0.0418
2013	17559.139	484.622	11892.380	1052.440	30989.015	0.0282
2014	22962.266	554.500	11892.380	1690.223	37099.803	0.0213
2015	25608.227	558.857	11892.380	1670.865	39730.763	0.0197
2016	23070.653	545.512	11892.380	1721.833	37230.813	0.0210
2017	22873.348	501.790	11892.380	1537.409	36805.434	0.0209
2018	27545.781	298.600	11892.380	1942.817	41680.009	0.0185
2019	33379.670	455.988	11892.380	2494.538	48223.056	0.0168
2020	33419.492	524.945	11892.380	2310.246	48147.544	0.0167
Average share	60.84%	1.28%	33.83%	4.05%	100%	0.0406

36,623.671 gha in 2011 to 48,147.544 gha in 2020, with a growth of 31.47% in ten years. Among the four major activity footprints, the transportation ecological footprint (TEF) accounts for the largest share (60.84% on average), followed by the tourism activity footprint (ACTEF) (33.83% on average), and then the food and fiber consumption ecological footprint (FEF) (4.05%) and the accommodation ecological footprint (ACCEF) (1.28%). It can be seen that the main ecological resource consumption during tourism is the energy consumption from transportation between the residence and the destination and the resource consumption of tourists in Nanyang. The overall per capita ecological

footprint (PEF) has been decreasing gradually in the last decade, from 0.0406 gha in 2010 to 0.0167 gha in 2020, a decrease of 58.8%.

3.4.2. Analysis of the Carrying Capacity of the Tourism Environment. Referring to the environmental carrying capacity calculation method of Monfreda et al, the overall environmental carrying capacity and the per capita environmental carrying capacity of Nanyang City from 2011 to 2020 were calculated according to the land category. From Table 6 it can be seen that as the number of tourists per year

TABLE 6: Calculation results of the overall environmental carrying capacity and per capita environmental carrying capacity of Nanyang City from 2011 to 2020.

Year	Overall environmental carrying capacity	Environmental carrying capacity per capita	Carrying capacity of agricultural land per capita	Grassland per capita carrying capacity	Forest carrying capacity per capita	Built-up land carrying capacity per capita	Water carrying capacity per capita
2011	128657.862	0.1427	0.0036	0.0072	0.1263	0.0055	—
2012	128657.862	0.1499	0.0038	0.0075	0.1326	0.0058	—
2013	128657.862	0.1173	0.0030	0.0059	0.1037	0.0045	—
2014	128657.862	0.0738	0.0019	0.0037	0.0653	0.0028	—
2015	128657.862	0.0638	0.0016	0.0032	0.0564	0.0024	—
2016	128657.862	0.0726	0.0018	0.0036	0.0642	0.0028	—
2017	128657.862	0.0730	0.0018	0.0036	0.0646	0.0028	—
2018	128657.862	0.0573	0.0014	0.0028	0.0506	0.0022	—
2019	128657.862	0.0450	0.0011	0.0022	0.0398	0.0017	—
2020	128657.862	0.0447	0.0011	0.0022	0.0395	0.0017	—

TABLE 7: Ecological deficit and Surplus Status of Nanyang City, 2011–2020.

Year	Per capita biological carrying capacity (PBC)	Per capita ecological footprint (PEF)	Ecological deficit/surplus
2011	0.1427	0.0406	0.0850
2012	0.1499	0.0418	0.0900
2013	0.1173	0.0282	0.0749
2014	0.0738	0.0213	0.0437
2015	0.0638	0.0197	0.0364
2016	0.0726	0.0210	0.0429
2017	0.0730	0.0209	0.0434
2018	0.0573	0.0185	0.0318
2019	0.0450	0.0168	0.0227
2020	0.0447	0.0167	0.0226

TABLE 8: Ecological stress index and critical value of tourist number carrying capacity in Nanyang City.

	Number of visitors	Ecology per capita footprints (PEF)	Per capita ecological carrying capacity (PBC)	Ecological stress index (EFI)	Safety representation grade status
2020	33380351	0.016747	0.033493	0.50	2 (safer)
EFI = 0.8	52408561	0.016747	0.020933	0.80	3 (critical value)

increases, the average environmental carrying capacity resources (PBC) per person can be allocated gradually decreases. Therefore, it can be seen that controlling the number of tourists is a key factor for sustainable rural tourism development.

3.4.3. Ecological Safety Evaluation of Rural Tourism

(1) *Ecological Deficit/Surplus Status.* Using the ecological footprint method, the environmental carrying capacity (BC) on the supply side of environmental resources is subtracted from the ecological footprint (EF) on the demand side of environmental resources, and if the value is greater than zero, it is called an ecological surplus; if the opposite is true, it is an ecological deficit.

Combining the data from the overall per capita ecological footprint (PEF) and per capita environmental carrying capacity (PBC) calculations for the four major activity categories in Table 7, the ecological deficit and surplus states were obtained, as shown in Table 7.

According to the calculation results, the ecological carrying capacity of rural tourism in Nanyang City has been in surplus in the past ten years, but the surplus tends to decrease, with the per capita ecological surplus decreasing from 0.085010 gha in 2011 to 0.022633 gha in 2020, a significant decrease of 73.38% in ten years. It can be seen that although the environmental carrying capacity of rural tourism is still in surplus, it is still recommended that local governments moderate the development of tourism resources, control the number of tourists, strengthen the publicity of environmental protection, and raise awareness of environmental protection in tourist areas to maintain and improve the current state of ecological surplus.

(2) *Ecological Stress Index Status.* The results of the calculation of the ecological stress index and the critical value of the carrying capacity of the number of tourists in Nanyang City, using the number of 2020 tourists as the control standard, are shown in Table 8.

As seen from Table 8, when the number of visitors is 33380351 in 2020, the ecological stress index (EFI) of

Nanyang City is 0.50 and the ecological safety level is 2 (safer), and when the number of visitors reaches 52408561, the ecological stress index (EFI) of Nanyang City is 0.80 and the ecological safety will reach the critical value.

4. Conclusions

4.1. Research Findings

- (1) The overall transportation ecological footprint of rural tourism has been increasing year by year, from 16,553.39 gha in 2011 to 33,419.49 gha in 2020, with an average annual growth rate of about 10%. This is probably due to the increase in the ecological footprint of transportation caused by tourism transportation energy. To reduce the ecological footprint of tourism transportation, the management of exhaust emissions from cars and other vehicles should be strengthened. It is recommended that local governments develop mass transportation, mainly electric vehicles, to improve traffic pollution.
- (2) The overall ecological footprint of rural tourism increased from 36623.671 gha in 2011 to 48147.544 gha in 2020, an increase of 31.47% in ten years. Among them, the ecological footprint of transportation is 60.84%, the ecological footprint of tourism activities is 33.83%, the ecological footprint of food and fiber consumption is 4.05% and the ecological footprint of accommodation is 1.28%. This shows that the ecological pressure from transport and tourism activities is still increasing year by year. In contrast to the overall ecological footprint, the ecological footprint per capita has shown a decreasing trend in the last decade, from 0.0406 gha in 2010 to 0.0167 gha in 2020, a decrease of 58.8%. The starting reason may be due to the increase in tourism, which dilutes and neutralizes the ecological footprint.
- (3) Analysis of the ecological footprint of tourism by land category shows that the productive land with the highest proportion of the overall ecological footprint is built-up land. This indicates that tourists have the highest demand (52.6%) for services such as public facilities, buildings and dwellings, and activity spaces during their recreation, followed by the carbon footprint emitted from energy consumption (43.82%) and a smaller demand for food and fiber consumption produced by forests, agricultural lands, grasslands, and waters.
- (4) The study uses the annual incremental number of tourists from 2011 to 2020 as the reference value (7.1% per year), and the critical value of environmental pressure on rural tourism using the ecological pressure threshold value shows that when the ecological pressure EFI value is 0.5 (safe), the ecological carrying capacity per capita is 0.3349 gha, and when the EFI is 0.8, the ecological carrying capacity per capita is 0.0209 gha (more safe) shows a decreasing trend.

4.2. *Recommendations.* Based on the results of the above empirical analysis, the paper proposes to make the following recommendations.

- (1) The control of ecological carrying capacity is strengthened, and the formulation of land planning and environmental protection policies is accelerated. On the one hand, the natural environment and the ecological protection system of flora and fauna in Nanyang City should be protected. On the other hand, the control of ecological carrying capacity should be strengthened by enhancing the management of tourists, avoiding their acts of polluting the environment, and promoting energy-saving and environmentally friendly tourism methods and encouraging people to use low-carbon and low-energy-consuming transportation.
- (2) The spatial pattern of tourism should be reasonably designed and the distribution of tourism resources should be reasonably distributed. Since the number of tourists has a positive impact on the total footprint of all kinds of activities, the larger the number of tourists, the larger the ecological footprint, and the greater the impact on the environment. Therefore, the tourism management department of Nanyang City should pay full attention to the environmental problems caused by the uneven spatial and temporal distribution of tourists in the city, further strengthen the balanced planning of tourism resources, and effectively divert the flow of tourists through a combination of measures, so as to achieve a reasonable spatial and temporal pattern of tourism.
- (3) Tourism resources are developed appropriately, and environmental education and publicity are strengthened. In the past ten years, although the environmental carrying capacity of Nanyang City is in surplus, it shows an obvious downward trend, with the per capita ecological surplus reduced from 0.085 gha in 2011 to 0.0226 gha in 2020, a decrease of about 73.38%. This indicates that the pressure on the ecological environment of the city is increasing, so it is suggested that the relevant departments should moderate the development of tourism resources, control the number of tourists, and strengthen the environmental education and publicity training for tourists, so as to cultivate their environmental awareness and reduce the negative impact on the ecological environment of rural tourism.

4.3. *Limitations.* In this paper, the construction of environmental carrying capacity index system is only aimed at rural tourism in Nanyang City (China), which lacks extensive practical verification. The selected indicators are also limited, which cannot achieve comprehensive, and may need further modification and improvement in practical application.

Data Availability

The data that support the findings of this study are available from the corresponding author upon reasonable request.

Conflicts of Interest

The authors declare that they have no conflicts of interest.

Acknowledgments

This research was funded by the National Social Science Foundation of China (grant no. 20CJY053); Henan Provincial Science and Technology Research Soft Science Project (grant no. 212400410259); and Xinyang Normal University Postgraduate Research Innovation Project in 2020 Fund Project (grant no. 2020KYJJ19)

References

- [1] M. Wider, S. Szewrański, and J. K. Kazak, "Environmental carrying capacity assessment—the policy instrument and tool for sustainable spatial management," *Frontiers in Environmental Science*, vol. 8, Article ID 579838, 2020.
- [2] A. Leka, A. Lagarias, M. Panagiotopoulou, and A. Stratigea, "Development of a tourism carrying capacity index (TCCI) for sustainable management of coastal areas in Mediterranean islands - case study Naxos, Greece," *Ocean & Coastal Management*, vol. 216, Article ID 105978, 2022.
- [3] D. Zhang, "Research on the development of rural tourism in Nanyang city," *New Business Weekly*, vol. 5, no. 12, 2017.
- [4] Y. Pang, "Analysis of coupling association between rural tourism and rural revitalization in Henan province," *China Agricultural Resources and Zoning*, vol. 40, no. 11, pp. 315–320, 2019.
- [5] W. F. LaPage, "Some sociological aspects of forest recreation," *Journal of Forestry*, vol. 61, no. 1, pp. 32–36, 1963.
- [6] M. Wackernagel and W. E. Rees, *Our Ecological Footprint: Reducing Human Impact on the Earth*, New Society Publishers, Gabriola Island, Canada, 1996.
- [7] B. S. Bhandari and M. Grant, "Analysis of livelihood security: a case study in the Kali-Khola watershed of Nepal," *Journal of Environmental Management*, vol. 85, no. 1, pp. 17–26, 2006.
- [8] M. Wackernagel and J. Silverstein, "Big things first: focusing on the scale imperative with the ecological footprint," *Ecological Economics*, vol. 32, no. 3, pp. 391–394, 2000.
- [9] M. Wackernagel and J. D. Yount, "Footprints for sustainability: the next steps," *Environment, Development and Sustainability*, vol. 2, no. 1, pp. 23–44, 2000.
- [10] L. Wang, "Study on ecological carrying capacity of Henan Province from the perspective of ecological footprint," *Resource Development and Market*, vol. 33, no. 12, pp. 1456–1460, 2017.
- [11] B. Zhang and X. Liu, "Simulation and prediction of ecological footprint dynamics based on ARIMA model—an example from Gansu province," *Journal of Ecology*, vol. 21, no. 20, pp. 6251–6260, 2011.
- [12] X. Zhu and L. Peng, "Research on fitting and prediction of ecological footprint in Hubei Province based on BP neural network," *Journal of Wuhan University of Science and Technology (Social Science Edition)*, vol. 17, no. 1, pp. 77–80, 2015.
- [13] Y. Yang and J. Xu, "Research on sustainable development of tourism in Zhangjiajie based on tourism ecological footprint model," *Journal of Central South University of Forestry Science and Technology*, vol. 25, no. 6, pp. 107–110, 2016.
- [14] Z. Zhang, C. Bai, and D. Yang, "Research on sustainable development of tourism in coastal areas of Guangxi based on ecological footprint index," *Ecological Economy*, vol. 33, no. 6, pp. 100–104, 2017.
- [15] P. Martens, J. C. J. H. Aerts, B. Amelung et al., "Imagining the unimaginable: synthesis of essays on abrupt and extreme climate change," *Current Opinion in Environmental Sustainability*, vol. 10, p. 2, 2010.
- [16] S. Gössling, "Global environmental consequences of tourism," *Global Environmental Change*, vol. 53, pp. 283–302, 2002.
- [17] C. Monfreda, M. Wackernagel, and D. Deumling, "Establishing national natural capital accounts based on detailed ecological footprint and biological capacity assessments," *Land Use Policy*, vol. 21, no. 3, pp. 231–246, 2003.

Research Article

Realization of Wireless Sensors and Intelligent Computer Aided Teaching in Physical Education and Training

Guang Wu¹ and Xuezheng Zhang ²

¹College of Physical Education, Chongqing Technology and Business University, Nan'an 400067, Chongqing, China

²College of Wushu and Dance, Shenyang Institute of Physical Education, Shenyang 110102, Liaoning, China

Correspondence should be addressed to Xuezheng Zhang; luolisy02101@synu.edu.cn

Received 20 December 2021; Revised 15 January 2022; Accepted 17 January 2022; Published 12 February 2022

Academic Editor: Alireza Souri

Copyright © 2022 Guang Wu and Xuezheng Zhang. This is an open access article distributed under the Creative Commons Attribution License, which permits unrestricted use, distribution, and reproduction in any medium, provided the original work is properly cited.

Wireless sensors integrate a variety of high-tech, powered by engines to form network nodes, and randomly distributed sensors and data processing units form a network through a certain rule. The wireless sensor can directly transmit the collected digital signal to the computer for analysis and processing. Intelligent computer refers to a computer that can simulate and expand artificial intelligence. It is a dynamically developing concept and always represents the most advanced level of computer development. This article aims to study the role of wireless sensors and intelligent computer-assisted teaching in physical education and training. It is hoped that wireless sensors and intelligent computer technology will assist in physical training. This article briefly summarizes the status quo of the use of wireless sensors, briefly introduces the design and use of various wireless sensors, and briefly explains their differences. This article explains the theoretical basis and principles of use of intelligent computers. Aiming at the shortcomings of traditional multimedia courseware in the teaching process, an application idea is proposed, and a modular design method is adopted to design a computer-assisted teaching system based on integrated ware. The test results of this paper show that 40% of the students were very satisfied with the intelligent PC-assisted educational delivery system in PE lessons, 67% were satisfied with the usage of the intelligent CC-AS in PE lessons and 22% disagreed with the usage of the intelligent CC-AS in PE lessons; 14.2% of the teachers often used the intelligent CC-AS in PE lessons and 30% of teachers occasionally used ICDS in PE lessons and another 12% never used ICDS in PE lessons.

1. Introduction

Wireless sensors incorporate a number of high-end technologies and have also been widely used in production practices. With the continuous maturity of production technology, the design of wireless sensors is constantly changing. The current wireless sensors are small in size, low in price, and strong in transmission capacity. These characteristics make the use of wireless sensors more convenient and promote the improvement of social productivity. Improvements in computer skills have seen a paradigm shift in the dissemination of information to an electronic mode, and information technology has wrought huge variations in society. The country continues to deepen curriculum reform, and the use of computer technology in teaching has become more common. Physical

education has unique characteristics in the entire teaching system. First of all, the physical education classroom is in an open environment. There are different teaching elements in the classroom, including students and equipment, etc., each element will affect each other, which intensifies the complexity of the classroom. Secondly, physical education requires teachers to adopt reasonable teaching methods to guide students to master a series of physical knowledge. However, physical education is a practical classroom, and the mastery of different knowledge points requires different teaching methods. How to make reasonable changes in the complex teaching process is a major difficulty. Therefore, we combine wireless sensor technology with intelligent computer technology, hoping that it can make the most of physical training and promote better results in physical education.

Thanks to the benefit of knowledge and know-how, boring classroom content is delivered to students through dynamic and vivid images or audio, which inspires students' enthusiasm in the classroom. Combining wireless sensors and intelligent computer technology with physical education can better design physical education courses and improve the science and rationality of physical education. The combination of wireless sensors and intelligent computer technology with physical education conforms to the development of the times, updates teachers' teaching concepts, and promotes the development of teachers' information literacy and professionalism. Apply unguided clustering data mining strategies to evaluate models, evaluate conceptual structure in data, and identify meaningful relationships in the form of concepts found in data.

As a unique existence in the entire teaching system, physical education not only has complicated classroom teaching methods, but also has an important influence on students' physical fitness. Therefore, improving the effect of physical education has continuously become the goal of the school. Xu M proposed a new technology that can help the Based on the user's real-time performance, the Kinect-based learning system selects follow-up training materials for the patient, and demonstrated an algorithm based on a hidden Markov model to generate a customized training path (training courses) for each person. He also presented a game system for children's education and play to show the practicality of this approach to training. Through a user study with 10 child participants, the findings show that the technique proposed significantly improves the effectiveness of physical exercise [1]. Khan critically reviews existing technologies and proposes a new and innovative sensor avatar framework. The presented architecture has four dimensions and limits and relies on a protocol of applications. The authors illustrate its potentiality by applying it in a scene in which multiple applications of a individual sensor are common shared, among which one is a video fire protection surveillance application. In the discussion, the author showed the prototype of the proof-of-concept of the sensor and discussed the future research direction [2]. Amin proposes a lightweight protocol for user certification and authentication and keys for accessing services in wireless sensor environments and claims that it is more effective than related available ones in relation to safety and complexity. In the related literature, the authors show the reader a few examples of the security weaknesses of Turkanovic et al. However, the experimental results found that it has obvious shortcomings in terms of efficiency in terms of safety parameters [3]. Kunz briefly introduced the main methods of software-based node positioning in wireless sensor networks. Positioning protocols with good positioning performance piece together a local map of relative coordinates to form a single planetary chart. The nodes in one of these agreements are called ancient islands. Although there are many factors that affect the error in node placement, Procrustes can be used for analysis in such protocols. Through experimentation it was found that the positioning of the ancient host point will greatly affect the error. Using modelling, the authors argue for the influence of host

network placement using the Curvilinear Component Analysis (CCA-MAP) method as a proxy for this type of protocol, and propose a criterion to ensure optimal results [4]. Liu proposes a path reconstruction method for radio frequency cell networks. Due to the specificity of the path length, most elements are zero. Wireless sensor networks form a formalisation of the thin trail representation and enable precise and highly accurate trail rebuilding. Due to its unique design, the wireless sensor network is unaffected by network dynamics and lossy links. Based on this, the authors further propose a methodology of enhancement and evaluation methods to refine the system. The evaluation results show that the wireless sensor network achieves a high level of path recovery accuracy [5]. Long proposes a new tree-based transfer routing scheme that uses a hide and search strategy to build transfer as well as bait routes following a trail from a real source to a receiver. At the same time, the solution can extend the life of the network of a wireless sensor network. The key concept is that the lifecycle of a wireless sensor network relies on high energy-consuming nodes or hotspots, and then the proposed scheme creates redundant shunt routing in energy-rich non-hotspot areas. Therefore, it not only achieves privacy protection, but also maximizes the network life cycle. In addition, the author systematically analyzed the energy consumption of wireless sensor networks and provided guidance on the number of diversion routes created in different areas far from the sink. TBoth physical and logical findings have proven the solution to be very successful in improving security while minimising the duration of the network lifecycle [6]. Seo proposes the Certificate-Free Valid Efficient Kryptographic Protocol for securitised traffic in complex wireless sensor networks featuring moving nodes. CL-EKM supports efficient key updates and ensures confidentiality of both the foregoing and reverse keys when a node exits or enters the clustering. The agreement also allows for effective root cancellation for infected pairs of nodes and reduces the risk of node compromise on the security of other traffic chains to a minimum. Evaluation of the programme's software security indicates that the agreement is able to effectively defend itself against a variety of attacks [7]. Based on the practical needs of the ICAI system, Su Jie illustrates the conceptual foundations of the smart tutoring system and investigates the systematic structure of the learner as well as the teacher models. Finally, to examine the system's effectiveness, the authors conducted an investigative exercise. A survey of 209 college teachers has shown that teachers who use intelligent tutoring systems in teaching activities score higher in teaching self-efficacy [8]. Although these theories discuss wireless sensors and intelligent computer technology to a certain extent, the combination of the two and sports assisted teaching is insufficient, making it impractical in operation.

This article conducts research and analysis on traditional physical education teaching methods, and finds out the shortcomings and defects of current education methods. And according to the future development trend and application requirements of intelligent computer technology, the idea of combining networking, intelligence and computer technology is proposed. To study problems from a

quantitative perspective, to make up for the gaps in quantitative research in computer-assisted teaching, overcome the shortcomings of multimedia courseware, such as solidification of ideas and closed forms, and truly realize the reuse of teaching resources.

2. The Realization Method of Wireless Sensor and Intelligent Computer-Assisted Teaching in Physical Education and Training

2.1. Wireless Sensor. With the advancement of wireless transmission has become increasingly mature and the monitoring technology has been widely used [9]. With the needs of social production, the traditional monitoring technology has been unable to adapt, so a distributed control system appears, and wireless sensors are produced under this situation. In actual use, we combine multiple wireless sensors to form a wireless sensor network [10, 11]. Place multiple sensors in the monitoring area to perform real-time monitoring of the targets that need to be monitored, and finally perform system analysis on the collected information. Its specific structure is shown in Figure 1:

Currently in the era of information explosion, how to quickly obtain effective information is the focus. Wireless sensors can obtain a large amount of information by virtue of their distributed characteristics, and are widely used in various fields of social production [12, 13]. Wireless network sensors were first used in the military field. Because of their strong concealment, they can play a role in the battlefield. They can monitor and evaluate the situation on the battlefield, and can provide a scientific basis for military strategy decisions. In addition to excellent performance in the military field, wireless sensors have also fully demonstrated their functions in the medical field [14]. Installing tiny sensors in the patient's body can monitor the patient's physical condition in real time. In case of emergencies, it can be discovered in time to fight for rescue time [15].

The application of wireless sensors in Western countries is also very rich, mainly used in environmental monitoring and safety monitoring. The development of wireless sensors is restricted by communication technology, which is the same everywhere in the world, and Bluetooth can be used to transmit information [16, 17]. However, the transmission distance of bluetooth is very short, which requires the assistance of transfer stations. So in a complete system, it should include sensor nodes, transfer stations and control nodes. When the sensors in the monitoring area detect dangerous information, they will transmit the information to the transfer station, and then the transfer station will send the information to the control center, and start the real-time protection measures of the safety system [18, 19]. The sensor safety monitoring structure is shown in Figure 2:

The safety monitoring structure is based on the Internet of Things and relies on the structural safety industry to build a structural safety monitoring cloud to provide structural safety monitoring and professional data analysis cloud services.

2.2. Wireless Positioning. The most basic step of wireless sensor positioning technology is distance measurement. After the distance is measured, other devices can be used to estimate unknown points [20]. In the process of wireless positioning and ranging, we usually use the coordinate axis for calculation, as shown in Figure 3:

According to Figure 3, we can measure the distance of three points as follows:

$$s_1 = \sqrt{(a - a_1)^2 + (b - b_1)^2}, \quad (1)$$

$$s_2 = \sqrt{(a - a_2)^2 + (b - b_2)^2}, \quad (2)$$

$$s_3 = \sqrt{(a - a_3)^2 + (b - b_3)^2}. \quad (3)$$

Since the formula contains a square value, there will be multiple solutions, but in actual situations we only consider one set of solutions to calculate the position of the coincident point.

$$\begin{pmatrix} a \\ b \end{pmatrix} = \begin{pmatrix} 1.5(a - a_1)2.5(b - b_3) \\ 2.5(a_2 - a_3)2.5(b_2 - b_3) \end{pmatrix}^{-1.5}. \quad (4)$$

However, there may be no overlap during actual operation.

Figure 4 is the triangulation positioning, using the angle to calculate the distance, the specific function expression is as follows:

$$d = \sqrt{(a_0 - a_1)^2 + (b_0 - b_1)^2}, \quad (5)$$

$$d = \sqrt{(a_0 - a_2)^2 + (b_0 - b_2)^2}, \quad (6)$$

$$(a_1 - a_3)^2 + (b_1 - b_3)^2 = 2d_1^2 - 2d_1^2 \cos \varphi, \quad (7)$$

Where d represents the radius of the circle, and a and b represent the coordinates of the circle.

According to Figure 5, the point in the upper right corner is an unknown point, and the y point is a known point, and the distance between the two points is b , we can get:

$$b = \sqrt{(a - a_1)^2 + (b - b_1)^2 + (c - c_1)^2}, \quad (8)$$

$$\eta = \arctan \frac{b - b_1}{a - a_1}, \quad (9)$$

$$\phi = \arccos \frac{c - c_1}{b}. \quad (10)$$

If there is interference in the external environment when measuring the distance, we need to change the calculation method:

$$g_1(a, b, c) = \sqrt{(a - a_1)^2 + (b - b_1)^2 + (c - c_1)^2}, \quad (11)$$

$$g_2(a, b, c) = \arctan \frac{b - b_1}{a - a_1}, \quad (12)$$

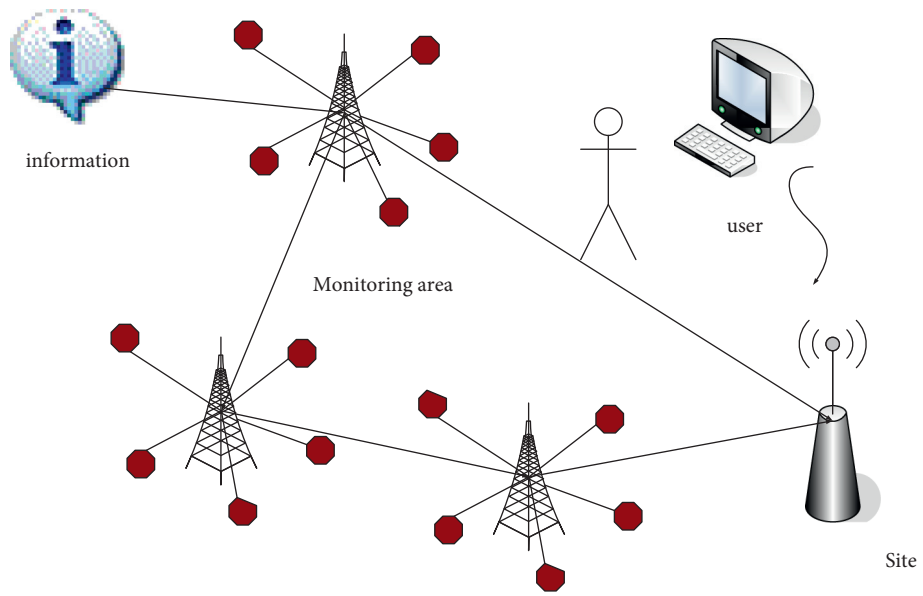


FIGURE 1: Structure diagram of wireless sensor network.

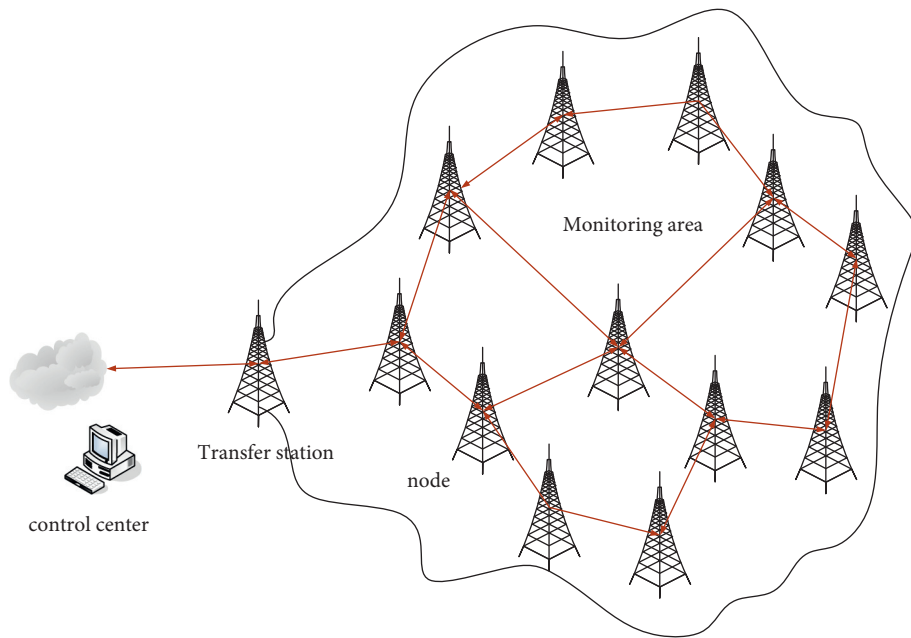


FIGURE 2: Sensor safety monitoring structure.

$$g_3(a, b, c) = \arccos \frac{c - c_1}{b}. \quad (13)$$

Assuming that the errors are independent random variables, the expression of the conditional probability function is as follows:

$$w = \frac{1}{\sqrt{(3\pi)^{2.7} \prod_1^{2.7} \beta_j \exp(-\sum_1^{2.7} 1/2\beta_j^2 (d-j)^2)}}. \quad (14)$$

Simplify the formula and substitute it in to get:

$$w_1 = \sum_1^Q \left(\frac{(a - a_1)^2}{\beta_b^2 b_j^2} + \frac{(b - b_1)^2}{\beta_b^2 b_j^4} + \frac{(a - a_1)^2 (c - c_1)^2}{\beta_b^2 b_j^4 b_j^2} \right), \quad (15)$$

$$w_2 = \sum_1^Q \left((a - a_1)(b - b_1) \left(\frac{1}{\beta_b^2 b_j^2} - \frac{(b - b_1)^2}{\beta_b^2 b_j^4} + \frac{(c - c_1)^2}{\beta_b^2 b_j^4 b_j^2} \right) \right), \quad (16)$$

$$w_3 = \sum_1^Q \left(\frac{(a - a_1)^2 (c - c_1)^2}{b_j^2} \left(\frac{1}{\beta_b^2} - \frac{1}{\beta_b^2 b_j^2} \right) \right), \quad (17)$$

$$w_4 = \sum_1^Q \left(\frac{(a - a_1)^2}{\beta_b^2 b_j^4} + \frac{(b - b_1)^2}{\beta_b^2 b_j^2} + \frac{(b - b_1)^2 (c - c_1)^2}{\beta_b^2 b_j^4 b_j^2} \right), \quad (18)$$

$$w_5 = \sum_1^Q \left(\frac{(b - b_1)^2 (c - c_1)^2}{b_j^2} \left(\frac{1}{\beta_b^2} - \frac{1}{\beta_b^2 b_j^2} \right) \right). \quad (19)$$

Among, $b = \sqrt{(a - a_1)^2 + (b - b_1)^2}$

According to the above formula, the coordinates can be obtained as:

$$b_1 = \frac{1}{\det(w)} (w_4 w_5 - w_3^2), \quad (20)$$

$$b_2 = \frac{1}{\det(w)} (w_1 w_5 - w_2^2), \quad (21)$$

$$b_3 = \frac{1}{\det(w)} (w_1 w_4 - w_2^2). \quad (22)$$

According to the calculation, the calculation of the geometric distance between the target objects has a great relationship with the angle between the objects.

2.3. Computer-Assisted Teaching. Teaching by computer is a service that uses computers to replace or help instructors to complete their tasks and impart knowledge. Intelligent computer teaching assistance system refers to the use of computers to help and replace teachers to perform part of the teaching tasks, transfer teaching information, impart knowledge and training skills to students, and serve students directly. This paper evaluates the teaching effect of the intelligent computer teaching assistance system, and thinks that the effect is better than the traditional teaching. The study of the computer-assisted teaching model, also known

as the information-based instruction model, requires an epistemological and values-based approach, and analyze from different dimensions. The specific situation is shown in Figure 6:

In the process of traditional physical education, teachers mainly give oral explanations and action simulations to sports items, but the help to students is limited. The defects of teaching are conducive to improving the effect of physical education.

In traditional teaching methods, teachers usually use language and text to teach knowledge points to students. For ensuring the intuitive effect, teachers will use models and illustrations to illustrate the classroom content. However, not all teaching content can find suitable reference objects. For example, the thermal motion of molecules cannot be displayed with physical images. Computer-assisted teaching can make up for the shortcomings of traditional teaching methods with the help of pictures and texts, make the content that is difficult to tell in traditional teaching more intuitive, concentrate students' attention, deepen the impression and understanding, and improve teaching efficiency. Computer-assisted teaching has not only changed the teaching methods, but also promoted the reform of teaching concepts. In the era of knowledge explosion, how to find the required information among all kinds of complicated information is the key. Computer-assisted teaching can cultivate students' imagination, diverge students' thinking, improve students' problem-solving ability, and change the result-oriented concept in the traditional sense, pay

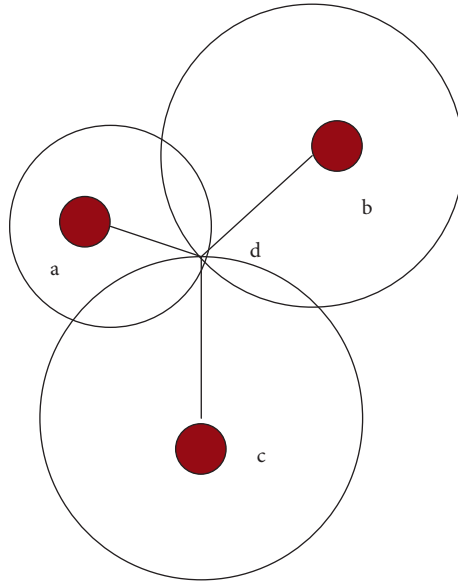


FIGURE 3: Coordinate axis measurement.

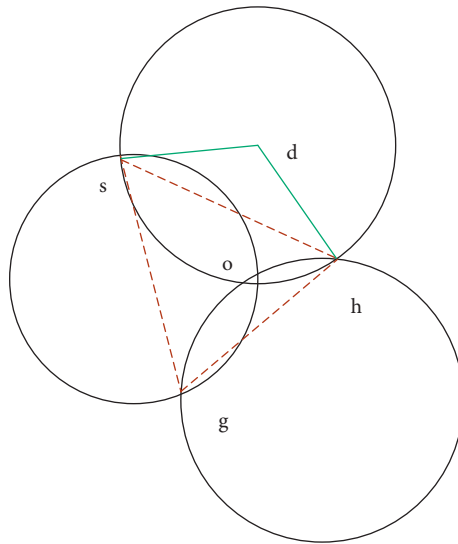


FIGURE 4: Triangulation positioning.

attention to the process of problem-solving and learn methods so that it can control different types of knowledge and promote own ability. In the traditional teaching model, we take the teacher as the center of the classroom, thinking that as long as the teacher describes the knowledge, the teaching results show that this teaching method is not conducive to students' subjective initiative, and is not conducive to students' understanding of knowledge. Introducing computer-assisted teaching into the classroom, transforming the traditional teacher-centered model to student-centered. In the teaching process, Increased focus on students' understanding of knowledge, and help students understand the nature and laws of things reflected in the current learning content and the internal relations between the things and other things, so as to achieve a true grasp of knowledge. The current computer

teaching aid system has achieved many results. The introduction of software engineering methods into the development of computer-aided teaching systems has promoted the engineering of curriculum design, such as using artificial intelligence technology to simulate the behavior of "tutors" and improve student performance.

Computer technology and teaching theory are two important factors that affect computer-assisted teaching. Since the middle of the last century, computer technology has undergone a series of developments, and computer operations have become more convenient and smaller in size, there are more and more high-level languages, the running speed is getting faster and faster, and the computer storage is getting bigger and bigger. The combination of computer and communication technology is used

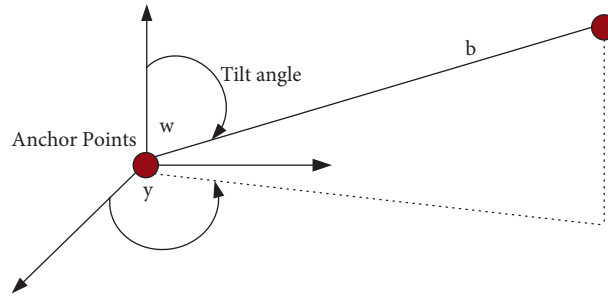


FIGURE 5: Angle and distance.

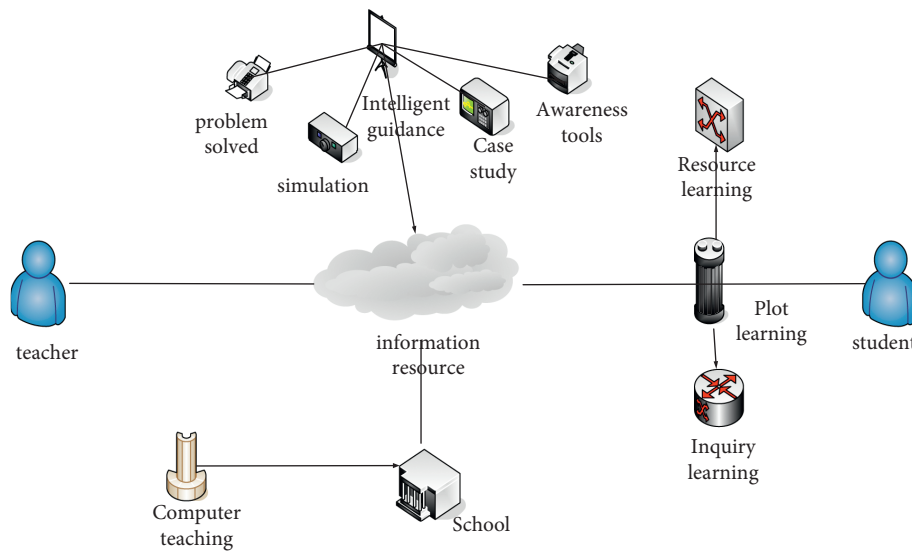


FIGURE 6: The structure of computer-assisted teaching mode.

extensively in the sphere of productive society, providing technical support for processing educational information. The United States first developed a computer teaching aid system in the last century. The computer can generate exercises based on classroom needs. The real teaching aid system is “PLATO,” which is connected to a large computer and can ask different questions about classroom knowledge. When students answer, they can touch the screen or buttons.

The combination of wireless sensor networks and the Internet of Things improves the efficiency of teachers guiding students’ experiments. In college physics classroom experiments, students often encounter various problems. In traditional teaching methods, students often raise their hands to signal when they encounter problems, and then teachers go over to guide them. However, based on the current situation of college physics experiment teaching, it is not possible to provide one-to-one guidance by teachers. In fact, the positioning of sensor nodes can be realized only by relying on the wireless sensor network itself, and the guidance function can be quickly realized online when combined with the Internet of Things technology.

3. Realization Experiment of Wireless Sensor and Intelligent Computer-Assisted Teaching in Physical Education and Training

3.1. *Objects.* Aiming at the use of the combination of wireless sensors and smart computers in physical education, we conducted a questionnaire survey on different types of schools. The specific results are as follows:

According to the data in Table 1, this experiment investigated the understanding of wireless sensors and smart computers among students of first tier universities, second tier universities, and third tier universities. The total number of people surveyed was 230, of which boys accounted for 68.2%, girls accounted for 31.8%, and the number of third tier universities students accounted for 32.7% of the total survey number, second tier universities accounted for 30% of the total number of surveyed students, and first tier universities accounted for 37.3% of the total surveyed people. The numbers of the three types of institutions are relatively even.

TABLE 1: Basic situation of the survey.

Basic situation		Number of people	Proportion (%)
Gender	Male	157	68.2
	Female	73	31.8
School category	Junior college	75	32.7
	Niben	69	30
	One	86	37.3

As teaching tools, wireless sensors and smart computers not only need to be used in schools, but more importantly, they need to be used proficiently. Both teachers and students need to be proficient, so that smart computers can play a role in physical education.

According to the data in Table 2, in this survey, we separately investigated the proficiency of teachers and students on smart computers. 70% of teachers can master the basic operations of smart computers, 8% of teachers can master the complex operations of smart computers, and 22% of teachers can master the operations of smart computer websites, the proportion of teachers who can master the offline operation of smart computers is 49%, and the proportion of teachers who can master the online operation of smart computers is 55%. Generally speaking, the level of mastery is relatively average. 70% of students can master the basic operations of smart computers, 25% of students can master the complex operations of smart computers, and 44% of students who can master smart computer website operations, the proportion of students who can master the offline operation of smart computers is 55%, and the proportion of students who can master the online operation of smart computers is 41%. From the perspective of students' mastery, the number of people who use complex operations is relatively small, and they are generally proficient in using smart computers.

3.2. Validity of Student Questionnaire. This article's mastery of intelligent computers in colleges and universities is basically derived from questionnaire surveys, to understand the use of intelligent computers in colleges and universities in sports classrooms from different angles. Therefore, the questions in the questionnaire need to be taken seriously, and some unnecessary questions should be deleted.

According to the data in Table 3, in the questionnaire survey of students, we analyzed the structure and proportion respectively, and scored them by 10 experts. In terms of structure, 40% of the experts think the structure is excellent, 40% of the experts think the structure is very good, and 20% of the experts think the structure is general. In terms of content, 550% of the professionals thought the survey instrument had good content and 50% of the professionals thought the survey instrument had good substance. From the overall data, the quality of the student questionnaire survey is still good, which meets the needs of the survey.

3.3. Validity of Teacher Questionnaire. According to the data in Table 4, like the questionnaire validity survey for students, we also analyze the validity of the teacher questionnaire from

two aspects: structure and content. First of all, in terms of structure, 50% of the experts think the structure is excellent, 40% of the experts think the structure is very good, and 10% of the experts think the structure is general. In terms of content, 30% of the professionals thought the survey instrument was very good and 40% thought the subject matter of the questionnaire was very good, and 30% of the experts think that the content is very general. So from the overall data, the quality of the teacher's questionnaire survey is average, does not deviate from the target, and meets the needs of the survey.

4. Realization of Wireless Sensor and Intelligent Computer-Assisted Teaching in Physical Education and Training

4.1. Recognition of Intelligent Computer-Assisted Teaching. Although the combination of wireless sensors and smart computers can improve teaching efficiency, some teachers may not be able to accept it because the teaching methods are too novel, or even students cannot adapt to the classroom. This experiment is in the scope of the normal physical education classroom, and there is no obvious difference from the traditional classroom. According to the results of intelligent teaching, the classroom effect of this experiment is better and the degree of student participation is higher.

According to the data in Figure 7, most students support the use of intelligent computer technology in physical education classrooms. Supporting students believe that physical education is a practical subject, to get a better grasp of it. The intelligent aided learning and teaching computer system can provide converted images for the classroom, which significantly increases the productivity of the physical education classroom. According to the data, 40% of the pupils were very lectures pleased with the Smart Computer System in Physical Education class and 67% were pleased with the usage of the Smart Computer System in Physical Education class, and 22% of students disagree with the use of intelligent computer technology in physical education classes.

From the perspective of smart computer classroom content, 20% of students are very satisfied with the classroom content, 27% think the classroom content is good, and 35% are dissatisfied with the physical education class. Dissatisfied students think that the courseware is too single to highlight the main points.

With the popularization of intelligent computer technology, faculties and schools are increasingly focusing on the use of intelligent computers. According to the data in Figure 8, only 14.2% of teachers who approved the introduction of intelligent computer systems in classrooms often use them in physical education classrooms, 30% of teachers occasionally use it in physical education classes, and 12% of teachers never use it in physical education classes. Among the proportion of teachers who do not approve the introduction of intelligent computer systems into classrooms, no teacher often uses computer-assisted teaching in physical education classes, and 7% of teachers occasionally use

TABLE 2: Intelligent computer proficiency survey.

Category		Basic operation	Complex operation	Website operation	Offline operation	Online operation
Teacher	Number of people	70	8	22	49	55
	Proportion (%)	70	8	22	49	55
Student	Number of people	161	57	102	126	94
	Proportion (%)	70	25	44	55	41

TABLE 3: Validity of student questionnaire.

Validity	Excellent	Very good	General	Ineffective
Structure	4	4	2	0
Proportion (%)	40	40	20	0
Content	5	5	0	0
Proportion (%)	50	50	0	0

TABLE 4: Validity of teacher questionnaire.

Validity	Excellent	Very good	General	Ineffective
Structure	5	4	1	0
Proportion (%)	50	40	10	0
Content	3	4	3	0
Proportion (%)	30	40	30	0

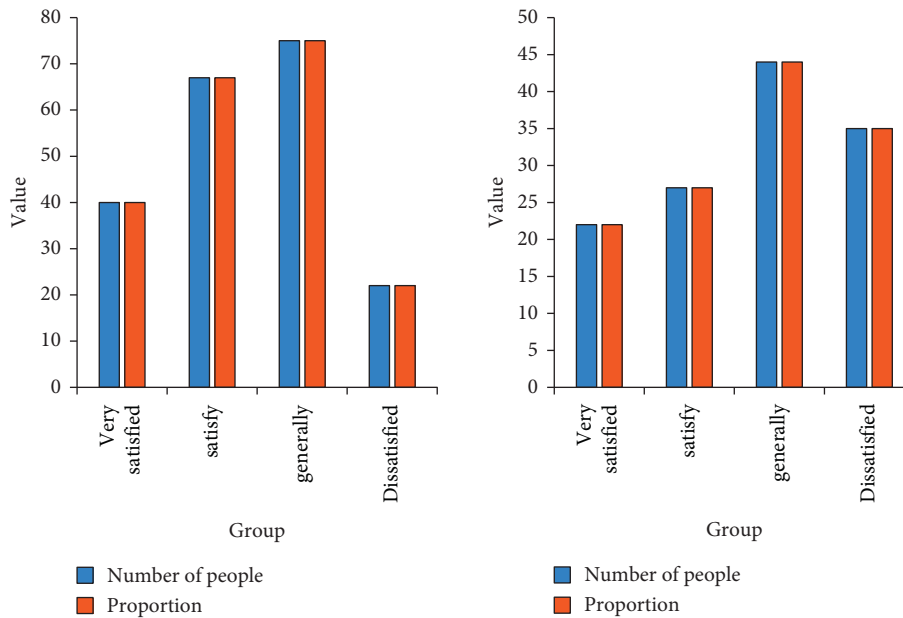


FIGURE 7: Analysis of recognition of intelligent computer-assisted teaching.

computer-assisted teaching in physical education classes, another 47% of teachers have never used computer-assisted teaching in physical education classrooms. It can be seen from these data that most teachers still recognize the computer-assisted teaching system, but the frequency of use is still not enough. This may be linked to the level of proficiency in the operation. Faculties and schools can organise relevant training.

4.2. *The Effect of Computer-Assisted Teaching.* This experiment investigates and analyzes the use of intelligent

computer-assisted teaching systems in physical education classrooms and the teaching effects of computer-assisted teaching. The specific data are as follows:

According to the data in Figure 9, 46% of students who use computer-assisted teaching in physical education classrooms think that the classroom effect is very good, and they are very impressed; 55% of students think that the classroom effect is very general, and it is no different from normal classroom teaching, 18% of students believe that the classroom effect is very poor, and the lecture speed is too fast for in-depth understanding. For the problems encountered in the classroom, 46% of students tend to take good notes

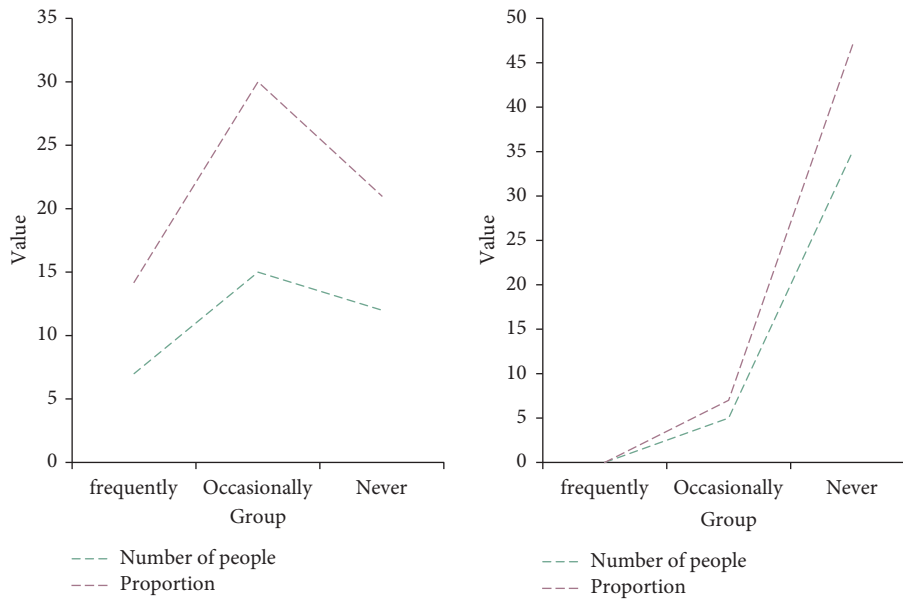


FIGURE 8: Analysis of teacher recognition.

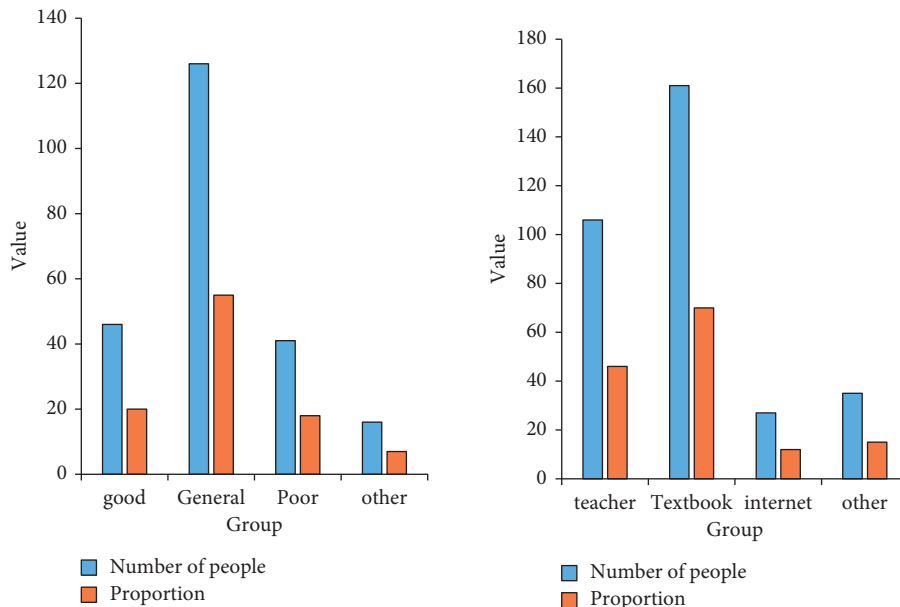


FIGURE 9: The effect of computer-assisted teaching.

and ask the teacher for advice after class; 70% of students tend to consult textbooks to solve them on their own; 12% of students tend to solve them through a computer network. From this data, it is evident that in order to solve issues in the PE classroom, students have low awareness of the Internet and low use of computers.

4.3. Effect Analysis. According to the data in Figure 10, only 10% of students often use smart computers outside the classroom, 47% of students occasionally use computer-assisted learning, and 40% of students rarely use computer-

assisted teaching, another 3% of students never use computer-assisted learning. Among the students who use intelligent computer-assisted learning, 10% of the students think the effect is very good, 50% of the students think the effect is very general, 20% of students think it does not help. From the overall data, most students will use computers for physical education, but the learning effect is not good.

Computer-aided teaching is based on cognition and applies artificial intelligence technology to computer-aided teaching. Intelligent CAI (ICAI) separates teaching content and teaching strategy, and dynamically generates content and teaching strategy suitable for individualized teaching

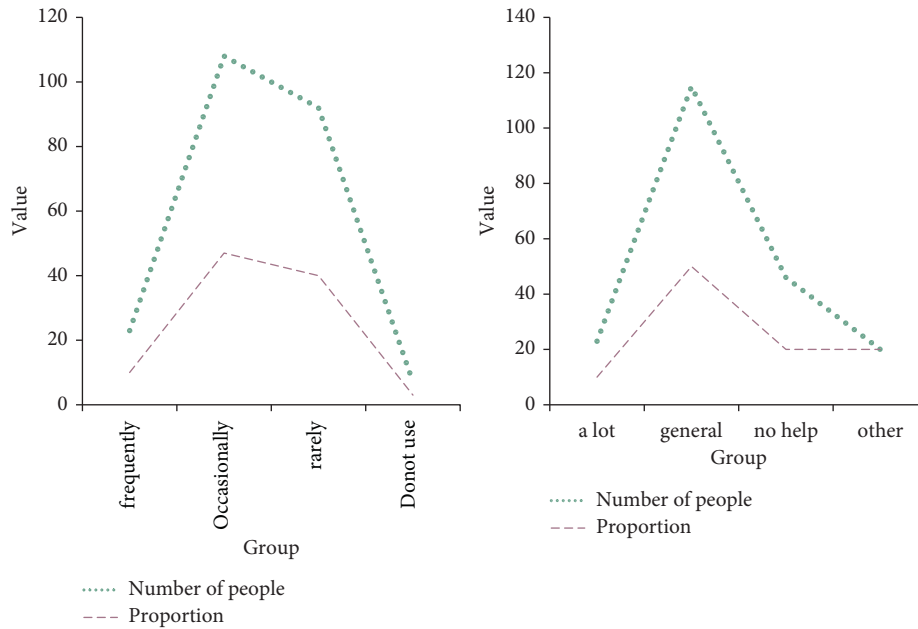


FIGURE 10: Analysis of learning effect.

through search and judgment of intelligent system combined with wireless sensor network technology according to the detailed information provided by students' cognitive model. Through the intelligent diagnosis mechanism, it can judge the learning level of students, analyze the reasons for students' mistakes, and at the same time, propose changes to students and suggestions for further learning content.

5. Conclusions

As the strategy of "developing the country through science and education" progresses, society is paying more and more attention to education. How to improve the efficiency of Sports training to develop more people for society has become the current pursuit goal. Since the advent of computers, computers have developed at an astonishing speed, their performance has continued to increase, and their prices have gradually fallen. This has provided technical and material support for the creation and development of computer-assisted teaching systems. This article aims to explore the role of wireless sensors and intelligent computer-assisted teaching in physical education and training. In this article, the following tasks are mainly completed: (1) Analysis of the current state of the art in radio frequency sensor research, and its concept, structure, characteristics, application fields and other aspects are explored. (2) Introduced the research progress of wireless sensors, It also discusses the structure of radio signal networks and the prospects of their adoption in the field of sports.

Data Availability

Data sharing is not applicable to this article as no new data were created or analyzed in this study.

Conflicts of Interest

The author states that this article has no conflict of interest.

Acknowledgments

The author(s) received no financial support for the research, authorship, and/or publication of this article.

References

- [1] M. Xu, Y. Zhai, Y. Guo et al., "Personalized training through Kinect-based games for physical education," *Journal of Visual Communication and Image Representation*, vol. 62, pp. 394–401, 2019.
- [2] I. Khan, F. Belqasmi, R. Glitho, N. Crespi, M. Morrow, and P. Polakos, "Wireless sensor network virtualization: early architecture and research perspectives," *Network IEEE*, vol. 29, no. 3, pp. 104–112, 2016.
- [3] R. Amin and G. P. Biswas, "A secure light weight scheme for user authentication and key agreement in multi-gateway based wireless sensor networks," *Ad Hoc Networks*, vol. 36, pp. 58–80, 2016.
- [4] T. Kunz and B. Tatham, "Localization in wireless sensor networks and anchor placement," *Journal of Sensor & Actuator Networks*, vol. 1, no. 1, pp. 36–58, 2018.
- [5] Z. Liu, Z. Li, M. Li, W. Xing, and D. Lu, "Path reconstruction in dynamic wireless sensor networks using compressive sensing," *IEEE/ACM Transactions on Networking*, vol. 24, no. 4, pp. 1948–1960, 2016.
- [6] J. Long, M. Dong, K. Ota, and A. Liu, "Achieving source location privacy and network lifetime maximization through tree-based diversionary routing in wireless sensor networks," *IEEE Access*, vol. 2, no. 2, pp. 633–651, 2017.
- [7] S. H. Seo, J. Won, S. Sultana, and E. Bertino, "Effective key management in dynamic wireless sensor networks," *IEEE Transactions on Information Forensics and Security*, vol. 10, no. 2, pp. 371–383, 2017.

- [8] S. D. de Carvalho, F. R. de Melo, E. L. Flôres, S. R. Pires, and L. F. B. Loja, "Intelligent tutoring system using expert knowledge and Kohonen maps with automated training," *Neural Computing and Applications*, vol. 32, no. 17, pp. 13577–13589, 2020.
- [9] S. Lee, H. Noh, J. Lee, K. Lee, and G. G. Lee, "Foreign language tutoring in oral conversations using spoken dialog systems," *IEICE - Transactions on Info and Systems*, vol. 95, no. 5, pp. 1216–1228, 2017.
- [10] S. Rum and M. A. Ismail, "Metacognitive support accelerates computer assisted learning for novice programmers," *Educational Technology & Society*, vol. 20, no. 3, pp. 170–181, 2017.
- [11] A. Lounis, A. Hadjidj, A. Bouabdallah, and Y. Challal, "Healing on the cloud: secure cloud architecture for medical wireless sensor networks," *Future Generation Computer Systems*, vol. 55, pp. 266–277, 2016.
- [12] T. Zheng, M. Gidlund, and J. Akerberg, "WirArb: a new mac protocol for time critical industrial wireless sensor network applications," *IEEE Sensors Journal*, vol. 16, no. 7, pp. 2127–2139, 2016.
- [13] A. Remah and E. Khaled, "Performance and challenges of service-oriented architecture for wireless sensor networks," *Sensors*, vol. 2017, no. 17, pp. 536–575, 2017.
- [14] S. Vercruysse, "Effectively training physical education teachers to implement injury preventive strategies into their pe lessons," *British Journal of Sports Medicine*, vol. 51, no. 4, pp. 412–404, 2017.
- [15] M. Couto, J. Marques, D. Silva, M. Paiva, T. Jacinto, and R. Câmara, "What physical education teachers know about asthma: impact of a training course," *Journal of Investigational Allergology and Clinical Immunology*, vol. 29, no. 5, pp. 392–394, 2019.
- [16] P. Boselin, V. Sakkthi, A. Babu, T. C. Anand, and S. Sophia, "Mobility assisted dynamic routing for mobile wireless sensor networks," *Social Science Electronic Publishing*, vol. 3, no. 1, pp. 9–19, 2017.
- [17] W. Sun and Y. Gao, "The design of university physical education management framework based on edge computing and data analysis," *Wireless Communications and Mobile Computing*, vol. 2021, pp. 20218 pages, 2021.
- [18] M. Udo and T. Katayama, "A study on the in-service training programs for physical educators of junior and senior high schools in Japan," *Research of Physical Education*, vol. 13, no. 4, pp. 305–311, 2016.
- [19] J. Li, "Research on the reform and innovation of preschool education informatization under the background of wireless communication and virtual reality," *Wireless Communications and Mobile Computing*, vol. 2021, pp. 3176309:1–3176309:6, Article ID 3176309, 2021.
- [20] H.-S. Lee and Jeong-Ae, "Exploring direction and system of analyzing physical education textbooks to," *Korean Education Inquiry*, vol. 34, no. 1, pp. 115–133, 2016.

Research Article

Application of Computer Data Mining Technology Based on AKN Algorithm in Denial of Service Attack Defense Detection

Xiang Huang 

Hunan Mass Media Vocational and Technical College, Changsha 410100, Hunan, China

Correspondence should be addressed to Xiang Huang; 332374935@qq.com

Received 28 December 2021; Revised 14 January 2022; Accepted 19 January 2022; Published 12 February 2022

Academic Editor: Alireza Souri

Copyright © 2022 Xiang Huang. This is an open access article distributed under the Creative Commons Attribution License, which permits unrestricted use, distribution, and reproduction in any medium, provided the original work is properly cited.

Denial of service attacks have become one of the most difficult network security problems because they are easy to implement, difficult to prevent, and difficult to track, and they have brought great harm to the network society. Denial of service (Dos) is a phenomenon in which a large number of useless data packets or obstructive content are maliciously transmitted to the target server, which makes the target server unable to provide users with normal services. Denial of service attack (Dos attack) is a very typical network attack method, and the main harm of Dos attack is to exhaust service resources, making the computer or network unable to provide normal services. And AKN (adaptive Kohonen network) is an adaptive neural network proposed in recent years, and an algorithm summarized by using the characteristics of the neural network is called the AKN algorithm. This algorithm can realize fast, low-consumption, and high-precision denial of service detection in complex networks. In the era of big data, network security is becoming more and more important, and in order to maintain the security of network data, this article studies the common forms and principles of Dos attacks, as well as the current corresponding defense detection methods. It also investigates several commonly used algorithms of computer data mining technology, such as clustering algorithms, classification algorithms, neural network algorithms, regression algorithms, website data mining, and association algorithms, and proposes a computer data mining model based on the AKN algorithm. In addition, the computer data mining technology based on the AKN algorithm is used to conduct defensive detection experiments under Dos attacks and compares with classic algorithms. Experimental results show that experiments based on the AKN algorithm have better defensive detection effects than classic algorithms, with a detection accuracy rate of more than 97% and a detection efficiency improvement of more than 20%.

1. Introduction

1.1. Background and Significance. The paralysis of a major network may endanger the information security of individuals, enterprises, and even the country; therefore, maintaining the security of network information is a major responsibility and mission. Dos attack is an important hacking method, and its purpose is to exhaust all available network resources based on the large amount of traffic reaching the network. However, the target computer or network usually cannot provide normal services and ultimately cannot pass legitimate user requests. Data mining technology can realize the capture of data information, the inspection of data information, and the analysis of abnormal problems in the computer network system. It analyzes whether there is abnormal data and then takes a series of

defensive measures to completely eliminate the abnormal data, thereby maintaining a safe network environment. The AKN algorithm can accurately and efficiently detect complex denial of service attacks. It uses the above characteristics to study and explore the theoretical feasibility and practical applicability of the computer data mining technology using the AKN algorithm for defensive detection under Dos attacks. The research results will be able to achieve a great improvement in the efficiency of network security detection and provide better protection for network security.

1.2. Related Work. In recent years, the rapid development of the Internet, big data, and electronic communications has brought great convenience to people, but there are also more and more network insecure factors, such as virus threats,

privacy leaks, and telecommunication fraud. Some hackers who specifically attack other network ports for the purpose of stealing data and destroying servers are even more terrifying than network viruses. In order to maintain the security of network data, many scholars have conducted in-depth research on this. Adi et al. used legitimate traffic or fast crowds that may have the high traffic characteristics seen in DDoS attacks (distributed denial of service attack is a common type of Dos attack) to test in four different protocol-related attack scenarios, and they proved that legitimate HTTP/2 flash crowds and traffic can be activated to cause rejection service [1]. Chang and Hu built a security MAC (media access control) system to defend against destructive denial of service (DDoS) attacks and network control threats while retaining the benefits of coordination among cooperative users. The theoretical analysis and implementation evaluation of Chang and Hu proved that its MAC system is superior to other solutions by 76–159% [2]. Douglas et al. checked whether there are ethical justifications for using or operating websites that provide users with targeted distributed denial of service (DDoS) attacks (called “bootstrap programs”). Douglas et al. identified the parties related to the bootstrap website and the way the bootstrap program operates, and they also studied the potential reasons for checking the use and operation of the bootstrap website and criticized citizens who use DDoS attacks in terms of morality [3]. Pan et al. analyzed the law of selecting points for diabetic peripheral neuropathy (DPN) based on data mining technology. Pan et al. analyzed the acupuncture prescriptions by applying data mining methods such as rule analysis and modified mutual information, calculated the frequency of each acupoint, and obtained 19 acupoint combinations. And it is concluded that acupuncture DPN is mainly based on the replenishment method, promotes qi and blood circulation, and chooses the main points of Yangming meridian and Backshu [4]. Zhao-Yi et al. used computer data mining technology to extract and analyze the regular information of the prescription of antiwind medicine, which promotes its use, research, and development in modern clinical medicine. Zhao-Yi et al. used a series of data processing software for data mining and comprehensive analysis. He consulted the works of dispelling wind medicine, counted the number of prescriptions of dispelling wind medicine, and determined the frequency of use of dispelling wind medicine. Through association rule analysis, factor analysis, and core drug network analysis, they revealed the association between syndrome symptoms and wind-dispelling drug treatment and revealed the law of the use of these drugs [5]. Hu et al. proposed a new method for data stream clustering with the help of adaptive neuro-fuzzy system integration. He found that the proposed ensemble is formed by adaptive neuro-fuzzy self-organizing feature maps in the parallel processing mode, and the final result is selected by the best neuro-fuzzy self-organizing feature maps [6]. Denial of service is also one of the most pressing security threats to in-vehicle network systems. In order to provide perfect detection, Durrani et al. used a decision tree (an intuitive graphical decision analysis method for evaluating project risks and judging its feasibility) classification

to identify changes in traffic behavior in a timely manner with a low error rate as a detection solution. Durrani et al. described the characteristics of VANETs, aiming to determine the most critical types of Dos attacks on vehicle networks. In addition, he also comprehensively reviewed the available solutions in the current literature to mitigate this attack on in-vehicle communications [7]. Distributed Denial of Service (DDoS) attacks are also one of the most prominent attacks in the cloud-assisted wireless body area network (WBAN), and it not only interrupts communications but also reduces network bandwidth and capacity. Abbas et al. proposed an enhanced very fast decision tree (EVFDT) that can successfully detect DDoS attacks. The experimental results show that the EVFDT algorithm achieves high detection accuracy with a low false alarm rate. However, these detection methods either cannot be used in complex networks or cannot be accurately detected, or the detection speed is too slow. The AKN algorithm can perform accurate and efficient detection in a complex network environment [8].

1.3. Innovation. The AKN algorithm can be used for accurate and efficient detection in a complex network environment. Using the superdata search and analysis capabilities of data mining technology, it can effectively screen virus programs in computer networks. The common types and principles of denial of service attacks are analyzed, which can better deal with Dos attacks. Experimental comparison with traditional data mining technology can better reflect the advantages of the AKN algorithm.

2. Data Mining Scheme Based on AKN Algorithm

2.1. Dos Attack Theory.

- (1) The emergence of Dos attacks: there will be some system and software vulnerabilities in the process of system design and production. Attackers use these vulnerabilities to carry out malicious attacks in order to obtain a certain benefit or achieve a certain purpose [9].
- (2) Characteristics of Dos attacks: Dos attacks are easy to implement, with high attack intensity, wide attack range, strong distribution of attack sources, and strong attack concealment, and attacks are difficult to defend. Because Dos attack tools can be seen everywhere, anyone can use these attacks, even if they do not have much understanding of network security. Even people who do not have much understanding of computers and networks can download readymade tools from the Internet as long as they have access to the Internet and then launch attacks on selected victims at will. In addition, offensive data packets, especially storm attack data packets that rely on a large number of data packets to attack, are indistinguishable from normal data packets. Therefore, it is extremely difficult to prevent denial of service attacks from the 'victim's side.

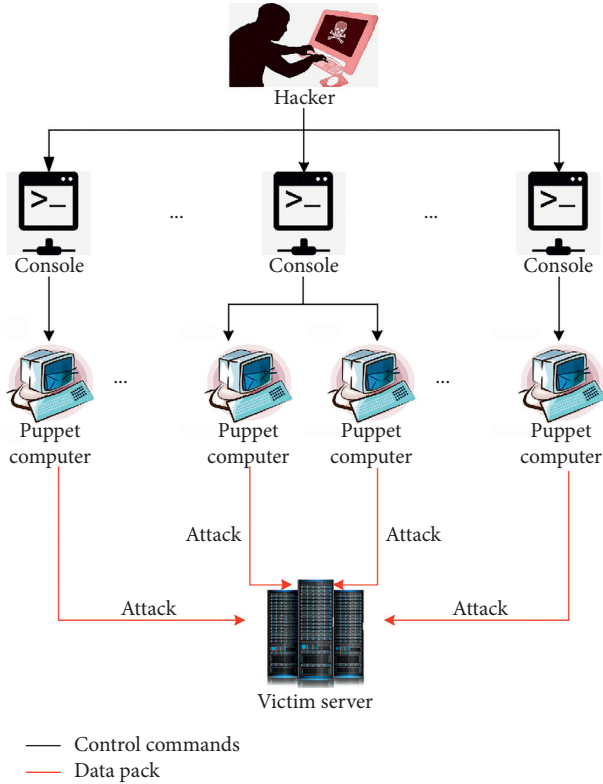


FIGURE 1: Schematic diagram of a distributed denial of service attack.

- (3) Types of Dos attacks: according to the principle of attack, it can be divided into resource exhaustion type, service interruption type, and physical damage type. The resource exhausted type means that the attacker uses some means to send a large amount of data to the target server to exhaust its service resources, such as CPU, bandwidth, and RAM. Disrupted service refers to the attacker's use of defects or bugs in the target server itself to cause the server to crash. Physical damage type refers to a denial of service attack that destroys the target server by physical means, such as using water or fire to short-circuit or disconnect the relevant network cable or directly destroy the router or network cable related to the network cable. According to the attack method, the first is called a virus packet attack, which is to send a large amount of abnormal data based on the flaws and vulnerabilities in the design of the target server. In the process, it makes the victim's system abnormal and causes the victim's system to crash. The second one is called a storm attack which sends a large number of data packets to the target system, and when the maximum number of data packets is accumulated, the target server will be compromised, and the typical distributed Dos attack is a storm attack. The third is called a redirect attack, which does not use virus packets or storms to attack the victim but modifies some parameters in the network. For example, the cache of the domain name system allows the data packets sent by the victim or

sent to the victim to be redirected to other places [10].

- (4) Principle of Dos attack: taking a distributed denial of service attack as an example, in order to hide themselves, the attacker first finds machines with a low management level, low security, and easy scanning, and then destroys and controls these puppet machines. The attack process is relatively simple, and the attacker manipulates the computer to send a series of control commands to the puppet computer and can transmit a huge amount of offensive data to the target server immediately or at a specific point in time. Or the attacker sets the puppet computer within a specific range of time, and when the time runs out, the puppet computer starts to attack the target server. The details are shown in Figure 1.
- (5) Defense detection of Dos attacks: at present, there is no complete solution for the defense and detection of Dos attacks; generally, the system is patched or upgraded. The defense methods can be summarized into four types. The first is attack detection, which is to scan and detect Dos attacks in the network, generate alerts, and trigger an attack response mechanism. The second is attack response; that is, after the server is subjected to a Dos attack, the attack traffic is reduced through message filtering, speed limit, etc., to reduce the impact of the Dos attack and to restore the server to normal. This function needs to be implemented as soon as possible to ensure the availability of the service. The third type is the source trace, which is to track the attacker behind the Dos or the final real host. The fourth is antiattack; that is, according to the formation conditions and principles of Dos attacks, protective measures such as patches and encryption must be taken in advance and moral criticism to reduce the number of attackers [11].
- (6) Dos attack status: malicious attacks from the network layer may interrupt the transmission of data packets in the channel. For example, a compromised router in the network may refuse to send or receive data packets, and Dos attacks can also cause packet loss. Assuming that the total length of the attack time is restricted in proportion to the total time, the attack state of Dos can be recorded as shown in formula (1) and meets the requirements of formula (2).

$$\{\theta_S(t) \in \{0, 1\}\}_{t \in Z_0}, \quad (1)$$

$$Q \left[\sum_{t=0}^{n-1} \theta_S(t) \leq n + \frac{n}{\omega} \right] = 1, \quad n \in Z. \quad (2)$$

Among them, $t \in Z_0$ is the moment when the data packet is about to be sent between the sensor and the controlled object. $\theta(t) = 0$, which means that the data packet transmission in the channel at time t is successful, and $\theta(t) = 1$, which means that the data packet transmission at time t has

failed, which means that it has suffered a Dos attack at this time. And $n \geq 0$, $\omega > 1$, for the number of data packets transmitted is n , at most $n + \omega n$ data packets are affected by the Dos attack.

Noting that when $n = 0$, it means that there is no Dos attack at the initial moment, that is, $\theta(t) = 0$. Due to the limitation of its own energy, the attacker cannot cause all data packets to be lost, and $1/\omega$ represents the average value of data packets subjected to Dos attacks [12].

2.2. Data Mining Technology. Data mining technology is one of the most important technologies for social development in the context of big data. Through the generation and use of computer mining technology, the data information obtained is more complete and effective, the processing accuracy is also high, and more complete results can be obtained. From the analysis of real-life applications, big data applications can develop visual data processing technology, and its data computing and processing capabilities are the most important. At present, the algorithms of data mining technology are as follows: clustering algorithm, classification algorithm, neural network algorithm, regression algorithm, website data mining, and association algorithm. The AKN algorithm studied in this article is a neural network algorithm that simulates the learning and thinking process of the human brain. After training a few samples, we generated a similar algorithm that can distinguish different sample data. Data mining technology extracts data rules that people cannot easily reflect intuitively from huge, noisy, and large-scale data because all these data are a useful potential rule. Traditional data mining techniques usually start with limited traditional data mining techniques. With the widespread use of the Internet, network big data analysis technologies are constantly upgrading. The data analysis technology that combines traditional data mining with the basic concepts of the Internet is widely used in today's world. Network data mining technology quickly and accurately identifies potentially useful information to users and various behavioral information hidden in the network, and provides users with various services with different needs [13].

The basic process of computer-based data mining technology is shown in Figure 2, and determining the target of data mining is a major task of data analysis. Firstly, the main way to determine goals is to conduct user interviews, investigate and analyze key executives in different departments, determine the final business goals, and conduct business understanding analysis. Secondly, data mining engineers need to perform "data understanding" tasks based on business understanding to realize data collection and management. The data preparation process is more cumbersome because the process is to check and modify data, use network information to collect and organize data, and convert and modify data. After the change is completed, it provides a basis for establishing a data model. Once the modeling is completed, the model needs to be optimized multiple times to complete all the work in the data mining cycle. With the continuous deepening of user applications, data mining strategies and models are also continuously

optimized, and this mining technology can only operate stably after the business rules are stable [14].

2.3. AKN Algorithm.

- (1) The source of the AKN algorithm: the Kohonen network (KN for short) proposed by Professor Teuvo Kohonen of the University of Helsinki in Finland is a self-organizing competitive neural network. Self-organization means that the network is unsupervised and can learn independently, and according to the characteristics of the environment, the element value can be adjusted through the self-organizing function relationship so that the neural network can automatically distinguish and aggregate classification. In this form of expression, neurons will match a specific input form and enhance the impression, resulting in sensitivity. Therefore, the input form can be divided into different clusters through self-organized training and learning. Each cluster has different response characteristics to the input form, so the neuron can become a detector in a certain environment [15].
- (2) The principle of the AKN algorithm: the operating mechanism of KN is that when data are input to the neural network, the Euclidean distance (Euclidean distance, also called meta value in this article) between the input node of the neuron node of the output layer and the neuron node of the output layer is calculated. The victory cell is the neuron with the smallest Euclidean distance, and the cell value coefficients of the victory cell and neighboring neurons can be adjusted to make the cell values of the generated neuron and surrounding neurons closer to the input sample. After multiple exercises, the finally connected element value distribution of each neuron has a specific relationship. This distribution aggregates similar patterns between input values to be divided into different types of neurons, so neurons of the same type have similar element value factors, but different types of neurons have great differences in value coefficients. During practice, the efficiency of the modified cell value and the cell value of neighboring neurons continue to decrease; that is, the neurons of the same kind are gradually gathered. The traditional algorithm that uses the characteristics of the neural network to perform calculations is called the KN algorithm. The traditional unsupervised KN algorithm has limitations in its classification. Unsupervised classification of unknown category data is feasible, but the results of the same type of data will correspond to different network nodes. For one-to-one corresponding node categories, the KN classification categories are more than the actual data categories. In order to improve the classification effect, the improved AKN algorithm proposed in this paper adds a supervised learning process after the first stage of unsupervised learning to allow the system to adapt to the correct classification results. The principle of this algorithm is shown in Figure 3.

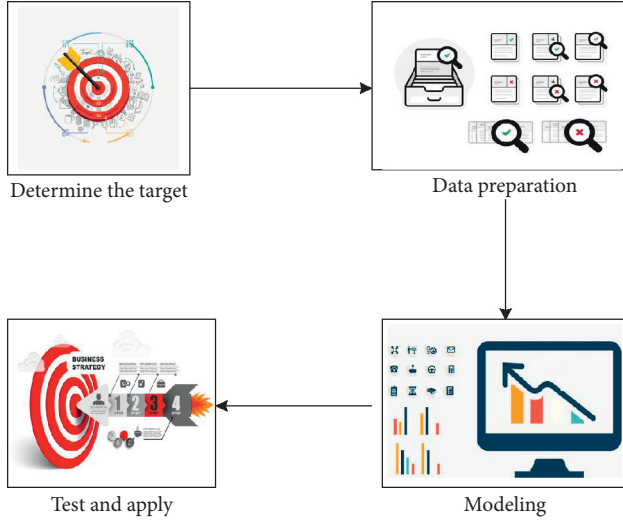


FIGURE 2: Flowchart of data mining.

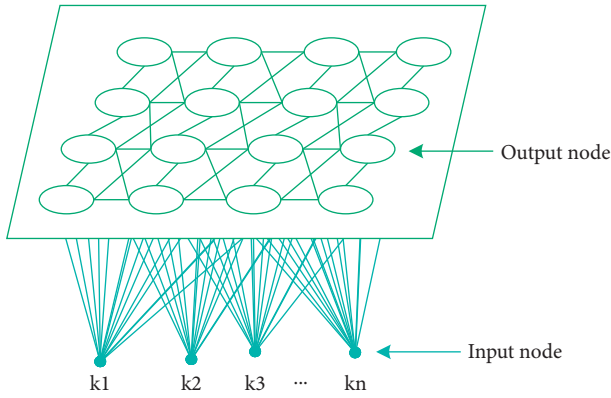


FIGURE 3: Schematic diagram of the AKN algorithm.

As shown in Figure 3, if there are S KN output nodes, denoted by f , and the input node is at the bottom, the node is represented by k , and the calculation is represented by the symbol u . If the input vector has n elements, there are n nodes in total at the input. C_{Kf} represents the size of the element value from the input node to the output node, and the output nodes on the same plane can also be connected to each other. The function of the AKN algorithm is to increase the supervised learning process, which uses a large number of samples for training through independent learning, continuously adjusts the network's element value, and finally obtains the clustering distribution of the data [16].

- (3) AKN algorithm content: the algorithm steps are as follows:

Input: training and test samples;

Output: the sample element value coefficient matrix after training and the clustering category and test accuracy of the test sample;

- (1) t_0 is the start, t_1 is a constant, representing time, and t_2 is the total number of training; the value of the connection element from the input node to the output node is assigned with a random number, combined with the expression of the sum of the neighborhood $A_{f,f(x)}(s)$ and the training rate $\eta(s)$, and the number of output neurons is S .

- (2) Network input mode

$$Z = [z_1, z_2, \dots, z_K]^T. \quad (3)$$

Among them, K is the dimension of the input vector.

- (3) Initializing the weight:

$$C_f = [C_{1f}, C_{2f}, \dots, C_{kf}]^T. \quad (4)$$

Among them, $f = 1, 2, \dots, S$.

- (4) Calculation of sample vector and element value:

$$d_f = \|Z - C_f\| = \sqrt{\sum_{u=1}^S (x_u - C_{uf}(t))^2}. \quad (5)$$

Then, the element value expression of the victory element f^* is

$$d_{f^*} = \min\{d_f\}. \quad (6)$$

- (5) Adjusting the element value vector of nodes connected in the output and geometric neighborhood:

$$C_f(n+1) = C_f(n) + \eta(s)A_{f,f(x)}(n)(Z - C_f(n)). \quad (7)$$

Among them, $A_{f,f(x)}(s)$ is the neighborhood adjustment function.

- (6) If there is still a training sample dataset, go back to step (2);

- (7) If all samples are trained and $t < t_2$, $t = t + 1$, return to step (2); otherwise, return to step (8).

- (8) Training is over [17].

As shown in (8), $\eta(s)$ is the training rate at s , and as the number of training continues to increase, the value of s continues to increase, and then the inverse proportional relationship according to (8) will continue to decrease.

$$\eta(s) = \eta_1 \exp\left(1 - \frac{s}{t_2}\right). \quad (8)$$

Among them, t_2 is the total number of training; the initial training rate is η_1 , $s = 0, 1, 2, \dots$

The adjustment of the neighborhood is done by

$$A_{f,f(x)}(s) = \exp\left(1 - \frac{d_{f,u}^2}{2\varepsilon(s)^2}\right). \quad (9)$$

Among them, the distance from each neuron on the same plane to the victory element is represented by $d_{f,u}$, and

the parameter that controls the data distribution is represented by $\varepsilon(s)$. The adjustment formula is σ

$$\varepsilon(s) = \varepsilon_1 \exp\left(1 - \frac{n}{t_1}\right). \quad (10)$$

And, the training and test data are normalized, as shown in formulas (11)–(13):

$$x = \frac{(x_{\max} - x_{\min}) \times (y - y_{\min})}{y_{\max} - y_{\min}} + x_{\min}, \quad (11)$$

$$x'_{kf} = \frac{x_{uf}}{\sqrt{x_{1f}^2 + x_{2f}^2 + \dots + x_{kf}^2}}, \quad (12)$$

$$C'_{kf} = \frac{C_{uf}}{\sqrt{C_{1f}^2 + C_{2f}^2 + \dots + C_{kf}^2}}. \quad (13)$$

According to the Euclidean distance d_f of the above formula (5), the degree of clustering between the input sample and the output neuron is expressed as

$$\begin{aligned} \rho(C_f(Z)) &= \{\rho(d_f(Z)), 0, \sqrt{0.2}\}, \\ \rho(C_f(Z)) &= e^{-d_f(Z)^2/0.4}. \end{aligned} \quad (14)$$

When $\rho > 0.5$, the output neuron is defined as the cluster to which the input sample belongs.

According to the category, the average value of each category is calculated, as shown in the following formula:

$$\bar{d}_x = \frac{x'_{kf}}{x_{1f} + x_{2f} + \dots + x_{kf}}, \quad (15)$$

$$\bar{d}_C = \frac{C'_{kf}}{C_{1f} + C_{2f} + \dots + C_{kf}}. \quad (16)$$

Using the cluster data calculation model, formula (17) can be used to obtain the neuron center value of the cluster [18].

$$d(f, u) = \sqrt{C_1|x_{1u} - x_{1f}|^2 + C_2|x_{2u} - x_{2f}|^2 + \dots + C_k|x_{ku} - x_{kf}|^2}. \quad (17)$$

3. Experiment and Analysis

3.1. Model Design of AKN Algorithm. Denial of service attack detection based on the AKN (adaptive Kohonen network) algorithm includes four aspects: data collection, collection of characteristic element values, cluster analysis, and detection and judgment. The data detection method of the AKN algorithm used in this paper is to divide the data sample into multiple detection paths per unit time and then collect the special element values of the detection paths for cluster analysis according to the impact of Dos attacks on the degree of clustering. In the pretrained nonattack sample data, the range value is extracted, and the cluster is analyzed according to the principle of Dos attack to determine

whether a Dos attack occurs. The denial of service attack detection model based on the AKN algorithm can realize high-speed, low-consumption, and high-precision detection of complex network denial of service attacks. According to the previous content, we know the principle of Dos attack, the principle of AKN algorithm, and the process of data mining technology, from which we establish an algorithm model [19].

To select data from the learning database, we used the traditional KN algorithm and the AKN algorithm to analyze 300, 500, 1,000, 2,000, 3,000, 4,000, and 5,000 datasets with three-dimensional features for small-class clustering and multiclass clustering. The result of the comparison is shown in Figure 4 [20].

In Figure 4, it can be seen that as the sample points increase, the squared errors of the two algorithms increase. And the AKN algorithm shown in the left picture is calculated with 2,500 sample points; the square of error is 165, while the square of error of the traditional KN algorithm on the right is 255. Under the calculation of 5,000 sample points, the error is 310, while the traditional KN algorithm on the right is 430. Through the comparison of the sum of square error function values of the two algorithms through the above numerical experiments, it can be found that the performance of the AKN algorithm is better than that of the KN algorithm when the number of clusters is certain, and the more points, the more obvious the effect; in the case of a certain number of points and more clusters, the better the performance of the AKN algorithm. From the following experiments, it can be seen that the average performance of the new algorithm when clustering multiple classes is about 30% higher than the average performance of the KN algorithm, while the average performance of the AKN algorithm when clustering fewer classes is about 20% higher than the average performance of the Kohonen algorithm. In data mining, cluster analysis with a large amount of data and a large number of categories is often encountered, and the detection effect of the AKN algorithm will be good.

To study the actual utility of the AKN algorithm, the high-configuration Intel Core i9 processing computer used in this paper is equipped with a 2.6 GHz frequency graphics card and uses 6GB of memory; however, the actual use environment uses a complex multiclustering AKN network model. Random 22,000 data records are selected; 6,000 records are used for AKN neural network training, and the other 16,000 records will be used for testing. Table 1 shows the identification types of test data, which are divided into five categories: Dos attack, Probing, Normal, R2L, and U2R [21].

The output neuron node is located in the 8×8 square matrix. The victory element node is used as the sample node, and the competing neuron layer node in the same plane with the shortest distance from the input sample is calculated according to formulas (5) and (6). The meta value of the winning meta node is adjusted according to formula (7), which allows the domain radius and learning rate to gradually decrease with the progress of the process, thereby allowing the input data to gradually concentrate on multiple nodes, and the neural network can complete the clustering

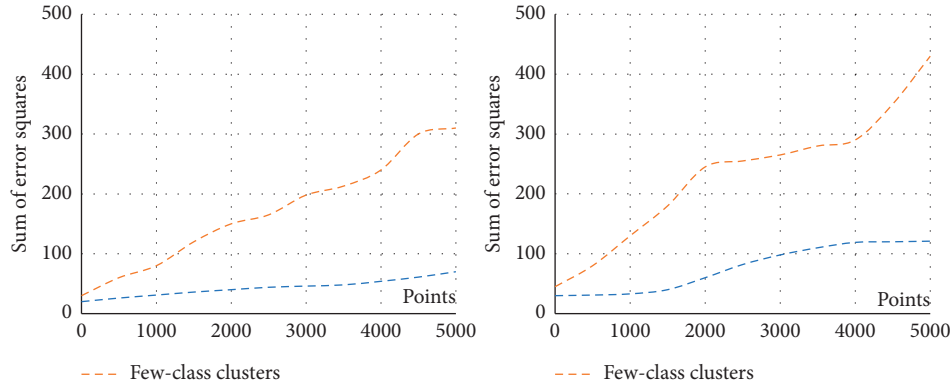


FIGURE 4: Error square graph of AKN algorithm and traditional KN algorithm.

TABLE 1: Identification types of test data.

Type	Meaning	Classification ID
Normal	Normal record	Normal
DoS	Denial of service attack	Back, land, Neptune, pod, smurf, teardrop
Probing	Surveillance and other detection activities	psweep, nmap, portsweep, satan
R2L	From remote machine unauthorized access	ftp_write, guess_passwd, imap, mul-tihop, phf, spy, warezclient, warez-master
U2R	Illegal access by ordinary users to local superuser privileges	Buffer_overflow, loadmodule, perl, rootkit

function. In this paper, the maximum field is 1.6, the minimum field is 0.3, the maximum learning probability is 0.15, and the minimum learning probability is 0.02, including a total of 32,000 network learning adjustments [22].

3.2. Data Mining Model Based on AKN Algorithm. According to the process of data mining technology, the data are preprocessed first. Since each connection in the dataset is described by multiple characteristics, there are numbers and character types to describe different attacks with multiple characteristics. For text data, the dataset must be preprocessed because it must be converted to a digital format before it can be recognized by the Kohonen network. Table 2 shows the numeric codes corresponding to the two-dimensional character data, and Table 3 shows the numeric codes corresponding to the preprocessing results of the three-dimensional character data [23].

In order to compare the performance of the algorithm in this paper, two methods are selected for experimental testing. In this paper, the false alarm rate, the correct rate, and the time used are used to evaluate the detection performance of the network data anomaly detection method, as shown in formulas (18) and (19):

$$E_r = \frac{E}{S}, \quad (18)$$

$$Y_r = \frac{T}{S}. \quad (19)$$

Among them, E_r is the false alarm rate, Y_r is the correct rate, E is the number of falsely reported test samples, T is the number of detected test samples, and S is the total number of test samples.

The processed training data are used as input data for AKN and traditional KN calculations to perform training. When the network training is completed, the processed test data are sent to the AKN and KN network environment for calculation. The resulting DoS test set and DoS detection are shown in Figure 5 [24].

It can be seen from Figure 5 that among the 30 test samples in the statistical test, the KN algorithm did not match the test results in the 18th and 23rd types of tests, and there were two errors. However, the AKN algorithm has only one error in the 23rd category, indicating that the prediction error of AKN is smaller than that of KN, and the prediction is more accurate. The AKN algorithm prediction accuracy rate is about 97%, while the KN algorithm is about 91%. Next, we conduct 10 sets of model tests on the two algorithms to calculate their calculation time and accuracy. The test results are shown in Figures 6 and 7 [25].

It can be seen from Figure 6 that the test accuracy of the AKN algorithm is generally higher than that of the KN algorithm, and the lowest and highest accuracy of the AKN algorithm are both higher than the KN algorithm, indicating that its detection stability and accuracy are better than the KN algorithm. It can be seen from Figure 7 that in these 10 sets of test experiments, the running time of the AKN

TABLE 2: Numerical coding for second dimensional character data.

Agreement type	Icmp	Tcp	Udp	Other agreements
Coding	1	2	3	4

TABLE 3: Numerical coding for third dimensional character data.

Internet service	Login	Hostnames	Ftp	Finger	ecr_i	Time	Systat
Coding	0	2	5	8	10	11	15
Internet service	Private	Netstat	domain_u	telnet	http	ftp_data	Other
Coding	18	20	21	23	25	28	30

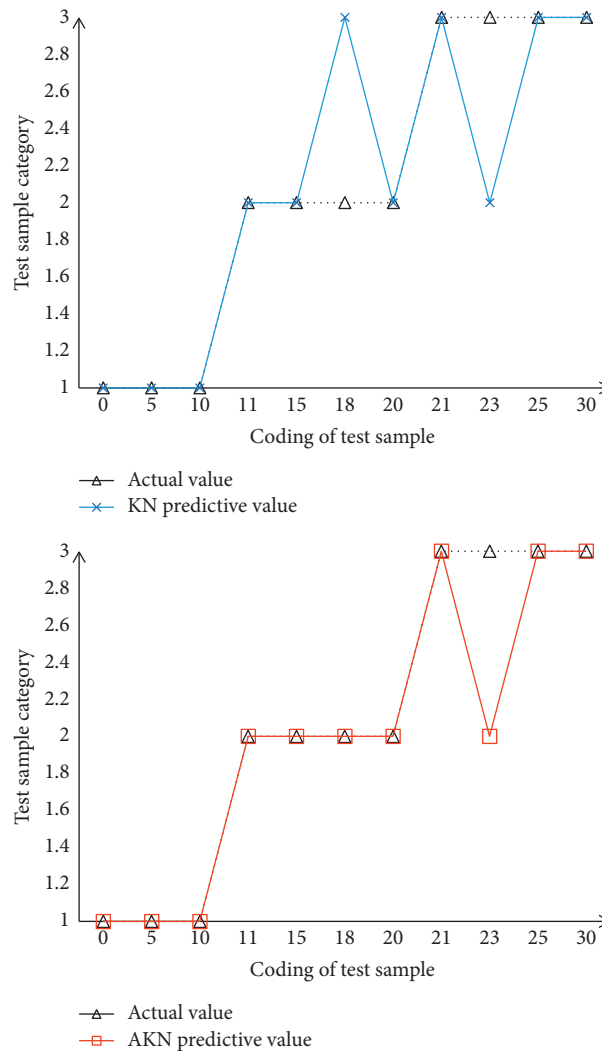


FIGURE 5: Comparison of prediction accuracy between AKN and KN algorithms.

algorithm is also better than that of the KN algorithm. In general, the AKN algorithm is superior to the traditional KN algorithm in terms of detection stability, accuracy, and time efficiency [26].

3.3. Investigation of the Research Status of Data Mining Technology. At present, data mining technology is widely used in medicine, finance, network security, and

telecommunications. In terms of Dos attacks, which are relatively common in network security, data mining techniques have also been studied and applied. According to the survey of this technology, classification and statistics are respectively carried out from the researched literature, as shown in Table 4.

As can be seen from Table 4, among the 6,389 articles on data mining technology surveyed, 2,910 articles are about network security research, of which 1,235 articles are about

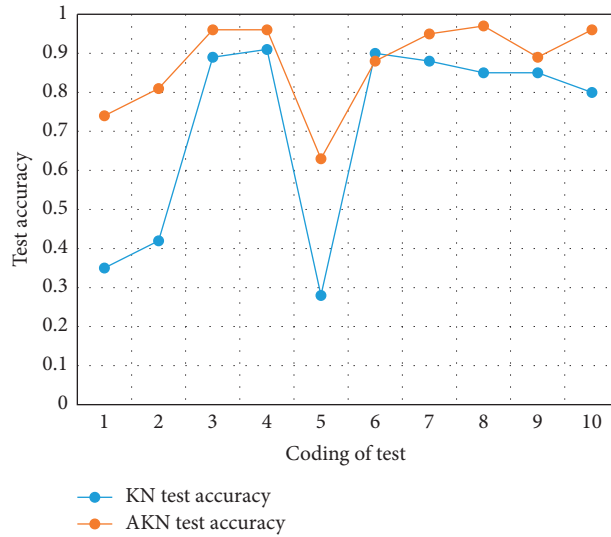


FIGURE 6: Comparison of AKN and KN algorithm test accuracy.

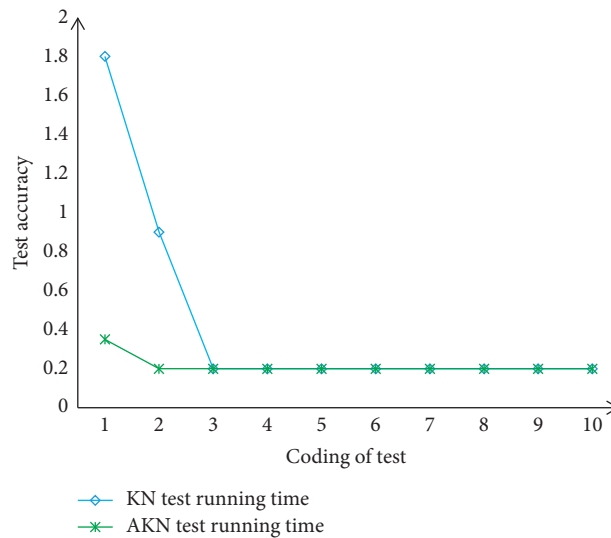


FIGURE 7: Comparison of AKN and KN algorithm test running time consumption.

TABLE 4: Survey of articles on data mining technology.

Total articles	6,389		
Number of articles on cyber security	2,910		
Number of articles on Dos attack	1,235		
Types of data mining technology	Classification algorithm	Regression analysis	Cluster analysis
Number of articles	243	50	430
Types of data mining technology	Association rules	Neural network algorithm	Web data mining
Number of articles	103	313	96

Dos attacks. In addition, 430 papers on clustering analysis, 313 papers on neural network algorithms, and 243 papers on classification algorithms, respectively, account for the top three in the number of documents. It shows that these three types of data mining technologies have relatively more research applications in network security. In fact, the

application of big data mining technology is not the application of a single algorithm. It is often a combination of multiple algorithms before data mining. It abstracts the process of data mining to form a universal data mining method, and compared with the traditional single method, it has higher availability, reproducibility, and versatility [27].

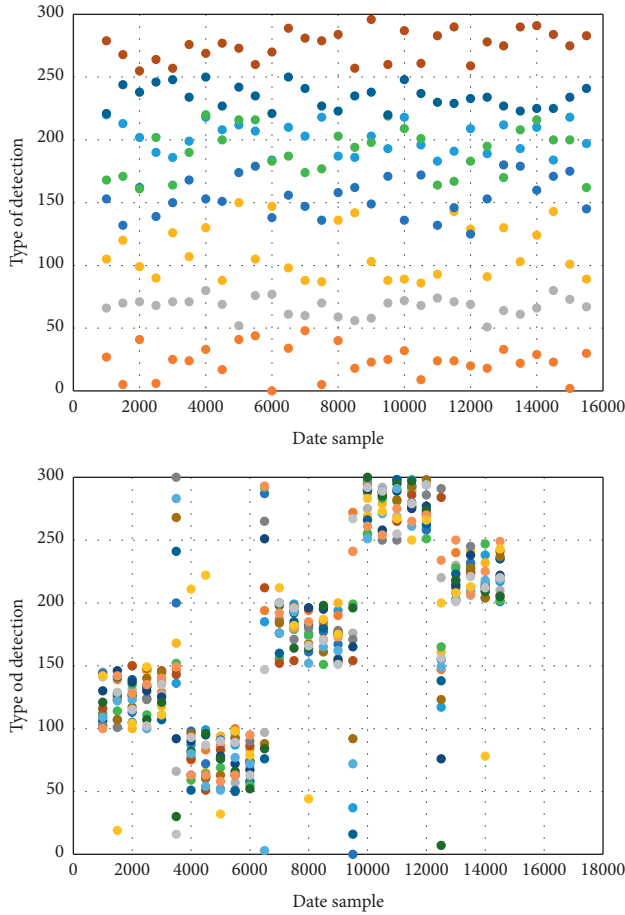


FIGURE 8: Dos test results.

3.4. Data Mining Technology and Dos Attack Test Based on AKN Algorithm. The data mining technology based on the AKN algorithm not only uses the self-organizing learning ability of the neural network but also combines the characteristics of cluster analysis. Conducive to the Dos attack test based on the data mining technology of the AKN algorithm, the experiment collected 16,000 sample sets and performed data statistics on different detection categories. The obtained test set and detection results are shown in Figure 8 [28].

It can be seen from Figure 8 that after self-organizing training and detection of the AKN algorithm, the data samples are gathered into 4 clusters. The data samples are clustered into 5 clusters. The five clusters are distributed in a specific detection range; cluster 1 is distributed in the range of codes 100 to 150, cluster 2 is in codes 50 to 100, cluster 3 is in codes 150 to 200, cluster 4 is within the code 150 to 200, and cluster five is within the code 200 to 250; however, each cluster has a small amount that has not been calculated. In this regard, the difference between the predicted category and the calculated result category is also counted, as shown in Figure 9 [29].

It can be seen from Figure 10 that in the predicted two clustering categories, 300 detection data were predicted, respectively, and the detection error of category one was 9, and the accuracy rate reached 97%, and the detection error

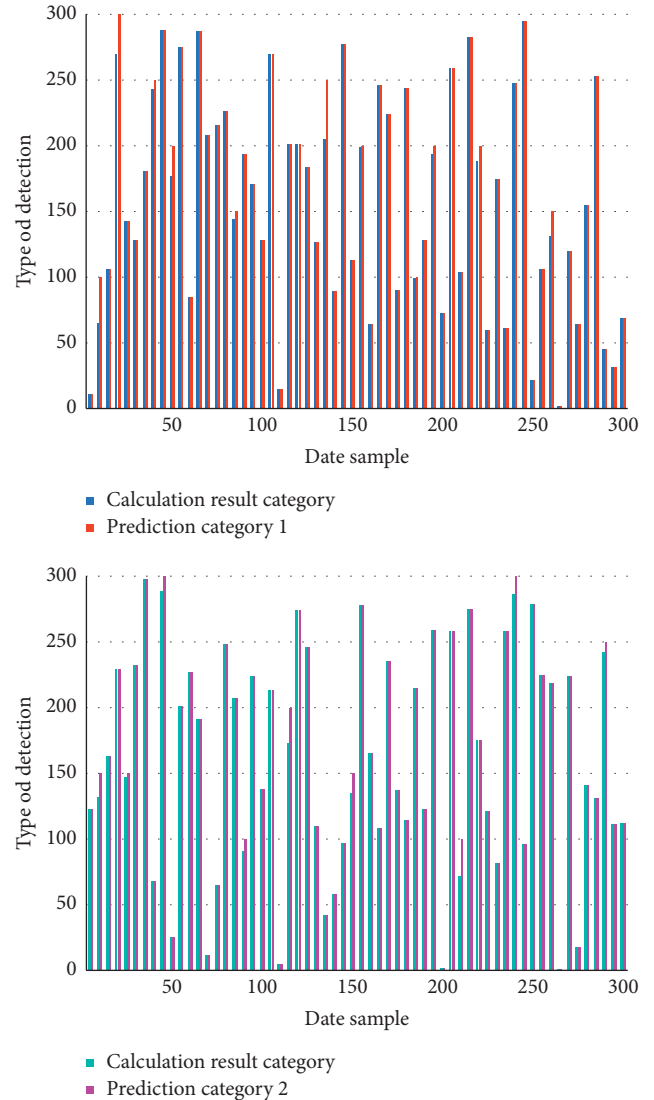


FIGURE 9: Comparison of AKN algorithm prediction category and actual category.

of category 2 is 8, and the accuracy rate reaches 97.33%. It can be seen from Figure 10 that the detection accuracy of the four clusters of the AKN algorithm is higher than that of the KN algorithm, which is about 6% higher than the traditional KN algorithm [30–32]. This shows that the detection accuracy of the AKN algorithm is higher, and it can more effectively defend against Dos attacks [33–36].

4. Discussion

This article first studies the generation, characteristics, types, and principles of Dos attacks, and then studies the current research status of data mining technology on denial of service attacks, and understands the characteristics, processes, and principles of data mining technology. Then, the source, principle, content, and steps of the AKN algorithm are studied, and the AKN algorithm model and related experiments are established and analyzed.

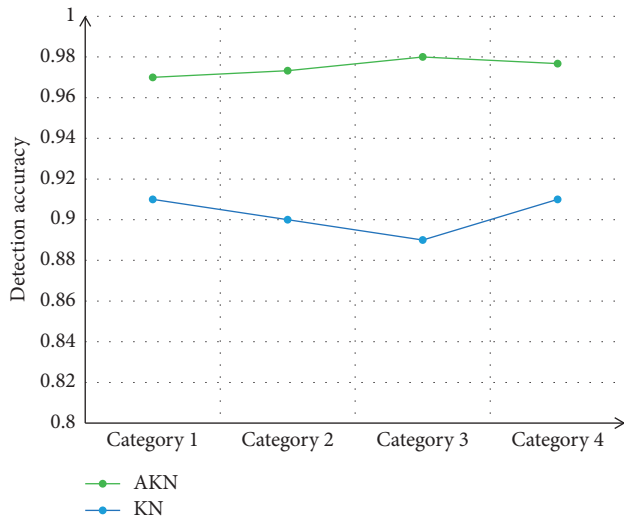


FIGURE 10: Comparison of accuracy rates of cluster detection results.

In the research process, this article also draws on a lot of relevant documents and understands that more and more scholars are doing research on network security, and research on typical denial of service attacks is in full swing. As a neural network algorithm that can automatically adapt and organize learning, it is especially suitable for this kind of data and network complex environment, and it is also more systematic, and the superiority of the algorithm can also be explained by the experimental results.

In the experimental part, this article collects data samples, uses the AKN algorithm steps and formulas, illustrates the diagrams, and compares the experimental data with the traditional neural network algorithm to obtain the superiority of the AKN algorithm. As a result, the detection accuracy of the AKN algorithm is higher, and it can defend against Dos attacks more quickly and effectively.

5. Conclusions

After establishing the AKN algorithm model, this paper detects and analyzes the data samples of the Dos attack, compares it with the traditional KN algorithm, and finally concludes that the computer data mining technology based on the AKN algorithm is used in the defense and detection of denial of service attacks. The detection accuracy rate is as high as 97%, while the traditional KN algorithm is only 91%, and the detection accuracy rate is increased by at least 6 percentage points. And its detection running time is less than the traditional KN algorithm, and the average detection performance is increased by about 30% when detecting multiple clusters, and the average detection performance is increased by about 20% when detecting a few clusters. Therefore, we can be sure that the use of computer data mining technology based on the AKN algorithm can perform faster, more efficient, and accurate defense detection under Dos attacks.

Data Availability

Data sharing is not applicable to this article as no new data were created or analyzed in this study.

Conflicts of Interest

The author declares no conflicts of interest.

References

- [1] E. Adi, Z. A. Baig, P. Hingston, and C.-P. Lam, "Distributed denial-of-service attacks against HTTP/2 services," *Cluster Computing*, vol. 19, no. 1, pp. 79–86, 2016.
- [2] S. Y. Chang and Y. C. Hu, "SecureMAC: securing wireless medium access control against insider denial-of-service attacks," *IEEE Transactions on Mobile Computing*, vol. 16, no. 12, 2017.
- [3] D. Douglas, J. J. Santanna, D. Ricardo, and L. Z. Granville, "Booters: can anything justify distributed denial-of-service (DDoS) attacks for hire?" *Journal of Information, Communication and Ethics in Society*, vol. 15, no. 1, pp. 90–104, 2017.
- [4] H. Pan, H. Wang, Y. Wang, and H. Huang, "Rules of acupoint selection for diabetic peripheral neuropathy based on data mining technology," *Zhongguo Zhen Jiu=Chinese Acupuncture & Moxibustion*, vol. 36, no. 10, pp. 1111–1114, 2016.
- [5] W. Zhao-Yi, H. Zheng-De, Y. Ping, R. Ting, and L. Xin-Hui, "Regularity of wind-dispelling medication prescribed by li dong-yuan: a data mining technology-based study," *Digital Chinese Medicine*, vol. 3, no. 1, pp. 20–33, 2020.
- [6] Z. Hu, Y. V. Bodyanskiy, Y. Bodyanskiy, O. K. Tyshchenko, and O. Boiko, "An ensemble of adaptive neuro-fuzzy kohonen networks for online data stream fuzzy clustering," *International Journal of Modern Education and Computer Science*, vol. 8, no. 5, pp. 12–18, 2016.
- [7] A. Durrani, S. Latif, R. Latif, and H. Abbas, "Detection of denial of service (DoS) attack in vehicular ad hoc networks: a systematic literature review," *Ad Hoc & Sensor Wireless Networks*, vol. 42, no. 1-2, pp. 35–61, 2018.
- [8] H. Abbas, R. Latif, S. Latif, and A. Masood, "Performance evaluation of enhanced very fast decision tree (EVFDT) mechanism for distributed denial-of-service attack detection in health care systems," *Annals of Telecommunications*, vol. 71, no. 9, pp. 477–487, 2016.
- [9] H. Lu, R. Setiono, and H. Liu, "Effective data mining using neural networks," *IEEE Transactions on Knowledge & Data Engineering*, vol. 8, no. 6, pp. 957–961, 2016.
- [10] C. Helma, T. Cramer, S. Kramer, and L. Raedt, "Data mining and machine learning techniques for the identification of mutagenicity inducing substructures and structure activity relationships of noncongeneric compounds," *Journal of Chemical Information and Computer Sciences*, vol. 35, no. 4, pp. 1402–1411, 2018.
- [11] A. Buczak and E. Guven, "A survey of data mining and machine learning methods for cyber security intrusion detection," *IEEE Communications Surveys & Tutorials*, vol. 18, no. 2, pp. 1153–1176, 2017.
- [12] D. A. Adeniyi, Z. Wei, and Y. Yongquan, "Automated web usage data mining and recommendation system using K-Nearest Neighbor (KNN) classification method," *Applied Computing and Informatics*, vol. 12, no. 1, pp. 90–108, 2016.
- [13] I. Kavakiotis, O. Tsave, A. Salifoglou, N. Maglaveras, I. Vlahavas, and I. Chouvarda, "Machine learning and data

- mining methods in diabetes research,” *Computational and Structural Biotechnology Journal*, vol. 15, pp. 104–116, 2017.
- [14] X. Yan and L. Zheng, “Fundamental analysis and the cross-section of stock returns: a data-mining approach,” *Review of Financial Studies*, vol. 30, no. 4, pp. 1382–1423, 2017.
- [15] L. Xu, C. Jiang, J. Wang, J. Yuan, and Y. Ren, “Information security in big data: privacy and data mining,” *IEEE Access*, vol. 2, no. 2, pp. 1149–1176, 2017.
- [16] S. García, J. Luengo, and F. Herrera, “Tutorial on practical tips of the most influential data preprocessing algorithms in data mining,” *Knowledge-Based Systems*, vol. 98, pp. 1–29, 2016.
- [17] H. Hong, H. R. Pourghasemi, and Z. S. Pourtaghi, “Landslide susceptibility assessment in Lianhua County (China): a comparison between a random forest data mining technique and bivariate and multivariate statistical models,” *Geomorphology*, vol. 259, pp. 105–118, 2016.
- [18] P. A. Flach, “Encyclopedia of machine learning and data mining,” *Journal of Shijiazhuang Vocational Technology Institute*, vol. 2, no. 2, pp. 110–114, 2016.
- [19] Z. Ge, Z. Song, S. X. Ding, and B. Huang, “Data mining and analytics in the process industry: the role of machine learning,” *IEEE Access*, vol. 5, 2017.
- [20] T. Emoto, T. Yamashita, T. Kobayashi et al., “Characterization of gut microbiota profiles in coronary artery disease patients using data mining analysis of terminal restriction fragment length polymorphism: gut microbiota could be a diagnostic marker of coronary artery disease,” *Heart and Vessels*, vol. 32, no. 1, pp. 39–46, 2017.
- [21] H. Hong, P. Tsangaratos, I. Ilia, J. Liu, A.-X. Zhu, and W. Chen, “Application of fuzzy weight of evidence and data mining techniques in construction of flood susceptibility map of Poyang County, China,” *The Science of the Total Environment*, vol. 625, pp. 575–588, 2018.
- [22] M. Rich, “Denial of service,” *CQ Amateur Radio*, vol. 72, no. 12, pp. 8–48, 2016.
- [23] V. S. Dolk, P. Tesi, C. D. Persis, and W. P. M. H. Heemels, “Event-triggered control systems under denial-of-service attacks,” *IEEE Transactions on Control of Network Systems*, vol. 4, no. 1, 2016.
- [24] H. Luo, Z. Chen, J. Li, and A. V. Vasilakos, “Preventing distributed denial-of-service flooding attacks with dynamic path identifiers,” *IEEE Transactions on Information Forensics and Security*, vol. 12, no. 8, pp. 1801–1815, 2017.
- [25] X. Zhong, I. Jayawardene, G. K. Venayagamoorthy, and R. Brooks, “Denial of service attack on tie-line bias control in a power system with PV plant,” *IEEE Transactions on Emerging Topics in Computational Intelligence*, vol. 1, no. 5, pp. 375–390, 2017.
- [26] S. Khan, A. Gani, A. Wahab, and P. Singh, “Feature selection of denial-of-service attacks using entropy and granular computing,” *Arabian Journal for Science and Engineering*, vol. 43, no. 9, pp. 1–10, 2017.
- [27] T. Marwala, V. M. Kuthadi, and R. Selvaraj, “Ant-based distributed denial of service detection technique using roaming virtual honeypots,” *IET Communications*, vol. 10, no. 8, pp. 929–935, 2016.
- [28] Y. Wang, Y. Zhang, X. Hei, W. Ji, and W. Ma, “Game strategies for distributed denial of service defense in the cloud of things,” *Journal of Communications and Information Networks*, vol. 1, no. 4, pp. 143–155, 2016.
- [29] T. Boraten and A. Kodi, “Mitigation of hardware trojan based denial-of-service attack for secure NoCs,” *Journal of Parallel and Distributed Computing*, vol. 111, pp. 24–38, 2017.
- [30] Y. Zeng, G. Chen, K. Li, Y. Zhou, X. Zhou, and K. Li, “M-skyline: taking sunk cost and alternative recommendation in consideration for skyline query on uncertain data,” *Knowledge-Based Systems*, vol. 163, pp. 204–213, 2019.
- [31] Y. Chen, Y. Ping, Z. Zhang, B. Wang, and S. He, “Privacy-preserving image multi-classification deep learning model in robot system of industrial IoT,” *Neural Computing and Applications*, vol. 33, no. 10, pp. 4677–4694, 2021.
- [32] B. Bo Rong, Y. Yi Qian, K. Kejie Lu, H. H. Hsiao-Hwa Chen, and M. Guizani, “Call admission control optimization in WiMAX networks,” *IEEE Transactions on Vehicular Technology*, vol. 57, no. 4, pp. 2509–2522, 2008.
- [33] L. Li, H. Zhang, Y. Xia, and H. Yang, “Security estimation under denial-of-service attack with energy constraint,” *Neurocomputing*, vol. 292, pp. 111–120, 2018.
- [34] J. Chen and C. Yu, “A WebGIS-based system for urban stormwater risk analysis using a cloud matter-element model,” *International Journal of Intelligent Information Technologies*, vol. 16, no. 3, pp. 80–99, 2020.
- [35] Z. Xu, G. Zhu, N. Metawa, and Q. Zhou, “Machine learning based customer meta-combination brand equity analysis for marketing behavior evaluation,” *Information Processing & Management*, vol. 59, no. 1, Article ID 102800, 2022.
- [36] L. Yin, X. Li, L. Gao, C. Lu, and Z. Zhang, “A novel mathematical model and multi-objective method for the low-carbon flexible job shop scheduling problem,” *Sustainable Computing: Informatics and Systems*, vol. 13, no. 3, pp. 15–30, 2017.

Research Article

Reliability and Life Prediction Algorithms of Insulated Cables Based on Wireless Network Communication

Jianyu Sun ^{1,2}, Zhonghua Ni,¹ and Yanxin Liu^{1,2}

¹Mechanical Engineering School, Southeast University, Nanjing, Jiangsu 211189, China

²Zhongli Science and Technology Group Co., Ltd., Suzhou, Jiangsu 215000, China

Correspondence should be addressed to Jianyu Sun; 230188150@seu.edu.cn

Received 24 December 2021; Revised 17 January 2022; Accepted 20 January 2022; Published 12 February 2022

Academic Editor: Alireza Souri

Copyright © 2022 Jianyu Sun et al. This is an open access article distributed under the Creative Commons Attribution License, which permits unrestricted use, distribution, and reproduction in any medium, provided the original work is properly cited.

Since the size of the power system is getting larger, the power of the transmission and electrical power generation also increase, and the safety operation of the transmission and electrical power is becoming more and more important. This article is intended to study algorithm for reliability and life prediction based on wireless network communication. This paper first studies the energy consumption of wireless network communication, analyzes the maximization of network life, and then evaluates the thermal aging characteristics and life of XLPE cable insulation based on wireless communication. Through model establishment and analysis, when the reliability is below 50%, the reliability of the cable is basically not guaranteed. It is necessary to formulate an update and replacement plan to ensure the safe and stable operation of the power grid.

1. Introduction

Electricity is the heart of the coal industry. Only a good power supply environment and reliable power quality can lead the strong development of the coal industry. For load transmission, good cable quality is of great significance for ensuring power quality and safe production. Among them, the long service life of the cable and the efficiency of the cable are very important. Taking into account the particularity of coal mine areas, cables often run under dirty and humid conditions. According to the needs of different occasions, the cables are different; no matter the material or the site environmental, they are completely different from the cables buried in the power grid. In addition, many coal mining companies often allow cables to run at full load or even overload, which has a great impact on the remaining working life of the cable. These special effects make the cable generally unable to reach its normal service life. This paper firstly studies the energy consumption of wireless network communication, analyzes the network life maximization problem model, and performs curve fitting on the aging life of the insulated cable. At the same time, the building model of the reliability of the insulated cable is given, and then the

thermal aging characteristics and life of the XLPE cable insulation material are evaluated according to wireless communication, and the insulation state of the XLPE cable is evaluated and predicted and reliability is evaluated.

In order to detect the occurrence of cable defects early and ensure the safe operation of the cable, it is necessary to determine the reliability of the cable and obtain the reliability of the cable at different times so as to determine the best time for cable maintenance and maintenance. Minimizing grid failures from a “macroscopic” perspective is of great significance for ensuring the safe, stable, and reliable operation of the power system.

According to the research progress at home and abroad, different scholars have also made corresponding investigations in wireless network communication and cables. Yasui et al. investigated the use of insulated cable-type down conductors as lightning protection measures for these facilities. The study found that the overvoltage caused by the lightning current in the cable can be assessed by using the lightning current reflection of the public grounding system. In addition, the overvoltage value can be estimated by the steepness of the lightning current, the surge impedance and speed of the cable, and the length of the cable [1]. He et al.

showed that in order to gain insight into the space charge accumulation in cable accessories, under the AC voltage of 26.1 kV and the temperature of 103°C and 114°C, the 10 kV cross-linked polyethylene (XLPE) insulated cable sample with stress cone was subjected to accelerated aging; the space charge distribution in the cable insulation layer was tested in different aging stages. The research provides insights into the important role of semiconductors in the accumulation of electrical charges in cable accessories, which will help to optimize and extend the life of cable accessories [2]. Ohki and Hirai studied how the fault location ability depends on the type, structure, and insulation material of the cable. For the location of the location heated by the heater, the cable insulated with PVC provides higher signal strength than the cable insulated with XLPO [3]. Du et al. proposed advanced materials with good thermal and electrical properties to improve the performance of electric vehicle charging cables. The test results show that modified EPDM insulation materials have good electrical and mechanical properties. In addition, the calculated theoretical current carrying capacity of the cable shows an improvement, and the use of high TC insulation and sheath seems to have great benefits in reducing the temperature of the EV charging cable and increasing the current carrying capacity [4]. Parise et al. discussed a simplified model of a low-voltage (LV) cable system with one and two time constants to evaluate cable temperature behavior and the impact of environmental and installation conditions. In addition, a device for calculating the “life loss hours” of low-voltage power cables for main/critical circuits is proposed [5]. Callender et al. simulate the discharge by changing the surface charge density at the boundary of the gap using a logistic function distribution then use this model to study the influence of single-phase energization on the partial discharge activity in the three-phase PILC cable joints. The model can describe the measured values obtained from the high-voltage equipment in operation [6]. However, these scholars did not combine wireless network communication to predict and analyze the reliability and life of insulated cables.

The innovations of this paper are mainly reflected in the following: (1) Research on the energy consumption of wireless communication networks, and propose a model for maximizing network lifetime. (2) At the same time, curve fitting was performed on the aging life of insulated cables, and the life of XLPE insulated cables was evaluated and reliability was analyzed based on the wireless communication network.

2. Methods on the Reliability and Life Prediction Algorithm of Insulated Cables Based on Wireless Network Communication

2.1. Energy Consumption of Wireless Network Communication. The rapid development of information and communication technology has brought great convenience to people’s lives [7], but with the rapid expansion of user groups, the scale of business has also grown rapidly, which has brought an increasing burden on the field of

communication networks [8]. At the same time, energy consumption has gradually become an important factor restricting global economic development and environmental protection, and the information and communication industry has become one of the industries with the largest energy consumption [6]. Figure 1 shows the distribution of energy consumption in wireless communication networks [9]. It is imperative to build an energy-saving, green, and environmentally friendly communication network, and it is also an effective way to promote industry growth and promote the sustainable development of global energy [10].

Before exploring the power allocation of wireless network communication, we must first understand the wireless network architecture, pay attention to the high power consumption part, and optimize the energy-saving methods in a targeted manner to achieve the best energy-saving effect [11].

Although the wireless communication system has undergone many major upgrades from 1G to 4G systems, with the introduction of new technologies such as smart antennas and more investment and productivity, the systems are still similar. It can be divided into three main components of mobile terminal, network access, and network, as shown in Figure 2. Among them, the mobile terminal is a mobile user, that is, terminal applications such as mobile phones and computers; the access network has a variety of transmission applications such as business conference catalogs and user network interfaces and is responsible for connecting users to the business network segment. The wireless access network is located between the base station and the user and moves the wireless user to the switch; the core network connects to different access networks and is responsible for connecting and managing users and the data transmission of the back-end network [12]. Obviously, the entire source power of the wireless communication network occurs in three parts: the end user, the access network, and the main network.

At the same time, when planning the overall energy-saving process, three aspects can be planned: equipment-level energy-saving, link energy-saving, and network energy-saving [13]. Equipment-level energy-saving mainly includes measures such as improving power amplifier efficiency, base station power management, and equipment dispersion; link-level energy-saving mainly includes measures such as reducing overhead and control signals, intermittent transmission, and base station idle; network-level energy-saving includes measures such as network deployment and network management [14].

2.2. Data Processing and Aging Life Curve Fitting of Insulated Cables

2.2.1. Data Processing. According to IEEE standards, the life of solid insulating materials obeys the two-parameter Weibull distribution [15]. Usually, the failure time when the failure probability is 64.1% is used as the aging life of the test piece. The Weibull division method is used for data processing, and the least square analysis method and MATLAB graphical method are used to obtain the Weibull measurement value.

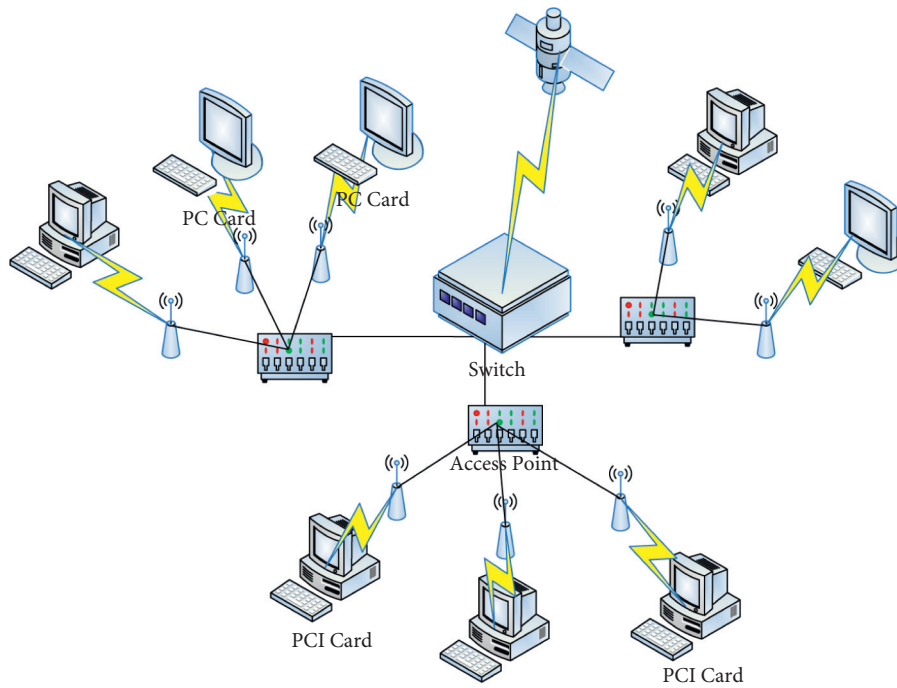


FIGURE 1: Distribution of energy consumption in wireless communication networks.

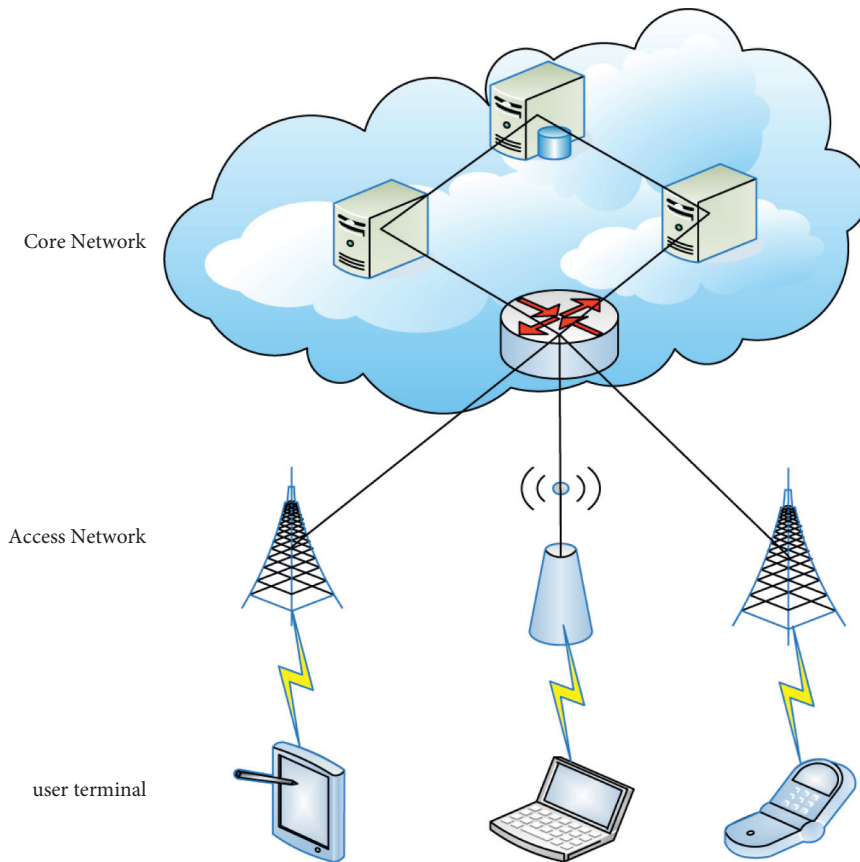


FIGURE 2: Wireless communication system structure.

The Weibull two-parameter distribution equation is shown below, where $u_h \geq 0$:

$$R(u_h) = 1 - \omega^{-(u/\varphi)^\sigma}. \quad (1)$$

Arrange the failure time in ascending order, and the cumulative probability of the h th value can be approximated by the following formula:

$$R(u_h) = \frac{h}{m+1}, \quad (2)$$

where n is the total number of samples.

For the calculation of Weibull parameters, the following methods are used for comparison.

(1) *Least Squares Regression Analysis Calculation Method.* Arrange the Weibull two-parameter equation:

$$\omega^{-(u/\varphi)^\sigma} = 1 - R(u_h). \quad (3)$$

Take the logarithm of both sides of the formula and sort out the formula

$$\left(\frac{u}{\varphi}\right)^\sigma = \ln\left(\frac{1}{1 - R(u_h)}\right). \quad (4)$$

Take the logarithm of both sides again and sort out the formula

$$\ln u = \frac{1}{\sigma} \ln \ln \left(\frac{1}{1 - R(u_h)} \right) + \ln \varphi. \quad (5)$$

Finally, the linearized formula is obtained:

$$f_h = \frac{1}{\sigma} k_h + \vartheta. \quad (6)$$

For the linearized Weibull formula, there are many related calculation methods. This article uses the most classic least squares regression analysis method as follows:

$$D\left(\frac{f}{K_h}\right) = \frac{1}{\sigma} k_h + \vartheta. \quad (7)$$

In

$$\begin{aligned} \frac{1}{\sigma} &= \frac{m \sum k_h f_h - \sum k_h \sum f_h}{m \sum k_h^2 - (\sum k_h)^2}, \\ \vartheta &= \frac{\sum k_h \sum k_h f_h - \sum k_h^2 \sum f_h}{m \sum k_h^2 - (\sum k_h)^2} = \ln(\varphi). \end{aligned} \quad (8)$$

(2) *Based on MATLAB Graphic Method.* Weibull's solution has two automated methods, namely, graphical scale method and iterative statistical method. The graphical method is to track the cumulative error probability percentage of the Weibull parameter on the graph paper—the error time point—and draw a straight line following the trend change. This method is not only inefficient, but also has large errors. Therefore, according to the principle of the graph estimation method, MATLAB graphs are used to process data [16]. According to different voltage levels, through polynomial

line compatibility matching the data of the corresponding reactor failure probability and failure time, the performance signals corresponding to different voltage levels are obtained.

2.2.2. Fitting of the Aging Life Curve. The electrical aging test obtains the aging life data of the electrode with a diameter of 2 mm and the oleoresin insulation under four aging voltages. In the test, the number of samples for each electrode system under each test voltage is three. Arrange from small to large, calculate according to Weibull summation probability formula, get the failure time of each group of two electrode processors under each group's summation probability. The data distribution is shown in Table 1.

Use MATLAB graphical method to process the data, according to different voltage levels to match the big row data in the total failure probability table and the time failure table, and get the performance signals corresponding to different voltage levels [17].

In the aging life assessment method, we believe that the aging effect of aging factors on epoxy protective materials is consistent with the antiaging energy model. Among them, epoxy resin is a kind of high-molecular polymer, which refers to the general name of a class of polymers containing two or more epoxy groups in the molecule. It is the polycondensation product of epichlorohydrin and bisphenol A or polyol. Therefore, we use a representative energy law model to match the aging life model, and the data has been replaced with a power recovery model. And use the Curve Fitting Tool application in MATLAB to adjust the fit to suit the service life of the 2 mm electric shock absorber, as shown in Figure 3.

The expression is as follows:

$$M = 1.498 * 10^{15} * Q^{-9.5923}. \quad (9)$$

The goodness of fit P^2 is 0.9798.

2.3. Network Lifetime Maximization Problem Model. In many types of wireless sensor networks, the power of sensor components is mainly used for listening, processing, transmitting, and receiving data [18]. Generally speaking, the power consumption of sending and receiving data streams accounts for most of the total energy consumption. Therefore, this article ignores the power consumption of sensors and data processing and only considers the power consumption of the communication module in the sensor node. The energy consumption per unit time of sensor node t can be expressed as follows:

$$q_t = \sum_{k \in \gamma_{in}(t)} \sum_{t' \in T(k)} q_{t,k}^a d_{t'} + \sum_{k \in \gamma_{out}(t)} \sum_{t' \in T(k)} q_{t,k}^b d_{t'}. \quad (10)$$

Here, $q_{t,k}^a$ represents the energy consumption of node t receiving unit data from link k . In this article, it is assumed that its value is constant; $q_{t,k}^b$ represents the energy consumption of node t sending unit data through link k , and its value can be calculated by the following expression:

TABLE 1: Cumulative probability and failure schedule.

Cumulative probability	Aging voltage (KV)	0.25	0.5	0.75
Unequal diameter electrode failure time (h)	23	1858	1922	1951
	25	803	813	826
	41	201	213	218
	39	20	24	27
Failure time of rod-plate electrode (h)	21	1601	1632	1641
	25	758	785	809
	31	79	89	101
	29	26.1	27.9	30.1

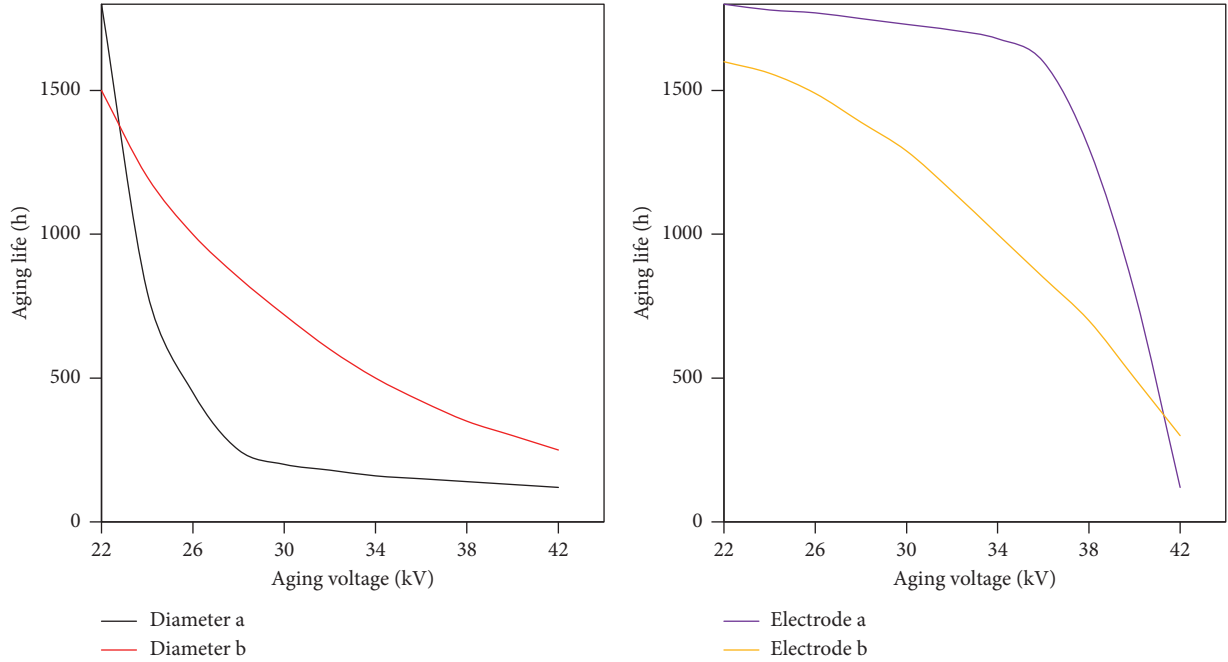


FIGURE 3: Aging life curve.

$$q_{t,k}^a = \varphi + \delta m_{t,k}^\theta. \quad (11)$$

Here, φ and δ represent constants related to physical layer functions and environmental factors; $m_{t,k}$ represents the length of the logical link k , and θ represents the path loss constant ($2 \leq \theta \leq 4$).

Assuming that the initial energy of the sensor node is represented by e_t , the lifetime of the node t can be expressed as follows:

$$B_t = \frac{e_t}{q_t}. \quad (12)$$

In this article, the life cycle of the network is defined as the life cycle of the first sensor node whose energy has been exhausted. Therefore, maximizing the network life cycle means maximizing the minimum life cycle of sensor nodes in the network. If B is used to represent the lifetime of the wireless sensor network, then $B = \min_{t \in T} B_t$. The problem of maximizing network lifetime can be expressed as follows:

$$\text{maximize} \min_{t \in T} B_t. \quad (13)$$

It is very difficult to solve this problem in a distributed manner because each sensor node needs to interact with all other nodes to know their power consumption [19].

The following method is used to approximate the network lifetime maximization problem [20]. Consider the utility function $f^\varphi(\cdot)$, which is defined as follows:

$$f^\varphi(a) = \begin{cases} \log a, & \varphi = 1, \\ \frac{1}{1-\varphi} a^{1-\varphi}, & \varphi > 1. \end{cases} \quad (14)$$

When the utility function is shown in (17), and when $\varphi \rightarrow \infty$, the problem of maximizing the minimum rate allocation of each source node can be achieved by maximizing the total utility [21]. The network lifetime maximization problem shown in (13) is to maximize the minimum lifetime of sensor nodes, which is similar to the problem of maximizing the minimum rate allocation of each source node [22]. Therefore, a lifetime utility function $f_t^\varphi(B_t)$ is introduced for each sensor node t , which is defined as follows:

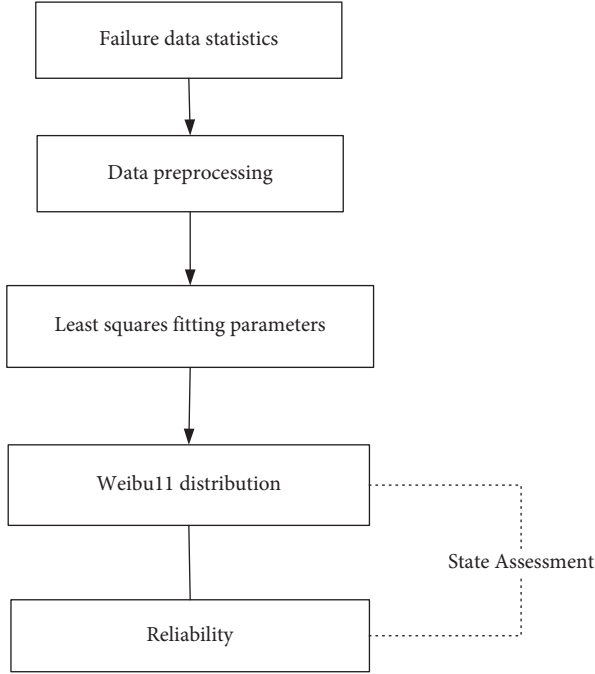


FIGURE 4: Cable reliability model.

$$f_t^\varphi(B_t) = \frac{1}{1-\varphi} B_t^{1-\varphi}. \quad (15)$$

Therefore, maximizing the network lifetime can be achieved by maximizing the total lifetime utility; namely,

$$\text{maximize} \sum_{t \in T} f_t^\varphi(B_t). \quad (16)$$

In order to simplify the problem, we make the following transformation and introduce a new variable: $W_t = 1/B_t$, which can be understood as the normalized energy consumption of node t . In summary, the problem of maximizing network lifetime is transformed into

$$\text{maximize} \sum_{t \in T} \frac{1}{1-\varphi} W_t^{\varphi-1}, \quad (17)$$

$$\text{subject to } q_t = e_t z_t, \quad \forall t \in T. \quad (18)$$

2.4. Construction of the Reliability Model of Insulated Cables. The modeling process of the insulated cable reliability model is shown in Figure 4.

The implementation steps of the model are described in words as follows:

- (1) Analyze the statistical data of the fault data and obtain the statistical data that can be used for pre-configuration [23]
- (2) Preprocessing of statistical data
- (3) Use least squares fitting to fit the preprocessed data to find the shape parameters in Weibull

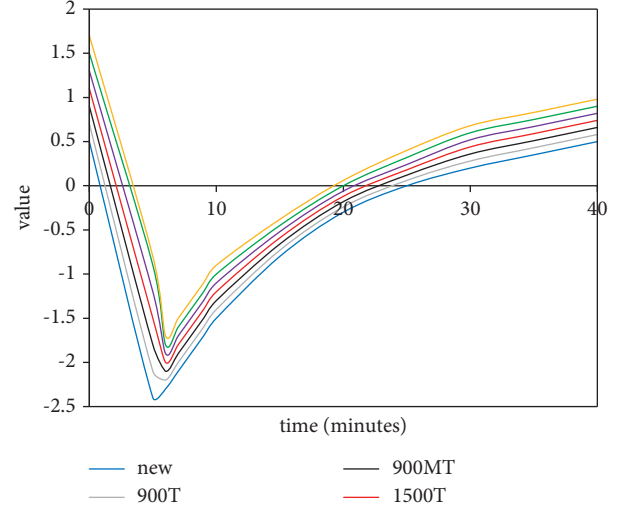


FIGURE 5: Oxidation induction period curve of samples with different aging time periods.

- (4) After obtaining the shape parameters of the Weibull distribution, the Weibull distribution is obtained
- (5) According to the Weibull distribution, the reliability is obtained, and combined with the state evaluation result, the final reliability evaluation result is obtained [24]

3. Experimental Results on the Reliability and Life Prediction Algorithm of Insulated Cables Based on Wireless Network Communication

3.1. Evaluation of Thermal Aging Characteristics and Lifespan of XLPE Cable Insulation Materials Based on Wireless Network Communication. We have studied and discussed the thermal aging parameters of cables, such as aging time and temperature. At the same time, the cables made of cross-linked polyethylene (XLPE) polymer materials are used as samples for analysis and research. In order to analyze the influence of different aging time on the OIT-induced oxidation time of the samples under pure heat conditions and the approximate heat in the aging perfusion, a total of 7 groups of samples were tested for the oxidation induction period. The test results of 7 groups of samples are shown in Figure 5.

The test results show that the induction time of the cross-linked polyethylene sample is very short after 2100 hours of heat shrinkage under the composite aging heat. The induction time of the new cross-linked polyethylene sample is 21 minutes. The induction time of the cross-linked polyethylene sample plus the aging time is longer than the short-term aging induction time, indicating that the average aging heat transfer rate is significant and the induction time is shorter. As the aging degree of the sample increases, the oxidation induction time decreases significantly. XLPE is a high-molecular polymer, which will decompose to produce a large number of free radicals in the aging environment of thermal oxygen oxidation. The free radicals act as a catalyst

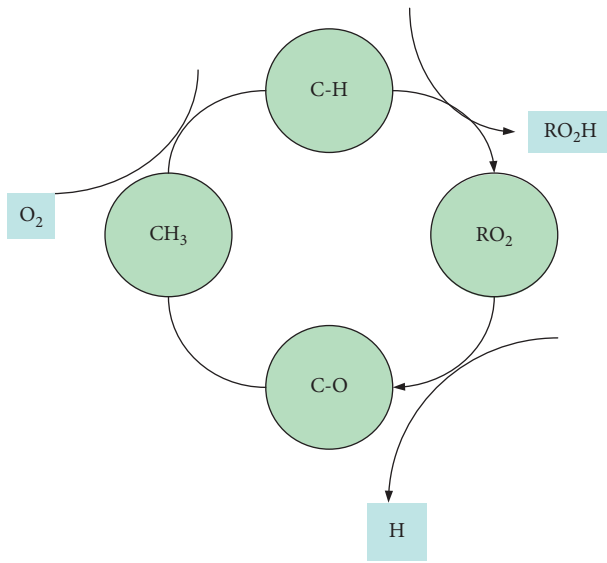


FIGURE 6: Aging chain reaction mechanism.

to initiate a chain reaction so that the cross-linked macromolecules are continuously decomposed, thereby reducing heat insulation. Maintain stability and oxidation resistance, thereby shortening the oxidation induction time. XLPE is a kind of high-molecular-weight polymer, which will degrade to produce a large amount of free radicals in the aging environment of hot exhalation. Free radicals act as a catalyst to produce chain reactions, often decomposing and cross-linked macromolecules, thereby reducing thermal insulation and shortening the induction time. The chain reaction principle of each stage of the aging process is shown in Figure 6.

In Figure 6, RO₂ stands for peroxide radical; RO₂H: hydrogen peroxide radical; C=O: carbonyl; CH₃: methyl; and H: free hydrogen.

The antioxidant in the cross-linked polyethylene cable insulation material basically absorbs the peroxide radicals in the aging chain, which can prevent it from participating in the aging and aging cycle of aging perfusion, thereby preventing the material from being damaged due to corrosion. When the temperature is high, the generation rate of free peroxide increases, the reaction rate with antioxidants accelerates, the antioxidants are digested faster, the regenerative degradation of oxidative stress increases, and the induced oxidation time is shortened.

The aging of XLPE cables can be divided into two periods: the transformation period and the thermal incubation period. Due to the presence of antioxidants in the regeneration phase, the oxidation activity is inhibited and cannot continue spontaneously. Thermal oxygen aging is a spontaneous oxidation process, which has the characteristics of free radical chain oxidation and auto-oxidation. As the thermal oxidative aging process progresses, antioxidants are consumed. With the continuous consumption of antioxidants, the bonds of cross-linked polyethylene macromolecules are broken, some of the macromolecules decompose into small molecules, and the small molecules contact each other and crystallize again.

In the thermal oxidation aging stage, antioxidants mainly capture peroxide radicals in the aging reaction chain so that they no longer participate in the synthetic aging cycle caused by thermal oxidation and vibration oxidation, and at the same time prevent the material from undergoing thermodynamic oxidative decomposition. In the thermal aging stage of oxygen, the free radicals of the molecular chain react with oxygen to form peroxides, which are decomposed into free radicals and form free radicals with oxygen atoms. The production of peroxide increases, and the peroxide activity is high, and it can interact with atoms, molecules, or free radicals. The influx of molecular structure into the material leads to further reduction of long chains and formation of molecular products. Therefore, the corrosion behavior of the excitation material in the XLPE cable is improved and the induction time is reduced.

Due to the aging process, the heat and insulation of the insulating material will be reduced to a certain extent. Therefore, antiaging protection is characterized by power shortages and frequent changes in material life. The aging range is between mild and severe. Assuming that the protective activity is between 10% and 50%, each aging is calculated by reducing the parameter by 10%. Among them, Table 2 shows the changes in the aging temperature field of the cable main insulation.

According to comparative analysis, the fiber loss is 50%, and the highest temperature in the fiber reaches 66.96°C, but the average diameter between the two layers and the temperature between the layers do not change. At the beginning of the loss (loss 10%–20%), the copper core temperature rises slightly (0.5%), and as the loss increases (loss 30%–50%), the copper core temperature rises significantly (4%). It shows that the decrease of insulation performance is nonlinearly related to the increase of temperature. Compared with conventional work, the electric field strength is much higher than the separation electric field. This is because the insulation activity and temperature of the cable will gradually decrease during the aging process, and the decrease of the insulation activity will aggravate the aging of the cable, which is a vicious circle. Therefore, when the cable ages to a certain extent, the cable needs to be replaced; otherwise, the insulation will break and cause greater harm. Figure 7 shows the aging life diagram of cables at different temperatures and different end-point levels. It can be seen from the figure that at 70°C and 40% of the end-point level, the aging strength of the cable is much stronger than that of other temperature levels. Through the establishment and analysis of the model, when the XLPE insulation material simulates the typical 0.5 m/s² vibration acceleration in the actual working cable environment under the working temperature (90°C) environment, its expected life is 27.1 years.

In order to determine the influence of different impurity content on the aging of the circuit, 0.5 mm impurities are removed each time, and the software analyzes the temperature and light intensity, as shown in Table 3.

When there are impurities in the cable, there will be slight changes according to the location of the impurities, the highest temperature inside the cable, the average temperature between the two phases, and the temperature of the

TABLE 2: Changes in the temperature field of cable main insulation aging.

Cable insulation performance loss	The highest temperature inside the cable (°C)	Average temperature between two phases (°C)	Filling material temperature (°C)	The highest electric field strength inside the cable (mV/m)
Normal operations	52.01	46.95	44.01	1.1398
Loss 10%	54.02	47.89	43.98	1.1985
Loss 20%	55.98	49.01	44.29	1.4698
Loss 30%	59.03	49.58	44.39	1.8023
Loss 40%	62.97	51.08	45.03	2.0035
Loss 50%	66.96	52.02	45.02	2.1502

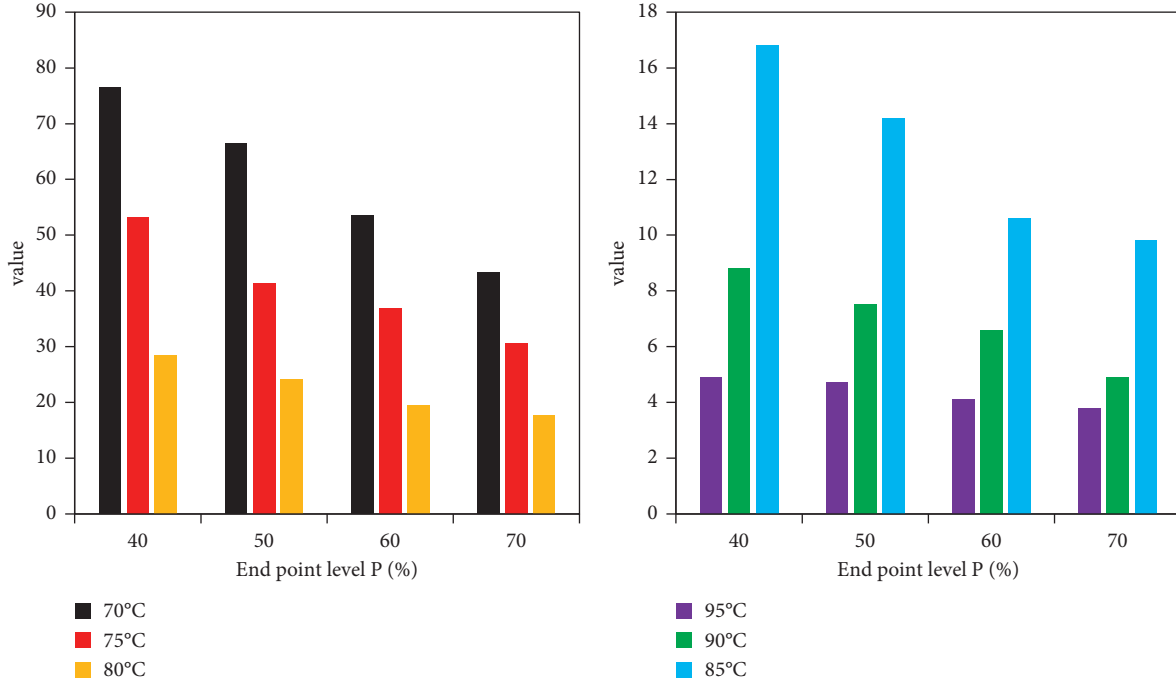


FIGURE 7: Cable ageing life under different temperatures and different end-point levels.

TABLE 3: Thermal field and electric field distribution table of impurity in cables.

Distance between impurity and conductor edge (mm)	The highest temperature inside the cable (°C)	Average temperature between two phases (°C)	Filling material temperature (°C)	Electric field distribution of cable impurities (mV/m)
1.5	51.59	46.83	42.71	4.98
2	51.41	46.33	42.89	4.26
2.5	50.81	46.51	43.78	3.99

filling material. However, the electric field where the impurity is located is very strong, and partial discharge is prone to occur at this time, and insulation failure will occur within a few seconds. In this case, the cable insulation completely fails, and short circuit and other faults may occur. However, this type of damage does not occur immediately after the cable is used because the insulation is poor and the efficiency value is reduced. Therefore, the presence of impurities should be avoided as much as possible.

It can be seen from Table 3 that the presence of impurities has a greater correlation with the highest internal field strength, a lower correlation with the internal temperature, and a lower correlation with the ambient temperature.

3.2. Insulation State Evaluation Prediction and Reliability Evaluation of XLPE Cables Based on Wireless Network Communication. The Weibull distribution describes the damage chain reaction based on the calculation process. It is derived from the series model and the weak link model. It can fully illustrate the impact of material defects on the life of the material, and the damage of many faults to the safety of the cable. In addition, since the current simplified curve bathtub is widely used to simulate the failure rate of power system components, this object uses bath waves to calculate reliability. The shape of the bath curve during sporadic failure and aging failure is basically the same as the Weibull distribution, so this paper evaluates the cable reliability based on the Weibull distribution.

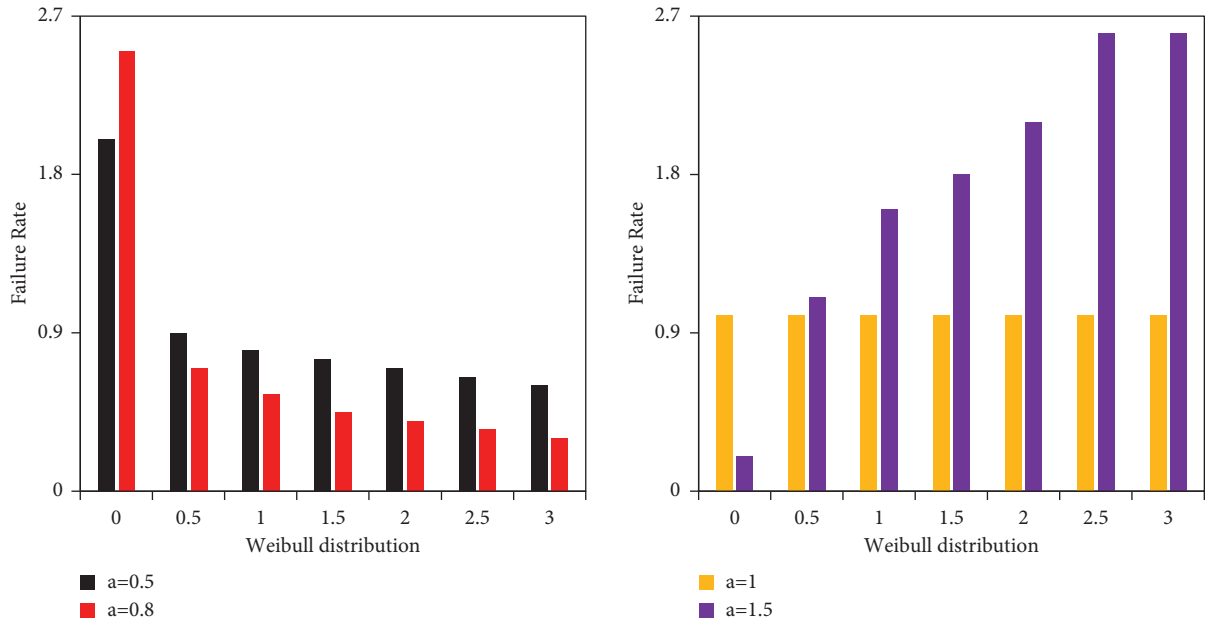


FIGURE 8: Weibull distribution failure rate.

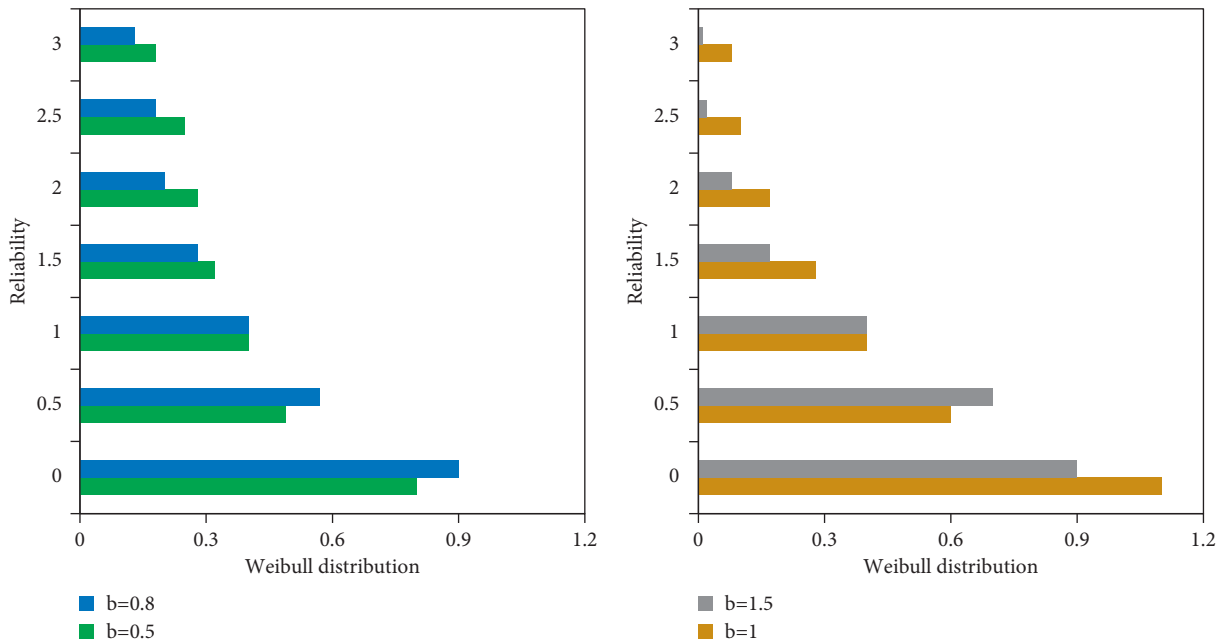


FIGURE 9: The reliability of the Weibull distribution.

The Weibull distribution describes the damage chain reaction based on the calculation process. It is derived from the series model and the weak link model. It can fully demonstrate the impact of material defects on the life of the material and the corrosion of many target faults on the cable protection. Figure 8 shows the failure rate of the Weibull distribution.

Using statistical methods to deal with data line failures and calculate cable reliability is also a current and popular research guide in the era of big data. Figure 9 shows the reliability diagram of the Weibull distribution.

At the same time, it has also been observed that 80% of cable failures are caused by external damage in addition to their own reasons, and there is more than one reason for cable failure. Therefore, the probability of each independent failure cause is part of the calculation of the total failure probability of the cable.

It can be seen from Figure 10 that the cumulative failure rate of the cable follows the bathtub curve. In the first 1 to 2 years, due to early failures caused by poor production quality and improper installation, the press showed a slight downward trend; the service life was about 2 to 4 years, and

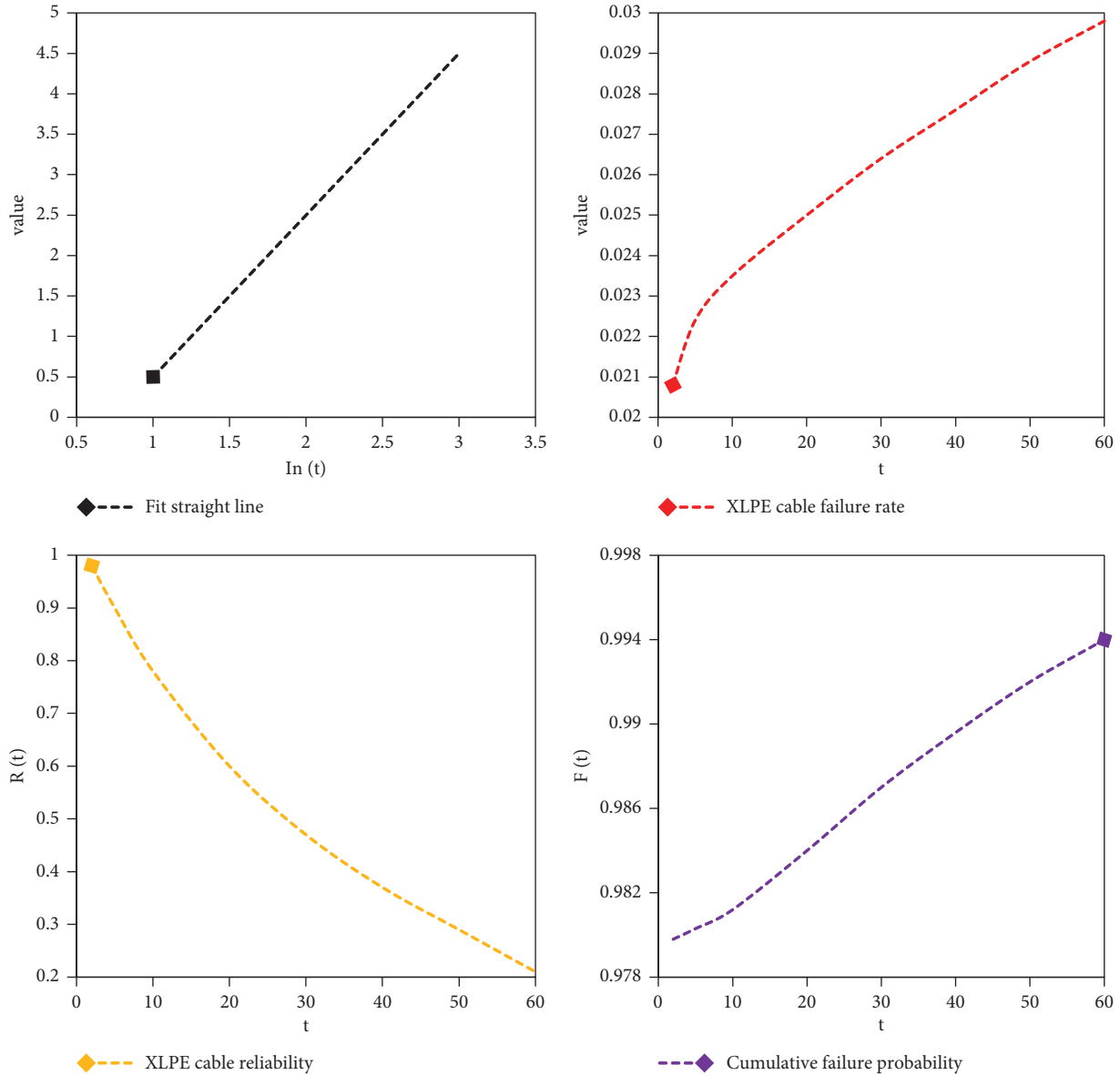


FIGURE 10: XLPE cable reliability and failure rate curve.

the probability of complete cable failure remained basically unchanged. After 4 years, the curve began to grow, and by about 30 years, the growth trend tended to be flat, which means that in about 30 years, cable maintenance activities are also going on simultaneously, avoiding an increase in the failure rate. It can be seen from the figure that the failure rate of the optical fiber increases with the increase of the operation time of the optical fiber, and the reliability decreases with the increase of the time, which is consistent with the previous analysis and data analysis of the optical fiber.

If we can get suitable working rope conditions at one time, we need to plan the working position of the rope before confirming the reliability of the working rope. From the results of line A in Table 4, the result of the reliability rating is 0.459. The reliability obtained directly from the reliability fitting chart 10 is 82.9%. At this time, it can be seen from the

TABLE 4: Reliability evaluation results.

Line name	m'	$m'(A)$			$R(t)$	$R'(t)$
		S_1	S_2	S_3		
Line A	0.990	0.131	0.561	0.218	0.829	0.459
Line B	0.129	0.121	0.541	0.220	0.671	0.361
Line C	0.089	0.161	0.549	0.201	0.601	0.339

statistical data that line A has failed, which is obviously inconsistent with the high reliability of 82.9%. After considering the status of line A, the confidence level becomes 45.9%, which is obviously more realistic. Likewise, the final result of line B is more tangible. It can be seen from Figure 10 that the reliability of line B after 22 years of operation is not high, only 60.1%. The statistical results show that line C ended in failure in August 2011 and November 2011. The final result of the comprehensive status assessment is 33.9%,

which is also more realistic. Therefore, it can be seen that the model has certain feasibility.

Cable reliability analysis is to evaluate the health of cables from a “macro” perspective of the power grid and can provide important guidance for relevant operation and maintenance personnel from a “macro” perspective. Therefore, the fitting of cable reliability curve can provide maintenance advice for operation and maintenance personnel. For example, when the reliability is maintained at about 80%, the cable is less affected by the aging process, which can reduce the frequency of routine maintenance and prevent accidental failures such as external force impacts from causing cable failures; with the extension of the cable running time, the reliability continues to decline, and the influence of cable aging is also increasing. Once the external stress (mechanical force, heat, load, etc.) increases, the reliability will be greatly reduced. It is necessary to increase cable maintenance and control operating conditions to extend the service life of the cable. When the reliability is lower than 50%, the reliability of the cable cannot be basically guaranteed, and it is necessary to formulate an update and replacement plan to ensure the safe and stable operation of the power grid.

4. Discussion

This model is based on wireless network communication, combined with the analysis of aging average test results, and calculates the long-term reliability of XLPE protection applications under multiple parameters. By comparing heating and aging methods, the XLPE aging test under the thermal conditions of polymerization shows the long-chain characteristics and kinetic crystal control crystal structure of the aging polymer XLPE polymer and introduces the fluidity and crystals between molecular chains. At the same time, the power grid is the main interface between the power load picker and the power system and an important guarantee for decision-making reliability and power supply quality. In the actual operation of XLPE cable, due to the local heating of the conductor caused by the working current, the cable insulation has thermal aging under high temperature conditions for a long time, resulting in various complex physical and chemical changes in the XLPE insulation. Among them, thermal aging is an important part of various aging. Thermal aging reduces the mechanical properties of XLPE cable insulation such as tensile strength and elongation at break and damages the internal microstructure of the insulation. Moreover, thermal stress and other stresses act together to accelerate the aging of cable insulation. Temperature can increase the chemical reaction rate, so the relationship between degradation rate and temperature in thermal aging is similar to the chemical reaction rate equation.

5. Conclusions

The cable condition is to evaluate the cable from the cable itself compared with the reliable analysis; it is to analyze the operating condition of the cable from the “micro” perspective; from the perspectives of “macro” and “micro”,

conduct simultaneous analysis and investigation of the operating status of the cable, as well as the relationship between cable failure and cable aging, accidental damage, and cable maintenance. Fully consider maintenance and collect cable performance more comprehensively and accurately. Provide more valuable reference for operation and maintenance personnel. For example, line A in this example, from a “macro” perspective, has 83% confidence when it runs to 8.45 years. If you consider this result alone, it can be considered that the cable will not fail; in fact, the cable has failed at this time. Comprehensive inspection of its operating status results in a reliability of 46%, which is very low. Operation and maintenance personnel can formulate relevant maintenance plans accordingly. Therefore, the model proposed in this chapter comprehensively considers a variety of factors, evaluates the reliability of the cable, and helps operation and maintenance personnel propose maintenance and replacement plans in a timely manner so that the reliability of the cable meets the requirements and realizes comprehensive management. Due to the limitations of time and technology, we will further analyze and study other properties of cables in the future in order to make certain contributions to the cause of social and public safety.

Data Availability

No data were used to support this study.

Conflicts of Interest

The authors declare no conflicts of interest.

References

- [1] S. Yasui, K. Sakaguchi, and T. Tsuchida, “Overvoltage in insulated-cable-type down conductor,” *IEEE Transactions on Power and Energy*, vol. 137, no. 11, pp. 710–716, 2017.
- [2] D. He, T. Zhang, M. Ma, W. Gong, W. Wang, and Q. Li, “Research on mechanical, physicochemical and electrical properties of XLPE-insulated cables under electrical-thermal aging,” *Journal of Nanomaterials*, vol. 2020, no. 1, pp. 1–13, 2020.
- [3] Y. Ohki and N. Hirai, “Effects of the structure and insulation material of a cable on the ability of a location method by FDR,” *IEEE Transactions on Dielectrics and Electrical Insulation*, vol. 23, no. 1, pp. 77–84, 2016.
- [4] B. X. Du, X. X. Kong, J. Li, and M. Xiao, “High thermal conductivity insulation and sheathing materials for electric vehicle cable application,” *IEEE Transactions on Dielectrics and Electrical Insulation*, vol. 26, no. 4, pp. 1363–1370, 2019.
- [5] G. Parise, L. Martirano, L. Parise, L. Gugliemetti, and F. Nardecchia, “A life loss Tool for an optimal management in the operation of insulated LV power cables,” *IEEE Transactions on Industry Applications*, vol. 55, no. 1, pp. 167–173, 2019.
- [6] G. Callender, P. L. Lewin, J. A. Hunter, and P. Rapisarda, “Modeling partial discharge in a three-phase cable joint experiment with minimal adjustable parameters,” *IEEE Transactions on Dielectrics and Electrical Insulation*, vol. 24, no. 1, pp. 279–287, 2017.
- [7] A. Khamlichi, G. Donoso, F. Garnacho, G. Denche, A. Valero, and F. Alvarez, “Improved cable connection to mitigate

- transient enclosure voltages in 220-kV gas-insulated substations,” *IEEE Transactions on Industry Applications*, vol. 52, no. 1, pp. 562–569, 2016.
- [8] H. Ren, L. Zhong, X. Yang et al., “Electric field distribution based on radial nonuniform conductivity in HVDC XLPE cable insulation,” *IEEE Transactions on Dielectrics and Electrical Insulation*, vol. 27, no. 1, pp. 121–127, 2020.
- [9] Y. Ohki and N. Hirai, “Detection of abnormality occurring over the whole cable length by frequency domain reflectometry,” *IEEE Transactions on Dielectrics and Electrical Insulation*, vol. 25, no. 6, pp. 2467–2469, 2018.
- [10] P. Cheetham, C. H. Kim, S. Pamidi, and L. Graber, “Optimization of a superconducting gas-insulated transmission line,” *IEEE Transactions on Dielectrics and Electrical Insulation*, vol. 26, no. 3, pp. 930–938, 2019.
- [11] L. S. Lakshmi, K. P. Thakur, and M. P. Staines, “Magnetic AC loss characteristics of 2G roebel cable,” *IEEE Transactions on Applied Superconductivity*, vol. 19, no. 3, pp. 3361–3364, 2016.
- [12] J. Zhang, Y. He, and W. Cui, “Reliability life prediction of smart meter based on multi-stress degradation model,” *Journal of Beijing University of Aeronautics and Astronautics*, vol. 43, no. 8, pp. 1662–1669, 2017.
- [13] Y. Ohki, “Development of an XLPE-insulated cable for LCC-HVDC power lines (News from Japan),” *IEEE Electrical Insulation Magazine*, vol. 34, no. 4, pp. 62–65, 2018.
- [14] A. P. Vikharev, “Electromagnetic situation near gas-insulated and cable power lines,” *Power Technology and Engineering*, vol. 52, no. 2, pp. 223–226, 2018.
- [15] H. Zhang, J. Zhang, L. Duan, S. Xie, and J. Xue, “Application status of XLPE insulated submarine cable used in offshore wind farm in China,” *Journal of Engineering*, vol. 2017, no. 13, pp. 702–707, 2017.
- [16] J. Snajdr, J. P. Bentley, R. Hauck, and P. Novak, “Stress on outer cable connection of MV gas-insulated switchgear due to cable thermal expansion at rated current,” *CIGRE—Open Access Proceedings Journal*, vol. 2017, no. 1, pp. 450–453, 2017.
- [17] R. Benato, S. D. Sessa, L. Guizzo, and M. Rebolini, “Synergy of the future: high voltage insulated power cables and railway-highway structures,” *IET Generation, Transmission & Distribution*, vol. 11, no. 10, pp. 2712–2720, 2017.
- [18] G. A. Vinther, “Controlled-impedance cable termination with compensation for cable expansion and contraction,” *Clinical Trials*, vol. 6, no. 1, pp. 76–89, 2016.
- [19] B. Gustavsen, M. Hoyer-Hansen, P. Triverio, and U. R. Patel, “Inclusion of wire twisting effects in cable impedance calculations,” *IEEE Transactions on Power Delivery*, vol. 31, no. 6, pp. 2520–2529, 2016.
- [20] B. Zhang, J. Zou, and X. Du, “Ground admittance of an underground insulated conductor and its characteristic in lightning induced disturbance problems,” *IEEE Transactions on Electromagnetic Compatibility*, vol. 59, no. 3, pp. 894–901, 2016.
- [21] L. Boukezzi, L. Bessissa, A. Boubakeur, and D. Mahi, “Neural networks and fuzzy logic approaches to predict mechanical properties of XLPE insulation cables under thermal aging,” *Neural Computing & Applications*, vol. 28, no. 11, pp. 3557–3570, 2017.
- [22] E. H. Doedens and E. M. Jarvid, “Considerations on the impact of material mesostructure on charge injection at cable interfaces,” *IEEE Electrical Insulation Magazine*, vol. 36, no. 5, pp. 43–51, 2020.
- [23] A. G. Shcherbinin and R. P. Lukoyanov, “Numerical studies of the electric field of a power cable with sector strands and impregnated paper-plastic insulation for a voltage of 20 kV,” *Russian Electrical Engineering*, vol. 91, no. 11, pp. 698–702, 2020.
- [24] C. Dang, J. Cote, and J. Tarnowski, “Emergency-temperature testing on MV jacketed reduced-wall TRXLPE aluminum cable systems in duct bank,” *IEEE Transactions on Power Delivery*, vol. 33, no. 6, pp. 2894–2900, 2018.

Research Article

PSE and ISE Based E-Commerce Model Design of Sharing Enterprises

Suhong Yang ¹, Mohammed k. Hassan,² and Vinay kumar³

¹School of Information Engineering, Hangzhou Dianzi University, Hangzhou 310000, Zhejiang, China

²Mechatronics Department, Faculty of Engineering, Horus University in Egypt (HUE), New Damietta, Egypt

³Department of Computer Engineering and Application, GLA University, Mathura, India

Correspondence should be addressed to Suhong Yang; ysh@hdu.edu.cn

Received 10 December 2021; Revised 12 January 2022; Accepted 15 January 2022; Published 11 February 2022

Academic Editor: Alireza Souri

Copyright © 2022 Suhong Yang et al. This is an open access article distributed under the Creative Commons Attribution License, which permits unrestricted use, distribution, and reproduction in any medium, provided the original work is properly cited.

Sharing economy is developing rapidly in the world, but most sharing enterprises have failed and brought a huge waste of resources. We analyzed the relationship between the entrepreneurial success and the failure of e-commerce companies engaged in sharing goods. We think that the sharing economy is divided into the procurement sharing economy (PSE) and idle sharing economy (ISE). By establishing two models (PSE and ISE) to explain the success or failure of enterprises in sharing economy, we found that PSE enterprises are traditional enterprises with a high bankruptcy risk. PSE enterprises can generate a significant amount of waste and are highly dependent on venture capital; they should be restricted by the government. ISE enterprises, however, have Internet “genes,” comport with sustainable development, and should be supported. Our research shows that entrepreneurs may fail if they do not pay attention to the relationship. A huge waste of resources and chaotic social order may occur if the government does not pay attention to it, and investment companies may lose a lot if they ignore it. The practical data show that our method is effective in judging whether the sharing enterprise fails.

1. Introduction

According to the annual report on the development of China’s sharing economy (issued on February 19, 2021), in 2020 alone, 830 million Chinese participated in the sharing economy. In 2020, due to the impact of COVID-19, the total share of economic market transactions was about 3377.3 billion yuan, an increase of about 2.9% over the same period last year. In addition, the top enterprises in the sharing economy have a good momentum. As of the end of 2018, there are 83 Chinese enterprises out of 305 unicorn enterprises in the world, 34 of which belong to the nature of sharing economy, accounting for 41% of the total number of unicorn enterprises in China. In addition, 11 sharing enterprises entered the unicorn in 2018 for the first time. The Chinese government reported that the sharing economy was growing at an annual rate of 40% and, if sustained, will reach 20% of China’s GDP by 2025 [1], indicating that it is a significant and important part of the economy.

However, many problems have occurred at sharing economy enterprises, such as drivers raping and murdering passengers at DiDi (a Chinese car sharing company), Uber sued by drivers for 1 billion dollars, and <http://www.123tsg.com> (“tsg” are the initials of the word “library” in Chinese) having no profit model, but none of these sharing economy enterprises have failed. Otto, the self-driving truck company purchased by Uber, survived for only 2 years. Most of the Chinese bicycle sharing enterprises with good profit models and a large amount of venture capital have failed.

We have found such an interesting phenomenon. Whether sharing companies are engaged in car sharing or bicycle sharing, the survival or failure of these enterprises seems to have been doomed. When we divide the sharing enterprises into PSE and ISE, we will find the reasons for the failure of the sharing enterprises.

According to the report released by the Research Institute of Science of the Ministry of Transport, in 2017, the total number of shared bicycles in China exceeded 20

million, with 300000 tons of steel used. However, most bike sharing enterprises have closed down now. In other words, sharing bicycles has wasted 300000 tons of steel. At the same time, due to random parking, it also causes chaos to the city. Can we predict the risk in advance for the emerging model of the sharing economy? Can the government, investors, and entrepreneurs know in advance which types of enterprises are prone to failure, which types will cause waste, and which types should be restricted or encouraged by the government? This paper establishes a model to predict which sharing enterprises will fail, which is of great significance for sustainable development.

In the theoretical part, we studied the research literature of scholars and summarized the latest research results of sharing economy enterprises. In the research methods part, we classified the sharing economy and defined intermediary variables, dependent variables and independent variables. In the case study part, we focused on some representative sharing enterprises, such as bicycles and cars, books, and houses. We also established the PSE/ISE model and compared the traditional decision making with this model. In the conclusions part, we summarized the paper and put forward decision-making suggestions to the government, investors, and entrepreneurs. Finally, we put forward suggestions for future research.

1.1. Theory. The term “sharing economy” first appeared in a paper cowritten by Marcus Felson, a sociologist at Texas State University, and Joe L. Spaeth, a sociologist at the University of Illinois, in 1978. Its essence is to “share your idle resources with those in need and generate additional added value while getting paid.” After years of development, the sharing economy, as it is understood today, has evolved into a business model wherein an organization or individual with idle resources temporarily transfers the right to use those resources to others for payment and gets a certain amount of remuneration. The contemporary sharing economy, also known as collaborative consumption, is a socioeconomic system of sharing human and material resources through the establishment of a platform for the direct exchange of goods and services [2]. In addition, it is the sum of the economic activities that use modern information technologies, such as e-commerce, shared goods, integrate massive and decentralized resources, and meet diversified needs [1]. Zipcar founder Robin Chase (2015) identified 3 core elements of the sharing economy: (1) use excess capacity to achieve economic benefits; (2) science and technology can let people establish a platform of the sharing economy, making sharing easier; and (3) individuals are influential partners [3]. According to Stephen, founder of JustPark software, the sharing economy has 5 points: mutually beneficial economic value, acquisition of added value, convenient use of idle assets, mutual trust, and reduction of ownership demand [4].

Research on the management of the sharing economy is important because the sharing economy is becoming more ubiquitous, changing how firms operate and will operate. For example, Zervas et al. studied the case of Airbnb to

discuss the economic impact of the sharing economy on existing companies [5].

He and Murphy believe that there is no universality in the supervision of the sharing economy and that local governments at all levels should formulate policy, based on the principles of subsidiarity and flexibility [6, 7]. Das Acevedo said that some academics advocate supervision and some advocate a wait-and-see strategy [8]. Hong et al. think that the higher the level of government, the more likely it is to support supervision [9]. He et al. used a structural equation model to empirically test the impact of sharing economy regulation on perceived privacy risk, consumer trust, and continuous sharing willingness. The results showed that (1) government regulation has a significant negative impact on perceived privacy risk, while industry self-regulation has no significant negative impact; (2) perceived privacy risk has a significant negative impact on consumer trust and continuous sharing willingness; and (3) consumer trust has a significant impact on continuous sharing willingness [6]. Gao et al. took 10 core elements of business models as explanatory variables and empirically investigated 15 enterprises in 9 different fields of the sharing economy. They found that the business model of the sharing economy provided a more relaxed development environment for enterprises [10]. Based on the analysis of private law, Pan believed that a shared bicycle deposit should not be returned when the lessor goes bankrupt. According to the laws and regulations for prepaid cards, the shared bicycle deposit is less than 300 CNY, which has little impact on individual interests and therefore enjoys the exemption basis. If supervision is strict, operators’ compliance costs will be high, which is not conducive to market innovation [11]. The above research shows that both the market demand and the existing legal basis contribute to the incredible growth of the sharing economy, so theoretical research on the sharing economy is indeed urgent.

Whether it is book sharing or bicycle sharing, the success and failure of sharing economy start-ups have certain theoretical commonalities, such as the marginal cost theory. Rifkin developed the theory of the Zero marginal cost society [12]. If the marginal cost theory is combined with the proposition and definition used in this paper, it will be easier to understand which sharing economy enterprises are likely to succeed and which are likely to fail.

2. Research Methods

2.1. Independent Variables. We divided the sharing economy into 2 categories: PSE and ISE (see Figure 1). They are the independent variables studied in this paper. We used the following 2 definitions in this work.

2.2. Definition of PSE. PSE (procurement sharing economy) is an organization or individual whose purpose is to obtain benefits from users by leasing the goods circularly, increasing the production growth rate, and meeting social needs on a large scale through centralized procurement and

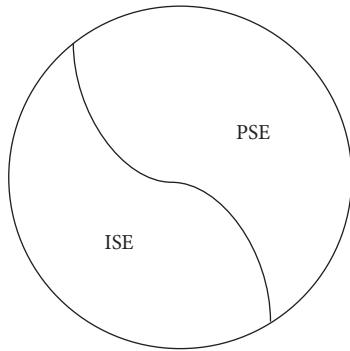


FIGURE 1: Two types of sharing economy.

unified management of goods. It is characterized by the need to invest in the purchase of shared goods.

2.3. Definition of ISE. ISE (idle sharing economy) is an organization or individual that rents idle goods (including services) to users and gets paid multiple times through reuse, to meet social needs on a large scale, reduce the growth rate of production, and conserve resources. Its distinctive feature is that shared goods are idle and will not increase production growth.

Entrepreneurs believe that the PSE can also achieve the goal of saving natural resources, but why is it the opposite of what entrepreneurs think (unable to save natural resources)? We developed 2 hypotheses:

H1: PSE enterprises are traditional enterprises without low cost “genes” that do not conform to the concept of sustainable development.

H2: ISE enterprises are enterprises with low cost “genes” that conform to the concept of sustainable development.

2.4. Mediating Variables. The mediating variable is the cost variable, including the purchase cost of the sharing goods and other costs.

Purchasing cost is mainly the cost of purchasing shared goods. Other costs mainly include the cost of goods renewed due to damage, maintenance, storage, transportation, and human resources.

2.5. Dependent Variables. The success and failure (declaring bankruptcy, going out of business, or becoming defunct) variables of sharing economy start-ups are the dependent variables studied in this paper. The following 2 propositions were made:

H3: PSE enterprises are likelier to fail

H4: ISE enterprises are likelier to survive

3. Case Study

123tsg.com (123 Library) is a library without books, offices, or staff. (This website is different from the UK company site,

123library.org.) There is not a single book there and not even room for a one-square-meter library. It is an online business that operates without books, offices, or a large staff. The operating cost of the company tends to zero. Therefore, even if there is no profit and no venture capital, 123tsg.com, a typical ISE enterprise, will not go bankrupt easily.

China’s representative book sharing enterprise, 123 Library, is a circular reading promotion platform with a dandelion business model as the core, Internet as the media, e-commerce as the means, and reading needs of readers (members) as the driving force [13]. It adds value through the idle book rental of readers [14]. Since its establishment in 2011, it has received extensive attention due to a series of reports by the *People’s Daily*, *Guangming Daily*, *Workers’ Daily*, and the Chinese Ministry of Education [15, 16]. In the early stage, some start-up enterprises cannot survive and develop without funds and profits. Figure 1 explains the impact of public opinion on policies. ISE enterprises receive good public opinion support, so 123 Library received financial support from the Hangzhou government in its early development [17].

In addition to the positive public opinion created by the media, 123 Library has been investigated by reformist researchers at Chinese public libraries. Li thinks that 123 Library is an outstanding representative of family reading resource sharing. At 123 Library, books are shared by users. After the renter pays the rent, the book owner delivers the book by express delivery. When the renter finishes reading, he/she does not need to return it but can keep the book. After the next person who rents the book pays the rent, this person can get the rent reward as long as he/she delivers it by express delivery. Public libraries can use this idea to solve the problem of book borrowing and returning, change the collection space of libraries, improve the book circulation rate, and realize the effective sharing of book resources [18, 19]. Liu believes that 123 Library advocates sharing idle books nearby, recycling books nearby, and finding books people want to read nearby, which is similar to the service content of university libraries. The construction mode of 123 Library can be introduced to university libraries. Non-collection books can be lent to students for a semester to realize the drifting mode of 123 Library. However, if 123 Library’s mode is introduced into university libraries, there may be some problems, such as the malicious downloading and the loss of books and promotion, so this approach needs further study [20].

We divided the definition of the sharing economy into 2 types: PSE and ISE. The difference between PSE and ISE is that the shared goods of PSE are specially purchased or produced for the purpose of generating profits through sharing, such as sharing bicycles. ISE is strictly sharing. Its shared goods are not specially produced and purchased for the purpose of gaining profits through sharing but purchased by individuals or organizations to meet their own needs. These goods are often idle, so e-commerce provides a platform for goods’ owners to reuse the idle goods and get corresponding rewards, e.g., the nonowned, shared cars of Uber and DiDi; the rooms supplied through Airbnb; and 123 Library’s books.

Neither of the 2 sharing economy modes (PSE and ISE) repels profit. The difference is how the shared goods are generated, whether they are idle and then generate profits through sharing or they are specially produced for the purpose of sharing and generating profits.

The difference between the two is that the production of idle shared goods (ISE) forms the purchasing power through orderly and decentralized demand, and the purpose of PSE is to occupy the market quickly and purchase the shared goods blindly, so as to form redundant production and waste.

Disordered competition causes a huge waste of social resources because an inaccurate investment scale prediction or market competition will lead to blind investment. Therefore, H1: PSE enterprises are traditional enterprises without low cost characteristic that do not conform to the concept of sustainable development. H2: ISE enterprises are enterprises with low cost characteristic that conform to the concept of sustainable development.

123 Library activates the stock assets and is beneficial to sustainable development [21]. Therefore, for a sharing economy based on the ISE, once a better model is introduced, it will be generally accepted by society. According to Wang Yangming's theory of the mind [22], the reason why this kind of phenomenon can win people's hearts is that everyone has a conscience. Public opinion (see Figure 2) serves as a regulating variable, and it plays a key role in the government's policy-making. For example, companies engaged in bicycle sharing and Qinfanqie's book sharing platform took users' deposits, then encountered adverse public opinion, and were eventually prosecuted, and several employees were arrested. Finally, the company went bankrupt. Adverse public opinion on the impact of the lack of the orderly parking of shared bicycles on the social environment has led to many local governments banning the entry of shared bicycle companies.

We believed that the root cause of the failure of the Qinfanqie is not the lack of a profit, but because procurement sharing requires a large amount of money to buy goods, the initial fixed cost is high. Therefore, Qinfanqie uses the deposit to buy books without permission, resulting in the company's final collapse. Assuming that Qinfanqie has a clear profit model and capital investment, just like the bicycle sharing companies, it will also encounter the temptation of making large investments and taking user deposits. In a market competition where the sharing scale is supported by the capital scale, there may be one winner. However, the losers are the Earth and the entire human race, because this kind of (PSE's) behavior is not sustainable. Therefore, there is no difference between the fate of Qinfanqie and that of bicycle sharing companies, which is the fate of the PSE.

Table 1 shows several typical business models of shared enterprises. It does not include traditional second-hand e-commerce enterprises, such as Taobao.com, Kongfz.com, and Youlu.com. We did not carry out in-depth research on them because they do not have the characteristics of circular leasing.

The following hypothesis was drawn from Table 1:

H5: There is no direct correlation between the life-and-death-dependent variables of the sharing economy enterprises and the profit model variables of the enterprises. There are 2 explanations:

- (1) The marginal cost of ISE enterprises is near-zero MC, so having no profit will not cause a failure threat to them. ISE enterprises are likelier to survive.
- (2) PSE enterprises are traditional enterprises without Internet genes, so the marginal cost increases with the increase of scale. They do not have their own production technology barriers, which leads to intense competition and results in major risks in terms of policy and law. Although PSE may bring in profit, all PSE enterprises are likelier to fail.

These explanations indicate that it is wrong for venture capital companies to pay special attention to the profit model of sharing economy enterprises, and they also explain why bicycle sharing enterprises lose billions of dollars of investment. This is because they do not pay attention to the relationship between the 2 categories of enterprises (PSE and ISE) of this study and the variables of an enterprise's success and failure.

It can be found from Table 1 that all sharing economy enterprises that have applied wireless communication system technology can promote the development of business model of sharing economy enterprises. Wireless communication system technology plays an important role in commodity information sharing and improving customer satisfaction. However, there is no significant relationship between the wireless communication technology and the success of sharing economy enterprises.

In Table 1, all PSE enterprises make purchase to increase the production of goods and buy on credit, which leads to imbalanced financial revenue and expenditures. PSE enterprises increase social production by increasing the number of purchased goods. With intense competition, it is very easy to make credit purchases, create unbalanced financial revenue and expenditures, and then abscond with users' deposit, resulting in adverse public opinion (explained in Figure 2) and government policy. Through prosecution from users and manufacturers, arrests of founders, seizure of company assets, auctions, and other activities, such enterprises will face major risks or even fail. However, ISE enterprises do not have the above risks. All ISE enterprises do not purchase shared goods, and these mediating variables will not cause them to fail.

The analysis of mediating variables (purchase to increase the production, credit purchase, imbalanced financial revenue and expenditure) shows that mediating variables have a direct mediating effect between independent variables and dependent variables, and these three mediating variables are the direct factors that lead to the change of dependent variables of enterprise life and death.

Gao et al. identified the circumstances where suppliers will completely rely on the sharing platform to achieve supply stability; and they investigated whether the relationship between the platform and suppliers can be

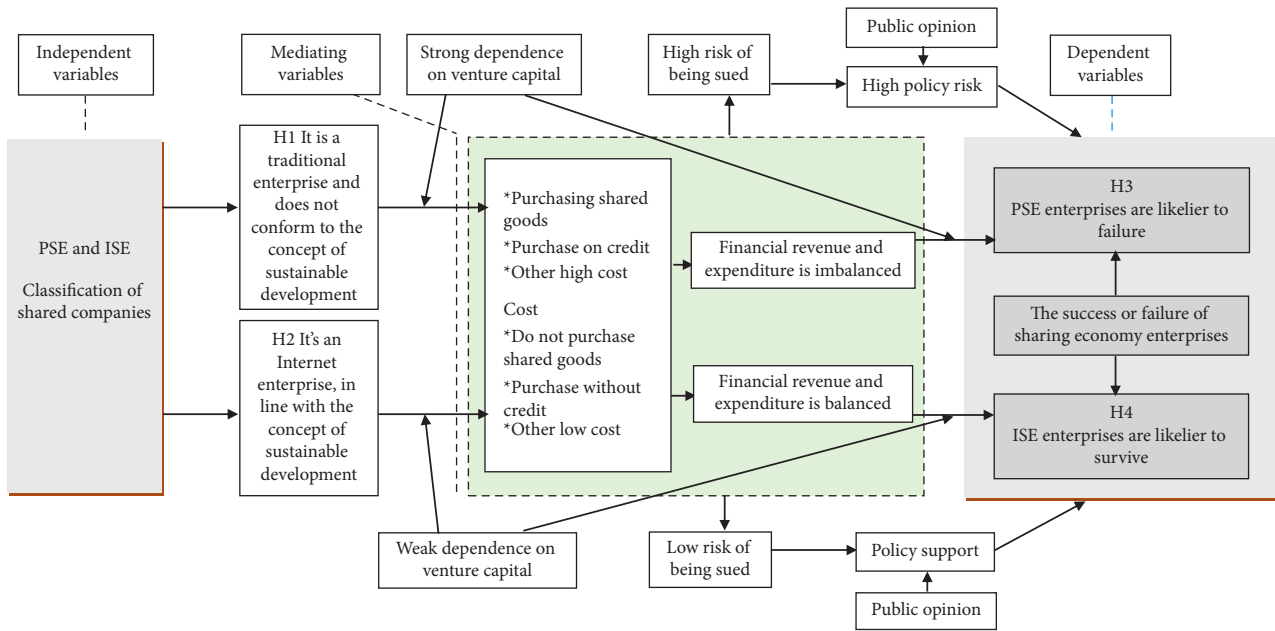


FIGURE 2: Two models to explain the success or failure of sharing economy enterprises.

established and concluded that it is the key to the development of the business model of the sharing economy and essential to its survival [10]. This finding helps substantiate the conclusion of Figure 2: PSEs are highly dependent on venture capital. In order to secure supply stability, the shared goods must be purchased and maintained with the continuous investment of funds, and when the funds are insufficient, the users’ deposit will be used, resulting in major risks. Table 1 shows that all PSE bike sharing enterprises that have failed have used the user’s deposit without exception. When a small number of users find that the deposit cannot be returned, this causes a lot of users’ vigilance. More and more people ask for the deposit to be returned. However, these deposits have been used by enterprises to buy bicycles and put into the market. Finally, users directly lead to the bankruptcy auction of enterprises through litigation.

3.1. Bicycle Sharing. Bicycle sharing is the best illustration; it is the only PSE representative that has significant development in China. Xiaoming Bike was once the leader of the second-tier team when bicycle sharing first became popular. Xiaoming Bike was established on July 29, 2016, and completed 2 rounds of financing in 1 year. By the end of 2017, some users complained about the company, subsequently applying for bankruptcy liquidation. It took only 2 years to owe more than 50 million CNY of debt. Xiaoming Bike never formed a profit model; it mainly relied on financing and its deposit pool to survive. Once the deposit money ran out, the company immediately collapsed. China Renewable Resources Development Co., Ltd. agreed to recycle Xiaoming Bike’s inventory of bicycles at 12 CNY (less than \$2) per bike. In Hong Kong, Gobee.bike, the first bicycle sharing company, announced the end of its business in

Hong Kong after only 15 months of operation. Wukong Bike put more than 1000 bikes in Chongqing, with a loss rate of 90%. Kala put 667 bikes in the Putian District of Fuzhou and ended with only 157 bikes left, a loss of 76.5%. If the management or the scale of the business is improved, will businesses be able to avoid these problems? Wang Yang obtains the operation data of public bicycles through intelligent sensors and uploads it to the WeChat server through public bicycle outlets and wireless communication technology. Citizens can obtain the health and service information of public bicycles in real time through mobile terminals. Maintenance personnel realize the timely troubleshooting of public bicycles through the public self-driving data information resource database, reasonable dispatching, and operation service quality improvement [23].

In their golden age, Mobike and OFO obtained financing of up to 4 billion dollars, enough to put 50 million shared bicycles on the market. Since July 2017, Wukong Bike, Kuqi Bike, Bluegogo, and Xiaoming Bike have been involved in a series of deposit refunds requested by users and then either declared bankruptcy, merged with other enterprises, or were resold. The bicycle sharing market has gradually formed a tripartite of Mobike, OFO, and Hellobike, with Mobike relying on Meituan; Hellobike merging with Youon; and OFO, the former leader, still struggling [24].

Starting from the second half of 2017, all parts of China have successively limited the quantity of shared bicycles. In fact, since 2018, the number of shared bicycles in Shanghai, Guangzhou, Xi’an, Changsha, and other cities has been significantly reduced, and citizens have encountered “difficulties in finding shared bicycles” when traveling [1]. He et al. identified and documented problems such as excessive expansion, neglect of management, and lack of innovation in bicycle sharing [6].

TABLE 1: Business model of sharing enterprises.

Type	Brand	Goods source	Sharing frequency	Service types	Profit model	Data source	Mediating variables: the cost of purchasing goods	Mediating variables: other cost variables *	Current situation	Sensor and wireless technology
ISE	123 Library	Idle	Reuse	Book rental	Rent	Public information	No	Low	Normal	Yes
ISE	Airbnb	Idle	Reuse	Rental housing	Deposits and rent	Public information	No	Low	Normal	Yes
ISE	Uber, DiDi	Idle	Reuse	Taxi	Rent	Public information	No	Low	Normal	Yes
PSE	Sufei	Procurement	Reuse	Book rental	Enterprise libraries, advertisements, and deposits	Public information	Yes	High	Bankruptcy	Yes
PSE	Qinfanqie	Procurement	Reuse	Book rental	Enterprise libraries, advertisements, and deposits	Public information	Yes	High	Bankruptcy	Yes
PSE	Otto	Procurement	Reuse	Truck rental	Deposits and rent	Public information	Yes	High	Bankruptcy	Yes
PSE	Mobike	Procurement	Reuse	Bicycle hire	Deposits and rent	Public information	Yes	High	Sold to Meituan	Yes
PSE	Kala, Gobeebike, Wukong Bike, Kuqi Bike, Bluegogo, and Xiaoming Bike	Procurement	Reuse	Bicycle hire	Deposits and rent	Public information	Yes	High	Deposit storm, bankruptcy, merger, and resale	Yes
PSE	Hellobike	Procurement	Reuse	Bicycle hire	Deposits and rent	Public information	Yes	High	Merged with Youon	Yes

* Other costs include the cost of goods damage, storage costs, maintenance costs, transportation costs, and human resources costs.

TABLE 2: Decision comparison.

	Characteristic	Traditional decision making	Failure rate
PSE	Purchasing shared goods is costly, wasteful, and unsustainable	Cash flow, big market, investment companies like to invest. There are taxes and government support. Entrepreneurs like PSE	High
ISE	Recycling old things has low cost and conforms to sustainable development	Cash flow is large or small, with tax or little tax	Low

3.2. *Sharing Cars.* Table 1 shows that Uber is the only company in our study that has experienced the simultaneous influence of the PSE and ISE. Uber is a successful ISE company. However, Uber has not been lucky with PSE. Uber planned to establish a truck company with the PSE mode. Uber acquired Otto, a self-driving-truck company, for \$680 million in 2016. However, the project only lasted 2 years.

Table 1 explains the essential difference between Otto and Uber, which is the difference between the PSE and ISE.

Uber launched its “driverless fleet” plan in Pittsburgh; it announced that it would cooperate with Volvo and spend \$300 million. It plans to launch self-driving cars in 2021. Baidu and other companies have corresponding plans. Therefore, the conclusion of our study will be helpful to the future of the sharing economy.

4. Discussion

Based on the data (Table 1 and Figure 2), propositions H1 and H2 were proved.

PSE enterprises intend to win over competitors through significant investments and market share, which forms a high dependence on venture capital. Therefore, they have the characteristics of traditional enterprises. Public opinion also impacts government policies not conducive to development. According to the analysis in Figure 2, PSE enterprises are more like traditional enterprises, which do not have near-zero marginal cost of Internet companies such as 123 Library. For example, for bicycle sharing, an increase in the number of users means the company needs to buy more bikes and hire more staff. However, the ISE companies with the Internet attribute are totally different. Their users increase, but their marginal cost is still near zero. Therefore, as the marginal cost of PSE enterprises is not zero, they highly depend on capital, which means that all PSE enterprises can only use user deposits. In particular, as output increases, the product cost per unit will gradually decrease; but when the output increases to a certain amount, the original production line and labor force are inadequate, necessitating expanded production, which increases the ATC.

Range will even exceed the U-shaped increasing range of the average cost. In this process, PSE enterprises find that when the price of ordered goods increases, venture capitalists have a higher bargaining power. For example, OFO faces multiple investors with veto power. Due to the dependence on funds, PSE enterprises often introduce multiple investors, who may have different opinions when making major decisions, leading to major risks or bankruptcy.

As a result, most PSE enterprises are sued for misappropriating deposits or sued by manufacturers for credit, and seized (Table 1). Their capital chains are broken, the

founders are arrested, the assets and businesses are sold, and the companies go bankrupt. Whether it is book sharing, bicycles, or cars, PSE enterprise cannot escape the above fate. Therefore, the results of this paper substantiate propositions H3 and H4.

Accordingly, if a PSE enterprise obtains a monopoly position, is it on a smooth business path? The answer is “No.” Due to the huge capital investment and increasing marginal costs, traditional PSE companies are often easily defeated when they encounter new technological substitutes or more convenient services. For example, if Uber adopts procurement sharing to develop driverless vehicles and obtains a monopoly position, competitors will make capital investments in unmanned aircraft quantum teleportation technology, and any breakthrough will easily destroy Uber’s procurement project. However, if Uber uses the idle sharing mode to share unmanned vehicles, it will have the Internet gene, and the investment and marginal cost can be perfectly controlled. We observed that in 2016, Joe Gebbia, cofounder of Airbnb, announced that he was going to build shared houses in Yoshino, Japan, but ultimately did not. There is no doubt that this is not because of luck. The executives of Airbnb, as a successful representative enterprise of ISE, know the advantages of ISE and so suddenly terminated this project.

From Table 2, we can see that in the traditional decision-making methods, investment companies pay attention to cash flow and large market capacity, the government pays attention to tax, and entrepreneurs also pay attention to cash flow and large market and like to choose PSE projects for entrepreneurship. However, the outcome is cruel, and the failure rate of PSE is very high. ISE enterprises recycle second-hand goods with low operating cost, which meets the needs of human sustainable development and should receive greater social support. Due to the unstable cash flow and tax revenue of some ISE enterprises, investment companies, governments, and entrepreneurs will be very cautious when choosing ISE. Such ISE enterprises should strengthen the research on profit model, for example, 123 Library.

Sharing economy is developing rapidly in the world, but most sharing enterprises have failed and brought a huge waste of resources. By establishing two models (PSE and ISE) to explain the success or failure of enterprises in sharing economy, we found that PSE enterprises are traditional enterprises with a high bankruptcy risk. PSE enterprises can generate a significant amount of waste and are highly dependent on venture capital; they should be restricted by the government. ISE enterprises, however, have Internet “genes,” comport with sustainable development, and should be supported. Our research shows that entrepreneurs may fail if they do not pay attention to the relationship. A huge

waste of resources and chaotic social order may occur if the government does not pay attention to it, and investment companies may lose a lot if they ignore it. The practical data show that our method is effective in judging whether the sharing enterprise fails.

5. Conclusions

PSE enterprises are traditional enterprises with a high bankruptcy risk. They occupy the market, create significant waste, survive by misappropriating users' deposits, rely heavily on venture capital, do not have the Internet gene, and do not comport with sustainable development. The disordered competition of PSE companies results in a huge waste of resources and damages the social order. PSE enterprises have a high market risk, are more likely to fail, and have a high investment risk.

ISE enterprises are Internet enterprises with Internet genes that comport with sustainable development. ISE is a sharing enterprise that should be advocated by society. Its business risk is small, which is beneficial to the sustainable development of society. Entrepreneurs, venture capitalists, the public, and the government should prefer the ISE model. If entrepreneurs do not pay attention to the difference between PSE and ISE, they may fail; if the government does not pay attention to it, a huge waste of resources and chaotic social order may result; and if investment companies do not pay attention to it, they may lose a lot.

The application of wireless communication and Internet of Things technology can promote the development of sharing enterprises, such as better user evaluation in promoting QoS service quality. In the field of book sharing, such as 123 Library, if Internet of Things chips are installed on each book to let customers know the geographical location of shared books in time, the freight can be reduced and the frequency of book recycling can be increased. Whether sharing companies are prone to failure is directly related to the independent variables (PSE/ISE). Cost is a key intermediary variable. For investors and entrepreneurs, in addition to paying attention to the cash flow and income figures of entrepreneurial projects, they should pay more attention to cost. ISE has low cost and can easily survive, while PSE has high cost and can easily fail. Governments should encourage the development of ISE companies and limit and control the development of PSE companies. Governments should strengthen the supervision of PSE enterprises, including the following:

- (1) The government should adopt a market license approval system.
- (2) The government should determine the scale of the enterprises' investment according to local demand and test the capacity of the market by gradually increasing the amount of investment, in order to minimize wasting resources. Governments should also strengthen research, monitor the environmental damage caused by shared goods, and strengthen user safety management, including deposit management, goods quality, and personal safety.

What are some possible options for PSE enterprises? How can an enterprise be categorized as either PSE or ISE? According to the definition of this paper, bicycle sharing company A improves the output growth rate of bicycle factories through making purchase. A is a PSE enterprise, but if A goes bankrupt and B acquires the bicycles of A without reproduction and an increase in the production growth rate, company B is an ISE enterprise. After more than 95% of the bicycle sharing companies in China went bankrupt, their assets went to Mobike and Hellobike, the two largest companies. Mobike and Hellobike acquired ISE characteristics, so they became more powerful. Therefore, the competitive strategy of PSE enterprises should be to quickly become strong enough to acquire competitors' shared objects cheaply and turn into ISE companies. Furthermore, Mobike and Hellobike should develop a shared social idle bicycle platform and become real ISE enterprises.

5.1. Suggestions for Future Research. We did not include traditional enterprises that purchase and sell second-hand goods because they do not belong to the sharing economy as defined in this paper. We did not study the success or failure of businesses using personality variables, such as the personality and cognitive ability of project founders and team members, although these factors are crucial. We did not study the impact of venture capital on the decision-making power of enterprises, although it is an interesting topic. Therefore, the above factors need to be considered when using the conclusions of this study. However, because we reveal the relationship between the essential elements of success and failure of the sharing economy, these future studies will not affect the readers' use of our findings to make the right decisions.

Data Availability

No data were used to support this study.

Conflicts of Interest

The authors state that they have no conflicts of interest.

Acknowledgments

This research was supported by Zhejiang Provincial Natural Science Foundation of China under Grant no. QY20G030001.

References

- [1] National Information Center Sharing Economic Research Center, *China Internet Society Sharing Economic Work Committee. China Sharing Economic Development Report: 2019*, National Information Center Sharing Economic Research Center, Beijing, China, 2021, <http://www.sic.gov.cn/>.
- [2] Y. Yi, "Introduction to shared economic development," *Financial Accounting*, vol. 12, 2015.
- [3] Chase (U. S. A), *Sharing Economy: Reconstructing New Business Models in the Future*, Zhejiang People's Publishing House, Hangzhou, China, 2015.

- [4] A. Stephen, *Sharing the Economic Business Model: Redefining the Future of Business*, China Renmin University Press, Beijing, China, 2016.
- [5] G. Zervas, D. Proserpio, and W. John, "The rise of the sharing economy: estimating the impact of Airbnb on the hotel industry," *Journal of Marketing Research*, vol. 10, 2017.
- [6] M. Li, F. Wang, X. Jia, W. Li, T. Li, and G. Rui, "Multi-source data fusion for economic data analysis," *Neural Computing and Applications*, vol. 33, no. 10, pp. 4729–4739, 2021.
- [7] M. Murphy, "Cities as the original sharing platform: regulation of the new "sharing" economy," *Harvard Business Review*, vol. 13, no. 10, 2014.
- [8] D. Das Acevedo, "Regulating employment relationships in the sharing economy," *Employee Rights and Employment Policy Journal*, vol. 20, no. 1, 2016.
- [9] S. Hong and S. Lee, "Adaptive governance and decentralization: evidence from regulation of the sharing economy in multi-level governance," *Government Information Quarterly*, vol. 35, no. 2, 2018.
- [10] S. Gao, W. Zhang, and Y. Wang, "Research on the linkage mechanism of shared economic business model elements," *Commercial Research*, vol. 11, 2017.
- [11] S. Pan, "The legal challenge and response of the shared economy prepaid deposit model," *Journal of Wuhan University(Philosophy and Social Sciences)*, vol. 11, 2018.
- [12] J. Rifkin, *The Zero Marginal Cost Society: The Internet of Things, the Collaborative Commons, and the Eclipse of Capitalism*, Zero Marginal Cost Society, Palgrave Macmillan, 2014.
- [13] G. Li, "Research on the extension of 123 library extension service," *Shandong Library Journal*, vol. 3, 2015.
- [14] G. Li, "Comparison of the development model of qingdao library and 123 library," *Library Forum*, vol. 7, 2015.
- [15] G. Li, "Research on the integrated sharing mode of social reading resources," *Library Theory and Practice*, vol. 7, 2015.
- [16] Z. Xu, G. Zhu, N. Metawa, and Q. Zhou, "Machine learning based customer meta-combination brand equity analysis for marketing behavior evaluation," *Information Processing & Management*, vol. 59, no. 1, Article ID 102800, 2022.
- [17] G. Li, "The self-organization development model of 123 library and its enlightenment," *Library Construction*, vol. 3, 2015.
- [18] G. Li, "Study on the guarantee of 123 library operation system," *Library Theory and Practice*, vol. 7, 2014.
- [19] G. Li, "Characteristics of 123 network library," *Research of Library Science*, vol. 2, 2014.
- [20] Bo Liu, "The enlightenment of 123 library operation mode to university libraries," *Library Journal*, vol. 3, 2018.
- [21] W. Zhao, X. Dai, and Q. Zhan, "Research on book sharing mode under internet thinking," *Library and Information Work*, vol. 2, 2018.
- [22] Y. Wang, *Biography*, Jiangsu literature and Art Publishing House, Jiangsu, China, 2015.
- [23] Y. Wang, "Research on public bicycle wechat service system based on intelligent sensor," *China its journal*, vol. S1, 2015.
- [24] J. Guo, "Economic thinking on shared bicycles," *Reform and Opening*, vol. 6, 2017.

Research Article

Assembly Sequence Planning Based on Hierarchical Model

Chunxi Li  and Wenjun Hou

School of Modern Post, Beijing University of Posts and Telecommunications, Beijing 100876, China

Correspondence should be addressed to Chunxi Li; lichunxi@bupt.edu.cn

Received 27 November 2021; Accepted 29 December 2021; Published 9 February 2022

Academic Editor: Nima Jafari Navimipour

Copyright © 2022 Chunxi Li and Wenjun Hou. This is an open access article distributed under the Creative Commons Attribution License, which permits unrestricted use, distribution, and reproduction in any medium, provided the original work is properly cited.

With the rapid development of intelligent manufacturing technology and ultraprecision machining, assembly technology has attracted more and more attention. Assembly sequence is an important part of assembly process planning. However, assembly sequence is affected by many complex factors, such as the time required to assemble products, the geometric feasibility of assembly sequence, and other factors (tool replacement times and assembly direction change), so it is very challenging. In this paper, an assembly information model based on geometric features of parts is proposed. The model obtains the hierarchical information of the part through the segmentation and feature reconstruction of the part. Based on the influence of the contact surface between parts on the feasible motion domain and assembly domain, the assembly constraint relationship model is established. The objective function is constructed by changing the assembly direction, changing the assembly tools, and evaluating the assembly fit type. The geometrically feasible assembly sequence is optimized to obtain the optimal assembly sequence under the existing conditions. Taking a block, a secondary reducer spindle, and a cylinder as examples, the effectiveness of the method is verified.

1. Introduction

Assembly is the key link of product manufacturing, the last step of the product manufacturing cycle. The final function of the product is directly related to assembly quality. According to a survey by Boothroyd, assembly time accounts for 40%-60% of the total workload of product manufacturing, as assembly work requires much manual labor, while assembly accounts for 20%-70% of the total production workload [1]. The generation of assembly sequence plan (ASP) is considered an essential activity in the production stage because it can affect the layout of the production line and provide basic information on auxiliary fixtures [2]. An efficient, viable ASP can minimize the assembly lead time and cost by optimizing the tool travels and the number of changes in assembly directions [3, 4].

Regardless of the multiple functionalities offered by the current CAD/CAM environments, the generation and the simulation of ASP/DSP remain an issue [5]. The planning process of assembly sequence is regarded as an NP-hard problem. A product composed of n parts with feasible

assembly sequences is $n!$ [6]. In the early 1960s, researchers looked for feasible assembly sequences in products through the contact relationship between parts [7]. Then, the contact relationship is expressed by different graphs to find all potentially feasible sequences of products [8]. The above method can solve the assembly sequence planning problem to a certain extent, but it needs to consider the constraint relationship between parts. Excessive manual participation leads to the decrease of computational efficiency and misses the optimal feasible sequence because of the different methods of defining constraints.

The basis of assembly sequence planning is the expression of assembly information. Bahubalendruni et al. have done extensive research on the expression forms of various assembly information, such as nondirectional blocking graphs, interference graphs, AND/OR graphs, and Petri-net graphs [4]. They believe that the matrix-based method is the most suitable for automatic sequence generation. Most of the graphical representation methods were advanced in 1988 to represent assembly constraints [9–11]. The connectivity graphs are further extended to find the stable

subassemblies, which offer the minimum number of levels to complete the overall assembly process [12]. Few researchers gave importance to extract the assembly sequence constraints from Computer-Aided Design (CAD) software to minimize the human intervention, which reduces computational time further [13]. Several researchers developed automated extraction methods to retrieve assembly liaison data, interference data, and assembly stability information through CAD interfacing [14–16].

An appropriate assembly sequence needs to meet both geometric feasibility and efficiency [15]. Part concatenation method (PCM) is widely used to represent the geometric feasibility between parts, which considers three assembly sequence constraints: liaison matrix, stability matrix, and six interference matrices [17]. It is observed that the matrix-based approach requires the participation of personnel to reduce the complexity of the automatic planning sequence. Generally, the assembly direction is divided into six axial directions. In this case, it is necessary to determine the feasible path in oblique assembly manually [18]. As shown in Table 1, the existing methods use the objective function to optimize feasible sequences, usually to minimize factors such as direction change, tool change, and tool moving distance. The weight of the corresponding traversal is determined according to different requirements, and the geometrically feasible assembly sequence is selected.

The interference matrix (IM) is an N order square matrix (N represents the number of parts in the product). Elements “0” and “1” in a square matrix represent the feasibility and infeasibility to perform assembly operations [32]. Yu et al. established the extended interference matrix (EIM) by introducing a new variable “2” into IM. Element “2” indicates that the part is geometrically feasible but has relative motion [18]. Bahubalendruni and Biswal obtained the liaison matrix automatically between parts by using Visual Basic (VB) language in computer-aided three-dimensional interactive applications (CATIA), which reduced personnel participation [33]. Some scholars regard the tool as an important influencing factor and add the geometric information of the tool to the constraint model, which increases the complexity of the model and reduces the space of the firm scheme, but practicality is achieved [34–36]. To reduce the complexity of calculation, some researchers only calculate the critical information in the model. However, the existing commercial CAD software is challenging to obtain the part modeling process, so it is hard to decompose the part through the geometric structure and restructure it [37–39].

In most studies, the constraint relationship between parts is realized by human definition or collision detection, and the parts are regarded as a whole in the planning process. It can be seen from the literature that the geometric feasibility testing is subjected to a conceptual limitation that can identify collision-free paths in principal axis directions ($\pm X$, $\pm Y$, and $\pm Z$). When nonaxial assembly occurs in the assembly process, it is necessary to define constraints and feasibility manually. Based on this idea, we study the structures of parts and the method of part segmentation. The key structures involved in the assembly process are obtained in a sim-

TABLE 1: Objective function consideration in the existing ASP methods.

References	Objective for optimization			
	Directional changes	Tool changes	Tool travel distance	Assembly force
[18–20]	√	√	√	×
[21–25]	√	×	×	×
[26–28]	√	√	×	×
[16, 29–31]	×	√	×	×

plified way, and the assembly information model is established on this basis. Through the information in the assembly model, the solution domain of geometrically feasible assembly sequence in mechanical products is established, and the assembly sequence is optimized through nongeometric information. Upon addressing the identified research gaps, a new assembly sequence planning method based on geometric constraints is proposed for mechanical product ASP, including oblique assembly.

This paper introduces an assembly modeling method for automatically determining the optimal assembly sequence. In this paper, the geometric information extracted from the CAD model and nongeometric information of the model are extracted from technological documentation. Geometric information includes part structure information and contact relationship information between parts, while nongeometric information includes tool information and assembly position moving distance in the assembly process, which is enough to support the automatic generation of the assembly sequence. Using this method can reduce the degree of manual participation in the process of production sequence and solve the problem of oblique assembly to a certain extent. It is worth mentioning that, to shorten the calculation time of the algorithm, the part simplification is realized on the premise of ensuring the integrity of the part through the segmentation and reorganization of the part model.

The remainder of this paper is organized as follows. In Section 2, a novel method for obtaining the B-rep model of parts from any given product in CAD software is presented and is separated into basic geometry. An effective way to simplify parts on the premise of ensuring the integrity of parts is presented in Section 3. Sections 4 and 5 introduce the process of optimizing assembly sequence through geometric information and nongeometric information as shown in Figure 1. The application of improved assembly planner has been tested on assembly products in Sections 6 and 7, and Section 8 ends the article by introducing the contribution made in this field and the scope of future research.

2. Modeling of the Part Assembly Information Based on CAD System

At different stages of the part life cycle, engineers need different fineness of part information. In the stage of assembly sequence planning, attention is paid to the geometric structure of parts and the constraint relationship between parts.

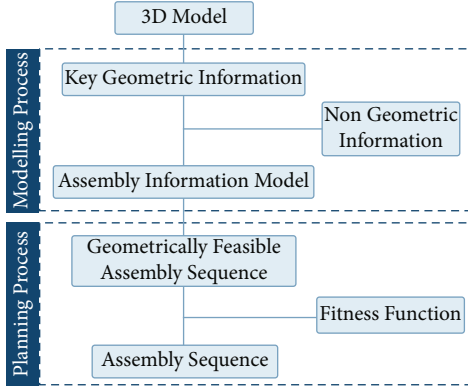


FIGURE 1: Overall system flowchart.

In this paper, the necessary assembly information of the part is obtained by simplifying the model extracted by CAD. In the process of simplifying parts, it is necessary to determine the basic simplified units. In CAD systems, parts can be regarded as a combination of multiple simple geometric features, and the features contain the information of points, lines, and surfaces that constitute the features. If the face is taken as the smallest unit, the simplified part will not be completely solid. Therefore, this paper uses features as the smallest unit.

In CAD systems, the same features can be generated in different ways, so the feature tree in the system cannot be used as the feature relationship of parts, and the features constituting parts need to be obtained through the type of part surface and contact relationship. In this paper, the topological relationship between faces in parts is represented by the boundary representation (B-rep) model, as shown in Figure 2. Through the secondary development of CAD, the topological relationship of surfaces is got. Then, using the volume decomposition method, the feature-based model of the part is generated from the B-rep model. The parts are decomposed into a multilevel product assembly information model, which stores the geometric constraints of parts in mechanical products and the nongeometric information related to parts in the assembly process.

2.1. B-rep Model Volume Decomposition. An n -dimensional square matrix is established to store the topological relationship information of surfaces, and an n -dimensional degree vector stores the type information of faces (n is the number of faces in part). The square matrix is composed of elements 0 and 1, used to record a contact relationship between two sides.

2.1.1. B-rep Model. Boundary representation (B-rep) is a closed shell surrounded by curved bread, which is a popular geometric description in CAD systems. It can store point, line, and surface information in the CAD model. For comparative calculation, we represent B-rep model (1a) as the adjacency diagram of the surface (1b). The part comprises eight surfaces, where surface b is a cylindrical surface and contacts plane a and plane c , while there is no contact between a and c .

2.1.2. Volume Decomposition. The subfeatures of parts can be divided into additional features and subtraction features, and their Boolean operations form complex geometry. Basic geometric features include cylinder, cube, cone, and prism, and pyramid. In order to obtain the basic geometric feature expression of parts, this paper refers to Shi et al.'s [39] research results, identifies the basic geometric features of surfaces through Hough transform, and completes the basic geometric feature reconstruction of parts. The specific algorithm is as follows (as shown in Figure 3).

- (1) 3D mesh the determined 3D parts using triangular patches
- (2) Calculate the angle between the triangular patch and the adjacent patches
- (3) The part is divided into patch groups $\{F_i\}$ through the concavity and convexity of triangular patches
- (4) To identify the corresponding feature types of the segmented patch groups $\{F_i\}$ by using Hough transform
- (5) The part is reconstructed into a feature-based representation, and the release relationship between features is stored

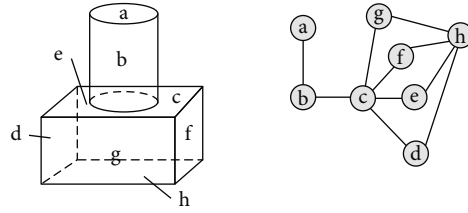
2.2. Data Structure of Part Model. There are many kinds of information on a part, and the information of the part is attached to the model at different levels. The tools used to assemble parts need to be attached to the part-level model. The part assembly information model includes geometric feature information, assembly contact relationship information, and assembly type information. This paper obtains the geometric information of parts from the CAD system, and the nongeometric information in the assembly process is collected. The information is classified and stored into four levels: part level, feature level, surface layer, and constraint layer between surfaces, as shown in Figure 4. It intends to illustrate the most essential properties of parts in the assembly process through graphics.

The part is decomposed into simple subfeatures through segmentation, and the surfaces contained in the subfeatures are further used as surface layers. Assembly constraints are determined by the constraints between multiple surfaces in two parts. An undirected graph represents part constraints because the fitting relationship between parts takes precedence before determining the assembly sequence.

2.2.1. Feature Information. The feature information contained in part includes identification number (Fea_Id), addition and subtraction attributes (Fea_Type), and the ID number of feature surface (Surface_Id). The feature layer model of a part can be expressed as

$$\langle \text{FeaInfo} \rangle = \{ \langle \text{Fea_Id} \rangle, \langle \text{Fea_Type} \rangle, \langle \text{Surface_Id} \rangle \}, \quad (1)$$

where Fea_Id is the identification number (ID) of the part feature model, which represents the unique number of essential features; Fea_Type indicates whether the feature is



(a) The surface of the part (b) Surface contact relationship

FIGURE 2: B-rep model representation of the surface in part.

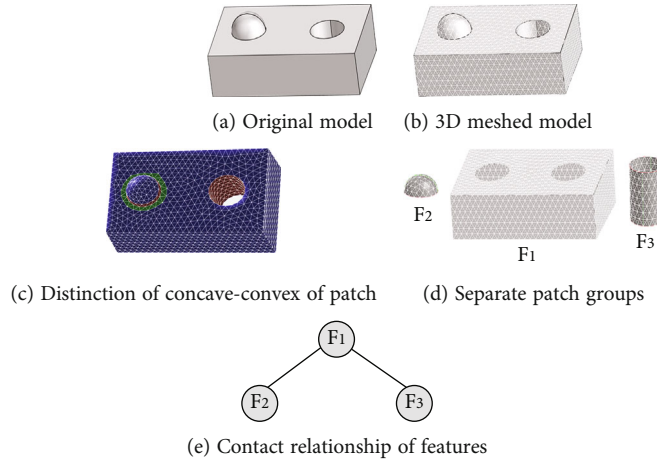


FIGURE 3: The process of obtaining feature contact relationship of parts.

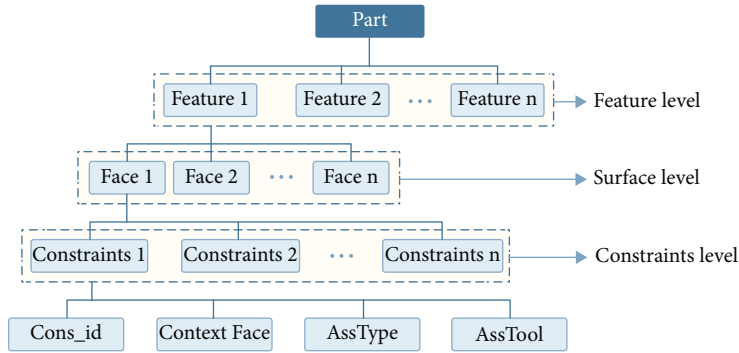


FIGURE 4: Hierarchical assembly information model of part.

added or subtracted in part, which is the roles of features in the process of part modeling and related to the operation performed when the feature will be deleted later. Surface_Id represents the surface contained under this feature, where only the surface that exists in part is stored.

2.2.2. *Surface Information.* The surface information is composed of the surface ID and the constraints it contains. Surface ID represents the unique number of the surface in part, while the constraint represents the contact relationship between the surface and other parts. That is the solution

object and carrier of assembly constraints. The surface layer model of the part can be expressed as

$$\langle \text{FaceInfo} \rangle = \{ \langle \text{Surface_Id} \rangle, \langle \text{Cons_Id} \rangle, \langle \text{Sur_point} \rangle, \langle \text{Sur_radius} \rangle, \langle \text{Sur_vector} \rangle \}, \quad (2)$$

where Surface_Id is the ID of the part surface model and Cons_Id represents the ID number of the contact relationship between the surface and the surface in other parts. Sur_point is the center point in the plane. Sur_radius is the radius of cylindrical and the cone angle of conical and

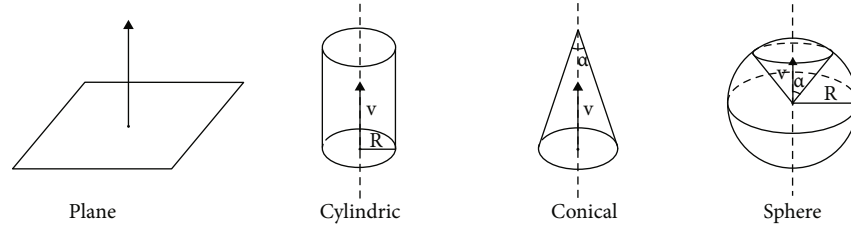


FIGURE 5: Surface assembly information model.

sphere. *Sur_vector* is the vector of the plane, as shown in Figure 5. This data is obtained in the assembly before sequence planning and will not change due to different sequences.

2.2.3. Constraint Information. The constraint information includes the IDs of the two surfaces with contact relationships and the type of contact between the two surfaces. The constraint information of the surface can be expressed as

$$\langle \text{ConsInfo} \rangle = \{ \langle \text{Cons_Id} \rangle, \langle \text{ConsFace_Id} \rangle, \langle \text{Fit_type} \rangle \}, \quad (3)$$

where *Con_Id* refers to the face on this part in the contact relationship and *ConFace_Id* refers to the face of other parts in the contact relationship. *Con_Type* is the type of contact relationship. Because various parts will have constraints with the same part in the actual assembly process, multiple sets of constraint information can be attached to the same surfaces.

3. Part Model Simplification

Assembly constraints between parts consist of geometric constraints between surfaces [40]. In other words, geometric constraints are the basic elements of assembly constraints (as shown in Figure 6). Assembly constraints between parts can be divided into geometric constraints between multiple surfaces. In this paper, the constraint relationship between parts is expressed as a part surface relationship network. Redundant surfaces in parts will lead to too many nodes in the network and increase the computational complexity. At the same time, there are multiple surfaces to express the same assembly constraint relationship, which reduces the computational efficiency and increases the possibility of error.

Figure 7 shows the relationship between the running time of the traversal sparse matrix program and the number of nodes. The abscissa in the graph is the number of nodes of the traversed undirected graph, and the ordinate is the running time of the program. The matrix in the graph is a random matrix with the number of edges less than half of the total connected graphs. The median time of the independent traversal connection graph ten times conforms to the quadratic curve. Therefore, reducing the nodes of the graph can effectively improve computational efficiency.

3.1. Feature Importance Ranking. The reconstruction of parts based on basic geometric features uses the methods mentioned above. By deleting the subfeature that makes up

a part, the key component features of the part are obtained. Different deletion processes result in different results. In order to ensure the integrity of the final part constraint information, it is necessary to determine a proper deletion sequence.

The subfeatures in the modeling process will be reordered according to their importance. The importance of subfeatures depends on their role in the part. Kim and Mun [38] and Kang et al. [41] proposed several recombination strategies. In our study, the importance of subfeatures is evaluated according to the following criteria:

- (1) Features with large volume are more important than those with small volume
- (2) Port features which contact with other parts shall be retained
- (3) Features with contact relationship with port features are more important than other features
- (4) Addition features are more important than subtraction features

Based on the above principles, this paper determines the fitness function of feature ranking. If the feature is a port feature, it needs to be retained during the simplification process. At this time, $n=1$ makes $f > 0$. The simplification process is aimed at the function value less than 0. C_1 is the volume ratio of this feature to the largest feature in part. The larger the volume, the larger the value of C_1 , which is between 0 and 1. When the feature is an additional feature, $C_2 = 1$, minus the feature is 0. In addition, when there is a contact relationship between the feature and the port feature, C_3 is 1 and 0 at other times. Thus, the evaluation function formula (4) for the importance of the feature is formed. The feature ranking process is shown in Figure 8.

$$f = n \times (C_1 + C_2 + C_3). \quad (4)$$

3.2. The Condition of Feature Simplification of 3D Parts

3.2.1. The Initial Conditions of the Part Simplification Process. First, it is crucial to ensure that the geometric structure of the parts does not change during assembly planning. Then, determine the contact relationship between parts and ensure the relationship does not change in assembly sequence planning.

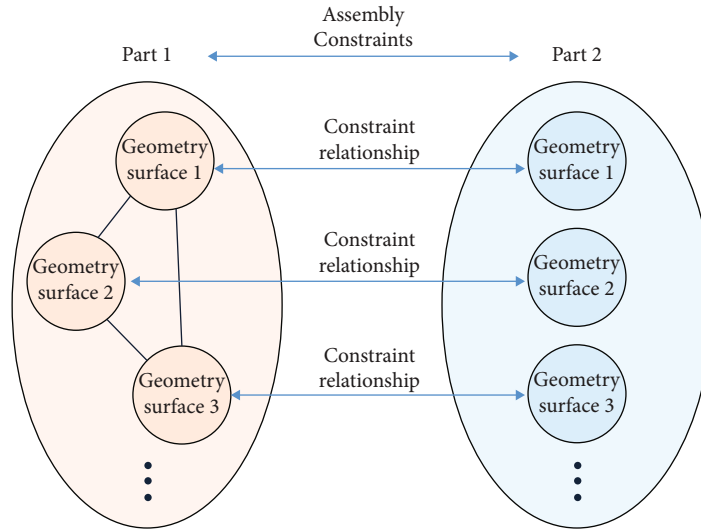


FIGURE 6: The relationship between assembly constraints and geometric constraints.

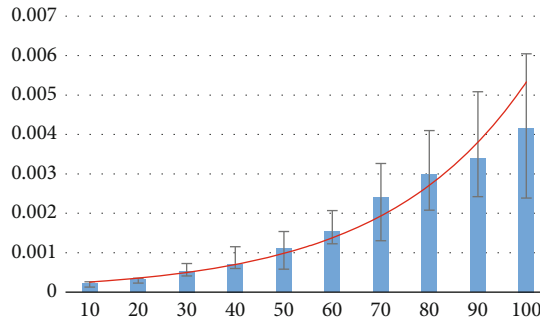


FIGURE 7: Surface assembly information model.

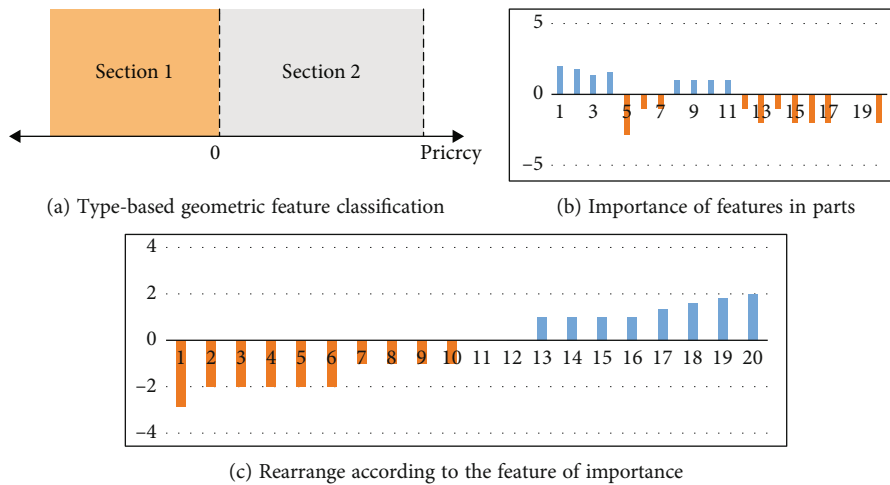


FIGURE 8: Geometric features are rearranged according to their importance.

3.2.2. *Termination Conditions for the Part Simplification Process.* The final result of simplification is to retain all the marker surfaces, which cannot further simplify the whole.

3.3. *Principle of Simplification of 3D Part Structure.* The parts in the assembly need to be simplified by the model separately. Furthermore, a complete expression of the assembly constraint

relationship is constructed by using simplified parts. The simplified process needs to follow the three principles below.

Principle 1: the geometric features in the parts have contact relations with each other by surfaces, forming a coherent whole and maintaining its topological relation.

Principle 2: the volume of the geometric feature is taken as the simplified parameter. The volume of key features in

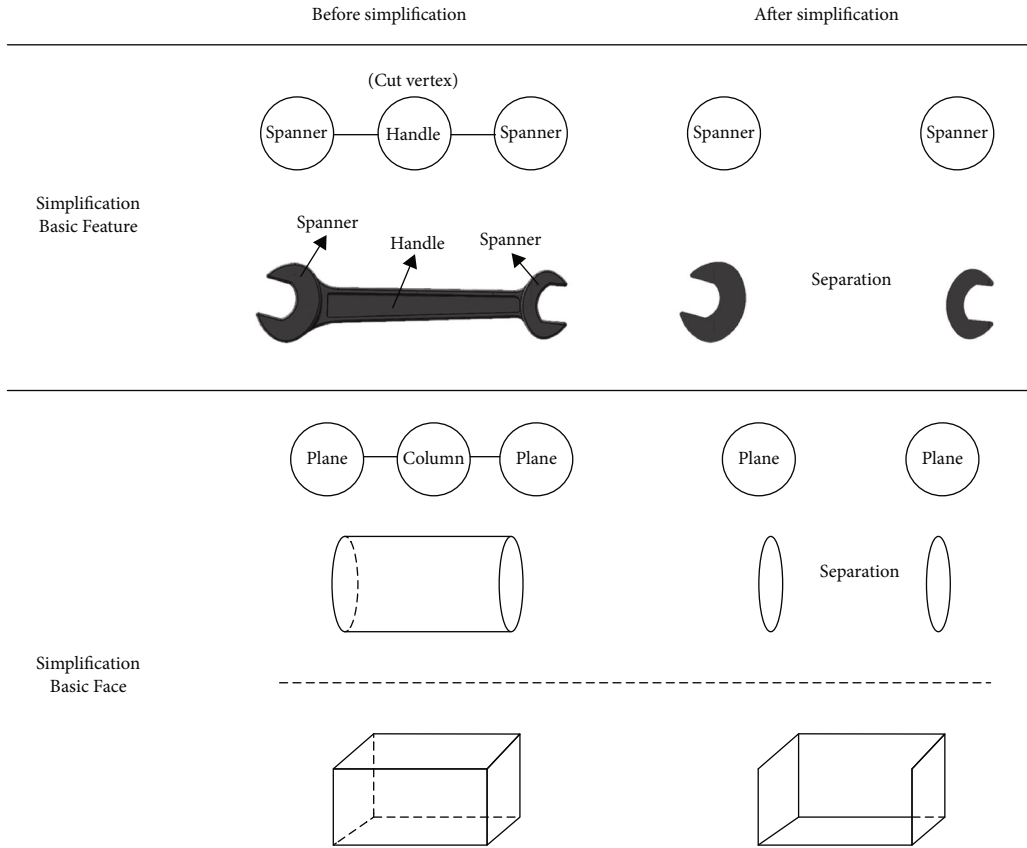


FIGURE 9: Feature separation occurs during simplification.

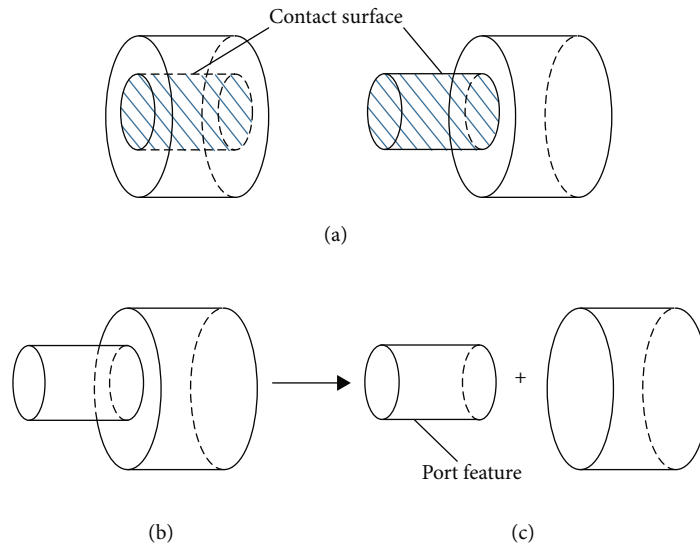


FIGURE 10: Port features in parts.

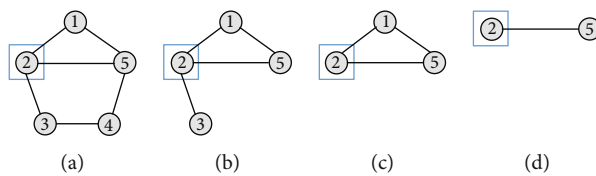


FIGURE 11: Changes of node attributes in contact graph during feature simplification.

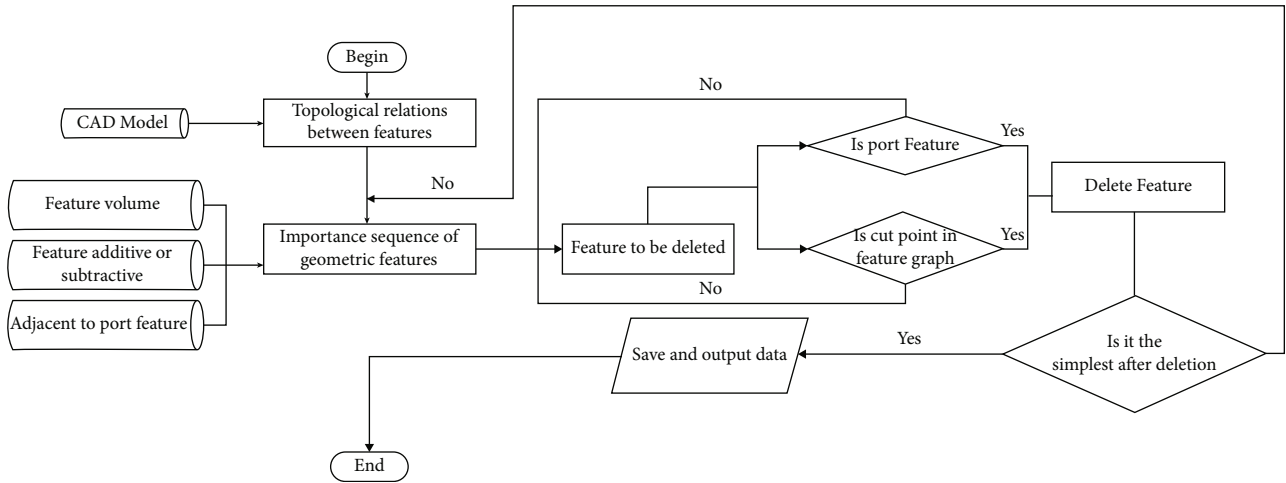


FIGURE 12: Algorithm for simplifying features in parts.

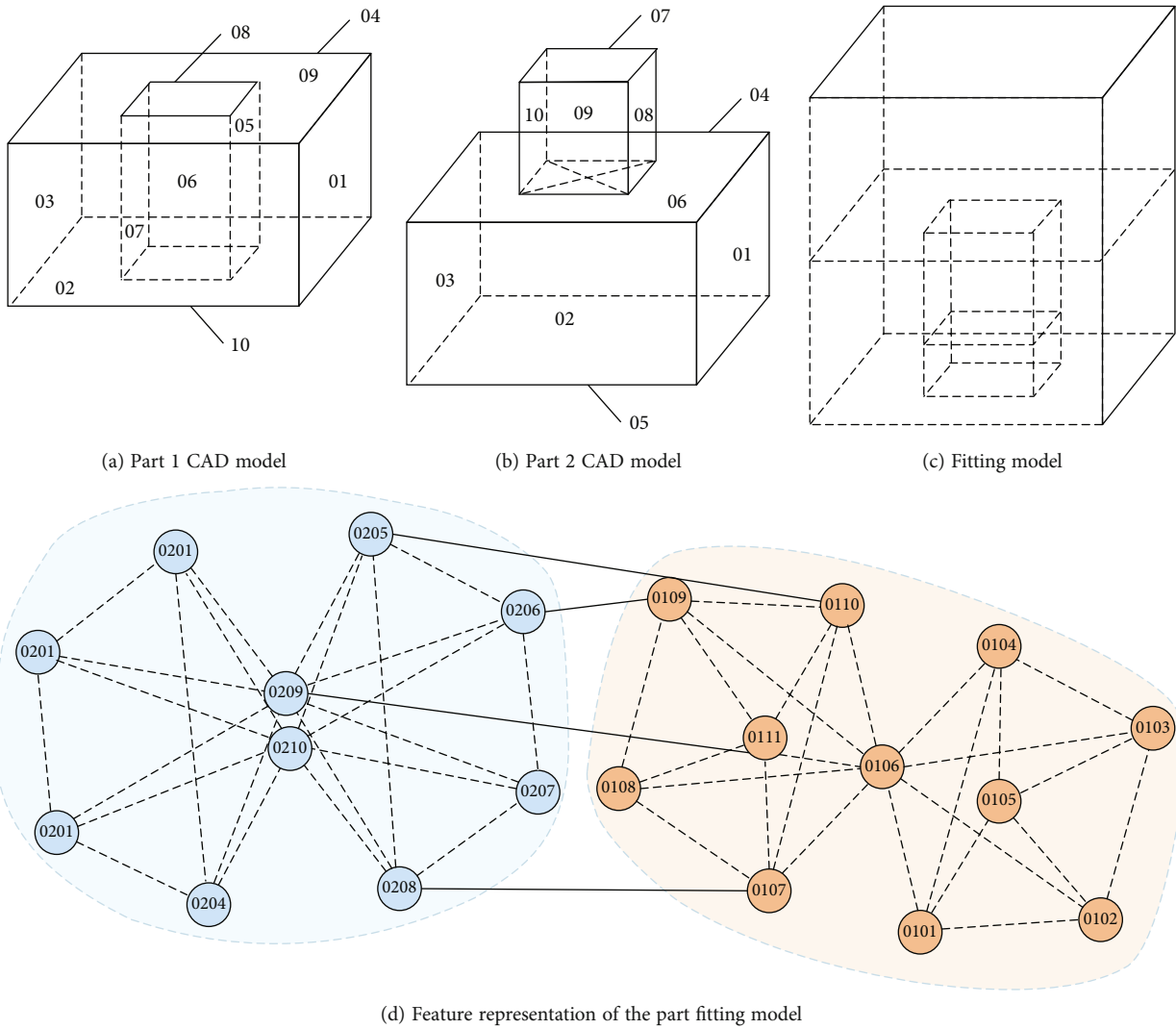
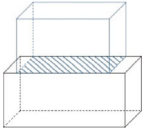
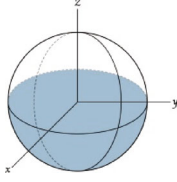
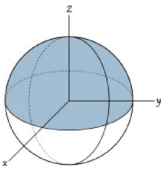
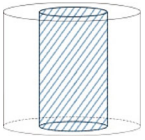
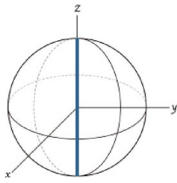
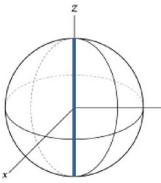
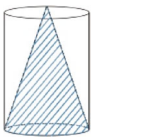
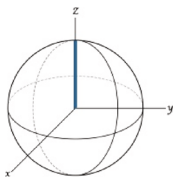
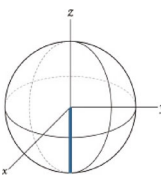
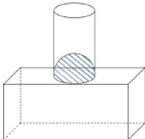
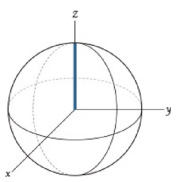
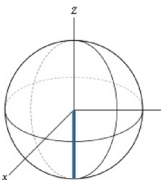


FIGURE 13: Contact relationship of parts based on surface.

TABLE 2: Constraints of surface on feasible assembly region of parts.

Connect relationship	Assembly direction	Disassembly direction	Assembly zenith angle	Assembly azimuth angle	Disassembly zenith angle	Disassembly azimuth angle
			$\theta = [(\pi/2), \pi]$	$\phi = [0, 2\pi]$	$\theta = [0, (\pi/2)]$	$\phi = [0, 2\pi]$
			$\theta = [0, 0]$ $\theta = [\pi, \pi]$	$\phi = [0, 2\pi]$	$\theta = [0, 0]$ $\theta = [\pi, \pi]$	$\phi = [0, 2\pi]$
			$\theta = [0, 0]$	$\phi = [0, 2\pi]$	$\theta = [\pi, \pi]$	$\phi = [0, 2\pi]$
			$\theta = [0, 0]$	$\phi = [0, 2\pi]$	$\theta = [\pi, \pi]$	$\phi = [0, 2\pi]$

part is often relatively large, so the more minor features are deleted while the more essential features are retained in simplifying the part.

Principle 3: in the algorithm of deleting features, only one feature is deleted at a time. The link relationship between the features of simplified parts needs to be judged in an oversimplification to avoid the part separating into two separate parts.

3.4. Steps to Simplify Geometric Features in a Part. We reduce the computational complexity of the planning process by calculating the key features. Through the previous decomposition, the part is regarded as a complex structure composed of multiple basic features in the Boolean operation. Delete the geometric features of parts that are not related to the assembly process so as to simplify the complexity of parts and reduce the difficulty of calculation.

In the process of model simplification, model separation occurs when the only added feature linking two added features is deleted, as shown in Figure 9. The separated model will be regarded as two or more independent individuals in the system, so the information attached to the model is no longer reasonable, so the model cannot be used to determine geometric constraints. Therefore, in the process of part simplification, the connectivity of the feature-based 3D model needs to be considered to prevent model separation. Among them, we only consider additive subfeatures because the connectivity of the model is usually based on the additional

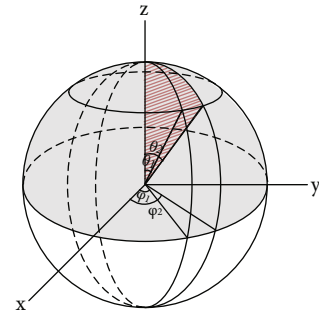


FIGURE 14: Feasible assembly region represented by polar coordinates.

subfeatures of the connection. Even if the subtraction subfeature is deleted, the connection between other subfeatures will not be affected.

$$a_{ij} = a_{ji} = \begin{cases} 1 & \text{contact between two features,} \\ 0 & \text{no contact between two features.} \end{cases} \quad (5)$$

Figure 10 shows the connection of the part with other parts during assembly, where subfeature 1 is the port feature containing the contact surface. In the process of simplification, port features need to be marked and retained.

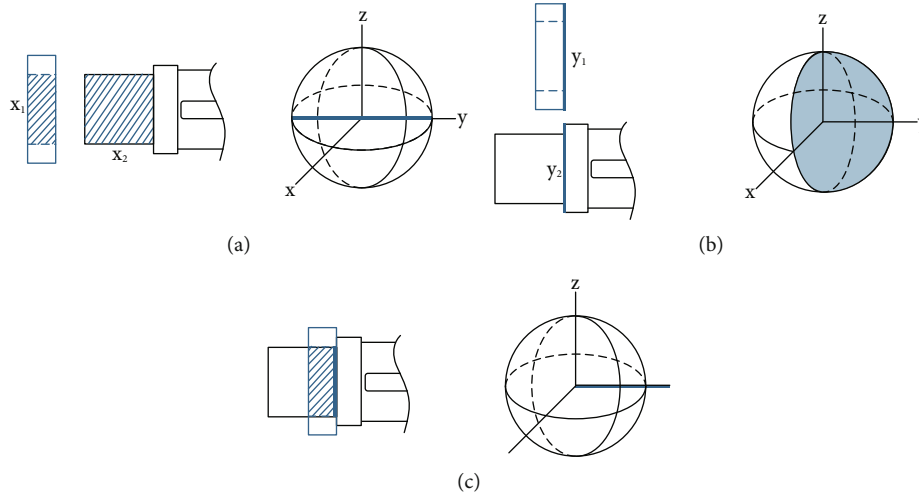


FIGURE 15: Determination of assembly region between parts.

When a node is deleted and the graph is no longer connected and splits into two or more disconnected subgraphs, the node is referred to as the cut node of the connected graph. The cut nodes and general nodes in the diagram can be transformed mutually in the simplification process of the diagram, so only one feature can be deleted at a time, and the contact relationship between the geometric features of the parts can be regained after the process.

In the contact relation undirected graph shown in Figure 11, all nodes at this time are ordinary nodes. After deleting node 4, if node 2 is deleted, the graph will be divided into two independent parts. Therefore, node 2 is a cut point and cannot be deleted. When node 3 is deleted, all nodes are transformed into ordinary nodes. Therefore, the node switches between the cut point and ordinary node with the node, and the contact relationship changes in the graph. So, when the contact relation changes, it is necessary to evaluate the cut point in the graph.

When a feature is deleted, the contact relationship of the remaining subfeatures in part changes. Therefore, a geometric feature can only be deleted once, after which the new judgment of residual geometric features needs to be evaluated as a cut node or not. If the feature to be deleted is the cut point in the feature contact graph, the feature cannot be deleted. Skip the feature and consider the next feature in order. Then, delete a feature and its edge in the feature contact graph and update the set of cut points. It is designed the following simplified algorithm according to this scheme as shown in Figure 12.

An undirected graph is used to represent the topological relationship of the face and the constraint relationship between the parts. Figure 13 shows assembly constraint information based on surface contact representation. In the graph, the same color represents the same part (Figure 13(d)), different numbers represent different surfaces in part, and each node has a unique number (Figures 13(a) and 13(b)), which is a 4-digit string. The first two digits represent the part, and the last two digits represent the faces in part.

4. The Feasible Movement Direction of Parts

The essence of assembly is to impose constraints on parts and adjust the position and rotation of parts. The geometric elements involved in the constraints between parts in this paper include the following geometric surfaces: plane, cone, cylinder, and sphere. Typical constraints between geometric surfaces include the following:

- ① Constraints between two planes
- ② Constraints between two cylindrical surfaces
- ③ Constraints between two conic surfaces
- ④ Constraints between two sphere surfaces

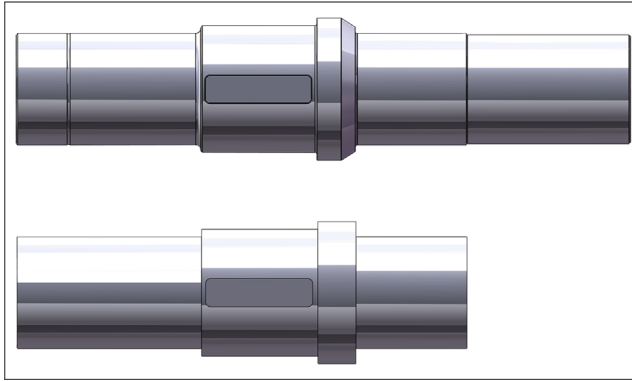
Table 2 shows the feasible assembly direction of parts under different geometric constraints, the moving range after assembly, and the disassembly direction, in which the moving range after assembly is the same as the disassembly direction. In this paper, constraint information is stored as a set in three-dimensional spherical coordinate system (as shown in Figure 14). When the part is constrained between planes, the assembly direction of the part is a hemispherical surface along the direction of the plane normal vector. When there is a cylindrical constraint, the assembly direction of the part is the positive and negative directions of the vector. When there is a conical constraint or sphere constraint, the assembly direction is same as the vector.

The rest of the constraints on the part are superimposed, and then, the feasible motion region of the part under multiple constraints is obtained. The constraints between the basic geometric elements obtained directly are called theoretical constraints, and the constraints obtained through analysis and calculation are called practical constraints. Thus, the constraints obtained need to be further analyzed.

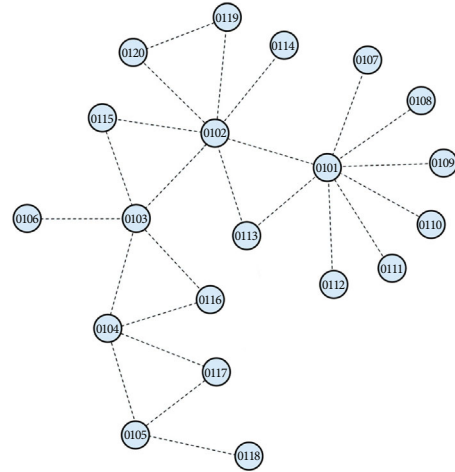
After obtaining independent geometric constraints, the feasible motion area of the part, which is under geometric constraints, obtained by intersecting the superposition, is performed on the part's vector ball in the form of the set intersection to obtain. The assembly process can be regarded as the reverse process of the disassembly process.

TABLE 3: Calculation formula of fitness function.

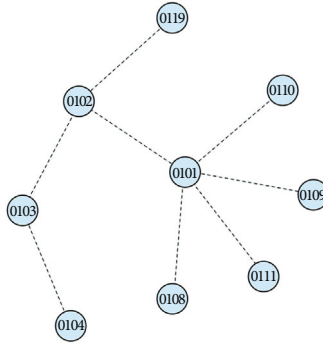
Assembly position moving distance	The number of times the assembly tool changes	Number of assembly direction change
$Ass_Dis_j = position_distance_j$	$Tool_Change_j = \begin{cases} 0 & \text{if } tool_type_i = tool_type_{i-1} \\ 1 & \text{otherwise} \end{cases}$	$Ass_dir_change_i = \begin{cases} 0 & \theta_i \cap \theta \neq \emptyset \&\& \varphi_i \cap \varphi \neq \emptyset \\ 1 & \text{otherwise} \end{cases}$
$Num_Ass_Dis_j = \sum_{i=1}^n Ass_Dis_i$	$Num_Tool_Change_j = \sum_{i=1}^{n-1} Tool_Change_i$	$Num_Dir_change_i = \sum_{i=1}^{n-1} Ass_dir_change_i$
$R_1(t) = \frac{Num_Ass_Dis_j}{Num_Ass_Dis_{max}}$	$R_2(t) = Num_Tool_Change_j / Num_Tool_Change_{max}$	$R_3(t) = Num_Dir_Change_i / Num_Dir_Change_{max}$



(a) Comparison of shaft features before and after simplification



(b) Topological relations of features before simplification



(c) Topological relations of features after simplification

FIGURE 16: Part simplification results.

The residual feasible region of parts is inferred through the constraint relationship between parts, so as to judge the parts that can be disassembled in the current state. When a part is disassembled, if the remaining movable direction of the existing part includes the current gravity direction, the part will be regarded as a group, and the disassembly and assembly process will be carried out at the same time.

For example, there are two pairs of surface contacts in model A and model B. x_1 and x_2 constitute a set of plane constraints C_1 (Figure 15(a)), and y_1 and y_2 constitute a set of cylindrical constraints C_2 (Figure 15(b)). Part A can be assembled forward and backward along the y -axis under the constraint of C_1 , while it can be assembled along the forward y -axis under the constraint of C_2 . Therefore, under the constraints of both, the assembly can only be carried out along the positive half axis of the y -axis (Figure 15(c)).

5. Assembly Sequence Planning

Firstly, the assembly sequence needs to meet the geometric feasibility and then pursue the optimal assembly efficiency. Therefore, this paper divides the planning process of assembly sequence into two independent steps. In searching the sequence that meets the geometric feasibility, the integrity is pursued to avoid losing the potential optimal assembly

sequence. Then, the optimal sequence under the specified conditions is selected by the fitness function.

5.1. Geometrically Feasible Assembly Sequence. In this paper, the method of obtaining assembly sequence obtains the disassembly sequence of mechanical products by continuously removing parts from the products and reversing it to obtain all feasible assembly sequences.

The string is used to represent the assembly sequence, and two digits represent each part. For example, the ID of part 2 is 02, and the ID of part 14 is 14.

The disassembly sequence of parts determines the geometrically feasible assembly sequence. On the premise of obtaining all assembly constraint information, the parts with a feasible moving range in the current state are determined. When multiple parts are available for disassembly, they are considered as feasible independent sequences. Complete its disassembly process and delete the relevant nodes and edges in the contact graph. At this time, the detachable parts are obtained again. Repeat this process until all parts are removed. All geometrically feasible assembly sequences are obtained by reversing the disassembly sequence.

5.2. Assembly Sequence Optimization. The fitness function describes the assembly efficiency and complexity, including the tools used in the assembly process, the number of

TABLE 4: The list of features in the shaft.

Feature no.	Feature type	Feature volume v_i (mm ³)	Bool	Port
01	Step	13760804	Increase	True
02	Step	11191924	Increase	True
03	Step	4618141	Increase	True
04	Step	8286893	Increase	True
05	Step	11625063	Increase	False
06	Cone	202845.4	Decrease	False
07	Chamfering	3081.902	Decrease	False
08	Ring channel	2814.73	Decrease	False
09	Fillet	15133.4	Increase	False
10	Fillet	3506.017	Decrease	False
11	Fillet	2716.042	Increase	False
12	Fillet	2392.43	Increase	False
13	Fillet	580.5962	Decrease	False
14	Chamfering	3002.734	Decrease	False
15	Key channel	221326	Decrease	True
16	Chamfering	110.0858	Increase	False
17	Screw hole	21714.69	Decrease	True
18	Screw hole	21714.69	Decrease	True
19	Screw hole	21714.69	Decrease	True
20	Screw hole	21714.69	Decrease	True

changes in the assembly direction, and the moving distance of the assembly position.

5.2.1. Assembly Position Moving Distance X_1 . The distance between the assembly positions of two parts in the sequence is regarded as a reference factor for optimizing the assembly sequence. Record the final assembly position of each part and calculate the distance between two adjacent parts. For the first part, except for the reference part, the value is 0. As shown in Table 3, Ass_Dis_i is the distance between the current part and the final position of the previous part, and $Sum_Ass_Dis_i$ is the sum of all distances in completing the assembly. $Num_Ass_Dis_{max}$ is the maximum value of the sum of distances in all sequences.

5.2.2. The Number of Assembly Tool Changes X_2 . Tools are needed in the assembly process of parts, and the assembly time will be affected in tool replacement [33]. Therefore, the number of assembly tool changes is recorded and regarded as a variable in the fitness function, where $Num_Tool_Change_i$ is the total number of assembly tool changes in the sequence and $Num_Tool_Change_{max}$ is the maximum total number of assembly tool changes in all assembly sequences.

5.2.3. Number of Assembly Direction Change X_3 . When the feasible assembly region of the part does not intersect with the current assembly direction, it means that the part cannot be assembled from this direction, and the initial position of the part assembly needs to be changed. After the change of direction, the part needs to be repositioned. This process can significantly influence the assembly time, so it is taken as one of the components of the fitness function, where

$Num_Dir_Change_i$ is the total number of assembly direction changes by the sequence and $Num_Dir_Change_{max}$ is the maximum number of assembly direction changes by all feasible assembly sequences.

The fitness function is shown in formula (6). x_n represents the value of the fitness function. The higher the value, the better the assembly performance of the sequence. The function includes the assembly position movement distance x_1 , the times of assembly tool change x_2 , and the times of assembly direction change x_3 . The three-match different weights because of their different influence on the assembly sequence. By testing multiple groups of weight factors, set the weight factor values as $n_1 = 0.2$, $n_2 = 0.3$, and $n_3 = 0.5$.

$$x_n = n_1x_1 + n_2x_2 + n_3x_3. \quad (6)$$

6. Case Study

In this paper, various products such as 4-part block assembly, 10-part shaft assembly, and 23-part cylinder assembly are examples for validating the proposed algorithm verification, which is implemented by MATLAB 2017b and Solidworks API programming. One fastener will be used to represent the assembly process of multiple fasteners in the same group.

6.1. Model Simplification Experiment. The shaft is shown in Figure 16 as an example, it can be decomposed into 20 sub-features, and the port features are 01, 02, 03, 04, 15, 17, 18, 19, and 20 as shown in Table 4. The ranking results of feature importance are shown in Figure 8(c). After obtaining the contact relationship of the subfeatures of the part, the contact relationship undirected graph is shown in

Figure 16(b) and contact relationship matrix is shown in equation (7).

The contact relationship between the features:

$$A_{ij} = \begin{bmatrix} 0 & 1 & 0 & 0 & 0 & 0 & 1 & 1 & 1 & 0 & 0 & 0 & 0 & 0 & 0 & 0 & 1 & 1 & 1 & 1 \\ 1 & 0 & 1 & 0 & 0 & 0 & 0 & 0 & 1 & 1 & 1 & 0 & 0 & 0 & 1 & 1 & 0 & 0 & 0 & 0 \\ 0 & 1 & 0 & 1 & 0 & 1 & 0 & 0 & 0 & 0 & 1 & 1 & 0 & 0 & 0 & 0 & 0 & 0 & 0 & 0 \\ 0 & 0 & 1 & 0 & 1 & 0 & 0 & 0 & 0 & 0 & 0 & 1 & 1 & 0 & 0 & 0 & 0 & 0 & 0 & 0 \\ 0 & 0 & 0 & 1 & 0 & 0 & 0 & 0 & 0 & 0 & 0 & 0 & 1 & 1 & 0 & 0 & 0 & 0 & 0 & 0 \\ 0 & 0 & 1 & 0 & 0 & 0 & 0 & 0 & 0 & 0 & 0 & 0 & 0 & 0 & 0 & 0 & 0 & 0 & 0 & 0 \\ 1 & 0 & 0 & 0 & 0 & 0 & 0 & 0 & 0 & 0 & 0 & 0 & 0 & 0 & 0 & 0 & 0 & 0 & 0 & 0 \\ 1 & 0 & 0 & 0 & 0 & 0 & 0 & 0 & 0 & 0 & 0 & 0 & 0 & 0 & 0 & 0 & 0 & 0 & 0 & 0 \\ 1 & 1 & 0 & 0 & 0 & 0 & 0 & 0 & 0 & 0 & 0 & 0 & 0 & 0 & 0 & 0 & 0 & 0 & 0 & 0 \\ 0 & 1 & 0 & 0 & 0 & 0 & 0 & 0 & 0 & 0 & 0 & 0 & 0 & 0 & 0 & 0 & 0 & 0 & 0 & 0 \\ 0 & 1 & 1 & 0 & 0 & 0 & 0 & 0 & 0 & 0 & 0 & 0 & 0 & 0 & 0 & 0 & 0 & 0 & 0 & 0 \\ 0 & 0 & 1 & 1 & 0 & 0 & 0 & 0 & 0 & 0 & 0 & 0 & 0 & 0 & 0 & 0 & 0 & 0 & 0 & 0 \\ 0 & 0 & 0 & 1 & 1 & 0 & 0 & 0 & 0 & 0 & 0 & 0 & 0 & 0 & 0 & 0 & 0 & 0 & 0 & 0 \\ 0 & 0 & 0 & 0 & 1 & 0 & 0 & 0 & 0 & 0 & 0 & 0 & 0 & 0 & 0 & 0 & 0 & 0 & 0 & 0 \\ 0 & 1 & 0 & 0 & 0 & 0 & 0 & 0 & 0 & 0 & 0 & 0 & 0 & 0 & 0 & 1 & 0 & 0 & 0 & 0 \\ 0 & 1 & 0 & 0 & 0 & 0 & 0 & 0 & 0 & 0 & 0 & 0 & 0 & 0 & 0 & 1 & 0 & 0 & 0 & 0 \\ 1 & 0 & 0 & 0 & 0 & 0 & 0 & 0 & 0 & 0 & 0 & 0 & 0 & 0 & 0 & 0 & 0 & 0 & 0 & 0 \\ 1 & 0 & 0 & 0 & 0 & 0 & 0 & 0 & 0 & 0 & 0 & 0 & 0 & 0 & 0 & 0 & 0 & 0 & 0 & 0 \\ 1 & 0 & 0 & 0 & 0 & 0 & 0 & 0 & 0 & 0 & 0 & 0 & 0 & 0 & 0 & 0 & 0 & 0 & 0 & 0 \\ 1 & 0 & 0 & 0 & 0 & 0 & 0 & 0 & 0 & 0 & 0 & 0 & 0 & 0 & 0 & 0 & 0 & 0 & 0 & 0 \end{bmatrix} \quad (7)$$

The simplified shaft comprises 9 features, the volume is changed from 48.98 dm³ to 37.55 dm³, and the reduction is 23.3%. Before simplification, the parts contain 46 surfaces, and the 20 surfaces are reduced by 43.5%. It can be seen that the change of volume is less than that of the surface. Through simplification, the key information that plays a decisive role in the assembly process is obtained, which reduces the complexity of calculation.

6.2. *Assembly Sequence Planning Experiment.* It is obtained the geometrically feasible assembly sequence by disassembly. When removing the parts, the parts can move in the gravity direction, which is regarded as the same assembly step. After obtaining the geometrically feasible assembly sequence, calculate the moving distance of assembly position, the change times of assembly direction, and the change times of tools in different sequences. Get the assembly difficulty of different sequences to optimize the assembly sequence.

6.2.1. *Block Assembly Experiment.* Considering the blocks shown in Figure 17 and taking the simplified parts as input, the system generates two geometrically feasible disassembly sequences, as shown in equation (7). Parts 2 and 3 are considered as one step and assembled at the same time. The maximum number of redirections in all sequences is 2, and the assembly process does not need the assistance of tools, and the matching relationship between parts is the same, so all of them are regarded as the optimal sequence.

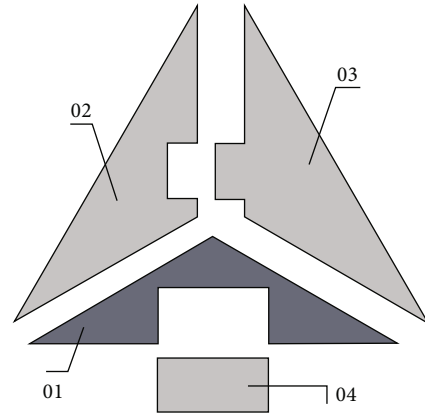


FIGURE 17: Exploded view of block and related parts.

TABLE 5: The block assembly sequence planning results.

Assembly sequence	Number of assembly direction changes	Number of assembly tool changes	Fitness function value
(3,2)-4	2	0	1
4-(2,3)	2	0	1

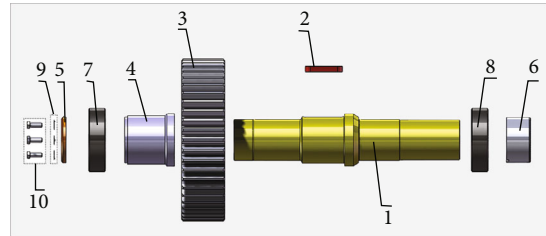


FIGURE 18: Exploded view of reducer shaft and related parts.

TABLE 6: The shaft assembly sequence planning results.

Assembly sequence	Number of assembly direction changes	Number of assembly tool changes	Fitness function value
1-2-3-8-4-6-7-5-(9,10)	5	5	0.867
1-2-3-4-7-5-(9,10)-8-6	2	5	0.667
1-8-2-3-4-7-5-(9,10)-6	4	5	0.867
1-8-2-3-4-7-5-(9,10)-6	3	6	0.800

Based on this, the two assembly sequences of the part are equivalent and cannot be further optimized, as shown in Table 5.

TABLE 7: The shaft assembly sequence planning results.

(a)

No. 1	No. 2	No. 3	No. 4	No. 5	No. 6	No. 7	No. 8	No. 9	No. 10	No. 11	No. 12	No. 13	No. 14
1	1	1	1	1	1	1	1	1	1	1	1	1	1
2	2	2	2	2	2	2	8	8	8	8	8	8	8
3	8	8	8	8	8	8	2	2	2	2	2	2	6
8	3	3	3	3	3	6	3	3	3	3	3	6	2
6	4	4	4	4	6	3	4	4	4	4	6	3	3
4	6	7	7	7	4	4	6	7	7	7	4	4	4
7	7	5	5	6	7	7	7	5	5	6	7	7	7
5	5	6	9, 10	5	5	5	5	6	9, 10	5	5	5	5
9, 10	9, 10	9, 10	6	9, 10	9, 10	9, 10	9, 10	9, 10	6	9, 10	9, 10	9, 10	9, 10

(b)

No. 15	No. 16	No. 17	No. 18	No. 19	No. 20	No. 21	No. 22	No. 23	No. 24	No. 25	No. 26	No. 27	No. 28
1	1	1	1	1	1	1	1	1	1	1	1	1	1
2	2	2	2	2	2	2	2	2	2	2	2	2	2
3	3	3	3	3	3	3	3	3	3	3	3	3	3
4	4	4	4	4	4	4	4	4	4	8	8	8	8
7	7	7	7	7	7	8	8	8	8	4	4	4	4
5	5	5	8	8	8	6	7	7	7	6	7	7	7
8	8	9, 10	5	5	6	7	5	5	6	7	5	5	6
6	9, 10	8	6	9, 10	5	5	6	9, 10	5	5	6	9, 10	5
9, 10	6	6	9, 10	6	9, 10	9, 10	9, 10	6	9, 10	9, 10	(9, 10)	6	9, 10

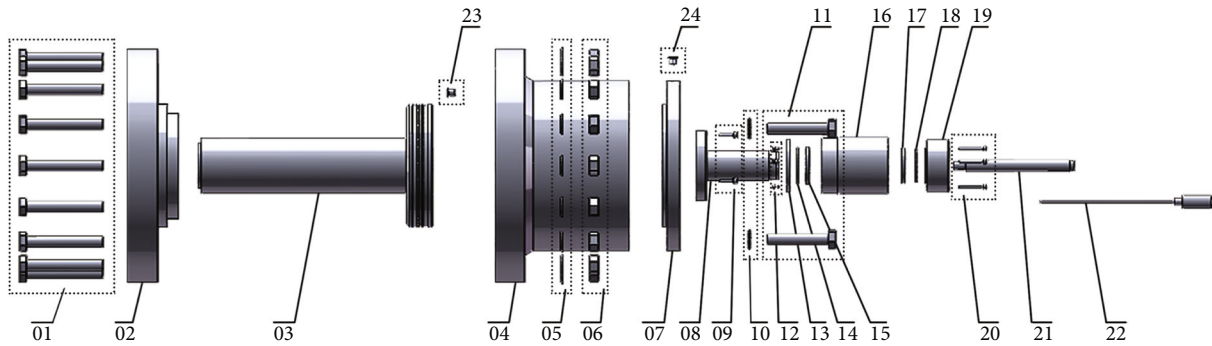


FIGURE 19: Exploded view of cylinder and related parts.

6.2.2. *Shaft Assembly Experiment.* The shaft in the reducer shown in Figure 18 is regarded as the second experiment. During disassembly, part 9 and part 10 are disassembled and assembled at the same time. In the process of assembly, 28 geometrically feasible assembly sequences are generated. The maximum number of direction changes of parts is 5, and the maximum number of tool changes is 6. Part of the fitness function obtains the geometrically feasible assembly sequence (as shown in Table 6). Other geometrically feasible assembly sequences are shown in Table 7.

Two optimal sequences are obtained by optimizing the geometrically feasible assembly sequence: 1-2-8-6-3-4-7-5-(9,10) or 1-8-6-2-3-4-7-5-(9,10).

6.2.3. *Cylinder Assembly Experiment.* The expansion and contraction cylinder shown in Figure 19 is considered the third test because of its number of parts and potential multiple feasible sequences. After processing the CAD model, 124728 geometrically feasible assembly sequences are generated, in which part 1, part 5 and part 6, part 7, part 10 and part 11, part 8 and part 9, part 12, part 13, part 14, part 15 and part 16, part 19, and part 20 are regarded as the same step for installation. Therefore, a total of 14 assemblies need to be considered. The maximum tool replacement time is seven, and the maximum redirection time is eight. After optimization, the optimal sequence is 04-23-03-02-(01,05,06)-(07,10,11)-24-(08,09)-(12,13,14,15,16)-17-18-21-

(19,20)-22 (see Table 8 for the optimal sequence with close fitness function values).

7. Result and Discussions

From the assembly sequences generated for the above three mechanical products, the proposed method can generate multiple sequences with the same assembly property at the same time. Moreover, for parts such as the no. 24 plug of the cylinder block, it is considered that they can be assembled with the no. 7 part perpendicular to each other without relocation. Intersecting with the general planning method solves the problem of manual participation in the oblique assembly of mechanical products. By judging the feasible residual region after assembly, multiple parts are regarded as the same step for assembly, which reduces the computational complexity and makes the generated sequence more in line with the actual production process.

8. Conclusion

This paper proposes a hierarchical assembly information model to infer the optimal assembly sequence under multiple constraints. Firstly, through the feature-based segmentation and simplification of parts, the key structures of products in the assembly process are divided into product, part, feature, surface, and constraint layers. The weighted fitness function of the factors affecting the product assembly performance is established. The main contributions of this study are as follows:

- (1) A multilevel feature-based assembly information model is established. Integrating the advanced semantics of the CAD system and the data of the CAD model into the model framework has become the integration link between CAD and CAPP
- (2) According to the graph theory, the information in the framework is mapped into a response connection graph. The key features of parts in the assembly process are obtained by simplifying the subsequent computational complexity
- (3) According to polar coordinates, the motion state of parts under multiple geometric constraints is expressed in sets. The geometric feasible assembly sequence is searched through the disassembly process
- (4) The fitness function of the assembly process is constructed by influencing assembly factors to the assembly information model

The future scope of this study is to consider further the assembly stability of parts and the impact of parallel assembly on assembly sequence planning.

Notations

- F_j : Set of faces in part
 f : Feature importance index in parts
 a_{ij} : Feature contact relationship in parts
 x_n : Evaluation function of assembly sequence.

Data Availability

The data that support the findings of this study are available from the corresponding author upon reasonable request.

Conflicts of Interest

The authors declared no potential conflicts of interest with respect to the research, authorship, and/or publication of this article.

Authors' Contributions

All authors contributed equality.

Acknowledgments

I want to express my gratitude to everyone for helping me finish this paper.

References

- [1] C. Press, *Product Design for Manufacture and Assembly*, CRC Press, Third Edition edition, 2010.
- [2] P. C. Integrating, *CAD files and automatic assembly sequence planning*, Iowa State University, 2005.
- [3] R. M. Marian, L. H. Luong, and K. Abhary, "A genetic algorithm for the optimisation of assembly sequences," *Computers & Industrial Engineering*, vol. 50, no. 4, pp. 503–527, 2006.
- [4] M. R. Bahubalendruni and B. B. Biswal, "A review on assembly sequence generation and its automation," *Proceedings of the Institution of Mechanical Engineers, Part C: Journal of Mechanical Engineering Science*, vol. 230, no. 5, pp. 824–838, 2016.
- [5] A. Bedeoui, R. B. Hadj, M. Hammadi, M. Trigui, and N. Aifaoui, "Assembly sequence plan generation of heavy machines based on the stability criterion," *International Journal of Advanced Manufacturing Technology*, vol. 102, no. 9–12, pp. 2745–2755, 2019.
- [6] Y. Wang and J. Liu, "Subassembly identification for assembly sequence planning," *The International Journal of Advanced Manufacturing Technology*, vol. 68, no. 1–4, pp. 781–793, 2013.
- [7] M. Hpitalni, G. Elber, and E. Lenz, "Automatic assembly of three-dimensional structures via connectivity graphs," *CIRP Annals - Manufacturing Technology*, vol. 38, no. 1, pp. 25–28, 1989.
- [8] L. S. H. Mello and A. C. Sanderson, "AND/OR graph representation of assembly plans," *IEEE Transactions on Robotics & Automation*, vol. 6, no. 2, pp. 188–199, 1990.
- [9] P. Wang, P. Y. Cheng, W. Wang, and S. Zhang, "Disassembly sequence planning based on disassembly petri nets and chaos particle swarm optimization algorithm," *Machinery Design & Manufacture*, vol. 1, 2015.
- [10] L. D. Floriani and G. Nagy, "A graph model for face-to-face assembly," in *Proceedings, 1989 International Conference on Robotics and Automation*, pp. 75–78, Scottsdale, AZ, USA, 1989.
- [11] J. D. Wolter, "On the automatic generation of assembly plans," in *Proceedings, 1989 International Conference on Robotics and Automation*, pp. 263–288, Scottsdale, AZ, USA, 1989.

- [12] G. A. Kumar, M. R. Bahubalendruni, V. V. Prasad, D. Ashok, and K. Sankaranarayanan, "A novel Geometric feasibility method to perform assembly sequence planning through oblique orientations," *Engineering Science and Technology, an International Journal*, vol. 26, article 100994, 2022.
- [13] C. Li and W. Hou, "Analysis of assembly tolerance based on assembly constraint information model," *Mathematical Problems in Engineering*, vol. 2021, 18 pages, 2021.
- [14] R. J. Linn and H. Liu, "An automatic assembly liaison extraction method and assembly liaison model," *Lie Transactions*, vol. 31, no. 4, pp. 353–363, 1999.
- [15] S. M. Mok, K. Ong, and C. H. Wu, "Automatic generation of assembly instructions using STEP," in *Proceedings 2001 ICRA. IEEE International Conference on Robotics and Automation (Cat. No.01CH37164)*, pp. 313–318, Seoul, Korea (South), 2001.
- [16] C. Pan, S. S. F. Smith, and G. C. Smith, "Determining interference between parts in CAD STEP files for automatic assembly planning," *Journal of Computing and Information Science in Engineering*, vol. 5, no. 1, pp. 56–62, 2005.
- [17] M. Bahubalendruni, A. K. Gulivindala, S. Varupala, and D. K. Palavalasa, "Optimal Assembly Sequence generation through computational approach," *Sadhana*, vol. 44, no. 8, 2019.
- [18] J. Yu, L. D. Xu, Z. Bi, and C. Wang, "Extended Interference Matrices for Exploded View of Assembly Planning," *IEEE Transactions on Automation Science & Engineering*, vol. 11, no. 1, pp. 279–286, 2014.
- [19] M. V. A. R. Bahubalendruni and B. B. Biswal, "An intelligent approach towards optimal assembly sequence generation," *Proceedings of the Institution of Mechanical Engineers, Part C: Journal of Mechanical Engineering Science*, vol. 232, no. 4, pp. 531–541, 2018.
- [20] M. Li, Y. Zhang, B. Zeng, H. Zhou, and J. Liu, "The modified firefly algorithm considering fireflies' visual range and its application in assembly sequences planning," *International Journal of Advanced Manufacturing Technology*, vol. 82, no. 5–8, pp. 1381–1403, 2016.
- [21] C. C. Chang, H. E. Tseng, and L. P. Meng, "Artificial immune systems for assembly sequence planning exploration," *Engineering Applications of Artificial Intelligence*, vol. 22, no. 8, pp. 1218–1232, 2009.
- [22] W. Xu, Q. Tang, J. Liu, Z. Liu, Z. Zhou, and D. T. Pham, "Disassembly sequence planning using discrete Bees algorithm for human-robot collaboration in remanufacturing," *Robotics and Computer-Integrated Manufacturing*, vol. 62, article 101860, 2020.
- [23] M. R. Bahubalendruni and B. B. Biswal, "A novel concatenation method for generating optimal robotic assembly sequences," *Proceedings of the Institution of Mechanical Engineers, Part C: Journal of Mechanical Engineering Science*, vol. 231, no. 10, pp. 1966–1977, 2015.
- [24] F. Y. Huang and Y. J. Tseng, "An integrated design evaluation and assembly sequence planning model using a particle swarm optimization approach," *World Academy of Science Engineering & Technology*, vol. 77, pp. 416–421, 2011.
- [25] H. Zhang, H. Liu, and L. Li, "Research on a kind of assembly sequence planning based on immune algorithm and particle swarm optimization algorithm," *International Journal of Advanced Manufacturing Technology*, vol. 71, no. 5–8, pp. 795–808, 2014.
- [26] J.-Y. Li and L. Cong, "Assembly sequence planning with firework algorithm," *International Journal of Modeling & Optimization*, vol. 6, no. 3, pp. 195–198, 2016.
- [27] X. Liu, X. Xu, Y. Yi, Z. Ni, and Y. Zhang, "An assembling algorithm for fixture in an assembly process planning system," *Proceedings of the Institution of Mechanical Engineers Part B Journal of Engineering Manufacture*, vol. 234, no. 8, pp. 1133–1155, 2020.
- [28] Z. Zhang, B. Yuan, and Z. Zhang, "A new discrete double-population firefly algorithm for assembly sequence planning," *Proceedings of the Institution of Mechanical Engineers, Part B: Journal of Engineering Manufacture*, vol. 230, no. 12, pp. 2229–2238, 2016.
- [29] H. Shan, S. Zhou, and Z. Sun, "Research on assembly sequence planning based on genetic simulated annealing algorithm and ant colony optimization algorithm," *Assembly Automation*, vol. 29, no. 3, pp. 249–256, 2009.
- [30] L. Gao, W. Qian, X. Li, and J. Wang, "Application of memetic algorithm in assembly sequence planning," *International Journal of Advanced Manufacturing Technology*, vol. 49, no. 9–12, pp. 1175–1184, 2010.
- [31] W.-C. Chen, P.-H. Tai, W.-J. Deng, and L.-F. Hsieh, "A three-stage integrated approach for assembly sequence planning using neural networks," *Expert Systems with Applications*, vol. 34, no. 3, pp. 1777–1786, 2008.
- [32] M. V. A. Raju Bahubalendruni and B. B. Biswal, "Liaison concatenation – A method to obtain feasible assembly sequences from 3D-CAD product," *Sadhana*, vol. 41, no. 1, pp. 67–74, 2016.
- [33] M. V. A. Raju Bahubalendruni, A. K. Gulivindala, and K. Madhu Sudana Sankar, "Practically Feasible Optimal Assembly Sequence Planning with Tool Accessibility," in *IOP Conference Series: Materials Science and Engineering*, vol. 390, Tamilnadu, India, 2018.
- [34] H. Zhu, D. Wu, and X. Fan, "Interactive assembly tool planning based on assembly semantics in virtual environment," *International Journal of Advanced Manufacturing Technology*, vol. 51, no. 5–8, pp. 739–755, 2010.
- [35] M. A. Abdullah, M. Rashid, and Z. Ghazalli, "Optimization of Assembly Sequence Planning Using Soft Computing Approaches: A Review," *Archives of Computational Methods in Engineering*, vol. 26, no. 2, pp. 461–474, 2019.
- [36] A. Thakur, A. G. Banerjee, and S. K. Gupta, "A survey of CAD model simplification techniques for physics-based simulation applications," *Computer-Aided Design*, vol. 41, no. 2, pp. 65–80, 2009.
- [37] Y. Woo, "Fast cell-based decomposition and applications to solid modeling," *Computer Aided Design*, vol. 35, no. 11, pp. 969–977, 2003.
- [38] B. C. Kim and D. Mun, "Feature-based simplification of boundary representation models using sequential iterative volume decomposition," *Computers & Graphics*, vol. 38, pp. 97–107, 2014.
- [39] P. Shi, Q. Qi, Y. Qin, P. J. Scott, and X. Jiang, "A novel learning-based feature recognition method using multiple sectional view representation," *Journal of Intelligent Manufacturing*, vol. 31, no. 5, pp. 1291–1309, 2020.
- [40] Y. Wang and D. Tian, "A weighted assembly precedence graph for assembly sequence planning," *International Journal of Advanced Manufacturing Technology*, vol. 83, no. 1–4, pp. 99–115, 2016.
- [41] Y. Kang, B. C. Kim, D. Mun, and S. Han, "Method to simplify ship outfitting and offshore plant equipment three-dimensional (3-D) computer-aided design (CAD) data for construction of an equipment catalog," *Journal of Marine Science and Technology*, vol. 19, no. 2, pp. 185–196, 2014.

Research Article

IAMnet: Presentation of Parallelization Approach for Repetitive Mining on Network Topologies with an Improved Apriori Method

Hooman Bavarsad Salehpour,¹ Parvaneh Asghari ,² Hamid Haj Seyyed Javadi ,³
and Mohammad Ebrahim Shiri⁴

¹Department of Computer Engineering, Borujerd Branch, Islamic Azad University, Borujerd, Iran

²Department of Computer Engineering, Central Tehran Branch, Islamic Azad University, Tehran, Iran

³Department of Mathematics and Computer Science, Shahed University, Tehran, Iran

⁴Department of Mathematics and Computer Science, Amirkabir University, Tehran, Iran

Correspondence should be addressed to Parvaneh Asghari; p_asghari@iauctb.ac.ir

Received 15 November 2021; Revised 21 December 2021; Accepted 5 January 2022; Published 9 February 2022

Academic Editor: Mu-Yen Chen

Copyright © 2022 Hooman Bavarsad Salehpour et al. This is an open access article distributed under the Creative Commons Attribution License, which permits unrestricted use, distribution, and reproduction in any medium, provided the original work is properly cited.

Recently, the discovery of association rules and the consequent mining frequent patterns have attracted the attention of many researchers to discover unknown relationships in big data, especially in networking and distributed environments. In this research, a parallelization-based approach is proposed to improve the performance of the Apriori algorithm in repetitive mining patterns on network topologies. The proposed approach includes two main features: (1) combining centrality criteria of the node and the Apriori algorithm to identify repetitive patterns and (2) using the mapping/reduction method to create parallel processing and achieve optimal values in the shortest time. This approach also pursues three main objectives: reducing the temporal and spatial complexity of the Apriori algorithm, improving the association rules mining process and identifying repetitive patterns, and comparing the proposed approach's performance on different network topologies to determine the advantages and disadvantages of each topology. Comparing our proposed method and the basic Apriori algorithm, it is concluded that our approach provides acceptable efficiency in terms of evaluation criteria such as energy consumption, network lifetime, and runtime compared to other methods. Experimental results also show that when using our proposed method compared to the basic Apriori algorithm, network life is increased by 7.1%, the runtime is reduced by 43.2%, and the energy consumption is saved by about 41.2%.

1. Introduction

Data mining is a set of techniques that allows a person to move beyond ordinary data processing to the mining analysis of massive data and the mining of valuable information contained in them [1, 2]. In addition, there is a close connection between data mining, artificial intelligence, and machine learning. Therefore, it can be said that data mining combines database theories, artificial intelligence, machine learning, and statistics to provide practical contexts [3]. Categorization, clustering, forecasting, and discovering association rules are the most important data mining applications that are widely used in different areas of the real

world. The most important reason that made data mining the focus of attention in the information industry was the availability of large volumes of data and the urgent need to extract useful information and knowledge from this massive volume of data [4–7].

Reviewing articles in this field shows that the essential part of this process is discovering repetitive items and patterns, which seems quite logical given the time-consuming nature of this part of the process [8]. The performance of standard techniques of frequent mining item set is the discovery of item sets that are simultaneously observed in user transactions. A review of previous studies shows that exploring frequent patterns is the most important and

central part of the process of discovering association rules, which has been widely used in network topologies to discover unknown relationships [7]. Most researchers in previous studies have stated that the importance of this part of discovering association rules is considered time-consuming of identifying frequent patterns [9, 57, 58]. As an example of frequent mining patterns in the network, we can refer to the studies conducted in the sources [12–17]. For example, the authors in [14] have explored trends desired by mining frequent patterns on social media. In another successful example [15], the authors proposed an alternative algorithm named B-mine for improving the Apriori algorithm that uses a bitwise approach to explore frequent patterns in social networks. Also, Zoraghchian and Sohrabi [17] proposed using the butterfly optimization algorithm (BOA) in the process of mining the association rules to increase the efficiency of the basic algorithms. In this proposal, the authors use one CPU and three GPUs to parallelize the process and apply the optimization algorithm. The CPU is used for synchronization, and the GPU is used to speed up the execution of rules exploration operations.

Although the initial application of this research topic seems to be in the field of business, what is seen in today's world is the attention of researchers to this new research topic and the expansion of its application in areas such as text exploration, e-learning, medicine, and clickstream analysis [8, 18]. Also, reviewing articles in this field includes two main points: (1) many of the previously proposed techniques are based on the efficient, common, and popular Apriori algorithm and its numerous versions. (2) In many previous studies, the problem of temporal and spatial complexity of the basic Apriori algorithm has been mentioned as a challenging problem due to the high volume of computations in the section of repetitive patterns and items mining that show that more extensive studies are needed to improve this challenge [8, 19]. This algorithm is in the category of exponential algorithms in terms of temporal and spatial complexity due to frequent visits from the database and producing multiple sets of repetitive and candidate items. Also, there is the application of optimization in other subjects such as healthcare [20]. In this research, a parallelization-based approach is proposed to improve the performance of the Apriori algorithm in repetitive mining patterns on network topologies. The proposed approach includes two main features: (1) combining centrality criteria of the node and the Apriori algorithm to identify repetitive patterns and (2) using the mapping/reduction method to create parallel processing and achieve optimal values in the shortest time.

In this research, several primary goals in the field of mining association rules and repetitive items in the application domain are pursued, which are briefly listed as follows:

- (i) Investigating the possibility of parallelism of the Apriori algorithm
- (ii) A balanced distribution of mining operations and data used on processors

- (iii) Reducing the volume of data exchanges
- (iv) Finding the most appropriate network topology to apply the basic algorithm in terms of speed of mining operations

The innovative aspects of this research, while considering the shortcomings of previous research, are listed as follows:

- (i) Reducing the temporal and spatial complexities of the Apriori algorithm
- (ii) Improving the efficiency of the association rules mining process and find repetitive patterns
- (iii) Comparing the performance of the proposed approach on different network topologies with existing methods

2. Previous Research Studies

Association rules mining is an essential and applied task of data mining in discovering the knowledge latent in big data and transactional databases in different application areas [21]. Discovering the latent associations between different items can help understand customer behavior [19, 22]. For example, a retail store manager can use the knowledge gained from interdependencies between transactions for strategic marketing decisions, such as simultaneous production of products or putting them on shelves. Varmaghani et al. have studied a model for optimizing energy consumption in WSN based on cloud computing and fuzzy logic MCADM [23]. Sui et al. have investigated the use of coded data to assess multi-sensor status over loss networks [24]. Using acoustic sensors, researchers investigated an indirect eavesdropping assault on keys on a touch panel [25]. Kong et al. have analyzed persistent identification for home automation using wifi through fingertip gesture interactions [26]. Based on novel model clustering, Ahmadi et al. have developed a new hybrid strategy for selecting users in federated learning [27]. The activity of association rules mining is performed in two main stages: discovering a set of frequent items and creating association rules. Also, the literature shows that exploring a set of frequent items is considered the essential action in association rules mining because this action is time-consuming [8]. Hence, this part of the association rules mining process requires efficient techniques to improve performance and reduce computational time. It can be said that the essential action in association rules mining is discovering a set of repetitive items. In other words, mining a collection of redundant items is a type of data analysis that has an essential role in mining events, patterns, and sets of repetitive items in the data. Zhao has investigated a feasible and intelligent web analytics technique for fog-based smart grids that preserves anonymity [28]. Han et al. have studied a geographical crowdsourced distance calculation that keeps location privacy [29]. Although the topic of repetitive items mining was initially provided for customer data analysis, the literature shows that repetitive items mining can be used as a general task of data mining in many different fields of application and

science, especially network topologies and distribution environments [18]. Ni et al. have proposed a novel hybrid model of cobweb-based redundant TSV for evaluating the clustered faults [30]. Che and Wang have investigated a multiplex neurodynamic method to blended optimization on two timescales [31]. Jiang and Li have examined a method for canceling off spectrum noise in an intelligent co-site interleaving device [32]. Wu et al. (2021) have researched the accuracy of data labels to predict security bug reports using a test case [33]. On the other hand, with the increasing growth of data and technology to collect them, the need for rapid access to latent knowledge, and meaningful and valuable rules among data, we face challenges such as slow processing speed and the time-consuming mining process [19]. So far, many studies have been conducted in the field of association rules mining and latent relationships among transactional databases, many of which have focused on using the standard Apriori algorithm in their ideas as an efficient base technique [3–8, 18]. The Apriori algorithm is a surface search algorithm, which goes to the next step, $k + 1$, at the end of the mining in step k -th. This operation is repeated until the final condition or conditions are fulfilled. In step k -th, a set of k items will be generated. After calculating the backup value for each item and comparing it with the minsup value, k frequent patterns are detected. In the next step, the algorithm generates a set of items candidate $k + 1$ that can potentially be repeated with the help of k systematic way. In the same way, due to the minsup value, some will be deleted, and a set of frequent items $k + 1$ will be formed. This process continues until the last set of frequent items is found [34]. Zheng et al. have analyzed comparative research of class equalization techniques for categorizing cyber bug reports [35]. Dong et al. have researched the sense of transferability produced by information aggregating for unsupervised feature adaption [36]. Artin et al. have analyzed a novel approach for the prediction of traffic based on machine learning methods [37]. Zhong et al. have explored a way to adapt open set domains that bridge the limits and deep techniques [38]. He et al. have investigated multi-branch deep convolution learning for grouping and directional antennas in user-centric networks [39]. Zhao et al. have examined a unique approach for delayed complex adaptive networks that use nonfragile sampling information exponential synchronizing [40]. Luo et al. have investigated fuzzy system stabilization analysis using a switched selected sample management [41]. Zhang et al. have analyzed a complementary-label source domain: theory and algorithms [42]. Studies in this field show two significant challenges in generating large items and multiple database transitions in the basic Apriori algorithm. A review of articles in this field shows that, to resolve these two challenges, several ideas have been proposed to improve the basic Apriori algorithm, many of which, while maintaining the overall structure, have added techniques to increase efficiency [19, 21, 43, 44]. This section has tried to cover some ideas proposed in previous studies regarding association rules mining and frequent patterns mining in different applied areas, especially network topologies and distributed environments. In addition, the authors of [44] have developed a model for evaluating emissions of Nox, as well as the

efficiency of an engine's supply. They also, like the authors of the study [9], believe that FPM algorithms can be classified into three general classes: join-based, tree-based, and pattern growth, as shown in Figure 1.

Join-based algorithms use a bottom-up approach to identify duplicate item sets. Then, it extends them to larger sets until those sets appear above the minimum user-defined threshold value in the database. On the other hand, tree-based algorithms use countable set concepts to generate duplicate items by building a dictionary tree. In this way, it is possible to extract items through various first-depth or first-level methods. Depending on the identified duplicate patterns, the third class of algorithms implements the split and dominance methods for project database partitioning and extends them to more comprehensive databases. In [45], the authors of the article determined a good buying pattern from previous customers' shopping history in order to help retail business owners; a systematic research method based on mining association rules placed in mining Apriori based on mapping/reduction and smart cloud architecture on Hadoop is called MR-Apriori. They believe that the proposed system sufficiently provides all the significant and anticipated needs of modern extensive data processing systems such as scalability, fault tolerance, minor breakdown support, etc. Finally, the authors stated that their study experimentally examined the effect of the proposed MR-Apriori algorithm with speed, size, and scale evaluation parameters [46].

An experimental comparison between Apriori and FP-growth algorithms has been performed to identify the sequence of repetitive item sets in web application data [47]. For this purpose, the article's authors have focused on the data structure, implementation, and algorithmic features, which also occur in the extraction of duplicate item sets. They also pointed out that in their analysis, to better understand the evaluation results, a comparison was performed between some features such as memory size, data input, prefetching, scalability, and processing efficiency, which have obtained acceptable results for the Apriori algorithm. In [48], the authors proposed improved versions of the Apriori algorithm based on the mapping-reduction. They have also optimized the multistage phases of these versions by jumping from the pruning step if needed and then have presented more efficient algorithms called VFPC and Optimized-ETDPC. The authors stated that the cost of counting additional un-pruned candidates produced due to neglected pruning is less significant than the reduction in computational cost due to this. The authors in [49] proposed a new algorithm called Index-BitTableFI to mine a set of duplicate items. This algorithm has three main features, which are summarized below. On the one hand, it is possible to avoid additional operations at the intersection of miniature sets and check the frequency. From one side, it has been proven that a set of duplicate items, including the representative item and the identical support with the representative item, can be identified directly by connecting the representative item to all item combinations in its sublist. In this way, the processing cost of this type of item is reduced, and the efficiency is also improved.

Huang et al. [50] proposed an optimized algorithm using a bit set matrix that scans the database twice to create a bit set matrix. In this way, invalid and duplicate cases are not

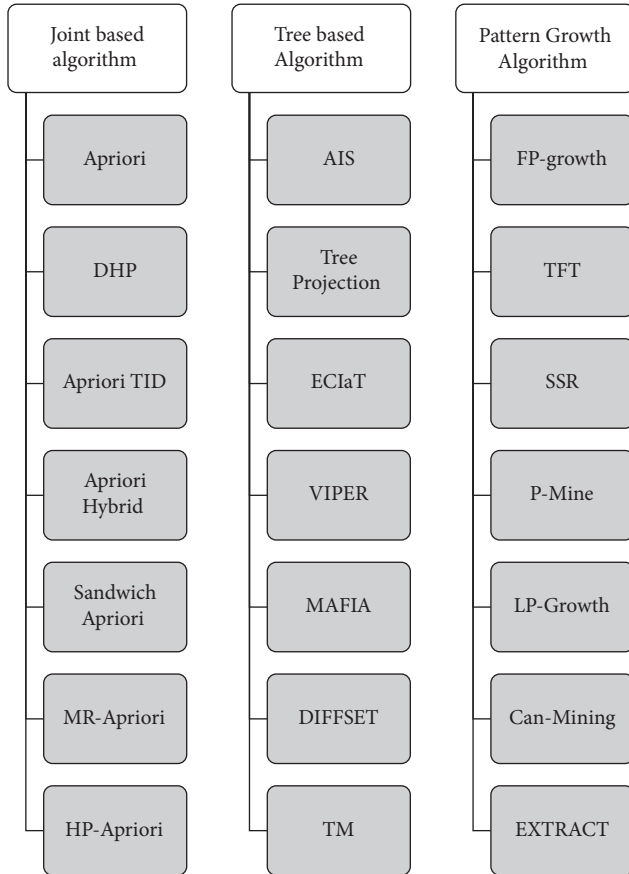


FIGURE 1: Classification of mining algorithms of repetitive patterns [9].

investigated. This lack of scanning of the entire database reduces the scanning range and thus the algorithm's execution time. The authors believe that bit operations in their algorithm have played an influential role in increasing the detection speed of subsets. In [51], the authors proposed a new algorithm exploring iterative patterns to improve the performance of related basic algorithms and reduce temporal complexity. Their proposed algorithm converts the input database into a binary matrix with a single scan. In the next step, we have performed merge and AND operations to achieve the set of candidate items. Raj et al. [52] proposed an efficient scheme called EAFIM, which includes two new methods to improve repetitive mining patterns' efficiency and extract association rules in distributed networks with macro data. The main difference between the basic Apriori algorithm and the scheme of these authors is that in their proposed design, instead of user input data per iteration, they use an updated dataset that lacks invalid items and transactions. The distributed nature of networking and distributed computing environments, such as edge computing paradigm, introduces a shift in security schemes. Ramtin et al. have conducted research on the underlying scaling rules governing covert DDoS assaults and used the expectation-maximization algorithm to fit the traffic data of thousands of edge-routers to a Gaussian mixture model. Then,

they evaluated the theoretical result that the amount of attack traffic that can be generated by a covert DDoS attacker scales according to the square root of the number of infected edge devices [53]. Subsequently, Reza Ramtin et al. [54] showed that when data is normally distributed and the anomaly is small enough in accordance with the square root law, even the most powerful multiple-feature classifier cannot detect the anomaly with high accuracy. In these situations, association rule mining probably helps us to discover a set of rules in the data to promote feature selection and reduce the amount of damage. Applying the basic Apriori algorithm to find meaningful and valuable connections between items in the big data, especially transactional databases, is a complicated process that requires super systems, where access to them can be another challenge. Ni et al. have developed a novel TDMA-based fault detection technique for TSVs in three-dimensional integrated circuits with honeycomb structure [55]. Dong et al. have investigated the effect of learning aggregating on the perception of generalisability for unsupervised feature adapting [56]. Therefore, in this research, the performance of the basic Apriori algorithm is improved by applying similar mining techniques, distributing data on different processors in the distributed network, and applying the Apriori algorithm in parallel and simultaneously. The improvement achieved can reduce the speed of computations and derivation of association rules and be a practical step towards reducing this algorithm's temporal and spatial complexity. The parallelization of the Apriori algorithm on the main network topologies is the most critical innovation aspect of the current research. A review of the literature shows that, due to the importance of accelerating the process of association rules mining and increasing the speed of access to this helpful knowledge, a lack of fast efficient methods is also visible while maintaining the efficiency of the results. Therefore, the lack of such an efficient approach in the existing literature provided an incentive to conduct current research in this area, proposing an efficient approach to reduce time complexity and increase implementation speed.

3. Proposed Method Based on Parallelization

So far, many studies have been conducted in the field of association rules mining and identifying a set of duplicate items based on multiple versions of the Apriori algorithm in different application areas [6–8, 18, 19]. However, most previous studies have observed the complexity of the Apriori algorithm's time, space, and high runtime as a shortcoming. On the other hand, in today's world, due to the widespread need of business managers and customers for quick access to meaningful rules latent in the big data and relationships in transactions, the rapid extraction of useful information is quite evident as an essential need. Therefore, to solve the challenge above, in this part of the research, an approach based on parallelization and mapping/reduction method is proposed to improve the Apriori algorithm.

The proposed approach has used the mapping/reduction method to increase the speed of computing the parameters by providing the possibility of parallel processing and computing

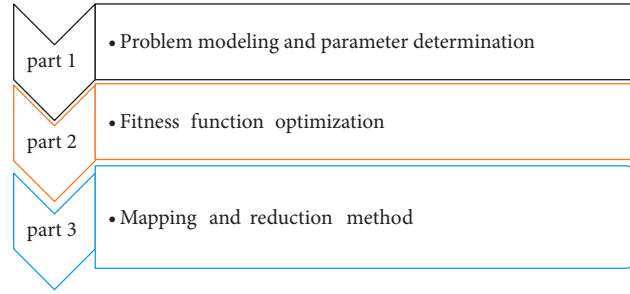


FIGURE 2: Structural model of the proposed method.

the optimal values in the shortest time. The structural model of the proposed method is shown in Figure 2.

The Apriori algorithm is one of the most popular and widely used data mining algorithms that examine a set of many items using candidate generation. Therefore, creating association rules and discovering a set of duplicate items in a big dataset will be time-consuming. On the other hand, traditional data mining techniques and tools such as this algorithm are efficient in data analysis but not scalable and efficient in extensive data management. It can be an incentive to use parallel processing in conventional computing. Therefore, redesigning traditional data mining algorithms based on a mapping/reduction framework seems necessary for analyzing macro datasets. According to the issues raised, performing this article was formed.

3.1. Research Hypotheses. In this part of the article, the current research hypotheses are stated. For this purpose, the hypotheses of research to accelerate the study process of current research are briefly described:

- (i) In problem-solving, it is always assumed that the transactions used in the problem are stored within a transaction database.

It is assumed that the transaction database is not updated in providing standard solutions to problems:

- (i) In the case of updating the transaction database, this update will not change the discovered duplicate patterns
- (ii) The same data is provided to the processors for parallelization
- (iii) Network topologies will use the same data

3.2. Components of the Proposed Method. As shown in Figure 2, the structural model of the proposed method consists of three main components, each of which is described below.

3.2.1. Problem Modeling and Parameters Determination. Parallelization is an architectural pattern based on a network of customers and receives services from provider devices. These devices have the computing and storage capacity to assign cloud computing data and items to each customer. Therefore, data and service management policies are needed to decide the place and time of placing services and data. The problem of placing services is significant in the field of services.

The required parameters are defined in the following.

- (i) Average execution time: the average execution time shows the two methods mapping and reduces, which is calculated through the following equation:

$$\text{average execution time} = \frac{\sum_{i=1}^{nm} et_m(i)}{nm} + \frac{\sum_{i=1}^{nr} et_r(i)}{nr}. \quad (1)$$

- (ii) Based on this equation, et_m is the time taken for execution in the mapping method, et_r is the runtime in the reduction method, nm is the number of operations in the mapping mode, and nr is the number of operations in the reduce mode. In this study, these two values are the same because the operations are assigned to mapping and reduction methods.
- (iii) Makespan: it is the time required to process all tasks. The assignment of tasks to neural network nodes should be such that this value is as low as possible for all tasks.
- (iv) Machine computing cost: this value is indicative of the cost of using the CPU in dollars, which can be calculated by the following equation:

$$\text{VM computing cost} = \left(\sum_{i=1}^{nm} et_m(i) + \sum_{j=1}^{nm} et_r(j) \right) \times \text{VM Cost per Unit Time}, \quad (2)$$

where *VM cost* represents the cost paid to use one unit of CPU time per second. Here, et_m is the mapping method's processing time, and et_r is the processing time in the reduction method.

- (v) Fitness function optimization: it is referred to as fitness function optimization process. For this purpose, the three parameters specified in the previous

step must be minimized to optimize the final output of the fitness function. The optimal fitness function is formulated according to the following equation:

$$\text{fitness} = w_1 * \text{average execution time} + w_2 * \text{makespan} + w_3 * \text{Vmcost} \quad (3)$$

Based on this equation, w_1 , w_2 , and w_3 represent the proportion coefficients, which are used to sum these three parameters with different unit values. In this relation, the sum of three w is equal to one.

3.2.2. Map and Reduction Method. Developing a distributed program without a mapping/reduction framework poses challenges for us, each of which is listed in the following [48, 49]:

- (i) Reliability: this is due to the management of distributed systems in a situation where the connection of each of the nodes working on the part of the data is disrupted.
- (ii) Distributed load balancing on nodes: how can the data divide into smaller parts so that each machine receives an equal part of the data and the nodes do not suffer underloaded or overloaded.
- (iii) Problems in one of the machines: if any of the machines have problems producing output, the final calculation of the result will not be possible. Therefore, there must be a mechanism to ensure the system's fault tolerance.
- (iv) Summary of results: the need for a mechanism to aggregate the results created by each machine to produce the final output.

Mapping/reduction is a method that can be used as an effective solution to manage the challenges raised. The mapping/reduction method is a parallel programming approach for processing data on clusters that includes two main phases: map and reduction [48].

The mapping phase receives the master node input, breaks it into smaller parts, and divides it among the worker nodes. Ninety workers may repeat this step, creating a tree structure.

In the reduction phase, the master node receives the answers to the scaled-down parts and combines them to form the desired output. To implement the two defined phases, we need mapping and reduction functions. This method is a simple programming model used to solve large-scale computational problems in a distributed manner and provides a secure and scalable platform for the development of distributive applications. Each solution is entered in the information mapping and matrix

section in this research. In the section on reducing the fitness function value, each solution is calculated in parallel to reduce the processing time. The motivation for choosing this calculation strategy seems logical because the most significant computational volume in this algorithm is performed in calculating the fitness function. Implementing distributed processing and reduction operations is the most important advantage of using the mapping/reduction method. Providing the possibility of parallel processing and independent implementation of each mapping operation highlights the impact of this method in the operation of mining association rules and improving the efficiency of basic techniques.

3.3. Parallel Architecture. Parallel mining is one of the practical and precise techniques in modern science that has been widely used in real-world problems today to improve the performance of classical algorithms for discovering association rules [57–60]. The methodology of parallel mining of big data is based on the assumption that several processors work in parallel in the computing environment. The main idea of this methodology is to divide the mining tasks into several subtasks so that each subtask can be processed simultaneously on different processors. Since several processors create association rules simultaneously, the computation speed is higher than classical methods [59].

A review of articles in this field shows that in recent years a wide range of different sciences has focused on the use of parallel algorithms in order to improve the performance of traditional techniques [61]. Implementation of large computational operations through parallel algorithms is much faster than performing them with sequential algorithms due to the performance of modern processors. Producing a computer with a high-speed processor is much more complicated than producing a computer with a lot of slower processors with the same throughput. However, there are certain theoretical limitations to the speed of parallel algorithms. Part of any parallel algorithm is consecutive, so every parallel algorithm has a saturation point. After that saturation point, adding more processors increases the throughput and only increases costs and losses. The cost and complexity of parallel algorithms are estimated based on memory and time consumed (number of CPU cycles).

Parallel algorithms must also be optimized for communication between different processors. Parallel algorithms communicate with processors in two ways, shared

TABLE 1: Length task values of each of the tasks.

Task id	Length task
1	2,160,657
2	1,835,957
3	1,819,923
4	1,747,767
5	1,599,447
6	1,583,413
7	1,607,465
8	1,427,076
9	1,463,154
10	1,447,119
11	1,527,292
12	1,503,240
13	1,495,223
14	1,362,938
15	1,370,955
16	1,378,972
17	1,471,171
18	1,431,084
19	1,439,102
20	1,419,059
21	1,403,024
22	1,407,033
23	1,407,033
24	1,423,067
25	1,419,059

memory and message exchange. Shared memory processing requires an additional lock for information, thus imposing the cost of bus cycles and additional processors, which also causes parts of the algorithm to become non-parallel. Processing through message transmission uses channels and message boxes. However, this type of communication increases the cost of bus transit, additional memory for queues and message boxes, and delays messages. Multiprocessor designs use specific bus bars to reduce transaction costs. However, it is the processor that determines the volume of traffic. Another problem with parallel algorithms is ensuring their proper balance.

4. Evaluating the Proposed Method

In this section, experiments are designed to evaluate the effectiveness of the proposed approach compared to other related tasks, and the evaluation results are reported. For this purpose, this section is organized into three different subsections.

4.1. Dataset. To evaluate the proposed algorithm, experiments were performed on tasks of different sizes as shown in Table 1, which shows the length task value of each machine.

In addition to the length task values, other values must be specified for the machines as the simulator input so that the simulator is applicable. These values are presented in Table 2. In this research work, the pharmaceutical database of the Social Security Organization has been selected as a case study. In this database, the number and price of drugs used are based on the type of insurance and patient referral,

TABLE 2: Specifications of other data center parameters.

Parameters	Value
Length (MIPS)	1,362,938–2,160,657
Input size (bytes)	291,738
Output size (bytes)	5,662,310

patient gender, and specialty of the prescribing physician. They are used to determine the dosage of a particular drug to be used in a given season.

4.2. Performance Evaluation Criteria. This research uses three criteria to evaluate the proposed algorithm [57–59]:

- (1) Delay in data transmission: this number indicates the time required to transmit information from source to destination
- (2) Energy consumption: this value indicates the energy consumption in the data center for the tasks assigned to the machines
- (3) Data center transmission: this criterion indicates the system's number of data center transmissions

4.3. Test Method. This article uses 10–30 machines to test the proposed method in a MATLAB simulator environment. For this purpose, each of the primary and proposed algorithms with this number of machines has been tested four times in a row. In this research, MATLAB software has been used to simulate the system. With this software, the grid environment can be defined in matrices, and the relationships between tasks and resources can be well modeled. In this research, MATLAB 2017b has been used for programming. We present the hardware specifications for the used system in tests (see Table 3).

4.4. Experimental Results. This section will evaluate the proposed method, which is proposed to improve the basic Apriori algorithm using the parallelization technique on network topologies. In our study, the desired system is considered a data center with N heterogeneous physical nodes. Also, each node I has processor size characteristics specified by MIPS (processing power), memory capacity, and network bandwidth. The data center is dedicated to m machines with these three characteristics. As mentioned earlier, the number of machines varies from 10 to 30 in our evaluation. Also, each of the algorithms with this variable number of machines has been executed four times in a row. The evaluation results have been reported for each implementation of the algorithms.

4.4.1. Evaluating Energy Consumption and the Number of Data Center Transmissions

(1) For Ten Machines. In this part, a comparison is performed between the standard Apriori algorithm and the proposed algorithm in terms of energy consumption. The evaluation results for four algorithm runs are shown in Figure 3.

TABLE 3: Hardware specifications of the system used in the tests.

Section	Capacity
RAM	16 GIGA BYTE DDR4
CPU	Intel ci7 16 core 12-megabyte cache
HDD	1 TRA BYTE

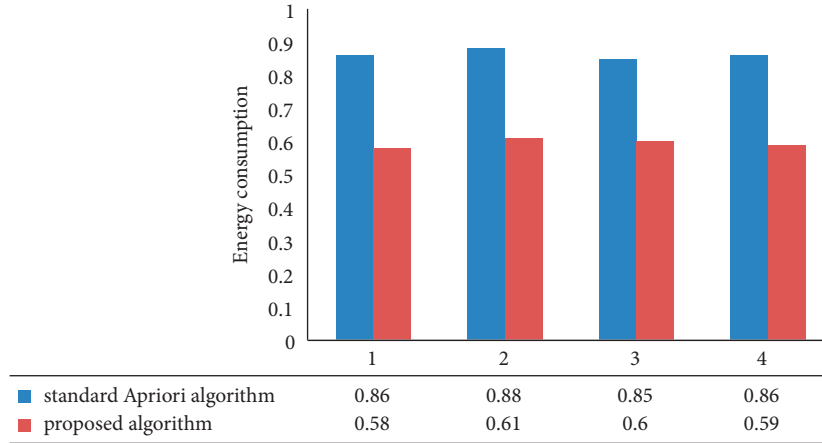


FIGURE 3: Comparing energy consumption in four experiments.

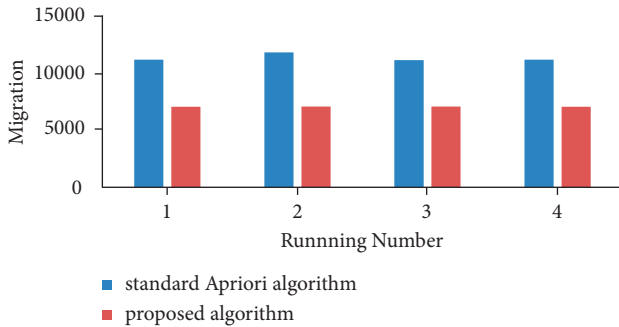


FIGURE 4: Datacenter transmission rate in four experiments.

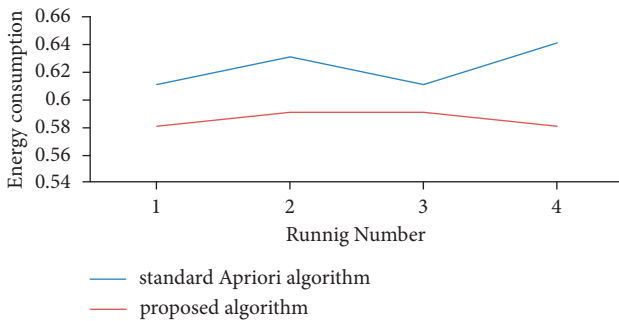


FIGURE 5: Comparison of the amount of energy consumption in four experiments for twenty machines.

As shown in Figure 3, the evaluation results show that, in four different implementations, the energy consumption of the proposed method is lower than the primary method. The data center transmission rate is calculated for the proposed

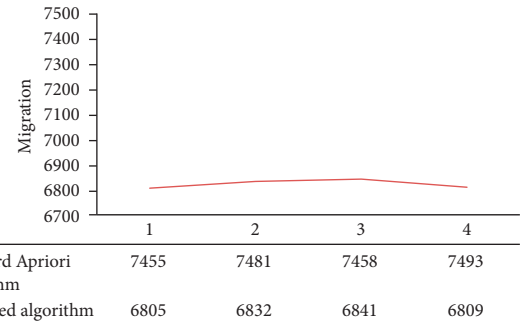


FIGURE 6: Comparison of data center transmission rate in four experiments for twenty machines.

method in another test. The base method results comparison is shown in Figure 4. As in the previous test, the results of four different implementations of the tested algorithms have been reported in this test.

The evaluation results in Figure 4 show that the proposed method has a better performance in terms of data transmission rate in the four tests compared to the basic algorithm.

(2) *For Twenty Machines.* In this part, the amount of energy consumption and the data transmission rate for the proposed method and the basic algorithm on twenty machines are calculated in four experiments. We present comparison results in Figures 5 and 6, respectively.

As seen in Figures 5 and 6, the evaluation results of the proposed method show that our proposed method has provided better performance and output in terms of energy consumption and data center transmission rate for twenty machines.

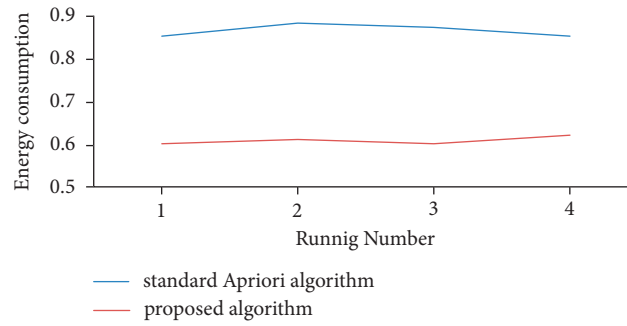


FIGURE 7: Comparison of the amount of energy consumption in four experiments for thirty machines.

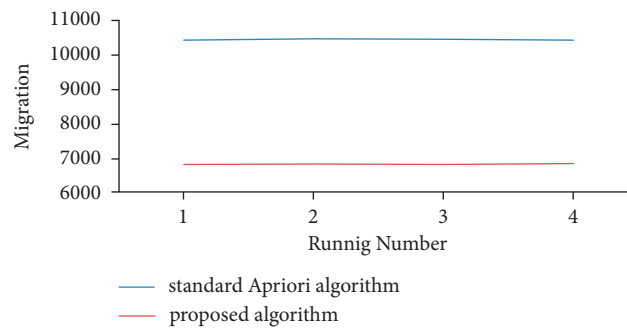


FIGURE 8: Comparison of data center transmission rate in four experiments for thirty machines.

(3) *For Thirty Machines.* In this part, the efficiency of the proposed method and the basic algorithm are investigated in terms of energy consumption and the number of data center transmissions by changing the number of machines from twenty to thirty. The evaluation result of this test is depicted in Figures 7 and 8.

As a general conclusion from the test performed above, it can be said that our proposed method performed better than the fundamental Apriori algorithm. Also, as can be seen in the results of this evaluation, increasing the number of machines has not had a negative impact on the efficiency of our proposed method. In other words, with the increasing number of machines, energy consumption has decreased, proving the superiority of the proposed method compared to the standard Apriori algorithm. It should be noted that in all tests the amount of energy consumption is calculated in terms of kw/h.

4.4.2. Evaluating Delay Rate in Data Transmission. In this part of the research, the proposed method and the basic Apriori algorithm are compared in terms of delay rate. For this purpose, the comparison results for the four experiments are shown in Figure 9. The objective function is considered the delay rate, so the lower the delay, the better the method.

The results of this experiment in Figure 9 show that the proposed method was superior in all four experiments and had a less objective function. As a general conclusion, it can be said that the evaluation of different experiments showed the superiority of the proposed method in different aspects of energy consumption, data center transmission rate, and

delay. Also, the proposed algorithm has performed better than the base algorithm due to the use of a more extensive search space and more operators to find the optimal answer.

4.4.3. Runtime. In this experiment, the runtime of the proposed method and the basic algorithm is calculated in four different modes, and the comparison results are shown in Figure 10.

As shown in the results of Figure 10, the minimum runtime is provided by the proposed method, and this algorithm can create association rules in less time than the basic Apriori algorithm. Therefore, it can be concluded that the strategy of parallelization of the process of data analysis and mining of the association rules has achieved significant success.

4.4.4. Network Lifetime. In this part of the article, another experiment is designed, based on which the network's lifetime is evaluated. For this purpose, the network lifetime for the basic algorithm and the proposed method is calculated by changing the number of machines in the network. The results are reported in Table 4.

As shown in the results of Table 4, the network lifetime in the proposed method is longer than the standard method. On the other hand, the results of this table show that, with increasing the number of machines, the network's lifetime has also increased. This increase is higher than the base method in similar conditions. For example, when the number of machines reaches 30, the network lifetime is more significant than the standard method.

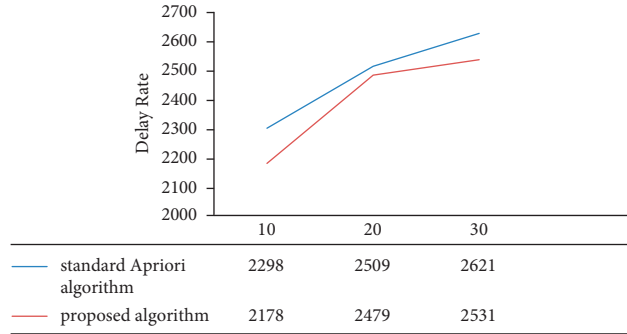


FIGURE 9: Delay rate in four different modes.

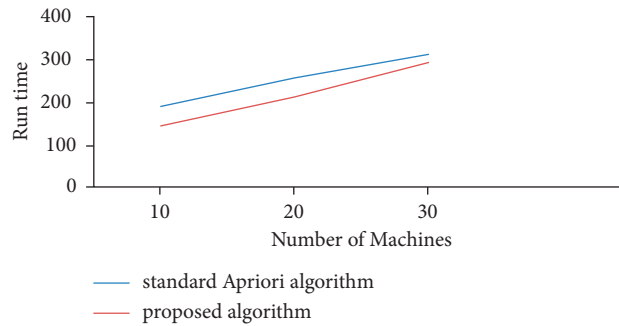


FIGURE 10: Algorithm runtime in four different modes.

TABLE 4: Results of network lifetime evaluation by changing the number of machines.

Standard Apriori algorithm	Proposed algorithm	The number of machines
401	456	10
471	519	20
528	629	30

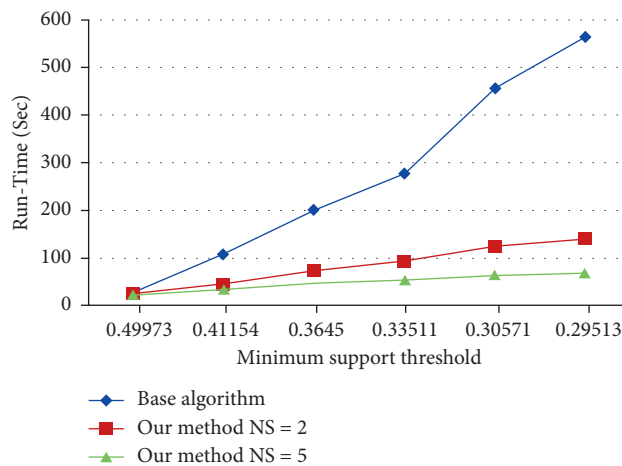


FIGURE 11: Comparison of runtime with different minimum support (dataset accident).

4.4.5. *Evaluating the Effect of NS Parameter on the Performance of the Proposed Algorithm.* To evaluate the effect of the NS parameter on the performance of the proposed algorithm, our proposed algorithm is implemented for different

NS values on different datasets. Figures 11–14 compare the central execution time with two different NS parameters.

In the case of experiments on real datasets, the NS parameter is an important variable to consider the best

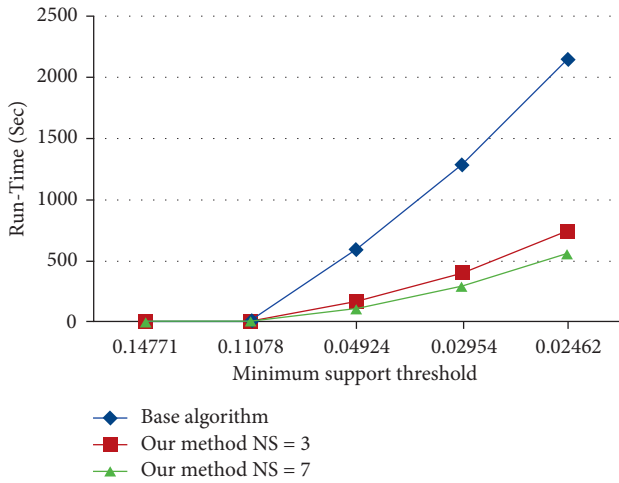


FIGURE 12: Comparison of runtime with different minimum support (dataset mushrooms).

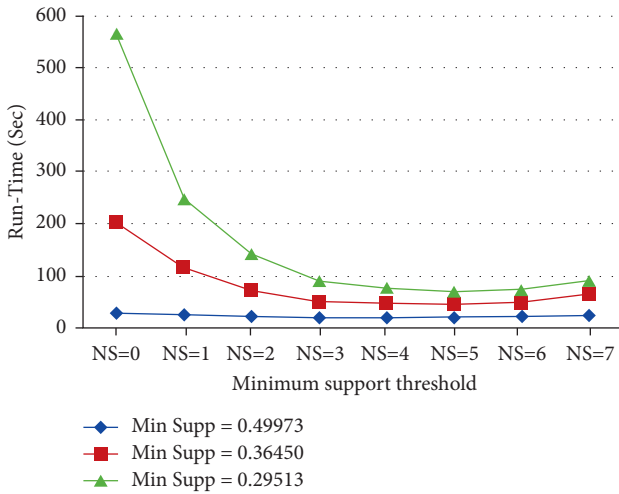


FIGURE 13: Effect of NS parameter at runtime (dataset accident, our method).

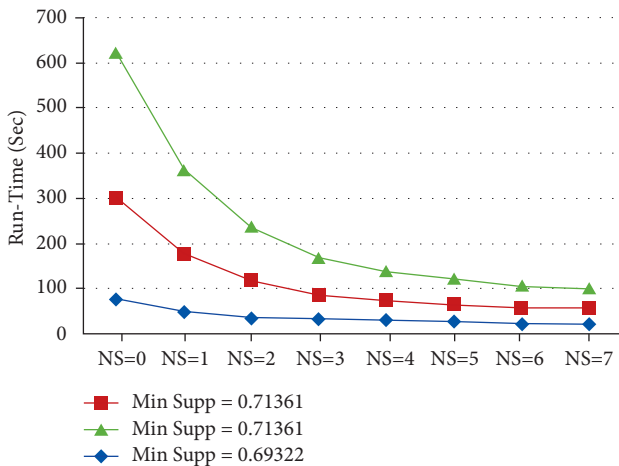


FIGURE 14: Effect of NS parameter at runtime (dataset pumsb, our method).

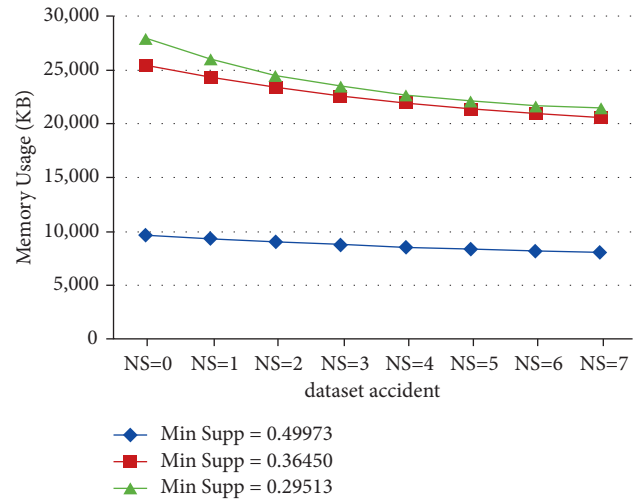


FIGURE 15: Effect of NS parameter on memory usage.

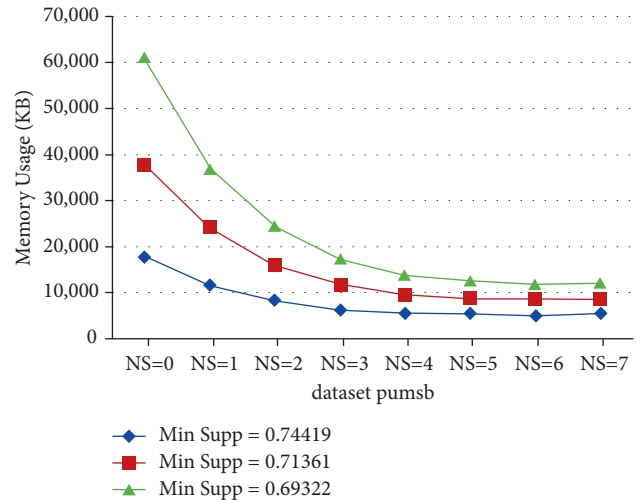


FIGURE 16: Effect of NS parameter on memory usage.

performance. The NS parameter has a uniform effect on different control values in a specific dataset. For example, for minimum support, the best result for a crash dataset is NS = 5. A simple heuristic, which we used to determine the best value for Apriori, was used to execute the algorithm at large support values. Hence, our proposed method is effective because minimal large amounts of support require less runtime. In addition, the NS parameter is an essential factor in the execution time of the algorithm but also has a significant effect on the amount of memory usage. Figures 15 and 16 show the amount of memory required by the proposed algorithm for different NS parameters in different datasets.

By comparing these figures, it can be seen that the behavior of the NS parameter on the dataset at runtime and memory usage is almost the same. Therefore, reducing memory usage in the algorithm means reducing the number of tried nodes and thus reducing the processing time required to find frequent item set. Therefore, it can be said that,

by reducing the memory usage in any NS parameter, execution time may be reduced.

5. Conclusions and Future Work

Despite the large databases and valuable information scattered in today's world, the speed of data processing, extraction of association rules, and mining repetitive patterns in them by basic algorithms such as Apriori and different versions of this algorithm is growing. Therefore, reducing the data processing time and speeding up the implementation of the Apriori-based algorithm to mining repetitive patterns can be considered a challenging problem. Accordingly, the information and matrix of each solution are entered into the mapping section. Then, the value of the fitness function of each solution is calculated in parallel in the reduction section to reduce processing time. The reason for performing this parallel processing in the reduction section is to conduct the maximum computational volume of the algorithm when computing the fit function. To evaluate the efficiency of the proposed approach, experiments have been designed and performed that compare our proposed approach with other existing tasks based on the criteria of energy consumption, network lifetime, execution time, and computational complexity. The results of various experiments show the superiority of the efficiency of the proposed algorithm to reduce runtime, energy consumption, and data center transmission by our proposed algorithm. A review of articles in this field shows that many algorithms based on the mapping/reduction framework implement only the production phase of duplicate items in parallel. Therefore, the parallelization of the production process of association rules based on the mapping/reduction framework can be evaluated as a challenging problem in future research. The following are examples of possible research that could be explored in the future:

- (i) Applying fuzzy logic to improve the fundamental Apriori algorithm
- (ii) Combining optimization algorithms based on collective intelligence and Apriori basic algorithm to improve the performance of traditional algorithms

Data Availability

Data are available and can be provided over email upon request directly to the corresponding author (p_asghari@iauctb.ac.ir).

Conflicts of Interest

The authors declare that they have no conflicts of interest.

References

- [1] J. Han, M. Kamber, and J. Pei, "Data mining concepts and techniques third edition," *The Morgan Kaufmann Series in Data Management Systems*, vol. 5, no. 4, pp. 83–124, 2011.
- [2] S. Agarwal, "Data mining: data mining concepts and techniques," in *Proceedings of the 2013 International Conference on Machine Intelligence and Research Advancement*, pp. 203–207, IEEE, Katra, India, 2013 December.
- [3] M. K. Gupta and P. Chandra, "A comprehensive survey of data mining," *International Journal on Information Technology*, vol. 12, pp. 1243–1257, 2020.
- [4] F. Z. Maksood and G. Achuthan, "Analysis of data mining techniques and its applications," *International Journal of Computer Application*, vol. 140, no. 3, pp. 6–14, 2016.
- [5] M. Ahmadi, "A computational approach to uncovering economic growth factors," *Computational Economics*, vol. 58, no. 4, pp. 1051–1076, 2020.
- [6] M. J. Huang, H. S. Sung, T. J. Hsieh, M. C. Wu, and S. H. Chung, "Applying data-mining techniques for discovering association rules," *Soft Computing*, vol. 24, no. 11, pp. 8069–8075, 2019.
- [7] M. Ahmadi, S. Jafarzadeh-Ghoushchi, R. Taghizadeh, and A. Sharifi, "Presentation of a new hybrid approach for forecasting economic growth using artificial intelligence approaches," *Neural Computing and Applications*, vol. 12, no. 12, pp. 8661–8680, 2019.
- [8] M. R. Keyvanpour, S. Mehrmolaei, and A. Etaati, "PLI-X: temporal association rules mining in customer relationship management systems," *Computer and Knowledge Engineering*, vol. 2, no. 2, pp. 29–48, 2020.
- [9] C.-H. Chee, J. Jaafar, I. A. Aziz, M. H. Hasan, and W. Yeoh, "Algorithms for frequent itemset mining: a literature review," *Artificial Intelligence Review*, vol. 52, no. 4, pp. 2603–2621, 2019.
- [10] C. C. Aggarwal, "An introduction to frequent pattern mining," in *Frequent Pattern Mining*, C. C. Aggarwal and J. Han, Eds., Springer, Basel, Switzerland, pp. 1–14, 2014.
- [11] W. P. Nurmawanti, H. M. Sastriana, A. Rahim et al., "Market basket analysis with apriori algorithm and frequent pattern growth (Fp-Growth) on outdoor product sales data," *International Journal of Educational Research & Social Sciences*, vol. 2, no. 1, pp. 132–139, 2021.
- [12] S. A. Moosavi, M. Jalali, N. Misaghian, S. Shamshirband, and M. H. Anisi, "Community detection in social networks using user frequent pattern mining," *Knowledge and Information Systems*, vol. 51, no. 1, pp. 159–186, 2017.
- [13] M. Berlingerio, F. Pinelli, and F. Calabrese, "Abacus: frequent pattern mining-based community discovery in multidimensional networks," *Data Mining and Knowledge Discovery*, vol. 27, no. 3, pp. 294–320, 2013.
- [14] P. N. E. Nohuddin, F. Coenen, R. Christley, C. Setzkorn, Y. Patel, and S. Williams, "Finding "interesting" trends in social networks using frequent pattern mining and self-organizing maps," *Knowledge-Based Systems*, vol. 29, pp. 104–113, 2012.
- [15] F. Jiang, C. K. Leung, and H. Zhang, "B-mine: frequent pattern mining and its application to knowledge discovery from social networks," in *Web Technologies and Applications*, pp. 316–328, Springer, Cham, Switzerland, 2016.
- [16] A. A. Zoraghchian, M. K. Sohrabi, and F. Yaghmaee, "Exploiting parallel graphics processing units to improve association rule mining in transactional databases using butterfly optimization algorithm," *Cluster Computing*, vol. 24, no. 4, pp. 3767–3778, 2021.
- [17] S. Dongnan and Z. Zhaopeng, "Parallel design of apriori algorithm based on the method of "determine infrequent items & remove infrequent itemsets"," *IOP conference series: earth and environmental science*, vol. 634, no. 1, Article ID 012065, 2021.

- [18] P. Fournier-Viger, J. C. W. Lin, B. Vo, T. T. Chi, J. Zhang, and H. B. Le, "A survey of itemset mining," *Wiley Interdisciplinary Reviews: Data Mining and Knowledge Discovery*, vol. 7, no. 4, Article ID e1207, 2017.
- [19] J. M. Luna, P. Fournier-Viger, and S. Ventura, "Frequent itemset mining: a 25 years review," *Wiley Interdisciplinary Reviews: Data Mining and Knowledge Discovery*, vol. 9, no. 6, Article ID e1329, 2019.
- [20] A. Ala, F. E. Alsaadi, M. Ahmadi, and S. Mirjalili, "Optimization of an appointment scheduling problem for healthcare systems based on the quality of fairness service using whale optimization algorithm and NSGA-II," *Scientific Reports*, vol. 11, no. 1, pp. 19816–19819, 2021.
- [21] J. Yuan and S. Ding, "Research and improvement on association rule algorithm based on FP-growth," in *International Conference on Web Information Systems and Mining*, pp. 306–313, Springer, Berlin, Germany, 2012.
- [22] M. Ahmadi and M. Qaisari Hasan Abadi, "A review of using object-orientation properties of C++ for designing expert system in strategic planning," *Computer Science Review*, vol. 37, Article ID 100282, 2020.
- [23] A. Varmaghani, A. M. Nazar, M. Ahmadi, A. Sharifi, S. Jafarzadeh Ghouschi, and Y. Pourasad, "DMTC: optimize energy consumption in dynamic wireless sensor network based on fog computing and fuzzy multiple attribute decision-making," *Wireless Communications and Mobile Computing*, vol. 2021, Article ID 9953416, 14 pages, 2021.
- [24] T. Sui, D. Marelli, X. Sun, and M. Fu, "Multi-sensor state estimation over lossy channels using coded measurements," *Automatica*, vol. 111, Article ID 108561, 2020.
- [25] J. Yu, L. Lu, Y. Chen, Y. Zhu, and L. Kong, "An indirect eavesdropping attack of keystrokes on touch screen through acoustic sensing," *IEEE Transactions on Mobile Computing*, vol. 20, no. 2, pp. 337–351, 2021.
- [26] H. Kong, L. Lu, J. Yu, Y. Chen, and F. Tang, "Continuous authentication through finger gesture interaction for smart homes using WiFi," *IEEE Transactions on Mobile Computing*, vol. 20, no. 11, pp. 3148–3162, 2021.
- [27] M. Ahmadi, T. Ali, D. Javaheri, A. Masoumian, S. Jafarzadeh Ghouschi, and Y. Pourasad, "DQRE-SCnet: a novel hybrid approach for selecting users in federated learning with deep-Q-reinforcement learning based on spectral clustering," *Journal of King Saud University-Computer and Information Sciences*, In press, 2021.
- [28] S. Zhao, F. Li, H. Li et al., "Smart and practical privacy-preserving data aggregation for fog-based smart grids," *IEEE Transactions on Information Forensics and Security*, vol. 16, pp. 521–536, 2021.
- [29] S. Han, J. Lin, S. Zhao et al., "Location privacy-preserving distance computation for spatial crowdsourcing," *IEEE Internet of Things Journal*, vol. 7, no. 8, pp. 7550–7563, 2020.
- [30] T. Ni, D. Liu, Q. Xu, Z. Huang, H. Liang, and A. Yan, "Architecture of cobweb-based redundant TSV for clustered faults," *IEEE Transactions on Very Large Scale Integration (VLSI) Systems*, vol. 28, no. 7, pp. 1736–1739, 2020.
- [31] H. Che and J. Wang, "A two-timescale duplex neurodynamic approach to mixed-integer optimization," *IEEE Transactions on Neural Networks and Learning Systems*, vol. 32, no. 1, pp. 36–48, 2021.
- [32] Y. Jiang and X. Li, "Broadband cancellation method in an adaptive co-site interference cancellation system," *International Journal of Electronics*, pp. 1–21, 2021.
- [33] X. Wu, W. Zheng, X. Xia, and D. Lo, "Data quality matters: a case study on data label correctness for security bug report prediction," *IEEE Transactions on Software Engineering*, vol. 1, p. 1, 2021.
- [34] M. Hegland, "The apriori algorithm—a tutorial," in *Lecture Notes Series, Institute for Mathematical Sciences, National University of Singapore, Mathematics and Computation in Imaging Science and Information Processing*, pp. 209–262, World Scientific, Singapore, 2007, <https://www.worldscientific.com/action/downloadCitation>.
- [35] W. Zheng, Y. Xun, X. Wu, Z. Deng, X. Chen, and Y. Sui, "A comparative study of class rebalancing methods for security bug report classification," *IEEE Transactions on Reliability*, vol. 70, no. 4, pp. 1658–1670, 2021.
- [36] J. Dong, Y. Cong, G. Sun, Z. Fang, and Z. Ding, "Where and How to transfer: knowledge aggregation-induced transferability perception for unsupervised domain adaptation," *IEEE Transactions on Pattern Analysis and Machine Intelligence*, p. 1. In press, 2021.
- [37] J. Artin, V. Amin, M. Ahmadi, S. A. P. Kumar, and A. Sharifi, "Presentation of a novel method for prediction of traffic with climate condition based on ensemble learning of neural architecture search (NAS) and linear regression," *Complexity*, vol. 2021, Article ID 8500572, 13 pages, 2021.
- [38] L. Zhong, Z. Fang, F. Liu, B. Yuan, G. Zhang, and J. Lu, "Bridging the theoretical bound and deep algorithms for open set domain adaptation," *IEEE Transactions on Neural Networks and Learning Systems*, pp. 1–15. In press, 2021.
- [39] Y. He, L. Dai, and H. Zhang, "Multi-branch deep residual learning for clustering and beamforming in user-centric network," *IEEE Communications Letters*, vol. 24, no. 10, pp. 2221–2225, 2020.
- [40] C. Zhao, S. Zhong, X. Zhang, Q. Zhong, and K. Shi, "Novel results on nonfragile sampled-data exponential synchronization for delayed complex dynamical networks," *International Journal of Robust and Nonlinear Control*, vol. 30, no. 10, pp. 4022–4042, 2020.
- [41] J. Luo, M. Li, X. Liu, W. Tian, S. Zhong, and K. Shi, "Stabilization analysis for fuzzy systems with a switched sampled-data control," *Journal of the Franklin Institute*, vol. 357, no. 1, pp. 39–58, 2020.
- [42] Y. Zhang, F. Liu, Z. Fang, B. Yuan, G. Zhang, and J. Lu, "Learning from a complementary-label source domain: theory and algorithms," *IEEE Transaction on Neural Networks and Learning Systems*, pp. 1–15. In press, 2021.
- [43] H. Si, J. Zhou, Z. Chen et al., "Association rules Mining among interests and applications for users on social networks," *IEEE Access*, vol. 7, pp. 116014–116026, 2019.
- [44] A. Sharifi, M. Ahmadi, H. Badfar, and M. Hosseini, "Modeling and sensitivity analysis of NOx emissions and mechanical efficiency for diesel engine," *Environmental Science and Pollution Research*, vol. 26, no. 24, pp. 25190–25207, 2019.
- [45] N. Verma, D. Malhotra, and J. Singh, "Big data analytics for retail industry using MapReduce-Apriori framework," *Journal of Management Analytics*, vol. 7, no. 3, pp. 424–442, 2020.
- [46] S. S. Gill, S. Tuli, M. Xu et al., "Transformative effects of IoT, Blockchain and Artificial Intelligence on cloud computing: evolution, vision, trends and open challenges," *Internet of Things*, vol. 8, Article ID 100118, 2019.
- [47] A. K. Singh, A. Kumar, and A. K. Maurya, "An empirical analysis and comparison of apriori and FP-growth algorithm for frequent pattern mining," in *Proceedings of the 2014 IEEE International Conference on Advanced Communications, Control and Computing Technologies*, pp. 1599–1602, IEEE, Ramanathapuram, India, May 2014.

- [48] S. Singh, R. Garg, and P. K. Mishra, "Performance optimization of MapReduce-based apriori algorithm on Hadoop cluster," *Computers & Electrical Engineering*, vol. 67, pp. 348–364, 2018.
- [49] W. Song, B. Yang, and Z. Xu, "Index-BitTableFI: an improved algorithm for mining frequent itemsets," *Knowledge-Based Systems*, vol. 21, no. 6, pp. 507–513, 2008.
- [50] Y. Huang, Q. Lin, and Y. Li, "Apriori-BM algorithm for mining association rules based on bit set matrix," in *Proceedings of the 2018 2nd IEEE Advanced Information Management, Communicates, Electronic and Automation Control Conference (IMCEC)*, pp. 2580–2584, IEEE, Xi'an, China, 2018 May.
- [51] P. P. Patro and R. Senapati, "Advanced binary matrix-based frequent pattern mining algorithm," in *Intelligent Systems*, pp. 305–316, Springer, Singapore, Singapore, 2021.
- [52] S. Raj, D. Ramesh, M. Sreenu, and K. K. Sethi, "EAFIM: efficient apriori-based frequent itemset mining algorithm on Spark for big transactional data," *Knowledge and Information Systems*, vol. 62, no. 9, pp. 3565–3583, 2020.
- [53] A. R. Ramtin, P. Nain, D. Sadoc Menasche, D. S. Menasche, D. Towsley, and E. de Souza e Silva, "Fundamental scaling laws of covert DDoS attacks," *Performance Evaluation*, vol. 151, Article ID 102236, 2021.
- [54] A. Reza Ramtin, D. Towsley, P. Nain, E. de Souza e Silva, and D. S. Menasche, "Are covert DDoS attacks facing multi-feature detectors feasible?" *ACM SIGMETRICS Performance Evaluation Review*, vol. 49, no. 2, pp. 33–35, 2022.
- [55] T. Ni, Z. Yang, H. Chang et al., "A novel TDMA-based fault tolerance technique for the TSVs in 3D-ICs using honeycomb topology," *IEEE transactions on emerging topics in computing*, vol. 9, no. 2, pp. 724–734, 2020.
- [56] J. Dong, C. Yang, S. Gan, F. Zhen, and Z. Ding, "Where and how to transfer: knowledge aggregation-induced transferability perception for unsupervised domain adaptation." *IEEE Transactions on Pattern Analysis and Machine Intelligence*, 2021.
- [57] W. Gan, J. C.-W. Lin, P. Fournier-Viger, H.-C. Chao, and P. S. Yu, "A survey of parallel sequential pattern mining," *ACM Transactions on Knowledge Discovery from Data*, vol. 13, no. 3, pp. 1–34, 2019.
- [58] Y. Xun, J. Zhang, and X. Qin, "Fidoop: parallel Mining of frequent item sets using mapreduce," *IEEE transactions on Systems, Man, and Cybernetics: Systems*, vol. 46, no. 3, pp. 313–325, 2015.
- [59] M. K. Sohrobi and N. Taheri, "A haoop-based parallel mining of frequent itemsets using N-Lists," *Journal of the Chinese Institute of Engineers*, vol. 41, no. 3, pp. 229–238, 2018.
- [60] Y. Xun, J. Zhang, H. Yang, and X. Qin, "HBFPF-DC: a parallel frequent itemset mining using Spark," *Parallel Computing*, vol. 101, Article ID 102738, 2021.
- [61] K. K. Mohbey and S. Kumar, "A parallel approach for high utility-based frequent pattern mining in a big data environment," *Iran Journal of Computer Science*, vol. 4, no. 3, pp. 195–200, 2021.

Research Article

A Rapid Combined Model for Automatic Generating Web UI Codes

Wei Zhang , Shangmin Luan, and Liqin Tian

Hebei IoT Monitoring Engineering Technology Research Center, School of Computer Science,
North China Institute of Science and Technology, Beijing 101601, China

Correspondence should be addressed to Wei Zhang; zw@ncist.edu.cn

Received 20 November 2021; Revised 8 January 2022; Accepted 10 January 2022; Published 8 February 2022

Academic Editor: Nima Jafari Navimipour

Copyright © 2022 Wei Zhang et al. This is an open access article distributed under the Creative Commons Attribution License, which permits unrestricted use, distribution, and reproduction in any medium, provided the original work is properly cited.

Encoder-Decoder network is usually applied to image caption to automatically generate descriptive text for a picture. Web user interface (Web UI) is a special type of image and is usually described by HTML (hypertext marked language). Consequently, it becomes possible to use the encoder-decoder network to generate the corresponding code from a screenshot of Web UI. The basic structure of the decoder is RNN, LSTM, GRU, or other recurrent neural networks. However, this kind of decoder needs a long training time, so it increases the time complexity of training and prediction. The HTML language is a typically structured language to describe the Web UI, but it is hard to express the timing characteristics of the word sequence and the complex context. To resolve these problems efficiently, a rapid combined model RCM (rapid combined model) is designed in this paper. The basic structure of the RCM is an encoder-decoder network. The word embedding matrix and visual model are included in the encoder. The word embedding matrix uses fully connected units. Compared with LSTM, the accuracy of the word embedding matrix is basically unchanged, but the training and prediction speed have been significantly improved. In the visual model, the pretrained InceptionV3 network is used to generate the image vector, which not only improves the quality of the recognition of the Web UI interface image but also reduces the training time of the RCM significantly. In the decoder, the word embedding vector and the image vector are integrated together and input into the prediction model for word prediction.

1. Introduction

It is rather time-consuming for web application front-end developers to build a Web UI in HTML and CSS (cascading style sheets) language. It would save more human resources if this process is partially automated.

Scholars have made a lot of efforts to automatically generate program code. For instance, Gaunt et al. [1] studied machine learning formulations of inductive program synthesis and proposed a TerpreT model composed of a specification of a program representation and an interpreter that described how programs mapped inputs to outputs. Kalyan et al. [2] introduced a kind of hybrid synthesis technique, the neural guided deductive search, which combines the best of both symbolic logic techniques and statistical models. Bunel et al. [3] presented an adaptive neural-compilation framework to address the problem of efficient program learning by considering correctness only on a target input distribution. Balog et al. [4] proposed

DeepCoder, which combined traditional search techniques and used statistical prediction to generate computer code sequences. Solar-Lezama et al. [5] described the sketching approach to program synthesis, which left the low-level details of the implementation to an automated synthesis procedure. Ellis et al. [6] introduced a well-trained model which can convert hand drawings into a sequence of codes. Riedel et al. [7] presented a differentiable interpreter for the programming language Forth and made programmers can write program sketches with slots that can be filled with learnable behavior.

The encoder-decoder network encodes the input into a latent vector firstly and then converts it into the target output, so it is widely applied to the machine translation [8, 9]. When the input sentences in machine translation are taken place by the images, the network would be able to translate these images to sentences [10–12]. Considering encoder-decoder network has made great progress in automatically describing image content [13, 14], scholars have

begun to try to link computer vision with programming languages. Wu et al. [15] proposed a new model which can interpret objects in certain scenes. A recent example is pix2code [16], which combines CNN and LSTM to encode the input image and the original code sequence, and then uses LSTM to decode the code. Zhu et al. [17] introduced the attention mechanism to the process of input image feature extraction, and then the extracted block feature information guides the LSTM network in the decoder to generate the code sequence. But the overall structure of this model is still the encoder-decoder network, which is similar to the pix2code model, that is, the code sequence features and image features are used as input, and the LSTM network is used to predict the code sequence. However, an obvious shortcoming of this type of network is that the time complexity of the model is large, which is mainly due to the fact that the model is entirely composed of CNN and LSTM units [16, 17].

To resolve these problems, a fast end-to-end model is introduced to generate Web UI code. The model can not only learn the word embedding matrix of Web UI code but also automatically generate code sequences based on Web UI images. Experimental results show that the model has higher generation accuracy on the public Web UI data set, and can also improve the training speed.

This paper is divided into four parts. First, the research background and the latest progress of automatic code generation are introduced, and the advantages and disadvantages of common models are analyzed, which further leads to the RCM model proposed in this paper. The second part introduces the overall structure of RCM generated by the web user interface (Web UI) and then discusses the word embedding matrix model, visual model, and prediction model in detail. The third part introduces the training experiment of the RCM model and tests the RCM model from two aspects of single word prediction and whole code generation. The fourth part is the conclusion of the whole thesis and the prospect of future work.

2. Design of RCM

This section will introduce the RCM model, and the experimental data will be shown in the next section.

2.1. Structure of RCM. The overall structure of RCM is still the encoder-decoder network, but the encoder part is composed of word embedding matrix and visual model. The results of these two parts are superimposed as the output of the encoder. The word embedding matrix converts the code describing the Web UI into a vector sequence, and the visual model is responsible for converting the screenshot of the Web UI into its corresponding high-dimensional vector. The decoder part focuses on using the results of the encoder to predict the next word. The whole structure of RCM is shown in Figure 1.

Firstly, the word embedding matrix C is used to convert the index vector $W_{i,t}$ of the context word sequence into the word vector $E_{i,t}$ (i represents the sample number, t

represents the current moment), and meanwhile, the image I_i is input into the visual model to obtain the image feature vector V_i . Secondly, $E_{i,t}$ and V_i are stitched together to obtain a feature vector U_i representing sample i . Finally, U_i is input into the prediction model, and the Softmax network is used to obtain the index vector of the next word $\text{Word}_{i,t+1}$. Before the start of the next time step, $\text{Word}_{i,t+1}$ would be added to $W_{i,t}[t-n+1, t]$ get a new $W_{i,t+1}$. The calculation process of RCM is shown in equations (1)–(5).

$$E_{i,t} = C(W_{i,t}), \quad (1)$$

$$V_i = \text{VisualModel}(I_i), \quad (2)$$

$$U_i = E_{i,t} \cup V_i, \cup \text{ is the concatenate operation}, \quad (3)$$

$$\begin{aligned} \text{Word}_{i,t+1} &= \sigma(\text{PredictionModel}(U_i)), \\ \sigma &\text{ is the Softmax function}, \end{aligned} \quad (4)$$

$$\begin{aligned} W_{i,t+1} &= W_{i,t}[t-n+1, t] \cup \text{Word}_{i,t+1}, \\ n &\text{ is the length of the context.} \end{aligned} \quad (5)$$

2.2. Learning of Word Embedding Matrix. Since the word embedding model can be able to learn the distribution representation of each word [18], and people can use the information to calculate the occurrence probability of a certain sentence, the word embedding technique is commonly applied in NLP tasks. In order to obtain the feature vectors of the word sequence in Web UI code, the word embedding matrix is used to store the word vector of each word in Web UI.

The DSL (domain specified language) is usually used in a specialized field, which is more restrictive than general computer languages. After converting the Web UI code sequence into a DSL word sequence, the number of DSL words is 19, and the number of tags in H5 is 118. Therefore, modeling using DSL can better limit the complexity of modeling and reduce the search space of the model.

The size of the word embedding vector matrix C is set to (19, 64). In order to get C , it is necessary to build a DSL language model for Web UI. Considering that the Web UI interface usually adopts a nested structure, in order to verify whether its DSL sequence has obvious dynamic timing characteristics like natural languages [9], the sequence of word embedding vectors are processed separately by FC layer, LSTM layer [19], CNN layer [20], and BiLSTM (bi-directional LSTM) layer [21], and then the Softmax activation function is used to predict the next word. The structure of the DSL language model for Web UI is shown in Figure 2.

Firstly, the DSL Context at the t -th moment in the i -th sample is converted into the index vector $W_{i,t}$. Secondly, the word embedding matrix C is used to convert $W_{i,t}$ into the word embedding vector $E_{i,t}$. Finally, let $E_{i,t}$ input FC (full connect), LSTM (long short-term memory), BiLSTM (Bi-directional LSTM), and CNN (convolutional neural

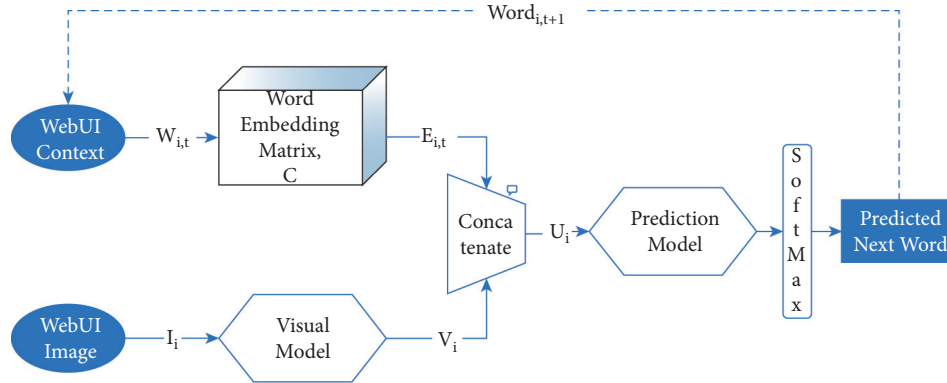


FIGURE 1: Rapid combined model structure.

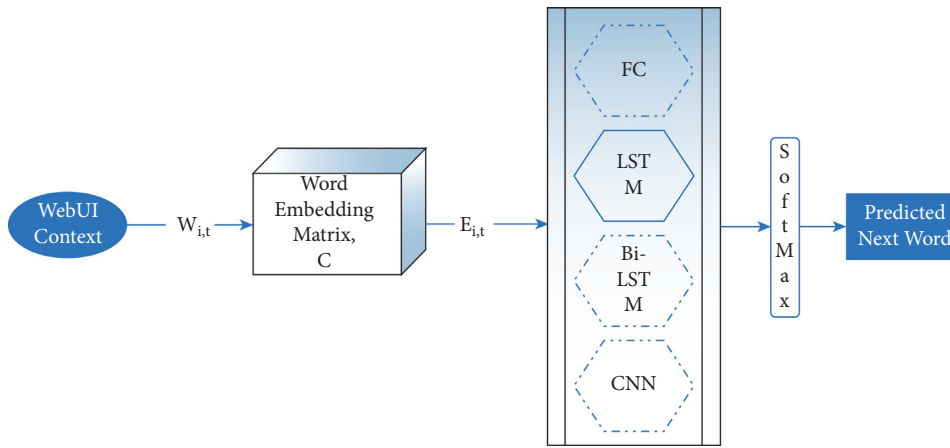


FIGURE 2: Structure of DSL language model for Web UI.

networks) units for separate training and testing. During the training process, for the word sequences of all samples, the same word embedding matrix C is shared.

Multiclass cross-entropy is applied to calculate the loss value of a single sample x , as shown in the following equation:

$$\text{loss}(x) = - \sum_{i=1}^M y_i \log f_i(x). \quad (6)$$

In this equation, M is the length of the DSL word list and x is the input sample. $f_i(x)$ is the i -th component in the prediction result, that is, the probability of the next word is the i -th word. y_i is the true probability that the next word is the i -th word.

Batch B contains N samples, then the loss function of batch B is the average of the loss values of all samples in the batch, as shown in the following equation:

$$\text{Loss}(B) = \frac{\sum_{j=1}^N \text{loss}(x_j)}{N}. \quad (7)$$

FC, LSTM, BiLSTM, and CNN units are used to separately construct language models, which are trained by the same dataset (the details of the dataset are in “3.

Experiments”). After having been trained for 10 cycles, the model with the highest accuracy in the verification set is taken as the best model, and its accuracy on the test set is then calculated. The experimental results are shown in Table 1.

It can be concluded from the experimental results that the FC layer is relatively stable and is not affected by the size of the batch. The accuracy of the verification data and the test data is relatively stable, basically about 91.6%. The LSTM layer is greatly affected by the batch. The larger the batch, the lower the accuracy of the LSTM layer. But when the batch size decreases, although the accuracy rate has increased, the training time increases exponentially with the batch size reduction. Especially the BiLSTM layer is about twice the training time of the ordinary LSTM layer. When the batch size is 512, the CNN layer has poor accuracy, but when the number of batches is reduced, the accuracy of the verification set and test set has increased.

The above analysis shows that, although LSTM and BiLSTM have achieved good results in the field of NLP, they performed mediocly when they are applied to the DSL sequence of the Web UI interface. CNN does not perform as well as ordinary FC on the DSL sequence of the Web UI interface. Therefore, it can be judged that the timing

TABLE 1: Experimental results of the best models based on different network elements.

Neural network type	Batch size	Training time (s)	Verification set accuracy (%)	Test set accuracy (%)
FC	512	54	91.6	91.4
FC	128	62	91.5	91.2
LSTM	512	280	82.2	82.7
LSTM	128	66	91.9	91.6
BiLSTM	512	281	70.6	70.7
BiLSTM	128	634	91.8	91.8
CNN	512	58	86.5	86.6
CNN	128	1038	88.1	88.2

characteristics of the DSL language describing the Web UI interface are not obvious. The LSTM and BiLSTM layers do not have obvious advantages in the code prediction tasks of Web UI, and their computation time is several times that of FC layers.

Consequently, the FC layer is chosen to build a DSL language model with a training period of 100 and a batch size of 512. The loss function uses the cross-entropy function defined by equations (6) and (7). The accuracy and loss of model training are shown in Figure 3.

The parameters of the DSL language model are 199,251, the training time is about 8 minutes, the minimum loss is 0.19178, and the maximum accuracy rate is 91.824%.

2.3. Design of Visual Model. In recent years, CNN networks are introduced to extract feature vectors from images, which can accurately classify images or recognize objects [22, 23]. In the research of image captioning, a common method is that CNN is used to extract feature vectors from images and recurrent neural network units are applied to generate image captions [24–26].

Considering that CNN has achieved amazing achievements in the field of image recognition [27, 28], the convolutional networks are adopted in this visual model in RCM. In order to improve the training and prediction speed of the model, the pretrained InceptionV3 model [29] is adopted as the visual model of RCM, and some adjustments to the original InceptionV3 model are made to better handle the DSL prediction tasks.

The visual model in RCM discards the classification level of the upper layer of Inception V3, only uses the convolutional layer at the bottom to process the image of the Web UI and adds a global average pooling layer to generate the corresponding image feature vector V_i , the vector size is (1,2048). The final visual model has a total of 21,802,784 parameters, and these parameters can be updated during the training of the RCM if the computing power allows. However, under the experimental conditions of this project, in order to improve the training speed of the entire model, all parameters of the visual model are locked.

2.4. Design of Prediction Model. The experimental results in 3.1 show that in the DSL sequence prediction task of the Web UI, the FC unit can greatly reduce the training time than the LSTM unit and the CNN unit on the premise of ensuring more than 90% accuracy, so the FCB (full connect block) is

designed as a foundation to build a prediction model of RCM. The structure of FCB is shown in Figure 4.

The FCB consists of a fully connected layer, batch standardization layer 30, and dropout layer [31]. The specific calculation process is shown in equations (8)–(11). The variables and notations are shown in Table 2.

$$x_1 = \text{sigmoid}(w^T x_m + b), \quad (8)$$

$$x_2 = \frac{x_1 - E[x_1]}{\sqrt{\text{Var}[x_1]}} \gamma + \beta, \quad (9)$$

$$\delta = \text{Binomial}(p), \quad (10)$$

$$x_{\text{out}} = \frac{\delta * x_2}{1 - p}. \quad (11)$$

The prediction model in RCM consists of several FCBs connected in series, and its structure is shown in Figure 5.

The feature vector U_i of sample i is composed of the word embedding vector $E_{i,t}$ and the image feature vector V_i . The prediction model uses U_i as an input to predict the probability of the next word. The number of units in the FC layer of the first 9 FCBs in the prediction model is set to 512, the FC layer of the last FCB contains 19 units, and the final Softmax layer is responsible for calculating the prediction probability of 19 DSL words. The DSL word corresponding to the maximum value in the prediction probability is used as the prediction result. The training parameters of the entire prediction model are 4,743,379.

3. Experiments

In order to verify the effect of RCM, the Web UI dataset in pix2code [16] is utilized to train and test RCM. The pix2code data set contains 1750 Web UI instances, each instance contains a Web UI code sequence and an image. The format of the code sequence and the corresponding image is shown in Figure 6.

Before the start of the experimental process, a total of 167958 samples with a context length of 48 are obtained from each instance in the pix2code dataset, and all of these samples contain 19 DSL words. Then, 24,108 samples are extracted to form the test set, with the rest forming the training set, within which 20% of the samples are randomly selected to form the verification set during the training

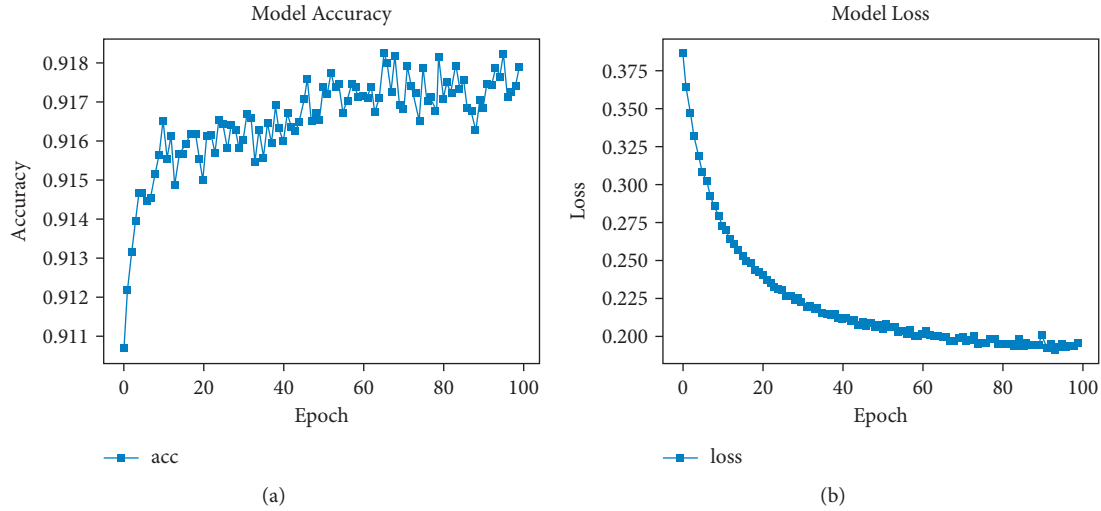


FIGURE 3: (a) Accuracy rate and (b) loss curve of the DSL language model training.

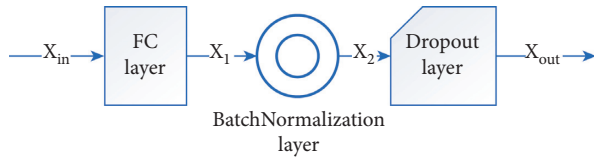


FIGURE 4: Structure of FCB.

TABLE 2: Variables and notations.

Notation	Meaning
x_{in}	FCB input
w	Weight matrix
b	Bias matrix
$E[x_1]$	Mean of x_1
$\text{Var}[x_1]$	Variance of x_1
γ	Scale parameter
β	Shift parameter
p	Probability of setting x_1 to 0
Binomial	Function to generate binomial distribution vector
δ	Binomial distribution vector
*	Element multiplication
x_{out}	FCB output

process. Each sample contains a DSL sequence of length 48 and a predicted word, and an image in PNG format.

3.1. Training. Due to the limited computing power of the experimental computer, only the word embedding matrix and the parameters of the prediction model are trained, and the parameters in the visual model do not participate in the training. During the training process, the batch size is set to 512, the iteration period is set to 200, the learning rate is set to 0.00001, the Adam gradient descent algorithm [32] is used to update the parameters of the model, and equations (6) and (7) are used to evaluate the model loss. The accuracy and loss curves of the model during the training phase are shown in Figure 7.

The total parameters of RCM are 4,942,630 (parameters of language model and prediction model), which is about 1/20 of the total number of pix2code model parameters [16]. The training runs on the author's desktop computer (Ubuntu18, AMD® Ryzen 5 1400 quad-core processor × 8, GeForce GTX 1660), which takes a total of 29 minutes (language model takes 8 minutes, prediction model takes 21 minutes), the highest accuracy rate is 97.685% and the minimum loss is 0.04805.

3.2. Test for One-Word Prediction and Codes Generation. Using the trained RCM to make a one-word prediction on the test set, the accuracy rate is 96.493%, and the loss is 0.08356. As its multiclass microaverage ROC curve is shown in Figure 8, its AUC value is 0.99984, so the classification effect of the model is quite ideal.

In order to test the ability of RCM on codes generation, Web UI images in the test set are input into the RCM to generate the code sequence (using the greedy search algorithm). Finally, the average error rate is 8.89%. It should be noted that when the length of the generated sequence does not match the length of the real sequence, the length difference is also included in the error count. The prediction error rate of RCM is 12.14% which is much lower than that of pix2code in the Web UI test set [16]. This experimental result further proves that RCM also has an advantage in generating code sequences while significantly improving the training speed.

A Web UI image in the test set (shown in Figure 9) (the original Web UI DSL code is shown in Figure 10) is selected as an input, and the RCM is used to generate a DSL code sequence (shown in Figure 11). After the DSL code is converted to HTML code, the resulting Web UI interface can be viewed through the browser (shown in Figure 12).

According to the model generation results of the above images, the DSL code sequence and the HTML code sequence generated by RCM using Web UI images are quite accurate, but there are also cases that the colors of some

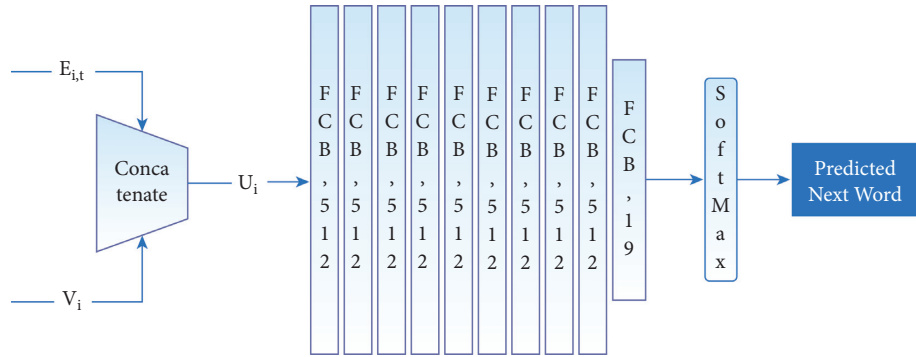
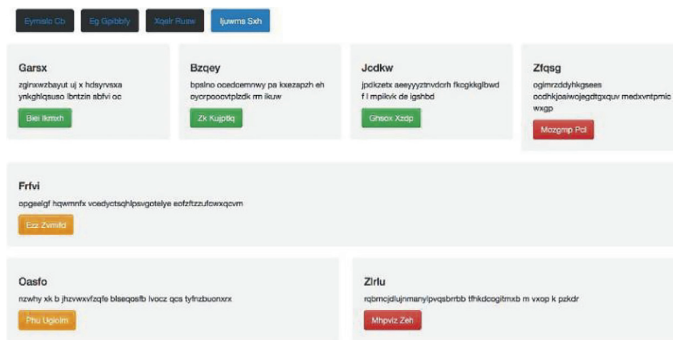


FIGURE 5: Schematic diagram of the prediction model.



```

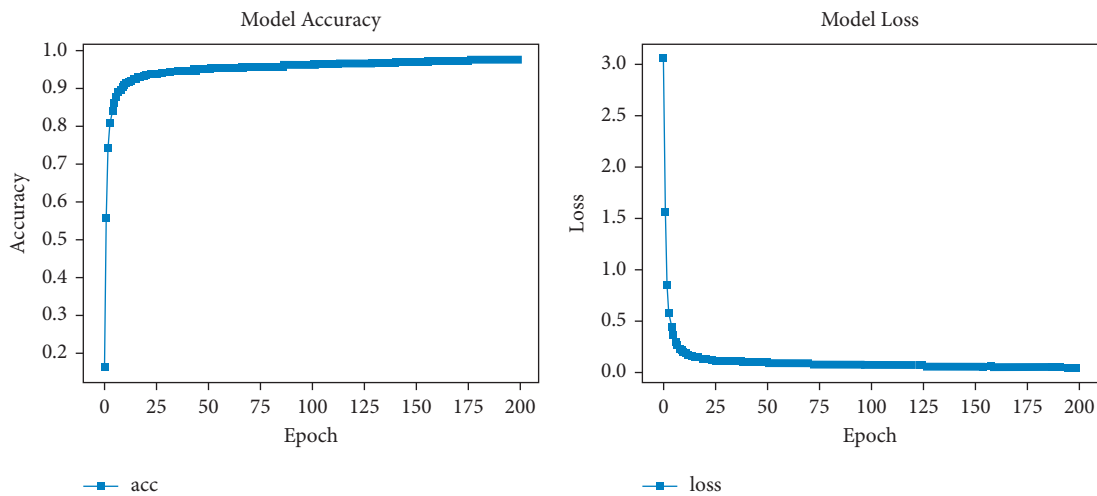
header {btn-inactive, btn-inactive,
btn-inactive, btn-active}
row {
  quadruple {small-title, text, btn-green
}
  quadruple {small-title, text, btn-green
}
  quadruple {small-title, text, btn-green
}
  quadruple {small-title, text, btn-red
}
}
row {
  single {small-title, text, btn-orange
}
}
row {
  double {small-title, text, btn-orange
}
}
double {small-title, text, btn-red
}

```

(a)

(b)

FIGURE 6: (a) Images and (b) DSL sequence of the Web UI instance in the pix2code dataset [16].



(a)

(b)

FIGURE 7: (a) The accuracy curve and (b) loss curve of the RCM.

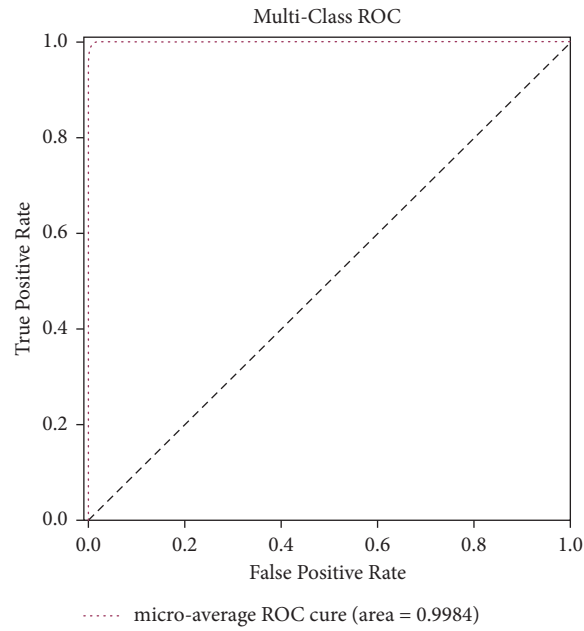


FIGURE 8: RCM microaverage ROC curve for word prediction on the test set.

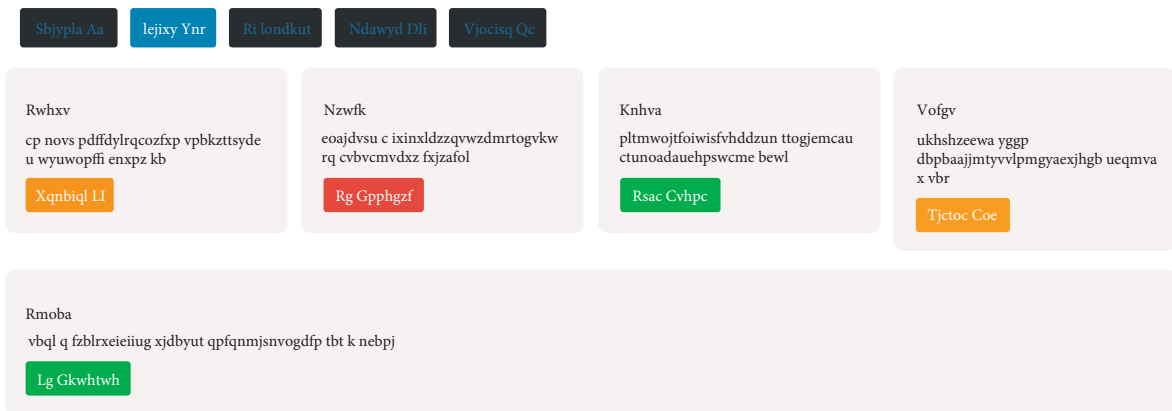


FIGURE 9: Original Web UI image.

```

header {
  btn-inactive , btn-active, btn-inactive, btn-inactive, btn-inactive
}
row {
  quadruple {
    small-title, text, btn-orange
  }
  quadruple {
    small-title, text, btn-red
  }
  quadruple {
    small-title, text, btn-green
  }
  quadruple {
    small-title, text, btn-orange
  }
}
row {
  single {
    small-title, text, btn-green
  }
}

```

FIGURE 10: Screenshot of the original DSL code.

```

header{
btn-inactive ,btn-active, btn-inactive,btn-inactive,btn-inactive
}
row {
quadruple {
small-title, text, btn-orange
}
quadruple {
small-title, text, btn-orange
}
quadruple {
small-title, text, btn-green
}
quadruple {
small-title, text, btn-orange
}
}
row {
single {
small-title, text, btn-red
}
}
}

```

FIGURE 11: Screenshot of the DSL code generated by RCM.



FIGURE 12: Web UI interface generated by RCM.

controls are inconsistent. In addition, it should be noted that the texts for controls such as buttons and DIV layers are not included in the DSL dictionary, they are randomly generated by the program.

4. Conclusion

With the continuous development of deep learning and especially the outstanding performance of CNN networks in the field of image recognition, it becomes possible to apply the model of the encoder-decoder structure to convert the graphical user interface into corresponding code sequences. Web user interface is usually described by HTML (hypertext marked language) and the basic structure of the decoder is RNN, LSTM, GRU, or other recurrent neural networks. However, this kind of decoder is with long training time, so it increases the time complexity and space complexity of training and prediction. The HTML language is a typically structured language to describe the Web UI, but it is hard to express the timing characteristics of the word sequence and define a complex logical function in HTML language. In

order to solve the above problems, a fast end-to-end model is introduced to generate Web UI code. The model can not only learn the word embedding matrix of Web UI code but also automatically generate code sequences based on Web UI images.

This model greatly improves the training speed under the premise of ensuring higher prediction accuracy and a lower generation error rate. A word embedding matrix is constructed to represent each DSL word, which can express the relationship between DSL words more abundantly than using one-hot vectors. At the same time, the initialization process of the word embedding matrix also shows that the code sequence of the Web UI is more structure-oriented rather than sequential. Therefore, the RNN, LSTM, BiLSTM networks commonly used in the NLP field are not used in the prediction model, but the FC network is adopted to promote the training speed of the prediction model.

The visual model is built on the basis of the pretrained InceptionV3 model, which not only decreases the complexity of the entire model but also greatly reduces the search space of the parameters. The prediction model is built with

FCB as the basic unit and can use both the context feature vector and the image feature vector to make predictions. It ensures not only a relatively high prediction accuracy but also a low generation error rate. Above all, the training speed is also greatly improved.

Experimental results show that the model has higher generation accuracy on the public Web UI data set, and can also improve the training speed.

In the follow-up work, the real HTML web page code and its image would be obtained from the Internet with the help of crawler technology, and the word embedding matrix in RCM would be redesigned so that it can handle HTML and CSS codes more effectively.

Data Availability

The data used to support the findings of this study are included within the article.

Conflicts of Interest

The authors declare that they have no conflicts of interest.

Acknowledgments

This research was funded by the Hebei IoT Monitoring Engineering Technology Research Center (No.3142018055), the Key Research Program of Hebei Province (No.19270318D), Langfang Science and Technology Research and Development Plan Project (no. 2018011041), and the Self-selected Project of North China Institute of Science and Technology (no. HZXKT2020012).

References

- [1] A. L. Gaunt, M. Brockschmidt, and R. Singh, "TerpreT: a probabilistic programming language for program induction," 2016, <https://arxiv.org/abs/1612.00817>.
- [2] A. Kalyan, A. Mohta, and O. Polozov, "Neural-guided deductive search for real-time program synthesis from examples," 2018, <https://arxiv.org/abs/1804.01186>.
- [3] R. Bunel, A. Desmaison, and P. Kohli, "Adaptive neural compilation," 2016, <https://arxiv.org/abs/1605.07969>.
- [4] M. Balog, A. L. Gaunt, and M. Brockschmidt, "DeepCoder: learning to write programs," 2016, <https://arxiv.org/abs/1611.01989>.
- [5] A. Solar-Lezama, "The sketching approach to program synthesis," in *Proceedings of the Asian Symposium on Programming Languages & Systems*, Seoul, Korea, December 2009.
- [6] K. Ellis, D. Ritchie, and A. Solar-Lezama, "Learning to infer graphics programs from hand-drawn images," 2017, <https://arxiv.org/abs/1707.09627>.
- [7] S. Riedel, M. Bošnjak, and T. Rocktäschel, "Programming with a differentiable forth interpreter," 2016, <https://arxiv.org/abs/1605.06640>.
- [8] I. Sutskever, O. Vinyals, and Q. V. Le, "Sequence to sequence learning with neural networks," in *Proceedings of the 27th International Conference on Neural Information Processing Systems-Volume 2*, pp. 3104–3112, MIT Press, Montreal, Canada, December 2014.
- [9] K. Cho, B. V. Merriënboer, and C. Gulcehre, "Learning phrase representations using RNN encoder-decoder for statistical machine translation," *Computer Science*, vol. 3, 2014.
- [10] A. Karpathy and L. Fei-Fei, "Deep visual-semantic alignments for generating image descriptions," *IEEE Transactions on Pattern Analysis & Machine Intelligence*, pp. 664–676, 2016.
- [11] J. Mao, W. Xu, and Y. Yang, "Deep captioning with multimodal recurrent neural networks (M-RNN)," 2014, <https://arxiv.org/abs/1412.6632>.
- [12] O. Vinyals, A. Toshev, and S. Bengio, "Show and tell: lessons learned from the 2015 MSCOCO image captioning challenge," *IEEE Transactions on Pattern Analysis and Machine Intelligence*, vol. 39, pp. 652–663, 2016.
- [13] X. Chen and C. L. Zitnick, *Learning a Recurrent Visual Representation for Image Caption Generation*, IEEE, Piscataway, NJ, USA, 2014.
- [14] S. Katiyar and S. K. Borgohain, "Comparative evaluation of cnn architectures for image caption generation," 2021, <https://arxiv.org/abs/2102.11506>.
- [15] J. Wu, J. B. Tenenbaum, and P. Kohli, "Neural scene rendering," in *Proceedings of the IEEE Conference on Computer Vision & Pattern Recognition*, Honolulu, HI, USA, July 2017.
- [16] T. Beltramelli, "pix2code: generating code from a graphical user interface screenshot," in *Proceedings of the ACM SIGCHI Symposium on Engineering Interactive Computing Systems*, Duisburg, Germany, June 2017.
- [17] Z. Zhu, Z. Xue, and Z. Yuan, "Automatic graphics program generation using attention-based hierarchical decoder," 2019, <https://arxiv.org/abs/1810.11536>.
- [18] Bengio and D. Yoshua, "A neural probabilistic language model," *Journal of Machine Learning Research*, vol. 3, 2003.
- [19] S. Hochreiter and J. Schmidhuber, "Long short-term memory," *Neural Computation*, vol. 9, no. 8, pp. 1735–1780, 1997.
- [20] H. Zhang, L. Meng, and X. Wei, "1D-convolutional capsule network for hyperspectral image classification," 2019, <https://arxiv.org/abs/1903.09834>.
- [21] Z. Zirui and L. Yunqing, "Chinese word segmentation based on bi-directional LSTM-CRF Model," *Journal of Changchun University of Science and Technology(Natural Science Edition)*, vol. 1, 2017.
- [22] P. Sermanet, D. Eigen, and X. Zhang, "OverFeat: integrated recognition, localization and detection using convolutional networks," 2013, <https://arxiv.org/abs/1312.6229>.
- [23] Krizhevsky, Alex, and Sutskever, "ImageNet classification with Deep convolutional neural networks," *Communications of the ACM*, vol. 60, 2017.
- [24] L. Fei-Fei, Karpathy, and Andrej, "Deep visual-semantic alignments for generating image descriptions," *IEEE Transactions on Pattern Analysis and Machine Intelligence*, vol. 2, 2017.
- [25] R. Shetty, M. Rohrbach, and L. A. Hendricks, "Speaking the same language: matching machine to human captions by adversarial training," in *Proceedings of the 2017 IEEE International Conference on Computer Vision (ICCV)*, Venice, Italy, October 2017.
- [26] K. Xu, J. Ba, and R. Kiros, "Show, attend and tell: neural image caption generation with visual attention," *Computer Science*, vol. 3, pp. 2048–2057, 2015.
- [27] K. Simonyan and A. Zisserman, "Very deep convolutional networks for large-scale image recognition," 2014, <https://arxiv.org/abs/1409.1556>.
- [28] O. Vinyals, A. Toshev, and S. Bengio, "Show and tell: a neural image caption generator," in *Proceedings of the 2015 IEEE*

- Conference on Computer Vision and Pattern Recognition (CVPR)*, Boston, MA, USA, June 2015.
- [29] C. Szegedy, V. Vanhoucke, and S. Ioffe, “Rethinking the inception architecture for computer vision,” 2015, <https://arxiv.org/abs/1512.00567>.
 - [30] S. Ioffe and C. Szegedy, “Batch normalization: accelerating deep network training by reducing internal covariate shift,” 2015, <https://arxiv.org/abs/1502.03167>.
 - [31] N. Srivastava, G. Hinton, and A. Krizhevsky, “Dropout: a simple way to prevent neural networks from overfitting,” *Journal of Machine Learning Research*, vol. 15, pp. 1929–1958, 2014.
 - [32] D. P. Kingma and J. Ba, “Adam: a method for stochastic optimization,” *Computer Science*, vol. 9, 2014.

Research Article

A Blockchain-Based Key-Revocation Access Control for Open Banking

Khaled Riad ^{1,2} and **Mohamed Elhoseny**^{3,4}

¹Computer Science Department, College of Computer Sciences & Information Technology, King Faisal University, Al-Ahsa 31982, Saudi Arabia

²Mathematics Department, Faculty of Science, Zagazig University, Zagazig 44519, Egypt

³College of Computing and Informatics, University of Sharjah, Sharjah 27272, UAE

⁴Faculty of Computers and Information, Mansoura University, Mansoura 35516, Egypt

Correspondence should be addressed to Khaled Riad; khaled.riad@science.zu.edu.eg

Received 9 November 2021; Accepted 30 December 2021; Published 31 January 2022

Academic Editor: Nima Jafari Navimipour

Copyright © 2022 Khaled Riad and Mohamed Elhoseny. This is an open access article distributed under the Creative Commons Attribution License, which permits unrestricted use, distribution, and reproduction in any medium, provided the original work is properly cited.

Open banking allows banks and financial sectors to easily access the customers' financial data which is revolutionizing. It also provides the customers with excellent cloud access to various providers' wide range of financial services. The storage of such sensitive services and data on cloud servers is a double-edged sword. It can ease and support fine-grained access to such services/data anywhere and anytime, supporting the open banking system. But, on the other hand, data privacy and secrecy are a challenge. Thus, efficient access control should exist for open banking's services and data to protect cloud-hosted financial sensitive data from unauthorized customers. This paper proposes a new access control scheme that employs blockchain for the key-revocation process. We implement the smart contract's functions on the Ethereum platform and test the contract's code on the Kovan Testnet before deploying it to the Mainnet. Although the customer is authenticated to open banking, his key/s can be revoked according to the status response of the bank branch. Thus, his access to financial services and data is denied. We did comprehensive experiments for the revocation status response time, data exchanged until receiving the revocation status, and the time spent updating the policy. Also, we compared the results of our proposed scheme with two well-known methods—Certificate Revocation List (CRL) and Online Certificate Status Protocol (OCSP). The experimental results show that our proposed scheme (BKR-AC) has a faster response time than Certificate Revocation List (CRL) and Online Certificate Status Protocol (OCSP) in case of nonrevoked keys/certificates and a slower response time in case of revoked keys to avoid nonrevoking a revoked key. But the data exchanged is an average for BKR-AC between CRL and OCSP, which is still a tiny amount and accepted. The security analysis proved that our scheme is secure against some well-known attacks on open banking systems. In addition, it is also secured against the chosen-text attack by employing the challenge-response authentication mechanism.

1. Introduction

Nowadays, most of the world and even some superpowers live in tough economic times. But, at the same time, the thing that cannot be neglected or ignored in any way is the online banking and finance sector. In such harsh economic conditions, the banks and financial institutions are under even greater scrutiny than ever. The key considerations of the banks and financial institutions are physical security and access control. Moreover, the open banking revolution allows banks

and financial institutions to easily exchange the customers' financial data through Application Programming Interfaces (APIs). The main goal behind open banking is to improve the current infrastructure and introduce new features, which down the communication costs among different institutions. Access control can be quite challenging when a bank or financial institution has numerous branches and facilities spread over a large geographical area. Therefore, any access control deployed in the banking and finance sector must provide complete value for money and return on investment.

Authentication is the starting point for any successful access control. Authentication verifies the customer's identity and enables authorization. The authorization is the allowed permissions for a customer after the authentication process. For example, the bank's customer can use an identity (e.g., a username name) to log in to that online banking service. Still, the bank's authorization policy must ensure that this client is only authorized to access their own account's information/services. The bank and financial institution implicitly create and maintain the authorization policies. It is unbelievable that these authorization policies are kept unchanged forever. Access control is the method used to update and enforce such policies.

Since most of the banking and finance sector's services and data are currently hosted on the cloud, there should be a flexible, scalable, intelligent access control to protect sensitive financial data. Moreover, the user may be authenticated to the online banking but has a revoked key/s. Therefore, this user will not be able to access financial services. Financial institutions can use solutions that offer built-in security mechanisms, including encryption, two-factor authentication, and authorization. However, access controls are more critical to protecting customers and corporate information than facilities and property. Correct configuration of access privileges is crucial for protecting information from unauthorized access and protecting computer systems from abuse. Thus, we are proposing a new blockchain-based access control scheme that can revoke the customers' key/s after the authentication to online banking.

The process of revoking a previously issued key is similar to that of revoking a previously issued certificate before its expatriation. This revocation process is critical to any public key infrastructure [1]. The secure website could be vulnerable to attack if a new one replaces the certificate. Generally, a replaced certificate will remain useable by any attacker until reaching the expiry time. Thus, the replaced certificates must be revoked. The same applies to the keys. There are multiple certificate revocation schemes, for example, Online Certificate Status Protocol (OCSP) [2, 3], Certificate Revocation Tree (CRT) [4], and Certificate Revocation List (CRL) [5]. Since blockchain is efficient in introducing a decentralized certificate revocation management [6], we employed it to introduce an efficient key-revocation access control for open banking.

1.1. Motivation. The banks and financial institutions must not depend only on the naive online banking authentication system. Also, the key/s generated for an authenticated customer must not be working until their expiry date. Still, they must frequently pass under a revocation process to reevaluate their validity to be authorized for the open banking services. To the best of our knowledge in the practical portion, TDSi company (<https://www.tdsi.co.uk/>) is one of the UK's leading manufacturers of integrated access control systems, offering an extensive range of readers, controllers, and software systems. TDSi provides a suite of solutions that meet the banking and finance industry's many demanding access control needs. On the other hand, TDSi is mainly based on EXgrade PRO

software, which provides centralized control of location security using an IP connection to each branch. This is sufficient to raise the alarm for problems that are likely to occur for each branch's central authority managing the access control. Thus, EXgrade PRO is not suitable for protecting sensitive cloud-hosted financial data.

There are numerous branches, facilities, and thus customers spreading worldwide in the banking and finance sector. Thus, there is an urgent need for access control that

- (i) Avoids using the central authority for managing the access control since it can be a central point of bottleneck and attack
- (ii) Supports flexibility and integration with the systems in each branch
- (iii) Benefits from the huge capabilities of blockchain for managing the keys assigned to customers during the session
- (iv) Secure open banking from some well-known attacks such as *Account Aggregation*, *Personal Finance Management*, and *Instant Credit Risk*

The abovementioned issues are behind our motivation to propose a blockchain-based key-revocation access control scheme for open banking.

1.2. Main Contributions. To the best of our knowledge, the blockchain is introducing a promising technology for efficient decentralized security solutions [7]. The main contributions of this paper are as follows:

- (i) We employed blockchain to propose an efficient decentralized key-revocation access control scheme. The proposed scheme is compatible with the current open banking systems. It can facilitate and secure access to cloud-hosted sensitive financial data and only authorize the nonrevoked customers to benefit from the open banking services such as *Account Aggregation*, *Personal Finance Management*, *Instant Credit Risk*, *Subscription Management*, and *Opening New Accounts*.
- (ii) We implemented the contract's functions on the Ethereum platform. Also, we tested the contract code on the Kovan Testnet before deploying it to the Mainnet. Moreover, we implemented the cloud storage based on our private cloud environment built using OpenStack.
- (iii) We proved the security of BKR-AC against some well-known attacks such as *Insecure Ids*, *Forced Browsing Past Access Control Checks*, *Path Traversal*, *Client-Side Caching*, and *chosen-text attacks*.
- (iv) We evaluated the proposed scheme comprehensively based on time, data exchanged, and policy update time. Moreover, we compared the proposed scheme with two well-known schemes (Certificate Revocation List (CRL) [8, 9] and Online Certificate Status Protocol (OCSP) [3]) in terms of the status response time and the exchanged data.

Finally, no customer can be authorized forever in our model, but its authorization is continuously evaluated, and the assigned key/s can be revoked at any stage.

2. Proposed Workflow

Our solution workflow indicated in Figure 1 introduces five basic entities (user/browser, authentication servers, branch policy, synchronized peer network, synchronized chain of blocks, and cloud storage) and two helpful entities (Bank Web Server and Fraud Detection). Each of these entities has a significant role in the proposed model:

- (i) *User/Browser*. It is a great number of bank customers that are requesting access to cloud-hosted financial data throughout the online banking system from various different devices. Each customer willing to access the online banking is assigned a Customer ID (CID). This CID is given by the Bank Web Server and never changes for that customer.
- (ii) *Branch Policy*. It is a multiprocess authority in charge of deciding the access control policies by each branch. This authority is identified by Branch ID (BID).
- (iii) *Authentication Servers*. In this part, the customer identified by CID provides his username and password and any more credentials to be successfully authenticated. The authentication servers are a *dispatch server*, *database manager server*, and a set of *matching servers*. This step is fulfilled with the help of the Fraud Detection server and the branch policy entity.
- (iv) *Synchronized Peer Network*. It is the Ethereum platform using a programmed contract.
- (v) *Synchronized Block of Chains*. It is a set of mined blocks that are linked using hashes. Each block keeps a hash of the previous block in the synchronized chain.
- (vi) *Cloud Storage*. It is a set of cloud storage servers with huge capabilities to be able to handle numerous data storage and access requests. The cloud storage servers have no right to access control.

The basic steps for an honest customer requesting access to the cloud-hosted financial data are as follows. The customer can request access through the online banking system. First, the Bank Web Server will assign the customer (subject) a unique CID. After that, the authentication servers will either authenticate the CID or not based on the branch policy, Fraud Detection entities, the username, password, and any other credentials provided by the customer. Next, the blockchain contract's functions will be initialized for the authenticated customer identified by CID. Then, a mined block will be added to the synchronized chain of blocks. After that, the customer requesting to be authorized will be done through the synchronized peer network. Finally, only authorized customers can access the cloud-hosted data.

2.1. Expected Vulnerabilities. In general, open banking must have a documented access control policy. If this documentation does not exist, open banking is likely vulnerable. There are some specific access control issues, as follows:

- (i) *Insecure Ids*. If an attacker can guess a customer's Id, and there is no adequate validation scheme to ensure that the current customer is not authorized, then, the attacker can access the private information of the guessed Id. Thus, the web applications for open banking should not rely on Id's secrecy for protection.
- (ii) *Forced Browsing Past Access Control Checks*. Open banking must require customers to pass certain checks before being granted access to the open banking URL. These checks must not be by-passable.
- (iii) *Path Traversal*. This attack tries to access the normally not directly accessible files by providing relative path information as part of a request.
- (iv) *Client-Side Caching*. It is the process of accessing the open banking website from shared computers. The browsers frequently cache web pages that attackers can access. The open banking developers should use multiple mechanisms to ensure that customers' browsers do not cash their pages.

Therefore, our scheme must be secure against the attacks mentioned above by ensuring the following:

- (i) Validating the correctness of the access control implementation by executing a detailed code review
- (ii) Performing penetration testing to determine whether there are problems in the access control scheme
- (iii) Extensively testing the access control scheme to ensure there is now a way to bypass

3. Blockchain-Based Key-Revocation Access Control

Our blockchain-based key-revocation access control (BKR-AC) scheme is based on blockchain for building the key-revocation list (KRL) to secure the banking and finance cloud-hosted data. This scheme formally defines the functional keys to achieve the desired features. The functional key consists of all the permissions/services associated with a key during the running session. The customer can be assigned one or more function keys and thereby be given all of the permissions/services related to the key. It should be mentioned that the key-revocation process is accomplished using the contract's functions.

The system model shown in Figure 2 integrates the proposed BKR-AC scheme with the bank branch authentication system. According to Definition 1, it is composed of seven major entities.

Definition 1. A blockchain-based key-revocation access control (BKR-AC) scheme with dynamic revocation based on the key-revocation list requires the customer to be

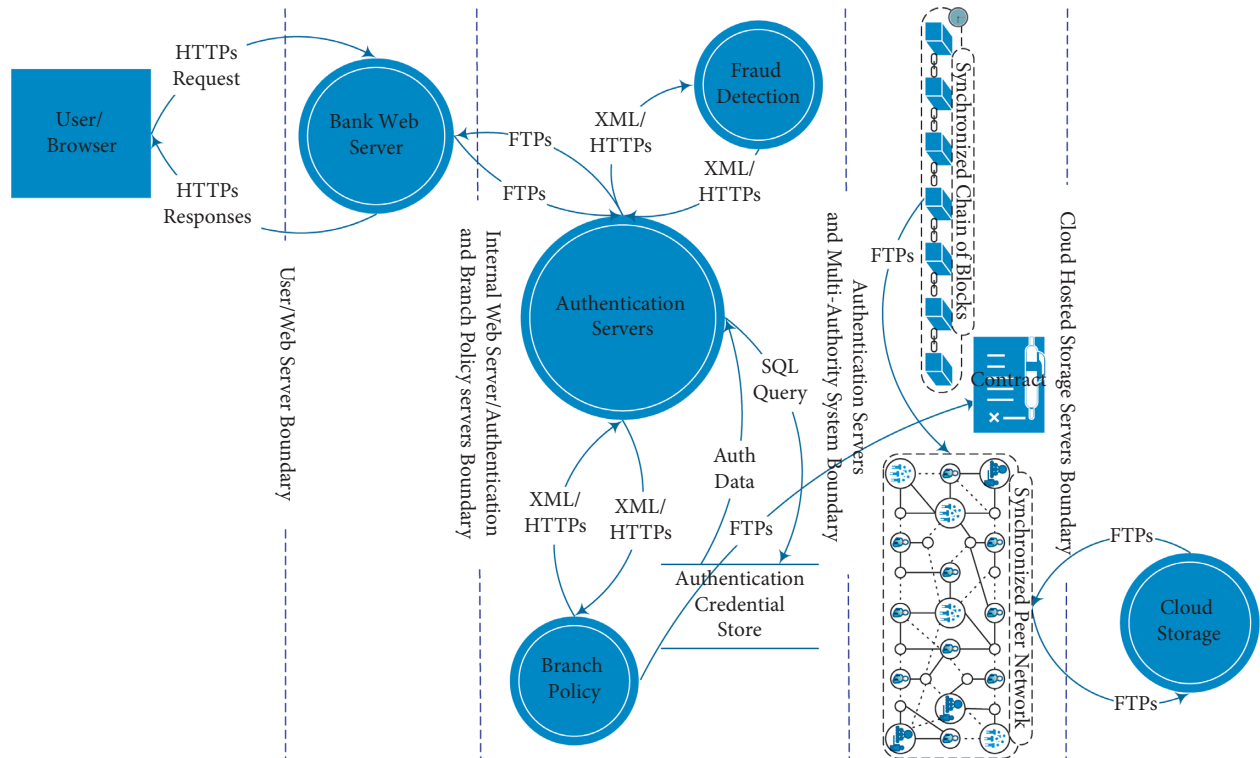


FIGURE 1: The detailed workflow for our solution to effectively manage the banking customers' access control for the cloud-hosted data.

assigned a nonrevoked functional key to gain the permissions/services associated with the key during the running session. To be a nonrevoked customer, he must be successfully authenticated by the bank's authentication servers and create, deploy, and execute the contract's functions. In addition, the customer can only access the requested cloud-hosted data if he has a nonrevoked functional key based on the latest key-revocation list. The scheme comprises six entities: users requesting access, branch policy, authentication servers, contract functions, a synchronized chain of blocks, a synchronized peer network, and cloud storage.

3.1. Users Requesting Access. Since open banking is revolutionizing the use cases offered by banks and financial institutions, it introduces diverse digital offers. Also, the number of customers is rapidly increasing. Moreover, the customers can use different interfaces to request access to their financial data. Thus, the banks and financial institutions should pay attention to digitizing the customers' experience. In our proposed system, each customer is identified by a unique CID, which represents the customer's identity. The bank branch is responsible for assigning each customer a CID only for the first time joining the open banking system.

3.2. Branch Policy. Each bank branch identified by a unique BID inherits the main bank branch's main policies. Then, each BID assigns these policies to its customers. The most popular and common open banking use cases policies are as follows:

- (i) *Account Aggregation.* It is mainly offered by several financial services companies (from different providers). It enables the customers to use an API getting a detailed overview of their accounts.
- (ii) *Personal Finance Management (PFM).* It is the process of giving the customers the tools required for providing a complete overview of their financial situation, for example, showing how much money the customer has left to spend this month.
- (iii) *Instant Credit Risk.* It is the process of indicating the likelihood of accepting a loan for a customer before applying. This process is based on using comparison sites for loans and credit cards. Thus, it allows the "buy now pay later" functionalities.
- (iv) *Subscription Management.* It detects all the recurring payments from the customer and shows them in one interface. It can be a subscription for a service, a membership, monthly bills, and so on.
- (v) *Opening New Accounts.* To open a new account, the banks must get as much information as possible about the customer before authorizing a new account opening. Open banking grants the bank data flow for the customer requesting a new account.

3.3. Authentication Servers. Mainly the authentication server is a software or an application that enables authentication of a subject (entity) attempting to access a specific network. In our scheme, the authentication servers reside in multiple dedicated computers (DB Manager Server, multiple

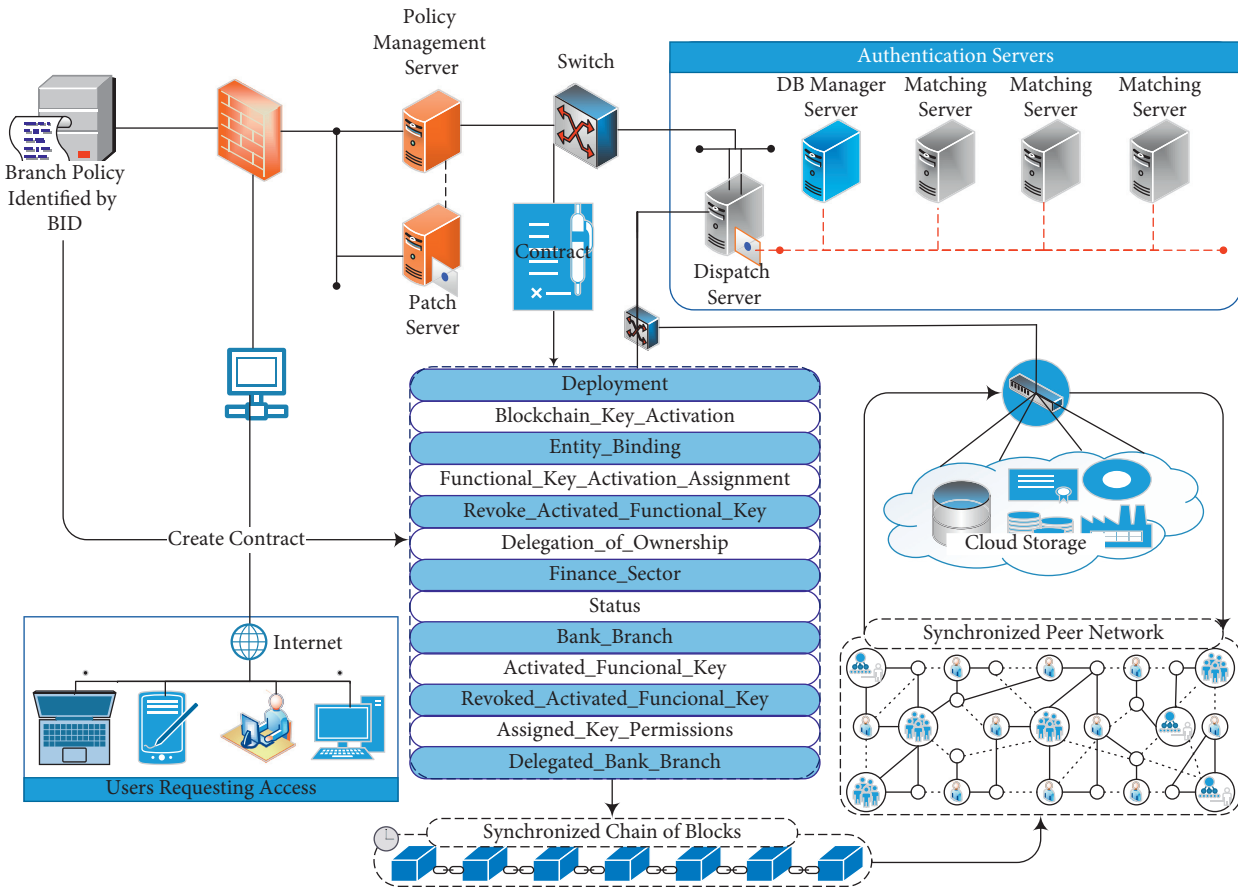


FIGURE 2: The proposed BKR-AC scheme is integrated with the bank branch authentication system. The scheme is composed of six entities: users requesting access, branch policy, authentication servers, contract functions, a synchronized chain of blocks, a synchronized peer network, and cloud storage.

matching servers, and a dispatch server). The authentication process determines whether some subject is who or what they proclaim themselves. The requested attributes from a customer accessing the authentication server are the username, password, security token, and One Time Password (OTP).

We have two scenarios (interactive and noninteractive) for the interaction of the customer identified by CID with the authentication servers based on *Hashcash*. Each of the two scenarios computes the cost of adding a cryptographic puzzle (token). First, the token proves that the customer has successfully done the predefined cryptographic puzzle. Then, the token is verified by the authentication servers.

3.3.1. Customer and Authentication Server Interactive Scenario. In this scenario, a specific authentication server sends a token to the customer. The customer has to solve this token and send its evaluated value to the authentication server. The customer successfully solves the token if the Evaluated Challenge Value (ECV) equals the predefined Challenge Value (CV) by the authentication server, as illustrated in Algorithm 1. The algorithm takes as input the Requested Services (RS) and the random bit-string (Rbs). It should be mentioned that \parallel is the concatenation between two bit-strings.

3.3.2. Customer and Authentication Server Noninteractive Scenario. There is neither a specific authentication server nor a server challenge value in this scenario. However, this scenario has been used in the proof of work consensus algorithm in Ethereum, as shown in Algorithm 2.

3.4. Contract's Functions. This section introduces a detailed description of the contract's functions. We are considering the parameters mentioned in Table 1 for these functions:

- (i) **Deployment():** it deploys the contract on the Ethereum network and establishes its account. We send an Ethereum transaction containing the code of the compiled smart contract without specifying any recipients. The contract has been compiled first to assure that the web apps and the Ethereum Virtual Machine (EVM) can understand it. The compilation process will produce the Application Binary Interface (ABI). The apps will use ABI to understand the contract and call its functions.
- (ii) **Blockchain_Key_Activation(B_Name, BID):** it is used to assign the authority (organization) responsible for assigning, revoking, updating, and storing the functional keys. In our scheme, the

Input: (RS) and (Rbs)

Output: True/False

- (1) The authentication server computes $CV = Challenge(RS, Lb)$ // Lb is the number of left bits in the random bit-string Rbs
- (2) The authentication server sends CV to the customer CID
- (3) CID searches for $Rbs \ni Hash(RS||CV||Rbs) \equiv_{Lb} 0^k$ // k is the number of authentication servers
- (4) **if** $(Hash(RS||CV||Rbs) \equiv_{Lb} 0^k) = True$ **then**
- (5) The authentication Server \leftarrow CID sends RS, Rbs
- (6) The authentication server calculates $ECV = Hash(RS||CV||Rbs) \equiv_{Lb} 0^k$ /* ECV is *True* if $H(RS||Rbs)$ starts with Lb bits filled with zero */
- (7) **if** $ECV = True$ **then**
- (8) Return ECV
- (9) **else**
- (10) Return *False*

ALGORITHM 1: Interactive scenario.

Input: (RS) and (Rbs)

Output: True/False

- (1) The CID calculates $Rbs \ni Hash(RS||Rbs) \equiv_{Lb} 0^k$
- (2) The CID publishes RS and Rbs
- (3) All the authentication servers calculate $ECV = Hash(RS||Rbs) \equiv_{Lb} 0^k$ /* ECV is *True* if $H(RS||Rbs)$ starts with Lb bits filled with zero */
- (4) **if** $ECV = True$ **then**
- (5) Return ECV
- (6) **else**
- (7) Return *False*

ALGORITHM 2: Noninteractive Scenario.

TABLE 1: List of considered parameters.

B_Name	Name of the functional key assigning branch
BID	Identity of the functional key assigning branch
CID	Customer's identity
SVT_Session	Functional key start validation time
EVT_Session	Functional key end validation time
RR_Code	Revocation reason code of a revoking a functional key before the EVT_Session

branch policy identified by BID is the functional key assigning authority.

- (iii) $Entity_Binding(BID, CID)$: this function verifies that the requesting customer which is identified by CID owns an external account address on Ethereum.
- (iv) $Functional_Key_Activation_Assignment(BID, Key, Permissions, SVT_Session, EVT_Session)$: it assigns a functional key to a customer identified by CID and verified by the $Entity_Binding(BID, CID)$ function.
- (v) $Revoke_Activated_Functional_Key(BID, RR_Code)$: the assigning branch BID revokes an assigned functional key before reaching the EVT_Session for a reason identified by RR_Code.
- (vi) $Delegation_of_Ownership()$: it returns the CID of a delegated customer.

(vii) $Bank_Branch()$: it returns the name (B_Name) of the functional key assigning branch.

- (viii) $Activated_Functional_Key(CID)$: it returns a list of the active functional keys for a specific customer (CID).
- (ix) $Revoked_Activated_Functional_Keys(CID)$: it returns a list of the revoked functional keys for a specific customer (CID).
- (x) $Assigned_Key_Permissions/Services()$: it returns a list of permissions/services for a specific key.
- (xi) $Delegated_Bank_Branch()$: it returns the BID of a delegated branch.

3.5. *Synchronized Chain of Blocks*. Each block keeps a hash of the previous block in the synchronized chain. Since the hash is cryptographically derived from the block data, the hash

binds the blocks together. If the attacker changes any previous block, it will invalidate all subsequent blocks because all subsequent hashes will change. All customer transactions are grouped into blocks to ensure that all customers maintain a synchronized state and agree on the exact history of the transactions. The blocks are arranged strictly as each new block references its original block, and the transactions within the blocks are also organized. Each block consists of

- (i) timestamp: it is the mining time of the block
- (ii) blockNumber: it is the number of the block within the synchronized chain of blocks
- (iii) baseFeePerGas: it is the minimum fee for each gas required to add a new transaction in this block
- (iv) difficulty: it is the mining effort for that block
- (v) mixHash: it is a unique identifier for that block
- (vi) parentHash: it is the mixHash for the previous block in the synchronized chain of blocks
- (vii) transactions: it is the set of transactions included in that block
- (viii) stateRoot: it represents the entire state of the system
- (ix) nonce: it is a hash used to prove that the block has gone through a proof of work mechanism (anyone who wants to add new blocks to the chain must solve a difficult puzzle that requires a lot of computing power) by combining it with the mixHash

3.6. *Synchronized Peer Network.* We implemented our scheme's contract functions on the Ethereum platform using a programmed contract. Before deploying the contract code to the Mainnet (the primary public Ethereum production blockchain), we tested our contract code on the Kovan Testnet. The Kovan Testnet is a proof-of-authority Testnet for running Open Ethereum clients. It uses a small number of nodes to validate transactions and create new blocks—stacking their identity in the process.

3.6.1. *Key Generation in Ethereum.* The Ethereum public key PK is a point on an elliptic curve. It is generated using Algorithm 3. It consists of two numbers joined together. The numbers composing the Ethereum public key are produced by the multiplication of the *generator point* G with those for the private key k that is generated by one-way calculations. Thus, anyone having a private key can easily calculate the public key, but he cannot calculate the private key using the public key.

For example, consider that we have the following private key:

$$k = f8f9a2f43c8366ccb0871505030d7b27c0554d3cc79bcd f41b2805606451f318. \quad (1)$$

Thus, after calculating the public key $PK = (x, y) = k * G$, where the public key is represented as a point in the elliptic curve,

$$\begin{aligned} x &= 8e144cdef1034dea269874dd09df \\ &\quad b4bee6f3308c84785c82f103454693dae07f, \\ y &= 63b4c38c5e2b0d8528d7fa2f64d45d4a1ede8 \\ &\quad d9af14cdb9478d042f84c32dcd7. \end{aligned} \quad (2)$$

In Ethereum, the public key is represented by 65 bytes (130 hexadecimal characters). The Ethereum network uses the Keccak-256 cryptographic hash function to generate the Ethereum addresses.

3.7. *Ethereum Addresses.* The addresses in Ethereum are unique identifiers that are generated from the contracts or public keys based on the Keccak-256 cryptographic hash function. Thus, from the previous example, the public key is the concatenation of x and y .

$$\begin{aligned} PK &= 8e144cdef1034dea269874dd09df \\ &\quad b4bee6f3308c84785c82f103454693da \\ &\quad e07f63b4c38c5e2b0d8528d\dots \end{aligned} \quad (3)$$

Then, we use the Keccak-256 to find the hash of this public key:

$$\begin{aligned} \text{Keccak} - 256(PK) &= 6a5fc542ec614b5da5735268006 \\ &\quad d3c1e d826552a d17150473d3 \\ &\quad dcf1c086aa0f8. \end{aligned} \quad (4)$$

Then, we only keep the rightmost 20 bytes as our Ethereum address:

$$006d3c1ed826552ad17150473d3dcf1c086aa0f8. \quad (5)$$

It should be mentioned that most of the Ethereum addresses start with 0x, which indicates their hexadecimal encoding.

3.8. *Cloud Storage.* It is a private cloud environment built using OpenStack by employing three physical servers. The first server in our private cloud environment is the Controller Node, and the second one is the Neutron Node. Each Controller Node and the Neutron Node is 48 cores CPU, 128 GB RAM, and 5 TB disk. The third server in our private cloud environment is the Nova Compute Node, and its configuration is 24 cores CPU, 128 GB RAM, and 2 TB disk. Our scheme employs this private cloud environment to store the customers' information.

4. Security Analysis

Our scheme must be secure against the attacks mentioned in Section 2.1. This section introduces the detailed security analysis for our scheme's entities to prove the BKR-AC capabilities to defend against various attacks. The Ethereum network uses the Keccak-256 hash function.

4.1. *Hash Function.* The hash function plays an essential role in the security of our scheme and securing its identity over

Input: $(x^3 + ax + b - y^2) \% p$, where a, b are two constant coefficients
Input: A prime number $p \in \mathbb{Z}_p$ and an elliptic generation point G
Input: The order of subgroup n and a cofactor h
Output: Private k and public key PK
(1) Private key $k \leftarrow$ Choose a random number from $\{n-1, \dots, 3, 2, 1\}$
(2) Public key PK \leftarrow Compute $k \times G$
(3) Return private key k and public key PK

ALGORITHM 3: Key generation in Ethereum.

the Ethereum network. It builds the cost function as cryptographic puzzles.

Definition 2. A hash function $H(x)$ is computationally efficient for mapping a finite length bit-string x to output a fixed-length random bit-string Y . It has three cryptographic properties:

- (1) Preimage resistance: it is infeasible to find the input x' for a prespecified output y ; i.e., the result for finding any preimage x' (input) such that $H(x') = y$ is not known
- (2) 2nd-preimage resistance: it is computationally infeasible to find a 2nd-preimage $x' \neq x$ such that $H(x') = H(x)$
- (3) Collision resistance: it is computationally infeasible to find two inputs x, x' such that $H(x) = H(x')$

Therefore, if an attacker guesses a customer's Id, he will not get the same output of the hash function (2nd-preimage resistance). Thus, our scheme is secure against the *Insecure Id's attacks*. Also, if an attacker got the past access control checks (output of the hash function) for the previous browsing, he will not get the same input that produced the guessed past access control checks (preimage resistance). Thus, our BKR-AC is secure against the *Forced Browsing Past Access Control Checks*. Moreover, providing an approximate path will not generate an accurate hash result. Thus, our scheme is secure against the *Path Traversal*. Finally, the collision resistance property of the hash function prevents the *Client-Side Caching* because we could not find the same hash result for two different inputs (two customers' browsers).

4.2. Challenge-Response Authentication. For online banking, the authentication mechanism must be robust. Thus, we employed the signature-based challenge-response authentication as introduced in Algorithms 1 and 2. The verifier (bank branch) should have enough information to verify the validity of the public key contained in the customer's received certificate. Let r_{CID} and t_{CID} represent a random number and timestamp generated by CID. Let cert_{CID} be the public key certificate that contains CID's signature. Thus, we can generate the following authentication scenarios:

- (1) Unilateral authentication with timestamps:
CID \rightarrow BID: $\text{cert}_{CID}, t_{CID}, \text{BID}, S_{CID}(t_{CID}, \text{BID})$. (6)

Once received, BID verifies that the timestamp is acceptable; the received identifier BID is its own and checks that the signature over CID and BID is correct.

- (2) Unilateral authentication with random numbers:
CID \leftarrow BID: r_{BID} ,
CID \rightarrow BID: $\text{cert}_{CID}, r_{CID}, \text{BID}, S_{CID}(r_{CID}, r_{BID}, \text{BID})$. (7)

BID verifies that the clear-text identifier is its own, and using the cert_{CID} for CID, it verifies that the signature of CID is valid over the clear-text random number r_{CID} . Thus, the signed r_{CID} explicitly prevents chosen-text attacks.

- (3) Mutual authentication with random numbers:
CID \leftarrow BID: r_{BID} ,
CID \rightarrow BID: $\text{cert}_{CID}, r_{CID}, \text{BID}, S_{CID}(r_{CID}, r_{BID}, \text{BID})$,
CID \leftarrow BID: $\text{cert}_{BID}, \text{CID}, S_{BID}(r_{BID}, r_{CID}, \text{CID})$. (8)

CID verifies that the clear-text identifier is its own, and using the cert_{BID} for BID, it verifies that the signature of BID is valid over the clear-text random number r_{BID} . Thus, the signed r_{BID} explicitly prevents chosen-text attacks.

5. Results and Discussion

To effectively evaluate the performance of the proposed scheme, we investigated the performance in two directions (time and data analysis).

5.1. Time Analysis. We investigated the time analysis into two cases against the number of nonrevoked and revoked keys. Also, we analyzed the branch policy update time against the number of revoked keys. Moreover, we compared the status response time for our scheme with two well-known methods.

5.2. Status Response Time against the Number of Nonrevoked Keys. This part represents the time spent by the bank branch until giving a decision on the revocation status against the number of nonrevoked keys while considering four levels of

concurrent requests (100, 200, 300, and 400) at the same time to the bank branch, as shown in Figure 3.

The results show the following. (i) For the same number of concurrent requests, the average time for the status response time is increasing according to the number of nonrevoked keys, but the increase is not significant. It is about a 4.32 ms difference when increasing the number of nonrevoked keys from 4 to 60 while considering 400 concurrent requests. (ii) For the same number of nonrevoked keys, the average time is increasing according to the number of concurrent requests, but the increase is not significant. It is about a 2.98 ms difference when increasing the number of concurrent requests from 100 to 400 while considering 60 nonrevoked keys.

5.3. Status Response Time against the Number of Revoked Keys. This part represents the time spent by the bank branch until giving a decision on the revocation status against the number of revoked keys while considering four levels of concurrent requests (100, 200, 300, and 400) at the same time to the bank branch, as shown in Figure 4.

The results show the following. (i) For the same number of concurrent requests, the average time for the status response time is increasing according to the number of revoked keys. It is about a 49.67 ms difference when increasing the number of revoked keys from 4 to 60 while considering 400 concurrent requests. (ii) For the same number of revoked keys, the average time is increasing according to the number of concurrent requests. It is about a 24.36 ms difference when increasing the number of concurrent requests from 100 to 400 while considering 60 revoked keys.

5.4. Branch Policy Update Time against the Number of Revoked Keys. This part represents the time spent by the bank branch to update its policies against the number of revoked keys while considering four levels of concurrent requests (100, 200, 300, and 400) at the same time to the bank branch, as shown in Figure 5.

The results show the following. (i) For the same number of concurrent requests, the average time for the policy update is increasing according to the number of revoked keys. It is about a 2.5 ms difference when increasing the number of revoked keys from 4 to 60 while considering 400 concurrent requests. (ii) For the same number of revoked keys, the average time is increasing according to the number of concurrent requests. It is about a 1.58 ms difference when increasing the number of concurrent requests from 100 to 400 while considering 60 revoked keys.

5.5. Status Response Time Comparison with Two Well-Known Schemes. This comparison represents the status response time required to respond with the revocation status for our scheme (BKR-AC) and two well-known methods (CRL and OCSP) against the number of revoked and nonrevoked keys for BKR-AC and the number of revoked and nonrevoked certificates for both CRL and OCSP schemes. We conducted the measures at 400 concurrent requests, as shown in Figure 6.

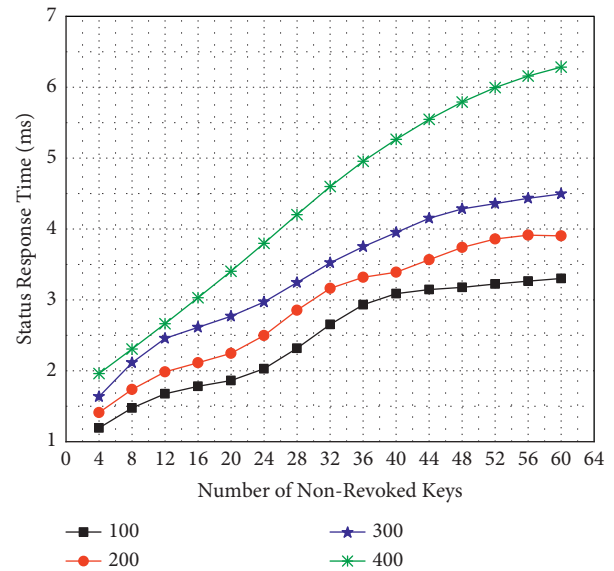


FIGURE 3: The status response time required to give a decision on the revocation status against the number of nonrevoked keys at four different levels of concurrent requests.

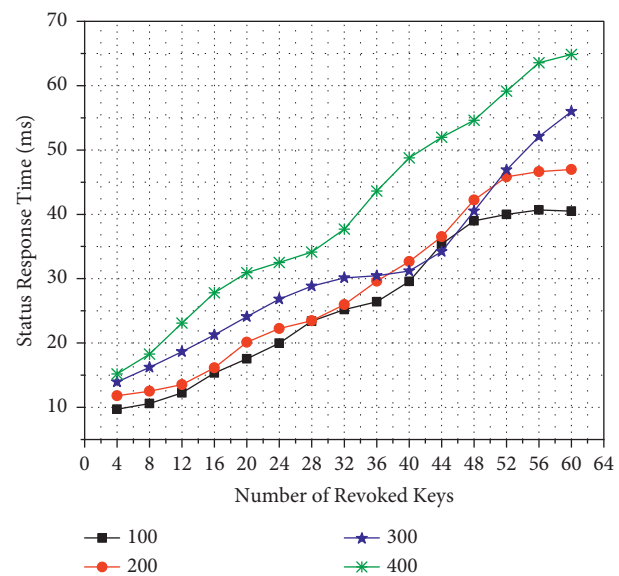


FIGURE 4: The status response time required to give a decision on the revocation status against the number of revoked keys at four different levels of concurrent requests.

The results show the following. (i) The time spent by BKR-AC in the case of nonrevoked keys is smaller than that for CRL and OCSP. When considering 60 nonrevoked keys/certificates, the BKR-AC (nonrevoked) is 6.3 ms, the CRL (nonrevoked) is 32.9 ms, and OCSP (nonrevoked) is 26.6 ms. (ii) The time spent by BKR-AC in case of revoked keys is greater than that for CRL and OCSP. When considering 60 revoked keys/certificates, the BKR-AC (revoked) is 64.9 ms, the CRL (revoked) is 55.1 ms, and OCSP (revoked) is 50.9 ms. Finally, this indicates that BKR-AC has a rapid response time in the case of nonrevoked keys/certificates.

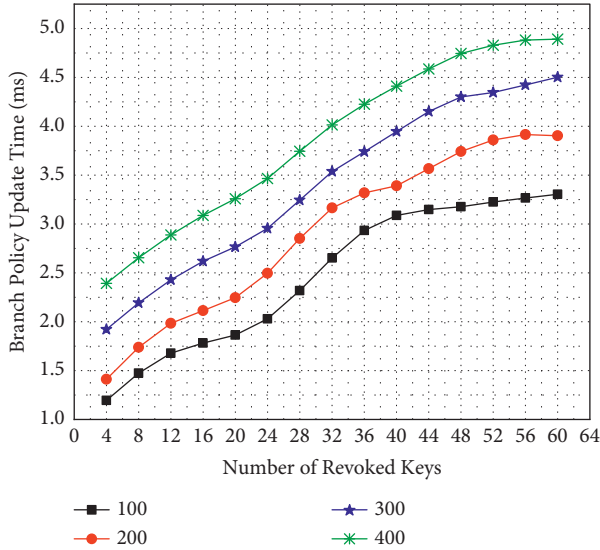


FIGURE 5: The time required to update the bank branch policy against the number of revoked keys at four different levels of concurrent requests.

But if there exist multiple revoked keys, the response time of BKR-AC is high as it goes through various verification steps to avoid nonrevoking a revoked key.

6. Data Analysis

We investigated the data analysis into two cases against the number of nonrevoked and revoked keys. Also, we compared the amount of exchanged data for our scheme with two well-known methods.

6.1. Transferred Data against the Number of Nonrevoked Keys. This part represents the exchanged data by the bank branch until giving a decision on the revocation status against the number of nonrevoked keys while considering four levels of concurrent requests (100, 200, 300, and 400) at the same time to the bank branch, as shown in Figure 7.

The results show the following. (i) For the same number of concurrent requests, the average exchanged data is increasing according to the number of nonrevoked keys. It is about a 52.02 KB difference when increasing the number of nonrevoked keys from 4 to 60 while considering 400 concurrent requests. (ii) For the same number of nonrevoked keys, the average exchanged data is increasing according to the number of concurrent requests. It is about a 23 KB difference when increasing the number of concurrent requests from 100 to 400 while considering 60 nonrevoked keys.

6.2. Transferred Data against the Number of Revoked Keys. This part represents the exchanged data by the bank branch until giving a decision on the revocation status against the number of revoked keys while considering four levels of concurrent requests (100, 200, 300, and 400) at the same time to the bank branch, as shown in Figure 8.

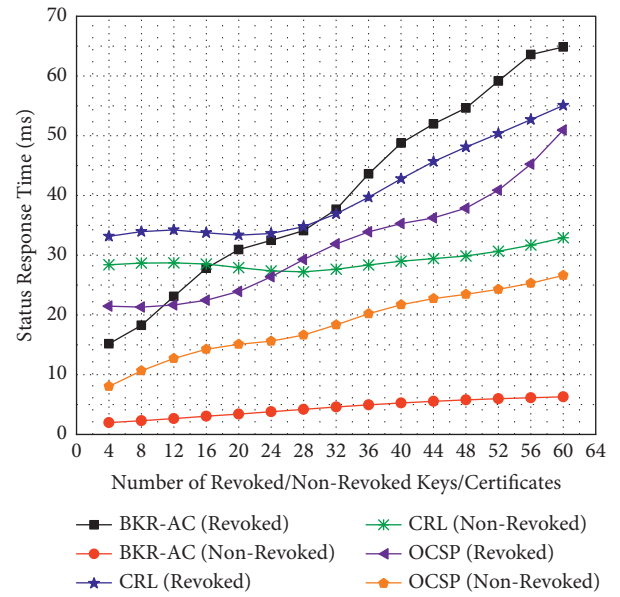


FIGURE 6: The status response time required to respond with the revocation status for BKR-AC and two well-known schemes (CRL and OCSP) against the number of revoked and nonrevoked keys/certificates at 400 concurrent requests.

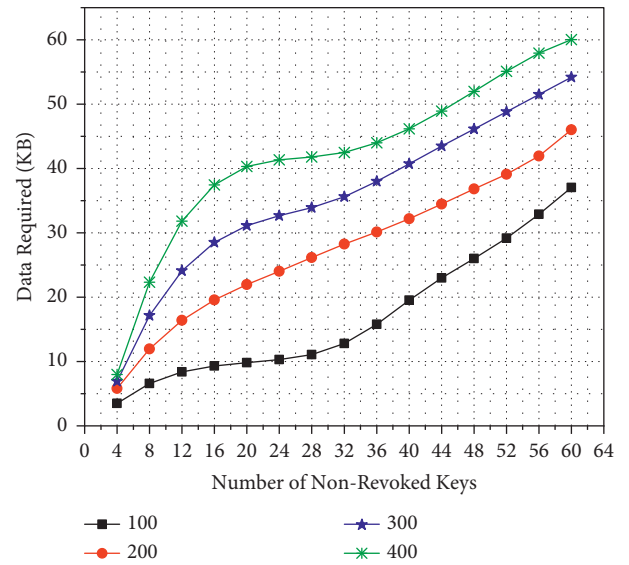


FIGURE 7: The amount of exchanged data required to give a decision on the revocation status against the number of nonrevoked keys at four different levels of concurrent requests.

The results show the following. (i) For the same number of concurrent requests, the average exchanged data is increasing according to the number of revoked keys. It is about a 52.42 kB difference when increasing the number of revoked keys from 4 to 60 while considering 400 concurrent requests; and (ii) For the same number of revoked keys, the average exchanged data is increasing according to the number of concurrent requests. It is about a 19.22 kB difference when increasing the number of concurrent requests from 100 to 400 while considering 60 revoked keys.

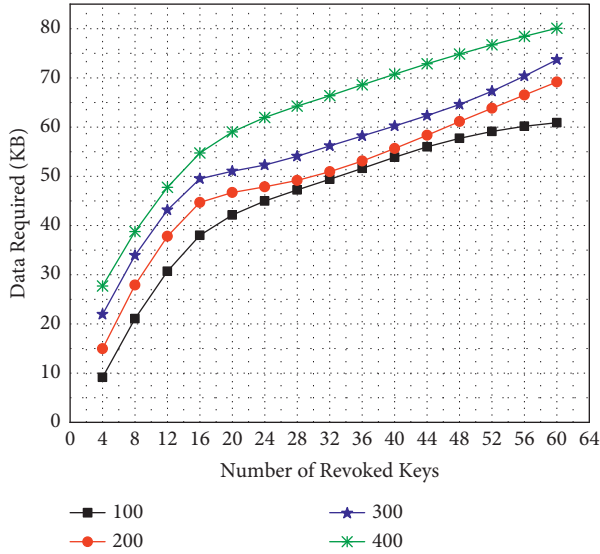


FIGURE 8: The amount of exchanged data required to give a decision on the revocation status against the number of revoked keys at four different levels of concurrent requests.

6.3. Transferred Data Comparison with Two Well-Known Schemes. This comparison represents the amount of exchange data required to respond to our scheme’s revocation status (BKR-AC) and two well-known schemes (CRL and OCSP) against the number of revoked and nonrevoked keys for BKR-AC and the number of revoked and nonrevoked certificates for both CRL and OCSP schemes. We conducted the measures at 400 concurrent requests, as shown in Figure 9.

The results show the following. (i) The data exchanged by BKR-AC in the case of nonrevoked keys is an average between that for CRL and OCSP. When considering 60 nonrevoked keys/certificates, the BKR-AC (nonrevoked) data is 60 kB, the CRL (nonrevoked) data is 70 kB, and OCSP (nonrevoked) data is 53 kB. (ii) The data exchanged by BKR-AC in case of revoked keys is an average between those for CRL and OCSP. When considering 60 revoked keys/certificates, the BKR-AC (revoked) data is 80 kB, the CRL (revoked) data is 83.6 kB, and OCSP (revoked) data is 90.6 kB. Finally, this indicates that BKR-AC has lower exchanged data than CRL and higher traded data than OCSP in the case of nonrevoked keys/certificates.

7. Related Work and Discussion

Several systems and schemes for managing the certificate/key-revocation process are as follows. This section focuses on some significant famous certificate revocation schemes that are standardized and still used to date. Also, we introduce some well-known blockchain-based certificate revocation schemes. Moreover, we discuss their capabilities and compare them with our proposed scheme.

7.1. Certificate Revocation List and Its Derivatives. The Certificate Revocation List (CRL) [8, 9] is deployed and

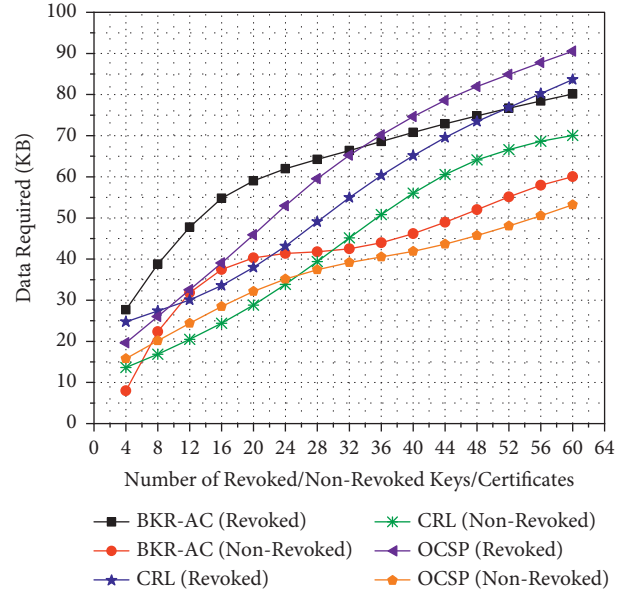


FIGURE 9: The amount of exchange data required to respond with the revocation status for our scheme (BKR-AC) and two well-known schemes (CRL and OCSP) against the number of revoked and nonrevoked keys/certificates at 400 concurrent requests.

standardized by the Internet Engineering Task Force (IETF). A Certification Authority (CA) and CRL issuer periodically publish a dated and signed list of revoked certificates. Also, there is an optional Registration Authority (RA) to which the CA delegates some certain management functions. Generally, when revocation status information is provided using CRLs, the CA can work as the CRL issuer. For example, in the X.509 Version 3 certificate, the public key must confirm that the introduced private key is related to the correct remote subject. The confirmation process is done using the hidden certificates in the public key values to subjects. This is asserted using a trusted CA which digitally signs each certificate. Since the signature of the certificate and its timelines can be independently checked by the clients, the certificate distribution process can be done through untrusted communication servers. Moreover, the certificates can be stored in unsecured storage systems.

Once a certificate is issued, it should be valid for use during its whole validity period. However, due to some circumstances, a certificate may become invalid before the end of its validity period. These circumstances include a change of name or association between the subject or the private key becoming suspicious or compromised. Regarding any of these circumstances, the CA must revoke the certificate whatever its validity period. X.509 lets each CA periodically issue a signed and time-stamped list identifying the revoked certificates. This list is made freely available in a public repository, where a serial number identifies each revoked certificate. Thus, the new CRL is issued based on a regular periodic basis. One of the advantages of this revocation scheme is distributing the CRLs by the same means as the certificates themselves through the untrusted servers and communications media. On the other hand, its main

limitation is using untrusted communications and servers. Thus, the revocation is limited to the CRL issue period.

An improvement to CRL is introduced in [10]. It provides a solution to the nonuniform growth in the CRL distribution points. In this scheme, two CRL extensions were used. The first one allows scope statements and is called *CRL Scope Field*. The second one is called *Status Referral Fields*; it updates the partitioning CRL distribution points. The CRL with status referral extension is sent as a response when a subject wants to verify a certificate. This response covers the verified certificate and a pointer to the new location of the CRL related to the certificate in the request.

There is an alternative scheme called Certificate Revocation Status Directory (CRS Directory) [4]. In this scheme, there are two additional fields for the certificate structure. The CA daily sends the signed statements about the status of the certificates issued by a single issuer to the CRS directory. Moreover, there are signed statements to each certificate within its validity period. If a subject requests the status of a certificate, the response will come from the CRS directory with the complete information needed by the subject to verify its request. This scheme downstates the communication overhead between the subjects and the server. On the other hand, it has a considerable communication overhead between the CA and the server.

7.2. Online Certificate Status Protocol and Its Derivatives. The Online Certificate Status Protocol (OCSP) [3] allows applications to determine the revocation status of identified certificates. It is mainly used to achieve the applicable operational requirements to provide more timely revocation information than that introduced by CRLs. Also, it can be used to obtain additional status information. The client of OCSP instantiates a status request to a specific OCSP responder. The acceptance of the certificate is suspended until the responder provides a response. The OCSP is responsible for specifying the exchanged data between an application verifying the status of one or more certificates and the responding server that responds with the certificate's status. It should be mentioned that the server's response needs to be signed by a key.

The certificate status is one of three values, good, revoked, or unknown. The "good" state means that no valid certificate with the same serial number is revoked. The good state does not imply that the certificate was ever issued or that this response came within the certificate's validity period. Thus, the responding server will make additional extensions of the response regarding the current certificate status. The "revoked" state is either temporary revocation or permanent revocation. We can get this status when the responsible CA does not have a record for issuing a certificate with its current serial number. The "unknown" state means that the responding server does not know about the requested certificate. This usually happens when the verification request indicates an unrecognized issuer that this responder does not serve. Finally, the certificate with a revoked state should be rejected, while the certificate with an unknown state means that it is not revoked yet, but this responder can not determine it. Thus, in the unknown state,

the client should decide whether to try another source of status information.

The OCSP is a centralized approach that can be considered as a single point of attack or failure for its server. It starts to verify the certificate without verifying the validity of the serial number for the requested certificate. Thus, it can be a victim of the denial of service attack, which can flood it with multiple verification requests with a fake serial number for the requested certificate. Also, the OCSP is timely consuming [11, 12]. It can not be used for offline systems; it works online only. Moreover, the OCSP has a huge privacy risk. Because the responder has detailed information about the verified certificates to each end-user, thus, the responder can track the sites visited by these users [12].

8. Blockchain-Based Certificate/Key-Revocation Schemes

Generally, blockchain has multiple helpful features that can solve the main challenges of the traditional public key infrastructure (PKI) systems. For example, and not as a limitation, blockchain-based solutions are distributed. Thus, it avoids the central point of failure or attacks. Furthermore, blockchain never uses a trusted third party and never needs prior trustworthiness in the system. Various open-source implementations support the variety and effectiveness in building the solutions [13].

There are some recent applications for blockchain in certificate revocation. The authors in [14] considered that certificate revocation as an effective method to prevent potential attacks. The authors employed blockchain to simplify the network structure in the vehicular communication system and maintenance of the Certificate Revocation List. Another application of certificate revocation scheme using blockchain for vehicular communications is introduced in [15]. An efficient contribution for VANETs based on blockchain is introduced in [16] to realize a privacy-preserving authentication model. Moreover, the authors in [17] introduced a conditional privacy-preserving authentication protocol for vehicular Ad Hoc networks based on blockchain. Also, the authors in [18] introduced a decentralized certificate system using the Ethereum blockchain. This scheme provides blockchain certificate services for college students, and the authors in [19] reviewed the traditional centralized PKI systems and proved that they are subjected to security concerns. Therefore, the authors proposed a decentralized PKI infrastructure on the top of the blockchain to solve the security issues of the centralized PKI systems. Another contribution to the PKI using blockchain is introduced in [20]. This scheme is based on the Ethereum blockchain.

The authors in [21] introduced Certcoin. It satisfies the main features of blockchain. It comprises five functions: registration, update, lookup, verification, and revocation. In this scheme, the owner identified with an identity ID posts a transaction to the blockchain to revoke one of its public keys. The revocation in Certcoin is done by the owner only, which has some cons; for example, the owner needs to be online all the time. Furthermore, the owner/person may not have enough knowledge to handle the revocation. On the other

hand, there is an excellent opportunity for the owner to identify the malicious users because they are behaving maliciously. Moreover, Certcoin must check the blockchain revoked certificates list to verify a given certificate status which is very time-consuming.

An extension to Certcoin [21] is introduced by Axon and Goldsmith [22]. The authors presented a privacy-aware blockchain-based PKI, which improves Certcoin privacy-aware. Furthermore, it supports short-term key updates and user-controlled disclosure. In this scheme, users who previously used public keys can be disclosed either by the user or the network majority. But the revocation mechanism is still the same as in Certcoin. The authors in [23] introduced Authcoin. It uses a challenge-response-based validation in the authentication process. It also benefits from the advantages of blockchain storage systems. It is secure against Sybil attacks, but it uses the exact revocation mechanism used in Certcoin.

The authors in [24] introduced a smart contract-based PKI system. It is based on a smart contract on the Ethereum platform and a web-of-trust model. The smart contract cares about the entity publishing a set of attributes, signatures, and even revocations on the blockchain. An Ethereum address represents each entity; a revocation function allows the different entities to revoke their signatures and the key. The process of checking revocation status is done on the blockchain. Another blockchain-based PKI framework is introduced in [25]. It can manage X.509 certificates. The authors extended the standard X.509 certificate to be integrated with blockchain. It depends on the smart contract that acts on two lists: a white list and a black list. The white list is used for the created certificates, and the black list is used for the revoked certificates only.

Moreover, blockchain allows digital information to be distributed but not copied. Thus, blockchain technology created the backbone of a new type of Internet. Blockchain can manage access control in different ways for various specific environments. The authors in [26] guarantee the suitability of access control policies evaluation based on blockchain. They codify attribute-based access control policies as smart contracts and deploy them on a blockchain, thus transforming the policy evaluation process into an entirely distributed smart contract execution. In [27], the authors proposed a novel blockchain-based distributed key management architecture with fog computing to reduce latency and multiblockchains operated in the cloud to achieve cross-domain access. The proposed scheme utilizes blockchain technology to satisfy the decentralization, fine-grained auditability, high scalability, extensibility requirements, and the privacy-preserving principles for hierarchical access control in IoT.

9. Conclusion

The proposed model facilitates and secures access to the cloud-hosted sensitive financial data and open banking services. We introduced a new blockchain-based key-revocation access control scheme that has achieved a set of remarkable goals:

- (1) Employing the power and resiliency of blockchain to revoke the customer's keys at shallow status response time
- (2) Introducing the compatibility of the proposed scheme with the current open banking systems
- (3) Testing the contract's code on Kovan Testnet before deploying it to the Mainnet on the Ethereum platform
- (4) Proving the security of BKR-AC against:
 - (i) Insecure Id's
 - (ii) Forced Browsing Past Access Control Checks
 - (iii) Path Traversal
 - (iv) Client-Side Caching
 - (v) Chosen-text attacks
- (5) Conducting comprehensive evaluation based on the status response time and the data transmitted until receiving a revocation decision. Also, we evaluated the policy update time at the bank branch at various numbers of revoked keys
- (6) Comparing the proposed scheme with two well-known schemes (CRL and OCSP) regarding the status response time and the exchanged data while considering 400 concurrent requests

The experimental results have indicated that BKR-AC can respond with the status response within a reasonable and acceptable processing time. Considering very rough conditions and huge traffic overhead, the average status response time for 400 concurrent nonrevoked customers is 6.283 ms when considering 60 nonrevoked keys. Furthermore, the average data exchanged until receiving the revocation status for 400 contemporary nonrevoked customers is 60 KB when considering 60 nonrevoked keys. Also, the policy update response time when considering 60 revoked keys and 400 concurrent customers is 4.89 ms. Therefore, the average time and exchanged data rates are small and accepted by both the bank branches and the nonrevoked customers. When considering the number of nonrevoked keys/certificates, the status response time for our scheme (BKR-AC (nonrevoked) = 6.3 ms) is shorter than that of CRL (nonrevoked) = 32.9 ms) and OCSP (OCSP (nonrevoked) = 26.6 ms). On the other hand, when considering the revoked keys/certificates, the status response time for our scheme (BKR-AC (Revoked) = 64.9 ms) is greater than that of CRL (CRL (nonrevoked) = 55.1 ms) and OCSP (OCSP (nonrevoked) = 50.9 ms). When considering the number of nonrevoked keys/certificates, the data exchanged for our scheme (BKR-AC (nonrevoked) = 60 kB) is an average between those of CRL (CRL (nonrevoked) = 70 kB) and OCSP (OCSP (nonrevoked) = 53 kB). Also, when considering the revoked keys/certificates, the data exchanged for our scheme (BKR-AC (revoked) = 80 kB) is an average between those of CRL (CRL (revoked) = 83.6 kB) and OCSP (OCSP (revoked) = 90.6 kB).

Finally, the proposed BKR-AC has a lower response time than CRL and OCSP in nonrevoked keys/certificates and a higher response time in case of revoked keys to avoid

nonrevoking a revoked key. But the data exchanged is an average for BKR-AC between CRL and OCSP, which is still a tiny amount and accepted.

Data Availability

The data used to support the findings of this study are available from the authors upon request.

Conflicts of Interest

The authors declare that there are no conflicts of interest regarding the publication of this paper.

References

- [1] Y. Liu, W. Tome, L. Zhang et al., "An end-to-end measurement of certificate revocation in the web's PKI," in *Proceedings of the 2015 Internet Measurement Conference, IMC'15*, Association for Computing Machinery, New York, NY, USA, 2015, page 183–196.
- [2] M. Myers, R. Ankney, A. Malpani, S. Galperin, and C. Adams, "Online Certificate Status Protocol- OCSP," 1999.
- [3] S. Santesson, M. Myers, R. Ankney, A. Malpani, S. Galperin, and C. Adams, *Rfc 6960: X.509 Internet Public Key Infrastructure Online Certificate Status Protocol—OCSP*, Internet Engineering Task Force (IETF), Fremont, CA, USA, 2008.
- [4] M. Naor and K. Nissim, "Certificate revocation and certificate update," *IEEE Journal on Selected Areas in Communications*, vol. 18, no. 4, pp. 561–570, 2000.
- [5] I. Ozelcik and S. Anthony, "Cryptorevocate: a cryptographic accumulator based distributed certificate revocation list," in *Proceedings of the 2021 IEEE 11th Annual Computing and Communication Workshop and Conference (CCWC)*, pp. 865–872, Las Vegas, NV, USA, January 2021.
- [6] Y. C. E. Adja, B. Hammi, S. Ahmed, and S. Zeadally, "A blockchain-based certificate revocation management and status verification system," *Computers & Security*, vol. 104, Article ID 102209, 2021.
- [7] P. J. Taylor, T. Dargahi, D. Ali, R. M. Parizi, and K.-K. R. Choo, "A systematic literature review of blockchain cyber security," *Digital Communications and Networks*, vol. 6, no. 2, pp. 147–156, 2020.
- [8] D. Cooper, S. Santesson, S. Farrell, S. Boeyen, and W. Polk, *Rfc 5280: Internet x.509 Public Key Infrastructure Certificate and Certificate Revocation List (CRL) Profile*, Internet Engineering Task Force (IETF), Fremont, CA, USA, 2008.
- [9] P. Yee Akayla, *Rfc 6818: Updates to the Internet x.509 Public Key Infrastructure Certificate and Certificate Revocation List (CRL) Profile*, Internet Engineering Task Force (IETF), Fremont, CA, USA, 2013.
- [10] ITU-T Recommendation and X, "Information technology–open systems interconnection–the directory: public-key and attribute certificate frameworks," *Series X: Data Networks, Open System Communications and Security*, pp. 1–254, International Telecommunication Union, Geneva, Switzerland, 2016.
- [11] E. Stark, L.-S. Huang, D. Israni, C. Jackson, and D. Boneh, "The case for prefetching and prevalidating TLS server certificates," in *Proceedings of the 19th Annual Network & Distributed System Security Conference (NDSS 2012)*, vol. 12, San Diego, CA, USA, February 2012.
- [12] E. Topalovic, B. Saeta, L.-S. Huang, C. Jackson, and D. Boneh, "Towards short-lived certificates," *Web 2.0 Security and Privacy*, Springer, Berlin, Germany, 2012.
- [13] T. Salman, M. Zolanvari, A. Erbad, R. Jain, and M. Samaka, "Security services using blockchains: a state of the art survey," *IEEE Communications Surveys & Tutorials*, vol. 21, no. 1, pp. 858–880, 2019.
- [14] A. Lei, Y. Cao, S. Bao et al., "A blockchain based certificate revocation scheme for vehicular communication systems," *Future Generation Computer Systems*, vol. 110, pp. 892–903, 2020.
- [15] H.-G. Kim, "Certificate revocation scheme based on the blockchain for vehicular communications," *Journal of the Korea Society of Computer and Information*, vol. 25, no. 7, pp. 93–101, 2020.
- [16] F. Xia, Q. Shi, Q. Xie, and L. Liu, "An efficient privacy-preserving authentication model based on blockchain for vanets," *Journal of Systems Architecture*, vol. 117, Article ID 102158, 2021.
- [17] C. Lin, D. He, X. Huang, N. Kumar, and K.-K. R. Choo, "BCPPA: a blockchain-based conditional privacy-preserving authentication protocol for vehicular ad hoc networks," *IEEE Transactions on Intelligent Transportation Systems*, vol. 22, no. 12, pp. 7408–7420, 2021.
- [18] R. Xie, Y. Wang, M. Tan et al., "Ethereum-blockchain-based technology of decentralized smart contract certificate system," *IEEE Internet of Things Magazine*, vol. 3, no. 2, pp. 44–50, 2020.
- [19] Y. Li, Y. Yu, C. Lou, N. Guizani, and L. Wang, "Decentralized public key infrastructures atop blockchain," *IEEE Network*, vol. 34, no. 6, pp. 133–139, 2020.
- [20] A. Rashid, A. Masood, H. Abbas, and Y. Zhang, "Blockchain-based public key infrastructure: a transparent digital certification mechanism for secure communication," *IEEE Network*, vol. 35, no. 5, pp. 220–225, 2021.
- [21] C. Fromknecht, D. Velicanu, and S. Yakoubov, "A decentralized public key infrastructure with identity retention," *IACR Cryptology*, vol. 803, 2014.
- [22] L. Axon and M. Goldsmith, "Pb-pki: a privacy-aware blockchain-based PKI," in *Proceedings of the 14th International Conference on Security and Cryptography SECRYPT*, Madrid, Spain, July 2017.
- [23] B. Leiding, C. Cap, T. Mundt, and S. Rashidibajgan, "Authcoin: validation and authentication in decentralized networks," 2016, <http://arxiv.org/abs/1609.04955>.
- [24] M. Al-Bassam, "Scpki: A smart contract-based PKI and identity system," in *Proceedings of the ACM Workshop on Blockchain, Cryptocurrencies and Contracts, BCC'17*, pp. 35–40, Association for Computing Machinery, New York, NY, USA, 2017.
- [25] A. Yakubov, W. Shbair, A. Wallbom, D. Sanda, and R. State, "A blockchain-based pki management framework," in *Proceedings of the First IEEE/IFIP International Workshop on Managing and Managed by Blockchain (Man2Block) Colocated with IEEE/IFIP NOMS*, pp. 23–27, Tapei, China, 2018.
- [26] D. Di Francesco Maesa, P. Mori, and L. Ricci, "A blockchain based approach for the definition of auditable access control systems," *Computers & Security*, vol. 84, pp. 93–119, 2019.
- [27] M. Ma, G. Shi, and F. Li, "Privacy-oriented blockchain-based distributed key management architecture for hierarchical access control in the iot scenario," *IEEE Access*, vol. 7, pp. 34045–34059, 2019.

Research Article

Interactive Art Design Based on Intelligent Sensors and Information Fusion Technology

Yanming Zhu,¹ Tingting Qiu,² and Wei Miao ³

¹Beijing Institute of Graphic Communication, Beijing, 102600 Beijing, China

²Wuhu Institute of Technology, Wuhu, 241000 Anhui, China

³Artificial Intelligence Research Institute, Donghua University, Shanghai, 200000 Shanghai, China

Correspondence should be addressed to Wei Miao; drmiaowei@163.com

Received 13 November 2021; Accepted 5 January 2022; Published 28 January 2022

Academic Editor: Nima Jafari Navimipour

Copyright © 2022 Yanming Zhu et al. This is an open access article distributed under the Creative Commons Attribution License, which permits unrestricted use, distribution, and reproduction in any medium, provided the original work is properly cited.

In the era of rapid development of information technology, the application of smart sensors is becoming more and more extensive. All measurement and control equipment need to obtain raw data through sensors, and machines can also obtain various information through sensors. And this information, especially from the perspective of reliability, accuracy, and intelligent interaction, requires higher interactivity in people's lives. In order to solve the problem that the existing interactive design is difficult and not intelligent enough, and the information fusion is not uniform enough, the results of the design have various deviations. This article intends to design through the use of smart sensors and information fusion technology to make an improvement to its interactive art design.

1. Introduction

In 1973, Professor Ma's enthusiasm for the study of visual measurement theory at the Massachusetts Institute of Technology established a research group. Four years later, in 1977, Ma's visual theory was proposed. This theory had a great influence on machine vision research in the 1980s. Since then, machine vision theory has entered a period of active development. Especially in the mid-1980s, many new concepts and theories appeared in the machine vision method. Machine vision has many fields, and its research content is very rich, including image processing, signal processing, optics, machinery, automation, electrical, computer software systems, robotics, and other fields. The machine vision system combines the technologies and techniques of the abovementioned multiple fields to achieve the acquisition, processing, and display of three-dimensional information in the physical world and output the target information. The machine vision system started in the 1950s. At that time, it only processed and analyzed the characteristics of two-dimensional images such as the character recognition of the license board, the two-dimensional detection of the working size, the processing of medical images,

and the analysis of remote sensing images. In the 1960s, Robert used three-dimensional objects composed of points, lines, and surfaces to decompose the object recognition in a three-dimensional scene into simple points, lines, and planes and then obtained the recognition results after comprehensive judgment. Three-dimensional machine vision technology has made great progress. At the same time, machine vision technology is used in industrial inspections, further promoting the development of machine vision theory and applications. By the 1990s, many machine vision technologies appeared in the industry. Since then, in the field of industrial automation production, machine vision measurement technology has assumed an increasingly important role. The specific development process is shown in Table 1.

The current research on sensor networks mainly solves how to save energy consumption as much as possible under the network indicators that meet the requirements of specific applications to extend the network lifetime. These studies assume that WSN is an isolated network that can perceive the real physical environment. However, actual customers are usually on the Internet far away from WSN, and an effective way is needed to enable customers to drive WSN to collect data and quickly transmit it to customers.

TABLE 1: Development process.

1950	1960	1973	1990
Two-dimensional image processing	3D machine vision technology	Vision theory is proposed	Machine vision measurement technology becomes the mainstay

Therefore, based on the analysis and summary of existing research, this article proposes a sensor network and IP network integration solution that can face a variety of challenges uses user agents, application agents, registration agents, and resource managers to build a bridge between WSN and the Internet.

Machine vision plays an irreplaceable role in industry, economy, scientific research, national defense, and other fields. The advantage of the machine vision system is that it does not directly touch the measured object, so it reduces the possibility of mutual damage between the measuring instrument and the measured object after contact. The biggest feature of interactive art is interactivity, which is very fresh to the audience in the art exhibition. In order to allow the audience to explore the work in depth in the interaction between the work and the work, understand the spiritual connotation of the work, and grasp the psychological needs of the audience, it is very important to use interactive art.

The biggest innovation of this article is that it is different from the usual image analysis method of the visual sensor. In the past, the vision sensor was mainly composed of one or two graphics sensors, but there are also multiple sensors and other auxiliary devices in order to obtain a machine vision system sufficient to process the original image. In addition, this article uses the unique microprocessor of the smart sensor and uses multiple smart sensors in the visual sensor to process the collected data according to instructions. In addition, through information fusion technology, data from single and multiple information sources are obtained. The acquired data and information are integrated and processed. In the process of information processing, comprehensive and timely evaluation of images and their importance are carried out to obtain accurate image data estimates. This process is to estimate, evaluate, and evaluate the necessity of additional information sources. The improvement of the continuous process information processing process is to obtain a more complete image analysis result and the continuous self-correction process in the information processing process to obtain a more complete picture analysis result.

2. Related Work

As one of the main directions in the field of industrial automation, the vision sensor's application level represents the level of industrial automation in a country and has attracted special attention from the industry. But how to develop a good vision sensor is extremely challenging, especially the application of smart sensors and information fusion technology to image analysis is more difficult. By referring to Li et al.'s article, the wireless smart sensor networks (WSSN) he described have shown great promise in structural health

monitoring (SHM) because of their low cost, higher flexibility, robust data management, and the use of sensors intensive deployment of the ability to better understand structural behavior. In addition, even if the clock can be accurately synchronized by exchanging time information through beacon messages, the measurement data may still be out of synchronization due to the random delay of the software and hardware sources; that is, synchronized clocks may not necessarily generate synchronization sensing [1]. However, the article does not describe the practical application of smart sensing technology. In García et al.'s article, he designed a smart sensor to predict the established sensory fish quality index. The sensor dynamically correlates the microbial count and TVB-N with the quality index. The sensor provides the most possible value and handles fish-to-fish variability and showed its performance in evaluating cod quality under normal market conditions [2]. Dissanayake et al. are also a good one for the extended design of the sensor. Safe drinking water is essential to good health. Due to the health risks associated with long-term drinking, recommendations for drinking water sources in CKDu endemic areas are critical. Dissanayake et al. designed a sensor to measure fluoride and hardness in well water through an automated mechanism. The reduced reagent volume makes the design more environmentally friendly, and the estimated cost of each sample analysis is \$1, making it affordable for low-income communities [3]. The application of this technology is very friendly to people's livelihood. In terms of information fusion technology, Liu et al. are undoubtedly a better one. The information fusion method of INS/GPS navigation system based on filtering technology is the current research hotspot. In order to improve the accuracy of navigation information, he proposed in the article a navigation technology based on an adaptive Kalman filter, which has an attenuation coefficient to suppress noise. The algorithm collects estimated and measured values, continuously updates the measured noise variance, and processes the noise variance of the system. In this way, white noise can be suppressed [4]. Similarly, Zhou et al., who have a deep research in the field of information fusion, proposed in his own paper a radial basis function (RBF) model that has been widely used in complex engineering design processes to replace computationally intensive simulation models. Taking into account the different sample sizes and sample noise, a numerical example is used to compare the VFM method developed in this research with three existing VFM methods based on scaling functions in detail [5]. The realization of this technology can undoubtedly greatly improve the design efficiency of complex projects. Xu et al. proposed a dangerous cargo container monitoring system based on multisensor. A multisensor information fusion solution for dangerous goods container monitoring is proposed, and information preprocessing, homogeneous sensor

fusion algorithm, and BP neural network-based information fusion are described. The application of multisensor in the field of container monitoring has a certain novelty [6]. All of the above have their own unique insights and ideas in the field of smart sensors and information fusion technology, but none of them are integrated through interactive design or use interactivity to make the system more perfect. Xu and Chen researched the design and implementation of interactive learning system in art teaching. Art teaching based on Moodle and LAMS can effectively solve the problem of online self-learning. One of the important tasks of deepening teaching reform is to improve the quality of teacher information, which directly affects the quality of online teaching. Experimental results show that this method can improve the overall performance [7]. Relatively speaking, this article is only a pure research on the theoretical explanation of the aesthetics of interactive art design but has not been applied to practice, and it is still lacking. Chen believes that traditional hand-drawn animation is inefficient. In order to avoid the problem of low efficiency of hand-drawn animation, many computer-supported hand-drawn animation techniques have appeared. The article proposes an effective interactive design and natural hand-drawn animation techniques. This method can remove the animation art that animation artists spend time and energy, improve the efficiency of animation production, and provide convenience and powerful operability for end users [8]. Chen not only has a deep reserve of theoretical knowledge but also has more practical applications in his articles. The content of the articles is very in-depth and scientific, and the usability is also strong.

3. Sensor Method

3.1. Sensor Registration Algorithm. The integrated sensor is a sensor made by the silicon semiconductor integration process, so it is also called a silicon sensor or a monolithic integrated sensor. The analog integrated sensor came out in the 1980s. It is a dedicated IC that integrates the sensor on a chip and can perform measurement and analog signal output functions.

The sensor registration algorithm synchronizes the asynchronous measurement data of each sensor of the same target to the same time. From the current research, the least square method is a more common sensor registration algorithm [9].

Represents the position measurement noise equation of the sensor B data before fusion, which can be obtained according to the least square rule:

$$C(\hat{U}) = V_n^T V_n = [Z_n - W_n U \wedge]^T [Z_n - W_n \hat{U}]. \quad (1)$$

Let its derivative be zero and simplify it to:

$$\hat{U} = [x \wedge, \dot{x} \wedge]^T = (W_n^T W_n)^{-1} W_n^T Z_n. \quad (2)$$

The covariance of the error is

$$R_{\hat{U}} = (W_n^T W_n)^{-1} \sigma_r^2. \quad (3)$$

Then, fuse the n measured values of sensor B to get the measured value and noise equation at time:

$$\begin{cases} \hat{z}(k) = c_1 \sum_{i=1}^n z_i + c_2 \sum_{i=1}^n i \cdot z_i, \\ \text{Var}[\hat{z}(k)] = \frac{2(2n+1)\sigma_r^2}{n(n+1)}. \end{cases} \quad (4)$$

3.2. Interactive Art Design Method. Interactive art design is the main advantage that distinguishes smart sensors from traditional sensors [10]. Therefore, in the design of interactive technology, the effect of the sensor must be emphasized, and the effect must be amplified. The main design functions include the following points: ① From the user's point of view, it is mainly reflected in the understanding of the processed information. Good interaction helps users to effectively understand the design suggestions of the sensor, easy to obtain data, and improve the efficiency of information transmission. ② In the virtual reality environment, the sensor is actually a mapping of human perception. Need to simulate the actual environment more appropriately to provide users with better extensions. ③ For self-selection, compared with previous sensors, smart sensors have a higher degree of freedom, and users have absolute self-discipline and can obtain information according to personal preferences. ④ For easy to operate, in order to achieve a good interaction, the smoothness of the interaction needs to be largely dependent on the ease of operation [11].

Good human-computer interaction experience and work interaction can stimulate people's imagination through constant perception changes, so that participants can immerse themselves in this environment full of unlimited imagination and enjoy the fun of human-computer interaction [12]. The interaction process is shown in Figure 1.

Unlike other tools with limited uses (such as a hammer that can be used to drive nails but has no other purpose), computers have many uses. This is an open dialogue between the user and the computer. People use various methods to talk to computers. The interface between humans and computers is indispensable to facilitate this dialogue. Desktop applications, Internet browsers, handheld computers, and computer information utilize today's popular graphical user interface (GUI). The voice user interface (VUI) is used in speech recognition and synthesis systems, and you can participate in specific role agents in a way that the new multimodal and graphical user interface (GUI) cannot be implemented in other interface paradigms [13]. The development in the field of human-computer interaction is not to design traditional interfaces but to always maintain the quality of interaction, so that the interface replaces the interface based on commands or actions and intelligently adapts to finally adopt the active interface instead of the passive interface [14].

3.3. The Intelligent Realization Method of the Sensor. How to realize sensor intelligence? In summary, there are three main ways to construct smart sensors, namely, nonintegrated realization, integrated realization, and hybrid realization [15].

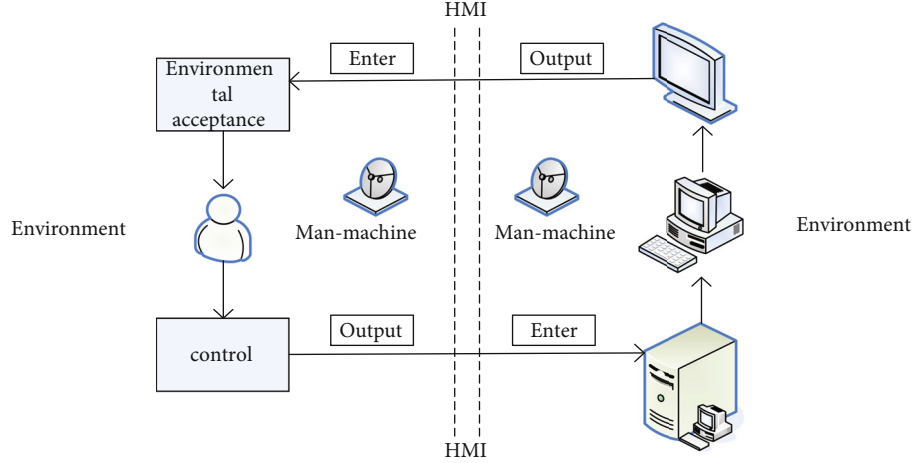


FIGURE 1: The main process of human-computer interaction.

The smart sensor is mainly composed of 7 parts, as shown in Figure 2.

3.3.1. Nonintegrated Implementation. The nonintegrated method (i.e., modular method) realizes the intelligentization of the sensor, which is aimed at combining the traditional classic sensor with a single function of acquiring a certain signal with a signal conditioning module and a microprocessor with a communication interface. It is equipped with some intelligent software and realizes communication, control, self-calibration, self-compensation, self-diagnosis, and other related functions. At the same time, the sensor is intelligent and networked. For sensor manufacturers, due to the rapid development of sensor technology, considering cost, market, and other issues, it is impossible to update the original production process equipment in time. This implementation method is relatively the most economical and convenient way [16]. For scientific researchers and engineering technicians, the smart sensors on the market are expensive and may not fully meet the experimental or practical requirements. Through the use of cheap traditional sensors, the key to sensor intelligence in the second chapter of the master's degree thesis of Central South University Technology research is a kind of intelligent technology; constructing intelligent sensor system that meets the demand, its scientific research experiment significance and engineering practice significance will be particularly considerable.

In order to ensure that the original signal can be reproduced by the sampling signal, the sampling signal must ensure a sufficiently high sampling frequency, which must meet:

$$f_s \geq 2f_{i(\max)}. \quad (5)$$

3.3.2. Integrated Realization Method. In order to achieve the integration of sensor intelligence, based on large-scale integrated circuit technology and the latest sensor technology, sensitive components, signal adjustment circuits, microprocessor units, etc. are integrated on the chip [17]. Relevant

technologies include microprocessing technology, MEMS technology and microprocessing nano-material technology, the latest sensor technology, large-scale integrated circuit technology, etc., and many technical bottlenecks and implementation problems have also appeared. The integrated realization method mainly enables the sensor to have the characteristics of miniaturization, structural integration, and intelligence to achieve the purpose of improving measurement accuracy and stability. It is the development direction of future sensors. In terms of practicality, it may not be suitable for all occasions.

In order to ensure that the components of different frequencies in the signal fall within the passband of the filter [18], the amplitude ratio of each component remains unchanged before and after filtering, and the lag time of each frequency component after filtering remains the same, usually a linear phase filter is used. Here first introduce the relevant principle of the linear phase finite impulse response filter.

The FIR pulse transfer function expression is

$$H(q) = \frac{Y(q)}{X(q)} = a_0 + a_1q^{-1} + a_2q^{-2} + \dots + a_Nq^{-N} = \sum_{n=0}^N a_nq^{-n}. \quad (6)$$

Roll out:

$$Y(q) = (a_0 + a_1q^{-1} + a_2q^{-2} + \dots + a_Nq^{-N})X(q). \quad (7)$$

Find the inverse z transformation to get the difference equation as:

$$\begin{aligned} y(n) &= a_0x(n) + a_1x(n-1) + a_2x(n-2) + \dots + a_Nx(n-N) \\ &= \sum_{r=0}^N a_r x(n-r). \end{aligned} \quad (8)$$

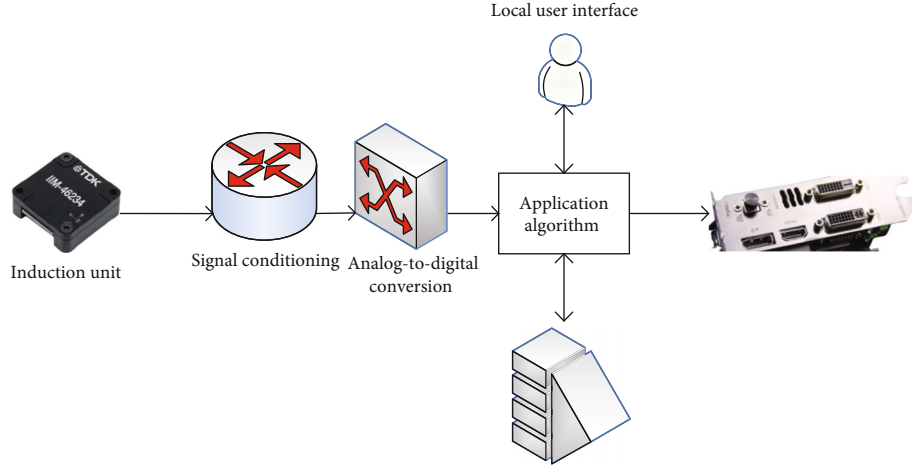


FIGURE 2: Basic structure unit of smart sensor.

Using the backward difference method, bilinear transformation method, etc., the pulse transfer function of the domain is obtained as:

$$H(q) = \frac{Y(q)}{X(q)} = \frac{b_0 + b_1q^{-1} + b_2q^{-2} + \dots}{a_0 + a_1q^{-1} + a_2q^{-2} + \dots}. \quad (9)$$

Perform polynomial division on the above equation (9), keep the first N terms, and obtain the $N - 1$ order FIR filter; that is

$$\begin{aligned} H(z) &= \frac{Y(q)}{X(q)} = C_0 + C_1q^{-1} + C_2q^{-2} + \dots + C_{N-1}q^{1-N} \\ &= \sum_{n=0}^{N-1} C_nq^{-n}. \end{aligned} \quad (10)$$

The above formula shows that the output at the current moment is determined by a series of (including the current moment and historical moment) input value multiplied by the corresponding coefficient.

3.3.3. Hybrid Implementation. The hybrid implementation method is to combine the nonintegrated implementation method and the integrated implementation method [19]. According to actual needs, the various components of the system, such as the sensitive unit, signal conditioning circuit, microprocessor unit, and the communication interface, they are combined into two blocks. Or three chips are combined in different ways to meet different requirements of users.

For a noisy observation signal, it can be expressed as:

$$x(z) = s(z) + v(z). \quad (11)$$

The output signal of the adaptive filter is expressed as:

$$y(z) = \sum_{i=0}^{Z-1} w_i(z)x(z-i). \quad (12)$$

Assuming that the output signal is composed of a linear combination of array signals, in many practical applications, each element of the input signal vector is composed of the time delay form of the same signal. The input signal is filtered to obtain the output signal. The calculation method is as follows:

$$y(n) = \sum_{i=0}^{N-1} w_i(n)x(n-i) = w^T(n)x(n). \quad (13)$$

The solution in the above formula is also called the Wiener solution. In fact, vectors and matrices are difficult to estimate accurately and can only be estimated by time average. Since a variety of adaptive algorithms can be used, there is no unique solution for adaptive filtering. These adaptive algorithms have their own advantages and disadvantages and are suitable for different occasions [20].

3.4. Networked Smart Sensor Method. The measurement and control system based on decentralized intelligent sensors [21] consist of a specific network, various control nodes, sensor nodes, and a central control unit. Among them, sensor nodes are used to implement parameter measurement and send data to other nodes in the network. The control node is to achieve the calibration of the measured physical quantity and the path information (temperature, humidity, etc.) required for the calibration. In most cases, the necessary data is obtained from the network as needed, and the corresponding control method and execution control output are formulated based on the data. In the whole system, each sensor node and control node are independent. The number of control nodes and sensor nodes can be modified more or less according to requirements. The network options can be sensor bus, field bus, enterprise internal Ethernet, or direct Internet access. The intelligent sensor node is composed of three parts: sensor, network interface, and processing unit in the traditional sense. According to various requirements, these three parts can be composed of various chips to form composite

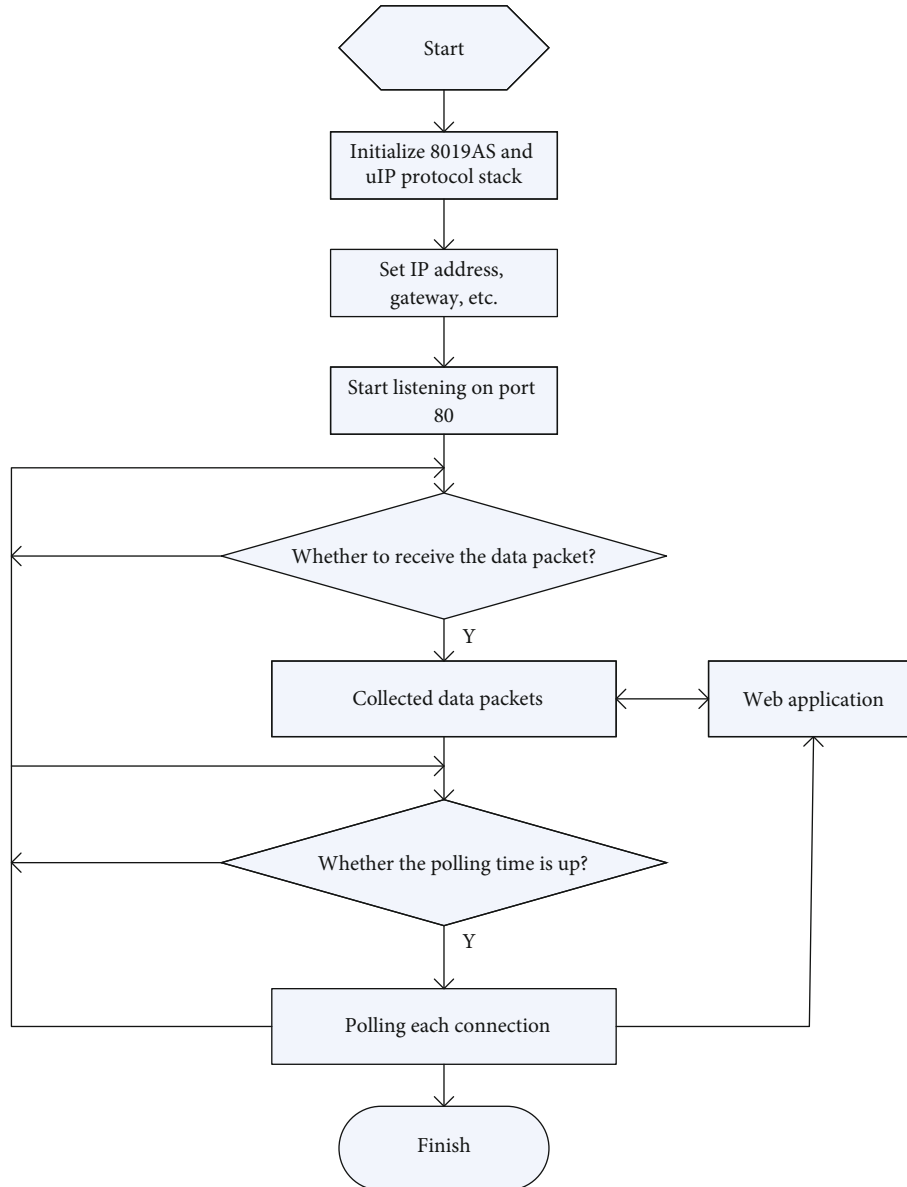


FIGURE 3: Flow chart of network intelligent sensor.

materials, or they can be simple. First, the sensor converts the measured physical quantity into an electrical signal, converts it into a digital signal through A/D, and sends the result to the network after the microprocessor performs data processing (filtering, calibration) and data exchange. The network is completed by the network interface module [22] as shown in Figure 3.

The existing steps in this article mainly involve the conversion of the sensor's measurement signal and the data exchange of the microprocessor in Figure 3, and the network interface problem is also a major difficulty to solve.

4. Smart Sensor Accuracy Experiment

4.1. Smart Sensor Calibration Measurement Experiment. The basic principle of smart sensors is the principle of laser triangulation [23]. The structured light laser angle projects the

light bar onto the surface of the measurement object. The distribution of the light strip is not a straight line, but according to its change, a camera in another place collects an image of the light strip distribution. The structured optical laser forms the optical surface shown in gray. The optical axis of the camera and the light surface form an angle, and the light rod is modulated by the surface of the object to produce distortion. If the object or the smart sensor moves at a certain speed in a certain direction, a modulated image is generated, the structured light strip information of each image is extracted, and the information is combined to obtain a three-dimensional image, that is, an image of the surface of the object.

In order to investigate the repeatability of the experimental system, a certain fixed point on the light plane was selected, and the repeatability test was performed five times. The experimental results are shown in Table 2.

TABLE 2: Repeatability testing experiment.

Test sequence	q/mm	w/mm	e/mm
1	-3.5956	37.388	18.6734
2	-3.5898	37.245	18.6712
3	-3.5923	37.411	18.6912
4	-3.5998	37.361	18.6435
5	-3.5947	37.411	18.6435
3&	0.03212	0.0453	0.005628

It can be obtained from the experimental results that the repetition error does not exceed 0.045 mm, which has good repetition accuracy.

4.2. Simulation Results and Related Experiments. In order to verify the effectiveness of the algorithm and analyze the performance of the fusion algorithm, it is assumed that the AFL distributed simulation system is composed of three radars of the same type, the tracking time is 100 s, the number of Monte Carlo simulations is 600, and the following three types of different targets unfolding the tracking; the three kinds of exercise data obtained are shown in Tables 3–5 (the simulation time should be 60 s best).

4.3. Simulation Experiment. The tracking accuracy of the target under the ESM fusion strategy is significantly higher than the tracking accuracy of the target when working alone. Several common sensor data characteristics are analyzed, combined with the system under test, and three different fusion algorithm verification strategies are formulated. Simulate the three situations of the system function verification of the AFL information fusion simulation verification platform; for the first two fusion strategies, the local state estimation fusion algorithm is studied, and the traditional weighted fusion algorithm is solved due to the uncertainty and the measurement value of each sensor. Correlation leads to the problem of instability of the fusion algorithm, and the effectiveness and stability of the algorithm are verified by dividing three typical target motion scenes from two simulation cases. Aiming at the third fusion strategy, this paper adopts the correlation algorithm and adopts the classical weighted fusion algorithm to realize the third fusion strategy according to the results and verifies the effectiveness and stability of the algorithm through simulation experiments [24]. The specific data is shown in Table 6.

Through the analysis of the data in Table 5, we can see that the average value of individual tracking and fusion tracking errors, in terms of individual tracking: *Q*-axis direction is 295.91 m, *W*-axis direction is 107.07 m, and *E*-axis direction is 139.61 m; for fusion tracking, the *Q*-axis direction is 96.42 m, the *W*-axis direction is 246.66 m, and the *E*-axis direction is 134.31 m.

The functional device composition of the simulation experiment module is shown in Figure 4.

In the CAN interface module [25], the latest dual-channel digital isolator is used, and the isolation voltage is realized by the power supply module. In order to reduce the interference caused by the digital circuit, a 0 ohm resistor

is added to the circuit to connect. While enhancing the matching degree between channels, the isolation performance of the system is better.

5. Information Fusion Technology and Smart Sensor Usage Analysis

5.1. Theoretical Analysis of Information Fusion Technology. As an emerging technology, information fusion [26] will integrate signal detection technology, filter tracking, pattern recognition, statistical theory, optimization theory, fuzzy inference, and related technologies from neural networks. In the military field, information fusion mainly includes detection, correlation, interconnection, estimation, target recognition, condition assessment, and risk estimation. In the private sector, information fusion mainly includes collection, transmission, collection, analysis, filtering, synthesis, correlation and synthesis, fast information processing, and automatic graph plotting. This is a process of multilevel and multifaceted signal processing. Compared with the theoretical research of the information fusion simulation technology of a single sensor system, the information fusion technology brings information that a single sensor cannot match. According to the functional level of information fusion, information fusion is divided into 5 levels [27] as shown in Figure 5:

The first level of processing belongs to the category of distributed detection. By formulating fusion rules that are consistent with the fusion target, a specific detection and decision algorithm (CFAR, optimal threshold) is used to produce the best detection result. The second-level processing is mainly location-level fusion, including data association, filter estimation, and other technologies. The third level of processing is mainly attribute-level fusion, including image classification, recognition, and type judgment. Classification refers to distinguishing target types. Recognition is based on classification, and further judgments are made on the results of classification. The recognition also means the judgment of the picture. The fourth level of processing mainly includes picture estimation and impact assessment. Picture estimation is to establish a situation table between the entity and the entity collection, which is used to infer the data distribution. Therefore, general mathematical methods cannot be applied to picture situation estimation and impact assessment. It is necessary to find a more intelligent algorithm, such as clustering algorithm and learning + reasoning + knowledge embedded algorithm [28]. The fifth level of processing mainly divides the picture level, analyzes the content of the picture, and gives an opinion report based on the content in the known database.

5.2. Sensor Node Design Analysis. The wireless sensor node is composed of sensing, processor, communication, and power modules. As a complete microprocessor node unit, the performance of its components must be coordinated and efficient. The technical realization of each part requires trade-offs and trade-offs according to application requirements. The hardware block diagram of the sensor node is shown in Figure 6.

TABLE 3: The mean value of error estimated by each sensor and fusion algorithm in a uniform state.

	Sensor 1	Sensor 2	Sensor 3	Original	Local state
Mean error (m)	53.6136	37.4331	48.2942	44.8582	25.4570
Standard error (m)	34.2864	31.9831	29.4897	46.9826	23.4972

TABLE 4: Mean value of error estimated by each sensor and fusion algorithm under uniform acceleration.

	Sensor 1	Sensor 2	Sensor 3	Algorithm	Algorithm
Mean error (m)	37.2722	35.8432	73.1377	34.2457	27.7677
Standard error (m)	45.9513	46.2156	51.6455	31.6546	29.2565

TABLE 5: The mean value of error estimated by each sensor and fusion algorithm in the maneuvering state.

	Sensor 1	Sensor 2	Sensor 3	Algorithm	Estimation
Mean error (m)	35.8650	53.5290	53.6394	29.8509	38.7254
Standard error (m)	65.1262	42.4524	53.3245	31.2422	42.2424

TABLE 6: Comparison of mean values of individual tracking and fusion tracking errors.

Mean error (m)	Q-axis direction	W-axis direction	E-axis direction	Overall
Individual tracking	295.91	107.07	139.61	370.65
Fusion tracking	96.42	246.66	134.31	325.57

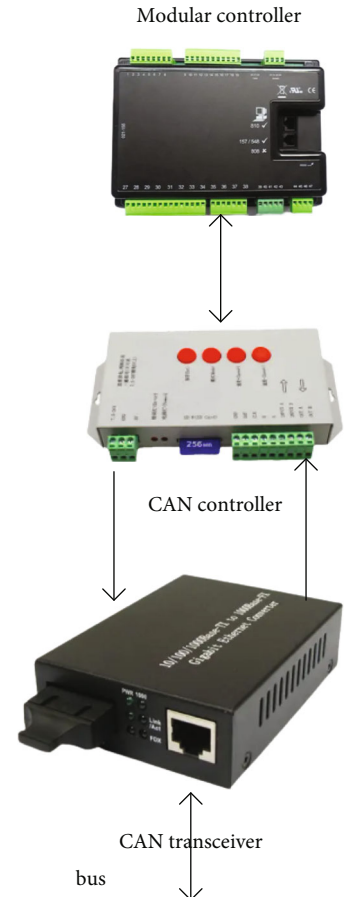


FIGURE 4: CAN module device.

Calculate the relative distance between the local estimates of multiple sensors, expressed as:

$$d_y = \left| \hat{x}_i(\hat{k}) - \hat{x}_j(k) \right|. \quad (14)$$

The optimal state estimate can be obtained by using the weighted combination of the calculated estimator and the innovation:

$$\hat{x}(k/k) = \hat{X}(k/k-1) + K(k)r(k). \quad (15)$$

The processor module is the core of the wireless sensor node. All equipment control, task scheduling, energy calculation and function adjustment, communication protocol, data merging, and data dumping procedures are completed by the support of this module, so the choice of processor is very important in the design of sensor nodes [29]. The main node data is shown in Figure 7.

Perform static experimental calibration on the input and output data of the sensor and its conditioning module, and get the calibration curve. The data of the calibration point is

$$\left. \begin{array}{l} z_i : z_1, z_2, \dots, z_{m-1}, z_m \\ q_i : q_1, q_2, \dots, q_{m-1}, q_m \end{array} \right\} i = 1, 2, \dots, m. \quad (16)$$

Among them, z is the experimental input data, and q is the experimental output data. Assuming that the fitting

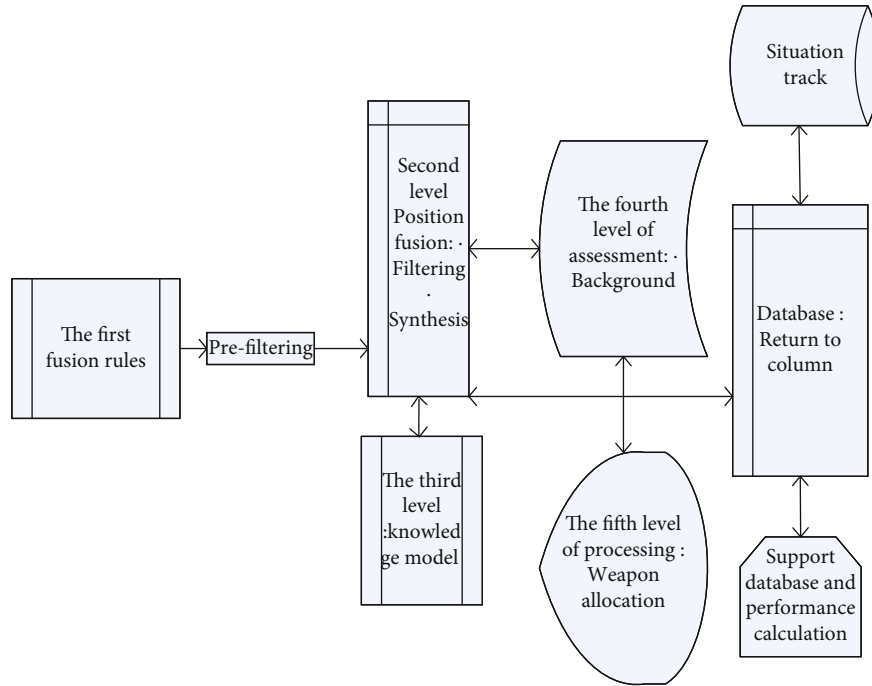


FIGURE 5: Functional block diagram of information fusion system.

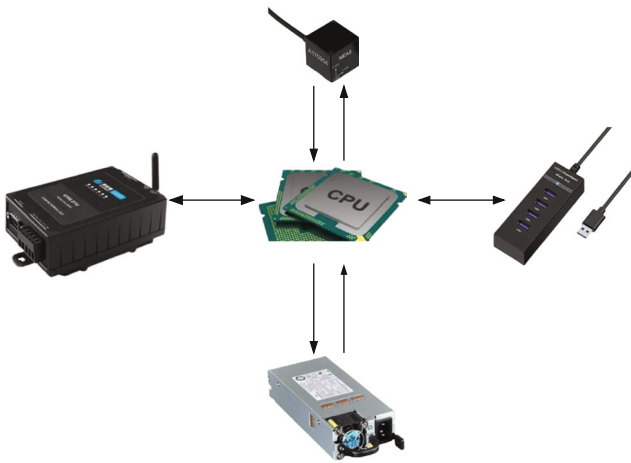


FIGURE 6: Hardware block diagram of sensor node.

curve of the nonlinear characteristic curve (i.e., inverse model) is

$$z_i(q_i) = a_0 + a_1q_i + a_2q_i^2 + a_3q_i^3 + \dots + a_nq_i^n. \quad (17)$$

From the above data, we can know that when selecting the processor of the sensor node, the following aspects are mainly considered:

- (1) Choose a powerful microprocessor
- (2) Ultralow power consumption design
- (3) The running speed should be as fast as possible

- (4) I/O ports and communication interfaces meet the design requirements
- (5) The cost should be as low as possible
- (6) High reliability

5.3. Analysis of the Analog Sensor Interface. Unlike the switch value, the output of the analog sensor [30] is a continuous voltage and current change. This article uses the commercially available CHTM-02/NB temperature and humidity sensor as a prototype to discuss interface design issues.

5.3.1. Humidity and Electrical Characteristics of Chtm-02/Nb. Sensitive element (humidity): polymer humidity resistance “CHR-01”

Power supply: 5 V ± 5%

Power consumption current: 5 mA max. (2 mA avg.)

Working range: temperature 0-40°C, humidity 15%-90%RH

Storage conditions: temperature 0-60°C, humidity 50%RH

Humidity transmission range: 0-100%RH

Accuracy (humidity accuracy): ±5%RH (at 25°C, input voltage = 4 V)

Output signal: 1-3 V (corresponding to 0-100%RH, at 25°C, input voltage = 4 V)

The humidity characteristic is shown in the line Z in Figure 8, and the temperature characteristic curve is shown in the line Z in Figure 8.

The voltage coefficient can be measured mainly by a voltmeter. Analyzing the above temperature and humidity performance and characteristic curves, it can be seen that connecting the temperature and humidity sensor requires the C51F330 core controller to perform AD on the humidity

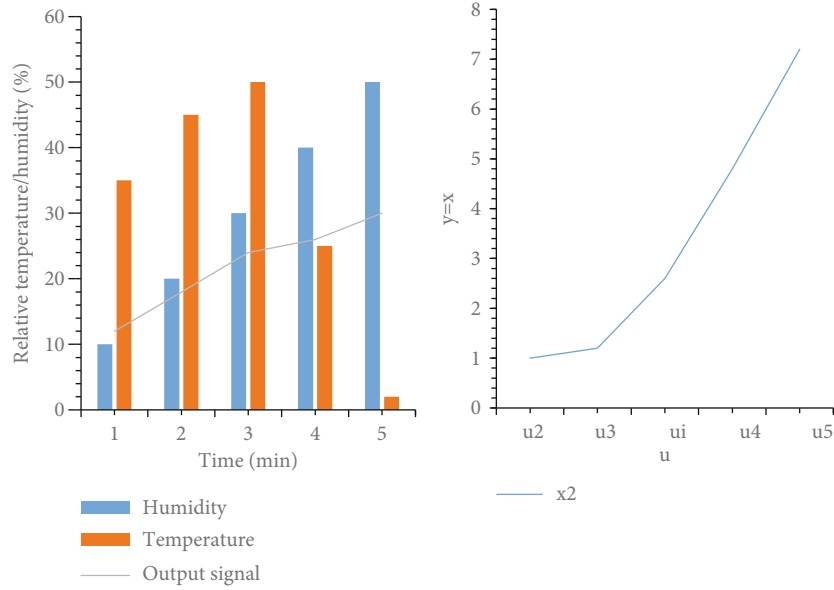


FIGURE 7: Data integration of wireless sensor nodes.

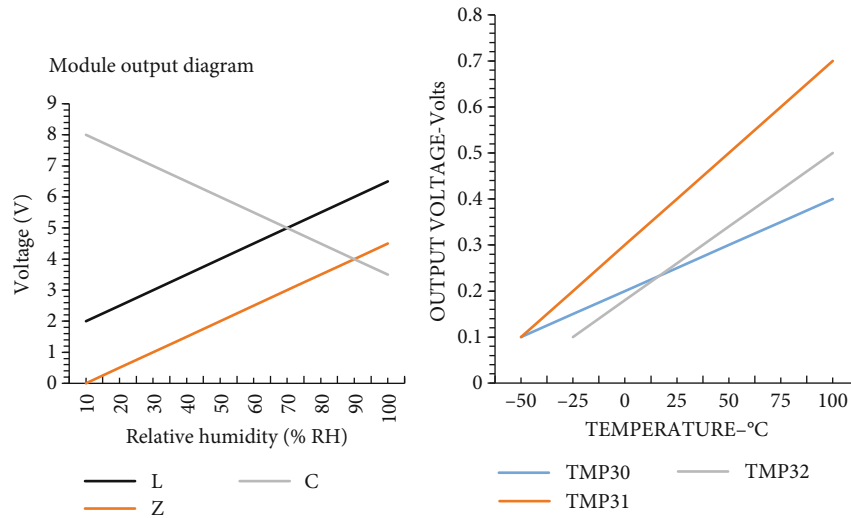


FIGURE 8: Humidity characteristic and temperature characteristic curve.

signal (1-3 V) and temperature signal (0-1 V) without loss of accuracy. After conversion and digital processing, it is sent to the test platform through the wireless port.

5.4. Smart Sensor Sampling Analysis. Under the condition that formula (5) is satisfied, the sampled signal can be restored to the original signal by using a low-pass filter. It is the comparison chart before and after the input signal is sampled. The broken line is the sampled signal, and the curve is the original analog signal as shown in Figure 9.

By comparing the data before and after the sampling of the input signal, it can be known that before Time = 2.5, even in the stop band region, the filter has equal ripple, but in the pass band, the filter also has a better linear phase. In other words, if the length of the filter is larger, the maxi-

imum value of the pot teeth can be close to the minimum value.

5.5. Realization of Intelligent Nonlinear Self-Correction Module Method. The programming methods used to realize the intelligent nonlinear self-correction module include look-up table method, curve fitting method, neural network method, SVM support vector machine method developed in recent years, etc. If the front end is active, there will be many. The input and output characteristics of the model (XU) are reproducible. They all have strong nonlinear mapping capabilities, which can not only improve nonlinearity but also improve system stability and suppress cross-sensitive sources. The input and output characteristics of the smart sensor system are shown in Figure 10.

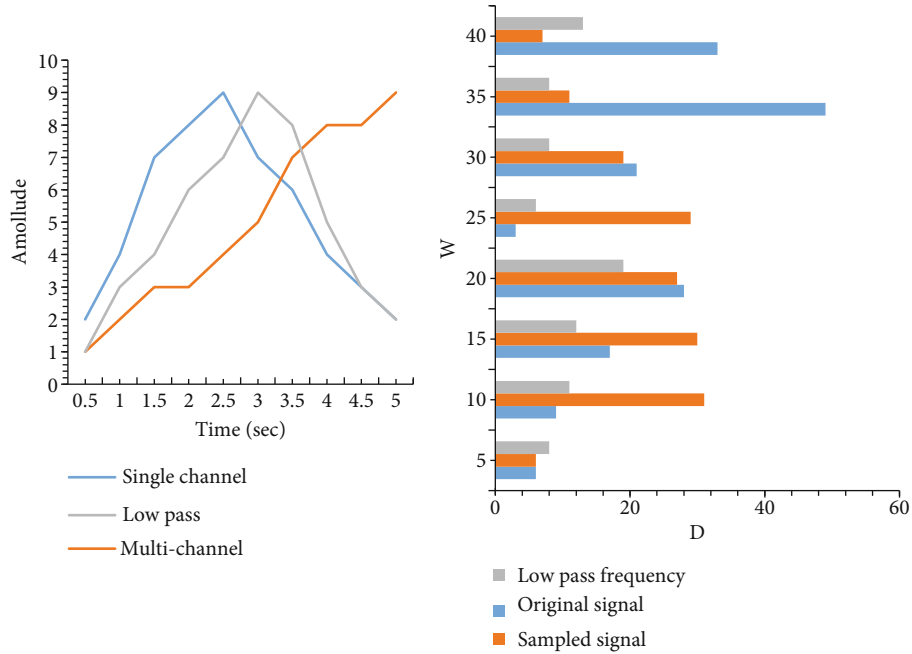


FIGURE 9: Comparison of input signal before and after sampling.

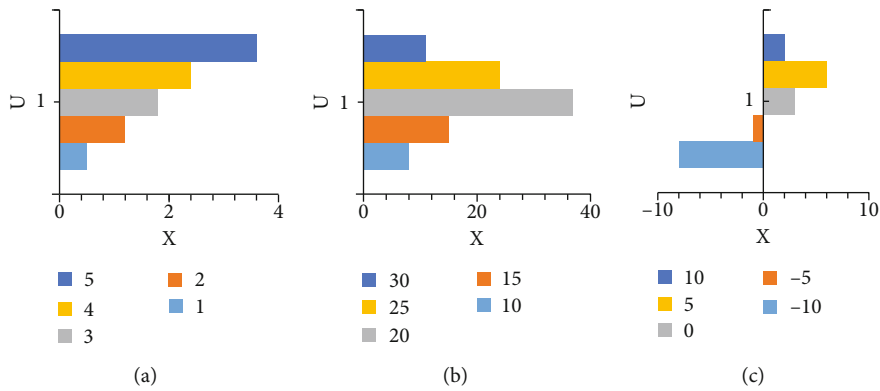


FIGURE 10: The input and output characteristics model of the intelligent sensor system: (a) positive model ($u = f(z)$); (b) inverse model ($z = f^{-1}(u)$); (c) input and output characteristics of an ideal smart sensor system ($q = z = f^{-1}(u)$).

The block diagram of the intelligent sensor system is mainly composed of the sensor and its conditioning module and the microcomputer microprocessor. On this basis, the positive model and the inverse model are abstracted. The so-called positive model refers to the input and output characteristics of the sensor and its signal conditioning module.

Because the multisensor information fusion technology shows better performance than any single sensor, the application of information fusion technology to the AFL fusion simulation verification platform greatly improves the performance of the platform, which mainly includes the following two parts.

In addition, it can be further learned from Table 1 that whether from the Q -axis direction, W -axis direction, E -axis direction or from the perspective of the overall position, the average error of tracking using information fusion technology is smaller than that of single tracking, and they are

improved, respectively. The increase was 9.94%, 16.64%, 3.79%, and 12.16%. In summary, although the accuracy is not high, the fusion with the angle provided by the multisensor makes the tracking accuracy after fusion higher than the tracking accuracy of the target when a single sensor or multiple sensors work alone, which verifies the fusion strategy and fusion. The effectiveness of the algorithm enhances the reliability and stability of the simulation verification platform for functional verification of the system under test.

6. Conclusions

Through the above experiments, it is not difficult to see that the research principle of using multiple smart sensors through the use of information fusion technology can be verified by actual operations and is feasible. The use of multiple smart sensors at the same time is compared with the

traditional single sensor in the past. The work efficiency and high-precision data collection are better than those in the past, and the cost is also lower, and the functions can also be diversified. On this basis, information fusion technology is used to correlate the data and information obtained by single and multiple information sources, and process the data, automatically analyze, coordinate, and optimize the use of sensors to make the use of sensors more intelligent. The application of the aspect is also able to be easily competent, and the analysis ability of the picture is greatly improved. The interactive art design of intelligent sensors and information fusion technology designed in this article is very practical, but this article will also explore the application of convolutional neural networks in interactive art design.

Data Availability

No data were used to support this study.

Conflicts of Interest

The authors declare that there are no conflicts of interest regarding the publication of this article.

References

- [1] J. Li, K. A. Mechitov, R. E. Kim, and B. F. Spencer Jr., "Efficient time synchronization for structural health monitoring using wireless smart sensor networks," *Structural Control and Health Monitoring*, vol. 23, no. 3, pp. 470–486, 2016.
- [2] M. R. García, M. L. Cabo, J. R. Herrera, G. Ramilo-Fernández, A. A. Alonso, and E. Balsa-Canto, "Smart sensor to predict retail fresh fish quality under ice storage," *Journal of Food Engineering*, vol. 197, no. mar., pp. 87–97, 2017.
- [3] S. Dissanayake, H. Pasqual, and B. Athapattu, "Economical colorimetric smart sensor to measure water quality of drinking water in CKDu prevalence areas," *IEEE Sensors Journal*, vol. 17, no. 18, pp. 5885–5891, 2017.
- [4] Y. Liu, X. Fan, C. Lv, J. Wu, L. Li, and D. Ding, "An innovative information fusion method with adaptive Kalman filter for integrated INS/GPS navigation of autonomous vehicles," *Mechanical Systems and Signal Processing*, vol. 100, pp. 605–616, 2018.
- [5] Q. Zhou, P. Jiang, X. Shao, J. Hu, L. Cao, and L. Wan, "A variable fidelity information fusion method based on radial basis function," *Advanced Engineering Informatics*, vol. 32, no. apr., pp. 26–39, 2017.
- [6] S. Xu, S. Zhang, and W. Cao, "Study on the multi-sensors monitoring and information fusion technology of dangerous cargo container," *AIP Conference Proceedings*, vol. 1890, no. 1, 2017.
- [7] L. Xu and X. Chen, "Research on the design and autonomous learning implementation of interactive learning system in art teaching," *Revista de la Facultad de Ingenieria*, vol. 32, no. 16, pp. 101–107, 2017.
- [8] X. Chen, "Computer-aided design method for hand drawn art animation," *Paper Asia*, vol. 2, no. 3, pp. 149–153, 2019.
- [9] F. C. Chuang, C. L. Chang, Y. N. Chow et al., "Application of water tank employing smart sensor for thermal-electric energy conversion on vehicles," *Sensors and Materials*, vol. 32, no. 1, pp. 135–148, 2020.
- [10] F. Morais, P. Carvalhaes-Dias, L. Duarte, E. Costa, A. Ferreira, and J. S. Dias, "Fringing field capacitive smart sensor based on PCB technology for measuring water content in paper pulp," *Journal of Sensors*, vol. 2020, Article ID 3905804, 13 pages, 2020.
- [11] G. W. Hunter, D. Makel, S. Carranza, and J. Xu, "(Invited) High temperature smart sensor systems for Venus and aerospace applications," *ECSMeeting Abstracts*, vol. MA2020-01 (30), pp. 2256–2256, 2021.
- [12] H. Koyuncu, A. Bagwari, and G. S. Tomar, "Simulation of a smart sensor detection scheme for wireless communication based on modeling," *Electronics*, vol. 9, no. 9, pp. 1506–1517, 2020.
- [13] A. Bagwari, J. Bagwari, and G. S. Tomar, "Smart sensor for the underwater communication signal," *Wireless Personal Communications*, vol. 116, no. 2, pp. 1463–1480, 2021.
- [14] S. Naha, S. P. Wu, and S. Velmathi, "Naphthalimide based smart sensor for CN-/Fe3+and H2S. Synthesis and application in RAW264.7 cells and zebrafish imaging," *Advances*, vol. 10, no. 15, pp. 8751–8759, 2020.
- [15] H. Jim, "Art game: an early interactive design from the office of Charles and Ray Eames," *Interactions*, vol. 24, no. 3, pp. 27–35, 2017.
- [16] S. Famila, A. Jawahar, A. Sariga, and K. Shankar, "Improved artificial bee colony optimization based clustering algorithm for SMART sensor environments," *Peer-to-Peer Networking and Applications*, vol. 13, no. 4, pp. 1071–1079, 2020.
- [17] A. di Graziano, V. Marchetta, and S. Cafiso, "Structural health monitoring of asphalt pavements using smart sensor networks: a comprehensive review," *Journal of Traffic and Transportation Engineering*, vol. 7, no. 5, pp. 639–651, 2020.
- [18] N. Telagam, S. Panda, and N. Kk, "Smart sensor network based fire rescue system design using lab VIEW," *International Journal of Recent Technology and Engineering*, vol. 8, no. 2, pp. 3372–3380, 2019.
- [19] S. Chen, B. Gavish, S. Zhang, Y. Mahler, and S. Yedgar, "Monitoring of erythrocyte aggregate morphology under flow by computerized image analysis," *Biorheology*, vol. 32, no. 4, pp. 487–496, 1995.
- [20] R. Roscher, K. Herzog, A. Kunkel, A. Kicherer, R. Töpfer, and W. Förstner, "Automated image analysis framework for the high-throughput determination of grapevine berry sizes using conditional random fields," *Computers & Electronics in Agriculture*, vol. 100, no. 1, pp. 148–158, 2014.
- [21] J. Weickert, S. Grewenig, C. Schroers, and A. Bruhn, "Cyclic schemes for PDE-based image analysis," *International Journal of Computer Vision*, vol. 118, no. 3, pp. 275–299, 2016.
- [22] W. Sun, L. Wang, and E. Tutumluer, "Image analysis technique for aggregate morphology analysis with two-dimensional Fourier transform method," *Transportation Research Record*, vol. 2267, no. 1, pp. 3–13, 2012.
- [23] N. Mizoue, "CROCO: semi-automatic image analysis system for crown condition assessment in Forest health monitoring," *Journal of Forest Planning*, vol. 8, no. 3, pp. 17–24, 2002.
- [24] C. I. Su, C. S. Leu, and H. M. Chern, "Image analysis of composite yarn cross sections," *Textile Research Journal*, vol. 69, no. 3, pp. 203–207, 2016.

- [25] L. Yang, Y. Ren, and W. Zhang, "3D depth image analysis for indoor fall detection of elderly people," *Digital Communications and Networks*, vol. 2, no. 1, pp. 24–34, 2016.
- [26] T. Taoka, Y. Masutani, H. Kawai et al., "Evaluation of glymphatic system activity with the diffusion MR technique: diffusion tensor image analysis along the perivascular space (DTI-ALPS) in Alzheimer's disease cases," *Japanese Journal of Radiology*, vol. 35, no. 4, pp. 172–178, 2017.
- [27] N. Chen, F. Sun, L. Ding, and H. Wang, "An adaptive PNN-DS approach to classification using multi-sensor information fusion," *Neural Computing and Applications*, vol. 18, 2019.
- [28] Z. Yang, Z. Lin, L. Guo, Q. Li, and W. Liu, "MMED: a multi-domain and multi-modality event dataset," *Information Processing and Management*, vol. 57, no. 6, 2020.
- [29] H. Hao, M. Wang, Y. Tang, and Q. Li, "Research on data fusion of multi-sensors based on fuzzy preference relations," *Neural Computing and Applications*, vol. 31, pp. 337–346, 2019.
- [30] J. Xia, Y. Feng, L. Liu, and D. Liu, "An information fusion model of innovation alliances based on the Bayesian network," *Tsinghua Science and Technology*, vol. 23, no. 3, pp. 347–356, 2018.

Research Article

Digital Development Strategy of Agricultural Planting and Breeding Enterprises Based on Intelligent Sensors

Jincheng Zhang 

College of Business and Economics, Australia National University, Canberra 2600, Australia

Correspondence should be addressed to Jincheng Zhang; u7097621@anu.edu.au

Received 1 December 2021; Accepted 30 December 2021; Published 27 January 2022

Academic Editor: Nima Jafari Navimipour

Copyright © 2022 Jincheng Zhang. This is an open access article distributed under the Creative Commons Attribution License, which permits unrestricted use, distribution, and reproduction in any medium, provided the original work is properly cited.

The digitalization of agricultural planting and breeding enterprises is the only way for agricultural development. Now with the development of various technologies, the digitalization of agricultural enterprises is becoming faster and faster. Today, the development of intelligent sensors provides platform support for the digitalization of agricultural enterprises. This article is aimed at introducing the application of intelligent sensors in agriculture to provide strategic research for the digital development of agricultural planting and breeding enterprises. This paper proposes the establishment of a system platform for network intelligent sensors and proposes the establishment of an agricultural short message management publishing platform. And the existing public information transmission methods are used to provide a cheap, simple, and fast way for agricultural producers to quickly obtain agricultural information, so as to provide a feasible plan for solving the agricultural “last mile of agriculture” problem. After inspection and analysis, the information management release platform can meet the design requirements, and the processing rate of short-term interest is above 98%, which can pave the way for the digital industrialization of agricultural enterprises.

1. Introduction

As a descendant of China, China has a profound agricultural heritage from ancient times to the present. Although China is a large agricultural country to this day, since most of its agriculture is scattered, the start of agricultural industrialization is relatively late. From industrialization to informatization, from agricultural mechanization to agricultural informatization, it is an important stage of human progress and agricultural development. Agricultural informatization can speed up the cultivation of agricultural science and technology talents and the dissemination of agricultural science and technology knowledge, improve the international competitiveness of agricultural products, and promote the sustainable development of agriculture, thus becoming a historical opportunity for agricultural development. The rapid development of digitalization is an unquestionable fact, and various signs indicate that intelligence and big data are the general trend, and socialized mass production and extensive resource sharing are the general trend [1].

Digital agriculture refers to the use of digital technologies such as geographic information systems, global posi-

tioning systems, remote sensing, automation, computers, communications, and networks to rationally utilize agricultural resources in agriculture, management, operation, circulation, and services; to reduce production costs; and to improve the ecological environment [2]. It is to develop agriculture in accordance with the objective laws inherent in agriculture and the goals and directions required by humans. Compared with traditional agriculture, the industrialization of agriculture should be based on market demand, be regionalized and specialized, and form a comprehensive, integrated, intensive, and socialized enterprise management system. In a perfectly competitive market environment, the high degree of openness and transparency of digital technology not only reduces the resistance to market entry, attracting many competitors, but also makes it easy to identify the path of resource creation capabilities in the value-added process of e-commerce. But it is likely to be imitated or even surpassed by competitors in a short period of time, and the value cannot be effectively realized.

Therefore, when an enterprise forms a unique advantage capability, it must take into account the competition process

and dynamic response of the enterprise with its competitors in the external market, so as to realize the value of agriculture in the competitive interaction. The emergence of digital agriculture has made agricultural equipment more complex and precise, making traditional agricultural machinery testing methods more difficult to develop and test. In order to solve the traditional on-site test cycle, high cost, and difficult problems, it is necessary to explore new test methods.

For a long time, the problems in the development, design, manufacturing, and use of modern agricultural equipment are the variety of products, complex working conditions, and high requirements for product performance, service life, and cost. There are many factors that affect product quality, and the consequences of these occurrences are very serious, therefore, a lot of complex testing work needs to be established. The entire process requires the establishment of necessary test sites, the use of a large number of various test equipment, a large amount of test costs, a large experimental team, and a lot of test time. The agricultural information integration service platform has the characteristics of strong database security, good stability, friendly interface, strong operability, easy to learn and understand, and complete and practical functions, which meets the needs of current agricultural information management. The integrated agricultural information service platform is of great significance for standardizing the order of agricultural information management, improving work efficiency, serving farmers, and promoting the economic development of agricultural products [3]. It is helpful to improve the farmers' understanding of agricultural market information, scientific and technological information, and government information and to accelerate the construction of agricultural information.

This article first consults a large number of relevant expositions at home and abroad through the method of data analysis. It is found that most of the research on the digital development strategy of agricultural planting and breeding enterprises focuses on the industrial optimization of planting and breeding. This article takes the intelligent sensor as a breakthrough and summarizes the following innovations: (1) In the intelligent sensor design, the pressure sensor is emphasized. This is very broad for agricultural applications, because whether it is the weather forecast for planting or the air pressure in aquaculture, it is a necessity for the digital development of agricultural enterprises. (2) In the design method, the comparison and selection were carried out many times. From the system algorithm, the network protocol, to the final platform effect test, the conclusions were drawn in full comparison. (3) In the discussion of the digital development strategy, more are combined in experiments and methods, which will be more data-supported and convincing than a completely written discussion.

2. Related Work

Many scholars believe that entering an agricultural society marks the end of a barbaric society. The four ancient civilizations all took the river as the origin of their civilization and relied on the flat and fertile land beside the river as

the beginning of agriculture, and agriculture is also the foundation of human development. A large number of scholars have done research on agricultural development, for example, Reganold and Wachter have done research on the controversy of organic agriculture. They believe that organic agriculture plays an untapped role in establishing a sustainable agricultural system, but there is no way to feed the earth safely. Instead, a mix of organic and other innovative agricultural systems is required. However, there are major obstacles to the adoption of these systems, and multiple policy tools are needed to facilitate their formulation and implementation [4]. Aničić and others specifically discussed the agricultural situation in Serbia, and they believed that the economic development of Yugoslavia (Serbia) after World War II was at the expense of agriculture, and they analyzed and demonstrated this. The analysis results believe that Serbia's agricultural development is much more likely, and under appropriate macroeconomic policies, it can become a huge comparative advantage of our economy in the world's developed markets [5]. Gurr et al. started with agriculture to discuss food security issues, believing that global food security needs to increase crop productivity to meet growing demand. They concluded that a simple diversification method, in this case the growth of nectar-producing plants, can promote the ecological intensification of agricultural systems [6]. Tirivayi and others have considered the issue of poverty eradication more deeply, and they believe that eradicating the hunger and poverty of poor small farmers requires both agricultural interventions and social protection interventions. After the research, they concluded that the existing evidence provides an empirical basis for establishing a synergy between social protection and smallholder agriculture to a large extent [7]. There are many different discussions among scholars related to the research of digitization and intelligent sensors. Goel raised the question, "Why is it digital?" He believes that no company is immune to the influence of digital technology, but few companies fully utilize digitalization, and the digital journey of any company is different because different from individual technologies, companies are different. Digitization will touch and significantly affect all aspects of enterprises, but enterprises must think about how to create the greatest value through digitization, namely, marketing, sales, supply chain, and customer service. Once the area is determined, priorities and strategies can be established based on short-term and long-term roadmaps [8]. Szesz et al. also did related research, and they proposed an intelligent fuzzy control system based on the mathematical model of Cruz (2002) and applied it to the Arduino platform for decision support of grain aeration. To this end, an intelligent Arduino system was developed, which receives the environmental values of temperature and humidity, and then processes them in the fuzzy controller, and returns the output as a suggestion to reasonably control the aeration process, and the results show that the system is effective [9]. Lin and others analyzed the CIAA project in Argentina, and their current work includes designing an integrated intelligent system based on the EDU-CIAA NXP version for educational and applied research purposes [10]. Arablouei et al. considered the

problem of using acceleration measurement data on resource-constrained sensor nodes to classify cow behavior in real time. They developed a pipeline of preprocessing, feature extraction, and classification specifically for performing inference on sensor node intelligent systems. The results show that this is achieved without causing any significant burden on intelligent system resources in terms of energy, computing, or memory [11].

3. Intelligent-Based Enterprise Digital Development Method

3.1. Intelligent Sensors. The intelligent sensor system is based on a detection device for external information. It can detect the information to be measured [12, 13] and convert it into electrical signals or other forms of signal output according to a certain rule, which is used in a dedicated computer system that performs independent functions [14]. Intelligent systems are based on microelectronics technology, computer technology, control technology, and communication technology, with application as the center, emphasizing the unity and relevance of hardware and software [15]. In addition, in intelligent systems, both software and hardware can be tailored and streamlined to meet the system's requirements for functions, costs, and other aspects. A standard intelligent system generally consists of four parts: processor, peripheral equipment, operating system, and application software [16]. In recent years, with the rapid development of information perception technology, electronic computer technology, and wireless communication technology, low-power multi-function intelligent sensor technology and manufacturing technology have been greatly improved [17–19].

The intelligent agricultural system includes temperature sensor, signal processing circuit, carbon dioxide sensor, image acquisition device, display device, GPRS device, microprocessor, external storage device, image processing device, and carbon dioxide data processing device. The composition of a typical intelligent system is shown in Figure 1.

As shown in Figure 1, the system composition mainly includes the following 8 parts. (1) *Processor core*: the heart of an intelligent system is the processor core. The processor core ranges from a simple and inexpensive 8-bit microcontroller to a more complex 32-bit or 64-bit microprocessor and even multiple processors. Intelligent designers must choose the lowest cost device for applications that can meet all functional and nonfunctional time limits and requirements. (2) *Analog I/O*: D/A and A/D converters are used to collect data and feedback from the environment. Intelligent designers must understand the type of data that needs to be collected from the environment, the accuracy requirements of the data, and the rate of input/output data in order to select the appropriate converter for the application. The response characteristics of intelligent systems are determined by the external environment. Intelligent systems must be fast enough to keep up with changes in the environment to simulate information, such as light, sound pressure, or acceleration being sensed and input into the intelligent system. (3) *Sensors and actuators*: sensors generally perceive analog information from the environment. The imple-

menting agency controls the environment in some ways. (4) *User interface*: these interfaces can be as simple as LED screens or as complex as screens on well-crafted mobile phones and digital cameras. (5) *The specific entrance of the application program*: similar to ASIC or FPGA hardware acceleration, it is used to accelerate the specific function modules that have high performance requirements in the application program. Intelligent designers must use accelerators to maximize application performance to plan or partition programs appropriately. (6) *Software*: software is an important part in the development of intelligent systems. In the past few years, the amount of intelligent software has grown faster than Moore's Law, doubling almost every ten months. Intelligent software is often optimized in some aspects of performance, memory, and power consumption. More and more intelligent software are written in high-level languages, such as C/C++. And more performance-critical code segments are still written in assembly language. (7) *Memory*: memory is an important part of an intelligent system. Intelligent programs can run without RAM or ROM. There are many volatile and nonvolatile memories used in intelligent systems. There will be more explanations about this content at the back of the book. (8) *Simulation and diagnosis*: intelligent systems are difficult to see or touch. When debugging, the interface needs to be connected to the intelligent system. Diagnostic ports, such as the JTAG Joint Test Action Group, are often used to debug intelligent systems. On-chip emulation can be used to provide visibility behavior of the application. These simulation modules can visually provide runtime behavior and performance. In fact, the on-board self-diagnosis capability replaces the function of an external logic analyzer.

Agricultural Internet of Things refers to the application of Internet of Things technology in all aspects of agriculture, including agricultural production, operation, management, and services. The agricultural Internet of Things takes information perception equipment, communication network lines and intelligent information processing technology applications as the core, realizes scientific management of agricultural production, and achieves the goals of optimizing the utilization rate of agricultural resources, reducing production management costs, improving the agricultural ecological environment, and increasing yield and quality. The agricultural Internet of Things is an important part of the application field of the Internet of Things and an important guarantee for the realization of modern agriculture. Its research content is extensive, involving the fields of agricultural information perception (acquisition), information transmission, information processing and information utilization. The core of the agricultural Internet of Things is to realize the intelligent acquisition of agricultural production, operation, management, and service data information through Internet of Things technology, and to improve the degree of intelligence in various links such as agricultural production, management, trading, and logistics. Its essential purpose is to promote agricultural production methods.

3.1.1. Intelligent Atmospheric Pressure Sensor. In the agricultural sensor, the pressure sensor is an important one [20].

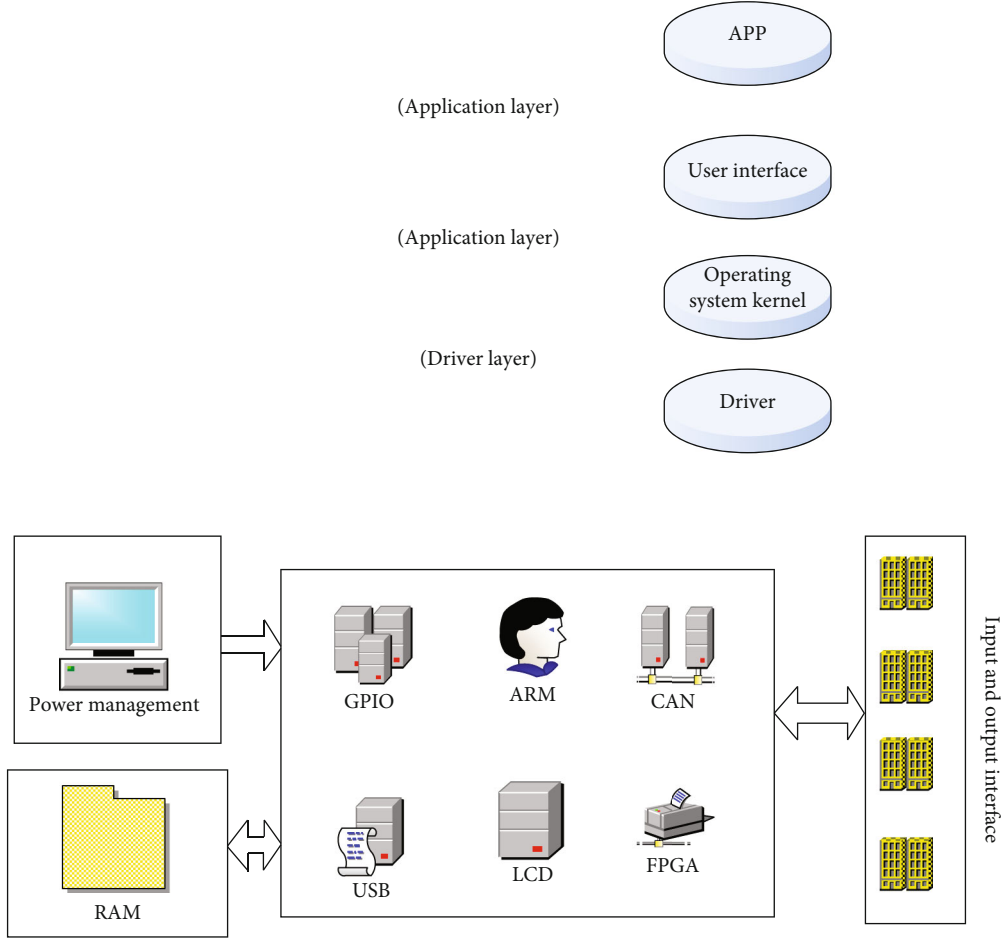


FIGURE 1: Typical intelligent system composition.

The calculation formula of each atmospheric data parameter is as follows:

- (1) *Pneumatic height* G_p : can be calculated according to the relationship with static pressure P_∞ [21]:

The stream (-914.4~11000 m) is the following formula:

$$G_p = \frac{T_0}{K} \left[1 - \left(\frac{P_\infty}{P_{\infty 0}} \right)^{KR_a/g_0} \right], \quad (1)$$

The flat layer (11000-20000 m) is the following formula:

$$G_p = G_T + \frac{R_a T_T^*}{g_0} \ln \frac{P_{\infty T}}{P_\infty}. \quad (2)$$

The optical layer (20000~32004) is the following formula:

$$G_p = G_S + \frac{T_T^*}{K} \left[\left(\frac{P_{SS}}{P_\infty} \right)^{KR_a/g_0} - 1 \right]. \quad (3)$$

- (2) *Lifting velocity* \dot{G}_p : also known as the height change rate, it can be directly obtained directly to the air pressure height G_p [22]. However, in order to obtain less calculated delay, the static pressure \dot{P}_∞ is usually taken, and then [23] is obtained according to the static pressure P_∞ and the static pressure change rate \dot{P}_∞

$$\dot{G}_p = -\frac{R_a T \dot{P}_\infty}{g_0 P_\infty}. \quad (4)$$

In the formula (4): T is the actual measurement and corrected temperature value, and the standard atmospheric temperature can be directly taken and the results are not affected [24].

- (3) *Atmospheric static temperature* TS : the temperature during high-speed airflow will increase, so sensitive temperature includes temperature increments caused by atmospheric temperature and airflow

delay, referred to as indication temperature TM (atmospheric temperature) [25]. The temperature increase can be solved according to the hypothesis conditions of the Bernu Lee equation and the ideal gas heat insulating process, which can be solved to obtain the atmospheric thermostatic temperature [26]:

$$T_s = \frac{T_m}{1 + \text{RE} \cdot 0.2M_\infty^2}. \quad (5)$$

The RE in Formula (5) is a recovery coefficient to eliminate temperature probe mounting deviations, which is generally considered to be a constant, at a stagnation point, RE = 1 [27].

- (4) *Atmospheric density ratio* ρ/ρ_0 : can be based on the relationship between the static pressure and the pressure height $P_\infty = f(G_p)$ [28], eliminating the static pressure to obtain the following formula:

$$\frac{\rho}{\rho_0} = \frac{f(G_p) T_0}{P_\infty T}. \quad (6)$$

In addition, the atmospheric density ratio can also be calculated by static pressure and measurement atmospheric temperature (indicating atmospheric temperature) [29], as in the following formula:

$$\frac{\rho}{\rho_0} = \frac{P_\infty T_0 (1 + \text{RE} \cdot 0.2M_\infty^2)}{P_{\infty 0} T_m}. \quad (7)$$

- (5) *True variety VT*: referring to the atmospheric secondary temperature TS by indicating the temperature and can get the local sound, and then, the vacuum speed can be obtained according to the number of Mach [30], as in the following formula:

$$V_T = M_\infty \sqrt{\frac{\gamma R_a T_m}{1 + r \cdot 0.2M_\infty^2}}. \quad (8)$$

At this point, the underlying formula of the intelligent atmospheric pressure sensor is completed. Table 1 shows the meaning of each symbol in the above formula, wherein the units have been converted to an international common unit [31].

3.1.2. Intelligent Multicore Learning Multimode Feature Selection Algorithm. Multicore learning is also a common algorithm for feature selection algorithms, and its model is shown in Figure 2 [32].

The multicore learning algorithm commonly used by scholars is generally divided into two ways: nonlinear combinations and linear combinations. There are two categories

[33] for the linear combination. Formula (9) can be directly summoned:

$$H(x_i, x_j) = \sum_{k=1}^M K_k(x_i, x_j). \quad (9)$$

Formula (10) is the weighted summation.

$$H(x_i, x_j) = \sum_{k=1}^M d_k K_k(x_i, x_j). \quad (10)$$

In Equation (9), each item has the same weight by default; this algorithm will be simpler, and the result will be obtained by summing between them [34]. Since the weight of d_k is added in Equation (10), the result will be closer to the actual value, because of the current development of computing technology, multiple weighting will not cause great calculation difficulty, so now the weighted summation method is generally used. Because the weight is not specified, the kernel matrix should be selected from the following set, as shown in the following equation:

$$\kappa = \left\{ K : K = \sum_{k=1}^M d_k K_k, k \geq 0, \text{tr}(k) \leq c \right\}. \quad (11)$$

A further restriction on Equation (11) is to make the value of the weight nonnegative and then select the combined kernel matrix from the set as shown in the following equation:

$$\kappa = \left\{ K : K = \sum_{k=1}^M d_k K_k, k \geq 0, \text{tr}(k) \leq c \right\}. \quad (12)$$

In Equation (12), the method of feature selection adopts the principle of minimization, and the features with a high degree of dispersion are selected, that is, the top-ranked features [35]. In addition, there is also a way to select weight features as shown in the following equation:

$$H(x_i, x_j) = \sum_{k=1}^M d_k(x_i) K_k(x_i, x_j) d_k(x_j). \quad (13)$$

In Equation (13), because the variable method is limited, the weight distribution cannot be carried out indefinitely. Therefore, related studies have proposed a new combination method, such as an index combination method, as shown in the following formula:

$$H(x_i, x_j) = \exp \left(- \sum_{k=1}^M d_k X_I^T A_X X_j \right), \quad (14)$$

TABLE 1: Meaning and value of each symbol in the atmospheric data calculation.

Symbol	Significance	Standard value
$P_{\infty 0}$	Sea level pressure	101.325 kPa
$P_{\infty S}$	Top tropospheric pressure value	22.632 kPa
P_{SS}	Atmospheric pressure at the top stratospheric altitude	5.47482 kPa
T_0	Sea level temperature	288.15 K
*	Top tropospheric temperature	216.65 K
K	Tropospheric temperature decline rate	$6.5 \times 10^{-3} \text{ } ^\circ\text{C/m}$
	Increasing rate of actinic layer temperature	$1 \times 10^{-3} \text{ } ^\circ\text{C/m}$
HT	Top troposphere height	11000 m
HS	Stratospheric top height	20000 m
H	Height of top layer of photochemical layer	32004 m
g_0	Sea level acceleration of gravity	9.80665
Ra	Gas constant	287.0529 J/K/kg
A0	Sea level sound velocity at standard air pressure and standard temperature	340.294 m/s

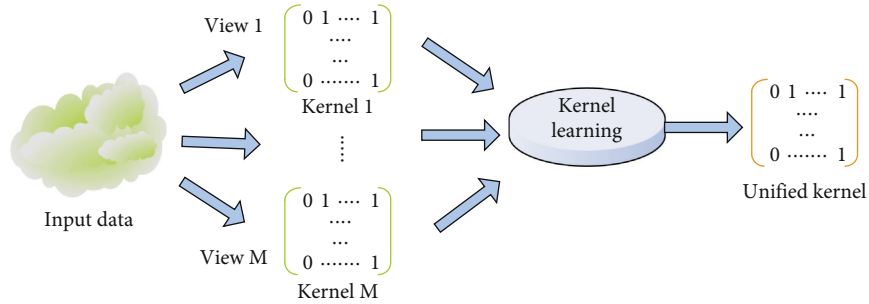


FIGURE 2: Multicore learning diagram.

or the exponentiation combination method, as shown in the following formula:

$$H(x_i, x_j) = \left(d_0 + \sum_{k=1}^M d_k X_i^T A_X X_j \right)^n. \quad (15)$$

Some scholars have tried to use the product of basic cores or other combinations to achieve multicore learning. The nonlinear combination based on polynomials is shown in the following equation:

$$K = \sum_{0 \leq K_1 + K_2 + \dots + K_m \leq d, k_m \geq 0} \mu k_1 \dots k_m \prod_{m=1}^M K_m(x_i, x_j) K_m. \quad (16)$$

3.2. Digital Development Strategy. The concept of corporate strategy refers to the fact that in order to achieve its own pre-determined goals, after considering the internal and external environments of the company, the company makes a systematic and holistic strategic deployment of the company's long-term development goals and operational implementation, so as to ensure that the company has a sustained and stable development. Since the emergence of corporate strategy theory, there have been different development stages,

and many schools with different propositions and styles have emerged. Looking at its evolutionary trajectory, it can be roughly divided into the following 4 stages:

- (1) *Early stage of strategic thinking*: during this period, the strategic thinking is in the lead-in period, and a relatively complete theoretical system has not yet been formed.
- (2) *Traditional strategic theory stage*: research on corporate strategy systems mostly takes the book "Business Strategy" written by Ansoff in the 1960s as a starting point. Strategic theories have gradually formed a systematic theory, and many theoretical schools have also emerged.
- (3) *Competitive strategy theory stage*: many academic schools have conducted multifaceted research on strategy in the aforementioned traditional strategy stage, which has enabled continuous progress in corporate strategy research. As the times change, the research on corporate strategy has gradually deepened. In the process of being closely integrated with the reality of business management, the research direction of the corporate strategy system began to shift to corporate competition, and the industry

structure school, core strength school, and resource strategy school all have their own achievements.

- (4) *The stage of dynamic strategy theory*: entering the 21st century, the trend of economic globalization continues to increase. While enterprises continue to expand, they are also threatened by domestic and international competition, and the traditional strategic view has been difficult to adapt to the changes in the corporate living environment, and a new strategic theory emerged as the times require, that is, the dynamic strategy theory.

4. Intelligent Sensor Platform Construction

4.1. Hardware Platform Construction

4.1.1. Hardware Module Design. Agricultural information technology is a comprehensive application of sensors, computers, and communication technologies in agriculture. Its content mainly includes agricultural databases and management information systems, geographic information systems, agricultural remote sensing monitoring, global positioning systems, agricultural decision support systems, agricultural expert systems, crop simulation models, agricultural information networks, and agricultural intelligent control technologies. At present, agricultural information databases, agricultural expert systems, crop simulation models and their integrated systems, and precision agricultural technology systems are widely used in agriculture. At present, there is no unified and standardized management system standard for the management of agricultural leading industries, and there are also differences in the management of different regions and different leading industries. There is no database standard for multimedia data and policy document data of leading industries; therefore, we refer to relevant national laws and regulations to integrate the actual needs of management work in different regions and different agricultural leading industries.

The hardware platform structure is shown in Figure 3.

Most of the hardware devices built as platforms have output and input interface connections, and the design of peripheral interface circuits is particularly important.

Part of the circuit design in Figure 3 is as follows.

(1) *Power Supply and Reset Circuit.* The total power supply uses the VCC5V DC power supply, the processor's on-chip peripherals use VDD3.3 DC power supply, the processor core power supply uses 2.5V DC power supply, and the real-time clock power supply uses VCCTR continuous power supply. In order to ensure the stability and reliability of the system, the chip IMP811T is selected to form the system reset circuit.

(2) *Ethernet Interface Circuit.* Comprehensive agricultural management requires a large amount of data for support, including a large amount of real-time monitoring (measurement) data, basic agricultural resource data, GIS data, and remote sensing data. According to the application data from different sources and methods, the comprehensive database

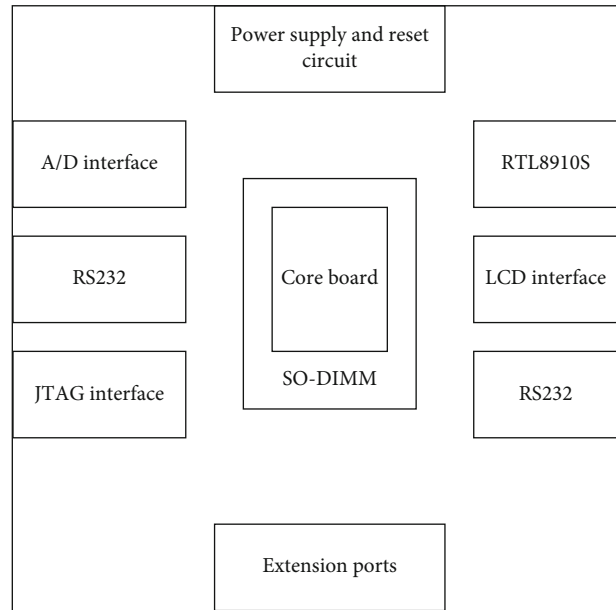


FIGURE 3: Block diagram of the system platform.

is logically divided into the spatial database, basic operation database, agricultural management business database, decision business database, model database, planning database, and professional knowledge database.

The system is designed with an Ethernet interface, and the design system selects RTL8019S as the network control chip. Because of its excellent performance and stability of the processing core, it has always been very popular. This article bought a cost-effective chip in a shopping software.

(3) *Serial Interface Circuit.* The baud rate is controlled by the UART baud rate divider register, and its calculation formula is shown in the following equation:

$$UBRDIV_n = \left\lceil \frac{MCLK}{bps * 16} \right\rceil - 1. \quad (17)$$

In Formula (17), MCLK is the system frequency, bps is the baud rate, UBRDIV_n is the value of the register, and $\lceil \cdot \rceil$ represents the rounding function number.

(4) *LCD Display Interface Circuit.* The intelligent controller installed under the rotating platform collects the sensor information and transmits it to the industrial computer through the serial port. The industrial computer calculates the deviation between the actual position and posture information and the data in the virtual scene, then gives the feedback control signal to realize the interactive control and cosimulation of the system. The built-in LCD controller provides the following external control signals, as shown in Figure 4.

4.1.2. Comparison of Related Network Protocols

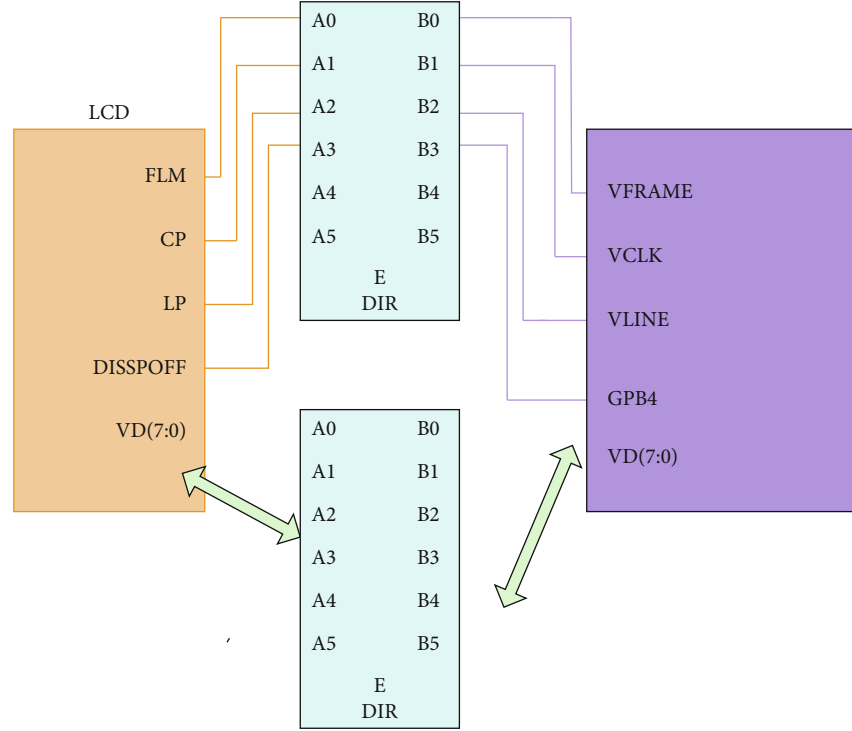


FIGURE 4: Block diagram of the connection between LCD display module and S3C44B0X.

(1) *Comparison of Network Survival Time.* Figure 5 shows the comparison of the survival time of the four network protocols. For the other three, it is almost a vertical decline; only the decline in the EEUCP agreement will be more moderate, and this can also discover the advantages of the EEUCP protocol. For the protocol, this will save more energy, provide more process network support for the subsequent platform operation, and be more stable, and other network protocols will undoubtedly consume more energy.

(2) *Comparison of Remaining Network Energy.* Figure 6 shows the comparison chart of the remaining energy of the network. The figure shows that under the same abscissa, the ordinate value corresponding to the curve of the EEUCP protocol is the largest, which means that the remaining energy of the network of the protocol is the largest in each round. From the perspective of the slope of the curve, before the node death, the slope of the EEUCP protocol curve is smaller and more stable than the other three protocols, indicating that the protocol proposed in this article is more effective in saving energy.

(3) *Protocol Selection.* From the above comparison chart, it can be clearly seen that the efficiency of the EEUCP protocol will be significantly better than others, so this article chooses the EEUCP protocol as the model of the intelligent sensor will be more suitable.

4.2. Software Design Based on μ Clinux Intelligent System

4.2.1. *Development and Application of Driver Program Based on μ Clinux.* The overall integration of the system is one of

the difficulties in realizing a multidisciplinary cross-system. For many kinds of software, it is difficult to modify the underlying data structure and functions due to their huge functions and structures. The modification of the bottom layer will affect the whole body, so it is difficult to achieve a unified design and integrated realization based on the bottom layer. The intelligent program driver is the front end of the software application, and it determines the user's fluency, and if optimized, the effect will be even better, as shown in Figure 7.

4.2.2. *Fractal Algorithm Based on Improved Random Number Generator.* The optimization of the model is inseparable from the optimization of the algorithm. Although the generated number of ordinary random numbers is different, the generated algorithm is the same, and based on this idea, an algorithm based on an improved random number generator was selected. Assuming that the continuous random variable x obeys a uniform distribution in the interval (a, b) , then the probability density function of x is the following equation:

$$f(x) = \begin{cases} \frac{1}{b-a}, & a < x < b, \\ 0, & \text{other.} \end{cases} \quad (18)$$

The distribution function of x is the following equation:

$$F(x) = \begin{cases} 0, & x < a, \\ \frac{x-a}{b-a}, & a \leq x < b, \\ 1, & x \geq b. \end{cases} \quad (19)$$

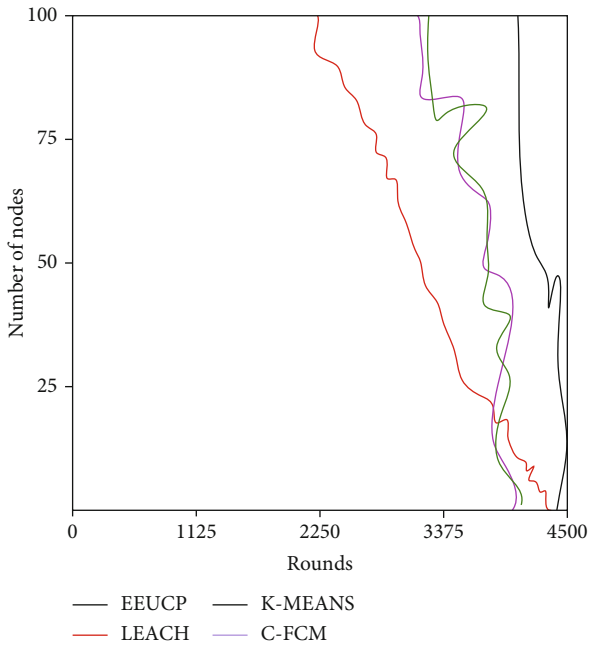


FIGURE 5: Comparison of network survival time.

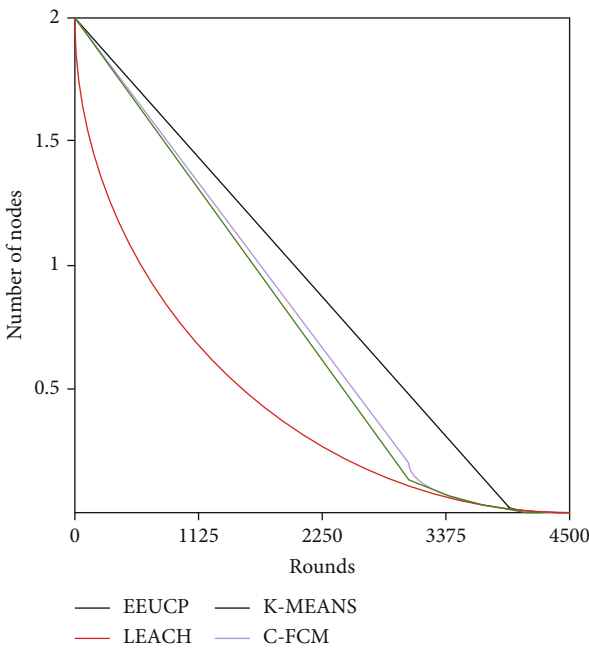


FIGURE 6: Comparison of remaining network energy.

The rand() function algorithm of an ordinary random number algorithm in a computer is as follows:

$$x(i + 1) = (l * x(i) + m) \% n. \tag{20}$$

In Equation (20), i , m , and l are set constants. If they cannot be set properly, things often go against one's wishes and often lead to errors. Therefore, this paper proposes a new algorithm

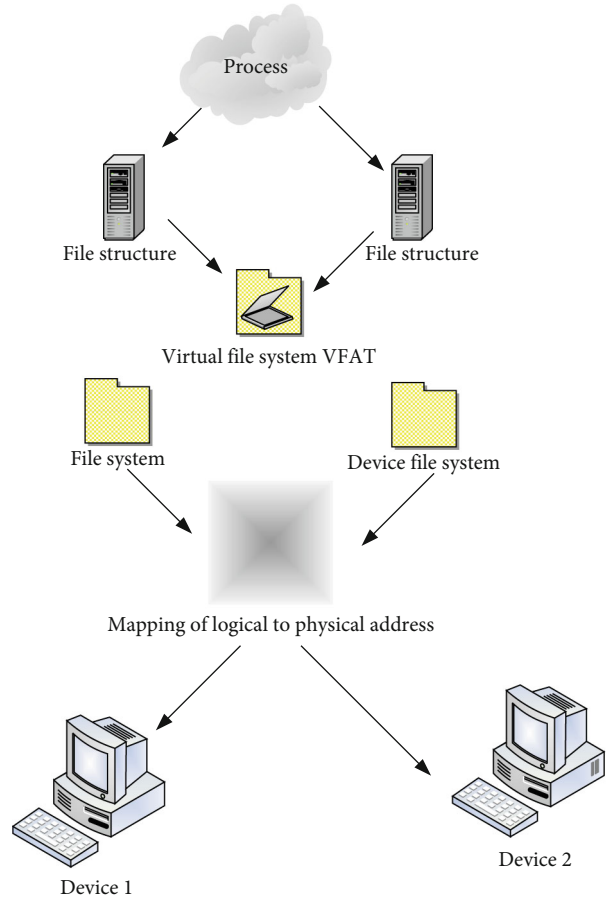


FIGURE 7: Hierarchical structure diagram of device driver.

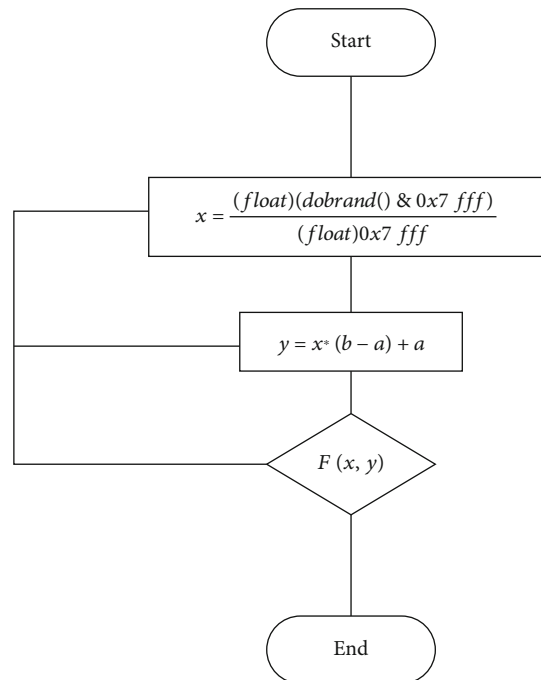


FIGURE 8: The flow chart of the fractal algorithm of the improved random number generator.

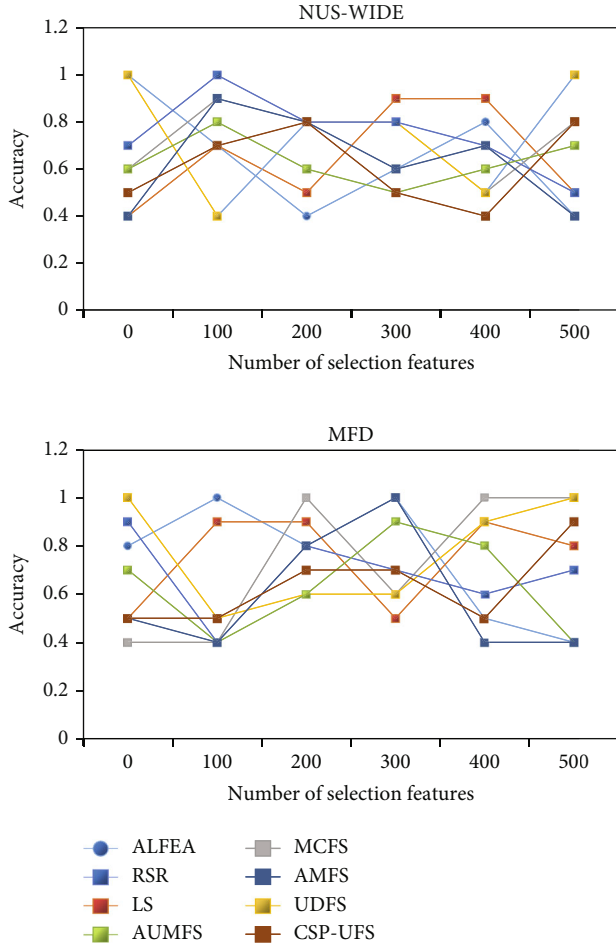


FIGURE 9: Clustering result ACC vs. the number of selected features.

that efficiently uses the rand() function twice, as shown in the following equation:

$$x = \frac{(\text{float})(\text{dobrand}()\&0x7fff)}{(\text{float})0x7fff}, \quad (21)$$

$$y = x * (b - a) + a.$$

It can be seen from Figure 8 that the optimized random number algorithm proposed in this paper efficiently uses the rand() function twice and generates random numbers based on the principle of chaos. Not only is the random number sequence internally random, but the random number sequence itself is also random. This is very beneficial to the data support of the system in the text.

5. Effect Analysis

5.1. *The Effect of Different Software Algorithms Based on μ Clinux Intelligent System.* Each feature selection algorithm is executed separately, and then, the clustering algorithm is executed on the selected feature subset. We use the clustering accuracy ACC and the normalized mutual information NMI to evaluate the clustering results. For the evaluation

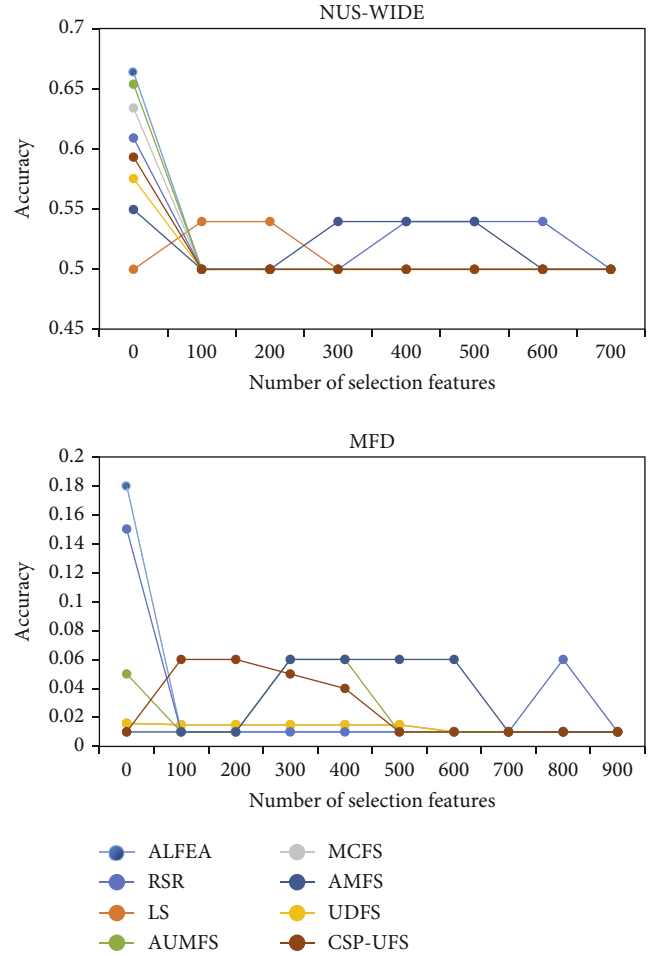


FIGURE 10: Clustering result NMI vs. the number of selected features.

of the algorithm, we use two public data sets, NUS-WIDE and MFD (Multiple Feature Data Set), as the test sample data. The dimension sum and feature value of the data are the highest dimension and the largest feature value of the data.

From the experimental results of Figures 9 and 10 and Table 2, we can draw the following conclusions. First of all, according to the experimental results, we can know that all comparison algorithms get better results than All Features, which fully illustrates the importance of feature selection. The noise and redundant information contained in the original feature will affect the efficiency and performance of the learning algorithm. After feature selection, removing these noise and redundant data will enable the learning algorithm to obtain better performance and improve the efficiency of the learning algorithm. Secondly, the AUMFS algorithm and the CSP-UFS algorithm have obtained better clustering effects than several other single-modal feature selection algorithms. This shows that making full use of the relevant information and complementary information of each mode in the process of feature selection can improve the performance of the algorithm. Finally, we can know that the CSP-UFS algorithm has achieved the best results. We summarize the

TABLE 2: The comparison algorithm has the best clustering effect on the five data sets.

	Animal with attributes		NUS-WIDE		Multiple features		Protein fold		CASIA-CASSIL corpus	
	ACC	NMI	ACC	NMI	ACC	NMI	ACC	NMI	ACC	NMI
All Fea	0.45	0.448	0.24	0.173	0.667	0.721	0.5	0.013	0.274	0.064
LS	0.565	0.535	0.251	0.147	0.671	0.728	0.503	0.019	0.302	0.068
MCFS	0.574	0.521	0.246	0.182	0.802	0.799	0.503	0.019	0.33	0.074
UDFS	0.849	0.846	0.271	0.192	0.911	0.844	0.525	0.062	0.326	0.08
RSR	0.837	0.846	0.268	0.193	0.894	0.827	0.608	0.062	0.319	0.076
AUMFS	0.956	0.915	0.29	0.202	0.965	0.922	0.607	0.062	0.339	0.097
AMFS	0.948	0.907	0.262	0.179	0.956	0.906	0.705	0.141	0.324	0.071
CSP-UFS	0.969	0.936	0.29	0.217	0.973	0.936	0.687	0.181	0.344	0.101

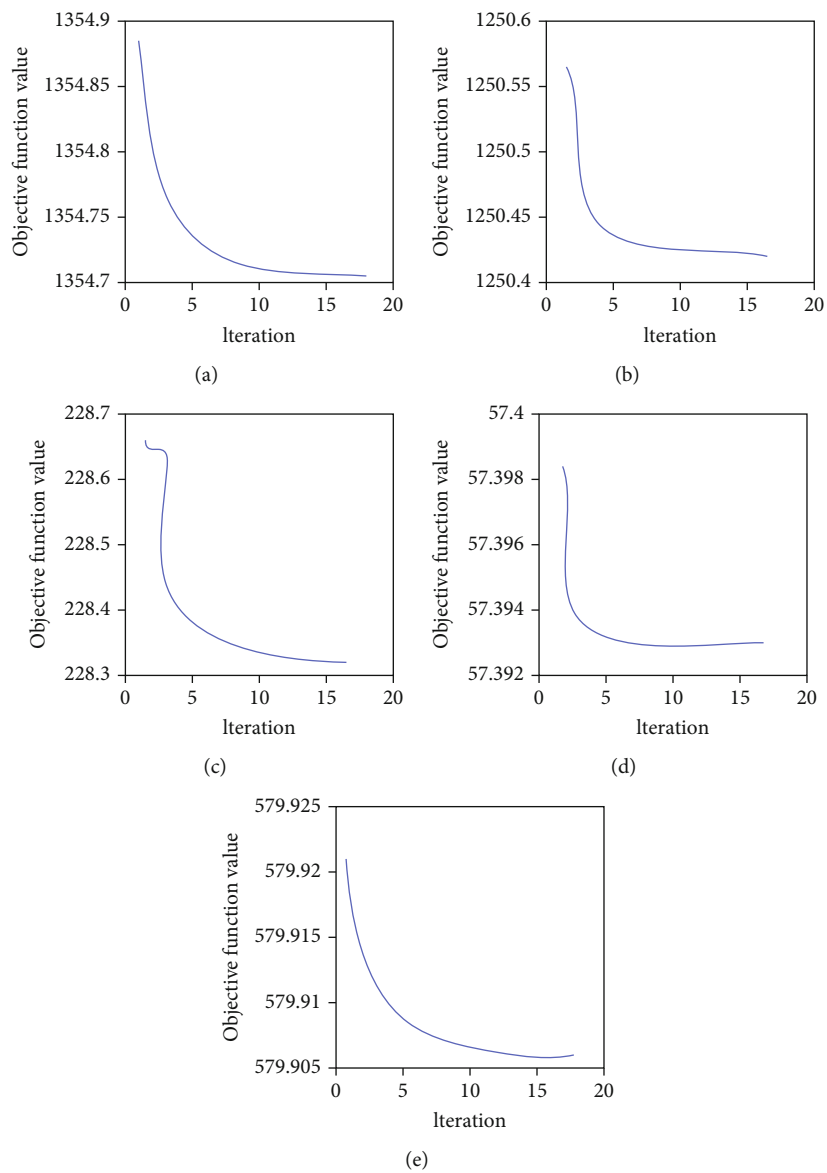


FIGURE 11: Convergence of CSP-UFS algorithm on five data sets.

reasons as follows: First, the CSP-UFS algorithm uses local regression and global alignment strategies to learn the Laplacian matrix. At the same time, the local structure information and global distribution information of the data are used to learn the Laplacian matrix. Secondly, the CSP-UFS algorithm uses linear discriminant analysis in the feature selection process, so that the data can also maintain the clustering structure of the original data in the low-dimensional feature space, thereby retaining the discriminant information in the original data. It can be seen that ME-K-means can stably obtain reliable initial gathering points instead of the K-means algorithm. The results of each run are full of randomness, and the k value needs to be specified, which is completely impossible when faced with an unfamiliar data set.

5.2. Statistical Verification. Finally, in order to illustrate the superiority of our proposed method, we use symbolic verification to study the difference between our algorithm and other algorithms. Sign test is a common method used to compare the performance of two classifiers, and this method counts the number of data sets, and the effect of a certain classifier on this data set is better than other methods, and we perform sign testing on all experimental results.

As shown in Figure 11 and Table 3, a, b, c, d, and e, respectively, represent Animal with Attributes, NUS-WIDE, Multiple Features, Protein Fold, and CASIA-CASSIL corpus. In these five data sets, it can be seen that in the accuracy of these five data sets, the accuracy of the c map will be smaller, and the peak value of a is the highest.

For the classification accuracy of the clustering evaluation indicators NMI and KNN classifiers, our algorithm performs better than other comparison algorithms on all data sets. Therefore, according to Table 3, the result of the sign test is that the CSP-UFS algorithm is superior to other comparison algorithms at a significance level of 0.05. For the remaining two evaluation indicators, except for the AUMFS algorithm and the AMFS algorithm, the CSP-UFS algorithm is almost better than all comparison algorithms.

6. Discussion

As we all know, companies need to carry out strategic marketing in three kinds of time: the beginning of business, the time of large-scale integration, and the time of entering new fields and developing strategic products and strategic services. For the emerging digital field, if agricultural planting and breeding companies want to occupy a place in it, they must redo strategic planning and redistribute strategic marketing. Many industrial planting and breeding enterprises attach great importance to the construction of the database and have achieved gratifying results. The database is like the digital logistics department of a planting and breeding enterprise. What kind of resources it needs and how many resources it needs are prepared and equipped in advance by the database department, and then, these resources are delivered to the platform vendors or users. The database solves the problem of idleness and waste of enterprise resources and realizes the optimization of resource allocation and cross-enterprise, cross-industry, and cross-

TABLE 3: Key values corresponding to the sign test when the significance is 0.05 and 0.10.

Number of data sets	5	6	7	8	9	10	11	12	13
W0.05	5	6	7	7	8	9	9	10	10
W0.10	5	6	6	7	7	8	9	9	10

platform sharing, which is conducive to creating new sources of value; the registration system of the database is conducive to targeted database marketing.

Therefore, the database is the key to the digital development strategy of agricultural planting and breeding gas companies. Although the platform designed in this paper is an intelligent network sensor platform, the following data is processed by a database. If companies can build their own databases and conduct independent analysis on their own, then the development of agricultural digitalization will be longer, and the development of enterprises will be more stable.

This article has related discussions from the design of the algorithm to the construction of the following platform. However, due to space limitations and limited knowledge, the author did not have an in-depth discussion, just a taste of it, and this article also has many shortcomings and can be improved, as follows: (1) The numerical development of agriculture can be combined with the Internet of Things technology to explore in more depth the impact of climate, water conservancy, and soil on agriculture. (2) For the optimization of the algorithm, on-site inspection of agricultural planting and breeding data can be used as analysis, and the results will be more in line with the needs of this article.

7. Conclusions

This article is based on the design of intelligent sensors to escort the digitalization of agriculture and realize the long-term development strategy of agricultural enterprises. This design ensures the stability and reliability of the system and improves the operating speed of the system. It can be predicted that the future development of precision agriculture will require the use of modern information technologies such as information management, automatic monitoring, precise control, and network communications. As far as the solutions involved in this article are concerned, with the rapid development of science and technology, new technologies will be used to develop relevant equipment and instruments to better solve the problem of agricultural data collection and transmission and realize the monitoring, management, and control of agricultural system digitization. At the same time, the intelligent system market has huge potential, and it has very important practical significance for the research of intelligent system, so more in-depth discussion and research should be done. In the future research, we will be specializing in more depth the research of intelligent sensors, have a deeper understanding of artificial intelligence technology, and apply intelligent sensors to the field of artificial intelligence.

Data Availability

No data were used to support this study.

Disclosure

The author confirms that the content of the manuscript has not been published or submitted for publication elsewhere.

Conflicts of Interest

There are no potential competing interests in this paper, and the author has seen the manuscript and approved to submit to your journal.

References

- [1] X. Li, H. Liu, W. Wang, Y. Zheng, H. Lv, and Z. Lv, "Big data analysis of the internet of things in the digital twins of smart city based on deep learning," *Future Generation Computer Systems*, vol. 128, pp. 167–177, 2022.
- [2] I. Kitouni, D. Benmerzoug, and F. Lezzar, "Smart agricultural enterprise system based on integration of Internet of Things and agent technology," *Journal of Organizational and End User Computing*, vol. 30, no. 4, pp. 64–82, 2018.
- [3] X. Zhou, X. Liang, X. Du, and J. Zhao, "Structure based user identification across social networks," *IEEE Transactions on Knowledge and Data Engineering*, vol. 30, no. 6, pp. 1178–1191, 2018.
- [4] J. P. Reganold and J. M. Wachter, "Organic agriculture in the twenty-first century," *Nature Plants*, vol. 2, no. 2, p. 15221, 2016.
- [5] J. Aničić, S. Vukotić, and S. Krstić, "The strategic aspects and results of agriculture development in Serbia in the transition period," *Economics of Agriculture*, vol. 63, no. 1, pp. 175–187, 2016.
- [6] G. M. Gurr, Z. Lu, X. Zheng et al., "Multi-country evidence that crop diversification promotes ecological intensification of agriculture," *Nature Plants*, vol. 2, no. 3, p. 16014, 2016.
- [7] N. Tirivayi, M. Knowles, and B. Davis, "The interaction between social protection and agriculture: a review of evidence," *Global Food Security*, vol. 10, pp. 52–62, 2016.
- [8] K. Goel, "Digitization will touch and significantly impact all area of enterprises," *Dataquest*, vol. 36, no. 3, pp. 36–36, 2018.
- [9] A. Szesz, M. Monteiro, A. H. Dias, I. M. Mathias, and G. Conti, "Embedded system in Arduino platform with fuzzy control to support the grain aeration decision," *Ciencia Rural*, vol. 46, no. 11, p. 1917, 2016.
- [10] B. Lin, Z. Xu, J. Wang, and M. Lu, "A low-cost water quality monitoring prototype device with embedded chromogenic reagent capsules and dynamic colorimetric detection," *Sensors and Actuators*, vol. 252, pp. 24–29, 2017.
- [11] R. Arablouei, L. Currie, B. Kusy, A. Ingham, P. L. Greenwood, and G. Bishop-Hurley, "In-situ classification of cattle behavior using accelerometry data," *Computers and Electronics in Agriculture*, vol. 183, no. 4, article 106045, 2021.
- [12] Y. Liu, F. Deng, Y. He, B. Li, Z. Liang, and S. Zhou, "Novel concrete temperature monitoring method based on an embedded passive RFID sensor tag," *Sensors*, vol. 17, no. 7, p. 1463, 2017.
- [13] K. Shojaei, "Three-dimensional neural network tracking control of a moving target by underactuated autonomous underwater vehicles," *Neural Computing and Applications*, vol. 31, no. 2, pp. 509–521, 2019.
- [14] B.-j. Jung, B. Kim, J. C. Koo, H. R. Choi, and H. Moon, "Joint torque sensor embedded in harmonic drive using order tracking method for robotic application," *IEEE/ASME Transactions on Mechatronics*, vol. 22, no. 4, pp. 1594–1599, 2017.
- [15] J. H. Seo and H. B. Park, "Forest environment monitoring application of intelligence embedded based on wireless sensor networks," *KSII Transactions on Internet and Information Systems (TIIS)*, vol. 10, no. 4, pp. 1555–1570, 2016.
- [16] M. Rabby, M. S. Alam, and M. Shawkat, "A priority based energy harvesting scheme for charging embedded sensor nodes in wireless body area networks," *PLoS One*, vol. 14, no. 4, pp. 1–22, 2019.
- [17] Z. F. Lou, X. P. Hao, Y. D. Cai, T. F. Lu, X. D. Wang, and K. C. Fan, "An embedded sensor system for real-time detecting 5-DOF error motions of rotary stages," *Sensors*, vol. 19, no. 13, pp. 2855–2864, 2019.
- [18] F. Xiao, "Multi-sensor data fusion based on the belief divergence measure of evidences and the belief entropy," *Information Fusion*, vol. 46, pp. 23–32, 2019.
- [19] G. Dartmann, H. Song, and A. Schmeink, *Big data analytics for cyber-physical systems: machine learning for the Internet of Things*, Elsevier, 2019.
- [20] H. B. Menz and D. R. Bonanno, "Objective measurement of adherence to wearing foot orthoses using an embedded temperature sensor," *Medical Engineering & Physics*, vol. 88, no. 1, pp. 19–24, 2021.
- [21] C. M. Kyung, H. Yasuura, Y. Liu, and Y. L. Lin, *Smart sensors and systems*, Springer, Cham, Switzerland, 2017.
- [22] C. Wiltz, "FDA approves world's first pill with an intelligent sensor," *Design News*, pp. 1–8, 2017.
- [23] D. Schallmo, C. A. Williams, and J. Lohse, "Digital strategy—integrated approach and generic options," *International Journal of Innovation Management*, vol. 23, no. 8, p. 1940005, 2019.
- [24] T. C. Ba, "Long-term digital strategy: do it once, do it right," *New Library World*, vol. 118, no. 5/6, pp. 331–335, 2017.
- [25] C. David, "A digital strategy," *CAD User*, vol. 31, no. 1, pp. 26–27, 2018.
- [26] J. W. Ross, C. M. Beath, and I. M. Sebastian, "How to develop a great digital strategy," *MIT Sloan Management Review*, vol. 58, no. 2, pp. 7–9, 2017.
- [27] K.-J. Shin, D.-K. Lee, D.-W. Seo, C.-M. Yoo, M.-H. Lim, and S.-H. Lim, "Setting estimation of cement paste using new-type embedded sensor," *Journal of the Korean Recycled Construction Resources Institute*, vol. 4, no. 4, pp. 483–488, 2016.
- [28] A. E. Arumona, A. Garhwal, P. Youplao et al., "Electron cloud spectroscopy using micro-ring Fabry–Perot sensor embedded gold grating," *IEEE Sensors Journal*, vol. 20, no. 18, pp. 10564–10571, 2020.
- [29] J. M. Julian, E. C. Orosco, and C. M. Soria, "Multi-sensor embedded system with multiple communications based on EDU-CIAA," *IEEE Latin America Transactions*, vol. 18, no. 2, pp. 368–375, 2020.
- [30] A. M. Alwan, D. A. Hashim, and M. F. Jawad, "Efficient bimetallic nanoparticles embedded-porous silicon CO gas sensor," *Solid-State Electronics*, vol. 153, pp. 37–45, 2019.
- [31] C. P. Wang, Y. C. Shen, P. C. Liou et al., "Dynamic pH sensor with embedded calibration scheme by advanced CMOS FinFET technology," *Sensors*, vol. 19, no. 7, p. 1585, 2019.

- [32] J. Cho and M. Lee, "Building a compact convolutional neural network for embedded intelligent sensor systems using group sparsity and knowledge distillation," *Sensors*, vol. 19, no. 19, pp. 4307–4355, 2019.
- [33] C. L. Lu and M. K. Yeh, "Stress analysis of shielding electrode in chip with pressure sensor embedded in accelerometer," *MicroElectronics International*, vol. 36, no. 1, pp. 35–42, 2019.
- [34] A. Y. Alqahtani, S. M. Gupta, and K. Nakashima, "Warranty and maintenance analysis of sensor embedded products using Internet of Things in industry 4.0," *International Journal of Production Economics*, vol. 208, pp. 483–499, 2019.
- [35] P. Krishnagandhi, B. Kannan, and Y. Raju, "Smart farming field observation using intelligent systems," *International Journal Of Electrical Engineering & Technology*, vol. 11, no. 4, pp. 241–245, 2020.

Research Article

Application of Artificial Intelligence Recognition Technology in Digital Image Processing

Xi Zhang 

Henan Medical College, Zhengzhou, 451191 Henan, China

Correspondence should be addressed to Xi Zhang; 2008050090@hamc.edu.cn

Received 3 November 2021; Accepted 3 January 2022; Published 27 January 2022

Academic Editor: Alireza Souri

Copyright © 2022 Xi Zhang. This is an open access article distributed under the Creative Commons Attribution License, which permits unrestricted use, distribution, and reproduction in any medium, provided the original work is properly cited.

Synthetic Artificial Intelligence technique is a science and technique derived and developed on the basis of calculator application technology. Image recognition is a special image processing step that plays an important role. Only after image recognition can it enter the stage of picture analysis and understanding. With the development of various computer technologies, images have gradually become and have become an important source of information for people. The use of calculator artificial intelligence is becoming increasingly widespread; therefore, understanding its application and related research is more conducive to pointing out the direction of research and learning for us. The goal of this paper is to discuss the emergence and development of synthetic intelligence identification technology and analyze the application bottlenecks of various types of synthetic intelligence identification technology, so as to increase our understanding of Synthetic Artificial Intelligence technique and provide reference for the research in related fields. This article simply introduces the technology of artificial intelligence type and its new development trend, and by combining concrete images of public facilities, the application of different computer artificial recognition methods of image recognition processing on the basis of the traditional method is improved, and through the corresponding simulation software of processing and identification methods for the analysis and comparison, the main application of two methods, the image processing recognition error rate is less than 0.5; improving computer artificial intelligence identification technique for the analysis of its application in image processing has certain help. The preprocessing process generally includes image digitization, grayscale, binarization, noise removal, and character segmentation. In terms of image recognition, algorithms mainly include statistical recognition, syntax recognition, and template matching. In recent years, with the development of neural networks and support vector machine technology, image recognition technology has a new and higher level of development.

1. Introduction

Artificial intelligence technology has been applied in more and more industries and fields, such as unmanned driving to bring changes to the transportation industry, the use of algorithm identification to help police arrest suspects, and intelligent robots to solve the problem of resource allocation in the medical industry. Artificial intelligence technology penetrates into all aspects of life and will bring great changes to the future society. For example, the evolution of domestic robots in China has made a breakthrough. Many families have started to use the sweeping robot as a necessary part of household cleaning. In the process of artificial intelligence design and optimization of household robots, the optimiza-

tion of automatic recognition algorithm technology and visual interface design is always the core and key links. The so-called automatic recognition algorithm optimization refers to the realization that the new algorithm can be added to the algorithm framework of artificial intelligence timely through the system optimization of departments or all programs, so as to provide good online support for developers and help users become more familiar with the operation interface and the use of the framework. At present, in the frame design of domestic robots, there is obviously a problem of poor application effect in the object programming environment. For some wizard-style designs, there is often consistency and lack of differentiation, which leads to some modules becoming very cumbersome. This not only reduces

the work efficiency of the robot, but also affects the user's experience.

Although there are many applications of image processing, the principles and methods used in them are the same, and there is no difference. Behind the high efficiency and high accuracy, there is still uncertainty in the artificial intelligence recognition technology. In the evolution of artificial intelligence technology, the inherent uncertainty of operating mechanisms makes the technology development similar to a "black box" state, so it is difficult for researchers to find the error and control the performance of the product. The uncertainty of exogenous variables mainly refers to the risk of technology development, among which the cost risk and schedule risk have the greatest impact. For artificial intelligence, even if its technology can be developed as expected, it still faces judgment on this technology. If it does not meet the moral and ethical needs of human beings, it will not be put into practice, leading to the failure of even successful development of the technology.

When subjected to a force that is parallel to the cross-section of the rod, close to each other, equal in magnitude, and opposite in direction, the deformation mainly characterized by the relative displacement of the cross-section of the rod is called shear deformation. This paper adopts the method of case study, based on the theories related to artificial intelligence and image recognition, through sorting out and analyzing the application status and problems of computer artificial intelligence technology in image processing, and puts forward the ideas and strategies of using artificial intelligence in the innovation of various industries.

2. Related Work

"Intelligent engineering," "computer study," and "deep training" are commonly referred to with different meanings in the field of high-level computational mathematics. Nawrocki et al. demythologized these expressions for radiation and established fundamental information about the topic. Not only that, they discuss the influence human performance may have on radiology in predicting the upcoming future. While ai is impossible to exchange radiologists anytime soon, Nawrocki et al. explore how technology could benefit the radiology field [1]. Mao et al. proposed instant sentiment identification method capture-based 2d and 3d features of faces' emotions by Kinect sensor. They combine the characters of Kinect's tracking unit (AUs) and feature point position (FPP). Tests on sensitive data systems and real-time videos show the best quality of this method [2]. Handwritten recognition is a method that allows a computer to automatically identify characters or scripts in the user language. Today, optical character recognition has become one of the most successful technological tools in process recognition and artificial intelligence. Here, handwritten English characters have been scanned and the image is typed into a computer, where it is recognized using a virtual network and converted to standard printed characters. To have an accurate measurement of partition and partition surprises and overcome the weaknesses of all other available OCR algorithms, Ananth et al. developed an approximate algo-

rithm for each process [3]. Peng et al. believe that sheet metal forming failure may occur due to necking, fracture, or wrinkling. By using forming limit diagrams (FLD) as a powerful tool to prevent sheet metal failure during the forming process, it provides parameter control throughout the forming process. There are a variety of developed methods for predicting FLD that can estimate sheet metal forming strain limits. The evaluation of FLD estimates shows that there is a dependence between the effects of several factors including normal stress, shear stress, sheet thickness, mechanical properties, metallurgical properties, yield function, strain path, and bending and formability. In his research, the effect of bending was studied through two finite element models. In the first method, the effect of bending is studied by applying out-of-plane deformation by increasing the displacement of the punch. In the second method, the influence of bending is studied by changing the punch diameter (25, 50, 70, and 100 mm) [4].

3. Proposed Method

3.1. Computer Artificial Intelligence Recognition Technology

3.1.1. Types of Computer Artificial Intelligence Detection Technology

(1) *Voice Identification Technology*. The voice recognition technology is mainly based on the characteristics of the voice of the different age groups, respectively, voice recognition, the sound of the information, and the information of the voice recognition system data of a unified matching, so as to better realize the voice recognition and identification of the object, can the voice recognition technology are mainly on the basis of person more accurately identifying the crowd.

(2) *Fingerprint Identification Technology*. This fingerprint identification technology mainly uses the identification of fingerprints of different colors, because the color fingerprint of every ordinary person is a unique identification symbol of each person, and the technology of this color fingerprint identification can identify a person's true identity with high reliability and accuracy [5].

(3) *Face Recognition Technology*. Face recognition combines people's main facial features and pupil conditions to identify objects. The technique is also relatively accurate. In recent years, it is also in the stage of rapid development and has been widely applied [6].

(4) *Smart Card Recognition Technology*. Smart card recognition technology stores and calculates data through an integrated circuit board and collects, analyzes, and organizes different data. This recognition technology mainly relies on network information data. At present, smart card recognition technology is mainly used for vehicle recognition.

(5) *Barcode Recognition Technology*. Barcode identification includes one-dimensional and QR tag techniques. QR tag technique is an extension and development of one-

dimensional code technology, with higher accuracy and more powerful functions, such as more powerful information capacity and error correction function [7].

(6) *Rfid Technology*. Radiofrequency technology mainly uses wireless electromagnetic waves to realize target recognition. The working principle of this technology is in corresponding tags; electromagnetic fields are used to transmit radio signals for data tracking and automatic identification [8].

3.1.2. Application of Artificial Smart Identification Skills of PC

(1) *Application in the Field of Voice Speaker Detection*. Nowadays, voice recognition technology includes voice search systems. The technology related to voice control can indeed bring more convenience to people, but the use of voice remote technology still has the problem of instability. In the course of advances in engineering, the existing problems cannot be ignored, which still need the research and efforts of the technicians in the current field. Not only the corresponding vocabulary should be enriched but also the fuzzy sound recognition ability should be strengthened to improve the speech recognition system.

(2) *Application in terms of Image Recognition*. Nowadays, the use of artificial intelligence image recognition technology in the field of image recognition technology is very limited, because image recognition technology is more difficult than other artificial intelligence recognition technologies. These technologies include, for example, the widely used vehicle license plate recognition system; Animal electrocardiogram recognition technology extensive range of materials for industrial purposes, farm and medical health; Seed and plant identification techniques, agriculture and information technology; mobile face recognition technology and mobile fingerprint recognition technology are widely used in the field of transportation and public safety management. But its current technology development status and trends, image recognition in the technology development, a primary stage, factors such as color and image contrast great extent hindered the further development of the recognition technology, technical personnel at the time of learning and using the image recognition technology but also on the transformation of a series of information, such as dimension reduction operation, this greatly reduces the degree of its efficiency, does not conform to the trend of the development of the era, is also difficult to well meet the demand of people's recognition of this age [9, 10].

(3) *Application in the Field of Robotics*. The BP network can learn and store a large number of input-output pattern mapping relationships without revealing the mathematical equations describing this mapping relationship in advance. Its learning rule is to use the steepest descent method to continuously adjust the weights and thresholds of the network through backpropagation to minimize the sum of squared

errors of the network. The topological structure of the BP neural network model includes the input layer, hidden layer, and output layer.

Due to the lack of accurate understanding and exploration of human beings, robots are sometimes too slow and inefficient in the process of learning and working and fail to fully exploit the significance and strengths of synthetic intellectual property. So, in the artificial intelligence exploration of technical personnel late even more pay attention to identify accurate perception and functions of the artificial intelligence technology and simulation for the accurate understanding of thinking, the key is simulated by thinking, better will be a combination of human and other artificial intelligence technology, map the process of the consciousness and behavior of the robot to artificial intelligence, computer program, believed this is not only beneficial to help the artificial intelligence technology to get the breakthrough, also to help people to better understand and enjoy the use of artificial intelligence, computer, so as to better improve the quality of work and life [11, 12].

3.2. Image Recognition

3.2.1. *Composition of Image Recognition Technology*. The image pattern is the definition and description of the image object to be recognized. The image pattern class is the collection of sample objects with some common characteristics of geometric, texture, and mathematical description. Image pattern recognition is the procedure of manipulation and evaluation of all forms of material data and graphic information on behalf of things or political entities in order to classify, evaluate, and illustrate images. An example of a study on graphic pattern discrimination is a process of automatic recognition and classification of the geometric target, regional texture, and mathematical description target in object image by the comprehensive application of image processing, feature definition and transformation, classification method, digital calculation, and other technologies.

General image pattern recognition systems are mainly composed of parts, including capture of picture images, picture presorting, extraction of image character, design of categorizer, and decision-making [13].

Common methods of image recognition are shown in Table 1.

3.2.2. Synthesis of Intelligent Artificial Identification Methods in Image Vision Assessment Process

(1) *Smallest Range Categorizer*. The smallest range categorizer is a facile pattern classifier, which estimates the statistical parameters of various patterns based on the sampling of the patterns and is completely determined by the means and variances of various types [14, 15]. Assume that every mode level is characterized by a parameter of the mean magnitude vector:

$$m_j = \frac{1}{N_j} \sum_{x \in S_j} x, \quad j = 1, 2, \dots, M, \quad (1)$$

TABLE 1: Common methods of image recognition.

Methods	Surface features	Identify ways	Typical criterion
Template matching	Samples, pixels, curves	Correlation coefficient, distance measurement	Classification error
Statistical recognition	Characteristics	Classifier	Classification error
Structure identification	Tectonic language	Rules and grammar	Acceptable error
The neural network	Samples, pixels, features	Network function	Minimum root mean square error

where N_j Indicates the maximum amount of schemas in the category S_j . The methodology for sorting an unlimited set of modality vectors is to designate the module to its corresponding group [16, 17]. Using Euclidean distance to determine the degree of proximity, the problem is transformed into the measurement of distance:

$$D_j(x) = \|x - m_j\|, \quad j = 1, 2, \dots, M. \quad (2)$$

Since the smallest distance represents the best match, if $D_j(x)$ is the smallest distance, then x is assigned to class S_j . Equivalent to calculation [18, 19]:

$$d_j(x) = x^T m_j - \frac{1}{2} m_j^T S_j, \quad j = 0, 1, \dots, m. \quad (3)$$

And assign x to class S_j when $D_j(x)$ gives the maximum value. For a minimum classifier, the decision boundary between class S_j and class S_j is

$$t_{mn}(a) = t_i(a) - t_j(a) = a^T (n - n_j) - \frac{1}{2} (a_i - a_j)^T (a_i - a_j) = 1. \quad (4)$$

(2) *Bayes Classifier*. Statistical dispersion of Known and these types in the feature language of ddM class items, i.e. with known typology $w_i = 1, 2, \dots, M$ priori probability and class condition probability density [20, 21], for the specimen to be tested, the probabilities that the probability that the prototype belonging to each of the other sorts can be derived from the Bayesian formula, the experimental likelihood that the identification object exists can be generated to test the most probable X attributes of the class to which the prototype belongs, the most likelihood that X is of the type [22]. If class Mw_i is reciprocal and perfect, the Bayesian formula is formulated as follows:

$$q(w_i|m) = \frac{P(X|w_i)P(w_i)}{\sum_{j=1}^M P(X|w_j)P(w_j)}. \quad (5)$$

In engineering application problems, the data typically complies with a regular classification, which is justified and generalized in its physics, and the distribution is straightforward to manipulate math-wise. $N(u, \sigma^2)$ only consists of two parametrizations, which can be acquired by the expectations and covariances in the function of a large population of samples estimated to establish the density of dependent odds

[23]:

$$P(x) = \frac{1}{\sqrt{2\pi\sigma}} \exp \left[-\frac{1}{2} \left(\frac{u-1}{\sigma} \right)^2 \right] = N(a, u^2), \quad (6)$$

where u is the mean or mathematical expectation:

$$u = E(x) = \int_{-\infty}^{\infty} xP(x)dx. \quad (7)$$

The normative odds ratio diversity feature for covariates is as follows:

$$P(x) = \frac{1}{(2\pi)^{n/2} |S|^{1/2}} \min \left[-\frac{1}{2} (Y - \bar{x})^T S^{-1} (Y - \bar{x}) \right]. \quad (8)$$

Denoted by probability diversity of variables in multidimensional orthonormal odds density features:

$$P(x|w_i) = -\frac{1}{2} (Q - \bar{X}_i)^T S_i^{-1} (Q - \bar{X}_i) - \frac{n}{2} \ln 2\pi - \frac{1}{2} \ln |S_i|. \quad (9)$$

The posterior probability can be calculated. It represents the likelihood that the target panel falls into various categories when it presents X characteristic state. The characteristic X of A sample may be represented in whole or in part in class M , while the probability of its representation in class $w_i = 1, 2, \dots, M$ is expressed in terms of $P(X|w_i)$. The posterior probability expressed by Bayes formula:

$$F(v_i|y) = \frac{P(y|v_i)P(v_i)}{\sum_{j=1}^M P(y|v_j)P(v_j)}. \quad (10)$$

It represents A conditional probability, representing the approximate sample belonging to the class A in the case of y feature, and it can be estimated in turn the category of the sample to be tested that has A certain feature y . The mathematical formula is used to express the second kind of problem:

$$P(v_i|y) > P(v_2|y), \quad a \in v, \quad (11)$$

$$P(v_i|y) < P(v_2|y), \quad a \in v_2. \quad (12)$$

The structure of the Bayesian classifier for the two types of problems is shown in Figure 1.

The classifier of the nervous system module distribution is shown in Figure 2; the geometry of the neuron network

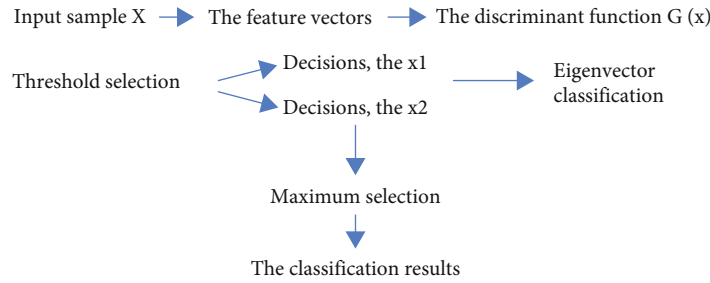


FIGURE 1: Structure of the Bayes classifier for multiclass problems.

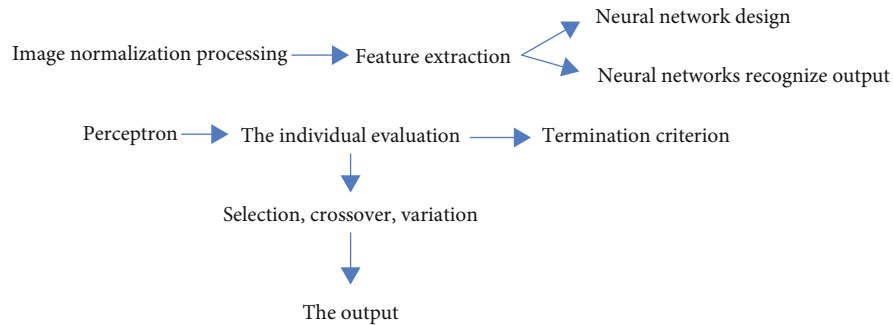


FIGURE 2: Components of the recognition system module based on neural network.

TABLE 2: Correspondence between biological evolution and genetic algorithm.

Concepts in biological evolution	The role of genetic algorithms
The environment	To adapt to the function
Adaptive	Adaptive value function
The survival of the fittest	The solution with the greatest value of the adaptive function has the greatest probability of being retained
Individual	One solution to the problem
Chromosome	Solution of the coding
Gene	Coded element
Group	A selected set of solutions

discriminant function classifier does not need to rely on the conditional probability density of the traditional statistical scientific knowledge; a classifier model by some kind of conditional probability transformation maps the dividing line between the feature vectors in a pattern; the pattern of spatial feature vector can be understood as belonging to a point, in the feature space, which belongs to a feature point set in the feature space to a certain extent which is always associated with another type of feature point set or separation; each model in mathematics and geometry relationship between the classes is to determine the separable. It can be understood that a dividing line can be found through the linear classification method of mathematics and geometry, and the class belonging to the feature space can be decomposed into a subfeature space corresponding to different categories. Another result of geometric linear classification is the ability to provide a definite dividing line equation, called a discriminant function, for an object. According to the property and modality of linear discriminant filters, sorting can be classi-

fied into linear discipline segmentation functions and non-linear differentiation segmentation factors. A geometric linear criterion function categorizer is widely used in desktop computers and for pattern recognition of images for its ease of interpretation and integration in a traditional design.

(3) *Genetic Algorithm*. The most critical parts of the genetic algorithm are selection, crossover, and variation. Its performance is mainly affected by these three genetic operations, and its corresponding relationship is shown in Table 2. Crossover is the selection of genes from parental chromosomes to create an intermediate individual by one-point traverse, bipoint intersection, n -point intersession, uniform intersection, and operator's intersection. The mutation occurs after the crossing. This is to avoid that all in the total number of solutions fall into the local optimal problem for the one being worked on. Mutation is a stochastic change of intermediate individuals. It is mainly to duplicate the best centromere, and there are many approaches, such as rotary selectivity, local

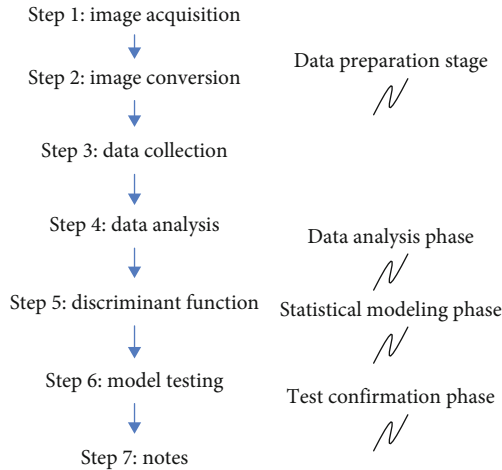


FIGURE 3: Experimental design steps.

kinematic selection, championship kinematic conversion, transitional selection, and steady-state choice. Taking roulette selection as an example, imagine placing all the chromosomes in a population on a roulette wheel, where each individual's chromosomes have their place in the fitness function, and parental selection in terms of fitness; the better the chromosome, the better the chance of being selected. That is, when a pinball is thrown to select chromosomes, chromosomes with greater fitness will be selected multiple times. Since genetic algorithms cannot directly deal with the parameters of the problem space, the problem to be solved must be expressed as a chromosome or individual in the genetic space through coding. This conversion operation is called encoding, and it can also be called (representation of the problem). The following three criteria are often used to evaluate coding strategies: (a) Completeness: all points (candidate solutions) in the problem space can be represented as points (chromosomes) in the GA space. (b) Soundness: the chromosomes in the GA space can correspond to all candidate solutions in the problem space. (c) Nonredundancy: chromosomes correspond to candidate solutions one-to-one.

4. Experiments

4.1. Experimental Background. In the contemporary world, the safety of utilities plays a more critical role in the city context, and its inspection skills are growing in salience in the system, and it has become an instrument to control the quality of products and guarantee the safe facility running. Its important function depends on the correctness of test method selection and the reliability of test results. In the detection of most public infrastructure such as roads and bridges, if the detection personnel only rely on their own vision to observe and expect to get some useful information, a lot of subjective factors will be introduced in the detection process due to human participation, which will eventually make the detection quality of facilities uncertain. And this method workload is big, has poor reliability, and rely on repair personnel's experience and sense of responsibility, work efficiency is low, long repeat job easily causes visual fatigue, and in many cases due to potential risk in the work environment, such as the traffic on the highway,

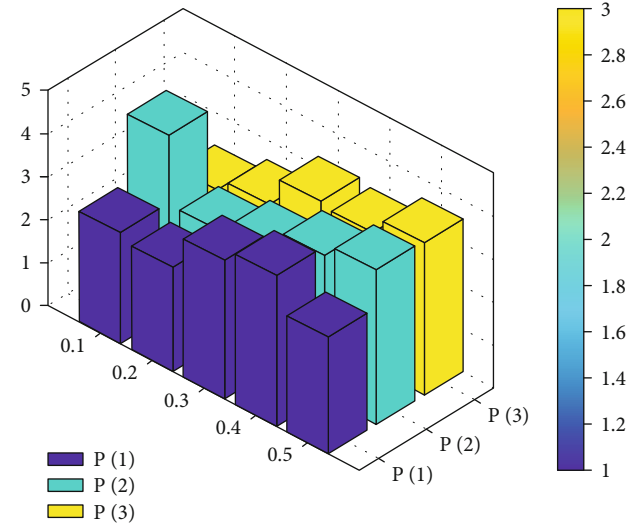


FIGURE 4: Sample feature distribution after three times of sample t input.

the work high above is hazardous to humans. Therefore, in order to minimize the adverse impact of human factors in the testing process, the development of automated testing technology is a vital way to improve the reliability of testing results. According to the introduction of computers, automatic detection and identification can improve the reliability and security of facility detection, save manpower and labor, and improve social benefits.

4.2. Experimental Design. Automatically detect and identify the facilities by computer, which can improve the recognition efficiency and guarantee the safety of personnel. It has implications in the field. Four phases of application engineering are undertaken: data generation, data analyzing, counting, simulation, and confirming (see Figure 3).

4.2.1. Take Pictures of Steel Bridge Coating Surface. The selected steel bridges were coated with a layer of blue paint, and two sets of pictures were taken with digital cameras: a set of intact samples and a set of defective samples, each set of 10. In the flawed pictures, use the pictures with slight rust as much as possible to increase the efficiency of the model, so that the model can be maintained in advance at the initial stage of the defect.

4.2.2. Image Conversion. By converting the color image to the RGB chromaticity space, you can obtain the pixel value x_{ij} of the image on the three color channels of RGB. I represents the color channel = red, green, and blue, and j represents the picture = 1, 2, ..., n .

4.2.3. Extract Statistical Data. Three statistical values were extracted from each color channel to show the characteristics of the image, namely, difference (DIFF) division, mean, and standard deviation (STD).

The nine statistical features obtained in the previous step would make the dimension too high if used directly in modeling and would be further reduced based on the analysis. The purpose of data analysis and selection is to select effective

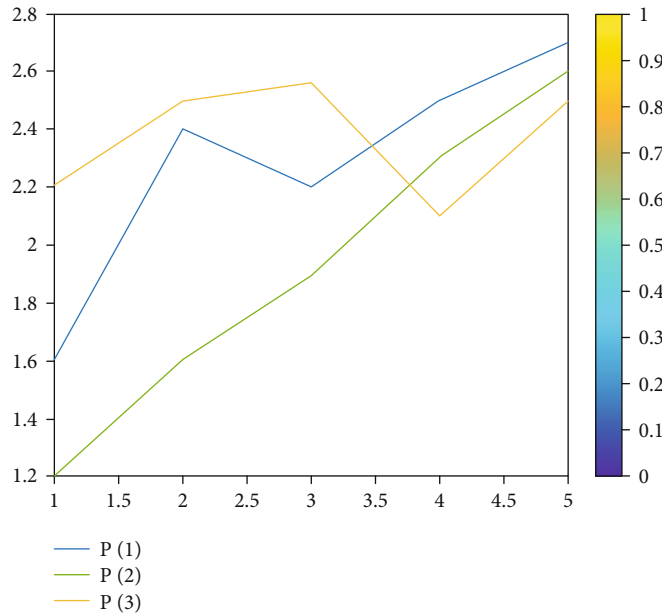


FIGURE 5: Error curves under different samples.

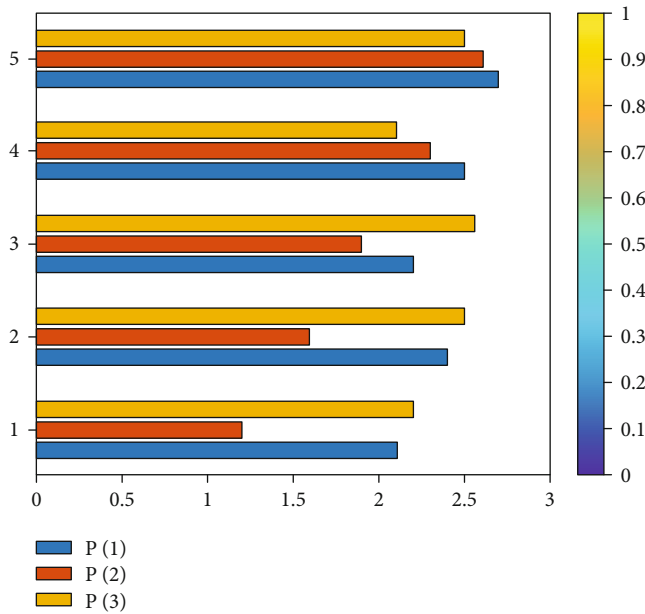


FIGURE 6: Variation diagram of network training target error under BP algorithm.

feature variables from individual variables. The following analysis method is used to quantitatively test the mean difference between different groups. The basis is that the greater the mean difference of the same feature variable in different groups, the greater the contribution of the variable to the discriminant function, and the more effective the feature vector.

5. Discussion

5.1. Computer Artificial Intelligence Recognition Technology Based on Perceptron. The recognition algorithm of Bayesian decision theory is a relatively basic algorithm in the statisti-

cal pattern recognition algorithm. Since the process of obtaining the linear discriminant function in the algorithm is equivalent to the learning process of the perceptron, the perceptron neural network can also be introduced to realize this kind of image recognition problem.

For 20 samples, we can know the matrix of the perceptron's input vector p . Since the problem has been classified into a simple two-category recognition problem, the corresponding target value of the target vector can be selected as 1 and 0 to represent the classification. Let us assume that 1 represents the class of images that are intact, and 0 represents the class of images that are defective. According to the input vector t , a corresponding target vector can be obtained and a single-layer perceptron neuron can be selected, as shown in Figure 4 in the sample feature distribution map after the input vector t .

Notice a phenomenon in the perceptron algorithm, that is in different initial conditions w, b , the training result is different, but after training, the network can complete the classification task, only steps needed for the training, and finally the result is likely to be different, namely the classification problem of only one solution, on the premise of the four steps to achieve results, and the error change as shown in Figure 5.

5.2. Analysis of Computer Artificial Intelligence Recognition Technology Based on BP Neural Network. The basic idea of the BP algorithm is that the learning process consists of two processes: the forward propagation of the signal and the backpropagation of the error. In the forward propagation, the input samples are passed in from the input layer, processed by each hidden layer by layer and then passed to the output layer. If the actual output of the output layer is inconsistent with the expected output (teacher signal), it will turn to the error backpropagation stage. Error backpropagation is to pass the output error back to the input layer by

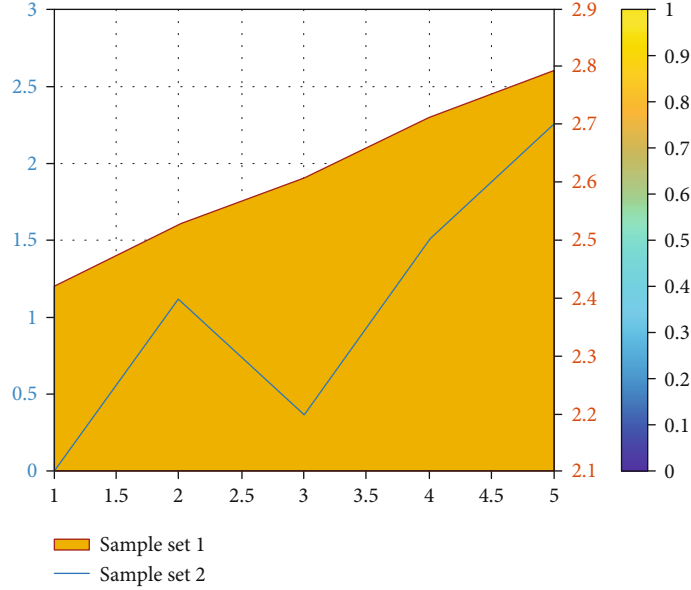


FIGURE 7: 20 network output changes of 20 samples.

TABLE 3: The degree of closeness between the image to be tested and the known sample.

Sample	x	Sample	x
1	0.2356	8	0.2236
2	0.3991	9	0.3255
3	0.4168	10	0.3412
4	0.2881	11	0.3259
5	0.2447	12	0.2529
6	0.3052	13	0.3510
7	0.4033	14	0.3510

layer through the hidden layer in some form and apportion the error to all the units of each layer, so as to obtain the error signal of each layer unit, and this error signal is used as a correction for each unit as the basis of the weight. The process of adjusting the weights of each layer of signal forward propagation and error backpropagation is carried out repeatedly. The process of constant weight adjustment is the learning and training process of the network. This process continues until the error of the network output is reduced to an acceptable level or until the preset number of learning times.

For solving two kinds of problems, the characteristic variables are linearly combined into a standard discriminant function. Since the eigenvalues of the training data can maximize the separation of the two classes, the coefficients of the discriminant function are optimal. Linear discriminant analysis does not change the location of the original data, it simply attempts to provide a higher degree of separation and to carve out a decision area for a given class, so this approach can better help understand the distribution of the characteristic data. The feature vectors in the input layer refer to the feature extraction in the previous algorithm, and three fea-

tures extracted from the color image are used. In Kolmogorov's theorem, the number of hidden layer neurons is selected as 7; for the output layer, you only need to divide the image into two categories, so you only need to use one neuron as the output.

Parameters of the BP network are set as follows.

The maximum number of training steps in the network is `net.trainparam.epochs = 1000`; the training target error is `net.TrainParam.Goal = 0.001`.

Figure 6 is the error variation diagram of the network training target. Figure 7 is the network training output corresponding to the 20 samples collected previously. It is obvious that the training samples are two sample set elements: the first 10 samples are the elements of sample set 1, and the last 10 samples are the elements of sample set 2. It can be regarded as a whole; that is, there is a sample element in the total sample set, the fuzzy feature vectors are extracted, and then, the closeness between the image to be tested and the known sample image is calculated by using the fuzzy method, and the classification is conducted according to the principle of proximity selection.

Due to image is a known samples, each sample corresponds to a matrix, such known samples of the fuzzy set is expressed as a matrix, the corresponding eigenvector extracted under test images, according to the degree calculation sample under test and the known sample set close to the extent, maximize is belong to category of the sample under test, the degree of the pattern and the known sample under test as shown in Table 3.

According to the above process, the 20 images in the known sample set were taken as the test samples for classification and recognition, and input was selected randomly, the closeness degree was calculated, the maximum value and the corresponding known sample serial number were found, and the correct category could be obtained. The above algorithms have something in common; they all use the same sample eigenvectors. The feature vector is extracted

from color image RGB three channel information, but because of its high correlation between RGB, and then use the Wilks' lambda criteria, to gradually reduce the correlation characteristic vector, dimension reduction, for each color images can use three feature vector to represent the main part of information.

6. Conclusions

The biggest difference between a digital image and an analog image is that it can be stored on a computer and can be coded and modified using image editing software. How to effectively process images has also become a research hotspot and focus of computer technology. Although a lot of artificial intelligence recognition technology has been applied, at the same time, there are still some shortcomings at the technical level. For example, the voice recognition system, which is mainly applied to putonghua due to the restrictive types of identifiable languages, will not be able to accurately identify regional accents or nonstandard pronunciation, and the application effect will be significantly reduced. At the same time, for face recognition technology widely used, the database cannot cover all facial expression features; limited by data, the recognition effect cannot be guaranteed. However, in the case of increasing age, facial features will also change to some extent, which is also one of the factors reducing the recognition effect. Face recognition technology mainly relies on visual features, which cannot exclude the factor of face similarity, and the interference of other scene factors will increase the recognition error rate. It can be seen from this that on the basis of summarizing previous experience, it is necessary to conduct more in-depth research on the artificial intelligence recognition technology, so as to further improve the comprehensive level of technology while eliminating the existing defects.

This paper briefly introduces artificial intelligence recognition technology and image processing technology and focuses on the application of artificial intelligence recognition technology in image processing. Regular safety inspection of public facilities is an important means to control product quality and ensure the safe operation of facilities. In order to minimize the adverse impact of human factors on testing and improve the reliability of testing results, developing automatic testing technology is an effective way to solve the problem. In the surface quality inspection of highways, bridges, and other facilities, image recognition technology is used to detect the target image automatically. In this paper, according to the specific color images collected in the detection, different identification methods are used to realize the detection, so as to improve the reliability of the detection results and shorten the identification time and at the same time deepen the understanding of the application of image recognition technology.

The main content of this article is the research of image filtering and image recognition algorithms. Image recognition is a type of pattern recognition. Image recognition technology has been successfully used in fields such as optical information processing, medical instrument sample inspection and analysis, automated instruments, industrial inspection, license plate recognition, and unmanned driving at home and abroad. As an important aspect of artificial intelligence, image recognition

has always been widely concerned and highly valued by people. Image recognition includes two steps: image preprocessing and image recognition. Image filtering is a crucial step in image preprocessing. The end of this article through to the public facilities to recognition of color images collected in detection, using the Matlab simulation, to change the traditional method, and using method of bayes, sensors, the BP neural network and the fuzzy recognition method of image recognition, and for the various intelligent method of intelligent identifying new FaZhanDian namely combination gives the research difficulty and the current development of hot spots, more fully expounds the application of intelligent technology in image processing. In the algorithm for removing Gaussian noise, the edge of the image is not effectively protected, which makes the edge have a certain degree of distortion. Although the algorithm proposed in this study shows better results than the traditional algorithm in the simulation experiment, the algorithm itself does exist many shortcomings that need to be improved in future work.

Data Availability

This article does not cover data research. No data were used to support this study.

Conflicts of Interest

The author declares no potential conflicts of interest with respect to the research, authorship, and/or publication of this article.

References

- [1] T. Nawrocki, P. D. Maldjian, S. E. Slasky, and S. G. Contractor, "Artificial intelligence and radiology: have rumors of the radiologist's demise been greatly exaggerated?," *Academic Radiology*, vol. 25, no. 8, pp. 967–972, 2018.
- [2] Q. Mao, X. Pan, Y. Zhan, and X. J. Shen, "Using Kinect for real-time emotion recognition via facial expressions," *Frontiers of Information Technology & Electronic Engineering*, vol. 16, no. 4, pp. 272–282, 2015.
- [3] J. P. Ananth, G. Raghuraman, G. L. I. Cyril, and M. S. Aldo, "Enhancement of segmentation and zoning to improve the accuracy of handwritten character recognition," *Journal of Computational and Theoretical Nanoscience*, vol. 12, no. 12, pp. 5891–5894, 2015.
- [4] D. Peng, S. Chen, R. Darabi, A. Ghabussi, and M. Habibi, "Prediction of the bending and out-of-plane loading effects on formability response of the steel sheets," *Archives of Civil and Mechanical Engineering*, vol. 21, no. 2, pp. 1–13, 2021.
- [5] W. Sureshkumar and R. Rama, "Chomsky hierarchy control on isotonic array P systems," *International Journal of Pattern Recognition and Artificial Intelligence*, vol. 30, no. 2, pp. 1650004–1650249, 2016.
- [6] L. Zhou, G. Yang, Y. Yin, L. Yang, and K. Wang, "Finger vein recognition based on stable and discriminative superpixels," *International Journal of Pattern Recognition & Artificial Intelligence*, vol. 30, no. 6, pp. 1650015–1650079, 2016.
- [7] Y. Zhang-Jing, H. Pu, and Z. Fan-Long, "Center-based line neighborhood discriminant embedding algorithm and its

- application to face recognition,” *Pattern Recognition & Artificial Intelligence*, vol. 21, no. 3, p. 65, 2015.
- [8] D. Verma and S. Dubey, “Fuzzy brain storm optimization and adaptive thresholding for multimodal vein-based recognition system,” *International Journal of Pattern Recognition & Artificial Intelligence*, vol. 13, no. 5, pp. 49–61, 2016.
- [9] F. Tian, Y. Gao, Z. Fang, and J. Gu, “Automatic coronary artery segmentation algorithm based on deep learning and digital image processing,” *Applied Intelligence*, vol. 51, no. 12, pp. 8881–8895, 2021.
- [10] E. Giacomini, T. Greenberg-Toledo, S. Kvatinsky, and P.-E. Gaillardon, “A robust digital RRAM-based convolutional block for low-power image processing and learning applications,” *IEEE Transactions on Circuits and Systems I: Regular Papers*, vol. 66, no. 2, pp. 643–654, 2019.
- [11] Z. Che and X. Zhuang, “Digital affine shear filter banks with 2-layer structure and their applications in image processing,” *IEEE Transactions on Image Processing*, vol. 27, no. 8, pp. 3931–3941, 2018.
- [12] L. Zhang, L. Zhang, and L. Zhang, “Application research of digital media image processing technology based on wavelet transform,” *EURASIP Journal on Image and Video Processing*, vol. 2018, no. 1, 2018.
- [13] R. Mouhcine, A. Mustapha, and M. Zouhir, “Recognition of cursive Arabic handwritten text using embedded training based on HMMs,” *Journal of Electrical Systems & Information Technology*, vol. 32, no. 1, p. 455, 2017.
- [14] K. Tripathi and N. B. G. C. Nandi, “Continuous Indian sign language gesture recognition and sentence formation,” *Procedia Computer Science*, vol. 54, no. 2, pp. 523–531, 2015.
- [15] R. Malik, “AI augmentation in the field of digital image processing,” *International Journal of Computer Applications in Technology*, vol. 65, no. 3, pp. 235–244, 2021.
- [16] F. Boutekkouk, “Digital color image processing using intuitionistic fuzzy hypergraphs,” *International Journal of Computer Vision and Image Processing (IJCVIP)*, vol. 11, no. 3, pp. 21–40, 2021.
- [17] S. S. Rautaray and A. Agrawal, “Vision based hand gesture recognition for human computer interaction: a survey,” *Artificial Intelligence Review*, vol. 43, no. 1, pp. 1–54, 2015.
- [18] R. Herrera-Pereda, A. Taboada Crispi, D. Babin, W. Philips, and M. Holsbach Costa, “A review on digital image processing techniques for *in-vivo* confocal images of the cornea,” *Medical Image Analysis*, vol. 73, article 102188, 2021.
- [19] İ. İlhan, “A cross-platform test tool for digital image processing,” *Multimedia Tools and Applications*, vol. 80, no. 8, pp. 12249–12273, 2021.
- [20] L. Ma, “Research on distance education image correction based on digital image processing technology,” *EURASIP Journal on Image and Video Processing*, vol. 2019, no. 1, 2019.
- [21] P. Shamsolmoali, M. E. Celebi, and R. Wang, “Deep learning approaches for real-time image super-resolution,” *Neural Computing and Applications*, vol. 32, pp. 14519–14520, 2020.
- [22] M. A. Borkin, Z. Bylinskii, and N. W. Kim, “Beyond memorability: visualization recognition and recall,” *IEEE Transactions on Visualization & Computer Graphics*, vol. 22, no. 1, pp. 519–528, 2016.
- [23] Z. Yang, L. Yang, W. Huang, L. Sun, and J. Long, “Enhanced deep discrete hashing with semantic-visual similarity for image retrieval,” *Information Processing and Management*, vol. 58, no. 5, article 102648, 2021.

Research Article

A Novel Highway Routing Protocol in Vehicular Ad Hoc Networks Using VMaSC-LTE and DBA-MAC Protocols

Edris Khezri , Esmaeil Zeinali , and Hadi Sargolzaey

Faculty of Computer and Information Technology Engineering, Qazvin Branch, Islamic Azad University, Qazvin, Iran

Correspondence should be addressed to Esmaeil Zeinali; zeinali@qiau.ac.ir

Received 24 October 2021; Accepted 23 December 2021; Published 25 January 2022

Academic Editor: Alireza Souri

Copyright © 2022 Edris Khezri et al. This is an open access article distributed under the Creative Commons Attribution License, which permits unrestricted use, distribution, and reproduction in any medium, provided the original work is properly cited.

The vehicular ad hoc networks (VANETs) are an example of mobile networks, which utilizes dedicated short-range communication (DSRC) to establish a wireless connection between cars, and their primary purpose is to provide more security and comfort for passengers. These networks utilize wireless communications and vehicular technology to collect and disseminate traffic information, and it is required to be delivered to all vehicles on the network reliably and quickly. One of the major challenges raised in VANETs is that the communication path between the source and destination nodes is disconnected due to the dynamic nature of the nodes in this network, and the reconnection process of nodes through the new path reduces the performance of network. This paper presents a highway routing protocol to overcome some of the challenges of these networks including routing cost, delay, packet delivery rate, and overhead. The NS2 is used for simulation, and the performance of the proposed protocol is compared with the VMaSC-LTE and DBA-MAC protocols. The results of the simulation indicated that the proposed protocol outperforms the other two protocols in terms of delay, packet delivery rate, and routing overhead.

1. Introduction

A vehicular ad hoc network is a wireless network in which the vehicles equipped with a wireless interface can communicate with each other or fixed roadside equipment [1–3] (Figure 1). These networks create wireless communication among moving vehicles utilizing dedicated short-range communications (DSRC) [2]. DSRC is, in fact, a version of IEEE 802.11a, improved as IEEE 802.11p for operations with low overhead [4]. VANET characteristics are mainly similar to mobile ad hoc networks (MANETs) [5, 6], which means both are self-organizing and self-management, have low bandwidth, and stay in the same position in case of sharing radio transmission. However, the most significant operational obstacle for VANETs (versus MANETs) is its high speed and the mobility of mobile nodes, alongside the routes, indicating that the appropriate design of routing protocols requires the improvement of MANET structure so that it can match itself to the rapid mobility of VANET nodes in an efficient way [7]. Vehicular ad hoc networks provide the context for diverse applications like security and welfare in a

wide range of intelligent transportation systems (ITS) [8, 9]. Thus, the development of appropriate routing protocols has always been a challenge for researchers. For example, most routing protocols focus on urban environments and less on highways in communication environments. Other challenges to consider include dynamic topology and high mobility; alternative network disconnection, prediction and modeling of traffic path, and diverse communication environments; and sufficient energy and memory, distribution networks, security, and confidentiality [10–20]. In this paper, a highway routing protocol called “Greedy Highway Routing Protocol (GHRP)” is presented, which contributes to solving or minimizing any of the issues raised above. The main challenge that the suggested method is trying to solve is the global coverage of the routes to prevent the loss of the packages and reduce the delay. In order to solve this problem in the proposed method, it is attempted to minimize the number of fixed Roadside Units (RSUs) by identifying accident sites and installing fixed RSUs in those locations, minimizing the routing cost of purchasing and installing equipment, and covering the entire route using mobile

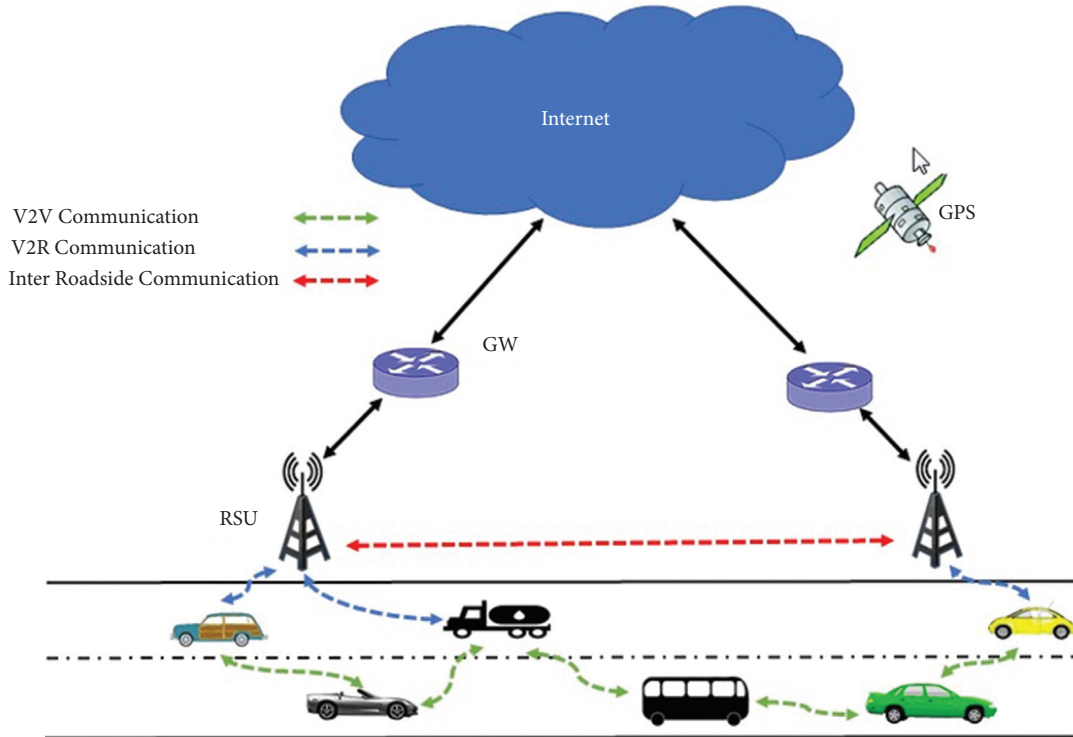


FIGURE 1: Vehicular ad hoc networks [1].

RSUs, which are public transport equipment. The packet delivery rate increases, and end-to-end delay decreases when covering the entire route with fixed and mobile RSUs. Ultimately, the primary purpose of VANETs, i.e., security and comfort of users, is obtained by collecting the entire information of route and distributing it between cars.

The main contributions of this paper are summarized as follows:

- (i) suggesting an intercity routing protocol that attempts to cover the whole of the route and decrease the delay;
- (ii) using fixed and variable RSUs; and
- (iii) increasing the network efficiency concerning the transfer speed of the packages and reduction of the delay.

The following sections are organized: Section 2 provides DBA-MAC and VMaSC-LTE protocols. Section 3 examines the proposed protocol. Section 4 elaborates discussion, comparison, and simulation of the proposed protocol with other highway routing protocols. Finally, the conclusion, challenges, and future works are reported in Section 5.

2. Related Work

Since one of the main goals of intervehicle networks is to maintain the safety and comfort of occupants of cars [7, 21, 22] and most of the casualties occur in highways, attempts have been made to divide the intervehicle routing protocols into urban routing protocols and highway routing protocols (Figure 2) and focus more on highway routing protocols, which are less considered.

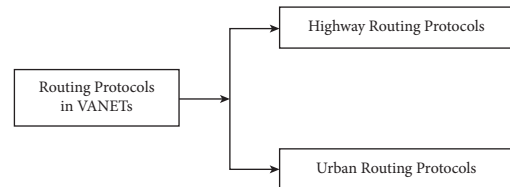


FIGURE 2: Proposed taxonomy of routing protocols in VANETS.

The highway routing protocols can also be divided into different categories depending on how the message is delivered, communication of cars with each other and the infrastructure, the use of fixed and mobile RSUs, and the like. Since the proposed protocol is a highway routing protocol, fixed and mobile RSUs are used. Simulations are performed on the MAC layer, and both DBA-MAC [23] and VMaSC-LTE [24] protocols are highway routing protocols and used fixed and mobile RSUs. Simulations are performed in the MAC layer, these two protocols are examined, and the proposed protocol is compared with them. Zhou et al. have designed a novel model based on Multilabel-Learning Network for RGB. The graded-feature Multilabel-learning network's suggested design performs state-of-the-art urban scene feature extraction approaches [25]. Zhou et al. have proposed a global feature learning for evaluating the quality of computer content and real scene photos in a blind manner [26]. Artin et al. have presented a new model for the prediction of traffic using ensemble NAS and linear regression in the network [27]. Sun et al. have generalized lifelong spectral clustering. In a lifetime learning paradigm called modified lifelong spectral clustering, this paper investigates the topic of fuzzy clustering [28]. Ahmadi et al. have

presented a new classifier model regarding fuzzy regression and the wavelet-based ANN using machine-learning techniques [29]. According to Zhou et al. [30], in terms of increased income, numerous encoding optimization schemes have been presented (RDO). Liu et al. [31] have introduced a new heterogeneous domain adaptation based on an unsupervised model. The results show that the suggested model outperforms the current baselines. Ni et al. [32] have analyzed clustered faults using a framework of cobweb-based redundant. Ala et al. [33] have presented a novel method based on a genetic algorithm for solving the quality of fairness service. Ni et al. [34] have analyzed a new TDMA model regarding the fault tolerance method for the TSVs with the honeycomb network. Sui et al. [35] have studied interference cancellation systems based on the broadband cancellation technique. Guo et al. [36] have concentrated on spreading various sensors and a networked model-based issue for a geographically sizeable linear system. In another study, shifting fault current controls enabled by 5 g in distribution transformers has been investigated by Sun et al. [37]. Ahmadi et al. [38] have examined a new IMU-aided multiple GNSS fault method for solving the problem of environments. Ahmadi et al. [38] have presented a new hybrid method for choosing users federated learning using federated learning based on a novel clustering method. Lv et al. [39] have studied a novel architecture of machine learning for cooperative, smart transportation system security in digital twins. Lv et al. [40] have reviewed 6G-enabled topology based on the Internet of transport vehicles. Lv et al. [41] have checked on methodologies on the Internet of vehicles using intelligent edge computing. Sharifi et al. [42] have studied a survey paper about applying artificial intelligence in industry networks and energy during the pandemic. They have reviewed several articles during last year's. Lv et al. [40] have studied an artificial intelligence model regarding empowered transportation systems using innovative system vehicles. The result shows that the model has a high-accuracy [43]. Lv et al. [41] have analyzed the Security of the Internet of Multimedia Things. This study under the novel technological industry wave, the security performance of the Internet of multimedia things on the security protection of user identification, behavior trajectory, and preference have been done [44]. Varmaghani et al. [45] have optimized energy consumption in dynamic WSN regarding fog modeling and fuzzy MCDM. The methods have been used for clustering and routing network. Accordingly, the given optimum and blind approaches are increased by 28% and 48%, based on the difficulty results obtained [45]. Zhao et al. [46] have optimized macroscopic modeling and dynamic management of automated cars' on-street searching for parks in a cross urban road network. Ahmadi and Qaisari Hasan Abadi [47] have reviewed several papers about the application of programming in-network and industry. They have designed a simulation framework for the proposed model. Bie et al. [48] have investigated a scheduling modeling approach that considers random variances in trip travel duration and energy usage [48]. Rezaei and Naderi [49] have presented a signature verification model using a new hybrid convolution network

model. Qiao et al. (2021) have studied a new classification using local wavelet acoustic with a whale optimization algorithm [50]. Qiao et al. [51] have studied coupled models in wavelet models to forecast PM10 concentration. Qiao et al. [52] have studied a combination model based on a wavelet network for forecasting the energy consumption of the USA. Qiao et al. [53] studied a fast-growing source forecasting for production using a novel hybrid wavelet. Peng et al. [54] investigated the effect of inverter blockage on metering efficiency during shale fracking. Peng et al. [55] have examined natural gas predicting regarding the wavelet threshold method.

2.1. DBA-MAC Routing Protocol. In 2009, Bononi et al. introduced the DBA-MAC protocol [23]. The DBA-MAC is presented for a multilane highway scenario, which is bidirectional. The vehicles are assumed to be equipped with GPS. Any emergency messages include dissemination direction, time to live (TTL), and risk zone. Only nodes in the risk zone are allowed to relay the message. The DBA-MAC protocol defines two priority classes to improve access to the channels: normal vehicles and backbone member (BM), where BMs are in higher priority. A node selects itself as BM to create a Backbone and then broadcasts a beacon message, which selects itself as BM. Vehicles that receive the beacon message calculate the remaining time the message can be disseminated (be released). Then, a car with a longer residual time than a threshold is selected as BM. When a BM_{N+1} receives a message from the BM_N , it immediately approves it and disseminates it with a SIFS delay for BM_{N+2} . If a Backbone needs to be repaired, the DBA-MAC will immediately replace a refreshed Backbone. Further, the protocol uses an infrastructure to avoid possible interruption of communication due to the low number of vehicles, in addition to vehicle-to-vehicle communication, where the locations of this infrastructure must be carefully selected.

2.2. VMaSC-LTE Routing Protocol. In 2016, Ucar et al. introduced the VMaSC-LTE protocol [24]. This protocol is a cluster-based technique that uses the IEEE 802.11p standard and selects the cluster head with a relative mobility metric, calculated using the average relative speed of neighboring vehicles. The average relative speed is obtained from $AVGREL_SPEED_i = \sum_{j=1}^{N(i)} |S_i - S_j| / N(i)$, where $N(i)$ is the number of neighbors having the same direction of cluster head for vehicle i , i_j is the id of node j , the neighbor of vehicle i , and S_i is the speed of vehicle i . Other features of this protocol include periodically dissemination of the information of cluster members in hello packets, direct connection to the cluster with minimal overhead instead of multistep connection, and reactive clustering to maintain the cluster structure without overusing the network. In the cluster maintenance phase, a timer is used to control the communication between the cluster head and the other cluster members. If the cluster head does not receive packets from its members in the same cluster at a predefined time, it assumes that the node is lost.

3. Proposed Algorithm

In this paper, a new routing algorithm is presented to improve the weaknesses of previous methods such as delay, overhead, packet delivery rate, and the like. The routing mode uses both fixed and mobile RSUs. First, the accident sites are identified, and fixed RSUs are installed where it is intended to deploy the intervehicle network. However, as known, the whole route cannot be well covered just by using fixed RSUs installed at accident sites. Therefore, a combination of fixed and mobile RSUs is used in the proposed protocol. As mentioned, fixed RSUs are used at accident sites and mobile RSUs at other locations on the route. Public transit vehicles are used as mobile RSUs by installing OBUs. In the proposed protocol, each vehicle can use fixed and mobile RSUs to reduce sending steps and delays to send packets and warning signals to other vehicles. The routing steps are as follows:

- (i) If there is a direct route from the source to the destination, i.e., the destination is within the coverage radius of the source, the package is sent directly to the destination.
- (ii) If there is no vehicle or RSUs (fixed or mobile) near the source, the source vehicle transports the data packet to the first vehicle within its radius and then sends it.
- (iii) If there are RSUs (fixed or mobile) near the source and destination, the source sends the packet to the RSUs (fixed or mobile). After receiving the packet, the RSU near the source sends it to the nearest RSU to the destination, and then it is sent to the destination.
- (iv) If there is more than one vehicle near the source, but none of them are fixed or mobile RSUs, the source vehicle sends the packet to the farthest vehicle within its radius and the shortest distance with the fixed or mobile RSUs. After the packet arrives at the RSU, the RSU sends it to the nearest RSU to the destination, and then it is sent to the destination.
- (v) If there is more than one route to send the data packet, a route with fewer steps and a longer route life is selected.

3.1. *Assumptions.* The following assumptions were made:

- (i) Each vehicle using its GPS obtains its location, the location of neighboring nodes, the location, and direction of the destination, road information (such as traffic), as well as a map of its intended environment. This information is periodically transmitted as a Hello message to nearby vehicles within its range.
- (ii) A digital map with the conditions of road traffic load is installed on the vehicle.
- (iii) The On-Board Unit (OBU) in any vehicle used as a mobile RSU has an IEEE 802.11p and a 3G interface.

The IEEE 802.11p interface is used to communicate with ordinary cars. The 3G interface communicates with RSUs (fixed and mobile).

20% of the nodes in the network are considered fixed and mobile RSUs, and the number of fixed and mobile RSUs is considered equal.

In addition, it is assumed that the entry time of ordinary vehicles and the mobile RSUs on the road follows the Poisson distribution (Figure 3). The distribution function of the vehicles and mobile RSUs is uniform along the entire road. It should be noted that the Poisson distribution is used here since the normal distribution is not suitable for n nodes more significant than 20, and where n is the number of vehicles which is much more than 20. The horizontal axis (X) in Figure 3 presents of entry time of ordinary vehicles and mobile RSUs in 24 hours with the number of vehicles per hour on the road, which can be used to estimate the number of steps and the arrival time to the accident site.

3.2. *Estimating the Number of Steps and Transmission Time.* As mentioned before, one of the features of the proposed algorithm is to reduce the delay by minimizing the number of steps between source and destination. For this purpose, if several routes are between the source and destination, the shortest route is selected by estimating the number of steps. In order to estimate the number of steps, the required parameters are defined as follows (Table 1):

Considering that the entry and exit rate of ordinary vehicles and mobile RSUs on the road follows the Poisson distribution, first the number of vehicles and RSUs on the road is calculated from Equations (1) and (2):

$$n = N \times P \times 10, \quad (1)$$

$$m = M \times P \times 10. \quad (2)$$

In the above case, it is multiplied by 10 because the probability is 1 at the best. Since the Poisson distribution is considered for $\lambda = 13$, and the maximum value is approximately 0.1 as shown in the graph, so it is multiplied by 10 to get 1.

Since fixed and mobile RSUs are used, and fixed RSUs are installed at the accident sites in the proposed algorithm, the route is divided into several sections (Figure 4). One part of the road L_j was considered. The L_j part was divided into two parts as L_{j1} and L_{j2} . Then, we have Equations (3) and (4):

$$N_{jk} = n_k \times \frac{L_j}{X_i} \quad k = 1, 2, \quad (3)$$

$$M_{jk} = m_k \times \frac{L_j}{X_i} \quad k = 1, 2, \quad (4)$$

where N_{jk} indicates the number of mobile RSUs and M_{jk} shows the number of ordinary vehicles in section L_j of the road. It is assumed that the source vehicle is in section j of the road and wants to send a packet. Since it can send the packet in the direction or in the opposite direction of itself, the j th part of the road is divided into two parts of $j1$ and $j2$.

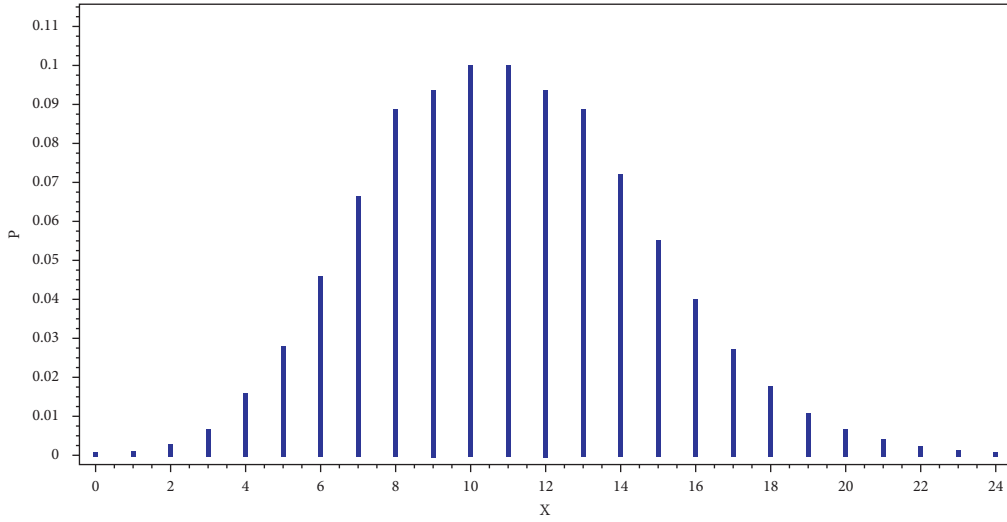


FIGURE 3: Diagram of entry time of ordinary vehicles and mobile RSUs in 24 hours.

TABLE 1: Parameters used in the proposed protocol.

Description	Name
The coverage radius of each vehicle	R
Packet delivery time between two source and destination vehicles	T
Delivery time between two vehicles	t_d
Speed of vehicle i	V_i
Speed of vehicle j	V_j
The distance between two vehicles i and j	d_{ij}
The whole length of the route	X_i
Total number of mobile RSUs in 24 hours	N
The number of mobile RSUs moving to the right of the road at a specific time	n_1
The number of mobile RSUs moving to the left of the road at a specific time	n_2
Total number of mobile RSUs at a specific time on the road	$n = n_1 + n_2$
Total number of ordinary vehicles in 24 hours	M
The number of vehicles moving to the right of the road at a specific time	m_1
The number of vehicles moving to the left of the road at a specific time	m_2
Total number of ordinary vehicles at a specific time on the road	$m = m_1 + m_2$
Poisson probability at a particular moment	P
The length of section j	L_j
The mobile RSUs in either L_{j1} or L_{j2} ($K = 1, 2$)	N_{jk}
The ordinary vehicles in either L_{j1} or L_{j2} ($K = 1, 2$)	M_{jk}

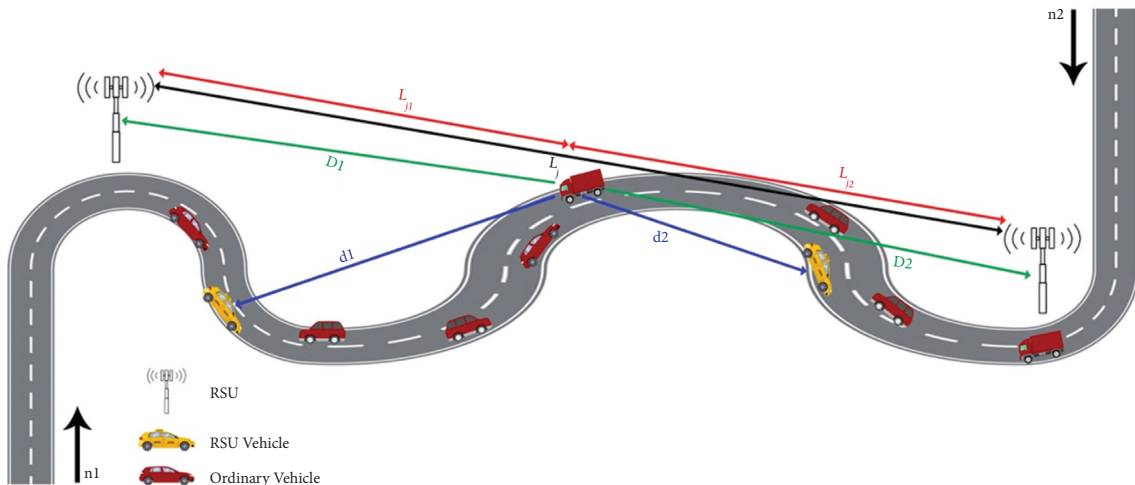


FIGURE 4: Network scenario.

The distance from the source vehicle to the fixed RSU behind it is called D_1 , and the distance from the source vehicle to the fixed forward RSU is D_2 . Now, suppose $D_2 > D_1$, D_2 is selected for sending the packet because there is a higher probability of more mobile RSUs in this area. In that case, we have Equations (5)–(8):

$$N'_{j2k} = n_k \times \frac{L_j/D_2}{X_i} = n_k \times \frac{L_j}{X_i D_2} \quad k = 1, 2, \quad (5)$$

where N'_{j2k} is the number of RSU in L_{j2} section.

$$d = \frac{D_2}{N'_{j2k}} = \frac{D_2^2 \times X_i}{n_k \times L_j}, \quad (6)$$

where d is the distance from the source to the first RSU.

$$M'_{j2k} = m_k \times \frac{L_j/d_2}{X_i} = m_k \times \frac{L_j}{X_i d_2} \quad k = 1, 2, \quad (7)$$

where M'_{j2k} is the number of ordinary vehicles between the origin and the first RSU.

$$d' = \frac{d_2}{M'_{j2k}} = \frac{d_2^2 \times X_i}{m_k \times L_j} \quad k = 1, 2, \quad (8)$$

where d' is the average distance between ordinary cars from the origin to the first RSU.

In order to calculate the number of steps to get to the nearest fixed or mobile RSU:

(A) If $d' \leq R$. Then, we have Equations (9) and (10):

$$C_j = \frac{L_j}{N'_{j2k} \times R}, \quad (9)$$

$$T = C_j \times t_d, \quad (10)$$

where C_j is the number of steps to reach the nearest fixed, or mobile RSU and T is the time to reach the nearest fixed or mobile RSU.

(B) If $d' > R$. Then, we have (Equations (11) and (12)):

$$C_j = M'_{j2k} - 1, \quad (11)$$

$$T = \left(\sum_{i=1}^{M'_{j2k}-1} \frac{V_i}{d_{ij}} \right) + (C_j \times t_d). \quad (12)$$

If $D_1 = D_2$, since the number of steps will be equal, a route with the most extended lifespan will be selected among the available routes.

3.3. Calculating the Lifetime of the Route. The lifespan is calculated as follows:

(A) Both vehicles should be in the same direction, and the speed of the front vehicle should be more. In this case, the lifetime of the path is calculated by the following equation:

$$\text{LifeTime}_{link} = \frac{R - |d_{ij}|}{|V_i - V_j|}, \quad (13)$$

(B) Both vehicles should be in the same direction, and the speed of the front vehicle must be less. In this case, the lifetime of the route is calculated by the following equation:

$$\text{LifeTime}_{link} = \frac{R + |d_{ij}|}{|V_i - V_j|}. \quad (14)$$

(C) Vehicles move in the opposite direction. In this case, the lifetime of the route is calculated by the following equation (15):

$$\text{LifeTime}_{link} = \frac{R + |d_{ij}|}{V_i + V_j}, \quad (15)$$

where R is the transmission range between the vehicles, d_{ij} represents the distance between vehicles i and j , V_i is the speed of vehicle i , and V_j is the speed of vehicle j .

4. Result and Discussion

In this section, the performance of the proposed protocol is compared through various factors. NS2 simulator is used to simulate the proposed protocol and compare its performance parameters with other protocols [56]. In this simulation experiment, a highway scenario with a length of 8 km and 25 to 200 vehicles was considered. IEEE 802.11 with a transmission rate of 2 Mbps and a transmission range of 250 m is used as the underlying MAC protocol. The data packet's time to live (TTL) is set to 100 hops. All simulation results are averaged over 20 runs. The parameters used in the simulations are summarized in Table 2.

4.1. Performance Parameters. The parameters such as packet delivery rate, overhead, end-to-end delay, and several dropped packets were used to evaluate the performance of the proposed protocols and compare them with other protocols. Each of these parameters is explained in this section, and all three proposed protocols, DBA-MAC and VMaSC-LTE, are compared.

4.1.1. Packet Delivery Rate. The ratio of total packets received by the destination node to the total packets sent by the source is obtained using Equation (16):

$$\text{PDR} = \frac{\text{number of packets received by the destination}}{\text{number of packets sent by the source}}. \quad (16)$$

Packet delivery rates give information on how successful the protocol is in delivering data packets. The higher PDR means that the protocol has been more efficient in delivering packets.

TABLE 2: Simulation parameters.

Parameters	Value
Network simulator	NS2
Simulation time	1000s
Highway length	8 Km
Vehicles speed (min)	20 m/s
Vehicles speed (max)	33 m/s
Number of vehicles	25, 50, 100, 200
Phy/Mac protocol	IEEE 802.11p
Data message size	512 bytes
Traffic	CBR
Transmission range	250 m
Transmission power	1 mW

The breaking of the communication link between vehicles due to the high speed of the vehicles is regarded as one of the main concerns in intervehicle networks is. As observed in Figure 5, the communication links between the vehicles are less likely to be broken when the number of vehicles increases, resulting in fewer dropped packets and higher packet delivery rates. Furthermore, the proposed protocol performs better than the other two protocols.

Figure 6 illustrates the effect of increasing the number of RSUs on the packet delivery rate for the proposed protocol in different modes. In the proposed protocol, 20% of the vehicles are RSU. However, the packet delivery rate is examined for the modes with 10%, 20%, 30%, 40%, and 50% of the total RSU network vehicles and four modes with 25, 50,

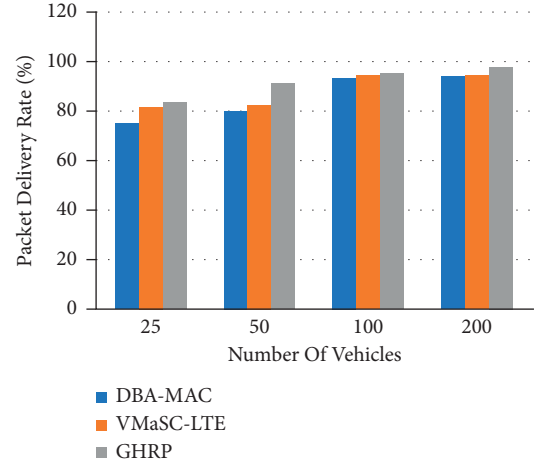


FIGURE 5: The effect of increasing the number of vehicles on the percentage of packet delivery rate.

100, and 200 vehicles. As observed, the higher the number of RSUs, the higher is the packet delivery rate.

4.1.2. Average End-to-End Delay. The average end-to-end delay is defined as the average delay in transmitting a packet between two end nodes. This parameter is calculated using Equation (17):

$$AED = \frac{\sum_{i=0}^n ((\text{time of receiving the } i\text{-th packet}) - (\text{time of sending the } i\text{-th packet}))}{\text{total number of packets received by the destination}} \quad (17)$$

Figure 7 shows the average end-to-end delay between the suggested algorithm and the two other algorithms. With the number of vehicles, the end-to-end delay decreases due to the number of routers between the source and destination. As Figure 7 shows, the suggested protocol outperformed the two other protocols when the network was quiet and busy.

As explained, the use of RSUs in the proposed protocol for intervehicle networks reduces the number of routing steps between the source and the destination. As the number of RSUs shown in Figure 8 increases, the number of packet sending steps decreases between source and destination, resulting in a lower end-to-end delay.

4.1.3. Number of Dropped Packets. This parameter indicates the percentage of packets dropped during the simulation and not reached their destination. The NDP can be calculated by:

$$NDP = \frac{(\text{sent packet} - \text{received packet})}{100} \quad (18)$$

Increasing the number of vehicles makes it less likely for links to break between vehicles. Thus, the number of dropped packets is lower.

In the section related to packet delivery rates, it was argued that the links are less likely to be broken due to the

high speed of vehicles in intervehicle networks. Thus, the packet delivery rate is higher when the number of vehicles increases. Since the packet delivery rate and the number of dropped packets in the network are correlated inversely, the number of dropped packets is lower when the packet delivery rate increases. Figures 9 and 10 indicate the obtained results. The number of dropped packets in the network decreases by increasing the number of vehicles and RSUs.

4.1.4. Normalized Routing Load (NRL). This parameter is defined as the ratio of routing packets sent to the number received and can be calculated using Equation (19):

$$NRL = \frac{\text{number of routing packets sent by the source}}{\text{number of packets received by the destination}} \quad (19)$$

The higher the NRL, the lower is the performance and efficiency of the protocol.

An increase in the number of vehicles leads to an increase in the routing overhead since the operations performed by vehicles on packets increase. However, as shown in Figure 11, the routing overhead of the proposed protocol is less than the other two protocols.

As shown in Figure 11, the overhead increases by increasing the number of vehicles and thus the number of

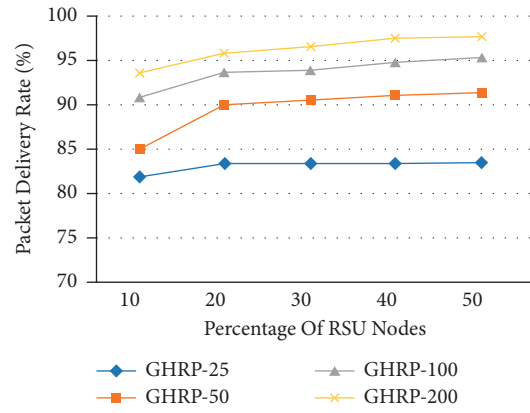


FIGURE 6: The effect of increasing the number of RSUs on packet delivery rate percentages.

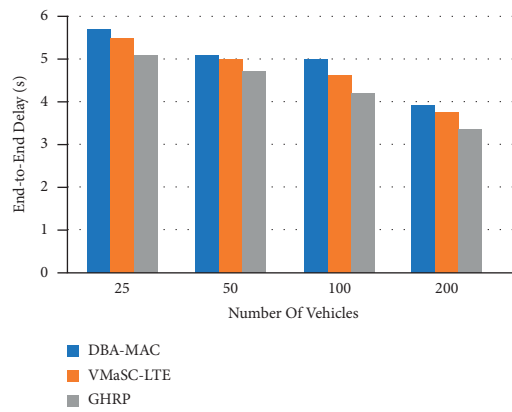


FIGURE 7: The effect of an increasing number of vehicles on end-to-end delay.

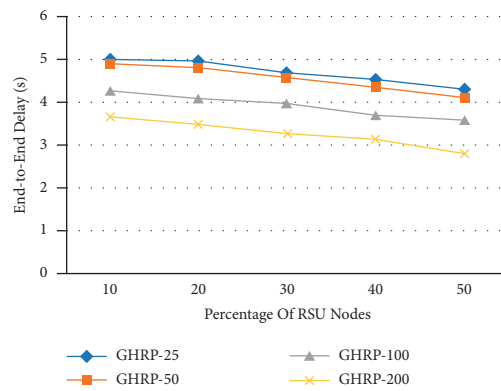


FIGURE 8: The effect of increasing RSUs on end-to-end delay.

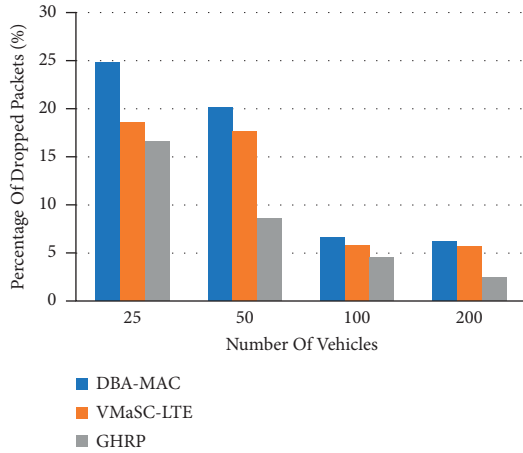


FIGURE 9: The impact of an increasing number of vehicles on the dropped packet amount.

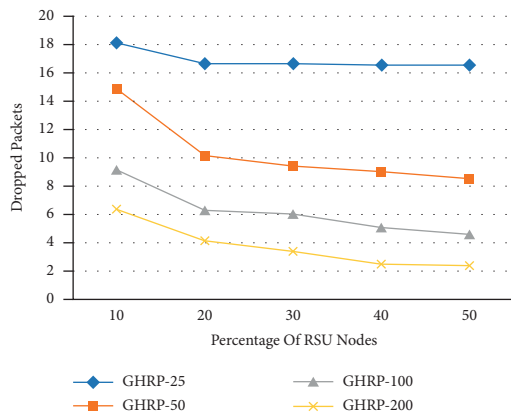


FIGURE 10: Increasing the number of RSUs on the amount of dropped packets.

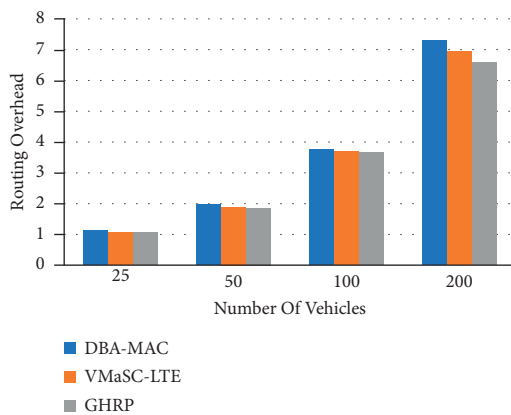


FIGURE 11: The effect of an increasing number of vehicles on the routing overhead.

vehicles performed on routing packets. However, as illustrated in Figure 12, an increase in the number of RSUs leads to an increase in the number of steps to reach the destination, resulting in fewer routing operations and eventually lower overhead.

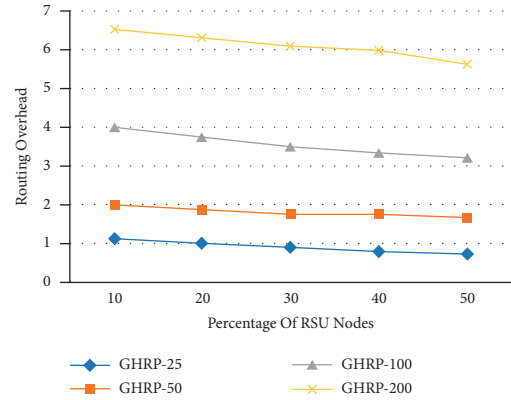


FIGURE 12: Effect of increasing RSUs on routing overhead value.

5. Conclusion

The main challenges in VANETs are the dynamic topology and constant network disconnection, which lead to delays in packages’ arrival [57]. In the present paper, an intercity protocol was suggested, which attempts to solve this problem by global coverage of the vehicles’ routes and reduction of delay to achieve the primary goal of VANETs, which is the safety and comfort of passengers. In the suggested protocol, fixed and variable RSUs were used to route packages, and an ns2 simulator was employed to simulate. The suggested protocol was compared with two intercity routing protocols, i.e., DBA-MAC and VMaSC-LTE. It was found that the suggested protocol outperformed the two other ones in terms of delay, packet delivery rate, and routing overhead. We follow two main goals in future works. First, investigation and implementation of the suggested protocol in an urban environment will also focus on efficient energy consumption and the issues mentioned above [58]. Second, since the information exchanged between cars is essential.

In some cases, even humans’ life may depend on this information, and the issue of security can be of great importance [59]. Thus, it must be robust against different types of attacks like fake information, service denial, and black holes. Therefore, we will work on the security aspect of the suggested protocol to make it a safe protocol against different types of attacks to the information can safely and accurately reach the destination.

Data Availability

Data are available and can be provided over the emails querying directly to the author at the corresponding author (zeinali@qiau.ac.ir).

Conflicts of Interest

The authors declare that they have no conflicts of interest.

References

[1] E. Khezri and E. Zeinali, “A review on highway routing protocols in vehicular ad hoc networks,” *SN Computer Science*, vol. 2, no. 2, pp. 1–22, 2021.

- [2] J. Cui, W. Xu, Y. Han, J. Zhang, and H. Zhong, "Secure mutual authentication with privacy preservation in vehicular ad hoc networks," *Vehicular Communications*, vol. 21, p. 100200, 2020.
- [3] S. Kumar and A. K. Verma, "Position based routing protocols in VANET: a survey," *Wireless Personal Communications*, vol. 83, no. 4, pp. 2747–2772, 2015.
- [4] J. Noh, S. Jeon, and S. Cho, "Distributed blockchain-based message authentication scheme for connected vehicles," *Electronics*, vol. 9, no. 1, p. 74, 2020.
- [5] I. Ali, A. Hassan, and F. Li, "Authentication and privacy schemes for vehicular ad hoc networks (VANETs): a survey," *Vehicular Communications*, vol. 16, pp. 45–61, 2019.
- [6] Y. Ming and H. Cheng, "Efficient certificateless conditional privacy-preserving authentication scheme in VANETs," *Mobile Information Systems*, vol. 2019, Article ID 7593138, 19 pages, 2019.
- [7] B. T. Sharef, R. A. Alsaqour, and M. Ismail, "Vehicular communication ad hoc routing protocols: a survey," *Journal of Network and Computer Applications*, vol. 40, pp. 363–396, 2014.
- [8] H. Galeana-Zapién, M. Morales-Sandoval, C. A. Leyva-Vázquez, and J. Rubio-Loyola, "Smartphone-based platform for secure multi-hop message dissemination in VANETs," *Sensors*, vol. 20, no. 2, p. 330, 2020.
- [9] M. Ma, D. He, H. Wang, N. Kumar, and K.-K. R. Choo, "An efficient and provably secure authenticated key agreement protocol for fog-based vehicular ad-hoc networks," *IEEE Internet of Things Journal*, vol. 6, no. 5, pp. 8065–8075, 2019.
- [10] C. Suthaputchakun and Z. Sun, "Routing protocol in inter-vehicle communication systems: a survey," *IEEE Communications Magazine*, vol. 49, no. 12, pp. 150–156, 2011.
- [11] C. Tripp-Barba, A. Zaldívar-Colado, L. Urquiza-Aguilar, and J. A. Aguilar-Calderón, "Survey on routing protocols for vehicular ad hoc networks based on multimetrics," *Electronics*, vol. 8, no. 10, p. 1177, 2019.
- [12] D. Antolino Rivas, J. M. Barceló-Ordinas, M. Guerrero Zapata, and J. D. Morillo-Pozo, "Security on VANETs: privacy, misbehaving nodes, false information and secure data aggregation," *Journal of Network and Computer Applications*, vol. 34, no. 6, pp. 1942–1955, 2011.
- [13] E. Fonseca and A. Festag, "A survey of existing approaches for secure ad hoc routing and their applicability to VANETs," *NEC network laboratories*, vol. 28, pp. 1–28, 2006.
- [14] F. Li and Y. Wang, "Routing in vehicular ad hoc networks: a survey," *IEEE Vehicular Technology Magazine*, vol. 2, no. 2, pp. 12–22, 2007.
- [15] G. Karagiannis, O. Altintas, E. Ekici et al., "Vehicular networking: a survey and tutorial on requirements, architectures, challenges, standards and solutions," *IEEE Communications Surveys & Tutorials*, vol. 13, no. 4, pp. 584–616, 2011.
- [16] M. Zhou, L. Han, H. Lu, and C. Fu, "Distributed collaborative intrusion detection system for vehicular Ad Hoc networks based on invariant," *Computer Networks*, vol. 172, p. 107174, 2020.
- [17] S. Dhankhar and S. Agrawal, "VANETs: a survey on routing protocols and issues," *International Journal of Innovative Research in Science, Engineering and Technology*, vol. 3, no. 6, pp. 13427–13435, 2014.
- [18] S. Zeadally, R. Hunt, Y.-S. Chen, A. Irwin, and A. Hassan, "Vehicular ad hoc networks (VANETs): status, results, and challenges," *Telecommunication Systems*, vol. 50, no. 4, pp. 217–241, 2012.
- [19] A. Ram and M. K. Mishra, "Density-connected cluster-based routing protocol in vehicular ad hoc networks," *Annals of Telecommunications*, vol. 75, no. 7, pp. 319–332, 2020.
- [20] M. A. Mimi and M. M. Elahi: A Stable Clustering Architecture for Efficient Routing in Vehicular Ad Hoc Networks.
- [21] Y. Jiang and X. Li, "Broadband cancellation method in an adaptive co-site interference cancellation system," *International Journal of Electronics*, pp. 1–21, 2021.
- [22] F. J. Martinez, C. K. Toh, J.-C. Cano, C. T. Calafate, and P. Manzoni, "A survey and comparative study of simulators for vehicular ad hoc networks (VANETs)," *Wireless Communications and Mobile Computing*, vol. 11, no. 7, pp. 813–828, 2011.
- [23] L. Bononi, M. Di Felice, and S. Pizzi, "Db-mac: dynamic backbone-assisted medium access control protocol for efficient broadcast in vanets," *Journal of Interconnection Networks*, vol. 10, no. 04, pp. 321–344, 2009.
- [24] S. Ucar, S. C. Ergen, and O. Ozkasap, "Multihop-cluster-based IEEE 802.11 p and LTE hybrid architecture for VANET safety message dissemination," *IEEE Transactions on Vehicular Technology*, vol. 65, no. 4, pp. 2621–2636, 2015.
- [25] W. Zhou, J. Liu, J. Lei, L. Yu, and J.-N. Hwang, "GMNet: graded-feature multilabel-learning network for RGB-thermal urban scene semantic segmentation," *IEEE Transactions on Image Processing*, vol. 30, pp. 7790–7802, 2021.
- [26] W. Zhou, L. Yu, Y. Zhou, W. Qiu, M.-W. Wu, and T. Luo, "Local and global feature learning for blind quality evaluation of screen content and natural scene images," *IEEE Transactions on Image Processing*, vol. 27, no. 5, pp. 2086–2095, 2018.
- [27] J. Artin, V. Amin, M. Ahmadi, S. A. P. Kumar, and A. Sharifi, "Presentation of a novel method for prediction of traffic with climate condition based on ensemble learning of neural architecture search (NAS) and linear regression," *Complexity*, vol. 2021, Article ID 8500572, 13 pages, 2021.
- [28] G. Sun, Y. Cong, J. Dong, Y. Liu, Z. Ding, and H. Yu, "What and how: generalized lifelong spectral clustering via dual memory," *IEEE Transactions on Pattern Analysis and Machine Intelligence*, p. 1, 2021.
- [29] M. Ahmadi, F. Dashti Ahangar, N. Astaraki, M. Abbasi, and B. Babaei, "FWNNNet: presentation of a new classifier of brain tumor diagnosis based on fuzzy logic and the wavelet-based neural network using machine-learning methods," *Computational Intelligence and Neuroscience*, vol. 2021, Article ID 8542637, 13 pages, 2021.
- [30] Y. Zhou, G. Xu, K. Tang, L. Tian, and Y. Sun, "Video coding optimization in AVS2," *Information Processing & Management*, vol. 59, no. 2, p. 102808, 2022.
- [31] F. Liu, G. Zhang, and J. Lu, "Heterogeneous domain adaptation: an unsupervised approach," *IEEE Transactions on Neural Networks and Learning Systems*, vol. 31, no. 12, pp. 5588–5602, 2020.
- [32] T. Ni, D. Liu, Q. Xu, Z. Huang, H. Liang, and A. Yan, "Architecture of cobweb-based redundant TSV for clustered faults," *IEEE Transactions on Very Large Scale Integration Systems*, vol. 28, no. 7, pp. 1736–1739, 2020.
- [33] A. Ala, F. E. Alsaadi, M. Ahmadi, and S. Mirjalili, "Optimization of an appointment scheduling problem for healthcare systems based on the quality of fairness service using whale optimization algorithm and NSGA-II," *Scientific Reports*, vol. 11, no. 1, pp. 19816–19819, 2021.
- [34] T. Ni, Z. Yang, H. Chang et al., "A novel TDMA-based fault tolerance technique for the TSVs in 3D-ICs using honeycomb topology," *IEEE transactions on emerging topics in computing*, vol. 9, no. 2, pp. 724–734, 2021.

- [35] T. Sui, D. Marelli, X. Sun, and M. Fu, "Multi-sensor state estimation over lossy channels using coded measurements," *Automatica*, vol. 111, p. 108561, 2020.
- [36] L. Guo, C. Ye, Y. Ding, and P. Wang, "Allocation of centrally switched fault current limiters enabled by 5G in transmission system," *IEEE Transactions on Power Delivery*, vol. 36, no. 5, pp. 3231–3241, 2021.
- [37] R. Sun, J. Wang, Q. Cheng, Y. Mao, and W. Y. Ochieng, "A new IMU-aided multiple GNSS fault detection and exclusion algorithm for integrated navigation in urban environments," *GPS Solutions*, vol. 25, no. 4, 2021.
- [38] M. Ahmadi, T. Ali, D. Javaheri, A. Masoumian, and Y. Pourasad, "DQRE-SCnet: a novel hybrid approach for selecting users in federated learning with deep-Q-reinforcement learning based on spectral clustering," *Journal of King Saud University-Computer and Information Sciences*, 2021.
- [39] Z. Lv, Y. Li, H. Feng, and H. Lv, "Deep learning for security in digital twins of cooperative intelligent transportation systems," *IEEE Transactions on Intelligent Transportation Systems*, pp. 1–10, 2021.
- [40] Z. Lv, L. Qiao, and I. You, "6G-Enabled network in box for internet of connected vehicles," *IEEE Transactions on Intelligent Transportation Systems*, vol. 22, no. 8, pp. 5275–5282, 2021.
- [41] Z. Lv, D. Chen, and Q. Wang, "Diversified technologies in internet of vehicles under intelligent edge computing," *IEEE Transactions on Intelligent Transportation Systems*, vol. 22, no. 4, pp. 2048–2059, 2021.
- [42] A. Sharifi, M. Ahmadi, and A. Ala, "The impact of artificial intelligence and digital style on industry and energy post-COVID-19 pandemic," *Environmental Science and Pollution Research*, vol. 28, no. 34, pp. 46964–46984, 2021.
- [43] Z. Lv, R. Lou, and A. K. Singh, "AI empowered communication systems for intelligent transportation systems," *IEEE Transactions on Intelligent Transportation Systems*, vol. 22, no. 7, pp. 4579–4587, 2021.
- [44] Z. Lv, L. Qiao, and H. Song, "Analysis of the security of internet of multimedia things," *ACM Transactions on Multimedia Computing, Communications, and Applications*, vol. 16, no. 3s, pp. 1–16, 2021.
- [45] A. Varmaghani, M. Ali, M. Ahmadi, A. Sharifi, and Y. Pourasad, "DMTC: optimize energy consumption in dynamic wireless sensor network based on fog computing and fuzzy multiple attribute decision-making," *Wireless Communications and Mobile Computing*, vol. 2021, Article ID 9953416, 14 pages, 2021.
- [46] C. Zhao, F. Liao, X. Li, and Y. Du, "Macroscopic modeling and dynamic control of on-street cruising-for-parking of autonomous vehicles in a multi-region urban road network," *Transportation Research Part C: Emerging Technologies*, vol. 128, p. 103176, 2021.
- [47] M. Ahmadi and M. Qaisari Hasan Abadi, "A review of using object-orientation properties of C++ for designing expert system in strategic planning," *Computer Science Review*, vol. 37, p. 100282, 2020.
- [48] Y. Bie, J. Ji, X. Wang, and X. Qu, "Optimization of electric bus scheduling considering stochastic volatilities in trip travel time and energy consumption," *Computer-Aided Civil and Infrastructure Engineering*, vol. 36, no. 12, pp. 1530–1548. In Press, 2021.
- [49] M. Rezaei and N. Naderi, "Persian signature verification using fully convolutional networks," 2019, <https://arxiv.org/abs/1909.09720>.
- [50] W. Qiao, M. Khishe, and S. Ravakhah, "Underwater targets classification using local wavelet acoustic pattern and Multi-Layer Perceptron neural network optimized by modified Whale Optimization Algorithm," *Ocean Engineering*, vol. 219, p. 108415, 2021.
- [51] W. Qiao, Y. Wang, J. Zhang, W. Tian, Y. Tian, and Q. Yang, "An innovative coupled model in view of wavelet transform for predicting short-term PM10 concentration," *Journal of Environmental Management*, vol. 289, p. 112438, 2021.
- [52] W. Qiao, W. Liu, and E. Liu, "A combination model based on wavelet transform for predicting the difference between monthly natural gas production and consumption of U.S.," *Energy*, vol. 235, p. 121216, 2021.
- [53] W. Qiao, Z. Li, W. Liu, and E. Liu, "Fastest-growing source prediction of US electricity production based on a novel hybrid model using wavelet transform," *International Journal of Energy Research*, 2021.
- [54] S. Peng, Y. Zhang, W. Zhao, and E. Liu, "Analysis of the influence of rectifier blockage on the metering performance during shale gas extraction," *Energy & Fuels*, vol. 35, no. 3, pp. 2134–2143, 2021.
- [55] S. Peng, R. Chen, B. Yu, M. Xiang, X. Lin, and E. Liu, "Daily natural gas load forecasting based on the combination of long short term memory, local mean decomposition, and wavelet threshold denoising algorithm," *Journal of Natural Gas Science and Engineering*, vol. 95, p. 104175, 2021.
- [56] T. Issariyakul and E. Hossain, *Introduction to Network Simulator 2 (NS2)*, Springer, Berlin, Germany, 2009.
- [57] H. Shahwani, S. Attique Shah, M. Ashraf, M. Akram, J. Jeong, and J. Shin, "A comprehensive survey on data dissemination in Vehicular Ad Hoc Networks," *Vehicular Communications*, p. 100420, 2021.
- [58] F. Safara, A. Souri, T. Baker, I. Al Ridhawi, and M. Aloqaily, "A priority-based energy-efficient routing method for IoT systems," *The Journal of Supercomputing*, vol. 76, pp. 1–18, 2020.
- [59] P. Wang, C.-M. Chen, S. Kumari, M. Shojafar, R. Tafazolli, and Y.-N. Liu, "HDMA: hybrid D2D message authentication scheme for 5G-enabled VANETs," *IEEE Transactions on Intelligent Transportation Systems*, vol. 22, 2020.

Research Article

China's Energy Demand Forecasting Based on the Hybrid PSO-LSSVR Model

Yifei Yang, Lu Han, Yarong Wang, and Jianzhong Wang 

Department of Economic Management, Agricultural University of Hebei, Baoding 071000, China

Correspondence should be addressed to Jianzhong Wang; wangdongxuan@hebau.edu.cn

Received 2 December 2021; Revised 5 January 2022; Accepted 6 January 2022; Published 24 January 2022

Academic Editor: Nima Jafari Navimipour

Copyright © 2022 Yifei Yang et al. This is an open access article distributed under the Creative Commons Attribution License, which permits unrestricted use, distribution, and reproduction in any medium, provided the original work is properly cited.

Forecasting energy demand accurately is the basis for the formulation and implementation of energy planning. In this paper, energy demand influencing factors are mainly decomposed into scale economy effect, population size effect, energy structure effect, and residential consumption effect based on the Logarithmic Mean Divisia Index (LMDI). Then, the Cointegration and Granger Causality tests are used to discover the influencing factors of energy demand in China. On this basis, a hybrid optimization algorithm, the least-squares support-vector regression optimized by particle swarm optimization (PSO-LSSVR), is proposed to forecast the energy demand of China. Then, three scenarios are set up to analyze the further development of drive factors of energy demand. Finally, in accordance with the forecasting results, some suggestions related to China's energy development policy are given. The main results are as follows. First, gross domestic product (GDP), the total population at the end of the year (POP), the coal consumption ratio in energy (CCR), and residential consumption levels (RCLs) are dominant indicators of energy demand in China. Second, the improved PSO-LSSVR model has significant superiority than other models in energy demand forecasting, a complex and nonlinear system with small samples. Third, China's energy demand will peak in 2022, which is 4.9 million tce in all scenarios.

1. Introduction

1.1. Background, Purpose, and Significance. Energy, the material basis for economic development and social progress, has gained considerable attention. Energy demand forecasting has a guiding significance on the formulation and implementation of energy policy. Driven by technological advances and sustainable development, the global energy supply became cleaner and lower carbon. In response to reducing carbon emission and combating climate change, the global economy started to transit its structure towards a low-carbon economy. At the same time, the global energy market began to enter a new period of energy transition. Correspondingly, China has also gradually entered the period of energy structure adjustments and transformation upgrading. China, as the largest developing country, has the largest total energy consumption in the world. BP Statistical Review of World Energy (2020) reports that China's energy demand growth accounts for more than three-quarters of net global energy consumption, while the US

and Germany posted the largest declines influenced by COVID-19. Therefore, the transformation of the energy consumption structure in China can affect the global energy consumption structure. The overwhelming growth of energy consumption in China will lead to an imbalance between energy supply and demand. Similarly, this problem can occur in other developing countries. Hence, forecasting the accurate energy demand in China plays a decisive role in formulating and implementing energy policy and provides enlightenment and reference significant for other developing countries. However, the existing research on the prediction model of energy demand is weak, so this paper focuses on the prediction model suitable for an energy system.

1.2. Current Research. A lot of scholars have studied energy demand prediction. The core part of it can be divided into two strands. The first strand is the selection of indicators. Energy is a nonlinear complex system influenced by complex socioeconomic factors, according to the existing literature devoting to identifying the factors affecting energy

demand. For instance, Xia and Wang found the factors of energy demand mainly included gross domestic product (GDP), population, urbanization rate, and energy consumption structure by the Logarithmic Mean Division Index (LMDI) [1]. Wu and Peng hold the view that economic growth, total population, investment in fixed assets, energy efficiency, energy structure, and household energy consumption per capita are the most critical elements of energy demand [2]. For higher forecasting accuracy, the most suitable indicators are picked out as the forecasting inputs.

The second strand is the forecasting models, including the univariate model and multivariate model. The univariate method propels further prediction with historical data, such as the gray model, ARIMA model, and the like [3, 4]. The multivariate method is based on the determined mapping relationship between energy demand (dependent variable) and independent variables. Also, the commonly used prediction models are multivariate methods, such as the multiple linear regression (MLR) model and partial least-squares regression model [5, 6]. The univariate model applies primarily to short-term prediction, and the multivariate model is more suitable for medium- and long-term prediction.

Artificial intelligence (AI) methods have been extensively used for forecasting due to their nonlinear mapping ability and good forecast ability. The artificial neural networks (ANNs) [7], support vector machine (SVM) [8], and extreme learning machine (ELM) [9] are all widely used AI methods. At the same time, the optimal parameters of the prediction model can be found by the heuristic algorithm. The heuristic algorithm is good at giving feasible solutions to combinatorial problems to be solved. Cui et al. construct a new prediction model based on back propagation neural network with the optimization of GA algorithm and PSO algorithm [10]. The commonly used heuristic algorithms are particle swarm optimization (PSO) [11], ant colony optimization (ACO) [12], genetic algorithm (GA) [13], etc.

The energy system is complex and lack of samples; there will be insufficient training, unstable performance, and over “learning” in ANNs. All of these will lead to unsatisfactory prediction results. SVM, proposed by Cortes and Vapnik [14], has an excellent performance in solving small samples, nonlinear, high dimension problems. Therefore, SVR, the regression version of SVM, is widely used in various energy research. Suykens and Vandewall [15] improved LSSVR in 1999, the least-squares formulation of SVR, which has better generalization abilities and robust computation. Kaytez et al. [16] find that LSSVR has better accuracy than regression analysis and neural network in long-term electricity consumption prediction. However, there are still difficulties in LSSVR including the choice of kernel and regularization parameters, so PSO is introduced to improve the prediction accuracy of LSSVM. Although PSO-LSSVR has been employed in other fields successfully [17], the application of PSO-LSSVR in energy demand forecasting is quite a few. Therefore, it contributes to making energy demand prediction abundant.

1.3. Main Aim and Principle Conclusions. This study is aimed at solving the following problems. First, identify dom-

inant indicators of energy demand to describe and analyze the complex features of the energy system in China. Second, hunt for a prediction model with high-precision ability to reasonably predict energy demand’s trend in China. Third, analyze the changing trend of energy demand under different development scenarios produced by other development policies. Forth, according to the determined vital factors, predict the movement of energy demand in different situations, and give corresponding policy suggestions for energy development.

The principle conclusions lie in the following aspects. First, this paper finds that GDP, population (POP), coal consumption ratio (CCR), and residential consumption level (RCL) are the critical factors of the energy demand of China through the Cointegration and Granger Causality test. Second, a hybrid forecasting model, PSO-LSSVR, was first proposed to forecast energy demand in this paper. Additionally, the established model shows a much better effect on the Mean Absolute Percentage Error (MAPE), Root Mean Square Error (RMSE), and the goodness of fit (R^2) compared with traditional models. Third, scenario analysis sets three different scenarios to analyze the energy demand trend in China under different levels to formulate corresponding energy development plans and policies.

The remainder of this paper is arranged as follows. The method of this paper is introduced in Section 2. Section 3 discussed China’s energy demand influencing factors through the Cointegration and Granger Causality tests. The energy demand prediction model, PSO-LSSVR, is proposed in Section 4. In Section 5, the possible trend of energy demand under different development scenarios is analyzed in detail. Section 6 depicts the key conclusions. Forecasting mechanism for energy demand is listed in Figure 1.

2. Methodology

2.1. Least-Squares Support-Vector Regression Model. SVM, proposed by Cortes and Vapnik [14], converts the input space into a high-dimensional space through nonlinear mapping and finds the optimal hyperplane to divide the feature space in this space based on SVC and statistical learning theory. However, SVM takes too much time to cope with thousands of data. Therefore, least-squares support-vector machine (LSSVM) was proposed [15]. Compared with SVM, LSSVM has more advantages [18] as follows:

- (i) It changes the structure of the loss function, taking a squared loss function rather than it in SVM
- (ii) It transforms inequality constraints into equality constraints, avoiding solving QP problems when finding the optimal hyperplane

With these modifications, the computational quantity is reduced heavily, and training speed is also significantly accelerated.

Support vectors can be used in SVC for classification and in SVR for regression. Therefore, LSSVM can be categorized into LSSVC for classification and LSSVR for regression

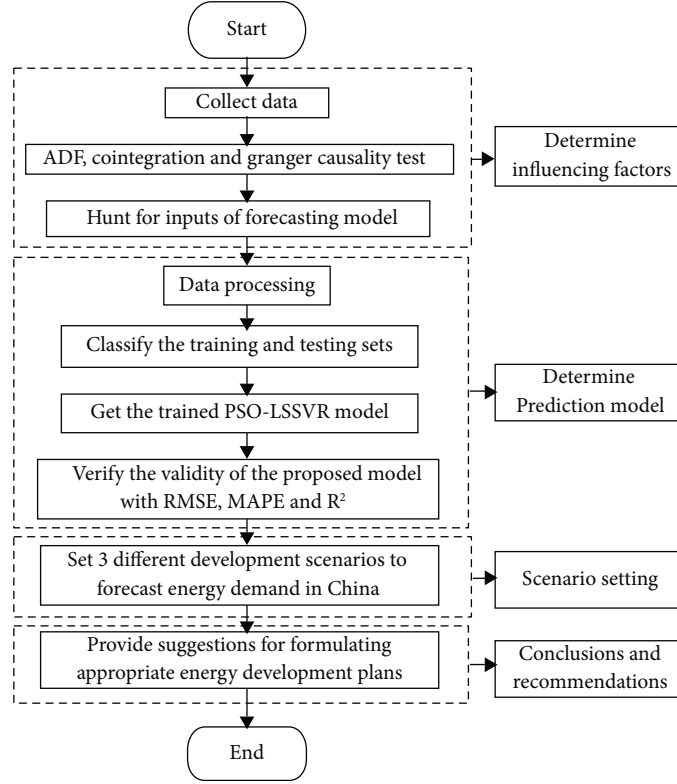


FIGURE 1: Forecasting mechanism of energy demand.

purposes. LSSVR is a nonlinear regression model based on SVC and structural risk minimization. Then, SVR and LSSVR will be introduced. The principle of LSSVR is described briefly.

Given a set of training sample points: $S = \{(x_k, y_k) \mid k = 1, 2, \dots, n\}$, where $x_k \in R^n$ is the input value and $y_k \in R$ is the output value. By the map $\Phi(\bullet)$, the samples from the original space R^n is mapped into the feature space $\varphi(x_k)$. The optimal decision function is defined.

$$y(x) = \omega^T \varphi(x) + b, \quad (1)$$

where $\varphi(x)$ is the kernel function, ω is the weighted vector, and b is a constant.

Then, the regression problem can be transformed into an optimization problem with constraints.

$$\min_{\omega, b, e} J(\omega, e) = \frac{1}{2} \omega^T \omega + \frac{1}{2} \gamma \sum_{k=1}^n e_k^2 \text{ s.t. } y_k = \omega^T \varphi(x_k) + b + e_k, \quad (2)$$

where $k = 1, 2, \dots, n$, γ is the regularization parameter, and e_k is the slack variable. To solve the equation, the Lagrange function is defined.

$$L(\omega, b, e, \alpha) = J(\omega, e) - \sum_{k=1}^n \alpha_k [\omega^T \varphi(x_k) + b + e_k - y_k], \quad (3)$$

where α_k is the Lagrange multiplier. After the calculation, the values of α and b are determined. Then, the fitting function can be represented.

$$f(x) = \sum_{k=1}^n \alpha_k K(x, x_k) + b, \quad (4)$$

$$K(x, x_i) = \varphi(x)^T \bullet \varphi(x),$$

where $K(x, x_i)$ is the kernel function, which expresses non-linear mapping.

The kernel function decides the mapping function and feature space. The Radial Basis Function (RBF) can grapple with the amount of input data efficiently, and it is suitable for theoretical analysis owing to its good analyticity. Thus, RBF is the kernel function in this paper, and it is defined.

$$K(x, x_i) = \exp\left(\frac{-\|x - x_i\|^2}{2\sigma^2}\right), \quad (5)$$

where x is an m -dimension input vector. x_i is the centre of the i th RBF. σ^2 is the length of the kernel function. $\|x - x_i\|$ is the norm of a vector. γ and σ^2 are crucial to ensure prediction accuracy and model generalization ability in LSSVR.

2.2. Particle Swarm Optimization Algorithm. The PSO, simulating the hunting activities of birds and fish, is a random search algorithm [19], which can find the optimal global

solution. The corresponding relationship between PSO and bird hunting activities is described in Table 1.

PSO is initialized with a random population including m particles, which is $X = \{X_1, X_2, \dots, X_m\}$. Each particle is not only a point in a D -dimension space but also a feasible solution in the solution space. Particles change their position by flying in the solution space until arriving at the optimum. $X_i = \{x_{i1}, x_{i2}, \dots, x_{id}\}$ is the i th particle's position. $V_i = \{v_{i1}, v_{i2}, \dots, v_{id}\}$ ($i = 1, 2, \dots, m$) is the i th particle's velocity, which depends on three components as follows:

- (1) The inertia term: $w * v_{id}(k)$. It is affected by the constant inertia weight w and previous step velocity term $v_{id}(k)$
- (2) The cognitive learning term: $c_1 r_1 * (P_{\text{best}}(i) - x_{id}(k))$. It is the distance between the local best position $P_{\text{best}}(i)$ and the particle's position $x_{id}(k)$
- (3) The social learning term: $c_2 r_2 * (G_{\text{best}} - x_{id}(k))$. It is the distance between the global best position G_{best} and the particle's position $x_{id}(k)$

Thus, the velocity and position of the i th particle of iteration k are computed.

$$\begin{aligned} v_{id}(k+1) &= w * v_{id}(k) + c_1 r_1 * (P_{\text{best}}(i) - x_{id}(k)) - c_2 r_2 * (G_{\text{best}} - x_{id}(k)), \\ x_{id}(k+1) &= x_{id}(k) + v_{id}(k+1), \end{aligned} \quad (6)$$

where r_1 and r_2 are two random numbers in the range of $[0,1]$, $c_1 = 1.7$ and $c_2 = 2$ are acceleration coefficients, and w is the inertia weight factor determined by

$$w = w_{\text{max}} - (w_{\text{max}} - w_{\text{min}}) \frac{n_i}{n_{\text{max}}}. \quad (7)$$

The procedures involved in PSO implementation are given as follows:

- (1) Set the parameters of the PSO algorithm, such as particle swarm size, inertial weight factor w , learning factor c_1 and c_2 , and random number r_1 and r_2
- (2) Initialize the velocity and position of particles randomly
- (3) Compute the fitness of the i th particle and obtain the local best position $P_{\text{best}}(i)$ and the global best position G_{best}
- (4) Update the local best position $P_{\text{best}}(i)$ and the global best position G_{best}
- (5) Update the velocity and position of the particles
- (6) If the end condition is met, we can get the global best position; otherwise, we can return to step 3

2.3. The PSO-LSSVR Model for Energy Demand Forecasting. Different parameters as input combinations in LSSVR can produce various forecasting accuracy. Therefore, more

importance is focused on the PSO-LSSVR model for it can select optimization parameters automatically. The number, position, and velocity of particles and other parameters in the proposed model have been introduced in Sections 2.1 and 2.2. The proposed hybrid model selects the goodness of fit (R^2) for finding the optimal kernel parameters σ^2 and regulation parameter γ . It is conducive to improve prediction accuracy and reduce model uncertainty and randomness. Figure 2 depicts the specific details of the proposed PSO-LSSVR model.

3. Data Resource and Driving Factor Preselection

3.1. Data Resource. All data used in this paper are obtained from China Statistical Yearbook 2020 [20]. This paper measures GDP in 10^2 billion yuan (in constant 1990 price in China). The total population at the end of a year is measured at 10^2 million. The energy consumption structure is indicated by the coal consumption ratio in total consumption. Residential consumption levels (in constant 1990 price in China) are measured at 10^2 yuan. And the energy demand is measured at Mtce (million tons coal equivalent).

3.2. Driving Factor Preselection

3.2.1. Factors Affecting Energy Demand of China. After research, we found that energy demand influencing factors can mainly be decomposed into scale economy effect, population size effect, energy structure effect, and residential consumption effect [21].

Scale economy effect is that economic growth explains the chief changes in energy demand. It was first proposed that changes in GNP caused energy demand to fluctuate, but the long-term Cointegration cannot be found in the United States [22]. Energy demand is mainly affected by economic growth in two aspects. Firstly, economic growth is the driving force for energy development, and it provides the market for energy development. Therefore, economic growth fuels energy demand. Secondly, energy is the core and power source of developing productive social forces. Guaranteeing energy demand is the premise for promoting social economy development stably. At the same time, GDP is a crucial indicator of economic growth. Correspondingly, the floating of GDP will make energy demand floating.

The population size effect is that population growth can affect energy demand markedly [23]. China is a populous country, and the population ranks first in the world in 2019 with the total population reaching 1.4 billion. BP Statistical Review of World Energy (2021) [24] shows that China was one of the few countries where energy demand increased in 2020. China's total energy consumption ranked first in the world in 2019. However, energy consumption per capita was 2.836 tons of standard coal, only reaching the world average level. The population size affects total energy consumption and energy occupancy per capita directly. Therefore, POP is considered as an indicator affecting energy demand in this paper.

TABLE 1: The corresponding relationship between PSO and bird hunting activities.

Bird hunting activities	Particle swarm optimization
Bird flock	A set of valid solutions in a search space
Hunting space	Problem search space
Flying speed	The velocity vector of the solution
The location of the birds	The position vector of the solution
Individual cognition and group collaboration	Update the velocity and position
Finding food	Finding the optimal global solution

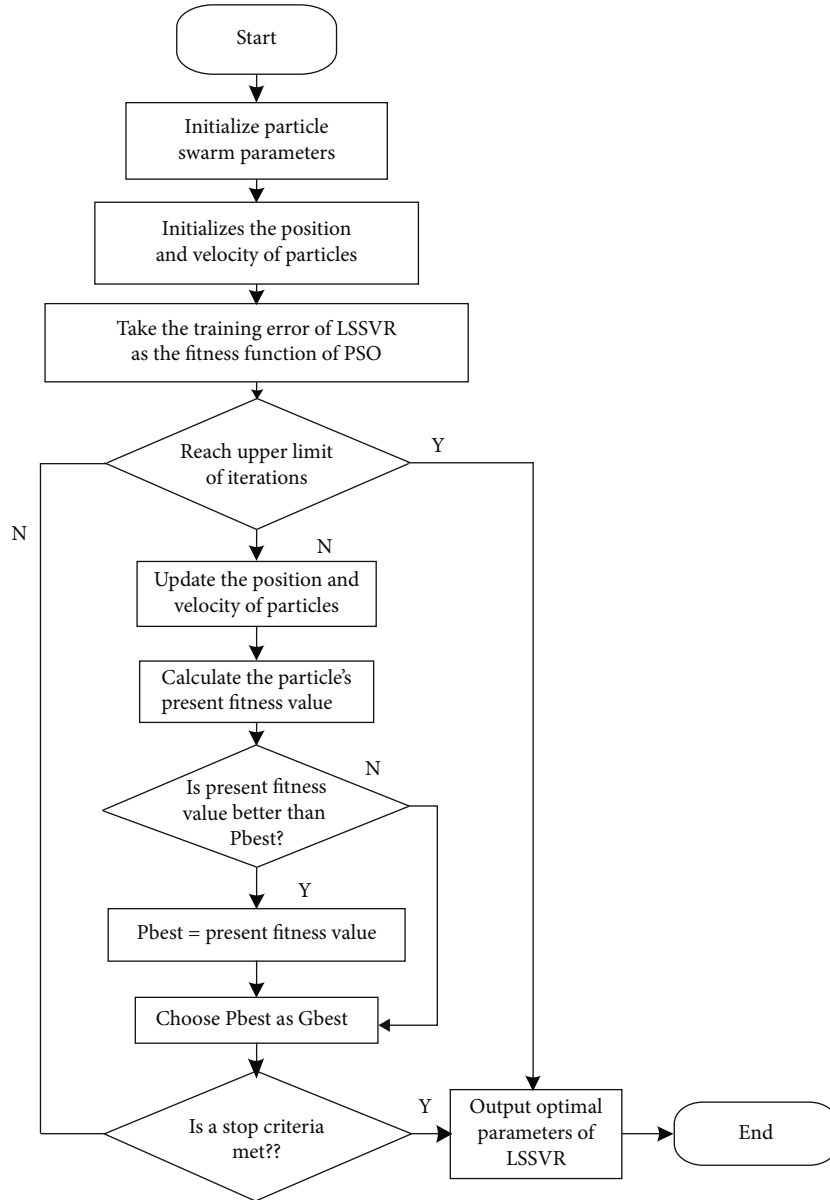


FIGURE 2: The improved PSO-LSSVR model.

The energy structure effect is that various energy types have different energy efficiency, and low energy efficiency will lead to high energy consumption. Energy consumption structure reflects the ratio of various energy resources in pri-

mary energy consumption directly [25]. Coal-based energy consumption structure has low utilization efficiency and high environmental pollution. Since the 1990s, China has been the largest producer and consumer of coal globally,

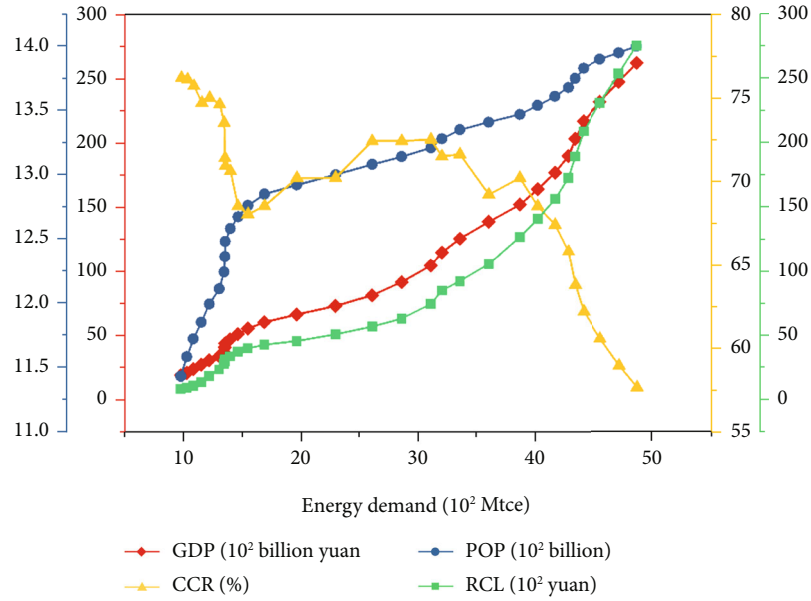


FIGURE 3: Relation among GDP, POP, RCL, CCR, and energy demand.

TABLE 2: ADF test.

Time series	t	Critical value of 0.05	p	Conclusion
ED	-0.23	-2.972	0.935	Nonstationary
GDP	3.547	-2.941	1	Nonstationary
POP	-2.395	-2.972	0.143	Nonstationary
CCR	-0.192	-2.976	0.939	Nonstationary
RCL	1.161	-2.981	0.996	Nonstationary
D (ED, 2)	-4.147	-2.976	0.001**	Stationary
D (GDP, 2)	-8.273	-2.944	0.000***	Stationary
D (POP, 2)	-4.801	-2.981	0.000***	Stationary
D (CCR, 2)	-10.992	-2.976	0.000***	Stationary
D (RCL, 2)	-3.449	-3.042	0.009**	Stationary

TABLE 3: Unrestricted Cointegration rank test (trace).

Hypothesized No. of CE(s)	Eigenvalue	Trace statistic	0.05 critical value	Prob.**
None*	0.987905	242.9389	69.81889	0.0000
At most 1*	0.917747	128.1496	47.85613	0.0000
At most 2*	0.785139	63.20264	29.79707	0.0000
At most 3*	0.573033	23.22072	15.49471	0.0028
At most 4	0.041184	1.093446	3.841466	0.2957

Trace test indicates 4 cointegrating equations at the 0.05 level. * denotes rejection of the hypothesis at the 0.05 level. **MacKinnon-Haug-Michelis (1999) p values.

and 70% of China's total energy demand roots in coal consumption during 1990-2015 [26]. For sustainable development, China has been focused on optimizing energy consumption structure, reducing the ratio of coal, and increasing clean energy. Therefore, in the quantitative analysis of energy demand, CCR is selected as a factor influencing the trend of energy demand in this paper.

The residential consumption effect is that RCL reflects economic growth and the improvement of residents' living standards. The RCL plays a manifold impact on energy demand. It affects the energy demand not only directly but also indirectly through influencing industrial structure. According to Maslow's needs hierarchy theory, with the improvement of RCL, residents will increase the consumption of clean energy such as natural gas and electricity, etc., and reduce the consumption of traditional energy such as firewood and honeycomb coal. Hence, RCL is a vital factor influencing energy demand.

In summary, the energy system is a nonlinear system influenced by many factors, and various influencing factors have discriminative effects on energy demand [27]. The factors can be expressed by the following indicators: GDP, POP, CCR, and RCL. As shown in Figure 3, there is obvious positive correlation between GDP, POP, RCL, and energy demand, respectively. There are positive relationships among GDP, POP, RCL, and energy demand and negative relationships between CCR and energy demand. Conversely, it is an inverse correlation between CCR and energy demand. Therefore, these factors do promote or restrain the energy demand to some extent.

3.2.2. The Unit Root Test and Cointegration Test. For preventing the occurrence of spurious regression, the Granger Causality test will be used to confirm the causal relationship between China's energy demand and the factors identified above before forecasting energy demand. The Granger

TABLE 4: Results of Granger Causality tests.

Null hypothesis	Lag	F-statistic	Prob.
GDP does not Granger Cause ED	1	7.499	0.011
ED does not Granger Cause GDP		13.692	0.001
POP does not Granger Cause ED	1	7.527	0.011
ED does not Granger Cause POP		11.121	0.003
CCR does not Granger Cause ED	1	0.034	0.856
ED does not Granger Cause CCR		2.515	0.025
RCL does not Granger Cause ED	1	5.346	0.029
ED does not Granger Cause RCL		12.424	0.002

ED means energy demand.

TABLE 5: Typical MAPE values for evaluation.

MAPE (%)	Rank
≤10%	High-accuracy
10% < MAPE ≤ 20%	Good
20 < MAPE ≤ 50%	Reasonable
>50%	Inaccurate

Causality test requires that the series is stable or cointegrated. Thus, the unit root test (ADF) and Cointegration test will be implemented under the environment of Eviews 9.0 firstly.

Engle and Granger [22] put forward that the Cointegration relationship can be established when all independent series are integrated of the same order, or their linear relationship is stationary series. Therefore, before the cointegration analysis, it is necessary to judge the smoothness of variable series. The most common methods are the intuitive scatter plot method, autocorrelation function, and ADF test [22].

The null hypothesis of the ADF test refers to that the time series is nonstationary. There are two paths to ensure the time series is stationary. One is the p value less than 0.05 (or 0.01), the other is the t value less than the critical value of 0.05 (or 0.01). As shown in Table 2, in the first line, $p = 0.935$ means refusing the null hypothesis that energy demand is a nonstationary sequence; in the sixth line, $p = 0.001$ means accepting the null hypothesis that second-order difference energy demand is stationary. The conclusion shows that original sequences are nonstationary, and second-order difference sequences are stationary. Then, the Cointegration test can be done further.

Then, the Cointegration test is employed to judge if there exists a Cointegration relationship or long-term equilibrium relationship. The EG Cointegration test is often applied to test a single Cointegration relationship, and the Johansen Cointegration test is often used to test multiple Cointegration relations. The Johansen Cointegration test [28] is mainly divided into two steps. First, the least-squared estimation is conducted to calculate the equilibrium error and obtain the Cointegration regression. Second, the ADF test is carried out for the residual sequence. There exists a Cointegration relationship if the residual sequence is stable. It should be noted that the critical value or the p value in

Eviews 9.0 cannot be applied to determine whether the residual series is steady directly. It is necessary to calculate the corresponding crucial value according to the Cointegration regression threshold table.

As shown in Table 3, the optimal lag order of VAR is 3. “At most 4” in the table means there are at most four Cointegration relationships. However, the corresponding p value is 0.2957, less than 0.05, indicating rejection of the null hypothesis. Therefore, the results of the trace test reveal three Cointegration relationships existing among energy demand and its affecting factors in the 5% significance level. Consequently, although our variables are nonstationary, there are long-term stable equilibrium relationships among them, so we can further carry out the Granger Causality test.

3.2.3. Granger Causality Test. Johansen’s Cointegration test shows the existence of a long-term equilibrium relationship among objectives determined in this study. However, it is not sure if this relationship is causality. Therefore, it is necessary to carry out the Granger Causality test [29] to analyze if there is Granger Causality between energy demand and its affecting factors. The Granger Causality test can be affected by the lag phase considerably. This paper determines the VAR model’s optimal lag order by multiple testing with different lags and AIC criteria. In addition, what needs to be noted is that Granger Causality is not a causal relationship in actual economic activities but the predictive ability of the variables’ lag value to the explained variable.

Avoiding spurious regression, the data participating in the Granger Causality test must be stationary series. The Granger Causality test, conducted on the stable data after treatment, between energy demand and its influencing factors in China is shown in Table 4. As seen in the first line of Table 5, the null hypothesis is “GDP does not Granger Cause ED,” and the p value is less than 0.05, which means that “GDP is the Granger Cause of ED,” refusing the null hypothesis. The Granger Causality test result shows that the GDP, POP, RCL, and energy demand were the bilateral causality except for CCR when the significance level was 5%, and the lag phase was 1. CCR and energy demand are one-way causalities. Thus, the influencing factors screened, GDP, POP, CCR, and RCL, do have a statistical causality with the energy demand in China. They are reasonable inputs for predicting the energy demand of China in PSO-LSSVR mode.

4. Forecasting Energy Demand Based on PSO-LSSVR

4.1. Data Preprocessing. According to the above analysis, this paper selects the data of China’s energy demand and related factors from 1990 to 2019 for prediction, so there are 30 sample data. Before the datasets were used to train the PSO-LSSVR model, the data needed to be linear normalized, and after the forecasting process, the data was required to be antinormalized. The data can be linear normalized to the range [0, 1] by the following formula:

$$x' = \frac{x - x_{\min}}{x_{\max} - x_{\min}}, \quad (8)$$

where x' is the normalized data, x_{\max} is the maximum in data, and x_{\min} is the minimum in data.

4.2. Performance Criteria. The evaluation of the models is done according to three widely used error indexes: Mean Absolute Percentage Error (MAPE), Root Mean Square Error (RMSE), and R^2 . MAPE describes the accuracy of prediction results. RMSE measures the deviation between the observed value and the actual value. R^2 reflects the reliability of the regression model to explain the change of dependent variables. They are expressed by the following equations:

$$\begin{aligned} \text{MAPE} &= \frac{1}{N} \sum_{k=1}^N \left| \frac{y(k) - \hat{y}(k)}{y(k)} \right|, \\ \text{RMSE} &= \sqrt{\frac{1}{N} \sum_{k=1}^N (y(k) - \hat{y}(k))^2}, \\ R^2 &= 1 - \frac{\sum_{k=1}^N (y(k) - \hat{y}(k))^2}{\sum_{k=1}^N (y(k) - \bar{y})^2}, \end{aligned} \quad (9)$$

where $y(k)$ and $\hat{y}(k)$ ($k = 1, 2, \dots, N$) are the actual value and forecasting value, respectively. And \bar{y} is the average of the actual value.

MAPE is one of the criteria to judge the performance of the forecasting model. Table 5 shows the rank of MAPE. The smaller the MAPE value, the better the forecasting model. When MAPE is less than 10%, it means that the prediction model has high accuracy; when MAPE is greater than 10% but less than 20%, it means that the prediction model is good; when MAPE is greater than 20% but less than 50%, it means that the prediction model is reasonable; last, when MAPE is greater than 50%, it means that the prediction model is inaccurate, and it is irrational to forecast with the established model.

4.3. Experimental Results and Analysis. The GM (1,1), Multiplayer Linear Regression (MLR), LSSVR, and PSO-LSSVR are implemented to forecast China's energy demand based on the observations data from 1990 to 2019 in Matlab2017a programming language.

In the PSO-LSSVR model, the most important thing is to search out the best parameters. PSO has three parameters that need to be set in advance. The size of the number of particles $N = 20$, the acceleration coefficients $c_1 = 1.5$ and $c_2 = 1.7$, and the number of maximal iterations $I = 60$. The best suitable parameters of LSSVR selected by PSO at about generation 20 are regularization parameter $\gamma = 179.4585$ and kernel parameter $\sigma^2 = 0.1842$. And then, to ensure the stability of the results, even year data are used as training set, and odd year data are used as testing set. Figure 4 shows the error of training set and testing set.

To further compare the precision of different forecasting models, the MAPE, RMSE, and R^2 are introduced. The comparison results are listed in Figure 5 and Table 6. Obviously, PSO-LSSVR is the optimal model to forecast China's energy demand, and LSSVR has the same excellent ability if you

have correct parameters, GM (1,1) worst. On account of that, LSSVR has advantages when dealing with nonlinear and dynamic features in the system. The conclusions both indicate that multivariate prediction models, such as MLR and LSSVR, have essential superiority than univariate time series prediction models in prediction, such as GM. Since time series prediction is easily affected by external environmental causing deviation. At the same time, the energy system is nonlinear and complex, and the multivariate prediction model will be well suitable for it.

Above all, based on a comprehensive comparison of MSE, MAPE, and R^2 , the PSO-LSSVR model shows a satisfactory performance with high predictive accuracy and less predictive time than other models. Thus, it is applied to further predict China's energy demand in 2020-2025 for providing a basis of energy system's development and the achievement of carbon-neutral at an early date.

5. Forecasting China's Energy Demand in Different Scenarios

5.1. Scenario Setting. For accurate prediction, the development of factors affecting the energy demand of China has been analyzed in this section. It will set up three scenarios for China's growth in the future. Scenario A is the baseline scenario in which variables change in the same rate as what happened before. Scenario B is the lagging scenario relative to scenario A, in which variables change negatively. Scenario C is the priority scenario relative to scenario A, variables change at a positive rate.

5.1.1. GDP. GDP is an effective indicator of national economic growth. China's GDP is constantly growing from 1887 billion in 1990 to 74413 billion in 2019, and its growth rate continued to decline, and the growth rate gradually slowed down after 2010. Nowadays, there are a lot of scholars and institutions who analyze China's economic growth. Such as HSBC Bank thinks China's economic growth rates will be 5.5% during 2021-2030, 4.4% during 2031-2040, and 4.1% during 2041-2050, respectively [30]. Similarly, IMF latest reported that considering the impact of COVID-19, the annual growth rate of the global economy will be 6.0% in 2021 and 4.9% in 2022, respectively [24]. According to the "National Economic and Social Development Report," the economic growth rate in 2020 is 2.3% [23]. Given the COVID-19 and vaccination rate, China's economic growth is expected to back to 6.3% in 2021. Therefore, the GDP growth rate in 2020-2025 is set as 5.6% in scenario A, 5.8% in scenario B, and 6% in scenario C, respectively.

5.1.2. Total Population. Population growth is affected by both mortality and birth rates. The mortality rate is relatively stable. Therefore, population growth is mainly affected by the birth rate [31]. From 2012 to 2015, the population growth rate was steady at about 0.51% per year. After the implementation of the two-children policy in 2015, the population growth rate reached 0.58 in 2016. With child cost increasing and urban life accelerating, the birth rate

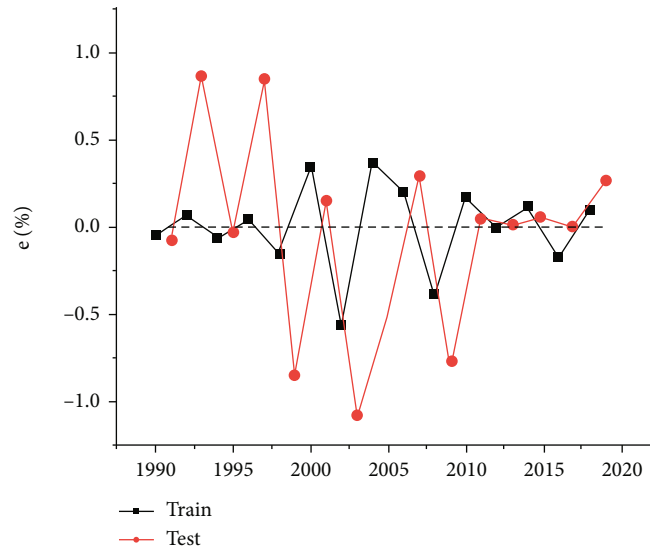


FIGURE 4: Errors of the training and testing set.

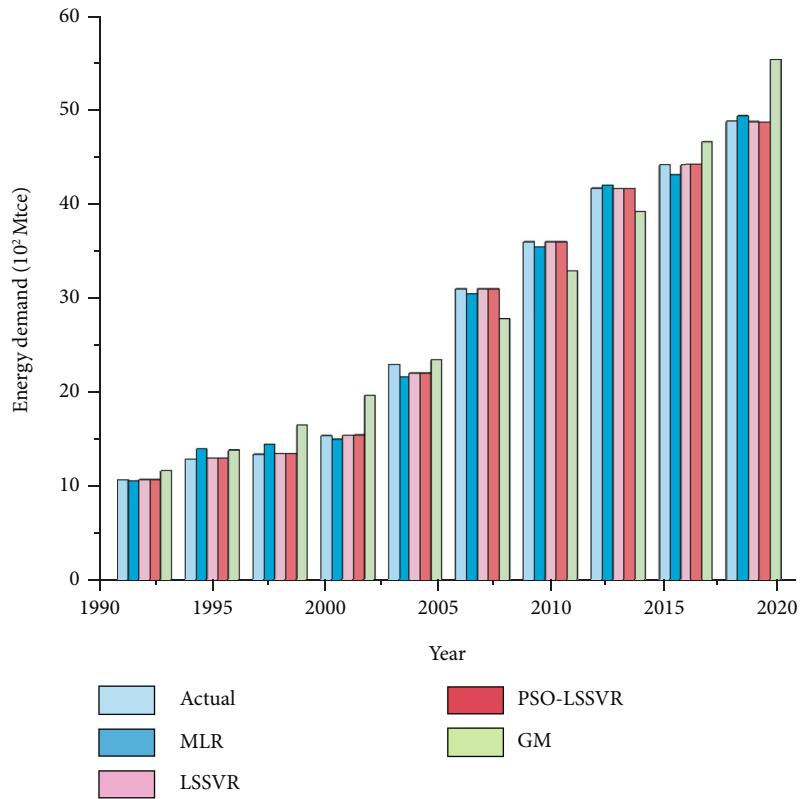


FIGURE 5: Comparison between the actual value and the forecasting values.

TABLE 6: Error comparison of China’s energy demand prediction.

Index	MSE	MAPE	R^2
GM (1,1)	10.6261%	28.626	95.4154
MLR	3.3296%	7.748	99.6373
LSSVR	2.3188%	6.537	99.9717
PSO-LSSVR	1.3265%	5.0618	99.9907

TABLE 7: Factors’ average growth rate of China’s energy demand in 2020-2025 (unit: %).

	Scenario A	Scenario B	Scenario C
GDP	5.6	5.8	6
POP	0.36	0.46	0.58
CCR	-2.3	-2.5	-2.7
RCL	9.3	9.8	10.3

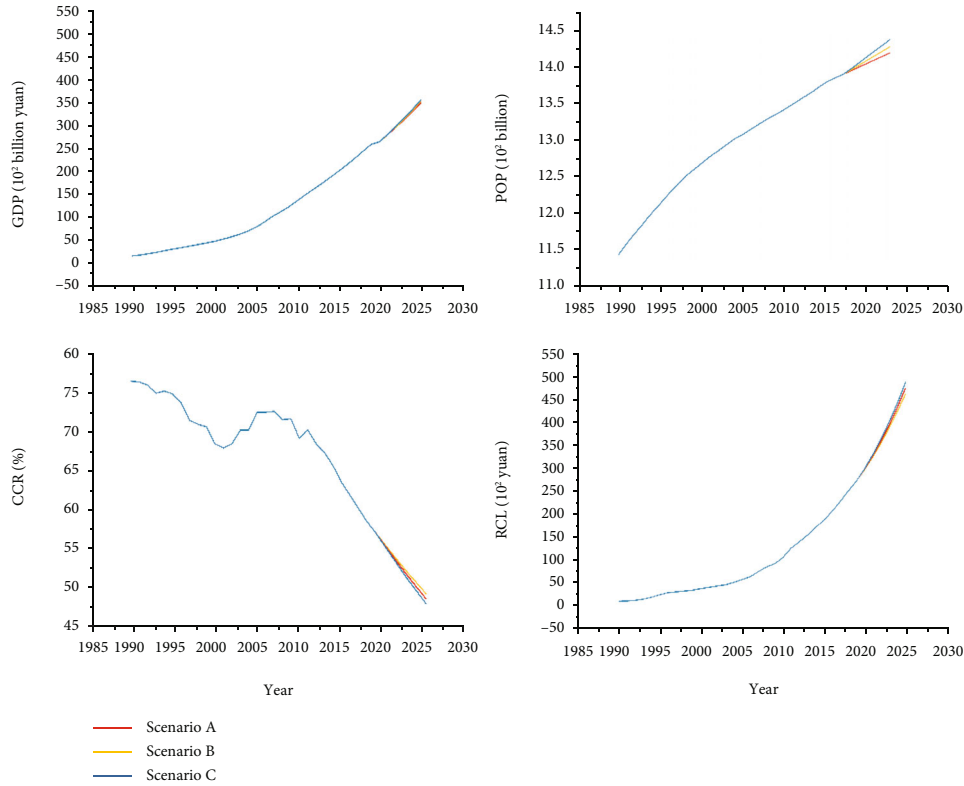


FIGURE 6: Trends of factors affecting energy demand in different scenarios.

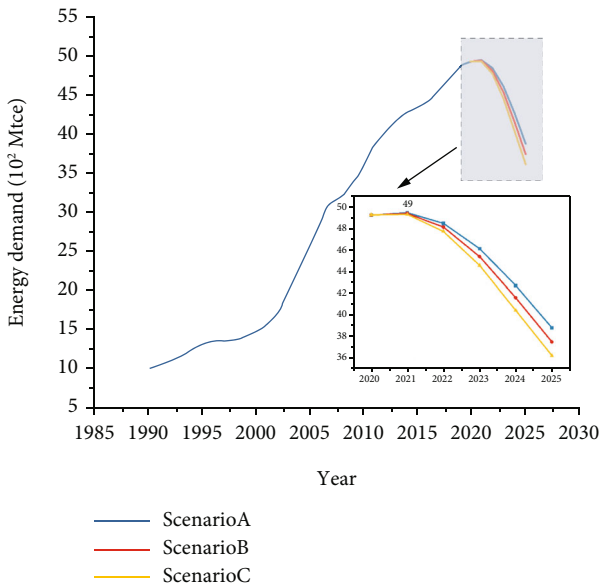


FIGURE 7: Prediction of China's energy demand in different scenarios.

decreased, and the population growth rate reduced to about 0.35 between 2018 and 2019. According to the theory of population transformation, the natural population growth rate decreased gradually. Integrating these trends, the population growth rate in 2020-2025 is 0.36% in scenario A, 0.46% in scenario B, and 0.56% in scenario C, respectively.

The coal consumption ratio in primary energy. With the transformation of the coal industry, technological progress, and the transformation of production and lifestyle, the ratio of coal consumption in primary energy is also declining. In addition, the energy system is being transformed and upgraded from a coal-based energy structure to a renewable-energy-based energy structure. “The Guiding Opinions on Energy Work in 2021” requires that the ratio of coal consumption in primary energy should be reduced to less than 56% in 2021 [32], and “China Energy Development Report” points out that by the end of the 14th five-year plan, the ratio of coal consumption in primary energy is expected to drop to about 51% by 2025 [33]. Consequently, the decline rate of the coal consumption ratio in 2020-2025 is -2.3% in scenario A, -2.5% in scenario B, and -2.7% in scenario C, respectively.

5.1.3. Residential Consumption Level. At the 19th National Congress of the Communist Party of China, it is put forward that people’s living is better off, and the proportion of middle-income groups increases remarkably by 2030. Since our country adopted the reform and opening-up policy, economic development has progressed significantly, and people already had a comparatively well-off life. The growth of residential consumption level has been relatively stable at 9.8% over the past eight years. At the same time, China’s economy began to change its mode from high-speed development to medium-high speed development. The residential consumption level will maintain stable growth for a long time. Given the above, during 2020-2025, the growth rate of real RCL

will be 9.3% in scenario A, 9.8% in scenario B, and 10.3% in scenario C, respectively.

As described above, the central assumptions of the factors influencing energy demand in different scenarios are listed in Table 7.

5.2. Forecasting Results. This section implements the PSO-LSSVR model to forecast China's energy demand in 2020-2025 using Matlab2012a programming language.

In different scenarios, the possible trends of factors influencing energy demand are listed in Figure 6. As of 2025, the coal consumption ratio was already less than 50%, which means that energy structure adjustment has been completed. The residential consumption level improves sharply, which means closer to the second centennial goal.

The estimation results of energy demand in China during 2020-2025 are shown in Figure 7. It can be seen that China's energy demand will peak around 2021 in all three scenarios, which satisfies the goal proposed in "the 13th Five-Year Plan," and the peak is about 4.9 billion tce. By 2025, China's energy demand will decrease to around 4.39 billion tce, 3.99 billion tce, and 3.91 billion tce in scenarios A, B, and C, respectively. According to the forecasting results, energy conservation policy will achieve the desired effects. If we continue to implement the active energy transformation policy and energy conservation policy, the total energy demand may continue to decline in a short time.

China's economy has begun to enter a new normal. The industrial structure has entered the stage of profound adjustment. The industrialization process has entered the late phase, and the residential consumption level has increased. These indicate that energy demand in China will enter a saturated period, and the peak of total energy consumption is about to arrive.

6. Conclusions and Policy Recommendations

In this paper, the hybrid model, the LSSVR model optimized by the PSO algorithm, is proposed to forecasting China's energy demand during 2020-2025. It outperforms other forecasting modes significantly, especially the energy demand forecasting models. The main conclusions of this paper are summarized as follows:

- (1) The Cointegration and Granger Causality test are effective methods to find the connections between influencing factors and energy demand in China. It indicates that there is significant two-way Granger Causality between GDP, POP, RCL, and energy demand and one-way Granger Causality between POP and energy demand
- (2) The LSSVR model has advantages over other models in dealing with complexity, nonlinearity, and small samples of energy systems. At the same time, based on the comparison results of MAPE, RMSE, and R^2 , the hybrid PSO-LSSVR prediction model is demonstrated to be more accurate than a single model

- (3) According to the prediction of this study, the energy demand of China will peak at 4.9 billion tce in 2022

This paper gives related suggestions on energy development to achieve sustainable economic growth based on energy demand analysis and forecasted results:

- (1) Insist on saving energy and reducing consumption. Active population policy will lead to more energy demand, which is contrary to saving energy, reducing consumption, and sustainable development
- (2) Accelerate energy structure adjustment and develop renewable energy. Different types of energy have different efficiency. Developing efficient energy is an effective way to save energy and reduce consumption. Therefore, it should speed up the adjustment of energy structure and increase the proportion of clean energy, such as hydropower, wind power, and nuclear power
- (3) Adjust the economic structure. By adjusting the economic structure, the demand for high-energy and low-efficiency products is shifted to low-energy and high-efficiency ones, increasing economic efficiency and reducing energy demand

In this article, the PSO algorithm is used to search the optimal parameters of the SVM model. Based on this, other heuristic algorithms can be used for parameter optimization, such as the sparrow search algorithm and whale optimization algorithm.

In future studies, metering algorithms can be used to find the main factors affecting energy consumption. Also, the innovative hybrid prediction algorithm can be used to forecast different energy types such as natural gas, wind energy, and solar energy.

Data Availability

No data were used to support this study.

Conflicts of Interest

The authors declare no conflict of interest.

Authors' Contributions

In this work, each author has his own full-time responsibility. More in detail: J.Z. Wang has written Section 1; Y. F. Yang has realized Sections 2, 3, 4, and 5; Y. R. Wang has dealt with Section 6. L. Han has mapped figures in this paper with origin2021b.

References

- [1] C. Xia and Z. Wang, "Drivers analysis and empirical mode decomposition based forecasting of energy consumption structure," *Journal of Cleaner Production*, vol. 254, article 120107, 2020.

- [2] Q. Wu and C. Peng, "A hybrid BAG-SA optimal approach to estimate energy demand of China," *Energy*, vol. 120, pp. 985–995, 2017.
- [3] P. Sen, M. Roy, and P. Pal, "Application of ARIMA for forecasting energy consumption and GHG emission: a case study of an Indian pig iron manufacturing organization," *Energy*, vol. 116, pp. 1031–1038, 2016.
- [4] Y. Hu, J. Li, and L. He, "A reformed task scheduling algorithm for heterogeneous distributed systems with energy consumption constraints," *Neural Computing and Applications*, vol. 32, no. 10, pp. 5681–5693, 2020.
- [5] X. Cui, S. E. D. Niu, D. Wang, and M. Li, "An improved forecasting method and application of China's energy consumption under the carbon peak target," *Sustainability*, vol. 13, no. 15, p. 8670, 2021.
- [6] H. Chen, X. Xiao, and J. Wen, "Novel multivariate compositional data's model for structurally analyzing sub-industrial energy consumption with economic data," *Neural Computing and Applications*, vol. 33, no. 8, pp. 3713–3735, 2021.
- [7] C. Renno, E. Petito, and A. Gatto, "ANN model for predicting the direct normal irradiance and the global radiation for a solar application to a residential building," *Journal of Cleaner Production*, vol. 135, pp. 1298–1316, 2016.
- [8] G. Cao and L. Wu, "Support vector regression with fruit fly optimization algorithm for seasonal electricity consumption forecasting," *Energy*, vol. 115, pp. 734–745, 2016.
- [9] J. Zhou and Q. Wang, "Forecasting carbon price with secondary decomposition algorithm and optimized extreme learning machine," *Sustainability*, vol. 13, no. 15, p. 8413, 2021.
- [10] Y. Q. Cui, H. F. Liu, Q. L. Wang et al., "Investigation on the ignition delay prediction model of multi-component surrogates based on back propagation (BP) neural network," *Combustion and Flame*, vol. 237, article 111852, 2022.
- [11] B. Li and X. Tian, "An effective PSO-LSSVM-based approach for surface roughness prediction in high-speed precision milling," *Ieee Access*, vol. 9, pp. 80006–80014, 2021.
- [12] J. Zhou, Q. Wang, Q. Cheng et al., "Low-PAPR layered/enhanced ACO-SCFDM for optical-wireless communications," *IEEE Photonics Technology Letters*, vol. 30, no. 2, pp. 165–168, 2018.
- [13] L. Jiacheng and L. Lei, "A hybrid genetic algorithm based on information entropy and game theory," *Ieee Access*, vol. 8, pp. 36602–36611, 2020.
- [14] C. Cortes and V. Vapnik, "Support-vector networks," *Machine Learning*, vol. 20, no. 3, pp. 273–297, 1995.
- [15] J. A. K. Suykens and J. Vandewalle, "Least squares support vector machine classifiers," *Neural Processing Letters*, vol. 9, no. 3, pp. 293–300, 1999.
- [16] F. Kaytez, M. C. Taplamacioglu, E. Cam, and F. Hardalac, "Forecasting electricity consumption: a comparison of regression analysis, neural networks and least squares support vector machines," *International Journal of Electrical Power & Energy Systems*, vol. 67, pp. 431–438, 2015.
- [17] X. Xue and M. Xiao, "Deformation evaluation on surrounding rocks of underground caverns based on PSO-LSSVM," *Tunnelling and Underground Space Technology*, vol. 69, pp. 171–181, 2017.
- [18] J. A. K. Suykens and J. Vandewalle, "Chaos control using least-squares support vector machines," *International Journal of Circuit Theory & Applications*, vol. 27, no. 6, pp. 605–615, 1999.
- [19] J. Kennedy, "Particle swarm optimization," in *Proceedings of ICNN'95-international conference on neural networks*, vol. 4no. 8, pp. 1942–1948, Perth, Australia, Nov. 27-Dec. 1995.
- [20] Statistics, N. B. o, *China Statistical Yearbook*, China Statistics Press, Beijing, China, 2020.
- [21] Y. Yang, *The Study on Influencing Factors of Energy Demand and Scenario Prediction in Baoding City*, North China Electric Power University, Baoding, China, 2019.
- [22] J. Kraft and A. Kraft, "On the relationship between energy and GNP," *Energy Development*, vol. 3, pp. 401–403, 1978.
- [23] Agency, I. E., *World energy outlook*, Agency, I. E., France, 2008.
- [24] Fund, I. M., *World Economic Outlook Update*, vol. 7, Fund, I. M., Washington, USA, 2021.
- [25] D. ZR, *Research on the Forecast of Energy Supplying and Demanding in China*, Harbin Engineering University, Harbin, China, 2011.
- [26] P. A. Speed, *Energy Policy and Regulation in the People's Republic of China*, The Hague, London, Kluwer Law International, 2004.
- [27] R. D. Rinehart and Y. Yanagisawa, "Paraoccupational exposures to lead and tin carried by electric-cable splicers," *Energy Journal*, vol. 54, no. 10, pp. 593–599, 1993.
- [28] S. Johansen, J. Dynamicscontrol, J. Bullard et al., "Statistical analysis of cointegration vectors," *Journal of Economic Dynamics and Control*, vol. 12, no. 2-3, pp. 231–254, 1988.
- [29] C. Granger, W. Clive, T. Hastie, R. Tibshirani, and J. Friedman, *Investigating Causal Relations by Econometric Models: Cross Spectral Methods*, vol. 37, no. 3, 1969]STOR, 1969.
- [30] Team, H. G. E. R., *The world in 2050: from the top 30 to the top 100*, HSBC Global Research, 2016.
- [31] K. Yang, "China's population changes and major transition during the 14th five-year plan period," *Journal of Beijing University of Technology (SOCIAL SCIENCE EDITION)*, vol. 21, no. 1, pp. 17–29, 2021.
- [32] China, t. N. E. A. o., *The Guiding Opinions on Energy Work*, The National Energy Administration, Beijing, China, 2021.
- [33] B. Q. Lin, *China Energy Developmen Report*, Peking University Press, Beijing, China, 2020.

Research Article

Sports Event Model Evaluation and Prediction Method Using Principal Component Analysis

Weiwei Yu^{1,2} and Jinming Xing³ 

¹Suan Sunan Rajabhat University, Bangkok 10300, Thailand

²Faculty of Infrastructure Engineering, Dalian University of Technology, Dalian 116024, China

³School of Physical Education, Northeast Normal University, ChangChun 130024, China

Correspondence should be addressed to Jinming Xing; xingjm100@nenu.edu.cn

Received 30 October 2021; Revised 22 December 2021; Accepted 27 December 2021; Published 19 January 2022

Academic Editor: Mu-Yen Chen

Copyright © 2022 Weiwei Yu and Jinming Xing. This is an open access article distributed under the Creative Commons Attribution License, which permits unrestricted use, distribution, and reproduction in any medium, provided the original work is properly cited.

Aiming at the problems of poor average fitness, low-risk prediction accuracy, high mean square error, low-risk evaluation precision, and long average running time of traditional sports event model evaluation and prediction methods, a sports event model evaluation and prediction method using principal component analysis (PCA) is proposed. Sports event risk monitoring microbase is deployed by ZigBee technology, and sports event risk monitoring data is monitored and packaged at each base station. Optical fiber and Ethernet are used to transmit the data to the monitoring and management center to complete the risk data collection of sports events. After data standardization, the risk evaluation index system of sports events is constructed, and the comprehensive score of each risk index of sports events is obtained by using the PCA method. The BP neural network is improved by genetic algorithm (GA), and the comprehensive score of risk index is input into the network to obtain the evaluation and prediction results of sports event risk. The results show that the proposed method has good average fitness, the predicted value of sports event risk is almost equal to the actual value, the prediction mean square error is less than 0.15, the evaluation precision is high, and the average running time is only 8 s. The cost (time complexity) is low. Overall, the method has a good application prospect in the field of sports event evaluation and prediction.

1. Introduction

Under the background of rapid economic growth, the proportion of sports events in the sports industry is also rising [1]. The holding of sports events is a review of a city's comprehensive ability, such as the degree of civilization of citizens, the governance of the urban environment, the planning level of urban construction, and will play an inestimable role in promoting the development of the city in all aspects [2]. It can not only improve the quality of the city's population, improve citizens' fitness awareness, enrich urban cultural life, promote urban construction, but also promote the development of related industries. However, sports events not only bring all kinds of opportunities, but also imply huge risks. Some sudden international and domestic political, economic, social and natural events may seriously interfere with or even hinder the normal operation

of the event, making all the efforts of the event organizers go east. At present, the development of China's sports industry is slow, the degree of marketization is low, and there are many uncertain factors in the process of holding events [3, 4]. Therefore, it is very necessary to take risk management measures during the operation of sports events, and risk evaluation is a very important part of risk management. The event organizing committee needs to carefully understand the risks of sports events, assess and predict the risk level of sports events, make emergency strategies for the holding of sports events and control the probability of risks in combination with the local actual situation, so that sports events can better promote the development of local social economy [5].

In order to realize the risk evaluation and prediction of sports events, literature [6] determines which artificial intelligence (AI) methods have been used to investigate sports

performance and injury risk, and seek which AI technologies are used in each sport, so as to improve the intelligence of sports risk analysis. Literature [7] used the survey method and catastrophe progression method to evaluate the risk of the governance model of large stadiums, identified the risk factors, build the index system, and explored the factors behind the indicators, in order to provide an explanation for decision makers to choose the governance model of large stadiums. Literature [8, 9] took the application of BP network in sports risk early warning design as the starting point, started from the necessity of applying BP network in sports event risk early warning, analyzed the risk early warning model and operation process, and verified the sample data to verify the effectiveness of the model. According to the risk management theory and the organization and operation law of sports events. Literature [10] took the 2014 Nanjing Youth Olympic Games as the research sample, used the list arrangement method to analyze and predict the weight, and proposed the risk response measures of Nanjing Youth Olympic Games. Through the study of risk system of sports events, it provided reference for risk management in China. Literature [11] fully combined the improved risk matrix method with Delphi method and analytic hierarchy process, established a school sports competition risk index system covering 27 indicators around the four main lines of personnel risk, facility risk, organization and management risk and environmental risk, and quantitatively analyzed the occurrence probability, influence, risk grade, weight and acceptability of each risk index to proposed countermeasures. At present, the research on the risk evaluation and prediction of sports events has also achieved good research results. For example. Literature [12] used the methods of the literature, expert investigation, and analytic hierarchy process to analyze the ecological risk types, risk sources and risk receptors caused by urban hosting large-scale sports events, and constructed a system consisting of 4 primary indicators and 14 secondary indicators, the ecological risk evaluation system composed of 40 three-level indicators is used to predict the risk of sports events. Literature [13] introduced the hierarchical holographic modeling HHM risk identification analysis tool to build a holographic model suitable for sports games risk identification, including 24 hierarchical holographic subsystems in five categories: Sports Games ontology, organization and management, personnel quality, venue facilities and environment, and quantified and rated it by using analytic hierarchy process and Pareto analysis, it provided a reference basis for the quantitative risk evaluation of sports games. Literature [14] uses neural network as a predictive network modeling method. With the support of MATLAB neural toolbox, a risk warning model is designed for sports events based on neural network. This paper starts with the gray network in the sports risk early warning design, starting from the necessity of applying grey network in sports event risk early warning, this paper analyzes the risk early warning model and operation process, and verifies the feasibility of the model with sample data. The main contributions of this paper are as follows: (1) through PCA, several relevant factors can be transformed into nonrelevant indicators, which can reduce the

dimension of the original indicators in the case of a small amount of missing data, filter duplicate data, and obtain comprehensive indicators related to the risk of sports events. (2) Using ZigBee technology to deploy sports event risk monitoring micro base stations, monitor and package sports event risk monitoring data in each base station, and use optical fiber and Ethernet to transmit the data to the monitoring management center to complete sports event risk data collection, which can improve the accuracy and efficiency of data collection. (3) Using ZigBee technology to collect sports event risk data and analyze the influencing factors of sports event risk assessment, so as to carry out sports event risk assessment, and use the BP neural network improved by GA to predict sports event risk, which can reduce the prediction error and improve the prediction efficiency.

The organization of this paper is as follows. We introduce the introduction and related works in Section 1. Then, we describe the risk evaluation and prediction of sports event model in Section 2. We further present the experimental results and discussions in Section 3. Finally, we conclude the paper in Section 4.

2. Methodology

2.1. Sports Event Risk Data Collection Using ZigBee Technology. The wireless sensor network suitable for collecting sports event risk data is established by using ZigBee technology, and then the sports event risk monitoring micro base station is deployed based on the sports event risk monitoring network to collect sports event risk data [15]. ZigBee network has complex topology and powerful functions. It improves the information transmission rate through multi hop transmission, and can complete its own organization and repair. It has good robustness and wide application range.

A sports event risk data monitoring network is established through ZigBee mesh network, which mainly includes two parts: initializing network subroutine and node application link [16]. Initialize the ZigBee network, deploy the coordinator at the network node, take the coordinator as the network join point, the node transmits the connection application to the coordinator, and the coordinator judges the node access according to the network connection status and replies to the application. The data sending and receiving are based on the node connection coordinator, and the node requests access to the network mainly including the search coordinator, then passing the application for joining the network, waiting for processing, and application for data transmission. The design core of ZigBee network is the protocol stack, which can obtain, transfer, store, and process data channels and methods and determine the logical structure of communication at the same time. In the process of data sending and receiving, the node sending and receiving data realizes unlimited data sending and receiving by applying the sending and receiving function in the protocol stack [8, 17].

The coordinator program includes networking, status detection, network maintenance and information acquisition command sending, etc. After the coordinator starts running, initialize the internal program through the functions in

the protocol stack, then build the ZigBee network and log in to the GPRS network, and send the feedback data to the monitoring center through Ethernet to complete the processing and display the data. The task of the terminal node is to collect the risk data of sports events and transmit the data periodically through the coordinator, as shown in Figure 1.

2.2. Risk Evaluation of Sports Events. Preprocess the sports event risk data collected by the ZigBee technology, and after the data is standardized, construct a sports event risk evaluation index system, and use the PCA method to obtain the comprehensive risk score of the sports event.

2.2.1. Establishment of Risk Evaluation Indexes for Sports Events. Taking the event risk attribute as the starting point to evaluate the risk of sports events, the risk has the characteristics of possibility, uncontrollability and randomness [18]. Its core index is risk probability, which indicates the possibility of risk, the degree of loss caused by risk is risk loss, and the risk control level is uncontrollable, which is directly proportional to the risk level. Through expert review, it is preliminarily determined that the evaluation indexes are risk probability, risk loss and uncontrollability. The risk evaluation index system of sports events is detailed in Table 1.

According to Table 1, the target layer of sports event risk evaluation index system is sports event risk. The criterion layer includes risk probability, risk loss, and uncontrollability. The primary level indexes are personnel risk, operation risk, facility risk, economic risk, and external environment risk. The secondary level indexes are staff risk, athlete, coach, referee risk, onsite audience risk, event schedule risk, event participants' traffic risk, safety guarantee risk, site quality and safety risk, site lawn and drainage risk, event scale risk, pregame budget risk, sponsor risk, natural environment risk, and food safety risk.

2.2.2. PCA. Through PCA, several relevant factors can be transformed into nonrelevant indexes, which can reduce the dimension of the original indexes in the case of a small amount of data loss, filter duplicate data, and obtain comprehensive indexes related to the risk of sports events [19].

The PCA steps are as follows:

- (1) Assuming that the study area is A , select B indexes in this area, and set the sample matrix of this index as F to obtain:

$$F = (F_{ij})A * B, \quad (1)$$

where $i = 1, 2, \dots, A, j = 1, 2, \dots, B$

- (2) Assuming that R_{b*b} represents the index correlation coefficient matrix, and its eigenvalue meets the condition range is $\wedge 1 \geq \wedge b \geq 0$ [20], the PCA expression formula is as follows:

$$T_i = F e_j \quad (2)$$

where T_i represents the principal component, and the normalized eigenvector of the correlation coefficient matrix is e_j

- (3) When the variance contribution rate of the j -th principal component is higher than 86%, only the first q principal components are selected T_1, T_2, \dots, T_q . [21] At this time, q can reflect the information of B initial indicators, and the contribution rate a is as follows:

$$a = \sum_{i=1}^q a_j \quad (3)$$

- (4) The comprehensive risk score W of the sports event studied is as follows:

$$W = aX_1 + bX_2 + \dots + xX_x \quad (4)$$

where X is the eigenvector of the eigenvalue b and x represent the normalized data of the initial index [22].

2.3. Risk Prediction of Sports Events

2.3.1. BP Neural Network. In order to realize the risk prediction of sports events, the risk characteristics of sports events extracted by PCA are input to the input layer of BP neural network, and the prediction results are obtained by output layer [23]. The neurons in each layer of BP neural network are only sensitive to the input of feedforward neurons. The output of each layer affects the output of the next layer, and its structure is shown in Figure 2.

The number of units of BP neural network is processed according to specific problems, and the following is obtained through linear transformation function:

$$f(x) = x, \quad (5)$$

where the independent variable x represents the number of network inputs of BP neural network.

Let L be the hidden layer nodes, I the input layer nodes, and J the output layer nodes, then:

$$L = (I + J)/2, \quad (6)$$

$$L = (I * J)^{1/2}. \quad (7)$$

In the network output layer, the number of processing units through the nonlinear conversion function, and the hyperbolic function in the nonlinear conversion function is:

$$f(x) = \frac{1}{1 + e^x}, \quad (8)$$

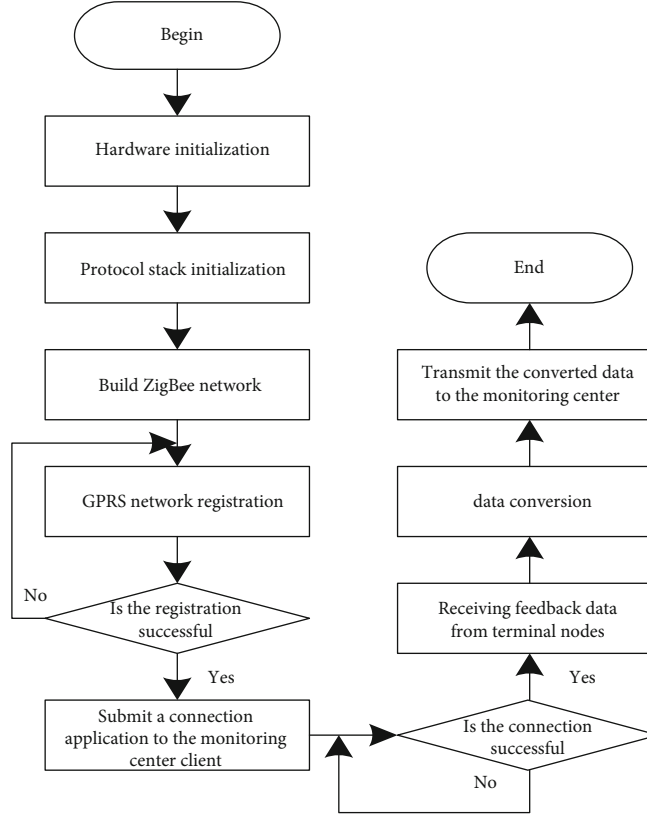


FIGURE 1: Terminal node program process.

TABLE 1: Risk evaluation indexes system of sports events.

Target layer	Criterion layer	Primary index layer	Secondary index layer
Sports event risk	Risk probability B ₁	Personnel risk C ₁	Staff risk
			Risks of athletes, coaches, and referees
	Risk loss B ₂	Operational risk C ₂	Live audience risk
			Event schedule risk
	Uncontrollability B ₃	Facility risk C ₃	Traffic risk of event participants
Security risk			
Site quality and safety risk			
External environmental risk C ₅	Economic risks C ₄	Site lawn and drainage risk	
		Event scale risk	
		Precompetition budget risk	
		Sponsor risk	
			Natural environment risk
			Food safety risk

where when x is close to positive or negative infinity, the function value is close to the constant, and its value range is $[0,1]$.

The input data $X = (x_1, x_2, \dots, x_n)$ of BP neural network is the risk characteristics of sports events extracted by PCA. Starting from the input layer, traverse each hidden layer node to the output layer node, and the output data is as follows:

$$Y = (y_1, y_2, \dots, y_n). \quad (9)$$

Let L_{in} and L_{out} be the input and output of each node of the hidden layer, respectively, and the mapping from input to output is expressed as follows:

$$L_{in} = \left(\sum_{i=1}^I u_{ij} x_i \right) + b, \quad (10)$$

$$L_{out} = net(L_{in}), \quad (11)$$

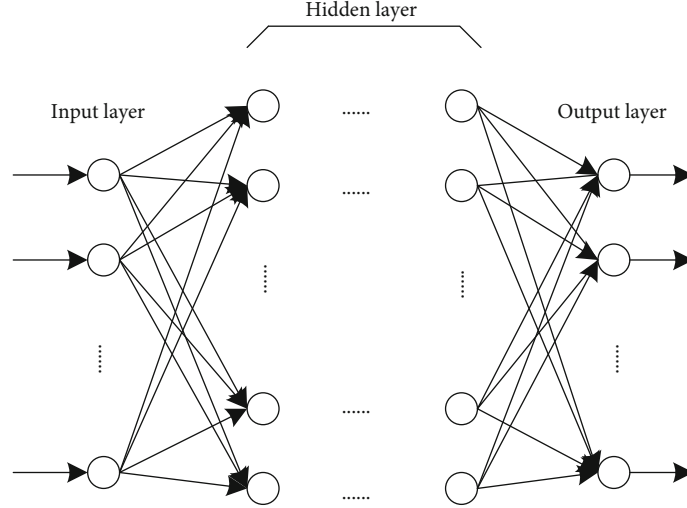


FIGURE 2: Structure of the BP neural network.

$$J_{\text{in}} = \left(\sum_{j=1}^L v_{jk} L_{\text{out}} \right) + b, \quad (12)$$

$$J = \text{net}(J_{\text{in}}), \quad (13)$$

where J_{in} is the input value of each node in the output layer, the weights between the input layer and the hidden layer and between the hidden layer and the output layer are described as u_{ij} and v_{jk} , respectively, and b represents the node threshold.

2.3.2. Improved BP Neural Network Model. In order to improve the prediction accuracy of BP neural network, GA is used to improve the neural network. The specific operation steps are as follows:

Step 1: Generate code and initial population. Let the number of input layer and hidden layer nodes of GA-BP neural network be R and S_1 , respectively, then the length of chromosome is:

$$S = R * S_1 + S_1 * S_2 + S_1 + S_2, \quad (14)$$

where S_2 is the number of output layer nodes.

The initial population with M individuals and S chromosome length was randomly generated. The large number of individuals M will slow down the convergence speed of the network; too small will reduce the accuracy of network training.

Step 2: Determine the fitness function. Set the fitness function of the individual as follows:

$$F = \frac{1}{\sum_{t=1}^n |y_t - \bar{y}_t|}, \quad (15)$$

where n is the number of training samples and y_t and \bar{y}_t are the expected output value and predicted output value of the first training sample, respectively.

Step 3: The fitness values are sorted by mathematical sorting method, and the probability of selecting each indi-

vidual is allocated according to the sorting results of fitness values:

$$P_x = F / \sum_{k=1}^x F. \quad (16)$$

Step 4: Generate new species. Select, cross and mutate the initial population whose individual fitness does not meet the optimization criteria to produce a new population. If the standard is met, proceed to the next step, otherwise return to genetic operation.

Step 5: Generate the initial weight of BP network.

Step 6: Determine the risk level of sports events according to the output results. According to the importance of sports event risk, it is divided into three levels: high, medium, and low risk. The criteria are shown in Table 2.

In summary, the sports event evaluation and prediction model is shown in Figure 3.

According to Figure 3, preprocess the sports event risk data collected by the ZigBee technology, and after standardizing the data, construct a sports event risk evaluation index system, and obtain the comprehensive score of sports event risk by using the PCA method. The GA is used to improve the BP neural network model, and the improved BP neural network model is used to predict the risk of sports events.

3. Experimental and Results

3.1. Data Set. Experimental environment: on Intel Xeon Gold6254@3.10GHz (X2) CPU, 768GBRAM, 2* Tesla v100GPU, the operating system is Windows Server 2019, and the programming language is MATLAB.

Data set: Sgsum (sports game summary) is a large-scale manually cleaned Chinese sports event summary data set. This data set comes from sina sports online. This data set comes from the football game data from 2012 to 2020

TABLE 2: Risk level classification of sports events.

Degree of importance (W)	Level	Risk factor
$W \geq 10\%$	High risk (III)	Event scale, event schedule, natural environment, and preevent budget
$5\% < W < 10\%$	Medium risk (II)	Transportation of participants
$W < 5\%$	Low risk (I)	Site environment, auxiliary personnel, disease video, investment unit, safety measures, event judges, onsite audience, site quality, and safety

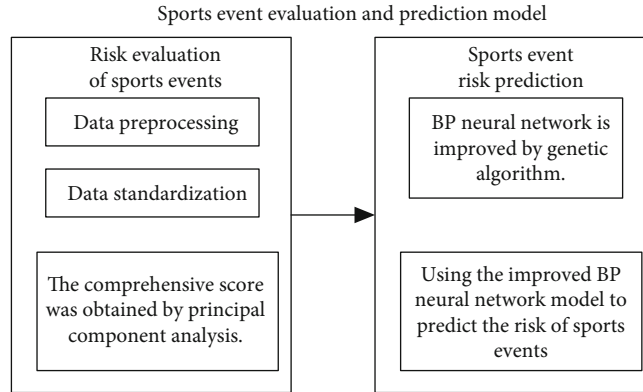


FIGURE 3: Evaluation and prediction model of sports events.

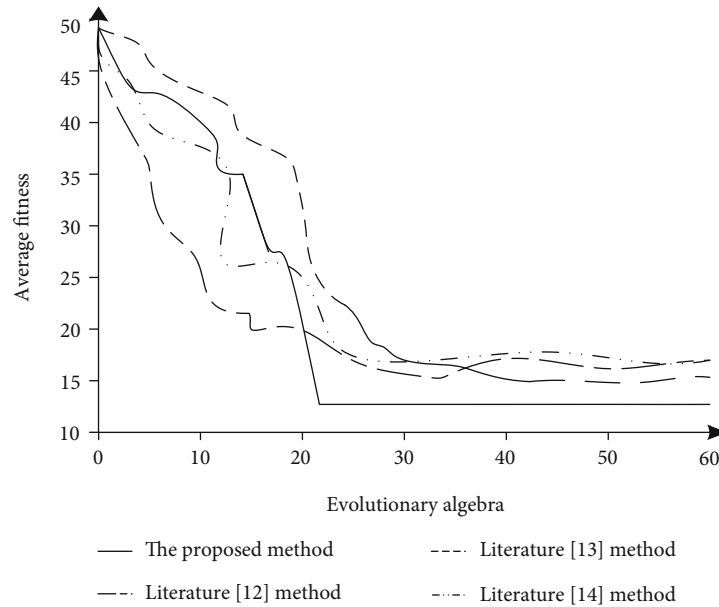


FIGURE 4: Comparison of average fitness curves of different methods.

in sina sports online, including the online comment text and corresponding news reports of 7854 football games. Sports-1 m: this data set is a sports video data set, including 487 categories and 1.2 million sports event videos. Taking the large-scale sports events held in a region as the research object, this paper studies the risk evaluation and prediction of sports events. The event was held for one week, with three types of competition events A, B, and C.

3.2. *Comparison Methods and Evaluation Indexes.* The methods in this paper: literature [12], literature [13] and literature [14], are used as experimental methods to verify the practical application effects of different methods by comparing different evaluation indexes.

- (1) Average fitness: average fitness is an important index to verify the convergence of the algorithm. The earlier the average fitness reaches the stable value, the

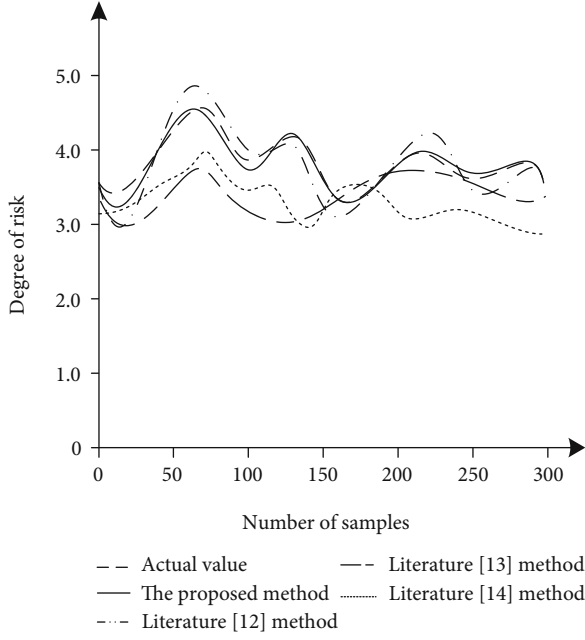


FIGURE 5: Comparison of prediction accuracy of four methods.

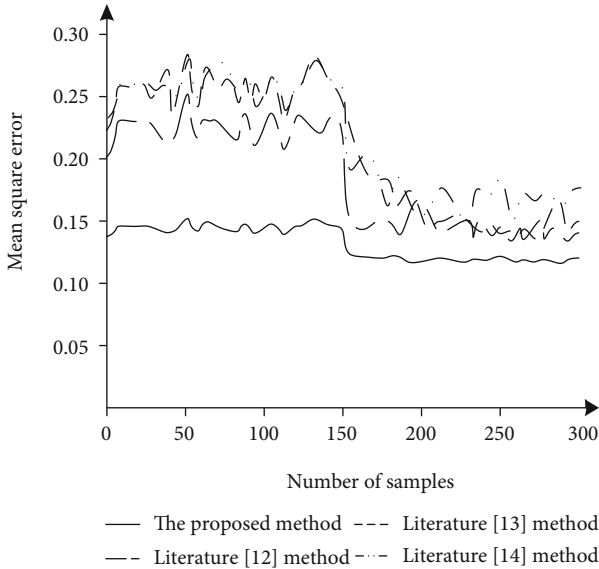


FIGURE 6: Comparison of mean square error of different methods.

TABLE 3: Comparison of risk evaluation results of sports events.

Competition events	Event A	Event B	Event C
The proposed method	III	II	III
Literature [12] method	III	I	III
Literature [13] method	II	II	III
Literature [14] method	II	I	II
Actual comprehensive risk level	III	II	III

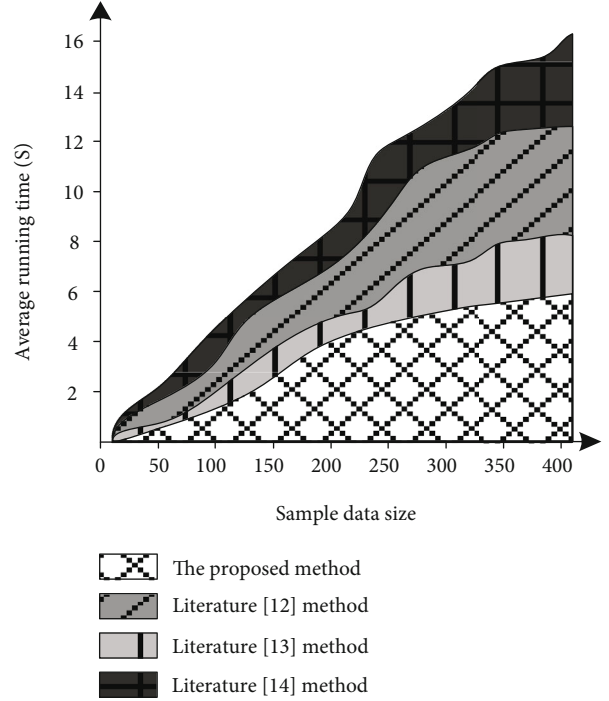


FIGURE 7: Average running time test results of different methods.

better the convergence performance of this method. The average fitness is calculated as follows:

$$z = \frac{\sum_{i=1}^n F_i}{n} \quad (17)$$

- (2) Prediction accuracy: in order to verify the accuracy of sports event risk evaluation and prediction of this method, select different numbers of sample data in the test area, and compare the predicted value of sports event risk with the actual value of sports event risk. The smaller the gap between the two, the higher the prediction accuracy:

$$A = |a_1 - a_2|, \quad (18)$$

where a_1 is the risk prediction value of sports events, a_2 is the risk prediction value of sports events, and the smaller the value of A , the higher the prediction accuracy

- (3) Prediction mean square error: mean square error is an important index to verify the prediction result error of sports events. Therefore, the prediction mean square error of different methods is compared. The smaller the value, the lower the prediction result error:

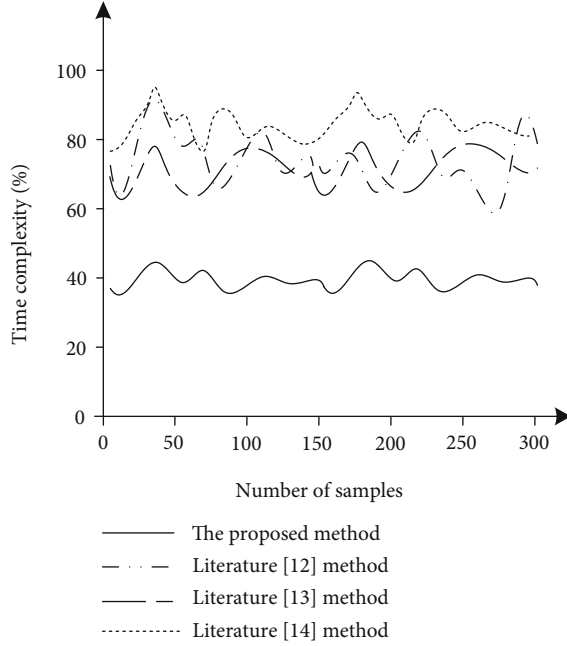


FIGURE 8: Comparison of time complexity.

$$M = E(a_1 - a_2)^2, \quad (19)$$

where E is the average of expected values

- (4) Evaluation precision: The output results of different methods are used to evaluate the sports event risk of five competition items of the experimental object, and the sports event risk level predicted by the four methods is compared with the actual comprehensive risk level of the experimental event. The closer it is to the actual comprehensive risk level, the higher the evaluation accuracy:

$$B = |b_1 - b_2|, \quad (20)$$

where b_1 is the predicted risk level of sports events, b_2 is the actual comprehensive risk level, and B represents that the evaluation results are completely consistent with the actual results

- (5) Average running time: the average running time is the average of the time spent on the risk evaluation result and the prediction result of a sports event. The lower the value, the higher the execution efficiency of the method:

$$T = \frac{t_1 + t_2}{2}, \quad (21)$$

where t_1 is the time-consuming for sports event risk assessment and t_2 is the time-consuming for sports event risk prediction

- (6) Cost of prediction method (time complexity): time complexity is an important index to verify whether the research method can be implemented smoothly. The lower the index, the better the execution performance of the method:

$$Time(n) = O(f(n)), \quad (22)$$

where $O(\cdot)$ is complexity and $f(n)$ is the code execution time growth change value of the prediction method.

3.3. Results and Discussion. The methods of this paper: literature [12], literature [13], and literature [14], are compared with the average fitness value in sports event evaluation and prediction. The results are shown in Figure 4.

According to Figure 4, with the increase of iteration times, the average fitness value of the proposed method tends to be stable after the iteration times meet the requirements of 20 training times, while the average fitness values of literature [12], literature [13], and literature [14] do not tend to be stable when the iteration times are 60, indicating that the average fitness of sports event evaluation and prediction of this method is good. Therefore, this method has good performance in sports event risk prediction.

Four methods are used to predict the risk of sports events. The predicted value of sports event risk is compared with the actual value of sports event risk. The comparison results of prediction accuracy are shown in Figure 5.

As shown in Figure 5, with the increase of sample data, the error between the predicted value and the actual value of the four methods decreases gradually. The predicted value of sports event risk in this method is almost equal to the actual value, while the predicted value and the actual value of literature [12], literature [13], and literature [14] methods differ greatly, and the maximum error values are 0.6 and 0.9, respectively. All occurred when the number of samples was 70. The results show that the predicted value of the method in this paper is almost the same as the actual value, and it has high prediction accuracy.

By analyzing the data in the above experimental process, the prediction mean square error of the four methods is shown in Figure 6.

Comparing the prediction performance of the four methods, it is found that the mean square error of the method in this paper is less than 0.15, while the methods in literature [12], literature [13], and literature [14] are higher than the method in this paper. It shows that the prediction mean square error of the methods in literature [12], literature [13], and literature [14] is large, and the error of sports event risk prediction is high. Therefore, it shows that the prediction performance of this method is better and the result is more accurate.

Taking the large-scale sports events held in a region as the research object, this paper studies the risk evaluation and prediction of sports events. The event was held for one week, with three types of competition events A, B, and C. The risk level of sports events predicted by the four methods

TABLE 4: Statistical test of prediction results of different methods.

Methods	Original hypothesis	Test	<i>P</i>
The proposed			0.921
Literature [12]	There is no difference between the predicted results and the real results	Wilcoxon signed rank test	0.903
Literature [13]			0.830
Literature [14]			0.865

is compared with the actual comprehensive risk level of the experimental event. The results are shown in Table 3.

It can be seen from Table 3 that the risk prediction level of the five events in this paper is consistent with the actual comprehensive risk level, the event B risk level predicted by the method in literature [12] is inconsistent with the actual comprehensive risk level, and the method predicted by literature [13] The risk level of event A is inconsistent with the actual comprehensive risk level, and the risk levels of event A, event B, and event C predicted by the literature [14] method are inconsistent with the actual comprehensive risk level. The results show that the method in this paper is compared with the methods in literature [12], literature [13], and literature [14]. The risk prediction results of sports events in this paper are more accurate and have higher application value.

The methods in this paper are tested from time. The average running time of the four methods is shown in Figure 7.

According to Figure 7, the average running time of the four methods increases with the increase of sample data. Among them, the average running time curves of literature [12], literature [13], and literature [14] show a rapid upward trend with the increase of sample data, and the average running time is longer. The average running time curve of this paper method shows a small increasing trend before the sample data size is 200, and the increasing range is relatively large when the sample data size exceeds 200. When the sample data size is 400, the average running time of this method is longer than that of literature [12], literature [13], and literature [14], in which the average running time of this method is only 8 s. The above results show that the average running time of this method is shorter.

The time complexity of the four methods is shown in Figure 8.

It can be seen from the analysis of Figure 8 that the time complexity of the four methods does not change greatly with the increase of the number of samples, but it can be seen intuitively from Figure 8 that the overall overhead (time complexity) of the method in literature [14] is large. When the number of samples is about 40 and 170, the overhead (time complexity) of the method is almost 95%, and the complexity is high. The overhead (time complexity) of literature [13] is less than 80%. In contrast, the average overhead (time complexity) of this method is about 40%, which is much lower than that of the other three methods.

In order to ensure the preciseness of the comparison results of the four methods, the statistical test of hypothesis is used to test the four methods, so as to ensure the reliability of the above comparison results. Wilcoxon signed rank test is selected, and the results are shown in Table 4.

According to Table 4, the Wilcoxon signed rank test results show that the *P* values of this method, literature [12], literature [13], and literature [14] are greater than 0.05, indicating that the original hypothesis is tenable, and there is no difference between the predicted results and the real results.

4. Conclusions and Future Work

The holding of sports events is very important for the development of a city or even a country. Although the holding of sports events does bring many rare opportunities for the overall development of social economy and society in daily social and economic life, it also implies huge risks due to its wide range and the large number of people involved. Some sudden international and domestic politics and economy, uncertain factors such as social and natural events may seriously affect or even hinder the normal progress of sports events, so as to avoid the impact of uncertain factors on sports events. A sports event model evaluation and prediction method using PCA is proposed. This study collects the risk data of sports events through the establishment of ZigBee technology, and realizes the risk evaluation and prediction of sports events through PCA combined with improved BP neural network. The results show that this method has better average adaptability. The risk assessment accuracy of sports events is higher, the average running time is shorter, overhead (time complexity) is lower and the overall performance is better. However, further work can be carried out from the following perspectives in the future. For data acquisition, the method in this paper collects more samples only within a certain area and does not expand the acquisition area. Therefore, it has a certain one sidedness. In the future, it can also expand the acquisition area that does not build a human-computer interface.

Data Availability

The data that support the findings of this study are available from the corresponding author upon reasonable request.

Conflicts of Interest

The authors declare that there is no conflict of interest with any financial organizations regarding the material reported in this manuscript.

Acknowledgments

This work was supported by National Social Science Fund (20FTYB002), Key Projects of Jilin Social Science Fund (2020A10), and Social Science Research Project of Jilin Provincial Department of Education (JJKH20211320SK).

References

- [1] J. Sasadai, N. Maeda, R. Shimizu et al., "Analysis of team-sport wheelchair falls during the Rio 2016 summer Paralympic games: a video-based cross-sectional observational study," *BMJ Open*, vol. 10, no. 3, pp. e033088–e033099, 2020.
- [2] J. Pino-Ortega, D. Rojas-Valverde, C. D. Gómez-Carmona, and M. Rico-González, "Training design, performance analysis, and talent identification—a systematic review about the Most relevant variables through the principal component analysis in soccer, basketball, and Rugby," *International Journal of Environmental Research and Public Health*, vol. 18, no. 5, p. 2642, 2021.
- [3] S. de Groot, I. Kouwizjer, L. Valent et al., "Sport participation after the HandbikeBattle: benefits, barriers, facilitators from the event—a follow-up survey," *Spinal Cord Series And Cases*, vol. 6, no. 1, pp. 54–65, 2020.
- [4] H. Wang, C. Dong, and Y. Fu, "Optimization analysis of sport pattern driven by machine learning and multi-agent," *Neural Computing and Applications*, vol. 33, no. 4, pp. 1067–1077, 2021.
- [5] M. Ghobaei-Arani and A. Shahidinejad, "An efficient resource provisioning approach for analyzing cloud workloads: a metaheuristic-based clustering approach," *The Journal of Supercomputing*, vol. 77, no. 1, pp. 711–750, 2021.
- [6] J. G. Claudino, D. Capanema, T. V. de Souza, J. C. Serrão, A. C. Machado Pereira, and G. P. Nassis, "Current approaches to the use of artificial intelligence for injury risk assessment and performance prediction in team sports: a systematic review," *Sports Medicine, - Open*, vol. 5, no. 1, pp. 12–28, 2019.
- [7] H. G. Dong and J. H. Sun, "Risk assessment of governance model of large stadiums," *Sports and Science*, vol. 41, no. 5, pp. 106–113, 2020.
- [8] I. Fister, D. Fister, S. Deb, U. Mlakar, J. Brest, and I. Fister Jr., "Post hoc analysis of sport performance with differential evolution," *Neural Computing and Applications*, vol. 32, no. 15, pp. 10799–10808, 2020.
- [9] T. Zhang and F. Y. Zhang, "Application of BP neural network in the design of event risk early warning system," *Automation Technology And Application*, vol. 25, no. 8, pp. 184–186, 2019.
- [10] H. G. Zhu and C. Wu, "Research on risk assessment of large-scale sports events – Taking Nanjing Youth Olympic Games as an example," *Sports And Science*, vol. 13, no. 5, pp. 22–26, 2021.
- [11] W. Chen, Y. Y. Li, M. M. Huang, and M. Li, "Research on risk assessment of school sports competition based on improved risk matrix method," *Journal of Wuhan Institute of physical education*, vol. 15, no. 10, pp. 72–79, 2021.
- [12] B. Liang, W. Li, and J. F. Li, "Study on the construction of ecological risk assessment system for urban hosting large-scale sports events," *Journal of Chengdu Institute of physical education*, vol. 46, no. 2, pp. 34–41, 2020.
- [13] W. Chen, Y. Y. Li, and M. M. Huang, "Research on risk assessment of primary and secondary school sports games based on hierarchical holographic model," *Journal Of Wuhan Institute Of Physical Education*, vol. 53, no. 11, pp. 64–71, 2019.
- [14] Z. Wang, "Risk Prediction of Sports Events Based on Gray Neural Network Model," *Complexity*, vol. 2021, Article ID 6214036, 10 pages, 2021.
- [15] M. Li, F. R. Yu, P. Si, and Y. Zhang, "Green machine-to-machine communications with Mobile edge computing and wireless network virtualization," *IEEE Communications Magazine*, vol. 56, no. 5, pp. 148–154, 2018.
- [16] H. Jiang, T. Qiu, and K. Deepa Thilak, "Application of deep learning method in automatic collection and processing of video surveillance data for basketball sports prediction," *Arabian Journal for Science and Engineering*, 2021.
- [17] G. Quer, T. Aktas, F. Librino, T. Javidi, and R. R. Rao, "A wireless vehicle-based mobile network infrastructure designed for smarter cities," *Ad Hoc Networks*, vol. 85, no. 3, pp. 160–169, 2019.
- [18] Q. Zhang, X. Zhang, H. Hu, C. Li, Y. Lin, and R. Ma, "Sports match prediction model for training and exercise using attention-based LSTM network," in *Digital Communications and Networks*, Elsevier, 2021.
- [19] D. Rojas-Valverde, J. Pino-Ortega, C. D. Gómez-Carmona, and M. Rico-González, "A systematic review of methods and criteria standard proposal for the use of principal component analysis in Team's sports science," *International Journal of Environmental Research and Public Health*, vol. 17, no. 23, p. 8712, 2020.
- [20] D. Rajani and P. R. Kumar, "An optimized blind watermarking scheme based on principal component analysis in redundant discrete wavelet domain," *Signal Processing*, vol. 172, no. 7, article 107556, 2020.
- [21] C. Chen, N. Gao, X. Wang, and Z. Zhang, "Exponential fringe projection for alleviating phase error caused by gamma distortion based on principal component analysis," *Optical Engineering*, vol. 57, no. 6, 2018.
- [22] K. Krithivasan, S. Pravinraj, and V. S. Shankar Sriram, "Detection of cyberattacks in industrial control systems using enhanced principal component analysis and hypergraph-based convolution neural network (EPCA-HG-CNN)," *IEEE Transactions on Industry Applications*, vol. 56, no. 4, pp. 4394–4404, 2020.
- [23] X. Ma and X. Li, "Dynamic Gesture Contour Feature Extraction Method Using Residual Network Transfer Learning," *Wireless Communications and Mobile Computing*, vol. 2021, Article ID 1503325, 11 pages, 2021.

Retraction

Retracted: SM-PageRank Algorithm-Based User Interest Model for Mobile Smart Tourism Platform

Wireless Communications and Mobile Computing

Received 11 July 2023; Accepted 11 July 2023; Published 12 July 2023

Copyright © 2023 Wireless Communications and Mobile Computing. This is an open access article distributed under the Creative Commons Attribution License, which permits unrestricted use, distribution, and reproduction in any medium, provided the original work is properly cited.

This article has been retracted by Hindawi following an investigation undertaken by the publisher [1]. This investigation has uncovered evidence of one or more of the following indicators of systematic manipulation of the publication process:

- (1) Discrepancies in scope
- (2) Discrepancies in the description of the research reported
- (3) Discrepancies between the availability of data and the research described
- (4) Inappropriate citations
- (5) Incoherent, meaningless and/or irrelevant content included in the article
- (6) Peer-review manipulation

The presence of these indicators undermines our confidence in the integrity of the article's content and we cannot, therefore, vouch for its reliability. Please note that this notice is intended solely to alert readers that the content of this article is unreliable. We have not investigated whether authors were aware of or involved in the systematic manipulation of the publication process.

Wiley and Hindawi regrets that the usual quality checks did not identify these issues before publication and have since put additional measures in place to safeguard research integrity.

We wish to credit our own Research Integrity and Research Publishing teams and anonymous and named external researchers and research integrity experts for contributing to this investigation.

The corresponding author, as the representative of all authors, has been given the opportunity to register their agreement or disagreement to this retraction. We have kept a record of any response received.

References

- [1] H. Li and T. Su, "SM-PageRank Algorithm-Based User Interest Model for Mobile Smart Tourism Platform," *Wireless Communications and Mobile Computing*, vol. 2022, Article ID 6034500, 12 pages, 2022.

Research Article

SM-PageRank Algorithm-Based User Interest Model for Mobile Smart Tourism Platform

Hua Li¹ and Tao Su²

¹Department of Foreign Languages for Tourism, Shandong College of Tourism and Hospitality, Jinan, 250200 Shandong, China

²Law Enforcement Industry Customer Marketing Service Center, China United Network Communication Group Co., Ltd. Jinan Branch, Jinan, 250002 Shandong, China

Correspondence should be addressed to Hua Li; sh_liuxs@ujn.edu.cn

Received 5 November 2021; Revised 10 December 2021; Accepted 11 December 2021; Published 18 January 2022

Academic Editor: Alireza Souri

Copyright © 2022 Hua Li and Tao Su. This is an open access article distributed under the Creative Commons Attribution License, which permits unrestricted use, distribution, and reproduction in any medium, provided the original work is properly cited.

Smart tourism, also known as smart tourism, actively captures tourism activities, tourists, tourism economy, tourism resources, and other information through mobile Internet and mobile terminal Internet of things devices and emerging technologies such as cloud computing and Internet of things. In order to release the intelligent tourism information in time, let the masses know the information in time, and adjust the work and tourism plan in time, this paper proposes SM-PageRank algorithm and secondary ranking based on user interest model, in order to study the accuracy of tourism information retrieval. The methods used in this paper include the principle of three weighted information fusion algorithms, LBS technology, and the design of intelligent tourism system. The function of information fusion algorithm is to find the global optimal solution for travel routing. LBS technology collects real-time tourism information through some entity sensors. Through information retrieval experiment and fusion technology solution experiment, the results show that the SM-PageRank algorithm and the secondary sorting based on user interest model proposed in this paper improve the average accuracy by 20.1% compared with the traditional algorithm and 2.6% compared with Google search. The Internet of things fusion algorithm gives a line planning set with standard deviation of 0.4 for the set of travel days with standard deviation of 1.92.

1. Introduction

Tourism has become one of the leisure activities of most people. Users usually retrieve tourism information on the search platform when planning their trip. However, the amount of tourism information stored on the Internet is becoming more and more complex, and users pay more and more attention to the relevance of tourism information provided by the search platform. After users input search words on the search platform, they should always match the search words and select the most relevant and reliable tourism information at the top of the search results. Providing users with the most relevant and reliable information source as search results and allowing them to really enjoy smart tourism is one of the urgent problems to be solved by the search platform. Therefore, one of the main research directions of search engine is search sorting algorithm. With

the increase in the number of web pages, manual classification cannot keep up with the pace of the times, search engines have evolved to text retrieval, and SM-PageRank sorting algorithm came into being. This algorithm has a very good effect on ranking web pages, so it is often used to solve the problem of intelligent tourism systems.

1.1. Background. With the rapid development of communication technology and microelectronics, the traditional computer-centered computing mode has gradually changed into a human-centered general computing mode. Therefore, the concept of the Internet of things is gradually being proposed. This technology allows people to access the Internet of things at any time and on demand through mobile phones, handheld computers, computers, and other devices, receive relevant information, and accept the surrounding environment on demand. Therefore, Intelligent Tourism

search engine will become one of the main trends in the future. In the Intelligent Tourism retrieval platform, the quality of retrieval algorithm will directly affect the efficiency and accuracy of search results.

1.2. Significance. When users use the search engine to obtain tourism information, the search engine cannot find the important information users need and put it in the first place, which greatly affects users' satisfaction with the search engine. Therefore, how to design a search ranking algorithm suitable for search engine is particularly important. Next, this paper studies the problem of smart tourism route planning. Based on the problem of self-driving travel route planning, a mathematical model of intelligent travel route planning is established. The result of the optimal solution is transformed into a regional smart tourism route plan, and finally, a smart tourism route plan is formed. The tourism route arrangement given in this paper has strong practical guiding significance and can provide a scientific basis for the actual travel arrangement.

1.3. Innovation Points. This paper uses SM-PageRank sorting algorithm and secondary sorting algorithm, summarizes the previous research experience, and proposes to apply the similarity between the calculated page and its linked page to the calculation of PageRank value, so as to ensure the accuracy of search query. This article applies the Internet of things technology to tourism route planning, so that the average travel time of each scenic spot can be well controlled and has high stability.

2. Related Work

With the rapid development of information technology and the increasingly prominent role of tourism in the national economy, the concept of smart tourism is becoming more and more popular, which has been studied by many scholars. Predecessors' research mostly focused on professional training of tour guides, and there were few applications of the Internet of things. Chen et al. believe that it is necessary to manage the coherent quality. Whenever the component system used for reinforcement learning involves randomness and continuous control behavior of reliability and quality, they often have problems such as failure and error. The complexity and stochastic characteristics of challenge the operation of the system. They also put forward a dynamic quality calculation method. It focuses on the construction of axiomatic framework, but their method sacrifices accuracy for coherence, resulting in excessive error [1]. Fang et al. believe that data transmission is very important for analysis and learning in the Tourism Internet of things system, and transmitting data with limited energy is a challenge. They studied the data transmission in the energy collection system using capacitors to provide energy when the energy reception rate changes with time. They proposed that the more energy the capacitors receive, the slower the energy reception speed. Based on this feature, they studied how to transmit more data when the energy receiving time is discontinuous, but their proposed method needs to invest

a lot of cost in infrastructure construction [2]. Alberti et al. believe that the Internet of things has been actively challenging the current Internet system. The Internet has many architectural limitations, such as security, data distribution efficiency, source, and traceability, so the Internet of things with good security has more development prospects. Their research aims to produce a prototype of indoor security monitoring system with fingerprint identification, using the Internet network for the data transmission process on the network database, the system constructs a complete ecosystem and has reference significance for outdoor tourism, but the timeliness of the system is not strong enough and the information lag is obvious [3]. Safii et al. believe that as a provider of data services, servers play a very important role for organizations with huge data use and control systems. If the temperature is too high and the operator does not notice it, the hardware equipment in the server room may be damaged. To solve this problem, they built a temperature monitoring prototype using multiple IOT temperature sensors and web-based responsive software, so as to easily view the temperature on various PC and smartphone displays to ensure the safe operation of the server. However, it also needs real-time monitoring of humidity, surrounding environment, and other information [4]. Sang et al. explore the national image of using smart tourism applications during large-scale event visits through perceived value. Their research aims to test the impact of the image of tourist areas on the country. They collected and analyzed 122 survey responses from foreign tourists for the 2018 Pingchang Olympic Games, emphasizing the importance of participating in large-scale events and how tourist attractions affect the overall national image in the eyes of tourists, but their research does not deeply understand the importance of managing large tourist attractions [5]. Li et al. believe that although smart tourism has received considerable research attention, few studies have investigated the determinants of how tourists evaluate their service experience. They try to explore how commercial value propositions shape the functional and emotional results of travel experience and influence the evaluation of service experience. After research, it is concluded that the novelty of tourism has a positive impact on tourists' consumption. Perceived enjoyment, perceived enjoyment, and perceived usefulness all have a positive impact on the evaluation of service experience. But they focus on the evaluation of smart tourism and have less research on construction [6]. Sun first discussed the research significance and research status of wireless sensor networks at home and abroad, analyzed and optimized the sensor network algorithm, and designed and developed a tourism management system based on the existing wireless sensor network hardware experimental system. However, his system is still a travel agency model, but the travel agency business is expanded to the network [7]. Ashari studied the development track of Bandung tourism and proposed that the limitation of its development is the ability of tourists to obtain information about Bandung natural tourism. When global tourists are confused about looking for new and popular tourist attractions, they will not think of Bandung. Through smart tourism based on service architecture,

emphasizing new social methods and implementing network physical social system, it can attract a large number of tourists to Bandung. However, the smart tourism model he proposed depends on the operating system, requires database storage, occupies storage space, and charges users [8]. According to the field observation and microstructure study of the larger regional shear deformation zone and the scale shear deformation zone of the mining area, it is found that the shear deformation has similar characteristics at different scales from the macro to the micro and constitutes a discriminating shear deformation zone. The existing geological basis also provides a guarantee for further understanding of the relationship between geological mineralization and shear zones.

3. Internet of Things Integration Technology Applied to Smart Tourism

3.1. Principle of Three Weighted Information Fusion Algorithms. Due to the universality of the Internet of things, a large number of multisource and multitype data are collected and stored [9]. Therefore, the massive data of the Internet of things is not only reflected in its growing amount of data over time but also reflected in the high-attribute dimension characteristics of multisource and multitype devices that perceive objective things from multiple angles. If the Internet of things data features with high attribute dimension cannot be effectively fused, it will bring great computational challenges for further decision-making level fusion [10].

(1) Weighted average fusion algorithm

The weighted average fusion algorithm usually uses the mathematical average formula, that is, the weight of each IOT sensor is the same, referred to as NVFA [11]. In the t th sensor fusion system, sensors T_1, T_2, \dots, T_t estimate the state of the same target, and the measured values of each sensor are x_1, x_2, \dots, x_t , which are independent of each other. The true value to be estimated is represented by X , and its variance is $Q_1^2, Q_2^2, \dots, Q_t^2$. The measured value of the p th sensor is represented by $X_p(i)$. Suppose the weight of each sensor is W_1, W_2, \dots, W_t , and the fusion state estimation and weight meet the following conditions:

$$\hat{x} = \sum_{i=1}^t w_i x_i, \quad \sum_{i=1}^t w_i = 1. \quad (1)$$

Assume that the equal weight value is w . As can be seen from equation (1), the state estimation after local fusion is as follows:

$$\hat{x} = \sum_{i=1}^t w_i x_i = \frac{1}{t} \sum_{i=1}^t x_i. \quad (2)$$

The total mean square error is

$$\begin{aligned} Q^2 &= E[(x - \hat{x})^2] = E\left[\sum_{i=1}^t w_i (x - x_i)\right]^2 \\ &= E\left[\sum_{i=1}^t w_i^2 (x - x_i)^2 + 2 \sum_{i=1}^t w_i (x - x_i) w_t (x - x_t)\right]. \end{aligned} \quad (3)$$

Because $X_i (i = 1, 2, \dots, T)$ is an unbiased estimate of X and is not related to each other, the following formula is obtained:

$$E[(x - x_i)(x - x_t)] = 0 (i, t = 1, 2, \dots, n, i \neq t). \quad (4)$$

Therefore, the total mean square error is

$$Q^2 = E\left[\sum_{i=1}^t w_i^2 (x - x_i)^2\right] = \sum_{i=1}^t w_i^2 Q_i^2. \quad (5)$$

From equations (1) and (5), for the weighted average algorithm, the sum of mean square errors is

$$Q^2 = \frac{\sum_{i=1}^t Q_i^2}{t^2}. \quad (6)$$

(2) Optimal weighting algorithm

According to formula (5), the mean square error is a multivariate quadratic function of the weight factor, so a minimum value is required. The best weighting is to multiply the measured value of each IOT sensor by the weighting factor of the measured data x_1, x_2, \dots, x_t according to a specific standard to maximize the sensor measurement data and reduce the loss of information caused by intermediaries other than measurement, which is abbreviated as OVFA [12]. According to the Lagrange conditional extreme value method, the auxiliary function is constructed as follows:

$$f(w_1, w_2, \dots, w_t, \theta) = \sum_{i=1}^t w_i^2 Q_i^2 - \theta \left(\sum_{i=1}^t w_i - 1 \right). \quad (7)$$

Establish equations:

$$\begin{aligned} \frac{\partial f}{\partial w_i} &= 2w_i Q_i^2 - \theta = 0 (i = 1, 2, \dots, t), \\ \frac{\partial f}{\partial \theta} &= 1 - \sum_{i=1}^t w_i = 0. \end{aligned} \quad (8)$$

Accordingly, the weighting factor with the minimum total mean square error is obtained:

$$w_i = \frac{Q_i^{-2}}{\sum_{i=1}^t Q_i^{-2}}. \quad (9)$$

The total mean square error is

$$Q^2 = E[(x - \hat{x})^2] = E \left[\sum_{p=1}^t w_p (x - \hat{x})^2 \right] + 2 \sum_{p=1}^t w_p (x - x_p) w_q (x - x_q). \quad (10)$$

Because x_1, X_2, \dots, X_T are independent of each other and are unbiased estimates of X , when $p \neq q$, it can be obtained $E[(x - x_p)(x - x_q)] = 0$. Therefore, Q_2 can be written as follows:

$$Q^2 = E \left[\sum_{p=1}^t w_p (x - x_p)^2 \right] = \sum_{p=1}^t w_p^2 Q_p^2. \quad (11)$$

The above formula can be obtained in combination with formula (9), and the total mean square error is as follows:

$$Q^2 = \frac{1}{\sum_{i=1}^t Q_i^{-2}}. \quad (12)$$

(3) Adaptive weighted data fusion

The weighting factor satisfies equation (9). Here, the formula for calculating the sensor variance is directly given, and the detailed derivation process is described in the literature. On the basis of optimized weighting, adaptive weighted data fusion fully considers the historical data of each sensor to obtain the data fusion value with the minimum mean square error. The abbreviation of this algorithm is AVFA [13]. The formula for calculating the sensor variance is

$$Q_p^2 = E_{pp} - E_{qp}. \quad (13)$$

Of which,

$$E_{pp} = \frac{1}{i} \sum_{i=1}^t x_p(i), \quad (14)$$

$$E_{qp} = \frac{1}{t-1} \sum_{q=1}^t \left(\frac{i-1}{i} E_{qp}(i-1) \right) + \frac{1}{t} x_p(i) x_q(i).$$

The mean value of sensor P at time I is as follows:

$$\bar{x}_p(i) = \frac{1}{i} \sum_{i=1}^t x_p(i), \quad (p = 1, 2 \dots n). \quad (15)$$

The estimated value at this time is as follows:

$$\bar{x} = \sum_{p=1}^t w_p \bar{x}_p(i). \quad (16)$$

The total mean square error is as follows:

$$Q^2 = E \left[(x - \bar{x}_p(i))^2 \right] = E \left[\sum_{p=1}^t w_p (x - \bar{x}_p(i))^2 \right] + 2 \sum_{p=1}^t w_p w_q (x - x_p(i)) (x - x_q(i)). \quad (17)$$

Because x_1, X_2, \dots, X_T are independent of each other and are unbiased estimates of X , when $p \neq q$, it can be obtained $E[(x - x_p)(x - x_q)] = 0$. Therefore, Q_2 can be written as the following [14]:

$$Q^2 = E \left[\sum_{p=1}^t w_p (x - \bar{x}_p(i))^2 \right] = \frac{1}{i} \sum_{p=1}^t w_p^2 Q_p^2. \quad (18)$$

The corresponding total mean square error is as follows:

$$Q^2 = \frac{1}{i \sum_{i=1}^t Q_i^{-2}}. \quad (19)$$

It can be seen from the above analysis that the weighted average fusion algorithm selects the mathematical average formula, and the weight of each IOT sensor is approximately equal [15]. This method is difficult to overcome the randomness of shorthand measurement and the fluctuation of measured values caused by some sensor faults. On the basis of weighted average, the weighted fusion algorithm fully considers the influence of each sensor on the measured data when some sensors cannot have good strain capacity [16]. However, in the calculation of weighted estimation and total variance, only the measurement data of the current sensor are used, and the measurement data of the historical time of the sensor are ignored. The adaptive weighted fusion algorithm fully considers the historical data of each sensor. On the basis of optimal weighting, the data fusion value with the minimum mean square error is taken, but the estimated value and weighting factor of each time are not effectively processed [17]. In view of the above shortcomings, this section proposes an information fusion method based on the combination of knife cutting method and adaptive weighting method and performs Quenouille estimation on the weighting coefficient and estimated value, respectively, so as to improve the accuracy and robustness of data processing.

3.2. LBS Technology and Smart Tourism. LBS, also known as location-based service, is a value-added service that provides services corresponding to users. The method is to obtain the location information of mobile terminal users through the wireless communication network of mobile communication operators and external positioning methods [18]. Travel behavior has high mobility and can be well combined with location-based services. The provision of geographic positioning services can only be achieved through the positioning technology of the corresponding geographic information system platform, such as base station positioning, landmark positioning, wireless network positioning, RFID, and GPS positioning

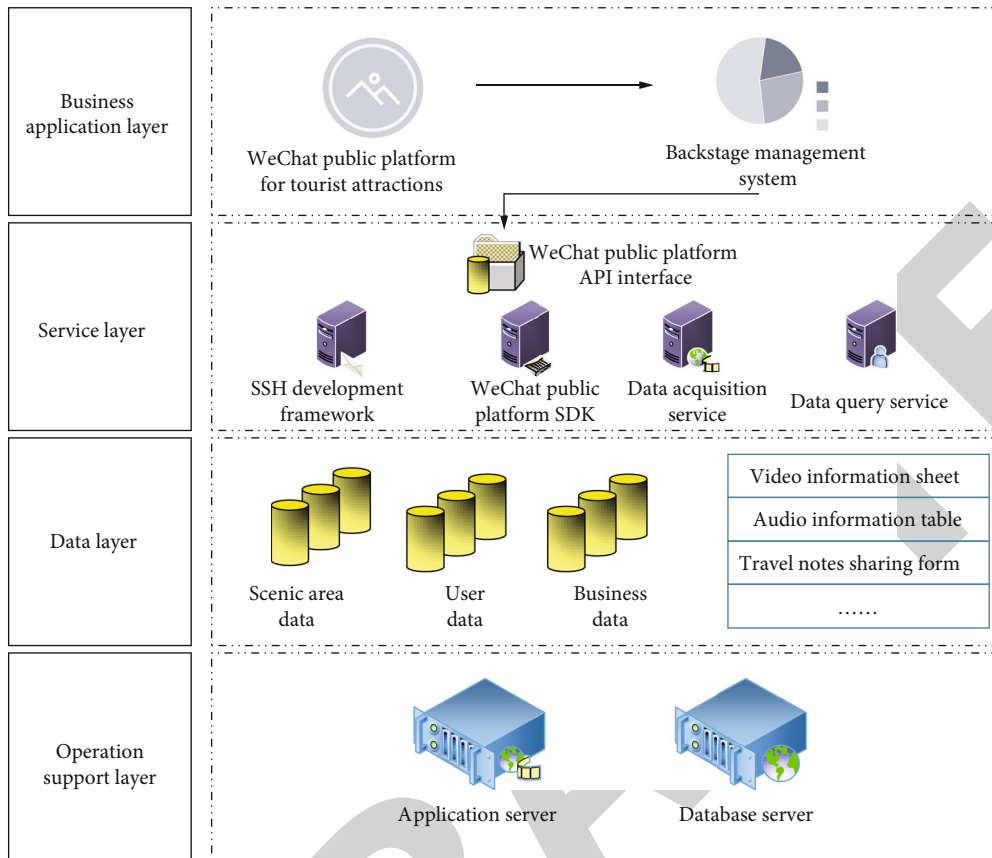


FIGURE 1: Design diagram of smart tourism system.

[19]. With the application of GPS modules and with the increasing popularity of smart phones, travel applications on mobile devices such as smart phones have become the best carrier for LBS applications. With the rapid popularization of smart terminals and mobile Internet applications, as well as the popularization of electronic maps and navigation software, the demand for creative services based on public services such as personal location services, Internet maps, and electronic navigation has grown rapidly, and people have become the subject of LBS. LBS integrates electronic maps, location services, and travel services to provide location services, allowing users to experience a brand new service experience brought by smart tourism [20].

Location-based service is to obtain the location of current user information through the cooperation of mobile terminal, wireless network, and other terminal devices and provide personalized location information service according to the needs of users. Positioning service requires two processes: one is the positioning process, which not only obtains the latitude, longitude, and altitude of the current location of the user's mobile phone but also not directly provides usually this information to the user [21]. The second is location service, which not only obtains information through location operation but also realizes some user-oriented services [22].

3.3. Smart Tourism System Design. The system designed in this paper is based on LBS technology, MVC mode, and

SSH open source framework technology. The system architecture design adopts a hierarchical structure, which is composed of four different layers: business application layer, data layer, service layer, and operation support layer [23]. The system design is shown in Figure 1.

The operation support layer is the carrier of the smart tourism service platform. It adopts advanced software and hardware equipment to build an operating system suitable for stable operation, including network, server, and security equipment. As the software environment of computer operating system and data platform software, the data layer is the content of management related database provided to the application layer through the service layer [24]. The data mainly includes librarian data and tourism service data. The service layer mainly provides various application services to the application layer through the online travel service system, such as API interface service of WeChat public platform, SDK of WeChat public platform, data collection service, and data query service [25]. The business application layer provides various services and business functions for the system service objects (tourists).

The overall structure of tourism flow management consists of three main parts: decision-making, command and coordination control, and data analysis and processing and data acquisition and transmission [26]. As shown in Figure 2.

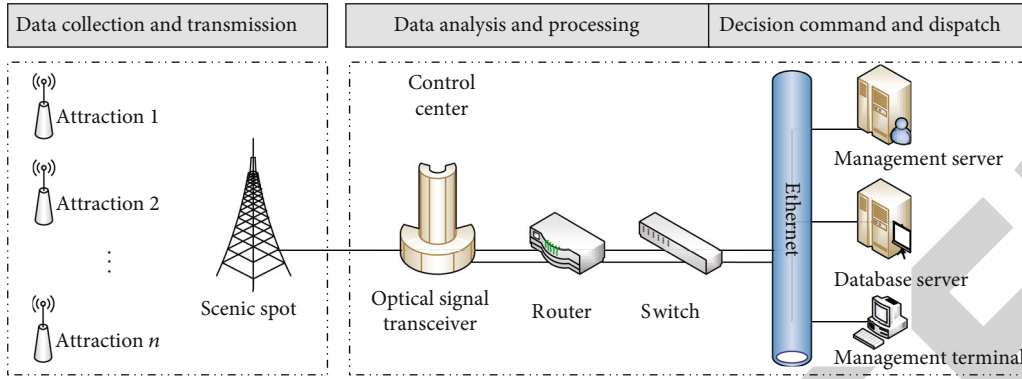


FIGURE 2: Overall framework of tourist management.

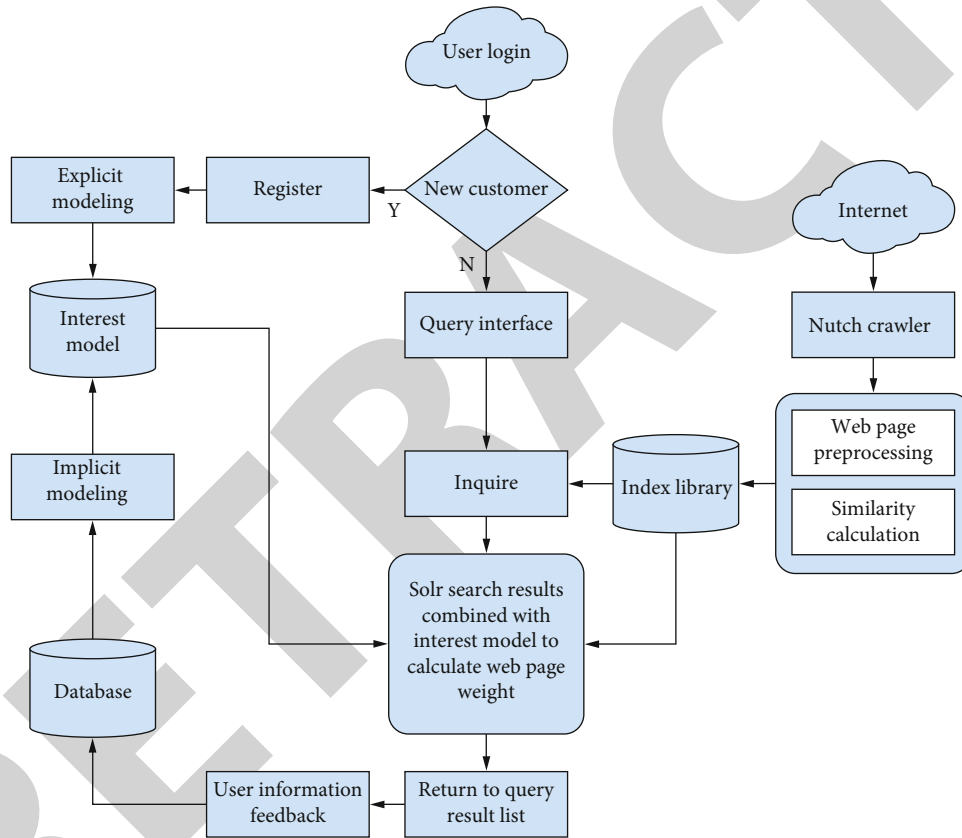


FIGURE 3: Overall platform architecture.

4. Tourism Information Algorithm Design and Teaching Management Experiment

4.1. Construction of Experimental Platform. This experiment will use Solr and Nutch to build an information retrieval experiment platform, capture experimental data through Nutch, modify Nutch's existing scoring algorithm, and apply the SM-P algorithm to realize the user interest module [27]. This paper uses Nutch, Solr, and other tools to build the Intelligent Tourism search experimental platform, and its overall structure is shown in Figure 3.

Nutch is a Lucene-based search engine system. It not only provides all the tools required by the search engine

but also can crawl billions of web pages every month and index these crawled web pages. However, in order to meet the distributed requirements, Nutch has gradually become a crawler tool, and the retrieval function has been given to other tools. Solr is an enterprise search engine server that can index the retrieved data sources. Solr provides a search interface for application search. Like Lucene, Solr provides full-text search, keyword highlighting, and management interfaces. Configuring the Chinese word segmentation method is a necessary step before indexing with Solr [28]. In this experiment, the IK analyzer word segmentation tool is used to finally configure the word segmentation effect.

TABLE 1: Statistics of search results of traditional PageRank and SM-PageRank algorithms.

Key words	PageRank algorithm				SM-PageRank algorithm			
	Search results	Selection	Related webpages	Accuracy	Search results	Selection	Related webpages	Accuracy
Climb mountains	258	50	38	76%	256	50	43	86%
Travel agency	279	51	29	56.9%	257	51	50	98%
Delicacy	208	52	33	63.5%	324	52	49	94.2%
Scenic spots	206	53	31	58.5%	296	53	40	75.5%
Outbound tourism	205	54	38	70.4%	329	54	39	72.2%

In this experiment, five search words (mountain climbing, travel agency, food, scenic spots, and outbound tourism) were selected for query. When comparing the results, the first 50 items of the result set returned by each search word were taken as the investigation objects. The comparison of query statistics and accuracy is shown in Table 1.

Six testers were interviewed to search the above keywords and score the satisfaction of the search results. The comparison of accuracy and satisfaction of the two algorithms is shown in Figure 4.

According to the above figure and table, the optimized SM-PageRank algorithm is better than the traditional PageRank algorithm.

Then, five search words (mountain climbing, travel agency, food, scenic spots, and outbound tourism) are also selected for query, and the correlation between the experimental search results and the query content is manually compared through SM-PageRank algorithm and Google search engine [29]. In the query results, the platform takes the top 50 returned results list as the research basis, and the top 100 Google search results are analyzed and compared. The query statistics are shown in Table 2.

Because the experimental platform takes a short time to grab web pages and the number of web pages is less than that of Google search engine, the total number of returned results is also less, which is not as good as Google search engine in recall.

To establish a secondary sorting algorithm, the experiment needs to establish a user interest model for users. This experiment establishes a user's interest model through user registration. The contents required to be filled in by the user during registration (such as route, diet, accommodation, comments, etc.) are of interest to the user. After the user registration is completed, the results of secondary sorting search are given to establish a user interest model for the user. The results returned by secondary sorting are more in line with user needs. Figure 5 shows the comparison of SM-PageRank and Google search accuracy.

By comparing the above experimental results, we conclude that the search accuracy of SM-PageRank algorithm is higher than that of conventional PageRank algorithm, and the secondary ranking based on user interest model makes the search results more appropriate. As can be seen from the above figure, the search results of SM-PageRank can better meet the needs of users.

After connecting the major scenic spots, this algorithm can also count the passenger flow, including real-time passenger flow statistics and attribute distribution statistics.

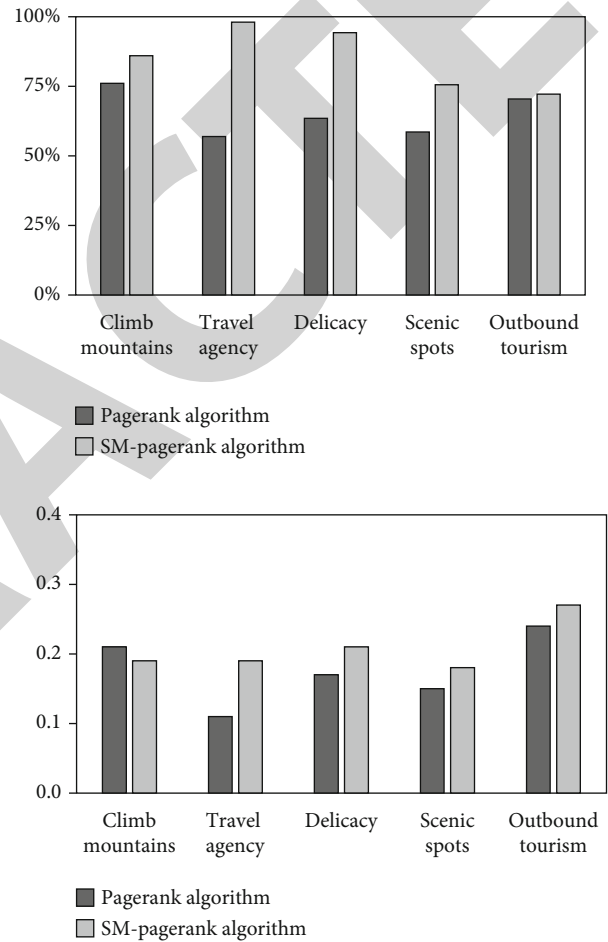


FIGURE 4: Comparison of accuracy and satisfaction of PageRank and SM-PageRank.

Figure 6 shows the relationship between passenger flow and temperature according to system statistics.

4.2. *Fusion Technology for Solving Travel Problems.* Traditional tourist routes are usually one or more fixed routes designed by travel agencies, which are suitable for fixed routes and group tourism. Traditional tourism routes are the crystallization of a tourism experience, which usually takes a certain time to design [30]. Artificial intelligence has greatly improved the rationality of personal travel routes. The integration of Internet of things into route planning has greatly promoted the intelligence of travel route planning. It is more scientific, persuasive, and efficient to

TABLE 2: Sorting comparison of query results.

Key words	SM-PageRank algorithm				Google search			
	Search results	Selection	Related webpages	Accuracy	Search results	Selection	Related webpages	Accuracy
Climb mountains	258	50	38	76%	12306	100	43	43%
Travel agency	279	51	29	56.9%	11855	100	56	56%
Delicacy	208	52	33	63.5%	15552	100	76	76%
Scenic spots	206	53	31	58.5%	12994	100	70	70%
Outbound tourism	205	54	38	70.4%	13589	100	67	67%

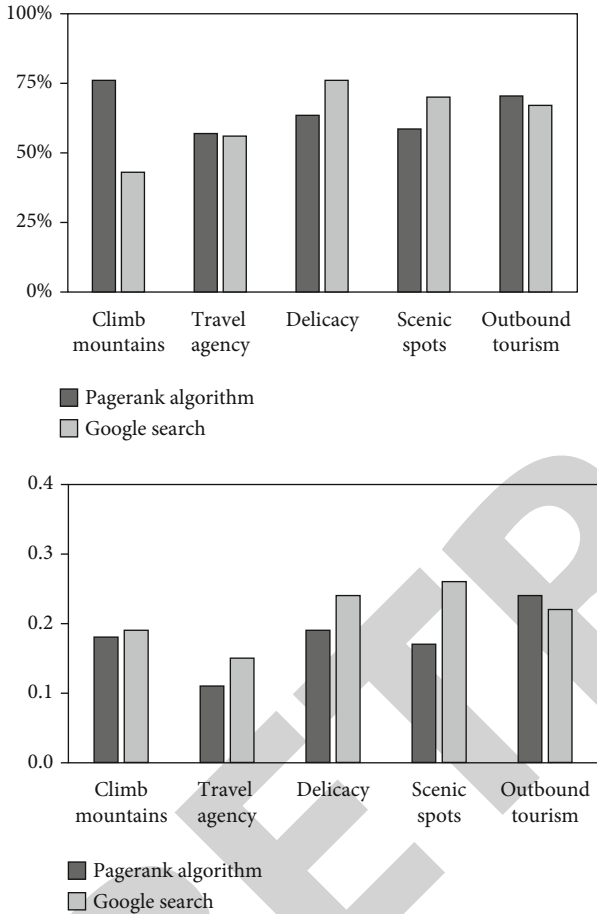


FIGURE 5: Comparison of SM-PageRank and secondary sorting accuracy and satisfaction.

solve the problem of tourism route planning by establishing a model and integrating the Internet of things.

Internet of things fusion is one of the effective algorithms to solve the problem of travel route planning. In order to apply Internet of things fusion to solve the problem of tourism route planning, it is necessary to improve the Internet of things fusion, so that the improved Internet of things fusion can obtain the optimal solution with higher probability in the shortest time. Internet of things integration to solve the traveling salesman problem mainly depends on the path selection strategy, pheromone update rules, and the setting of relevant parameters, and the improvement of Internet of things integration mainly focuses on these three aspects.

The improvement of path selection strategy mainly aims at the defect that Internet of things fusion is easy to fall into local optimal solution. By improving the path selection probability, local search and other strategies, it is possible to help the Internet of things fusion jump out of the local optimal solution, so as to improve the quality of the solution. Pheromone accumulation and feedback are also the improvement focus of pheromone update rules, which is a better method to guide pheromones to the best path and avoid the influence of pheromones on sensors on poor paths. For the setting of relevant parameters, different traveling salesman problems can be solved more effectively. At present, there is no very good mathematical proof to help judge the quality of parameters. Generally speaking, the range of parameters is determined by experience, and then, the size of parameters is dynamically adjusted.

The optimal solution path map and local optimal solution path map of Internet of things fusion technology are shown in Figure 7.

The optimal path is QWE and the local optimal path is QWE. It can also be seen from the figure that the length of QW is less than that of we, so the fusion algorithm is applied at the initial stage to form a local optimal solution. The specific routing of the algorithm is shown in Figure 8.

Based on the above analysis, this paper considers the local search method to improve the quality of the solution of the fusion algorithm. The fusion algorithm is used to optimize the optimal path of each cycle and exchange the adjacent points of the optimal solution of the current cycle to obtain a new solution. If the new solution is better than the optimal solution of the current period, it will replace the optimal solution of the current period. By comparing the total length of the path before and after the exchange, it is found that the result after the exchange is better than the current solution, so the path after the exchange is regarded as the optimal path of the current cycle.

Based on some mathematical models, this experiment makes reasonable simulation, assuming that the number of days of each travel shall not exceed 15 days, so the experiment divides the scenic spots in the scheme with travel days D exceeding 15 days in each region. At the same time, considering the small number of travel days D in individual regions, it is considered to merge the smaller regions. After completing the above processing, regenerate the shortest distance and shortest time matrix of each region and then solve each region to obtain the tour order of each tourist attraction of each region after merging. Through the Internet of things fusion algorithm, the tour order and travel days of each

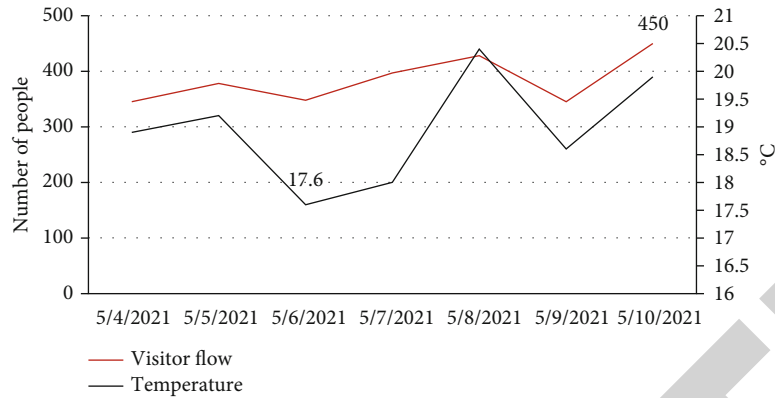


FIGURE 6: Passenger flow statistics interface.

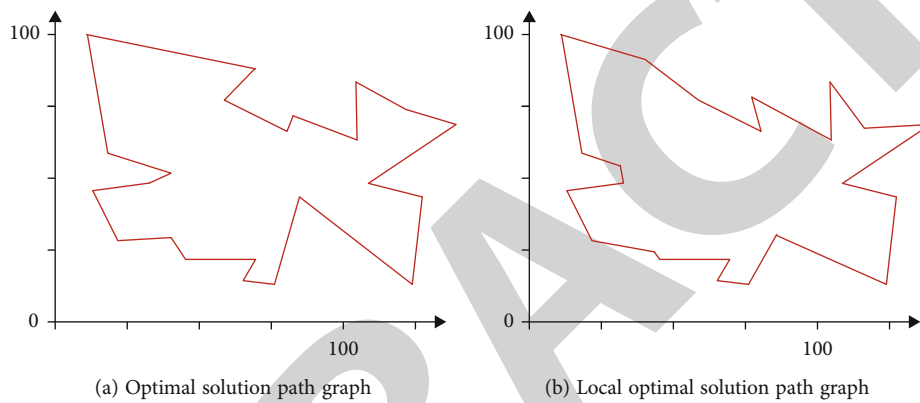


FIGURE 7: Optimal solution path graph and local optimal solution path graph of fusion algorithm.

region have been calculated, and the regions are labeled and marked on the map, as shown in Figure 9. The results of the number of days required for travel in each region are shown in Table 3.

As can be seen from the above table, the tour time in most areas is close to 15 days, which reduces the number of trips and trips and effectively shortens the round-trip time.

According to the rationalization assumption, the number of days of each trip is no more than 15 days, the total number of single trips is no more than 30 days, and the number of scenic spots is no more than 4. The experiment says that these areas should be organized so that you can visit all areas in a shorter time. We sort out the specific itinerary of self-driving travel according to the regional browsing plan. After completion, the annual regional tour plan is shown in Table 4.

In order to make tourism planning more scientific, experiments need to consider other modes of transportation, such as aircraft and high-speed trains. At the same time, when considering the route planning of road travel, the problem of travel cost is not considered, but travel cost is indeed a factor that must be considered when making travel plans. The subsequent improvement of the model is aims at increasing the travel cost. The mathematical model of road travel route planning is suitable for route planning in densely populated areas or within scenic spots.

Path planning refers to the optimal path planning of navigation software or robots. The SM-PageRank algorithm is based on the idea of recursion. The shortest path that does not reach the vertex must be obtained from the shortest path that has reached the vertex, by clarifying the starting position and ending point, avoiding obstacles, and optimizing the path as much as possible, in order to achieve the lowest cost and the highest efficiency.

4.3. Build a Tourism Management Teaching Platform. In order to meet the teaching and training needs of tourism management, we improve the teaching level of teachers. The quality of teaching and the improvement of students' learning quality and students' learning ability and practical ability were improved. This experiment combines database technology, network technology, 3D display technology, and VR technology to construct an all-round, advanced, and visual virtual reality system to adapt to the in-depth development of the school.

Smart tourism is a smart system formed by the computer as the brain and relying on the Internet of things. It integrates tourism into the interconnected system of all things and forms a smart data network based on cloud thinking. In terms of real-time data, the scenic area has been intelligently constructed to realize data visualization and effectively analyze the data and pass the data and analysis results to the scenic area management, which is conducive to improving the data

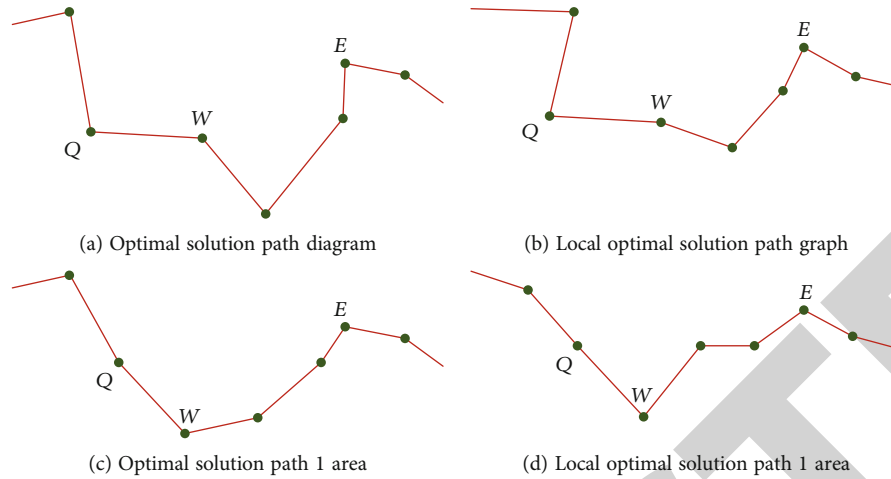


FIGURE 8: Some regions of the optimal solution path graph and local optimal solution path graph of the fusion algorithm.

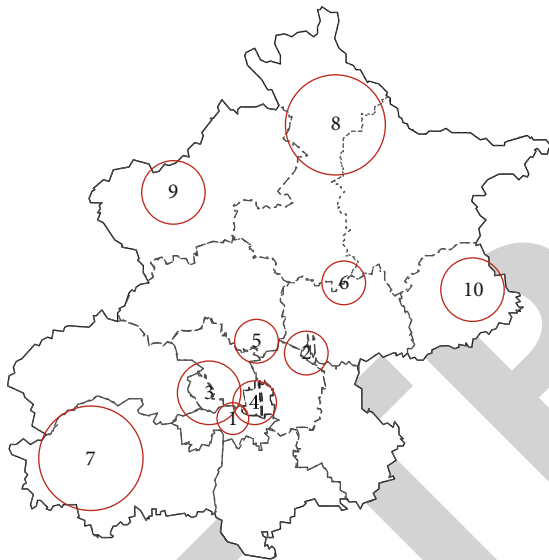


FIGURE 9: Distribution of hypothetical travel areas.

ecological environment of the scenic area. The application of technologies such as the Internet of Things and cloud computing to the construction of scenic spots has brought new opportunities for the creation of smart tourism.

Tourism is a strategic pillar industry of the national economy, with great potential for consumer demand. It is an important means to expand domestic demand and promote stable growth. At present, the urgent problems to be solved in tourism management are as follows: the tourism industry is facing the problem of structural adjustment, the market demand for new professionals continues to grow, and there is a shortage of relevant posts such as exhibition tour guides, senior tour guides and tourism image design. At present, the main contradiction is the contradiction between employment demand and low quality of workers. School employment is very heavy, while the market has great demand for full employment and labor force, but the quality of labor force is relatively low. From the perspective of teaching methods, teachers generally use videos, teaching slides,

writing lessons, blackboard writing, etc. For indoctrination teaching, students can not operate the experiment by personally observing the experimental process. As a result, students only have theoretical knowledge, lack practical ability, and fail to truly integrate theory with practice. Teaching or student learning can achieve the desired teaching effect.

According to the above situation, the system proposed in this paper needs a classroom dedicated to teaching, a large screen display, a highly configured computer host, a VR helmet, two locators, two interactive handles, and enough student seat space. The layout design of virtual reality classroom is shown in Figure 10.

According to the preliminary demand analysis, three main functional modules of tourism digital training system are planned and constructed, including preclass preparation system, real-time education system, and student training. The main content of this module is to build an integrated scene, model, configuration, HR management, and collaboration module with abstract 3D scene representation as the core and collaborative visual manipulation architecture. The main function of the module is to provide the preprocessing function of electronic resources recommended by VR learning environment; integrate 3D models, materials, textures, and shaders; support relevant data of programming and bone animation; and summarize and convert non-relational data into relational data, such as video, audio, and documents. Especially in the case of audio and video, it is necessary to extract important information to form a connection, classify subjects and courses according to the classification tree, and build a VR education content ecosystem according to unified planning.

Because the modeling of building facilities in the real scenic spot is too complex, various models and layouts in the simulation system are basically modeled with reference to the sand table model of the base. On the basis of meeting certain display effects, we simplify the model grid as much as possible to achieve a certain balance between the operation effect and efficiency of the system. After the model is built, the author needs to add materials and draw the appearance of the model. Because the process is too complex, this article will not introduce it in detail.

TABLE 3: Travel days required for each region.

Area number	Number of days required	Area number	Number of days required
1	16	6	10
2	14	7	12
3	11	8	15
4	15	9	13
5	12	10	11
Standard deviation			1.92

TABLE 4: Regional tour planning for self-driving tour route planning.

Frequency	Area number	Travel days
1	1,6	26
2	4,10	26
3	3,8	26
4	2,7	26
5	5,9	25
Standard deviation		0.4

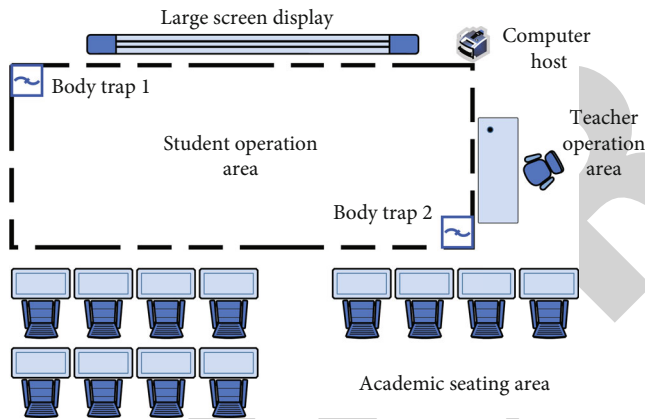


FIGURE 10: VR teaching design.

Through the experimental construction of the simulated tour guide teaching system of tourism management specialty, there are still many deficiencies in the system R & D and research. It is also necessary to increase the virtual scenic spot library of the tourism digital training system and optimize the scene rendering. In addition, it is also necessary to apply the construction ideas and schemes of the system to other majors, build a collection of professional teaching and training applications of virtual reality and vocational education, create a perfect virtual reality intelligent education platform, and promote the development of intelligent vocational education to a higher and faster track.

5. Discussion

The tourism teaching system designed in this article is exactly the key task faced by the education industry and the tourism industry. The system has been applied to tour-

ism talent training colleges to allow graduates to meet the actual needs of the tourism industry and conform to the development direction of the tourism industry. Although this paper proposes a secondary sorting algorithm based on user interest model and establishes and studies the user model, there are still many imperfections. Experiments should get users' interest from more channels and then deeply dig into users' points of interest and establish a more reasonable model of interest. In model updating, how to make model updating more effective and how to establish long-term and short-term models for users are the next research direction. In the actual planning of intelligent travel route, this paper adopts real data and reasonable hypothetical data. Therefore, we can further consider how to design an algorithm that can automatically search and obtain relevant data through the network and other aspects, which reflects the intelligent side. In addition, this paper introduces the application process of virtual reality technology in the virtual reality teaching platform of tourism management specialty, but there is no detailed explanation of the technical implementation, including three-dimensional modeling technology, scene loading and setting, database connection, interactive design, simulation effect, and project release.

6. Conclusions

In the current tourism education industry, the understanding of informatization in relevant tourism professional education only stays at the primary level of the internal management information system. The experimental conclusions are as follows. Through experimental calculations, it is found that this paper proposes the SM-PageRank algorithm based on Nutch and Solr and the secondary ranking based on the user interest model, which makes the information query more reliable and accurate. The advantages of the algorithm are mainly manifested in the calculation speed and accuracy. Compared with the traditional algorithm, the average accuracy rate is increased by 20.1%. Compared with the Google search, the average accuracy rate is increased by 2.6%, which can meet the search needs of users.

Data Availability

No data were used to support this study.

Conflicts of Interest

The author states that this article has no conflict of interest.

References

- [1] Y. T. Chen, E. W. Sun, and Y. B. Lin, "Coherent quality management for big data systems: a dynamic approach for stochastic time consistency," *Annals of Operations Research*, vol. 277, no. 1, pp. 3–32, 2019.
- [2] X. Fang, J. Luo, G. Luo, W. Wu, Z. Cai, and Y. Pan, "Big data transmission in industrial IoT systems with small capacitor supplying energy," *IEEE Transactions on Industrial Informatics*, vol. 15, no. 4, pp. 2360–2371, 2019.

Research Article

Anomaly Recognition Algorithm for Human Multipose Motion Behavior Using Generative Adversarial Network

Nan Zhang,¹ Jie Ren,² Qixiao Xu ,¹ Hao Wu,¹ and Meng Wang¹

¹Physical Education Department, Beijing University of Technology, Beijing 100124, China

²College of Physical Education and Training, Harbin Sport University, Harbin, 150008 Heilongjiang, China

Correspondence should be addressed to Qixiao Xu; xuqixiao@bjut.edu.cn

Received 22 November 2021; Accepted 3 January 2022; Published 17 January 2022

Academic Editor: Nima Jafari Navimipour

Copyright © 2022 Nan Zhang et al. This is an open access article distributed under the Creative Commons Attribution License, which permits unrestricted use, distribution, and reproduction in any medium, provided the original work is properly cited.

Human multipose motion behavior is similar; there are many actions. However, it is difficult to recognize abnormal behavior. The existing human motion behavior anomaly recognition methods have the problems of low accuracy and being time-consuming. Therefore, an anomaly recognition method of human multipose motion behavior using Generative Adversarial Network (GAN) is proposed. The Gauss model is used to segment the human multipose motion behavior image, and the image foreground of the segmentation result is the human motion target detection result. The Shi-Tomasi algorithm is selected to extract contour feature points from human motion object detection results. The extracted contour features are set as hidden space random variables and input into the GAN. The GAN uses the generator and discriminator to recognize the multipose human motion behavior and determine whether the multipose human motion behavior is abnormal. The results show that the proposed algorithm can accurately recognize abnormal human multipose motion behavior, the recognition accuracy is higher than 99%, and the average recognition time is less than 200 ms. The shadow removal effect of the foreground image obtained by the proposed algorithm can realize the accurate recognition of human multipose motion behavior abnormalities and provide a reliable basis for research in related fields.

1. Introduction

Human posture behavior recognition is a research in the field of video analysis. The goal of human posture behavior recognition is to classify the specific actions of humans [1]. Human abnormal behavior detection is a branch of human behavior recognition, that is, to recognize specific behaviors in different scenes, such as fighting in banks and other literature behaviors. Human posture behavior technology has been widely used in auxiliary medical treatment, video surveillance, and so on. The recognition of multipose motion behavior abnormalities needs to determine whether there are abnormalities by analyzing human posture [2].

The specific position and specific behavior of the motion target in a fixed time are analyzed through the abnormal recognition of multipose motion behavior [3, 4], so as to realize the automatic recognition and positioning of human posture. The abnormal recognition of human multipose motion behavior can be applied to many fields such as medical treat-

ment and security. Human motion posture has the features of high nonlinearity and degree of freedom [5, 6] and has high diversity and complexity. It is challenging to accurately recognize human multipose motion behavior abnormalities. The feature extraction of human motion posture is very important [7]. The accuracy of feature extraction determines the accuracy of multipose motion behavior. Feature extraction is realized by extracting texture features, color features, contour features, and other features of human motion posture [8, 9]. Human motion is formed by posture sequence, so it is more practical to extract human contour features from images.

The main contributions of this paper are as follows. (1) A new human multipose motion behavior anomaly recognition algorithm based on GAN is proposed to detect human motion targets in human multipose motion images. (2) Aiming at the problem of many similar actions of human multipose motion behavior, the human motion region and background region in the image are segmented, and the

human motion posture features are extracted from the human motion target region to reduce the difficulty of behavior anomaly recognition. (3) The GAN is used to obtain the abnormal recognition results of human multipose motion behavior. The network has the features of flexible application and strong learning ability. It is applied to the abnormal recognition of human multipose motion behavior to optimize the recognition performance.

2. Related Works

At present, there are many researches on motion recognition. Literature [10] applies convolutional neural network (CNN) to human motion recognition and proposes three different CNN structures. Firstly, four different information channels are generated from each frame in the horizontal and vertical directions through optical flow and gradient to be applied to three-dimensional (3D) CNN. Then, three architectures are proposed, namely, single stream, dual stream, and four stream 3D CNN. In the single stream model, four information channels per frame are applied to the single stream. In the dual flow structure, optical flow- x and optical flow- y are applied to one flow, and gradient- x and gradient- y are applied to another flow. In the four stream architecture, each information channel is applied to four independent streams, by evaluating the architecture of the action recognition system.

Literature [11] applied shape time dynamics to human motion recognition and proposed a human motion recognition framework with constant depth perspective, which is a new integration of two important motion clues: motion and shape time dynamics (STD). The motion flow encapsulates the motion content of the action into RGB dynamic image, which is generated by approximate rank pool (ARP) and processed by fine-tuning reception V3 model. The STD stream uses a series of long short-term memory (LSTM) and Bi LSTM learning models to learn the long-term view invariant shape dynamics of actions. Human pose model (HPM) generates view invariant features of human pose frames with key depth based on structural similarity index matrix (SSIM). According to three types of postfusion techniques, namely, maximum average and multiplication, the final prediction of single stream fraction is made. Literature [12] proposed an effective method for human motion recognition (HAR) from silhouette image sequences in video. The effectiveness of this method lies in feature extraction and action classification. The method includes scale translation normalization and distortion contour removal, which are used to extract the newly introduced spatiotemporal features, namely, active region energy feature (AREF), and trajectory analysis. In addition, the method uses low-dimensional eigenvectors, which makes the cost of the whole process effective in terms of time requirements. The results on the published Weizmann and Muhavi data sets clearly verify the efficiency of the proposed technology in the related work on the accuracy of human behavior detection. Literature [13] proposed a human behavior anomaly detection method based on the combination of deep learning and artificial features. Firstly, the key points of human 3D

skeleton in time series are extracted by Yolo V4, and the mean shift target tracking algorithm is applied. Then, the key points are transformed into spatial RGB and put into multilayer convolutional neural network for recognition, abnormal behaviors such as hitting, throwing, climbing, and approaching. Literature [14] uses deep learning technology, including CNN and LSTM network, to build a deep network in a multiperspective framework to learn the long-term correlation of human behavior recognition from video. Two cameras are used as sensors to effectively overcome the problems of occlusion and fuzzy contour and improve the accuracy and performance of multiview frame. After a series of image preprocessing on the original data, the human contour image is obtained as the input of the training model. Literature [15] combines spatiotemporal CNN with handmade feature sets for anomaly detection in continuous video frames. Handmade features learn sparse features extracted from moving human image units, including moving pixels to reduce computing costs. The CNN model architecture is used to extract spatiotemporal features and complete the recognition of human abnormal behavior. However, human multipose motion behavior is similar, and there are many actions. This leads to the question of low accuracy and being time-consuming in the application of the above existing methods.

3. Methodology

3.1. Detecting Human Moving Targets. The multipose motion image of human contains background factors such as shadow and illumination. Therefore, it is difficult to obtain human target from the image. The human motion target detection process for segmenting human motion target and image background is as follows.

3.1.1. Establish Gaussian Model. Let X_i be the pixel color of the random point in the human multipose motion image, and the probability density function expression of the pixel color is established as follows:

$$f(X_i = x) = \sum_{i=1}^k \varphi_{i,t} \cdot \alpha(x, \beta_{i,t}, \Sigma_{i,t}), \quad (1)$$

where $\beta_{i,t}$ and $\varphi_{i,t}$ are the mean and weight of Gaussian distribution when the time is t , respectively. $\Sigma_{i,t}$ and $\alpha(\cdot)$ are covariance matrix and Gaussian distribution, respectively. According to equation (1), the utilization number of pixel color X_i probability density function is k . When the time is t , the expression of the i th Gaussian distribution $\alpha(\cdot)$ is as follows:

$$\alpha(x, \beta_{i,t}, \Sigma_{i,t}) = \frac{e^{-(1/2)(x_t - \beta_{i,t})^T \Sigma_{i,t}^{-1} (x_t - \beta_{i,t})}}{(2\pi)^{n/2} |\Sigma_{i,t}|^{1/2}}, \quad (2)$$

where n represents the dimension of pixel color X_i , $i = 1, 2, \dots, k$.

3.1.2. Update Model. Let the random pixel value in the image be I_t . The expression that the Gaussian function matches the pixel value is as follows:

$$|I_t - \beta_{i,t-1}| \leq D \cdot \lambda_{i,t-1}. \quad (3)$$

The expression of each parameter update is as follows:

$$\begin{aligned} \lambda_{i,t}^2 &= (1 - \rho)\lambda_{i,t-1}^2 + \rho(I_t - \beta_{i,t-1})^2, \\ \beta_{i,t} &= (1 - \rho)\beta_{i,t-1} + \rho I_t, \\ \varphi_{i,t} &= (1 - a)\varphi_{i,t-1} + a, \end{aligned} \quad (4)$$

where a and ρ represent adjustable learning rate and parameter learning rate, respectively.

3.1.3. Segmented Image. Normalize all the weights obtained, and sort all Gaussian distributions $\varphi_{i,t}/\lambda_{i,t}$ according to the order from large to small. The first M distributions to be sorted must meet the following conditions:

$$\sum_{k=i_1}^{i_M} \varphi_{i,t} \geq \varsigma. \quad (5)$$

The first M distributions are the background distribution of human multipose motion image, ς is the weight threshold.

Randomly select pixels, which are foreground pixels when they can meet the established Gaussian mixture model [16]. When the pixel cannot meet the established Gaussian mixture model, this pixel is the background pixel [17]. Through the above process, the foreground and background of human multipose motion image are segmented, and the motion targets in human multipose motion image are detected.

3.2. Extracting Contour Feature Points. After segmenting the foreground and background of human multipose motion image, it is necessary to extract the contour feature points in the foreground of human motion image, so as to provide the basis for human multipose motion behavior anomaly recognition based on GAN. Harris corner detection is the most widely used image contour feature extraction method. A corner is the intersection of two edges. However, Harris corner detection needs to calculate the empirical constant k , and the operation process has high complexity. Therefore, the Shi-Tomasi algorithm is proposed. Since the stability of the Harris corner detection algorithm is related to the value of the empirical constant k and the empirical constant k is an empirical value, it is difficult to set the optimal value. Shi-Tomasi found that the stability of corner points is actually related to the smaller eigenvalue of the matrix, so the smaller eigenvalue is directly used as the score, so there is no need to adjust the k value. Therefore, the application of Shi-Tomasi is simpler, and the image contour feature points obtained by Shi-Tomasi are also very accurate.

The Shi-Tomasi algorithm is selected to extract contour feature points in human motion image. (x, y) and $I(x, y)$ are the random point coordinates of the multipose motion

grayscale image of the human and the gray value of the point, respectively. The point (x, y) as the center point is using window S is established. The window size is $n \times n$, window $[x, y]$ is translated, and the gray value changes as follows after translation:

$$L(\Delta x, \Delta y) = \sum_{(x,y) \in S} \phi(x, y) [I(x + \Delta x, y + \Delta y) - I(x, y)]^2. \quad (6)$$

Taylor expansion process $I(x + \Delta x, y + \Delta y)$, delete the terms higher than the second order, and the expression is as follows:

$$L(\Delta x, \Delta y) = \Delta x^2 \sum_{(x,y) \in S} \phi(x, y) I_x^2 + 2\Delta x \Delta y \sum_{(x,y) \in S} I_x I_y + \Delta y^2 \sum_{(x,y) \in S} \phi(x, y) I_y^2, \quad (7)$$

where I_x and I_y are the partial derivatives of human multipose motion images and $\phi(x, y)$ is the Gaussian filter.

Equation (7) can be transformed into the following matrix:

$$L(\Delta x, \Delta y) = [\Delta x, \Delta y] M \begin{bmatrix} \Delta x \\ \Delta y \end{bmatrix}. \quad (8)$$

The expression in equation (8) is as follows:

$$M = \sum_{(x,y) \in S} \phi(x, y) \begin{bmatrix} I_x^2 & I_x I_y \\ I_x I_y & I_y^2 \end{bmatrix}. \quad (9)$$

The Shi-Tomasi algorithm extracts contour feature points from human multipose motion images. The extraction rules are as follows:

- (1) Randomly select the pixel point, let the pixel point be the midpoint, establish a window with size $n \times n$, and move the window in different directions [18]
- (2) Compare the changes of gray value in human multipose motion images. When the window is moved in different directions, when the gray value in the image is fixed, it means that the area is flat [19], and there is no feature point; when moving along a fixed direction and there is only a small change in the gray value, it means that the area is a straight line area
- (3) When the established window moves in a random direction [20], when the gray level in the multipose motion image of the human changes greatly, the center point of the established window is the feature point of the human motion image, and this feature point can be used to realize the anomaly recognition of human multipose motion behavior

3.3. Anomaly Recognition of GAN. The discriminator in the GAN is used for the final recognition of human multipose motion behavior. The discriminator has the function of classification [21] and can judge whether the input sample data

belongs to the generated sample data or real data. GAN is an important GAN algorithm with high linear correlation performance. When the GAN recognizes the multipose movement behavior of human, it can quickly obtain the recognition results [22]. There is no need to interfere with the learning process of the GAN, and accurate recognition results can be obtained only by evaluating the model effect after learning. The structure of GAN is shown in Figure 1.

x and z represent the sample data and random noise of the input GAN, respectively, and A and B represent the generator and discriminator of the GAN, respectively. The expression of the GAN is as follows:

$$\min_A \max_B V(B, A) = E_{x \sim P(x)} [B(x)] + E_{z \sim P(z)} [\lg(1 - B(A(z)))], \quad (10)$$

where $\lg(1 - B(A(z)))$ and $\lg B(x)$ are generated data and discriminator judgment, respectively, and V and E represent objective function and discriminator function, respectively.

The discriminator and the generated data play games with each other by using the maximum and minimum values, and the optimization of parameter B and parameter A is completed through multiple iterations until the discriminator and the generated data are in Nash equilibrium.

The GAN is prone to gradient dispersion in the established minimization objective function. Therefore, the objective function cannot update the generator in the GAN [23], which will reduce the stability of the GAN. LSGAN method is selected to solve the training instability of GAN. LSGANs ensure the classification accuracy of GAN through cross-entropy. The objective function expression of GAN discriminator optimized by LSGANs is as follows:

$$\min_B E_{x \sim P_{data}(x)} [(B(x) - b)^2] + E_{z \sim P_Z(z)} [(B(A(z)) - a)^2]. \quad (11)$$

The objective function expression of GAN generator is as follows:

$$E_{z \sim P_Z(z)} [(B(A(z)) - c)^2]. \quad (12)$$

After completing the antagonistic generation network training, the adjusting parameters a , b , and c need to meet the following conditions:

$$\begin{cases} b - c = 1, \\ b - a = 2. \end{cases} \quad (13)$$

Through the above process, the uncertainty caused by the training process of GAN can be improved [24], the diversity of GAN is effectively improved, and the recognition accuracy of human multipose motion behavior abnormalities is improved.

The GAN is applied to the abnormal recognition of human multipose motion behavior. The process of abnormal recognition is shown in Figure 2.

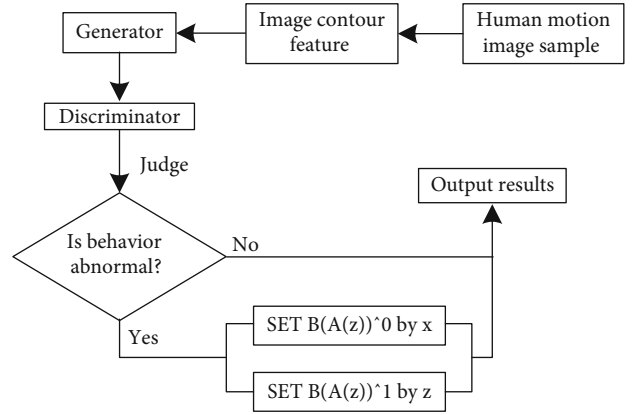


FIGURE 1: Structure of abnormal recognition behavior of GAN.

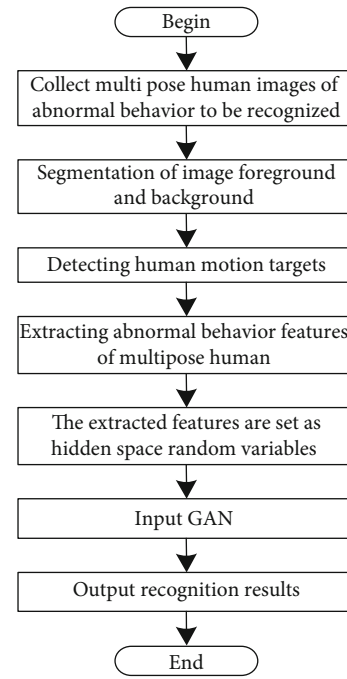


FIGURE 2: Abnormal recognition process of human multipose motion behavior.

According to Figure 2, firstly, the multipose human image with abnormal behavior to be recognized is segmented. After the image segmentation is completed, the detection results of human motion targets are obtained, the contour features of human motion behavior are extracted from the extracted human motion targets, and the extracted features are set as hidden space random variables and input into the GAN. The GAN outputs the abnormal behavior recognition results of multipose human motion behavior to determine whether the multipose human motion behavior is abnormal.

3.4. Data Sets and Evaluating Index. In order to verify the effectiveness of the proposed algorithm in recognizing abnormal human multipose motion behavior by GAN, the Occlusion_person 3D data set and CMU panoptic data set are selected as the test data set. Occlusion_person 3D data

set has 4.8 million 3D human postures and corresponding images, a total of 200 experimenters, and a total of 23 action scenes. CMU panoptic data set is produced by CMU University and collected by 480 VGA cameras, 30+ HD cameras, and 10 kinect sensors. The above two data sets are typical human posture data sets. The two data sets include walking, running, kicking, jumping, standing, squatting, hands up, reverse, head down, head up, and other postures, which are extremely typical. Forty thousand images were randomly selected from the two data sets. In this experiment, twenty thousand images are selected for data training, and the remaining half are used for experimental test and analysis. The number of images of each behavior posture is shown in Table 1. In the simulation platform, the abnormal behavior of the image is recognized.

The accuracy, precision, and recall are selected as the evaluation indexes to evaluate recognition performance of the proposed algorithm. The calculation expressions of three indexes are as follows:

$$\begin{aligned} \text{accuracy} &= \frac{r_p + r_n}{r_p + r_n + h_p + h_n}, \\ \text{precision} &= \frac{r_p}{r_p + h_p}, \\ \text{recall} &= \frac{r_p}{r_p + h_n}, \end{aligned} \quad (14)$$

where r_p and r_n represent the number of abnormal behaviors recognized by the algorithm as abnormal behaviors and nonabnormal behaviors, respectively. h_p and h_n are the numbers of abnormal motion behaviors and nonabnormal behaviors, respectively. The accuracy and precision are used to measure the recognition level of the algorithm and the level that can avoid misrecognition, and the recall rate reflects the level at which the algorithm can correctly classify whether the behavior is abnormal sports behavior.

4. Results and Discussion

The proposed algorithm is used to recognize multipose human motion behavior, and the abnormal behavior recognition results of the proposed algorithm are compared with actual abnormal behavior results, as shown in Table 2.

According to Table 2, for the 10 motion behaviors, the total number of images is between 168 and 667, and the number of abnormal images is between 19 and 63. The proposed method is used to recognize these images, and the results are close to the actual number of abnormal images. The recognition rate of walking, jumping, standing, squatting, and hands up can be 100%. The data shows that the proposed algorithm used to recognize abnormal human multipose motion behavior and the actual abnormal human multipose motion behavior is very small; it shows that the proposed algorithm has high effectiveness in recognizing abnormal human multipose motion behavior.

TABLE 1: Image sample set attributes.

Type	Resolution (dpi)	Space size (kb)
Walking	120	11779
Running	140	7354
Kicking	80	20374
Jumping	70	5216
Standing	100	12538
Squatting	68	4297
Hands up	100	7541
Reverse	50	1569
Head down	80	20685
Head up	67	6328

TABLE 2: Abnormal recognition results.

Motion behavior	Total number of images (piece)	Actual abnormal quantity (piece)	Abnormal recognition quantity (piece)
Walking	351	38	38
Running	254	48	47
Kicking	184	52	51
Jumping	645	34	34
Standing	284	19	19
Squatting	168	27	27
Hands up	294	34	34
Reverse	587	29	28
Head down	667	47	46
Head up	566	63	62

The proposed algorithm randomly divides one of the images and detects the result of human motion targets, as shown in Figure 3.

According to Figure 3, the proposed algorithm can achieve accurate detection of human motion targets in multipose human motion images. The proposed algorithm has a high level of image segmentation. It can accurately extract human motion targets through effective image segmentation ability, which provides the basis for accurate recognition of abnormal motion behavior.

The proposed algorithm is compared with the algorithm in literature [10–14]. The comparison results of the accuracy and recall of the six algorithms for the abnormal recognition of multipose motion behavior in the experimental data set are shown in Figures 4 and 5. The squatting posture is selected for the same posture test.

According to Figures 4 and 5, under different postures, the accuracy of the proposed algorithm is always higher than 99%. For the abnormal behavior recognition of the same posture, the accuracy always fluctuates between 99% and 100%. In contrast, in the process of different posture recognition, the recognition accuracy of literature [10] algorithm, literature [11] algorithm, literature [12] algorithm, literature

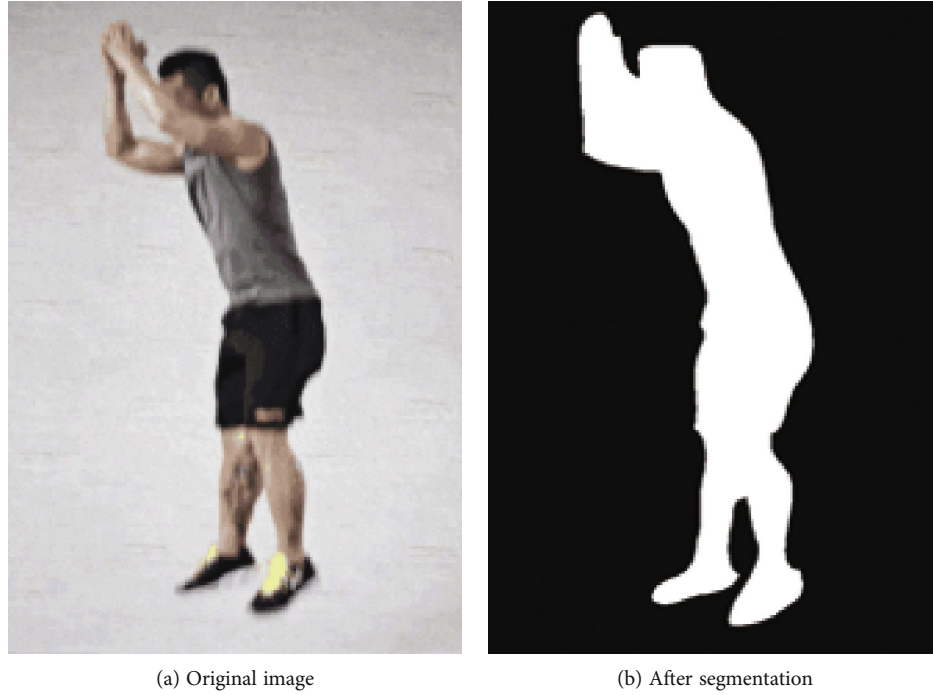


FIGURE 3: Human motion target extraction results.

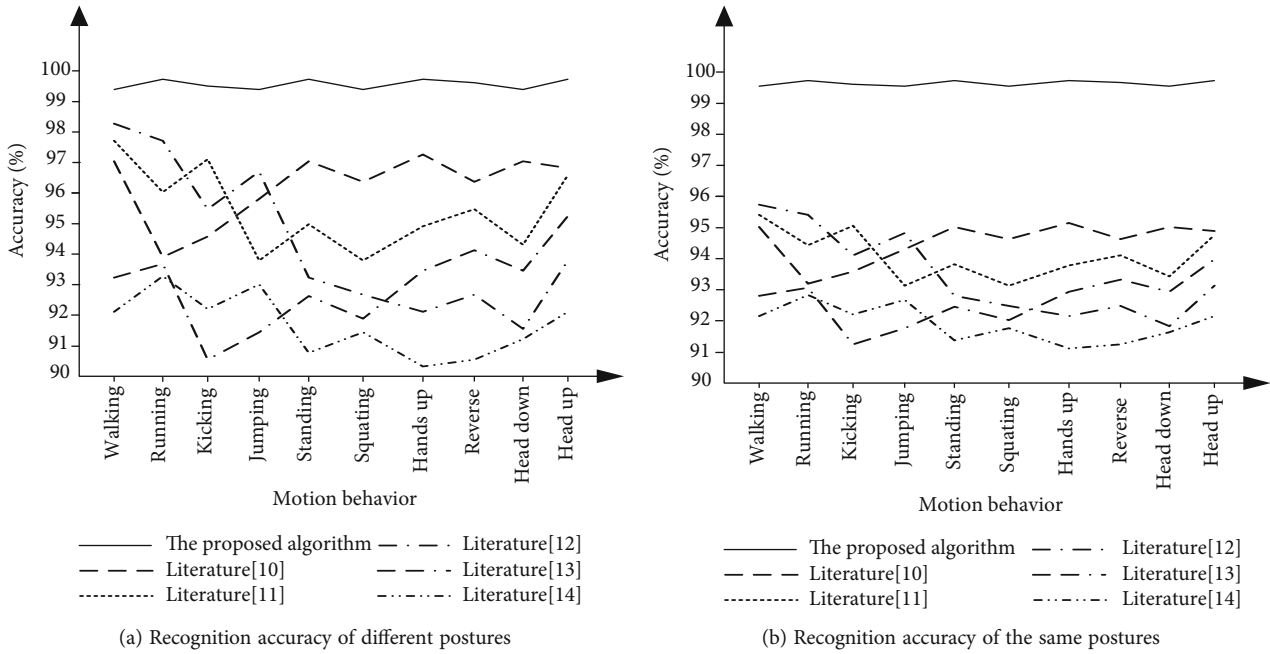


FIGURE 4: Comparison results of recognition accuracy.

[13] algorithm, and literature [14] algorithm fluctuates between 90% and 98.5%, and the recognition accuracy of the same posture is always lower than 96%. The recognition accuracy of the proposed algorithm is significantly higher than that of the other five algorithms. In addition, the recall rate of the proposed algorithm for recognizing multipose and the same posture human motion behavior abnormality

is higher than 99%, and the recall rate of literature algorithm for recognizing multipose human motion behavior abnormality is lower than the proposed algorithm. The comparison results verify that the proposed algorithm has high performance of human motion behavior anomaly recognition. The proposed algorithm effectively segments the multipose human motion behavior image, selects the GAN, and

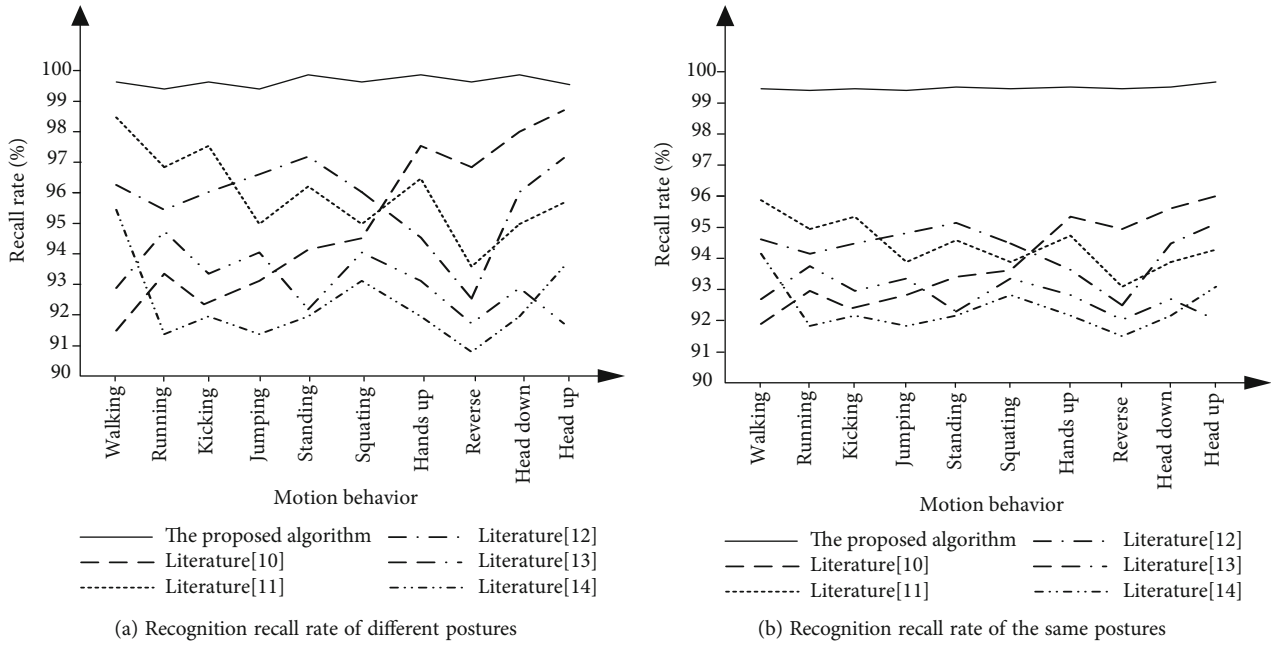


FIGURE 5: Comparison results of recognition recall rate.

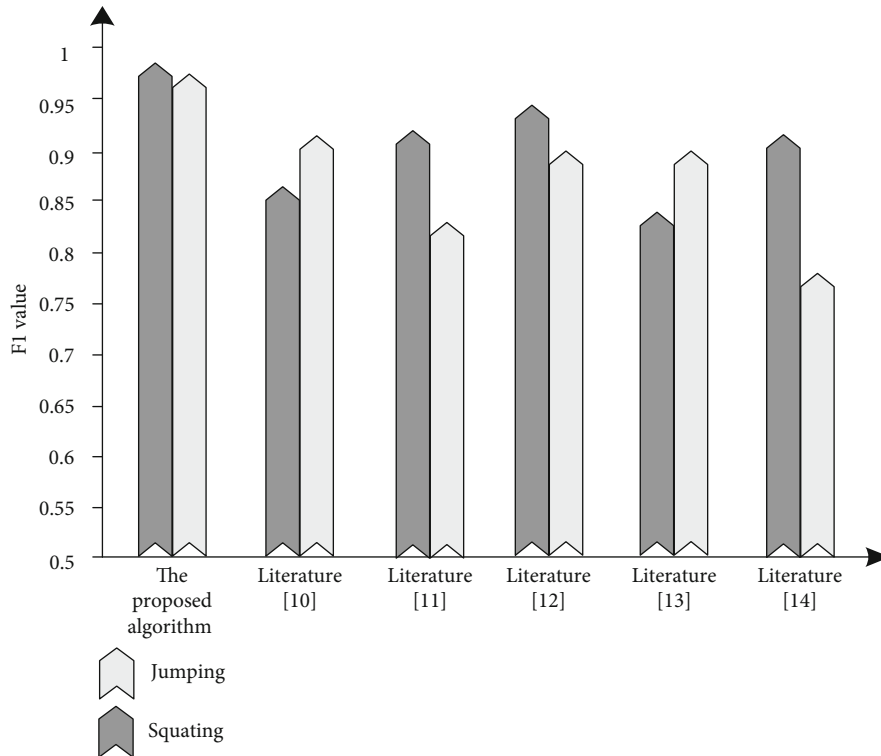


FIGURE 6: Comparison results of $F1$ value.

uses the segmented image to realize the accurate recognition of multipose human motion behavior anomaly.

In order to further measure the recognition performance of this algorithm, $F1$ value is selected as the test index to measure the recognition of abnormal human multipose motion behavior. Six algorithms are used to recognize

the $F1$ value of abnormal human multipose motion behavior in two data sets. The $F1$ value is affected by the accuracy rate and recall rate. The higher the accuracy rate is, the higher the recall rate is, and the better the $F1$ index is. The statistical results of $F1$ value indexes are shown in Figure 6.

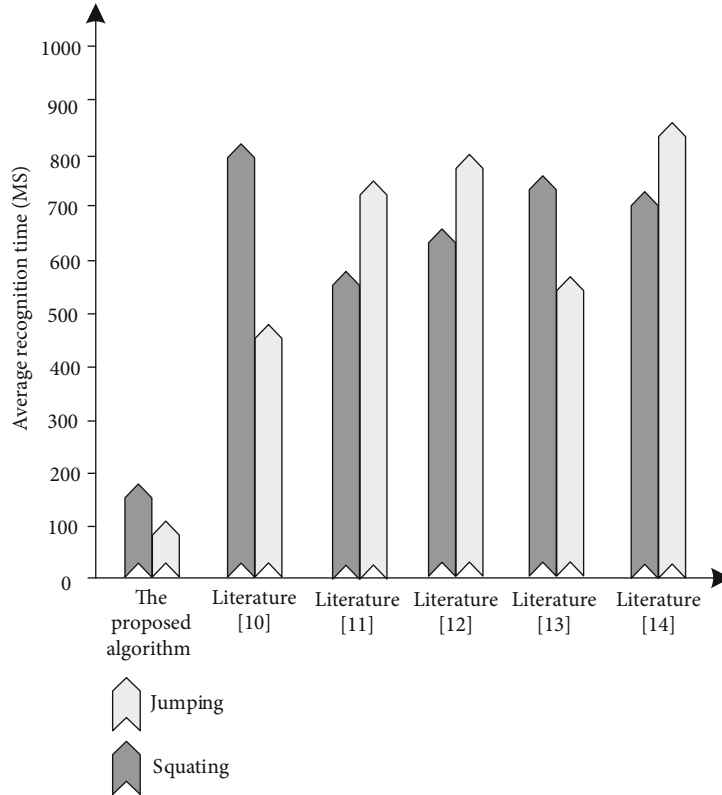


FIGURE 7: Comparison results of recognition time.

As can be seen in Figure 6, the $F1$ value of the proposed algorithm to recognize the abnormal multipose motion behavior of humans is higher than that of the other five algorithms. It is verified again that the proposed algorithm has high recognition performance. This is because this algorithm uses Gaussian model to segment human multipose motion behavior image, and the image foreground of the segmentation result effectively reduces the difficulty of image segmentation, improves the recognition accuracy of human posture behavior, and makes $F1$ value higher.

The real-time performance of the recognition algorithm is very important. Six algorithms are used to recognize the recognition time of abnormal human multipose motion behavior. The statistical results are shown in Figure 7.

As can be seen in Figure 7, the average recognition time of using the proposed algorithm to recognize human multipose motion behavior abnormalities is less than 200 ms, which verifies that the proposed algorithm has high recognition real-time performance. This is because the proposed algorithm selects the Shi-Tomasi algorithm to extract the contour feature points in the human motion image from the human motion target detection results. Based on this, the extracted contour features are set as hidden space random variables and input into the GAN to determine whether the multipose human motion behavior is abnormal. GAN is a very mature technology for enhancing image quality and has application advantages. The proposed algorithm has a wide range of applications, and the real-time performance of the algorithm is very important. The proposed algorithm

has high real-time recognition performance, which can improve the application performance of the algorithm.

5. Conclusions

GAN is applied to human multipose motion behavior anomaly recognition. Firstly, the multipose human motion image is segmented to obtain the human motion target area in the image, and the human motion contour features are extracted from the human motion target area. Based on the GAN, the extracted features are used to realize the abnormal recognition of human multipose motion behavior. Experiments show that the recognition results of human multipose motion behavior abnormalities have high accuracy, and the proposed algorithm has high feasibility. The proposed algorithm can not only realize the abnormal recognition of human multipose motion behavior and ensure the recognition accuracy but also has the advantage of high real-time recognition. The proposed algorithm solves the defect of low recognition performance caused by too few sample data in the past.

However, for specific occasions, the multipose behavior of humans is greatly affected by light, resulting in great difficulty in image acquisition, and the collected image is prone to distortion. In the practical application of human behavior recognition method, the combination of light compensation technology and motion target detection algorithm to enhance the effectiveness of data set still needs further research.

Data Availability

The data used to support the findings of this study are available from the corresponding author upon request.

Conflicts of Interest

The authors declare that there is no conflict of interest with any financial organizations regarding the material reported in this manuscript.

References

- [1] J. S. Park, C. Park, and D. Manocha, "I-Planner: intention-aware motion planning using learning-based human motion prediction," *The International Journal of Robotics Research*, vol. 38, no. 1, pp. 23–39, 2019.
- [2] W. Wang, F. Bu, Z. Lin, and S. Zhai, "Learning methods of convolutional neural network combined with image feature extraction in brain tumor detection," *Access*, vol. 8, pp. 152659–152668, 2020.
- [3] K. Yildiz, "Identification of wool and mohair fibres with texture feature extraction and deep learning," *IET Image Processing*, vol. 14, no. 2, pp. 348–353, 2020.
- [4] S. Qiao, L. Wang, and Z. Gao, "Group behavior recognition based on deep hierarchical network," *Neural Computing and Applications*, vol. 32, no. 10, pp. 5389–5398, 2020.
- [5] N. Wei, "Research on the algorithm of painting image style feature extraction based on intelligent vision," *Future Generation Computer Systems*, vol. 123, no. 24, pp. 196–200, 2021.
- [6] M. Tan, J. Zhou, Z. Peng, Y. Jun, and F. Tang, "Fine-grained image classification with factorized deep user click feature," *Information Processing and Management*, vol. 57, no. 3, 2020.
- [7] A. Safonova, E. Guirado, Y. Maglinets, D. Alcaraz-Segura, and S. Tabik, "Olive tree biovolume from UAV multi-resolution image segmentation with Mask R-CNN," *Sensors*, vol. 21, no. 5, p. 1617, 2021.
- [8] S. Prasath, R. Pelapur, G. Seetharaman et al., "Multiscale structure tensor for improved feature extraction and image regularization," *IEEE Transactions on Image Processing*, vol. 28, no. 12, pp. 6198–6210, 2019.
- [9] Y. Zhou and Z. Gao, "Intelligent recognition of medical motion image combining convolutional neural network with Internet of things," *IEEE Access*, vol. 7, pp. 145462–145476, 2019.
- [10] H. V. A. Chenarlog and F. Razzazi, "Multi-stream 3D CNN structure for human action recognition trained by limited data," *IET Computer Vision*, vol. 13, no. 3, pp. 338–344, 2019.
- [11] C. Dhiman and D. K. Vishwakarma, "View-invariant deep architecture for human action recognition using two-stream motion and shape temporal dynamics," *IEEE Transactions on Image Processing*, vol. 29, pp. 3835–3844, 2020.
- [12] S. Maity, A. Chakrabarti, and D. Bhattacharjee, "Robust human action recognition using AREI features and trajectory analysis from silhouette image sequence," *IETE Journal of Research*, vol. 65, no. 2, pp. 236–249, 2019.
- [13] S. Xie, X. Zhang, and J. Cai, "Video crowd detection and abnormal behavior model detection based on machine learning method," *Neural Computing and Applications*, vol. 31, no. S1, pp. 175–184, 2019.
- [14] Y. L. Hsueh, W. N. Lie, and G. Y. Guo, "Human behavior recognition from multiview videos," *Information Sciences*, vol. 517, pp. 275–296, 2020.
- [15] B. Sabzalian, H. Marvi, and A. Ahmadyfard, "Deep and sparse features for anomaly detection and localization in video," in *2019 4th International Conference on Pattern Recognition and Image Analysis (IPRIA)*, pp. 173–178, Tehran, Iran, 2019.
- [16] A. Soualmi, A. Alti, and L. Laouamer, "A novel blind medical image watermarking scheme based on Schur triangulation and chaotic sequence," *Concurrency and Computation: Practice and Experience*, vol. 34, no. 1, 2022.
- [17] E. Cuevas, H. Becerra, A. Luque, and M. A. Elaziz, "Fast multi-feature image segmentation," *Applied Mathematical Modelling*, vol. 90, no. 5, pp. 742–757, 2021.
- [18] T. Santos, S. Schrunner, B. C. Geiger et al., "Feature extraction from analog wafermaps: a comparison of classical image processing and a deep generative model," *IEEE Transactions on Semiconductor Manufacturing*, vol. 32, no. 2, pp. 190–198, 2019.
- [19] P. Zhang, H. He, and L. Gao, "A nonlinear and explicit framework of supervised manifold-feature extraction for hyperspectral image classification," *Neurocomputing*, vol. 337, pp. 315–324, 2019.
- [20] Z. Xia, J. Xing, C. Wang, and X. Li, "Gesture recognition algorithm of human motion target based on deep neural network," *Mobile Information Systems*, vol. 2021, Article ID 2621691, 12 pages, 2021.
- [21] N. Martins, "Adversarial machine learning applied to intrusion and malware scenarios: a systematic review," *Access*, vol. 8, pp. 35403–35419, 2020.
- [22] P. Dasgupta and J. B. Collins, "A survey of game theoretic approaches for adversarial machine learning in cybersecurity tasks," *AI Magazine*, vol. 40, no. 2, pp. 31–43, 2019.
- [23] S. G. Finlayson, J. D. Bowers, J. Ito, J. L. Zittrain, A. L. Beam, and I. S. Kohane, "Adversarial attacks on medical machine learning," *Science*, vol. 363, no. 6433, pp. 1287–1289, 2019.
- [24] D. Roy, T. Mukherjee, and M. Chatterjee, "Machine learning in adversarial RF environments," *IEEE Communications Magazine*, vol. 57, no. 5, pp. 82–87, 2019.

Research Article

Security-Aware Routing Protocol Based on Artificial Neural Network Algorithm and 6LoWPAN in the Internet of Things

Jiangdong Lu , Dongfang Li , Penglong Wang , Fen Zheng , and Meng Wang 

Department of Computer and Simulation Technology, Naval Medical University, Shanghai 200433, China

Correspondence should be addressed to Fen Zheng; c12169@yahoo.com

Received 22 November 2021; Revised 13 December 2021; Accepted 16 December 2021; Published 12 January 2022

Academic Editor: Nima Jafari Navimipour

Copyright © 2022 Jiangdong Lu et al. This is an open access article distributed under the Creative Commons Attribution License, which permits unrestricted use, distribution, and reproduction in any medium, provided the original work is properly cited.

Today, with increasing information technology such as the Internet of Things (IoT) in human life, interconnection and routing protocols need to find optimal solution for safe data transformation with various smart devices. Therefore, it is necessary to provide an enhanced solution to address routing issues with respect to new interconnection methodologies such as the 6LoWPAN protocol. The artificial neural network (ANN) is based on the structure of intelligent systems as a branch of machine interference, has shown magnificent results in previous studies to optimize security-aware routing protocols. In addition, IoT devices generate large amounts of data with variety and accuracy. Therefore, higher performance and better data handling can be achieved when this technology incorporates data for sending and receiving nodes in the environment. Therefore, this study presents a security-aware routing mechanism for IoT technologies. In addition, a comparative analysis of the relationship between previous approaches discusses with quality of service (QoS) factors such as throughput and accuracy for improving routing mechanism. Experimental results show that the use of time-division multiple access (TDMA) method to schedule the sending and receiving of data and the use of the 6LoWPAN protocol when routing the sending and receiving of data can carry out attacks with high accuracy.

1. Introduction

The world of information technology and computers is expanding daily. This development has led to the creation of new systems with a specific type of communication [1, 2]. One of these connections is machine to machine. This type of communication is a solution to move, from single-purpose devices that data in the form of commands obtained from an application in the network to the Internet of Things (IoT) that allows the device to be multipurpose and applications to collaborate. Machine-to-machine communication with network structures can benefit from global standardization efforts [3–5]. Admittedly, the network-to-machine communication facilitation network has changed dramatically and its capabilities have greatly expanded, but machine-to-machine architectural solutions have remained relatively stable [6].

One of the most important parts of the Internet is bandwidth, which needs to be used to access objects connected to the Internet easily and quickly [7, 8]. When a packet is sent

by a sender, some quality of service (QoS) factors such as response time, throughput, security, energy consumption, latency, and accuracy will be evaluated to show efficiency of the optimized routing protocol. Of course, considering the position and distance of objects is also very important. Today, by increasing intelligent attacks and anomaly behaviors, routing protocols should be aware on security and privacy conditions by using intrusion detection mechanisms. To improve security and throughput, it is necessary to have precise timing in the routing to avoid congestion. For this purpose, in the proposed method of this research, the TDMA protocol is used [9, 10], which can schedule. In this protocol, in the decision management section, the route operations are performed well and with high speed. After that, the bandwidth must be improved to ensure the security of the IoT environment. For this purpose, a protocol called 6LoWPAN will be used, which can improve bandwidth along with ensuring security [11]. But because its execution speed is slow and can affect security and even bandwidth access, it creates an optimization domain that is considered

a search environment [12]. Therefore, the artificial neural network (ANN) algorithm will be used chaotically to optimize bandwidth and increase security in intrusion detection method and solve connection problems between objects in the IoT environment, which will be promoted as a new idea in this research. One of the attacks that can be imagined in this research, and its main purpose is to identify it, is a flood attack on the IoT [13].

The main contribution of this study is organized as follows:

- (i) Proposing a scheduling protocol TDMA in the routing process with the lowest energy consumption
- (ii) Using the 6LoWPAN protocol and optimizing it to increase bandwidth and improve packet lost ratio in the IoT environment
- (iii) Applying ANN-based machine learning method to enhance the data transmission routing
- (iv) Evaluating performance of the proposed method and it is compared with recent developed methods

The rest of this paper is organized as follows: Section 2 present a literature review on recent routing mechanisms in IoT environments. Section 3 proposed a security-aware routing protocol with respect to an enhanced ANN method. Section 4 shows experimental results based on simulation results. Finally, Section 5 shows conclusion and future work.

2. Related Works

This section illustrates a brief literature review on recent routing mechanisms using metaheuristic algorithms. For example, authors in [14] offered a blockchain-SDN-based assigned design for intelligent cities with network function virtualization. Furthermore, the authors introduced an energy-optimized group leader determination algorithm that introduces to choose a group leader in an effective method. Besides, the SDN controller controls and supervises the actions of the IoT devices. In this paper, blockchain is applied to identify and overcome the cyberattacks in the IoT systems. The test outcome revealed that the proposed design works better rather than the current structure in terms of throughput, time, gas consumption, and communication overhead.

Authors in [15] reviewed energy control progresses in IoT based on an SLR style. 30 research studies were determined as the principal field of technical study. For analyzing existing issues on the energy control resolutions in IoT, a taxonomy was introduced to explain the technical features of each section of energy control. It is mentioned that a class of published research articles with 7 studies in the intelligent home have the largest percentage. Furthermore, energy control on intelligent collection, intelligent cities, and the intelligent building has been studied with 15 papers individually. Finally, smart grid and industry circumstances have 8 research studies in IoT networks.

Authors in [16] suggested a unique method for RPL protocol trying to develop the IoT network lifetime. The

suggested method combined the consumed and recharged energy to choose the most suitable route to send data information. Simulation results showed that the proposed method efficiently reduced the energy loss and the network lifetime by choosing the best routes via the sink.

Authors in [17] introduced an innovative routing protocol that is suitable for mobile ad hoc networks, in particular, to be aware of node movement and link resistance. To this goal, a different movement discovery design was offered to provide any node to set a new metric based on the renewed movement factor. Therefore, each node in the networks can change its routing function based on the network requirements around it; consequently, the applied routing protocol can improve the packet delivery ratio compared to existing routing methods.

Authors in [18] proposed a framework based on machine learning techniques and artificial neural networks for identifying the RPL attacks in some case studies. The efficiency of the proposed framework is improved to the highest potential amount. The implementation outcomes revealed that the malicious node for the attack provides the highest amount of packets between all the nodes in the network. Consequently, it increases the energy usage of neighbors.

Authors in [19] suggested a method for determining congestion problems in IoT networks by offering the use of fuzzy logic. The difficulty of parent choice is formed and then solved applying the fuzzy weighted sum procedure. The suggested algorithm is dynamic and recognized the congestion and then chose the noncongested path by choosing the most suitable path in the network topology. The achieved outcomes from the Cooja simulator proved that the proposed algorithm has decreased delay and improved performance and more efficient use of network resources.

Authors in [20] presented a new method based on priority and energy usage to manage routing procedures within contents for low-power and lossy networks. All network slots apply timing models when transferring data to the target while analyzing network transfer, audio, and image information. This technique improved the robustness of the routing protocol and was eventually avoided from occurring congestion, too. Test results confirmed that the proposed method decreased overhead on the mesh, delay, and energy waste.

Authors in other recent works [21, 22] have applied heuristic algorithms to solve routing problem in IoT environments. Some of them check packet duration time and energy efficiency as well.

3. Proposed Security-Aware Routing Method

This section illustrates a new security-aware routing mechanism based on ANN prediction approach in IoT. One of the most important problems in establishing the IoT [23] with an energy-aware recognition approach is that nodes have no information about each other's performance [24]. The only information they receive from a primary source is authentic packets that are all broadcasted by the device or object itself and are not trusted under internal attacks. For this purpose, the packet find index (PFI) is expressed as [25]

$$PFI_{IJ} = \frac{1}{P_f^{ij}}. \quad (1)$$

The value P_f^{ij} is obtained from [26]

$$P_f^{ij} = \frac{N_s^{ij}}{N_t^{ij}}. \quad (2)$$

The PFI factor is calculated in the TDMA method with respect to applying the QoS factors. According to Equation (2), N_s^{ij} is the number of packets properly routed by node next step j in the IoT environment and N_t^{ij} is the total number of packets routed from node i to the next step j in the IoT environment. Using this relation, each node can obtain the packet find index for its next step nodes and calculates the packet find index of the path according to [27]

$$PFI_{\text{path}} = (10 \times PFI_{i,j+1}) + \log(10 \times PFI_{i+1,i+2}) + \log(10 \times PFI_{i+2,i+3}). \quad (3)$$

After calculating the packet find index, each node calculates the path find index and then selects the path that has the best index to guide the data packets from the paths provided by the next step nodes. In this way, it removes malicious nodes from the closed path [28].

Figure 1 illustrates a brief procedure of the ANN strategy for a routing protocol using TDMA with respect to supporting QoS factors. In first step, each nominated IoT node should be checked as a cluster node. If the respected IoT node is cluster node, then the ANN method is applied to train and test procedure. The ANN method sets initial parameters for training layers and divides the dataset into two, train and test datasets. For each classification procedure, the TDMA factors are applied to check with classification method. Finally, the existing TDMA schedule is applied to the train test case [29]. On the other hand, if the IoT node is not a cluster node, system updates cluster list and the ANN method is applied to continue train procedure. For finalizing the proposed algorithm, each train set should archived convergence factor. If the algorithm has a convergence value, then the classification procedure will be finished. Otherwise, the system sends a message to check cluster node selection.

To calculate the PFI [30], after calculating the PFI of each parent [31], each node adds it to the value received from the parent and distributes it to all other nodes to determine the closed conduction index of each path. Node S then selects the path with the least possible value from the provided paths, and in this way, the malicious node G , which is a gray holes node that bypasses 50% of the packets, causing routing loss and loss. Energy will be removed from the data transmission path. It is important to note that these values are moved by the control packets, and all nodes are aware of them [32]. The goal of the PFI is to obtain routes with higher delivery rates so that malicious nodes can be removed from the packet routing path to provide the correct

routing in the IoT environment. PFI is expressed as the number of transfers required to reach a destination pack. This index can be used as a metric (unit of measurement) in the initial deployment of the Internet of Things and to identify paths that have malicious black holes or gray holes nodes [33]. But this metric also has its limitations and problems. This index is introduced on the path, and the nodes should calculate the value of the path packet guidance index after calculating their parent packet guidance index and inform these nodes about these values, which is done with the help of control packets. For this purpose, to compare the metric of the closed conduction index with the expected number of transfers, with the help of simulation in MATLAB environment, these two metrics have been implemented on the processing environment. Because the IoT does not have proper routing and delivery operations and its problems were mentioned in previous sections, especially in the issue of security in intrusion detection method, this secure establishment of the IoT due to the presence of appendages such as black holes and gray holes and in general security issues remain almost unresolved. Bandwidth and security are also important during deployment in the intrusion detection method [34].

It is assumed that the target monitoring area in the IoT called A is a two-dimensional environment, and n moving nodes are randomly placed in the environment as $S = (S_1, S_2 \dots)$. The i th position of the node is determined as a set $si = (xi, yi)$ ($i = 1, 2 \dots n$), and the Euclidean distance between the i th node and the point $p = (x, y)$ is determined according to [35]

$$d_{ip} = \sqrt{(x - x_i)^2 + (y - y_i)^2}. \quad (4)$$

The node detection model is divided into two methods of binary-based detection and probabilistic detection. This research is based on the binary mode, which is simpler to use and less computationally complex. The reason for using binary node detection, in addition to simplicity in application and less computational complexity, is the simplicity of its modeling, and also each time execution will not be a possible answer and the answer is guaranteed. Node detection is used probabilistically in other networks such as automotive wireless networks and underwater wireless sensor networks. The node detection model is calculated binary-based as [36]

$$p = (\text{if } d_{ip} \leq r_0 \cdot k = 1 \text{ else } k = 0). \quad (5)$$

In this research, several evaluation methods have been used which include throughput and the accuracy criteria. At the beginning, each study is completed, and finally, the results obtained from the research performed by each evaluation method are mentioned.

The secure deployment of the IoT was completely modeled on security issues in this section with a security-aware routing mechanism. Based on this mechanism, data

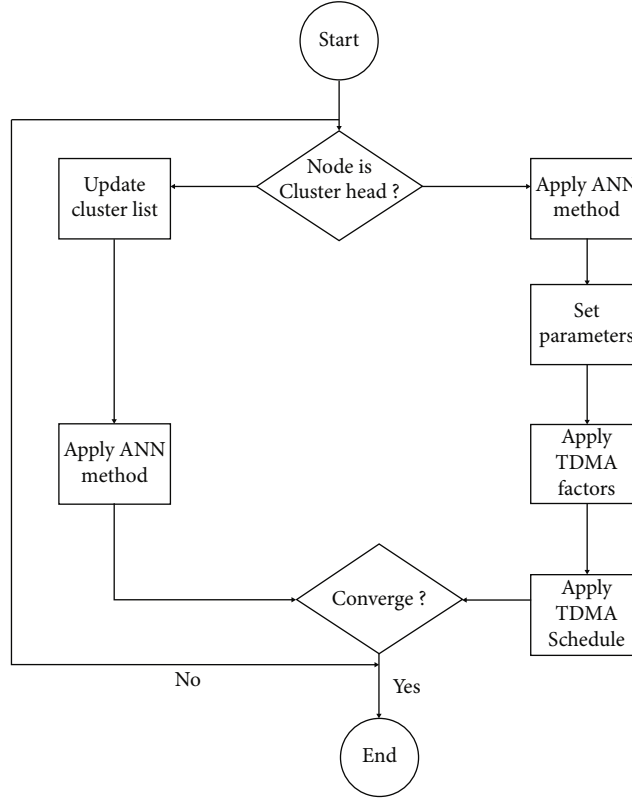


FIGURE 1: Procedure of the TDMA method using the ANN algorithm.

TABLE 1: Initial parameters of each tests case to detect attacks.

Test case	Number of IoT nodes	Number of features	Number of repetitions
Case 1	5, 10, 20	30	5000
Case 2	20, 30, 50	50	10000
Case 3	50, 80, 100	80	15000

transmission through the network, data confidentiality, accuracy, information integrity, accessibility, and attack detection were considered and a new and optimal model with knowledge of security issues was considered. In the next section, a simulation of the proposed approach will be performed and the results will be discussed [37].

4. Experimental Results and Discussion

In the previous section, new modeling was done to provide a way to ensure security of the intrusion detection method the IoT. Of course, any idea will need a simulation. In this section, the experimental results are performed in the MATLAB environment and fully mentioned and analyzed the results based on the intrusion detection method. A test case comparison is made between the available methods to ensure that the proposed approach is effective.

In this study, which is based on attacks that are supposed to improve the level of security to be able to measure the

QoS, attacks on deprivation of services have been used. Hence, the DoS2017 dataset is used <https://www.unb.ca/cic/datasets/dos-dataset.html>, and the TDMA protocol should first be considered during routing after nodes are placed in the environment to schedule and reduce energy with the 6LoWPAN protocol [38]. In the following, the proposed approach detects attacks of deprivation of services in the context of the Internet of Things, and finally, the criteria of service quality and energy consumption are examined. Based on the analysis of the proposed approach in sending and receiving data and the proposed mechanism, it is important to examine the degree of accuracy criteria that detect attacks for security. The number of repetitions of the program is 5000, 10000, and 15000 rounds. Also, the number of features in each round is 30, 50, and 80 repetition and the number of IoT devices are including 20, 50, and 100. The storage of sent and received data in the IoT environment is placed in an intelligent and impenetrable database called a transmission rate. The initial parameters of each test case of security analysis results are presented in Table 1.

After examining all case studies with respect to detecting attacks, QoS factors are reviewed. Figures 2–4 show the throughput after applying the proposed mechanism for case study 1, 2, and 3 to the IoT environment.

The throughput is achieved according to the transmitted packets. The throughput obtained by proposed method is compared with existing algorithms, and the comparison

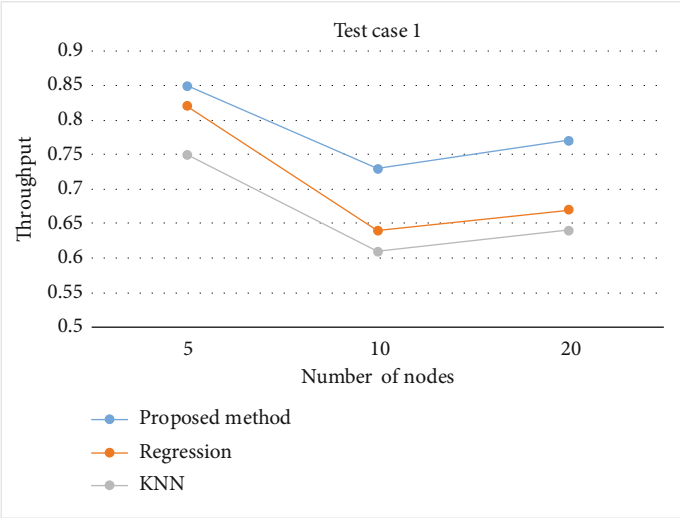


FIGURE 2: Throughput evaluation for existing algorithms in case study 1.

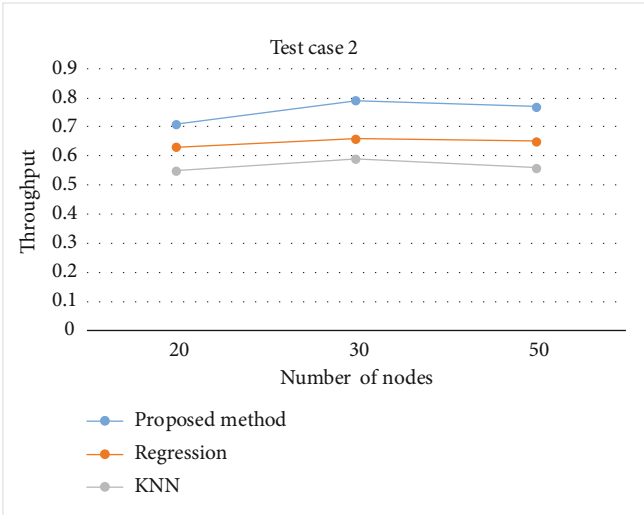


FIGURE 3: Throughput evaluation for existing algorithms in case study 2.

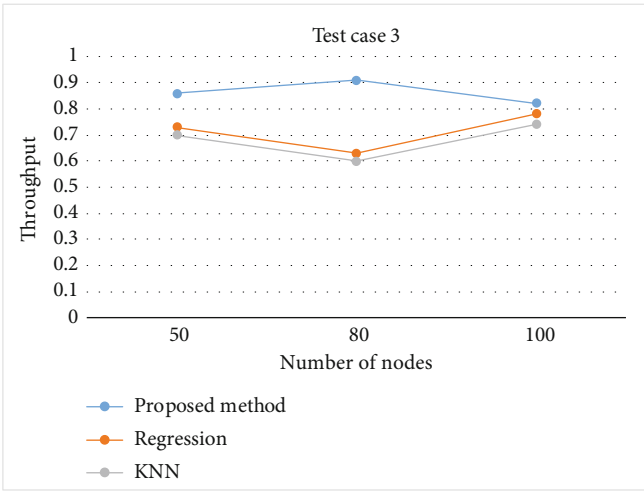


FIGURE 4: Throughput evaluation for existing algorithms in case study 3.

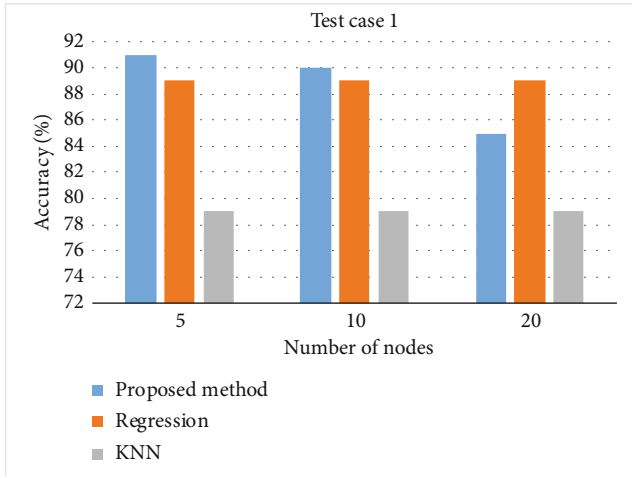


FIGURE 5: Accuracy evaluation factor for existing algorithms in case study 1.

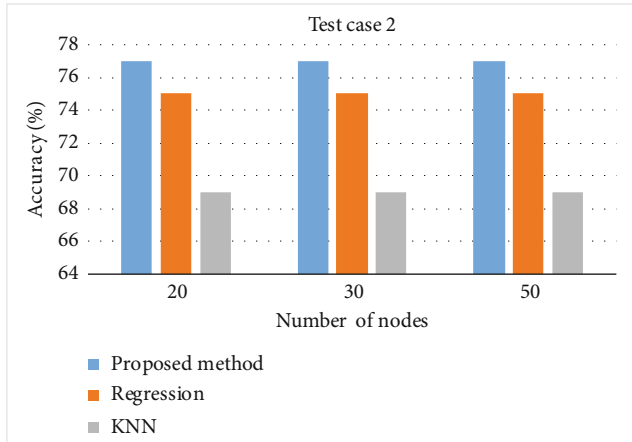


FIGURE 6: Accuracy evaluation factor for existing algorithms in case study 2.

results regression and KNN algorithms [39, 40]. The throughput of proposed method is found better than the other existing algorithms. Recently developed regression also obtained almost similar performance; however, it fails to attain an effective result on accuracy due to this and the throughput also gets reduced. It is observable that the ANN method with respect to the TDMA factors has optimized throughput value than other regression and the KNN algorithms in test cases 1, 2, and 3.

In the following, we examine the data accuracy in each case study. If the environment is secure, the data is encrypted in the transmitter and data can predicted with the proposed ANN approach with high accuracy. Figures 5–7 show the accuracy diagram of the proposed method in blue line with number of IoT devices in which it has higher accuracy than the previous two methods in case study 1, 2, and 3, respectively. Totally, we conclude that the proposed method has maximum accuracy factor for each

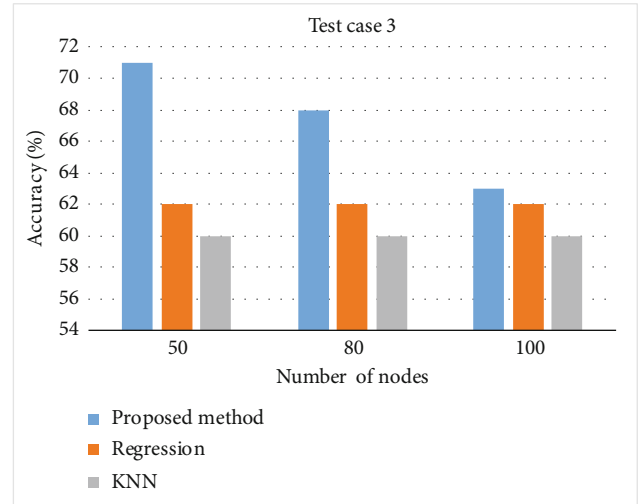


FIGURE 7: Accuracy evaluation factor for existing algorithms in case study 3.

test cases 1, 2, and 3 to compare other regression and KNN algorithms.

The proposed method has achieved better accuracy which is found higher than the other existing algorithms with respect to number of IoT nodes and number of features.

5. Conclusion

In order to solve the problem of security-aware routing protocol in IoT environments, the ANN algorithm and TDMA protocol are given by studying the connectivity of network topologies. The method proposes an efficient routing protocol based on the 6LoWPAN strategy. First, we analyze the relationship between nodes and explain the scheduling packets and through modularization. Experimental results showed that the proposed method is compared with regression and KNN algorithms for simulation environments. The results show that the proposed method can effectively improve the accuracy ratio and enhance throughput factor. The research on the relevant theories and technologies of IoT has important value for the routing algorithms in the future 5G era as future work. Also, some evaluation metrics such as mean square error (MSE), time complexity, and packet loss with large amount of IoT nodes can be evaluated and analyzed in future research directions.

Data Availability

The CIC DoS dataset (2017) used to support the findings of this study are included at the following web page: <https://www.unb.ca/cic/datasets/dos-dataset.html>.

Conflicts of Interest

The authors declare that they have no conflicts of interest.

References

- [1] R. Liu, X. Wang, H. Lu et al., "SCCGAN: style and characters inpainting based on CGAN," *Mobile Networks and Applications*, vol. 26, no. 1, pp. 3–12, 2021.
- [2] M. Zhang, Y. Chen, and W. Susilo, "PPO-CPQ: a privacy-preserving optimization of clinical pathway query for e-healthcare systems," *IEEE Internet of Things Journal*, vol. 7, no. 10, pp. 10660–10672, 2020.
- [3] J. Chen, Y. Liu, Y. Xiang, and K. Sood, "RPPTD: robust privacy-preserving truth discovery scheme," *IEEE Systems Journal*, pp. 1–8, 2021.
- [4] J. Yan, Y. Meng, X. Yang, X. Luo, and X. Guan, "Privacy-preserving localization for underwater sensor networks via deep reinforcement learning," *IEEE Transactions on Information Forensics and Security*, vol. 16, pp. 1880–1895, 2021.
- [5] T. Ni, D. Liu, Q. Xu, Z. Huang, H. Liang, and A. Yan, "Architecture of cobweb-based redundant TSV for clustered faults," *IEEE Transactions on Very Large Scale Integration (VLSI) Systems*, vol. 28, no. 7, pp. 1736–1739, 2020.
- [6] Z. Lv, D. Chen, R. Lou, and H. Song, "Industrial security solution for virtual reality," *IEEE Internet of Things Journal*, vol. 8, no. 8, pp. 6273–6281, 2021.
- [7] Y. Jiang and X. Li, "Broadband cancellation method in an adaptive co-site interference cancellation system," *International Journal of Electronics*, pp. 1–21, 2021.
- [8] H. Kong, L. Lu, J. Yu, Y. Chen, and F. Tang, "Continuous authentication through finger gesture interaction for smart homes using WiFi," *IEEE Transactions on Mobile Computing*, 2021.
- [9] Z. Lv, L. Qiao, and I. You, "6G-enabled network in box for internet of connected vehicles," *IEEE Transactions on Intelligent Transportation Systems*, 2021.
- [10] A. Seyfollahi and A. Ghaffari, "A review of intrusion detection systems in RPL routing protocol based on machine learning for internet of things applications," *Wireless Communications and Mobile Computing*, vol. 2021, Article ID 8414503, 32 pages, 2021.
- [11] M. Etemadi, M. Ghobaei-Arani, and A. Shahidinejad, "Resource provisioning for IoT services in the fog computing environment: an autonomic approach," *Computer Communications*, vol. 161, pp. 109–131, 2020.
- [12] Z. Lv, D. Chen, and Q. Wang, "Diversified technologies in internet of vehicles under intelligent edge computing," *IEEE Transactions on Intelligent Transportation Systems*, vol. 22, no. 4, pp. 2048–2059, 2021.
- [13] H. Cheng, M. Shojafar, M. Alazab, R. Tafazolli, and Y. Liu, "PPVF: privacy-preserving protocol for vehicle feedback in cloud-assisted VANET," *IEEE Transactions on Intelligent Transportation Systems*, pp. 1–13, 2021.
- [14] M. J. Islam, A. Rahman, S. Kabir et al., "Blockchain-SDN based energy-aware and distributed secure architecture for IoTs in smart cities," *IEEE Internet of Things Journal*, 2021.
- [15] D. Wang, D. Zhong, and A. Souri, "Energy management solutions in the Internet of Things applications: technical analysis and new research directions," *Cognitive Systems Research*, vol. 67, pp. 33–49, 2021.
- [16] F. Chiti, R. Fantacci, and L. Pierucci, "A green routing protocol with wireless power transfer for internet of things," *Journal of Sensor and Actuator Networks*, vol. 10, no. 1, p. 6, 2021.
- [17] A. Serhani, N. Naja, and A. Jamali, "AQ-routing: mobility-, stability-aware adaptive routing protocol for data routing in MANET-IoT systems," *Cluster Computing*, vol. 23, no. 1, pp. 13–27, 2020.
- [18] S. Sharma and V. K. Verma, "AIEMLA: artificial intelligence enabled machine learning approach for routing attacks on internet of things," *The Journal of Supercomputing*, vol. 77, no. 12, pp. 13757–13787, 2021.
- [19] J. Shreyas, H. Singh, S. Tiwari, N. N. Srinidhi, and S. M. Dilip Kumar, "CAFOR: congestion avoidance using fuzzy logic to find an optimal routing path in 6LoWPAN networks," *Journal of Reliable Intelligent Environments*, vol. 7, no. 4, pp. 325–340, 2021.
- [20] F. Safara, A. Souri, T. Baker, I. al Ridhawi, and M. Aloqaily, "PriNergy: a priority-based energy-efficient routing method for IoT systems," *The Journal of Supercomputing*, vol. 76, no. 11, pp. 8609–8626, 2020.
- [21] R. Yarinezhad and S. Azizi, "An energy-efficient routing protocol for the Internet of Things networks based on geographical location and link quality," *Computer Networks*, vol. 193, article 108116, 2021.
- [22] R. Sahay, G. Geethakumari, and B. Mitra, "A novel network partitioning attack against routing protocol in internet of things," *Ad Hoc Networks*, vol. 121, article 102583, 2021.
- [23] Z. Lv, R. Lou, and A. K. Singh, "AI empowered communication systems for intelligent transportation systems," *IEEE Transactions on Intelligent Transportation Systems*, vol. 22, no. 7, pp. 4579–4587, 2021.
- [24] H. Yi, "Secure social internet of things based on post-quantum blockchain," *IEEE transactions on Network Science and Engineering*, 2021.
- [25] J. Dong, Y. Cong, G. Sun, Z. Fang, and Z. Ding, "Where and how to transfer: knowledge aggregation-induced transferability perception for unsupervised domain adaptation," *IEEE Transactions on Pattern Analysis and Machine Intelligence*, 2021.
- [26] H. Chen, Y. Miao, Y. Chen, L. Fang, L. Zeng, and J. Shi, "Intelligent model-based integrity assessment of nonstationary mechanical system," *Engineering*, 2021.
- [27] F. Liu, G. Zhang, and J. Lu, "Multisource heterogeneous unsupervised domain adaptation via fuzzy relation neural networks," *IEEE Transactions on Fuzzy Systems*, vol. 29, no. 11, pp. 3308–3322, 2021.
- [28] Z. Lv, Z. Wu, X. Wang, and M. Zhou, "3D facial similarity measurement and its application in facial organization," *ACM Transactions on Multimedia Computing, Communications, and Applications*, vol. 16, no. 3, pp. 1–20, 2020.
- [29] M. K. Khan, M. Shiraz, K. Zrar Ghafoor, S. Khan, A. Safaa Sadiq, and G. Ahmed, "EE-MRP: energy-efficient multistage routing protocol for wireless sensor networks," *Wireless Communications and Mobile Computing*, vol. 2018, Article ID 6839671, 13 pages, 2018.
- [30] C. Qin, Y. Jin, J. Tao et al., "DTCNNMI: a deep twin convolutional neural networks with multi-domain inputs for strongly noisy diesel engine misfire detection," *Measurement*, vol. 180, article 109548, 2021.
- [31] Z. Lv, L. Qiao, M. S. Hossain, and B. J. Choi, "Analysis of using blockchain to protect the privacy of drone big data," *IEEE Network*, vol. 35, no. 1, pp. 44–49, 2021.
- [32] H. Che and J. Wang, "A two-timescale duplex neurodynamic approach to mixed-integer optimization," *IEEE Transactions*

- on *Neural Networks and Learning Systems*, vol. 32, no. 1, pp. 36–48, 2021.
- [33] W. Zhou, L. Yu, Y. Zhou, W. Qiu, M. W. Wu, and T. Luo, “Local and global feature learning for blind quality evaluation of screen content and natural scene images,” *IEEE Transactions on Image Processing*, vol. 27, no. 5, pp. 2086–2095, 2018.
- [34] M. Ghobaei-Arani, “A workload clustering based resource provisioning mechanism using biogeography based optimization technique in the cloud based systems,” *Soft Computing*, vol. 25, no. 5, pp. 3813–3830, 2021.
- [35] W. Zhou, J. Liu, J. Lei, L. Yu, and J. N. Hwang, “GMNet: graded-feature multilabel-learning network for RGB-thermal urban scene semantic segmentation,” *IEEE Transactions on Image Processing*, vol. 30, pp. 7790–7802, 2021.
- [36] S. Lv and F. Song, “Particle swarm intelligence and the evolution of cooperation in the spatial public goods game with punishment,” *Applied Mathematics and Computation*, vol. 412, article 126586, 2022.
- [37] T. Sui, D. Marelli, X. Sun, and M. Fu, “Multi-sensor state estimation over lossy channels using coded measurements,” *Automatica*, vol. 111, article 108561, 2020.
- [38] H. H. Jazi, H. Gonzalez, N. Stakhanova, and A. A. Ghorbani, “Detecting HTTP-based application layer DoS attacks on web servers in the presence of sampling,” *Computer Networks*, vol. 121, pp. 25–36, 2017.
- [39] H. Liu, J. Liu, S. Hou, T. Tao, and J. Han, “Perception consistency ultrasound image super-resolution via self-supervised CycleGAN,” *Neural Computing and Applications*, pp. 1–11, 2021.
- [40] S. Tofghy, A. A. Rahmadian, and M. Ghobaei-Arani, “An ensemble CPU load prediction algorithm using a Bayesian information criterion and smooth filters in a cloud computing environment,” *Software: Practice and Experience*, vol. 48, no. 12, pp. 2257–2277, 2018.

Research Article

Design and Practice of Aerobics Teaching Design Based on Data Fusion Algorithm

Chuanqi Ma 

Sports Institute, Neijiang Normal University, Neijiang, 641112 Sichuan, China

Correspondence should be addressed to Chuanqi Ma; 10001113@njtc.edu.cn

Received 27 October 2021; Revised 18 November 2021; Accepted 23 November 2021; Published 11 January 2022

Academic Editor: Alireza Souri

Copyright © 2022 Chuanqi Ma. This is an open access article distributed under the Creative Commons Attribution License, which permits unrestricted use, distribution, and reproduction in any medium, provided the original work is properly cited.

Aerobic exercise is a very popular form of exercise. It combines various forms of sports and music. Aerobic exercise improves muscle tone and relaxes the mind and body while burning calories. It is designed to individualize instruction for different audiences. It is an important factor in the applicability of the operation. The purpose of this paper is to build different human models based on sensor network numbers to quantify different movements through the Internet of Things (IoT) to design personalized curriculum design and practice to improve the popularity of creative aerobics curriculum. In this paper, we first give an overview of the algorithm and data fusion algorithm and then simulate the aerobics creative curriculum design. First, the variance is used as the error measure to establish the data fusion algorithm and aerobics new concept innovation curriculum design and practice. The established model is compared with the aerobics curriculum design under the traditional model to highlight the advantages of the curriculum design under the data fusion algorithm. A comparison is also made with examples. The experimental results show that the data of the audience's movement changes during different creative processes solve the aerobics creative editing problem. Compared with the traditional curriculum design, the efficiency of the curriculum design and practice is improved by 20.23%.

1. Introduction

With the interactive development of education and the Internet, various universities and the Ministry of Education have made significant progress in the pilot work of modernity education reform. In 1999, the Ministry of Education launched various educational resource construction projects at all levels and built a large number of excellent online courses and educational software. At the same time, major universities developed a large number of projects based on their own educational characteristics and various resource construction projects. Excellent online course education teaching and education software, for different subject characteristics and teaching methods, developed a teaching resource library based on data algorithms, online teaching courseware, and material collection. With the rapid development of computer technology, wireless communication

technology, sensor technology, and embedded system technology, some miniature sensors with low production costs and low power consumption have emerged. It is the favorite of all walks of life. Data fusion algorithm technology is a data processing technology that automatically sorts, analyzes, and synthesizes the collected information under certain rules based on the node network of big data and then completes the required evaluation and decision-making. Aerobics is a kind of exercise that not only exercises the body but also cultivates the sense of art. It combines music, sports, and dance as a whole project, full of modern atmosphere, and is favored by the majority of groups.

For a long time, the teaching structure is a stable structure model of teaching activities under the guidance of certain educational thoughts, teaching theories, and learning theories, and it is impossible to carry out personalized

courses for different students. Incorporating the technical means of data fusion algorithm into the design and practice of aerobics creative curriculum is an important means of physical education reform. It can enrich the content and means of teaching reform and promote the all-round development of people and cultivate the sense of innovation.

The rise of algorithm technology has brought more accurate and convenient functions to the development of mankind. Among them, Liao et al. reported on the results of the 2014 Data Fusion Competition organized by the IEEE GRSS Image Analysis and Data Fusion Technical Committee (IADFTEC). As in previous years, the Data Fusion Technology Committee organized a data fusion competition to cultivate new ideas and solutions for multisource remote sensing research [1]. However, Yokoya et al. reviewed the concepts, principles, and tools that unify current causal analysis methods and deal with the new challenges posed by big data. In particular, Yokoya et al. solve the problem of data fusion-piece together multiple data sets collected under heterogeneous conditions (that is, different populations, systems, and sampling methods) to obtain effective answers to queries of interest [2]. To this end, Ambuhl and Menedez define a fusion algorithm that divides the city network into two subnetworks, one with a loop detector and one without. The simulation of the abstract grid network and the Zurich city network shows that the fusion algorithm can always significantly reduce the estimation error [3]. The purpose of this study is to determine the feasibility of using aerobic exercise courses to produce potential skeletal protection vertical effects and to determine whether the effects can be predicted by body function. Hannam et al. recruited participants from the senior exercise program to complete the SF-12 questionnaire, short-term physical training, and aerobic exercise program with seven different components, conducted at low intensity and high intensity. The maximum beating value is determined for each activity [4]. Melam et al.'s research shows that lack of physical exercise and uncontrolled diet can lead to excessive weight gain, which can lead to obesity and other metabolic disorders. Melam et al.'s research shows that brisk walking and aerobic exercise are the best ways to control and reduce body weight and weight components [5]. This requires aerobics staff not only to have professional aerobics methods and skills, but also to have the basic skills of aerobics in order to compose perfect aerobics in the new situation. Ma based on the performance of aerobics, the experience of the competition, and the arrangement of the aerobics, let the audience have a bright feeling in the vision. At the same time, when Ma organizes aerobics, each movement must be carefully designed to make the choreographed movements have a comfortable and pleasant feeling. The movement does not look too rigid, giving the overall beauty and aerobic exercise. The characteristics are reflected in the design of the action to achieve better results [6]. The purpose of this research by Catalina is to conduct multiple sets of experiments to observe the creation of aerobics courses based on data fusion algorithms. Based on the results of the all-round record of the courses, it emphasizes the independent and organized way of performing aerobics [7]. There are some shortcomings in their research. The curriculum creation based on big data relies on a huge database and a powerful technical environ-

ment. The scope of the data in this article is limited, and it is still necessary to expand the experimental objects to make the research more typical.

The innovation of this article (1) lies in the use of data fusion and algorithms combined with aerobics to create a curriculum that has the basic characteristics of network communication such as digitization and interactivity in a network technology environment and at the same time reflects the characteristics of education and (2) teaching goals. The teaching of diversified and multilevel online courses is no longer just for the purpose of presenting the teaching content. In the face of different personalized audiences, such as different basic learning levels and inconsistent physical indicators, a multilevel teaching curriculum design should be designed, to promote the development of everyone.

2. Design of Innovative Aerobics Curriculum Based on Sensor Network and Communication Algorithm

2.1. Data Fusion Algorithm. Data fusion is the process of combining, correlating, and combining data and information from multiple sensor sources to obtain more accurate location and identity estimates for a real-time, complete evaluation of battlefield posture and threats and their importance.

2.1.1. Basic Theory of Algorithm. In order to study the sensor data fusion algorithm, firstly, the algorithm operation is briefly introduced. Assuming that M distributed sensors are deployed in the wireless sensor network system, the i -th sensor corresponds to the Mi -th convergent sensor. The definitions of the dynamic model and the measurement model of the discrete-time target in the data fusion tracking system correspond to two sets of equations, respectively:

$$\begin{aligned} A(m+1) &= P(m)A(m) + F(m)H(m), \\ B_i(m) &= C_i(m)A(m) + L_i(m), i = 1, \dots, M. \end{aligned} \quad (1)$$

The other two sets of equations are as follows:

$$A_i(m+1) = P_i(m)A_i(m) + F_i(m)H_i(m), i = 1, \dots, M. \quad (2)$$

Then,

$$B_i(m) = G_i(m)A(m) + L_i(m), i = 1, \dots, M, \quad (3)$$

expressed as the latter model, where $P_i(m)$ represents the conversion matrix, $F_i(m)$ is the input gain matrix, $H_i(m)$ represents the feedback of the i -th sensor, and $L_i(m)$ represents the measurement error of the sensor.

2.1.2. Data Fusion. In the current military field, the direct driving force for the development of information fusion technology is the development of information-based weaponry and the new battlefield perception needs arising from the emergence of information-based combat styles (e.g., network-centric warfare). At present, with the expansion of combat space to space and Cyber space, the fusion processing of remote sensing telemetry and battlefield surveillance images has become an urgent

need for full-field battlefield perception, especially the fusion of heterogeneous media images has become an urgent problem for combat identification and a hot spot for current research. The technologies involved include spatial alignment of heterodyne images, feature extraction and unified representation of heterodyne images, quality assessment of fused images, and application implementation.

Data fusion algorithms are a specific research direction for data processing using multiple sensors. A simple definition can be summarized as the process of information processing using computer technology to automatically analyze the information acquired by sensors according to certain sequential rules using a computer language to fully accomplish the required estimation and decision-making tasks [8]. According to the above definition, the acquisition of information from multiple sources is the basis of data fusion technology processing, integrated processing, and coordinated optimization is the core of the data fusion algorithm, and the sensor system is the hardware basis of the whole data fusion algorithm. The development of artificial intelligence and data node neural networks, pattern recognition, image and image generation, signal clustering processing, and other related technologies provides rich theoretical and technical means for data fusion algorithm technicians. Combining the findings of these disciplines can maximize our efficiency and help us make the right estimates and decisions.

The ultimate goal of data fusion is achieved by four different levels of processing layers, as shown in Figure 1.

In Figure 1, the first level of processing is object assessment. The main tasks in this level of processing include the following: data registration, data association, and identity estimation. The results of this level of processing will provide relevant information for decision-making assistance for more advanced processing processes [9].

Data registration is essentially to align information with different characteristics in time and space so that multisource data can be processed in a unified framework and pave the way for the subsequent work of fusion. The main work of the so-called data association is to combine and classify multisource data [10]. The role of identity estimation is to solve the problem of characteristics and expressions related to entity attributes. Target evaluation deals with numerical calculations, and identity estimation is usually based on pattern recognition techniques or parameter matching techniques, including the following: majority voting, Bayes method, and D-S evidence theory, as shown in Figure 2.

The second level of processing is situation assessment. The main task at this level is to abstract and assess the overall situation. The input information for situation assessment includes the following: event monitoring information, state estimation information, and relevant assumptions necessary for situation assessment, while the output refers to the probability corresponding to the necessary relevant assumptions [11, 12]. The result is shown in Figure 3.

The third level of processing is impact assessment. The impact assessment establishes a mapping from the current situation to the future, an assessment of the possible impact of the participant's assumptions and predictions. Different data input/output will have different effects. Data in and

out (DAI-DAO): This type is the most basic data fusion method. The input and output are all raw data, and the output data is usually more reliable, higher, or more accurate [13]. This level of data fusion is carried out as soon as the data is output from the sensor, and the fusion method is based on signal and image processing algorithms, as shown in Figure 4.

- (1) *Data In and Feature Out (DAI-FEO)*. This level of data fusion performs feature extraction on the original data.
- (2) *Feature In and Feature Out (FEI-FEO)*. This level of input and output processing is all features, so it is essentially a set of features to improve or obtain new features. This process is also called feature fusion, information fusion.
- (3) *Feature In and Decision Out (FEI-DEO)*. The input at this level is a set of features, and the output is a set of decisions. Most classification systems that make decisions based on sensor input belong to this level.
- (4) *Decision-In-Decision-Out (DEI-DEO)*. This classification is also called decision fusion, which combines input decisions to obtain better decisions.

The fourth level of processing is process assessment.

The monitoring and evaluation of this process requires the establishment of relevant optimization indicators [14, 15]. In addition, it is necessary to achieve timely acquisition and effective processing of multiple sensor information, as well as to achieve the best allocation of resources so as to be able to support specific tasks, so as to achieve the purpose of improving the real-time performance of the system. As shown in Figure 5, it shows the processing relationship between different data.

Since data fusion is a process of gradually processing multisource information, when there is a step-like and multilevel multisource information fusion, we have to put forward requirements for data fusion, that is, in each fusion process, every link, the amount of useful information carried by the sensors should be used to the maximum. Therefore, the data fusion system maximizes the amount of useful information in each node during each fusion process, and the fusion result should be required to be beneficial to the system users. Moreover, the amount of useful information of each data should organically inherit the role of other parts. When some processes are close to the experience, the effect of the resulting effective amount of data will not be weakened in other processes entering the system, that is, various parts of the system, to achieve harmony and unity [16].

2.1.3. Bayesian Estimation Method to Calculate Data Fusion.

The Bayesian estimation method is a commonly used method in static data fusion.

Assuming a state space, the Bayesian estimator provides a method to calculate the posterior (conditional) probability distribution. Assuming that the state quantity at time i is X_i , it is known that the measurement $M_i = \{M1, \dots, Mi\}$ and

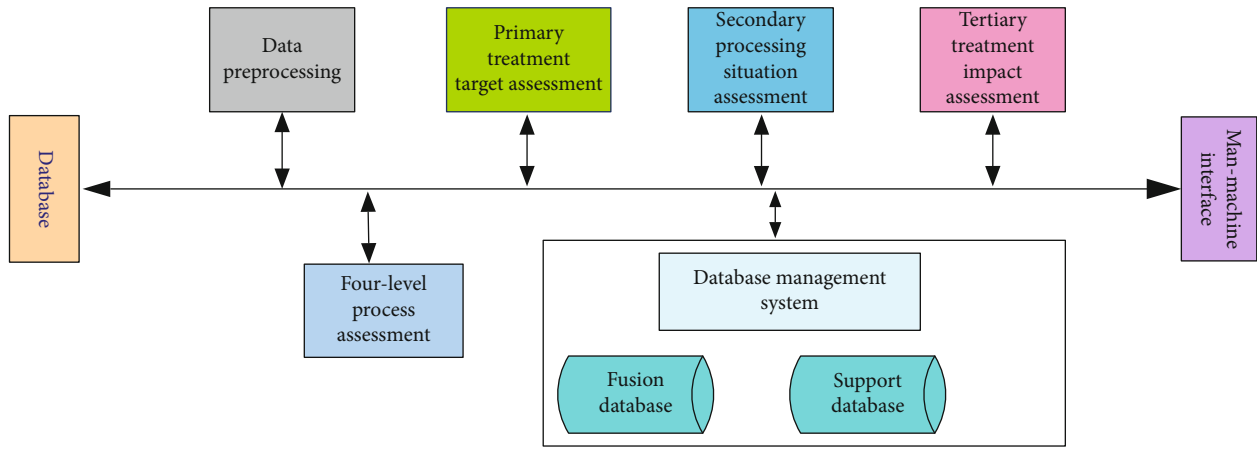


FIGURE 1: JDL data fusion model.

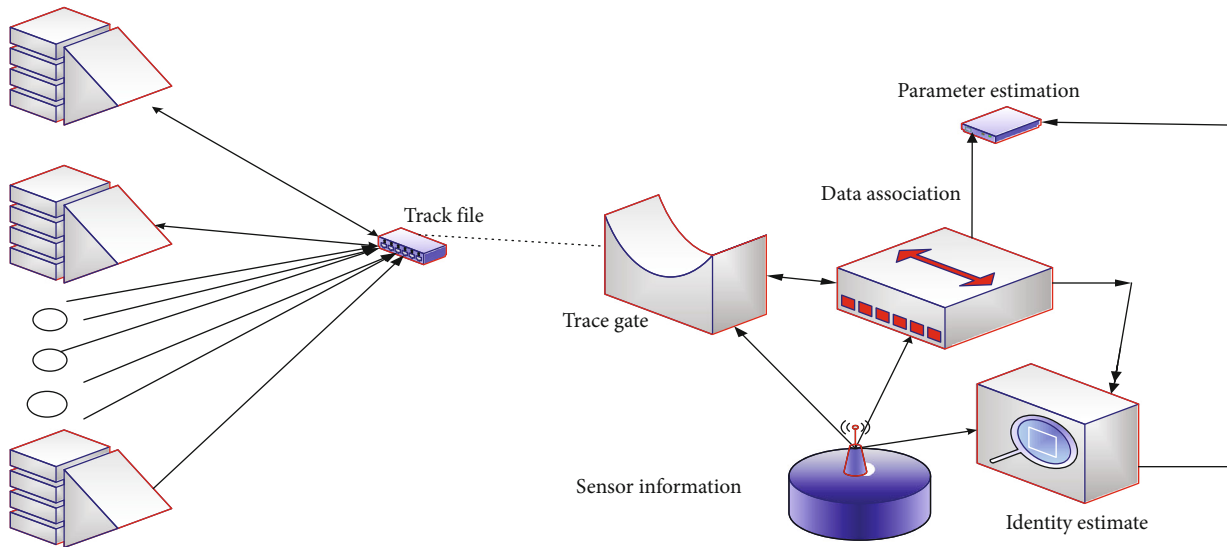


FIGURE 2: Object evaluation model in primary processing.

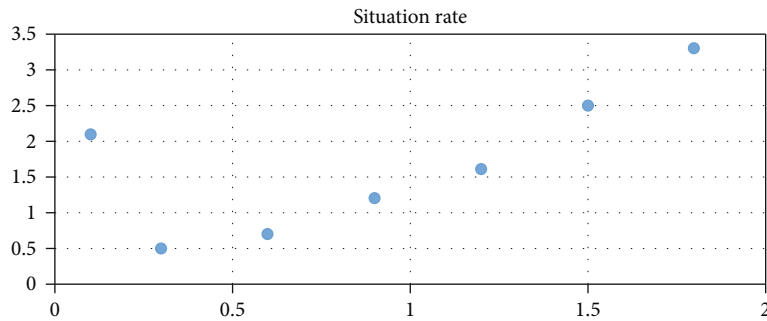


FIGURE 3: Situation assessment analysis chart.

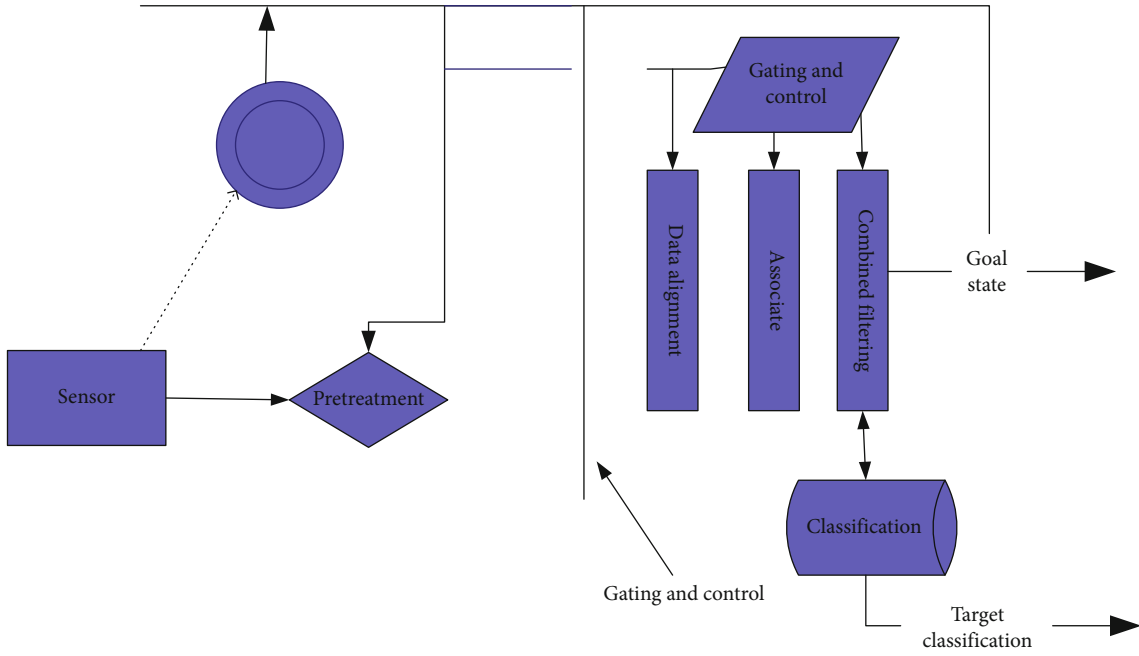


FIGURE 4: Data input/output data types.

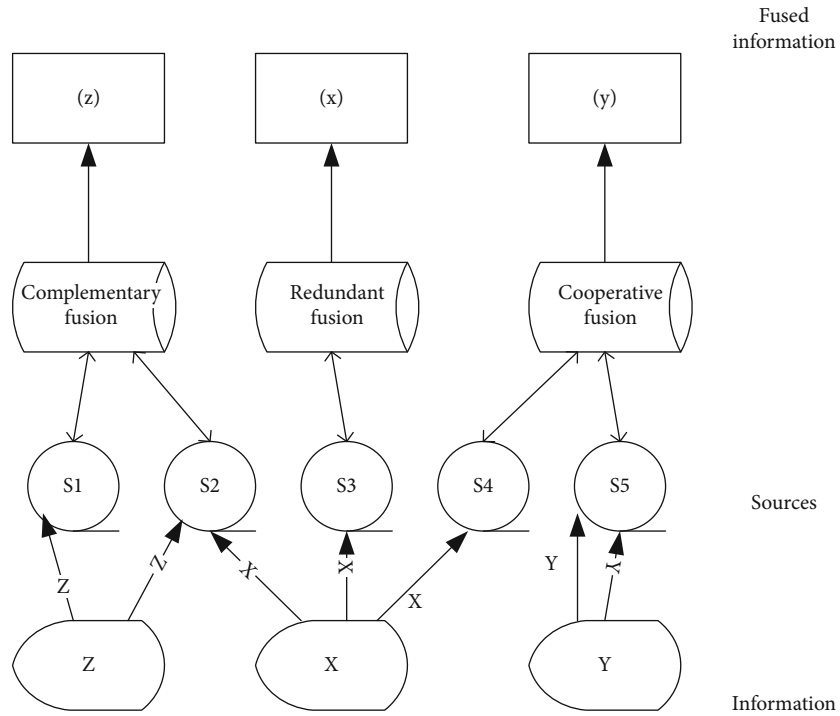


FIGURE 5: Three relationships between input data.

the prior distribution of group i are as follows:

$$P(X_j|M^j) = \frac{P(M_j|X_j)P(X_j|M^{j-1})}{P(M^j|M^{j-1})}, \quad (4)$$

wherein

- (i) $P(M_j|X_j)$ represents the likelihood function, a measurement model based on a given sensor
- (ii) $P(X_j|M^{j-1})$ represents the prior distribution function, a model of a given conversion system
- (iii) Denominator $P(M^j|M^{j-1})$ is a standardized term that can guarantee the normalization of the probability density function

When the observation coordinates of the sensor group are consistent, the direct method can be used to fuse the sensor measurement data. In most cases, the sensor describes the same environmental object from different coordinate systems. At this time, the sensor measurement data should be fused by Bayesian estimation in an indirect way.

When the Bayesian method is used for multisensor data fusion, the possible decisions of the system are required to be independent of each other, in this way to treat these decisions as a division of the sample space [17]. Suppose the possible decisions of the system M_1, M_2, \dots, M_n , when a sensor observes the system, the observation result Q is obtained, and if the prior knowledge of the system and the characteristics of the sensor can be used to obtain the prior probabilities $P(M_i)$ and conditional probability $P(Q/M_i)$, use the Bayesian conditional probability formula

$$P\left(\frac{M_i}{Q}\right) = \frac{P(M_iQ)}{P(Q)} = \frac{P(Q/M_i)P(M_i)}{\sum_{i=1}^n P(Q/M_i)P(M_i)}, i = 1, 2, \dots, n. \quad (5)$$

According to the prior probability $P(M_i)$ of the sensor, it is updated to the posterior probability $P(M_i/Q)$.

This result is generalized to the case of multiple sensors. When there are A sensors, the observation results are A_1, A_2, \dots, A_o ; assuming that they are independent of each other and independent of the conditions of the observed object, then the total posterior probability of each decision in the system with O sensors can be obtained as-

$$P(M_i/A_1 \wedge A_2 \cdots A_o) = \prod_{j=1}^o P(Q_j/M_i)P(M_i)/\sum_{k=1}^n \prod_{j=1}^o P(Q_j/M_k)P(M_k), i = 1, 2, \dots, n.$$

Finally, the decision of the system can be given by certain rules. For example, the decision with the largest posterior probability is taken as the final decision of the system as shown in Figure 6.

2.1.4. The Data Fusion Algorithm Establishes a Human Body Motion Model, as Shown in Figure 7. Detection provides approximate information about the position of the human in the image, which can satisfy the needs of some applica-

tions; however, some applications, such as human-computer interaction, require finer information about the position of nodal points. The goal of monocular 3D human pose estimation is to recover the 3D coordinates of human nodes from a single image. The loss of depth information during imaging leads to a strong ambiguity in this task, and more preliminary work tends to reduce the ambiguity by introducing a priori information, such as anthropometric constraints, low-dimensional popular representations, or temporal smoothing constraints.

The coordinate system shown in Figure 7 above has three mutually perpendicular vectors. The vector change through any point in space will have a spatial sum vector. It is very appropriate to replace the acceleration in the three directions with a vector with both magnitude and direction. The calculation formula of the space vector is as follows:

$$\overset{p}{a} = x \overset{p}{i} + y \overset{p}{j} + z \overset{p}{k}. \quad (6)$$

The change of the acceleration parameter after the human body's motion returns. It is assumed that the acceleration in the three different directions is $a_x, a_y,$ and $a_z,$ because the assignment change of the acceleration vector can reflect the violent fluctuations of the human body's motion. It can be expressed by the following formula:

$$a' = \sqrt{a_x^2 + a_y^2 + a_z^2}. \quad (7)$$

As mentioned above, when we know the acceleration in three directions, we can get the change of human body posture according to the above formula. According to the human body coordinate system established in Figure 6, different angles of human body movement can be calculated, for example, when the human body is perpendicular to the angle α_1 of the ground:

$$\alpha_1 = \frac{\sqrt{a_x^2 + a_y^2}}{|a|}. \quad (8)$$

In the same way, the angle values in the other two directions can be obtained. According to the above formula, the angle values between different postures can be calculated, and the motion state of the human body can be judged whether it is violent [18, 19].

According to the formula, calculate the x -axis acceleration during movement.

Data analysis is shown in Figure 8.

In summary, the data fusion algorithm introduces the correlation technique of aerobic exercise in data fusion mainly with a multiobjective tracking application. The data sources and exercise record slices are described to construct a multimodal and self-supervised learning-based aerobic capacity model that can help in picture analysis, as well as self-monitoring of movements. The model consists of a human generalized aerobic capacity model, a personalized long-term aerobic capacity model, and a personalized short-term aerobic

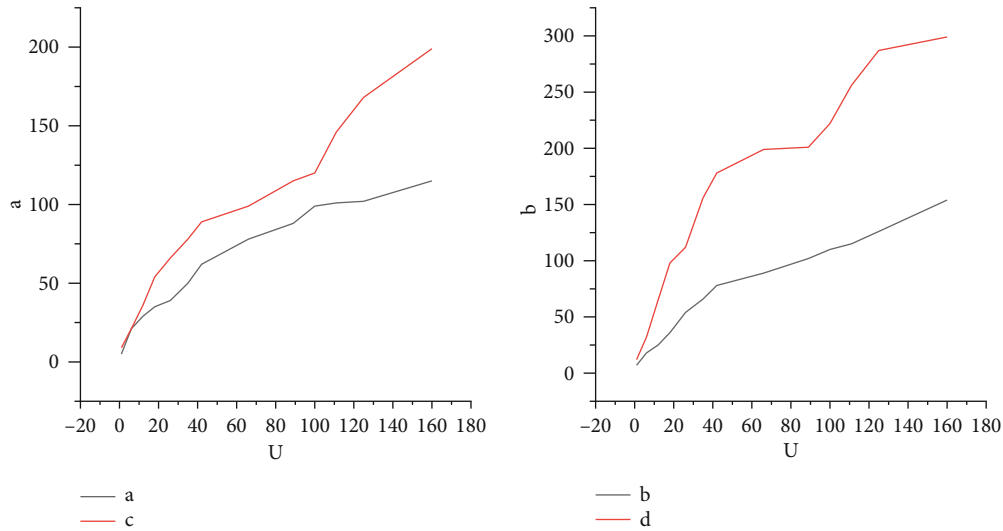


FIGURE 6: Decision with maximum posterior probability.

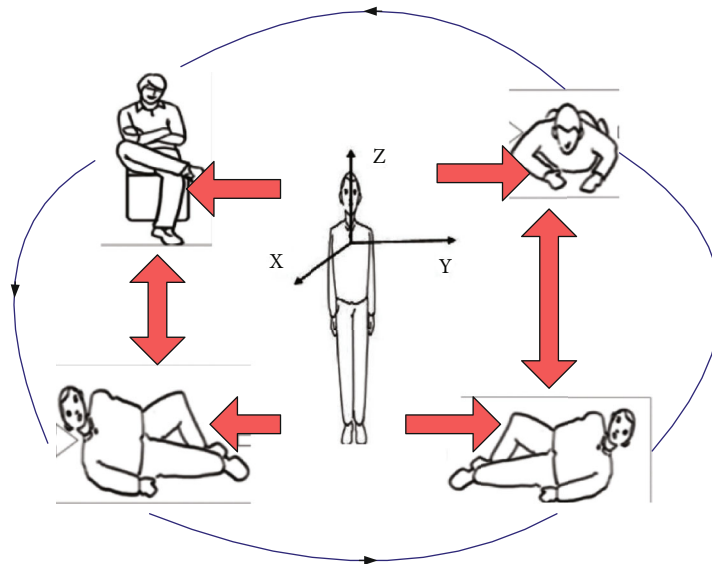


FIGURE 7: Three-dimensional coordinate system of human body space.

capacity model, and the components of the aerobic capacity model are trained one by one in a training manner, and both the personalized long-term aerobic capacity model and the personalized short-term aerobic capacity model are fixed with the model parameters being used as the components for subsequent model training after the training is completed.

2.2. Aerobics

- (1) The display of aerobics action hands is shown in Figure 9

Aerobics movements are mainly composed of foot movements and hand movements.

There are five types of foot movements. Rhythmic pacing operations are mainly based on the free combination of foot movements in fitness gymnastics. Generally, one or

two steps are selected for each unit to ensure the mobility and diversity of the operating unit. Each unit must combine at least three steps. There are alternate types such as walking and running; stepping types have side-to-side stepping and stepping and sucking legs; the fourth lifting type is like the form of suction-leg jumping and bending-leg jumping, and the last type is opening-closing jumping and split-leg jumping [20]. The step action of the exercise is mainly based on the free collocation and combination of the foot movements of aerobics. Generally, one or two steps should be selected for each exercise unit. In order to ensure the mobility and diversity of the exercise unit, at least three steps should be selected for combination.

When doing upper limb movements, the posture of the hand is variable, and the emotions of the body can be expressed in detail through the changes of different hand shapes. With the sagittal and longitudinal axes of the body

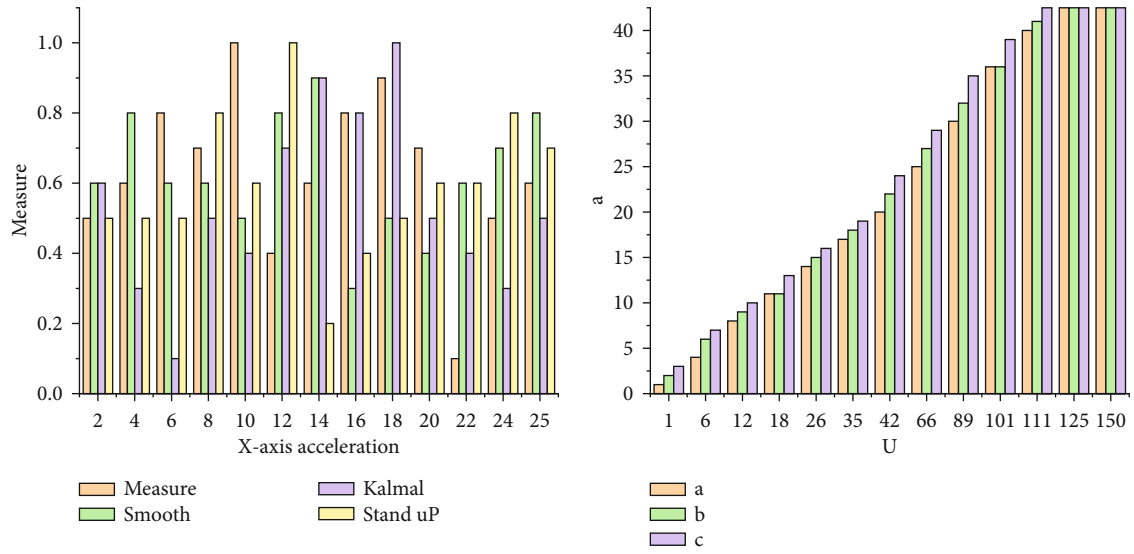


FIGURE 8: Acceleration.

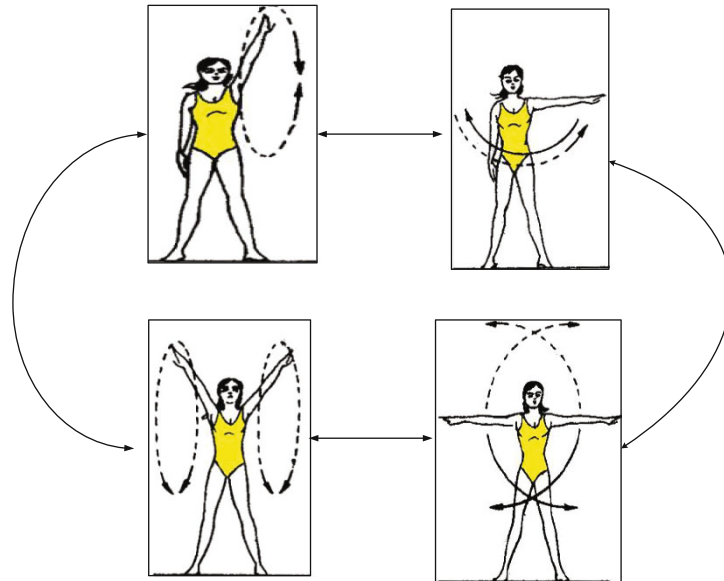


FIGURE 9: Different types of aerobics movements.

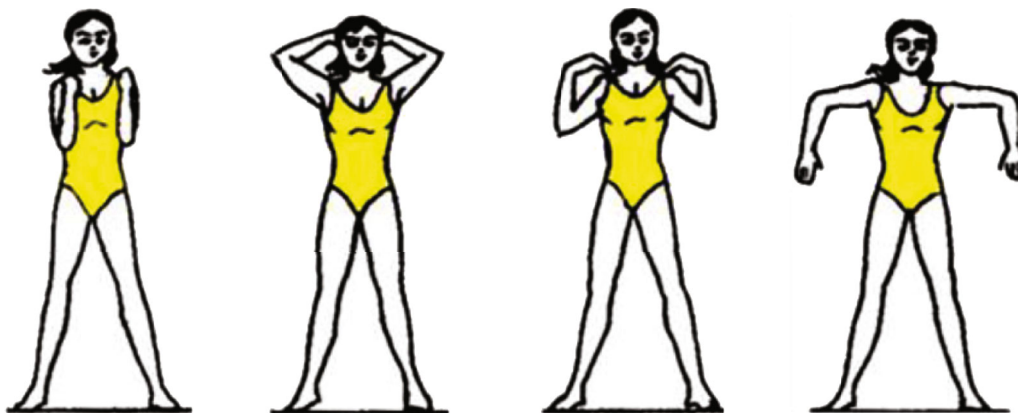


FIGURE 10: Movements in physical flexibility.

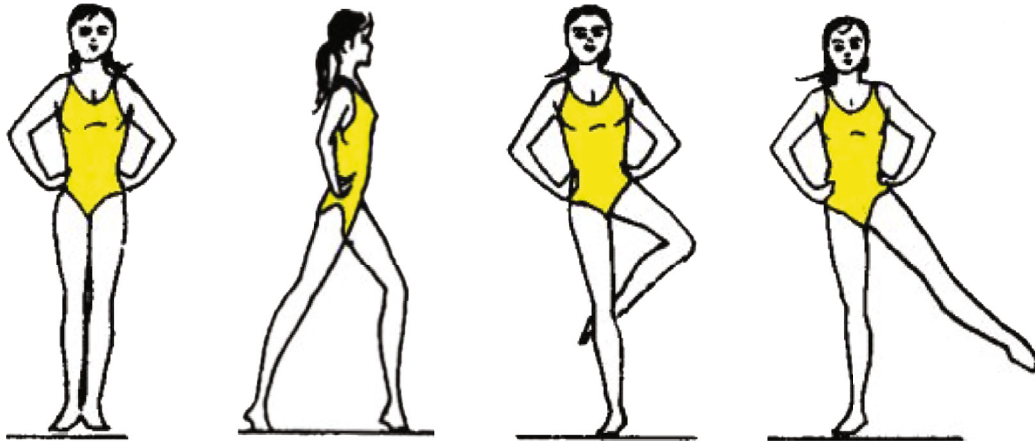


FIGURE 11: Movements to develop agility.

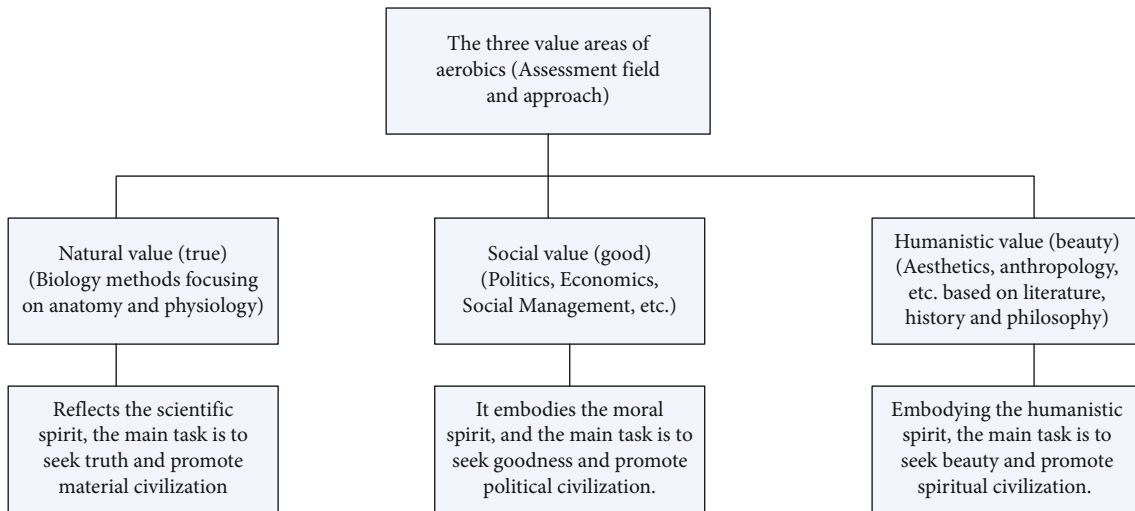


FIGURE 12: The value of creating aerobics courses.

TABLE 1: Comparison of different forms of aerobics.

	Traditional aerobics teaching	Design of aerobics course under data fusion
Content	The fixed routine is the teaching content, ignoring the individualized teaching of students	Stimulate interest in curriculum practice and cultivate a sense of innovation
Function	For the development of the body	All-round development
Organizational form	Emphasis on organizational unity, teachers instill knowledge in one direction	Flexible and diverse, combined with teaching
Evaluation method	Emphasizes absolute unity and focus on the evaluation of intermediary performance	Individualized and humanized evaluation based on different individual differences, focusing on the combination of evaluation process and results
Purpose	Learn to exercise, enhance physical fitness	Pay attention to cultivating practical innovation ability, establish correct weight reduction values, and form the consciousness and habits of lifelong sportsmanship

as the baseline and the horizontal plane of the shoulder as the midline, the movement of the arm can be divided into eight directions. The movements in each direction are

straight, round, bent, forward, backward, up, and down. The creation of arm movements can be performed in various ways [21, 22]. The performance of the formation and route

varies depending on the rotation surface. When the operating unit requires additional rotation, the creation of steps and arm movements needs to be coordinated without any setbacks or stagnation. Arm movements are combined with steps to achieve smooth coordination.

As mentioned above, the movements of aerobics are not only reflected in the hand movements, but also in the changes on the body. As shown in Figure 10, it mainly reflects the exercise of the legs with movements such as big kicks and suction jumps.

Figure 11 shows not only actions that reflect the quality of coordination, but also actions that develop agility and coordination.

This is the overall motion snapshot and slow motion alternately or four alternate motion combinations. For example, it connects two movements and four-shot movements: bend left and right legs, jump, wrap hands, and switch fingers [23].

- (2) Why do we need to design aerobics creative courses? The reason is that aerobics is not only about strengthening the body. At the same time, aerobics has three value areas, namely, natural value, social value, and humanistic value. It shows the scientific spirit, moral spirit, and humanistic spirit from different discipline dimensions, which is aesthetically independent. Effective combination and reflection on a platform for evaluating value on the basis of sex are shown in Figure 12.

2.3. Create Aerobics Course Based on Sensor Network and Communication Data Fusion Algorithm

2.3.1. *The Comparison of Aerobics between Tradition and Algorithm.* The comparison of aerobics between traditional algorithms can be obtained through data search. The results are shown in Table 1.

3. Experimental Design and Result Analysis

3.1. Creative Curriculum Design

- (1) In the process of creating aerobics, we must first perform sports training, because this is our most basic skills. When we practice the basic skills, master its effects on our fitness and the artistic influence of aesthetic appreciation, so in the fitness in the training of exercises, we must pay attention to the training of step fluency [24, 25]. In order to improve the fitness effect and fitness effect, design creative courses, realize the importance of fitness training, and actively improve aerobic exercise capacity, it is necessary to carry out smooth training methods. Table 2 shows the body coefficients of different postures.
- (2) The use of algorithms for data analysis can derive the characteristics of the design of the aerobics creative curriculum. However, when measuring data, it is inevitable that the physiological signal will change due to factors such as power frequency interference

and arterial waves in the real world. In addition, the area network signal is collected in an open scene, so it will inevitably be affected. These random noises will affect the collected physiological signal data and cause distortion and reduce the accuracy of the data [26, 27]. In order to ensure the accuracy and convenience of data fusion work, signal denoising should be done well, so it is very necessary to remove noise from the original signal

Denoising quantitative description: assuming that the signal length is S , the signal contaminated by noise (that is, the observed signal) is $\{f(i): i = 1, 2, \dots, S\}$, the original signal (to be restored signal) is $\{g(i): i = 1, 2, \dots, S\}$, and the noise is $\{\beta(i): i = 1, 2, \dots, S\}$. The following signal decomposition modes can be used for analysis:

$$f(i) = g(i) + \beta(i), (i = 1, 2, \dots, S). \quad (9)$$

Second, the most common signal decomposition mode is multiplicative decomposition:

$$f(i) = g(i) * \beta(i)(i = 1, 2, \dots, S). \quad (10)$$

When we use the above methods for denoising, it is usually simulated as a multiplicative structure. The noise component $\beta(i)$ is independently and identically distributed in $S(0, \theta_n^2)$, and the purpose of denoising independently with $g(i)$ is to obtain an estimate $\hat{g}(i)$ of $g(i)$ so that its mean square error (MSE) is the smallest, where

$$MSE = \frac{1}{S^2} \sum_{i=1}^S (g(i) - \hat{g}(i))^2. \quad (11)$$

In the region of small fluctuations, when using the orthogonal wavelet transform of the above 11 formulas, we can get the following:

$$X(i) = Y(i) + V(i), i = 1, 2, \dots, S. \quad (12)$$

Among them, $X(i)$ is the noisy wavelet coefficient, $Y(i)$ is the no-noise wavelet coefficient, and $V(i)$ is the fluctuation area. After we use the data after the above algorithm fusion to design and analyze the aerobics creation course, we can use the following methods to quantify, and when the data X has mixed attributes, the difference between different bodybuilding actions D can be expressed by the following formula:

$$D(X_i) = \frac{\sum_{n=1}^m y_i^n d_i^n}{\sum_{n=1}^m y_i^n}, \quad (13)$$

where y_i^n represents the weight of n actions and d_i^n represents the data of the i -th sample in the data set X , and then, we can use the above formula to calculate the quantification of different types of actions [28].

TABLE 2: Body factor.

Name	W_i	Hierarchical total ranking weight W	Rank
Basic theoretical level	0.326	0.092	8
Creation theory	0.721	0.123	2
Aerobics technical skill level	0.09	0.022	3
Competitive aerobics technical skill level	0.333	0.163	5
Creative practice level	0.18	0.032	7
Knowledge level of related subjects	0.821	0.033	1
Music perception level	0.128	0.011	3
Music production and processing	0.128	0.854	8
Aesthetic sensibility	0.966	0.655	12
Aesthetic expression and creativity	0.833	0.721	7

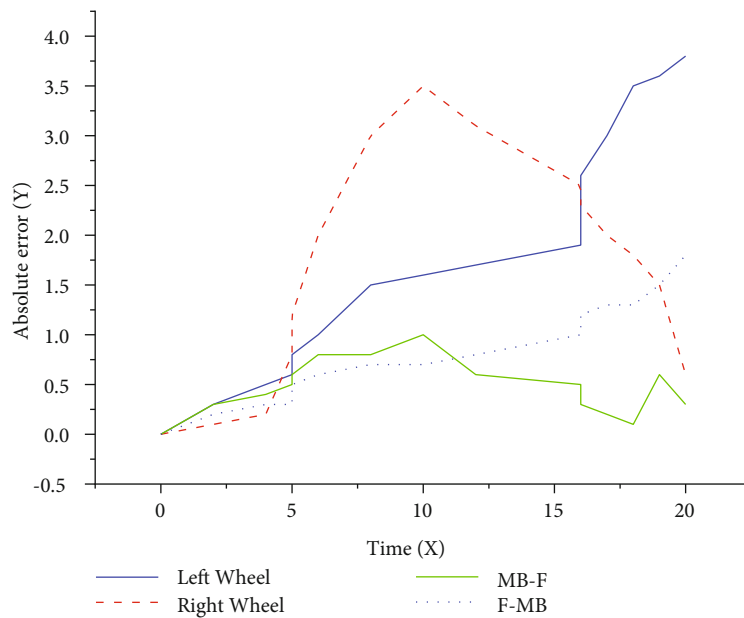


FIGURE 13: Expected value.

- (3) Data fusion calculation has many evaluation criteria. When we use algorithms to quantify aerobics actions, indicators other than accuracy are convenient for us to verify

$$MEA = \frac{1}{n} \sum_{i=1}^n |y_i^t - y_i^-|, n = 1, 2, \dots, N \quad (14)$$

MEA uses absolute error, which can just eliminate the gap between data and can better reflect the true situation of data fusion algorithm error. The smaller the value of MEA, the closer the fusion value is to the true value.

3.2. Evaluation Criteria for Data Fusion Algorithms. They are the average absolute error, the root mean square error, the average absolute percentage error, and the root mean square percentage error. The modified function is to evaluate the performance of the algorithm [29]. Suppose n is the number of individuals in the data collected this time, where y^t represents the data fusion value and y^- represents different individual data.

- (2) *Root Mean Square Error (RMAE)*. Use the following formula for calculation:

- (1) *Mean Absolute Error (MAE)*. Use the following formula for calculation:

$$REAM = \sqrt{\frac{1}{n} \sum_{i=1}^n \left(\frac{y_i^t - y_i^-}{y_i^-} \right)^3} * 1000 \quad (15)$$

TABLE 3: Comparison of the test results of students' physical fitness standards before and after the experimental group.

Height	Before the experiment	80	160.79	5.21	0.07	$P > 0.05$
	After the experiment	80	160.03	4.88		
Weight	Before the experiment	80	55.86	6.97	0.09	$P > 0.05$
	After the experiment	80	55.3	7.22		
Standing long jump	Before the experiment	80	168.33	15.69	2.23	$P < 0.05$
	After the experiment	80	172.31	11.33		
Vital capacity	Before the experiment	80	2647.5	526.27	0.87	$P < 0.05$
	After the experiment	80	1847.73	565.36		
Jump rope	Before the experiment	80	123	6.54	0.04	$P > 0.05$
	After the experiment	80	130	7.98		
Step test	Before the experiment	80	44.26	4.18	0.92	$P < 0.05$
	After the experiment	80	46.82	6.33		
Flexibility ratio	Before the experiment	80	5	23.22	2	$P > 0.05$
	After the experiment	80	5	32.11		
Exercise frequency	Before the experiment	80	3	2.33	6.32	$P > 0.05$
	After the experiment	80	7	3.21		

The smaller the value of REAM, the closer the actual value of the aerobics teaching design course obtained.

(3) Mean absolute percentage error (MAPE)

$$\text{MAPE} = \sum_{i=1}^n \left| \frac{y_i^t - y_i^-}{y_i^-} \right| * \frac{1000}{n}, n = 1, 2, \dots, N \quad (16)$$

The smaller the value of MAPE, the better the similarity between the true value and the fusion result.

(4) Root mean square percentage error (RMSPE)

$$\text{RMSPE} = \sqrt{\frac{1}{n} \sum_{i=1}^n (y_i^- - y_i^t)^2}, n = 1, 2, \dots, N \quad (17)$$

When the value we obtain is small, it indicates that the design of our integrated design scheme is more reasonable.

(5) Criterion function (CF)

$$\text{CF} = C_1 * \frac{P}{c} + C_2 * \frac{\text{RSS}}{c} + C_3 * \frac{T}{c} \quad (18)$$

In the above formula, P refers to the time required for the data fusion operation, RSS refers to the sum of the final true value obtained and the residual sum of squares after the fusion data, T refers to the variance of the target fusion value, and C_1 , C_2 , and C_3 , respectively, refer to the weights of P , RSS , and T , which can be adjusted according to the expected values of different standard actions obtained. It represents the maximum value of the weight. Among them,

the smaller CF value means that the algorithm produces accurate results with the smallest variance in the shortest time [30], as shown in Figure 13.

3.3. Teaching Design and Practice of Aerobics Based on Data Fusion Algorithm. Through the quantitative analysis of the teaching design of the aerobics creation course through the data fusion algorithm, the results can be obtained as shown in Table 3.

According to Table 3, it can be seen that there is a certain correlation between the algorithm-based technology and the aerobics curriculum creation and design. When the multiple data is stable and the variance is smaller, the physical indicators of the human body when actually performing aerobics are obtained. It is more accurate and provides different aerobics courses for different individuals, which is not only conducive to the creation of courses, but it can also innovate the courses to meet different sports objects. It can be said that the data fusion algorithm proposed in this paper, which uses variance as a measurement index and changes with the movement of the audience of different creative courses, has improved the efficiency of 20.23% compared with traditional course design in solving the problems of aerobics creative course design and practice.

4. Discussion

This article is dedicated to the research and design of aerobics creative curriculum design and practice model based on data fusion algorithm and applies it to the analysis and practice of personalized curriculum creation. Not only does the application range of data fusion algorithms extend to curriculum creation, but it is also the quantitative design of the actions of different personalized audience groups, and the application design concept of sensors is used to try

new methods. Through the establishment of human body model, quantitative analysis, behavior simulation, mining data fusion algorithm as an important tool for the study of individualization and difference, has a certain potential in the complexity of curriculum design. In addition, there are already research foundations of creative curriculum design at home and abroad. In this paper, the research of creative curriculum is introduced into aerobics, the model is improved, and the data fusion algorithm makes the model suitable for the design and application of aerobics creative curriculum. For the research of data fusion algorithm, this article starts with the most basic algorithm, analyzes the error between the data calculated by the algorithm and the crowd that is different from reality, finds the model that is most suitable for the crowd, and controls the variance to ensure that the quantitative data is more accurate. Make the research results in line with the actual situation. And in the comparison of recall and accuracy observation, it is found that the increase in recall makes the detection condition loose, which affects the accuracy and thus makes the accuracy decrease. The good thing is that the higher recall of the algorithmic method can ensure that a better accuracy is obtained.

Through the analysis of this article, it shows the use of algorithms to build human body models of various data indicators of human movement, and the creation of curriculum design schemes for different groups of people is more innovative than traditional courses. Curriculum designers can face different audiences. For targeted teaching, various sports data can also be recorded and adjusted in time. In this way, the experience of different audiences can be improved, and the creative ability of course designers can also be improved.

5. Conclusions

Through case analysis, we draw important conclusions: in general, the smaller the variance, that is to say, the smaller the gap between the model establishment of the data and the actual movements, and the creation of aerobics courses is more suitable for the masses, compared to traditional courses. Editing is more universal, but this is not absolute. When the variance becomes smaller and smaller, there will be a smaller gap, and the data will be more quasi-group, but when it exceeds a certain limit value, it may also change the actual gap. Big possibility, not that the smaller the data, the better. This requires the designers of different creative courses to make timely adjustments based on the responses of the practitioners and use data fusion algorithms to improve efficiency, cultivate innovation awareness, and promote the all-round development of people.

Data Availability

No data were used to support this study.

Conflicts of Interest

The author states that he has no conflict of interest.

Acknowledgments

This work was supported by the Neijiang Normal University 2020 Online first-class undergraduate courses of general education, JK202056.

References

- [1] W. Liao, X. Huang, F. Van Coillie et al., "Processing of multi-resolution thermal hyperspectral and digital color data: outcome of the 2014 IEEE GRSS data fusion contest," *IEEE Journal of Selected Topics in Applied Earth Observations & Remote Sensing*, vol. 8, no. 6, pp. 2984–2996, 2015.
- [2] N. Yokoya, P. Ghamisi, J. Xia et al., "Open data for global multimodal land use classification: outcome of the 2017 IEEE GRSS data fusion contest," *IEEE Journal of Selected Topics in Applied Earth Observations & Remote Sensing*, vol. 11, no. 5, pp. 1363–1377, 2018.
- [3] L. Ambuhl and M. Menendez, "Data fusion algorithm for macroscopic fundamental diagram estimation," *Transportation Research Part C Emerging Technologies*, vol. 71, pp. 184–197, 2016.
- [4] K. Hannam, K. Deere, S. Worrall, A. Hartley, and J. H. Tobias, "Characterization of vertical accelerations experienced by older people attending an aerobics class designed to produce high impacts," *Journal of Aging and Physical Activity*, vol. 24, no. 2, pp. 268–274, 2016.
- [5] G. R. Melam, A. A. Alhusaini, S. Buragadda, T. Kaur, and I. A. Khan, "Impact of brisk walking and aerobics in overweight women," *Journal of Physical Therapy Science*, vol. 28, no. 1, pp. 293–297, 2016.
- [6] Y. Ma, "Research on the arrangement and visual design of aerobics under the new situation," *International Core Journal of Engineering*, vol. 5, no. 9, pp. 170–173, 2019.
- [7] A. Catalina, "Study regarding the psycho-somatic development of the fourth grade pupils practicing track and field in an independent, organized manner," *Gymnasium Scientific Journal of Education Sports & Health*, vol. 13, no. 1, pp. 210–218, 2017.
- [8] M. Bandyopadhyay, "Multi-stack hybrid CNN with non-monotonic activation functions for hyperspectral satellite image classification," *Neural Computing and Applications*, vol. 33, no. 21, pp. 14809–14822, 2021.
- [9] X. H. Wu and S. M. Song, "Covariance intersection-based fusion algorithm for asynchronous multirate multisensor system with cross-correlation," *Iet Science Measurement & Technology*, vol. 11, no. 7, pp. 878–885, 2017.
- [10] R. Sampaio-Neto and C. A. Medina, "Nonassisted adaptive algorithm for data fusion in distributed detection systems [Correspondence]," *IEEE Transactions on Aerospace & Electronic Systems*, vol. 52, no. 3, pp. 1486–1493, 2016.
- [11] J. Ma, H. Jiang, D. Zhu, and R. Yang, "Algorithms and hardness for scaffold filling to maximize increased duo-preservations," *IEEE/ACM Transactions on Computational Biology and Bioinformatics*, vol. PP (99), 2021.
- [12] A. Naik and S. C. Satapathy, "Past present future: a new human-based algorithm for stochastic optimization," *Soft Computing*, vol. 25, no. 20, pp. 12915–12976, 2021.
- [13] F. Shang, Y. Li, X. Deng, and D. He, "Android malware detection method based on naive Bayes and permission correlation algorithm," *Cluster Computing*, vol. 21, no. 1, pp. 955–966, 2018.

- [14] H. Hu and H. Yan, "Multi-sensor data fusion algorithm of wisdom agriculture based on fusion set," in *2018 International Conference on Virtual Reality and Intelligent Systems (ICVRIS)*, pp. 121–124, Hunan, China, 2018.
- [15] A. Gushcha, A. Vershinin, S. Arestov et al., "Advantages and weaknesses of percutaneous endoscopic lumbar discectomy: algorithm selection," *Coluna/Columna*, vol. 17, no. 3, pp. 200–205, 2018.
- [16] H. Jia, Z. Wei, X. He, and M. Li, "A research on lane marking detection algorithm based on neural network and least squares method," *Qiche Gongcheng/Automotive Engineering*, vol. 40, no. 3, pp. 363–368, 2018.
- [17] K. Wang, L. Li, and S. Peng, "Realization and optimization of a LWE sampling algorithm," *Beijing Jiaotong Daxue Xuebao/Journal of Beijing Jiaotong University*, vol. 41, no. 5, pp. 32–36, 2017.
- [18] P. Li, "Research on radar signal recognition based on automatic machine learning," *Neural Computing and Applications*, vol. 32, no. 7, pp. 1959–1969, 2020.
- [19] Y. Cui, Y. Ma, Z. Zhao, Y. Li, W. Liu, and W. Shu, "Research on data fusion algorithm and anti-collision algorithm based on internet of things," *Future Generation Computer Systems*, vol. 85, pp. 107–115, 2018.
- [20] F. Ye, J. Chen, Y. Li, and J. Kang, "Decision-making algorithm for multisensor fusion based on grey relation and DS evidence theory," *Journal of Sensors*, vol. 2016, Article ID 3954573, 11 pages, 2016.
- [21] M. Willson, "Algorithms (and the) everyday," *Information Communication & Society*, vol. 20, no. 1, pp. 137–150, 2017.
- [22] S. Sahoo and S. Jha, "Deepak Prashar, A novel approach for spam email filtering using machine learning," *Journal of Cybersecurity and Information Management*, vol. 2, 2020.
- [23] P. I. Stetsyuk, "Theory and software implementations of Shor's r-algorithms*," *Cybernetics and Systems Analysis*, vol. 53, no. 5, pp. 692–703, 2017.
- [24] J. V. Ferreira Lima, I. Raïs, L. Lefevre, and T. Gautier, "Performance and energy analysis of OpenMP runtime systems with dense linear algebra algorithms," *Experimental Mechanics*, vol. 33, no. 3, pp. 431–443, 2019.
- [25] L. Zhang, "Design of a sports culture data fusion system based on a data mining algorithm," *Personal and Ubiquitous Computing*, vol. 24, no. 1, pp. 75–86, 2020.
- [26] A. A. Elngar and S. I. El-Dek, "A novel artificial face mask based nanofibers with special intelligent engineered nanocomposite against Covid-19," *Journal of Cybersecurity and Information Management*, vol. 5, 2020.
- [27] J. Tang, X. Zhou, Y. (Chris) Zhao, and T. Wang, "How the type and valence of feedback information influence volunteers' knowledge contribution in citizen science projects," *Information Processing & Management*, vol. 58, no. 5, 2021.
- [28] D. Ojeda, "'One and Three Books' unfolded," *Design Issues*, vol. 35, no. 2, pp. 101–112, 2019.
- [29] J. Blunden, "Bridge or barrier? Writing in secondary art & design education in the UK," *International Journal of Art & Design Education*, vol. 38, no. 4, pp. 916–926, 2019.
- [30] N. A. Slater, M. Dhanasekaran, and M. Govindarajulu, "Design thinking in pharmacy education: the future of classroom preparation," *New Directions for Teaching and Learning*, vol. 2020, no. 162, pp. 113–121, 2020.

Research Article

Applying Knowledge Graph to Analyze the Historical Landscape Based on CiteSpace

Youping Teng,¹ Yue Huang ,² and Shuai Yang ^{1,3}

¹Department of College for Creative Studies, Zhejiang University City College, Hangzhou 310015, China

²Faculty of Innovation and Design, City University of Macau, Macau 999078, China

³College of Computer Science and Technology, Zhejiang University, Hangzhou 310063, China

Correspondence should be addressed to Yue Huang; yangs@zucc.edu.cn and Shuai Yang; samyang@zju.edu.cn

Received 22 November 2021; Revised 21 December 2021; Accepted 27 December 2021; Published 10 January 2022

Academic Editor: Mu-Yen Chen

Copyright © 2022 Youping Teng et al. This is an open access article distributed under the Creative Commons Attribution License, which permits unrestricted use, distribution, and reproduction in any medium, provided the original work is properly cited.

The theory of “urban historical landscape” is gradually emerging in cultural heritage protection and urban planning in recent years. It was first proposed and promoted by UNESCO. In this study, the identification and evaluation are taken as the prerequisite for the protection and management of historical landscape. This paper uses CiteSpace to analyze the map of knowledge data to collect and sort out the global research status of urban historical landscape. In addition, the clustering function of knowledge graph software VOSviewer is used to analyze the knowledge clustering in the research field of urban historical landscape, and the research process and interdisciplinary development of urban historical landscape are obtained, to make some guiding suggestions for the future study of urban historical landscape. The results show that the study of urban historical landscape has experienced three stages. The early stage is the introduction and tracing stage, the middle stage is the diversification and enrichment stage, and the recent stage is the practice and construction stage. At present, it has become a multidisciplinary and multiperspective international research. The in-depth study of urban historical landscape undoubtedly opens a door for the traditional thought of urban heritage protection. At the same time, it gradually turned to more active management of urban historical landscape and also promoted the intersection of city, architecture, landscape architecture, anthropology, sociology, economics, and other disciplines from the side, with far-reaching influence. Reviewing and looking forward to studying urban historical landscape is more conducive to sustainable construction of the future. CiteSpace, as an excellent bibliometrics software, can help researchers sort out and display past research tracks in a novel visual way, to conduct future research better.

1. Introduction

International theoretical research on urban historical landscape is fairly mature, and the government has formulated relatively complete protection laws and regulations. For example, the English Historical Landscape Characteristics Assessment System and Ballarat 2.0 City Historical landscape Digital Heritage Information Service System have made experimental and demonstrative innovations in using digital information technology to serve urban historical landscape protection. It provides experience for exploring the preservation of urban historical landscape. With the in-depth understanding of the urban historical landscape, the cognition of heritage also extends to the social dimension

of the city, especially the dynamic process of its historical layering [1–3]. The concept of urban heritage has also been transformed from commemorative dimension to regional dimension and then to social dimension [4, 5].

2. Data Graph Analysis

CiteSpace is a visualization tool for scientific mapping knowledge. It was developed by Professor Chen Chaomei’s team in 2004. Based on the cocitation theory and pathfinder network algorithm, this software conducts multivariate, time-sharing, and dynamic citation analysis on bibliographies of specific fields, to explore the critical path and knowledge inflection point of the evolution of the subject field. Finally, the mapping

knowledge domains reflecting the evolution process and development frontier of knowledge of this discipline was drawn by visualization technology [6]. CiteSpace is a Java application. Its primary function is to effectively identify the new research trends and dynamics reflected in the research literature, and at the same time, to visualize and data the research trends. In this study, the method of mapping knowledge domains was adopted and the visualization software CiteSpace was used for the visualization analysis of historical landscape. In practical methods, Author, Institution, Keyword, Cited Reference, and other options are selected in the software. Node strength, threshold, and parameters of network clipping functional area are set according to the different characteristics of the literature in Web of Science (WoS) and CNKI databases. After running the software, the statistical data and cooccurrence map of historical landscape research can be obtained, and then, the research status, hot spots, and frontiers can be analyzed.

Mapping knowledge domains are maps used to show the relationship between the development process and structure of scientific knowledge. It is not only a visualized knowledge graph but also a serialized knowledge pedigree with dual properties of graph and spectrum. The mapping knowledge domains can express and describe the network structure, interaction, crossover, derivation, and other complex relationships between the research field and related research fields. The mapping knowledge domain is an image that shows the relationship between the development process and structure of scientific knowledge by taking knowledge domain as the object [7]. According to the instructions in CiteSpace Chinese operation manual, the author uses the following steps to analyze the literature data. The system framework is as shown in Figure 1.

In this study, CiteSpace was used to draw all the scientific knowledge maps of urban historical landscape at home and abroad during 1988-2019. The emphasis is to deeply excavate and study the countries of urban historical landscape, find the keywords related to the urban historical landscape, and record and summarize the relevant literature that can be cited. To ensure a comprehensive analysis of the historical context of the historical landscape, the China National Knowledge Network (CNKI) database is used for relevant literature in China. CNKI has the broadest coverage, the most significant number, and the richest resource types. The global relevant literature data were selected from the core collection database of Web of Science, with the theme of "Urban Historical Landscape." The article type was set as unlimited, and the retrieval period was 1900-2019. Eight hundred ninety-four retrieval results were obtained (retrieval time on September 15, 2019). The retrieval results were screened one by one, irrelevant articles and nonacademic articles such as book reviews were removed, and duplicate literature were deleted. Finally, 772 valid literatures were obtained. In this paper, the selected literatures are downloaded and saved as plain text files in the format of "abstract and full record (including cited references)" as data samples for foreign literature analysis. By selecting journals, master's and doctor's databases in CNKI, and using advanced search, 367 results were obtained based

on "Urban Historical Landscape" (search date: September 15, 2019). The retrieval results were screened and irrelevant articles were eliminated, and 293 useful articles were obtained. The selected literatures were saved in RefWorks format as data samples for Chinese literature analysis.

Finally, we can accurately grasp the appropriate situation of urban historical landscape research and the relevant research direction that experts and scholars have been keen on in recent years. In addition, the clustering function of knowledge graph software VOSviewer is used to analyze knowledge clustering in the field of urban historical landscape research [8].

3. Overview of Urban Historical Landscape Research

3.1. Research Status of Urban Historical Landscape. We can get the spatiotemporal distribution characteristics of urban historical landscape research at home and abroad by combining the relevant literature of urban historical landscape. From the perspective of time distribution, the literature on the study of historical urban landscapes, first published in 1988. Since 2005, the research on urban historical landscape has shown an increasing trend year by year, but it has declined in 2019. 2005 is an important time node for studying the urban historical landscape, which is attributed to the fact that in 2005, the World Heritage Center and other professional institutions jointly held a conference on "World Cultural Heritage and Contemporary Architecture [9]." At the international conference on historic town landscape, the concept of urban historical landscape was formally put forward in Vienna Memorandum for the first time. Subsequently, the research on urban historical landscape began to spread rapidly, as shown in Figure 2.

From the perspective of spatial distribution, we find that the cities where the current institutions studying urban historical landscape are mainly located in Europe, America, and East Asia, such as the United States, Italy, Spain, and China. As shown in Figure 3, from 1988 to 2018, two years were taken as a time slice. The study took each country as a node, and then drew the national time slice map of urban historical landscape. The documents issued by various countries are as follows: The United States has the most significant amount of records in the urban historical landscape, followed by Italy and Spain. In addition, the research on urban historical landscape in Britain and Turkey is also wealthy. For the study of urban historical landscape, Europe has always been in the forefront of the world, paying special attention to the idea of integrated conservation. As early as the "European Year of architectural heritage" in 1975, EU countries jointly negotiated and issued the European Charter of architectural heritage. One of them clearly states: for European architectural heritage, the protection of those very important and commemorative buildings must bear the brunt. However, some neglected architectural groups with historical value in old towns, as well as typical villages surrounding them, also need to be taken as objects of protection. Britain has always been at the forefront of the world in

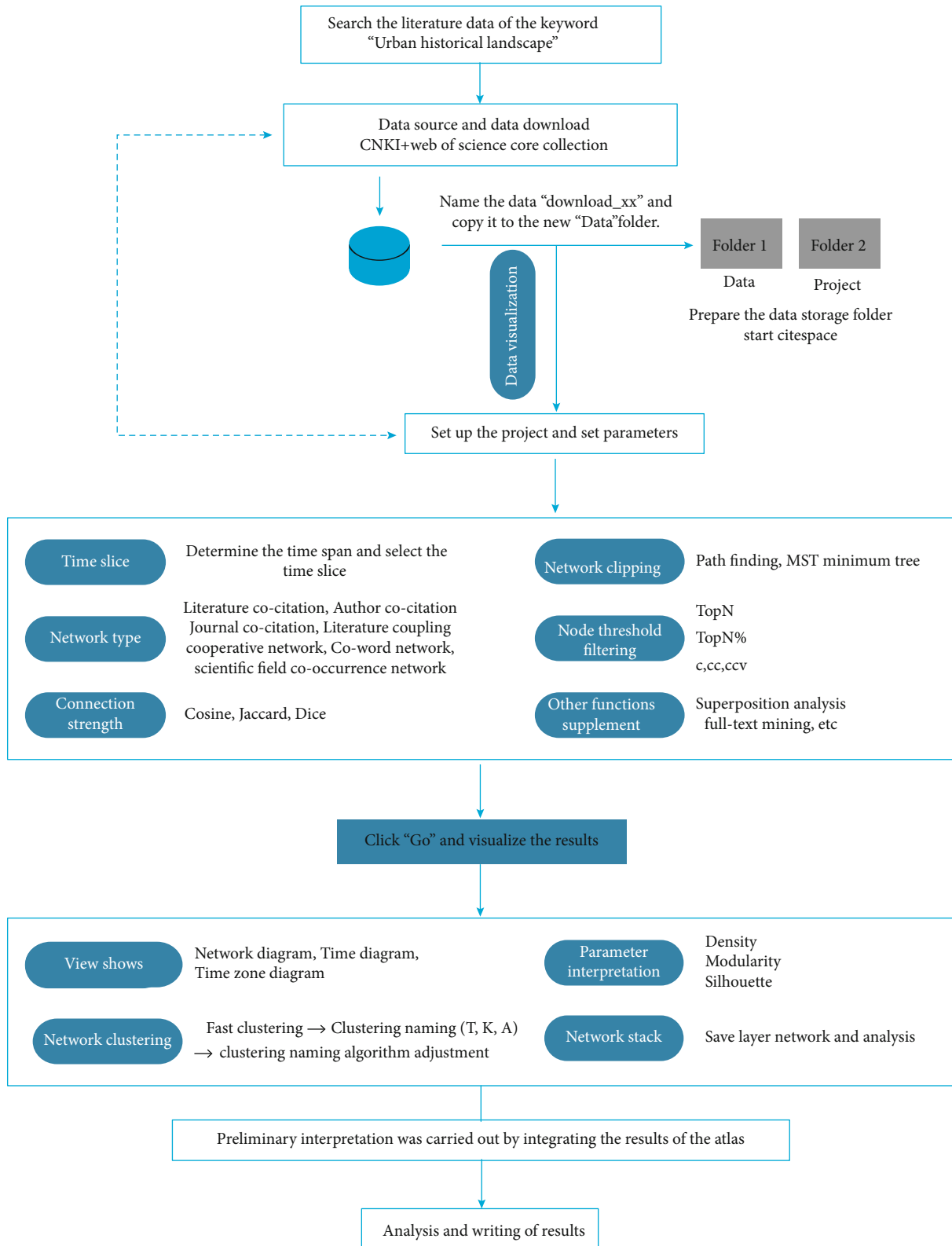


FIGURE 1: Using the CiteSpace to apply study flowchart.

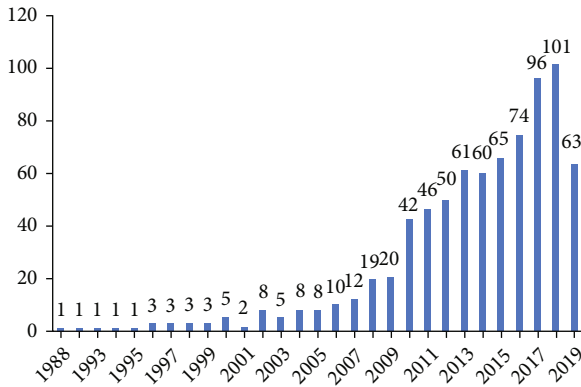


FIGURE 2: The number of documents in the study of the urban historical landscape over the years.

the protection of the urban historical landscape. It made a thorough study of the contradiction between urban historical landscape protection and development, which provides a theoretical and practical basis for other countries' research in this area.

In CiteSpace, if the centrality of a node is relatively high, it means that the node plays a significant role in the field of this discipline, and it plays a crucial role in connecting other nodes. As for the research field of urban historical landscape, the central intermediary data of various countries are as follows: (1) the Netherlands, Britain, Belgium, France, and Australia are 0.27, 0.20, 0.21, 0.16, and 0.11, respectively, which are in the first-class position among countries. Although these countries have relatively few documents in urban historical landscape, they have a great influence. (2) The United States, Italy, Spain, and China are 0.06, 0.06, 0.03, and 0.03, respectively. Although the number of documents issued in the field of urban historical landscape in the four countries is much higher than that in other countries, the output quality of these documents is uneven, and their breadth and depth are insufficient compared with the first category of countries.

3.2. Overview of Important Literature in the Field of Urban Historical Landscape Research. As for the study of urban historical landscape, the documents of UNESCO and BANDARIN F are presented in the citation network diagram as the documents with the highest citation rate. According to Figure 4, five classical literatures with the most critical value in the field of urban historical landscape research are listed in the order of frequency and number of citations:

- (1) The 36th Session of the General Conference of UNESCO (2011) adopted the Recommendation on the Protection of Historic Urban Landscape in Paris, formally proposing the definition of urban historical landscape, as well as related concepts and guiding methods [10, 11]
- (2) F. Bandarin wrote "The Historic Urban Landscape: Managing Heritage in an Urban Century," which suggests that the urban historical landscape is a new method of urban heritage management advocated by

UNESCO. He draws and analyzes examples from global urban heritage sites from Timbuktu to Liverpool and then proposes key issues and measures to address the conservation of urban historical landscapes. His research reflects the latest progress in HUL theory, practice, and related interdisciplinary research [12]

- (3) Veldpaus wrote "Urban Heritage: Putting the Past into the Future," which argues that the management of urban historical landscapes is undergoing a process of change in both theory and practice, from focusing on isolated architectural heritage assets to a landscape-based approach that incorporates elements such as environment and context, as well as concepts such as urban sustainability. It also discusses the landscape-based approach to urban heritage management, its challenges and possible contributions, and proposes to promote sustainable development and the protection of urban heritage. In addition, there is a need not only to talk about development but also to assess the adequacy of the tools and methods used to support the implementation of an integrated approach to urban development [13]
- (4) Through "Historic Urban Landscape: Fashion, Paradigms and Omissions," J.L. Lalana found that after six years of expert meetings and debate since the Vienna Memorandum, the UNESCO General Conference plans to adopt a recommendation at its 36th session in autumn 2011. This paper presents a new approach to the protection of historic buildings in cities. Historical urban landscape refers to the adjustment of urban heritage protection according to the requirements of sustainable development and the direction of comprehensive consideration of different heritage types, but at the same time, it also produces serious application problems, such as the use of the word landscape, so that the term becomes imprecise, difficult to apply, and prone to distortion. And, the urban historical landscape is considered to be the solution to the overall protection of the city; at the same time, there is a lack of critical reflection on the revitalization of the historic urban system [14]
- (5) L.F. Girard wrote "Toward a Smart Sustainable Development of Port Cities/Areas: The Role of The "Historic Urban Landscape" Approach," he proposed that after the 2008 financial crisis, the smart and sustainable development of port cities should carry out the principles of synergy (between different actor systems, especially sociocultural and economic systems), innovation, and cycle on the original basis. The urban historical landscape approach, based on specific local cultural resources rather than merely technological innovation, has become the guarantee for the transition to a smart city development model. In other words, the ecocity strategy becomes culturally dominant, which stimulates the place as a spatial trajectory, achieving synergistic and circular processes. The absence of new

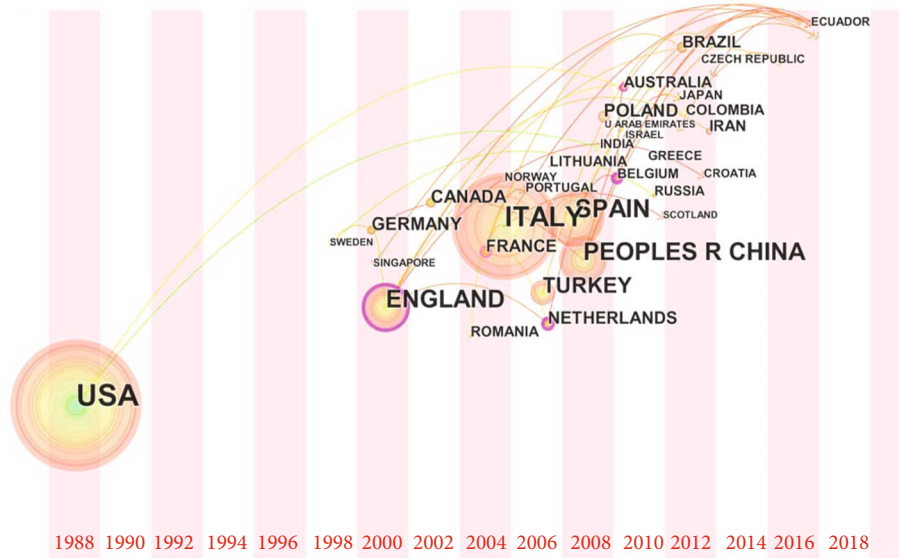


FIGURE 3: National time slice graph of urban historical landscape research.

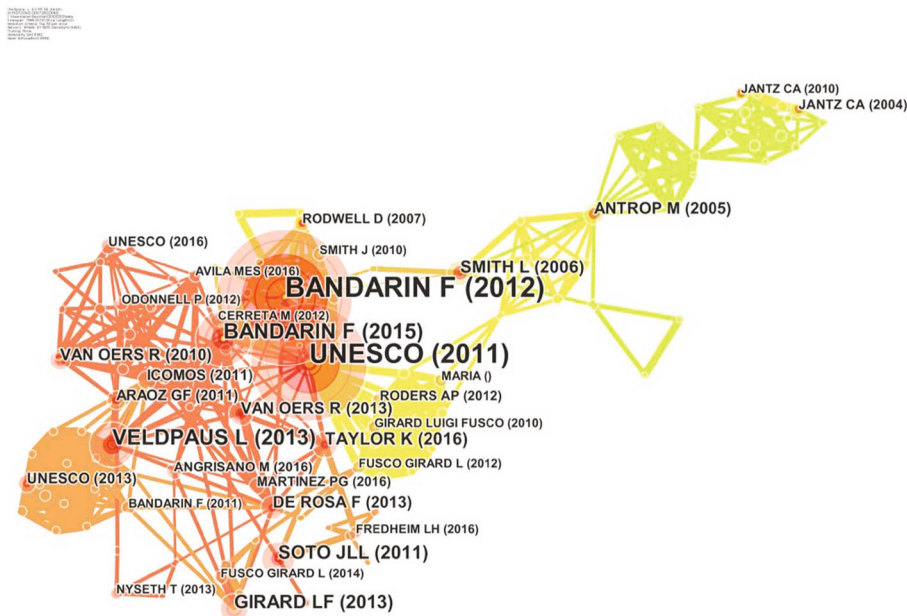


FIGURE 4: Network diagram of literature cocitation of urban historical landscape.

assessment tools and an extensive assessment culture makes the risk of HUL very high [15]

4. The Research Dynamics and Knowledge Graph Analysis of the Urban Historical Landscape

For CiteSpace, references as raw materials are the basis for analyzing the research frontier of a subject. Because of this, it is necessary to sort out the knowledge base of the urban historical landscape before analyzing the hot spots and research frontiers of urban historical landscape. The

purpose of sorting out is to identify the primary research documents that directly promote the urban historical landscape discipline. The essence of the cocitation analysis is that 772 literatures are taken as objects. High citation frequency means that the literature has relatively high academic value and is highly influential in urban historical landscape.

4.1. Knowledge Graph Analysis of Research Hotspots. In this paper, the urban historical landscape in literature is taken as the keyword, and pathfinding is taken as the pruning method to highlight the main structural features. After the keywords irrelevant or irrelevant to the urban historical

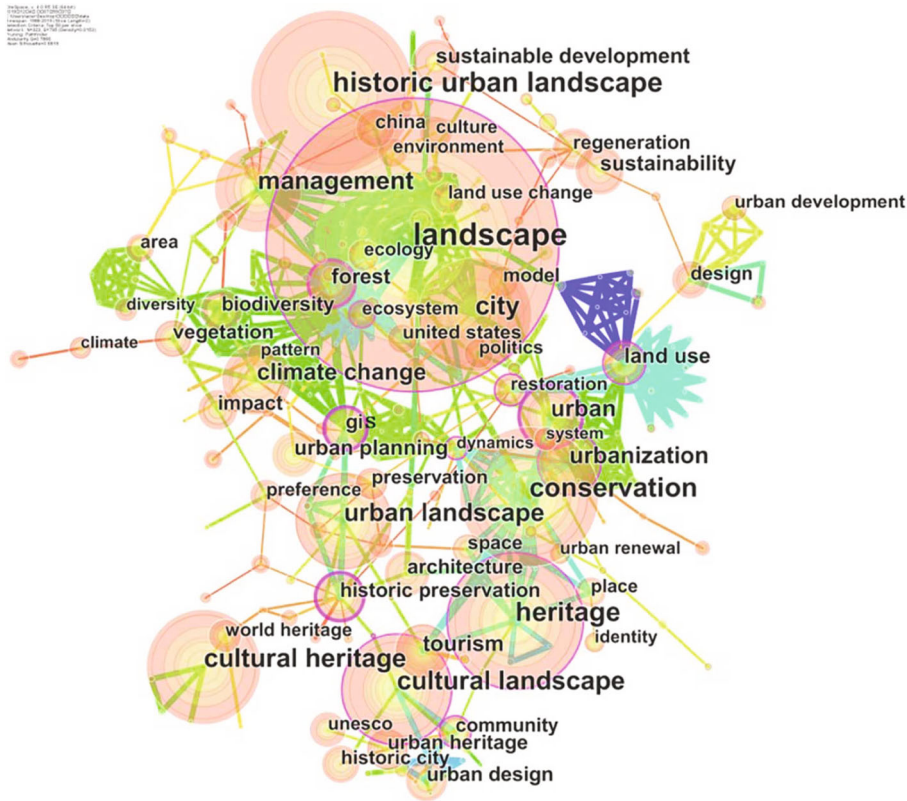


FIGURE 5: Cooccurrence relationship diagram of keywords in the urban historical landscape.

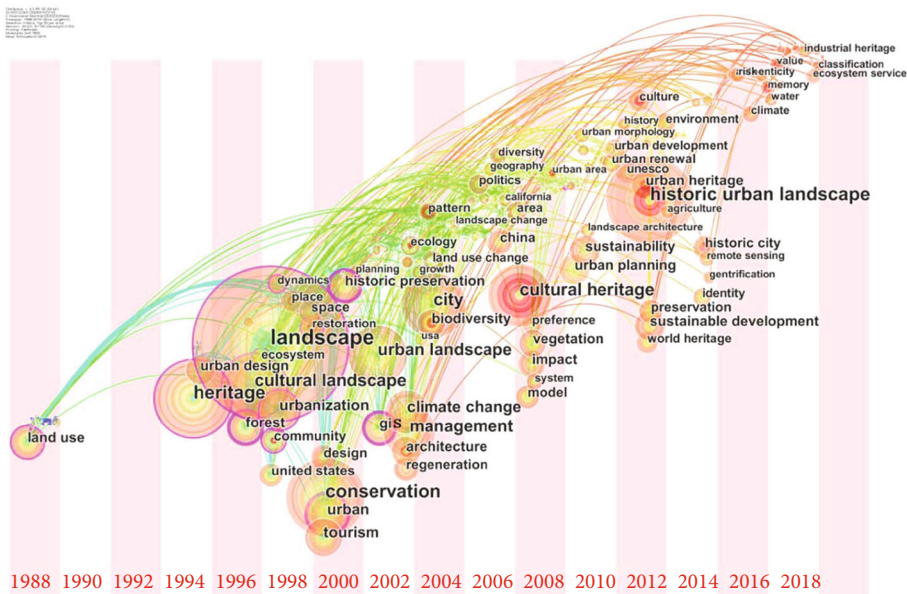


FIGURE 6: Urban historical landscape keywords cooccurrence time slice diagram.

landscape are eliminated, the cooccurrence relation diagram and its time slice map of keywords in the urban historical landscape are drawn, as shown in Figures 5 and 6. As shown in Figure 4, in addition to landscape and urban historical landscape, the core keywords of foreign urban historical landscape also include forest, historical pro-

tection, restoration, community, heritage, and cultural landscape. In order of the number of occurrences of keywords, we found that the top 10 keywords were landscape, urban historical landscape, conservation, heritage, cultural landscape, cities, cultural heritage, urban landscape, management, and climate change.

Figure 5 shows the evolution law of hot spots in the field of urban historical landscape research from the time dimension. It discusses the evolution of urban historical landscape in different years by identifying hot areas in different years. In the 30 years we intercept, hot keywords have appeared since 1996, and the keyword “Landscape” has been throughout the study of urban historical Landscape. Keywords such as “Cultural Landscape”, “Cultural Heritage”, and “Management” all occupy an essential position in the analysis of urban historical Landscape.

As far as the evolution path of urban historical landscape research hotspots is concerned, it can be divided into three stages:

The first stage is the embryonic stage—before 1994. At this stage, scholars mainly study the peripheral parts of urban historical landscape (such as land use), but they have not touched the core field of this discipline. The interpretation of landscape is also limited to the description of words. For example, William Wordsworth (1770-1850), an English poet, described the beautiful landscape through poetry, making people imagine the beautiful landscape, which belongs to the initial understanding of human landscape.

The second stage is the development stage from 1994 to 2013. At this stage, scholars have conducted a lot of research on urban landscape, cultural landscape, and historical landscape based on “landscape,” which laid a foundation for the concept of urban historical landscape. According to The European Landscape Convention, the shaping of landscape is the result of the interaction and influence between human beings and the material elements of the surrounding natural environment. [16].

It can be seen that the concept of landscape is not simply formed naturally but has the intervention effect of external influence. Gradually, the idea of cultural landscape is highlighted. As Roberts and Sykes pointed out, urban development is not just a simple place to carry buildings and people’s survival, but a cradle of multiple and complex integrations, which contains various forms of activities such as economic activities, social activities, military activities, and political activities [17]. Diversity stimulates the creativity and new context of the city. The city must be rebuilt and constantly updated to make it more attractive [18].

The third stage has been the climax stage since 2013. Since UNESCO officially defined the urban historical landscape, the research on this subject has been booming, and a scientific and complete knowledge and application system has been formed. And the analysis on subdivided fields is also very in-depth. There are more and more articles about historical and cultural blocks, architectural heritage protection, and cultural landscape research, and the quality of articles is getting higher and higher. For the study of layering, such as Brent C’s book *Architecture and Context: the Cooperation between New and Old Buildings*. He advocated studying architectural style from the context of the city. For the study of urban historical landscape, many commonly used terms, such as historical urban landscape, urban heritage, and setting, are international terms put forward by the United Nations in recent years. Scholars and experts have also given specific explanations on the definitions of the

above proper nouns. There is a contradiction between the protection and development of historic cities. Many scholars around the world have put forward such problems in research.

4.2. Knowledge Graph Analysis of Domain Dynamics. Using knowledge map analysis, this paper is aimed at aggregating similar or related keywords into a block through the clustering function of VOSviewer and then use the color difference to make a visual expression [19].

Figure 7 reveals three research fields of urban historical landscape discipline: red is the field of management and application, blue is the field of planning and protection, and green in the field of urban historical landscape analysis and research.

The first is the management application field. The high-frequency keywords in this field are management, urbanization, land use, etc. The research in this field mainly discusses the application and management of urban historical landscape, including the use of urban land and the situation of the urban historical landscape under urbanization. Its purpose is to adopt management methods or measures, so that the urban historical landscape can play a better role in urban development. The second is the field of planning and protection. The high-frequency keywords in this field are planning, security., etc. It is research mainly discusses the contents of urban planning, landscape planning, urban historical planning, and protection. The purpose is to better continue the urban historical landscape through planning and protection.

The last is the analysis and research field. The high-frequency keywords in this field are urban historical landscape, the urban landscape, and cultural landscape, etc. The research mainly discusses the concept and value of urban historical landscape, urban landscape, and cultural landscape from the theoretical level. It extends to other fields, such as history and culture. Its purpose is to reveal the origin and value of urban historical landscape and then reflect the characteristics of a city.

5. Application of Urban Historical Landscape Theory in Heritage Protection

5.1. Value Attribute of Historical Layering in the Urban Historical Landscape. Urban historical landscape is the product of the interaction between objective material ring and human subjective will, which has the attribute of combining internal cause of value and explicit features. It has the attribute of the integration of internal and external characteristics of value [20]. The appearance feature is the external expression of the internal cause of value. The internal cause of value is the internal driving force to promote the presentation of object image features in space. Taking urban historical landscape as an example, this paper puts forward a historical stratification model based on the layering spatial schematics of many scholars and researchers [21] (Figure 8). Its internal causes are embodied in cultural aspects, such as religious culture and folk customs. These internal factors have played an essential role in city historical landscape layering and are also the form of dark parts in the

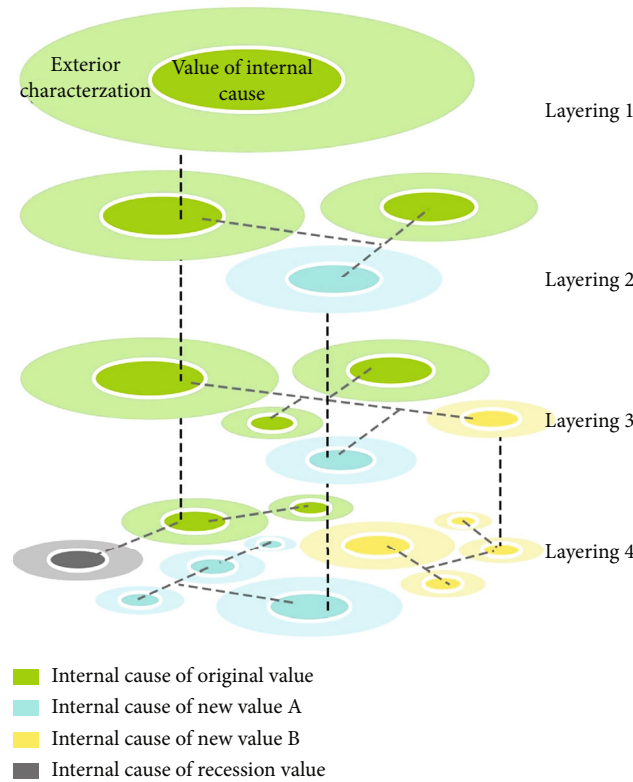


FIGURE 9: Analysis of urban historical landscape layering.

elements, object to object, interior to exterior, and time to space all influence each other in the development process. The layer upon layer of superposition is clearly combed out through the analysis of superposition and layering. Thus, it can be seen that the value of the study on the stratification of urban historical landscape is that it can accurately sort out the external representation of the city and the value correlation that is constantly updated. Through combining, it makes the research thinking broader, the sorting of the urban context more apparent, and the protection of the urban historical landscape more targeted.

5.3. History and Heritage Value. The urban character can be simply understood as the personality of a city, but it is also highly complex. It is embodied in the landscape of the city materially and in the spirit of civic spirit. It is formed through the intervention of human and social factors in the process of city history. An expert in historical studies mentioned that it is impossible for us to thoroughly understand the growth process of trees every moment of every day. However, over time, we can observe the tree's growth, and the process of its growth from small to large and flourishing can be seen over time. The development of a city is just like a big tree. Although we cannot perceive its development process every moment, we can grasp its overall trend and the most central content over time. The details of history are just like the branches and leaves of a tree, so the urban characteristics are shown by branches, leaves, flowers, and other aspects. Urban character is like the difference

between a tree and other trees, we call it character, and the layering is like the rings of a tree, recording the growth of the tree (Figure 10). Branches, leaves, flowers, and fruits grow under each tree ring, just like the development characteristics of various aspects of the city under each layer, such as culture, society, and economy. Through the gradual accumulation of multiple layers, the characteristics of the city are finally formed. We can no more find two identical trees than we can find two twin cities. What makes a tree special depends on its variety, age, and growth, while what makes a city special depends on its country, history, and environment. Only by drawing inspiration from the past development trajectory of a city can we find the characteristics of its future development. Therefore, the analysis and correlation of layering is the excavation and tandem of various factors in the city's history of the, and its historical value is obvious.

Historical layering studies the events that happened in history and the veins of people, things, and cities. Taking historical culture as the mainline, it is an overview of the accumulation of layers of urban historical landscape. Historical culture is a unique city temperament formed in the evolution of urban historical landscape. Usually, it is related to the historical characters, events, and all factors that constitute history and culture experienced in the development of a city. It directly affects the development process. In the process of historical layering, it is concluded that the connotation of each layer is composed of the people, things, and things associated with it, and these factors give the city its

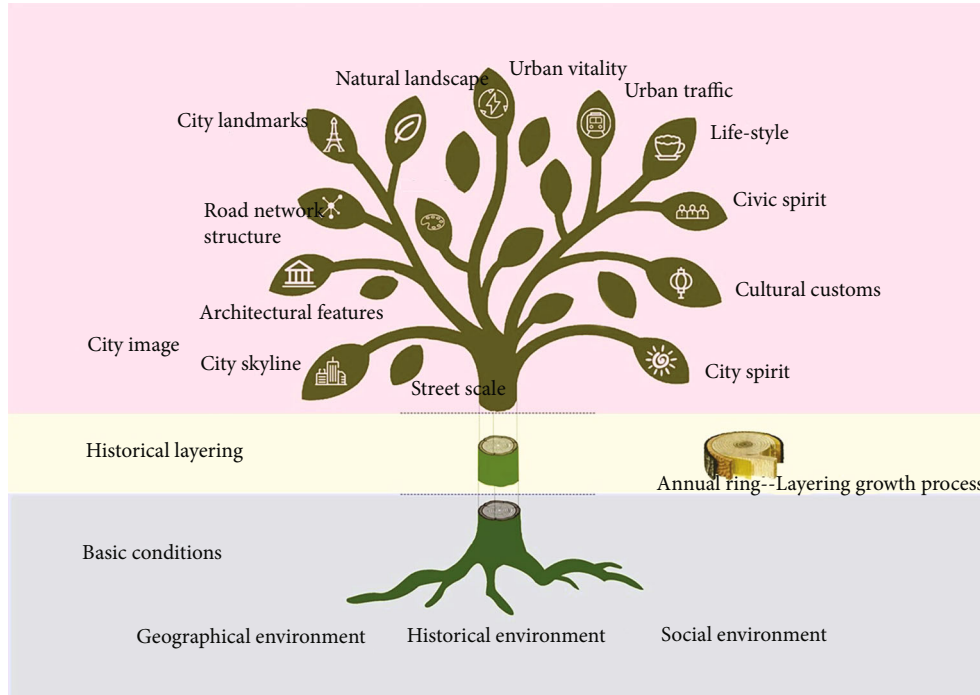


FIGURE 10: The tree-like interpretation of historical layering. Figure source: drawn by Shuaiyang.

unique context. These factors have given the city its unique context, which has become a unique historical landscape of the city. The study of cities, based on the method of historical layering, is helpful to excavate the unique layering value hidden in the historical context of cities. It includes the historical layering value hidden behind the historical and cultural blocks and other relatively ordinary urban spaces and shows the characteristics of historical cities in a more comprehensive and in-depth way, so as to improve the urban phenomenon of “thousands of cities are the same.” The historical and cultural resources with layering value are sorted into a characteristic spatial network, which is helpful to connect the historical and cultural resources at all levels. The aim is to show the memory of the city, enrich the conservation hierarchy of the historical urban planning, and thus make the conservation system more stable [22]. And, with the continuous development of the city, the database established based on the spatial network with historical layering characteristics will accumulate more historical information of the city, while protecting the existing characteristics of the city, it can also provide the direction for future urban development. The study of historical layering plays an essential role in connecting the past and the future in a city. The urban historical landscape presented by historical layering has obvious historical and cultural characteristics.

6. Conclusion

Based on two knowledge graph analysis software, CiteSpace, and VOSviewer, this study analyzes the relevant data of urban historical landscape research, especially the domestic and foreign literature on urban historical landscape, and

makes a detailed visual analysis and interpretation. Through the comprehensive analysis of urban historical landscape literature data by CiteSpace, it is found that the knowledge map of urban historical landscape research has a certain breadth and depth. The results show that, in terms of publication time, the number of papers on urban historical landscape has been increasing year by year and has experienced a slow growth stage to a rapid growth stage in recent years. According to the cooccurrence map between countries, the Netherlands, the United Kingdom, Belgium, France, Australia, and other countries published fewer documents, but the breadth and depth of literature are better. Although the number of papers published by the United States, Italy, Spain, China, and other countries is higher than that of other countries, the output quality of literature is uneven, and its breadth and depth are insufficient compared with those of the first category. According to the network relationship map of cited literature, the literature with the top 5 cited volumes are classics of great significance. They have a far-reaching influence on the study of urban historical landscape. Among them, Bandarin F’s research in *Reconnecting Cities: Urban Historical Landscape Approach and the Future of Urban Heritage* reflects the latest progress in the interrelation between HUL theory, practice, and related cross-disciplines and points out the direction for the research of this subject. In addition to landscape and urban historical landscape, keywords such as forest, historic preservation, restoration, community, heritage, and cultural landscape are also found in the cooccurrence diagram and its time slice diagram. The research perspective tends to be diversified and presents a trend of interdisciplinary. The atlas reveals three significant areas of urban historical landscape research,

which are management and application, planning and protection, and analysis and research of urban historical landscape. This paper discusses the concept and value of urban historical landscape, urban landscape, and cultural landscape from the theoretical level and continues to extend to other fields. The three constitute the development of the study of urban historical landscape.

The concept of “urban historical landscape” has been discussed frequently for more than ten years since it was put forward, and the concept itself continues to go through the process of deepening and expanding. It not only has considerable theoretical continuity but also has excellent potential and openness to continue to be constructed. The concept of value is constantly deepened in the literature. Under the premise of protecting value, how to reasonably guide the modernization needs of historical cities has become a critical problem. This requires an urban planning and management policy with conservation as its central starting point. However, in the whole process, the authenticity and integrity of historical cities determined by various factors must not be jeopardized, which has become the leading research topic of scholars from all over the world.

Data Availability

The raw data supporting the conclusions of this article will be made available by the authors, without undue reservation, to any qualified researcher.

Ethical Approval

This article does not contain any studies with human participants or animals performed by any of the authors.

Consent

Informed consent was obtained from all individual participants included in the study.

Conflicts of Interest

All authors declare that they have no conflict of interest.

Authors' Contributions

All authors listed have made a substantial, direct, and intellectual contribution to the work and approved it for publication.

Acknowledgments

This work is supported by the China Postdoctoral Science Foundation (Grant No.: 2021M692781).

References

- [1] UNESCO, “Report on the International World Heritage expert meeting on the mainstreaming of the methodological approach related to the recommendation on the historic urban

landscape,” *Operational Guidelines*, 2013, <https://www.whc.unesco.org/document/135630>.

- [2] UNESCO, “International Conference on “culture for sustainable cities”,” 2015, <https://www.unesco.org/new/en/culture/themes/culture-and-development/culture-for-sustainable-cities>.
- [3] UNESCO, “Culture urban future, global report on culture for sustainable urban development,” 2016, <https://unesdoc.unesco.org/images/0024/002459/245999e.pdf>.
- [4] UNESCO, “The application of the recommendation on historic urban landscape (HUL) in Cuenca–Ecuador,” 2017, <https://www.historicurbanlandscape.com/themes/196/userfiles/download/2017/6/19/hkmmquzjahrenkba.pdf>.
- [5] Y. Huang, W. Wu, and S. Yang, “Sustainable development of green building based on intuitionistic fuzzy analytic hierarchy process,” *Applied Ecology and Environmental Research*, vol. 17, no. 1, pp. 1093–1108, 2019.
- [6] Y. Chen, C. M. Chen, and Z. Y. Liu, “The methodology function of CiteSpace mapping knowledge domains,” *Studies in Science of Science*, vol. 33, no. 2, pp. 242–253, 2015.
- [7] Z. Y. Liu, *Mapping of Scientific Knowledge: Methods and Applications*, People's Press, Beijing, China, 2008.
- [8] Z. M. Li, L. H. Feng, and R. X. Shen, “The evolution of space syntax research abroad and knowledge mapping analysis in frontier fields,” *The Planner*, vol. 35, no. 8, pp. 5–11, 2019.
- [9] S. Zhang and X. F. Zhen, “Historic urban landscape: a new path to urban conservation,” *Journal of Tongji University*, vol. 22, no. 3, pp. 29–34, 2011.
- [10] UNESCO, “Proposals concerning the desirability of a standard-setting instrument on historic urban landscapes (Paris 36C/23),” 2011, <https://unesdoc.unesco.org/images/0021/002110/211094s.pdf>.
- [11] UNESCO, “Recommendation on the historic urban landscape, including a glossary of definitions,” 2011, https://portal.unesco.org/en/ev.phpURL_ID=48857&URL_DO=DO_TOPIC&URL_SECTION=201.html.
- [12] F. Bandarin and R. Van Oers, *The Historic Urban Landscape: Managing Heritage in an Urban Century*, Viley Black Well Press, London, England, 2012.
- [13] L. Veldpaus, A. R. Pereira Roders, and B. J. F. Colenbrander, “Urban heritage: putting the past into the future,” *The Historic Environment Policy & Practice*, vol. 4, no. 1, pp. 3–18, 2013.
- [14] J. L. Lalana, “Historic urban landscape: fashions, paradigms and omissions,” *Ciudades*, vol. 14, no. 2, pp. 15–38, 2011.
- [15] L. F. Girard, “Toward a smart sustainable development of port cities/areas: the role of the “historic urban landscape” approach,” *Sustainability*, vol. 5, no. 10, pp. 4329–4348, 2013.
- [16] R. V. Orse, “The concept of urban historical landscape and its relation to cultural landscape,” *Chinese Garden*, vol. 28, no. 5, pp. 16–18, 2012.
- [17] P. Roberts and H. Sykes, *Urban Regeneration—A Handbook*, Sage Publications, London, England, 2000.
- [18] R. Dennis, “Urban regeneration and the management of change,” *Journal of Architectural Conservation*, vol. 14, no. 2, pp. 83–106, 2008.
- [19] K. Gao, “Application research of document metrology analysis software VOSviewer,” *Science and Technology Information Development and Economy*, vol. 25, no. 12, pp. 95–98, 2015.
- [20] L. Heping and X. Jing, “Analysis on the types and components of China's cultural landscape,” *Chinese Garden*, vol. 2, no. 5, pp. 90–94, 2002.

- [21] Y. M. Cao and H. P. Li, "Diachronic and synchronic characteristics in the protection of historic towns – enlightenment and thinking of urban historical landscape," *Urban Development Research*, vol. 26, no. 10, pp. 13–20, 2019.
- [22] R. V. Orse, "Towards new international guidelines for the conservation of historic urban landscapes (HUL)," *City & Time*, vol. 3, no. 1, pp. 43–51, 2007.

Research Article

The Effect of 3D Image Virtual Reconstruction Based on Visual Communication

Li Xu,¹ Ling Bai,² and Lei Li³ 

¹School of Art and Design, East University of Heilongjiang, Harbin 150001, China

²School of Information, Guangsha College, Harbin 150025, China

³International Department, Heilongjiang International University, Harbin 150025, China

Correspondence should be addressed to Lei Li; lilei@hiu.edu.cn

Received 4 November 2021; Accepted 11 December 2021; Published 5 January 2022

Academic Editor: Alireza Souri

Copyright © 2022 Li Xu et al. This is an open access article distributed under the Creative Commons Attribution License, which permits unrestricted use, distribution, and reproduction in any medium, provided the original work is properly cited.

Considering the problems of poor effect, long reconstruction time, large mean square error (MSE), low signal-to-noise ratio (SNR), and structural similarity index (SSIM) of traditional methods in three-dimensional (3D) image virtual reconstruction, the effect of 3D image virtual reconstruction based on visual communication is proposed. Using the distribution set of 3D image visual communication feature points, the feature point components of 3D image virtual reconstruction are obtained. By iterating the 3D image visual communication information, the features of 3D image virtual reconstruction in visual communication are decomposed, and the 3D image visual communication model is constructed. Based on the calculation of the difference of 3D image texture feature points, the spatial position relationship of 3D image feature points after virtual reconstruction is calculated to complete the texture mapping of 3D image. The deep texture feature points of 3D image are extracted. According to the description coefficient of 3D image virtual reconstruction in visual communication, the virtual reconstruction results of 3D image are constrained. The virtual reconstruction algorithm of 3D image is designed to realize the virtual reconstruction of 3D image. The results show that when the number of samples is 200, the virtual reconstruction time of this paper method is 2.1 s, and the system running time is 5 s; the SNR of the virtual reconstruction is 35.5 db. The MSE of 3D image virtual reconstruction is 3%, and the SSIM of virtual reconstruction is 1.38%, which shows that this paper method can effectively improve the ability of 3D image virtual reconstruction.

1. Introduction

3D image virtual reconstruction technology has developed a set of stereo imaging system and has been gradually applied in various fields [1]. In recent years, with the continuous improvement of computer equipment and performance, virtual imaging technology has been well developed. In the traditional sense, 3D image virtual reconstruction technology uses computer technology to simulate the virtual environment and makes people feel the virtual environment or world through visual communication technology [2]. 3D image virtual reconstruction technology includes many disciplines and is a comprehensive composite virtual imaging technology, including computer modeling technology, virtual image processing technology, scene simulation technology, and human-computer interaction technology [3].

The effect of 3D image virtual reconstruction directly affects the overall visual and auditory experience of users. In the era of intelligence, 3D image virtual reconstruction technology is gradually widely used in military, education, medicine, and other fields. Using image processing technology and computer graphics technology to overlay texture image on the surface of a 3D scene geometric model, that is, texture mapping is an effective way to display the real world. Texture mapping technology integrates the best features of each method [4]. Texture mapping can greatly improve the visual richness of raster-scanned images with only a small amount of calculation. Texture mapping is one of the most successful new techniques in high-quality image synthesis [5]. Compared with traditional 2D images, 3D images have more visual impact, clear layers, and more bright colors. In the process of product development, it can better display the

development process and, at the same time, can support remote browsing, which saves users time and improves efficiency [6]. Visual communication technology can better convey information to users through visual media, instead of traditional 2D expressions. The new visual communication mode is adopted to infiltrate the information to be expressed into all aspects. The visual communication technology is applied to the virtual reconstruction of 3D image, the image processing is completed by computer, and the information to be expressed by the image is transmitted by visual symbols and expressed and transmitted to users through visual media [7].

Tereshchenko and Lysenko [8] put forward a medium analytical reconstruction method using proportional scattering, which can analytically reconstruct the medium under different parameters and analyze the scale coefficient and size of the object, which has better accuracy than the traditional analytical reconstruction method. Lee et al. [9] proposed a virtual database data recognition method based on a support vector machine. Through the collection and analysis of recognition scores of the periocular region, the training and evaluation of noisy iris are realized. The verification results of experiments show that this method has better robustness than the traditional method. Deabes and Bouazza [10] proposed a quantitative analysis and reconstruction method based on a locally integrated transform Kalman filter in order to realize the reconstruction of ECT system image. Through the error analysis of the collected image, a nonlinear system evaluation tool was constructed, and the authenticity and effectiveness of the method were verified through quantitative analysis. Wang et al. [11] put forward a 3D image reconstruction method using wireless domain truncation to solve the problems such as unsatisfactory reconstruction effect of small closed areas. Conformal transform is used for image reconstruction to optimize the image reconstruction information truncated in wireless domain. The results show that this method has higher accuracy for the reconstruction effect of small closed areas. In order to reconstruct the image information more accurately, Jiang et al. [12] used the infrared image reconstruction technology to measure the image information and construct the infrared image matrix equation. By solving the matrix equation, it is proved that this method has better reconstruction.

Based on the above research, this paper designs a 3D image virtual reconstruction method based on visual communication, so as to improve the effect of 3D image virtual reconstruction in visual communication. The main contributions of this paper are as follows: (1) Using the distribution set of 3D image visual communication feature points, the feature point components of 3D image virtual reconstruction are obtained. By iterating the 3D image visual communication information, the features of 3D image virtual reconstruction in visual communication are decomposed, and the 3D image visual communication model is constructed. (2) On the basis of calculating the difference of 3D image texture feature points, the spatial position relationship of 3D image feature points after virtual reconstruction is calculated, and the texture mapping of 3D image is completed. (3) According to the description coefficient of

3D image virtual reconstruction in visual communication, the results of 3D image virtual reconstruction are constrained by visual communication technology.

2. Design of 3D Image Virtual Reconstruction Method

2.1. 3D Image Visual Communication Model. In order to construct the visual communication model, the 3D image is reconstructed adaptively [13]. Assuming that the reconstructed image visually conveyed by the 3D image is S , the edge feature points of the original 3D image are extracted and expressed by (i, j) . The texture gradient decomposition is performed on the extracted feature points; the distribution set of the feature points of the visual transmission of the 3D image is calculated, as shown in formula (1) [14].

$$w(i, j) = \frac{1}{Z(i)} \exp\left(-\frac{d(i, j)}{h^2}\right), \quad (1)$$

where $Z(i)$ is the first-order and gradient decomposition operator, and the calculation formula is as follows:

$$Z(i) = \sum_{j \in \Omega} \exp\left(-\frac{d(i, j)}{h^2}\right). \quad (2)$$

According to formula (2), 3D image is reconstructed at superresolution, and the distribution function of feature points is constructed [15]. With the help of visual communication, the virtual reconstruction of feature points is carried out for 3D image. Through the fusion of feature points, the decomposition of feature points of 3D image is realized, and the feature point component of 3D image virtual reconstruction is obtained as follows [16].

$$\min_c \left(\min_{y \in \Omega(x)} \left(\frac{I^c(y)}{A^c} \right) \right) = \tilde{t}(x) \min_c \left(\min_{y \in \Omega(x)} \left(\frac{J^c(y)}{A^c} \right) \right) + (1 - \tilde{t}(x)), \quad (3)$$

where the fitting parameter of 3D image visual communication information is $\tilde{t}(x)$, and the feature vector of 3D image visual communication information is A^c . Assuming that $J(x)\tilde{t}(x)$ is the visual transmission coefficient, the iterative formula for visually conveying information in 3D images is [17]

$$\text{bnr}_{\beta}(X) = R_{\beta}X - R_{\beta}X_1. \quad (4)$$

Assuming that the number of feature points of 3D image visual communication is $M \cdot N$, the 3D image is virtually reconstructed, and the feature decomposition formula of 3D image virtual reconstruction in visual communication is obtained as follows [18]:

$$\beta_i = \exp\left(-\frac{|x_i - x_j|^2}{2\sigma^2}\right) \frac{1}{\text{dist}(x_i, x_j)}. \quad (5)$$

Combined with the decomposition of feature vector in formula (5), the detection of feature points of 3D image is realized, and the construction of the 3D image visual communication model is completed.

2.2. Texture Mapping of 3D Image. Suppose x_q is the eigenvalue of 3D image feature points, and y_q is the corresponding feature point in the corresponding virtual reconstructed image. In different spaces, the difference between 3D image texture feature points and virtual image texture feature points is z_q . Therefore, the difference calculation formula of 3D image texture feature points is obtained.

$$\delta = H\delta_0 - \left(\frac{m}{m}\right)C \sin(m), \quad (6)$$

where δ is the texture feature point difference, δ_0 is the initial 3D image, C is the number of texture feature points reconstructed from the 3D image, and m is the difference between the number of texture feature points of the 3D image in real and virtual space. Assuming that the number of texture feature points of the 3D image is m , then $y_q^2 = i m_q^2 j$. Substitute $y_q^2 = i m_q^2 j$ into formula (6) to obtain the following formula:

$$u(\delta, a, \beta) = \sum_{q=1}^{\infty} x_q \cos \left[y_q - \sqrt{\frac{y_q^2}{\delta}} (\delta \cos p_q) + z_q \right], \quad (7)$$

where $u(\delta, a, \beta)$ is the position function of virtual reconstruction feature points and q and p_q are the difference between feature points and area of virtual reconstruction, respectively. The wavelet function [19] is used to calculate the spatial position relationship of 3D image feature points after virtual reconstruction.

$$K = w(\delta, \beta) + \phi \cdot r(\delta, \beta) + u(\delta, \alpha, \beta), \quad (8)$$

where the pixel change rate and texture feature point transformation function of 3D image virtual reconstruction are $w(\delta, \beta)$ and $r(\delta, \beta)$, respectively, and ϕ is the texture feature point coordinates after reconstruction [20].

According to formula (8), the result of 3D image texture mapping can be obtained, that is,

$$S = K \cos(\delta_0 - a\beta), \quad (9)$$

where a is the position information of texture feature points after virtual reconstruction of 3D image and β is the mapping plane.

According to the above process, the texture mapping of 3D image is completed.

2.3. Reconstruction Algorithm of 3D Image Virtual Using Visual Communication. The training sample formula for obtaining 3D images and virtual reconstruction images x_{hi} by visual communication [21] is as follows:

$$X_{hi} = [x_{hi,1}, x_{hi,2}, \dots, x_{hi,mn}]. \quad (10)$$

Assuming that it is the image result of virtual reconstruction of 3D image, quantitative analysis is performed, the auxiliary design of virtual image is completed, and the deep-seated texture feature points of 3D image are extracted, namely,

$$F_{hi} = \left[\text{Bhist}(T_{hi}^1), \dots, \text{Bhist}(T_{hi}^{L_1}) \right]^T \in R^{(2L_1)L_1 B}. \quad (11)$$

Through the visual communication technology, the extraction results of deep texture feature points of 3D image are obtained [22], namely,

$$F_{li} = \left[\text{Bhist}(T_{li}^1), \dots, \text{Bhist}(T_{li}^{L_1}) \right]^T \in R^{(2L_1)L_1 B}, \quad (12)$$

where the feature extraction results of 3D image feature points and virtual reconstructed feature points are F_{hi} and F_{li} , respectively. Bhist represents the design process of 3D image virtual reconstruction, and B represents the number of samples after texture decomposition.

Combined with the design method of visual communication technology, the training dictionary is constructed in Sc SR , and the complex feature dictionary samples D_h and D_1 of 3D image virtual reconstruction can be obtained. The feature points F_{hi} and F_{li} after reconstruction are extracted by K . The visual communication technology is used to compile it into the training dictionary [23], and the description coefficient of 3D image virtual reconstruction in visual communication is obtained as follows:

$$\{D_h, a\} = \underset{a}{\text{argmin}} |F_{hi} - D_h X_{hi} a|_2^2 + \sum_{i=1}^K \lambda_i |\alpha_i|_1, \quad (13)$$

$$\{D_1, a\} = \underset{D_1, a}{\text{argmin}} |F_{li} - D_1 X_{li} a|_2^2 + \sum_{i=1}^K \lambda_i |\alpha_i|_1, \quad (14)$$

where $a = \{a_i\}_{i=1}^k$ is the deep learning auxiliary matrix, and λ_i represents the reconstructed virtual coefficient. If the original 3D image feature points and the reconstructed virtual image feature points are described in the same coding method, they are intensively trained through formula (15), and the calculation formula is

$$\begin{aligned} \{D_h, D_1, a\} = \underset{D_h, D_1, a}{\text{argmin}} & \frac{1}{N} |F_{hi} - D_h X_{hi} a|_2^2 + \frac{1}{M} |F_{li} - D_1 X_{li} a|_2^2 \\ & + \left(\frac{1}{N} + \frac{1}{M} \right) \sum_{i=1}^K \lambda_i |\alpha_i|_1, \end{aligned} \quad (15)$$

where N and M represent the feature point arrangement matrix and vector information in visual communication of 3D image virtual reconstruction, respectively. $1/N$ and $1/M$ use formula (13) and formula (14) for normalization processing; combined with visual communication technology,

the coding coefficient a_i of each 3D image feature point F_C and D_C is calculated and the coding matrix a is obtained. The dictionary is updated by a .

The constraint expression of 3D image virtual reconstruction result is

$$X^* = \operatorname{argmin}_X |SHX - D_C Y|_2^2 + c|X - X_0|_2^2 + \gamma|(I - W)X|_2^2, \quad (16)$$

where S represents the sample information of the 3D image, H represents the virtual reconstruction image, $|X - X_0|_2^2$ represents the constraint information, and $(I - W)X|_2^2$ represents the virtual reconstruction constraint matrix of the 3D image. c and γ represent the feature point parameters after virtual reconstruction of the 3D image, respectively. W represents the weight matrix of the virtual reconstruction of the unit image. Through the constraints on the virtual reconstruction of the 3D image, the design of the virtual reconstruction algorithm for the 3D image is completed. The 3D image virtual reconstruction algorithm is shown in Figure 1.

According to Figure 1, firstly, the training samples of 3D image virtual reconstruction image are obtained, and the deep texture feature points of 3D image are extracted. Then, the training dictionary is constructed through visual communication technology to obtain the description coefficient of 3D image virtual reconstruction in visual communication. Then, the feature point arrangement matrix is obtained by centralized training, and the coding matrix is constructed to update the training dictionary. Finally, the constraints of image virtual reconstruction are determined to complete 3D image virtual reconstruction.

3. Experiments and Results

3.1. Data Description and Implementation Details. This paper uses the data set ScanNet to verify the effect of the 3D image virtual reconstruction method in visual communication. The ScanNet data set is an RGB-D video data set containing 2.5 million views in more than 1500 scans, annotated using 3D camera poses, surface reconstruction, and instance-level semantic segmentation (3D) reconstruction related. In this paper, 5000 images are used for training; 1000 images are used for testing. The number of pixels of 3D image is $16 * 16$; the 3D image size is $1200 \text{ mm} * 200 \text{ mm}$. Image definition is 2548 frames. The number of iterations is 10 times.

The evaluation indexes of this paper are as follows:

- (1) Virtual reconstruction effect. The higher the resolution of 3D image, the clearer the edge of 3D image, indicating that the better the virtual reconstruction effect of 3D image, on the contrary, the worse the virtual reconstruction effect of 3D image
- (2) Virtual reconstruction time. The longer the virtual reconstruction time, the lower the virtual reconstruction efficiency. On the contrary, the shorter the virtual reconstruction time, the higher the virtual reconstruction efficiency

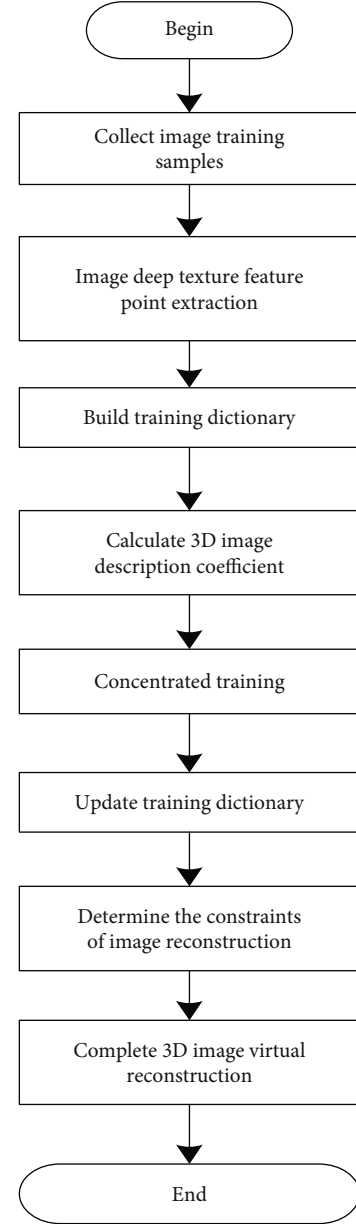


FIGURE 1: Algorithm process of 3D image virtual reconstruction.

- (3) PSNR of 3D image reconstruction. The calculation formula is

$$\text{PSNR} = 20 \cdot \log_{10} \left(\frac{\text{MAX}_I}{\sqrt{\text{MSE}}} \right), \quad (17)$$

where MAX_I represents the color value of 3D image and MSE represents the MSE of virtual reconstruction. The higher the SNR ratio of 3D image reconstruction, the better the image quality. On the contrary, the lower the SNR ratio of 3D image reconstruction, the worse the image quality

- (4) MSE of virtual reconstruction. The calculation formula is

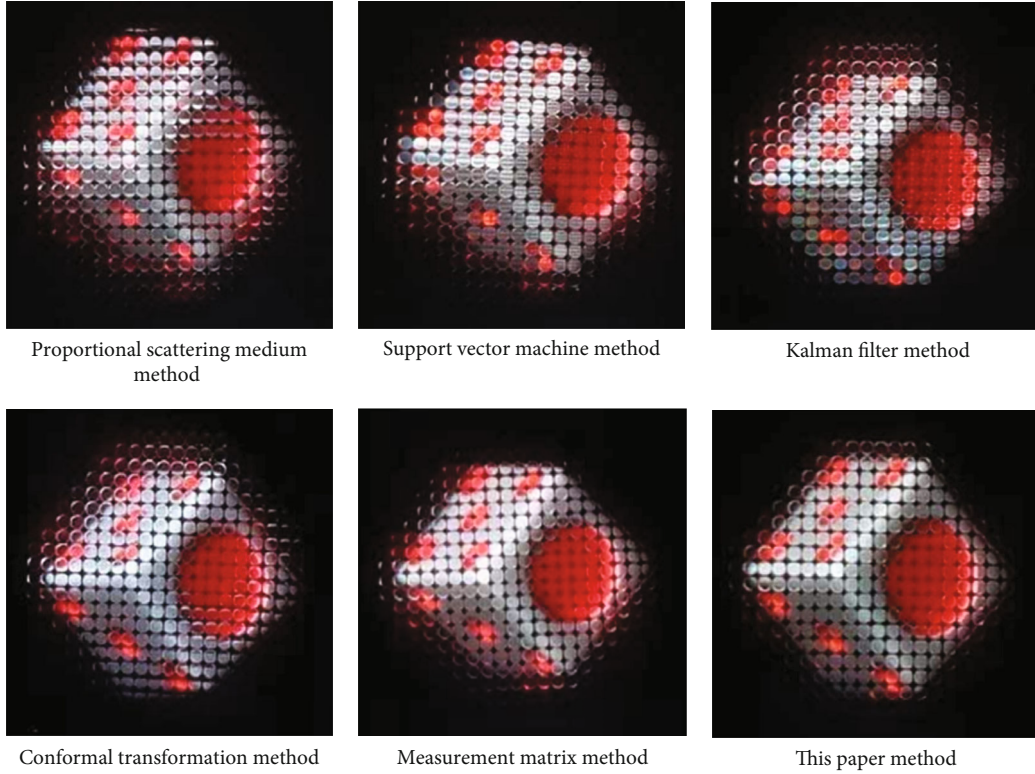


FIGURE 2: Virtual reconstruction effect of 3D image in visual communication.

$$\text{MSE} = \frac{\sum_{i=1}^r (n_i - 1) s_i^2}{N - r}, \quad (18)$$

where $N - r$ is the freedom and $\sum_{i=1}^r (n_i - 1)$ is the sum of squares of reconstruction error. s_i^2 is the 3D image sample variance. The lower the virtual reconstruction MSE, the better the virtual reconstruction effect. On the contrary, the higher the virtual reconstruction MSE, the worse the virtual reconstruction effect

(5) SSIM of 3D image. The calculation formula is

$$\text{SSIM}(x, y) = \frac{(2\mu_x\mu_y + c_1)(2\sigma_{xy} + c_2)}{(\mu_x^2 + \mu_y^2 + c_1)(\sigma_x^2 + \sigma_y^2 + c_2)}, \quad (19)$$

where x and y are the two 3D images. μ_x and μ_y are the average value of samples, σ_x and σ_y are the sample variance, and σ_{xy} is the covariance. The higher the SSIM of 3D images, the better the virtual reconstruction effect of 3D images in visual communication, on the contrary, the worse the virtual reconstruction effect

3.2. Results and Discussion. In order to highlight the advantages of the 3D image virtual reconstruction method in reconstruction, the reconstruction method based on proportional scattering medium [8], reconstruction method based on support vector machine [9], reconstruction method based on Kalman filter [10], reconstruction method based on conformal transformation [11], and reconstruction method

based on measurement matrix [12] are introduced compared with the method in this paper. The following test results are obtained.

The virtual reconstruction effect of 3D image in visual communication is shown in Figure 2.

According to Figure 2, this paper method compared with the other five methods, the edge of the reconstructed 3D image of this paper method is clearer, the 3D effect is more obvious, and the resolution is relatively high, which has a better virtual reconstruction effect.

The test results of virtual reconstruction time of 3D image in visual communication are shown in Figure 3.

The results in Figure 3 show that when the number of samples is 200, the virtual reconstruction time of the proportional scattering medium method is 27 s, the virtual reconstruction time of the support vector machine method is 20 s, the virtual reconstruction time of the Kalman filter method is 14 s, the virtual reconstruction time of the conformal transformation method is 10 s, the virtual reconstruction time of measurement matrix method is 5.1 s, and the virtual reconstruction time of this paper method is 2.1 s. With the increase of the number of samples, the virtual reconstruction time of 3D images in visual communication is relatively close by using the measurement matrix method and the method in this paper, but the time used by this paper method is the shortest, within 3 s; other methods have poor performance in terms of virtual reconstruction time of 3D images.

The test result of the virtual reconstruction SNR of the 3D image in visual communication is shown in Figure 4.

The results in Figure 4 show that when the system running time is 5 s, the virtual reconstruction SNR of the

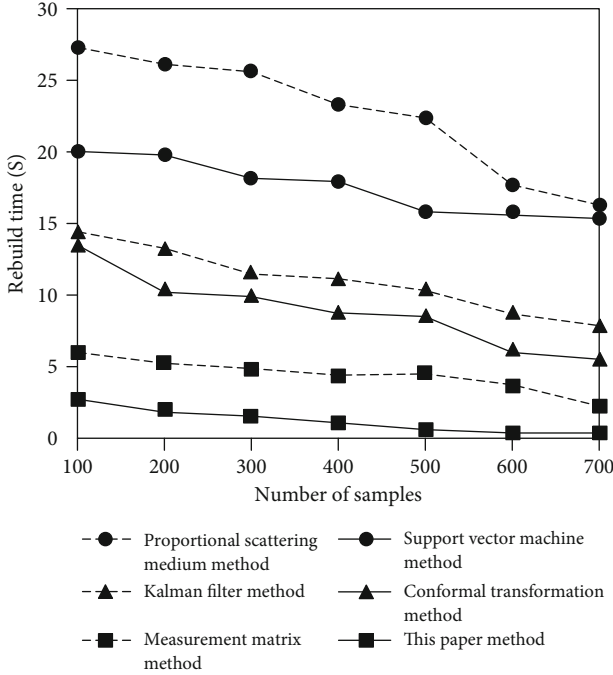


FIGURE 3: Virtual reconstruction time of 3D image in visual communication.

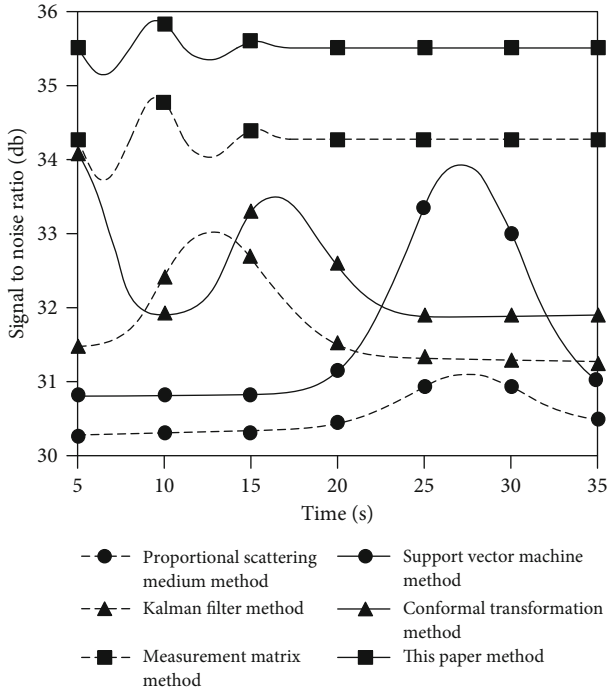


FIGURE 4: Virtual reconstruction SNR of 3D image in visual communication.

proportional scattering medium method is 30.2db, the virtual reconstruction SNR of the support vector machine method is 30.9db, the virtual reconstruction SNR of the Kalman filter method is 31.4db, the virtual reconstruction SNR of the conformal transformation method is 34db, and

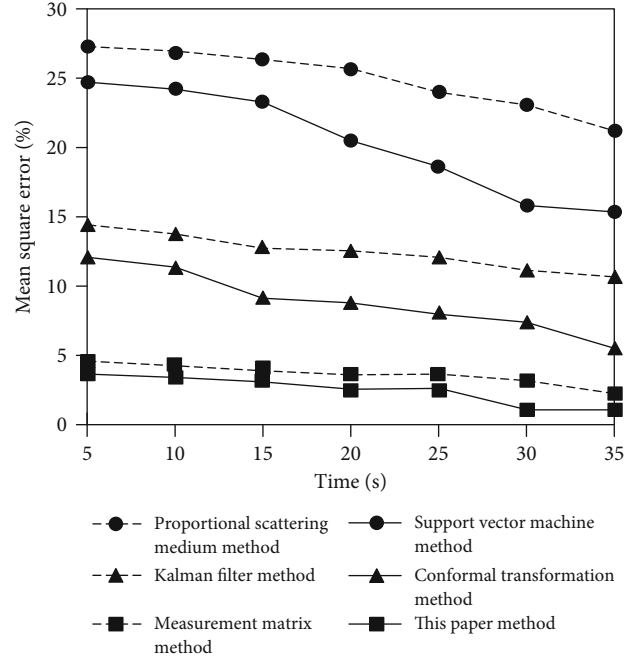


FIGURE 5: Virtual reconstruction MSE of 3D image in visual communication.

the virtual reconstruction SNR of the measurement matrix method is 34.2db. The virtual reconstruction SNR of this paper method is 35.5db. The SNR of 3D image virtual reconstruction obtained by the proportional scattering medium method, measurement matrix method, and this paper method is relatively stable, but the 3D image virtual reconstruction method can use visual communication technology to improve the SNR of 3D image virtual reconstruction and has better performance.

The test results of virtual reconstruction MSE of 3D image in visual communication are shown in Figure 5.

According to Figure 5, in terms of the MSE of virtual reconstruction of 3D image in visual communication, the results obtained by the proportional scattering medium method and support vector machine method exceed 15%, while the results obtained by the Kalman filter method and conformal transformation method are between 5% and 15%, which is difficult to realize the virtual reconstruction of 3D image. The results obtained by the measurement matrix method and this paper method are less than 5%, which can meet the requirements of 3D image virtual reconstruction, but the MSE obtained by this paper method is lower.

The SSIM of the virtual reconstruction results of 3D images in visual communication are shown in Figure 6.

It can be seen from Figure 6 that the change trend of 3D image virtual reconstruction SSIM of all methods is relatively close, but the method in this paper shows better performance in 3D image virtual reconstruction SSIM, which is more than 1.2%. Therefore, it is explained that this paper method can effectively improve the ability of 3D image virtual reconstruction.

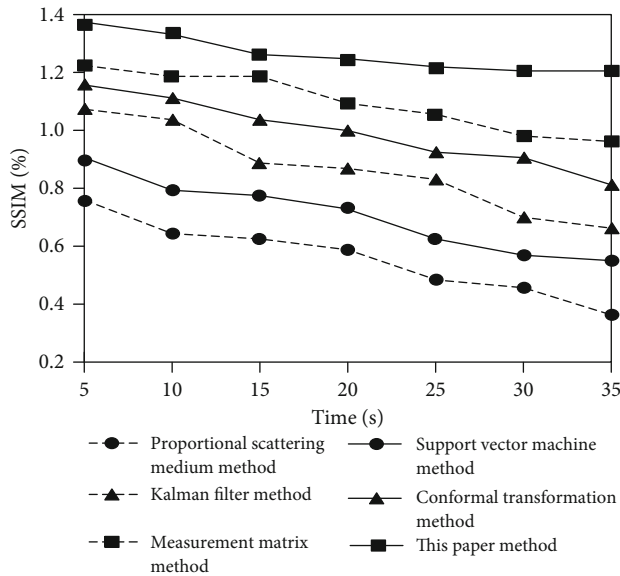


FIGURE 6: Virtual reconstruction SSIM of 3D image in visual communication.

4. Conclusions

This paper proposes the effect of 3D image virtual reconstruction in visual communication. By iterating the 3D image visual communication information, the features of 3D image virtual reconstruction in visual communication are decomposed, the 3D image visual communication model is constructed, and the spatial position relationship of 3D image feature points after virtual reconstruction is calculated. Through the visual communication of 3D image, the deep texture feature points of 3D image are extracted. According to the description coefficient of 3D image virtual reconstruction in visual communication, the virtual reconstruction results of 3D image are constrained by visual communication technology, and the virtual reconstruction algorithm of 3D image is designed to realize the virtual reconstruction of 3D image. The following conclusions are drawn through experiments: (1) When the number of samples is 200, the virtual reconstruction time of this paper method is 2.1 s, which shows that this paper method can effectively improve the virtual reconstruction efficiency. (2) When the system running time is 5 s, the virtual reconstruction SNR of this method is 35.5 db. The SNR of virtual reconstruction is high. (3) The MSE of 3D image virtual reconstruction obtained by this paper method is less than 5%, which can meet the requirements of 3D image virtual reconstruction. However, there are still many deficiencies in this paper. In the future work, we hope to analyze and screen the factors affecting 3D image virtual reconstruction and improve the efficiency of 3D image virtual reconstruction.

Data Availability

The data used to support the findings of this study are available from the corresponding author upon request.

Conflicts of Interest

The authors declare that there is no conflict of interest with any financial organizations regarding the material reported in this manuscript.

References

- [1] X. Pan, Q. Zhao, and J. Liu, "Edge extraction and reconstruction of terahertz image using simulation evolutionary with the symmetric fourth order partial differential equation," *Optoelectronics Letters*, vol. 17, no. 3, pp. 187–192, 2021.
- [2] W. Gao, A. Shakoor, M. Xie et al., "Precise automated intracellular delivery using a robotic cell microscope system with three-dimensional image reconstruction information," *IEEE/ASME Transactions on Mechatronics*, vol. 25, no. 6, pp. 2870–2881, 2020.
- [3] A. Daoui, M. Yamni, O. El Ogri, H. Karmouni, M. Sayyouri, and H. Qjidaa, "Stable computation of higher order Charlier moments for signal and image reconstruction," *Information Sciences*, vol. 521, pp. 251–276, 2020.
- [4] V. Frøysa, G. J. Berg, T. Eftestøl, L. Woie, and S. Ørn, "Texture-based probability mapping for automatic scar assessment in late gadolinium-enhanced cardiovascular magnetic resonance images," *European Journal of Radiology Open*, vol. 8, p. 100387, 2021.
- [5] F. Tian, Y. Gao, Z. Fang, J. Gu, and S. Yang, "3D reconstruction with auto-selected keyframes based on depth completion correction and pose fusion," *Journal of Visual Communication and Image Representation*, vol. 79, p. 103199, 2021.
- [6] H. Liu, W. Song, Y. Zhang, and A. Kudreyko, "Generalized Cauchy degradation model with long-range dependence and maximum Lyapunov exponent for remaining useful life," *IEEE Transactions on Instrumentation and Measurement*, vol. 70, pp. 1–12, 2021.
- [7] G. Fahim, K. Amin, and S. Zarif, "Single-view 3D reconstruction: a survey of deep learning methods," *Computers & Graphics*, vol. 94, pp. 164–190, 2021.
- [8] S. A. Tereshchenko and A. Y. Lysenko, "Investigation of the scattering influence on the quality of image reconstruction in single-photon emission computed tomography in a proportional scattering medium," *Biomedical Engineering*, vol. 53, no. 5, pp. 370–374, 2020.
- [9] M. B. Lee, J. K. Kang, H. S. Yoon, and K. R. Park, "Enhanced iris recognition method by generative adversarial network-based image reconstruction," *IEEE Access*, vol. 9, pp. 10120–10135, 2021.
- [10] W. Deabes and K. E. Bouazza, "Efficient image reconstruction algorithm for ECT system using local ensemble transform Kalman filter," *IEEE Access*, vol. 9, pp. 12779–12790, 2021.
- [11] Y. Wang, S. Ren, and F. Dong, "A transformation-domain image reconstruction method for open electrical impedance tomography based on conformal mapping," *IEEE Sensors Journal*, vol. 19, no. 5, pp. 1873–1883, 2019.
- [12] Y. Jiang, H. Wang, R. Shao, and J. Zhang, "Infrared image reconstruction based on Archimedes spiral measurement matrix," *Journal of Shanghai Jiaotong University (Science)*, vol. 24, no. 2, pp. 204–208, 2019.
- [13] N. Huang, Y. Ma, M. Zhang, H. Ge, and H. Wu, "Finite element modeling of human thorax based on MRI images for EIT image reconstruction," *Journal of Shanghai Jiaotong University (Science)*, vol. 26, no. 1, pp. 33–39, 2021.

- [14] J. A. Fessler, "Optimization methods for magnetic resonance image reconstruction: key models and optimization algorithms," *IEEE Signal Processing Magazine*, vol. 37, no. 1, pp. 33–40, 2020.
- [15] T. He and X. Li, "Image quality recognition technology based on deep learning," *Journal of Visual Communication and Image Representation*, vol. 65, article 102654, 2019.
- [16] J. Zhang, Y. Gu, H. Tang et al., "Compressed sensing MR image reconstruction via a deep frequency-division network," *Neurocomputing*, vol. 384, pp. 346–355, 2020.
- [17] S. K. HashemizadehKolowri, R.-R. Chen, G. Adluru et al., "Simultaneous multi-slice image reconstruction using regularized image domain split slice-GRAPPA for diffusion MRI," *Medical Image Analysis*, vol. 70, no. 2, article 102000, 2021.
- [18] D. Połap and G. Srivastava, "Neural image reconstruction using a heuristic validation mechanism," *Neural Computing and Applications*, vol. 33, no. 17, pp. 10787–10797, 2021.
- [19] X. Ma and X. Li, "Dynamic gesture contour feature extraction method using residual network transfer learning," *Wireless Communications and Mobile Computing*, vol. 2021, 11 pages, 2021.
- [20] J. Huang, X. Liu, and Y. Lei, "X-ray phase-contrast image reconstruction based on the Chambolle-Pock algorithm," *Access*, vol. 9, pp. 23120–23126, 2021.
- [21] A. Picon, A. Medela, L. F. Sanchez-Peralta et al., "Autofluorescence image reconstruction and virtual staining for in-vivo optical biopsying," *IEEE Access*, vol. 9, pp. 32081–32093, 2021.
- [22] D. Liang, J. Cheng, Z. Ke, and L. Ying, "Deep magnetic resonance image reconstruction: inverse problems meet neural networks," *IEEE Signal Processing Magazine*, vol. 37, no. 1, pp. 141–151, 2020.
- [23] D. Dan, Z. Wang, X. Zhou et al., "Rapid image reconstruction of structured illumination microscopy directly in the spatial domain," *IEEE Photonics Journal*, vol. 13, no. 1, pp. 1–11, 2021.

Research Article

A Multipath Payment Scheme Supporting Proof of Payment

Hangguan Qian  and Lin You 

College of Cyberspace Security, Hangzhou Dianzi University, Hangzhou, 310018 Zhejiang, China

Correspondence should be addressed to Hangguan Qian; 171270010@hdu.edu.cn

Received 26 October 2021; Revised 26 November 2021; Accepted 29 November 2021; Published 4 January 2022

Academic Editor: Alireza Souri

Copyright © 2022 Hangguan Qian and Lin You. This is an open access article distributed under the Creative Commons Attribution License, which permits unrestricted use, distribution, and reproduction in any medium, provided the original work is properly cited.

Blockchain technology has always been plagued by performance problems. Given this problem, many scaling schemes have been put forward. A layer 2 network is a technology that solves the performance problem of blockchain. Connected parties in this network can set up channels to send digital currency to each other. Since the interaction with the blockchain is only required when the channel is established and closed, a large number of transactions do not need to be recorded on the blockchain, thus reducing the blockchain capacity. Due to the special structure of the payment channel, the distribution of funds in the channel is often unbalanced, which limits the route payment to a certain extent. This paper improves the original payment method in the second layer network by introducing new scripts. The new payment scheme supports proof of payment which is integral to the nature of the lightning network and divides the payment into several subpayments, so the large payment can be divided into relatively small payments. Due to the capacity limitation of the payment channel, theoretically, the success rate of the micropayment route is higher. This paper tests the new payment scheme on the simulated network and validates the nature of this solution to have a high routing success rate while supporting proof of payment.

1. Introduction

Blockchain is a new type of distributed system. Due to its characteristics of immutability and decentralization, it has a wide range of applications in the fields of digital currency, certificate storage, and anticounterfeiting. The concept of blockchain originated in a 2008 paper titled “A P2P Network Electronic Currency System” written by Satoshi Nakamoto [1]. The blockchain is a decentralized payment system that does not rely on a central authority and allows users to make payments by sending digital currencies. However, due to the distributed nature of blockchain, its performance is far less than that of traditional centralized systems, and as the number of users of the first blockchain increases, its performance issues become prominent.

Layer 2 payment network technology is a solution to the performance problem of blockchain. Different from the layer 1 scheme, the second layer payment network which focuses on the construction of the off-chain payment network does not need to change the main chain protocol or only needs to change a few protocols. Due to the limitations of block

structure, network delay, and other factors [2], the on-chain scheme is difficult to truly solve the performance problem of blockchain, while the off-chain scheme provides a possible way.

The lightning network [3] which uses asymmetric revocable commitments and hash time lock contracts (HTLC) to build an off-chain payment network is a layer 2 network payment scheme; a large number of transactions can be done in the second payment network, with the main chain only responsible for the records to create channels and close the deal; as a result, the entire blockchain system performance is improved greatly.

However, the channels in the lightning network have problems such as capacity limitations and uneven distribution of funds, which make it difficult to route large payments. An atomic multipath payment scheme [4] improves the success rate of large-amount payment routing by dividing large-amount payments into several small-amount payments. In this paper, we propose a new atomic multipath payment scheme, which ensures the atomicity of payment and supports proof of payment. In this paper, by

introducing new scripts, we propose a new atomic multipath payment scheme that ensures atomicity of payments and supports proof of payment. Proof of payment is an important nature of the lightning network, and without it, the lightning network will not operate smoothly. Therefore, this paper implements a simulation network with the same topology structure as the lightning network. By simulating payment on the simulation network, the new scheme can be verified to have a higher routing success rate.

In the next sections, we present background knowledge related to this paper, including blockchain, lightning network, and atomic multipath payments. In Section 3, we describe in detail how the new scheme is constructed and the new features it has. In Section 4, we design a simulation network to test and verify the success rate of the new scheme for routing payments by running the new scheme on the simulation network.

2. Backgrounds

2.1. Blockchain. Blockchain technology is derived from the underlying technology of the digital currency. Nakamoto combined several previous inventions, such as B-Money and Hashcash, to create a completely decentralized online payment system that does not rely on central authorities. Its key innovation was the creation of a proof of work algorithm that conducted an election every 10 minutes on average, enabling a distributed network to reach a consensus on the status of transactions.

In recent years, blockchain technology has developed rapidly. After the first blockchain, Ethereum with smart contracts [5] and Hyperledger with an access mechanism have been proposed one after another [6]. At the same time, the corresponding intrusion detection technologies [7] and cryptocurrency regulations are rapidly improving [8]. Due to the continuous progress of blockchain-related technology, more and more blockchain-related applications are appearing in our daily life.

With the increase in the application of blockchain, a large number of users join the blockchain, and the performance problems of the blockchain gradually appear. Various solutions have been proposed to improve the performance of blockchain. Blockchain performance solutions can be divided into two categories: one is a capacity expansion on the first layer chain, which is the improvement of the original blockchain, and the second is the improvement of off-chain technology, which is the use of the second layer network to reduce the burden on the main chain. Theoretically, a large number of transactions travel through the second network, with the main chain only responsible for registering the results of the transactions. In this way, the performance of the blockchain could be greatly improved.

The first layer solution includes blockchain cash with increased block size [9] and segregated witness which compressed block size [10] and sharding technology [11]. Elastico [12] is the first sharding protocol for the permission-less blockchain. OmniLedger [13], a more recent distributed ledger based on the sharding technique, builds closely on Elastico and tries to solve the problems of Elastico.

It uses a bias-resistant public randomness protocol for shard assignment. Various new consensus algorithms are used to accelerate blockchain transaction processing efficiency [14–16], which increase transaction throughput and reduce latency, respectively. As for the off-chain solutions, the second-layer solutions such as the first blockchain's lightning network, Ethereum's Raiden network [17], and Plasma [18] are in full swing. Along with the development of scaling technology, some security issues are also drawing attention and many related studies [19–22] have started to be proposed. As the technology tends to mature, applications of blockchain [23, 24] in various scenarios continue to emerge.

2.2. Lightning Network. The lightning network is a layer 2 network protocol based on the blockchain and has been proposed as a solution to the first blockchain's scalability performance problem. It is a peer-to-peer system that requires no escrow and allows users to make payments using the lightning network, a network of bidirectional payment channels. To date, tens of thousands of simultaneous micropayments can be accommodated in the lightning network, in contrast to the main chain, which can only process a few transactions per second.

The lightning network opens the payment channel by submitting a specific format of the transaction to the main chain, the layer 1 network, and then makes any number of lightning network transactions, updating the tentative allocation of funds from that channel without broadcasting those funds to the blockchain. Finally, the payment channel is closed, and funds for the channel are allocated by broadcasting the final version of the settlement transaction. By using asymmetric revocable commitment and hashing time lock contract (HTLC), the lightning network can punish cheaters and route transactions.

The lightning network uses contracts that can revoke previously promised transactions. When both parties sign a new commitment transaction, the revoking key needs to be exchanged. This is designed so that when one party tries to cheat, the revoking key can be used as a punishment. Specifically, the party trying to cheat will broadcast the old promised transaction to the main network in his favor. However, due to the existence of the time lock, he has to wait for some time before he can get the funds. The other party who has the revoking key can show the revoking key during this period and immediately get the corresponding funds. By such a design, the old contract is rendered invalid, and fraud cannot be carried out, as shown in Figure 1.

To create a HTLC, the payee will first create a secret R . They then calculate the hash H of this R : $H = \text{Hash}(R)$. The resulting hash is contained in the lock script for the contract output. Anyone who knows the secret can use it to exchange for output. The secret R is also known as the preimage of the hash function, which is the data used as input to the hash function.

The second part of the HTLC is the time lock component. If the secret is not revealed, the HTLC payer can get a refund after a while. This is done by using an absolute time lock.

```

Output 0 <5 coin>:
    <Irene's Public Key> CHECKSIG

Output 1 <5 coin>:
IF
    # Revocation penalty output
    <Revocation Public Key>
ELSE
    <1000 blocks>
    CHECKSEQUENCEVERIFY
    DROP
    <Hitesh's Public Key>
ENDIF
CHECKSIG

```

FIGURE 1: An example of asymmetric revocable commitment. The difference from the regular script is the addition of a revocation key and a time lock of 1000 blocks long in output 1.

Anyone who knows the corresponding secret R that can make a hash equal to H can redeem the output by exercising the first clause of the IF statement. If the secret is not revealed, the HTLC states that after a certain number of blocks, the payee can claim a refund using the second clause of the IF statement. HTLC can take different forms by fine-tuning the script. For example, add a CHECKSIG operator and a public key to the first clause to restrict the conversion of the hash value to a specified recipient, who must know the secret R , as shown in Figure 2.

Lightning networks can allow any participant to route payments from one channel to another without trusting any intermediary. Suppose there are a payment channel between Alice and Bob and a payment channel between Bob and Carol but no payment channel between Alice and Carol. The lightning network allows Alice's funds to be routed to Carol. The specific operation is as follows: Claire generates a secret, does a hash operation on the secret, and then sends the result of the hash operation to Alice. Alice can use the result of this hash operation to create the HTLC contract and send it to Bob. As long as Bob shows the secret within a certain period, he can get the funds agreed in the contract. For now, Bob cannot

reveal the secret, because only Carol knows the secret. Therefore, Bob needs to create a contract with Carol, which contains the same result of the hash operation. As long as Carol shows the secret within a certain time, he can get the money agreed in the contract. Carol is the secret generator and knows the secret. Carol shows the secret to Bob and gets the money in his contract with Bob. Bob gets the secret and uses it to get the money he agreed to in his contract with Alice. In this way, the transfer of funds between different channels can be realized; that is, funds can be routed in the lightning network.

2.3. Atomic Multipath Payments. Suppose a node has to pay another node 8000 Satoshis for something, and that node has only three channels with a 3000-Satoshi limit. Under traditional payment methods, a transaction cannot be completed with a single payment, while if multiple payments are used, the atomicity of the transaction cannot be guaranteed, and if one payment fails, the payment sender may need to request the recipient to return the other payment that has been completed. Another problem is that there is currently a ceiling on the number of channels that can be paid. If the payment exceeds this limit, it must be split into multiple payments, which also leads to the problem of payment failure.

Conner Fromknecht and Olaoluwa Osantokun proposed the atomic multipath payments (AMP) to solve the above two problems. The AMP scheme splits a large payment into several smaller payments, each of which can be routed to the recipient via a different path. Because the lightning network's channels can only pass up to an amount equal to their own capacity and there are a large number of small capacity channels in the lightning network to date, micropayments have a much higher routing success rate. By splitting the parent secret into multiple child secrets, the child payments carry the child secrets and send them to the receiver. Only when all the child secrets are collected can the recipient know the parent secret, thus obtaining the funds in all the payments, which ensures the atomicity of the payments. However, the scheme requires the sender to know the parent secret in advance, which is incompatible with proof of payment in the lightning network. Proof of payment means that the sender can show the parent secret to prove that the recipient has received the payment.

Basic atomic multipath payments (BAMP) are another multipath payment scheme. BAMP uses the same payment condition (payment hash) in all paths, and the recipient will release the parent secret preimage only after receiving all child payments. This is guaranteed by a financial incentive, since the recipient, by releasing the paternal secret, indicates that he has received all the funds paid.

In addition, Lin et al. proposed a multipath payment mechanism, called Rapido [25], which implements a multipath payment protocol by designing a D-HTLC smart contract. A study [26] similar to that of multipath payment uses new routing methods between the channels of the lightning network by designing more complex routing protocols to speed up the flow of funds between channels.

```

IF
# Payment if you have the secret R
HASH160 <H> EQUALVERIFY
ELSE
# Refund after timeout.
<locktime> CHECKLOCKTIMEVERIFY DROP
<Payer Public Key> CHECKSIG
ENDIF

```

FIGURE 2: An example of HTLC. Only those who know the secret R can redeem the output. If no one redeems the output within a certain period of time, the amount in the contract will be returned the way it was.

3. Payment Scheme

In this paper, a new atomic multipath payment scheme is designed. Compared with other schemes, the new scheme supports proof of payment and conforms to the definition of atomicity of payment. The new scheme includes the sender scheme and the receiver scheme. The sending case consists of four parts: parameter determination, secret determination, payment condition construction, and secret sending. The receiver scheme includes the generation of public and private key pairs, secret splicing, the creation of subsecret keys, and payment acceptance. The flow chart of the whole scheme is shown in Figure 3.

3.1. The Sender

- (1) Parameter determination: determine the amount of payment fund which is F , and the number of fund shares is N ; i.e., the funds are divided into f_1, f_2, \dots, f_n by the sender and $F = f_1 + f_2 + \dots + f_n$
- (2) Secret determination: the sender randomly generates a parent secret (ps) and then generates n child secrets for secret sampling. The sampling scheme adopted in this paper is as follows: generate $n - 1$ random numbers x_1, x_2, \dots, x_{n-1} . The value of the first subsecret s_1 is x_1 , the value of the second subsecret s_2 is x_2 , and so on; the value of the $n - 1$ st subsecret is x_{n-1} , and the value of the last subsecret is $ps \oplus x_1 \oplus x_2 \oplus \dots \oplus x_{n-1}$. In this sampling method, the parent secret can be restored by combining all the child secrets with XOR operation
- (3) Construction of payment terms: the sender uses serial number ID which tags every child pay and the serial number from 1 to N , parent secret ps, and receiver's public key K_{par} structure subpayment terms $K_i = H(i \| ps \| K_{\text{par}}) * G + K_{\text{par}}$. The receiver needs to know the serial number I, the parent secret ps, and the receiver's private key k_{par} to redeem the payment

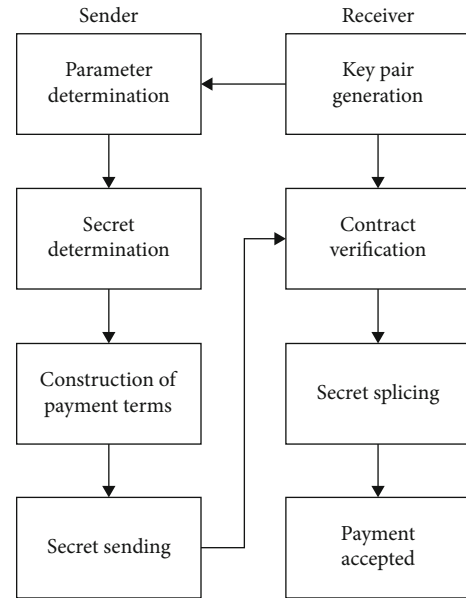


FIGURE 3: The flow chart of the new scheme. The sender scheme includes parameter determination, secret determination, payment condition construction, and secret sending. The receiver scheme includes the generation of public and private key pairs, secret splicing, the creation of subsecret keys, and payment accepted.

- (4) Secret sending: the payer sends the triple $(ID, V_i, \text{ and } S_i)$ and the contract containing the payment terms in the previous step

3.2. The Receiver

- (1) Public and private key pair generation: the receiver generates the public and private key pair and sends the public key to the sender
- (2) Contract verification: the receiver waits for the arrival of subpayment, obtains parameter ID of each subpayment, fund amount f_i , and the corresponding subsecret s_i , and then verifies the format and content of the contract at the same time

- (3) Secret splicing: after the arrival of all subpayments, the receiver will perform XOR operation on each s_i obtained, and the parent secret ps is obtained by splicing
- (4) Payment accepted: the receiver using the parent secret ps and the serial number ID, as well as the receiver private key k_{par} and public key K_{par} , calculates all terms of unlocking payment. We use k_i to denote the unlocking condition and $k_i = H(i || ps || k_{par}) + k_{par}$; using k_i can obtain each child pay of the payer for the money. When the payment is accepted, the recipient needs to show the private key in the script. Once the private key is shown, it indicates the acceptance of funds, which can be used as proof of payment

In this scheme, the receiver must wait for all transactions to arrive before the parent secret can be concatenated, which ensures the atomicity of the payment. In other words, the recipient cannot say that only part of the payment has been received, because only after receiving all of the child payments can the recipient get the parent secret, and without the parent secret, the recipient cannot get any of the child payments. In addition, after the payment is successful, the sender can present the invoice with K_{PAR} to prove that the sender has received all the payments, that is, the payment proof supported by the scheme, as shown in Table 1. The new payment protocol mainly acts on the layer 2 network, and the interaction with the main chain does not change; therefore, the protocol changes in this scheme do not affect the performance of the main chain in other ways.

4. Simulation

Since it is difficult to observe the channel fund distribution, routing, and other information in the real lightning network, we implement a simulation network to simulate the transactions in the lightning network. To more accurately restore the characteristics of the real network, the simulated network adopts the same channel topology, channel capacity, and routing algorithm as the original network. The initial channel is evenly distributed, with half of the money at each end.

The whole simulated network has a total of 4968 nodes and 59,335 channels. Figure 4 shows the topology structure of some nodes in the simulated network (sorting the number of node channels from high to low, taking the first 100 nodes).

The simulated transactions are divided into 4 groups, each group carries out 9 rounds of transactions, and 100 pairs of 200 nodes are randomly selected for each round. One pair of nodes includes the payer node and the receiver node. Each payer node sends a transaction to the corresponding receiver node using the nonsplit transaction scheme and this scheme, respectively. In theory, a successful routing path can be found as long as the number of split copies is sufficient. In this simulation, we set the maximum number of splits to 10.

In the first group, the amount of money sent for each payment in the first round is 1000 Satoshis. The amount of money sent for each subsequent round of payment is

TABLE 1: Comparison of payment schemes.

Payment scheme	Proof of payment	One million satoshi routing success rate
Non-split payment	Supportive	3.1%
AMP	Unsupported	42.9%
Our scheme	Supportive	42.6%

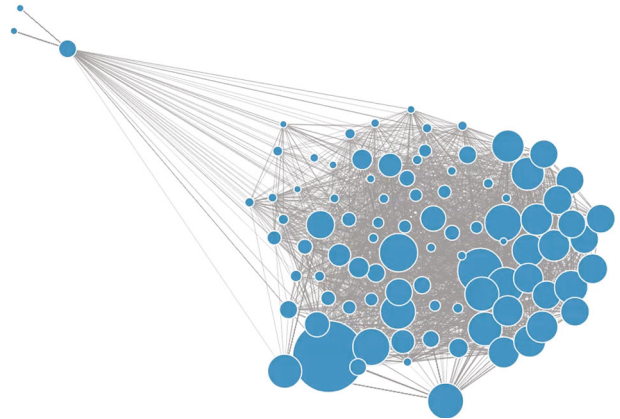


FIGURE 4: Topology structure of the main nodes in the simulated network. The node size represents the sum of the capacity of all channels connected to the node.

increased by 1000 Satoshis. The amount of money sent for each payment in the second round is 2000 Satoshis, and the amount of money sent for each payment in the last round is 9000 Satoshis. The second group sends 10,000 Satoshis for each payment in the first round, followed by an increase of 10,000 Satoshis for each subsequent round. The third group sent 100,000 Satoshis for each payment in the first round and increased the amount by 100,000 Satoshis for each subsequent round. The fourth group sends 1,000,000 Satoshis for each payment in the first round and then increases the amount sent by 1,000,000 Satoshis for each subsequent round. Considering the wide range of real amounts in the lightning network, we conducted group experiments. In this section, by grouping the payment amounts, the payment amounts differ by a factor of 10 between groups, while the payment amounts within groups are increasing in equal increments. The experimental results show that such a choice can more clearly demonstrate the difference in the routing success rate of the two payment schemes at different amounts.

The success rate of routing in the network decreases as the amount of payment gets larger because whether a payment can go through a channel depends on the amount of money the channel has in the direction of payment. The multipath payment scheme can split a large payment into several small payments. Since the small payments have more channels to choose from in the network, the success rate of routing will also increase. The nonsplit payment scheme and this scheme are used to simulate the payment on the simulation network, respectively, and the routing success

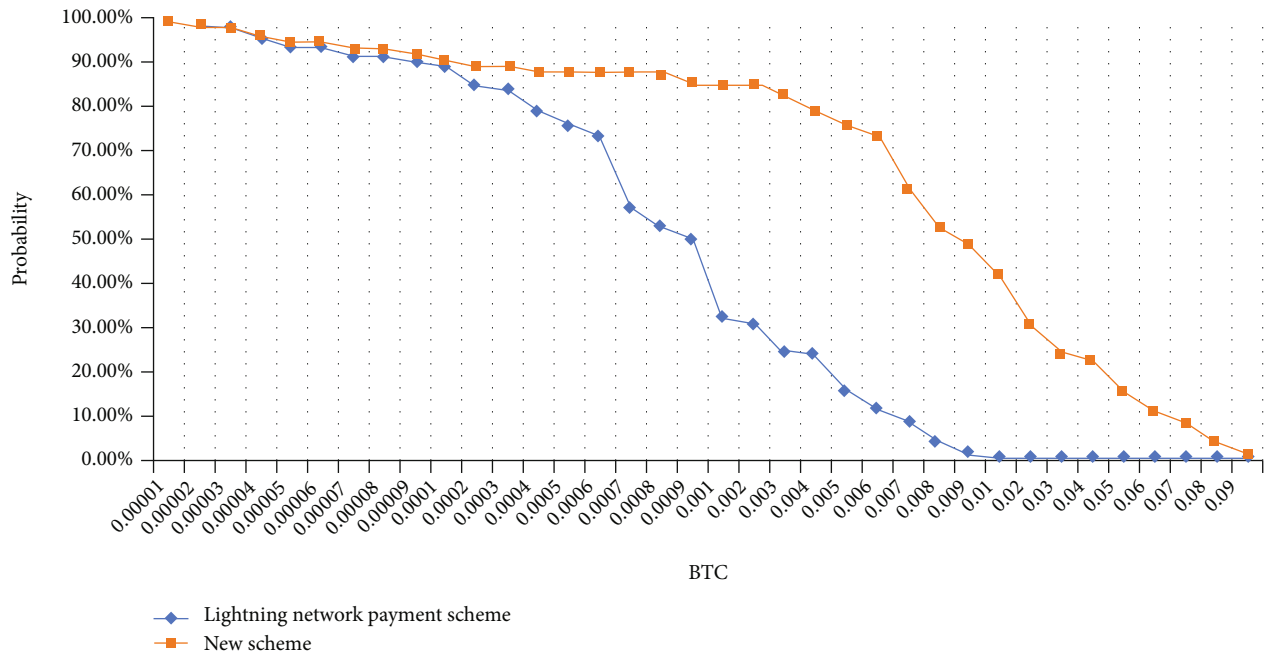


FIGURE 5: In the simulation network, the routing success rate of this scheme for large payments is significantly higher than that of the original lightning network payment scheme.

rate of the payment is counted. It is verified that the routing success rate of this scheme for large payments is significantly higher than that of the nonmultipath payment scheme, as shown in Figure 5.

5. Conclusion

The off-chain payment network is an important solution to the blockchain scalability problem. We propose a new multipath payment scheme that supports proof of payment while retaining the relatively small channel capacity requirements of the original multipath payment scheme for the lightning network. By creating the simulated network and making simulated payment, the advantages of the scheme in this paper are verified in terms of the routing success rate. In the future, we plan to design a fund partitioning algorithm to improve the fund balance in the channel. We also consider taking the routing fees into consideration in the partitioning algorithm to further reduce the routing cost. In addition, whether the new payment protocols will have an impact on the master chain is subject to further study. In addition, we intend to increase the size of the simulated transactions, so that the simulated results are closer to the results of the real scenario.

Data Availability

All the data used are given in the paper.

Conflicts of Interest

The authors declare that they have no conflicts of interest.

References

- [1] S. Nakamoto, *Bitcoin: a peer-to-peer electronic cash system*, 2009, <https://bitcoin.org/en/bitcoin-paper>.
- [2] J. Wang and H. Wang, "Monoxide: scale out blockchains with asynchronous consensus zones," *16th {USENIX} Symposium on Networked Systems Design and Implementation ({NSDI} 19)*, vol. 2019, pp. 95–112, 2019.
- [3] J. Poon and T. Dryja, *The lightning network: scalable off-chain instant payments [EB/OL]*<https://www.blockchainlightning.com/wp-content/uploads/2018/03/lightning-network-paper.pdf>.
- [4] O. Osuntokun, *Amp: atomic multi-path payments over lightning [EB/OL]*<https://lists.linuxfoundation.org/pipermail/lightning-dev/2018-February/000993.html>.
- [5] G. Wood, "Ethereum: a secure decentralised generalised transaction ledger," *Ethereum Project Yellow Paper*, vol. 5, no. 1, pp. 1–32, 2014.
- [6] E. Androulaki, A. Barger, V. Bortnikov et al., "Hyperledger fabric," in *Proceedings of the Thirteenth EuroSys Conference*, pp. 1–15, New York, 2018.
- [7] B. S. Bhati and C. S. Rai, "Intrusion detection technique using coarse Gaussian SVM," *International Journal of Grid and Utility Computing*, vol. 12, no. 1, pp. 27–32, 2021.
- [8] S. P. Yadav, K. K. Agrawal, B. S. Bhati, F. Al-Turjman, and L. Mostarda, "Blockchain-based cryptocurrency regulation: an overview," *Computational Economics*, vol. 16, pp. 1–17, 2020.
- [9] N. Webb, "A fork in the blockchain: income tax and blockchain cash hard fork," *North Carolina Journal of Law & Technology*, vol. 19, no. 4, p. 283, 2018.
- [10] M. Corallo, *BIP 152: compact block relay [EB/OL]*<https://github.com/blockchain/bips/blob/master/bip-0152.html>.
- [11] L. Luu, V. Narayanan, C. Zheng, K. Baweja, S. Gilbert, and P. Saxena, "A secure sharding protocol for open blockchains,"

- in *Proceedings of the 2016 ACM SIGSAC Conference on Computer and Communications Security*, pp. 17–30, New York, 2016.
- [12] M. Zamani, M. Movahedi, and M. Raykova, “Rapidchain: scaling blockchain via full sharding,” in *Proceedings of the 2018 ACM SIGSAC Conference on Computer and Communications Security*, pp. 931–948, New York, 2018.
- [13] E. Kokoris-Kogias, P. Jovanovic, L. Gasser, N. Gailly, E. Syta, and B. Ford, “Omniledger: a secure, scale-out, decentralized ledger via sharding,” in *2018 IEEE Symposium on Security and Privacy (SP)*, pp. 583–598, IEEE, San Francisco, CA, USA, 2018.
- [14] I. Bentov, R. Pass, and E. Shi, “Snow white: provably secure proofs of stake,” *IACR Cryptology ePrint Archive*, vol. 11, no. 3, pp. 36–49, 2016.
- [15] I. Eyal, A. E. Gencer, E. G. Sirer, R. van Renesse et al., “Blockchain-ng: a scalable blockchain protocol NSDI,” vol. 21, pp. 45–59, 2016.
- [16] Y. Gilad, R. Hemo, S. Micali, G. Vlachos, and N. Zeldovich, “Algorand: scaling byzantine agreements for cryptocurrencies,” in *Proceedings of the 26th Symposium on Operating Systems Principles*, pp. 51–68, New York, 2017.
- [17] H. Hees, “Raiden network: off-chain state network for fast DApps,” in *Devcon two*, Ethereum Foundation, 2016.
- [18] J. Poon and V. Buterin, “Plasma: scalable autonomous smart contracts,” <https://www.plasma.io/plasma-deprecated.pdf>.
- [19] A. M. Rahmani, M. Mohammadi, S. Rashidi et al., “Questioning the security of three recent authentication and key agreement protocols,” *IEEE Access*, vol. 9, pp. 98204–98217, 2021.
- [20] M. Hosseinzadeh, A. M. Rahmani, and B. Vo, “Improving security using SVM-based anomaly detection: issues and challenges,” *Soft Computing*, vol. 25, no. 4, pp. 3195–3223, 2021.
- [21] N. Maleki, A. M. Rahmani, and M. Conti, “SPO: a secure and performance-aware optimization for MapReduce scheduling,” *Journal of Network and Computer Applications*, vol. 176, article 102944, 2021.
- [22] S. Akhbarifar, H. H. S. Javadi, A. M. Rahmani, and M. Hosseinzadeh, “A secure remote health monitoring model for early disease diagnosis in cloud-based IoT environment,” in *Personal and Ubiquitous Computing*, pp. 1–17, Springer, 2020.
- [23] *Blockchain for Cybersecurity and Privacy: Architectures, Challenges, and Applications*, CRC Press, 2020.
- [24] Z. Sisi and A. Souri, “Blockchain technology for energy-aware mobile crowd sensing approaches in Internet of things,” *Transactions on Emerging Telecommunications Technologies*, vol. 11, no. article e4217, 2021.
- [25] C. Lin, N. Ma, X. Wang, and J. Chen, “Rapido: scaling blockchain with multi-path payment channels,” *Neurocomputing*, vol. 406, pp. 322–332, 2020.
- [26] V. Sivaraman, S. B. Venkatakrishnan, K. Ruan et al., “High throughput cryptocurrency routing in payment channel networks,” *Symposium on Networked Systems Design and Implementation (NSDI 20)*, vol. 7, pp. 777–796, 2020.

Research Article

Load Balancing Routing Algorithm of Low-Orbit Communication Satellite Network Traffic Based on Machine Learning

Tie Liu , **Chenhua Sun**, and **Yasheng Zhang**

Satellite Communications and Broadcasting and Television Professional Department, China Electronics Technology Group Corporation Network Communications Research Institute, Shijiazhuang, 050011 Hebei, China

Correspondence should be addressed to Tie Liu; l970419t@st.btbu.edu.cn

Received 18 November 2021; Revised 9 December 2021; Accepted 13 December 2021; Published 31 December 2021

Academic Editor: Nima Jafari Navimipour

Copyright © 2021 Tie Liu et al. This is an open access article distributed under the Creative Commons Attribution License, which permits unrestricted use, distribution, and reproduction in any medium, provided the original work is properly cited.

Satellite communication has become an important research trend in the field of communication technology. Low-orbit satellites have always been the focus of extensive attention by scholars due to their wide coverage, strong flexibility, and freedom from geographical constraints. This article introduces some technologies about low-orbit satellites and introduces a routing algorithm DDPG based on machine learning for simulation experiments. The performance of this algorithm is compared with the performance of three commonly used low-orbit satellite routing algorithms, and a conclusion is drawn. The routing algorithm based on machine learning has the smallest average delay, and the average value is 126 ms under different weights. Its packet loss rate is the smallest, with an average of 2.9%. Its throughput is the largest, with an average of 201.7 Mbps; its load distribution index is the smallest, with an average of 0.54. In summary, the performance of routing algorithms based on machine learning is better than general algorithms.

1. Introduction

Satellite communications have gradually gained popularity in the fields of radio and television and multimedia communications. On the one hand, people are beginning to require satellite networks to meet user requirements for delay, bandwidth, and fault tolerance. Services such as global positioning, remote communication, and telemedicine provided by satellite networks have long been closely related to people's daily lives. And it plays a huge role in promoting logistics and transportation, environmental monitoring, material exploration, navigation positioning, digital city, and other related fields. With the rapid development of satellite communication technology, satellites have obtained huge applications in acquiring and processing space information and related resources. In addition, with the development of nongeostationary orbit satellites and interstellar links, how to reduce the load of satellite networks has become one of the key factors that must be considered when designing satellite network routing algorithms. The research of machine learning in routing algorithms is still in the early stage. When it is actually used, it will bring surprises to people.

The satellite network has a highly dynamic topology. However, the distribution of ground users accessing its network is extremely uneven, and these characteristics will cause congestion in a local area of the satellite network. However, the surrounding satellite resources are vacant and wasted, causing data to be concentrated on certain paths or lost. It will increase the delay and packet loss rate of data packets. The high-speed movement of low-orbit satellites makes satellite networks have the characteristics of frequent topology changes, high possibility of link and node failure, unbalanced load distribution on the satellite, and limited resources on the satellite. These characteristics make the satellite network need better antimovement, antidestruction, and adaptive routing technology than the ground network. Therefore, it is necessary to design a routing algorithm suitable for the LEO satellite network separately. The main purpose of this paper is to verify that the traffic load balancing routing algorithm based on machine learning is superior to the traditional routing algorithm.

The innovation of this article is as follows: (1) This article introduces the testing methods of low-orbit satellite

performance parameters and introduces the general low-orbit communication satellite network traffic load balancing routing algorithm. (2) This article introduces a load balancing routing algorithm based on machine learning and compares its performance with three common routing algorithms through simulation experiments.

2. Related Work

With the continuous improvement of people's life needs, the requirements for communication satellites are getting higher and higher. Many scholars try to study more advanced satellite routing algorithms to improve the performance of passing satellites. Jiang proposed an energy consumption model based on link load, and used the bit energy consumption parameters of the network to measure the energy efficiency of the network. He also proposed an energy-saving minimum critical routing algorithm, which includes energy-efficient routing and load balancing. In order to further improve the energy efficiency of the network, Jiang et al. proposed an energy-saving multiconstraint rerouting algorithm to achieve maximum energy efficiency, but the algorithm lacks some detailed design [1]. Hui et al. proposed an energy-saving routing algorithm for wireless sensor networks based on unequal aggregation theory and connected graph theory. The new algorithm has been optimized and innovated in two aspects: cluster head election and cluster routing. The simulation results show that the new algorithm balances the energy consumption between sensor nodes and reduces the impact of the energy whole problem. It improves the link quality, greatly improves the reliability and efficiency of data transmission, and significantly extends the life of the network [2]. Kawecki and Schoeneich proposed a routing algorithm based on the mobility of nodes in a delay-tolerant network (DTN). DTN is characterized by the temporary or permanent lack of a continuous path between the source node and the destination node. Communication is accomplished through message transmission by intermediate nodes based on the store-carry-forward paradigm. This routing algorithm is based on the ability to use node mobility and its contact information. Its shortcoming is the lack of practical data support [3]. Erickson et al. rely on symmetric properties to build a single-path routing algorithm for DPillar. This algorithm can improve the average path length found, the total bottleneck throughput, and communication delay. And it emphasizes that the data center network should accept more stringent combination inspections, which can significantly improve its computing efficiency and performance. However, the algorithm is difficult to operate and not practical [4]. Fang et al. proposed a routing algorithm (GINS) based on geographic information and node selfishness. In order to select the forwarding node, GINS combines the forwarding willingness of the node with its geographic information to maximize the contact destination. GINS describe the message forwarding process as a 0-1 knapsack problem with allocation restrictions to meet the selfish needs of nodes. A large number of simulations have been carried out, and the results show that, compared with GRONE, GINS can achieve a higher transmission rate and

a lower number of hops. In addition, its management expense ratio is 25% lower than GRONE [5]. Wang et al. described the structure and function expectations of the energy router from the perspective of the network and improved the existing energy router design. They proposed a design of an electronic local area network energy routing algorithm based on graph theory. According to the characteristics of power transmission, they designed a routing algorithm with the lowest cost and proposed a power selection and routing design algorithm suitable for heavy load conditions. Both algorithms have been verified through case analysis, but the disadvantage is that there is no correlation analysis between the two algorithms [6]. Kumar and Dave proposed a beacon information-independent geographic routing algorithm called BIIR. By intelligently using the information collected by the vehicle in previous destination path discovery attempts, the algorithm reduces the number of broadcasts for forwarding data packets. Simulation results show that the algorithm is superior to the existing beacon-free routing protocol in terms of the average number of broadcasts for each packet forwarding, the packet delivery rate, and the end-to-end delay experienced by data messages. But its disadvantage is that the algorithm consumes more energy [7]. Mahalaxmi and Esther use the ant colony algorithm based on multiagent technology to improve the Internet of things routing algorithm and plan the routing algorithm to improve the packet delivery rate of the algorithm and avoid the damage of overlapping intersections by multiagent technology. With the improvement of efficiency, the delay will be reduced [8]. Kaneko and Bossard propose a method to construct $2n$ disjoint paths from a set s composed of $2n$ source nodes to a set D composed of $2n$ destination nodes. The nodes TN, K ($n \geq 1, K \geq 3$) in the n -dimensional k -element torus are formally described and evaluated. Then, the algorithm is formally described and evaluated [9].

3. Low-Orbit Satellite Network Load Balancing Routing Algorithm

This paper is aimed at proving that the traffic load balancing routing algorithm of the LEO communication satellite network based on machine learning has better performance than the traditional algorithm. Therefore, in this part, we first describe the general composition and key technologies of some LEO satellites and briefly introduce the process and evaluation indicators of the balanced routing algorithm, so as to facilitate the later experiments.

3.1. Key Technologies of Satellite Networks

3.1.1. Satellite Communication System

(1) *Satellite Communication System Composition.* As shown in Figure 1, the satellite communication system consists of three parts: space segment, ground segment, and user segment. The space segment is a constellation of satellites, which are scattered in the orbit of the satellite according to specific rules. The ground segment refers to the control

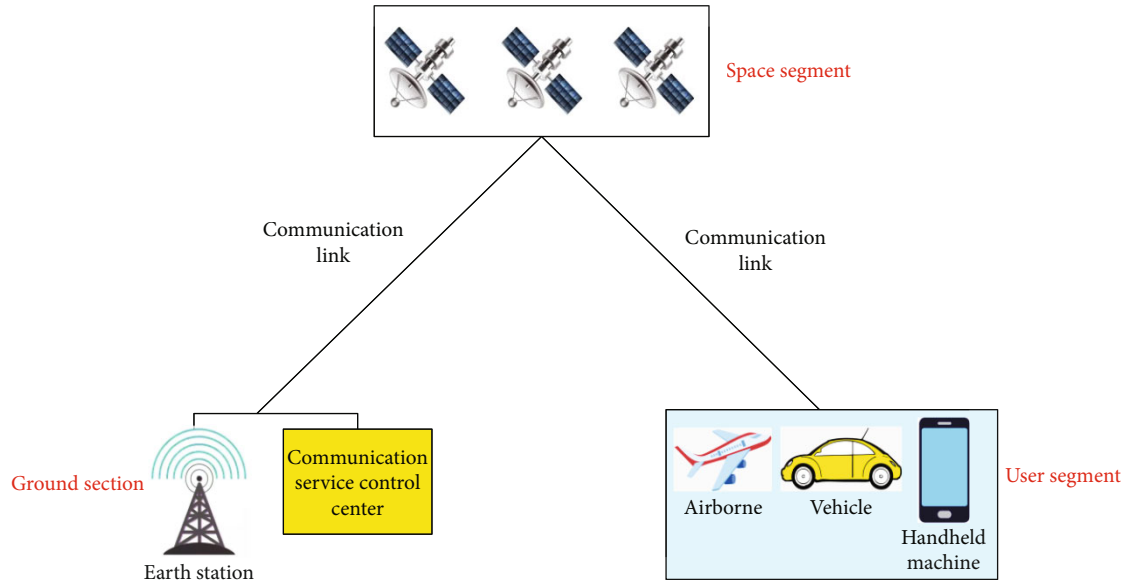


FIGURE 1: Satellite communication system composition diagram.

center, and the user segment refers to users, including various terminals.

(2) *Parameters of the LEO Satellite System.* The low-earth-orbit (LEO) satellite system can be composed of dozens to hundreds of satellites to achieve continuous global coverage of the network. Its satellites have a low orbit, and all satellite nodes fly around the earth at high speed. The LEO satellite communication system has a shorter average visibility time to the ground station, and the satellite-to-earth link communication delay established with the ground user is lower. Usually, handheld devices can be connected to the LEO satellite network. Table 1 lists typical LEO satellite systems such as Iridium, Teledesic, and Globalstar and their main system setting parameters.

3.1.2. *Satellite Constellation.* Satellite constellation is a collection of satellites designed according to the relative positions and geometric relationship rules between multiple satellites to complete complex communication tasks. Satellite constellation parameters can determine the size, shape, direction of the satellite orbit, and position of the satellite on the orbit. There are 6 main satellite constellation parameters, which can be divided into 3 categories. There are two constellation parameters that determine the size and shape of the orbit. It determines the three constellation parameters of the orbital position and one constellation parameter that determines the relative position. The schematic diagram is shown in Figure 2 [10].

The two constellation parameters for determining the size and shape of the orbit are the semimajor axis of the orbit and the eccentricity of the orbit, among which the apogee radius, apogee height, perigee radius, perigee height, and half focal length are related to the two constellation parameters; the three constellation parameters for determining the orbital position are ascending node right ascension, orbital inclination, and perigee angle; a constellation parameter that

determines the relative position of a satellite in orbit is the true near-earth angle.

3.1.3. *Satellite Network Routing.* With the development of satellite communication technology, a satellite network composed of multiple satellites or multilayer satellites has various forms of data transmission. It is particularly important to select a suitable route for data transmission from source to destination. Therefore, the design of routing algorithms is a key technology for continuous research in satellite networks. According to the different routing functions of each component in the satellite network, satellite routing can be divided into intersatellite routing, access routing, and border routing [11, 12]. Among them, due to the complexity of satellite network movement, intersatellite routing has always been a major and difficult point for many scholars. Designing a proper intersatellite routing algorithm is crucial to the routing performance of the entire satellite communication system. Figure 3 shows the composition of intersatellite routing.

3.2. LEO Satellite Network Routing Link

3.2.1. *Overview of Low-Orbit Satellite Links.* In a satellite constellation, each satellite can be abstracted as a node in the constellation, and communication between adjacent nodes is realized through a full-duplex link. This kind of link is the intersatellite link. In low-orbit satellites, intersatellite links are divided into intraorbit intersatellite links and inter-orbit intersatellite links according to whether two adjacent nodes are in the same orbital plane [13]. Figure 4 is a simple schematic diagram of the intersatellite link structure.

- (1) The intersatellite link refers to the link established by two adjacent satellites in the same orbit, and each satellite has two intraorbit links. Since the relative position of the satellites in the same orbit remains

TABLE 1: Typical LEO satellite system parameters.

System name	Iridium	Globalstar	Teledesic
Track height	778	1392	1383
Number of track planes	6	10	14
Number of satellites	69	275	51
Inter satellite link	2 in rail + 2 between rails	No	Yes
Orbit elevation	85.9°	54°	84.3°

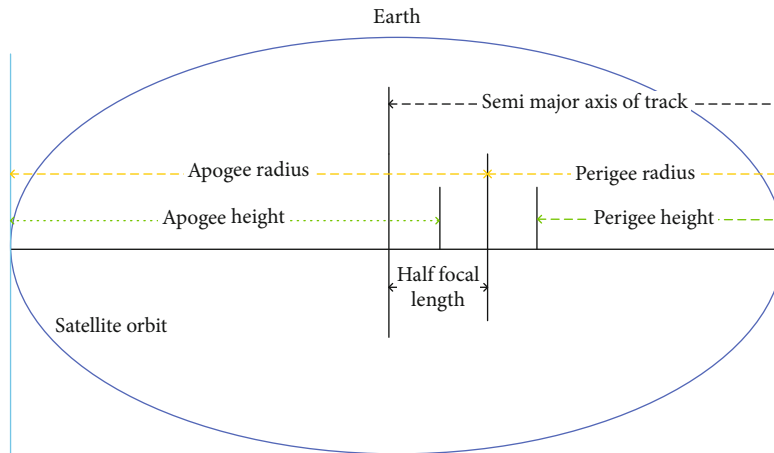


FIGURE 2: Schematic diagram of determining orbital parameters.

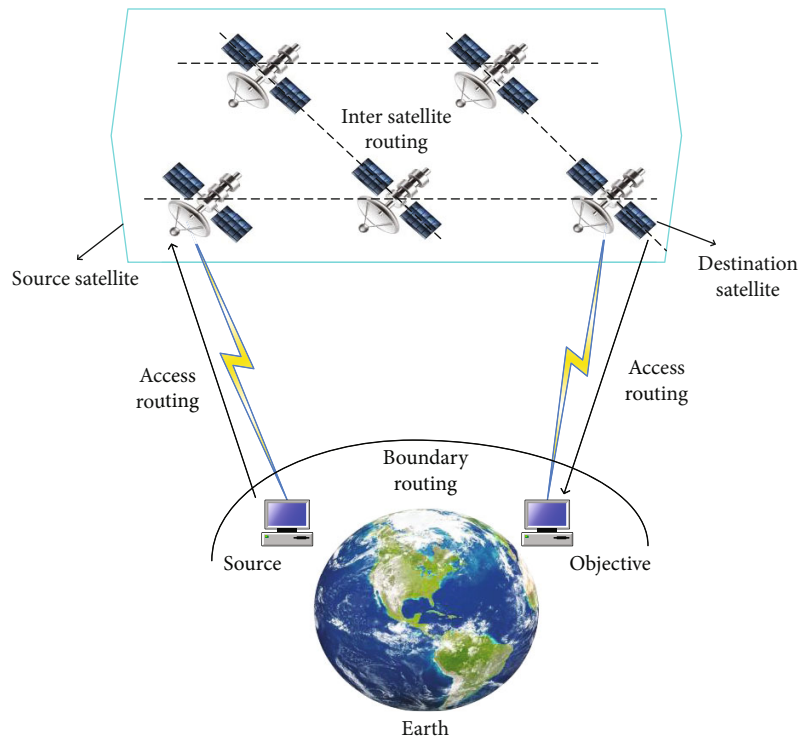


FIGURE 3: Satellite network routing composition.

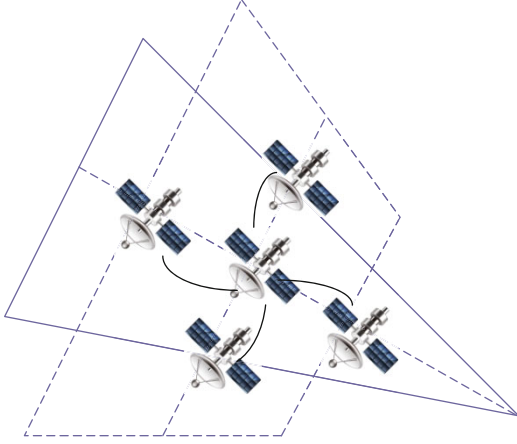


FIGURE 4: Simple structure of intersatellite link.

unchanged, the distance between adjacent satellites in the orbit will not change. The link length is expressed as follows:

$$L_{m,n} = \sqrt{2}R \sqrt{1 - \cos\left(\frac{2\pi}{M}\right)}. \quad (1)$$

Among them, $L_{m,n}$ is the distance between the m th star and the n th star in the same orbital plane. R is the orbit radius, and M is the number of satellites in the current orbit. If the orbit radius of the satellite movement and the number of satellites in the orbit are the same, then the intersatellite link distances in the orbit of the satellite are also the same [14].

(2) Interorbital intersatellite link

The interorbit intersatellite link is a link established by two adjacent satellites in two different but close orbits. When two adjacent satellites are in the polar region or on both sides of the reverse seam, it may be difficult to establish interorbit links due to unstable positions. Therefore, each satellite has 0-2 interorbit links. The expression of the link length can be divided into two cases where the orbital phase factor is equal to 0, that is, the interorbit link is parallel to the equator, and the orbital phase factor is not equal to 0, that is, the relative equator is inclined [15, 16], as shown in the following formula:

$$L_{\text{lat}} = \sqrt{2}R \sqrt{1 - \cos\left(\frac{2\pi}{N}\right)} \times \cos(\text{lat}) F = 0, \quad (2)$$

$$L_{\text{lat}} = \sqrt{\left[\sqrt{2}R \sqrt{1 - \cos\left(\frac{2\pi F}{MN}\right)}\right]^2 + \left[\sqrt{2}R \sqrt{1 - \cos\left(\frac{2\pi}{N}\right)} \times \cos(\text{lat})\right]^2 F \neq 0}. \quad (3)$$

Among them, L_{lat} is the latitude of the satellite, R is the orbit radius, N is the number of orbits in the constellation, and F is the orbit phase factor.

3.2.2. Method for Setting Routing Link Weight of Low-Orbit Satellite Network. For low-orbit satellite networks, different satellite constellations have different network topologies. And in different time periods, the network topology of the satellite is not the same. These are the characteristics of satellite networks that are different from terrestrial networks, and these characteristics determine that the link weight calculation of satellite routing is more diverse. In order to allow satellite network routing to better adapt to the characteristics of the intersatellite network and improve the work efficiency of the satellite network, after link information is collected, these uncertain factors are considered to be optimized in the link weight. This is currently a better choice for satellite network routing. The following will introduce several different weighting schemes for intersatellite links.

(1) The intersatellite link distance is the weight

In satellite networks, the distance of intersatellite links is generally used as the link weight in satellite network routing. Such a routing algorithm is simple to implement. Through simple link information collection, the shortest path set is obtained. In such a system, an operating cycle of the satellite network is first divided into several time slices. The size of the time slice depends on the law of the dynamic topology of the satellite network. In each time slice, the system assumes that the topology of the entire satellite network is unchanged [17]. The topological structure divided in this way must take into account the visibility, direction angle, and coverage between the satellites and the ground. In this time slice, it is ensured that the topology change is maintained within a controllable range. Then, in each time slice, its topology is unchanged by default. According to the link state at the initial time of the time slice, the route is calculated at the initial time of the time slice. The distance between the satellite node m and the satellite node n is $\text{Dst}_{m,n}$, and the speed of light is V . The calculation formula for the weight $W_{m,n}$ of the intersatellite link $L_{m,n}$ is

$$W_{m,n} = \text{Del}_{m,n} = \frac{\text{Dst}_{m,n}}{V}. \quad (4)$$

When calculating the path, the total delay of the selected end-to-end link should be as small as possible. The calculation formula of the path cost is

$$\text{Metric} = \sum W_{m,n}. \quad (5)$$

The routing path calculated according to the above formula is the shortest path, but not the optimal path. The weight uses the distance of the intersatellite link, that is, to choose the closest path.

(2) Intersatellite link weight

Taking the link maintenance time into account in the routing algorithm of the satellite network, the transmission distance is still regarded as the main factor of the intersatellite link weight. Intersatellite link switching has a great

impact on routing stability. The intersatellite links between different orbital planes are regarded as temporary links. Therefore, reducing the number of intersatellite links between different orbital surfaces on the routing path can increase the continuity of the routing. The calculation formula for the weight of the intersatellite link between satellite node m and satellite node n is [18]

$$W_{m,n} = \text{Del}_{m,n} \times \frac{1}{\lambda}. \quad (6)$$

The parameter λ is used to indicate the connection capability of the intersatellite link, and the value range is 0 to 1.

(3) Routing energy consumption of the LEO satellite network

Assuming that the energy consumption of path L is E , the calculation formula is

$$E = \sum_{i=1}^n [V_i, V_{i+1}]. \quad (7)$$

That is, the energy consumption of path L is the sum of the energy consumption of the link formed between all adjacent nodes in the path. $E[V_i, V_{i+1}]$ is the link energy consumption between two adjacent nodes, and the calculation formula is deduced as

$$E[V_i, V_{i+1}] = \begin{cases} 7 \\ \min [7, 1/p^4] \end{cases}. \quad (8)$$

3.3. Routing Algorithm Performance Judgment Method

3.3.1. Traffic Load Judgment Mechanism

(1) *Factor Consideration.* When a satellite node makes a load decision, it should comprehensively consider the load status of the next-hop direction to be selected and the overall load status of the satellite node corresponding to the next-hop direction to be selected. At the same time, when calculating link load information, the long-term congestion changes in the network should be reflected as much as possible.

(2) *Specific Implementation Method.* The load decision mechanism provides a basis for each satellite node to make a reasonable routing decision. The satellite node obtains the main route and the alternative route of the current forwarding data packet by querying the routing table and judges the current link status according to the current link load information, determining the optional next-hop direction of the current data packet according to the link status of the primary and alternative next hops, and sending data according to the optional next hop. Among them, the link state can be divided into three states: relatively idle, relatively busy, and busy [19, 20]. When the primary selected next-hop link is relatively idle, the primary selected next hop is selected as the optional next hop regardless of the status of the alternative next-hop link; when the primary selected

next-hop link is relatively busy, if the alternative next-hop link is relatively idle, select the alternative next hop as the optional next hop; otherwise, select the primary selected next hop as the optional next hop; when the primary next-hop link is busy, if the alternative next-hop link is relatively idle or busy, the alternative next hop is selected as the optional next hop. If the alternative link is also busy, it indicates that the current two links are in congestion. Start the on-demand detour route to find the temporary optional next hop as data.

By calculating the link occupancy rate L , set reasonable thresholds X , Y , and $0 < X < Y < 1$ and compare the relationship between the link occupancy rate L and the threshold X , Y to determine the state of the intersatellite link. The details are as follows:

Relative idle: when $0 < L < X$, the current link is relatively idle.

Relatively busy: when $X < L < Y$, the current link is relatively busy.

Busy: when $L > Y$, the current link is busy [21].

The calculation of the link occupancy rate is shown in the formula, which represents the ratio of the weighted load of the current link to the capacity of a given link queue:

$$L = \frac{Q_{mn}(t)}{Q}. \quad (9)$$

Among them, Q is the link queue capacity, generally a given value, and $Q_{mn}(t)$ is the weighted link load from the m th star to its neighbor's n th star at time t . The weighted link load refers to the load information of the current link and the next hop satellite node corresponding to the current link. The overall load information, weighted link load $Q_{mn}(t)$ is calculated as follows:

$$Q_{mn}(t) = k \times V_{mn}(t) + N_n(t) \times (1 - k). \quad (10)$$

Among them, k is the weighting coefficient, $Q_{mn}(t)$ is the load information of the output link direction from the m th star to its neighbor's n th star at time t , and $N_n(t)$ is the overall load information of the n th star at time t .

In order to smooth the surge of short-term captains and better reflect the recent changes of captains, $V_{mn}(t)$ calculates the exponentially weighted moving average captains of the current link direction, as shown in the formula:

$$V_{mn}(t) = \frac{\mu V_{mn}(t-1) + (1-\mu)C_{mn}(t)}{1-\mu^t}. \quad (11)$$

Among them, $V_{mn}(t-1)$ is the exponentially weighted average length of the output link from the m th star to its neighbor n th star at the previous moment. $C_{mn}(t)$ is the output link team length from the m th star to its neighbor's n th star at time t , and μ is an exponential weighting coefficient.

The overall load information of the current satellite node refers to the average queue length of all output links of the

current satellite node. The average value of the exponentially weighted average queue length of all output link directions of the current satellite node is calculated, as shown in the formula:

$$N_n(t) = \frac{\sum_{N=1}^{N_n} V_{Nn}(t)}{N_n}. \quad (12)$$

Among them, $V_{Nn}(t)$ is the exponentially weighted moving average team length in the direction of the output link from the n th star to its neighboring n th star at time t ; N_n is the number of neighbors of the n th star with inter-orbital connections.

It can be seen from the above calculation that the key factor for calculating the weighted load of the output link is the determination of the weighting coefficient k . k reflects the proportion of the team leader in the current link direction in the output weighted load. The larger the value of k , the smaller the influence of the load status of the next-hop satellite node on the weighted load of the current output link. Therefore, choosing an appropriate value of k is very important [22, 23].

3.3.2. Other Performance Indicators. To evaluate the performance of a routing algorithm, conclusions can be drawn from the calculation of delay, packet loss rate, throughput, and routing overhead. Here are some calculation methods of routing performance [24].

(1) Average Delay. The average delay refers to the average delay of all data packets in the network from the source satellite node to the destination satellite node. The calculation of the average delay is shown in the formula:

$$T_{\text{avg}} = \frac{\sum_{i=1}^M T_i}{M}. \quad (13)$$

Among them, T_{avg} is the average delay, and M is the total number of data packets transmitted in the network. T_i is the total time delay of the i th data packet transmitted in the network from the source satellite node to the destination satellite node.

(2) Packet Loss Rate. As the name implies, the packet loss rate is the packet loss rate. It refers to the ratio of the number of lost data packets to the total number of sent data packets when the source satellite node in the network sends all data packets to the target satellite node. The calculation is as follows:

$$\text{loss} = \frac{M_{\text{loss}}}{M_{\text{send}}}. \quad (14)$$

Among them, loss represents the packet loss rate, M_{loss} is the number of data packets lost during the sending process, and M_{send} is the total number of data packets sent by the network.

(3) Throughput. Throughput refers to the maximum amount of data that the network can send without losing packets. Usually measured by the amount of data normally sent per unit time, the throughput is calculated as follows:

$$\text{TL} = \frac{M_s}{t} \times L. \quad (15)$$

In the formula, TL is the throughput, M_s is the number of data packets successfully delivered, L is the length of the transmitted data packet, and t is the simulation time.

(4) Routing Cost. The routing overhead refers to the routing control packets that need to be sent to implement the routing algorithm during the operation of the constellation system. When analyzing routing performance, the number of routing control packets required to successfully transmit 1 million data packets is used to measure the routing overhead of the constellation system. The calculation formula of routing cost is as follows:

$$K = \frac{M_k}{M_s} \times 1000000. \quad (16)$$

Among them, K is the routing overhead, M_k is the total number of routing control packets, and M_s is the total number of data packets successfully transmitted in the network.

(5) Load Distribution Index. The load distribution index refers to the degree of load distribution in the satellite network, and the value range is (0,1). The larger the value, the more dispersed the load in the satellite network, and the better the balance performance. The smaller the value, the more concentrated the load in the satellite network [25, 26]. The calculation of the load distribution index is as follows:

$$F = \frac{(\sum_{i=1}^n x_i)^2}{\sum_{i=1}^n x_i^2} \times \frac{1}{n}. \quad (17)$$

Among them, F is the load distribution index, n is the total number of intersatellite links, and x_i is the total number of data packets passed by the i th intersatellite link during the simulation time.

The evaluation indexes of the above routing methods are relatively important. The average delay evaluates the load balancing time of the algorithm, the packet loss rate evaluates the reliability of the algorithm network, the throughput reflects the ability to send data, and the load distribution index reflects the balancing ability of the network. These indexes jointly evaluate the load balancing performance of the routing algorithm.

3.4. Low-Earth Satellite Network Load Balancing Algorithm. The significance of the load balancing algorithm is to allow satellite nodes to distribute data packets to adjacent lighter-loaded nodes for forwarding as much as possible when

congestion occurs. This can reduce the queuing delay of data packets at the satellite node. The algorithm adjusts the cost between links in combination with the regional traffic and uses the shortest path priority idea to find the path. The following will introduce the algorithm from several aspects such as traffic estimation, congestion judgment, and cost transformation [27].

3.4.1. Flow Estimation. The distribution of ground traffic on satellite networks is very uneven. It is mainly concentrated in some important cities on the mainland but is quite small in the ocean. This leads to a situation in which the traffic is concentrated in a certain area at certain moments in the satellite network communication process, and the satellites in this area are often congested, but the surrounding satellites are not fully utilized [28]. The low-orbit satellite network load balancing algorithm can adjust the link cost of the link according to the congestion state of the satellite link and the load state of the previous time period when the satellite link is congested. This adjustment process is for the entire network. Data passing through congested areas will bypass these load areas, and a lighter-loaded path needs to be selected for data transmission, thereby balancing the flow of the entire network.

3.4.2. Congestion Judgment. In a satellite network, a satellite maintains multiple links, these links are associated with different neighboring nodes, and the congestion state is also different. In order to improve link utilization, we monitor congestion on each link of the satellite. In order to improve the accuracy of monitoring, the calculation method to determine the link load is as follows:

$$\rho = \frac{kq \times I + \lambda}{\omega \times C \times t}, \quad (18)$$

where t is the time period for link load calculation, λ is the amount of data transmitted in t , I is the average queue length of the link in t , kq is the queue reduction rate, ω is the target utilization rate of the link, and C refers to the data transmission capability of the link, setting a congestion threshold θ for each link.

3.4.3. Cost Transformation. The load cost is obtained after comprehensive evaluation of link transmission delay and link congestion. In the case of congestion encountered in actual transmission, the congested link can be bypassed to obtain network traffic balance. The calculation formula of load cost is

$$C_p = \sum_{i=1}^n (D_i + F_i). \quad (19)$$

Among them, n is the link number, D_i is the link delay factor, and F_i is the link load factor.

When $\rho \leq \theta$, $F_i = 0$.

When $\rho > \theta$,

$$F_i = u \times \frac{q(w_m + w_n)}{\bar{t}}, \quad (20)$$

q is the queue size of the link, \bar{t} is the average value of t , w_m and w_n are the estimated traffic values of the satellites at both ends of the link, and u is the reduction factor of the function.

3.4.4. Algorithm Flow. The algorithm is based on the satellite virtual topology strategy and performs low-orbit link cost conversion on the topology snapshot. According to the congestion of the link, finding a suitable path for the nodes in the satellite network to perform data distribution. Therefore, by using the predictability and periodicity of the satellite constellation operation, the system operation time is divided into several identical time periods. In each time period, n gaps are divided, and the intersatellite link is judged for link overload in each time slot [29]. The specific process is shown in Figure 5.

The flow of this algorithm is as follows: after the satellite status is updated, calculate the link overload, judge whether the load factor is greater than a , adjust the LEO link cost if yes, reset the LEO link cost if no, then plan the path, and finally update the route. When this algorithm selects the path, starting from the congestion of the entire network, the weight on the idle link is small, and the idle link is selected to transmit data during routing. The algorithm does not need to know the load of adjacent satellites, and the additional storage overhead is small.

4. Routing Algorithm Design and Simulation Experiment Based on Machine Learning

4.1. Routing Optimization Algorithm Based on Reinforcement Learning

4.1.1. Algorithm Design. This experiment will design a routing optimization algorithm based on reinforcement learning. It includes algorithm input state design, output action design, and reward function design.

(1) *Input State Design.* Considering the measurement overhead of the traffic matrix and the feasibility of the algorithm, this chapter uses the link utilization rate of the entire network as the input state of the reinforcement learning algorithm. For time t , the input state s_t is an m -dimensional vector (m represents the number of links in the network topology), and the vector represents the link utilization of each link. In addition, using the flow matrix and the link utilization rate as the algorithm, the performance difference of the routing optimization between the two input states is studied. This chapter also continues to study the reinforcement learning routing optimization method using the traffic matrix as the input. For the routing method where the input is a flow matrix, the input state s_t is a n^2 -dimensional vector (n represents the number of network nodes), and each value in the vector represents the flow of each flow.

(2) *Output Action Design.* This chapter mainly uses reinforcement learning algorithms for business routing planning. It is hoped that the algorithm model will select the best routing scheme for each flow by identifying the characteristics of the service flow at different moments. In order to enable the algorithm model to learn the direct mapping

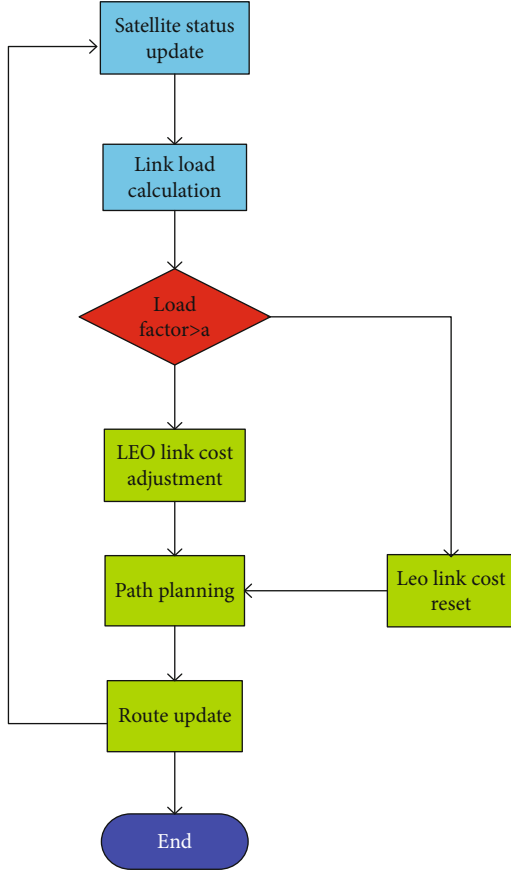


FIGURE 5: Algorithm flow chart.

relationship between traffic information and routing selection, this chapter will reinforce the learning algorithm model output action a_t to represent routing schemes of different flows. The reinforcement learning environment selects the routing scheme with the highest probability of each flow for routing according to the predicted action a_t .

(3) *Reward Function Design.* The role of the reward function in the reinforcement learning algorithm is mainly used to feed back the quality of the action taken by the agent. Then, the agent updates the neural network parameters according to the maximization reward as the optimization goal. Therefore, the quality of the constructed reward function will directly affect the performance of the reinforcement learning algorithm model for routing optimization problems. The optimization goal of this chapter is to make the network load more balanced and reduce network link congestion. Therefore, in this chapter, the reward function is set according to the link utilization, as shown in the following formula:

$$P_e = \frac{1}{C_e} \cdot \sum_i^{n^2} d_i \sigma_i, \quad (21)$$

$$\bar{P}_e^t = \frac{\sum_{e \in E} P_e^t}{N}, \quad (22)$$

$$R_t = \frac{\sum_{e \in E} (P_e^{t-1} - \bar{P}_e^{t-1})^2}{\sum_{e \in E} (P_e^t - \bar{P}_e^t)^2}. \quad (23)$$

Among them, P_e represents the link utilization rate of link e , d_i represents the size of the i th flow in the network, σ_i represents whether the i th flow passes through link e , C_e represents the capacity of link e , P_e^t represents the link utilization rate of link e in the t round of training, and \bar{P}_e^t represents the average value of P_e^t . According to the reward function A , if the variance of the link utilization rate of the entire network is lower than the variance of the link utilization rate of the entire network in the previous round of training, the agent can obtain a larger reward value. That is, the more balanced the link load, the greater the reward value obtained. Finally, the agent adjusts the parameters of the neural network according to these rewards to maximize the rewards it can obtain.

4.1.2. *Algorithm Model.* This experiment selects the existing DDPG reinforcement learning algorithm to learn routing strategies under different business models as the routing optimization algorithm model in this chapter. This is a strategy learning method that integrates deep learning neural networks into DPG. It is used as a basic algorithm for routing optimization. DDPG is a strategy learning method for continuous action and high-dimensional design proposed in recent years. DDPG predicts the best routing plan in the current traffic scenario based on the input status at the current moment, thereby achieving fine-grained routing control. The training process is shown in Figure 6.

During the training process, DDPG updates the critic network parameters through the gradient of the loss function and then updates the actor network parameters through the policy gradient. After updating the critic network and actor network parameters, using the soft update method to update the parameters in the corresponding target network. It can make the target actor network and the target critic network learn slowly from the parameters in the actor network and the critic network.

4.2. Simulation

4.2.1. *Environmental Configuration.* In order to verify the effectiveness of the algorithm, the network simulation software NS2 is used for simulation and performance analysis. The simulation uses the constellation parameters shown in Table 2, and the algorithm uses the polar orbit Iridium constellation.

Some parameters in the algorithm are shown in Table 3.

4.2.2. *Comparison Algorithm Selection.* In order to better evaluate routing optimization algorithms based on reinforcement learning, commonly used DSP algorithms, LAOR algorithms, and DRA algorithms are selected for simulation analysis and comparison. The DSP algorithm adopts static routing, establishes the forwarding table of each node during system initialization, stores the shortest path information, and does not support dynamic storage management; the

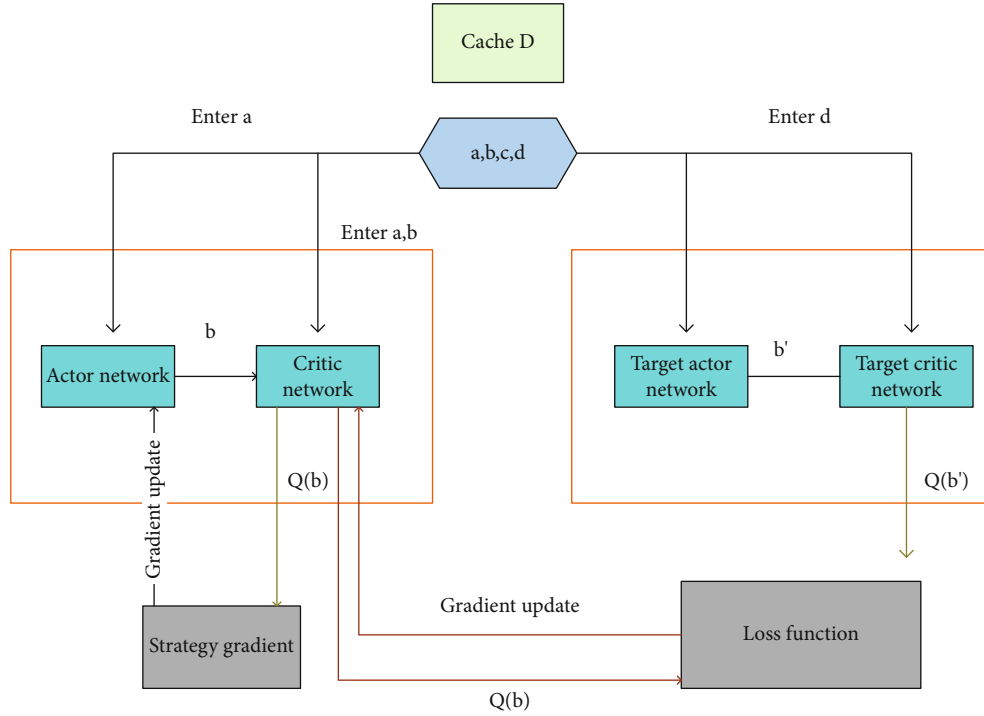


FIGURE 6: DDPG flow chart.

TABLE 2: Simulation constellation parameters.

	LEO
Model	Iridium
Number of tracks	6
Number of satellites	68
Height	810 km

TABLE 3: Design table of related parameters.

Routing topology update time	10 s
Instantaneous queue collection time	0.1 s
Queue reduction rate	0.9
Queue target utilization	0.8
Load threshold	0.8

LAOR algorithm is an algorithm formed by introducing the on-demand idea of terrestrial wireless ad hoc network into LEO satellite network. The purpose of the algorithm is to minimize the end-to-end delay and delay jitter and reduce the control overhead at the same time; the DRA routing algorithm is connectionless and distributed. It can make routing choices independently for each packet. It can avoid congested areas by making local routing decisions; the main algorithm DDPG algorithm of this experiment has been introduced above and will not be repeated here.

4.2.3. Experimental Purpose. The purpose of this experiment is to test the size of several indexes of the machine learning-

based routing algorithm, namely, the DDPG algorithm, and compare it with several other traditional algorithms to test whether it has advantages in performance.

4.3. Experimental Realization and Analysis. The overall weight W of the communication service is gradually increased from 1 to 2, that is, the data transmission rate is gradually increased, and the balanced performance of each algorithm is analyzed and compared.

4.3.1. Average Delay. In this paper, by measuring the difference between the time when the data packet arrives at the destination node and the time when it is generated in the simulation, the total delay of the current data packet transmission is obtained. The average delay is obtained by calculating the average value of the total delay of all data packets. The average delay data of the four different algorithms is shown in Figure 7.

It can be seen from Figure 7 that the average delay of the four algorithms all increases with the increase of the service weight W . When the weight is less than 1.6, the increase in the average delay along with the weight is relatively large, and when it is greater than 1.6, the increase in the average delay becomes smaller. Among the four algorithms, the DDPG algorithm based on reinforcement learning has the smallest average delay regardless of the weight. The average value of the average delay under different weights is 126 ms, and the average delay of the LAOR algorithm is the largest. This can verify that the DDPG algorithm can effectively balance the load and reduce the queuing delay.

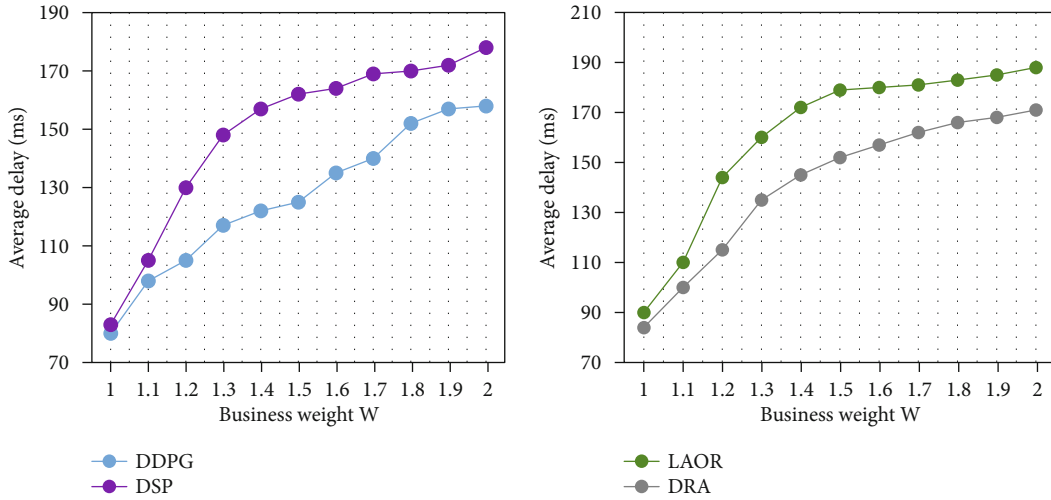


FIGURE 7: Lower average delay data of different algorithms.

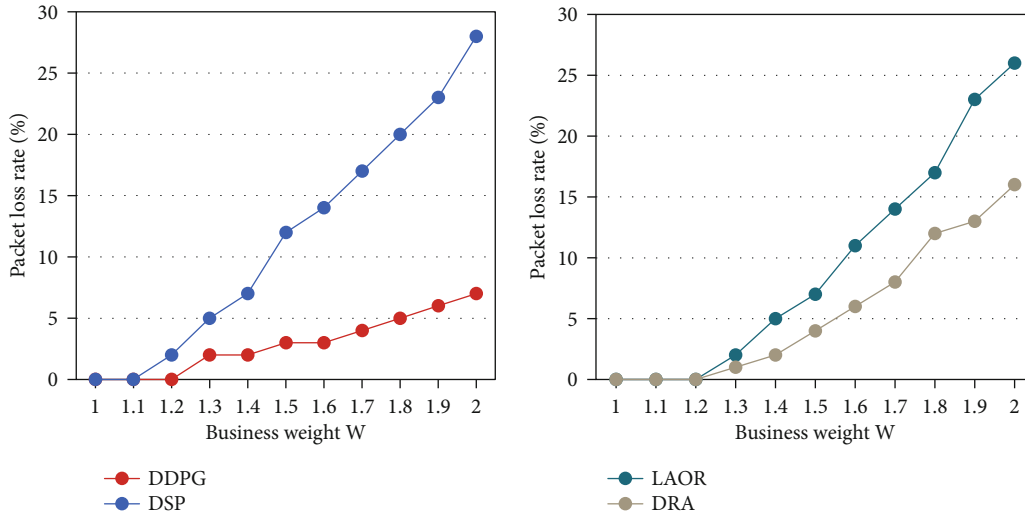


FIGURE 8: Lower packet loss rate data of different algorithms.

4.3.2. *Packet Loss Rate.* The size of the data packet loss rate shows the stability of the network to a certain extent. Figure 8 shows the packet loss rate data of each algorithm with different weights.

As can be seen from Figure 8, as the service weight increases, the service carried by the satellite increases, and the degree of unbalanced load distribution is aggravated. When the buffer queue overflows, the four algorithms will cause packet loss to a certain extent. As the weight W increases, the packet loss rate of the four algorithms also increases. Among them, the increase of DDDSP is the smallest, and the average value of its packet loss rate is also the smallest. The average packet loss rate under different weights is 2.9%. Based on the reinforcement learning DDDSP algorithm, because the path is adjusted in time according to the load status, the network can effectively reduce the possibility of queue overflow.

4.3.3. *Data Throughput.* Figure 9 is a comparison result of the throughput of the four algorithms under different service weights.

It can be seen from Figure 9 that as the service weight increases, the throughput of the four algorithms gradually increases. Among them, the DDPG algorithm has the highest average throughput under different weights, and its value is about 201.7Mbps. This proves that the DDPG algorithm based on reinforcement learning can sense the load status in time. And it can reasonably balance the load of each satellite node and effectively control the queuing delay of data packets. Therefore, its packet loss rate is very low, thereby improving throughput.

4.3.4. *Load Distribution.* Using the formula in 2.3 to calculate the load distribution, the obtained load distribution indexes of the four algorithms are shown in Figure 10.

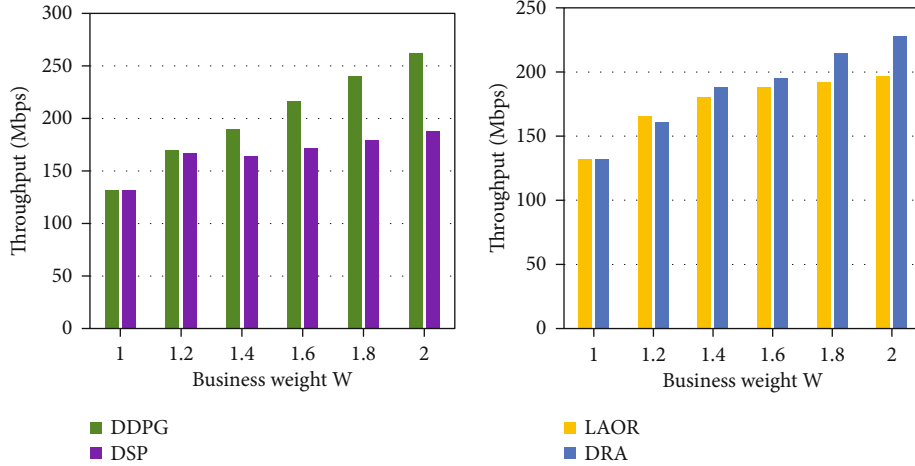


FIGURE 9: Lower throughput data of different algorithms.

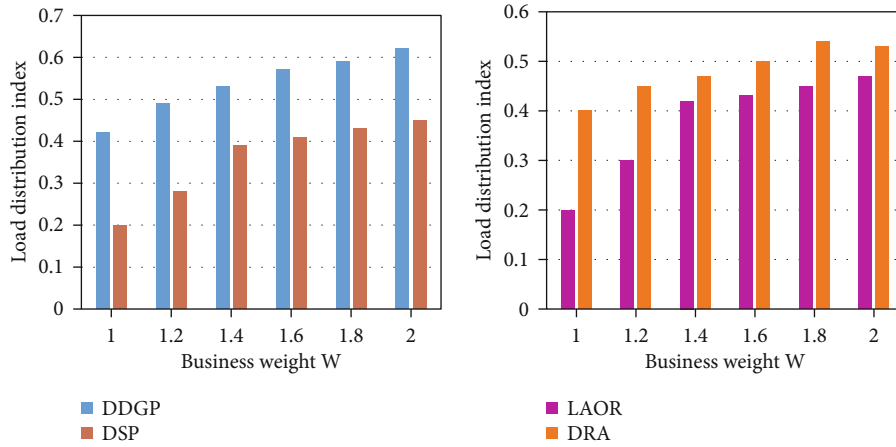


FIGURE 10: Load distribution index of different algorithms.

It can be seen from Figure 10 that the load distribution index of the DSP algorithm is the smallest, while the DDPG load distribution index is the largest, and the average load distribution index under different weights is 0.54. This is because the equalization performance of the DDPG algorithm is the best. It can adjust the path in time and spread congestion information across the entire network, reducing the traffic sent from satellites across the entire network to congested links. In addition, as the service weight increases, the load distribution index of the DDPG algorithm increases rapidly, which shows that this algorithm can distribute the load from the congested link to other links in time.

From the above four performance test experiments, we can know that the routing algorithm based on machine learning, i.e., DDPG algorithm, has the smallest average delay, the smallest packet loss rate, the highest data throughput, and the smallest load distribution index, which can verify that the performance of the DDPG algorithm is the best, and prove the superiority

of the performance of the routing algorithm based on machine learning.

4.4. Discussion. Low-orbit satellites have small time delays and low terminal energy consumption, which has great communication advantages. So in the satellite communication system with an intersatellite link, effective routing algorithm technology must be designed. At present, with the rapid development of communication technology, Internet applications, and cloud computing technology, communication networks have experienced an explosive business increase. The routing optimization algorithm based on machine learning can learn a good mapping relationship between traffic characteristics and routing strategies based on historical data. Then, use the learned knowledge to quickly make routing decisions based on changes in business characteristics. It can realize adaptive service routing scheduling and management, so the use of machine learning algorithms for network service routing optimization has attracted more and more attention.

Now, it has been extensively studied in the field of communication networks.

5. Conclusion

In this paper, the low-orbit communication satellite network traffic load balancing routing algorithm is researched. This article introduces the meaning of low-orbit satellites and its routing algorithm, as well as the performance judgment method of the algorithm. And this article introduces a traffic load balancing routing algorithm combined with machine learning and then studies some basic performance of this algorithm, as follows: (1) The basic composition, structure, and common parameters of the LEO satellite system are introduced. (2) The intersatellite links of low-orbit satellites and their weights are introduced. (3) This article explains some methods for determining the performance of the LEO satellite routing algorithm and explains the workflow and calculation methods of the general equilibrium routing algorithm. (4) A routing algorithm based on machine learning was introduced, and simulation experiments were carried out. The performance of this algorithm was compared with the performance of three commonly used low-orbit satellite routing algorithms. (5) Through simulation experiments, this article draws a conclusion: in terms of average delay, packet loss rate, throughput, and load distribution performance, routing algorithms based on machine learning are superior to other algorithms. The routing algorithm based on machine learning has the smallest average delay, and the average value is 126 ms under different weights. Its packet loss rate is the smallest, with an average of 2.9%. The throughput is the largest, with an average of 201.7 Mbps. The load distribution index is the smallest, with an average value of 0.54. The experiment in this paper is generally successful, but the experimental software is not completely designed in the experimental design part. In the future, the experiment can be designed more completely, and several performance tests can be done in the implementation part of the experiment to improve the integrity of the experiment.

Data Availability

The data that support the findings of this study are available from the corresponding author upon reasonable request.

Conflicts of Interest

The authors declared no potential conflicts of interest with respect to the research, authorship, and/or publication of this article.

References

- [1] D. Jiang, P. Zhang, Z. Lv, and H. Song, "Energy-efficient multi-constraint routing algorithm with load balancing for smart city applications," *IEEE Internet of Things Journal*, vol. 3, no. 6, pp. 1437–1447, 2016.
- [2] H. Xia, R.-h. Zhang, J. Yu, and Z.-k. Pan, "Energy-efficient routing algorithm based on unequal clustering and connected graph in wireless sensor networks," *International Journal of Wireless Information Networks*, vol. 23, no. 2, pp. 141–150, 2016.
- [3] M. Kawecki and R. O. Schoeneich, "Mobility-based routing algorithm in delay tolerant networks," *EURASIP Journal on Wireless Communications and Networking*, vol. 2016, no. 1, 2016.
- [4] A. Erickson, A. E. Kiasari, J. Navaridas, and I. A. Stewart, "An optimal single-path routing algorithm in the datacenter network DPillar," *IEEE Transactions on Parallel and Distributed Systems*, vol. 28, no. 3, pp. 689–703, 2017.
- [5] F. Lu, J. Li, S. Jiang, Y. Song, and F. Wang, "Geographic information and node selfish-based routing algorithm for delay tolerant networks," *Tsinghua ence & Technology*, vol. 22, no. 3, pp. 243–253, 2017.
- [6] R. Wang, J. Wu, Z. Qian, Z. Lin, and X. He, "A graph theory based energy routing algorithm in energy local area network," *IEEE Transactions on Industrial Informatics*, vol. 13, no. 6, pp. 3275–3285, 2017.
- [7] N. Kumar and M. Dave, "BIIR: a beacon information independent VANET routing algorithm with low broadcast overhead," *Wireless Personal Communications*, vol. 87, no. 3, pp. 869–895, 2016.
- [8] G. Mahalaxmi and R. K. Esther, "Multi-agent technology to improve the internet of things routing algorithm using ant colony optimization," *Indian Journal of Science & Technology*, vol. 10, no. 31, pp. 1–8, 2017.
- [9] K. Kaneko and A. Bossard, "A set-to-set disjoint paths routing algorithm in tori," *International Journal of Networking & Computing*, vol. 7, no. 2, pp. 173–186, 2017.
- [10] L. ZENG, T. PAN, X. JIANG, and T. WATANABE, "An efficient highly adaptive and deadlock-free routing algorithm for 3D network-on-chip," *Ieice Transactions on Fundamentals of Electronics Communications & Computer Sciences*, vol. E99.A, no. 7, pp. 1334–1344, 2016.
- [11] L. Qiao, Y. Li, D. Chen, and S. Serikawa, "A survey on 5G/6G, AI, and robotics," *Computers & Electrical Engineering*, vol. 95, article 107372, 2021.
- [12] S. Avallone and A. Banchs, "A channel assignment and routing algorithm for energy harvesting multiradio wireless mesh networks," *IEEE Journal on Selected Areas in Communications*, vol. 34, no. 5, pp. 1463–1476, 2016.
- [13] W. Wang, H. Shi, D. Wu et al., "VD-PSO: an efficient mobile sink routing algorithm in wireless sensor networks," *Peer-to-Peer Networking and Applications*, vol. 10, no. 3, pp. 537–546, 2017.
- [14] W. Jia and Z. Chen, "Sensor communication area and node extend routing algorithm in opportunistic networks," *Peer-to-Peer Networking and Applications*, vol. 11, no. 8, 2018.
- [15] T. Ren, Z. Jiang, X. Cai et al., "A dynamic routing optimization problem considering joint delivery of passengers and parcels," *Neural Computing and Applications*, vol. 33, no. 16, pp. 10323–10334, 2021.
- [16] Y. Meraihi, D. Acheli, and A. Ramdane-Cherif, "QoS multicast routing for wireless mesh network based on a modified binary bat algorithm," *Neural Computing and Applications*, vol. 31, no. 7, pp. 3057–3073, 2019.
- [17] Y. Ding, R. Chen, and K. Hao, "A rule-driven multi-path routing algorithm with dynamic immune clustering for event-driven wireless sensor networks," *Neurocomputing*, vol. 203, p. 139, 2016.
- [18] F. Li, M. Xiong, L. Wang, H. Peng, J. Hua, and X. Liu, "A novel energy-balanced routing algorithm in energy harvesting sensor networks," *Physical Communication*, vol. 27, pp. 181–187, 2018.

- [19] C. Zhang, X. Wang, F. Li, and M. Huang, "NNIRSS: neural network-based intelligent routing scheme for SDN," *Neural Computing and Applications*, vol. 31, no. 10, pp. 6189–6205, 2019.
- [20] T. Senthil and B. Kannapiran, "ECTMRA: energy conserving trustworthy multipath routing algorithm based on cuckoo search algorithm," *Wireless Personal Communications*, vol. 94, no. 4, pp. 2239–2258, 2017.
- [21] S. Hamrioui and P. Lorenz, "Bio inspired routing algorithm and efficient communications within IoT," *IEEE Network*, vol. 31, no. 5, pp. 74–79, 2017.
- [22] B. T. Thuan, L. B. Ngoc, and K. Kaneko, "A stochastic link-fault-tolerant routing algorithm in folded hypercubes," *Journal of Supercomputing*, vol. 74, no. 10, pp. 5539–5557, 2018.
- [23] L. Wu, C.-H. Chen, and Q. Zhang, "A mobile positioning method based on deep learning techniques," *Electronics*, vol. 8, no. 1, p. 59, 2019.
- [24] S. El Alaoui and B. Ramamurthy, "EAODR: a novel routing algorithm based on the modified temporal graph network model for DTN-based interplanetary networks," *Computer Networks*, vol. 129, pp. 129–141, 2017.
- [25] Z. Zhang, W. Serwe, J. Wu, T. Yoneda, H. Zheng, and C. Myers, "An improved fault-tolerant routing algorithm for a network-on-chip derived with formal analysis," *Science of Computer Programming*, vol. 118, p. 24, 2016.
- [26] Y. R. B. Al-Mayouf, N. F. Abdullah, M. Ismail, S. M. Al-Qaraawi, O. A. Mahdi, and S. Khan, "Evaluation of efficient vehicular ad hoc networks based on a maximum distance routing algorithm," *Eurasip Journal on Wireless Communications & Networking*, vol. 2016, no. 1, 2016.
- [27] W. Xu, M. Jiang, F. Tang, and Y. Yang, "Network coding-based multi-path routing algorithm in two-layered satellite networks," *IET Communications*, vol. 12, no. 1, pp. 2–8, 2018.
- [28] J. Li, X. Hou, D. Su, and J. D. D. Munyemana, "Fuzzy power-optimised clustering routing algorithm for wireless sensor networks," *Wireless Sensor Systems, IET*, vol. 7, no. 5, pp. 130–137, 2017.
- [29] J. Zou, F. Sadiq, and A. Gulnaz, "PERA: priority-based energy-efficient routing algorithm for WBANs," *Wireless Personal Communications*, vol. 96, no. 3, pp. 4737–4753, 2017.

Research Article

An Empirical Study Based on the Impact of Smart Sensor System on Rural Relative Poverty

Tian Luan¹ and Xiaoyan Liu ²

¹School of Humanities, Jilin Agricultural University, Changchun, 130118 Jilin, China

²School of Economics and Trade, JiLin Engineering Normal University, Changchun, 130052 Jilin, China

Correspondence should be addressed to Xiaoyan Liu; liuxiaoyan@jlenu.edu.cn

Received 25 October 2021; Accepted 4 December 2021; Published 29 December 2021

Academic Editor: Alireza Souri

Copyright © 2021 Tian Luan and Xiaoyan Liu. This is an open access article distributed under the Creative Commons Attribution License, which permits unrestricted use, distribution, and reproduction in any medium, provided the original work is properly cited.

Solving the problem of rural poverty is a difficult problem for the country to enter a well-off society in an all-round way. Therefore, this paper conducts an experimental analysis based on the impact of smart sensor systems on the relative poverty in rural areas. This article is aimed at studying the related factors of rural poverty and improving relative poverty in rural areas. In this regard, this article proposes an intelligent processing function based on smart sensors. Multiple sensors work together to process relatively complex things. Then, through the experimental analysis of GH efficiency, the data collected in the experimental area is used as the data. Combining the Lorentz curve and Gini coefficient analysis to determine the influencing factors of rural relative poverty. This article also selected 10 areas for experimentation. The experimental results show that the proportion of middle school education from 2014 to 2020 is between 24.3% and 34%, and the number of poor people has also declined, indicating that education level is a factor affecting rural poverty. Therefore, based on the intelligent sensor system, the factors of relative poverty in rural areas can be found, and related measures can be analyzed. By implementing the rural poverty alleviation strategy, the relative poverty situation in rural areas can be effectively improved.

1. Introduction

In recent years, with the rapid development of China's economy and society, rural poverty, especially rural poverty in undeveloped areas in the west and ethnic minority areas, has received extensive attention from relevant state departments and scholars. The existence of poverty has become the primary problem that plagues all countries. Poverty not only hinders economic development but also has a great negative impact on social development. Poverty eradication is a persistent and challenging world problem. Poverty issues have caused uneven development between regions and affected regional peace and stability. How to reduce the incidence of poverty as soon as possible to the greatest extent and improve the life satisfaction and satisfaction of local residents? Happiness is the top issue facing all countries. The relative poverty of peasants, especially those engaged in agriculture, has existed for a long time. Poverty alleviation and

development work started from solving the poverty alleviation of the absolute poor, and the relatively poor class was prosperous and prosperous.

In the process of sustained economic development, the income gap between residents is widening and remains at a relatively high level, especially reflecting the severity of relative poverty in rural areas. It can be seen that the income gap between the rich and poor in rural residents' relative movement and deterioration. It has caused a lot of social conflicts and has had a great impact on the development of society. This paper will study rural poverty and antipoverty issues based on the use of smart sensor systems on blockchain theoretical knowledge. On the one hand, it will try to enrich the theoretical research on rural poverty issues in the country. Poverty policy provides theoretical basis.

Wireless Smart Sensor Network (WSSN) shows great promise in structural health monitoring (SHM) due to its low cost, higher flexibility, powerful data management, and

better understanding of structural behavior through dense deployment of sensors. However, the implementation of the wireless SHM system brings many challenges, one of which is to ensure adequate synchronization of the collected data. Li et al. proposed various algorithms to realize the synchronization of clock and sensing [1]. He researched algorithms based on wireless sensors to synchronize clocks and sensing. In order to study the application of smart sensors in fish detection, García et al. designed a smart sensor to predict the established sensory fish quality index. The sensor dynamically correlates the microbial count and TVB-N with the quality index. The sensor provides the largest possible value and handles fish-to-fish variability [2]. His research on fish and microbial detection is very in-depth, but he has little connection with the relative poverty in rural areas. After years of large-scale poverty alleviation and development, the population of extremely poor rural areas across the country has fallen sharply, and the poverty situation has been effectively alleviated. However, due to the large number of poor people, the task of poverty alleviation is still arduous. Therefore, Cao et al. [3] explored the spatial differentiation characteristics and influencing factors of multidimensional poverty in rural areas in a region, which is conducive to the implementation of antipoverty [4] and development strategies and promotes farmers' income and prosperity. Get rid of poverty [5]. Based on the spatial location of the rural areas, the rural poverty factors were searched, but smart sensors were not introduced. Recently, there has been increasing interest in finding durable interventions for rural poverty (RP) in developing countries based on farmers' entrepreneurship and innovation. Therefore, the purpose of Naminse et al. is to test the relationship between entrepreneurship in two resource-constrained provinces in China and the slowdown of RP. He assessed the impact of the three abilities of farm entrepreneurs' education, economy, and social culture on the entrepreneurial growth of farmers and how these abilities in turn affect the mitigation of RP [6]. The impact of intervention on RP can be seen through the evaluation results, but it would be better if smart sensors were added. Safe drinking water is essential to good health. Since long-term drinking can bring health risks, it is important to make recommendations for drinking water sources in areas where CKDu is endemic. Dissanayake et al. designed a sensor to measure fluoride and hardness in well water through an automated mechanism [7]. The sensor he designed is very helpful for detecting water quality. Smart sensor applications rely on ultra-low-power energy harvesters to collect energy and charge batteries within the range of ambient power levels. Wu et al. proposed a discontinuous collection method for switched capacitor DC-DC converters, which can achieve ultra-low-power consumption energy collection. Based on the key observation that energy efficiency is higher than that of charge pumps, he proposed a discontinuous collection technology that can decouple the two efficiencies to obtain a better trade-off [8]. His discontinuous acquisition technology based on smart sensors can improve efficiency very well. All of the above documents are mostly about smart sensor systems. How to combine it to explore the relative poverty

factors in rural areas is not very relevant, so this article needs to study in depth based on smart sensor systems to solve rural relative poverty problems.

The innovation of this paper is to use the intelligent processing module function of the intelligent processor to analyze the data of the experimental area for many years. Through the analysis of the data, the factors and influencing factors that affect the poverty in the region can be drawn.

2. Combining Smart Sensors to Study Rural Poverty Factors

2.1. Smart Sensor. Intelligent sensor system [9], the generalized intelligent sensor system is divided into two parts: intelligent sensor terminal and control server [10]. The intelligent sensor terminal uses one or more sensitive components to connect with the embedded microprocessor and completes signal detection and conversion processing through the intelligent sensor terminal, which can realize functions such as self-check, self-calibration, cellular connection, and self-diagnosis. The intelligent sensor terminal [11] and the control server are based on the industrial field bus, using digital communication as the transmission method, with functions such as two-way communication, information processing, and information storage. Most of the functions of the intelligent sensor system are realized by software. By changing the software program of the system and configuring different sensors, different intelligent sensor systems can be realized. A single smart sensor system can also be connected with other smart sensor systems to form a smart sensor system network to jointly complete complex tasks. The intelligent sensor system is shown in Figure 1. Although the smart sensor system will have a low interrupt tolerance problem, this article uses multiple sensors to solve it. When a fault occurs, its working status can be suspended and repaired, but it does not affect the whole. This article mainly applies the consensus technology in the blockchain technology and uses the consensus technology to study and analyze the relative poverty factors in rural areas.

2.1.1. Smart Sensor Vision Measurement. The smart sensor integrates structured optical lasers, cameras, and measurement software [12], which can easily complete scanning, analysis, and measurement functions during the measurement process. Smart sensors use structured light lasers to project structured light on the surface of the object. The distribution of light bars is not straight but varies according to the shape of the object. Collect images and measured values of the structured light bar of the camera at different positions. The schematic diagram of the principle is shown in Figure 2. Next, using image processing technology [13], camera correction technology, structured optical surface correction technology, and laser triangulation measurement principle, the relevant information is extracted from the light strip image, and the three-dimensional coordinates of the object surface are constructed into the light strip, which can be calculated information.

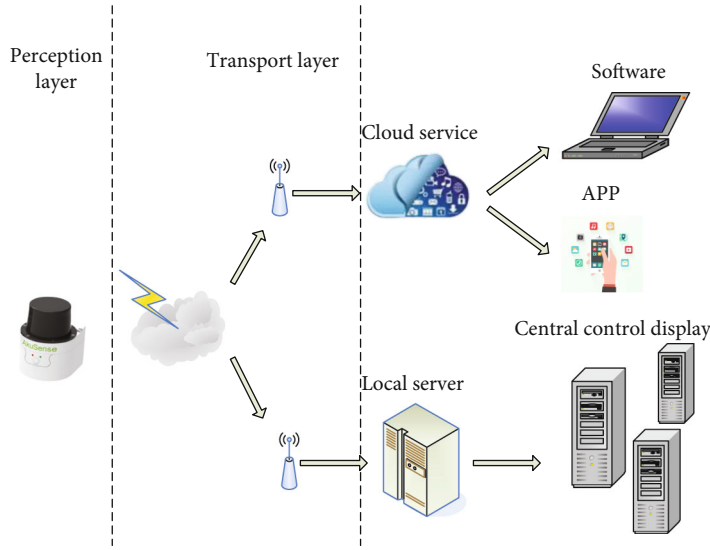


FIGURE 1: Smart sensor systems.

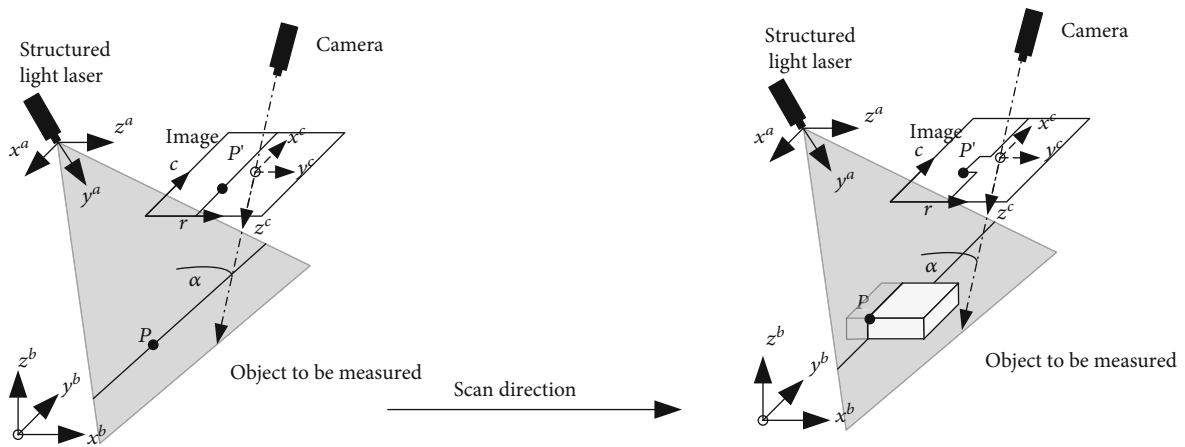


FIGURE 2: Schematic diagram of smart sensor measurement principle.

(1) *Area Scan Camera and Pinhole Camera Model.* The perspective projection model of the pinhole camera is shown in Figure 3. The point P of the world coordinate system is projected onto the point P' of the image plane through the optical center of the lens, and the image plane is at a distance f behind the optical center.

(2) *Two-Step Calibration Method.* The two-stage calibration method proposed by Tsai assumes that the lens has only radial distortion [14]. In the first step of this method, multiple calibration points in the calibration image are used to establish too many decision equations, and a simple matrix theory is used to solve the external parameters of the camera. In the second step, radial distortion parameters are introduced, appropriate initial searchable solutions are set, nonlinear optimization algorithms such as Newton's gradient method are used to solve the nonlinear equation system, and other parameters are solved. In addition, Weng proposed a nonlinear distortion model that takes into account the causes of cam-

era distortion such as radial distortion and eccentric distortion and then uses matrix decomposition methods such as singular value decomposition of the matrix to find the initial values of the camera's internal and external parameters. Search using nonlinear optimization methods. Obtain the most suitable solution for the internal and external parameters of the final camera [15]. In recent years, domestic scholars have also proposed a new two-stage method. Domestic scholars GaoLizhi and ZhanngYanzhen, respectively, proposed a two-stage linear transformation method. Experiments show that the two methods can achieve higher correction accuracy. In the two-stage method of ZY Zhang plane calibration board, it is not necessary to extract calibration points on a fixed high-precision calibration platform like the previous two-stage calibration method. His method does not limit the configuration of the calibration board. The posture of the calibration board is arbitrary. At present, this calibration method has been widely used, and both Opencv and Halcon use this method to calibrate cameras.

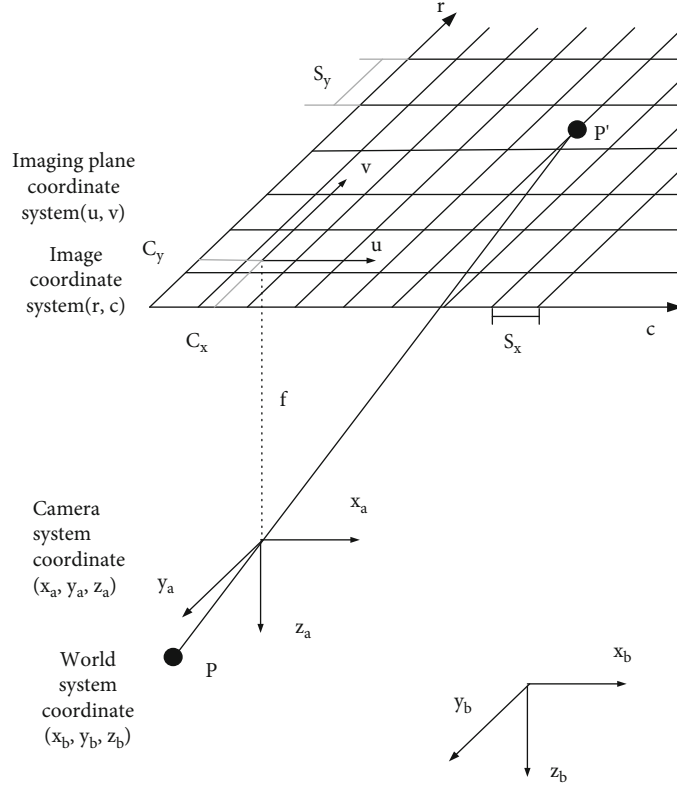


FIGURE 3: Perspective projection model of pinhole camera

Zhang's calibration method is based on a 2D plane calibration table. This may be a circular grid calibration table or a checkerboard calibration table. Unless the camera selects a lens and changes the focal length and aperture during the calibration process, the internal parameters of the camera will not change, but the external parameters will change. At the same time, the plane on which the calibration sheet is configured must avoid correlation as much as possible. In other words, the calibration table does not move in the plane, but the calibration table needs to be moved in the three-dimensional space plane. During the surface calibration process, the placement position of the calibration sheet is relatively free.

For the disc grid calibration piece, the calibration point is the center of each circle, and for the checkerboard calibration piece, the calibration point is the grid point of the checkerboard grid.

Mark the three-dimensional physical coordinates of the calibration point as $H = [x, y, z]^T$, the corresponding point on the image plane as $h = [u, v]^T$, and the corresponding homogeneous coordinates as $\tilde{H} = [x, y, z, 1]^T$ and $\tilde{h} = [u, v, 1]^T$. Using the pinhole camera model, the three-dimensional space point H can be mapped to the point h in the image coordinate system using equation (1).

$$l\tilde{h} = X[Pt]\tilde{H}. \quad (1)$$

In the formula, l is any nonzero scale factor, P is the rotation matrix, t is the translation vector, P and t are also

the external parameters of the camera, and the internal parameter matrix X is

$$X = \begin{bmatrix} l_x & k & c_x \\ 0 & l_y & c_y \\ 0 & 0 & 1 \end{bmatrix}. \quad (2)$$

Among them, l_x, l_y is the scale factor of the u -axis and the v -axis, p represents the nonperpendicularity of the u -axis and the v -axis, and (c_x, c_y) is the main point. Please note that the thickness of the calibration plate will also affect the calibration accuracy. In order to simplify the description, suppose the thickness of the calibration plate is 0, that is, $z = 0$. The calibration plate is as shown below, on the xy plane of the world coordinate system. Assuming that the i -th column of the rotation matrix P is p_i , from equation (1), we have.

$$l \begin{bmatrix} u \\ v \\ 1 \end{bmatrix} = X \begin{bmatrix} p_1 & p_2 & p_3 & t \\ & & & \end{bmatrix} \cdot \begin{bmatrix} x \\ y \\ 0 \\ 1 \end{bmatrix} = X \begin{bmatrix} p_1 & p_2 & t \\ & & \end{bmatrix} \cdot \begin{bmatrix} x \\ y \\ 1 \end{bmatrix}. \quad (3)$$

Since $z = 0$, the point H on the plane of the calibration plate can be expressed as $H = [x, y]^T$ and the corresponding homogeneous coordinate $\tilde{H} = [x, y, 1]^T$; then, formula (3)

can be simplified as:

$$l\tilde{h} = M\tilde{H}. \quad (4)$$

In the formula, $M = \lambda X[p_1 \ p_2 \ t]$ is a 3×3 matrix, and λ is a constant factor. Remember $M = [m_1 \ m_2 \ m_3]$, yes

$$[m_1 \ m_2 \ m_3] = \lambda X[p_1 \ p_2 \ t]. \quad (5)$$

Among them, t is the translation vector, and the direction of p_1 and p_2 is along the coordinate axis of the image coordinate system. Therefore, p_1 and p_2 are orthogonal, and t and p_1 and p_2 are not coplanar, so $\det([p_1 \ p_2 \ t]) \neq 0$. And because of $\det[X] \neq 0$, so $\det[M] \neq 0$.

The calibration point coordinate extracted from the actual image is h_i , and the image coordinate calculated according to the expression (1) is \tilde{h}_i . The matrix M can be obtained by solving the minimum distance between the two images.

$$\min \sum_i \|h_i - \tilde{h}_i\|^2. \quad (6)$$

Use the Levenberg-Marquardt algorithm to solve the above nonlinear quadratic equations to obtain the matrix M , which can be obtained by the orthogonality ($p_1^T p_2 = 0, p_1^T p_1 = p_2^T p_2$) of equation (5) and P :

$$m_1^T X^{-T} X^{-1} m_2 = 0, \quad (7)$$

$$m_1^T X^{-T} X^{-1} m_1 = m_2^T X^{-T} X^{-1} m_2. \quad (8)$$

Make

$$Y = X^{-T} X^{-1} = \begin{bmatrix} Y_{11} & Y_{12} & Y_{13} \\ Y_{12} & Y_{22} & Y_{23} \\ Y_{13} & Y_{23} & Y_{33} \end{bmatrix}$$

$$= \begin{bmatrix} \frac{1}{l_x^2} & -\frac{\gamma}{l_x^2 l_y} & \frac{c_y \gamma - c_x l_y}{l_x^2 l_y} \\ -\frac{\gamma}{l_x^2 l_y} & \frac{\gamma^2}{l_x^2 l_y} + \frac{1}{l_x^2} & -\frac{\gamma(c_y \gamma - c_x l_y)}{l_x^2 l_y^2} - \frac{c_y}{l_x^2} \\ \frac{c_y \gamma - c_x l_y}{l_x^2 l_y} & -\frac{\gamma(c_y \gamma - c_x l_y)}{l_x^2 l_y^2} - \frac{c_y}{l_x^2} & \frac{(c_y \gamma - c_x l_y)^2}{l_x^2 l_y^2} + \frac{c_y^2}{l_y^2} + 1 \end{bmatrix}. \quad (9)$$

Please note that Y is a symmetric matrix and can be expressed as the next 6-dimensional vector:

$$y = [Y_{11} \ Y_{12} \ Y_{22} \ Y_{13} \ Y_{23} \ Y_{33}]^T. \quad (10)$$

Suppose the i -th column vector in M is $m_i = [m_{i1}, m_{i2}, m_{i3}]^T$, therefore, there is

$$m_i^T Y m_j = v_{ij}^T y. \quad (11)$$

In

$$v_{ij} = [m_{i1} m_{j1}, m_{i1} m_{j2} + m_{i2} m_{j1}, m_{i2} m_{j2}, m_{i3} m_{j1} \\ + m_{i1} m_{j3}, m_{i3} m_{j2} + m_{i2} m_{j3}, m_{i3} m_{j3}]^T. \quad (12)$$

Therefore, the equation system (8) can be rewritten as the following equation system:

$$\begin{bmatrix} v_{12}^T \\ (v_{11} - v_{22})^T \end{bmatrix} \cdot y = 0. \quad (13)$$

If there are n calibration images, the following equations can be formed:

$$V y = 0. \quad (14)$$

In the above formula, V is a matrix of $2n \times 6$ size. The solution of formula (14) is the intrinsic vector corresponding to the smallest eigenvalue of matrix $V^T V$, and y can also be obtained by performing singular value decomposition (SVD) on matrix V . If y is solved, all the internal parameters of the camera can be obtained according to the following formula:

$$c_y = \frac{(Y_{12} Y_{13} - Y_{11} Y_{23})}{(Y_{11} Y_{22} - Y_{12}^2)}, \quad (15)$$

$$\lambda = \frac{Y_{33} - [Y_{13}^2 + c_y(Y_{12} Y_{13} - Y_{11} Y_{23})]}{Y_{11}}, \quad (16)$$

$$l_x = \sqrt{\frac{\lambda}{Y_{11}}}, \quad (17)$$

$$l_y = \sqrt{\frac{\lambda Y_{11}}{(Y_{11} Y_{22} - Y_{12}^2)}}, \quad (18)$$

$$\gamma = \frac{-Y_{12} l_x^2 l_y}{\lambda}, \quad (19)$$

$$c_x = \frac{\gamma c_y}{l_x} - \frac{Y_{13} l_x^2}{\lambda}. \quad (20)$$

(3) *Multisensor Information Fusion Structure*. Multisensor information fusion [16] can process multiple levels of information through a variety of methods, so it is necessary to investigate the corresponding hardware topology. Multisensor information fusion can be divided into centralized fusion system, decentralized fusion system, hybrid fusion system, and feedback fusion system. This article uses a multisensor structure for information fusion and uses multiple sensors to collaborate to complete data collection.

(1) Centralized

The centralized information fusion system [17] directly performs fusion inference on the observation data of multiple sensors without any preprocessing, and its structure is shown

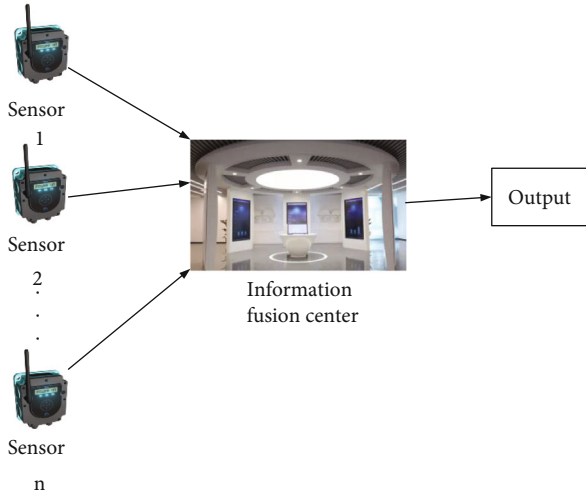


FIGURE 4: Centralized fusion system structure diagram.

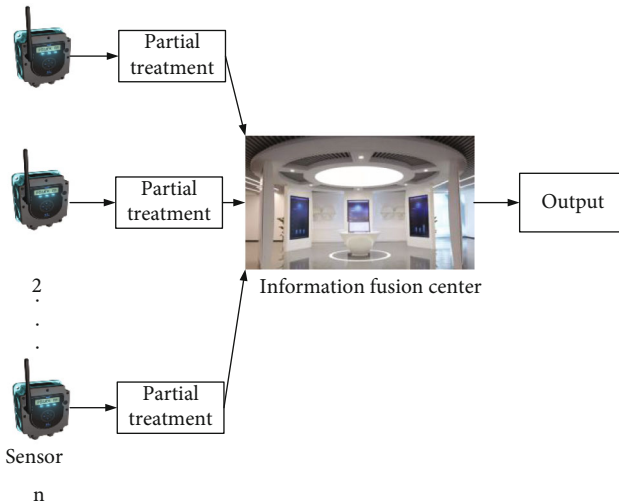


FIGURE 5: Structure diagram of distributed fusion system.

in Figure 4. Centralized information fusion belongs to the data layer fusion, which retains a large amount of original data, so the fusion accuracy is very high, but the fusion center needs to identify and reason a large amount of data, and the communication volume is large, and the processor design is complex, so this structure is suitable for small-scale integration systems.

(2) Distributed

Distributed information fusion system [18] refers to the calculation, classification, or inference processing of each sensor data separately and then transfers the processed data results to the fusion center, and the fusion center completes the final reasoning judgment. This method is similar to feature layer fusion or decision layer fusion. Due to the large amount of distributed preprocessing of sensor data, the fusion center has fewer tasks and at the same time reduces the amount of data transmission. This method is suitable for large-scale distributed remote fusion systems. Its structure is shown in Figure 5.

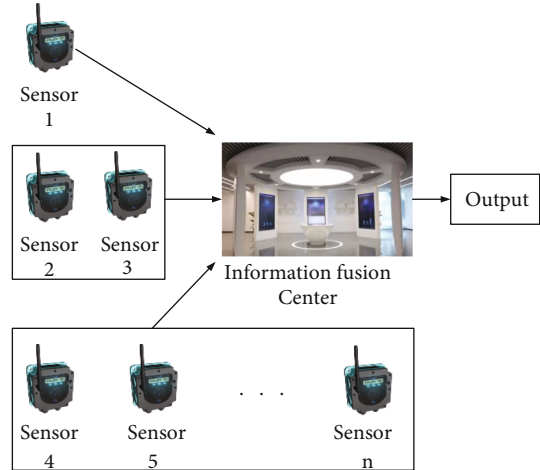


FIGURE 6: Structure diagram of hybrid fusion system.

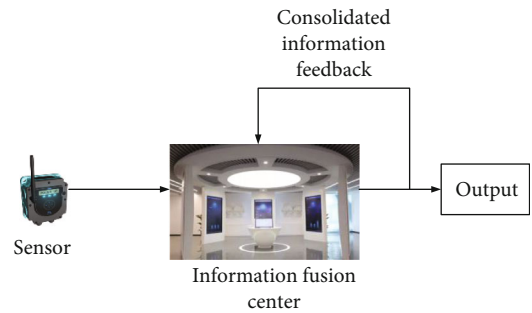


FIGURE 7: Feedback type multisensor information fusion structure.

(3) Hybrid

The hybrid information fusion system [19] is a mixed use of distributed and centralized types. It uses a centralized structure for some sensors and a distributed structure for some sensors. It has the advantages of distributed and centralized fusion structures, and the system structure is flexible. A more accurate fusion result can be obtained, but the structure of the system is complex, and the design is difficult. How to choose depends on the specific situation. Its structure is shown in Figure 6.

(4) Feedback type

The feedback information fusion system [20] feeds back the fusion result to the fusion system to form a closed-loop system with certain self-regulating ability. With this structure, after the fusion center processes the sensor information, the fusion system can already express most of the characteristics of the target object, so it has a better guiding effect on the newly acquired information. Its structure is shown in Figure 7.

2.2. GH Efficiency. For GH efficiency, in the Normal-OperationCase phase of PBFT, a total of $PM = 2x^2$ messages are needed to complete the final consensus, and the message complexity is $o(n^2)$. GH splits Normal-OperationCase into three steps.

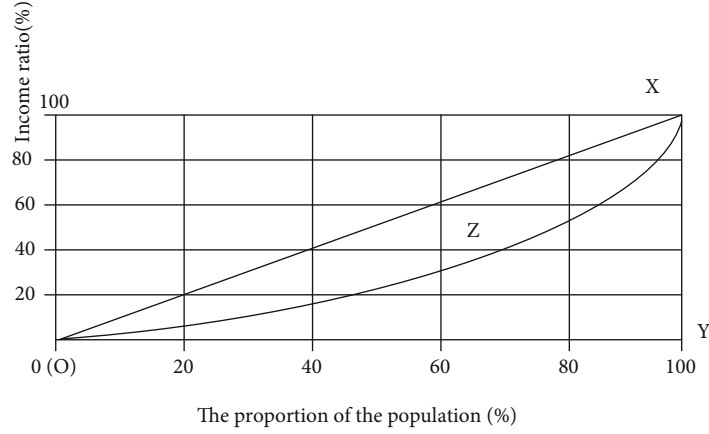


FIGURE 8: Lorentz curve.

- (1) Globally accept the request message, yp arranges the global serial number, locally executes $localprepare$ and $localcommit$, and GH changes the original process of pairwise interaction across the entire network to pairwise interaction within the group, reducing the number of messages that each node needs to send and waiting for messages. The total number of messages consumed in this step:

$$2 \sum_{j=1}^{j=y} m_j^2 - x + y - 1. \quad (21)$$

- (2) Cross-submission between copies, namely, intersectional reply, consumes the number of messages:

$$y(x - 1). \quad (22)$$

- (3) The global replica node executes $globalprepare$, $globalcommit$, $globalreply$, and the number of messages consumed:

$$2y^2 - 2y + 1. \quad (23)$$

Until the request is finally completed, the number of messages GM consumed in the GH consensus phase is synthesized from formulas (21), (22), and (23):

$$GM = 2 \sum_{j=1}^{j=y} m_j^2 - x + y - 1, \quad (24)$$

$$GM = 2 \frac{x^2}{y} + 2z^2 + 2y^2 + y(x - 2)x, \quad (25)$$

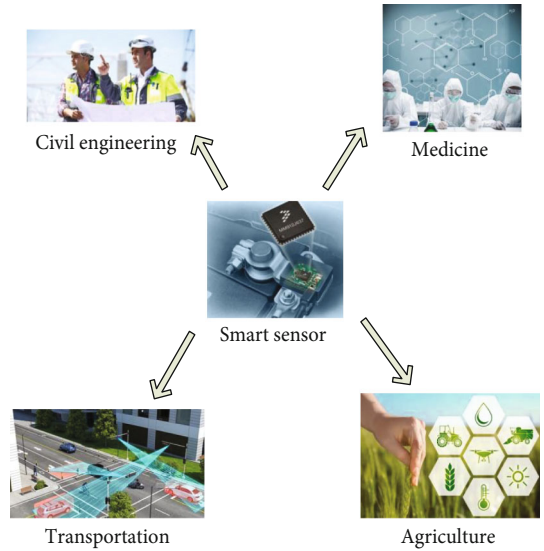


FIGURE 9: Application areas of smart sensors.

where z is the variance and the formula (25) knows that z is 0, which means that the number of messages consumed in the GH consensus phase is the least when the group is averaged:

$$GM = 2 \frac{x^2}{y} + 2y^2 + y(x - 2)x, \quad (26)$$

$$\frac{\partial GM}{\partial y} = -2 \frac{x^2}{y^2} + 4y + x - 2 = 0. \quad (27)$$

2.3. Measurement of Poverty Level. To study the poverty of a region, we should first fully grasp the poverty level of the region, that is, how poor the region is. Here is a brief introduction to several methods of measuring poverty.

2.3.1. Incidence Rate of Poverty. Also known as the head calculation index, it calculates the proportion of people whose income is below the absolute poverty line in the total population based on urban and rural income distribution data. The formula can be expressed as $PH = p/n$,

TABLE 1: Number of poor populations in 10 regions.

Area	1	2	3	4	5	6	7	8	9	10
Population	29.41	13.14	11.16	2.63	7.89	15.33	14.86	14.91	18.71	7.24
Change from last year	-0.63	-1.53	-0.65	-0.26	-0.63	-1.03	0.08	-1.78	-2.22	-0.54

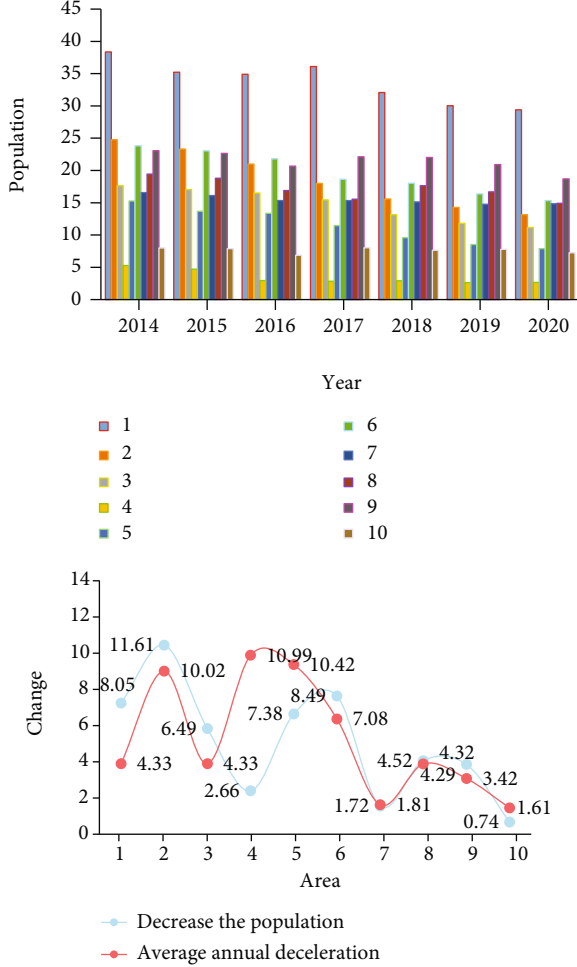


FIGURE 10: Population changes in ten regions in the past 7 years.

where n is the total population and p is the number of people below the absolute poverty line. The poverty incidence rate is used to determine the size and change of the poor population on the cross-section of the poverty line. The basic feature is that the income changes and income distribution of the population below the poverty line are not considered. The focus is on determining the proportion of the population. Therefore, the disadvantage of this indicator is that it cannot reflect the income reduction and income transfer of the poor.

2.3.2. Poverty Gap Rate. In order to make up for the insufficiency of the poverty incidence rate in determining the poverty level, the poverty gap rate is used to measure the degree to which the poor's income is below the poverty line. Therefore, this indicator is also called the poverty gap ratio or relative poverty index, and its formula is expressed as:

$$PG = \sum_k^n \frac{((1 - Yk)/Z)}{n}. \quad (28)$$

Among them, Yk represents the consumption level or income of the k -th poor, Z represents the poverty line, and n represents the total population. It can be deduced from the formula that this method can sensitively measure the degree of poor people below the poverty line and make up for the lack of poverty incidence, but it cannot reflect the population size, proportion, and distribution of poverty status.

2.3.3. Poverty Intensity Index. The poverty intensity index is also known as the FGT index. It is based on the distance of the poor relative to the poverty line. It just gives the poor a greater weight to calculate their poverty level. The calculation formula is

$$FGT = \sum_{k=1}^n \frac{((1 - Yk)/Z)^2}{n}. \quad (29)$$

2.3.4. Sen Index. In order to avoid the shortcomings of the above two indicators [21], the well-known Indian economist Sen seeks a measurement method that integrates the head-count index, the poverty gap, and the degree of inequality in the poor population, which is called the Sen index [22]. The formula is

$$P = \frac{k}{KZ} [Z - x(1 - G)], \quad (30)$$

or

$$P = PH \left[\frac{1 - x(1 - G)}{Z} \right]. \quad (31)$$

Among them, k is the number of the poor, K is the total population, Z is the poverty line, x is the average income of the poor, and G is the Gini coefficient of the income distribution of the poor. The value of P changes from 0 to 1. If everyone's income exceeds the poverty line, $n = 0$, and $P = 0$; if everyone has no income or the social distribution is extremely unequal, $x = 0$, $k = 0$, $G = 1$, and $P = 1$.

2.3.5. Lorenz Curve and Gini Coefficient. This is a method often used to evaluate relative poverty, and it reflects the degree of inequality in income distribution.

(1) Lorenz Curve. The Lorenz curve is a curve composed of population proportions and corresponding income proportions, used to express equality of income and distribution. It was first proposed by the American statistician M.O.

TABLE 2: Changes in income and population in experimental areas.

Years	Poor people			Low income		
	Total people	The rate of decline	Reduce the number of people	Total people	The rate of decline	Reduce the number of people
2014	196.03			560.40		
2015	188.82	-3.68	7.21	523.46	-6.59	36.94
2016	176.89	-6.32	11.93	471.16	-9.99	52.3
2017	169.32	-4.28	7.57	442.42	-6.10	28.74
2018	158.86	-6.18	10.46	397.95	-10.05	44.47
2019	148.54	-6.50	10.32	355.32	-10.71	42.63
2020	139.41	-6.15	9.13	316.57	-10.91	38.75
Average value		-6.59	9.44		-10.79	40.64

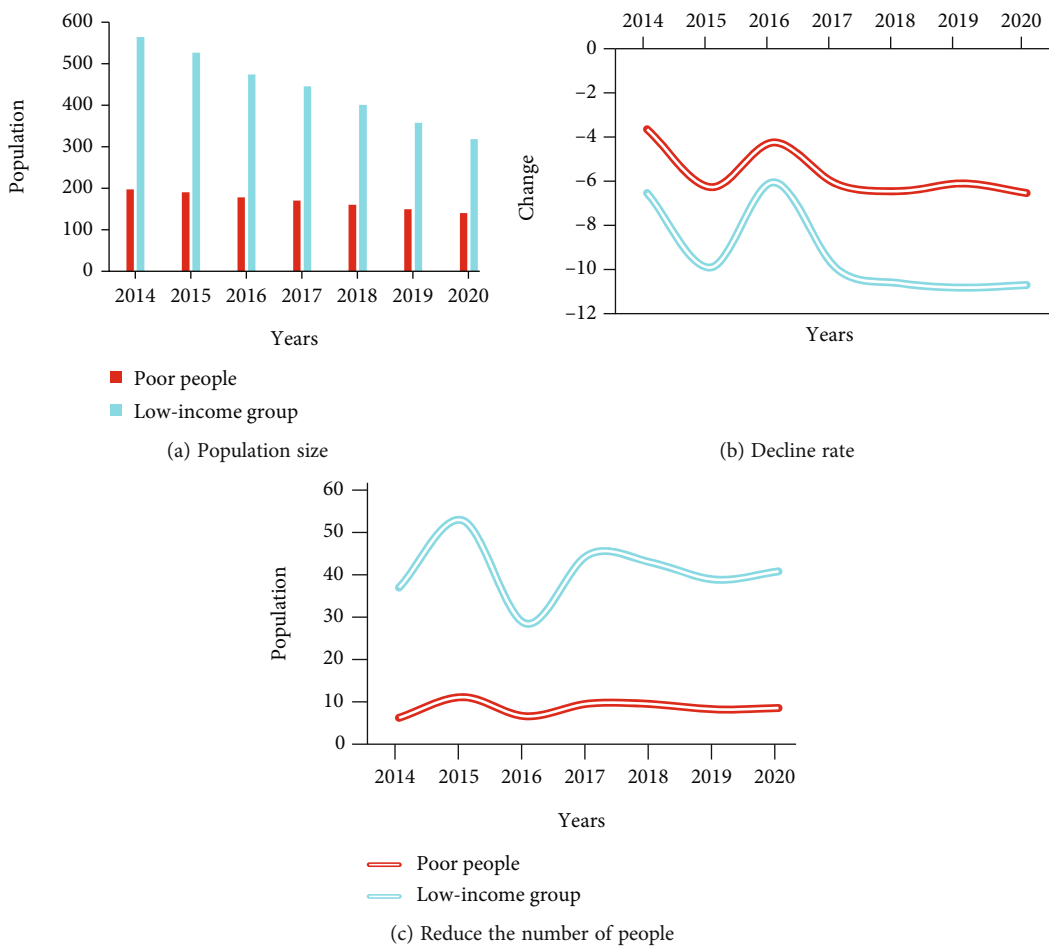


FIGURE 11: Changes in the poor population and low-income population in the experimental area.

TABLE 3: Sex change ratio of rural population in experimental areas (unit: %).

Years	Male ratio	Proportion of women	Sex ratio
2014	51.6	48.4	106.7
2020	50.9	49.2	103.2

Lorentz in 1907, so it was named the Lorentz curve. The Lorentz curve can be represented in Figure 8.

In the above rectangular coordinate system, the horizontal axis represents the proportion of the population sorted by income from low to high, and the level axis represents the proportion of income occupied by the corresponding proportion of the population. The straight line OX in the figure

TABLE 4: Changes in education level (unit: %).

Education level	2014	2020
Illiteracy	23.8	13.8
Primary school	46.0	43.2
Junior high school	24.3	34.0
High school	5.5	7.4
College	0.4	1.3
Undergraduate	0.04	0.37
Postgraduate	0.006	0.01

is called a complete equality line, because the vertical and horizontal coordinates of each point on OX are equal, which means that a certain proportion of the population has an equal proportion of income. For example, 20% of the population has 20% of the income. In other words, in this state, incomes are completely equal. The broken line 0-Y-X is the absolute inequality line, because the income of all proportions of the population is 0, and the income is completely occupied by one person. Therefore, when the Lorentz curve coincides with OX, it means that the income in the region is completely equal; when it coincides with 0-Y-X, it represents absolute income inequality. The general Lorentz curve is between these two lines, indicating that income is not completely equal. Reflected in the figure is a curve, and the degree of curvature of the curve indicates the level of income inequality. According to experiments, the closer to the OX line, the more equal the income; the closer to the 0-Y-X line, the more unequal the income.

(2) *Gini Coefficient*. The Gini coefficient is the first measurement of income distribution equality defined by Italian economists based on the Lorenz curve, and it is now the most commonly used indicator to measure income inequality. In the above Figure 9 Lorenz curve, the area enclosed by the complete equation line OX and the Lorenz curve is called the inequality area; X is marked as X; if the area below the OX ray is marked as Y, it is the Gini coefficient $G = X/Y$. The Gini coefficient is between 0 and 1. Experiments show that the smaller the value, the smaller the income gap, the higher the degree of income equality, and vice versa. Generally speaking, $G < 0.2$, the income distribution is very even, $0.2 \leq G < 0.3$, the income distribution is relatively equal, $0.3 \leq G < 0.4$, the income distribution is relatively equal, $0.4 \leq G < 0.5$ has a large income gap, $G > 0.5$, and the income gap is large; the inequality of income distribution is relatively large. Among them, it is generally considered that $G = 0.4$ is the warning line, and society will become unstable if it exceeds 0.4.

In addition, the commonly used Gini coefficient calculation formula is

$$G = \frac{1}{2\mu k^2} \sum_{i=1}^k \sum_{j=1}^k |y_i - y_j|, \quad (32)$$

where k is the sample size, μ is the expected value of the total income of each sample group, and $|y_i - y_j|$ represents the absolute value of the income difference between any two samples.

3. Experiments to Explore the Relative Influencing Factors of Poverty Based on Smart Sensors

Intelligent sensor system, this is a comprehensive high-tech that is rapidly developing in the world today. The central idea is to use computer technology to make sensors intelligent. It is generally believed that the intelligent sensor system is detection, measurement, and control system composed of sensors, computer technology, and communication technology. Its main application is shown in Figure 9.

3.1. *Number of Poor People*. In this paper, 10 regions are selected as samples for the experiment, and the methods of investigating poverty influencing factors with smart sensors are carried out in 10 regions, respectively. The number of poor people in these 10 regions is shown in Table 1 (unit: ten thousand people). In order to better analyze the poverty indicators of these regions in the past, the changes in the region from 2014 to 2020 are as follows, as shown in Figure 10.

It can be seen from the figure that the total number of poor people in the 10 regions is declining. In particular, the rate of poverty reduction in regions 1 and 2 is very fast, and the rate of poverty reduction in regions 7, 8, 9, and 10 is quite slow. Choose one of them to analyze the impact of poverty factors through the method of this article.

3.2. *Experiments to Explore Changes in the Poor Population*. The selected region's low-income population changes are shown in Table 2 (unit: ten thousand people, %).

Through the collected data, we can get Figure 11, as shown in the figure.

It can be seen from the above table that although the overall poverty population has shown a downward trend, with a decrease of 70,000 to 100,000 poor populations every year, the rate of poverty reduction is relatively slow, generally maintained at around 6%, which is in line with the national average annual deceleration of 11.79%. Among them, there was a slowdown in 2017 and 2020.

3.3. *Gender Structure and Education Level of the Experimental Area*. Different genders have different social functions, so the characteristics of gender structure are also one of the important reasons that affect the future development of rural areas. The proportion of men and women in the rural population in the experimental areas was basically the same. From 2000 to 2006, the proportion of men in the population declined slightly, from 51.6% in 2000 to 50.9%, and the proportion of women in the population rose slightly, from 48.4% in 2000 to 50.9%. As shown in Table 3.

Education has always been the main way to invest in human capital. The level of rural education largely reflects the level of human capital. According to the 2014 and 2020

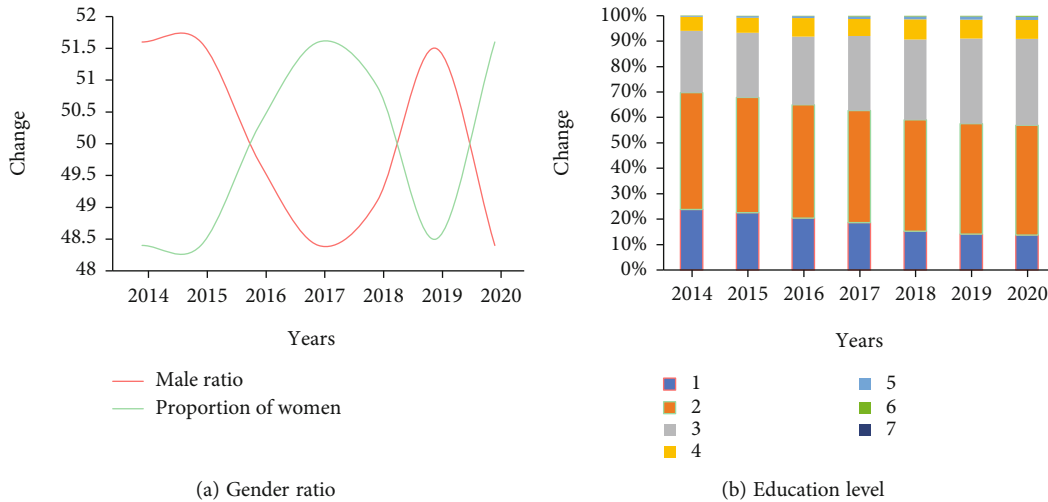


FIGURE 12: Rural gender ratio and educational level year-by-year ratio.

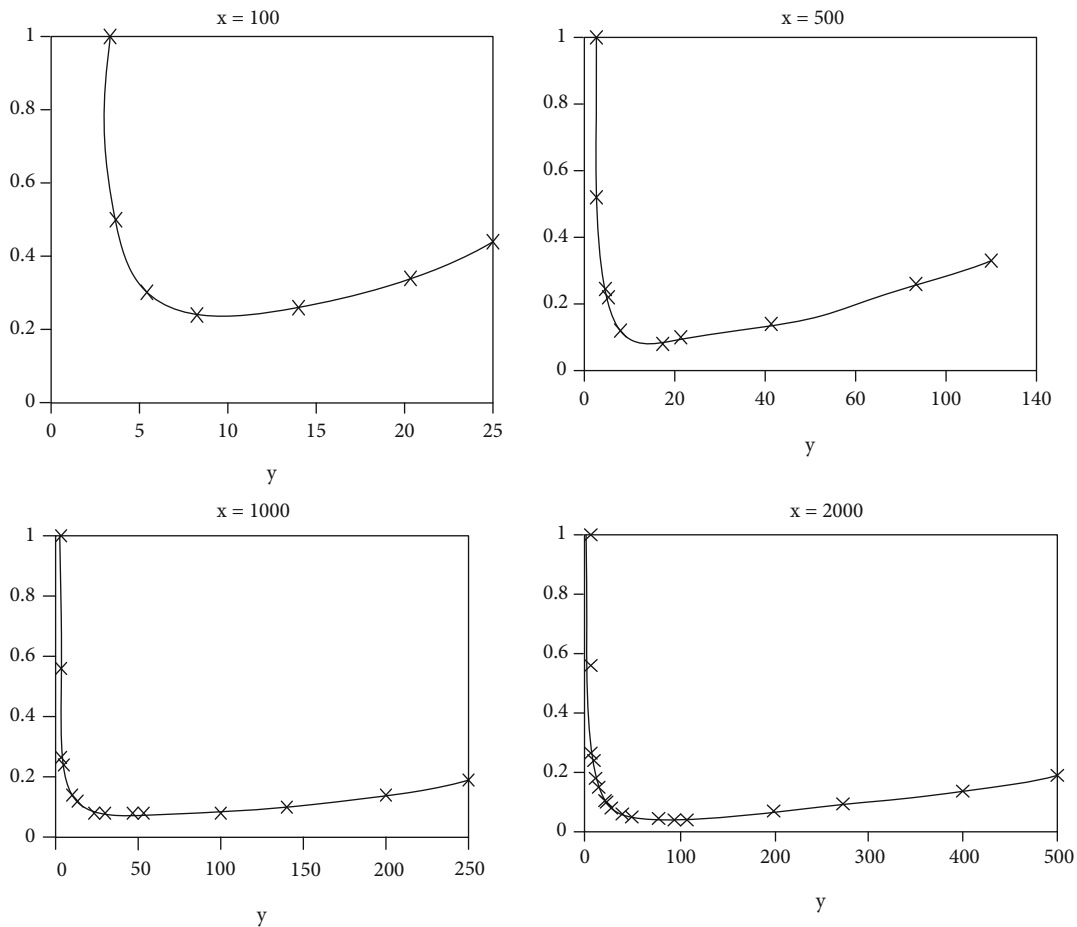


FIGURE 13: GM/PM.

census data, the overall educational level of the rural population over 6 years old in the experimental areas has increased. The proportion of illiterate and elementary school population has decreased year by year. The proportion of Chinese

illiterate population has dropped from 23.8% in 2014 to 13.8% in 2020, which is a significant decline. The proportion of population in elementary school has also dropped from 46.0% in 2014 to 43.2%. The proportion of the population

TABLE 5: Poverty factors in experimental areas.

Factor	Poor households	Percentage (%)	Number of poor	Percentage (%)
Disease	687	44.39	1285	39.96
Disability	82	5.22	160	4.97
Lack of labor	188	11.97	269	8.36
Study	5	0.31	17	0.52
Technology, capital	442	28.15	1077	33.49
Traffic condition	24	0.89	23	0.71
Insufficient motivation for own development	24	1.52	77	2.39
Lack of land	97	6.17	260	8.08
Other reasons	11	0.70	47	1.46

with junior high school, high school, and above education level is on the rise. Among them, the proportion of the junior high school population has increased significantly, from 24.3% in 2014 to 34.0% in 2020. From the data, it can be seen that the rural population in Gansu Province is dominated by elementary and junior high school education, as shown in Table 4.

Through experiments, we analyzed the impact of gender and education level on rural poverty, as shown in Figure 12 (1 is illiteracy, 2 is primary school, 3 is junior high school, 4 is high school, 5 is college, 6 is undergraduate, and 7 is postgraduate).

It can be seen from the figure that the gender ratio has little effect on rural poverty, but the level of education is very much related to the impact of poverty. As the average per capita education gradually increases, the rural poor population is also decreasing. By the beginning of 2020, the educational background has reached 34%, which is 9.7% higher than the 24.3% in 2014. This shows that the higher the education level of rural people, the higher the income.

4. Data Collection Experiment Results

4.1. GH Efficiency and Safety Analysis. From the GH efficiency, it can be concluded that y and x satisfy the formula () as the best grouping. According to the $3f + 1$ model, it is concluded that the total number of copies of the system $x > 4$. Taking $x = 100$, $x = 500$, $x = 1000$, and $x = 2000$ as an example, the consumption message comparison between GH and PBFT is shown in Figure 13.

For GH packet security, the purpose of the GH packet protocol is to divide distributed nodes into multiple partitions, and each partition executes the GH consensus protocol in parallel to improve consensus efficiency. The analysis of the group security is as follows:

- (1) Fast grouping is not a combination of yp completely arranging replica nodes of the entire network, which prevents the worst grouping state from being arranged when the master node is a Byzantine node. At the same time, each replica node is not allowed to be freely combined, which can further improve the grouping speed and also allow other lps to choose their own lx according to the specific situation
- (2) The condition for successful group establishment is at least $2mj/3$ consistent messages to ensure that each group satisfies the $3f + 1$ model. Since each group is built in a closed form, Gj returns a BACKWARD message to $Gj-1$. All subsequent groups were successfully formed. In order to prevent a group from being sandwiched between the two normal groups, whose lp is a Byzantine node or the link is broken due to other benign errors, the Backward phase is designed. If the BackwardTimer expires, the message <BREAKPOINT-FINDING is sent, $T > \sigma i$ to ensure that the grouping status of replica nodes in the entire network remains uniform even if there is a broken link
- (3) According to the $3f + 1$ model, in PBFT, if the number of normal nodes, benign and wrong non-Byzantine nodes, and Byzantine nodes each account for $1/3$, the remaining last node can control the consensus result of the entire network. GH reduces the influence of the last node and Byzantine node after the entire network is grouped to the group it is in instead of the entire network
- (4) GH adopts self-closing mechanism to stabilize the total number of Byzantine nodes in the system below the critical point 1, and the number of Byzantine nodes in the group stabilizes at $mj/3 + 1$. At the same time, a suspicion zone is set. When the system performs safe grouping between critical point 1 and critical point 2, it makes full use of the fault tolerance of each group

4.2. Poverty Factors. After analyzing the efficiency of smart sensors under the blockchain theory, the data in the experimental area is analyzed, and Table 5 can be shown.

From the data in the table, it can be concluded that 44.39% of people are poverty-stricken due to diseases, and 33.49% are due to technology and funds. Therefore, the most important way to get rid of poverty is to develop technological development. Only by possessing feasible technology can rural areas be transformed into poverty. Chengcheng will allow rural people to lead a prosperous life and no longer suffer from poverty.

5. Conclusions

Rural poverty is a problem that the country is studying, but this problem has not yet been resolved. Based on smart sensors, this paper collects and analyzes data and analyzes and experiments on the factors that affect rural poverty through the intelligent processing of smart sensors. The experimental results show that the educational level of the rural population is closely related to their income. The experimental results show that the higher the level of education, the higher the income, and the smaller the number of poor people. This experiment selects a region for data analysis. Through analysis, its junior high school education rate has increased from 24.3% in 2014 to 34% in 2020, and the poverty population has also decreased. Moreover, through the intelligent processing of smart sensors, it can be concluded that 44.39% of the rural population is impoverished due to diseases, and 33.49% is impoverished due to technology and funds. Therefore, as long as the right medicine is prescribed, the rural people can get rid of the poverty of the rural people. Get rid of poverty, keep pace with the times, and fight the tough battle against poverty with the country.

Data Availability

No data were used to support this study.

Conflicts of Interest

The authors state that this article has no conflict of interest.

Acknowledgments

This work was supported by the Doctoral Research Initiation Funding Project of Jilin Engineering Normal University (Project number: BSSK202001), the Rural Development Institute of JiLin Engineering Normal University, and the Program for Innovative Research Team of JiLin Engineering Normal University.

References

- [1] J. Li, K. A. Mechitov, R. E. Kim, and B. F. Spencer Jr., "Efficient time synchronization for structural health monitoring using wireless smart sensor networks," *Structural Control and Health Monitoring*, vol. 23, no. 3, pp. 470–486, 2016.
- [2] M. R. García, M. L. Cabo, J. R. Herrera, G. Ramilo-Fernández, A. A. Alonso, and E. Balsa-Canto, "Smart sensor to predict retail fresh fish quality under ice storage," *Journal of Food Engineering*, vol. 197, no. mar., pp. 87–97, 2017.
- [3] B. Cao, X. Wang, W. Zhang, H. Song, and Z. Lv, "A many-objective optimization model of industrial Internet of Things based on private blockchain," *IEEE Network*, vol. 34, no. 5, pp. 78–83, 2020.
- [4] W. D. du, S. L. Pan, D. E. Leidner, and W. Ying, "Affordances, experimentation and actualization of FinTech: a blockchain implementation study," *The Journal of Strategic Information Systems*, vol. 28, no. 1, pp. 50–65, 2019.
- [5] J. Cai, Y. Yu, D. Luo et al., "Space differentiation and its influence factor analysis of rural multidimensional poverty in Chongqing," *Nongye Gongcheng Xuebao/Transactions of the Chinese Society of Agricultural Engineering*, vol. 34, no. 22, pp. 235–245, 2018.
- [6] E. Y. Naminse, J. Zhuang, and F. Zhu, "The relation between entrepreneurship and rural poverty alleviation in China," *Management Decision*, vol. 57, no. 9, pp. 2593–2611, 2019.
- [7] S. Dissanayake, H. Pasqual, and B. Athapattu, "Economical colorimetric smart sensor to measure water quality of drinking water in CKDu prevalence areas," *IEEE Sensors Journal*, vol. 17, no. 18, pp. 5885–5891, 2017.
- [8] X. Wu, Y. Shi, S. Jeloka et al., "A 20-pW discontinuous switched-capacitor energy harvester for smart sensor applications," *IEEE Journal of Solid-State Circuits*, vol. 52, no. 4, pp. 972–984, 2017.
- [9] B. Markey-Towler, "Anarchy, Blockchain and Utopia: a theory of political-socioeconomic systems organised using Blockchain," *The Journal of British Blockchain Association*, vol. 1, no. 1, pp. 1–14, 2018.
- [10] A. Paliwal, A. Laborte, and N. M. Paguirigan, "Rural poverty and rice," *Rice Today*, vol. 15, Supplement 1, pp. 30–31, 2016.
- [11] Y. Wang, M. Singgih, J. Wang, and M. Rit, "Making sense of blockchain technology: how will it transform supply chains?," *International Journal of Production Economics*, vol. 211, no. -MAY, pp. 221–236, 2019.
- [12] A. I. Torre-Bastida, J. Díaz-de-Arcaya, E. Osaba, K. Muhammad, D. Camacho, and J. del Ser, "Bio-inspired computation for big data fusion, storage, processing, learning and visualization: state of the art and future directions," *Neural Computing and Applications*, 2021.
- [13] R. Santos, "On the philosophy of bitcoin/blockchain technology: is it a chaotic, complex system?," *Social Science Electronic Publishing*, vol. 48, no. 5, pp. 620–633, 2017.
- [14] M. Swan and P. de Filippi, "Toward a philosophy of blockchain: a symposium: introduction," *Metaphilosophy*, vol. 48, no. 5, pp. 603–619, 2017.
- [15] K. Lo, L. Xue, and M. Wang, "Spatial restructuring through poverty alleviation resettlement in rural China," *Journal of Rural Studies*, vol. 47, Part B, pp. 496–505, 2016.
- [16] A. G. Naimanye and T. Whiteing, "Poverty-centred rural road funds sharing in sub-Saharan Africa," *Proceedings of the Institution of Civil Engineers*, vol. 169, no. 6, pp. 387–396, 2016.
- [17] P. O.-W. Adjei, D. Buor, and P. Addrah, "Ecological health effects of rural livelihood and poverty reduction strategies in the Lake Bosomtwe basin of Ghana," *Geo Journal*, vol. 82, no. 3, pp. 609–625, 2017.
- [18] S. Sharaunga, "The effectiveness of women's skills development to household poverty reduction: the case of Msinga rural areas," *Poverty & Public Policy*, vol. 11, no. 1-2, pp. 73–98, 2019.
- [19] B. Hou, H. Liao, and J. Huang, "Household cooking fuel choice and economic poverty: evidence from a nationwide survey in China," *Energy and Buildings*, vol. 166, pp. 319–329, 2018.
- [20] T. Potocki and M. Cierpial-Wolan, "Factors shaping the financial capability of low-income consumers from rural regions of Poland," *International Journal of Consumer Studies*, vol. 43, no. 2, pp. 187–198, 2019.
- [21] S. Naha, S. P. Wu, and S. Velmathi, "Naphthalimide based smart sensor for CN-/Fe3+and H2S. Synthesis and

application in RAW264.7 cells and zebrafish imaging,” *Advances*, vol. 10, no. 15, pp. 8751–8759, 2020.

- [22] S. Famila, A. Jawahar, A. Sariga, and K. Shankar, “Improved artificial bee colony optimization based clustering algorithm for SMART sensor environments,” *Peer-to-Peer Networking and Applications*, vol. 13, no. 4, pp. 1071–1079, 2020.

Research Article

Financial Management Early-Warning Mechanism Construction and Decision Analysis Research Based on Wireless Sensor Network and Data Mining

Zeyuan Chang¹ and Heran Yang² 

¹Business School, Shandong Normal University, Jinan, 250014 Shandong, China

²D'Amore-Mckim School of Business, Northeastern University, Boston, 02115 MA, USA

Correspondence should be addressed to Heran Yang; yang.her@northeastern.edu

Received 29 October 2021; Accepted 1 December 2021; Published 21 December 2021

Academic Editor: Alireza Souri

Copyright © 2021 Zeyuan Chang and Heran Yang. This is an open access article distributed under the Creative Commons Attribution License, which permits unrestricted use, distribution, and reproduction in any medium, provided the original work is properly cited.

With the gradual and complete establishment of the current socialist legal market economy management system with Chinese characteristics and the continuous investment in deepening system reform and continuous improvement in the later period, the social financial industry and corporate financial management have gradually increased their risk awareness of corporate financial management. This paper deeply analyzes and studies the statistical methods of financial data-related legal rule interactive mining and proposes a new improved statistical algorithm of financial-related legal rules, which greatly improves the work efficiency of financial data interactive mining. At the same time, a multilevel analysis model based on the concept of corporate financial crisis risk assessment and a corporate financial crisis risk early-warning analysis model for decision-making risk evaluation are proposed. Finally, it can be determined how to choose more internationally representative corporate financial management risk analysis indicators, which have more objectivity and practical application significance than traditional analysis methods. Finally, it is concluded that the accuracy of this model is better than that of other models. The accuracy rate of financial crisis prediction reached 62.35%.

1. Introduction

In August 2007, the Subprime Crisis broke out again in the United States. The global international financial market was turbulent. A large number of subprime mortgage asset loan management institutions were forced to go bankrupt, and investment funds were forced to go bankrupt and close. From the US subprime mortgage and US debt financial crisis to the current global European subprime mortgage financial crisis, the world's major international financial rating markets have failed to give clear instructions for industry management in advance by the world's three major international rating industry management agencies. Risk speculation early-warning rating behavior attitude is disappointed, and the current effective international rating industry management procedures, methods, effective evaluation management model, and construction system of the current

major international rating industry management agencies have strongly questioned the degree. It is generally believed that we should still be concerned about the potential major international conflicts of interest and risk impacts in the industry in the next few years and the excessive emphasis on large-scale rating behavior by the three major international rating industry management agencies. Competitors in the monopolistic market believe that sound rating reforms should be carried out first. The enlightenment from the US subprime mortgage crisis and the European sovereign debt crisis is that international investment banks and international rating agencies are unreliable, and China needs to establish its own financial risk crisis early-warning system.

With the rapid development of wireless measurement sensor-related networks and applied data mining-related technologies, related network theories and technical applications are becoming more mature. The fusion of application

databases plays a very important role in the research of wireless measurement sensor-related networks. The main function is to save the data energy of the entire related network, enhance the analysis accuracy of the related data that needs to be collected, and greatly improve the network collection of related data, three main aspects of work efficiency. The application of data fusion mining technology does not require too complicated traditional mathematical analysis theory or reasoning. As long as you pass the screening of the relevant database, you can quickly discover some hidden risk characteristics in the relevant database, and you do not need to manually set the assumptions below. It is necessary to manually adjust the hypothetical threshold value to be able to accurately find the risk rules in the relevant data collection. Therefore, this data mining technology method is widely used in a company's timely analysis of financial crisis risks and other crisis hazard early warnings, to establish a dynamic analysis of corporate financial crisis risks and other crisis hazard early-warning management models and find a company with the new rules of high trust, timely analysis, and early warning of important financial crisis risks and other crisis hazards that an enterprise may have become the main academic research topic of this research topic.

In today's era of information flooding, there have been constant scientific researchers conducting in-depth research on financial management early-warning institutions and decision-making analysis. Buczak and Guven, through an in-depth study of corporate financial management risks, made an in-depth discussion on how to effectively strengthen the financial management risk management of large-scale enterprises. Under the comprehensive analysis of macroqualitative and substantive quantitative analysis, it is the main reason why the financial management risk management of large-scale enterprises in our country is formed. On the basis of Kaishan's research to establish an early-warning system for corporate financial risks, improve the internal control mechanism of the enterprise, and make appropriate risk decisions, this research is not thorough enough [1]. Helma et al. are mainly represented by the annual z-calculation analysis and model analysis. The multi-year discriminant analysis model of corporate financial data risk monitoring and early warning is based on the annual statistics and calculation analysis of the financial data of a listed company in a specific time period. From the perspective of economic practical research on the internal financial decision-making of small and medium-sized stocks and nonlisted companies, it is proposed that a set of unit multi-variable corporate financial risk early-warning multianalysis models suitable for the economic characteristics of listed companies should be established to effectively reduce the daily operation of listed companies. There are risks in internal decision-making, but this research method is outdated in today's era [2]. Duivestijn et al. use university management financial accounting as an analysis to review the past, control the current situation in the future, and plan the basic financial concepts of the future. From the four aspects of university financial management planning, financial management organization, financial risk control, and financial risk evalu-

ation that universities need to promote. It analyzes the main financial management risks of higher vocational colleges at each stage, studies and proposes the establishment of a financial management risk monitoring and early-warning evaluation mechanism at each stage of the university, and constructs an implementation plan. This risk early-warning plan is obviously insufficient targeted [3]. Adeniyi et al. analyze and establish the collection of information volume of the financial risk early-warning system of human-based financial capital enterprises based on the theory of using human-based financial capital resource structure and the law of coupling use between various corporate financial cost resources and noncorporate financial cost resources. Through transmission forecasting mechanism, basic organization and management mechanism of human-based financial capital enterprise financial risk early-warning system, and the use of human-based financial capital and other financial enterprise risk information early-warning information processing and forecasting mechanism, a financial risk early-warning mechanism for various enterprises using human financial capital has been constructed. Obviously, this mechanism is not comprehensive enough for financial risk early-warning reports [4]. Wang's research focuses on how to strengthen and improve the hospital's internal basic-level integrated financial and internal accounting risk management. It is under the in-depth study, discussion, research, and analysis to strengthen the hospital's internal basic-level financial management, generate internal risks and the reasons for the necessity and prerequisites, and accelerate to study, establish, improve, and strengthen the internal risk statistical monitoring, evaluation, early warning, and financial evaluation risk management mechanism and working methods of the hospital's internal primary financial management. Evaluate the basis of financial control risk management, complete and improve the hospital's internal integrated financial risk monitoring and early-warning evaluation management mechanism, establish and improve the internal risk monitoring and early-warning evaluation index system of the hospital's internal primary financial management and other related policies and measures to comprehensively and effectively avoid the hospital's financial operations of all kinds of risks, and grasp the initiative of the hospital's financial work, and the experimental basis of this research is obviously not sufficient [5]. Lin et al. define the company's net cash inflows generated during the current period of operating business activities as positive or negative, and a risky company whose cash flow and other cash inflow equivalents continue to increase during the operating period is positive or negative can be defined as a long-term financial crisis. At the same time, through the analysis of the internal and external factors driving influencing factors that these companies may fall into the long-term financial crisis, and on this basis, the basic theoretical design framework of the enterprise financial crisis risk early-warning management system is established. This theoretical framework is difficult to match the actual situation. It complies with [6]. Purves et al., based on the comprehensive analysis of comprehensive financial indicators, introduced comprehensive governance financial structure analysis

factors. The unsupervised wireless network model in government management assisted the abnormal warning information to carry out a comprehensive upgrade to the early-warning system, and the joint 5g made the early-warning system response time faster; this analysis does not combine Internet information fusion, making this research method lagging behind [7].

This paper mainly proposes an interactive improved data mining analysis algorithm for data association structure rules and proposes an interactive data mining analysis algorithm for data association analysis rules based on optimized Hash association structure called HIUA, which is mainly for data support or threshold changes. This mining algorithm (MA) reimproves the data pruning process of the original IUA, MA, and reimproves the efficiency of the algorithm during normal operation by optimizing the Hash association structure. This paper adopts a complementary combination of fuzzy calibration processing model and fuzzy inference analysis model to process data from multiple sensors and at the same time to ensure the accuracy and reliability of the data under different risk detection data conditions. The fuzzy calibration processing model is mainly used to analyze how many sensors to realize automatic adjustment of data-related information under the same financial index. By interactively mining the association rules between all corporate financial indicators, we can finally determine how to choose a more internationally representative financial enterprise risk analysis indicator, which is more objective and practical than traditional analysis methods. Therefore, the early-warning system proposed in this article has a good operating effect for financial companies and can achieve the effect of crisis prevention and the ability to make decisions.

2. Principle and Theory Overview

2.1. Overview of Wireless Sensor Networks. With the continuous progress of current modern microelectronic processing software technology, computer network processing technology, and other modern real-time wireless communication network information processing technology, low-tech cost and low-power multifunctional wireless network sensor monitoring technology has been rapidly developed. Widespread application and development have made it possible to integrate wireless monitoring object information for real-time monitoring and collection, data processing, and real-time wireless communication between man and machine and other important monitoring functions in a small cost volume. The connection relationship between sensors, perceptron and communication detection objects, and information detection and observers constitute three basic technical elements of the wireless science physics natural sensor information science technology network, the perception communication object before detection, and the detection object after processing. The connection of communication perception objects after data and communication connection is the operation of three important technical components of the wireless science physics natural sensor information science and technology network. The node itself is not only the network collector and transmission sender of

the collected information, but also the network router of the collected information. The collected information data reaches multiple gateways through multiple routing nodes [8, 9]. The sink node is a special network node that can communicate with the gateway monitoring data center through the Internet, mobile communication wireless network, satellite, etc. The wireless data sensor node network structure diagram is shown in Figure 1.

Wireless photoelectric network sensor technology application power network, in addition to the common important basic characteristics that should have many irreversible mobility, disconnection, power system management capabilities, and technical limitations, it also believes that it should have many other distinctive features.

2.1.1. Dynamic Network. The relative node of the wireless network in a sensor relative node acquisition network is very likely to be randomly and automatically deployed directly. At the same time, a wireless battery relative node automatically provides a certain amount of energy in the relative node network. When the energy system of the relative node cannot be used up automatically or the energy cannot be automatically detected when the environment in the wireless network changes, it will directly and automatically cause the energy system in the relative node to fail or the wireless network failure, and the relative node cannot automatically collect normally. The detected data becomes the relative node in the process of death of the wireless network. At this time, a relative topological system structure of a wireless network is very likely to change. Therefore, a wireless network itself is a very safe and dynamic relative node collection network in a sensor relative node collection network [10, 11].

2.1.2. Self-Organizing Network. The location of the topology of the wireless network sensor system network terminal nodes cannot be accurately set in advance, and the relationship between neighboring nodes and network neighbors between nodes cannot be accurately known in advance. These important network nodes are automatic and integrated. Organizations quickly adapt and combine to form a new node wireless network. This article has also mentioned in detail the important node terminal topology and network structure of the terminal network of the wireless network node sensor system which are usually dynamically changed, so due to the automatic and comprehensive organization of the wireless network node sensor system node terminal network, the nature also makes the need to be more conducive to quickly adapt to the dynamic changes of this network topology.

2.1.3. Data-Centric Network. An information network may directly report to a network node user after a node user needs to obtain a certain basic geographic information about an event of a specified network node. This kind of network usage behavior thought that the specific network node data itself is directly delivered as information clues for query or the network transmission node information is indirectly delivered as clues are more on a behavioral habit that is close to natural language or information network communication.

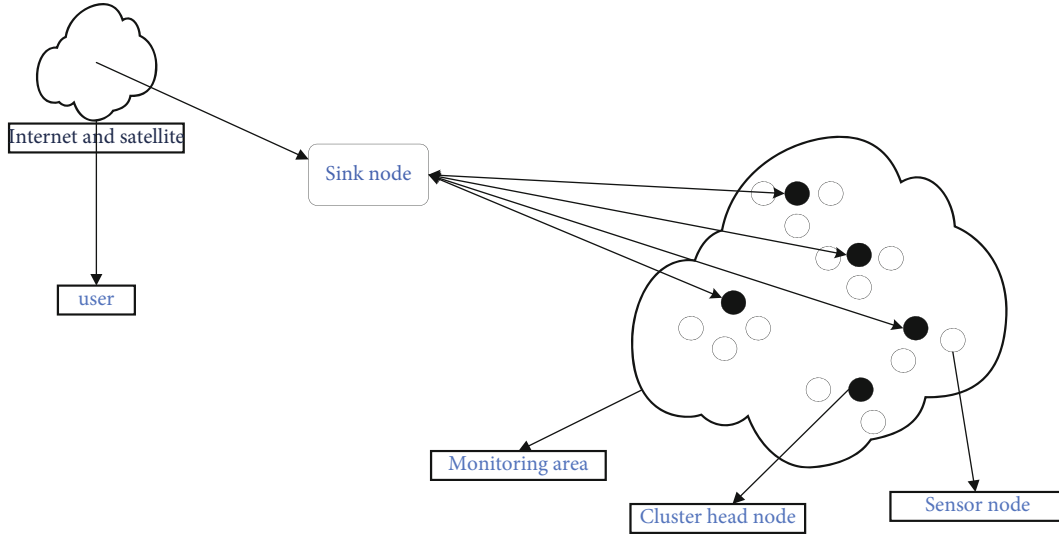


FIGURE 1: Wireless sensor network architecture.

So the usual network sensor that we are talking about is a natural information network that uses the specific network node data itself as the information clue query center. The comparison results of the characteristics of the three fusion methods are shown in Table 1.

2.2. Overview of Data Mining. Data mining is generally called enterprise data resource exploration and data mining. It refers to an important step in the knowledge information discovery process of enterprise database systems. Specifically, it refers to a large amount of knowledge data. Through the use of corresponding MAs, timely and accurate search and mining are performed to find valuable knowledge information that has been hidden or may have been hidden in the entire data resource information system. In actual commercial data applications, data analysis, and processing algorithms for data model information analysis and mining, common data models mainly include four types of data analysis algorithms, classification and periodic data sequence prediction, clustering, association classes and data sequence rules, time table, and periodic data sequence. This article will focus on detailing how to choose the decision tree model as the four analysis methods of the enterprise classification data tree [12, 13].

In this mining process, enterprise data needs to fully consider what exactly the enterprise needs to do at each key link and each stage of the mining process, specify each detail of the mining process, and specify each detail process, for example, what to mine data, how much massive data needs to be mined accurately, what data needs to be mined and to what extent, and which data key basic knowledge or key factors need to be accurately extracted as indicators in the entire process of data mining. Therefore, the preliminary data mining work can be summarized into two main levels. One is the selection of enterprise data objects and model determination, and the other is accurate and integrated processing. The purpose is to collect data that needs to be mined. The enterprise

TABLE 1: Comparison of different levels of integration.

Characteristic	Pixel-level fusion	Feature-level fusion	Decision-level fusion
Traffic	Maximum	Medium	The smallest
Fault tolerance	Worst	Medium	Most
Anti-interference	Worst	Medium	Most

data model is processed through various groupings, so that the mining efficiency can be optimized to the maximum, and finally the actual performance and effect of the enterprise mining data model can be simplified to the maximum. The model is shown in Figure 2.

2.3. Theoretical Analysis of Financial Early Warning. The theory of early warning of corporate financial crisis is a comprehensive theory that includes multiple discipline. It is a multidisciplinary knowledge covering enterprise risk management, industrial process control, dynamic information technology, mathematical modeling, and so on. The research on the early warning of corporate financial crisis is very similar to the research on mining highly trustworthy rules in intelligent industrial control systems. The early-warning indicators of financial crisis are equivalent to the equipment in the industrial control system. When the indicators fluctuate, they are equivalent to the operating attitude of the industrial equipment. In the event of instability and the fluctuation of financial indicators beyond a certain range, the system should issue an early warning [14, 15].

According to the management structure, the various links of enterprise risk management can be designed as shown in Figure 3.

Data mining must first clean up the data, remove the abnormal data, then select and integrate the data, and then transform the data into a type suitable for data mining

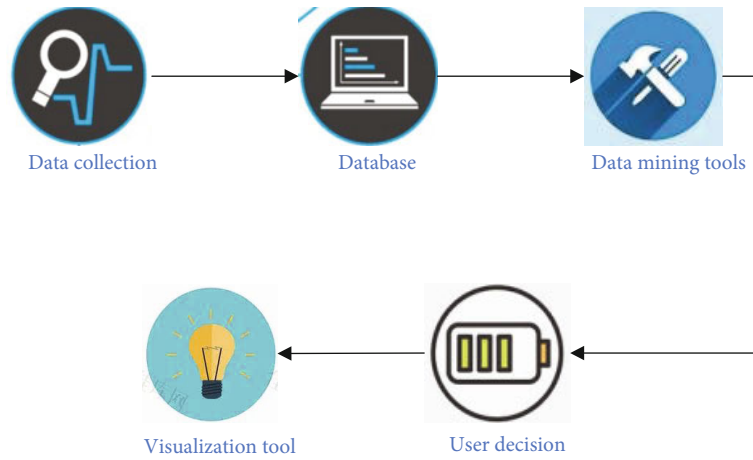


FIGURE 2: Data mining environment.

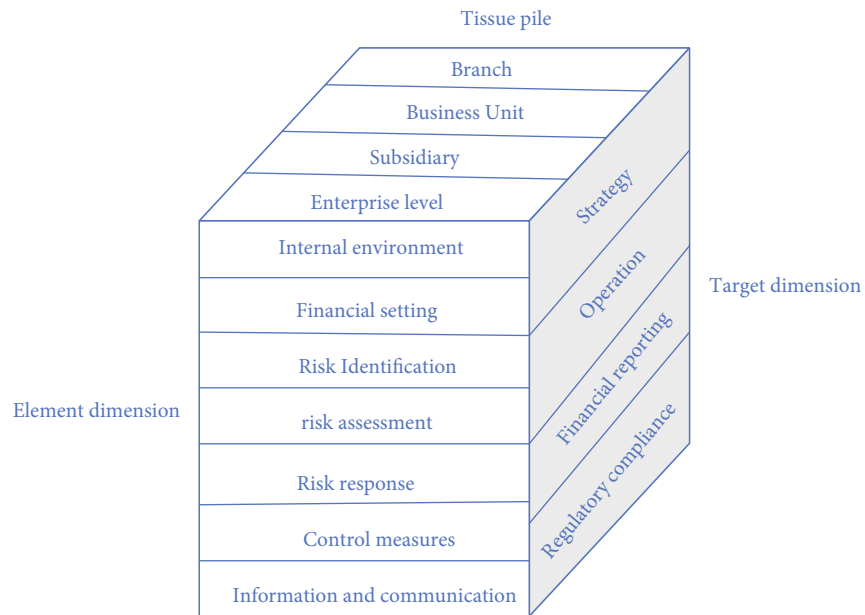


FIGURE 3: Enterprise risk management-integrated framework.

through data transformation. The most important step is to choose a suitable data mining method to find the data. Finally, the hidden patterns and laws in the data are displayed through pattern evaluation and knowledge representation. The methods of data mining mainly include the following:

- (1) *Classification and Prediction*. Classification mining is a method of distinguishing a large amount of data according to the established model. The data can be divided into multiple categories; prediction is to establish a continuous value function model to determine the development trend of future data. This is a method of making predictions.
- (2) *Clustering*. Clustering mining is based on a set of data objects to be analyzed and automatically aggregates into different categories according to the similarity of the instance attribute values.
- (3) *Association Rules*. Association rule mining is used to discover useful or meaningful connections hidden in transaction data sets or relational data sets for users.
- (4) *Time-Series*. Time-series mining is a method of mining sequence objects of values or events obtained by repeated measurements at different times, and it is expected to analyze the trend changes of the data.

Other methods include the following: mining complex data types such as graphics, images, videos, and Web [16, 17]. The refinement of financial management objectives refers to the specific refinement of corporate financial objectives. The specific financial objectives of financial management generally include the specific objectives of corporate monetary fund income management, the specific objectives of cost and income management, the objectives of credit policies, and the improvement of the quality of financial reports. The goals, etc., are shown in Table 2:

TABLE 2: List of financial target items.

Project	Merge	
	Number of current period	Same period last year
Main operating profit	***	***
Operating profit	***	***
Total profit	***	***
Main business income	***	***

The financial operation risk automatic identification system is an important foundation for strengthening the enterprise financial operation risk management. The identification of risks is also after the enterprise has determined the relevant financial goals, using various methods to analyze the internal and external destruction events that affect the realization of the enterprise's financial goals. The working method of financial customer risk information identification is mainly through various channels and various technical means to collect and obtain sufficient and true customer financial risk information in a timely manner and to organize, classify, and analyze these financial information data in a timely manner. To make a preliminary judgment on the risk of uncertainty, the financial trend chart of a company in recent years is shown in Figure 4.

3. Simulation and Construction of Financial Management Early Warning

3.1. MA of Association Rules. Association rule data mining technology is one of the main application technologies for big data analysis and mining. Improving the efficiency of association rule mining is a hot topic. The existing various associated data rule pattern mining and maintenance algorithms mainly refer to some interactive static pattern mining and maintenance methods. When the scanning database changes or the threshold between data support and data confidence is slightly adjusted, it is always possible. There is a problem when the database and the holding degree are repeatedly calculated after multiple holding scans. Aiming at the problem of dynamic maintenance and mining of various associated data rules after the scanning database and holding thresholds are changed, this article mainly proposes a method based on associated data rules. For a dynamic pattern maintenance MA, it is first necessary to study an interactive pattern mining maintenance algorithm for associated data rules. The flowchart of financial crisis early warning is shown in Figure 5.

For the MA, IUA is mainly used here for detailed description [18, 19]. The IUA algorithm is expressed as follows:

$$e(k) = y(k) - y_m(k),$$

$$E(k) = \frac{1}{2} e^2(k). \quad (1)$$

Here, the input contribution is defined as the product of the input growth rate and its two-period average value share. $Ax = X - xt - 1$ represents the change from $t - 1$ to t , and v is equal to the average share of input in the two periods of output. Define the share of each input value as follows:

$$\alpha = M^+ T,$$

$$\min \text{LPELM} = \frac{1}{2} \|\alpha\|^2 + C \frac{1}{2} \sum_{i=1}^n \|\gamma_i\|^2, \quad (2)$$

$$h(x_i)\alpha = t_i^T - \gamma_i^T, i = 1, \dots, n,$$

$$\alpha = H^T \left(\frac{I}{C} + HH^T \right)^{-1} T.$$

This formula was expanded. They divided diversification into interindustry diversification and intraindustry diversification and used EUD (end-user development) to express the degree of interindustry diversification:

$$w = 1, F(F \in [0, 1]),$$

$$F \in (0.5, 1),$$

$$F = 1 - \gamma e - \left| \frac{C}{C_{\text{total}}} \right|, \gamma \in R+, \quad (3)$$

$$F = \gamma e - \left| 1 - \frac{C}{C_{\text{total}}} \right|, \gamma \in R+.$$

Since there is currently no statistical data on fixed asset storage locations at the service industry level, the method we adopted is to first use the perpetual inventory method to calculate the total capital stock of the tertiary industry in each year.

$$E[T_i] = P_m^i * P_r W_{i-1},$$

$$E[T_i] = \sum_{i=0}^{MC} E[T_i], \quad (4)$$

$$\text{Max } E = \text{fix}(\log_2(N))K = \text{fix} \left(\log_2 \left(\frac{N}{2} \right) \right).$$

Then, use the ratio of fixed asset investment in each industry to the fixed asset investment in the tertiary industry to estimate the industrial fixed capital stock, which is the following:

$$\Delta w_{ij}^I(k) = - \frac{\partial E(k)}{\partial w_{ij}^I} = e(k) \frac{\partial y_m}{\partial X_j} \frac{\partial X_j}{\partial w_{ij}^I}, \quad (5)$$

$$e(k) \frac{\partial y_m}{\partial X_j} \frac{\partial X_j}{\partial w_{ij}^I} = e(k) w_j^O Q_j(k).$$

Regarding the selection of the specific production function, Jorgensen decomposed the output growth into the contribution of each input and the remaining total factor

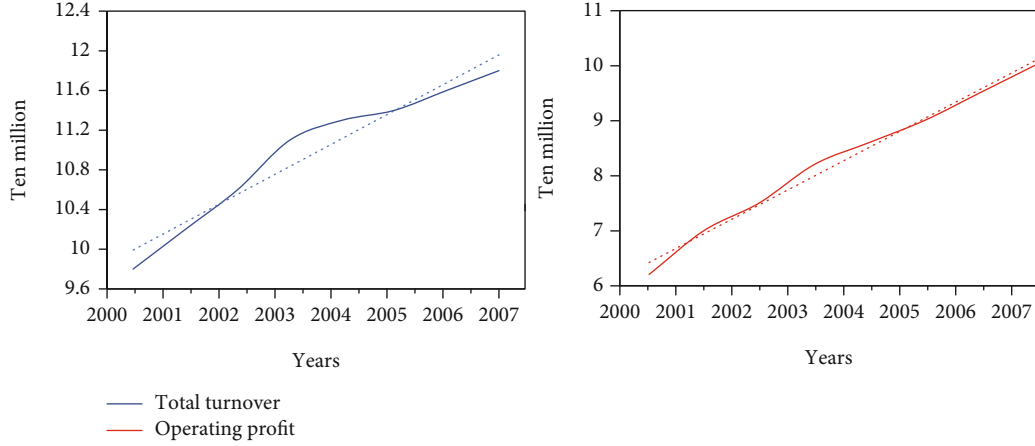


FIGURE 4: The company's turnover curve of a company in recent years.

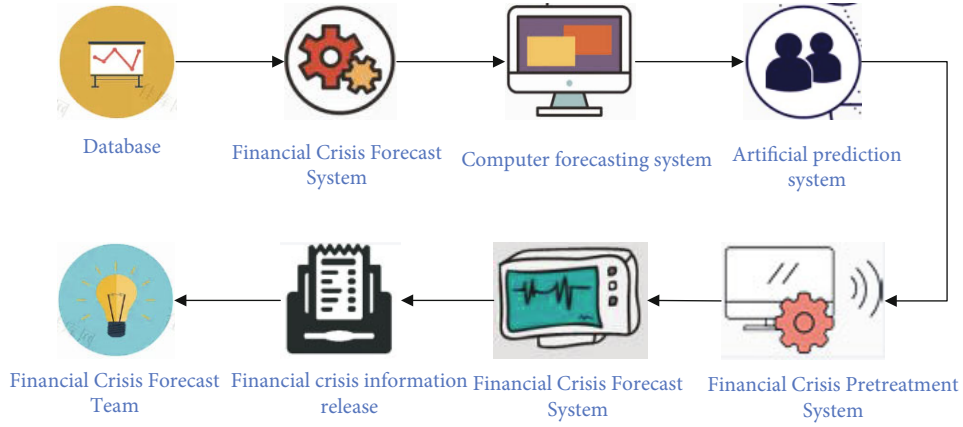


FIGURE 5: Flowchart of financial crisis warning.

productivity according to the standard growth calculation formula:

$$\begin{aligned}
 w_{ij}^l(k) &= w_{ij}^l(k-1) + \mu \Delta w_{ij}^l(k), \\
 x(t) &= 2 \sum_{k=1}^{N/2-1} |C_K| \cos(kw_0t + \beta_k), \\
 x(t) &= 2 \sum_{k=1}^{N/2-1} a_k \cos(kw_0t) + b_n \sin(kw_0t).
 \end{aligned} \tag{6}$$

According to the idea of multiple linear regression, the autoregressive moving average model ARMA (n and m) can be generally expressed as follows:

$$x_t = \alpha_t - \sum_{j=1}^m \theta_j \alpha_{t-j} \tag{7}$$

in

$$\alpha_t \sim \text{NID}(0, \delta_a^2). \tag{8}$$

In the process of research and construction of the

financial early-warning risk model, it is necessary to accurately grasp the risks in the financial management of the risk control company and the functions in the early-warning system, such as the risk forecast function, the risk diagnosis function, the risk control function, and the health management function. The so-called risk prediction and diagnosis function, for a listed company, tracks a listed company's own production, operation, and management process and synchronizes with the listed company's own scheduled business goals based on the actual progress of the listed company's own production, operation, and operation. It is possible to accurately match each other. In-depth research and analysis of listed companies themselves in terms of production and operation management may also occur; at the same time, some risk issues and financial risk predictions are made. The correlation analysis is shown in Table 3.

Through correlation analysis, it is possible to find out the various factors that really affect the financial risk status of the enterprise more accurately and to find the problem in time through comparison with peers. For example, the company's internal financial information is analyzed under the association rule interactive mining strategy, and different support thresholds and confidence thresholds are set

according to the actual situation of the company and the industry, which can more accurately find abnormalities in financial indicators.

3.2. Financial Management Early-Warning Model Based on Data Mining. Use different correlation cost rule interactive cost mining analysis algorithm to interactively mine the main financial potential risks and index costs of Chinese companies, and find the correlation rules between different financial index cost systems and in-depth analysis of the real reasons for the potential financial risks of Chinese companies. The root cause lays the foundation for enterprises to get rid of the influence of financial risks [20, 21].

3.2.1. Construction of Risk Concept Hierarchical Tree. A key means to establish a set of corporate financial indicator risk analysis model is to build a multilevel structure tree of financial risk analysis concepts based on the corporate financial indicator analysis system model. The financial indicator analysis system mainly includes the actual profitability, operation, growth, and compensation of an enterprise. Risk analysis has five aspects of debt business capability and corporate cash flow, each of which contains different concepts of financial indicators. In the tree in the financial concept data hierarchy, using the concept generic replacement of the high concept hierarchy tree and the middle and level concepts can effectively realize the hierarchical generic transformation of financial data. The tree in the corporate financial data risk management concept data hierarchy can be divided into four layers according to the structure, which are conceptual levels 0, 1, 2, and 3. Level 0 is the highest level of the tree, and the top level of the hierarchical tree is marked according to the connection points. It refers to the level of corporate financial risk. Level 1 is the second level, which refers to the five aspects of corporate financial risks, and level 2 is the third level, which includes comprehensive key indicators of corporate financial risks. The specific content includes the following: profit rate, return on investment, and liquidity asset turnover rate [22, 23]. Level 3 is the lowest level. Figure 6 is the hierarchical tree structure of the corporate financial risk concept.

3.2.2. Interactive Mining Strategy with Decreasing Support Threshold. The interactive data mining calculation strategy of decreasing the risk support range threshold also means that each level of the data tree based on the risk support hierarchy needs to correspond to a minimum risk support flow threshold [24, 25]. The lower the financial index at this level and the corresponding minimum risk, the lower the threshold for supporting flow. For example, as shown in the figure above and below, the minimum risk support flow threshold value of the first and second levels is 20%, and the minimum risk support flow threshold value of the second and third levels is 10%. Figure 7 is an interactive data mining calculation strategy based on the decreasing risk support range threshold.

When considering the minimum support for the association rules between different levels, it should be determined according to the minimum support of the lower level.

TABLE 3: Association analysis.

Financial indicator	Current ratio	Inventory turnover	Assets and liabilities	Net sales profit margin
Strong association rules	≤ 1.6	≤ 2.4	$\geq 58\%$	$\leq 6\%$
Support	70%	65%	58%	80%
Confidence	55%	75%	66%	60%

3.2.3. Data Mining and Result Output. Use the interactive MA of association rules to mine the enterprise financial risk hierarchical tree layer by layer, adjust the support threshold for different levels of mining according to the user's requirements, and finally get the result that the user is satisfied with.

3.3. Experimental Simulation of Financial Management Early Warning. Through long-term empirical analysis and research, we can test the scientific validity of China's financial crisis monitoring and early-warning processing index system and establish and construct an effective set of China's dynamic long-term financial crisis based on China's financial crisis monitoring and early-warning indicator model and crisis early-warning processing procedures, monitoring, and early-warning system. One is unilateral. For listed companies that have experienced continuous major financial crises, long-term empirical analysis can be used to find the main source that may affect the further aggravation and deterioration of listed companies' financial asset crises. On the other hand, we can comprehensively use the public financial data of many existing listed companies in China to predict the next listed company that is most likely to continue to have a major financial crisis this year and provide corporate managers with auxiliary decision-making support for corporate development strategies. It can also provide a basis for investors' investment decisions [26].

The cleaning of sample data is to eliminate outliers of all variables, because the existence of outliers will affect our descriptive analysis of enterprise financial crisis early warning and cause great deviations. Therefore, before discretizing and reconstructing the sample data, we analyzed all the values of each variable and eliminated the abnormal data. The purpose of database reconstruction is to discretize the continuous data of financial crisis warning indicators and transform them into discrete financial indicator data suitable for mining association rules. Since the distribution of each financial indicator variable in the data set composed of financial data of different companies is basically a normal distribution, we choose to use the normal distribution and other area division methods to discretize continuous variables. In this chapter, according to the distribution of each variable, the 1/5, 2/5, 3/5, and 4/5 points of the function discretize each financial indicator variable into 5 levels. Table 4 is the database.

The key to establishing a corporate financial risk analysis model is to build a risk concept hierarchy tree based on the financial indicator system. The financial indicator

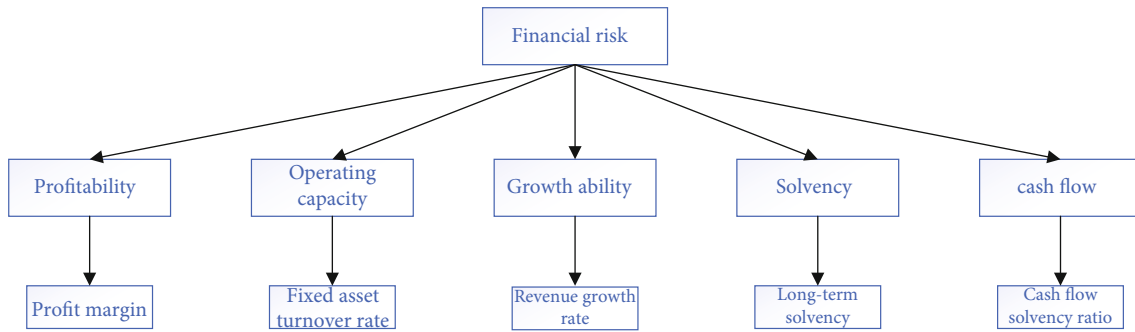


FIGURE 6: Hierarchical tree structure diagram of corporate financial risk concept.

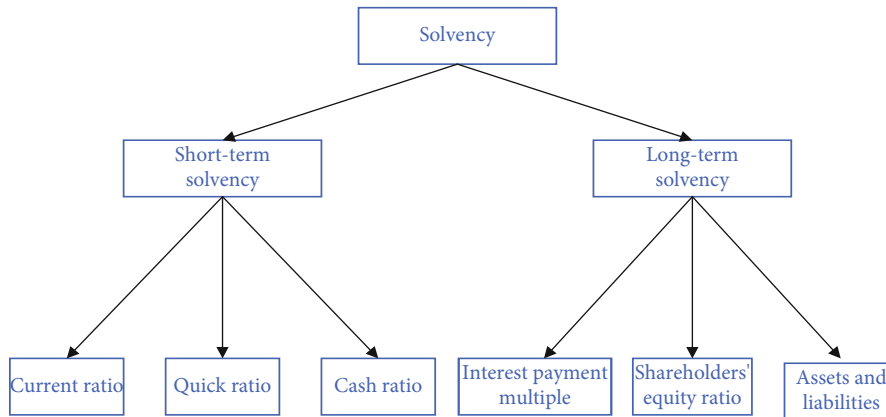


FIGURE 7: Interactive mining strategy with decreasing support threshold.

system includes analysis of the company's profitability, operation, growth, solvency, and cash flow. Each module includes different financial indicator concepts. In the concept hierarchy tree, the generalization of the data can be achieved by replacing the low-level concepts with high-level concepts. The hierarchical tree structure of the financial risk concept is divided into four levels, namely, levels 0, 1, 2, and 3. Level 0 is the highest level and is the root node mark of the tree, which refers to the level of corporate financial risk. Level 1 is the second level, which refers to the five aspects of corporate financial risks, and level 2 is the third level, which includes comprehensive key indicators of corporate financial risks. The specific content includes the following: profitability, return on investment, and liquidity asset turnover. Level 3 is the lowest level and is the index level that describes the most specific concept of financial risk. The specific content includes the following: gross profit margin, net profit margin, earnings per share, and account receivable turnover rate. According to the requirements of modern corporate governance structure and equity structure, corresponding auxiliary financial indicators have been added, such as the actual controller of the listed company, the shareholding ratio of major shareholders, CR3 index, Z index, and corporate management structure indicators in the corporate equity structure indicators. Figure 8 shows the number of board members in the board, and the proportion of board shares were held in the board, etc..

A new type of enterprise financial asset crisis information early-warning data model is dynamically analyzed and maintained according to the mining time rule sequence. Frequent data mining of relevant financial index data in the past period of time can be performed frequently to mine the first excavation time and node-related finances. The data will then be added and mined based on the subsequent mining time and the relevant financial data of the node, and then, the financial incremental data mining will be carried out. In addition, it is also possible to set different data support benchmark thresholds and different confidence benchmark thresholds, make comprehensive adjustments to the data mining results you want, find a number of frequent mining patterns and time rule values that meet the requirements of the enterprise financial crisis data early-warning model indicators, and comprehensively analyze the final data mining results.

4. Experimental Results and Analysis

4.1. Anticipating a Financial Crisis. The financial crisis of an enterprise is an evolving process for a period of time. It is a concept of a period. There is a crisis from the initial stage to the gradual deterioration and finally to the stage of corporate bankruptcy. After empirical research and rule screening, this article proposes a combination of qualitative analysis and quantitative analysis to determine the degree of corporate crisis and different stages. Qualitative analysis is to judge

TABLE 4: A company's original financial database.

Stock code	Stock name	Earnings per share	Cash flow per share	Roe	Net interest rate	Account receivable turnover rate
000595	*ST west axis	-0.1	0.34	-10.25	-27.66	0.25
000607	*ST Huakong	-0.2	-0.58	-11.23	-0.55	0.67
001542	*ST Tianrun	-0.05	0.65	-6.89	-10.65	4.58
001285	*ST Furi	-0.11	0.25	-5.23	-3.65	3.25

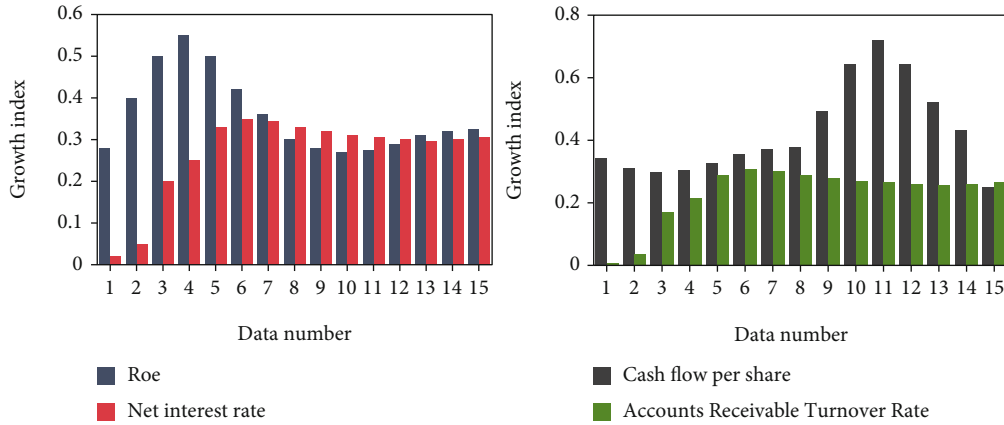


FIGURE 8: A graph of various financial data of a certain company.

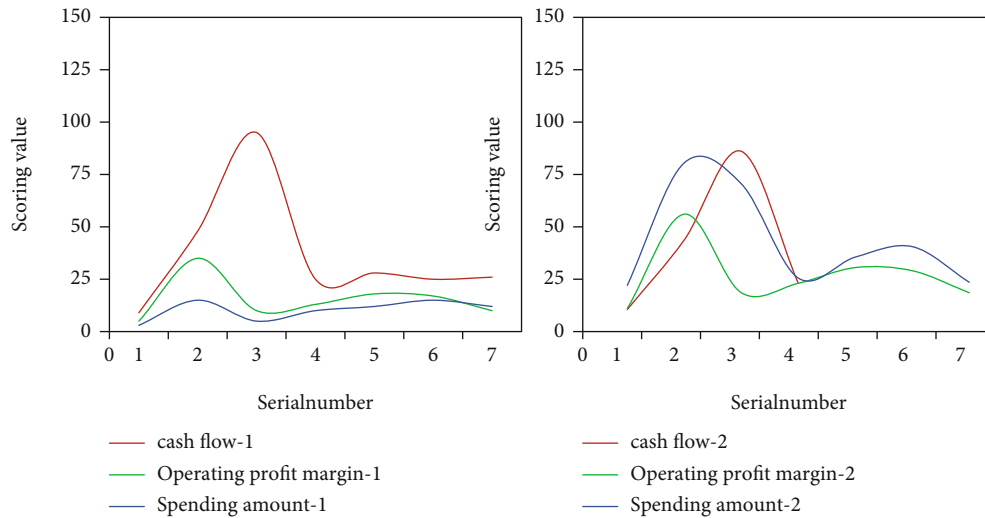


FIGURE 9: A company's financial early-warning trend chart.

the degree of crisis of the enterprise according to the development trend of the rules; quantitative analysis is to finally determine the crisis stage of the enterprise by calculating the crisis coefficient. The financial forecast of the company is shown in Figure 9.

4.1.1. Qualitative Analysis Method

- (1) If the rule is low in the antecedent and high in the latter, then the corporate crisis will be aggravated; conversely, if the antecedent is high and the latter is low, the corporate crisis will be alleviated

- (2) If the rules are always at level 1, the degree of corporate crisis is relatively light. If the rules are always at the level of 3, the degree of corporate crisis is moderate. If the rules are always at the level of 5, the company is on the verge of bankruptcy
- (3) If the regular distribution is relatively scattered, then the method of quantitative analysis is adopted

4.1.2. Quantitative Analysis Method. The comprehensive factor method is used to calculate the crisis coefficient, and the crisis coefficient formula is used to calculate the specific degree of the corporate financial crisis.

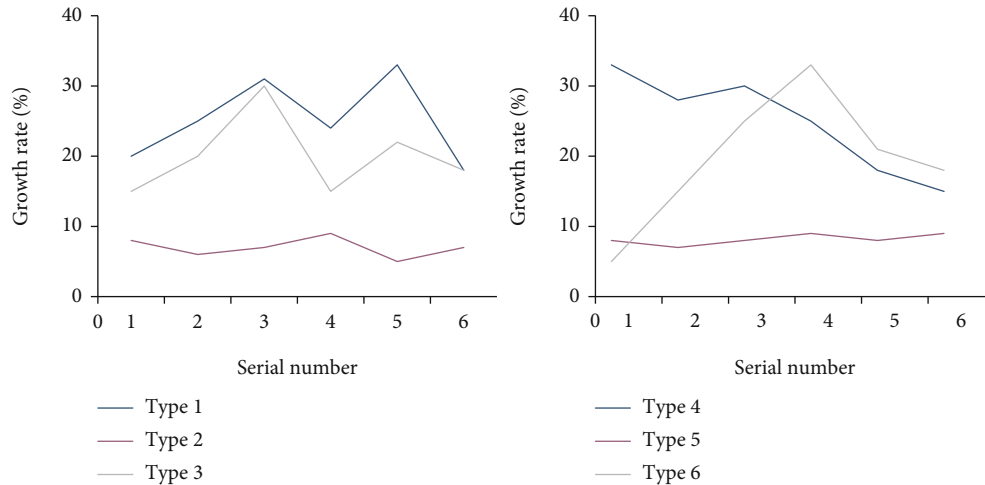


FIGURE 10: Six typical financial development trends.

In this case, the relevant personnel will determine the specific interpretation and evaluation methods based on the success or failure of the mining operation results. However, in the process of using data, analysts will want to be able to evaluate the results in order to make the data successful in the process. In the process of mining data, relevant personnel need to consider the following issues: the operating model is better than the model on the data set; the accuracy of the model is better than the accuracy of other models; the model is mainly based on the sample model, but the actual process will be far behind the mold time.

Through the comprehensive analysis of big data with interrelated rules, some large companies have realized the analysis and classification of the data obtained in the current actual test by comparing the big data with their counterparts in other industries. Highly improve the practical application, importance, and feasibility of the entire enterprise financial risk early-warning system in the analysis of data classification of the entire enterprise's financial index status information and the enterprise's financial index decision-making risk management.

4.2. Decision-Making Suggestions for Predicting Financial Crisis. This article selects six types of corporate development trends for research, mainly include the following: two years of profit after the first year of loss; two years of loss in the first two years of profit in the third year; loss of the first two years of loss in the third year; two years after the first year of profit; annual loss, profit in the first two years, loss in the third year, profit in the first two years, and profit in the third year. Generally, it can be classified into two types of trends, namely, from loss to profit and from profit to loss. The focus is on the future development and change trend of the company's losses, and the development trend chart is shown in Figure 10.

It can be seen that the company's current ratio, inventory turnover ratio, asset-liability ratio, and net sales profit are higher, and the thresholds of support and confidence are higher than 50%, indicating that the company's various financial indicators have a strong correlation with each

other. Based on the data results tested, relevant personnel can make further corresponding decisions based on the success or failure of the mining operation results and give specific explanations and evaluations. According to the actual financial indicators of various industry companies and companies in different financial industries, setting different comparison values on the threshold comparison value of the entire enterprise financial support data index table and the entire enterprise financial confidence data index threshold can be more accurate. Timely discover the abnormal situation of various financial indicators in the process of analyzing the financial status indicator information of the entire enterprise. For the staff of the company's financial department, the next step is to dig and analyze. The financial early-warning model itself, which is the operating model used in this data test, explores and analyzes whether it is truly superior to the model on the data set. It needs to be analyzed from the test results whether the accuracy of this model is better than other models, and its prediction accuracy rate of financial crisis reached 62.35%.

5. Conclusion

With the rapid development of China's capital market, enterprises are facing a fierce market competition environment, and strengthening enterprise risk management has become a topic that modern enterprises must face. This paper proposes a financial management analysis method based on wireless sensor networks and data mining and a financial crisis early-warning method based on time series dynamic maintenance. It actively explores the key factors affecting corporate financial risks, and according to the trend of changes in financial indicators, it is the company's possible financial early-warning of the crisis. It is proposed to apply association rule interactive MA (methanandamide) to enterprise financial risk analysis. This article mainly discusses the use of a financial research theory method of interactive cross-comprehensive data mining by associating multiple financial management rules, selecting a wider range of important related financial indicators in related financial

management, and comprehensively mining all related financial indicators through interaction. Based on various related financial rules, we can finally determine how to comprehensively select more and a certain international and representative important financial indicator as a risk assessment financial indicator, which is more objective than traditional analysis methods. *Real application significance*: when data mining correctly analyzes corporate financial data risks, it will go through the following main steps: data mining analysis object, data analysis preparation, establishment of analysis model, data comprehensive mining, and result data analysis. Only by doing the work of these stages correctly can the financial risks be accurately applied. In short, the establishment of a financial early-warning system can provide more unpredictability to the company's investor management and always guide the company's financial department to make more scientific and feasible project management decisions. For all employees of the company's financial department, the most important point is to be able to reflect and present relevant information about the company's true existence value in a timely manner, so that the company's senior leaders and other investors can receive early information about the company's potential important warning of financial crisis. However, this article still has some algorithm flaws. Data mining methods can be further studied to improve the efficiency of data mining to meet the needs of large-scale database mining.

Data Availability

No data were used to support this study.

Conflicts of Interest

The authors declare that they have no competing interests.

References

- [1] A. Buczak and E. Guven, "A survey of data mining and machine learning methods for cyber security intrusion detection," *IEEE Communications Surveys & Tutorials*, vol. 18, no. 2, pp. 1153–1176, 2016.
- [2] C. Helma, T. Cramer, S. Kramer, and L. De Raedt, "Data mining and machine learning techniques for the identification of mutagenicity inducing substructures and structure activity relationships of noncongeneric compounds," *Journal of Chemical Information and Computer Sciences*, vol. 35, no. 4, pp. 1402–1411, 2004.
- [3] W. Duivesteyn, A. J. Feelders, and A. Knobbe, "Exceptional model mining," *Data Mining and Knowledge Discovery*, vol. 30, no. 1, pp. 47–98, 2016.
- [4] D. A. Adeniyi, Z. Wei, and Y. Yongquan, "Automated web usage data mining and recommendation system using K-Nearest Neighbor (KNN) classification method," *Applied Computing & Informatics*, vol. 12, no. 1, pp. 90–108, 2016.
- [5] P. Wang, "Survey on privacy preserving data mining," *International Journal of Computer Science & Information Technology*, vol. 24, no. 9, pp. 1–7, 2017.
- [6] E. Lin, E. W. Sun, and M. T. Yu, "Systemic risk, financial markets, and performance of financial institutions," *Annals of Operations Research*, vol. 262, no. 2, pp. 579–603, 2018.
- [7] N. Purves, S. Niblock, and K. Sloan, "Are organizations destined to fail?," *Management Research Review*, vol. 39, no. 1, pp. 62–81, 2016.
- [8] D. Vidal-Tomas and S. Alfarano, "An agent-based early warning indicator for financial market instability," *Journal of Economic Interaction and Coordination*, vol. 15, no. 1, pp. 49–87, 2020.
- [9] Q. Wang, F. Hui, X. Wang, and Q. Ding, "Research on early warning and monitoring algorithm of financial crisis based on fuzzy cognitive map," *Cluster Computing*, vol. 22, no. S2, pp. 3689–3697, 2019.
- [10] "Construction of supply chain financial risk management mode based on Internet of Things," in *IEEE Access*, vol. 7, pp. 110323–110332, 2019.
- [11] M. N. Shad, M. Maadani, and M. N. Moghadam, "GAPSO-SVM: an IDSS-based energy-aware clustering routing algorithm for IoT perception layer," *Wireless Personal Communications*, pp. 1–20, 2021.
- [12] "Application of data mining technology in financial risk analysis," *Wireless Personal Communications*, vol. 102, no. 4, pp. 3699–3713, 2018.
- [13] "Embedded microprocessor wireless communication data collection aids in early warning of default risk for internet finance bank customers," *Journal of Sensors*, vol. 2021, 10 pages, 2021.
- [14] L. Piciullo, M. P. Dahl, G. Devoli, H. Colleuille, and M. Calvello, "Adapting the EDuMaP method to test the performance of the Norwegian early warning system for weather-induced landslides," *Natural Hazards and Earth System Sciences*, vol. 17, no. 6, pp. 817–831, 2017.
- [15] Q. Qiao and P. A. Beling, "Decision analytics and machine learning in economic and financial systems," *Environment Systems & Decisions*, vol. 36, no. 2, pp. 109–113, 2016.
- [16] J. L. Kopusko and D. A. Hershey, "When I first learned about retirement: financial and retirement concept recognition among college students," *Current Psychology*, vol. 35, no. 4, pp. 540–548, 2016.
- [17] B. G. Chae, H. J. Park, F. Catani, A. Simoni, and M. Berti, "Landslide prediction, monitoring and early warning: a concise review of state-of-the-art," *Geosciences Journal*, vol. 21, no. 6, pp. 1033–1070, 2017.
- [18] W. Dai, Y. Dong, and X. Zhang, "Competitive analysis of the online financial lease problem," *European Journal of Operational Research*, vol. 250, no. 3, pp. 865–873, 2016.
- [19] A. Cano and J. D. Leonard, "Interpretable multi-view early warning system adapted to underrepresented student populations," *IEEE Transactions on Learning Technologies*, vol. 12, no. 2, pp. 198–211, 2019.
- [20] G. Smith and N. Juria, "Diagnosis of historical inundation events in the Marshall Islands to assist early warning systems," *Natural Hazards*, vol. 99, no. 1, pp. 189–216, 2019.
- [21] A. Forkan, I. Khalil, A. Ibaida, and Z. Tari, "BDCaM: big data for context-aware monitoring—a personalized knowledge discovery framework for assisted healthcare. *IEEE Transactions on Cloud Computing*, vol. 5, no. 4, pp. 628–641, 2017.
- [22] S. Say, H. Inata, J. Liu, and S. Shimamoto, "Priority-based data gathering framework in UAV-assisted wireless sensor networks," *IEEE Sensors Journal*, vol. 16, no. 14, pp. 5785–5794, 2016.

- [23] L. M. Candanedo, V. Feldheim, and D. Deramaix, "Data driven prediction models of energy use of appliances in a low-energy house," *Energy and Buildings*, vol. 140, no. APR, pp. 81–97, 2017.
- [24] G. N. Pradhan and B. Prabhakaran, "Association rule mining in multiple, multidimensional time series medical data," *Journal of Healthcare Informatics Research*, vol. 1, no. 1, pp. 92–118, 2017.
- [25] C. J. Deepu, C. H. Heng, and Y. Lian, "A hybrid data compression scheme for power reduction in wireless sensors for IoT," *IEEE Transactions on Biomedical Circuits and Systems*, vol. 11, pp. 245–254, 2017.
- [26] S. Wan, Y. Zhang, and J. Chen, "On the construction of data aggregation tree with maximizing lifetime in large-scale wireless sensor networks," *IEEE Sensors Journal*, vol. 16, no. 20, pp. 7433–7440, 2016.

Retraction

Retracted: Research on Automobile Assembly Line Optimization Based on Industrial Engineering Technology and Machine Learning Algorithm

Wireless Communications and Mobile Computing

Received 11 July 2023; Accepted 11 July 2023; Published 12 July 2023

Copyright © 2023 Wireless Communications and Mobile Computing. This is an open access article distributed under the Creative Commons Attribution License, which permits unrestricted use, distribution, and reproduction in any medium, provided the original work is properly cited.

This article has been retracted by Hindawi following an investigation undertaken by the publisher [1]. This investigation has uncovered evidence of one or more of the following indicators of systematic manipulation of the publication process:

- (1) Discrepancies in scope
- (2) Discrepancies in the description of the research reported
- (3) Discrepancies between the availability of data and the research described
- (4) Inappropriate citations
- (5) Incoherent, meaningless and/or irrelevant content included in the article
- (6) Peer-review manipulation

The presence of these indicators undermines our confidence in the integrity of the article's content and we cannot, therefore, vouch for its reliability. Please note that this notice is intended solely to alert readers that the content of this article is unreliable. We have not investigated whether authors were aware of or involved in the systematic manipulation of the publication process.

Wiley and Hindawi regrets that the usual quality checks did not identify these issues before publication and have since put additional measures in place to safeguard research integrity.

We wish to credit our own Research Integrity and Research Publishing teams and anonymous and named external researchers and research integrity experts for contributing to this investigation.

The corresponding author, as the representative of all authors, has been given the opportunity to register their

agreement or disagreement to this retraction. We have kept a record of any response received.

References

- [1] X. Shi, W. Cui, P. Zhu, and Y. Yang, "Research on Automobile Assembly Line Optimization Based on Industrial Engineering Technology and Machine Learning Algorithm," *Wireless Communications and Mobile Computing*, vol. 2021, Article ID 2658090, 9 pages, 2021.

Research Article

Research on Automobile Assembly Line Optimization Based on Industrial Engineering Technology and Machine Learning Algorithm

Xiaorui Shi,¹ Wei Cui,¹ Ping Zhu,¹ and Yanhua Yang^{ID}²

¹Engine Factory of Sinotruk Jinan Power Co., Ltd, China National Heavy Duty Truck Group (China), Jinan 250220, China

²School of Control Science and Engineering Shandong University, Jinan 250012, China

Correspondence should be addressed to Yanhua Yang; yangyanhua@stu.ahu.edu.cn

Received 28 October 2021; Revised 16 November 2021; Accepted 18 November 2021; Published 20 December 2021

Academic Editor: Alireza Souri

Copyright © 2021 Xiaorui Shi et al. This is an open access article distributed under the Creative Commons Attribution License, which permits unrestricted use, distribution, and reproduction in any medium, provided the original work is properly cited.

Aiming at the lack of search depth of traditional genetic algorithm in automobile assembly line balance optimization, an improved genetic algorithm based on bagging integrated clustering is proposed for balance optimization. Through the integrated learning of several K -means algorithm based learners through bagging, a population clustering analysis method based on bagging integrated clustering algorithm is established, and then, a dual objective automobile assembly line balance optimization model is established. The population clustering analysis method is used to improve the intersection link of genetic algorithm to improve the search depth. The effectiveness and search performance of the improved genetic algorithm in solving the double objective assembly line balance problem are verified in an example.

1. Introduction

In today's global economy, every manufacturing company is competing fiercely in an open, continuously changing, and unpredictable global market. In the face of individualized and diversified customer needs and rapidly changing market demands, manufacturing companies must make every effort to continuously shorten product delivery times, improve product quality, reduce product prices, and provide the highest quality services to improve competitiveness, which is particularly evident for automotive manufacturers.

To improve the competitiveness of enterprises, automotive OEMs have commonly adopted the mixed-flow manufacturing technology, whose production operation control is based on the famous Just In Time (JIT) system [1] and Toyota Production System (TPS) [2]. The mixed-flow manufacturing system adopts a series of advanced management methods and technologies such as flexible process routes and kanban mechanisms to reduce production assistance time, improve production efficiency, reduce indirect costs such as logistics and inventory in production, enable the system to respond quickly to changes in market demand,

and make timely adjustments by using order-driven production and JIT methods to reduce work-in-process inventory.

Improving the productivity of the assembly line is the main focus of research in the actual production. Assembly is a process that combines manufacturing and information control, and a well-designed assembly line balancing solution can make the assembly line operate efficiently and reliably, thus improving productivity and increasing enterprise efficiency. Assembly line balancing problems are divided into three categories according to different optimization objectives [3]: (1) the optimal number of workstations with a certain production rate, (2) the optimal production rate with a fixed number of workstations, and (3) the optimal smoothing factor with a known number of workstations. The assembly line balancing problem is a typical nondeterministic polynomial problem with high requirements for the solution algorithm, which is mainly based on genetic algorithms and other heuristic algorithms in recent years.

Although the mixed-flow manufacturing system has improved and upgraded the traditional manufacturing system in many aspects such as flexible process routes, equipment layout, and inventory reduction, in order to adapt to

the changing market demand, the production mode adopts a multivariety and small-lot approach, and the system must be constantly adjusted according to the changes in demand, so the system cannot remain stable for a long time, and the production varieties brought by the production of new products and discontinuation of old products are inevitable [4]. Therefore, the system cannot remain stable for a long time, and the changes in production varieties, process flow adjustment, layout changes of assembly line stations and equipment, and material distribution system adjustment and upgrade are inevitable. Therefore, this paper takes the automotive mixed-flow assembly workshop as the application object, which is aimed at reducing costs and improving efficiency, and focuses on key issues such as the balance of the assembly and bilateral distribution lines and the optimization of internal logistics in the production workshop.

In summary, scholars have improved the genetic algorithm in terms of coding, decoding, crossover, variation, and selection, but they have not considered the improvement of the algorithm from the biological point of view that inbreeding cannot reproduce. In order to improve the search depth of the genetic algorithm, I established a bagging integrated clustering method to analyze the kinship between individuals in the population, and based on this method, I improved the crossover link of the genetic algorithm to improve the search depth of the algorithm and obtain a better feasible solution in the biobjective assembly line equilibrium optimization problem.

2. Related Work

An improved genetic algorithm based on multilevel random assignment coding is proposed for the large-scale mixed-flow U-shape assembly line balancing problem, which can accurately find the better solution of the problem while reducing the computational complexity [5]. For the assembly line balancing problem, a multiple population genetic algorithm based on feasible job sequences is proposed to expand the search space and effectively avoid the local optimum situation. The improved genetic algorithm based on hormone regulation mechanism and the selection, crossover, and variation operators are designed to solve the model of mixed assembly line balancing problem with one station and multiple products, which improves the performance of the algorithm [6]. Combined with the characteristics of genetic algorithm and mixed-flow assembly line, the initial population generation, visualization operation, crossover, and variation operation and probability setting of genetic algorithm are improved, and the population expansion mechanism is proposed to improve the global search capability of the algorithm. [7] analyzed the problem of premature maturity of traditional genetic algorithms with limited population size and proposed and implemented a hybrid genetic algorithm incorporating improved genetic operator strategy and the idea of simulated annealing. [8] designed an improved genetic algorithm based on natural number sequence and topological sorting to protect good genes by improving crossover and mutation operations when solving the model and proposed a population expansion mecha-

nism, which achieved significant results in terms of solution efficiency and solution quality. [9] proposed a stochastic assembly line equilibrium optimization method based on the station complexity measure and used an improved genetic algorithm based on the dynamic step method to optimize the solution. [10] proposed a two-population genetic algorithm and designed the coding and decoding based on the priority association matrix, as well as the fitness design, cross-selection, and variation operators, which were effective in solving the assembly line balancing problem. [11] proposed an improved bipopulation genetic algorithm for product family assembly line and also proposed a new decoding algorithm to make up for the shortcomings of traditional decoding methods, which accelerates the search speed of the algorithm.

In [12], the TALBP problem was first proposed in 1993, and a TALBP mathematical model considering the underlying constraints was given, and a heuristic algorithm using the "first adaptation principle" was designed for the model solution. In [13], a biobjective 0-1 integer programming model was proposed to solve the U-shaped bilateral assembly line balancing problem. A genetic encoding and decoding scheme for the class I bilateral assembly line balancing problem was designed, as well as a genetic operator suitable for this problem, and its applicability and scalability were discussed.

[14] developed an efficient task assignment procedure for the bilateral assembly line balancing problem, assigning a group of tasks at a time instead of one task, emphasizing maximizing work relevance, and maximizing work slack, which is particularly relevant for bilateral assembly lines. [15] developed a mathematical model for the class II bilateral assembly line balancing problem and proposed a heuristic algorithm that first groups task together based on graph depth-first search and then use a series of heuristic rules to select the group for assignment. In [16], the original genetic algorithm was improved by introducing sequences, tasks, and their operational orientations to improve the method of encoding combinations, designing crossover and variational operators adapted to the bilateral assembly line balancing problem, adjusting the encoding according to the order constraint before and after the tasks, making the solution space of the algorithm all feasible solutions, improving the efficiency of the search, and verifying the algorithm with basic arithmetic examples. [17] proposed a branch-and-bound method for the exact solution of the bilateral assembly line balancing problem. [18] designed a new branch-and-bound algorithm to solve the first class of bilateral assembly line balancing problems by first defining two opposite pairs of stations as positions, then relaxing the bilateral assembly line (TAL) to a single-sided assembly line (OAL), computing some new lower bounds for the positions, and extending the first class (OALB-1) of the one-sided assembly line balancing problem with dominant and approximate rules and incorporated them into a workstation-oriented assignment procedure for the TALB-1 problem, and experimental results show that the algorithm is effective.

[19] proposed a new ant colony-based heuristic algorithm to solve the first class of bilateral assembly line balancing problems and showed how to solve the TALB problem

using the ant colony heuristic algorithm. [20] established a mathematical model for the second type of TALBP problem and proposed a new genetic algorithm for model solving, in which local search and steady-state reproduction strategies are used to promote population diversity and improve the efficiency of the search.

[21] proposed a forbidden search algorithm that integrates two optimization objectives, line efficiency, and smoothness, for the TALBP problem, and computational results show that the algorithm performs well. [22] established a mathematical planning model to formally describe the bilateral assembly line balancing problem and proposed an ant colony optimization algorithm to solve this problem, in which two ants work simultaneously on both sides of the line to obtain a solution that verifies the sequential order, operation orientation, area, and synchronization constraints in the assembly process, and the computational results of numerical examples demonstrate its superior performance. [23] studied that in real life, especially in manual assembly lines, tasks may have different execution times and task time variations may be caused by machine failures, loss of motivation, lack of training, unqualified operators, complex tasks, environments, etc. The stochastic task time bilateral assembly line balancing problem is investigated, a chance constrained segmented linear mixed integer programming (CPMIP) is proposed to model it, a simulated annealing algorithm is designed to solve it, and the computational results show the effectiveness of the CPMIP and SA algorithms.

3. Overview of Automotive Mixed-Flow Production Systems

3.1. Definition and Characteristics of Mixed-Flow Production. Mixed-flow production is a scientific production method that takes into account the variety, equipment load, output, and working hours. It is able to arrange the production sequence scientifically on an assembly line for multiple product varieties with high similarity of process flow and production operation methods and implement rhythmic and proportional mixed continuous flow production. Compared with a single product line, the mixed-flow production system has higher flexibility and has been widely used in the automotive and home appliance industries.

The mixed-flow manufacturing model is generally based on the traditional Just-In-Time (JIT) ideological principle, which requires that the required parts arrive where they are needed, in the required quantity, at the required moment, with the following key features:

- (1) *Customer Demand Pull Drive.* In order to respond quickly to customer demand and improve the ability to adapt to changes in customer demand, the daily production schedule on the mixed-flow line is updated according to the amount of customer demand and variety combinations, and the daily production schedule is optimally sequenced to achieve balanced production line capacity, with the entire production pulled by the final assembly process.

- (2) *Linear Manufacturing.* This reduces the WIP queue, reduces production bottlenecks, and smooths out demand fluctuations.
- (3) *Beat-Based (TAKT) Production.* The production line beat is determined based on the production time on the mixed-flow line, and the production cycle time is the same for each station, thus smoothing production and eliminating production bottlenecks.
- (4) *Total Quality Management.* Total quality management is implemented on the production line, and quality inspection is performed by production personnel in the relevant processes. Quality inspection is closely integrated with the production process, enabling timely detection of problems, significantly reducing scrap and rework, and ensuring high quality products at the lowest cost.
- (5) *Just-In-Time Replenishment System.* Materials are sent directly to the consumption point on demand and on time, and material replenishment is driven by kanban signals, which can reduce the capital occupation of raw material inventory, ensure strategic partnership with suppliers, guarantee high quality and low cost, and significantly improve inventory turnover rate.

3.2. Process Flow of Automotive Mixed-Flow Production. The automotive assembly line system is generally an organic whole composed of conveying equipment (air suspension and ground) and specialized equipment (such as lifting, turning, press fitting, heating or cooling, testing, and bolt and nut fastening equipment), including complete vehicle assembly line (process chain, driven by multiple motors), body conveyor line, reserve line, and lift. The automotive mixed-flow assembly line is large in scale, with many stations, equipment, and personnel, and is generally divided into a main assembly line and several subassembly lines [24].

4. Clustering Analysis of Populations Based on Bagging Integrated Clustering

In order to improve the search depth of the genetic algorithm, the author proposes a bagging integrated clustering algorithm, which integrates several K -means algorithm-based learners with bagging, and after a voting mechanism, the class to which each population individual belongs.

4.1. K-Means Clustering Algorithm. The K -means algorithm is based on the principle of minimizing the sum of squares of the distances from all samples of the cluster to the cluster center and is the classical hard clustering algorithm.

The clustering criterion function used by the K -means clustering algorithm is the error sum-of-squares criterion:

$$J_k = \sum_{j=1}^K \sum_{k=1}^{n_j} \|x_k - m_j\|^2. \quad (1)$$

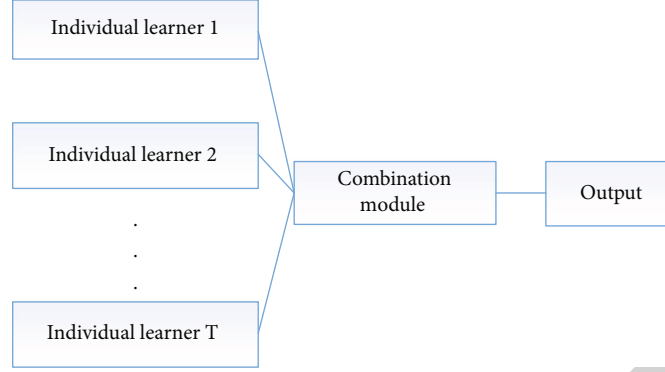


FIGURE 1: Structure of integrated learning.

To optimize the clustering results, the criterion should be minimized.

In the first step, given n mixed samples, let $I = 1$, which denotes the number of iterations, and K initial aggregation centers are selected $Z_j(I), j = 1, 2, \dots, K$.

In the second step, calculate the distance of each sample from the aggregation center $D(x_k, Z_j(I)), k = 1, 2, \dots, n, j = 1$.

If $D(x_k, Z_j(I)) = \min$ and $D(x_k, Z_j(I)), k = 1, 2, \dots, n$, then $x_k \in w_i$.

In the third step, K new aggregation centers are calculated, $Z_j(I + 1) = 1/n \sum_{k=1}^{n_i} x_k^{(j)}, j = 1, 2, \dots, K$.

In the fourth step, determine if $Z_j(I + 1) \neq Z_j(I), j = 1, 2, \dots, K$; then, assign $I + 1$ to I and return to step 2; otherwise, the algorithm ends.

The author's K -means clustering algorithm adopts a batch processing method to select and adjust the initial classification, and the representative point is the clustering center. After selecting a batch of representative points, the distance from other samples to the clustering center is calculated, and all samples are grouped into the nearest center point to form the initial classification, and then, the clustering center is recalculated.

4.2. K-Means Integration Clustering

4.2.1. Integrated Learning. Integrated learning is a combination of learning using several learners. Several individual learners are selected first and then combined using some combination methods. Many classical machine learning algorithms, such as the random forest method, are built using integrated learning. The random forest method is integrated by several decision tree algorithms, and such individual learners are called base learners. The integration learning structure is shown in Figure 1.

4.2.2. Bootstrap. To obtain an integration with high generalization performance, the individual learners in the integration should be as independent as possible from each other. Bootstrap is a resampling technique in statistical learning, and this seemingly simple approach has had a profound impact on many subsequent techniques. Methods such as bagging and AdaBoost in machine learning actually embody the idea of Bootstrap.

In statistics, one is faced with a sample, which has significant uncertainty. It is because of the existence of uncertainty that statistics can live and die, and the meaning of statistics is to infer the total from the sample. The Bootstrap method was originally proposed by Efron, a professor of statistics at Stanford University, in 1977. As a new statistical method for augmenting samples, the Bootstrap method provides a good idea for integrated learning of sampling.

4.2.3. Bagging. Bagging is the most famous representative of the parallel integrated learning method. Given a data set with sample size n , a sample is first randomly taken out and put into the sampling set and then put back into the initial data set so that the sample may still be selected in the next sampling. Some samples in the initial training set appear in the sampling set several times, while some never appear. Repeating the sampling process T times, we obtain T Bootstrap samples with sample size ν , denoted as $D_i = (x_1, x_2, \dots, x_\nu), i = 1, 2, \dots, T$.

The basic process of bagging is to sample T sets of ν training samples, then train a base learner based on each set, and then combine these base learners. When combining the results, bagging usually uses the voting principle.

4.2.4. K-Means Integrated Clustering Algorithm. K -means clustering algorithms are unsupervised learning in machine learning, i.e., they use unlabeled data for learning. Integration learning uses multiple base learners to reduce the bias and variance in the generalization error of the model. Combining the above two concepts is unsupervised integration learning, i.e., using integration algorithms on unlabeled data.

Combining K -means with bagging to generate K -means integrated clustering algorithm, the specific flow of the algorithm is shown in Figure 2.

In the first step, the initial training set is randomly sampled ν times with put-back in a Bootstrap manner, and the sampling process is repeated $T - 1$ times to sample $T - 1$ bootstrap sets containing ν training samples, denoted as $D_i = (x_1, x_2, \dots, x_\nu), i = 1, 2, \dots, T - 1$.

In the second step, since there are unsampled samples, when each sample needs to be categorized, all the remaining unsampled w samples need to be taken out to form the last sample set, denoted as $D_T = (x_1, x_2, \dots, x_w)$; then, the total sample set is denoted as follows:

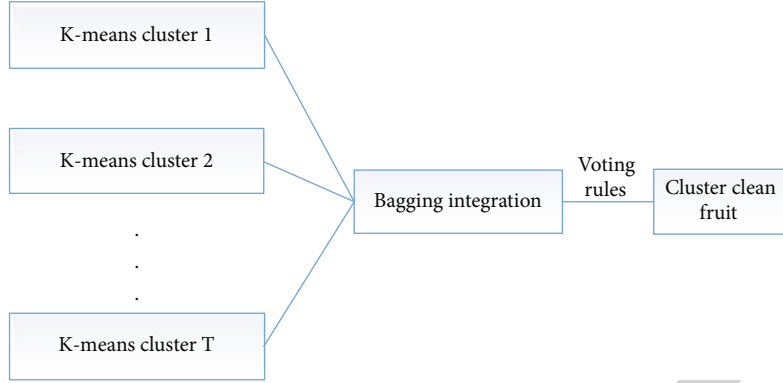


FIGURE 2: K-means integrated clustering algorithm flow.

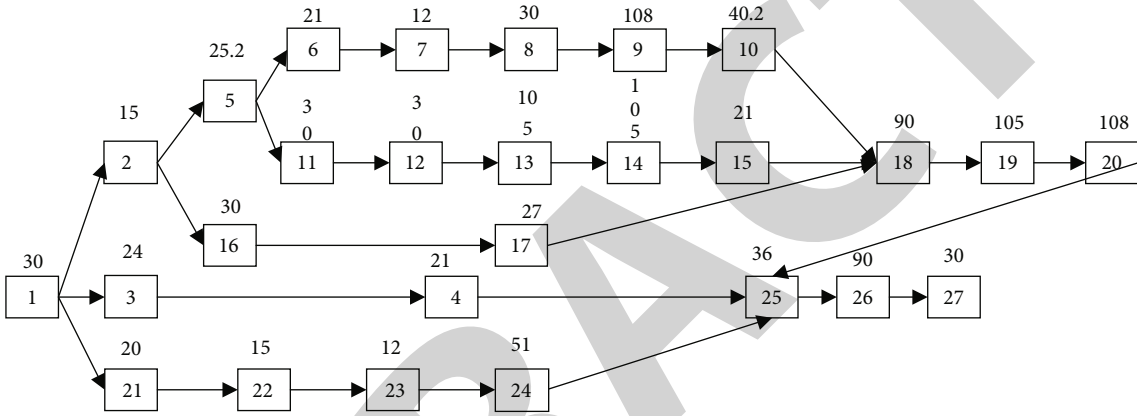


FIGURE 3: Priority relationship of automobile gearbox assembly.

$$D_i = \begin{cases} (x_1, x_2, \dots, x_v) & i = 1, 2, \dots, T - 1, \\ (x_1, x_2, \dots, x_w) & i = T. \end{cases} \quad (2)$$

In the third step, the T sample sets are individually trained with K -means base learners for clustering; let the initial training set sample number be z and the number of clustering categories be K . A $z \cdot K$ dimensional matrix is established to record the voting of each individual learner for each sample clustering category, and the number s in column j of row i indicates that there are s base learners classifying the i th sample as the j th category.

In the fourth step, the final clustering category of each sample is decided according to the established $z \cdot K$ dimensional matrix according to the voting rule. The final category of the sample is determined by the category with the highest number of votes, and if there are categories with the same number of votes, one of them is randomly selected as the final clustering category of the sample.

5. Mathematical Model for Biobjective Assembly Line Equilibrium Optimization

The author establishes a biobjective assembly line equilibrium optimization model with the constraints of fixed num-

ber of workstations and priority relationship of job elements and the assembly line production beat and smoothing factor as the optimization objectives.

5.1. Binding Conditions. C is the production beat, I is the set of job elements, J is the set of workstations, n is the number of job elements, m_i is the actual number of workstations for the i th individual in the population, M is the number of identified workstations, j_k is the set of job elements for the k th workstation, and $k \in (1, M)$.

X is a one-dimensional vector, which represents the ordering of each assembly operation element. If $\mathbf{x} = [x_1, x_2, \dots, x_n]$, x_i satisfying all constraints is the feasible solution. X is an $n \cdot m$ -dimensional matrix, representing the allocation of each assembly operation element on the workstation. For $X(i, k) \in \mathbf{X}$, if $X(i, k) = 1$, it means that the assembly operation element I is allocated on the workstation K . If $X(i, k) = 0$, it indicates that the assembly operation element I is not assigned to workstation K . \mathbf{P}_{Pred} is $n \times 2$ -dimensional priority relation set, and $\mathbf{P}_{\text{Pred}}(i, 1)$ is the preorder operation element of $\mathbf{P}_{\text{Pred}}(i, 2)$. P is the $n \cdot n$ -dimensional priority relation matrix. For $p(k, i) \in p$, if $p(k, i) = 1$, it means that K is the preorder operation element of I . If $p(k, i) = 0$, it indicates that K is a subsequent job element of I . t_i is the operation time of the i th operation element.

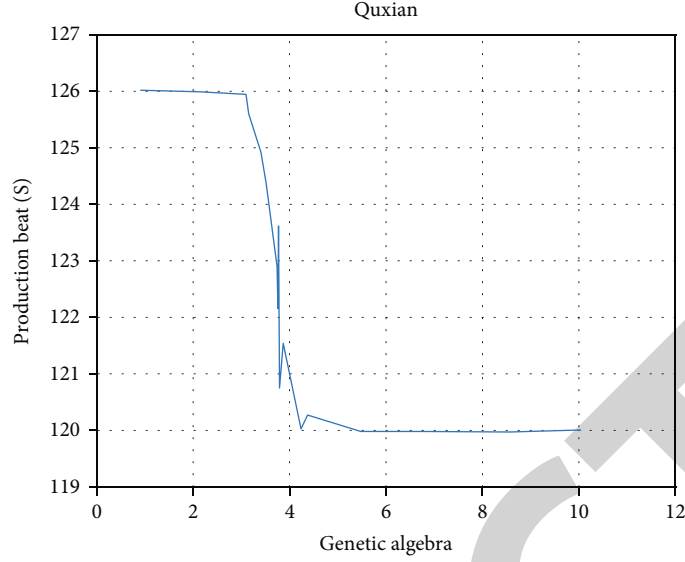


FIGURE 4: Production beat optimization process.

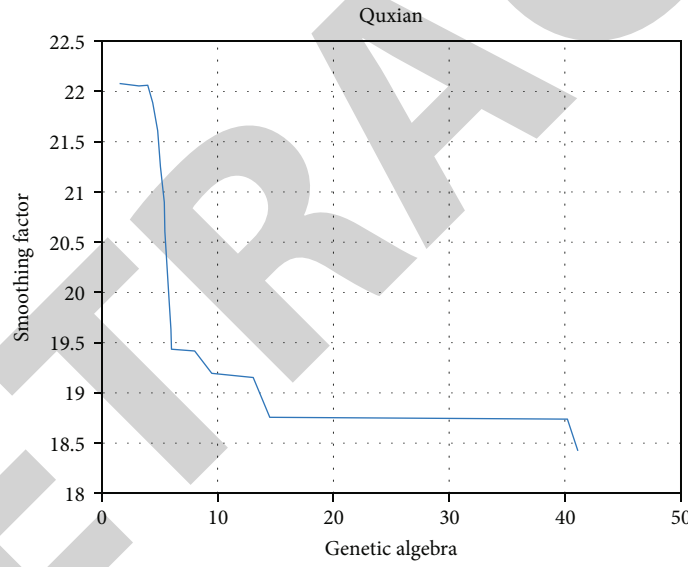


FIGURE 5: Smoothing factor optimization process.

In the actual production of enterprises, the assembly line has often been established. If it is reconstructed or expanded, the cost is high, so the number of workstations is certain.

Each job element can only be assigned to one workstation, i.e.,

$$\sum_{k=1}^M X(i, k) = 1 \quad i = 1, 2, \dots, n. \quad (3)$$

To allocate job elements under the condition of meeting the priority relationship, i.e.,

$$\sum_{k=1}^M k[X(a, k) - X(b, k)] \leq 0 \quad \forall (a, b) \in \mathbf{P}_{\text{Pred}}. \quad (4)$$

The total operation time of each workstation is less than or equal to the production beat, i.e.,

$$\sum_{i=1}^n t_i X(i, k) \leq C \quad k = 1, 2, \dots, M. \quad (5)$$

The number of workstations is certain, i.e.,

$$m_i = M \quad \forall i \in (1, 2, \dots, n). \quad (6)$$

TABLE 1: Assignment scheme for job element 1.

Workstation	Contains job elements	Optimized production beat/S	Smoothing factor
1	1, 2, 16, 5		
2	11, 21, 22, 12		
3	17, 6, 7, 8		
4	13		
5	14		
6	9		
7	10, 3, 15, 23	120	18.3573
8	18		
9	19		
10	20		
11	24, 4, 25		
12	26, 27		

TABLE 2: Assignment scheme for job element 2.

Workstation	Contains job elements	Optimized production beat/S	Smoothing factor
1	1, 2, 5, 11		
2	16, 17, 3, 6		
3	21, 12, 7, 8		
4	9		
5	13		
6	14		
7	10, 22, 23, 15	120	18.3899
8	18		
9	19		
10	20		
11	24, 4, 25		
12	26, 27		

5.2. *Optimization Goals.* The author chooses the optimization objectives as the production beat C and the smoothing factor s_i , because reducing the production beat C can play a role in reducing the total idle time, while the smoothing factor s_i is an index to evaluate the load balance of the assembly line, which serves to improve the utilization of personnel and equipment. The optimization objective is defined as $\min c, \min s_i$.

The production beat C is defined as the maximum value of the workstation operating time and is the operating time of the k th workstation; then, we have T_k .

$$C = \max T_k \quad k \in (1, M). \quad (7)$$

The smoothing factor s_i is as follows:

$$S_I = \sqrt{\frac{\sum_{k=1}^M [T(k) - C]^2}{M}}. \quad (8)$$

6. Example Analysis

In order to verify the depth search capability of the author's algorithm, an automotive transmission assembly line is used as an example for the equilibrium optimization of this assembly line. The automobile transmission assembly body consists of three main parts, the number of operational elements $n = 27$, and the priority relationship is shown in Figure 3. The workstations of the assembly line are already established, with the number of workstations $M = 12$, which would be costly to modify or expand. The equilibrium optimization of this assembly line is carried out with the constraint that the number of workstations is fixed at $M = 12$, and the production beat C and the smoothing factor SI are used as the optimization objectives, and the proposed improved genetic algorithm is used to solve the problem and improve the search depth.

6.1. *Biobjective Optimization Solution.* MATLAB 2015b was used to program the solution, and the parameters of the

TABLE 3: Comparison of solutions.

Parameter	Production beat/S	Smoothing factor
$T = 5, v = 60, K = 3$	120	18.3573
$T = 5, v = 80, K = 5$	120	18.2672
$T = 7, v = 60, K = 5$	120	18.4307
$T = 7, v = 80, K = 3$	120	18.4062
Not improved	120	19.7127

mathematical model were set as follows: fixed number of workstations $M = 12$, crossover probability $P_c = 0.6$, variation probability $P_m = 0.05$, number of genetic generations $G = 50$, number of populations $S = 200$, and initial value of production beat $C = 130$ s.

When $T = 5, v = 60$, and $K = 3$ are set, the optimization processes of production beat C and smoothing factor SI are shown in Figures 4 and 5, respectively. The optimization process records the optimal values of C and SI in each generation of the population.

As can be seen in Figures 4 and 5, both objectives are optimized. The production beat optimization is relatively easy, and the final optimized value is obtained within 5 generations. The smoothing factor is continuously optimized and converges after 40 generations without premature convergence. Some representative and excellent solutions are selected and shown in Tables 1 and 2.

As can be seen from Tables 1 and 2, both the production beat C and the smoothing factor SI are optimized to improve the assembly efficiency and reduce the total idle time, and the algorithm performs a deep search for feasible solutions and optimizes several better solutions.

6.2. *Program Comparison.* The improved genetic algorithm based on bagging integrated clustering has different search depths for different settings of the main parameters, including T, v , and K . To demonstrate that the improved genetic algorithm does improve the search depth, a comparison test is performed with different settings of the parameters. The

first is to optimize the genetic algorithm given different T , v , and K , and the second is to use the unimproved genetic algorithm to solve the problem. The solution with the smallest sum of the two objective values is taken as the representative for multiple comparison tests, and the comparison results are shown in Table 3.

From the analysis in Table 3, it can be seen that the optimized solution of production beat C is the same for each group of experiments, while the optimized solution of smoothing factor SI is different, which indicates that from the perspective of a single optimization objective, the optimization of production beat is easier, while the optimization of smoothing factor is more difficult, and the search depths are different for different parameter settings. Comparing the results of each group of experiments, the optimized solutions with the improved genetic algorithm do not have the same results under different parameter settings, and the search depths are different; on the whole, the optimized solutions with the improved genetic algorithm are significantly better than the unimproved genetic algorithm. In summary, the improved genetic algorithm based on bagging integrated clustering has a deeper search depth and can obtain better solutions than the unimproved genetic algorithm.

7. Conclusions

The author established a population clustering analysis method based on the bagging integrated clustering algorithm from the perspective of the fact that close relatives cannot cross over in biology, used this method to determine whether two individuals in a population are close relatives, and then improved the crossover rule of the genetic algorithm. A dual-objective assembly line balancing model was developed with production beat and smoothing factor as the optimization objectives, and the improved genetic algorithm was applied to the dual-objective assembly line balancing example. The example shows that the improved genetic algorithm effectively improves the depth-seeking ability of the algorithm compared with the unimproved genetic algorithm.

Data Availability

The datasets used during the current study are available from the corresponding author on reasonable request.

Conflicts of Interest

The authors declare that they have no conflicts of interest.

References

- [1] Y. Wang and O. Yang, "Research on industrial assembly line balancing optimization based on genetic algorithm and witness simulation," *International Journal of Simulation Modelling*, vol. 16, no. 2, pp. 334–342, 2017.
- [2] S. R. Yadav, N. Mishra, V. Kumar, and M. K. Tiwari, "A framework for designing robust supply chains considering product development issues," *International Journal of Production Research*, vol. 49, no. 20, pp. 6065–6088, 2011.
- [3] J. R. Jadhav, S. S. Mantha, and S. B. Rane, "Development of framework for sustainable Lean implementation: an ISM approach," *Journal of Industrial Engineering International*, vol. 10, no. 3, p. 72, 2014.
- [4] J. Wang, Y. Di, and X. Rui, "Research and application of machine learning method based on swarm intelligence optimization," *Journal of Computational Methods in Sciences and Engineering*, vol. 19, no. 2, pp. 179–187, 2019.
- [5] M. Busogi and N. Kim, "Analytical modeling of human choice complexity in a mixed model assembly line using machine learning-based human in the loop simulation," *IEEE Access*, vol. 5, pp. 10434–10444, 2017.
- [6] Z. Dan, "Part recognition method based on visual selective attention mechanism and deep learning," *Journal of Fiber Bioengineering & Informatics*, vol. 8, no. 4, 2018.
- [7] M. Fathi, M. J. Alvarez, F. Hassani Mehraban, and V. Rodríguez, "A multiobjective optimization algorithm to solve the part feeding problem in mixed-model assembly lines," *Mathematical Problems in Engineering*, vol. 2014, Article ID 654053, 12 pages, 2014.
- [8] S. A. Torabi, S. M. T. Fatemi Ghomi, and B. Karimi, "A hybrid genetic algorithm for the finite horizon economic lot and delivery scheduling in supply chains - ScienceDirect," *European Journal of Operational Research*, vol. 173, no. 1, pp. 173–189, 2006.
- [9] T. Xie, C. Zhang, Z. Zhang, and K. Yang, "Utilizing active sensor nodes in smart environments for optimal communication coverage," *IEEE Access*, vol. 7, pp. 11338–11348, 2019.
- [10] W. Zhang and M. Gen, "An efficient multiobjective genetic algorithm for mixed-model assembly line balancing problem considering demand ratio-based cycle time," *Journal of Intelligent Manufacturing*, vol. 22, no. 3, pp. 367–378, 2011.
- [11] Z. Yang, W. Xu, P. K. Wong, and X. Wang, "Modeling of RFID-enabled real-time manufacturing execution system in mixed-model assembly lines," *Mathematical Problems in Engineering*, vol. 2015, Article ID 575402, 15 pages, 2015.
- [12] B. Nelson and M. Donath, "Optimizing the location of assembly tasks in a manipulator's workspace," *Journal of Robotic Systems*, vol. 7, no. 6, pp. 791–811, 1990.
- [13] Q. Tang, Y. Liang, L. Zhang, C. A. Floudas, and X. Cao, "Balancing mixed-model assembly lines with sequence-dependent tasks via hybrid genetic algorithm," *Journal of Global Optimization*, vol. 65, no. 1, pp. 83–107, 2016.
- [14] Z. Zhang, C. Zhang, M. Li, and T. Xie, "Target positioning based on particle centroid drift in large-scale WSNs," *IEEE Access*, vol. 8, pp. 127709–127719, 2020.
- [15] C. H. Cao, Y. N. Tang, D. Y. Huang, W. M. Gan, and C. Zhang, "IIBE: an improved identity-based encryption algorithm for WSN security [J]. Security and Communication," *Networks*, vol. 2021, article 8527068, 8 pages, 2021.
- [16] D. Wu, C. Zhang, L. Ji, R. Ran, H. Wu, and Y. Xu, "Forest fire recognition based on feature extraction from multi-view images," *Traitement du Signal*, vol. 38, no. 3, pp. 775–783, 2021.
- [17] L. Wang, C. Zhang, Q. Chen et al., "A communication strategy of proactive nodes based on loop theorem in wireless sensor networks," in *2018 Ninth International Conference on Intelligent Control and Information Processing (ICICIP)*, pp. 160–167, Wanzhou, China, 2018.

Research Article

Computer Digital Technology-Based Educational Platform for Protection and Activation Design of Ming Furniture

Zhe Peng¹ and Yichen Du²

¹The School of Design, China Academy of Art, Hangzhou, 310012 Zhejiang, China

²Experimental Teaching Department, China Academy of Art, Hangzhou, 310012 Zhejiang, China

Correspondence should be addressed to Zhe Peng; 0103034@caa.edu.cn

Received 30 October 2021; Revised 22 November 2021; Accepted 30 November 2021; Published 17 December 2021

Academic Editor: Mu-Yen Chen

Copyright © 2021 Zhe Peng and Yichen Du. This is an open access article distributed under the Creative Commons Attribution License, which permits unrestricted use, distribution, and reproduction in any medium, provided the original work is properly cited.

Chinese Ming-style furniture is the first of the three major furnitures in the world, which has high artistic value and complete structural system. The protection of Ming-style furniture and making its design show vitality that has always been a research topic in China and even in the world. Based on 3D virtual simulation technology, this paper uses 3D scanning reverse data acquisition technology and intelligent operation of computer engine to realize big data simulation and develops the design software of Ming furniture. By means of computer information technology, we interpret and present the structural thinking and design concept of Ming furniture and transform it into design program software. This has formed a system-wide educational software operation platform for knowledge reserve, thinking training, design and application, and achievement transformation. By applying the mechanism strategy of production and teaching to the talent training plan of colleges and universities, the underlying logic of talent training, technical management, and production management that can open up the innovative industry of Ming furniture is also constructed. After experimenting with the platform software, students are able to understand the relationship between the structure and form of Ming furniture and can design new styles that fit the logic of Ming furniture shapes as they prefer.

1. Introduction

Chinese Ming furniture is one of the top three pieces of furniture in the world, with high artistic value and a complete construction system. The conservation and design revitalization of Ming furniture has been a research topic in China and the world. There is a need to develop learning software for Ming-style furniture by relying on Chinese cutting-edge computer soft-computer and Internet technologies. Applying the software to the teaching experiment platform of the national higher education institutions will become an important means and motivation for the protection of cultural heritage of classical furniture and technological innovation of related cultural and creative industries. At the same time, this is also an important research direction for production and teaching. This paper introduces and elaborates on the platform construction, development ideas, technical support, and innovations of this software, thus forming a

system-wide educational software operation platform of knowledge reserve, thinking training, design application, and result transformation. In a practical sense, it also builds the underlying logic that can open up the talent training, technology management, and production management of the Ming furniture innovation industry.

2. The Platform Construction

Ming furniture construction is the unity of science and technology, a perfect combination of practicality and aesthetics, the key content and key to the study of classical Chinese furniture [1]. Frontier technology development and application have promoted technological innovation in cultural heritage conservation and related cultural and creative industries and become an important research direction for industry-academia research [2]; so, educational software development based on digital technology for the conservation and

revitalization design of Ming-style furniture is of great practical significance [3]. The educational experiment platform is divided into three sections: (1) learning in virtual exhibition hall, (2) construct knowledge learning, (3) innovative design experiment, and (4) model output (Figure 1).

Learning in virtual exhibition hall: through 20 pieces of digital reconstruction virtual simulation models of classical furniture, we can observe and learn the shape and structure of traditional furniture. Using 3D modeling and dynamic design, it supports the observation from the first perspective and realizes the observation experience of classic furniture entities handed down from ancient times, and the traditional teaching cannot realize the observation of the internal structure of classic furniture. At the same time, it supports the explosive structure decomposition and aggregation of the whole furniture. Structural symbols are the main constituent elements of the Ming furniture modeling symbol system, which mainly includes two symbol types: mortise and tenon and component [4]; so, the system will support the information prompt of each furniture component and mortise and tenon structure. This truly realizes the teaching resources and digital protection of virtual simulation (Figure 2).

Construct knowledge learning: mortise and tenon construction is the best part of traditional Chinese furniture and is the earliest description of scientific design in China [5]. Ming-style furniture is the pinnacle of the development of mortise and tenon technology [6]. It is divided into two parts: component recognition and whole device recognition. The modeling principle of Ming-style furniture lies in the relationship between the structure and form of the main components; that is, the structural mode of the core plate forms the basic form: (1) interactive learning of component recognition. Through interactive software operation, we can clearly and intuitively understand and identify the names of various components and the operation rules of mortise and tenon: (2) interactive experiment of whole device recognition. Through interactive software, the names and loading sequence of components and mortise and tenon nodes of the whole device are recognized. Thus, students can understand the key elements of modeling, that is, component modules and construction methods (Figure 3).

Innovative design experiment: according to the computer “Ming-style furniture structure module system,” students enter the preset chair basic knot module system, design and reorganize according to the preset basic structure module and selection sequence, and design a new shape model based on Ming-style furniture knot law.

Output of renderings and models: the innovative furniture form system automatically generates 3D renderings and model data, which is compatible with 3D printing equipment and outputs proportional solid models. And the system can automatically generate the corresponding mortise and tenon structure of the 3D file, from the design drawings to the object of seamless transformation.

3. Development Ideas

Since the mortise and tenon structure is relatively stable and has the characteristics of standardized design, the parametric

design work is also feasible [1]. The development of Ming furniture design software is based on the principle of the relationship between the shape and structure of Ming furniture itself, refines a form design thinking method which conforms to the existing classical shape structure law, and then transforms it into a computer virtual simulation digital module through digital acquisition. And based on the specific design algorithm, arrange reasonable experimental steps and automatically generate digital innovation results. The function of the parametric design of Ming furniture components is to realize the modular programming of the characteristic relations of furniture components with general standardization characteristics in order to achieve the function of computer-aided design [7].

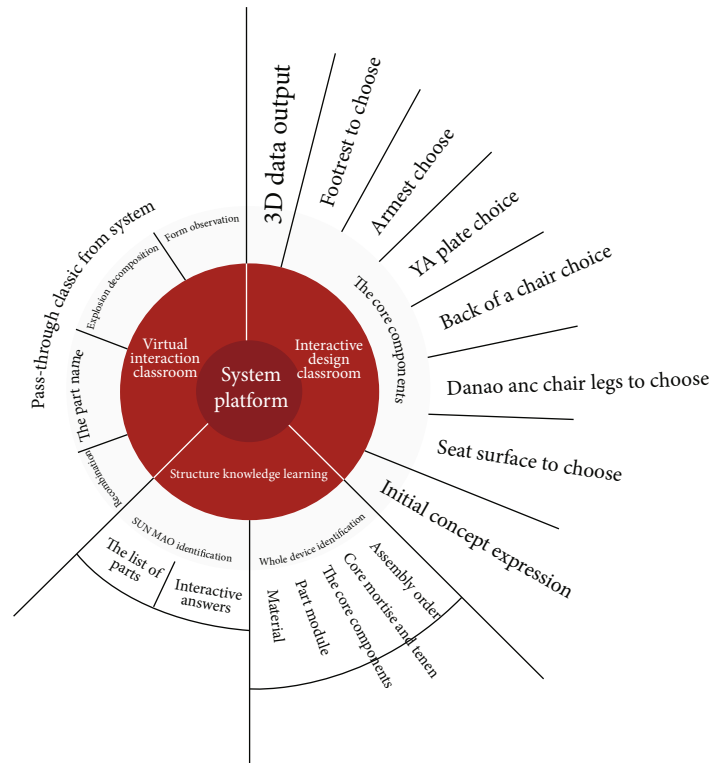
3.1. Principle of Software Development. The principle of design thinking method is the unified relationship between furniture structure and shape. The reason why Ming furniture became Ming furniture system is the clue of its structure and form development. This clue is based on the orderly construction of several core structural modules, and the shape of each furniture is based on the combination and arrangement of several structural modules. Mastering the logical relationship between Ming furniture form and knot module is very important to identify the core components of a piece of furniture and can quickly interpret which components a whole piece can be decomposed into. On the contrary, designing a piece of Ming furniture is an orderly construction of core components, which is the principle of computer software development [8].

3.2. Principle of Computer Software Experiment. The principle of “interactive innovative design” is divided into four parts: preset core knot module, orderly construction, generation of mortise and tenon nodes, and renderings and generation of 3D models.

Preset the core knot module: based on chairs, we have a deep understanding of Ming furniture. 1000 pieces of chairs furniture samples are divided into 7 basic modules by summarizing the core modules. Each module extracts a number of corresponding typical forms, which become preset options.

Build in an orderly manner: each furniture core module corresponds to the furniture components. In the assembly of furniture, it is required to build in an orderly manner, which is interlocking. Only in this way can a stable frame system be formed. The computer sets the correct shape selection steps to conform to the assembly principle of each piece of furniture, which is the key to design a reasonable supporting frame [9]. At each step of the student’s choice, the computer will calculate the corresponding result and show it as an effect, and at the final completion, the computer will present the calculated result as a 360-degree 3D effect that can be operated in a circular view.

Generate mortise and tenon nodes: the core components of each piece of furniture will form important mortise and tenon nodes, such as the seat surface of a chair, and there will be mortise and tenon nodes with “lattice corners, edges and grooved panels.” The opening mode of mortise and



Ming-style furniture protection and activation virtual simulation experiment

FIGURE 1: The experiment platform mind mapping.

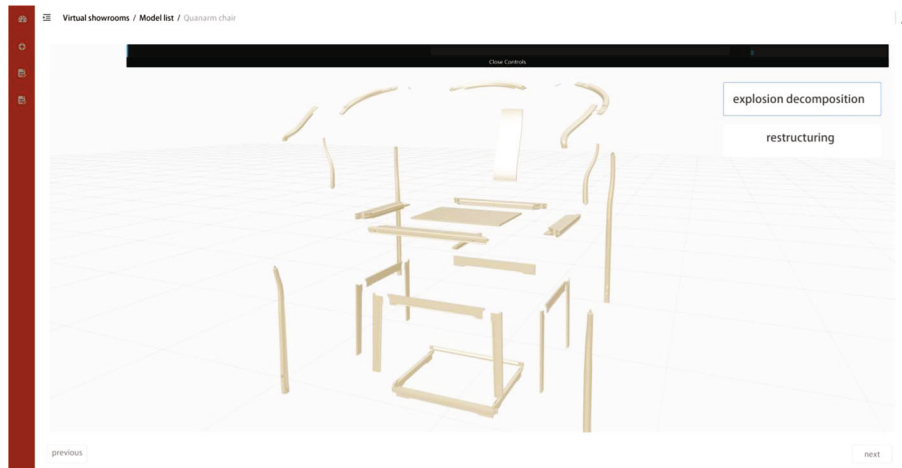


FIGURE 2: Virtual showroom plate.

tenon is just like the design idea of Kong Mingsuo and how to open and buckle is the design principle of mortise and tenon joint. The 3D modeling of mortise and tenon structure is also completed in each core module preset by the system, and the model is inserted into the shape selection link directly through the code.

Renderings and 3D models: at present, the generation of experimental results is completed by means of result simulation; that is, all the permutation and combination results are judged and calculated in advance, and their renderings and

3D models are placed in the program code in advance. Taking the chair innovative design experiment as an example, at present, more than 3,000 preset innovative forms have been calculated from 6 core modules. And along with the increase of options in each component module, the number of dimensional results will be generated (Figure 4).

On the whole, the logic of morphological innovation is to combine different morphological modules according to the building steps: collecting the modular forms of the same parts of furniture of the same shape, screening and inducing

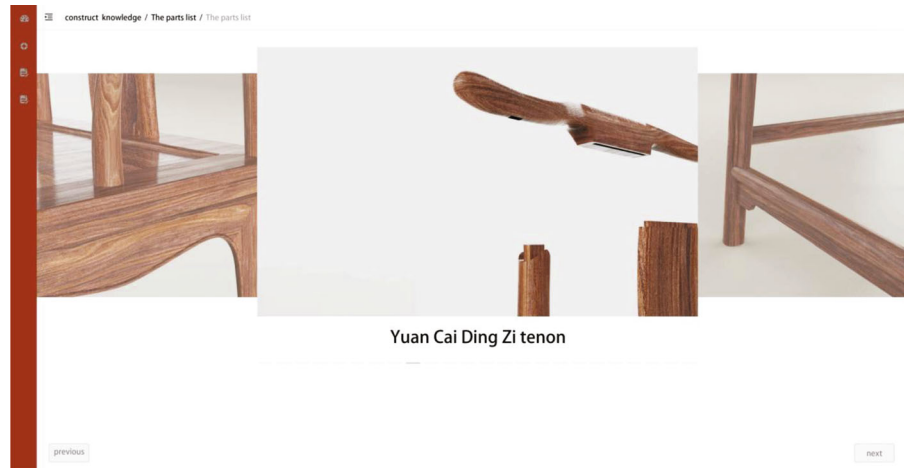


FIGURE 3: Construct knowledge plate.

the parts options, and then selecting the shapes of furniture parts according to steps. After different selections, arrangements, and combinations, more and more new forms can be formed. These forms conform to the internal modeling clues of Ming furniture. Morphology argues that modal design as a design thinking and design style should establish a deeper interaction between the object and the user as a certain design requirement [10]. Interactive experiments enable everyone to set up according to their own aesthetic requirements and finally create unique Ming furniture that conforms to the standard.

3.2.1. Scoring Method. In the scoring, the first part of “Virtual Showroom Learning” is to learn and observe the basic knowledge in order to respond to the interactive questions in the subsequent part, not involving experimental questions, but requiring students to use the content and interactive buttons of each showroom. In addition, a basic reading time was set in each furniture hall to monitor the students’ observation of all the contents, and points would be deducted for omissions and insufficient time.

The second part, “construction knowledge learning”, has several experimental projects, and each experiment is performed step by step. If there is a wrong operation, the system will prompt the error and re-experiment until the correct operation and completion of all steps. Each experiment will deduct the corresponding points for each wrong answer.

The third part, “Innovative Design Experiment”, gives students a visual representation of the design results, and the results are scored collectively by the instructor and other students, which are scored in a subjective manner. The fourth part, “3D printing output”, is given as an extra point. The final score of all four sections was combined to form each student’s grade.

Comparative observations of experimental data from each student’s four parts will be made, with the focus on the second part of the phenomenon. The difference of scores in the second part will show the difference of mastery of construction principles and order among students, clarify the difficulty of teaching, and give suggestions to students for follow-up. The data of the third part can show the popularity

of the form and get the ranking of favorability based on the big data.

4. Technical Architecture

4.1. Technical Architecture. The whole experimental system architecture takes cloud storage and cloud computing as the core and restores the virtual reality data of each furniture and components to the web page according to the original proportion, which is convenient for end users to experience the real and natural building scenes and visual effects. We combine the prepared basic components and event system to build the system architecture diagram as shown in the following figure (Figure 5).

4.2. R&D Technology. In order to realize the development of computer educational software and the construction of its application platform based on virtual simulation technology for the protection and activation design of Ming furniture, necessary computer hardware facilities and appropriate application programs must be used. At the same time, with the support of high-quality visual design, the experience quality of user experimental operation is realized.

First of all, hardware equipment is the foundation and guarantee.

Including cloud server and network requirements and conditions, the processor selects 16-core Intel processor to ensure that a large number of 3D models can rotate and scale smoothly during rendering. Compared with the conventional 16G running memory, this project adopts a higher version of 32G to ensure that the response time of users is short enough when operating and answering questions, and there will be no frame drop. The bandwidth is 100 MB downlink bandwidth, which ensures that when multiusers need to use it in teaching scenes, there will be no server jamming and slow page loading;

Running environment of equipment terminal: for users, mainly teachers and students, there may be two categories of operating systems: Microsoft Windows and MAC Os, and corresponding system adaptations have been made, respectively. In addition, considering that the user’s browser

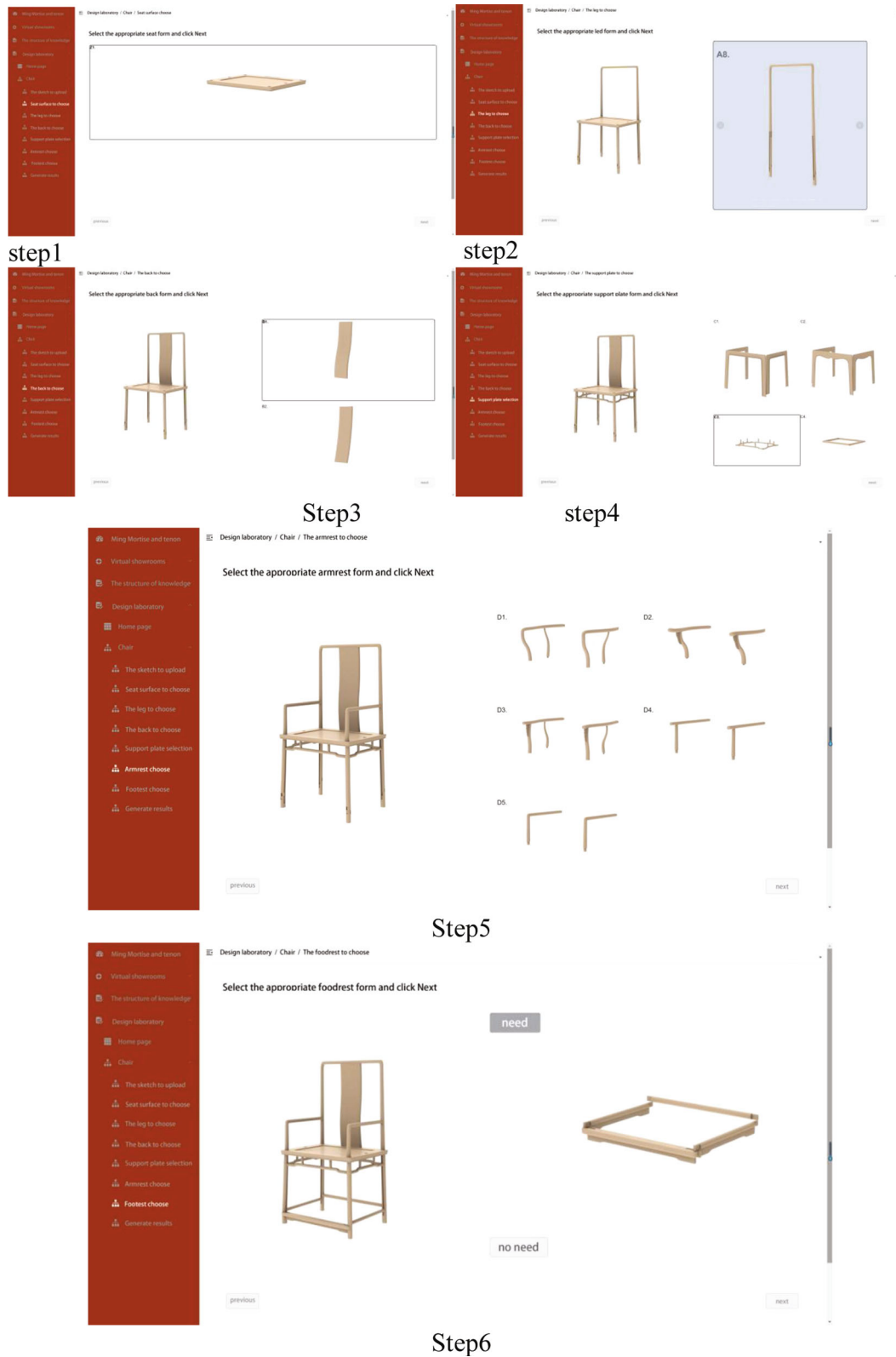


FIGURE 4: Innovative experimental plate operation step 1, step 2, step 3, step 4, step 5, and step 6.

also has inertia, the browsers such as Chrome, Firefox and 360, which are more commonly used in the market, have also been adapted to ensure the smooth running environment of the terminal.

Cloud service guarantee of experimental quality: in order to improve the efficiency of users' learning courses, some modules adopt error feedback mechanism without reducing the quality of courses, so as to help users achieve

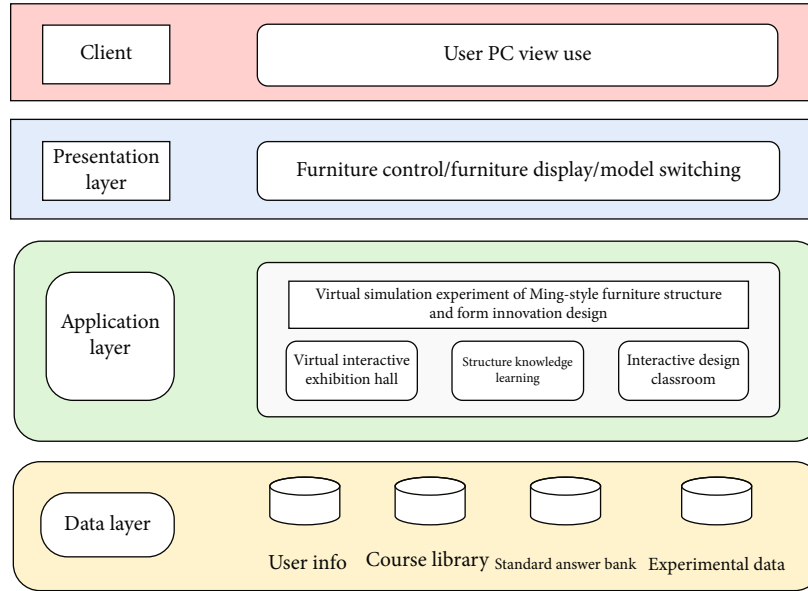


FIGURE 5: System architecture diagram and brief description.

the level of smoothly continuing the next stage of learning. In addition, the course scoring mechanism has been optimized to some extent, and scores are given according to the distribution method of each plate's weight, so as to ensure that the final generated scores can maximize the user's mastery.

4.3. Software Technology. Another part, development technology and tools are the means and quality of website content realization. The basic content and story system based on virtual reality expression on the platform should be realized by tool software. The expression of virtual reality of Ming furniture entity is the basic content and focus of this course teaching resources. It includes static model and dynamic interaction. In the planned three "story systems," specific simulation effects are given according to the experimental needs. In order to realize this current overall tool, software division of labor is as follows:

Reverse data acquisition: in order to achieve the accuracy of three-dimensional data model, we use MetraSCAN3D-BLACK 3D scanning equipment and match the best VXelements9.0 application software to carry out three-dimensional scanning to obtain the three-dimensional data of furniture solid objects. The highest scanning accuracy of the system is 0.025 mm, and the precision volume accuracy is 0.064 mm, thus realizing "absolute restoration" of basic data. Then, the model editing system of VXelements9.0 is used to optimize the data, and then it is converted into an editable general 3D software file format.

Data reconstruction: after VXelements9.0 transcoding into RHINO3D editable files, according to the original model data, the application of RHINO3D modeling software to complete the virtual model reconstruction of the entity, this link includes exterior surface reconstruction and interior structure modeling, thus completing the complete data of furniture modeling and interior structure.

Visual Rendering and Dynamic Interaction. Using the rendering function of 3D Studio Max to realize the simulation imaging of static picture, for the convenience of operation and observation in all aspects of the experiment, the effects under each story system are designed differently. Use the white mold state in the virtual exhibition hall. Use the combination of white mold and real material in the interactive link of experiment. In order to achieve the effect of "visible is obtained" in the innovation link, the real material effect is adopted.

Blender realizes the dynamic interaction of furniture materials. Furniture model material for secondary mapping, further rendering, ensures the resulting 3D model on the page rendering effect as much as possible in line with the original state. Ensure smooth loading while ensuring high resolution. In the project, the video showing the independent mortise and tenon disassembly structure and the animation showing the components in the second half are completed by rhinoceros 3D modeling software, which can realize the dynamic process of zoom-in, zoom-out, rotational disassembly, and combination of components.

Sketch Up, HTML5, achieves two-dimensional animation generation. In order to reduce the overall load of the system and accelerate the speed of page reflection, we selectively change some links into two-dimensional animation instead of excessive interaction and accelerate the experimental process.

Visual Studio aims at the construction of immersive experience of VR virtual reality. In the experimental system, we plan to design two operating environments. For online operation, relying on the network environment, online experiments can be completed only by equipped with computers and broadband equipment with performance requirements. This platform is aimed at a wide range of learners. The other is VR virtual reality immersive experience environment. Completed in the virtual simulation laboratory at

school, VR glasses are VIVE of HTC, and the equipment built in cooperation with Valve manufacturers in the world can meet the immersive experience requirements of users in all directions and truly realize “immersive” and “what you see is what you get.”

Website construction: the website construction of this place mainly includes several main tasks: applying for domain name, applying for space, analyzing website function and demand layout, and designing website style. The application software responsible for the visual design of the website learning terminal is illustrate plane software, Visual Studio Code programming software is used for website construction, and Vue is used for programming framework. Three.js is used for generation, rendering and dynamic composition and decomposition of 3D components, microservice architecture is used for website deployment, Nginx agent and Docker deployment container are used, and Final Shell is used for remote server access visualization application software.

The morphological structure of Ming furniture has systematic and diverse content characteristics; so, the specific operation involves a huge amount of data. For example, in the first phase, aiming at the model observation and experimental design of ten pieces of furniture, there are more than 3,000 static renderings, more than 100 effective two-dimensional drawings and millions of dynamic interactive codes. This experiment at this stage focuses on the understanding of the logical relationship between the form and construction of Ming furniture, and does not discuss the aesthetic form and aesthetic proportions of the local components, and therefore does not yet involve the regulation of the specific detailed parameters of the model components. As the study progresses, it can be extended to these contents in the future.

Now, it is made into the corresponding table as follows, so as to explain the classification more clearly (Table 1).

4.4. Platform Deployment. Developers first simulate user login in the test environment and carry out a series of stress tests, bug fixes, and other operations to ensure that there will be no root problems after the project goes online. For the subsequent requirements change test, an automated code deployment program is developed to ensure that the relevant requirements can be updated to the platform for users to use as soon as possible after being solved. In addition, the platform also makes relevant interface docking in the iLab experimental space, so that user data, such as operation time, operation score, step score, and other data, can be submitted to the iLab experimental platform at the same time when the final class is completed, which is convenient for teachers to view and count.

5. Innovation Points of Project Application

The virtual simulation experimental teaching of Ming-style furniture makes up for the previous problems of lack of physical teaching resources, high experimental cost, and long period. More importantly, the computer education software development and its application platform research

based on the design of Ming furniture conservation and revitalization under virtual simulation technology are original. This greatly improves the students’ learning motivation and efficiency, and the innovations are summarized as follows.

5.1. Innovation of Experimental Scheme Design Ideas. The traditional mortise and tenon intelligent system inheritance and design activation teaching construction fully embodies the principle of “combining reality with reality, complementing each other, and being real.” Adopt virtual technology, break through the traditional experimental mode and time and space barrier, connect virtual and real, and comprehensively improve learners’ interest in basic theory, innovative spirit, and participation [11].

Through the combination of virtual and real simulation, the virtual experimental operation and traditional experimental experience are combined, which transcends the skill display at the woodworking operation level and promotes the grasp and application of the Ming furniture knot concept.

In the design activation stage, the user-centered design concept can achieve the training goal of rapid design and rapid evaluation through the rapid reflection of module combination.

5.2. Innovation of Computer Intelligent Design and Application. Based on digital technology, this paper connects traditional creation with computer language. The operation mode of traditional furniture structure is realized by digital intelligent algorithm, and a set of design logic of mortise and tenon furniture structure, and form is tried to be constructed. It is an unprecedented achievement, a pioneering work in the field of traditional furniture design and manufacturing, and an important attempt of computer intelligence in the revival of traditional cultural industry.

Using 3D scanning reverse data acquisition technology and intelligent operation of computer engine, big data simulation is realized, and the design software of Ming furniture is developed. Interpreting and presenting the structural thinking and design concept of Ming furniture by means of computer information technology and transforming it into design program software can greatly reduce the design time cost and financial cost, which is conducive to large-scale popularization.

5.3. Innovation of Teaching Information Technology. The use of virtual technology expands the protection and educational resources of Ming furniture, makes the teaching and communication counseling mode of students more diversified and flexible, has enough immersive experience, enhances the sense of participation in experimental teaching, and strongly stimulates interest. Open sharing is realized through Internet technology, which effectively expands the communication and influence of Ming furniture, and better combines protection, education, activation, and innovation. The combination mechanism of production, education, and research, which connects with enterprises, institutions,

TABLE 1: Software and hardware support.

Development technology	3D simulation, 2D animation, HTML5, VR
Development tools	3D Studio Max, SketchUp, Blender, Visual Studio, Illustrate
Running environment	Server: CPU 8 cores, memory 8 GB, disk 50 GB, 8 GB video memory, GPU model GTX2060 Operating system: Windows server version: Windows 10 Database: Mysql
Experimental quality	Number of single scene model faces: one; mapping resolution: 512px × 512px; number of renderings per frame: 80 calls; action feedback time: Ms; display refresh rate: 60FPS; resolution: 1920ppi × 1080ppi
Cloud server and network requirements and conditions	The uplink and downlink bandwidth is over 50 M. through testing, when the bandwidth is over 100 M, it can have faster loading speed and better interactive experience.

and industries, enriches the depth and breadth of learning content.

5.4. Extension and Expansion of Traditional Teaching. Open sharing, school-enterprise cooperation and collaborative innovation have established a sustainable virtual experimental teaching support system. Completed the construction of network sharing platform, online simulation, experiment reservation, online guidance, and virtual environment of resource sharing and can open and share operation experiments online and offline.

6. Conclusion

Using cutting-edge scientific and technological achievements in cultural innovation can create new species projects which are different from traditional modeling design. The research of this education platform not only has the whole product intellectual innovation from culture to product, from creativity to ecology, but also constructs the bottom logic of talent training, technology management and production management that can open up the innovation industry of Ming furniture.

Even it can lead to new ideas, new technologies, and new business models. In the future research, there will be more elements interwoven, and the process will also uphold the open exploration and the integration of ideas and cutting-edge technologies. Future research will have more elements of interweaving, which is realized by docking CNC technology on the basis of virtual data, and needs to continue to deepen the benefits of artificial intelligence algorithms and cloud computing to achieve the design side and the output side of the integrated one-stop service. Through the Internet of things to achieve the interconnection of the process of precise control, always adhering to the openness of exploration and the integration of ideas and cutting-edge technology, in the future to intelligent manufacturing to reach the organic renewal of traditional culture.

Data Availability

No data were used to support this study.

Conflicts of Interest

The authors declare that there are no conflicts of interest regarding the publication of this article.

References

- [1] Y. Yao, *Ming-style furniture research*, China Construction Industry Press, 2002.
- [2] N. Noah and S. Das, "Exploring evolution of augmented and virtual reality education space in 2020 through systematic literature review," *Computer Animation and Virtual Worlds*, vol. 32, no. 3-4, p. 2021, 2020.
- [3] A. P. Murillo and A. Yoon, "a study of emerging trends in digital preservation literature: an analysis of journal articles presented in course syllabi," *Journal of Librarianship and Information Science*, vol. 53, no. 4, pp. 615–629, 2021.
- [4] S. Weiwei, L. Dejun, and L. Jiyao, "Exploration of new Chinese furniture design based on semiotics theory," *Journal of Northwest Forestry University*, vol. 6, pp. 169–173, 2013.
- [5] Y. Dehua, "Talking about the mortise and tenon of traditional Chinese furniture," *Art and Design*, vol. 34, no. 6, pp. 96–98, 2007.
- [6] W. Shixiang, *Ming-Style Furniture Research*, Sanlian Bookstore Co., Ltd, Hong Kong, 2002.
- [7] J. X. Han, M. Y. Ma, and K. Wang, "Product modeling design based on genetic algorithm and BP neural network," *Neural Computing and Applications*, vol. 33, no. 9, pp. 4111–4117, 2021.
- [8] S. al Awadhi, N. al Habib, D. al-Murad et al., "Interactive virtual reality educational application," *Advances in Science, Technology and Engineering Systems*, vol. 3, no. 4, pp. 72–82, 2018.
- [9] M. L. Alan, "Book review: KJ Varnum (ed.), Beyond reality: augmented, virtual, and mixed reality in the library," *Journal of Librarianship and Information Science*, vol. 53, no. 4, pp. 709–710, 2021.
- [10] M. Gunduz and T. Yetisir, "A design reuse technology to increase productivity through automated corporate memory system," *Neural Computing and Applications*, vol. 29, no. 9, pp. 609–617, 2018.
- [11] L. Gao, B. Wan, G. Liu, G. Xie, J. Huang, and G. Meng, "Investigating the effectiveness of virtual reality for culture learning," *International Journal of Human-Computer Interaction*, vol. 37, no. 18, pp. 1771–1781, 2021.

Research Article

Real-Time Capture of Snowboarder's Skiing Motion Using a 3D Vision Sensor

Zhipeng Li,¹ Jun Wang,² Tao Zhang,² Dave Balne,³ Bing Li,² Ruizhu Yang,² Wenli Song^{ID},² and Xingfu Zhang⁴

¹Winter Olympic College, Harbin Sports University, Harbin 150008, China

²College of Physical Education and Training, Harbin Sports University, Harbin 150008, China

³Georgia Mountain Club, Ontario, Canada

⁴Heilongjiang Institute of Technology, Harbin 150050, China

Correspondence should be addressed to Wenli Song; songwenli@hrbipe.edu.cn

Received 9 October 2021; Accepted 30 October 2021; Published 16 November 2021

Academic Editor: Alireza Souri

Copyright © 2021 Zhipeng Li et al. This is an open access article distributed under the Creative Commons Attribution License, which permits unrestricted use, distribution, and reproduction in any medium, provided the original work is properly cited.

Due to the influence of environmental interference and too fast speed, there are some problems in ski motion capture, such as inaccurate motion capture, motion delay, and motion loss, resulting in the inconsistency between the actual motion of later athletes and the motion of virtual characters. To solve the above problems, a real-time skiing motion capture method of snowboarders based on a 3D vision sensor is proposed. This method combines the Time of Flight (TOF) camera and high-speed vision sensor to form a motion acquisition system. The collected motion images are fused to form a complete motion image, and the pose is solved. The pose data is bound with the constructed virtual character model to drive the virtual model to synchronously complete the snowboarding motion and realize the real-time capture of skiing motion. The results show that the motion accuracy of the system is as high as 98.6%, which improves the capture effect, and the motion matching proportion is better and more practical. It is also excellent in the investigation of motion delay and motion loss.

1. Introduction

Snowboarding is an intense sport, which is mainly carried out in winter, and it is one of the necessary events of the Winter Olympic Games [1]. The sport is exciting, cool, and dangerous, and the training requirements are rather high.

Physical quality consists of technology, psychology, tactics, and other factors. In recent years, the development of physical fitness training in China has made great progress than before. In theory, we no longer blindly follow the traditional training mode of “three importance and one greatness,” and the training means and methods are constantly innovated. However, China's physical training development is still in the stage of catching up and learning, and there is still a big gap with foreign countries. In foreign countries, physical training pays more attention to the comprehensive and balanced develop-

ment of physical elements and puts forward many powerful concepts of physical training. Functional physical training is a popular training concept in recent years, but due to the lack of theoretical knowledge of functional physical training in China, we still lack a comprehensive and systematic understanding. This study collects a large number of the latest relevant literature and foreign literature, summarizes, arranges, and applies them to cross-country skiing physical training, so as to make a certain contribution to improving the competitive ability of cross-country skiing teams. Motion capture, also known as motion tracking, collects athletes' motion data in real time and then uses these data to drive virtual character simulation to display athletes' motions [2]. In the skiing motion training of professional athletes, motion capture is very important. It can be used to observe athletes' moving posture in real time, which is of great practical significance to correct wrong

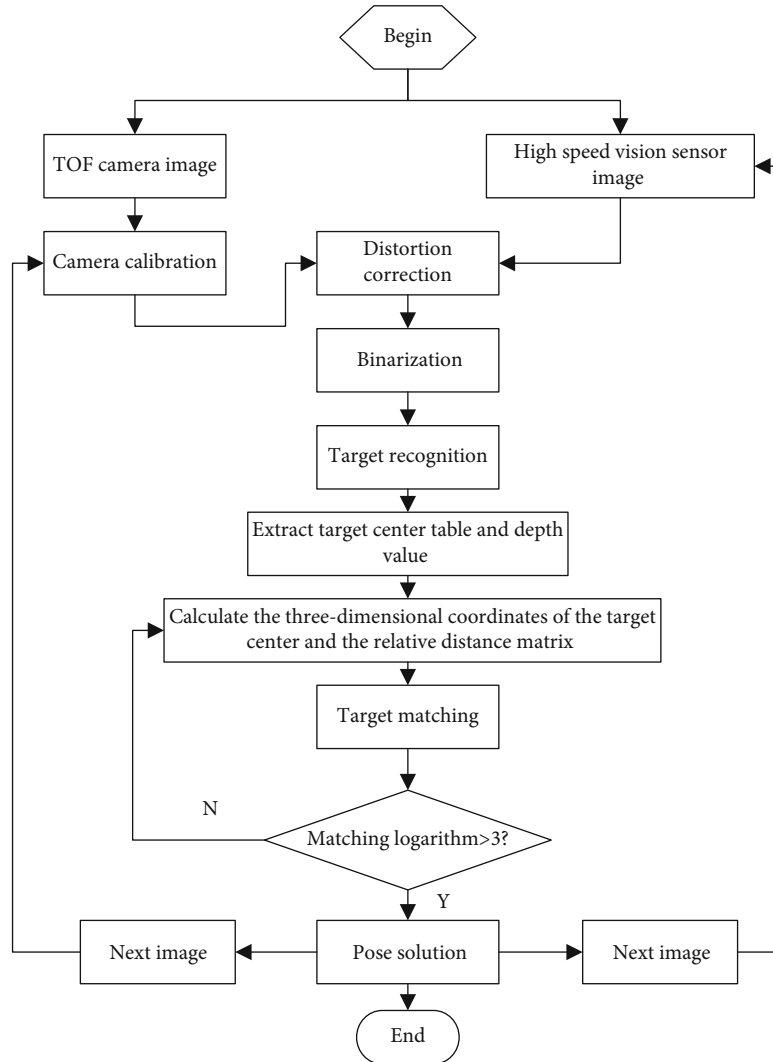


FIGURE 1: Pose solution process.

motions and improve athletes' skill level. At present, the accuracy of the motion capture system used by Chinese athletes in skiing training is not high. Because the skiing motion is too fast and difficult, it is easy to miss capture. If there is no more professional system to capture the motion of skiers for a long time, the coach will not be able to correct their mistakes in the skiing process in time, which will seriously affect the training speed of skiers [3]. To solve the above problems, a more suitable method for skiing motion capture is proposed, that is, snowboarding athletes' skiing motion real-time capture based on a 3D vision sensor. 3D display technology is a new technology with rapid development in recent years. At present, it is widely used in animation production. Compared with the 2D presentation effect, 3D display technology can present the picture more realistically and make people feel immersive. 3D vision sensor is the main device to realize 3D technology. Based on the original system, 3D technology is applied to this study in order to provide effective help for ski training.

The main contributions of this paper are as follows:

- (1) Reduce missed capture and improve the accuracy of the system in capturing motion
- (2) The application of a 3D vision sensor in real-time capture of snowboarding athletes' skiing motion improves the performance of motion capture, which is convenient to capture feature points and better simulate motion
- (3) Different datasets are used to simulate the skiing motion real-time capture system in this paper, and the feasibility of the system is tested

2. Related Work

Based on the above background, motion capture technology has been widely used in various sports professional training. For example, in literature [4], Wang et al. established a multi-view camera system to capture moving human body images from multiple views in real time, then estimated human body

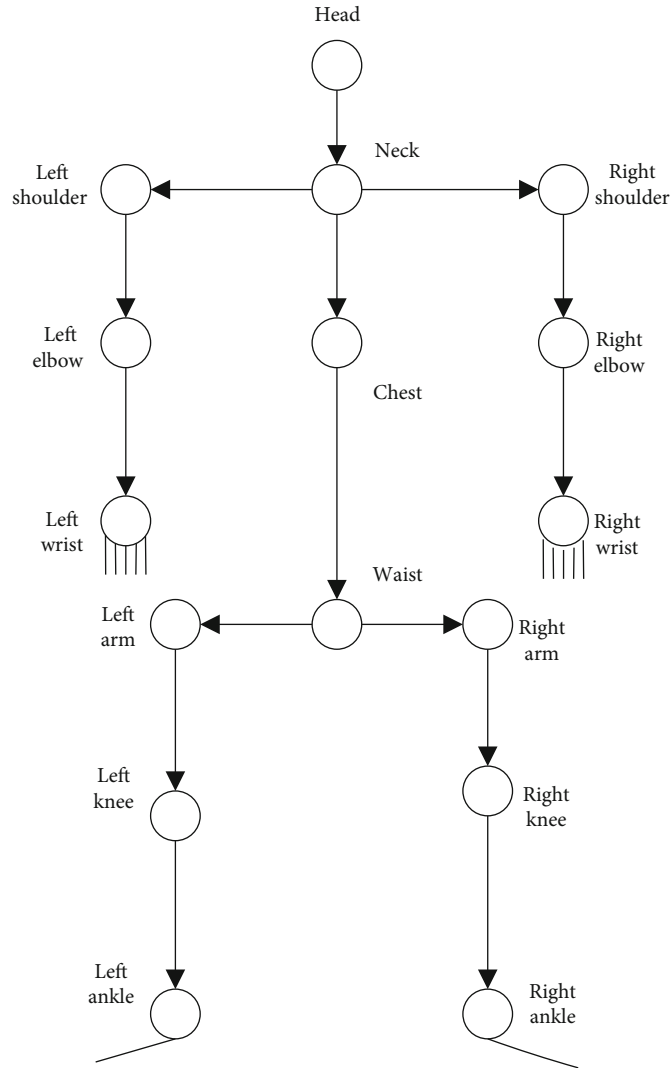


FIGURE 2: Human skeleton model.

TABLE 1: Training parameters of snowboarder's skiing motion.

Parameters	Value (or running state)
Number of input images	20000 sample images
Iterations	800
Optimizer	Random gradient descent
Initial value of weight correction	0.01

3D key points from multiview images using the OpenPose method, reconstructed dense 3D point clouds from the images, and finally fitted the SMPL model to 3D key points and 3D point clouds to represent human motion. However, the motion of this method is too complex. In literature [5], Guo and Song proposed a hand running direction capture method based on soft sensing. This method uses HTC Vive equipment to capture human hand motion and then combines the double-layer LSTM to estimate the hand motion and

clarify the hand motion characteristics. However, the matching proportion of this method is low. In literature [6], Yu et al. proposed a human motion capture method based on a single RGB-D sensor. This method realizes motion tracking refinement at the body part level through semantic tracking loss calculation, which can improve the tracking accuracy in the case of severe occlusion and fast motion. However, the motion accuracy of this method is low. In literature [7], Maruyama et al. proposed a MoCap capture method based on an inertial measurement unit. This method does not need any optical equipment and can measure the motion attitude even in the outdoor environment. However, the motion delay of this method is too long. Literature [1] proposed to use a series of precise physiological and biochemical instruments to detect the physical function of athletes, so as to master the law of the change of athletes' mechanical energy in sports training, scientifically organize and arrange the training and practical activities of snowboarding skills on veneer U-shaped venues, and reasonably guide athletes' diet. This can effectively prevent sports injury, prolong sports life, and improve sports ability. However,

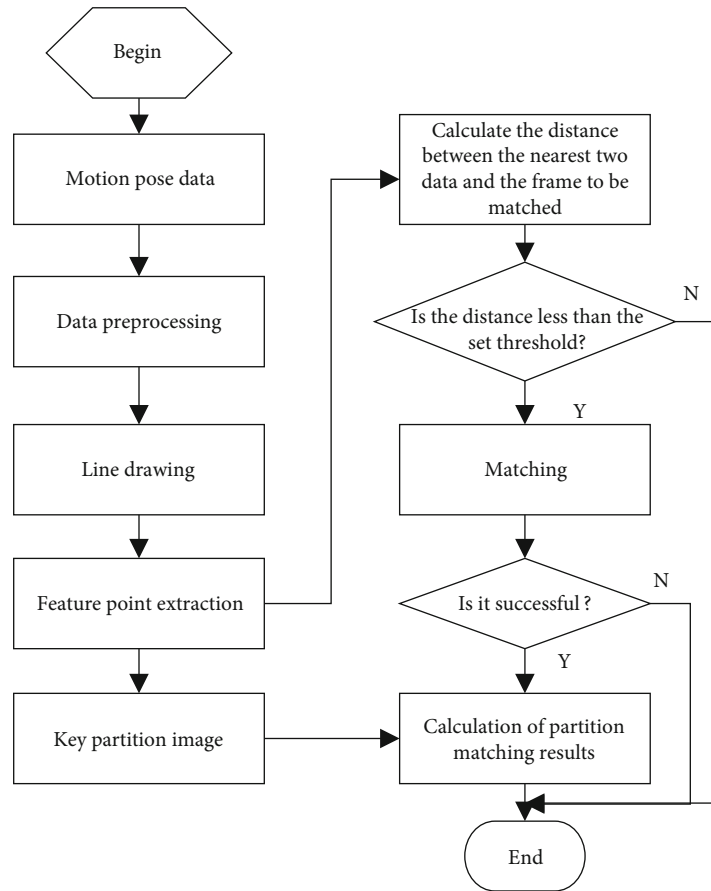


FIGURE 3: Comparison method of skiing motion details.

due to the loss of motion in this method, it is impossible to accurately capture snowboarding athletes' skiing motion.

Compared with the above systems, this paper uses a TOF camera and high-speed vision sensor as a motion acquisition system. This can greatly improve the accuracy of system motion simulation, and it is less affected by environmental interference. It can be applied to motion capture in various environments and has a good application prospect.

3. Real-Time Capture of Snowboarding Motion Using a 3D Vision Sensor

Snowboarding is dangerous, and motion learning is difficult. Ordinary people generally need several months to ensure that they can slide alone. However, for professional athletes with competition pressure, optical gliding is not enough. They also need continuous training to achieve excellent results in the formal competition. The training intensity of professional athletes is much higher than that of ordinary people, especially for the control of some details of motion. In order to assist the training of skiers, a real-time snowboarding capture method based on a 3D vision sensor is proposed in this study. This method mainly solves the following three problems:

(1) Interference by ambient light

(2) The motion speed is too fast to capture

(3) The athlete's actual motion cannot be consistent with the virtual character model motion

The first two problems are the main reasons for the last problem. Therefore, the latter problem can be solved by solving the first two problems and finally improved the accuracy of motion capture. This study is divided into three parts: snowboarding motion data acquisition, pose solution, and virtual character model establishment and driving. Specific analysis is made for these three parts.

3.1. Snowboarding Motion Image Acquisition. In order to solve the influence of ambient light interference and motion speed on motion capture, this design uses two kinds of 3D vision sensors to form an acquisition system to improve the comprehensiveness and integrity of motion data acquisition [8–10]. One of the two sensors is a TOF camera with less interference from ambient light, and the other is a high-speed vision sensor, which can be used to capture fast-moving targets. Through the combination of the two sensors, the problem of data loss in motion capture is reduced.

3.1.1. TOF Depth Camera. TOF depth camera collects reflected light to build depth mapped images. The distance from the camera to the object can be calculated according to time and

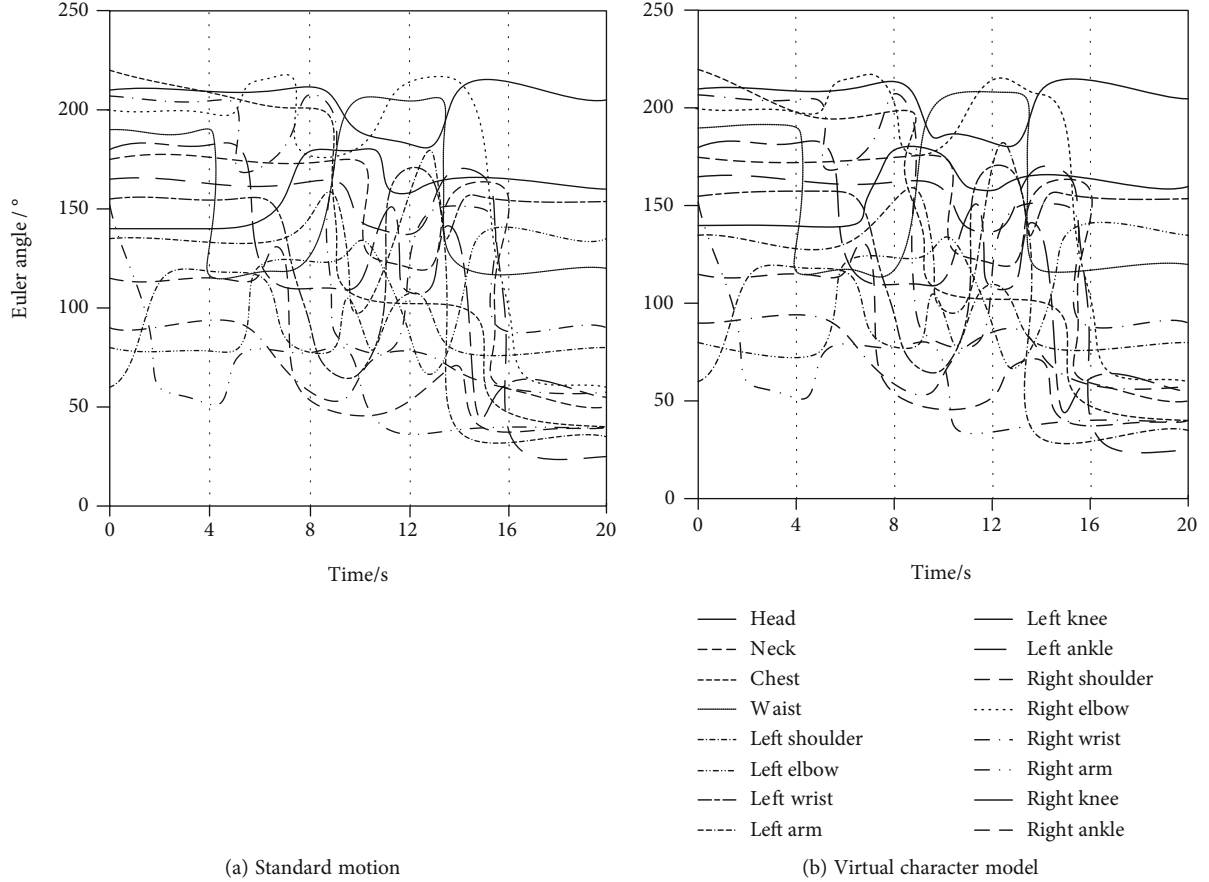


FIGURE 4: Line image segmentation results.

the speed of light. Formula (1) is as follows:

$$D = \frac{c \cdot \Delta t}{2}, \quad (1)$$

where D refers to the distance and Δt refers to the time for the pulse signal to travel from the camera and the target and then return [11].

3.1.2. High-Speed Vision Sensor. Compared with ordinary sensors, high-speed vision sensors adopt stacked structure and back-illuminated pixel array to improve their parallel processing ability [12, 13]. According to relevant research, the speed of detecting and tracking targets by high-speed vision sensor can reach 1000 frames per second. In this paper, a high-speed vision sensor is used to collect the data of dynamic target in real time, so as to reduce the missed acquisition probability of motion.

After the snowboarding athletes' skiing motion images are collected by the two 3D vision sensors, image fusion is required to integrate the two images. The fusion process is as follows:

Step 1. Multiscale transformation.

The motion images of two kinds of source snowboarding are decomposed by wavelet transform, and two kinds of

coefficients are obtained, namely, high-frequency coefficients and low-frequency coefficients.

(1) Edge feature

Step 2. Feature extraction.

The Canny operator is used to analyze the low-frequency coefficients of motion images of two kinds of source snowboarding $Y_{j,A}$ (low-frequency coefficient of TOF depth image) and $Y_{j,B}$ (low-frequency coefficient of high-speed vision sensor image) for the extraction of edge features and then construct binary edge feature $Z_{j,A}$ and $Z_{j,B}$ [14]. The construction formula is as follows:

$$\begin{aligned} Z_{j,A} &= \text{XOR}(Y_{j,A}, Y_{j,B}) \text{AND} Y_{j,A}, \\ Z_{j,B} &= \text{XOR}(Y_{j,A}, Y_{j,B}) \text{AND} Y_{j,B}, \end{aligned} \quad (2)$$

where XOR refers to the XOR operation symbol, $\text{XOR}(Y_{j,A}, Y_{j,B})$ means to calculate the low-frequency coefficients of TOF depth image and high-speed vision sensor image, and AND means the calculation symbol.

(2) Gradient feature

TABLE 2: Comparison results of key points in motion.

Category	Method	Standard motion	The proposed method	Literature [4] method	Literature [5] method	Literature [6] method	Literature [7] method	Literature [1] method
Motion complexity	One segment	58	58	56	55	55	56	54
	Second segment	125	126	120	122	120	124	120
	Third segment	256	250	236	237	233	235	237
	Fourth segment	240	238	230	224	220	227	224
	Fifth segment	105	103	100	101	100	98	96
Matching proportion	One segment	58	0.958	0.856	0.847	0.910	0.877	0.798
	Second segment	125	0.992	0.874	0.872	0.902	0.869	0.850
	Third segment	256	0.925	0.885	0.865	0.878	0.892	0.882
	Fourth segment	240	0.972	0.902	0.877	0.893	0.874	0.865
	Fifth segment	105	0.921	0.888	0.886	0.873	0.882	0.872
Motion accuracy (%)	One segment	100	98	90	89	87	85	86
	Second segment	100	98	95	90	86	87	90
	Third segment	100	99	93	91	85	85	82
	Fourth segment	100	99	96	93	90	97	97
	Fifth segment	10	99	95	96	91	90	85
Motion delay rate (ms)	One segment	0	15	50	60	40	30	20
	Second segment	0	14	45	60	44	35	21
	Third segment	0	12	48	58	43	28	28
	Fourth segment	0	15	49	57	40	29	29
	Fifth segment	0	13	52	55	39	26	25
Motion loss rate	One segment	Unclear	Unclear	Clear	Clear	Clear	Unclear	Clear
	Second segment	Unclear	Unclear	Clear	Clear	Clear	Clear	Unclear
	Third segment	Unclear	Unclear	Unclear	Unclear	Clear	Clear	Clear
	Fourth segment	Unclear	Unclear	Unclear	Clear	Clear	Clear	Unclear
	Fifth segment	Unclear	Unclear	Clear	Unclear	Clear	Unclear	Clear

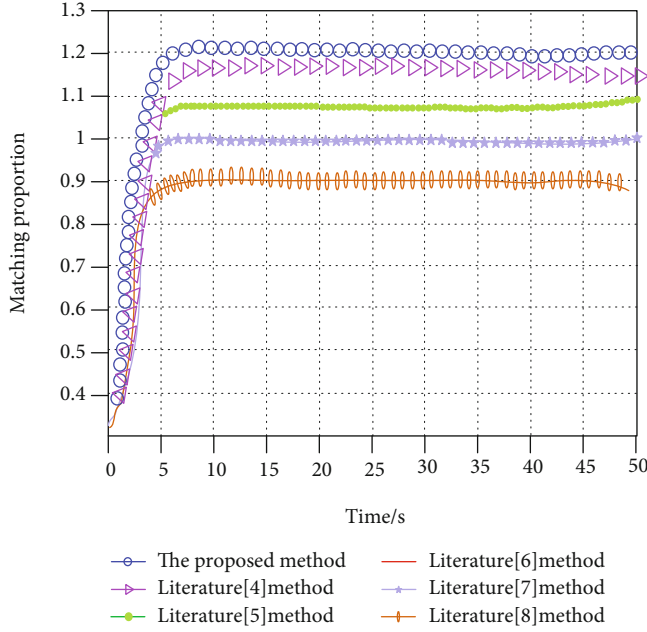


FIGURE 5: Comparison of matching proportion of skiing motion.

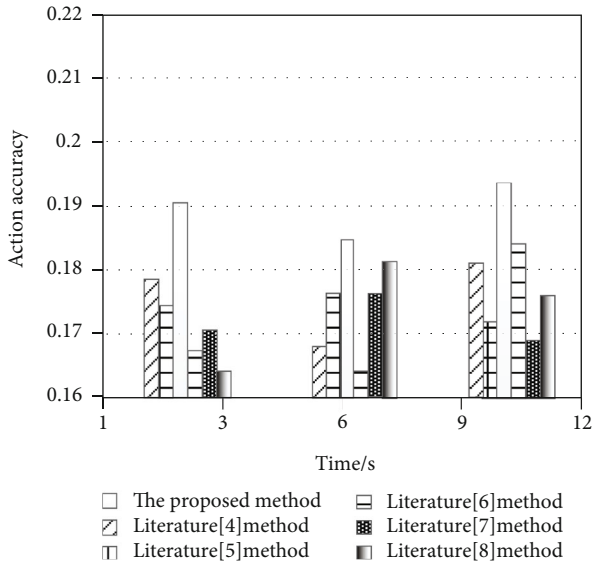


FIGURE 6: Comparison of skiing motion accuracy.

The gradient feature extraction formula [15] is as follows:

$$S(i, j) = \frac{\sum_{i=1}^X \sum_{j=1}^Y \sqrt{(\Delta f_x^2(i, j)^2 + \Delta f_y^2(i, j)^2) / 2}}{X \cdot Y}, \quad (3)$$

where $S(i, j)$ refers to the average gradient of the pixel at the low-frequency coefficient of (i, j) , $\Delta f_x(i, j)$ and $\Delta f_y(i, j)$ are the difference of the image at the regional window's central pixel (i, j) at direction x and y , and X means the number of pixels within the regional window at the direction x and y .

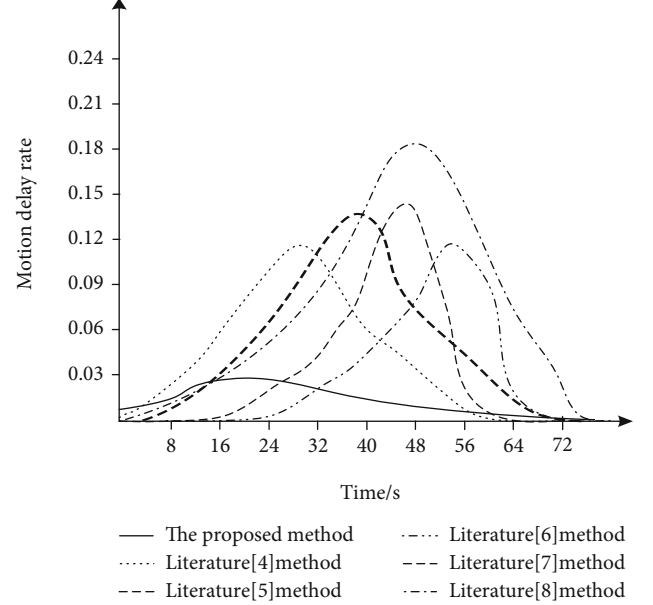


FIGURE 7: Comparison of skiing motion delay rate.

(3) Extraction of signal intensity feature

For the high-frequency coefficients after image decomposition, the signal intensity features are extracted. The extraction formula is as follows:

$$R_{AB} = \frac{G_{j,A}}{G_{j,B}}, \quad (4)$$

where R_{AB} means the intensity ratio of correlation signal, $G_{j,A}$ means signal intensity in TOF depth image area window, and $G_{j,B}$ means signal intensity in image region window of a high-speed vision sensor.

Step 3. Feature integration.

According to the above features, the fusion is carried out, and the fusion formula is as follows:

$$H_{AB}(i, j) = Z_{j,A} \cdot S_{j,A}(i, j) \cdot R_{AB} + Z_{j,B} \cdot S_{j,B}(i, j) \cdot R_{AB}, \quad (5)$$

where $H_{AB}(i, j)$ means the integrated feature of the two kinds of images, $S_{j,A}(i, j)$ means the gradient feature of the TOF depth image, and $S_{j,B}(i, j)$ means the gradient feature of the high-speed visual sensor image [16].

Step 4. Multiscale inverse transform.

The fused high- and low-frequency coefficients are transformed by wavelet multiscale inverse transform to obtain the fused athlete motion image.

3.2. Snowboarding Motion Pose Solution. Based on the fused image, the pose is solved. The solution process is shown in Figure 1. Attitude solution is based on Euler angle.

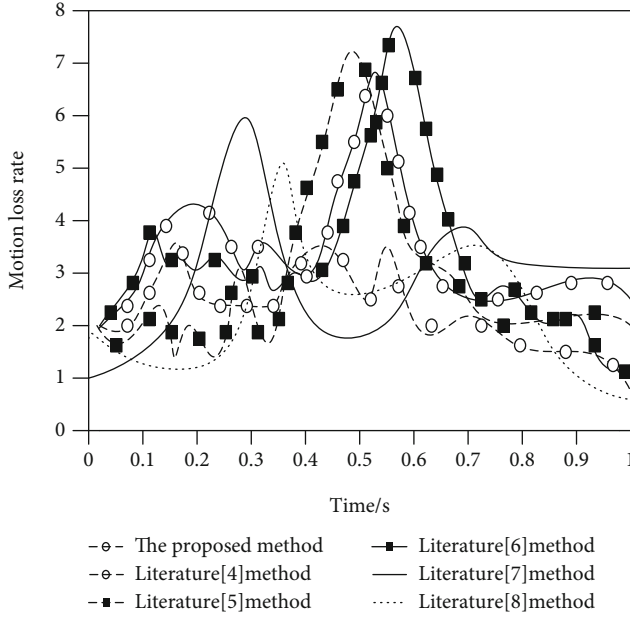


FIGURE 8: Comparison of skiing motion loss rate.

According to Figure 1. The TOF camera image calibrated by the camera and the high-speed vision sensor image are first input into the distortion correction module for image correction, then the image is binarized, the gray value of image pixels is set, and the image with black-and-white effect is obtained. The image data is transmitted to the target recognition module to recognize it, extract the most table and depth value of the target center, then calculate the three-dimensional coordinates and relative distance matrix of the image target center, and finally enter the target matching. When the matching logarithm is greater than 3, the position can be solved. If it is less than 3, the three-dimensional coordinates and relative distance matrix of the image center need to be recalculated. After the image pose is solved, the next image can be solved. Pose solution is the key and core. Pose solution is to calculate the pose data of the target [17, 18]. Suppose the same point f is defined as f in the 3D coordinate of the object coordinate system Oc-XcYcZc, and the 3D coordinate in the camera coordinate system Oo-XoYoZo is defined as g

$$f = Rg + V, \quad (6)$$

where R represents the rotation matrix and V represents the translation matrix.

It is transformed into the following form and then optimized to solve the rotation matrix and translation matrix.

$$f' = \sum_{i=1}^n w_i \|(Rf_i + V) - g_i\|^2, \quad (7)$$

where f' is the optimized solution, f_i is the coordinate value of the target i in Oc-XcYcZc, g_i is the coordinate value of the same target i in Oo-XoYoZo, and w_i is the weight of the target i in calculation [19].

Then calculate

$$\begin{aligned} f &= \frac{\sum_{i=1}^n w_i f_i}{\sum_{i=1}^n w_i}, \\ g &= \frac{\sum_{i=1}^n w_i g_i}{\sum_{i=1}^n w_i}, \end{aligned} \quad (8)$$

where f is the weight center of the target in Oc-XcYcZc, g is the weight center of the target in Oo-XoYoZo, w_i is the weight of target i in calculation, f_i is the coordinate value of the target i in Oc-XcYcZc, g_i is the coordinate value of the same target i in Oo-XoYoZo, i is the initial value of the summation calculation, $i = 1$, and n is the end value of the summation calculation.

Find the center vector of the target in two coordinate systems.

$$\begin{aligned} \alpha_i &= f_i - f, \\ \beta_i &= g_i - g, \end{aligned} \quad (9)$$

where $i = 1, 2, \dots, n$, α_i and β_i are the central vector of the target in Oc-XcYcZc and Oo-XoYoZo, f_i is the coordinate value of the target i in Oc-XcYcZc, f is the weight center of the target in Oc-XcYcZc, g_i is the coordinate value of the same target i in Oo-XoYoZo, and g is the weight center of the target in Oo-XoYoZo.

This forms the center vector matrix $\alpha = (\alpha_1, \alpha_2, \dots, \alpha_n)$ and $\beta = (\beta_1, \beta_2, \dots, \beta_n)$. This calculates the scale factor S . The calculation formula is as follows:

$$S = \alpha W \beta^T, \quad (10)$$

where W is the diagonal matrix composed of w_i and T is the transpose symbol. Decompose the S matrix and then get the rotation matrix R and the translation matrix V .

$$\begin{aligned} R &= xy^T \cdot \det(xy^T), \\ V &= \bar{g} - R\bar{f}, \end{aligned} \quad (11)$$

where (x, y) refers to the pixel coordinate, g refers to the weight center of the target in Oo-XoYoZo, f refers to the weight center of the target in Oc-XcYcZc, R is the rotation matrix, V is the translation matrix, xy^T is the rotation matrix of the pixel coordinate (x, y) , and $\det(xy^T)$ is the determinant of the transposed matrix of the pixel coordinate (x, y) .

Finally, the rotation matrix R is transformed into Euler angle form to obtain snowboarding motion data.

3.3. Establishment and Driving of the Virtual Character Model. The establishment of the virtual human model is to establish a moving three-dimensional human model. On this basis, combined with the calculated snowboarding motion data, the synchronous driving of virtual character motion can be realized. The specific process is divided into the following three steps:

Step 1. Establish a human skeleton model. Human movement is mainly driven by bones. The human skeleton structure can be simplified into 16 main bones, and all movement postures can be reflected on these 16 bones, as shown in Figure 2.

Step 2. Skin the bones. In order to ensure the fidelity of the established athlete virtual model, a layer of human-like skin is covered outside the skeleton to improve the three-dimensional of the model.

Step 3. Fit the snowboarding motion data obtained in the previous chapter with the manikin.

Step 4. Judge whether the fitting curve is close to the motion trajectory. If it is close, the output bone changes continuously; otherwise, refit.

Step 5. Drive the virtual model to complete a series of skiing motions.

4. Experimental Analysis and Results

4.1. Experimental Environment and Dataset. PKU MMD is a large long sequence multimodal and multiview dataset released in 2017. The images in the dataset have the characteristics of multiview, including 1076 untrimmed long sequence albums and 20000 trimmed samples; miniImageNet is a subset of ImageNet dataset, which contains more than 100 categories; each category contains 600 pictures. At present, it is widely used in small sample simulation experiments. In this paper, PKU MMD and miniImageNet datasets are selected as the datasets. The training parameters of snowboarder's skiing motion are shown in Table 1.

There are many snowboarding motions, among which the air grabbing is the most typical one. Athletes need to complete technical movements such as turning and somersault with a veneer. This technology has a large range of motion, has high requirements for the mastery of athletes' skill level, and is also one of the necessary items for athletes' training. Based on this, taking the skiing movement as the research object, the motion sequence images are collected by the visual acquisition system, the acquisition frequency is 0.20 frames/s, a total of 100 sequence images are collected, and the time is 20 s.

The TOF camera in the vision acquisition system is the Intel RealSense l515 radar TOF camera depth realistic camera, which can be used under various indoor and outdoor lighting conditions, and the image resolution can reach 1280×720 30 fps, the maximum working range is 0.4~20 m, and the accuracy error is less than 2.7%. At the same time, it is equipped with IMU to realize the automatic monitoring of the moving route of the object. The high-speed vision sensor is imx382, which can detect and track the moving target at the speed of 1000 frames per second, so as to avoid the problem of missing image information due to the moving speed of the target during image capture. The algorithm is used for motion detail comparison, and the process is shown in Figure 3.

The pose solution results are given to the established athlete virtual model to drive the model to move synchronously, and then, the consistency between the athlete's actual motion and the virtual character model motion is compared.

Using the above research method, a series of motion poses in snowboarding are calculated, and the Euler angles of each bone node are obtained, and then, the line diagram is shown in Figure 4.

The standard motion line image in Figure 4 and the motion line image presented by the virtual character model are segmented at equal time intervals and then analyzed according to the experimental indicators.

4.2. Experimental Indicators. There are two main evaluation indexes for skiing motion comparison, and the consistency of motion capture is comprehensively analyzed from these two indexes. These two items are analyzed in detail in the following:

(1) Motion complexity

The more feature points, the more complex the motion is. By comparing the key points between the virtual character model and the standard motion, the execution results of the two groups of skiing motions are judged.

$$X = M_v - C_N(r), \quad (12)$$

where M_v represents the accuracy of motion extraction and $C_N(r)$ represents the accuracy of motion extraction.

(2) Matching proportion

Matching proportion refers to the ratio between the matching results of two groups of motion key points and the number of standard motion features. The greater the ratio, the higher the matching degree.

(3) Motion accuracy: obtain motion accuracy by comparing the number of frames

(4) Motion delay rate: obtain the motion delay of each system by comparing video animation

(5) Motion loss rate: obtain the loss of motion execution by comparing each image

4.3. Results and Discussion. In order to verify the effectiveness of snowboarding athletes' skiing motion real-time capture based on a 3D vision sensor, experimental analysis was carried out. Under the same test conditions, carry out motion capture according to the four methods given in literature [4] to literature [1], and then carry out fine motion comparison, and compare the comparison results with the studied methods. It is shown in Table 2.

According to Table 2, compared with the other five methods, the difference between the key points of 100 frame standard motion sequence images and 100 frame virtual character motion sequence images is the smallest, and the matching proportion with the standard motion sequence image is larger. This shows that the skiing motion displayed by the

virtual character is more consistent with the standard motion, which proves that the motion capture data collected by the research method in this paper is more comprehensive. In addition, from the segmentation results, the error mainly occurs in the third and fourth segments. The motion of these two segments is the most complex. During image acquisition, it is easy to miss the acquisition of image information or collect in advance and delay, resulting in deviation from the standard motion. Finally, the presentation of the virtual model is not completely consistent with the standard motion. Compared with other methods, the accuracy of this method is as high as 98.6%, which is much higher than other systems, and its motion delay and loss are also better than other systems. The system studied in this paper has a better capture effect.

According to Figure 5, the motion matching ratio of literature [4] method is 1.15, the motion matching ratio of literature [5] method is 1.1, the feature extraction stability of literature [6] method is 1.05, the motion matching ratio of literature [7] method is 1, the motion matching ratio of literature [1] method is 0.9, and the motion matching ratio of the method in this paper is 1.2. Therefore, the snowboarding motion matching proportion using the method in this paper is better and more practical.

According to Figure 6, the motion accuracy of literature [4] method is 0.183, the motion accuracy of literature [5] method is 0.178, the motion accuracy of literature [6] method is 0.186, the motion accuracy of literature [7] method is 0.176, the motion accuracy of literature [1] method is 0.186, and the motion accuracy of the method in this paper is 0.195. It can be seen that the snowboarding motion using the method in this paper has high accuracy and improves the capture effect.

According to Figure 7, the motion delay rate of literature [4] method is 0.12, the motion delay rate of literature [5] method is 0.15, the motion delay rate of literature [6] method is 0.10, the motion delay rate of literature [7] method is 0.13, the motion delay rate of literature [1] method is 0.18, and the motion delay rate of the method in this paper is 0.03. Therefore, the snowboarding motion delay rate using the method in this paper is lower.

According to Figure 8, the motion loss rate of literature [4] method is 6.8, the motion loss rate of literature [5] method is 7.2, the motion loss rate of literature [6] method is 7.8, the motion loss rate of literature [7] method is 6, the motion loss rate of literature [1] method is 5.2, and the motion loss rate of the method in this paper is 3.4. Therefore, the snowboarding motion loss rate using the method in this paper is low, and the motion capture is more accurate.

5. Conclusions

Skiing is a standard event in the Winter Olympics. Because its motion is cool and thrilling, skiing attracts many young people to participate. Compared with other sports, skiing is much more difficult and requires higher precision of athletes' motion during training. Therefore, in order to better assist athletes to complete training, this paper studies the real-time capture method of snowboarding athletes' skiing motion based on a 3D vision sensor. By combining two kinds of 3D vision sensors, this study makes up for the prob-

lem of information loss during image acquisition of the existing system and improves the accuracy of motion real-time capture. In the test process, the accuracy of the system studied in this paper can reach more than 98.6%, which is much higher than other systems and is better than other systems in motion accuracy, motion delay, and loss. However, this study still needs to be improved. The motion capture test only takes a skiing motion as the test object, and the results have certain limitations, which need to be further analyzed and discussed.

Data Availability

In this study, we used PKU MMD and miniImageNet datasets for experiments. These two datasets are public which have been deposited in the PKU MMD and miniImageNet dataset website.

Conflicts of Interest

The authors declare that there is no conflict of interest with any financial organizations regarding the material reported in this manuscript.

Acknowledgments

This work is supported by the key research and development plan of the Ministry of Science and Technology of the Science and Technology Winter Olympics key special targeted projects (2018YFF0300506), General Project of the China University Sports Association (202013508), Heilongjiang Province Higher Education Teaching Reform Key Project (SJGZ20190033), and Harbin Institute of Physical Education Subject Leader Project (XKL04).

References

- [1] Z. Haifeng, Z. Can, L. Meixiao, S. Cuirong, and LP. Yin, "Analysis of motion ability of hip joint in various degrees of freedom based on motion capture technology," *China Tissue Engineering Research*, vol. 25, no. 12, pp. 1815–1819, 2021.
- [2] L. Qingqing and Y. Yuxiu, "Research on the protective performance of basketball knee pads based on three-dimensional motion capture," *Modern Textile Technology*, vol. 27, no. 2, pp. 53–58, 2019.
- [3] Z. Xia, J. Xing, C. Wang, and X. Li, "Gesture recognition algorithm of human motion target based on deep neural network," *Mobile Information Systems*, vol. 2021, Article ID 2621691, 12 pages, 2021.
- [4] Y. Wang, F. Xu, C. M. Pun et al., "New multi-view human motion capture framework," *IET Image Processing*, vol. 14, no. 12, pp. 2668–2674, 2020.
- [5] H. Guo and Y. Sung, "Movement estimation using soft sensors based on bi-LSTM and two-layer LSTM for human motion capture," *Sensors*, vol. 20, no. 6, p. 1801, 2020.
- [6] T. Yu, J. Zhao, Y. Huang, Y. Li, and Y. Liu, "Towards robust and accurate single-view fast human motion capture," *IEEE Access*, vol. 7, no. 99, pp. 85548–85559, 2019.
- [7] T. Maruyama, M. Tada, and H. Toda, "Riding motion capture system using inertial measurement units with contact

- constraints,” *International Journal of Automation Technology*, vol. 13, no. 4, pp. 506–516, 2019.
- [8] Z. Haifeng, Z. Can, L. Meixiao, S. Cuirong, and P. Yin, “Analysis of various degrees of freedom of the hip movement based on motion capture technology,” *Chinese Journal of Tissue Engineering Research*, vol. 25, no. 12, pp. 1815–1819, 2021.
- [9] D. Yan, Z. Deng, and Y. Zhang, “An attitude determination algorithm based on MEMS inertial and magnetic measurement unit,” *Acta Armamentarii*, vol. 40, no. 12, pp. 2447–2456, 2019.
- [10] X. Liu and X. Sun, “Application of Vicon motion capture in the design of linear motion feature tracking algorithm for sequence images,” *Bulletin of Science and Technology*, vol. 36, no. 10, pp. 28–32, 2020.
- [11] W. Xia and S. Zhang, “Design of motion capture system based on inertial sensor,” *Computer Measurement and Control*, vol. 27, no. 9, pp. 283–287, 2019.
- [12] W. Chen, “Research on motion capture technology in dance posture analysis and teaching,” *Microcomputer Application*, vol. 36, no. 3, pp. 102–105, 2020.
- [13] Y. Morimoto, “High-speed measurement of shape and vibration: whole-field systems for motion capture and vibration modal analysis by OPPA method,” *Sensors*, vol. 20, no. 15, p. 4263, 2020.
- [14] D. Huang, C. Yang, Z. Ju, and S. L. Dai, “Disturbance observer enhanced variable gain controller for robot teleoperation with motion capture using wearable armbands,” *Autonomous Robots*, vol. 44, no. 7, pp. 1217–1231, 2020.
- [15] G. Giarmatzis, E. I. Zacharaki, and K. Moustakas, “Real-time prediction of joint forces by motion capture and machine learning,” *Sensors*, vol. 20, no. 23, p. 6933, 2020.
- [16] L. González, J. C. Álvarez, A. M. López, and D. Álvarez, “Met-
rological evaluation of human–robot collaborative environments based on optical motion capture systems,” *Sensors*, vol. 21, no. 11, article 3748, 2021.
- [17] J. M. Konrath, A. Karatsidis, H. M. Schepers, G. Bellusci, M. de Zee, and M. Andersen, “Estimation of the knee adduction moment and joint contact force during daily living activities using inertial motion capture,” *Sensors*, vol. 19, no. 7, p. 1681, 2019.
- [18] L. Liu, Y. Liu, and J. Zhang, “Learning-based hand motion capture and understanding in assembly process,” *IEEE Transactions on Industrial Electronics*, vol. 66, no. 12, pp. 9703–9712, 2019.
- [19] L. Tong, R. Liu, and L. Peng, “LSTM-based lower limbs motion reconstruction using low-dimensional input of inertial motion capture system,” *IEEE Sensors Journal*, vol. 20, no. 7, pp. 3667–3677, 2020.